

Cover Picture

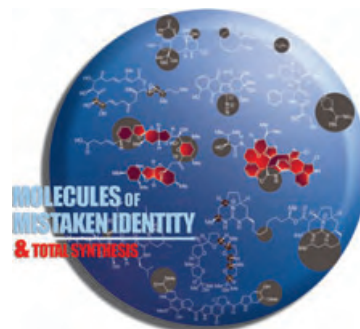
**Oliver M. T. Pearce, Kerry D. Fisher, Julia Humphries,
Leonard W. Seymour,* Alberto Smith, and Benjamin G. Davis***

Sugar-specific mechanisms of cell transfection can be created by the controlled glycosylation of the surfaces of adenoviruses, which have an icosahedral structure, as depicted in the cover picture. In their Communication on page 1057 ff., L. W. Seymour, B. Davis, and co-workers describe how derivatives of adenoviruses with galactose or mannose selectively transfect human macrophages rather than the standard human endothelia and how this dramatic retargeting holds promise for gene therapy.



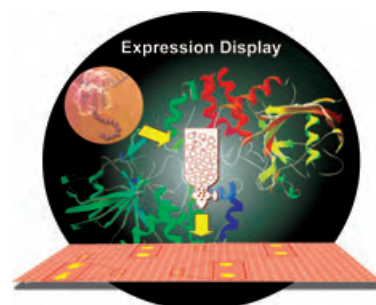
Natural Products Synthesis

To err is human! Even with modern analytical methods mistakes can be made in the structural elucidation of natural products. K. C. Nicolaou and S. A. Snyder show how chemical synthesis can help to solve these molecular puzzles in their Review on page 1013 ff.



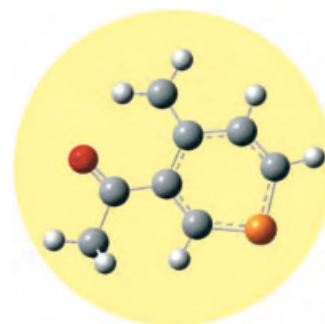
Enzyme Selection

In their Communication on p. 1048 ff. S. Q. Yao et al. describe a new method for the simultaneous selection of mRNA-bound enzymes and for their identification with the aid of a DNA-microarray.



Phosphorus Compounds

A simple access to the rare β -functional phosphinine compounds from readily available phospholide ions is described by F. Mathey and J. Grundy in their Communication on p. 1082 ff.





The following Communications have been judged by at least two referees to be “very important papers” and will be published online at www.angewandte.org soon:

Stuart L. Schreiber,* Chuo Chen, Xiaodong Li,
Christopher S. Neumann, Michael M.-C. Lo
Convergent Diversity-Oriented Synthesis of Small-Molecule Hybrids

Ralf Haiges,* Jerry A. Boatz, Robert Bau, Stefan Schneider,
Thorsten Schroer, Muhammed Yousufuddin, Karl O. Christe*
Polyazide Chemistry: The First Binary Group 6 Azides, $\text{Mo}(\text{N}_3)_6$, $\text{W}(\text{N}_3)_6$, $[\text{Mo}(\text{N}_3)_7]^-$, and $[\text{W}(\text{N}_3)_7]^-$ and the $[\text{NW}(\text{N}_3)_4]^-$ and $[\text{NMo}(\text{N}_3)_4]^-$ Ions

Hans A. Bechtel, Jon P. Camden, Davida J. Ankeny Brown,
Marion R. Martin, Richard N. Zare,* Konstantin Vodopyanov
Effects of Bending Excitation on the Reaction of Chlorine Atoms with Methane

Liang Deng, Hoi-Shan Chan, Zuowei Xie*
Synthesis, Reactivity, and Structural Characterization of the First 14-Vertex Carborane

Xuejun Liu, Gaosheng Chu, Robert A. Moss,* Ronald R. Sauer,*
Ralf Warmut*
Fluorophenoxycarbene Inside a Hemicarcerand: A Bottled Singlet Carbene

Silvio Aime,* Carla Carrera, Daniela Delli Castelli, Simonetta Geninatti Crich, Enzo Terreno
Light-On/Light-Off of Cells Labeled with MRI-PARACEST Agents

News

B. L. Feringa Receives Spinoza Award _____ 996 Novartis Award to J. S. Clark and J. P. Clayden _____ 996

Books

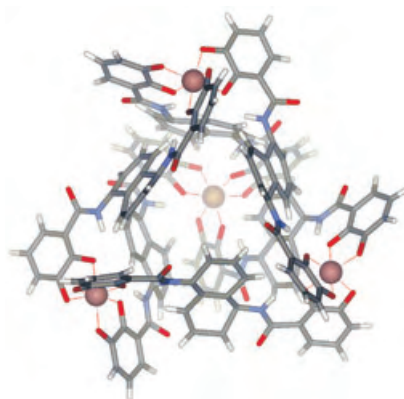
Palladium Reagents and Catalysts Jiro Tsuji reviewed by S. S. Stahl _____ 997
Biophysical Chemistry Alan Cooper reviewed by M. Kahms _____ 998

Highlights

Supramolecular Chemistry

A. Lützen* _____ 1000–1002

Self-Assembled Molecular Capsules—
Even More Than Nano-Sized Reaction
Vessels



Far from exhausted is the potential of molecular capsules (a tetranuclear gallium complex is shown as an example). Previously these self-assembled units served as receptors and tiny reaction vessels. In recent work they were used as sensitizers in photochemically induced reactions and as catalysts for rearrangements.

Reviews

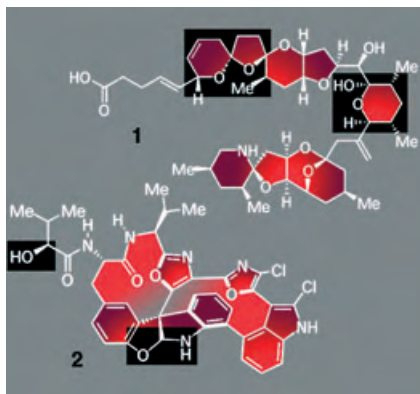
NMR Tomography

P. C. Lauterbur* _____ 1004–1011

All Science Is Interdisciplinary—From
Magnetic Moments to Molecules to Men
(Nobel Lecture)

Merely by chance, says Paul Lauterbur, one of the recipients of the Nobel Prize for Physiology or Medicine in 2003, were NMR imaging techniques his main research focus for many years. In his Nobel Lecture, he describes important

facets of his life and his scientific carrier that led him from silicones to the clinical application of NMR spectroscopy and later to the question of how chemistry can help in explaining biology.



It is a commonly held belief that the process of assigning structures to newly isolated natural products (see picture) is a relatively routine endeavor, one that offers little opportunity for adventure and does not require the art of chemical synthesis. This Review seeks to question the veracity of such a position and makes the case that there is plenty of room in the process of structural elucidation for intellectual challenge, chemical synthesis, and drama.

Natural Products Synthesis

K. C. Nicolaou,*

S. A. Snyder _____ 1012–1044

Chasing Molecules That Were Never There: Misassigned Natural Products and the Role of Chemical Synthesis in Modern Structure Elucidation

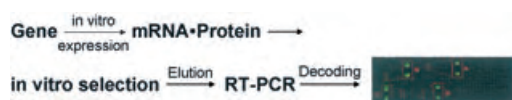
Communications

Analytical Methods

Y. Hu, G. Y. J. Chen,

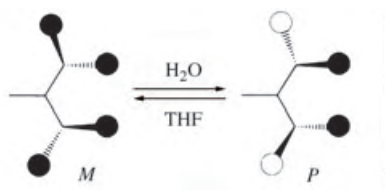
S. Q. Yao* _____ 1048–1053

Activity-Based High-Throughput Screening of Enzymes by Using a DNA Microarray

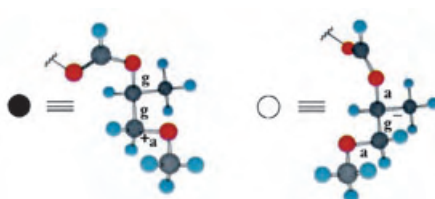


The expression display method is developed, which combines two techniques, ribosome display and DNA microarray, to express a mixture of proteins from their corresponding cDNA. Upon functional selection using an activity-based probe,

multiple target enzymes are simultaneously isolated and subsequently identified by hybridization to a DNA microarray (see scheme; RT=reverse transcription, PCR=polymerase chain reaction).



Staying in shape: The second and third generations of a new dendron system switch from left-handed to right-handed helical conformations upon a change in solvent from THF to water (picture; left).



This inversion occurs in tandem with conformational shifts about the O–C–C–O bonds of a subset of terminating glycol chains, from *gauche, gauche⁺, anti* to *anti, gauche⁻, anti* (picture; right).

Conformational Analysis

A. L. Hofacker,

J. R. Parquette* _____ 1053–1057

Dendrimer Folding in Aqueous Media: An Example of Solvent-Mediated Chirality Switching

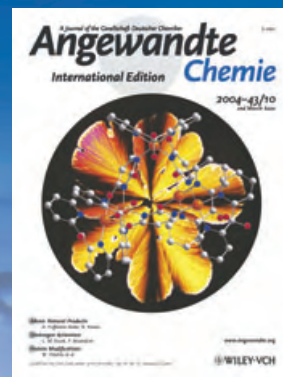
For the USA and Canada:

ANGEWANDTE CHEMIE International Edition (ISSN 1433-7851) is published weekly by Wiley-VCH PO Box 191161, D 69451 Weinheim, Germany. Air freight and mailing in the USA by Publications Expediting Inc. 200 Meacham Ave., Elmont, NY 11003. Periodicals

postage paid at Jamaica NY 11431. US POSTMASTER: send address changes to *Angewandte Chemie*, Wiley-VCH, 111 River Street, Hoboken, NJ 07030. Annual subscription price for institutions: US\$ 4948.00/4498.00 (valid for print and electronic / print or electronic delivery); for individuals who are personal members of a

national chemical society, or whose institution already subscribes, or who are retired or self-employed consultants, print only: US\$ 394.00. Postage and handling charges included. All Wiley-VCH prices are exclusive VAT.

The best in chemistry – for more than a hundred years



A Journal of the Gesellschaft Deutscher Chemiker

Angewandte International Edition Chemie

www.angewandte.org

1888: The beginning
of a success story

Constant Innovations

- 1962:** First issue of the International Edition
- 1976:** Graphical abstracts
- 1979:** Cover pictures
- 1988:** Centenary of Angewandte
- 1989:** Routine use of color
- 1991:** New section: Highlights
- 1992:** Computerized editorial tracking system
- 1995:** Internet service for readers
- 1998:** Regular press service; full-text online
- 2000:** New section: Essays; EarlyView: Communications available online ahead of the printed version
- 2001:** New section: Minireviews
- 2002:** Online submission of manuscripts
- 2003:** Weekly publication; new section: News; new layout
- 2004:** Backfiles (1962-1997); ManuscriptXpress: Online system for authors and referees



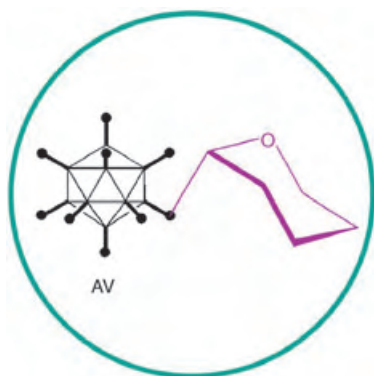
Angewandte's advisors...

Hartmut Wiezer
Clariant International AG,
Sulzbach am Taunus

» **Angewandte Chemie** is a highly acknowledged international chemical journal. Its attraction is based on excellence in content and presentation. It is a pleasure to commit myself to further the quality and success of **Angewandte Chemie**. «

Angewandte Chemie International Edition is
a journal of the German Chemical Society (GDCh)



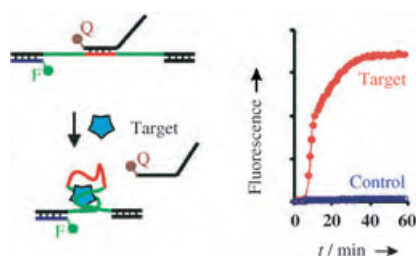


A sugar-specific transfection mechanism is introduced by the glycosylation of adenoviruses (AVs, see picture), and manipulation of the glycosylation pattern allows the selective transfection of human macrophages in favor of the usual target. This dramatic retargeting holds promise for the fine-tuning of adenoviruses for applications such as gene therapy.

Glycoviruses

O. M. T. Pearce, K. D. Fisher,
J. Humphries, L. W. Seymour,*
A. Smith, B. G. Davis* — 1057 – 1061

Glycoviruses: Chemical Glycosylation
Retargets Adenoviral Gene Transfer



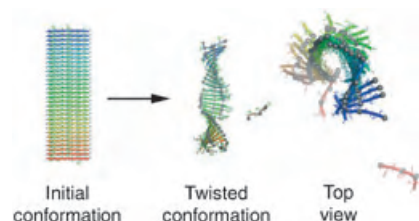
Picking out probes: A novel approach permits isolation of standard DNA aptamers by in vitro selection and conversion into fluorescence signaling probes. This method comprises the isolation of DNA aptamers capable of duplex-to-complex structure switching and labeling the derived aptamers with a pair of short DNA strands with a fluorophore F and a quencher Q to create a reporter system for real-time sensing (see picture).

Fluorescent Probes

R. Nutiu, Y. Li* — 1061 – 1065

In Vitro Selection of Structure-Switching
Signaling Aptamers

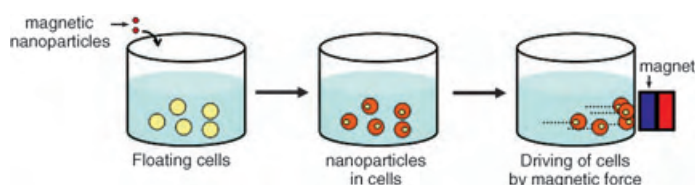
Modeling the mechanisms of protofibril twisting: Molecular-dynamics simulations of simian viral peptide aggregates show that β sheets of 10 to 30 chains form left-handed helical ribbons with saddlelike curvature (see picture). These structures are highly dynamic, with oscillations around an average twist angle of $9\text{--}10^\circ$, and a pitch of 15–20 nm, depending on β -sheet length. The peptides studied are key to viral entry into host cells.



Peptide Modeling

P. Soto, J. Cladera, A. E. Mark,
X. Daura* — 1065 – 1067

Stability of SIV gp32 Fusion-Peptide
Single-Layer Protofibrils as Monitored by
Molecular-Dynamics Simulations



Cells in motion: Multifunctional nanoparticles, with a unique combination of magnetic and fluorescent properties, coupled with biocompatibility are prepared. The uptake of the magnetic nano-

particles by cells is investigated, and an external “magnetic motor effect” on the cells containing the nanoparticles is observed (see scheme).

Bionanotechnology

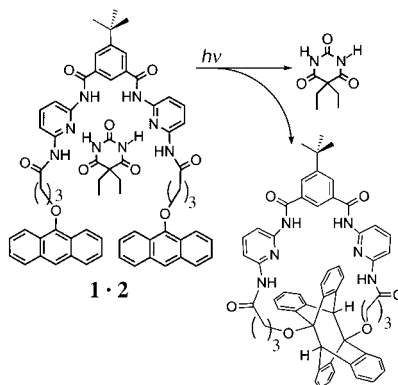
T.-J. Yoon, J. S. Kim, B. G. Kim, K. N. Yu,
M.-H. Cho,* J.-K. Lee* — 1068 – 1071

Multifunctional Nanoparticles Possessing
A “Magnetic Motor Effect” for Drug or
Gene Delivery

Host–Guest Chemistry

Y. Molard, D. M. Bassani, J.-P. Desvergne,*
P. N. Horton, M. B. Hursthouse,
J. H. R. Tucker* — 1072–1075

Photorelease of an Organic Molecule in
Solution: Light-Triggered Blockage of a
Hydrogen-Bonding Receptor Site

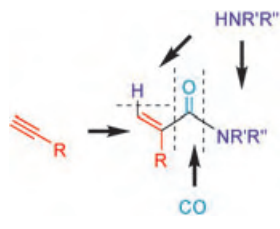


Bathed in light, the acyclic receptor **1** that binds a neutral guest molecule through hydrogen bonding (**1·2**) undergoes an intramolecular anthracene photodimerization reaction to yield a macrocyclic structure. The dramatic change in the structure of **1** from open to cyclic affects the binding properties of the receptor sites and leads to the exclusion of the guest molecule.

Radical Carbonylation

Y. Uenoyama, T. Fukuyama, O. Nobuta,
H. Matsubara, I. Ryu* — 1075–1078

Alkyne Carbonylation by Radicals:
Tin-Radical-Catalyzed Synthesis of
 α -Methylene Amides from 1-Alkynes,
Carbon Monoxide, and Amines

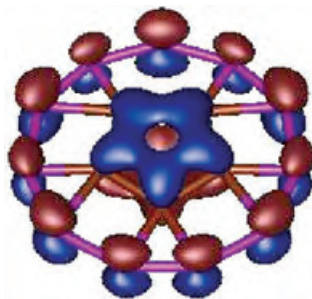


A convergent synthesis of α -methylene amides exploits a hybrid radical/ionic concept in which radical carbonylation of alkynes is followed by ionic trapping of the resulting carbonyl-containing radical species with amines (see scheme). The reaction of substituted terminal alkynes with pressurized CO, Bu_3SnH , and 2,2'-azobisisobutyronitrile in the presence of a large excess of amines gave good yields of the corresponding α -methylene amides.

Computer Chemistry

S. Erhardt, G. Frenking,* Z. Chen,
P. von R. Schleyer* — 1078–1082

Aromatic Boron Wheels with More than
One Carbon Atom in the Center:
 C_2B_8 , $\text{C}_3\text{B}_9^{3+}$, and $\text{C}_5\text{B}_{11}^+$

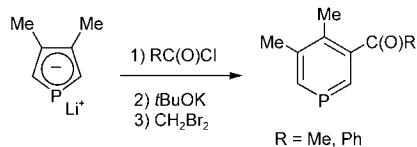


Computational exploration of carboranes of formula $\text{C}_n\text{B}_{m+1}^{q+}$ reveals that more than one hypercoordinated carbon atom can be enclosed by a peripheral ring comprising a suitable number of boron atoms. The C_2B_8 , $\text{C}_3\text{B}_9^{3+}$, and $\text{C}_5\text{B}_{11}^+$ species (the LUMO of the latter is shown) are stabilized by substantial Hückel π aromaticity. Furthermore, multicenter σ bonding helps bind the inner carbon units to the boron perimeters, though they can freely rotate relative to one another.

Phosphorus Heterocycles

J. Grundy, F. Mathey* — 1082–1084

One-Pot Conversion of Phospholide Ions
into β -Functional Phosphinines



Only a few β -functional phosphinines are known. As a result, the reactivity of this class of compounds is almost unexplored. A straightforward access to such compounds from the readily available phospholide ions is described (see scheme) and the reaction mechanism is explored by theoretical methods.

Simply mixing the complex $[\{\text{RuCl}_2(1,3,5\text{-C}_6\text{H}_3\text{iPr}_3)\}_2]$ (**1**) with PCy_3 is sufficient to generate a catalyst suitable for highly efficient atom-transfer radical addition and polymerization reactions at exceptionally low temperatures (see scheme). The steric congestion at the metal caused by the bulky ligands is thought to be essential for the reactivity of the catalyst.

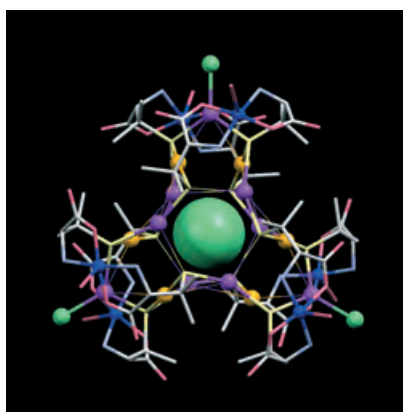


Living Polymerization

L. Quebatte, M. Haas, E. Solari,
R. Scopelliti, Q. T. Nguyen,
K. Severin* _____ **1084–1088**

Atom-Transfer Radical Reactions under Mild Conditions with $[\{\text{RuCl}_2(1,3,5\text{-C}_6\text{H}_3\text{iPr}_3)\}_2]$ and PCy_3 as the Catalyst Precursors

All three coinage metals are present in the supramolecular compound created from D-penicillamine (D-H₂pen) by stepwise reaction with Au^I, Ag^I, and Cu^{II} in the presence of Cl[−]. In this compound, 20-nuclear monocationic $[\text{Au}_6\text{Ag}_8\text{Cu}_6\text{Cl}(\text{H}_2\text{O})_5(\text{D-pen})_{12}]^+$ and 21-nuclear monoanionic $[\text{Au}_6\text{Ag}_9\text{Cu}_6\text{Cl}_4(\text{H}_2\text{O})_6(\text{D-pen})_{12}]^-$ (see picture) supramolecular cages, each of which accommodates a Cl[−] ion (green), are linked so as to form a giant rock-salt-like lattice structure.

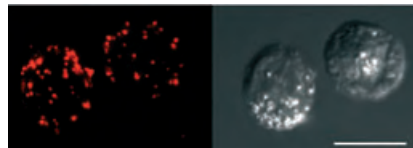


Supramolecular Chemistry

A. Toyota, T. Yamaguchi,
A. Igashira-Kamiyama, T. Kawamoto,
T. Konno* _____ **1088–1092**

A Rock-Salt-Like Lattice Structure Consisting of Monocationic and Monoanionic Au^I/Ag^I/Cu^{II} Supramolecular Cages of D-Penicillamine

Patch work: Through attachment of chromatic polydiacetylene (PDA) nanopatches onto the plasma membrane, real-time visualization of surface processes in living cells is possible (see picture; scale bar: 10 μm). The membrane-incorporated polymer patches did not adversely affect cell vitality for several hours and responded to structural perturbations of the

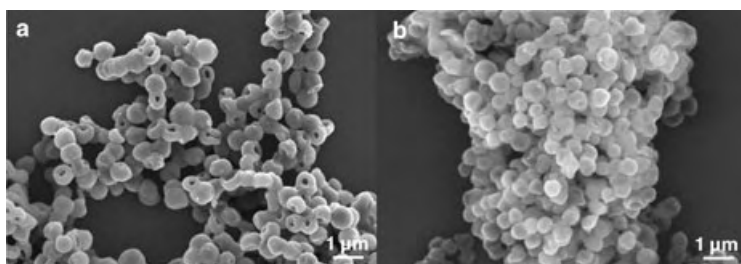


plasma membrane both through induction of fluorescence as well as by undergoing blue–red color changes.

Cell Imaging

Z. Orynbayeva, S. Kolusheva, E. Livneh,
A. Lichtenshtein, I. Nathan,
R. Jelinek* _____ **1092–1096**

Visualization of Membrane Processes in Living Cells by Surface-Attached Chromatic Polymer Patches



Interior decorating: Polymerization of styrene sulfonate monomers on the inner surface of polyelectrolyte hollow capsules results in polymers having molecular weights an order of magnitude higher

than those produced in solution. The shape of the capsules after polymerization can be manipulated by varying the styrene sulfonate content (see SEM images; a: 25 wt %, b: 40 wt %).

Materials Science

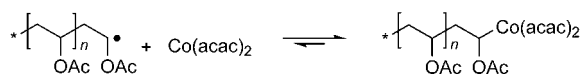
W. S. Choi, J.-H. Park, H. Y. Koo, J.-Y. Kim,
B. K. Cho, D.-Y. Kim* _____ **1096–1101**

“Grafting-From” Polymerization inside a Polyelectrolyte Hollow-Capsule Microreactor

Radical Polymerization

A. Debuigne, J.-R. Caille,
R. Jérôme* 1101–1104

Highly Efficient Cobalt-Mediated Radical
Polymerization of Vinyl Acetate



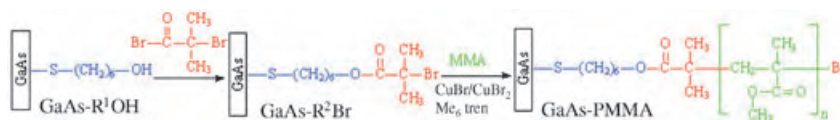
Reversible end-capping of the growing polymer chains to form dormant species (see scheme) lowers the radical concentration. Thus, cobalt(II) acetylacetonate efficiently controls the bulk radical polymerization of vinyl acetate. The molar

mass of the poly(vinyl acetate) increases linearly with monomer conversion, polydispersity is as low as 1.15, and polymerization can be resumed by preformed vinyl acetate oligomers. acac = acetylacetonate.

Surface Polymerization

Q. J. Cai, G. D. Fu, F. R. Zhu, E.-T. Kang,*
K.-G. Neoh 1104–1107

GaAs–Polymer Hybrids Formed by
Surface-Initiated Atom-Transfer Radical
Polymerization of Methyl Methacrylate



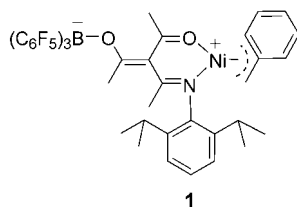
A sulfanylhexasanol coupling agent is crucial for the preparation of GaAs–poly-(methyl methacrylate) (PMMA) hybrids by surface-initiated atom-transfer radical polymerization (ATRP) of methyl meth-

acrylate (see scheme) as it passivates the GaAs surface and also immobilizes the ATRP initiator. The surface states of GaAs are not significantly affected by the ATRP process.

Homogeneous Catalysis

Y. Chen, G. Wu,
G. C. Bazan* 1108–1112

Remote Activation of Nickel Catalysts for
Ethylene Oligomerization

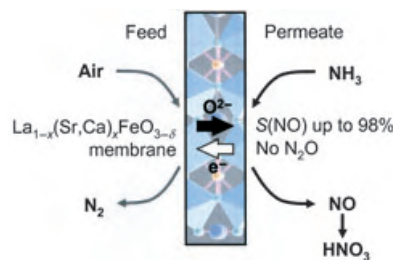


Remote control: A novel molecular design is described and used to probe the activation of transition-metal-based ethylene polymerization and oligomerization initiators by the action of a Lewis acid across an electronically delocalized structural unit. Compound **1** which has a Lewis acid attached to a site removed from the trajectory of the incoming substrate, shows high activity for ethylene oligomerization.

Ammonia Oxidation

J. Pérez-Ramírez,*
B. Vigeland 1112–1115

Perovskite Membranes in Ammonia
Oxidation: Towards Process
Intensification in Nitric Acid Manufacture



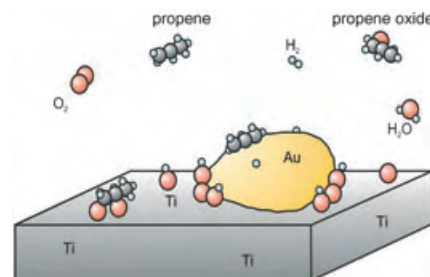
Intensified nitric acid production is possible when NH₃ is oxidized with Ca- and Sr-substituted lanthanum ferrite perovskites in a membrane reactor with NO selectivities of up to 98% (see picture). In this new process atmospheric N₂ is rejected by the oxygen-conducting membrane, expensive noble metal catalysts are unnecessary, and no environmentally harmful N₂O is produced.

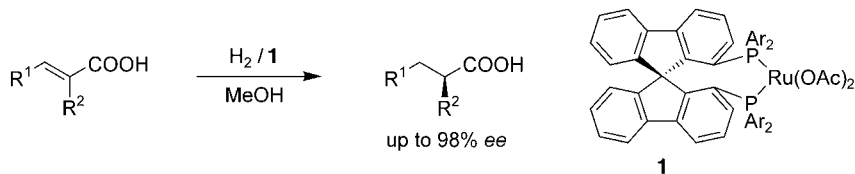
Heterogeneous Catalysis

T. A. Nijhuis,* T. Visser,
B. M. Weckhuysen 1115–1118

The Role of Gold in Gold–Titanium
Epoxidation Catalysts

Gold can activate propene or influence titania such that a reaction occurs in which bidentate propoxy species are formed on the catalyst (see picture). In the absence of gold this reaction is not possible. This observation brings the understanding of this unique catalyst system one step further.





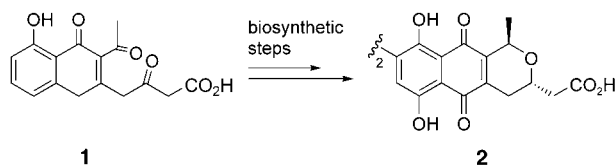
High and wide: The high rigidity and large dihedral angle of chiral, spirobifluorene-based diphosphane ligands lead to excellent reactivity and enantioselectivity in the

ruthenium-catalyzed asymmetric hydrogenation of α,β -unsaturated carboxylic acids (see scheme).

Asymmetric Catalysis

X. Cheng, Q. Zhang, J.-H. Xie, L.-X. Wang, Q.-L. Zhou* 1118–1121

Highly Rigid Diphosphane Ligands with a Large Dihedral Angle Based on a Chiral Spirobifluorene Backbone



Compelling evidence for the intermediacy of the free β -keto acid **1**, rather than the corresponding enzyme-bound thiolate as previously proposed, in the biosynthesis of the antibiotic actinorhodin (**2**) was obtained from studies of the enantioselective

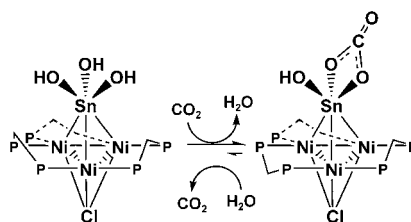
reduction of a range of β -keto acids by the engineered strain of *S. coelicolor* CH999/pIJ5675. This excellent whole-cell biotransformation system gave the desired *S* β -hydroxy acids with >95% ee.

Biotransformation

K. I. Booker-Milburn,* R. Gillan, M. Kimberley, T. Taguchi, K. Ichinose, G. R. Stephenson, Y. Ebizuka, D. A. Hopwood 1121–1125

Enantioselective Reduction of β -Keto Acids with Engineered *Streptomyces coelicolor*

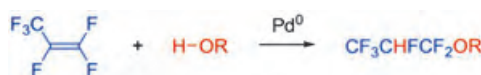
Tin caps: A straightforward synthetic pathway leads to a series of trihydroxy tin capped trinuclear nickel clusters. The $\text{Sn}(\text{OH})_3$ groups of the clusters resist oligomerization. They display high nucleophilicity leading to reversible formation of an η^2 -carbonato tin capped cluster in the presence of CO_2 (see scheme) and ring opening of 1,2-epoxybutane to the corresponding tin coordinated diolate.



Cluster Compounds

E. Simón-Manso, C. P. Kubiak* 1125–1128

A Trihydroxy Tin Group That Resists Oligomerization in the Trinuclear Nickel Cluster $[\text{Ni}_3(\mu\text{-P}, \text{P}'\text{-PPh}_2\text{CH}_2\text{PPh}_2)_3(\mu_3\text{-L})(\mu_3\text{-Sn}(\text{OH})_3)]$



No vinyl ether by-products are formed in the palladium(0)-complex catalyzed hydroalkoxylation of hexafluoropropene (see scheme). Saturated hydrofluoroethers are selectively synthesized with

alcohols or phenols under neutral conditions in the presence of $[\text{Pd}(\text{PPh}_3)_4]/\text{dppb}$. dppb = 1,4-bis(diphenylphosphanyl)butane.

Hydrofluoroethers

Y. Matsukawa,* J. Mizukado, H.-d. Quan, M. Tamura, A. Sekiya 1128–1130

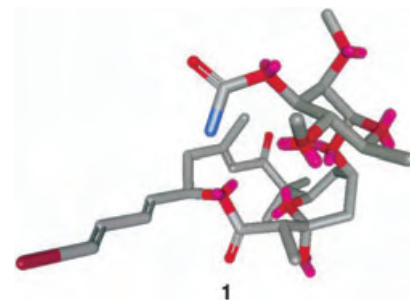
Palladium(0)-Catalyzed Hydroalkoxylation of Hexafluoropropene: Synthesis of Hydrofluoroethers under Neutral Conditions

Natural Product Synthesis

I. Paterson,* G. J. Florence,
A. C. Heimann,
A. C. Mackay _____ **1130–1133**

Stereocontrolled Total Synthesis of
(–)-Aurisides A and B

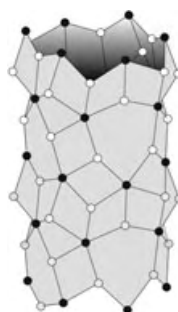
An expedient total synthesis of aurisides A and B (**1**), unusual cytotoxic macrolide glycosides isolated from the Japanese sea hare *D. auricularia*, takes advantage of a highly convergent aldol-based route for the stereocontrolled construction of the common macrolide core. This is followed by α -selective glycosylation to introduce the sugar moieties.



Oxidic Nanotubes

S. V. Krivovichev,* V. Kahlenberg, R. Kaindl,
E. Mersdorf, I. G. Tananaev,
B. F. Myasoedov _____ **1134–1136**

Nanoscale Tubules in Uranyl Selenates



An inorganic oxo salt, $K_5[(UO_2)_3(SeO_4)_5](NO_3)(H_2O)_{3.5}$, forms a structure based on nanoscale uranyl selenate tubules (see picture; ● $\{UO_7^{8-}\}$ bipyramids, ○ $\{SeO_4^{2-}\}$ tetrahedra). The interiors of the nanotubules are occupied by K^+ ions and H_2O molecules.

Sources

Product and Company Directory

You can start the entry for your company in “Sources” in any issue of *Angewandte Chemie*.

If you would like more information, please do not hesitate to contact us.

Wiley-VCH Verlag – Advertising Department

Tel.: ☎ 62 01 - 60 65 65

Fax: ☎ 62 01 - 60 65 50

E-Mail: MSchulz@wiley-vch.de

Service

Vacancies _____ **1137**

Keywords _____ **1138**

Authors _____ **1139**

Preview _____ **1141**



B. L. Feringa Receives Spinoza Award

The Spinoza Award of the Netherlands Organisation for Scientific Research (NWO) is considered by some as the Dutch Nobel Prize. The award has been presented annually since 1995 to three or four researchers from The Netherlands of any academic discipline. Each award winner receives a research grant of € 1 500 000. Benedictus de Spinoza (1632–1677), after whom the award is named, was a Jewish Dutch philosopher of Portuguese origin whose name stands for the freedom of the researcher in the face of restrictions posed by institutions.



B. Feringa

Ben Feringa (University of Groningen, The Netherlands) is one of four award winners for 2004. His research focuses on stereochemistry and encompasses organic synthesis, asymmetric catalysis, molecular switches and motors, self-assembly, and nanosystems. Feringa completed his PhD in 1978 in Groningen under the guidance of H. Wynberg on the topic of asymmetric phenol oxidation and then worked for Shell in Amsterdam and Sittingbourne (UK). He returned as a lecturer to the University of Groningen in 1984 and became full professor there in 1988. Since 2003 he has been Jacobus H. van 't Hoff Professor of Molecular Sciences. Feringa is a member of the Academic Advisory Board of *Advanced Synthesis & Catalysis* and the author of a book on molecular switches.^[1a] He

recently reported in *Angewandte Chemie* on the direct visual measurement of the stereoselectivity of a catalytic reaction by using liquid crystals.^[1b] In 1999 he discussed in a Review the state of asymmetric synthesis in chiral crystals and through photochemistry with circularly polarized light, as well as mechanisms for the amplification of chirality.^[1c]

Novartis Award to J. S. Clark and J. P. Clayden

Novartis has awarded the Novartis European Young Investigator Award in Chemistry since 2002. The award, with a monetary value of SFr 100 000, is presented annually to scientists resident in Europe and under the age of 40 who have made outstanding achievements in organic or bioorganic chemistry. The recipients for 2004 are J. Stephen Clark (University of Nottingham, UK) and Jonathan P. Clayden (University of Manchester, UK).

Stephen Clark studied chemistry at the University of Edinburgh (UK) and completed his PhD in 1988 on natural products synthesis under the supervision of A. B. Holmes at the University of Cambridge (UK). He then joined the research group of D. A. Evans (Harvard University, USA). In 1990 he took up a position as lecturer at the University of Nottingham, where he has been Professor of Organic Chemistry since 2001. His research interests include the total synthesis of natural products and the development of stereoselective methods for the synthesis of carbo- and heterocycles, as well as metal-mediated and asymmetric catalytic reactions. Clark received the award for the development of new synthetic methods based on carbenoids and metathesis, and their application in natural products synthesis. In *Angewandte Chemie* he



J. S. Clark

reported on the synthesis of polycyclic ethers by double ring-closing metathesis.^[2]

Jonathan Clayden studied chemistry at the University of Cambridge and completed his PhD there in 1992 under the guidance of S. Warren. He then carried out postdoctoral research with M. Julia at the Ecole Normale Supérieure in Paris. In 1994 he became a lecturer at the University of Manchester, where he has been professor since 2001. His research covers various aspects of organic synthesis and stereochemistry, for example, asymmetric synthesis, atropisomerism, organolithium chemistry, conformation control, and remote stereocontrol. The award recognizes his development of new synthetic methods based on dearomatization reactions and non-biaryl atropisomers. He described dearomatizing disrotatory electrocyclic ring-closing reactions of lithiated *N*-benzoyloxazolidines in *Angewandte Chemie*,^[3a] and his Communication on the use of dipole moments to control the relative orientation of functional groups will be published in issue 8/2005.^[3b]



J. P. Clayden

- [1] a) B. L. Feringa, *Molecular Switches*, Wiley-VCH, Weinheim, **2001**; b) R. Eelkema, R. A. van Delden, B. L. Feringa, *Angew. Chem.* **2004**, *116*, 5123; *Angew. Chem. Int. Ed.* **2004**, *43*, 5013; c) B. L. Feringa, R. A. van Delden, *Angew. Chem.* **1999**, *111*, 3624; *Angew. Chem. Int. Ed.* **1999**, *38*, 3418.
- [2] J. S. Clark, O. Hamelin, *Angew. Chem.* **2000**, *112*, 380; *Angew. Chem. Int. Ed.* **2000**, *39*, 372.
- [3] a) J. Clayden, S. Purewal, M. Helliwell, S. J. Mantell, *Angew. Chem.* **2002**, *114*, 1091; *Angew. Chem. Int. Ed.* **2002**, *41*, 1049; b) M. S. Betson, J. Clayden, H. K. Lam, M. Helliwell, *Angew. Chem. Int. Ed.*, January 14, **2005**, DOI: 10.1002/anie.200461787.

Self-Assembled Molecular Capsules—Even More Than Nano-Sized Reaction Vessels

Arne Lützen*

Keywords:

homogeneous catalysis · molecular capsules · photochemical sensitizers · self-assembly · supramolecular chemistry

The inclusion of molecules in defined cavities implies the exciting possibility of subsequent modification, since the included molecule is greatly affected by the specific steric conditions and arrangement of functional groups in the cavity. In analogy to enzyme-catalyzed reactions, such complexes can result in accelerated reactions or even in completely new reactions. Container molecules like cryptophanes and (hemi-)carcerands can encapsulate small molecules and even facilitate the formation of and studies on reactive compounds such as cyclobutadiene, benzyne, cycloheptatetraene, and *anti*-Bredt bridgehead olefins within their interior.^[1]

Although synthetic organic chemistry has had tremendous success in the last years^[2] the huge effort associated with the fabrication of complicated structures is a severe limitation. An attractive alternative is the application of synthetic strategies in which covalent bonds are not formed, but rather reversible, self-assembly processes dictated by “weak” intermolecular interactions such as hydrogen bonds and metal coordination lead to complex structures.^[3] This strategy has a number of benefits: The high degree of convergence usually makes this synthesis easier than that of the covalently assembled analogue (if such a structure is indeed conceivable). Depending on the reaction conditions,

the assembly is highly precise, because these equilibrium-controlled processes are self-controlling and self-repairing, and the resulting thermodynamically stable aggregates often show interesting dynamic behavior. In addition, cooperative effects are often observed such that after an initial rate-determining nucleation, the assembly is rapid since the formation of several bonds becomes easier than formation of just one.

Following this approach, capsular aggregates could also be obtained.^[4] Figures 1–3 show some examples of capsules that can not only stabilize reactive species or molecules in uncommon conformations through encapsulation but also act as molecular reaction vessels for encapsulated substrates. The first examples were described in the late 1990s by the group of J. Rebek, Jr. with their hydrogen-bonded assemblies^[5] (Figure 1). They demonstrated that Diels–Alder reactions could be accelerated and even catalyzed within the so-called softball **1**.^[6] Several years later the same group found that the cylindrical capsule **2** can be used to control reactions like the formation of amides in a very elegant manner. Small differences in the encapsulation of single reactants and reagents lead to a temporary compartmentalization of the species involved in this model transformation.^[7c]

Similar results were obtained with supramolecular metal complexes prepared by self-assembly.^[8] Figure 2 shows systems described by Fujita et al., which were used as molecular reaction chambers.^[8d,9] Stoichiometric [2+2] cycloadditions could be performed in both hexanuclear palladium(II) complexes **3** and **4**, leading to products that could not

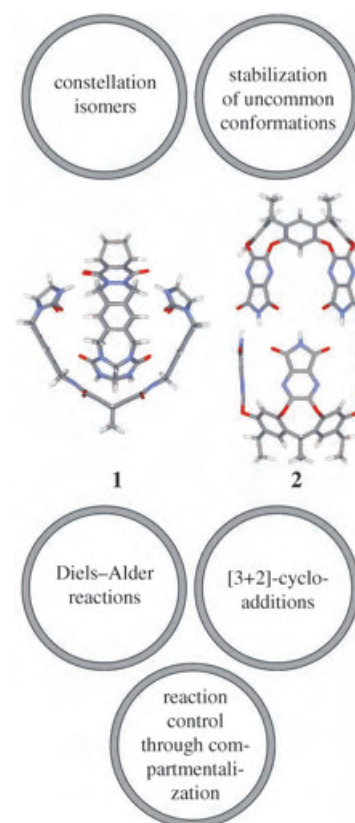


Figure 1. PM3-minimized structures of softball **1** and the cylindrical capsule **2** from the group of J. Rebek, Jr. and some of the successful applications of these dimeric aggregates.^[6,7] The long alkyl chains of the glycoluril units of **1** and of the lower rim of the resorcin[4]arenes in **2** have been omitted.

be obtained without the capsules.^[9b,c] Furthermore, **3** could be employed as an inverse phase-transfer reagent in Wacker oxidations of styrene derivatives in aqueous solution.^[9a] Recently, M. Fujita and co-workers were able to add another interesting feature to this

[*] Priv.-Doz. Dr. A. Lützen
Institute of Pure and Applied Chemistry
University of Oldenburg
P.O. Box 2503
26111 Oldenburg (Germany)
Fax: (+49) 441-798-3706
E-mail: arne.luetzen@uni-oldenburg.de

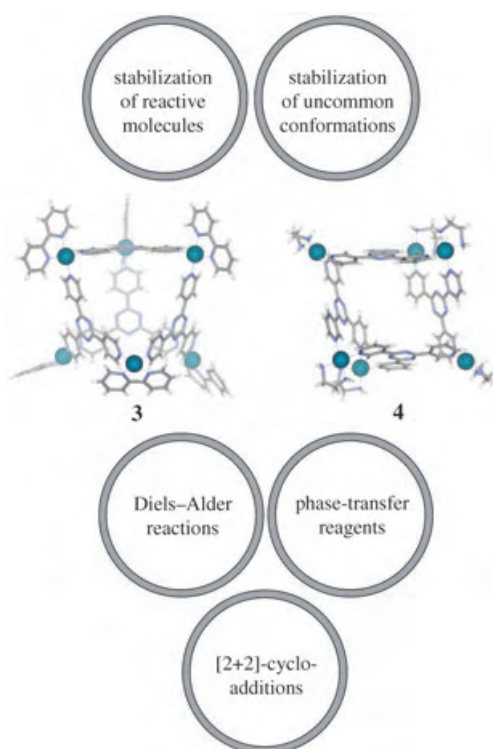


Figure 2. X-ray crystal structures of the hexanuclear metal coordination compounds **3** and **4** synthesized by M. Fujita et al. and some of their applications.^[8d,9] Counterions, solvent molecules, and guest molecules have been omitted. Complex **3** is shown with 2,2-bipyridine ligands; however, most of the studies were performed with ethylene diamine as the chelating ligand.

list of applications: they used capsule **3** as a sensitizer in photochemically induced oxidations of encapsulated adamantane molecules.^[10] The assumption is that the triazene ligand is photochemically excited in the first step. Subsequent electron transfer from one of the four encapsulated adamantane molecules to the host cage leads to the formation of a proton, an adamantyl radical, and a deep-blue radical anion of **3** (in fact, the former overall twelve-fold positively charged complex is transformed into an overall eleven-fold positively charged radical). Finally, these reactive species are then quenched by oxygen and water to give regenerated capsule **3** and the encapsulated oxidation products (Scheme 1).

A common problem in the application of molecular capsules as reaction vessels is that the products themselves are typically good guests. Consequently, the product inhibits further reaction, and the host does usually not show catalytic activity. This was also the case

for the C–H activation mediated by an iridium complex encapsulated by the tetranuclear supra-molecular gallium compound **5** (Figure 3), which was reported by Bergman, Raymond et al. only a few months ago.^[11] More recently they have circumvented this problem in an extremely elegant manner. Again they employed the highly charged anionic assembly **5**, whose spectacular properties, for example, its special affinity to sterically complementary ammonium ions and its “structural memory”, were already demonstrated in the past.^[12] In this new account they describe another important application: aza-Cope rearrangements can be accelerated within this capsule by a factor of almost 1000 and can even be performed in a catalytic fashion (Scheme 2).^[13] This reaction is not necessarily one of the most important chemical transformations, but the authors were clever to choose it because the previously reported properties of the capsule fit this reaction almost perfectly. The substrate, the quaternary ammonium ion **6**, is an excellent guest for the anionic capsule. The confining cavity of **5** forces **6** to adopt a conformation that is barely populated in bulk solution but very favorable for the desired rearrange-

ment. The reversible rearrangement gives iminium ion **7**, which, like **6**, is a good guest. Subsequently the included

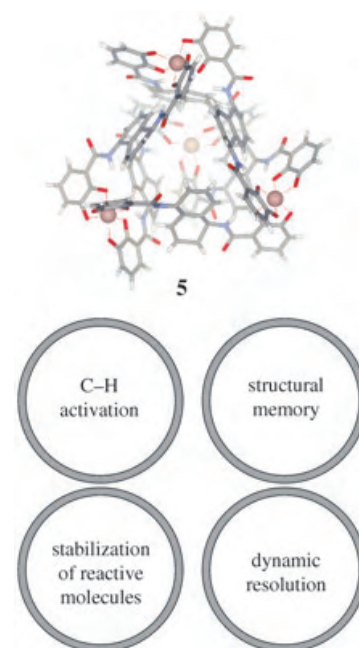
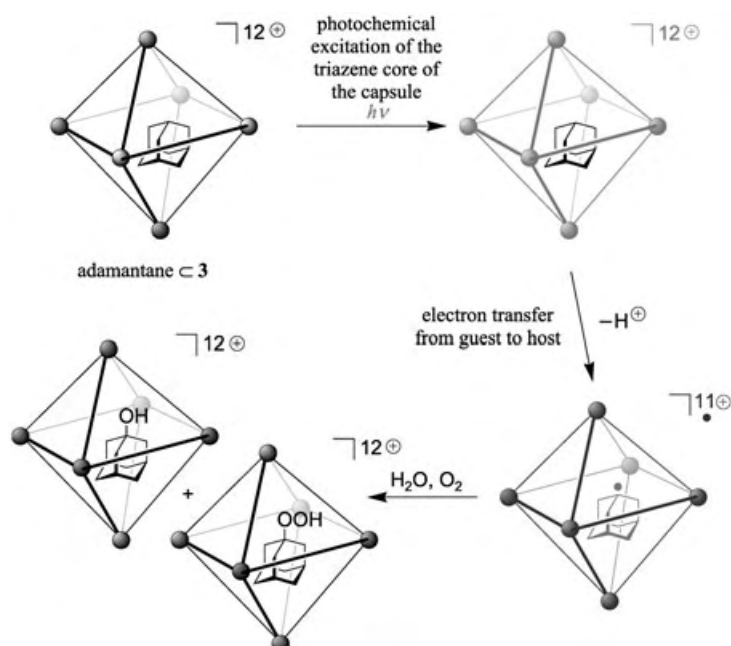
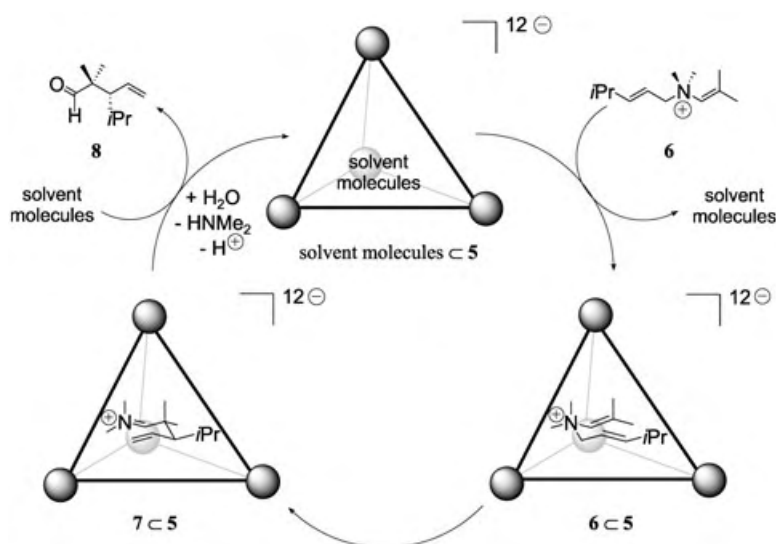


Figure 3. X-ray crystal structure of the tetranuclear gallium complex ($\Delta,\Delta,\Delta,\Delta$)-**5** synthesized by Raymond et al. and some of the applications achieved with these supramolecular assemblies.^[8a,11,12] Counterions, solvent molecules, and the guest molecule have been omitted for clarity.



Scheme 1. In the photochemically induced oxidation of adamantane encapsulated in **3**, capsule **3** acts as a sensitizer. Although four molecules of adamantane are encapsulated in **3**, only one undergoes the reaction shown.



Scheme 2. Catalytic cycle of the aza-Cope rearrangement within **5**. Since **5** was used in racemic form, **8** was also obtained as a racemate, even though only one enantiomer is shown above.

product equilibrates with the free product in the bulk solution. Free **7** undergoes irreversible hydrolysis in the aqueous solution to furnish neutral aldehyde **8**, which is not a good guest for **5** and thus does not compete with **6** for encapsulation. Alternatively, one could also consider that **7** is hydrolyzed inside the cavity almost instantaneously, because water is able to enter the cavity rather easily. The resulting aldehyde **8** is then subsequently exchanged for **6**. In both cases, the catalytic cycle is completed.

It is possible to create molecular capsules with distinct properties that meet the requirements of a given reaction—even though the exact mechanism of guest exchange is not yet fully understood and the activity of the catalyst is far less than that of enzymes. It will be very interesting to see which reaction will be studied next within anionic, cationic, or neutral self-assembled molecular capsules. The topic of stereochemical control of reactions within chiral aggregates will certainly be addressed in future work in this area.

- [1] Some recent reviews: a) A. Jasat, J. C. Sherman, *Chem. Rev.* **1999**, 99, 931–967; b) R. Warmuth, M. A. Marvel, *Eur. J. Org. Chem.* **2001**, 423–437; c) R. Warmuth, J. Yoon, *Acc. Chem. Res.* **2001**, 34,

- 95–105; two new examples: d) P. Roach, R. Warmuth, *Angew. Chem.* **2003**, 115, 3147–3150; *Angew. Chem. Int. Ed.* **2003**, 42, 3039–3042; e) J.-L. Kedelhué, K. J. Langenwalter, R. Warmuth, *J. Am. Chem. Soc.* **2003**, 125, 973–986.
- [2] a) K. C. Nicolaou, E. J. Sorensen, *Classics in Total Synthesis*, Wiley-VCH, Weinheim, **1996**; b) K. C. Nicolaou, S. A. Snyder, *Classics in Total Synthesis II*, Wiley-VCH, Weinheim, **2003**.
- [3] Some reviews: a) J.-M. Lehn, *Angew. Chem.* **1990**, 102, 1347–1362; *Angew. Chem. Int. Ed. Engl.* **1990**, 29, 1304–1319; b) J. S. Lindsey, *New J. Chem.* **1991**, 15, 153–180; c) D. S. Lawrence, T. Jiang, M. Levett, *Chem. Rev.* **1995**, 95, 2229–2260; d) D. Philp, J. F. Stoddart, *Angew. Chem.* **1996**, 108, 1242–1286; *Angew. Chem. Int. Ed. Engl.* **1996**, 35, 1154–1196; f) M. C. T. Fyfe, J. F. Stoddart, *Acc. Chem. Res.* **1997**, 30, 393–401; h) L. M. Greig, D. Philp, *Chem. Soc. Rev.* **2001**, 30, 287–302.
- [4] F. Hof, S. L. Craig, C. Nuckolls, J. Rebek, Jr., *Angew. Chem.* **2002**, 114, 1556–1578; *Angew. Chem. Int. Ed.* **2002**, 41, 1488–1508.
- [5] a) J. Rebek, Jr., *Chem. Soc. Rev.* **1996**, 255–264; b) M. M. Conn, J. Rebek, Jr., *Chem. Rev.* **1997**, 97, 1647–1668; c) J. Rebek, Jr., *Acc. Chem. Res.* **1999**, 32, 278–286; d) J. Rebek, Jr., *Chem. Commun.* **2000**, 637–643.
- [6] a) J. Kang, J. Rebek, Jr., *Nature* **1997**, 385, 50–52; b) J. Kang, G. Hilmersson, J. Santamaría, J. Rebek, Jr., *J. Am. Chem. Soc.* **1998**, 120, 3650–3656.

- [7] a) T. Heinz, D. M. Rudkevich, J. Rebek, Jr., *Angew. Chem.* **1999**, 111, 1206–1209; *Angew. Chem. Int. Ed.* **1999**, 38, 1136–1139; b) S. Körner, F. C. Tucci, D. M. Rudkevich, T. Heinz, J. Rebek, Jr., *Chem. Eur. J.* **2000**, 6, 187–195; c) J. Chen, S. Körner, S. C. Craig, D. M. Rudkevich, J. Rebek, Jr., *Nature* **2002**, 415, 385–386; d) J. Chen, J. Rebek, Jr., *Org. Lett.* **2002**, 4, 327–329; e) A. Shivanyuk, J. Rebek, Jr., *Angew. Chem.* **2003**, 115, 708–710; *Angew. Chem. Int. Ed.* **2003**, 42, 684–686.
- [8] Some recent reviews: a) D. L. Caulder, K. N. Raymond, *Acc. Chem. Res.* **1999**, 32, 975–982; b) S. Leininger, B. Oleynyuk, P. J. Stang, *Chem. Rev.* **2000**, 100, 853–908; c) G. F. Swiegers, T. J. Malefetsse, *Chem. Rev.* **2000**, 100, 3483–3537; d) M. Fujita, K. Umamoto, M. Yoshizawa, N. Fujita, T. Kusakawa, K. Biradha, *Chem. Commun.* **2001**, 509–518; e) B. J. Holliday, C. A. Mirkin, *Angew. Chem.* **2001**, 113, 2076–2098; *Angew. Chem. Int. Ed.* **2001**, 40, 2022–2043; f) S. R. Seidel, P. J. Stang, *Acc. Chem. Res.* **2002**, 35, 972–983.
- [9] a) H. Ito, T. Kusakawa, M. Fujita, *Chem. Lett.* **2000**, 598–599; b) T. Kusakawa, M. Yoshizawa, M. Fujita, *Angew. Chem.* **2002**, 114, 1403–1405; *Angew. Chem. Int. Ed.* **2002**, 41, 1347–1349; c) M. Yoshizawa, Y. Takeyama, T. Okano, M. Fujita, *J. Am. Chem. Soc.* **2003**, 125, 3243–3247; d) T. Kusakawa, T. Nakai, T. Okano, M. Fujita, *Chem. Lett.* **2003**, 284–285.
- [10] M. Yoshizawa, S. Miyagi, M. Kawano, K. Ishiguro, M. Fujita, *J. Am. Chem. Soc.* **2004**, 126, 9172–9173.
- [11] D. H. Leung, D. Fiedler, R. G. Bergman, K. N. Raymond, *Angew. Chem.* **2004**, 116, 981–984; *Angew. Chem. Int. Ed.* **2004**, 43, 963–966.
- [12] a) D. L. Caulder, R. E. Powers, T. N. Parac, K. N. Raymond, *Angew. Chem.* **1998**, 110, 1940–1943; *Angew. Chem. Int. Ed.* **1998**, 37, 1840–1843; b) M. Ziegler, J. L. Brumaghim, K. N. Raymond, *Angew. Chem.* **2000**, 112, 4285–4287; *Angew. Chem. Int. Ed.* **2000**, 39, 4119–4121; c) M. Ziegler, A. V. Davis, D. W. Johnson, K. N. Raymond, *Angew. Chem.* **2003**, 115, 689–692; *Angew. Chem. Int. Ed.* **2003**, 42, 665–668; d) D. Fiedler, D. H. Leung, R. G. Bergman, K. N. Raymond, *J. Am. Chem. Soc.* **2004**, 126, 3674–3675.
- [13] D. Fiedler, R. G. Bergman, K. N. Raymond, *Angew. Chem.* **2004**, 116, 6916–6919; *Angew. Chem. Int. Ed.* **2004**, 43, 6748–6751.

NMR Tomography

All Science Is Interdisciplinary—From Magnetic Moments to Molecules to Men (Nobel Lecture)**

Paul C. Lauterbur*


Keywords:

imaging techniques · NMR spectroscopy · Nobel Lecture

Biography

My ancestors apparently emigrated from Europe in the middle of the 19th century; the Lauterburs probably from Luxembourg, and my mother's people, Wagners and Weingartners, from Baden-Baden in Germany or nearby. They settled in northern Ohio, where my mother's father, Hans Christian Wagner, married Margaret (Maggie) Weingartner. They lived in Tiffin, Ohio when I was a child, where they had raised my mother, Gertrude Frieda Wagner, her twin brother Joseph, and their youngest child, who became a nun with the name Mary Monica. Nearby lived my grandfather Paul Lauterbur who married a woman of Irish descent, Margaret Hillan. They eventually moved south to Sidney, Ohio and had a number of children, of whom my father, Edward Joseph Lauterbur, was the youngest. He later married Gertrude Wagner (the families seem always to have been acquainted) and they had four children, Thomas who died shortly after birth, me, my younger brother Edward Joseph Lauterbur II (Joe) and my sister Margaret. We grew up in a house in Sidney complete with a series of dogs, and as the years went by, birds, turtles, newts, fish, snakes, and other animals, and with interesting yards full of trees, bushes and flowers, as well as a nearby park, open spaces, and neighbors, some of whom did not resent children trespassing on their property. It was, in memory, an idyllic time. My father worked in the town, as an engineer and part-owner of the Peerless Bread Machinery Company, and my mother kept house with help of a young woman who did some domestic chores and sometimes cared for the children. Although I attended a parochial school, Holy Angels School, I recall little of it except that the nuns who taught there seemed to value order and discipline over all else, which made it especially desirable to evade their control. More influential in my later interests was, I believe, my aunt Anna Lauterbur, who taught in Burriss Laboratory School at Ball State Teachers College (now Ball State University) in Muncie, Indiana, just west of the Ohio–Indiana border. She was fascinated by natural history, always kept a terrarium in her elementary school classroom, and gave me a subscription to the magazine *Natural History*. A very gentle person, always willing to listen to a child, she was my favorite aunt.

My parents' hobby was horseback riding, and so they bought a farm outside of town, and we moved there just as I was transferring to the public high school. The farm, with an old but remodeled house, a barn, various outbuildings, fields, woods, and a little creek, was a small paradise to a teen-age



boy, even though I acquired many duties, such as caring for the horses, mowing the lawn, cultivating the garden, and helping with harvesting. There was also time, of course, for hunting and fishing, collecting snakes, turtles, and caterpillars to raise to butterflies or moths, and for general exploration. School was now more interesting also. Not only did I take up the game of chess as a freshman, but I beat the local

[*] Prof. Dr. P. C. Lauterbur
Department of Chemistry
University of Illinois
600 St. Mathews Ave., A 554 CLSL, Urbana, IL 61801 (USA)
E-mail: pcl@uiuc.edu

[**] Copyright© The Nobel Foundation 2003. We thank the Nobel Foundation, Stockholm, for permission to print this lecture.

champions at it, to their great disgust because they were seniors, and then moved on to play a local adult expert, one of the teachers. Classes were a mixture of pleasure and boredom. One of my teachers, who taught biology and chemistry, had the foresight to excuse me and some of my classmates, who were members of the local science club, from his lectures, so that we were free to use the time to do experiments, both standard and wild, in the school lab. He also had the courage to intervene when some of the dangerous ones came to the attention of the school authorities and we could have been expelled.

I met him again recently, and his son recalled that when told of my Nobel Prize, he said, "I always knew he would do something like that". After graduating from high school, I went on to Case Institute of Technology, an engineering school now part of Case Western Reserve University, in Cleveland, Ohio, about 200 miles north-east of Sidney. My father had recommended it, because, as he observed, he didn't know what scientists did for a living, but engineers could always get a job. But, given a choice of majors, I chose chemistry.

I had had so-called "chemistry sets" of simple chemicals and apparatus since my earliest years (I particularly liked the pungent smell of burning sulfur), and my own home laboratories even before high school. The curriculum at Case was quite general, including all forms of science (except biology) and engineering, including civil, electrical, mechanical, and chemical, and all of the related technologies such as surveying, mechanical drawing, as well as seemingly endless labs of all kinds, for which I have always been grateful. In addition to the excitement and drudgery of academics, there were also the pleasures and stresses of fraternity life, girls, and culture, as well as new friends and foods. Continuing my habit of doing things a little differently than expected, I wrote a Senior Thesis on my attempt to make an organosilicon free radical, but the advisor for it was an organic chemist who specialized in natural products.

When I graduated (with a BSc in chemistry, because I did not qualify for an engineering degree as I had replaced a Unit Operations laboratory course with a graduate course in Quantum Chemistry), I was tired of lectures and professors, and determined to get back to lab work. I knew little about graduate study and the structure of a scientific career, so I accepted an offer to work for the Dow Corning Corporation in their Mellon Institute laboratories, where the emphasis was more scientific than technical. I was also told that I could take graduate courses at the University of Pittsburgh free as an Institute employee. There was much interesting work, I found, in our group at the Institute. Organosilicon synthesis, theories of rubber elasticity, techniques of vacuum distillation, elastomer testing, all were new to me and endlessly stimulating. I was particularly fascinated by the puzzle of how small particles strengthened rubber.^[1] I even managed to overcome my distaste for academics and took a few courses.

It had long been known that "carbon black" dramatically improved the properties of natural or synthetic organic rubbers, and it had been found that the same was true for silicone elastomers if small particles of silica were used instead of carbon, but it was not clear whether surface

chemistry was involved or simply physical properties. I addressed one aspect of the problem by substituting phthalocyanine dyes for silica, and they worked perfectly, with their effectiveness decreasing as predicted when the particle size was increased by recrystallization from liquid hydrogen fluoride. Unfortunately, I never achieved a theoretical understanding of the effect, despite intense study of elastomer theory, but I had bright blue rubber and skin.

During that period, I also began to learn about nuclear magnetic resonance (NMR) from various visitors and speakers and to read a little about that new form of spectroscopy as well. It seemed ideally suited, even at that early date, for investigating the structures and electron distributions in molecules, and various physical properties of materials. Therefore, as part of my graduate education at the University of Pittsburgh, in addition to a "literature seminar" on interstellar molecules, I gave one on a paper describing NMR properties of rubber. Before I could begin a planned collaboration on the hydrogen NMR spectroscopy of silicon compounds, however, my deferments came to an end and I was drafted into the Army and my eventual assignment was proposed to be in the SPP (Scientific and Professional Personnel) program, which my BSc and two years of work experience qualified me for.

First, however, I was assigned by mistake to a tank battalion at Fort Knox, Kentucky. After hastily correcting that error, I was given eight weeks of minimal basic training and was assigned to the SPP program, as planned, at the Army Chemical Center in Edgewood, Maryland. My specific assignment there was in the Medical Laboratories, where I learned to operate an electron microscope to measure the properties of small aerosol particles meant to carry chemical warfare agents deep into the lungs, and I also proposed, and began to set up, a light-scattering apparatus to quantitate vapor adsorption on aerosol particles. Another aspect of my duties was to capture and weigh experimental animals meant for the testing of chemical weapons, so that I became skilled, for example, at catching goats in an open field, for which my farm experience was useful.

In time, I learned, from a fellow draftee in my barracks, a Columbia PhD, that his unit had purchased an NMR machine, but didn't know how to use it. I said, "Hey, I know all about that!", and managed a transfer to help set it up, and arranged for one of my science club buddies, Marlan Shepard, from high school, who had also just been drafted, to join me in the lab, where, among others, we had a drafted Harvard PhD in physical chemistry, Norbert Muller, later a professor at Purdue for many years. We got to work enthusiastically, and I eventually published four papers^[3-6] from our work there, which had turned into a rather unusual opportunity for a young soldier. Perhaps, even more important for my future, I received at least second-hand scraps of a Harvard education, especially the attitudes towards scientific work, from Nobby Muller.

When I was mustered out of the Army, I had to decide where to go next. I even considered regular full-time graduate school, but the appeal of Mellon Institute as a familiar supportive working environment won out, especially after my group agreed to buy me my own NMR machine. When I

returned to the Institute I arranged that requisition, tested the machine on a standard organosilicon compound (polydimethylsiloxane) at the manufacturer's laboratory and factory, and impatiently did the initial installation itself when the machine was delivered. The first critical experiments I did, however, were on ^{13}C NMR by retuning the instrument, as I had calculated that, if ^{29}Si resonances could be seen, so could those of ^{13}C , and a much larger variety of stable carbon compounds existed than of silicon compounds.

My first work in that area, a broad survey of carbon compounds,^[4] led to many other publications on various classes of organic chemicals,^[5,6,8,10] work that absorbed much of my attention for several years and eventually provided the basis for my PhD dissertation. Finally completing those requirements was stimulated in part by my learning of an academic job offer to me that was planned but never made, because the department learned that I did not yet have the degree, and I had begun to be dissatisfied with Mellon Institute because of some restrictions they had placed on my activities. After I obtained that degree, I looked at several opportunities and selected one in academia, because, as I remarked, "I wanted to be free to try any silly thing I decided to do". One unexpected feature of the job offer, at the State University of New York at Stony Brook, was that it was for the rank of associate professor, so that I went directly to that level, and almost automatic tenure soon after, without even a postdoctorate appointment. I set up an NMR lab there, and also began to learn the duties and problems of university life while helping to build the department and the institution, and especially, learning to work with students, by that time having gotten over my own distaste for professors by becoming one myself.

During the academic year 1969–1970, I took my first sabbatical leave, spending it in Palo Alto, California, in the group of John Baldeschwieler in the Chemistry Department at Stanford. In addition to the scientific opportunities and satisfactions, there were personal activities as well. I had married Rose Mary Caputo in 1962, and although she was not in good health, we sometimes visited San Francisco and we had two children, Dan and Sharon (who later renamed herself Sharyn) who enjoyed the nearly perpetual summer there. I had an undergraduate student doing work back in Stony Brook who began a new project in my lab there, calculating hypothetical ^{13}C NMR spectra of denatured proteins from data for amino acid spectra. Two graduate students, José Ramirez and Skip Hutton, also remained to continue their research, mostly of isotope effects on NMR spectra,^[11] and I flew back to Stony Brook almost once a month to stay in touch with these activities.

Back in Stanford, I was trying some new NMR-related things. I went up to the Syntex research labs nearby and began research on ^3H NMR spectroscopy of tritium-labeled pharmaceuticals. Only one paper on tritium NMR spectroscopy of organic compounds, by George Tiers, had appeared, so our discovery that one of the "standards" provided to us by Syntex was apparently not labeled in the position they thought it was, interfered with our publishing those observations in the limited time we had available, but led to my later setting up a lab, with a chemistry colleague at Stony Brook, to

do more such work. I also began collaborative studies at Varian Associates, in that manufacturer's service labs, of natural-abundance ^{13}C NMR spectroscopy of the protein lysozyme in their experimental new superconducting spectrometer, and published the first paper on that subject. I was also working in a lab in the Stanford Medical Center to learn to label a protein, ribonuclease A, with ^{13}C at each of its four methionine residues for eventual NMR studies. And, I suppose just to keep busy, I was working with my host, John Baldeschwieler, and Barry Shapiro, a previous visitor to his group and friend of mine from Mellon Institute days, to commercialize ^{13}C -isotope-enrichment technology developed at Los Alamos National Laboratories. We even started a company, "Kivatec", to use Los Alamos underground distillation methods for that purpose.

It is clear that I was actively beginning to consider biomedical NMR spectroscopy as a new area for application of my skills and knowledge of NMR, partly stimulated by the activities of Oleg Jardetzky, a new member of the Stanford faculty. My intense and detailed involvement in biomedical applications of NMR came, however, from an entirely unexpected direction.

After I returned to Stony Brook, by a long, leisurely automobile drive from California with my family, and settled in again to my department (where I found the same arguments continuing that had been going on when I left) an unexpected event occurred. It had its beginning several years earlier, when a field service engineer for Varian, the leading NMR company, saw an opportunity and asked for my opinion on his idea of starting his own company to make or distribute specialized NMR equipment and supplies. His business plan seemed reasonable, and I encouraged him to go ahead. For a time the company thrived, and I was a member of the Board of Directors.

In May of 1971, however, some other members of the board compared notes with the company's banker and found that the company had engaged in some very dubious business practices and was, in fact, bankrupt. At a hastily called Board meeting, appropriate actions were weighed, and the banker, there as a guest, threatened to close the company that day unless someone he trusted could be persuaded to take over as President, Chairman of the Board, and Chief Executive Officer. I was the only academic on the Board, the semester had just ended, and the others believed that I was free for the summer, so that I was asked to take the job. I agreed, flew to the company headquarters in New Kensington, Pennsylvania, near Pittsburgh, at the beginning of each week and back to Stony Brook and my family and students for the weekend.

The developments at the company could supply the plot for a novel, but the incident that is important for my purpose here is that a postdoc arrived with tumor-bearing rats to check the proton NMR relaxation times of their tumors and normal tissues and organs. I was there to observe the experiments, and noted that large and consistent differences were obtained for specimens from all parts of the sacrificed animals and that the experiments seemed well-done. Some individuals were speculating that similar measurements might supplement or replace the observations of cell structure in tissues by pathologists, but the invasive nature of the animal procedure

was distasteful to me, the data too complex, and the sources of differences too obscure, to be relied upon for medical decisions. As I pondered the problem that evening, I realized that there might be a way to locate the precise origins of NMR signals in complex objects, and hence to form an image of the distributions of the nuclei in two or even three dimensions. That story, and its consequences, is told more fully elsewhere.

Shortly afterwards, I returned to my university for the fall semester, and a colleague took over my company responsibilities. The beginning of the new academic year was a very busy time, and I found some quiet moments to test my ideas about a mathematical approach to such imaging during attendance at seminars and then to consider practical aspects of the idea as the semester proceeded. In the meantime, I began dropping in on the new medical library of the university, which I passed each morning on the way to work, to spend a few minutes reading, in journals and books, about new developments, problems, and questions in medicine that a new imaging method might address. As I became more confident that these techniques could be both practical and useful, I gradually reoriented most of my research in that direction, then spent almost 30 years on developing the techniques and applications of NMR imaging, while chemistry as such became mostly a subject to be taught to students.

An exception, later to be significant, was my general interest in evolution and the origin of life, a topic that I addressed in guest lectures at my university and in selected teaching experiments for undergraduate laboratories. During this period, of course, my children were growing up, as they do, but my marriage was disintegrating. I began to be recognized for my imaging work, and my earlier scientific accomplishments began to be overshadowed by this new direction. At the same time, my efforts to expand the imaging studies, now named MRI by medical doctors, began to be seriously inhibited by administrative and political problems at Stony Brook. My marriage ended in divorce, and I formed a new personal attachment with Joan Dawson, an American physiologist, working at University College, London, whose field was muscle biophysics and physiology, as studied mostly by NMR. If we were to be together, either she needed a new position at Stony Brook or we both needed new jobs elsewhere. After looking at several possibilities, and getting married in 1984, we accepted offers at the University of Illinois.

We moved to Urbana in 1985, with a new baby and high hopes for our professional lives, which were immediately dashed. A plan to share our time between the Urbana and Chicago campuses was foreclosed by technical and political problems in Chicago, and my intended equipment in Urbana, a new whole-body MRI machine associated with a hospital there, was unavailable because of a legal dispute. That problem was never resolved. The hospital eventually sold the machine, but I obtained a small animal-scale machine from the university and began new experiments. My laboratory was organized as the Biomedical Magnetic Resonance Laboratory, initially located in a rented building near campus. When the landlord, a hospital, decided to demolish the building to further its own plans, a small new building was built for my laboratory.

In the late nineteen nineties, that building, including my office, my laboratories, my staff, and all of my equipment, including that provided from university funds in 1985 and those items purchased from external grants over the years, were transferred to another university operation. My wife and I considered looking for new positions, but, in addition to having spent a great deal of time and money building a house, our daughter was in a very good high school, so we stayed. I had a joint appointment in the Department of Chemistry, and moved there, because I had already begun to think about a new approach to the origin of biology from chemistry and wanted to pursue that line of research. Thus, by the time the long-awaited Nobel Prize for MRI was awarded, I had left that field for another (and my daughter had entered college). I am now not only actively pursuing my new research interests, but learning the new skills in time management required of a Nobel Laureate.

Science

The title is not a tribute to some trendy hybrid field, but an introduction to a lecture on a Nobel Prize for Physiology or Medicine that is shared by a chemist and a physicist. Few events could illustrate more clearly the blending both at the boundaries, and sometimes through the bodies, of our disciplines. For that is what they are, disciplines, not natural categories with rigid boundaries to be defended against intrusions, but guides to instruction and efficient administration.

Historically, the record is clear. Chemistry, for example, was cobbled together from mystical alchemy, metallurgy, physics, mineralogy, medicine, and cookery, eliminating incompatibilities as it evolved and consolidated into a more-or-less unified discipline. Physics has been formed, and enriched, by contributions from astronomy, mechanics, mathematics, chemistry, and other sciences. We have recently observed the rationalization of much of biology by chemistry, with the help of physics.

Nuclear magnetic resonance began within physics, at a confluence among particle physics, condensed matter physics, spectroscopy, and electromagnetics. The discovery of ways to observe the subtle properties of atomic nuclei in solids, liquids, and eventually gases, earned Felix Bloch and Edward Purcell a Nobel Prize in Physics in 1952. Applications to studies of molecular motions and structures began almost immediately. The discoverers themselves, it is told, even used their own bodies as samples. In an early predecessor to MRI, Jay Singer measured blood flow in a human arm, and actual medical measurements were started when Erik Odeblad, a Swedish MD, constructed apparatus and devised methods to study very small quantities of human secretions for medical purposes. Biological studies followed, in other labs, using animal tissues, including hearts, and entire small animals.

In 1971, Raymond Damadian observed that some malignant tissue, obtained from tumors implanted into rats, had longer NMR relaxation times than many normal tissues. This observation caught the attention of several people, and Hollis decided to attempt to confirm and extend it by a study of a

related system, Morris hepatomas in rats, readily available to him at Johns Hopkins University. At one point, a postdoctoral fellow in his laboratory, Leon Saryan, brought some of the animals to the small company in western Pennsylvania which had actually carried out the earlier Damadian work. There, the rats were sacrificed and dissected and the tissue samples studied by NMR. I happened to be present to observe the entire process, for reasons described before, and, as a chemist not ordinarily involved with animal experiments, found them rather distasteful. All such NMR experiments were subject to error from nonuniformities in sample composition, the static magnetic field, and the radiofrequency magnetic field. However, the differences in the NMR signals from one tissue to another, normal as well as diseased, seemed robust in the experiments I observed. I thought they might actually be reproducible and useful, especially if the signal intensities, relaxation times, etc. could be measured from outside the living body with sufficient spatial resolution.

That evening, over dinner, it occurred to me that, as the frequencies of NMR signals depended on the local magnetic field, there might be a general way to locate them in a nonuniform magnetic field. I knew, however, that the strength of a static field could not have a unique value in each location in three dimensions, but that the complex shape of such a field could be represented by an expansion in a set of functions such as those provided by the correction fields ("shim" fields) available on NMR machines to cancel unwanted magnetic field nonuniformities, term by term, with linear gradients, quadratic ones, etc. Could this be the answer? A little reflection made me doubt it. I recalled that single-center expansions of molecular wave functions had been tried in quantum chemistry, but converged on useful solutions slowly and poorly. An alternative occurred to me. What if one used a large set of simple linear gradients, oriented in many directions in turn in three dimensions? I knew of no examples in any field. This was early September 1971, and X-ray computer tomography was not yet widely known, and neither had I encountered the similar ideas that were being tested in radioastronomy by Bracewell and in electron microscopy by Herman and Gordon, and by others in different fields. Nor did I know of any mathematics to solve such problems, but I recalled another idea from quantum chemistry, that when equations were not solvable in analytic form, an iterative method, in which approximate solutions were compared to known properties and systematically adjusted to a closer and closer fit, could be used.

To test this idea, I wrote down numbers such as 1s and 0s in small arrays 4×4 or even 8×8 square and added them along the vertical and horizontal directions, representing the one-dimensional data that would be generated by linear magnetic field gradients perpendicular to those directions; data at 45° and 135° was generated similarly. The "data" could then be "back-projected" across the image space as a series of bands and summed where they crossed, from which the trial image of summed intensities could be projected in each of the original directions for comparison with the actual "data", and modified by added or multiplicative terms to agree with it. The procedure might then be repeated, in hopes that the next computed trial image would be a closer approximation on

each cycle to the synthetic original one. I asked local mathematicians whether such a procedure was known and would work. All said they knew of no examples, and some said it was obviously valid, while others said it was clear that it would not converge, so I just tried it myself, with pencil and paper calculations. The result, with such simple mathematical "phantoms" (test objects) at least, was that the calculations converged very rapidly indeed. Later, a computer scientist with whom I had consulted came across a paper in a subsequent issue of a journal that used exactly my algorithm. This simultaneously validated the method and eliminated my claims to priority. I later learned that much work on the so-called "reconstruction from projections" problem had been published, by many people in many contexts, in recent years, almost all done independently in different fields. My real interest, however, was in the magnetic resonance imaging problem, and that remained unique.

I then turned my attention to the question of whether there would be enough NMR signal-to-noise ratio with large enough radiofrequency coils to surround a human body and the low magnetic fields I thought might be practical in resistive magnets over such large volumes. The standard reference, *Nuclear Magnetism*, by Abragam provided equations that suggested that the answer was favorable. At about the same time, my review of the magnet literature revealed that resistive magnets with fields of the order of 1000 G (0.1 T) and diameters of about 1 m could be constructed and operated economically with enough field uniformity to support the NMR experiments I had in mind.

Before I could start my research, there was another matter to resolve. A patent attorney at the company had advised me to do no experiments at my university, as they would compromise my patent position. He and I had been actively working on preparing patent application documents, in exchange for his fee of a percentage of any financial returns that might result. Unfortunately, a business dispute developed between us in connection with the company, and he declined to continue with our agreement. When that happened, I made a patent disclosure to my university, which in turn sent it to the organization they used to evaluate such documents and prepare patent applications.

In the meantime, I began experiments, preparing test objects by attaching 1-mm diameter glass melting point capillaries to the inside of 5-mm glass NMR sample tubes, the capillaries filled with ordinary water (H_2O) and the outer tubes with heavy water (D_2O). The reason for the D_2O was to roughly match the magnetic susceptibility across the sample so that the capillary signals would be less distorted than they would have been with air in that space. I first tried three capillaries, but the signals were too complex for easy interpretation, so I tried just two. I also tried using the linear gradients in the magnetic field supplied by the appropriate shim controls on a small analytical NMR spectrometer in the Chemistry Department, with 5-mm sample tubes filled with ordinary water. As expected, their projections were half-ellipses, or semicircles for the proper adjustment of the strength of the gradient.

For an actual test of the image mathematics on real data, I attached a paper disc, marked at intervals of 45° , to the outer

tube containing two capillaries and rotated it to orientations of 0, 45, 90 and 135° relative to the gradient direction while recording the NMR signal on a pen and ink recorder. I then digitized the recordings by measuring the height of the curves at intervals with a ruler and recording the numbers on a piece of paper, with the intervals corresponding to the projections of a square grid for each angle. The numbers were then transferred manually to punch cards that could be fed to a reader attached to the departmental instrument control computer, originally intended only to operate an X-ray diffractometer for single crystal structure determinations. Its memory (ferrite cores) was so limited that all calculations had to be made in integer (fixed point) mode, and intermediate results had to be punched out on a deck of cards to be reentered later for the next step, and each subprogram had to be kept on a separate deck of punched cards. The final result was then printed by a typewriter as a 20 × 20 array of numbers, and the “image” produced by hand-drawn contours on that array.

This seems tedious on later description but was exciting then because the whole process and its results were being encountered for the first time, especially as I recognized that the “pictures” were a new kind of image, based on principles completely different from those behind other imaging methods. To emphasize this point, I coined the new word “zeugmatography” (zeugma, Greek: connection, yoke) as a description, checking with a classical scholar for its fidelity to ancient roots and with a speaker of contemporary Greek to ensure that the meaning of “zeugma” had not shifted during later centuries.

Reassured, I used it in a manuscript I wrote for the journal *Nature*, which was summarily rejected. I felt this was a mistake, not because I foresaw all of the medical applications that would follow, but because of the physical uniqueness of the concept. I was also trying to think of another example that would work in practice, but it was to be over a quarter of a century later that an example, involving the differential shift of the spectra of two closely spaced atoms in an inhomogeneous electric field, was published, but the authors did not notice the similarities. My appeal to *Nature* was followed by submission of a revised version of my manuscript containing references to cancer and other more obviously relevant topics, and this time it was accepted.^[14] (Almost thirty years later, *Nature* publicly celebrated its appearance there.) Slightly earlier, I had presented my results in a short contributed paper at an American Physical Society meeting, which then had a policy of accepting any meeting talk by a member, but it was attended by only a handful of listeners, one of whom was a graduate student who told me that his professor had done the same thing, but I never found any evidence that he had. A similar pattern repeated itself several times in later years, with people telling me that they had the same ideas but had not followed them up with experiments and publication.

This work, and its subsequent elaborations, became the subject of my lectures afterward at most meetings I attended, including seminars. Before I began describing it in detail everywhere, however, the university's agent rejected the patent application because they felt that it could not generate enough funds to pay for the application process. I then asked

my university for permission to pursue the application independently but never received a reply. I was not in a financial position to quit my job and defy the university, and the grace period for applying for a US patent after publication had nearly expired, so I abandoned that idea and decided instead to encourage others to pursue this new technology, inviting everyone interested to visit my laboratory to observe our efforts and learn from us. People did come, from industry, academia, and government laboratories, foreign and domestic, and I began supplying a bibliography of such work to all and helping to organize meetings on the subject to compare our methods and results. Among these people were Professor Raymond Andrew and members of his group at Nottingham University, and Drs. Mansfield, Moore, and others there, as well as representatives of medical instrument companies and medical doctors and medical physicists themselves. As I hoped, interest began building as many other groups were involved.

We continued our work, which shortly involved graduate students and postdoctoral fellows as well as undergraduate research students, and, as I had hoped, more contributions were published by other laboratories, with some remarkable early images from Waldo Hinshaw in Andrew's group at Nottingham. As the depth and breadth of application grew, both large and small companies began to see opportunities, and within less than ten years commercial instruments began to come to market, large enough to hold a human being and to support true clinical research. Competitive pressures among physicians, industrial interest, and multiplying applications and techniques began to generate the explosive growth that was to characterize the past twenty years, leading, among other things, to the recognition of this phenomenon by the Royal Swedish Academy of Sciences. I and my group continued to make contributions through this period as well, some of them significant, but the most gratifying experiences emotionally were those when a stranger would volunteer “you saved my daughter's life”, or “your machine saved me from an unnecessary operation”. By the end of the millennium, despite the continuing excitement of the field, almost thirty years of a detour from chemistry to medical imaging began to pall, and I changed my focus to a field of chemical research, just in time for my past to catch up with me in the form of a Nobel Prize. All detours should be so productive!

The following list of references [1–63] is a selection out of 319 publications.

Received: October 22, 2004

- [1] “Filler Phenomena in Silicone Rubber”: E. L. Warrick, P. C. Lauterbur, *Ind. Eng. Chem.* **1955**, 47, 485–491.
- [2] “Nuclear Magnetic Resonance Field Shifts of Si29 in Various Materials”: G. R. Holzman, P. C. Lauterbur, J. H. Anderson, W. Koth, *J. Chem. Phys.* **1956**, 25, 172–173.
- [3] “Nuclear Magnetic Resonance Spectra of Phosphorus Compounds”: N. Muller, P. C. Lauterbur, J. Goldenson, *J. Am. Chem. Soc.* **1956**, 78, 3557–3561.
- [4] “¹³C Nuclear Magnetic Resonance Spectra”: P. C. Lauterbur, *J. Chem. Phys.* **1957**, 26, 217–218.

- [5] "Some Applications of C^{13} Nuclear Magnetic Resonance Spectra to Organic Chemistry": P. C. Lauterbur, *Ann. N. Y. Acad. Sci.* **1958**, 70, 841–857.
- [6] "Anisotropy of the C^{13} Chemical Shift in Calcite": P. C. Lauterbur, *Phys. Rev. Lett.* **1958**, 343.
- [7] " Sn^{119} Nuclear Magnetic Resonance Spectra": J. J. Burke, P. C. Lauterbur, *J. Am. Chem. Soc.* **1961**, 83, 326–331.
- [8] "Magnetic Shielding and the Electronic Structures of Aromatic Molecules": P. C. Lauterbur, *Tetrahedron Lett.* **1961**, 274–279.
- [9] "Nuclear Magnetic Resonance Spectra of Elements Other than Hydrogen and Fluorine": P. C. Lauterbur in *Determination of Organic Structures by Physical Methods*, Vol. 2 (Eds.: F. C. Nachod, W. D. Phillips), Academic Press, New York, **1962**, chap. 7, pp. 465–533.
- [10] " ^{13}C Nuclear Magnetic Resonance Spectroscopy. VI. Azines and Methyl Azines": P. C. Lauterbur, *J. Chem. Phys.* **1965**, 43, 360–363.
- [11] "Solvent Isotope Effects on Chemical Shifts of Ions in Aqueous Solutions": A. Loewenstein, J. Shporer, P. C. Lauterbur, J. E. Ramirez, *J. Chem. Soc. Chem. Commun.* **1968**, 214–215.
- [12] "Pseudorotation in Trigonal-Bipyramidal Molecules": P. C. Lauterbur, F. Ramirez, *J. Am. Chem. Soc.* **1968**, 90, 6722–6726.
- [13] " ^{13}C NMR Spectroscopy of Biopolymers": P. C. Lauterbur, E. J. Runde, B. L. Blitzer in *Magnetic Resonances in Biological Research* (Ed.: C. Franconi), Gordon and Breach, London, **1971**, pp. 355–364.
- [14] "Image Formation by Induced Local Interactions: Examples Employing Nuclear Magnetic Resonance": P. C. Lauterbur, *Nature* **1973**, 242, 190–191.
- [15] "Zeugmatographic High Resolution Nuclear Magnetic Resonance Spectroscopy. Images of Chemical Inhomogeneity within Microscopic Objects": P. C. Lauterbur, D. M. Kramer, W. V. House, Jr., C.-N. Chen, *J. Am. Chem. Soc.* **1975**, 97, 6866–6868.
- [16] "In Vivo Zeugmatographic Imaging of Tumors": P. C. Lauterbur, C.-M. Lai, J. A. Frank, C. S. Dulcey, Jr., *Physics in Canada* 32, Special July Issue: Digest of the Fourth International Conference on Medical Physics, Abstract 33.11, **1976**.
- [17] "NMR Studies of the Protein–Solvent Interface": P. C. Lauterbur, B. V. Kaufman, M. K. Crawford in *Biomolecular Structure and Function* (Ed.: P. F. Abris), Academic Press, New York, **1978**, pp. 329–351.
- [18] "Augmentation of Tissue Water Proton Spin–Lattice Relaxation Rates by In Vivo Addition of Paramagnetic Ions": P. C. Lauterbur, M. H. Mendonca Dias, A. M. Rudin in *Frontiers of Biological Energetics* (Eds.: P. O. Dutton, J. Leigh, A. Scarpa), Academic Press, New York, **1978**, pp. 752–759.
- [19] "The Sensitivity of the Zeugmatographic Experiment Involving Human Samples": D. I. Hoult, P. C. Lauterbur, *J. Magn. Reson. A* **1979**, 34, 425–433.
- [20] "On Two Approaches to 3D Reconstruction in NMR Zeugmatography": R. B. Marr, C.-N. Chen, P. C. Lauterbur in *Mathematical Aspects of Computed Tomography*, Vol. 8 (Eds.: G. T. Herman, F. Natterer), Springer, Berlin, **1981**, pp. 225–240.
- [21] "The Use of Paramagnetic Contrast Agents in NMR Imaging. II. In Vivo Studies": M. H. Mendonca Dias, P. C. Lauterbur, E. J. Brown, Jr., *Abstracts First Annual Meeting of the Society of Magnetic Resonance in Medicine*, Boston, **1982**, pp. 105–106.
- [22] "Aspects of Cardiac Diagnosis Using Synchronized NMR Imaging": E. Heidelberg, S. B. Petersen, P. C. Lauterbur, *Eur. J. Radiol.* **1983**, 3, 281–285.
- [23] "NMR Technology for Medical Studies": T. F. Budinger, P. C. Lauterbur, *Science* **1984**, 226, 288–298.
- [24] "Ferromagnetic Particles as Contrast Agents for Magnetic Resonance Imaging": M. H. Mendonca Dias, M. L. Bernardo, Jr., R. N. Muller, V. Acuff, P. C. Lauterbur, *Abstracts Fourth Annual Meeting of the Society of Magnetic Resonance in Medicine*, London, **1985**, p. 887.
- [25] "Cancer Detection by Nuclear Magnetic Resonance Zeugmatographic Imaging": P. C. Lauterbur, *Accomplishments in Cancer Research*, 1985 Prize Year, General Motors Cancer Research Foundation, J. B. Lippincott Co., Philadelphia, **1986**; also in *Cancer* **1986**, 57, pp. 1899–1904.
- [26] "Microscopic NMR Imaging": P. C. Lauterbur, L. Kyle Hedges, *Abstracts XXIII Congress Ampere on Magnetic Resonance*, Rome, **1986**, pp. 24–27.
- [27] "SLIM: Spectral Localization By Imaging": X. Hu, D. N. Levin, P. C. Lauterbur, T. Spraggins, *Magn. Reson. Med.* **1988**, 8, 314–322.
- [28] "Three Dimensional Electron Spin Resonance Imaging": R. K. Woods, G. Bacic, P. C. Lauterbur, H. M. Swartz, *J. Magn. Reson. A* **1989**, 84, 247–254.
- [29] "Relaxivity and Stabilities of Metal Complexes of Starburst Dendrimers: A New Class of MRI Contrast Agents": E. Wiener, P. C. Lauterbur, *Works-in-Progress Abstracts, Ninth Annual Meeting of the Society of Magnetic Resonance in Medicine*, New York, **1990**, p. 1106.
- [30] "NEUROVISION: A Software Tool for Functional MRI Neuroimaging Analysis": C. S. Potter, M. Banich, N. Cohen, A. Kramer, P. C. Lauterbur, H. D. Morris, *Abstracts SMRM/SMRI Functional MRI of the Brain Workshop*, Arlington, **1993**, p. 243.
- [31] "ChickScope: An Interactive MRI Classroom Curriculum Innovation for K-12": B. C. Bruce, B. O. Carragher, B. M. Damon, M. J. Dawson, J. A. Eurell, C. D. Gregory, P. C. Lauterbur, M. M. Marjanovic, B. Mason-Fossum, H. D. Morris, C. S. Potter, U. Thakkar, *Comput. Edu. J.* **1997**, 29, pp. 73–87.
- [32] "Principles of Magnetic Resonance Imaging: A Signal Processing Perspective": Z.-P. Liang, P. C. Lauterbur, IEEE, Piscataway, **1999**.
- [33] "The Structure of Chemical Matter and the Germs of Life": *Second Astrobiology Symposium*, NASA Ames Research Laboratory, **2002**, poster.
- [34] "The Chemical Origins of Biologies: Bootstrapping toward Life": P. C. Lauterbur, still unpublished.
- [35] "On The Signs of CH and HH Coupling Constants": P. C. Lauterbur, R. J. Kurland, *J. Am. Chem. Soc.* **1962**, 84, 3405.
- [36] "Stable Isotope Distributions by NMR Zeugmatography": P. C. Lauterbur, *Proceedings of the First International Conference on Stable Isotopes in Chem., Biol. and Med., U.S.A.E.C. CONF-730525*, **1973**, p. 255–260.
- [37] "Magnetic Resonance Zeugmatography": P. C. Lauterbur, *Pure Appl. Chem.* **1974**, 46, 149–157.
- [38] "Reconstruction from Selectively Excited Signals in Nuclear Magnetic Resonance Zeugmatography": P. C. Lauterbur, W. V. House, Jr., D. M. Kramer, C.-N. Chen, F. W. Porretto, C. S. Dulcey, Jr. in *Image Processing for 2-D and 3-D Reconstruction from Projections: Theory and Practice in Medicine and the Physical Sciences*, Opt. Soc. Am., **1975**, p. MA10-1-2.
- [39] "Water Proton Spin–Lattice Relaxation Times in Normal and Edematous Dog Lungs": P. C. Lauterbur, J. A. Frank, M. J. Jacobson, *Physics in Canada* 32, Special July Issue: Digest of the Fourth International Conference on Medical Physics, Abstract 33.9, **1976**.
- [40] "Nuclear Magnetic Resonance Zeugmatography for Medical Imaging": C.-M. Lai, W. V. House, Jr., P. C. Lauterbur, *Proceedings of IEEE Electro/78 Conference, Session 30, Technology for Non-Invasive Monitoring of Physiological Phenomena*, **1978**, paper 2.
- [41] " ^{31}P Spectroscopic Zeugmatography of Phosphorus Metabolites": P. Bendel, C.-M. Lai, P. C. Lauterbur, *J. Magn. Reson. A* **1980**, 38, 343–356.
- [42] "Zeugmatography by Reconstruction from Projections": P. C. Lauterbur, C.-M. Lai, *IEEE Trans. Nucl. Sci.* **1980**, 27, 1227–1231.

- [43] "True Three Dimensional Nuclear Magnetic Resonance Zeugmatographic Images of a Human Brain": D. M. Kramer, J. S. Schneider, A. M. Rudin, P. C. Lauterbur, *Neuroradiology* **1981**, *21*, 239–244.
- [44] "Nuclear Magnetic Resonance Zeugmatographic Imaging of the Heart: Application to the Study of Ventricular Septal Defect": M. A. Heneghan, T. M. Biancaniello, E. Heidelberger, S. B. Petersen, M. J. Marsh, P. C. Lauterbur, *Radiology* **1982**, *143*, 183–186.
- [45] "Three-dimensional Nuclear Magnetic Resonance Zeugmatographic Imaging of Surgical Specimens": M. H. Mendonca Dias, W. J. Mann, J. Chumas, M. L. Bernardo, Jr., P. C. Lauterbur, *Biosci. Rep.* **1982**, *2*, 713–717.
- [46] "3D Synchronized Proton NMR Imaging of the Beating Heart": E. Heidelberger, S. B. Petersen, P. C. Lauterbur, *Abstracts First Annual Meeting of the Society of Magnetic Resonance in Medicine*, Boston, **1982**, pp. 72–73.
- [47] "Gas Phase ^{19}F NMR Zeugmatography: A New Approach to Lung Ventilation Imaging": E. Heidelberger, P. C. Lauterbur, *Abstracts First Annual Meeting of the Society of Magnetic Resonance in Medicine*, Boston, **1982**, pp. 70–71.
- [48] "The Use of Paramagnetic Contrast Agents in NMR Imaging. I. Preliminary in vitro Studies": M. H. Mendonca Dias, P. C. Lauterbur, A. M. Rudin, *Abstracts First Annual Meeting of the Society of Magnetic Resonance in Medicine*, Boston, **1982**, pp. 103–104.
- [49] "Rapid Medium-Resolution 3-D NMR Zeugmatographic Imaging of the Head": M. L. Bernardo, P. C. Lauterbur, *Eur. J. Radiol.* **1983**, *3*, 257–263.
- [50] "True 3-D Imaging of Limbs by NMR Zeugmatography with Off-Resonance Irradiation": R. N. Muller, M. J. Marsh, M. L. Bernardo, P. C. Lauterbur, *Eur. J. Radiol.* **1983**, *3*, 286–290.
- [51] "Theory and Simulation of NMR Spectroscopic Imaging and Field Plotting by Projection Reconstruction Involving an Intrinsic Frequency Dimension": P. C. Lauterbur, D. N. Levin, R. B. Marr, *J. Magn. Reson. A* **1984**, *59*, 536–541.
- [52] "Experimental Example of NMR Spectroscopic Imaging by Projection Reconstruction Involving an Intrinsic Frequency Dimension": M. L. Bernardo, Jr., P. C. Lauterbur, L. K. Hedges, *J. Magn. Reson. A* **1985**, *61*, 168–174.
- [53] "Microscopic NMR Imaging of the Magnetic Fields Around Magnetite Particles": P. C. Lauterbur, M. L. Bernardo, Jr., M. H. Mendonca Dias, L. K. Hedges, *Works-in-Progress Abstract, Fifth Annual Meeting of the Society of Magnetic Resonance in Medicine*, Montreal, **1986**, pp. 229–230.
- [54] "Image Reconstruction": R. K. Woods, W. B. Hyslop, R. B. Marr, P. C. Lauterbur in *EPR Imaging and In Vivo EPR* (Eds.: G. R. Eaton, S. S. Eaton, K. Ohno), CRC, Boca Raton, **1991**, pp. 91–117.
- [55] "Simultaneous 3D-Localized, ^{31}P Spectroscopy of Brain and Muscle in the Intact Head of the Living Rat Using the SLIM Technique": E. S. Fletcher, C. D. Gregory, H. Lee, W. T. Greenough, P. C. Lauterbur, M. J. Dawson, *Works-in-Progress Abstracts, Ninth Annual Meeting of the Society of Magnetic Resonance in Medicine*, New York, **1990**, p. 1332.
- [56] "Effects of Restricted Diffusion on Microscopic NMR Imaging": W. B. Hyslop, P. C. Lauterbur, *J. Magn. Reson. A* **1991**, *94*, 501–510.
- [57] "Constrained Reconstruction Methods in MR Imaging": Z.-P. Liang, F. E. Boada, R. T. Constable, E. M. Haacke, P. C. Lauterbur, M. R. Smith, *Magn. Reson. Med.* **1992**, *4*, 67–185.
- [58] "RF Microcoils with Micron-scale Feature Sizes for NMR Microscopy": T. L. Peck, R. L. Magin, L. LaValle, I. Adesida, P. C. Lauterbur, *Abstracts 12th Annual Meeting of the Society of Magnetic Resonance in Medicine*, New York, **1993**, p. 296.
- [59] "Dendrimer-Based Metal Chelates: A New Class of MRI Contrast Agents": E. C. Wiener, M. W. Brechbiel, H. Brothers, R. L. Magin, O. A. Gansow, D. A. Tomalia, P. C. Lauterbur, *Magn. Reson. Med.* **1994**, *31*, 1–8.
- [60] "Is There a Role for Interactive Brain Mapping Over the World Wide Web?": P. C. Lauterbur, C. S. Potter, C. D. Gregory, H. D. Morris, *Abstracts International Symposium on Brain Mapping*, Oiso, **1996**, p. 42.
- [61] "Apparent Water Diffusion Measurements in Electrically Stimulated Neural Tissue": V. Gulani, G. A. Iwamoto, P. C. Lauterbur, *Magn. Reson. Med.* **1999**, *41*, pp. 241–246.
- [62] "Lactate Quantitation in a Gerbil Brain Stroke Model by GSLIM of Multiple-Quantum-Filtered Signals": J. A. Kmiecik, C. D. Gregory, Z.-P. Liang, P. C. Lauterbur, M. J. Dawson, *Magn. Reson. Imaging* **1999**, *9*, 539–543.
- [63] "Apparent Diffusion Tensor Measurements in Myelin Deficient Rat Spinal Cords": V. Gulani, A. G. Webb, I. D. Duncan, P. C. Lauterbur, *Magn. Reson. Med.* **2001**, *45*, 191–195.

Natural Products Synthesis

Chasing Molecules That Were Never There: Misassigned Natural Products and the Role of Chemical Synthesis in Modern Structure Elucidation

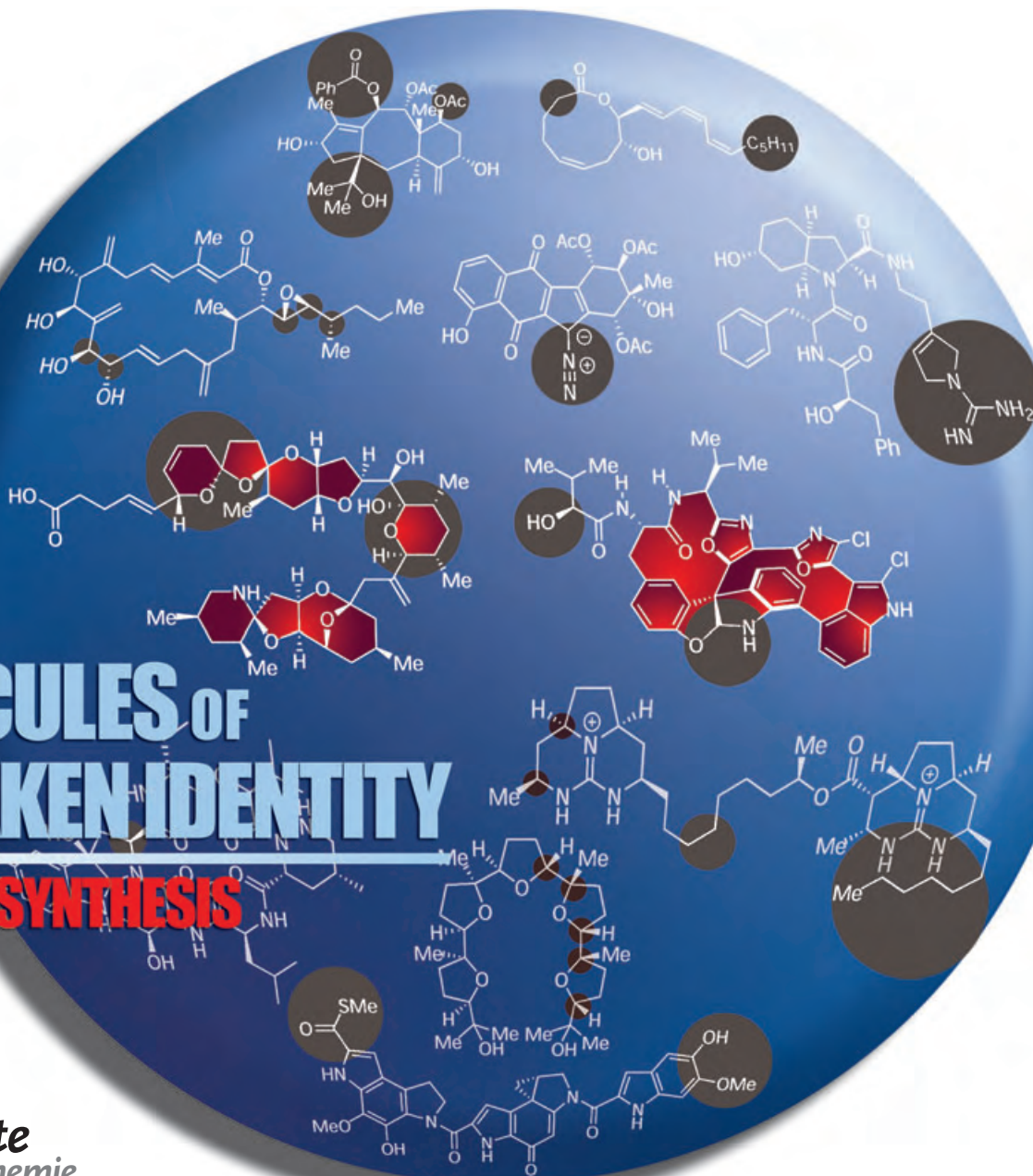
K. C. Nicolaou and Scott A. Snyder*

Keywords:

azaspiracid-1 · diazonamide A ·
natural products · revised structures ·
total synthesis

MOLECULES OF MISTAKEN IDENTITY & TOTAL SYNTHESIS

Angewandte
Chemie



Over the course of the past half century, the structural elucidation of unknown natural products has undergone a tremendous revolution. Before World War II, a chemist would have relied almost exclusively on the art of chemical synthesis, primarily in the form of degradation and derivatization reactions, to develop and test structural hypotheses in a process that often took years to complete when grams of material were available. Today, a battery of advanced spectroscopic methods, such as multidimensional NMR spectroscopy and high-resolution mass spectrometry, not to mention X-ray crystallography, exist for the expeditious assignment of structures to highly complex molecules isolated from nature in milligram or sub-milligram quantities. In fact, it could be argued that the characterization of natural products has become a routine task, one which no longer even requires a reaction flask! This Review makes the case that imaginative detective work and chemical synthesis still have important roles to play in the process of solving nature's most intriguing molecular puzzles.

1. Introduction

During all of the 19th century and most of the early half of the 20th century, natural product structure elucidation was an art that depended almost entirely on the power of chemical synthesis, or, more specifically, on the effectiveness of degradation or derivatization processes, to reveal the architectural design of a molecule. Assuming both that gram quantities of the substance under investigation were available and that the chemical transformations employed proceeded along expected lines, researchers of that era might have expected to solve their molecular puzzles after a few years of painstaking effort. The assignment of absolute or relative configuration was, of course, essentially out of the question in most cases.

Needless to say, this intellectually difficult and physically tedious approach had its limitations, and was often attended with errors. For example, during the 1920s there was tremendous interest in establishing the structures of a number of steroids. Although a formidable task that stymied many, two researchers in Germany, Wieland and Windaus, rose to the challenge and unraveled several of the key structural motifs of these molecules, leading them to propose a number of architectures, such as structure **1** for cholesterol (Figure 1).^[1] So impressed was the chemical community with this work that it ultimately served as part of the basis for their separate receipt of the Nobel Prize in Chemistry in 1927 and 1928, respectively. Unfortunately, as anyone today can instantly recognize, their proposals had a number of inaccuracies in terms of the core structure—mistakes that were revealed in 1932 when Bernal obtained the first X-ray crystal structure of a steroid (ergosterol (**2**), Figure 1).^[2]

Nevertheless, the near-exclusive use of chemical synthesis for structural elucidation did score a number of remarkable successes, such as correct assignments for the natural products quinine (**4**)^[3] and haemin (**5**)^[4] prior to the start of World War II, and strychnine (**6**) in 1946 (Figure 2).^[5] Equally

From the Contents

1. Introduction	1013
2. The State of Modern Structure Elucidation	1015
3. The Ramifications of Structural Misassignments	1026
4. Misassignment Case Studies	1029
5. Summary and Outlook	1037

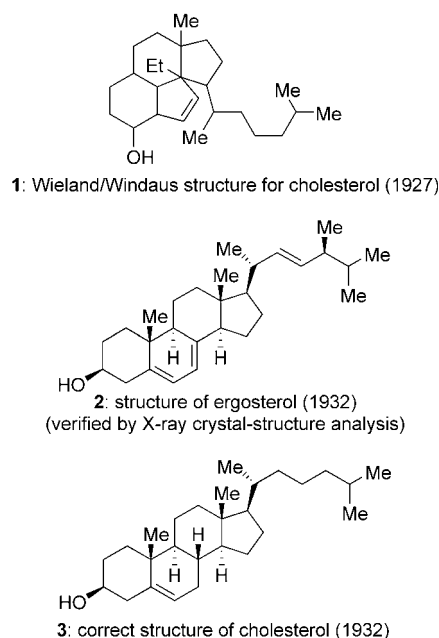


Figure 1. A classical misassignment: Wieland and Windaus were awarded the Nobel Prize in Chemistry in 1927 and 1928, respectively, for deriving structures of natural products, such as their proposed structure **1** for cholesterol.

[*] Prof. Dr. K. C. Nicolaou, Dr. S. A. Snyder
Department of Chemistry and
The Skaggs Institute for Chemical Biology
The Scripps Research Institute
10550 North Torrey Pines Road, La Jolla, CA 92037 (USA)
Fax: (+1) 858-784-2469
E-mail: kcn@scripps.edu
and
Department of Chemistry and Biochemistry
University of California, San Diego
9500 Gilman Drive, La Jolla, CA 92093 (USA)

important, if not more so, these efforts also served as the principle driving force for the discovery of new chemical reactivity. Indeed, much of our present knowledge regarding heterocyclic chemistry was established through structural work directed towards the targets shown in Figure 2, among

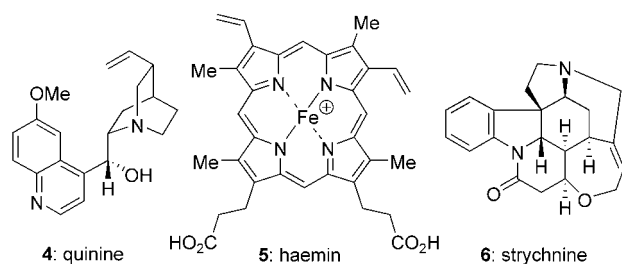
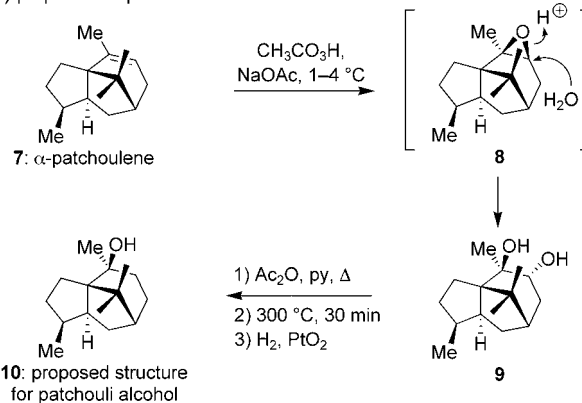


Figure 2. Quinine (4), haemin (5), and strychnine (6): The elucidation of the structures of these natural products inspired a great deal of new chemistry.

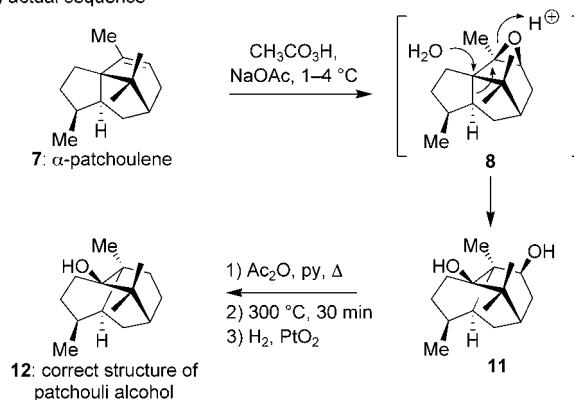
others, just as work focused on confirming the connectivities of the steroids afforded insight into how carbon–carbon bonds could be forged and cleaved. Phrased differently, as recently formulated by Doering: “In the beginning, the isolation of chemicals from natural sources provided an unceasing stimulus to the creation and development of science.”^[6]

By contrast, total synthesis played almost no role as a vehicle for chemical discovery during these early days. Instead, it served as the means to obtain a final proof of structure once degradative work had been completed, under the belief that if synthetically derived material matched its natural counterpart in all respects, then the proposed structure must be correct. This assumption was an accurate one for the most part, though it, too, could lead to misassignments. A classic example resides in work directed towards patchouli alcohol, a natural product that had been assigned structure **10** (Scheme 1) in 1961 by Büchi and his colleagues at the Massachusetts Institute of Technology (MIT) after several years of careful study.^[7] In 1962, the Büchi group felt that they had confirmed their structural proposal by obtaining synthetic material that corresponded fully to authentic patchouli alcohol in just four steps from another natural product, α -patchoulene (**7**).^[8] As shown in Scheme 1 a, those operations were: 1) epoxidation of the double bond in **7** followed by nucleophilic ring opening to generate diol **9**; 2) acetylation of

a) proposed sequence



b) actual sequence



Scheme 1. The total synthesis of patchouli alcohol by Büchi et al. caused faith to be placed in the wrong structure for the natural product (they postulated **10** instead of **12**). The error occurred as a result of an unexpected skeletal rearrangement.

the resulting secondary alcohol; 3) thermally induced elimination of the newly formed acetate; and 4) hydrogenation of the resulting olefin.

Although this synthesis should have provided the final verdict on the structure of patchouli alcohol, the case was reopened a year later when Dunitz and his colleagues at the Eidgenössische Technische Hochschule Zürich obtained an X-ray crystal structure of a diester derivative that suggested that **12**, rather than **10**, was the structure of patchouli alcohol.^[9] What had happened? Well, the problem did not



K. C. Nicolaou was born in Cyprus and educated in England and the USA. He is currently Chairman of the Department of Chemistry at The Scripps Research Institute, and is also Professor of Chemistry at the University of California, San Diego. His impact on chemistry, biology, and medicine is reflected in nearly 600 publications and 57 patents, and he has trained hundreds of graduate students and postdoctoral fellows. His *Classics in Total Synthesis* series, co-authored with Erik J. Sorensen and Scott A. Snyder, is a source of inspiration for students and organic chemists around the world.



Scott A. Snyder, born in Palo Alto, California, received his BA in chemistry from Williams College in 1999. He completed his PhD in May 2004 at The Scripps Research Institute with K. C. Nicolaou on the total synthesis of diazonamide A and is currently an NIH postdoctoral fellow with E. J. Corey at Harvard University. He is co-author of *Classics in Total Synthesis II* and has contributed to over 30 publications, review articles, book chapters, and patents. He received predoctoral fellowships from the National Science Foundation, Pfizer, and Bristol-Myers Squibb.

lie with the crystal structure or with the sequence employed by the MIT team. Instead, the discrepancy resulted from an unanticipated skeletal rearrangement that had occurred in the Büchi synthesis when **7** was treated with peracid, an operation that fortuitously generated the correct architecture of the natural product as represented by **11**.^[10] A lucky coincidence, indeed!

By the late 1960s, the chances of encountering such an unanticipated outcome during efforts towards structure elucidation dropped precipitously as the “classical” chemical approach was gradually replaced by a far more accurate battery of nondestructive methods, such as nuclear magnetic resonance (NMR), ultraviolet (UV), and infrared (IR) spectroscopy, circular dichroism (CD), and mass spectrometry (MS).^[11] Today, these methods have grown both in number and power to the extent that a researcher seeking to characterize a few milligrams of an unknown natural product would probably rely entirely on spectroscopic techniques to obtain a complete structural assignment. The benefits, at least based on some recently assigned natural product structures, are clear: Far more complex molecules can be tackled in far less time, even when the compounds are isolated in miniscule amounts. Furthermore, for synthetic chemists, discovery has become intricately linked to processes other than degradation, such as total synthesis. Even as early as 1963, the chemical community keenly perceived the power of these changes, as evidenced by the following remarks:

If penicillin were discovered today ... the scientific problems of studying a pure crystalline compound with a molecular weight of about 350 would not have been nearly so difficult. The conclusion is that a good graduate student would probably work out the structure of penicillin in a day or so. Just a generation ago, that same scientific feat took the best of us years of intensive work.

John C. Sheehan (1982)^[12]

We have now reached the stage where often we have insufficient material for a retention sample; where crystallization is not worth attempting; where determination of a melting point may be a prohibitive waste of material; and yet, where we have learned more about the structure of that molecule than we did years ago with grams of substance.

Carl Djerassi (1980)^[13]

While it is undeniable that organic chemistry will be deprived of one special and highly satisfying kind of opportunity for the exercise of intellectual *élan* and experimental skill when the tradition of purely chemical structure elucidation declines, it is true too that the not infrequent dross of such investigations will also be shed; nor is there any reason to suppose that the challenge for the hand and the intellect must be less, or the fruits less tantalizing, when chemistry *begins* at the advanced vantage point of an established structure.

R. B. Woodward (1963)^[5d]

At the same time, these advances have also left some (especially those who “grew up” during the classical era) with

a lingering sense that something important and valuable has been lost, that the practice of structure elucidation can never again provide the drama it once did:

Today ... spectroscopic methods have almost entirely supplanted this classical approach, and therewith deprived the science of a rich inexhaustible source of unpremeditated discoveries.

W. von E. Doering (1999)^[6]

Until the mid-1960s, structure determination was an art that could be likened to solving a complicated detective case, but with the spectacular advancement in spectroscopy it has become less inspiring, and since the mid-1980s, in most cases, structure determination has become rather “routine”.

Koji Nakanishi (1991)^[14]

In any event, progress can not be reversed, and, at present, our spectroscopic abilities have converted chemical synthesis into its own highly specialized and rewarding discipline, one that has little to do with structure elucidation apart from the assignment of absolute or relative stereochemistry in those cases where spectroscopy or X-ray crystallography can not provide the answer. We might be able to gauge the current state of the field of structural elucidation by considering molecules such as palytoxin (**13**, Figure 3), a compound whose highly ornate architecture was established almost completely by spectroscopic means with synthesis filling in the missing stereochemical information.^[15] A number of other examples could also be used as a barometer. To mention just one, synthesis has not yet made its final mark on amphidinolide N (**14**). With nine unassigned stereocenters, the correct structure is one of 512 possible isomers!^[16]

Certainly a rosy picture, but is it completely accurate? Are structural elucidations mostly uneventful endeavors? Have spectroscopic techniques made the process of characterization one almost devoid of errors? Is there no role for total synthesis beyond stereochemical assignment? Herein we address these issues and hope to succeed in convincing you not only that chemical synthesis still has much to offer, but also that there is a long way to go before natural product characterization can be considered a process devoid of adventure, discovery, and, yes, even unavoidable pitfalls.

2. The State of Modern Structure Elucidation

As a starting point for tackling some of the questions listed above, we searched a variety of scientific databases for a series of keyword terms, such as “structural misassignment” and “revised structure”, to ascertain just how frequently natural products have been incorrectly assigned during the past few years.^[17] We expected to find only a few errors, with most of these arising from a misassigned stereocenter or two, and those in only the most complex or unique of structures. The actual output proved to be very different. Limiting our search to literature published from January 1990 to April 2004, we uncovered the existence of well over 300 structural revisions, many of which extended far beyond simple stereo-

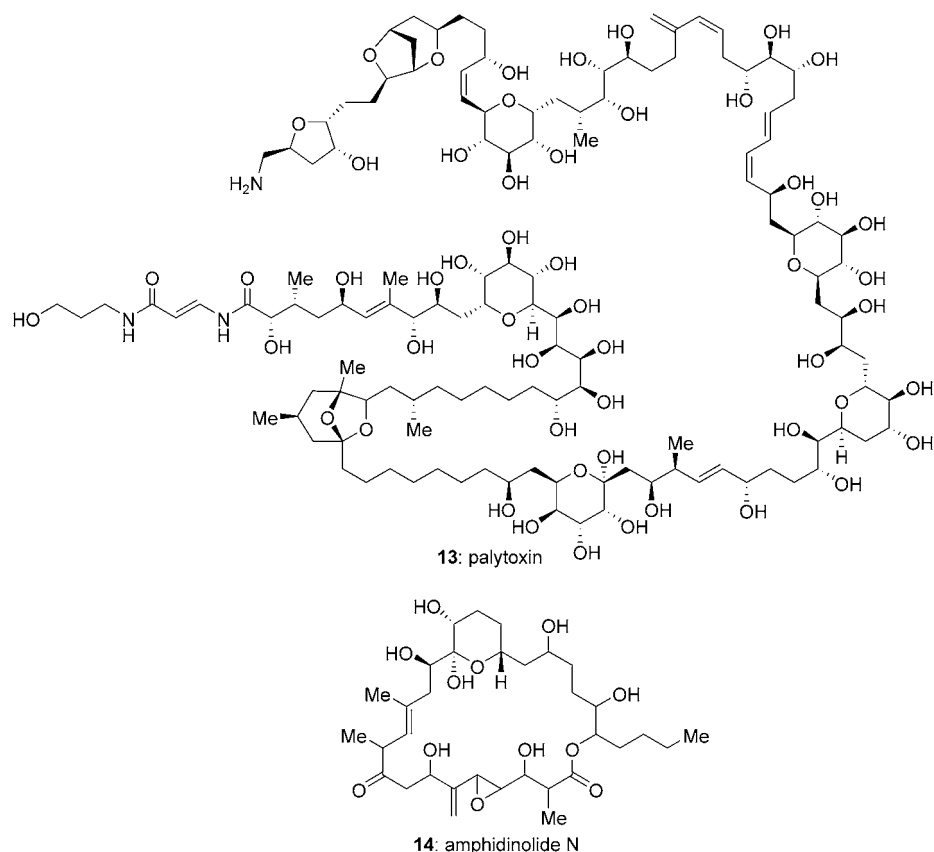


Figure 3. Determination of absolute/relative configuration: the last frontier of chemical-structure elucidation? The structure of palytoxin (**13**) was ultimately determined by chemical synthesis. In the proposed structure of amphidinolide N (**14**) the configurations of nine stereocenters remain unassigned.

chemical problems into the realm of profound, and sometimes complete, constitutional changes. Tables 1 to 8 present 50 members of this collection in no particular order. Amazingly, the examples cover virtually every compound class, including steroids, terpenes, indole alkaloids, and peptides, and encompass molecules of all sizes and levels of stereochemical complexity.

Clearly, this diverse array of structures reveals that mistakes are still a common occurrence despite our present advantages. But why do so many errors occur? The answer certainly does not place into question the skills of the scientists who made the original structural determination. On the contrary, it is amazing just how many complicated natural products have been assigned correctly, especially when only limited material was available or the natural substance in question was unlike any other ever observed. Instead, the number of errors simply reflects the fact that *every* method for assignment has its weaknesses, some of which can not be resolved even if every other tool for structural elucidation is also applied.

For example, although X-ray crystallography is traditionally viewed as an infallible technique, it can occasionally lead to misassignments because it does not reveal the positions of hydrogen atoms (those shown in any crystal structure have always been drawn in). Consequently, it is sometimes difficult

to discern between O atoms and NH groups, as discussed at some length with an example in Section 4. X-ray crystallography can also confuse the identity of atoms within certain functional groups devoid of hydrogen atoms. Table 4 shows an example in which the assignment of a C atom instead of an N atom (a cyano rather than a diazo group) led to a long-standing incorrect structure for the kinamycins.^[70–72]

NMR spectroscopy, too, can only provide so much of the overall picture, especially in the case of molecules with insufficient hydrogen atoms to obtain the ^1H , ^{13}C correlations needed to assign their deeper domains properly. Many of the structural revisions in the tables fall into this category, even though a number of powerful two-dimensional techniques, such as INEPT, HMBC, HMQC, and TOCSY, were applied. In some cases, even NMR spectroscopy is of little use as a tool despite its awesome power, and more basic methods, such as IR spectroscopy, become the principal source of structural information. Such was the case with the unnamed coumarin shown in Table 2, a compound whose structure proved exceedingly difficult to ascertain considering its relatively small size.^[39,40]

Of course, structural assignments are rarely based on just one method and are typically the culmination of a careful refinement process that considers a variety of architectural possibilities, pruned only when new information is added to the overall picture. Consequently, assignment errors are often the result of faith placed in spectroscopic data that is actually spurious, as incorrect structures that should have been excluded early in the process can then survive. For example, in their effort to assign a structure to halipeptin A (see Table 1), the research group of Gomez-Paloma used high-resolution mass spectrometric data obtained by the fast-atom bombardment (FAB) technique to identify its molecular formula. Their finding ($\text{C}_{31}\text{H}_{54}\text{N}_4\text{O}_8$) was then combined with information from other sources (primarily NMR spectroscopy) to generate a proposed structure that included a unique four-membered ring linked to a carbonyl group at the core of the molecule.^[27] However, upon reinvestigation of the molecular formula a year later by using a different high-resolution mass spectrometric technique (electron-spray ionization, ESI), the data now suggested that the molecular formula $\text{C}_{31}\text{H}_{54}\text{N}_4\text{O}_6\text{S}$ was a far better match for halipeptin A (i.e., the exchange of two oxygen atoms for a sulfur atom). Consequently, a very different structural assignment for the central portion of the molecule resulted.^[28] A similar type of mass spectrometric error was responsible the misassignment of a portion of didemnis-

Table 1: Selected structures of misassigned natural products and proposed structural revisions.

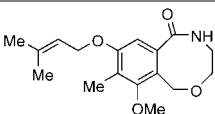
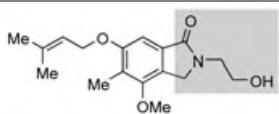
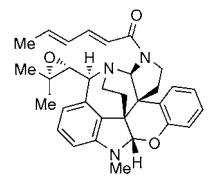
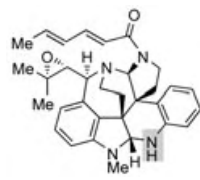
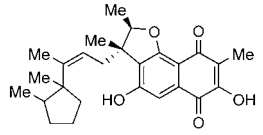
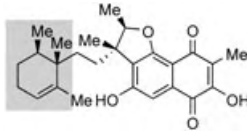
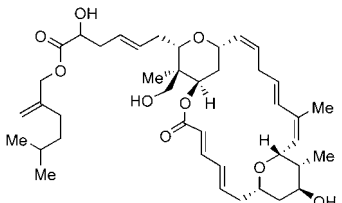
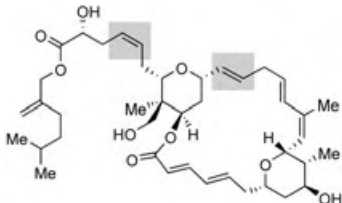
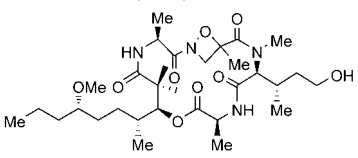
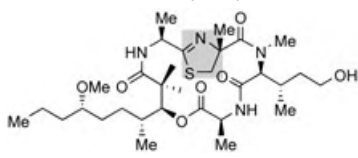
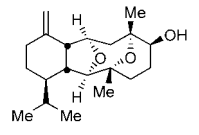
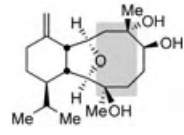
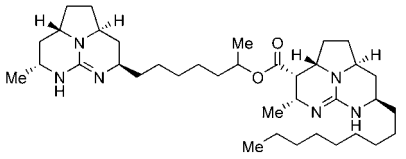
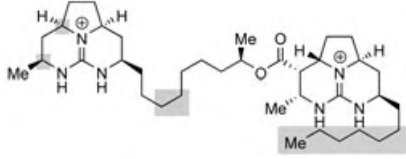
Proposed structure	Methods used in original assignment	Revised structure and basis for revision	Verified by total synthesis
 porritoxin Suemitsu et al. (1992) ^[18]	NMR UV IR MS	 2D NMR experiments Horiuchi et al. (2002) ^[19]	Cornella and Kelly (2004) ^[20]
 nomofungin Hemscheidt et al. (2001) ^[21]	NMR UV IR CD MS	 comparison with literature data for another natural product Stoltz et al. (2003) ^[22]	no
 neomarinone Fenical et al. (2000) ^[23]	NMR UV IR MS	 2D NMR spectroscopy and feeding experiments Moore et al. (2003) ^[24]	no
 lasonolide A McConnell et al. (1994) ^[25]	NMR IR MS	 chemical synthesis Lee et al. (2002) ^[26]	Lee et al. (2002) ^[26]
 halipeptin A Gomez-Paloma et al. (2001) ^[27]	NMR UV IR MS derivatization	 reevaluation of MS data and chemical synthesis Gomez-Paloma et al. (2002) ^[28]	no
 sclerophytin A Sharma and Alam (1988) ^[29]	NMR IR MS	 2D NMR spectroscopy and chemical synthesis Paquette et al. (2000) ^[30]	Overman, Paquette, et al. (2001) ^[31]
 batzelladine F Faulkner et al. (1997) ^[32]	NMR UV IR MS	 reevaluation of MS data and chemical synthesis Cohen and Overman (2001) ^[33]	Cohen and Overman (2001) ^[33]

Table 2: Selected structures of misassigned natural products and proposed structural revisions.

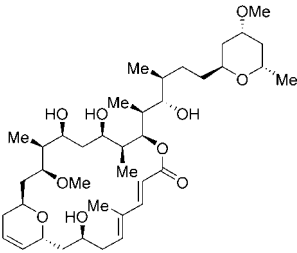
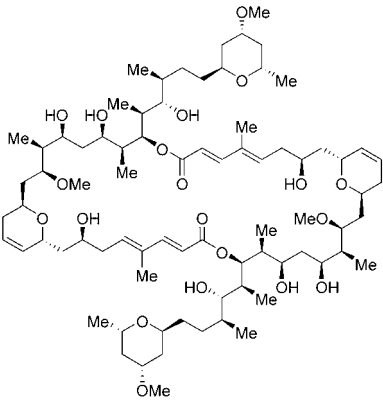
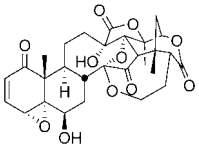
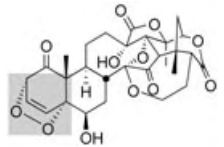
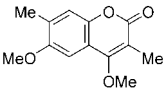
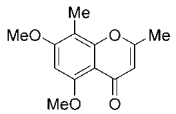
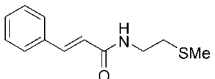
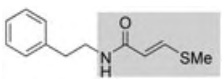
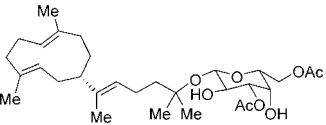
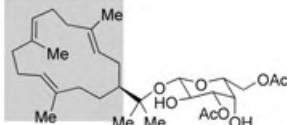
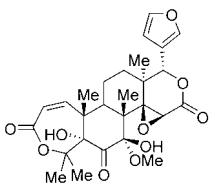
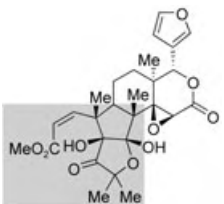
Proposed structure	Methods used in original assignment	Revised structure and basis for revision	Verified by total synthesis
 <p>swinholide A Carmely and Kashman (1985)^[34]</p>	NMR UV IR MS	 <p>reisolation and reexamination Kitagawa et al. (1990)^[35]</p>	Paterson et al. (1994) ^[36]
 <p>physalin K Ramachandra Row et al. (1980)^[37]</p>	NMR EA UV IR CD MS derivatization	 <p>isolation of related compounds and more detailed spectroscopic investigations Kawai et al. (1995)^[38]</p>	no
 <p>unnamed coumarin Atta-Ur-Rahman et al. (1991)^[39]</p>	NMR UV IR MS	 <p>chemical synthesis Kalinin and Snieckus (1998)^[40]</p>	Kalinin and Snieckus (1998) ^[40]
 <p>sinharine Hofer et al. (1992)^[41]</p>	NMR UV IR MS	 <p>chemical synthesis Johnson et al. (1994)^[42]</p>	Johnson et al. (1994) ^[42]
 <p>calyculaglycoside A Rodríguez et al. (1997)^[43]</p>	NMR UV IR MS degradation	 <p>isolation of related compounds, biogenetic considerations, and degradation Rodríguez et al. (2001)^[44]</p>	no
 <p>harrisonin Nakanishi et al. (1976)^[45]</p>	NMR UV IR CD MS	 <p>X-ray crystallography and 2D NMR spectroscopy Fischer et al. (1997)^[46]</p>	no

Table 3: Selected structures of misassigned natural products and proposed structural revisions.

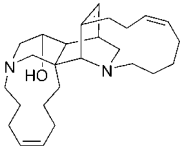
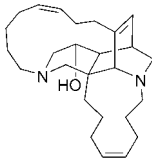
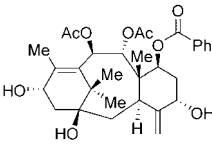
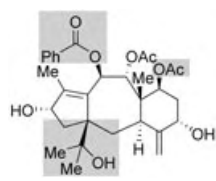
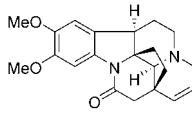
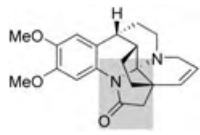
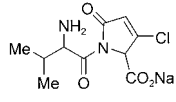
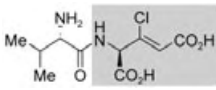
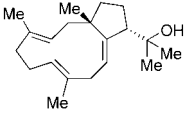
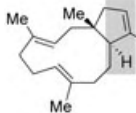
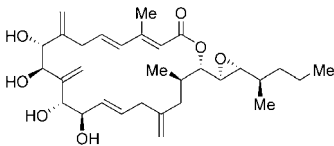
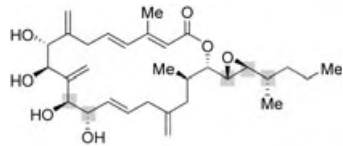
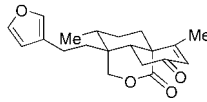
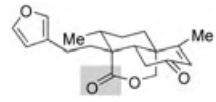
Proposed structure	Methods used in original assignment	Revised structure and basis for revision	Verified by total synthesis
 xestocyclamine A Crews et al. (1993) ^[47]	NMR IR MS	 isolation of related compounds and reevaluation Rodríguez and Crews (1994) ^[48]	no
 brevifoliol Tachibana et al. (1991) ^[49]	NMR IR MS	 reisolation and reexamination Georg et al. (1993) ^[50]	no
 isoschizogamine Renner and Fritz (1965) ^[51]	NMR EA UV IR derivatization	 reisolation and 2D NMR spectroscopy Hájíček et al. (1998) ^[52]	Hubbs and Heathcock (1999) ^[53]
 FR900148 Kuroda et al. (1980) ^[54]	NMR EA IR derivatization	 reisolation and reexamination Yasuda and Sakane (1991) ^[55]	no
 palominol Rodríguez et al. (1990) ^[56]	NMR IR MS derivatization	 isolation of related compounds and comparison of spectra Shin and Fenical (1991) ^[57]	Corey and Kania (1998) ^[58]
 (+)-amphidinolide A Kobayashi et al. (1991) ^[59]	NMR UV IR CD MS derivatization	 chemical synthesis Trost and Harrington (2004) ^[60]	Trost and Harrington (2004) ^[60]
 sacacarin Maciel et al. (1998) ^[61]	NMR UV IR MS	 chemical synthesis Grossman and Rasne (2001) ^[62]	Grossman and Rasne (2001) ^[62]

Table 4: Selected structures of misassigned natural products and proposed structural revisions.

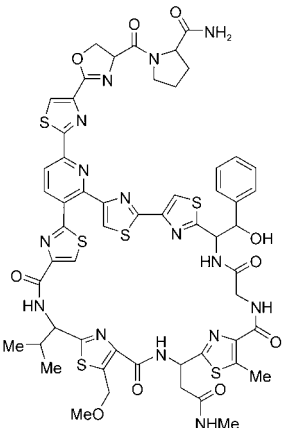
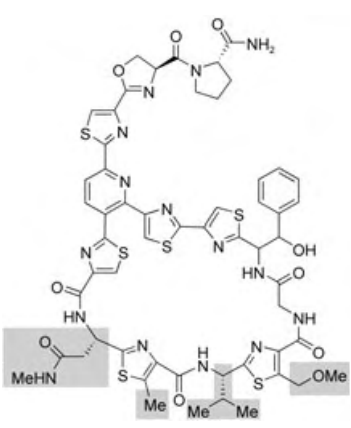
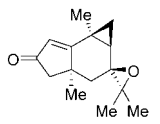
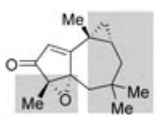
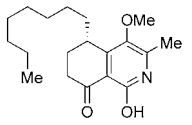
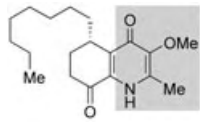
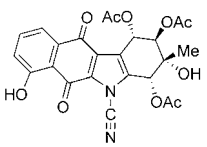
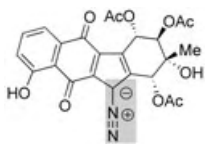
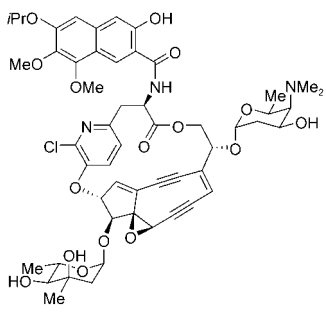
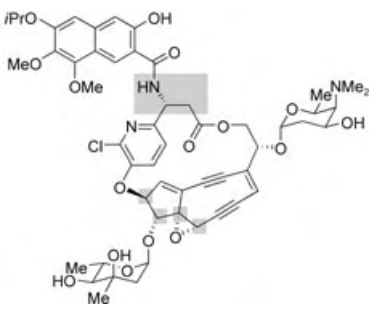
Proposed structure	Methods used in original assignment	Revised structure and basis for revision	Verified by total synthesis
 <p>GE2270A Ferrari et al. (1991)^[63]</p>	NMR EA UV IR MS degradation	 <p>degradation and chemical synthesis Tavecchia et al. (1995)^[64]</p>	no ^[65]
 <p>caespitenone Asakawa et al. (1980)^[66]</p>	NMR UV IR MS derivatization	 <p>2D NMR spectroscopy Asakawa et al. (1993)^[67]</p>	no
 <p>antidesmone Bringmann et al. (1999)^[68]</p>	NMR UV CD IR MS derivatization	 <p>feeding experiments Bringmann et al. (2000)^[69]</p>	no
 <p>kinamycin C Ômura et al. (1973)^[70]</p>	X-ray crystallography NMR UV IR MS degradation derivatization	 <p>2D NMR spectroscopy and chemical synthesis Gould et al. (1994)^[71] and Dmitrienko et al. (1994)^[72]</p>	no
 <p>kedarcidin chromophore Leet et al. (1992)^[73]</p>	NMR UV IR MS degradation derivatization	 <p>chemical synthesis Hirama et al. (1997)^[74]</p>	no ^[75]

Table 5: Selected structures of misassigned natural products and proposed structural revisions.

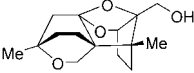
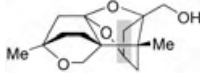
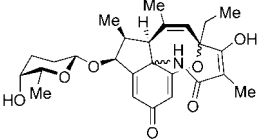
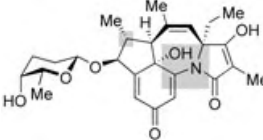
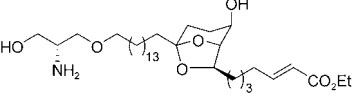
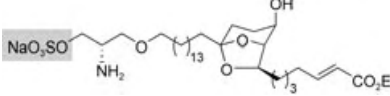
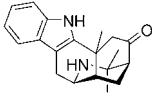
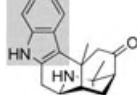
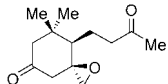
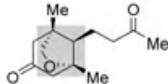
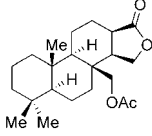
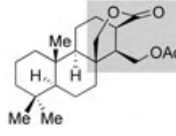
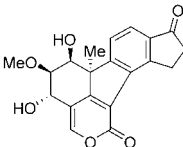
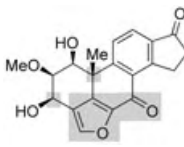
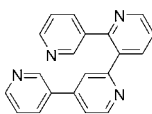
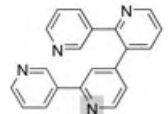
Proposed structure	Methods used in original assignment	Revised structure and basis for revision	Verified by total synthesis
 sporol Tempesta et al. (1986) ^[76]	NMR IR MS	 NMR spectroscopy and chemical synthesis Ziegler et al. (1988) ^[77]	Ziegler et al. (1992) ^[78]
 tetrapetalone A Hirota et al. (2003) ^[79]	NMR UV IR MS derivatization	 ¹ H- ¹⁵ N HMBC spectroscopy Hirota et al. (2003) ^[80]	no
 (+)-didemniserinolipid B Jiménez et al. (1999) ^[81]	NMR UV IR MS	 MS and chemical synthesis Ley et al. (2002) ^[82]	Ley et al. (2002) ^[82]
 (+)-aristolasicone Husson et al. (1988) ^[83]	NMR UV IR CD MS derivatization	 X-ray crystallography and chemical synthesis Borschberg et al. (1991) ^[84]	Borschberg et al. (1991) ^[84]
 annuionone A Macías et al. (1998) ^[85]	NMR IR MS	 reevaluation of NMR spectroscopic data Takikawa et al. (2003) ^[86]	Takikawa et al. (2003) ^[86]
 aplyroseol-14 Taylor and Toth (1997) ^[87]	NMR MS	 chemical synthesis Arnó et al. (2003) ^[88]	Arnó et al. (2003) ^[88]
 TAEMC161 Nakajima et al. (2000) ^[89]	NMR UV IR MS	 comparison with literature data for another natural product Wipf and Kerekes (2003) ^[90]	no
 nemertelline Kern et al. (1976) ^[91]	NMR MS	 X-ray crystallography and chemical synthesis Zoltewicz and Cruskie (1995) ^[92]	Zoltewicz et al. (1995) ^[93]

Table 6: Selected structures of misassigned natural products and proposed structural revisions.

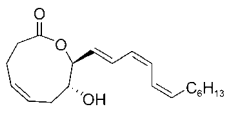
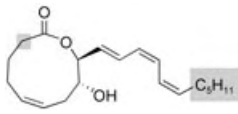
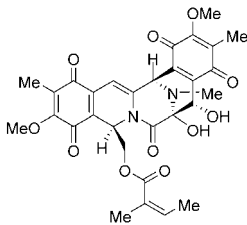
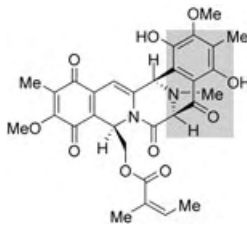
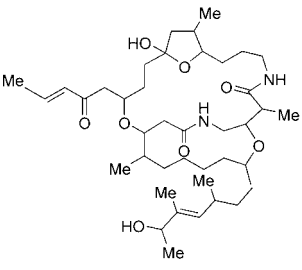
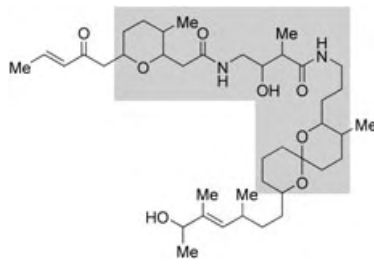
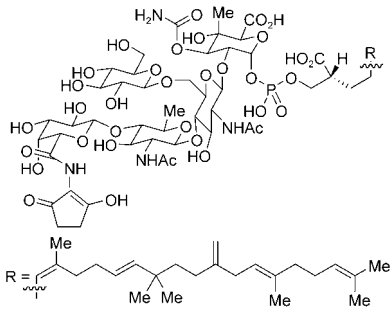
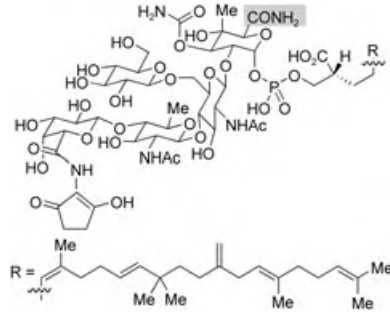
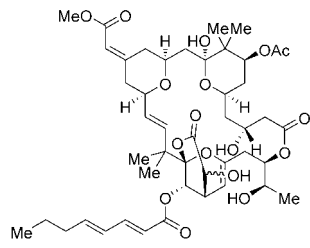
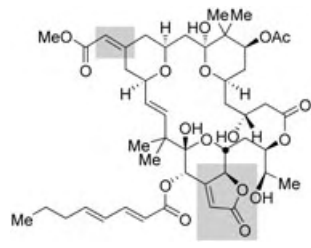
Proposed structure	Methods used in original assignment	Revised structure and basis for revision	Verified by total synthesis
 <p>ascidiatrienolide A Lindquist and Fenical (1989)^[94]</p>	NMR UV IR MS	 <p>chemical synthesis Holmes et al. (1993)^[95]</p>	Holmes et al. (1993) ^[95]
 <p>renieramycin H Parameswaran et al. (1998)^[96]</p>	NMR UV IR MS	 <p>2D NMR spectroscopy and X-ray crystallography Saito et al (2001)^[97]</p>	no
 <p>bistramide A Hawkins et al. (1989)^[98]</p>	NMR MS	 <p>reisolation and reevaluation Ireland et al. (1992)^[99]</p>	no
 <p>moenomycin A Riemer et al. (1981)^[100]</p>	NMR MS degradation derivatization	 <p>MS and 2D NMR spectroscopy Fehlhaber et al. (1990)^[101]</p>	no
 <p>bryostatin 3 Pettit et al. (1983)^[102]</p>	NMR UV MS	 <p>2D NMR spectroscopy Schaufelberger et al. (1991)^[103]</p>	Yamamura et al. (2000) ^[104]

Table 7: Selected structures of misassigned natural products and proposed structural revisions.

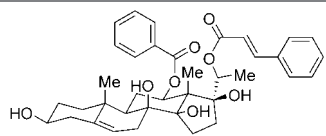
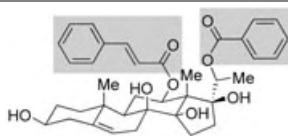
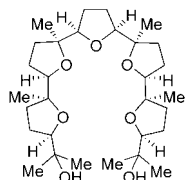
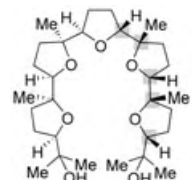
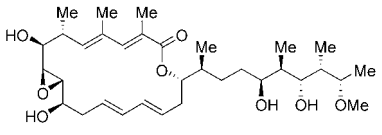
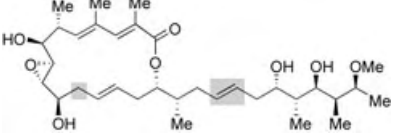
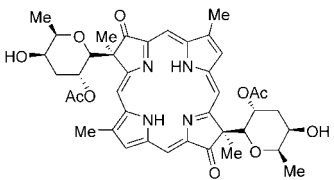
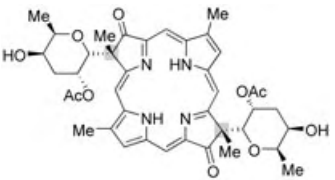
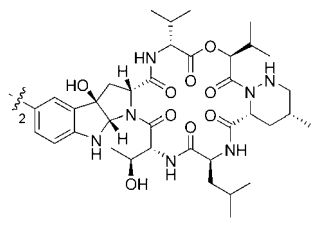
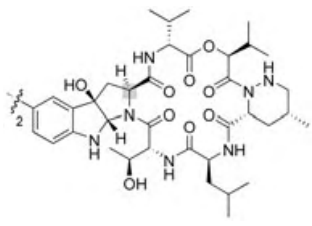
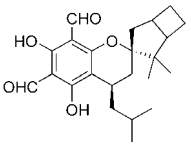
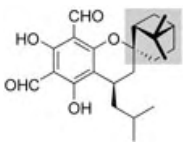
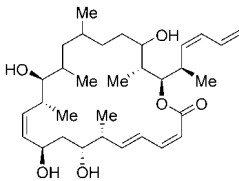
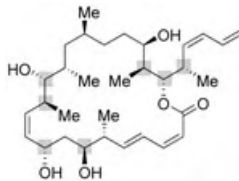
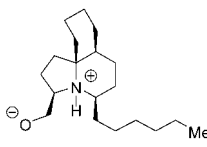
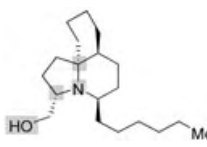
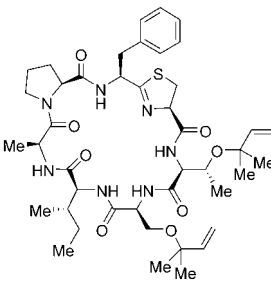
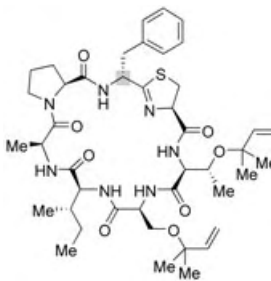
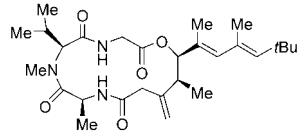
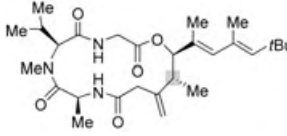
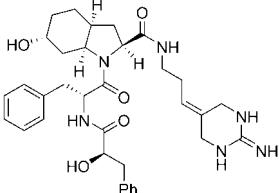
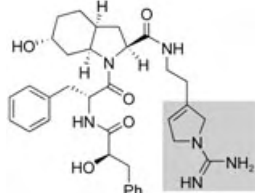
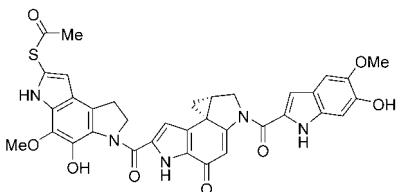
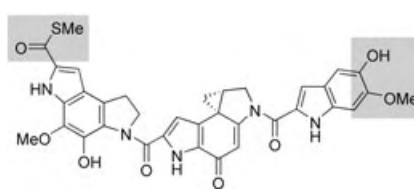
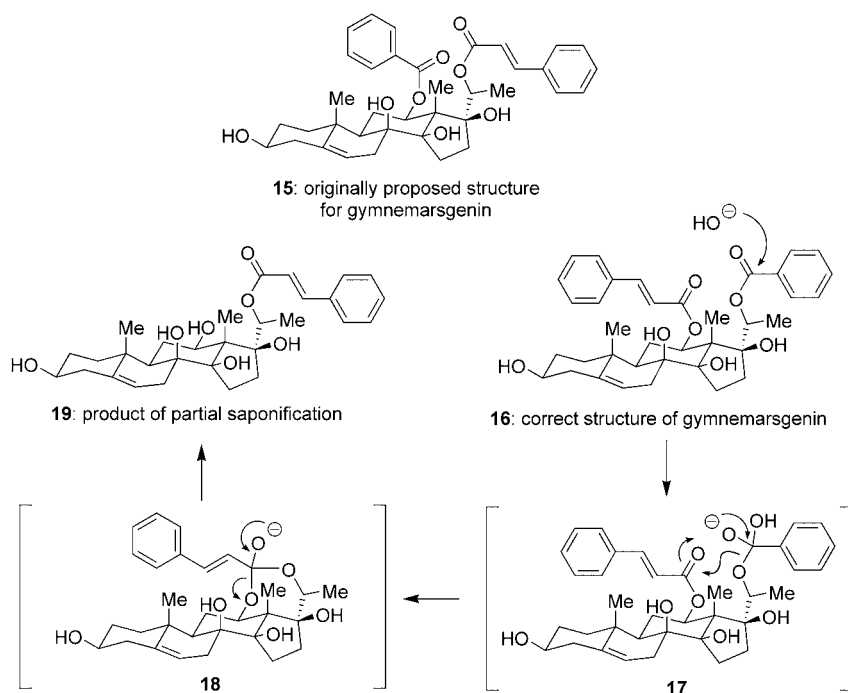
Proposed structure	Methods used in original assignment	Revised structure and basis for revision	Verified by total synthesis
 gymnemarsgenin Zhou et al. (1989) ^[105]	NMR UV IR MS degradation	 NMR spectroscopy Cordell et al. (1995) ^[106]	no
 glabrescol Reynolds et al. (1995) ^[107]	NMR IR MS	 chemical synthesis Morimoto et al. (2000) ^[108b]	Morimoto et al., Xiong and Corey (2000) ^[108b, c]
 FD-891 Eguchi, Kakinuma, et al. (2002) ^[109c]	NMR UV IR MS degradation	 chemical synthesis and comparison with literature data for another natural product Eguchi, Kakinuma, et al. (2004) ^[110]	no
 (+)-tolyporphin A Moore et al. (1992) ^[111]	NMR UV MS derivatization	 chemical synthesis and NMR spectroscopy Kishi et al. (1999) ^[112]	Wang and Kishi (1999) ^[113]
 himastatin Leet et al. (1996) ^[114]	NMR UV IR MS degradation derivatization	 chemical synthesis Kamenecka and Danishefsky (1998) ^[115]	Kamenecka and Danishefsky (1998) ^[115]
 robustadial A Nakanishi et al. (1984) ^[116]	NMR UV IR CD MS degradation derivatization	 chemical synthesis Cheng and Snyder (1988) ^[117]	Salomon et al. (1988) ^[118]

Table 8: Selected structures of misassigned natural products and proposed structural revisions.

Proposed structure	Methods used in original assignment	Revised structure and basis for revision	Verified by total synthesis
 dictyostatin 1 Pettit et al. (1995) ^[119]	NMR UV IR MS	 reisolation and reexamination Paterson et al. (2004) ^[120]	no
 lepadiformine Biard et al. (1994) ^[121]	NMR IR MS derivatization	 chemical synthesis Kibayashi et al. (2000) ^[122]	Kibayashi et al. (2000) ^[122]
 trunkamide A Ireland, Bowden, et al. (1996) ^[123]	NMR UV IR MS degradation derivatization	 chemical synthesis Wipf and Uto (2000) ^[124]	Wipf and Uto (2000) ^[124]
 antillatoxin Gerwick et al. (1995) ^[125]	NMR CD UV IR MS	 chemical synthesis Shioiri et al. (1999) ^[126]	Shioiri et al. (1999) ^[126]
 oscillarin Martin et al. (1996) ^[127]	NMR MS	 chemical synthesis Hanessian et al. (2004) ^[128]	Hanessian et al. (2004) ^[128]
 yatakemycin Igarashi et al. (2003) ^[129]	NMR UV IR MS	 chemical synthesis Boger et al. (2004) ^[130]	Boger et al. (2004) ^[130]



Scheme 2. Potential characterization pitfalls: A degradation reaction leads to an internal migration, and the structure **15** is therefore assigned (erroneously) to the steroid natural product gymnemarsgenin (**16**).

inolipid B (Table 5), although the revision in this case involved a much smaller constitutional change.^[81,82]

In other instances, the collected spectroscopic data might have led to the right assignment, if a chemical method had not led to a mistake. Such was the case in the attempt to assign a structure to the steroid natural product gymnemarsgenin (Table 7), whereby a final degradative reaction seeking to cleave only one of the two ester groups was employed to assist in confirming the positions of these functionalities within the molecule. Unfortunately, this experiment led the original research team to propose an incorrect structure (**15**, see Scheme 2), as an internal migration reaction occurred under the conditions used, an outcome that was not recognized until well after publication.^[105,106]

We could fill pages with the stories behind some of these reassignments. Rather than doing this, we encourage you to explore independently those examples that interest you most, as they provide a rich source of potential research projects and a wealth of interesting problems as to how one might attempt to discern between the original and revised structures. Instead, we use the examples in Tables 1 to 8 to make the case that chemical synthesis still has a major role to play in structural assignments, especially structural revisions. Indeed, for over half of the reassignments in this sample (27), chemical synthesis was required to reach a revised architecture, and in 22 cases it was total synthesis that indicated that there was a problem in the first place. Many of these examples involved the process of establishing/revising the configuration of stereocenters, as hinted above, but that should not give the false impression that such a correction involved little work. For example, the research group of Lee had to prepare a

number of structural isomers of lasonolide A (Table 1) before they realized its true constitution.^[25,26] Similarly, Trost and Harrington synthesized ten different diastereomers of amphidinolide A (see Table 3) to assure themselves of its identity, as differences in the chemical-shift values in the NMR spectra were only slight, and no natural sample was available to enable a direct comparison.^[59,60]

In other cases, chemical synthesis served to confirm a given motif. For example, apart from using a different mass spectrometric experiment to reassign the structure of halipeptin A, the Gomez-Paloma team also synthesized a model compound bearing the newly proposed thiazoline motif so that they could compare its spectroscopic properties to those of the natural product.^[28] Similarly, Hiram and co-workers prepared a substantial portion of the kedarcidin chromophore (Table 4) to convince themselves of

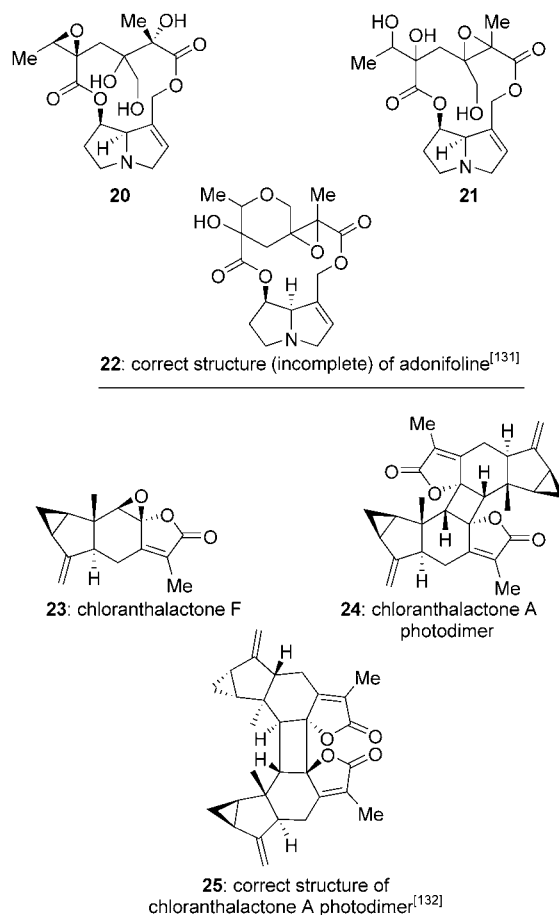


Figure 4. Selected examples of natural products isolated independently by two different research groups, each of whom proposed a structure. In each case it was ultimately shown that neither proposal was correct.

the altered connectivity and configuration that they intended to propose in its revised architecture.^[74] It is inconceivable, of course, that all these corrections could have been made without chemical synthesis.

Thus, given our present state, the question becomes: Can anything be done to limit the number of mistakes made in structural assignments? In our opinion, apart from perhaps the isolation of more sample, there is only modest room for improvement without the introduction of more powerful spectroscopic techniques. However, one type of unfortunate error could potentially be avoided if chemists were to deposit all their spectral data into a universal database similar to that used for X-ray crystal structures: namely, the proposal of an incorrect structure for a natural product that has already been isolated and characterized. There are five examples in the tables in which this situation occurred: nomofungin, TAEMC151, FD-891, renieramycin H, and the unnamed coumarin. Figure 4 shows two additional examples, whereby different research teams isolated the same natural product independently and proposed different structures (and names) for that compound, only for it to be recognized later that they were both in error.^[131,132] Perhaps all these mistakes (and much work) could have been avoided if it was easier to determine through a computer search engine whether a given natural product had already been isolated and/or independently characterized. Access to spectra (not just tables of data)

could certainly assist in the assignment of newly isolated members of a given class of natural products and should facilitate the structural reassignment process in those instances in which an error has occurred.

Finally, for a considerable number of natural products whose originally proposed structures have been called into question through total synthesis, a revised assignment has yet to be made. Figure 5 shows just a few of these unsolved mysteries, some of which have been lingering without an alternative structure for a number of years.

3. The Ramifications of Structural Misassignments

While the story behind any individual reassignment of the structure of a natural product can afford insight into the weaknesses of a particular method used for its initial assignment, it is rare that such a misassignment does not also incur a number of palpable and sometimes far-reaching consequences. Of these, the most serious might be the temptation to develop inaccurate biosynthetic proposals for entire classes of compounds.

For example, in 1925 Pummerer et al. showed that the one-electron oxidation of *p*-cresol with $K_3[Fe(CN)_6]$ afforded the dimeric product **28** (Scheme 3), whose formation was rationalized as the coupling of two radicals (**26a** and **26b**)

followed by a spontaneous cyclization. This structural assignment was further supported by the subsequent reaction of the compound with acid and acetic anhydride to generate the biaryl system **29**.^[147] Although the Pummerer ketone (**28**) is not a natural product, the assignment of its structure was important because its identity and mode of formation served as the basis for a number of biosynthetic pathways proposed over the next 30 years, such as that proposed by Robinson for morphine (**34**).^[148]

These ideas would all be turned upside down in 1955. Unable to formulate a mechanism by which compound **28** could be converted into **29** and uncertain of why the cyclization step required for the formation of **28** from **27** would occur at ambient temperature, Barton^[148] proposed an alternative pathway for the reaction (Scheme 3). He suggested that the true structure of the Pummerer ketone was the product **31** derived from the union of the two carbon-centered radicals **26b** and **26c**. Compound **29** could then be formed from **31** simply by an acid-induced dienone–phenol

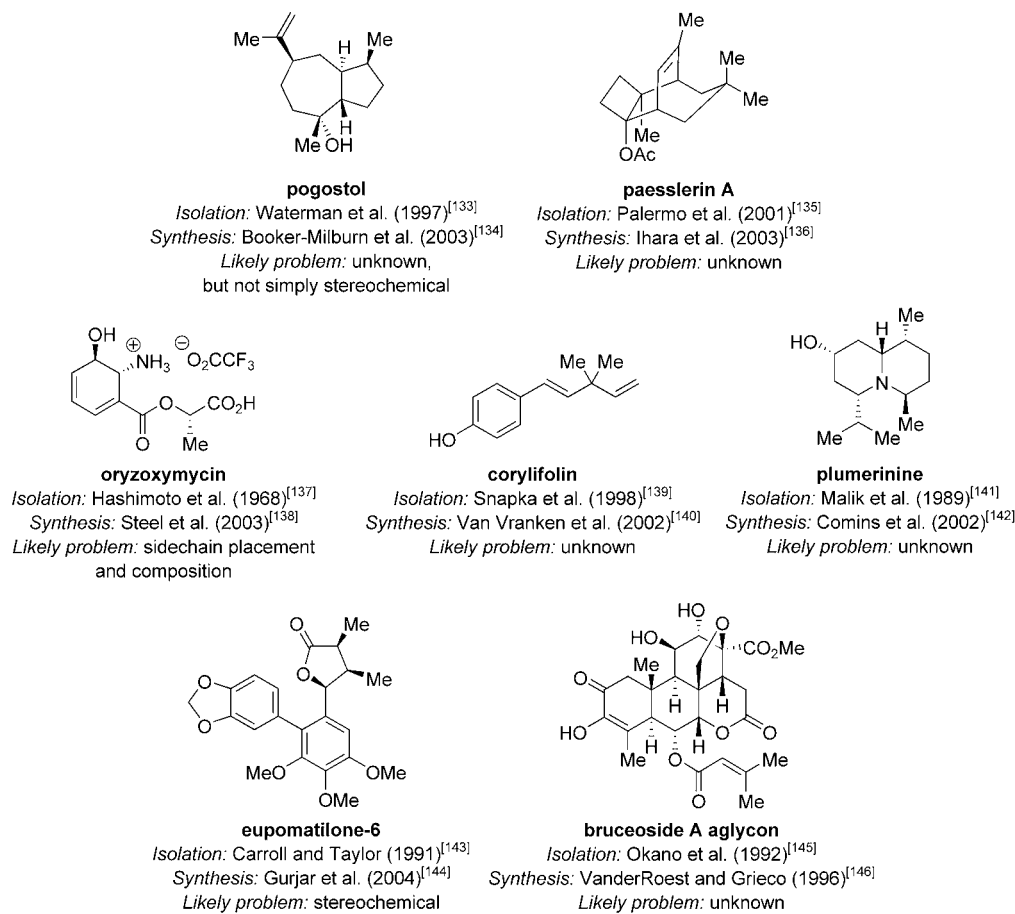
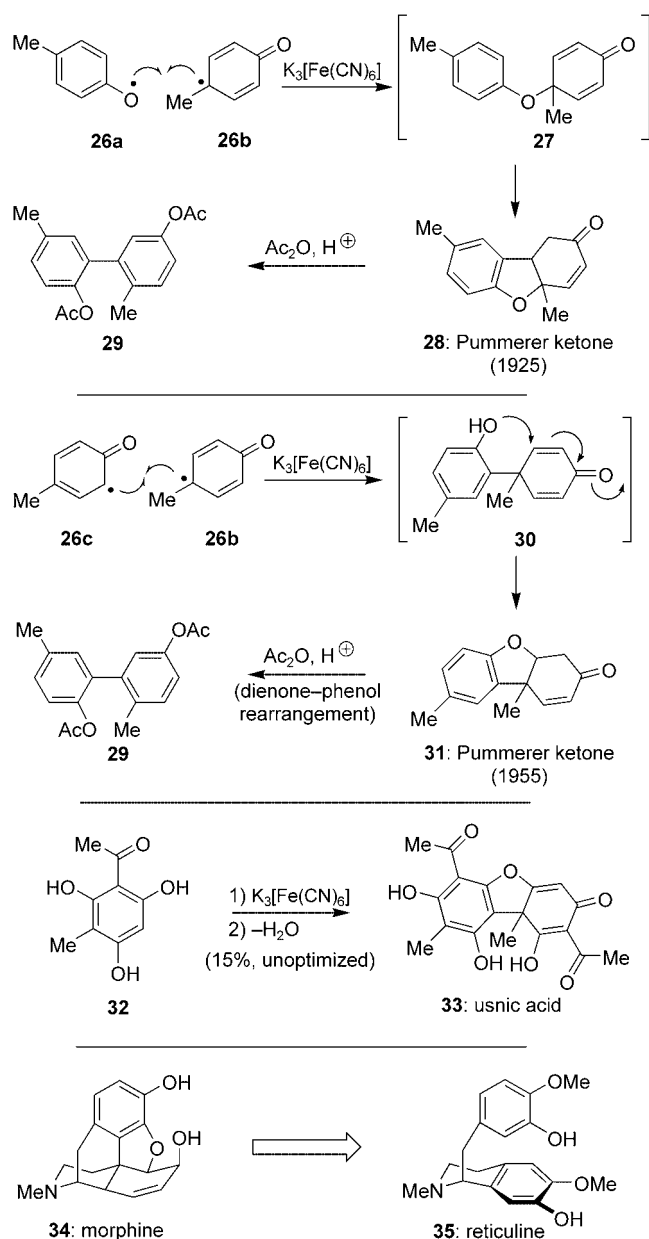


Figure 5. Unsolved mysteries: natural products whose proposed structures have been disproved by synthesis, but are awaiting a revised proposal.

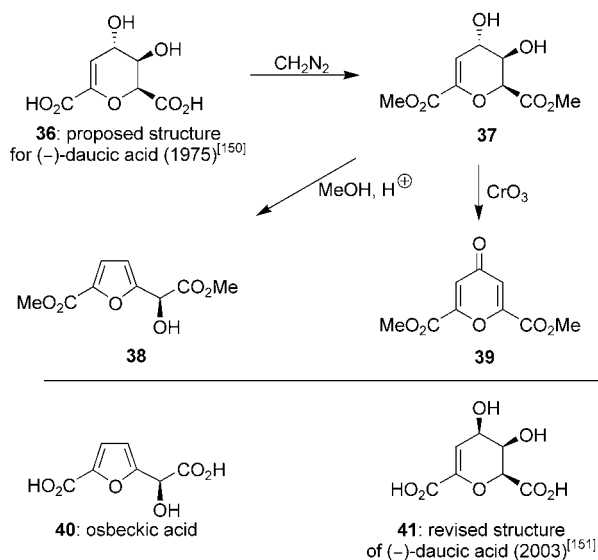


Scheme 3. A structural misassignment for the Pummerer ketone served as the basis for numerous errors regarding the biosynthesis of natural products such as morphine (**34**). Barton's reexamination of this problem led to a structural revision with important ramifications, including a two-step total synthesis of usnic acid (**33**).

rearrangement. Within a few weeks, laboratory experiments proved him right, and he was able to extend the validity of his alternate mechanism and the new structure for the Pummerer ketone to a number of other areas, such as the synthesis of the lichen-derived natural product usnic acid (**33**) in just two steps from **32**. Barton also used his mechanism to formulate a biosynthetic pathway for morphine that was entirely different from those previously proposed, with benzyloquinoline alkaloid **35** as a likely starting substrate. Although unknown at the time, compound **35** was isolated as a natural product a few years later (named reticuline)^[149] and shown through

feeding experiments to be intimately involved in the biosynthesis of morphine.

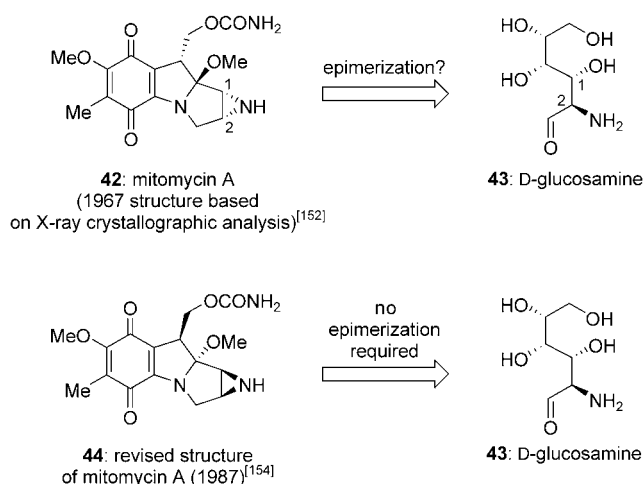
Such major revisions to biosynthetic pathways occur with some frequency today. Although there are several elegant examples we could cite, perhaps one of the most interesting comes from recent work by the research group of Lichtenthaler that disproved a structure established by Barton himself! The natural product in question is daucic acid, which was first assigned structure **36** (Scheme 4) based primarily on



Scheme 4. Although many aspects of Barton's original proposed structure for daucic acid (**36**) were accurate, the structure was ultimately proven to be incorrect in 2003 through chemical synthesis.

its conversion into compounds such as **37**, **38**, and **39**, the second of which fully matched a diester of another natural product, osbeckic acid (**40**).^[150] In 2003, the Lichtenthaler team was not entirely convinced that the configurations of the C2 and C3 stereocenters proposed earlier by Barton were correct, so they synthesized all possible stereoisomers of daucic acid and proved that **41** was the actual structure.^[151] The fact that daucic acid has a D-lyxo configuration, rather than the D-xylo configuration originally proposed, has a number of implications for the biosynthetic pathways through which plants generate such dicarboxylic acids, a line of study that is still being investigated today.

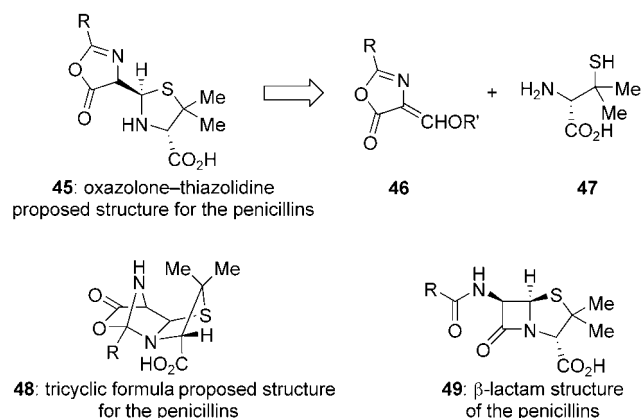
Sometimes, though, it need not be an entire pathway that is wrong. Confusion can also arise when a proposed structure appears incongruent with known biosynthetic data. A good example of such a phenomenon comes from the story of the mitomycins, an especially important group of natural products, one of which (mitomycin C) is employed clinically as an anticancer agent. In 1967, their structures were fully assigned (including their absolute configurations) based on a battery of spectroscopic methods and X-ray crystallography.^[152] The structure of one of these agents, mitomycin A (**42**), is shown in Scheme 5. A few years later this assignment seemed questionable in light of some feeding experiments that revealed D-glucosamine (**43**) as the source of most of the "right-hand"



Scheme 5. Although established by X-ray crystallography, the absolute configuration of the structure assigned to mitomycin A (**42**) in 1967 did not make sense in light of biosynthetic feeding experiments. This discrepancy would not be reconciled for 20 years.

domain of the molecule. If this were true, a number of the stereocenters of this building block would have to be epimerized to produce a mitomycin architecture with the absolute configuration corresponding to **42**.^[153] Why was there this discrepancy? As it turns out, the original X-ray crystal structure of mitomycin A provided the wrong absolute configuration (as determined by the R-factor-ratio test). In 1987, a crystal of better quality was obtained, and the structural and biosynthetic data were finally reconciled with the revised structure **44**.^[154]

Incorrectly assigned natural products not only complicate the determination of biosynthetic schemes, but can have additional costs in terms of time and money if effort is devoted toward their synthesis. Perhaps one of the earliest and best illustrations of this point is the truly profound body of resources brought to bear by the American and British governments on the problem of synthesizing penicillin during World War II in the hopes of increasing its supply. Since these were the days before the β -lactam structure **49** (Scheme 6) of



Scheme 6. Debate surrounding the structure of the penicillins had a profound effect on synthetic approaches to their total synthesis both during and after World War II.

this agent was verified by Crawford-Hodgkin by X-ray crystallography,^[155] the lack of certainty regarding its actual constitution led synthetic chemists of the period to pursue a number of potential penicillin structures in the laboratory. Famous examples include the oxazolone-thiazolidine architecture **45** favored principally by Robinson and a tricyclic alternative **48** that was advocated at one point by Woodward.^[12] Each of these structures calls for a unique synthetic approach (such as the connection of **46** and **47** to generate **45**). However, since neither comes even close to matching the true architecture of the target molecule, it is not surprising that the millions of dollars and hundreds of years' worth of human effort invested in their synthesis during the war afforded few dividends on the penicillin-supply front.^[156] Indeed, fermentation remained the only viable source of these powerful antibiotics until the late 1950s, when Sheehan and his colleagues at MIT finally completed a total synthesis after developing a number of novel synthetic methods for the purpose.^[12]

Similar chances exist today for a synthetic chemist to devote effort to the synthesis of a proposed structure that bears little relationship to the actual architecture of the natural product, even though it has been assigned based on a number of advanced spectroscopic techniques unavailable during the 1940s and 1950s. Several of the natural products listed in the eight tables in Section 2 would certainly fit this bill. As a further example, consider the series of structures **50–52** proposed between 1982 and 1992 for the relatively complex and stereochemically rich natural product carzinophilin (Figure 6).^[157–159] These proposals are certainly quite

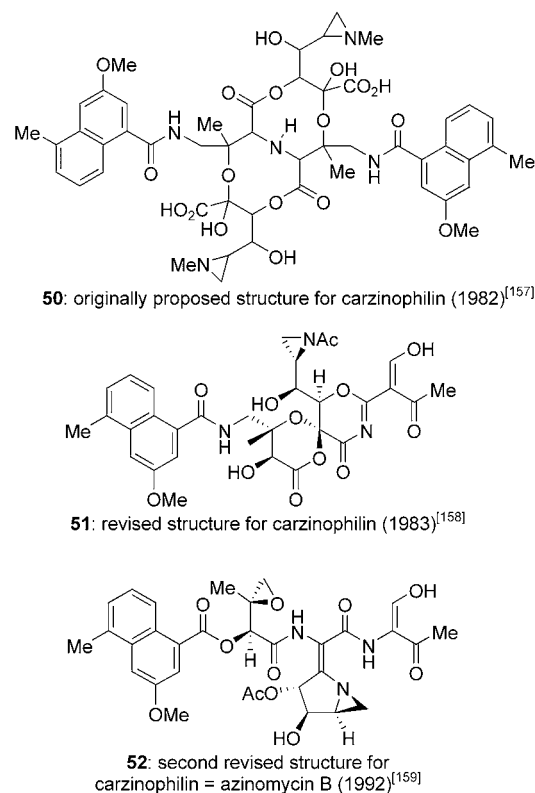


Figure 6. Progression of structural assignments for carzinophilin.

disparate, as no structural element apart from the terminal aromatic motif is shared by all.^[160]

However, a structural reassignment that involves a much smaller alteration to the molecular architecture can throw a synthetic approach into a similar degree of disarray. A good illustration resides in the elucidation of the structure of the liminoid insect antifeedant azadirachtin. In 1975, the research group of Nakanishi correctly determined most of its architecture based exclusively on spectroscopic methods and proposed structure **53** (Figure 7).^[161] By the mid-1980s,

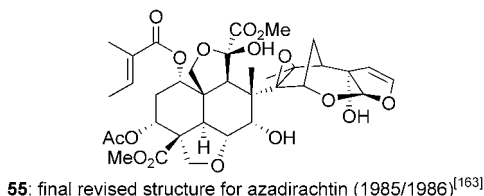
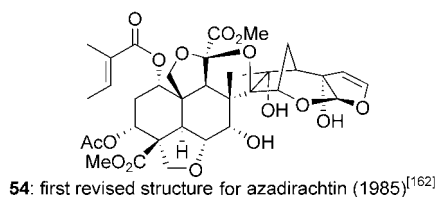
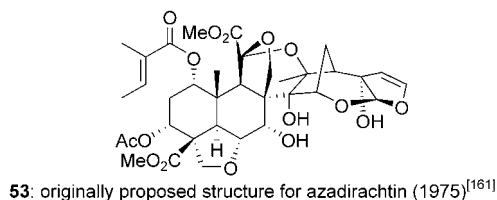
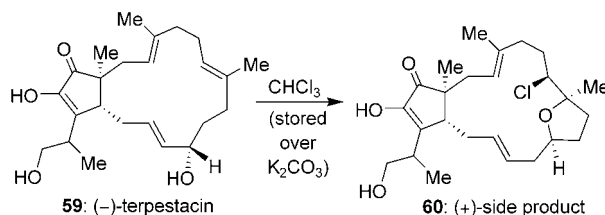
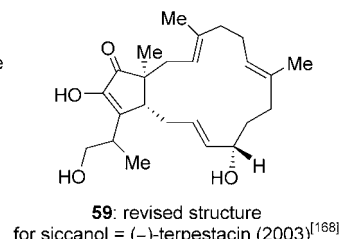
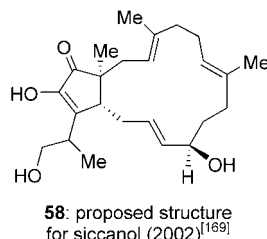
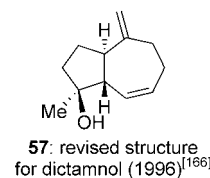
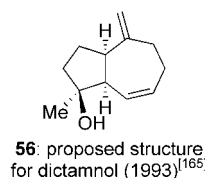


Figure 7. Progression of structural assignments for the limonoid insect-antifeedant azadirachtin.

however, the isolation of some structurally related compounds began to suggest that some elements of the central core were inaccurate. These findings led ultimately to a series of reassignments, first by Ley and co-workers in 1985, who proposed structure **54**,^[162] and then by teams led by Ley and Kraus a few months later, who finally proposed structure **55** based on X-ray crystallography in the former case and NMR spectroscopy in the latter.^[163] Although apparently subtle, these changes are profound in terms of the strategies that one would probably employ for the synthesis of the different structures, especially considering that most published strategies at the time these revisions were made sought to build the azadirachtin structure by connecting fragments corresponding to its “left-” and “right-hand” domains.^[164]

Arguably, the misassignment of the configuration of a single stereocenter can have similar ramifications. For example, if a stereocenter at a ring junction is incorrectly assigned, as happened with the natural product dictamnol (**57**, Scheme 7), then a completely new synthetic approach might be required.^[165–167] Similarly, in an age driven by the use of asymmetric reactions to establish stereocenters, a stereochemical error in another part of the molecule could have an impact on the strategy/catalyst design. A recent example is a total synthesis reported by Chan and Jamison at MIT^[168] that



Scheme 7. When misassigned stereocenters occur at critical positions, such as ring junctions, profound alterations in the synthetic strategies are typically required to access the revised structure.

showed that the proposed structure **58** of siccanol^[169] was incorrect and that the natural product is identical to (-)-terpestacin (**59**).^[170]

As a final note, the process by which the structure of (-)-terpestacin (**59**) was assigned is also worth mentioning, since a number of problems were caused by what is normally a routine step in the characterization process: determination of the sign of its optical rotation. Terpestacin (**59**) was originally reported to have a positive optical-rotation value in chloroform. In 2002, the research group of Myers at Harvard University synthesized the same enantiomer, only to obtain a negative value when they measured its optical rotation in the same solvent.^[171] What was the problem? The chemists who had isolated **59** stored their chloroform over K_2CO_3 , a practice which generated enough elemental chlorine to convert terpestacin (**59**) into **60**, a product whose optical-rotation value is positive!

4. Misassignment Case Studies

Structural misassignments, as with all errors in science, also have an emotional component. Certainly a researcher would be disturbed to discover that an assignment he or she had made was incorrect, just as he or she would probably be pleased to find out that his or her proposal had been verified. Since our research group is not directly engaged in the process of isolation and/or characterization, we can not comment on how a scientist feels in such a position from a first-hand perspective. We know, however, what it is like as a synthetic

chemist to be in the midst of a total synthesis or at its “end”, only to find out that the molecule we were chasing was never there! In this section, we present two personal accounts that hopefully convey a sense of these emotions, and we hope to show how misassignments can lead to some benefits as well. We want to reiterate, however, that these case studies are not meant to point any blame at structural chemists or indicate frustration with their efforts. Quite on the contrary, these pioneers work wonders with often incredibly complex puzzles, frequently under severe constraints of material and time (present cases included).

4.1. Case Study 1: Diazonamide A

The tale of the marine natural product diazonamide A began in 1991 when the research groups of Fenical and Clardy first communicated its structure (i.e. **66**, Scheme 8) in the *Journal of the American Chemical Society*.^[172] From that moment forward, this molecule enraptured the synthetic community in a way that few others ever match, primarily by virtue of its highly intricate and structurally novel architecture and its potential as a new weapon in the fight against cancer. Over the course of the next decade, nearly a dozen research groups initiated campaigns to synthesize its diabolically

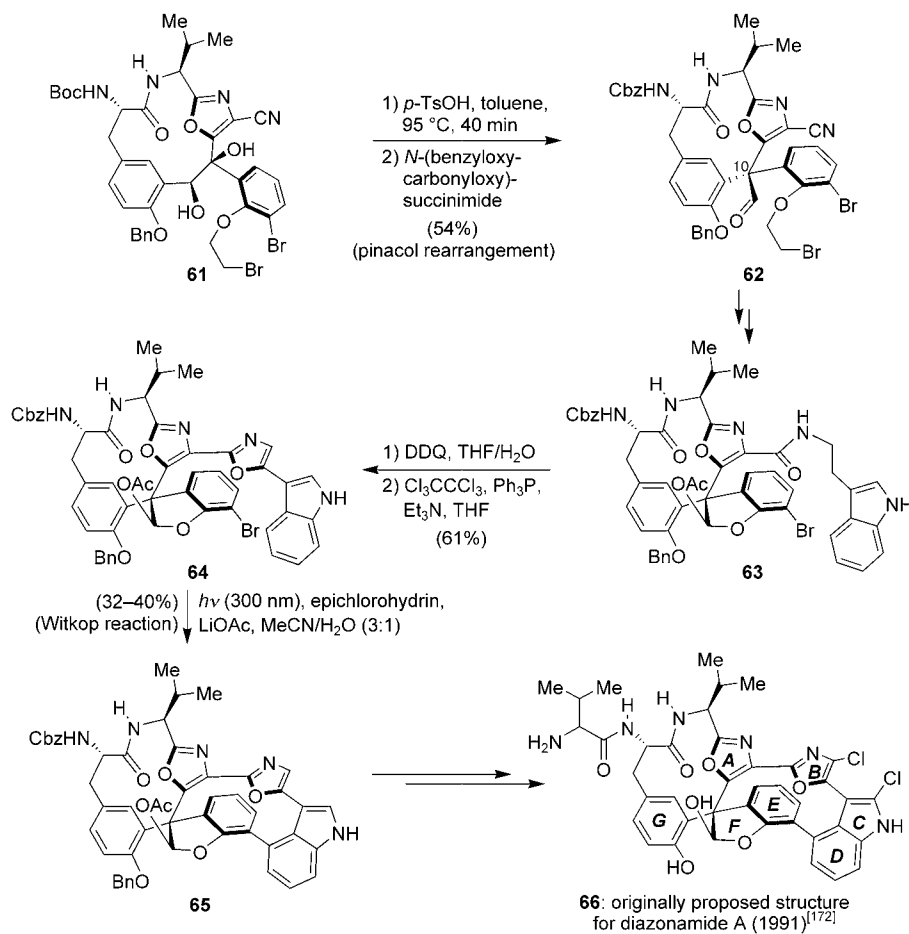
complex structural elements and explore its chemical biology more fully.^[173]

Our own journey of discovery began in June of 1999, when we embarked on the total synthesis of diazonamide A, armed with what we thought was a carefully designed synthetic strategy. Unfortunately, the next few months would teach us what a number of teams before us had already learned: the synthesis of the individual domains, such as the indole ring or an oxazole subunit, was relatively simple, but joining these fragments together to form even one of the two 12-membered rings was astonishingly difficult.^[174]

When the synthetic community at large is fully mobilized, however, few challenges in total synthesis remain unanswered for long. At the end of 2001, a team led by Harran at the Southwestern Medical Center in Dallas was finally able to assemble all the disparate subunits of diazonamide A,^[175] by using a creative strategy featuring two powerful reactions to forge the formidable macrocyclic domains of the molecule (Scheme 8). The first was an acid-induced pinacol rearrangement of chiral diol **61**. In this step, contraction of the 13-membered ring in **61** led to the formation of the 12-membered AG macrocycle and the daunting C10 quaternary center at the heart of the molecule. The second key reaction was an inventive use of the Witkop photocyclization. This operation converted **64** into **65** with complete atropselectivity as a result

of π stacking between the B and E rings in the starting material. With these domains in place, a few finishing touches then converted **65** into diazonamide A; or at least into what was supposed to be diazonamide A (**66**). Instead, chemical synthesis had uncovered yet another example of a structural misassignment!

What had gone wrong? The story is certainly an interesting one. During the early stages of their structural-elucidation efforts, the Fenical and Clardy groups worked exceedingly hard to obtain a crystal structure for diazonamide A to support their assignment of a structure that was unlike that of any other natural product ever isolated. Although that task would ultimately prove impossible with diazonamide A, the conversion of diazonamide B (**67**, Figure 8), a structural relative with similar NMR, UV, and IR spectroscopic data, into a *p*-bromobenzamide derivative provided a beautifully crystalline solid. The structure of this derivative (**68**) verified much of the anticipated general diazonamide skeleton with only one exception: the presence of an acetal moiety bridging the F and G rings. This outcome was surprising, as NMR spectroscopic data seemed to indicate the existence of an open hemiacetal instead (as drawn for structure **67**) based on a small coupling constant between what was assigned as the hydrogen atom at C11 and a hydrogen atom that underwent isotope



Scheme 8. The creative synthetic route of Harran and co-workers led to the proposed structure of diazonamide A (**66**), but the spectral data did not match those of the natural product.

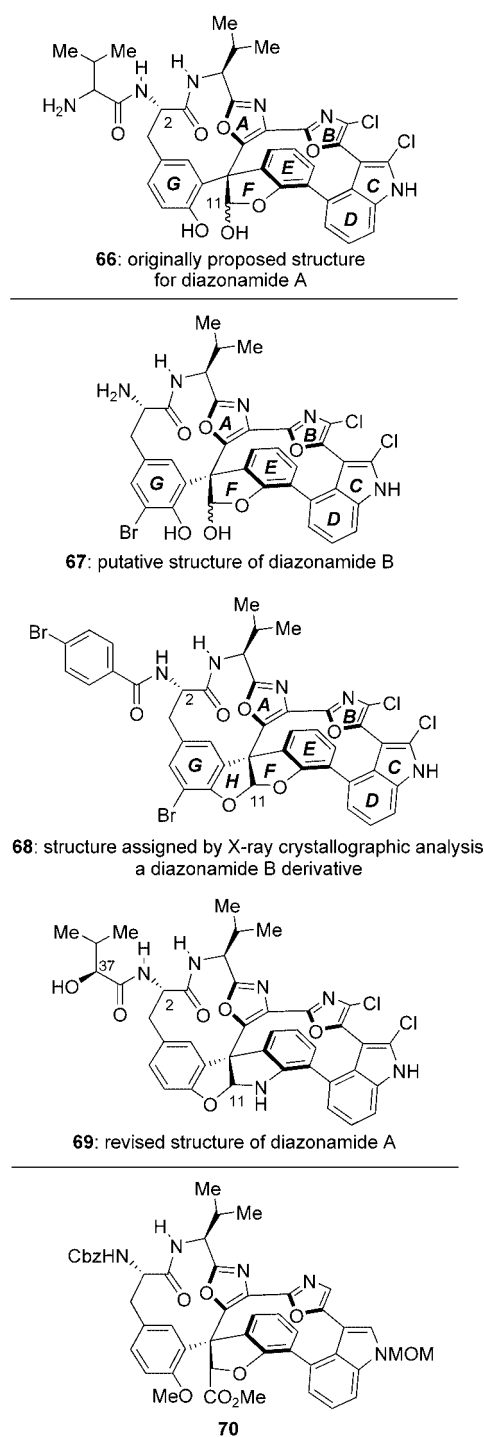


Figure 8. Basis for the structural misassignment and reassignment of diazonamide A.

exchange with D_2O . Needing to reconcile this incongruity, the Fenical and Clardy groups proposed that the closed acetal observed in crystal structure **68** was an artifact resulting from the conditions employed to attach the *p*-bromobenzamide group to **67**. Thus, if a hemiacetal was accepted for the F ring of diazonamide A, then the one element of diazonamide A which the X-ray crystal-structure analysis of **68** could not reveal, namely, the amino acid tethered at the C2 position,

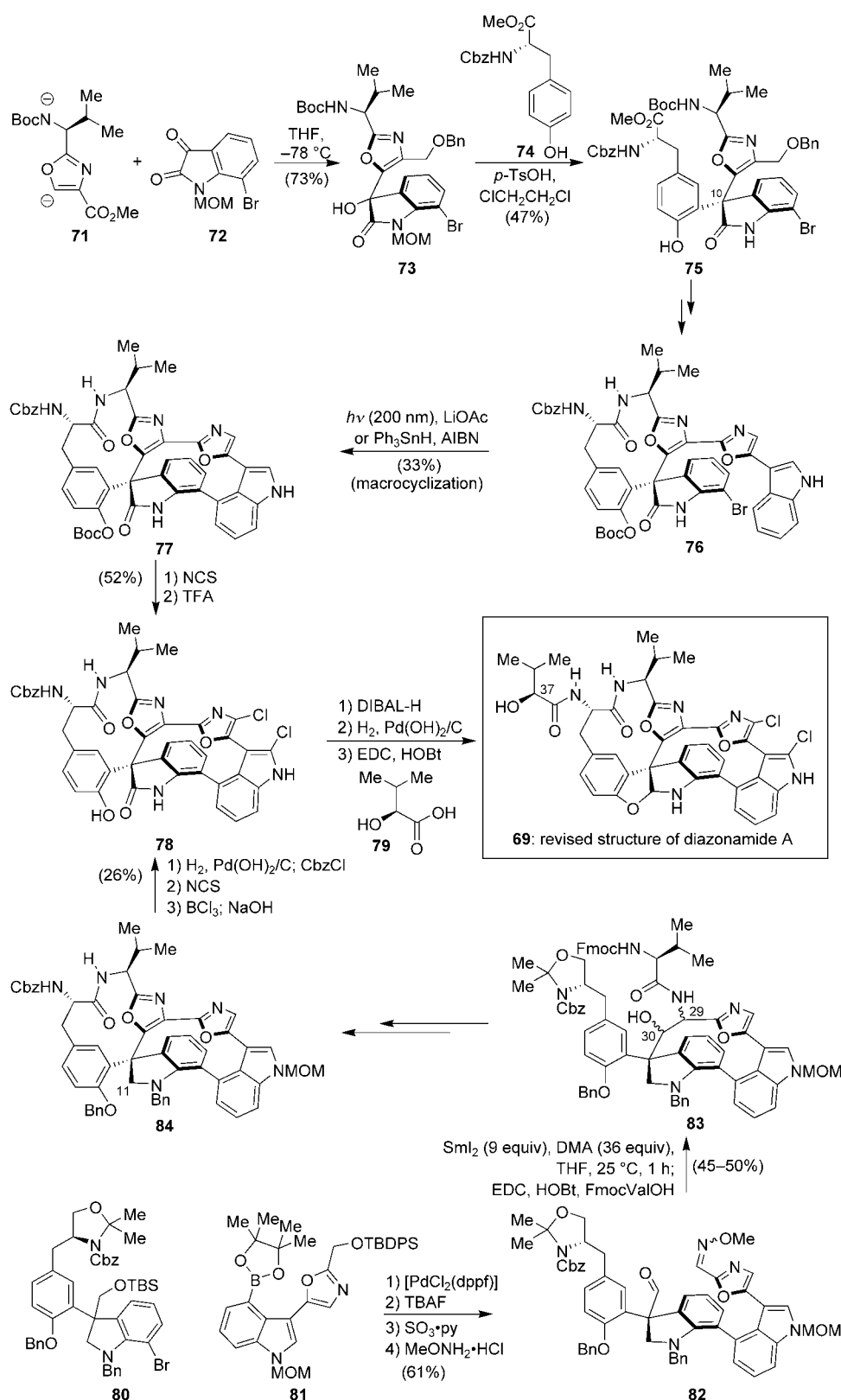
must be a valine residue. This hypothesis would agree with a signal observed by mass spectrometry corresponding to $[M + H - H_2O]^+$. As a result of these observations, diazonamide A was assigned structure **66**.^[172]

Armed with the knowledge that both the X-ray crystal structure of **68** and the formula derived from the mass spectrometric data of diazonamide A corresponded to the loss of a molecule of water, the research group of Harran speculated that perhaps the correct structure for the natural product differed from **66** simply through the presence of a closed acetal. This alternate compound would contain all the critical elements of the crystal structure **68** and would thus have a signal in the mass spectrum corresponding directly to $[M + H]^+$. Admirably, this compound was immediately synthesized by the Harran team, but, once again, the physical data of the synthetic material failed to correlate with data obtained from the natural sample of diazonamide A.^[175] Where was the problem?

The answer resided in the assignment of the crystal structure that gave **68**. By computational analysis, the Harran group subsequently determined that the oxygen atom in the F ring of **68** (and thus in **66**) should really be an NH group within an aminal system, as in the revised structure **69**. Consequently, a second modification somewhere else in the molecule was required to account for the mass spectrometric profile of diazonamide A. The obvious site for a change was that occupied by the terminal group attached to the amine functionality at C2. If this fragment was 2-hydroxyisovaleric acid, as shown in **69**, then all of the previously incongruent data would appear to be reconciled. Thus, the misassignment was the result of a series of logical deductions stemming from a single piece of bad evidence; now it was up to synthesis to prove whether or not the new proposal was correct.

With little question, this structural reassignment sent shockwaves to all the research groups that had been attempting to synthesize this molecule when it was first published in the last December issue of *Angewandte Chemie* in 2001.^[175] Although we certainly admired the beautiful synthesis of Harran and his team as well as the logic behind the proposed structural revision, our initial reaction could only be described as intense disappointment and frustration. Not only did the molecule that we had been pursuing for over two years not exist, but we were uncertain whether we could even apply any part of our developed sequence in a new drive to access **69**, since this new structure was constitutionally different from **66** at a key position. These feelings were magnified by a certain sense of irony in that we had just overcome a major synthetic hurdle which had held us back for a couple of months, finally reaching the advanced and critical intermediate **70** (Figure 8) that we thought was only a few steps away from the final target.

For a few days, we were unsure of just how to proceed. Questions running through our minds included whether or not we should go ahead and complete the originally proposed structure even though it did not represent the natural substance, and just how we should attempt to tackle the “new” diazonamide A. The team took advantage of the convenient timing of the Christmas holiday and came back together in January of 2002 with a clear battle plan. We would



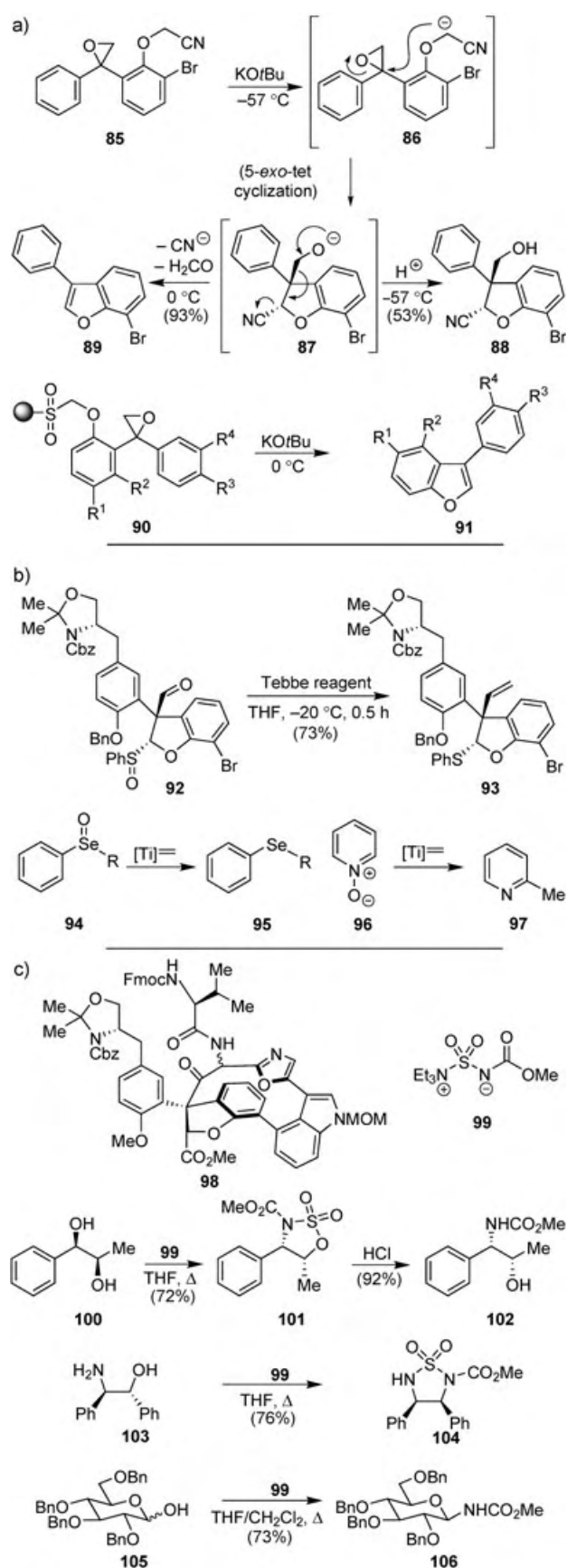
Scheme 9. The two synthetic routes developed by the Nicolaou group to verify **69** as the correct structure of diazonamide A and ultimately establish the configuration at C37.

tackle the new molecule from two different angles: one based on the order of macrocycle construction that the Harran team had employed to great success, and the other based on key

explorations recently led to the discovery that the Burgess reagent is remarkably effective at mediating a number of nondehydrative transformations, such as the formation of

elements of the strategy we had already developed to access the original structure **66**. It would take a year for both of these plans to reach fruition following the development of some novel synthetic strategies and tactics. Finally the correct structure of diazonamide A was proved to be **69** and the absolute configuration of its C37 stereocenter was established.^[176,177] The key elements of these two total syntheses are summarized in Scheme 9. Of particular note are the construction of the quaternary carbon center with its adjoining aromatic systems in the first synthesis of diazonamide A, and the application of a novel SmI₂-promoted hetero-pinacol cyclization sequence to create the heteroaromatic core in the second.^[178,179]

Reflecting on our project as a whole, we realize now that the frustration we felt at the end of 2001, although understandable, was misplaced. The misassignment of diazonamide A turned out to be more of a reward than a punishment, even though it extended the duration of the project by several months. Indeed, had the correct structure **69** been known from the outset, we would probably have learned much less. For example, our work towards the “incorrect” F ring led us to design a novel 5-*exo*-tet cyclization reaction to form the quaternary stereocenter of the target molecule (namely, to synthesize **88**). When tweaked properly, this reaction can also deliver 3-aryl benzofurans, such as **89**, in a controlled manner (Scheme 10a).^[180] Furthermore, during work on manipulating this ring system we found that titanocene methyldiene compounds can deoxygenate sulfoxides and selenoxides, and can convert pyridine *N*-oxides into 2-methylpyridines (Scheme 10b).^[181] None of these discoveries would have been made if we had been working with indoles or oxindoles instead. Similarly, had we not encountered difficulties in our efforts to form the A ring of **66** from intermediate **98** with the Burgess reagent (**99**; Scheme 10c), we might never have been inspired to explore the chemistry of this reagent further. These

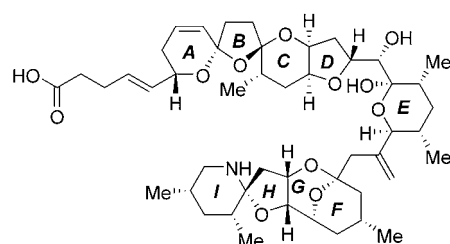


Scheme 10. a)–c) During the synthesis of the originally proposed structure of diazonamide A, a number of new synthetic methodologies were discovered.

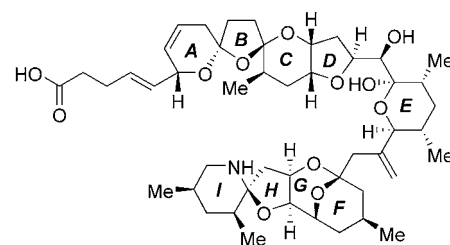
sulfamides from 1,2-diols, α - and β -glycosylamines from carbohydrates, and cyclic sulfamides from 1,2-aminoalcohols.^[182] We also may never have been inspired to devise two distinct strategies to reach diazonamide A (**69**) in such a short period of time. That alone was a unique and highly rewarding experience.

4.2. Case Study 2: Azaspiracid-1

Our second adventure in the area of structural revision through chemical synthesis concerns the natural product azaspiracid-1, the flagship member of a family of marine toxins identified as the causative agents of several incidents of rather severe shellfish poisoning (termed the azaspiracid syndrome). First isolated in 1996 as a 2-mg sample from 20 kg of mussel meat by the research group of Yasumoto, the structure of azaspiracid-1 was elucidated within a relatively short period of time through the careful application of sophisticated spectroscopic techniques. Azaspiracid-1 was assigned the structure **119** in 1998 (Figure 9).^[183] These pioneering studies, however, failed to unveil the absolute configuration of the molecule and the relative stereochemistry between its ABCDE and FGHI domains.



119: originally proposed structure for azaspiracid-1



121: revised structure of azaspiracid-1

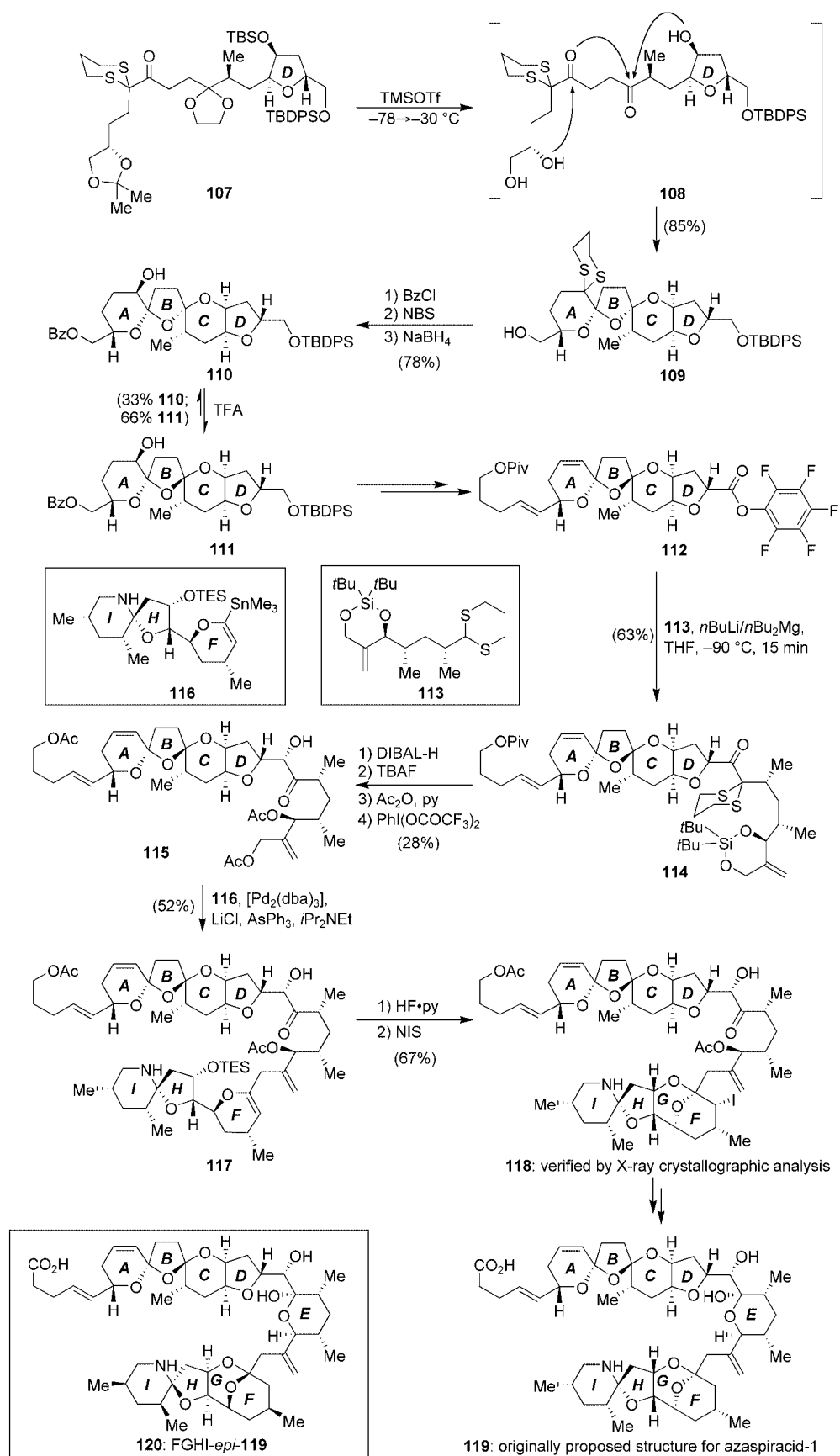
Figure 9. The revised structure of azaspiracid-1 (**121**): far more than just a simple change.

Just like diazonamide A, this molecule quickly caught the attention of the synthetic community because of its structural uniqueness. Of particular interest are an unusual azaoxaspiro ring fused to a 2,9-dioxabicyclo[3.3.1]nonane system, and a trioxadispiroketal framework attached to a tetrahydrofuran ring. Indeed, the first reports on synthetic studies towards structural subunits of this formidable synthetic target already began to appear within months of its structure being disclosed.^[184] A team in our research group also began exploring means by which to construct this molecule, with a

full assault beginning in 2001 after some other projects had been completed.^[185]

By the end of 2002 we were able to construct the 9 rings and 20 stereogenic centers of structure **119** through the route summarized in Scheme 11.^[186] Key features of the chemistry developed included a TMSOTf-induced cascade spirocyclization to form the tetracyclic ABCD system **109** from the linear precursor **107**, a subsequent directed epimerization step to generate the correct ABCD stereostructure (**110**→**111**), and fragment coupling steps that made use of a dithiane subunit (**112**+**113**→**114**) and a Stille reaction (**115**+**116**→**117**). Nevertheless, as you might have already guessed, when we finally reached the coveted structure **119**, the properties of the synthesized material did not match those of the natural product. The same news awaited us when we arrived at the FGHI epimer of **119** (i.e. **120**) through an identical route by using the enantiomer of **116**.

At first, we thought this unexpected outcome reflected the fact that something had gone wrong in our reaction sequence: that a stereocenter had been inverted by accident or that an unintended rearrangement had taken place. These fears were quickly allayed when we obtained an X-ray crystal structure for compound **118**, an intermediate six steps from the end of the sequence. This result verified that all the preceding steps had gone according to plan. Thus, barring an unknown problem during the final operations, our synthesis had revealed that the proposed



Scheme 11. Selected highlights of the synthesis by Nicolaou and co-workers of the originally proposed structure **119** of azaspiracid-1.

structure for azaspiracid-1 was incorrect. Where the problem(s) lay, however, was far from obvious. It would take us another year of intensive investigations involving synthetic and degradative work (the latter in collaboration with the research group of Satake of Tohoku University), a series of frustrating close calls, and the unearthing of some subtle clues before we were finally able to determine that the solution was structure **121** (Figure 9). This assignment was ultimately verified by total synthesis.^[187]

Our first foray into the identification of the correct structure of azaspiracid-1, as guided by discussions with Professor Satake (a member of the team that isolated the compound), sought to evaluate the orientation of the hydroxy group at C20, since a cloud of doubt surrounded its original assignment. This task proved quite easy to accomplish by using advanced intermediates from our developed sequence, and within a few days we were able to generate both **122** and **123** (Figure 10), the C20 epimers of our originally synthesized

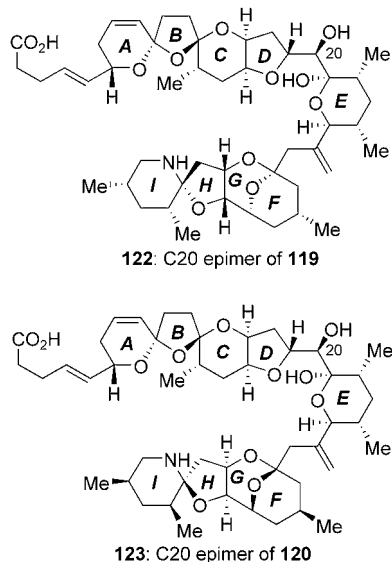
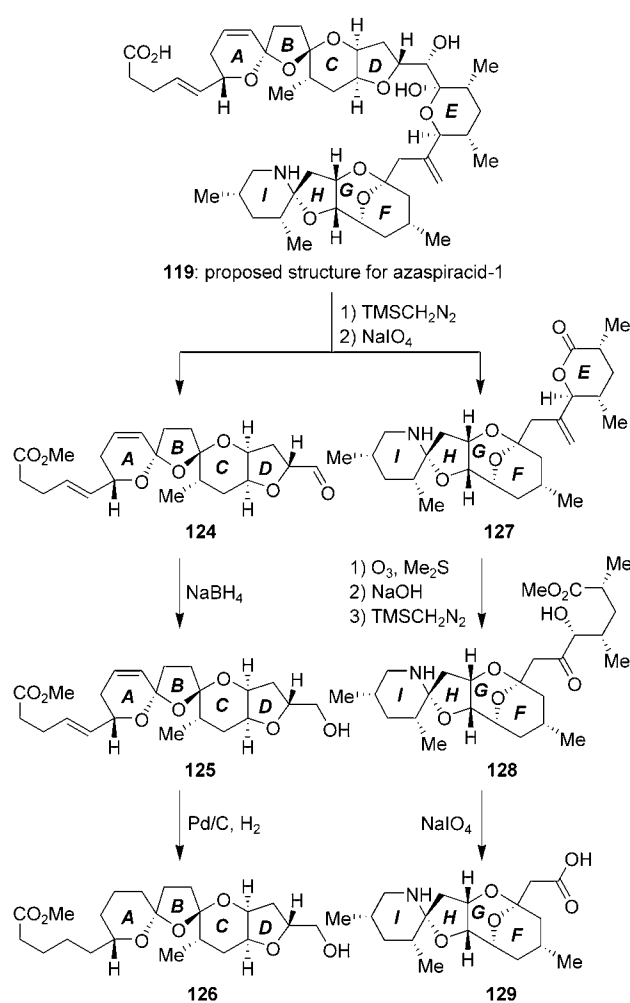


Figure 10. The search for the correct structure of azaspiracid-1: The problem does not lie with the configuration at C20.

compounds **119** and **120**. Despite their ready accessibility, however, compounds **122** and **123** brought us no closer to the ultimate goal, for their spectroscopic data bore as many differences to those of the natural sample as the data of the substances we had made before. Clearly, we needed to adopt a much more systematic and rational strategy to pinpoint the location and nature of the errors; guesswork would only waste time and material resources.

Fortunately, a classical approach to structure elucidation made a crucial contribution to this analysis. The Satake group provided the information needed by degrading and derivatizing natural azaspiracid-1 (the originally minuscule supplies of which had been somewhat enriched by a series of additional isolations) into an array of fragments corresponding to both the “upper” (**124**, **125**, and **126**) and “lower” domains (**127**, **128**, and **129**) of the molecule (Scheme 12). Consequently, our next goal became the preparation of synthetic material that



Scheme 12. Chemical degradation and derivatization of azaspiracid-1: The structures of all compounds are based on the originally assigned structure **119** of azaspiracid-1. (Only one of the four possible absolute configurations based on the original drawings of Satake et al. is shown.)

corresponded to these products for comparison purposes. We expected that we could then immediately locate the site (or sites) of the structural errors. We also hoped that these endeavors would help define the relative configuration of the ABCDE and FGHI domains as well as reveal the absolute configuration of each fragment and thus of the entire structure.

We began our studies by focusing on the “lower” half of the structure. Within a few weeks we had synthesized two compounds which corresponded to the degradation product represented in Scheme 12 as **127**: the compound with the configuration shown in Scheme 12 and its FGHI epimer **130** (Figure 11). Of these two diastereomers, only **130** was a perfect match with the degradation product. Thus, we now knew that there were no structural misassignments in this region of the molecule, and we knew what the relative configuration was within the EFGHI domain. To ascertain the absolute configuration, we then generated **129** through total synthesis. Since the optical rotation of **129** proved to be equal in value but opposite in sign to that of the degradation

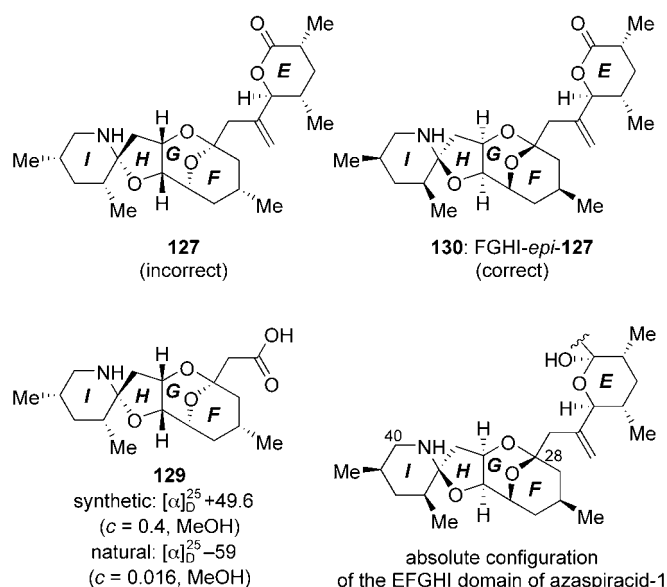


Figure 11. Determination of the relative configuration within the EFGHI domain and the absolute configuration of the FGHI domain of azaspiracid-1.

product, we could then assign with confidence structure **130** to the EFGHI fragment (Figure 11).

With the “bottom” half of the molecule secured, we then focused our attention on the “upper” framework. Now the true adventure would begin. Aware that the structural error(s) must lie within this domain, we began our detective work with an analysis of synthetic materials corresponding to the degradation fragment **125** (Scheme 12). That precise structure had already been synthesized, and, as expected, it did not match the sample derived from the natural product. Interestingly, however, most of the spectroscopic discrepancies seemed to reside within a single domain of this fragment: the A ring. Yet, despite careful investigations of this structural region, the required correction remained a mystery, since the use of 2D NMR spectroscopic techniques failed to provide any conclusive hints.

As is often the case, nature had already solved the problem for us: Hopmann and Faulkner had isolated and characterized a natural product, lissoketal (**131**, Figure 12), whose NMR spectroscopic data were beautifully reminiscent of those of the A-ring region of compound **125** derived from natural azaspiracid-1.^[188] Therefore, we expected that the structural problem with azaspiracid-1 might reside

simply in the positioning of the A-ring double bond, with **132** being the correct target structure! Filled with excitement that synthetic azaspiracid-1 would soon be in our grasp, we prepared **132** as quickly as we could. Its NMR spectrum would, unfortunately, knock the wind out of our sails, as although the A-ring signals now appeared to be mostly correct, the chemical shifts of a number of other resonances were still incorrect. The fact that we were still dealing with the wrong structure was further confirmed when the double bonds in **132** were hydrogenated to give the fully saturated compound **126**, whose ¹H NMR spectrum also differed from that of the hydrogenated derivative of the degradation product.

We now had to go back to the drawing board. Although we had conclusively established the positioning of both double bonds within the azaspiracid-1 framework, we were now left with 128 possible structures for the ABCD domain, since we could not be confident in the assignment of any of the seven stereogenic centers. Not even an army of chemists could hope to prepare such an array of compounds in a timely manner, even with unlimited funding (which we certainly did not have)! The problem seemed insurmountable, but again we were helped by a clue from nature. That piece of information related to thermodynamic stability. During the handling of both azaspiracid-1 itself and the ABCD fragments derived through degradation we noted that the ABC double-spiroketal unit was stable under acidic conditions. By contrast, our synthetic compounds that should correspond to this portion of the molecule had only fleeting lifetimes when exposed to a pH value less than 5, because of epimerization at the C13

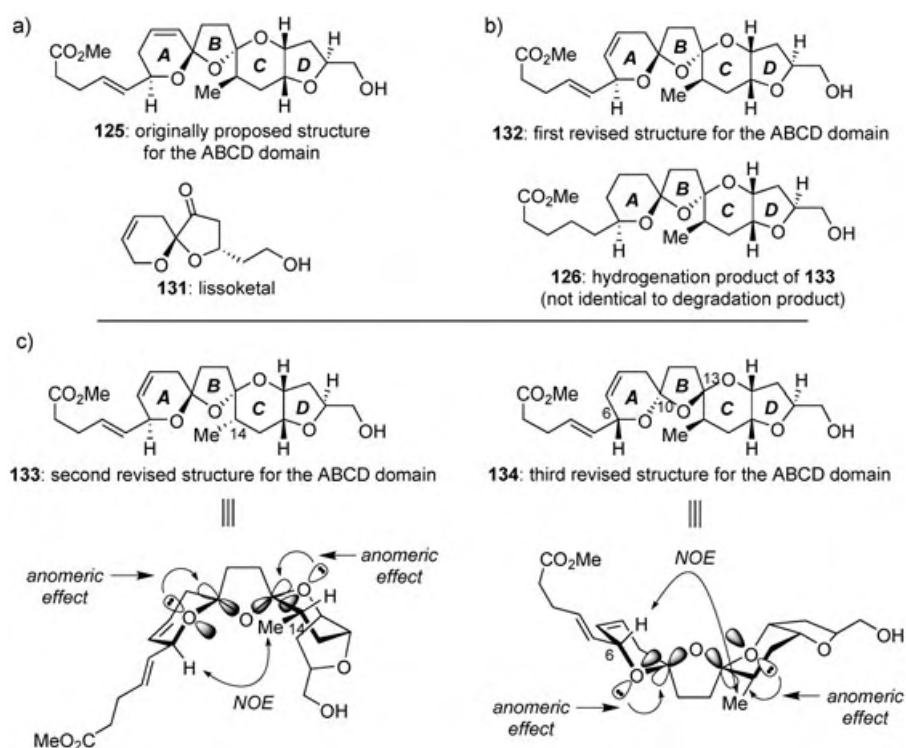


Figure 12. Final steps a)–c) in the assignment of the structure **134** to the ABCD domain of azaspiracid-1. The differences in all of the proposed structures versus the original assignment have been highlighted.

center. This tidbit of information suggested that the problem might lie in this region. Indeed, molecular models pointed to structure **133** as a possible candidate for the degradation product, since it would be favored by a double anomeric effect (an advantage that our original targets did not have) and would be likely to exhibit the obligatory NOE reported for the natural product (see Figure 12c). However, once again chemical synthesis would prove this intuition to be false, as synthetic intermediates encountered en route to **133** were not stable.

There was still one more chance for success. What if we inverted the C6 stereocenter in the A ring? Molecular modeling studies suggested that this variant, **134** (Figure 12c), would exhibit both a double anomeric effect and the required NOE, whereas alterations to any of the other potentially relevant stereocenters in this domain (i.e. C10, C13, and C14) appeared less promising. Our next move was, therefore, to synthesize compound **134** as quickly as possible, and this time the ^1H NMR spectrum fully matched that of the degradation product!

This outcome was certainly welcome after nearly a year of intense study, but one question remained: What was the absolute configuration of this domain? Only synthesis could answer this question, as the limited amount of material derived from degradation reactions corresponding to the ABCD region of the natural product did not permit the accurate measurement of its optical rotation. Which enantiomer to use was a gamble: a bet that we would ultimately lose, for the wrong stereoisomer was completed first! After a final retreat (and in the knowledge that we would soon prevail) we advanced on the alternate “upper-domain” fragment, and on Monday, May 10, 2004 at 9.00 a.m. one of us (K.C.N.) returned from a meeting in Moscow to discover a set of matching ^1H NMR spectra (Figure 13), which indicated that azaspiracid-1 had finally been synthesized and that its correct structure was **121** (Figure 9)! This data was accompanied by a note written half in Greek and half in English from Dr. Theocharis Koftis, one of the azaspiracid-1 team (Figure 14): “It contains some $n\text{Bu}_4\text{NOH}$, but the odyssey is over!”

In this long campaign, one which filled us at times with great excitement and at times with intense disappointment, the goal was finally reached through the power of chemical synthesis in a manner not too dissimilar from that used decades ago for structural elucidation.^[187] Although spectroscopy revealed most features of the structure of azaspiracid-1 with an amazingly small amount of material, ultimately it

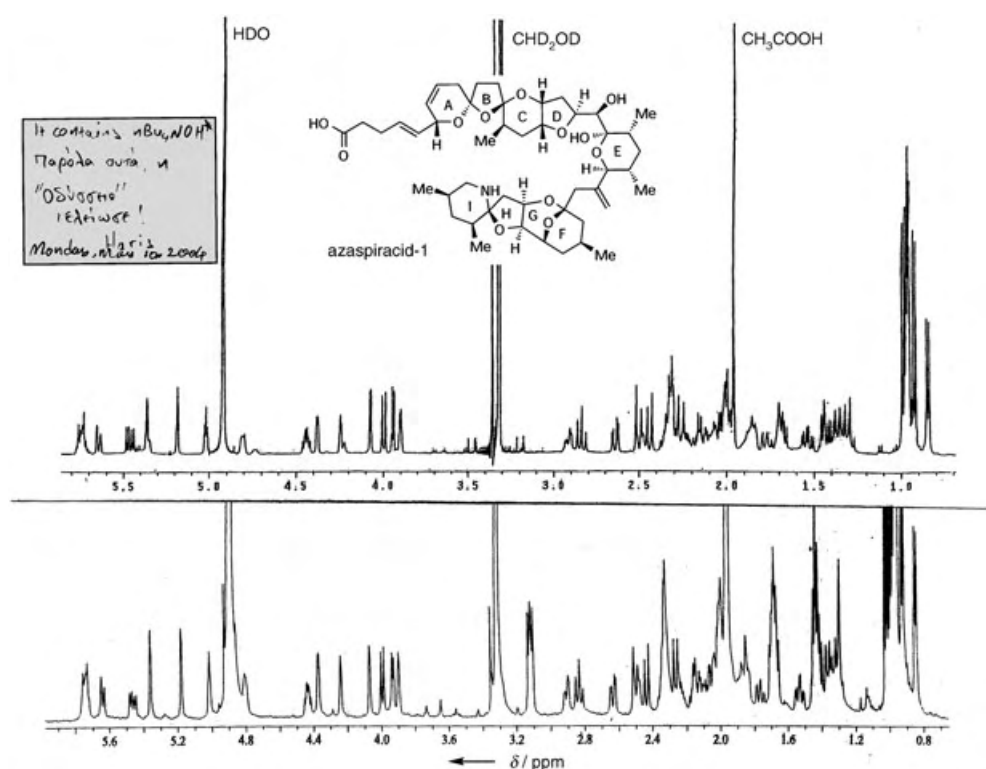


Figure 13. Correlation of NMR spectra of natural (top) and synthetic (bottom) azaspiracid-1 (not exactly to the same scale).



Figure 14. The “finalists” of the triumphant team proudly display the azaspiracid-1 structure and their flags. From left to right: Taotao Ling, Wenjun Tang, Goran Petrovic, Theocharis Koftis, Stepan Vyskocil, Michael Frederick.

could not do it all. Only when spectroscopy was combined with synthesis were all the details finally resolved.

5. Summary and Outlook

Although the past half century has witnessed a remarkable improvement in our ability to isolate and characterize

complex natural products, mistakes are still a relatively common occurrence. However, as the stories in Section 4 relating to our own experiences hopefully indicate, this state of affairs is far from catastrophic. Indeed, structural misassignments clearly provide opportunities for synthetic chemists to make discoveries through total synthesis, and certainly show that there is still adventure to be had in the process of structure assignment. It will be interesting to see just what the next half century will bring in terms of the isolation and synthesis of natural products. Only time will tell, but we can be certain that as long as chemists continue to isolate new and diverse substances from nature, there will be plenty of challenges for our intellectual and physical skills. Moreover, much new science awaits discovery during the struggle to synthesize such new molecular puzzles.^[189,190]

List of Abbreviations

AIBN	2,2'-azobisisobutyronitrile
Bn	benzyl
Boc	<i>tert</i> -butoxycarbonyl
Bz	benzoyl
Cbz	benzyloxycarbonyl
CD	circular dichroism
dba	<i>trans,trans</i> -dibenzylideneacetone
DDQ	2,3-dichloro-5,6-dicyano-1,4-benzoquinone
DIBAL-H	diisobutylaluminum hydride
DMA	<i>N,N</i> -dimethylacetamide
4-DMAP	4-dimethylaminopyridine
dppf	1,1'-(diphenylphosphanyl)ferrocene
EA	elemental analysis
EDC	1-(3-dimethylaminopropyl)-3-ethylcarbodiimide hydrochloride
Fmoc	9-fluorenylmethoxycarbonyl
HOBt	1-hydroxybenzotriazole
INEPT	insensitive nuclei enhanced by polarization transfer
MOM	methoxymethyl
NBS	<i>N</i> -bromosuccinimide
NCS	<i>N</i> -chlorosuccinimide
NIS	<i>N</i> -iodosuccinimide
NOE	nuclear Overhauser enhancement
py	pyridine
TBAF	tetra- <i>n</i> -butylammonium fluoride
TBDPS	<i>tert</i> -butyldiphenylsilyl
TBS	<i>tert</i> -butyldimethylsilyl
TES	triethylsilyl
Tf	trifluoromethanesulfonyl
TFA	trifluoroacetic acid
THP	tetrahydropyranyl
TMS	trimethylsilyl
Ts	4-toluenesulfonyl

It is with great pride and pleasure that we thank our collaborators, whose names appear in the references cited and whose contributions made the work described so rewarding and enjoyable. We gratefully acknowledge the National Institutes of Health (USA), the Skaggs Institute for Chemical

Biology, American Bioscience, Amgen, Novartis, Bristol-Myers Squibb (fellowship to S.A.S.), CaPCURE, the George E. Hewitt Foundation, Pfizer (fellowship to S.A.S.), and the National Science Foundation (fellowship to S.A.S.) for supporting our research programs.

Received: June 3, 2004

- [1] To explore these assignments further, see the Nobel Prize website: <http://www.nobel.se/chemistry>.
- [2] J. D. Bernal, *Nature* **1932**, 129, 721.
- [3] a) P. Rabe, *Ber. Dtsch. Chem. Ges.* **1908**, 41, 62; b) P. Rabe, E. Ackerman, W. Schneider, *Ber. Dtsch. Chem. Ges.* **1907**, 40, 3655; for the first total synthesis of quinine, see: c) R. B. Woodward, W. E. Doering, *J. Am. Chem. Soc.* **1944**, 66, 849; d) R. B. Woodward, W. E. Doering, *J. Am. Chem. Soc.* **1945**, 67, 860–874.
- [4] H. Fischer, K. Zeile, *Justus Liebigs Ann. Chem.* **1929**, 468, 98.
- [5] a) L. H. Briggs, H. T. Openshaw, R. Robinson, *J. Chem. Soc.* **1946**, 903–908; b) R. Robinson, *Experientia* **1946**, 2, 28; for the first total synthesis of strychnine, see: c) R. B. Woodward, M. P. Cava, W. D. Ollis, A. Hunger, H. U. Daeniker, K. Schenker, *J. Am. Chem. Soc.* **1954**, 76, 4749–4751; d) R. B. Woodward, M. P. Cava, W. D. Ollis, A. Hunger, H. U. Daeniker, K. Schenker, *Tetrahedron* **1963**, 19, 247–288; see also: e) Robert Burns Woodward: Artist and Architect in the World of Molecules (Eds.: O. T. Benfey, P. J. T. Morris), Chemical Heritage Foundation, Philadelphia, **2001**, p. 470.
- [6] W. von E. Doering in H. Hopf, *Classics in Hydrocarbon Chemistry*, Wiley-VCH, Weinheim, **2000**, p. 547.
- [7] G. Büchi, R. E. Erickson, N. Wakabayashi, *J. Am. Chem. Soc.* **1961**, 83, 927–938.
- [8] G. Büchi, W. D. MacLeod, *J. Am. Chem. Soc.* **1962**, 84, 3205–3206.
- [9] a) M. Dobler, J. D. Dunitz, B. Gubler, H. P. Weber, G. Büchi, O. J. Padilla, *Proc. Chem. Soc. London* **1963**, 383; b) G. Büchi, W. D. MacLeod, O. J. Padilla, *J. Am. Chem. Soc.* **1964**, 86, 4438–4444.
- [10] Interestingly, one could actually consider the birth of organic synthesis to be the product of a structural misassignment. In 1828, Friedrich Wöhler was attempting to synthesize ammonium isocyanate (NH₄OCN), which actually has the structure NH₄NCO. When he took a bottle of what he thought was silver isocyanate (actually silver cyanate), added ammonium chloride, and heated, urea resulted, an outcome that he did not intend, but one which was fortuitous nonetheless. For an interesting discussion on Wöhler's synthesis of urea, see: P. S. Cohen, S. M. Cohen, *J. Chem. Educ.* **1996**, 73, 883–886.
- [11] a) K. Nakanishi in *Comprehensive Natural Products Chemistry*, Vol. 1 (Eds.: D. H. R. Barton, K. Nakanishi, O. Meth-Cohn), Elsevier, Amsterdam, **1999**, pp. xxiii–xl; b) C. Djerassi, *Pure Appl. Chem.* **1975**, 41, 113–144; for an interesting recent account on two misassignments in inorganic chemistry, see: c) J. A. Labinger, S. J. Weininger, *Angew. Chem.* **2004**, 116, 2664–2672; *Angew. Chem. Int. Ed.* **2004**, 43, 2612–2619.
- [12] J. C. Sheehan, *The Enchanted Ring: The Untold Story of Penicillin*, MIT Press, Cambridge, **1984**, p. 224.
- [13] C. Djerassi, *Steroids Made It Possible* (Ed.: J. I. Seeman), American Chemical Society, Washington, DC, **1990**, p. 205 (Profiles, Pathways and Dreams Series).
- [14] K. Nakanishi, *A Wandering Natural Products Chemist* (Ed.: J. I. Seeman), American Chemical Society, Washington, D.C., **1991**, p. 230 (Profiles, Pathways and Dreams Series). The quote is on page 87. For a further insightful analysis of the state of the art of

- total synthesis in 1974, see: A. Eschenmoser, *Naturwissenschaften* **1974**, *61*, 513–525.
- [15] a) L. L. Klein, W. W. McWhorter, S. S. Ko, K.-P. Pfaff, Y. Kishi, D. Uemura, Y. Hirata, *J. Am. Chem. Soc.* **1982**, *104*, 7362–7364; b) S. S. Ko, J. M. Finan, M. Yonaga, Y. Kishi, D. Uemura, Y. Hirata, *J. Am. Chem. Soc.* **1982**, *104*, 7364–7367; c) H. Fujioka, W. J. Christ, J. K. Cha, J. Leder, Y. Kishi, D. Uemura, Y. Hirata, *J. Am. Chem. Soc.* **1982**, *104*, 7367–7369; d) J. K. Cha, W. J. Christ, J. M. Finan, H. Fujioka, Y. Kishi, L. L. Klein, S. S. Ko, J. Leder, W. W. McWhorter, K.-P. Pfaff, M. Yonaga, D. Uemura, Y. Hirata, *J. Am. Chem. Soc.* **1982**, *104*, 7369–7371; for a detailed account of this synthesis, see: K. C. Nicolaou, E. J. Sorensen, *Classics in Total Synthesis: Targets, Strategies, Methods*, VCH, Weinheim, **1996**, chap. 36, p. 798.
- [16] M. Ishibashi, N. Yamaguchi, T. Sasaki, J. Kobayashi, *J. Chem. Soc. Chem. Commun.* **1994**, 1455–1456.
- [17] Our SciFinder search terms included: revised structure, structural reassignment, misassigned structure, incorrect structure, putative structure, tentative structure, and structural revision. Interestingly, each of these searches produced quite a different set of results, and well over 1000 hits were obtained overall for the period of January 1990 to March 2004.
- [18] R. Suemitsu, K. Ohnishi, M. Horiuchi, A. Kitaguchi, K. Odamura, *Phytochemistry* **1992**, *31*, 2325–2326.
- [19] M. Horiuchi, T. Maoka, N. Iwase, K. Ohnishi, *J. Nat. Prod.* **2002**, *65*, 1204–1205.
- [20] I. Cornella, T. R. Kelly, *J. Org. Chem.* **2004**, *69*, 2191–2193.
- [21] A. S. Ratnayake, W. Y. Yoshida, S. L. Mooberry, T. K. Hemscheidt, *J. Org. Chem.* **2001**, *66*, 8717–8721.
- [22] J. A. May, R. K. Zeidan, B. M. Stoltz, *Tetrahedron Lett.* **2003**, *44*, 1203–1205. Nomofungin is identical to the natural product communesin B, which had been isolated and characterized almost a decade earlier: A. Numata, C. Takahashi, Y. Ito, T. Takada, K. Kawai, Y. Usami, E. Matsumura, M. Imachi, T. Ito, T. Hasegawa, *Tetrahedron Lett.* **1993**, *34*, 2355–2358.
- [23] I. H. Hardt, P. R. Jensen, W. Fenical, *Tetrahedron Lett.* **2000**, *41*, 2073–2076.
- [24] J. A. Kalaitzis, Y. Hamano, G. Nilsen, B. S. Moore, *Org. Lett.* **2003**, *5*, 4449–4452.
- [25] P. A. Horton, F. E. Koehn, R. E. Longley, O. J. McConnell, *J. Am. Chem. Soc.* **1994**, *116*, 6015–6016.
- [26] a) E. Lee, H. Y. Song, J. W. Kang, D.-S. Kim, C.-K. Jung, J. M. Joo, *J. Am. Chem. Soc.* **2002**, *124*, 384–385; b) E. Lee, H. Y. Song, J. M. Joo, J. W. Kang, D. S. Kim, C. K. Jung, C. Y. Hong, S. Jeong, K. Jeon, *Bioorg. Med. Chem. Lett.* **2002**, *12*, 3519–3520; c) H. Y. Song, J. M. Joo, J. W. Kang, D.-S. Kim, C.-K. Jung, H. S. Kwak, J. H. Park, E. Lee, C. Y. Hong, S. Jeong, K. Jeon, J. H. Park, *J. Org. Chem.* **2003**, *68*, 8080–8087. In this reassignment not only was an error found in the proposed structure, but the sign of the optical rotation reported for the natural product was also incorrect.
- [27] A. Randazzo, G. Bifulco, C. Giannini, M. Bucci, C. Debitus, G. Cirro, L. Gomez-Paloma, *J. Am. Chem. Soc.* **2001**, *123*, 10870–10876.
- [28] C. Della Monica, A. Randazzo, G. Bifulco, P. Cimino, M. Aquino, I. Izzo, F. De Riccardis, L. Gomez-Paloma, *Tetrahedron Lett.* **2002**, *43*, 5707–5710.
- [29] P. Sharma, M. Alam, *J. Chem. Soc. Perkin Trans. 1* **1988**, 2537–2540.
- [30] a) L. A. Paquette, O. M. Moradei, P. Bernardelli, T. Lange, *Org. Lett.* **2000**, *2*, 1875–1878; b) D. Friedrich, R. W. Dotsch, L. A. Paquette, *Org. Lett.* **2000**, *2*, 1879–1882; for the full account of this reassignment, see: c) D. Friedrich, L. A. Paquette, *J. Nat. Prod.* **2002**, *65*, 126–130; for another synthesis of the originally assigned structure of sclerophytin A, see: d) L. E. Overman, L. D. Pennington, *Org. Lett.* **2000**, *2*, 2683–2686.
- [31] a) F. Gallou, D. W. C. MacMillan, L. E. Overman, L. A. Paquette, L. D. Pennington, J. Yang, *Org. Lett.* **2001**, *3*, 135–137; for the full account of these total syntheses, see: b) P. Bernardelli, O. M. Moradei, D. Friedrich, J. Yang, F. Gallou, B. P. Dyck, R. W. Dotsch, T. Lange, L. A. Paquette, *J. Am. Chem. Soc.* **2001**, *123*, 9021–9032; c) D. W. C. MacMillan, L. E. Overman, L. D. Pennington, *J. Am. Chem. Soc.* **2001**, *123*, 9033–9044; for a personal account of one of these research programs, see: d) L. A. Paquette, *Chem. Rec.* **2001**, *1*, 311–320; e) L. A. Paquette, *Chemtracts* **2002**, *15*, 345–366.
- [32] A. D. Patil, A. J. Freyer, P. B. Taylor, B. Carté, G. Zuber, R. K. Johnson, D. J. Faulkner, *J. Org. Chem.* **1997**, *62*, 1814–1819.
- [33] a) F. Cohen, L. E. Overman, *J. Am. Chem. Soc.* **2001**, *123*, 10782–10783. Earlier work by other groups had revised the stereostructure of the left-hand guanidine portion of batzelladine F, but the carbon framework was not corrected: b) G. P. Black, P. J. Murphy, A. J. Thornhill, N. D. A. Walshe, C. Zanetti, *Tetrahedron* **1999**, *55*, 6547–6554; c) B. B. Snider, M. V. Busuyek, *J. Nat. Prod.* **1999**, *62*, 1707–1711; d) K. Nagasawa, H. Koshino, T. Nakata, *Tetrahedron Lett.* **2001**, *42*, 4155–4158.
- [34] S. Carmely, Y. Kashman, *Tetrahedron Lett.* **1985**, *26*, 511–514.
- [35] a) M. Kobayashi, J. Tanaka, T. Katori, M. Matsuura, I. Kitagawa, *Tetrahedron Lett.* **1989**, *30*, 2963–2966; b) I. Kitagawa, M. Kobayashi, T. Katori, M. Yamashita, J. Tanaka, M. Doi, T. Ishida, *J. Am. Chem. Soc.* **1990**, *112*, 3710–3712; c) M. Kobayashi, J. Tanaka, T. Katori, M. Matsuura, M. Yamashita, I. Kitagawa, *Chem. Pharm. Bull.* **1990**, *38*, 2409–2418; d) M. Kobayashi, J. Tanaka, T. Katori, I. Kitagawa, *Chem. Pharm. Bull.* **1990**, *38*, 2960–2966; e) M. Doi, T. Ishida, M. Kobayashi, I. Kitagawa, *J. Org. Chem.* **1991**, *56*, 3629–3632.
- [36] a) I. Paterson, J. D. Smith, R. A. Ward, J. G. Cumming, *J. Am. Chem. Soc.* **1994**, *116*, 2615–2616; b) I. Paterson, K.-S. Yeung, R. A. Ward, J. G. Cumming, J. D. Smith, *J. Am. Chem. Soc.* **1994**, *116*, 9391–9392; for the full account of this total synthesis, see: c) I. Paterson, J. G. Cumming, R. A. Ward, S. Lamboley, *Tetrahedron* **1995**, *51*, 9393–9412; d) I. Paterson, J. D. Smith, R. A. Ward, *Tetrahedron* **1995**, *51*, 9413–9436; e) I. Paterson, R. A. Ward, J. D. Smith, J. G. Cumming, K.-S. Yeung, *Tetrahedron* **1995**, *51*, 9437–9466; f) I. Paterson, K.-S. Yeung, R. A. Ward, J. D. Smith, J. G. Cumming, S. Lamboley, *Tetrahedron* **1995**, *51*, 9467–9486; for a later total synthesis of swinholid A, see: g) K. C. Nicolaou, K. Ajito, A. P. Patron, H. Khatuya, P. K. Richter, P. Bertinato, *J. Am. Chem. Soc.* **1996**, *118*, 3059–3060; h) K. C. Nicolaou, A. P. Patron, K. Ajito, P. K. Richter, H. Khatuya, P. Bertinato, R. A. Miller, M. J. Tomaszewski, *Chem. Eur. J.* **1996**, *2*, 847–868; for a review of these two syntheses, see: K. C. Nicolaou, S. A. Snyder, *Classics in Total Synthesis II: More Targets, Strategies, Methods*, Wiley-VCH, Weinheim, **2003**, chap. 3, p. 639.
- [37] L. Ramachandra Row, K. S. Reddy, N. S. Sarma, T. Matsuura, R. Nakashima, *Phytochemistry* **1980**, *19*, 1175–1181.
- [38] a) B. Makino, M. Kawai, Y. Iwata, H. Yamamura, Y. Butsugan, K. Ogawa, M. Hayashi, *Bull. Chem. Soc. Jpn.* **1995**, *68*, 219–226; for the structural revision of another member of this family, see: b) B. Makino, M. Kawai, T. Ogura, M. Nakanishi, H. Yamamura, Y. Butsugan, *J. Nat. Prod.* **1995**, *58*, 1668–1674; for the structural revision of another physalin, whose proposed structure was based on a misassigned degradation product, see: c) M. Kawai, T. Ogura, Y. Butsugan, T. Taga, M. Hayashi, *Tetrahedron* **1991**, *47*, 2103–2110.
- [39] T. H. Al-Tel, M. H. A. Zarga, S. S. Sabri, M. Feroz, N. Fatima, Z. Shah, Atta-Ur-Rahman, *Phytochemistry* **1991**, *30*, 3081–3085.
- [40] A. V. Kalinin, V. Snieckus, *Tetrahedron Lett.* **1998**, *39*, 4999–5002. This revised structure is that of isoeugenetin methyl ether, a derivative of the natural product isoeugenetin that had been

- prepared nearly fifty years earlier: a) H. Schmid, A. Bolleter, *Helv. Chim. Acta* **1949**, *32*, 1358–1360; b) H. Schmid, A. Bolleter, *Helv. Chim. Acta* **1950**, *33*, 917–922.
- [41] H. Greger, O. Hofer, H. Kählig, G. Wurz, *Tetrahedron* **1992**, *48*, 1209–1218.
- [42] W. M. Johnson, S. W. Littler, C. R. Strauss, *Aust. J. Chem.* **1994**, *47*, 751–756; for a later total synthesis of sinharine and a discussion of the original misassignment, see: S. Hinterberger, O. Hofer, H. Greger, *Tetrahedron* **1994**, *50*, 6279–6286.
- [43] O. M. Cobar, A. D. Rodríguez, O. L. Padilla, J. A. Sánchez, *J. Org. Chem.* **1997**, *62*, 7183–7188.
- [44] Y.-P. Shi, A. D. Rodríguez, O. L. Padilla, *J. Nat. Prod.* **2001**, *64*, 1439–1443.
- [45] I. Kubo, S. P. Tanis, Y.-W. Lee, I. Miura, K. Nakanishi, A. Chapya, *Heterocycles* **1976**, *5*, 485–498.
- [46] M. S. Rajab, J. K. Rugutt, F. R. Fronczek, N. H. Fischer, *J. Nat. Prod.* **1997**, *60*, 822–825.
- [47] J. Rodríguez, B. M. Peters, L. Kurz, R. C. Schatzman, D. McCarley, L. Lou, P. Crews, *J. Am. Chem. Soc.* **1993**, *115*, 10436–10437.
- [48] J. Rodríguez, P. Crews, *Tetrahedron Lett.* **1994**, *35*, 4719–4722.
- [49] F. Balza, S. Tachibana, H. Barrios, G. H. N. Towers, *Phytochemistry* **1991**, *30*, 1613–1614.
- [50] a) G. I. Georg, S. R. Gollapudi, G. L. Grunewald, C. W. Gunn, R. H. Himes, B. K. Rao, X.-Z. Liang, Y. W. Mirhom, L. A. Mitscher, D. G. Vander Velde, Q.-M. Ye, *Bioorg. Med. Chem. Lett.* **1993**, *3*, 1345–1348; b) G. I. Georg, Z. S. Cheruvallath, D. Vander Velde, Q.-M. Ye, L. A. Mitscher, *Bioorg. Med. Chem. Lett.* **1993**, *3*, 1349–1350; for a slightly later publication leading to the same structural revision based on X-ray crystallographic analysis of a related compound, see: c) G. Appendino, L. Barboni, P. Gariboldi, E. Bombardelli, B. Gabetta, D. Viterbo, *J. Chem. Soc. Chem. Commun.* **1993**, 1587–1589; in concurrent work, a group (which included some of the initial isolation chemists) identified the transposition of the acetate and benzoate units originally at C7 and C10, respectively, but not the constitutional change: d) A. Chu, J. Zajicek, G. H. N. Towers, C. M. Soucy-Breau, N. G. Lewis, R. Croteau, *Phytochemistry* **1993**, *34*, 269–271.
- [51] a) U. Renner, H. Fritz, *Helv. Chim. Acta* **1965**, *48*, 308–317; for the earlier report of the isolation of isoschizogamine, see: b) U. Renner, P. Kernweisz, *Experientia* **1963**, *19*, 244–246.
- [52] J. Hájicek, J. Taimr, M. Budesínský, *Tetrahedron Lett.* **1998**, *39*, 505–508.
- [53] J. L. Hubbs, C. H. Heathcock, *Org. Lett.* **1999**, *1*, 1315–1317.
- [54] a) Y. Kuroda, M. Okuhara, T. Goto, M. Yamashita, E. Iguchi, M. Kohsaka, H. Aoki, H. Imanaka, *J. Antibiot.* **1980**, *33*, 259–266; b) Y. Kuroda, M. Okuhara, T. Goto, M. Okamoto, M. Yamashita, M. Kohsaka, H. Aoki, H. Imanaka, *J. Antibiot.* **1980**, *33*, 267–271.
- [55] a) N. Yasuda, K. Sakane, *J. Antibiot.* **1991**, *44*, 801–802. Interestingly, the structure of FR900148 was questioned earlier based on the isolation of a potential biosynthetic precursor, but was not revised: b) L. Chaiet, B. H. Arison, R. L. Monaghan, J. P. Springer, J. L. Smith, S. B. Zimmerman, *J. Antibiot.* **1984**, *37*, 207–210.
- [56] J. Cáceres, M. E. Rivera, A. D. Rodríguez, *Tetrahedron* **1990**, *46*, 341–348.
- [57] a) J. Shin, W. Fenical, *J. Org. Chem.* **1991**, *56*, 3392–3398; for a follow-up article by the original isolation chemists on the structural assignment, see: b) A. D. Rodríguez, A. L. Acosta, H. Dhasmana, *J. Nat. Prod.* **1993**, *56*, 1843–1849.
- [58] a) E. J. Corey, R. S. Kania, *Tetrahedron Lett.* **1998**, *39*, 741–744; for a later total synthesis of palominol, see: b) H. Miyaoka, Y. Isaji, H. Mitome, Y. Yamada, *Tetrahedron* **2003**, *59*, 61–75.
- [59] a) J. Kobayashi, M. Ishibashi, H. Hirota, *J. Nat. Prod.* **1991**, *54*, 1435–1439; for the original publication on the isolation, see: b) J. Kobayashi, M. Ishibashi, H. Nakamura, Y. Ohizumi, T. Yamasu, T. Sasaki, Y. Hirata, *Tetrahedron Lett.* **1986**, *27*, 5755–5758; for a review on this family of natural products, see: c) M. Ishibashi, J. Kobayashi, *Heterocycles* **1997**, *44*, 543–572.
- [60] a) B. M. Trost, P. E. Harrington, *J. Am. Chem. Soc.* **2004**, *126*, 5028–5029; for earlier syntheses of the originally proposed structure, see: b) H. W. Lam, G. Pattenden, *Angew. Chem.* **2002**, *114*, 526–529; *Angew. Chem. Int. Ed.* **2002**, *41*, 508–511; c) R. E. Maleczka, L. R. Terrell, F. Geng, J. S. Ward, *Org. Lett.* **2002**, *4*, 2841–2844; d) B. M. Trost, J. D. Chisholm, S. T. Wroblewski, M. Jung, *J. Am. Chem. Soc.* **2002**, *124*, 12420–12421.
- [61] M. A. M. Maciel, A. C. Pinto, S. N. Brabo, M. N. Da Silva, *Phytochemistry* **1998**, *49*, 823–828.
- [62] R. B. Grossman, R. M. Rasne, *Org. Lett.* **2001**, *3*, 4027–4030.
- [63] a) E. Selva, G. Beretta, N. Montanini, G. S. Saddler, L. Gastaldo, P. Ferrari, R. Lorenzetti, P. Landini, F. Ripamonti, B. P. Goldstein, M. Berti, L. Montanaro, M. Denaro, *J. Antibiot.* **1991**, *44*, 693–701; b) J. Kettenring, L. Colombo, P. Ferrari, P. Tavecchia, M. Nebuloni, K. Vékey, G. G. Gallo, E. Selva, *J. Antibiot.* **1991**, *44*, 702–715.
- [64] a) P. Tavecchia, P. Gentili, M. Kurz, C. Sottani, R. Bonfichi, S. Lociuero, E. Selva, *J. Antibiot.* **1994**, *47*, 1564–1567; for the full account of this structural revision, see: b) P. Tavecchia, P. Gentili, M. Kurz, C. Sottani, R. Bonfichi, E. Selva, S. Lociuero, E. Restelli, R. Ciabatti, *Tetrahedron* **1995**, *51*, 4867–4890.
- [65] For synthetic work which nearly reached this target molecule, see: T. Suzuki, K. Nagasaki, K. Okumura, C. Shin, *Heterocycles* **2001**, *55*, 835–840.
- [66] Y. Asakawa, A. Yamamura, T. Waki, T. Takemoto, *Phytochemistry* **1980**, *19*, 603–607.
- [67] M. Tori, K. Nakashima, M. Toyota, Y. Asakawa, *Tetrahedron Lett.* **1993**, *34*, 3751–3752.
- [68] A. Buske, S. Busemann, J. Mühlbacher, J. Schmidt, A. Porzel, G. Bringmann, G. Adam, *Tetrahedron* **1999**, *55*, 1079–1086.
- [69] G. Bringmann, J. Schlauer, H. Rischer, M. Wohlfarth, J. Mühlbacher, A. Buske, A. Porzel, J. Schmidt, G. Adam, *Tetrahedron* **2000**, *56*, 3691–3695.
- [70] S. Ômura, A. Nakagawa, H. Yamada, T. Hata, A. Furusaki, T. Watanabe, *Chem. Pharm. Bull.* **1973**, *21*, 931–940.
- [71] S. J. Gould, N. Tamayo, C. R. Melville, M. C. Cone, *J. Am. Chem. Soc.* **1994**, *116*, 2207–2208.
- [72] S. Mithani, G. Weeratunga, N. J. Taylor, G. I. Dmitrienko, *J. Am. Chem. Soc.* **1994**, *116*, 2209–2210.
- [73] a) J. E. Leet, D. R. Schroeder, S. J. Hofstead, J. Golik, K. L. Colson, S. Huang, S. E. Klover, T. W. Doyle, J. A. Matson, *J. Am. Chem. Soc.* **1992**, *114*, 7946–7948; b) J. E. Leet, D. R. Schroeder, D. R. Langley, K. L. Colson, S. Huang, S. E. Klover, M. S. Lee, J. Golik, S. J. Hofstead, T. W. Doyle, J. A. Matson, *J. Am. Chem. Soc.* **1993**, *115*, 8432–8443.
- [74] S. Kawata, S. Ashizawa, M. Hirama, *J. Am. Chem. Soc.* **1997**, *119*, 12012–12013.
- [75] The Myers group has synthesized the complete kedarcidin chromophore aglycon enantioselectively in protected form, thus verifying its revised connectivities and stereostructure: A. G. Myers, P. C. Hogan, A. R. Hurd, S. D. Goldberg, *Angew. Chem.* **2002**, *114*, 1104–1109; *Angew. Chem. Int. Ed.* **2002**, *41*, 1062–1067.
- [76] D. G. Corley, G. E. Rottinghaus, M. S. Tempesta, *Tetrahedron Lett.* **1986**, *27*, 427–430.
- [77] F. E. Ziegler, A. Nangia, M. S. Tempesta, *Tetrahedron Lett.* **1988**, *29*, 1665–1668.
- [78] a) F. E. Ziegler, C. A. Metcalf, G. Schulte, *Tetrahedron Lett.* **1992**, *33*, 3117–3120; for the full account of this total synthesis, see: b) F. E. Ziegler, C. A. Metcalf, A. Nangia, G. Schulte, *J. Am. Chem. Soc.* **1993**, *115*, 2581–2589.

- [79] T. Komoda, Y. Sugiyama, N. Abe, M. Imachi, H. Hirota, A. Hirota, *Tetrahedron Lett.* **2003**, *44*, 1659–1661.
- [80] T. Komoda, Y. Sugiyama, N. Abe, M. Imachi, H. Hirota, H. Koshino, A. Hirota, *Tetrahedron Lett.* **2003**, *44*, 7417–7419.
- [81] N. González, J. Rodríguez, C. Jiménez, *J. Org. Chem.* **1999**, *64*, 5705–5707.
- [82] H. Kiyota, D. J. Dixon, C. K. Luscombe, S. Hettstedt, S. V. Ley, *Org. Lett.* **2002**, *4*, 3223–3226.
- [83] C. Kan-Fan, J.-C. Quirion, I. R. C. Bick, H.-P. Husson, *Tetrahedron* **1988**, *44*, 1651–1660.
- [84] a) R. Güller, M. Dobler, H.-J. Borschberg, *Helv. Chim. Acta* **1991**, *74*, 1636–1642; for the full account of this total synthesis, see: b) J.-C. Quirion, H.-P. Husson, C. Kan, O. Laprévotte, A. Chiaroni, C. Riche, S. Burkard, H.-J. Borschberg, I. R. C. Bick, *J. Org. Chem.* **1992**, *57*, 5848–5851; for total syntheses of related alkaloids whose structures were also revised, see: c) S. Burkard, H.-J. Borschberg, *Helv. Chim. Acta* **1991**, *74*, 275–289; d) R. Güller, H.-J. Borschberg, *Helv. Chim. Acta* **1991**, *74*, 1643–1653.
- [85] F. A. Macías, R. M. Varela, A. Torres, R. M. Oliva, J. M. G. Molinillo, *Phytochemistry* **1998**, *48*, 631–636.
- [86] H. Takikawa, K. Isono, M. Sasaki, F. A. Macías, *Tetrahedron Lett.* **2003**, *44*, 7023–7025.
- [87] W. C. Taylor, S. Toth, *Aust. J. Chem.* **1997**, *50*, 895–902.
- [88] M. Arnó, M. A. González, R. J. Zaragoza, *J. Org. Chem.* **2003**, *68*, 1242–1251.
- [89] E. Sakuno, K. Yabe, T. Hamasaki, H. Nakajima, *J. Nat. Prod.* **2000**, *63*, 1677–1678.
- [90] P. Wipf, A. D. Kerekes, *J. Nat. Prod.* **2003**, *66*, 716–718. TAEMC161 is actually the phytotoxin natural product viridiol, which had been isolated and characterized more than 30 years earlier: J. S. Moffatt, J. D. Bu'Lock, T. H. Yuen, *Chem. Commun.* **1969**, 839.
- [91] W. R. Kem, K. N. Scott, J. H. Duncan, *Experientia* **1976**, *32*, 684–686.
- [92] J. A. Zoltewicz, M. P. Cruskie, *Tetrahedron* **1995**, *51*, 11401–11410.
- [93] a) M. P. Cruskie, J. A. Zoltewicz, K. A. Abboud, *J. Org. Chem.* **1995**, *60*, 7491–7495; for a later total synthesis of nemertelline, see: b) A. Bouillon, A. S. Voisin, A. Robic, J.-C. Lancelot, V. Collot, S. Rault, *J. Org. Chem.* **2003**, *68*, 10178–10180.
- [94] N. Lindquist, W. Fenical, *Tetrahedron Lett.* **1989**, *30*, 2735–2738.
- [95] a) M. S. Congreve, A. B. Holmes, A. B. Hughes, M. G. Looney, *J. Am. Chem. Soc.* **1993**, *115*, 5815–5816; for a later total synthesis of ascidiatrienolide A, see: b) A. Fürstner, M. Schlede, *Adv. Synth. Catal.* **2002**, *344*, 657–665.
- [96] P. S. Parameswaran, C. G. Naik, S. Y. Kamat, B. N. Pramanik, *Indian J. Chem. Sect. B* **1998**, *37*, 1258–1263.
- [97] N. Saito, H. Sakai, K. Suwanborirux, S. Pummangura, A. Kubo, *Heterocycles* **2001**, *55*, 21–28. These researchers were the first to note that renieramycin H is identical to cribrastatin 4, a compound isolated independently by Pettit et al. and characterized by using X-ray crystallographic analysis: G. R. Pettit, J. C. Knight, J. C. Collins, D. L. Herald, R. K. Pettit, M. R. Boyd, V. G. Young, *J. Nat. Prod.* **2000**, *63*, 793–798.
- [98] a) B. M. Degnan, C. J. Hawkins, M. F. Lavin, E. J. McCaffrey, D. L. Parry, D. J. Watters, *J. Med. Chem.* **1989**, *32*, 1354–1359; for the original isolation, see: b) D. Gouiffès, S. Moreau, N. Helbecque, J. L. Bernier, J. P. Hénichart, Y. Barbin, D. Laurent, J. F. Verbist, *Tetrahedron* **1988**, *44*, 451–459. Bistramide A has also been named bistratene A; for a later isolation of other family members, see: c) J.-F. Biard, C. Roussakis, J.-M. Kornprobst, D. Gouiffès-Barbin, J.-F. Verbist, P. Cotelte, M. P. Foster, C. M. Ireland, C. Debitus, *J. Nat. Prod.* **1994**, *57*, 1336–1345.
- [99] M. P. Foster, C. L. Mayne, R. Dunkel, R. J. Pugmire, D. M. Grant, J.-M. Kornprobst, J.-F. Verbist, J.-F. Biard, C. M. Ireland, *J. Am. Chem. Soc.* **1992**, *114*, 1110–1111.
- [100] a) P. Welzel, F.-J. Witteler, D. Müller, W. Riemer, *Angew. Chem.* **1981**, *93*, 130–132; *Angew. Chem. Int. Ed. Engl.* **1981**, *20*, 121–123; b) P. Welzel, B. Wietfeld, F. Kunisch, T. Schubert, K. Hobert, H. Duddeck, D. Müller, G. Huber, J. E. Maggio, D. H. Williams, *Tetrahedron* **1983**, *39*, 1583–1591.
- [101] H.-W. Fehlhaber, M. Girg, G. Seibert, K. Hobert, P. Welzel, Y. Van Heijenoort, J. Van Heijenoort, *Tetrahedron* **1990**, *46*, 1557–1568.
- [102] G. R. Pettit, C. L. Herald, Y. Kamano, *J. Org. Chem.* **1983**, *48*, 5354–5356.
- [103] a) D. E. Schaufelberger, G. N. Chmurny, J. A. Beutler, M. P. Koleček, A. B. Alvarado, B. W. Schaufelberger, G. M. Muschik, *J. Org. Chem.* **1991**, *56*, 2895–2900; b) G. N. Chmurny, M. P. Koleček, B. D. Hilton, *J. Org. Chem.* **1992**, *57*, 5260–5264.
- [104] K. Ohmori, Y. Ogawa, T. Obitsu, Y. Ishikawa, S. Nishiyama, S. Yamamura, *Angew. Chem.* **2000**, *112*, 2376–2379; *Angew. Chem. Int. Ed.* **2000**, *39*, 2290–2294.
- [105] a) J.-J. Chen, S.-X. Qiu, Z.-X. Zhang, J. Zhou, *Acta Bot. Yunnanica* **1989**, *11*, 203–208; b) S.-X. Qiu, Z.-X. Zhang, J. Zhou, *Acta Bot. Sin.* **1990**, *32*, 936–942.
- [106] S.-X. Qiu, L.-Z. Lin, Y. Nan, P. Lin, J.-J. Chen, Z.-X. Zhang, J. Zhou, G. A. Cordell, *Phytochemistry* **1995**, *40*, 917–921.
- [107] W. W. Harding, P. A. Lewis, H. Jacobs, S. McLean, W. F. Reynolds, L.-L. Tay, J.-P. Yang, *Tetrahedron Lett.* **1995**, *36*, 9137–9140.
- [108] Three groups synthesized the proposed structure of glabrescol independently at roughly the same time: a) H. Hioki, C. Kanehara, Y. Ohnishi, Y. Umemori, H. Sakai, S. Yoshio, M. Matsushita, M. Kodama, *Angew. Chem.* **2000**, *112*, 2652–2654; *Angew. Chem. Int. Ed.* **2000**, *39*, 2552–2554; b) Y. Morimoto, T. Iwai, T. Kinoshita, *J. Am. Chem. Soc.* **2000**, *122*, 7124–7125; c) Z. Xiong, E. J. Corey, *J. Am. Chem. Soc.* **2000**, *122*, 4831–4832. Reference [108b] included a revision of the structure and the first reported total synthesis of the true glabrescol. A few months later, a second and more efficient total synthesis of the revised structure was reported: d) Z. Zhong, E. J. Corey, *J. Am. Chem. Soc.* **2000**, *122*, 9328–9329; for an attempt to use molecular modeling to predict the correct structure of glabrescol, see: e) B. R. Bellenie, J. M. Goodman, *Tetrahedron Lett.* **2001**, *42*, 7477–7479.
- [109] For the original isolation and elucidation of parts of the structure, see: a) M. Seki-Asano, T. Okazaki, M. Yamagishi, N. Sakai, K. Hanada, K. Mizoue, *J. Antibiot.* **1994**, *47*, 1226–1233; b) M. Seki-Asano, Y. Tsuchida, K. Hanada, K. Mizoue, *J. Antibiot.* **1994**, *47*, 1234–1241; for the assignment of the stereostructure FD-891, see: c) T. Eguchi, K. Kobayashi, H. Uekusa, Y. Ohashi, K. Mizoue, Y. Matsushima, K. Kakinuma, *Org. Lett.* **2002**, *4*, 3383–3386.
- [110] T. Eguchi, K. Yamamoto, K. Mizoue, K. Kakinuma, *J. Antibiot.* **2004**, *57*, 156–157. The revised structure is exactly the same as that of the natural product BE-45653: H. Ogawa, S. Nakajima, H. Suzuki, K. Ojiri, H. Suda, *Jpn. Kokai Tokkyo Koho*, **1997**, 0987285.
- [111] a) M. R. Prinsep, F. R. Caplan, R. E. Moore, G. M. L. Patterson, C. D. Smith, *J. Am. Chem. Soc.* **1992**, *114*, 385–387; b) M. R. Prinsep, G. M. L. Patterson, L. K. Larsen, C. D. Smith, *Tetrahedron* **1995**, *51*, 10523–10530.
- [112] a) T. G. Minehan, Y. Kishi, *Angew. Chem.* **1999**, *111*, 972–975; *Angew. Chem. Int. Ed.* **1999**, *38*, 923–925; b) T. G. Minehan, L. Cook-Blumberg, Y. Kishi, M. R. Prinsep, R. E. Moore, *Angew. Chem.* **1999**, *111*, 975–977; *Angew. Chem. Int. Ed.* **1999**, *38*, 926–928.
- [113] W. Wang, Y. Kishi, *Org. Lett.* **1999**, *1*, 1129–1132.

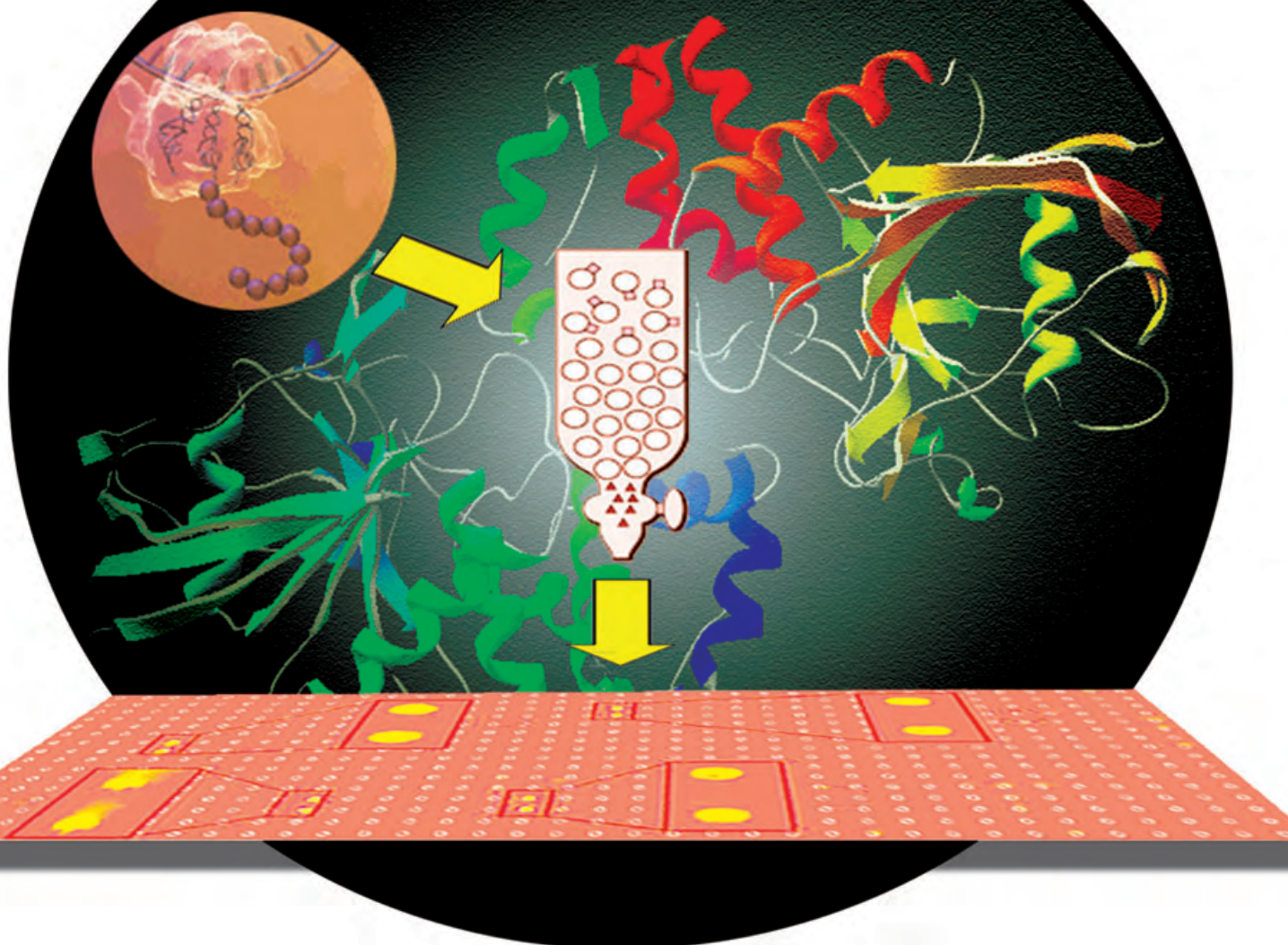
- [114] For the original isolation and elucidation of parts of the structure, see: a) K. S. Lam, G. A. Hesler, J. M. Mattei, S. W. Mamber, S. Forenza, K. Tomita, *J. Antibiot.* **1990**, *43*, 956–960; b) J. E. Leet, D. R. Schroeder, B. S. Krishnan, J. A. Matson, *J. Antibiot.* **1990**, *43*, 961–966; for the assignment of the stereostructure of himastatin, see: c) J. E. Leet, D. R. Schroeder, J. Golik, J. A. Matson, T. W. Doyle, K. S. Lam, S. E. Hill, M. S. Lee, J. L. Whitney, B. S. Krishnan, *J. Antibiot.* **1996**, *49*, 299–311.
- [115] a) T. M. Kamenecka, S. J. Danishefsky, *Angew. Chem.* **1998**, *110*, 3164–3166; *Angew. Chem. Int. Ed.* **1998**, *37*, 2993–2995; b) T. M. Kamenecka, S. J. Danishefsky, *Angew. Chem.* **1998**, *110*, 3166–3168; *Angew. Chem. Int. Ed.* **1998**, *37*, 2995–2998; for the full account of this work, see: c) T. M. Kamenecka, S. J. Danishefsky, *Chem. Eur. J.* **2001**, *7*, 41–63.
- [116] R.-s. Xu, J. K. Snyder, K. Nakanishi, *J. Am. Chem. Soc.* **1984**, *106*, 734–736.
- [117] Q. Cheng, J. K. Snyder, *J. Org. Chem.* **1988**, *53*, 4562–4567; for an earlier total synthesis of the originally proposed structure of robustadiol A, see: K. Lal, E. A. Zarate, W. J. Youngs, R. G. Salomon, *J. Am. Chem. Soc.* **1986**, *108*, 1311–1312.
- [118] a) R. G. Salomon, K. Lal, S. M. Mazza, E. A. Zarate, W. J. Youngs, *J. Am. Chem. Soc.* **1988**, *110*, 5213–5214; for a full account of this synthesis, see: b) R. G. Salomon, S. M. Mazza, K. Lal, *J. Org. Chem.* **1989**, *54*, 1562–1570; for more recent total syntheses of the robustadiols, see: c) S. Koser, H. M. R. Hoffmann, D. J. Williams, *J. Org. Chem.* **1993**, *58*, 6163–6165; d) S. Bissada, C. K. Lau, M. A. Bernstein, C. Dufresne, *Can. J. Chem.* **1994**, *72*, 1866–1869; e) I. R. Aukrust, L. Skatteboel, *Acta Chem. Scand.* **1996**, *50*, 132–140; for a synthesis of robustadiol A dimethyl ether, see: f) M. Majewski, G. Bantle, *Tetrahedron Lett.* **1989**, *30*, 6653–6656; g) M. Majewski, N. M. Irvine, G. W. Bantle, *J. Org. Chem.* **1994**, *59*, 6697–6702.
- [119] For the original isolation and elucidation of parts of the structure, see: a) G. R. Pettit, Z. A. Cichacz, F. Gao, M. R. Boyd, J. M. Schmidt, *J. Chem. Soc. Chem. Commun.* **1994**, 1111–1112; for the determination of parts of the stereostructure of dictyostatin 1, see: b) G. R. Pettit, Z. A. Cichacz, US Patent 5430053, **1995** [*Chem. Abst.* **1995**, *123*, 139562]; for some information on its biological activity, see: c) R. A. Isbrucker, J. Cummins, S. A. Pomponi, R. E. Longley, A. E. Wright, *Biochem. Pharmacol.* **2003**, *66*, 75–82.
- [120] I. Paterson, R. Britton, O. Delgado, A. E. Wright, *Chem. Commun.* **2004**, 632–633.
- [121] J. F. Biard, S. Guyot, C. Roussakis, J. F. Verbist, J. Vercauteren, J. F. Weber, K. Boukef, *Tetrahedron Lett.* **1994**, *35*, 2691–2694.
- [122] a) H. Abe, S. Aoyagi, C. Kibayashi, *J. Am. Chem. Soc.* **2000**, *122*, 4583–4592; b) H. Abe, S. Aoyagi, C. Kibayashi, *Angew. Chem.* **2002**, *114*, 3143–3146; *Angew. Chem. Int. Ed.* **2002**, *41*, 3017–3020; for the full account of this total synthesis, see: c) C. Kibayashi, S. Aoyagi, H. Abe, *Bull. Chem. Soc. Jpn.* **2003**, *76*, 2059–2074; for earlier total syntheses of the proposed structure of lepadiformine that did not point to a definitive structural alternative, see: d) W. H. Pearson, Y. Ren, *J. Org. Chem.* **1999**, *64*, 688–689; e) K. M. Werner, J. M. de los Santos, S. M. Weinreb, M. Shang, *J. Org. Chem.* **1999**, *64*, 686–687; f) K. M. Werner, J. M. de los Santos, S. M. Weinreb, M. Shang, *J. Org. Chem.* **1999**, *64*, 4865–4873; g) H. Abe, S. Aoyagi, C. Kibayashi, *Tetrahedron Lett.* **2000**, *41*, 1205–1208; for later total syntheses of the revised structure of lepadiformine, see: h) P. Sun, C. Sun, S. M. Weinreb, *Org. Lett.* **2001**, *3*, 3507–3510; i) T. J. Greshock, R. L. Funk, *Org. Lett.* **2001**, *3*, 3511–3514; j) P. Sun, C. Sun, S. M. Weinreb, *J. Org. Chem.* **2002**, *67*, 4337–4345; for a review of one of these research programs, see: k) S. M. Weinreb, *Acc. Chem. Res.* **2003**, *36*, 59–65.
- [123] A. R. Carroll, J. C. Coll, D. J. Bourne, J. K. MacLeod, T. M. Zabriskie, C. M. Ireland, B. F. Bowden, *Aust. J. Chem.* **1996**, *49*, 659–667.
- [124] a) P. Wipf, Y. Uto, *J. Org. Chem.* **2000**, *65*, 1037–1049; for their synthesis of the originally proposed structure, see: b) P. Wipf, Y. Uto, *Tetrahedron Lett.* **1999**, *40*, 5165–5169; for later total syntheses of the revised structure of trunkamide A, see: c) B. McKeever, G. Pattenden, *Tetrahedron Lett.* **2001**, *42*, 2573–2577; d) B. McKeever, G. Pattenden, *Tetrahedron* **2003**, *59*, 2713–2727; e) J. M. Caba, I. M. Rodriguez, I. Manzanares, E. Giral, F. Albericio, *J. Org. Chem.* **2001**, *66*, 7568–7574.
- [125] J. Orjala, D. G. Nagle, V. L. Hsu, W. H. Gerwick, *J. Am. Chem. Soc.* **1995**, *117*, 8281–8282.
- [126] a) F. Yokokawa, H. Fujiwara, T. Shioiri, *Tetrahedron Lett.* **1999**, *40*, 1915–1916; for the full account of this work, see: b) F. Yokokawa, H. Fujiwara, T. Shioiri, *Tetrahedron* **2000**, *56*, 1759–1775; for earlier syntheses of the proposed structure of antillatoxin that did not lead to the proposal of a definitive structural alternative, see: c) F. Yokokawa, T. Shioiri, *J. Org. Chem.* **1998**, *63*, 8638–8639; d) J. D. White, R. Hanselmann, D. J. Wardrop, *J. Am. Chem. Soc.* **1999**, *121*, 1106–1107.
- [127] S. Konetschny-Rapp, H.-W. Krell, U. Martin, World patent 96/11941, **1996** [*Chem. Abst.* **1996**, *124*, 315175].
- [128] S. Hanessian, M. Tremblay, J. F. W. Petersen, *J. Am. Chem. Soc.* **2004**, *126*, 6064–6071.
- [129] Y. Igarashi, K. Futamata, T. Fujita, A. Sekine, H. Senda, H. Naoki, T. Furumai, *J. Antibiot.* **2003**, *56*, 107–113.
- [130] M. E. Tichenor, D. B. Kastrinsky, D. L. Boger, *J. Am. Chem. Soc.* **2004**, *126*, 8396–8398; for earlier studies relating to the chemical biology of this interesting natural product, see: J. P. Parrish, D. B. Kastrinsky, S. E. Wolkenberg, Y. Igarashi, D. L. Boger, *J. Am. Chem. Soc.* **2003**, *125*, 10971–10976.
- [131] For the correction of the two incorrect structures, see: a) L. Witte, L. Ernst, V. Wray, T. Hartmann, *Phytochemistry* **1992**, *31*, 1027–1028; for the earlier misassignments, see: b) J. G. Urones, P. B. Barcala, I. S. Marcos, R. F. Moro, M. L. Esteban, A. F. Rodriguez, *Phytochemistry* **1988**, *27*, 1507; c) F. Bohlmann, C. Zdero, J. Jakupovic, M. Grenz, V. Castro, R. M. King, H. Robinson, L. P. D. Vincent, *Phytochemistry* **1986**, *25*, 1151–1159; see also: d) E. Roeder, *Phytochemistry* **1990**, *29*, 11–29.
- [132] For the correction of the two incorrect structures, see: a) H. Okamura, T. Iwagawa, M. Nakatani, *Bull. Chem. Soc. Jpn.* **1995**, *68*, 3465–3467; for the earlier misassignments, see: b) Y. Takeda, H. Yamashita, T. Matsumoto, H. Terao, *Phytochemistry* **1993**, *33*, 713–715; c) M. Uchida, Y. Koike, G. Kusano, Y. Kondo, S. Nozoe, C. Kabuto, T. Takemoto, *Chem. Pharm. Bull.* **1990**, *28*, 92–102; d) M. Uchida, G. Kusano, Y. Kondo, S. Nozoe, T. Takemoto, *Heterocycles* **1978**, *9*, 139–144.
- [133] T. C. Fleischer, R. D. Waigh, P. G. Waterman, *J. Nat. Prod.* **1997**, *60*, 1054–1056.
- [134] K. I. Booker-Milburn, H. Jenkins, J. P. H. Charmant, P. Mohr, *Org. Lett.* **2003**, *5*, 3309–3312.
- [135] M. F. Rodríguez Brasco, A. M. Seldes, J. A. Palermo, *Org. Lett.* **2001**, *3*, 1415–1417.
- [136] K. Inanaga, K. Takasu, M. Ihara, *J. Am. Chem. Soc.* **2004**, *126*, 1352–1353.
- [137] T. Hashimoto, S. Kondo, H. Naganawa, T. Takita, K. Maeda, H. Umezawa, *J. Antibiot.* **1974**, *27*, 86–87.
- [138] M. E. Bunnage, T. Ganesh, I. B. Masesane, D. Orton, P. G. Steel, *Org. Lett.* **2003**, *5*, 239–242.
- [139] N. J. Sun, S. H. Woo, J. M. Cassady, R. M. Snapka, *J. Nat. Prod.* **1998**, *61*, 362–366.
- [140] J. B. Perales, N. F. Makino, D. L. Van Vranken, *J. Org. Chem.* **2002**, *67*, 6711–6717.
- [141] S. N. Kazmi, Z. Ahmed, W. Ahmed, A. Malik, *Heterocycles* **1989**, *29*, 1901–1906.

- [142] D. L. Comins, X. Zheng, R. R. Goehring, *Org. Lett.* **2002**, *4*, 1611–1613.
- [143] A. R. Carroll, W. C. Taylor, *Aust. J. Chem.* **1991**, *44*, 1615–1626.
- [144] M. K. Gurjar, J. Cherian, C. V. Ramana, *Org. Lett.* **2004**, *6*, 317–319.
- [145] N. Fukamiya, M. Okano, M. Miyamoto, K. Tagahara, K.-H. Lee, *J. Nat. Prod.* **1992**, *55*, 468–475.
- [146] J. M. VanderRoest, P. A. Grieco, *J. Org. Chem.* **1996**, *61*, 5316–5325.
- [147] R. Pummerer, H. Puttfarcken, P. Schopflocher, *Ber. Dtsch. Chem. Ges. B* **1925**, *58*, 1808–1820.
- [148] a) D. H. R. Barton, A. M. Defflorin, O. E. Edwards, *Chem. Ind.* **1955**, 1039; b) D. H. R. Barton, A. M. Defflorin, O. E. Edwards, *J. Chem. Soc.* **1956**, 530–532; for an engaging overview of this work, see: D. H. R. Barton, *Half a Century of Free Radical Chemistry*, Cambridge University Press, Cambridge, **1993**, p. 164.
- [149] a) E. Brochmann-Hanssen, B. Nielsen, *Tetrahedron Lett.* **1965**, *7*, 1271–1274; b) A. R. Battersby, G. W. Evans, *Tetrahedron Lett.* **1965**, *7*, 1275–1278.
- [150] D. H. R. Barton, B. D. Brown, D. D. Ridley, D. A. Widdowson, A. J. Keys, C. J. Leaver, *J. Chem. Soc. Perkin Trans. 1* **1975**, 2069–2076; see also: A. J. Keys, C. J. Leaver, D. H. R. Barton, B. D. Brown, D. A. Widdowson, *Nature* **1971**, *232*, 423–424.
- [151] a) F. W. Lichtenthaler, K. Nakamura, J. Klotz, *Angew. Chem.* **2003**, *115*, 6019–6023; *Angew. Chem. Int. Ed.* **2003**, *42*, 5838–5843; b) F. W. Lichtenthaler, J. Klotz, K. Nakamura, *Tetrahedron: Asymmetry* **2003**, *14*, 3973–3986.
- [152] For the initial assignment based on X-ray crystallography and other methods, see: a) J. S. Webb, D. B. Cosulich, J. H. Mowat, J. B. Patrick, R. W. Broschard, W. E. Meyer, R. P. Williams, C. F. Wolf, W. Fulmor, C. Pidacks, J. E. Lancaster, *J. Am. Chem. Soc.* **1962**, *84*, 3185–3187; b) J. S. Webb, D. B. Cosulich, J. H. Mowat, J. B. Patrick, R. W. Broschard, W. E. Meyer, R. P. Williams, C. F. Wolf, W. Fulmor, C. Pidacks, J. E. Lancaster, *J. Am. Chem. Soc.* **1962**, *84*, 3187–3188; c) A. Tulinsky, *J. Am. Chem. Soc.* **1962**, *84*, 3188–3190; d) A. Tulinsky, J. H. van den Hende, *J. Am. Chem. Soc.* **1967**, *89*, 2905–2911.
- [153] a) U. Hornemann, M. J. Aikman, *J. Chem. Soc. Chem. Commun.* **1973**, 88–89; b) U. Hornemann, J. P. Kehrer, C. S. Nunez, R. L. Ranieri, *J. Am. Chem. Soc.* **1974**, *96*, 320–322.
- [154] N. Hirayama, K. Shirahata, *Acta. Crystallogr. Sect. B* **1987**, *43*, 555–559.
- [155] For a detailed account of the British–American penicillin project, see: *The Chemistry of Penicillin* (Eds.: H. T. Clarke, J. R. Johnson, R. Robinson), Princeton University Press, Princeton, **1949**, p. 1094.
- [156] Interestingly, two attempts to synthesize penicillin from compounds of type **46** and **47** did lead to miniscule amounts of the natural product through an unanticipated rearrangement. However, the yield was too low for this method to replace fermentation as the primary source of the penicillin during the war.
- [157] J. W. Lown, C. C. Hanstock, *J. Am. Chem. Soc.* **1982**, *104*, 3213–3214.
- [158] a) M. Onda, Y. Konda, A. Hatano, T. Hata, S. Ômura, *J. Am. Chem. Soc.* **1983**, *105*, 6311–6312; b) M. Onda, Y. Konda, A. Hatano, T. Hata, S. Ômura, *Chem. Pharm. Bull.* **1984**, *32*, 2995–3002.
- [159] M. E. Salvati, E. J. Moran, R. W. Armstrong, *Tetrahedron Lett.* **1992**, *33*, 3711–3714. These researchers were also the first to recognize problems with the molecular formula proposed earlier for carzinophilin (see: P. England, K. H. Chun, E. J. Moran, R. W. Armstrong, *Tetrahedron Lett.* **1990**, *31*, 2669–2672; E. J. Moran, R. W. Armstrong, *Tetrahedron Lett.* **1991**, *32*, 3807–3810) and to recognize that carzinophilin is identical to azinomycin B, a compound isolated a few years earlier but thought, at the time, to have a different molecular formula: a) K. Nagaoka, M. Matsumoto, J. Oono, K. Yokoi, S. Ishizeki, T. Nakashima, *J. Antibiot.* **1986**, *39*, 1527–1532; b) K. Yokoi, K. Nagaoka, T. Nakashima, *Chem. Pharm. Bull.* **1986**, *34*, 4554–4561.
- [160] For the total synthesis of azinomycin A, see: R. S. Coleman, J. Li, A. Navarro, *Angew. Chem.* **2001**, *113*, 1786–1789; *Angew. Chem. Int. Ed.* **2001**, *40*, 1736–1739; for the most advanced synthetic studies towards azinomycin B/carzinophilin, see: M. Hashimoto, M. Matsumoto, S. Terashima, *Tetrahedron* **2003**, *59*, 3019–3040 and ensuing publications in this series.
- [161] P. R. Zanno, I. Miura, K. Nakanishi, D. L. Elder, *J. Am. Chem. Soc.* **1975**, *97*, 1975–1977.
- [162] J. N. Hilton, H. B. Broughton, S. V. Ley, Z. Lidert, E. D. Morgan, H. S. Rzepa, R. N. Sheppard, *J. Chem. Soc. Chem. Commun.* **1985**, 968–971.
- [163] a) H. B. Broughton, S. V. Ley, A. M. Z. Slawin, D. J. Williams, E. D. Morgan, *J. Chem. Soc. Chem. Commun.* **1986**, 46–47; b) W. Kraus, M. Bokel, A. Klenk, H. Pöhl, *Tetrahedron Lett.* **1985**, *26*, 6435–6438; for the full account of these final structural investigations, see: c) D. A. H. Taylor, *Tetrahedron* **1987**, *43*, 2779–2787; d) C. J. Turner, M. S. Tempesta, R. B. Taylor, M. G. Zagorski, J. S. Termini, D. R. Schroeder, K. Nakanishi, *Tetrahedron* **1987**, *43*, 2789–2803; e) J. N. Bilton, H. B. Broughton, P. S. Jones, S. V. Ley, Z. Lidert, E. D. Morgan, H. S. Rzepa, R. N. Sheppard, A. M. Z. Slawin, D. J. Williams, *Tetrahedron* **1987**, *43*, 2805–2815; f) W. Kraus, M. Bokel, A. Bruhn, R. Cramer, I. Klaiber, A. Klenk, G. Nagl, H. Pöhl, H. Sadlo, B. Vogler, *Tetrahedron* **1987**, *43*, 2817–2830.
- [164] For reviews on synthetic work towards azadirachtin, see: a) S. V. Ley, A. A. Denholm, A. Wood, *Nat. Prod. Rep.* **1993**, *10*, 109–157; b) S. V. Ley, *Pure Appl. Chem.* **1994**, *66*, 2099–2102; for our own work towards this target, see: c) K. C. Nicolaou, M. Follmann, A. J. Roecker, K. W. Hunt, *Angew. Chem.* **2002**, *114*, 2207–2210; *Angew. Chem. Int. Ed.* **2002**, *41*, 2103–2106; d) K. C. Nicolaou, A. J. Roecker, M. Follmann, R. Baati, *Angew. Chem.* **2002**, *114*, 2211–2214; *Angew. Chem. Int. Ed.* **2002**, *41*, 2107–2110; e) K. C. Nicolaou, A. J. Roecker, H. Monenschein, P. Guntupalli, M. Follmann, *Angew. Chem.* **2003**, *115*, 3765–3770; *Angew. Chem. Int. Ed.* **2003**, *42*, 3637–3642.
- [165] N. Takeuchi, T. Fujita, K. Goto, N. Morisaki, N. Osone, K. Tobinaga, *Chem. Pharm. Bull.* **1993**, *41*, 923–925.
- [166] D. P. Piet, R. V. A. Orru, L. H. D. Jenniskens, C. van de Haar, T. A. van Beek, M. C. R. Franssen, J. B. P. A. Wijnberg, A. de Groot, *Chem. Pharm. Bull.* **1996**, *44*, 1400–1403. Prior to the publication of this article, the isolation group had reported a total synthesis of dictamnol that verified the originally proposed structure. Their synthesis had indeed provided synthetic dictamnol, but only because their use of the strongly acidic Jones reagent caused epimerization at one bridgehead carbon atom to produce the required *trans*-fused hydroazulene system of the revised structure: T. Koike, K. Yamazaki, N. Fukumoto, K. Yashiro, N. Takeuchi, S. Tobinaga, *Chem. Pharm. Bull.* **1996**, *44*, 646–652.
- [167] For other total syntheses of dictamnol, see: a) G. L. Lange, A. Merica, M. Chimanikire, *Tetrahedron Lett.* **1997**, *38*, 6371–6374; b) G. L. Lange, C. Gottardo, A. Merica, *J. Org. Chem.* **1999**, *64*, 6738–6744; c) P. A. Wender, M. Fuji, C. O. Husfeld, J. A. Love, *Org. Lett.* **1999**, *1*, 137–139.
- [168] J. Chan, T. F. Jamison, *J. Am. Chem. Soc.* **2003**, *125*, 11514–11515.
- [169] Y. Nishishi, C.-H. Lim, C. Tanaka, H. Miyagawa, T. Ueno, *Biosci. Biotechnol. Biochem.* **2002**, *66*, 685–688.
- [170] a) M. Oka, S. Iimura, Y. Narita, T. Furumai, M. Konishi, T. Oki, Q. Gao, H. Kakisawa, *J. Org. Chem.* **1993**, *58*, 1875–1881; b) S. Iimura, M. Oka, Y. Narita, M. Konishi, H. Kakisawa, Q. Gao, T. Oki, *Tetrahedron Lett.* **1993**, *34*, 493–496.

- [171] a) A. G. Myers, M. Siu, F. Ren, *J. Am. Chem. Soc.* **2002**, *124*, 4230–4232; for other total syntheses of terpestacin, see: b) K. Tatsuta, N. Masuda, H. Nishida, *Tetrahedron Lett.* **1998**, *39*, 83–86; c) K. Tatsuta, N. Masuda, *J. Antibiot.* **1998**, *51*, 602–606; the latter synthesis suffered from the same problem with the optical-rotation measurement.
- [172] N. Lindquist, W. Fenical, G. D. Van Duyne, J. Clardy, *J. Am. Chem. Soc.* **1991**, *113*, 2303–2304.
- [173] For highlights of previous synthetic studies towards the diazonamides, see: a) V. Wittmann, *Nachr. Chem.* **2002**, *50*, 477–482; b) T. Ritter, E. M. Carreira, *Angew. Chem.* **2002**, *114*, 2601–2606; *Angew. Chem. Int. Ed.* **2002**, *41*, 2489–2495.
- [174] a) K. C. Nicolaou, S. A. Snyder, K. B. Simonsen, A. E. Koumbis, *Angew. Chem.* **2000**, *112*, 3615–3620; *Angew. Chem. Int. Ed.* **2000**, *39*, 3473–3478; b) K. C. Nicolaou, X. Huang, N. Giuseppone, P. Bheema Rao, M. Bella, M. V. Reddy, S. A. Snyder, *Angew. Chem.* **2001**, *113*, 4841–4845; *Angew. Chem. Int. Ed.* **2001**, *40*, 4705–4709.
- [175] a) J. Li, S. Jeong, L. Esser, P. G. Harran, *Angew. Chem.* **2001**, *113*, 4901–4906; *Angew. Chem. Int. Ed.* **2001**, *40*, 4765–4770; b) J. Li, A. W. G. Burgett, L. Esser, C. Amezcua, P. G. Harran, *Angew. Chem.* **2001**, *113*, 4906–4909; *Angew. Chem. Int. Ed.* **2001**, *40*, 4770–4773.
- [176] K. C. Nicolaou, M. Bella, D. Y.-K. Chen, X. Huang, T. Ling, S. A. Snyder, *Angew. Chem.* **2002**, *114*, 3645–3649; *Angew. Chem. Int. Ed.* **2002**, *41*, 3495–3499.
- [177] K. C. Nicolaou, P. Bheema Rao, J. Hao, M. V. Reddy, G. Rassias, X. Huang, D. Y.-K. Chen, S. A. Snyder, *Angew. Chem.* **2003**, *115*, 1795–1800; *Angew. Chem. Int. Ed.* **2003**, *42*, 1753–1758.
- [178] For a review of these two syntheses, see: K. C. Nicolaou, S. A. Snyder, *Classics in Total Synthesis II: More Targets, Strategies, Methods*, Wiley-VCH, Weinheim, **2003**, chap. 20, p. 639; for the full account of our efforts towards diazonamide A, see: a) K. C. Nicolaou, S. A. Snyder, X. Huang, K. B. Simonsen, A. E. Koumbis, A. Bigot, *J. Am. Chem. Soc.* **2004**, *126*, 10162–10173; b) K. C. Nicolaou, S. A. Snyder, N. Giuseppone, X. Huang, M. Bella, M. V. Reddy, P. Bheema Rao, A. E. Koumbis, P. Giannakakou, A. O'Brate, *J. Am. Chem. Soc.* **2004**, *126*, 10174–10182; c) K. C. Nicolaou, D. Y.-K. Chen, X. Huang, T. Ling, M. Bella, S. A. Snyder, *J. Am. Chem. Soc.* **2004**, *126*, 12888–12896; d) K. C. Nicolaou, J. Hao, M. V. Reddy, P. Bheema Rao, G. Rassias, S. A. Snyder, X. Huang, D. Y.-K. Chen, W. E. Brenzovich, N. Giuseppone, P. Giannakakou, A. O'Brate, *J. Am. Chem. Soc.* **2004**, *126*, 12897–12906.
- [179] A third total synthesis of diazonamide A was recently completed by the Harran group: A. W. G. Burgett, Q. Li, Q. Wei, P. G. Harran, *Angew. Chem.* **2003**, *115*, 5111–5116; *Angew. Chem. Int. Ed.* **2003**, *42*, 4961–4966.
- [180] K. C. Nicolaou, S. A. Snyder, A. Bigot, J. A. Pfefferkorn, *Angew. Chem.* **2000**, *112*, 1135–1138; *Angew. Chem. Int. Ed.* **2000**, *39*, 1093–1096.
- [181] K. C. Nicolaou, A. E. Koumbis, S. A. Snyder, K. B. Simonsen, *Angew. Chem.* **2000**, *112*, 2629–2633; *Angew. Chem. Int. Ed.* **2000**, *39*, 2529–2533.
- [182] a) K. C. Nicolaou, X. Huang, S. A. Snyder, P. Bheema Rao, M. Bella, M. V. Reddy, *Angew. Chem.* **2002**, *114*, 862–866; *Angew. Chem. Int. Ed.* **2002**, *41*, 834–838; b) K. C. Nicolaou, D. A. Longbottom, S. A. Snyder, A. Z. Nalbandian, X. Huang, *Angew. Chem.* **2002**, *114*, 4022–4026; *Angew. Chem. Int. Ed.* **2002**, *41*, 3866–3870; c) K. C. Nicolaou, S. A. Snyder, A. Z. Nalbandian, D. A. Longbottom, *J. Am. Chem. Soc.* **2004**, *126*, 6234–6235; for the full account of this work, see: d) K. C. Nicolaou, S. A. Snyder, D. A. Longbottom, A. Z. Nalbandian, X. Huang, *Chem. Eur. J.* **2004**, *10*, 5581–5606.
- [183] M. Satake, K. Ofuji, H. Naoki, K. J. James, A. Furey, T. McMahon, J. Silke, T. Yasumoto, *J. Am. Chem. Soc.* **1998**, *120*, 9967–9968; for the later isolation of some structurally related compounds, see: K. Ofuji, M. Satake, T. McMahon, K. J. James, H. Naoki, Y. Oshima, T. Yasumoto, *Biosci. Biotechnol. Biochem.* **2001**, *65*, 740–742.
- [184] a) R. G. Carter, D. J. Weldon, *Org. Lett.* **2000**, *2*, 3913–3916; b) J. Aiguade, J. Hao, C. J. Forsyth, *Tetrahedron Lett.* **2001**, *42*, 817–820; c) J. Hao, J. Aiguade, C. J. Forsyth, *Tetrahedron Lett.* **2001**, *42*, 821–824; d) A. B. Dounay, C. J. Forsyth, *Org. Lett.* **2001**, *3*, 975–978; e) J. Aiguade, J. Hao, C. J. Forsyth, *Org. Lett.* **2001**, *3*, 979–982; f) C. J. Forsyth, J. Hao, J. Aiguade, *Angew. Chem.* **2001**, *113*, 3775–3779; *Angew. Chem. Int. Ed.* **2001**, *40*, 3663–3667.
- [185] a) K. C. Nicolaou, P. M. Pihko, N. Diedrichs, N. Zou, F. Bernal, *Angew. Chem.* **2001**, *113*, 1302–1305; *Angew. Chem. Int. Ed.* **2001**, *40*, 1262–1265; b) K. C. Nicolaou, W. Qian, F. Bernal, N. Uesaka, P. M. Pihko, J. Hinrichs, *Angew. Chem.* **2001**, *113*, 3775–3779; *Angew. Chem. Int. Ed.* **2001**, *40*, 4068–4071.
- [186] a) K. C. Nicolaou, Y. Li, N. Uesaka, T. V. Koftis, S. Vyskocil, T. Ling, M. Govindasamy, W. Qian, F. Bernal, D. Y.-K. Chen, *Angew. Chem.* **2003**, *115*, 3771–3776; *Angew. Chem. Int. Ed.* **2003**, *42*, 3643–3648; b) K. C. Nicolaou, D. Y.-K. Chen, Y. Li, W. Qian, T. Ling, S. Vyskocil, T. V. Koftis, M. Govindasamy, N. Uesaka, *Angew. Chem.* **2003**, *115*, 3777–3781; *Angew. Chem. Int. Ed.* **2003**, *42*, 3649–3653.
- [187] a) K. C. Nicolaou, S. Vyskocil, T. V. Koftis, Y. M. A. Yamada, T. Ling, D. Y.-K. Chen, W. Tang, G. Petrovic, M. Frederick, Y. Li, M. Satake, *Angew. Chem.* **2004**, *116*, 4412–4418; *Angew. Chem. Int. Ed.* **2004**, *43*, 4312–4318; b) K. C. Nicolaou, T. V. Koftis, S. Vyskocil, G. Petrovic, T. Ling, Y. M. A. Yamada, T. Ling, W. Tang, M. Frederick, *Angew. Chem.* **2004**, *116*, 4418–4424; *Angew. Chem. Int. Ed.* **2004**, *43*, 4318–4324.
- [188] C. Hopmann, D. J. Faulkner, *Tetrahedron Lett.* **1997**, *38*, 169–170.
- [189] For a recent review on the types of discoveries that can emanate from programs in total synthesis, see: K. C. Nicolaou, S. A. Snyder, *Proc. Natl. Acad. Sci. USA*, **2004**, *101*, 11929–11936.
- [190] Note added in proof (17 January 2005): Since the submission of this Review, a number of additional structural revisions of natural products have been reported. Most involve stereochemical misassignments, but several are more profound. Rather than cite these works (as there are many), we suggest using a search engine such as SciFinder with terms such as “misassigned structure”, “revised structure”, and “structural revision” if you wish to explore this area further. Should a future review on this subject appear from other authors, hopefully these examples, as well as others not expounded upon here, will be presented in more detail.

Communications

Expression Display



Upon selection by using an activity-based small-molecule probe, multiple target mRNA-bound enzymes are isolated simultaneously and identified by hybridization to a DNA microarray. The back ground shows the structure of a protein tyrosine phosphate from the Protein Databank. For more information on this method called expression-display see the Communication by S. Q. Yao et al. on the following pages.

Activity-Based High-Throughput Screening of Enzymes by Using a DNA Microarray**

Yi Hu, Grace Y. J. Chen, and Shao Q. Yao*

Remarkable advances in genomics have been accomplished, including the development and application of the DNA microarray technology,^[1] and the recent completion of the Human Genome Project.^[2] Consequently, the enormous amount of genetic information at an organism's transcriptional level is now becoming available. This situation has created the tremendous challenge to develop new techniques capable of studying the between 100 000 and 1 000 000 functionally expressed proteins estimated in the human proteome alone.^[3] Despite numerous innovations, to date, no single proteomic technique can encompass the diverse functionalities of proteins in a proteome. For example, two-dimensional gel electrophoresis (2D-GE), coupled with mass spectrometry, is primarily used to study the relative abundance, but not enzymatic activity, of proteins expressed in a biological sample.^[4] Other techniques have been developed for proteome-wide analysis of protein structure,^[5] localization,^[6] and interactions.^[7,8] One of them, the protein microarray, offers the chance to study a variety of protein activities in a large scale.^[9] However, the development of this technology is largely hampered by the cost and effort needed to generate many functional proteins in sufficient purity, as well as a lack of microarray-compatible assays available to screen for different proteins, for example, enzymes spotted in a microarray.^[10,11]

Enzymes are arguably the most important class of proteins, practically involved in every biological process in the cellular machinery. Many classes of enzymes, for example, proteases, kinases, and phosphatases, are linked to a variety of diseases. Traditionally, enzymes have been individually screened, identified, and characterized.^[12] Recently, activity-based approaches have been reported for the study of enzymes in a proteome-wide scale.^[13] However, these methods are based on electrophoretic and other chromatographic

separation methods,^[14,15] and require mass spectrometry for individual protein identification, which makes them less than ideal for high-throughput studies.

Protein-display technologies, which allow the generation of a large pool of encoded proteins, their display for functional selection, and rapid decoding of their structures, are particularly useful for large-scale analysis of protein activity.^[16] One such technology, ribosome display, allows the *in vitro* expression of $> 10^{13}$ proteins in a cell-free translation reaction and at the same time the proteins are "tagged" with their own coding mRNAs.^[17] Although display technologies are primarily used to "evolve" proteins from a large pool of related ones (typically analogues of parental proteins generated by mutagenesis), in recent years, they have been modified to express the entire collection of proteins encoded by the complementary DNA (cDNA) in an organism.^[18] Herein, we show that proteins, when expressed from a cDNA library and properly displayed (e.g. by ribosome display), are also useful for the activity-based screening of enzymes, which, when combined with the DNA microarray technology, could provide an extremely powerful strategy for the high-throughput identification and characterization of enzymes belonging in the same class(es) and, in future, other classes of non-enzyme proteins.

Our strategy, named "Expression Display", expresses proteins (in the form of ribosomal complexes with their own coding mRNAs) in a single mixture from a cDNA library (Figure 1 a). Upon functional selection of enzymes belonging in the same class (e.g. PTPs) with a suitable activity-based small-molecule probe (Figure 1 b), again in a single reaction mixture in the presence of other unrelated proteins, the isolated mixture (containing the desired enzymes still associated with their mRNAs) is subsequently "decoded", in a high-throughput manner, by hybridization to a DNA microarray (which contains the spatially addressable, entire genetic complement of the cDNA library) (Figure 1 c,d). Noted that, although the DNA-microarray technique has been used for genome-wide screening of DNA-binding sequences of transcription factors,^[19] DNA methylation,^[20] and histone deacetylation,^[21] as well as for the decoding of protein ligands generated from encoded combinatorial libraries,^[22,23] our work is, to our knowledge, the first example where it is used for high-throughput decoding of expressed proteins (from their mRNAs).

We chose ribosome display over other display technologies (e.g. phage display and mRNA display) for protein expression and encoding, as it is *in vitro*-based (allowing $> 10^{13}$ proteins in a library) and simple to perform (does not require DNA/RNA derivatization with puromycin^[24]). To demonstrate the strategy, yeast tyrosine phosphatases were chosen as targets because the yeast proteome is well studied, and an activity-based probe targeting PTPs is available.^[25]

To ensure that ribosome display expresses, isolates, and decodes functional proteins from a pool of other proteins, we constructed a model system in which streptavidin and EGFP (enhanced green fluorescent protein; 100-fold excess) were displayed. Upon enrichment with biotin, the mRNA corresponding to streptavidin was preferentially isolated and confirmed (see Supporting Information). We tested whether

[*] G. Y. J. Chen, Prof. Dr. S. Q. Yao
Department of Chemistry
National University of Singapore
3 Science Drive 3, Singapore 117543 (Republic of Singapore)
Fax: (+65) 6779-1691
E-mail: chmyaosoq@nus.edu.sg

Y. Hu, G. Y. J. Chen, Prof. Dr. S. Q. Yao
Department of Biological Sciences
National University of Singapore
14 Science Drive 4, Singapore 117543 (Republic of Singapore)

[**] Funding support was provided by the National University of Singapore (NUS) and the Agency for Science, Technology and Research (A*STAR) of Singapore. S.Q.Y. is the recipient of the 2002 Young Investigator Award (YIA) from the Biomedical Research Council (BMRC).



Supporting information for this article is available on the WWW under <http://www.angewandte.org> or from the author.

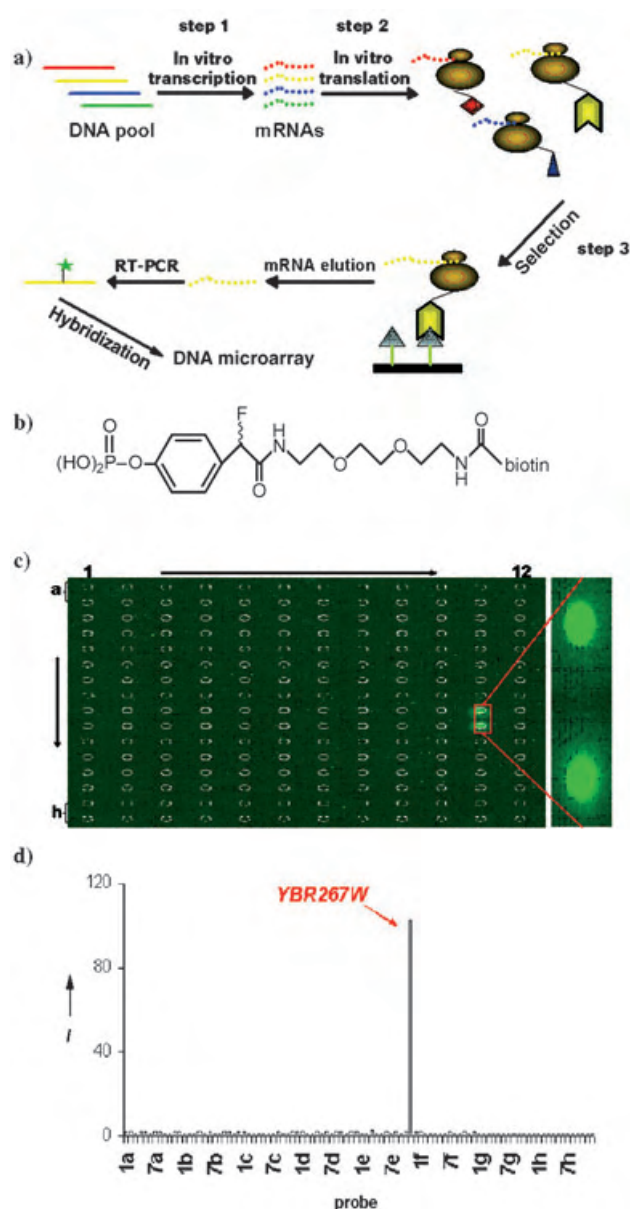


Figure 1. a) Schematic representation of expression display; RT = reverse transcription, PCR = polymerase chain reaction, see text for full details. b) The structure of the activity-based probe specific for protein tyrosine phosphatases (PTPs). c) The hybridization of Cy3-labeled reverse transcripts from in vitro selection onto a “decoding” DNA microarray containing 96 yeast ORFs (in duplicate). The spotting pattern is highlighted by white circles. The numbering of spots, their corresponding genes, and relative fluorescence intensities are in the Supporting Information. The positive spots, representing YBR267W (in duplicate), are highlighted in the enlargement. d) Relative fluorescence intensities (*I*) of spots from the DNA microarray after hybridization. The intensity values of replicate spots were averaged.

a ribosome-displayed, mRNA-tethered PTP could be isolated from other proteins with the activity-based probe (shown in Figure 1b), and subsequently identified by a microarray spotted with individual “decoding” DNAs (that is, complementary to the mRNAs tethered to the protein library). We isolated plasmids containing 96 different yeast open-reading frames (ORFs), one of which is YBR267W, encoding a known

PTP (i.e. positive control). To ensure that all genes were equally represented in the DNA library, all yeast ORFs were individually amplified with the same pair of primers. Subsequently, multistep reassembly PCR was performed to introduce suitable spacers/linkers, as well as the T7 promoter/terminator and other components essential for ribosome display. Removal of the stop codon in the genes is optional, but it was carried out throughout our experiments to maximize the yield of displayed proteins.^[17] Upon pooling into a single mixture, the resulting DNA library was transcribed and translated to generate a mixture of ribosome-displayed proteins from the 96 genes (Step 1 in Figure 1a). Subsequently, streptavidin magnetic beads immobilized with a biotinylated activity-based probe (Figure 1b) were used to isolate any PTP present in the mixture (Step 2). The probe reacts irreversibly with PTPs (as well as some alkaline phosphatases;^[25]) in a highly specific, activity-dependent manner. The washing steps were optimized to remove any residual protein–ribosome–mRNA complex from the beads without causing dissociation of the complex itself. The mRNAs from the probe-bound complexes were subsequently eluted and purified. To decode (Step 3), the isolated mRNAs were reversely transcribed to generate the corresponding fluorescently labeled cDNAs which were then hybridized to the “decoding” DNA microarray, and identified by virtue of the location of fluorescent spots on the array (Figure 1c,d). The DNA microarray (constructed in house), contains individual cDNA from all 96 yeast genes. Results showed that the only fluorescent spot on the microarray was that of YBR267W (i.e. the positive hit). A control hybridization experiment with a Cy3-labeled PCR product obtained using mRNAs before ribosome display/selection showed a fairly homogeneous distribution of fluorescent spots throughout the array (data not shown). In a separate experiment, isolated mRNAs (after Step 2) were reversely transcribed, amplified by PCR, and cloned into pCR2.1-TOPO vector (Invitrogen), subsequent DNA sequencing showed: 10 out of 10 randomly chosen clones corresponded to the YBR267W gene. When sodium orthovanadate, a potent tyrosine phosphatase inhibitor, was added to the incubation mixture during expression display (i.e. at Step 2), the selection of YBR267W was abolished (see Supporting Information). Together, all these lines of evidence validated our strategy, that is, enzymes expressed from a cDNA library using ribosome display could be preferentially isolated on the basis of their enzymatic activity (by the aid of a suitable activity-based probe) and subsequently identified, in high-throughput, by hybridization to a DNA microarray.

To assess whether expression display could be used for high-throughput proteomics mass screening of enzymes in a class-specific manner, we applied our strategy to a yeast cDNA library containing 384 different yeast ORFs, including multiple previously characterized PTPs (four in total; including YBR267W, YDL230W, YFR028C, and YPR073C), non-PTP phosphatases (see below), other classes of enzymes (proteases, kinases, oxidoreductases), and non-enzyme proteins. Once again, all genes were individually PCR-amplified and assembled before pooling to ensure equal representation in the library. Upon in vitro transcription and translation, the mixture containing the ribosome-display proteins was subject

to activity-based enrichment, in a single reaction, using the same small-molecule probe. The isolated mixture was reversely transcribed, amplified with Cy3-labeled dNTPs, and hybridized to a “decoding” DNA microarray (containing 384 cDNAs) for parallel identification of PTPs (Figure 2a): upon subtraction of background fluorescence, the only significantly fluorescent spots identified from the microarray were from those genes encoding the four PTPs (Figure 2b). The identities of these genes were independently confirmed by DNA sequencing, as described above. The enzymatic activities of the corresponding proteins were further confirmed by successful labeling of the individually purified proteins with the probe in a gel-based experiment, as well as inhibition experiments with sodium orthovanadate (see

Supporting Information). Noticeably, the relative intensity of the fluorescent spots in Figure 2a,b (with 384 genes) was considerably weaker than those in Figure 1c,d (with 96 genes), presumably a result of the decreased expression of each protein from a larger cDNA library (theoretically fourfold less expression from the same translation mixture, assuming equal expression among different genes).

The small-molecule probe used in the above experiments is highly specific towards PTPs.^[25] To assess whether proteins identified from expression display retain a similar fidelity as defined by the probe (in the specific targeting of PTPs), we included in the reaction mixture other non-PTP phosphatases. As shown in Figure 2c, within a single round of selection, only the four PTPs emerged as positive hits, as their fluorescence intensities were clearly enriched over those of the eighteen non-PTP phosphatases proteins, as well as the rest of proteins in the library. Together, with the availability of new activity-based probes,^[26–28] our strategy may be readily modified to accommodate different classes of enzymes which confer either highly specific or broad-based specificities, thus providing a novel and general means in high-throughput enzymology.

In conclusion, we have demonstrated that expression display could be used for high-throughput screening and identification of proteins on the basis of their enzymatic activities: with an activity-based probe, we have shown, for the first time, multiple enzymes in the same class (e.g. PTPs), when expressed (from a cDNA library together with other proteins) in a single mixture as ribosome-displayed complexes, could be isolated, and subsequently identified, in high throughput, using DNA microarray as the “decoding” platform (this is also the first example of protein decoding). In our experiments, all genes were individually cloned before pooling into a single cDNA library to preserve their diversity and equal distribution, and to unambiguously validate our strategy. Other cDNA libraries, either commercially available or constructed using standard cloning techniques, should be equally amendable. Our strategy is unique in a number of ways when compared with existing proteomic techniques: 1) it differs from the electrophoretic/chromatographic protein profiling methods (including activity-based methods;^[13–15,25–28]) by allowing high-throughput identifications of enzymes without the need for mass spectrometry; 2) by avoiding the need for parallel cloning, expression, purification, and characterization of proteins (as in the case reported in ref. [12]), it could (in principle) routinely express, screen, and identify thousands (if not millions/billions) of proteins, all in a single reaction mixture; 3) by utilizing RT-PCR for the amplification of isolated mRNAs and subsequently decoding by hybridization, it should in principle provide a very low detection limit for target proteins. What remains unaddressed from this study, is the maximum number of different proteins allowed in the strategy? Clearly, from our results, shown in Figure 2, with a single round of protein selection (e.g. no amplification of the input protein amount), the fluorescence intensity of positive hits (from DNA microarray screening) decreased concomitantly with the increasing cDNA library size. However, with the easy adaptation of multiple rounds of protein enrichment (as in the case of ribosome display, and

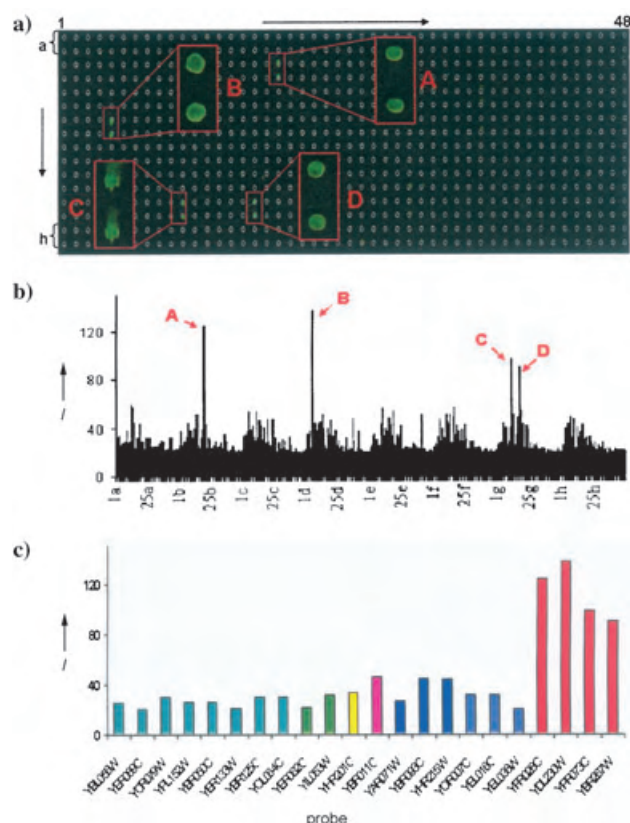


Figure 2. Rapid identification of multiple yeast PTPs using expression display. a) The hybridization of Cy3-labeled reverse transcripts from *in vitro* selection onto a “decoding” DNA microarray containing 384 yeast ORFs (in duplicate). The spotting pattern is highlighted by white circles. The numbering of spots, their corresponding genes, and relative fluorescence intensities are given in the Supporting Information. The positive spots are highlighted in the enlargements. Four positives were identified as A: YFR028C, B: YDL230W, C: YPR073C, and D: YBR267W, corresponding to the four positive PTPs in the cDNA library. b) Relative fluorescence intensities (*I*) of spots from the DNA microarray after hybridization. The intensity values of replicate spots were averaged. The four positive PTPs are labeled (A–D). c) Comparison of relative fluorescence intensities of the four PTPs (red) to those of other phosphatases in the cDNA library, including eight Ser/Thr phosphatases (cyan), two DL-glycerol phosphatases (green), one exopolyphosphatase (yellow), one inorganic pyrophosphatase (pink), three acid phosphatases (dark blue), and three phosphatase homologues (light blue).

other display technologies), the capacity of our strategy may be greatly expanded, thus making it possible in future to “display” and screen all proteins, including low-abundant ones, present in a proteome (> 1 000 000 proteins).

Experimental Section

DNA constructs: Details of the cloning are described in Supporting Information. Briefly, yeast ORFs were amplified from plasmids of ExClones (Invitrogen, USA) with the following primers: Exclone-YF (5'-GCGGCGGCCATATGGAATTCAGCTGACCACC-3') and Exclone-YR (5'-GGCGGCTGCTCTTCCGCATCCCCGGGAA-TTGCCATGCCA-3'), which removed the stop codon from each ORF, and presumably maximized the yield of ribosome-displayed proteins.^[17] However, it was shown previously that, without removal of the stop codon, ribosome display also worked.^[29] A spacer was amplified from amino acids 211–299 of gene III of filamentous phage M13mp19 with the primers Y-spacer-F (5'-GGGGATGCGGAA-GAGCAGCCGCCCTCAACCTCTGTCAAT-3') and Spacer-R (5'-CCGCACACCAGTAAGGTGTGCGGTATCACCAG-TAGCACC-3'), and subsequently ligated to the amplified yeast ORFs: both the ORF and the spacer were digested by Sap I (NEB, USA) at 37°C for 2 h and subsequently ligated with T4 ligase (NEB) overnight at 16°C. The ligation products were amplified first by two primers, Y-SDA (5'-AGACCACAACGGTTTCCCTCTAGAAA-TAATTTTGTAACTTTAAGAAGGAGATATATCCATG-GAATTCAGCTGACCACC-3') and Spacer-R, followed by amplification with primers Y-T7B (5'-ATACGAAATTAATACGACTCACTATAGGGAGACCACAACGG-3') and Spacer-R. All final constructs were re-amplified with the primers Y-T7B and Spacer-R, if necessary. Streptavidin and EGFP genes were constructed similarly (Supporting Information).

In vitro transcription and translation: Depending on the experiments, different DNA constructs were pooled proportionally to obtain a master mixture. 1–6 µg of the mixture was transcribed with the RiboMAX large-scale RNA production system T7 (Promega) for 4 h at 37°C. The mRNAs were purified by an RNeasy mini kit (Qiagen). The resulting transcripts were translated in vitro with an *E. coli* translation system (Roche) in the presence of magnesium acetate (10 mM), anti-ssrA (5.6 µM; 5'-TTAAGCTGCTAAAGCG-TAGTTTTCGTCGTTTGCGACTA-3') and rRNasin (0.5 µL 40 U µL⁻¹; Promega). The translation was performed in a 35 µL reaction for 7 min at 37°C, before stopping by immediately transferring the product into an ice-cold binding buffer (220 µL) containing Tris-acetate (50 mM; pH 7.5 Tris = 2-amino-2-(hydroxymethyl)-1,3-propanediol), NaCl (150 mM), magnesium acetate (50 mM), Tween 20 (0.1% (v/v)), bovine serum albumin (0.1 mg mL⁻¹) and heparin (2 mg mL⁻¹).

In vitro selection: The small-molecule probe^[25] (50 µL, 300 µM) was incubated with Streptavidin MagneSphere paramagnetic particles (50 µL; Promega) for 30 min at room temperature with gentle shaking, followed by washing with 1 × PBS (three times; PBS = phosphate buffered saline) to remove any excessive free probe. Subsequently, the above translation mixture, premixed with the binding buffer, was incubated with the beads for 2 h on ice. For the control selection with streptavidin/EGFP, immobilized iminobiotin agarose (20 µL; Pierce) were added to translation mixture and incubated for 1 h on ice. After incubation, the beads (agarose for streptavidin reaction) were washed four times with a washing buffer containing Tris-acetate (50 mM; pH 7.5), NaCl (150 mM), magnesium acetate (50 mM) and Tween 20 (0.1% (v/v)). The washing conditions were optimized to remove residual, displayed proteins without breaking the ribosome complexes. Subsequently, mRNAs were released from the ribosome ternary complexes at room temperature with an elution buffer containing Tris-acetate (50 mM; pH 7.5), NaCl (150 mM) and EDTA (20 mM; EDTA = N,N'-(1,2-ethanediyl)bis[(N-carboxymethyl)-

glycine]). The eluted mRNAs were purified by RNeasy mini kit (Qiagen).

RT-PCR: Reverse transcription was performed using AMV reverse transcriptase (Promega) with the primer, Spacer-R, according to the supplier's recommendation. PCR was performed using Taq polymerase (Promega) in the presence of 5% (v/v) dimethyl sulfoxide (5 min at 95°C, followed by 25 cycles of 30 s at 95°C, 30 s at 50°C and 2.5 min at 72°C, with a final 10 min of extension at 72°C). PCR products were analyzed by agarose gel electrophoresis. For fluorescent labeling of RT-PCR product, Cy3-dCTP (Amersham Biosciences) was incorporated into PCR products according to the supplier's recommendation. The fluorescent DNAs were subsequently used as probes for DNA microarray hybridization. For direct cloning and DNA sequencing, see the Supporting Information.

DNA microarray: All DNA templates used for spotting the “decoding” DNA microarrays were amplified, in 96-well formats with primers Y-T7B and Spacer-R, from plasmids containing the corresponding yeast ORFs from Exclones. DNA spotting and hybridization were performed as described elsewhere,^[30] with the following modifications: yeast ORFs were spotted in duplicate onto 75 × 25 mm polylysine-coated glass slides using a CHIPWRITER arrayer (Virtek), followed by incubation in a humid chamber overnight at room temperature. After rehydration, blocking, and denaturing, the slides were dried and ready for DNA hybridization. The probes were the Cy3-labeled reverse transcripts from earlier in vitro selection experiments. The hybridization chambers were kept in a humid environment at 60°C for 2–4 h or overnight. After washing, the slides were analyzed by ArrayWoRx scanner (Applied Precision). The values of signal intensity of duplicate spots were averaged for each ORF (Supporting Information).

Received: August 11, 2004

Published online: November 11, 2004

Keywords: analytical methods · DNA microarrays · enzymes · proteomics · ribosome display

- [1] D. J. Lockhart, E. A. Winzler, *Nature* **2000**, *405*, 827–836.
- [2] J. C. Venter, *Science* **2001**, *291*, 1304–1351.
- [3] S. Fields, *Science* **2001**, *291*, 1221–1224.
- [4] R. Aebersold, M. Mann, *Nature* **2003**, *422*, 198–207.
- [5] S. K. Burley, *Nat. Struct. Biol.* **2000**, *7*, 932–934.
- [6] W. K. Huh, J. V. Falvo, L. C. Gerke, A. S. Carroll, R. W. Howson, J. S. Weissman, E. K. O'Shea, *Nature* **2003**, *425*, 686–691.
- [7] A. C. Gavin, M. Bosche, R. Krause, P. Grandi, M. Marzioch, A. Bauer, J. Schultz, J. M. Rick, A. M. Michon, C. M. Cruciat, M. Remor, C. Hofert, M. Schelder, M. Brajenovic, H. Ruffner, A. Merino, K. Klein, M. Hudak, D. Dickson, T. Rudi, V. Gnau, A. Bauch, S. Bastuck, B. Huhse, C. Leutwein, M. A. Heurtier, R. R. Copley, A. Edelmann, E. Querfurth, V. Rybin, G. Drewes, M. Raida, T. Bouwmeester, P. Bork, B. Seraphin, B. Kuster, G. Neubauer, G. Superti-Furga, *Nature* **2002**, *415*, 141–147.
- [8] Y. Ho, A. Gruhler, A. Heilbut, G. D. Bader, L. Moore, S. L. Adams, A. Millar, P. Taylor, K. Bennett, K. Boutillier, L. Y. Yang, C. Wolting, I. Donaldson, S. Schandorff, J. Shewnarane, M. Vo, J. Taggart, M. Goudreaux, B. Musk, C. Alfarano, D. Dewar, Z. Lin, K. Michalickova, A. R. Willems, H. Sassi, P. A. Nielsen, K. J. Rasmussen, J. R. Andersen, L. E. Johansen, L. H. Hansen, H. Jespersen, A. Podtelejnikov, E. Nielsen, J. Crawford, V. Poulsen, B. D. Sorensen, J. Matthiesen, R. C. Hendrickson, F. Gleeson, T. Pawson, M. F. Moran, D. Durocher, M. Mann, C. W. V. Hogue, D. Figgeys, M. Tyers, *Nature* **2002**, *415*, 180–183.
- [9] G. MacBeath, S. L. Schreiber, *Science* **2000**, *289*, 1760–1763.
- [10] G. Y. J. Chen, M. Uttamchandani, Q. Zhu, G. Wang, S. Q. Yao, *ChemBiochem* **2003**, *4*, 336–339.

- [11] G. Y. J. Chen, M. Uttamchandani, R. Y. P. Lue, M. L. Lesai-cherre, S. Q. Yao, *Curr. Top. Med. Chem.* **2003**, 3, 705–724.
- [12] M. R. Martzen, S. M. McCraith, S. L. Spinelli, F. M. Torres, S. Fields, E. J. Grayhack, E. M. Phizicky, *Science* **1999**, 286, 1153–1155.
- [13] N. Jessani, B. F. Cravatt, *Curr. Opin. Chem. Biol.* **2004**, 8, 54–59.
- [14] Y. Liu, M. P. Patricelli, B. F. Cravatt, *Proc. Natl. Acad. Sci. USA* **1999**, 96, 14694–14699.
- [15] G. C. Adam, J. Burbaum, J. W. Kozarich, M. P. Patricelli, B. F. Cravatt, *J. Am. Chem. Soc.* **2004**, 126, 1363–1368.
- [16] M. Li, *Nat. Biotechnol.* **2000**, 18, 1251–1256.
- [17] J. Hanes, A. Pluckthun, *Proc. Natl. Acad. Sci. USA* **1997**, 94, 4937–4942.
- [18] S. Zozulya, M. Lioubin, R. J. Hill, C. Abram, M. L. Gishizky, *Nat. Biotechnol.* **1999**, 17, 1193–1198.
- [19] V. R. Iyer, C. E. Horak, C. S. Scafe, D. Botstein, M. Snyder, P. O. Brown, *Nature* **2001**, 409, 533–538.
- [20] B. van Steensel, S. Henikoff, *Nat. Biotechnol.* **2000**, 18, 424–428.
- [21] D. Robyr, Y. Suka, I. Xenarios, S. K. Kurdستاني, A. Wang, N. Suka, M. Grunstein, *Cell* **2002**, 109, 437–446.
- [22] S. Melkko, J. Scheuermann, C. E. Dumelin, D. Neri, *Nat. Biotechnol.* **2004**, 22, 568–574.
- [23] N. Winssinger, J. L. Harris, B. J. Backes, P. G. Schultz, *Angew. Chem.* **2001**, 113, 3254–3258; *Angew. Chem. Int. Ed.* **2001**, 40, 3152–3155.
- [24] R. Roberts, J. W. Szostak, *Proc. Natl. Acad. Sci. USA* **1997**, 94, 12297–12302.
- [25] For synthesis of the probe used in this study, see: Q. Zhu, X. Huang, G. Y. J. Chen, S. Q. Yao, *Tetrahedron Lett.* **2003**, 44, 2669–2672. It should be noted a similar PTP probe was first reported by Lo et al. (L. C. Lo, T. L. Pang, C. H. Kuo, Y. L. Chiang, H. Y. Wang, J. J. Lin, *J. Proteome Res.* **2002**, 1, 35–40).
- [26] Q. Zhu, A. Girish, S. Chattopadhyaya, S. Q. Yao, *Chem. Commun.* **2004**, 1512–1513.
- [27] S. Saghatelian, N. Jessani, A. Joseph, M. Humphrey, B. F. Cravatt, *Proc. Natl. Acad. Sci. USA* **2004**, 101, 10000–10005.
- [28] E. W. S. Chan, S. Chattopadhyaya, R. C. Panicker, X. Huang, S. Q. Yao, *J. Am. Chem. Soc.* **2004**, 126, 14435–14446.
- [29] L. C. Mattheakis, R. R. Bhatt, W. J. Dower, *Proc. Natl. Acad. Sci. USA* **1994**, 91, 9022–9026.
- [30] <http://www.microarrays.org/protocols.html>.

Dendrimer Folding in Aqueous Media: An Example of Solvent-Mediated Chirality Switching**

Amanda L. Hofacker and Jon R. Parquette*

Allosteric proteins exhibit highly nonlinear responses to external stimuli that cause small perturbations of a particular parameter to effect very large changes in protein structure and function.^[1] This behavior is a direct consequence of the structural cooperativity that correlates the conformational equilibria of multiple subunits within the protein structure.^[2] Such allosteric phenomena are commonly observed in biomacromolecules and are critical for their function. There are relatively few synthetic materials, however, that exhibit this conformational cooperativity.^[3] The creation of such conformational adaptability in synthetic systems requires the allosteric transmission of local structural or chiral information to the next hierarchical level of structural organization. We have recently developed a dendrimeric system that adopts a compact, helical shape governed by the *syn,syn* conformational preference of the pyridine-2,6-dicarboxamide repeat unit.^[4] We report herein that water-soluble versions of these dendrons fold in water. Furthermore, the terminal pentaethylene glycol chains and the dendron secondary structure exhibit highly correlated conformational equilibria. Accordingly, solvent-induced conformational fluctuations of the terminal pentaethylene glycol chains are correlated with an inversion in the sense of helical chirality expressed by the dendrons.^[5]

Information transfer in folded synthetic systems usually occurs through inter-^[6] or intramolecularly^[7] self-organized assemblies through an ensemble of noncovalent interactions. Polar protic solvents such as water typically disrupt hydrogen bonding and electrostatic interactions, thereby compromising the stability of such assemblies. For example, elements of peptide secondary structure, independent of the global protein structure, exhibit only marginal stability in pure water.^[8] Similarly, many synthetic foldamers exhibit less stable conformations in water.^[9] However, any potential biological application of folded synthetic materials requires an ability to adopt conformational order in aqueous media.

The conformational preference of the pyridine-2,6-dicarboxamide repeat unit in our folded dendrons is a result of intramolecular hydrogen bonding present in the *syn,syn* conformation, as well as an electrostatic destabilization of

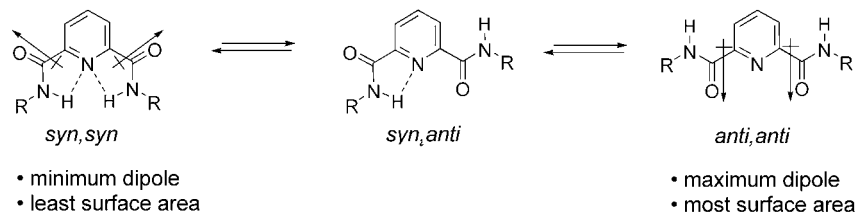
[*] A. L. Hofacker, Prof. J. R. Parquette
Department of Chemistry, The Ohio State University
100 W. 18th Ave., Columbus, OH 43210 (USA)
E-mail: parquett@chemistry.ohio-state.edu

[**] We thank Professor Heather Allen and Dr. Gang Ma for assistance with the IR spectroscopic studies. This work was supported by the National Science Foundation (CHE-0239871).



Supporting information for this article is available on the WWW under <http://www.angewandte.org> or from the author.

the alternative *syn,anti* and *anti,anti* conformations. Previous studies strongly suggest that tighter packing of the dendritic chains in poor solvents plays an important role in the folded



conformation of these dendrons.^[10] Although water should disrupt the hydrogen bonding interactions of the *syn,syn* conformation and decrease the energetic cost of the larger dipole moments of the *syn,anti* and *anti,anti* conformations, the packing effect should nevertheless dominate, as the propensity of hydrophobic regions to minimize their exposure to solvent ultimately results in a hydrophobic collapse of the dendritic structure.

Chiral pentaethylene glycol **1**, prepared from ethyl L-lactate, was installed at the periphery of the dendrons to impart solubility in water (Figure 1).^[6b,9a] Dendrons **2–4** exhibited moderate solubility in water, and excellent solubility in organic media. However, millimolar solutions of dendrons in water exhibited a lower critical solution temperature (LCST) that induced clouding and precipitation upon heating to $\approx 25\text{--}30^\circ\text{C}$.^[9a,11]

The circular dichroism (CD) spectra of **2** featured an intense negative couplet centered at $\approx 316\text{ nm}$ (Figure 2b) in THF and in water, the latter case being slightly lower in magnitude relative to that from the sample in THF. This bisignet signal results exclusively from the excitonic coupling of the $\pi \rightarrow \pi^*$ transitions of the anthranilate chromophores, which are polarized along the axis containing C3 and C6 (Figure 2a).^[4d] The presence of the negative couplet indicates that the first generation dendron **2** adopts an *M*-type helical conformation, relating the anthranilate chromophores in both THF and in water. This observation highlights the importance of packing interactions in determining the conformational properties of the dendron.

The second generation dendron **3** exhibited a negative couplet in THF comparable in magnitude with that of dendron **2**, which also indicates an *M* helical bias. However, the negative couplet was replaced by an equally intense positive couplet in aqueous media, which indicates that an *M* \rightarrow *P* helical transition occurred in water. The third-generation dendron **4** also displayed a similar *M* \rightarrow *P* helical transition upon going from THF to water. Varying the THF/H₂O ratio for **3** and **4** at 25°C revealed *M* \rightarrow *P* crossover points in the range of 10–20% THF for **3** and 30–40% THF for **4** (Supporting Information).

The positive components of the CD couplets in water for **3** and **4** were decreased in amplitude relative to the negative branches at shorter wavelengths. The unsymmetrical appearance of these couplets is a consequence of the increased chromophore congestion that occurs in poor, structure-collapsing solvents and is commonly observed for this dendrimer system.^[4] Such structural congestion induces further mixing of the couplet transitions with other transitions within the dendron, which results in desymmetrized couplet intensities.^[12]

The amphiphilic nature of the dendrons creates a tendency for aggregation to occur in water, and to a lesser degree, in THF. Comparison of the hydrodynamic radii (R_h) of **2–4**, measured by DOSY NMR spectroscopy,^[13] to the calculated van der Waals radii^[14] (R_{vdW}) indicates that significant aggregation occurred in D₂O solution,^[15] whereas monomeric species were present in [D₈]THF (Table 1). Aggregation has been shown to play a significant role in the conformational equilibria of chiral molecules^[16] and introduces the possibility for intermolecular excitonic coupling^[17] in the CD spectra. Therefore, CD and UV/Vis spectra were recorded for **2–4** as a function of concentration in THF and H₂O (Supporting Information). The UV/Vis and CD spectra of all dendrons were essentially invariant over a 100-fold concentration range (10^{-4} to 10^{-6} M), thereby ruling out aggregation as a source of or contributing factor to the *M* \rightarrow *P* helical inversion.

Previous vibrational spectroscopic studies showed that poly(oxyethylene) (POE) chains experience an increased preference for the C–C *gauche* conformation, whereas only a small increase in the C–O *anti*

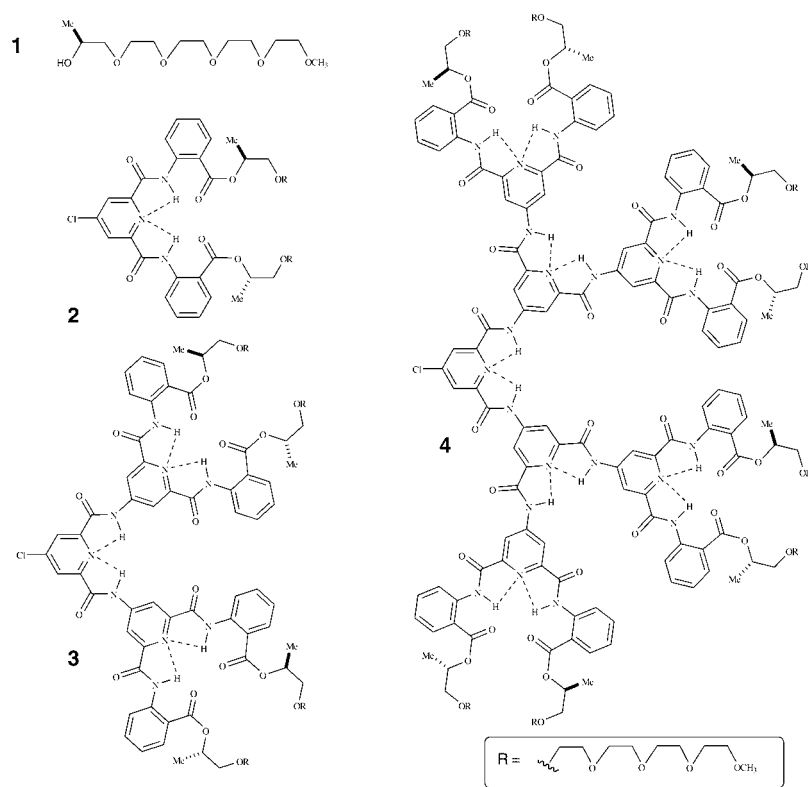


Figure 1. Water-soluble dendrons with chiral, pentaethylene glycol termini.

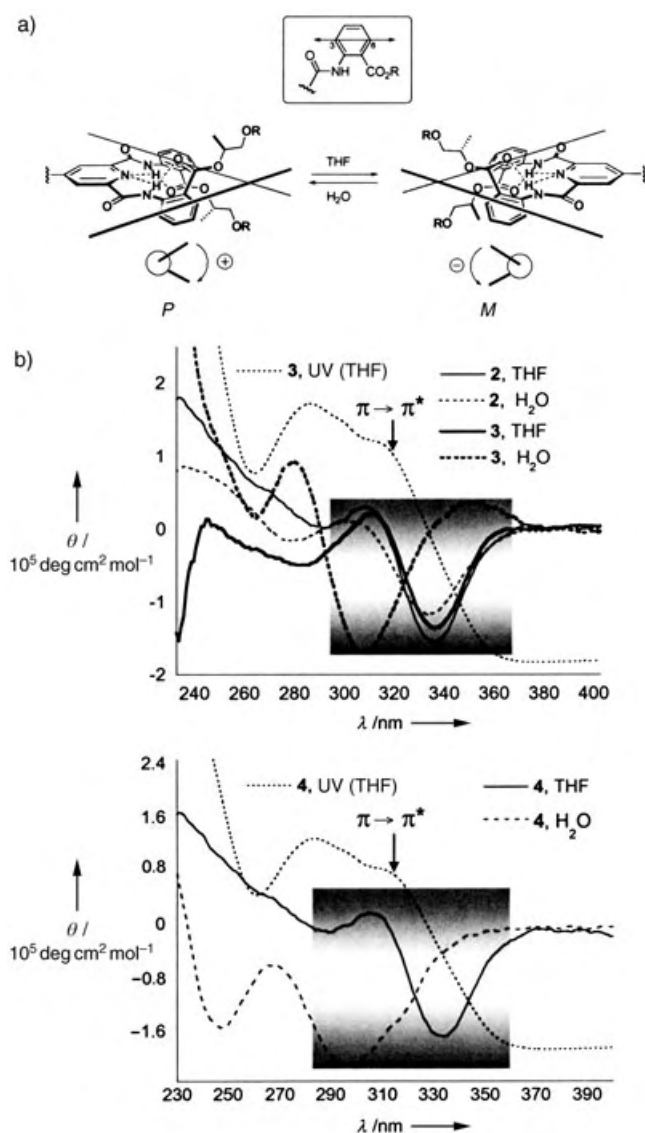


Figure 2. a) Direction of electronic transition dipole moments of the $\pi \rightarrow \pi^*$ transition at 316 nm and corresponding sign of CD couplet. b) CD spectra of dendrons **2–4** in H_2O and THF. Spectra are normalized with respect to concentration and the number of chiral terminal groups.

Table 1: Experimentally determined (R_h) and calculated (R_{vdw}) hydrodynamic radii [Å]

Compound	R_h ([D ₈]THF ^[a])	R_h (D ₂ O ^[b])	R_{vdw} ^[c]
2 (3.5 mM)	5.8	19.7	5.80
3 (3.6 mM)	8.4	43.9 ^[d]	7.45
4 (3.4 mM)	8.3	52.8 ^[e]	9.48

[a] DOSY NMR spectroscopy, 27 °C. [b] DOSY NMR spectroscopy, 10 °C. [c] Van der Waals radii, calcd. [d] Measured in [D₈]THF/D₂O (10%). [e] Measured in [D₈]THF/D₂O (2%).

population occurs upon progression from nonpolar to aqueous media.^[18] The preferred conformation of the *anti, gauche* O–C–C bond pair in water is consistent with the solid-state structure of the POE helix.^[19]

The effect of solvent on the conformational preference of the terminal glycol chains of **3** was investigated by IR spectroscopy with the key bands at 1355–1360 cm^{-1} (A), and 1335–1320 cm^{-1} (B) for the respective *gauche* and *anti* C–C conformations; and with those at 1310–1297 cm^{-1} (C), and 1290–1295 cm^{-1} (D) for the *gauche* and *anti* C–O conformations, respectively.^[18c] The disappearance of the C–C *anti* band (B) and the slight increase in the C–O *anti* band (D) upon going from [D₈]THF^[20] to H_2O for glycol chain **1** (Figure 3a) closely mirrors the spectroscopic behavior

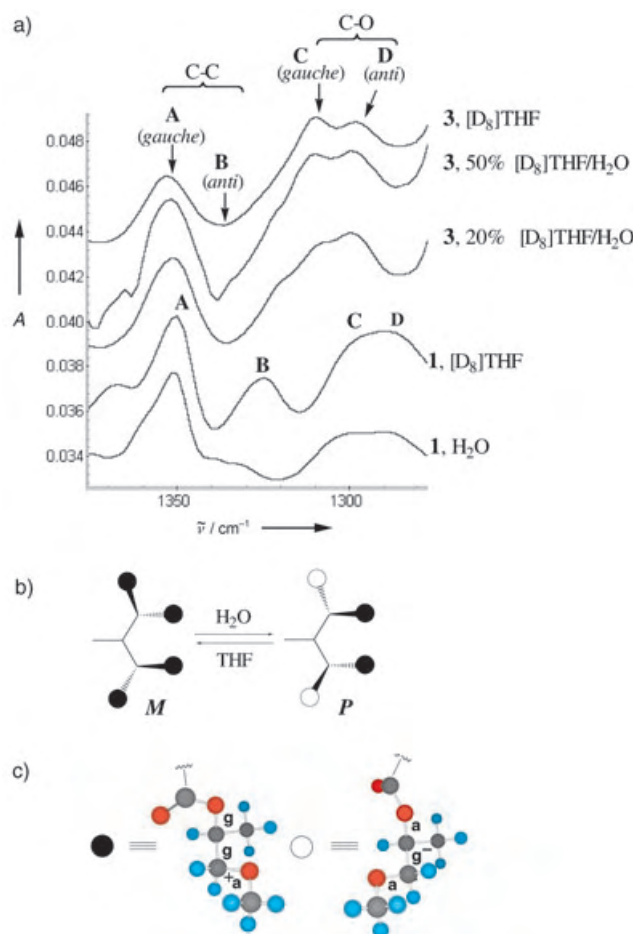


Figure 3. a) IR spectra of **1** and **3** as a function of solvent, measured with a horizontal ZnSe crystal and a 45° single bounce attenuated total reflection (ATR) accessory (20% [D₈]THF in H_2O was necessary to attain the 25-mm concentrations of **3** required for IR spectroscopy). b) Schematic depiction of the lowest-energy conformers of **3** ($R = \text{Me}$). c) Conformation of terminal glycol chains in CHCl_3 (left) and H_2O (right) as predicted by conformational searching (MM3).

reported for other POE oligomers.^[18] Molecular dynamics simulations estimate that similar observations for POE represent an increase in the C–C *gauche* population from 76% in benzene to 100% in water.^[21] However, in contrast to **1**, dendron **3** exhibits a significant increase in the C–O *anti* band (D) as water is added, whereas the C–C *anti* band (B) is missing from the spectra at all H_2O /[D₈]THF ratios.

These observations indicate that the solvation of **3** in water induces a *gauche* \rightarrow *anti* conformational shift about the

C–O bond. Furthermore, a strong preference for the C–C *gauche* conformation exists for the dendrons at all solvent ratios, in contrast to the parent glycol chain **1** and POE. The fact that the C–C *gauche* preference of dendron **3** is stronger than it is for POE or **1** suggests the occurrence of correlated motions among the terminal glycol chains that shift the conformational equilibria toward the lower energy C–C *gauche* arrangement.^[4c]

Monte Carlo conformational searching of **3** (R = Me) with the GB/SA solvation model^[22] predicts an *M* helical bias in CHCl₃^[23] whereas a *P* helix is preferred in water, in accord with the CD studies (Figure 4). Closer inspection of each of the lowest-energy conformers reveals that the *M*→*P* helical inversion is correlated with a shift of two of the four glycol

chains from *gauche, gauche*⁺, *anti* to *anti, gauche*[−], *anti* conformations around the respective O–C–C–OMe bonds (Figure 3b). The uniformly *gauche*[±] preference of all the C–C bonds in both water and CHCl₃ and the corresponding conformational shift of two O–C bonds from *gauche* to *anti* upon going from CHCl₃ to water is consistent with the observed vibrational data.

The results of this study demonstrate that these dendrons not only adopt a stable folded state in aqueous media, but also exhibit correlated chain–chain and dendron–chain conformational equilibria. The correlated chain–chain motions induce a shift in equilibrium of the terminal chains toward the lower-energy *gauche* state, in contrast to the case of an isolated chain (**1**). Similarly, solvent-induced conformational fluctuations of the terminal chains are coupled with dendron helical secondary structure through correlated dendron–chain motions. This work suggests the potential of folded dendrimers to exhibit nonlinear conformational responses to localized structural perturbations.

Received: June 11, 2004

Revised: November 5, 2004

Published online: January 5, 2005

Keywords: amphiphiles · chirality · circular dichroism · dendrimers · IR spectroscopy

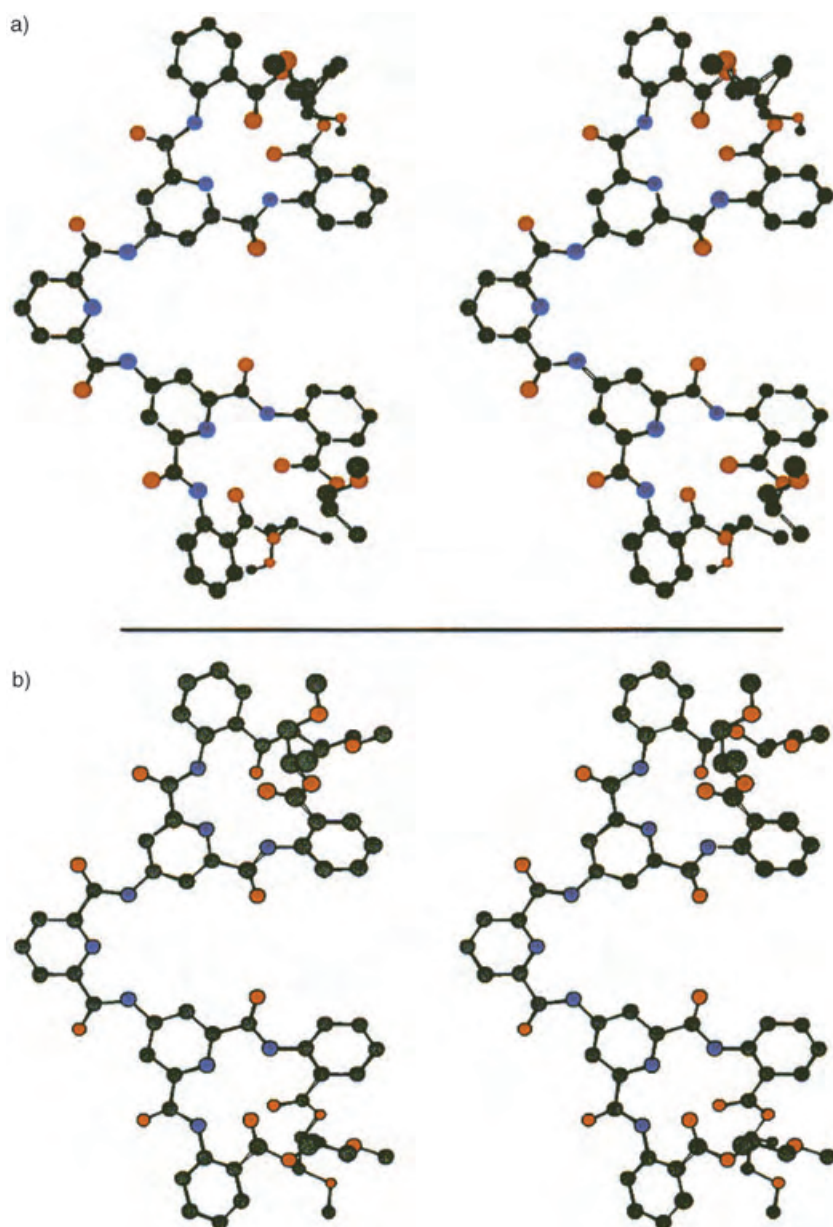


Figure 4. Stereograms of the lowest-energy conformers determined by Monte Carlo conformational searching (MM3) using the GB/SA solvation model for a) CHCl₃ (*M* helicity) or b) H₂O (*P* helicity) as implemented in MacroModel 8.5.

- [1] a) J. M. Yon, D. Perahia, C. Ghelis, *Biochimie* **1998**, *80*, 33; b) O. Jardetzky, *Prog. Biophys. Mol. Biol.* **1997**, *65*, 171; c) D. Kern, E. R. P. Zuiderweg, *Curr. Opin. Struct. Biol.* **2003**, *13*, 748.
- [2] K. L. Mayer, M. R. Earley, S. Gupta, K. Pichumani, L. Regan, M. J. Stone, *Nat. Struct. Biol.* **2003**, *10*, 962.
- [3] For a recent review of conformational cooperativity in helical linear polymers, see: E. Yashima, K. Maeda, T. Nishimura, *Chem. Eur. J.* **2004**, *10*, 42.
- [4] a) B. Huang, M. A. Prantil, T. L. Gustafson, J. R. Parquette, *J. Am. Chem. Soc.* **2003**, *125*, 14518; b) B. Huang, J. R. Parquette, *J. Am. Chem. Soc.* **2001**, *123*, 2689; c) J. Recker, D. J. Tomcik, J. R. Parquette, *J. Am. Chem. Soc.* **2000**, *122*, 10298; d) P. Gandhi, B. Huang, J. C. Gallucci, J. R. Parquette, *Org. Lett.* **2001**, *3*, 3129.
- [5] For selected examples of solvent-mediated chirality inversion, see: a) V. V. Borovkov, G. A. Hembury, Y. Inoue, *Angew. Chem.* **2003**, *115*, 5568; *Angew. Chem. Int. Ed.* **2003**, *42*, 5310; b) K. Morino, K. Maeda, E. Yashima, *Macromolecules* **2003**, *36*, 1480; c) H. Nakashima, M. Fujiki, J. R. Koe, M. Motonaga, *J. Am. Chem. Soc.* **2001**, *123*, 1963; d) H. Nakako, R. Nomura, T. Masuda, *Macromolecules* **2001**, *34*, 1496; e) S. E. Boiadjev, D. A. Lightner, *J. Am. Chem. Soc.* **2000**, *122*, 378.
- [6] a) L. Brunsveld, E. W. Meijer, A. E. Rowan, R. J. M. Nolte, *Top. Stereochem.* **2003**, *24*, 373; b) L. Brunsveld, H. Zhang, M. Glasbeek, J. A. J. M. Vekemans, E. W. Meijer, *J. Am. Chem. Soc.* **2000**, *122*, 6175.
- [7] a) T. Nakano, Y. Okamoto, *Chem. Rev.* **2001**, *101*, 4013; b) M. M. Green, J.-W. Park, T. Sato, A. Teramoto, S. Lifson, R. L. B. Selinger, J. V. Selinger, *Angew. Chem.* **1999**, *111*, 3328; *Angew. Chem. Int. Ed.* **1999**, *38*, 3139.

- [8] a) C. A. Rohl, R. L. Baldwin, *Methods Enzymol.* **1998**, 295, 1; b) M. Goodman, A. S. Verdini, C. Toniolo, W. D. Phillips, F. A. Bovey, *Proc. Natl. Acad. Sci. USA* **1969**, 64, 444.
- [9] For some leading references, see: a) M. T. Stone, J. S. Moore, *Org. Lett.* **2004**, 6, 469; b) I. Huc, *Eur. J. Org. Chem.* **2004**, 17; c) T. L. Raguse, J. R. Lai, S. H. Gellman, *J. Am. Chem. Soc.* **2003**, 125, 5592; d) A. J. Zych, B. L. Iverson, *J. Am. Chem. Soc.* **2000**, 122, 8898; e) Y. Hamuro, J. P. Schneider, W. F. DeGrado, *J. Am. Chem. Soc.* **1999**, 121, 12200.
- [10] J. R. Parquette, *C. R. Chim.* **2003**, 6, 779.
- [11] Clouding was observed at 25–30°C at mM concentrations visually and by UV/Vis spectroscopy, but not at the μM concentrations used for the CD studies. Polyethylene glycol also exhibits a LCST: S. Saeki, N. Kuwahara, M. Nakata, M. Kaneko, *Polymer* **1976**, 17, 685.
- [12] For a discussion, see: G. Gottarelli, S. F. Mason, G. Torre, *J. Chem. Soc. B* **1970**, 1349.
- [13] J. K. Young, G. R. Baker, G. R. Newkome, K. F. Morris, C. S. J. Johnson, *Macromolecules* **1994**, 27, 3464.
- [14] Calculated by using increments described in: J. T. Edward, *J. Chem. Educ.* **1970**, 47, 261.
- [15] Small amounts of $[\text{D}_8]\text{THF}$ and lower temperatures were necessary to obtain the mM concentrations required for DOSY NMR spectroscopy in D_2O . The degree of aggregation is likely to be significantly lower at the μM concentrations required for the CD studies.
- [16] For examples in which CD is enhanced by aggregation, see: a) A. R. A. Palmans, J. A. J. M. Vekemans, E. E. Havinga, E. W. Meijer, *Angew. Chem.* **1997**, 36, 2763; *Angew. Chem. Int. Ed. Engl.* **1997**, 36, 2648; b) C. Nuckolls, T. J. Katz, T. Verbiest, S. Van Elshocht, H. G. Kuball, S. Kiesewalter, A. J. Lovinger, A. Persoons, *J. Am. Chem. Soc.* **1998**, 120, 8656; c) C. Nuckolls, T. J. Katz, L. Castellanos, *J. Am. Chem. Soc.* **1996**, 118, 3767; d) D. W. Huang, S. Matile, N. Berova, K. Nakanishi, *Heterocycles* **1996**, 42, 723.
- [17] V. V. Borovkov, T. Harada, Y. Inoue, R. Kuroda, *Angew. Chem. Int. Ed.* **2002**, 114, 1436; *Angew. Chem. Int. Ed.* **2002**, 41, 1378.
- [18] a) S. A. Wahab, H. Matsuura, *Phys. Chem. Chem. Phys.* **2001**, 3, 4689; b) R. Begum, T. Yonemitsu, H. Matsuura, *J. Mol. Struct.* **1998**, 447, 111; c) R. Begum, H. Matsuura, *J. Chem. Soc. Faraday Trans.* **1997**, 93, 3839.
- [19] Y. Takahashi, H. Tadokoro, *Macromolecules* **1973**, 6, 672.
- [20] $[\text{D}_8]\text{THF}$ is transparent in this region. Changes in the relative peak intensities represent shifts in population ratios, but not actual population ratios.
- [21] K. Tasaki, *Macromolecules* **1996**, 29, 8922.
- [22] As implemented in MacroModel 8.5. For the GB/SA model, see W. C. Still, A. Tempczyk, R. C. Hawley, T. Hendrickson, *J. Am. Chem. Soc.* **1990**, 112, 6127.
- [23] Because an *M* helical bias was observed by CD for dendrons 3–4 in all organic solvents studied (i.e., CH_2Cl_2 , CH_3CN , THF), we employed the GB/SA model for chloroform to model the conformational behavior in THF.

Glycoviruses: Chemical Glycosylation Retargets Adenoviral Gene Transfer**

Oliver M. T. Pearce, Kerry D. Fisher, Julia Humphries, Leonard W. Seymour,* Alberto Smith, and Benjamin G. Davis*

Gene therapy of infectious, vascular, and multifactorial diseases employs a variety of viruses, which each have specific qualities that make them suitable for their chosen application.^[1] Gene therapy provides a means to exploit knowledge generated under the human genome project by the use of gene delivery vectors to supplement the function of missing or mutated genes. Some applications of gene therapy require therapeutic gene delivery to specific diseased cells, such as the cystic fibrotic epithelia for treatment of cystic fibrosis,^[2] whereas others accommodate transgene expression within nondiseased cells such as muscle cells or liver hepatocytes in a so-called “cell factory” approach^[3,4] In both applications, successful delivery of the virus requires precise target-cell specificity, an ability to evade neutralizing antibodies, and increased blood circulation to the target cell or tissue. Control of these properties is one of the major challenges facing viral gene therapy today.^[5]

The adenovirus (AV) is a commonly used vector for therapeutic gene therapy.^[6] It has an icosahedral structure with 12 protruding fiber proteins,^[7] each of which comprise a knob domain that binds through a three-way interaction with the coxsackie adenovirus receptor (CAR) of target cell membranes.^[7,8] CAR binding is currently the major route of infection, although nonspecific integrin-mediated uptake is also known.^[8] In both cases, critical lysine residues exposed on

[*] Dr. K. D. Fisher, Dr. L. W. Seymour
Department of Clinical Pharmacology
University of Oxford
Radcliffe Infirmary
Woodstock Road, Oxford, OX2 6HE (UK)
Fax: (+44) 1865-224-538
E-mail: len.seymour@clinical-pharmacology.oxford.ac.uk
O. M. T. Pearce, Dr. B. G. Davis
Chemistry Research Laboratory
University of Oxford
Mansfield Road, Oxford, OX1 3TA (UK)
Fax: (+44) 1865-285-002
E-mail: ben.davis@chem.ox.ac.uk
Dr. J. Humphries, Dr. A. Smith
Academic Department of Surgery
Cardiovascular Division
St Thomas' Hospital
Kings College London
London, SE1 7EH (UK)

[**] We thank the UK Biotechnology and Biological Sciences Research Council for the award of a studentship (O.M.T.P.), Mrs Sue Phipps, Mr Oliver Hayward, and Mrs Barbara Sawyer for invaluable technical assistance, and Dr. Karl Harrison for elegant graphics.



Supporting information for this article is available on the WWW under <http://www.angewandte.org> or from the author.

the virus capsid,^[9] particularly on the knob domain and fiber protein, are responsible for successful interaction and cellular uptake and gives AV a broad tropism of infection.^[10] We reasoned that a more-precisely targeted adenoviral vector might be possible if capsid lysine residues could be modified so that normal infection pathways (Figure 1 a) were disrupted and a new cell-specific infection was induced (Figure 1 b).

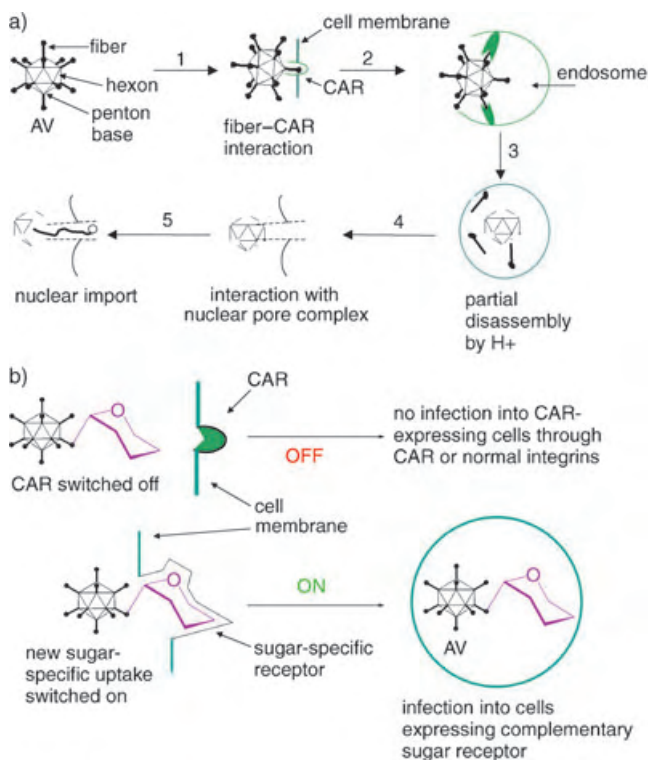


Figure 1. a) Currently accepted mechanism of adenovirus (AV) transfection through coxsackie adenovirus receptor (CAR).^[7b] Lysine residues on fiber proteins are believed to be highly involved in the protein–protein interaction.^[9] 1) Interaction with CAR-expressing cell; 2) receptor-mediated endocytosis; 3) internalization; 4) trafficking to nuclear pore through microtubules; 5) further disassembly and import of viral DNA through interaction of terminal protein with host nuclear pore complex. b) Proposed effect of glycosylation of AV with carbohydrates acting as biological switches.

For this viral retargeting we chose carbohydrates, which play a critical role in cellular trafficking.^[11] Interactions of carbohydrates with cellular receptors are often highly precise,^[12] and important, elegant approaches have explored the potential of glycosylated nonviral gene vectors.^[13–17] Control of glycosylation also influences protein delivery;^[18–21] indeed, we recently showed that carbohydrates are powerful targeting

moieties in a novel protein drug-delivery system called LEAPT (lectin-directed enzyme-activated prodrug therapy).^[22] However, to the best of our knowledge, artificial viral glycosylation in gene delivery has not been explored and we show here that chemically glycosylated AVs are dramatically retargeted.

Careful control of conditions allowed three different levels of glycosylation—high (H), medium (M), and low (L)—of the approximately 1800 available surface lysines.^[23–26] The use of different 2-imino-2-methoxyethyl-1-thioglycosides (IMEs, **1**)^[27,28] allowed both galactosylation (Gal) and mannosylation (Man) to create six novel glycosylated AV structures: Man_H-AV, Man_M-AV, Man_L-AV, Gal_H-AV, Gal_M-AV, and Gal_L-AV (Figure 2).

Remarkably, adenovirus appears very robust under these conditions of chemical glycosylation, and following purification by means of a Microspin S-400HR column, yields of up to 91 %^[29] of intact adenovirus were obtained. PicoGreen analysis,^[30] size-exclusion HPLC, photon correlation spectroscopy (PCS), and measurements of zeta potentials revealed that viral integrity is maintained in the purified virus after glycosylation and that size-exclusion spin column purification successfully removed degraded particles.^[31] HPLC chromatograms^[31] for purified, modified, and unmodified samples showed no differences in retention times which is consistent with the undisturbed virus and correlates with results of titrations using PicoGreen. PCS was used to examine the effects of modification of AV particles on their size and aggregation and showed a clear increase in diameter (for example, AV = 120 ± 6 nm, whereas Man_H-AV = 204 ± 27 nm). Interestingly, this diameter (≈ 200 nm) is consistent with the diameter of adenovirus^[31] if the diameter is measured from the tip of protruding fiber proteins, which are not usually detected by PCS. Glycosylation of AV fiber therefore appears to significantly enhance detection and particle measurement. Zeta potentiometry revealed similar levels of surface charges for AV and Man_H-AV (or Gal_H-AV) which is consistent with the conversion of surface lysines ($pK_a \approx 11$) into amidines, which are also basic ($pK_a \approx 15–17$).^[32]

SDS-PAGE (sodium dodecylsulfate polyacrylamide gel electrophoresis) was used to determine the levels and locations of glycosylation for all six glycoviruses. Heavily glycosylated structures (Man_H-AV and Gal_H-AV) showed significant differences in protein mass for hexon, penton-base, and fiber proteins (Figure 3 a and b). The presence of sugars was confirmed by the cleavage of diols by periodic acid followed by staining with Pro-Emerald stain (Figure 3 b).^[33] Concanavalin A (ConA) affinity chromatography^[34] revealed a high affinity for Man_H-AV but not Gal_H-AV^[35] or AV. Indeed, only upon addition of a mannose-rich buffer did the

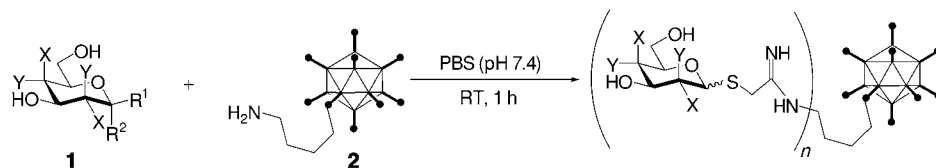


Figure 2. Glycosylation of adenovirus (**2**) with IME reagents (**1**). (1 a = Gal: X = OH, Y = H, R¹ = SCH₂C(NH)OMe, R² = H; 1 b = Man: X = H, Y = OH, R¹ = H, R² = SCH₂C(NH)OMe). PBS = phosphate-buffered saline solution.

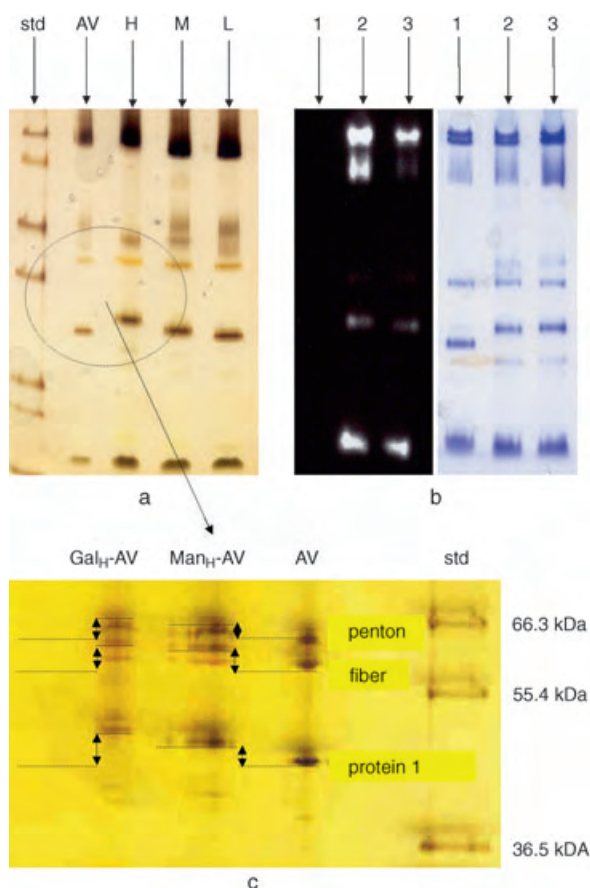


Figure 3. a) Characterization of glycosylation of Man-AV by SDS-PAGE with silver stain (std = standard, AV = adenovirus, H = high, M = medium, L = low). b) Glycoproteins, 1 = AV, 2 = Gal_H-AV, 3 = Man_H-AV, revealed with Pro-Emerald 488 stain (left) and with coomassie brilliant-blue protein stain (right). c) Expanded view shows more-detailed levels of progressive, tuneable glycosylation. Man_H-AV particles were also retained on a ConA affinity column which is consistent with mannosylation.^[31]

mannosylated Man_H-AV particles elute.^[31] SDS-PAGE, which revealed the location of glycosylation, also allowed an estimation of the number of sugars that were attached to each protein (Table 1). For both Man- and Gal-modified structures, a comparison of the theoretical number of exposed lysine moieties^[23–26] with the calculated increases in weight and the percentage of glycosylated lysines showed that Gal_H-AV = 93 ± 3%, Gal_M-AV = 40 ± 1.5%, and Gal_L-AV = 7 ± 0.2%. Man_H-AV displayed a percentage that is comparable with Gal_H-AV, whereas Man_M-AV and Man_L-AV showed

slightly lower values compared to the corresponding Gal-modified structures.^[36]

As lysine residues that are present on AV fiber proteins are required for effective interaction of AV with CAR and membrane integrins,^[9] we considered that increasing the level of glycosylation from low to high would in turn decrease AV transfection ability through CAR. We successfully demonstrated this reduction (Figure 4a) by using a luciferase-expressing AV mutant.^[37] Man_H-AV and Gal_H-AV (shown as

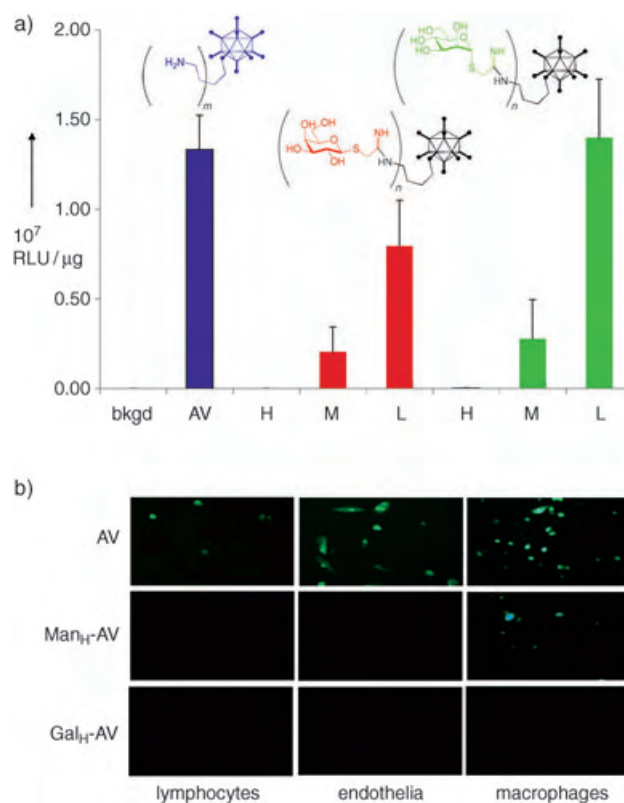


Figure 4. a) Effect of glycosylation in vitro on usual transduction mechanism of adenovirus in coxsackie adenovirus receptor (CAR)-expressing A549 (lung carcinoma) cell lines (RLU = relative light units). Red bars indicate galactosylated AV and green bars indicate mannosylated AV. H, M, and L indicate the high, medium, and low levels, respectively, of glycosylation within sugar modification. The left-hand column indicates the level of background fluorescence (bkgd). The number of naturally occurring lysine residues per virus particle is 22 200. b) The retargeting of mannosylated adenovirus (Man_H-AV) is selective for macrophages, which express the mannose receptor. Unmodified virus (AV) is used as a positive control and galactosylated virus (Gal_H-AV) is used as a negative control.

Table 1: Predicted levels of glycosylation on major virus capsid proteins.

Protein	Number of repeats/virus	Estimated number of lysine residues	Estimated number of sugars/protein (for Gal-AV)		
			H	M	L
Fiber	24	15	14	5	2
Penton	12	20	14	3	nd ^[a]
Hexon	720	30	28	12	2
Total		22 200	20 700 ^[b] ± 700	8800 ^[b] ± 300	1490 ^[b] ± 40

[a] Not detected. [b] Based on calculated increases in weight. See main text for details.

H in Figure 4a) showed a dramatic reduction with no significant transfection ability above the background signal in A549 cells.

With the successful modulation of transfection in A549 cells observed, we next examined the retargeting of Gal_H-AV and Man_H-AV green fluorescent protein^[37]

(GFP)-expressing reporter virus in three types of cell that are found in the human blood system, namely, lymphocytes, macrophages, and endothelial cells (Figure 4b). The CAR mechanism in Gal_H-AV and Man_H-AV was removed by modification. Endothelial cells^[38] were not transfected by either, whereas AV remained active. Lymphocytes, which are not transfected by AV,^[39] were used as a negative control. A small amount of AV transfection was seen in the lymphocyte sample owing to the presence of contaminating monocytes.^[40,41] Finally, transfection of macrophages by means of retargeting through the mannose receptor^[18,20] was examined by using Man_H-AV. Excitingly, significant transduction was observed with Man_H-AV.^[42] AV also showed transfection of macrophages possibly through integrin binding.^[8] Gal_H-AV showed no transduction of macrophages which suggests that Man_H-AV transduction is a specific, sugar-mediated uptake.^[43]

For the first time, by the use of controlled and precise glycosylation chemistry we have successfully modified the fragile structure of AV with carbohydrates and modulated its function. AV transfection can now be adapted to carbohydrate–protein receptor interactions as putative lysine glycosylation “switches off” normal receptor pathways and “switches on” specific sugar-mediated pathways; the clear potential in therapy is under investigation.

Received: August 31, 2004

Revised: November 23, 2004

Keywords: carbohydrates · cell recognition · drug delivery · glycosylation · viruses

- [1] D. Grimm, M. A. Kay, *Curr. Gene Ther.* **2003**, 3, 281.
- [2] P. C. Zamecnik, M. K. Raychowdhury, D. R. Tabatadze, H. F. Cantello, *Proc. Natl. Acad. Sci. USA* **2004**, 101, 8150.
- [3] R. Xu, H. Li, L.-y. Tse, H.-f. Kung, H. Lu, S. L. Lam Karen, *Curr. Gene Ther.* **2003**, 3, 65.
- [4] G. J. Bauerschmitz, A. Kanerva, M. Wang, I. Herrmann, D. R. Shaw, T. V. Strong, R. Desmond, D. T. Rein, P. Dall, D. T. Curiel, A. Hemminki, *Int. J. Cancer* **2004**, 111, 303.
- [5] D. Luo, *Trends Biotechnol.* **2004**, 22, 101.
- [6] C. Volpers, S. Kochanek, *J. Gene Med.* **2004**, 6, S164.
- [7] C. San Martin, R. M. Burnett, *Curr. Top. Microbiol. Immunol.* **2003**, 272, 57.
- [8] O. Meier, F. Greber Urs, *J. Gene Med.* **2004**, 6, S152.
- [9] J. Howitt, C. W. Anderson, P. Freimuth, *Curr. Top. Microbiol. Immunol.* **2003**, 272, 331.
- [10] J. Roy-Chowdhury, M. S. Horwitz, *Mol. Ther.* **2002**, 5, 340.
- [11] R. A. Dwek, T. D. Butters, F. M. Platt, N. Zitzmann, *Nat. Rev. Drug Discovery* **2002**, 1, 65.
- [12] H.-J. Gabius, H.-C. Siebert, S. Andre, J. Jimenez-Barbero, H. Ruediger, *ChemBioChem* **2004**, 5, 740.
- [13] P. Midoux, C. Mendes, A. Legrand, J. Raimond, R. Mayer, M. Monsigny, A. C. Roche, *Nucleic Acids Res.* **1993**, 21, 871.
- [14] P. Erbacher, A. C. Roche, M. Monsigny, P. Midoux, *Bioconjugate Chem.* **1995**, 6, 401.
- [15] T. Ferkol, J. C. Perales, F. Mularo, R. W. Hanson, *Proc. Natl. Acad. Sci. USA* **1996**, 93, 101.
- [16] I. Fajac, S. Grosse, P. Briand, M. Monsigny, *Gene Ther.* **2002**, 9, 740.
- [17] T. Nakai, T. Kanamori, S. Sando, Y. Aoyama, *J. Am. Chem. Soc.* **2003**, 125, 8465.
- [18] M. R. Lennartz, F. S. Cole, P. D. Stahl, *J. Biol. Chem.* **1989**, 264, 2385.
- [19] B. Friedman, K. Vaddi, C. Preston, E. Mahon, J. R. Cataldo, J. M. McPherson, *Blood* **1999**, 93, 2807.
- [20] S. J. Lee, S. Evers, D. Roeder, A. F. Parlow, J. Risteli, L. Risteli, Y. C. Lee, T. Feizi, H. Langen, M. C. Nussenzweig, *Science* **2002**, 295, 1898.
- [21] B. G. Davis, M. A. Robinson, *Curr. Opin. Drug Discovery Dev.* **2002**, 5, 279.
- [22] M. A. Robinson, S. T. Charlton, P. Garnier, X.-T. Wang, S. S. Davis, A. C. Perkins, M. Frier, R. Duncan, T. J. Savage, D. A. Wyatt, S. A. Watson, B. G. Davis, *Proc. Natl. Acad. Sci. USA* **2004**, 101, 14527.
- [23] C. R. O'Riordan, A. Lachapelle, C. Delgado, V. Parkes, S. C. Wadsworth, A. E. Smith, G. E. Francis, *Hum Gen Ther.* **1999**, 10, 1349.
- [24] M. J. van Raaij, A. Mitraki, G. Lavigne, S. Cusack, *Nature* **1999**, 401, 935.
- [25] F. K. Athappilly, R. Murali, J. J. Rux, Z. Cai, R. M. Burnett, *J. Mol. Biol.* **1994**, 242, 430.
- [26] R. Neumann, J. Chroboczek, B. Jacrot, *Gene* **1988**, 69, 153.
- [27] Y. C. Lee, C. P. Stowell, M. J. Krantz, *Biochemistry* **1976**, 15, 3956.
- [28] C. P. Stowell, Y. C. Lee, *Methods Enzymol.* **1982**, 83, 278.
- [29] Yields determined from the total DNA present in the sample by PicoGreen analysis.
- [30] Adenoviral capsid proteins exist as homodimers or homotrimers that can be disrupted easily by the addition of a denaturant such as sodium dodecylsulphate (SDS) or guanidinium chloride. The level of destruction of the adenovirus was analyzed by the PicoGreen method (see Supporting Information), whereas spin column purification would have removed degraded viral particles. PicoGreen analysis of DNA solution levels is routinely used to indirectly calculate the number of viral particles present in solution and has the advantage of high sensitivity, which is useful when protein concentrations are too low for accurate analysis as is often the case with adenoviral titrations. PicoGreen analysis performed on intact viral particles showed only background fluorescence. By comparison of viral samples after glycosylation with the unglycosylated batch, we are able to determine the effect of glycosylation on the structure of adenoviruses.
- [31] See Supporting Information.
- [32] V. Borisenko, M. S. Sansom, G. A. Woolley, *Biophys. J.* **2000**, 78, 1335.
- [33] Purchased from Molecular Probes (www.probes.com).
- [34] Purchased from Galab.
- [35] The retention time for the galactosylated particles was slightly longer than that for the unmodified particles owing to a nonspecific interaction.
- [36] See Supporting Information.
- [37] M. L. Read, K. H. Bremner, D. Oupicky, N. K. Green, P. F. Searle, L. W. Seymour, *J. Gene Med.* **2003**, 5, 232.
- [38] S. A. Nicklin, D. J. Von Seggern, L. M. Work, D. C. Pek, A. F. Dominiczak, G. R. Nemerow, A. H. Baker, *Mol. Ther.* **2001**, 4, 534.
- [39] M. S. Horwitz, *J. Gene Med.* **2004**, 6, S172.
- [40] G. M. Graziani-Bowering, J. M. Graham, L. G. Filion, *J. Immunol. Methods* **1997**, 207, 157.
- [41] This method was used to isolate lymphocytes and monocytes in high purity. The authors comment on the inevitability of contamination owing to both types exhibiting high heterogeneity for the method. Lymphocyte stimulation may also occur here.
- [42] Relative transgene expression levels for Man_H-AV based on RLU (relative light units) are around 40% of the AV level in macrophage but 0% of AV transfection in A549 (A549: AV 1.2×10^7 , Man_H-AV 0; macrophage: AV 1.1×10^9 , Man_H-AV 4.5×10^8).

- [43] Given the similarly high glycosylation levels of Man_H-AV ($90 \pm 3\%$) and Gal_H-AV ($93 \pm 3\%$), we believe that the possibility of low-level normal mode infection being present in Man_H-AV but not in Gal_H-AV is unlikely. Nonetheless, to discount the possibility of low-level normal mode infection, we confirmed the mannose-dependent nature of Man_H-AV transfection through the use of 1% mannose solution, which completely ablated transgene expression to background levels. Transfection by unmodified AV was not affected by 1% mannose solution.

Fluorescent Probes

In Vitro Selection of Structure-Switching Signaling Aptamers**

Razvan Nutiu and Yingfu Li*

Signaling aptamers are aptamer probes that couple target binding to fluorescent-signal generation. These molecular sensors have potential applications in biosensing, proteomics, and drug discovery.^[1] Here we describe a new in vitro selection approach for generating unmodified DNA aptamers that can be immediately transformed into effective signaling probes without the need for further optimization.

Standard aptamers can be easily generated by the technique of in vitro selection.^[2] However, for biosensing applications, postselection modifications must be carried out in order to convert the aptamer concerned into a signaling probe. Although several conversion strategies have been reported,^[3] the modification processes often require lengthy optimization steps to ensure that the affinity and specificity of the original aptamer is not lost upon labeling and that the modified signaling aptamer is able to significantly modulate the fluorescent signal upon target binding.

An alternative method is to create signaling aptamers directly by in vitro selection. Jhaveri et al. have reported the only signaling-aptamer selection method by which signaling aptamers labeled with a single fluorophore can be created.^[4]

However, their results showed that even if the selected aptamers were capable of target binding, a significant number of them failed to induce a concomitant fluorescence change upon target binding, presumably due to the insubstantial alteration of fluorescence properties of the attached fluorophore. More recently, the same group published a selection method for the optimization of signaling properties of molecular beacons containing a fluorophore–quencher pair.^[5] It is conceivable, as the authors have already suggested in their report, that this method could be adapted to the selection of signaling-aptamer probes that detect nonnucleic acid targets. Encouraged by their work, we conducted an in vitro selection study for deriving signaling aptamers that function by the structure-switching mechanism previously described by us for the rational design of signaling aptamers.^[6]

The structure-switching idea takes advantage of the universal ability of any aptamer to adopt two different structures: a duplex structure with an antisense DNA and a complex structure with the cognate target. We have shown that an aptamer can switch structures from duplex to complex upon target addition and, if the aptamer is labeled with a fluorophore and the antisense DNA is labeled with a quencher (denoted QDNA), the structure-switching process can be synchronized to fluorescence signaling.^[6] However, fine-tuning of the QDNA represents a major challenge in the design of structure-switching signaling aptamers, as many QDNA sequences must be tested before a suitable signaling-aptamer system can be established. Therefore, we sought to overcome this problem by utilizing the power of in vitro selection. The strategy described in this report permits the creation of standard aptamers that are encoded with a duplex-to-complex switching capability and can be converted into signaling probes immediately upon their isolation.

The selection strategy is shown in Figure 1. A special DNA library (Figure 1a) was used that contained a central 15-nucleotide fixed-sequence domain (red) flanked by two random-sequence domains (green) of 10 and 20 nucleotides, each further flanked by primer-binding sequences (black). The central fixed-sequence domain was designed to be complementary to an antisense oligonucleotide biotinylated at its 5'-end (denoted BDNA). This arrangement permitted immobilization of the DNA library onto avidin-coated beads through DNA hybridization (step 1 of Figure 1b; see the Supporting Information for more details regarding the library design). We also added two short oligonucleotides, P1 and P2, to prevent the involvement of the primer-binding sequences in the tertiary folding of eventual aptamers. To demonstrate our concept, we used four standard NTPs (nucleoside triphosphates; blue star) as the potential aptamer targets. The immobilized DNA assembly was then exposed to a solution of a mixture of NTPs, each at 0.1 mM (step 2). Aptamers able to form the DNA/target complex should switch from the bead-bound state to the solution. These molecules were then collected and amplified by PCR (step 3). The reverse primer contained a ribonucleotide (R) at its 3'-end to create a chimeric antisense strand prone to NaOH-mediated cleavage, which permitted the isolation of the sense strand by gel electrophoresis (step 4). The recovered sense DNA was reannealed to BDNA, P1, and P2 and used for the

[*] R. Nutiu, Prof. Dr. Y. Li
Department of Biochemistry and Department of Chemistry
McMaster University
Hamilton, ON, L8N 3Z5 (Canada)
Fax: (+1) 905-522-9033
E-mail: liying@mcmaster.ca

[**] We thank the entire Li group as well as Dr. Eric Brown and Dr. Gerard Wright for insightful discussions. This study was funded by the Canadian Institutes of Health Research (CIHR) and the Natural Sciences and Engineering Research Council of Canada. Y.L. holds a Canada Research Chair. R.N. received a CIHR Doctoral Research Award.



Supporting information for this article (library design and experimental details) is available on the WWW under <http://www.angewandte.org> or from the author.

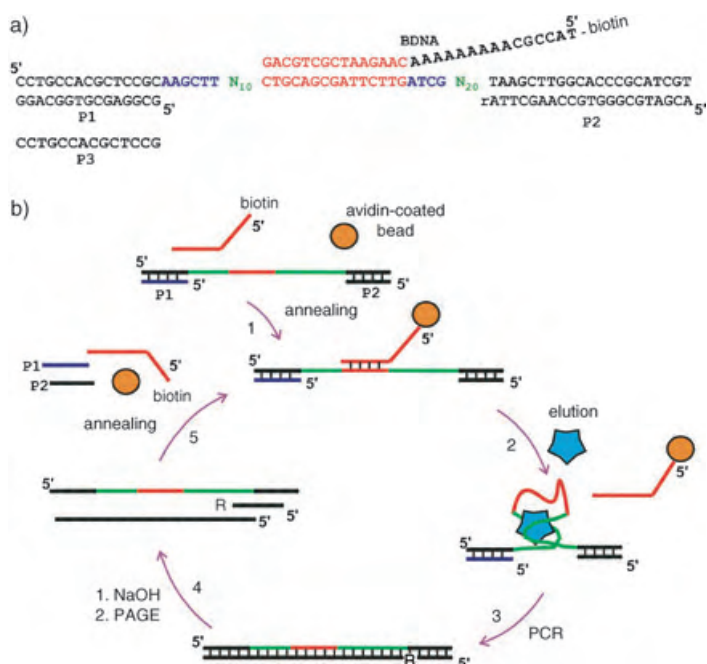


Figure 1. In vitro selection of structure-switching aptamers. a) DNA library design. b) In vitro selection scheme.

next round of selection (step 5). It is noteworthy that BDNA and P1 were intended as the eventual sequences for carrying a quencher and a fluorophore, respectively, so that upon completion of in vitro selection, the selected aptamers could be immediately converted into signaling molecules.

The switching activity, defined as the ratio of the fraction of DNA eluted by the targets over that by selection buffer only, was measured for each selection round (Figure 2a). By the 14th round, the DNA population exhibited significant switching activity. Upon testing, generation 14 (G14) was found to be responsive only to ATP. Next, G14 was subjected to four parallel selections, one for each NTP (at 0.1 mM). After two more rounds, the ATP-binding population (ATP-G16) showed an eightfold ATP-dependent switching activity. Similarly, a sixfold GTP-dependent switching activity was observed for GTP-G17. In contrast, both the CTP and UTP populations failed to register any significant activity after several more rounds of selection. Subsequently, ATP-G16 and GTP-G18 were cloned and sequenced.

Based on sequence alignment, three sequence classes were found in the ATP population and one class in the GTP population (Figure 2b). Four individual ATP-binding (ATP1.1, ATP2.1, ATP2.5, and ATP3.1) and three GTP-binding (GTP1.1, GTP1.2, and GTP1.5) molecules were chemically synthesized and assessed for signaling abilities. At this point, the BDNA was modified with a 4,4-dimethylaminoazobenzene-4'-carboxylic acid (DABCYL) moiety (Q) at the 3'-end and renamed QDNA, and P1 was labeled with fluorescein (F) at the 5'-end and renamed FDNA (Figure 3a). Each DNA assembly (made of the synthetic aptamer, FDNA, QDNA, and P2) successfully signaled the presence of the cognate target, with an increase in fluorescence intensity upon target addition (Figure 3b). For each aptamer, the fluores-

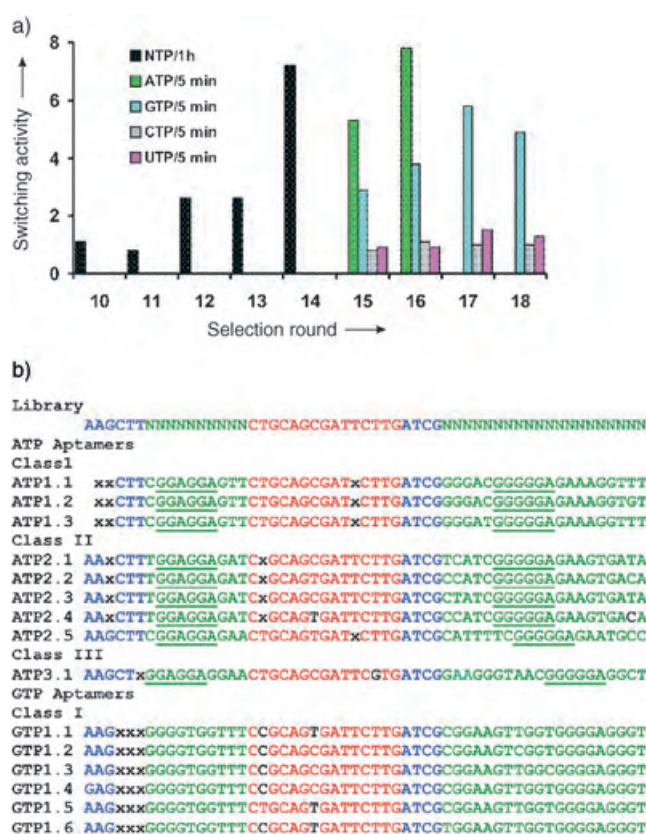


Figure 2. In vitro selection results. a) Progression of in vitro selection. b) The isolated aptamers. The primer binding sites are not shown; "x" represents deletions. Black letters in the central constant region represent mutations relative to the original sequence. The green letters represent the random domain, the red letters represent the central anti-sense-binding domain, and the blue letters represent initially present fixed nucleotides. ATP = adenosine 5'-triphosphate, GTP = guanosine 5'-triphosphate, CTP = cytidine 5'-triphosphate, UTP = uridine 5'-triphosphate.

cence intensity increased markedly when the cognate NTP target was introduced while it remained unchanged upon the addition of the noncognate target. (For clarity, the noncognate target data are only shown for ATP1.1 and GTP1.2.) We found that ATP1.1 and GTP1.2 have the best signaling performance within each relevant group.

To further confirm the structure-switching nature of each aptamer, we conducted an equilibrium-shifting experiment, as shown in Figure 4 for ATP1.1 as an example. Two aptamer-containing solutions A and B (data series in gray and black, respectively) were used. For both solution A and solution B, we first incubated FDNA, P2, and ATP1.1 for 10 min in the absence of QDNA and ATP. Because of the lack of QDNA, the fluorescence intensity of each solution was at its maximum. Then, 1 mM ATP was added to solution B while no ATP was added to solution A. The fact that both solutions maintained the same level of fluorescence intensity indicates that the binding of ATP to the aptamer did not alter its fluorescence intensity. Upon the addition of QDNA after 20 minutes, the fluorescence intensity of both solutions decreased. However, the target-containing solution (solution B) experienced a much smaller reduction in fluorescence

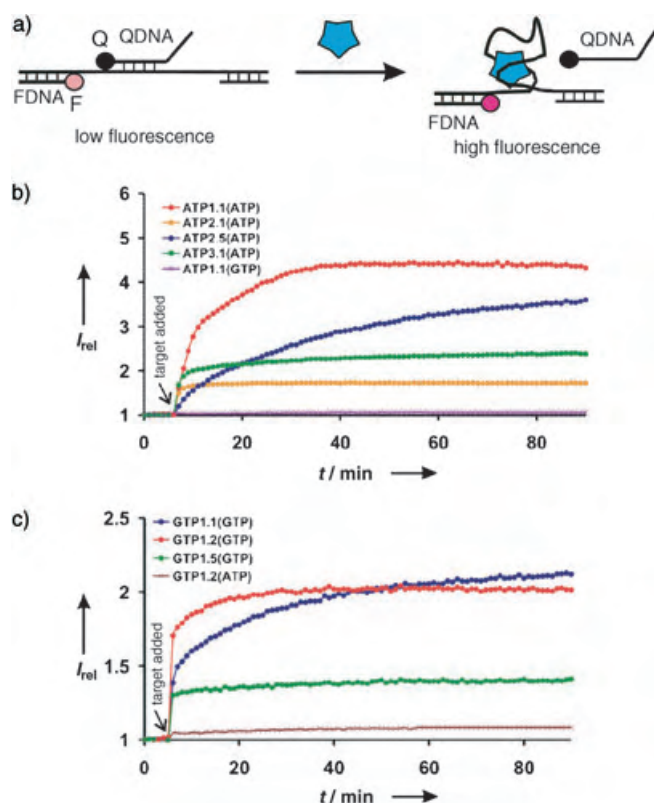


Figure 3. Converting selected aptamers into fluorescent reporters. a) DNA modification and signaling scheme. b) and c) Signaling profiles of four ATP-binding and three GTP-binding aptamers, respectively. I_{rel} relative fluorescence intensity.

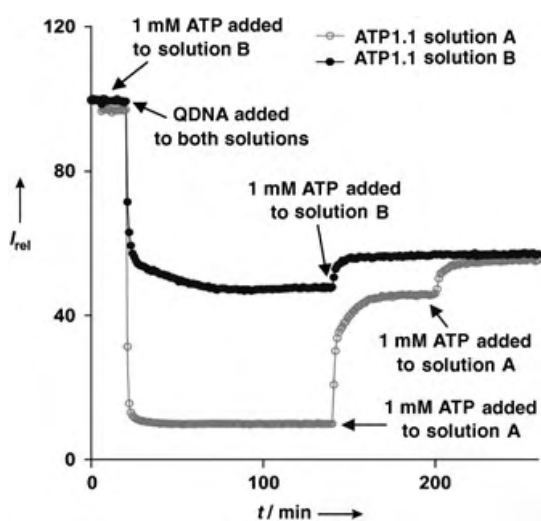


Figure 4. Proof of structure switching by an equilibrium-shifting experiment.

intensity than the target-lacking solution (solution A). The data are consistent with the formation of the aptamer–ATP complex in solution B and the significant reduction in the number of QDNA–aptamer duplexes in solution B as compared to solution A. After 140 minutes, 1 mM ATP was added to each solution. For solution B, only a small increase of fluorescence intensity was observed, a fact suggesting that the

aptamer's target-binding site was largely saturated prior to the addition of the extra ATP. In stark contrast, a significant increase in fluorescence intensity was observed in solution A, which is indicative of a structure transition from the aptamer–QDNA duplex to the aptamer–ATP complex. Finally, when further 1 mM ATP was added to solution A (therefore both solutions contained the same concentrations of ATP and DNA species), solution A reached the same level of fluorescence seen with solution B. The same level of fluorescence reached by both solutions in the end with different orders of ATP and QDNA additions indicates that the switch between the duplex structure and the complex structure is an equilibrium process.

To explore the possibility of multicolor detection of different analytes in the same solution, we kept ATP1.1 unchanged and altered the sequence of the 5'-primer-binding domain of GTP1.2 (the new construct is now named GTP1.2Cy3), to bind a different FDNA labeled with indodicarbocyanine 3 (Cy3; FDNA was renamed Cy3DNA; see the sequences in the Supporting Information). Next, we exposed the mixture of FDNA, Cy3DNA, ATP1.1, GTP1.2Cy3, QDNA, and P2 to 1 mM ATP and 1 mM GTP in different orders (Figure 5 a–c). First, we incubated the mixture without any target to get a background reading. Then we added the ATP (Figure 5 a) or the GTP (Figure 5 c) or both (Figure 5 b) and recorded the fluorescence for 30 minutes. Finally, we added the second target (GTP in Figure 5 a and ATP in Figure 5 c) and recorded the signal for a further 30 minutes. In all three cases, both aptamers correctly indicated the cognate target independently of the presence of the second, uncognate target.

To conclude, we have demonstrated that *in vitro* selection can be carried out to generate structure-switching aptamers that can be immediately transformed into probes able to report target binding by fluorescence signaling. Moreover, we have demonstrated that two different signaling aptamers can work simultaneously in the same solution, thereby offering the possibility of multiplex detection. It is also worth commenting that although our aim in this study was to create signaling aptamers, the same selection method is equally attractive for standard aptamer selections, especially in cases where small molecules serve as aptamer targets (for which filter-based selection cannot be used) because our new method eliminates the need for target immobilization for creation of an affinity column.

All our selected aptamers share a common structural feature due to the design of the initial library: the nucleotides critical for target binding are arranged into two sequence motifs spanning the central fixed-sequence domain (Figure 2 b). This arrangement closely resembles the “self-assembled” aptamers previously reported.^[3b,c]

Interestingly, all our ATP-binding aptamers contain two stretches of nucleotides (underlined green nucleotides in Figure 2 b) that constitute the ATP-binding site of a previously isolated ATP-binding DNA aptamer.^[7,8] This observation indicates that we have rediscovered the same ATP-binding aptamer. This is not completely surprising as other studies have revealed that *in vitro* selection often offers a repeated solution to a given problem.^[9] The isolation of the

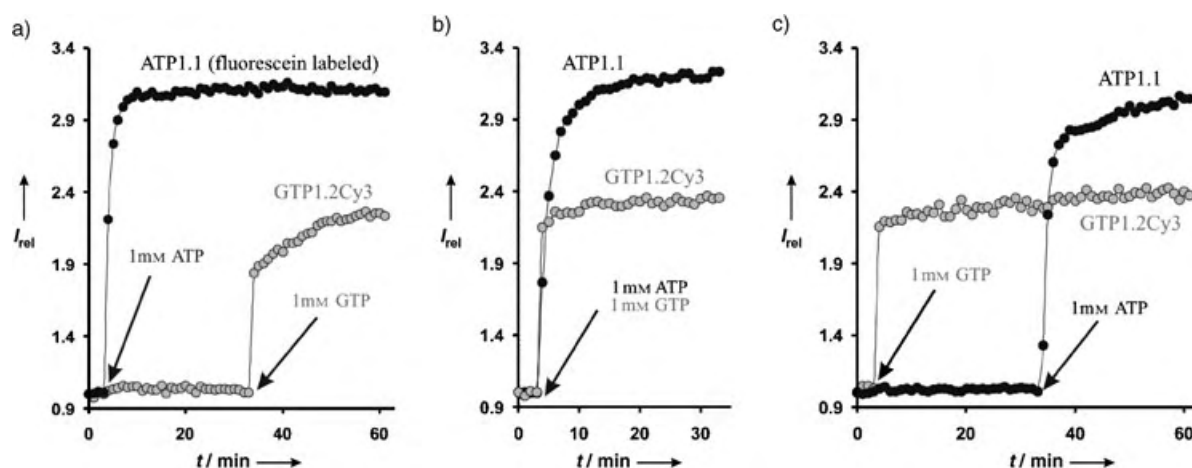


Figure 5. Two-color detection of ATP and GTP in a single solution. ATP1.1 is labeled with fluorescein, GTP1.2 is labeled with Cy3, and QDNA contains a DABCYL moiety as a quencher for both fluorophores. a) Addition of ATP followed by addition of GTP. b) Simultaneous addition of ATP and GTP. c) Addition of GTP followed by addition of ATP.

same aptamer motif in different laboratories from different library designs (a continuous stretch of random-sequence nucleotides in the previous study; two stretches of random-sequence nucleotides flanking a constant-sequence region in the current study) and two different selection strategies (the target ATP was immobilized on a column to retain the aptamer sequences from a DNA library in the previous study; the DNA library was immobilized on a column through DNA hybridization and ATP was used to elute the aptamer sequences in the current study) may suggest that these underlined nucleotides form a small but highly optimized binding site for ATP. The small size of the aptamer means its high abundance in the initial library and the optimal binding site should make it fit for survival during the selection process. The recurrence of the aptamer could also be a result of our choice to use a small-size library that could not lead to isolation of larger and more complex aptamers. We also notice that each selected structure-switching aptamer family shows a very high degree of conservation in most nucleotides located outside of the target-binding motifs, a result suggesting that these nucleotides may help the structure-switching process.

All of our aptamers were able to generate an easily detectable fluorescence signal; however, these directly converted signaling aptamers could achieve only limited fluorescence enhancement (4.5-fold with the best ATP-binding aptamer ATP1.1 and twofold with the best GTP-recognizing aptamer GTP1.2). Although our best signaling aptamers exhibited a signaling magnitude comparable to some of the known aptamer sensors obtained by rational design strategies (1.5-fold in ref. [3a], threefold in ref. [3d] and ref. [3h], fivefold in ref. [3j]), the best rationally designed signaling aptamers can produce a fluorescence enhancement as high as 14-fold.^{[3b], [6a]} It is conceivable that the signaling performance of our signaling aptamers can be improved by carrying out optimization experiments (such as using an extended FDNA or QDNA that can place F and Q in close proximity). It is also important to point out that all the selected aptamers involuntarily acquired one or two mutations or deletions in the BDNA-binding domain during the in vitro selection

process (Figure 2b), which obviously leads to the formation of a weaker aptamer–BDNA duplex for easier structure switching. However, it also gives a higher fluorescence background for the signaling system. Based on this observation, we believe that better signaling aptamers could be derived in future in vitro selection efforts by conducting the duplex-formation step (steps 1 and 5 in Figure 1b) at an elevated temperature (22°C was used in the current study) to eliminate the sequences with weakened duplex structures.

Our selection failed to generate DNA aptamers that bind CTP or UTP. Although precise reasons for this failure could not be determined at this point, we speculate that this might have been caused by our choice of a DNA library containing only 30 random nucleotides. It is quite possible that potential CTP- and UTP-binding aptamers require considerably more nucleotides and our starting library simply did not meet this requirement. Another possibility is that these two nucleotides may inherently be poor aptamer targets. It remains to be determined whether CTP- and UTP-binding aptamers can be derived by using more complex libraries.

Received: August 31, 2004

Revised: October 18, 2004

Published online: January 11, 2005

Keywords: aptamers · fluorescence · in vitro selection · nucleic acids · sensors

- [1] a) S. D. Jayasena, *Clin. Chem.* **1999**, *45*, 1628–1650; b) L. S. Green, C. Bell, N. Janjic, *Biotechniques* **2001**, *30*, 1094–1110; c) M. Famulok, M. Blind, G. Mayer, *Chem. Biol.* **2001**, *8*, 931–939; d) P. Burgstaller, A. Jenne, M. Blind, *Curr. Opin. Drug Discov. Dev.* **2002**, *5*, 690–700; e) X. Fang, A. Sen, M. Vicens, W. Tan, *ChemBioChem* **2003**, *4*, 829–834; f) R. Nutiu, J. M. Yu, Y. Li, *ChemBioChem* **2004**, *5*, 1139–1144; g) J. Srinivasan, S. T. Cload, N. Hamaguchi, J. Kurz, S. Keene, M. Kurz, R. M. Boomer, J. Blanchard, D. Epstein, C. Wilson, J. L. Diener, *Chem. Biol.* **2004**, *11*, 499–508.
- [2] a) C. Tuerk, L. Gold, *Science* **1990**, *249*, 505–510; b) A. D. Ellington, J. W. Szostak, *Nature* **1990**, *346*, 818–822.

- [3] a) S. Jhaveri, R. Kirby, R. Conrad, E. Maglott, M. Bowser, R. T. Kennedy, G. Glick, A. D. Ellington, *J. Am. Chem. Soc.* **2000**, *122*, 2469–2473; b) R. Yamamoto, T. Baba, P. K. Kumar, *Genes Cells* **2000**, *5*, 389–396; c) M. N. Stojanovic, P. de Prada, D. W. Landry, *J. Am. Chem. Soc.* **2000**, *122*, 11547–11548; d) N. Hamaguchi, A. Ellington, M. Stanton, *Anal. Biochem.* **2001**, *294*, 126–131; e) M. N. Stojanovic, P. de Prada, D. W. Landry, *J. Am. Chem. Soc.* **2001**, *123*, 4928–4931; f) J. J. Li, X. Fang, W. Tan, *Biochem. Biophys. Res. Commun.* **2002**, *292*, 31–40; g) J. R. Babendure, S. R. Adams, R. Y. Tsien, *J. Am. Chem. Soc.* **2003**, *125*, 14716–14717; h) K. Yamana, Y. Ohtani, H. Nakano, I. Saito, *Bioorg. Med. Chem. Lett.* **2003**, *13*, 3429–3431; i) E. J. Merino, K. M. Weeks, *J. Am. Chem. Soc.* **2003**, *125*, 12370–12371; j) M. N. Stojanovic, D. M. Kolpashchikov, *J. Am. Chem. Soc.* **2004**, *126*, 9266–9270.
- [4] S. Jhaveri, M. Rajendran, A. D. Ellington, *Nat. Biotechnol.* **2000**, *18*, 1293–1297.
- [5] M. Rajendran, A. D. Ellington, *Nucleic Acids Res.* **2003**, *31*, 5700–5713.
- [6] a) R. Nutiu, Y. Li, *J. Am. Chem. Soc.* **2003**, *125*, 4771–4778; b) R. Nutiu, Y. Li, *Chem. Eur. J.* **2004**, *10*, 1868–1876.
- [7] D. E. Huizenga, J. W. Szostak, *Biochemistry* **1995**, *34*, 656–665.
- [8] C. H. Lin, D. J. Patel, *Chem. Biol.* **1997**, *4*, 817–832.
- [9] a) K. Salehi-Ashtiani, J. W. Szostak, *Nature* **2001**, *414*, 82–84; b) D. Saran, J. Frank, D. H. Burke, *BMC Evol. Biol.* **2003**, *3*, 26; c) R. P. Cruz, J. B. Withers, Y. Li, *Chem. Biol.* **2004**, *11*, 57–67.

Peptide Modeling

Stability of SIV gp32 Fusion-Peptide Single-Layer Protofibrils as Monitored by Molecular-Dynamics Simulations**

Patricia Soto, Josep Cladera, Alan E. Mark, and
Xavier Daura*

Amyloid fibrils are filamentous structures formed from peptides and proteins of widely varied sequence and

length.^[1,2] Such noncovalent assemblies are at the heart of a wide range of diseases including Alzheimer's and Creutzfeldt-Jakob disease (CJD) in humans, and bovine spongiform encephalopathy (BSE) in cattle.^[3] These protein-conformational diseases are particularly intriguing, because, given appropriate conditions, the formation of amyloid aggregates appears to be a generic property of constituent polypeptides and is largely independent of their source.^[3] The biophysical factors that determine whether specific sequences will form stable amyloid suprastructures are largely unknown. Furthermore, high-resolution structural data has proved difficult to obtain because the fibrils are insoluble and noncrystalline.^[1] X-ray diffraction patterns from amyloid fibers are consistent with a cross- β structure.^[4] This, in conjunction with information from solid-state NMR spectroscopic analysis,^[5] cryoelectron microscopy, and image processing,^[6] has led to the proposal of models for amyloid protofilaments that consist of multilayered, helical β sheets. The structural features of the fibrillar forms of different proteins are very similar. This suggests that fibrils form by a common mechanism, and that the elucidation of the assembly process in one system will shed light on amyloid formation in general.^[1-3] Herein we report atomistic molecular-dynamics (MD) simulations performed in explicit solvent to investigate the supramolecular organization of a single-layer protofibril formed from the simian immunodeficiency virus wild-type (SIVwt) peptide.

The SIVwt peptide corresponds to the N-terminal region of the SIV transmembrane glycoprotein 32 (gp32) (GVFVLGFLGFLA). It is involved in triggering the fusion of viral and target cell membranes, which facilitates entry of the virus into the cell.^[7] This 12-residue peptide is very hydrophobic, a property shared with the A β (30-40) C-terminal segment of the amyloid peptide responsible for Alzheimer's disease. A β (30-40) is in the so-called functional domain required for cytotoxicity and has been shown to adopt a β -strand conformation and to form parallel β sheets.^[8] The close relationship between amyloid peptides and HIV fusion peptides has been reported previously.^[9]

Based primarily on IR spectroscopic data, the SIVwt peptide has been reported to form aggregated β structures.^[10,11] From their analysis of SIVwt peptides with attenuated total reflectance spectroscopy (ATR), Martin et al. reported an IR band typical of β aggregates that contain strong hydrogen bonds.^[10] Interestingly, such aggregates have spectroscopic characteristics indistinguishable from those of amyloid fibrils. We noted that samples for the ATR studies were prepared by drying solutions of peptides in dimethyl sulfoxide (DMSO) onto the ATR crystal. Thus, the concentration of the fusion peptide was very high, and little DMSO remained in the sample. However, when dissolved in an aqueous buffer, the retroviral fusion peptides formed large, colloidal aggregates,^[10,11] which are spectroscopically identical to those formed in DMSO at low DMSO/peptide molar ratios. Moreover, these aggregates present the same spectroscopic features of the peptide aggregates that form upon peptide-mediated membrane fusion.

The fact that this peptide forms β aggregates in DMSO provides a unique opportunity to study the process of fibril formation in atomic detail with MD simulation techniques.

[*] Prof. X. Daura
Catalan Institution for Research and Advanced Studies (ICREA)
Institute of Biotechnology and Biomedicine
Universitat Autònoma de Barcelona
08193 Bellaterra, Barcelona (Spain)
Fax: (+34) 93-581-2011
E-mail: xavier.daura@uab.es
P. Soto, Prof. A. E. Mark
Groningen Biomolecular Sciences and Biotechnology Institute (GBB)
Department of Biophysical Chemistry, University of Groningen
9747 AG Groningen (The Netherlands)
Prof. J. Cladera
Biophysics Unit
Department of Biochemistry and Molecular Biology
Universitat Autònoma de Barcelona
08193 Bellaterra, Barcelona (Spain)

[**] This work was supported by the Spanish MCyT/FEDER, reference BIO2003-02848. We thank S. Ventura for critical reading of the manuscript.

Owing to its low atom density, DMSO is a much less expensive solvent to simulate than water. This means that it is possible to study the collective properties of large-scale aggregates in explicit solvent.

Figure 1 shows that the parallel β -sheet aggregates spontaneously adopt a helical suprastructure in the simulations. For pb10 (a protofibril construct with 10 parallel chains;

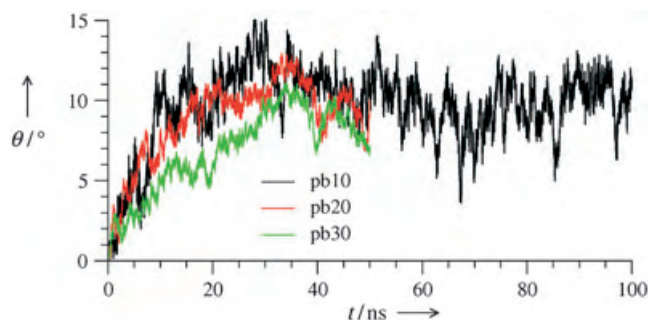


Figure 1. Twist angle per peptide chain in simulations of pb10, pb20, and pb30 as a function of time. The twist angle θ was calculated as $\theta = \arccos(\mathbf{u}_m \cdot \mathbf{u}_n) / (n - m + 1)$, in which \mathbf{u} is the unit vector from the α -C atom of residue 1 to that of residue 12 for each chain, and m and n are the first and last chains respectively, in an aggregate with five or more interstrand hydrogen bonds. (These were chains 2–7 in pb10, chains 7–19 in pb20, and chains 5–20 in pb30.)

see experimental section) the β sheet twists away from the initial planar conformation during the first 20 ns. A dynamic equilibrium is then established involving partial unwinding and rewinding of the suprastructure. The helical twist per chain oscillates between $\approx 5^\circ$ and $\approx 15^\circ$. The average twist angle is 10° , and the average helical pitch is 15 nm (calculated for chains 2–7 over the interval of 20–100 ns). Fraying was observed at the ends of the structure, and chains 1, 8, 9, and 10 have less than five hydrogen bonds to their neighbors after 30 ns. Pb20 and pb30 (constructs with 20 and 30 parallel chains, respectively) behave similarly to pb10. The average twist angle and average pitch are 10° and 16 nm for pb20, and 9° and 20 nm for pb30, over the interval of 20–50 ns. As with pb10, only the chains with an average of five interstrand hydrogen bonds or more (7–19 in pb20 and 5–20 in pb30) were included in these estimates. The final structure of pb30 is shown in Figure 2. In all three cases, the ends of the sheet tend to adopt a higher twist angle than the central section. Thus, modeling short fragments would overestimate the degree of twist; indeed, the twists of pb10 and pb20 are slightly greater than that of pb30. In addition, fragments at the ends are found to orient in a different direction to the main axis of the protofibril (helix bending), while still maintaining a helical twist.

The supramolecular structure observed in the simulations can be described as a left-handed twisted ribbon with saddlelike curvature.^[12] The chirality of the constituent chains renders this structure more thermodynamically stable than a helical ribbon.^[2,12] In the simulations, we observed a cooperative twisting of the β sheet until a maximum twist angle was reached. At the point of maximum stress in the geometry, there was a subsequent relaxation toward a smaller

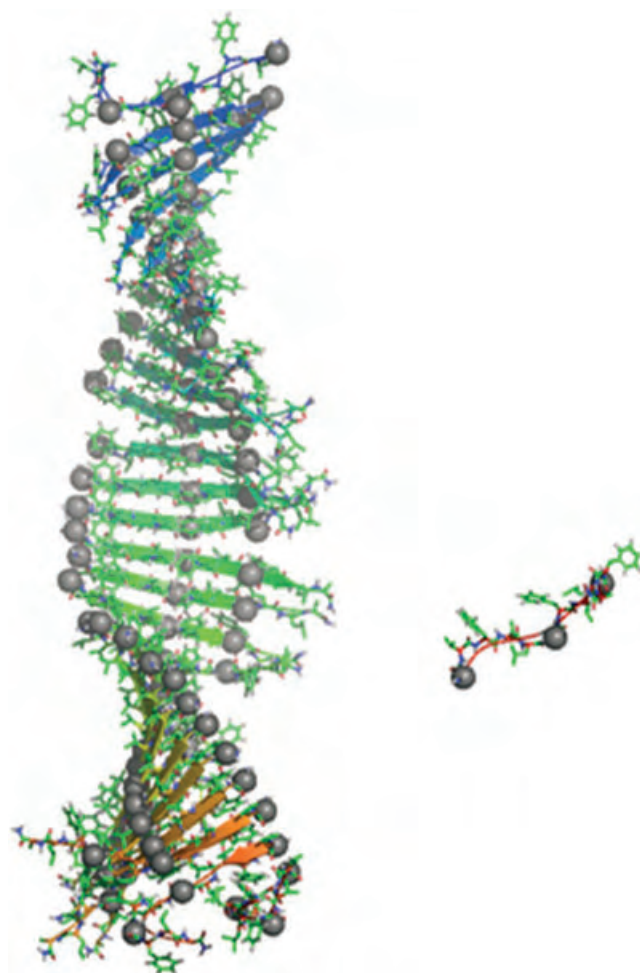


Figure 2. The protofibril pb30 at 50 ns. One terminal chain has dissociated (right). The average twist angle per chain is 9° , and the average pitch (P) is 20 nm at 20–50 ns. The pitch is calculated as $P = N_c \times D_c$, in which N_c is the number of peptide chains per 360° turn and D_c is the translation per chain along the long fibril axis. N_c and D_c are calculated only for intact chains (those bearing at least five or more interstrand hydrogen bonds. See Figure 1).

angle, followed by alternating partial unwinding/rewinding events around an equilibrium twist angle. The average twist angle of the ribbon, $\approx 9^\circ$, may be compared with twist angles of $\approx 0.5^\circ$ to $\approx 2.5^\circ$ suggested for multilayered amyloid fibrils,^[6,13] with an angle of $\approx 7^\circ$ proposed for a speculative model of bilayered β 2-microglobulin fibrils,^[14] and with twist angles ranging from 0° to $\approx 30^\circ$ for single-layer β -sheet motifs in proteins.^[15,16]

The cross- β structure of amyloid fibrils inferred from diffraction data (β strands of the precursor polypeptides are perpendicular to, and ribbonlike β sheets are parallel to the fibril axis)^[6] is compatible with either a parallel or antiparallel arrangement of the polypeptide strands. Packing depends on the sequence of the polypeptide, and the nature of the interactions between the side chains of neighboring strands. It was recently suggested that an increase of the amphiphilicity of the A β (16–22) peptide changes the β sheet structure in the fibrils from antiparallel to parallel.^[17] To test the effect of chain orientation on the stability and twisting of the SIVwt

protofibril, a simulation of 10 antiparallel chains in DMSO was performed. A rapid loss of interchain hydrogen bonding was observed (results not shown). After 50 ns, only two adjacent chains had more than five interstrand hydrogen bonds. Therefore, the results suggest that the parallel β sheet arrangement is most stable and that nonpolar interactions between side chains dominate.^[18]

We believe that this is the first example in which the spontaneous twisting of a protofibril into an *equilibrium* twisted-ribbon suprastructure has been observed. Recently, Fishwick et al.^[19] claimed to have simulated the spontaneous twisting of 20-membered β sheets formed by glutamine-rich peptides with an implicit solvent model. However, the large structural changes observed in the extremely short simulations (100 ps) cast serious doubt on the reliability of the results. In other computational studies of amyloid protofibrils, a specific twist has simply been imposed on the ribbon structure with simulations serving only to relax the initial conformation.^[20] Our work demonstrates that it is possible to model stable protofibril structures at an atomic level. Studies of the spontaneous aggregation of this peptide into extended β sheet structures are under way.

Experimental Section

Four systems were simulated. Three were β -sheet constructs containing 10 (pb10), 20 (pb20), and 30 (pb30) parallel SIVwt chains. The construct pb10 was simulated for 100 ns, pb20 and pb30 for 50 ns. The initial arrangement of the β sheets was planar. The average distance between facing α -C atoms was 0.4 nm. The long axis of the β sheet was ~ 4 nm for pb10, ~ 8 nm for pb20, and ~ 12 nm for pb30. Each β sheet was placed in a periodic cuboid of $8 \times (D+4) \times 7$ nm³ (D = length of the long axis) and solvated with DMSO.^[21] A fourth system consisting of 10 peptide chains in an antiparallel arrangement (ab10) was also simulated to test the effect of the orientation of the peptide on the stability of the protofibril. All simulations were performed with the GROMACS software^[22] and the GROMOS 43 A1 force field.^[23] The end groups of the peptide were neutral (H_2N^- , $-\text{CONH}_2$) in accordance with experimental data. The temperature and pressure were coupled to external baths^[24] at 300 K and 1 bar with relaxation times of 0.1 and 0.5 ps, respectively. Bond lengths were constrained with the LINCS algorithm.^[25] The equations of motion were integrated with the leap-frog algorithm with a time step of 2 fs. Nonbonding interactions were evaluated with a twin-range cutoff of 0.8/1.4 nm, and a charge-group pair list updated every 10 time steps.

Received: September 9, 2004

Published online: January 3, 2005

Keywords: aggregation · molecular dynamics · peptides · protein models · protofibrils

- [1] R. Tycko, *Curr. Opin. Chem. Biol.* **2000**, *4*, 500.
- [2] S. Zhang, D. M. Marini, W. Hwang, S. Santoso, *Curr. Opin. Chem. Biol.* **2002**, *6*, 865.
- [3] C. M. Dobson, *Philos. Trans. R. Soc. London Ser. B* **2001**, *356*, 133.
- [4] M. Sunde, C. C. Blake, *Q. Rev. Biophys.* **1998**, *31*, 1.
- [5] A. T. Petkova, Y. Ishii, J. J. Balbach, O. N. Antzutkin, R. D. Leapman, F. Delaglio, R. Tycko, *Proc. Natl. Acad. Sci. USA* **2002**, *99*, 16742.
- [6] J. L. Jiménez, E. J. Nettleton, M. Bouchard, C. V. Robinson, C. M. Dobson, H. R. Saibil, *Proc. Natl. Acad. Sci. USA* **2002**, *99*, 9196.
- [7] M. Horth, B. Lambrecht, M. C. L. Khim, F. Bex, C. Thiriart, J. M. Ruyschaert, A. Burny, R. Brasseur, *EMBO J.* **1991**, *10*, 2747.
- [8] O. N. Antzutkin, J. J. Balbach, R. D. Leapman, N. W. Rizzo, J. Reed, R. Tycko, *Proc. Natl. Acad. Sci. USA* **2000**, *97*, 13045.
- [9] a) T. Pillot, M. Goethals, B. Vanloo, C. Talussot, R. Brasseur, J. Vandekerckhove, M. Rosseneu, L. Lins, *J. Biol. Chem.* **1996**, *271*, 28757; b) W. M. Wojtowicz, M. Farzan, J. L. Joyal, K. Carter, G. J. Babcock, D. I. Israel, J. Sodroski, T. Mirzabekov, *J. Biol. Chem.* **2002**, *277*, 35019; c) A. Saez-Cirion, J. L. Nieva, W. R. Gallaher, *AIDS Res. Hum. Retroviruses* **2003**, *19*, 969; d) L. M. Gordon, P. W. Mobley, W. Lee, S. Eskandari, Y. N. Kaznessis, M. A. Sherman, A. J. Waring, *Protein Sci.* **2004**, *13*, 1012.
- [10] I. Martin, M. C. Dubois, F. Defrise-Quertain, T. Saermark, A. Burny, R. Brasseur, J. M. Ruyschaert, *J. Virol.* **1994**, *68*, 1139.
- [11] a) J. Cladera, I. Martin, J. M. Ruyschaert, P. O'Shea, *J. Biol. Chem.* **1999**, *274*, 29951; b) J. L. Nieva, S. Nir, A. Muga, F. M. Goñi, J. Wilschut, *Biochemistry* **1994**, *33*, 3201.
- [12] R. Oda, I. Huc, M. Schmutz, S. J. Candau, F. C. MacKintosh, *Nature* **1999**, *399*, 566.
- [13] a) K. Lu, J. Jacob, P. Thiagarajan, V. P. Conticello, D. G. Lynn, *J. Am. Chem. Soc.* **2003**, *125*, 6391; b) T. S. Burkoth, T. L. S. Benzinger, V. Urban, D. M. Morgan, D. M. Gregory, P. Thiagarajan, R. E. Botto, S. C. Meredith, D. G. Lynn, *J. Am. Chem. Soc.* **2000**, *122*, 7883.
- [14] M. I. Ivanova, M. R. Sawaya, M. Gingery, A. Attinger, D. Eisenberg, *Proc. Natl. Acad. Sci. USA* **2004**, *101*, 10584.
- [15] C. Chothia, T. Hubbard, S. Brenner, H. Barns, A. Murzin, *Annu. Rev. Biophys. Biomol. Struct.* **1997**, *26*, 597.
- [16] For a more in-depth review on fibril morphologies, see: L. C. Serpell, *Biochim. Biophys. Acta* **2000**, *1502*, 16.
- [17] D. J. Gordon, J. J. Balbach, R. Tycko, S. C. Meredith, *Biophys. J.* **2004**, *86*, 428.
- [18] a) S. Ventura, E. Lacroix, L. Serrano, *J. Mol. Biol.* **2002**, *322*, 1147; b) M. López de la Paz, K. Goldie, J. Zurdo, E. Lacroix, C. M. Dobson, A. Hoenger, L. Serrano, *Proc. Natl. Acad. Sci. USA* **2002**, *99*, 16052; c) S. Ventura, J. Zurdo, S. Narayanan, M. Parreno, R. Mangués, B. Reif, F. Chiti, E. Giannoni, C. M. Dobson, F. X. Aviles, L. Serrano, *Proc. Natl. Acad. Sci. USA* **2004**, *101*, 7258.
- [19] C. W. G. Fishwick, A. J. Beevers, L. M. Carrick, C. D. Whitehouse, A. Aggeli, N. Boden, *Nano Lett.* **2003**, *3*, 1475.
- [20] a) L. Li, T. A. Darden, L. Bartolotti, D. Kominos, L. G. Pedersen, *Biophys. J.* **1999**, *76*, 2871; b) W. M. Hwang, D. M. Marini, R. D. Kamm, S. Q. Zhang, *J. Chem. Phys.* **2003**, *118*, 389.
- [21] H. Liu, F. Müller-Plathe, W. F. van Gunsteren, *J. Am. Chem. Soc.* **1995**, *117*, 4363.
- [22] a) H. J. C. Berendsen, D. van der Spoel, R. van Drunen, *Comput. Phys. Commun.* **1995**, *91*, 43; b) E. Lindahl, B. Hess, D. van der Spoel, *J. Mol. Model.* **2001**, *7*, 306.
- [23] a) X. Daura, A. E. Mark, W. F. van Gunsteren, *J. Comput. Chem.* **1998**, *19*, 535; b) W. F. van Gunsteren, S. R. Billeter, A. A. Eising, P. H. Hünenberger, P. Krüger, A. E. Mark, W. R. P. Scott, I. G. Tironi, *Biomolecular Simulation: The GROMOS96 Manual and User Guide*, vdf Hochschulverlag AG an der ETH, Zürich, and BIOMOS BV, Groningen, **1996**.
- [24] H. J. C. Berendsen, J. P. M. Postma, W. F. van Gunsteren, A. DiNola, J. R. Haak, *J. Chem. Phys.* **1984**, *81*, 3684.
- [25] B. Hess, H. Bekker, H. J. C. Berendsen, J. G. E. M. Fraaije, *J. Comput. Chem.* **1997**, *18*, 1463.

Multifunctional Nanoparticles Possessing A “Magnetic Motor Effect” for Drug or Gene Delivery**

Tae-Jong Yoon, Jun Sung Kim, Byung Geol Kim, Kyeong Nam Yu, Myung-Haing Cho,* and Jin-Kyu Lee*

Magnetic ferrite nanoparticles (usually called ferrofluid) have been widely used in various applications, such as smart seal magnetic circuits,^[1] audio speakers,^[2] and magnetic domain detectors.^[3] Recently, magnetic nanoparticles have been suggested for many new applications in high-density magnetic data storage,^[4] magnetic resonance imaging,^[5] catalyst supporters,^[6] and biomedical applications, such as magnetic carriers for bioseparation,^[7] enzyme and protein immobilization,^[8] and contrast-enhancing media.^[9] Transmission electron microscopy (TEM) or magnetic resonance imaging (MRI) have been used to observe magnetic nanoparticles incorporated within cells. However, TEM or MRI are not convenient for in situ monitoring, and thus a sensitive and easy technique for monitoring the nanoparticles in cells in situ is desirable. Confocal laser scanning microscopy (CLSM) is a highly sensitive detection technique specific to the fluorescence wavelength of the dye used. Incorporation of a fluorescent dye into the nanoparticle would enable the detection and monitoring, in situ, of the movement of the nanoparticles under an external magnetic field, for example.

Nanoparticles have been coated with a shell of stable and biocompatible material, such as silica (SiO_2), to avoid potential toxic effects on cells.^[10–12] Incorporation of a fluorescent dye into the silica shell seemed a good choice to

us. The polyvinylpyrrolidone (PVP) method has been applied to particles having ionic surface charges to generate a sol–gel silica coating with thickness which can be altered by varying the amount of tetraethoxysilane (TEOS) loaded.^[13] Herein, we report the preparation, employing a modified PVP method, of cobalt ferrite magnetic nanoparticles coated with a shell of amorphous silica, which contains luminescent organic dyes, such as rhodamine B isothiocyanate (RITC, orange, $\lambda_{\text{max(em)}} = 555 \text{ nm}$) or fluorescein isothiocyanate (FITC, green, $\lambda_{\text{max(em)}} = 518 \text{ nm}$) on the inside of the silica shell and biocompatible poly(ethylene glycol) (PEG) on the outside. We wished to determine whether the fluorescence characteristics of the organic dye could be used in conjunction with CLSM to compare the efficiency of uptake into cells of magnetic nanoparticles with and without PEG modification. Monitoring the movement of doped cells under an external magnetic field was also investigated because of its potential use in bioseparation and related applications.

Water-soluble bare cobalt ferrite magnetic nanoparticles of average size about 9 nm, synthesized by a slight modification of the co-precipitation method from $\text{FeCl}_3 \cdot 6\text{H}_2\text{O}$ and $\text{CoCl}_2 \cdot 6\text{H}_2\text{O}$ in hot basic NaOH solution,^[14] were stabilized with PVP to make them homogeneously dispersed in ethanol. The mixed solution of TEOS and dye-modified silane compound, synthesized from 3-aminopropyltriethoxysilane (APS) and dye-isothiocyanate,^[15] was polymerized on the surface of PVP-stabilized cobalt ferrites by adding ammonia solution as a catalyst to form organic-dye-incorporated cobalt ferrite–silica core–shell nanoparticles. The ratio of the concentrations of cobalt ferrite magnetic nanoparticles (Co ferrite MNPs) and TEOS was optimized to prevent the homogeneous nucleation of silica and to control the silica-shell thickness of the core–shell Co ferrite–silica MNPs. The TEM images in Figure 1 of silica-coated Co ferrite MNPs

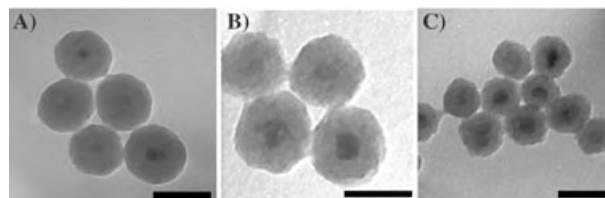


Figure 1. TEM images of Co ferrite–silica (core–shell) MNPs with controlled shell thicknesses. A) TEOS/MNP = 0.12 mg/4 mg, scale bar = 100 nm, B) TEOS/MNP = 0.06 mg/4 mg, scale bar = 50 nm, C) TEOS/MNP = 0.03 mg/4 mg, scale bar = 50 nm. As the ratio of TEOS/MNP (w/w) decreases, the shell thickness decreases.

prepared using different ratios of TEOS/MNP show that the thickness of the silica shell can be precisely controlled to produce core–shell nanoparticles with diameters ranging from 30 to 80 nm as the amount of TEOS was increased from 0.03 to 0.12 mg. The crystallinity and magnetic properties of the core material did not change upon coating with silica (see Supporting Information). PEG was easily attached to the silica-shell surface by adding PEG– $\text{Si}(\text{OMe})_3$ solution after the shell formation was complete (see Supporting Information). This approach could be directly applied to the

[*] T.-J. Yoon,^[†] B. G. Kim, Prof. J.-K. Lee
Materials Chemistry Laboratory
School of Chemistry
Seoul National University
Seoul, 151-747 (Korea)
Fax: (+82) 2-882-1080
E-mail: jinklee@snu.ac.kr

J. S. Kim,^[†] K. N. Yu, Prof. M.-H. Cho
Laboratory of Toxicology
College of Veterinary Medicine and
School of Agricultural Biotechnology
Seoul National University
Seoul, 151-747 (Korea)
Fax: (+82) 2-873-1268
E-mail: mchotox@snu.ac.kr

[†] These authors contributed equally to this work.

[**] This work is supported by Nano Systems Institute-National Core Research Center (NSI-NCRC), Korea Science and Engineering Foundation (KOSEF). T.-J.Y., J.S.K., B.-G.K., and K.N.Y. are grateful for the award of a BK21 fellowship. We thank Prof. Seung Bum Park for his valuable comments and Ms. Eun Jung Kang for her help with CLSM investigations. “Magnetic motor effect”: cell movement as a result of applying an external magnetic field to cells containing magnetic nanoparticles.

Supporting information for this article is available on the WWW under <http://www.angewandte.org> or from the author.

synthesis of dye-labeled and surface-modified core-shell magnetic nanoparticles, MNP-SiO₂(RITC or FITC) and MNP-SiO₂(RITC or FITC)-PEG. Attachment of PEG did not significantly change the size of the nanoparticles (determined by TEM measurements). The average diameter of the organic-dye-labeled Co ferrite-silica (core-shell) MNPs used in this study was about 50 nm as shown in Figure 1 B.

Although photobleaching is a common problem when fluorescent dyes are used, no significant photobleaching was observed in our rigid matrix system, as reported for a similar embedded system,^[16] and thus fluorescence intensity could be used to quantitatively analyze the quantity of core-shell nanoparticles incorporated into cells. The CLSM images in Figure 2 show breast cancer cells (MCF-7) after 24 h of

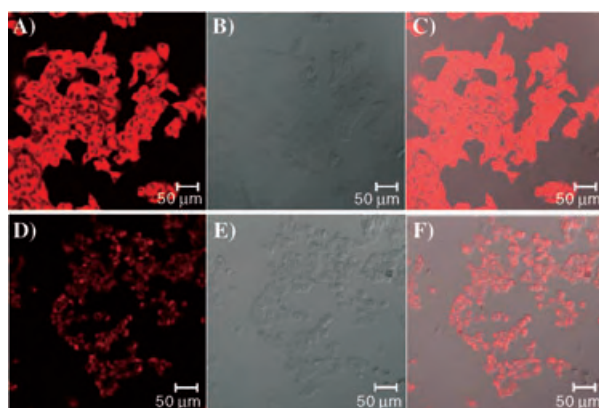


Figure 2. CLSM images of breast cancer cells after growth in media containing MNP-SiO₂(RITC)-PEG (A–C) or MNP-SiO₂(RITC) nanoparticles (D–F). (A and D: fluorescence images; B and E: bright-field images; C and F: overlay of the fluorescence and bright-field images).

growth in media containing MNP-SiO₂(RITC)-PEG (PEG-modified nanoparticle, Figure 2 A–C) and MNP-SiO₂(RITC) (unmodified, Figure 2 D–F). From the overlay images (Figure 2 C and F) of the fluorescence images (Figure 2 A and D) and bright-field images (Figure 2 B and E), respectively for both samples, it seems that the surface modification by PEG enhances the incorporation of Co ferrite MNP into cells. Thus all subsequent experiments were conducted using MNP-SiO₂(RITC)-PEG.

If dyes having different fluorescence emission wavelengths are used, the position of the nanoparticles containing different dyes could be selectively monitored simultaneously at the respective emission wavelength. The CLSM images in Figure 3 show breast cancer cells (MCF-7) containing MNP-SiO₂(RITC)-PEG or MNP-SiO₂(FITC)-PEG clearly emitting at different wavelengths, with orange light from RITC and green light from FITC. By changing the focus distances, CLSM could “slice” the cell images at different *z* positions to clearly show that emission did not emerge from the organic-dye-labeled core-shell MNPs adsorbed on the cell membrane surface, but from what was delivered into the cytoplasm of living cells. It was also confirmed that core-shell MNPs could not penetrate the nucleus as there was no emission from the nucleus (Figure 3 B and E).

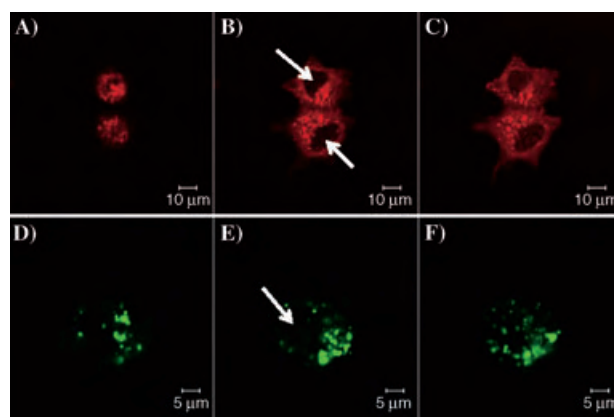


Figure 3. CLSM z-sectioned images of breast cancer cells obtained by using MNP-SiO₂(RITC)-PEG (A–C) and MNP-SiO₂(FITC)-PEG (D–F). (A and D: top slices; B and E: middle slices; C and F: bottom slices). The white arrows indicate the position of nucleus.

For the time-dependent studies of the uptake of MNP-SiO₂(RITC)-PEG nanoparticles by live MCF-7 cells, the cells were attached to a glass cover slip, a culture solution containing MNP-SiO₂(RITC)-PEG nanoparticles was loaded onto the cover slip and CLSM fluorescence images were taken every 5 minutes (Figure 4). As time elapsed, the

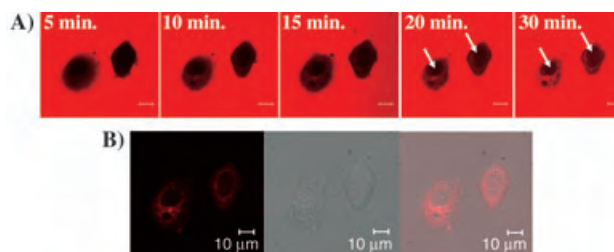


Figure 4. MCF-7 cells mixed with a culture of MNP-SiO₂(RITC)-PEG solution. Cells were recorded for 30 min with a video camera and up to 48 h by time-elapse photography. A) Representative pictures captured at 5 min intervals. As time elapsed, we could clearly determine the location of the nucleus (white arrow). B) After saturation with MNP-SiO₂(RITC)-PEG, the media was removed and the cell sample carefully washed. The CLSM measurements show fluorescent emissions only from the internalized MNP-SiO₂(RITC)-PEG nanoparticles. (left: fluorescence image; middle: bright-field image; right: merged image).

dark cytoplasm region in the cell faded and turned into an orange emissive region owing to the uptake of MNP-SiO₂(RITC)-PEG, and the position of the nucleus became clearly visible (Figure 4 A). The cell was saturated with dye-labeled core-shell nanoparticle within 30 min, and no significant intensity difference in the cytoplasm area nor emission from the nucleus region were detected during the next 48 h. After saturation, the culture solution containing the excess of MNP-SiO₂(RITC)-PEG nanoparticles was removed and the sample carefully washed with a new culture solution (that did not contain MNP-SiO₂(RITC)-PEG nanoparticles). Subsequent CLSM measurement of the sample showed that the fluorescent emissions came from the internalized MNP-

SiO₂(RITC)-PEG nanoparticles (Figure 4B); all the emission from the culture solution containing MNP-SiO₂(RITC)-PEG nanoparticles around the cells was removed. The internalization process seems to follow the mechanism of normal endocytosis, which allows the internalization of core-shell MNPs into various cells including mammalian lung normal cells (NL-20), lung cancer cells (A-549), and breast cancer cells (MCF-7). After they had been subjected to 24 h starvation, MCF-7, NL-20, and A-549 cells were treated with MNP-SiO₂(RITC or FITC)-PEG, and the cell viability was measured by a 3-(4,5-dimethylthiazol-2-yl)-2,5-diphenyltetrazolium bromide (MTT) assay. In this condition, the cell viability was maintained at greater than 90% in all groups indicating that the Co ferrite-silica core-shell MNPs, MNP-SiO₂(RITC or FITC)-PEG, do not show acute cytotoxicity at the level of a few tenths of a microgram (80 µg mL⁻¹) within 48 h.

Once we were convinced by fluorescence experiments and inductively coupled plasma atomic emission spectrometry (ICP-AES) measurements that a considerable quantity of the MNPs were incorporated into cells (uptake about 10⁵ nanoparticles per cell), we attempted to monitor the movement of cells containing MNPs under an external magnetic field (Figure 5)—this movement is anticipated to be an advantageous property of MNPs for real biological applications, such as cell separation and drug- or gene-delivery carrier.

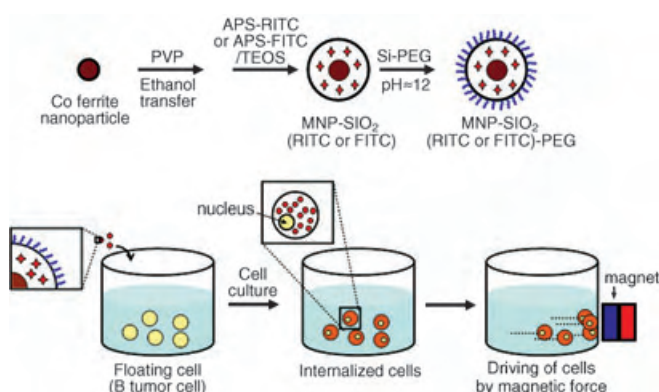


Figure 5. Schematic illustration of the overall synthetic procedure for MNP-SiO₂(RITC)-PEG and the movement of cells containing magnetic nanoparticles by an external magnetic force.

Microscope images in Figure 6 were captured every 0.2 s from the video camera focused in the area near the container wall (about 1 cm away) while an external magnetic field was applied with a commercial Nd-Fe-B magnet (≈ 0.3 Tesla) on the outside of the Petri dish (upper-left position in Figure 6), containing floating B tumor cells internalized with MNP-SiO₂(RITC)-PEG nanoparticles. As observed in the captured microscope images of Figure 6, B tumor cells that had sunk to the bottom of the Petri dish moved relatively slowly at a speed of approximately 0.2 mm s⁻¹, probably owing to interaction with the bottom surface. However, floating cells moved very fast at a speed of approximately 1.0 mm s⁻¹. When the external magnet was removed and reapplied to the outside of Petri dish, the movement of cells was halted and restarted

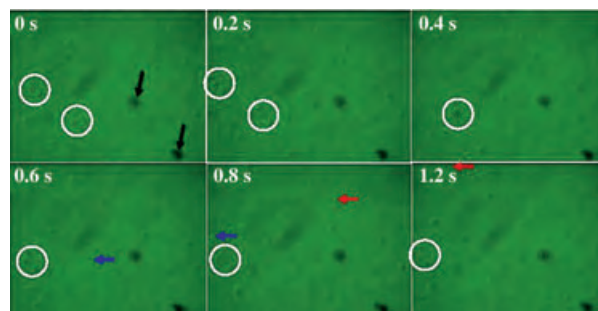


Figure 6. Optical microscope images of floating B tumor cells. Images were captured every 0.2 seconds (see video in Supporting Information). The external magnetic field direction is towards the upper-left corner, and B tumor cells that had sunk to the bottom of the dish moved relatively slowly to that direction (white circles), while floating B tumor cells moved much faster (blue and red arrows). The black arrows denote the standard direction of cell movements at the bottom surface of the dish.

again. Moving the position of external magnet could also easily change the direction of the cell movement. To our knowledge, this is the first clear observation of the “magnetic motor effect”: cell movement as a result of applying an external magnetic field to cells containing magnetic nanoparticles. Surprisingly, the speed of the cell movement is quite fast, confirming that the amount of internalized MNPs in our system was sufficiently high to show a magnetic motor effect while not causing any cytotoxicity.

In summary, the organic-dye-labeled Co ferrite-silica (core-shell) magnetic nanoparticles have been prepared by a modified polyvinylpyrrolidone (PVP) method and the sol-gel process. The thickness of the silica shell could be easily controlled by adjusting the ratio of magnetic nanoparticle to tetraethoxysilane (TEOS) and dye-modified silane. Core-shell magnetic nanoparticles could also be labeled with two different organic dyes, such as rhodamine B isothiocyanate (RITC) and fluorescent isothiocyanate (FITC), and the nanoparticle surface could be modified with bio-inert poly(ethylene glycol) (PEG) groups, providing multifunctional magnetic and optical properties along with biocompatibility. We investigated the internalization efficiencies of MNP-SiO₂(RITC or FITC), and MNP-SiO₂(RITC or FITC)-PEG in various in vitro cell studies and clearly observed the external magnetic motor effect on floating cells internalized with MNPs. These basic results on core-shell MNPs are expected to lead to applications in cell separation, biological labeling and detection, and drug and gene delivery.

Experimental Section

FeCl₃·6H₂O, CoCl₂·6H₂O, and Fe(NO₃)₃·9H₂O (Sigma-Aldrich), RITC and FITC organic dyes (Fluka), APS, TEOS, and PEG-Si(OMe)₃ (Gelest) were used without further purification.

MNP-SiO₂(RITC or FITC)-PEG: Cobalt ferrite solution (34.7 mL, 20 mg MNP mL⁻¹ solution in water) was added to polyvinylpyrrolidone solution (PVP; 0.65 mL; *M*_n 55,000 Da, 25.6 g L⁻¹ in H₂O), and the mixture was stirred for 1 day at room temperature. The PVP-stabilized cobalt ferrite nanoparticles were separated by addition of aqueous acetone (H₂O/acetone = 1/10, v/v) and centrifugation at 4000 rpm for 10 min. The supernatant solution was removed, and

the precipitated particles were redispersed in ethanol (10 mL). Multigram-scale preparation of PVP-stabilized cobalt ferrite nanoparticles was easily reproduced in this modified synthetic method. Trimethoxysilane modified by rhodamine B isothiocyanate (RITC) was prepared from 3-aminopropyltriethoxysilane (APS) and rhodamine B isothiocyanate under nitrogen using a standard Schlenk line technique.^[10,15] A mixed solution of TEOS and RITC-modified trimethoxysilane (TEOS/RITC-silane molar ratio = 0.3/0.04) was injected into the ethanol solution of PVP-stabilized cobalt ferrite. Polymerization initiated by adding ammonia solution (0.86 mL; 30 wt % by NH_3) as a catalyst produced cobalt ferrite-silica core-shell nanoparticles containing organic dye. These nanoparticles were dispersed in ethanol and precipitated by ultra-centrifugation (18000 rpm, 30 min). The purified core-shell nanoparticles (45 mg) were redispersed in absolute ethanol (10 mL) and then treated with 2-[methoxy(polyethyleneoxy)propyl]trimethoxysilane (PEG-Si(OMe)₃; 125 mg, 0.02 mmol), $\text{CH}_3\text{O}(\text{CH}_2\text{CH}_2\text{O})_{6-9}\text{CH}_2\text{CH}_2\text{CH}_2\text{Si}(\text{OCH}_3)_3$, at pH \approx 12 (adjusted with NH_4OH). The resulting MNP-SiO₂(RITC)-PEG was washed and centrifuged in EtOH several times and characterized by IR spectroscopy (C-H stretching band at 2800–2900 cm^{-1}). MNP-SiO₂(FITC)-PEG could also be prepared by a similar method by using FITC-silane instead of RITC-silane. All the prepared nanoparticles were characterized by TEM, FT-IR, UV/Vis absorption and emission spectroscopy, and vibrating sample magnetometer (VSM) measurements.

Cell culture: Breast cancer cells (mammary gland adenocarcinoma, MCF-7), normal human bronchial epithelial cells (NL-20), and lung cancer cells (A-549) were from American Type Culture Collection. MCF-7 cells were grown in DMEM (Cambrex Bio Science) containing 10% FBS (v/v) and MNP-SiO₂(RITC or FITC)-PEG (40 μL , 2 mg mL^{-1}). NL-20 and A-549 were grown in RPMI (Cambrex Bio Science) under the same conditions. All cells were cultured in Lab-Tek glass chamber slides (Nalge Nunc International) to facilitate fluorescence emission by confocal laser scanning microscopy (CLSM).

MTT assay: The cells were incubated in a 96-well plate. At the end of the incubation period, 3-(4,5-dimethylthiazol-2-yl)-2,5-diphenyltetrazolium bromide (MTT; 50 μL , Sigma-Aldrich) in pH = 7.2 phosphate buffered saline (PBS; 0.2 mg mL^{-1}) was added to each well (final concentration of 0.4 mg mL^{-1}) and cultures were incubated in 5% CO_2 for 4 h at 37°C. Then the culture medium was carefully removed by pipetting, and the formazan crystals generated by dehydronase activity in mitochondria, which only occurs in living cells, were dissolved in DMSO (150 μL) for analysis. After 10 min agitation on a shaker, absorbance was measured at 490 nm and 620 nm for test and reference solutions, respectively.

CLSM: 3D image reconstructions of organic-dye-labeled nanoparticles were obtained with a Zeiss LSM 510 CLSM equipped with a computer-controlled scan stage. An argon laser for RITC excitation at 543 nm (488 nm for FITC) was used for imaging. For each cell, more than 10 optical planes were scanned by changing the focal length to detect the nanoparticles at different locations within the cell. In experiments involving live cells, an exclusive culture chamber was used to maintain a cell culture temperature of 37°C.

Determination of the quantity of nanoparticles in cells: The total number of cells in the magnetic motor experiment (Figure 6) was estimated to be 4.0×10^5 by using a hemacytometer chamber. ICP-AES measurement, after the cells containing nanoparticles were destroyed and nanoparticles were completely dissolved with concentrated HCl, reveals the quantity of cobalt ion in each cell to be approximately 10^{-13} mmol. From calculation, each 9-nm CoFe_2O_4 nanoparticle contains about 10^{-18} mmol of Co ions. Therefore, the number of magnetic nanoparticles in each cell in our magnetic motor effect experiments can be estimated to be of the order of 10^5 .

Keywords: bioinorganic chemistry · fluorescent probes · hybrid materials · magnetic properties · nanotechnology

- [1] K. Furumura, H. Sugi, Y. Murakami, H. Asai, US patent 4598914, **1986**.
- [2] J. A. King, US patent 4,017,694, **1977**.
- [3] a) D. H. Han, H. L. Luo, Z. Yang, *J. Magn. Magn. Mater.* **1996**, *161*, 376–378; b) H. Fujiwara, *J. Appl. Phys.* **1993**, *73*, 5757–5762.
- [4] a) Q. Song, Z. J. Zhang, *J. Am. Chem. Soc.* **2004**, *126*, 6164–6168; b) H. Zeng, J. Li, J. P. Liu, Z. L. Wang, S. Sun, *Nature* **2002**, *420*, 395–398; c) C. Liu, B. Zou, A. J. Rondinone, Z. J. Zhang, *J. Am. Chem. Soc.* **2000**, *122*, 6263–6267.
- [5] a) J. M. Perez, L. Josephson, T. O'Loughlin, D. Högemann, R. Weissleder, *Nat. Biotechnol.* **2002**, *20*, 816–820; b) J. M. Perez, T. O'Loughlin, F. J. Simeone, R. Weissleber, L. Josephson, *J. Am. Chem. Soc.* **2002**, *124*, 2856–2857; c) L. Babes, B. Denizot, G. Tanguy, J. J. L. Jeune, P. Jallet, *J. Colloid Interface Sci.* **1999**, *212*, 474–482.
- [6] T. J. Yoon, W. Lee, Y. S. Oh, J. K. Lee, *New J. Chem.* **2003**, *27*, 227–229.
- [7] a) P. S. Doyle, J. Bibette, A. Bancaud, J. Viovy, *Science* **2002**, *295*, 2237; b) H. Gu, P. Ho, K. W. T. Tsang, L. Wang, B. Xu, *J. Am. Chem. Soc.* **2003**, *125*, 15702–15703; c) D. Wang, J. He, N. Rosenzweig, Z. Rosenzweig, *Nano Lett.* **2004**, *4*, 409–413.
- [8] a) D. Cao, P. He, N. Hu, *Analyst* **2003**, *128*, 1268–1274; b) T. Mirzabekov, H. Kontos, M. Farzan, W. Marasco, J. Sodroski, *Nat. Biotechnol.* **2000**, *18*, 649–654; c) J. P. Chen, W. S. Lin, *Enzyme Microb. Technol.* **2003**, *32*, 801–811; d) K. Nishimura, M. Hasegawa, Y. Ogura, T. Nishi, K. Kataoka, H. Handa, M. Abe, *J. Appl. Phys.* **2002**, *91*, 8555–8556; e) I. Willner, E. Katz, *Angew. Chem. Int. Ed.* **2003**, *42*, 4576–4588.
- [9] a) E. X. Wu, H. Tang, K. K. Wong, J. Wang, *J. Magn. Reson. Imaging* **2004**, *19*, 50–58; b) J. M. Perez, L. Josephson, R. Weissleder, *ChemBioChem* **2004**, *5*, 261–264.
- [10] Y. Lu, Y. Yin, B. T. Mayers, Y. Xia, *Nano Lett.* **2002**, *2*, 183–186.
- [11] M. A. Correa-Duarte, M. Giersig, N. A. Kotov, L. M. Liz-Marzán, *Langmuir* **1998**, *14*, 6430–6435.
- [12] a) A. Kros, M. Gerritsen, V. S. I. Sprakel, N. A. J. M. Sommerdijk, J. A. Jansen, R. J. M. Nolte, *Sens. Actuators B* **2001**, *81*, 68–75; b) Y. Shchipunov, *J. Colloid Interface Sci.* **2003**, *268*, 68–76.
- [13] a) C. Graf, D. L. J. Vossen, A. Imhof, A. van Blaaderen, *Langmuir* **2003**, *19*, 6693–6700.
- [14] a) D. Zins, V. Cabuil, R. Massart, *J. Mol. Liq.* **1999**, *83*, 217–232; b) M. H. Sousa, F. A. Tourinho, J. Depeyrot, G. J. da Silva, M. C. F. L. Lara, *J. Phys. Chem. B* **2001**, *105*, 1168–1175.
- [15] a) N. A. M. Verhaegh, A. van Blaaderen, *Langmuir* **1994**, *10*, 1427–1438; b) A. van Blaaderen, V. Vrij, *Langmuir* **1992**, *8*, 2921–2931.
- [16] a) S. Santra, P. Zhang, K. Wang, R. Tapeç, W. Tan, *Anal. Chem.* **2001**, *73*, 4988–4993; b) K. P. McNamara, Z. Rosenzweig, *Anal. Chem.* **1998**, *70*, 4853–4859.

Received: September 7, 2004

Published online: January 5, 2005

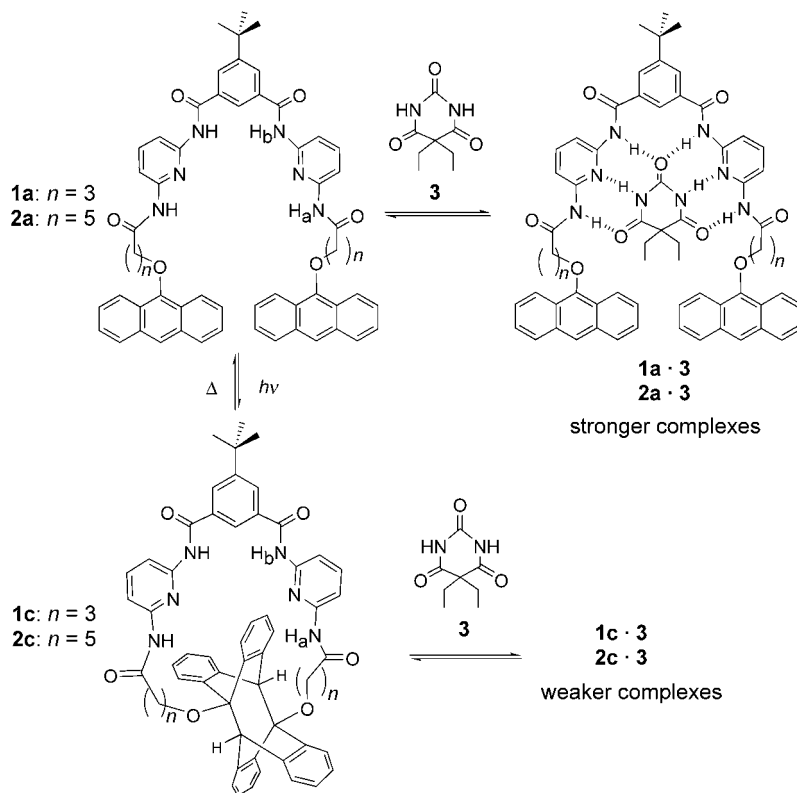
Photorelease of an Organic Molecule in Solution: Light-Triggered Blockage of a Hydrogen-Bonding Receptor Site**

Yann Molard, Dario M. Bassani, Jean-Pierre Desvergne,* Peter N. Horton, Michael B. Hursthouse, and James H. R. Tucker*

The selective recognition of a guest by a molecular host is a fundamental process whose understanding has led to the design of systems that are capable of controlled associative/dissociative behavior.^[1] Such systems rely on an external physical or chemical stimulus to modulate reversible intermolecular forces that are responsible for the association of two or more species, and they are ubiquitous to all living organisms, wherein they play a vital role in complex signal-transmission, regulation, and amplification processes. There are now several examples of receptor molecules that contain photoresponsive units for which the strength of a binding interaction with a particular guest species in solution can be controlled by light.^[2] The vast majority of these receptors rely on a photochromic auxiliary to impart a light-induced structural modification of a crown-ether-like cavity. Although the flexibility of the crown ether units facilitates the modulation of their binding properties, such systems have so far been focused on the binding of metal ions, whereas reports of photoresponsive receptors that bind organic species through multiple hydrogen-bonding interactions are rare.^[2c,3]

Herein, we demonstrate how light controls the binding affinity of a hydrogen-bonding receptor towards a neutral organic molecule to such an extent that the bound guest (barbital) is effectively released upon photoirradiation.

Receptors **1a** and **2a** (Scheme 1; **a** denotes acyclic) were synthesized through a five-step reaction pathway starting from anthrone and were fully characterized (see Supporting Information).^[4] Each receptor was designed to contain two



Scheme 1. Receptors **1a** and **2a** bind barbital (**3**) strongly in solution; photoirradiation of the receptors gives the macrocycles **1c** and **2c**, which are weaker binders of **3**.

pyridine-2,6-diamide units connected by a phenyl spacer group to generate a motif that has been shown to bind barbital (**3**) strongly in chlorinated solvents through six complementary hydrogen bonds.^[5] The binding site was connected by an alkyl spacer group of variable length to two anthracene units, which were expected to undergo the well-characterized and thermally reversible $4\pi+4\pi$ photocycloaddition reaction through an intramolecular pathway^[6] to result in a change in the structure of the receptor from acyclic to macrocyclic. Anthracene photodimerization is particularly versatile as it can proceed smoothly in a range of solvents.^[6a]

As expected, both receptors **1a** and **2a** bound barbital strongly in chlorinated organic solvents to give complexes of 1:1 stoichiometry as determined by ^1H NMR spectroscopy. The addition of one equivalent of **3** to a solution of **1a** in CDCl_3 (8.5 mM) induced downfield shifts in the two signals that correspond to the four NH protons of the receptor (from $\delta = 8.04$ to 9.62 ppm for H_a ; from $\delta = 8.40$ to 9.88 ppm for H_b). The addition of further amounts of **3** brought about no further significant changes to the spectrum which indicates the

[*] Dr. D. M. Bassani, Dr. J.-P. Desvergne
Laboratoire de Chimie Organique et Organométallique
Université Bordeaux I
351, Cours de la Libération, 33405 Talence (France)
Fax: (+33) 5-4000-6994
E-mail: jp.desvergne@lcoo.u-bordeaux1.fr

Dr. Y. Molard, Dr. J. H. R. Tucker
Department of Chemistry
University of Exeter
Stocker Road, Exeter EX44QD (UK)
Fax: (+44) 1392-263-434
E-mail: j.h.r.tucker@ex.ac.uk

Dr. P. N. Horton, Prof. M. B. Hursthouse
EPSRC National Crystallography Service
School of Chemistry, University of Southampton
Highfield, Southampton SO171BJ (UK)

[**] Financial support for this work was provided by the EPSRC (GR/S07438/01 to Y.M.)

Supporting information for this article is available on the WWW under <http://www.angewandte.org> or from the author.

formation of a strongly bound 1:1 complex. As shown in Figure 1, the addition of **3** to a solution of **2a** in CH₂Cl₂ (2.15×10^{-5} M) did not affect the anthracene ¹L_a absorption band (300–400 nm) in the UV/Vis spectrum of the receptor,^[2b] but

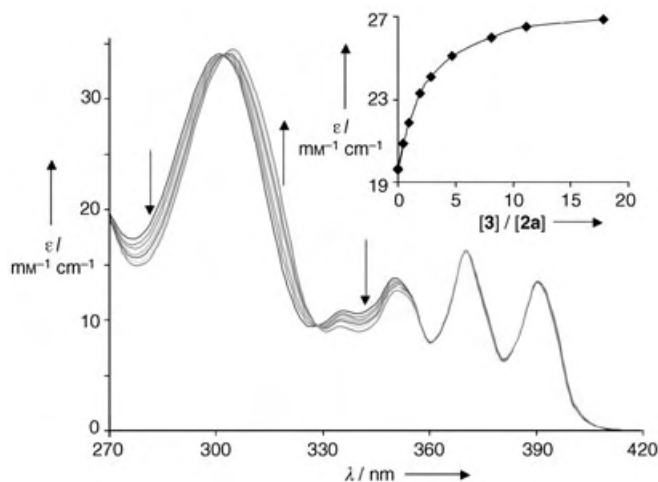


Figure 1. The binding of **3** by receptor **2a** as followed by UV/Vis spectroscopy; [**2a**] = 2.15×10^{-5} M with additions of 0, 0.5, 1, 2, 3, 5, and 8 equivalents of **3**. The inset shows the increase in the observed molar absorption coefficient (ϵ) at $\lambda = 315$ nm upon addition of **3**.

induced a bathochromic shift in the pyridine band (from $\lambda_{\text{max}} = 298$ to 304 nm) which reflects a bonding interaction between the guest and both pyridine units.^[7] The binding constants $K = [\text{complex}]/[\text{host}] \times [\text{3}]$ (host = **1a** or **2a**) were determined for each receptor by using the Letagrop program.^[8] The values (Table 1) are in the same range as those for previously described acyclic barbiturate receptors in chlorinated solvents.^[5a,c]

Table 1: Binding constants for the complexation of barbitol (**3**) by the receptors in their acyclic (**1a** and **2a**) and macrocyclic forms (**1c** and **2c**).

Receptor	$K [\text{M}^{-1}]$	
	Acyclic form (a)	Cyclic form (c)
1	$38\,000 \pm 2500^{[a]}$	$38 \pm 6^{[b]}$
2	$27\,000 \pm 3000^{[a]}$	$8320 \pm 575^{[a]}$

[a] Determined by UV/Vis spectroscopy measurements in CH₂Cl₂, receptor concentration $\approx 2 \times 10^{-5}$ M. [b] Determined by ¹H NMR spectroscopy measurements in CD₂Cl₂, receptor concentration = 1.7×10^{-3} M.

Continued irradiation (Hg lamp, lead filter) of solutions of **1a** and **2a** (5×10^{-4} M) in degassed dichloromethane during five hours resulted in the disappearance of the ¹L_a anthracene band in the absorption spectra of the receptors. Upon removal of the solvent, the photodimers **1c** and **2c** (Scheme 1, **c** denotes cyclic) were isolated as air-stable solids in essentially quantitative yield according to the ¹H NMR spectra of **2a** in CDCl₃ before and after photoirradiation (Figure 2, see Supporting Information for ¹H NMR spectra of **1a** and **1c**). The new signal at $\delta = 4.43$ ppm (Figure 2b) corresponds to the two bridgehead protons on the photodimer subunit and

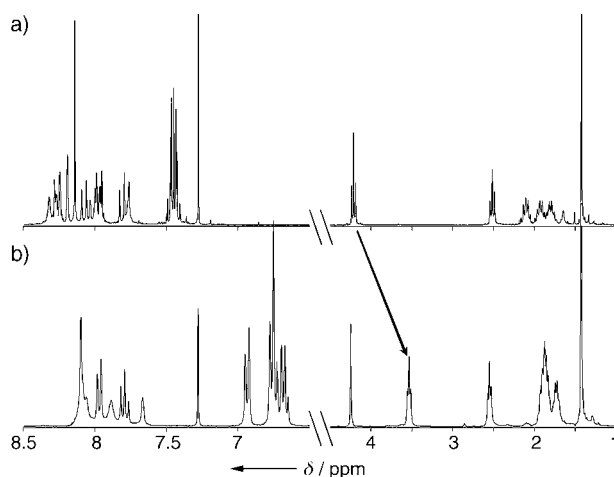


Figure 2. ¹H NMR spectra of **2a** in CDCl₃ before and after photoirradiation: a) initial spectrum of **2a** and b) spectrum after 5 h (compound **2c**).

confirms the $4\pi+4\pi$ photocycloaddition reaction between the central rings on each anthracene unit.^[2b] A close inspection of the ¹H NMR spectral pattern for the aromatic resonances of **1c** and **2c** suggests a head-to-tail (HT) structure rather than the anticipated head-to-head (HH) structure.^[9] This was confirmed by X-ray diffraction studies of crystals of **1c** and **2c**, which were grown from CDCl₃ and THF/hexane, respectively (Figure 3).^[10] A plausible explanation is the much lower

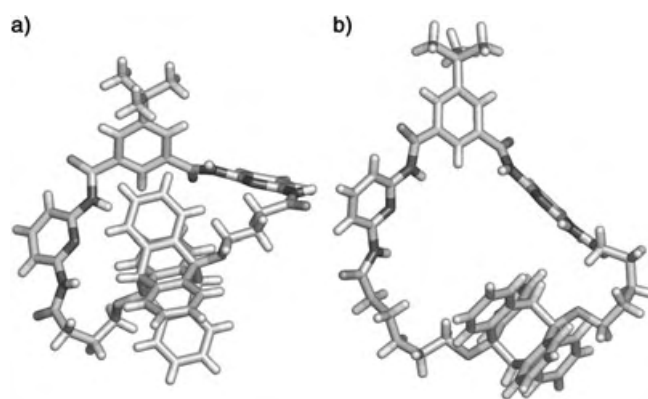


Figure 3. Representations of the head-to-tail structures of a) **1c** (tri-clinic, space group $P\bar{1}$) and b) **2c** (monoclinic, space group $C2/c$) obtained by X-ray crystallography. Solvent molecules (CDCl₃ for **1c** and THF for **2c**) have been omitted for clarity.

thermal stability of 9-alkoxy-substituted anthracene HH photodimers,^[6b] which, if formed, would be expected to undergo a relatively rapid thermal retrocyclization reaction to yield the starting materials. In the case of **1c** (Figure 3a), the size and shape of the binding cavity are strongly affected by the four bulky *ortho*-xylene units of the photodimer. Furthermore, one of the four N–H bonds points away from the cavity. In **2c** (Figure 3b), although all six hydrogen-bonding groups point inwards, the binding site is distinctly

nonplanar with an angle of $77.5(2)^\circ$ between the pyridine planes.

Preliminary studies revealed that **1c** and **2c** are fairly stable at room temperature (as usually observed for HT anthracene photodimers^[6b]), but can be switched back to the starting materials (open form) upon gentle heating (e.g., after heating a solution of **1c** in toluene at $\approx 80^\circ\text{C}$ for two days, $\geq 90\%$ of the starting material **1a** was regenerated).

To assess the photoswitched binding behavior of these systems, the binding of barbital by the two photoproducts was evaluated by ^1H NMR spectroscopy (**1c**) and by UV/Vis spectroscopy (**2c**). It was immediately apparent that the binding between **3** and **1c** was much weaker than with its acyclic counterpart because in contrast to **1a**, a large excess of guest was required to bring about significant changes to the NMR spectra. Figure 4 depicts the aromatic and aliphatic

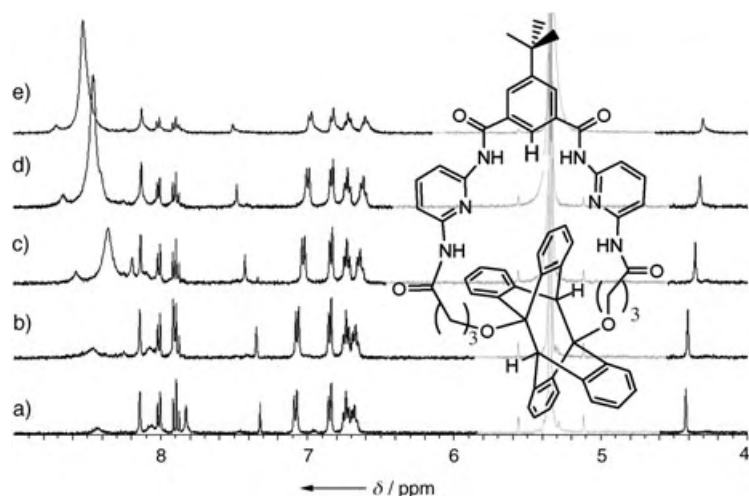


Figure 4. Evolution of the ^1H NMR spectrum of **1c** in CD_2Cl_2 upon addition of **3**. [**1c**] = $1.7 \times 10^{-3} \text{ M}$ and remains constant during the titration. a) **1c**, b) [**3**]/[**1c**] = 1, c) [**3**]/[**1c**] = 6, d) [**3**]/[**1c**] = 11, and e) [**3**]/[**1c**] = 15.

regions of the ^1H NMR spectra of **1c** in CD_2Cl_2 (1.7 mm) in the presence of increasing amounts of **3**. Upon the addition of 15 equivalents of barbital, changes were observed in the signals for the protons of the photoadduct: the bridgehead protons moved upfield from $\delta = 4.42$ to 4.29 ppm , the proton at C-2 of the isophthaloyl group shifted from $\delta = 7.32$ to 7.52 ppm , and the amide protons H_a and H_b (see Scheme 1) underwent relatively small downfield shifts (H_a : from $\delta = 7.82$ to 8.56 ppm), which is consistent with a weak hydrogen-bonding interaction. The binding constant for a 1:1 complex was calculated from the chemical shift values for proton H_a by using the EQNMR program.^[11] The value obtained ($K = 38 \text{ M}^{-1}$, Table 1) confirms that photodimerization of **1a** dramatically affects the ability of **1c** to form a strong complex with barbital, with an approximately 1000-fold decrease observed in the binding constant. An explanation for this change can be obtained from the X-ray crystal structure of **1c** (Figure 3a), which clearly shows that it is impossible for the receptor to accommodate barbital within its cavity. Instead, it

is likely that, at any one time, only one side of the guest is weakly bound by one pyridinediamide unit, whereas the other unit is blocked by the photoadduct. The value of the binding constant is, in fact, lower than those obtained for unhindered three-point hydrogen-bonding interactions with the pyridine-2,6-diamide motif in chlorinated solvents.^[12]

As found for the **1a/1c** system, photodimerization of **2a** into **2c** lowers the binding constant with barbital (Table 1), but the decrease is less significant at approximately threefold, with $K_{(2a)}/K_{(2c)} = 3.3 \pm 0.6$. From the crystal structure of **2c** (Figure 3b), it is clear that the longer spacer unit prevents the photoadduct from blocking the cavity and enables the guest to be stabilized by six hydrogen bonds. This was borne out by the ^1H NMR spectra in CDCl_3 which indicated relatively large shifts of the signals for the protons H_a and H_b upon addition of approximately one equivalent of barbital (from $\delta = 7.88$ and 8.05 ppm to 9.23 and 9.61 ppm , respectively). The presence of **3** also has a strong influence on the excited-state behavior of **1a** and **2a**. In particular, the observed decrease in the quantum yield for photodimerization (0.07 and 0.07 versus 0.01 and 0.05 for the formation of **1c** and **2c** in the absence and presence of **3**, respectively) probably reflects a lowered photoreactivity of the complexes **1a·3** and **2a·3**.

Finally, a photoirradiation experiment was performed on the **1a/1c** system in the presence of barbital to examine whether photoswitched binding could be observed in situ. A solution of **1a** in CD_2Cl_2 ($5 \times 10^{-4} \text{ M}$) which contained 0.95 equivalents of **3** (to ensure that the guest was fully complexed) was continuously irradiated and monitored by ^1H NMR spectroscopy over time (see Supporting Information). The study revealed that the signal for the proton of the imide group of barbital shifted upfield from $\delta = 12.16 \text{ ppm}$ (before irradiation) to $\delta = 9.79 \text{ ppm}$ (after 3 h irradiation). At the same time, the signals for the receptor changed from those of almost fully complexed **1a** (H_a and H_b signals at $\delta = 9.20$ and 9.47 ppm respectively) to those of essentially uncomplexed **1c** (H_a and H_b signals at $\delta = 7.82$ and 8.41 ppm , respectively; signal for the proton at C-2 of the isophthaloyl group at $\delta = 7.31 \text{ ppm}$). These observations are consistent with the ejection of the guest from the receptor upon photodimerization [Eq. (1)].



In conclusion, these studies have shown how light can be used to control both the binding and the in situ release of a neutral guest molecule through structural changes to a hydrogen-bonding receptor. The latter, designed to bind barbital and other biologically relevant molecules such as urea derivatives, offers the possibility to photoregulate the release of such species in a reversible manner.

Received: September 10, 2004

Revised: October 13, 2004

Published online: January 11, 2005

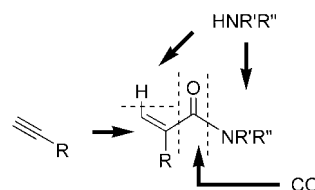
Keywords: host–guest systems · molecular devices · molecular recognition · photochemistry · supramolecular chemistry

- [1] a) J.-M. Lehn, *Supramolecular Chemistry, Concepts and Perspectives*, VCH, Weinheim, **1995**; b) G. Cooke, *Angew. Chem.* **2003**, *115*, 5008; *Angew. Chem. Int. Ed.* **2003**, *42*, 4860.
- [2] For examples and reviews of photochemically controlled host-guest systems, see: a) K. Kimura, H. Sakamoto, M. Nakamura, *Bull. Chem. Soc. Jpn.* **2003**, *76*, 225; b) G. McSkimming, J. H. R. Tucker, H. Bouas-Laurent, J.-P. Desvergne, S. J. Coles, M. B. Hursthouse, M. E. Light, *Chem. Eur. J.* **2002**, *8*, 3331, and references therein; c) A. Bacchi, M. Carcelli, C. Pelizzi, G. Pelizzi, P. Pelagatti, D. Rogolino, M. Tegoni, C. Viappiani, *Inorg. Chem.* **2003**, *42*, 5871, and references therein; d) For cyclodextrin systems, see: A. Mulder, A. Jukovic, J. Huskens, D. N. Reinhoudt, *Org. Biomol. Chem.* **2004**, *2*, 1748, and references therein; e) For a hydrogen-bonding system that binds an organic cation, see: C. A. Hunter, M. Togrul, S. Tomas, *Chem. Commun.* **2004**, 108.
- [3] For examples of related photochemically controlled processes that involve hydrogen bonding, see: a) S. Yagai, T. Nakajima, T. Karatsu, K. Saitow, A. Kitamura, *J. Am. Chem. Soc.* **2004**, *126*, 11500; b) Y. Vida Pol, R. Suau, E. Perez-Inestrosa, D. M. Bassani, *Chem. Commun.* **2004**, 1270, and references therein; c) L. N. Lucas, J. van Esch, R. M. Kellogg, B. L. Feringa, *Chem. Commun.* **2001**, 759; d) M. S. Vollmer, T. D. Clark, C. Steinem, M. R. Ghadiri, *Angew. Chem.* **1999**, *111*, 1703; *Angew. Chem. Int. Ed.* **1999**, *38*, 1598; e) F. Würther, J. Rebek, Jr., *Angew. Chem.* **1995**, *107*, 503; *Angew. Chem. Int. Ed. Engl.* **1995**, *34*, 446; f) M. Irie, O. Miyatake, K. Uchida, T. Eriguchi, *J. Am. Chem. Soc.* **1994**, *116*, 9894.
- [4] **1a**: FAB-MS: m/z calcd for $C_{58}H_{53}N_6O_6$: 929.4027 [$M^+ + H$]; found: 929.4015; elemental analysis calcd (%) for $C_{58}H_{52}N_6O_6 \cdot 0.5 H_2O$: C 74.26, H 5.69, N 8.96; found: C 74.44, H 5.65, N 8.88. **2a**: FAB-MS: m/z calcd for $C_{62}H_{61}N_6O_6$: 985.4653 [$M^+ + H$]; found: 985.4659; elemental analysis calcd (%) for $C_{62}H_{60}N_6O_6 \cdot 0.5 H_2O$: C 74.90, H 6.18, N 8.45; found: C 74.95, H 6.14, N 8.35.
- [5] a) S.-K. Chang, A. D. Hamilton, *J. Am. Chem. Soc.* **1988**, *110*, 1318; b) S.-K. Chang, D. Van Engen, E. Fan, A. D. Hamilton, *J. Am. Chem. Soc.* **1991**, *113*, 7640; c) I. Aoki, T. Harada, T. Sakaki, Y. Kawahara, S. Shinkai, *J. Chem. Soc. Chem. Commun.* **1992**, 1341; d) I. Aoki, Y. Kawahara, T. Sakaki, T. Harada, S. Shinkai, *Bull. Chem. Soc. Jpn.* **1993**, *66*, 927.
- [6] a) H. Bouas-Laurent, A. Castellan, J.-P. Desvergne, R. Lapouyade, *Chem. Soc. Rev.* **2000**, *29*, 43; b) H. Bouas-Laurent, A. Castellan, J.-P. Desvergne, R. Lapouyade, *Chem. Soc. Rev.* **2001**, *30*, 248.
- [7] Preliminary studies indicate that complexation leads to a quenching of the fluorescence emission from both receptors which is possibly a result of conformational changes.
- [8] a) L. G. Sillen, B. Warnqvist, *Ark. Kemi* **1968**, *31*, 377; b) L. G. Sillen, B. Warnqvist, *Ark. Kemi* **1968**, *31*, 315.
- [9] a) H. D. Becker, *Chem. Rev.* **1993**, *93*, 145; b) H.-D. Becker, V. Langer, *J. Org. Chem.* **1993**, *58*, 4703.
- [10] CCDC-249540 and CCDC-249539 (**1c** and **2c**, respectively) contain the supplementary crystallographic data for this paper. These data can be obtained free of charge from The Cambridge Crystallographic Data Centre via www.ccdc.cam.ac.uk/data_request/cif.
- [11] M. J. Hynes, *J. Chem. Soc. Dalton Trans.* **1993**, 311.
- [12] A. D. Hamilton, D. Van Engen, *J. Am. Chem. Soc.* **1987**, *109*, 5035.

Alkyne Carbonylation by Radicals: Tin-Radical-Catalyzed Synthesis of α -Methylene Amides from 1-Alkynes, Carbon Monoxide, and Amines**

Yoshitaka Uenoyama, Takahide Fukuyama,
Osamu Nobuta, Hiroshi Matsubara, and Ilhyong Ryu*

Radical reactions have become an important tool in organic synthesis.^[1] Radical carbonylation is a useful method for the preparation of a variety of carbonyl compounds.^[2] We previously reported that acyl-radical cyclization onto an imine nitrogen atom provides a useful route to lactam rings.^[3] We also recently found that intramolecular trapping of an α -ketenyl radical by an amino group leads to the formation of cyclic amides.^[4] Acrylamides and derivatives thereof are employed in a wide range of organic reactions, which include nucleophilic additions, cycloaddition reactions, and radical reactions, to name just a few.^[5] They are also extensively used in the synthesis of polymeric materials.^[6] The goal of this work was to develop a novel synthesis of acrylamide derivatives by taking advantage of a hybrid radical/ionic reaction involving the radical carbonylation of alkynes and subsequent ionic trapping of the resulting carbonyl-containing radical species by amines (Scheme 1).^[7,8]



Scheme 1. A convergent synthesis of 2-substituted acrylamides.

Thus, when 1-octyne was treated with propylamine (50 molequiv) and pressurized CO (85 atm) in the presence of 30 mol % tributyltin hydride and 20 mol % 2,2'-azobisisobutyronitrile (AIBN), the reaction proceeded smoothly [Eq. (1)]. *N*-Propyl-2-hexylacrylamide (**3a**) was obtained in 82 % yield after isolation by flash chromatography on silica gel with EtOAc as eluent. α -Stannylmethylene amide **4a**

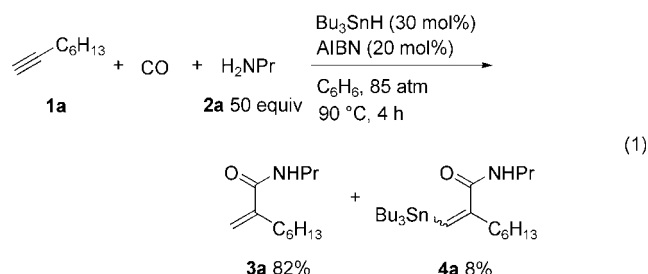
[*] Y. Uenoyama, Dr. T. Fukuyama, O. Nobuta, Dr. H. Matsubara, Prof. I. Ryu
Department of Chemistry
Faculty of Arts and Sciences
Osaka Prefecture University
Sakai, Osaka 599-8531 (Japan)
Fax: (+81) 72-254-9695
E-mail: ryu@ms.cias.osakafu-u.ac.jp

[**] This work was supported by Grant-in-Aid for Scientific Research (B) from JSPS. Technical support of Library & Science Information Center, Osaka Prefecture University for the computational study is gratefully acknowledged.



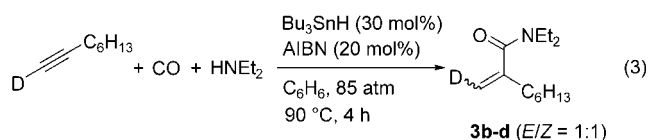
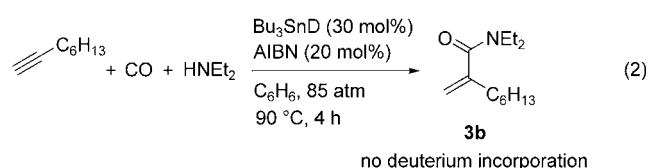
Supporting information for this article is available on the WWW under <http://www.angewandte.org> or from the author.

(8%), formed as a byproduct, can be converted to **3a** by protodestannylation with MeOH and Me₃SiCl (room temperature, 10 min). The amount of tributyltin hydride can be reduced to 20 mol%, which gave 75% yield of **3a**, whereas with 10 mol% of tributyltin hydride chain propagation is not so sufficient and the yield of **3a** decreased to 49%. We also tested PhSH instead of Bu₃SnH, but the reaction gave a complex mixture containing **3a** in only low yield.



A variety of primary and secondary amines were examined for use in this reaction, and all proved to work well (Table 1). Terminal alkynes with hydroxy, chloro, phenylsulfide, acetoxy, and benzyloxy functionalities can be efficiently carbonylated to give the corresponding α -methylene amides in good to excellent yields (entries 3–9). The carbonylation of phenylacetylene (**1i**) in the presence of pyrrolidine gave the corresponding amide **3j**, albeit in rather modest yield (entry 10). In the case of substrate **1j** with two alkynyl moieties, the reaction proceeded chemoselectively on the terminal alkyne to provide the corresponding amide **3k** (entry 11).

To obtain some insight into the reaction mechanism, we conducted labeling experiments with tributyltin deuteride [Eq. (2)] and 1-deuterated 1-octyne [Eq. (3)]. Deuterium incorporation was not observed in the first case, but it was detected in the second case, which is consistent with a scenario in which an amine hydrogen atom is transferred to the vinylic position of the product.



A tin-radical-catalyzed hybrid radical/ionic mechanism is proposed in Scheme 2. Addition of tributyltin radical to the alkyne terminus generates a vinyl radical, which then undergoes carbonylation to generate an α -ketenyl radical. Inter-molecular trapping of the α -ketenyl radical by amines affords

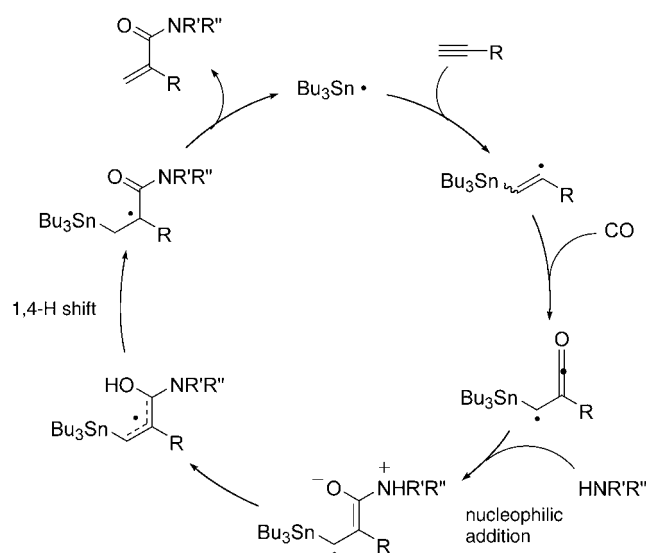
Table 1: Synthesis of α -methylene amides by tin-radical-catalyzed carbonylation of 1-alkynes.^[a,b]

$ \begin{array}{c} \text{R-C}\equiv\text{C}\text{H} + \text{CO} + \text{HNR}'\text{R}'' \xrightarrow[\text{C}_6\text{H}_6, 85 \text{ atm}, 90^\circ\text{C}, 4 \text{ h}]{\text{Bu}_3\text{SnH (30 mol\%)} \\ \text{AIBN (20 mol\%)}} \\ \text{O}=\text{C}(\text{NR}'\text{R}'')\text{C}(\text{R})\text{CH}_2 \\ \text{1} \quad \quad \quad \text{2} \quad \quad \quad \text{3} \end{array} $				
Entry	Alkyne	Amine	Product	Yield [%] ^[c]
1		H ₂ NPr		82
	1a	2a	3a	
2		HNEt ₂		75
	1a	2b	3b	
3		HNEt ₂		74
	1b	2b	3c	
4		HNEt ₂		76
	1c	2b	3d	
5				69
	1d	2c	3e	
6		H ₂ NPr		82
	1e	2a	3f	
7				92
	1f	2d	3g	
8				69
	1g	2e	3h	
9				89
	1h	2f	3i	
10				56
	1i	2d	3j	
11		H ₂ NPr		63
	1j	2a	3k	

[a] Alkyne **1** (1 mmol), amine **2** (50 mmol), Bu₃SnH (0.3 mmol), AIBN (0.2 mmol), CO (85 atm), benzene (20 mL), 90°C, 4 h. [b] Generally, less than 10% of the α -stannylmethylene amide **4** was formed as by-product. [c] Yields after isolation by flash chromatography on SiO₂.

1-hydroxyallyl radicals. A subsequent 1,4-H migration^[9] to give α -keto followed by β -fission leads to the formation of α -methylene amides and regenerates tributyltin radical.^[10]

To obtain further insight into the unusual radical 1,4-H shift, DFT calculations were carried out for the isomerization



Scheme 2. A hybrid radical/ionic mechanism for tin-catalyzed carbonylation of alkynes leading to 2-substituted acrylamides.

of a 1-hydroxyallyl radical ($\text{HO}(\text{H}_2\text{N})\text{C}=\text{CCH}(\cdot)\text{SnH}_3$) to the corresponding enol radical ($\text{H}_2\text{NC}=\text{OCH}(\cdot)\text{CH}_2\text{SnH}_3$).^[11] As shown in Figure 1, the 1,4-H migration is predicted to be exothermic by 80.0 kJ mol^{-1} , and the reaction via a five-membered cyclic transition state is a possible reaction pathway for the proposed 1,4-H shift.

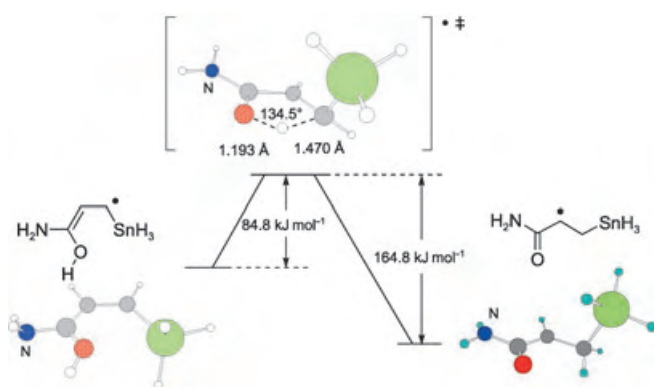


Figure 1. Optimized structures and energy barriers for the 1,4-H shift calculated at the CCSD(T)/DZP//B3LYP/DZP level of theory.

In summary, we have reported a new method for the carbonylation of alkynes, which is unique in being catalyzed by tributyltin radicals. Ionic trapping of the α -ketenyl radical by amines and radical 1,4-H shift from the resulting 1-hydroxyallyl radical are the keys to the success of the reaction. Thus, the radical/polar crossover process provides a new route for the carbonylation of alkynes without the use of transition-metal catalysis.

Experimental Section

AIBN (33.9 mg, 0.21 mmol), benzene (20 mL), 1-octyne (**1a**, 113.6 mg, 1.03 mmol), propylamine (**2a**, 4.1 mL, 50 mmol), and

Bu_3SnH (82.6 mg, 0.28 mmol) were placed in a 50-mL stainless steel autoclave. The autoclave was closed, purged three times with carbon monoxide, pressurized with 85 atm of CO, and then heated at 90°C for 4 h. Excess CO was discharged at room temperature. The solvent was removed under reduced pressure. The residue was purified by flash chromatography on silica gel (gradient from hexane to hexane/EtOAc 2:1) to give **3a** (169.9 mg, 82 %), (*E*)-**4a** (28.4 mg, 6 %), and (*Z*)-**4a** (10.8 mg, 2 %).

Received: September 11, 2004

Keywords: alkynes · amides · carbonylation · radical reactions · tin

- [1] For reviews on radical chemistry, see a) *Radicals in Organic Synthesis*, Vols. 1 and 2 (Eds.: P. Renaud, M. P. Sibi), Wiley-VCH, Weinheim, **2001**; b) D. P. Curran, N. A. Porter, B. Giese, *Stereochemistry of Radical Reactions*, VCH, Weinheim, **1996**; c) W. B. Motherwell, D. Crich, *Free Radical Chain Reactions in Organic Synthesis*, Academic Press, London, **1992**.
- [2] For reviews on radical carbonylations, see a) I. Ryu, N. Sonoda, *Angew. Chem.* **1996**, *108*, 1140; *Angew. Chem. Int. Ed. Engl.* **1996**, *35*, 1050; b) I. Ryu, N. Sonoda, D. P. Curran, *Chem. Rev.* **1996**, *96*, 177; c) I. Ryu, *Chem. Soc. Rev.* **2001**, *30*, 16; See also a review on acyl radicals: c) C. Chatgililoglu, D. Crich, M. Komatsu, I. Ryu, *Chem. Rev.* **1999**, *99*, 1991.
- [3] a) I. Ryu, K. Matsu, S. Minakata, M. Komatsu, *J. Am. Chem. Soc.* **1998**, *120*, 5838; b) C. Falzon, I. Ryu, C. H. Schiesser, *Chem. Commun.* **2002**, 2338; c) I. Ryu, H. Miyazato, H. Kuriyama, K. Matsu, M. Tojino, T. Fukuyama, S. Minakata, M. Komatsu, *J. Am. Chem. Soc.* **2003**, *125*, 5632; d) M. Tojino, N. Ostuka, T. Fukuyama, H. Matsubara, C. H. Schiesser, H. Kuriyama, H. Miyazato, S. Minakata, M. Komatsu, I. Ryu, *Org. Biomol. Chem.* **2003**, *1*, 4262.
- [4] M. Tojino, Y. Uenoyama, T. Fukuyama, I. Ryu, *Chem. Commun.* **2004**, 2482.
- [5] a) T. Tatee, K. Narita, S. Kurashige, S. Ito, H. Miyazaki, H. Yamanaka, M. Mizugaki, T. Sakamoto, H. Fukuda, *Chem. Pharm. Bull.* **1986**, *34*, 1643; b) O. Kitagawa, K. Aoki, T. Inoue, T. Taguchi, *Tetrahedron Lett.* **1995**, *36*, 593; c) C. Andres, J. P. Duque-Soladana, R. Pedrosa, *J. Org. Chem.* **1999**, *64*, 4282.
- [6] Recent reviews: a) M. J. Caulfield, G. G. Qiao, D. H. Solomon, *Chem. Rev.* **2002**, *102*, 3067; b) S. Y. Lee, S. J. Park, Y. Lee, S. H. Lee, *Biopolymers* **2003**, *10*, 281.
- [7] For radical carbonylations of alkynes, see a) S. Nakatani, J. Yoshida, S. Isoe, *J. Chem. Soc. Chem. Commun.* **1992**, 880; b) D. P. Curran, J. Sisko, A. Balog, N. Sonoda, K. Nagahara, I. Ryu, *J. Chem. Soc. Perkin Trans. 1* **1998**, 1591; c) T. Fukuyama, Y. Uenoyama, S. Oguri, N. Otsuka, I. Ryu, *Chem. Lett.* **2004**, *33*, 854. See also refs. [3c,3d,4].
- [8] For related Pd-catalyzed transformations, see a) S. Torii, H. Okumoto, M. Sadakane, H. X. Long, *Chem. Lett.* **1991**, 1673; b) B. E. Ali, A. El-Ghanam, M. Fettohi, J. Tijani, *Tetrahedron Lett.* **2000**, *41*, 5761; c) B. E. Ali, J. Tijani, *Appl. Organomet. Chem.* **2003**, *17*, 921; d) U. Matteoli, A. Scrivanti, V. Beghetto, *J. Mol. Catal. A* **2004**, *213*, 183.
- [9] Examples of radical 1,4-H shifts: a) M. Gulea, J. M. López-Romero, L. Fensterbank, M. Malacria, *Org. Lett.* **2000**, *2*, 2591; b) P. C. Montevecchi, M. C. Navacchia, *Tetrahedron Lett.* **1996**, *37*, 6583; c) D. Crich, S. Sun, J. Brunckova, *J. Org. Chem.* **1996**, *61*, 605; d) S.-H. Chen, S. Huang, Q. Gao, J. Golik, V. Farina, *J. Org. Chem.* **1994**, *59*, 1475.
- [10] As for the formation of tin-containing by-product **4a**, hydrogen abstraction from 1-hydroxyallyl radical may be a possible reaction course. For a recent mechanistic study on a related system, see A. L. J. Beckwith, V. W. Bowry, W. R. Bowman, E.

Mann, J. Parr, J. M. D. Storey, *Angew. Chem.* **2004**, *116*, 97; *Angew. Chem. Int. Ed.* **2004**, *43*, 95.

- [11] Gaussian98 (Revision A.7), M. J. Frisch, G. W. Trucks, H. B. Schlegel, G. E. Scuseria, M. A. Robb, J. R. Cheeseman, V. G. Zakrzewski, J. A. Montgomery, R. E. Stratmann, J. C. Burant, S. Dapprich, J. M. Millam, A. D. Daniels, K. N. Kudin, M. C. Strain, O. Farkas, J. Tomasi, V. Barone, M. Cossi, R. Cammi, B. Mennucci, C. Pomelli, C. Adamo, S. Clifford, J. Ochterski, G. A. Petersson, P. Y. Ayala, Q. Cui, K. Morokuma, D. K. Malick, A. D. Rabuck, K. Raghavachari, J. B. Foresman, J. Cioslowski, J. V. Ortiz, B. B. Stefanov, G. Liu, A. Liashenko, P. Piskorz, I. Komaromi, R. Gomperts, R. L. Martin, D. J. Fox, T. Keith, M. A. Al-Laham, C. Y. Peng, A. Nanayakkara, C. Gonzalez, M. Challacombe, P. M. W. Gill, B. G. Johnson, W. Chen, M. W. Wong, J. L. Andres, M. Head-Gordon, E. S. Replogle, J. A. Pople, Gaussian, Inc., Pittsburgh, PA, **1998**.

Computer Chemistry

Aromatic Boron Wheels with More than One Carbon Atom in the Center: C_2B_8 , $C_3B_9^{3+}$, and $C_5B_{11}^{+***}$

Stefan Erhardt, Gernot Frenking,* Zhongfang Chen, and Paul von Ragué Schleyer*

Dedicated to Professor Reinhardt Ahlrichs on the occasion of his 65th birthday

A large number of molecules with planar tetracoordinated carbon centers have now been characterized, both experimentally and computationally.^[1] When the constituent atoms “fit” satisfactorily, both geometrically and electronically, even higher carbon hypercoordination can be achieved.^[2] The first example was discovered computationally as a rather stable local minimum: CB_6^{2-} (D_{6h}) has a central planar hexacoordinate carbon center surrounded by a six-membered boron ring as well as six π electrons.^[2a] While structures with planar

penta- and heptacoordinate carbon centers have also been described, there are limits.^[2b] An eight-membered boron ring is too large to bind a carbon atom in the center.^[2b] However, planar octacoordination can be achieved with central atoms that are larger than carbon. Newly prepared B_{10} to B_{15} planar clusters are the most recent examples.^[3] These neutral and charged boron species B_n^{q+} also exhibit Hückel $(4n+2)\pi$ -electron aromaticity.^[3] The central atom in planar hypercoordinate compounds may also be a transition metal: Frenking and co-workers predicted theoretically the six- π -electron, aromatic, metal-centered, planar cations $[Fe(Sb_5)]^+$ and $[Fe(Bi_5)]^+$.^[4]

Can more than one planar hypercoordinated carbon atom reside inside a binary planar ring system of the type C_nX_m (in which X represents any other atom)? A single carbon enclosed by a B_8 (or a larger boron ring) does not reside in the center and binds to only a few boron atoms at the inner rim.^[2b] This positioning leaves space available for a second carbon atom to join the first. Indeed, C_2B_8 is just such a species (Figure 1 a). By means of extensive computational exploration of $C_nB_m^{q+}$, possibilities with various compositions and charges, q , we also have located concentric borocarbon minima, with three- ($C_3B_9^{3+}$) and five-membered carbon rings ($C_5B_{11}^{+}$) inside boron circumferences. We searched unsuccessfully for a $C_nB_m^{q+}$ stationary point with a C_4 ring in the center. However, both the planar D_{3h} $C_3B_9^{3+}$ trication (Figure 1 c), with a central carbon triangle and six π electrons, as well as the C_{2v} $C_5B_{11}^{+}$ cation (Figure 1 e), with central C_5 cycle and ten π electrons are minima.^[5] The bonding (σ and π) and the properties of these new aromatic molecules (Figure 1) are intriguing.

Figure 1 a, c, and e provide an overview of the geometrical details of the C_2B_8 (D_{2h}), $C_3B_9^{3+}$ (D_{3h}), and $C_5B_{11}^{+}$ (C_{2v}) minima, respectively, calculated at the B3LYP/6-311 + G(2df) density functional level by using the Gaussian 03 program.^[6,7] These species have structural and bonding features in common. Single bonds more or less normal in length (i.e., 1.53 Å for C–C, 1.60 Å for C–B,^[8] and about 1.65 for B–B) are shown with solid lines in Figure 1, whereas dashed lines identify C–B contacts at significantly longer interatomic distances (and imply participation in multicenter bonding). Hence, the carbon atoms of the central C_2 , C_3 , and C_5 units are more strongly bound to some of the perimeter boron atoms than to others. This influences the B–B distances in the outer rings, which vary over a range of 0.15 Å. In contrast the C–C interatomic distances are all near 1.50 Å (the shortest length is 1.487 Å for the C_2 unit in C_2B_8). While one planar tetracoordinate carbon is clearly present in $C_5B_{11}^{+}$ (Figure 1 e), the long C–B distances complicate the assignment of coordination numbers to the carbon atoms. When these long contacts are counted, the carbon atoms in Figure 1 a and c are all planar pentacoordinate, while those in Figure 1 e are either penta- or tetracoordinate. Note that B_{12} , which is isoelectronic with $C_3B_9^{3+}$, has a quasi-planar equilibrium geometry with lower symmetry (C_{3v}).^[3b]

Remarkably, the C_2 , C_3 , and C_5 units in C_2B_8 , $C_3B_9^{3+}$, and $C_5B_{11}^{+}$, respectively, are highly fluxional and rotate readily inside the perimeters of their boron rings. The behavior of C_2B_8 is much like a compass needle swinging around seeking

[*] Dipl.-Chem. S. Erhardt, Prof. Dr. G. Frenking
Fachbereich Chemie
Philipps-Universität Marburg
Hans-Meerwein-Strasse, 35039 Marburg (Germany)
Fax: (+49) 6421-282-5566
E-mail: frenking@chemie.uni-marburg.de
Dr. Z. Chen, Prof. P. v. R. Schleyer
Department of Chemistry
University of Georgia
Athens, GA (USA)
Fax: (+1) 706-542-7514
E-mail: schleyer@chem.uga.edu

[**] The research at Marburg has been supported by the Deutsche Forschungsgemeinschaft. The work at Georgia was supported by National Science Foundation Grant CHE-0209857.

Supporting information for this article is available on the WWW under <http://www.angewandte.org> or from the author.

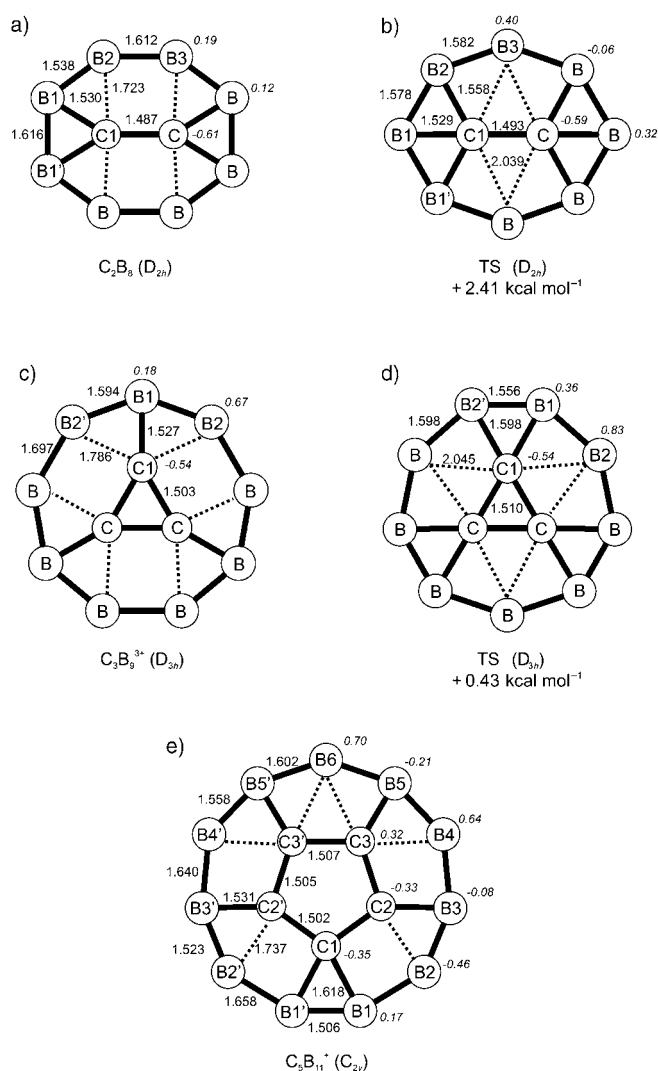


Figure 1. B3LYP/6-311+G(2df) geometries of $C_nB_m^{q+}$ molecules (interatomic distances in Å, natural charges (NBO) are in italics). a) Equilibrium structure of C_2B_8 ; b) transition structure of C_2B_8 for rotation of the C_2 moiety in the molecular plane; c) equilibrium structure of $C_3B_9^{3+}$; d) transition structure of $C_3B_9^{3+}$ for rotation of the C_3 cycle in the molecular plane; e) equilibrium structure of $C_5B_{11}^+$.

its orientation, but the C–C entity remains strongly bound to its perimeter during the rotation. The barrier is only $2.41 \text{ kcal mol}^{-1}$ (with zero-point energy (ZPE) corrections) and involves a D_{2h} transition structure (Figure 1 b) with planar tetracoordinated carbon centers. Each carbon center is too weakly bound ($r = 2.039 \text{ Å}$) to the two remaining outer boron atoms to have fully developed planar hexacoordination.

The barrier for the counter rotation of the outer boron ring and the inner C_3 triangle in $C_3B_9^{3+}$ is only $0.43 \text{ kcal mol}^{-1}$ with ZPE corrections; the transition structure (Figure 1 d) is highly symmetric (D_{3h}). Astonishingly, the rotation of the C_5 cycle within the B_{11} perimeter in $C_5B_{11}^+$ is essentially free. We could not locate any transition state for rotation at the B3LYP/6-311+G(2df) level. A C_s transition state was located at the lower B3LYP/6-31G(d) level (harmonic imaginary frequency $6i \text{ cm}^{-1}$), but this only was $0.06 \text{ kcal mol}^{-1}$ higher in energy than the C_{2v} equilibrium structure.

The bonding situation in these compounds is peculiar: the total carbon–boron interaction energies are large both in the initial and the rotation transition states. During the rotations that are nearly barrier-less, the multicenter B–C binding interactions transform gradually from one arrangement to the other. Note that more B–C contacts exist in the transition states than in the minima (compare Figure 1 b with 1 a and 1 d with 1 c), which helps lower the energy barriers.

The borocarbon systems (Figure 1) all follow the Hückel $4n+2$ electron rule. C_2B_8 and $C_3B_9^{3+}$ have six π electrons, whereas $C_5B_{11}^+$ has ten. Figure 2 shows the occupied π mo-

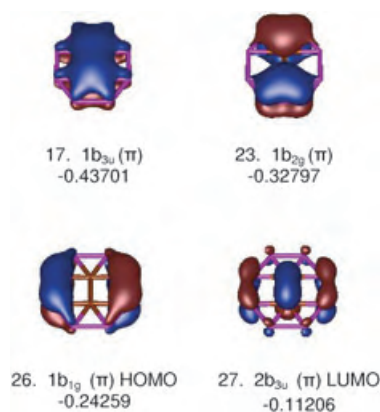


Figure 2. Plot of the occupied π MOs and the LUMO of C_2B_8 . Orbital energies are given in Hartrees.

lecular orbitals (MOs) and the lowest unoccupied molecular orbital (LUMO) of C_2B_8 . The full set of occupied valence MOs and the three lowest-lying vacant orbitals are given in the Supporting Information. The three occupied π orbitals (Figure 2, MOs 17, 23, and 26) are akin to the π MOs of benzene.^[9] The $C_3B_9^{3+}$ trication has 18 occupied valence MOs (all are depicted in the Supporting Information). The three occupied π orbitals (also akin to benzene), the degenerate σ highest occupied molecular orbital (HOMO), and the three lowest-lying empty orbitals with π symmetry are shown in Figure 3. $C_5B_{11}^+$ has 26 occupied valence MOs (see the

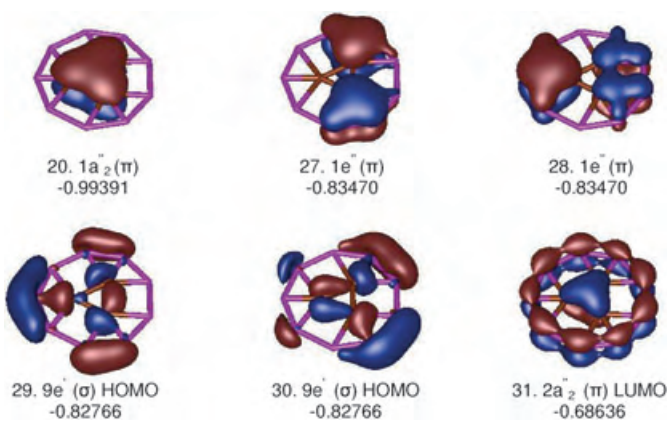


Figure 3. Plot of the occupied π MOs, the degenerate σ HOMO, and the LUMO of $C_3B_9^{3+}$. Orbital energies are given in Hartrees.

Supporting Information), five of which have π symmetry and the typical pattern of a ten- π -electron, Hückel, aromatic system. In addition, Figure 4 depicts the five lowest-lying empty orbitals, which also have π symmetry.

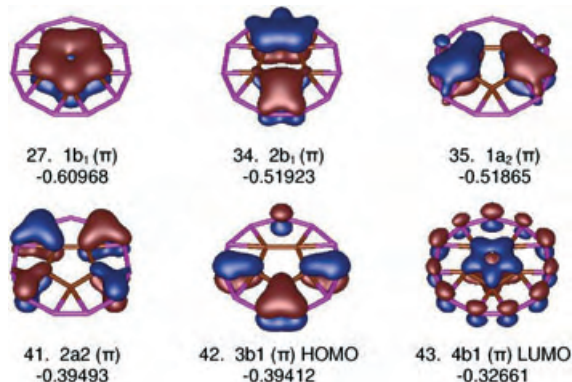


Figure 4. Plot of the occupied π MOs and the LUMO of $C_5B_{11}^+$. Orbital energies are given in Hartrees.

While the lowest-lying π MO of C_2B_8 (Figure 2, MO 17) is centered on the two inner carbon atoms, it also extends over the eight peripheral boron atoms. In contrast, the lowest-energy π MOs of $C_3B_9^{3+}$ (Figure 3, MO 20) and of $C_5B_{11}^+$ (Figure 4, MO 27) only involve the central carbon rings. While these resemble the π MO of the cyclopropenyl cation, $C_3H_3^+$, and the lowest π MO of the cyclopentadienyl anion, the analogy is imperfect because of the higher-lying multi-node π MOs of the borocarbons. These MOs are not occupied in the simple carbon rings, which accounts for their shorter C–C bond lengths. The higher-lying borocarbon π MOs (Figure 2, MOs 23 and 24 for C_2B_8 ; Figure 3, MOs 27 and 28 for $C_3B_9^{3+}$; Figure 4 MOs 34, 35, 41, and 42 for $C_5B_{11}^+$) have nodal planes through the carbon rings, but contribute to the C–B bonding.

The σ -bonding situations in C_2B_8 , $C_3B_9^{3+}$, and $C_5B_{11}^+$ are similar. C_2B_8 has 13 and $C_3B_9^{3+}$ 15 occupied σ MOs; both correspond to the number of bonds with normal lengths shown in Figure 1. The 21 occupied σ MOs of $C_5B_{11}^+$ also correspond to the solid bonds in Figure 1 if the C1B1B1' triangle (with the longer C–B bonds) is assigned three-center two-electron character. In addition, the long C–B interactions (1.737 to 2.045 Å) in all minima and transition structures in Figure 1 arise from π and the electron-deficient σ bonding. Note that without such delocalized bonding interactions, a number of the boron atoms in each species would only be bicoordinate.^[10] Inspection of the valence orbitals of the rotational transition states of C_2B_8 and $C_3B_9^{3+}$ (depicted in the Supporting Information) show that the σ and π orbitals change only slightly in comparison with the equilibrium forms although there are significant differences between the atomic partial charges and interatomic distances (Figure 1).

If the long contacts are included, all the carbons in these species are planar four- to six-coordinate, but their total Wiberg bond indices (WBI) range from 3.8 to 3.9. Thus, the octet rule is not violated. If the atomic electronegativity values are used, the natural charges of the carbons are

negative and the boron atoms positive. Even in the $C_3B_9^{3+}$ trication, the charge on the carbon atom is negative (−0.54) while that on each boron atom is positive (+0.18 and +0.67), that is, the total charges are −1.62 on the C_3 moiety and +4.62 on the B_9 ring.

As C_2B_8 does not have the requisite higher symmetry, the MOs are not degenerate. The two highest-lying π MOs (Figure 2, MOs 23 and 26) differ significantly in energy. Hence, we also optimized planar $C_2B_8^{2+}$ (in which the HOMO, π MO 26, is empty), but for the resulting cyclic four- π D_{2h} structure one imaginary frequency was obtained, whose vector pointed to out-of-plane deformation. Thus, planar cyclic four- π $C_2B_8^{2+}$ is not a viable species. Although the three lowest-lying empty orbitals of C_2B_8 also have π symmetry, the $C_2B_8^{2-}$ dianion and $C_2B_8^{4-}$ tetraanion (with eight and ten π electrons, respectively) are both transition states with imaginary frequencies pointing out-of-plane.

Similar results were obtained for the eight- π -electron $C_3B_9^+$. The higher lying degenerate $1e''$ π MOs (MO 27 and 28) do not constitute the HOMO of 10π $C_3B_9^{3+}$. (The degenerate σ HOMO $17e'$, Figure 3, is slightly higher in energy.) The $2a_2''$ LUMO of $C_3B_9^{3+}$ is a nondegenerate π orbital with an aesthetically pleasing concentric antibonding π -MO pattern between the C_5 and B_9 rings. We optimized the geometry of planar $C_3B_9^+$, in which the latter orbital is occupied. Although it has an electronic structure consistent with D_{3h} symmetry, the resulting planar eight- π -electron $C_3B_9^+$ monocation was not a minimum. Its one imaginary frequency corresponds to an out-of-plane C_{3v} distortion.

More details concerning the aromaticity in these intriguing $C_nB_m^{q+}$ compounds were revealed by the total NICS (nucleus independent chemical shifts)^[11] and by analyzing their dissected CMO (canonical molecular orbital) contributions (calculated with the NBO 5.0 program).^[12] NICS points were calculated in the centers (and above) of all the unique rings. The resulting NICS grids display the diatropic (shielded) points in red and paratropic (deshielded) points in green. NICS plots of C_2B_8 are given in Figure 5 as an example (those for $C_3B_9^{3+}$ and $C_5B_{11}^+$ are given in the Supporting Information). The total NICS plots (Figure 5a), as well as the plots of all the π MO contributions together (Figure 5b), show all the rings to be aromatic. In contrast, the contributions from all the σ orbitals are small and often paratropic (Figure 5c and Supporting Information). Hence, the aromaticity of these borocarbons is dominated by the π , rather than the σ , contributions.

In conclusion, it is possible that more than one directly joined planar hypercoordinated carbon atom can be enclosed by a peripheral ring comprising a suitable number of boron atoms. The C_2B_8 , $C_3B_9^{3+}$, and $C_5B_{11}^+$ species described here (Figure 1) are stabilized by substantial Hückel π aromaticity, judging from the NICS behavior (Figure 5). In addition, multicenter σ bonding helps bind the inner carbon units to the boron perimeters. These molecules are highly fluxional. Remarkably, the inner C_2 as well as the C_3 and C_5 units and outer boron rings can rotate quite freely with regard to one another. These unusual planar clusters are stable when the constituent atoms fit nicely, both geometrically and electronically. The original idea^[13] for stabilizing such planar clusters

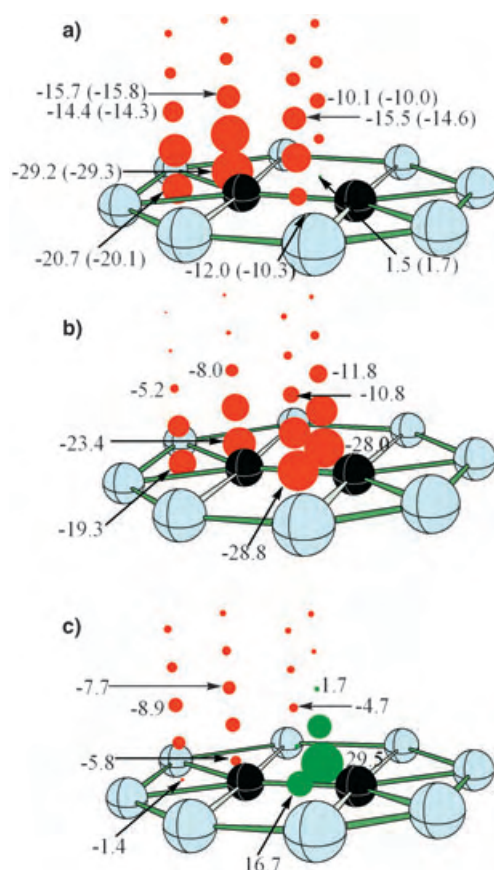


Figure 5. a) Plots of total NICS contributions, b) contributions from all π orbitals, and c) contributions from σ orbitals at the individual ring centers and up to 2 Å above C_2B_8 (D_{2h}) calculated at the GIAO-B3LYP/6-31G(d) level. The total NICS values at GIAO-B3LYP/6-311 + G(2df) are given in parentheses. The red and green colors denote negative (diatropic) and positive (paratropic) NICS values, respectively.

with hypercoordinate central atoms, which was later experimentally confirmed,^[14] should guide the design of additional intriguing structures. While all the structures in Figure 1 are local minima fulfilling both the electronic and geometrical requirement for good bonding, they are not the global minima for the given compositions. Isomers with the carbon atoms on the outside are lower in energy, but they have neither the aesthetic appeal nor the remarkable fluxional characteristics of the structures described here.

Received: September 13, 2004

Revised: November 11, 2004

Keywords: aromaticity · boron · carboranes · density functional calculations

- [1] For recent reviews, see a) K. Sorger, P. v. R. Schleyer, *THEOCHEM* **1995**, 338, 317–346; b) D. Röttger, G. Erker, *Angew. Chem.* **1997**, 109, 840–856; *Angew. Chem. Int. Ed. Engl.* **1997**, 36, 812–827; c) L. Radom, D. R. Rasmussen, *Pure Appl. Chem.* **1998**, 70, 1977–1984; d) W. Siebert, A. Gunale, *Chem. Soc. Rev.* **1999**, 28, 367–371; e) R. Choukroun, P. Cassoux, *Acc. Chem.*

Rex. **1999**, 32, 494–502; f) V. I. Minkin, R. M. Minyaev, R. Hoffmann, *Russ. Chem. Rev.* **2002**, 71, 869–892.

- [2] a) K. Exner, P. v. R. Schleyer, *Science* **2000**, 290, 1937–1940; b) Z. X. Wang, P. v. R. Schleyer, *Science* **2001**, 292, 2465; c) Z.-X. Wang, P. v. R. Schleyer, *Angew. Chem.* **2002**, 114, 4256–4259; *Angew. Chem. Int. Ed.* **2002**, 41, 4082–4085; d) T. N. Gribanova, R. M. Minyaev, V. I. Minkin, *Mendeleev Commun.* **2001**, 169–170; e) R. M. Minyaev, T. N. Gribanova, *Russ. Chem. Bull.* **2000**, 109, 783–796; f) R. M. Minyaev, T. N. Gribanova, A. G. Starikov, V. I. Minkin, *Dokl. Chem.* **2002**, 382, 41–45; g) R. M. Minyaev, T. N. Gribanova, A. G. Starikov, V. I. Minkin, *Mendeleev Commun.* **2001**, 213–214; h) V. I. Minkin, R. M. Minyaev, *Mendeleev Commun.* **2004**, 43–46; i) S. D. Li, C. Q. Miao, G. M. Ren, *Eur. J. Inorg. Chem.* **2004**, 2232–2234.
- [3] a) H. J. Zhai, A. N. Alexandrova, K. A. Birch, A. I. Boldyrev, L.-S. Wang, *Angew. Chem.* **2003**, 115, 6186–6190; *Angew. Chem. Int. Ed.* **2003**, 42, 6004–6008; b) H.-J. Zhai, B. Kiran, J. Li, L.-S. Wang, *Nat. Mater.* **2003**, 2, 827–833.
- [4] M. Lein, J. Frunzke, G. Frenking, *Angew. Chem.* **2003**, 115, 1341–1345; *Angew. Chem. Int. Ed.* **2003**, 42, 1303–1306.
- [5] We calculated neutral C_5B_{10} (among other $C_nB_m^{q+}$ species) because the total number of valence electrons (50) and the expected number of π electrons (10) leaves 40 valence electrons for the σ framework. For a cyclic species of C_5B_{10} , one would need 20 electrons for ten B–B bonds and ten electrons for five C–C bonds, thus leaving ten electrons for carbon–boron bonding. The latter ten electrons could be used for five CB_2 moieties, that is, there would be five three-center two-electron bonds for the bonding between the carbon and boron cycles. Planar (D_{5h}) C_5B_{10} is a transition state; the vectors of the imaginary frequency point to an out-of-plane distortion.
- [6] The geometries have been optimized at the B3LYP level by using 6-311 + G(2df) basis sets. The nature of the stationary points was examined by calculating the Hessian matrices at the B3LYP/6-311 + G(2df) level. All the calculations have been carried out with the Gaussian03 program.^[7]
- [7] Gaussian03 (Revision A.1), M. J. Frisch, G. W. Trucks, H. B. Schlegel, G. E. Scuseria, M. A. Robb, J. R. Cheeseman, J. A. Montgomery, Jr., T. Vreven, K. N. Kudin, J. C. Burant, J. M. Millam, S. S. Iyengar, J. Tomasi, V. Barone, B. Mennucci, M. Cossi, G. Scalmani, N. Rega, G. A. Petersson, H. Nakatsuji, M. Hada, M. Ehara, K. Toyota, R. Fukuda, J. Hasegawa, M. Ishida, T. Nakajima, Y. Honda, O. Kitao, H. Nakai, M. Klene, X. Li, J. E. Knox, H. P. Hratchian, J. B. Cross, C. Adamo, J. Jaramillo, R. Gomperts, R. E. Stratmann, O. Yazyev, A. J. Austin, R. Cammi, C. Pomelli, J. W. Ochterski, P. Y. Ayala, K. Morokuma, G. A. Voth, P. Salvador, J. J. Dannenberg, V. G. Zakrzewski, S. Dapprich, A. D. Daniels, M. C. Strain, O. Farkas, D. K. Malick, A. D. Rabuck, K. Raghavachari, J. B. Foresman, J. V. Ortiz, Q. Cui, A. G. Baboul, S. Clifford, J. Cioslowski, B. B. Stefanov, G. Liu, A. Liashenko, P. Piskorz, I. Komaromi, R. L. Martin, D. J. Fox, T. Keith, M. A. Al-Laham, C. Y. Peng, A. Nanayakkara, M. Challacombe, P. M. W. Gill, B. Johnson, W. Chen, M. W. Wong, C. Gonzalez, J. A. Pople, Gaussian, Inc., Pittsburgh, PA, **2003**.
- [8] C. H. Suresh, N. Koga, *J. Phys. Chem. A* **2001**, 105, 5940–5944.
- [9] The in-plane node, the condition for a π orbital, is not counted.
- [10] The work presented herein may be compared with a recent MO analysis of C_5^{2-} and alkaline-metal coordinated analogues that contain a planar tetracoordinate carbon atom at the center: a) G. Merino, M. A. Mendez-Rojas, A. Vela, *J. Am. Chem. Soc.* **2003**, 125, 6026–6027; b) G. Merino, M. A. Mendez-Rojas, H. I. Beltrán, C. Corminboeuf, T. Heine, A. Vela, *J. Am. Chem. Soc.* **2004**, 126, 16160–16169. We thank one referee for pointing the work out to us.
- [11] P. v. R. Schleyer, C. Maerker, A. Dransfeld, H. Jiao, N. v. E. Hommes, *J. Am. Chem. Soc.* **1996**, 118, 6317–6318.

- [12] a) J. A. Bohmann, F. Weinhold, T. C. Farrar, *J. Chem. Phys.* **1997**, *107*, 1173–1184; b) T. Heine, P. v. R. Schleyer, C. Corminboeuf, G. Seifert, R. Reviakine, J. Weber, *J. Phys. Chem. A* **2003**, *107*, 6470–6475. The MO–NICS analyses were at the GIAO B3LYP/6-31G(d) level. The total NICS values calculated at this level are comparable to those calculated at GIAO-B3LYP/6-311+G(2df) level (See the Supporting Information).
- [13] P. v. R. Schleyer, A. I. Boldyrev, *J. Chem. Soc. Chem. Commun.* **1991**, 1536–1538.
- [14] a) X. Li, L. S. Wang, A. I. Boldyrev, J. Simons, *J. Am. Chem. Soc.* **1999**, *121*, 6033–6038; b) L. S. Wang, A. I. Boldyrev, X. Li, J. Simons, *J. Am. Chem. Soc.* **2000**, *122*, 7681–7687; c) X. Li, H. F. Zhang, L. S. Wang, G. D. Geske, A. I. Boldyrev, *Angew. Chem.* **2000**, *112*, 3776–3779; *Angew. Chem. Int. Ed.* **2000**, *39*, 3630–3633.

Phosphorus Heterocycles

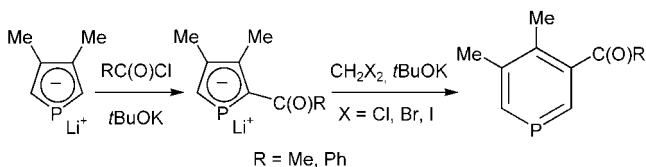
One-Pot Conversion of Phospholide Ions into β -Functional Phosphinines

Joanna Grundy and François Mathey*

Although the first β -functional phosphinine, a 3-phosphaphenol, was synthesized by Märkl et al. as early as 1977,^[1] only a few such compounds are known,^[2] particularly if we exclude a series of polyfunctional derivatives obtained by [4+2] cycloaddition between 1-phosphadienes or synthetic equivalents and functional alkynes.^[3] As a result, the reactivity of this class of compounds is almost unexplored.^[4] Herein, we describe a straightforward access to such compounds from the readily available phospholide ions.

In 1997, we described a simple method which converts α -unsubstituted into α -functional phospholides.^[5] This method has been applied to the synthesis of 2-acylphospholides.^[6] In the course of a systematic investigation of the reactivity of these species, we discovered that their reaction with dihalomethanes unexpectedly leads to the formation of 3-acylphosphinines (Scheme 1).

The whole sequence takes place at room temperature or below. The reaction is best run with dibromomethane. The 3-



Scheme 1.

[*] J. Grundy, Prof. F. Mathey
UCR-CNRS Joint Research Chemistry Laboratory
Department of Chemistry
University of California Riverside
Riverside, CA 92521-0403
E-mail: fmathey@citrus.ucr.edu

functional phosphinines appear to be the sole products of the transformation as determined by monitoring the reaction mixture by ³¹P NMR spectroscopy. Whatever the nature of the β -substituent, the ³¹P resonance signal is observed at $\delta = 188 \pm 1$ ppm (CDCl₃) as for the 3-unsubstituted species.^[7] This observation underlines the weakness of the electronic interaction between phosphorus and the functional *meta* substituent. The phosphinines are purified by chromatography on silica gel or by distillation in a Kugelrohr apparatus. They were completely characterized by NMR spectroscopy and mass spectrometry. The final yields of isolated products based on the starting 1-phenyl-3,4-dimethylphosphole (three reactions in one pot) remain modest (8–20%), probably because of substantial losses during the purification procedure. We have also checked that the conversion into phosphinine does not take place in the absence of the functional substituent.

Since we had no precise idea about the mechanism of formation of these functional phosphinines, we decided to investigate various possibilities by DFT calculations at the B3LYP/6-311+G(d,p) level^[8] using the Gaussian03 package.^[9] We decided to check the possibility of a carbenoid mechanism. We admitted the formation of a carbenoid species by deprotonation of the P-CH₂X unit of the initially formed 1-haloalkylphosphole. The process was modeled using the anion derived from 1-chloromethyl-2-acetylphosphole. The theoretical investigation of the reaction pathway suggested that the conversion into phosphinine proceeded by the initial opening of the phosphole ring, to give the 1-chloro-6-acetyl-2-phosphahexatriene anion as a first intermediate. The transition state (one imaginary frequency) between the phosphole and the phosphahexatriene anions was computed to lie 25.3 kcal mol⁻¹ higher in energy than the starting phosphole anion (zero-point energy (ZPE) included). Thus, this mechanism was discarded because it needed too much energy to be operative at RT and provided no explanation for the role of the acyl substituents.

It is possible to deprotonate one methyl group of 3,4-dimethylphosphole sulfides^[10] or borane complexes.^[11] We thus decided to investigate the possibility of a similar deprotonation in the present case, the role of the electron-withdrawing functional groups being to facilitate this deprotonation. The process was modeled using the anion derived from 1-chloromethyl-2-acetyl-3-methylphosphole **A**. The computed structure is shown in Figure 1. The exocyclic C=CH₂ unit has a strong double bond character (1.371 Å), the internal C1–C2 bond is essentially a single bond (1.450 Å), thus the negative charge is mainly localized at C1. Since, C1, P7, C8, and Cl11 are coplanar and the C1–C8–Cl11 angle is 153°, the geometrical situation is ideal for a S_N2 backside attack of C1 onto C8–Cl11, leading to the bicyclic phosphirane **B** whose computed structure is shown in Figure 2. The transition state between **A** and **B** (one imaginary frequency, intrinsic reaction coordinate (IRC) calculations) was computed to lie 13.8 kcal mol⁻¹ higher in energy than the starting anion. Thus, this pathway is acceptable both in terms of energy and because it rationalizes the role of the functional substituent. We detected no acceptable pathway between the bicyclic phosphirane **B** and the final phosphinine. But we noted that H10 lies only at 2.433 Å from O12 and bears a

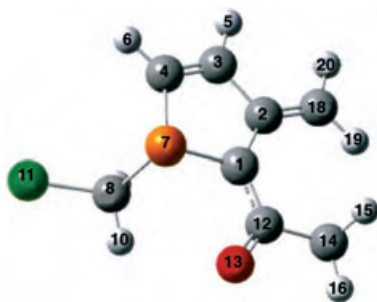


Figure 1. Computed structure of the anion **A** derived from 1-chloromethyl-2-acetyl-3-methylphosphole. Selected interatomic distances [Å], angles, and torsion angles [°]: C1...C8 2.825, C8-C11 1.851, C2-C18 1.371, C1-C2 1.450, C1-C12 1.415; C1...C8-Cl11 153.0, C1-P7-C8-Cl11 173.7. Gray C, green Cl, orange P, red O.

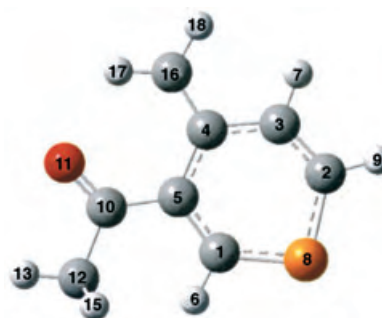
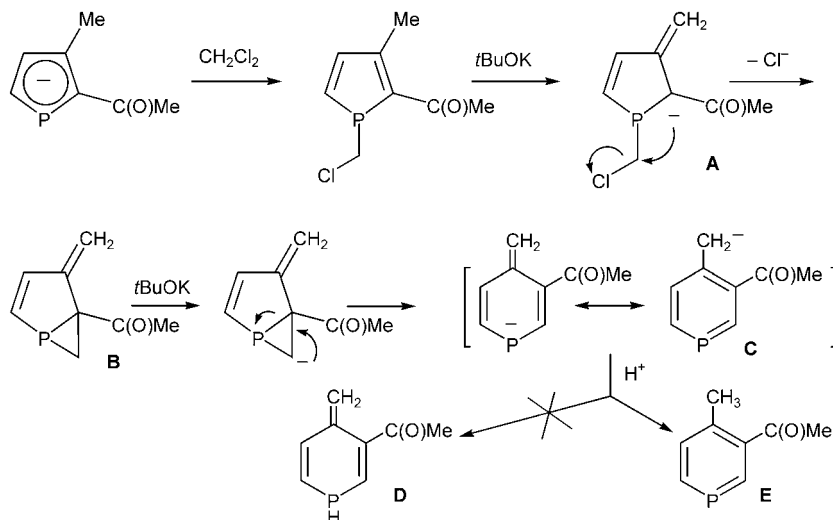


Figure 3. Computed structure of phosphinine anion **C**. Selected bond lengths [Å] and angles [°]: C1-P8 1.740, C2-P8 1.797, C1-C5 1.403, C2-C3 1.354, C3-C4 1.465, C5-C4 1.483, C4-C16 1.368; C1-P8-C2 97.6. Gray C, orange P, red O.

significantly higher positive Mulliken charge than H9 (+0.068 versus +0.014). We thus investigated the conversion of the phosphirane anion obtained from **B** by abstraction of H10 into the corresponding phosphinine anion **C** whose computed structure is shown in Figure 3. The exocyclic C=CH₂ unit has a strong double bond character (C4–C16 1.368 Å). The negative charge appears to be essentially localized at phosphorus (−0.47) and at the carbon center of the exocyclic =CH₂ group (C16 −0.49). The conversion of the anion derived from **B** into **C** is equivalent to the ring opening of a phosphirane anion and is extremely easy.^[12] The first transition state between the anion of **B** and **C** lies very close to the starting anion and is only 2.3 kcal mol^{−1} higher in energy than the starting product. The phosphinine anion is more stable than the phosphirane anion by 59.6 kcal mol^{−1} (ZPE included). The protonation of **C** can either occur at the phosphorus center to give **D**, or at the exocyclic =CH₂ group to give **E** (Scheme 2). However, the phosphinine **E** is more stable than **D** by 26.7 kcal mol^{−1} and thus, will be the sole final product of the reaction by a protonation–deprotonation equilibrium. The mechanism of the conversion is thus well established and is summarized in Scheme 2.

What the DFT calculations show is that the methyl β-substituent (this was partly verified using 2,5-diphenylphos-



Scheme 2.

pholide ion whose ring expansion fails) and the electron-withdrawing functional group that activates the methyl are necessary. Within the limits of these requirements, numerous variations on the functional substituent are still possible (a preliminary experiment has shown that the ring expansion works with the ethoxycarbonyl α-substitution).

Experimental Section

Synthesis of 3-acetyl-4,5-dimethylphosphinine: 1-Phenyl-3,4-dimethyl phosphole (1.88 g, 10 mmol) was stirred with lithium wire (0.14 g, 20 mmol) in THF (20 mL) for about 3 h. After removal of excess lithium by filtration, PhLi was quenched by the addition of AlCl₃ (3.33 mmol, 0.45 g) at −30 °C and warming the stirred solution to ambient temperature over 1 h. The reaction solution was cooled to −78 °C and acetyl chloride (10 mmol, 0.68 mL) was added, the solution was then warmed to room temperature over about 7 min, then *t*BuOK (2.24 g, 20 mmol) was added. The reaction solution was cooled to −78 °C and CH₂Br₂ (10 mmol, 0.70 mL) was added, then the mixture stirred at ambient temperature for ca. 3 h. The crude product was extracted with diethyl ether (3 × 10 mL) and column chromatography on silica gel with hexane:diethyl ether 90:10 to give the pure 3-acetyl-4,5-dimethylphosphinine as a colorless oil (0.13 g, 7.8% yield).

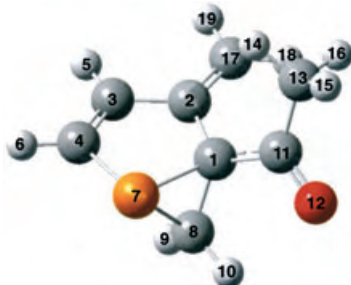


Figure 2. Computed structure of bicyclic phosphirane **B**. Significant bond lengths [Å] and angles [°]: C1-C8 1.501, C2-C17 1.342, C1-C2 1.504, C1-C11 1.506; C1-P7-C8 46.6. Gray C, orange P, red O.

^1H NMR (300 MHz, CDCl_3): δ = 8.53 (dd, 1H, $^2J_{\text{PH}}$ = 37 Hz, $^4J_{\text{HH}}$ = 3 Hz, PCH), 8.39 (dd, 1H, $^2J_{\text{PH}}$ = 34 Hz, $^4J_{\text{HH}}$ = 3 Hz, PCH), 2.55 (s, 3H, COCH_3), 2.45 (s, 3H, CH_3), 2.30 ppm (d, $^4J_{\text{PH}}$ 4 Hz, 3H, CH_3); ^{31}C NMR (75 MHz, CDCl_3): δ = 205.7 (CO), 155.7 (d, $^1J_{\text{PC}}$ = 50 Hz, PCH), 148.0 (d, $^2J_{\text{PC}}$ = 15 Hz, C_β), 147.3 (d, $^1J_{\text{PC}}$ = 52 Hz, PCH), 144.7 (d, $^2J_{\text{PC}}$ = 15 Hz, C_β), 134.5 (d, $^3J_{\text{PC}}$ = 19.2 Hz, C_γ), 30.8 (s, CH_3), 24.1 (d, $^3J_{\text{PC}}$ = 3.1 Hz, CH_3), 18.1 ppm (CH_3); ^{31}P NMR (121 MHz, CDCl_3 , external standard 85% H_3PO_4): δ = 188.5 ppm; Mass spectrum: m/z 166 [M^+], (80%), 151 [$M^+ - \text{Me}$] (59%), 123 [$M^+ - \text{COMe}$] (100%).

Synthesis of 3-benzoyl-4,5-dimethylphosphinine: 3-Benzoyl-4,5-dimethylphosphinine was prepared using the procedure described above, with benzoyl chloride (10 mmol, 1.16 mL) instead of acetyl chloride. However instead of chromatographic separation the crude reaction mixture was distilled at 175 °C, 10^{-2} mbar over 8 h using a Glaskugelrohr 51 (Büchi) to give the pure 3-benzoyl-4,5-dimethylphosphinine (0.50 g, 22% yield) as a colorless oil, which turned yellow immediately on contact with air. ^1H NMR (300 MHz, CDCl_3): δ = 8.60 (dd, 1H, $^2J_{\text{PH}}$ = 36.9 Hz, $^4J_{\text{HH}}$ = 3 Hz, PCH), 8.37 (dd, 1H, $^2J_{\text{PH}}$ = 34.8 Hz, $^4J_{\text{HH}}$ = 3 Hz, PCH), 7.81–7.43 (m, 5H, Ph), 2.50 (s, 3H, CH_3), 2.22 ppm (d, $^4J_{\text{PH}}$ = 3.6 Hz, 3H, CH_3); ^{31}C NMR (75 MHz, CDCl_3): δ = 199.2 (CO), 155.6 (d, $^1J_{\text{PC}}$ = 50 Hz, PCH), 148.8 (d, $^1J_{\text{PC}}$ = 52.4 Hz, PCH), 146.2 (d, $^2J_{\text{PC}}$ = 15.4 Hz, C_β), 144.5 (d, $^2J_{\text{PC}}$ = 15.1 Hz, C_β), 136.5 (s, ipso C(Ph)), 135 (d, $^3J_{\text{PC}}$ = 19 Hz, C_γ), 133.8, 130.2, 128.7 (3s, CH(Ph)), 24.1 (d, $^3J_{\text{PC}}$ = 3 Hz, CH_3), 18.7 ppm (CH_3); ^{31}P NMR (121 MHz, CDCl_3 , external standard 85% H_3PO_4): δ = 187.4 ppm; Mass spectrum: m/z 228 [M^+] (62%), 105 [PhCO], 100%; Exact mass: calcd: 228.0704; found: 228.0738.

Received: September 16, 2004

Revised: November 10, 2004

Published online: January 20, 2005

Keywords: density functional calculations · heterocycles · phosphinines · phosphorus · reaction mechanisms

- Cossi, G. Scalmani, N. Rega, G. A. Petersson, H. Nakatsuji, M. Hada, M. Ehara, K. Toyota, R. Fukuda, J. Hasegawa, M. Ishida, T. Nakajima, Y. Honda, O. Kitao, H. Nakai, M. Klene, X. Li, J. E. Knox, H. P. Hratchian, J. B. Cross, C. Adamo, J. Jaramillo, R. Gomperts, R. E. Stratmann, O. Yazyev, A. J. Austin, R. Cammi, C. Pomelli, J. W. Ochterski, P. Y. Ayala, K. Morokuma, G. A. Voth, P. Salvador, J. J. Dannenberg, V. G. Zakrzewski, S. Dapprich, A. D. Daniels, M. C. Strain, O. Farkas, D. K. Malick, A. D. Rabuck, K. Raghavachari, J. B. Foresman, J. V. Ortiz, Q. Cui, A. G. Baboul, S. Clifford, J. Cioslowski, B. B. Stefanov, G. Liu, A. Liashenko, P. Piskorz, I. Komaromi, R. L. Martin, D. J. Fox, T. Keith, M. A. Al-Laham, C. Y. Peng, A. Nanayakkara, M. Challacombe, P. M. W. Gill, B. Johnson, W. Chen, M. W. Wong, C. Gonzalez, J. A. Pople, Gaussian, Inc., Pittsburgh, PA, **2003**.
- [10] F. Mathey, *Tetrahedron* **1974**, *30*, 3127–3137; F. Mathey, *Tetrahedron* **1976**, *32*, 2395–2400.
- [11] N. H. Tran Huy, F. Mathey, *Organometallics* **1994**, *13*, 925–928.
- [12] This point is discussed in: “Three-membered Rings.1. Phosphiranes and Phosphirenes”: F. Mathey, M. Regitz in *Phosphorus–Carbon Heterocyclic Chemistry: The Rise of a New Domain* (Ed.: F. Mathey), Elsevier, Oxford **2001**, pp. 17–55.

- [1] G. Märkl, G. Adolin, F. Kees, G. Zander, *Tetrahedron Lett.* **1977**, 3445–3448. For another synthesis, see: K. H. Dötz, A. Triliomis, K. Harms, *Tetrahedron* **1993**, *49*, 5577–5597.
- [2] 3-Chloro and 3-bromo: G. Märkl, K. Hock, *Tetrahedron Lett.* **1983**, *24*, 2645–2648; 3- CO_2Me : G. Märkl, G. Dorfmeister, *Tetrahedron Lett.* **1987**, *28*, 1093–1096; 3- PPh_2 : G. Märkl, C. Dörge, Th. Riedl, F.-G. Klärner, C. Lodwig, *Tetrahedron Lett.* **1990**, *31*, 4589–4592; 3-alkynyl: G. Märkl, S. Dorsch, *Tetrahedron Lett.* **1995**, *36*, 3839–3842.
- [3] D. G. Holah, A. N. Hughes, K. L. Knudsen, R. Perrier, *J. Heterocycl. Chem.* **1988**, *25*, 155–160; G. Märkl, C. Dörge, *Angew. Chem.* **1990**, *102*, 106–107; *Angew. Chem. Int. Ed. Engl.* **1990**, *29*, 106–107; H. Trauner, E. De la Cuesta, A. Marinetti, F. Mathey, *Bull. Soc. Chim. Fr.* **1995**, *132*, 384–393; N. Avarvari, P. Le Floch, F. Mathey, *J. Am. Chem. Soc.* **1996**, *118*, 11978–11979; N. Avarvari, P. Le Floch, L. Ricard, F. Mathey, *Organometallics* **1997**, *16*, 4089–4098.
- [4] As far as we know, the nucleophilic substitution of 3-halophosphinines by lithium amides is the only reaction of 3-functional phosphinines that has been described to date: G. Märkl, K. Hock, *Tetrahedron Lett.* **1983**, *24*, 5055–5058.
- [5] S. Holand, M. Jeanjean, F. Mathey, *Angew. Chem.* **1997**, *109*, 98–100; *Angew. Chem. Int. Ed. Engl.* **1997**, *36*, 98–100.
- [6] P. Toullec, F. Mathey, *Synlett* **2001**, 1977–1979.
- [7] J.-M. Alcaraz, F. Mathey, *Tetrahedron Lett.* **1984**, *25*, 4659–4662.
- [8] A. D. Becke, *J. Chem. Phys.* **1993**, *98*, 5648–5652; C. T. Lee, W. T. Yang, R. G. Parr, *Phys. Rev. B* **1988**, *37*, 785–789.
- [9] Gaussian03 (Revision A.1), M. J. Frisch, G. W. Trucks, H. B. Schlegel, G. E. Scuseria, M. A. Robb, J. R. Cheeseman, J. A. Montgomery, Jr., T. Vreven, K. N. Kudin, J. C. Burant, J. M. Millam, S. S. Iyengar, J. Tomasi, V. Barone, B. Mennucci, M.

Living Polymerization

Atom-Transfer Radical Reactions under Mild Conditions with $[\{\text{RuCl}_2(1,3,5\text{-C}_6\text{H}_3\text{iPr}_3)_2\}]$ and PCy_3 as the Catalyst Precursors**

Laurent Quebatte, Michel Haas, Euro Solari,
Rosario Scopelliti, Quoc T. Nguyen, and Kay Severin*

The complex $[\text{RuCl}_2(p\text{-cymene})(\text{PCy}_3)]$ (**1**) has emerged as a versatile catalyst precursor for synthetically important transformations such as ring-closing^[1] and ring-opening olefin-metathesis reactions^[2] and atom-transfer radical polymerizations (ATRP).^[3] An attractive feature of this catalyst is the fact that it can be prepared in situ from commercially available $[\{\text{RuCl}_2(p\text{-cymene})\}_2]$ (**2**) and PCy_3 . Somewhat surprising was the observation by Demonceau and co-workers that complex **1**—despite its good activity in ATRP reactions—fails to catalyze atom-transfer radical additions

[*] L. Quebatte, Dr. M. Haas, Dr. E. Solari, Dr. R. Scopelliti,
Dr. Q. T. Nguyen, Prof. K. Severin
Institut des Sciences et Ingénierie Chimiques
École Polytechnique Fédérale de Lausanne (EPFL)
1015 Lausanne (Switzerland)
Fax: (+41) 21-693-9305
E-mail: kay.severin@epfl.ch
Dr. Q. T. Nguyen
Institute of Materials, EPFL
1015 Lausanne (Switzerland)

[**] This work was supported by a postdoctoral fellowship from the Ministère de la Culture, de l'Enseignement Supérieur et de la Recherche, Luxembourg (M.H.) and by the Swiss National Science Foundation. We thank Prof. Harm-Anton Klok (EPFL) for his support with the GPC measurements.



Supporting information for this article is available on the WWW under <http://www.angewandte.org> or from the author.

(ATRA) of CCl_4 to olefins,^[4] although ATRP and ATRA are mechanistically very similar.^[5] Herein, we show that by replacing the (*p*-cymene)ruthenium complex **2** with the tris(isopropyl)benzene complex $[\text{RuCl}_2(1,3,5\text{-C}_6\text{H}_3\text{Pr}_3)_2]$ (**3**) it is possible to catalyze both ATRP and ATRA reactions under exceptionally mild conditions with high efficacy.

Activation of **1** is thought to proceed by a thermally or photochemically induced replacement of the arene ligand.^[1–3,6] We reasoned that a sterically more demanding π ligand might facilitate this replacement due to steric congestion with the PCy_3 ligand. The commonly used hexamethylbenzene complex $[\text{RuCl}_2(\text{C}_6\text{Me}_6)_2]$ was not considered because of its low solubility and because it had been reported that the reaction with PCy_3 does not give the monomeric complex $[\text{RuCl}_2(\text{C}_6\text{Me}_6)(\text{PCy}_3)]$.^[7] Instead, we focused on the tris(isopropyl)benzene complex **3**, which can be obtained easily from **2** by arene exchange.^[8]

First, we investigated the ATRP of methyl methacrylate (MMA) by using ethyl 2-bromo-2-methylpropionate as the initiator and a mixture of **3** and PCy_3 as the catalyst precursors ($\text{3/PCy}_3/\text{initiator/MMA} = 1:2:4:1600$). The reaction was carried out at a temperature of only 50°C , which is significantly below the $80\text{--}85^\circ\text{C}$ commonly employed for ruthenium-catalyzed MMA polymerizations.^[3,9,10] After 24 h, PMMA could be isolated in 90% yield. The polymer was found to have a very narrow molecular-weight distribution of $\bar{M}_w/\bar{M}_n = 1.19$ (\bar{M}_n and \bar{M}_w are the number-average and weight-average molecular mass, respectively; $\bar{M}_n = 35\,000$, initiation efficiency $f = 1.03$).^[11] Furthermore, a linear relationship of $\ln([M]_0/[M])$ versus time was observed ($[M]$ is the concentration of the monomer; see the Supporting Information), which suggests that polymerization had occurred in a controlled fashion. A radical mechanism is supported by the observed tacticity of *rr:mm:mm* = 63:30:7 and the fact that the reaction was completely inhibited by galvinoxyl. A comparison of the initial turnover frequencies (TOF)^[12] revealed that under these mild conditions, the new catalyst **3/PCy** ($\text{TOF} = 59\text{ h}^{-1}$) is one order of magnitude more active than the previously reported system **2/PCy** ($\text{TOF} = 5\text{ h}^{-1}$), which was considered to be one of the most active Ru-based catalyst systems described so far.^[13] Ethyl methacrylate can likewise be polymerized by **3/PCy** at 50°C in a controlled fashion (yield after 24 h: 89%, $\bar{M}_n = 40\,200$, $\bar{M}_w/\bar{M}_n = 1.10$, $f = 1.01$).^[11] Reactions with butyl acrylate as the monomer gave also a very high yield (99%) but revealed a bimodal molecular-weight distribution ($\bar{M}_n = 158\,500$, $\bar{M}_w/\bar{M}_n = 3.36$, $f = 0.32$).^[14] Reactions with styrene, on the other hand, gave only low amounts of polymer (yield: 9%). It should be noted, however, that the ATRP of styrene is generally carried out at temperatures above 100°C .^[9]

Encouraged by the success of the new catalyst system in ATRP reactions, we investigated the ATRA of CCl_4 and of CHCl_3 to styrene. Again, the catalyst was prepared in situ by mixing **3** with two equivalents of PCy_3 (**3**/styrene/ CHCl_3 or $\text{CCl}_4 = 1:300:450$). Two reactions were carried out in toluene at 40°C : one in the presence of a light source of moderate intensity, the other in the dark. Reactions with CCl_4 gave nearly zero conversions, whereas a conversion of 65% (yield: 63%) was observed after 24 h for reactions with CHCl_3 that

had no influence from a light source. These results were surprising in view of the higher intrinsic reactivity of CCl_4 but in accordance with the observation that complex **1** is not able to promote the addition of CCl_4 to styrene.^[4]

The time course of reactions between styrene and CHCl_3 catalyzed by complex **3** in the presence of one and two equivalents of PCy_3 is depicted in Figure 1 ($[\text{3}] = 1\text{ mol}\%$).

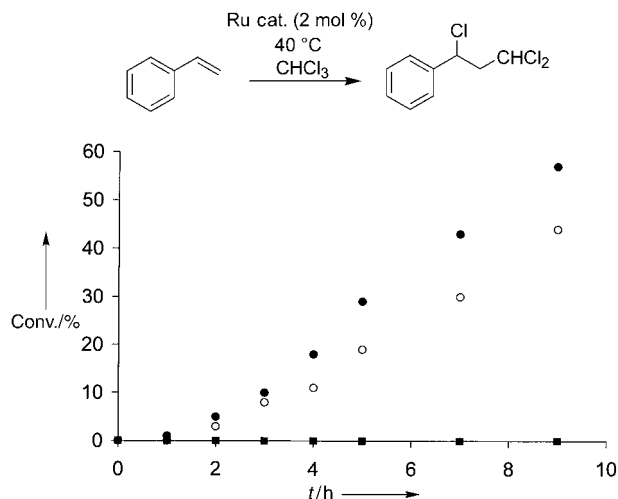


Figure 1. Time course of reactions between styrene and CHCl_3 catalyzed by **3** + 2 PCy_3 (●), **3** + 1 PCy_3 (○), and **2** + 2 PCy_3 (■). Reaction conditions: **2** or **3**/styrene/ $\text{CHCl}_3 = 1:100:150$; [**2**] or [**3**] = 13.8 mm , toluene, 40°C , no light. The conversion is based on the consumption of styrene as determined by GC.

An induction period is clearly visible, which indicates that catalyst activation must take place. A Ru/ PCy_3 ratio of 1:1 is advantageous, although the reaction rates at a later stage of this reaction (4–9 h) are similar to the reaction rates observed when substoichiometric amounts of PCy_3 are present. As in the case of the polymerization reactions, the nature of the π ligand was found to be crucial: reactions performed with the *p*-cymene complex **2** instead of the tris(isopropyl)benzene complex **3** gave zero conversion.^[15]

To test the scope and the limitations of the new catalyst system, **3/PCy**, we investigated ATRA reactions with different olefins (Table 1). The CHCl_3 adducts of the aromatic olefins *p*-chlorostyrene, *p*-methoxystyrene, 1-vinylnaphthalene, and styrene (entries 1–4) were obtained in yields of between 69 and 95% with a ruthenium catalyst concentration of 2–6 mol% at 40°C (entries 1–3) or 60°C (entry 4). It should be noted that for a Ru-based catalyst, synthetically useful yields above 80% have been described only for the carbene complex $[\text{RuCl}_2(\text{CHPh})(\text{PCy}_3)_2]$ (2.5–7.5 mol%, $65\text{--}80^\circ\text{C}$).^[16] Using a substrate/**3** ratio of 1000:1, we were able to obtain the CHCl_3 adduct of styrene in 57% yield after two weeks. This corresponds to 285 turnovers per ruthenium atom, which is, to the best of our knowledge, the highest value ever reported.^[17] MMA is a less suited substrate because polymerization becomes a significant side reaction, in accordance with the results described above (entry 5).

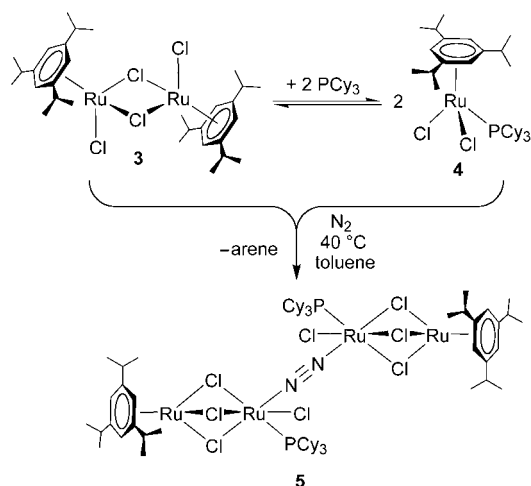
To obtain more information about the mode of activation for reactions with the new catalyst system, we examined

Table 1: ATRA reactions catalyzed by **3**/PCy₃ or by **5**.

Entry	Cat.	Substr. A	Substr. B	T [°C]	t [h]	Conv./Yield [%]
1	3 /PCy ₃	styrene	CHCl ₃	40	48	95/91 ^[a]
2	3 /PCy ₃	<i>p</i> -chlorostyrene	CHCl ₃	40	48	93/84 ^[a]
3	3 /PCy ₃	<i>p</i> -methoxystyrene	CHCl ₃	40	48	98/95 ^[b]
4	3 /PCy ₃	1-vinylnaphthalene	CHCl ₃	60	48	73/69 ^[b]
5	3 /PCy ₃	MMA	CHCl ₃	40	48	92/15 ^[a]
6	5	styrene	CHCl ₃	40	1	25/19 ^[c]
7	5	styrene	CHCl ₃	40	48	88/93 ^[c]
8	5	styrene	CCl ₄	40	2	99/98 ^[d]
9	5	MMA	CCl ₄	40	5	89/65 ^[d]
10	5	1-decene	CCl ₄	40	5	67/66 ^[d]

[a] **3**/PCy₃/olefin/CHCl₃ = 1:2:100:150, [**3**] = 13.8 mM; [b] **3**/PCy₃/olefin/CHCl₃ = 3:6:100:150, [**3**] = 41.4 mM; [c] **5**/olefin/CHCl₃ = 1:200:300; [**5**] = 6.9 mM; [d] **5**/olefin/CCl₄ = 1:600:900; [**5**] = 2.3 mM. All reactions were performed in toluene. The conversion (conv.) is based on the consumption of the olefin and the yield is based on the formation of product as determined by GC or ¹H NMR spectroscopy after the time given.

solutions of **3** and PCy₃ in [D₈]toluene by ¹H and ³¹P NMR spectroscopy. At room temperature, an equilibrium between **3**, PCy₃, and the monomeric complex [RuCl₂(1,3,5-C₆H₃iPr₃)(PCy₃)] (**4**) was rapidly established, with 25 % of the ruthenium being present in the form of **3** and 75 % in the form of the monomer **4** (Scheme 1). This reaction was



Scheme 1. In the presence of PCy₃, the dimeric complex **3** is in equilibrium with the monomeric complex **4**. Partial loss of the arene ligand leads to the formation of the tetranuclear complex **5**.

followed by slow liberation of the arene ligand. At 40 °C, this displacement proceeded with a half-life of *t*_{1/2} = 5 h. When the reaction mixture was allowed to cool to room temperature, an orange, crystalline complex precipitated. This compound was identified as the tetranuclear complex **5** based on elemental and crystallographic analysis.^[18] For comparison, the reaction between the *p*-cymene complex **1**, and arene displacement required significantly harsher reaction conditions (*t*_{1/2} = 13 h, 60 °C). When the heating was stopped after 12 h, an orange complex precipitated. Again, the results of the elemental analysis suggested that a

tetranuclear dinitrogen complex (**6**) of low solubility had formed.

Complex **5** represents the first structurally characterized product of an arene-displacement reaction with [{RuCl₂(arene)}₂] and PCy₃ (see Figure 2). A plausible mechanism of formation is the liberation of trisopropylbenzene from **4** to generate [RuCl₂(PCy₃)]_n, which subsequently reacts with unconverted **3** and N₂ to give the mixed, chloro-bridged complex **5**.^[19] The two {(1,3,5-C₆H₃iPr₃)Ru(μ-Cl)₃RuCl(PCy₃)N} fragments are related by a crystallographic inversion center. The dinitrogen ligand bridges the fragments in a nearly linear fashion (Ru1-N1-N1A = 174.9(3)°) and the N–N bond length of 1.120(4) Å is similar to that reported for other complexes with Ru–N≡N–Ru units.^[20] The Ru–Cl (Ru1/Ru2–Cl1/Cl2/Cl3 = 2.41–2.53 Å, Ru1–Cl4 = 2.3759(6) Å) and the Ru–P (2.3121(7) Å) bond lengths are within the expected range.

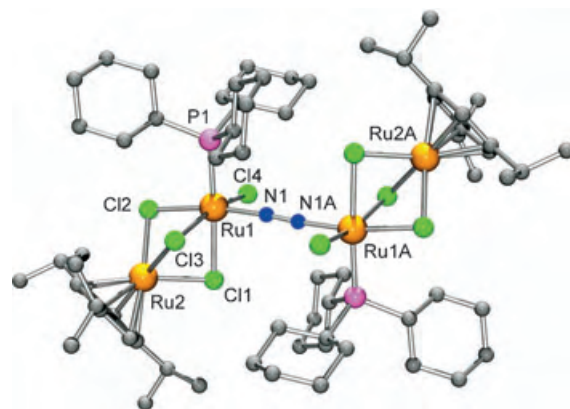


Figure 2. Molecular structure of complex **5** in the crystal. The hydrogen atoms and the solvent molecules are omitted for clarity.

The tetranuclear complex **5** is a very active ATRA catalyst. For the addition of CHCl₃ to styrene, for example, a yield of 19 % was observed after only one hour at 40 °C (Table 1, entry 6). The final yield after 48 h was similar to that found for **3**/PCy₃ (entry 7). Interestingly, complex **5** can also effect the addition of CCl₄ to olefins (entries 8–10). The observed TOFs are comparable to those of the best ATRA catalysts described so far, despite the low reaction temperature.^[21] In this context it is interesting to note that two other complexes containing a {Ru–N≡N–Ru} structural motif were reported to catalyze atom-transfer radical reactions.^[21a,22] For both complexes it was suggested that catalyst activation proceeds by a CCl₄-induced loss of the N₂ ligand, and a similar mode of activation appears likely for reactions with **5**.

Since the mixture of **3** and PCy₃ was inactive for CCl₄ additions, CCl₄ seemed to interfere with catalyst activation. Control experiments showed that this is indeed the case. CCl₄ was found to react immediately with PCy₃ to give a trichloromethylphosphonium salt.^[23] The phosphine is thus

removed from the equilibrium between **3** and **4**, thus preventing the formation of the catalytically active ruthenium complex.

In summary, we have demonstrated that a mixture of complex **3** and PCy₃ can be used to efficiently catalyze atom-transfer radical reactions at exceptionally low temperatures. Less than 0.07 mol % of complex **3** is required to quantitatively polymerize methacrylates in a controlled fashion at 50 °C. For the ATRA of the notoriously difficult substrate CHCl₃ to aromatic olefins, synthetically useful yields of > 80 % can be obtained with only 1–3 mol % of complex **3** at 40 °C. We have evidence that catalyst activation proceeds by a PCy₃-induced substitution of the arene ligand, and for the first time a product of such a reaction has been structurally characterized.

Experimental Section

Synthesis of complex 5: Complex **3** (100 mg, 133 μmol) was added to a solution of PCy₃ (37.3 mg, 133 μmol) in toluene (10 mL). The solution was stirred for 4 h at 40 °C and then allowed to cool to room temperature. After one week, orange crystals formed, which were collected and washed with pentane (yield: 78.3 mg, 70 %). Elemental analysis calcd (%) for C₆₆H₁₁₄Cl₈N₂P₂Ru₄·2 C₆H₅CH₃: C 51.39, H 7.01, N 1.50; found: C 51.53, H 6.95, N 1.15. The same complex was obtained in reactions with a 3/PCy₃ ratio of 1:2, but the yields were lower. NMR spectra were not recorded owing to the low solubility of **5** in benzene or toluene. In chlorinated solvents the decomposition of **5** was observed.

General polymerization procedure: The monomer and a solution of the initiator in toluene (ethyl 2-bromo-2-methylpropionate for acrylates and 1-bromoethylbenzene for styrene; 0.1 M) were added to a Schlenk tube that contained the ruthenium complex **2** or **3** (6.25 μmol) and PCy₃, such that the molar ratios [Ru]/[initiator]/[monomer] were 1:2:800. *n*-Octane (50 μL) was added as the internal standard for GC measurements. Immediately after the components had been mixed, the tube was placed in a thermostatted oil bath (50 °C), which was shielded from light. After a given period of time, the mixture was cooled and diluted with THF (6 mL). The polymer was then precipitated with hexane (acrylates) or with methanol (styrene), isolated, and dried under vacuum. Remaining traces of catalyst were removed by dissolving the polymer in toluene and by adding silica gel. After the silica gel had been removed, the solvent was removed by evaporation and the polymer was dried in vacuum. All reactions were performed under an atmosphere of dry nitrogen and with freshly distilled substrates and solvents. The molecular weights and the molecular-weight distributions of the polymers were determined by gel permeation chromatography (DMF, 60 °C) with PMMA standards. The conversions were determined by GC and the yields by mass.

Received: September 18, 2004

Published online: January 20, 2005

Keywords: homogeneous catalysis · living polymerization · polymers · ruthenium

Chem. **2000**, *606*, 55–64; c) A. Hafner, A. Mühlebach, P. A. van der Schaaf, *Angew. Chem.* **1997**, *109*, 2213–2216; *Angew. Chem. Int. Ed. Engl.* **1997**, *36*, 2121–2124; d) A. Demonceau, A. W. Stumpf, E. Saive, A. F. Noels, *Macromolecules* **1997**, *30*, 3127–3136; e) A. W. Stumpf, E. Saive, A. Demonceau, A. F. Noels, *J. Chem. Soc. Chem. Commun.* **1995**, 1127–1128; f) A. Demonceau, A. F. Noels, E. Saive, A. J. Hubert, *J. Mol. Catal.* **1992**, *76*, 123–132.

- [3] a) F. Simal, D. Jan, L. Delaude, A. Demonceau, M.-R. Spirlet, A. F. Noels, *Can. J. Chem.* **2001**, *79*, 529–535; b) F. Simal, S. Seville, L. Hallet, A. Demonceau, A. F. Noels, *Macromol. Symp.* **2000**, *161*, 73–85; c) F. Simal, D. Jan, A. Demonceau, A. F. Noels in *Controlled/Living Radical Polymerization* (Ed.: K. Matyjaszewski), ACS Symposium Series 768, ACS, Washington, **2000**, chap. 16; d) F. Simal, A. Demonceau, A. F. Noels, *Angew. Chem.* **1999**, *111*, 559–562; *Angew. Chem. Int. Ed.* **1999**, *38*, 538–540.
- [4] F. Simal, A. Demonceau, A. F. Noels, *Tetrahedron Lett.* **1999**, *40*, 5689–5693.
- [5] a) M. Kamigaito, T. Ando, M. Sawamoto, *Chem. Rev.* **2001**, *101*, 3689–3745; b) K. Matyjaszewski, J. Xia, *Chem. Rev.* **2001**, *101*, 2921–2990.
- [6] For an early report on arene-replacement reactions of [RuCl₂(*p*-cymene)(PR₃)₂] complexes see: M. A. Bennett, A. K. Smith, *J. Chem. Soc. Dalton Trans.* **1974**, 233–241.
- [7] M. A. Bennett, T.-N. Huang, J. L. Latten, *J. Organomet. Chem.* **1984**, *272*, 189–205.
- [8] J. W. Hull Jr., W. L. Gladfelter, *Organometallics* **1984**, *3*, 605–613.
- [9] For some recent examples of Ru-catalyzed ATRP reactions see: a) T. Opstal, F. Verpoort, *Angew. Chem.* **2003**, *115*, 2982–2985; *Angew. Chem. Int. Ed.* **2003**, *42*, 2876–2879; b) L. Delaude, S. Delfosse, A. Richel, A. Demonceau, A. F. Noels, *Chem. Commun.* **2003**, 1526–1527; c) T. Opstal, K. Couchez, F. Verpoort, *Adv. Synth. Catal.* **2003**, *345*, 393–401; d) F. Simal, S. Delfosse, A. Demonceau, A. F. Noels, K. Denk, F. J. Kohl, T. Weskamp, W. A. Herrmann, *Chem. Eur. J.* **2002**, *8*, 3047–3052; e) M. Kamigaito, Y. Watanabe, T. Ando, M. Sawamoto, *J. Am. Chem. Soc.* **2002**, *124*, 9994–9995; f) B. De Clercq, F. Verpoort, *Macromolecules* **2002**, *35*, 8943–8947; g) B. De Clercq, F. Verpoort, *J. Mol. Catal. A* **2002**, *180*, 67–76; S. Hamasaki, M. Kamigaito, M. Sawamoto, *Macromolecules* **2002**, *35*, 2934–2940; h) Y. Watanabe, T. Ando, M. Kamigaito, M. Sawamoto, *Macromolecules* **2001**, *34*, 4370–4374; i) T. Ando, M. Kamigaito, M. Sawamoto, *Macromolecules* **2000**, *33*, 5825–5829.
- [10] The ruthenium complex [RuH₂(PPh₃)₄] was reported to catalyze the controlled polymerization of MMA at 30 °C, but significantly higher catalyst concentrations (MMA/Ru = 200:1) and reaction times (300 h) were required: H. Takahashi, T. Ando, M. Kamigaito, M. Sawamoto, *Macromolecules* **1999**, *32*, 6455–6461.
- [11] Generally, values below 1.0 are observed. Currently, we have no explanation for this discrepancy.
- [12] The initial TOF was calculated from the conversion of MMA per ruthenium atom after 6 h as determined by gas chromatography.
- [13] Some copper complexes are also able to catalyze the ATRP of MMA at ambient temperatures, but the catalyst concentrations are generally higher (MMA/Cu ≈ 100:1). See for example: a) D. P. Chatterjee, U. Chatterjee, B. M. Mandal, *J. Polym. Sci. Part A* **2004**, *42*, 4132–4142; b) D. M. Haddleton, D. Kukulj, D. J. Duncalf, A. M. Heming, A. J. Shooter, *Macromolecules* **1998**, *31*, 5201–5205.
- [14] Bimodal GPC profiles have previously been observed in ATRP reactions with ruthenium catalysts and butyl acrylate as the monomer: O. Tutusaus, S. Delfosse, F. Simal, A. Demonceau, A. F. Noels, R. Núñez, C. Viñas, F. Teixidor, *Inorg. Chem. Commun.* **2002**, *5*, 941–945.

[1] a) A. Fürstner, T. Müller, *J. Am. Chem. Soc.* **1999**, *121*, 7814–7821; b) A. Fürstner, L. Ackermann, *Chem. Commun.* **1999**, 95–96.

[2] a) J. Baran, I. Bogdanska, D. Jan, L. Delaude, A. Demonceau, A. F. Noels, *J. Mol. Catal. A* **2002**, *190*, 109–116; b) D. Jan, L. Delaude, F. Simal, A. Demonceau, A. F. Noels, *J. Organomet.*

- [15] At higher temperatures or upon photochemical activation, the ATRA of CHCl_3 to styrene was also observed for reactions with **1** and PCy_3 .
- [16] a) B. T. Lee, T. O. Schrader, B. Martín-Matute, C. R. Kauffman, P. Zhang, M. L. Snapper, *Tetrahedron* **2004**, *60*, 7391–7396; b) J. A. Tallarico, L. M. Malnick, M. L. Snapper, *J. Org. Chem.* **1999**, *64*, 344–345.
- [17] To the best of our knowledge, the highest turnover number (TON) for a Ru-catalyzed addition of CHCl_3 to styrene was reported for the complex $[\text{Cp}^*\text{RuCl}(\text{PPh}_3)_2]$ (TON = 207, 85 °C, 24 h; Cp^* = pentamethylcyclopentadienyl): F. Simal, L. Włodarczyk, A. Demonceau, A. F. Noels, *Eur. J. Org. Chem.* **2001**, 2689–2695.
- [18] Crystal data for $5 \cdot 2 \text{C}_6\text{H}_5\text{CH}_3 \cdot \text{C}_{80}\text{H}_{130}\text{Cl}_8\text{N}_2\text{P}_2\text{Ru}_2$, $M_r = 1869.68$, monoclinic, space group $P2(1)/c$, $a = 13.1038(8)$, $b = 19.3979(10)$, $c = 17.8631(8)$ Å, $\alpha = 90$, $\beta = 109.074(5)$, $\gamma = 90^\circ$, $V = 4291.2(4)$ Å³, $Z = 2$, $\rho_{\text{calcd}} = 1.447 \text{ g cm}^{-3}$, $\mu = 1.018 \text{ mm}^{-1}$, $F(000) = 1932$, crystal dimensions $0.19 \times 0.18 \times 0.13 \text{ mm}^3$. Data collection: KM4/Sapphire CCD, $T = 140(2) \text{ K}$, $\text{MoK}\alpha$ radiation, $\lambda = 0.71073$ Å, $\theta = 3.20\text{--}25.02^\circ$, $-15 \leq h \leq 15$, $-23 \leq k \leq 23$, $-20 \leq l \leq 21$, 24640 reflections collected, 7567 independent reflections, $R_{\text{int}} = 0.0329$, semi-empirical absorption correction (MULABS), max./min. transmission: 0.9485/0.7504. Refinement: $N_{\text{ref}} = 7567$, $N_{\text{par}} = 473$, $R_1 [I > 2\sigma(I)] = 0.0252$, wR_2 (all data) = 0.0601, largest difference peak 0.475 e Å^{-3} , largest difference minimum -0.673 e Å^{-3} . Structure solution and refinement by SHELX97 (G. M. Sheldrick, SHELX97, Programs for Crystal Structure Analysis, University of Göttingen, Göttingen (Germany), **1998**). H atoms were placed in calculated positions by using the riding model. CCDC-247810 contains the supplementary crystallographic data for this paper. These data can be obtained free of charge from The Cambridge Crystallographic Data Centre via www.ccdc.cam.ac.uk/data_request/cif.
- [19] For some recent publications about mixed, halogeno-bridged complexes see: a) S. Gauthier, R. Scopelliti, K. Severin *Organometallics* **2004**, *23*, 3769–3771; b) S. Gauthier, L. Quebatte, R. Scopelliti, K. Severin, *Chem. Eur. J.* **2004**, *10*, 2811–2821; c) S. Gauthier, L. Quebatte, R. Scopelliti, K. Severin, *Inorg. Chem. Commun.* **2004**, *7*, 708–712; d) K. Severin, *Chem. Eur. J.* **2002**, *8*, 1514–1518, and references therein.
- [20] a) L. Bonomo, C. Stern, E. Solari, R. Scopelliti, C. Floriani, *Angew. Chem.* **2001**, *113*, 1497–1500; *Angew. Chem. Int. Ed.* **2001**, *40*, 1449–1452; b) V. Rodriguez, I. Atheaux, B. Donnadiou, S. Sabo-Etienne, B. Chaudret, *Organometallics* **2000**, *19*, 2916–2926; c) D. G. Gusev, F. M. Dolgushin, M. Y. Antipin, *Organometallics* **2000**, *19*, 3429–3434; d) K. Abdur-Rashid, D. G. Gusev, A. J. Lough, R. H. Morris, *Organometallics* **2000**, *19*, 1652–1660; e) R. A. T. M. Abbenhuis, I. del Río, M. M. Bergshoef, J. Boersma, N. Veldman, A. L. Spek, G. van Koten, *Inorg. Chem.* **1998**, *37*, 1749–1758.
- [21] For highly active ATRA catalysts see reference [14] and: a) L. Quebatte, R. Scopelliti, K. Severin, *Angew. Chem.* **2004**, *116*, 1546–1550; *Angew. Chem. Int. Ed.* **2004**, *43*, 1520–1524; b) O. Tutusaus, C. Viñas, R. Núñez, F. Teixidor, A. Demonceau, S. Delfosse, A. F. Noels, I. Mata, E. Molins, *J. Am. Chem. Soc.* **2003**, *125*, 11830–11831; c) T. Opstal, F. Verpoort, *New J. Chem.* **2003**, *27*, 257–262; d) B. De Clercq, F. Verpoort, *J. Organomet. Chem.* **2003**, *672*, 11–16; e) O. Tutusaus, S. Delfosse, A. Demonceau, A. F. Noels, C. Viñas, F. Teixidor, *Tetrahedron Lett.* **2003**, *44*, 8421–8425; f) R. A. Gossage, L. A. Van de Kuil, G. van Koten, *Acc. Chem. Res.* **1998**, *31*, 423–431.
- [22] I. del Río, G. van Koten, M. Lutz, A. L. Spek, *Organometallics* **2002**, *21*, 361–364.
- [23] PPh_3 shows similar reactivity: R. Appel, *Inorg. Synth.* **1986**, *24*, 107–109.

A Rock-Salt-Like Lattice Structure Consisting of Monocationic and Monoanionic Au^IAg^ICu^{II} Supramolecular Cages of D-Penicillamine**

Atsushi Toyota, Tadashi Yamaguchi, Asako Igashira-Kamiyama, Tatsuya Kawamoto, and Takumi Konno*

Over the past decade, considerable interest has been devoted to the controlled synthesis of metallosupramolecular species, such as finite coordination rings and cages and infinite coordination polymers, not only because of their intriguing structural diversity but also because of their potential as new functional materials.^[1] While the most common approach to obtain metallosupramolecules is based on the self-assembly of multidentate organic ligands and metal ions, our synthetic strategy has been directed toward the use of metal complexes with sulfur-containing aminocarboxylates such as L-cysteinate (L-cys) and D-penicillamine (D-pen) as building blocks, which are aggregated by forming S-bridged structures with transition metal ions.^[2] Recently, we have found that the six-coordinate complexes [Co(L-cys-*N,S*)(en)₂]⁺ (en = ethylenediamine) and [Re^VO(D-pen-*N,S*)(D-pen-*N,O,S*)][−] can bind to Ag^I ions not only through thiolato groups but also through pendant carboxylate groups to produce a variety of supramolecular structures, including 1D helix and 2D sheet.^[2b-d] This result showed the suitability of L-cys and D-pen metal complexes as favorable building blocks that adopt various binding modes toward transition metal ions.

To expand the range of mixed-metal supramolecular architectures constructed from simple sulfur-containing aminocarboxylates, we investigated the binding ability of the two-coordinate Au^I complex [Au(D-pen-*S*)₂]^{3−},^[3] which was prepared as a model of gold-based antiarthritis drugs. In this complex, two D-pen ligands coordinate to a linear Au^I center only through thiolato groups, thus leaving two amino and two carboxylate groups as potential binding sites for additional metal ions, besides two coordinated thiolato groups. Here we report that the stepwise reaction of [Au(D-pen-*S*)₂]^{3−} with Ag^I and Cu^{II} in the presence of Cl[−] (Scheme 1) creates a

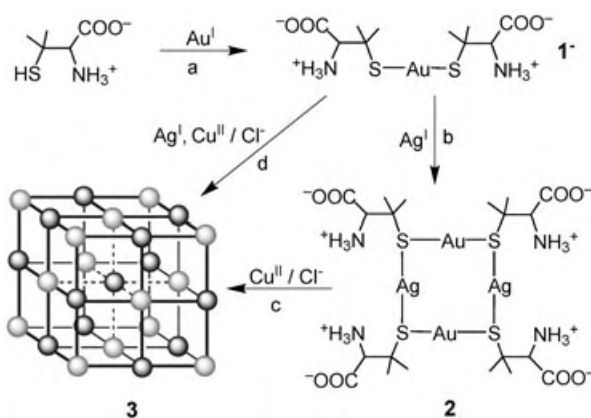
[*] A. Toyota, Dr. A. Igashira-Kamiyama, Dr. T. Kawamoto, Prof. T. Konno
Department of Chemistry
Graduate School of Science
Osaka University
Toyonaka, Osaka 560-0043 (Japan)
Fax: (+81) 6-6850-5765
E-mail: konno@ch.wani.osaka-u.ac.jp

Dr. T. Yamaguchi
Department of Chemistry
School of Science and Engineering
Waseda University
Shinjuku-ku, Tokyo 169-8555 (Japan)

[**] This work was supported by a Grant-in-Aid for Scientific Research on Priority Area (no. 16033235) from the Ministry of Education, Culture, Sports, Science, and Technology.



Supporting information for this article is available on the WWW under <http://www.angewandte.org> or from the author.



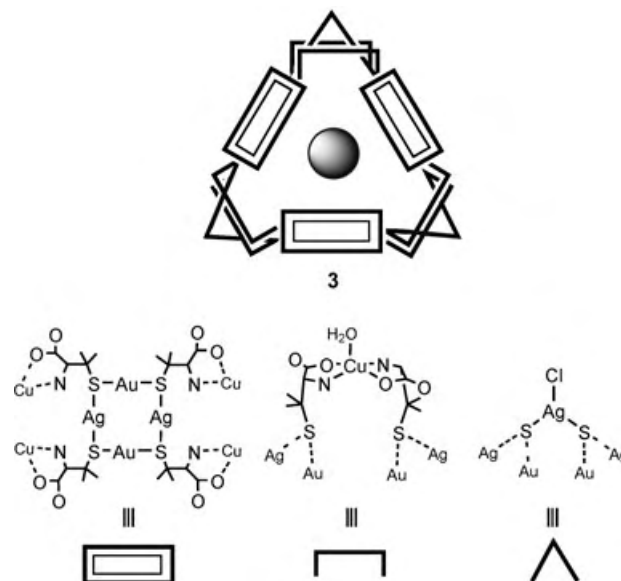
Scheme 1. Synthetic routes to **3** by way of **1** and **2**. a) $[\text{AuCl}\{\text{S}(\text{CH}_2\text{CH}_2\text{OH})_2\}]$ in methanol; b) AgNO_3 in water; c) CuCl_2 in aqueous acetate buffer; d) AgNO_3 , $\text{Cu}(\text{NO}_3)_2 \cdot 3\text{H}_2\text{O}$, and NH_4Cl in aqueous acetate buffer.

metallo-supramolecular architecture containing all three coinage metals, gold(I), silver(I), and copper(II). While several metal compounds with two of the three coinage metals have been prepared,^[4] to our knowledge, incorporation of Au^{I} , Ag^{I} , and Cu^{II} in one supramolecular structure is unprecedented. Remarkably, this product was found to be composed of monocationic 20-nuclear $\text{Au}_6^{\text{I}}\text{Ag}_6^{\text{I}}\text{Cu}_6^{\text{II}}$ and monoanionic 21-nuclear $\text{Au}_6^{\text{I}}\text{Ag}_6^{\text{I}}\text{Cu}_6^{\text{II}}$ supramolecular cages encapsulating a Cl^- ion, which are regularly coupled to each other to construct a unique rock-salt-like lattice structure comprising huge monocationic and monoanionic metallo-supramolecules.

Treatment of $(\text{NH}_4)[\text{Au}(\text{D-Hpen})_2]$ (**1**)^[5] with AgNO_3 in a 1:1 ratio rapidly gave a photoluminescent white powder (**2**).^[6] Compound **1** is sparingly soluble in water at neutral pH, but shows good solubility in acidic or basic aqueous solution. X-ray fluorescence spectrometry confirmed the presence of Au and Ag in **2**, and its elemental analytical data were in good agreement with the 1:1 stoichiometry of $\text{Ag}[\text{Au}(\text{D-Hpen})_2]$. The ^1H and ^{13}C NMR spectra of **2** in D_2O (1M Na_2CO_3), each of which exhibits only a single set of signals, are very similar to those of **1**. However, the ^{13}C NMR signal ($\delta = 54.33$ ppm) due to the tertiary C atom adjacent to the S atom is strongly shifted downfield relative to the corresponding signal for **1** ($\delta = 51.02$ ppm). This suggests that in solution Ag^{I} ions are connected to $[\text{Au}(\text{D-Hpen-S})_2]^-$ through S atoms, compatible with the tendency of soft Ag^{I} ions to coordinate to soft thiolato groups. Accordingly, **2** is assumed to be the neutral $\text{Au}_2^{\text{I}}\text{Ag}_2^{\text{I}}$ complex $[\text{Au}_2\text{Ag}_2(\text{D-Hpen-S})_4]$ in which two $[\text{Au}(\text{D-Hpen-S})_2]^-$ molecules are linked by two Ag^{I} atoms through S atoms to form a $\text{Au}_2^{\text{I}}\text{Ag}_2^{\text{I}}\text{S}_4$ square (Scheme 1). Consistent with this assumption, the electrospray mass spectrum (ES-MS) of **2** in methanol:water (1:1/ Na_2CO_3) gave a main signal at $m/z = 1201$, the calculated molecular mass and the isotopic distribution of which match well with those for $[\text{Au}_2\text{Ag}_2(\text{D-Hpen-S})(\text{D-Hpen-S})_3]^-$. If this proposed structure is correct, **2** is expected to bind with a third metal ion by using the four free N,O arms to form a metalloaggregate composed of $[\text{Au}_2\text{Ag}_2(\text{D-Hpen-S})_4]^{4-}$ square units. Indeed, when **2** was treated with an excess of CuCl_2 in an aqueous buffer solution (pH 6.2), blue cubelike crystals of **3** were isolated from the

blue reaction solution. While the quite poor solubility of **3** precluded its characterization in solution, the presence of Au, Ag, and Cu atoms and D-pen ligands was revealed by the X-ray fluorescence, IR ($\nu_{\text{CO}} = 1600\text{ cm}^{-1}$), UV/Vis (broad band at ca. 615 nm), and CD (broad positive band at ca. 595 nm) spectroscopy in the solid state, together with the elemental analysis. The structure of **3**, which crystallizes in the cubic space group $P2_13$, was established by single-crystal X-ray crystallography.^[7]

The asymmetric unit of **3** contains one-third of two crystallographically independent $\text{Au}^{\text{I}}\text{Ag}^{\text{I}}\text{Cu}^{\text{II}}$ clusters with D-pen ligands (**3a** and **3b**), besides lattice water molecules (see Supporting Information). As shown in Scheme 2 and Figure 1,



Scheme 2. Representation of the anionic cluster **3a**.

the entire cluster **3a** consists of three distorted square units of $[\text{Au}_2\text{Ag}_2(\text{D-pen-S})_4]^{4-}$, in which two Au^{I} and two Ag^{I} atoms are alternately bridged by four S atoms from four D-pen²⁻ ligands (av Au–S 2.301(5), Ag–S 2.485(4) Å, S–Au–S 171.8(2), S–Ag–S 152.7(2)°). The three $[\text{Au}_2\text{Ag}_2(\text{D-pen-S})_4]^{4-}$ units are linked by six Cu^{II} atoms through NH_2 and COO^- groups to form a cyclic cage structure (av Cu–N 1.99(2), Cu–O 1.90(2) Å). In this structure, six Cu^{II} and six Ag^{I} ions are arranged to form an outer and an inner twisted trigonal prism, respectively, and six Au^{I} atoms are located between them. Each Cu^{II} atom is chelated in a planar fashion by two N,O arms from two different $[\text{Au}_2\text{Ag}_2(\text{D-pen-S})_4]^{4-}$ units in a *trans* geometry, while its apical site is occupied by a water molecule (av Cu–O 2.44(2) Å). This $\text{Au}_6^{\text{I}}\text{Ag}_6^{\text{I}}\text{Cu}_6^{\text{II}}$ cage structure is sustained by three additional Ag^{I} atoms, each of which is trigonally coordinated by two S atoms from two different $[\text{Au}_2\text{Ag}_2(\text{D-pen-S})_4]^{4-}$ units and a Cl^- atom (av Ag–S 2.558(5), Ag–Cl 2.406(5) Å). In addition, one Cl^- ion is encapsulated in the center of the cage and has short contacts with the six inner Ag^{I} atoms (av Ag...Cl 3.072(4) Å). Thus, **3a** is a 21-nuclear monoanionic cage cluster with a diameter of about 16 Å and a height of about 12 Å, which is composed of 6 Au^{I} , 9 Ag^{I} , and

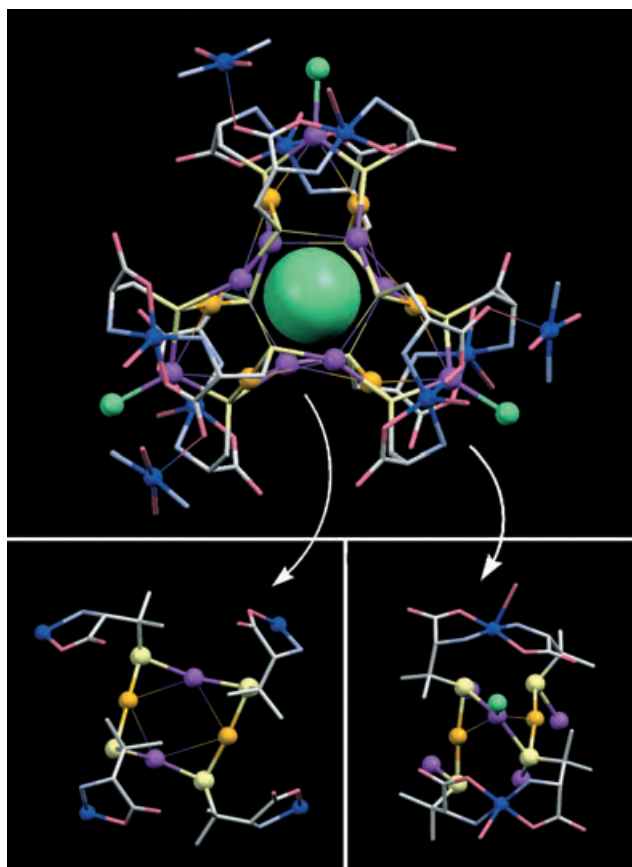


Figure 1. Top: stereoview of the anionic cluster **3a** bound by three Cu^{II} ions from the three adjacent cationic clusters **3b**: Au orange, Ag purple, Cu blue, Cl green, S yellow, O pink, N light blue, C light gray. Lower: structural details.

6 Cu^{II} ions in combination with 12 D-pen^{2-} ligands, 4 Cl^- atoms, and 6 H_2O molecules. Of note is the presence of 18

metallophilic $\text{Au}\cdots\text{Ag}$ interactions with distances of 2.880(2)–3.249(2) Å in **3a**,^[4b–d] together with six $\text{Ag}\cdots\text{S}$ interactions (2.875(5)–2.936(5) Å), which complete the rigid $\text{Au}_6^{\text{I}}\text{Ag}_9^{\text{I}}\text{S}_{12}$ core structure. The structure of cluster **3b**, which also encapsulates a Cl^- atom at the center of the cage (av $\text{Ag}\cdots\text{Cl}$ 3.140(5) Å), appears to be virtually the same as that of cluster **3a** (Figure 2). However, in **3b** the cage consisting of three $[\text{Au}_2\text{Ag}_2(\text{D-pen-S})_4]^{4-}$ units (av Au-S 2.298(5), Ag-S 2.472(5) Å, S-Au-S 173.5(2), S-Ag-S 157.2(2)°) and six Cu^{II} ions is bound by two $[\text{Ag}(\text{H}_2\text{O})]^{+}$ moieties (av Ag-S 2.534(6), Ag-O 2.34(2) Å), which are disordered in two of three positions, in place of three $[\text{AgCl}]^0$ moieties in **3a**. Thus, **3b** is composed of 6 Au^{I} , 8 Ag^{I} , and 6 Cu^{II} ions in combination with 12 D-pen^{2-} ligands, one Cl^- atom, and two H_2O molecules, which construct a 20-nuclear monocationic cage structure. In **3b** only three of six *trans*- CuN_2O_2 planes are coordinated by apical water molecules (Cu-O 2.30(1) Å), each of which forms a hydrogen bond to the carboxylato O atom of the adjacent monoanionic cluster of **3a** ($\text{O}\cdots\text{O}$ 2.85(2) Å).^[8] The apical positions of the remaining three *trans*- CuN_2O_2 planes are bound by three COO^- groups from three different monoanionic clusters with a Cu-O distance of 2.38(1) Å. As a result, the monoanionic and monocationic cage clusters are connected to each other such that each anionic/cationic cage is octahedrally surrounded by six cationic/anionic cages to form a rock-salt-like lattice structure with a volume that is about 200 times larger than that of NaCl (Figure 3).^[8,9]

The EPR spectrum of a solid sample of **3** at 77 K displays a simple isotropic signal with $g=2.12$, consistent with the presence of Cu^{II} ions. Furthermore, a very weak half-field transition band is observed, which is indicative of the presence of a weak magnetic exchange interaction between two adjacent Cu^{II} centers.^[10] The weak antiferromagnetic character of the interaction between Cu^{II} centers was revealed by the magnetic measurements for **3** in the temperature range of 2 to 300 K. The plot of $\chi_{\text{m}}T$ versus T is almost constant in

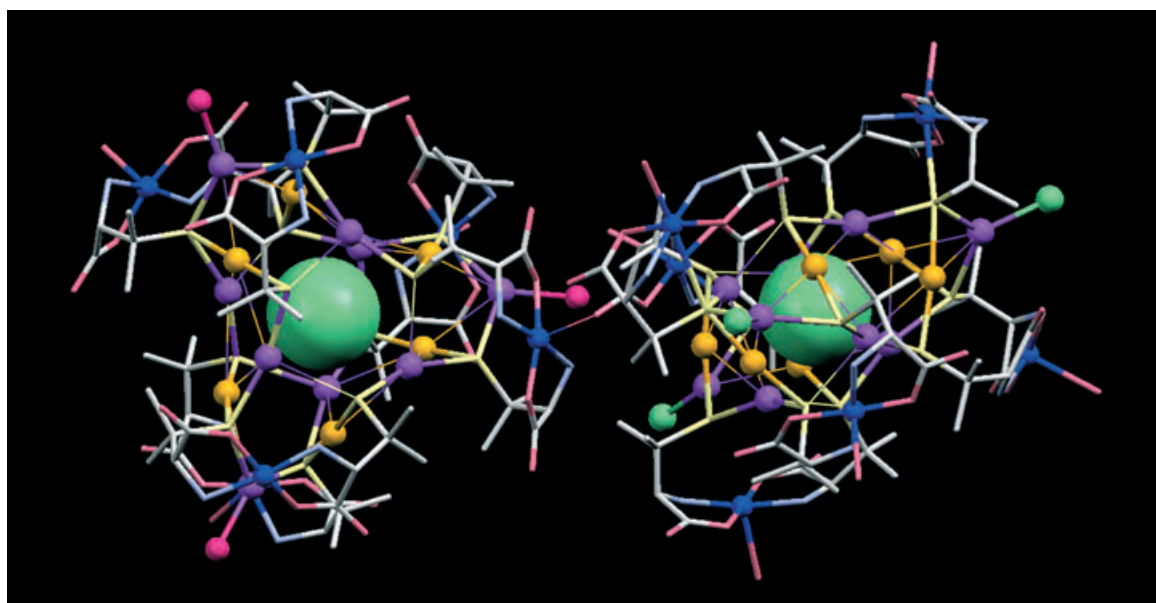


Figure 2. Stereoview of the cationic cluster **3b** (left) linked with the anionic cluster **3a** (right): Au orange, Ag purple, Cu blue, Cl green, S yellow, O pink, N light blue, C light gray.

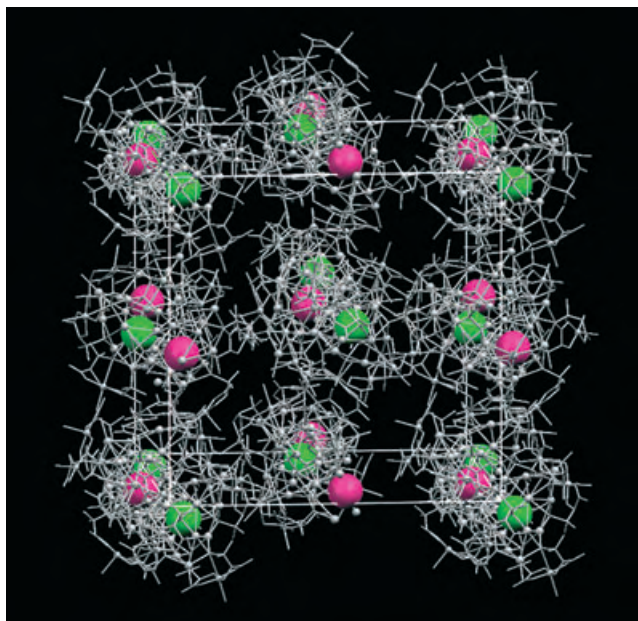


Figure 3. Rock-salt-like lattice structure of **3**. Green balls: central Cl^- ions in anionic clusters **3a**, pink balls: central Cl^- ions in cationic clusters **3b**.

the range of 300 to 40 K with a $\chi_m T$ value of about $4.72 \text{ cm}^3 \text{ K mol}^{-1}$, which is slightly smaller than the spin-only value of $5.05 \text{ cm}^3 \text{ K mol}^{-1}$ for the magnetically dilute 12 Cu^{II} centers, and then decreases sharply to $4.10 \text{ cm}^3 \text{ K mol}^{-1}$ at 2 K on lowering the temperature.

When one equivalent of AgNO_3 was added to the reaction mixture of **2** and CuCl_2 , **3** was obtained in higher yield, as expected from the presence of additional Ag^{I} atoms that support the cage structure in **3**. On the other hand, the use of $\text{Cu(NO}_3)_2 \cdot 3\text{H}_2\text{O}$ instead of CuCl_2 did not afford **3**, and a green–blue powder was obtained instead. Thus, the Cl^- ion incorporated in the center of each cage is essential for the formation of **3**. Interestingly, **3** was also produced by the one-pot reaction of **1** with a mixture of AgNO_3 and $\text{Cu(NO}_3)_2 \cdot 3\text{H}_2\text{O}$ in the presence of NH_4Cl (Scheme 1).^[11,12]

In summary, $(\text{NH}_4)[\text{Au}(\text{D-Hpen})_2]$ (**1**) readily reacts with Ag^{I} to afford $[\text{Au}_2\text{Ag}_2(\text{D-Hpen-S})_4]$ (**2**) as a white solid, which further reacts with Cu^{II} in the presence of Cl^- ions to produce blue crystals of $\text{Au}^{\text{I}}\text{Ag}^{\text{I}}\text{Cu}^{\text{II}}$ complex **3**. Thus, $[\text{Au}(\text{D-pen-S})_2]^{3-}$ can bind to both soft and hard metal ions using two amino and two carboxylate groups, besides two coordinated thiolato groups. Compound **3** was found to be a remarkable heterometallic aggregate comprising two kinds of supramolecular cages, $[\text{Au}_6\text{Ag}_8\text{Cu}_6\text{Cl}(\text{H}_2\text{O})_5(\text{D-pen})_{12}]^+$ and $[\text{Au}_6\text{Ag}_9\text{Cu}_6\text{Cl}_4(\text{H}_2\text{O})_6(\text{D-pen})_{12}]^-$, each of which accommodates a Cl^- ion. Although several metallocages templated by a Cl^- ion have been reported,^[13] **3** is the first example of a supramolecular cage involving three coinage metal ions, Ag^{I} , Au^{I} , and Cu^{II} . The overall charge of each cage in **3** is ingeniously regulated by the attachment of $[\text{AgCl}]^0$ or $[\text{Ag}(\text{H}_2\text{O})]^+$ fragments, such that the 20-nuclear monocationic and the 21-nuclear monoanionic cage clusters combine to generate an unprecedented 1:1 supramolecular salt with a rock-salt-like lattice structure. Finally, the results demonstrate that heterometallic supra-

molecular species exhibiting unique structures and multiple supramolecular interactions can be created exclusively from simple sulfur-containing aminocarboxylates by stepwise combination with appropriate transition metal ions. Work is in progress to construct other supramolecular structures based on **1** and **2** in combination with other transition metal ions.

Experimental Section

3: A solution of CuCl_2 (23 mg, 0.17 mmol) in an acetate buffer solution (pH 6.2, 150 mL) was added to a colorless solution containing **2** (50 mg, 0.04 mmol) and Na_2CO_3 (25 mg) in water (10 mL). The green mixture was stirred at RT overnight, during which time the solution turned blue. The blue solution was concentrated to ca. 10 mL and allowed to stand at RT for several days. The resulting blue cubelike crystals were collected by filtration. Yield: 24 mg (42% based on Au); elemental analysis (%) calcd for $[\text{Au}_6\text{Ag}_8\text{Cu}_6\text{Cl}(\text{H}_2\text{O})_5(\text{D-pen})_{12}][\text{Au}_6\text{Ag}_9\text{Cu}_6\text{Cl}_4(\text{H}_2\text{O})_6(\text{D-pen})_{12}] \cdot 13.5 \text{ H}_2\text{O}$ ($\text{C}_{120}\text{H}_{265}\text{Ag}_{17}\text{Au}_{12}\text{Cl}_5\text{Cu}_{12}\text{N}_{24}\text{O}_{72.5}\text{S}_{24}$): C 15.82, H 2.93, N 3.69; found: C 15.54, H 2.88, N 3.65. The addition of 1 equiv of AgNO_3 (7 mg, 0.04 mmol) to the above green mixture led to the formation of blue crystals in higher yield (72% based on Au).

Received: October 5, 2004

Published online: January 3, 2005

Keywords: aggregation · cage compounds · S ligands · supramolecular chemistry · transition metals

- [1] a) S. Leininger, B. Olenyuk, P. J. Stang, *Chem. Rev.* **2000**, *100*, 853–908; b) G. F. Swiegers, T. J. Malefetse, *Chem. Rev.* **2000**, *100*, 3483–3537; c) B. J. Holliday, C. A. Mirkin, *Angew. Chem.* **2001**, *113*, 2076–2097; *Angew. Chem. Int. Ed.* **2001**, *40*, 2022–2043; d) M. D. Ward, J. A. McCleverty, J. C. Jeffery, *Coord. Chem. Rev.* **2001**, *222*, 251–272; e) C. Janiak, *Dalton Trans.* **2003**, 2781–2804.
- [2] a) T. Konno, M. Hattori, T. Yoshimura, M. Hirotsu, *Chem. Lett.* **2000**, 852–853; b) T. Konno, T. Yoshimura, K. Aoki, K. Okamoto, M. Hirotsu, *Angew. Chem.* **2001**, *113*, 1815–1818; *Angew. Chem. Int. Ed.* **2001**, *40*, 1765–1768; c) T. Konno, T. Kawamoto, R. Kuwabara, T. Yoshimura, M. Hirotsu, *Chem. Lett.* **2002**, 304–305; d) T. Konno, Y. Shimazaki, T. Yamaguchi, T. Ito, M. Hirotsu, *Angew. Chem.* **2002**, *114*, 4905–4909; *Angew. Chem. Int. Ed.* **2002**, *41*, 4711–4715; e) T. Konno, *Bull. Chem. Soc. Jpn.* **2004**, *77*, 627–649.
- [3] a) J. Vivente, M.-T. Chicote, P. González-Herrero, P. G. Jones, *J. Chem. Soc. Dalton Trans.* **1994**, 3183–3187; b) D. J. Leblanc, J. F. Britten, Z. Wang, H. E. Howard-Lock, C. J. L. Lock, *Acta Crystallogr. Sect. C* **1997**, *53*, 1763–1765.
- [4] a) E. J. Fernández, J. M. López-de-Luzuriaga, M. Monge, M. A. Rodríguez, O. Crespo, M. C. Gimeno, A. Laguna, P. G. Jones, *Chem. Eur. J.* **2000**, *6*, 636–644; b) M. A. R. Omary, M. A. Omary, J. P. Fackler, Jr., *Inorg. Chim. Acta* **2002**, *334*, 376–384; c) E. J. Fernández, A. Laguna, J. M. López-de-Luzuriaga, M. Monge, P. Pykkö, N. Runeberg, *Eur. J. Inorg. Chem.* **2002**, 750–753; d) V. J. Catalano, S. J. Horner, *Inorg. Chem.* **2003**, *42*, 8430–8438; e) Q.-H. Wei, G.-Q. Yin, L.-Y. Zhang, L.-X. Shi, Z.-W. Mao, Z.-N. Chen, *Inorg. Chem.* **2004**, *43*, 3484–3491.
- [5] A white crystalline sample of **1** was prepared in 84% yield from Au^{I} and D-Hpen according to a modified literature method^[3b] using chloro(thiodiethanol)gold(I) instead of chloro(tetrahydrothiophene)gold(I). Elemental analysis (%) calcd for $\text{NH}_4[\text{Au}(\text{D-Hpen})_2] \cdot 11/3 \text{ H}_2\text{O}$ ($\text{C}_{10}\text{H}_{31.3}\text{AuN}_3\text{O}_{7.67}\text{S}_2$): C 20.80, H 5.47, N 7.28; found: C 20.84, H 5.14, N 7.23; ^1H NMR (270 MHz, $\text{D}_2\text{O}/1\text{M}$

- Na₂CO₃): δ = 1.30 and 1.61 (CH₃), 3.47 ppm (CH); ¹³C NMR (68 MHz, D₂O/1M Na₂CO₃): δ = 31.06 and 37.99 (CH₃), 51.02 (SC), 70.71 (CH), 177.22 ppm (COO).
- [6] A solution of AgNO₃ (0.23 g, 1.36 mmol) in water (24 mL) was added to a stirred solution of **1** (0.80 g, 1.39 mmol) in water (12 mL), which gave a white precipitate immediately. After stirring at RT for 90 min, followed by cooling in an ice bath for 30 min, the resulting white powder of **2** was collected by filtration and washed with water and methanol. Yield: 0.83 g (95%); elemental analysis (%) calcd for [Au₂Ag₂(DHPen)₄·4H₂O (C₂₀H₄₈Ag₂Au₂N₄O₁₂S₄): C 18.85, H 3.80, N 4.40; found: C 18.75, H 3.62, N 4.50; ¹H NMR (270 MHz, D₂O/1M Na₂CO₃): δ = 1.40 and 1.64 (CH₃), 3.36 ppm (CH); ¹³C NMR (68 MHz, D₂O/1M Na₂CO₃): δ = 31.22 and 38.11 (CH₃), 54.33 (SC), 71.00 (CH), 180.52 ppm (COO). Excitation of a solid sample of **2** at 308 nm at RT and 77 K gave a strong emission band at 709 and 672 nm, respectively.
- [7] Crystal structure analysis for **3**: Bruker SMART-1000 CCD-based diffractometer, T = 213 K, MoK α radiation (λ = 0.71069 Å). The structure was solved by the Patterson method with DIRDIF92 (PATY) and refined by full-matrix least-squares techniques on F^2 using SHELXL-93. Hydrogen atoms were not included in the calculations. C₁₂₀H₂₆₅Ag₁₇Au₁₂Cl₅Cu₁₂N₂₄O_{72.5}S₂₄, M_r = 9111.12 crystal size 0.2 × 0.2 × 0.1 mm³, cubic, space group $P2_13$, a = 32.749(2) Å, V = 35124(3) Å³, Z = 4, ρ_{calcd} = 1.723 g cm⁻³, μ = 6.851 mm⁻¹, ω -2 θ scan mode, 2 θ_{max} = 50.0, 221 649 reflections collected, 20 699 independent reflections, 15 791 observed reflections ($I > 2\sigma(I)$), 880 parameters, semiempirical absorption corrections with SADABS, max./min. transmission 0.478/0.345, $R1$ ($I > 2\sigma(I)$) = 0.055, $wR2$ (all data) = 0.174, Flack parameter 0.010(6), residual electron density 3.34/−1.55 e Å⁻³ (the peaks larger than 1.5 e Å⁻³ were found in the vicinity of heavy atoms). The disordered Ag and O atoms in cluster **3b** were refined with a site occupancy factor of 2/3, which gave satisfactory thermal parameters. CCDC 247589 contains the supplementary crystallographic data for this paper. These data can be obtained free of charge from the Cambridge Crystallographic Data Centre via www.ccdc.cam.ac.uk/data_request/cif.
- [8] Each *trans*-[CuN₂O₂(H₂O)] moiety of **3b** is triply hydrogen bonded to the adjacent *trans*-[CuN₂O₂(H₂O)] moiety of **3a** through COO_(3b)⋯H₂O_(3a) (2.82(2) Å) and COO_(3a)⋯H₂N_(3b) (2.86(2) Å), besides COO_(3a)⋯H₂O_(3b) (2.85(2) Å). The distance between the encapsulated Cl⁻ ions in **3a** and **3b** connected by hydrogen bonds (Cl_(3a)⋯Cl_(3b) 17.015(6) Å) is comparable with that for connection by a Cu–O_{COO} coordination bond (Cl_(3a)⋯Cl_(3b) 16.145(6) Å). Furthermore, the *cis* angles among the encapsulated Cl⁻ ions in **3a** and **3b** are roughly close to the octahedral angle of 90° (Cl_(3a)–Cl_(3b)–Cl_(3a) = 80.13(2)–100.75(3)°, Cl_(3b)–Cl_(3a)–Cl_(3b) = 79.73(3)–100.33(3)°).
- [9] Once isolated from the mother liquor, a crystalline sample of **3** loses water molecules of solvation, as revealed by the loss of surface luster. The powder X-ray diffraction pattern of a dried sample of **3** shows small peaks, indicative of the collapse of the lattice structure after the removal of solvating water molecules. Thermogravimetric (TGA) analysis shows a gradual weight loss of 16.5% up to 85°C, followed by a quick weight loss of 20.1% at around 145°C (see Supporting Information). The remaining weight at 150°C is 62.5%, which corresponds well with that of the Au, Ag, Cu, and S atoms in **3** (62.9% calcd). This implies that the pyrolysis of organic groups and dehydration are complete in a relatively low temperature range.
- [10] K. Yamada, S. Yagishita, H. Tanaka, K. Tohyama, K. Adachi, S. Kaizaki, H. Kumagai, K. Inoue, R. Kitaura, H.-C. Chang, S. Kitagawa, S. Kawata, *Chem. Eur. J.* **2004**, *10*, 2647–2660.
- [11] A solution of AgNO₃ (0.15 g, 0.87 mmol) in an acetate buffer solution (pH 6.2, 150 mL) was added to a solution of **1** (0.50 g, 0.87 mmol) in an acetate buffer solution (150 mL). After stirring at RT for 30 min, a solution containing Cu(NO₃)₂·3H₂O (0.42 g, 1.7 mmol) and NH₄Cl (0.05 g) in an acetate buffer (150 mL) was added. The mixture was stirred at RT overnight, concentrated to ca. 110 mL, and then allowed to stand at RT for several days to give blue crystals of **3** (0.42 g, 67% based on Au).
- [12] All crystalline samples of **3** obtained from different synthetic routes showed identical IR spectra. Furthermore, eight crystals selected from independent synthetic crops had identical unit-cell parameters, and four of them gave the same X-ray analytical data.
- [13] a) P. D. Beer, P. A. Gale, *Angew. Chem.* **2001**, *113*, 502–532; *Angew. Chem. Int. Ed.* **2001**, *40*, 486–516; b) D. Rais, J. Yau, D. M. P. Mingos, R. Vilar, A. J. P. White, D. J. Williams, *Angew. Chem.* **2001**, *113*, 3572–3575; *Angew. Chem. Int. Ed.* **2001**, *40*, 3464–3467; c) A. Kamiyama, T. Kajiura, T. Ito, *Chem. Lett.* **2002**, 980–981; d) R. Vilar, *Angew. Chem.* **2003**, *115*, 1498–1516; *Angew. Chem. Int. Ed.* **2003**, *42*, 1460–1477; e) C. W. Liu, C.-M. Hung, H.-C. Haia, B.-J. Liaw, L.-S. Liou, Y.-F. Tsai, J.-C. Wang, *Chem. Commun.* **2003**, 976–977.

Visualization of Membrane Processes in Living Cells by Surface-Attached Chromatic Polymer Patches**

Zulfiya Orynbayeva, Sofiya Kolusheva, Etta Livneh, Alexandra Lichtenshtein, Ilana Nathan, and Raz Jelinek*

The plasma membrane constitutes a critical platform for diverse biological processes, such as ligand recognition,^[1] drug action,^[2] vesicle fusion and endocytosis,^[3] and pore-formation

[*] Dr. Z. Orynbayeva, Dr. S. Kolusheva, Dr. R. Jelinek
Ilse Katz Center for Meso- and Nano-Scale Science and Technology
and
Department of Chemistry
Ben Gurion University
Beersheva 84105 (Israel)
Fax: (+972) 8-647-2943
E-mail: razj@bgu.ac.il
Prof. E. Livneh
Immunology and Microbiology
Ben Gurion University, Beersheva 84105 (Israel)
A. Lichtenshtein, Prof. I. Nathan
Clinical Biochemistry
Ben Gurion University and Soroka University Medical Center
Beersheva 84105 (Israel)

[**] We are grateful to Dr. Rina Jeger, Dr. Aviva Kiriati (Ben Gurion University), and Dr. Vladimir Kiss (Weizmann Institute of Sciences) for assistance with the microscopy experiments. Financial assistance from the Reimund Staedler Minerva Center for Mesoscopic Macromolecular Engineering, funded through the BMBF, is acknowledged.



Supporting information for this article is available on the WWW under <http://www.angewandte.org> or from the author.

by membrane-active peptides.^[4] Many of these membrane processes involve perturbations that affect the structural or dynamic properties of the phospholipid bilayers, or result in changes to the cell membrane or its morphology.^[5] Numerous membrane studies employing model systems have been reported,^[6] and varied techniques have been developed for imaging surface phenomena in living cells. Almost all the imaging methods are based on radioactive or fluorescent labels^[7] or employ semiconductor quantum dots^[8] that target specific molecules or biochemical pathways. However, microscopic imaging of localized plasma-membrane interactions and bilayer perturbations in living cells has not been achieved. Such information would greatly contribute towards understanding diverse cell-surface processes and their effects on membrane constituents.

Herein we show that attachment of polydiacetylene (PDA) nanopatches onto cell surfaces facilitates visualization and analysis of membrane-perturbing events in living cells. Conjugated PDA assemblies exhibit unique chromatic properties. PDA vesicular aggregates and films have been shown to undergo distinct blue–red colorimetric changes owing to conformational transitions in the conjugated (ene–yne) polymer backbone, induced by external structural perturbations.^[9] Furthermore, PDA also exhibits interesting fluorescence properties; no fluorescence is emitted by the initially polymerized blue-phase PDA, while the red-phase PDA strongly fluoresces at 560 nm and at 640 nm.^[10] The chromatic transformations of PDA have also occurred in biological contexts: recent studies have demonstrated that blue–red transitions could be induced by membrane-active compounds in vesicle assemblies of phospholipid bilayers incorporated within the PDA matrixes.^[11]

As a proof-of-concept for construction of PDA-labeled living cells, monocytic U937 leukemic cells were incubated with vesicles composed of dimyristoylphosphatidylethanolamine (DMPE), dimyristoylphosphatidylglycerol (DMPG), and the diacetylene monomer 10,12-tricosadiynoic acid (mole ratio among the components 1:1:3), and subsequent short (10–20 s) irradiation at 254 nm induced polymerization of the PDA nanopatches. The phospholipid constituents were found to be essential for PDA attachment to the cell membrane, and a fluorescence resonance energy transfer (FRET) experiment confirmed the occurrence of significant fusion between the DMPE/DMPG/PDA vesicles and the plasma membrane (see Supporting Information). Surface attachment of DMPE/DMPG/PDA vesicles that were irradiated and polymerized prior to addition to the cell is generally feasible (thus eliminating the UV-irradiation step which is detrimental to the cells). This procedure, however, yielded a much smaller degree of vesicle surface attachment (possibly owing to the rigidity of the already-polymerized PDA framework) and furthermore induced chromatic transformations within the vesicles upon cell binding.

A critical question pertaining to the usefulness of the new PDA–cell system concerns the effect of vesicle attachment on cell survival. We carried out both a trypan-blue exclusion assay^[12] and acridine-orange/ethidium bromide double staining^[13] to evaluate the percentage of live PDA-treated U937 cells following the incubation and polymerization

(Figure 1). The cell vitality data obtained from the two assays clearly show that most of the PDA-labeled cells survived for more than three hours after the treatment. At longer time periods the percentage of dead and pre-apoptotic cells increased, probably owing to the vesicle fusion processes, the UV irradiation, and the absence of various necessary nutrients in the buffer medium.

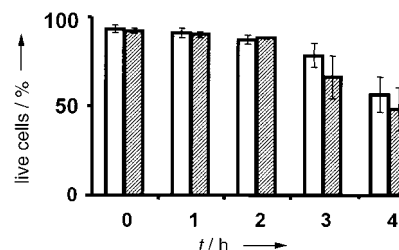


Figure 1. Percentage of live PDA-labeled cells, calculated at different times after incubation of the U937 cells in the presence of phospholipid/polymer nanopatches and subsequent polymerization. Cell viability was determined by the trypan-blue assay (white bars)^[12] and the acridine-orange/ethidium bromide assay (shaded bars).^[13]

The surface topography and membrane morphology of the PDA-treated U937 cells were examined by scanning electron microscopy (SEM, Figure 2A,B) and transmission

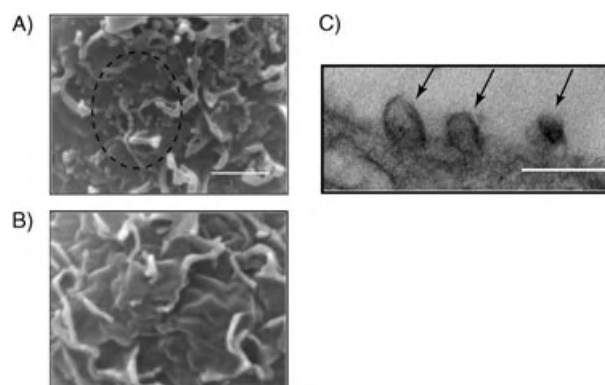


Figure 2. SEM images depicting: A) part of the membrane surface of the PDA-labeled cells showing nanopatches. The broken oval highlights a region with a large number of the patches (scale bar: 1 μ m); B) part of the membrane surface of an untreated U937 cell (same scale as (A)); C) TEM image depicting a thin section of the PDA-labeled cell membrane showing fused PDA particles (indicated with arrows; scale bar: 200 nm).

electron microscopy (TEM, Figure 2C). Magnification of the membrane surface by SEM reveals an abundance of small bright patches of 50–100 nm in size localized at the cell surface (Figure 2A). These nanopatches appeared only when the U937 cells were placed in suspensions containing phospholipid/PDA vesicles and were not observed on surfaces of untreated cells (Figure 2B). A representative thin-section TEM image of a PDA-labeled cell in Figure 2C clearly shows irregular patches protruding from the membrane leaflet, most likely corresponding to the dense PDA particles.^[14] These darker structures were conspicuous on membranes of the

PDA-labeled cells but were not observed in TEM experiments of native U937 cells.

PDA-labeled U937 cells were used to investigate membrane interactions of biological and pharmaceutical molecules (see Figure 3 and Figure 4). Figure 3 depicts laser confocal microscopy images of the chromatic cells. Unperturbed PDA-labeled cells did not emit any fluorescence (Figure 3A) since the surface-incorporated PDA assemblies in their initial blue phase are not fluorescent.^[10] However, addition of lidocaine, a local anesthetic, to the cell suspension resulted in the appearance of fluorescent spots concentrated exclusively on the cell surface (Figure 3B). Lidocaine, similar to other anesthetic substances, is believed to increase bilayer fluidity,^[15] which induces the structural transformation of the PDA nanopatches into the fluorescent red phase (Figure 3B). Modification of bilayer fluidity by lipophilic substances was shown to induce dramatic chromatic transitions in model phospholipid/PDA vesicles.^[16] Importantly, bilayer fluidization induced by the lidocaine employed in this case did not give rise to immediate cell lysis, as determined by the trypan-blue cell viability assay (data not shown). Similar to lidocaine, membrane perturbations by polymyxin-B (PMB), a cytotoxic membrane-active peptide,^[17] produced striking fluorescence images (Figure 3C). The extended fluorescence view shown in Figure 3C (containing superposition of cell-surface slices extracted over a 2- μm width) depicts abundant spots distributed on the cell surface, most likely corresponding to locations of plasma-membrane disruption induced by the peptide.

The chromatic cell platform was used to study other membrane-perturbing processes, such as the interaction of lipid vesicles with cellular membranes.^[18] Figure 3D and E feature the confocal microscopy images recorded at different times after addition of vesicles composed of dimyristoylphosphatidylcholine (DMPC) and cholesterol to the PDA-labeled cells. The microscopy image in Figure 3D was recorded approximately five minutes after mixing the PDA-labeled cells with DMPC/cholesterol dispersion and shows faint fluorescent patches most likely indicating the onset of interactions between the vesicles and the bilayer membrane of the U937 cells. Greater abundance of fluorescent areas with higher intensities was recorded approximately thirty minutes after addition of DMPC/cholesterol dispersion to the chromatic cells (Figure 3E). The appearance of increasingly intense fluorescent domains on the membrane is ascribed to the local destabilization of the membrane through cholesterol-promoted binding.^[19]

The unique colorimetric properties of PDA can be further exploited for the analysis of membrane interactions. Figure 4A depicts photographs of the PDA-labeled cells before and after interaction with oleic acid, a membrane-fluidizing agent.^[20] The sedimented cells before treatment had the intense blue color of the polymer patches attached to the cell membrane (Figure 4A, left image). However, immediately after incubating the cells with oleic acid, the cell suspension turned red (Figure 4A, right image) owing to fluidization of the plasma membrane. Importantly, examination of the cells treated with oleic acid under a microscope (data not shown) indicated significant swelling on the cells, most likely a result

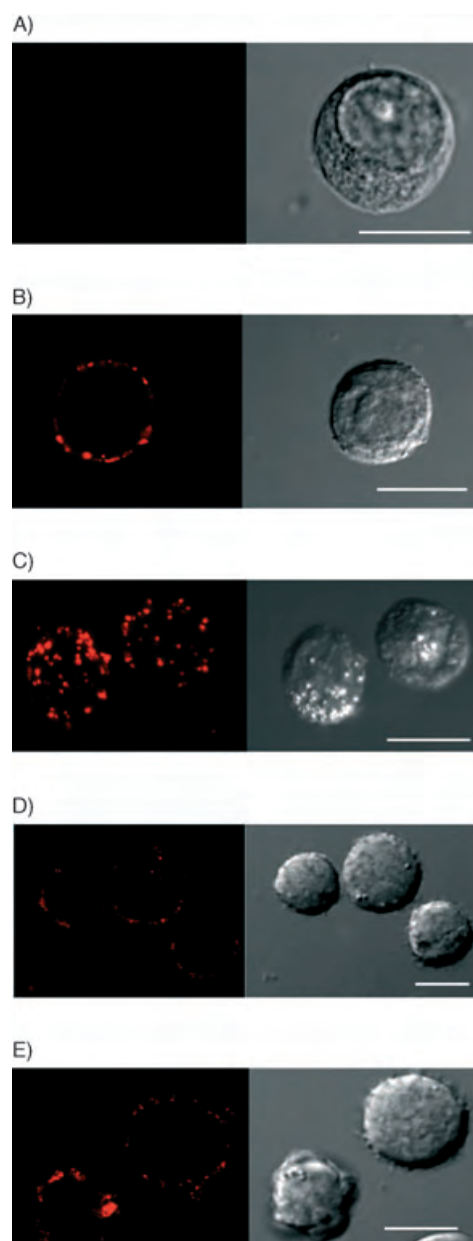


Figure 3. Confocal microscopy fluorescence images recorded using an LP 560 nm filter (left) and transmission differential interference contrast (DIC) microscopy images (right) of PDA-labeled U937 cells. Scale bars in all images correspond to 10 μm . A) Initially prepared unperturbed PDA-labeled cells: no fluorescence emitted from the blue-phase PDA patches; B) Addition of lidocaine (1 mM) to the hybrid cell suspension. C) Addition of PMB (50 μM). An extended fluorescence image is shown (superposition of four membrane slices). D and E) Interaction of DMPC/cholesterol vesicles (0.1 mM final lipid concentration) with the PDA-labeled cells either 5 min (D) or 30 min (E) after mixing of DMPC/cholesterol vesicles with PDA-labeled cells.

of membrane disruption by the fatty acid, which is consistent with the colorimetric data in Figure 4.

Figures 4B–D indicate that visible spectroscopy could be employed for studying cell-membrane processes by using the PDA-labeled cells. The spectra of the parent blue PDA-labeled cells displayed the typical maxima at around 650 nm (solid lines, Figure 4B and C). Addition of oleic acid to the

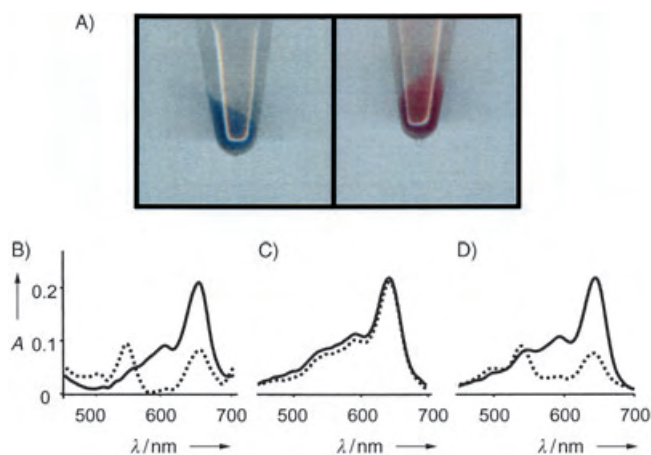


Figure 4. Photographs of tubes containing PDA-labeled cells. The cells were sedimented to improve visible observation. Left tube: blue cells before treatment; right tube: cells after incubation with oleic acid (180 μM). UV/Vis spectra: B) PDA-labeled cell suspension before (solid line) and after (broken line) addition of oleic acid, final concentration 180 μM ; C) PDA-labeled cell suspension before (solid line) and after (broken line) addition of poly-L-lysine, final concentration 1 $\mu\text{g mL}^{-1}$; D) Cell-free DMPE/DMPC/PDA vesicle suspension before (solid line) and after (broken line) addition of poly-L-lysine, final concentration 1 $\mu\text{g mL}^{-1}$.

PDA-labeled cells gave rise to a pronounced blue-to-red transition and accordingly the emergence of a dominant peak at around 540 nm (broken line, Figure 4B). The color transition of PDA is most likely related to the increased fluidity of the lipid membrane induced by oleic acid.

The visible spectroscopy data in Figure 4C and D further facilitate evaluating the critical issue of whether the chromatic transitions observed in the PDA-labeled cells were due to plasma-membrane perturbations induced by membrane-active compounds, rather than induced by direct interactions with the phospholipid/PDA particles attached to the cells (these interactions would clearly attract much less biological interest). Figure 4C depicts the spectrum resulting from addition of high-molecular-weight (84 kDa) poly-L-lysine (PL), a polypeptide with a high positive charge,^[21] to the PDA-labeled cells. Figure 4C clearly demonstrates that no colorimetric change was observed when PL was added to the suspension of PDA-labeled cells. In contrast, PL gave rise to an immediate and dramatic blue–red transformation of free lipid/PDA vesicles (not attached to cells) in an aqueous solution (Figure 4D). This color change arises from the strong electrostatic interactions between the positively charged polypeptide and the phospholipid/PDA vesicles.^[11] The comparison between the spectroscopic results of PDA-labeled cells (Figure 4C) and cell-free vesicles (Figure 4D) indicates that PL only marginally interacted with the plasma-membrane-embedded PDA moieties, which are protected by cell-surface carbohydrate residues that hinder access of the large polypeptide to the membrane. Furthermore, the absence of immediate colorimetric change after mixing the cells with PL (Figure 4C) suggests that PL does not induce significant initial disruption of the cell membrane, even though this polypeptide is known to eventually give rise to cell lysis.^[22]

In summary, we have constructed new chemically engineered cells through attachment of chromatic polydiacetylene nanopatches onto the plasma membrane. These hybrids facilitated visualization and investigation of surface processes in living cells. The membrane-incorporated polymer patches did not adversely affect cell vitality for several hours and responded to structural perturbations of the plasma membrane both through induction of fluorescence as well as by undergoing blue–red color changes. The new chromatic cell platform is generic by nature and conceptually different from other cellular imaging techniques. In essence, the fluorescent/colorimetric polydiacetylene patches do not report upon specific biomolecular targets within the cell surface (or cell interior) but rather respond to processes and surface interactions that give rise to structural and dynamic modifications of the plasma membrane. This approach makes possible microscopic imaging and quantitative spectroscopic analyses of biological events occurring in real time within the membranes of living cells. PDA-labeled cells were constructed in our laboratories using other cell types, including epithelial MCF-7 cells, Chinese hamster ovarian (CHO) cells, erythrocytes, and others (manuscript in preparation). The new chromatic cell system could find wide applicability including studying plasma-membrane fusion and vesicle budding processes.

Received: October 22, 2004

Published online: January 10, 2005

Keywords: cell imaging · fluorescent probes · membrane processes · scanning probe microscopy · vesicles

- [1] J. M. Berg, J. L. Tymoczko, L. Stryer, *Biochemistry*, Freeman, New York, **2002**.
- [2] R. C. Srivastava, S. B. Bhise, S. S. Mathur, *Adv. Colloid Interface Sci.* **1984**, *20*, 131–161.
- [3] J. M. Besterman, R. B. Low, *Biochem. J.* **1983**, *210*, 1–13.
- [4] A. S. Ladokhin, M. E. Selsted, S. H. White, *Biophys. J.* **1997**, *72*, 1762–1766.
- [5] M. Terasaki, K. Miyake, P. L. McNeil, *J. Cell Biol.* **1997**, *139*, 63–74.
- [6] M. J. Zuckermann, J. H. Ipsen, L. Miao, O. G. Mouritsen, M. Nielsen, J. Polson, J. Thewalt, I. Vattulainen, H. Zhu, *Methods Enzymol.* **2004**, *383*, 198–229.
- [7] a) D. K. Struck, R. E. Pagano, *J. Biol. Chem.* **1980**, *255*, 5404–5410; b) T. Arvinte, P. L. Steponkus, *Biochemistry* **1988**, *27*, 5571–5677.
- [8] M. Bruchez, M. Moronne, P. Gin, S. Weiss, A. P. Alivisatos, *Science* **1998**, *281*, 2013–2016. See also M. Green *Angew. Chem.* **2004**, *116*, 4221–4223; *Angew. Chem. Int. Ed.* **2004**, *43*, 4129–4131.
- [9] a) H. Ringsdorf, B. Schlarb, J. Venzmer, *Angew. Chem.* **1988**, *100*, 117–162; *Angew. Chem. Int. Ed. Engl.* **1988**, *27*, 113–158; b) S. Okada, S. Peng, W. Spevak, D. Charych, *Acc. Chem. Res.* **1998**, *31*, 229–239; c) D. Charych, Q. Cheng, A. Reichert, G. Kuziemko, M. Stroh, J. O. Nagy, W. Spevak, R. C. Stevens, *Chem. Biol.* **1996**, *3*, 113–120.
- [10] T. Kobayashi, M. Yasuda, S. Okada, H. Matsuda, H. Nakanishi, *Chem. Phys. Lett.* **1997**, *267*, 472–480.
- [11] a) D. Charych, J. O. Nagy, W. Spevak, M. D. Bednarski, *Science* **1993**, *261*, 585–588; b) S. Okada, R. Jelinek, D. Charych, *Angew. Chem.* **1999**, *111*, 678–682; *Angew. Chem. Int. Ed.* **1999**, *38*, 655–

- 659; c) S. Kolusheva, L. Boyer, R. Jelinek, *Nat. Biotechnol.* **2000**, *18*, 225–227; d) S. Kolusheva, T. Shahal, R. Jelinek, *Biochemistry* **2000**, *39*, 15851–15859.
- [12] R. L. P. Adams in *Cell Culture for Biochemists, Vol. 8* (Eds.: R. H. Burdon, P. H. van Knippenberg), Elsevier, Amsterdam, **1990**, p. 64.
- [13] J. Grossmann, J. M. Maxson, C. M. Whitacre, D. E. Orosz, N. A. Berger, C. Fiocchi, A. D. Levine, *Am. J. Pathol.* **1998**, *153*, 53–62.
- [14] J. Song, Q. Cheng, R. C. Stevens, *Chem. Phys. Lipids* **2002**, *114*, 203–214.
- [15] a) D. Papahadjopoulos, K. Jacobson, G. Poste, G. Shepherd, *Biochim. Biophys. Acta* **1975**, *394*, 504–519; b) E. C. Kelusky, C. P. Smith, *Biochemistry* **1983**, *22*, 6011–6017.
- [16] D. Evrard, E. Touitou, S. Kolusheva, Y. Fishov, R. Jelinek, *Pharm. Res.* **2001**, *18*, 943–949.
- [17] R. L. Danner, K. A. Joiner, M. Rubin, W. H. Patterson, N. Johnson, K. M. Ayers, J. E. Parrillo, *Antimicrob. Agents Chemother.* **1989**, *33*, 1428–1434.
- [18] a) R. E. Pagano, L. Huang, C. Wey, *Nature* **1974**, *252*, 166–167; b) K.-D. Lee, S. Nir, D. Papahadjopoulos, *Biochemistry* **1993**, *32*, 889–899.
- [19] M. J. Hope, K. R. Bruckdorfer, C. A. Hart, J. A. Lucy, *Biochem. J.* **1977**, *166*, 255–263.
- [20] S. S. Funari, F. Barcelo, P. V. Escriba, *J. Lipid Res.* **2003**, *44*, 567–575.
- [21] W. Hartmann, H.-J. Galla, *Biochim. Biophys. Acta* **1978**, *509*, 474–490.
- [22] R. A. Jorquera, J. Berrios, J. Sans, C. Vergara, D. J. Benos, J. G. Reyes, *Biol. Cell* **2002**, *94*, 233–241.

Materials Science

“Grafting-From” Polymerization inside a Polyelectrolyte Hollow-Capsule Microreactor**

Won San Choi, Jeong-Ho Park, Hye Young Koo,
Ju-Young Kim, B. K. Cho, and Dong-Yu Kim*

Over the last decade versatile, electrostatic layer-by-layer (LbL) assembly methods involving polyelectrolytes^[1–5] have been widely used in the preparation of hollow capsules. These capsules can be fabricated by the stepwise adsorption of polyelectrolytes with charges that are opposite from their aqueous media onto templating cores, especially organic or inorganic particles and biopolymers,^[6] followed by dissolution

of the templating cores to give polyelectrolyte hollow capsules that are replicas of the templates.^[7–10]

A variety of microcapsules with customized physicochemical properties can be produced by incorporating one or more functional components, such as nanoparticles, biomacromolecules, lipids, photosensitive dyes, inorganic crystals, and multivalent ions, onto the capsule wall or into the interior of the capsule.^[11–15] Hollow capsules consisting of alternating layers of strong and weak polyelectrolytes can also be used for the targeted encapsulation and controlled release of macromolecules by tuning the porosity upon changing the pH value.^[16,17] Most of these studies have focused on the development of synthetic methodologies and the characterization of the hollow capsules. Relatively little attention has been directed to reactions in the confined interior of these hollow capsules.^[18–20] In these studies, hollow capsules were used as microreactors for spatially restricted inorganic synthesis. However, only a limited number of reports have appeared that demonstrate that polymerization inside hollow capsules could provide new opportunities for tuning the properties of the products. For example, polyelectrolyte-loaded capsules have been used to tune the physicochemical properties of the products formed in the interior of a nanoreactor capsule,^[21,22] and enzyme-loaded capsules have been employed for the synthesis of polymers within microcapsules.^[23,24]

Recently, the so-called “grafting-from” polymerization technique has attracted a great deal of attention because polymer brushes can be generated with high grafting densities of surface-attached neutral macromolecules, as well as polyelectrolytes.^[25–27] Grafting-from polymerization at solid surfaces can be performed directly at the surface by using an immobilized initiator and various polymerization techniques. The initiator system is immobilized on the surface of a solid substrate and the polymer layer is then generated by polymerization in situ. To date, these grafting-from polymers or polymer brushes have been largely prepared on flat substrates.

Herein we report the grafting-from polymerization to generate end-attached polyelectrolyte brushes inside a hollow-capsule microreactor. To the best of our knowledge, polymer brushes grown from the inner wall of hollow capsules have not yet been reported. This novel fabrication method for hollow capsules was performed by preparing polyelectrolyte hollow capsules whose inner layer was coated with a water-soluble initiator, followed by polymerization of a styrene sulfonate (SS) monomer on the inner wall. The shape of the capsules after polymerization could be controlled by varying the SS content. Furthermore, we also demonstrate that these hollow capsules can be used as a novel submicroreactor to control polymerization behavior.

Figure 1 shows the fabrication of polyelectrolyte hollow capsules with initiator bound on the inner wall, and the grafting-from polymerization. Poly(allylamine hydrochloride) (PAH) and poly(styrene sulfonate) (PSS) were used as the positive and negative polyelectrolytes, respectively, and potassium peroxodisulfate (KPS) was used as the water-soluble initiator. The capsule reactors were fabricated by the layer-by-layer (LbL) assembly technique^[28–30] on sacrificial

[*] W. S. Choi, J.-H. Park, H. Y. Koo, J.-Y. Kim, Prof. B. K. Cho, Prof. D.-Y. Kim
Center for Frontier Materials
Department of Materials Science and Engineering
Gwangju Institute of Science and Technology
1 Oryong-dong, Buk-gu, Gwangju 500-712 (Korea)
Fax: (+82) 62-970-2304
E-mail: kimdy@gist.ac.kr

[**] This work was supported by a Korea Research Foundation Grant (KRF-2003-041-D00215).

Supporting information for this article is available on the WWW under <http://www.angewandte.org> or from the author.

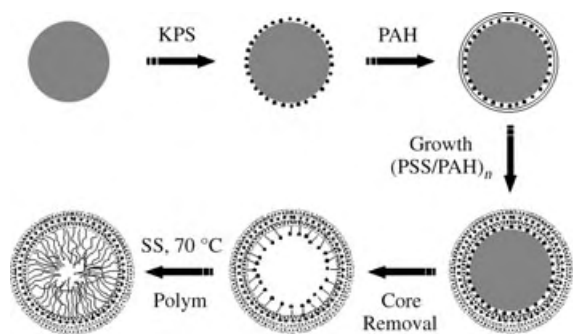


Figure 1. Schematic representation of the procedures used for fabricating initiator-coated hollow capsules and grafting-from polymerization inside the capsules.

colloidal particles, followed by decomposition of the cores in HCl solution. The amount of initiator bound onto the capsules was estimated to be about 57% of the original amount by measurement of the amount of free initiator extracted. The water-soluble monomer styrene sulfonate (SS) was subsequently dispersed in a suspension of initiator-bound hollow capsules. PSS was then grown by a grafting-from polymerization method at 70°C for four hours. The SS monomers are selectively polymerized inside the capsule reactors only, because the initiator is present only at the inner wall of the hollow capsules. After polymerization, the immobilized polymers bound to the interior of the hollow capsules were released by treatment with HCl to characterize them further. Figure 2 summarizes the ζ potential recorded

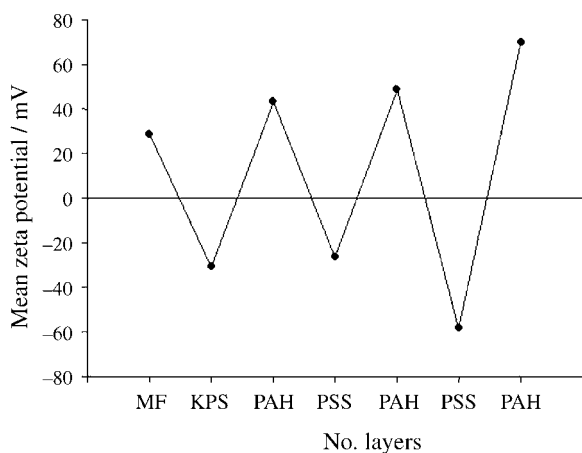


Figure 2. ζ potential as a function of layer number for MF particles coated with KPS(PAH/PSS)₂PAH. Experiments were repeated three times for each measurement and the average value was used. The line shown is to guide the eye and has no other meaning.

with layer deposition for the KPS(PAH/PSS)₂PAH system. The ζ potential alternates between positive and negative values, thereby indicating the successful recharging of the particles coated with the polyelectrolyte layers after deposition of each layer.

To confirm the immobilization of KPS at the inner wall of the hollow capsules the temperature-dependent magnetiza-

tion of the hollow capsules with and without KPS was measured with a superconducting quantum interference device (SQUID) magnetometer: the generation of radical species arising from the dissociation of KPS would allow the detection of a change of magnetization. As shown in Figure 3,

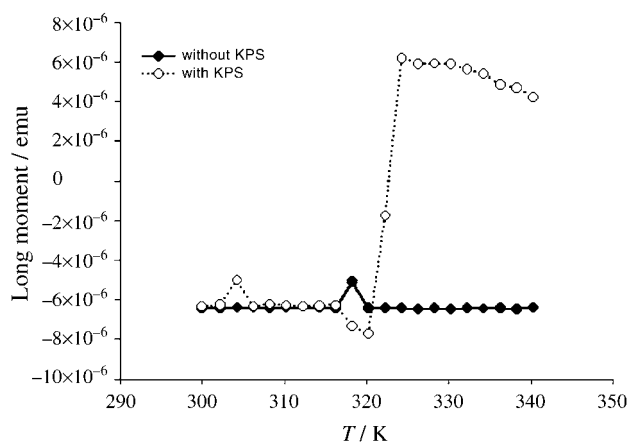


Figure 3. The SQUID measurements of hollow capsules without and with KPS in a solution with SS monomer. The latter case shows a dramatically increased magnetic moment at 320 K as a result of activation and propagation of the KPS initiator, whereas the former case does not.

while no change in magnetic moment was observed between 300 and 340 K for the hollow capsules without KPS, a sudden jump in magnetization was observed at 322 K for the hollow capsules with KPS, which is close to the typical initiation temperature of KPS. These observations mean that radical species—unpaired electrons—are produced upon dissociation of KPS, and that these species subsequently propagate. Therefore, the detection of magnetization is direct evidence that KPS is bound to the inner wall of the hollow capsules and could play a role as a polymerization initiator.

Figure 4 shows SEM micrographs of the polyelectrolyte-coated particles and the corresponding hollow capsules obtained after removing the melamine formaldehyde (MF) core and drying on a silicon wafer. The drying process forms creases and folds in the shells as they collapse. Essentially no residual MF could be detected by SEM.

These hollow capsules were dispersed in a solution of the SS monomer. The polymerization was carried out with different SS contents at 70°C for four hours. After the polymerization, the capsules were separated from the solution of the SS monomers by centrifugation; their shapes were found to be dependent on the initial SS content. Figure 5 shows SEM micrographs of hollow capsules after polymerization in solutions containing 25 wt % (Figure 5a) and 40 wt % (Figure 5b) of SS monomer. The latter shows “semi-spherical” capsules because sufficient polymers (PSS) have been produced to fill the capsules, whereas the former shows “caved-in” capsules as a result of insufficient amounts of polymer inside the capsules. The size of the “caved-in” and “semispherical” capsules is about 600 and 800 nm, respectively.

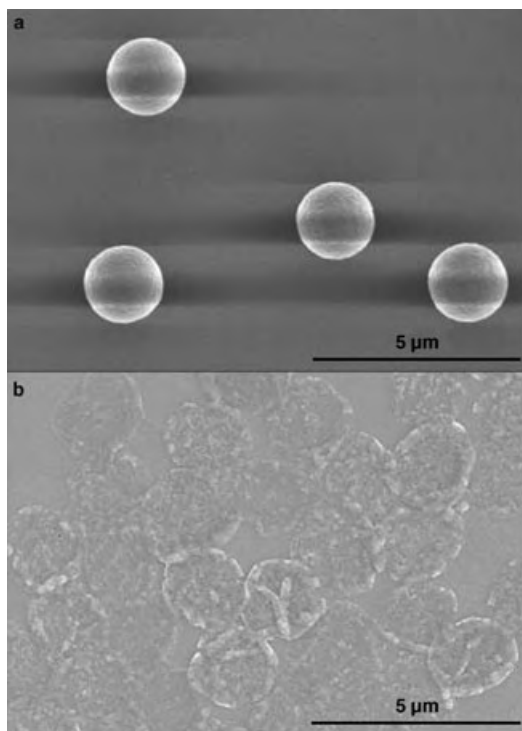


Figure 4. SEM micrographs of a) an MF particle coated with KPS/(PAH/PSS)₂PAH, and b) the corresponding hollow shell obtained after removal of the MF core by treatment with HCl.

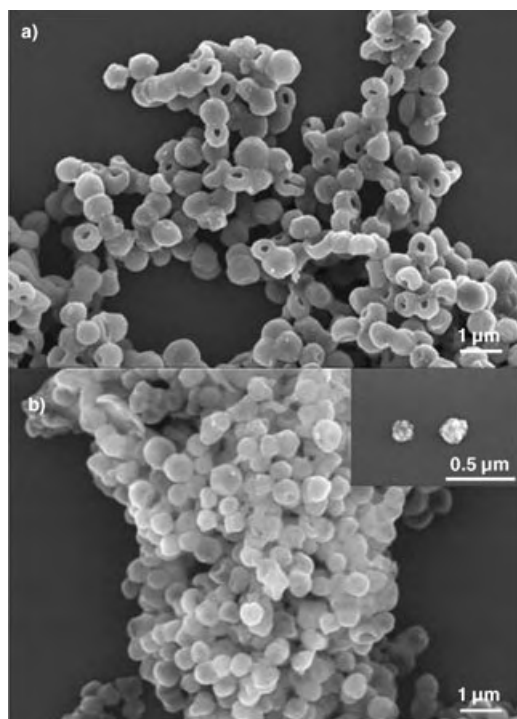


Figure 5. SEM micrographs of the polymer-containing capsules: a) “caved-in” capsules (25 wt% SS monomer); b) “semispherical” capsules (40 wt% SS monomer). Hollow capsules without SS monomer undergo severe shrinkage at 70 °C (inset).

The hollow capsules shrink after polymerization: their size was reduced from a diameter of 1.87 μm to about 200 nm after heating to 70 °C for four hours in the absence of SS monomer (inset in Figure 5). It has been reported that heating can cause shrinkage of the surface area by 20% leading to a reduction in the diameter of the capsules and an increase in wall thickness as a result of the breaking and re-forming of ion pairs, thus yielding a more three-dimensional configuration of the polymer.^[7] In our case, the shrinkage is more severe because of the prolonged heating and the thinner polyelectrolyte walls and indicate that the higher the monomer content the less the shrinkage of the capsules. It seems that the polymer chains on the interior of the capsule walls play an important role as a shrinkage-resistant framework. The shape of the “caved-in” particles is similar to that of erythrocytes, and these types of “caved-in” particles are known to show excellent properties when used as a plastic pigment in paper coating. The high-shear viscosity of the “caved-in” particles is lower than that of a spherical particle, and their sheet gloss, print gloss, and opacity are higher than those of spherical particles because of their shape.^[31]

Field-emission transmission electron microscopy (FE-TEM) measurements were performed to examine the interior structure of the polymer-grown capsules. In the case of the “caved-in” capsules, the dark ring region corresponds to a polymer brush shell structure. The FE-TEM image of the “caved-in” case clearly shows hollows in the capsules, and, as expected, the semispherical case (Figure 6 b and 6 d) shows no evidence of a hollow. The FE-TEM analysis clearly reveals that the polymer brushes grow from the inner surface of the hollow capsules and are bound to the interior of the hollow capsule where they act as a shrink-resistant frame. It has been reported that the capsule shape can be stabilized by the formation of an insoluble, stiff, gel-like structure in the capsule interior which contains residual MF and PSS.^[32] In our case, however, the capsule shapes are stabilized by the soluble polymers grown from the inner wall, and the shapes are

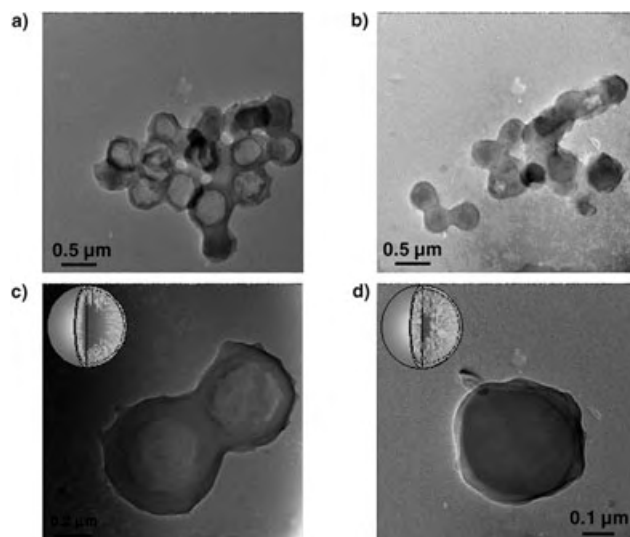


Figure 6. TEM micrographs of polymer-containing capsules as a function of monomer content: a), c) “caved-in” capsules (25 wt% SS monomer); b), d) “semispherical” capsules (40 wt% SS monomer).

determined by the amount of polymer present inside the capsules.

We also investigated the influence of the confined interior of our hollow capsules on the detailed polymerization behavior. Although polymerization behavior, such as the molecular weight and molecular-weight distribution of the polymers formed, in a bulk reaction space has been extensively investigated both theoretically and experimentally over a long period of time, there are only a few, limited methods available for controlling the polymerization behavior of common monomers. It would therefore be significant for the field of polymerization if such behavior could be manipulated by easily controllable factors, such as the confining geometry. We used our initiator-bound hollow capsules to investigate whether the confined nanospace and surface anchoring could be used to control the polymerization behavior. To do so, we polymerized PSS by using four different approaches to form “floating-outside” polymers, which are obtained from free-floating initiators outside the hollow capsules, “floating-inside” polymers, which are obtained from free-floating initiators inside the hollow capsules, “immobilized-outside” polymers, which are grown from the outer surface of highly cross-linked MF particles, and “immobilized-inside” polymers, which are grown from the inner surface of the capsules. The floating and immobilized polymers were collected after treatment with HCl. Polyelectrolyte shells are semipermeable,^[28–30] and therefore small molecules such as an initiator and a monomer can easily penetrate through the shell wall, while large molecules, such as polymers, cannot. However, even large molecules can penetrate the shell wall when the polyelectrolyte shell has an open form, such as under acid conditions.^[17] Thus, treatment with 0.5 M HCl permitted the interior polymers to be collected by opening the shell. After this treatment, the capsules were separated from the dangling polymer by centrifugation. Figure 7 shows a comparison of the molecular weights of the four types of polymers obtained inside and outside of the hollow capsules; 40 wt % of SS monomer was used in all cases. The floating-inside polymers have a molecular weight and PDI that are about twice those of the floating-outside polymers. This result indicates that some confined-space effects may exist. However, surprisingly, the immobilized-inside polymers grown from the inner surface have a molecular weight that is an order of magnitude higher than both the floating-inside and the floating-outside polymers. This kind of unusual polymerization behavior inside small capsules has not been reported until now.

To investigate the immobilization effect, SS monomers were polymerized on an initiator-bound MF surface. Highly cross-linked MF particles were used in this case. These immobilized-outside polymers have a higher molecular weight than the floating-outside polymers, but the difference is not as much as between the immobilized-inside and floating-inside cases (Figure 7b). Thus, the immobilization effect alone cannot explain the unusually high molecular weight of the immobilized-inside polymers. Even though the detailed mechanism responsible for this behavior is not yet clear, on the basis of the results described above we believe that this extraordinary molecular weight behavior results

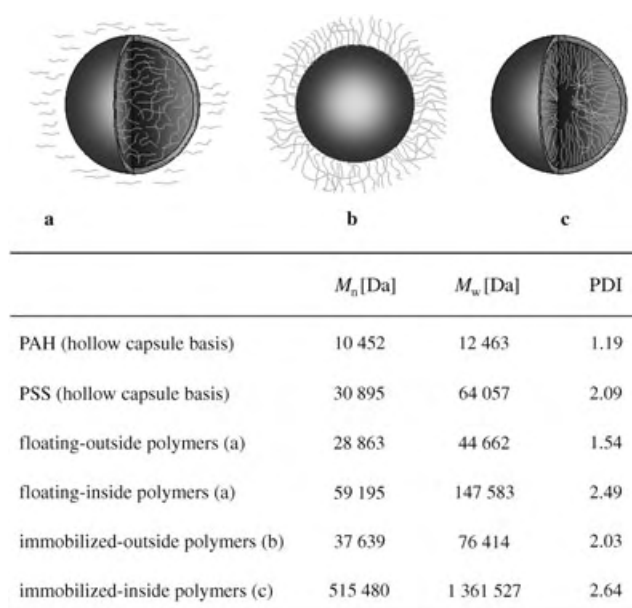


Figure 7. Schematic representation and comparison of molecular weights and polydispersity index (PDI) of a) floating-outside and floating-inside polymers, b) immobilized-outside polymers obtained on a colloidal surface, and c) immobilized-inside polymers obtained in a confined space.

from both immobilization and confined-space effects. A further detailed examination of these effects is currently under way. We also expect that this kind of polymerization behavior could be further controlled by varying the capsule size. If this can be achieved, it might open up a new route to the development of “tunable microreactors”, which could control a variety of chemical and polymerization reactions.

In conclusion, the hollow capsules reported here serve as a microreactor for the efficient polymerization of SS monomers in grafting-from polymerization inside the capsules. The hollow capsules formed after the grafting-from polymerization show either caved-in or semispherical shapes. The shape of the capsules after polymerization is strongly dependent on the initial SS content, thus implying the possibility to control the shape of the resulting nanoparticles in our system. The immobilized polymers obtained in the confined space have a much higher molecular weight than polymers produced in bulk solution as a result of both immobilization and confined-space effects. Thus, the polyelectrolyte hollow capsules reported here successfully serve as a unique microreactor for the polymerization and also allow the manipulation of the shape of the nanoparticles.

Experimental Section

PSS ($M_w = 70\,000$), PAH ($M_w = 15\,000$), KPS, and SS monomer were purchased from Aldrich. Weakly and highly cross-linked MF particles were purchased from Microparticle (GmbH) and Fluka, respectively. The water used in all experiments was prepared in a three-stage Milli-Q plus 185 purification system and had a resistivity higher than 18 MΩ cm. The capsule reactors (KPS (2.3 mg)/(PAH (1 mg mL^{−1})/PSS (1 mg mL^{−1}))/PAH were fabricated by the LbL assembly technique^[28–30] on MF (0.12 mL) colloidal particles with a diameter

of 1.87 μm , followed by decomposition of the MF cores in 0.15 M HCl solution ($\text{pH} < 1$). The detailed procedure for the formation of initiator-bound hollow capsules is as follows: an aqueous KPS solution (2 mL, 2.3 mg in water) was added to an aqueous suspension (0.12 mL) of positively charged MF particles (10 wt %). The dispersion was gently agitated for 15 min to allow the KPS to adsorb onto the MF particles. The mixture was then centrifuged at 10000 g for 4 min, the supernatant removed, and water (2 mL) added. The particles were then redispersed by gentle shaking. The centrifugation/wash/dispersion cycle was repeated three times to ensure removal of any free KPS from the solution. After formation of the KPS layer outside the MF cores, PAH and PSS polyelectrolyte layers were deposited by an established LbL assembly technique.^[28–30] The polyelectrolyte assembling conditions, including the centrifugation/wash/dispersion cycle, were the same as described above (1 mg mL^{-1} , 0.5 M NaCl). After deposition of five layers of polyelectrolytes, the template MF core was removed by treatment with 0.15 M HCl ($\text{pH} < 1$) to give initiator-bound hollow capsules.

For the estimation of the amount of KPS initiator bound to the inner wall of the capsules, free initiator molecules were extracted and quantified follows: an aqueous solution of KPS (2.3 mg in 2 mL of water) was added to an aqueous suspension (0.12 mL) of positively charged MF particles (10 wt %). After adsorption of the KPS onto the MF particles, the dispersion was centrifuged, the supernatant containing free KPS collected, and water (2 mL) added. The particles were then redispersed by gentle shaking. The centrifugation/wash/dispersion cycle was repeated several times to ensure collection of the free KPS from the solution. The collected solution of free KPS was evaporated and the weight of the residue was measured. For each measurement, experiments were repeated five times and the average value was used. The measured weight was about 1 mg; therefore, the approximate amount of initiator bound to the MF cores was about 1.3 mg (57 % of the original amount).

The water-soluble monomer styrene sulfonate (SS; 40 wt %, 44 mg) was subsequently dispersed in a suspension (1.5 mL, 0.03 wt %) of the initiator-bound hollow capsules. 25 and 40 wt % SS, relative to the MF emulsion weight, was used as the monomer. Polymerization was carried out at 70 °C for 4 h.

Floating-inside and floating-outside polymers obtained from free-floating initiators inside and outside the hollow capsules were polymerized under the same conditions as described above; 40 wt % of SS monomer (44 mg) and KPS (2.3 mg) were dispersed in a suspension of the hollow capsules. Immobilized-outside polymers were obtained on the initiator-bound MF surface; a solution of KPS (2 mL) was added to an MF suspension (0.12 mL). The KPS adsorption procedure was the same as described above. After adsorption, the particles were separated from the KPS solution by centrifugation, followed by several washing cycles with water. SS monomer (40 wt %, 44 mg) was dispersed in a suspension (1.5 mL, 1.5 wt %) of KPS-bound MF particles. Polymerization was carried out under the same conditions as described above. For separation of all these polymers from the capsules the particles were dispersed in 0.5 M HCl for 20 min to allow the collection of the polymers. The dangling polymers (immobilized-inside and immobilized-outside) were collected by gently stirring the dispersion for 20 min and then centrifugation at 10000 g for 4 min. Finally, the supernatant containing the polymerized PSS was collected. To collect floating-outside polymers, the suspension containing the polymers was centrifuged in an aqueous medium and the supernatant containing the polymers was collected. To collect floating-inside polymers, the suspension containing the polymers was centrifuged in an aqueous medium and then the precipitate was dispersed in 0.5 M HCl for 20 min; the collection process was the same as described above.

The surface charge was measured on an OTSUKA (ELS 8000) apparatus. The FE-SEM micrographs were obtained with a Hitachi (S-4700) microscope. The FE-TEM measurements were performed on a Philips (TECNAI F20) microscope operating at 200 kV. Samples

were prepared by applying a drop of the capsule solution onto a carbon-coated copper grid. The molecular weights and their PDI values were measured by gel-permeation chromatography (GPC, Breeze System 500 Series). SQUID measurements were performed on a Quantum design (MPMS XL) device with scan temperatures from 300 K to 340 K at 10 K min^{-1} in 2 K increments (21 steps).

Received: June 15, 2004

Revised: October 20, 2004

Published online: January 3, 2005

Keywords: materials science · microreactors · polyelectrolytes · polymerization

- [1] G. Decher, J. Hong, *Macromol. Chem. Macromol. Symp.* **1991**, 46, 321–328.
- [2] S. Park, M. F. Rubner, A. M. Mayes, *Langmuir* **2002**, 18, 9600–9604.
- [3] G. Decher, *Science* **1997**, 277, 1232–1237.
- [4] P. Bertrand, A. Jonas, A. Laschewsky, R. Legras, *Macromol. Rapid Commun.* **2000**, 21, 319–348.
- [5] P. T. Hammond, *Curr. Opin. Colloid Interface Sci.* **2000**, 4, 430–442.
- [6] F. Caruso, *Adv. Mater.* **2001**, 13, 11–22.
- [7] S. Leporatti, C. Gao, A. Voigt, E. Donath, H. Möhwald, *Eur. Phys. J. E* **2001**, 2, 13–20.
- [8] C. Gao, H. Möhwald, J. Shen, *Adv. Mater.* **2003**, 15, 930–933.
- [9] F. Caruso, D. Trau, H. Möhwald, R. Renneberg, *Langmuir* **2000**, 16, 1485–1488.
- [10] F. Caruso, C. Schüller, D. G. Kurth, *Chem. Mater.* **1999**, 11, 3394–3399.
- [11] S. Moya, E. Donath, G. B. Sukhorukov, M. Auch, H. Bäuml, H. Lichtenfeld, H. Möhwald, *Macromolecules* **2000**, 33, 4538–4544.
- [12] Z. Dai, A. Voigt, S. Leporatti, E. Donath, L. Dähne, H. Möhwald, *Adv. Mater.* **2001**, 13, 1339–1342.
- [13] F. Caruso, M. Spasova, V. Salgueirino, L. M. Liz-Marzan, *Adv. Mater.* **2001**, 13, 1090–1094.
- [14] G. B. Sukhorukov, L. Dähne, J. Hartmann, E. Donath, H. Möhwald, *Adv. Mater.* **2000**, 12, 112–115.
- [15] K. Kamata, Y. Lu, Y. Xia, *J. Am. Chem. Soc.* **2003**, 125, 2384–2385.
- [16] G. Ibarz, L. Dähne, E. Donath, H. Möhwald, *Adv. Mater.* **2001**, 13, 1324–1327.
- [17] G. B. Sukhorukov, A. A. Antipov, A. Voigt, E. Donath, H. Möhwald, *Macromol. Rapid Commun.* **2001**, 22, 44–46.
- [18] D. G. Shchukin, I. L. Radtchenko, G. B. Sukhorukov, *J. Phys. Chem. B* **2003**, 107, 86–90.
- [19] D. G. Shchukin, I. L. Radtchenko, G. B. Sukhorukov, *Mater. Lett.* **2003**, 57, 1743–1747.
- [20] I. L. Radtchenko, M. Giersig, G. B. Sukhorukov, *Langmuir* **2002**, 18, 8204–8208.
- [21] L. Dähne, S. Leporatti, E. Donath, H. Möhwald, *J. Am. Chem. Soc.* **2001**, 123, 5431–5436.
- [22] C. S. Peyratout, H. Möhwald, L. Dähne, *Adv. Mater.* **2003**, 15, 1722–1726.
- [23] R. Ghan, T. Shutava, A. Patel, V. John, Y. Lvov, *Macromolecules* **2004**, 37, 4519–4524.
- [24] T. Shutava, Z. Zheng, V. John, Y. Lvov, *Biomacromolecules* **2004**, 5, 914–921.
- [25] J. Ruhe, W. Knoll, *Supramolecular Polymers*, Marcel Dekker, New York, **2000**.
- [26] X. Guo, M. Ballauff, *Langmuir* **2000**, 16, 8719–8726.
- [27] X. Guo, A. Weiss, M. Ballauff, *Macromolecules* **1999**, 32, 6043–6046.
- [28] Y. Lvov, A. A. Antipov, A. Mamedov, H. Möhwald, G. B. Sukhorukov, *Nano Lett.* **2001**, 1, 125–128.

- [29] G. B. Sukhorukov, E. Donath, H. Lichtenfeld, E. Knippel, M. Knippel, A. Budde, H. Möhwald, *Colloids Surf. A* **1998**, *137*, 253–266.
- [30] A. A. Antipov, G. B. Sukhorukov, E. Donath, H. Möhwald, *J. Phys. Chem. B* **2001**, *105*, 2281–2284.
- [31] F. Hoshino, M. Nakano, T. Yanagihara, *Preprints of the Seventh Polymeric Microspheres Symposium* **1992**, 197.
- [32] G. B. Sukhorukov, D. G. Shchukin, W. F. Dong, H. Möhwald, V. V. Lulevich, O. I. Vinogradova, *Macromol. Chem. Phys.* **2004**, *205*, 530–535.

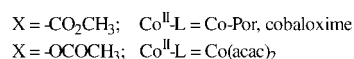
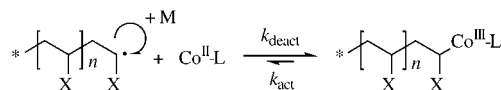
Radical Polymerization

Highly Efficient Cobalt-Mediated Radical Polymerization of Vinyl Acetate**

Antoine Debuigne, Jean-Raphaël Caille, and Robert Jérôme*

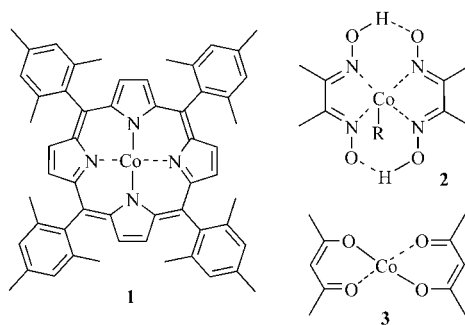
In the last decades, rapidly increasing attention has been paid to so-called macromolecular engineering, that is, the synthesis of novel polymeric materials with well-defined molecular parameters. In this respect, controlled radical polymerization (CRP) proved to be a suitable strategy, because of its mild experimental conditions and tolerance to water. Nowadays, nitroxide-mediated polymerization (NMP),^[1] atom-transfer radical polymerization (ATRP),^[2] and radical addition–fragmentation chain-transfer (RAFT)^[3] are among the more popular CRP techniques. All of them rely on the same concept, which consists of decreasing the radical concentration in the medium and thus the probability of irreversible termination. This is achieved by reversible conversion of the growing macroradicals P^\bullet to dormant species PX . The persistent-radical effect (PRE) is the origin of the high propensity of the radicals to undergo reversible deactivation rather than self-coupling reactions.^[4]

The lability of the cobalt–carbon bond under thermal and photolytic treatment,^[5] and thus the reversibility of its cleavage, make cobalt complexes suitable candidates for PRE^[6] and regulation of CRP. The first example of cobalt-mediated radical polymerization (CMRP), reported by Wayland et al., was the radical polymerization of acrylates in the presence of cobalt porphyrin complexes such as (tetramesitylporphyrinato)cobalt complex **1** [Co(TMP)].^[7,8] The cobalt complex reversibly end-caps the growing polymeric radicals under heating, which accounts for the equilibrium between dormant ($P\text{--Co}^{\text{III}}\text{L}$) and active species (P^\bullet) shown in Scheme 1. In this process, the oxidation state of the metal



Scheme 1. Equilibrium between dormant and active species in CMRP of acrylates and vinyl acetate.

species alternates between two and three. Later, more efficient halogenated cobalt porphyrin complexes were designed, synthesized, and used to improve the polymerization kinetics.^[9] Moreover, the process was extended to alkylcobaloximes **2**, which are suitable photoinitiators for CMRP of acrylates.^[10] However, in spite of all these improvements, CMRP remains restricted to the polymerization of acrylates. Other monomers, such as methacrylates and styrene, predominantly undergo hydrogen elimination and are accordingly involved in catalytic chain-transfer polymerization (CCTP).^[11] More dramatically, vinyl acetate (VAC) polymerization is completely inhibited by the cobalt porphyrin complexes.^[12]



We tested cobalt(II) acetylacetonate complex **3**, which is commercially available, cheap, and reasonably soluble in acrylic monomers, in the radical polymerization of *n*-butyl acrylate (*n*BuA) and vinyl acetate initiated by 2,2'-azo-bis(4-methoxy-2,4-dimethyl valeronitrile) (V-70) at 30 °C. In contrast to cobalt porphyrin complexes and cobaloximes, **3** is unable to mediate and control the radical polymerization of *n*-butyl acrylate. Indeed, formation of chains with high molar mass and broad molar mass distribution at low conversion is clear indication of an uncontrolled process (Table 1, entry 1).

[*] A. Debuigne, Prof. R. Jérôme
 Center for Education and Research on Macromolecules (CERM)
 University of Liège
 Sart-Tilman, B6, 4000 Liège (Belgium)
 Fax: (+32) 4-366-3497
 E-mail: rjerome@ulg.ac.be

Dr. J.-R. Caille
 Solvay Research and Technology
 rue de Ransbeek 310, 1120 Brussels (Belgium)

[**] The authors gratefully acknowledge Solvay for financial support. They are grateful to V. Bodart and F. Declercq (Solvay) and C. Detrembleur (F.N.R.S.) for fruitful discussions. They thank Wakko for providing them with V-70. They are also indebted to the “Belgian Science Policy” for financial support in the frame of the “Inter-university Attraction Poles Programme (PAI V/03)—Supramolecular Chemistry and Supramolecular Catalysis”.

Supporting information for this article is available on the WWW under <http://www.angewandte.org> or from the author.

Table 1: Bulk radical polymerization of vinyl acetate and *n*-butyl acrylate in the presence of [Co(acac)₂].

Entry	M	[M]/[Co]	t [h]	Z ^[c] [%]	$M_{n,SEC}$ ^[d] [10 ³ g mol ⁻¹]	$M_{n,theor}$ ^[e] [10 ³ g mol ⁻¹]	M_w/M_n
1	<i>n</i> BuA ^[a]	348	2	< 1			
			3	5	35.0	2.4	2.20
			5	8	39.7	3.9	2.00
2	VAc ^[b]	542	16	29	13.0	13.6	1.13
			18	42	17.9	19.9	1.17
			20	49	20.4	22.8	1.19
			22	56	22.8	26.2	1.22
			24	64	25.4	30.1	1.21
3	VAc ^[b]	813	13	16	13.0	11.2	1.11
			14	22	19.9	15.4	1.13
			15.5	33	26.5	23.1	1.15
			17	42	33.3	29.4	1.17
			19	55	41.8	38.4	1.20
4	VAc ^[b]	1626	22	70	51.4	49.0	1.23
			14	56	70.5	78.4	1.22
5	VAc ^[b]	2168	14	60	99.0	112.0	1.33

[a] Bulk polymerization of *n*BuA at 30°C, [Co(acac)₂]/[V-70] = 1. [b] Bulk polymerization of VAc at 30°C, [Co(acac)₂]/[V-70] = 6.5. [c] The monomer conversion Z is determined gravimetrically after removal of the unconverted monomer in vacuo. [d] Determined by size-exclusion chromatography (SEC) with polystyrene calibration. [e] $M_{n,theor} = ([M]_0/[Co]_0) \times M_{mono} \times Z$.

When the polymerization of vinyl acetate (VAc) is conducted in the presence of **3** under the same experimental conditions, no polymer is formed for at least 12 h at 30°C (Table 1, entries 2 and 3). However, the polymerization of vinyl acetate starts after this period of time, and a controlled process is observed, as assessed by the linear increase of the molar mass with monomer conversion (Figure 1). As

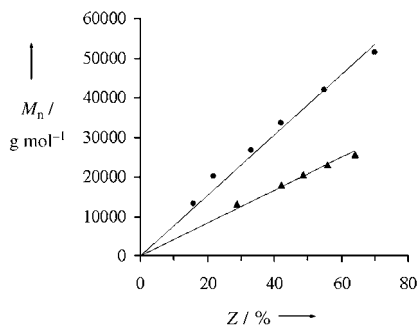


Figure 1. Dependence of PVAc molar mass M_n on monomer conversion Z for bulk polymerization of vinyl acetate at 30°C. [VAc]/[Co(acac)₂] = 542 (▲) and 813 (●) (Table 1, entries 2 and 3).

expected, the molar mass of poly(vinyl acetate), PVAc, is controlled by the [VAc]/[Co(acac)₂] ratio; higher molar masses are obtained at higher molar ratios of monomer to Co complex (Figure 1). Therefore, appropriate choice of the [VAc]/[Co(acac)₂] ratio allows PVAc to be prepared with molar masses as high as 70 000 and 99 000 g mol⁻¹, with reasonably low polydispersities (Table 1, entries 4 and 5). As a rule the polydispersity is very narrow ($1.1 \leq M_w/M_n \leq 1.2$) throughout the polymerization. The slight but significant increase in polydispersity with monomer conversion is observed in any controlled radical processes as result of irreversible termination reactions and, in this case, possible

transfer reactions to monomer and/or polymer. Further evidence for the pronounced efficacy of this cobalt complex in mediating the radical polymerization of vinyl acetate can be found in the good agreement between experimental and theoretical molar masses ($M_{n,theor}/M_{n,SEC} = 1 \pm 0.12$, Table 1). The theoretical values were calculated under the assumption that one polymer chain is growing per [Co(acac)₂] unit, according to the mechanism proposed by Wayland and co-workers for the CMRP of acrylates (Scheme 1).^[7]

The CMRP of vinyl acetate was also initiated at higher temperature (60°C) by AIBN instead of V-70 in the presence of [Co(acac)₂]. Under these conditions, the molar mass again increases with monomer conversion, the polymerization rate is higher, but the experimental molar masses are higher than predicted ($M_{n,theor}/M_{n,SEC} \approx 0.5$), which is evidence for higher probability of irreversible chain termination. Con-

sistently, the molar mass distribution is much broader ($M_w/M_n = 2.0$ –3.5).

The kinetics of this CMRP of vinyl acetate are first-order in monomer, as assessed by the linear dependence of $\ln([M]_0/[M])$ versus time (Figure 2). This observation confirms that the macroradical concentration remains essentially constant and that irreversible termination reactions do not play a

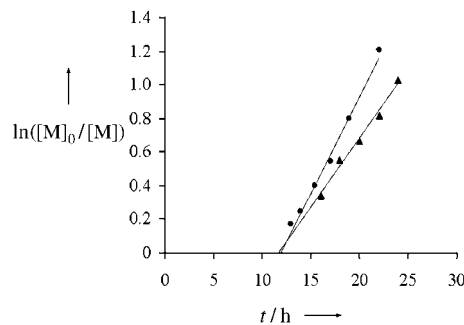


Figure 2. Time dependence of $\ln([M]_0/[M])$ for the bulk polymerization of vinyl acetate at 30°C. [VAc]/[Co(acac)₂] = 542 (▲) and 813 (●) (Table 1, entries 2 and 3). [M]₀ and [M] are the vinyl acetate concentration at times 0 and t, respectively.

major role. In contrast to acrylates, an induction period of several hours is systematically observed in the radical polymerization of VAc, which would be the time for the radicals generated in situ to convert Co^{II} into Co^{III}–P. During this nonproductive period, a drastic change in the color of the medium, from purple to dark brown-green, is observed, consistent with the suggested change in oxidation state of the cobalt complex.

Vinyl acetate oligomers ($M_n = 1300$ g mol⁻¹, $M_w/M_n = 1.13$), preformed in bulk at 30°C with V-70 in the presence of [Co(acac)₂], were collected and purified by repeated

precipitation in heptane, and finally used as macroinitiators for vinyl acetate polymerization. Resumption of the VAc polymerization was successful, as assessed by the shift of the SEC chromatograms with time towards lower elution volumes, a polydispersity that remains narrow, and a very small amount of unconverted macroinitiator (Figure 3). This obser-

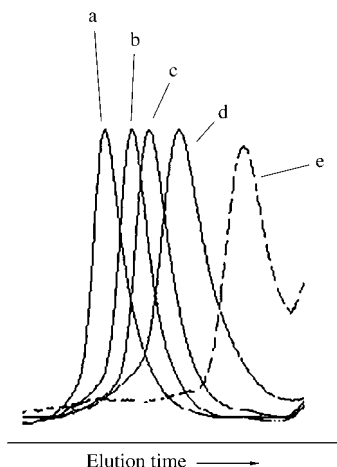


Figure 3. Size-exclusion chromatograms for PVAc initiated at 30°C by a preformed PVAc macroinitiator end-capped by $[\text{Co}(\text{acac})_2]$. $[\text{VAc}]/[\text{PVAc-Co}] = 319$. a) $M_n = 24\,300$, $M_w/M_n = 1.11$, 57% conversion; b) $M_n = 13\,300$, $M_w/M_n = 1.24$, 30% conversion; c) $M_n = 9\,900$, $M_w/M_n = 1.16$, 20% conversion; d) $M_n = 5\,800$, $M_w/M_n = 1.13$, 10% conversion; e) PVAc macroinitiator, $M_n = 1\,300$, $M_w/M_n = 1.13$.

vation paves the way for the synthesis of block copolymers by sequential polymerization of VAc and any comonomer whose polymerization is controlled by the same initiator/Co complex system. This may be a restriction, because the Co complex that controls VAc polymerization is not necessarily effective in the polymerization of other monomers, such as acrylates. In that case, exchange of Co complexes is required between the consecutive polymerization steps.

As mentioned previously, vinyl acetate polymerization is inhibited by cobalt porphyrin,^[12] which reacts irreversibly with the very reactive radicals of the VAc type. In this particular case, the equilibrium is completely shifted towards the dormant form. However, quite an appropriate balance is established between dormant and active species by $[\text{Co}(\text{acac})_2]$, with an instantaneous concentration of active chains low enough to impart control on the polymerization. In case of acrylates, the deactivation rate of the propagating radicals into dormant species is very low compared to the rate of propagation, and this leads rapidly to a large number of active chains. This drastic change in the position of the dormant/active species equilibrium when VAc is substituted for *n*BuA can be explained by the more pronounced leaving character and the lower reactivity of the polyacrylate radicals, as result of a stabilizing substituent.

Finally, ^{13}C NMR analysis of PVAc confirmed that the Co complex has no influence on the stereoregularity of the polymer formed by the radical process.^[13]

Up to now only few systems were able to mediate the polymerization of vinyl acetate with more or less success, such

as degenerative chain transfer with alkyl iodides,^[14] ATRP,^[15] and RAFT with xanthates^[16] and dithiocarbamates,^[17] whereas cobalt-mediated radical polymerization was inactive.

In the light of the results reported herein, the role of the ligand in CMRP is essential. This technique, restricted to acrylates, until now, can be tuned by the appropriate choice of ligand (e.g., substitution of acetylacetonate for porphyrin) and extended even to reluctant monomers such as VAc. This is expected to renew interest in CMRP and its extension to other vinylic monomers. Moreover, this very efficient control of vinyl acetate polymerization paves the way to macromolecular engineering of poly(vinyl acetate) and directly derivatized poly(vinyl alcohol), including tailored telechelic polymers and block and graft copolymers of different architectures.

Experimental Section

Vinyl acetate and *n*-butyl acrylate were dried over calcium hydride, degassed by several freeze/thaw cycles, distilled under reduced pressure, and stored under argon. Cobalt(II) acetylacetonate (> 98%, Merck), 2,2'-azobisisobutyronitrile (AIBN, Fluka) and 2,2'-azobis(4-methoxy-2,4-dimethyl valeronitrile) (V-70, Wako) were used as received.

General procedure: V-70 (200 mg, 0.65 mmol) and $[\text{Co}(\text{acac})_2]$ (25.7 mg, 0.1 mmol) were placed in a 30 mL flask and degassed by three vacuum/argon cycles. Dry, degassed vinyl acetate (5 mL, 54.2 mmol) was then added by syringe under argon. The purple mixture was stirred and heated at 30°C. After a few hours, the color changed from purple to dark brown-green. No polymerization occurred for at least 12 h, after which the viscosity of the solution increased substantially. Samples were withdrawn at different reaction times, and monomer conversion was determined by weighing the collected polymer after removal of the unconverted monomer in vacuo. The same procedure was used for *n*-butyl acrylate (5 mL, 34.8 mmol) polymerization initiated by V-70 (31 mg, 0.1 mmol).

PVAc oligomers (110 mg, 0.085 mmol, $M_{n,\text{SEC}} = 1300 \text{ g mol}^{-1}$, $M_w/M_n = 1.13$) were prepared according to the general procedure and collected at low monomer conversion by repeated precipitation in heptane. They were dissolved in degassed vinyl acetate (2.5 mL, 27.1 mmol) and heated at 30°C to resume the controlled radical polymerization.

Received: July 16, 2004

Revised: October 11, 2004

Published online: January 11, 2005

Keywords: cobalt · ligand effects · polymerization · radical reactions · vinyl acetate

- [1] C. J. Hawker, A. W. Bosman, E. Harth, *Chem. Rev.* **2001**, *101*, 3661.
- [2] K. Matyjaszewski, J. Xia, *Chem. Rev.* **2001**, *101*, 2921.
- [3] G. Moad, J. Chiefari, Y. K. Chong, J. Krstina, R. T. A. Mayadunne, A. Postma, E. Rizzardo, S. H. Thang, *Polym. Int.* **2000**, *49*, 993.
- [4] H. Fischer, *Chem. Rev.* **2001**, *101*, 3581.
- [5] a) J. Halpern, *Acc. Chem. Res.* **1982**, *15*, 238; b) F. T. T. Ng, G. L. Rempel, C. Mancuso, J. Halpern, *Organometallics* **1990**, *9*, 2762; c) D. C. Woska, Z. D. Xie, A. A. Gridnev, S. D. Ittel, M. Fryd, B. B. Wayland, *J. Am. Chem. Soc.* **1996**, *118*, 9102.
- [6] B. E. Daikh, R. G. Finke, *J. Am. Chem. Soc.* **1992**, *114*, 2938.

- [7] B. B. Wayland, G. Poszmik, S. L. Mukerjee, M. Fryd, *J. Am. Chem. Soc.* **1994**, *116*, 7943.
- [8] Z. Lu, M. Fryd, B. B. Wayland, *Macromolecules* **2004**, *37*, 2686.
- [9] B. B. Wayland, L. Basicckes, S. L. Mukerjee, M. Wei, M. Fryd, *Macromolecules* **1997**, *30*, 8109.
- [10] L. D. Arvanitopoulos, M. P. Greuel, H. J. Harwood, *Polym. Prepr.* **1994**, *35*, 549.
- [11] A. A. Gridnev, S. D. Ittel, *Chem. Rev.* **2001**, *101*, 3611.
- [12] N. S. Enikolopyan, B. R. Smirnov, G. V. Ponomarev, I. M. Belgovskii, *J. Polym. Sci. Polym. Chem. Ed.* **1981**, *19*, 879.
- [13] More details on the tacticity analysis can be found in the Supporting Information.
- [14] M. Kamigaito, M. Sawamoto, *Polym. Prepr.* **2002**, *43*, 179.
- [15] a) A. Tsuyoshi, M. C. Iovu, K. Matyjaszewski, *Macromolecules* **2003**, *36*, 9346; b) M. Wakioka, K.-Y. Baek, T. Ando, M. Kamigaito, M. Sawamoto, *Macromolecules* **2002**, *35*, 330.
- [16] a) E. Rizzardo, J. Chiefari, R. T. A. Mayadunne, G. Moad, S. H. Thang, *Polym. Prepr.* **1999**, *40*, 342; b) E. Rizzardo, J. Chiefari, R. T. A. Mayadunne, G. Moad, S. H. Thang, *ACS Symp. Ser.* **2000**, *768*, 278; c) E. Rizzardo, J. Chiefari, R. Mayadunne, G. Moad, S. Thang, *Macromol. Symp.* **2001**, *174*, 209.
- [17] M. Destrac, D. Charmot, X. Franck, S. Z. Zard, *Macromol. Rapid Commun.* **2000**, *21*, 1035.

Surface Polymerization

GaAs–Polymer Hybrids Formed by Surface-Initiated Atom-Transfer Radical Polymerization of Methyl Methacrylate

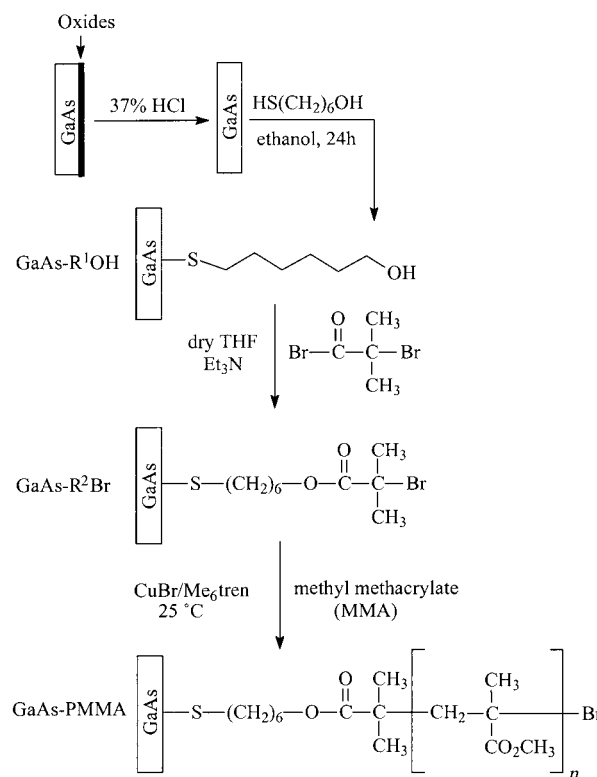
Qin Jia Cai, Guo Dong Fu, Fu Rong Zhu,
En-Tang Kang,* and Koon-Gee Neoh

Semiconductor–polymer hybrids prepared by incorporating polymer brushes on semiconductor substrates have attracted considerable attention in recent years. The hybrids have unique surface and interface properties,^[1–10] and allow the fabrication of nanopatterns.^[11–16] Popular strategies for incorporating polymer brushes on substrates include the “top-down” or “grafting-to” approach, in which macromolecules are tethered directly onto the surface of a substrate, and the “bottom-up” or “grafting-from” approach, which attempts to grow polymer brushes from initiators anchored on a substrate surface. The latter approach can result in more densely

packed polymer brushes.^[17] Ionic (anionic^[18–20] and cationic^[6,21]), ring-opening,^[11,22–26] radical,^[17,27,28] nitroxide-mediated radical,^[1] and atom-transfer radical^[3–6,29,30] polymerizations have been used for surface graft polymerizations. Among these techniques, atom-transfer radical polymerization (ATRP) allows the preparation of well-defined polymers and polymer architectures, and exhibits good tolerance for functional groups and stability against impurities.^[5,6]

Semiconductor–polymer hybrids prepared by surface-initiated polymerization on silicon substrates,^[1–7] carbon nanotubes,^[8–10] and germanium nanoparticles^[31] have been reported. GaAs–polymer hybrids with well-ordered polymer brushes have potential applications in advanced GaAs-based semiconductor devices,^[32] chemical sensors,^[33] and biomaterials.^[34] Recent developments in the preparation of Au–polymer hybrids by surface-initiated ATRP^[16,35,36] and GaAs–organic hybrids from self-assembled monolayers (SAMs) of alkane thiols on GaAs^[37] have inspired us to synthesize GaAs–polymer hybrids by ATRP. We also hoped that a dense, well-defined, and covalently bonded polymer nanofilm would help to stabilize the surface states^[37,38] associated with this compound semiconductor.

We prepared GaAs–polymer hybrids by surface-initiated ATRP of methyl methacrylate (MMA) from ATRP initiators covalently immobilized on the (100)-oriented GaAs single-crystal surfaces. This process allows the preparation of GaAs–polymer hybrids with well-defined, covalently tethered polymer brushes. The strategy for preparing GaAs–polymer hybrids by ATRP is shown in Scheme 1. A nearly stoichiometrically pure GaAs surface with reactive sites (dangling



Scheme 1. Covalent immobilization of ATRP initiators on the GaAs surface and surface-initiated ATRP to form the GaAs-PMMA hybrids.

[*] Q. J. Cai, G. D. Fu, Prof. E.-T. Kang, Prof. K.-G. Neoh
Department of Chemical and Biomolecular Engineering
National University of Singapore
Kent Ridge, Singapore 119260 (Singapore)
Fax: (+65) 6779-1936
E-mail: cheket@nus.edu.sg

Q. J. Cai, Dr. F. R. Zhu
Institute of Materials Research and Engineering
3 Research Link, Singapore 117602 (Singapore)



Supporting information for this article is available on the WWW under <http://www.angewandte.org> or from the author.

bonds) was obtained after the oxides on a 3 cm² GaAs(100) wafer were removed by treatment with concentrated HCl (37%) for two minutes.^[38] The GaAs substrate was subsequently immersed in a 5 mM ethanol solution of 6-sulfanyl-1-hexanol (which had been subjected to three freeze–pump–thaw cycles) for 24 h at room temperature to form the hydroxy-terminated GaAs surface (GaAs-R¹OH). The GaAs surface with immobilized ATRP initiators (GaAs-R²Br) was obtained by immersing the GaAs-R¹OH substrate in a 0.1 M THF solution of 2-bromoisobutryl bromide containing 0.1 M triethylamine for two minutes under argon. GaAs–polymer hybrids were finally prepared by surface-initiated ATRP of MMA on the GaAs-R²Br surface in a continuously stirred solution containing 5.3 mL of MMA, CuBr (14.3 mg, 0.1 mmol), CuBr₂ (2.2 mg, 0.01 mmol), and tris[2-(dimethylamino)ethyl]amine^[39] (Me₆tren, 26 μ L, 0.11 mmol), for between 4 and 21 h at room temperature under argon.

Figure 1a shows the As3d and Ga3d core-level spectra of the (100)-oriented GaAs single-crystal surface after HCl etching, as measured by X-ray photoelectron spectroscopy (XPS). The As3d core-level spectrum shows a spin-orbit-split doublet, with binding energies (BEs) at about 40.7 eV (3d_{5/2}) and 41.4 eV (3d_{3/2}), attributable to the GaAs species.^[40] The Ga3d core-level spectrum has a peak component at a BE of about 19.0 eV associated with the GaAs species.^[40] The As and Ga oxide species are absent in both spectra, thereby indicating that they have been completely removed by the treatment with concentrated HCl (Supporting Information).

Figure 1b shows the As3d and Ga3d core-level spectra of the GaAs-R¹OH surface. The presence of As–S (BEs of about 42.0 eV (3d_{5/2}) and 42.7 eV (3d_{3/2})) and Ga–S (BE of about 19.7 eV) species on the GaAs surface,^[41–43] and the fact that only one chemical state of sulfur is observed (S2s core-level spectrum can be curve-fitted with only one peak component at a BE of about 225.5 eV, which is associated with the sulfide species^[40]), suggest that the GaAs-R¹OH surface consists of 6-sulfanyl-1-hexanol coupled covalently by As–S and Ga–S bonds. The thickness of the hydroxythiol layer could not be determined with sufficient accuracy by ellipsometry.

Figure 1c shows the wide scan and Br3d core-level spectra of the GaAs-R²Br surface. The successful immobilization of the bromoester initiators on the GaAs surface is verified by the appearance of a Br3d spin-orbit-split doublet with BEs of about 70 eV (3d_{5/2}) and 71 eV (3d_{3/2}).^[40] (The BE assignments for the various elemental species and chemical states are provided in the Supporting Information.) The resulting GaAs-R²Br substrate has a uniform film thickness of about 0.7 nm, as measured by ellipsometry at five different locations on the surface of a 3-cm² GaAs substrate. The surface roughness (*R_a*) of the GaAs-R²Br substrate, as determined from the atomic force microscopy (AFM) image, remains practically unchanged from that of the starting GaAs surface (Table 1). The density of the coupling agent/initiator species was estimated from the linear contribution of ethyl 2-bromo-2-methylpropionate (1.33 g mL^{−1}) and 1-butanethiol (0.84 g mL^{−1}).^[44] Thus, from the density (~1.1 g mL^{−1}) and the molecular weight (282 g mol^{−1}) of the coupling agent/initiator species, the surface-graft density was estimated to be

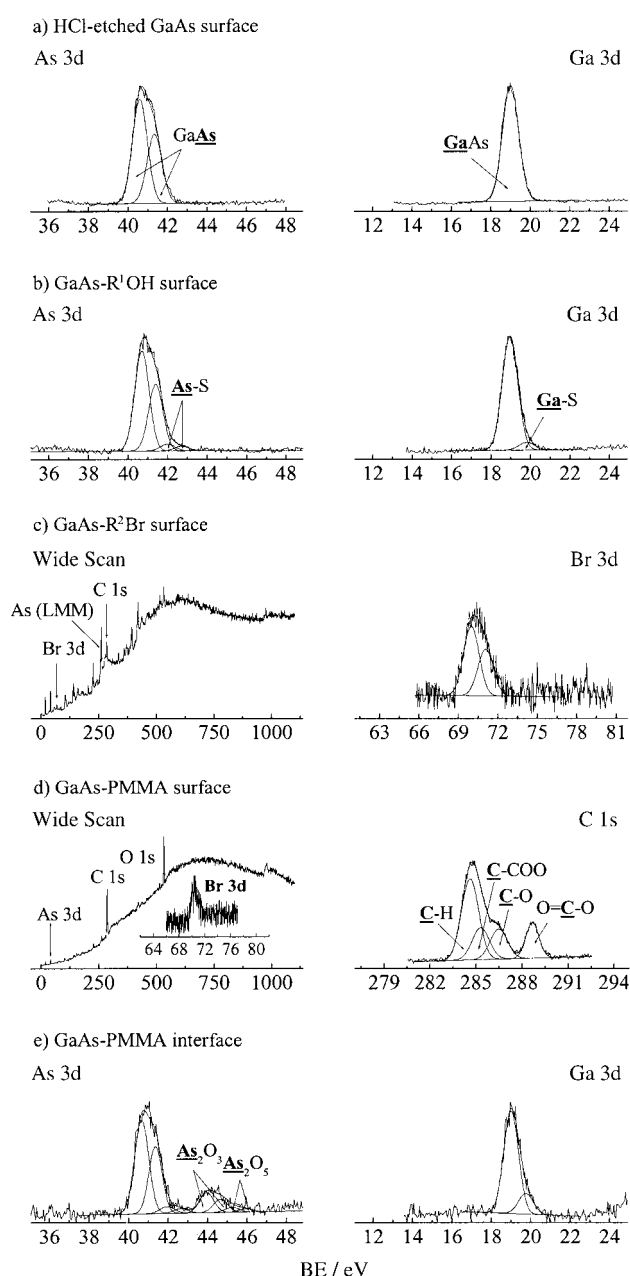


Figure 1. XPS core-level and wide-scan spectra of a) the HCl-etched GaAs surface, b) the GaAs-R¹OH surface, c) the GaAs-R²Br surface, d) the GaAs-PMMA hybrid (sample PMMA1, Table 1) surface, and e) the GaAs-PMMA hybrid interface (sample PMMA1, Table 1).

about 1.6 units nm^{−2}, which is similar to that of SAMs of alkane thiols on GaAs surfaces reported previously.^[37]

After the surface-initiated ATRP of MMA on the GaAs-R²Br surface for 21 h at room temperature, the GaAs substrate with surface-grafted MMA polymer (PMMA)—the GaAs-PMMA hybrid—was washed/extracted continuously for 8 h with a large volume of THF, which is a good solvent for PMMA, to remove the physically adsorbed PMMA and reactant residues. The resulting GaAs-PMMA hybrid, with a PMMA film thickness of about 29 nm, as measured by ellipsometry, has a water contact angle of about 69° (GaAs-PMMA4, Table 1). This contact angle is similar to

Table 1: Thickness and surface roughness of the PMMA films grafted on the GaAs (100) substrates.^[a]

Sample	<i>t</i> [h] ^[b]	Thickness [nm] ^[c]	DP ^[d]	<i>R_a</i> [nm] ^[e]
HCl-etched GaAs	–	–	–	0.56
GaAs-R ² Br	–	0.7	–	0.52
GaAs-PMMA1	4	9	120	0.43
GaAs-PMMA2	8	20	270	0.58
GaAs-PMMA3	12	24	320	0.53
GaAs-PMMA4	21	29	390	0.63

[a] Reaction conditions for fabricating GaAs-PMMA hybrids: [MMA]:[CuBr]:[CuBr₂]:[Me₆tren] = 500:1:0.1:1.1 at room temperature under argon. [b] Reaction time. [c] The film thickness was measured by ellipsometry. [d] The average degree of polymerization (DP) was estimated based on a surface initiator density of about 1.6 units nm⁻², a PMMA density of 1.1 g cm⁻³, an MMA molecular weight of 100 g mol⁻¹, and the corresponding PMMA film thickness. [e] *R_a* is the arithmetic mean of surface roughness calculated from the roughness profile of the AFM image.

that of the PMMA homopolymer (about 71°).^[45] As shown in Table 1, the thickness of the grafted PMMA film in the resulting GaAs-PMMA hybrids increases with an increase in polymerization time, which suggests that the growth of the PMMA chains occurs by a controlled process. This proposal was further supported by an approximately linear increase in the average degree of polymerization (DP) of PMMA homopolymer with MMA monomer conversion (see Supporting Information) for concurrent polymerizations with the free initiator (ethyl 2-bromo-2-methylpropionate) in solution. Since the average cross-sectional area of the PMMA chain prepared by surface-initiated ATRP is 1.8–2.0 nm²^[35,36] and the surface initiator density is about 1.6 units nm⁻², the surface initiator efficiency of the present system is estimated to be about 30%. Together with a PMMA thickness of 29 nm (sample GaAs-PMMA4, Table 1), a PMMA density of 1.1 g cm⁻³,^[36] and an MMA molecular weight of 100 g mol⁻¹, the average DP of the PMMA graft chain was estimated to be about 390. This value is also similar to those obtained from homopolymerizations in solution (see Supporting Information).

XPS was again used to characterize the PMMA polymer brushes grafted onto the GaAs surface. Figure 1 d shows the high-resolution C1s core-level spectrum of the GaAs-PMMA1 sample surface (Table 1). The C1s core-level line shape is dominated by that of PMMA.^[46] The spectrum consists of four peak-components with BEs at 284.6 eV for the aliphatic hydrocarbons (C–C and C–H species), 285.3 eV for the C–COO species, 286.4 eV for the C–O species, and 288.6 eV for the O=C–O species.^[46] The [C–H/C–C]:[C–COO]:[C–O]:[O=C–O] molar ratio, as determined from the C1s spectral component area ratio, is 2.8:1.2:1.1:1. This ratio deviates somewhat from the theoretical ratio of 2:1:1:1 for PMMA, probably as a result of contributions of the underlying initiator and thiol coupling-agent to the aliphatic hydrocarbon species, as the PMMA film thickness (~9 nm) is comparable to the sampling depth of the XPS technique (see below). With an increase in PMMA film thickness, the surface composition approaches that of pure PMMA. The inset in Figure 1 d shows the Br3d core-level spectrum of the

GaAs-PMMA1 sample surface (Table 1). The persistence of the Br signal is consistent with the fact that the growth of the PMMA chain from the surface is a surface-initiated polymerization process with a living characteristic.

The chemical states of the GaAs-PMMA hybrid interface with a PMMA film thickness of about 9 nm (sample GaAs-PMMA1, Table 1) were also investigated by XPS. Since the probing depth of the XPS technique for hydrocarbon polymers is 10 nm,^[47] the As3d and Ga3d signals of the hybrid should originate mainly from the uppermost surface of the GaAs substrate after the grafting of about 9 nm of PMMA. Only a trace amount of As oxide and no Ga oxide species were observed in the XPS spectra of the GaAs-PMMA interface (Figure 1 e), which suggests that the surface-initiated ATRP has a minimal effect on the chemical states of the GaAs surface and that the surface-coupled 6-sulfanyl-1-hexanol also serves as a passivation layer for the GaAs surface.

The surface morphology of the GaAs-PMMA hybrid and the HCl-etched GaAs was studied by AFM. Figure 2 a,b show

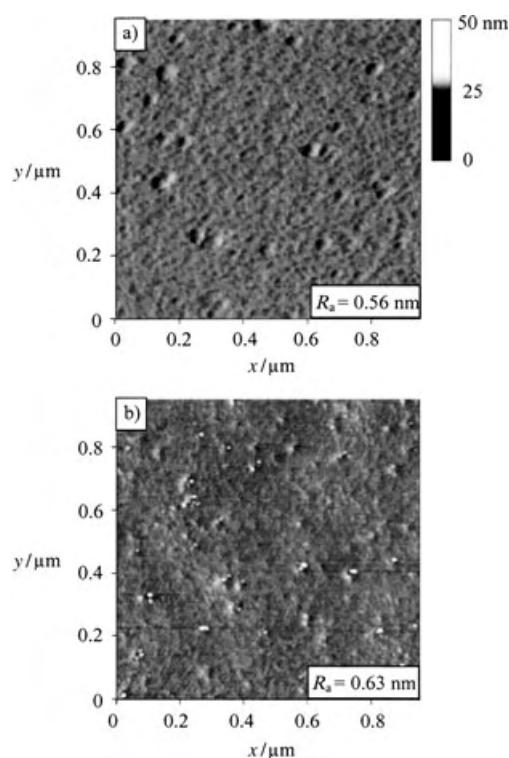


Figure 2. AFM images of a) the HCl-etched GaAs surface and b) the GaAs-PMMA hybrid surface (sample GaAs-PMMA4, Table 1).

the respective AFM images of the HCl-etched GaAs and the GaAs-PMMA hybrid surfaces (sample GaAs-PMMA4, Table 1). The surface roughness (*R_a* ~ 0.63 nm) of the GaAs-PMMA hybrid is similar to that of the original HCl-etched GaAs surface (*R_a* ~ 0.56 nm). The nanoscopic uniformity of the GaAs-PMMA hybrid surface can be attributed to the well-defined PMMA brushes prepared by the surface-initiated ATRP.

The process of surface-initiated ATRP of MMA on the GaAs-R²Br surface was further verified by two parallel experiments. These experiments involved 1) immersion of the GaAs-R¹OH substrate in a continuously stirred MMA monomer solution containing CuBr (14.3 mg, 0.1 mmol), CuBr₂ (2.2 mg, 0.01 mmol), and Me₆tren (26 μ L, 0.11 mmol), and 2) immersion of the GaAs-R²Br substrate in a continuously stirred MMA monomer solution without CuBr, CuBr₂, and Me₆tren, for 12 h at room temperature. No change in the thickness of the organic layer was detected by ellipsometry for samples from both experiments, which is consistent with the fact that surface-initiated ATRP of MMA occurs only in the presence of both the surface initiator and the Cu catalyst.

In summary, surface-initiated ATRP on a functionalized GaAs single-crystal surface has allowed the successful preparation of GaAs-PMMA hybrids at room temperature. The surface states of the GaAs substrate are not significantly affected by the ATRP process. The sulfanyhexanol coupling-agent acts as a covalently bonded ATRP initiator and it also passivates the GaAs surface by the formation of covalent Ga-S and As-S bonds. Thus, the present study provides a simple approach for the preparation of GaAs-polymer hybrids with well-defined polymer brushes and preserved interfacial states.

Received: August 6, 2004

Revised: November 17, 2004

Published online: January 11, 2005

Keywords: arsenic · gallium · polymerization · radical reactions · surface states

- [1] P. Mansky, Y. Liu, E. Huang, T. P. Russell, C. Hawker, *Science* **1997**, 275, 1458.
- [2] A. Sidorenko, S. Minko, K. Schenk-Meuser, K. Duschner, M. Stamm, *Langmuir* **1997**, 13, 770.
- [3] M. Ejaz, S. Yamamoto, K. Ohno, Y. Tsujii, T. Fukuda, *Macromolecules* **1998**, 31, 5934.
- [4] M. Husseman, E. E. Malmström, M. McNamara, M. Mate, D. Mecerreyes, D. G. Benoit, J. L. Hedrick, P. Mansky, E. Huang, T. P. Russell, C. J. Hawker, *Macromolecules* **1999**, 32, 1424.
- [5] K. Matyjaszewski, P. J. Miller, N. Shukla, B. Immaraporn, A. Gelman, B. B. Luokala, T. M. Siclován, G. Kickelbick, T. Vallant, H. Hoffman, T. Pakula, *Macromolecules* **1999**, 32, 8716.
- [6] B. Zhao, W. J. Brittain, *J. Am. Chem. Soc.* **1999**, 121, 3557.
- [7] X. Kong, T. Kawai, J. Abe, T. Iyoda, *Macromolecules* **2001**, 34, 1837.
- [8] Z. Yao, N. Braidy, G. A. Botton, A. Adronov, *J. Am. Chem. Soc.* **2003**, 125, 16015.
- [9] S. Qin, D. Qin, W. T. Ford, D. E. Resasco, J. E. Herrera, *J. Am. Chem. Soc.* **2004**, 126, 170.
- [10] H. Kong, C. Gao, D. Yan, *J. Am. Chem. Soc.* **2004**, 126, 412.
- [11] M. Husemann, D. Mecerreyes, C. J. Hawker, J. L. Hedrick, R. Shah, N. L. Abbott, *Angew. Chem.* **1999**, 111, 685; *Angew. Chem. Int. Ed.* **1999**, 38, 647.
- [12] M. Husseman, M. Morrison, D. Benoit, J. Frommer, C. M. Mate, W. D. Hinsberg, J. L. Hedrick, C. J. Hawker, *J. Am. Chem. Soc.* **2000**, 122, 1844.
- [13] J. W. Park, E. L. Thomas, *J. Am. Chem. Soc.* **2002**, 124, 514.
- [14] T. A. von Werne, D. S. Germack, E. C. Hagberg, V. V. Sheares, C. J. Hawker, K. R. Carter, *J. Am. Chem. Soc.* **2003**, 125, 3831.
- [15] L. Ionov, S. Minko, M. Stamm, J. F. Gohy, R. Jérôme, A. Scholl, *J. Am. Chem. Soc.* **2003**, 125, 8303.
- [16] M. Kaholek, W. K. Lee, B. LaMattina, K. C. Caster, S. Zauscher, *Nano Lett.* **2004**, 4, 373.
- [17] O. Prucker, J. Rühe, *Macromolecules* **1998**, 31, 592.
- [18] N. Tsubokawa, H. Ueno, *J. Appl. Polym. Sci.* **1995**, 58, 1221.
- [19] R. Jordan, A. Ulman, J. F. Kang, M. H. Rafailovich, J. Sokolov, *J. Am. Chem. Soc.* **1999**, 121, 1016.
- [20] M. K. D. Ingall, C. H. Honeyman, J. V. Mercure, P. A. Bianconi, R. R. Kunz, *J. Am. Chem. Soc.* **1999**, 121, 3607.
- [21] R. Jordan, A. Ulman, *J. Am. Chem. Soc.* **1998**, 120, 243.
- [22] M. Weck, J. J. Jackiw, R. R. Rossi, P. S. Weiss, R. H. Grubbs, *J. Am. Chem. Soc.* **1999**, 121, 4088.
- [23] N. Y. Kim, N. L. Jeon, I. S. Choi, S. Takami, Y. Harada, K. R. Finnie, G. S. Girolami, R. G. Nuzzo, G. M. Whitesides, P. E. Laibinis, *Macromolecules* **2000**, 33, 2793.
- [24] A. Juang, O. A. Scherman, R. H. Grubbs, N. S. Lewis, *Langmuir* **2001**, 17, 1321.
- [25] N. L. Jeon, I. S. Choi, G. M. Whitesides, N. Y. Kim, P. E. Laibinis, Y. Harada, K. R. Finnie, G. S. Girolami, R. G. Nuzzo, *Appl. Phys. Lett.* **1999**, 75, 4201.
- [26] M. R. Buchmeiser, F. Sinner, M. Mupa, K. Wurst, *Macromolecules* **2000**, 33, 32.
- [27] M. Niwa, M. Date, N. Higashi, *Macromolecules* **1996**, 29, 3681.
- [28] B. de Boer, H. K. Simon, M. P. L. Werts, E. W. van der Vegte, G. Hadziioannou, *Macromolecules* **2000**, 33, 349.
- [29] X. Huang, M. J. Wirth, *Macromolecules* **1999**, 32, 1694.
- [30] H. Mori, A. Böker, G. Krausch, A. H. E. Müller, *Macromolecules* **2001**, 34, 6871.
- [31] R. S. Tanke, S. M. Kauzlarich, T. E. Patten, K. A. Pettigrew, D. L. Murphy, M. E. Thompson, H. W. H. Lee, *Chem. Mater.* **2003**, 15, 1682.
- [32] S. M. Sze, *Physics of Semiconductor Devices*, 2nd ed., Wiley, New York, **1981**.
- [33] F. Seker, K. Meeker, T. F. Kuech, A. B. Ellis, *Chem. Rev.* **2000**, 100, 2505.
- [34] E. Sackmann, M. Tanaka, *Trends Biotechnol.* **2000**, 18, 58.
- [35] J. B. Kim, M. L. Bruening, G. L. Baker, *J. Am. Chem. Soc.* **2000**, 122, 7616.
- [36] R. R. Shah, D. Merceyces, M. Husemann, I. Rees, N. L. Abbott, C. J. Hawker, J. L. Hedrick, *Macromolecules* **2000**, 33, 597.
- [37] C. W. Sheen, J. X. Shi, J. Martensson, A. N. Parikh, D. L. Allara, *J. Am. Chem. Soc.* **1992**, 114, 1514.
- [38] K. Adlkofer, M. Tanaka, *Langmuir* **2001**, 17, 4267.
- [39] J. Queffelec, S. G. Gaynor, K. Matyjaszewski, *Macromolecules* **2000**, 33, 8629.
- [40] J. F. Moulder, W. F. Stickel, P. E. Spol, K. D. Bomben, in *Handbook of X-ray Photoelectron Spectroscopy* (Ed.: J. Chastain), Perkin-Elmer, Eden Prairie, MN, **1992**, p. 61.
- [41] C. J. Spindt, D. Liu, K. Miyano, P. L. Meissner, T. T. Chiang, T. Kendelewicz, I. Lindau, W. E. Spicer, *Appl. Phys. Lett.* **1989**, 55, 861.
- [42] T. Hou, C. M. Greenlief, S. W. Keller, L. Nelen, J. F. Kauffman, *Chem. Mater.* **1997**, 9, 3186.
- [43] A. Shaporenko, K. Adlkofer, L. S. O. Johansson, M. Tanaka, M. Zharnikov, *Langmuir* **2003**, 19, 4992.
- [44] *Aldrich Handbook of Fine Chemicals and Laboratory Equipment: 2003–2004*, Sigma-Aldrich Chem. Co., Milwaukee, WI, p. 327 and p. 842.
- [45] P. J. Eaton, P. Graham, J. R. Smith, J. D. Smart, T. G. Nevell, J. Tsiouklis, *Langmuir* **2000**, 16, 7887.
- [46] G. Beamson, D. Briggs, *High Resolution XPS of Organic Polymers. The Scienta ESCA Database*, Wiley, New York, **1993**, p. 118.
- [47] D. Briggs, *Surface Analysis of Polymers by XPS and Static SIMS*, Cambridge University Press, Cambridge, **1998**, p. 36.

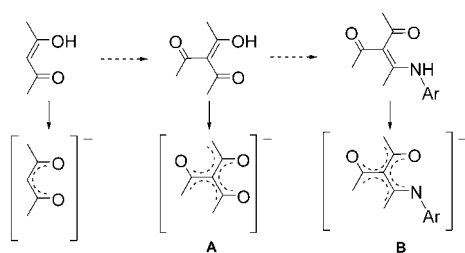
Remote Activation of Nickel Catalysts for Ethylene Oligomerization**

Yaofeng Chen, Gang Wu, and Guillermo C. Bazan*

An important consideration in the design of homogenous transition-metal initiators for the oligomerization and polymerization of olefins concerns the mode of activation. While neutral initiators are becoming increasingly available,^[1] the majority are cationic species generated upon addition of a strong Lewis acid, in the presence or absence of an alkylating agent, to a neutral organometallic precursor. The most typical activators are alkylaluminoxanes^[2] and well-defined Lewis acids, such as $B(C_6F_5)_3$.^[3] For example, $B(C_6F_5)_3$ reacts with $[Cp_2ZrMe_2]$ ($Cp = C_5H_5$) to give $[Cp_2ZrMe(MeB(C_6F_5)_3)]$.^[4] The dynamics of the resulting cation/anion pair, such as dissociation equilibria or the ability of the olefin to displace the anion, are important in determining the availability of the active site and the overall reactivity towards the unsaturated organic substrate.^[3,5]

Zwitterionic initiators, which provide an intermediate choice between cationic and neutral species for specifying reactivity and functionality tolerance, are fewer in number.^[6–10] In the case of $[(H_3C)C[N(C_6H_5)]C[O-B(C_6F_5)_3]-[N(C_6H_5)]-\kappa^2N,N']Ni(\eta^3-CH_2C_6H_5)]$, the Lewis acid attaches to a site removed from the trajectory of the incoming substrate and no dissociative process is required for initiation or propagation of oligomerization or polymerization reactions.^[11] This complex has found utility in the design of tandem copolymerization reactions for producing branched polyethylene from ethylene alone.^[12]

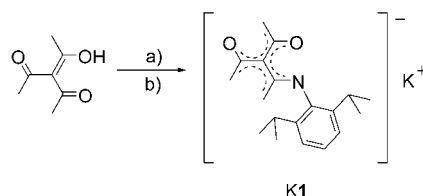
Herein we provide a design for a ligand with an electronically delocalized conduit that extends the distance between the metal and the site of Lewis acid attachment. Our rationale begins with the well-known bidentate acetylacetonate (acac) ligand, which forms readily from 4-hydroxypent-3-ene-2-one. Extension of the framework by addition of an acetyl group at the internal carbon atom yields commercially available triacetyl methane (3-(1-hydroxyethylidene)-2,4-pentanedione), which, upon deprotonation, is anticipated to yield the delocalized structure **A** in Scheme 1. Replacement of one of the oxygen atoms by an aryl-substituted nitrogen group provides 3-[1-(arylamino)ethylidene]pentane-2,4-dione derivatives and anionic structures, such as **B** (Scheme 1). On the basis of additional steric bulk from the aromatic unit, we anticipated π coordination to nickel complexes. However, it also seemed plausible that a strong and large Lewis acid



Scheme 1. General ligand design.

would prefer binding to an O site and force π coordination to the nickel.

Condensation of 2,6-diisopropylaniline with triacetyl methane in toluene using a catalytic amount of *p*-toluenesulfonic acid provides 3-[1-(2,6-diisopropylphenylamino)ethylidene]pentane-2,4-dione. The 2,6-diisopropylphenyl group was chosen for its stabilization of reactive nickel centers and tendency to increase the molecular weight of the products of ethylene addition reactions.^[13] Subsequent deprotonation with KH in THF provides the potassium salt of the ligand (**K1**) in 46% overall yield starting from triacetyl methane (Scheme 2).



Scheme 2. Synthesis of the potassium salt of the ligand (**K1**); a) 2,6-diisopropylaniline, *p*-toluenesulfonic acid monohydrate, toluene; b) KH, THF.

1H and ^{31}P NMR spectroscopy show that the reaction of **K1** with $[Ni(\eta^1-CH_2C_6H_5)Cl(PMe_3)_2]$ ^[14] provides an organometallic compound which contains the organic fragment in **K1**, an η^1 -benzyl group (1H NMR: $\delta = 7.68$ ppm), and a coordinated trimethylphosphine ligand. These data do not allow for unambiguous determination of the ligand coordination mode. Single crystals of the product suitable for X-ray diffraction studies were obtained from a solution of pentane (Figure 1).^[15] The product is therefore **2**, as shown in Scheme 3. The nickel center has a distorted square-planar coordination geometry with the 3-[1-(2,6-diisopropylphenyl-imino)ethyl]acetylacetonate ligand bound through the two oxygen atoms at nearly equal Ni–O separations (1.889(2) and 1.8982(19) Å). The bond lengths, C1–O1 (1.269(3) Å), C3–O2 (1.276(3) Å), C1–C2 (1.411(4) Å), and C2–C3 (1.399(4) Å), are intermediate between those of typical single and double bonds. The coplanar disposition of C1, C2, C3, O1, and O2 atoms is consistent with a delocalized electronic structure.

The addition of one equivalent $B(C_6F_5)_3$ to **2** was monitored by NMR spectroscopy in C_6D_6 . Quick formation of a new organometallic product is detected, which contains a coordinated trimethylphosphine ligand (1H NMR: $\delta =$

[*] Dr. Y. Chen, Dr. G. Wu, Prof. Dr. G. C. Bazan
Departments of Chemistry and Materials
Center for Polymer and Organic Solids
The University of California, Santa Barbara, CA 93106 (USA)
Fax: (+1) 805-893-4120
E-mail: bazan@chem.ucsb.edu

[**] This work was supported by the US Department of Energy (Grant Number: DE-FG03098ER14910).

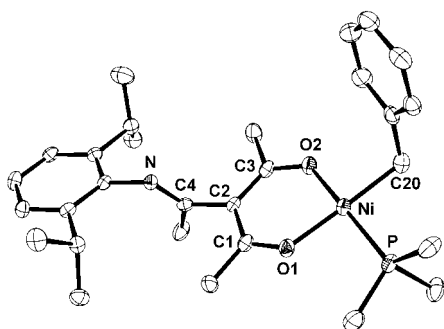
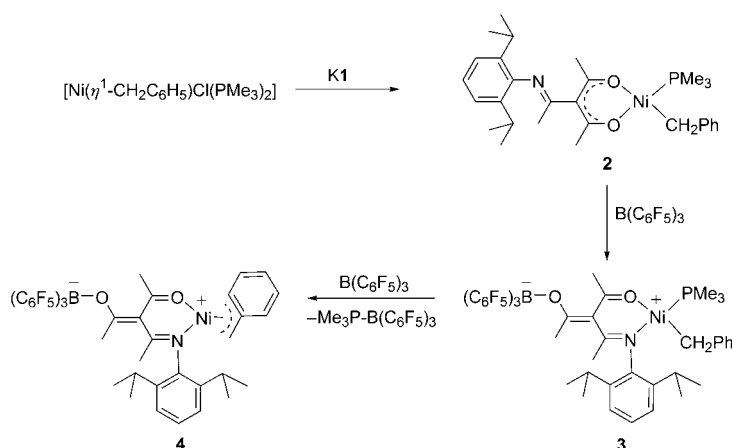


Figure 1. ORTEP drawing of **2**; thermal ellipsoids set at 50% probability, hydrogen atoms are omitted for clarity.



Scheme 3. Synthesis of compounds **2**, **3**, and **4**.

0.46 ppm; ^{31}P NMR: $\delta = -7.92$ ppm), $\text{B}(\text{C}_6\text{F}_5)_3$ (^{11}B NMR: $\delta = -12.55$ ppm), and an $\eta^1\text{-CH}_2\text{C}_6\text{H}_5$ fragment (^1H NMR: $\delta = 7.40$ ppm). Single crystals formed directly from the C_6D_6 solution and the solid-state structure was determined by crystallographic methods (Figure 2).^[15] These data indicate that the molecular structure of **3** is as shown in Scheme 3, where one of the carbonyl groups binds $\text{B}(\text{C}_6\text{F}_5)_3$. The transformation from **2** to **3** requires for the ligand to change its binding mode. Our current thinking is that this process is likely from a small amount of the NO bound regioisomer of **2**, which is in equilibrium with the OO bound counterpart. Coordination of the oxygen center to boron drives the equilibrium to the NO isomer. Although the product may be a mixture of *E*- and *Z*-isomers, only the isomer that minimizes steric interactions between the bulky 2,6-diisopropylphenyl substituent and $\text{B}(\text{C}_6\text{F}_5)_3$ is observed.

The structural parameters in **3** offer insight into bond localization and charge distribution. The C2–C3 separation (1.371(5) Å) is consistent with a double bond, whereas the C2–C1 (1.466(5) Å) and C2–C4 (1.486(5) Å) separations reveal substantial single-bond character. This localized bonding in the chelating ring forces C2 away from the O1–C1–C4–N plane. The nickel center is also removed from this plane (0.95 Å) and the overall six-member cyclic structure adopts a boat-like conformation (Figure 2b).^[16] These observations are consistent with the bond order of **3** shown in Scheme 3 and

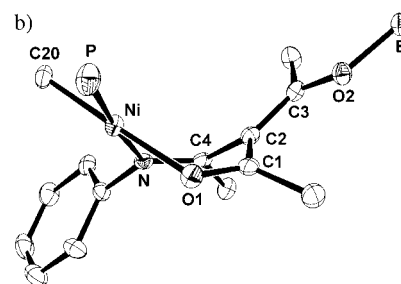
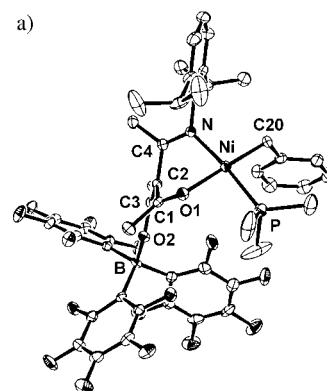
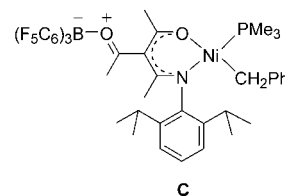


Figure 2. ORTEP diagrams of the molecular structure of compound **3**. a) Complete structure and b) the environment close to the nickel center. Thermal ellipsoids are set at 50% probability, hydrogen atoms are omitted for clarity.

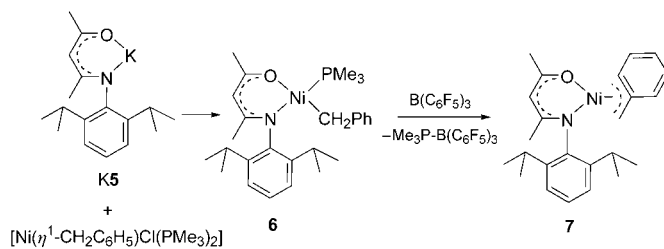
indicate that a contribution from structure **C** is not significant. As a result, we expect a zwitterionic structure for **3** with a large partial positive charge on the nickel center.



A new complex is formed on addition of one equivalent of $\text{B}(\text{C}_6\text{F}_5)_3$ to **3** along with a white precipitate which corresponds to $\text{Me}_3\text{P-B}(\text{C}_6\text{F}_5)_3$. The same products are formed by addition of two equivalents $\text{B}(\text{C}_6\text{F}_5)_3$ to **2**. Characterization by ^1H , ^{13}C , ^{11}B and ^{19}F NMR spectroscopy shows that the nickel-containing product forms nearly quantitatively and contains the fragment corresponding to ligand **1**, $\text{B}(\text{C}_6\text{F}_5)_3$ (^{11}B NMR: $\delta = -13.25$ ppm) and an $\eta^3\text{-benzyl}$ ligand (^1H NMR: $\delta = 6.26$ ppm). Based on these data we propose that the reaction removes the trimethylphosphine from the coordination sphere of nickel and yields **4** (see Scheme 3). Repeated efforts to structurally characterize **4** were not successful.

Two ketoaryliminato compounds (**6** and **7**) were prepared to provide a baseline measure for reactivity towards ethylene and to provide a comparison of ligand structures. As shown in

Scheme 4, the reaction of potassium 4-(2,6-diisopropylphenylimino)acetylacetonate (**K5**) with $[\text{Ni}(\eta^1\text{-CH}_2\text{C}_6\text{H}_5)\text{Cl}(\text{PMe}_3)_2]$ provides a new compound, **6**. NMR spectroscopy indicates that the compound contains the organic fragment in



Scheme 4. Synthesis of compounds **6** and **7**.

K5, an η^1 -benzyl group (^1H : NMR $\delta = 7.90$ ppm) and a coordinated trimethylphosphine ligand.^[17] Single crystals of **6** were grown from a pentane solution (Figure 3).^[15] A distorted

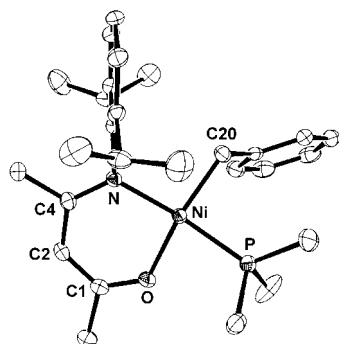


Figure 3. ORTEP diagram of the molecular structure of compound **6**, thermal ellipsoids are set at 50% probability, hydrogen atoms are omitted for clarity.

square-planar coordination geometry is observed, with the 4-(2,6-diisopropylphenylimino)acetylacetonate ligand coordinating by the nitrogen and oxygen atoms. The Ni–O and Ni–N bond lengths are 1.907(2) and 1.954(2), respectively. As in the case of **2**, the ligand fragment coordinated to Ni in **6** displays a delocalized electronic framework. For example, the bond lengths, C1–O (1.288(3) Å), C4–N (1.329(4) Å), C1–C2 (1.373(4) Å), and C2–C4 (1.410(4) Å), are intermediate between those of typical single and double bonds, and the C1, C2, C4, O, and N atoms are coplanar.

Comparison of the structures of **3** and **6** shows the influence of $\text{B}(\text{C}_6\text{F}_5)_3$ -carbonyl coordination on the ligand electronic structure. Compared with **6**, compound **3** contains longer C1–C2 and C2–C4 bonds and shorter C1–O1 and C4–N bonds (for **3**, C1–O1 1.241(4) Å, C4–N 1.288(5) Å). By this remote attachment of the Lewis acid, the bonding in the ligand becomes considerably more localized. It is also of note that the Ni–O bond (1.974(3) Å) in **3** is about 0.07 Å longer than that in **6** (1.907(2) Å), which reveals that the borated ligand in **3** is a poorer donor.

The addition of $\text{B}(\text{C}_6\text{F}_5)_3$ to **6** in toluene results in the formation of $\text{Me}_3\text{P-B}(\text{C}_6\text{F}_5)_3$ and a new product **7**, which ^1H and ^{13}C NMR spectroscopy show contains the fragment in ligand **5** and an η^3 -benzyl ligand (^1H NMR: 6.68 ppm). Based on these results we propose that the net reaction involves borane–phosphine complexation and a hapticity increase by the benzyl ligand to fill the vacant coordination site. The final product is thus compound **7** in Scheme 4.

Addition of 100 psi (689.476 kPa) ethylene above a solution of **4** in toluene at 30°C results in the quick consumption of the ethylene, with an activity of 1450 kg product/mol Ni h. When 2 equivalents of $\text{B}(\text{C}_6\text{F}_5)_3$ are added as a “scrubbing agent”, the activity increases to 5450 kg product/mol Ni h. The products are a distribution of ethylene oligomers with an internal olefin structure. Similar products and activities are found by addition of $\text{B}(\text{C}_6\text{F}_5)_3$ to **2** under ethylene. For example, the catalytic system produced by **2** and 3 equivalents of $\text{B}(\text{C}_6\text{F}_5)_3$ displays an activity of 3130 kg product/mol Ni h. No reaction occurs with **2** alone since the trimethylphosphine blocks coordination of ethylene. The activity of compound **7** towards ethylene under similar reaction conditions is only 51 kg product/mol Ni h. Therefore, the decreased electron density at the nickel center in **3**, relative to **7**, results in a substantial increase of reactivity.

In summary, addition of $\text{B}(\text{C}_6\text{F}_5)_3$ to **2** results in a change of the binding mode of ligand **1** and in the coordination of a carbonyl functionality to boron. Direct attachment of $\text{B}(\text{C}_6\text{F}_5)_3$ to the “pendant” imino nitrogen in **2** is discouraged by the steric bulk of the diisopropylphenyl substituent. The conversion from **2** into **3** changes the binding mode of ligand **1** from LX (L = neutral two-electron donor, X = one-electron ligand in the covalent model)^[18] to L_2 , thereby removing electron density from the nickel center. The bonding parameters of **3** are consistent with little electron delocalization within the ligand framework. Removing the PMe_3 in **3** with $\text{B}(\text{C}_6\text{F}_5)_3$ induces an η^1 to η^3 hapticity change in the benzyl ligand to provide **4**, which is an effective ethylene oligomerization initiator. While we recognize that there are structural differences, the much higher reactivity of **4**, relative to **7**, highlights the effect of the reduced electron density at nickel. It is noteworthy that the Lewis acid makes its influence across the Ni–N–C–C–C–O structural unit.

Experimental Section

All manipulations were performed under a nitrogen atmosphere. Toluene and THF were distilled from benzophenone ketyl, and pentane was dried over Na/K alloy. The toluene for reactions with ethylene use was purchased from Aldrich (anhydrous grade) and purified further over Na/K alloy. Tris(pentafluorophenyl)boron was provided by Boulder Scientific Company, and purified further by sublimation. Ethylene (99.99%) was purchased from Matheson Trigas and purified by passing through Agilent moisture and oxygen/moisture traps. Triacetylmethane (3-(1-hydroxyethylidene)-2,4-pentanedione) and 2,6-diisopropylaniline were purchased from Aldrich and used without further purification. 4-(2,6-Diisopropylphenylimino)acetylacetone (**5**) was prepared from condensation of 2,6-diisopropylaniline with acetylacetone in benzene using a catalytic amount of *p*-toluenesulfonic acid.^[19] NMR spectra were recorded on a Varian 200, 400, or Bruker 200 spectrometers. ^1H NMR spectra were calibrated using signals from the solvent and are reported downfield

from tetramethylsilane (TMS) referenced to residual solvent ^1H signals. ^{11}B NMR, ^{19}F NMR, and ^{31}P NMR spectra were calibrated and reported downfield from external $\text{BF}_3\cdot\text{OEt}_2$, CFC_3 , and H_3PO_4 , respectively. Mass spectrometric analyses were obtained using a VG70 magnetic sector instrument. Elemental analyses were performed by Analytic Lab, Marine Science Institute, University of California, Santa Barbara.

1: 3-(1-hydroxyethylidene)-2,4-pentanedione (1.02 g, 7.2 mmol), 2,6-diisopropylaniline (1.06 g, 6.0 mmol), *p*-toluenesulfonic acid monohydrate (200 mg), and toluene (25 mL) were placed in a 50-mL flask equipped with Dean–Stark apparatus. After refluxing overnight, the solvent was removed under vacuum, and the residue was extracted with hexane (60 mL). The volume of the solution was then concentrated to approximately 5 mL, and cooled to -20°C to give a white solid (0.95 g, 53% yield, m.p. 103°C); ^1H NMR (200 MHz, C_6D_6 , 25°C): $\delta = 14.23$ (br s, 1H; NH), 7.15–6.95 (m, 3H; imine-ph-H), 2.98 (septet, $J = 6.8$ Hz, 2H; *i*Pr-CH), 2.19 (br s, 3H; CH_3 in acetyl), 2.10 (br s, 3H; CH_3 in acetyl), 1.75 (s, 3H; CH_3), 1.01 (d, $J = 6.6$ Hz, 6H; *i*Pr- CH_3), 0.99 ppm (d, $J = 6.6$ Hz, 6H; *i*Pr- CH_3); ^{13}C NMR (100 MHz, CDCl_3 , 25°C): $\delta = 199.59$ (br s, carbonyl), 166.21 (imine), 145.67, 132.77, 128.87, 123.98 (ph-C), 114.57 (ethylene), 31.67 (br s, CH_3 in acetyl), 28.77 (*i*Pr-CH), 24.66 (*i*Pr- CH_3), 22.75 (*i*Pr- CH_3), 18.06 ppm (CH_3); HRMS (EI): m/z calcd for $\text{C}_{19}\text{H}_{27}\text{NO}_2$, 301.2042; found, 301.2047; Elemental analysis calcd (%) for $\text{C}_{19}\text{H}_{27}\text{NO}_2$: C 75.71, H 9.03, N 4.65; found: C 75.60, H 8.87, N 4.79.

K1: KH (64 mg, 1.6 mmol) was added to 3-[1-(2,6-diisopropylphenylamino)ethylidene]pentane-2,4-dione (452 mg, 1.5 mmol) in THF (5 g). After stirring for 3 h at room temperature, the reaction mixture was filtered, and the solvent was removed under vacuum. Trituration with pentane for 1 h gave the potassium salt (**K1**) as a white solid (441 mg, in 87% yield). ^1H NMR (200 MHz, $\text{C}_6\text{D}_6/\text{THF}$ (10/1), 25°C): $\delta = 7.13$ –6.98 (m, 3H; imine-ph-H), 2.22 (s, 6H; CH_3 in acetyl), 1.98 (s, 3H; CH_3), 1.80 (septet, $J = 7.2$ Hz, 2H; *i*Pr-CH), 1.24 (d, $J = 6.8$ Hz, 6H; *i*Pr- CH_3), 1.13 ppm (d, $J = 6.8$ Hz, 6H; *i*Pr- CH_3).

2: **K1** (290 mg, 0.85 mmol) and $[\text{Ni}(\eta^1\text{-CH}_2\text{C}_6\text{H}_5)\text{Cl}(\text{PMe}_2)_2]$ (288 mg, 0.85 mmol) were stirred in THF (5 g) for 3 h at room temperature. The reaction mixture was then filtered, the filtrate collected, and the THF removed under vacuum. The residue was extracted with pentane (25 g). The solution was concentrated to approximately 4 mL and cooled to -35°C to yield a yellow solid (360 mg, 80% yield). ^1H NMR (400 MHz, C_6D_6 , 25°C): $\delta = 7.68$ (d, $J = 7.2$ Hz, 2H; benzyl-ph- $\text{H}^{2,6}$), 7.25–7.11 (m, 6H; imine-ph-H and benzyl-ph- $\text{H}^{3,4,5}$), 3.06 (septet, $J = 6.8$ Hz, 2H; *i*Pr-CH), 2.18 (s, 3H; CH_3 in acetyl), 2.07 (d, $J = 6.8$ Hz, 2H; benzyl- CH_2), 1.92 (s, 3H; CH_3 in acetyl), 1.62 (s, 3H; CH_3), 1.16 (d, $J = 6.8$ Hz, 6H; *i*Pr- CH_3), 1.15 (d, $J = 6.8$ Hz, 6H; *i*Pr- CH_3), 0.76 ppm (d, $J = 10.0$ Hz, 9H; PCH_3); ^{13}C NMR (100 MHz, C_6D_6 , 25°C): $\delta = 184.96$, 183.98 (carbonyl), 169.87 (imine), 149.97, 147.14, 136.89, 129.13, 128.82, 124.41, 123.97, 123.44 (ph-C), 118.63 (ethylene), 28.46 (*i*Pr-CH), 27.88 (CH_3 in acetyl), 27.25 (CH_3 in acetyl), 24.56 (CH_3), 24.45 (*i*Pr- CH_3), 23.79 (*i*Pr- CH_3), 12.92 (d, $J = 28$ Hz, PCH_3), 12.28 ppm (d, $J = 26$ Hz, benzyl- CH_2); ^{31}P NMR (162 MHz, C_6D_6 , 25°C): $\delta = -6.79$ ppm; Elemental analysis calcd (%) for $\text{C}_{29}\text{H}_{42}\text{NO}_2\text{P}_2\text{Ni}$: C 66.18, H 8.04, N 2.66; found: C 66.11, H 7.40, N 2.82.

3: Compound **2** (10.5 mg, 0.02 mmol) and one equivalent of $\text{B}(\text{C}_6\text{F}_5)_3$ (10.2 mg, 0.02 mmol) were mixed in C_6D_6 (0.9 mL). After 1 h, the solution was filtered, and ^1H , ^{19}F , ^{11}B and ^{31}P NMR spectra of the filtrate were recorded. The spectra indicated the nearly quantitative formation of complex **3**. ^1H NMR (400 MHz, C_6D_6 , 25°C): $\delta = 7.40$ (d, $J = 8.0$ Hz, 2H; benzyl-ph- $\text{H}^{2,6}$), 7.18–7.05 (m, 6H; imine-ph-H and benzyl-ph- $\text{H}^{3,4,5}$), 2.46 (s, 3H; CH_3 in acetyl), 2.12 (s, 3H; CH_3), 1.47 (s, 3H; $\text{CH}_3\text{-CO-B}(\text{C}_6\text{F}_5)_3$), 0.94 (br d, $J = 4.8$ Hz, 6H; *i*Pr- CH_3), 0.46 ppm (d, $J = 10.0$ Hz, 9H; PCH_3), *i*Pr-CH, benzyl- CH_2 and one of *i*Pr- CH_3 not observed; ^{19}F NMR (376 MHz, C_6D_6 , 25°C): $\delta = -133.83$, -157.97 , -163.91 ppm; ^{31}P NMR (162 MHz, C_6D_6 , 25°C): $\delta = -7.92$ ppm; ^{11}B NMR (161 MHz, C_6D_6 , 25°C): $\delta = -12.55$ ppm. Single crystals suitable for X-ray analysis formed after three days.

4: Compound **2** (52.6 mg, 0.10 mmol) and two equivalents of $\text{B}(\text{C}_6\text{F}_5)_3$ (102 mg, 0.20 mmol) were mixed in C_6H_6 (4.0 g). The color of the solution changed from orange to red immediately along with the formation of white precipitate. After stirring for 1 h, hexane (1.0 g) was added to the mixture and the reaction mixture was filtered after 15 min. The C_6H_6 and hexane were removed from the filtrate under vacuum, which gave a red solid product (91 mg, 94% yield). ^1H NMR (400 MHz, C_6D_6 , 25°C): $\delta = 7.27$ (t, $J = 7.6$ Hz, 1H; benzyl-ph- H^4), 7.00 (t, $J = 7.6$ Hz, 1H; imine-ph- H^4), 6.96 (d, $J = 7.4$ Hz, 2H; imine-ph- $\text{H}^{3,5}$), 6.90 (t, $J = 7.6$, 2H; benzyl-ph- $\text{H}^{3,5}$), 6.26 (d, $J = 7.0$ Hz, 2H; benzyl-ph- $\text{H}^{2,6}$), 2.88 (septet, $J = 6.8$ Hz, 2H; *i*Pr-CH), 2.01 (br s, 3H; CH_3 in acetyl), 1.80 (s, 3H; CH_3), 1.48 (br s, 3H; $\text{CH}_3\text{-CO-B}(\text{C}_6\text{F}_5)_3$), 1.31 (d, $J = 6.8$ Hz, 6H; *i*Pr- CH_3), 0.96 (s, 2H; benzyl- CH_2), 0.85 ppm (d, $J = 6.8$ Hz, 6H; *i*Pr- CH_3); ^{13}C NMR (50 MHz, C_6D_6 , 25°C): $\delta = 184.93$, 174.46, 151.30, 146.48, 140.41, 138.76, 138.05, 135.41, 129.59, 125.05 and 116.25 (carbonyl, imine and ph-C), 107.94 (ethylene), 31.06, 29.27 and 25.07 (CH_3 in acetyl, $\text{CH}_3\text{-CO-B}(\text{C}_6\text{F}_5)_3$ and CH_3), 28.61 (*i*Pr-CH), 24.89 (*i*Pr- CH_3), 24.09 (*i*Pr- CH_3), 23.46 ppm (benzyl- CH_2); ^{19}F NMR (C_6D_6 , 376 MHz, 25°C): $\delta = -133.79$, -158.13 , -164.29 ppm; ^{11}B NMR (C_6D_6 , 161 MHz, 25°C): $\delta = -13.25$ ppm; Elemental analysis calcd (%) for $\text{C}_{44}\text{H}_{33}\text{NO}_2\text{BF}_{15}\text{Ni}$: C 54.92, H 3.46, N 1.46; found: C 53.71, H 3.51, N 1.45.

6: Compound **6** was prepared in 90% yield from potassium 4-(2,6-diisopropylphenylimino)acetylacetonate by the same method for preparing **2**. ^1H NMR (400 MHz, C_6D_6 , 25°C): $\delta = 7.90$ (d, $J = 7.2$ Hz, 2H; benzyl-ph- $\text{H}^{2,6}$), 7.08–6.97 (m, 6H; imine-ph-H and benzyl-ph- $\text{H}^{3,4,5}$), 5.13 (s, 1H; CH), 4.07 (septet, $J = 6.8$ Hz, 2H; *i*Pr-CH), 1.81 (s, 3H; CH_3), 1.59 (s, 3H; CH_3), 1.40 (d, $J = 6.8$ Hz, 6H; *i*Pr- CH_3), 1.21 (d, $J = 7.2$ Hz, 6H; *i*Pr- CH_3), 0.81 (s, 2H; benzyl- CH_2), 0.66 ppm (d, $J = 9.6$ Hz, 9H; PCH_3); ^{13}C NMR (100 MHz, C_6D_6 , 25°C): $\delta = 176.42$ (carbonyl), 166.02 (imine), 147.79, 142.16, 130.36, 127.99, 126.01, 124.02, 123.60, 123.60 (ph-C), 98.29 (ethylene), 28.63 (*i*Pr-CH), 26.64 (CH_3), 26.02 (CH_3), 25.07 (*i*Pr- CH_3), 24.86 (*i*Pr- CH_3), 12.55 (d, $J = 26$ Hz, PCH_3), 10.04 ppm (d, $J = 24$ Hz, benzyl- CH_2); ^{31}P NMR (162 MHz, C_6D_6 , 25°C): $\delta = -13.26$ ppm; Elemental analysis calcd (%) for $\text{C}_{27}\text{H}_{40}\text{NOPNi}$: C 66.96, H 8.33, N 2.89; found: C 67.56, H 8.51, N 3.02.

7: $\text{B}(\text{C}_6\text{F}_5)_3$ (153 mg, 0.30 mmol) in toluene (2 g) was added to **6** (145 mg, 0.30 mmol) in toluene (2 g). The color of solution changed from orange to dark red, and a white precipitate formed after several minutes. After stirring for 1 h, 1 g hexane was added to the mixture and the reaction mixture was filtered after 15 min. Solvents were removed from the filtrate under vacuum and the residue was extracted with hexane (1 g). The hexane was removed under vacuum to afford 114 mg of **7** in 93% yield. ^1H NMR (400 MHz, C_6D_6 , 25°C): $\delta = 7.46$ (t, $J = 7.6$ Hz, 1H; benzyl-ph- H^4), 7.08–7.05 (m, 5H; imine-ph-H and benzyl-ph- $\text{H}^{3,5}$), 6.68 (dd, $J = 8.0$ Hz, 2H; benzyl-ph- $\text{H}^{2,6}$), 4.85 (s, 1H; CH), 3.85 (septet, $J = 6.8$ Hz, 2H; *i*Pr-CH), 1.70 (s, 3H; CH_3), 1.42 (d, $J = 6.8$ Hz, 6H; *i*Pr- CH_3), 1.41 (s, 3H; CH_3), 1.13 (d, $J = 6.8$ Hz, 6H; *i*Pr- CH_3), 0.70 ppm (s, 2H; benzyl- CH_2); ^{13}C NMR (100 MHz, C_6D_6 , 25°C): $\delta = 178.30$ (carbonyl), 165.22 (imine), 151.91, 140.10, 134.91, 127.62, 125.67, 124.05, 116.92, 107.65 (ph-C), 97.71 (ethylene), 28.88 (CH_3), 28.56 (*i*Pr-CH), 27.09 (CH_3), 24.68 (*i*Pr- CH_3), 24.53 (*i*Pr- CH_3), 23.06 ppm (benzyl- CH_2); Elemental analysis calcd (%) for $\text{C}_{24}\text{H}_{31}\text{NONi}$: C 70.62, H 7.65, N 3.43; found: C 70.42, H 7.53, N 3.48.

Typical reaction with ethylene: Compound **4** (5 μmol) in toluene (0.50 g) was added to a 70-mL glass reactor charged with toluene (27.50 g). The reactor was assembled and brought out of the glove box. After stirring the solution at 30°C for 2 min, ethylene was fed continuously for 20 min under a pressure of 100 psi (689.476 kPa). The reaction was quenched by release of ethylene pressure and addition of acetone (1 mL). The solvent was removed to afford a viscous oil, which was further dried under high vacuum overnight. The yield was measured by weighing the viscous oil or by weighing the

entire reaction assembly before and after reaction; the two techniques are in agreement to within $\pm 5\%$.

Received: August 12, 2004

Published online: January 12, 2005

Keywords: ethylene oligomerization · homogeneous catalysis · Lewis acids · nickel · zwitterionic compounds

- [1] S. D. Ittel, L. K. Johnson, M. Brookhart, *Chem. Rev.* **2000**, *100*, 1169–1204.
- [2] W. Kaminsky, H. Sinn, *Transition Metals and Organometallics as Catalyst for Olefin Polymerization*, Springer, Berlin, **1988**.
- [3] E. Y.-X. Chen, T. J. Marks, *Chem. Rev.* **2000**, *100*, 1391–1434.
- [4] X. Yang, C. L. Stern, T. J. Marks, *J. Am. Chem. Soc.* **1991**, *113*, 3623–3625.
- [5] a) G. Fink, W. Fenzl, R. Mynott, *Z. Naturforsch. B* **1985**, *40*, 158–166; b) D. E. Richardson, N. G. Alameddine, M. F. Ryan, T. Hayes, J. R. Eyler, A. R. Siedle, *J. Am. Chem. Soc.* **1996**, *118*, 11244–11253; c) F. Schaper, A. Geyer, H. H. Brintzinger, *Organometallics* **2002**, *21*, 473–483; d) C. R. Landis, K. A. Rosaaen, D. R. Sillars, *J. Am. Chem. Soc.* **2003**, *125*, 1710–1711.
- [6] M. Bochmann, S. J. Lancaster, O. B. Robinson, *J. Chem. Soc. Chem. Commun.* **1995**, 2081–2082.
- [7] Y. Sun, R. E. v. H. Spence, W. E. Piers, M. Parvez, G. P. A. Yap, *J. Am. Chem. Soc.* **1997**, *119*, 5132–5143; b) X. Song, M. Bochmann, *J. Organomet. Chem.* **1997**, *545–546*, 597–600.
- [8] Y. H. Kim, T. H. Kim, N. Y. Kim, E. S. Cho, B. Y. Lee, D. M. Shin, Y. K. Chung, *Organometallics* **2003**, *22*, 1503–1511.
- [9] C. C. Lu, J. C. Peters, *J. Am. Chem. Soc.* **2002**, *124*, 5272–5273.
- [10] a) B. Temme, G. Erker, J. Karl, H. Luftmann, R. Fröhlich, S. Kotila, *Angew. Chem.* **1995**, *107*, 1867–1869; *Angew. Chem. Int. Ed. Engl.* **1995**, *34*, 1755–1757; b) J. W. Strauch, G. Erker, G. Kehr, R. Fröhlich, *Angew. Chem.* **2002**, *114*, 2662–2664; *Angew. Chem. Int. Ed.* **2002**, *41*, 2543–2546; c) For review see: G. Erker, *Acc. Chem. Res.* **2001**, *34*, 309–317; G. Erker, *Chem. Commun.* **2003**, 1469–1476.
- [11] B. Y. Lee, G. C. Bazan, J. Vela, Z. J. A. Komon, X. Bu, *J. Am. Chem. Soc.* **2001**, *123*, 5352–5353.
- [12] a) Z. J. A. Komon, X. Bu, G. C. Bazan, *J. Am. Chem. Soc.* **2000**, *122*, 12379–12380; b) Z. J. A. Komon, G. M. Diamond, M. K. Leclerc, V. Murphy, M. Okazaki, G. C. Bazan, *J. Am. Chem. Soc.* **2002**, *124*, 15280–15285; c) R. W. Barnhart, G. C. Bazan, T. Mourey, *J. Am. Chem. Soc.* **1998**, *120*, 1082–1083; d) G. C. Bazan, G. Rodriguez, A. J. Ashe III, S. Al-Ahmad, C. Müller, *J. Am. Chem. Soc.* **1996**, *118*, 2291–2292.
- [13] a) S. A. Svejda, L. K. Johnson, M. Brookhart, *J. Am. Chem. Soc.* **1999**, *121*, 10634–10635.
- [14] E. Carmona, M. Paneque, M. L. Poveda, *Polyhedron* **1989**, *8*, 285–291.
- [15] a) Crystal data for **2**: $C_{29}H_{42}NO_2PNi$, $M_r = 526.32$, monoclinic, space group $P2_1/c$, $a = 13.270(2)$, $b = 26.931(4)$, $c = 7.9511(13)$ Å, $\beta = 99.479(3)^\circ$, $V = 2802.7(8)$ Å³, $Z = 4$, orange, crystal size $0.3 \times 0.15 \times 0.1$ mm³, $Mo_{K\alpha}$, $\lambda = 0.71073$ Å, $T = 117(1)$ K, $R = 5.57\%$, $wR = 12.78\%$ for 4582 unique reflections with $I > 2\sigma(I)$. Crystal data for **3**: $C_{53}H_{42}D_6BF_{15}NO_2PNi$, $M_r = 1122.42$, triclinic, space group $P\bar{1}$, $a = 10.7104(11)$, $b = 17.4223(17)$, $c = 27.722(3)$ Å, $\alpha = 94.128(2)$, $\beta = 91.465(2)$, $\gamma = 101.601(2)^\circ$, $V = 5049.9(9)$ Å³, $Z = 4$, yellow, crystal size $0.25 \times 0.2 \times 0.1$ mm³, $Mo_{K\alpha}$, $\lambda = 0.71073$ Å, $T = 117(1)$ K, $R = 6.68\%$, $wR = 15.45\%$ for 14927 unique reflections with $I > 2\sigma(I)$. Crystal data for **6**: $C_{27}H_{40}NOPNi$, $M_r = 484.28$, triclinic, space group $P\bar{1}$, $a = 9.5913(8)$, $b = 11.4579(10)$, $c = 13.7938(12)$ Å, $\alpha = 108.936(2)$, $\beta = 90.072(3)$, $\gamma = 111.424(2)^\circ$, $V = 1322.4(2)$ Å³, $Z = 2$, orange, crystal size $0.25 \times 0.2 \times 0.15$ mm³, $Mo_{K\alpha}$, $\lambda = 0.71073$ Å, $T = 117(1)$ K, $R = 4.19\%$, $wR = 10.00\%$ for 5050 unique reflections with $I > 2\sigma(I)$. b) CCDC-245971 (**2**), CCDC-245972 (**3**), and CCDC-245973 (**6**) contain the supplementary crystallographic data for this paper. These data can be obtained free of charge from The Cambridge Crystallographic Data Centre via www.ccdc.cam.ac.uk/data_request/cif.
- [16] J. Feldman, S. J. Mclain, A. Parthasarathy, W. J. Marshall, J. C. Calabrese, S. D. Arthur, *Organometallics* **1997**, *16*, 1514–1516.
- [17] The synthesis and reactivity of the related complex [(2,6-*i*Pr₂(C₆H₃)NC(CH₃)=CHCOCH₃)Ni(PPh₃)Ph] was recently published: D. Zhang, G. Jin, L. Weng, F. Wang, *Organometallics* **2004**, *23*, 3270–3275.
- [18] R. H. Crabtree, *The Organometallic Chemistry of the Transition Metals*, Wiley, New York, **1994**.
- [19] X. He, Y. Yao, X. Luo, J. Zhang, Y. Liu, L. Zhang, Q. Wu, *Organometallics* **2003**, *22*, 4952–4957.

Ammonia Oxidation

**Perovskite Membranes in Ammonia Oxidation:
Towards Process Intensification in Nitric Acid
Manufacture*****Javier Pérez-Ramírez* and Bent Vigeland*

Ammonia is oxidized over PtRh alloy gauzes to form NO as the first step in the industrial production of nitric acid, a process that has remained practically unchanged for over 80 years. The reaction typically yields 94–96 % NO and 4–6 % by-products (N_2O and N_2) at 1073–1223 K.^[1] Major drawbacks associated with the platinum-based catalysts are: 1) high production cost, 2) metal loss in the form of volatile oxides necessitate efficient metal recovery (Pd catchment) and refining systems, and 3) the production of N_2O , an environmentally harmful gas. Nitric acid manufacture is the largest single source of N_2O in the chemical industry (125×10^6 t CO_2 -equiv per annum), and the development and implementation of abatement technology for this gas is required.^[2] The above aspects have stimulated research towards replacing noble metals by oxide catalysts for NH_3 oxidation. Oxides may offer the advantage of lower investment, simpler manufacture, and reduced N_2O emission.^[2,3] A vast number of patent applications have claimed promising performance of spinels or perovskites in the reaction, preferably containing Co, but also Fe, Mn, Bi, or Cr.^[3] Laboratory, pilot, and industrial tests have typically been carried out in fixed-bed reactors with oxides in the form of

[*] Dr. J. Pérez-Ramírez
Yara Technology Centre Porsgrunn
Catalysis and Nitric Acid Technology
P.O. Box 2560, 3908 Porsgrunn (Norway)
Fax: (+47) 2415-8213
E-mail: javier.perez.ramirez@yara.com
Dr. B. Vigeland
Norsk Hydro, Corporate Research Centre, Materials Development
P.O. Box 2560, 3908 Porsgrunn (Norway)

[**] This research was supported by Yara International ASA.

particles, pellets, or monoliths. Several key aspects have prevented the industrial implementation of oxide catalysts: 1) relatively low NO selectivity (< 90%), 2) rapid deactivation under relevant reaction conditions, and 3) the lower optimal operating temperature compared to noble metal catalysts causes difficulties with the steam balance in a revamped plant.^[2]

Herein we present the first lanthanum ferrite-based perovskite membranes for ammonia oxidation, with which NO selectivities up to 98% and no N₂O formation were attained. Our strategy was to combine in a single membrane reactor the separately reported properties of the above perovskites as oxygen conductors^[4] and catalysts for NH₃ oxidation.^[5] Accordingly, the applied configuration, depicted in Figure 1, integrates the separation of O₂ from air at the

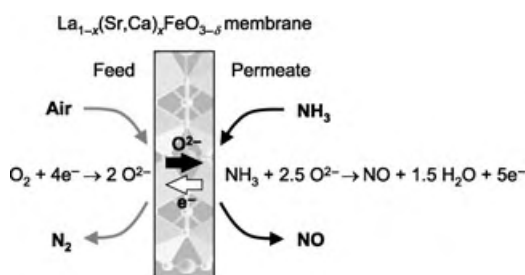


Figure 1. NH₃ oxidation to NO with mixed conducting membranes.

feed side by transport through oxygen vacancies in the mixed conducting membrane, and the reaction of oxygen with ammonia on the membrane surface at the permeate side. The surfaces of the membrane at the feed and permeate sides function as reduction ($O_2 \rightarrow 2O^{2-}$) and oxidation ($NH_3 \rightarrow NO$) catalysts, respectively. This gives rise to a radically intensified process for nitric acid manufacture, as large amounts of inert N₂ (2/3 of the total flow in today's plants) are excluded.

Important features of perovskite membranes in ammonia oxidation include oxygen flux $J(O_2)$, selectivity to NO $S(NO)$, and chemical stability in reducing and oxidizing atmosphere at high temperature. These interrelated parameters can be tailored by tuning the degree of calcium and strontium substitution in lanthanum ferrite-based perovskites $La_{1-x}(Sr,Ca)_xFeO_{3-\delta}$. A higher degree of substitution x increases the number of oxygen vacancies δ and thus the oxygen flux, but at the expense of lower chemical stability.^[4,6,7] Furthermore, La substitution by alkaline earth cations in the perovskite structure is also known to influence the catalytic properties of these mixed oxides.^[3] This can be caused by variation in the charge and/or coordination of 3d cations, changes in surface chemical composition, and development of microheterogeneities at the catalyst surface.

The preparation and characterization of the perovskite powders and the applied procedure for testing the membranes in the form of dense disks are described in the Experimental Section. For a $La_{0.8}Sr_{0.2}FeO_{3-\delta}$ membrane disk as an illustrative example, Figure 2 shows the typical dependence of NO selectivity and O₂ flux on the inlet NH₃ flow at different temperatures. In the temperature range investigated, NO

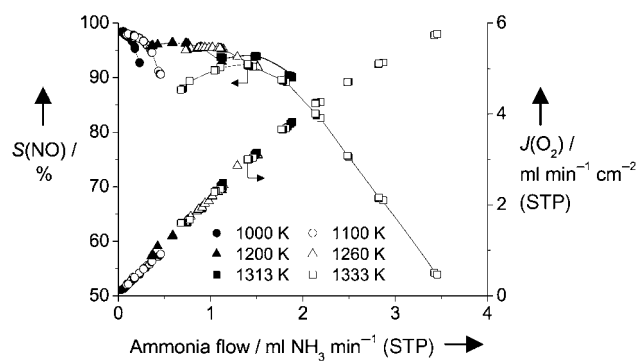


Figure 2. NO selectivity and O₂ flux versus inlet ammonia flow at different temperatures for a $La_{0.8}Sr_{0.2}FeO_{3-\delta}$ membrane.

selectivities in the range of 90–100% can be obtained by adjusting the inlet NH₃ flow. No N₂O was formed (< 10 ppm) in these experiments, and N₂ was the only N-containing by-product. Ammonia conversion (80–95%) increases with increasing temperature and decreases at high ammonia flow rates. The oxygen flux is expected to increase with temperature at a fixed oxygen potential gradient. Under our experimental conditions, however, the oxygen flux is almost exclusively controlled by the ammonia flow rate and thus independent of temperature. The NO selectivity, however, is dependent on temperature, and moreover exhibits a maximum with the inlet ammonia flow. As expected, the NO selectivity decreases in favor of N₂ under conditions of excess ammonia as a result of favorable recombination of adsorbed NH_x fragments.^[3,8] The additional observation of decreasing selectivity at low ammonia flow rates, which gives rise to the maximum, is attributed to partial oxidation on the hot reactor walls of NH₃ bypassing the membrane with excess oxygen recombining and escaping the membrane surface. The faster reaction at high temperature explains the decrease in the maximum NO selectivity when going from 1000 K (98%) to 1333 K (92%). Implicitly, with these membrane materials, higher NO selectivities than those displayed in Figure 2 would have been obtained if wall effects could be excluded. The shift of the NO selectivity maximum to lower ammonia molar flow with decreasing temperature reflects the reduced oxygen flux (at constant oxygen potential) at lower temperatures.

Figure 3 shows the maximum NO selectivity and corresponding oxygen flux as functions of the degree of substitution of Ca and Sr in the lanthanum ferrite perovskites at 1200 K. As expected, the oxygen flux is proportional to the degree of substitution. The maximum NO selectivity (95–96%) does not depend on the type and degree of substitution within this range, and this indicates similar catalytic performance of these membrane compositions. Wu et al.^[5] studied NH₃ oxidation at 1073 K in a fixed-bed reactor with catalyst particles and reported optimal NO selectivities ($\approx 95\%$) for $x = 0.2-0.7$ in $La_{1-x}Sr_xFeO_3$. For the membrane reactor described herein, the optimum degree of substitution is determined by a combination of maximum flux with absolute chemical stability under process conditions. This optimum degree of substitution of Sr and Ca probably lies in the range of $x = 0.1-0.2$.

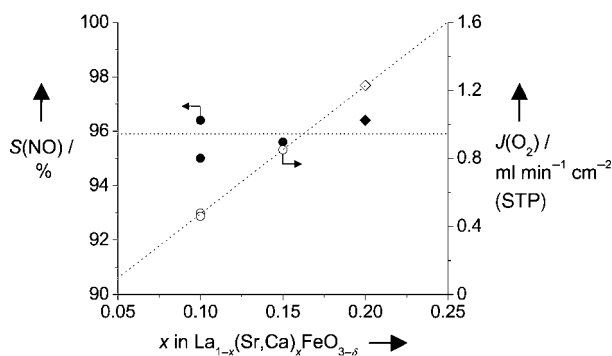


Figure 3. Maximum NO selectivity (solid symbols) and corresponding oxygen flux (open symbols) at 1200 K versus the degree of substitution in Ca- (circles) and Sr-substituted (diamonds) lanthanum ferrite perovskites.

The above results demonstrate the potential of Ca- and Sr-substituted lanthanum ferrite membranes for the high-temperature oxidation of ammonia; the NO selectivities of up to 98% are comparable to those of state-of-the-art PtRh alloys.^[1,2] In addition, formation of undesirable N₂O is totally suppressed. The implementation of an ammonia oxidation process based on oxygen-conducting membranes would constitute a major step change in nitric acid production (a top-ten product in the bulk chemicals industry) and have a strong impact on the fertilizer industry. Apart from the superior NO selectivity, in situ separation of O₂ from air by membranes enables extremely compact and intensified production units, as N₂ represents about 70% of the total flow in a current plant. The reduction in total flow would allow a drastic size decrease in key plant units, including the absorption tower and the tail-gas train, as well as intensification in piping. Moreover, energy savings for compression of the NO_x gas before the absorption step, which requires high pressure, further contributes to an improved nitric acid production process. In summary, a more efficient and sustainable process can be attained, which is especially attractive for nitric acid production that is decentralized from large existing plants.

Our current research for further implementation of membrane technology in ammonia oxidation focuses on scaling up membrane disks to monolithic membranes, with which surface areas in the range of 2000–3000 m² per cubic meter of reactor can be obtained, depending on cell size and wall thickness.^[9] The reactor design involves the distribution of ammonia and air in a monolithic structure with square channels in a chess-board pattern (one channel for ammonia and the four surrounding channels for air). The significantly increased surface area to reactor volume ratio of monoliths will enable application of substantially higher ammonia concentrations on the permeate side compared to the disk configuration used in the present study.

Experimental Section

Lanthanum ferrite-based perovskites La_{1-x}A_xFeO_{3-δ} (A = Ca, Sr; x = 0.1–0.2) were prepared by a conventional wet complexation route with citric acid. Standardized solutions (1 M) of the metal nitrates were

mixed with citric acid in a molar ratio of acid to total cations of 3. The resulting solution was slowly heated to 433 K (40 K h⁻¹) to ensure complete complexation and left overnight at this temperature to dry. After further heating to 773 K for 5 h in flowing air to remove organic matter and final calcination at 1173 K for 10 h, all powders were single-phase perovskites as evidenced by XRD. The particle size, obtained by laser scattering, was in the range of 0.1–0.5 μm. Dense membrane disks (>95% of theoretical density) were made by uniaxial pressing and sintering at 1573 K. After final grinding and polishing, membrane disks with a diameter of 10 mm (≈80 mm²) and a thickness of ≈0.9 mm were obtained. The disks were mounted in a quartz microreactor, sketched in Figure 4, which was heated to

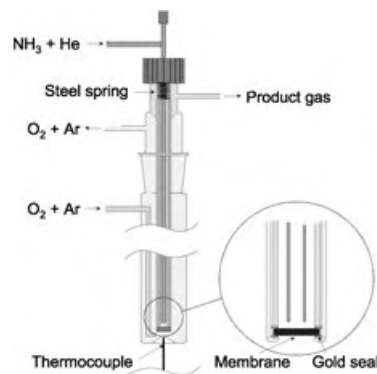


Figure 4. Quartz reactor used in the membrane tests.

1333 K for sealing with gold rings. The oxidation of ammonia was investigated at 1000–1333 K by feeding an equimolar O₂/Ar mixture to the feed side, and NH₃/He mixtures to the permeate side. The inlet ammonia flow was varied in the range of 0.05–4.5 ml min⁻¹ (STP), with a total flow of 130 ml min⁻¹ (STP). Product gases were analyzed on-line with a mass spectrometer and a gas chromatograph. Freedom from leakages was verified by the absence of Ar on the permeate side. The NO selectivity was obtained from the concentrations at the reactor outlet according to $S(\text{NO}) = c(\text{NO}) / [c(\text{NO}) + 2c(\text{N}_2\text{O}) + 2c(\text{N}_2)]$. The oxygen flux $J(\text{O}_2)$ was determined from the measured concentrations of all O-containing species. Stable membrane performance over the typical testing period (10 days) was verified by periodically repeating measurements under selected temperature/flow conditions.

Received: September 17, 2004

Published online: January 13, 2005

Keywords: heterogeneous catalysis · membranes · oxidation · perovskite phases · reactive separation

- [1] a) S. L. Hansforth, J. N. Tilley, *Ind. Eng. Chem.* **1934**, 26, 1287; b) E. Wagner, T. Fetzner in *Handbook of Heterogeneous Catalysis*, Vol. 4 (Eds.: G. Ertl, H. Knözinger, J. Weitkamp), VCH, Weinheim, **1997**, pp. 1748–1761; c) R. J. Farrauto, C. H. Bartholomew, *Fundamentals of Industrial Catalytic Processes*, Chapman & Hall, London, **1997**, p. 481.
- [2] J. Pérez-Ramírez, F. Kapteijn, K. Schöffel, J. A. Moulijn, *Appl. Catal. B* **2003**, 44, 117, and references therein.
- [3] V. A. Sadykov, L. A. Isupova, I. A. Zolotarskii, L. N. Bobrova, A. S. Noskov, V. N. Parmon, E. A. Brushtein, T. V. Telyatnikova, V. I. Chernyshev, V. V. Lunin, *Appl. Catal. A* **2000**, 204, 59.
- [4] Y. Teraoka, H. Zhang, S. Furukawa, N. Yamazoe, *Chem. Lett.* **1985**, 1743.

- [5] Y. Wu, T. Yu, B. Dou, C. Wang, X. Xie, Z. Yu, S. Fan, Z. Fan, L. Wang, *J. Catal.* **1989**, *120*, 88.
- [6] J. E. ten Elshof, H. J. M. Bouwmeester, H. Verweij, *Solid State Ionics* **1996**, *89*, 81.
- [7] Y. Takeda, K. Kajiura, S. Naka, M. Takano in *Proceedings of the 3rd International Conference on Ferrites* (Eds.: H. Watanabe, S. Iida, M. Sugimoto), Japan, **1982**, 414.
- [8] a) J. M. Bradley, A. Hopkinson, D. A. King, *J. Phys. Chem.* **1995**, *99*, 17 032; b) J. Pérez-Ramírez, E. V. Kondratenko, V. A. Kondratenko, M. Baerns, *J. Catal.* **2004**, *127*, 90.
- [9] a) F. Kapteijn, J. J. Heiszwolf, T. A. Nijhuis, J. A. Moulijn, *Cattech* **1999**, *3*, 24; b) A. Stankiewicz, J. A. Moulijn, *Ind. Eng. Chem. Res.* **2002**, *41*, 1920.

Heterogeneous Catalysis

The Role of Gold in Gold–Titania Epoxidation Catalysts**

T. Alexander Nijhuis,* Tom Visser, and
Bert M. Weckhuysen

Catalysts consisting of gold nanoparticles on titania supports have received considerable attention over the past years as novel systems for the direct and selective epoxidation of propene.^[1–3] A process to directly epoxidize propene is highly desirable as the currently available processes are not optimal. The chlorohydrin process is being phased out because of environmental concerns, and each of the hydroperoxide processes [styrene monomer/propylene oxide (SM/PO) and propylene oxide/*tert*-butanol, (PO/TBA)] produces a by-product (styrene and *tert*-butanol, respectively) in a fixed amount, thus making the production capacity less flexible.

Gold–titania catalysts are able to epoxidize propene in the presence of a mixture of hydrogen and oxygen under very mild conditions (323–373 K and atmospheric pressure). Although these catalyst systems are highly selective, two main problems need to be addressed. The conversion remains quite low (typically below 2 %, although conversions of up to 10 % have been reported with certain promoters^[4]) and the hydrogen efficiency is insufficient, typically 30 %.^[5]

Understanding the mode of operation of the catalyst would be a great help in improving the catalyst performance. The general assumption is that a reaction takes place, in which a peroxide species is formed from hydrogen and oxygen on

gold particles, and the propene would then be epoxidized over Ti sites.^[3,6] It is known that titania acts as an epoxidation catalyst in the liquid phase when hydrogen peroxide is the oxidant.^[7] It has also been shown that gold catalysts are capable of producing hydrogen peroxide from hydrogen and oxygen.^[8] However, attempts to prove that this reaction occurs during the gas-phase epoxidation of propene with hydrogen and oxygen have so far been unsuccessful. Our ongoing Raman spectroscopy study of the catalyst has not yet shown the presence of any peroxide species during the reaction, even though the sensitivity of Raman spectroscopy towards peroxides is high.^[9]

The low yield of product obtained from gold–titania catalysts is usually explained by a strong adsorption of propene oxide on the catalyst.^[4,5] In this work the adsorption behavior of propene, propene oxide, and related species on titania and gold–titania is investigated by use of IR spectroscopy to get a better understanding of the events on the catalyst surface, and to thus allow the development of a reaction mechanism and a better catalyst.

Prior to the spectroscopic study, the catalyst activity was verified.^[9] the epoxidation activity of the catalyst comprising 1 wt % Au on P25 titania was 0.9 % conversion, 99 % selectivity at 323 K, and a gas hourly space velocity (GHSV) of 6000 h^{−1} (mixture of 10 % O₂, H₂, and propene in He). This catalyst performance is comparable to the reported activity for similar catalysts.^[1,3,10]

When the adsorption and subsequent desorption of propene on the bare titania P25 support was measured, no bands remained, thus indicating a completely reversible physical adsorption. This is in full agreement with the observation of Mul and co-workers.^[11] However, when the same experiment was performed with the Au/TiO₂ catalyst, the adsorption was no longer reversible. In Figure 1 the IR spectra of both samples after desorption of physisorbed propene are shown. Evidence of residual species on the surface of the Au/TiO₂ catalyst is clearly visible in the corresponding spectrum, whereas for titania only a small decrease in the absorption at 1650 cm^{−1} is observed owing to a slight decrease in water content, which also causes a negative

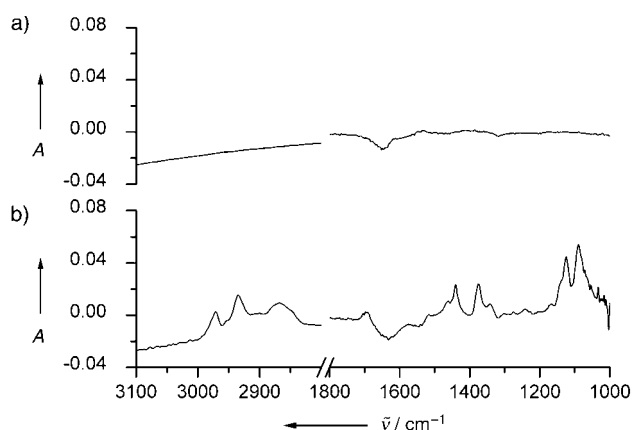


Figure 1. IR spectra of adsorbed species on the a) titania support and on the b) gold-on-titania catalyst after adsorption and subsequent desorption of propene (323 K; 100 spectra averaged).

[*] Dr. ir. T. A. Nijhuis, Dr. T. Visser, Prof. Dr. ir. B. M. Weckhuysen
Department for Inorganic Chemistry and Catalysis
Debye Institute, Utrecht University
Sorbonnelaan 16, 3584 CA Utrecht (The Netherlands)
Fax: (+31) 30-251-1027
E-mail: x.nijhuis@chem.uu.nl

[**] NWO/STW is kindly acknowledged for the VIDI grant supporting the research of T.A.N. NWO/CW is acknowledged for the VICI grant for B.M.W.

background at higher wavenumbers. In the IR spectrum of the gold-on-titania catalyst, bands appear at 2970, 2935, 2870, 1460, 1440, 1375, 1340, 1130, and 1090 cm^{-1} . As the catalyst was exposed only to propene, it is apparent that gold plays a more elaborate role in this catalyst system than was generally assumed, namely, that the gold is just providing peroxide for the epoxidation with propene on titania. The bare titania on which the propene was adsorbed was titania from a blank catalyst preparation (i.e., prepared in the same way as the gold catalyst but without the addition of AuCl_3). Therefore the different adsorption behavior of propene can only originate from the gold and not from changes to the titania during the preparation of the catalyst.

The bands in the 1050–1150- cm^{-1} region are characteristic of C–O–Ti stretching vibrations,^[11,12] thus indicating that an adsorbed species remains on the titania support. To make the identification of this residual species more facile, experiments were performed in which different components were adsorbed and desorbed on the P25 support. Propene oxide, 1,2-propanediol, 1-propanol, and 2-propanol all adsorbed irreversibly on (i.e., reacted with) titania. The spectra of species remaining after adsorption/desorption are given in Figure 2a. In the CH stretching region, the main bands that can be observed are usually assigned as $\nu_{\text{as}}(\text{CH}_3)$ at 2970, $\nu_{\text{as}}(\text{CH}_2)$ 2935, $\nu_{\text{s}}(\text{CH}_3)$ 2900, and $\nu_{\text{s}}(\text{CH}_2)$ at 2870 cm^{-1} . In the CH bending region $\delta_{\text{as}}(\text{CH}_3)/\delta(\text{CH}_2)$ at 1460, $\delta_{\text{s}}(\text{CH}_3)$ at 1375, and $\delta(\text{CH})$ at 1335 cm^{-1} can be assigned. The bands at 1090 and 1140 cm^{-1} can be assigned as the C–O–Ti stretching vibra-

tions for primary and secondary carbon atoms, respectively. The structures of the most likely species as they are formed on the titania surface are given in Figure 2b.

When the difference spectrum for propene adsorbed/desorbed on the gold-on-titania catalyst in Figure 1 is compared to the spectra in Figure 2, it is clearly quite similar to that of the species on the surface of titania after adsorption of propene oxide or propanediol. The source of the oxygen atom in this component is unclear, but it probably originates from titania O or OH groups. The formation of this species can only be explained by considering a key role played by gold: propene adsorbs onto gold, and this adsorbed and activated species then reacts with surface O(H) groups of the titania. Alternatively, the gold might influence the reactivity of the nearby titania, thus making it react more easily with propene. The fact that the intensities of the peaks of the spectrum in Figure 1b are relatively low (absorbance is about 20 times lower than that in Figure 2), can be easily explained by the relatively low gold loading of 1 wt %, which makes only a small portion of the titania surface available for a reaction with propene. This can be observed in the TEM micrograph in Figure 3 in which the gold particles occupy only a small part of the titania.

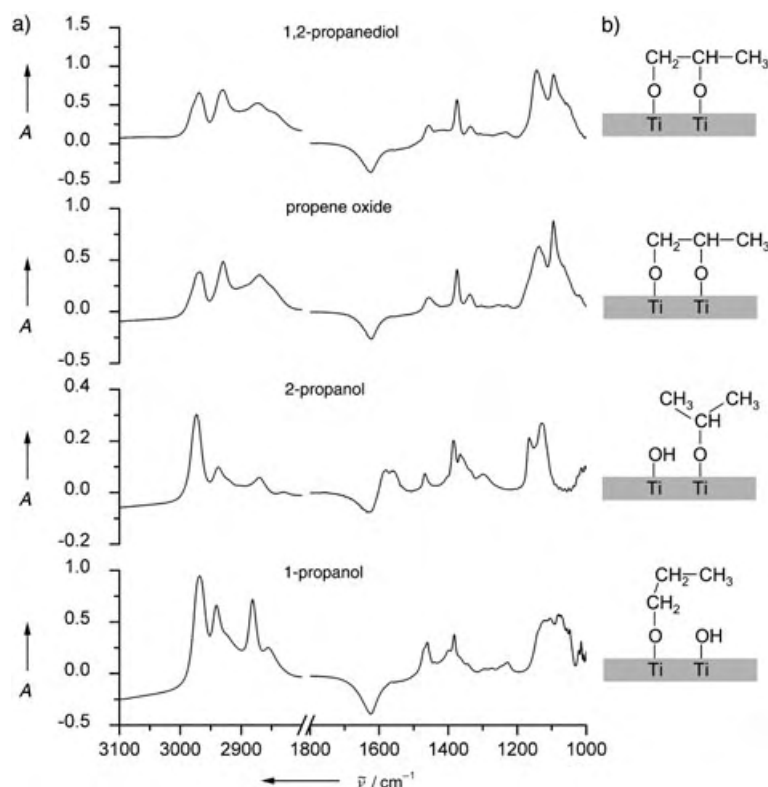


Figure 2. a) IR spectra after adsorption and subsequent desorption of 1,2-propanediol, propene oxide, 2-propanol, and 1-propanol on titania (323 K). b) Most likely structures of the adsorbate species that correspond to the IR spectra in a) (20 spectra averaged).

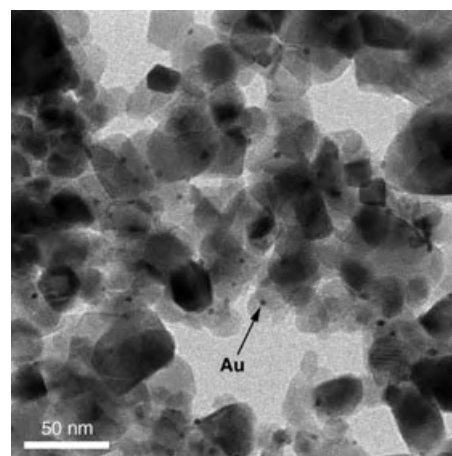


Figure 3. TEM micrograph of 1 wt % gold on titania (P25) catalyst.

The only real difference between the spectrum in Figure 1b and the spectra in Figure 2 for adsorbed propene oxide and 1,2-propanediol is the intensities of the bands at 1440 and 1370 cm^{-1} . Over time, the intensity of these bands increases further, even when the catalyst is kept in a helium gas stream, whereas the intensity of the other bands decrease very slowly (Figure 4). In addition, a broad band appears at 1500–1550 cm^{-1} . The bands that grow in intensity can be attributed to carbonate/carboxylate species.^[13,14] The fact that the intensities of the CH stretching bands do not increase supports this assignment. The formation of carbonates/carboxylates can be explained by the slow oxidation of bidentate propoxy species. This oxidation reaction must be catalyzed by the gold particles, as it is not observed when the bidentate propoxy species is formed on bare titania by the adsorp-

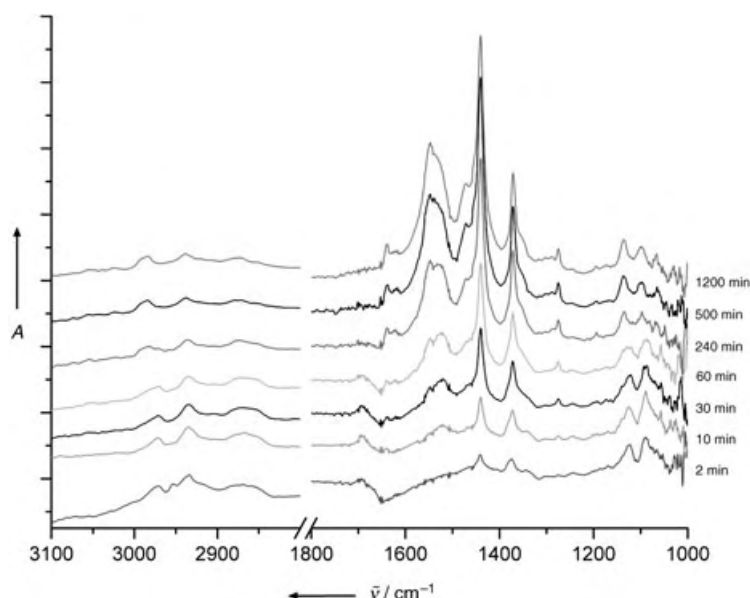


Figure 4. Spectra that demonstrate the gradual oxidation of a bidentate propoxy species on the gold–titania catalyst. Spectra were recorded from 2 to 1200 min after exposure of the catalyst to propene for 2 min (323 K; 10 spectra averaged).

tion of propene oxide or 1,2-propanediol. Furthermore, formation of carbonates/carboxylates may partly explain why gold–titania catalysts slowly lose activity during epoxidation. The fact that a calcination procedure removes these species from the surface^[13] concurs with the observation that the catalyst largely regains its activity for epoxidation after calcination. Additional evidence that these carbonate/carboxylate species are key to the deactivation of the catalyst comes from the fact that they could not be observed on a catalyst consisting of gold on a dispersed titania support.^[9] This type of catalyst is known to be much more stable towards deactivation.^[3,15]

An additional experiment was performed in which a mixture of gas comprising 10% propene, 10% oxygen, 10% hydrogen, and the rest helium was fed to the Au/TiO₂ sample for only 3 min. Figure 5 shows the IR spectrum of the adsorbed species 3 min after removal of the propene feed. The presence of hydrogen and oxygen results in much more intense bands of the bidentate propoxy species in a shorter time. In the presence of hydrogen/oxygen it is observed that the bidentate propoxy species is slowly oxidized on the catalyst surface (similar to the situation evinced in Figure 4). However, the rate at which the bidentate propoxy bands decrease in intensity is slightly higher, thus indicating that desorption occurs. The species formed by the oxidation of the bidentate propoxy species in the presence of hydrogen and oxygen are a little different as bands at 1350 and 1720 cm⁻¹ also appear. Increasing the temperature to 373 K results in the complete disappearance of the bands of the bidentate propoxy species (only the carbonate/carboxylate bands remain), which was not the case when a similar experiment was performed in a helium stream. It is likely then that hydrogen and oxygen aid the desorption of this species. Further work is needed to verify whether the desorbing species is indeed propene oxide. However, this assumption

seems likely to be the case, as propene oxide is the only product in catalytic experiments carried out under mild conditions.

In summary, the role of gold in the epoxidation of propene is more than that generally assumed, namely, that gold merely provides a peroxide species, which subsequently epoxidizes propene on the titania sites. An IR spectroscopic study has shown that the presence of gold nanoparticles on titania catalyzes a reaction between propene and the titania sites. A bidentate propoxy species is produced, similar to that formed when propene oxide is absorbed on titania. The gold particles also catalyze a consecutive oxidation of the bidentate propoxy species to form carbonate/carboxylate species, which is possibly the cause of catalyst deactivation. In the presence of hydrogen and oxygen the bidentate propoxy species can desorb from the catalyst surface. Therefore it is likely this species is a reaction intermediate in the epoxidation of propene.

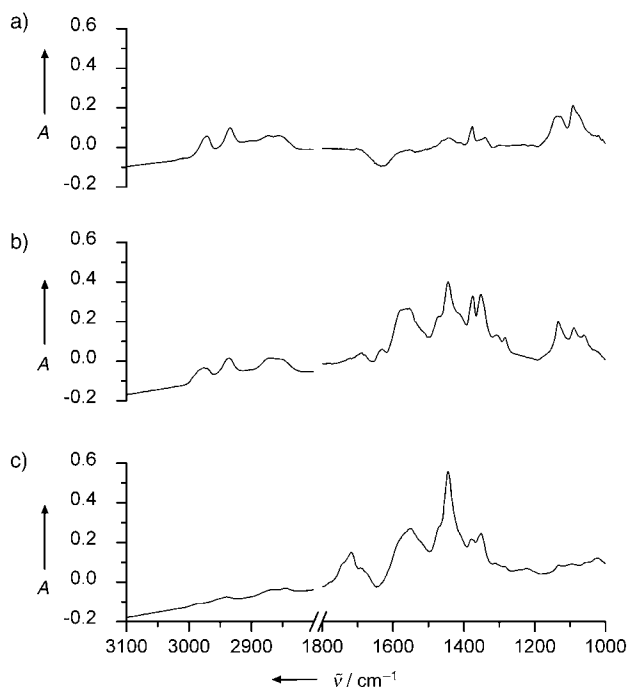


Figure 5. Spectra recorded after 3 min passage of a gas stream comprising 10% propene, 10% H₂, 10% O₂, and He (323 K). a) 3 min after removal of propene; b) after 3 h; c) 30 min after the temperature was increased to 373 K (50 spectra averaged).

Experimental Section

Highly dispersed gold-on-titania catalysts were prepared by a deposition/precipitation method. A solution of AuCl₃ in water was slowly added to a stirred suspension of P25 titania in water. The pH of the water was kept at 9.5 with aqueous ammonia. After the catalyst had been aged for 30 min, it was filtered and washed three times with deionized water. The catalyst was dried in air overnight at 393 K and calcined for 4 h at 673 K (10 K min⁻¹ heating and cooling rate). TEM

analysis showed a narrow size distribution for the gold particles (3.2–4.2 nm), although there were a few smaller and larger particles, all of which were in the range of 2–6 nm. X-ray fluorescence (XRF) analysis showed the amount of chlorine on the catalyst (a known promoter) to be lower than the detection limit of 7 ppm. The only contaminant present in a significant quantity was nickel (200 ppm), which was also present in the P25 used. Catalytic testing showed a propene oxide yield of up to 0.5 % at 323 K and a space velocity of 6000 h⁻¹ with a gas mixture of 10 % propene, 10 % hydrogen, and 10 % oxygen in helium.

Adsorption experiments were performed with a Perkin Elmer Spectrum One IR transmission spectrometer with self-supporting catalyst wafers of 100–120 micrometer thickness (pressed at 1.5 ton from powdered catalyst). Prior to the adsorption–desorption experiment the samples were dried in situ by heating them to 573 K in helium, and then the samples were cooled to 323 K. For liquids, adsorption measurements were performed by pumping either 400 µL h⁻¹ of liquid in a He stream of 25 mL min⁻¹ (at 353 K) fed through an IR cell for 10 min, after which only helium was fed, and the desorption was measured. Propene adsorption was measured similarly with a gas stream of 5 mL min⁻¹ of propene in 25 mL min⁻¹ of helium. During the desorption in helium, spectra were measured until no changes were observed. The spectra of the samples at 323 K prior to the adsorption were used as background.

Received: September 20, 2004

Published online: January 13, 2005

Keywords: epoxidation · gold · IR spectroscopy · propene · titania

- [1] A. K. Sinha, S. Seelan, S. Tsubota, M. Haruta, *Top. Catal.* **2004**, 29, 95–102.
- [2] A. E. Stangland, K. B. Stavens, R. P. Andres, W. M. Delgass, *J. Catal.* **2000**, 191, 332–347.
- [3] T. A. Nijhuis, B. J. Huizinga, M. Makkee, J. A. Moulijn, *Ind. Eng. Chem. Res.* **1999**, 38, 884–891.
- [4] A. K. Sinha, S. Seelan, S. Tsubota, M. Haruta, *Angew. Chem.* **2004**, 116, 1572–1574; *Angew. Chem. Int. Ed.* **2004**, 43, 1546–1548.
- [5] A. Zwijnenburg, M. Makkee, J. A. Moulijn, *Appl. Catal. A* **2004**, 270, 49–56.
- [6] C. Sivadinarayana, T. V. Choudhary, L. L. Daemen, J. Eckert, D. W. Goodman, *J. Am. Chem. Soc.* **2004**, 126, 38–39.
- [7] M. G. Clerici, G. Bellussi, U. Romano, *J. Catal.* **1991**, 129, 159–167.
- [8] P. Landon, P. F. Collier, A. J. Papworth, C. J. Kiely, G. J. Hutchings, *Chem. Commun.* **2002**, 2058–2059.
- [9] T. A. Nijhuis, T. Visser, B. M. Weckhuysen, unpublished results.
- [10] T. Hayashi, K. Tanaka, M. Haruta, *J. Catal.* **1998**, 178, 566–575.
- [11] G. Mul, A. Zwijnenburg, B. van der Linden, M. Makkee, J. A. Moulijn, *J. Catal.* **2001**, 201, 128–137.
- [12] V. Sanchez Escribano, G. Busca, V. Lorenzelli, *J. Phys. Chem.* **1990**, 94, 8939–8945.
- [13] M. A. Bollinger, M. A. Vannice, *Appl. Catal. B* **1996**, 8, 417–443.
- [14] M. Maciejewski, P. Fabrizioli, J. D. Grunwaldt, O. S. Becker, A. Baiker, *Phys. Chem. Chem. Phys.* **2001**, 3, 3846–3855.
- [15] N. Yap, R. P. Andres, W. N. Delgass, *J. Catal.* **2004**, 126, 156–170.

Highly Rigid Diphosphane Ligands with a Large Dihedral Angle Based on a Chiral Spirobifluorene Backbone**

*Xu Cheng, Qi Zhang, Jian-Hua Xie, Li-Xin Wang, and Qi-Lin Zhou**

Asymmetric catalysis is undoubtedly a powerful, economically feasible tool for the synthesis of optically active organic compounds both in the laboratory and on a production scale. The design and synthesis of chiral phosphane ligands have played a significant role in the development of efficient, transition-metal-catalyzed asymmetric reactions.^[1] In the last decades, a large number of chiral diphosphane ligands, such as diop,^[2] binap,^[3] josiphos,^[4] duphos,^[5] pennphos,^[6] bisp,^[7] p-phos,^[8] and tangphos,^[9] have been prepared and used in asymmetric catalysis with excellent enantioselectivities. Since there are no universal ligands and catalysts for asymmetric transformations, and most asymmetric reactions are substrate dependent, the search for chiral ligands that are more efficient in terms of high enantioselectivity and high turnover number (TON) remains one of the most important goals in asymmetric catalysis.

Although many structural features should be taken into consideration in the design of new chiral ligands, a certain degree of rigidity of the ligand and catalyst has been shown to be one of the most significant factors for obtaining high enantioselectivity.^[10] For instance, in the “privileged” chiral catalysts containing a binap ligand, the highly rigid, atropisomeric, C_2 -symmetric binaphthyl structure fixes the conformation of the seven-membered heterometallocyclic ring of its metal complexes and determines the orientations of the *P*-phenyl groups, which ultimately exert steric influence on the binding substrate.^[11] As modifications of binap, a number of diphosphane ligands with a narrower dihedral angle have been designed, for example biphemp,^[12] segphos,^[13] tunaphos,^[14] synphos,^[15] and naphphos,^[16] which have provided a better enantiocontrol in several well-established catalytic reactions.^[17] In contrast, ligands with a wider dihedral angle than that of binap have rarely been explored.^[18] Herein we report the synthesis of the new spirobifluorene-based diphosphane ligands (SFDPs) **1** with an extremely high rigidity and

[*] X. Cheng, Q. Zhang, Dr. J.-H. Xie, Prof. L.-X. Wang, Prof. Q.-L. Zhou
State Key Laboratory and
Institute of Elemento-organic Chemistry
Nankai University
Tianjin 300071 (China)
Fax: (+ 86) 222-350-6177
E-mail: qlzhou@nankai.edu.cn

[**] We thank the National Natural Science Foundation of China, the Major Basic Research Development Program (Grant G2000077506), the Ministry of Education of China, and the Committee of Science and Technology of Tianjin for financial support.

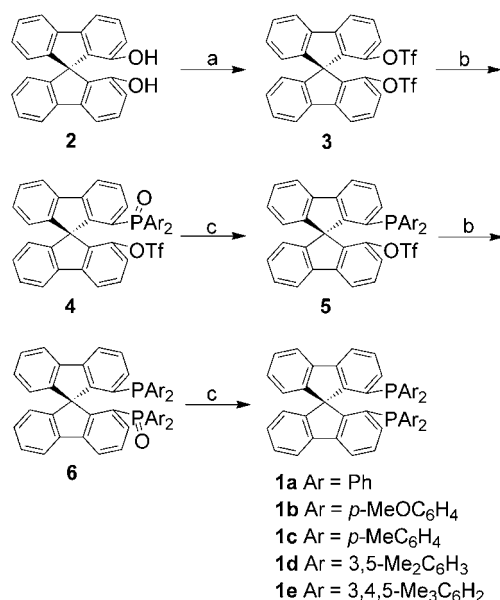


Supporting information for this article is available on the WWW under <http://www.angewandte.org> or from the author.

large dihedral angle based on a spirobifluorene backbone, the structural characterization of a Pd complex, and their application in ruthenium-catalyzed asymmetric hydrogenation of α,β -unsaturated carboxylic acid, with high activity and excellent enantioselectivity.

While molecules with a 9,9'-spirobifluorene structure have been widely applied in molecular electronics,^[19] light-emitting materials,^[20] enantioselective molecular recognition,^[21] and other areas,^[22] the use of chiral ligands with a 9,9'-spirobifluorene backbone for asymmetric catalysis has not yet been reported. Recently, we reported the synthesis of optically pure 9,9'-spirobifluorene-1,1'-diol (SBFOL, **2**).^[23] The diphosphane ligands **1** can be synthesized from SBFOL. Thus, (*R*)-(**2**) was first converted into the ditriflate (*R*)-**3** in quantitative yield. This compound was then directly subjected to diphosphanylation with diarylphosphanes in the presence of a nickel catalyst following the method of Cai et al.^[24] for the synthesis of binap, although no coupling reaction occurred. We therefore attempted Hayashi's stepwise strategy^[25] to introduce phosphanyl groups and found that it works nicely. Monophosphanylation of ditriflate (*R*)-**3** with diarylphosphane oxide in the presence of a Pd complex of dppb, followed by reduction with trichlorosilane, generated (*R*)-1-(diarylphosphanyl)-1'-trifluoromethanesulfonyloxy-9,9'-spirobifluorene ((*R*)-**5**). The second diarylphosphanyl group was introduced by repeating the above two-step protocol. The target diphosphanes (*R*)-**1** were obtained in 50–60% overall yield (Scheme 1). Following the same procedure, the diphosphanes (*S*)-**1** were also synthesized from (*S*)-9,9'-spirobifluorene-1,1'-diol.

A crystal of the complex $[\text{PdCl}_2((R)\text{-1a})]$ suitable for X-ray diffraction was grown and analyzed.^[26] As can be seen from Figure 1, the complex has a square-planar configuration and the eight-membered heterometalocyclic ring formed by the chelate coordination of SFDP to palladium is highly rigid. The perpendicular spirobifluorene structure is distorted: in $[\text{PdCl}_2((R)\text{-1a})]$, the P-Pd-P bite angle is 96.7° , which is



Scheme 1. Synthesis of ligands **1**: a) Ti_2O , pyridine, CH_2Cl_2 , -15°C , 3 h; b) $\text{Pd}(\text{OAc})_2$ (5 mol %), dppb (5 mol %), $i\text{Pr}_2\text{EtN}$, Ar_2POH , DMSO, 100°C , 1 h; c) HSiCl_3 , $i\text{Pr}_2\text{EtN}$, toluene, 110°C , 8 h.

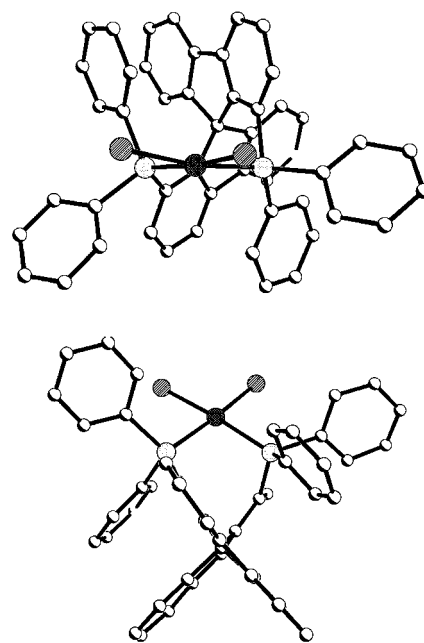
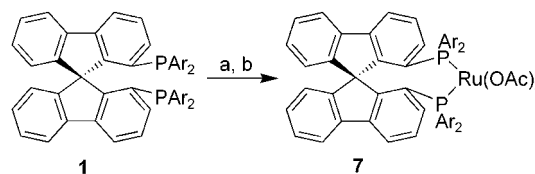


Figure 1. Crystal structure of $[\text{PdCl}_2((R)\text{-1a})]$. Solvent and hydrogen atoms have been omitted for clarity.

greater than that of $[\text{PdCl}_2((R)\text{-binap})]$ (92.7°).^[11c] In addition, one *P*-phenyl group on each phosphorus atom lies parallel to the fluorene ring of the bifluorene moiety; the distances between the centers of the *P*-phenyl rings and the benzo rings of bifluorene are 3.5 and 3.6 Å, respectively, thereby indicating π - π stacking interactions between the *P*-phenyl rings and the fluorenes, as also observed in $[\text{PdCl}_2((R)\text{-binap})]$.^[11c] The Pd-P (2.28 and 2.30 Å) and Pd-Cl (2.33 and 2.36 Å) bond lengths in $[\text{PdCl}_2((R)\text{-1a})]$ are in the typical range for dichloropalladium complexes bearing diphosphane ligands.^[27]

The efficiency of the chiral SFDP ligands in the enantioselective, ruthenium-catalyzed hydrogenation of α,β -unsaturated carboxylic acids, which is a very useful reaction in organic and industrial synthesis, was investigated.^[28] The catalysts **7** were prepared as red powders from $[\{\text{RuCl}_2(\text{C}_6\text{H}_6)_2\}]$ and **1** in DMF followed by the addition of NaOAc (Scheme 2).^[29] The catalysts $[\text{Ru}(\text{OAc})_2((R)\text{-1})]$ ((*R*)-**7**) show a single resonance signal in their ^{31}P NMR spectra ($\delta = 64$ –67 ppm).

Although significant progress has been achieved in asymmetric hydrogenation of α -arylacrylic acid and other α,β -unsaturated carboxylic acids,^[8,30] the asymmetric hydrogenation of cinnamic acid derivatives is still a challenge.^[30c,31] The catalyst $[\text{Ru}(\text{OAc})_2((R)\text{-1a})]$ ((*R*)-**7a**) was initially tested in the hydrogenation of α -methylcinnamic acid at a substrate-



Scheme 2. Preparation of catalysts $[\text{Ru}(\text{OAc})_2((R)\text{-1})]$ ((*R*)-**7**):

a) $[\{\text{RuCl}_2(\text{C}_6\text{H}_6)_2\}]$ (0.56 equiv.), DMF; b) NaOAc (10 equiv.), MeOH.

to-catalyst (S/C) ratio of 400 in MeOH under 6 atm of H₂ at room temperature over 48 h. The hydrogenation product α -methylhydrocinnamic acid was obtained in 93 % yield with 60 % *ee* (Table 1, entry 1). This result is better than that

Table 1: Asymmetric hydrogenation of α -methylcinnamic acid derivatives.^[a]

Entry	R	Cat.	t [h]	Yield [%] ^[b]	<i>ee</i> [%] ^[c]
1	H	(R)- 7a	48	93	60
2	H	(R)- 7b	48	89	45
3	H	(R)- 7c	30	91	70
4	H	(R)- 7d	24	93	87
5	H	(R)- 7e	18	91	94
6	<i>p</i> -Me	(R)- 7e	22	93	90
7	<i>m</i> -Me	(R)- 7e	20	93	97
8	<i>o</i> -Me	(R)- 7e	22	91	95
9	<i>p</i> -OMe	(R)- 7e	25	91	94
10	<i>m</i> -OMe	(R)- 7e	20	92	94
11	<i>o</i> -OMe	(R)- 7e	24	90	94
12	<i>p</i> -Cl	(R)- 7e	10	91	94
13	<i>m</i> -Cl	(R)- 7e	12	94	92
14	<i>o</i> -Cl	(R)- 7e	9	90	93
15	<i>m</i> -Br	(R)- 7e	12	90	95
16	<i>o</i> -Br	(R)- 7e	12	93	95
17	<i>p</i> -CF ₃	(R)- 7e	9	90	92
18	<i>o</i> -CF ₃	(R)- 7e	8	94	92
19	<i>o</i> -NO ₂	(R)- 7e	30	93	92
20	2-naphth	(R)- 7e	18	95	93

[a] Conditions: [substrate] = 0.25 mol L⁻¹ in MeOH, S/C = 400, *p*_{H₂} = 6 atm, *T* = 25–28 °C. [b] Conversions were quantitative for all reactions. All hydrogenated products were fully characterized (see Supporting Information). [c] *ee* was determined by HPLC analysis of the respective anilide with a chiral column (see Supporting Information). The predominant configuration of α -methylhydrocinnamic acid is *S*. All other saturated acids have positive rotations.

obtained with [Ru(OAc)₂((*R*)-binap)] (48 h, 29 % yield, 30 % *ee*).^[30c] A systematic investigation of the effect of the substituents in ligands **1** showed that the introduction of 3,4,5-trimethylphenyl groups in (*R*)-**1e** dramatically increased the activity and enantioselectivity of the catalyst (18 h, 94 % *ee*; Table 1, entry 5). A variety of α -methylcinnamic acid derivatives were hydrogenated under these mild conditions using catalyst (*R*)-**7e** with excellent enantioselectivities. The results summarized in Table 1 represent the highest enantioselectivity yet achieved in the asymmetric hydrogenation of α -methylcinnamic acid.^[30c,31]

The asymmetric hydrogenation of tiglic acid and its derivatives was also examined with catalyst **7**. The results are summarized in Table 2. In contrast to the hydrogenation of α -methylcinnamic acid, all catalysts **7** provided high enantioselectivities (Table 2, entries 1–5). It was found that the highly enantioselective hydrogenation can be performed even when the S/C ratio is increased to 10000 (Table 2, entry 7). Different tiglic acid derivatives can be hydrogenated with catalyst **7d** with excellent enantioselectivities (Table 2, entries 8–12). These results are comparable to, or better than, those obtained with [Ru(OAc)₂(binap)]^[30a] and other catalysts.^[30c,32]

Table 2: Asymmetric hydrogenation of tiglic acid derivatives.^[a]

Entry	R ¹	R ²	Cat.	<i>t</i> [h]	Yield [%]	<i>ee</i> [%] ^[b]
1	Me	Me	(<i>R</i>)- 7a	16	92	96
2	Me	Me	(<i>R</i>)- 7b	16	85	96
3	Me	Me	(<i>R</i>)- 7c	16	91	94
4	Me	Me	(<i>R</i>)- 7d	16	92	97
5	Me	Me	(<i>R</i>)- 7e	12	85	97
6 ^[c]	Me	Me	(<i>R</i>)- 7d	30	90	98
7 ^[d]	Me	Me	(<i>R</i>)- 7d	100	94	98
8	Et	Me	(<i>R</i>)- 7d	24	94	96
9	<i>n</i> Pr	Me	(<i>R</i>)- 7d	30	91	96
10	<i>n</i> Pr	Et	(<i>R</i>)- 7d	40	82	94
11	<i>n</i> Bu	Me	(<i>R</i>)- 7d	35	92	96
12	<i>i</i> Bu	Me	(<i>R</i>)- 7d	40	88	97

[a] Conditions: see footnote [a] in Table 1. [b] *ee* was determined by HPLC analysis of the respective anilide with a chiral column (AD-H); the predominant configuration is *S* for all products. [c] [substrate] = 0.625 mol L⁻¹, S/C = 1000. [d] [substrate] = 6.25 mol L⁻¹, S/C = 10000, 50 °C.

In conclusion, SFDP, a new type of highly rigid diphosphane ligands with a large dihedral angle, has been synthesized based on a chiral spirobifluorene backbone. Their ruthenium complexes are highly efficient catalysts for asymmetric hydrogenation of α,β -unsaturated carboxylic acids. The excellent activity and enantioselectivity of these ruthenium complexes in the hydrogenation of α -methylcinnamic acid derivatives and tiglic acid derivatives indicate that these highly rigid ligands might be more widely applicable in asymmetric catalytic reactions.

Received: September 22, 2004

Revised: November 25, 2004

Keywords: asymmetric catalysis · chirality · hydrogenation · phosphines · spirobifluorenes

- [1] a) For reviews, see: a) *Comprehensive Asymmetric Catalysis*, Vols. I–III (Eds.: E. N. Jacobsen, A. Pfaltz, H. Yamamoto), Springer, Berlin, **1999**; b) W.-J. Tang, X.-M. Zhang, *Chem. Rev.* **2003**, *103*, 3029.
- [2] H. B. Kagan, T.-P. Dang, *J. Am. Chem. Soc.* **1972**, *94*, 6429.
- [3] A. Miyashita, A. Yasuda, H. Takaya, K. Toriumi, T. Ito, T. Souchi, R. Noyori, *J. Am. Chem. Soc.* **1980**, *102*, 7932.
- [4] A. Togni, C. Breutel, A. Schnyder, F. Spindler, H. Landert, A. Tijani, *J. Am. Chem. Soc.* **1994**, *116*, 4062.
- [5] M. J. Burk, J. R. Lee, J. P. Martinez, *J. Am. Chem. Soc.* **1994**, *116*, 10847.
- [6] Q. Jiang, Y. Jiang, D. Xiao, P. Cao, X. Zhang, *Angew. Chem.* **1998**, *110*, 1203; *Angew. Chem. Int. Ed.* **1998**, *37*, 1100.
- [7] T. Imamoto, J. Watanabe, W. Yoshiyuki, H. Masuda, H. Yamada, H. Tsuruta, S. Matsukawa, K. Yamaguchi, *J. Am. Chem. Soc.* **1998**, *120*, 1635.
- [8] C.-C. Pai, C.-W. Lin, C.-C. Lin, C.-C. Chen, A. S. C. Chan, *J. Am. Chem. Soc.* **2000**, *122*, 11513.
- [9] W. Tang, X. Zhang, *Angew. Chem.* **2002**, *114*, 1682; *Angew. Chem. Int. Ed.* **2002**, *41*, 1612.
- [10] T. P. Yoon, E. N. Jacobsen, *Science* **2003**, *299*, 1691.
- [11] a) K. Toriumi, T. Ito, H. Takaya, T. Souchi, R. Noyori, *Acta Crystallogr. Sect. B* **1982**, *38*, 807; b) K. Mashima, K. Kusano, T. Ohta, R. Noyori, H. Takaya, *J. Chem. Soc. Chem. Commun.*

- 1989, 1208; c) F. Ozawa, A. Kubo, Y. Matsumoto, T. Hayashi, *Organometallics* **1993**, 12, 4188.
- [12] a) R. Schmid, M. Cereghetti, B. Heiser, P. Schönholzer, H.-J. Hansen, *Helv. Chim. Acta* **1988**, 71, 897.
- [13] T. Saito, T. Yokozawa, X. Zhang, N. Sayo (Takasago International Corporation), US Patent 5,872,273, **1999**.
- [14] Z.-Z. Zhang, H. Qian, J. Longmire, X.-M. Zhang, *J. Org. Chem.* **2000**, 65, 6223.
- [15] a) S. D. de Paule, N. Champion, V. Vidal, J.-P. Genêt, P. Dellis (SYNDEM), FR 2830254, **2001**; b) C. C. Pai, Y. M. Li, Z. Y. Zhou, A. S. C. Chan, *Tetrahedron Lett.* **2002**, 43, 2789.
- [16] G. Michaud, M. Bulliard, L. Ricard, J.-P. Genêt, A. Marinetti, *Chem. Eur. J.* **2002**, 8, 3327.
- [17] For examples, see: a) S. Wu, W. Wang, W. Tang, M. Lin, X. Zhang, *Org. Lett.* **2002**, 4, 4495; b) S. D. de Paule, S. Jeulin, V. Ratovelomanana-Vidal, J.-P. Genêt, N. Champion, P. Dellis, *Tetrahedron Lett.* **2003**, 44, 823; c) S. D. de Paule, S. Jeulin, V. Ratovelomanana-Vidal, J.-P. Genêt, N. Champion, G. Deschaux, P. Dellis, *Org. Process Res. Dev.* **2003**, 7, 399; d) B. H. Lipshutz, K. Noson, W. Chrisman, A. Lower, *J. Am. Chem. Soc.* **2003**, 125, 8779.
- [18] X. Zhang, K. Mashima, K. Koyano, N. Sayo, H. Kumobayashi, S. Akutagawa, H. Takaya, *Tetrahedron Lett.* **1991**, 32, 7283.
- [19] a) J. M. Tour, R.-L. Wu, J. S. Schumm, *J. Am. Chem. Soc.* **1990**, 112, 5662; b) J. Pei, J. Ni, X.-H. Zhou, X.-Y. Cao, Y.-H. Lai, *J. Org. Chem.* **2002**, 67, 8112.
- [20] a) U. Bach, D. Lupo, P. Comte, J. E. Moser, F. Weissortel, J. Salbeck, H. Spreitzer, M. Gratzel, *Nature* **1998**, 395, 583; b) J. Krüger, R. Plass, M. Grätzel, P. J. Cameron, L. M. Peter, *J. Phys. Chem. B* **2003**, 107, 7536.
- [21] a) V. Alcazar, F. Diederich, *Angew. Chem.* **1992**, 104, 1503; *Angew. Chem. Int. Ed. Engl.* **1992**, 31, 1521; b) D. K. Smith, F. Diederich, *Chem. Commun.* **1998**, 2501; c) A. Tejada, A. I. Oliva, L. Simón, M. Grande, M.-C. Caballero, J. R. Morán, *Tetrahedron Lett.* **2000**, 41, 4563.
- [22] a) J.-H. Fournier, T. Maris, J. D. Wuest, *J. Org. Chem.* **2003**, 68, 241; b) C. Poriel, Y. Ferrand, P. Le Maux, C. Paul, J. Rault-Berthelot, G. Simonneaux, *Chem. Commun.* **2003**, 2308.
- [23] X. Cheng, G.-H. Hou, J.-H. Xie, Q.-L. Zhou, *Org. Lett.* **2004**, 6, 2381.
- [24] D. Cai, J. F. Payack, D. R. Bender, D. L. Hughes, T. R. Verhoeven, P. J. Reider, *Org. Synth.* **1998**, 76, 6.
- [25] Y. Uozumi, A. Tanahashi, S.-Y. Lee, T. Hayashi, *J. Org. Chem.* **1993**, 58, 1945.
- [26] Crystal data for $[\text{PdCl}_2((R)\text{-1a})(\text{CH}_2\text{Cl}_2)]$: $\text{C}_{50}\text{H}_{36}\text{Cl}_4\text{P}_2\text{Pd}$, $M_r = 925.70$, yellow block, $0.35 \times 0.24 \times 0.20$ mm, orthorhombic, space group $P2_12_12_1$, $a = 12.146(11)$ Å, $b = 16.915(18)$ Å, $c = 22.05(2)$ Å, $\alpha = 90^\circ$, $\beta = 90^\circ$, $\gamma = 90^\circ$, $V = 4530(8)$ Å³, $\rho_{\text{calc}} = 1.357$ g cm⁻³, $\mu = 0.791$ mm⁻¹, $F(000) = 1878$, $Z = 4$, $\text{MoK}\alpha$ radiation, $\lambda = 0.71073$ Å, $T = 293$ K, θ scan range $1.91 < \theta < 25.00^\circ$. Reflections collected 7408, 6617 unique reflections, $R_1 = 0.0836$. CCDC-256882 contains the supplementary crystallographic data for this paper. These data can be obtained free of charge via www.ccdc.cam.ac.uk/conts/retrieving.html (or from the Cambridge Crystallographic Data Centre, 12 Union Road, Cambridge CB2 1EZ, UK; fax: (+44)1223-336-033; or deposit@ccdc.cam.ac.uk).
- [27] a) W. L. Steffen, G. J. Palenik, *Inorg. Chem.* **1976**, 15, 2432; b) T. Hayashi, M. Konishi, Y. Kobori, M. Kumada, T. Higuchi, K. Hirotsu, *J. Am. Chem. Soc.* **1984**, 106, 158.
- [28] a) R. Noyori, *Asymmetric Catalysis in Organic Synthesis*, Wiley, **1994**, p. 28; b) I. Kitagawa, K. Ohsashi, N. I. Baek, M. Sakaami, M. Yoshikawa, H. Shibuya, *Chem. Pharm. Bull.* **1997**, 45, 786.
- [29] M. Kitamura, M. Tokunaga, R. Noyori, *J. Org. Chem.* **1992**, 57, 4053.
- [30] a) T. Ohta, H. Takaya, M. Kitamura, K. Nagai, R. Noyori, *J. Org. Chem.* **1987**, 52, 3174; b) X. Zhang, T. Uemura, K. Matsumura, N. Sayo, H. Kumobayashi, H. Takaya, *Synlett* **1994**, 501; c) T. Uemura, X.-Y. Zhang, K. Matsumura, N. Sayo, H. Kumobayashi, T. Ohta, K. Nozaki, H. Takaya, *J. Org. Chem.* **1996**, 61, 5510; d) P. G. Jessop, R. R. Stanley, R. A. Brown, C. A. Eckert, C. L. Liotta, T. T. Ngo, P. Pollet, *Green Chem.* **2003**, 5, 123.
- [31] I. Yamaka, M. Yamaguchi, T. Yamagishi, *Tetrahedron: Asymmetry* **1996**, 7, 3339.
- [32] a) J. P. Genêt, C. Pinel, V. Ratovelomanana-Vidal, S. Mallart, X. Pfister, L. Bischoff, M. C. de Andrade, S. Darses, C. Galopin, J. A. Laffitte, *Tetrahedron: Asymmetry* **1994**, 5, 675; b) T. Benincori, E. Cesarotti, O. Piccolo, F. Sanniccolo, *J. Org. Chem.* **2000**, 65, 2043.

Biotransformation

Enantioselective Reduction of β -Keto Acids with Engineered *Streptomyces coelicolor***

Kevin I. Booker-Milburn,* Rebecca Gillan,
Meriel Kimberley, Takaaki Taguchi, Koji Ichinose,
G. Richard Stephenson, Yutaka Ebizuka, and
David A. Hopwood

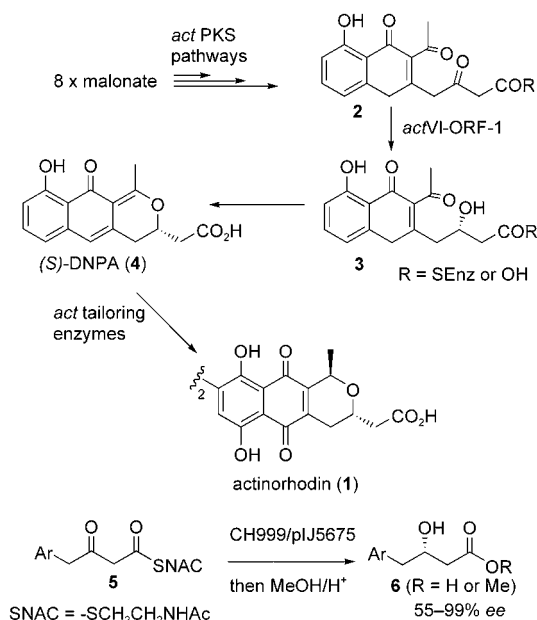
The soil bacterium *Streptomyces coelicolor* has long been studied owing to its production of antibiotics, the most significant of which is the dimeric benzoisochromanequinone

[*] Dr. K. I. Booker-Milburn, R. Gillan, Dr. M. Kimberley
School of Chemistry
University of Bristol
Cantock's Close, Bristol BS8 1TS (UK)
Fax: (+44) 117-929-8611
E-mail: k.booker-milburn@bristol.ac.uk
Dr. T. Taguchi, Prof. K. Ichinose,^[†] Prof. Y. Ebizuka
Graduate School of Pharmaceutical Sciences
The University of Tokyo
Hongo, Bunkyo-ku, Tokyo 113-0033 (Japan)
Dr. G. R. Stephenson
Wolfson Materials and Catalysis Centre
School of Chemical Sciences and Pharmacy
University of East Anglia
Norwich, Norfolk, NR4 7TJ (UK)
Prof. Sir D. A. Hopwood
John Innes Centre
Norwich Research Park
Colney, Norwich, Norfolk, NR4 7UH (UK)

[†] Current address:
Research Institute of Pharmaceutical Sciences
Musashino University
Shinmachi, Nishitokyo, Tokyo 202-8585 (Japan)

[**] This work was supported by the BBSRC (research grant 7/B14735), the EPSRC, the Royal Society (Joint Project grant 11701), Grants-in-Aid for Scientific Research on Priority Areas from the Ministry of Education, Science, Sports, and Culture of Japan (Genome Biology 1414210), and the Japan Society for the Promotion of Science (JSPS Research Fellowship for Young Scientists). We also thank Dr. John Crosby, Dr. Russell Cox, and Prof. Tom Simpson (University of Bristol) for useful discussions. We thank Emma Brennand (UEA) for some preliminary synthetic work.

actinorhodin (ACT, **1**). *S. coelicolor* is generally regarded as the best genetically characterized of all the streptomycete bacteria. Recently its complete genomic sequence was published.^[1] Over the years a clear picture has emerged for the biosynthesis of the skeleton of **1**.^[2] It is generally accepted that **2** (or the phenol tautomer of **2**) is assembled from eight malonate units by a type II polyketide synthase (PKS). Whether **2** is released at this stage from the PKS as the free β -keto acid ($R = OH$) or is subject to further biotransformations as the enzyme-bound thiolate ($R = SEnz$) is a matter for speculation (see below). Reduction of **2** is thought to lead to the hydroxy acid **3**, which then undergoes cyclization followed by dehydration to give the yellow pigment (*S*)-DNPA (**4**, 4,10-dihydro-9-hydroxy-1-methyl-10-oxo-3*H*-naphtho[2,3*c*]pyran-3-(*S*)-acetic acid). Significantly, **4** has been isolated from both mutant^[3] and recombinant^[4] strains of *S. coelicolor*, thus strongly implicating its role as a true intermediate in ACT biosynthesis. It is thought that **4** then undergoes a series of enzyme-controlled reduction, oxidation, hydroxylation, and dimerization steps, which result in the formation of **1** (Scheme 1). A number of genes thought to encode the

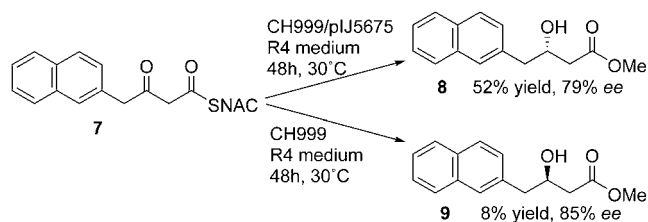


Scheme 1. Biosynthesis of actinorhodin **1** and feeding studies with SNAC derivatives.

various enzymes have been identified (*act* tailoring genes), but at this stage the likely intermediates in the biosynthesis of **4** have yet to be confirmed. The reduction of **2** is believed to occur by the action of a reductase (RED1) encoded by the *actVI-ORF-1* gene. Good evidence for this hypothesis was first obtained by Floss and co-workers,^[3] who found that the B1 mutant strain of *S. coelicolor* accumulated significant quantities of **4**. More recently we showed^[4] that a recombinant strain (CH999/pIJ5660) of *S. coelicolor* containing *actPKS* and *actVI-ORF-1* genes resulted in the production of **4** on fermentation in a liquid medium. A further strain was engineered from the plasmid pIJ5660, from which the

ketosynthase (KS) gene *actI-ORF-1* had been deleted. This new strain (CH999/pIJ5675) did not have the ability to synthesize the polyketide skeleton from which **2** is derived, but could still express RED1 and thus serve as a whole-cell reduction medium. A number of *N*-acetylcysteamine β -ketothioester (SNAC) substrates were fed to this strain. They underwent enantioselective reduction to the corresponding β -hydroxy acids with moderate to high *ee* values (analyzed as the methyl esters **6**, $R = Me$). The fact that a range of nonnatural SNAC derivatives proved to be substrates for RED1, but that other β -ketoesters were not, provided convincing evidence at the time for the likely existence of **2** as the thiolate ($R = SEnz$). These results led us to conclude that “NAC thioesters are required for recognition by the *actVI-ORF-1* reductase and/or they are required for successful transport across the cell membrane”.^[5] Herein we present results from further study that demonstrate that this statement is likely to be incorrect and that CH999/pIJ5675 is a much more general biotransformation system than previously thought.

In our previous studies on biotransformations with CH999/pIJ5675, it was found that some of the SNAC substrates underwent reduction with only moderate enantioselectivities. For example, the naphthyl substrate **7** was produced with just 55% *ee*. This low value was initially proposed to be a result of a lack of stereoselectivity of RED1. Previously we determined *ee* values by converting the reduced products into Mosher ester derivatives and analyzing the diastereomers by NMR spectroscopy. On reinvestigation of this reduction with a number of *act* strains it was found that the *ee* values of the derived hydroxyesters could be determined more reliably by HPLC on a chiral phase.^[6] For example, the reduction of **7** with CH999/pIJ5675, followed by esterification, gave the *S* β -hydroxyester **8** as before, but the *ee* value was determined more accurately to be 79%, a result that was confirmed by repeated biotransformations. We were intrigued to find that the biotransformation of **7** with the host CH999 as a control gave the *R* β -hydroxyester **9** with 85% *ee* in consistently low chemical yield (Scheme 2). The fact that



Scheme 2. Reduction of **7** with CH999/pIJ5675 and CH999.

the opposite absolute stereochemistry predominates in this case indicates that **7** is reduced by one or more non-*act* reductases within CH999. It is therefore very likely that the less-than-optimal *ee* values obtained previously with CH999/pIJ5675 and SNAC derivatives can be explained by the action of a non-*act* reductase, which competes with RED1 for the SNAC substrates.

At about this time we were able to demonstrate^[7] the functional expression of RED1 in *E. coli* and were intrigued to find that the reduction of **5** (Ar = Ph) appeared to proceed, following initial hydrolysis, to give the free β -keto acid **6**. This result prompted us to embark on an investigation into the generality of the CH999/pIJ5675 strain as a whole-cell biotransformation system for the enantioselective reduction of β -keto acids to the corresponding *S*- β -hydroxy acids (Table 1). A range of β -keto acids were prepared by

when yields are expressed based on recovered decarboxylated ketone. RED1 proved to be very tolerant of methoxy substitution at various positions on the aryl ring. Only when an alkenyl substituent was introduced at the *ortho* position (in **10**, Table 1, entry 9) was no reduction observed. This alkenyl compound **10** was prepared with the aim of synthesizing an analogue of **2** with an aryl methyl ketone moiety. Unfortunately, all attempts to convert **10** into the corresponding ketone (e.g. ozonolysis) proved fruitless, as the resulting product underwent spontaneous cyclization to a naphthyl derivative. It is reasonable to speculate that the failure of **10** to undergo reduction could be explained by the fact that the RED1 active site is likely to possess a binding domain that recognizes the polar methyl ketone residue in **2** rather than the lipophilic alkenyl group in **10**.^[8]

However, it was encouraging to note that the saturated cyclohexyl-substituted β -keto acid (Table 1, entry 10) and the *n*-pentyl-substituted β -keto acid (Table 1, entry 11) underwent clean reduction to the corresponding *S*-hydroxy acids with high enantioselectivity. It is particularly interesting to observe that this latter β -keto acid has been reported to undergo reduction to the *R*-hydroxy acid with baker's yeast.^[9] These examples demonstrate the potential of RED1 for the reduction of non-aryl or non-actinorhodin-like substrates. In all cases biotransformation to the β -hydroxy acids occurred with essentially complete stereoselectivity, as evidenced by HPLC on a chiral phase and by comparison with synthetic samples of the racemates. The absolute stereochemistry was found to be *S* in all cases, as proved by correlation either with known compounds or with the *R*-enantiomers, which were synthesized by Noyori hydrogenation^[10] of the appropriate β -ketoesters.

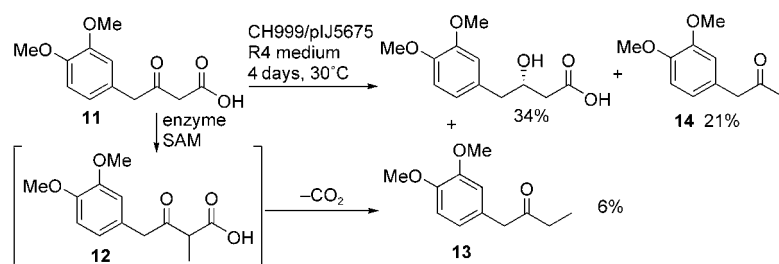
Reduction of the β -keto acid **11** also proved interesting. Along with the hydroxy acid and the decarboxylated ketone **14**, the ethyl ketone **13**^[11] was obtained consistently as a minor component (5–6% yield). This ethyl ketone is probably formed by the adventitious action of an (*S*)-adenosylmethionine(SAM)-dependent methyltransferase on the β -keto acid **11**. It is likely that **11** is methylated to give **12**, which then undergoes decarboxylation to provide **13** (Scheme 3). No trace of the proposed methylated β -keto acid **12** was ever detected, despite several repeats of this biotransformation.

Table 1: Enantioselective reduction of β -keto acids with engineered *S. coelicolor* (CH999/pIJ5675).

Entry	Substrate	Product	Yield [%]	ee [%]
1 ^[b]			80	> 99
2			77	97
3			24 (42) ^[a]	99
4 ^[b]			61 (72) ^[a]	99
5			43 (59) ^[a]	98
6 ^[b]			40 (56) ^[a]	98
7			34 (45) ^[a]	> 99
8 ^[b]			59 (80) ^[a]	99
9 ^[b]			41 ^[c]	
10			54	99
11 ^[d]			52	> 95

[a] Based on recovered decarboxylated ketone. [b] Fed as sodium salts. [c] In addition to 25% recovered **10**. [d] ee value determined by NMR spectroscopic analysis of Mosher ester derivative.

hydrolysis of the corresponding methyl esters, which themselves were prepared by general routes that we used previously for the synthesis of SNAC derivatives. These β -keto acids were then fed to CH999/pIJ5675 as the free acids and/or the sodium salts (0.8-mmol scale). Not unexpectedly, many of the β -keto acids proved to be labile towards decarboxylation, and in certain cases better results were obtained with the sodium salts. However, many of the lower yields were a reflection of unavoidable decarboxylation rather than the efficiency of the reductase itself, as is clear



Scheme 3. Proposed ethyl ketone formation with SAM-dependent methyltransferase.

This methyltransferase is probably encoded somewhere on the CH999 host genome.^[12] Strong evidence in favor of this hypothesis was found when **11** was incubated with the CH999 host strain and only **14** (26 %) and **13** (5 %) were obtained. No ethyl ketone products were detected from any of the biotransformations carried out with the other substrates in this study, thus suggesting that this methyltransferase has a high degree of substrate specificity.

In summary, a variety of aryl- and alkyl-substituted β -keto acids have been shown to be excellent substrates for RED1 from *S. coelicolor*. The products are formed in reasonable to good yields with complete selectivity for the *S* enantiomer. These results demonstrate that the engineered *S. coelicolor* strain CH999/pIJ5675 is a useful whole-cell biotransformation system for the reduction of β -keto acids with an enantioselectivity that is opposite to that of baker's yeast. Furthermore, these results, in conjunction with protein functional expression studies, provide the first clear evidence that the free β -keto acid **2** ($R=OH$) is the likely RED1 substrate in the biosynthesis of **1**, rather than an enzyme-bound β -keto-thioester (**2**, $R=SEnz$) as previously thought. In vitro studies with purified RED1 are ongoing, and the results will be reported in the near future.

Experimental Section

Typical procedure: A suspension of CH999/pIJ5675 spores suspended in glycerol (15 μ L) and thiostrepton solution (30 mM in DMF, 15 μ L) was added to an R4 medium (10 mL) in a 25-mL universal tube under sterile conditions. The solution was incubated on an orbital shaker (30°C, 220 rpm) for 3 days to form a seed culture. Six 500-mL conical flasks were then each charged with an R4 medium (50 mL), thiostrepton solution (5 μ L), and seed culture (3 mL). A single flask containing CH999/pIJ5660 spores^[4] was prepared in a similar way to be incubated simultaneously as an indicator of secondary-metabolite production. The cultures were incubated on a shaker (30°C, 220 rpm) until the indicator had turned dark brown (approximately 2 days). 4-(Naphthalen-2-yl)-3-oxobutanoic acid (0.18 g, 0.79 mmol) was dissolved in methanol (6 mL), and 1 mL of this solution added to each of the six flasks of CH999/pIJ5675 culture, which were then returned to the shaker and incubated for a further 4 days. The resulting solutions were filtered to remove cell debris, combined, and acidified to pH 3. The solution was extracted with ethyl acetate (3 \times 100 mL), and the combined organic extracts were washed with water (2 \times 50 mL) and brine (2 \times 50 mL). The extracts were dried ($MgSO_4$), and the solvent was removed in vacuo to yield a brown solid. Purification by flash chromatography (eluant: 70 % ethyl acetate/40–60 petroleum ether) gave (*S*)-3-hydroxy-4-(naphthalen-2-yl)butyric acid as a white solid (0.14 g, 77 %). M.p.: 126–127°C (lit.: 126–128°C^[13]); $[\alpha]_D^{25} +1.17$ ($c=1.03$, $CHCl_3$); IR (neat): $\tilde{\nu}_{max}=3406, 2923,$

1695 cm^{-1} ; 1H NMR (400 MHz, CD_3OD): $\delta=2.56$ (dd, $J=10.4, 5.3$ Hz, 1H, $CHCO_2H$), 2.63 (dd, $J=10.4, 2.3$ Hz, 1H, $CHCO_2H$), 2.98 (dd, $J=8.5, 3.9$ Hz, 1H, $CHAr$), 3.03 (dd, $J=8.5, 4.4$ Hz, 1H, $CHAr$), 4.33–4.41 (m, 1H, $CHOH$), 7.29 (dd, $J=5.3, 0.9$ Hz, 1H, ArH), 7.31–7.36 (m, 2H, ArH), 7.59 (s, 1H, ArH), 7.67–7.71 ppm (m, 3H, ArH); ^{13}C NMR (100 MHz, CD_3OD , Me_4Si): $\delta=40.9$ (CH_2CO_2H), 43.8 (CH_2Ar), 69.8 ($CHOH$), 126.0 (CH), 126.2 (CH), 126.3 (CH), 127.7 (CH), 127.9 (CH), 128.1 (CH), 128.3 (CH), 133.3 (C), 134.7 (C), 138.8 (CCH_2), 175.3 ppm (CO_2H); MS (EI): m/z : 230 ($[M]^+$, 50 %), 212 (34), 167 (25), 142 (100), 128 (15), 115 (46), 89 (29), 83 (55), 71 (41), 63 (15).

Received: September 22, 2004

Published online: January 11, 2005

Keywords: bioorganic chemistry · biosynthesis · enantioselectivity · enzymes · reduction

- [1] S. D. Bentley, K. F. Chater, A. M. Cerdano-Tarraga, G. L. Challis, N. R. Thomson, K. D. James, D. E. Harris, M. A. Quail, H. Kieser, D. Harper, A. Bateman, S. Brown, G. Chandra, C. W. Chen, M. Collins, A. Cronin, A. Fraser, A. Goble, J. Hidalgo, T. Homsby, S. Howarth, C. H. Huang, T. Kieser, L. Larke, L. Murphy, K. Oliver, S. O'Neil, E. Rabbinowitsch, M. A. Rajandream, K. Rutherford, S. Rutter, K. Seeger, D. Saunders, S. Sharp, R. Squares, S. Squares, K. Taylor, T. Warren, A. Wietzorrek, J. Woodward, B. G. Barell, J. Parkhill, D. A. Hopwood, *Nature* **2002**, 417, 141–147.
- [2] a) D. A. Hopwood, M. J. Bibb, K. F. Chater, T. Kieser, C. J. Bruton, H. M. Kieser, D. J. Lydiate, C. P. Smith, J. M. Ward, H. Schrempf, *Genetic Manipulation of Streptomyces. A laboratory Manual*, The John Innes Foundation, Norwich, **1985**; b) P. L. Bartel, C. B. Zhu, J. S. Lampel, D. C. Dosch, S. P. Connors, J. M. Beale, P. J. Keller, C. Chang, H. G. Floss, *J. Bacteriol.* **1990**, 172, 4816–4826; c) R. McDaniel, S. Ebert-Khosla, D. A. Hopwood, C. Khosla, *Science* **1993**, 262, 1546–1550; d) M. A. Fernández-Moreno, M. Martínez, J. L. Cabarello, K. Ichinose, D. A. Hopwood, F. Malpartida, *J. Biol. Chem.* **1994**, 269, 24854; e) D. A. Hopwood, *Chem. Rev.* **1997**, 97, 2465–2497, and references therein.
- [3] S. P. Cole, B. A. M. Rudd, D. A. Hopwood, C.-J. Chang, H. G. Floss, *J. Antibiot.* **1987**, 40, 340–347.
- [4] K. Ichinose, C. M. Surti, T. Taguchi, F. Malpartida, K. I. Booker-Milburn, G. R. Stephenson, Y. Ebizuka, D. A. Hopwood, *Bioorg. Med. Chem. Lett.* **1999**, 9, 395–400.
- [5] C. E. Anson, M. J. Bibb, K. I. Booker-Milburn, C. Clissold, P. J. Haley, D. A. Hopwood, K. Ichinose, W. P. Revill, G. R. Stephenson, C. M. Surti, *Angew. Chem.* **2000**, 112, 230–233; *Angew. Chem. Int. Ed.* **2000**, 39, 224–227.
- [6] Chiralcel OD column; heptane/2-ProH/trifluoroacetic acid (90:10:0.1) for acids; heptane/2-ProH (9:1) for esters.
- [7] T. Taguchi, T. Itoh, M. R. Kimberley, K. I. Booker-Milburn, G. R. Stephenson, Y. Ebizuka, K. Ichinose, unpublished results.
- [8] T. Taguchi, K. Kunieda, M. Takeda-Shitaka, D. Takaya, N. Kawano, M. R. Kimberley, K. I. Booker-Milburn, G. R. Stephenson, H. Umeyama, Y. Ebizuka, K. Ichinose, *Bioorg. Med. Chem.* **2004**, 12, 5917–5927.
- [9] M. Utaka, H. Watabu, H. Higashi, T. Sakai, S. Tsuboi, S. Torii, *J. Org. Chem.* **1990**, 55, 3917–3921.
- [10] G. Capozzi, S. Roelens, S. Talamo, *J. Org. Chem.* **1993**, 58, 7932–7936.
- [11] Selected data for **13**: IR (neat): $\tilde{\nu}_{max}=2926, 2853, 1713\text{ cm}^{-1}$; 1H NMR (400 MHz, $CDCl_3$, Me_4Si): $\delta=1.02$ (t, $J=4.6$ Hz, 3H, CH_3), 2.47 (q, $J=4.6$ Hz, 2H, CH_2), 3.62 (s, 2H, CH_2), 3.87 (6H, 2 \times CH_3), 6.71 (d, $J=1.2$ Hz, 1H, ArH), 6.75 (dd, $J=5.2, 1.2$ Hz,

¹H, ArH), 6.84 ppm (d, $J = 5.2$ Hz, 1H, ArH); ¹³C NMR (100 MHz, CDCl₃, Me₄Si): $\delta = 7.7$ (CH₃), 35.0 (CH₂CH₃), 49.4 (CH₂CO), 55.8 (CH₃OAr), 55.9 (CH₃OAr), 112.2 (CH), 112.4 (CH), 121.3 (CH), 126.9 (CCH₂), 148.0 (COCH₃), 149.0 (COCH₃), 209.4 ppm (CO); MS (EI): m/z : 208 ($[M]^+$, 12%), 151 (82), 107 (6), 87 (11), 83 (100), 57 (11).

- [12] Two putative methyltransferases (ORFs (open reading frames) SCO2170 and SCO2098) have been identified on the *S. coelicolor* genome (from reference [1]).
- [13] D. I. Barron, P. T. Bysouth, R. W. Clarke, A. R. Copley, O. Stephenson, D. K. Vallance, A. M. Wild, *J. Med. Chem.* **1968**, *11*, 1139–1144.

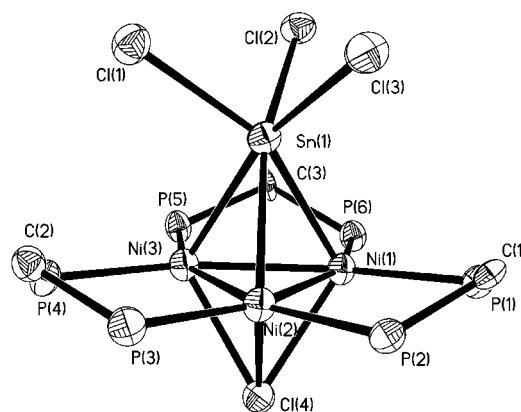


Figure 1. ORTEP diagram of complex **1** (thermal ellipsoids set at 50 % probability). Selected bond lengths [Å] and angles [°]: Sn(1)–Cl(3) 2.457(3), Sn(1)–Cl(2) 2.466(3), Sn(1)–Cl(1) 2.473(3), Sn(1)–Ni(2) 2.5960(16), Sn(1)–Ni(3) 2.6185(16), Ni(1)–Ni(2) 2.4593(18), Ni(1)–Ni(3) 2.4829(18), Ni(2)–Ni(3) 2.4825(16), Ni–P(average) 2.2180(18); Cl(3)–Sn(1)–Cl(2) 88.36(9), Ni(2)–Ni(1)–Ni(3) 60.30(5), P(1)–Ni(1)–Sn(1) 107.20(10), P(6)–Ni(1)–Sn(1), 108.91(10).

Cluster Compounds

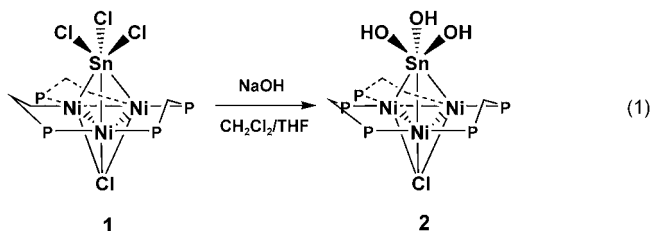
A Trihydroxy Tin Group That Resists Oligomerization in the Trinuclear Nickel Cluster $[\text{Ni}_3(\mu\text{-P,P'-PPh}_2\text{CH}_2\text{PPh}_2)_3(\mu_3\text{-L})-(\mu_3\text{-Sn(OH)}_3)]^{**}$

Eugenio Simón-Manso and Clifford P. Kubiak*

The conversion of tin chloride reagents into the corresponding hydroxides typically results in the formation of oligomeric tin oxides.^[1–3] We report herein the preparation and reactivity of a trinuclear nickel cluster that is capped by a $\mu_3\text{-Sn(OH)}_3$ group. This is a rare example of a complex that contains an intact trihydroxy tin group, thus allowing the study of the chemistry of tin hydroxides without interference from competing reactions that form oligomeric tin oxides.

The trichlorostannyl-capped cluster $[\text{Ni}_3(\mu\text{-dppm})_3(\mu_3\text{-Cl})(\mu_3\text{-Sn(Cl)}_3)]$ (**1**; dppm = bis(diphenylphosphino)methane) is a dark-green diamagnetic species, the $^{31}\text{P}\{^1\text{H}\}$ NMR spectrum of which displays a singlet at $\delta = -2.3$ ppm that is flanked by satellites arising from coupling to the trichlorostannyl group ($^2J_{(^{31}\text{P}-^{119}\text{Sn},^{117}\text{Sn})} = 138$ Hz (unresolved)). The properties of cluster **1** are similar to the closely related μ -iodo-capped cluster that was reported recently.^[4] The molecular structure of the trichlorostannyl-capped cluster **1** is presented in Figure 1. The three chlorine atoms of the $\mu_3\text{-SnCl}_3$ are staggered with respect to the three nickel atoms, resulting in an approximately octahedral coordination environment at the tin atom and approximate C_{3v} symmetry for the cluster.

Cluster **1** may be converted into the trihydroxystannyl-capped cluster $[\text{Ni}_3(\mu\text{-dppm})_3(\mu_3\text{-Cl})(\mu_3\text{-Sn(OH)}_3)]$ (**2**) in high yield by treatment with in situ hydrolyzed NaH in a $\text{CH}_2\text{Cl}_2/\text{THF}$ solvent mixture [Eq. (1)]. Use of NaH provides higher yields than direct use of NaOH, most likely because the NaH powder gives more highly dispersed NaOH than the poorly soluble NaOH pellets.



Cluster **2** is a deep-blue diamagnetic solid whose $^{31}\text{P}\{^1\text{H}\}$ NMR spectrum displays a singlet with satellites at $\delta = -0.1$ ppm ($^2J_{(^{31}\text{P}-^{119}\text{Sn},^{117}\text{Sn})} = 122$ Hz (unresolved)). The unit cell of crystals of **2** has three independent molecules per unit cell and was solved in space group $P3$. The molecular structure of **2** is presented in Figure 2. The structure reveals a $\mu_3\text{-Sn(OH)}_3$ group capping a triangular Ni_3 cluster in a staggered conformation. Overall, the bond parameters of **2** are quite similar to the $\mu_3\text{-SnCl}_3$ -capped precursor **1** and the cluster $[\text{Ni}_3(\mu\text{-dppm})_3(\mu_3\text{-I})(\mu_3\text{-SnCl}_3)]$.^[4] However, the solid-state crystal structure of **2** reveals that the clusters are organized in pairs with the two Sn(OH)_3 groups facing each other in a crystallographically imposed threefold staggered conformation (Figure 3).

The face-to-face arrangement of pairs of Sn(OH)_3 groups suggests partial intermolecular hydrogen bonding in the solid state. The intermolecular distances between pairs of O atoms of the hydroxy groups (Figure 3 A) fall in the narrow range of 2.983(10)–3.003(10) Å. This is at the long end of the range

[*] Dr. E. Simón-Manso, Prof. C. P. Kubiak
Department of Chemistry & Biochemistry
University of California-San Diego
La Jolla, CA 92093-0358 (USA)
Fax: (+1) 858-534-5383
E-mail: ckubiak@ucsd.edu

[**] The authors thank DOE (DE-FG03-99ER14992) and NSF (CHE-0315593) for support of this research. L = Cl, Br.

Supporting information for this article (ORTEP diagram for complex **6**, spectroscopic data, and MS data) is available on the WWW under <http://www.angewandte.org> or from the author.

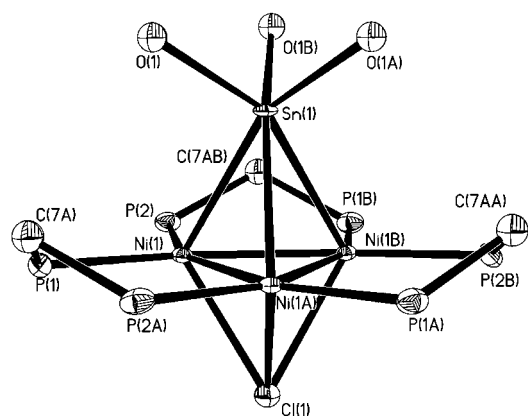


Figure 2. ORTEP diagram of complex **2** (thermal ellipsoids set at 50 % probability). Selected bond lengths [Å] and angles [°]: Sn(1)–O(1) 2.039(7), Sn(1)–Ni(1) 2.6355(17), Ni–P(average) 2.193(3), Ni(1)–Cl(1) 2.429(4), Ni(1)–Ni(1A) 2.451(2); O(1)–Sn(1)–O(1A) 94.0(3), O(1)–Sn(1)–Ni(1) 105.4(2), Ni(1)–Sn(1)–Ni(1A) 55.41(5), Ni(1)–Ni(1A)–Ni(1B) 60.0.

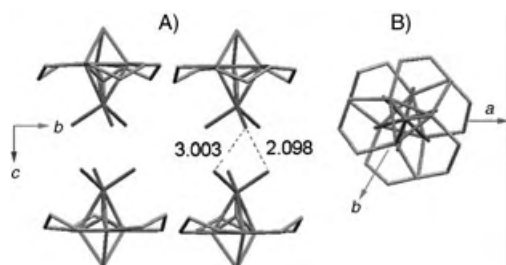


Figure 3. Packing diagram for the crystal structure of complex **2** showing the pairing-up of the clusters: A) side view, B) top view.

normally associated with relatively weak O–H...O hydrogen bonding.^[5] The fact that the μ_3 -Sn(OH)₃ group of the cluster **2** resists oligomerization is likely to be the result of the considerable steric influences of the {Ni₃(dppm)₃} framework. A space-filling diagram of the structure of **2** shows that the μ_3 -Sn(OH)₃ group sits in a hydrophobic pocket created by the phenyl rings of the three dppm ligands (Figure 4).

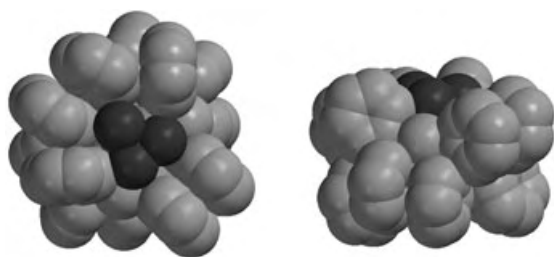
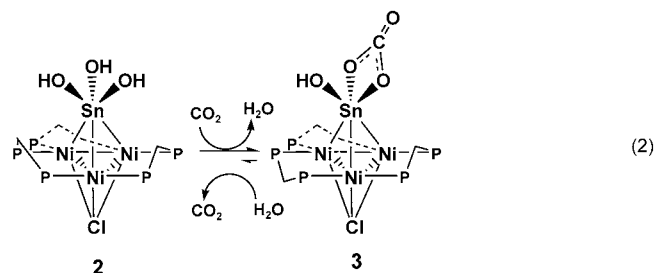


Figure 4. Two projections of the space-filling diagram of the structure of complex **2**; the three oxygen atoms of the μ_3 -Sn(OH)₃ groups are shown in darker gray.

The μ_3 -Sn(OH)₃ group of cluster **2** exhibits nucleophilic addition to carbon dioxide and epoxides. Bubbling CO₂ through solutions of complex **2** in CH₂Cl₂ or THF results in

an immediate color change from deep-blue to purple and the quantitative formation of the η^2 -carbonate complex **3** [Eq. (2)].



Characteristic bands for carbonate, $\tilde{\nu}_{\text{CO}} = 1634$ and 1669 cm^{-1} , are observed in the solid-state and solution IR spectra of cluster **3**. The ³¹P{¹H} NMR spectrum is a singlet flanked by two satellites at $\delta = +1.1 \text{ ppm}$ ($^2J_{^{31}\text{P}-^{119}\text{Sn},^{117}\text{Sn}} = 128 \text{ Hz}$ (unresolved)). Formation of the carbonate cluster is accompanied by H₂O elimination, and the reaction between the μ_3 -Sn(OH)₃ cluster **2** and the μ_3 -Sn(OH)(η^2 -CO₃) cluster **3** is completely reversible [Eq. (2)]. The molecular structure of cluster **3** is presented in Figure 5.

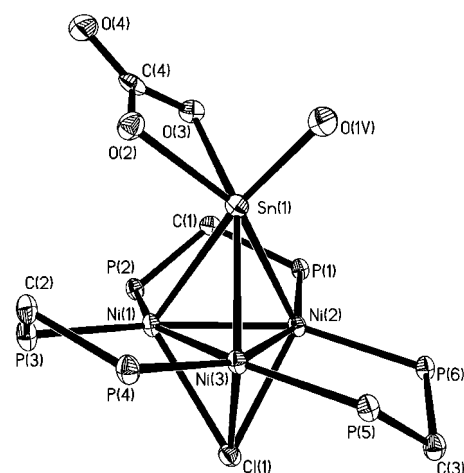
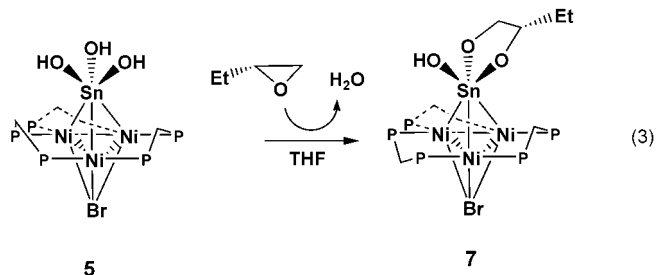


Figure 5. ORTEP diagram for complex **3** (thermal ellipsoids set at 50 % probability). Selected bond lengths [Å] and angles [°]: Sn(1)–O(3) 2.121(3), Sn(1)–Ni(3) 2.5197(7), Ni(1)–Ni(3) 2.4344(8), Ni(1)–Cl(1) 2.4705(14), Ni(3)–Cl(1) 2.3543(13), O(4)–C(4) 1.223(6), O(2)–C(4) 1.325(6); O(1V)–Sn(1)–O(3) 90.39(9), O(3)–Sn(1)–O(2) 61.80(13), Ni(3)–Sn(1)–Ni(2) 57.42(2), Ni(2)–Ni(1)–Ni(3) 61.01(3), O(3)–C(4)–O(2) 111.8(4).

The carbonate-capped cluster **3** exhibits one of the most distorted angles yet observed in a carbonate complex, $\angle \text{O(3)–Sn(1)–O(2)} = 61.80(13)^\circ$, and a highly distorted octahedral coordination geometry around the tin atom.^[6] The carbonate group is also highly distorted from ideal D_{3h} symmetry (ideal: all C–O ≈ 1.28 – 1.29 Å) with longer C–O bond lengths for the oxygen atoms coordinated to tin (average: $1.330(3) \text{ Å}$), and a shorter C–O bond lengths for the uncoordinated oxygen atom ($1.223(6) \text{ Å}$). The O(3)–C(4)–O(2) bond angle is narrow (111.8°), reflecting a strained four-membered ring.

Cluster **2** also undergoes ring-opening addition of 1,2-epoxybutane to give the 1,2-diolate tin cluster $[\text{Ni}_3(\mu\text{-PPh}_2\text{CH}_2\text{PPh}_2)_3(\mu_3\text{-Cl})(\mu_3\text{-Sn}(\text{OH})(\eta^2\text{-O-CH}_2\text{CH}(\text{C}_2\text{H}_5)\text{-O}))]$ (**4**). Cluster **4** was characterized by mass spectrometry and NMR spectroscopy (see Supporting Information). This reaction results in isomeric mixtures, and we were unable to isolate a suitable crystal of **4** for X-ray characterization. However, the closely related $\mu_3\text{-Br}$ derivative $[\text{Ni}_3(\mu\text{-PPh}_2\text{CH}_2\text{PPh}_2)_3(\mu_3\text{-Br})(\mu_3\text{-Sn}(\text{OH})_3)]$ (**5**; prepared from $[\text{Ni}_3\{\mu\text{-P,P'-dppm}\}_3(\mu_3\text{-Br})(\mu_3\text{-SnBr}_3)]$ (**6**), see Experimental Section) reacts with 1,2-epoxybutane to afford the 1,2-diolate cluster $[\text{Ni}_3(\mu\text{-PPh}_2\text{CH}_2\text{PPh}_2)_3(\mu_3\text{-Br})\{\mu_3\text{-Sn}(\text{OH})(\eta^2\text{-OCH}_2\text{-CH}(\text{C}_2\text{H}_5)\text{O})\}]$ (**7**) as a crystalline material [Eq. (3)].



Cluster **7** is a turquoise-blue diamagnetic solid, and its $^{31}\text{P}\{^1\text{H}\}$ NMR spectrum displays a singlet with satellites at $\delta = -1.9$ ppm ($^2J_{(^{31}\text{P}-^{119}\text{Sn},^{117}\text{Sn})} = 98$ Hz (unresolved)). The molecular structure of complex **7** shows a $\text{OCH}_2\text{CH}(\text{C}_2\text{H}_5)\text{O}$ diolate group coordinated to the tin atom in a chelated η^2 fashion (Figure 6). The large thermal parameter for the C(5) atom in the direction perpendicular to the O(1)-O(2)-C(5)-C(4) plane is the result of superposition of two different orientations of the molecule in the crystal lattice. The centrosymmetric $P2_1/c$ space group confirms the presence of a 50:50 *R/S* racemic mixture in the crystal.

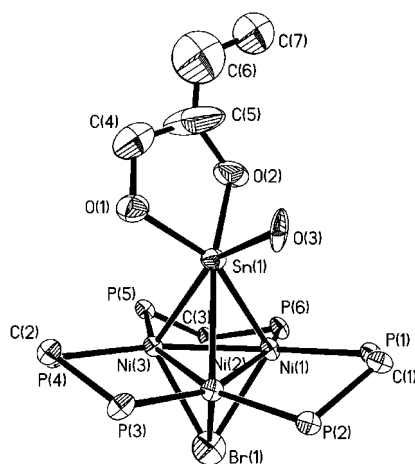


Figure 6. ORTEP diagram for complex **7** (thermal ellipsoids set at 50 % probability). Selected bond lengths [Å] and angles [°]. Ni(1)-Ni(3) 2.4307(14), Ni(1)-Br(1) 2.4470(16), Ni(1)-Sn(1) 2.6238(12), Ni(2)-Sn(1) 2.6173(12), Ni(3)-Sn(1) 2.5873(11), Sn(1)-O(2) 2.020(7), Sn(1)-O(1) 2.043(7), Sn(1)-O(3) 2.178(7); Ni(3)-Ni(1)-Ni(2) 59.60(4), Ni(3)-Ni(1)-Sn(1) 61.44(4), Ni(3)-Ni(2)-Ni(1) 60.17(4).

Complexes **2** and **5** constitute rare examples of tin trihydroxy compounds. A search of more than 250 000 structures in the Cambridge Crystallographic Data Center^[7-9] does not yield any structurally characterized compounds that have an intact $\text{Sn}(\text{OH})_3$ fragment. The search recalls only one example of a $\text{Sn}(\eta^2\text{-CO}_3)$ group. Of course, the usual tendency for such groups is to dimerize or even polymerize.^[1-3]

In conclusion, we report a straightforward synthetic pathway that leads to a new series of trihydroxy tin trinuclear nickel clusters. The reactivity of these clusters is centered at the octahedrally coordinated tin atom. The $\text{Sn}(\text{OH})_3$ groups of clusters **2** and **5** resist oligomerization and display high nucleophilicity leading to reversible formation of an η^2 -carbonato-tin-capped cluster in the presence of CO_2 and ring opening of 1,2-epoxybutane to the corresponding tin-coordinated diolate.

Experimental Section

1: A solution of SnCl_2 (274 mg, 1.46 mmol) dissolved in THF was added to a mixture of $[\text{Ni}(\text{cod})_2]$ (400 mg, 1.46 mmol; cod = cyclo-octadiene), dppm (845 mg, 2.2 mmol), and $[\text{Ni}(\text{acac})_2]$ (186 mg, 0.73 mmol; acac = 2,4-pentanedione) in THF (20 mL). The solution turned dark-green immediately and a green precipitate appeared. The solid was collected by filtration and washed with diethyl ether. Recrystallization from CH_2Cl_2 /diethyl ether gave pure **1** (690 mg, 59 %). Elemental analysis (%) calcd for $\text{C}_{75}\text{H}_{66}\text{Cl}_4\text{Ni}_3\text{P}_6\text{Sn}$: C 56.66, H 4.18; found: C 56.29, H 4.88; $^{31}\text{P}\{^1\text{H}\}$ NMR (121 MHz, $[\text{D}_8]\text{THF}$, 295 K): $\delta = -2.3$ ppm (s, sat. $^2J_{(^{31}\text{P}-^{119}\text{Sn},^{117}\text{Sn})} = 138$ Hz (unresolved)).

2: Solid NaH (10 mg, 0.416 mmol) was suspended in a solution of **1** (200 mg, 0.125 mmol) dissolved in a mixture of CH_2Cl_2 /THF (3:2). Water (8 μL , 0.444 mmol) was injected through a septum into this suspension and H_2 evolved. After 2 h the reaction was complete (followed by ^{31}P NMR spectroscopy). The solvent was evaporated to dryness, and the residue was kept under vacuum overnight. Extraction with CH_2Cl_2 and evaporation of the solvent gave a deep-blue solid (150 mg, 73 %). Elemental analysis (%) calcd for $\text{C}_{77}\text{H}_{71}\text{Cl}_3\text{Ni}_3\text{O}_3\text{P}_6\text{Sn}$ (**2**- CH_2Cl_2): C 56.69, H 4.39; found: C 56.47, H 4.62. $^{31}\text{P}\{^1\text{H}\}$ NMR (121 MHz, $[\text{D}_8]\text{THF}$, 295 K): $\delta = -0.1$ ppm (s, sat. $^2J_{(^{31}\text{P}-^{119}\text{Sn},^{117}\text{Sn})} = 122$ Hz (unresolved)). IR (KBr): $\nu_{\text{OH}} = 3658$ cm^{-1} (br).

3: Carbon dioxide was bubbled through a solution of **2** (100 mg, 0.06 mmol) dissolved in CH_2Cl_2 (5 mL). The color of the solution changed from deep-blue to deep-purple immediately. Complete conversion was verified by ^{31}P NMR spectroscopy. Elemental analysis (%) calcd for $\text{C}_{77}\text{H}_{69}\text{Cl}_3\text{Ni}_3\text{O}_4\text{P}_6\text{Sn}$ (**3**- CH_2Cl_2): C 56.23, H 4.19; found: C 56.40, H 4.67; $^{31}\text{P}\{^1\text{H}\}$ NMR (121 MHz, $[\text{D}_8]\text{THF}$, 295 K): $\delta = 1.1$ ppm (s, sat. $^2J_{(^{31}\text{P}-^{119}\text{Sn},^{117}\text{Sn})} = 128$ Hz (unresolved)). IR (KBr): $\nu = 1634, 1669$ cm^{-1} .

5: Using cluster **6** as starting material (see below) and the same synthetic procedure described for cluster **2**, compound **5** was obtained as a deep-blue solid (110 mg, 64 %). Elemental analysis (%) calcd for $\text{C}_{75}\text{H}_{69}\text{BrNi}_3\text{O}_3\text{P}_6\text{Sn}$: C 57.05, H 4.40; found: C 58.34, H 4.95. $^{31}\text{P}\{^1\text{H}\}$ NMR (121 MHz, $[\text{D}_8]\text{THF}$, 295 K): $\delta = -1.1$ ppm (s, sat. $^2J_{(^{31}\text{P}-^{119}\text{Sn},^{117}\text{Sn})} = 115$ Hz (unresolved)); IR (KBr): $\nu_{\text{OH}} = 3668$ cm^{-1} (br).

$[\text{Ni}_3\{\mu\text{-P,P'-dppm}\}_3(\mu_3\text{-Br})(\mu_3\text{-SnBr}_3)]$ (**6**): Solid SnBr_2 (≈ 5 mg) was added to a suspension of KBr (42 mg, 0.36 mmol) in a solution of **1** (200 mg, 0.125 mmol) dissolved in THF (10 mL). After two days the reaction was complete (verified by ^{31}P NMR spectroscopy) and the color of the solution had changed from dark-green to brown-green. The volume was reduced by evaporation under vacuum to 5 mL, and diethyl ether (5 mL) was added. The solid was collected by filtration and washed with diethyl ether (175 mg, 75 %). Elemental analysis (%) calcd for $\text{C}_{79}\text{H}_{74}\text{Br}_4\text{Ni}_3\text{OP}_6\text{Sn}$ (**6**-THF): C 51.57, H 4.02; found: C

52.11, H 4.13. $^{31}\text{P}\{^1\text{H}\}$ NMR (121 MHz, $[\text{D}_8]\text{THF}$, 295 K): $\delta = -2.1$ (s, sat. $^2J_{(^{31}\text{P}-^{119}\text{Sn}, ^{117}\text{Sn})} = 140$ Hz (unresolved)).

7: 1,2-Epoxybutane (30 mg, 0.22 mmol) was added to a solution of cluster **5** (250 mg, 0.16 mmol) in THF (10 mL). The solution was gently heated and an immediate color change from deep-blue to turquoise was observed. The ^{31}P NMR spectrum shows no signal for the starting cluster **5** and only one singlet at $\delta = -1.9$ ppm (185 mg, 63 %).

MALDI-MS $[\text{Ni}_3(\text{dppm})_3\text{Br}\{\text{Sn}(\text{OH})[\text{OCH}_2\text{CH}(\text{C}_2\text{H}_5)\text{O}]\text{H}\}]^+$ 1633 m/z ; $^{31}\text{P}\{^1\text{H}\}$ NMR (121 MHz, $[\text{D}_8]\text{THF}$, 295 K): $\delta = -1.9$ ppm (s, sat. $^2J_{(^{31}\text{P}-^{119}\text{Sn}, ^{117}\text{Sn})} = 98$ Hz (unresolved)).

CCDC-250075–CCDC-250079 (**1**, **2**, **3**, **6**, and **7**) contain the supplementary crystallographic data for this paper. These data can be obtained free of charge from the Cambridge Crystallographic Data Centre via www.ccdc.cam.ac.uk/data_request/cif.

Received: September 27, 2004

Published online: January 4, 2005

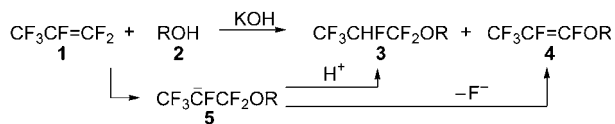
Keywords: carbon dioxide activation · cluster compounds · nickel · ring opening · tin

-
- [1] E. N. Suci, B. Kuhlmann, G. A. Knudsen, R. C. Michaelson, *J. Organomet. Chem.* **1998**, 556, 41.
 - [2] J. Janssen, J. Magull, H. W. Roesky, *Angew. Chem.* **2002**, 114, 1425; *Angew. Chem. Int. Ed.* **2002**, 41, 1365.
 - [3] M. A. Edelman, P. B. Hitchcock, M. F. Lappert, *J. Chem. Soc. Chem. Commun.* **1990**, 1116.
 - [4] B. K. Breedlove, P. E. Fanwick, C. P. Kubiak, *Inorg. Chem.* **2002**, 41, 4306.
 - [5] F. A. Cotton, G. Wilkinson in *Advanced Inorganic Chemistry*, 5th ed., Wiley, **1988**, pp. 90–94.
 - [6] T. Kimura, T. Sakurai, M. Shima, *Acta Crystallogr. Sect. B* **1982**, 38, 112.
 - [7] F. H. Allen, W. D. S. Motherwell, *Acta Crystallogr. Sect. B* **2002**, 58, 407.
 - [8] F. H. Allen, *Acta Crystallogr. Sect. B* **2002**, 58, 380.
 - [9] I. J. Bruno, J. C. Cole, P. R. Edgington, M. Kessler, C. F. Macrae, P. McCabe, J. Pearson, R. Taylor, *Acta Crystallogr. Sect. B* **2002**, 58, 389.
-

Palladium(0)-Catalyzed Hydroalkoxylation of Hexafluoropropene: Synthesis of Hydrofluoroethers under Neutral Conditions**

Yasuhisa Matsukawa, Junji Mizukado, Hengdao Quan, Masanori Tamura, and Akira Sekiya*

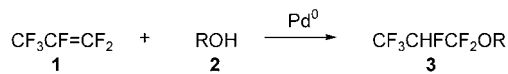
The development of alternatives to chlorofluorocarbons (CFCs) and hydrochlorofluorocarbons (HCFCs) has become an important and urgent issue. Hydrofluoroethers (HFEs) are excellent candidates as environmentally friendly replacements for refrigerants, cleaning solvents, or blowing agents characterized by low ozone-depletion and global-warming effects^[1] HFEs (R_FCHFCF_2OR) can be synthesized regioselectively by the addition of an alcohol to an industrially available fluorinated alkene such as tetrafluoroethylene (TFE) or hexafluoropropene (HFP; **1**) under strongly basic conditions.^[2] However, the β -fluorinated carbanion intermediates **5**, formed by the addition of alkoxides to fluorinated alkene **1**, lead to the production of unsaturated vinyl ethers **4** by β -fluoride elimination (Scheme 1).^[3]



Scheme 1. Hydroalkoxylation of HFP (**1**) under basic conditions.

In light of these environmental and safety aspects, we decided to investigate a new, alternative process to produce saturated ethers selectively under neutral conditions without the need for a basic medium. Here, we describe a novel Pd⁰-catalyzed hydroalkoxylation of the fluorinated alkene HFP (**1**) (Scheme 2).

Our first attempt to hydroalkoxylate HFP with trifluoroethanol in the presence of Pd^{II} salts such as PdCl₂ and



Scheme 2. Pd⁰-catalyzed hydroalkoxylation of HFP (**1**).

[*] Dr. Y. Matsukawa, Dr. J. Mizukado, Dr. H.-d. Quan, Dr. M. Tamura,
Dr. A. Sekiya
Research Institute for Sustainable Chemical Innovation
National Institute of Advanced Industrial Science and Technology
(AIST)
1-1-1 Higashi, Tsukuba, Ibaraki 305-8565 (Japan)
Fax: (+81) 29-861-4771
E-mail: y.matsukawa@aist.go.jp

[**] This research was supported by the New Energy and Industrial Technology Development Organization (NEDO)

Supporting information for this article is available on the WWW under <http://www.angewandte.org> or from the author.

$\text{Pd}(\text{OAc})_2$, the Wacker process, was unsuccessful.^[4] However, we found that Pd catalysts containing phosphane ligands, such as $[\text{PdCl}_2(\text{PPh}_3)_2]$ and $[\text{PdCl}_2(\text{P}(c\text{Hex})_3)_2]$, gave the expected ether $\text{CF}_3\text{CHF}(\text{CF}_2\text{OCH}_2\text{CF}_3)$ (**3a**) in 42 % and 49 % yield, respectively, after 72 h at 150 °C. Interestingly, the hydroalkoxylation of **1** was efficiently catalyzed by the Pd^0 complex $[\text{Pd}(\text{PPh}_3)_4]$, even at ambient temperature, provided that HFP was bubbled continuously through the system (Table 1).^[5]

Table 1: Pd^0 -catalyzed hydroalkoxylation of HFP (**1**).^[a]

Entry	ROH	t [h]	Product	Yield [%] ^[b]
1	$\text{CF}_3\text{CH}_2\text{OH}$ (2a)	18	3a	72
2	$\text{CF}_3\text{CF}_2\text{CH}_2\text{OH}$ (2b)	18	3b	73
3	$(\text{CF}_3)_2\text{CHOH}$ (2c)	18	3c	99
4 ^[c]	2c	46	3c	100
5	$\text{CCl}_3\text{CH}_2\text{OH}$ (2d)	18	3d	92
6 ^[d]	CH_3OH (2e)	24	3e	67
7 ^[d]	$\text{CH}_3\text{CH}_2\text{OH}$ (2f)	24	3f	46
8 ^[e]	PhCH_2OH (2g)	18	3g	9
9	$\text{C}_6\text{H}_5\text{OH}$ (2h)	18	3h	76
10 ^[f]	2h	3	3h	99
11	$\text{C}_6\text{F}_5\text{OH}$ (2i)	77	3i	41
12 ^[f]	2i	18	3i	100

[a] Unless otherwise specified, reactions of **1** (excess) with **2** (2 mmol) in acetonitrile (5 mL) were carried out in the presence of 5 mol % of $[\text{Pd}(\text{PPh}_3)_4]$ at room temperature. [b] Yields based on alcohols **2** calculated from the ^{19}F and ^1H NMR spectra with 1,4-bis(trifluoromethyl)benzene as an internal standard. [c] The reaction was carried out in the presence of 1 mol % of $[\text{Pd}(\text{PPh}_3)_4]$. [d] Acetonitrile (15 mL) was used as the solvent. [e] Production of trace amounts of benzaldehyde (3 %) was observed. [f] The reaction was conducted at 40–50 °C.

The reaction of an excess of HFP with acidic haloalcohols proceeded at room temperature to afford the corresponding ethers in good to excellent yields (Table 1, entries 1 to 5). In the case of poorly acidic alcohols, the corresponding ethers were obtained in only moderate yields (Table 1, entries 6 and 7). The reaction with benzyl alcohol (**2g**) gave ether **3g** in low yield (Table 1, entry 8).

The reaction with phenol (**2h**) also gave the ether $\text{CF}_3\text{CHF}(\text{CF}_2\text{OC}_6\text{H}_5)$ (**3h**) in 76 % yield (Table 1, entry 9). In the case of pentafluorophenol (**2i**), the reaction required a longer time and the ether $\text{CF}_3\text{CHF}(\text{CF}_2\text{OC}_6\text{F}_5)$ (**3i**) was obtained in only 41 % yield (Table 1, entry 11). At 40–50 °C these two phenol derivatives gave the corresponding ethers **3h** and **3i** in almost quantitative yields (Table 1, entries 10 and 12).

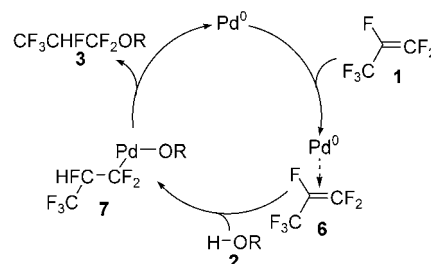
1,4-Bis(diphenylphosphanyl)butane (dppb) proved to be an effective ligand for the Pd^0 -catalyzed hydroalkoxylation of HFP—the $[\text{Pd}(\text{PPh}_3)_4]/\text{dppb}$ system enhanced the yields of the hydroalkoxylation with poorly acidic alcohols dramatically (Table 2).

Our results indicate the importance of the ability of the alcohols to act as a proton source and the electron donation from electron-rich Pd^0 species to HFP, which is enhanced by dppb. We propose the reaction mechanism for the Pd^0 -catalyzed hydroalkoxylation of HFP shown in Scheme 3.^[6] The electron-deficient alkene HFP coordinates to the electron-rich Pd^0 center to generate the η^2 -complex **6**. Subsequent

Table 2: Pd^0 -catalyzed hydroalkoxylation in the presence of dppb.^[a]

Entry	ROH	t [h]	Product	Yield [%] ^[b]
1	$\text{CF}_3\text{CH}_2\text{OH}$ (2a)	21	3a	84
2	$\text{CF}_3\text{CF}_2\text{CH}_2\text{OH}$ (2b)	21	3b	86
3	CH_3OH (2e)	24	3e	83
4	$\text{CH}_3\text{CH}_2\text{OH}$ (2f)	24	3f	78
5	PhCH_2OH (2g)	24	3g	82

[a] All reactions of **1** (excess) with **2** (2 mmol) in acetonitrile (15 mL) were carried out in the presence of 5 mol % of $[\text{Pd}(\text{PPh}_3)_4]$ and 10 mol % of dppb at room temperature. [b] Yields based on alcohols **2** calculated from the ^{19}F and ^1H NMR spectra with 1,4-bis(trifluoromethyl)benzene as an internal standard.



Scheme 3. Plausible mechanism for the Pd^0 -catalyzed hydroalkoxylation.

addition of a proton from alcohols **2** would give the intermediate **7**. Reductive elimination would then afford fluoroether **3** and regenerate the Pd^0 center. Continuous addition of **1** and dppb should enhance the formation of **6** and improve the yield. While acidic, fluorinated alcohols and phenols would stabilize intermediates **7**, the steric bulk of **2c** and **2d** might enhance the reductive elimination.

In summary, we have developed a Pd^0 -catalyzed hydroalkoxylation of a fluorinated alkene with various alcohols. This is the first example of the synthesis of saturated ethers by the addition of an alcohol to a $\text{C}=\text{C}$ double bond in the presence of a palladium(0) catalyst. In this process, which is performed under neutral conditions, saturated hydrofluoroethers are selectively obtained without any formation of vinyl ethers. This procedure might be the basis for an asymmetric synthesis of hydrofluoroethers. Studies of the scope and limitations of this reaction, as well as its mechanistic details, are in progress.

Received: October 5, 2004

Published online: January 11, 2005

Keywords: alcohols · fluorinated alkenes · green chemistry · hydroalkoxylation · palladium

[1] A. Sekiya, S. Misaki, *J. Fluorine Chem.* **2000**, *101*, 215.

[2] a) A. L. Henne, M. A. Smook, *J. Am. Chem. Soc.* **1950**, *72*, 4378; b) J. D. Park, W. M. Sweeney, S. L. Hopwood, Jr., J. R. Lacher, *J. Am. Chem. Soc.* **1956**, *78*, 1685; c) R. E. A. Dear, E. E. Gilbert, *J. Chem. Eng. Data* **1969**, *14*, 493; d) A. V. Fokin, V. A. Komarov, A. F. Kolomiets, A. I. Rapkin, O. V. Verenikin, T. M. Potarina, *Izv. Akad. Nauk SSSR Ser. Khim.* **1977**, *9*, 2141 [*Chem. Abstr.*

- 1977, 88, 22065]; e) J. Murata, M. Tamura, A. Sekiya, *Green Chem.* **2002**, 4, 60.
- [3] a) K. Okuhara, H. Baba, R. Kojima, *Bull. Chem. Soc. Jpn.* **1962**, 35, 532; b) H. Harada, N. Ishikawa, *J. Fluorine Chem.* **1978**, 11, 87.
- [4] For a recent review on Pd^{II}-catalyzed Wacker-type hydroalkoxylation, see: M. Beller, J. Seayad, A. Tillack, H. Jiao, *Angew. Chem.* **2004**, 116, 3448; *Angew. Chem. Int. Ed.* **2004**, 43, 3368, and references therein.
- [5] For the Pd⁰-catalyzed hydroalkoxylation of dienes or allenes to afford oligomerization products via cyclic palladium intermediates, see: a) E. J. Smutny, *J. Am. Chem. Soc.* **1967**, 89, 6793; b) H. Yagi, E. Tanaka, H. Ishiwatari, M. Hidai, Y. Uchida, *Synthesis* **1977**, 334; c) A. Krotz, F. Vollmüller, G. Stark, M. Beller, *Chem. Commun.* **2001**, 195; d) Y. Inoue, Y. Ohtsuka, H. Hashimoto, *Bull. Chem. Soc. Jpn.* **1984**, 57, 3345; For Pd⁰-catalyzed pronucleophilic addition to methylenecyclopropanes to afford allylic ethers via π -allyl palladium intermediates, see: e) D. H. Camacho, I. Nakamura, S. Saito, Y. Yamamoto, *Angew. Chem.* **1999**, 111, 3576; *Angew. Chem. Int. Ed.* **1999**, 38, 3365.
- [6] For an “anti-Wacker”-type mechanism for the hydroalkoxylation of diynes, see: D. H. Camacho, S. Saito, Y. Yamamoto, *Tetrahedron Lett.* **2002**, 43, 1085.

Natural Product Synthesis

Stereocontrolled Total Synthesis of (–)-Aurisides A and B**

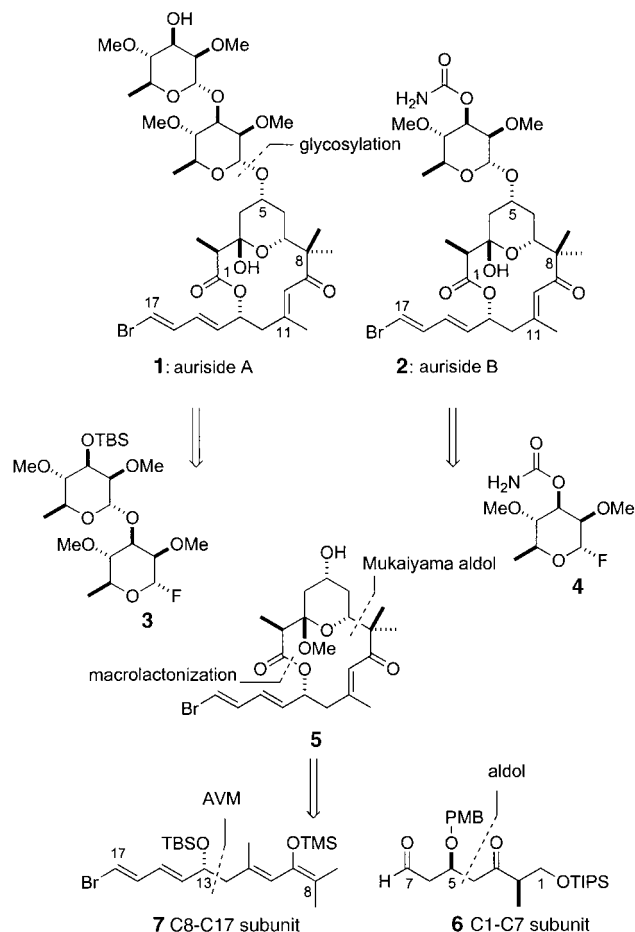
Ian Paterson,* Gordon J. Florence, Annekatrin C. Heimann, and Angela C. Mackay

Aurisides A (**1**) and B (**2**) are unique marine polyketides isolated in 1996 by Yamada and co-workers from the Japanese sea hare *Dolabella auricularia*,^[1a] an organism that has proved to be a rich source of bioactive secondary metabolites.^[2] Initial biological screening of **1** and **2** highlighted significant cytotoxicity, with IC₅₀ values against HeLa S₃ cervical cancer cell lines of 0.17 and 1.2 µg mL^{–1}, respectively. The aurisides are 14-membered glycosylated macrolides that contain a six-membered hemiacetal ring, an *E*-trisubstituted enone with an *E,E* bromodiene side chain appended at C13, and different sugar moieties attached at C5 (Scheme 1).

The unusual structure of the aurisides, combined with their biological activity and low natural abundance (0.8 mg of **1** was obtained from 278 kg of *D. auricularia*), has generated

growing interest in these compounds as synthetic targets.^[1b,3] In 1998, the Yamada group reported a synthesis of the aglycon unit, confirming their initial stereochemical assignment. The low yield of their route was the result of several problematic steps in its late stages.^[1b] Herein, we report the first total synthesis of aurisides A (**1**) and B (**2**) by appropriate attachment of the required sugar residue, which involves a highly convergent and expedient aldol-based route for the stereocontrolled construction of the common macrolide core.

As outlined in Scheme 1, our synthetic strategy relied on a late-stage, α -selective glycosylation of the equatorial C5



Scheme 1. Retrosynthetic analysis for the aurisides.

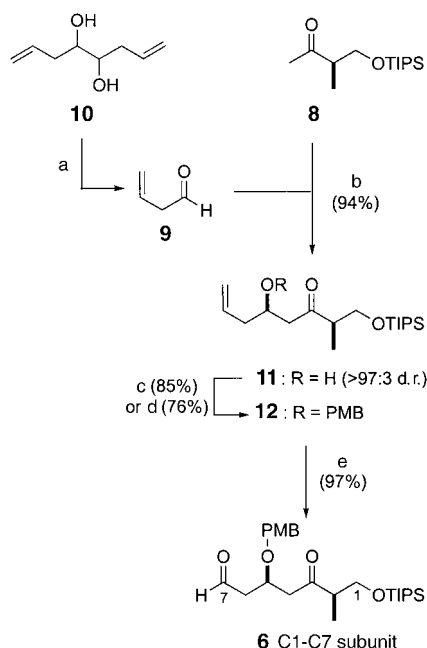
alcohol in lactone **5** with the fluorosugar **3** or **4**, each derived from L-rhamnose. The macrocyclic lactone, in turn, was envisaged to arise from a stereocontrolled Mukaiyama aldol coupling between aldehyde **6** (C1–C7) and silyl enol ether **7** (C8–C17) containing a bromodiene terminus, followed by a suitable macrolactonization step. Introduction of the remote C13 stereocenter in **7** was planned to rely on the application of an asymmetric vinylogous Mukaiyama (AVM) aldol reaction,^[4] while the C5 center in **6** would also be installed by a suitable aldol reaction.^[5]

As shown in Scheme 2, the synthesis of the C1–C7 subunit **6** began with a highly stereoselective boron-mediated aldol reaction of the readily available methyl ketone **8**^[6] with 3-

[*] Prof. Dr. I. Paterson, Dr. G. J. Florence, A. C. Heimann, Dr. A. C. Mackay
University Chemical Laboratory
Lensfield Road, Cambridge, CB2 1EW (UK)
Fax: (+44) 1223-336-362
E-mail: ip100@cam.ac.uk

[**] This research was supported by the EPSRC, Emmanuel College, Cambridge (Research Fellowship to G.J.F.), the EC (Network HPRN-CT-2000-18), and Merck Research Laboratories.

Supporting information for this article is available on the WWW under <http://www.angewandte.org> or from the author.

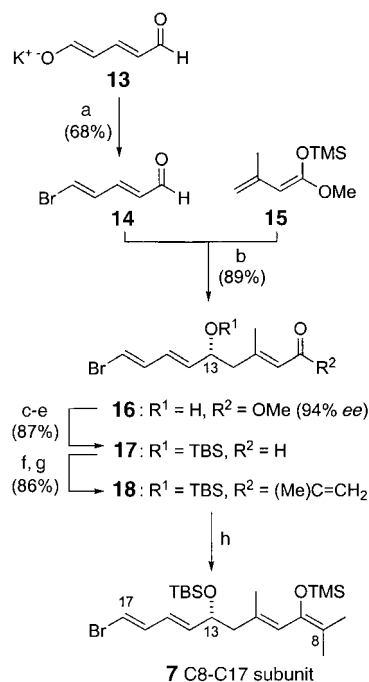


Scheme 2. Synthesis of the C1–C7 subunit **6**. a) NaIO_4 , CH_2Cl_2 , pH 4 buffer, 0°C , 3 h; b) 1. $(+)$ - Ipc_2BCl , Et_3N , Et_2O , 0°C , 1 h; 2. **9**, CH_2Cl_2 , $-78^\circ\text{C} \rightarrow -27^\circ\text{C}$, 2.5 h; 3. H_2O_2 (30% aq), pH 7 buffer, MeOH , $0^\circ\text{C} \rightarrow \text{RT}$, 1 h; c) PMBTCA, TfOH (0.3 mol%), Et_2O , room temperature, 3 h; d) PMBTCA, $\text{Sc}(\text{OTf})_3$ (1 mol%), PhMe , 0°C , 15 min; e) O_3 , NaHCO_3 , CH_2Cl_2 , -78°C , 10 min; then PPh_3 , $-78^\circ\text{C} \rightarrow \text{RT}$, 3 h. $\text{Ipc} =$ isopinocampheyl, PMBTCA = *para*-methoxybenzyltrichloroacetimidate, Tf = trifluoromethanesulfonyl, TIPS = triisopropylsilyl.

butenal (**9**), derived from the oxidative cleavage of 1,2-glycol **10**.^[7] Enolization of **8** with $(+)$ - $\text{Ipc}_2\text{BCl}/\text{Et}_3\text{N}$,^[6,8] followed by the addition of a freshly prepared anhydrous solution of **9** at -78°C , provided the corresponding 1,4-*syn* aldol adduct **11** (94%, >97:3 d.r.). Treatment of **11** with PMBTCA in the presence of catalytic TfOH in Et_2O at room temperature afforded the PMB ether **12** in 85% yield.^[9] Alternatively, use of $\text{Sc}(\text{OTf})_3$ in toluene at 0°C provided **12** in 76% yield on a multigram scale,^[10] with decreased by-product formation. Subsequent ozonolysis of **12** with reductive PPh_3 workup gave the 1,5-ketoaldehyde **6** in 97% yield.

Synthesis of the C8–C17 subunit **7** (Scheme 3) commenced with the bromination of potassium glutacetaldehyde (**13**),^[11] according to the method of Duhamel and co-workers.^[12] Treatment of **13** with Br_2 and PPh_3 provided the corresponding *E,E* bromodienal **14** (68%). The stage was now set for the critical AVM reaction between **14** and silyl dienolate **15**^[13] to introduce the C13 stereocenter, along with the 10*E*-trisubstituted alkene functionality.^[5,14] Gratifyingly, treatment of aldehyde **14** with $[(R)\text{-binol-Ti}(\text{OiPr})_2]$ (50 mol%) in THF at -78°C , generated in situ from (R) -binol and $\text{Ti}(\text{OiPr})_4$, followed by addition of silyl dienolate **15** provided the vinylogous aldol adduct **16** exclusively in 89% yield and 94% *ee*.

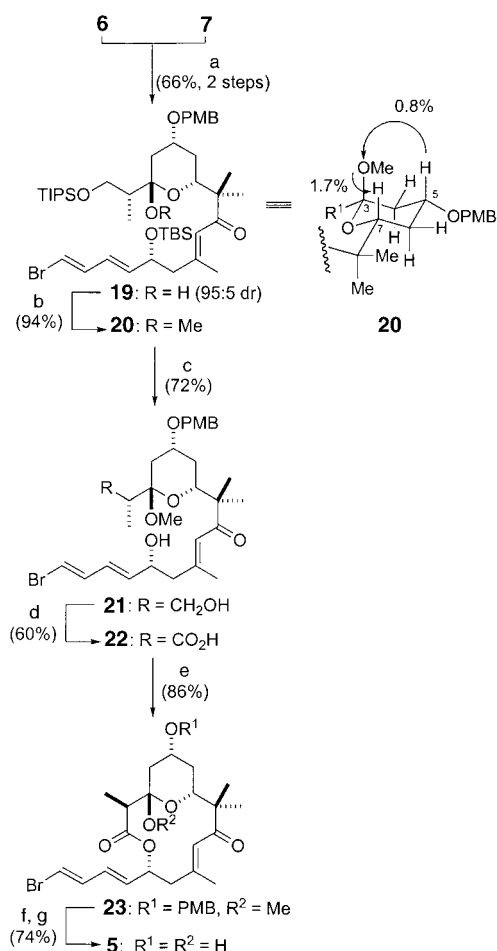
TBS ether formation on the alcohol **16** was followed by conversion into aldehyde **17** by treatment with DIBAL. Subsequent reoxidation with MnO_2 proceeded in 87% yield. Addition of isopropenyl magnesium bromide to **17** and oxidation of the resulting alcohol with MnO_2 provided



Scheme 3. Synthesis of the C8–C17 subunit **7**. a) Br_2 , PPh_3 , CH_2Cl_2 , $0^\circ\text{C} \rightarrow \text{RT}$, 4 h; b) $\text{Ti}(\text{OiPr})_4$ (50 mol%), (R) -binol (50 mol%), CaH_2 , THF, -78°C , 72 h; c) TBSCl , imidazole, CH_2Cl_2 , room temperature, 4 h; d) DIBAL, CH_2Cl_2 , -78°C , 2 h; e) MnO_2 , Et_2O , room temperature, 3 h; f) $\text{CH}_2=\text{CH}(\text{Me})\text{MgBr}$, THF, $-78^\circ\text{C} \rightarrow 0^\circ\text{C}$, 1.5 h; g) MnO_2 , Et_2O , room temperature, 5 h; h) *L*-Selectride, CaH_2 , THF, -78°C , 15 min; $\text{TMSCl-Et}_3\text{N}$, $-78^\circ\text{C} \rightarrow -20^\circ\text{C}$, 45 min. Binol = 1,1'-bi(2-naphthol), TBS = *tert*-butyldimethylsilyl, DIBAL = diisobutylaluminum hydride, *L*-Selectride = lithium tri-*sec*-butylborohydride, TMS = trimethylsilyl.

enone **18** (86%), anticipated as a direct precursor to the silyl enol ether **7**. Initial attempts at this transformation employing Chan hydrosilylation,^[15] $\text{LiAlH}_4/\text{CuI}/\text{TMSCl}$,^[16] or the Stryker reagent^[17] proved unsuccessful. However, when **18** was subjected to *L*-Selectride in THF at -78°C , regioselective 1,4-reduction of the less sterically encumbered enone was observed. The resultant enolate was quenched with TMSCl to provide the C8–C17 subunit **7**, which was used directly in the subsequent coupling step.

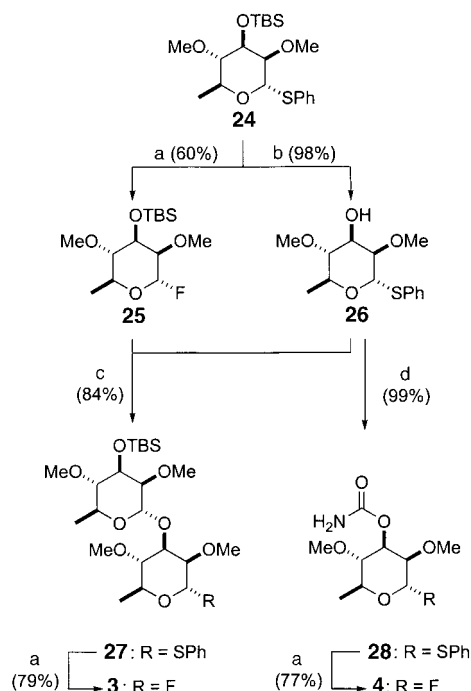
With key subunits **6** and **7** in hand, attention was focused on their Mukaiyama-type aldol union to introduce the C7 stereocenter, relying on 1,3-*anti* induction from the C5 ether through an open transition state, following the Evans polar model,^[18] thus completing the carbon backbone of aglycon **5** (Scheme 4). In practice, exposure of **6** and **7** to $\text{BF}_3 \cdot \text{Et}_2\text{O}$ in CH_2Cl_2 at -95°C provided the adduct in 66% yield (from **18**) with 95:5 d.r. which was present in solution in the closed hemiacetal form **19**. Treatment of **19** with PPTS, $(\text{MeO})_3\text{CH}$, and MeOH cleanly provided methyl acetal **20**. To confirm the stereochemistry of **20**, irradiation of 5-H provided a diagnostic NOE interaction with the C3-OMe, consistent with their 1,3-diaxial relationship, whereas irradiation of the C3-OMe in turn, provided a further NOE interaction with 7-H. Cleavage of the silyl ethers with TASF in wet DMF gave diol **21** (72%).^[19] Selective oxidation of the C1 terminus to *seco* acid **22** was next attempted and required careful optimization. Under the conditions developed by Piancatelli and co-work-



Scheme 4. Synthesis of the auriside aglycon **5**. a) $\text{BF}_3 \cdot \text{OEt}_2$, CaH_2 , CH_2Cl_2 , -95°C , 10 min; b) PPTS (20 mol %), $\text{CH}(\text{OMe})_3$, MeOH, room temperature, 4 h; c) TASF, H_2O , DMF, $0 \rightarrow 15^\circ\text{C}$, 5 h; d) 1. TEMPO, $\text{PhI}(\text{OAc})_2$, MeCN, pH 7 buffer, 6 h; 2. NaClO_2 , NaH_2PO_4 , $t\text{BuOH}$, H_2O , 2-methyl-2-butene, room temperature, 30 min; e) 1. 2,4,6-trichlorobenzoyl chloride, Et_3N , PhMe, room temperature, 1 h; 2. DMAP, room temperature, 4 h; f) DDQ, CH_2Cl_2 , pH 7 buffer, room temperature, 30 min; g) $p\text{TsOH} \cdot \text{H}_2\text{O}$, THF, H_2O , room temperature, 16 h. PPTS = pyridinium *p*-toluenesulfonate, TASF = (diethylamino)sulfur trifluoride, DMF = *N,N*-dimethylformamide, TEMPO = 4-amino-2,2,6,6-tetramethylpiperidine-1-oxyl, DMAP = 4-*N,N*-dimethylaminopyridine, DDQ = 2,3-dichloro-5,6-dicyano-1,4-benzoquinone, *pTsOH* = *para*-toluenesulfonic acid.

ers,^[20] treatment of **21** with TEMPO and $\text{PhI}(\text{OAc})_2$ in MeCN/pH7 buffer (5:1) provided the intermediate aldehyde, which was further oxidized with NaClO_2 to give **22** in 60% yield. This intermediate readily underwent Yamaguchi macrolactonization to provide the desired 14-membered macrocycle **23** cleanly (86%).^[21] Cleavage of the PMB ether with DDQ and hydrolysis of the methyl acetal then afforded auriside aglycon **5** in 74% yield. At this stage, the ^1H and ^{13}C NMR spectroscopic data and specific rotation agreed with those reported by the Yamada group.^[1b]

With aglycon **5** in hand, attention was now directed toward the preparation of the activated fluorosugar units **3** and **4** (Scheme 5). Following work reported by the Nicolaou group, a nine-step sequence starting from L-rhamnose was

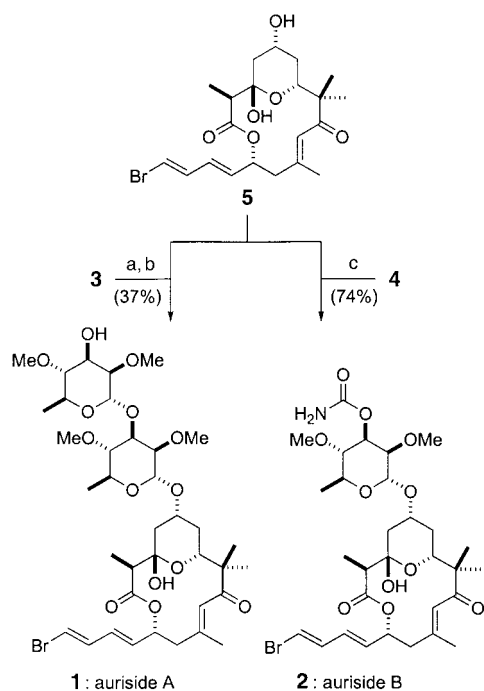


Scheme 5. Synthesis of fluorosugar units **3** and **4**. a) DAST, NBS, -15°C , 15 min; b) TBAF, THF, $0^\circ\text{C} \rightarrow \text{RT}$, 4 h; c) SnCl_4 , AgClO_4 , molecular sieves (4 Å), Et_2O , $0^\circ\text{C} \rightarrow \text{RT}$, 4 h; d) $\text{Cl}_3\text{CC}(\text{O})\text{NCO}$, CH_2Cl_2 , room temperature, 1 h; K_2CO_3 , MeOH, room temperature, 2 h. DAST = (diethylamino)sulfur trifluoride, NBS = *N*-bromosuccinimide, TBAF = tetrabutylammonium fluoride.

used to access common precursor **24**.^[22,23] Formation of the disaccharide **3** began with the activation of **24** with DAST/NBS to provide exclusively α -fluorosugar **25** in 60% yield.^[24] Mukaiyama glycosylation between **25** and **26**,^[25] obtained by deprotection of **24** with TBAF, provided **27** as the α -anomer exclusively (84%). Activation of **27** with DAST/NBS then afforded **3** in 79% yield. The fluorosugar **4** required for auriside B (**2**) was readily synthesized in 77% yield by treatment of **26** with trichloroacetyl isocyanate to afford carbamate **28** (99%),^[26] followed by activation with DAST/NBS.

Completion of the total synthesis, as shown in Scheme 6, required the coupling of aglycon **5** with either activated sugar **3** or **4** to directly provide auriside A (following silyl deprotection) and auriside B, respectively. Under the Mukaiyama protocol, the reaction of **3** and **5** followed by desilylation with $\text{HF} \cdot \text{pyr}$ afforded (–)-auriside A (**1**) in 37% yield ($[\alpha]_D^{20} = -16.3$ ($c = 0.033$ in MeOH) Ref. [1a] -43.0 ($c = 0.050$ in MeOH)). Similarly, the reaction of **4** and **5** proceeded smoothly to afford (–)-auriside B in 74% yield ($[\alpha]_D^{20} = -21.6$ ($c = 0.10$ in MeOH), Ref. [1a] -30.0 ($c = 0.090$ in MeOH)). In each case, analytical data (^1H , ^{13}C NMR and IR spectroscopy, MS, and specific rotation) for the synthetic material were in excellent agreement with those reported for natural aurisides A and B, allowing confirmation of the relative and absolute configurations of these compounds.^[27]

In conclusion, we have completed an expedient total synthesis of (–)-aurisides A and B that proceeds in 18 steps (1.7% overall yield) and 17 steps (3.5% overall yield),



Scheme 6. Completion of the total synthesis of aurisides A (**1**) and B (**2**). a) SnCl_2 , AgClO_4 , molecular sieves (4 Å), Et_2O , $0^\circ\text{C} \rightarrow \text{RT}$, 16 h; b) $\text{HF}:\text{py}$, THF, $0^\circ\text{C} \rightarrow \text{RT}$, 16 h; c) SnCl_2 , AgClO_4 , molecular sieves (4 Å), Et_2O , $0^\circ\text{C} \rightarrow \text{RT}$, 8 h.

respectively. By building the *E,E* bromodiene of the side chain into the silyl enol ether **7**, the key Mukaiyama aldol coupling with aldehyde **6** delivers the advanced intermediate **19** in a highly convergent manner. This can then be converted into the aurisides by α -selective glycosylation of the derived macrolide core **5** with the fluorosugars **3** and **4**. This work also highlights an efficient enantioselective vinylogous Mukaiyama aldol reaction, which in tandem with our diastereoselective boron-mediated aldol methodology provides a rapid synthetic entry into this structurally unique class of bioactive marine macrolides.

Received: October 11, 2004

Published online: January 21, 2005

Keywords: aldol reaction · antitumor agents · glycosylation · natural products · total synthesis

- [1] a) H. Sone, H. Kigoshi, K. Yamada, *J. Org. Chem.* **1996**, *61*, 8956; b) H. Sone, K. Suenaga, Y. Bessho, T. Kondo, H. Kigoshi, K. Yamada, *Chem. Lett.* **1998**, 85.
- [2] For examples of other bioactive and structurally unique secondary metabolites isolated from *Dolabella auricularia*, see: a) dolastatins: G. R. Pettit, Y. Kamano, C. L. Herald, Y. Fujii, H. Kizu, M. R. Boyd, F. E. Boettner, D. L. Doubek, J. M. Schmidt, J.-C. Chapuis, C. Michel, *Tetrahedron* **1993**, *49*, 9151; H. Sone, T. Shibata, T. Fujita, M. Ojika, K. Yamada, *J. Am. Chem. Soc.* **1996**, *118*, 1874; b) dolabelides: M. Ojika, T. Nagoya, K. Yamada, *Tetrahedron Lett.* **1995**, *36*, 7491; c) dolabellin: H. Sone, T. Kondo, M. Kiryu, H. Ishiwata, M. Ojika, K. Yamada, *J. Org. Chem.* **1995**, *60*, 4774.

- [3] a) M. Romero-Ortega, D. A. Colby, H. F. Olivo, *Tetrahedron Lett.* **2002**, *43*, 6439; b) H. F. Olivo, F. Velazquez, M. Romero, Y. Rios, *Abstr. Pap. Am. Chem. S.* 225: 311-ORGN, Part 2, MAR 2003; c) D. Y. Gin, H. M. Nguyen, *Abstr. Pap. Am. Chem. S.* 225: 245-ORGN Part 2, MAR 2003.
- [4] I. Paterson, R. D. M. Davies, A. C. Heimann, R. Marquez, A. Meyer, *Org. Lett.* **2003**, *5*, 4477.
- [5] For a review, see: C. J. Cowden, I. Paterson, *Org. React.* **1997**, *51*, 1.
- [6] Methyl ketone **8** was prepared in 96% yield over three steps from methyl(*R*)-3-hydroxy-2-methylpropionate: 1) TIPSCl, imidazole, CH_2Cl_2 , room temperature, 16 h; 2) $\text{MeONHMe}\cdot\text{HCl}$, $i\text{PrMgCl}$, THF, -20°C , 1 h; 3) MeMgBr , THF, 0°C , 1 h. We have previously reported the use of *ent*-**8** in the context of our spongistatin work: I. Paterson, R. M. Oballa, *Tetrahedron Lett.* **1997**, *38*, 8241.
- [7] 1,2-Glycol **10** was prepared from glyoxal (Sn, allyl bromide, sonication, room temperature, 3 h): a) M. T. Crimmins, S. J. Kirincich, A. J. Wells, A. L. Choy, *Synth. Commun.* **1998**, *28*, 3675; b) M. T. Crimmins, A. L. Choy, *J. Am. Chem. Soc.* **1999**, *121*, 5653.
- [8] a) I. Paterson, J. M. Goodman, M. Isaka, *Tetrahedron Lett.* **1989**, *30*, 7121; b) I. Paterson, J. M. Goodman, M. A. Lister, R. C. Schumann, C. K. McClure, R. D. Norcross, *Tetrahedron* **1990**, *46*, 4663.
- [9] T. Iverson, D. R. Bundle, *J. Chem. Soc. Chem. Commun.* **1981**, 1240.
- [10] A. N. Rai, A. Basu, *Tetrahedron Lett.* **2003**, *44*, 2267.
- [11] Potassium glutacetaldehyde **13** was prepared from pyridinium-1-sulfonate in 61% yield: J. Becher, *Synthesis* **1980**, 589.
- [12] a) D. Soulez, G. Ple, L. Duhamel, P. Duhamel, *J. Chem. Soc. Chem. Commun.* **1995**, 563; b) D. Soulez, G. Ple, L. Duhamel, *J. Chem. Soc. Perkin Trans. 1* **1997**, 1639.
- [13] J. Savard, P. Brassard, *Tetrahedron* **1984**, *40*, 3455.
- [14] For a review of the vinylogous aldol reaction, see: G. Casiraghi, F. Zanardi, G. Appendino, G. Rassu, *Chem. Rev.* **2000**, *100*, 1929.
- [15] T. H. Chan, G. Z. Zheng, *Tetrahedron Lett.* **1993**, *34*, 3095.
- [16] E. C. Ashby, J.-J. Lin, R. Kovar, *J. Org. Chem.* **1976**, *41*, 1939.
- [17] W. S. Mahoney, D. M. Brestensky, J. M. Stryker, *J. Am. Chem. Soc.* **1988**, *110*, 291.
- [18] D. A. Evans, M. J. Dart, J. L. Duffy, M. G. Yang, *J. Am. Chem. Soc.* **1996**, *118*, 4322.
- [19] K. A. Scheidt, H. Chen, B. C. Follows, S. R. Chemler, D. S. Coffey, W. R. Roush, *J. Org. Chem.* **1998**, *63*, 6436; under other silyl deprotection conditions, complete decomposition of **20** was observed.
- [20] A. DeMico, R. Margarita, L. Parlanti, A. Vescovi, G. Piancatelli, *J. Org. Chem.* **1997**, *62*, 6974.
- [21] J. Inanaga, K. Hirata, T. Saeki, T. Katsuki, M. Yamaguchi, *Bull. Chem. Soc. Jpn.* **1979**, *52*, 1989.
- [22] For a Review, see: K. C. Nicolaou, H. J. Mitchell, *Angew. Chem.* **2001**, *113*, 1624; *Angew. Chem. Int. Ed.* **2001**, *40*, 1576.
- [23] a) R. E. Dolle, K. C. Nicolaou, *J. Am. Chem. Soc.* **1985**, *107*, 1691; b) R. E. Dolle, K. C. Nicolaou, *J. Am. Chem. Soc.* **1985**, *107*, 1695.
- [24] K. C. Nicolaou, A. Chucholowski, R. E. Dolle, J. L. Randall, *J. Chem. Soc. Chem. Commun.* **1984**, 1155.
- [25] T. Mukaiyama, Y. Murai, S. Shoda, *Chem. Lett.* **1981**, 431.
- [26] P. Kocovsky, *Tetrahedron Lett.* **1986**, *27*, 5521.
- [27] Copies of ^1H and ^{13}C NMR spectra for aglycon **5** and aurisides A (**1**) and B (**2**) are provided in the Supporting Information.

Nanoscale Tubules in Uranyl Selenates**

Sergey V. Krivovichev,* Volker Kahlenberg,
Reinhard Kaindl, Edgar Mersdorf, Ivan G. Tananaev,
and Boris F. Myasoedov

Since the discovery of carbon nanotubes in 1991,^[1] a great deal of attention has been devoted to the synthesis and characterization of inorganic nanotubes.^[2] In particular, oxidic nanotubes exhibit interesting properties and hold promise for potential applications. Such nanotubes have been prepared for a variety of chemical systems, including vanadium oxides,^[3] titania,^[4] niobium oxides,^[5] and rare-earth oxides.^[6] One of the most accepted models of formation of nanotubes is the rolling and folding-up of single-layer sheets of the corresponding prototype lamellar materials.^[2c,7] Thus, it is generally possible to prepare nanotubes and nanoscrolls from any lamellar material that can be exfoliated into separate nanosheets.^[7] Among inorganic materials, layered structures are especially prevalent for hexavalent uranium oxo compounds^[8] owing to the strong tendency of the U^{6+} ion to form linear uranyl ions, UO_2^{2+} . This tendency leads to a highly anisotropic distribution of chemical bonds within $\{U^{VI}O_n\}$ coordination polyhedra,^[9] and, in particular, favors their condensation through longer U–O bonds lying in the equatorial plane relative to the uranyl ions. Despite the abundance of layered structures for U^{VI} oxo compounds, there are no reports of their ability to form tubular objects. Here, we report the synthesis and structure of $K_5[(UO_2)_3(SeO_4)_5](NO_3)(H_2O)_{3.5}$ (**1**), which is a new compound based upon nanoscale uranyl selenate tubules.

The uranyl selenate-nitrate **1** was obtained as small, greenish-yellow, transparent crystals (Figure 1) from the room-temperature reaction of uranyl nitrate, K_2CO_3 , and H_2SeO_4 in aqueous solution.^[10] The structure of **1**^[11] was found to be highly unusual for inorganic oxo compounds with triangular and tetrahedral oxoanions such as NO_3^- , SeO_3^{2-} , SO_4^{2-} , SeO_4^{2-} , CrO_4^{2-} , MoO_4^{2-} , PO_4^{3-} , AsO_4^{3-} , etc. It is based upon tubules parallel to the *a* axis that consist of corner-sharing $\{UO_7^{8-}\}$ pentagonal bipyramids and $\{SeO_4^{2-}\}$ tetra-

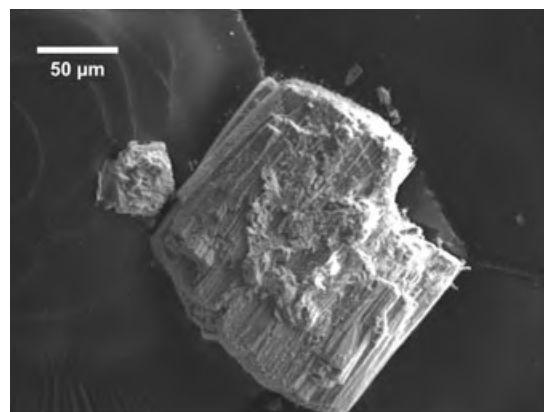


Figure 1. SEM image of a crystal of **1**.

dra (Figure 2). Each $\{UO_7^{8-}\}$ pentagonal bipyramid shares its five equatorial corners with adjacent $\{SeO_4^{2-}\}$ tetrahedra, whereas each $\{SeO_4^{2-}\}$ tetrahedron is linked to three adjacent

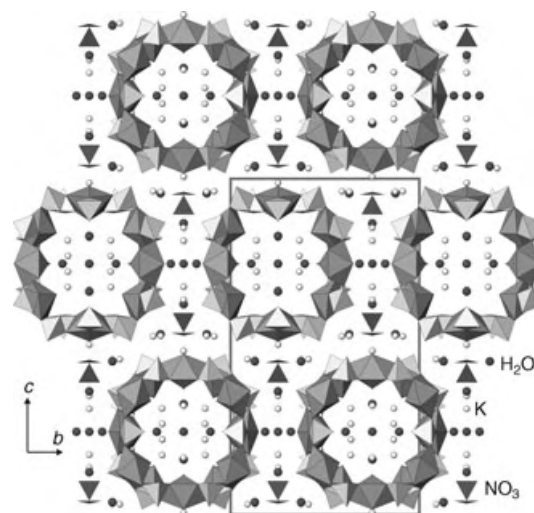


Figure 2. Crystal structure of **1** projected along the *a* axis. $\{UO_7^{8-}\}$ bipyramids are dark grey, $\{SeO_4^{2-}\}$ tetrahedra are light grey.

uranyl bipyramids. The composition of the tubule is $[(UO_2)_3(SeO_4)_5]^{4-}$, with a U/Se ratio of 3:5. The interiors of the tubules are occupied by K^+ ions and H_2O molecules, and there are additional K^+ ions and H_2O molecules, as well as NO_3^- groups, between the tubules. Within the $\{UO_7^{8-}\}$ bipyramids, the U–O bonds corresponding to the uranyl cations are in the range of 1.75–1.77 Å, whereas 2.36 to 2.45 Å are observed for the equatorial U–O bonds. The mean Se–O bond lengths within the $\{SeO_4^{2-}\}$ tetrahedra are in the range of 1.625–1.624 Å. The bond-valence sums for the U^{6+} and Se^{6+} positions^[9] are in the range of 5.75–6.24 valence units. The $\{UO_7^{8-}\}$ bipyramids are distorted, with a nonplanar arrangement of the equatorial U–O bonds that is undoubtedly a consequence of the tubular character of the uranyl selenate unit.

The size of the uranyl selenate $[(UO_2)_3(SeO_4)_5]^{4-}$ tubules in the structure of **1** is on the nanoscale. The external diameter

[*] Prof. Dr. S. V. Krivovichev
Department of Crystallography, St. Petersburg State University
University Emb. 7/9, 199034 St. Petersburg (Russia)
Fax: (+43) 512-5072926
E-mail: skrivovi@mail.ru

Prof. Dr. V. Kahlenberg, Dr. R. Kaindl, E. Mersdorf
Institut für Mineralogie und Petrographie
Universität Innsbruck
Innrain 52, 6020 Innsbruck (Austria)
Dr. I. G. Tananaev, Acad. B. F. Myasoedov
Institute of Physical Chemistry
Russian Academy of Sciences
Leninskiy prospect 31, 119991 Moscow (Russia)

[**] This work was financially supported by the Austrian Science Fund (FWF) (project M771-N10). We thank Prof. Dr. Ulrich Griesser for his help with the IR measurements.

of the tubule is 17 Å (1.7 nm), whereas its internal diameter, measured as the distance between the closest oxygen atoms across the cavity, is 7.4 Å (0.74 nm). The latter value provides a crystallographic free-diameter of 4.7 Å, which is similar to those of the small-pore zeolites^[12] and other molecular sieves such as titanosilicate ETS-4.^[13]

The topology of the $[(\text{UO}_2)_3(\text{SeO}_4)_5]^{4-}$ nanoscale tubules found in the structure of **1** can be described by means of a nodal representation that is especially suitable for the description of structures based upon coordination polyhedra of two types.^[14] In this approach, the $\{\text{UO}_7^{8-}\}$ bipyramids and $\{\text{SeO}_4^{2-}\}$ tetrahedra are symbolized by black and white vertices, respectively, and the vertices are linked by a line segment if two respective polyhedra share a common oxygen atom. The black-and-white graph corresponding to the topological structure of the $[(\text{UO}_2)_3(\text{SeO}_4)_5]^{4-}$ tubule is shown in Figure 3a; its idealized, unfolded version is given in Figure 3b. To obtain the tubular graph corresponding to the $[(\text{UO}_2)_3(\text{SeO}_4)_5]^{4-}$ tubule (Figure 3a, c), one has to cut the graph into tapes along the lines indicated in Figure 3b, fold the tape, and glue its sides accordingly.

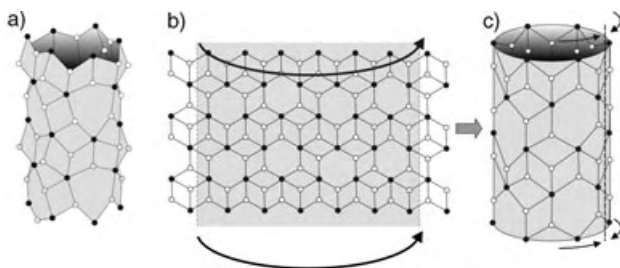


Figure 3. Nodal representation of the uranyl selenate tubule in the structure of **1** (a), its prototype 2D graph (b), and its idealized folded version (c). $\{\text{UO}_7^{8-}\}$ bipyramids and $\{\text{SeO}_4^{2-}\}$ tetrahedra are symbolized by black and white vertices, respectively.

Most of the inorganic nanotubes known have a prototype layered material from which they can be (at least theoretically) obtained by exfoliation of single-layer sheets and their folding up into a tube. The same holds for the uranyl selenate nanoscale tubules observed in the structure of **1**. The 3:5 black-and-white graph shown in Figure 3b is an underlying topology for a number of $[(\text{UO}_2)_3(\text{TO}_4)_5]^{4-}$ sheets found in the structures of inorganic oxo salts where T is S,^[15] Cr,^[16] or Se.^[17] However, to define the topology of a sheet by means of its nodal representation is not enough to define its complete topological structure.^[16,17] The point is that each $\{\text{TO}_4^{2-}\}$ tetrahedron in the sheet is three-connected, that is, it shares three of its four corners with adjacent $\{\text{UO}_7^{8-}\}$ bipyramids, thus leaving the fourth corner unshared. This gives rise to four classes of geometrical isomers of the $[(\text{UO}_2)_3(\text{TO}_4)_5]^{4-}$ sheets that differ in the orientation sequences of the tetrahedra (see ref. [16] for more details). Interestingly, none of the geometrical isomers observed in the layered phases corresponds directly to tetrahedra orientation of the uranyl selenate tubule observed in **1**. Exactly four of the five tetrahedra forming the tubule have their unshared corners oriented outside relative to the wall, whereas only one is oriented

inside. This specificity of the topological structure of the tubule is a consequence of its cylindrical topology.

To be able to fold up into a tube, uranyl selenate units must possess geometrical flexibility. It has been shown^[18] that the structural units observed in the structures of uranyl compounds with tetrahedral TO_4^{2-} oxoanions (T = S, Cr, Se, Mo) are very flexible. This results in a variety of topologically different structures^[14] and a number of reconstructive^[19] and displacive^[20] phase transitions. It is therefore not surprising that the U-O-T links are flexible enough to permit folding of a layered fragment into a tubule.

We note that the $[(\text{UO}_2)_3(\text{SeO}_4)_5]^{4-}$ tubules observed in the structure of **1** cannot be referred to as nanotubes as this term is reserved for materials with the corresponding morphology,^[2c] that is, for free-standing, nanoscale tubular objects. However, all known examples of tubular objects found in inorganic systems have their counterparts in the world of nanotubes (e.g. vanadium oxide nanotubes,^[3,21] molybdenum sulfide nanotubes,^[22] etc.). It should be mentioned that single crystals composed of highly ordered arrays of single-walled carbon nanotubes have also been obtained.^[23] Remškar^[24] has reported that nanotubes with diameters less than a few tenths of a micrometer show a strong tendency to self-assemble, that is, to form ordered, crystalline structures that can be observed by X-ray diffraction techniques. These observations indicate that the fabrication of free-standing uranium oxido nanotubes is highly likely under the appropriate conditions. This opens up a new area of research on uranium and actinide nanomaterials with possible applications in nanotechnology. In particular, this may lead to new solutions for the problem of utilization of depleted uranium, hundreds of thousands of tons of which is now stored by nuclear powers such as the U.S. and Russia.

In conclusion, we have succeeded in preparing a new inorganic material with a structure based upon nanoscale uranyl selenate tubules. It is the first example of a nanotubular structure observed for uranium compounds and the first example of an ordered nanotubular object observed in the structures of inorganic oxo salts.

Received: October 19, 2004

Published online: January 11, 2005

Keywords: nanotubes · oxides · selenium · solid-state structures · uranium

[1] S. Iijima, *Nature* **1991**, 354, 56.

[2] a) R. Tenne, M. Homyonfer, Y. Feldman, *Chem. Mater.* **1998**, 10, 3225; b) W. Tremel, *Angew. Chem.* **1999**, 111, 2311; *Angew. Chem. Int. Ed.* **1999**, 38, 2175; R. Tenne, *Chem. Eur. J.* **2002**, 8, 5297; c) G. R. Patzke, F. Krumeich, R. Nesper, *Angew. Chem.* **2002**, 114, 2554; *Angew. Chem. Int. Ed.* **2002**, 41, 2446; d) R. Tenne, *Angew. Chem.* **2003**, 115, 5280; *Angew. Chem. Int. Ed.* **2003**, 42, 5124; e) C. N. R. Rao, M. Nath, *Dalton Trans.* **2003**, 1; f) M. Remškar, *Adv. Mater.* **2004**, 16, 1497.

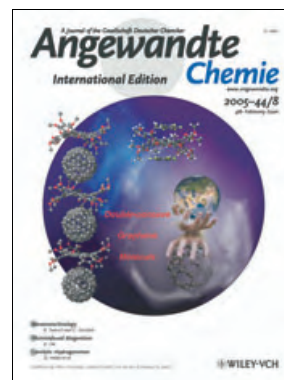
[3] M. E. Spahr, P. Bitterli, R. Nesper, M. Müller, F. Krumeich, H. U. Nissen, *Angew. Chem.* **1998**, 110, 1339; *Angew. Chem. Int. Ed.* **1998**, 37, 1263; F. Krumeich, H.-J. Muhr, M. Niederberger, F. Bieri, B. Schnyder, R. Nesper, *J. Am. Chem. Soc.* **1999**, 121, 8324; A. Doble, K. Ngala, S. Yang, P. Y. Zavalij, M. S. Wittingham,

- Chem. Mater.* **2001**, *13*, 4382–4386; V. Petkov, P. Y. Zavalij, S. Lutta, M. S. Wittingham, V. Parvanov, S. Shastri, *Phys. Rev. B* **2004**, *69*, 085410; L. Krush-Elbaum, D. M. News, H. Zeng, V. Derycke, J. Z. Sun, R. Sandstrom, *Nature* **2004**, *431*, 672.
- [4] P. Hoyer, *Adv. Mater.* **1996**, *8*, 857; G. H. Du, Q. Chen, R. C. Che, Z. Y. Yuan, L.-M. Peng, *Appl. Phys. Lett.* **2001**, *79*, 3702; Q. Chen, W. Zhou, G. Du, L.-M. Peng, *Adv. Mater.* **2002**, *14*, 1208.
- [5] G. B. Saupe, C. C. Waraksa, H.-N. Kim, Y. J. Han, D. M. Kashak, D. M. Skinner, T. E. Mallouk, *Chem. Mater.* **2000**, *12*, 1556; G. Du, Q. Chen, Y. Yu, W. Zhou, L.-M. Peng, *J. Mater. Chem.* **2004**, *14*, 1437.
- [6] M. Yada, C. Taniguchi, T. Torikai, T. Watari, S. Furuta, H. Katsuki, *Adv. Mater.* **2004**, *16*, 1448.
- [7] M. Wörle, F. Krumeich, F. Bieri, H.-J. Muhr, R. Nesper, Z. Anorg. Allg. Chem. **2002**, *628*, 2778; Y. D. Li, X. L. Li, R. R. He, J. Zhu, Z. X. Deng, *J. Am. Chem. Soc.* **2002**, *124*, 1411; C. Ye, G. Meng, Z. Jiang, Y. Wang, G. Wang, L. Zhang, *J. Am. Chem. Soc.* **2002**, *124*, 15180; S. Zhang, L.-M. Peng, Q. Chen, G. H. Du, G. Dawson, W. Z. Zhou, *Phys. Rev. Lett.* **2003**, *91*, 256103; J. Wang, Y. Li, *Adv. Mater.* **2003**, *15*, 445; R. Ma, Y. Bando, T. Sasaki, *J. Phys. Chem. B* **2004**, *108*, 2115.
- [8] P. C. Burns, M. L. Miller, R. C. Ewing, *Can. Mineral.* **1996**, *34*, 845; P. C. Burns, *Rev. Mineral.* **1999**, *38*, 23; P. M. Almond, T. E. Albrecht-Schmitt, *Inorg. Chem.* **2003**, *42*, 5693.
- [9] P. C. Burns, R. C. Ewing, F. C. Hawthorne, *Can. Mineral.* **1997**, *35*, 1551.
- [10] **1**: K_2CO_3 (0.045 g, 0.33 mmol), 40% H_2SeO_4 (0.15 mL, 1.46 mmol), and $(\text{UO}_2)(\text{NO}_3)_2 \cdot 6\text{H}_2\text{O}$ (0.17 g, 0.34 mmol) were dissolved in 2 mL of distilled H_2O and stirred until the mixture was completely homogeneous. The solution was then poured into a watch glass and was kept at 60 °C for about 30 min. An additional 0.2 mL of H_2O was then added and the solution was left to evaporate in a fumehood. Greenish-yellow crystals of **1** were formed in 10% yield within about 24 h. The compound was characterized by semiquantitative electron microprobe analysis. IR and Raman spectra were recorded and the presence of uranyl ions, selenate, and nitrate groups was confirmed.
- [11] Crystallographic data for **1**: $\text{K}_5[(\text{UO}_2)_3(\text{SeO}_4)_5](\text{NO}_3)(\text{H}_2\text{O})_{3.5}$; $M_r = 1845.42 \text{ g mol}^{-1}$, plate-like crystal, $0.05 \times 0.06 \times 0.02 \text{ mm}^3$, orthorhombic, $Pnmm$, $a = 11.2048(10)$, $b = 18.2132(19)$, $c = 32.364(3) \text{ \AA}$, $V = 6604.7(11) \text{ \AA}^3$, $Z = 8$, $\rho_{\text{calc}} = 3.712 \text{ g cm}^{-3}$, $2\theta_{\text{max}} = 49.80^\circ$, $\lambda(\text{MoK}\alpha) = 0.71073 \text{ \AA}$, ω -scan (1° per image) at $\phi = 0^\circ$ (STOE IPDS II), 293 K, 32 004 measured reflections, 5875 independent reflections, 4657 reflections with $|F_o| \geq 4\sigma_F$ ($R_{\text{int}} = 0.120$, $R_\sigma = 0.063$), numerical absorption correction (programs X-Shape and X-Red, STOE, Darmstadt, **1998**), structure solution by direct methods, full-matrix least-squares refinement (263 parameters) on $|F^2|$, no treatment of H atoms (programs SIR-97^[24] and SHELXL-97 (G. M. Sheldrick, program for the refinement of crystal structures, Göttingen, **1997**)), $R_1 = 0.080$, $wR_2 = 0.168$ for observed reflections, $R_1 = 0.103$, $wR_2 = 0.177$ for all data, max./min. electron density: 4.406/–1.982. Further details of the crystal structure investigations may be obtained from the Fachinformationszentrum Karlsruhe, 76344 Eggenstein-Leopoldshafen, Germany (fax: (+49) 7247-808-666; e-mail: crysdata@fiz-karlsruhe.de), on quoting the depository number CSD-414481.
- [12] C. Baerlocher, W. M. Meier, D. H. Olson, *Atlas of Zeolite Structure Types*, Elsevier, Dordrecht, **2001**.
- [13] S. M. Kuznicki, *Large-pored crystalline titanium molecular sieve zeolites*, **1989**, U. S. Patent No. 4853 202.
- [14] a) S. V. Krivovichev, C. L. Cahill, P. C. Burns, *Inorg. Chem.* **2002**, *41*, 34; b) S. V. Krivovichev, P. C. Burns, *J. Solid State Chem.* **2003**, *170*, 106; c) S. V. Krivovichev, C. L. Cahill, P. C. Burns, *Inorg. Chem.* **2003**, *42*, 2459; d) S. V. Krivovichev, *Crystallogr. Rev.* **2004**, *10*, 185.
- [15] S. V. Krivovichev, P. C. Burns, *Radiochemistry* **2004**, *46*, 441.
- [16] S. V. Krivovichev, P. C. Burns, *Z. Kristallogr.* **2003**, *218*, 683; S. V. Krivovichev, P. C. Burns, *Z. Kristallogr.* **2003**, *218*, 725.
- [17] S. V. Krivovichev, V. Kahlenberg, *Z. Anorg. Allg. Chem.* **2004**, *630*, 2736; S. V. Krivovichev, V. Kahlenberg, *J. Alloys Compd.* **2004**, in press.
- [18] S. V. Krivovichev, *Radiochemistry* **2004**, *46*, 434.
- [19] E. V. Nazarchuk, S. V. Krivovichev, S. K. Filatov, *Radiochemistry* **2004**, *46*, 438.
- [20] S. V. Krivovichev, T. Armbruster, D. Yu. Chernyshov, P. C. Burns, E. V. Nazarchuk, W. Depmeier, *Microporous Mesoporous Mater.* **2004**, in press.
- [21] P. Millet, J. Y. Henry, F. Mila, J. Galy, *J. Solid State Chem.* **1999**, *147*, 676.
- [22] M. Remškar, A. Mrzel, Z. Skraba, A. Jesih, M. Ceh, J. Demšar, P. Stadelmann, F. Levy, D. Mihailovic, *Science* **2001**, *292*, 479.
- [23] R. R. Schlitter, J. W. Seo, J. K. Gimzewski, C. Durkan, M. S. M. Saifullah, M. E. Welland, *Science* **2001**, *292*, 1136.
- [24] A. Altomare, G. Cascarano, C. Giacovazzo, A. Gualardi, *J. Appl. Crystallogr.* **1993**, *26*, 343.

Cover Picture

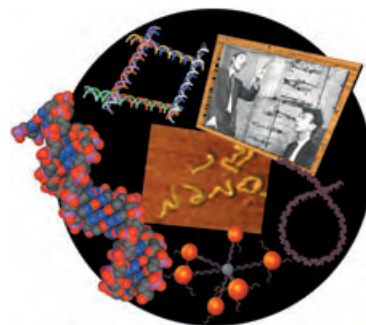
Zhaohui Wang, Florian Dötz, Volker Enkelmann, and Klaus Müllen*

Highly twisted permethoxylated hexa-*peri*-hexabenzocoronene forms inclusion complexes with hexafluorobenzene and fullerene guest molecules. In addition to the “double-concave” surface which allows its coordination to suitable guest molecules on both sides, the flexible methoxy groups at the periphery of this host molecule adjust their orientation to the size and shape of the guest molecules. Further details are reported in the Communication by K. Müllen et al. on page 1247 ff.



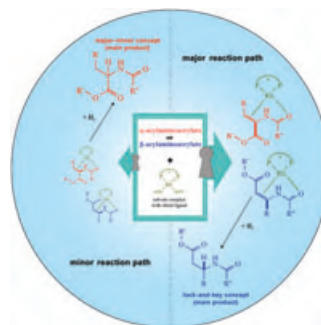
Bionanotechnology

The DNA sequence contains codes directing interactions and recognition processes on the nanometer scale. B. Samorì and G. Zuccheri demonstrate in their Review on page 1166 ff. how these codes can be identified and exploited.



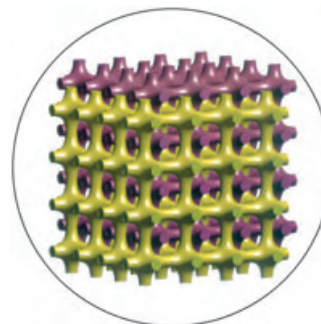
Asymmetric Catalysis

D. Heller et al. demonstrate in their Communication on page 1184; ff. that it is the “major” substrate complexes, which were characterized by X-ray single-crystal analysis, which lead to the major product in the asymmetric hydrogenation of β -acylaminoacrylates.



Porous Materials

The morphology of the skeletal silica network known as the plumber's nightmare is described in the Communication by U. Wiesner et al. on page 1226 ff. The approach is simple and takes place by a block-copolymer-directed sol-gel synthesis.





The following Communications have been judged by at least two referees to be “very important papers” and will be published online at www.angewandte.org soon:

Rimane Aoun, Jean-Luc Renaud, Pierre H. Dixneuf, Christian Bruneau*
Concomitant Monoreduction/Hydrogenation of Unsaturated Cyclic Imides to Lactams Catalyzed by Ruthenium Precursors

M. Maue, T. Schrader*
A Color Sensor for Catecholamines

Stuart L. Schreiber*, Chuo Chen, Xiaodong Li, Christopher S. Neumann, Michael M.-C. Lo
Convergent Diversity-Oriented Synthesis of Small-Molecule Hybrids

Ralf Haiges*, Jerry A. Boatz, Robert Bau, Stefan Schneider, Thorsten Schroer, Muhammed Yousufuddin, Karl O. Christe
Polyazide Chemistry: Preparation and Characterization of Binary Group 6 Azides.

Hans A. Bechtel, Jon P. Camden, Davida J. Ankeny Brown, Marion R. Martin, Richard N. Zare*, Konstantin Vodopyanov
Effects of Bending Excitation on the Reaction of Chlorine Atoms with Methane

Liang Deng, Hoi-Shan Chan, Zuowei Xie*
Synthesis, Reactivity, and Structural Characterization of the First 14-Vertex Carborane

Obituary

Ernst-Ulrich Franck (1920–2004): Fluids at High Pressures and Supercritical Temperatures

F. Hensel ————— 1156

Books

Metal-Catalyzed Cross-Coupling Reactions

Armin de Meijere, François Diederich

reviewed by F. Glorius ————— 1157

Experiments, Models, Paper Tools

Ursula Klein

reviewed by J. A. Berson ————— 1157

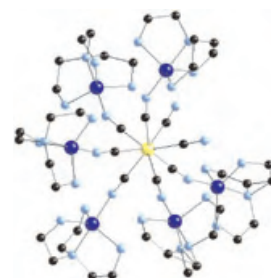
Highlights

Photoinduced Magnetism

A. Dei* ————— 1160–1163

Photomagnetic Effects in Polycyanometallate Compounds: An Intriguing Future Chemically Based Technology?

Out of the blue: Photoinduced magnetism in polymeric “Prussian Blue” analogues is a well understood phenomenon that can even occur near room temperature. The lessons learned are now being transferred to the synthesis of molecular cyanide-bridged single-molecule magnets (see picture; Mo yellow, C black, N blue, Cu purple) whose magnetic properties change drastically on light irradiation.

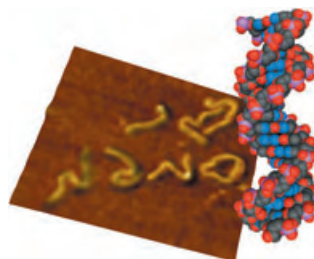


Reviews

Bionanotechnology

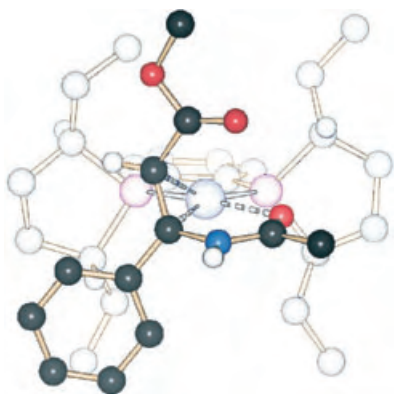
B. Samorì,* G. Zuccheri — 1166–1181

DNA Codes for Nanoscience



A question of scale: The interaction and recognition processes of DNA have been traditionally described on the Ångström scale. Embedded in DNA are also informational codes that control these processes on the nanoscale (see picture). Nanoscience can take advantage of these codes to control the self-assembly of biological and nonbiological molecules or their orientation on surfaces.

Communications



Five catalyst–substrate complexes of the type $[\text{Rh}(\text{chiral ligand})(\beta\text{-dehydroamino acid derivative})\text{BF}_4]$ were characterized for the first time by X-ray analysis (see example). Low-temperature NMR spectroscopy proved that three of these complexes are “major” substrate complexes, which lead to the main product in asymmetric hydrogenation, contrary to the known classical examples with analogous α -dehydroamino acid derivatives.

Catalytic Hydrogenation



H.-J. Drexler, W. Baumann, T. Schmidt, S. Zhang, A. Sun, A. Spannenberg, C. Fischer, H. Buschmann, D. Heller* _____ **1184–1188**

Are β -Acylaminoacrylates Hydrogenated in the Same Way as α -Acylaminoacrylates?

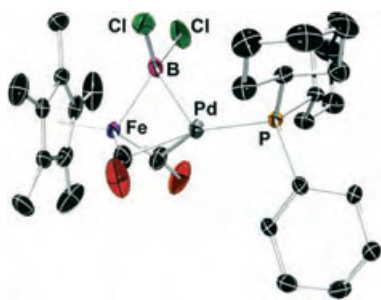


In great shape: Star-shaped telechelic oligomers can be coupled with a junction unit to yield amorphous copolyester-urethane networks, which are not only biodegradable but can also be fixed in a new, temporary shape after they have been processed into a permanent shape. The permanent shape can be recovered by heating (see picture). Such polymer networks may find application in ophthalmology.

Shape-Memory Polymers

A. Alteheld, Y. Feng, S. Kelch, A. Lendlein* _____ **1188–1192**

Biodegradable, Amorphous Copolyester-Urethane Networks Having Shape-Memory Properties



Building bridges: The combination of the Lewis acidic dichloroboryl complex $[(\eta^5\text{-C}_5\text{Me}_5)\text{Fe}(\text{CO})_2\text{BCl}_2]$ and a Lewis basic $[\text{Pd}(\text{PR}_3)]$ fragment gives the first dinuclear monoboryl complex with a symmetric μ, η^2 bridging BR_2 ligand (see structure). The dative nature of the palladium–boron bonding interaction makes the dinuclear compound a rare example of a transition-metal borane complex.

Boryl Complexes



H. Braunschweig,* K. Radacki, D. Rais, G. R. Whittell _____ **1192–1194**

A Boryl Bridged Complex: An Unusual Coordination Mode of the BR_2 Ligand

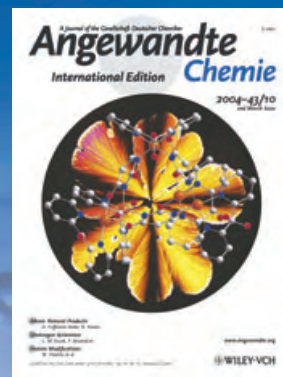
For the USA and Canada:

ANGEWANDTE CHEMIE International Edition (ISSN 1433-7851) is published weekly by Wiley-VCH PO Box 191161, D 69451 Weinheim, Germany. Air freight and mailing in the USA by Publications Expediting Inc. 200 Meacham Ave., Elmont, NY 11003. Periodicals

postage paid at Jamaica NY 11431. US POSTMASTER: send address changes to *Angewandte Chemie*, Wiley-VCH, 111 River Street, Hoboken, NJ 07030. Annual subscription price for institutions: US\$ 4948.00/4498.00 (valid for print and electronic / print or electronic delivery); for individuals who are personal members of a

national chemical society, or whose institution already subscribes, or who are retired or self-employed consultants, print only: US\$ 394.00. Postage and handling charges included. All Wiley-VCH prices are exclusive VAT.

The best in chemistry – for more than a hundred years



A Journal of the Gesellschaft Deutscher Chemiker
Angewandte Chemie
International Edition

www.angewandte.org

1888: The beginning
of a success story

Constant Innovations

- 1962:** First issue of the International Edition
- 1976:** Graphical abstracts
- 1979:** Cover pictures
- 1988:** Centenary of Angewandte
- 1989:** Routine use of color
- 1991:** New section: Highlights
- 1992:** Computerized editorial tracking system
- 1995:** Internet service for readers
- 1998:** Regular press service; full-text online
- 2000:** New section: Essays; EarlyView: Communications available online ahead of the printed version
- 2001:** New section: Minireviews
- 2002:** Online submission of manuscripts
- 2003:** Weekly publication; new section: News; new layout
- 2004:** Backfiles (1962-1997); ManuscriptXpress: Online system for authors and referees



Angewandte's advisors...

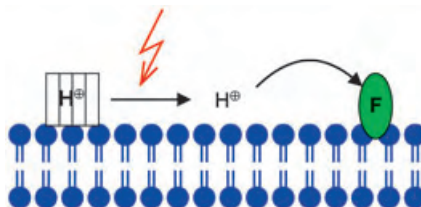
Richard N. Zare
Stanford University

» Size does matter, as well as shape, motion, composition, and chemical complexity. I read **Angewandte Chemie** each week to learn about the latest, most exciting developments in the world of chemistry. «

Angewandte Chemie International Edition is
a journal of the German Chemical Society (GDCh)



Large jumps in pH on the nanosecond timescale can be achieved upon one- and two-photon flash photolysis of novel coumarinylmethyl esters, which are phototriggers for H^+ (see scheme, F = pH-sensitive fluorescence indicator). The compounds are excellent tools for the study of rapid H^+ -triggered processes, for example, proton migration along membrane surfaces.

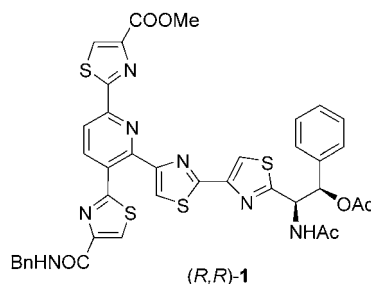


Photoactivatable Compounds

D. Geißler, Y. N. Antonenko, R. Schmidt, S. Keller, O. O. Krylova, B. Wiesner, J. Bendig, P. Pohl, V. Hagen* _____ **1195–1198**

(Coumarin-4-yl)methyl Esters as Highly Efficient, Ultrafast Phototriggers for Protons and Their Application to Acidifying Membrane Surfaces

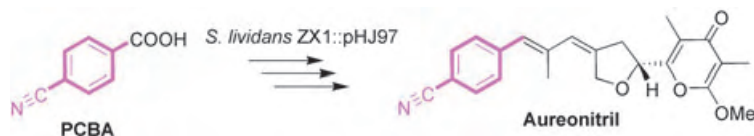
Two birds were killed with one stone by the synthesis of the trisubstituted pyridine (*R,R*)-**1** and its diastereoisomer. In a short synthetic sequence for the construction of the GE 2270 thiazolyl peptides, 2,3,6-tri-bromopyridine was converted into pyridine **1** in only four steps (Bn = benzyl). In addition, the absolute and relative configuration of a major degradation product of GE 2270A was proven.



Natural Products

G. Heckmann, T. Bach* _____ **1199–1201**

Synthesis of the Heterocyclic Core of the GE 2270 Antibiotics and Structure Elucidation of a Major Degradation Product



Tapping nature's biosynthetic potential: Formation of the rare *p*-nitro benzoate precursor of aureothin, a mixed polyketide metabolite of *Streptomyces thioluteus*, requires two key enzymes: a *p*-amino benzoate synthase and an *N*-oxygenase. Feeding of surrogates to engineered block

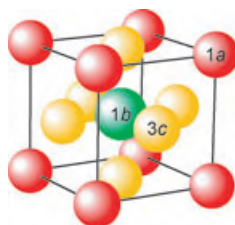
mutants (e.g. *S. lividans* ZX1::pHJ97) reveals that the iterative modular aureothin polyketide also accepts *p*-cyano benzoate as the starter, which is subsequently processed to the nitrile analogue of aureothin, aureonitrile, which has improved cytostatic properties.

Antitumor Agents

M. Ziehl, J. He, H.-M. Dahse, C. Hertweck* _____ **1202–1205**

Mutasynthesis of Aureonitrile: An Aureothin Derivative with Significantly Improved Cytostatic Effect

Cutting corners: The perovskite-like ternary nitrides MFe_3N of the iron- and platinum-group metals are theoretically investigated. All eight compounds are predicted as being ferromagnetic, with saturation moments between 7.1 and 9.2 μ_B per formula unit, and with larger M atoms preferentially occupying the corner position 1a (see picture). Two ternary nitrides, yet to be made, are predicted as lucrative synthetic goals.



Ternary Nitrides

J. von Appen, R. Dronskowski* _____ **1205–1210**

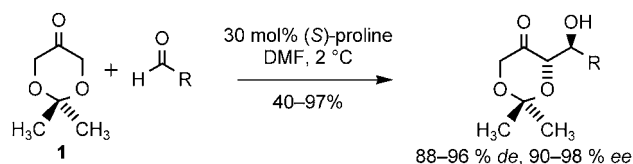
Predicting New Ferromagnetic Nitrides from Electronic Structure Theory: $IrFe_3N$ and $RhFe_3N$



Asymmetric Synthesis

D. Enders,* C. Grondal — 1210–1212

Direct Organocatalytic De Novo Synthesis of Carbohydrates



One small step for a catalyst: A biomimetic asymmetric synthesis of carbohydrates was accomplished by a proline-catalyzed aldol reaction of 2,2-dimethyl-1,3-dioxan-5-one as the methylene com-

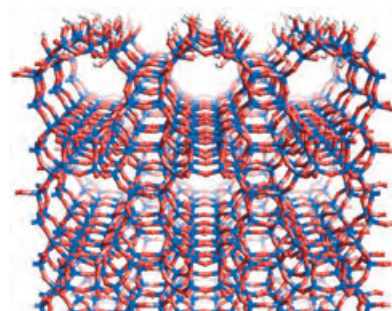
ponent with various aldehydes. This new organocatalytic C_3+C_n strategy leads directly to selectively protected simple sugars and amino sugars.

Solid-State Chemistry

M. E. Chiu, B. Slater,*
J. D. Gale — 1213–1217

Simulating the Dissolution and Growth of Zeolite beta C

A simple model of zeolite growth and dissolution has been constructed. Lattice-energy calculations suggest that both growth and dissolution, progressing through attachment or leaching of monomeric units, involves a number of exothermic and endothermic steps. Oligomeric units may play a key role in overcoming the most endothermic (rate-determining) steps of crystal growth associated with the pictured high-energy structure.

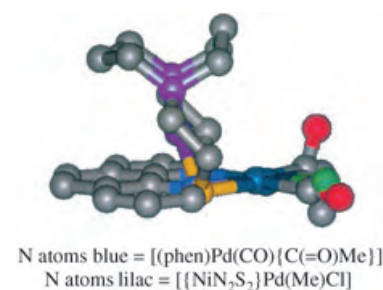


Nickel Complexes

M. V. Rampersad, S. P. Jeffery,
J. H. Reibenspies, C. G. Ortiz,
D. J. Darensbourg,
M. Y. Darensbourg* — 1217–1220

N_2S_2Ni Metallothiolates as a Class of Ligands that Support Organometallic and Bioorganometallic Reactivity

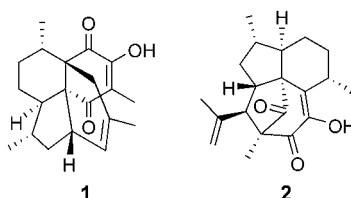
It hinges on the ligand: The electron-donor ability of NiN_2S_2 ligands is compared to that of traditional diphosphine and diimine ligands. Structural comparison of NiN_2S_2 and *o*-phenanthroline (phen) complexes of $\{W(CO)_4\}$ and $\{PdX_2\}$ units shows asymmetry imposed by the hinge bonding of the NiN_2S_2 S donors (see superimposed structures) which favors stereo- and regioselective substrate addition.



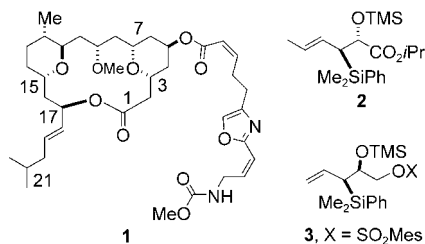
Natural Product Synthesis

D. C. Harrowven,* D. D. Pascoe,
D. Demurtas, H. O. Bourne — 1221–1222

Total Synthesis of (–)-Colombiasin A and (–)-Elisapterosin B



Intramolecular cycloaddition reactions are central in the total syntheses of colombiasin A (1) and elisapterosin B (2) described, which use (–)-dihydrocarvone as the starting material. A Moore rearrangement of a vinylcyclobutene is used to initiate the cycloaddition.

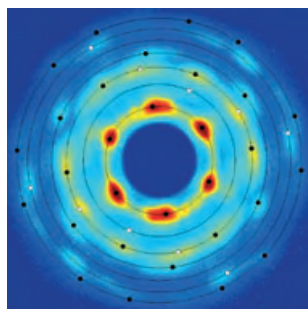


A convergent and enantioselective total synthesis of (+)-leucascandrolide (1) was accomplished in 17 steps. Central to this synthesis is the rapid and efficient integration of the bispyran moiety into **1** using two consecutive [4 + 2] annulation reactions between an aldehyde and the chiral silanes **2** and **3** (TMS = trimethylsilyl, Mes = mesityl = 2,4,6-trimethylphenyl).

Natural Product Synthesis

Q. Su, J. S. Panek* — 1223 – 1225

Total Synthesis of (+)-Leucascandrolide A



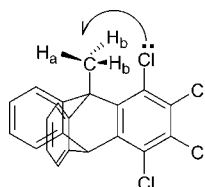
Pipe-dream realized: The as-made nanocomposite derived from a block-copolymer-directed sol-gel synthesis consists of silica networks embedded in an organic matrix. Calcination of the structure at high temperatures gives a final skeletal silica network consistent with the morphology called plumber's nightmare (point group $Im\bar{3}m$; see small-angle X-ray scattering (SAXS) pattern of an inverse form of this morphology).

Porous Materials

A. Jain, G. E. S. Toombes, L. M. Hall, S. Mahajan, C. B. W. Garcia, W. Probst, S. M. Gruner, U. Wiesner* — 1226 – 1229

Direct Access to Bicontinuous Skeletal Inorganic Plumber's Nightmare Networks from Block Copolymers

Bonding out of the blue: Strong evidence of the occurrence of specific hydrogen bonds, the so called blue-shifting hydrogen bonds, between hydrogen atoms of CH_3 in 9-methyltrityptenes and halogen substituents in the *peri* position (see scheme) comes from low-temperature 1H NMR measurements that yield the $^1J(C,H)$ values for the individual CH_3

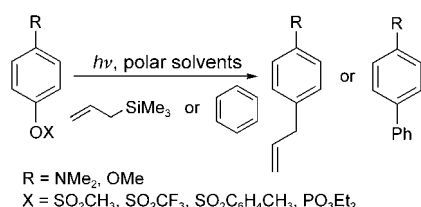


protons, as well as from natural bond orbital analysis and DFT calculations of the geometries and J couplings.

Hydrogen Bonds

T. Ratajczyk, I. Czernski, K. Kamińska-Trela, S. Szymanski,* J. Wojcik* — 1230 – 1232

$^1J(C,H)$ Couplings to the Individual Protons in a Methyl Group: Evidence of the Methyl Protons' Engagement in Hydrogen Bonds



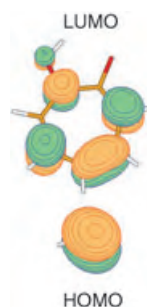
Photochemical cleavage of Ar–O bonds in phenyl esters substituted with electron-donating groups offers a convenient method for the arylation of alkenes and arenes. The reaction proceeds by an S_N1 mechanism via a triplet phenyl cation to form allylbenzene or biphenyl derivatives under mild conditions (see scheme).

Synthetic Methods

M. De Carolis, S. Protti, M. Fagnoni,* A. Albini* — 1232 – 1236

Metal-Free Cross-Coupling Reactions of Aryl Sulfonates and Phosphates through Photoheterolysis of Aryl–Oxygen Bonds

Coupling drives the rotation: A theoretical study of proton-transfer dynamics of 5-methyltropone (5MTR) has identified a long-range mechanical interaction. Methyl group rotation can be driven by proton transfer because of coupling between hyperconjugation and tautomerization within 5MTR (see HOMO–LUMO interaction). A quantum-mechanical mechanism is presented in which this molecule undergoes a conformational change.



Molecular Dynamics

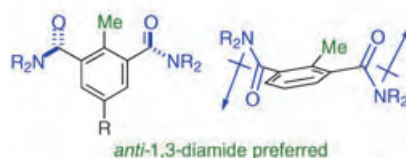
H. Ushiyama,* K. Takatsuka* — 1237 – 1240

Methyl Group Rotation Driven by Proton Transfer through a Long-Range Chemical Interaction

Conformational Analysis

M. S. Betson, J. Clayden,* H. K. Lam,
M. Helliwell 1241–1244

Using Dipoles to Control the
Directionality of Functional Groups:
Syn- and *Anti*-Oriented Benzene-1,3-
dicarboxamides



Poles apart: The relative orientation of a pair of functional groups—amides in this case—can be controlled by the choice of the substituent that lies between them. Groups which are effectively cylindrically symmetrical (Me, Cl) allow direct interac-



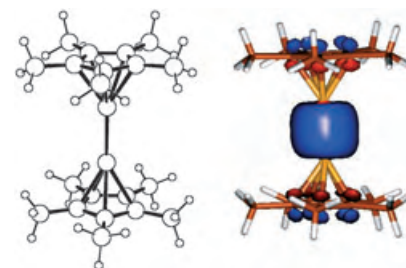
tion between the dipoles of the amides and induce an *anti* orientation, whereas polar groups (OCOR, OSO₂R, SO₂R) interact with the dipole of both amides to yield a *syn* orientation (see picture).

Metal–Metal Bonds

D. del Río, A. Galindo,* I. Resa,
E. Carmona* 1244–1247

Theoretical and Synthetic Studies on
[Zn₂(η⁵-C₅Me₅)₂]: Analysis of the Zn–Zn
Bonding Interaction

More than 1 g of the dizinc compound [Zn₂(η⁵-C₅Me₅)₂] can be readily obtained in a single preparation. Density functional calculations reveal that the Zn–Zn bond is relatively strong and derives mainly from interaction between the Zn 4s orbitals (see picture).

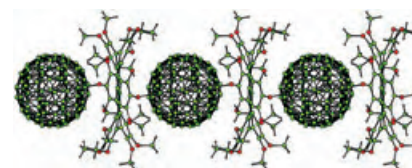


Noncovalent Interactions

Z. Wang, F. Dötz, V. Enkelmann,
K. Müllen* 1247–1250

“Double-Concave” Graphene:
Permethoxylated Hexa-*peri*-
hexabenzocoronene and Its Cocrystals
with Hexafluorobenzene and Fullerene

Extremely nonplanar permethoxylated hexa-*peri*-hexabenzocoronene can be prepared by using a facile ferric chloride cyclodehydrogenation procedure. The combination of a rigid “double-concave” aromatic core with 18 flexible methoxy groups at the periphery makes it a remarkable host molecule, as revealed by single-crystal analysis of its crystalline



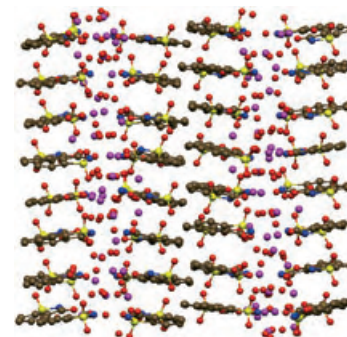
inclusion complexes with hexafluorobenzene and fullerene guest molecules (see crystal structure).

Structure Elucidation

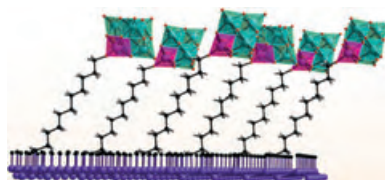
P. Naumov,* G. Jovanovski, O. Grupče,
B. Kaitner, A. D. Rae,
S. W. Ng 1251–1254

Solid-State Structure and Temperature/
Evacuation-Induced Dehydration of
Sodium Saccharinate 1.875 Hydrate

Sweet solution: The *P*2₁/*n* (*Z* = 64) structure of the commercial sweetener sodium saccharinate, which has an unusually large unit cell of 15.6 nm³, is an occupational and displacive modulation of an idealized *C*2/*m* (*Z* = 8) structure that results from a structural misfit. This determination (see picture) shows—after more than 150 years of use of the compound as a food additive—that it is better regarded as a 1.875 hydrate than a dihydrate.



Covalent ties: The polyoxometalate $(n\text{Bu}_4\text{N})_3[(\text{MeO})\text{TiW}_5\text{O}_{18}]$ is easily anchored to alkanol-functionalized surfaces of porous and single-crystal silicon (see picture, polyhedra: polyoxometalate, dark blue: Si surface). Scanning tunneling microscopy reveals the growth of 35–50 nm diameter islands on functionalized Si(111), which suggests that the immobi-

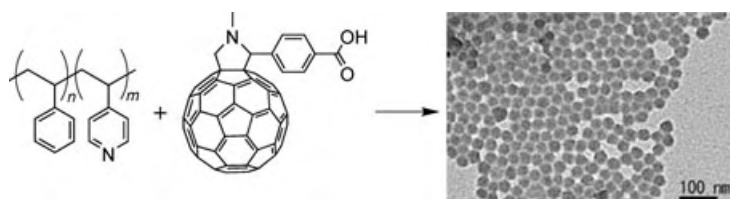


lized polyoxometalates act as nucleation sites for electrostatic aggregation.

Surface Chemistry

R. J. Errington,* S. S. Petkar,
B. R. Horrocks, A. Houlton, L. H. Lie,
S. N. Patole _____ 1254–1257

Covalent Immobilization of a TiW_5
Polyoxometalate on Derivatized Silicon
Surfaces



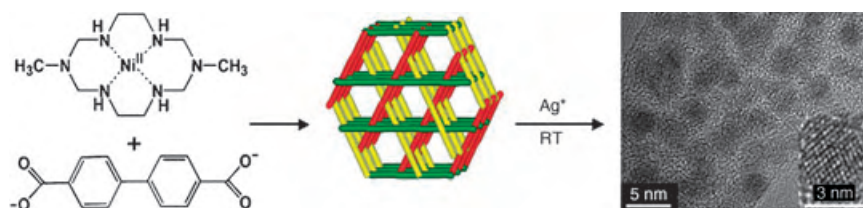
On the starting block: Polystyrene-*block*-poly(4-vinylpyridine) and a [60]fullerene carboxylic acid combine to form spherical supramolecular aggregates (see picture), the size and morphology of which can be

controlled by changing the block composition ratio in the copolymer. The method is generally applicable to the construction of organic nanoparticles.

Supramolecular Chemistry

N. Fujita, T. Yamashita, M. Asai,
S. Shinkai* _____ 1257–1261

Formation of [60]Fullerene Nanoclusters
with Controlled Size and Morphology
through the Aid of Supramolecular Rod-
Coil Diblock Copolymers



Hi ho silver! Coordination polymer chains assembled from a Ni^{II} hexaazamacrocyclic and sodium 4,4'-biphenyldicarboxylate can be packed to form a porous framework (see picture). Nanocomposites of silver particles and matrix can be prepared

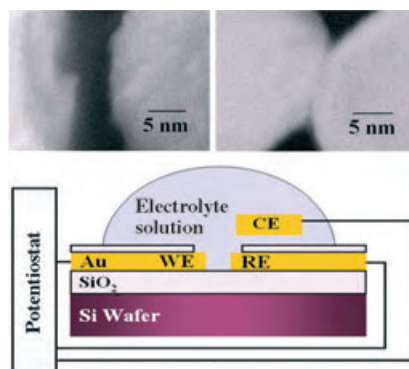
by immersing the framework in AgNO_3 solution, and the matrix-free silver nanoparticles (≈ 3 nm) isolated by treatment of the solid with boiling diethyl ether containing oleic acid.

Crystal Engineering

H. R. Moon, J. H. Kim,
M. P. Suh* _____ 1261–1265

Redox-Active Porous Metal–Organic
Framework Producing Silver
Nanoparticles from Ag^{I} Ions at Room
Temperature

Potential feedback: Metallic electrodes with controlled gap widths ranging from about 10 nm down to several angstroms (as determined by SEM measurements) can be fabricated electrochemically by using a simple potential feedback system with a unique electrode configuration (see picture). The working principle is based on the potential distribution in the electric double-layer. The process is simple, controllable, and reproducible.



Nanotechnology

J. Xiang, B. Liu, S.-T. Wu, B. Ren, F.-Z. Yang,
B.-W. Mao, Y. L. Chow,
Z.-Q. Tian* _____ 1265–1268

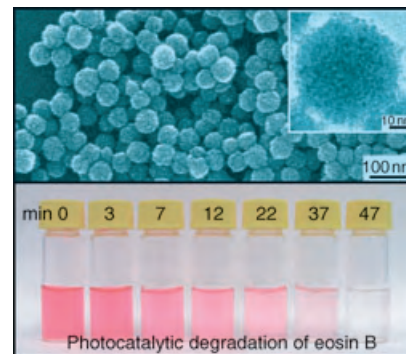
A Controllable Electrochemical
Fabrication of Metallic Electrodes with a
Nanometer/Angstrom-Sized Gap Using
an Electric Double Layer as Feedback

Nanostructures

J.-S. Hu, L.-L. Ren, Y.-G. Guo, H.-P. Liang,
A.-M. Cao, L.-J. Wan,*
C.-L. Bai* ————— **1269–1273**

Mass Production and High Photocatalytic
Activity of ZnS Nanoporous
Nanoparticles

Self-assembly of hexagonal 3–5-nm ZnS nanocrystals can be used for the large-scale production of zinc sulfide nanoporous nanoparticles (NPNPs). The uniform, spherical NPNPs are monodisperse and have surface areas on the order of $156 \text{ m}^2 \text{ g}^{-1}$. The ZnS NPNPs are more effective photocatalysts than Degussa P25 titania or ZnS nanocrystals in the photo-degradation of eosin B at ambient temperature (see picture).



Angewandte Chemie International Edition
WILEY-INTERSCIENCE®
DISCOVER SOMETHING GREAT

"Hot Papers" are chosen by the Editors for their importance in a rapidly evolving field of high current interest. A preview with the graphical abstracts of these articles can be found on the *Angewandte Chemie* homepage in Wiley InterScience at www.angewandte.org.

All articles in *Angewandte Chemie* are published online several weeks ahead of print. They are found under the "EarlyView" link on the journal's homepage in Wiley InterScience.

Angewandte

Service

Keywords ————— **1274**

Authors ————— **1275**

Preview ————— **1277**

Corrigendum

Pd-Catalyzed Amination of Nucleoside
Arylsulfonates to yield *N*⁶-Aryl-2,6-
Diaminopurine Nucleosides

P. Gunda, L. M. Russon,
M. K. Lakshman* ————— **6372–6377**

Angew. Chem. Int. Ed. **2004**, 43

DOI 10.1002/anie.200460782

Some errors in the references cited in the published article were later noticed by the authors. The correct citations for references [1a, b], [3e], [6b], [16b], and [18] are provided below. The authors apologize for the oversight and any confusion it may have caused.

- [1] a) J. P. Wolfe, S. Wagaw, J.-F. Marcoux, S. L. Buchwald, *Acc. Chem. Res.* **1998**, 31, 805–818;
b) J. F. Hartwig, *Acc. Chem. Res.* **1998**, 31, 852–860.
- [3] e) F. De Riccardis, F. Johnson, *Org. Lett.* **2000**, 2, 293–295.
- [6] b) Y.-Z. Xu, Q. Zheng, P. F. Swann, *Tetrahedron Lett.* **1991**, 32, 2817–2820.
- [16] b) M. Havelková, D. Dvořák, M. Hocek, *Synthesis* **2001**, 1704–1710.
- [18] D. Zim, S. L. Buchwald, *Org. Lett.* **2003**, 5, 2413–2415.

Ernst-Ulrich Franck (1920–2004): Fluids at High Pressures and Supercritical Temperatures

The physical and chemical properties of supercritical fluids and supercritical fluid mixtures are of major scientific and technological interest and have therefore been the focus of a great deal of research over the past 50 years.



Ever-increasing sophistication in experimental high-pressure techniques coupled with new theoretical developments has resulted in an enhanced understanding of the behavior of supercritical fluids and the extension of their

scope of application. One of the towering pioneers in this development was Ernst-Ulrich Franck, Professor of Physical Chemistry at the Universität Karlsruhe (Germany), who died on December 21, 2004 in Karlsruhe at the age of 84.

Ernst-Ulrich Franck was born on August 2, 1920 in Hamburg. After graduating from high school in 1939 he studied chemistry—interrupted by several years of military service—at the Universität Göttingen (Germany), where he graduated in 1946. He completed his PhD in 1950 in Göttingen under the guidance of Prof. Arnold Eucken on transport properties of reacting gases.^[1]

Afterwards, as a research associate in Göttingen, Ernst-Ulrich Franck had a particular interest in water and aqueous solutions at high temperatures and pressures: a large and at that time still inadequately understood class of fluids. His name is directly connected with a number of outstanding achievements in

this field, including the breakthrough he made by drawing attention to the unique properties of dense supercritical steam as an electrolytic solvent.^[2] In 1961 he was offered the position of Professor of Physical Chemistry at the Universität Karlsruhe, which would soon become a world center of research on physical and chemical phenomena in fluids at high pressures and supercritical temperatures. His activities in Karlsruhe included pioneering research on phase equilibria and critical phenomena of fluid mixtures and on electrolytic properties of hydrothermal fluids, first attempts to understand the thermodynamic and electrical properties of supercritical metals and salts, and remarkable contributions to the understanding of high-pressure combustion and high-pressure flames.

Ernst-Ulrich Franck's pioneering contributions to the exploration of the fluid state of matter were recognized with many prizes and honors. These awards reflect not only universal respect and admiration for his scientific research, but also the remarkable breadth of his activities. They include the DECHEMA Medal of the Deutsche Gesellschaft für Chemisches Apparatewesen (1958), the Bunsen Medal of the Deutsche Bunsengesellschaft (1970), the P. W. Bridgman Medal of the International Association for High Pressure Research (1981), the Yeram S. Touloukian Award of the American Association of Mechanical Engineers (1988), the Abraham Gottlieb Werner Medal of the Deutsche Mineralogische Gesellschaft (1989), and the IAPWS Gibbs medal of the International Association for the Properties of Water and Steam (1999). He was also elected as a member of the Heidelberg Academy of Sciences (1975), the Leopoldina Acad-

emy (1978), and the Göttingen Academy of Sciences (1991), and received an honorary doctorate from the Philipps-Universität Marburg (1992) and honorary membership of the Deutsche Bunsengesellschaft (1996).

Franck's institute in Karlsruhe attracted students and scientists from around the world. He trained more than 80 doctoral students, and for numerous postdoctoral fellows and guest scientists from Europe and overseas his institute was a world-renowned center for high-pressure research on fluids. The results of 50 years of research were described in more than 200 publications. Franck's passionate interest in the properties of supercritical fluids continued after his retirement in 1988. Even then, he changed his research program only slightly. As emeritus professor he authored an impressive 63 publications. A summary in Franck's own words of the most important results on supercritical water can be found in reference [3].

Ernst-Ulrich Franck's scientific work has had an important influence on supercritical-fluid research and will have a continuing effect in the future. Those who have been fortunate and privileged enough to work with him as students, colleagues, or friends owe him a great debt of gratitude. We will miss him.

Friedrich Hensel
Universität Marburg (Germany)

- [1] E. U. Franck, E. Wicke, *Angew. Chem.* **1954**, 66, 701.
- [2] E. U. Franck, *Angew. Chem.* **1961**, 73, 309.
- [3] H. Weingärtner, E. U. Franck, *Angew. Chem.* **2005**, 117, DOI: 10.1002/ange.200462468; *Angew. Chem. Int. Ed.* **2005**, 44, DOI: 10.1002/anie.200462468.

Photomagnetic Effects in Polycyanometallate Compounds: An Intriguing Future Chemically Based Technology?

Andrea Dei*

Keywords:

cyanides · electron transfer · magnetic properties · photochemistry · single-molecule magnets

Molecular systems undergoing a reversible and controlled change of their physical properties following a change in an external parameter offer an appealing perspective for the realization of molecular-scale electronic devices.^[1,2] In particular, molecules showing photochromism are of potential interest as materials for optical data storage.^[3] Photochromism is defined as a light-stimulated reversible interconversion between two isomers which have different electronic absorption spectra. In practice, the photoinduced interconversion occurs by irradiating an absorption band of the starting material with an appropriate light source. The starting material can in turn be regenerated by irradiating an appropriate electronic transition of the photoinduced product. Since, in general, the two isomers have different free energies at any given temperature, the starting compound is often the more stable one. Therefore the photoinduction process yields a metastable product. A thermally induced relaxation process to the ground state may occur depending on the free-energy potential barrier of the relaxation process.

A dramatic extension of the perspectives of photochromism was given by the development of molecular mag-

netism,^[4,5] which lead to the discovery that the switching of the magnetic properties of a molecule and long-range magnetic-order effects can be induced by photoexcitation.^[6,7]

The number of coordination compounds showing photoinduced magnetic properties in the solid state is still limited to some dithienylethylene derivatives,^[8,9] tetracyanoethylene organometallic compounds,^[10] spin-cross-over,^[11,12] and valence-tautomeric complexes.^[13,14] In this framework the most promising perspectives are given by the so-called Prussian blue analogues, which have the general formula $A_2xM^{II}_{(1.5-x)}[M^{III}(CN)_6]$ ($x=0-1$; A = alkali metal ion; M^{II} , M^{III} = transition-metal ions). These compounds can be considered as metal complexes formed by a hexacyanometallate $[M(CN)_6]^{n-}$ unit, which can act as a hexamonomodentate ligand towards up to six different metal ions M' with the formation of three dimensional $M-CN-M'$ arrays. This property has been successfully exploited for the design of molecular-based magnets and several compounds showing spontaneous magnetization with high critical temperatures (T_c) have been obtained. Examples are $V[Cr(CN)_6] \cdot 2.8H_2O$ and $[Cr_{2.12}(CN)_6] \cdot 2.8H_2O$ with $T_c = 315$ K and 270 K, respectively.^[15,16]

Few years ago Hashimoto and co-workers discovered that long-range magnetic ordering in the compound $K_{0.2}Co_{1.4}[Fe(CN)_6] \cdot 6.9H_2O$ can be achieved by irradiation with red light at low

temperature, the original material being restored by blue light irradiation or by heating.^[17] This result was extremely important since it showed how the magnetic behavior of a molecular-based material can be controlled by light. It should be mentioned that it followed the discovery of the LIESST (light-induced excited-spin-state trapping) effect described some years before.^[6,7,11,12]

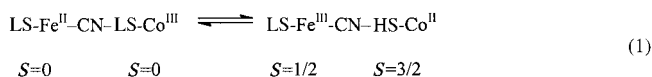
Further studies on several compounds of formula $A_2xCo_{(1.5-x)}[Fe(CN)_6] \cdot nH_2O$ (A = Na, Rb, Cs) have provided evidence for the rationalization of the observed phenomenon.^[18-24] Herein the main properties of some of them are summarized and discussed.

In an extremely simplified approach,^[18] it can be stated that the changes in the magnetic properties are associated with the photoinduced valence tautomeric interconversion [Eq. (1); LS = low spin, HS = high spin].

The pair of bridged metal centers on the left side of Equation (1) is diamagnetic while the pair on the right is paramagnetic. When the whole lattice is made up of paramagnetic pairs, the compound orders ferrimagnetically below 20 K. This situation is observed in $Co^{II}_{1.5}[Fe^{III}(CN)_6] \cdot 6H_2O$.^[19] The magnetic properties of this compound are not affected by the light since only paramagnetic pairs are present.

If a significant concentration of diamagnetic $Fe^{II}-Co^{III}$ pairs is introduced into the lattice, as in the low-temperature phase $Na_{0.4}Co^{II}_{0.3}Co^{III}$.

[*] Prof. Dr. A. Dei
INSTM Research Unit
LAMM Dipartimento di Chimica dell'
Università di Firenze
Via della Lastruccia 3
50019 Sesto Fiorentino, Firenze (Italy)
Fax: (+39) 055-457-3372
E-mail: andrea.dei@unifi.it



$[\text{Fe}^{\text{II}}(\text{CN})_6] \cdot 5\text{H}_2\text{O}$, then irradiation of the $\text{Fe}^{\text{II}} \rightarrow \text{Co}^{\text{III}}$ charge-transfer band (500–750 nm) at 5 K induces the valence tautomeric interconversion [Eq. (1)] which results in a change of the magnetism of the compound from paramagnetic to ferrimagnetic.^[20] The new magnetic state is stable for several days at 5 K. The original paramagnetic material is restored by heating to 130 K or by irradiation at 1319 nm at 5 K. The same behavior was observed in other sodium and rubidium derivatives, but not in the cesium ones.^[19–23]

The different oxidation-states in $\text{Co}_{1.5}^{\text{II}}[\text{Fe}^{\text{III}}(\text{CN})_6] \cdot 6\text{H}_2\text{O}$ and $\text{Na}_{0.4}\text{Co}_{0.3}^{\text{II}}\text{Co}^{\text{III}}[\text{Fe}^{\text{II}}(\text{CN})_6] \cdot 5\text{H}_2\text{O}$ are due to the different reducing power of the Co^{II} center in the two lattices. In all the above compounds the Fe^{III} and Fe^{II} ions are always bound to six carbon atoms from six cyanide ligands, whereas the hexacoordinate M^{II} metal ions (in the prussiate compounds of general formula $\text{M}_{1.5}^{\text{II}}[\text{Fe}^{\text{III}}(\text{CN})_6] \cdot n\text{H}_2\text{O}$) are bound to four cyanide nitrogen atoms.^[18–24] Their coordination polyhedron is completed by two water molecules. Under these conditions the Fe^{III} ion is not able to oxidize the Co^{II} ion. However, when alkali-metal cations A^+ are introduced into the structure, the $\text{M}^{\text{II}}/\text{Fe}^{\text{III}}$ ratio decreases and reaches the limiting value of 1 in the compounds of general formula $\text{AM}[\text{Fe}(\text{CN})_6]$. In this case the M^{II} metal ion is coordinated by six cyanide nitrogen donors and thus the Co^{II} ion can be oxidized by the Fe^{III} yielding an $\text{Fe}^{\text{II}}\text{-CN-Co}^{\text{III}}$ pair. When the introduction of the alkali-metal cation into the structure is only partial, the situation is critical, because only a partial substitution of the two water molecules in the coordination sphere of Co^{II} occurs, and thus the $\text{Fe}^{\text{III}}\text{-CN-Co}^{\text{II}}$ and $\text{Fe}^{\text{II}}\text{-CN-Co}^{\text{III}}$ species have similar energies and their relative stability is controlled by several parameters. As a result, $\text{Na}_{0.4}\text{Co}_{0.3}^{\text{II}}\text{Co}^{\text{III}}[\text{Fe}^{\text{II}}(\text{CN})_6]$ undergoes a thermally (entropy) induced valence tautomeric transition to $\text{Na}_{0.4}\text{Co}_{1.3}^{\text{II}}[\text{Fe}^{\text{III}}(\text{CN})_6]$ ($T_c = 260\text{ K}$).^[21] This transition is characterized by a large thermal hysteresis loop (40 K). (In addition, it was recently shown that such alkali-metal-doped compounds also undergo pressure-induced electron-transfer processes.^[25]) These results can be explained by the following observation:

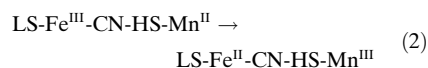
The Fe–C bond lengths do not change significantly (0.02 Å) in the electron-transfer process since the $\text{Fe}(t_{2g}^5) \rightarrow \text{Fe}(t_{2g}^6)$ change does not involve any σ^* bonding orbitals. However, an increase of 0.19 Å is observed in the Co–N bond lengths when the $\text{LS-Co}^{\text{III}}$ center is reduced to HS-Co^{II} since, in this $\text{Co}(t_{2g}^6) \rightarrow \text{Co}(t_{2g}^5e_g^2)$ change, the population of the σ^* orbitals is altered. Thus, as the temperature increases, the $\text{Fe}^{\text{III}}\text{-Co}^{\text{II}}$ species is favored by electronic and vibrational entropy contributions.

At low temperature the irradiation of the metal-to-metal charge-transfer (MMCT) band $\text{Fe}^{\text{II}} \rightarrow \text{Co}^{\text{III}}$ affords the metastable paramagnetic $\text{Fe}^{\text{III}}\text{-Co}^{\text{II}}$ species. The resulting large change in the Co–N bond lengths must be adsorbed by the surrounding lattice, which causes a high degree of network strain. This accommodation of the Co–N bond lengths involves the formation of a magnetic-phase domain and the metastable state is trapped owing to the high energy barrier associated with its relaxation to the original diamagnetic ground state (see below). As a result the metastable $\text{Fe}^{\text{III}}\text{-CN-Co}^{\text{II}}$ pair can be trapped by fast cooling at low temperatures (frozen-in effect).^[7] It was therefore rather surprising that $\text{Cs}_{0.97}\text{Co}[\text{Fe}(\text{CN})_6]_{0.97} \cdot 3.2\text{H}_2\text{O}$, where the diamagnetic pairs are dominant, is rather insensitive to light stimulation.^[23] Verdager and co-workers demonstrated that this result arises from the lack of flexibility of the crystal lattice, the interconversion processes at the first step require some structural vacancies.^[24] It was also suggested that all of the Co^{III} centers are surrounded by six N donors, which have a poor oxidizing power, whereas in the sodium and rubidium derivatives the same ions are coordinated, on average, by five N donors and one O donor. The calculated Franck–Condon excitation energies of the two states support this suggestion.^[26]

As mentioned above, the metastable states obtained upon irradiation are stable at 5 K for several days and the original ground state is regenerated by heating. The thermal relaxation curves cannot be fitted with the usual exponential law which characterizes the relaxation process of an excited state of diluted molecular systems, the curves in fact have a sigmoidal shape which

suggests the existence of an autocatalytic process.^[27] In addition, the metastable states show large magnetic hysteresis effects. All these properties are consistent with the existence of huge cooperative effects arising from strong intermolecular interactions. This situation means that the photoexcitation of any unit in the lattice induces the transformation of its surroundings, thus promoting the growth of a domain of molecules which are in the metastable state. The main consequence is that the potential barrier may be so large that at low temperatures the thermally activated relaxation process can be, in practice, precluded. These findings suggest the basis for a new systems for information storage.^[28]

As well as the cobalt prussiate complexes, the manganese analogues have also been studied.^[29] At room temperature the compound $\text{RbMn}[\text{Fe}(\text{CN})_6]$ contains antiferromagnetically coupled HS-Mn^{II} and $\text{LS-Fe}^{\text{III}}$ ions. As the temperature is decreased, an electron-transfer process occurs according to the valence tautomeric interconversion in Equation (2) thus affording ferromagnetically coupled Mn^{III} ions bridged by the $\text{NC-Fe}^{\text{II}}\text{-CN}$ diamagnetic moiety.



The transition involves a change of the unit cell of the solid which is caused by the strong distortion arising from the formation of the Mn^{III} species. At low temperature the compound behaves as a ferromagnet ($T_c = 10\text{ K}$). Light irradiation then induces the formation of the $\text{Fe}^{\text{III}}\text{-Mn}^{\text{II}}$ pairs as the metastable state and a photodemagnetization effect is observed. A significant photoinduced magnetization was detected for a Nd prussiate derivative, although the origin of the light effect has not yet been elucidated.^[30]

These significant results show the possibility of inducing ordered magnetic phases by light stimulation. It is important to stress, however, that the above mentioned systems require quite a long illumination time at very low temperature. Both these aspects were rather discouraging for the possible technological application of these compounds

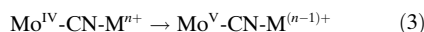
until the following spectacular result was obtained by Sato and co-workers.^[31]

The sodium cobalt prussiate derivatives undergo reversible entropy-driven valence-tautomeric transitions involving the $\text{Fe}^{\text{II}}\text{-CN-Co}^{\text{III}}$ diamagnetic pairs (low-temperature (LT) phase) and the $\text{Fe}^{\text{III}}\text{-CN-Co}^{\text{II}}$ paramagnetic pairs (high-temperature (HT) phase). A compound of formula $\text{Na}_{0.36}\text{Co}_{1.32}[\text{Fe}(\text{CN})_6] \cdot 5.6\text{H}_2\text{O}$ was found to exhibit a large thermal hysteresis with $T_{\text{c}\uparrow} = 230\text{ K}$ and $T_{\text{c}\downarrow} = 197\text{ K}$. Abrupt changes in the χT values begin at 225 K in the heating process (\uparrow) and at 205 K in the cooling process (\downarrow). The electronic spectra of the two tautomers are characterized by broad bands in the visible regions with absorption maxima at around 680 nm for the $\text{Fe}^{\text{II}}\text{-CN-Co}^{\text{III}}$ (LT) phase and 590 nm for the $\text{Fe}^{\text{III}}\text{-CN-Co}^{\text{II}}$ (HT) phase. A single-shot irradiation at 520 nm of the HT phase with a laser pulse (8 ns) at 205 K induced the complete transition to the LT phase. The reverse LT \rightarrow HT phase transition was obtained by irradiating the sample with a single shot at the same wavelength at 225 K. It is also remarkable that the photoinduced transition occurs only if the photon density of the laser pulse exceeds a critical threshold value. This means that the phase-transition occurs when the number of excited centers is higher than a threshold value necessary to cause a domino effect with the surrounding lattice. This result is extremely important since it shows that a photoinduced magnetization change can occur at high temperature provided that the system exhibits a large hysteresis loop.

It was found that in $\text{HS-Fe}^{\text{II}}_{1.5}[\text{Cr}^{\text{III}}(\text{CN})_6] \cdot 7.5\text{H}_2\text{O}$ the two paramagnetic metal ions experience a ferromagnetic interaction which is disconnected by irradiation.^[32] In the manganese(II) analogue the two metal ions experience antiferromagnetic interactions and the compound behaves as a ferrimagnet ($T_{\text{c}} = 67\text{ K}$).^[33] A mixed ferro-ferrimagnetic behavior characterizes the ternary derivatives $(\text{Mn}^{\text{II}}_x\text{Fe}^{\text{II}}_{1-x})_{1.5}[\text{Cr}^{\text{III}}(\text{CN})_6] \cdot z\text{H}_2\text{O}$ whose overall magnetization is determined by the ratio of ferromagnetic ($\text{Fe}^{\text{II}}\text{-Cr}^{\text{III}}$) and ferrimagnetic ($\text{Mn}^{\text{II}}\text{-Cr}^{\text{III}}$) contributions. This compound has a negative magnetization, but irradiation at 16 K in the

presence of a weak magnetic field (10 G) induces a change of the sign of the magnetization, thus affording a photoinduced magnetic pole inversion.^[34] Thermal treatment restored the starting material. This behavior is due to the photochromic properties of the $\text{Fe}^{\text{II}}\text{-CN-Cr}^{\text{III}}$ pairs.

A different strategy used for the synthesis of photomagnetic materials exploits light-sensitive polycyanometallate ligands. A small enhancement of the magnetization was observed using the $[\text{Fe}(\text{CN})_5\text{NO}]^{2-}$ complex,^[6,35] but more significant results were obtained using $[\text{W}^{\text{IV}}(\text{CN})_8]^{4-}$ and $[\text{Mo}^{\text{IV}}(\text{CN})_8]^{4-}$ precursors. Again the photomagnetic effects are due to valence tautomeric effects [Eq. (3)], the Mo^{V} center is paramagnetic ($S = 1/2$).^[36]



Laser irradiation of the MMCT $\text{Mo}^{\text{IV}}\rightarrow\text{Cu}^{\text{II}}$ band of $\text{Cu}_2[\text{Mo}(\text{CN})_8] \cdot 8\text{H}_2\text{O}$ induces an enhancement of the magnetization as a result of the light-induced conversion into $\text{Mo}^{\text{V}}\text{-CN-Cu}^{\text{I}}$.^[37]

Photomagnetic effects were also found in cobalt-octacyanotungstate derivatives. $\text{CsCo}[\text{W}(\text{CN})_8] \cdot \text{H}_2\text{O}$ undergoes a thermally induced phase transition with a large hysteresis loop ($T_{\text{c}\uparrow} = 216$, $T_{\text{c}\downarrow} = 167$).^[38] This transition is attributed to the valence-tautomeric interconversion of the diamagnetic $\text{LS-Co}^{\text{III}}\text{-NC-W}^{\text{IV}}$ pair (stable at low temperatures) into the paramagnetic $\text{HS-Co}^{\text{II}}\text{-NC-W}^{\text{V}}$ pair, which is dominant at high temperatures. Again the same electron-transfer process could also be induced by light irradiation in the MMCT $\text{W}^{\text{IV}}\rightarrow\text{Co}^{\text{III}}$ band at 5 K, resulting in a strong enhancement of the magnetization.

These recent results by few research groups provided the basis for potential applications in the next generation of information storage devices. Most of the studies to date have concerned polymeric systems, but these results allow molecular systems to be conceived. Molecules containing up to six paramagnetic metal ions coordinated to a polycyanometallate anion have been isolated.^[39] If such compounds are highly anisotropic, these molecules may behave as photochromic single-molecule magnets (SMMs).^[40] The way for

obtaining this kind of system has been recently traced by Marvaud, Mathonière, and co-workers.^[41] $[\{\text{Cu}(\text{tren})\text{NC}\}_6\text{Mo}(\text{CN})_2](\text{ClO}_4)_8 \cdot 4.5\text{H}_2\text{O}$ (Figure 1; tren = tris(2-aminoethyl)amine) was isolated and structurally

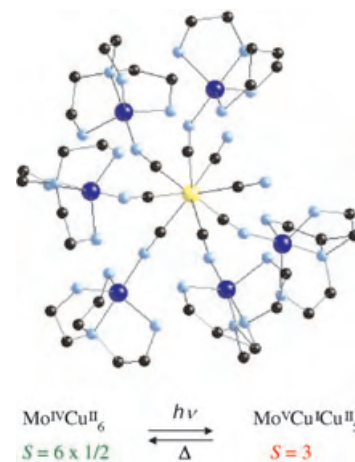


Figure 1. X-ray crystal structure of $[\{\text{Cu}(\text{tren})\text{NC}\}_6\text{Mo}(\text{CN})_2]^{8+}$ and an indication of the photoinduced changes. Hydrogen atoms, crystallization solvents, and counterions are omitted for clarity (Mo yellow, C black, N light blue, Cu dark blue).^[41]

characterized. The magnetic properties of this compound are consistent with a diamagnetic Mo^{IV} center surrounded by six weakly interacting $S = 1/2$ Cu^{II} ions. Once irradiated with a blue light, the magnetic properties change drastically, thus affording an $S = 3$ species. It was suggested that the light irradiation induces an electron transfer between the Mo^{IV} and one Cu^{II} ion, thus yielding a $\text{Mo}^{\text{V}}\text{Cu}^{\text{I}}\text{Cu}^{\text{II}}_5$ product in which the six paramagnetic centers experience a ferromagnetic interaction. The original compound can be restored by thermal treatment at 280 K. It can be easily anticipated that the developments of this strategy will allow the design and the synthesis of a family of discrete molecular systems showing peculiar photomagnetic properties.

Published online: January 14, 2005

- [1] B. L. Feringa, *Molecular Switches*, Wiley-VCH, Weinheim, Germany, 2001.
- [2] A. P. de Silva, N. D. McClenaghan, *Eur. J. Chem.* **2004**, 10, 574.

- [3] Special issue "Photochromism: Memories and Switches" M. Irie (Guest Ed.), *Chem. Rev.* **2000**, 100, 1683.
- [4] O. Khan, *Molecular Magnetism*, Wiley-VCH, Weinheim, **1993**.
- [5] *Magnetism: molecules to materials* (Eds.: J. S. Miller, M. Drillon), Wiley-VCH, Weinheim, **2001**.
- [6] P. Gütllich, Y. Garcia, T. Woike, *Coord. Chem. Rev.* **2001**, 219–221, 839.
- [7] O. Sato, *Acc. Chem. Res.* **2003**, 36, 692.
- [8] A. Fernandez-Acebes, J.-M. Lehn, *Chem. Eur. J.* **1999**, 5, 3285.
- [9] K. Takayama, K. Matsuda, M. Irie, *Chem. Eur. J.* **2003**, 9, 5605.
- [10] D. A. Pejakovic, C. Kitamura, J. S. Miller, A. J. Epstein, *Phys. Rev. Lett.* **2002**, 88, 57202.
- [11] P. Gütllich, A. Hauser, H. Spiering, *Angew. Chem.* **1994**, 106, 2109; *Angew. Chem. Int. Ed. Engl.* **1994**, 33, 2024.
- [12] P. Gütllich, Y. Garcia, H. A. Goodwin, *Chem. Soc. Rev.* **2000**, 29, 419.
- [13] O. Sato, S. Hayami, Z.-Z. Gu, K. Takahashi, R. Nakajima, A. Fujishima, *Chem. Phys. Lett.* **2002**, 355, 169.
- [14] C. Carbonera, A. Dei, J. F. Létard, C. Sangregorio, L. Sorace, *Angew. Chem.* **2004**, 116, 3198; *Angew. Chem. Int. Ed.* **2004**, 43, 3136.
- [15] S. Farley, T. Mallah, R. Ouhaes, P. Veillet, M. Verdaguer, *Nature* **1995**, 378, 701.
- [16] O. Sato, T. Iyoda, A. Fujishima, K. Hashimoto, *Science* **1996**, 271, 49.
- [17] O. Sato, T. Iyoda, A. Fujishima, K. Hashimoto, *Science* **1996**, 272, 704.
- [18] M. Verdaguer, *Science* **1996**, 272, 698.
- [19] O. Sato, Y. Einaga, A. Fujishima, K. Hashimoto, *Inorg. Chem.* **1999**, 38, 4405.
- [20] O. Sato, Y. Einaga, T. Iyoda, A. Fujishima, K. Hashimoto, *J. Electrochem. Soc.* **1997**, 144, L11.
- [21] O. Sato, Y. Einaga, T. Iyoda, K. Hashimoto, *J. Phys. Chem. B* **1997**, 101, 3903.
- [22] C. Cartier dit Moulin, F. Villain, A. Bleuzen, M.-A. Arrio, P. Saintctavit, C. Lomenech, V. Escax, F. Baudet, E. Dartyge, J.-J. Gallet, M. Verdaguer, *J. Am. Chem. Soc.* **2000**, 122, 6653.
- [23] A. Bleuzen, C. Lomenech, V. Escax, F. Villain, F. Varret, C. Cartier dit Moulin, M. Verdaguer, *J. Am. Chem. Soc.* **2000**, 122, 6648.
- [24] V. Escax, A. Bleuzen, J. P. Itié, P. Munsch, F. Varret, M. Verdaguer, *J. Phys. Chem. B* **2003**, 107, 4763.
- [25] V. Ksenofontov, G. Levchenko, S. Reianan, P. Gütllich, A. Bleuzen, V. Escax, M. Verdaguer, *Phys. Rev. B* **2003**, 68, 024415.
- [26] T. Kawamoto, Y. Asai, S. Abe, *Phys. Rev. Lett.* **2001**, 86, 348.
- [27] A. Goujon, O. Roubeau, F. Varret, A. Dolbecq, A. Bleuzen, M. Verdaguer, *Eur. Phys. J. B* **2000**, 14, 115.
- [28] J. C. Moore, E. J. Lochner, C. Ramsey, N. S. Dalal, A. E. Stiegman, *Angew. Chem.* **2003**, 115, 2847; *Angew. Chem. Int. Ed.* **2003**, 42, 2741.
- [29] H. Tokoro, S. Ohkoshi, K. Hashimoto, *Appl. Phys. Lett.* **2003**, 82, 1245.
- [30] G. Li, T. Akitsu, O. Sato, Y. Einaga, *J. Am. Chem. Soc.* **2003**, 125, 12396.
- [31] H. W. Liu, K. Matsuda, Z. Z. Gu, K. Takahashi, A. L. Cui, R. Nakajima, A. Fujishima, O. Sato, *Phys. Rev. Lett.* **2003**, 90, 167403.
- [32] S. Ohkoshi, Y. Einaga, A. Fujishima, K. Hashimoto, *J. Electroanal. Chem.* **1999**, 473, 245.
- [33] S. Ohkoshi, O. Sato, T. Iyoda, A. Fujishima, K. Hashimoto, *Inorg. Chem.* **1997**, 36, 268.
- [34] S. Ohkoshi, K. Hashimoto, *J. Am. Chem. Soc.* **1999**, 121, 10591.
- [35] Z.-Z. Gu, O. Sato, T. Iyoda, K. Hashimoto, A. Fujishima, *J. Phys. Chem.* **1996**, 100, 18289.
- [36] G. Rombaut, M. Verelst, S. Golhen, L. Ouahab, C. Mathonière, O. Kahn, *Inorg. Chem.* **2001**, 40, 1151.
- [37] S. Ohkoshi, N. Machida, Y. Abe, Z. J. Zhong, K. Hashimoto, *Chem. Lett.* **2001**, 312.
- [38] Y. Arimoto, S. Ohkoshi, Z. J. Zhong, H. Seino, Y. Mizohe, K. Hashimoto, *J. Am. Chem. Soc.* **2003**, 125, 9240.
- [39] V. Marvaud, C. Decroix, A. Scullier, F. Tuyères, C. Guyard-Duhayon, J. Vaissermann, J. Marrot, F. Gonnet, M. Verdaguer, *Chem. Eur. J.* **2003**, 9, 1692.
- [40] D. Gatteschi, R. Sessoli, *Angew. Chem.* **2003**, 115, 278; *Angew. Chem. Int. Ed.* **2003**, 42, 268.
- [41] J. M. Herrera, V. Marvaud, M. Verdaguer, J. Marrot, M. Kalisz, C. Mathonière, *Angew. Chem.* **2004**, 116, 5584; *Angew. Chem. Int. Ed.* **2004**, 43, 5468.

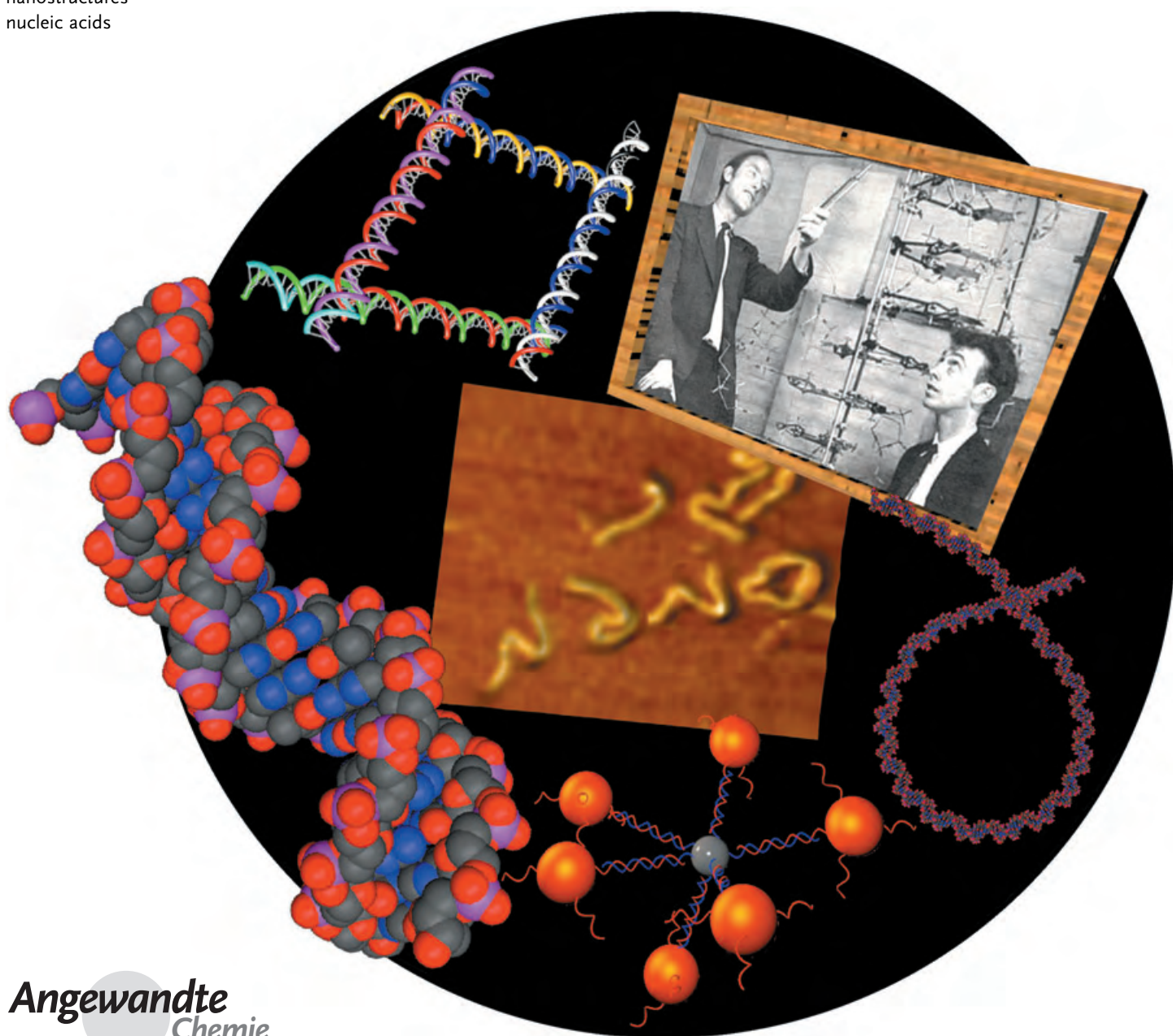
Bionanotechnology

DNA Codes for Nanoscience

Bruno Samorì* and Giampaolo Zuccheri

Keywords:

bionanotechnology · DNA ·
DNA–protein interactions ·
molecular recognition ·
nanostructures ·
nucleic acids

In memory of Claude HélèneAngewandte
Chemie

The nanometer scale is a special place where all sciences meet and develop a particularly strong interdisciplinarity. While biology is a source of inspiration for nanoscientists, chemistry has a central role in turning inspirations and methods from biological systems to nanotechnological use. DNA is the biological molecule by which nanoscience and nanotechnology is mostly fascinated. Nature uses DNA not only as a repository of the genetic information, but also as a controller of the expression of the genes it contains. Thus, there are codes embedded in the DNA sequence that serve to control recognition processes on the atomic scale, such as the base pairing, and others that control processes taking place on the nanoscale. From the chemical point of view, DNA is the supramolecular building block with the highest informational content. Nanoscience has therefore the opportunity of using DNA molecules to increase the level of complexity and efficiency in self-assembling and self-directing processes.

1. Introduction

In 2003, celebrations were held around the world in commemoration of the 50th anniversary of the discovery of the double-helical structure of DNA. Over these 50 years, the picture that Watson and Crick gave of the DNA structure in their historical paper in *Nature*^[1] has changed significantly. On analyzing DNA fiber diffraction data, they described a chain homogeneous in its canonical B-form structure, the most common in living organisms and in normal solution conditions. They had already envisaged that “the specific base pairing immediately suggests a possible copying mechanism for the genetic material.” On the other hand, a homogeneous straight chain could act only as a simple repository of the genetic information, with little function in itself. This picture was implying that the expression and the control of the genes would be delegated to proteins only. A more unified version is now finding more and more supporters: DNA itself also controls the expression of the genes through protein-recognition mechanisms that are based on the modulation of the DNA structure and dynamics along the chain. To date these recognition processes have been studied on small model systems (oligonucleotides) mostly by high-resolution techniques, such as X-ray crystallography and NMR spectroscopy. Research tools and methods common in the nanosciences now make it possible to study DNA interactive processes on the nano- and the microscale with molecules more similar to the substrates of the cellular processes. These methods led to the discovery that the codes contained in the DNA base sequence rule these interactive processes from the atomic scale of the single base-pair level to the nanometer and micrometer scale-lengths of the DNA superstructures.

The term “code” was defined by Trifonov as “any pattern or bias in the sequence which corresponds to one or another specific biological (biomolecular) function or interaction.”^[2] The codes of DNA are generally chemical in nature, mostly structural: it is the complementarity of the interaction between two aromatic systems that determines the base-pairing specificity. On a larger length scale, the composition of

From the Contents

1. Introduction	1167
2. The Base-Pairing Code for DNA Recognition on the Atomic Scale	1167
3. Structural Codes for DNA Recognition on the Nanoscale: Shape and Flexibility	1172
4. Summary and Outlook	1178

many local chain deformations in space drives, for instance, the wrapping of DNA around the histone proteins in nucleosomes in chromatin.

Herein we present an overview of the information codes embedded in

DNA. These can provide a toolbox of DNA recognition processes that can be used to switch self-organization along different length and energy scales. The field of DNA nanotechnology has relied to date exclusively on the base-pairing code but there is room for much more. After a brief survey of some of the major achievements, we will dwell longer on the more complex codes that can exploit multiple hierarchies of information in the self-assembling of more and more complex DNA-based nanostructures.

2. The Base-Pairing Code for DNA Recognition on the Atomic Scale

The pairing of complementary bases between DNA molecules or, similarly, between DNA and RNA or RNA and RNA, drives not only DNA replication, but also other biological functions, such as DNA transcription, translation, and repair. In nanoscience and nanotechnology methods have been developed that more and more extensively use this code to create tools and molecular constructions.

2.1 Base-Pairing in the Cell

The specific pairing of nucleobases is the main repository of genetic information of DNA. The Watson–Crick pattern of the possible hydrogen bonds and their geometry provides the basis for the encoding of genetic information in a robust code present in two copies in any double stranded DNA (dsDNA)

[*] Prof. B. Samori, Dr. G. Zuccheri
Department of Biochemistry “G. Moruzzi”
University of Bologna and
The National Institute for the Physics of the Matter (INFM)
Via Irnerio 48, 40126 Bologna (Italy)
Fax (+39) 051-209-4387
E-mail: bruno.samori@unibo.it

molecule. The fairly regular structure of the double helix requires a proper alignment of the bases and the exclusive pairing of a purinic with a pyrimidinic base, to create a 2-nm-wide helix.

The need of a perfect pairing for the millions of base pairs of genomic DNA requires a complex and robust control of matching, since many instances of short complementary sequences can be present and compete for the target sequence. Many proteins are used during recombination to make sure that any sub-optimal pairing is rejected (by making it unstable). On the other hand, for evolution to proceed, there must be a balance between genetic stability and rearrangements.^[3]

Base-pairing errors are also caused by damage in the DNA. DNA-damaging agents are present both exogenously in the environment and also endogenously as by-products of metabolic processes. Cells have evolved a number of ways to deal with breaks in the double-strand.^[4] Furthermore, certain normal processes, such as the recombination steps involved in the development of the lymphoid system in vertebrates, have the potential to create a high number of double-strand breaks.

2.2 Use of Base-Pairing for Nanoscience and Nanotechnology

The specific recognition between complementary stretches of nucleotides to form a Watson–Crick double-chain is being used more and more extensively in nanoscience to drive specific recognition processes that are used to assemble nanoscale constructions made of DNA only, of DNA and other components, or mainly of other components, in which the DNA is only used to promote the assembly. The presence of the DNA, with its controllable molecular properties, enables the creation of constructions with a predictable structure, which leads to ordered (regular) systems. The constructions can reach an impressive level of complexity, and, although being made of numerous DNA strands, assemble precisely.

The DNA base-pairing code is also used to perform calculations. Highly parallel solvers for specific problems and algorithms (such as, the Hamiltonian path) can be implemented through the use of DNA. The field of “DNA computing” is very young and very active, and is moving rapidly from simulations to realizations.^[5,6]

For all the applications of the DNA base-pairing code, affinity and specificity are particularly important. In biomolecular interactions that are based on shape complementarity, or steric fit between the two counterparts (enzyme–substrate, antigen–antibody, aptamer–small-molecule complexes) both high specificity and high affinity are achieved at the same time. A nonprecise steric fit between two surfaces results in significant energetic penalties. In the case of nucleic acid interactions, however, as the binding affinity for the chosen target sequence increases, the sequence specificity decreases. This situation is due to the fact that the recognition mode and the association between two nucleic acid chains is based on a one-dimensional (1D) nucleation-zipping mechanism.^[7,8] Steric fit and nucleation zipping differ dramatically. The slightest change in the shape of a key will totally impair its function. In an interaction that can be described by the three-dimensional (3D) concept of shape-complementarity, both affinity and specificity depend on the extent of steric fit, and are thus correlated. In contrast, a strong zip with one irregular or missing link can still be fastened with high affinity leaving out the small mismatched part. An increase in affinity through lengthening the complementary section of the zip does not compensate for the small loss of free energy arising from the mismatch, because the longer complex with the mismatch will be stabilized comparably. This mechanism results in a gradual decrease of nucleic acid hybridization specificity with increasing binding affinity: a scientist designing a nucleic acid probe or a molecular construction must bear in mind that a longer oligonucleotide is not always better, and that there might be alternative strategies for increasing the specificity and the affinity at the same time (see ref. [7] for an overview of some of these strategies.)

2.2.1 DNA-Based Molecular Constructions

Work done mainly by Ned Seeman's group^[9–13] (but also more recently in the Reif and Winfree groups^[14,15]) reveals the power of using the code in the nucleotide sequences of single-stranded DNA (ssDNA) to direct self-assembly processes. Large polymeric constructions (1D and 2D)^[16] or smaller oligomeric or monomeric objects can be prepared by the assembly of at least six different oligonucleotides into structures based on the blocked Holliday junction (Figure 1a). Computerized methods have been developed to



Bruno Samorì is Professor of Organic Chemistry at the School of Biotechnology of the University of Bologna. Up until 1990, he carried out researches with polarized spectroscopy techniques on the stereochemistry of synthetic organic molecules, (at the University of Bologna, with S. F. Mason at King's College, London, with I. Tinoco at the UC Berkeley). Since then, his research interests moved to the chemistry and biology of DNA superstructures, and, more recently, also to protein folding and mechanochemistry. He has been President of the Division of the Chemistry of the Biological Systems of the Italian Chemical Society and also of the Italian Society of Microscopic Sciences.



Giampaolo Zuccheri is full-time Researcher in the Department of Biochemistry of the University of Bologna. He received his “Laurea” in 1994 from the Faculty of Industrial Chemistry of the University of Bologna and his Ph.D. in Chemistry in 1998 from the University of Calabria, Italy. He has worked with Marcos Maestre (Lawrence Berkeley National Labs) and with Carlos Bustamante (then at the University of Oregon) and he is currently working with Bruno Samorì. His interests focus on the chemistry and biophysics of nucleic acids.

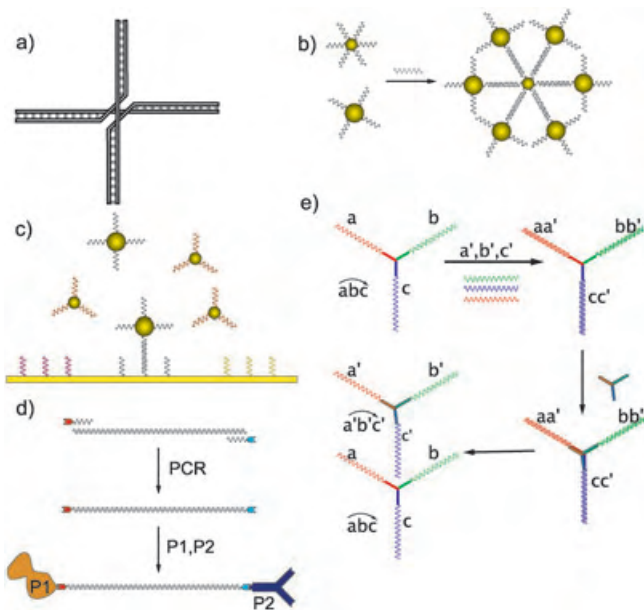


Figure 1. Examples of DNA-based nanoconstructions. a) A Holliday Junction is made by four arms of dsDNA joined at a crossover. In the naturally occurring junction (an intermediate in recombination) the crossover can migrate thanks to the sequence symmetry of the arms; in the blocked junctions, the building block for many of the constructions from the Seeman group, the position of the junction is fixed by breaking the symmetry of the sequence around the crossover point.^[16] b) Linking of oligonucleotide functionalized gold nanoparticles by an oligonucleotide motif, each half of which is complementary to one or the other particle-bound oligonucleotide.^[23] c) Gold nanoparticles can be specifically anchored on surface spots where oligonucleotides are attached. The assemble signal can be, similarly to (b), an oligonucleotide with each half complementary to the particle-bound or the surface-bound oligonucleotides.^[28] d) PCR-mediated introduction of unusual functionalities in a dsDNA segment of desired sequence and length as a method to prepare specifically designed DNA–protein hybrids.^[31] e) Self-replication of connectivity among oligonucleotides.^[32] Base pairing is used to localize three oligonucleotides in space with termini at the right distance for cross-linking. The base pairing on the preformed tri-linked template regulates the configuration of the assembly on the new tri-linked structure.

choose oligonucleotide sequences that could improve on the self-assembly specificity, by minimizing the possible frame-shift errors or the mismatches. These are some of the most serious sources of possible errors in the self-assembly, and which probably determine the upper limit for structural complexity. Atomic force microscopy (AFM) and classical biochemical techniques, such as electrophoresis, are used to characterize the building blocks and the constructed nano-objects. One of the peculiar properties of the DNA-based constructions born in the Seeman group is their rigidity. Being a fairly stiff polymer, DNA lends itself to the construction of braided structures with at least twice the rigidity of dsDNA (that is, with a persistence length (see Section 3.2) of up to 100 nm).^[9]

Shih and co-workers have recently reported the formation of a DNA octahedron, approximately 22 nm in diameter, through the folding of a very long (1699-nucleotide) ssDNA by a simple denaturation–renaturation procedure in the

presence of five 40-mer synthetic oligonucleotides.^[17] The methodology used to prepare the 1699-nucleotide-ssDNA (originally proposed by Stemmer and co-workers^[18]) is also remarkable: starting from synthetic oligodeoxynucleotides, a kilo-base-pair long template can be constructed by a polymerase-chain-reaction (PCR)-based method. The template is amplified in the context of a bacterial plasmid, and then later excised, thus allowing its production by cloning.

In this type of structure DNA does not “simply” have coding and structural functions, it can also have functional properties: at least two types of approaches have been used to create motion in DNA-only objects. DNA can undergo structural transitions in response to changes in its environment. Under appropriate conditions, an alternating GC sequence can undergo the B–Z transition resulting in a reversal of handedness of the double helix. Seeman and co-workers have employed this controlled and induced rotation to change the distance between objects in space.^[12] When these objects are labeled with fluorescent dyes, the motion can be easily followed studying their photophysical properties.

If nanoobjects result from the programmed assembly of a number of (long) oligonucleotides, then a second type of approach towards implementing motion can be based on a competitive reconstruction of the objects after the addition of other (more extensively) complementary DNA strands. This strategy has been used by Yurke and co-workers^[19] and by Feng and co-workers^[15] to drive controlled and cyclic motions in monomeric or polymeric (lattice-like) DNA objects. One of the main features of these motors is that they “burn” DNA, meaning that a full cycle of contraction–retraction requires the addition of two complementary oligonucleotides, and thus produces one double-strand of useless DNA in solution with the motor.

Yurke et al.^[19] presented a nanotweezer that very ingeniously could move objects in space if driven by the specific recognition of the base-pairing code. Similarly, the code might also be used to tell which of a series of different tweezers should close or open or where in space a DNA-tethered object should be taken to: all obtained simply by adding a few components in solution.

Feng and co-workers^[15] applied the strategy devised by Yurke et al. to the type of arrays invented by Seeman and co-workers. They obtained large flat objects that can be tightened or expanded by the addition of oligonucleotides, so that they might work as movers, as size-specific switchable filters, or in the mechanical release of complexed objects. Other research groups have presented examples where some of the various conformational transitions of DNA have been exploited to move objects around.^[6,13,20]

2.2.2 Exploiting the Code: DNA-Mediated Molecular Construction

After the pioneering idea of DNA-templated circuits presented by Robinson and Seeman,^[21] and the scheme for implementation of DNA-directed electrical wires by Di Mauro and Hollenberg,^[22] many examples of DNA objects and constructions have been reported: these are often hybrids

of DNA and other types of molecules, which range from small organic molecules to proteins or even synthetic polymers.

In these materials, DNA is mainly used as a structuring element, which drives the self-assembly of molecules that would not interact, or would do so in a disorderly fashion. After the chemical preparation of units which are properly designed to self-assemble into a molecule–oligonucleotide hybrid, it is often only necessary to mix the components together in the right stoichiometry to obtain the adducts.

The group of Mirkin has developed many techniques for arranging nanoparticles exploiting the code in oligonucleotides that are attached to them.^[23] The easiest way is to employ thiol-modified oligonucleotides (now available from commercial oligonucleotide providers) that attach strongly to clean gold surfaces.^[24] Fritschke and co-workers,^[25] Niemeyer and co-workers,^[26] and Mirkin and co-workers^[27] have provided examples where gold nanoparticles have been attached to flat gold surfaces thanks to the creation of a short stretch of dsDNA between nanoparticle-bound and surface-bound complementary oligonucleotides. In some of the examples, the two types of oligonucleotides are not complementary to each other, but are complementary to either half of a third oligonucleotide that can switch the anchoring of the soluble nanoparticles to the surface, when added to the solution (Figure 1c).^[27,28] The same strategy can be used to create ordered aggregates of different nanoparticles in solution, where a number of oligonucleotide-functionalized nanoparticles assemble as a response to the introduction of another oligonucleotide that serves as the “glue”, its two halves are complementary to the oligonucleotides anchored on the nanoparticles (Figure 1b).^[23]

Niemeyer and co-workers have investigated many DNA–streptavidin constructions: biotinylated oligonucleotides were obtained commercially, or from the derivatization of other commercially available modified oligonucleotides with hetero-bifunctional linkers.^[29] These complexes can also be used to bind other biotinylated products to the already established DNA–streptavidin complex, a virtue of the tetravalency of streptavidin (that could even be expanded). By following this strategy, a wide variety of complexes can be obtained, for instance biotinylated antibodies have been bound to the oligonucleotide-bound streptavidin, so that the antibody complex could then be driven to adsorb to a specific spot on a gold surface where the complementary oligonucleotide was tethered by a gold–sulfur bond.^[30]

To date, nanoscientists have mainly employed commercially available modified oligonucleotides that were brought onto the market for totally different purposes (mainly for molecular biology). The full power of synthetic chemistry have still to be unchained to the benefit of this field. A few remarkable examples of this power are already available: Abell and co-workers prepared asymmetric protein dumbbells through the use of custom prepared modified oligonucleotides that could bind proteins specifically and also work as PCR primers^[31] (Figure 1d). This result could be interpreted as an initial step towards the organized synthesis of replicas of the multiprotein factories found inside cells.

Another noteworthy example of the use of organic chemistry together with DNA coding has been presented by

von Kiedrowski and co-workers.^[32] By preparing a tridentate linker, they could assemble a Y-shaped tris oligonucleotide, an uncommon template. The template could link to three soluble complementary oligonucleotides in solution, these oligonucleotides could in turn cross-link to another tridentate linker in a stereochemically controlled fashion (Figure 1e). The entire process can be thought of as the replication of (stereochemically controlled) connectivity, a feat requiring a high degree of control.

Nanoelectronics has been one of the guiding lights for many nanoscience researches. The base-pairing code of DNA has been used for the assembly of nanoelectronic components, as shown, for example, in the sequence-specific single-DNA-molecule lithography of Keren and co-workers.^[33] The method involves the use of RecA, a protein that binds to an ssDNA molecule and facilitates its sequence-specific “invasion” inside a long dsDNA molecule. When Keren and co-workers turned a long DNA double-helix into a metallic nanowire by electroless metallization, the presence of the invading nucleoprotein complex (RecA polymerized on the single-stranded DNA) in a section of the chain served as a mask to prevent metallization of that part of the double-helix. Thus, the DNA-templated metal wire had an insulating gap whose precise location and length had been determined by the length and the sequence of the single-stranded section.

In another example of use of the DNA codes in nanoelectronics, carbon nanotubes have been derivatized with oligonucleotides. The base-pairing codes of different batches of tubes drive the assembly of families of tubes, to serve as electronic components.^[34] This self-assembly could also be interesting for creating nanostructured materials with exceptional mechanical properties, thanks to nanotubes, but that are also water soluble, thanks to the bound DNA.

Recently, DNA has also been coupled with synthetic polymers, in an attempt to realize hybrid materials that could exploit the base-pairing properties of DNA.^[35]

2.2.3 RNA and Synthetic Analogues of Natural Nucleic Acids

Storage of information through the pairing of bases is not a property of DNA only. The base-pairing of single-stranded RNA with DNA has been used to attach different oligonucleotides (and objects-bearing oligonucleotides) along the RNA chain.^[29] The RNA is effectively used as a master program. Alternatively, the interactions amongst RNA molecules themselves can be used for making unusual and complex structures held together by noncovalent bonds. The artificial modular assembly units that are used to form RNA nanoobjects have been termed tecto-RNA.^[36] These are self-assembling RNA building blocks that are designed and programmed to generate RNA super-architectures in a highly predictable manner for a wide range of applications.^[37]

There is currently much interest, also from the pharmaceutical industry, in small double-stranded RNAs (designated as small interfering RNAs or siRNAs) because they can be used for the sequence-specific silencing of gene expression through RNA interference in eukaryotic cells.^[38] Exogenously supplied siRNAs have potent and specific effects in reducing the expression of homologous endogenous genes. This gene-

silencing approach based on RNA interference might help to overcome efficiency problems of traditional antisense molecules.

Peptide nucleic acids (PNAs) are DNA or RNA synthetic mimics, in which the nucleobases are attached to a peptide-like (polyamide) uncharged backbone.^[39] PNA oligomers can form stable duplex structures with Watson–Crick complementary DNA and RNA (or PNA) oligomers, and they can also bind to targets in duplex DNA by helix invasion.^[40] Peter Nielsen, recognized as the inventor of PNA, has recently reviewed the applications of these molecules in chemistry, biology, and medicine, including drug discovery, genetic diagnostics, molecular recognition, and the origin of life.^[41]

PNA molecules that function as molecular beacons have been developed for the recognition of specific sequences within dsDNA without denaturation. Molecular beacons are sensitive fluorescent probes which hybridize selectively to designated DNA and RNA targets. With the aid of PNA “openers” (dehybridizing agents that open the double helix) molecular beacons were employed for the detection of a chosen target sequence in dsDNA and, in particular, to discriminate between complementary versus mismatched dsDNA sequences.^[42] PNA beacons are advantageous over DNA beacons because they can be used to analyze unpurified or non-deproteinized DNA samples. This feature of PNA beacons may find applications in the emerging area of fluorescent DNA diagnostics.^[43]

PNA has several useful characteristics, these include the ability to form triple helices and complexes with other topologies, the possibility of being chiral,^[44] and a stronger base-pairing in PNA–DNA hybrids than in regular dsDNA (because of the electric neutrality of the PNA backbone). These properties provide researchers with a wide spectrum of possibilities for the tailoring and the control of the specificity, the affinity, and the steric effects of the base-pair interaction.^[7]

Other recently developed DNA analogues, the locked nucleic acids (LNAs) are modified nucleotides that contains a 2'-O, 4'-C methylene bridge. This bridge, locked in 3'-endo conformation, restricts the flexibility of the ribofuranose ring and locks the structure into a rigid bicyclic formation, which confers an enhanced hybridization performance and an exceptional biological stability.^[45] An LNA probe forms a more stable hybrid with its target sequence than the corresponding DNA stand would.^[46] This increase in hybridization stability allows a significant broadening of the experimental conditions.^[47]

Eschenmoser and co-workers synthesized another type of nucleic acids called L- α -threofuranosyl oligonucleotides, or TNAs.^[48] They found that complementary TNA strands can form stable double helices and are capable of Watson–Crick base pairing with DNA, RNA, and TNA. A variety of DNA polymerases have been screened for activity on a TNA template, and several showed a surprisingly good ability to copy limited stretches of TNA.^[49]

Attempts have also been made at extending the concept of DNA base-pairing through the synthesis of a pseudoDNA containing bigger polycyclic bases.^[50]

2.2.4 DNA Chips and DNA Detection: The Reading of the Code and the Interplay Between Affinity and Specificity in the Base Pairing

One of the most established technical applications in which the base-pairing codes of DNA are exploited is genetic analysis. For research and diagnostic purposes, cells are scanned for the presence of genes, or for the level of expression of peculiar genetic products.^[51,52] Parallel genetic testing is currently performed on devices termed “sensing arrays” which consist of an array of “spots” on a surface. A different oligonucleotide is anchored to each spot and can base-pair with the DNA or RNA target or analyte molecules. The read-out of the hybridization is based on the introduction of fluorescent,^[51] electroactive,^[53] or nanoparticle labels^[28,54] to produce a measurable signal. Several attempts at the fully electronic detection of (labeled or unlabelled) nucleic acids and proteins have been performed,^[55] but the sensitivity is still far from optimal (more than 10^4 molecules of analyte required). Electrical-detection-based technologies will make the sensing-array technology suitable for simple-to-use, low-cost, point-of-care diagnostics, for applications in environmental analysis, biohazard and bioweapons detection, and for the detection of pathogens.

Many chemical strategies have been employed to immobilize nucleic acids at surfaces including electropolymerization, streptavidin–biotin interactions, gold–thiol links.^[56] Fully electronic methods that would detect unlabelled DNA molecules without the need for amplification of the target molecule (that is, that are not based on methods such as PCR) are now required. This important goal strongly depends on the development of 1) nanoscience-based strategies for signal enhancement, 2) methods to increase both the affinity and the specificity of the base-pairing recognition processes. While the former is a new field, much has already been done for the latter, and a particularly clear overview about the very special interplay between affinity and selectivity in nucleic acid interaction can be found in a recent article by Demidov and Frank-Kamenetskii.^[7] Some of the approaches used to increase simultaneously the affinity and specificity use oligonucleotides in novel topologies (e.g. circular, dendrimeric, nanoparticle-bound), while others employ newer types of oligonucleotide analogues (LNAs, PNAs).^[7]

2.2.5 The Need to Develop Further Strategies for the Synthesis of Bio-Nanotechnological Building Blocks

The room for expanding the applications of DNA to nanotechnology is mainly limited by the availability of suitable and efficient chemical strategies for the preparation, purification, and handling of the necessary building blocks.

The available techniques for solid-phase synthesis can prepare milligram amounts of oligonucleotides, much less if high purity, unusual length (more than, say, 40 nucleotides), or subsequent derivatization of the oligonucleotide is called for. The high cost for the preparation of gram amounts of numerous oligonucleotides is prohibitive. For the preparation and the purification of nucleic acids, organic chemists are beginning to employ techniques familiar to the biochemist

and the molecular biologist, such as gel electrophoresis and PCR. These techniques that have been developed and optimized for obtaining minute quantities of products, will have to be adapted for the growing needs of the scientific community. Extremely powerful methods based on the use of restriction endonucleases or DNA ligases (methods which are the envy of polymer chemists for their precision), will also need to be made more efficient before they can be used with large quantities of substrates. More proficient methods for the derivatization of surfaces and for cross-linking will be also needed.^[57] A great effort is required to adapt the available tools to the needs of a growing bio-nanotechnology community.

3. Structural Codes for DNA Recognition on the Nanoscale: Shape and Flexibility

The base sequence of a DNA segment also encodes the dynamics of the chain. DNA is continuously morphing into shapes and structures alternative to the canonical B-form, it is coiling in the cell nucleus, it is “swilling lazily around in a nourishing molecular soup of transcription factors and other regulatory proteins that are milling around the nucleus.”^[58]

Atomic force microscopy (AFM) imaging can give a particularly clear view of the apparently chaotic movements of a single DNA molecule. When a drop of solution containing a population of molecules of the same sequence and length is spread on the surface of a freshly-cleaved crystal of mica, and the resulting spread is imaged by AFM, the image can be like the micrograph in Figure 2. No two macromolecules have the same shape and conformation, in spite of being totally identical from any chemical or biochemical point of view. Contrary to the first impression, the apparently chaotic dynamics that leads to such a variety of shapes is not random.

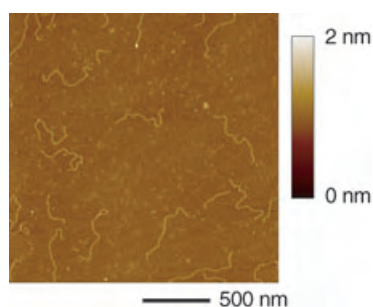


Figure 2. AFM image of a spread of DNA palindromic dimers obtained by dimerizing a restriction fragment excised out of plasmid pBR322 DNA. The 1878 base-pair long DNA molecules were spread on freshly cleaved muscovite mica from a solution of 4 mM HEPES buffer (pH 7.4), 10 mM NaCl, 2 mM MgCl₂ containing approximately 1 nM DNA molecules. Only the molecules completely inside the borders of the image and not presenting any anomalous structure (loops, kinks, bound objects) are used for digitally tracking the helical axis and for the subsequent curvature analysis. Smaller DNA fragments (or residual monomers) are recognized from their measured contour lengths, and subsequently neglected.

3.1. The DNA Shape Code: From the Ångström to the Nanometer Scale

The shape assumed in space and in time by a particular DNA molecule has been analyzed in terms of the superposition of the thermal fluctuations of the structure and the intrinsic, lowest energy structure of a chain with that sequence.^[59,60] The average structure of dsDNA depends on the sequence: the differences in the spatial arrangement imparted by the different base pairs along the chain give rise to deterministic modulations of the relative orientations of the average planes of the base pairs. These orientations are commonly expressed in terms of the base-step orientation parameters: roll, tilt, and twist (see Figure 3).

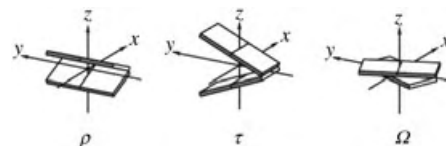


Figure 3. The dinucleotide step orientational parameters: roll (ρ), tilt (τ), and twist (Ω). The composition of the three rotations along the DNA chain gives rise to local and global curvatures.

Considerable effort has gone into defining sets of these parameters corresponding to the lowest energy structures directed by the sequence. Recently, Crothers has reviewed the approaches and the sets of values reported.^[61]

Table 1 gives the values that De Santis et al. defined on the basis of conformational energy minimization calculations,^[62] and then refined to fit experimental gel-retardation values.^[63,64] The roll, tilt, and twist values of the dinucleotide steps significantly deviate from the canonical B-form structure proposed by Watson and Crick^[1] and refined by Arnott and Hukins.^[65] Sets of angles like those in Table 1 (derived from nearest-neighbor simplifications of the chain properties)

Table 1: Values [°] for the dsDNA base-step orientational parameters.^[a]

5'-end	3'-end			
	A	C	G	T
Roll angles (ρ)				
A	−5.400	−2.500	1.000	−7.300
C	6.800	1.300	4.600	1.000
G	2.000	−3.700	1.300	−2.500
T	8.000	2.000	6.800	−5.400
Tilt angles (τ):				
A	−0.500	−2.700	−1.600	0.000
C	0.400	0.600	0.000	1.600
G	−1.700	0.000	−0.600	2.700
T	0.000	1.700	−0.400	0.500
twist angles (Ω):				
A	35.975	33.737	34.428	35.260
C	34.078	33.146	33.478	34.428
G	34.647	33.325	33.146	33.737
T	34.450	34.647	34.078	35.975

[a] See Figure 3.^[64,88] The 5'-end is in the left column from top to bottom and the 3'-end is from left to right across the row: for example, the roll angle for a 5'-TA-3' step is 8.0 degrees.

make it possible to easily predict the lowest energy chain conformation of a molecule from its sequence.

Positive or negative roll or tilt angles give rise to local bending of the double-helix axis. These local bends might lead to a zigzag pattern of the chain axis, which remains essentially straight, unless the bend occurs in phase with the double-stranded helical repeat. In this latter case, the bend might give rise to extended persistent curvatures that propagate from the Ångström to the nanometer scale.^[66] An example of large-scale curvature is the 211 base-pair segment from the kinetoplast DNA of the Trypanosomatidae Protozoan *Crithidia fasciculata*. This is the most highly curved natural DNA known. Its sequence (Figure 4c), is characterized by a

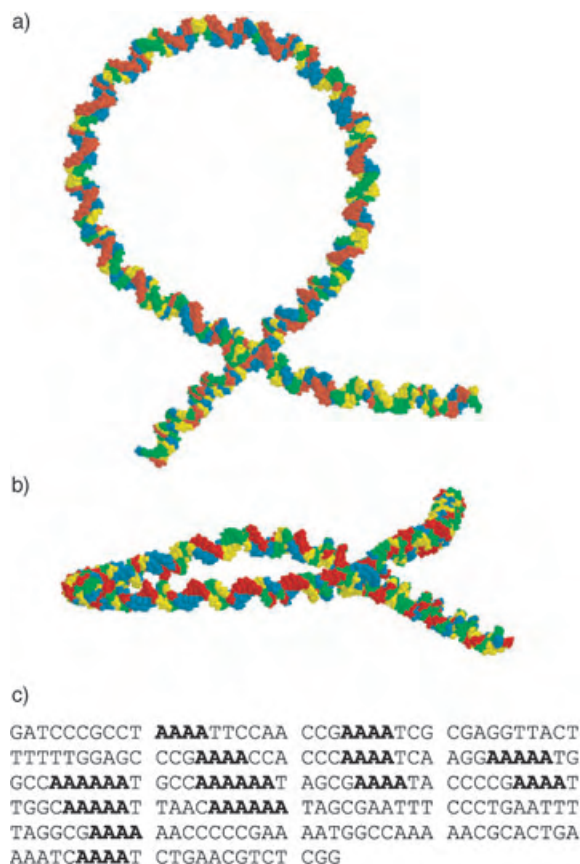


Figure 4. Predicted 3D structure of the curved segment of *Crithidia fasciculata*. (<http://archimede.chem.uniroma1.it/webdna.html>). a) View along a direction nearly perpendicular to the curvature plane, b) view along a direction almost parallel to the curvature plane, the segregation of adenines and thymine on the two faces of the curvature plane is clearly visible: red adenine, blue thymine, green guanines, yellow cytosines. c) The base sequence of the molecule shown in (a) and (b).

periodical recurrence of tracts of 3 to 6 adenine residues; the centers of most of these tracts are separated by 10 or 11 base pairs, that is, the average helical repeat. This distribution of the adenine tracts, perfectly phased with the helical winding, means that this short DNA segment has its lowest conformational energy when wrapped in a circle (Figure 4a,b). Experimental evidence of such a large curvature was first provided by Griffith et al.^[67]

Intrinsic curvatures have been monitored and studied by X-ray crystallography on very short double-stranded oligonucleotides.^[68] On longer DNA molecules, the curvatures have been studied by gel retardation,^[69,70] circularization kinetic,^[71,72] electron microscopy (EM),^[73] AFM,^[74,75] and have been simulated by molecular dynamics.^[76] Commonly, these experiments were carried out with dsDNA constructs with 1) anomalous flexibility sites, such as single-stranded stretches,^[75] internal loops arising from mismatches,^[70] a single nick,^[77] a double-stranded linker connecting triple-helix tracts,^[78] or 2) segments whose curvature was tailored and controlled by accurate phasing^[75] or unphasing,^[60,71] of adenine tracts with the helical periodicity. All these approaches to the study of intrinsic curvature are based on the determination of global parameters of the whole chain under investigation such as the persistence length, the end-to-end distance, or the cyclization J factor. Information about the sequence encoding and the molecular mechanisms that drives the formation of extended curvatures was inferred from the variations of the values of these global DNA parameters with respect to their values for reference sequences. A combinatorial approach has been proposed for this kind of study.^[71]

The trace of the trajectory of the double-helical axis of individual dsDNA chains deposited on a substrate can be recorded by EM or AFM. The intrinsic curvatures of dsDNA can thus be studied from the single-molecule point of view and it is possible to set up methods to map the intrinsic curvature along the chain of a natural DNA of any sequence. This investigation is carried out by computing the curvature from the angular chain deflections (Figure 5a) along a large number of profiles, averaging the values, and plotting these averaged values as a function of the (fractional) position along the chain (Figure 5b).^[74]

The intrinsic DNA curvatures can therefore be predicted theoretically and experimentally evaluated either as an average value for a particular DNA chain or as a localized value, mapped along the same chain. Despite these capabilities and many high-resolution NMR spectroscopy and X-ray studies of local bends in oligonucleotides, the description of the origin of large intrinsic curvatures at the atomic level remains disputed. No one doubts that a long-range curvature requires adenine tracts separated by a defined distance, and that it depends little on the nature of the sequences that separate the adenine tracts (see Figure 4c).^[79] It is not clear how the adenine tracts play a dominant role. The discussion has been mostly focused on the composition of the geometry parameters of the base pairs at the junctions of the adenine tracts with those of the rest of the chain.^[68,80] It is somewhat surprising that all different theoretical approaches based on nearest-neighbor models,^[63,81,82] reach very similar results in their description of the path of the helical axis in the nanoscale despite the different values they utilize for the base-step parameters (see also Table 1 and 2 in reference [61]).

We must therefore conclude that curvature is a long-range superstructural property that is more determined by the way the double helix selects, composes, and phases the local bends over different spatial scales; the individual parameters of the

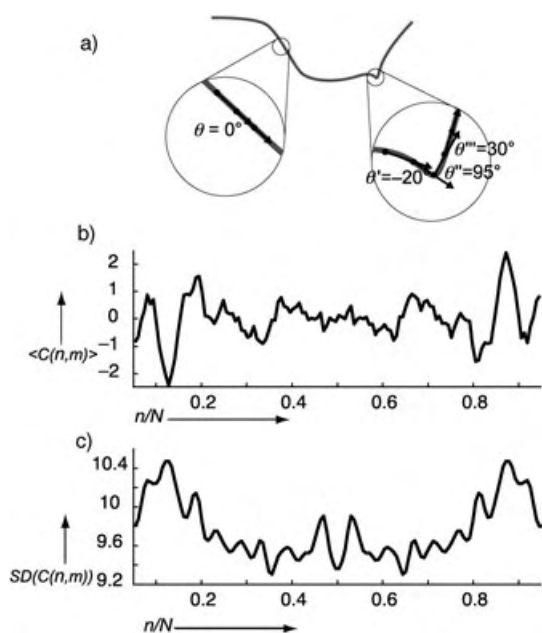


Figure 5. a) Method for quantifying the local DNA curvature from AFM images: the DNA chain axis is digitized in a segmented fashion and the local chain direction (and thus the curvature) is determined numerically; b) Plot of the experimental local DNA curvature (evaluated from the AFM images) along the chain of tail–tail palindromic dimers constructed using the EcoRV and the PstI sites of plasmid pBR322 DNA.^[74] The average local curvature $\langle C(n,m) \rangle$, in degrees (where n is the sequence position, $m = 2$ helical turns is the width of the averaging window) is plotted against the fractional position along the chain contour, n/N . The experimental plot has been made symmetrical by averaging the two equivalent halves to double the curvature information on the DNA sequence c) Plot of the experimental local DNA flexibility of the same DNA molecule evaluated as the standard deviation (SD) of the local chain curvature.

bends play a much less significant role. The nature of this structural code of DNA is thus not simply determined by the sequence (the words) but more subtly by the way the sequences are arranged along the chain (the language), with the notion that a certain flexibility in the sequence is allowed without producing serious changes in the average shape of the molecule.

3.2. The DNA Flexibility: From the Dinucleotide to the Micrometer Scale

The sequence in a DNA molecule determines not only the lowest energy profile of the molecule but also its local response to the thermal fluctuations. In this way the sequence controls the formation of conformers and superstructures. Note that a conformation, even if poorly populated, can play a crucial biological function. In fact, it can be recognized and selected to switch on processes that the most stable structures might not be able to activate. If our knowledge is limited to the lowest energy profiles, our chance of understanding functions might be limited. One of the experimental observables that gives insight into the accessible conformational space of a chain is its local axial flexibility, that is, the

tendency of the long axis of the double helix to deviate both locally and globally from a straight trajectory.

While there is satisfactory agreement on the determinants of DNA curvature (see Section 3.1), the issue of DNA flexibility is still under debate. The considerations that will follow reflect the point of view of the authors of the articles in question, and are certainly bound to require modification as more results become available.

The axial flexibility of the chains is controlled by the spatial arrangement of their sequences, in particular by van der Waals and electrostatic interactions between the adjacent base pairs.^[66,82–84] The electrostatic interactions are dominated by a large dipole on G–C pairs which is in contrast with a diffuse distribution of charge on A–T base-pairs.^[84,85] Adjacent A–T base-pairs can thus stack without displacement caused by electrostatic forces, whereas the repulsive dipoles in adjacent G–C base pairs lead to a slide displacement which results in a more positive roll angle.

Another factor that influences the general axial flexibility is the compressibility of both the major and minor grooves which results in the presence of exocyclic groups in the grooves.^[86] Recently, De Santis and co-workers showed that the axial flexibility is thermodynamically related to the melting temperature of a DNA tract when a first-order elasticity is assumed. This data can be easily obtained from the sequence by averaging the formal melting temperature assigned to each dinucleotide step. The results obtained by adopting such a dinucleotide flexibility scale satisfactorily explain the static and dynamic curvature dispersion of DNA images and the sequence-dependent thermodynamic stability of nucleosomes as well.^[64,74,87,88]

The axial flexibility of a chain in the nanometer length scale can be described in terms of its persistence length P , a parameter commonly used for defining a polymer bending rigidity. The parameter P is defined as the length over which the polymer axis direction is retained under thermal agitation. A number of techniques including light scattering,^[89] rotational diffusion,^[90] DNA cyclization kinetics,^[91] cryo-electron microscopy,^[60] as well as conventional electron microscopy^[92,44] and AFM^[93] have led to estimates for P of around 50 nm for mixed-sequence B-form DNA. The measured value of P , as determined by most techniques, depends not only on the intrinsic flexibility of the DNA molecule but also on the anisotropy of the axial flexibility which is due to its intrinsic curvature.^[60,94]

On the length scale of the dinucleotide steps, the axial flexibility (or bendability) has been estimated from the range of conformations adopted by the specific base steps in crystal structures of either DNA oligomers, or of DNA–protein complexes.^[82,95,96] In DNA oligomers, the deformations that force the DNA to bend locally (and make it possible to evaluate its bendability) are due to the lattice structure of the crystal. In DNA–protein complexes, the local bendability of the chain was demonstrated by the ability of the proteins to bend DNA at the binding positions. On this basis, the pyrimidine–purine steps were found to be more easily deformable than the purine–pyrimidine and purine–purine steps. The bendability of the dinucleotide steps decreases in the order $CG > CA(=TG) > TA > CC(=GG) > TC(=GA)$

> GC > TT(=AA) > GT(=AC) > CT(=AG) > AT. Olson and co-workers also deduced harmonic energy functions from the mean value and the dispersion of the base-pair step parameters.^[95,97]

Imaging methodologies that enable the trajectories of the DNA molecules under investigation to be visualized, make it possible to map not only the local intrinsic curvatures along the chain but also the local modulation of flexibility that is determined by the sequence. By evaluating the dispersion of the curvature values, flexibility plots, like that in Figure 5c, were generated for a population of symmetric molecules obtained by the dimerization of a tract of the DNA plasmid pBR322.^[74] These plots show that the local flexibility is generally higher where the molecule is more curved. This indicates that the sequence shapes the conformational space of the chain by modulating the intrinsic curvature and the flexibility in the same way. Molecular dynamics simulations (based on all-atom potentials) performed on oligonucleotide duplexes with adenine tracts indicate that they are essentially straight and rigid, and that the more bent and distorted steps (with respect to the canonical B-form) are more dynamically deformable.^[98]

There are 16 possible dinucleotides, of which 10 are symmetrically unique. The frequencies of these steps along the chain of the dimer shown in Figure 5 are reported in Figure 6. A good correlation with the flexibility results for the AA(=TT), TA, and AT steps. Anticorrelation is obtained instead for the CG, CA(=TG), and also the GC steps. This result is in contrast with the assignments of the bendability of the dinucleotide steps reported above. In fact, the crystal

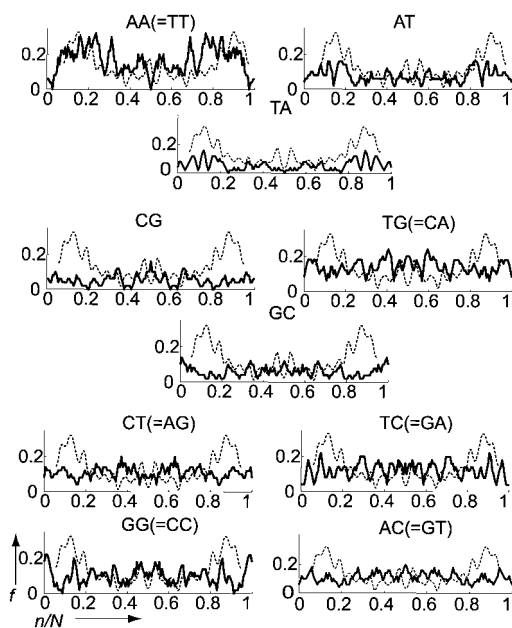


Figure 6. Plots of the dinucleotide steps frequencies along the chain of the dimeric molecules whose curvature and flexibility are plotted in Figure 5. The frequencies are evaluated with a spatial resolution similar to the curvature plots in Figure 5. *f* is the fractional step frequency, *n/N* is the fractional position along the chain contour. Superimposed on each plot (dashed trace, on an arbitrary scale) is the profile of the chain flexibility (as evaluated in Figure 5c), which is shown to enable correlations to be seen.

structures indicated the CG and CA(=TG) steps as the most bendable ones. As in the case of curvature, the flexibility assignments on the nanoscale can hardly be reconciled with those made by different techniques on the atomic scale. The following considerations can be made in an attempt to explain this disagreement: It can be argued that the currently available crystallographic data are not optimal. As the authors of these studies point out, the harmonic energy functions evaluated by them can change as new data accumulate.^[97] Furthermore, the oligonucleotides analyzed by X-ray diffraction contained tracts systematically GC-rich at the ends, and AT-rich in the central positions.^[99] This composition might have affected the statistical significance of the analysis. Additionally, the spread of the dinucleotide geometric parameters in the set of crystal structures (about a hundred) of the oligonucleotides correlates quite poorly with that of DNA–protein complexes.^[61] Nevertheless, both analyses indicate the CG and the CA (=TG) steps as particularly bendable, in marked disagreement with the results obtained on the nanoscale by AFM.^[74]

It can reasonably be expected that this disagreement is due to the averaging of the smaller-scale properties along the chain. Okonogi et al. identified the CG step as the most flexible and GC as the most inflexible, while the values of AT and TA were intermediate;^[100] the average of the CG and GC flexibility is lower than the average for the combined AT and TA steps. On this basis, sequences containing AT and TA steps were assigned as the most flexible of all dinucleotides.^[100] On the other hand, it must be taken into account that the helical structure does not only add and average the different contributions, rather it combines them according to their phase with respect to the helical repeat. In this way, a large local flexibility might be even obtained by appropriately phasing a number of steps that might not be the most bendable. Also the DNA curvature is determined more by the way the double helix selects, composes, and phases the local bends over different spatial scales, than by the extent of the individual deformations (see Section 3.1).

One other possible difference should be taken into account when the dinucleotide bendabilities obtained from X-ray diffraction analyses (as in refs. [82,95]) or from spectroscopic methods (as in ref. [100]) are compared with flexibility data obtained by AFM imaging. The molecules imaged by AFM have been transferred from the 3D space of the solution to the quasi-2D space of the substrate surface. This reduction of the degrees of freedom from a 3D to a 2D space could damp out-of-plane motions and emphasize in-plane flexibility. This effect is another source of disagreement between the measurements made over different length scales. At the same time, results from flattened DNA are particularly valuable in structural biology, since they mimic the restrictions that are expected to occur in DNA–protein complexes, where the DNA chain is confined on the protein surface. This intrinsic limitation of the AFM technique can be useful in shedding light on the topology of these complexes.

Other information about the DNA structural codes on the nanoscale comes from the structures of the complexes of DNA with architectural proteins, such as the histones (see Section 3.3). These complexes are analyzed by focusing on

how conformationally rigid and flexible sequences are combined to drive the positioning of the proteins on the DNA chain that wraps them. According to Travers, the results of this analysis agrees with the assignment of AT and TA as fairly flexible steps.^[86] The conclusion that TA is the most flexible step is supported by the very low stacking energy of this step, and by the data by Zhang and Crothers^[71] and by McConnell and Beveridge.^[98] This conclusion fits very well with the AFM data.

As far as the AA step is concerned, there seems to be an energy barrier that prevents it from adopting large distortions. On the other hand, the recent structure of the nucleosome core reported by Richmond and Davey,^[101] shows large distortions at the junctions between the AA tracts and the flanking sequences. On this basis, it is likely that the properties of the AA step depend greatly on its sequence content (A. A. Travers, personal communication). The high flexibility assigned to the AA step from AFM measurements might include contributions from the mechanical properties of the flanking positions.

In conclusion, the subtle intertwining of the DNA recognition mechanisms operating at different length scales is teaching us a lot about the structural basis of size-dependent molecular phenomena.

3.3. Indirect Read-Out in DNA–Protein Recognition

DNA-binding proteins can be classified in two groups. The first is that of the proteins, such as histones and histone-like proteins, which maintain the chromosome structure and drive its modification as required by the expression and regulation of the genome. DNA is wrapped around these proteins. The specificity of their binding is strictly related to the sequence-dependent curvature and flexibility of the DNA tracts involved. In particular, the standard free energies of competitive nucleosome-reconstitution experiments are satisfactorily predicted theoretically in terms of curvature and flexibility by adopting a statistical thermodynamic model.^[64,87,88]

The proteins of the second group are those involved in the regulation of the gene expression through their interaction with DNA control elements. These proteins can achieve rapid target location by initially binding to a nonspecific site on the DNA and then reaching the specific site by one dimensional diffusion or by intersegment transfer, or both.^[102] These proteins recognize their specific binding sites by sampling the specific contacts through a recognition mechanism called “direct read-out.”^[103,104] This is a recognition process at an atomic level of resolution. This very detailed sampling can take place at each position along the DNA chain or, more efficiently, only at certain positions, such as those in which the DNA can be more easily bent. This latter process implies that during the one dimensional diffusion along the DNA, the protein continuously bends the DNA chain into a particular local conformation and so tests the way in which the DNA conformation can change: this is the so-called “indirect read-out” mechanism that is based on the sampling of conformational and mechanical properties on the nanoscale.^[105]

Reporting their study on DNA bending by Cro protein,^[106] Bustamante et al. suggested that the dynamics of the one-dimensional diffusion along the DNA might be dominated by the propagation of “bending waves with the protein riding at their vertex.” The ease of DNA bending could signal the protein of its arrival at the specific locus. If the specific site requires less energy to distort, it will yield a more stable complex that allows time for the protein to check for sequence-specific contacts. The role of DNA bending in transcriptional regulation has been reviewed.^[103] The number of proteins that are recognized to bend DNA is constantly increasing and the idea that all DNA tracking proteins bend DNA is strengthening all the time. The coding for the indirect read-out is more flexible than that for sequence-specific direct read-out: a certain sequence can be replaced by an unrelated one, as long as it is as curved and flexible as the previous one.^[107]

Indirect read-out dominates the recognition processes of the architectural proteins of the first group. The same mechanism is just the first component of the recognition between the proteins of the second group and their specific sites. An example of an indirect recognition without the presence of the direct contacts (that is, recognition outside the van der Waals radii) is that of the FIS activator protein with its binding sites.^[108]

3.4. The Formation of Loops: An Effect of DNA Structural Codes

As shown by Griffith et al. for the highly curved *Crithidia fasciculata* DNA,^[67] the DNA shape and flexibility can facilitate the formation of loops, a superstructure that can control gene expression. In a DNA chain, these loops make it possible to mediate the interactions of units a long way apart in the primary structure.^[109] The formation of DNA loops (which can be directly observed by AFM imaging^[110]) depends on the appropriate phasing of base-pair deformability with the double-helical repeat. Matsumoto and Olson^[97] have simulated a naturally straight chain which contains intrinsically flexible and rigid dimer steps spaced by half-turn increments (5 base pairs apart) and have found that this will bend in a preferred direction, to form loops.

3.5. A Crystal Surface Can Read the Structural Codes of DNA

Macromolecules exert exceptional control over many growth and organization processes, such as the nucleation of inorganic compounds, phase stabilization, assembly, and pattern formation.^[111] Much effort is now paid to identifying the appropriate compatibilities and combinations of biological macromolecules with inorganic materials and to understanding how the organizational capabilities of biological molecules can be combined with inorganic systems in self-assembly processes. Examples of this research include, peptides with selectivity for binding to metal surfaces and metal oxide surfaces and those that can recognize and control the growth of an inorganic semiconductor surface, such as that of GaAs.^[112]

In addition to peptides and proteins, is it possible for a DNA chain to be recognized at the biological–inorganic interface? A straight DNA chain can rotate around its axis on the surface, so many possible orientations are expected to be equally probable and the chemical characteristics are averaged to a cylindrical symmetry. On the other hand, this rotation is somewhat hindered in an intrinsically curved segment.

The intrinsic DNA curvature also defines an average plane for the curved segment: the two faces of the DNA chain (on the two sides of the plane) are also chemically different owing to the different spatial distribution of the dinucleotide steps that give rise to the chain curvature.

A high-resolution molecular model of the lowest energy conformation of the *Crithidia fasciculata* fragment shows that the almost planar structure has one face that is A-rich while the other is T-rich. This arrangement is the result of the recurrence of the A-tract that is phased with the helical winding (see Figure 4b). In principle, this structure can deposit on mica on either of these two faces. Its direct observation (with the EM or the AFM) does not allow the preferred face of adsorption, if any, to be identified because it is not possible to read the direction of the sequence.

The strategy used to determine the preferred adsorption face is shown schematically in Figure 7a: the two faces of a square thin object (for example, a paper square), one black and one white, can only be distinguished by their colors, since

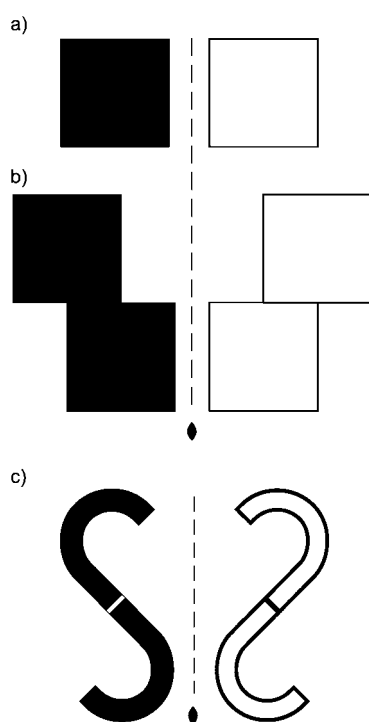


Figure 7. a) The oppositely colored faces of a thin square object can not be distinguished by form alone. b) The two oppositely colored faces of a chiral object obtained by fusing two copies of an object as in (a). In this case, the face (white or black) shown can be distinguished by the morphology of the object, even if the color could not be distinguished. c) A palindromic DNA dimer made with a curved DNA section is expected to have the same property as the model in (b) when flattened on a surface in a S-like shape: the face can be recognized without reading the direction of the base sequence.

they have the same shape. Likewise the distinguishing feature of DNA chains, the directions of the sequence, cannot be identified in EM or AFM images of the *Crithidia* segment. On the other hand, with the colored square, if a new object is built by linking two of these squares to make a chiral shape like that in Figure 7b, the two prochiral faces of this thin object can be distinguished on a purely morphological basis: just from their shape. By ligation of two *Crithidia* segments (Figure 7c) either in the tail–tail (PvuII–EcoRI–PvuII, solid trace in Figure 8) or in the head–head (NheI–SalI–NheI, dashed trace in Figure 8) orientation two palindromic dimers

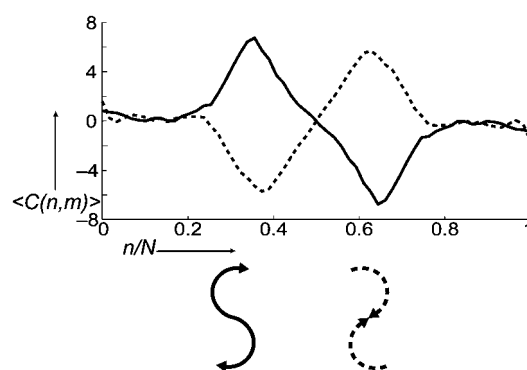


Figure 8. Plot of the experimental local DNA curvature (evaluated from the AFM images) along the chain of tail–tail (PvuII–EcoRI–PvuII, solid trace) and head–head (NheI–SalI–NheI, dashed trace) palindromic dimers constructed using the *Crithidia fasciculata* segment. The average local curvature, in degrees (over windows of approximately 2 helical turns, as in Figure 5b) are evaluated as a function of the fractional position along the chain contour, n/N . According to the signs of the local curvatures, the average shapes preferentially assumed by the tail–tail (S-type, solid line) and head–head (S*-type, dashed line) dimers are sketched.

were constructed. These DNA palindromic dimers of a strongly curved DNA segment are like the prochiral objects in Figure 7b. In fact, when the curved palindromic molecule in two dimensions assumes an S-like average shape (with its internal dyadic axis perpendicular to the surface), because of the segregation of A and T bases on the two faces of the monomeric curved tracts, its two prochiral faces expose either A-rich or T-rich sequences (Figure 7c). The face exposed to the crystal surface by a population of molecules deposited on mica can thus only be identified by AFM imaging of the palindromic dimers of the segment of interest, not of the segment itself. By analyzing the shape assumed by two large sets of the two palindromic dimers of the *Crithidia fasciculata* fragment (Figure 8) it was discovered that the face that both dimers expose preferentially to the mica is the T-rich one. A statistical analysis of these shapes demonstrated that the preference is such that one face was deposited between five and nine times more frequently than the other.^[113]

We believe that this effect should be interpreted as the recognition of a DNA superstructure based on an indirect read-out mechanism. The extent of this recognition effect is not directly controlled by the sequence but by the degree of curvature. In fact, from the analysis of average local curvatures of dimers of pBR322 restriction fragments, with sequences without the extensive phasing found in *Crithidia*

and therefore with only moderate curvatures, the same evidence of the presence of a surface recognition phenomenon was found, but with a smaller magnitude (B. Samorì, P. De Santis, unpublished results). The surface of a crystal such as mica does not recognize the base sequence itself but the periodicity of the adenine tracts: if the adenine tracts are not properly phased no extended curvature occurs and thus no significant segregation of complementary bases on well-defined faces is obtained. This recognition effect is therefore expected to be general for any curved dsDNA molecules. Further investigations are requested to discover the structural basis upon which this recognition process is based and, consequently, to decipher the underlying informational code.

We can hypothesize that a recognition process of this kind might have been relevant in the pre-cellular stages of the evolution of life. Inorganic surfaces have served as catalysts for prebiotic syntheses^[114] and also as templates for the self-organization of increasingly more complex biostructures.^[115]

4. Summary and Outlook

The DNA sequence encodes the nanoscale properties, superstructures, and recognition mechanisms that DNA exhibits. A nanoscientific point of view shows how the DNA double-helical structure acquires different qualities over different spatial scales. DNA achieves these qualities by behaving like an antenna that eliminates the “perturbations” that are out of phase and adds only those in phase.

Looking at biology from a nanoscientific point of view introduces us into the methodologies and the purposes that nature follows in its “engineering” of complex systems. As Horst Störmer says in his lectures: “nanoscale science is raising the lid on the biggest LEGO of the universe.”

While the biologists are also beginning to tackle their scientific topics from a nanoscientific point of view, nanoscience and nanotechnology are more and more inspired by biology and interested in DNA. The information content and the scale of complexity of DNA can introduce a higher level of complexity in self-assembling processes that also involve non-biological molecules.

DNA can also provide recognition processes whose selectivity and stringency can be modulated on different length scales, such as in the direct and indirect read-out mechanisms between DNA and proteins. Nanoscience and nanotechnology have already adopted the direct read-out strategy based on the base-pairing code as a handy tool. The other, more complex codes are at the moment just a source of inspiration for nanoscience. Investigations might open the possibility to exploit these codes in a similar fashion to the base pairing code. A toolbox of DNA recognition processes that could switch self-organization among different length and energy scales could be available. The discovery that DNA superstructures can be recognized by a crystal surface is a first step towards this goal: complex DNA-based self-assembling nanostructures^[10] could be tailored in a way to be recognized by a crystal surface. Two different hierarchies of information could be exploited at the same time. Further steps towards higher levels of complexity could also be made by using

DNA-binding proteins. DNA-based nanotraces on cationic crystal surfaces might be designed by assembling highly curved and straight DNA tracts, that are bound by proteins at consensus sequences.

Addendum

Since the submission of this manuscript, several interesting and relevant papers have been published. Sherman and Seeman showed the performance of a DNA walking device, where a DNA biped can stroll in a controlled manner on a DNA “sidewalk”.^[116] The fine degree of control of the motion is achieved thanks to the addition of oligonucleotides that bind the legs of the biped to specific locations on the sidewalk.

Mao et al. presented a fully autonomous DNA motor, which exploits an integrated DNA enzyme to produce cyclic motion.^[117] The nanomotor continues to cycle undisturbed between its open and closed states as long as the enzyme substrate is present in solution (unless a molecular brake is set). This is a true case of conversion of chemical energy into nanoscale motion in a fully synthetic device.

Surfaces, which play a major role in nanotechnology are also becoming an important part of DNA computation: Su and Smith described a surface DNA computer,^[118] while Reif and co-workers are applying DNA codes to cryptography.^[119]

The principles behind DNA assembly are becoming clearer as a result of the increasing number of experimental examples (such as the DNA tetrahedron of Goodman and co-workers^[120] or the rigid nanotriangle modules and arrays of Mao and co-workers^[121]). Winfree and co-workers have tried to define the thermodynamic rules for the correct assembly of nucleic acids sequences.^[122]

The very prolific group of Chengde Mao has also shown how to do nanoscale lithography using DNA arrays: once laid on a surface, the holes of the arrays can be filled with metal by high-vacuum evaporation. Removing the metal film, while leaving the DNA on the surface, yields a nanoscale-patterned metal structure that is a negative replica of the DNA array pattern.^[123]

On July 28th, 2004, Sir Francis Harry Compton Crick died.

Experimental work was supported by Ministero dell'Istruzione Università Ricerca, Programmi Biotechnologie Legge 95/95 (5%), and Progetti di Interesse Nazionale 2001–2003, Progetti Pluriennali Università di Bologna, and FISIR D.M. 16/10/20 Anno 1999 and ESF Eurocore “SONS” Programme for 2003–2006. We thank Pasquale De Santis (Rome) for helpful discussion and comments about the manuscript. We also thank Andrew Travers (Cambridge) for sharing unpublished work, for critically reading the manuscript, and for very helpful suggestions, especially about the comparative analysis of the flexibility of the TA and AA steps (Section 3.2). We thank Dr. Andrea Giro for help in preparation of the frontispiece graphics.

Received: January 28, 2004

Revised: April 12, 2004

Published Online: November 5, 2004

- [1] J. D. Watson, F. H. C. Crick, *Nature* **1953**, *171*, 737–738.
- [2] E. N. Trifonov, *Bull. Math. Biol.* **1989**, *51*, 417–432.
- [3] D. R. F. Leach in *DNA Recombination and Repair* (Eds.: P. J. Smith, C. J. Jones), Oxford University Press, Oxford, **1999**, pp. 1–15.
- [4] B. K. Singleton, P. A. Jeggo in *DNA Recombination and Repair* (Eds.: P. J. Smith, C. J. Jones), Oxford University Press, Oxford, **1999**, pp. 16–37.
- [5] a) L. M. Adleman, *Science* **1994**, *266*, 1021–1024; b) C. Mao, T. H. LaBean, J. H. Relf, N. C. Seeman, *Nature* **2000**, *407*, 493–496.
- [6] a) Y. Benenson, R. Adar, T. Paz-Elizur, Z. Livneh, E. Shapiro, *Proc. Natl. Acad. Sci. USA* **2003**, *100*, 2191–2196; b) Y. Benenson, T. Paz-Elizur, R. Adar, E. Keinan, Z. Livneh, E. Shapiro, *Nature* **2001**, *414*, 430–434.
- [7] V. V. Demidov, M. D. Frank-Kamenetskii, *Trends Biochem. Sci.* **2004**, *29*, 62–71.
- [8] V. A. Bloomfield, D. M. Crothers, I. Tinoco, *Nucleic Acids: Structures, Properties, and Functions*, University Science Books, Sausalito, **2000**.
- [9] P. Sa-Ardyen, A. V. Vologodskii, N. C. Seeman, *Biophys. J.* **2003**, *84*, 3829–3837.
- [10] N. C. Seeman, *Nature* **2003**, *421*, 427–431.
- [11] N. C. Seeman, *Annu. Rev. Biophys. Biomol. Struct.* **1998**, *27*, 225–248.
- [12] C. Mao, W. Sun, Z. Shen, N. C. Seeman, *Nature* **1999**, *397*, 144–146.
- [13] H. Yan, X. Zhang, Z. Shen, N. C. Seeman, *Nature* **2002**, *415*, 62–65.
- [14] a) E. Winfree, F. Liu, L. A. Wenzler, N. C. Seeman, *Nature* **1998**, *394*; b) H. Yan, T. H. LaBean, L. Feng, J. H. Reif, *Proc. Natl. Acad. Sci. USA* **2003**, *100*, 8103–8108; c) H. Li, S. H. Park, J. H. Reif, T. H. LaBean, H. Yan, *J. Am. Chem. Soc.* **2004**, *126*, 418–419; d) R. M. Dirks, M. Lin, E. Winfree, N. A. Pierce, *Nucleic Acids Res.* **2004**, *32*, 1392–1403.
- [15] L. Feng, S. H. Park, J. H. Reif, H. Yan, *Angew. Chem.* **2003**, *115*, 4478–4482; *Angew. Chem. Int. Ed.* **2003**, *42*, 4342–4346.
- [16] C. Mao, W. Sun, N. C. Seeman, *J. Am. Chem. Soc.* **1999**, *121*, 5437–5544.
- [17] W. M. Shih, J. D. Quispe, G. F. Joyce, *Nature* **2004**, *427*, 618–621.
- [18] W. P. Stemmer, A. Cramer, K. D. Ha, T. M. Brennan, H. L. Heyneker, *Gene* **1995**, *164*, 49–53.
- [19] B. Yurke, A. J. Turberfield, A. P. J. Mills, F. C. Simmel, J. L. Neumann, *Nature* **2000**, *406*, 605–608.
- [20] a) P. Alberti, J. L. Mergny, *Proc. Natl. Acad. Sci. USA* **2003**, *100*, 1569–1573; b) D. Liu, S. Balasubramanian, *Angew. Chem.* **2003**, *115*, 5912–5914; *Angew. Chem. Int. Ed.* **2003**, *42*, 5734–5736; c) C. M. Niemeyer, M. Adler, S. Lenhart, S. Gao, H. Fuchs, L. F. Chi, *ChemBioChem* **2001**, *2*, 260–264; d) C. M. Niemeyer, M. Adler, *Angew. Chem.* **2002**, *114*, 3933–3937; *Angew. Chem. Int. Ed.* **2002**, *41*, 3779–3783; e) J. W. J. Li, W. H. Tan, *Nano Lett.* **2002**, *2*, 315–318.
- [21] B. H. Robinson, N. C. Seeman, *Protein Eng.* **1987**, *1*, 295–300.
- [22] E. Di Mauro, C. P. Hollenberg, *Adv. Mater.* **1993**, *5*, 384–386.
- [23] C. A. Mirkin, R. L. Letsinger, R. C. Mucic, J. J. Storhoff, *Nature* **1996**, *382*, 607–609.
- [24] a) M. Hegner, P. Wagner, G. Semenza, *FEBS Lett.* **1993**, *336*, 452–456; b) S.-J. Park, A. A. Lazarides, C. A. Mirkin, P. W. Brazis, C. R. Kannewurf, R. L. Letsinger, *Angew. Chem.* **2000**, *112*, 4003–4006; *Angew. Chem. Int. Ed.* **2000**, *39*, 3845–3848; c) C. Bamdad, *Biophys. J.* **1998**, *75*, 1997–2003.
- [25] a) A. Csáki, R. Möller, W. Straube, J. M. Köhler, W. Fritzsche, *Nucleic Acids Res.* **2001**, *29*, E81; b) R. Möller, A. Csáki, J. M. Köhler, W. Fritzsche, *Nucleic Acids Res.* **2000**, *28*, E91.
- [26] a) C. M. Niemeyer, B. Ceyhan, P. Hazarika, *Angew. Chem.* **2003**, *115*, 5944–5948; *Angew. Chem. Int. Ed.* **2003**, *42*, 5766–5770; b) C. M. Niemeyer, B. Ceyhan, M. Noyong, U. Simon, *Biochem. Biophys. Res. Commun.* **2003**, *311*, 995–999.
- [27] L. M. Demers, D. S. Ginger, S. J. Park, Z. Li, S. W. Chung, C. A. Mirkin, *Science* **2002**, *296*, 1836–1838.
- [28] S. J. Park, T. A. Taton, C. A. Mirkin, *Science* **2002**, *295*, 1503–1506.
- [29] C. M. Niemeyer, W. Bürger, J. Peplies, *Angew. Chem.* **1998**, *110*, 2391–2395; *Angew. Chem. Int. Ed.* **1998**, *37*, 2265–2268.
- [30] C. M. Niemeyer, B. Ceyhan, *Angew. Chem.* **2001**, *113*, 3798–3801; *Angew. Chem. Int. Ed.* **2001**, *40*, 3685–3688.
- [31] J. M. Tomkins, B. K. Nabbs, K. Barnes, M. Legido, A. J. Blacker, R. A. McKendry, C. Abell, *ChemBioChem* **2001**, *2*, 375–378.
- [32] L. H. Eckardt, K. Naumann, W. M. Pankau, M. Rein, M. Schweitzer, N. Windhad, G. von Kiedrowski, *Nature* **2002**, *420*, 286.
- [33] K. Keren, M. Krueger, R. Gilad, G. Ben-Yoseph, U. Sivan, E. Braun, *Science* **2002**, *297*, 72–75.
- [34] K. A. Williams, P. T. Veenhuizen, B. G. de la Torre, R. Eritja, C. Dekker, *Nature* **2002**, *420*, 761.
- [35] a) K. J. Watson, S. J. Park, J. H. Im, S. T. Nguyen, C. A. Mirkin, *J. Am. Chem. Soc.* **2001**, *123*, 5592–5593; b) L. Zhu, P. S. Lukeman, J. W. Canary, N. C. Seeman, *J. Am. Chem. Soc.* **2003**, *125*, 10178–10179.
- [36] L. Jaeger, N. B. Leontis, *Angew. Chem.* **2000**, *112*, 2576–2580; *Angew. Chem. Int. Ed.* **2000**, *39*, 2521–2524.
- [37] L. Jaeger, E. Westhof, N. B. Leontis, *Nucleic Acids Res.* **2001**, *29*, 455–463.
- [38] S. M. Elbashir, J. Harborth, W. Lendeckel, A. Yalcin, K. Weber, T. Tuschl, *Nature* **2001**, *411*, 494–498.
- [39] P. E. Nielsen, M. Egholm, O. Buchart, *Bioconjugate Chem.* **1994**, *5*, 3–7.
- [40] V. V. Demidov, N. E. Broude, I. V. Lavrentieva-Smolina, H. Kuhn, M. D. Frank-Kamenetskii, *ChemBioChem* **2001**, *2*, 133–139.
- [41] P. E. Nielsen, *Mol. Biotechnol.* **2004**, *26*, 233–248.
- [42] H. Kuhn, V. V. Demidov, J. M. Coull, M. J. Fiandaca, B. D. Gildea, M. D. Frank-Kamenetskii, *J. Am. Chem. Soc.* **2002**, *124*, 1097–1103.
- [43] H. Kuhn, V. V. Demidov, B. D. Gildea, M. J. Fiandaca, J. C. Coull, M. D. Frank-Kamenetskii, *Antisense Nucleic Acid Drug Dev.* **2001**, *11*, 265–270.
- [44] S. Sforza, G. Haaima, R. Marchelli, P. E. Nielsen, *Eur. J. Org. Chem.* **1999**, 197–204.
- [45] M. Petersen, J. Wengel, *Trends Biotechnol.* **2003**, *21*, 74–81.
- [46] U. Christensen, N. Jacobsen, V. K. Rajwanshi, J. Wengel, T. Koch, *Biochem. J.* **2001**, *354*, 481–484.
- [47] D. Latorra, D. Hopkins, K. Campbell, J. M. Hurley, *Biotechniques* **2003**, *34*, 1150–1158.
- [48] a) K. Schöning, P. Scholz, S. Guntha, X. Wu, R. Krishnamurthy, A. Eschenmoser, *Science* **2000**, *290*, 1347–1351; b) A. Eschenmoser, *Science* **1999**, *284*, 2118–2124.
- [49] J. C. Chaput, J. K. Ichida, J. W. Szostak, *J. Am. Chem. Soc.* **2003**, *125*, 856–857.
- [50] a) H. Liu, J. Gao, S. R. Lynch, Y. D. Saito, L. Maynard, E. T. Kool, *Science* **2003**, *302*, 868–871; b) A. Marx, D. Summerer, *Angew. Chem.* **2004**, *116*, 1653–1654; *Angew. Chem. Int. Ed.* **2004**, *43*, 1625–1626.
- [51] E. M. Southern, *Methods Mol. Biol.* **2001**, *170*, 1–15.
- [52] M. J. Heller, *Annu. Rev. Biomed. Eng.* **2002**, *4*, 129–153.
- [53] a) E. Palecek, *Talanta* **2002**, *45*, 809–819; b) E. Palecek, F. Jelen, *Crit. Rev. Anal. Chem.* **2002**, *32*, 261–270; c) K. Kerman, M. Kobayashi, E. Tamiya, *Meas. Sci. Technol.* **2004**, *15*, R1–R11.

- [54] T. A. Taton, C. A. Mirkin, R. L. Letsinger, *Science* **2000**, 289, 1757–1760.
- [55] C. Guiducci, C. Stagni, G. Zuccheri, A. Bogliolo, L. Benini, B. Samorì, B. Riccò, *Biosens. Bioelectron.* **2004**, 19, 781–787.
- [56] R. Hölzel, N. Gajovic Eichmann, F. F. Bier, *Biosens. Bioelectron* **2003**, 18, 555–564.
- [57] M. C. Pirrung, *Angew. Chem* **2002**, 41, 1326–1341; *Angew. Chem. Int. Ed.* **2002**, 41, 1276–1289.
- [58] H. Pearson, *Nature* **2003**, 421, 310–312.
- [59] a) J. A. Schellman, S. C. Harvey, *Biophys. Chem.* **1995**, 55, 95–114; b) C. R. Calladine, H. R. Drew, *J. Mol. Biol.* **1996**, 257, 479–485.
- [60] J. Bednar, P. Furrer, V. Katritch, A. Z. Stasiak, J. Dubochet, A. Stasiak, *J. Mol. Biol.* **1995**, 254, 579–594.
- [61] D. M. Crothers, *Proc. Natl. Acad. Sci. USA* **1998**, 95, 15163–15165.
- [62] a) P. De Santis, A. Palleschi, M. Savino, A. Scipioni, *Biophys. Chem.* **1988**, 32, 305–317; b) P. De Santis, A. Palleschi, S. Morosetti, M. Savino in *Structure and Dynamics of Nucleic Acids, Proteins and Membranes* (Eds.: E. Clementi, S. Chin), Plenum, New York, **1986**, pp. 31–49.
- [63] P. De Santis, A. Palleschi, M. Savino, A. Scipioni, *Biochemistry* **1990**, 29, 9269–9273.
- [64] a) D. Boffelli, P. De Santis, A. Palleschi, G. Risuleo, M. Savino, *FEBS Lett.* **1992**, 300, 175–178; b) P. De Santis, A. Palleschi, M. Savino, A. Scipioni, *Biophys. Chem.* **1992**, 42, 147–152.
- [65] S. Arnott, D. W. Hukins, *J. Mol. Biol.* **1973**, 81, 93–105.
- [66] M. A. El Hassan, C. R. Calladine, *Philos. Trans. R. Soc. London* **1997**, 355, 43–100.
- [67] J. Griffith, M. Bleyman, C. A. Rauch, P. A. Kitchin, P. T. Englund, *Cell* **1986**, 46, 717–724.
- [68] R. E. Dickerson, D. Goodsell, M. L. Kopka, *J. Mol. Biol.* **1996**, 256, 108–125.
- [69] P. R. Hardwidge, R. B. Den, E. D. Ross, L. J. Maher, *J. Biomol. Struct. Dyn.* **2000**, 18, 219–230.
- [70] J. D. Kahn, E. Yun, D. M. Crothers, *Nature* **1994**, 368, 163–166.
- [71] Y. Zhang, D. M. Crothers, *Proc. Natl. Acad. Sci. USA* **2003**, 100, 3161–3166.
- [72] a) Y. Zhang, D. M. Crothers, *Biophys. J.* **2003**, 84, 136–153; b) P. De Santis, M. Fuà, M. Savino, C. Anselmi, G. Bocchinfuso, *J. Phys. Chem.* **1996**, 100, 9968–9976.
- [73] a) J. A. Cognet, C. Pakleza, D. Cherny, E. Delain, E. Le Cam, *J. Mol. Biol.* **1999**, 285, 997–1009; b) G. Muzard, B. Theveny, B. Revet, *EMBO J.* **1990**, 9, 1289–1298.
- [74] G. Zuccheri, A. Scipioni, V. Cavaliere, G. Gargiulo, P. De Santis, B. Samorì, *Proc. Natl. Acad. Sci. USA* **2001**, 98, 3074–3079.
- [75] C. Rivetti, C. Walker, C. Bustamante, *J. Mol. Biol.* **1998**, 280, 41–59.
- [76] W. K. Olson, V. B. Zhurkin, *Curr. Opin. Struct. Biol.* **2000**, 10, 286–297.
- [77] E. Le Cam, F. Fack, J. Menissier-de Murcia, J. A. Cognet, A. Barbin, V. Sarantoglou, B. Revet, E. Delain, G. de Murcia, *J. Mol. Biol.* **1994**, 235, 1062–1071.
- [78] T. Akiyama, M. E. Hogan, *Biochemistry* **1997**, 36, 2307–2315.
- [79] T. E. Haran, J. D. Kahn, D. M. Crothers, *J. Mol. Biol.* **1994**, 244, 135–143.
- [80] a) A. Barbic, D. P. Zimmer, D. M. Crothers, *Proc. Natl. Acad. Sci. USA* **2003**, 100, 2369–2373; b) D. Strahs, T. Schlick, *J. Mol. Biol.* **2000**, 301, 643–663.
- [81] A. Bolshoy, P. McNamara, R. E. Harrington, E. N. Trifonov, *Proc. Natl. Acad. Sci. USA* **1991**, 88, 2312–2316.
- [82] A. A. Gorin, V. B. Zhurkin, W. K. Olson, *J. Mol. Biol.* **1995**, 247, 34–48.
- [83] a) C. R. Calladine, *J. Mol. Biol.* **1982**, 161, 343–352; b) K. Yanagi, G. G. Prive, R. E. Dickerson, *J. Mol. Biol.* **1991**, 217, 201–214; c) M. A. Young, G. Ravishanker, D. L. Beveridge, H. M. Berman, *Biophys. J.* **1995**, 68, 2454–2468.
- [84] C. A. Hunter, *J. Mol. Biol.* **1993**, 230, 1025–1054.
- [85] a) C. A. Hunter, *Bioessays* **1996**, 18, 157–162; b) J. Gallego, A. R. Pascual-Teresa, M. T. Pisabarro, F. Gago in *QSAR and Molecular Modeling. Concepts, Computational Tools and Applications* (Eds.: F. Sanz, J. Giraldo, F. J. R. Manaut), Prous Science, Barcelona, **1995**, pp. 274–281.
- [86] A. A. Travers, *Philos. Trans. R. Soc. London Ser. A* **2004**, 362, 1423–1438.
- [87] C. Anselmi, G. Bocchinfuso, P. De Santis, M. Savino, A. Scipioni, *J. Mol. Biol.* **1999**, 286, 1293–1301.
- [88] C. Anselmi, P. De Santis, R. Paparcone, M. Savino, A. Scipioni, *Biophys. Chem.* **2002**, 95, 23–47.
- [89] E. S. Sobel, J. A. Harpst, *Biopolymers* **1991**, 31, 1559–1564.
- [90] P. J. Hagerman, *Annu. Rev. Biophys. Biophys. Chem.* **1988**, 17, 265–286.
- [91] a) D. Shore, R. L. Baldwin, *J. Mol. Biol.* **1983**, 170, 957–981; b) W. H. Taylor, P. J. Hagerman, *J. Mol. Biol.* **1990**, 212, 363–376.
- [92] C. Frontali, E. Dore, A. Ferrauto, E. Gratton, A. Bettini, M. R. Pozzan, E. Valdevit, *Biopolymers* **1979**, 18, 1353–1373.
- [93] T. Berge, N. S. Jenkins, R. B. Hopkirk, M. J. Waring, J. M. Edwardson, R. M. Henderson, *Nucleic Acids Res.* **2002**, 30, 2980–2986.
- [94] A. Scipioni, C. Anselmi, G. Zuccheri, B. Samorì, P. De Santis, *Biophys. J.* **2002**, 83, 2408–2418.
- [95] W. K. Olson, A. A. Gorin, X. J. Lu, L. M. Hock, V. B. Zhurkin, *Proc. Natl. Acad. Sci. USA* **1998**, 95, 11163–11168.
- [96] a) R. E. Dickerson, *Nucleic Acids Res.* **1998**, 26, 1906–1926; b) R. E. Dickerson, T. K. Chiu, *Biopolymers* **1997**, 44, 361–403.
- [97] A. Matsumoto, W. K. Olson, *Biophys. J.* **2002**, 83, 22–41.
- [98] K. J. McConnell, D. L. Beveridge, *J. Mol. Biol.* **2001**, 314, 23–40.
- [99] W. K. Olson, http://rutchem.rutgers.edu/~olson/Bdna_list.html, **1998**.
- [100] T. M. Okonogi, S. C. Alley, A. W. Reese, P. B. Hopkins, B. H. Robinson, *Biophys. J.* **2002**, 83, 3446–3459.
- [101] T. J. Richmond, C. A. Davey, *Nature* **2003**, 423, 145–150.
- [102] a) P. H. von Hippel, O. G. Berg, *J. Biol. Chem.* **1989**, 264, 675–678; b) R. Fickert, B. Muller-Hill, *J. Mol. Biol.* **1992**, 226, 59–68.
- [103] J. Perez-Martin, V. de Lorenzo, *Annu. Rev. Microbiol.* **1997**, 51, 593–628.
- [104] A. A. Travers, *DNA–Protein Interactions, 1st Ed.*, Chapman & Hall, London, New York, **1993**.
- [105] L. Jen-Jacobson, *Biopolymers* **1997**, 44, 153–180.
- [106] D. A. Erie, G. Yang, H. C. Schultz, C. Bustamante, *Science* **1994**, 266, 1562–1566.
- [107] B. Revet, S. Brahms, G. Brahms, *Proc. Natl. Acad. Sci. USA* **1995**, 92, 7535–7539.
- [108] I. K. Pemberton, G. Muskhelishvili, A. A. Travers, M. Buckle, *J. Mol. Biol.* **2002**, 318, 651–663.
- [109] K. Rippe, P. H. von Hippel, J. Langowski, *Trends Biochem. Sci.* **1995**, 20, 500–506.
- [110] a) C. Wyman, E. Grotkopp, C. Bustamante, H. C. Nelson, *EMBO J.* **1995**, 14, 117–123; b) K. Rippe, M. Guthold, P. H. von Hippel, C. Bustamante, *J. Mol. Biol.* **1997**, 270, 125–138; c) M. Barna, T. Merghoub, J. A. Costoya, D. Ruggero, M. Branford, A. Bergia, B. Samorì, P. P. Pandolfi, *Dev. Cell* **2002**, 3, 499–510.
- [111] a) N. C. Seeman, A. M. Belcher, *Proc. Natl. Acad. Sci. USA* **2002**, 99, 6451–6455; b) A. M. Belcher, X. H. Wu, R. J. Christensen, P. K. Hansma, G. D. Stucky, D. E. Morse, *Nature* **1996**, 381, 56–58; c) G. Falini, S. Albeck, S. Weiner, L. Addadi, *Science* **1996**, 271, 67–69.

- [112] a) S. Brown, *Proc. Natl. Acad. Sci. USA* **1992**, *89*, 8651–8655; b) S. Brown, *Nat. Biotechnol.* **1997**, *15*, 269–272; c) S. R. Whaley, D. S. English, E. L. Hu, P. F. Barbara, A. M. Belcher, *Nature* **2000**, *405*, 665–668.
- [113] B. Sampaiole, A. Bergia, A. Scipioni, G. Zuccheri, M. Savino, B. Samorì, P. De Santis, *Proc. Natl. Acad. Sci. USA* **2002**, *99*, 13566–13570.
- [114] R. Saladino, U. Ciambecchini, C. Crestini, G. Costanzo, R. Negri, E. Di Mauro, *ChemBioChem* **2003**, *4*, 514–521.
- [115] a) N. Lahav, S. Nir, A. C. Elitzur, *Prog. Biophys. Mol. Biol.* **2001**, *75*, 75–120; b) P. Szabó, I. Scheuring, T. Czárán, E. Szathmáry, *Nature* **2002**, *420*, 340–343; c) S. J. Sowerby, N. G. Holm, G. B. Petersen, *Biosystems* **2001**, *61*, 69–78; d) S. J. Sowerby, C. A. Cohn, W. M. Heckl, N. G. Holm, *Proc. Natl. Acad. Sci. USA* **2001**, *98*, 820–822; e) C. Anselmi, P. De Santis, R. Paparcone, M. Savino, A. Scipioni, *Origins Life Evol. Biosphere* **2004**, *34*, 143–149.
- [116] W. B. Sherman, N. C. Seeman, *Nano Lett.* **2004**, *4*, 1203–1207.
- [117] a) Y. Chen, C. Mao, *J. Am. Chem. Soc.* **2004**, *126*, 8626–8627; b) Y. Chen, M. Wang, C. Mao, *Angew. Chem.* **2004**, *116*, 3638–3641; *Angew. Chem. Int. Ed.* **2004**, *43*, 3554–3557.
- [118] X. Su, L. M. Smith, *Nucleic Acids Res.* **2004**, *32*, 3115–3123.
- [119] A. Gehani, T. LaBean, J. Reif in *Aspects of Molecular Computing* (Eds.: N. Jonoska, G. Paun, G. Rozenberg), Springer, Heidelberg, **2004**, pp. 167–188.
- [120] R. P. Goodman, R. M. Berry, A. J. Turberfield, *Chem. Commun.* **2004**, 1372–1373.
- [121] D. Liu, M. Wang, Z. Deng, R. Walulu, C. Mao, *J. Am. Chem. Soc.* **2004**, *126*, 2324–2325.
- [122] R. M. Dirks, M. Lin, E. Winfree, N. A. Pierce, *Nucleic Acids Res.* **2004**, *32*, 1392–1403.
- [123] Z. Deng, C. Mao, *Angew. Chem.* **2004**, *116*, 4160–4162; *Angew. Chem. Int. Ed.* **2004**, *43*, 4068–4070.

Quality counts...

The best of chemistry every week

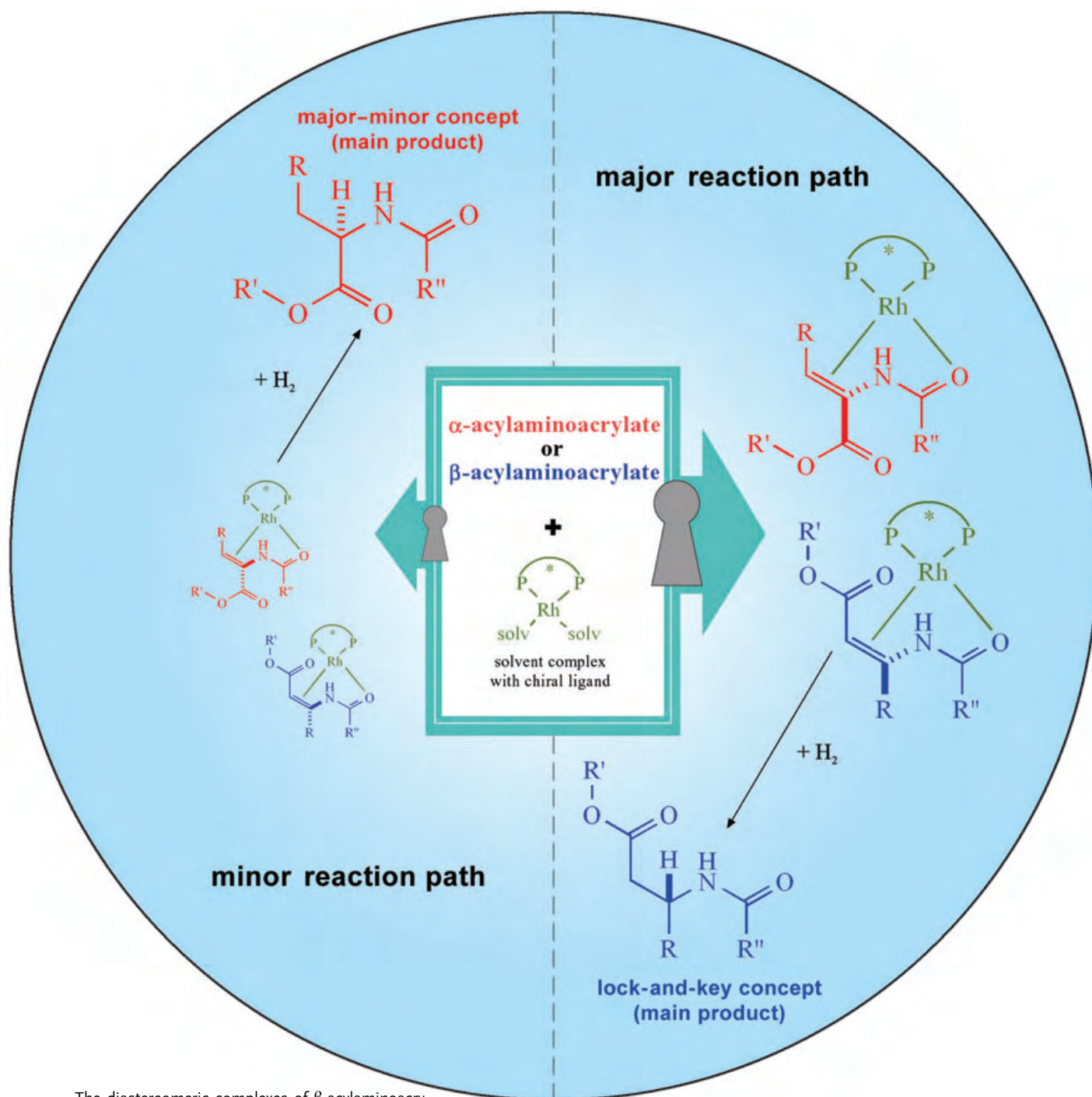
Wiley-VCH
P.O. Box 10 11 61
69451 Weinheim
Germany
Phone +49 (0) 6201-606-400
Fax +49 (0) 6201-606-184
e-mail: angewandte@wiley-vch.de
www.angewandte.org

Angewandte Chemie International Edition is a journal of the GDCh, the German Chemical Society

GDCh

WILEY-VCH

Communications



The diastereomeric complexes of β -acylaminoacrylates shown do not differ much in reactivity, in contrast to intermediates in the asymmetric hydrogenation of α -dehydroamino acids. As a result, the major intermediate determines the selectivity of the reaction in terms of the lock-and-key principle rather than the major-minor concept. D. Heller et al. describe the reaction mechanism in more detail on the following pages.

Are β -Acylaminoacrylates Hydrogenated in the Same Way as α -Acylaminoacrylates?*

Hans-Joachim Drexler, Wolfgang Baumann,
Thomas Schmidt, Songlin Zhang, Ailing Sun,
Anke Spannenberg, Christine Fischer,
Helmut Buschmann, and Detlef Heller*

Dedicated to Jack Halpern and John M. Brown

The synthesis of amino acids is still of current interest.^[1] In contrast to known and even industrially used homogeneously catalyzed hydrogenations of α -dehydroamino acid derivatives, the asymmetric hydrogenation of protected β -aminoacrylates has only lately moved into the focus of research.^[2] Meanwhile, catalytic systems have been described reaching high activities and substrate/catalyst ratios, which lead to practically enantiomerically pure β -amino acid derivatives; rhodium as a transition metal seems to be most suitable.^[3]

The asymmetric hydrogenation of α -dehydroamino acids was investigated intensively in the last decades, but there are still only a few indications of the reaction mechanism of β -dehydroamino acids. For the α -dehydroamino acids it is proposed that diastereomeric substrate complexes are formed from the solvent complex and the prochiral olefin in a preequilibrium. The diastereomeric substrate complexes react in a sequence of elementary steps—oxidative addition of hydrogen, insertion, and reductive elimination—to give the enantiomeric products. The research groups led by Halpern, Landis, and Brown were able to show that the major substrate complex present in distinct excess does not lead to the main enantiomer. The source of the enantioselectivity was identified as the extreme reactivity of the minor substrate complex.^[4] These results were generalized in the literature as the major/minor concept, and one can certainly call it a basic principle of homogeneous catalysis. The fundamental

idea of the extreme reactivity of one intermediate is reflected, for example, in the concept of “ligand-accelerated catalysis”.^[5] In addition to comprehensive kinetic and NMR spectroscopic studies, three X-ray structures of major substrate complexes support the mechanism, also referred to as the “anti lock-and-key motif”.^[4a,6]

Recently an alternative was found in studies on P,S ligands: a catalyst–substrate complex of an α -dehydroamino acid derivative, which was characterized by X-ray analysis, leads to the observed major enantiomeric form of the product.^[7] Since, on the one hand, a C_1 -symmetric ligand can in theory form four stereoisomeric substrate complexes coupled by inter- and possibly intramolecular equilibria, and, on the other hand, two sets of two substrate complexes lead to the two enantiomers, it is not certain that the one substrate complex detected by NMR spectroscopy and the isolated complex are identical.

First mechanistic investigations on the asymmetric hydrogenation of β -dehydroamino acid derivatives go back to Gridnev and Imamoto. They detected hydridoalkyl complexes at -100°C after the addition of methyl (*E*)-3-*N*-acetylamino-3-methylacrylate to the dihydrido solvent complex $[\text{RhH}_2(\text{L})(\text{MeOH})_2]\text{BF}_4$ (L = chiral bidentate phosphine ligand).^[8] Still, it is questionable whether such species are also stable under stationary hydrogenation conditions at room temperature. Nevertheless, kinetic and NMR investigations indicated that the reaction sequence of the asymmetric hydrogenation is in principle analogous to the hydrogenation of α -dehydroamino acid derivatives.^[9a]

The aim of this work is the in-depth mechanistic understanding of the rhodium-catalyzed asymmetric hydrogenation of β -acylaminoacrylates. The direct comparison to the known reaction mechanism of the hydrogenation of α -acylaminoacrylates is of special interest.

Catalyst–substrate systems particularly appropriate for mechanistic investigations are those for which the rate of product formation is independent of the substrate concentration, that is, the hydrogenation follows a zero-order rate law. For this borderline case of Michaelis–Menten kinetics characterized by preequilibria, only the stable catalyst–substrate complexes are present in the reaction solution during the hydrogenation; this can be proved easily by ^{31}P NMR spectroscopy.^[9] In contrast to the (*E*)- β -acylamino- β -arylacrylates, which are hydrogenated in a first-order reaction,^[3b] the *Z* substrates show the desired kinetic behavior. It should be possible to isolate and characterize such stable catalyst–substrate complexes. We succeeded with a complex formed from the substrate methyl (*Z*)-3-*N*-acetylamino-3-phenylacrylate (**1**). This complex, $[\text{Rh}((R,R)\text{-Et-duphos})(\text{1})]\text{BF}_4$, is the first rhodium complex with a β -acylaminoacrylate (see the Supporting Information).^[10]

Like the known cases with α -acylaminoacrylates,^[4a,6,7] the *Z* substrate is bound as a chelate to the rhodium through the double bond and the amide oxygen atom. This is particularly surprising, because the enantioselectivities for the hydrogenation of the *Z* isomers, which are in general lower than those of the *E* isomers, were explained by the nonchelating binding of the substrate caused by an intramolecular hydrogen bond in the substrate. Indeed, for several *Z* isomers these

[*] Dr. H.-J. Drexler, Dr. W. Baumann, Dipl.-Chem. T. Schmidt, Dr. A. Sun, Dr. A. Spannenberg, Dr. C. Fischer, Priv.-Doz. Dr. D. Heller
Leibniz-Institut für Organische Katalyse
an der Universität Rostock e.V.
Buchbinderstrasse 5/6, 18055 Rostock (Germany)
Fax: (+49) 381-466-9383
E-mail: detlef.heller@ifok.uni-rostock.de

Dr. S. Zhang
College of Chemistry and Environmental Science
Henan Normal University Xixiang
453007 Henan (China)

Dr. H. Buschmann
ESTEVE
Av. Mare de Deu de Montserrat 221
08041 Barcelona (Spain)

[**] We thank the Deutsche Forschungsgemeinschaft for their generous support as well as Prof. C. R. Landis for stimulating discussions. We especially thank C. Pribbenow for skilled technical assistance.

Supporting information for this article is available on the WWW under <http://www.angewandte.org> or from the author.

intramolecular hydrogen bonds^[11] were proven by X-ray crystal structures (see refs. [2, 12] and the Supporting Information). However, this interaction is apparently cancelled upon complexation of the substrate to the transition metal.

The hydrogenation of methyl (*Z*)-3-*N*-acetylamino-3-phenylacrylate (**1**) with the catalyst system Rh/(*R,R*)-Et-duphos (Et-duphos = 1,2-bis(2,5-diethylphosphoryl)benzene) in methanol at 25 °C and 1.0 bar overall pressure provides the *S* enantiomer in 85 % *ee* (59 % *ee* in isopropyl alcohol). In contrast, the isolated catalyst–substrate complex leads to the *R* enantiomer. Yet assigning the crystallized intermediate as either the major or minor substrate complex is not reasonable, since the ratio of the complexes at room temperature in both solvents is approximately 56:44 (³¹P NMR spectrum).

However, several complexes formed with the catalyst system Rh/(*S,S*)-dipamp (dipamp = 1,2-ethanediylbis[(2-methoxyphenyl)phenylphosphane]) and β-acetylamino-β-arylacrylates show ³¹P NMR signals for one substrate complex in great excess in methanol at room temperature (Table 1, column 2). Here, too, we were able to analyze these catalyst–substrate complexes by X-ray crystallography. The complexes

Table 1: [Rh((*S,S*)-dipamp)((*Z*)-β-acetylamino-β-arylacrylate)]BF₄ in methanol: ratios of the diastereomeric substrate complexes at different temperatures, enantioselectivities (25 °C, normal pressure), and reactivity ratios of the intermediates.

1 – 4

	R	[Major]/[minor] ratio (T)		S Sel. [% ee] (e.r.)	$k_{\text{maj}}/k_{\text{min}}$
1	C ₆ H ₅	90:10 (RT)	96:4 (−87°C)	50 (3.0)	0.33
2	<i>p</i> -ClC ₆ H ₄	88:12 (RT)	93:7 (−87°C)	38 (2.2)	0.30
3	<i>m</i> -NO ₂ C ₆ H ₄	81:19 (RT)	86:14 (−84°C)	20 (1.5)	0.35
4	<i>p</i> -MeC ₆ H ₄	91:9 (RT)		60 (4.0)	0.39

of methyl (*Z*)-3-*N*-acetylamino-3-(*p*-chlorophenyl)acrylate (**2**) and methyl (*Z*)-3-*N*-acetylamino-3-(*m*-nitrophenyl)acrylate (**3**) are shown in Figure 1 (see the Supporting Information for details). One peculiarity of all four substrate complexes is that the OMe group of the dipamp ligand interacts with the rhodium center as a hemilabile ligand. This type of coordination is often discussed but to the best of our knowledge has never been proven by X-ray analysis.^[13]

The four isolated substrate complexes each lead to the *S* enantiomer. Surprisingly, the *S* enantiomer is also the major product of the asymmetric hydrogenation in methanol (although the enantioselectivities are only 20–60 % *ee*, Table 1, column 4).

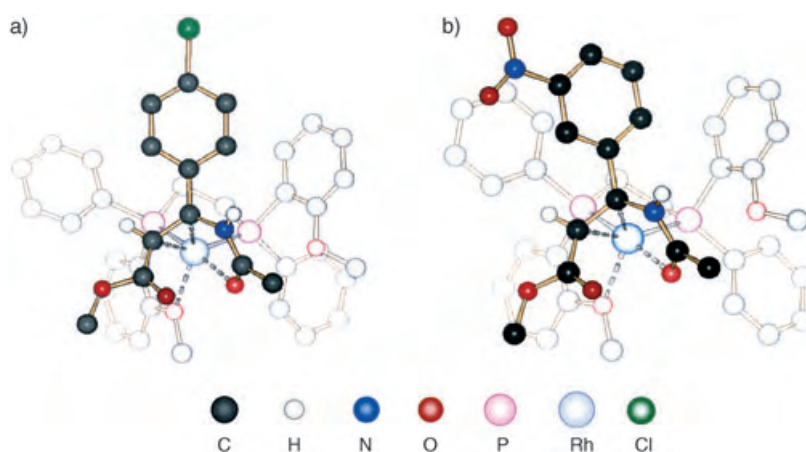


Figure 1. Structures of the cations in a) [Rh((*S,S*)-dipamp)(**2**)]BF₄ and b) [Rh((*S,S*)-dipamp)(**3**)]BF₄ determined by X-ray crystal structure analysis.

There are several ways to eliminate the possibility that only the minor substrate complexes crystallize, including complicated NOE measurements and solid-state NMR spectroscopy. However, we chose a different, simpler variant and tried to “freeze out” the interconversion between the diastereomeric catalyst–substrate complexes at low temperatures. It is crucial to this method that both of the substrate complexes are clearly detectable even at the lowest temperature employed (Table 1, column 3) and furthermore that the crystals are sufficiently soluble.

The results for the substrate methyl (*Z*)-3-*N*-acetylamino-3-(*p*-chlorophenyl)acrylate (**2**) are represented in Figure 2.^[14] When we dissolved single crystals of the substrate complex in a sealed NMR tube at approximately −90 °C, only the major substrate complex was visible in the spectrum at −83 °C (Figure 2a). When we allowed the very same NMR tube to warm over several hours to room temperature, both of the substrate complexes were again evident in the known ratio of 88:12 (Figure 2b, Table 1). The spectrum recorded after recooling this NMR tube is shown in Figure 2c. The agreement between the major/minor ratio determined at room temperature and at low temperature (Figure 2, Table 1) proves that the thermodynamic equilibrium between the substrate complexes has been reached in both cases.

Analogous results were obtained for the substrates methyl (*Z*)-3-*N*-acetylamino-3-phenylacrylate (**1**) and methyl (*Z*)-3-*N*-acetylamino-3-(*m*-nitrophenyl)acrylate (**3**) (see the Supporting Information). These findings support the unequivocal conclusion that the major substrate complexes crystallized. Thus, it has been proven for the first time that the substrate complex dominant in solution controls the stereochemistry of the product. This is in keeping with the lock-and-key mechanism known from enzyme catalysis.

The enantiomeric ratio is the result of two factors: the ratio of the concentrations of the intermediates ([major substrate complex]/[minor substrate complex]) as the first level of selection in the reaction sequence and the ratio of their reactivities (*k*_{maj}/*k*_{min}) as the second level of selection.^[15] In case of [Rh((*R,R*)-Et-duphos)(**1**)]BF₄ the selectivity must arise from the difference in reactivity of the diastereomeric

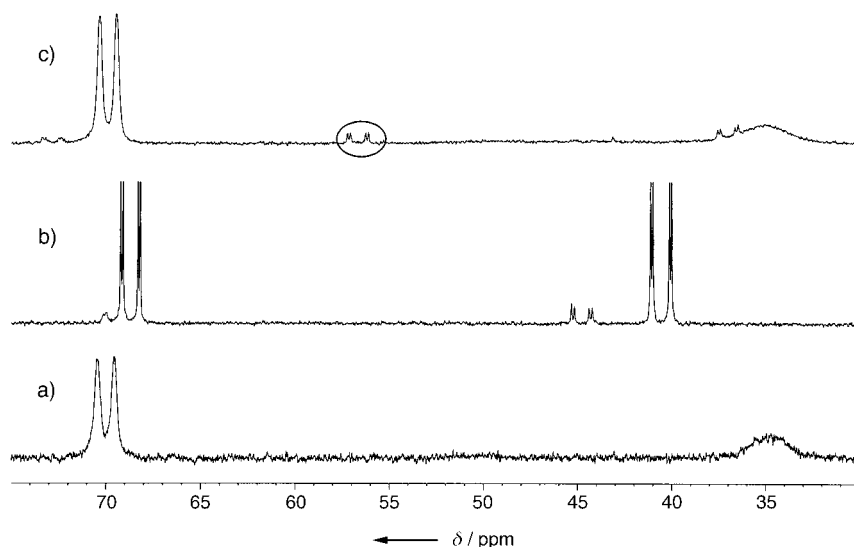


Figure 2. ^{31}P NMR spectra of a solution prepared from single crystals of $[\text{Rh}((S,S)\text{-dipamp})]\text{BF}_4$ dissolved at -90°C in methanol a) immediately after dissolving ($T = -83^\circ\text{C}$), b) after warming to 25°C and equilibration ($[\text{major}]/[\text{minor}] = 88:12$), and c) after recooling the sample from (b) to $T = -78^\circ\text{C}$ ($[\text{major}]/[\text{minor}] = 93:7$).

substrate complexes because their concentrations are roughly equal at room temperature (ratio 56:44). The experimentally determined enantiomer ratio is 12.3 in methanol (85 % *ee*) and 3.9 in isopropyl alcohol (59 % *ee*), which indicates that the difference in the reactivities of the two intermediates cannot be very great.

The situation is similar with dipamp as the ligand. For the examples investigated the diastereomer ratios of the catalyst–substrate complexes and the enantiomer ratios of products of the asymmetric hydrogenation indicate that in each case the minor substrate complex reacts approximately only three times faster than the major substrate complex (Table 1, column 5).^[16] The fact that the minor substrate complexes are only slightly more reactive than the major substrate complexes does not agree with the known ratios of reactivity of diastereomeric catalyst–substrate complexes containing α -acylaminoacrylates. Kinetic investigations of the hydrogenation of methyl (*Z*)-*N*-acetylaminocinnamate with $[\text{Rh}(\text{dipamp})(\text{MeOH})_2]^+$ resulted in a reaction rate for the minor substrate complex that was 580 times greater for the oxidative addition of hydrogen at 25°C than for the major substrate complex.^[4d] With chiraphos as the chiral ligand this difference in reactivity was estimated at more than 1000 when the analogous ethyl ester was the substrate.^[4c]

In conclusion we have determined that reaction sequence for the hydrogenations of β - and α -acylaminoacrylates with cationic rhodium(i) complexes is the same. For the first time catalyst–substrate complexes for several β -dehydroamino acid derivatives were characterized by X-ray structure analysis. The chelating binding of the prochiral olefin to rhodium occurs—as in the α -substituted analogues—through the double bond and the amide oxygen.

While in case of α -acylaminoacrylates the catalyst–substrate complex dominant in solution does not lead to the

major product of the asymmetric hydrogenation,^[17] in our study three single crystals unequivocally identified as major substrate complexes by low-temperature ^{31}P NMR spectroscopy show opposite behavior. The major intermediate determines the selectivity (lock-and-key principle). The main cause for this apparently lies in the slight difference in reactivities of the diastereomeric substrate complexes. The classic major/minor concept is based on the fact that the minor substrate complex is much more reactive than the major substrate complex, but this extreme difference in reactivity is not evident in the substrate complexes with β -acylaminoacrylates in this work. Therefore for the examples studied the complexation of the substrate as the first level of selection plays an even bigger role than previously assumed.

Received: August 19, 2004

Keywords: asymmetric catalysis · β -amino acids · catalyst–substrate complexes · hydrogenation · reaction mechanisms

- [1] a) J.-A. Ma, *Angew. Chem.* **2003**, *115*, 4426–4435; *Angew. Chem. Int. Ed.* **2003**, *42*, 4290–4299; b) N. Sewald, *Angew. Chem.* **2003**, *115*, 5972–5973; *Angew. Chem. Int. Ed.* **2003**, *42*, 5794–5795.
- [2] Review: H.-J. Drexler, J. You, S. Zhang, C. Fischer, W. Baumann, A. Spannenberg, D. Heller, *Org. Process Res. Dev.* **2003**, *7*, 355–361.
- [3] a) W. Tang, W. Wang, Y. Chi, X. Zhang, *Angew. Chem.* **2003**, *115*, 3633–3635; *Angew. Chem. Int. Ed.* **2003**, *42*, 3509–3511; b) J. You, H.-J. Drexler, S. Zhang, C. Fischer, D. Heller, *Angew. Chem.* **2003**, *115*, 942–945; *Angew. Chem. Int. Ed.* **2003**, *42*, 913–916; c) D. Pena, A. J. Minnaard, J. G. deVries, B. L. Feringa, *J. Am. Chem. Soc.* **2002**, *124*, 14552–14553; d) Y.-G. Zhou, W. Tang, W.-B. Wang, W. Li, X. Zhang, *J. Am. Chem. Soc.* **2002**, *124*, 4952–4953.
- [4] a) A. S. C. Chan, J. J. Pluth, J. Halpern, *J. Am. Chem. Soc.* **1980**, *102*, 5952–5954; b) J. M. Brown, P. A. Chaloner, *J. Chem. Soc. Chem. Commun.* **1980**, 344–346; c) J. Halpern in *Asymmetric Synthesis*, Vol. 5 (Ed.: J. D. Morrison), Academic Press, Orlando, **1985**, pp. 41–69; d) C. R. Landis, J. Halpern, *J. Am. Chem. Soc.* **1987**, *109*, 1746–1754; e) C. R. Landis, S. Feldgus, *Angew. Chem.* **2000**, *112*, 2985–2988; *Angew. Chem. Int. Ed.* **2000**, *39*, 2863–2866; f) S. Feldgus, C. R. Landis, *J. Am. Chem. Soc.* **2000**, *122*, 12714–12727.
- [5] D. J. Berrisford, C. Bolm, K. B. Sharpless, *Angew. Chem.* **1995**, *107*, 1159–1171; *Angew. Chem. Int. Ed. Engl.* **1995**, *34*, 1059–1064. (“The goal of channeling the catalysis through one particular complex is usually achieved by an overwhelming kinetic activity favoring that one complex over the many other complexes which assemble in solution. For ligand-accelerated processes with early transition metal complexes, this in situ selection of a highly reactive (and selective) metallic complex from a variety of thermodynamically dictated assemblies is a crucial requirement.”)

- [6] a) B. McCulloch, J. Halpern, M. R. Thomas, C. R. Landis, *Organometallics* **1990**, *9*, 1392–1395; b) H.-J. Drexler, S. Zhang, A. Sun, A. Spannenberg, A. Arrieta, A. Preetz, D. Heller, *Tetrahedron: Asymmetry* **2004**, *15*, 2139–2150.
- [7] D. Evans, F. E. Michael, J. S. Tedrow, K. R. Campos, *J. Am. Chem. Soc.* **2003**, *125*, 3534–3543.
- [8] M. Yasutake, I. D. Gridnev, N. Higashi, T. Imamoto, *Org. Lett.* **2001**, *3*, 1701–1704.
- [9] a) D. Heller, H.-J. Drexler, J. You, W. Baumann, K. Drauz, H.-P. Krimmer, A. Börner, *Chem. Eur. J.* **2002**, *8*, 5196–5202; b) D. Heller, H.-J. Drexler, A. Spannenberg, B. Heller, J. You, W. Baumann, *Angew. Chem.* **2002**, *114*, 814–817; *Angew. Chem. Int. Ed.* **2002**, *41*, 777–780; c) D. Heller, R. Thede, D. Haberland, *J. Mol. Catal. A* **1997**, *115*, 273–281.
- [10] CCDC 216557, CCDC 216558, CCDC 247714, CCDC 247715, CCDC 247716, and CCDC-247717 contain the supplementary crystallographic data for this paper. These data can be obtained free of charge via www.ccdc.cam.ac.uk/conts/retrieving.html (or from the Cambridge Crystallographic Data Centre, 12, Union Road, Cambridge CB21EZ, UK; fax: (+44)1223-336-033; or deposit@ccdc.cam.ac.uk).
- [11] W. D. Lubell, M. Kitamura, R. Noyori, *Tetrahedron: Asymmetry* **1991**, *2*, 543–554.
- [12] A. Chiaroni, C. Riche, F. Dumas, D. Potin, J. D'Angelo, *Acta Crystallogr. Sect. C* **1995**, *51*, 967–970.
- [13] a) J. A. Ramsden, T. D. W. Claridge, J. M. Brown, *J. Chem. Soc. Chem. Commun.* **1995**, 2469–2471; b) T. Imamoto, H. Tsuruta, Y. Wada, H. Masuda, K. Yamaguchi, *Tetrahedron Lett.* **1995**, *36*, 8271–8274.
- [14] The chloro compound was chosen because the absolute configuration of the main hydrogenation product has been proven by X-ray structure analysis and therefore the assignment of the HPLC-Chiralyser signals is definite.^[3b]
- [15] $[P]/[P^*] = [major\ substrate\ complex]/[minor\ substrate\ complex] (k_{maj}/k_{min})$; D. Heller, H. Buschmann, H.-D. Scharf, *Angew. Chem.* **1996**, *108*, 1964–1967; *Angew. Chem. Int. Ed.* **1996**, *35*, 1852–1854. An analogous equation with the stability constants resulting from the equilibrium treatment was already described by Halpern and Landis.^[4d] For the equation used here resulting from the steady-state treatment, the ratio of the stability constants must be replaced by the reciprocal values of the corresponding Michaelis constants.
- [16] These considerations apply only if the ratio of the diastereomeric substrate complexes determined under argon corresponds to that under hydrogen atmosphere. For the hydrogenation of methyl (Z)-N-acetylaminocinnamate with the dipamp catalyst this seems to be the case: D. Heller, H. Buschmann, *Top. Catal.* **1998**, *5*, 159–176.
- [17] For a detailed mechanistic study of the analogous hydrogenation with Ru catalysts, see: M. Kitamura, M. Tsukamoto, Y. Bessho, M. Yoshimura, U. Kobs, M. Widmalm, R. Noyori, *J. Am. Chem. Soc.* **2002**, *124*, 6649–6667.

Biodegradable, Amorphous Copolyester-Urethane Networks Having Shape-Memory Properties**

Armin Alteheld, Yakai Feng, Steffen Kelch, and
Andreas Lendlein*

Degradable polymers having a thermally induced shape memory can be fixed in a new, temporary shape after they have been processed into a permanent shape. They have great potential for biomedical applications, especially in the area of minimally invasive surgery.^[1] One example is the insertion of a bulky medical device in a compressed temporary shape through a small surgical incision. When the implant is heated above a switching temperature (T_{trans}), it returns to its application-relevant permanent shape. After a given time the device degrades, and a second surgery for its removal is not necessary.^[2,3]

Shape-memory polymers generally consist of two components: cross-links determining the permanent shape and switching segments fixing the temporary shape at temperatures below T_{trans} . Cross-linkage can be achieved either by physical interaction (e.g., in thermoplastic polymers) or by chemical bonds (e.g., in thermosets or photosets). In covalently cross-linked shape-memory polymer networks a maximum weight content of switching segments is possible. In contrast, thermoplastic materials must contain a sufficient amount of hard-segment-determining blocks so that a sufficient number of physical cross-links exist at temperatures above T_{trans} .^[4]

The blocks that determine the switching segment may display T_{trans} as either a melting temperature or a glass transition temperature. In biodegradable shape-memory polymers previously described as thermoplastic multiblock-copolymers^[3] or photoset AB polymer networks^[2,5] T_{trans} is the melting point of crystallizable oligo(ϵ -caprolactone) segments. Hydrogels with hydrophobic and crystallizable side chains as molecular switches also can show a thermoresponsive one-way shape-memory effect.^[6]

Based on noncrystallizable switching segments, completely amorphous shape-memory polymer networks having a glass transition temperature as T_{trans} can be designed. These networks are transparent, and they should show a more

[*] Dr. A. Alteheld, Dr. Dr. Y. Feng, Dr. S. Kelch, Prof. Dr. A. Lendlein
GKSS-Forschungszentrum Geesthacht GmbH
Institut für Chemie
Kantstrasse 55, 14513 Teltow (Germany)
Fax: (+49) 3328-352-452
E-mail: andreas.lendlein@gkss.de

[**] The authors thank Andreas Kastanja for the photos. This work was supported by the Bundesministerium für Bildung und Forschung (BioFuture award no. 0311867), by the Ministerium für Schule, Wissenschaft und Forschung, Nordrhein-Westfalen (fellowship for A.A.), and by mnemoScience GmbH, Aachen (Germany).



Supporting information for this article is available on the WWW under <http://www.angewandte.org> or from the author.

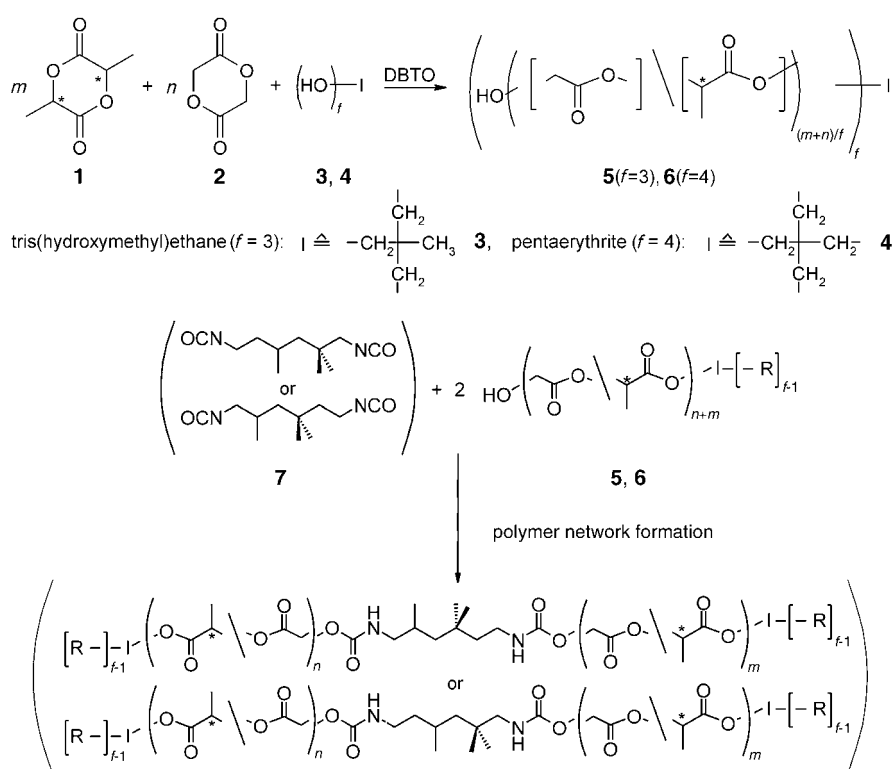
homogenous degradation than semicrystalline polymers since hydrolytic degradation occurs faster in amorphous regions than in crystalline ones.^[7–11] Both features are most relevant for certain medical applications and therapeutic methods. Transparency is required for applications like replacement of ocular tissue.^[12–15] The homogenous degradation behavior of amorphous aliphatic copolyesters qualifies them as preferred matrices in the area of controlled drug delivery.^[10]

However, the completely amorphous polymer networks with thermally induced shape-memory effects described in literature, such as poly(styrene)^[16] and poly(acrylate) resins,^[17] were not originally developed for medical applications and are not hydrolytically degradable. In this paper we report on, to our knowledge, the first amorphous, biodegradable, shape-memory polymer networks.

Our structural concept is based on polymer networks that are synthesized by coupling well-defined star-shaped telechelic oligomers with a low-molecular-weight junction unit. In this polymer network architecture the functionality of the cross-links is defined by the branch points of the telechelic precursor. The switching segment chains are formed by coupling the end groups of two different arms of the precursors. When the structure–property relationships are known, we will be able to adjust the macroscopic properties of the polymer networks to the specific requirements of each medical application by varying these structural parameters.

The amorphous shape-memory thermosets introduced in this communication were prepared from star-shaped hydroxy-telechelic co-oligoesters. The cross-linking reaction was performed by adding an isomeric mixture of 1,6-diisocyanato-2,2,4-trimethylhexane and 1,6-diisocyanato-2,4,4-trimethylhexane (**7**) as junction units (Scheme 1). The co-oligoester segments consist of oligo[*rac*-lactide)-*co*-glycolide] (**5,6**) synthesized by copolymerization of *rac*-dilactide (**1**, mixture of 93.8 mol % D,D- and L,L-dilactide and 6.2 mol % *meso*-dilactide) and diglycolide (**2**). The cross-link points were introduced by ring-opening polymerization of **1** and **2** with the initiators 1,1,1-tris(hydroxymethyl)ethane (**3**) and pentaerythritol (**4**), resulting in trifunctional and tetrafunctional netpoints, respectively. Poly(*rac*-lactide)s and poly[*rac*-lactide)-*co*-glycolide]s containing up to 75 mol % glycolide are amorphous.^[18] The T_{trans} values of the resulting shape-memory polymers are the glass transition temperatures T_g , which are between ca. 59 °C for poly(*rac*-lactide)^[19] and ca. 36 °C for poly(glycolide).^[20] The homo- and copolymers of **1** and **2** are established in biomaterial science and known to be biocompatible and biodegradable.^[21,22]

The obtained copolyester-urethane networks exhibited a gel content higher than 90 %. The degree of swelling of the copolyester-urethane networks increased with increasing chain length of the copolyester segment due to the lower



Scheme 1. Synthetic route to amorphous, biodegradable copolyester-urethane networks. I: initiator, f: functionality of initiator, R: oligo[*rac*-lactide)-*co*-glycolide] segment. DBTO = dibutyltin oxide.

cross-link density. The networks prepared from the three-armed oligomers **5** showed a higher degree of swelling than those from four-armed species **6** when the molecular weight of the oligomers was similar, indicating a lower cross-link density.

The thermal properties of polymer networks were characterized with differential scanning calorimetry (DSC) by cooling samples from the melt at 150 to -50°C at 10 K min^{-1} and reheating them to 150°C at 10 K min^{-1} . As expected, the optically clear materials did not show any crystallization or melting peak in DSC experiments. The T_g values (second heating run) of the copolyester-urethane networks were in the range between 48 and 66°C and about 10–50 K above the T_g values of the respective telechelic cooligomers **5** and **6** (Figure 1). For both types of polymer networks the T_g values were found to be around 55°C when the number average molecular weight (M_n) of the precursors was higher than 4000 g mol^{-1} . For lower M_n values, the T_g values of the networks prepared from four-armed precursors **6** are higher than those synthesized from three-armed precursors **5** and increase significantly with decreasing M_n . This effect is in agreement with the theory of Fox and Flory,^[23] which predicts an increase in T_g with decreasing molecular weight of the chain segments and increasing functionality of the netpoints. However, it must be noted that the chemical composition of the polymer networks (e.g. the diurethane content) depends drastically on the molecular weight of the precursors. Intermolecular interactions like H-bonding through the diurethane units and nonideal cross-linking because of

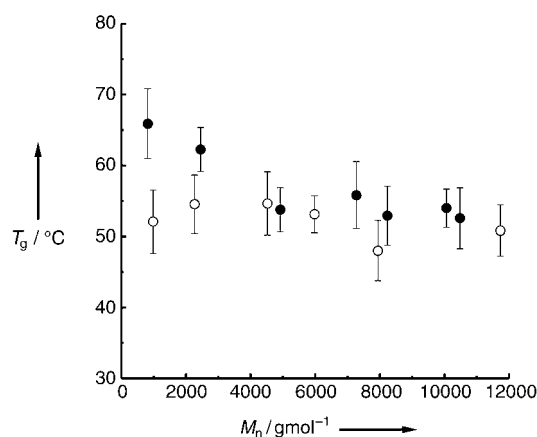


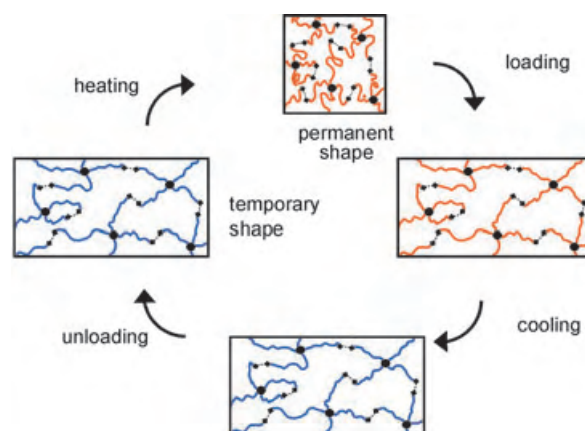
Figure 1. Glass transition temperature of copolyester-urethane networks (DSC) from the second heating cycle as a function of the molecular weight of the telechelic precursors M_n (determined by ^1H NMR spectroscopy). Copolyester-urethane networks: \circ : three-armed oligomers **5**, \bullet : four-armed oligomers **6**.

possible dangling chain ends or loop formation may also influence T_g . For biomedical applications the T_g value of the networks could potentially be adjusted around body temperature by increasing the glycolide content.

At 70°C , approximately 20°C above T_g , the polymer networks are in a rubber-elastic state, and no necking occurred in the stress-strain test. Young's modulus E and elongation at break ϵ_b depend on the segment length of the covalent network: with increasing molecular weight of the precursors, in other words, increasing chain lengths of the networks, E decreases and ϵ_b increases, respectively. The results of mechanical tests at 70°C showed that it was possible to realize deformations from the permanent to the temporary shape of up to 470%. The value for E decreased by a factor between 60 and 530 compared to that of identical sample measured at 25°C (Table 1). The value for ϵ_b decreased from 470% at 70°C to 250% at 25°C for the loosely cross-linked

material N-P-LG(17)-10000. The tensile stress at break σ_b increased by at least an order of magnitude when the measurement temperature was decreased from 70 to 25°C .

The shape-memory effect of amorphous biodegradable copolyester-urethane networks is illustrated in Scheme 2. In



Scheme 2. Illustration of shape-memory effect for amorphous, biodegradable copolyester-urethane networks prepared from oligo[(*rac*-lactide)-*co*-glycolide]tetrals **6** and low-molecular-weight diisocyanate **7**. —: oligo[(*rac*-lactide)-*co*-glycolide] segment, \blacklozenge : diurethane link, \bullet : netpoint.

the programming step, the amorphous polyurethane network was deformed from its permanent shape to its temporary shape at a high temperature ($T_{\text{high}} = 70^\circ\text{C}$), held in its deformed shape, and cooled below T_{trans} to T_{low} . After fixation of the deformed temporary shape was complete, the load was removed. In the recovery step the network was reheated above T_{trans} to T_{high} , and the original permanent shape was recovered. The macroscopic shape-memory effect of these materials is demonstrated in Figure 2. The complex transformation from the temporary shape ("SM") to the perma-

Table 1: Mechanical and shape-memory properties of biodegradable copolyester-urethane networks.^[a]

Network ^[b]	M_n [g mol ⁻¹] ^[c]	E [MPa] ^[d]	σ_b [MPa] ^[d]	ϵ_b [%] ^[d]	E [MPa] ^[e]	σ_b [MPa] ^[e]	ϵ_b [%] ^[e]	ϵ_m [%]	$R_f(1)$ [%]	$R_r(1)$ [%]	$\bar{R}_{x,2-5}$ [%]	$\bar{R}_{r,2-5}$ [%]
N-T-LG(17)-1000	980	330 ± 30	25.8 ± 1.4	90 ± 10	2.84 ± 0.53	1.80 ± 0.01	115 ± 30	n.d.	n.d.	n.d.	n.d.	n.d.
N-T-LG(15)-2000	2270	520 ± 150	20.2 ± 4.2	170 ± 30	1.84 ± 0.14	2.85 ± 0.43	250 ± 30	n.d.	n.d.	n.d.	n.d.	n.d.
N-T-LG(17)-5000	4500	490 ± 35	29.3 ± 4.7	165 ± 30	0.92 ± 0.23	3.78 ± 1.12	470 ± 75	50 ^[f]	91.5	98.5	94.5 ± 2.5	98.5 ± 1.0
N-T-LG(17)-6000	6000	345 ± 70	26.2 ± 1.2	305 ± 45	1.11 ± 0.25	1.84 ± 0.93	375 ± 65	100	94.5	> 99.0	94.5 ± 0.5	> 99.0 ± 0
N-T-LG(16)-8000	7900	600 ± 125	34.7 ± 0.3	150 ± 5	1.22 ± 0.14	2.67 ± 0.54	370 ± 10	100	95.5	> 99.0	91.0 ± 0.0	99.0 ± 0.5
N-T-LG(18)-12000	11 700	390 ± 35	24.2 ± 4.2	150 ± 5	0.77 ± 0.12	0.71 ± 0.33	875 ± 90	100	91.8	97.3	91.7 ± 0.1	96.9 ± 0.4
N-P-LG(17)-1000	820	340 ± 80	29.2 ± 4.8	100 ± 20	5.89 ± 0.78	3.23 ± 0.24	90 ± 10	n.d.	n.d.	n.d.	n.d.	n.d.
N-P-LG(18)-2000	2450	495 ± 145	26.1 ± 3.2	50 ± 10	2.62 ± 0.04	2.30 ± 0.45	180 ± 110	n.d.	n.d.	n.d.	n.d.	n.d.
N-P-LG(15)-5000	4900	375 ± 60	30.4 ± 5.3	240 ± 90	1.16 ± 0.12	2.90 ± 0.01	240 ± 10	50 ^[f]	90.5	> 99.0	91.0 ± 2.5	96.5 ± 1.5
N-P-LG(15)-7000	7300	420 ± 35	21.4 ± 5.3	180 ± 5	1.21 ± 0.19	2.38 ± 1.07	300 ± 130	100	92.0	> 99.0	92.5 ± 0.0	> 99 ± 0.0
N-P-LG(16)-8000	8200	350 ± 80	18.3 ± 3.3	265 ± 50	1.03 ± 0.26	1.75 ± 0.36	430 ± 115	100	96.0	> 99.0	97.0 ± 2.0	98.5 ± 1.5
N-P-LG(17)-10000	10000	340 ± 60	36.2 ± 5.9	250 ± 210	1.86 ± 0.35	3.51 ± 0.21	470 ± 5	100	96.5	92.5	95.0 ± 0.0	90.0 ± 1.0

[a] E : Young's modulus, σ_b : tensile stress at break, ϵ_b : elongation at break, $R_f(N)$: strain fixity rate, $R_r(N)$: strain recovery rate, N : number of cycles, $\bar{R}_{x,2-5}$: average R_x for the second to fifth cycle. [b] Polymer networks were denoted as N-T (tris(hydroxymethyl)ethane) or N-P (pentaerythritol) LG (glycolide content in precursors in wt%); approximate number average molecular weight M_n of precursors determined by ^1H NMR spectroscopy. [c] Molecular weight of the precursor was calculated from integration of the ^1H NMR signals of **1** (δ_{CH} : 5.00–5.30 ppm) and **2** (δ_{CH_2} : 4.50–4.90 ppm), and initiators **3** (δ_{CH_2} : 3.95–4.15 ppm) and **4** (δ_{CH_2} : 4.05–4.25 ppm). [d] Determined at 25°C . [e] Determined at 70°C . [f] Samples broke in the second cycle when $\epsilon_m = 100\%$. n.d.: not determined.

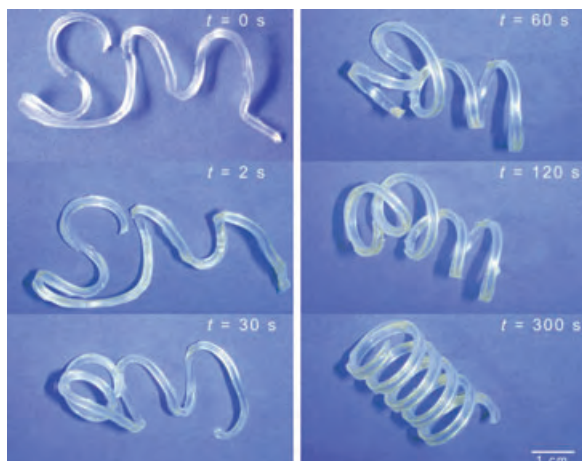


Figure 2. The series of photographs demonstrates the macroscopic shape-memory effect for a biodegradable copolyester-urethane network. The transition from the temporary shape ("SM") to the permanent shape ("corkscrew") took 300 s at 70°C.

nent shape ("corkscrew") took approximately 5 min at a temperature of 70°C.

The shape-memory properties of the polymer networks were quantified by cyclic, thermomechanical tensile experiments.^[4] The strain fixity rate R_f and the strain recovery rate R_r were calculated to quantify the fixation of the temporary and the recovery of the permanent shape of the polymer networks. R_f and R_r of all prepared networks were higher than 90% for all cycles (Table 1). The shape-memory properties varied slightly between the first and the second cycle due to segment-chain orientation and relaxation effects. After the second cycle, R_f and R_r reached almost constant values. The recovery stress was in the range of 0.8–1.0 MPa when polymer network N-P-LG(17)-10000 was heated to $T_h = 70^\circ\text{C}$ in its temporary shape ($\epsilon_m = 100\%$).

The mechanical properties of the polymer networks in their temporary shape (ϵ_u) are important characteristics for potential applications. For this purpose, a series of samples were programmed by elongating to ϵ_m and cooling to T_{low} , resulting in an elongation at the stress-free state ϵ_u . Figure 3 shows the effect of ϵ_u on the mechanical properties of the polymer network N-P-LG(17)-10000. Applying a deformation in the same direction as that used for forming the temporary shape resulted in a significant increase of E , while ϵ_u was lower than 100%. For higher values of ϵ_u no further increase could be observed. This behavior indicates that a certain preorientation of chain segments in the amorphous polymer networks leads to higher mechanical strength and a lower elongation at break ϵ_b .^[24]

The hydrolytic degradation experiments showed three major phases in the degradation of the polymer networks: the mass was unchanged during an induction phase (1), which was followed by a phase characterized by accelerated mass loss (2), and finally by a phase showing retarded mass loss (3). The degradation curves shown in Figure 4 indicate bulk degradation. Linear poly[(*rac*-lactide)-*co*-glycolide] (25% glycolide) microspheres with $M_n \approx 80\,000\text{ g mol}^{-1}$ degraded homogeneously, while the scaffold made from a copolymer with

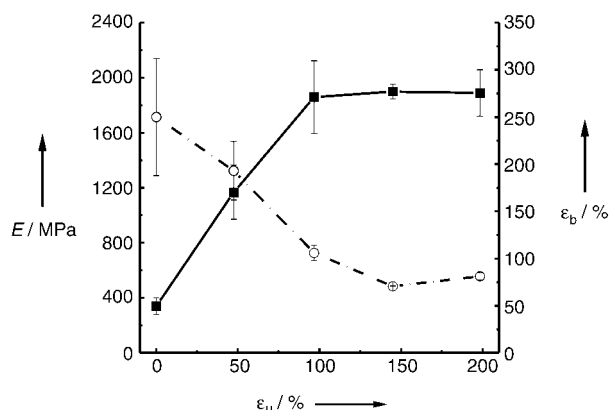


Figure 3. Young's modulus E (■) and elongation at break ϵ_b (○) for the network N-P-LG(17)-10000 in its temporary shape at 25°C as a function of elongation in the stress-free state ϵ_u after fixation in cyclic thermomechanical tensile experiments.

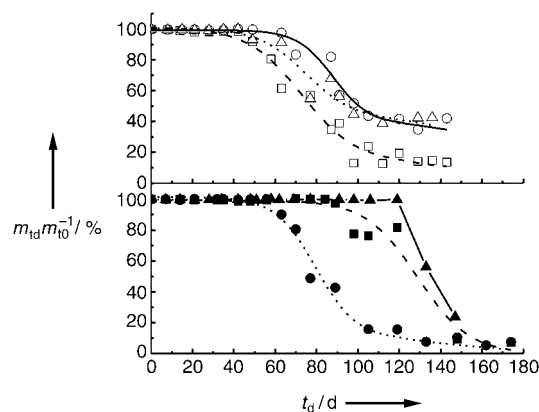


Figure 4. Hydrolytic degradation of copolyester-urethane networks in aqueous phosphate buffer solution (pH 7) at 37°C. Relative mass loss: ratio of mass m_{td} at degradation time t_d (in days) to the initial mass m_{t0} , for polymer networks with varying segment chain length and functionality of crosslinks. Copolyester-urethane networks: □: N-T-LG(17)-1000, ○: N-T-LG(17)-5000, △: N-T-LG(17)-6000, ■: N-P-LG(17)-1000, ▲: N-P-LG(17)-10000.

$M_n > 100\,000\text{ g mol}^{-1}$ showed an induction period of 48 d.^[10,25] The induction period is characterized by the diffusion of water into the polymer networks and the beginning of the hydrolytic degradation of the copolyester segment chains. The diffusion of water is influenced by the hydrophilicity of polymer networks which increases with increasing diurethane unit content and the glycolide content of the copolyester (Table 1 in the Supporting Information). The beginning cleavage of ester bonds led to an increase in the swelling capability. During this period the swollen and partly degraded chain segments were still connected to multifunctional netpoints. Copolyester-urethane networks from four-armed cooligomers **6** had an induction period of 60 to 125 d, while 45 to 65 d were characteristic for the polymer networks from the three-armed oligomers **5**, which reflects their lower crosslink density (Figure 4).

In summary, we have demonstrated that a series of copolyester-urethane networks are amorphous and biode-

gradable, and have shape-memory properties. The synthetic route to the polymer networks allows the adjustment of certain molecular parameters such as functionality of the crosslinks and the segment chain length. In this way, polymer networks with variable mechanical properties but nearly constant shape-memory properties (T_{trans} , R_f and R_r) could be obtained. The copolyester-urethane networks are transparent and undergo bulk degradation. Biodegradable, transparent biomaterials with shape memory may be crucial in the development of minimally invasive surgery in ophthalmology.

Experimental Section

5, 6: All polymerizations were carried out in bulk under nitrogen at 130°C. A mixture of 85 wt % *rac*-dilactide **1**, 15 wt % diglycolide **2**, and the initiators (**3** or **4**) was heated and stirred. When the melt became optically clear, dibutyltin oxide (0.2 wt %, DBTO) was added. After 5 days the reaction mixture was cooled to room temperature. The cooligomers were dissolved in a six- to tenfold excess of CH_2Cl_2 and then precipitated in hexane. The precipitate was washed with hexane and dried to constant weight at 80°C.

Synthesis of the copolyester-urethane network: The telechelic cooligomer was dissolved in a tenfold excess of CH_2Cl_2 under nitrogen. Compound **7** (molar ratio of isocyanato to hydroxy functional groups of 1.05) was added to the solution with stirring. After 5 min the reaction mixture was poured into teflon dishes and kept under nitrogen flow for 24 h at room temperature to evaporate the solvent carefully during formation of the polymer network. To complete film crosslinking, the films were kept at 80°C for further 4 days. The crude films were extracted with chloroform and dried to constant weight under vacuum (0.1 mbar) at 80°C.

Received: July 19, 2004

Published online: January 17, 2005

Keywords: amorphous materials · materials science · polymers · shape-memory polymers

- [15] A. W. Lloyd, R. G. A. Faragher, S. P. Denyer, *Biomaterials* **2001**, 22, 769.
- [16] K. Takeda, M. Akiyama, T. Yamamizu, *Angew. Makromol. Chem.* **1988**, 157, 123.
- [17] V. A. Stoy, F. T. Delahanty (Kingston Technologies, Inc.), EP0439892A2, **1990**.
- [18] A. Lendlein, *Chem. Unserer Zeit* **1999**, 33, 279.
- [19] M. Vert, P. Christel, F. Chabot, J. Leray in *Macromolecular Biomaterials* (Eds.: G. W. Hastings, P. Ducheyne), CRC, Boca Raton, **1984**, p. 119.
- [20] D. K. Gilding, A. M. Reed, *Polymer* **1979**, 20, 1459.
- [21] K. Yamaguchi, J. M. Anderson, *J. Controlled Release* **1993**, 24, 81.
- [22] L. Lu, A. G. Garcia, A. G. Mikos, *J. Biomed. Mater. Res.* **1999**, 46, 236.
- [23] a) T. G. Fox, P. J. Flory, *J. Appl. Phys.* **1950**, 21, 581; b) T. G. Fox, L. J. Loshaek, *J. Polym. Sci.* **1955**, 15, 371.
- [24] I. M. Ward in *Structure and Properties of Oriented Polymers*, Applied Science, London, **1975**, p. 256.
- [25] L. B. Wu, J. D. Ding, *Biomaterials* **2004**, 25, 5821.

- [1] F. El Feninat, G. Laroche, M. Fiset, D. Mantovani, *Adv. Eng. Mater.* **2002**, 4, 91.
- [2] A. Lendlein, A. Schmidt, R. Langer, *Proc. Natl. Acad. Sci. USA* **2001**, 98, 842, published online before print as USA 10.1073/pnas.031571398 at www.pnas.org.
- [3] A. Lendlein, R. Langer, *Science* **2002**, 296, 1673, published online before print on April 25, 2002 in (Science Express Reports) www.scienceexpress.org, Page 1/10.1126/science.1066102.
- [4] a) A. Lendlein, S. Kelch, *Angew. Chem.* **2002**, 114, 2138–2162; *Angew. Chem. Int. Ed.* **2002**, 41, 2034.
- [5] D. Rickert, A. Lendlein, A. M. Schmidt, S. Kelch, W. Roehlke, R. Fuhrmann, R. P. Franke, *J. Biomed. Mater. Res.* **2003**, 67, 722.
- [6] Y. Osada, A. Matsuda, *Nature* **1995**, 376, 219.
- [7] S. Li, *J. Biomed. Mater. Res.* **1999**, 48, 342.
- [8] I. Jabbal-Gill, W. Lin, O. Kistner, S. S. Davis, L. Illum, *Adv. Drug Delivery Rev.* **2001**, 51, 97.
- [9] C. Witschi, E. Doelker, *J. Controlled Release* **1998**, 51, 327.
- [10] E. R. Edelman, A. Nathan, M. Katada, J. Gates, M. J. Karnovsky, *Biomaterials* **2000**, 21, 2279.
- [11] M. Ramchandani, D. Robinson, *J. Controlled Release* **1998**, 54, 167.
- [12] L. Liu, H. Sheardown, *Biomaterials* **2005**, 26, 233.
- [13] M. J. Bruining, A. P. Pijpers, P. Kingshott, L. H. Koole, *Biomaterials* **2002**, 23, 1213.
- [14] D. F. Williams, *Sadhana* **2003**, 28, 563.

Boryl Complexes

**A Boryl Bridged Complex: An Unusual Coordination Mode of the BR_2 Ligand****

Holger Braunschweig, Krzysztof Radacki,
Daniela Rais, and George R. Whittell*

The chemistry of transition-metal boryl complexes has been the focus of intense research for well over a decade.^[1] Interest in this area has been driven by the intermediacy of these compounds in hydroboration^[2] and diboration^[3] reactions of unsaturated organic substrates, as well as selective C–H bond activation of hydrocarbons.^[4] Efforts to improve the catalytic efficiency of such processes have prompted numerous structural^[1a,b,e,g] and theoretical^[1c,d,f] investigations, with the aim of gaining a more comprehensive understanding of the nature of the metal–boron bond. The majority of structural data indicate a strong σ -donor ability of the BR_2 ligand, and indicate its absolute preference for terminal or near-terminal^[5] coordination. The species that have been structurally characterized are, however, almost exclusively^[5,6] mononu-

[*] Prof. Dr. H. Braunschweig, Dr. K. Radacki, Dr. D. Rais,
Dr. G. R. Whittell
Institut für Anorganische Chemie
Bayerische Julius-Maximilians-Universität Würzburg
Am Hubland, 97074 Würzburg (Germany)
Fax: (+49) 931-888-4623
E-mail: h.braunschweig@mail.uni-wuerzburg.de

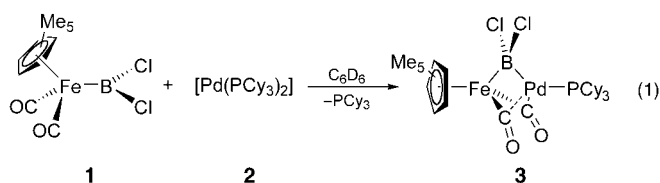
[**] This work was supported by the DFG and the EPSRC. D.R. thanks the Alexander von Humboldt Foundation for a postdoctoral fellowship. The authors thank Dr. C. Burschka for assistance with X-ray crystallography.



Supporting information for this article is available on the WWW under <http://www.angewandte.org> or from the author.

clear compounds, in which the possibility for the boryl ligand to adopt a bridging position is clearly precluded. Herein we present the synthesis and structural characterization of the first dinuclear monoboryl complex $[(\eta^5\text{-C}_5\text{Me}_5)\text{Fe}(\mu\text{-CO})_2(\mu\text{-BCl}_2)\text{Pd}(\text{PCy}_3)]$ (**3**) which features a (μ_2, η^2) symmetrically bridging BR_2 ligand.

The dichloroboryl precursor $[(\eta^5\text{-C}_5\text{Me}_5)\text{Fe}(\text{CO})_2\text{BCl}_2]$ (**1**) was prepared following a procedure established for the synthesis of its cyclopentadienyl analogue $[(\eta^5\text{-C}_5\text{H}_5)\text{Fe}(\text{CO})_2\text{BCl}_2]$,^[7] and isolated as analytically pure dark orange crystals. Monitoring the reaction of equimolar amounts of complex **1** and $[\text{Pd}(\text{PCy}_3)_2]$ (**2**)^[8] in C_6D_6 by multinuclear NMR spectroscopy revealed immediate consumption of the starting materials and predominant formation of a new compound, **3**, with concomitant liberation of tricyclohexylphosphine [Eq. (1)].



Analytically pure samples of compound **3** could be obtained as bright orange crystals by fractional crystallization from toluene/hexane at -30°C . The atom connectivity within the complex was ascertained by single-crystal X-ray diffraction (Figure 1).^[9] The analysis reveals the presence of two crystallographically independent molecules, **3a** and **3b**, in the asymmetric unit, both featuring an unprecedented symmetrically bridging dichloroboryl group linking the two transition-metal-containing fragments, $[(\eta^5\text{-C}_5\text{Me}_5)\text{Fe}(\text{CO})_2]$ and $[\text{Pd}(\text{PCy}_3)]$. Bridging coordination of typically monodentate

ligands, such as alkyl and more recently silyl groups, has precedent,^[10] and several examples of bridged borylene complexes have been reported.^[11] However, instances of bridging boryl groups are extremely scarce and limited to one mixed $\text{Rh}^{\text{I}}/\text{Rh}^{\text{III}}$,^[5b] and two Pt^{I} dimers^[5a] that feature a highly asymmetric, semibridging catecholboryl ligand.

The Fe–B bond lengths in **3** (2.095(4) Å, **3a**; 2.078(4) Å, **3b**) are considerably longer than that in $[(\eta^5\text{-C}_5\text{H}_5)\text{Fe}(\text{CO})_2\text{BCl}_2]$ (1.942(3) Å),^[7b] a situation consistent with the increased coordination number at boron, but shorter than that reported for $[(\eta^5\text{-C}_5\text{H}_5)\text{Fe}(\text{CO})_2\text{BCl}_2(4\text{-MeC}_5\text{H}_4\text{N})]$ (**4**, 2.1326(14) Å),^[7b] which features an almost ideally tetrahedrally coordinated boron atom. In **3**, the two carbonyl groups covalently linked to iron interact with the palladium center in a semibridging fashion (Pd–Fe–C(O) average: 61.5°)^[12] and, together with the bridging boryl group, bring the two metal centers into close proximity (Pd1–Fe1: 2.5310 Å, **3a**; Pd2–Fe2: 2.5436 Å, **3b**).

The geometry at boron is that of a heavily distorted tetrahedron. The most pronounced deviation from the ideal tetrahedral angle is for the Fe–B–Pd bond angle ($75.01(14)^\circ$, **3a**; $75.21(13)^\circ$, **3b**). This phenomenon is analogous to what is commonly observed in heterodinuclear carbene-bridged complexes,^[13] where the values for the M–CH₂–M' bond angle are in the range $74.0\text{--}87.4^\circ$.^[13c] The Pd–B bond lengths (2.062(4) Å, **3a**; 2.090(4) Å, **3b**) are comparable to those reported for the only two structurally characterized compounds that possess Pd–B bonds (2.006(9)–2.077(6) Å).^[14] These, however, are palladium(II) species, with terminally bound boryl ligands, that is, with a three-coordinate boron atom. In **3**, the palladium(0) fragment $[(\text{PCy}_3)\text{Pd}]$ binds to the BCl_2 group of complex **1**, thereby increasing the coordination number at boron to four. If these two factors are considered, it can be concluded that the Pd–B bond in the boryl bridged complex **3** is strong.

The structural parameters highlighted above are consistent with a symmetrical bridging mode of the boryl ligand in **3**, which greatly differentiates this complex from the semibridging catecholboryl species.^[5] Despite the undisputable bridging coordination of the boryl ligand in the catecholboryl compounds, only a highly asymmetric coordination is achieved in these systems, as a likely consequence of the lower Lewis acidity of the catecholboryl with respect to the dichloroboryl group.

A qualitative description of the bonding in complex **3** can be deduced from bonding schemes developed for related carbonyl systems^[15] and the aforementioned platinum and rhodium complexes^[5b] as well as preliminary theoretical calculations. Hence, the bridging unit in **3** can be formally viewed as resulting from a dative bond from the saturated boryl complex **1** to the $[(\text{Cy}_3\text{P})\text{Pd}]$ fragment and consequent back-donation of the $[(\text{Cy}_3\text{P})\text{Pd}]$ fragment into both the out of phase combination of the CO π^* orbitals and the empty orbital of π symmetry at boron.^[16] Furthermore, by virtue of the dative Pd–B interaction, boryl-bridged species **3** is a rare example of a transition-metal borane complex.^[17] Only three such compounds have been structurally authenticated.^[18]

The most striking spectroscopic feature of complex **3** is a strongly deshielded ^{11}B NMR resonance signal at $\delta =$

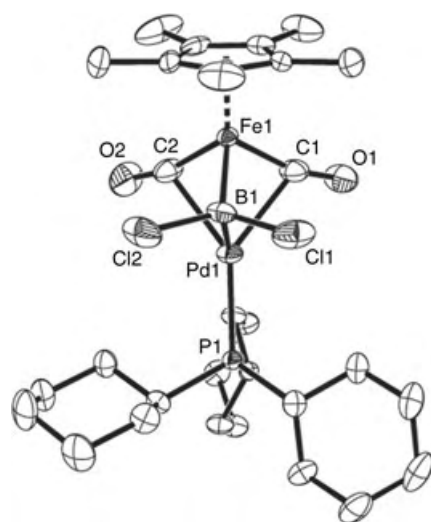


Figure 1. Molecular structure of **3** with selected bond lengths [Å] and angles [$^\circ$]. **3a**: Pd1–B1 2.062(4), Fe1–B1 2.095(4); Fe1–B1–Pd1 $75.01(14)$, Cl1–B1–Cl2 $111.4(2)$, Cl1–B1–Pd1 $111.2(2)$, Cl1–B1–Fe1 $120.8(2)$; **3b**: Pd2–B2 2.090(4), Fe2–B2 2.078(4); Fe2–B2–Pd2 $75.21(13)$, Cl3–B2–Cl4 $110.5(2)$, Cl3–B2–Pd2 $109.1(2)$, Cl3–B2–Fe2 $120.6(2)$.

72.2 ppm ($\omega_{1/2}$ = 616 Hz), which is only modestly high-field shifted with respect to that of **1** (δ = 94.9 ppm). Such a low-field value is extremely unusual for a four-coordinate boron atom, particularly if compared to that of the Lewis base adduct **4** (δ = 18.8 ppm). Compound **3** is moderately air- and moisture-sensitive in the solid state but extremely sensitive in solution. Under inert atmosphere, a solution of **3** in C₆D₆ slowly decomposes to **1** and metallic palladium. Upon heating at high temperatures (80 °C), the regeneration of **1** is accelerated and traces of free tricyclohexylphosphine ($\delta(^{31}\text{P})$ = 9.8 ppm) and of the Lewis base adduct **1**-PCy₃^[19] are detected in solution. Palladium is recovered in small amounts as palladium metal, but predominantly, as *trans*-[(C₆H₅)₂PdCl₂]₂,^[20] as judged from ³¹P NMR spectroscopy.

In conclusion, we have described the preparation of the first dinuclear monoboryl complex [(η^5 -C₅Me₅)Fe(μ -CO)₂(μ -BCl₂)Pd(PCy₃)] (**3**), the complex also features an unprecedented bridging BR₂ ligand. The dative nature of the palladium–boron interaction makes **3** a rare example of a transition-metal borane complex.

Received: October 27, 2004

Published online: January 20, 2005

Keywords: boranes · boron · boryl complexes · bridging ligands · palladium

- [1] a) H. Braunschweig, *Angew. Chem.* **1998**, *110*, 1882–1898; *Angew. Chem. Int. Ed.* **1998**, *37*, 1786–1801; b) G. J. Irvine, M. G. J. Lesley, T. B. Marder, N. C. Norman, C. R. Rice, E. G. Robins, W. R. Roper, G. R. Whittell, L. J. Wright, *Chem. Rev.* **1998**, *98*, 2685–2722; c) G. Frenking, N. Fröhlich, *Chem. Rev.* **2000**, *100*, 717–774; d) K. T. Giju, F. M. Bickelhaupt, G. Frenking, *Inorg. Chem.* **2000**, *39*, 4776–4785; e) H. Braunschweig, M. Colling, *Coord. Chem. Rev.* **2001**, *223*, 1–51; f) A. A. Dickinson, D. J. Willock, R. J. Calder, S. Aldridge, *Organometallics* **2002**, *21*, 1146–1157; g) S. Aldridge, D. L. Coombs, *Coord. Chem. Rev.* **2004**, *248*, 535–559.
- [2] a) K. Burgess, M. J. Ohlmeyer, *Chem. Rev.* **1991**, *91*, 1179–1191; b) I. Beletskaya, A. Pelter, *Tetrahedron* **1997**, *53*, 4957–5026.
- [3] T. B. Marder, N. C. Norman, *Top. Catal.* **1998**, *5*, 63–73.
- [4] R. E. Maleczka, Jr., F. Shi, D. Holmes, M. R. Smith III, *J. Am. Chem. Soc.* **2003**, *125*, 7792–7793, and references therein.
- [5] a) D. Curtis, M. J. G. Lesley, N. C. Norman, A. G. Orpen, J. Starbuck, *J. Chem. Soc. Dalton Trans.* **1999**, 1687–1694; b) S. A. Westcott, T. B. Marder, R. T. Baker, R. L. Harlow, J. C. Calabrese, K. C. Lam, Z. Lin, *Polyhedron* **2004**, *23*, 2665–2677.
- [6] For dinuclear complexes featuring bidentate boryl ligands, see: S. Aldridge, R. J. Calder, A. Rossin, A. A. Dickinson, D. J. Willock, C. Jones, D. J. Evans, J. W. Steed, M. E. Light, S. J. Coles, M. B. Hursthouse, *J. Chem. Soc. Dalton Trans.* **2002**, 2020–2026, and references therein.
- [7] a) S. Aldridge, R. J. Calder, R. E. Baghurst, M. E. Light, M. B. Hursthouse, *J. Organomet. Chem.* **2002**, *649*, 9–14; b) H. Braunschweig, K. Radacki, F. Seeler, G. R. Whittell, *Organometallics* **2004**, *23*, 4178–4180.
- [8] W. Kuran, A. Musco, *Inorg. Chim. Acta* **1975**, *12*, 187–193.
- [9] Crystal data for **3**: C₃₀H₄₈BCl₂FeO₂PPd *M*_r = 715.66, orange blocks, 0.40 × 0.30 × 0.28, monoclinic, space group *P*2(1), *a* = 12.1746(10), *b* = 18.3648(17), *c* = 14.4103(10) Å, α = 90.00, β = 94.502(9), γ = 90.00°, *V* = 3212.0(5) Å³, *Z* = 4, ρ_{calcd} = 1.480 g cm^{−3}, μ = 1.253 cm^{−2}, *F*(000) = 1480, *T* = 173 K; STOE-IPDS diffractometer with area detector, graphite-monochromated MoK α radiation. The structure was solved using direct methods, refined with the Shelx software package and expanded using Fourier techniques. All non-hydrogen atoms were refined anisotropically. Hydrogen atoms were assigned idealized positions and were included in structure-factor calculations. *R*₁ = 0.0373, *W*_R = 0.0746, 13 649 independent reflections [*2* θ = 53.9°] and 685 parameters. CCDC-253776 (**3**) contains the supplementary crystallographic data for this paper. These data can be obtained free of charge from the Cambridge Crystallographic Data Centre via www.ccdc.cam.ac.uk/data_request/cif.
- [10] P. Braunstein, N. M. Boag, *Angew. Chem.* **2001**, *113*, 2493–2499; *Angew. Chem. Int. Ed.* **2001**, *40*, 2427–2433, and references therein.
- [11] a) H. Braunschweig, T. Wagner, *Angew. Chem.* **1995**, *107*, 904–905; *Angew. Chem. Int. Ed. Engl.* **1995**, *34*, 825–826; b) H. Braunschweig, M. Müller, *Chem. Ber./Recueil* **1997**, *130*, 1295–1298; c) H. Braunschweig, C. Kollann, U. Englert, *Eur. J. Inorg. Chem.* **1998**, 465–468; d) M. Shimoi, S. Ikubo, Y. Kawano, K. Yasuro, K. Katoh, H. Ogino, *J. Am. Chem. Soc.* **1998**, *120*, 4222–4223; e) H. Braunschweig, C. Kollann, K. W. Klinkhammer, *Eur. J. Inorg. Chem.* **1999**, 1523–1529; f) H. Braunschweig, M. Colling, *J. Organomet. Chem.* **2000**, *614–615*, 18–26, and references therein; g) S. Aldridge, D. L. Coombs, C. Jones, *Chem. Commun.* **2002**, 856–857.
- [12] R. H. Crabtree, M. Lavin, *Inorg. Chem.* **1986**, *25*, 805–812.
- [13] a) T. V. Ashworth, J. A. K. Howard, M. Laguna, F. G. A. Stone, *J. Chem. Soc. Dalton Trans.* **1980**, 1593–1600; b) J. A. K. Howard, K. A. Mead, J. R. Moss, R. Navarro, F. G. A. Stone, P. Woodward, *J. Chem. Soc. Dalton Trans.* **1981**, 743–750; c) C. A. Mirkin, G. L. Geoffroy, P. D. Macklin, A. L. Rheingold, *Inorg. Chim. Acta* **1990**, *170*, 11–15, and references therein; d) M. Bergamo, T. Beringhelli, G. D'Alfonso, P. Mercandelli, M. Moret, A. Sironi, *Inorg. Chim. Acta* **2000**, *300–302*, 1022–1034, and references therein.
- [14] a) S.-Y. Onozawa, Y. Hatanaka, T. Sakakura, S. Shimada, M. Tanaka, *Organometallics* **1996**, *15*, 5450–5452; b) S.-Y. Onozawa, M. Tanaka, *Organometallics* **2001**, *20*, 2956–2958.
- [15] For MO calculations and a general scheme applicable to systems featuring “dative” M–M bonds and non-compensating, semi-bridging carbonyl ligands, see: R. D. Barr, T. B. Marder, A. G. Orpen, I. D. Williams, *J. Chem. Soc. Chem. Commun.* **1984**, 112–114.
- [16] For examples of nucleophilic reactivity of unsaturated, late-transition-metal complexes, see: B. V. Popp, J. L. Thorman, C. M. Morales, C. R. Landis, S. S. Stahl, *J. Am. Chem. Soc.* **2004**, *126*, 14832–14842, and references therein.
- [17] Early reports on transition-metal borane complexes have been proven incorrect, to some extent, by more recent studies, that have demonstrated the absence of any transition-metal–boron linkage in the reported species, a) H. Braunschweig, T. Wagner, *Chem. Ber.* **1994**, *127*, 1613–1614; b) H. Braunschweig, T. Wagner, *Z. Naturforsch. B* **1996**, *51*, 1618–1620; c) H. Braunschweig, C. Kollann, *Z. Naturforsch. B* **1999**, *54*, 839–842.
- [18] a) A. F. Hill, G. R. Owen, A. J. P. White, D. J. Williams, *Angew. Chem.* **1999**, *111*, 2920–2923; *Angew. Chem. Int. Ed.* **1999**, *38*, 2759–2761; b) M. R. St.-T. Foreman, A. F. Hill, A. J. P. White, D. J. Williams, *Organometallics* **2004**, *23*, 913–916; c) D. J. Mihalczik, J. L. White, J. M. Tanski, L. N. Zakharov, G. P. A. Yap, C. D. Incarvito, A. L. Rheingold, D. Rabinovich, *Dalton Trans.* **2004**, 1626–1634.
- [19] Spectroscopic data for **1**-PCy₃: ¹H NMR (64 MHz, C₆D₆, 25 °C): δ = 3.4 ppm (d, ¹*J*_{B-P} = 147 Hz); ³¹P NMR (162 MHz, C₆D₆, 25 °C): δ = −2.8 ppm (q, ¹*J*_{B-P} = 147 Hz).
- [20] V. V. Grushin, C. Bensimon, H. Alper, *Inorg. Chem.* **1994**, *33*, 4804–4806.

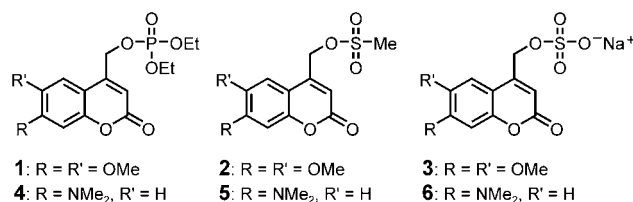
Photoactivatable Compounds

(Coumarin-4-yl)methyl Esters as Highly Efficient, Ultrafast Phototriggers for Protons and Their Application to Acidifying Membrane Surfaces**

Daniel Geißler, Yuri N. Antonenko, Reinhard Schmidt, Sandro Keller, Oxana O. Krylova, Burkhard Wiesner, Jürgen Bendig, Peter Pohl, and Volker Hagen*

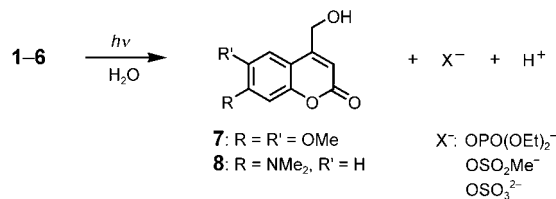
Protons play a crucial role in cellular signal transduction. They trigger protein conformational transitions and are coupling intermediates in electron transport phosphorylation, and their transmembrane gradients may serve as energy sources or stores. Kinetic studies of all these processes may be aided by photoactivatable proton precursors for the generation of rapid pH jumps. With these proton sources ("caged protons"), the spatial and temporal pH distribution can be controlled without diffusional mixing delays.^[1,2] Most of the precursors are nitrobenzyl derivatives, namely 2-nitrobenzaldehydes,^[3–5] as well as 2-nitrobenzyl and/or 1-(2-nitrophenyl)ethyl acetates,^[1] phosphates,^[6–8] tosylates,^[9,10] and sulfates.^[7,11] Their application is limited by the low efficiency of the activation in the long-wavelength UV/Vis range and the generation of reactive *o*-nitrosocarbonyl photoproducts.

Here we introduce (6,7-dimethoxycoumarin-4-yl)methyl (DMCM) diethyl phosphate (**1**), DMCM methanesulfonate (**2**), and sodium DMCM sulfate (**3**), as well as [7-(dimethylamino)coumarin-4-yl]methyl (DMACM) diethyl phosphate (**4**), DMACM methanesulfonate (**5**), and sodium DMACM sulfate (**6**) as a new class of phototriggers for protons that facilitates the study of proton-dependent biological processes (Scheme 1). Compound **1**, for example, has already been used to study H⁺ migration along lipid bilayers.^[12]



Scheme 1. Structures of the phototriggers 1–6.

Photocleavage of **1–6** is efficient and clean. It yields H⁺, the respective anion, and the strongly fluorescent **7** or **8** (Scheme 2). The esters themselves are only very weakly



Scheme 2. Photolysis of 1–6.

fluorescent as indicated by their particularly small fluorescence quantum yields (Table 1). Both the DMCM and the DMACM moieties have been introduced earlier for the

Table 1: Properties of 1–6.^[a]

Photo-trigger	$\lambda_{\text{abs}}^{\text{max}}$ [nm]	ϵ^{max} [M ^{−1} cm ^{−1}]	ϕ	$\lambda_{\text{f}}^{\text{max}}$ [nm]	ϕ_{f}	c_{s} [μM]
1 ^[b]	346	11 400	0.08	447	0.005	> 10 000
2 ^[c]	348	10 700	0.23	437	0.002	40 ^[b]
3 ^[d]	345	11 000	0.09	445	0.007	> 10 000
4 ^[b]	386	16 100	0.36	497	0.006	3700
5 ^[c]	388	17 100	0.79	487	0.002	100 ^[b]
6 ^[d]	382	14 700	0.46	506	0.008	> 10 000

[a] Long-wavelength absorption maxima $\lambda_{\text{abs}}^{\text{max}}$, extinction coefficient ϵ^{max} , photochemical quantum yield ϕ , fluorescence maxima $\lambda_{\text{f}}^{\text{max}}$, fluorescence quantum yield ϕ_{f} , and concentration at saturation c_{s} . [b] In acetonitrile/HEPES (5:95), pH 7.2. [c] In acetonitrile/HEPES (20:80), pH 7.2. [d] In HEPES, pH 7.2.

photoreversible inactivation of cyclic nucleotide monophosphates.^[13,14] The analogues (7-methoxycoumarin-4-yl)methyl (MCM) diethyl phosphate and methanesulfonate have been described previously,^[15,16] but they were not classified or used as phototriggers for protons.

Compounds **1**, **2**, **4**, and **5** were synthesized by esterification of the alcohols **7** and **8** with diethyl phosphoric acid chloride and methanesulfonic acid chloride, respectively, in CH₂Cl₂ in the presence of pyridine or triethylamine at 0 °C with yields of 53–68 %. The photoactivatable sulfates **3** and **6** were prepared by treatment of **7** and **8** with the triethylamine/SO₃ complex in dimethylformamide using the general method of Tserng and Klein.^[17,11] The yields were 77 % for **3** and only 16 % for **6** (see the Supporting Information for preparative details and analytical characterization).

[*] D. Geißler, S. Keller, Dr. O. O. Krylova, Dr. B. Wiesner, Prof. Dr. P. Pohl,^[†] Dr. V. Hagen

Forschungsinstitut für Molekulare Pharmakologie
Robert-Rössle-Strasse 10, 13125 Berlin (Germany)
Fax: (+49) 30-94793-159
E-mail: hagen@fmp-berlin.de

Prof. Dr. Y. N. Antonenko
A. N. Belozersky Institute of Physico-Chemical Biology
Moscow State University (Russia)
Prof. Dr. R. Schmidt
Institut für Physikalische und Theoretische Chemie
Johann Wolfgang Goethe-Universität Frankfurt/Main (Germany)
Prof. Dr. J. Bendig
Institut für Chemie
Humboldt-Universität zu Berlin (Germany)

[†] Present address:
Institut für Biophysik
Johannes Kepler Universität Linz (Austria)

[**] This work was supported by the Deutsche Forschungsgemeinschaft and the Fonds der Chemischen Industrie. We thank B. Gentsch for technical assistance and Dr. E. Krause for the mass spectra.

Supporting information for this article is available on the WWW under <http://www.angewandte.org> or from the author.

The absorption maxima of the DMACM esters **4–6** are more intense and red-shifted by 40 nm relative to those of the DMCM derivatives **1–3** at about 346 nm. Thus, efficient photolysis of the DMCM esters occurs at 330–365 nm and of the DMACM esters at 365–420 nm. Conceivably, the photocleavage proceeds in analogy to the conversion of MCM esters,^[16] by means of an S_N1 mechanism, including singlet-state activation, ion-pair formation, ion-pair separation, and subsequent hydroxylation. Because the reaction quantum yields should correlate with both the electron-donor strength of the substituent in position 7 of the coumarin chromophore (stabilization of the intermediate coumarinylmethyl carbocation) and the leaving-group ability, the reaction quantum yields were expected to be higher for the DMACM esters than for the DMCM esters and to increase in the order diethyl phosphates \approx sulfates $<$ methanesulfonates. The measured photochemical quantum yields (φ) for proton photorelease confirmed these predictions (Table 1).

The high quantum yield of **5** is unique for photoactivatable compounds with coumarinylmethyl moieties. The high quantum yield combined with the high extinction coefficient results in an unparalleled photosensitivity. By using φ multiplied by the molar absorptivity (ϵ) as a criterion for the overall sensitivity of photocleavage,^[1] the DMACM compounds **4–6** were confirmed to be the most sensitive phototriggers described so far. The $\varphi\epsilon^{\max}$ values of **1–3** (900–2400 M⁻¹ cm⁻¹) and of **4–6** (5800–13 500 M⁻¹ cm⁻¹) are very high. To illustrate the excellent photochemical properties of the coumarinylmethyl esters, H⁺ photorelease from **6** was compared with that from the commercially available 2-hydroxyphenyl 1-(2-nitrophenyl)ethyl phosphate (NPE-HPP) (Figure 1).

Exposure of **1** and **6** to femtosecond pulses of a mode-locked Ti:sapphire laser at 728 and 750 nm, respectively, caused a significant decrease of the fluorescence intensity of fluorescein isothiocyanate (FITC) dextran, indicating that photocleavage was possible with two-photon excitation as well (Figure 2). Sensitivity to two-photon photolysis has been described recently for photoactivatable (6-bromo-7-hydroxy-coumarin-4-yl)methyl compounds.^[18]

Proton sources relying on the 2-nitrobenzyl rearrangement provide H⁺ photorelease with rate constants of 2×10^7 s⁻¹ and $> 4 \times 10^7$ s⁻¹ for unbuffered and buffered solutions, respectively.^[19] The photolysis pathway of the coumarinylmethyl ester cleavage suggests reaction rates that are significantly higher. To check the hypothesis, we conducted time-resolved energy-dependent fluorescence measurements. Deconvolution of the experimentally determined decay curves of high-intensity single-pulse excitations (0.5 ns half-width) of **1**, **3**, **4**, and **6** revealed fluorescence contributions from the corresponding coumarinylmethyl alcohols **7** or **8**. Since both **7** and **8** were released within the duration of the excitation pulse, photolytic H⁺ formation occurred with a rate constant of at least 5×10^8 s⁻¹, that is, H⁺ was liberated within two nanoseconds or even faster.

The pK_a values of the corresponding acids of the sulfate (1.98),^[20] diethyl phosphate (0.71),^[21] and methanesulfonate group (−1.54)^[22] suggest that **1–3** are potent H⁺ sources in solutions down to pH 2 or 1. Acidifications by photolysis of

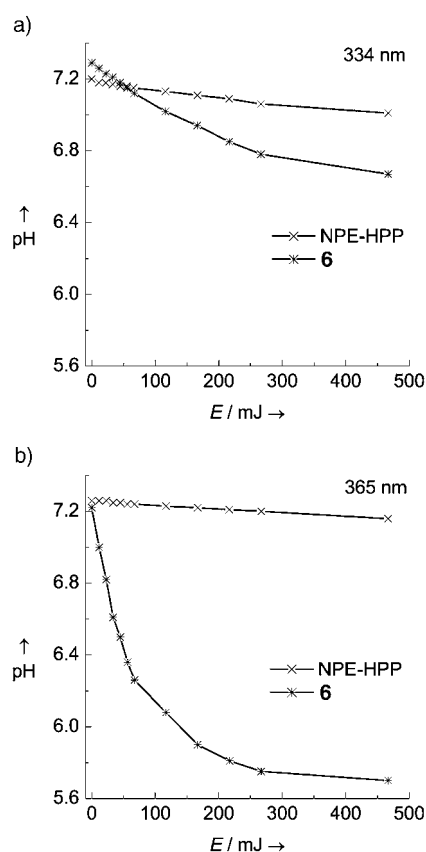


Figure 1. Comparison of the photosensitivity of H⁺ release from 25 μ M **6** and 25 μ M NPE-HPP in aqueous solution (pH 7.2; reaction volume: 2.8 mL) a) at 334 nm, b) at 365 nm. E = energy of irradiation.

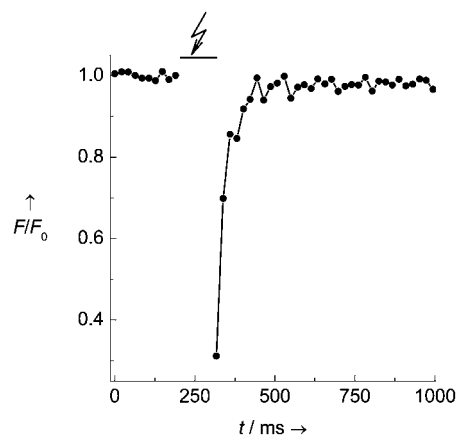


Figure 2. Photorelease of H⁺ from **6** upon two-photon excitation. A solution of **6** (500 μ M) was mixed with the pH-sensitive fluorescence indicator FITC dextran (750 nm) in CAPSO buffer solution (pH 9.0) and irradiated for 106 ms (black bar; CAPSO = 3-(cyclohexylamino)-2-hydroxy-1-propanesulfonic acid, sodium salt). The fluorescence intensity F of FITC dextran was recorded before and after irradiation. The fluorescence recovery was due to proton diffusion out of the irradiated area. F/F_0 = relative fluorescence intensity.

compounds **4–6** are somewhat restricted by the buffering capacity of the dimethylamino group in **4–6** or in the released alcohol **8** (pK_a = 2.0), but the photolytic pH drop is not

notably diminished as long as $\text{pH} > 2$. Large pH jumps may well be achieved with **1–6**. Thus, an aqueous 200 μM solution of **6** at pH 7.0 gave pH changes of three units in representative H^+ photorelease experiments (data not shown).

Despite their excellent photocharacteristics, **2** and **5** are less useful proton sources because their half-life in aqueous buffers (pH 7.2) is only 26.8 and 28.6 h, respectively. In contrast, within 24 h less than 0.5% of **1**, **3**, **4**, and **6** was hydrolyzed in 2-[4-(2-hydroxyethyl)-1-piperazinyl]ethanesulfonic acid (HEPES) buffer (pH 7.2) as indicated by HPLC. Since **3** and **6** are easily soluble in HEPES buffer and both **1** and **4** exhibit reasonable solubility in acetonitrile/HEPES (5:95; Table 1), their application for biophysical studies seems promising.

We have probed membrane partitioning of phototriggers **1**, **3**, **4**, and **6** by isothermal titration calorimetry (details see Supporting Information). Figure 3 shows dilution-corrected

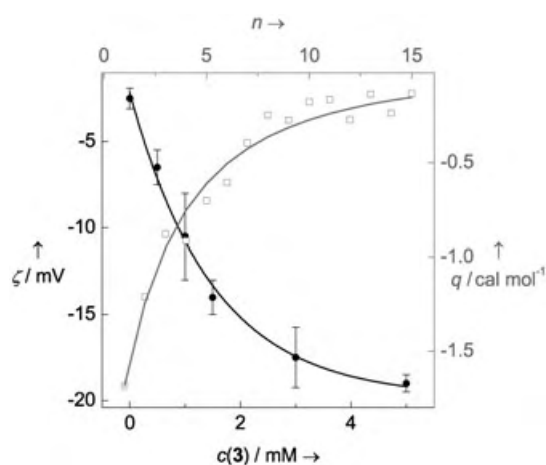


Figure 3. Membrane adsorption of the phototriggers. By titration of 20 μM **1** with 20 μL aliquots of 40 mM DPhPC (100 mM NaCl, 10 mM CAPSO, pH 9.0, 25 °C) the heats of reaction (q , squares) could be measured, normalized with respect to the molar amount of injectant, and plotted versus the injection number n . The best fit (gray line) yielded $\Delta H \approx -1 \text{ kcal mol}^{-1}$, $\Delta G^0 \approx -6 \text{ kcal mol}^{-1}$, and $\Delta S^0 \approx 16 \text{ cal mol}^{-1} \text{ K}^{-1}$. For **3** and **6** (not shown): $\Delta H \approx -2 \text{ kcal mol}^{-1}$, $\Delta G^0 \approx -5 \text{ kcal mol}^{-1}$, and $\Delta S^0 \approx 10 \text{ cal mol}^{-1} \text{ K}^{-1}$. Adsorption of **3** increased the electrophoretic mobility (monitored by a zeta-sizer, model DELSA 440 SX, Coulter Electronics, USA) of large unilamellar DPhPC vesicles (suspended in 20 mM NaCl, 10 mM HEPES, pH 7.1, 23 °C), which was used to calculate their ζ -potentials (circles with standard deviations).

data for compound **1**, from which the adsorption constant^[23] was obtained. For **1** and **4**, $K = 300 \pm 150 \text{ M}^{-1}$, whereas the two ionic species **3** and **6** bound somewhat less strongly with $K = 100 \pm 50 \text{ M}^{-1}$. The calorimetric data are consistent with measurements of electrophoretic mobility, which revealed roughly the same adsorption constants (Figure 3). The charge brought by adsorption of **3** to diphytanoyl-phosphatidylcholine (DPhPC) vesicles was monitored and used to calculate the electrical potential (ζ) at the shear plane of the vesicles.^[24,25] With increasing concentrations of **3**, the ζ -potential saturated at -20 mV (in 20 mM NaCl), indicating that the binding site for one molecule of **3** is at least 20 lipid molecules in size.

Proton release from membrane-anchored coumarin derivatives is an excellent tool to study the kinetics of acid-sensing membrane channels or other processes taking place at the membrane–water interface, for example, proton migration along the membrane surface.^[12] To quantify membrane surface acidification, horizontal planar lipid bilayers containing fluorescein-labeled lipids were placed on the top of an inverse fluorescence microscope.^[12] After membrane exposure to a UV flash, the response of the pH-sensitive dye (*N*-(fluorescein-5-thiocarbamoyl)-1,2-dihexadecanoyl-*sn*-glycero-3-phosphoethanolamine) was monitored from one leaflet or both leaflets, depending on whether the membrane was permeable for the caged compound.

Due to the high energetic barrier for membrane diffusion of charged compounds, photolysis of **6** mediated a rapid fluorescence decrease of fluorescein in one membrane leaflet only (Figure 4, α). Subsequent proton diffusion out of the

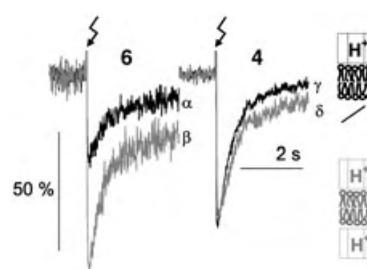


Figure 4. Sidedness of proton release upon flash photolysis. Addition of **6** (α) and **4** (γ) exclusively to the upper membrane leaflet induced a rapid drop in fluorescence (from F_0 to F) of the membrane-anchored pH-sensitive dye. In contrast to **4** (δ), **6** doubled the fluorescence drop (β) when added also to the compartment facing the lower membrane leaflet. The difference indicates that the membrane-impermeant compound **6** can be used to generate a transmembrane pH gradient, whereas the membrane-permeant compound **4** always acidifies both membrane leaflets similarly. After an initial acidification, fluorescence recovery was observed due to buffer or proton diffusion. The buffer solution contained 0.1 mM CAPSO, 100 mM NaCl, pH 9.0. Membranes were formed from a mixture of DPhPC and the fluorescent pH-sensitive dye (mass ratio 95:5) dissolved in *n*-decane. Fluorescence was collected from the central membrane region used for proton release by a UV flash.

region irradiated led to fluorescence recovery. Addition of **6** to the aqueous solutions on both sides of the membrane doubled the fluorescence drop because both interfaces were acidified (Figure 4, β). In contrast to the charged compounds **3** and **6**, we expected the hydrophobic diethyl phosphates **1** and **4** to be membrane-permeant. Consistently, addition of **4** to one or both compartments revealed the same pH drop (Figure 4, γ and δ).

The experiments in Figure 4 imply that the caged compound located in the aqueous phase contributes only negligibly to the interfacial acidification. This hypothesis was confirmed: the shift induced by **3** vanished when c_i (interfacial concentration) was diminished from ≈ 0.3 to about 0.04 mM while the bulk aqueous concentration was held constant (0.3 mM). To this end, a charged membrane was formed containing 50 mol% negatively charged lipids (diphytanoyl-phosphatidylserine, DPhPS). The Boltzmann distribution^[26]

predicts that the bulk concentration must be augmented to 2 mM to compensate for the electrostatic repulsion caused by the surface potential of -50 mV and to reestablish the initial c_i , which is in accord with our experimental observation (Figure 5). The same considerations hold for the sulfate **6**, which, due to the higher quantum yield, produced larger pH responses at the same concentration (Figure 5).

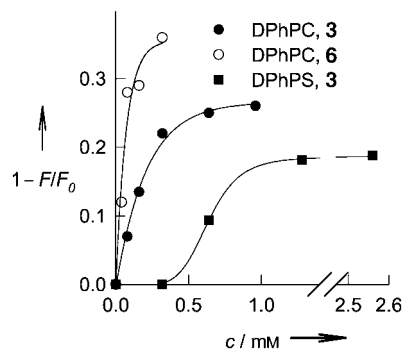


Figure 5. The increase in the H^+ concentration on the bilayer surface results exclusively from photolysis of phototriggers bound to the membrane. The relative fluorescence drop measured for negatively charged DPhPS bilayers (squares) was smaller than that for electroneutral DPhPC membranes (circles) due to electrostatic repulsion of the negatively charged **3** (filled symbols). As a result of the higher quantum yield, the efficiency of acidification mediated by **6** (open symbols) was higher. For conditions and a definition of F and F_0 see Figure 4.

Thus, coumarinylmethyl diethyl phosphates and coumarinylmethyl sulfates act as very sensitive and ultrafast phototriggers for protons, which can induce large pH jumps. Their membrane affinity can be exploited for investigation of the impact of membrane surface pH on signaling, folding, and transport. Leaflet specificity is achieved by choosing membrane-permeant (**1**, **4**) or membrane-impermeant (**3**, **6**) compounds. Moreover, the proton precursors **1**, **3**, **4**, and **6** will extend decisively the tools available for the study of spatial- and time-dependent aspects of other H^+ -triggered processes. Their biological applications are aided by long-wavelength UV/Vis-activation, which should minimize cell-damaging side effects.

Received: August 6, 2004

Keywords: membranes · photoactivatable compounds · photolysis · protecting groups · protons

- [6] J. H. Kaplan, B. Forbush, J. F. Hoffman, *Biochemistry* **1978**, *17*, 1929–1935.
- [7] J. E. T. Corrie, B. C. Gilbert, V. R. N. Munasinghe, A. C. Whitwood, *J. Chem. Soc. Perkin Trans. 2* **2000**, 2483–2491.
- [8] S. Khan, F. Castellano, J. L. Spudich, J. A. McCray, R. S. Goody, G. P. Reid, D. R. Trendham, *Biophys. J.* **1993**, *65*, 2368–2382.
- [9] F. M. Houlihan, A. Shugard, R. Gooden, E. Reichmanis, *Macromolecules* **1988**, *21*, 2001–2006.
- [10] F. M. Houlihan, O. Nalamasu, J. M. Kometani, E. Reichmanis, *J. Imaging Sci. Technol.* **1997**, *41*, 35–40.
- [11] A. Barth, J. E. Corrie, *Biophys. J.* **2002**, *83*, 2864–2871.
- [12] S. Serowy, S. M. Saparov, Y. N. Antonenko, W. Kozlovsky, V. Hagen, P. Pohl, *Biophys. J.* **2003**, *84*, 1031–1037.
- [13] T. Eckardt, V. Hagen, B. Schade, R. Schmidt, C. Schweitzer, J. Bendig, *J. Org. Chem.* **2002**, *67*, 703–710.
- [14] V. Hagen, S. Frings, B. Wiesner, S. Helm, U. B. Kaupp, J. Bendig, *ChemBioChem* **2003**, *4*, 434–442.
- [15] R. S. Givens, B. Matuszewski, *J. Am. Chem. Soc.* **1984**, *106*, 6860–6871.
- [16] B. Schade, V. Hagen, R. Schmidt, R. Herbrich, E. Krause, T. Eckardt, J. Bendig, *J. Org. Chem.* **1999**, *64*, 9109–9117.
- [17] K.-Y. Tserng, P. D. Klein, *J. Lipid Res.* **1977**, *18*, 491–495.
- [18] T. Furuta, S. S.-H. Wang, J. L. Dantzer, T. M. Dore, W. J. Bybee, E. M. Callaway, W. Denk, R. Y. Tsien, *Proc. Natl. Acad. Sci. USA* **1999**, *96*, 1193–1200.
- [19] M. Schwörer, J. Wirz, *Helv. Chim. Acta* **2001**, *84*, 1441–1458.
- [20] *CRC Handbook of Chemistry and Physics* (Ed.: D. R. Lide), CRC, Boca Raton, **1994**, p. 8–44.
- [21] V. I. Galkin, R. D. Sayakhov, A. R. Garifzyanov, R. A. Cherkasov, A. N. Pudovik, *Dokl. Chem. (Engl. Transl.)* **1991**, *318*, 114–116.
- [22] N. C. Marziani, M. Sampoli, M. Gonizzi, *J. Phys. Chem.* **1986**, *90*, 4347–4353.
- [23] H. Heerklotz, *J. Phys. Condens. Matter* **2004**, *16*, R441–R467.
- [24] T. I. Rokitskaya, M. Block, Y. N. Antonenko, E. A. Kotova, P. Pohl, *Biophys. J.* **2000**, *78*, 2572–2580.
- [25] E. E. Pohl, U. Peterson, J. Sun, P. Pohl, *Biochemistry* **2000**, *39*, 1834–1839.
- [26] R. M. Peitzsch, M. Eisenberg, K. A. Sharp, S. McLaughlin, *Biophys. J.* **1995**, *68*, 729–738.

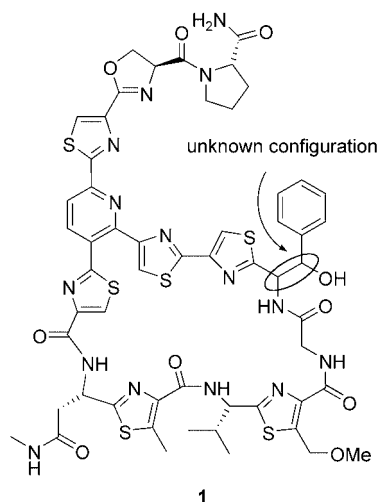
- [1] H. A. Lester, J. M. Nerbonne, *Annu. Rev. Biophys. Bioeng.* **1982**, *11*, 151–175.
- [2] M. Gutman, E. Nachliel, *Biochim. Biophys. Acta* **1990**, *1015*, 391–414.
- [3] G. Bonetti, A. Vecli, C. Viappiani, *Chem. Phys. Lett.* **1997**, *269*, 268–273.
- [4] C. Viappiani, S. Abbruzzetti, J. R. Small, L. J. Libertini, E. W. Small, *Biophys. Chem.* **1998**, *73*, 13–22.
- [5] K. Janko, J. Reichert, *Biochim. Biophys. Acta* **1987**, *905*, 409–416.

Natural Products

Synthesis of the Heterocyclic Core of the GE 2270 Antibiotics and Structure Elucidation of a Major Degradation Product**

Golo Heckmann and Thorsten Bach*

The thiazolyl peptide GE 2270A (**1**) was isolated in 1991 from *Planobispora rosea* ATCC 53733.^[1] The compound, like many other closely related GE 2270 thiazolyl peptides,^[2] shows

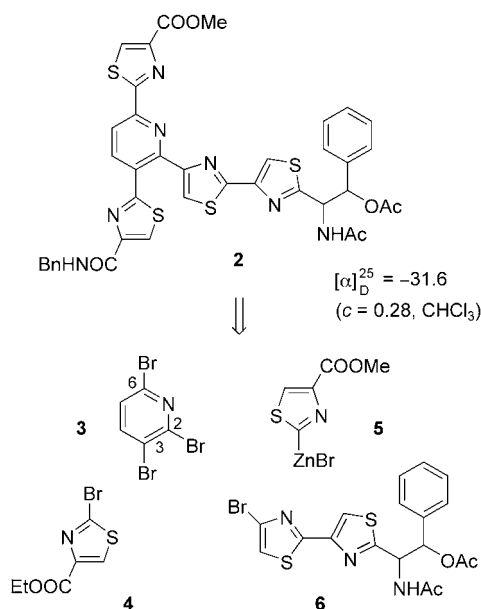


antibiotic activity by inhibiting the bacterial elongation factor (EF) Tu (GE 2270A: IC₅₀ = 5 nM).^[3] EF-Tu is a protein in bacteria cells that catalyzes the binding of aminoacyl-tRNA to the A site of the ribosome.^[4] In eukaryotes this function is carried out by the elongation factor EF-1 alpha, which is not inhibited by GE 2270A.^[5] The remarkable antibiotic activity and the demanding molecular architecture of the GE 2270 thiazolyl peptides make them interesting synthetic targets.^[6–8] A total synthesis of these compounds has not yet been reported.

The structure of GE 2270A was established in 1991^[1b] but corrected in 1995.^[9] The configurations of four of the six stereogenic centers could be elucidated by degradation reactions and by structure comparison with synthetic material.^[9] Only the configuration of the 1,2-amino alcohol in the eastern part of the molecule is not known. Herein we report a concise synthetic approach to the core structure of the

GE 2270 thiazolyl peptides and the synthesis of a degradation product that proves the absolute configuration of GE 2270A.

The degradation product **2** is depicted in Scheme 1. It was obtained from GE 2270A by Tavecchia et al. after hydrolysis with formic acid, treatment with Na₂CO₃/MeOH, aminolysis with benzylamine, and subsequent acetylation.^[9] The compound was characterized by UV/Vis, IR, and ¹H NMR spectroscopy as well as by its specific rotation (Scheme 1).



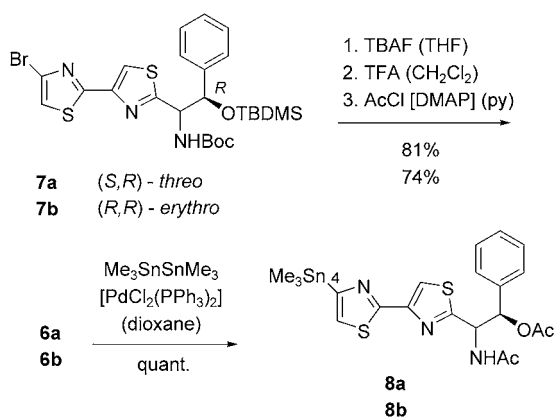
Scheme 1. Retrosynthetic disconnection of the GE 2270A degradation product **2** into the fragments **3–6**.

According to our strategy the central 2,3,6-trisubstituted pyridine moiety of the GE 2270 thiazolyl peptides should be synthesized from easily accessible 2,3,6-tribromopyridine (**3**)^[10] by three consecutive C–C bond-formation reactions. Pyridine **2** was used as a model system to establish our plan for the construction of the GE 2270 core. In the present case we hoped to address the 3-position of the pyridine by employing a regioselective bromine–lithium exchange reaction.^[11] The transmetalation step should be followed by a cross-coupling with a 2-bromothiazole (e.g. **4**). In subsequent cross-coupling reactions, positions 2 and 6 of the pyridine ring should be attacked nucleophilically.^[12,13] It was our opinion that the more easily accessible position 6 would be prone to regioselective substitution by a suitable zinc reagent (e.g. **5**). The final cross-coupling reaction should be performed with a zinc, tin, or boron reagent prepared from bromide **6**.

To elucidate the structure of the degradation product **2** it was necessary to use both possible diastereomeric bromides *threo*- and *erythro*-**6** in enantiomerically pure form. We started with the bithiazoles *threo*-(*S,R*)-**7** (**7a**) and *erythro*-(*R,R*)-**7** (**7b**), which were synthesized from enantiomerically pure (*R*)-mandelonitrile (Scheme 2). Bithiazole *erythro*-(*R,R*)-**7** (**7b**) was generated from the corresponding *erythro* amino alcohol in full analogy to the procedure used for the synthesis of the known compound **7a**.^[14] Cleavage of the *tert*-butyldimethylsilyl (TBDMS) protecting group with tetrabu-

[*] Dipl.-Chem. G. Heckmann, Prof. Dr. T. Bach
Lehrstuhl für Organische Chemie I
Technische Universität München
Lichtenbergstrasse 4, 85747 Garching (Germany)
Fax: (+49) 89-2891-3315
E-mail: thorsten.bach@ch.tum.de

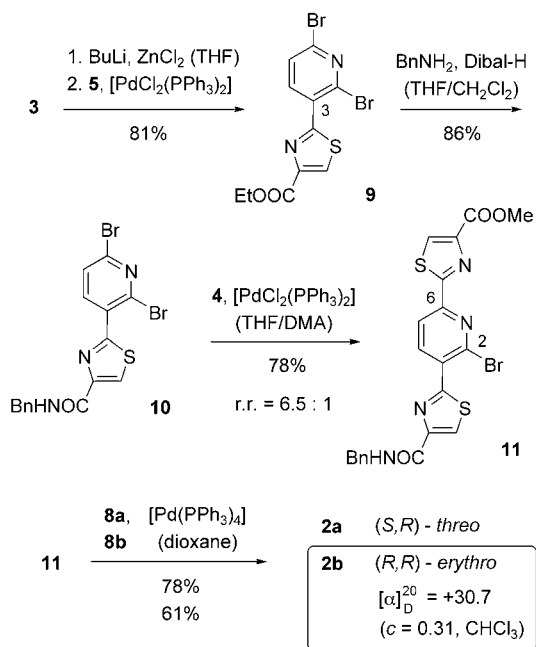
[**] This project was supported by the Deutsche Forschungsgemeinschaft (Ba 1372-9/1) and by the Fonds der Chemischen Industrie.



Scheme 2. Synthesis of the diastereomeric stannylated bithiazoles **8a** and **8b** from the precursors **7a** and **7b**.

tylammonium fluoride (TBAF) and removal of the *tert*-butoxycarbonyl (Boc) protecting group with trifluoroacetic acid (TFA) furnished the free amino alcohol, which was then doubly acetylated. The overall yields of these three steps for both diacetates **6a** (81%) and **6b** (74%) were satisfactory. The introduction of a metal in the 4-position of the bithiazole was best achieved by Pd-catalyzed stannylation with hexamethylditin at 80°C.^[8a] Attempts to zincate after bromine–lithium exchange at the 4-position were unsuccessful. The prepared stannanes **8a** and **8b** were used directly in the next reaction.

As we had hoped, tribromopyridine **3** was converted regioselectively into the 3-lithium compound and transmetalated to the zinc compound, which underwent a Negishi cross-coupling with the ethyl ester **4**^[15] (Scheme 3). This reaction



Scheme 3. Synthesis of the trisubstituted pyridines **2a** and **2b** from 2,3,6-tribromopyridine (**3**) and structure comparison with the known degradation product, which is assigned the structure *ent-2b*.

proceeded more smoothly than the cross-coupling with the analogous 2-bromothiazole *N*-benzylamide which was also attempted. In an additional step the amide was generated in good yield by treating ester **9** with *N*-benzylamine/diisobutylaluminum hydride (Dibal-H).^[16] The next cross-coupling reaction was preceded by reductive metalation of methyl 2-bromothiazole-4-carboxylate with zinc.^[17] The resulting zinc compound reacted with 2,6-dibromopyridine **10** in a Negishi cross-coupling. The regioselectivity was not completely perfect, and besides the desired 6-substituted 2-bromopyridine **11** the 2-substituted 6-bromopyridine was formed. The regioisomeric ratio (r.r.) was 6.5:1. It was necessary to apply an excess of the zinc compound to achieve a quantitative turnover. When we used 1.3, 1.8, and 2.2 equivalents of the zinc reagent, the yield of **11** increased under otherwise identical conditions from 41% to 52% to 62%. In the last case 20% of the starting material could be recovered. Finally, the inseparable mixture of regioisomers underwent a Stille cross-coupling with the stannanes **8a** and **8b**.^[18] The reaction proceeded well without complications at 80°C in dioxane. The mixture of regioisomers was separated by semipreparative HPLC.^[18]

The ¹H NMR spectra of the degradation product^[9] and of the *erythro* isomer **2b**^[18] match perfectly, whereas the spectra of the *threo* isomer **2a** exhibit significant differences. The differences are found mainly at the spin system of the N,O-diacetylated amino alcohol. The chemical shift of the CH(OAc)-proton of the degradation product was reported as δ = 6.20 ppm and its coupling constant as ³J = 8.0 Hz^[9] (**2a**: 6.32, ³J = 5.2 Hz; **2b**: 6.19, ³J = 8.0 Hz). The CH(NHAc) proton gives rise to a virtual triplet at δ = 5.60 ppm and ³J ≈ 8.1 Hz (**2a**: 5.66, dd, ³J = 8.8, 5.2 Hz; **2b**: 5.58, virt. t, ³J ≈ 8.4 Hz). The synthetic (*R,R*) enantiomer **2b** exhibited a positive specific rotation (Scheme 3, [α]_D²⁰ = +30.7 (c = 0.31, CHCl₃)), and consequently a (*S,S*) configuration could be assigned to the degradation product and also to the thiazolyl peptides GE2270. The absolute values of the specific rotation for **2b** (Scheme 3) and for the degradation product *ent-2b* (Scheme 1) are nearly identical, whereas for **2a** a specific rotation of [α]_D²⁰ = −2.9 (c = 0.56, CHCl₃) was determined.

The construction of the core fragment of the thiazolyl peptides GE2270 described herein should also be applicable to the synthesis of the natural product. The cross-coupling reactions allow a high degree of functionality within the different reaction partners and should facilitate the linkage of more complex building blocks. Studies in this direction and further optimization of the cross-coupling chemistry are currently being carried out.

Received: August 19, 2004

Published online: January 14, 2005

Keywords: asymmetric synthesis · cross-coupling · heterocycles · metalation · natural products

[1] a) E. Selva, G. Beretta, N. Montanini, G. S. Saddler, L. Gastaldo, P. Ferrari, R. Lorenzetti, P. Landini, F. Ripamonti, B. P. Goldstein, M. Berti, L. Montanaro, M. Denaro, *J. Antibiot.* **1991**, *44*,

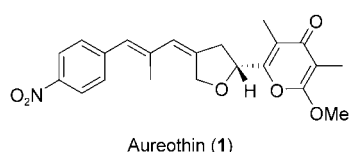
- 693–701; b) J. Kettenring, L. Colombo, P. Ferrari, P. Tavecchia, M. Nebuloni, K. Vékey, G. G. Gallo, E. Selva, *J. Antibiot.* **1991**, *44*, 702–715.
- [2] E. Selva, P. Ferrari, M. Kurz, P. Tavecchia, L. Colombo, S. Stella, E. Restelli, B. P. Goldstein, F. Ripamonti, M. Denaro, *J. Antibiot.* **1995**, *48*, 1039–1042.
- [3] a) P. H. Anborgh, A. Parmeggiani, *J. Biol. Chem.* **1993**, *268*, 24622–24628; b) E. Selva, N. Montanini, S. Stella, A. Soffientini, L. Gastaldo, M. Denaro, *J. Antibiot.* **1997**, *50*, 22–26; c) S. E. Heffron, F. Jurnak, *Biochemistry* **2000**, *39*, 37–45.
- [4] Overview: I. M. Krab, A. Parmeggiani, *Prog. Nucleic Acid Res. Mol. Biol.* **2002**, *71*, 513–551.
- [5] J. Clough, S. Chen, E. M. Gordon, C. Hackbarth, S. Lam, J. Trias, R. J. White, G. Candiani, S. Donadio, G. Romanò, R. Ciabatti, J. W. Jacobs, *Bioorg. Med. Chem. Lett.* **2003**, *13*, 3409–3414.
- [6] Modification of GE2270A: a) P. Tavecchia, M. Kurz, L. Colombo, R. Bonfichi, E. Selva, S. Lociuoro, E. Marzorati, R. Ciabatti, *Tetrahedron* **1996**, *52*, 8763–8774; b) ref. [5].
- [7] a) K. Okumura, H. Saito, C.-g. Shin, K. Umemura, J. Yoshimura, *Bull. Chem. Soc. Jpn.* **1998**, *71*, 1863–1870; b) K. Okumura, T. Suzuki, C.-g. Shin, *Heterocycles* **2000**, *53*, 765–770; c) T. Suzuki, A. Nagasaki, K. Okumura, C.-g. Shin, *Heterocycles* **2001**, *55*, 835–840.
- [8] Synthetic routes to the central pyridine core of related thiazoyl peptides: a) from 6-aminopyridone: T. R. Kelly, C. T. Jagoe, Z. Gu, *Tetrahedron Lett.* **1991**, *32*, 4263–4266; b) from a 1,5-diketone: M. A. Ciufolini, Y. C. Shen, *J. Org. Chem.* **1997**, *62*, 3804–3805; c) from a 3,6-disubstituted pyridone: K. Okumura, Y. Nakamura, C.-g. Shin, *Bull. Chem. Soc. Jpn.* **1999**, *72*, 1561–1569; d) by Bohlmann–Rahtz reaction: M. C. Bagley, K. E. Bashford, C. L. Hesketh, C. J. Moody, *J. Am. Chem. Soc.* **2000**, *122*, 3301–3313; M. C. Bagley, J. W. Dale, R. L. Jenkins, J. Bower, *Chem. Commun.* **2004**, 102–103; e) by [4+2] cycloaddition: K. C. Nicolaou, M. Nevalainen, B. S. Safina, M. Zak, S. Bulat, *Angew. Chem.* **2002**, *114*, 2021–2025; *Angew. Chem. Int. Ed.* **2002**, *41*, 1941–1945; C. J. Moody, R. A. Hughes, S. P. Thompson, L. Alcaraz, *Chem. Commun.* **2002**, 1760–1761; R. A. Hughes, S. P. Thompson, L. Alcaraz, C. J. Moody, *Chem. Commun.* **2004**, 946–948; K. C. Nicolaou, B. S. Safina, M. Zak, A. A. Estrada, S. H. Lee, *Angew. Chem.* **2004**, *116*, 5197–5202; *Angew. Chem. Int. Ed.* **2004**, *43*, 5087–5092.
- [9] P. Tavecchia, P. Gentili, M. Kurz, C. Sottani, R. Bonfichi, E. Selva, S. Lociuoro, E. Restelli, R. Ciabatti, *Tetrahedron* **1995**, *51*, 4867–4890.
- [10] H. J. den Hertog, E. Farenhorst, *Recl. Trav. Chim. Pays-Bas* **1948**, *67*, 380.
- [11] For the regioselectivity of the halogen–metal exchange reactions of 2,3- and 2,5-dibromopyridines, see: a) W. E. Parham, R. M. Piccirilli, *J. Org. Chem.* **1977**, *42*, 257–260; b) M. Mallet, G. Quéguiner, *Tetrahedron* **1985**, *41*, 3433–3440; c) G. J. Quallich, D. E. Fox, R. C. Friedmann, C. W. Murtiashaw, *J. Org. Chem.* **1992**, *57*, 761–764; d) F. Trécourt, G. Breton, V. Bonnet, F. Mongin, F. Marsais, G. Quéguiner, *Tetrahedron* **2000**, *56*, 1349–1360; e) T. Takahashi, Y. Li, P. Stepnicka, M. Kitamura, Y. Liu, K. Nakajima, M. Kotora, *J. Am. Chem. Soc.* **2002**, *124*, 576–582.
- [12] For the regioselectivity of cross-coupling reactions with a 3-acyl-2,6-dichloropyridine, see: W. Yang, Y. Wang, J. R. Corte, *Org. Lett.* **2003**, *5*, 3131–3134.
- [13] Selected monographs on cross-coupling reactions: a) *Metal-catalyzed Cross-coupling Reactions*, 2nd ed. (Eds.: A. de Meijere, F. Diederich), Wiley-VCH, Weinheim, **2004**; b) “Cross-Coupling Reactions—A Practical Guide”: Ed. N. Miyaura, *Top. Curr. Chem.* **2002**, *219*; c) J. J. Li, G. W. Gribble, *Palladium in Heterocyclic Chemistry*, Pergamon, Oxford, **2000**; d) L. Brandsma, S. F. Vasilevsky, H. D. Verkruijsse, *Application of Transition Metal Catalysts in Organic Synthesis*, Springer, Berlin, **1999**.
- [14] A. Spieß, G. Heckmann, T. Bach, *Synlett* **2004**, 131–133.
- [15] a) T. R. Kelly, F. Lang, *J. Org. Chem.* **1996**, *61*, 4623–4633; b) A. T. Ung, S. G. Pyne, *Tetrahedron: Asymmetry* **1998**, *9*, 1395–1407.
- [16] P.-Q. Huang, X. Zheng, X.-M. Deng, *Tetrahedron Lett.* **2001**, *42*, 9039–9041.
- [17] A. S. B. Prasad, T. M. Stevenson, J. R. Citineni, V. Nyzam, P. Knochel, *Tetrahedron* **1997**, *53*, 7237–7254.
- [18] A solution of bromopyridine **11** (27.4 mg, 53.0 μmol ; r.r. = 6.5:1), stannane **8b** (35.2 mg, 64.0 μmol), and tetrakis(triphenylphosphine)palladium(0) (6.1 mg, 10 μmol) in 1.5 mL of dioxane was stirred under an argon atmosphere for 16 h at 80 °C. Saturated ammonium chloride solution (15 mL) was added to the dark brown suspension, and the aqueous layer was extracted with CH_2Cl_2 (2×20 mL). The combined organic layers were dried (Na_2SO_4) and filtered. A small portion of silica gel was added, and the solvent was removed in vacuo. The residue was purified by flash chromatography (silica gel 60, 2×18 cm, solvent: ethyl acetate) and 26.5 mg (61 %) of the desired product (r.r. = 6.5:1) was obtained. To separate the regioisomers a portion of the product was purified by semipreparative HPLC (YMC, ODS-A, 250×20 ; MeCN/ H_2O 20:80 \rightarrow 100:0 in 30 min; flow = 15.0 mL min^{-1}). The desired product **2b** was isolated as a colorless solid. R_f = 0.43 (EtOAc); $[\alpha]_D^{20}$ = +30.7 (c = 0.31, CHCl_3); UV (MeCN/ H_2O = 89/20): λ_{max} = 302 nm; $^1\text{H NMR}$ ($[\text{D}_6]\text{DMSO}$, 360 MHz): δ = 1.75 (s, 3H), 2.00 (s, 3H), 3.90 (s, 3H), 4.46 (d, 3J = 6.1 Hz, 2H) 5.58 (virt. t, $^3J \cong 8.4$ Hz, 1H), 6.19 (d, 3J = 8.0 Hz, 1H), 7.21–7.40 (m, 10H), 7.90 (s, 1H), 8.29 (s, 1H), 8.34 (d, 3J = 8.2 Hz, 1H), 8.37 (s, 1H), 8.75 (d, 3J = 8.2 Hz, 1H), 8.75 (s, 1H), 8.84 (d, 3J = 8.6 Hz, 1H), 9.10 ppm (t, 3J = 6.2 Hz, 1H); $^{13}\text{C NMR}$ ($[\text{D}_6]\text{DMSO}$, 90 MHz): δ = 21.0 (q), 22.5 (q), 42.4 (t), 52.4 (q), 54.4 (d), 74.8 (d), 118.1 (d), 119.2 (d), 123.3 (d), 126.9 (d), 127.3 (d), 127.4 (d), 128.4 (d), 128.6 (d), 129.6 (s), 132.5 (d), 137.1 (s), 139.7 (s), 140.1 (d), 147.4 (s), 147.5 (s), 149.8 (s), 150.1 (s), 151.0 (s), 152.8 (s), 160.6 (s), 161.3 (s), 162.1 (s), 163.6 (s), 167.9 (s), 169.2 (s), 169.3 (s), 170.5 ppm (s), two aromatic CH signals overlap; HRMS (FAB): $\text{C}_{39}\text{H}_{32}\text{N}_7\text{O}_6\text{S}_4$ $[(M+H)^+]$ calcd: 822.1297, found: 822.1289.

Mutasyntesis of Aureonitrile: An Aureothin Derivative with Significantly Improved Cytostatic Effect**

Martina Ziehl, Jing He, Hans-Martin Dahse, and Christian Hertweck*

Polyketides constitute a highly diverse group of natural products that play a leading role in drug discovery.^[1] All polyketides are assembled from an acyl starter unit by repetitive Claisen condensations of extender units derived from malonyl coenzyme A (CoA) in a manner that closely parallels fatty acid biosynthesis.^[2] While the vast majority of polyketides are primed with acetate, a number of polyketide synthases (PKSs) utilize alternative starter units that enlarge polyketide diversity and provide the molecule with important structural and biological features.^[3] Consequently, the variation of starter units can be an efficient approach to yield complex natural product analogues with potentially improved activity, selectivity, availability, and fewer unwanted side effects. A strategy to achieve this goal is the addition of non-natural primers to a mutant, in which particular genes that code for the biosynthesis of the starter unit have been deleted. This technique, which suppresses the formation of the natural metabolites, is also referred to as “mutasyntesis”.^[4–7] In the PKS area this approach has been successful generating analogues of erythromycin,^[3,8,9] rifamycin,^[10] and enterocin.^[11] The most impressive example for mutational synthesis of a polyketide derivative to date is the engineered biosynthesis of the anthelmintic agent doramectin by exchanging the isobutyrate starter of avermectin for cyclohexanoate.^[12–14]

A highly unusual polyketide starter unit, *p*-nitro benzoate (PNBA), is employed in the biosynthesis of aureothin (**1**), a polyketide-shikimate hybrid metabolite from the soil bacterium *Streptomyces thioluteus*.^[15,16] Aureothin exhibits a vari-



[*] M. Ziehl, J. He, Dr. H.-M. Dahse, Dr. C. Hertweck
Hans-Knoell-Institute for Natural Products Research
Beutenbergstrasse 11a
07745 Jena (Germany)
Fax: (+49) 3641-656-705
E-mail: christian.hertweck@hki-jena.de

[**] Financial support by the DFG priority program SPP1152: “Evolution of metabolic diversity” (HE3469/2) is gratefully acknowledged. We thank Dr. U. Möllmann and Dr. A. Härtl for biological testing, and K.-D. Menzel and M. Steinacker for assistance with fermentation. We are also grateful to Prof. Xiufen Zhou of Shanghai Jiaotong University, China, and Prof. Jose Salas and Dr. Carmen Mendez, University of Oviedo, Spain, for the gifts of *S. lividans* ZX1 and *S. albus*, respectively.

ety of pharmacological properties, which include weak cytotoxic, antifungal, and antiviral activities.^[17] As a basis for engineering aureothin derivatives with altered bioactivity profiles, we recently cloned and analyzed the entire aureothin (*aur*) biosynthesis gene cluster.^[18] In addition to employing the rare PNBA starter unit, the multifunctional PKS enzyme complex has some peculiar features. First, the aureothin PKS does not have an obvious loading domain like that found in conventional bacterial type I PKS,^[3] and thus the priming mechanism is obscure. Possibly the primer is loaded directly onto the KS1 domain after activation by the putative acyl CoA ligase AurE. Second, contrary to the principle of colinearity, the first module (AurA) is used iteratively.^[18] Consequently, the KS of AurA has a double editing role, as it needs to tolerate the alternative PKS starter moiety before and after the first elongation cycle (Figure 1). Thus, using the aureothin PKS in precursor-directed biosynthesis would be intriguing.

Analyses of the *aur* genes suggested that the biosynthesis of PNBA involves a *p*-aminobenzoate (PABA) synthase, AurG, which converts chorismate into PABA, and a novel *N*-oxygenase, AurF, for the *N*-oxygenation of PABA.^[16] Thus, for the mutasyntesis of aureothin derivatives, two genes, *aurF* and *aurG*, were targeted for the construction of suitable null mutants (Figure 1). The PABA synthase gene *aurG* was successfully excised from the *aur* gene cluster on expression plasmid pHJ48 using the λ Red method.^[19,20] The resulting plasmid, pHJ97 (Figure 2), was introduced into the heterologous expression hosts *S. lividans* ZX1, by polyethyleneglycol (PEG) induced protoplast transformation, and *S. albus*, by intergeneric conjugation.^[21] The recombinant strains were fermented and their metabolic profiles monitored by thin layer chromatography (TLC) and HPLC/MS. Remarkably, the transconjugant *S. albus*::pHJ97 was still capable of aureothin biosynthesis, albeit in strongly reduced amounts. This result is in accord with the finding that not only one, but several PABA synthase genes may be present in a *Streptomyces* genome, including the essential PABA synthase genes required for folic acid synthesis.^[22,23] In contrast to the results obtained with *S. albus*, aureothin biosynthesis was completely abolished in *S. lividans* ZX1::pHJ97, and only upon administering synthetic PABA to the mutant, was aureothin production restored. It thus appears that the titer of PABA is strain-dependent and that PABA involved in folate biosynthesis does not interfere with the aureothin pathway. Another null mutant lacking the *N*-oxygenase gene was generated analogously to the *aurG* null mutant (Figure 2). Transfer of the manipulated gene cluster into *S. lividans* ZX1 resulted in a strain (*S. lividans* ZX1::pHJ79) that is incapable of producing aureothin in the absence of synthetic PNBA.^[16] This result underlines our earlier finding that PNBA, and not PABA, serves as starter unit and suggests that the aureothin synthase has a rather high primer specificity.

Expression of the mutated gene clusters in the *S. lividans* host appeared suitable for mutasyntesis, since the *aur* pathway could only be restored with exogenously supplied PABA or PNBA. To explore the substrate specificity of the *aur* PKS, first *p*-, *m*-, and *o*-PNBA were administered to a growing culture of *S. lividans* ZX1::pHJ79. Not surprisingly,

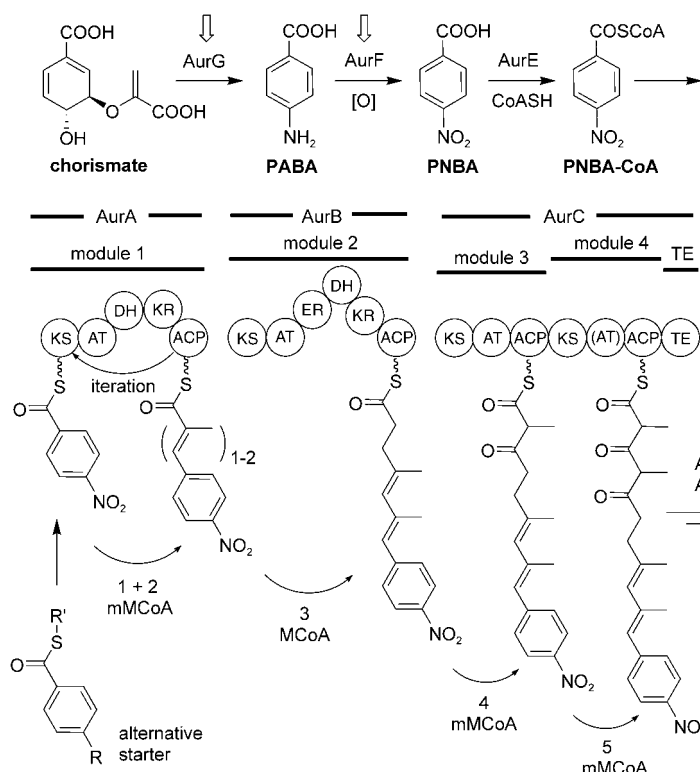


Figure 1. Model of aureothin biosynthesis starting from chorismate and the strategy for priming the type I PKS with alternative activated benzoates (R' : NAC, CoA). Key enzymes (AurF, AurG) involved in the biosynthesis of the starter unit (PNBA) are targets for mutasynthesis and highlighted with arrows.

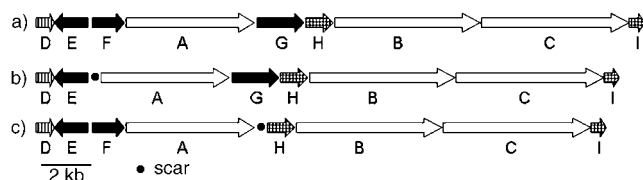


Figure 2. Organization of a) the entire *aur* gene cluster, as in pHJ48, b) *aurF* null mutant (pHJ79), and c) *aurG* null mutant (pHJ97); *aur*-ABC PKS genes, *aurD* regulator gene, *aurE* acyl-CoA ligase gene, *aurF* N-oxygenase gene, *aurG* PABA synthase gene, *aurH* P-450 monooxygenase gene, *aurI* O-methyl transferase gene.

only the *p*-substituted acid was used as substrate, while the regioisomers were not incorporated. In a series of further feeding experiments a variety of *p*-substituted PNBA surro-

gates were tested, either as free acids or as the corresponding *N*-acetyl cysteamine (NAC) thioesters, which were synthesized using the dicyclohexyl carbodiimide/4-dimethylaminopyridine (DCC/DMAP) method.^[24,25] The NAC adducts serve as activated acyl CoA mimics^[26] that may diffuse into the bacterial cells and bypass a potential bottleneck, the putative acyl CoA ligase AurE. Of the various *p*-substituted benzoic acids, *p*-iodo, *p*-bromo, *p*-chloro, and *p*-fluoro benzoate, as well as *p*-*N*-acetamido anthranilic acid and *p*-dimethylamino benzoate were probed on a 100-mL fermentation scale. Unfortunately, novel aureothin derivatives could not be detected in the crude extracts of these feeding experiments. Also, toluic acid and terephthalic acid monomethyl ester failed to incorporate. Strikingly though, addition of *p*-cyano benzoic acid to a culture of the *aurF* null mutant yielded a novel metabolite, which was detected by ESI-MS in the positive mode (m/z 378). Since only relatively low quantities of the new compound were produced, we tested if *p*-cyano benzoyl-SNAC would provide higher yields, as it does not need to be activated as an acyl CoA adduct by the ligase (Figure 3). However, the yield did not exceed that obtained with the free acid, which reveals that in this case acid activation by the ligase AurE is not a bottleneck.

To obtain sufficient quantities of the new compound for structure elucidation and biological testing, a medium-scale fermentation (50 L)

was performed. Fermentation broth and mycelium of the mutant supplemented with cyano benzoate were exhaustively extracted with ethyl acetate, and the crude extracts were subjected to sequential column chromatography on silica and sephadex LH-20. Final purification of the new compound was by preparative HPLC.

HR-MS and ^{13}C NMR spectroscopy corresponded to a molecular formula of $\text{C}_{23}\text{H}_{23}\text{NO}_4$. The presence of a nitrile moiety was confirmed by the ^{13}C NMR spectroscopy signal at $\delta = 142.14$ ppm, as well as the very characteristic IR band ($\nu_{\text{C}\equiv\text{N}}$) at 2223 cm^{-1} . Except for the signals of the aromatic protons, the ^1H NMR spectroscopic data of **1** and the new compound were very similar, and HH-COSY, HMQC, and HMBC data revealed the same connectivities. All spectroscopic (MS^n) and spectroscopic (IR, NMR) data support the

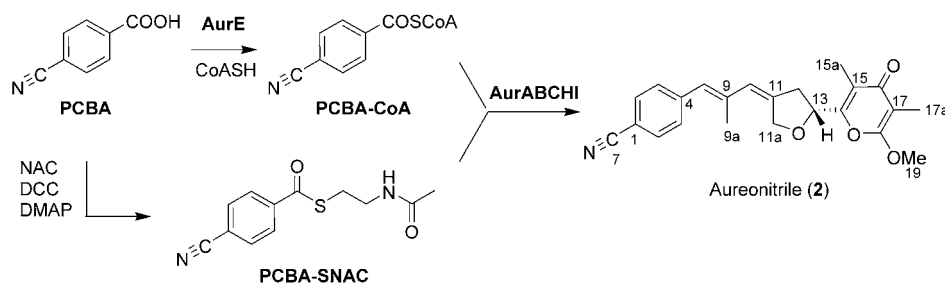


Figure 3. Mutasynthesis of aureonitrile with PCBA and PCBA-SNAC.

expected structure of an aureothin derivative substituted with a nitrile moiety instead of the nitro group. The new compound was thus named aureonitrile (**2**). In addition, NOE measurements revealed the same configuration for **2** as for aureothin. It is surprising that out of the number of *p*-substituted benzoates only *p*-cyano benzoate was tolerated by the PKS, but not related compounds with substituents that induce comparable $-I$ - and $-M$ effects, such as methyl carboxylate and *N*-acetamido. This observation may be rationalized by a similar charge distribution of nitrile and nitro groups.

Aureonitrile (**2**) was subjected to broad biological testing, with focus on antimicrobial and cytotoxic assays. While **2** shows only weak antibacterial activities, it has a reasonably high potency against fungal pathogens, for example *Candida albicans* (IC_{50} of 12.5 μM). The most remarkable results, however, were obtained in cytotoxicity and antiproliferative assays.

Most importantly, we observed a flat dose-response curve of the pyrones, which indicates a cytostatic effect (Figure 4).

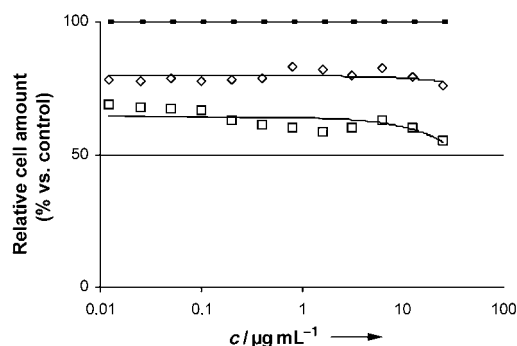


Figure 4. Cytostatic effect of aureothin (**1**; \diamond) and aureonitrile (**2**; \square) on adherent human cervix carcinoma HeLa cells. For control (\blacksquare) and for dilutions of **1** and **2**, the same number of cells was seeded per microplate well. After incubation (72 h) the relative amount of treated cells was monitored versus the control.

Compared to **1**, compound **2** shows a significantly enhanced activity ($>200\%$) against various tumor cell lines, such as HeLa and K-562, at a wide range of concentration. In contrast to classical anticancer drugs, which often exert unwanted cytotoxic effects in addition to cytostatic properties, the new generation of antitumor agents should show only cytostatic effects in a broad therapeutic window. Such drugs stop cell proliferation at the checkpoints of mitosis or interfere with DNA synthesis.^[27] Owing to the intriguing properties of **2**, in vivo assays and the elucidation of its molecular target are now underway.

In conclusion, we have successfully explored the potential of the iterative aureothin PKS for precursor-directed biosynthesis. For this purpose, suitable mutants were engineered, which also supported the biosynthetic model of PNBA generation via PABA involving a specific PABA synthase. For complementation of the mutants, a number of PNBA surrogates were tested as free acids, as well as the corresponding synthetic *N*-acetyl cysteamine thioesters. The iterative *aur* polyketide synthase, which lacks a loading domain, exhibits a rather high substrate specificity, besides PNBA it

only allows *p*-cyano benzoate to be further processed. However, the resulting fully characterized nitrile analogue of aureothin, shows significantly enhanced cytostatic effects against HeLa and K-562 tumor cells compared to the native compound in the range 50 $\mu\text{g L}^{-1}$ to 10 ng mL^{-1} . This result underlines the power of mutasynthesis towards polyketide derivatives with improved properties. Strain optimization and complementary synthetic approaches are currently underway to obtain larger quantities of aureonitrile.

Experimental Section

Construction of *aurG* null mutant: Deletion of *aurG* from the *aur* gene cluster was performed in analogy to the described method for inactivation of *aurF*^[16] using the λ Red method with primers *aurGF* (5'-AGG ACG ACC CCG CTC GAA CCG ACA GGG AGG CTC CCG ATG ATT CCG GGG ATC CGT CGA CC-3') and *aurGR* (5'-CTT GAA GCC CGT CGA ACG ACG GGC GGA ACG GCC GTA CTA TGT AGG CTG GAG CTG CTT C-3'). The polymerase chain reaction (PCR) product was introduced into *E. coli* BW25113/pIJ790 containing cosmid pHJ48, which includes the entire aureothin biosynthesis gene cluster, with concomitant substitution of the *aurG* gene by the extended spectinomycin resistance cassette. The inserted cassette was removed through expression of the FLP-recombinase in *E. coli*, to yield a 81 base pair (bp) "scar" in the preferred reading frame. The resulting plasmid, pHJ97, was then introduced into *S. albus* by intergeneric conjugation using *E. coli* ET12567 containing the RP4 derivative pUZ8002 or into *S. lividans* ZX1 by PEG-mediated protoplast transformation.

Synthesis of *p*-nitrobenzoyl-SNAC: Dimethylaminopyridine (0.82 mmol, 98 mg) *N*-acetyl cysteamine (6.1 mmol, 0.7 mL), and dicyclohexylcarbodiimide (4.43 mmol, 4.4 mL, 1M solution in dichloromethane) were sequentially added to a solution of (4 mmol, 593 mg) *p*-cyano benzoic acid in dry dichloromethane (24 mL) and dry THF (8 mL) at 0°C. The mixture was stirred for 10 min at 0°C and 3 days at room temperature. After filtration through celite the solution was passed through a short column of copper sulfate impregnated silica. PNBA-SNAC was purified by precipitation with petroleum ether. Yield: 594.4 mg (59%). ¹H NMR (300 MHz, CDCl₃): δ = 1.95 (s, 3H, CH₃); 3.24 (t, J = 6.5 Hz, 2H, S-CH₂), 3.51 (q, J = 6.3 Hz, 2H, CH₂-N), 5.94 (br s, 1H, NH-CO), 7.73 (d, J = 8.47 Hz, 2H), 8.01 ppm (d, J = 8.39 Hz, 2H); ¹³C NMR (75 MHz, CDCl₃): δ = 23.14 (CH₃), 29.03 (S-CH₂), 39.25 (CH₂-N), 116.87 (C-CN), 117.65 (CN), 127.69 (2C, Ar), 132.52 (2C, Ar), 139.75 (C-CO), 170.32 (N-CO), 190.75 ppm (CO-S); IR (film): $\tilde{\nu}$ = 2231 ($\nu_{\text{C}\equiv\text{N}}$), 1642, 1553 ($\nu_{\text{O}=\text{NH}}$, $\nu_{\text{C}=\text{C}}$), 919 cm^{-1} (γ_{CH} , Ar); HR-MS calcd for C₁₂H₁₃SN₂O₂: 249.0692; observed: 249.0696.

Fermentation and isolation of aureonitrile: All fermentations were performed in liquid M10 medium supplemented with apramycin (50 $\mu\text{g mL}^{-1}$) as described elsewhere.^[18] Precursors were added as sterile solutions in H₂O/DMSO (v/v = 75:25, c = 1 mg/100 μL). A *S. lividans*:pHJ79 seed culture was used to inoculate 50 L M10 (*apra*) medium in a stainless steel fermenter. The culture was pulse-fed with *p*-cyano benzoate (1.325 g) in two portions. After 5 days with constant stirring at 28°C mycelium and filtrate were separated and exhaustively extracted with ethyl acetate. The crude extracts were separated on silica by using a chloroform/methanol gradient as eluent and on sephadex by using methanol for elution. All fractions containing the main product were combined and further purified by RP-HPLC on a Phenomenex Luna C18 column (10 μ , 250 \times 21.2 mm) using a 80:20–100:0 acetonitrile/water gradient for elution over 10 min at a flow rate of 20 mL min^{-1} . Yield: 5.9 mg of a dark yellow solid. ¹H NMR (300 MHz, CDCl₃): δ = 1.84 (s, 3H, 17a-CH₃), 2.0 (s, 3H, 9a-CH₃), 2.01 (s, 3H, 15a-CH₃), 2.98 (m, 2H, 13-CH₂), 3.92 (s, 3H, O-CH₃), 4.71 (d, J = 14.2 Hz, 1H, 11a-CH₂), 4.84 (d, J = 14.2 Hz, 1H, 11a-CH₂), 5.12 (t, J = 6.9 Hz, 1H, 12-CH), 6.16 (s, 1H, 10-CH), 6.30 (s, 1H, 8-

CH), 7.32 (d, $J = 8.2$ Hz, 2H, Ar H3,H5), 7.61 ppm (d, $J = 8.3$ Hz, 2H, Ar H2, H6); ^{13}C NMR (75 MHz, CDCl_3): $\delta = 6.89$ (17a-CH₃), 9.42 (15a-CH₃), 17.65 (9a-CH₃), 38.27 (13-CH₂), 55.26 (O-CH₃), 70.10 (11a-CH₂), 73.33 (12-CH), 100.11 (17-C), 110.10 (1-C), 118.89 (4-C), 120.18 (15-C), 126.00 (10-CH), 128.72 (8-CH), 129.53 (Ar C3,C5), 132.00 (Ar C2, C6), 137.89 (9-C), 140.22 (11-C), 142.15 (CN), 154.72 (14-C), 162.09 (18-C), 180.60 ppm (16-C); IR (film): $\tilde{\nu} = 2223$ ($\nu_{\text{C}\equiv\text{N}}$), 1718 ($\nu_{\text{C=O}}$), 1662 ($\nu_{\text{C=O}}$), 1591, 1499, w ($\nu_{\text{C=C}}$), 915 cm^{-1} ($\nu_{\text{C-O-C}}$); HR-MS: calcd for $\text{C}_{23}\text{H}_{24}\text{NO}_4$: 378.1700; observed: 378.1705.

Antiproliferative and cytotoxic assay: Cells of K-562 (DSM ACC10), L-929 (DSM ACC2), and HeLa (DSM ACC57) were cultured in RPMI1640 medium (GIBCOBRL), supplemented with gentamicin sulfate (25 $\mu\text{g mL}^{-1}$; Cambrex), 10% heat inactivated fetal bovine serum (GIBCOBRL), and GlutaMAX-1 (GIBCOBRL) at 37°C in high density polyethylene flasks (NUNC). Aureothin (**1**) and aureonitrile (**2**) were dissolved in ethanol (10 mg mL^{-1}) before being diluted in RPMI1640. The adherent cells of L-929 and HeLa were harvested at the logarithmic growth phase after soft trypsinization, using 0.25% trypsin in PBS (phosphate buffer saline) containing 0.02% EDTA (Biochrom KG). For cytotoxicity assays, approximately 10000 HeLa cells per well of the 96-well microplates cells were seeded with RPMI1640 (0.2 mL) and pre-incubated for 48 h without **1** and **2**. After formation of a subconfluent monolayer, cells were treated with dilutions of **1** and **2** and incubated under physiological conditions (72 h at 37°C in a humidified atmosphere and 5% CO_2). For the antiproliferative assay, **1** and **2** were tested against L-929 and K-562. For each experiment approximately 10000 cells were seeded with RPMI1640 (0.1 mL) per well of the 96-well microplates and subsequently exposed to dilutions of **1** and **2** and incubated under physiological conditions for 72 h. The measurement of cytotoxicity and cell growth inhibition was based on registration of living cells after incubation with **1** and **2** versus untreated control. Non-adherent K-562 cells were analyzed by an electronic cell analyzer system CASY1 (Schärfe) as described elsewhere.^[28] Adherent L-929 and HeLa cells were fixed by glutaraldehyde (Merck) and stained with methylene blue (SERVA) for 15 min. After gentle washing the stain was eluted with HCl (0.2 mL, 0.33N) in the wells. The optical densities were measured at 660 nm in a SUNRISE microplate reader (TECAN).

Received: September 14, 2004

Published online: January 11, 2005

Keywords: antitumor agents · mutasynthesis · natural products · polyketides

- [1] D. O'Hagan, *The Polyketide Metabolites*, Ellis Horwood, Chichester, **1991**.
- [2] J. Staunton, K. J. Weissman, *Nat. Prod. Rep.* **2001**, *18*, 380.
- [3] B. S. Moore, C. Hertweck, *Nat. Prod. Rep.* **2002**, *19*, 70.
- [4] K. L. Rinehart, L. S. Shield, *Fortschr. Chem. Org. Naturst.* **1976**, *33*, 231.
- [5] K. L. Rinehart, *Pure Appl. Chem.* **1977**, *49*, 1361.
- [6] S. J. Daum, J. R. Lemke, *Annu. Rev. Microbiol.* **1979**, *33*, 241.
- [7] W. Wohlleben, S. Pelzer, *Chem. Biol.* **2003**, *10*, 1163.
- [8] K. Konishita, P. G. Williard, C. Khosla, D. E. Cane, *J. Am. Chem. Soc.* **2001**, *123*, 2495.
- [9] R. P. Desai, T. Leaf, Z. Hu, C. R. Hutchinson, A. Hong, G. Byng, *Biotechnol. Prog.* **2004**, *20*, 38.
- [10] D. Hunziker, T.-W. Yu, C. R. Hutchinson, H. G. Floss, C. Khosla, *J. Am. Chem. Soc.* **1998**, *120*, 1092.
- [11] J. A. Kalaitzis, M. Izumikawa, L. Xiang, C. Hertweck, B. S. Moore, *J. Am. Chem. Soc.* **2003**, *125*, 9290.
- [12] C. J. Dutton, S. P. Gibson, A. C. Goudie, K. S. Holdom, M. S. Pacey, J. C. Ruddock, J. D. Bu'Lock, M. K. Richards, *J. Antibiot.* **1991**, *44*, 357.

- [13] H. A. I. McArthur, *A Novel Avermectin, Doramectin—A Successful Application of Mutasynthesis*, Society for Industrial Microbiology, Fairfax, VA, **1998**.
- [14] T. A. Cropp, D. J. Wilson, K. A. Reynolds, *Nat. Biotechnol.* **2000**, *18*, 980.
- [15] Y. Hirata, H. Nakata, K. Yamada, K. Okuhara, T. Naito, *Tetrahedron* **1961**, 252.
- [16] J. He, C. Hertweck, *J. Am. Chem. Soc.* **2004**, *126*, 3694.
- [17] J. L. Schwartz, M. Tishler, B. H. Arison, H. M. Shafer, S. Omura, *J. Antibiot.* **1976**, *29*, 236.
- [18] J. He, C. Hertweck, *Chem. Biol.* **2003**, *10*, 1225.
- [19] K. A. Datsenko, B. L. Wanner, *Proc. Natl. Acad. Sci. USA* **2000**, *97*, 6640.
- [20] K. C. Murphy, K. G. Campellone, A. R. Poteete, *Gene* **2000**, *246*, 321.
- [21] T. Kieser, M. J. Bibb, M. J. Buttner, K. F. Chater, D. A. Hopwood, *Practical Streptomyces Genetics*, The John Innes Foundation, Norwich, UK, **2000**.
- [22] M. P. Brown, K. A. Aidoo, L. C. Vining, *Microbiology* **1996**, *142*, 1345.
- [23] J. M. Green, B. P. Nichols, *J. Biol. Chem.* **1991**, *266*, 12972.
- [24] B. Neises, W. Steglich, *Angew. Chem.* **1978**, *90*, 556.
- [25] C. J. Wilkinson, E. J. Frost, J. Staunton, P. F. Leadlay, *Chem. Biol.* **2001**, *8*, 1197.
- [26] J. Staunton, A. C. Sutkowski, *J. Chem. Soc. Chem. Commun.* **1991**, 1110.
- [27] S. N. Gardner, M. Fernandes, *J. Exp. Ther. Oncol.* **2004**, *4*, 9.
- [28] H.-M. Dahse, B. Schlegel, U. Gräfe, *Pharmazie* **2001**, *56*, 489.

Ternary Nitrides

Predicting New Ferromagnetic Nitrides from Electronic Structure Theory: IrFe_3N and $\text{RhFe}_3\text{N}^{}$** *Jörg von Appen and Richard Dronskowski**

The nitride phase Fe_4N has been the subject of intense experimental^[1–3] and also theoretical^[4,5] studies owing to its potential application as a high-density recording material. It is characterized by a large saturation magnetization of $208 \text{ emu g}^{-1[6]}$ close to $\alpha\text{-Fe}$ (218 emu g^{-1}), a low coercivity, and a chemical inertness that exceeds that of the metal itself. The perovskite-like crystal structure of Fe_4N ($a = 3.795 \text{ \AA}$)^[7] is given in Figure 1.

There have been some attempts to improve the magnetic properties of Fe_4N through atomic substitution, and some berthollide compounds of general type $\text{M}_x\text{Fe}_{4-x}\text{N}$ ($x < 1$) with

[*] J. von Appen, Prof. R. Dronskowski
Institut für Anorganische Chemie
Rheinisch-Westfälische Technische Hochschule
52056 Aachen (Germany)
Fax: (+49) 241-80-92642
E-mail: drons@hal9000.ac.rwth-aachen.de

[**] We thank Prof. Herbert Jacobs for valuable information, the Fonds der Chemischen Industrie for their support, and the Forschungszentrum Jülich for the usage of their computational resources.

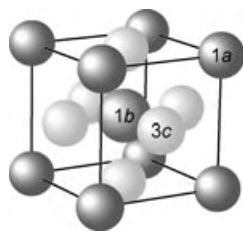


Figure 1. The crystal structure of Fe_4N in space group $Pm\bar{3}m$. The gray nitrogen atom occupies the very center (Wyckoff position $1b$), and the dark-gray/light-gray iron atoms are found at the corners ($1a$) and face centers ($3c$).

$M = \text{Mn},^{[8]} \text{Ru},^{[9]} \text{Os},^{[9]} \text{Co},^{[10]} \text{Ir},^{[9]} \text{Ag},^{[11]} \text{Zn}^{[12]}$ were reported. In addition, a few stoichiometrically precise phases MFe_3N with $M = \text{Ni},^{[1]} \text{Pd},^{[13]} \text{Pt},^{[1]} \text{Au},^{[11]}$ and $\text{In}^{[12]}$ are known. Upon substitution only Mn occupies both lattice sites ($1a$ and $3c$, see Figure 1) within the perovskite-like structure, all other metals exclusively replace the corner Fe atom such that these M atoms are coordinated by twelve nearest Fe neighbors.

To our knowledge, there is only a single Fe_4N -related report^[9] of the attempted replacement of Fe by its higher homologues Ru and Os (and also by Ir). No daltonide phase but only berthollide compounds $\text{M}_x\text{Fe}_{4-x}\text{N}$ with $x \leq 0.20$ were prepared. On the theoretical side, various studies have analyzed the role played by M guest atoms such as Ni and Pd,^[14–16] Pt,^[17] Mn,^[15,16] Ag and Au,^[18] Sn,^[16] Zn and In,^[19] Cu,^[20] Co, Cr, and Ti.^[21] These studies specifically targeted the theoretical lattice parameters and saturation moments of the compounds, some of which are still hypothetical. In addition, there is a recent theoretical report on a likewise hypothetical RuFe_3N ^[22] but, otherwise, there are no contributions on substituting Fe in Fe_4N by either Os, Rh, or Ir. To fill this important gap, we have examined the complete set of daltonide compounds MFe_3N of the iron- and platinum-group metals by means of total-energy density-functional calculations to determine stable atomic configurations, absolute stabilities, and also physical properties.

The atomic ordering of the iron- and platinum-group metals M over the $1a$ and $3c$ sites was analyzed. For this purpose, the total energies of statistically *disordered* compounds, designated $^{1a}(\text{M}_{1/4}\text{Fe}_{3/4})^{3c}(\text{M}_{3/4}\text{Fe}_{9/4})^{1b}(\text{N})$ —the Wyckoff superscripts indicate the positions in the disordered phase—were compared with two *ordered* configurations: The M atom may either exclusively replace the corner Fe atom, $^{1a}(\text{M})^{3c}(\text{Fe}_3)^{1b}(\text{N})$, or M may substitute one of the three facial Fe atoms, $^{1a}(\text{Fe})^{3c}(\text{MFe}_2)^{1b}(\text{N})$. The numerical results are given in Table 1 as *relative* energies with respect to the random occupation.

In the case of CoFe_3N , the energy differences between the three structural alternatives are so tiny that there is no preference for the small Co atom to occupy either $1a$ or $3c$ (or

to strive for both positions simultaneously); this already alludes to the similar behavior for the likewise small Mn atom in MnFe_3N . An increase in atomic size, however, clearly disfavors the facial $3c$ position (see Table 1, left energy column) for the heavier atoms Rh, Ir, Pd, and Pt. On the contrary, the corner $1a$ position is the most attractive one for these larger atoms, as shown by the strong energetic gains (see center energy column). This simple interpretation is in accord with independent suggestions^[23] relating the atomic ordering with two factors, namely the relative affinity of M and Fe for nitrogen and, more important, the differences in atomic sizes;

Table 1: Metallic radii r_M [Å], total energy differences ΔE [kJ mol^{−1}] between different atomic orderings relative to a random occupation, and the corresponding lattice parameters a [Å] of MFe_3N in the perovskite-like structure type.

Distribution	r_M	$^{1a}(\text{Fe})^{3c}(\text{MFe}_2)^{1b}(\text{N})$		$^{1a}(\text{M})^{3c}(\text{Fe}_3)^{1b}(\text{N})$		$^{1a}(\text{M}_{1/4}\text{Fe}_{3/4})^{3c}(\text{M}_{3/4}\text{Fe}_{9/4})^{1b}(\text{N})$	
		ΔE	a	ΔE	a	ΔE	a
Co	1.25	−2	3.79	−2	3.79	0	3.79
Ni	1.25	4	3.80	−16	3.80	0	3.80
Ru	1.34	−2	3.89	−11	3.85	0	3.88
Os	1.35	4	3.90	−7	3.82	0	3.88
Rh	1.34	10	3.91	−71	3.87	0	3.90
Ir	1.36	16	3.92	−79	3.85	0	3.91
Pd	1.38	33	3.94	−111	3.88	0	3.93
Pt	1.38	40	3.97	−149	3.88	0	3.95

the size of the $1a$ position was estimated as 1.42 Å whereas the value for the $3c$ site is only 1.28 Å.^[9] Qualitatively, the similarity of the metallic radii of Co and Ni to that of Fe (1.24 Å) therefore explains the minute energy differences between the different orderings for the $3d$ elements; for the larger (Rh, Ir) and largest (Pd, Pt) atoms, however, the corner $1a$ position is the optimum choice. Small deviations from this size rule (Ru and Os entries) must be related to differences in chemical affinities to nitrogen. Quantitatively, the well-characterized compounds PdFe_3N and PtFe_3N support our calculations.^[1,13] Indeed, both phases are described as following the $^{1a}(\text{M})^{3c}(\text{Fe}_3)^{1b}(\text{N})$ scheme, and their experimental lattice parameters of 3.866 and 3.857 Å are quite close to the theoretical ones (Table 1), the small theoretical overestimation being typical for the GGA method.^[24] In the following, we stick to this ordered $^{1a}(\text{M})^{3c}(\text{Fe}_3)^{1b}(\text{N})$ distribution.

The *absolute* stabilities of the MFe_3N family of compounds was studied with respect to plausible educt phases by theoretically determining the total electronic energies of all the participating elements.^[25] In addition, the nitride phase FeN which adopts the zinc blende type was included because theory indicates that this binary compound is enthalpically more stable than the elements, in accord with independent calorimetric measurements;^[26] in fact, the phase designated $\text{FeN}_{0.91}$ is the most exothermic iron nitride ($\Delta H_f \approx -50$ kJ mol^{−1}). Given the simple chemical reaction in Equation (1), the absolute energetic stabilities of MFe_3N over all competing phases result as Equation (2).



$$\Delta E = E(\text{MFe}_3\text{N}) - E(\text{FeN}) - 2E(\text{Fe}) - E(M) \quad (2)$$

MFe ₃ N		
Fe	Co	Ni
-2	7	-8
Ru	Rh	Pd
64	-23	-47
Os	Ir	Pt
108	2	-74

Figure 2. Theoretical reaction energies ΔE (kJ mol⁻¹) of MFe₃N with M being a Group VIII transition metal. Experimentally reported phases are highlighted in gray.

The theoretical reaction energies obtained are sketched in Figure 2. As expected, the reaction energies for the already synthesized compounds NiFe₃N, PdFe₃N, and PtFe₃N turn out to be *negative* and thus confirm the density-functional result to be correct because all three compounds have been reported as enthalpically stable phases. The fully ordered compounds MFe₃N with M = Ru, Os, Co, and Ir are all predicted to be unstable and, indeed, these have only been reported as non-stoichiometric, disordered phases (see above). Surprisingly, the phase RhFe₃N, yet to be made, seems theoretically to be an exothermic and ordered compound (see below). While it is hard to deduce a simple stability trend from Table 1, all the MFe₃N compounds (even the unstable ones) are predicted to be ferromagnetic (see below), with GGA saturation moments between 7.1 and 9.2 μ_B per formula unit; the theoretical value for Fe₄N is 10.3 μ_B . For a closer analysis, we focus on the energetically almost stable IrFe₃N and the energetically stable RhFe₃N phase.

The perovskite-like IrFe₃N exhibits a theoretical lattice parameter of $a = 3.85$ Å, which corresponds to an 0.9% lengthening in comparison to Fe₄N; for Fe₄N, theory finds $a = 3.817$ Å, only 0.6% larger than the experimental result. In IrFe₃N, the electronic ground state is the one of an itinerant ferromagnet, and the magnetization amounts to 9.0 μ_B per

formula unit, with local moments of approximately 0.92 μ_B for Ir and 2.68 μ_B for Fe. This situation needs to be compared with Fe₄N where local Fe moments of 3.01 and 2.44 μ_B are found for the 1a and 3c positions. The increase in the ⁵⁷Fe moment for IrFe₃N is a consequence of the very long Fe–Fe separations but the total moment of IrFe₃N is smaller since an Fe atom on the 1c position has been replaced by Ir.

Because the total energy of IrFe₃N is only slightly higher (that is, by +3 kJ mol⁻¹) than the sum of its educts, a possibly stable high-pressure phase must also be considered. Therefore, the total-energy calculations for IrFe₃N and all competing phases were repeated but using cell volumes that were allowed to vary around their equilibrium volumes. In addition, the already synthesized intermetallic compound FeIr₃[²⁷] (ReO₃ type) was considered as a competing phase; other competing compounds might be given by binary nitrides of iridium but no such compound has been reported to date, and theoretical investigations[²⁸] predict them to be unstable. The resulting energy–volume diagram is presented in the left part of Figure 3 (top). For a more convenient visualization of the transition pressures, the energy–volume diagram is converted into a free enthalpy–pressure diagram (Figure 3, top right). It is customary to replace the free enthalpy difference ΔG by an enthalpy difference ΔH because of the often minute entropy differences between solid-state materials. The pressure p is extracted from the energy–volume diagram by a simple numerical differentiation of a Murnaghan fit to this data, namely $p = -\partial E/\partial V$. The enthalpy H can be calculated by $H = E + pV$. The final enthalpy–pressure diagram is shown in the right part of Figure 3 (top).

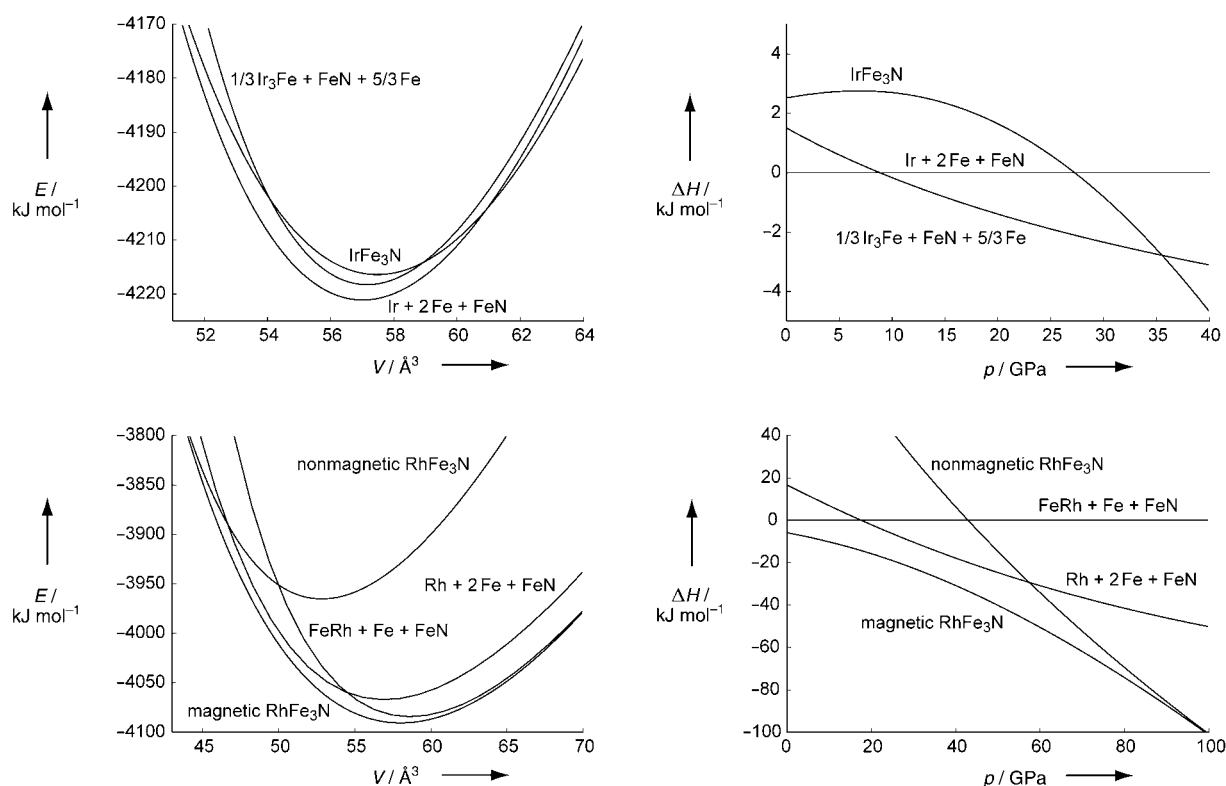


Figure 3. Energy–volume (left) and enthalpy–pressure diagram (right) for IrFe₃N (top) and RhFe₃N (bottom) and their respective competing phases.

At zero pressure, a mechanical mixture of the elemental Ir/Fe plus the binary phase FeN is the thermodynamically stable configuration; this is clear from both the energy–volume and enthalpy–pressure diagrams. At pressures above 9 GPa, the intermetallic compound FeIr₃ becomes enthalpically favorable and wins over Ir/Fe/FeN; at even higher pressures beyond 37 GPa, however, IrFe₃N turns out to be the thermodynamically stable phase. Because the energy–volume diagram of IrFe₃N shows a larger volume (as well as its higher energy) than those of the other two chemical alternatives, the existence of a transition pressure towards IrFe₃N requires a higher compressibility for this compound. Indeed, the calculated bulk modulus B_0 of IrFe₃N is only 204 GPa, which is smaller than the corresponding values of Fe (235 GPa), FeN (264 GPa), and Ir (326 GPa). Thus, IrFe₃N should be accessible for pressures higher than 37 GPa.

The energy minimization of RhFe₃N arrives at an equilibrium lattice parameter of 3.87 Å which is 1.4 % larger than the theoretical value for Fe₄N. The RhFe₃N saturation magnetization is predicted as 9.2 μ_B per formula unit, with local moments of 0.96 and 2.76 μ_B for Rh and Fe; the very large moment for Fe mirrors the increased lattice parameter. As mentioned before, RhFe₃N is more stable (by -23 kJ mol^{-1}) than its competitors FeN/Fe/Rh. To arrive at a full picture, energy–volume and enthalpy–pressure diagrams were generated for all the compounds as in the preceding case; these diagrams are shown in Figure 3 (bottom). In these plots, another competing phase was also included, namely the known ferromagnetic intermetallic compound FeRh^[29] (CsCl type); no binary Rh nitride seems to be stable.^[28] For illustrative purposes, a hypothetically nonmagnetic (that is, without any spin moments) RhFe₃N is also depicted in Figure 3 (bottom).

At zero pressure, the binary compound FeRh is slightly lower in enthalpy than Fe and Rh; nonetheless, magnetic RhFe₃N is still the most stable phase (by -7 kJ mol^{-1}) in this system. Owing to the larger equilibrium volume of FeRh, its enthalpy increases faster upon applying pressure than for the mechanical mixture Fe/Rh; therefore, above 18 GPa the composition Fe/Rh/FeN is already favored over Fe/FeRh/FeN. Nonetheless, the ferromagnetic, perovskite-like RhFe₃N is the stable phase over the entire range of pressures between 0 and 100 GPa. An important stabilizing factor of RhFe₃N is the onset of ferromagnetism (spin polarization) since the hypothetically nonmagnetic phase is less stable by $+122 \text{ kJ mol}^{-1}$. For very small volumes (below 45 Å^3), ferromagnetic and nonmagnetic RhFe₃N energetically coincide such that, by applying enormous pressures (above 100 GPa), the ferromagnetism can be mechanically quenched.

As has been alluded to already, the local magnetic moments reflect the expansion/compression of the lattices, a typical phenomenon observed in ferromagnetic compounds. The stronger the exchange splitting, the more effective is the shielding of the minority (β) spins by the majority (α) spins.^[30] Because the more diffuse β electrons are mainly responsible for the chemical bonding, the interatomic distances will increase for a better overlap.^[31] In other words, the continuous loss of magnetization upon applying pressure results from the suppressed exchange splitting by constraining the more diffuse β spins and the more localized α spins to the same spatial region. This effect is also the reason why the magnetic moments of the ³Fe atoms decrease in the order RhFe₃N > IrFe₃N > Fe₄N, a series that mirrors the shortening of the Fe–Fe separations.

A direct insight into the chemical bonding of RhFe₃N is presented in Figure 4 from DOS and COHP analyses: Within the non-spin-polarized calculation (top), a high DOS is found

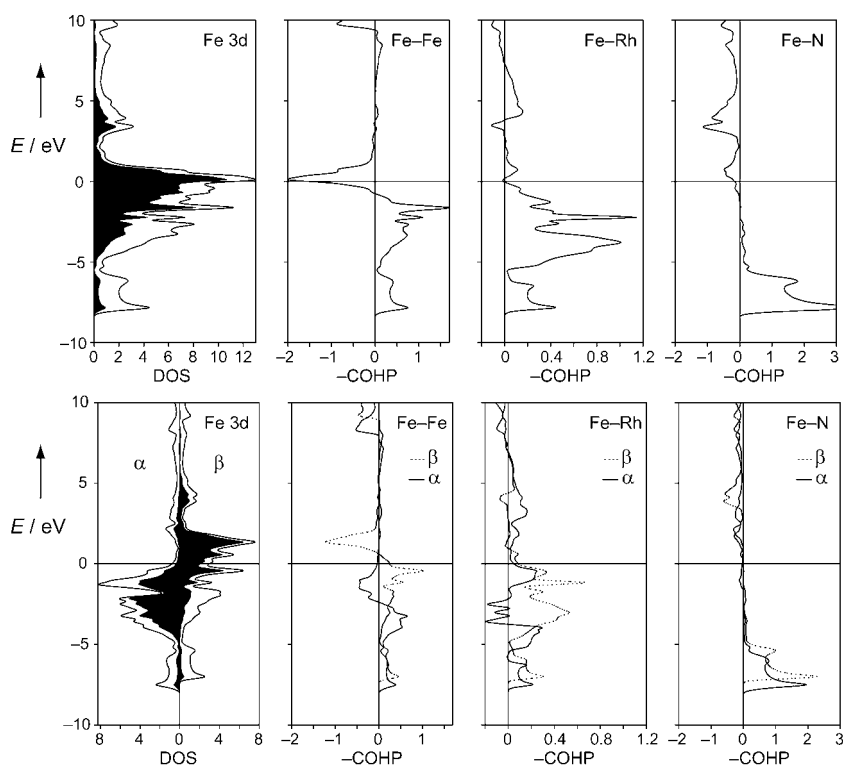


Figure 4. Total and local (Fe 3d) density-of-states (DOS) as well as crystal orbital Hamiltonian population (COHP) analysis for RhFe₃N on the basis of a non-spin-polarized (top) and a spin-polarized (bottom) GGA calculation.

at the Fermi level (horizontal line), mostly arising from Fe 3d contributions, a clear sign of electronic instability. Its source—very strong antibonding interactions in the highest occupied bands—is directly visible from the Fe–Fe COHP curves. In contrast, the Fe–Rh combination only reflects bonding interactions, as does the Fe–N combination (with the exception of tiny antibonding contributions at the Fermi level). The onset of spin polarization (bottom) leads to drastic changes. The DOS at the Fermi level shrinks significantly

because of the exchange splitting, moving the α spins to lower energies and the β spins to higher energies; however, the material stays metallic. While the bonding interactions for the Fe–N and also Fe–Rh combinations are not very much affected (the integrated COHP values stay almost the same), the antibonding Fe–Fe interactions at the Fermi level have been removed, thereby improving Fe–Fe bonding and stabilizing the ferromagnetic ground state of RhFe_3N .

Summarizing, electronic-structure calculations from first principles have been performed to investigate the structural stabilities of perovskite-like MFe_3N compounds of the iron- and platinum-group metals, derivatives of Fe_4N . There is a clear tendency, especially for the larger metal atoms M, to replace the corner Fe atom (1a position), and this effect is considered to be largely of geometrical and not of electronic origin. For all the compounds, a ferromagnetic ground state is found, and the saturation moments are slightly smaller than that of Fe_4N . Upon replacing the corner Fe atom by a larger M atom, the enlarged lattice parameter induces a higher moment for the remaining Fe atoms but this can not fully compensate the loss of the corner Fe atom in terms of magnetism. The ferromagnetic ground state results from an optimized bonding resulting from the removal of formerly Fe–Fe antibonding states at the Fermi level. Total-energy calculations reveal two unknown phases as worthwhile synthetic goals. While ferromagnetic RhFe_3N is an exothermic compound at ambient pressure and remains ferromagnetic up to 100 GPa, IrFe_3N may also be synthesized as a ferromagnetic material but only at pressures above 37 GPa.

Experimental Section

Theoretical Methods: The first-principles electronic-structure calculations of density-functional type were performed using the Vienna ab initio simulation package,^[32,33] plane-wave basis sets and ultrasoft pseudopotentials. The exchange-correlation energy was treated in the generalized gradient approximation (GGA).^[24] The plane-wave cut-off energies were chosen to be 500 eV. The Brillouin zone integrations were performed using the scheme of Monkhorst and Pack.^[34] Optimized structural models were obtained by relaxing all forces to values below $10^{-3} \text{ eV } \text{\AA}^{-1}$ and stresses below 1 kbar. To examine the structural behavior at high pressures, all total energies were recalculated under compression and expansion, and the lattice parameters were scaled in steps of 1% from 91–106% of the minimum geometries. Statistically disordered compounds were investigated by setting up a $3 \times 2 \times 2$ enlarged supercell containing 48 sites for metal atoms and 12 nitrogen atoms; the 12 M atoms were randomly placed on the 48 positions. The energy differences between differing configurations turned out to be very small, on the order of 1 kJ mol^{-1} or less. In addition, calculations based on the all-electron scalar-relativistic Linear Muffin–Tin Orbital (LMTO) theory^[35] in its tight-binding representation^[36] were undertaken using the TB-LMTO-ASA 4.7 program.^[37] A $20 \times 20 \times 20$ k mesh was used for the LMTO calculations. The chemical bonding situations were analyzed using the crystal orbital Hamilton population (COHP) technique.^[38]

Received: October 8, 2004

Published online: January 5, 2005

Keywords: density-functional calculations · ferromagnetism · nitrides · platinum-group metals

- [1] G. W. Wiener, J. A. Berger, *J. Met.* **1955**, 7, 360.
- [2] S. K. Chen, S. Jin, T. H. Tiefel, Y. F. Hsieh, E. M. Gyorgy, D. W. Johnson, Jr., *J. Appl. Phys.* **1991**, 70, 6247.
- [3] H. Jacobs, D. Rechenbach, U. Zachwieja, *J. Alloys Compd.* **1995**, 227, 10.
- [4] S. Matar, P. Mohn, G. Demazeau, B. Siberchicot, *J. Phys. (Paris)* **1988**, 49, 1761.
- [5] C. A. Kuhnen, R. S. de Figueiredo, V. Drago, E. Z. da Silva, *J. Magn. Magn. Mater.* **1992**, 111, 95.
- [6] C. Guillard, H. Creveaux, C. R. Hebd. *Seances Acad. Sci.* **1946**, 222, 1170.
- [7] G. W. Wiener, J. A. Berger, *Ann. Chim.* **1983**, 8, 533.
- [8] B. Siberchicot, S. F. Matar, L. Fournès, G. Demazeau, P. Hagenmüller, *J. Solid State Chem.* **1990**, 84, 10.
- [9] D. Andriamandroso, S. Matar, G. Demazeau, L. Fournès, *IEEE Trans. Magn.* **1993**, 29, 2.
- [10] S. Matar, L. Fournès, S. Chérubin-Jeanette, G. Demazeau, *Eur. J. Solid State Inorg. Chem.* **1993**, 30, 871.
- [11] R. S. de Figueiredo, J. Foct, *J. Magn. Magn. Mater.* **1997**, 173, 141.
- [12] C. A. Kuhnen, R. S. de Figueiredo, A. V. dos Santos, *J. Magn. Magn. Mater.* **2000**, 219, 58.
- [13] H. H. Stadelmaier, A. C. Fraker, *Trans. Metall. Soc. AIME* **1960**, 218, 571.
- [14] P. Mohn, K. Schwarz, S. Matar, G. Demazeau, *Phys. Rev. B* **1992**, 45, 4000.
- [15] C. A. Kuhnen, A. V. dos Santos, *J. Magn. Magn. Mater.* **1994**, 130, 353.
- [16] C. A. Kuhnen, A. V. dos Santos, *J. Alloys Compd.* **2000**, 297, 68.
- [17] S. Matar, P. Mohn, J. Kübler, *J. Magn. Magn. Mater.* **1992**, 104, 1927.
- [18] R. S. de Figueiredo, C. A. Kuhnen, A. V. dos Santos, *J. Magn. Magn. Mater.* **1997**, 173, 141.
- [19] C. A. Kuhnen, R. S. de Figueiredo, A. V. dos Santos, *J. Magn. Magn. Mater.* **2000**, 219, 58.
- [20] R. S. de Figueiredo, J. Foct, A. V. dos Santos, C. A. Kuhnen, *J. Alloys Compd.* **2001**, 315, 42.
- [21] A. V. dos Santos, C. A. Kuhnen, *J. Alloys Compd.* **2001**, 321, 60.
- [22] C. Paduani, *J. Magn. Magn. Mater.* **2004**, 278, 231.
- [23] C. Cordier-Robert, J. Foct, *Eur. J. Solid State Inorg. Chem.* **1992**, 29, 39.
- [24] J. P. Perdew in *Electronic Structure of Solids '91* (Eds.: P. Ziesche, H. Eschrig), Akademie Verlag, Berlin, **1991**, p. 11.
- [25] In general, enthalpy differences ΔH at zero pressure can be expressed as differences between calculated total electronic energies ΔE ; for absolute-zero temperature, ΔE also equals ΔG . If gaseous species are not involved, the approximate close correspondence between ΔE and ΔG holds for finite temperatures, too.
- [26] F. Tessier, A. Navrotsky, R. Niewa, A. Leineweber, H. Jacobs, S. Kikkawa, M. Takahashi, F. Kanamaru, F. J. DiSalvo, *Solid State Sci.* **2000**, 2, 457.
- [27] Z. Yu, *Acta Geol. Sin. (Engl. Transl.)* **1996**, 9, 27.
- [28] J. von Appen, R. Dronskowski, unpublished results.
- [29] L. Zsoltos, *Phys. Status Solidi A* **1967**, 20, K25.
- [30] G. A. Landrum, R. Dronskowski, *Angew. Chem.* **1999**, 111, 1481; *Angew. Chem. Int. Ed.* **1999**, 38, 1389; G. A. Landrum, R. Dronskowski, *Angew. Chem.* **2000**, 112, 1598; *Angew. Chem. Int. Ed.* **2000**, 39, 1560.
- [31] R. Dronskowski, *Adv. Solid State Phys.* **2002**, 42, 433.
- [32] G. Kresse, J. Hafner, *Phys. Rev. B* **1993**, 47, 558; G. Kresse, J. Hafner, *Phys. Rev. B* **1994**, 49, 14251.
- [33] G. Kresse, J. Furthmüller, *Comput. Mater. Sci.* **1996**, 6, 15; G. Kresse, J. Furthmüller, *Phys. Rev. B* **1996**, 55, 11169.
- [34] H. J. Monkhorst, J. D. Pack, *Phys. Rev. B* **1976**, 13, 5188.
- [35] O. K. Andersen, *Phys. Rev. B* **1975**, 12, 3060; H. Skriver, *The LMTO Method*, Springer, Berlin, **1984**; O. K. Andersen, *The*

Electronic Structure of Complex Systems (Eds.: P. Phariseau, W. M. Temmerman), Plenum, New York, **1984**.

[36] O. K. Andersen, O. Jepsen, *Phys. Rev. Lett.* **1984**, 53, 2571.

[37] G. Krier, O. Jepsen, A. Burkhardt, O. K. Andersen, The TB-LMTO-ASA program, version 4.7, Max-Planck-Institut für Festkörperforschung, Stuttgart, Germany.

[38] R. Dronskowski, P. E. Blöchl, *J. Phys. Chem.* **1993**, 97, 8617.

Direct Organocatalytic De Novo Synthesis of Carbohydrates**

Dieter Enders* and Christoph Grondal

Dedicated to Professor Wilhelm Keim
on the occasion of his 70th birthday

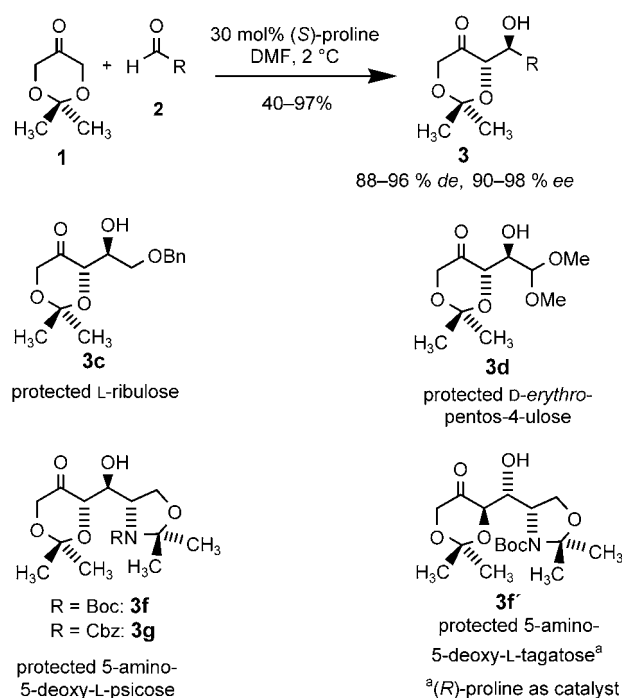
Carbohydrates are a class of natural products of great importance in chemical, biological, and medicinal research.^[1] Carbohydrates play a key role in many biological processes, for example, as components of glycoproteins, nucleic acids, glycolipids, peptido- and proteoglycans, and liposaccharides.^[2] They are both target molecules in modern organic synthesis and sources of enantiopure building blocks (chiron approach)^[3] and chiral auxiliaries.^[4] An extensive arsenal of methods for the de novo synthesis of carbohydrates is already available, but typically several synthetic steps and extensive protecting group manipulations are necessary.^[5] Recently, MacMillan et al. disclosed a “two-step” synthesis of aldohexoses based on an asymmetric proline-catalyzed aldol reaction.^[6] Nature also employs a stereoselective aldol reaction in the biosynthesis of carbohydrates; the carbohydrate skeleton is assembled by means of an enzyme-catalyzed aldol reaction of dihydroxyacetone phosphate (DHAP).^[7]

The application of DHAP in carbohydrate synthesis has been investigated quite intensively with biological methods in particular,^[8] but also chemical methods could be employed successfully with DHA and its derivatives as C₃ building blocks in asymmetric synthesis.^[9] A new challenge concerning syntheses with DHA as a C₃ building block is the development of organocatalytic methods. Barbas III et al. described a direct aldol reaction of DHA with different aldehydes, in which proline and various proline derivatives were used as

catalysts. While in part good diastereoselectivities were reached, the products turned out to be racemic in all cases.^[10]

We now report on the successful development of the first diastereo- and enantioselective organocatalytic aldol reaction with 2,2-dimethyl-1,3-dioxan-5-one (**1**, dioxanone)^[11] as a DHA equivalent and methylene component. When suitable aldehyde carbonyl components are employed, this biomimetic C₃+C_n strategy facilitates the direct assembly of selectively protected ketoses in one step.

For our first example we chose 2-methylpropanal (**2a**) as a model system for the aldol reaction with dioxanone and optimized the reaction conditions in terms of chemical yield, enantiomeric excess, and *anti/syn* ratio. The best reaction conditions so far call for (*S*)-proline as the catalyst, DMF as the solvent, and a temperature of 2 °C. The *anti* aldol product **3a** was obtained diastereoselectively with an excellent yield of 97 %, an *anti/syn* ratio of > 98:2, and a high enantiomeric excess of 94 % *ee*. Subsequently we were also able to show that the aldol reaction of **1** with the α -branched aldehydes **2a**, **b**, **d–g** proceeds with good to very good yields, excellent *anti/syn* ratios, and enantiomeric excesses in all cases (Scheme 1,



Scheme 1. (*S*)- and (*R*)-proline-catalyzed asymmetric aldol reaction of dioxanone with various aldehydes.

Table 1). When the linear aldehyde **2c** was employed, the aldol product **3c** was isolated in only moderate yield (40 %), but still excellent stereoselectivity (*anti/syn* = > 98:2, 97 % *ee*). The lower yield may be explained by the fact that linear aldehydes also undergo self-aldol condensation, which is in direct competition with the crossed-aldol reaction. The use of aromatic aldehydes as the carbonyl component reduced the diastereoselectivity. For example, the (*S*)-proline-catalyzed aldol reaction of **1** with *ortho*-chlorobenzaldehyde proceeded with a good yield of 73 % but with an *anti/syn*

[*] Prof. Dr. D. Enders, Dipl.-Chem. C. Grondal
Institut für Organische Chemie
RWTH Aachen
Professor-Pirlet-Strasse 1, 52074 Aachen (Germany)
Fax: (+49) 241-809-2127
E-mail: enders@rwth-aachen.de

[**] This work was supported by the Fonds der Chemischen Industrie (Kekulé fellowship for C.G.). We thank the companies Degussa AG, BASF AG, and Bayer AG for the donation of chemicals.

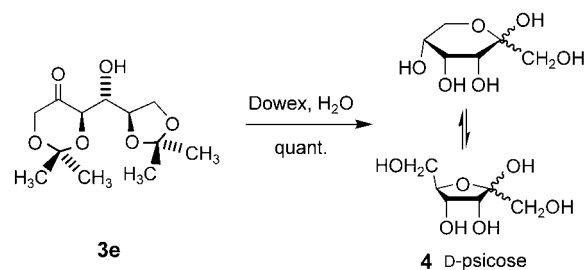
Table 1: (*S*)-proline-catalyzed asymmetric aldol reaction of dioxanone **1** with aldehydes **2** to form the aldol products **3** (see Scheme 1).^[a]

3	R	Yield [%] ^[b]	<i>anti/syn</i> [%] ^[c]	<i>ee</i> [%] ^[d]
a	CH(CH ₃) ₂	97	> 98:2	94
b	Cy ^[i]	86	> 98:2	90
c	CH ₂ OBn ^[i]	40	> 98:2	97
d	CH(OCH ₃) ₂	69	94:6	93
e		76	> 98:2	≥ 98 ^[e,f]
f		80	> 98:2	≥ 96 ^[g]
f'		31	> 98:2	≥ 96 ^[e,g]
g		80	> 98:2	≥ 96 ^[h]

[a] General reaction conditions: 2.3 mmol dioxanone, 2.3 mmol aldehyde, 30 mol % (*S*)-proline, 1.2 mL DMF, 2 °C, 6 d. [b] Yields of **3** isolated after flash chromatography on silica gel. [c] Determined by ¹H and ¹³C NMR spectroscopy. [d] Determined by HPLC on chiral stationary phases (Chiralpak AD, Chiralpak IA 5μ, Daicel IA, Daicel OJ, Whelk O1). [e] (*R*)-proline was used as the catalyst. [f] Based on the *ee* value of **2e**. [g] Based on the *ee* value of **2f**. [h] Based on the *ee* value of **2g**. [i] Abbreviations: Bn = benzyl, Boc = tert-butyloxycarbonyl, Cbz = benzyl-oxycarbonyl, Cy = cyclohexyl.

ratio of only 4:1 and enantiomeric excesses of 86 % *ee* (*anti*) and 70 % *ee* (*syn*). The aldol products **3** accessible directly by organocatalysis are selectively and partly orthogonal doubly protected sugars and amino sugars, for example, L-ribose (**3c**), D-erythro-pentos-4-ulose (**3d**), 5-amino-5-deoxy-L-psicose (**3f, g**), and 5-amino-5-deoxy-L-tagatose (**3f'**). In the case of **3d**, the stereoselective ketose reduction followed by acetal hydrolysis should lead to an aldose ("inversion strategy"),^[12] which will greatly expand the potential of this new protocol.

When we used the *S*-configured, enantiomerically pure NBoc- (**2f**) and NCbz-protected Garner aldehydes (**2g**), (*S*)-proline proved to be the appropriate catalyst, since high chemical yields (80 %), excellent *anti/syn* ratios (> 98:2), and high *ee* values (96 % *ee*) were obtained for the corresponding aldol products **3f** and **3g**. As expected, (*R*)-proline was not the appropriate catalyst for this aldol reaction because it led to a significant decrease in yield (31 %) although the diastereoselectivity remained high (for **3f'**). Consequently, (*R*)-proline was the appropriate catalyst for the reaction of α-branched *R*-configured aldehydes. This could be confirmed by the aldol reaction of **1** with the *R*-configured 2,3-*O*-(isopropylidene)-D-glyceraldehyde (**2e**).^[13] The double acetonide-protected D-psicose **3e**,^[14] which was obtained with 76 % yield in this way, was quantitatively deprotected with an acidic ion-exchange resin (Dowex W50X2-200) to give the parent D-psicose (**4**, Scheme 2). The identity of the ketohexose could be proven unambiguously by spectroscopic comparison (¹H and ¹³C NMR, HPLC, and optical rotation data) with an authentic, commercially available sample.



Scheme 2. Deprotection of **3e** to give D-psicose (**4**) (mixture of the four isomers α,β-D-psicofuranose and α,β-D-psicopyranose).

The formation of the *anti* aldol products **3** and the absolute configurations given are consistent with related proline-catalyzed aldol reactions.^[15] The absolute configurations were also confirmed by polarimetric comparison with independently synthesized aldol products.^[16] The observed relative topicity can be explained by the Houk–List model for proline-catalyzed aldol reactions with cyclic ketones, where an enamine intermediate and an intermolecular hydrogen bond play the decisive role (Figure 1).^[17]

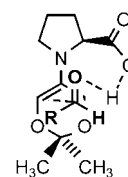
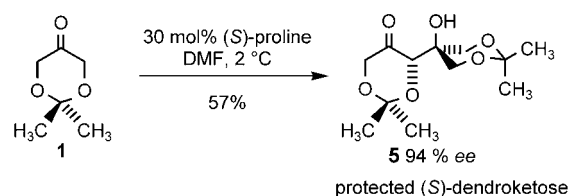


Figure 1. Postulated transition state (Houk–List model) for the (*S*)-proline-catalyzed one-step de novo synthesis of simple sugars and derivatives.

Further investigations revealed that under proline catalysis compound **1** underwent self-aldol condensation to give the adduct **5**, which represents a direct precursor of (*S*)-dendroketo (Scheme 3).^[18] The aldol addition proceeded with high enantioselectivity (94 % *ee*) and a moderate yield of 57 %. This observation shows that in principle ketones can act as carbonyl components under formation of quaternary stereogenic centers. It is unnecessary to point out that a simple change of (*S*)- to (*R*)-proline as catalyst leads to the opposite absolute configurations at the aldol C₃/C₄ centers (here (*R*)-dendroketo, see also **3e** and **3f'**).



Scheme 3. (*S*)-proline-catalyzed asymmetric self-aldol condensation of dioxanone **1** to give the double acetonide-protected (*S*)-dendroketo **5**.

In conclusion, our asymmetric, (*S*)-proline-catalyzed aldol reaction of the DHA equivalent **1** with various aldehydes generates the same relative and absolute configuration as the enzyme tagatose aldolase (TagA). Whereas the TagA catalyzed aldol reaction proceeds unselectively,^[19] our organocatalytic approach offers a viable alternative. As shown with the asymmetric synthesis of the rare ketosugar D-psicose (**4**) and related simple sugars and amino sugars, this new protocol

opens an impressively simple, biomimetic direct approach to selectively and differently protected simple carbohydrates and related compounds in practically one step. At present, we are optimizing and extending this procedure by varying the methylene and carbonyl components as well as the organo-catalyst.

Experimental Section

Unless otherwise stated, all chemicals are commercially available and were used without further purification. All new compounds were fully characterized (IR, NMR, MS, elemental analysis, optical rotation).

3e: Compound **1** (1.0 g, 7.69 mmol) was dissolved in dimethylformamide (4 mL) in a 10-mL round-bottomed flask, and (*R*)-proline (266 mg, 2.31 mmol) was added with stirring. The suspension was stirred for 30 min after which freshly prepared **2e** (1.0 g, 7.69 mmol) was added. The flask was evacuated, flushed with argon and stored at 2°C for 6 d. The suspension was quenched with sat. aq. ammonium chloride solution (2 mL) and extracted with ethyl acetate (3 × 5 mL). The combined organic layers were concentrated and purified by flash column chromatography using silica gel (diethyl ether/pentane, 2:1). Product **3e** (1.52 g, 76%) was obtained as a colorless oil. $[\alpha]_D^{24} = 126.8$ (*c* = 1.02 in CHCl₃); IR (CHCl₃): $\tilde{\nu}$ = 3461 (s), 3133 (s), 2988 (m), 2939 (m), 1747 (s), 1378 (s), 1224 (s), 1157 (m), 1069 (s), 990 (w), 948 (w), 889 (m), 853 (s), 758 cm⁻¹ (s); ¹H NMR (400 MHz, CDCl₃): δ = 1.33 (s, 3H, CCH₃), 1.37 (s, 3H, CCH₃), 1.47 (s, 6H, C(CH₃)₂), 2.96 (s, 1H, OH), 3.98–4.09 (m, 4H), 4.27–4.34 (m, 2H), 4.45 ppm (dd, *J* = 3.3 Hz, *J* = 1.3 Hz, 1H, CH); ¹³C NMR (125 MHz, CDCl₃): δ = 23.2 (CH₃), 24.5 (CH₃), 25.2 (CH₃), 26.3 (CH₃), 66.1 (CH₂), 66.7 (CH₂), 71.9 (CH), 74.9 (CH), 76.1 (CH), 100.5 (C(CH₃)₂), 109.2 (C(CH₃)₂), 206.9 ppm (CO); MS (CI, isobutane): *m/z* (%): 261 (1) [*M*⁺ + 1], 245 (82) [*M*⁺ – CH₃], 202 (15) [*M*⁺ – CO(CH₃)₂], 187 (41) [C₈H₁₁O₅⁺], 131 (32) [C₆H₁₁O₃⁺], 101 (100) [C₄H₅O₃⁺], 72 (14) [C₃H₄O₂⁺], 59 (50) [C₃H₇O⁺]; elemental analysis calcd for C₁₂H₂₀O₆ (%): C 55.37, H 7.74; found: C 55.02, H 7.73.

4: The aldol product **3e** (520 mg, 2 mmol) was stirred with 10 mL deionized water in a 10-mL round-bottomed flask, and Dowex W50X2-200 ion-exchange resin (350 mg) was added. After complete conversion (followed by TLC) the ion-exchange resin was removed by filtration over glass wool, and the aqueous solution was lyophilized, affording D-psicose (**4**) (360 mg, 100%). If necessary, D-psicose was purified using silica gel (ethyl acetate/methanol, 6:1). $[\alpha]_D^{24} = +3.02$ (*c* = 1.16 in H₂O); Lit.: $[\alpha]_D^{20} = +3.1$ (*c* = 1.62 in H₂O);^[20] ¹H NMR (400 MHz, D₂O) mixture of α,β -D-psicofuranose and α,β -D-psicopyranose: δ = 3.31 (d, *J* = 11.8 Hz), 3.43–3.71 (m), 3.81–3.95 (m), 4.07 (m), 4.20 ppm (dd, *J* = 7.7 Hz, *J* = 4.7 Hz); ¹³C NMR (125 MHz, D₂O): δ = 60.0 (CHOH), 61.4 (CHOH), 62.4 (CHOH), 62.9 (CH₂), 63.1 (CHOH), 63.3 (CH₂), 64.0 (CHOH), 64.2 (CHOH), 65.1 (CHOH), 65.5 (CH₂), 65.9 (CHOH), 69.0 (CH₂), 70.2 (CH₂), 70.3 (CH₂), 71.0 (CHOH), 71.7 (CHOH), 74.7 (CHOH), 82.7 (CHOH; CH₂), 97.6 (C(OH)OCH₂), 98.4 (C(OH)OCH₂), 103.2 (C(OH)OCH₂), 105.6 ppm (C(OH)OCH₂).

Received: October 26, 2004

Published online: January 14, 2005

Keywords: aldol reaction · amino sugars · asymmetric synthesis · carbohydrates · organocatalysis

- [1] a) K. C. Nicolaou, H. J. Mitchell, *Angew. Chem.* **2001**, *113*, 1625–1672, *Angew. Chem. Int. Ed.* **2001**, *40*, 1576–1624; b) *Carbohydrates Mimics* (Ed.: Y. Chapleur), Wiley-VCH, Weinheim, **1998**.
- [2] a) M. Sznajdman in *Bioorganic Chemistry: Carbohydrates* (Ed.: S. M. Hecht), Oxford University Press, New York, **1999**, pp. 1–

- 56; b) K. M. Koeller, C.-H. Wong, *Chem. Rev.* **2000**, *100*, 4465–4493; c) A. Varki, *Glycobiology* **1993**, *3*, 97–130.
- [3] S. Hanessian, *Total Synthesis of Natural Products: The “Chiron” Approach*, Pergamon, Oxford, **1983**.
- [4] H. Kunz, K. Rück, *Angew. Chem.* **1993**, *105*, 355–377; *Angew. Chem. Int. Ed. Engl.* **1993**, *32*, 336–358.
- [5] a) T. Ogawa, *Chem. Soc. Rev.* **1994**, *23*, 397–407; b) S. J. Danishefsky, M. T. Bilodeau, *Angew. Chem.* **1996**, *108*, 1482–1522; *Angew. Chem. Int. Ed. Engl.* **1996**, *35*, 1380–1520; c) S. Hanessian, *Preparative Carbohydrate Chemistry*, Marcel Dekker, New York, **1997**; d) T. Hudlicky, D. A. Entwistle, K. K. Pitzer, A. J. Thorpe, *Chem. Rev.* **1996**, *96*, 1195–1220.
- [6] a) A. B. Northrup, I. K. Mangion, F. Hettche, D. W. C. MacMillan, *Angew. Chem.* **2004**, *116*, 2004–2006; *Angew. Chem. Int. Ed.* **2004**, *43*, 2152–2154; b) A. B. Northrup, D. W. C. MacMillan, *Science* **2004**, *305*, 1752–1755.
- [7] M. Calvin, *Angew. Chem.* **1962**, *74*, 165–175; *Angew. Chem. Int. Ed. Engl.* **1962**, *1*, 65–75.
- [8] a) “Enolates, Organocatalysis, Biocatalysis and Natural Product Synthesis”: W.-D. Fessner in *Modern Aldol Reactions*, Vol. 1 (Ed.: R. Mahrwald), Wiley-VCH, Weinheim, **2004**, 201–272; b) C.-H. Wong, T. D. Machajewski, *Angew. Chem.* **2000**, *112*, 1206–1230; *Angew. Chem. Int. Ed.* **2000**, *39*, 1352–1375; c) W.-D. Fessner, C. Walter, *Top. Curr. Chem.* **1996**, *184*, 97–194; d) S. Takayama, G. J. McGarvey, C.-H. Wong, *Chem. Soc. Rev.* **1997**, *26*, 407–415; e) M. Schürmann, M. Schürmann, G. A. Sprenger, *J. Mol. Catal. B* **2002**, *8*, 19–20, 247–252.
- [9] Review: D. Enders, M. Voith, A. Lenzen, *Angew. Chem.* **2005**, *117*; *Angew. Chem. Int. Ed.* **2005**, *44*, in press.
- [10] a) A. Córdova, W. Notz, C. F. Barbas III, *Chem. Commun.* **2002**, 3024–3025; b) For an efficient proline-catalyzed aldol reaction of hydroxy acetone with aldehydes see: W. Notz, B. List, *J. Am. Chem. Soc.* **2000**, *122*, 7386–7387.
- [11] Dioxanone **1** can be synthesized easily by undergraduate students on a 1-mol scale from simple precursors and is also commercially available. a) D. Enders, M. Voith, S. J. Ince, *Synthesis* **2002**, 1775–1779; b) D. Enders, B. Bockstiegel, *Synthesis* **1989**, 493–496.
- [12] C. W. Borysenko, A. Spaltenstein, J. A. Straub, G. M. Whitesides, *J. Am. Chem. Soc.* **1989**, *111*, 9275–9276.
- [13] Freshly prepared **2e** was used for the aldol reaction due to its tendency for polymerization and racemization.
- [14] M. Majewski, P. Nowak, *J. Org. Chem.* **2000**, *65*, 5152–5160.
- [15] a) B. List, *Acc. Chem. Res.* **2004**, *37*, 548–557; b) B. List, L. Hoang, H. J. Martin, *Proc. Natl. Acad. Sci. USA* **2004**, *101*, 5839–5842; c) “Enolates, Organocatalysis, Biocatalysis and Natural Product Synthesis”: B. List in *Modern Aldol Reactions*, Vol. 1 (Ed.: R. Mahrwald), Wiley-VCH, Weinheim, **2004**, 161–200.
- [16] a) D. Enders, O. Prokopenko, G. Raabe, J. Runsink, *Synthesis* **1996**, 1095–1100; b) D. Enders, S. J. Ince, *Synthesis* **2002**, 619–624.
- [17] a) S. Bahmanyar, K. N. Houk, H. J. Martin, B. List, *J. Am. Chem. Soc.* **2003**, *125*, 2475–2479; L. Hoang, S. Bahmanyar, K. N. Houk, B. List, *J. Am. Chem. Soc.* **2003**, *125*, 16–17; c) S. Bahmanyar, K. N. Houk, *J. Am. Chem. Soc.* **2001**, *123*, 12911–12912.
- [18] H. C. Jarrell, W. A. Szarek, J. K. N. Jones, A. Dmytraczenko, E. B. Rathbone, *Carbohydr. Res.* **1975**, *45*, 151–159; b) W. A. Szarek, G. W. Schnarr, H. C. Jarrell, J. K. N. Jones, *Carbohydr. Res.* **1977**, *53*, 101–108.
- [19] a) W.-D. Fessner, O. Eyrish, *Angew. Chem.* **1992**, *104*, 76–78; *Angew. Chem. Int. Ed. Engl.* **1992**, *31*, 56–58; b) O. Eyrish, G. Sinerius, W.-D. Fessner, *Carbohydr. Res.* **1993**, *238*, 287–306; c) E. Garcia-Junceda, G. J. Shen, T. Sugai, C.-H. Wong, *Bioorg. Med. Chem.* **1995**, *3*, 945–953.
- [20] M. Steiger, T. Reichstein, *Helv. Chim. Acta* **1936**, *19*, 184–189.

Simulating the Dissolution and Growth of Zeolite Beta C**

May E. Chiu, Ben Slater,* and Julian D. Gale

Understanding how zeolites form on the atomic scale, under natural or laboratory conditions, remains a fundamental challenge to both experiment and theory. One goal of these studies is to control and manipulate the mechanism and rate of formation to produce tailored nanoporous materials whose unique framework architectures and voids provide channels or cages with exceptional reactive environments and sieving capabilities.^[1] One of the most enduring questions, despite many decades of very active research, concerns the role of primary building units (PBUs, that is, silicate monomers) and secondary building units (SBUs, that is, polymeric or oligomeric silicates) in the crystal-growth mechanism. For example, whereas NMR spectroscopy has been used extensively to identify units present in the mother liquor, the precise configurations, charge state, proportion of monomers to dimers and higher oligomers, and the role of these units within crystal growth remain controversial subjects.^[2–4] There is a clear need to determine the extent to which primary and secondary building units influence the mechanism and rate of growth, and the focus of the work described herein is to investigate layer assembly by monomers through atomistic computer-simulation techniques. We now relate how the dissolution and growth processes can be studied simultaneously and consider the implications of our results for monomer-mediated and monomer-with-oligomer growth.

Our model system to investigate growth and dissolution is zeolite beta C, a recently synthesized^[5] member of the zeolite beta family, first predicted by Treacy, Newsam, and co-workers,^[6] which exhibits a 3D interpenetrating 12-membered ring (MR) network. In previous work^[7] we examined the surface structure of the (100) face of zeolite beta C to rationalize observations from HREM measurement. Figure 1 shows the framework structure of zeolite beta C; only the

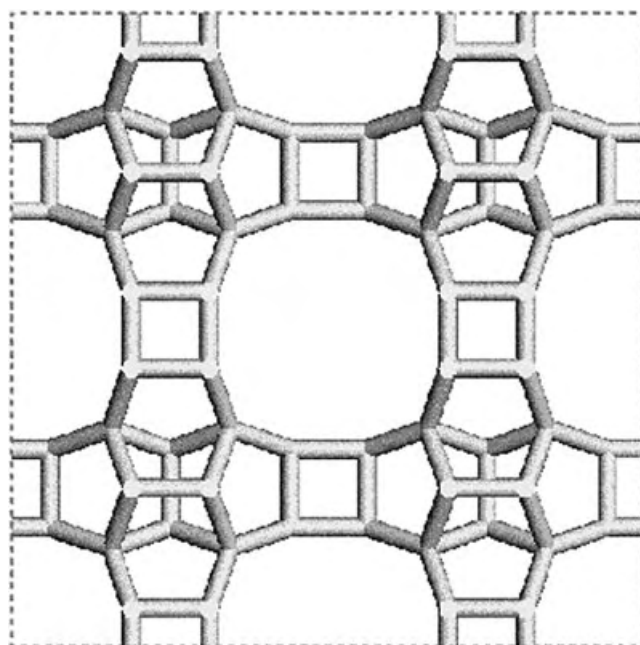


Figure 1. The unit cell and silicon-only framework of zeolite beta C viewed along [100]. Vertices indicate silicon atoms.

silicon atoms are shown, and the central 12-MR channel can be seen clearly in the center of the figure. We previously showed that two terminations imaged with HREM^[7] (Figure 2a, b, and c), could be explained by first-principle results. In particular, the absence of the surface structure (Figure 2e and h), which classical calculations predict to have equal stability to structures shown in Figure 2d and f (and g and i), can be rationalized through the formation of single- and double-4-rings and their subsequent reaction with the crystal surface. These calculations support the view that SBUs can play a part in the assembly of framework materials, but they pertain to a very small component of the growth process. It has been found that characteristic terminations are observed on crystal surfaces that correspond to thermodynamic minima; these surface architectures are long-lived states during the crystal-growth process, and hence intermediary structures are, by implication, relatively short-lived or not extant at any stage of the crystal layer assembly. Herein, we study the intermediate stages of growth and determine whether exotic terminating structures have similar stabilities (thermodynamically accessible) to those observed experimentally. We also assess whether the growth could be mediated by PBUs or SBUs.

Owing to the unit-cell size and density, coupled with the vast number of unique and hypothetical terminating surface structures that can be imagined, we were compelled to use the Born model of solids, which employs shell-model interionic potentials^[8] to model the crystal bulk and surface structure, in order to decrease simulation expense. All calculations were carried out with GULP3.0^[9] code to relax both bulk and surface configurations. Terminating silanol species are represented by two- and three-body potentials.^[10] Additionally, the surface energy is corrected for the presence of a solvent continuum through the newly implemented algorithm

[*] M. E. Chiu
Department of Chemistry, University of Cambridge
Lensfield Road, Cambridge, CB2 1EW (UK)

Dr. B. Slater
The Davy–Faraday Research Laboratory
The Royal Institution of Great Britain
21 Albemarle Street, London, W1S 4BS (UK)
Fax: (+44) 20-729-3569
E-mail: ben@ri.ac.uk

J. D. Gale
Nanochemistry Research Institute
Department of Applied Chemistry
Curtin University of Technology
P.O. Box U1987, Perth 6845 (Australia)

[**] B.S. would like to thank the Nuffield Foundation for providing a student bursary for M.C. J.D.G. acknowledges the support of the Government of Western Australia through a Premier's Research Fellowship.

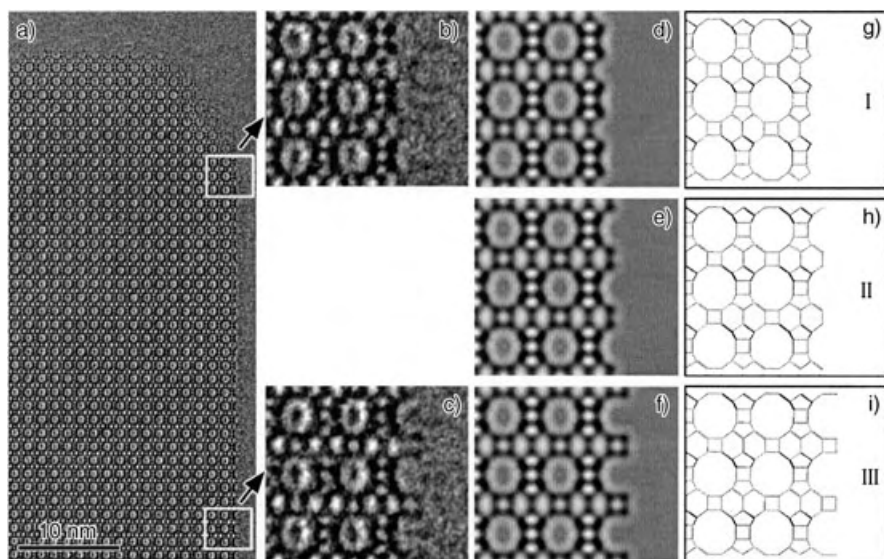


Figure 2. Comparison of high-resolution electron microscopy (HREM) and simulation results taken from Slater et al.^[7] Parts a), b), and c) are HREM images; g), h), and i) are simulation predictions. Parts d), e), and f) are simulated HREM patterns based on structure predictions g), h), and i), respectively.

COSMIC,^[11] which adapts the widely used COSMO^[12] approach for the treatment of 2D periodic surfaces. In this case, the solvation energy is determined based on a single-point calculation taking the dielectric constant of water to be 78.4. To model the crystal surface, a semi-infinite approach is used which is equivalent to the theoretical approach used in previous work.^[7] The model of the crystal surface is constructed with four layers of zeolite beta C, divided into an upper region (containing two layers) that is fully relaxed and a lower region (containing two layers), which is held fixed to represent the long-range potential of the underlying bulk material.

To survey the structures that can be sampled during growth, it is simpler to mimic a dissolution process rather than growth, so that possible geometries are revealed as each unit is removed. The structure shown in Figure 2h is used as the starting point for a hypothetical dissolution reaction. Note that the starting point is not important for structure generation as the purpose of the experiment is to generate “hypothetical” structures. Hence, there is no *deterministic* factor that controls which structures are sampled. A single-crystal-growth layer containing 32 silicon tetrahedra (equivalent to the number of formula units within the unit cell) is removed systematically by “dissolving” one silicon tetrahedron (T site) after another until the original starting configuration is regenerated. At each step, one silicon atom is selected from one of the symmetry-inequivalent surface-accessible sites. (Such sites are those that would be in contact with the solvent. In total, over 130 unique configurations were considered; in some instances, owing to fourfold symmetry equivalence, only one configuration needs to be considered for each step, but in the latter stages of the dissolution/growth model, up to 11 symmetrically distinct silicon atoms are exposed at the surface and hence 11 surface structures are

relaxed.) The accessibility of the surface sites is actually determined crudely with a search radius of 2.5 Å below the uppermost silicon site. Two of the four oxygen atoms bonded to the silicon are then selected and a charge-neutral SiO₂ fragment is displaced to the bottom of the upper (relaxed) layer. The corresponding symmetry-related fragment within the upper layer is displaced to the base of the lower (fixed) layer. This operation guarantees that the number of species within the lower region remains the same throughout the simulation, so that the surface energy and electrostatics are well-behaved. It also ensures that the newly created surface is nonpolar. Herein, we have restricted the study to monomeric units to decrease the configurational permutations to a computable quantity.

It is presumed that under typical hydrothermal synthesis conditions, the coordinatively unsaturated fragment and surface react with water, which heterolytically splits to form proton and hydroxide species that bind to the undercoordinated oxygen and silicon sites, respectively, such that no undercoordinated

sites are exposed on any of the intermediate structures that are generated. A charge-neutral fragment (SiO₂) would be expected to react with water to form dispersed PBUs (SiOH₄), which would be absorbed in a sol-gel layer above the hydroxylated surface. However, this contribution is not explicitly included in the model described herein. Driver software was developed to effect the stepwise displacement of neutral SiO₂ units which also reconstructs and hydroxylates surface structures to generate nonpolar surface terminations. The Helmholtz surface energy^[13] is calculated at each stage to evaluate surface stability. This calculation includes the energy required to dissociate water at the surface, to ensure that the surface energy describes the total work done per unit area in a closed Born–Haber cycle. The latter procedure has been used extensively,^[13, 14] and is described in detail in the report of Parker and co-workers.^[15]

Figure 3a describes the surface energy as a function of the number of T sites removed. Only the lowest-energy configuration is reported, and hence the configurations are notionally indicative of a minimum-energy pathway for dissolution or growth. As the crystal surface is dissolved, the surface becomes more enthalpically unstable until approximately 3/4 of a surface layer is dissolved; thereafter, dissolution is exothermic. The process of dissolution can be interpreted from a converse perspective, reading the graph from right to left, whereby the *growth* by monomer addition is described. The dissolution process is initially endothermic, and thereafter exothermic, which is qualitatively consistent with experimental observations.

The first point on the graph corresponds to the terminating structure given in Figure 2e or 2h. Interpreting the graph from left to right, it can be observed that the surface energy rises slightly for the first two T sites removed, rises sharply as a third site is removed, and finally drops to an energy

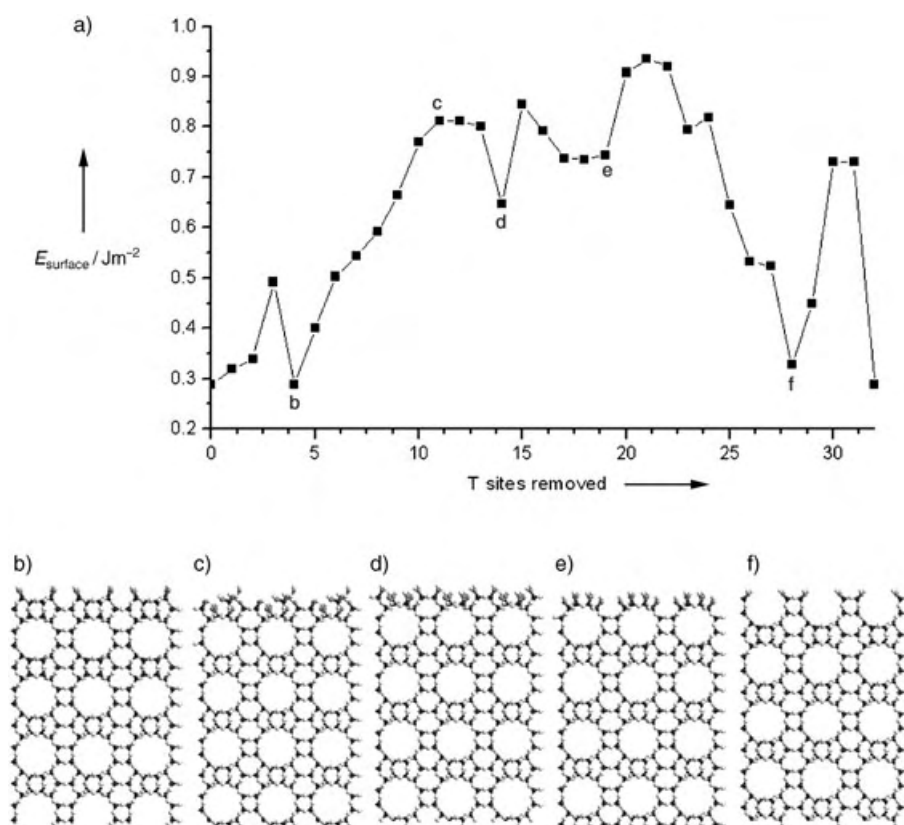


Figure 3. a) Surface energy as a function of the number of T sites removed with selected surface configurations. b)–f) Depictions of selected points along the minimum surface energy pathway, as indicated on the graph in part a). Silicon atoms are shown in black, lattice oxygen atoms in gray, hydrogen in white, and hydroxy oxygen atoms in dark gray. The surface shown is the (100) surface in cross section through the [100] axis. The top of each cross section represents the crystal terminating structure.

comparable with that of the starting structure. This process relates to the stepwise dissolution of a 4-ring expressed at the crystal surface. Removing the first two sites creates silicon sites with geminal hydroxy functions, whilst loss of the third T site creates a very unstable Si site bonded to three hydroxy groups (a trimeric species). Subsequent removal of T sites results in a general monotonic increase in the surface energy, accompanied by a rise in the density of silanol groups per unit area. Steps 11–13 are almost equivalent in energy, as are steps 17–19, suggesting that growth and dissolution occur with similar rates. After step 21, the general trend is for the surface energy to decrease rapidly, accompanied by a release of energy. Figure 3b–f illustrates five structures, selected from different regions of the dissolution process. Figure 3b shows a surface that is equivalent to that observed in HREM (Figure 2). Figure 3c shows a partially dissolved layer that is composed of 4- and 5-rings (common to beta and, for example, Mordenite zeolites) and a high density of intramolecular hydrogen-bonded silanol groups. Figure 3d shows a local minimum in the surface energy, in which the structure has been dissolved further to create a relatively atomically smooth surface. This can be further dissolved, with an energetic penalty, to the state shown in Figure 3e in which

the 12-MR channel system lies directly below the surface, protected by a very thin membrane of siliceous material. When this membrane is dissolved there is a substantial increase in energy, but subsequent dissolution is relatively facile and exothermic. The final structure formed (Figure 3f) is equivalent to that shown in Figure 2c,f, and i, and has an energy almost equivalent to those of the structures observed at steps 0 and 4 of Figure 3a. There are three global minima, and hence this exhaustive survey corroborates earlier assertions that terminations observed by microscopy techniques correspond to surface-energy minima. Notably, the most endothermic steps are those associated with the interruption of channels or cages (such as the 12-MR) or the formation of highly unstable species with three silanol groups bonded to a single silicon site.

By examining the growth process (Figure 3a right to left), it is clear that there is a substantial energetic penalty associated with the formation of a closed 12-MR channel—a process of clathration around the solvent/sol-gel mixture. However, once this barrier is overcome, the general trend is for the surface to become more stable, with

large decreases in surface energy that are associated with formation of closed loops, such as ring systems or channels.

A more detailed display of the energy changes (Figure 4) shows the net change in energy associated with removing (or in a contrary sense, adding) a T site from the surface. The energy changes are calculated *with respect to the previous step* and include corrections for the solvation energy. It is clear that the dissolution consists of mainly endothermic steps that have a maximum absolute energy of ≈ 2.9 eV. Reading the figure from right to left to interpret growth (taking into account that the 31st step is the first step of growth), again it can be seen that maximum endothermic energy change associated with stepwise growth is up to ≈ 2.9 eV. Note that the maxima associated with endothermic changes occur as isolated peaks and are accompanied by satellite exothermic troughs in the surface energy. One interpretation of these data is that these relatively unfavorable steps during growth (or dissolution) could be avoided if cooperative events, such as the dissolution or addition of dimeric (or higher-order oligomeric) species, occurred. The precise mechanism and rate-determining step of growth/dissolution would therefore be highly dependent on the distribution and population of oligomers within solution. Furthermore, it is well known from

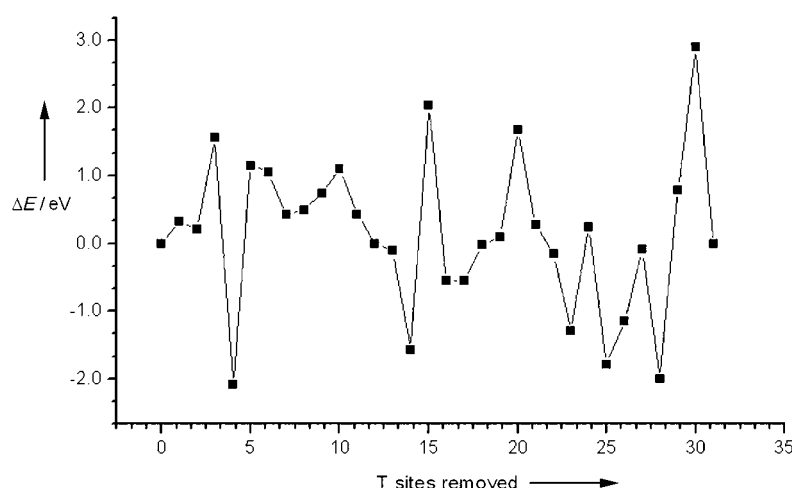


Figure 4. Change in energy for contiguous dissolution with respect to each previous step.

experiment that the distribution of oligomers is highly influenced by the pH value of the solution. Consequently, the role of oligomers in facilitating crystal growth may be a function of pH. A further complication is that the pH value rises during synthesis, a phenomenon that would tend to dissolve small unstable oligomeric species, thus creating more highly charged monomeric species. This suggests that at different stages of growth, crystal assembly may involve distinct species from those involved at lower pH values.

The maximum absolute enthalpy change of $+2.9 \text{ eV}$ ($\approx 280 \text{ kJ mol}^{-1}$) is clearly very large; however, the majority of enthalpy changes are much less than $+2.0 \text{ eV}$. Notwithstanding the magnitude of enthalpy changes, there are a number of factors missing from our model that would substantially lower the energy barrier for growth/dissolution. The present model for the solvent is an approximation, and needs to be enhanced to describe strong interactions, especially in sterically confined regions. Entropy changes of the solvent that arise from the ordering of water are probably larger than the change in the number of species, and may be of similar magnitude to vibrational entropy changes associated with the condensation of monomers to the surface. The solvation energy calculated for all structures was between 0.3 eV and 0.7 eV , though we expect that the solvation energy would increase upon relaxation, particularly for the least stable surfaces, which express a high density of silanol groups. Further details of the solvation of surfaces and all the structures assessed will be reported in a separate publication. We anticipate that most of these effects will systematically lower the surface energy and probably the energy difference between metastable surfaces as well. Correspondingly, the energy barriers should also be diminished. Almost certainly, of far greater significance to the accuracy of our calculations is the absence of pH effects and the mineralizer (fluoride), both of which will substantially lower the barrier to growth. Typical energy barriers measured for zeolitic materials that are relatively simple to synthesize are in the order of $\approx 0.5\text{--}1.4 \text{ eV}$,^[16–22] which when taken with the observation that beta C is difficult to synthesize, suggest that the energy barrier of $\approx 2.0\text{--}2.9 \text{ eV}$ may not be grossly in

error. However, we assume that the activation barrier associated with the surface and monomer/oligomeric complex is substantially smaller than the monomeric condensation barrier (calculated to be $\approx 0.4\text{--}1.0 \text{ eV}$).^[23] If oligomers alter the course of the minimum energy pathway by eliminating the most endothermic processes, then the barrier becomes close to $\approx 1 \text{ eV}$, in very reasonable agreement with measurements. Recent work by Mora-Fonz et al.^[24] suggests that the condensation enthalpy of two monomers is very low ($\approx -0.1 \text{ eV}$) and that the formation energy becomes more favorable in general as monomers condense onto large solution fragments. The use of this as a discriminator to indicate the upper bound for monomer-mediated growth would imply that only approximately half of the steps are viable, and that the supply of specific oligomers may control a substantial part of crystal assembly.

This work explores the enthalpy changes associated with monomeric growth and dissolution to assess whether there is evidence that growth (in particular) can proceed exclusively by addition of monomers, or whether oligomers are required to build the crystal. The results provide strong evidence that the barriers to growth are sufficiently low that one cannot discount the role of monomeric fragments during growth or dissolution. Our evidence suggests that many and possibly all of the stages of growth are thermally accessible, but oligomers may play a key role in overcoming the least-favorable (i.e., rate-determining) stages of growth. These include the assembly of double 4-rings at the crystal surface (indicated by Figure 4) through concerted condensation, for example, of dimeric or trimeric species with the crystal surface, or by reaction of larger preformed oligomers (such as double 4-rings) with the surface. It is clear that experimental data (e.g. NMR spectroscopy) relating to the distribution of oligomers within solution and their sensitivity to extra-framework cations, pH, and other synthesis parameters are needed before the role of PBUs and SBUs during growth can be definitively assigned. However, it is already known that the contents of solution can be manipulated or skewed, such as in the synthesis of purely siliceous zeolite A (which can be regarded as being made entirely from double 4-ring units), recently reported by Corma et al.,^[25,26] in which the unusually stable double 4-ring is presumed to be in excess of other fragments. Future simulation work will employ FP methods to estimate the barrier heights that govern the type of species that form in solution, at what rate, and the reactions of these species with zeolite surfaces.

Received: August 5, 2004

Published online: January 5, 2005

Keywords: crystal growth · solid-state structures · solvent effects · surface chemistry · zeolites

[1] C. S. Cundy, P. A. Cox, *Chem. Rev.* **2003**, *103*, 663.

[2] C. E. A. Kirschhock, R. Ravishankar, F. Verspeurt, P. J. Grobet, P. A. Jacobs, J. A. Martens, *J. Phys. Chem. B* **1999**, *103*, 4965.

- [3] C. T. G. Knight, S. D. Kinrade, *J. Phys. Chem. B* **2002**, *106*, 3329.
- [4] C. E. A. Kirschhock, R. Ravishankar, F. Verspeurt, P. J. Grobet, P. A. Jacobs, J. A. Martens, *J. Phys. Chem. B* **2002**, *106*, 3333.
- [5] Z. Liu, T. Ohsuna, O. Terasaki, M. A. Camblor, M. J. Diaz-Cabanas, K. Hiraga, *J. Am. Chem. Soc.* **2001**, *123*, 5370.
- [6] J. M. Newsam, M. M. J. Treacy, W. T. Koetsier, C. B. Degruyter, *Proc. R. Soc. London Ser. A* **1988**, *420*, 375.
- [7] B. Slater, C. Richard, A. Catlow, Z. Liu, T. Ohsuna, O. Terasaki, M. A. Camblor, *Angew. Chem.* **2002**, *114*, 1283; *Angew. Chem. Int. Ed.* **2002**, *41*, 1235.
- [8] M. J. Sanders, M. Leslie, C. R. A. Catlow, *J. Chem. Soc. Chem. Commun.* **1984**, 1271.
- [9] J. D. Gale, A. L. Rohl, *Mol. Simul.* **2003**, *29*, 291.
- [10] K. P. Schroder, J. Sauer, M. Leslie, C. R. A. Catlow, J. M. Thomas, *Chem. Phys. Lett.* **1992**, *188*, 320.
- [11] J. D. Gale, A. L. Rohl, in preparation.
- [12] A. Klamt, G. Schuurmann, *J. Chem. Soc. Perkin Trans. 2* **1993**, 799.
- [13] S. C. Parker, N. H. de Leeuw, S. E. Redfern, *Faraday Discuss.* **1999**, 381.
- [14] N. H. de Leeuw, F. M. Higgins, S. C. Parker, *J. Phys. Chem. B* **1999**, *103*, 1270.
- [15] S. D. Fleming, A. L. Rohl, S. C. Parker, G. M. Parkinson, *J. Phys. Chem. B* **2001**, *105*, 5099.
- [16] P. S. Singh, T. L. Dowling, J. N. Watson, J. W. White, *Phys. Chem. Chem. Phys.* **1999**, *1*, 4125.
- [17] R. T. Wilkin, H. L. Barnes, *Am. Mineral.* **2000**, *85*, 1329.
- [18] V. Nikolakis, E. Kokkoli, M. Tirrell, M. Tsapatsis, D. G. Vlachos, *Chem. Mater.* **2000**, *12*, 845.
- [19] C. S. Cundy, B. M. Lowe, D. M. Sinclair, *Faraday Discuss.* **1993**, 235.
- [20] J. N. Watson, L. E. Iton, R. I. Keir, J. C. Thomas, T. L. Dowling, J. W. White, *J. Phys. Chem. B* **1997**, *101*, 10094.
- [21] A. T. Davies, G. Sankar, C. R. A. Catlow, S. M. Clark, *J. Phys. Chem. B* **1997**, *101*, 10115.
- [22] S. Y. Yang, A. Navrotsky, *Microporous Mesoporous Mater.* **2002**, *52*, 93.
- [23] J. C. G. Pereira, C. R. A. Catlow, G. D. Price, *Chem. Commun.* **1998**, 1387.
- [24] M. J. Mora-Fonz, C. R. A. Catlow, D. W. Lewis, *Angew. Chem.* submitted **2004**.
- [25] A. Corma, F. Rey, M. J. Sabater, S. Valencia, Spanish patent number P200400662, Spain, **2004**.
- [26] A. Corma, F. Rey, J. Rius, M. J. Sabater, S. Valencia, *Nature* **2004**, *431*, 287.

N₂S₂Ni Metallothiolates as a Class of Ligands that Support Organometallic and Bioorganometallic Reactivity**

Marilyn V. Rampersad, Stephen P. Jeffery,
Joseph H. Reibenspies, Cesar G. Ortiz,
Donald J. Darensbourg, and Marcetta Y. Darensbourg*

That Cys-X-Cys tripeptide linkages can serve as tetradentate N₂S₂ ligands, utilizing carboxamido nitrogen and cysteinyl sulfur atoms as donors in metalloenzyme active sites, has recently been verified in several protein crystal structures.^[1–5] It was further discovered that the nickel-bound Cys-Gly-Cys NiN₂S₂ moiety of acetyl coA synthase binds through bidentate bridging thiolate groups to a second nickel center which mediates the organometallic reactions required of the biocatalyst (the assembly of CH₃⁺, CO, and SR[–] into the acetyl coA thioester CH₃C(=O)SR).^[1,2] The (Cys-Gly-Cys)Ni unit joins a host of synthetic NiN₂S₂ complexes that are known to form multimetal clusters through μ-SR interactions. Nature's control of binuclearity in the construction of an organometallic catalyst presents the intriguing possibility that the NiN₂S₂ complexes might be suitable for development as a novel class of ligands for organometallic chemistry and catalysis. To this end we have characterized a series of NiN₂S₂ complexes, four of which are shown in Figure 1, according to their electron-donating ability and stereochemical fea-

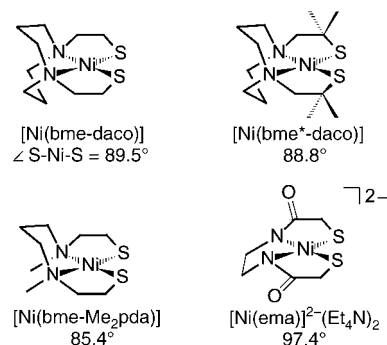


Figure 1. NiN₂S₂ complexes used as S-donor ligands; bme-daco = 1,5-(1,5-diazacyclooctane)di(ethylthiolate), bme*-daco = di(2-methyl-2-propylthiolate), bme-Me₂pda = N,N'-dimethyl-2,9-diazanonanedithiolate, ema^{4–} = 2,7-dioxo-3,6-diazaoctanedithiolate.

[*] M. V. Rampersad, S. P. Jeffery, Dr. J. H. Reibenspies, C. G. Ortiz, Prof. Dr. D. J. Darensbourg, Prof. Dr. M. Y. Darensbourg
Department of Chemistry
Texas A&M University
College Station, TX 77843 (USA)
Fax: (+1) 979-845-0158
E-mail: marcetta@mail.chem.tamu.edu

[**] We gratefully acknowledge the financial support from the National Science Foundation (CHE 01-11629 and CHE 02-34860) and the Robert A. Welch Foundation.



Supporting information for this article is available on the WWW under <http://www.angewandte.org> or from the author.

tures.^[6–9] These characteristics are contrasted to the classical ligands of organometallic chemistry, diphosphines and diimines. The results are presented herein along with an organometallic reaction principle that models steps in acetyl coA synthase as well as CO/olefin copolymerization catalysis.

According to Equation (1), NiN₂S₂ derivatives of tungsten tetracarbonyl were prepared from the labile-ligand complex, *cis*-[(piperidine)₂W(CO)₄].^[10] Vibrational mode assignments and ν(CO) stretching frequencies are listed in Table 1.

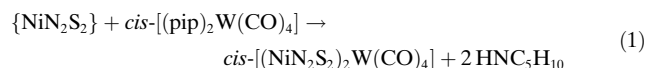


Table 1: IR data for [(NiN₂S₂)W(CO)₄] and [(L₂)W(CO)₄] complexes.^[a]

NiN ₂ S ₂ or L ₂	(A ₁)	(B ₁)	(A ₂)	(B ₂)
(bme-daco)Ni	1995	1871	1853	1819
(bme*-daco)Ni	1996	1871	1857	1816
(bme-Me ₂ pda)Ni	1993	1876	1843	1826
[Ni(ema)] ²⁻	1986	1853	1837	1791
dmpm ^[b]	2007	1885	1885	1863
bipy ^[c] or o-phen ^[d]	2006	1887	1870	1830
pip ^[e]	2000	1863	1852	1809

[a] ν(CO) cm⁻¹, DMF solution spectra; assignments under C_{2v} symmetry. [b] dmpm = dimethyl phosphinomethane. [c] bipy = bipyridine. [d] o-phen = o-phenanthroline. [e] pip = piperidine.

Of note is the similarity of the ν(CO) values for the W(CO)₄ derivatives containing neutral NiN₂S₂ units; the corresponding ν(CO) values for species with the dianionic complex, [Ni(ema)W(CO)₄]²⁻ are shifted negatively from these by 8 to 35 cm⁻¹, dependent on the vibrational mode compared. Thus as might be expected and as indicated by the CO stretching frequencies, this dianionic ligand transfers more electron density to the W(CO)₄ unit than the neutral NiN₂S₂ ligands.

Also listed in Table 1 are the ν(CO) values for *cis*-[(pip)₂W(CO)₄] and representative classical bidentate P- and N-donor ligands in [(LL)W(CO)₄] complexes. From this data we conclude that the electron-donating ability of neutral NiN₂S₂ S-donor ligands towards the {W(CO)₄} fragment is greater than that of diphosphines, and closer in donor ability to the o-phen and bipy ligands. The dianionic NiN₂S₂ ligand derived from the ema tetraanion is a significantly better donor. The electron-donating ability of these ligands to the W(CO)₄ moiety is: [Ni(ema)]²⁻ > {NiN₂S₂}⁰ > phen > (pip)₂ > bipy > dmpm. The molecular structures of three [(NiN₂S₂)W(CO)₄] complexes are presented as ball and stick drawings in Figure 2; for comparison, the structure of [(o-phenanthroline)W(CO)₄] is also shown.^[11] The orientation chosen for these depictions stresses the most prominent structural feature of the nickel dithiolates: the dihedral angle or hinge at the Ni(μ-S)₂W linkage that generates distinct asymmetry to the molecule. Thus, the C_{2v} symmetry used to assign the ν(CO) IR spectra holds only for the atom donor sets in the first coordination sphere; the overall symmetry from the molecular structure is C_s. The dihedral angles defined by the intersection of best planes of NiN₂S₂ and

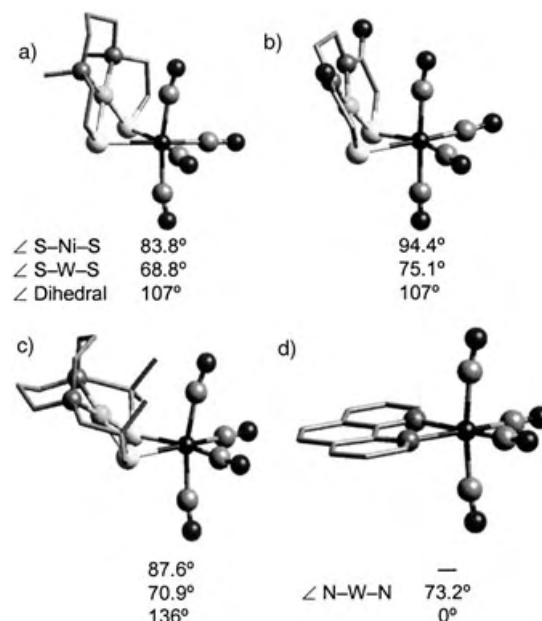


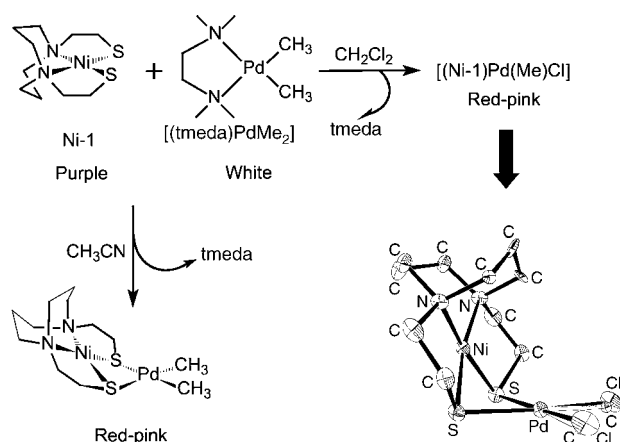
Figure 2. Ball-and-stick molecular structures of a) [Ni(bme-Me₂pda)W(CO)₄], b) [Ni(ema)W(CO)₄]²⁻, c) [Ni(bme*-daco)W(CO)₄], and d) [(o-phenanthroline)W(CO)₄]. The dihedral angle is for the intersection of the best planes of NiN₂S₂ and WS₂C₂.

WS₂C₂ are identical, 107°, for the relatively flat [Ni(ema)]²⁻ and the Ni(bme-Me₂pda) metallothiolate ligands, however, the steric bulk of the geminal dimethyl groups on the carbon α to the thiolate sulfur in the [(bme*-daco)Ni] complex opens the hinge to 136°. The Ni...W separations of [Ni(ema)W(CO)₄] (2.928 Å), [Ni(bme-Me₂pda)W(CO)₄] (3.033 Å), and [Ni(bme*-daco)W(CO)₄] (3.389 Å), reflect the different hinge angles of the complexes. There is some deviation from linearity of the CO groups closest to the NiN₂S₂ plane, however the observed angles do not correlate with steric bulk of the ligands. Note that the analogous CO groups in the phenanthroline derivative of {W(CO)₄} also bend away from the position of the substituent ligand, despite the fact that there is no possibility of a steric or lone-pair assist to this deformation.

Listed in Figure 2 are the S-W-S angles, the “bite angles” of the NiN₂S₂ bidentate ligands. The largest, 75.1° is for the rigid ema ligand; the more flexible, neutral ligands have bite angles of around 70°. In addition, the S-Ni-S angles of the tungsten-bound ligand, show only minor decreases from those S-Ni-S angles in the free ligand (Figure 1 and Figure 2). As the S-W bonds are longer than the S-Ni bonds, the S-W-S bite angles are from 15–22° smaller than the corresponding S-Ni-S angles of the free NiN₂S₂ ligands.

As the electron-donor abilities and the relatively flat form of the NiN₂S₂ ligands mimic diimine ligands we sought a model reaction for the purpose of contrasting organometallic reactivity supported by diimine and NiN₂S₂ ligands. A logical choice is the classical CO insertion process of interest in CO/olefin copolymerization catalysis. This reaction also serves as a biomimic of the CO insertion process of acetyl coA synthase. While the exogenous (that is, as related to the NiN₂S₂ moiety) nickel center is the active metal in both

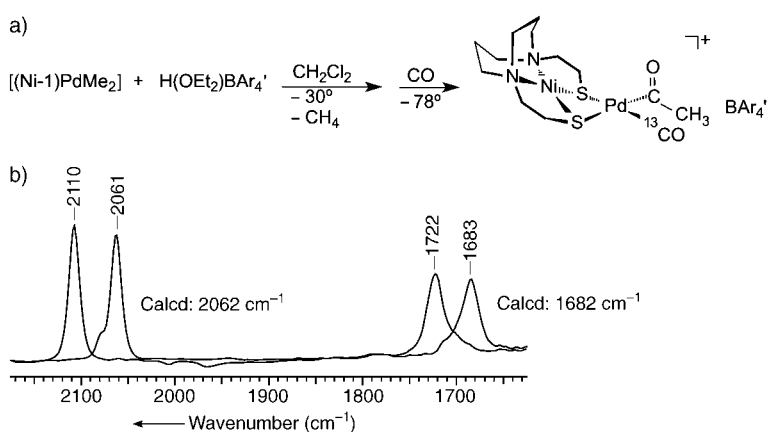
processes, the palladium analogue offers greater stability and the chance for isolating intermediates. The tmeda ligand-displacement route developed by Boersma, Van Koten, et al. for the preparation of diphosphine and diimine derivatives of $\{NiMe_2\}$ and $\{PdMe_2\}$ units, was used for the preparation of $[Ni(bme-daco)PdMe_2]$ Scheme 1.^[12] In CH_3CN , the red-pink product obtained is $[Ni(bme-daco)PdMe_2]$ as evidenced by mass spectral analysis. Unfortunately, high-quality crystals were not forthcoming. Crystals suitable for X-ray diffraction studies were acquired from the reaction performed in CH_2Cl_2 . These crystals analyzed as the chloro-methyl derivative $[Ni(bme-daco)Pd(Me)Cl]$ whose molecular structure is shown as a thermal ellipsoid plot in Scheme 1. In it, the NiN_2S_2 unit from $[(bme-daco)Ni]$ (Ni-1), binds to palladium through bridging sulfur interactions forming a square-planar $\{S_2Pd(Me)Cl\}$ unit in which the methyl



Scheme 1. Displacement of tmeda from $[(tmeda)PdMe_2]$ by $[Ni(bme-daco)]$ in CH_2Cl_2 and MeCN. The crystal structure of the product obtained in CH_2Cl_2 is also shown; tmeda = N,N,N',N' -tetramethyl-1,2-ethanediamine.

and chlorine atoms are disordered; they were modeled with 50% occupancy of each site. The dihedral angle between the two square planes is 101.3° , and the $Ni\cdots Pd$ separation is 2.802 \AA .

In accordance with the method of Brookhart et al., for the generation of an open site on an analogous $[(o\text{-phenanthroline})PdMe_2]$ ^[13] complex Scheme 2 depicts the reactivity of $[(Ni-1)PdMe_2]$ with acid ($HBAr'_4$; $Ar' = 3,5\text{-}(CF_3)_2C_6H_3$) in CH_2Cl_2 at $-30^\circ C$. On cooling this solution to $-78^\circ C$, purging with CO produced a compound with $\nu(CO)$ infrared bands at 2110 and 1722 cm^{-1} , assigned to a terminal and an acetyl CO group, respectively, consistent with the structure proposed in Scheme 2. With ^{13}C -labeled CO (95% enriched), shifts in both the terminal and the acetyl CO positions match the calculated predictions of $\nu(^{13}CO)$ bands, supporting the assignment (Scheme 2 b). For the analogous $[(o\text{-phen})Pd(CO)\{C(=O)Me\}]^+$, the $\nu(CO)$ bands are at 2127 (terminal CO) and 1745 cm^{-1} , (acetyl $C=O$),^[13] which reflects the poorer electron-donating ability of $o\text{-phen}$ compared with Ni-1 towards the Pd^{2+} center, as also seen with the $\{W(CO)_4\}$ probe moiety.



Scheme 2. a) Reaction of $[(Ni-1)PdMe_2]$ with acid and CO. b) IR spectra of the reaction product and of the ^{13}C -labeled product which agrees well with the calculated isotope-shift bands.

Isotopic labeling was also used to explore the exchange reaction of bound with free ^{13}CO in $[(Ni-1)Pd(CO)\{C(=O)Me\}]^+$ in CH_2Cl_2 . Under a ^{13}CO atmosphere over the course of 30 min at $-78^\circ C$, the IR spectrum of the solution showed approximately 75% enrichment of the terminal CO position while the acetyl ^{12}CO band remained the major species. Nevertheless, there was some build-up of a shoulder on the lower energy side of the 1722 cm^{-1} band which indicated minor incorporation of ^{13}CO into the acetyl position.

The facile nature of the terminal CO exchange with free ^{13}CO at $-78^\circ C$ deserves comment. As the processes which might create an open site, chelate ring-opening or CO dissociation, are expected to have activation barriers that could not be overcome at such low temperatures, we assume that CO exchange proceeds by an associative process. A similar five-coordinate intermediate would also account for the deinsertion process that is required for the apparent incorporation of some of the ^{13}C label into the acetyl site. On the other hand, the strength of the $Pd-S$ bond in the NiS_2Pd chelate system is unknown and the breaking of one NiS_2-Ni bond in the theoretical model of acetyl coA synthase was computed as a probably route for creating the open site required for CO uptake and catalysis.^[14] Further discussion at this time would just be speculation.

In 1995, Holm and Tucci demonstrated an essential feature of acetyl coA synthase, the coupling of a thiolate and a nickel-bound acetyl group using the $[(bipy)NiMe_2]$ complex which readily reacts with a RSH source forming $[(bipy)NiMe(SR)]$ with subsequent thioester formation upon introduction of CO gas.^[15] NaSMe was added to $[(Ni-1)Pd(CO)\{C(=O)Me\}]^+$ in CH_2Cl_2 at $-30^\circ C$. On warming the dark red solution to $22^\circ C$, over the course of 1 h, the IR spectrum showed diminished bands for the carbonyl groups of the $NiPd$ complex and growth of a band at 1686 cm^{-1} , consistent with that of a pure sample of $MeSC(=O)Me$. Whether the formation of the thioester occurred by nucleophilic attack of the $^-[SR]$ or reductive elimination of the acetyl requires further study.

These results suggest the NiN_2S_2 complexes which model a soft bidentate binding site for redox-active exogenous nickel centers in nature should also be considered as a new class of synthetic ligands for organometallic chemistry. An intriguing aspect of the ligands to be developed is the extensive stereochemical potentiality, best illustrated by the overlay of the $[(\text{Ni-1})\text{Pd}(\text{Me})\text{Cl}]$ with the $[(\text{phen})\text{Pd}(\text{CO})\{\text{C}(\text{=O})\text{Me}\}]^+$ complex, Figure 3.^[13] One face of the square planar $d^8\text{Pd}$

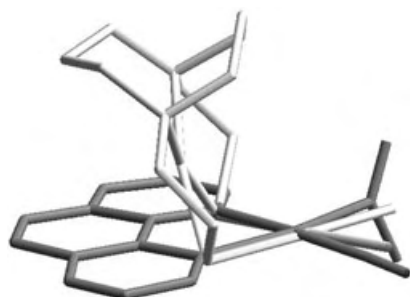


Figure 3. Cerius model overlay of $[(\text{Ni-1})\text{Pd}(\text{Me})\text{Cl}]$ (white) with the $[(\text{phen})\text{Pd}(\text{CO})\{\text{C}(\text{=O})\text{Me}\}]^+$ (gray) ion.

active metal center is flanked by the square plane of the NiN_2S_2 ligands in $[(\text{Ni-1})\text{Pd}(\text{Me})\text{Cl}]$, while the other is open. Substrates approaching the open site are expected to experience strong orientational preferences due to this feature and hence lead to regioselectivity. Chirality can also be introduced into the ligands at several places.

In conclusion, the $\nu(\text{CO})$ frequencies probed by the $\{\text{W}(\text{CO})_4\}$ and Pd-acetyl moieties indicate that NiN_2S_2 ligands are much better electron donors than conventional diphosphines and diimines, yet with the capability of stabilizing low-oxidation-state metals, such as W^0 and Pd^{II} . The NiN_2S_2 complex serves as a ligand to a Pd-alkyl metal center that undergoes CO addition and insertion reactions similar to those of Brookhart's catalyst. Moreover, the reactivity of the $[\text{NiN}_2\text{S}_2\text{Pd-alkyl}]$ complex with CO and an $[\text{SR}]$ source to produce a thioester is the first example of a heterobimetallic complex that is able to mimic the final step mediated by the acetyl coA synthase enzyme active site.

Experimental Section

See Supporting Information for all additional syntheses. CCDC-253549–253552 contain the supplementary crystallographic data for this paper. These data can be obtained free of charge via www.ccdc.cam.ac.uk/contents/retrieving.html (or from the Cambridge Crystallographic Data Centre, 12 Union Road, Cambridge CB21EZ, UK; fax: (+44) 1223-336-033; or deposit@ccdc.cam.ac.uk).

$[\text{Ni}(\text{bme}^*\text{-daco})\text{W}(\text{CO})_4]$: The yellow $[\text{W}(\text{CO})_4(\text{pip})_2]$ (0.12 g, 0.26 mmol) was dissolved in CH_2Cl_2 (20 mL) and heated to 40°C for 10 min under an N_2 atmosphere. To this was added dropwise a lilac-purple solution of $[\text{Ni}(\text{bme}^*\text{-daco})]$ (0.09 g, 0.26 mmol) dissolved in CH_2Cl_2 (10 mL). The resulting red-brown solution was heated for an additional 10 min at 40°C , and then stirred at 22°C ultimately producing a brown precipitate. The solvent and piperidine were removed under vacuum and the brown solid washed with benzene (25 mL \times 2) and diethyl ether (25 mL \times 2). The solid was extracted with CH_2Cl_2 and orange-red crystals were obtained from vapor diffusion of hexane into this solution, yield 0.11 g (65%) elemental

analysis (%) calcd for $\text{C}_{18}\text{H}_{28}\text{N}_2\text{Ni}_1\text{O}_4\text{S}_2\text{W}_1$: C 33.6, H 4.39, N 4.36; found: C 32.1, H 4.49, N 4.49. UV/Vis in DMF solution: $\lambda_{\text{max}}(\epsilon) = 306$ (5002), 372 (1382), 420 (1480), 504 nm (495).

Received: August 21, 2004

Keywords: acetyl coA synthase · bioinorganic chemistry · insertion · nickel · S ligands

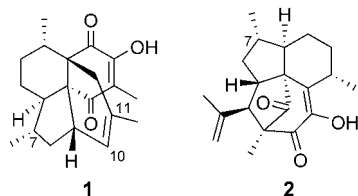
- [1] T. I. Doukov, T. M. Iverson, J. Seravalli, S. W. Ragsdale, C. L. Drennan, *Science* **2002**, 298, 567–572.
- [2] C. Darnault, A. Volbeda, E. J. Kim, P. Legrand, X. Vernède, P. A. Lindahl, J. C. Fontecilla-Camps, *Nat. Struct. Biol.* **2003**, 10, 271–279.
- [3] S. Nagashima, M. Nakasako, N. Dohmae, M. Tsujimura, K. Takio, M. Odaka, M. Yohda, N. Kamiya, I. Endo, *Nat. Struct. Biol.* **1998**, 5, 347–351.
- [4] W. Huang, J. Jia, J. Cummings, M. Nelson, G. Schneider, Y. Lindqvist, *Structure* **1997**, 5, 691–699.
- [5] V. Svetlitchni, H. Dobbek, W. Meyer-Klaucke, T. Meins, B. Thiele, P. Römer, R. Huber, O. Meyer, *Proc. Natl. Acad. Sci. USA* **2004**, 101, 446–451.
- [6] D. K. Mills, J. H. Reibenspies, M. Y. Darensbourg, *Inorg. Chem.* **1990**, 29, 4364–4365.
- [7] M. Y. Darensbourg, I. Font, M. Pala, J. H. Reibenspies, *J. Coord. Chem.* **1994**, 32, 39–49.
- [8] G. J. Colpas, M. Kumar, R. O. Day, M. J. Maroney, *Inorg. Chem.* **1990**, 29, 4779–4788.
- [9] H. J. Kruger, G. Peng, R. H. Holm, *Inorg. Chem.* **1991**, 30, 734–742.
- [10] D. J. Darensbourg, R. L. Kump, *Inorg. Chem.* **1978**, 17, 2680–2682.
- [11] H. Jinshun, C. Qingong, W. Manfong, L. Shimei, *J. Struct. Chem.* **1985**, 26, 69–71.
- [12] W. De Graaf, J. Boersma, J. J. Smeets, A. L. Spek, G. Van Koten, *Organometallics* **1989**, 8, 2907–2917.
- [13] F. C. Rix, M. Brookhart, P. S. White, *J. Am. Chem. Soc.* **1996**, 118, 4746–4764.
- [14] C. E. Webster, M. Y. Darensbourg, P. A. Lindahl, M. B. Hall, *J. Am. Chem. Soc.* **2004**, 126, 3410–3411.
- [15] G. C. Tucci, R. H. Holm, *J. Am. Chem. Soc.* **1995**, 117, 6489–6496.

Natural Product Synthesis

Total Synthesis of (–)-Colombiasin A and (–)-Elisapterosin B**

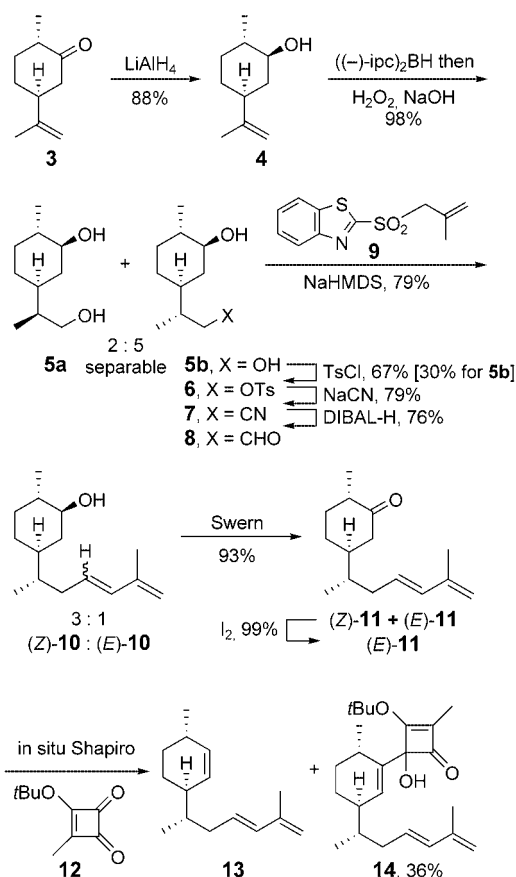
David C. Harrowven,* David D. Pascoe,
Daniela Demurtas, and Heather O. Bourne

Colombiasin A (**1**) and elisapterosin B (**2**) are recent additions to the family of diterpenes from the gorgonian octacoral *Pseudopterogorgia elisabethae*.^[1,2] Discovered by Rodriguez et al., their unusual molecular architecture soon attracted attention from the natural products community.^[3] Initially, colombiasin A proved the more popular target,^[4] with total syntheses being reported firstly by Nicolaou et al.^[5] and then by Kim and Rychnovsky.^[6] The latter report also describes the first total synthesis of (–)-elisapterosin B, a compound that exhibits strong antiparasitic activity against *Plasmodium falciparum*, the parasite responsible for the most severe forms of malaria.^[3] A synthesis of (+)-elisapterosin B by Rawal et al. followed soon after.^[7] Herein we describe total syntheses of both (–)-colombiasin A (**1**) and (–)-elisapterosin B (**2**)



in which a Moore rearrangement^[8] of vinylcyclobutene **14** is used to set up intramolecular [4+2]^[4-6] and [5+2]^[7,9] cycloaddition reactions leading to the target compounds.

Our synthesis of **14** (Scheme 1) began with (–)-dihydrocarvone (**3**), which was reduced to alcohol **4** using LiAlH₄. Hydroboration with ((–)-ipc)₂BH,^[10] followed by oxidative work-up gave diols **5** as a 5:2 mixture of diastereomers. These were separated by a combination of column chromatography and fractional crystallization. Sequential monotosylation to **6**, cyanide displacement to nitrile **7**, and DIBAL-H reduction to aldehyde **8** then allowed us to introduce the diene function by means of a Julia reaction with **9**.^[11] Higher yields were obtained using the Kocienski modification,^[12] these conditions giving **10** as a 3:1 mixture of *Z* and *E* isomers in 79% yield. Swern oxidation followed, and the resulting mixture of



Scheme 1. Synthesis of intermediate **14**; ipc = 2,6,6-trimethylbicyclo[3.1.1]hept-3-yl, NaHMDS = sodium hexamethyldisilazane, Ts = *p*-toluenesulfonyl, DIBAL-H = diisobutylaluminum hydride.

Z and *E* dienones **11** was equilibrated to (*E*)-**11** in near quantitative yield with catalytic iodine.

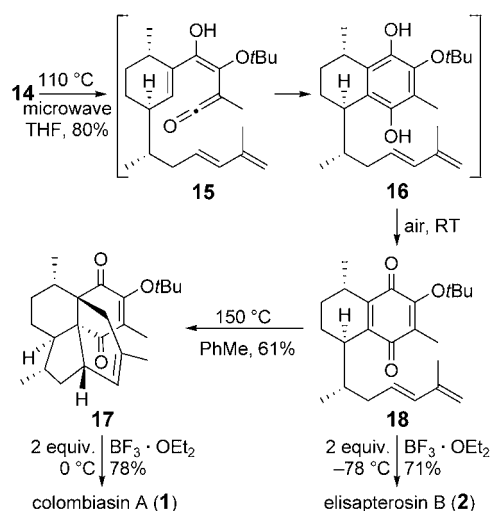
The next step, a Shapiro reaction between dienone (*E*)-**11** and squarate **12**,^[13] proved troublesome.^[14] Though the tosylhydrazone of (*E*)-**11** was readily formed and isolated, it gave triene **13** as the major product on treatment with butyllithium and addition of squarate **12**. By contrast, all attempts to prepare and isolate the corresponding trisylhydrazone (trisyl = triisopropylbenzenesulfonyl), either directly or indirectly,^[15] met with failure. Monitoring the reaction by NMR spectroscopy showed that the formation of the trisylhydrazone was facile at room temperature in CDCl₃, and that it subsequently decomposed on prolonged standing. Consequently, an in situ variant of the Shapiro reaction was developed (Scheme 1). Trisylhydrazine and (*E*)-**11** in THF were first stirred at ambient temperature for 2 h before the reaction mixture was cooled to –78 °C. Four equivalents of *n*BuLi were then added and the temperature raised to –20 °C. At this juncture squarate **12** was added, giving vinylcyclobutene **14** in 36% yield.

The stage was now set for a Moore rearrangement of **14** to hydroquinone **16**,^[8] a reaction that proceeded smoothly at 110 °C in THF under microwave irradiation (Scheme 2). After cooling to ambient temperature and stirring in air, quinone **18** was isolated in a satisfying 80% yield. Heating a toluene solution of **18** in the dark at 150 °C, either conven-

[*] Dr. D. C. Harrowven, D. D. Pascoe, D. Demurtas, Dr. H. O. Bourne
School of Chemistry
University of Southampton
Highfield, Southampton, SO17 1BJ (UK)
Fax: (+44) 2380-596-805
E-mail: dch2@soton.ac.uk

[**] Financial support from EPSRC, Pfizer, and the University of Southampton is gratefully acknowledged.

Supporting information for this article is available on the WWW under <http://www.angewandte.org> or from the author.



Scheme 2. Total syntheses of (–)-colombiasin A (**1**) and (–)-elisapterosin B (**2**) starting with **14**.

tionally or in the microwave oven, induced an intramolecular Diels–Alder cycloaddition to (–)-colombiasin A *tert*-butyl ether **17**.^[4–6] Attempts to effect removal of the protective group with TiCl_4 succeeded in that task,^[16] but also led to Markovnikov addition of HCl across the sensitive C10–C11 double bond.^[5] Deprotection with diethyl ether–trifluoroborane however, proceeded cleanly to complete a total synthesis of (–)-colombiasin A (**1**). Notably, exposing quinone **18** to diethyl ether–trifluoroborane induced both deprotection of the *tert*-butyl ether and an intramolecular [5+2] cycloaddition to give (–)-elisapterosin B (**2**);^[6] our synthetic samples of **1** and **2** exhibit physical and spectral characteristics identical to those reported for the natural products.^[1,2]

In conclusion, stereocontrolled syntheses of (–)-colombiasin A (**1**) and (–)-elisapterosin B (**2**) have been achieved, in twelve and eleven steps respectively from (–)-dihydrocarvone (**3**). The problematic C7 stereocenter was established by hydroboration with ((–)-*ipc*)₂BH, and the use of a *tert*-butyl protective group ensured that deprotection could be accomplished in high yield without disruption of the sensitive C10–C11 double bond.^[5] A distinctive feature of our approach is the use of a Moore rearrangement to set up intramolecular [4+2] and [5+2] cycloaddition reactions, leading to (–)-colombiasin A (**1**) and (–)-elisapterosin B (**2**) respectively. Studies are underway to further develop and improve the *in situ* Shapiro reaction and to apply the “reagent-free” rearrangement sequence in syntheses of related natural products such as elisapterosins A and D.^[2,3,17]

Received: October 11, 2004

Keywords: cycloaddition · diterpenes · marine natural products · rearrangement · total synthesis

[1] A. D. Rodríguez, C. Ramírez, *Org. Lett.* **2000**, *2*, 507–510.

[2] A. D. Rodríguez, C. Ramírez, I. I. Rodríguez, C. L. Barnes, *J. Org. Chem.* **2000**, *65*, 1390–1398.

- [3] a) A. D. Rodríguez, Y.-P. Shi, *Tetrahedron* **2000**, *56*, 9015–9023; b) A. D. Rodríguez, C. Ramírez, *J. Nat. Prod.* **2001**, *2*, 507–510.
- [4] a) D. C. Harrowven, M. J. Tyte, *Tetrahedron Lett.* **2001**, *42*, 8709–8711; b) J. H. Chaplin, A. J. Edwards, B. L. Flynn, *Org. Biomol. Chem.* **2003**, *1*, 1842–1844.
- [5] a) K. C. Nicolaou, G. Vassilikogiannakis, W. Mägerlein, R. Kranich, *Angew. Chem.* **2001**, *113*, 2543–2547; *Angew. Chem. Int. Ed.* **2001**, *40*, 2482–2486; b) K. C. Nicolaou, G. Vassilikogiannakis, W. Mägerlein, R. Kranich, *Chem. Eur. J.* **2001**, *7*, 5359–5371.
- [6] A. I. Kim, S. D. Rychnovsky, *Angew. Chem.* **2003**, *115*, 1305–1308; *Angew. Chem. Int. Ed.* **2003**, *42*, 1267–1270.
- [7] N. Waizumi, A. R. Stankovic, V. H. Rawal, *J. Am. Chem. Soc.* **2003**, *125*, 13022–13023.
- [8] a) J. O. Karlsson, N. V. Nguyen, L. D. Foland, H. W. Moore, *J. Am. Chem. Soc.* **1985**, *107*, 3392–3393; b) S. T. Perri, H. J. Dyke, H. W. Moore, *J. Org. Chem.* **1989**, *54*, 2032–2034; c) A. Enhnen, K. Karabelas, J. M. Heering, H. W. Moore, *J. Org. Chem.* **1990**, *55*, 1177–1185.
- [9] a) P. Walls, J. Padilla, P. Joseph-Nathan, F. Giral, J. Romo, *Tetrahedron Lett.* **1965**, 1577–1582; b) P. Joseph-Nathan, V. Mendoza, E. Garcia, *Tetrahedron* **1977**, *33*, 1573–1576; c) P. Joseph-Nathan, M. E. Garibay, R. L. Santillan, *J. Org. Chem.* **1987**, *52*, 759–763; d) T. A. Engler, C. M. Scheibe, R. Iyengar, *J. Org. Chem.* **1997**, *62*, 8274–8275.
- [10] a) H. C. Brown, P. V. Ramachandran, *J. Organomet. Chem.* **1995**, *500*, 1–19; b) D. S. Matteson, *Synthesis* **1986**, 973–985.
- [11] a) J. B. Baudin, G. Hareau, S. A. Julia, O. Ruel, *Tetrahedron Lett.* **1991**, *32*, 1175–1178; b) J. B. Baudin, G. Hareau, S. A. Julia, O. Ruel, *Bull. Soc. Chim. Fr.* **1993**, *130*, 336–357; c) J. B. Baudin, G. Hareau, S. A. Julia, R. Lorne, O. Ruel, *Bull. Soc. Chim. Fr.* **1993**, *130*, 856–878.
- [12] a) N. D. Smith, P. J. Kocienski, S. D. A. Street, *Synthesis* **1996**, 652–666; b) P. R. Blakemore, P. J. Kocienski, A. Morley, K. Muir, *J. Chem. Soc. Perkin Trans. 1* **1999**, 955–968; c) R. Bellingham, K. Jarowicki, P. Kocienski, V. Martin, *Synthesis* **1996**, 285–296.
- [13] M. W. Reed, D. J. Pollart, S. T. Perri, L. D. Foland, H. W. Moore, *J. Org. Chem.* **1988**, *53*, 2477–2482.
- [14] A. R. Chamberlin, S. H. Bloom, *Org. React.* **1990**, *39*, 1–83.
- [15] H. Berner, H. Vyplel, G. Schulz, G. Fischer, *Monatsh. Chem.* **1985**, *116*, 1165–1176.
- [16] R. H. Schlessinger, R. A. Nugent, *J. Am. Chem. Soc.* **1982**, *104*, 1116–1118.
- [17] G. Zanoni, M. Franzini, *Angew. Chem.* **2004**, *116*, 4942–4946; *Angew. Chem. Int. Ed.* **2004**, *43*, 4837–4841.

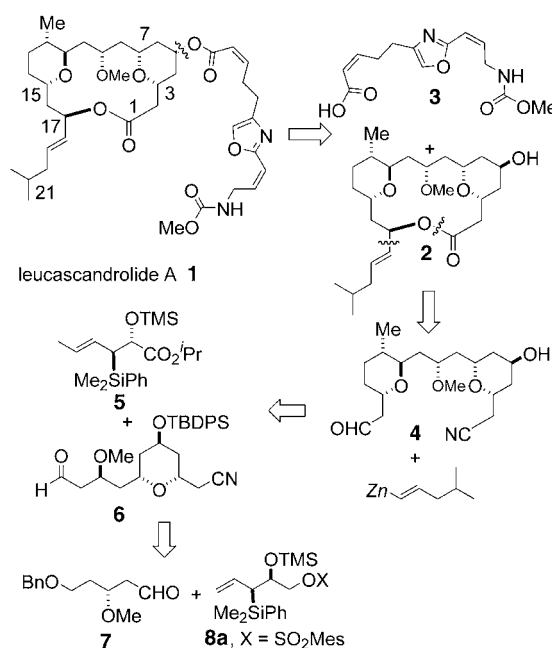
Natural Product Synthesis

Total Synthesis of (+)-Leucascandrolide A**

Qibin Su and James S. Panek*

Leucascandrolide A (**1**) is a bioactive metabolite isolated by Pietra and coworkers from the calcareous sponge *Leucascandra caveolata*, found off the east coast of New Caledonia in the Coral sea.^[1] Two-dimensional NMR experiments were used to determine the relative configuration of **1**, while its absolute configuration was assigned by employing a Mosher analysis at the C5-hydroxy group. This natural product possesses an 18-membered macrolide ring that includes two trisubstituted tetrahydropyran rings, and an unsaturated oxazole-containing side chain. Leucascandrolide A (**1**) displays significant in vitro cytotoxicity against human KB and P388 tumor cell lines with low IC₅₀ values (0.05 and 0.26 $\mu\text{g mL}^{-1}$, respectively) as well as strong inhibition of *Candida albicans*, a pathogenic yeast. Recent reports^[2] indicate that **1** is no longer available from its original natural source. It has been postulated that **1** is not a metabolite of *Leucascandra caveolata*, but rather of an opportunistic bacteria that colonized the sponge, as evidenced by the large amounts of dead tissue in the initial harvest of the marine organism. As a consequence, all known sources of the natural product have been depleted.^[2] This fact, the potent bioactivity, and the unique structure of **1** have led to much attention among the synthetic community. Following the first total synthesis by Leighton et al.,^[3] there have been additional reports detailing total,^[4] formal,^[5] and fragment syntheses.^[6]

Herein, we describe an enantioselective total synthesis of (+)-leucascandrolide A (**1**). This synthesis is highlighted by the rapid and efficient construction of the bispyran **4** which contains a *cis*- and a *trans*-2,6-disubstituted tetrahydropyran ring. These rings were assembled in two [4+2] annulation reactions between aldehydes **7** and **6** and our newly introduced chiral allylsilane **8a** and crotylsilane **5**,^[7] respectively. Our retrosynthetic analysis is illustrated in Scheme 1. Disconnection at the C5–ester bond reveals a macrolactone containing two pyran rings (**2**) and an oxazole-containing side chain **3**. Upon further analysis of the macrolide, we envisaged



Scheme 1. Retrosynthesis of **1**; SO₂Mes = 2-mesitylenesulfonate.

that the allylic alcohol could be obtained from the addition of an alkenyl zinc species to aldehyde **4**.

Recently, we have described a highly diastereomerically and enantiomerically controlled [4+2] annulation between aldehydes and *syn* allylsilane **8b**, which produces *trans*-2,6-disubstituted dihydropyrans (Table 1).^[8] Our attempt to

Table 1: Dihydropyran synthesis from aldehydes and allylsilanes **8**.

Entry	R	Silane	Product, yield [%] ^[a]	d.r. (<i>trans</i> : <i>cis</i>) ^[b]
1	<i>i</i> Pr	8a , X = SO ₂ Mes	9a , 90	1:25
2	PhCH ₂	8a , X = SO ₂ Mes	9b , 91	1:8
3	C ₄ H ₉	8a , X = SO ₂ Mes	9c , 85	1:16
4 ^[8]	<i>i</i> Pr	8b , X = Me	9d , 91	> 30:1
5 ^[8]	PhCH ₂	8b , X = Me	9e , 91	> 30:1
6 ^[8]	<i>c</i> -Hex	8b , X = Me	9f , 95	10:1

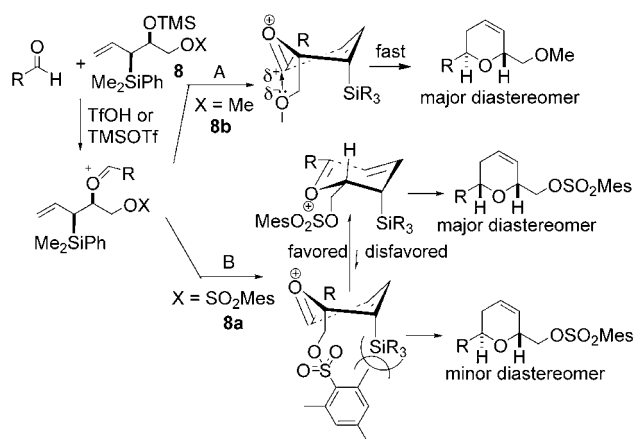
[a] Yields are based on pure materials isolated after chromatography on SiO₂. [b] The configuration of the pyran products was assigned by NOE measurements. The product ratio was determined by ¹H NMR spectroscopy (400 MHz).

rationalize such a stereochemical outcome of the annulation process is depicted in Scheme 2. When allylsilane **8b** reacts with the aldehyde, we suggested that stabilization of the oxocarbenium cation by the neighboring electron-rich methyl ether favored a twist-boat intermediate thus accelerating the formation of the *trans*-2,6-dihydropyran product (route A in Scheme 2). If this were the case, the complementary *cis*-2,6-dihydropyran adducts could also be obtained from a *syn* allylsilane if the ring formation process occurred predominantly through a chair-like transition state. We predicted this could be achieved by tuning the steric and stereoelectronic

[*] Q. Su, Prof. Dr. J. S. Panek
Department of Chemistry and
Center for Chemical Methodology and Library Development
Boston University
590 Commonwealth Ave., Boston, MA 02215 (USA)
Fax: (+1) 617-353-6466
E-mail: panek@chem.bu.edu

[**] Financial support for this research was obtained from the National Institutes of Health (GM055740), Johnson & Johnson, Merck Co., Novartis, Pfizer, and GlaxoSmithKline. The authors are grateful to Dr. Les A. Dakin and Neil F. Langille for helpful discussions on the preparation of side chain **3**, and to Dr. Julien Beignet for assistance with the preparation of the manuscript.

Supporting information for this article is available on the WWW under <http://www.angewandte.org> or from the author.



Scheme 2. Possible transition states for the [4+2] annulation of aldehydes with **8**.

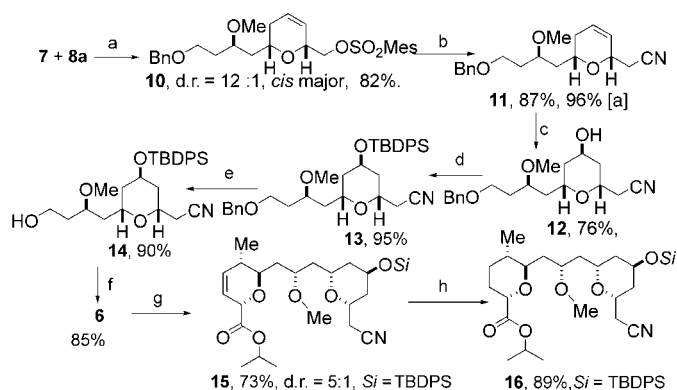
properties of the X substituent in the starting allylsilane **8**, for example by using a) an electron-withdrawing group X to minimize anchimeric assistance onto the oxocarbenium ion, and b) a sterically demanding functional group X to maximize destabilizing 1,2-diaxial interactions between X and the allylsilane moiety in the twist-boat conformer (route B in Scheme 2).

Accordingly, we evaluated the reactivity and selectivity of allylsilane **8a** bearing a mesitylsulfonate group in our [4+2] annulation (Table 1). The desired *cis*-2,6-dihydropyran products were obtained in very good yields and with high levels of diastereoselectivity (entries 1–3);^[9] the annulation using allylsilane **8b** to produce *trans*-2,6-dihydropyrans (entries 4–6)^[8] shows the generality of the methodology for synthesizing this class of heterocycles. Moreover, the reversal in the sense of diastereoselection, resulting from the subtle structural differences between the two allylsilanes, is in accordance with our proposed transition states (Scheme 2) and gives further insight into a plausible mechanism of this interesting [4+2] annulation.

We were then ready to exploit the accessibility of *cis*-2,6-dihydropyrans in the synthesis of leucascandrolide A (**1**). Gratifyingly, annulation between allylsilane **8a**^[10] and aldehyde **7**^[11] proceeded smoothly in the presence of TfOH to afford the desired dihydropyran **10** in good yield and with good diastereoselectivity (Scheme 3).^[12] The presence of the sulfonate in this product allowed an efficient one-carbon homologation through S_N2 displacement using NaCN to yield nitrile **11**.

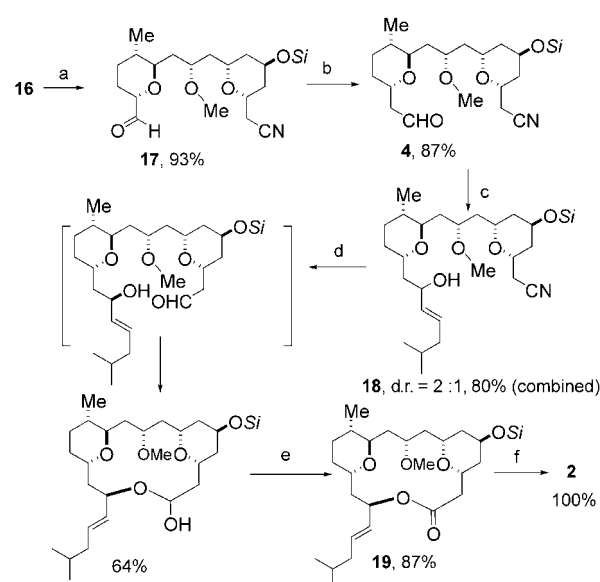
Oxymercuration of the double bond of **11** installed the C5-hydroxy group, as the single regio- and diastereomer **12**,^[13] which was protected as the TBDPS ether **13**. Subsequent debenzoylation with BCl₃ furnished the primary alcohol **14**, which was oxidized to aldehyde **6** using PCC.^[14] Next, the crucial [4+2] annulation between **6** and crotylsilane **5** was carried out with useful diastereoselectivity and in good yield to produce dihydropyran **15**,^[7a] which was hydrogenated to bispyran **16**.

Reduction of the isopropyl ester of **16** in presence of the nitrile group was conducted with complete chemoselectivity using DIBAL-H (2.1 equiv.) in Et₂O at –78 °C thus providing



Scheme 3. Reagents and conditions: a) TfOH, CH₂Cl₂, –78 °C; b) NaCN, DMF, 60 °C; c) mercury(II) trifluoroacetate, THF/H₂O, then NaBH₄ in NaOH (aq.); d) TBDPSCl, imidazole, DMF; e) BCl₃, CH₂Cl₂, –78 °C; f) PCC, CH₂Cl₂; g) **5**, TMSOTf, CH₂Cl₂, –50 °C; h) H₂, Pd/C. TfOH = trifluoromethanesulfonic acid, DMF = dimethylformamide, TBDPS = *tert*-butyldiphenylsilyl, PCC = pyridinium chlorochromate, TMSOTf = trimethylsilyl trifluoromethanesulfonate. [a] Yield based on recovered starting material.

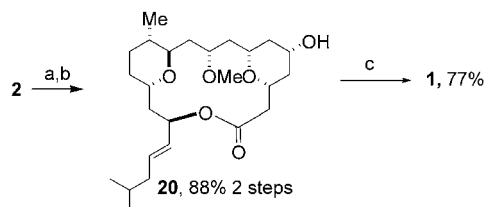
aldehyde **17** in high yield (Scheme 4). Homologation of the aldehyde group by a phosphorus-based olefination with methoxymethylenetriphenylphosphine and subsequent mercury acetate mediated hydrolysis of the resulting enol ether furnished aldehyde **4** in 87% over two steps.^[15] Finally, addition of an alkenyl zinc species to **4** afforded allylic alcohol **18** in good yield, albeit with disappointing diastereoselectivity.^[16] The diastereomers **18** were separated and the (17-*R*) alcohol obtained in 53% yield.



Scheme 4. Reagents and conditions. a) DIBAL-H, Et₂O, –78 °C; b) Ph₃P=CHOMe, THF, –78 °C to room temperature, then Hg(OAc)₂, THF/H₂O; c) in situ synthesis of the zinc reagent: 4-methyl-1-pentyne, CH₂Cl₂, [Cp₂Zr(H)Cl], room temperature; then ZnMe₂, –60 to 0 °C; then reaction with **4**, 0 °C; d) DIBAL-H, CH₂Cl₂, –78 °C, then HCl (aq., 1 N); e) PCC, CH₂Cl₂; f) TBAF, THF. DIBAL-H = diisobutylaluminum hydride, TBAF = tetrabutylammonium fluoride, Si = TBDPS.

Inspired by a spontaneous macroacetalization reported by Kozmin et al.,^[4a] we decided for a similar transformation of nitrile **18**. Therefore, careful addition of DIBAL-H to a solution of **18** in CH₂Cl₂ at –78°C followed by acidic hydrolysis of the resulting imine furnished a transient hydroxyaldehyde which spontaneously cyclized into the desired macrolactol. Oxidation to the macrolactone **19** using PCC followed by a TBAF-promoted deprotection of the C5-TBDPS ether provided macrolide **2** in excellent yield, establishing, at this stage, a formal total synthesis of leucascandrolide A (**1**).

It has been reported that it was difficult to achieve a direct acylation of the axially orientated C5-hydroxy group of **2**.^[4c] We therefore turned our attention to the Mitsunobu reaction^[17] to install the side chain at this center. Inversion of the configuration at C5 was achieved by a two-step oxidation–reduction sequence in excellent yield and with excellent selectivity (Scheme 5). Acid **3**^[6c] and macrolide **20** were then united smoothly under Mitsunobu conditions to conclude the total synthesis of leucascandrolide A (**1**); the physical and spectroscopic properties of our compound were identical to those reported for **1**.^[1,3]



Scheme 5. Reagents and conditions. a) Dess–Martin periodinane, pyridine, CH₂Cl₂; b) NaBH₄, MeOH, 0°C; c) **3**, PPh₃, DIAD, THF/benzene. DIAD = diisopropyl azodicarboxylate.

In summary, we accomplished a convergent and enantioselective total synthesis of (+)-leucascandrolide A (**1**) in 17 steps from available aldehyde **7** and allylsilane **8a**. The present synthesis features an efficient route to **4** using two consecutive [4+2] annulation reactions between aldehydes and our chiral allyl- and crotylsilanes for the rapid and efficient integration of the bispyran moiety into **1**. Thus, chiral organosilane reagents were shown to be of salient utility for synthesizing complex pyran-containing natural products. Moreover, studies toward the completion of structural analogues of **1** using this silane methodology are currently in progress in our laboratory.

Received: October 22, 2004

Published online: January 17, 2005

Keywords: allylsilanes · annulation · antitumor agents · asymmetric synthesis · natural products

[1] M. D'Ambrosio, A. Guerriero, C. Debitus, F. Pietra, *Helv. Chim. Acta* **1996**, *79*, 51.

[2] a) M. D'Ambrosio, M. Tato, G. Pocsfalvi, C. Debitus, F. Pietra, *Helv. Chim. Acta* **1999**, *82*, 347; b) M. D'Ambrosio, M. Tato, G. Pocsfalvi, C. Debitus, F. Pietra, *Helv. Chim. Acta* **1999**, *82*, 1135.

- [3] K. R. Hornberger, C. L. Hamblett, J. L. Leighton, *J. Am. Chem. Soc.* **2000**, *122*, 12894.
- [4] a) Y. Wang, J. Janic, S. A. Kozmin, *J. Am. Chem. Soc.* **2002**, *124*, 13670; b) A. Fettes, E. M. Carreira, *Angew. Chem.* **2002**, *114*, 4272; *Angew. Chem. Int. Ed.* **2002**, *41*, 4098; c) I. Paterson, M. Tudge, *Angew. Chem.* **2003**, *115*, 357; *Angew. Chem. Int. Ed.* **2003**, *42*, 343.
- [5] a) D. J. Kopecky, S. D. Rychnovsky, *J. Am. Chem. Soc.* **2001**, *123*, 8420; b) P. Wipf, J. T. Reeves, *J. Chem. Soc. Chem. Commun.* **2002**, 2066; c) D. R. Williams, S. V. Plummer, S. Patnaik, *Angew. Chem.* **2003**, *115*, 4064; *Angew. Chem. Int. Ed.* **2003**, *42*, 3934; d) M. T. Crimmins, P. Siliphaivanh, *Org. Lett.* **2003**, *5*, 4641.
- [6] a) M. T. Crimmins, C. A. Carroll, B. W. King, *Org. Lett.* **2000**, *2*, 597; b) P. Wipf, T. H. Graham, *J. Org. Chem.* **2001**, *66*, 3242; c) L. A. Dakin, N. F. Langille, J. S. Panek, *J. Org. Chem.* **2002**, *67*, 6812; d) L. A. Dakin, J. S. Panek, *Org. Lett.* **2003**, *5*, 3995.
- [7] a) H. Huang, J. S. Panek, *J. Am. Chem. Soc.* **2000**, *122*, 9836; for some other examples of pyran syntheses through Prins-type cyclization, see: b) S. D. Rychnovsky, S. Marumoto, J. J. Jaber, *Org. Lett.* **2001**, *3*, 3815; c) I. E. Markó, D. J. Bayston, *Synthesis* **1996**, 297.
- [8] Q. Su, J. S. Panek, *J. Am. Chem. Soc.* **2004**, *126*, 2425.
- [9] Other electron-withdrawing groups such as acetate, pivaloate, trifluoroacetate, benzoate, and methyl carbonate as X gave predominantly the *cis* isomers, however with lower diastereoselectivities and in lower yields.
- [10] For a high-yielding preparation of silane **8a**, see Supporting Information.
- [11] Aldehyde **7** was prepared in high yield from the known alcohol; see Supporting Information.
- [12] Using a less bulky sulfonate group (*p*-toluenesulfonate) as X in **8** produced the corresponding *cis* pyran with lower diastereoselectivity (d.r. = 9:1).
- [13] H. C. Brown, P. Geoghegan, Jr., *J. Am. Chem. Soc.* **1967**, *89*, 1522.
- [14] E. J. Corey, J. W. Suggs, *Tetrahedron Lett.* **1975**, 2647.
- [15] A. Maercker, *Org. React.* **1965**, *14*, 270.
- [16] P. Wipf, W. Xu, *Tetrahedron Lett.* **1994**, *35*, 5197.
- [17] O. Mitsunobu, *Synthesis* **1981**, 1.

Direct Access to Bicontinuous Skeletal Inorganic Plumber's Nightmare Networks from Block Copolymers**

Anurag Jain, Gilman E. S. Toombes, Lisa M. Hall, Surbhi Mahajan, Carlos B. W. Garcia, Wolfgang Probst, Sol M. Gruner, and Ulrich Wiesner*

The co-assembly of organic and inorganic materials into a wide variety of structures at the nanoscale represents one of the most promising and exciting avenues for development of novel multifunctional materials.^[1] A research area that has captivated researchers for some time is the synthesis and characterization of co-continuous nanostructures. Pioneering work in the field was done at Mobil Corp.^[2,3] where a surfactant template was used to obtain mesoporous silica-type materials with enormous surface areas and pores larger than those accessible with conventional zeolites. The approach has since then been advanced to much larger pore sizes by utilizing block copolymers as templates.^[4–7] The continuous nature of nanoscale channels combined with the unique structural and physical properties of these materials has sparked enormous interest for applications in areas such as catalysis, molecular separation, photonics, energy generation and storage, or electronics. Whereas most of the work in the field has been based on the so-called regular co-continuous structures in which the silica resides in the matrix of the bicontinuous mesophase,^[8–13] relatively few examples exist of the more challenging reverse mesophases^[14–17] in which the inorganic component forms the network channels. Moreover, all of these studies focused on cubic structures with $Ia\bar{3}d$ symmetry. Herein we report for the first time, to our knowledge, a simple approach to silica-based skeletal bicontinuous networks with $Im\bar{3}m$ symmetry in thick samples. Furthermore, the approach provides direct access to the

skeletal networks thereby rendering time consuming back-filling procedures unnecessary. The as-made nanocomposite derived from a block-copolymer-directed sol-gel synthesis consists of silica networks embedded in an organic matrix. The structure is robust enough to undergo calcination at high temperatures, which gives the final skeletal silica networks (also known as nano-relief structures). Small angle X-ray scattering (SAXS) and transmission electron microscopy (TEM) data are consistent with the plumber's nightmare morphology (point group $Im\bar{3}m$) based on the P minimal surface (see Figure 4).^[13,18,19] Proven modifications of the sol-gel process, to include transition-metal oxides,^[20] or extension of the approach to non-oxide ceramics, such as SiCN and SiC,^[21] may provide a unique approach to the straightforward design and fabrication of multifunctional skeletal networks in the future.

Many bicontinuous mesophases are based on minimal surfaces.^[22] Minimal surfaces, which have zero mean curvature all across the surface, result from the requirement of area-minimization of the intermaterial dividing surface of two dissimilar materials. A large variety of intertwined 3D continuous structures based on these minimal surfaces have been computed mathematically and, for several systems, realized experimentally.^[23,24] Extensive theoretical and experimental research has shown, however, that in classical block copolymers, energetic combined with space-filling requirements put considerable constraints on the equilibrium mesophases that can be obtained.^[25] Indeed, the double gyroid mesophase has been the only bicontinuous phase that has been found to be stable in diblock copolymer systems in a highly restricted parameter space.^[26] Similarly, most bicontinuous mesoporous inorganic materials obtained from organic templates also belong to the gyroid family.^[8–11] By careful manipulation of the polymer-ceramic interface utilizing organically modified silica precursors (ormocers) and working from organic solvents, we have recently shown the existence of a new bicontinuous cubic phase in bulk organic-inorganic hybrids and mesoporous materials derived from it that is consistent with the plumber's nightmare morphology.^[13,27] This result has opened the possibility for finding a variety of bicontinuous cubic phases by rationally altering the relative content of inorganic and organic components in the hybrids.^[28]

In contrast, the realization of the inverse bicontinuous structures where the inorganic components occupy the channels (that is, the minority volume fraction) has been much more challenging. Most approaches have been based either on thin films^[17] that cannot be easily extended to the bulk or negative replication of the parent mesophase which becomes the sacrificial mold.^[14–16] Negative replication using impregnation and other techniques, apart from being tedious, gives rise to large-scale imperfections and defects in the resulting strut networks. Herein we present a simple and direct approach to bicontinuous 3D connected robust network struts starting from a cubic bicontinuous bulk hybrid material for which structural data is consistent with the plumber's nightmare morphology that is subsequently heat-treated at high temperatures without loss of the structural symmetry.

[*] A. Jain, S. Mahajan, C. B. W. Garcia, U. Wiesner
Department of Materials Science and Engineering, Bard Hall
Cornell University
Ithaca, NY 14853 (USA)
Fax: (+1) 607-255-2365
E-mail: ubw1@cornell.edu

G. E. S. Toombes, S. M. Gruner
Department of Physics, Clark Hall
Cornell University, Ithaca, NY 14853 (USA)
L. M. Hall
Rose-Hulman Institute of Technology
Terre Haute, IN 47803 (USA)

W. Probst
Consulting & Education in Microscopy
Digital Imaging and Analysis, Essingen (Germany)

[**] The financial support of the National Science Foundation (Grant DMR-0072009) is gratefully acknowledged. The work made use of the Cornell Center for Materials Research (CCMR) electron microscopy facility, supported through the National Science Foundation Materials Research Science and Engineering Program (DMR-0079992), and the work was further supported by DOE grant DEFG02-97ER62443.

Monodisperse poly(isoprene-*b*-ethylene oxide) (PI-*b*-PEO), synthesized anionically (polydispersity < 1.1) with a total molecular weight of 19900 g mol⁻¹ and PEO volume fraction, f_{PEO} , of 0.15, was used as the structure-directing agent. The pure diblock copolymer exhibits a BCC morphology in the melt consisting of PEO spheres in a PI matrix. Sol-gel synthesis was carried out by mixing the polymer with ormocer precursor, (3-glycidyloxypropyl) trimethoxysilane (GLYMO) and aluminum *sec*-butoxide in a molar ratio of 80:20 following a procedure described elsewhere.^[7] The procedure used herein differs from that reported in that the evaporation of the solvents before the final condensation step was carried out in a rotating cylindrical Büchi evaporator under controlled vacuum. Assuming negligible phase mixing between the PI (density 0.91 g cm⁻³) and the inorganic/PEO microphases (density 1.4 g cm⁻³),^[29] the volume fraction of the PEO/inorganic phase in the as-made material was calculated to be 0.37. This is very close to the volume fraction of the PI channels (0.36 and 0.37) in the plumber's nightmare morphology.^[13,28] The as-made hybrid sample was then calcined by heating to 600 °C in several steps which pyrolyzed the organic components and left the bicontinuous skeletal networks of silica.

SAXS experiments were performed on both the as-made and calcined samples to determine the underlying symmetry of the nanostructured materials. Azimuthally integrated scattering profiles of X-ray scattering intensity, I , versus the magnitude of the scattering vector, $q = (4\pi/\lambda)\sin\theta$, where λ is the X-ray wavelength and 2θ is the scattering angle, for the as-made and the calcined samples are shown in Figure 1. As is typically the case for copolymer diffraction, the powder diffraction patterns yield too few orders to unambiguously assign a lattice symmetry. However, even a small number of rings allows the exclusion of most symmetries. The most intense and unambiguous reflections in Figure 1a have the distance ratios of $\sqrt{2}$, $\sqrt{6}$, $\sqrt{8}$, and $\sqrt{14}$. These ratios are consistent with the $Im\bar{3}m$ space group and inconsistent with the $Ia\bar{3}d$ gyroid-like symmetry. The unit cell size (73 nm) and relative peak intensities are quite similar to the more rigorously characterized regular structure that was assigned to the plumber's nightmare morphology.^[28] The scattering profile of the calcined material in Figure 1b differs considerably from the parent material. The most intense peaks have the distance ratios of $\sqrt{2}$, $\sqrt{4}$, $\sqrt{6}$, $\sqrt{8}$, and $\sqrt{12}$ with some scattering features also evident at $\sqrt{14}$. This is again consistent with the $Im\bar{3}m$ space group with a unit cell size of 47 nm. It corresponds to a shrinkage of the unit cell size by approximately 36% relative to the uncalcined material and is similar to calcination results on such block copolymer derived ormocer materials.^[28] The considerable change in the relative peak intensities is indicative of a significant variation in the structure factor of the calcined mesophase from the parent material. The plasticizing effect of the polymer chains on the ceramic in these materials was recently demonstrated by solid-state NMR spectroscopy.^[30] The changes in the scattering amplitude may reflect the ability of the ceramic to readjust and perfect the structure during calcination from the parent "flexible ceramic" nanocomposites.

In a number of calcined samples, individual crystallites were large enough that Bragg Peaks were observed (Fig-

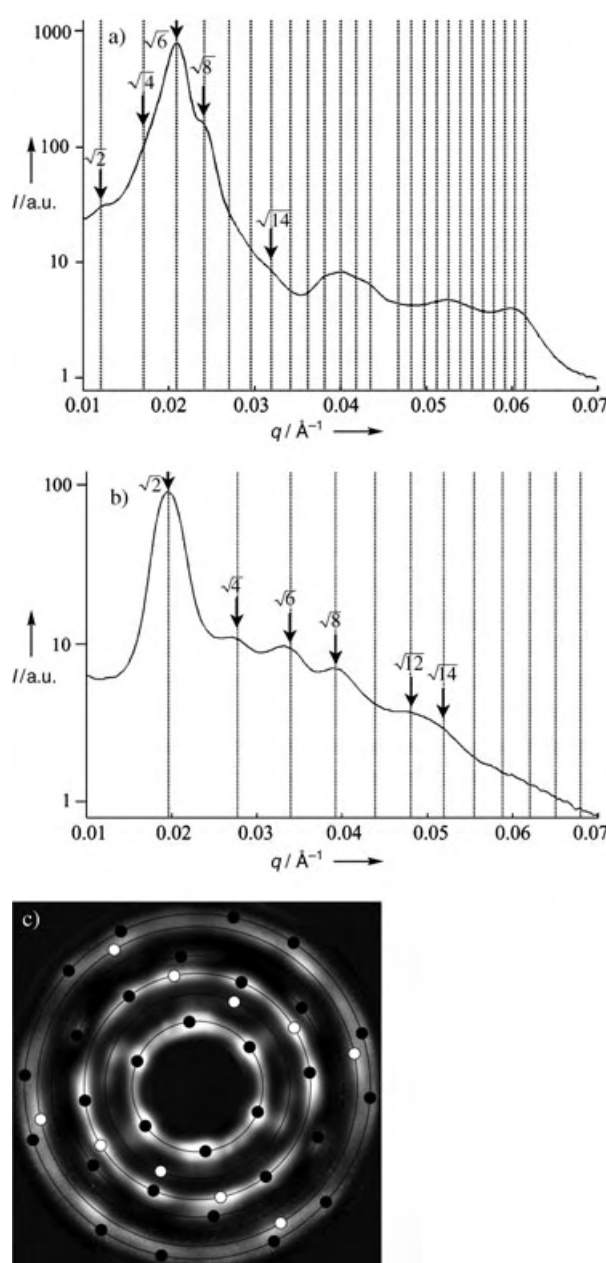


Figure 1. Azimuthally integrated scattering profile (X-ray intensity I versus scattering wave vector q) measured for the a) as-made and b) calcined samples. The vertical dotted lines correspond to the expected peaks for $Im\bar{3}m$ crystallographic space group. c) 2D SAXS pattern of the calcined sample. The markers correspond to the indexed peak positions for the calcined sample (see text for explanation). The radii of the circles q are given by $q = \sqrt{h^2 + k^2 + l^2}$, where h , k , and l are integers allowed by the $Im\bar{3}m$ symmetry group.

ure 1c). The pronounced sixfold symmetry of the diffraction image reflects the threefold symmetry ($\{111\}$ zone direction) of a cubic crystal. The black markers in Figure 1c locate the six $\sqrt{2}$ [110], six $\sqrt{8}$ [211], six $\sqrt{8}$ [220], and twelve $\sqrt{14}$ [321] peaks permitted in the $Im\bar{3}m$ space group. While there is no unique indexing for a diffraction pattern generated by multiple crystallites, most of the diffraction spots in Figure 1c were generated by a single crystallite. The white markers (zone direction [110]) illustrate how a second crystallite might

account for many of the remaining diffraction spots. Clearly, however, more than two crystallites contributed to the diffraction pattern. In other diffraction images, the fourfold symmetry axis of the $Im\bar{3}m$ space group has been observed (data not shown). These symmetries give us considerable confidence that the unit cell is cubic. The $\sqrt{2}$, $\sqrt{4}$, and $\sqrt{12}$ peaks eliminate the $Ia\bar{3}d$ (gyroid) space group while the space group $Pn\bar{3}m$ (double diamond) seems quite unreasonable given the systematic absence of $\sqrt{3}$, $\sqrt{9}$, and $\sqrt{11}$ peaks. The peaks and symmetries observed in the diffraction data are thus fully consistent with the $Im\bar{3}m$ (plumber's nightmare) space group.

The shrinkage of the unit cell volume and the association of the inorganic material with the minority fraction suggest that the calcined samples preserve the strut structure of the sample, which is the reverse of what has been observed when the PEO + inorganic component is the majority fraction. It is remarkable that calcination leaves behind the two discrete interwoven networks intact without collapsing on each other. We speculate that they are held in place by the grain boundaries. The absence of collapse of the network structure is corroborated by the high surface area indicated by nitrogen sorption/desorption measurements. Indeed, the calcined sample exhibits a nitrogen-sorption isotherm of type IV according to BDDT classification, with a specific surface area of $295 \text{ m}^2 \text{ g}^{-1}$ according to the Brunauer–Emmett–Teller (BET) method (data not shown).^[31]

To elucidate further the structure in real space, we have performed TEM on bulk, calcined, and solvent-dispersed samples. Figure 2a and b show two dark-field projections of the bulk as-made composite. The continuity of the silica networks (white struts) in the underlying structure is clearly observed in both images. The TEM image and its autocorrelation (inset) in Figure 2b indicate that the struts form a lattice of similar size to that determined by SAXS (some lattice distortion is expected from the sample and TEM

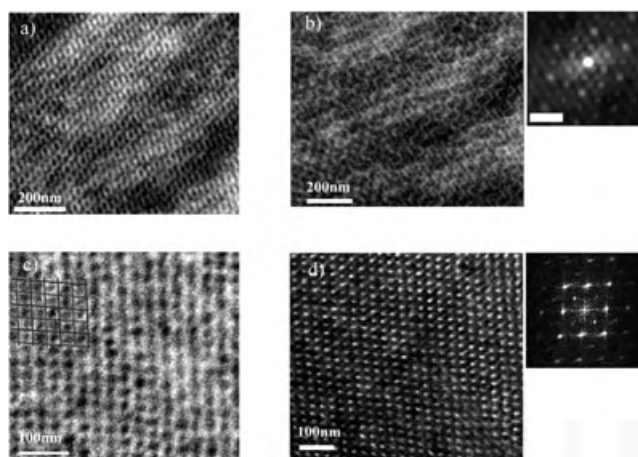


Figure 2. a) Dark-field TEM image of the as-made sample showing the continuous network structure. b) Dark-field image of the as-made sample showing network-struts. The inset shows the autocorrelation of the image; scale bar 100 nm. c) Dark-field image of the calcined sample. The black and the gray lines indicate the individual networks contained in the bicontinuous lattice. d) Bright-field image of the calcined sample. The inset shows the computed Fourier transform image.

specimen preparation method^[28]). Figure 2c shows a dark-field image of the calcined sample and indicates the individual networks that compose the mesophase. A bright-field image of the calcined sample is shown in Figure 2d. Despite minor distortion of the sample, the underlying lattice is clearly discernable. The peaks in the corresponding Fourier transform image (Figure 2d inset) give a consistent fit to a lattice of the $Im\bar{3}m$ space group with a side of 51 nm. This is within close tolerance of the value determined from SAXS.

The presence of the organic matrix around the silica channels can be used for dispersing the sample in an organic solvent, such as toluene. By sonicating a piece of the as-made sample in toluene, the network structure could be ripped apart and a colloidal solution was obtained. Such dispersion provides direct visualization of the network struts when viewed under TEM. Figure 3a–c show bright-field images of

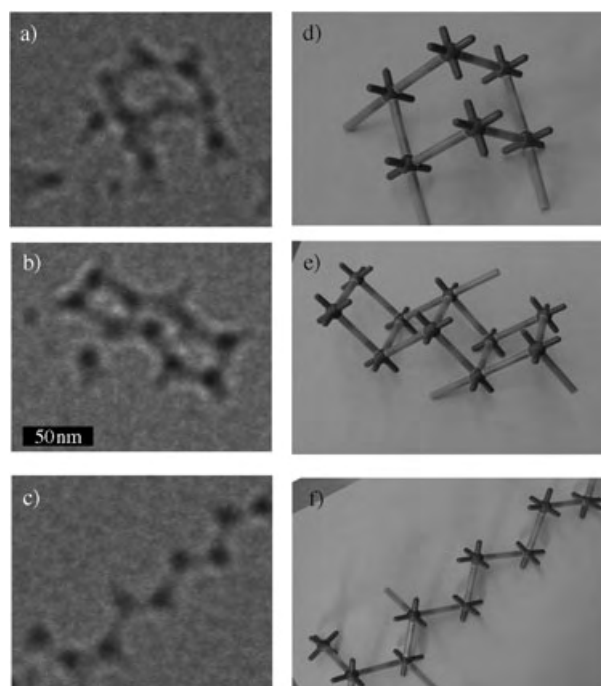


Figure 3. Bright-field TEMs of the broken network structure (a–c) dispersed in a toluene solution, and the corresponding projections from a bead–stick model (d–f). The scale bar in (b) is the same for all TEMs. The distance measured between the nodes are in accord with the expected value from SAXS and TEM measurements.

different broken network struts. The struts appear as light-gray lines connected together at junctions that resolve as dark spots in the TEM image. These images further confirm the skeletal character of the structure. As shown in Figure 3d–f, struts and junctions from a bead-and-stick model of the $Im\bar{3}m$ lattice can be assembled into matching projections.

In summary, we have demonstrated a simple and direct approach to thick samples of robust skeletal silica-based bicontinuous nanostructures. By using a combination of SAXS and TEM, the structure of the mesophase was found to be most consistent with the $Im\bar{3}m$ cubic space group associated with the plumber's nightmare morphology (Figure 4b) based on the “P” minimal surface (Figure 4a). The

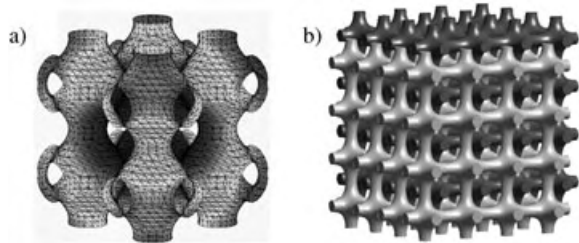


Figure 4. a) The "P" minimal surface. b) A skeletal structure of the plumber's nightmare with the networks occupying 37% of the volume.

existence of the bicontinuous structure in the reverse phase points towards the versatility and the generality of the phase space attainable by ormocer-derived organic-inorganic hybrid materials. Structural integrity was preserved in the thick samples after calcination although the inorganic constituent formed the minority phase. Nitrogen-sorption isotherms demonstrated a large surface area associated with these networks. These periodic and interconnected networks also have potential as photonic band-gap materials.^[32]

Experimental Section

SAXS data were collected on a Rigaku RU300 copper rotating-anode ($\lambda = 1.54 \text{ \AA}$) operated at 40 kV and 50 mA. X-rays were monochromatized with a Ni filter and focused using orthogonal Franks mirrors. SAXS patterns were collected with a homebuilt $1 \text{ K} \times 1 \text{ K}$ pixel CCD detector.^[33]

For TEM of the bulk samples, 50–100 nm sections were cut using a Leica Ultracut UCT microtome at 210 K (as-made composite) and 300 K (skeletal networks) and transferred to copper grids. TEM was performed on a Leo 922 Ω (tungsten filament) microscope at 200 kV using an objective aperture angle of 3.6 mrad. Images were taken in both the elastic filtering as well as the inelastic energy-loss imaging mode using a slow-scan CCD camera (lateral resolution $2 \text{ K} \times 2 \text{ K}$ pixels). A value of ΔE of 120–145 eV around the Si K edge was chosen for the images taken in the energy-loss mode. To image broken pieces of the network structure, samples were dispersed in toluene by stirring and sonication. The resulting colloidal suspension was transferred on carbon-coated grids. For ease in imaging, the grids were subjected to UV-ozonolysis/calcination to remove the organics before imaging under a JEOL 1200EX microscope operating at 120 kV in the bright-field mode.

Nitrogen adsorption and desorption isotherms were measured on a Micromeritics ASAP 2020 at 77 K after outgassing at 100 mPa for 15 h at 523 K.

Received: July 1, 2004

Revised: November 11, 2004

Published online: January 17, 2005

Keywords: block copolymers · ceramics · self-assembly · silicon · zeolite analogues

- [1] H. Eckert, M. D. Ward, *Chem. Mater.* **2001**, *13*, 3059.
- [2] C. T. Kresge, M. E. Leonowicz, W. J. Roth, J. C. Vartuli, J. S. Beck, *Nature* **1992**, *359*, 710.
- [3] A. Monnier, F. Schüth, Q. Huo, D. Kumar, D. Margolese, R. S. Maxwell, G. D. Stucky, M. Krishnamurthy, P. Petroff, A. Firouzi, M. Janicke, B. F. Chmelka, *Science* **1993**, *261*, 1299.
- [4] S. A. Bagshaw, E. Prouzet, T. J. Pinnavaia, *Science* **1995**, *269*, 1242.
- [5] D. Zhao, J. Feng, Q. Huo, N. Melosh, G. H. Fredrickson, B. F. Chmelka, G. D. Stucky, *Science* **1998**, *279*, 548.
- [6] L. Bronstein, E. Krämer, B. Berton, C. Burger, S. Förster, M. Antonietti, *Chem. Mater.* **1999**, *11*, 1402.
- [7] M. Templin, A. Franck, A. Du Chesne, H. Leist, Y. Zhang, R. Ulrich, V. Schädler, U. Wiesner, *Science* **1997**, *278*, 1795.
- [8] Y.-T. Chan, H.-P. Lin, C.-Y. Mou, S.-T. Liu, *Chem. Commun.* **2002**, *23*, 2878.
- [9] X. Liu, B. Tian, C. Yu, F. Gao, S. Xie, B. Tu, R. Che, L. Peng, D. Zhao, *Angew. Chem.* **2002**, *114*, 4032; *Angew. Chem. Int. Ed.* **2002**, *41*, 3876.
- [10] K. Flodstrom, V. Alfredsson, N. Kaellrot, *J. Am. Chem. Soc.* **2003**, *125*, 4402.
- [11] C. Yu, Y. Yu, D. Zhao, *Chem. Commun.* **2000**, *7*, 575.
- [12] D. Zhao, Q. Huo, J. Feng, B. F. Chmelka, G. D. Stucky, *J. Am. Chem. Soc.* **1998**, *120*, 6024.
- [13] A. C. Finnefrock, R. Ulrich, A. Du Chesne, C. C. Honeker, K. Schumacher, K. K. Unger, S. M. Gruner, U. Wiesner, *Angew. Chem.* **2001**, *113*, 1247; *Angew. Chem. Int. Ed.* **2001**, *40*, 1208.
- [14] B. Tian, X. Liu, L. A. Solovyov, Z. Liu, H. Yang, Z. Zhang, S. Xie, F. Zhang, B. Tu, C. Yu, O. Terasaki, D. Zhao, *J. Am. Chem. Soc.* **2004**, *126*, 865.
- [15] S. Che, A. E. Garcia-Bennett, X. Liu, R. P. Hodgkins, P. A. Wright, D. Zhao, O. Terasaki, T. Tatsumi, *Angew. Chem.* **2003**, *115*, 4060; *Angew. Chem. Int. Ed.* **2003**, *42*, 3930.
- [16] S. C. Laha, R. Ryoo, *Chem. Commun.* **2003**, *17*, 2138. See also F. Schüth, *Angew. Chem.* **2003**, *115*, 3730; *Angew. Chem. Int. Ed.* **2003**, *42*, 3604.
- [17] V. Z. H. Chan, J. Hoffman, V. Y. Lee, H. Iatrou, A. Avgeropoulos, N. Hadjichristidis, R. D. Miller, E. L. Thomas, *Science* **1999**, *286*, 1716.
- [18] D. A. Huse, L. Stanislas, *J. Phys.* **1988**, *49*, 605.
- [19] J. Seddon, R. Templar, *New Sci.* **1991**, *45*, 1769.
- [20] C. B. W. Garcia, Y. Zhang, F. DiSalvo, U. Wiesner, *Angew. Chem.* **2003**, *115*, 1564; *Angew. Chem. Int. Ed.* **2003**, *42*, 1526.
- [21] C. B. W. Garcia, C. Lovell, C. Curry, M. Faught, Y. Zhang, U. Wiesner, *J. Polym. Sci. Part B* **2003**, *41*, 3346.
- [22] E. L. Thomas, D. M. Anderson, C. S. Henkee, D. Hoffman, *Nature* **1988**, *334*, 598.
- [23] A good source for mathematical description and visualization of bicontinuous mesophases is available at <http://www.msri.org/publications/sgp/SGP/>
- [24] P. Ström, D. M. Anderson, *Langmuir* **1992**, *8*, 691.
- [25] I. W. Hamley, *The Physics of Block Copolymers*, Oxford University Press, Oxford, **1998**.
- [26] D. A. Hajduk, P. E. Harper, S. M. Gruner, C. C. Honeker, G. Kim, E. L. Thomas, L. J. Fetters, *Macromolecules* **1994**, *27*, 4063.
- [27] C. Garcia, R. Ulrich, M. Kamperman, A. Jain, U. Wiesner, unpublished results.
- [28] A. C. Finnefrock, R. Ulrich, G. E. S. Toombes, S. M. Gruner, U. Wiesner, *J. Am. Chem. Soc.* **2003**, *125*, 13084.
- [29] R. Ulrich, A. Du Chesne, M. Templin, U. Wiesner, *Adv. Mater.* **1999**, *11*, 141.
- [30] S. M. De Paul, J. W. Zwanziger, R. Ulrich, U. Wiesner, H. W. Spiess, *J. Am. Chem. Soc.* **1999**, *121*, 5727.
- [31] S. Brunauer, L. S. Deming, W. S. Deming, E. Teller, *J. Am. Chem. Soc.* **1940**, *62*, 1723.
- [32] M. Maldovan, A. M. Urbas, N. Yufa, W. C. Carter, E. L. Thomas, *Phys. Rev. B* **2002**, *65*, 165123.
- [33] M. W. Tate, S. M. Gruner, E. F. Eikenberry, *Rev. Sci. Instrum.* **1997**, *68*, 47.

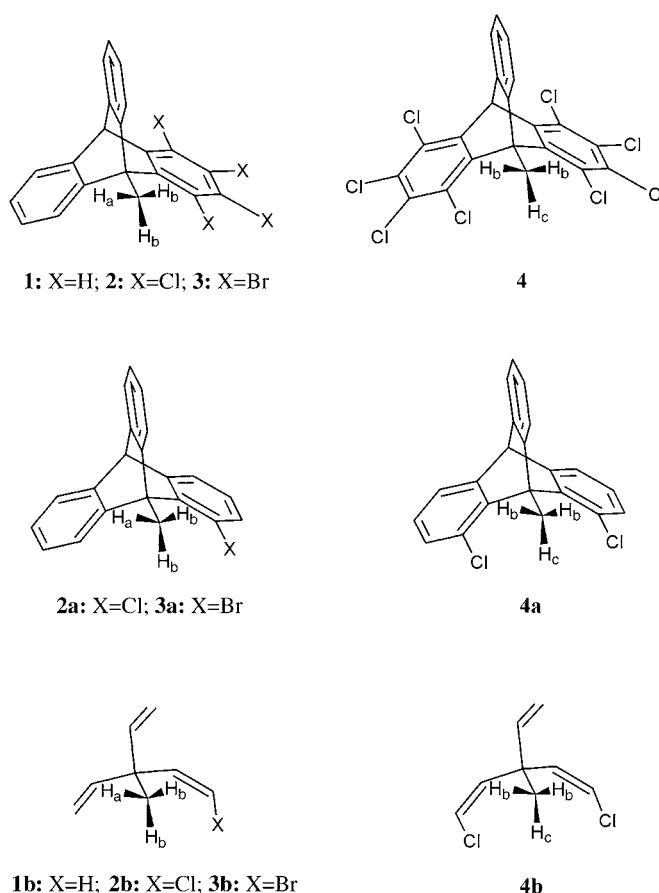
Hydrogen Bonds

$^1J(\text{C},\text{H})$ Couplings to the Individual Protons in a Methyl Group: Evidence of the Methyl Protons' Engagement in Hydrogen Bonds**

Tomasz Ratajczyk, Igor Czerski, Krystyna Kamienska-Trela, Sławomir Szymanski,* and Jacek Wojcik*

The exceptionally high torsional energy barriers, reaching 40 kJ mol^{-1} , for the methyl group in 9-methyltritycene derivatives bearing chlorine or bromine atoms in the *peri*-positions, allow the freezing out of the stochastic motion of the methyl rotor in these compounds on the timescale of NMR spectroscopy experiments in liquids.^[1–3] The measurements performed by us at ambient temperature for the parent 9-methyltritycene (**1**) as the reference molecule and in the range of 170–200 K for 1,2,3,4-tetrachloro-9-methyltritycene (**2**), 1,2,3,4-tetrabromo-9-methyltritycene (**3**), and 1,2,3,4,5,6,7,8-octachloro-9-methyltritycene (**4**; Scheme 1), yielded the $^1J(\text{C},\text{H})$ couplings to the individual methyl protons in all three halogeno derivatives. The protons of the methyl group in these compounds represent a first-order A_2B spin system with $^2J_{\text{H,H}}$ of approximately 12.5 Hz and a $|H_a - H_b|$ chemical shift difference of about 0.9–1.1 ppm, depending on the compound. This result allowed us to determine the $^1J(\text{C},\text{H})$ couplings directly from the corresponding ^{13}C satellite signals in ^1H spectra. The results are presented in Table 1.

In the parent methyltritycene **1** (in which the methyl protons are isochronous; Scheme 1) the $^1J(\text{C},\text{H})$ coupling of the methyl group (126.8 Hz) is similar to that in the methyl group of ethylbenzene (126.0 Hz).^[4] In compounds **2** and **3** the $^1J(\text{C},\text{H})$ value of approximately 131 Hz for protons H_b , which are close to the *peri* atom X (see Scheme 1) is considerably larger than that in **1**. For the *trans* disposed proton H_a which is remote from X, the coupling value is 124 Hz and is smaller than in **1**. In **4**, substitution of the second *peri* position with Cl causes further increase, up to the value of 135.5 Hz, of the



Scheme 1. Top row: Structures of the 9-methyltritycenes investigated. Middle row: model compounds for molecular geometry optimization. Bottom row: *cis* 1-halogeno-3-methyl-3-vinylpenta-1,4-dienes used as models for J coupling calculations.

coupling to the proton (H_c) which is close to the two chlorine atoms. In this compound, the $^1J(\text{C},H_b)$ couplings to the two remaining protons which have only one halogen atom at their neighborhood each are of 128 Hz. Thus, a close contact between a halogen atom and the proton involved in a C–H coupling causes a substantial increase of the $^1J(\text{C},\text{H})$ value.

The results can be interpreted in terms of a C–H...X ($X =$ halogen atom) interaction representing a specific, recently identified sort of hydrogen bonding.^[5a] For sp^3 carbon atoms, the distinctive feature of such a bonding is an electron-density transfer from the electron donor (X) to the σ^* orbital between the carbon atom and a substituent on the carbon atom that is remote from the donor.^[5a] The interaction has been termed hydrogen bonding because, as for the ordinary hydrogen bonds, it is associated with a characteristic modification of the C–H bond(s) proximate to X.^[5a] However, instead of a weakening typical for an ordinary hydrogen-bond, a strengthening/contraction is observed for such bonds.^[5a] Because this is reflected in a hyperchromic shift of the C–H stretching frequency, the effect is called blue-shifting hydrogen-bond.^[5a] It can also cause an enhancement of the corresponding $J(\text{C},\text{H})$ couplings.^[5a–c] The occurrence of such a bond has already been postulated in many intermolecular systems,^[5a–d] but its influence on the C–H coupling was usually much weaker

[*] Dr. J. Wojcik
Institute of Biochemistry and Biophysics
Polish Academy of Sciences
Pawinskiego 5a, 02-106 Warszawa (Poland)
Fax: (+48) 22-658-4683
E-mail: jacekw@ibb.waw.pl

T. Ratajczyk, I. Czerski, Prof. K. Kamienska-Trela, Prof. S. Szymanski
Institute of Organic Chemistry
Polish Academy of Sciences
Kasprzaka 44/52, 01-224 Warszawa (Poland)
Fax: (+48) 22-632-6681
E-mail: sszym@icho.edu.pl

[**] We thank Professor M. Jaszunski for insightful comments. The X-ray measurements were undertaken in the Crystallographic Unit of the Physical Chemistry Laboratory at the Chemistry Department of the University of Warsaw.

Supporting information for this article (synthesis, NMR measurements, computational methods, X-ray structure of compound **2**) is available on the WWW under <http://www.angewandte.org> or from the author.

(ca. 1 Hz or smaller^[5c,d]) than the effects reported herein. At variance with intermolecular systems, in an intramolecular case there are no reference values for the stretching frequencies and $^1J(\text{C,H})$ couplings of interest. Therefore, a series of indirect arguments is given below that speak in favor of the blue-shifting hydrogen bonds to occur in the systems presented.

We consider the RB3LYP/6-31G(D,P)-optimized geometrical data^[6] for **1** and for the appropriately simplified model compounds, that is, the 1-chloro- (**2a**), 1-bromo- (**3a**), and 1,5-dichloro- (**4a**) derivatives of 9-methyltritycene, (Scheme 1, middle). The calculated C–H bond length of 1.094 Å in the methyl group of the parent compound **1** is close to the value of 1.095 Å obtained by the same method for the methyl group in ethylbenzene. In agreement with expectations for the blue-shifting hydrogen-bond model, in **2a** and **3a** the C–H_b bonds near the halogen atom are shrunk to 1.090 Å while the length of the remote C–H_a bond remains the same as in **1**. The most significant contraction of the C–H bond, down to 1.085 Å, occurs in **4a** for the methyl proton H_c which is near to two chlorine atoms (with a distance of approximately 2.70 Å to each). For the two remaining protons in **4a** (protons H_b), the corresponding values are 1.091 Å and are close to those for protons H_b in **2a** and **3a**. Note that the DFT geometry of **2a** has been validated by the X-ray structure obtained for **2** (as far as the carbon atom positions are concerned; the experimental H atom positions are insufficiently accurate).^[7]

Further evidence of the occurrence of the C–H...X interaction is obtained from an analysis of the DFT J couplings calculated for the model *cis* and *trans* 1-halogeno-3-methyl-3-vinylpenta-1,4-dienes, (**2b–4b**, *cis* compounds shown in Scheme 1, bottom).^[8,9] The trends observed in the experimental J values are well reproduced by the couplings calculated for compounds of the *cis* configuration (Table 1). The couplings in *trans* compounds where the C–H...X interaction is not possible are very close to the DFT J coupling in the parent compound **1b** (122 Hz or slightly smaller). In all the cases the Fermi contact contribution is the main factor determining the coupling values (> 98 %) as well the changes occurring in them. The dia- and paramagnetic orbital dipole terms are small and their magnitudes remain constant through the whole series of the compounds studied.

For such 9-methyltritycene derivatives where the *peri* substituents do not have electron-donating properties, examples of the methyl group dynamics being frozen on the timescale of liquid-phase NMR spectroscopy are not known.^[2] Therefore, the strong steric repulsion alone, experienced by the methyl group in the transition state, is not enough to hinder the methyl rotation. When, as in the compounds investigated, the potential electron donors are present at a suitable distance, the ground torsional state can gain an extra stabilization through the hydrogen bonds engaging the methyl protons. This situation would explain the ease with which the methyl group rotation can be stopped, because in the transition state a similar stabilization could not be effected for geometrical reasons.

Table 1: $^1J(\text{C,H})$ Couplings to methyl protons in 9-methyltritycene derivatives.

Compound	$^1J(\text{C,H})$ (exp) [Hz]			Compound	$^1J(\text{C,H})$ (calcd) ^[a] [Hz]		
	H _a	H _b	H _c		H _a	H _b	H _c
1	126.8	–	–	1b	122.2	–	–
2	124	130.5	–	2b	118.8	124.2	–
3	124	131.5	–	3b	118.3	124.7	–
4	–	128.0	135.5	4b	–	121.2	129.5

[a] Calculated using truncated models of series **1b–4b** with the geometries optimized for **1** and models of series **2a–4a** (see text and Scheme 1).

The most direct evidence of the occurrence of the C–H...X hydrogen bonds stems from the natural bond orbital (NBO) analysis.^[10] In **2a**, an electron-density transfer from one of the three lone pairs of Cl to the remote σ^* orbital on the methyl carbon atom,^[5a] that is, to the σ^* orbital of the C–H_a bond situated *trans* to *peri*-Cl, does take place. (Note that, for the blue-shifting hydrogen-bond to be formed, the accepting orbital on carbon need not involve a C–H bond; in general, it can involve any properly situated C–Y bond^[5a] (see also the Supporting Information).) The corresponding NBO stabilization energy^[10] is 4.5 kJ mol^{–1}, this value can be used as a rough measure of the strength of the intramolecular hydrogen bond concerned. It seems likely that the decrease of the $^1J(\text{C,H}_a)$ coupling below the value in the parent system **1** is a response to this electron transfer.

The foregoing discussion sheds new light on the nature of factors that shape up the torsional potential of the methyl groups in the triptycenes investigated. Following the discovery of a novel dynamic effect, most clearly exhibited by strongly hindered methyl groups, the so called damped quantum rotation,^[3,11] a renewed interest in NMR spectroscopy studies of such systems can be expected.

Finally, effects similar to those described above were also found in 1,2,3,4-tetrachloro-9,10-dimethyltritycene (**5**) and 1,2,3,4-tetrabromo-9,10-dimethyltritycene (**6**). In 1,2,3,4-tetrafluoro-9-methyltritycene (**7**) the torsional energy barrier is not high enough to allow direct observation of the $^1J(\text{C,H})$ couplings of the individual methyl protons. For the CH...F grouping the NBO stabilization energy of only 2.5 kJ mol^{–1} was calculated for **7a**. Accordingly, the difference between the calculated $^1J(\text{C,H})$ couplings in **7b**, $^1J(\text{C,H}_b) - ^1J(\text{C,H}_a) = 4.5$ Hz, is noticeably smaller than the corresponding quantity for **2b** (5.4 Hz, see Table 1). This result is in a qualitative agreement with the relationship between the respective NBO stabilization energies. (For more details concerning compounds **5–7** see the Supporting Information.)

Received: July 21, 2004

Revised: August 27, 2004

Published online: January 17, 2005

Keywords: blue-shifting hydrogen bonds · density functional calculations · halogens · hydrogen bonds · NMR spectroscopy

[1] M. Nakamura, M. Oki, H. Nakanishi, O. Yamamoto, *Bull. Chem. Soc. Jpn.* **1974**, *47*, 2415–2419.

[2] M. Oki in *Reactivity and Structure Concepts in Organic Chemistry*, Vol. 30 (Eds.: K. Hafner, J. M. Lehn, C. W. Rees, P.

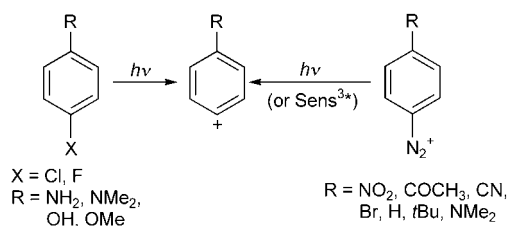
- von Rague Schleyer, B. M. Trost, R. Zahradnik), Springer, Berlin, **1993**, p. 84.
- [3] a) P. Bernatowicz, S. Szymanski, *Phys. Rev. Lett.* **2002**, *89*, 023004; b) I. Czerski, P. Bernatowicz, J. Jazwinski, S. Szymanski, *J. Chem. Phys.* **2003**, *118*, 7157–7160; c) P. Bernatowicz, I. Czerski, J. Jazwinski, S. Szymanski, *J. Magn. Reson.* **2004**, *169*, 284–292.
- [4] M. I. Watkins, G. A. Olah, *J. Am. Chem. Soc.* **1981**, *103*, 6566–6574.
- [5] a) K. Müller-Dethlefs, P. Hobza, *Chem. Rev.* **2000**, *100*, 143–167; b) X. Li, L. Liu, H. B. Schlegel, *J. Am. Chem. Soc.* **2002**, *124*, 9639–9647; c) M. P. M. Marques, A. M. Amorim da Costa, P. J. A. Ribeiro-Claro, *J. Phys. Chem. A* **2001**, *105*, 5292–5297; d) J. Wojcik, K. Kamienska-Trela, M. Pecul, E. Bartoszak-Adamska, S. I. Vdovenko, I. I. Gerus, *ChemPhysChem* **2004**, *5*, 159–165.
- [6] Gaussian03 (Revision B.04), M. J. Frisch, G. W. Trucks, H. B. Schlegel, G. E. Scuseria, M. A. Robb, J. R. Cheeseman, J. A. Montgomery, Jr., T. Vreven, K. N. Kudin, J. C. Burant, J. M. Millam, S. S. Iyengar, J. Tomasi, V. Barone, B. Mennucci, M. Cossi, G. Scalmani, N. Rega, G. A. Petersson, H. Nakatsuji, M. Hada, M. Ehara, K. Toyota, R. Fukuda, J. Hasegawa, M. Ishida, T. Nakajima, Y. Honda, O. Kitao, H. Nakai, M. Klene, X. Li, J. E. Knox, H. P. Hratchian, J. B. Cross, C. Adamo, J. Jaramillo, R. Gomperts, R. E. Stratmann, O. Yazyev, A. J. Austin, R. Cammi, C. Pomelli, J. W. Ochterski, P. Y. Ayala, K. Morokuma, G. A. Voth, P. Salvador, J. J. Dannenberg, V. G. Zakrzewski, S. Dapprich, A. D. Daniels, M. C. Strain, O. Farkas, D. K. Malick, A. D. Rabuck, K. Raghavachari, J. B. Foresman, J. V. Ortiz, Q. Cui, A. G. Baboul, S. Clifford, J. Cioslowski, B. B. Stefanov, G. Liu, A. Liashenko, P. Piskorz, I. Komaromi, R. L. Martin, D. J. Fox, T. Keith, M. A. Al-Laham, C. Y. Peng, A. Nanayakkara, M. Challacombe, P. M. W. Gill, B. Johnson, W. Chen, M. W. Wong, C. Gonzalez, J. A. Pople, Gaussian, Inc., Pittsburgh, PA, **2003**.
- [7] CCDC-245228 (2) contains the supplementary crystallographic data for this paper. These data can be obtained free of charge from The Cambridge Crystallographic Data Centre via www.ccdc.cam.ac.uk/data_request/cif.
- [8] Calculated using DeMoN program developed by V. G. Malkin, O. L. Malkina, D. R. Salahub, *Chem. Phys. Lett.* **1994**, *221*, 91–99. For further details see Supporting Information.
- [9] The geometry of the compounds was derived by partial truncation of the benzene rings in compounds of series **2a–4a** (see Scheme 1).
- [10] a) J. P. Foster, F. Weinhold, *J. Am. Chem. Soc.* **1980**, *102*, 7211; b) A. E. Reed, L. A. Curtiss, F. Weinhold, *Chem. Rev.* **1988**, *88*, 899–926.
- [11] S. Szymanski, *J. Chem. Phys.* **1999**, *111*, 288–299.

Metal-Free Cross-Coupling Reactions of Aryl Sulfonates and Phosphates through Photoheterolysis of Aryl–Oxygen Bonds**

Marco De Carolis, Stefano Protti, Maurizio Fagnoni,* and Angelo Albini*

Metal-mediated cross-coupling reactions have been extensively developed for the formation of aryl–carbon bonds. In these reactions, an aryl–halogen (mostly Br or I) or an aryl–oxygen bond is activated in the starting compound, for example, an aryl sulfonate^[1] can be used in the Suzuki–Miyaura procedure for the synthesis of biphenyls.^[2,3] A limitation of these syntheses is the severe experimental conditions that must be employed, such as an inert atmosphere, strictly anhydrous solvents, and the use of a base or a high temperature. Furthermore, although triflates are the most reactive precursors for the aryl sulfonate series they are less easily handled and are relatively expensive. Efforts to extend the reaction to the less reactive mesylates^[6] and tosylates have met with some success.^[1,6,7] Another class of reagents with a potential O-leaving group is the aryl phosphates, of which to our knowledge only a couple of examples have been reported. These involve coupling the phosphate with Grignard reagents in the presence of phosphane–nickel(II) complexes.^[8]

We have recently identified an alternative cross-coupling reaction, in which the aryl-substituted bond in the starting compound is cleaved heterolytically, rather than activated, by a photochemical reaction. For example, the photosensitized decomposition of diazonium salts allowed general access to a triplet phenyl cation^[9] (Scheme 1) which in turn reacted with olefins and aromatic compounds^[10] to generate aryl–carbon



Scheme 1. Photochemical generation of triplet phenyl cations.

[*] M. De Carolis, S. Protti, Dr. M. Fagnoni, Prof. A. Albini
Department of Organic Chemistry
University of Pavia
Via Taramelli 10, 27100 Pavia (Italy)
Fax: (+39) 0382-507-323
E-mail: fagnoni@unipv.it
angelo.albini@unipv.it

[**] Partial support of this work by Murst, Rome (Italy) is gratefully acknowledged.

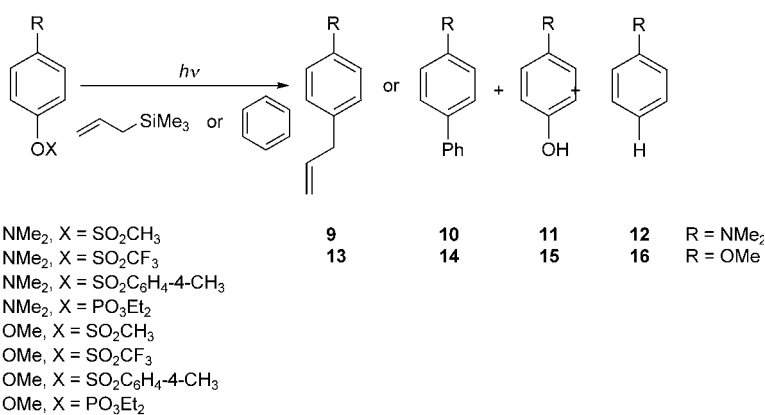


Supporting information for this article is available on the WWW under <http://www.angewandte.org> or from the author.

bonds. The electrophilic character of these salts limits the choice of nucleophiles that can be used in the photoarylation reactions, since there will be competing thermal reactions. However, aryl cations could also be photogenerated starting from electron-donating substituted aryl halides, such as chloro- or fluoroanilines,^[11] chlorophenols, and chloroanisoles^[12] (Scheme 1). Delocalization of the positive charge on the electron-donating substituents in the resulting aryl cation as well as the use of a polar medium resulted in efficient photoheterolysis. Extending the scope of this mild, metal-free cross-coupling reaction would greatly increase its synthetic significance.

We reasoned that the incorporation of O-leaving groups might also be beneficial in the aryl cation precursor, thus enabling the reaction to be applied to the readily available and versatile family of aryl esters. There are no precedents for such processes, and what is known about these compounds points to homolytic cleavage of the ArO–X bond, as exemplified by the (radical) photo-Fries reaction of organic esters.^[13] The photochemistry of their inorganic counterparts (aryl sulfonates and phosphates) has also not been extensively studied. Aryl tosylates were reported to undergo the photo-Fries reaction in polar solvents,^[14] but aryl triflates eliminated the triflate group both on irradiation in acetone^[15a] and under photoelectron transfer conditions (for example, from pentafluorophenyl triflate^[15b]), although this is known for a very limited number of cases. Furthermore, the nickel-mediated synthesis of biphenyl starting from phenyl triflate was favored in UV light.^[15c] The photolability of the aryl tosylates, like the aryl phosphates, has been known for 50 years and represents one of the first examples of photoinduced nucleophilic substitution.^[16] However, this photolability has remained limited to photohydrolysis in water,^[17] apart from the intramolecular process reported for alken-1-ylarylmethyl phosphates^[18a] and of bi- and triaryl phosphates,^[18b] where aryl-vinyl or aryl-aryl bonds are formed. Conversely, photofragmentation of the P–OAr bond occurred through resonant two-photon reactions on irradiation of the 4-methoxyphenyl-diethyl phosphate in cyclohexane.^[18c]

Therefore, we decided to investigate the photochemistry of *N,N*-dimethylamino- and methoxy-substituted phenyl sulfonates **1–3** and **5–7** as well as the phosphates **4** and **8**. These compounds are readily prepared from the corresponding phenols (see the Supporting Information) by irradiation in an argon-flushed polar solution in the presence of either allyltrimethylsilane (ATMS) or benzene (1M). The *N,N*-dimethylamino derivatives were found to decompose quantitatively (or close to) within 4–5 hours while the methoxy-derivatives needed 20–32 hours (Scheme 2, Table 1). We



Scheme 2. Arylation reactions by the irradiation of phenyl esters in the presence of allyltrimethylsilane or benzene.

Table 1: Photolysis of 4-*N,N*-dimethylamino esters **1–4** (0.05 M) in the presence of ATMS (1 M) or benzene (1 M).

Entry	Ester	Solvent	Nucleophile	Consumption [%]	t_{IRR} [h]	Yield ^[a] [%]		
						phenylated	11	12
1	1	MeCN	ATMS	100	4	9 , 95	–	–
2	1	TFE	ATMS ^[b]	100	4	9 , 100	–	–
3	1	H ₂ O/MeCN	ATMS ^[c]	100	4	9 , 100	–	–
4	1	TFE	benzene ^[b]	100	4	10 , 100	–	–
5	2	TFE	ATMS	73	5	9 , 15	81	–
6	2	TFE	benzene	84	5	10 , 19	56	5
7	3 ^[d]	^[d]	ATMS or benzene	29–85	5	^[d]	–	–
8	4	MeCN	ATMS	100	5	9 , 82	–	16
9	4	TFE	ATMS	100	5	9 , 100	–	–
10	4	H ₂ O/MeCN	ATMS ^[c]	100	5	9 , 100	–	–
11	4	TFE	benzene	85	5	10 , 96	–	4

[a] Yields determined by gas chromatography (GC) analysis based on consumed ester; for preparative results see the Experimental Section. [b] 0.2 M nucleophile. [c] ATMS at 0.5 M for solubility reasons. [d] No photoproducts detected by GC analysis under any of the conditions used for the other esters.

found that cross-coupling reactions had taken place in all cases and gave the corresponding allylated and phenylated derivatives. The product yield depended on the reagent used and on the solvent (MeCN, 2,2,2-trifluoroethanol (TFE), or H₂O/MeCN 1:5). Since acid was liberated in the process, the solutions were buffered by an equimolar amount of triethylamine (except when water was present in solution). Control experiments showed that thermal processes were not involved in the formation of the phenyl–carbon bonds.

Table 1 shows the results with dimethylaminophenyl esters as the substrates. In particular, photolysis of mesylate **1** in the presence of ATMS (1M) provided 4-(2-propenyl)-*N,N*-dimethylaniline (**9**) in almost quantitative yield.^[19] The formation of 4-phenyl-*N,N*-dimethylaniline (**10**) was quantitative in TFE in the presence of benzene; water/MeCN afforded the next highest yield (48 %), although photoreduction to *N,N*-dimethylaniline (**12**) was not negligible. However, triflate **2** gave a low yield of both **9** and **10** (15 and 19 %, respectively, in TFE), with deprotection to yield 4-hydroxy-*N,N*-dimethylaniline (**11**) being the main pathway. Tosylate **3** was more resistant to photodecomposition and no products were detected by gas chromatographic analysis (Table 1, entry 7).

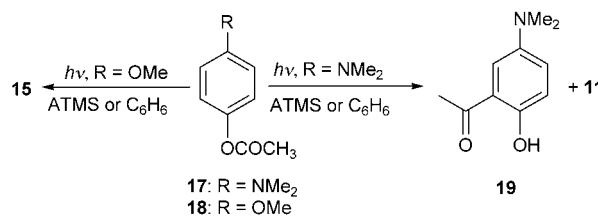
The performance of diethylphosphate **4** was very close to that of mesylate **1**. Allylated derivative **9** was produced in a quantitative yield when **4** was irradiated in TFE or MeCN/water while phenylated **10** was produced in a yield of 96 % in TFE and about 50 % in the other solvents. Phenylation was also examined in MeOH and no significant difference was observed when MeCN was used. The precursor that gave the best results was mesylate **1**, which gave equally good yields when lower amounts of both nucleophiles were employed (see Table 1, entries 2 and 4).

Since the conditions were different from those used in the original study on haloanilines,^[11] we tested the cross-coupling reactions of 4-chloro-*N,N*-dimethylaniline under these conditions for comparison. Formation of allylated **9** was quantitative in this case (ATMS could effectively be used at 0.2 M concentration), while phenylation of benzene occurred in a low to moderate yield (24–51 %). Again, reduction to *N,N*-dimethylaniline was the main competing process.

Methoxyphenyl esters **5–8** inefficiently absorbed the UV-B light used and reacted only sluggishly.^[22] Acetone (0.9 M) sensitization proved efficient even if irradiation times were four to six times longer than those of esters **1–4** (≈ 20 –30 hours).^[23,24] Photoreaction of mesylate **5** in the presence of ATMS yielded 4-(2-propenyl)anisole (**13**) and the yield increased from 17 % in acetonitrile to 100 % in aqueous acetonitrile^[25] (Scheme 2, Table 2). Phenylation of benzene

see Table 2, entry 4). Furthermore, the presence of oxygen only slightly affected the yield of **13** from **6** when the reaction was carried out in water/MeCN (Table 2, entry 5).

We then tested 4-(*N,N*-dimethylamino)phenyl (**17**) and 4-methoxyphenyl acetate (**18**) as representative organic esters (Scheme 3). Both compounds underwent photohomolysis of



Scheme 3. Photochemical reactions of phenyl acetates.

the acetyl group, and phenols **11** (14–45 %) and **15** (close to quantitative) were produced, as well as the photo-Fries product **19** (19–56 % yield) in the former case. Carrying out the irradiation in the presence of either ATMS (1 M) or benzene (1 M) did not affect the product distribution and no phenylation products were obtained.

Finally, precursors lacking electron-donating substituents were tested. Thus phenyl mesylate and phenyl triflate were photolyzed both in TFE and water/MeCN (the solvents which gave the best results in the previous cases) in the presence of the above nucleophiles, but neither allylbenzene nor biphenyl were formed.

The above data show that various phenyl sulfonates and phosphates with electron-donating substituents are suitable precursors for the photochemical phenylation of alkenes and arenes. Both mesylate **1** and phosphate **4** could be used for synthesizing *N,N*-dimethylamino derivatives **9** and **10** in quantitative yields, although concurrent paths dramatically lowered the arylation yield in the photodecomposition of triflate **2** and tosylate **3**. Also in the cases of the methoxyphenyl esters, triflate **6** was the best precursor for obtaining both **13** and **14**. The latter compound was also obtained in high yield from mesylate **5** and phosphate **8**,

while tosylate **7** gave complex mixtures. Phenyl esters performed better than phenyl halides in the arylation of arenes,^[26] where the latter precursors underwent reduction to a considerable extent (see below). The initiating photoheterolysis step liberated mineral acids during the reaction. The use of triethylamine as a buffer prevented the irradiated solutions from darkening and gave a clean reaction. Particularly noteworthy is that a mixed solvent containing water exerted a sufficient buffering effect.^[27]

The photoreactions of phenyl halides substituted with electron-donating groups^[11,12] and of benzenediazonium salts^[10] supports the theory that the arylation of esters results from the triplet state of the precursor. In this case, two

Table 2: Photolysis of 4-methoxy esters **5–8** in the presence of nucleophiles.

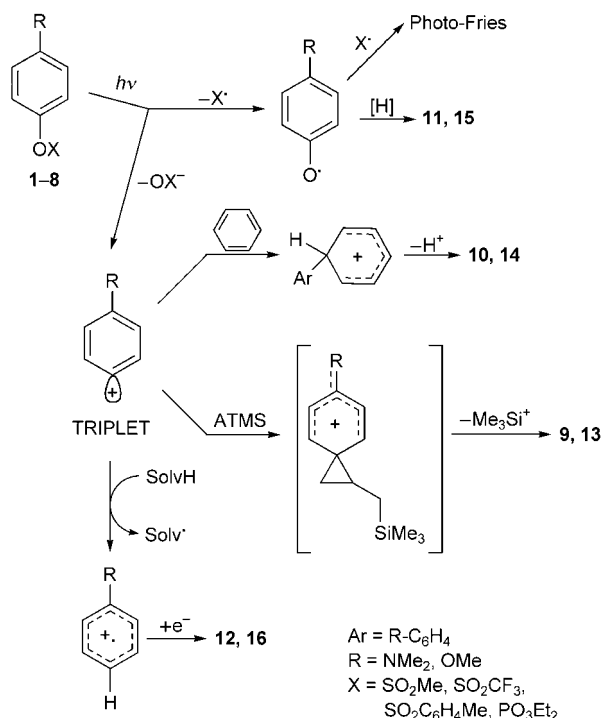
Entry	Ester	Solvent	Nucleophile	Consumption [%]	t_{IRR} [h]	Yield ^[a] [%]		
						phenylated	15	16
1	5	TFE	ATMS	79	30	13 , 73	–	6
2	5	H ₂ O/MeCN	ATMS ^[b]	100	24	13 , 100	–	–
3	5	H ₂ O/MeCN	benzene	100	24	14 , 58	–	8
4	6	TFE	ATMS	100	30	13 , 100 (48) ^[c]	–	–
5	6	H ₂ O/MeCN	ATMS ^[b,d]	100	24	13 , 90	–	9
6	6	TFE	benzene	100	28	14 , 97	–	–
7	6	H ₂ O/MeCN	benzene	100	24	14 , 74	–	9
8	7	TFE	ATMS	71	22	13 , 23	21	–
9	7	TFE	benzene	85	22	14 , 15	12	–
10	8	TFE	ATMS	100	30	13 , 44	–	12
11	8	TFE	benzene	100	24	14 , 96	–	–

[a] Yields determined by gas chromatographic (GC) analysis based on consumed ester; for preparative results see the Experimental Section. [b] ATMS at 0.5 M for solubility reasons. [c] 0.2 M nucleophile. [d] Under nondeaired conditions.

was less satisfactory, since the maximum yield of 4-phenylanisole (**14**) was 58 % both in water/MeCN and TFE. Triflate **6** gave moderate to excellent yields of both **13** and **14**, especially in TFE—a much better performance than both aminophenyl triflate **2** and methoxyphenyl mesylate **5**. Tosylate **7** gave complex mixtures with poor yields of the phenylation products (not exceeding 23 %), with deprotection being by far the main pathway. Again, TFE was the best solvent for the arylation reactions starting from phosphate **8**, and photoproducts **13** and **14** were isolated in 44 and 96 % yields, respectively.

Of the methoxyphenyl esters examined, triflate **6** gave the best results. The reaction proceeded fairly efficiently in TFE with a 0.2 M concentration of nucleophile (48 % with ATMS,

competitive cleavage paths operate (Scheme 4), with photolysis of the O–X bond forming a phenyloxy radical and photoheterolysis of the phenyl–O bond yielding a phenyl cation in the triplet state. The first pathway accounts both for



Scheme 4. Mechanistic paths in the photodegradation of esters **1–8**.

the formation of deprotected phenols **11** and **15** (important in the photolysis of triflate **2**) and for the photo-Fries reaction that occurs predominantly with acetate **17**. This route also probably has a role in the reactions with tosylates. The triplet phenyl cation formed in the second pathway adds selectively to π nucleophiles. Benzene rearomatization leads to biphenyls **10** and **14**, while elimination of a trimethylsilyl group by ATMS leads to allylbenzenes **9** and **13**.^[28] A competing reaction for the triplet cation is reduction by the solvent.^[31] The importance of this pathway depends on the starting material (and thus on the nature of the counterion XO^-) and of the π trap, as well as the solvent chosen. Among the aminophenyl esters reduction is significant particularly with the phosphate, while among the methoxyphenyl esters reduction is particularly significant with the mesylate and the triflate. However, in almost all cases it is possible to choose a solvent where reduction is minimized and arylation occurs in high or quantitatively yield, with TFE and MeCN/water (5:1) often being a good choice.

In summary, the photolysis of phenyl sulfonates and phosphates substituted with electron-donating groups is an appealing method for the phenylation of alkenes and arenes. The method is general and, when all the previous findings with phenyl halides and benzenediazonium salts are considered, compares favorably with metal catalysis^[32] in that mild conditions are employed. These reactions are also insensitive to oxygen and moisture (indeed, water can be used as a mixed

solvent) and avoids the use of bases or other aggressive reagents. In addition, a relatively low concentration of the π nucleophile is efficient (often 0.2 M, a 4:1 excess with respect to the ester), and expensive and often unstable catalysts are not required. The success of the reaction is based on the smooth photogeneration of the triplet phenyl cations and their selective reaction with π nucleophiles. Mechanistic studies on this previously unreported efficient photoheterolysis of the phenyl–oxygen bond of these esters are now underway.

Experimental Section

Typical procedure of the phenylation reactions through photoheterolysis of phenyl esters: A solution (18–30 mL) of ester **1–8** (0.05 M), triethylamine (TEA, 0.05 M), and benzene or ATMS (0.2 to 1 M) in the chosen solvent was poured in a quartz tube^[33] and purged for 10 min with argon, septum capped, and irradiated with six 15 W phosphor-coated lamps (range of emission 295–335 nm, maximum at 310 nm). The solution was concentrated in vacuo and purified by column chromatography (cyclohexane/ethyl acetate as eluants). In the reactions involving esters **5–8**, acetone (100 μ L per mL of solvent, 0.9 M) was added to the reaction mixture. When water/MeCN was used as the solvent, no TEA was added. The yields of isolated products consistently approached those determined by gas chromatographic analysis (Table 1 and Table 2); for example, compound **6** \rightarrow **13**, 80%; **6** \rightarrow **14**, 85%.

Received: July 27, 2004

Revised: October 13, 2004

Published online: January 12, 2005

Keywords: arylation · aryl cations · aryl esters · cross-coupling · photochemistry

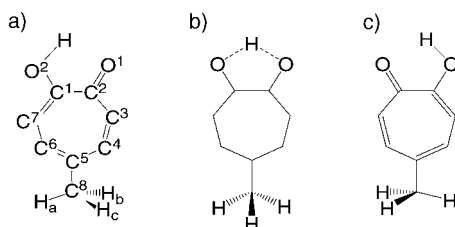
- [1] Z.-Y. Tang, Q.-S. Hu, *J. Am. Chem. Soc.* **2004**, *126*, 3058–3059, and references therein.
- [2] N. Miyaura, A. Suzuki, *Chem. Rev.* **1995**, *95*, 2457–2483; N. Miyaura, *Top. Curr. Chem.* **2002**, *219*, 11–59.
- [3] Very recently, biphenyls were obtained from aromatic ethers either by nickel-catalyzed cross-couplings with aryl Grignard reagents^[4] or ruthenium-mediated reactions with aryl boronates.^[5]
- [4] J. W. Dankwardt, *Angew. Chem.* **2004**, *116*, 2482–2486; *Angew. Chem. Int. Ed.* **2004**, *43*, 2428–2432.
- [5] F. Kakiuchi, M. Usui, S. Ueno, N. Chatani, S. Murai, *J. Am. Chem. Soc.* **2004**, *126*, 2706–2707, and references therein.
- [6] V. Percec, J.-Y. Bae, D. H. Hill, *J. Org. Chem.* **1995**, *60*, 1060–1065; V. Percec, G. M. Golding, J. Smidrkal, O. Weichold, *J. Org. Chem.* **2004**, *69*, 3447–3452.
- [7] A. H. Roy, J. F. Hartwig, *J. Am. Chem. Soc.* **2003**, *125*, 8704–8705; H. N. Nguyen, X. Huang, S. L. Buchwald, *J. Am. Chem. Soc.* **2003**, *125*, 11818–11819; A. Fürstner, A. Leitner, M. Mendez, H. Krause, *J. Am. Chem. Soc.* **2002**, *124*, 13856–13863; D. Badone, R. Cecchi, U. Guzzi, *J. Org. Chem.* **1992**, *57*, 6321–6323.
- [8] M. Tanaka, K. Chiba, M. Okita, T. Kaneko, K. Tagami, S. Hibi, Y. Okamoto, H. Shirota, M. Goto, H. Obaishi, H. Sakurai, Y. Machida, I. Yamatsu, *J. Med. Chem.* **1992**, *35*, 4665–4675; T. Hayashi, Y. Katsuro, Y. Okamoto, M. Kumada, *Tetrahedron Lett.* **1981**, *22*, 4449–4452.
- [9] In contrast to the singlet states, triplet phenyl cations behave as selective electrophiles and react with π , not n nucleophiles; see reference [10].

- [10] S. Milanese, M. Fagnoni, A. Albini, *Chem. Commun.* **2003**, 216–217.
- [11] B. Guizzardi, M. Mella, M. Fagnoni, M. Freccero, A. Albini, *J. Org. Chem.* **2001**, *66*, 6353–6363; M. Mella, P. Coppo, B. Guizzardi, M. Fagnoni, M. Freccero, A. Albini, *J. Org. Chem.* **2001**, *66*, 6344–6352; B. Guizzardi, M. Mella, M. Fagnoni, A. Albini, *Tetrahedron* **2000**, *56*, 9383–9389; B. Guizzardi, M. Mella, M. Fagnoni, A. Albini, *Chem. Eur. J.* **2003**, *9*, 1549–1555; A. Fraboni, M. Fagnoni, A. Albini, *J. Org. Chem.* **2003**, *68*, 4886–4893.
- [12] S. Protti, M. Fagnoni, M. Mella, A. Albini, *J. Org. Chem.* **2004**, *69*, 3465–3473.
- [13] J. W. Meyer, G. S. Hammond, *J. Am. Chem. Soc.* **1972**, *94*, 2219–2228; M. R. Sandner, E. Hedaya, D. J. Trecker, *J. Am. Chem. Soc.* **1968**, *90*, 7249–7254.
- [14] D. Bellus in *Advances in Photochemistry*, Vol. 8 (Eds.: J. N. Pitts, Jr., G. Hammond, W. A. Noyes, Jr.), Wiley-Interscience, New York, **1971**, pp. 109–159; J. L. Stratenus, E. Havinga, *Recl. Trav. Chim. Pays-Bas* **1966**, *85*, 434–436; E. Elhalem, B. N. Bailey, R. Docampo, I. Ujvari, S. H. Szajnman, J. B. Rodriguez, *J. Med. Chem.* **2002**, *45*, 3984–3999.
- [15] a) Y.-S. Chang, J.-S. Jang, M. L. Deinzer, *Tetrahedron* **1990**, *46*, 4161–4164; b) Q.-Y. Chen, Z.-T. Li, *J. Org. Chem.* **1993**, *58*, 2599–2604; c) S. Knapp, J. Albaneze, H. J. Schugar, *J. Org. Chem.* **1993**, *58*, 997–998.
- [16] E. Havinga, R. O. De Jongh, W. Dorst, *Recl. Trav. Chim. Pays-Bas* **1956**, *75*, 378–383.
- [17] R. S. Givens, L. W. Kueper III, *Chem. Rev.* **1993**, *93*, 55–66.
- [18] a) M. Nakamura, Y. Okamoto, S. Takamuku, *Chem. Commun.* **1996**, 209–210; b) M. Shi, K. Yamamoto, Y. Okamoto, S. Takamuku, *Phosphorus Sulfur Silicon Relat. Elem.* **1991**, *60*, 1–14; c) M. Nakamura, A. Ouchi, M. Miki, T. Majima, *Tetrahedron Lett.* **2001**, *42*, 7447–7449.
- [19] Palladium-catalyzed arylation of allyltrimethylsilane starting from aryl iodides led to allyl aromatic compounds in low to good selectivities according to the conditions used,^[20] whereas aryl triflates afforded arylated allylsilanes.^[21]
- [20] T. Jeffery, *Tetrahedron Lett.* **2000**, *41*, 8445–8449.
- [21] K. Olofsson, M. Larhed, A. Hallberg, *J. Org. Chem.* **1998**, *63*, 5076–5079.
- [22] Methoxyphenyl esters exhibited the long-wavelength band at 275–280 nm, with virtually no absorption at 310 nm, thus poorly matching the spectrum of the lamp (see Experimental Section). In contrast, aminophenyl esters strongly absorbed at 310 nm ($\epsilon \approx 1200\text{--}2500 \text{ mol}^{-1} \text{ dm}^3 \text{ cm}^{-1}$).
- [23] Some irradiations with mesylate **5** in the presence of ATMS were carried out under nonsensitized conditions at 254 nm and gave the same product distribution, although product **13** was not stable under prolonged irradiation. The use of the lamps at a wavelength of 310 nm prevented both product photodegradation and competitive absorption by benzene when this was used as the trap. A possible wavelength dependence of the reaction is under investigation.
- [24] In these acetone-sensitized reactions in the presence of ATMS, the Paternò-Büchi oxetane was found as a by-product in a variable amount, particularly in the case of phosphate **8**.
- [25] The presence of a protic polar medium (for example, water) could dramatically favor the photoheterolytic process, see: M. Freccero, M. Fagnoni, A. Albini, *J. Am. Chem. Soc.* **2003**, *125*, 13182–13190.
- [26] 4-Methoxybiphenyl was obtained only in 7% yield in aprotic solvent after irradiation of 4-chloroanisole in the presence of benzene (1M). In TFE the yield did not exceed 70%.
- [27] Triethylamine (0.05 M) buffers the acid liberated in the photolysis of the esters and avoids degradation and polymerization of the photoproducts, as indicated by experiments using cesium carbonate instead which led to the same product distribution.
- However, the use of the MeCN/water mixed solvent made the use of a base unnecessary, thus supporting the idea that electron transfer between the amine and the triplet state of the aromatic reagents (very short lived in the halides, reference [25] and presumably also of the esters) is not involved in the arylation reaction.
- [28] Attack of allyltrimethylsilane by cations is well known. The alternative formation of compounds **9** and **13** by a photo-generated aryl radical is excluded on two grounds. First, it has been reported that such a path operates only with strongly electrophilic aryl radicals (for example, 3,5-dinitrophenylradical^[29]) and, then, only with a poor yield. Moreover, β fragmentation of the adduct radical leading to allylated derivatives is usually observed with an $(\text{Me}_3\text{Si})_3\text{Si}$ group rather than with other alkyl- or aryl-substituted silanes.^[30] Second, purposely designed experiments disfavor this hypothesis. Thus, generation of an authentic 4-methoxyphenyl radical by photolysis of 4-bromoanisole in the presence of ATMS gave no allylated compounds but only anisole. Likewise, substituting 2,3-dimethylbutene for ATMS gave 2,3-dimethyl-3-(4-methoxyphenyl)-1-butene, 2,3-dimethyl-3-(4-methoxyphenyl)-2-(2,2,2-trifluoroethoxy)butane, 2,3-dimethyl-2-(4-methoxyphenyl)butane, and 2-(4-methoxyphenyl)-2-(2,2,2-trifluoroethoxy)-3,3-dimethylbutane from **5** in $\text{CF}_3\text{CH}_2\text{OH}/\text{Cs}_2\text{CO}_3$, in the same proportion as from 4-chloroanisole (see reference [12]). This reaction is difficult to envisage other than involving loss of a proton from (or solvent addition to) an adduct cation. (Further evidence is the fact that a cationic Wagner–Meerwein rearrangement has taken place in the last product).
- [29] F. Ek, L.-G. Wistrand, T. Frejd, *J. Org. Chem.* **2003**, *68*, 1911–1918.
- [30] L. Chabaud, P. James, Y. Landais, *Eur. J. Org. Chem.* **2004**, 3173–3199.
- [31] The role of solvents, and in particular of alcohols, as hydrogen donors (and not as nucleophiles) in the reaction with the triplet phenyl cation has been previously demonstrated, see Refs. [10–12].
- [32] In rare instances, the Suzuki coupling occurred under microwave irradiation in the absence of a catalyst, see: N. E. Leadbeater, M. Marco, *Angew. Chem.* **2003**, *115*, 1445–1447; *Angew. Chem. Int. Ed.* **2003**, *42*, 1407–1409.
- [33] Quartz allowed the absorption of all of the light emitted by the lamp.

Methyl Group Rotation Driven by Proton Transfer through a Long-Range Chemical Interaction**

Hiroshi Ushiyama* and Kazuo Takatsuka*

Proton transfer takes place ubiquitously in water, many organic compounds, proteins, DNA, and so on, and therefore it is a very fundamental chemical reaction that plays a vital role in biological processes and material sciences.^[1–3] Likewise, the internal rotation of the methyl group and its derivatives constitute a fundamental notion in the study of molecular structure and dynamics.^[4] Herein, we discuss an almost unidirectional interaction between these two dynamical elements, by which proton transfer can induce the internal rotation of a methyl group in a mutually remote site. Such an interaction can be typically found in the ground state of 5-methyltropolone (5MTR, Scheme 1). Reciprocating motion



Scheme 1. a) Stable structure of 5-methyltropolone (5MTR), b) the transition state, and c) the mirror image of a). The torsional angle θ of the methyl group is defined as the dihedral angle between the planes of C4–C5–C8 and C5–C8–H_a. $\theta = \pi$ and 0 for the structures a) and c), respectively. The irrelevant hydrogen atoms are omitted for clarity.

of the proton is mechanically transformed to rotational motion of the methyl group. This phenomenon is not only chemically surprising but interesting for the study of molecular machines.^[6–9] Also, this dynamic coupling interaction suggests that a large conformational change in a molecule can be triggered by relevant proton transfer processes.^[4] We have

found that the mechanism of this long-range interaction is quite generic and can be explained by quantum-mechanical interactions between the hyperconjugation of the methyl group and the tautomerization resulting from proton transfer.

Recently, in the fluorescence excitation and hole-burning spectra in the S₁–S₀ region of 5MTR, Nishi et al. found that the excitation of the internal rotational levels of the methyl group promotes proton tunneling.^[10,11] This finding suggests the existence of a very long-range interaction between proton tunneling and methyl internal rotation in the *excited state*. Inspired by this remarkable discovery, we studied the proton transfer dynamics in the *ground state* potential surface of 5MTR and other relevant molecules by different theoretical methods. We were looking for a long-range mechanical interaction and found an interesting interaction that is fundamentally essential to many aspects of molecular science.

The basic energetics of 5MTR are: The density functional theory (DFT) with the B3LYP functional using 6-31G** gives 0.219 eV for the transition state (the energy barrier from a) to c) via b) in Scheme 1), whereas for tropolone, that is, without the methyl group, it is 0.193 eV. On the other hand, the rotational barrier of the methyl group in the torsional angle, freezing all the other molecular geometries at the potential minimum, is 0.034 eV.^[12] Therefore the difference between the barrier heights of 5MTR and tropolone in their transition states comes from the rotational barrier of the methyl group. These values depend on the computational methods used, and DFT tends to give smaller values. However, the overall features estimated by other methods are all qualitatively common. We applied the restricted Hartree–Fock (RHF), Møller–Plesset perturbation theory (MP2), and configuration interaction with single and double excitations (CISD). The basic nature of the electronic structure is reflected in the bond lengths. The single bonds (C2–C3, C4–C5, and C6–C7) are about 1.42 Å, whereas the double bonds (C3=C4, C5=C6, and C7=C1) are shorter (1.37 Å). Bond alternation follows proton transfer, switching the sites of the single and double bonds; that is, tautomerization (Scheme 1). In other words, proton transfer has to surmount the potential barrier to perform such a tautomerization and large geometrical deformation.^[13] The bond C1–C2 is exceptional since it remains single and long during proton transfer.

To study the relevant dynamics, we carried out the full dimensional ab initio molecular dynamics at the RHF level of approximation.^[14,15] In our ab initio simulation, energies and potential derivatives were calculated with the RHF method of the 6-31G basis set. Even with the RHF method, full-dimensional dynamics are very time-consuming. We first sampled the position of each atom \mathbf{R}_{init} randomly around the optimized stable structure \mathbf{R}_{opt} within the range of $|\mathbf{R}_{\text{init}} - \mathbf{R}_{\text{opt}}| < 0.2$ Å. Each trajectory was integrated with zero initial momenta in terms of the locally analytic integrator.^[16] After the trajectories had been run for 10 fs, all the momenta were scaled to attain an aimed total amount of energy. We studied three cases having a total energy of 1.25 E_0 , 2.75 E_0 , and 4.25 E_0 , where E_0 is the vibrational zero point energy (4.205 eV) of 5MTR. Fifty trajectories were sampled for each energy. Although these energies are seemingly much higher than the transition state energy, proton transfer does not take

[*] Dr. H. Ushiyama, Prof. K. Takatsuka
Department of Basic Science
Graduate School of Arts and Sciences
The University of Tokyo, Komaba, 153-8902, Tokyo (Japan)
Fax: (+81) 3-5454-6588
E-mail: ushiyama@mns2.c.u-tokyo.ac.jp
kaztak@mns2.c.u-tokyo.ac.jp

[**] The authors thank Professors Jörn Manz and Keiichi Ogawa for valuable discussions. This work was supported in part by a Grant-in-Aid for Basic Science and the 21st Century COE Program for Frontier in Fundamental Chemistry from the Ministry of Education, Science, Culture, Sports, Science, and Technology of Japan. Support from JSPS for the Japan–Germany cooperative research project is also gratefully acknowledged.

Supporting information for this article is available on the WWW under <http://www.angewandte.org> or from the author.

place readily, since the energy is distributed over all the possible modes. Only 4 (for $1.25 E_0$), 13 (for $2.75 E_0$), and 20 (for $4.25 E_0$) trajectories out of the individual fifty samples realized proton transfer within 1 ps. Except for the clear difference in the frequencies of proton transfer, not much dependence on energy was observed. In particular, all proton transfers were always followed by methyl group rotation.

Herein, we define the moment of proton transfer as the instant when the relevant proton comes to the middle position between the two oxygen atoms. At this moment, bond alternation is not usually observed yet; however, 10–15 fs after this, the reorganization of the electronic structure follows. Thus, the proton undergoes transfer prior to tautomerization, and moreover, if the bond alternation does not follow successfully, the proton returns to the original site.^[13] On the other hand, it has been numerically confirmed that the electron density on the seven-membered ring is virtually unchanged before and after rotation of the methyl group. Thus, virtually no mechanical path exists through which internal rotation of the methyl group can transmit energy to the proton transfer site.

Figure 1 shows the change in the torsional angle of the methyl group after proton transfer, which has been averaged over the sampled trajectories of $2.75 E_0$. Around 30–40 fs

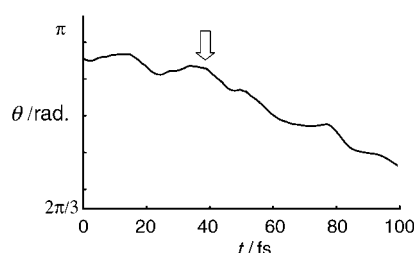


Figure 1. Time dependence of the torsional angle θ of the methyl group after proton transfers (see Scheme 1). The angles are statistically averaged over the different occasions of proton transfer observed in the trajectories of $2.75 E_0$. θ larger than π has been transformed to $2\pi - \theta$.

(marked with an arrow) after proton transfer, the methyl group begins to rotate, which changes the angle by 60° over approximately 100 fs. (For a more direct inspection a movie can be seen in the Supporting Information.) The rotation often continues and exceeds 60° because of inertia and slow intramolecular energy relaxation, although sometimes it stops at approximately this angle. If proton transfer does not occur, the torsional angle most frequently remains constant in this time scale. Since the tautomerization takes place 10–15 fs after the proton transfer, the methyl group begins to rotate after the tautomerization is finished. Although these estimated values are dependent on the quality of the adopted approximation, it is thus confirmed that methyl group rotation follows proton transfer. Therefore it is established that a quantum-mechanical mechanism is involved in the conformational change of this molecule, by which the in-plane reciprocating motion of the proton is unidirectionally transmitted to the rotational motion of the methyl group at a remote site.

We analyzed the mechanism of these correlated dynamics in terms of hyperconjugation within the molecule coupled with the tautomerization. Hyperconjugation is a classic concept in organic chemistry established by Dewar many years ago^[17,18] (refs. [5,19] give a more sophisticated treatment of hyperconjugation): A minus linear combination of the 1s atomic orbitals of two hydrogen atoms in a methyl group can behave somewhat like a 2p orbital and thereby can participate in a nearby π conjugation at an appropriate orientation. Therefore it is quite natural to consider that the hyperconjugation can couple with the π system of the seven-membered ring of tropolone and this interaction should be (positively or negatively) greatest when a pair of hydrogen atoms is positioned vertically to the tropolone plane. We shall call this pair in the upright position the vertical pair (VP).

Since the methyl group is regarded as an electron-donating functional group, the primary interaction between the methyl and π system should arise from the HOMO of the methyl group and the LUMO of tropolone. In practice, the methyl group is represented as methane in terms of its size and orientation in this study. As for another HOMO–LUMO interaction, the LUMO of methane is symmetric with respect to the molecular plane, whereas the HOMO of tropolone, which is a π orbital, is antisymmetric. Hence, this pairing results in virtually no interaction between these two orbitals.^[20] Figure 2 shows such a HOMO–LUMO interaction.

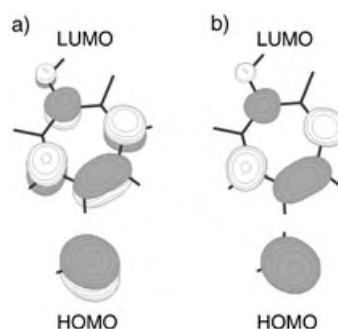


Figure 2. A HOMO (methyl group)–LUMO (tropolone) interaction representing coupling between hyperconjugation and tautomerization. a) A perspective view of 5-methyltropolone (5MTR) of Scheme 1 a from the side of the methyl group. b) Projection of a) onto the molecular plane.

Here, one of the HOMOs of methane, representing the methyl group is primarily composed of two 1s orbitals on two hydrogen atoms, which are perpendicular to the molecular plane, and looks just like a 2p orbital. (The two hydrogen atoms that are seen lie in the molecular plane and have nothing to do with hyperconjugation. One of them is responsible for the C–C bond between tropolone and the methyl group.) As is clearly seen in Figure 2b, the LUMO of tropolone has a large amplitude on the C4–C5 bond and has the right phase thus allowing a good overlap with the HOMO of the methyl group. On the other hand, the LUMO has a node inbetween C5 and C6, which should cancel or weaken the hyperconjugation. Besides, there is a large component of the tropolone's HOMO at C5–C6 (not shown graphically),

which induces an exchange repulsion with the HOMO of the methyl group (HOMO–HOMO interaction). Therefore the VP should be placed at the side of C4–C5, thus letting the methyl group sit comfortably with the tropolone π system. (The rotational barrier is estimated to be 0.034 eV.) Once the proton transfer, which is associated with tautomerization, takes place, the HOMO of the methyl group loses its stability and faces repulsion. (The LUMO of tropolone after proton transfer can be readily obtained as the mirror image of the LUMO in Figure 2.) To avoid this repulsion, the methyl group rotates by 60° to establish a new stable HOMO–LUMO interaction by placing the VP at the site of C5–C6, as in Scheme 1c.

This mechanism is qualitative, general, and robust. For instance, it is likely that the present dynamics will occur even if proton transfer proceeds by quantum-mechanical tunneling, as long as the associated wavepacket state can induce tautomerization. From this mechanism, certain theoretical deductions and predictions may be made. Figure 3 shows the

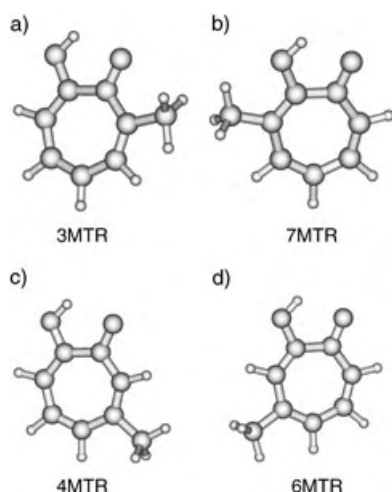


Figure 3. Stable structures of methyltropolones: a) 3-methyltropolone (3MTR) (0.082 eV), b) 7-methyltropolone (7MTR) (0.052 eV), c) 4-methyltropolone (4MTR) (0.038 eV), and d) 6-methyltropolone (6MTR) (0.042 eV). The values in parentheses are the height of their rotational barrier (0.034 eV for 5-methyltropolone).

stable structures of the methyltropolone derivatives: 3-methyltropolone (3MTR), 7-methyltropolone (7MTR), 4-methyltropolone (4MTR), and 6-methyltropolone (6MTR). Noting the orientation of the methyl group, the rotational barriers of the methyl group in these molecules as estimated by DFT are 0.082, 0.052, 0.038, and 0.042 eV, respectively. The primary reason for these orientations is that the VP of 3MTR avoids the node of the LUMO at C3–C4 preferring the simple LUMO at C2–C3. The orientation in 7MTR is interesting in that the VP seems to avoid the node of the LUMO formed inbetween C1 and O2 and prefers the simple LUMO component between C6–C7. It is easy to extend this view to 4MTR and 6MTR.

It can be readily seen that 3MTR and 7MTR are the proton-transfer product counterparts of each other as are 4MTR and 6MTR. This implies that proton transfer in 3MTR

should cause methyl rotation leading to the most stable orientation of 7MTR. Likewise, proton transfer in 7MTR should induce methyl rotation. A similar phenomenon should be the case for 4MTR and 6MTR. Thus, internal rotation of the methyl group can be induced at any site from C3 to C7.

Although our study was stimulated by the dynamics of 5MTR, we emphasize that the present phenomenon and its mechanism can be observed in other molecular systems. A simple example is methylmalonaldehyde (larger and more complicated systems, including intermolecular proton transfer, will be reported elsewhere).^[21] Figure 4 shows the

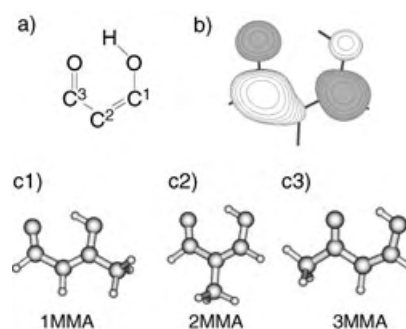


Figure 4. a) Molecular structure of malonaldehyde (MA), b) the LUMO of MA, and c1)–c3) the stable structures of 1-methylmalonaldehyde (1MMA) (0.054 eV), 2-methylmalonaldehyde (2MMA) (0.030 eV), and 3-methylmalonaldehyde (3MMA) (0.023 eV), respectively. The values in parentheses are the height of their rotational barriers.

structure of malonaldehyde, its LUMO, and the stable structures of 1-methylmalonaldehyde (1MMA), 2-methylmalonaldehyde (2MMA), and 3-methylmalonaldehyde (3MMA). The quantum-chemical origins of these orientations are almost completely the same as that of the methyltropolones. From Figure 4, it can be readily seen that the internal rotation of the methyl group at any position is induced by proton transfer, as long as the associated tautomerization can sufficiently couple with the hyperconjugation.

There is a simple rule to predict the orientation of a methyl group in bond alternation systems such as tropolone and linear polyene:^[22] The VP of a methyl group tends to be more stable at the site of a single-bond (the other side of the double-bond). Various explanations are possible for this preferred orientation; however, we account for it in terms of the following facts as observed in the above examples, a) the LUMO π orbital tends to have large components in single bonds, b) the LUMO π orbital tends to have a node on the double bonds, and c) at double-bond sites there are large components of the HOMO of the π system. These are just guiding principles to be confirmed with individual molecular orbital calculations. Also, many other secondary effects may exist that violate this “rule”. Where this rule holds, proton transfer or other dynamics that alter the position of single and double bonds within a molecule can induce the rotation of methyl groups at the relevant sites.

An important implication of the present finding is that proton transfer can trigger a large conformational change

through methyl group rotation.^[4] For example, if one of the hydrogen atoms in the methyl group is substituted with a large alkyl group, a large amplitude conformational change can be driven by a relevant proton transfer.

Protein motors are of interest to many biologists and chemists.^[23,24] They are usually assemblies of large molecules that tie molecular dynamics with biological functioning. Yet chemists are interested in far smaller elementary molecules that can potentially work as molecular machines or elements within one.^[6–9] The present dynamics, in which a reciprocating motion is transformed into a rotational motion on a molecular level, may be utilized as a molecular rotor or for transmission. The molecule 5MTR is very well-suited to such an application. Besides, it is interesting to recall that the interaction of the methyl group through tautomerization or bond alternation can be conveyed in principle to a very remote site through, for example, a linear polyene. However, for this mechanism to be applied to a molecular motor, one needs to introduce asymmetry into the methyl group so that it rotates only in one direction.^[25] Also, practical ways of continuously injecting energy into the proton transfer should be investigated so that the methyl group can be kept rotating.^[26] These studies are underway in our laboratory.

In summary, methyl group rotation can be driven by proton transfer because of coupling between hyperconjugation and tautomerization. This is important not only as a basic long-range interaction in fundamental chemistry but also as a mechanical transformation that can be utilized as an integral part of molecular machinery and stereochemistry.

Received: July 28, 2004

Published online: January 14, 2005

Keywords: ab initio calculations · conformation analysis · hyperconjugation · proton transfer · tautomerism

- [1] *Proton transfer in hydrogen-bonded systems* (Ed.: T. Bountis), Plenum, New York, **1992**.
- [2] V. A. Benderskii, D. E. Makarov, C. A. Wight, *Chemical Dynamics at Low Temperatures*, Wiley, New York, **1994**.
- [3] V. May, O. Kühn, *Charge and energy transfer dynamics in molecular systems*, Wiley-VCH, Berlin, **2000**.
- [4] It is well-known that a rather delicate interaction between two methyl groups in ethane (originally the so-called eclipsed and staggered conformations in 1,2-dichloroethane, S. Mizushima, Y. Morino, *Proc. Indiana Acad. Sci.* **1938**, *8*, 315; S. Mizushima, Y. Morino, *Bull. Chem. Soc. Jpn.* **1942**, *17*, 94–99) can induce methyl rotation resulting in a large conformational change. Yet, the physical origin of the rotational barrier in ethane is still under intensive study.^[5]
- [5] Y. Mo, W. Wu, L. Song, M. Lin, Q. Zhang, J. Gao, *Angew. Chem. Int. Ed.* **2004**, *43*, 1986–1990; *Angew. Chem.* **2004**, *116*, 2020–2024.
- [6] T. R. Kelly, H. De Silva, R. A. Silva, *Nature* **1999**, *401*, 150–152.
- [7] N. Koumura, R. W. J. Zijlstra, R. A. van Delden, N. Harada, B. L. Feringa, *Nature* **1999**, *401*, 152–155. This paper lists recent progress in designing various parts of molecular machines.
- [8] D. A. Leigh, J. K. Y. Wong, F. Dehez, F. Zerbetto, *Nature* **2003**, *424*, 174–179.
- [9] S. Hiraoka, K. Hirata, M. Shionoya, *Angew. Chem.* **2004**, *116*, 3902–3906; *Angew. Chem. Int. Ed.* **2004**, *43*, 3814–3818.

- [10] K. Nishi, H. Sekiya, H. Kawakami, A. Mori, Y. Nishimura, *J. Chem. Phys.* **1998**, *109*, 1589–1592.
- [11] K. Nishi, H. Sekiya, H. Kawakami, A. Mori, Y. Nishimura, *J. Chem. Phys.* **1999**, *111*, 3961–3969.
- [12] The ab initio calculations were performed with a Gaussian program package.
- [13] H. Ushiyama, K. Takatsuka, *J. Chem. Phys.* **2001**, *115*, 5903–5912.
- [14] K. Bolton, W. L. Hase, G. H. Peslherbe in *Modern Methods for Multidimensional Dynamics Computations in Chemistry* (Ed.: D. L. Thompson), World Scientific, Singapore, **1998**, pp. 143–189.
- [15] The ab initio molecular dynamics simulations were performed with a GAMESS program package. M. W. Schmidt, K. K. Baldridge, J. A. Boatz, S. T. Elbert, M. S. Gordon, J. H. Jensen, S. Koseki, N. Matsunaga, K. A. Nguyen, S. Su, T. L. Windus, M. Dupuis, J. A. Montgomery, *J. Comput. Chem.* **1993**, *14*, 1347–1363.
- [16] H. Ushiyama, Y. Arasaki, K. Takatsuka, *Chem. Phys. Lett.* **2001**, *346*, 169–176.
- [17] M. J. S. Dewar, *Hyperconjugation*, Ronald, New York, **1962**, p. 43.
- [18] A. Streitwieser Jr., *Molecular Orbital Theory for Organic Chemists*, Wiley, New York, **1961**.
- [19] H. Nakai, M. Kawai, *Chem. Phys. Lett.* **1999**, *307*, 272–276; H. Nakai, M. Kawai, *J. Chem. Phys.* **2000**, *113*, 2168–2174.
- [20] The actual LUMO of methane and HOMO of tropolone are provided visually in the Supporting Information.
- [21] H. Ushiyama, K. Takatsuka, to be published.
- [22] π -conjugation systems like benzene should not be included.
- [23] G. Tsiavalariis, S. Fujita-Becker, D. J. Manstein, *Nature* **2004**, *427*, 558–561.
- [24] M. Reconditi, M. Linari, L. Lucii, A. Stewart, Y. B. Sun, P. Boesecke, T. Narayanan, R. F. Fischetti, T. Irving, G. Piazzesi, M. Irving, V. Lombardi, *Nature* **2004**, *428*, 578–581.
- [25] For laser control of molecular chirality, see Y. Fujimura, L. González, K. Hoki, D. Kröner, J. Manz, Y. Ohtsuki, *Angew. Chem.* **2000**, *112*, 4785–4788; *Angew. Chem. Int. Ed.* **2000**, *39*, 4586–4588.
- [26] The methyl rotation is usually induced by both forward and backward proton transfers. Suppose, for instance, the methyl group at the stable orientation in 5MTR is rotated by a forward proton transfer. Upon completion of its 60° rotation, another proton transfer backward will make a further rotation.

Conformational Analysis

Using Dipoles to Control the Directionality of Functional Groups: *Syn*- and *Anti*-Oriented Benzene-1,3-dicarboxamides**

Mark S. Betson, Jonathan Clayden,* Ho Kam Lam, and Madeleine Helliwell

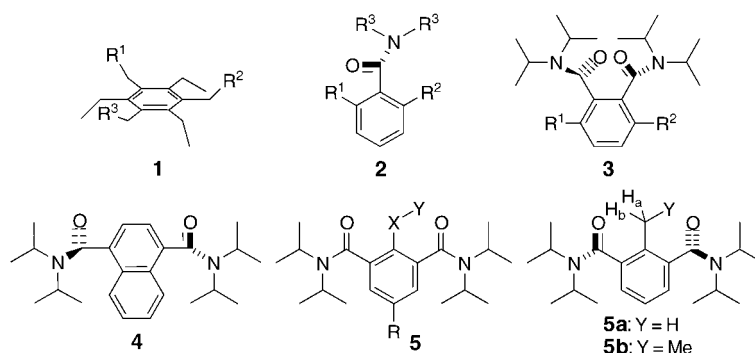
The control of conformation, which until quite recently was feasible only in cyclic compounds, now appears to be a realistic target for stereoselective synthesis^[1–3] alongside its traditional goal of controlling configuration. The relative spatial orientation of pairs or triads of functional groups attached to an aromatic ring can be used to modulate the binding properties of ligands, receptors, and sensors^[4–8] and the bulk properties of liquid crystals.^[9] From the crystallographic work of MacNicol et al.^[10,11] and the theoretical and dynamic NMR spectroscopic studies of Mislow and co-workers^[12] on polyalkylbenzenes, it has been generally assumed that the *syn* orientation of functions carried by an aromatic ring may be favored by interposing cylindrically unsymmetrical groups, such as ethyl or alkoxy, between them. A growing number of ligands of general structure **1** (Scheme 1) have been designed on this basis.^[4,13] It is clear that the 1,3-*syn* conformation of polysubstituted arenes is favored (usually^[14]) in the crystalline state,^[10,11,15] in metal–arene complexes (by NMR spectroscopic studies),^[12,16,17] and in calculated ground states.^[12,16] However, there is to date neither direct empirical evidence for the magnitude of the effect in solution nor data on the role of the intervening substituent.^[18]

Herein we present the first direct evidence from NMR spectroscopic studies that 1) a group interposed between two *meta*-related functions may indeed force them to adopt a *syn* orientation with high selectivity and 2) the magnitude of the effect is critically dependent on the nature of the group. We show that a pair of *meta*-related amide groups on an aromatic ring have a natural tendency to lie facing in opposite directions with a conformational selectivity of >95:5 *anti*. Their relative orientation may be completely inverted to >95:5 *syn*, but only if a polar group with an associated dipole is placed in between them—a polar group such as acetyl exerts a far more powerful effect than the widely used ethyl group. Steric effects alone are insufficiently powerful to overturn the preference of the amides to adopt an *anti* conformation.

The hydrogen-bonding and metal-binding capacity of secondary aromatic amides has earned them the pivotal role

in molecules designed to adopt specific conformations^[19] or to exhibit molecular recognition.^[20] However, rapid bond rotations in secondary amides frequently renders detailed studies of their conformational properties in solution difficult over the temperature ranges attainable in common solvents. Tertiary aromatic amides **2** (Scheme 1), which usually adopt conformations in which the plane of the amide is more or less perpendicular to the plane of the aromatic ring,^[21] undergo much slower bond rotations and are readily studied by dynamic NMR spectroscopic or saturation transfer techniques.^[22–24]

In the benzene-1,2-dicarboxamide **3**, the amide groups align themselves such that their carbonyl groups are oriented in opposite directions, whether for steric or electronic reasons (Scheme 1).^[25,26] We prepared simple benzene-1,4-dicarbox-



Scheme 1. Conformational preference in arene-1,2-, -1,3-, and -1,4-dicarboxamides.

amide and benzene-1,3-dicarboxamide derivatives **4** and **5a** by standard methods^[27] and found that a strong orientational preference also persists in these compounds. Conformers about the Ar–CO bond of *ortho*-substituted tertiary amides such as **4** and **5a** are expected to interconvert only slowly on the NMR timescale even at 25 °C,^[21,23] but their NMR spectra essentially show a single set of peaks at both 20 °C and –50 °C in CDCl₃. An X-ray crystal structure of **5a** (Figure 1 a) shows an *anti* alignment of the amides in the solid state.

The ¹H NMR spectrum (CDCl₃, 20 °C) of the closely related 2-ethyl-substituted isophthalamide **5b** shows a mixture of conformers in a ratio of approximately 5:1. The ethyl group of the major conformer is an ABX₃ system, while the equivalent signal in the minor conformer is a simple A₂X₃ quartet + triplet. As the *anti* conformer is chiral and the *syn* conformer is achiral, with a plane of symmetry lying through the ethyl group, these observations allow us to assign with certainty *anti* stereochemistry to the major conformer of **5b**. When the solvent is changed to CD₃OD, **4** and **5a** also show two conformers at 20 °C in a ratio of 6:1 for **4** and 2:1 for **5a**. We assume that the major conformer is still *anti*, although the lack of a stereochemical marker makes it impossible to assign the stereochemistry with certainty.

To probe further the influence of the substituent that lies between the two amides on their relative conformation, we prepared a series of isophthalamides **5a–s**.^[27] Where feasible, an isopropyl substituent was incorporated at the 5 position to act as a symmetry reporter—in the achiral *syn* conformers the

[*] Dr. M. S. Betson, Prof. J. Clayden, H. K. Lam, Dr. M. Helliwell
Department of Chemistry
University of Manchester
Oxford Road
Manchester M13 9PL (UK)
Fax: (44) 161-275-4612
E-mail: j.p.clayden@man.ac.uk

[**] We are grateful to the Leverhulme Trust for a grant and to Dr. Andrew Regan for assistance with molecular modeling studies.

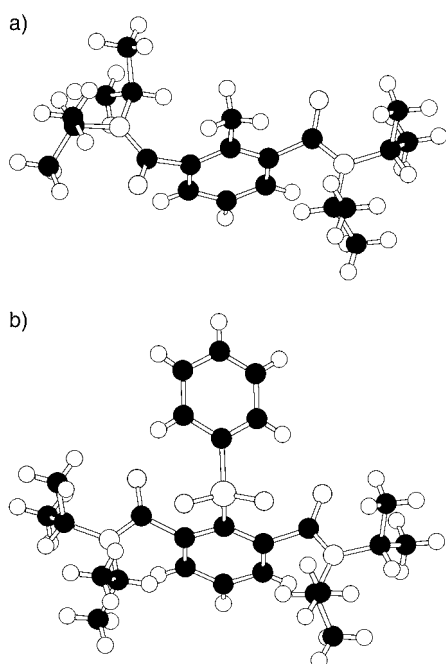


Figure 1. a) X-ray crystal structure of *anti*-5 (**5a**). b) X-ray crystal structure of *syn*-5 (**5s**).

isopropyl group will exhibit a homotopic pair of methyl groups, whereas in the chiral *anti* conformers its methyl groups may be a diastereotopic pair of 3H doublets. The conformational ratios, obtained by ^1H NMR spectroscopy in CDCl_3 at ambient temperature unless otherwise stated, are shown in Table 1.

These results show that the conformation of the isophthalamides is entirely dependent on the nature of the $-\text{X}-\text{Y}$ substituent interposed between the two amides groups, and to explain this it is necessary to consider the preferred orientation of this substituent. For substituents other than $-\text{X}-\text{Y} = \text{Me}$ (**5a**) or Cl (**5c**), steric hindrance between Y and the flanking amide groups requires that the Y group lie out of the plane of the ring. In *anti*-5, rotation about the $\text{Ar}-\text{X}$ bond leads to a pair of rapidly interconverting but identical

Table 1: Conformations of benzene-1,3-dicarboxamides

Entry	Compound	$-\text{X}-\text{Y}$	R	Ratio <i>anti</i> : <i>syn</i>	Notes
1	5a	Me	H	> 93:7	[a,b]
2	5a	Me	H	67:33	[a,c]
3	5b	Et	H	83:17	[d]
4	5c	Cl	H	> 95:5	[a]
5	5d	OMe	<i>i</i> Pr	57:43	[d]
6	5e	OBn ^[e]	<i>i</i> Pr	54:46	[d]
7	5f	OSEM ^[e]	<i>i</i> Pr	54:46	[d]
8	5g	O <i>i</i> Pr	<i>i</i> Pr	35:65	[d]
9	5g	O <i>i</i> Pr	<i>i</i> Pr	18:82	[d,f]
10	5h	OPh	H	35:65	[a]
11	5i	SMe	H	40:60	[a]
12	5j	SPh	H	35:65	[a]
13	5k	OAc	<i>i</i> Pr	< 7:93	[d]
14	5k	OAc	<i>i</i> Pr	< 7:93	[d,f]
15	5l	OBz ^[e]	<i>i</i> Pr	< 4:96	[d]
16	5m	$\text{OCOC}_5\text{H}_4\text{OMe}$	<i>i</i> Pr	< 4:96	[b,d]
17	5n	OTs ^[e]	<i>i</i> Pr	< 7:93	[d]
18	5o	OMs ^[e]	<i>i</i> Pr	14:86	[d]
19	5p	$\text{OCON}i\text{Pr}_2$	<i>i</i> Pr	< 4:96	[d]
20	5q	CONEt_2	<i>i</i> Pr	< 5:95	[d]
21	5r	SO_2Me	H	< 5:95	[a]
22	5s	SO_2Ph	H	< 5:95	[a,g]

[a] Stereochemical assignment unconfirmed, but proposed by analogy with related compounds. [b] X-ray crystal structure indicates *anti* stereochemistry in the solid state. [c] Ratio determined in CD_3OD . [d] Stereochemical assignment on the basis of topology of signals. [e] Bn = benzyl, SEM = 2-trimethylsilyloxyethoxymethoxy, Bz = benzoyl, Ts = *p*-toluenesulfonyl, Ms = methanesulfonyl. [f] Ratio determined in $(\text{CD}_3)_2\text{SO}$. [g] X-ray crystal structure indicates *syn* stereochemistry in the solid state.

conformers with Y always lying *syn* to one amide $\text{C}=\text{O}$ group and *anti* to the other, while in *syn*-5, rotation about $\text{Ar}-\text{X}$ leads to two rapidly interconverting diastereoisomeric conformers with either two *syn* or two *anti* interactions between Y and the amide $\text{C}=\text{O}$ groups (Figure 2). Thus whatever the nature of the interaction between Y and the amide groups, the interaction can be maximized in *syn*-5 (as Y can choose whether to be *syn* or *anti* to either $\text{C}=\text{O}$ or NR_2 of both amides simultaneously) whereas in *anti*-5 the $\text{Y}\cdots\text{amide}$ interaction is lessened because Y can have a favorable interaction only with one amide group at a time. Super-

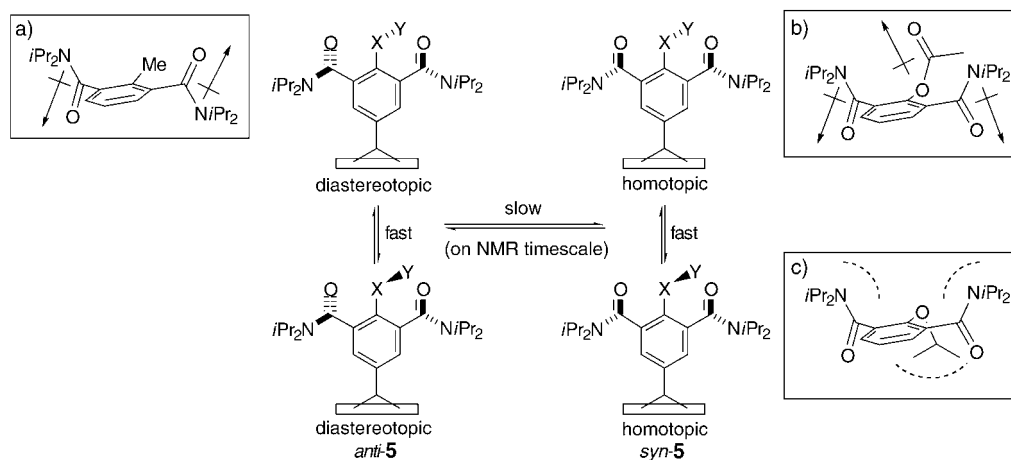


Figure 2. Factors governing the conformations in benzene-1,3-dicarboxamides.

imposed on this, direct interaction (i.e. one not mediated by -X-Y) between the amide groups, whether steric or electronic, must favor the *anti* conformer.

We already noted that in **5a** a single, presumably *anti*, conformer is indeed favored. The same is true for **5c**: both of the compounds have -X-Y groups which are essentially cylindrically symmetrical and therefore exert no conformational preference on the amide substituents. We therefore propose that in the absence of other conformational influences, a pair of *meta*-disposed amide groups will adopt a relative *anti* conformation presumably because of dipole repulsion between the two C=O groups (Figure 2a).^[28]

In **5b**, with -X-Y=-CH₂-Me, the *anti* preference is lessened because Y (=Me) can interact only weakly and probably by steric repulsion with the NR₂ groups of the amides; direct repulsion between the amide groups is still however dominant. However, in the series of ethers **5d–5h** the preference switches from *anti* to *syn*, with a weak correlation between the size of Y and the *syn* preference. In these ethers and in the sulfides **5i** and **5j**, repulsion between Y and the amide NR₂ groups is great enough to overcome their tendency to lie *anti* (Figure 2c), particularly in a polar solvent (Table 1, entry 9).

The greatest ability to overturn the *anti* preference is shown by the -X-Y groups in compounds **5k–5s**, which have in common the presence of an electronegative oxygen atom within the group Y. The role of the oxygen atom in controlling the relative conformation of the amides must be to provide a third directed dipole that can simultaneously oppose the dipoles of both amide groups, as illustrated in Figure 2b. The importance of the oxygen atom is underlined by the difference in conformational preference between the isopropyl ether **5g** and the acetate ester **5k**, both of whose -X-Y groups are sterically similar, and between the sulfides **5i,j** and the sulfones **5r,s** where the sulfones have even less ability to impose steric differentiation on the faces of the isophthalamide ring.

The X-ray crystal structure of sulfone **5s** (Figure 1b) confirms *syn* stereochemistry in the solid state. In the X-ray crystal structure of **5m**, however, the amides are aligned *anti*: a clear warning against the use of solid-state conformations to deduce the preferred structures in solution.^[14,29] Calculations^[30] of the conformations of **5a** (*anti* preferred by 2.9 kJ mol⁻¹), **5j** (*anti* and *syn* within 0.2 kJ mol⁻¹), and **5s** (*syn* preferred by 2.8 kJ mol⁻¹), though not **5k** (for which calculations predicted *anti* stereochemistry), agreed qualitatively with the reasoning in Figure 2.

To summarize, we have shown that by choosing carefully the nature of the substituent interposed between two functional groups, it is possible to control their relative orientation. We believe that the incorporation of polar substituents in polysubstituted arenes may play a greater role in the induction of *syn* orientations in future studies of sensors and ligands that contain these units.

Received: August 25, 2004

Revised: November 2, 2004

Published online: January 14, 2005

Keywords: amides · conformation analysis · dipoles · electrostatic interactions

- [1] R. W. Hoffmann, *Angew. Chem.* **2000**, *112*, 2134; *Angew. Chem. Int. Ed.* **2000**, *39*, 2054.
- [2] J. Clayden, A. Lund, L. Vallverdú, M. Helliwell, *Nature* **2004**, *431*, 966.
- [3] J. Clayden, *Chem. Commun.* **2004**, 127.
- [4] G. Hennrich, E. V. Anslyn, *Chem. Eur. J.* **2002**, *8*, 2219, and references therein.
- [5] A. Metzger, V. M. Lynch, E. V. Anslyn, *Angew. Chem.* **1997**, *109*, 911; *Angew. Chem. Int. Ed. Engl.* **1997**, *36*, 862.
- [6] L. A. Cabell, M. D. Best, J. J. Lavigne, S. E. Schneider, D. M. Perreault, M.-K. Monahan, E. V. Anslyn, *J. Chem. Soc. Perkin Trans. 2* **2001**, 315.
- [7] L. O. Abouderbala, W. J. Belcher, M. G. Boutelle, P. J. Cragg, J. W. Steed, D. R. Turner, K. J. Wallace, *Proc. Natl. Acad. Sci. USA* **2002**, *99*, 5001.
- [8] K. J. Wallace, W. J. Belcher, D. R. Turner, K. F. Syed, J. W. Steed, *J. Am. Chem. Soc.* **2003**, *125*, 9699, and references therein.
- [9] M. L. Bushey, A. Hwang, P. W. Stephens, C. Nuckolls, *J. Am. Chem. Soc.* **2001**, *123*, 8157.
- [10] D. D. MacNicol, A. D. U. Hardy, D. R. Wilson, *Nature* **1977**, *266*, 611.
- [11] D. D. MacNicol, J. J. McKendrick, D. R. Wilson, *Chem. Soc. Rev.* **1978**, *7*, 65.
- [12] D. J. Iverson, G. Hunter, J. F. Blount, J. R. Damewood, K. Mislow, *J. Am. Chem. Soc.* **1981**, *103*, 6073.
- [13] B. M. O'Leary, T. Szabo, N. Svenstrup, C. A. Schalley, A. Lützen, M. Schäfer, J. Rebek, *J. Am. Chem. Soc.* **2001**, *123*, 11519.
- [14] C. Walsdorff, K.-M. Park, J. Oh, K. Kim, *Acta Crystallogr. Sect. C* **1999**, *55*, 108.
- [15] J. A. Chudek, G. Hunter, R. L. MacKay, G. Farber, W. Weissensteiner, *J. Organomet. Chem.* **1989**, *377*, C69.
- [16] I. I. Schuster, W. Weissensteiner, K. Mislow, *J. Am. Chem. Soc.* **1986**, *108*, 6661.
- [17] G. Hunter, R. L. MacKay, P. Kremminger, W. Weissensteiner, *J. Chem. Soc. Dalton Trans.* **1991**, 3349.
- [18] *Anti* orientations of 1,4-difunctionalized arenes, presumably mediated by the preferred all-*anti* arrangement of two intervening ethyl groups, have been observed by NMR spectroscopy. See: K. V. Kilway, J. S. Siegel, *Tetrahedron* **2001**, *57*, 3615.
- [19] I. Huc, *Eur. J. Org. Chem.* **2004**, 17.
- [20] J.-M. Lehn, *Supramolecular Chemistry: Concepts and Perspectives*, VCH, Weinheim, **1995**.
- [21] P. Bowles, J. Clayden, M. Helliwell, C. McCarthy, M. Tomkinson, N. Westlund, *J. Chem. Soc. Perkin Trans. 1* **1997**, 2607.
- [22] W. H. Stewart, T. H. Siddall, *Chem. Rev.* **1970**, *70*, 517.
- [23] A. Ahmed, R. A. Bragg, J. Clayden, L. W. Lai, C. McCarthy, J. H. Pink, N. Westlund, S. A. Yasin, *Tetrahedron* **1998**, *54*, 13277.
- [24] R. A. Bragg, J. Clayden, G. A. Morris, J. H. Pink, *Chem. Eur. J.* **2002**, *8*, 1279.
- [25] J. Clayden, J. H. Pink, S. A. Yasin, *Tetrahedron Lett.* **1998**, *39*, 105.
- [26] For related observations with other functional groups, see: D. Casarini, L. Lunazzi, *J. Org. Chem.* **1996**, *61*, 6240; D. Casarini, L. Lunazzi, A. Mazzanti, *J. Org. Chem.* **1997**, *62*, 7592; D. Casarini, L. Lunazzi, A. Mazzanti, E. Foresti, *J. Org. Chem.* **1998**, *63*, 4991; U. Berg, T. Liljefors, C. Roussel, J. Sandström, *Acc. Chem. Res.* **1985**, *18*, 80; J. Lacour, D. Monchaud, J. Mareda, F. Favarger, G. Bernardinelli, *Helv. Chim. Acta* **2003**, *86*, 65.
- [27] Compounds with X-Y=OR (except OAr) were generally made by double anionic *ortho* Fries rearrangement (M. P. Sibi, V. Snieckus, *J. Org. Chem.* **1983**, *48*, 1935) from 4-isopropylphenol. Most other compounds were made from isophthalonitrile

through *ortho* lithiation and electrophilic quenching (M. P. Sibi, V. Snieckus, *J. Org. Chem.* **1983**, *48*, 1935). Full details will be reported in a future publication.

- [28] The decreased preference for the *anti* conformation in **5a** in a polar solvent (Table 1, entry 2) supports this explanation.
- [29] CCDC 232753, 232754, and 232755 (**5a**, **5m**, and **5s**) contain the supplementary crystallographic data for this paper. These data can be obtained free of charge from The Cambridge Crystallographic Data Centre via www.ccdc.cam.ac.uk/data_request/cif. For an X-ray crystal structure indicating *syn,syn* stereochemistry in a benzene-1,2,3-tricarboxamide, see: R. J. Mills, N. J. Taylor, V. Snieckus, *J. Org. Chem.* **1989**, *54*, 4372.
- [30] Molecular modeling studies were carried out using Macromodel with the MM2* force field. See: F. Mohamadi, N. G. J. Richards, W. C. Guida, R. Liskamp, M. Lipton, C. Caulfield, G. Chang, T. Hendrickson, W. C. Still, *J. Comput. Chem.* **1990**, *11*, 440.

Metal–Metal Bonds

Theoretical and Synthetic Studies on $[\text{Zn}_2(\eta^5\text{-C}_5\text{Me}_5)_2]$: Analysis of the Zn–Zn Bonding Interaction**

Diego del Río, Agustín Galindo,* Irene Resa, and Ernesto Carmona*

Recently we have characterized $[\text{Zn}_2(\eta^5\text{-C}_5\text{Me}_5)_2]$ (**1**), a molecular compound of zinc with a Zn–Zn bond.^[1] The unique nature of this compound warrants a study of its bonding and electronic properties. Herein, we provide details of a theoretical investigation of the Zn–Zn bonding interaction in **1**, along with further synthetic studies that result in the direct preparation of the compound on a gram scale.

Complex **1** formed unexpectedly during attempts to generate the half-sandwich ethyl derivative $[\text{Zn}(\text{C}_2\text{H}_5)(\eta^5\text{-C}_5\text{Me}_5)]$ (**2**) from $[\text{Zn}(\text{C}_5\text{Me}_5)_2]$ ^[2] and $[\text{Zn}(\text{C}_2\text{H}_5)_2]$. At -60°C

in pentane the reaction produced compound **2**, whereas upon mixing diethyl ether solutions of the two reactants at -10°C the dizinc compound **1** was isolated in moderate yields.^[1] Notably, compound **1** is also generated when $[\text{Zn}(\text{C}_5\text{Me}_5)_2]$ is treated with $[\text{Zn}(\text{C}_6\text{H}_5)_2]$ ^[3] in diethyl ether, under similar conditions; the related half-sandwich complex $[\text{Zn}(\eta^5\text{-C}_5\text{Me}_5)(\text{C}_6\text{H}_5)]$ is the other organometallic product of this transformation (see Experimental Section). The limitations of this synthesis of **1** prompted us to search for a more convenient procedure. Whereas $[\text{Zn}(\text{C}_5\text{Me}_5)_2]$ is recovered unaltered upon attempted reduction with Rieke zinc, the use of Na, K, K/naphthalene, or KH produces **1** in variable yields. Of these materials, potassium hydride appears to be the most useful reagent and allows the synthesis of **1** by an experimentally simple procedure, namely the reduction of $[\text{Zn}(\text{C}_5\text{Me}_5)_2]$ in tetrahydrofuran at -20°C , over a period of 2–3 h. Moreover, isolation of $[\text{Zn}(\text{C}_5\text{Me}_5)_2]$ is not necessary—the dizinc compound **1** may be prepared in quantities of over 1 g by the direct reaction of ZnCl_2 , KC_5Me_5 , and KH at room temperature (see Experimental Section).

The electronic structure and bonding properties of **1** were computed by a density functional theory approach at the B3LYP level (see Experimental Section and Supporting Information). The simplest model, the parent compound $[\text{Zn}_2(\eta^5\text{-C}_5\text{H}_5)_2]$ (**3**), was also calculated (see the Supporting Information). In view of the structural diversity of main-group metallocenes,^[4] several starting geometries, with and without symmetry, were investigated, resulting in different optimized structures. The use of the atomic coordinates obtained from the X-ray study,^[1] but with imposed C_{5h} and S_{10} symmetries, yielded optimized structures that are characterized by four and five imaginary frequencies, respectively. Subsequent optimization without symmetry constraints still gave four imaginary frequencies, all smaller than $30i\text{ cm}^{-1}$, but involving displacement of the Zn atoms. In an attempt to eliminate them, the optimization was repeated with the GDHIS algorithm and a finer grid for the integration step (see Supporting Information). The resulting optimized structure $[\text{Zn}_2(\eta^5\text{-C}_5\text{Me}_5)_2]$ (**1a**), is displayed in Figure 1.

However, two small imaginary frequencies of $13i$ and $12i\text{ cm}^{-1}$, which involve deviation of the two Zn atoms from the η^5 coordination mode, were still found. For the parent molecule **3** a related optimized structure, $[\text{Zn}_2(\eta^5\text{-C}_5\text{H}_5)_2]$ (**3a**), was obtained with three imaginary frequencies; $[\text{Zn}_2(\eta^3\text{-C}_5\text{H}_5)_2]$ (**3b**) was found to be a real minimum. In light of this

[*] Dr. D. del Río, I. Resa, Prof. Dr. E. Carmona
Instituto de Investigaciones Químicas
Departamento de Química Inorgánica
Consejo Superior de Investigaciones Científicas
Universidad de Sevilla
Avda. Américo Vespucio 49
Isla de la Cartuja, 41092 Sevilla (Spain)
Fax: (+34) 95-446-0565
E-mail: guzman@us.es

Prof. Dr. A. Galindo
Departamento de Química Inorgánica
Universidad de Sevilla
Apto 553, 41071 Sevilla (Spain)
Fax: (+34) 95-455-7153
E-mail: galindo@us.es

[**] Financial support from the DGESIC (Projects BQU2001-1995 and BQU2001-3715) and from the Junta de Andalucía is gratefully acknowledged. D.d.R. and I.R. thank the EU and Ministry of Education, respectively, for research grants.

Supporting information for this article is available on the WWW under <http://www.angewandte.org> or from the author.

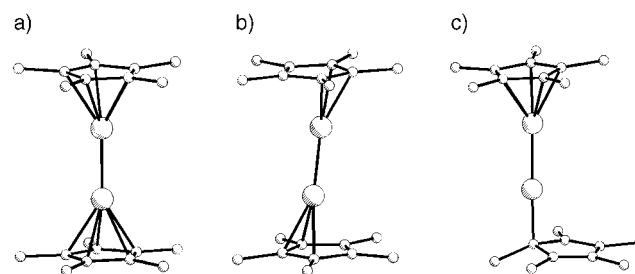


Figure 1. Optimized structures for $[\text{Zn}_2(\text{C}_5\text{Me}_5)_2]$: a) $[\text{Zn}_2(\eta^5\text{-C}_5\text{Me}_5)_2]$ (**1a**); b) $[\text{Zn}_2(\eta^3\text{-C}_5\text{Me}_5)_2]$ (**1b**); c) $[\text{Zn}_2(\eta^1\text{-C}_5\text{Me}_5)(\eta^5\text{-C}_5\text{Me}_5)]$ (**1c**). (H atoms omitted for clarity.)

result, the analogous structure for **1**, $[\text{Zn}_2(\eta^5\text{-C}_5\text{Me}_5)_2]$ (**1b**), was optimized and found to correspond to a real minimum on the potential energy surface (Figure 1).

To complete these studies, and having in mind the propensity of zirconocenes to adopt a slipped-sandwich or $\eta^5/\eta^1(\pi)$ structure,^[5] the optimization of a starting point with one η^5 - and one $\eta^1\text{-C}_5\text{Me}_5$ ring was considered appropriate. The resulting structure, **1c**, is also a real minimum (NImag = 0), and is presented in Figure 1. It is worth pointing out that the C_5H_5 analogue **3c** is not a stationary point; instead, all optimization attempts converge to the pseudoallylic structure **3b**.

The energy differences between the optimized structures of **1** are negligible ($\leq 0.1 \text{ kcal mol}^{-1}$), thereby indicating a flat energy surface in the gas phase. Therefore, the optimized structure **1a** can be employed for the description of the molecules of **1** despite the existence of two imaginary frequencies. It seems reasonable to assume that the specific packing found in the crystals of **1** may overcome this small energy difference (Supplementary Information). For this structure the computed bond distances and angles match the experimental values closely. In particular, the calculated Zn–Zn bond distance of 2.331 Å, without a doubt the most salient feature of this compound, compares very well with the value of 2.305(3) Å found by X-ray diffraction methods. Furthermore, the computed $(\text{C}_5\text{Me}_5)_{\text{centr.}}\text{-Zn-Zn}$ angle of 178.9° is also in excellent agreement with the average experimental value of 177.4(1)°. The calculated Zn–Zn bond length may be compared with values computed for other dizinc species that have been studied theoretically. For instance, the dizinc dihalides Zn_2X_2 (X = F, Cl, Br, I), computed at various levels of theory, display Zn–Zn bond lengths in the range 2.28–2.42 Å.^[6,7] In addition, ab initio studies for Zn_2H_2 lead to Zn–Zn distances of about 2.38 Å.^[7,8]

An important objective of the present study was the investigation of the unprecedented Zn–Zn bond of **1**. On the basis of previous analysis of $\{\text{M}(\text{C}_5\text{H}_5)\}$ fragments,^[9] including $\{\text{Zn}(\text{C}_5\text{H}_5)\}$,^[5a,10,11] the frontier orbitals for a $\{\text{Zn}(\eta^5\text{-C}_5\text{Me}_5)\}$ unit are the singly occupied HOMO (an antibonding combination of the a_1 , $\pi\text{-C}_5\text{Me}_5$ orbital and the zinc s and p_z orbitals) and a pair of degenerate orbitals that result from the combination of the e_1 $\pi\text{-C}_5\text{Me}_5$ and the $p_{x,y}$ metal orbitals. These qualitative arguments lead to a Zn–Zn bond derived from the interaction of the singly occupied HOMOs of two $\{\text{Zn}(\eta^5\text{-C}_5\text{Me}_5)\}$ fragments. However, DFT calculations reveal that the Zn–Zn bonding interaction resides in the HOMO–4, and that even if it has a contribution of Zn orbitals close to 60%, the metal–metal bond involves mostly the Zn 4s orbitals (more than 96%), with only a small contribution from the 4p orbitals (less than 4%). A simplified MO diagram that includes the HOMO–4 is provided in the Supporting Information. The higher-energy occupied orbitals (from HOMO–3 to HOMO) are quasi-degenerate and result from the in-phase and out-of-phase combinations of the e_1 C_5Me_5 orbitals, with very little participation from the d (<2%) and p (<0.5%) orbitals of Zn. The LUMO represents the antibonding zinc–zinc interaction and its major contributors are the 4s orbitals (89%), with minor participation of the C_5Me_5 (9%) and the Zn d orbitals (2%).

Figure 2 shows the calculated overlap population density of states (OPDOS) for **1a**.

The next target of this analysis was the estimation of the Zn–Zn bond energy in **1a**. A fragment-oriented approach^[12]

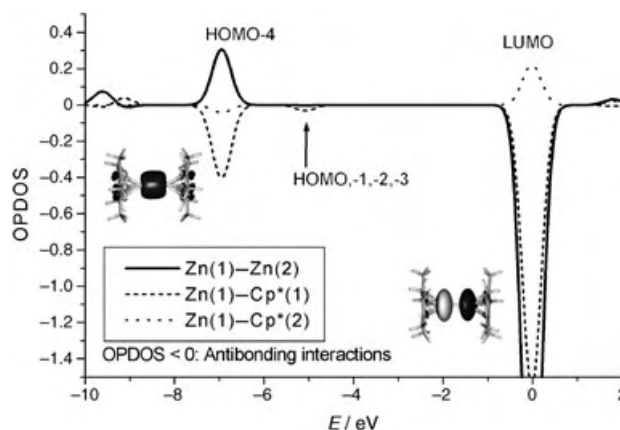


Figure 2. Calculated overlap population density of states (OPDOS) for $[\text{Zn}_2(\eta^5\text{-C}_5\text{Me}_5)_2]$ (**1a**). The insets display 3D representations of the HOMO–4 and the LUMO. The former clearly has a positive overlap population between the Zn atoms.

was adopted in which the metal–metal bond-dissociation energy (BDE) was calculated in two steps. Firstly, we computed the energy needed for “snapping” the metal–metal bond, $E(\text{Zn-Zn})$, and then the energy ER, gained when the isolated fragment relaxes from its original conformation to the optimal ground-state structure with imposed C_5 and C_{5v} symmetries for **1a** and **3a**, respectively (see Supporting Information). This approach allows the basis set superposition error (BSSE) associated with the Zn–Zn bond energy to be computed directly by the counterpoise method.^[13] The calculated BDEs for complexes **1a** and **3a** are given in Table 1, wherein they are broken down into their various

Table 1: Calculated Zn–Zn bond dissociation energy (BDE) for complexes **1a** and **3a**, with energy contributions [kcal mol^{-1}].

	$E(\text{Zn-Zn})^{\text{[a]}}$	ER	BSSE	BDE ^[b]
$[\text{Zn}_2(\eta^5\text{-C}_5\text{Me}_5)_2]$ (1a)	66.3	–1.2	–0.9	62.1
$[\text{Zn}_2(\eta^5\text{-C}_5\text{H}_5)_2]$ (3a)	66.7	–1.3	–0.8	62.5

[a] The computed bonding energies represent only the electronic contribution to the reaction enthalpies and do not include ZPE corrections. [b] Corrected for BSSE.

energy contributions (for further details, see the Supporting Information). The results obtained for the Zn–Zn bond energy in both complexes are analogous and are actually similar to the energies computed previously for related Zn–Zn bonds (about 59 kcal mol^{-1} for Zn_2H_2 ,^[7,8] and in the range 57–67 kcal mol^{-1} for the dihalides Zn_2X_2 with X = F, Cl, Br, I).^[6,7]

The final objective of our theoretical study was to ascertain the viability of a possible bridging hydride structure, $[\text{Zn}_2(\eta^5\text{-C}_5\text{Me}_5)_2(\mu\text{-H})_2]$ (**4a**). Attempts to optimize the structure of such a complex proved unsuccessful as the stationary

point found in all cases consists of two molecules of $[\text{Zn}(\eta^1\text{-C}_5\text{Me}_5)(\text{H})]$ (**5a**) that are kept together by means of dipole–dipole interactions. A graphical representation of the final optimized structure can be found in the Supporting Information. In contrast, if the optimization of the model $[\text{Zn}_2(\eta^5\text{-C}_5\text{H}_5)_2(\mu\text{-H})_2]$ is done under C_{2h} symmetry, complex **4b** can be found as a stationary point. However, this is characterized by six imaginary frequencies that involve displacement of the Zn atoms and breaking of the imposed molecular symmetry. If the symmetry constraints are removed the optimization converges, as in the case of C_5Me_5 , to two molecules of $[\text{Zn}(\eta^1\text{-C}_5\text{H}_5)(\text{H})]$ (**5b**). Even if the structure of complex **4b** is not a minimum on the potential energy surface we consider it useful to compare some of the structural parameters of this calculated model complex with the observed experimental values of **1**. In particular, the calculated Zn–Zn bond distance for **4b**, 2.498 Å, is appreciably longer than the experimentally observed value of 2.305(3) Å. This fact provides additional theoretical support for the $[\text{Zn}_2(\eta^5\text{-C}_5\text{Me}_5)_2]$ structure of **1**.

In summary, a rational, simple synthesis of $[\text{Zn}_2(\eta^5\text{-C}_5\text{Me}_5)_2]$ (**1**) has been developed. As **1** is so far the only organometallic compound of zinc that contains a Zn–Zn bond, it is expected that its availability will allow not only the study of its chemical properties but also its use as a starting material for the preparation of other Zn–Zn compounds, thereby contributing to the development of this previously unforeseen area of the chemistry. Theoretical calculations reveal that the Zn–Zn bond of **1** ($\approx 60 \text{ kcal mol}^{-1}$) is relatively strong, and derives mostly from the zinc 4 s orbitals, with very little participation of the zinc 4 p orbitals. Furthermore, a bridging hydride structure, $[\text{Zn}_2(\eta^5\text{-C}_5\text{Me}_5)_2(\mu\text{-H})_2]$, appears to be unattainable, whereas the calculated bond distances and angles for the optimized structure, $[\text{Zn}_2(\eta^5\text{-C}_5\text{Me}_5)_2]$, match the experimental X-ray diffraction values very closely.

Experimental Section

1: Tetrahydrofuran (50 mL) was added to a mixture of KC_5Me_5 (2.78 g, 16 mmol), ZnCl_2 (1.09 g, 8 mmol), and KH (0.32 g, 8 mmol) with careful exclusion of oxygen and moisture. The resulting suspension was stirred for about 3 h at room temperature and the solvent was then evaporated under reduced pressure. The residue was extracted with three portions of pentane (30 mL each). Crude $[\text{Zn}_2(\eta^5\text{-C}_5\text{Me}_5)_2]$ (**1**) was obtained as a pale yellow solid in about 60–80% yield (between 0.9 and 1.2 g) upon removal of the solvent in vacuo. This product was sufficiently pure for chemical studies but could be further purified by recrystallization from pentane, at -20°C , as reported previously.^[1] This operation provided highly crystalline material. We routinely followed the above synthetic procedure starting with 4–10 mmol of ZnCl_2 . ^1H NMR (C_6D_6 , 20°C): $\delta = 2.02 \text{ ppm}$; $^{13}\text{C}\{^1\text{H}\}$ NMR (C_6D_6 , 20°C): $\delta = 10.0$ (C_5Me_5), 108.8 ppm (C_5Me_5).^[1]

Reactions of $[\text{Zn}(\text{C}_5\text{Me}_5)_2]$ and ZnR_2 ($\text{R} = \text{C}_2\text{H}_5$, C_6H_5): Equimolar solutions of $[\text{Zn}(\text{C}_5\text{Me}_5)_2]$ and $[\text{Zn}(\text{C}_2\text{H}_5)_2]$ in $(\text{C}_2\text{D}_5)_2\text{O}$ were mixed in an NMR tube at -20°C . ^1H NMR monitoring revealed the formation of $[\text{Zn}_2(\eta^5\text{-C}_5\text{Me}_5)_2]$ (**1**) together with minor amounts of the half-sandwich compound $[\text{Zn}(\text{C}_2\text{H}_5)(\eta^5\text{-C}_5\text{Me}_5)]$.^[1] The formation of ethane was ascertained by GC analysis of the volatiles produced during different reaction runs. Similarly, $(\text{C}_2\text{D}_5)_2\text{O}$ solutions of $[\text{Zn}(\text{C}_5\text{Me}_5)_2]$ react readily with $[\text{Zn}(\text{C}_6\text{H}_5)_2]$ dissolved in the same solvent. However, in this case approximately equimolar mixtures of $[\text{Zn}_2(\eta^5\text{-C}_5\text{Me}_5)_2]$ and $[\text{Zn}(\eta^5\text{-C}_5\text{Me}_5)(\text{C}_6\text{H}_5)]$ were always generated.

The structures of all calculated complexes were computed within the density functional theory at the B3LYP^[14] level with the 6-31G** basis set for C and H atoms and 6-311G* for the Zn atoms. All the calculations were performed with the Gaussian-98 package.^[15] The GDIIS algorithm^[16] and a finer integration grid were used. Several starting geometries, with and without symmetry, were investigated for each complex, resulting in different optimized structures. For all of them vibrational frequency calculations by diagonalization of the analytically computed Hessian were computed. The number of imaginary frequencies (NImag) of each optimized structure is given in the text. The MO analysis was performed with the AOMix program.^[17] Further details are included in the Supporting Information.

Received: October 1, 2004

Published online: January 20, 2005

Keywords: bond energy · cyclopentadienyl ligands · density functional calculations · metallocenes · zinc

- [1] I. Resa, E. Carmona, E. Gutiérrez-Puebla, A. Monge, *Science* **2004**, 305, 1136.
- [2] R. Blom, J. Boersma, P. H. M. Budzelaar, B. Fischer, A. Haaland, H. V. Volden, J. Weidlein, *Acta Chem. Scand. Ser. A* **1986**, 40, 113.
- [3] a) D. K. Bretinger, C. E. Zybilla, in *Synthetic Methods of Organometallic and Inorganic Chemistry*, Vol. 5 (Eds.: D. K. Bretinger, W. A. Herrmann), Thieme, Stuttgart, **1999**, pp. 150–153; b) P. R. Markies, G. Schat, O. S. Akkerman, F. Bickelhaupt, W. J. J. Smeets, A. L. Spek, *Organometallics* **1990**, 9, 2243.
- [4] a) P. H. M. Budzelaar, J. J. Engelberts, J. H. van Lenthe, *Organometallics* **2003**, 22, 1562; b) T. P. Hanusa, *Organometallics* **2002**, 21, 2559; c) P. Jutzi, N. Burford, *Chem. Rev.* **1999**, 99, 969; d) P. Jutzi, N. Burford, *Metallocenes*, Wiley-VCH, Weinheim, Germany, **1998**.
- [5] a) A. Haaland, S. Samdal, N. V. Tverdova, G. V. Girichev, N. I. Giricheva, S. A. Shlykov, O. G. Garkusha, B. V. Lokshin, *J. Organomet. Chem.* **2003**, 684, 351; b) D. J. Burke, T. P. Hanusa, *J. Organomet. Chem.* **1996**, 512, 165; c) B. Fischer, P. Wijkens, J. Boersma, G. van Koten, W. J. J. Smeets, A. L. Spek, P. H. M. Budzelaar, *J. Organomet. Chem.* **1989**, 376, 223.
- [6] M.-S. Liao, Q.-E. Zhang, W. H. E. Schwarz, *Inorg. Chem.* **1995**, 34, 5597.
- [7] M. Kaupp, H. G. von Schnering, *Inorg. Chem.* **1994**, 33, 4179.
- [8] T. M. Greene, W. Brown, L. Andrews, A. J. Downs, G. V. Chertihin, N. Runeberg, P. Pyykkö, *J. Phys. Chem.* **1995**, 99, 7925.
- [9] E. Canadell, O. Eisenstein, *Organometallics* **1984**, 3, 759.
- [10] B. V. Lokshin, O. G. Garkusha, Yu. A. Borisov, N. E. Borisova, *Russ. Chem. Bull. Int. Ed.* **2003**, 52, 831.
- [11] V. M. Rayón, G. Frenking, *Chem. Eur. J.* **2002**, 8, 4693.
- [12] A. Rosa, A. W. Ehlers, E. J. Baerends, J. G. Snijders, G. te Velde, *J. Phys. Chem.* **1996**, 100, 5690.
- [13] S. F. Boys, F. Bernardi, *Mol. Phys.* **1970**, 19, 553.
- [14] a) A. D. Becke, *J. Chem. Phys.* **1993**, 98, 5648; b) C. Lee, Y. Wang, R. G. Parr, *Phys. Rev. B* **1988**, 37, 785.
- [15] Gaussian98 (Revision A.7), M. J. Frisch, G. W. Trucks, H. B. Schlegel, G. E. Scuseria, M. A. Robb, J. R. Cheeseman, V. G. Zakrzewski, J. A. Montgomery, R. E. Stratmann, J. C. Burant, S. Dapprich, J. M. Millam, A. D. Daniels, K. N. Kudin, M. C. Strain, O. Farkas, J. Tomasi, V. Barone, M. Cossi, R. Cammi, B. Mennucci, C. Pomelli, C. Adamo, S. Clifford, J. Ochterski, G. A. Petersson, P. Y. Ayala, Q. Cui, K. Morokuma, D. K. Malick, A. D. Rabuck, K. Raghavachari, J. B. Foresman, J. Cioslowski, J. V. Ortiz, B. B. Stefanov, G. Liu, A. Liashenko, P. Piskorz, I. Komaromi, R. Gomperts, R. L. Martin, D. J. Fox, T. Keith, M. A. Al-Laham, C. Y. Peng, A. Nanayakkara, C. Gonzalez, M.

Challacombe, P. M. W. Gill, B. G. Johnson, W. Chen, M. W. Wong, J. L. Andres, M. Head-Gordon, E. S. Replogle, J. A. Pople, Gaussian, Inc., Pittsburgh, PA, **1998**.

- [16] a) P. Csaszar, P. Pulay, *J. Mol. Struct.* **1984**, *114*, 31; b) Ö. Farkas, H. B. Schlegel, *J. Chem. Phys.* **1999**, *111*, 10806.
- [17] a) S. I. Gorelsky, A. B. P. Lever, *J. Organomet. Chem.* **2001**, *635*, 187; b) S. I. Gorelsky, AOMix program, rev. 5.62. <http://www.obligato.com/software/aomix>

Noncovalent Interactions

“Double-Concave” Graphene: Permethylated Hexa-*peri*-hexabenzocoronene and Its Cocrystals with Hexafluorobenzene and Fullerene**

Zhaohui Wang, Florian Dötz, Volker Enkelmann, and Klaus Müllen*

Polycyclic aromatic hydrocarbons (PAHs) represent a unique class of organic molecules since they combine the fascination of fullerene analogues with the outstanding materials properties of graphite and conducting polymers.^[1] Their planarity is often presumed to be their most significant geometric characteristic, however, the synthesis of molecules which are at variance with this structural truism has drawn persistent attention from many organic chemists, in particular in view of the total synthesis of fullerene.^[2] As a result of the remarkable inner strain of these bent π systems, most of the synthetic routes require extreme conditions such as flash vacuum pyrolysis (FVP), and therefore suffer from low yields and tedious chromatographic separation steps, although a few solution-phase synthesis have been reported.^[3]

Recently there has been an increasing interest in supramolecular fullerene chemistry because of its potential applications in chemistry, biology, and materials science.^[4] The design of host molecules capable of recognizing fullerenes is mainly based on a kind of complementary principle where the utilization of concave/convex interactions^[5] has resulted in

the emergence of a few macrocyclic fullerene receptors.^[6] Porphyrins and metalloporphyrins with planar π surfaces have also been shown to interact with the curved π surface of fullerenes, predominantly through van der Waals dispersion forces.^[7]

The arene-perfluoroarene stacking interactions, which have been shown to occur in numerous 1:1 complexes,^[8] are of substantial theoretical and practical importance because of their role in solid-state polymerization,^[9a] cross-linking of hydrogels,^[9b] molecular electronics^[9c] and liquid-crystal stabilization.^[9d]

Herein, we introduce a strongly twisted graphene molecule, namely, permethylated hexa-*peri*-hexabenzocoronene (permethylated HBC, **4**) with a remarkable “double-concave” conformation, as revealed by single-crystal analysis. The combination of a rigid “double-concave” aromatic core with eighteen flexible methoxy groups at the periphery suggests **4** is an ideal model compound for supramolecular host-guest chemistry. Accordingly, we elucidate the single-crystal structures of its crystalline inclusion complexes with hexafluorobenzene (HFB) and fullerene guest molecules, the self-assembly of which is controlled mainly by arene-perfluoroarene interactions and geometrically complementary van der Waals interactions, respectively.

Permethylated HBC **4** was prepared in three simple steps from commercially available starting materials (Scheme 1). The synthesis of the symmetric 3,3',4,4',5,5'-hexamethoxydiphenylacetylene (**2**) was based on a Stille-type coupling of 5-bromo-1,2,3-trimethoxybenzene (**1**) with bis-(tributylstannyl)acetylene. Subsequent cyclotrimerization of the diphenylacetylene with $[\text{Co}_2(\text{CO})_8]$ yielded the hexaphenylbenzene precursor molecule **3** bearing 18 alkoxy substituents. The remarkable oxidative cyclodehydrogenation of **3** was carried out under the established ferric chloride conditions.^[10] The crude products were purified by column chromatography to yield **4** as an orange solid in 52% yield for the last step (see Supporting Information).

Permethylated HBC **4** is the first persubstituted HBC derivative prepared. The additive effect of 18 donor groups to the outer phenyl rings should facilitate an oxidative ring closure whereas the complete substitution of the outer perimeter by alkoxy groups successfully prevents chlorination of the core. The absorption maximum of **4** shows a significant bathochromic shift of 37 nm with respect to the unsubstituted parent HBC as a consequence of the 18 electron-donating alkoxy substituents and the expected nonplanarity caused by steric congestion^[11] (see Supporting Information).

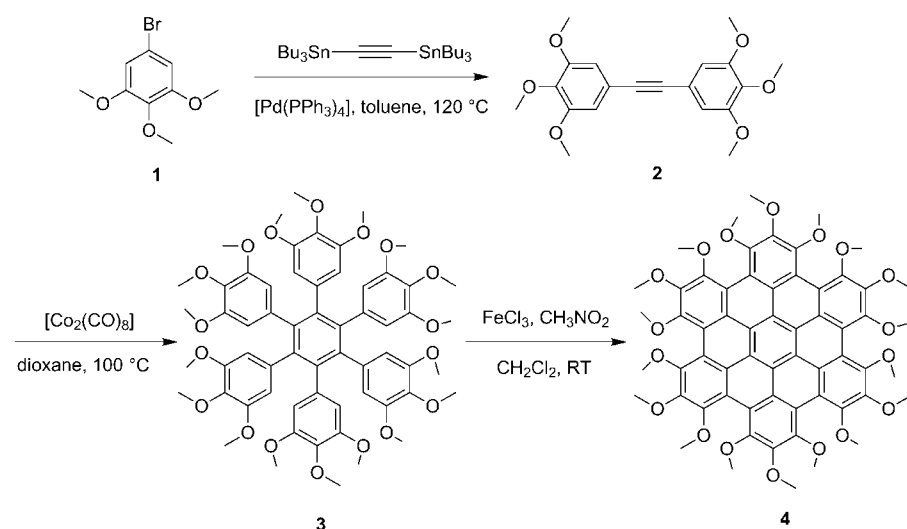
To determine the three-dimensional structure of **4**, crystals suitable for single-crystal X-ray structure analysis were obtained by slow evaporation of a solution of **4** in dichloromethane at room temperature.^[12] The crystal structure was found to be markedly nonplanar, thus reflecting the presence of pronounced *peri* interactions (Figure 1 a). The six carbon atoms of the central benzene ring are coplanar to within 0.014 Å. The steric congestion in the bay region forces the outer aromatic rings to flip up and down in an alternating manner with respect to the inner ring. A similar regular pattern is also observed for the orientation of the methoxy groups which alternately point up and down. The orientation

[*] Dr. Z. Wang, Dr. F. Dötz,^[†] Dr. V. Enkelmann, Prof. Dr. K. Müllen
Max Planck Institute for Polymer Research
Ackermannweg 10, 55128 Mainz (Germany)
Fax: (+49) 6131-379-351
E-mail: muellen@mpip-mainz.mpg.de

[†] Present address: BASF PolymerResearch
GKS/A-B001, 67056 Ludwigshafen (Germany)

[**] This work was financially supported by the Zentrum für Multifunktionelle Werkstoffe und Miniaturisierte Funktionseinheiten (BMBF 03N 6500), the EU-TMR project SISITOMAS, the Deutsche Forschungsgemeinschaft (Schwerpunkt Feldeffekttransistoren), and the EU project DISCEL (G5RD-CT-2000-00321). We thank R. Bauer for his help with graphical presentations.

Supporting information for this article (the synthesis of compound **4**, packing arrangement of the $[(\text{hfb})_2\text{C}]\text{4}$ complex, and UV/Vis absorption spectra of **4**) is available on the WWW under <http://www.angewandte.org> or from the author.



Scheme 1. Synthetic route to permethoxylated HBC (**4**).

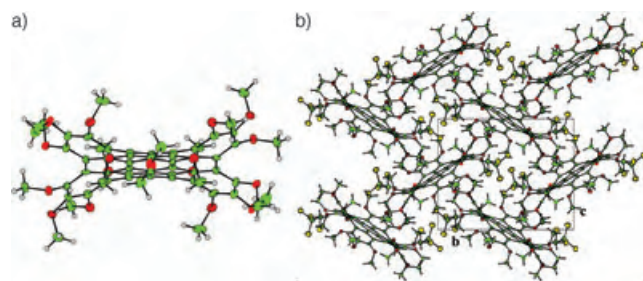


Figure 1. a) Single-crystal structure of **4**; b) herringbone packing arrangement of **4** in the solid state.

of the two *meta*-methoxy groups is found to coincide with that of the twisted phenyl ring, for example, in the case of a phenyl ring flipping down they are oriented in the same direction. The *para*-methoxy group is oriented in the opposite way.

The severe *peri* interactions destabilizing a planar D_{6h} form result in the molecule displaying two concave faces and adopting a centrosymmetric conformation. A similar alternating distortion is observed in perchlorocoronene.^[13] In contrast to perchlorocoronene which exhibits only a slight distortion ($\beta = 4.8^\circ$, β is the angle between the central aromatic ring and the distorted outer rings), **4** displays a significant deviation from the planar geometry, with a maximum angle of $\beta = 16.8^\circ$ (for comparison, the fullerene segment corannulene shows an angle of 23.6°).^[14]

Permethoxylated HBC (**4**) crystallizes in the common space group $P2_1/c$ and exhibits a herringbone-type structure with a large interplanar distance of 13.05 \AA . This packing is quite different from that of parent HBC and hexa-*tert*-butyl-HBC;^[15] the 18 overcrowded methoxy groups dramatically change the packing pattern from a face-to-face to an edge-to-face arrangement, since the interplanar distance of **4** is far too large to enable any intermolecular π - π interactions in the crystals (Figure 1b).

The extraordinary “double-concave” conformation classifies permethoxylated HBC (**4**) as a new host molecule.

Inclusion of hexafluorobenzene should be revealing since electron-deficient and electron-rich aromatic rings (for example, HFB and the central coplanar benzene ring of **4**, respectively) have an overwhelming preference for a face-to-face or π -stacked sandwich geometry because of favorable electrostatic quadrupole-quadrupole interactions. Furthermore, a space-filling model shows clearly that HFB fits perfectly into the cavity of **4** (Figure 2).

Crystals of the 2:1 complex $[(\text{hfb})_2 \supset \text{4}]$ possess an asymmetric unit with half a molecule of **4** (on a center of symmetry) and one HFB molecule. HFB and the central ring in **4** are not strictly parallel. As a consequence, the distance of the C atoms of HFB to the plane of **4** ranges from 3.27 to 3.37 \AA , and the F atoms of HFB

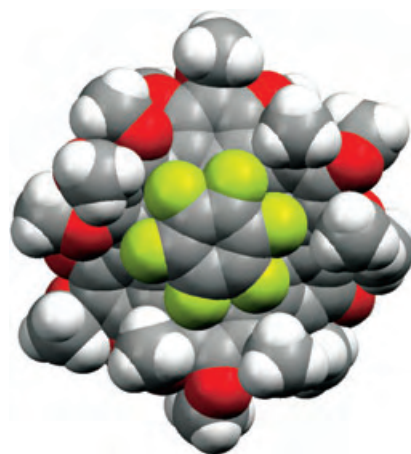


Figure 2. Space-filling model of the complex formed between HFB and **4**.

from 3.15 to 3.43 \AA . This distance is closer than the typical stacking separation in arene-perfluoroarene complexes (ca. 3.5 \AA), which indicates a strong interaction probably arising from the electron-donating effect of the methoxy groups (Figure 3). Adjacent sandwich complexes are off-set

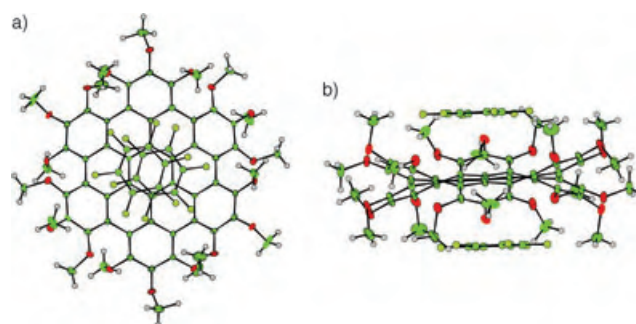


Figure 3. Single-crystal structure of the $[(\text{hfb})_2 \supset \text{4}]$ complex: a) top view and b) side view.

laterally from each other to give a tilted columnar arrangement, in contrast to the normal packing pattern of infinite stacks of alternating arene and perfluoroarene molecules. The close contacts between stacks of complexes consist of F...F interactions between the fluorine atoms at the ends of two neighboring HFB molecules. The F...F separation of 2.79 Å is comparable to a sum of the van der Waals radii of 2.90 Å.^[16] This packing preference reflects the combined effect of maximized electrostatic interactions with the two HFB molecules sandwiching the HBC molecules and compatible accommodation of HFB into the cavity formed by flexible surrounding methoxy groups.

The “double-concave” permethoxylated HBC (**4**) was expected to be geometrically complementary to the globular C₆₀ shape, and the inclusion of “thick” C₆₀ will also afford sufficient separation between HBC molecules and avoid steric crowding of the methoxy groups. Slow evaporation of the solvent from a solution of **4** and fullerene (1:1) in CS₂ yielded black crystals. The crystal structure is shown in Figure 4. The fullerene is positioned exactly on the central

molecules on both sides, the flexible methoxy groups at the periphery of **4** adjust their orientation to the size and shape of the guest molecules. Indeed, **4** possesses *D*_{3d} symmetry in the crystals of the fullerene complex, in contrast to the centrosymmetry in its dichloromethane solvates and the HFB complexes. A comparison of the crystal structures shows that the orientation of the 18 methoxy groups changes to provide a cavity into which the different guest molecules may be accommodated.

We have presented a novel approach to an extremely nonplanar persubstituted HBC derivative by using the facile cyclodehydrogenation procedure with ferric chloride at room temperature. X-ray single-crystal analysis revealed that permethoxylated HBC (**4**) has an extraordinary “double-concave” conformation in which the dramatic deviation from planarity arises because of steric congestion in the bay region. The remarkable propensity of guest molecules to change the self-assembly of this novel host molecule and the fascinating structures obtained in this way are intriguing in view of the design of new host–guest systems and materials, for example, based on functionalized fullerenes and perfluoroarenes. Attaching long alkyl chains onto the PAH core should give it liquid-crystalline properties.

Received: July 27, 2004

Keywords: crystal engineering · fullerenes · host–guest systems · noncovalent interactions · self-assembly

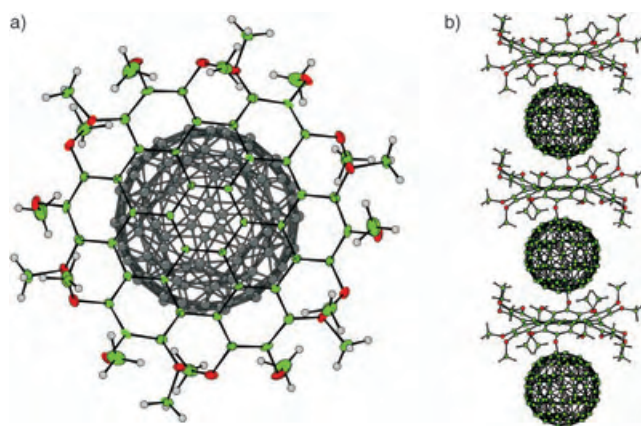


Figure 4. Single-crystal structure of the complex formed between fullerene and **4**: a) top view and b) side view of the columnar packing arrangement.

benzene ring of **4**, thus yielding a perfect columnar packing arrangement. This situation is in contrast to the porphyrin–fullerene complex which shows a zigzag arrangement of porphyrins, with fullerenes sandwiched in the clefts. As is often the case with fullerene structures, there is crystallographic disorder with rapid oscillation of the carbon atoms of the C₆₀ molecules;^[17] nevertheless, the disposition of **4** and the C₆₀ moieties is well resolved.

The closest approach of the C₆₀ carbon atoms to the central ring plane of **4** is 2.95 Å, which is significantly shorter than separations observed for normal π – π interactions.^[18] The unexpectedly strong interaction between a curved π surface and a flat π surface (central ring of **4**) may be explained in terms of van der Waals interactions and polar electrostatic interactions rather than as charge-transfer interactions.^[19]

It should be noted that in addition to the “double-concave” surface which allows the inclusion of suitable guest

- [1] a) E. Clar, *Polycyclic Hydrocarbons*, Academic Press, London, **1964**; b) M. Zander, *Polycyclische Aromaten*, B. G. Teubner, Stuttgart, **1995**.
- [2] a) Examples of nonplanar PAHs: S. Grimme, J. Harren, A. Sobanski, F. Vögtle, *Eur. J. Org. Chem.* **1998**, 1491; K. Shibata, A. A. Kulkarni, D. M. Ho, R. A. Pascal, Jr., *J. Am. Chem. Soc.* **1994**, *116*, 5983; R. A. Pascal, Jr., W. D. McMillan, D. V. Engen, R. G. Eason, *J. Am. Chem. Soc.* **1987**, *109*, 4660; H. M. Duong, M. Bendikov, D. Steiger, Q. Zhang, G. Sonmez, J. Yamada, F. Wudl, *Org. Lett.* **2003**, *5*, 4433; N. Kobayashi, T. Fukuda, K. Ueno, H. Ogino, *J. Am. Chem. Soc.* **2001**, *123*, 10740; b) for the total synthesis of fullerene and the synthesis of the bowl-shaped fullerene segment corannulene, see, for example: M. M. Boorum, Y. V. Vasil'ev, T. Drewello, L. T. Scott, *Science* **2001**, *294*, 828; H. E. Bronstein, N. Choi, L. T. Scott, *J. Am. Chem. Soc.* **2002**, *124*, 8870; T. J. Seiders, E. L. Elliott, G. H. Grube, J. S. Siegel, *J. Am. Chem. Soc.* **1999**, *121*, 7804; R. G. Lawton, W. E. Barth, *J. Am. Chem. Soc.* **1971**, *93*, 1730.
- [3] a) T. J. Seiders, K. K. Baldrige, J. S. Siegel, *J. Am. Chem. Soc.* **1996**, *118*, 2574; b) A. Sygula, P. W. Rabideau, *J. Am. Chem. Soc.* **2000**, *122*, 6323; c) H. A. Reisch, M. Bratcher, L. T. Scott, *Org. Lett.* **2000**, *2*, 1427.
- [4] A. Hirsch, *The Chemistry of the Fullerenes*, Thieme, Stuttgart, **1994**; F. Diederich, C. Thilgen, *Science* **1996**, *271*, 317; A. Hirsh, *Angew. Chem.* **2004**, *116*, 2380; *Angew. Chem. Int. Ed.* **2004**, *43*, 2326; F. Diederich, M. Gomez-Lopez, *Chem. Soc. Rev.* **1999**, *28*, 263; J. F. Nierengarten, *Top. Curr. Chem.* **2003**, *228*, 87; J. F. Nierengarten, *Angew. Chem.* **2001**, *113*, 3061; *Angew. Chem. Int. Ed.* **2001**, *40*, 2973.
- [5] F. Hajek, M. W. Hosseini, E. Graf, A. De Cian, J. Fischer, *Angew. Chem.* **1997**, *109*, 1830; *Angew. Chem. Int. Ed. Engl.* **1997**, *36*, 1760.

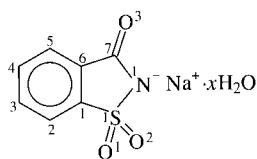
- [6] For examples, see: J. L. Atwood, G. A. Koutsantonis, C. L. Raston, *Nature* **1994**, 368, 229; T. Suzuki, K. Nakashima, S. Shinkai, *Chem. Lett.* **1994**, 699; T. Haino, M. Yanase, Y. Fukazawa, *Angew. Chem.* **1998**, 110, 1044; *Angew. Chem. Int. Ed.* **1998**, 37, 997; J. L. Atwood, L. J. Barbour, C. L. Raston, I. B. N. Sudria, *Angew. Chem.* **1998**, 110, 1029; *Angew. Chem. Int. Ed.* **1998**, 37, 981; T. Kawase, K. Tanaka, N. Fujiwara, H. R. Darabi, M. Oda, *Angew. Chem.* **2003**, 115, 1662; *Angew. Chem. Int. Ed.* **2003**, 42, 1624; M. Wang, X. Zhang, Q. Zheng, *Angew. Chem.* **2004**, 116, 856; *Angew. Chem. Int. Ed.* **2004**, 43, 838.
- [7] a) Y. Sun, T. Drovetskaya, R. D. Bolskar, R. Bau, P. D. W. Boyd, C. A. Reed, *J. Org. Chem.* **1997**, 62, 3642; b) M. M. Olmstead, D. A. Costa, K. Maitra, B. C. Noll, S. L. Phillips, P. M. Van Calcar, A. L. Balch, *J. Am. Chem. Soc.* **1999**, 121, 7090; c) P. D. W. Boyd, M. C. Hodgson, C. E. F. Rickard, A. G. Oliver, L. Chaker, P. J. Brothers, R. D. Bolskar, F. S. Tham, C. A. Reed, *J. Am. Chem. Soc.* **1999**, 121, 10487.
- [8] For reviews and examples, see: E. A. Meyer, R. K. Castellano, F. Diederich, *Angew. Chem.* **2003**, 115, 1224; *Angew. Chem. Int. Ed.* **2003**, 42, 1210; J. C. Collings, K. P. Roscoe, R. L. Thomas, A. S. Batsanov, L. M. Stimson, J. A. K. Howard, T. B. Marder, *New J. Chem.* **2001**, 25, 1410; M. Gdaniec, W. Jankowski, M. J. Milewska, T. Polonski, *Angew. Chem.* **2003**, 115, 4033; *Angew. Chem. Int. Ed.* **2003**, 42, 3903; S. W. Watt, C. Dai, A. J. Scott, J. M. Burke, R. L. Thomas, J. C. Collings, C. Viñey, W. Clegg, T. B. Marder *Angew. Chem.* **2004**, 116, 3123; *Angew. Chem. Int. Ed.* **2004**, 43, 3061.
- [9] a) G. W. Coates, A. R. Dunn, L. M. Henling, D. A. Dougherty, R. H. Grubbs, *Angew. Chem.* **1997**, 109, 290; *Angew. Chem. Int. Ed. Engl.* **1997**, 36, 248; G. W. Coates, A. R. Dunn, L. M. Henling, J. W. Ziller, E. B. Lobkovsky, R. H. Grubbs, *J. Am. Chem. Soc.* **1998**, 120, 3641; b) A. F. M. Kilbinger, R. H. Grubbs, *Angew. Chem.* **2002**, 114, 1633; *Angew. Chem. Int. Ed.* **2002**, 41, 1563; c) M. L. Renak, G. P. Bartholomeu, S. Wang, P. J. Ricatto, R. J. Lachiotte, G. C. Bazan, *J. Am. Chem. Soc.* **1999**, 121, 7787; W. J. Feast, P. W. Lovenich, H. Puschmann, C. Taliani, *Chem. Commun.* **2001**, 505; d) M. Weck, A. R. Dunn, K. Matsumoto, G. W. Coates, E. B. Lobkovsky, R. H. Grubbs, *Angew. Chem.* **1999**, 111, 2909; *Angew. Chem. Int. Ed.* **1999**, 38, 2741.
- [10] a) M. D. Watson, A. Fechtenkötter, K. Müllen, *Chem. Rev.* **2001**, 101, 1267; b) Z. Wang, M. D. Watson, J. Wu, K. Müllen, *Chem. Commun.* **2004**, 336.
- [11] Z. Wang, Z. Tomovic, M. Kastler, R. Pretsch, F. Negri, V. Enkelmann, K. Müllen, *J. Am. Chem. Soc.* **2004**, 126, 7794.
- [12] Data collections for the crystal-structure analysis were performed on a Nonius KCCD diffractometer equipped with a Cryostream cooler with graphite monochromated MoK α radiation. The structures were solved by direct methods (Shelx) and refined on *F* with anisotropic temperature factors for the non-hydrogen atoms. The H atoms were refined with fixed isotropic temperature factors in the riding mode. **4**·4CH₂Cl₂: C₃₂H₃₁Cl₄O₉, monoclinic, space group *P*2₁/*c*, *T* = 150 K, *a* = 14.6101(7), *b* = 13.0471(6), *c* = 16.2439(7) Å, β = 91.990(3)°, *V* = 3094.5(4) Å³, *Z* = 4, ρ_{calcd} = 1.505 g cm⁻³, μ = 0.438 mm⁻¹; 12418 reflections measured, of which 7485 were unique (*R*_{int} = 0.026) and 3661 were observed; *R* = 0.086, *R*_w = 0.0817. **4**·2C₆F₆: C₃₆H₂₇F₆O₉, triclinic, space group *P*1̄, *T* = 120 K, *a* = 11.1105(5), *b* = 11.7330(5), *c* = 13.0297(6) Å, α = 73.425(1), β = 88.923(1), γ = 75.098(1)°, *V* = 1570.2(2) Å³, *Z* = 2, ρ_{calcd} = 1.517 g cm⁻³, μ = 0.131 mm⁻¹; 29594 reflections measured, of which 8552 were unique (*R*_{int} = 0.048) and 5203 were observed; *R* = 0.0651, *R*_w = 0.0698. **4**·C₆₀: C₂₀H₉O₃, trigonal, space group *R*3̄, *T* = 120 K, *a* = 22.1940(7), *b* = 22.1940(7), *c* = 12.8191(5) Å, *V* = 5468.4(6) Å³, *Z* = 6, ρ_{calcd} = 1.624 g cm⁻³, μ = 0.110 mm⁻¹; 26529 reflections measured, of which 3375 were unique (*R*_{int} = 0.041) and 1687 were observed; *R* = 0.0872, *R*_w = 0.0967. The fullerene molecule was found to be disordered even at low temperatures such that no meaningful bonding geometry could be detected in the fullerene fragment. The strongest peaks observed in difference Fourier maps were included in the refinement. In the initial refinement cycles they were refined with a common isotropic temperature factor and variable occupancy factors. Additional difference Fourier peaks were added until the electron density in the C₆₀ fragment amounted to the expected value of 10 carbon atoms. In the last cycles of the refinement they were refined with isotropic temperature factors and the fixed occupancy factors which had been determined in the previous refinement cycles. CCDC-245390, CCDC-245391, and CCDC-245392 contain the supplementary crystallographic data for this paper. These data can be obtained free of charge via www.ccdc.cam.ac.uk/conts/retrieving.html (or from the Cambridge Crystallographic Data Centre, 12, Union Road, Cambridge CB21EZ, UK; fax: (+44) 1223-336-033; or deposit@ccdc.cam.ac.uk).
- [13] a) T. Baird, J. H. Gall, D. D. MacNicol, P. R. Mallinson, C. R. Michie, *J. Chem. Soc. Chem. Commun.* **1988**, 1471; b) G. A. Downing, C. S. Frampton, D. D. MacNicol, P. R. Mallinson, *Angew. Chem.* **1994**, 106, 1653; *Angew. Chem. Int. Ed. Engl.* **1994**, 33, 1587.
- [14] J. C. Hanson, C. E. Nordmann, *Acta Crystallogr. Sect. B* **1975**, 32, 1147.
- [15] a) R. Goddard, M. W. Haenel, W. C. Herndon, C. Krüger, M. Zander, *J. Am. Chem. Soc.* **1995**, 117, 30; b) P. T. Herwig, V. Enkelmann, O. Schmelz, K. Müllen, *Chem. Eur. J.* **2000**, 6, 1834.
- [16] R. S. Rowland, R. Taylor, *J. Phys. Chem.* **1996**, 100, 7384.
- [17] B. Narymbetov, H. Kobayashi, M. Tokumoto, A. Omerzu, D. Mihailovic, *Chem. Commun.* **1999**, 1511.
- [18] Graphite and typical arene/arene separation is in the range 3.3–3.5 Å, fullerene/arene approaches lie in the range 3.0–3.5 Å, calixarene/fullerene and related complexes 3.5–3.6 Å, however, a close approach 2.75 Å is observed for a porphyrin/fullerene assembly.^[7]
- [19] A toluene solution of C₆₀ and **4** shows UV/Vis spectra that are simply the superposition of the spectra of the two individual chromophores without a charge-transfer absorption band; however, it is still difficult to draw conclusions about whether or not charge-transfer interactions are important in crystals

Structure Elucidation

Solid-State Structure and Temperature/
Evacuation-Induced Dehydration of Sodium
Saccharinate 1.875 Hydrate**

Panče Naumov,* Gligor Jovanovski, Orhideja Grupče,
Branko Kaitner, A. David Rae, and Seik Weng Ng

The anion of saccharin^[1] is a polyfunctional ligand that binds to a plethora of metal ions.^[2,3] The solid hydrate of sodium saccharinate (“sodium saccharin” or “saccharinum soluble”; Scheme 1) is an edible chemical which constitutes more than



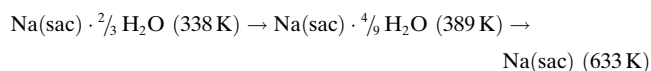
Scheme 1. The atom-labeling scheme for the monoclinic hydrate of sodium saccharinate.

half of the world’s artificial sweeteners, but which is suspected to be carcinogenic.^[1] Although the compound has been extensively used for more than 150 years, its exact structure has not been unequivocally established. In most chemical

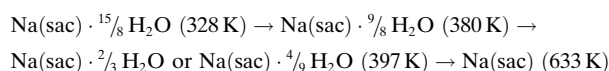
catalogues it is listed as the dihydrate $\text{Na}(\text{sac}) \cdot 2\text{H}_2\text{O}$ ($\text{sac} = \text{C}_7\text{H}_4\text{NO}_3\text{S}^-$). An earlier effort to determine its crystal structure failed because of an unusually large monoclinic unit cell^[4] and partial dehydration. Air-stable triclinic $\text{Na}(\text{sac}) \cdot \frac{2}{3}\text{H}_2\text{O}$ is obtained upon recrystallization from ethanol.^[5,6] Herein we report the first determination of the structure of the commercial artificial sweetener sodium saccharinate. The relative stability and the mechanisms of isobaric dehydration (heating at constant pressure) and isothermal dehydration (evacuation at constant temperature) of the two hydrates are also revealed.

Recrystallization of sodium saccharinate from different solvents yielded two hydrates. Whereas the physicochemical analysis of the hydrate obtained from 95 % ethanol was consistent with the triclinic $\text{Na}(\text{sac}) \cdot \frac{2}{3}\text{H}_2\text{O}$ described previously,^[5,6] the monoclinic hydrate that was obtained from water was identical to the unpurified commercial product. Precise thermoanalytical measurements of the latter showed 1.87 ($\frac{15}{8}$ by diffraction, see below) water molecules per formula unit.

The otherwise stable crystals of $\text{Na}(\text{sac}) \cdot \frac{2}{3}\text{H}_2\text{O}$ are dehydrated^[7] in two well-defined steps when heated under isobaric conditions. The intermediate $\text{Na}(\text{sac}) \cdot \frac{4}{9}\text{H}_2\text{O}$ exists in the interval 343–389 K (the peaks evident in the differential thermal analysis (DTA) traces are given in parentheses):



The crystals of $\text{Na}(\text{sac}) \cdot \frac{15}{8}\text{H}_2\text{O}$ are stable for months if stored in a closed vessel and not allowed to suffer mechanical damage. However, if they are exposed to dry air, placed in an evacuated container, or coarsely ground, they turn opaque. The isobaric dehydration of $\text{Na}(\text{sac}) \cdot \frac{15}{8}\text{H}_2\text{O}$ (see the Supporting Information) commences above room temperature ($> 303 \text{ K}$) and proceeds through two intermediates: $\text{Na}(\text{sac}) \cdot \frac{9}{8}\text{H}_2\text{O}$ (328–373 K) and $\text{Na}(\text{sac}) \cdot \frac{2}{3}\text{H}_2\text{O}$ or $\text{Na}(\text{sac}) \cdot \frac{4}{9}\text{H}_2\text{O}$ (the exact formula of the second intermediate could not be identified because of its instability at its formation temperature):



The changes in the IR spectra^[3,8] and the final spectra obtained after evacuation and moderate heating of $\text{Na}(\text{sac}) \cdot \frac{15}{8}\text{H}_2\text{O}$ are nearly identical (Figure 1). This observation indicates that the isobaric dehydration and the initial isothermal dehydration both proceed to give the same product, which was identified by thermal analysis to be $\text{Na}(\text{sac}) \cdot \frac{9}{8}\text{H}_2\text{O}$. Comparison of the infrared spectra obtained (Figure 2) confirms that the product is not the stable triclinic $\text{Na}(\text{sac}) \cdot \frac{2}{3}\text{H}_2\text{O}$. Figure 2 also shows that the isothermal dehydration commences more gradually than the isobaric one. The absence of additional spectral changes upon further evacuation indicates that prolonged isothermal evacuation does not affect $\text{Na}(\text{sac}) \cdot \frac{9}{8}\text{H}_2\text{O}$.

The crystallographic data for the two hydrates and a detailed discussion of the monoclinic structure are given in

[*] Dr. P. Naumov
International Center for Young Scientists
National Institute for Materials Science
1-1 Namiki, Tsukuba, Ibaraki 305-0044 (Japan)
Fax: (+81) 29-860-4706
E-mail: naumov.pance@nims.go.jp
Dr. P. Naumov, Prof. G. Jovanovski, Prof. O. Grupče
Institute of Chemistry
Faculty of Science
“Sv. Kiril i Metodij” University
P.O. Box 162, MK-1001 Skopje (Macedonia)
Prof. B. Kaitner
Chemistry Department
Laboratory of General and Inorganic Chemistry
Faculty of Science, University of Zagreb
Ul. kralja Zvonimira 8, HR-10002 Zagreb (Croatia)
Prof. A. D. Rae
Australian National University
Research School of Chemistry
Canberra, A.C.T. 0200 (Australia)
Dr. S. W. Ng
Department of Chemistry
University of Malaya, 50603 Kuala Lumpur (Malaysia)

[**] This study was performed through Special Coordination Funds for Promoting Science and Technology from the Ministry of Education, Culture, Sports, Science, and Technology of the Japanese Government. We also thank the Ministry of Education and Science of the Republic of Macedonia and the Ministry of Science of the Republic of Croatia for financial support.

Supporting information for this article is available on the WWW under <http://www.angewandte.org> or from the author.

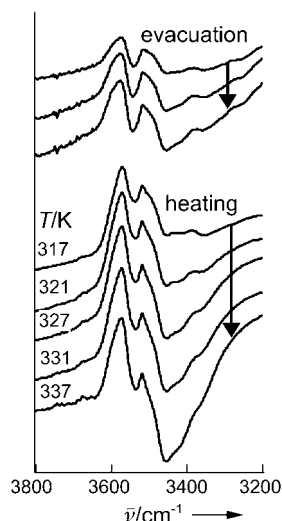


Figure 1. Effects of isothermal (evacuation) and isobaric (heating) dehydration on the $\nu(\text{OH})$ region in the difference IR spectrum of $\text{Na}(\text{C}_7\text{H}_4\text{NO}_3\text{S}) \cdot 15/8 \text{H}_2\text{O}$. For the isothermal dehydration, the difference spectra were obtained by subtraction of a reference spectrum of $\text{Na}(\text{sac}) \cdot 15/8 \text{H}_2\text{O}$ from the spectra of samples evacuated with a rotary oil pump for various times. For the isobaric dehydration, the difference spectra were obtained by subtraction of the initial spectrum of the $\text{Na}(\text{sac}) \cdot 15/8 \text{H}_2\text{O}$ from the spectra of the same sample heated at various temperatures.

the Supporting Information. The structure of the triclinic hydrate at 78 K is identical to the structure determined at room temperature.^[5] The crystal of the monoclinic $P2_1/n$ hydrate $\text{Na}_{64}(\text{C}_7\text{H}_4\text{NO}_3\text{S})_{64} \cdot 120 \text{H}_2\text{O}$ ($\text{Na}(\text{C}_7\text{H}_4\text{NO}_3\text{S}) \cdot 15/8 \text{H}_2\text{O}$, $a = 18.6998(1)$, $b = 28.5277(1)$, $c = 29.2257(3)$ Å, $\beta = 93.582(1)^\circ$, $V = 15560.4(2)$ Å³, $Z = 64$, $T = 95(2)$ K) may be regarded as an occupational and displacive modulation of an idealized (i) structure with $C2/m$ $Z = 8$ symmetry whereby $a_i = a$, $b_i = b/4$, and $c_i = c/2$. The large number of structurally different water molecules is confirmed by the matrix-isolation spectra of the partially deuterated compound.^[9] As shown in Figure 3, a large fraction of the structure can be described as a displacive modulation of the saccharinate anions away from the hypothetical idealized $C2/m$ structure in which all but the sulfonyl oxygen atoms of the saccharinate anions would lie on mirror planes and consequently strictly parallel to each other. Two sodium atoms (Na12 and Na13, see the Supporting Information) take the positions of two water molecules (O16 and O23) in the idealized structure. The resulting structural misfit results in three sodium atoms (Na12, Na15, Na16), four water molecules (O1, O2, O15, O23), and one saccharinate anion (I) being disordered over two

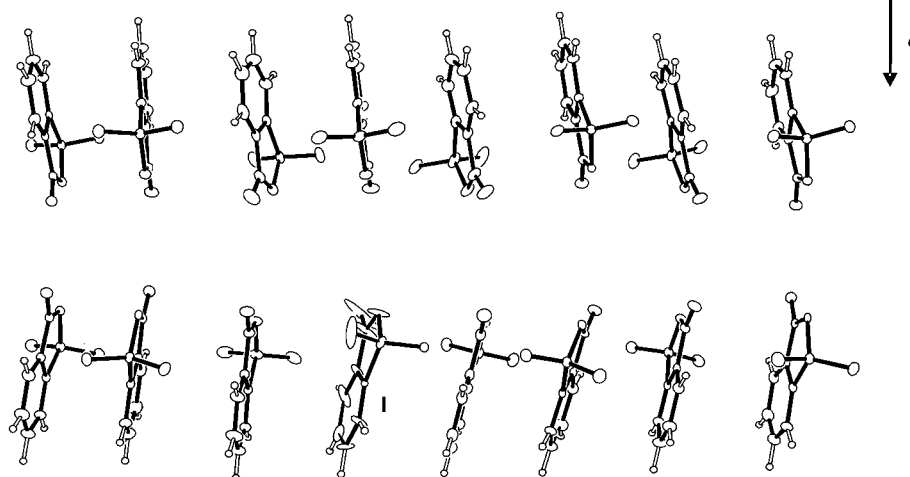


Figure 3. The positions of the 16 independent saccharinate anions relative to each other as viewed approximately normal to the bc -plane. Only the major part (occupancy 0.666(2)) of the disordered saccharinate ion I is shown.

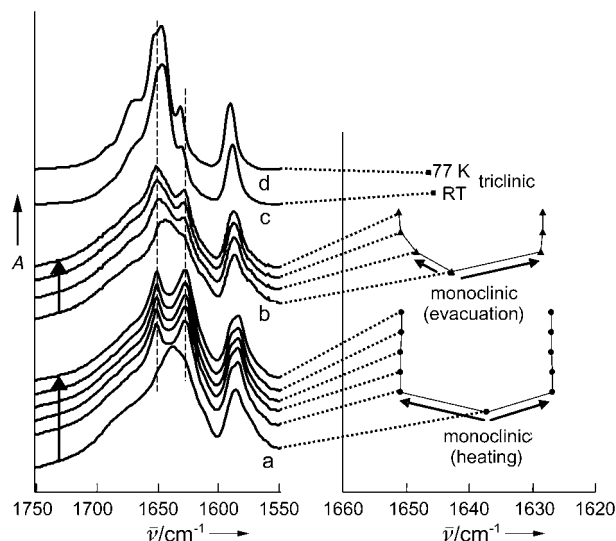


Figure 2. Changes (left) and temporal profiles of the positions (right) of the carbonyl stretching bands in the IR spectrum of $\text{Na}(\text{C}_7\text{H}_4\text{NO}_3\text{S}) \cdot 15/8 \text{H}_2\text{O}$ with isobaric (monoclinic: a, ●) and isothermal (monoclinic: b, ▲) dehydration. The spectra and values for $\text{Na}(\text{C}_7\text{H}_4\text{NO}_3\text{S}) \cdot 2/3 \text{H}_2\text{O}$ (■) at 298 K (c, RT) and 77 K (d) are also plotted for comparison.

positions with occupancies 0.334(2) and 0.666(2). The displacive modulations allow all the sodium atoms to be surrounded by six oxygen or nitrogen atoms, and all the water molecules to be at reasonable contact distances to the saccharinate anions. The ranges of the shortest distances of the ligands to the metal atoms are compiled in Table 1.

The crystal structure of $\text{Na}(\text{sac}) \cdot 9/8 \text{H}_2\text{O}$ obtained by dehydration of $\text{Na}(\text{sac}) \cdot 15/8 \text{H}_2\text{O}$ could not be determined because of reduced crystallinity. However, the splitting of the $\nu(\text{CO})$ mode in the IR spectra (1651 , 1627 cm^{-1} ; Figure 2) indicates that the saccharinate ions differentiate into two structural groups upon dehydration, with average^[3a] C–O

Table 1: Ranges of the metal-to-ligand distances in the structure of $\text{Na}(\text{C}_7\text{H}_4\text{NO}_3\text{S}) \cdot \frac{15}{8} \text{H}_2\text{O}$.

Parameter ^[a]	Range [Å]
$\text{Na} \cdots \text{O}_{1,2}$	2.289(12)–2.940(3)
$\text{Na} \cdots \text{O}_3$	2.214(2)–3.081(8)
$\text{Na} \cdots \text{N}_1$	2.435(3)–3.062(3)
$\text{Na} \cdots \text{O}(\text{water})$	2.200(6)–2.862(4)

[a] The atom labels refer to Scheme 1.

bond lengths of 1.222 and 1.238 Å. Moreover, the shift of the $\nu(\text{CO})$ modes of $\text{Na}(\text{sac}) \cdot \frac{9}{8} \text{H}_2\text{O}$ relative to $\text{Na}(\text{sac}) \cdot \frac{15}{8} \text{H}_2\text{O}$ reveals^[3] that upon dehydration the saccharinate residues of one group correspond more to the 1,2-benzisothiazol-3-one form while those of the other group are closer to the 1,2-benzisothiazolyl-3-olato form.

In the initial structure, the saccharinate ions are stacked into columns running parallel to the *b*-axis (Figure 4). The

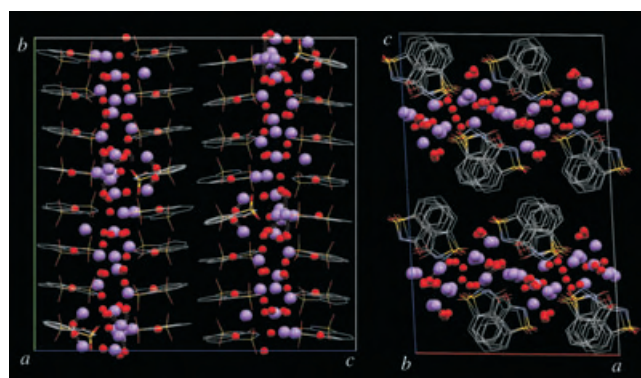


Figure 4. Ball-and-stick representation of the packing in the structure of $\text{Na}(\text{C}_7\text{H}_4\text{NO}_3\text{S}) \cdot \frac{15}{8} \text{H}_2\text{O}$. Water oxygen atoms and the sodium ions are colored red and purple, respectively. The hydrogen atoms are omitted for clarity.

metal ions and the water molecules fill up the space between the saccharinate columns. On the basis of the above findings and the structure of $\text{Na}(\text{sac}) \cdot \frac{15}{8} \text{H}_2\text{O}$, we suggest the following scenario for its initial dehydration: Removal of the loosely bound 48 water molecules from the unit cell during the first step, induced either by heating or by evacuation, causes the saccharinate ions to slide out of the stacks, presumably in the direction of their sulfonyl functional groups and towards the voids produced by the leaving water molecules. The sliding results in differentiation of the saccharinate ions into two groups, which differ in their distances to the metal ions and their ionicity, which is recorded as a splitting of the carbonyl band.

Experimental Section

Recrystallization of commercial sodium saccharinate (Merck, purity > 99%) from water by slow evaporation at ambient temperature yielded large colorless monoclinic crystal blocks of centimeter dimensions. The cell parameters corresponded with the compound prepared by neutralization of an aqueous solution of saccharin with sodium carbonate or sodium hydroxide^[10] and recrystallized from

water. The purity of the sample before and after the recrystallization was checked by elemental analysis and inductively coupled plasma/atomic emission spectroscopy (ICP-AES). The contents of the most likely impurities, potassium (62 and 11 ppm by ICP-AES) and ethanol (below the detection limit of 0.1 ppm by HS-GC/MS), were insignificant for the purposes of this study. The diffraction measurements were carried out on a $0.45 \times 0.25 \times 0.20 \text{ mm}^3$ specimen obtained by partial dissolution of a larger crystal in water. The triclinic compound was obtained in the form of smaller colorless crystals by recrystallization from 95% ethanol.

The thermogravimetry/differential scanning calorimetry (TG/DSC) curves were recorded in the 298–723 K range on a Rigaku ThermoPlus analyzer at a heating rate of 2 K min^{-1} using non-pulverized, freshly prepared crystals. The IR spectra were recorded on a Perkin–Elmer System 2000 interferometer (KBr pellets) using a low-temperature cell. The pellets were prepared under minimum dehydration. Diffraction measurements on the two crystals were carried out at 95 K on a Siemens CCD area-detector diffractometer equipped with the Rigaku low-temperature system.^[11] The triclinic structure was determined by direct phase determination^[12] and refined^[13] to $R = 0.0298$ for 4943 $I > 2\sigma(I)$ reflections ($wR_2 = 0.0805$) and $R = 0.0336$ for all 5570 ($wR_2 = 0.0823$) reflections (GOF = 1.080). For the monoclinic compound, the sphere of 246589 reflections measured to $2\theta = 55^\circ$ ($-24 < h < 24$, $-36 < l < 36$, $-37 < l < 37$) consisted of 35542 independent reflections. The structure was determined with SHELXS-97^[14] and refined with RAELS00.^[15,16] The structure (see the Supporting Information) is presented as an ORTEP^[17] diagram in Figure 3. CCDC 242403 and 242404 contain the supplementary crystallographic data for this paper. These data can be obtained free of charge from the Cambridge Crystallographic Data Centre via www.ccdc.cam.ac.uk/data_request/cif.

Received: June 22, 2004

Revised: October 31, 2004

Published online: January 5, 2005

Keywords: artificial sweeteners · hydrates · IR spectroscopy · structure elucidation · X-ray diffraction

- [1] a) J. M. Price, C. G. Biava, B. L. Oser, E. E. Vogin, J. Steinfeld, H. L. Ley, *Science* **1970**, *167*, 1131–1132; b) E. M. Garland, T. Sakata, M. J. Fisher, T. Masui, M. S. Cohen, *Cancer Res.* **1989**, *49*, 3789–3794; c) T. Masui, M. A. Mann, D. C. Borgeson, M. E. Garland, T. Okamura, H. Fujii, C. J. Pelling, M. S. Cohen, *Teratog. Carcinog. Mutagen.* **1993**, *13*, 225–235; d) N. Suzuki, H. Suzuki, *Cancer Res.* **1995**, *55*, 4253–4256.
- [2] a) P. Naumov, G. Jovanovski, *Struct. Chem.* **2000**, *10*, 19–33; b) P. Naumov, G. Jovanovski, *Vib. Spectrosc.* **2000**, *24*, 201–211; c) P. Naumov, G. Jovanovski, *J. Coord. Chem.* **2001**, *54*, 63–79; d) P. Naumov, G. Jovanovski, *Curr. Org. Chem.* **2001**, *5*, 1059–1077; e) P. Naumov, G. Jovanovski, J. V. Hanna, I. A. Razak, S. Chantrapromma, H.-K. Fun, S. W. Ng, *Inorg. Chem. Commun.* **2001**, *4*, 766–768; f) P. Naumov, G. Jovanovski, M. Ristova, I. A. Razak, S. Çakir, S. Chantrapromma, H.-K. Fun, S. W. Ng, *Z. Anorg. Allg. Chem.* **2002**, *628*, 2930–2939.
- [3] a) P. Naumov, G. Jovanovski, *J. Mol. Struct.* **2001**, *563*, 335–339; b) P. Naumov, G. Jovanovski, M. G. B. Drew, S. W. Ng, *Inorg. Chim. Acta* **2001**, *314*, 154–162; c) P. Naumov, G. Jovanovski, S. Z. Hu, I. H. Suh, I. A. Razak, S. Chantrapromma, H. K. Fun, S. W. Ng, *Acta Crystallogr. C* **2001**, *57*, 1016–1019.
- [4] G. Jovanovski, PhD thesis, University of Zagreb, **1981**.
- [5] G. Jovanovski, B. Kamenar, *Cryst. Struct. Commun.* **1982**, *11*, 247–249.
- [6] G. Jovanovski, O. Grupče, B. Šoptrajanov, *J. Mol. Struct.* **1990**, *219*, 61–66.

- [7] P. Naumov, G. Jovanovski, S. Abbrent, L.-E. Tergenius, *Thermochim. Acta* **2000**, *31*, 123–130.
- [8] The difference IR spectra in the $\nu(\text{OH})$ region were employed to avoid overlap with the strong bands of the reactant. The $\nu(\text{CO})$ mode of $\text{Na}(\text{sac}) \cdot ^{15}/_8 \text{H}_2\text{O}$ which splits into a doublet was found to be very sensitive to dehydration.
- [9] As the pronounced structural disorder precludes accurate location of the hydrogen atoms by X-ray diffraction, the structure of the stoichiometric water was additionally investigated with the isotopic matrix-isolation method (examples: a) G. Jovanovski, P. Naumov, O. Grupče, B. Kaitner, *Eur. J. Solid State Inorg. Chem.* **1998**, *35*, 231–242; b) P. Naumov, G. Jovanovski, *Solid State Sci.* **2000**, *2*, 249–256) from spectra of partially deuterated $\text{Na}(\text{sac}) \cdot ^{15}/_8 (\text{H},\text{D})_2\text{O}$ with low deuterium content ($x_{\text{D}} < 5\%$). The isotopically isolated HDO isotopomers exhibit a complex spectrum in the 2660–2280 cm^{-1} region (see the Supporting Information), to which 30 mixed Gaussian–Lorentzian component $\nu(\text{OD})$ bands with different intensities were fitted. This result indicates the structural dissimilarity of at least 30 structurally different water OH groups.
- [10] Attempted synthesis by metathesis in $\text{K}(\text{sac}) \cdot ^{2}/_3 \text{H}_2\text{O}$ results in mixed triclinic $\text{K}_2\text{Na}(\text{sac})_3 \cdot \text{H}_2\text{O}$: K. M. A. Malik, S. Z. Haider, M. A. Hossain, *Acta Crystallogr. C* **1984**, *40*, 1696–1698.
- [11] SAINT (Siemens Area Detector Integration Program), SMART (Siemens Molecular Analysis Research Tool); Siemens Analytical X-ray Instruments Inc., Madison, Wisconsin, USA, **1996**.
- [12] A. Altomare, G. Cascarano, C. Giacovazzo, A. Guagliardi, M. C. Burla, G. Polidori, M. Camalli, SIR92. Program for automatic solution of crystal structures by direct methods, *J. Appl. Crystallogr.* **1994**, *27*, 435–435.
- [13] G. M. E. Sheldrick, SHELXL-97, Structure refinement program, University of Göttingen, Germany, **1997**.
- [14] G. M. E. Sheldrick, SHELXS-97, Structure solution program, University of Göttingen, Germany, **1997**.
- [15] A. D. Rae, RAELS00. A comprehensive constrained least-squares refinement program; Australian National University, Canberra, Australia, **2000**.
- [16] The use of refinable coordinates defined relative to local orthonormal axial systems (a) A. D. Rae, *Acta Crystallogr. C* **1975**, *31*, 560–570; b) A. D. Rae, *Acta Crystallogr. C* **1975**, *31*, 570–574) allowed all the saccharinate anions in the asymmetric unit to be exactly the same and have exact local mirror symmetry. The thermal motion of each molecule was described by its own *TLX* parameterization (*T* is the translation tensor, *L* is the libration tensor, and *X* is the origin of libration), 15 variables per molecule. Both components of the disordered anion **I** were set to belong to the same *TLX* parameterization with the *T* value constrained to be isotropic. The remaining non-hydrogen atoms were refined as isolated anisotropic atoms. Hydrogen atoms were re-included in expected geometric positions after each refinement cycle and were given thermal parameters defined by those of the atoms to which they are attached. Some 792 variables were used to describe the refinement of 245 non-hydrogen atom sites and 132 hydrogen atom sites. In the final refinement cycle (see Supporting Information), the maximum Δ/σ value was 0.10. min./max. electron density: $-3.3/3.4 \text{ e}\text{\AA}^{-3}$ when all reflections were used. An uncorrelated 4% error in $|F(\text{h})|$ was included along with a counting statistic error for evaluating weights $w = [\sigma(F)^2 + (0.04F)^2]^{-1}$. The errors quoted for bond lengths and angles are conditional on the appropriateness of the various constraints and restraints.
- [17] C. K. Johnson, ORTEP. Oak Ridge National Laboratory, Oak Ridge, Tennessee, USA, **1976**.

Covalent Immobilization of a TiW_5 Polyoxometalate on Derivatized Silicon Surfaces**

R. John Errington, Sagar S. Petkar,
Benjamin R. Horrocks, Andrew Houlton, Lars H. Lie,
and Samson N. Patole*

Polyoxometalates (POMs) are discrete, molecular metal oxides with dimensions ranging from about one to tens of Ångströms, a wide variety of topologies and compositions, and an extensive range of chemical and electronic properties which, together with their thermal and oxidative stabilities, are leading to applications in catalysis, electrooptics, magnetism, medicine, and biology.^[1–3] Consequently, POMs are attractive as functional components of active materials. In recent years, systematic methods for POM synthesis and derivatization have been developed, providing an expanding range of robust “designer” components for “bottom-up” materials synthesis, and a major challenge now facing those engaged in POM research is to devise generic methods for constructing functional nanoscale architectures from these versatile building blocks.

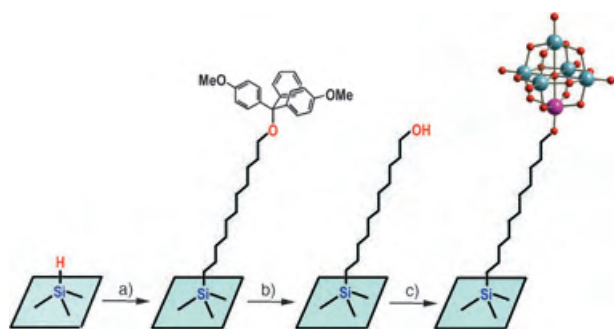
The self-assembly of organic monolayers on surfaces has developed over the last two decades into a powerful strategy for the construction of hierarchical structures from molecular components and, although self-assembled inorganic monolayers have received much less attention, several groups have investigated the incorporation of POMs into surface-confined structures. Ordered monolayers of POMs have been obtained on silver and gold by adsorption from solution,^[4,5] and evaporative solution deposition has been used to produce catalytically active POM layers on highly oriented pyrolytic graphite (HOPG).^[6–8] Hybrid organic–POM multilayered magnetic structures have been produced by Langmuir–Blodgett techniques,^[9–11] while electrostatic layer-by-layer assembly with cationic polyelectrolytes has produced more robust hybrid structures.^[12] These approaches rely upon either electrostatic interactions or ill-defined chemisorption for the assembly of POM monolayers or multilayers and, to our knowledge, the only example of well defined covalent attachment to a surface is that of a thiol-derivatized POM on gold nanoparticles.^[13] Our previous work has shown that monofunctional alkoxide POM derivatives $[(\text{RO})\text{MW}_5\text{O}_{18}]^{n-}$ ($\text{M} = \text{Ti, Zr, Nb}$) are accessible through hydrolytic aggregation reactions involving metal alkoxides.^[14] These species react

[*] Dr. R. J. Errington, Dr. S. S. Petkar, Dr. B. R. Horrocks,
Prof. A. Houlton, L. H. Lie, Dr. S. N. Patole
School of Natural Sciences, Chemistry
University of Newcastle upon Tyne, NE1 7RU (UK)
Fax: (+44) 191-222-6929
E-mail: John.Errington@ncl.ac.uk

[**] This work was supported by the EPSRC (Grant no. GR/N65028) and by the University of Newcastle upon Tyne. We are grateful to Dr. Lidija Siller and Satheesh Krisnamurthy of the School of Chemical Engineering and Advanced Materials, University of Newcastle upon Tyne for the XPS measurements.

with protic reagents HX to provide access to a range of new derivatives $[\text{XW}_5\text{O}_{18}]^{n-}$ (for example, $\text{X}=\text{OR}'$, OAr , O_2CMe , acac) and we now report the application of this chemistry to the covalent attachment of a TiW_5 hexametalate to single-crystal and porous silicon by reaction with alkanol surface monolayers.

The availability of robust, alkanol-derivatized silicon surfaces from hydrogen-terminated silicon^[15] provided the means to attach MW_5O_{18} molecular heterometal oxides to the silicon surface through covalent M-O-C alkoxide bonds by alcoholysis of the M-OR bond in $[(\text{RO})\text{MW}_5\text{O}_{18}]^{n-}$ (Scheme 1). From EXSY NMR spectroscopy experiments



Scheme 1. a) $\text{CH}_2=\text{CH}(\text{CH}_2)_9\text{O}(\text{DMT})$, toluene, reflux, 18 h; b) $\text{Cl}_3\text{CCO}_2\text{H}$, CH_2Cl_2 ; c) $0.05 \text{ M } (n\text{Bu}_4\text{N})_3[(\text{MeO})\text{TiW}_5\text{O}_{18}]$ (red O, blue W, purple Ti) in MeCN, 85 °C, 24 h. DMT = 1,ω-dimethoxytrityl.

we have determined that the rate of exchange between free methanol and the methoxide in $[(\text{MeO})\text{TiW}_5\text{O}_{18}]^{3-}$ is approximately 0.03 s^{-1} , so this comparatively inert POM was chosen as the adsorbate in these experiments in the expectation that the resulting POM-derivatized surfaces would be sufficiently stable for subsequent characterization.

Samples of single-crystal and porous silicon were functionalized with ω-hydroxyundecyl monolayers and then treated with acetonitrile solutions of $(n\text{Bu}_4\text{N})_3[(\text{MeO})\text{TiW}_5\text{O}_{18}]$ at 85 °C, washed with MeCN and dried. Figure 1 shows scanning tunneling microscopy (STM) images of a single-crystal Si(111) surface with a ω-hydroxyundecyl monolayer before and after treatment with a MeCN solution of $(n\text{Bu}_4\text{N})_3[(\text{MeO})\text{TiW}_5\text{O}_{18}]$ and washing with MeCN. Steps and terraces of the alkanol-modified surface are visible in Figure 1 a, while new features are clearly visible after treatment with the POM solution. X-ray photoelectron spectroscopy (XPS) analysis of the treated monolayer surface confirms the presence of W^{VI} and Ti^{IV} in oxide environments

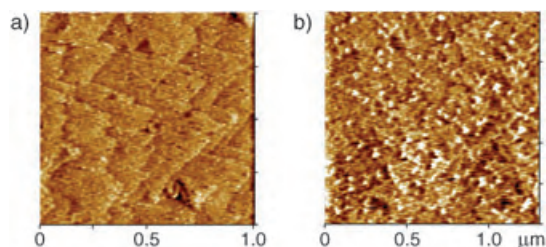


Figure 1. STM images of ω-hydroxyundecyl derivatized Si(111) surface before (a) and after (b) treatment with a MeCN solution of $(n\text{Bu}_4\text{N})_3[(\text{MeO})\text{TiW}_5\text{O}_{18}]$.

(Figure 2). The W $4f_{7/2}$ and $4f_{5/2}$ binding energies of 36.3 and 38.5 eV and the Ti $2p_{3/2}$ and $2p_{1/2}$ binding energies of 459.6 and 465 eV are comparable with those reported for electrostatically bound $[\text{SiW}_{12}\text{O}_{40}]^{4-}$ ions (binding energies = 35.3 and 37.3 eV)^[16] and for TiO_2 (binding energies = 458.9 and 464.6 eV).^[17]

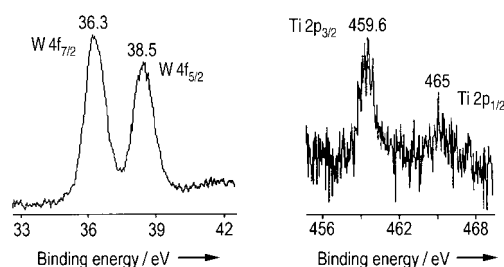


Figure 2. XPS analysis of ω-hydroxyundecyl derivatized Si(111) surface after treatment with $(n\text{Bu}_4\text{N})_3[(\text{MeO})\text{TiW}_5\text{O}_{18}]$.

To investigate the nature of the interactions between the POM anions and the organic monolayer in more detail, samples of porous silicon derivatized with ω-hydroxyundecyl groups were prepared and then treated with a solution of $(n\text{Bu}_4\text{N})_3[(\text{MeO})\text{TiW}_5\text{O}_{18}]$ in MeCN in a similar fashion to the single-crystal silicon. The FT-IR spectrum of $(n\text{Bu}_4\text{N})_3[(\text{MeO})\text{TiW}_5\text{O}_{18}]$ in the region $400\text{--}1200 \text{ cm}^{-1}$ is shown in Figure 3 a and the FT-IR difference spectrum between a ω-hydroxyundecyl derivatized porous silicon film and the original hydrogen-terminated silicon is shown in Figure 3 b. The difference FT-IR spectrum between the sample after and before treatment with the alkoxohexametalate is shown in Figure 3 c. A comparison of the $\nu(\text{OH})$ regions shows that the broad band at 3300 cm^{-1} becomes negative in Figure 3 c, which indicates loss of OH upon reaction between the alkanol surface and the TiOMe group. In addition, the appearance of bands from $\text{W}=\text{O}$ and $\text{W}-\text{O}-\text{W}$ of the POM at 958, 883, and 795 cm^{-1} confirm the presence of the oxoanion. The $\nu(\text{CH})$ region in Figure 3 c contains bands due to the $[n\text{Bu}_4\text{N}]^+$ ion in addition to the undecyl chains and the large peak at 1093 cm^{-1} is from $\text{Si}-\text{O}$, formed upon oxidation of residual SiH groups (see below).

The STM image in Figure 1 b shows the surface features to have diameters of 35–50 nm and profile analysis shows heights of approximately 4 nm. Assuming that the optimum packing of $[n\text{Bu}_4\text{N}]^+$ ions and $[(\text{MeO})\text{TiW}_5\text{O}_{18}]^{3-}$ ions is that observed in the crystal structure,^[14] the fraction of ω-hydroxyundecyl groups that would be required to react with the $\text{Ti}-\text{OMe}$ groups to achieve this packing density can be estimated by mapping the plane containing the methoxide oxygen atoms in the unit cell of $(n\text{Bu}_4\text{N})_3[(\text{MeO})\text{TiW}_5\text{O}_{18}]$ onto the Si(111) surface. As during preparation of the ω-hydroxyundecyl monolayer the packing constraints of the dimethoxytrityl-protected alkanol groups restrict functionalization to, at most, every second SiH site,^[18,19] the Si:POM ratio of 11.4:1 derived by this mapping would mean that only around 17.5% of available undecanol groups in the monolayer would be derivatized in the formation of a close-packed layer of $(n\text{Bu}_4\text{N})_3[(\text{RO})\text{TiW}_5\text{O}_{18}]$ ($\text{R}=\text{Si}(\text{CH}_2)_{11}$). This situation would leave residual undecanol groups on the surface,

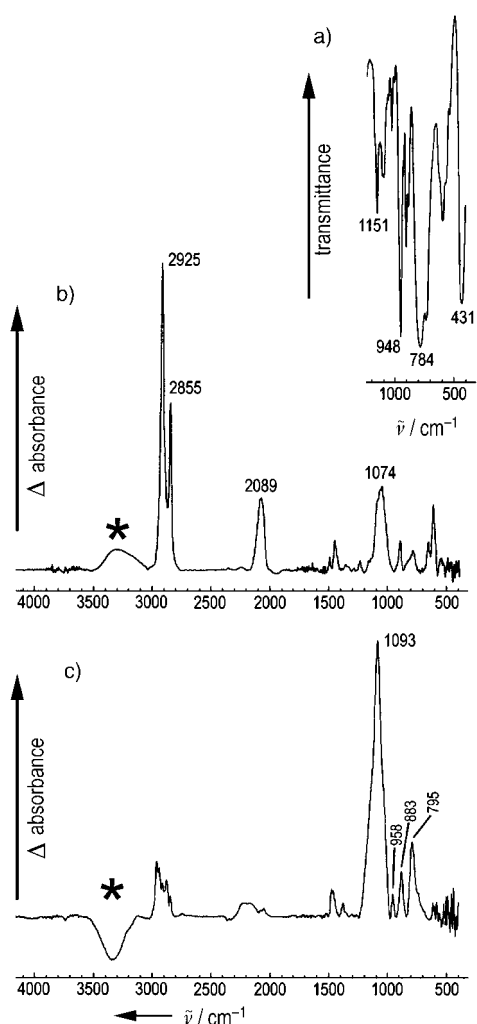


Figure 3. a) Section of the FT-IR spectrum of $(n\text{Bu}_4\text{N})_3[(\text{MeO})\text{TiW}_5\text{O}_{18}]$ as a Nujol mull, b) FT-IR difference spectrum between ω -hydroxyundecyl derivatized porous silicon film and hydrogen-terminated silicon, c) FT-IR difference spectrum between ω -hydroxyundecyl derivatized porous silicon film after and before treatment with $(n\text{Bu}_4\text{N})_3[(\text{MeO})\text{TiW}_5\text{O}_{18}]$; $\nu(\text{OH})$ regions marked with an asterisk.

while the remaining SiH groups may be susceptible to oxidation. The heights of the surface features in Figure 1b suggest greater than monolayer coverage in these areas, probably a result of electrostatic interactions. The unit cell volume ($Z=4$) of $(n\text{Bu}_4\text{N})_3[(\text{MeO})\text{TiW}_5\text{O}_{18}]\cdot 0.5\text{MeCN}$, is $6852(8)\text{ \AA}^3$ and, if the surface features observed in Figure 1b were composed of close-packed $[n\text{Bu}_4\text{N}]^+$ ions and $[(\text{RO})\text{TiW}_5\text{O}_{18}]^{3-}$ ions, they should therefore contain between 2000 and 4700 hexametallate ions together with their associated cations. If these larger features are indeed a result of a “surface crystallization” process it may be that electrostatic aggregation around an initial covalently bound POM serves to direct subsequent covalent attachment at other alkanol sites, which results in “island” growth. We are now investigating whether the degree of electrostatic aggregation can be controlled by ion exchange or by varying the POM solution concentration, the reaction times, or the washing process in attempts to move towards monolayer coverage.

In conclusion, these results demonstrate that covalent metal alkoxide bonding can be used to immobilize a polyoxometallate on alkanol-derivatized silicon surfaces, although further aggregation beyond the monolayer also occurs, probably through electrostatic interactions. After 6 h reaction time, the POMs were localized in clusters on the surface containing between 2000 and 5000 TiW_5 units, and further studies are in progress to investigate the factors affecting POM clustering and surface coverage. In an extension of this covalent approach to larger POMs our initial experiments with Keggin $[(\text{RO})\text{TiPW}_{11}\text{O}_{39}]^{4-}$ and Wells–Dawson $[(\text{R}_2\text{Si}_2\text{O})\text{P}_2\text{W}_{17}\text{O}_{61}]^{6-}$ derivatives appear promising and results will be described in due course.

Experimental Section

$(n\text{Bu}_4\text{N})_3[(\text{MeO})\text{TiW}_5\text{O}_{18}]$ was prepared as described elsewhere.^[14] STM images of silicon surfaces were collected in air and in constant current mode using a Multimode Nanoscope III (DI Digital Instruments). The Pt/Ir tips used for STM imaging were prepared by electrochemical etching of 80/20 Pt/Ir alloy wire in 1M HCl/saturated CaCl_2 using approximately 20 V a.c. FT-IR Spectra (unpolarized) of porous Si samples were obtained using a Biorad Excaliber series spectrometer fitted with mercury cadmium telluride (MCT) detector in the normal transmission alignment. Features owing to water vapor and CO_2 were minimized by purging the sample compartment with dry N_2 . Spectra of (modified minus hydrogen-terminated) porous silicon were referenced to an unetched piece of Si (100) wafer. The difference spectra (modified minus hydrogen-terminated) were then baseline corrected prior to the integration. The resolution was 2 cm^{-1} and 64 scans were summed and averaged.

Preparation of hydrogen-terminated Si (111) wafers: (111) Oriented silicon wafers (phosphorus-doped, n-type $1\text{--}20\text{ }\Omega\text{ cm}$ resistivity, Compant Technology) were first cut into 1 cm^2 pieces and then degreased with acetone. An oxide layer was formed by immersing the chips in freshly prepared “piranha” solution (4:1 v/v conc. H_2SO_4 :30% H_2O_2) for 1 h at 80°C . The oxide was removed and a hydrogen-terminated surface was formed by etching in N_2 -purged 40% w/v aqueous NH_4F for 3 min with the chip held in a vertical orientation as suggested elsewhere.^[20] Wafers were then rinsed for 20 s in deionized water (Millipore, nominal $18\text{ M}\Omega\text{ cm}$) and blown dry with N_2 .

Preparation of porous silicon: Porous silicon was formed by galvanostatic anodization of silicon wafers ((100) oriented; boron-doped, p-type, $10\text{ }\Omega\text{ cm}$ resistivity, Compant Technology). Chips ($\approx 1.0\text{ cm} \times 1.0\text{ cm}$) were degreased in acetone and then oxidised in freshly prepared “pirhana” solution (4:1 v/v conc. H_2SO_4 :30% H_2O_2) for at least 10 min at room temperature. The oxide was removed and a hydride layer was formed by a subsequent immersion in 48% w/w aqueous HF (10 min). Wafers were then rinsed for 20 s in deionized water (Millipore, nominal $18\text{ M}\Omega\text{ cm}$) and blown dry with N_2 . Ohmic contact to the back of the chip was made by rubbing with In/Ga eutectic. The chip was then placed in a polytetrafluoroethylene (PTFE) cell with an electrolyte consisting of a 1:1 v/v solution of 48% aqueous HF:ethanol and a current density of 12.7 mA cm^{-2} was applied until the charge passed reached 5.0 C cm^{-2} (ca. 6.5 min). The porous silicon was then washed in deionized water to remove ethanol and then immersed for a few seconds in 48% aqueous HF to remove any residual oxide. The chip was finally rinsed with distilled water and dried in a stream of dry N_2 .

Reaction between 1,ω-dimethoxytritylundecanol and porous silicon or Si(111) and subsequent deprotection: Porous silicon was treated with the protected alkene by heating in a 10% v/v solution of undecenol-DMT in toluene (predistilled over Na) under reflux for approximately 18 h under nitrogen. The chips were then rinsed with

toluene, CH_2Cl_2 ($\times 2$) and dried in a stream of N_2 . The presence of the monolayer was confirmed by normal transmission FT-IR spectroscopy (ν = aromatic C–H 3074, 3040, 3000 cm^{-1} , alkyl C–H 2927, 2854 cm^{-1} , C=C 1641, 1608, CH_2 (scissor) 1465 cm^{-1} . Washing with 3% trichloroethanoic acid in CH_2Cl_2 quantitatively removed all the bands associated with the DMT group and produced a broad band centred at about 3300 cm^{-1} assigned to $\nu(\text{OH})$.

Modification of Si(111) single-crystal chips was by the same method, except that it was not possible to obtain the FT-IR spectrum in the normal transmission alignment for reasons of instrumental sensitivity. After alkylation, the surface was washed with excess toluene and dried under N_2 before storing under N_2 prior to use.

Reaction between $(n\text{Bu}_4\text{N})_3[(\text{MeO})\text{TiW}_5\text{O}_{18}]$ and undecanol-derivatized Si: The undecanol-derivatized single-crystal or porous Si chips were immersed in a MeCN solution of $(n\text{Bu}_4\text{N})_3[(\text{MeO})\text{TiW}_5\text{O}_{18}]$ (0.05 M, 5 mL) under dry N_2 in a Schlenk flask. The flask was then heated to 85 °C for 6 h. After cooling, the chip was removed, washed with dry acetonitrile, and dried in a stream of dry N_2 .

Received: June 24, 2004

Revised: November 11, 2004

Keywords: alkoxides · polyoxometalates · surface chemistry · titanium · tungsten

- [1] M. T. Pope, A. Müller, *Angew. Chem.* **1991**, *103*, 56; *Angew. Chem. Int. Ed. Engl.* **1991**, *30*, 34.
- [2] *Polyoxometalates: From platonic solids to anti-retroviral activity* (Eds.: M. T. Pope, A. Müller), Kluwer, Dordrecht, Netherlands, **1994**.
- [3] *Polyoxometalate Chemistry: From topology via self-assembly to applications* (Eds.: M. T. Pope, A. Müller), Kluwer, Dordrecht, Netherlands, **2001**.
- [4] W. G. Klemperer, C. G. Wall, *Chem. Rev.* **1998**, *98*, 297.
- [5] M. Ge, B. Zhong, W. G. Klemperer, A. A. Gewirth, *J. Am. Chem. Soc.* **1996**, *118*, 5812.
- [6] B. Keita, L. Nadjio, *Surf. Sci. Lett.* **1991**, *254*, L443.
- [7] M. S. Kaba, I. K. Song, D. C. Duncan, C. L. Hill, M. A. Barteau, *Inorg. Chem.* **1998**, *37*, 398.
- [8] M. A. Barteau, J. E. Lyons, I. K. Song, *J. Catal.* **2003**, *216*, 236.
- [9] M. Clemente-Leon, C. Mingotaud, B. Agricole, C. J. Gomez-Garcia, E. Coronado, P. Delhaes, *Angew. Chem.* **1997**, *109*, 1143; *Angew. Chem. Int. Ed. Engl.* **1997**, *36*, 1114.
- [10] M. Clemente-Leon, E. Coronado, P. Delhaes, C. J. Gomez-Garcia, C. Mingotaud, *Adv. Mater.* **2001**, *13*, 574.
- [11] M. Clemente-Leon, B. Agricole, C. Mingotaud, C. J. Gomez-Garcia, E. Coronado, P. Delhaes, *Langmuir* **1997**, *13*, 2340.
- [12] S. Liu, G. D. Kurth, B. Bredenkotter, D. Volkmer, *J. Am. Chem. Soc.* **2002**, *124*, 12279.
- [13] C. R. Mayer, S. Neveu, V. Cabuil, *Angew. Chem.* **2002**, *114*, 519; *Angew. Chem. Int. Ed.* **2002**, *41*, 501.
- [14] W. Clegg, M. R. J. Elsegood, R. J. Errington, J. Havelock, *J. Chem. Soc. Dalton Trans.* **1996**, 681.
- [15] A. R. Pike, L. H. Lie, R. A. Eagling, L. C. Ryder, S. N. Patole, B. A. Connelly, B. R. Horrocks, A. Houlton, *Angew. Chem.* **2002**, *114*, 637; *Angew. Chem. Int. Ed.* **2002**, *41*, 615.
- [16] Y. Wang, C. Guo, Y. Chen, C. Hu, W. Yu, *J. Colloid Interface Sci.* **2003**, *264*, 176.
- [17] D. Gonbeau, C. Guimon, G. Pfister-Guillouzo, A. Levasseur, G. Meunier, R. Dormoy, *Surf. Sci.* **1991**, *254*, 81.
- [18] A. B. Sieval, B. v. d. Hout, H. Zuilhof, E. J. R. Sudhölter, *Langmuir* **2000**, *16*, 2987.
- [19] A. B. Sieval, B. v. d. Hout, H. Zuilhof, E. J. R. Sudhölter, *Langmuir* **2001**, *17*, 2172.
- [20] C. P. Wade, C. E. D. Chidsey, *Appl. Phys. Lett.* **1997**, *71*, 1679.

Formation of [60]Fullerene Nanoclusters with Controlled Size and Morphology through the Aid of Supramolecular Rod–Coil Diblock Copolymers**

Norifumi Fujita, Taketomo Yamashita, Masayoshi Asai, and Seiji Shinkai*

It is known that block copolymers can self-organize into a large number of phase-separated superlattices with characteristic dimensions that range from a few nanometers up to several micrometers.^[1] The interplay of supramolecular physics and chemistry has opened up several new approaches to the production of inorganic, organic, and biological superstructures and to their integration into functional units.^[2] Amphiphilic compounds are frequently utilized as functional matrices in the preparation of these superstructures.^[3] In the study of their applications, the importance of controlling the size of nanoparticles has been described; such control was successful particularly in the field of inorganic materials such as metal colloids, quantum dots, and cluster catalysts.^[1,4] Examples of controlling the size of their organic counterparts, however, are very limited so far,^[5] in spite of their wide range of applications in materials science.

When a solution of diblock copolymer PS(21 400)-*b*-P4VP(20 700) (**A**; PS = polystyrene, *b* = block, P4VP = poly(4-vinylpyridine)) is cast on a surface under appropriate conditions, a periodic lamellar structure about 20 nm in diameter is formed as a result of the amphiphilic nature of the copolymer.^[6] The very different surface basicities of the PS and P4VP domains allows acidic species only to be selectively assembled on the P4VP domain. For example, when the sol–gel reaction of tetraethoxysilane is carried out on this surface silica grows to form a string structure on the P4VP domain.^[6] Herein, we report a supramolecular approach using rod–coil diblock copolymers prepared from random-coil PS-*b*-P4VPs as hosts and [60]fullerene carboxylic acid as a guest that leads to the formation of spherical [60]fullerene nanoclusters with controlled size and morphology, which are changeable depending on the composition of the PS-*b*-P4VPs.^[7] The examples described herein would offer one of the most convenient practical methodologies (just by mixing) for the control and fabrication of [60]fullerene nanoparticles.

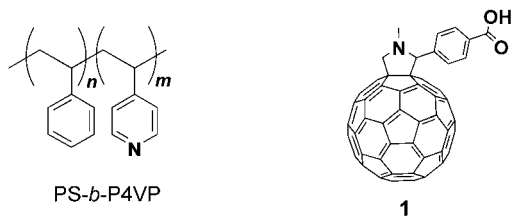
[*] Dr. N. Fujita, T. Yamashita, M. Asai, Prof. Dr. S. Shinkai
Department of Chemistry & Biochemistry
Graduate School of Engineering, Kyushu University
6-10-1 Hakozaki, Higashi-ku, Fukuoka 812-8581 (Japan)
Fax: (+81) 92-642-3611
E-mail: seijitcm@mbox.nc.kyushu-u.ac.jp

[**] Support was provided by the 21st Century COE Project, Functional Innovation of Molecular Informatics. We would like to thank H. Matsukizono and M. Fujita of Kyushu University for the DLS analysis and AFM measurements, respectively.



Supporting information for this article is available on the WWW under <http://www.angewandte.org> or from the author.

Polymer **A** (1.0 mg) and [60]fullerene carboxylic acid (**1**, 1.0 mg) were dissolved in 3-pentanone (1.0 mL), and sonicated for one minute at room temperature. The solution



became homogeneous and brown in color, thus indicating that **1** had interacted with polymer **A** (since **1** was only partially soluble in 3-pentanone without **A**). A carbon-coated copper grid was immersed in this solution for a few seconds and then dried under ambient conditions for 6 hours. After the sample had been dried in vacuo for 12 hours, it was analyzed by transmission electron microscopy (TEM) without staining.

TEM analysis revealed that the size and morphology of the generated spherical [60]fullerene clusters are quite uniform. Black spheres with a small distribution range of diameters (20–30 nm) are clearly recognized (Figure 1). The

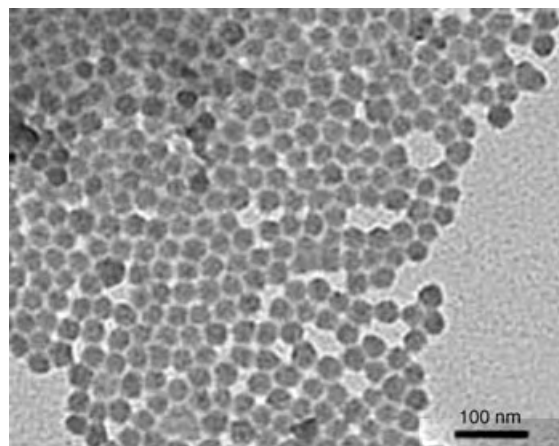


Figure 1. TEM image of polymer **A-1** composite.

samples observed by TEM were not stained, and therefore the black contrast is a result of electron absorption by the [60]fullerenes. Thus, one can propose that a carboxylic acid group in **1** interacts with a pyridine moiety in the P4VP block in polymer **A**, which adopts a rodlike rigid conformation because of the structural bulkiness of bound **1** (Figure 2). Thus, the random-coil structure of the P4VP block is transformed into a rodlike rigid structure and accompanied by a decrease in the solubility. The poor solubility of the [60]fullerene-complexed P4VP block and the high solubility of the PS block in 3-pentanone should result in the formation of the micelle-like superstructures seen in Figure 1. To further support this rationale we carried out TEM analysis of five reference samples prepared under similar conditions to those described above: **1** only, PS homopolymer with **1**, P4VP

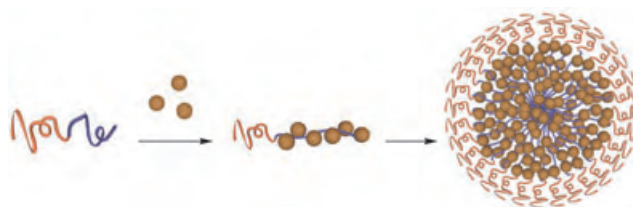


Figure 2. Schematic representation of the formation of supramolecular rod-coil polymers leading to the generation of micelles.

homopolymer with **1**, a mixture of PS and P4VP with **1**, and polymer **A** with unmodified [60]fullerene or with the methyl ester analogue of **1** (**2**, see the Supporting Information). None of these samples shows any spherical or periodic surface structure in the TEM images. Thus, the block composition in the macromolecule and the pyridine–carboxylic acid interaction are indispensable to the formation of such a unique spherical structure.

Spectral analysis of P4VP in the **A-1** composite gives an insight into the type of host–guest interactions occurring in this system. The 3-pentanone solvent was removed from the polymer **A-1** composite by evaporation, and the resultant brown solid was dried in vacuo and subjected to attenuated total reflectance (ATR) FTIR spectroscopic measurements. The ATR-FTIR spectra of the samples show the formation of the hydrogen bond between the pyridyl group in PS-*b*-P4VP and the carboxylic acid group in **1** very clearly. The **A-1** composites were prepared in different molar ratios of **1** (from 0.20 to 1.0 molar equivalents, where the molar equivalent is defined as the molar ratio of the carboxylic acid function in **1** with respect to the pyridyl function in polymer **A**). In the IR spectra (see the Supporting Information), a band at 1597 cm^{−1}, which is assigned to the ring-stretching vibration, is gradually shifted to 1609 cm^{−1}, which is assigned to the hydrogen-bonded pyridyl group.^[8] This shift induced by the interaction with the carboxylic acid group becomes larger as the molar ratio of added **1** increases. Samples containing more than 0.6 molar equivalents of **1** result in turbid solutions, which implies that all the pyridyl groups in polymer **A** cannot interact with **1**: at most, 0.6 molar equivalents of **1** can form a hydrogen bond with the pyridyl group in polymer **A**, probably as a result of steric crowding. Analysis of the C=O band in the same IR spectra clearly shows that hydrogen bonding between the pyridyl group in the block copolymer and **1** plays a key role in the formation of nanoparticles^[7a] (for details see the Supporting Information). The five samples prepared for the IR experiments were directly subjected to TEM analysis, and all the samples showed a spherical structure similar to that of the TEM image shown in Figure 1.

It is expected that the length of the homopolymer segments in PS-*b*-P4VPs would affect the size and morphology of the [60]fullerene clusters in the core of the micelle-like PS-*b*-P4VP-**1** composites. We thus tried to construct [60]fullerene superstructures with PS-*b*-P4VPs having block segments of different lengths. The [60]fullerene clusters were prepared according to the same conditions as above, where the molar ratio of **1** versus the pyridyl function in the P4VP segment is fixed to 0.6 molar equivalents. Table 1 summarizes

Table 1: Compositions of PS-*b*-P4VPs used and structural parameters of their composites with **1**.

PS- <i>b</i> -P4VP	M_n of PS and P4VP [g mol ⁻¹]	M_w/M_n of PS- <i>b</i> -P4VP	$m(\text{P4VP})/n(\text{PS})$	Morphology and size observed by TEM
polymer A	21 400/20 700	1.13	0.96	sphere, $d = 20\text{--}30$ nm
polymer B	31 900/13 200	1.08	0.41	sphere, $d = 20\text{--}25$ nm
polymer C	35 500/3680	1.06	0.10	sphere, $d = 15\text{--}20$ nm
polymer D	19 900/29 400	1.15	1.5	sphere and cylinder, $d = 40$ nm, $l = 200\text{--}300$ nm
polymer E	3300/18 700	1.14	5.6	—
polymer F	109 000/27 000	1.15	0.25	sphere, $d = 50\text{--}60$ nm

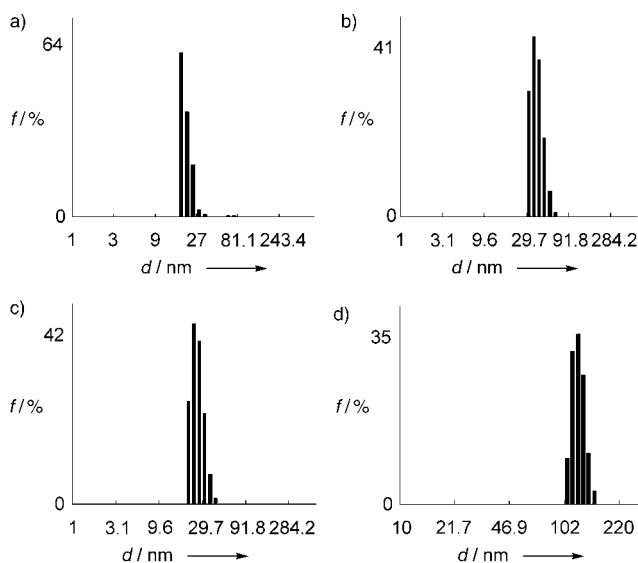
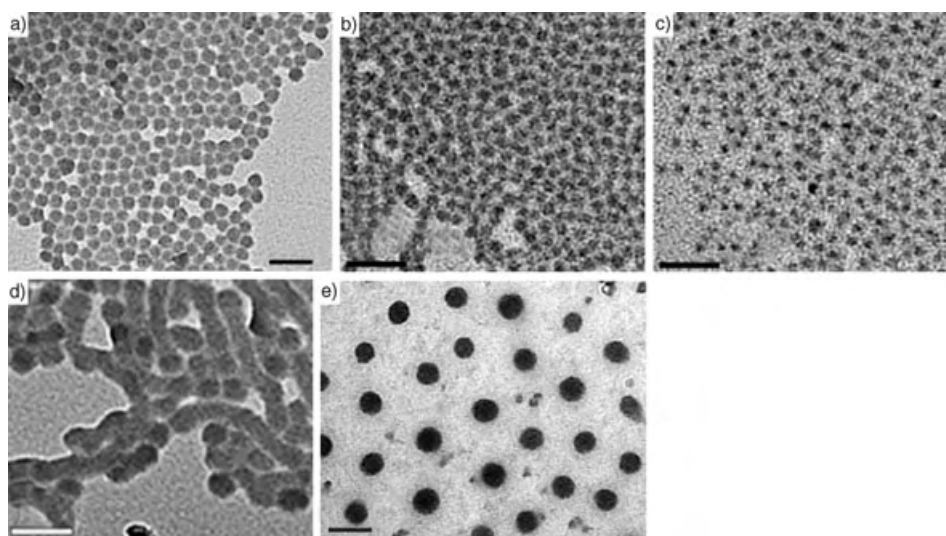
the structures of the PS-*b*-P4VPs used and the resultant size and morphology of the PS-*b*-P4VP-**1** composites observed by TEM. It is seen from Table 1 and Figure 3 that polymers **A–C**, which have a shorter P4VP segment length with respect to the PS segment length, tend to form spherical aggregates in which the diameter decreases from 20–30 to 20–25 to 15–20 nm, respectively, as length of the P4VP segment decreases from a P4VP/PS ratio of 0.96:1 to 0.41:1 to 0.10:1, respectively. The superstructure formed when the P4VP/PS ratio in the PS-*b*-P4VPs becomes larger changes to a mixture of sphere and cylinder, as seen in the case of polymer **D** (P4VP/PS = 1.5:1). Furthermore, polymer **E** with a P4VP/PS ratio of 5.6:1 does not form any superstructure, as observed by TEM (not shown). Polymer **F** with a P4VP/PS molar ratio of 0.25:1 also shows spherical morphology when it interacts with **1**.

The specific difference in the superstructure formed can be explained as follows. The [60]fullerenes tend to aggregate into a spherical structure that seems to be a priori the most stable (polymers **A–C**, and **F**) when the PS segment has sufficient length to induce solubility to the spherical [60]fullerene clusters. However, the PS domain cannot impart sufficient solubility to the spherical [60]fullerene clusters when the length of the PS segment is relatively short (polymer **D**), and the structure is transformed into a cylindrical morphology. This change results in a decrease in the surface area covered with the PS segment. In the case of polymer **E**,

the PS segment is so short that the superstructure requiring coverage by the solvophilic PS segment is no longer created. It is clear, therefore, that the structural morphologies of the composites are sharply correlated with the balance of the solubility of the [60]fullerene clusters and the length of the PS segments.

Dynamic light scattering (DLS) analysis provides information on

the diameter of the nanoparticles in solution. Figure 4 shows the size distribution of PS-*b*-P4VP-**1** composites in 3-pentanone solution, and indicates that the diameters of the composites are very narrowly distributed. The diameters of the spherical PS-*b*-P4VP-**1** composites prepared from poly-


Figure 4. DLS profiles of a) polymer **A-1**, b) polymer **B-1**, c) polymer **C-1**, and d) polymer **F-1** composites.

Figure 3. TEM images of PS-*b*-P4VP-**1** composites. a) Polymer **A-1**, b) polymer **B-1**, c) polymer **C-1**, d) polymer **D-1**, and e) polymer **F-1**. The scale bars correspond to 100 nm.

mers **B**, **C**, and **F** are larger than those determined by TEM. However, the diameter of the spherical PS-*b*-P4VP-**1** composites prepared from polymer **A** is almost the same as that determined by TEM. These discrepancies are rationalized as follows. In the PS-*b*-P4VP-**1** composites obtained from polymers **B**, **C**, and **F**, the molecular weights of the PS segments are sufficiently higher than those of the P4VP segments that the PS corona surrounding the [60]fullerene cluster can be extended into the bulk solution. This situation results in the diameters determined by DLS studies being larger than those determined by TEM. In the case of polymer **A**, however, the molecular weight of the PS segment is comparable to that of the P4VP segment and the PS corona is mainly distributed near the surface of the [60]fullerene cluster. As a result, the diameter of the **A-1** composite determined by DLS studies is nearly the same as that determined by TEM.

The size and morphology of the composites can be directly confirmed by scanning electron microscopy (SEM, Figure 5a), which supports the narrow size distribution of the polymer **A-1** composite. The diameter of the spherical nanoparticles seen in Figure 5a is comparable with that observed by DLS measurements. Furthermore, the AFM image of the **A-1** composite in Figure 5b also shows the spherical morphology with a diameter of about 20 nm. These results consistently support the view that the [60]fullerene clusters created from the PS-*b*-P4VP-**1** composites are stable both in solution and on the surface, even under ultrahigh vacuum conditions.

Mixing two different PS-*b*-P4VP copolymers with **1** provided a very interesting result. Firstly, it was confirmed from TEM analysis that when polymer **A** or **F**, which have long PS block segments, is mixed with **1** in 3-pentanone, the resultant composites show small or large black dots with diameters of 20–30 or 50–60 nm, respectively. Next, polymer **A** (1.0 mg), polymer **F** (1.0 mg), and **1** (2.4 mg) were dissolved together in 3-pentanone (2.0 mL). Interestingly, the TEM image of the sample prepared from this solution shows two different small and large black dots, with the smaller dots excluded from the peripheral area of the larger dots; thus, this finding clearly shows the presence of the PS corona region (Figure 6a). These observations imply that the two copolymers tend to aggregate with **1** separately, thus inducing an intriguing phase-separation phenomenon in the same solution. It is energetically unfavorable for polymers **A** and **F**,

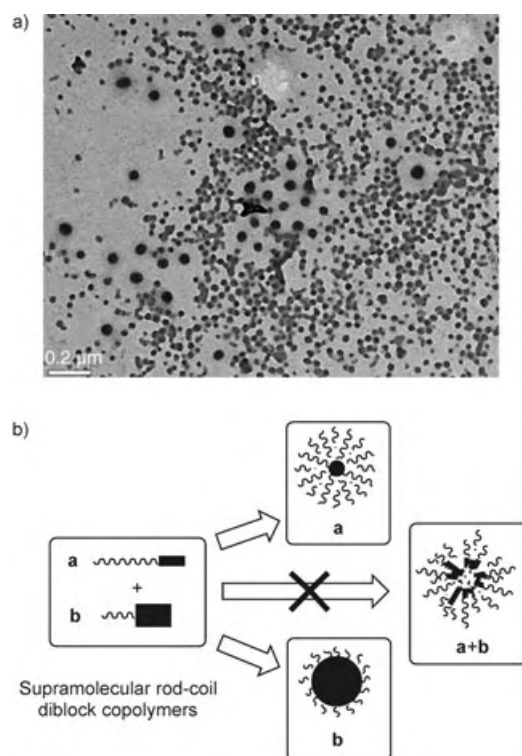


Figure 6. a) TEM image of the sample prepared from a mixture of **1** and polymers **A** and **F** in 3-pentanone. b) Schematic representation of “homo” aggregation processes.

which have different block compositions, to form a mixed aggregate in the 3-pentanone solution, because their rod-coil shapes are mismatched (Figure 6b). As a result, the formation of two “homo” aggregates is more stable than that of one “mixed” aggregate.

In summary, we have demonstrated the construction of novel supramolecular aggregates by utilizing the formation of hydrogen bonds between host block copolymers and a guest [60]fullerene carboxylic acid. Treatment of these supramolecular rod-coil diblock copolymers under appropriate conditions led to the creation of [60]fullerene nanoparticles with narrow distributions in size and morphology. This methodology is also applicable to the controlled construction of other organic nanoparticles. It is well-known that control of the size and morphology of nanoparticles plays an important role in nanomaterials chemistry; therefore, the methodology de-

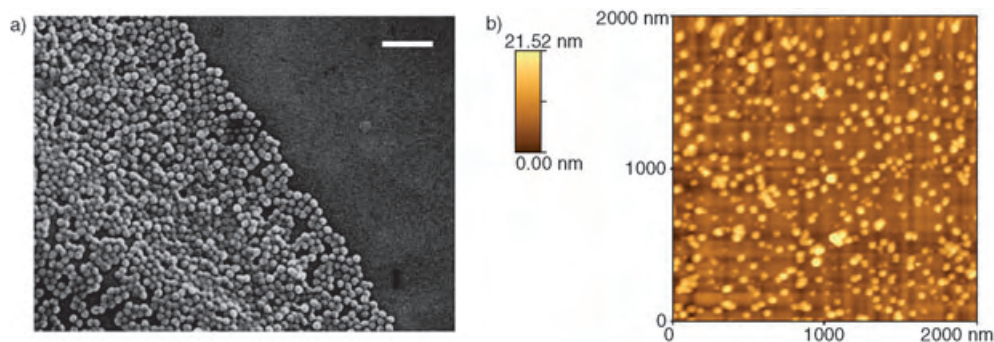


Figure 5. a) SEM and b) AFM images of polymer **A-1** composite. The scale bar in the SEM image corresponds to 200 nm and the side of the AFM image is 2 μm long.

scribed here should provide a novel approach to nanomaterials chemistry and functions. The organic nanoparticles obtained from these experiments should show interesting redox, electrochemical, and photochemical properties.

Experimental Section

The block copolymers and [60]fullerene carboxylic acid (**1**) were dissolved in 3-pentanone in a capped test tube and the mixture was sonicated (IUCHI, VS-150) in a water bath at room temperature at a power level of 150 W (50 kHz). The solution became homogeneous after 1 min. This sonication procedure did not affect the polymers or **1**, as confirmed by gel-permeation chromatography and mass spectrometry. A carbon-coated copper grid was immersed in the solution and dried under ambient conditions for 6 h. After drying the sample in vacuo for 12 h at room temperature, it was subjected to TEM observation.

Received: July 3, 2004

Revised: November 12, 2004

Published online: January 20, 2005

Keywords: block copolymers · fullerenes · host–guest systems · nanostructures · supramolecular chemistry

- [1] For recent reviews, see: a) S. Förster, T. Plantenberg, *Angew. Chem.* **2002**, *114*, 712–739; *Angew. Chem. Int. Ed.* **2002**, *41*, 688–714; b) S. Förster, M. Antonietti, *Adv. Mater.* **1998**, *10*, 195–217.
- [2] For recent work, see: D. M. Vriezema, J. Hoogboom, K. Velonia, K. Takazawa, P. C. M. Cristianen, J. C. Maan, A. E. Rowan, R. J. M. Nolte, *Angew. Chem.* **2003**, *115*, 796–800; *Angew. Chem. Int. Ed.* **2003**, *42*, 772–776, and references therein; for recent reviews, see: I. W. Hamley, *Angew. Chem.* **2003**, *115*, 1730–1752; *Angew. Chem. Int. Ed.* **2003**, *42*, 1692–1712.
- [3] For selected papers, see: a) Y. N. C. Chan, R. R. Schrock, R. E. Cohen, *Chem. Mater.* **1992**, *4*, 24–27; b) J. P. Spatz, S. Mößner, M. Möller, *Chem. Eur. J.* **1996**, *2*, 1552–1555; c) M. Antonietti, S. Förster, J. Hartmann, S. Oestreich, *Macromolecules* **1996**, *29*, 3800–3806; d) S. Klingelhöfer, W. Heitz, A. Greiner, S. Oestreich, S. Förster, M. Antonietti, *J. Am. Chem. Soc.* **1997**, *119*, 10116–10120; e) M. Moffitt, L. McMahon, V. Pessel, A. Eisenberg, *Chem. Mater.* **1995**, *7*, 1185–1192; f) M. Möller, J. P. Spatz, *Curr. Opin. Colloid Interface Sci.* **1997**, *2*, 177–187; g) V. Sankaran, J. Yue, R. E. Cohen, R. R. Schrock, *J. Am. Chem. Soc.* **1993**, *115*, 4409–4410; h) O. A. Platonova, L. M. Bronstein, S. P. Solodovnikov, I. M. Yanovskaya, E. S. Obolonkova, P. M. Valetsky, E. Wenz, M. Antonietti, *Colloid Polym. Sci.* **1997**, *275*, 426–431; i) A. V. Kabanov, S. V. Vinogradov, Y. G. Suzdaltseva, V. Y. Alakhov, *Bioconjugate Chem.* **1995**, *6*, 639–643.
- [4] R. Schlögl, S. Bee, A. Hamid, *Angew. Chem.* **2004**, *116*, 1656–1667; *Angew. Chem. Int. Ed.* **2004**, *43*, 1628–1637, and references therein.
- [5] H. Kasai, S. Okazaki, T. Hanada, S. Okada, H. Oikawa, T. Adschiri, K. Arai, K. Yase, H. Nakanishi, *Chem. Lett.* **2000**, 1392–1393, and references therein.
- [6] N. Fujita, H. Otsuka, A. Takahara, S. Shinkai, *Chem. Lett.* **2003**, *32*, 352–353.
- [7] For representative examples of self-assemblies of polymeric supramolecules, see: a) T. Kato, J. M. J. Fréchet, *Macromolecules* **1989**, *22*, 3818–3819; b) O. Ikkala, G. ten Brinke, *Science* **2002**, *295*, 2407–2409, and references therein.
- [8] a) A. Sidorenko, I. Tokarev, S. Minko, M. Stamm, *J. Am. Chem. Soc.* **2003**, *125*, 12211–12216; b) H. Peng, D. Chen, M. Jian, *Langmuir* **2003**, *19*, 10989–10992.

Redox-Active Porous Metal–Organic Framework Producing Silver Nanoparticles from Ag^I Ions at Room Temperature**

Hoi Ri Moon, Ji Hyun Kim, and Myunghyun Paik Suh*

Metal–organic framework (MOF) coordination polymers have been the focus of recent research interest because of their potential applications in molecular adsorption and separation processes,^[1] ion exchange,^[2] catalysis,^[3] sensor technology,^[4] and optoelectronics.^[5] They can be designed and assembled to generate cavities or channels of various sizes and shapes by the appropriate choice of building blocks.^[6] However, metal–organic open frameworks are often not robust, so they collapse when the guest molecules occupying the voids are removed, and thus applications are still very limited compared to those for zeolites.

The preparation of monodispersed silver nanoparticles has attracted great attention because they exhibit a strong surface plasmon resonance that depends on the particle size and shape.^[7] However, control of the size and shape of silver particles is much more difficult than that of gold or platinum particles.^[8] Metal nanoparticles are often prepared by accommodating micro- or mesoporous inorganic materials with metal compounds or metal nanocomposites, followed by reduction processes.^[8,9] The method requires a high temperature and long reaction time, and yet formation of small monodispersed (< 5 nm) silver particles is still very difficult. Calcination at higher than 450 °C and many subsequent washing steps are needed to obtain host-free nanoparticles from these matrixes. Silver nanoparticles can also be prepared by reduction of a solution of Ag^I ions with reducing agents such as borohydride in the presence of surfactant or polymers, but the method cannot prevent the formation of large aggregates of silver particles.^[10] Therefore, the preparation of monodispersed small silver nanoparticles under mild conditions without extra reduction processes would be very useful. However, it is extremely difficult to find an appropriate solid support that can reduce Ag^I ions to silver particles at ambient temperature.^[11] In particular, there has been no redox-active MOF for such a purpose.

Herein, we report the construction of the new MOF $[\text{Ni}(\text{C}_{10}\text{H}_{26}\text{N}_6)]_3(\text{bpdc})_3 \cdot 2\text{C}_5\text{H}_5\text{N} \cdot 6\text{H}_2\text{O}$ (**1**; bpdc = 4,4'-biphenyldicarboxylate) with permanent porosity, as well as

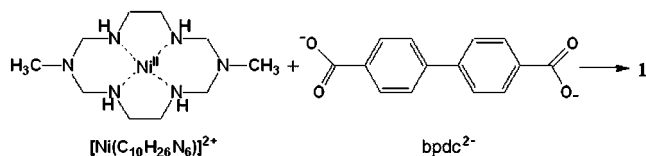
[*] H. R. Moon, J. H. Kim, Prof. Dr. M. P. Suh
School of Chemistry
Seoul National University
Seoul 151-747 (Republic of Korea)
Fax: (+82) 2-886-8516
E-mail: mpsuh@snu.ac.kr

[**] This work was supported by the Korea Institute of Science and Technology Evaluation and Planning (project no. M1-0213-03-0001). We thank Prof. J. W. Cheon of Yonsei University, Seoul, Korea for helpful discussions.



Supporting information for this article is available on the WWW under <http://www.angewandte.org> or from the author.

the room-temperature preparation of both silver nanoparticle/matrix composites and isolated silver nanoparticles (≈ 3 nm) by employing **1** as matrix. Compound **1** was constructed by packing of the linear coordination polymer chains formed from the nickel macrocyclic complex $[\text{Ni}(\text{C}_{10}\text{H}_{26}\text{N}_6)](\text{ClO}_4)_2$ and bpdc^{2-} ions in a water/pyridine mixture. Although various linear coordination polymers have



been prepared, those exhibiting permanent porosity are extremely rare.^[12,13] Previously, we reported a similar porous material, $[\text{Ni}(\text{cyclam})(\text{bpydc})] \cdot 5\text{H}_2\text{O}$ (**2**; cyclam = 1,4,8,11-tetraazacyclotetradecane; bpydc = 2,2'-bipyridyl-5,5'-dicarboxylate), which was assembled from $[\text{Ni}(\text{cyclam})](\text{ClO}_4)_2$ and bpydc^{2-} ions in water.^[13] However, **2** dissociated in the AgNO_3 solution to liberate $[\text{Ni}(\text{cyclam})]^{2+}$ ions because of the strong affinity of bpydc^{2-} for Ag^+ ions, and no silver nanoparticles were produced. Therefore, we now employ bpdc^{2-} ligands as the organic building block. We also use a different macrocycle $\text{C}_{10}\text{H}_{26}\text{N}_6$, since it can stabilize the Ni^{III} state better than the cyclam ligand.^[14] To the best of our knowledge, **1** is the first MOF coordination polymer that produces metallic silver from Ag^+ ions.

It is common that a framework with different topology results when any building block or solvent system is changed in self-assembly systems.^[6a,b] However, although we employed different metal and organic building blocks as well as a different solvent system in the present study from those used to prepare **2**,^[13] we obtained **1** with a similar structure to that of **2**. In the X-ray structure of **1** (Figure 1), linear polymer chains are formed by the coordination of bpdc^{2-} ligands to the Ni^{II} macrocycle in a bimonodentate fashion, and they extend in three different directions ([010], [001], and [101]) to construct a double network of threefold braids.^[15] The flat bpdc^{2-} ligand creates grooves between the macrocycles in a chain such that the macrocycles in the other chain fit into the

grooves, thus providing robustness of the framework. There are interchain $\text{CH} \cdots \pi$ interactions^[16] between the CH of the macrocycle and the phenyl rings of the bpdc^{2-} ligand ($\text{C} \cdots \text{H}$ distance, 3.442–3.662 Å; dihedral angles, 32.8–40.0°; see Supporting Information). The structure generates 1D channels with honeycomb-like windows of diameter 9.7 Å (effective size, 7.3 Å), which are filled with water and pyridine guest molecules.

Compound **1** is insoluble in water or organic solvents. The thermogravimetric analysis trace of **1** indicates that all guest molecules can be removed at 138°C and the apohost is stable up to 250°C. The X-ray powder diffraction (XRPD) pattern of the desolvated solid is the same as that of as-prepared **1** (Figure 2a and b), which indicates that the open structure is

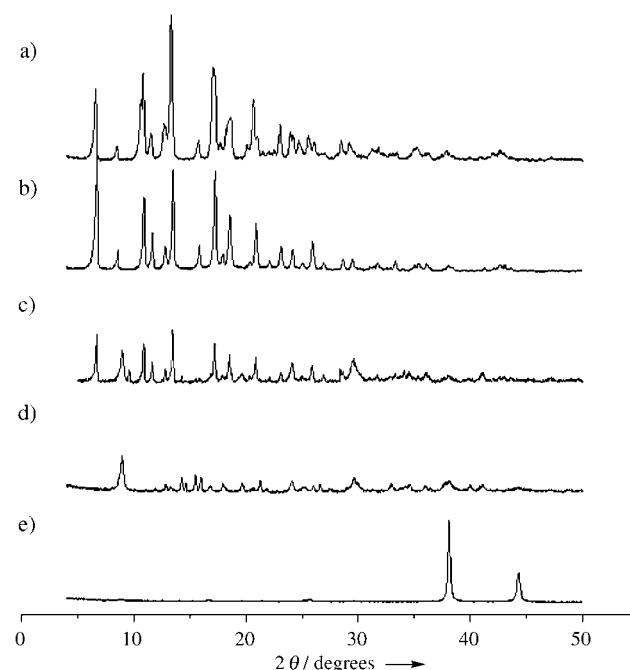


Figure 2. XRPD patterns for a) original host framework **1**, b) desolvated host framework prepared by drying **1** at 130°C for 1 h, c) desolvated host solid after immersion in a methanolic solution of AgNO_3 for 10 min, d) after immersion for 18 h, and e) host-free silver nanoparticles.

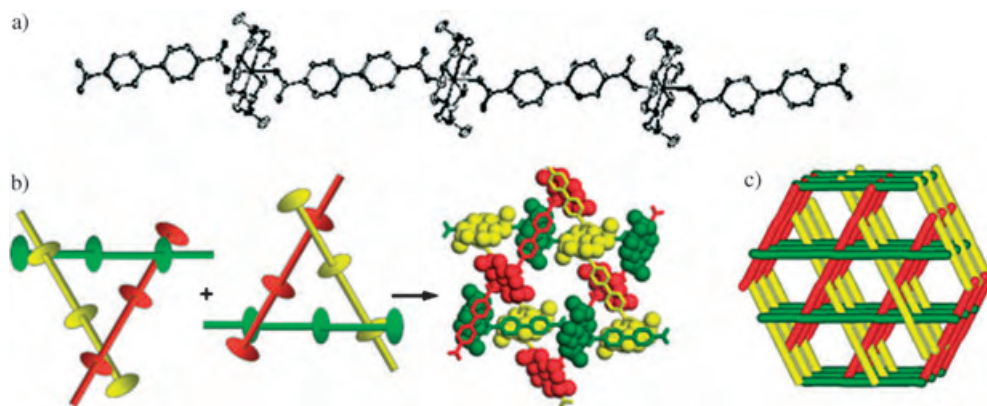


Figure 1. X-ray structure of **1**. a) Structure of the linear coordination polymer. b) Double network of threefold braids where macrocycles fit into the grooves created by bpdc^{2-} ligands. c) View showing the stacking of the linear chains to generate 1D channels.

robust even after removal of the guest molecules. The N_2 gas sorption data revealed a reversible type I isotherm as a consequence of the permanent porosity. The Langmuir surface area and pore volume estimated from the data are $691 \text{ m}^2 \text{ g}^{-1}$ and $0.390 \text{ cm}^3 \text{ g}^{-1}$ ($0.45 \text{ cm}^3 \text{ cm}^{-3}$), respectively, which compare favorably with those of zeolites (pore volume: $0.18\text{--}0.47 \text{ cm}^3 \text{ cm}^{-3}$).^[17]

A pink-colored desolvated framework was prepared by heating **1** at 130°C and 10^{-5} Torr for 1 h. Immersion of this product in a methanolic solution of AgNO_3 ($8.0 \times 10^{-2} \text{ M}$) at room temperature afforded a dark-brown host solid containing silver nanoparticles ($\approx 3 \text{ nm}$ diameter; Figure 3) as a result of the redox reaction between Ag^{I} ions and the Ni^{II} macrocycles of the host. Aqueous solvent should not be used for this reaction because the host framework dissociates in the AgNO_3 solution. The electron paramagnetic resonance (EPR) spectrum (Figure 4) of the resulting solid shows peaks at $g_{\perp} = 2.183$ and $g_{\parallel} = 2.024$, indicative of the tetragonally distorted Ni^{III} species,^[14,18] and a peak at $g = 2.005$ for metallic silver.^[19] X-ray photoelectron spectroscopy ($3d_{5/2}$ and $3d_{3/2}$ peaks for Ag, 368.0 and 374.1 eV, respectively; $2p_{3/2}$ and $2p_{1/2}$ peaks for Ni^{III} , 855.4 and 872.8 eV, respectively)^[20] and energy-dispersive X-ray spectroscopy data also indicate that Ag^0 and Ni^{III} coexist in the solid (see Supporting Information). The color change of the host solid from pink to dark brown must be attributed to the formation of Ni^{III} ions^[14] and the surface plasmons of spherical silver nanoparticles.^[21,22] The Ni^{III} species is in an uncommon oxidation state, but it can be stabilized by azamacrocyclic as a pseudooctahedral species.^[14] The Ag^{I} ions interact with the aromatic rings of the bpdc^{2-} ligands that form the channel surface of **1**,^[23] and the redox reaction between the Ag^{I} ions and the Ni^{II} ions incorporated in the host leads to the silver nanoparticles. To see if the silver nanoparticles can be formed only by the nonporous insoluble solid of the Ni^{II} macrocyclic complex, crystals of $[\text{Ni}(\text{C}_{10}\text{H}_{26}\text{N}_6)](\text{ClO}_4)_2$ (0.078 g, 0.16 mmol) were immersed in a methanolic solution of AgNO_3 (20 mL, $8.0 \times 10^{-2} \text{ M}$, 1.6 mmol) for several hours. The reaction did not produce silver nanoparticles, which indicates that both the redox-active Ni^{II} -macrocyclic component and the porous structure are necessary to obtain the nanoparticles.

In general, the size, shape, and crystallinity of the nanoparticles depend on the concentration of the metal ions, the temperature, and the type of solvent.^[24] However, these properties were not significantly affected by the range

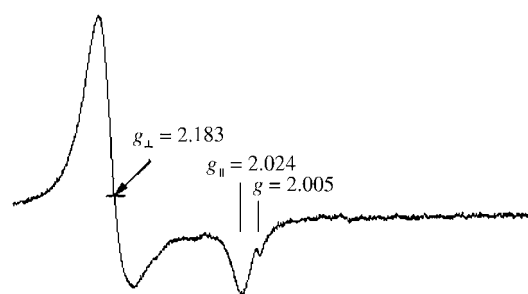


Figure 4. EPR spectrum measured at room temperature for the powder sample isolated after immersion of the desolvated solid of **1** in a MeOH solution of AgNO_3 ($8.0 \times 10^{-2} \text{ M}$).

of experimental conditions used in this study (metal ion concentration: $4.0 \times 10^{-3}\text{--}2.0 \times 10^{-1} \text{ M}$; solvent: MeCN, EtOH, or toluene), except that the lattice fringe of the silver nanoparticles became more distinct when the composites were prepared in a boiling methanolic solution of AgNO_3 (see Supporting Information).

The XRPD pattern (Figure 2) does not show formation of silver nanomaterials distinctly, even though the high-resolution (HR) TEM (Figure 3) images clearly showed incorporation of silver lattices in the matrix: when the desolvated solid of **1** was immersed in the Ag^{I} solution for 10 minutes, the isolated solid showed the same XRPD pattern as that of **1**, which indicates that the open framework structure was maintained. However, the XRPD pattern (Figure 2d) changed completely and became much weaker and broader after immersion of the host solid in the Ag^{I} solution for 18 hours. This observation suggests that the original host structure was destroyed. The silver peaks in these XRPD patterns are extremely weak, probably because the silver particles are too small (3 nm)^[25] and the number of silver crystals is too small compared with that of the host solid. Elemental analysis data (see Experimental Section) for the framework solid isolated after immersion in the AgNO_3 solution for 10 minutes indicate that the reaction stoichiometry of the Ni^{II} ion of the host and AgNO_3 is 1:1. Since the host framework becomes positively charged, it includes free NO_3^- ions as shown by the unsplit 1382 cm^{-1} peak in the IR spectra. The NO_3^- ions in the nanocomposite were partially exchanged with ClO_4^- ions when the solid was immersed in a methanolic solution of LiClO_4 for 48 hours (see Supporting Information).

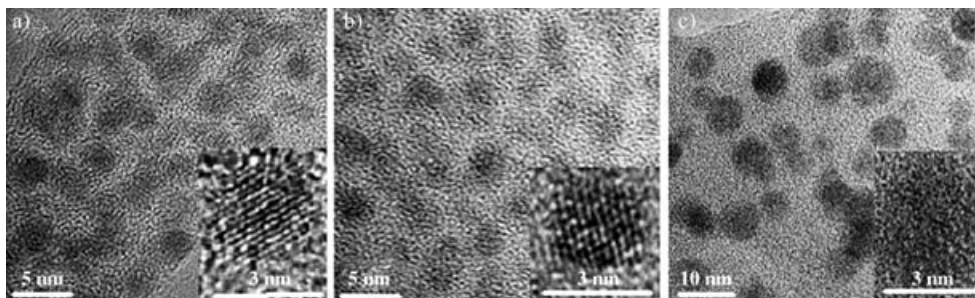


Figure 3. HRTEM images of the solid isolated after immersion of the desolvated **1** in a methanolic solution of AgNO_3 ($8.0 \times 10^{-2} \text{ M}$) at room temperature: a) for 10 min, b) for 18 h, and c) after removal of the host framework by heating the solid of (b) in dioctyl ether in the presence of oleic acid.

We cannot yet explain clearly how silver nanoparticles larger than the window size of the host framework channels formed or how they grew. However, on the basis of the present XRPD results and elemental analysis data, as well as the fact that the nonporous insoluble Ni^{II} -macrocyclic complex $[\text{Ni}(\text{C}_{10}\text{H}_{26}\text{N}_6)](\text{ClO}_4)_2$ did not produce silver nanoparticles, we suggest that the Ag^0 atoms initially collect in the channels, then diffuse into the surface of the host solid where they aggregate to form nanoparticles,^[21] which are stabilized by the bpdc^{2-} ligands as the immersion time progresses, until the framework structure is destroyed.^[26]

Host-free silver nanoparticles about 3 nm in diameter (Figure 3c), which might be capped with long-chain carboxylic acids, were isolated by treating the nanocomposite in boiling diethyl ether (at $\approx 290^\circ\text{C}$) in the presence of oleic acid. The XRPD pattern (Figure 2e) of the host-free silver nanoparticles exhibits intense peaks characteristic of crystalline silver at $2\theta = 38^\circ$ and 44° .^[25,27] When the host framework of the silver nanocomposite was destroyed with acid or heat without capping agents, the particles were significantly aggregated (see Supporting Information).

In conclusion, we have demonstrated that the present MOF is multifunctional: it acts as a porous material and also as a redox catalyst for the synthesis of silver nanoparticles (≈ 3 nm in diameter) at ambient temperature. We cannot yet explain clearly how silver nanoparticles larger than the window size of the framework channels form or how they grow, but further studies on the mechanistic aspects and the reduction of other metal ions will be performed.

Experimental Section

1: $[\text{Ni}(\text{C}_{10}\text{H}_{26}\text{N}_6)](\text{ClO}_4)_2$ ^[28] (0.098 g, 0.20 mmol) was dissolved in water/pyridine (6 mL, 2:1 v/v), and an aqueous solution (2 mL) of Na_2bpdc (0.07 g, 0.24 mmol) was added dropwise. The yellow solution was allowed to stand at room temperature until pale purple crystals formed which were isolated by filtration, washed with methanol, and dried in air. Yield: 95%. FTIR (Nujol mull): $\nu = 3370$ (m, br), 3169 (m), 1606 (w), 1586 (s), 1541 (m), 1018 (m), 833 (s), 771 (s) cm^{-1} ; UV/Vis (diffuse reflectance spectrum, λ_{max}): 509 nm. Elemental analysis: calcd for $\text{Ni}_3\text{C}_{82}\text{H}_{124}\text{N}_{20}\text{O}_{18}$ (%): C 53.12, H 6.74, N 15.11; found: C 51.66, H 7.01, N 15.01.

X-ray crystallography: Crystal data for **1**: $\text{Ni}_3\text{C}_{82}\text{H}_{124}\text{N}_{20}\text{O}_{18}$, $M_r = 1854.08$, triclinic, space group $P\bar{1}$, $a = 11.530$, $b = 15.663$, $c = 15.634$ Å, $V = 2295.4$ Å³, $Z = 1$, $T = 293$ K, $R_1 = 0.0618$ ($I > 2\sigma(I)$), $wR_2(F^2) = 0.1851$ ($I > 2\sigma(I)$), GOF = 1.017. CCDC 242970 (**1**) contains the supplementary crystallographic data for this paper. These data can be obtained free of charge via www.ccdc.cam.ac.uk/conts/retrieving.html (or from the Cambridge Crystallographic Data Centre, 12 Union Road, Cambridge CB2 1EZ, UK; fax: (+44) 1223-336-033; or deposit@ccdc.cam.ac.uk).

Preparation of silver nanocomposites: Framework **1** was desolvated at 130°C under vacuum (10^{-5} Torr) for 1 h, which resulted in a pink color. The desolvated solid (0.100 g, 0.16 mmol) was immersed in a methanolic solution (20 mL) of AgNO_3 (8.0×10^{-2} M, 1.6 mmol) at room temperature for 10 min, which resulted in a dark-brown solid, and kept immersed for an additional 18 h. The resulting dark-brown powder was isolated by filtration, washed with MeOH, and dried in air. Elemental analysis for the solid immersed in the AgNO_3 solution for 10 min: calcd for $[\text{Ni}(\text{C}_{10}\text{H}_{26}\text{N}_6)]_3(\text{bpdc})_3 \cdot 6\text{H}_2\text{O} \cdot 3\text{AgNO}_3$ ($\text{Ni}_3\text{C}_{72}\text{H}_{114}\text{N}_{21}\text{O}_{27}\text{Ag}_3$) (%): C 39.21, H 5.21, N 13.34; found: C 38.42, H 4.69, N 11.71; UV/Vis (diffuse reflectance spectrum, λ_{max}): 378, 449 nm; elemental analysis (%) for the solid

immersed for 18 h: found: C 25.50, H 2.79, N 9.95. The desolvated framework **1** (0.100 g, 0.16 mmol) was also immersed in 4.0×10^{-3} M (0.080 mmol) and 4.0×10^{-2} M (0.80 mmol) methanolic AgNO_3 solutions (20 mL) at room temperature for 10 min. The same experiments were carried out in boiling MeOH as well as in toluene, ethanol, and acetonitrile.

Isolation of host-free silver nanoparticles: The solid sample (0.11 g, 0.17 mmol based on Ni^{II}) isolated after immersion of the dried framework compound **1** in the AgNO_3 solution for 18 h was refluxed for 4 h in diethyl ether (10 mL) in the presence of oleic acid (0.18 g, 0.65 mmol). The solution became yellow as the host framework dissociated into the building blocks. The dark-brown powder was filtered off, washed with MeOH, and dried in air.

Received: July 23, 2004

Revised: September 1, 2004

Published online: January 12, 2005

Keywords: coordination polymers · host–guest systems · microporous materials · nanostructures · silver

- [1] a) N. L. Rosi, J. Eckert, M. Eddaoudi, D. T. Vodak, J. Kim, M. O’Keeffe, O. M. Yaghi, *Science* **2003**, *300*, 1127–1129; b) R. Kitaura, K. Seki, G. Akiyama, S. Kitagawa, *Angew. Chem.* **2003**, *115*, 444–447; *Angew. Chem. Int. Ed.* **2003**, *42*, 428–431; c) M. P. Suh, J. W. Ko, H. J. Choi, *J. Am. Chem. Soc.* **2002**, *124*, 10976–10977; d) K. S. Min, M. P. Suh, *Chem. Eur. J.* **2001**, *7*, 303–313; e) H. J. Choi, T. S. Lee, M. P. Suh, *Angew. Chem.* **1999**, *111*, 1490–1493; *Angew. Chem. Int. Ed.* **1999**, *38*, 1405–1408; f) J. W. Ko, K. S. Min, M. P. Suh, *Inorg. Chem.* **2002**, *41*, 2151–2157.
- [2] a) K. S. Min, M. P. Suh, *J. Am. Chem. Soc.* **2000**, *122*, 6834–6840; b) O. M. Yaghi, H. Li, *J. Am. Chem. Soc.* **1996**, *118*, 295–296.
- [3] a) J. S. Seo, D.-M. Whang, H.-Y. Lee, S. I. Jun, J.-H. Oh, Y.-J. Jeon, K.-M. Kim, *Nature* **2000**, *404*, 982–986; b) T. Sawaki, Y. Aoyama, *J. Am. Chem. Soc.* **1999**, *121*, 4793–4798.
- [4] a) M. Albrecht, M. Lutz, A. L. Spek, G. van Koten, *Nature* **2000**, *406*, 970–974; b) J. A. Real, E. Andrés, M. C. Muñoz, M. Julve, T. Granier, A. Bousseksou, F. Varret, *Science* **1995**, *268*, 265–267.
- [5] O. R. Evans, W. Lin, *Chem. Mater.* **2001**, *13*, 2705–2712.
- [6] a) H. J. Choi, M. P. Suh, *J. Am. Chem. Soc.* **1998**, *120*, 10622–10628; b) T. J. Prior, M. J. Rosseinsky, *CrystEngComm* **2000**, *2*, 128–133; c) M. P. Suh, H. J. Choi, S. M. So, B. M. Kim, *Inorg. Chem.* **2003**, *42*, 676–678; d) H. J. Choi, M. P. Suh, *Inorg. Chem.* **1999**, *38*, 6309–6312; e) J. Lu, A. Mondal, B. Moulton, M. J. Zaworotko, *Angew. Chem.* **2001**, *113*, 2171–2174; *Angew. Chem. Int. Ed.* **2001**, *40*, 2113–2116.
- [7] a) M. Malinsky, K. L. Kelly, G. C. Schatz, R. P. van Duyne, *J. Am. Chem. Soc.* **2001**, *123*, 1471–1482; b) T. R. Jensen, M. D. Malinsky, C. L. Haynes, R. P. van Duyne, *J. Phys. Chem. B* **2000**, *104*, 10549–10556.
- [8] S. Besson, T. Gacoin, C. Ricolleau, J.-P. Boilot, *Chem. Commun.* **2003**, 360–361.
- [9] a) M. Huang, A. Choudrey, P. Yang, *Chem. Commun.* **2000**, 1603–1604; b) S. Wang, D.-G. Choi, S.-M. Yang, *Adv. Mater.* **2002**, *14*, 1311–1314; c) J. Zhang, B. Han, Z. Hou, Z. Liu, J. He, T. Jiang, *Langmuir* **2003**, *19*, 7616–7620; d) Y. Plyuto, J.-M. Berquier, C. Jacquiod, C. Ricolleau, *Chem. Commun.* **1999**, 1653–1654.
- [10] a) L. Lu, H. Wang, Y. Zhou, S. Xi, H. Zhang, J. Hub, B. Zhao, *Chem. Commun.* **2002**, 144–145; b) D. L. Van Hying, W. G. Klempner, C. F. Zukoski, *Langmuir* **2001**, *17*, 3128–3135.
- [11] B. H. Hong, S. C. Bae, C.-W. Lee, S. Jeong, K. S. Kim, *Science* **2001**, *294*, 348–351.

- [12] S. Takamizawa, E. Nakata, H. Yokoyama, K. Mochizuki, W. Mori, *Angew. Chem.* **2003**, *115*, 4467–4470; *Angew. Chem. Int. Ed.* **2003**, *42*, 4331–4334.
- [13] E. Y. Lee, M. P. Suh, *Angew. Chem.* **2004**, *116*, 2858–2861; *Angew. Chem. Int. Ed.* **2004**, *43*, 2798–2801.
- [14] M. P. Suh, *Adv. Inorg. Chem.* **1997**, *44*, 93–146.
- [15] S. Lidin, M. Jacob, S. Anderson, *J. Solid State Chem.* **1995**, *114*, 36–41.
- [16] M. Nishio, M. Hirota, Y. Umezawa, *The CH- π Interaction: Evidence, Nature, and Consequences*, Wiley, New York, **1998**, pp. 52–56.
- [17] D. W. Breck, *Zeolite Molecular Sieves*, Wiley, New York, **1974**, chap. 8.
- [18] M. P. Suh, E. Y. Lee, B. Y. Shim, *Inorg. Chim. Acta* **1998**, 337–341.
- [19] a) H. Yamada, J. Michalik, H. Sadlo, J. Perlinska, S. Takenouchi, S. Shimomura, Y. Uchida, *Appl. Clay Sci.* **2001**, *19*, 173–178; b) J. Michalik, L. Kevan, *J. Am. Chem. Soc.* **1986**, *108*, 4247–4253.
- [20] a) C. D. Wagner in *Handbook of X-ray Photoelectron Spectroscopy. A Reference Book of Standard Data for Use in X-ray Photoelectron Spectroscopy* (Ed.: G. E. Muilenberg), Eden Prairie, Minnesota, **1979**, pp. 84, 85, 120, 121; b) Z. R. Yue, W. Jiang, L. Wang, H. Toghiani, S. D. Gardner, Jr., C. U. Pittman, *Carbon* **1999**, *37*, 1607–1618; c) A. Davidson, J. F. Tempere, M. Che, *J. Phys. Chem.* **1996**, *100*, 4919–4929.
- [21] A. S. Korchev, M. J. Bozack, B. L. Slaten, G. Mills, *J. Am. Chem. Soc.* **2004**, *126*, 10–11.
- [22] K. L. Kelly, E. Coronado, L. Zhao, G. C. Schatz, *J. Phys. Chem. B* **2003**, *107*, 668–677.
- [23] F. A. Cotton, G. Wilkinson in *Advanced Inorganic Chemistry*, 5th ed., Wiley, New York, **1988**, p. 945.
- [24] a) R. He, X. Qian, J. Yin, Z. Zhu, *J. Mater. Chem.* **2002**, *12*, 3783–3786; b) M. Yamada, H. Nishihara, *Langmuir* **2003**, *19*, 8050–8056; c) L. Lu, H. Wang, Y. Zhou, S. Xi, H. Zhang, J. Hu, B. Zhao, *Chem. Commun.* **2002**, 144–145.
- [25] a) P. V. Adhyapak, P. Karandikar, K. Vijayamohan, A. A. Athawale, A. Chandwadkar, *Mater. Lett.* **2004**, *58*, 1168–1171; b) L. Yang, G. H. Li, L. D. Zhang, *Appl. Phys. Lett.* **2000**, *76*, 1537–1539; c) A. Watanabe, H. Kozuka, *J. Phys. Chem. B* **2003**, *107*, 12713–12720.
- [26] a) L. Sordelli, G. Martra, R. Psaro, C. Dossi, S. Coluccia, *J. Chem. Soc. Dalton Trans.* **1996**, 765–770; b) F. Li, B. C. Gates, *J. Phys. Chem. B* **2003**, *107*, 11589–11596.
- [27] a) Y.-J. Han, J. M. Kim, G. D. Stucky, *Chem. Mater.* **2000**, *12*, 2068–2069; b) L.-Z. Wang, J.-L. Shi, W.-H. Zhang, M.-L. Ruan, J. Yu, D.-S. Yan, *Chem. Mater.* **1999**, *11*, 3015–3017; c) C. Damle, A. Kumar, M. Sastry, *J. Phys. Chem. B* **2002**, *106*, 297–302.
- [28] M. P. Suh, S.-G. Kang, *Inorg. Chem.* **1988**, *27*, 2544–2546.

A Controllable Electrochemical Fabrication of Metallic Electrodes with a Nanometer/Angstrom-Sized Gap Using an Electric Double Layer as Feedback**

Juan Xiang, Bo Liu, Sun-Tao Wu, Bin Ren,
Fang-Zu Yang, Bing-Wei Mao, Yuan L. Chow, and
Zhong-Qun Tian*

A pair of facing electrodes with a desired gap width ranging from several angstroms to several nanometers is a key structure in the domain of nanoscience and nanotechnology.^[1–10] For example, such a structure supported on a microchip provides a means to interface individual molecules or nanocrystals in integrated circuits.^[2–5] The fabricated gap should have a width that is controllable and can be set to meet the specific needs of the target molecules (0.5–2 nm scale) or nanocrystals (1–10 nm scale) whose electron-transport properties can be characterized in detail.^[6–10]

In the past few years, three methods have been developed for fabricating electrode pairs with nano-sized or angstrom-sized gaps for device applications.^[10–18] The first one, referred to as “break junction”, is based on the mechanical breaking of a metal wire into two electrodes with a certain gap.^[10,11] The involvement of mechanical forces in the fabrication procedure seems unlikely to be promising for manufacturing microchips, and, moreover, does not have the precision and flexibility to give the desired gap width. The second approach is based on electromigration of metal atoms, which is realized by passing a large electrical current through, and eventually breaking, a gold nanowire.^[12,13] This process can yield a stable electrode separation of 1 nm with high efficiency. The above two methods, however, have certain limitations in applicability. The metal nanowire to be broken on a chip should be very thin, around 20 nm, and nanowires of this diameter can only be fabricated by electron-beam lithography, which is not commonly available.

The third method, which is based on the principle of electrodeposition or electrodisolution, can overcome the above-mentioned disadvantages.^[14–19] By electrodepositing metal atoms onto a specific face of electrodes, one can sequentially narrow the gap from the original micrometer scale down to the domain of a few angstroms, or even connect

[*] Dr. J. Xiang, B. Liu, Dr. B. Ren, Dr. F.-Z. Yang, Prof. Dr. B.-W. Mao, Dr. Y. L. Chow, Prof. Dr. Z.-Q. Tian
State Key Laboratory of Physical Chemistry of Solid Surfaces
Xiamen University, 361005 Xiamen (China)
Fax: (+ 86) 592-208-5439
E-mail: zqtian@xmu.edu.cn
Prof. Dr. S.-T. Wu
Pen-Tung Sah Micro-Electro-Mechanical Systems Research Center
Xiamen University, 361005 Xiamen (China)

[**] This work was supported by the Natural Science Foundation (grant nos. 20021002 and 20328306) and the Ministry of Science and Technology of China (grant no. 2001CB610506). We sincerely thank N. J. Tao for helpful discussions.

two electrodes to form a quantum contact.^[14–19] This electrochemical method is more versatile than the break-junction and electromigration methods mentioned above, especially as the process can be reversed in the electrodisolution mode for controlled etching of metal atoms from a wire to solution, thus widening the gap from angstrom up to sub-micrometer scales. The most important feature of the electrochemical method is the use of a feedback system to precisely control the resultant gap width. Several experimental parameters, such as electrochemical current and electrolyte conductance, are critically dependent on the gap between two facing electrodes, especially when the gap is narrowed to below the sub-micrometer scale. The electrodeposition process can be stopped by switching off the potentiostat when the conductance reaches a preset value, which provides an accurate and reproducible way to control the gap width between 20 and 3 nm.^[16–19] Recently, Tao and co-workers developed a new method to fabricate a molecular-sized gap by using the tunneling current as feedback to precisely monitor electrochemical deposition/etching.^[15] When the gap is narrowed below 1 nm, a tunneling current occurs and increases exponentially with a further reduction in the gap width. They observed an interesting stepwise variation in the tunneling current during deposition and etching, which makes it possible to fabricate gaps with sub-angstrom precision. This method affords a great advantage in that it achieves a snug fitting of different molecules, which is an important feature in the fabrication of molecular electronics.^[2,20] However, this very promising method seems to have two insurmountable limitations. First of all, it is much more suitable for making a small gap (below 1 nm). Secondly, the four-electrode bipotentiostat to monitoring the tunneling-current feedback is custom-made to a special design and is not commercially available.

In view of the above limitations, it is desirable to develop a simpler and more versatile electrochemical method. Firstly, the method should be able to create gaps ranging from several angstroms to 10 nm, since this is the best scale for fitting designed molecules or growing a nanodot (nanocrystal) of semiconductors or other materials in-between the two electrodes in nanodevices. Secondly, the method should also have a much simpler feedback system that allows the adaptation of a commonly used electrochemical instrument, as this may persuade many research groups to use the method. We report here a chronopotentiometric method that readily allows the electrochemical fabrication of pairs of metallic electrodes with defined gap widths that range from several nanometers down to several angstroms. In this new approach, gap widths are fabricated for the first time by using both the electrode potential and also a universally available three-electrode potentiostat as feedback indicators. The process is simple, controllable, reproducible, and robust, and enables the rapid fabrication of a wide range of nanogaps without the need for any sophisticated instrumentation.

The fabrication involves two major steps—lithography and electrodeposition. First, a pair of facing gold electrodes supported on a SiO₂ chip is prepared with an electrode gap of about 2 μm by a conventional lithography technique (see inset of Figure 1). The wide electrode separation at this stage is not

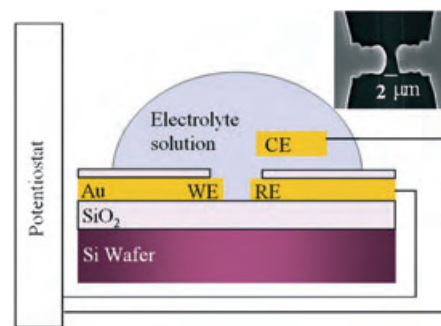


Figure 1. Schematic representation of the experimental setup. The inset shows a pair of facing gold electrodes fabricated on, and covered with, SiO₂, which allows only a small area of both electrodes to be exposed to a solution containing gold ions.

critical. The second step is to narrow the gap down to the nanometer scale by electrodepositing Au atoms onto the working electrode. In comparison with previous methods^[14–19] the present method has two major differences, namely, the electrode configuration and the feedback mode (see Figure 1). In our new design, the pair of facing electrodes serve as the working electrode (WE) and reference electrode (RE), respectively. This configuration differs from the conductance-feedback and current-feedback modes, which use both facing electrodes as WEs.^[14–19] Experiments were carried out on this unique electrode arrangement by applying a controlled current between the WE and the CE with a current source (a galvanostat).^[21] Metal atoms were deposited layer by layer on the WE face at a chosen constant current (I_{dep}) so as to narrow the gap width between the WE and the RE. The operation is controllable and the coating uniform. The potential difference between the WE and the RE (V_{gap}) was monitored continuously during the electrodeposition process, and was plotted as the chronopotentiometric curve shown in Figure 2a. The monitored V_{gap} was about -0.55 V at a deposition current (I_{dep}) of 0.1 mA cm^{-2} , and remained constant until the gap was narrowed below a certain value. The value of V_{gap} decreased irregularly with time, and finally approached zero, thus indicating that the WE and RE electrodes had become connected. This observation clearly demonstrates that V_{gap} can be used as a feedback to control the gap width. It was of special interest to examine the evolution of the gap when V_{gap} started to decrease according to the chronopotential response shown in Figure 2a. Figure 2b and 2c show SEM images of the gap at a preset chronopotential value of $V_{\text{gap}} = -0.55$ V (at the initial changing stage) and $V_{\text{gap}} = -0.01$ V (near the final stage) as indicated by the potential feedback, respectively. The gap width in the former is approximately 4.5 nm, while the latter shows the gap to be very small and beyond the resolution of SEM. Alternatively, the width of the gap can be estimated from the formula $I \propto V \exp(-ks)$, where I is the tunneling current, V the bias potential, s the gap width, and k a constant. Therefore, if we measure the I – V curve experimentally for the case shown in Figure 2c, and with a known k value, we can calculate s . The linear I – V curve for the gap in air (Figure 2d)

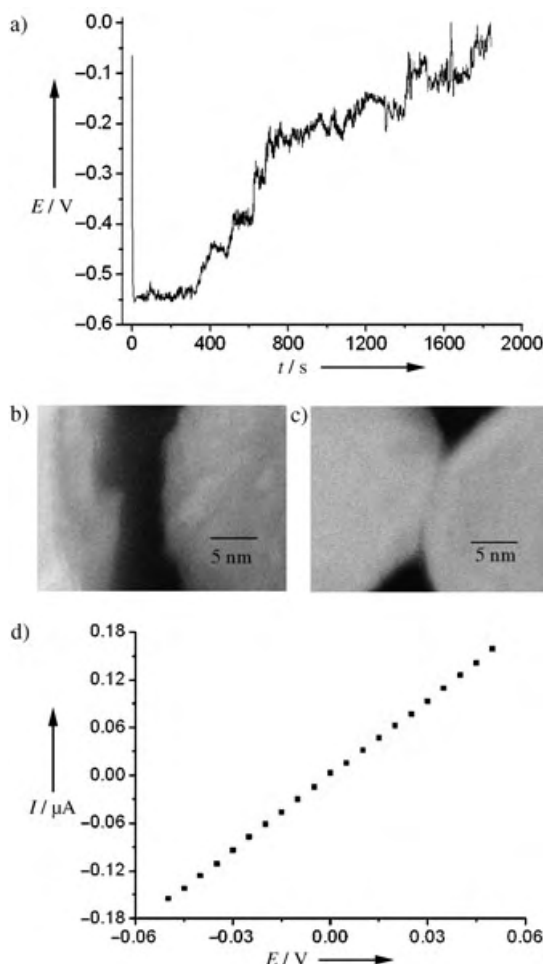


Figure 2. a) A chronopotential response curve during the whole electrodeposition process as Au is deposited on the WE. b) An SEM image of the gap at the preset V_{gap} of -0.55 V. c) An SEM image of the gap at the preset V_{gap} of -0.01 V. d) The corresponding I - V curve of the gap in (c).

enabled us to substitute k with an average of its values in vacuo^[22] and in solution,^[23] and calculate the gap width to be approximately 1.5 Å.

We then performed a set of experiments by presetting 12 potentials from -0.55 to -0.01 V as the feedback to control the nanogap fabrication, and then measured their I - V values.

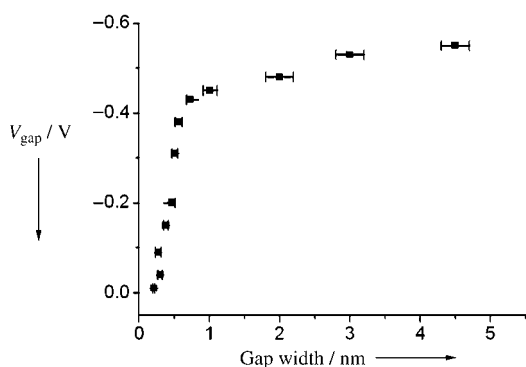


Figure 3. Correlation of the monitored gap width versus V_{gap} .

The value of V_{gap} is plotted against the gap width in Figure 3, which shows that the gap can be fabricated in a controlled manner over a range from 4.5 nm to 2 Å. This systematic experiment demonstrates that an electrode separation ranging from several angstroms to several nanometers can be constructed simply by choosing a preset potential. By measuring the potential difference between the WE and the RE, we are able to monitor the gap distance in a range smaller than 4.5 nm and perform a controlled deposition with sub-nanometer resolution.

Why, under the present electrode configuration, does V_{gap} start to decrease when the gap is narrowed down to around 5 nm (Figure 3)? This trend most probably results from the pattern of potential drops in the electrical double-layer. According to the Guoy-Chapman-Stern (GCS) model,^[24] a double layer consists of a compact layer (CL) with a sharp potential drop and a diffuse layer (DL) with a slow potential

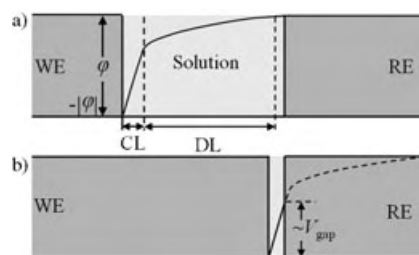


Figure 4. Representation of the working electrochemical principle when fabricating nano/angstrom-gap electrodes. The double layer consists of a compact layer (CL) and a diffuse layer (DL).

drop (Figure 4a). Since no potential drop occurs beyond the double-layer region when the gap is narrowed down to around the double-layer thickness, the RE (which acts as the potential probe) can be considered to penetrate into the double-layer region of the WE (Figure 4b). This arrangement provides a guide for presetting the V_{gap} value so that the termination of the electrodeposition process produces a desired gap width.

The electrolyte concentration can also critically influence the double-layer structure,^[24] which is another factor that contributes to the V_{gap} versus gap-width relationship. Since the fabrication of the largest gap width by our method is mainly determined by the double-layer structure, namely, the potential distribution and the layer thickness, one could also control the width by adjusting the electrolyte concentration. Figure 5 shows that when the concentration of the plating solution is diluted by 100 times and the potential is set at -0.6 V, the accessible gap width can be extended to 10 nm (Figure 5b). It should be noted that the potential distribution in the nanogap is much more complicated than that shown in Figure 4 because of many factors. For example, the double layer of the RE has not been taken into account in our preliminary model. A systematic investigation of this unique double layer is needed to gain a more-detailed picture.

In summary, we have demonstrated a simple potential-feedback system with a hitherto-untried electrode configuration to fabricate metallic electrodes with controlled gap

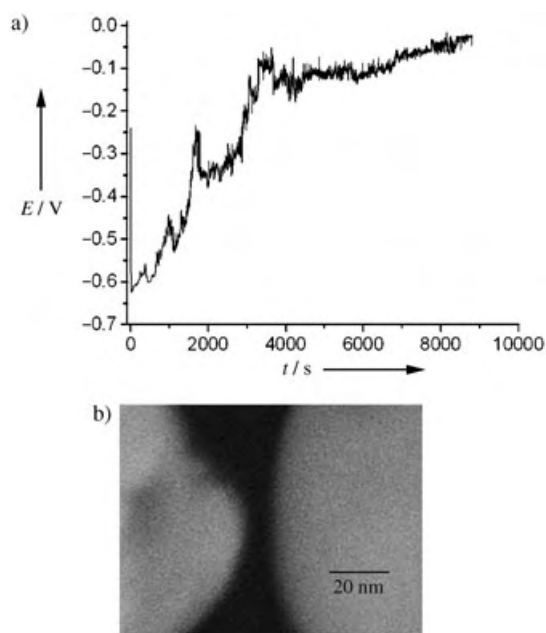


Figure 5. a) A chronopotential response curve during the whole electrodeposition process as Au is deposited on the WE. $I_{\text{dep}} = 0.1 \text{ mA cm}^{-2}$; the electroplating solution contains $0.15 \text{ } \mu\text{M}$ $\text{KAu}(\text{CN})_2$, $3 \text{ } \mu\text{M}$ $\text{K}_3\text{C}_6\text{H}_5\text{O}_7$, and $3 \text{ } \mu\text{M}$ KH_2PO_4 . b) An SEM image of the gap at the preset V_{gap} of -0.6 V .

widths over a wide range from about 10 nm down to several angstroms. The working principle is based on the potential distribution in the electric double-layer. The process is simple, controllable, and reproducible, and allows the rapid fabrication of electrode pairs with conventional equipment, which may persuade more research groups to use the method. This method has the potential of leading to three techniques for future studies in nanodevices, surface-enhanced Raman scattering (SERS), and electrochemical double-layers. A nanocrystal of various materials could be grown electrochemically to fuse the gap by simply changing the electroplating solution.^[25] It could also be used to study SERS of molecules located at the junction of two nanotips to determine which exhibits the highest activity.^[26] More importantly, one could use this controllable nanogap to investigate the double-layer structure in detail, which has been a key issue in electrochemistry for a long time.

Experimental Section

The electrode pair and nanogap fabrication: The pair of facing Au (99.99%) electrodes were fabricated by an optical-lithography technique on an n-type Si wafer of $\langle 111 \rangle$ orientation that was covered with 2- μm , thermally oxidized silicon layer. The initial separation was typically 2 μm . The electrochemical fabrication of the nanogap electrodes was realized by using a CHI631A electrochemical workstation (CHI Co., USA). The deposition current in chronopotentiometry was 0.1 mA cm^{-2} . The electroplating solution was $15 \text{ } \mu\text{M}$ $\text{KAu}(\text{CN})_2$, with 0.3 mM $\text{K}_3\text{C}_6\text{H}_5\text{O}_7$ and 0.3 mM KH_2PO_4 as supporting electrolytes. These optimized experimental parameters, especially the current density, ensure that the Au deposits in a uniform and compact manner, which ensures a reasonably good stability of the fabricated nanogap in both solution and air. When the electroplating solution

was diluted by a factor of 100, that is, the electroplating solution was $0.15 \text{ } \mu\text{M}$ $\text{KAu}(\text{CN})_2$ with $3 \text{ } \mu\text{M}$ $\text{K}_3\text{C}_6\text{H}_5\text{O}_7$ and $3 \text{ } \mu\text{M}$ KH_2PO_4 , the largest fabricated gap width was about 10 nm. All solutions were prepared with analytical grade reagents and Milli-Q water. The nanogap electrodes with a gap larger than 1 nm were characterized with a LEO1530 scanning electron microscope (LEO Co., Germany). The nanogap electrodes with gaps smaller than 1 nm were characterized with a Keithley 4200 semiconductor characterization system to measure the corresponding I - V curve of the gap.

Received: August 26, 2004

Published online: January 12, 2005

Keywords: electrochemistry · electrodes · gold · nanostructures · nanotechnology

- [1] A. Nitzan, M. A. Ratner, *Science* **2003**, *300*, 1384.
- [2] C. Joachim, J. K. Gimzewski, A. Aviram, *Nature* **2000**, *408*, 541.
- [3] W. J. Liang, M. P. Shores, M. Bockrath, J. R. Long, H. Park, *Nature* **2002**, *417*, 725.
- [4] J. Park, A. N. Pasupathy, J. I. Goldsmith, C. Chang, Y. Yaish, J. R. Petta, M. Rinkoski, J. P. Sethna, H. D. Abruna, P. L. McEuen, D. C. Ralph, *Nature* **2002**, *417*, 722.
- [5] C. A. Mirkin, M. A. Ratner, *Annu. Rev. Phys. Chem.* **1992**, *43*, 719.
- [6] Y. Selzer, M. A. Cabassi, T. S. Mayer, D. L. Allara, *J. Am. Chem. Soc.* **2004**, *126*, 4052.
- [7] D. Porath, A. Bezryadin, S. De Vries, C. Dekker, *Nature* **2000**, *403*, 635.
- [8] B. Q. Xu, N. J. Tao, *Science* **2003**, *301*, 1221.
- [9] V. Rajagopalan, S. Boussaad, N. J. Tao, *Nano Lett.* **2003**, *3*, 851.
- [10] M. A. Reed, C. Zhou, C. J. Muller, T. P. Burgin, J. M. Tour, *Science* **1997**, *278*, 252.
- [11] J. Reichert, R. Ochs, D. Beckmann, H. B. Weber, M. Mayor, H. von Lohneysen, *Phys. Rev. Lett.* **2002**, *88*, 176804.
- [12] H. Park, A. K. L. Lim, A. P. Alivisatos, J. Park, P. L. McEuen, *Appl. Phys. Lett.* **1999**, *75*, 301.
- [13] H. Park, J. Park, A. K. L. Lim, E. H. Anderson, A. P. Alivisatos, P. L. McEuen, *Nature* **2000**, *407*, 57.
- [14] H. X. He, S. Boussaad, C. Z. Li, N. J. Tao, *J. Electroanal. Chem.* **2002**, *522*, 167.
- [15] C. Z. Li, H. X. He, N. J. Tao, *Appl. Phys. Lett.* **2000**, *77*, 3995.
- [16] A. F. Morpurgo, C. M. Marcus, D. B. Robinson, *Appl. Phys. Lett.* **1999**, *74*, 2084.
- [17] Y. V. Kervennic, H. S. J. van der Zant, A. F. Morpurgo, L. Gurevich, L. P. Kouwenhoven, *Appl. Phys. Lett.* **2002**, *80*, 321.
- [18] Y. Kashimura, H. Nakashima, K. Furukawa, K. Torimitsu, *Thin Solid Films* **2003**, *438*, 317.
- [19] M. M. Deshmukh, A. L. Prieto, Q. Gu, H. Park, *Nano Lett.* **2003**, *3*, 1383.
- [20] F. R. F. Fan, Y. X. Yao, L. T. Cai, L. Cheng, J. M. Tour, A. J. Bard, *J. Am. Chem. Soc.* **2004**, *126*, 4035.
- [21] A. J. Bard, L. R. Faulkner, *Electrochemical Methods: Fundamentals and Applications*, 2nd ed., Wiley, New York, **2001**, chap. 8.
- [22] W. Schmickler, D. Henderson, *J. Electroanal. Chem.* **1990**, *290*, 283.
- [23] A. Vaught, T. W. Jing, S. M. Lindsay, *Chem. Phys. Lett.* **1995**, *236*, 306.
- [24] A. J. Bard, L. R. Faulkner, *Electrochemical Methods: Fundamentals and Applications*, 2nd ed., Wiley, New York, **2001**, chap. 13.
- [25] H. X. He, J. S. Zhu, N. J. Tao, L. A. Nagahara, I. Amlani, R. Tsui, *J. Am. Chem. Soc.* **2001**, *123*, 7730.
- [26] Z. Q. Tian, B. Ren, *Annu. Rev. Phys. Chem.* **2004**, *55*, 197.

Mass Production and High Photocatalytic Activity of ZnS Nanoporous Nanoparticles**

Jin-Song Hu, Ling-Ling Ren, Yu-Guo Guo, Han-Pu Liang, An-Min Cao, Li-Jun Wan,* and Chun-Li Bai*

Environmental problems associated with organic pollutants and toxic water pollutants provide the impetus for sustained fundamental and applied research in the area of environmental remediation. Semiconductor photocatalysis offers the potential for complete elimination of toxic chemicals through its efficiency and potentially broad applicability.^[1] Various new compounds and materials for photocatalysis have been synthesized in the past few decades. A successful example is TiO₂, a metal oxide often used as a catalyst in photochemistry, electrochemistry, environmental protection, and in the battery industry.^[2]

Recently, transition-metal sulfides, in particular ZnS and CdS, have been intensively studied because of their unique catalytic functions compared to those of TiO₂.^[2,3] These studies have revealed that ZnS nanocrystals (NCs) are good photocatalysts as a result of the rapid generation of electron-hole pairs by photoexcitation and the highly negative reduction potentials of excited electrons. The photocatalytic properties occur not only in the photoreductive production of H₂ from water and the photoreduction of CO₂,^[4] but also in the phototransformation of various organic substrates such as the oxidative formation of carbon-carbon bonds from organic electron donors, *cis-trans* photoisomerization of alkenes, and the photoreduction of aldehydes and their derivatives.^[5] The notable finding in nonmetalized ZnS photocatalysis is an irreversible two-electron-transfer photoreduction of organic substrates.^[6] A favorable shift of the optical response into the visible region occurs subsequent to the doping of transition metal or rare-earth metal ions, such as Ni²⁺ and Cu²⁺; therefore, ZnS NCs can also be used as effective catalysts for photocatalytic evolution of H₂ and photoreduction of toxic ions under visible-light irradiation.^[7]

An important application of ZnS is as a photocatalyst in environmental protection through the removal of organic

pollutants and toxic water pollutants. ZnS nanomaterials have been used for the photocatalytic degradation of organic pollutants such as dyes, *p*-nitrophenol, and halogenated benzene derivatives in wastewater treatment.^[8] However, the applications of ZnS NCs in photocatalysis are limited to a considerable degree because of the high cost of their large-scale production, coupled with the tremendous difficulties in separation, recovery, and recycling in industrial applications. Nevertheless, the studies have demonstrated that nanoporous materials with high surface-to-volume ratios can be successfully used in various catalysis, environmental engineering, and sensor systems.^[9] Some nanoporous materials with regular shapes such as porous nanowires, nanotubes, spheres, and nanoparticles have been successfully prepared by chemical or physical methods,^[10] most of which use templates that are intrinsically high in cost and with low production yield. Therefore, the development of cost-effective methods suitable for the large-scale synthesis of ZnS nanoporous nanostructures with high catalytic activity and easy separation represents a critical challenge to their practical applications.

Herein, we report a simple procedure for mass production by using a low-cost, self-assembly synthetic route to produce ZnS nanoporous nanoparticles (NPNPs) composed of building blocks comprising hexagonal wurtzite ZnS nanocrystals of several nanometers in diameter. The advantages of the present protocol are: 1) high surface-to-volume ratios with effective prevention of further aggregation of the nanoparticles, so as to retain high catalytic activities; 2) the profitability of size-quantized, nanometer-sized semiconductor particles with higher redox potentials as a result of the increase in band-gap energy (the energy difference between the lowest unoccupied and highest occupied molecular orbitals),^[1,2] which in turn enhances the charge-transfer rates in the system and drastically reduces the volume recombination, that is, radiationless recombination of the electron-hole pair within the semiconductor particle;^[11] 3) easier separation and recycling than those obtainable with common NCs because of the larger diameters of NPNPs; and 4) good dispersity and useful dimension without the requirement of constant stirring or a "dark" reaction for adsorption of substrates. In addition, we demonstrate that the ZnS NPNP is an excellent photocatalyst with higher photodegradation efficiency of eosin B in environmental protection than that of TiO₂ nanoparticles.

ZnS NPNPs were prepared by a facile solution-phase thermal decomposition route in the presence of poly(*N*-vinyl-2-pyrrolidone) (PVP). The fine structural details of ZnS NPNPs were investigated by using TEM. Figure 1a shows a low-magnification TEM image of a ZnS sample, which indicates that the sample is composed of a large quantity of well-dispersed spherical nanoparticles with uniform size and shape. The average size of these particles estimated from the TEM image is about 60 nm, which is in good agreement with the result measured by dynamic light scattering (not shown). A typical scanning electron microscope (SEM) image of the sample is presented in Figure 1b, in which the morphology of spherical nanoparticles is also clearly visible. The surface of every particle is rough and with many smaller particles. The high-magnification TEM image in Figure 1c shows many

[*] J.-S. Hu,^[‡] L.-L. Ren, Y.-G. Guo,^[‡] H.-P. Liang,^[‡] A.-M. Cao,^[‡] Prof. Dr. L.-J. Wan, Prof. Dr. C.-L. Bai
Institute of Chemistry
Chinese Academy of Sciences (CAS)
Beijing 100080 (China)
Fax: (+86) 10-6255-8934
E-mail: wanlijun@iccas.ac.cn
clbai@iccas.ac.cn

[‡] Also in the Graduate School of the CAS, Beijing (China)

[**] This work was supported by the National Natural Science Foundation of China (Nos. 20025308 and 20177025), the National Key Project on Basic Research (Grant G2000077501), and the Chinese Academy of Sciences. We thank Dr. L. Jiang for his help in the writing of this manuscript.

Supporting information for this article is available on the WWW under <http://www.angewandte.org> or from the author.

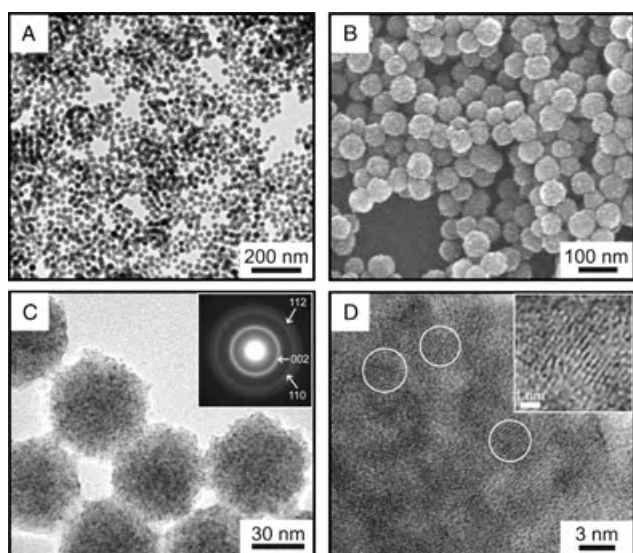


Figure 1. a) Low-magnification TEM image, b) SEM image, c) high-magnification TEM image, and d) HRTEM image of ZnS NPNPs. The inset in (c) is the electron diffraction pattern. The inset in (d) shows the enlarged lattice fringes.

spots with a clear contrast difference in each individual nanoparticle. This observation further confirms that these NPNPs consist of smaller NCs with a size of 3–5 nm which are assembled in a nanoporous structural configuration. A selected-area electron diffraction (ED) pattern of ZnS NPNPs is presented in the inset of Figure 1c. The ED pattern shows a set of concentric rings instead of sharp spots as a result of the small crystallites. The diffraction rings have been indexed to (002), (110), and (112) planes of the hexagonal ZnS phase (JCPDS No. 80-0007). A representative high-resolution TEM (HRTEM) image of ZnS NPNPs in Figure 1d, with an inset image taken on the outside of the particles, shows the lattice fringes of nanocrystals in nanoparticles with a spacing of 0.31 nm, which corresponds to an interplanar distance of the (002) plane of hexagonal ZnS.

The XRD patterns shown in Figure 2 are for ZnS NPNPs obtained at 150 and 180 °C. The diffraction patterns of the two samples are very similar and are in good agreement with hexagonal ZnS (space group: $P6_3/m$ (186)) with lattice constants $a = 3.777$ and $b = 6.188$ Å (JCPDS No. 80-0007). This result illustrates that a heating temperature of 150 °C is sufficient to produce a high-temperature-stable hexagonal ZnS phase in this system. The significant broadening of the diffraction peaks is ascribed to the very small crystallite size within ZnS NPNPs, similar to the case reported in the literature.^[12] Moreover, energy-dispersive X-ray (EDX) analysis of ZnS NPNPs (see the Supporting Information) shows two peaks for the elements Zn and S, in addition to the C, O, and Cu derived from the carbon-coated copper TEM grid. These observations show the product is composed of hexagonal ZnS.

Brunauer–Emmett–Teller (BET) gas sorptometry measurements were conducted to examine the porous nature of the ZnS NPNPs. Figure 3 shows the N_2 adsorption/desorption isotherm and the pore-size distribution (inset) of ZnS NPNPs.

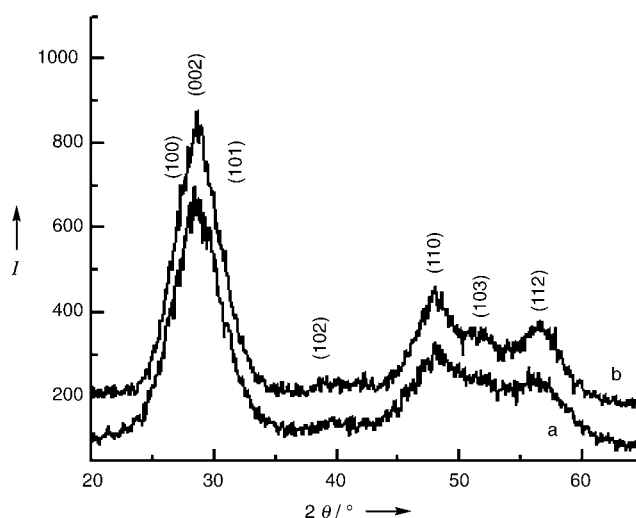


Figure 2. X-ray diffraction pattern of ZnS NPNPs acquired at a) 150 °C and b) 180 °C.

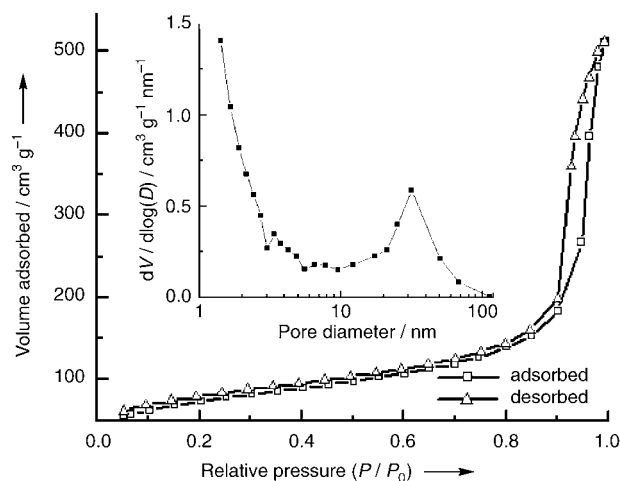


Figure 3. Nitrogen adsorption/desorption isotherm and Barrett–Joyner–Halenda (BJH) pore size distribution plot (inset) of ZnS NPNPs.

The isotherms are identified as type IV, which is characteristic of mesoporous materials. The pore-size distribution obtained from the isotherm indicates a number of pores less than 5 nm in the sample. These pores presumably arise from the spaces among the small nanocrystallites within a ZnS NPNP. The large pores of around 30 nm are attributed to the interparticle spaces. The sharp distribution of the mesopores around 30 nm suggests that the NPNPs have high monodispersity. The BET specific surface area of the sample was calculated from N_2 isotherms at -196.6 °C, and was found to be as much as about 156.1 m² g⁻¹. The single-point total volume of pores at $P/P_0 = 0.9926$ was 0.59 cm³ g⁻¹. The extremely high BET surface area and large total pore volume strongly support the fact that the nanoparticles have a nanoporous structure.

In a series of further experiments we discovered that PVP not only contributed to stabilizing the NPNP assembly but also exerted vigorous control over the formation of the spherical geometry. If no PVP was in the reaction solution,

the small nanoparticles generated initially by the decomposition of complex precursors tended to rapidly aggregate in a random manner, thus leading to the formation of an agglomerate cross-linked by numerous irregular particles (see the Supporting Information). As such, no distinct spherical nanoparticles could be observed. The addition of PVP into the reaction system at a molar ratio of PVP to zinc precursor of 0.04:1 resulted in the sample being mainly composed of spherical particles with plenty of defects that were only partially cross-linked. This finding indicates that the initial nanoparticles tend to assemble into spherical aggregates in the presence of PVP, and any further agglomeration is essentially inhibited by PVP. An increase in the amount of PVP improved the ability to form spherical aggregates and effectively prevented the aggregates from agglomeration. In a typical example in which the molar ratio of PVP to zinc was increased to 0.08, the sample consisted substantially of nanoparticles with regular spherical shape. Therefore, it is clear from the formation process that each spherical particle was produced by aggregation of many smaller nanometer-scale crystallites with a diameter of about 3–5 nm. These spherical nanoparticles were well-separated and had uniform size and shape, such as those shown in Figure 1 a and b.

ZnS has been used as a semiconductor-type photocatalyst for the photoreductive dehalogenation of halogenated benzene derivatives, photocatalytic degradation of water pollutants, and photocatalytic reduction of toxic metal ions.^[4–7] To demonstrate the potential applicability of the present ZnS NPNPs in these applications we investigated their photocatalytic activity relative to those of ZnS NCs prepared by a literature method^[4e] and of a commercial photocatalyst (Degussa P25 titania), with the photocatalytic degradation of eosin B as a test reaction. The characteristic absorption of eosin B at 517 nm was chosen as the monitored parameter for the photocatalytic degradation process. Figure 4 shows the

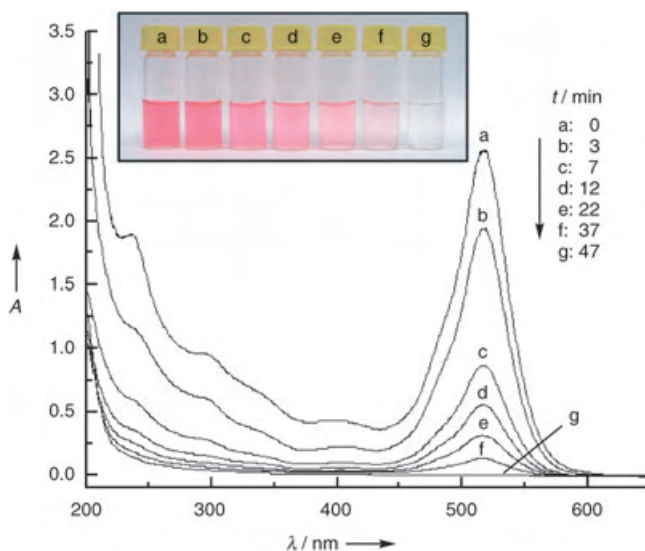


Figure 4. Absorption spectrum of a solution of eosin B (5.0×10^{-5} M, 30 mL) in the presence of ZnS NPNPs (10 mg) under exposure to UV light.

absorption spectrum of an aqueous solution of eosin B (initial concentration: 5.0×10^{-5} M, 30 mL) in the presence of ZnS NPNPs (10 mg) under exposure to UV light for various durations. The absorption peaks corresponding to the eosin B molecule, such as the sharp peak at 517 nm, diminish gradually as the exposure time increases and completely disappear after about 40 minutes. No new absorption bands appear in either the visible or ultraviolet regions, which indicates the complete photodegradation of eosin B. The color-change sequence in the sample during this process is shown in the inset of Figure 4, from which it is clear that the intense pink color of the starting solution gradually disappears with increasingly longer exposure times.

A further comparative experiment was carried out to investigate the catalytic activity. The solution of eosin B was subjected to a series of experimental conditions: a) with Degussa P25 titania (10 mg), in the dark; b) without catalyst, with UV light; c) with ZnS NCs (10 mg), in the dark; d) with ZnS NPNPs (10 mg), in the dark; e) with Degussa P25 titania (10 mg) and UV light; f) with ZnS NCs (10 mg) and UV light; and g) with ZnS NPNPs (10 mg) and UV light. The results are illustrated in Figure 5. Under the experimental conditions

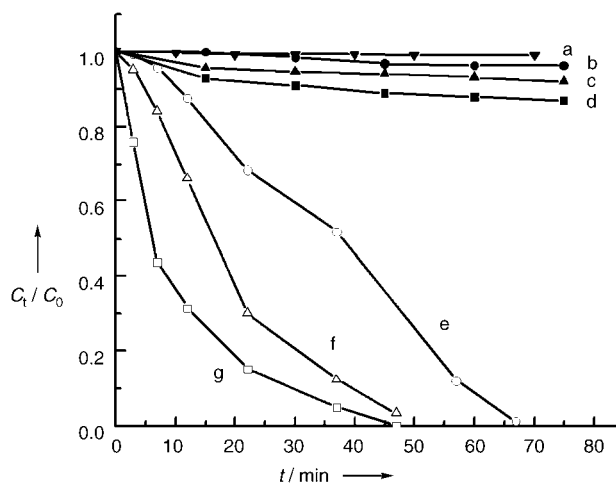


Figure 5. Photodegradation of eosin B (5.0×10^{-5} M, 30 mL) under different conditions: a) with Degussa P25 titania (10 mg), in the dark; b) without any catalyst, with UV light; c) with ZnS NCs (10 mg), in the dark; d) with ZnS NPNPs (10 mg), in the dark; e) with Degussa P25 titania (10 mg) and UV light; f) with ZnS NCs (10 mg) and UV light; g) with ZnS NPNPs (10 mg) and UV light.

from (a) to (d), the photocatalytic effect on the solution degradation without catalysts but under exposure to UV light is almost the same as that with catalyst but no exposure to UV light. For example, a slight decrease in the concentration of eosin B was detected in the absence of any catalyst (curve b). Exposure to UV light for 1.5 h resulted in only 5% degradation of this compound. A slight decrease in the concentration of eosin B took place in the presence of ZnS NPNPs (curve d) and ZnS NCs (curve c) in the dark, compared to that in the presence of Degussa P25 (curve a) in the dark. This decrease may be mainly ascribed to the adsorption of eosin B on the porous nanostructures, although without exposure to UV light. The concentration of he

eosin B solution hardly changed after mixing the solution with catalysts for 15 minutes, which indicates that the adsorption of eosin B on nanostructured catalysts reached an equilibrium state. However, from the data in curves e (Degussa P25), f (ZnS NCs), and g (ZnS NPNPs), it is clearly seen that, under identical conditions with exposure to UV light, the ZnS NPNP photocatalyst shows much greater activity than that of Degussa P25 or ZnS NCs. The degradation of eosin B in the ZnS NPNPs follows first-order kinetics. Exposure of the solution of eosin B to UV light for about 40 minutes resulted in complete decolorization. This difference in the photocatalytic activity between ZnS NPNPs and Degussa P25 can be explained by the larger specific surface area of the former (ca. $156.1 \text{ m}^2 \text{ g}^{-1}$ versus Degussa P25 powder ca. $45 \text{ m}^2 \text{ g}^{-1}$), and hence the stronger adsorption of the ZnS NPNPs to the molecules of eosin B. The photocatalytic superiority of ZnS NPNPs over ZnS NCs may be influenced by the unwanted aggregation of ZnS NCs during the reaction, which leads to a rapid decrease in the active surface area, while ZnS NPNPs maintain an excellent porous nanostructure and are effectively prevented from aggregating. A more detailed understanding of the photocatalytic activity of ZnS NPNPs is currently under way.

In conclusion, we have developed a simple and robust method to produce ZnS nanoporous nanoparticles on a large scale. These NPNPs are uniform spheres, monodispersed in size at around 60 nm in diameter, and are formed by a self-assembly process of hexagonal ZnS nanocrystals of 3–5-nm size as building blocks. They possess a specific surface area on the order of $156 \text{ m}^2 \text{ g}^{-1}$, which leads to substantially more effective photocatalytic performance compared to that of Degussa P25 titania or ZnS NCs, as demonstrated in the photodegradation of eosin B at ambient temperature. A combination of their unique features of high surface-to-volume ratios, monodispersion, and rich photocatalytic and luminescent properties suggests that these ZnS NPNPs will find many interesting applications in semiconductor photocatalysis, inorganic light-emitting diodes (ILEDs), solar cells, environmental remediation, and nanodevices.

Experimental Section

Preparation of ZnS NPNPs: Zinc acetate, thiourea, and ethylene glycol were obtained from Beijing Chemical Reagent Ltd., China, in the highest purity and used directly without further purification. Poly(*N*-vinyl-2-pyrrolidone) (PVP, $M_w = 58000$) was obtained from Sigma-Aldrich Chemical Co., USA. Ultrapure water with a resistivity of $18.2 \text{ M}\Omega \text{ cm}$, produced by using a Milli-Q apparatus (Millipore), was used in all the experiments. ZnS NPNPs were produced by a precursor thermolysis route in the presence of ethylene glycol as the reaction medium. In a typical experiment, zinc acetate (6 mmol) and thiourea (12 mmol) were dissolved in ethylene glycol (150 mL). PVP (4.8 g) was then added to the solution with stirring and, after its complete dissolution, the clear solution was heated to 150°C . After about 10 min the solution turned milky white, which indicated the initial formation of ZnS nanocrystals. The mixture was maintained at $150 \pm 5^\circ\text{C}$ for 3 h and the color of the reaction solution became milky white mixed with light yellow. The ZnS NPNPs obtained were separated from the reaction mixture by centrifugation, and washed several times with ultrapure water and ethanol to remove the

impurities and PVP. Finally, the ZnS NPNPs were dried in a vacuum oven (ca. 0.1 MPa) for 6 h prior to being characterized.

Preparation of ZnS NCs: ZnS nanocrystallites were prepared by using the method described in the literature.^[4c] Briefly, the ZnS NC samples were prepared in an argon atmosphere by mixing equal amounts of aqueous 0.05 M solutions of ZnSO_4 and Na_2S in an ice bath with stirring. TEM images showed that the so-prepared ZnS NCs had a diameter ranging from 3 to 5 nm, and easily aggregated.

Characterization: For TEM observation, the samples were redispersed in water or ethanol by ultrasonic treatment and dropped on carbon-copper grids. TEM images were collected by using a JEOL JEM 2010F microscope working at 200 kV and equipped with an energy-dispersive X-ray analyzer (Phoenix). A Hitachi S-4300F scanning electron microscope (SEM) was used to investigate the morphology of the hollow spheres.

X-ray powder diffraction (XRD) measurements were carried out with a Rigaku D/max-2500 instrument using filtered $\text{Cu}_{K\alpha}$ radiation. The nitrogen adsorption and desorption isotherms at 77 K were measured using a Micrometrics ASAP 2010 system after the sample was degassed in vacuum at 130°C overnight. A Shimadzu UV-1601PC spectrophotometer was used to record the UV/Vis spectra of various samples.

Photocatalytic activity measurement: A cylindrical pyrex flask (capacity ca. 40 mL) was used as the photoreactor vessel. The reaction system containing eosin B ($\text{C}_{20}\text{H}_6\text{Br}_2\text{N}_2\text{Na}_2\text{O}_9$, Sigma-Aldrich Chemical Co.; $5.0 \times 10^{-5} \text{ M}$, 30 mL) and ZnS NPNP catalyst (10 mg) was magnetically stirred in the dark for 15 min to reach the adsorption equilibrium of eosin B with the catalyst, and then exposed to light from a Philips HPK high-pressure Hg lamp (125 W). Commercial TiO_2 (Degussa P25, Degussa Co.) was adopted as the reference with which to compare the photocatalytic activity under the same experimental conditions. UV/Vis absorption spectra were recorded at different intervals to monitor the reaction.

Received: September 21, 2004

Published online: January 14, 2005

Keywords: nanostructures · photocatalysis · self-assembly · semiconductors · zinc

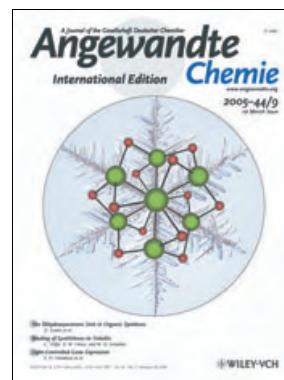
- [1] a) M. R. Hoffmann, S. T. Martin, W. Choi, D. W. Bahnemann, *Chem. Rev.* **1995**, 95, 69–96; b) M. Anpo, M. Takeuchi, *J. Catal.* **2003**, 216, 505–516.
- [2] a) I. Salem, *Catal. Rev. Sci. Eng.* **2003**, 45, 205–296; b) A. L. Linsebigler, G. Lu, J. T. Yates, Jr., *Chem. Rev.* **1995**, 95, 735–758.
- [3] a) S. Yanagida, K. Mizumoto, C. J. Pac, *J. Am. Chem. Soc.* **1986**, 108, 647–654; b) S. Yanagida, T. Azuma, Y. Midori, C. J. Pac, H. Sakurai, *J. Chem. Soc. Perkin Trans. 2* **1985**, 1487–1493; c) W. F. Shangguan, A. Yoshida, *J. Phys. Chem. B* **2002**, 106, 12227–12230; d) G. Q. Guan, T. Kida, K. Kusakabe, K. Kimura, X. M. Fang, T. L. Ma, E. Abe, A. Yoshida, *Chem. Phys. Lett.* **2004**, 385, 319–322.
- [4] a) H. Fujiwara, H. Hosokawa, K. Murakoshi, Y. Wada, S. Yanagida, *Langmuir* **1998**, 14, 5154–5159; b) A. Koca, M. Sahin, *Int. J. Hydrogen Energy* **2002**, 27, 363–367.
- [5] a) S. Yanagida, H. Kawakami, Y. Midori, H. Kizumoto, C. J. Pac, Y. Wada, *Bull. Chem. Soc. Jpn.* **1995**, 68, 1811–1823; b) M. Kanemoto, T. Shiragami, C. J. Pac, S. Yanagida, *J. Phys. Chem.* **1992**, 96, 3521–3526; c) T. Shiragami, H. Ankyu, S. Fukami, C. J. Pac, S. Yanagida, H. Mori, H. Fujita, *J. Chem. Soc. Faraday Trans.* **1992**, 88, 1055–1061; d) S. Marinković, N. Hoffmann, *Eur. J. Org. Chem.* **2004**, 3102–3107; e) G. Hörner, P. John, R. Kunne, G. Twardzik, H. Roth, T. Clark, H. Kisch, *Chem. Eur. J.* **1999**, 5, 208–217.
- [6] a) S. Yanagida, Y. Ishimaru, Y. Miyake, T. Shiragami, C. J. Pac, K. Hashimoto, T. Sakata, *J. Phys. Chem.* **1989**, 93, 2576–2582;

- b) S. Yanagida, H. Kizumoto, Y. Ishimaru, C. J. Pac, H. Sakurai, *Chem. Lett.* **1985**, 141.
- [7] a) I. Tsuji, A. Kudo, *J. Photochem. Photobiol. A* **2003**, *156*, 249–252; b) A. Kudo, M. Sekizawa, *Catal. Lett.* **1999**, *58*, 241–243; c) A. Kudo, M. Sekizawa, *Chem. Commun.* **2000**, 1371–1372; d) O. Hamanoi, A. Kudo, *Chem. Lett.* **2002**, 838–839.
- [8] a) J. Dai, Z. Jiang, W. Li, G. Bian, Q. Zhu, *Mater. Lett.* **2002**, *55*, 383–387; b) H. Yin, Y. Wada, T. Kitamura, S. Yanagida, *Environ. Sci. Technol.* **2001**, *35*, 227–231; c) C. L. Torres-Martínez, R. Kho, O. I. Mian, R. K. Mehra, *J. Colloid Interface Sci.* **2001**, *240*, 525–531; d) Y. Wada, H. Yin, T. Kitamura, S. Yanagida, *Chem. Commun.* **1998**, 2683–2684; e) X. Wang, S. O. Pehkonen, A. K. Ray, *Ind. Eng. Chem. Res.* **2004**, *43*, 1665–1672.
- [9] a) J. C. Yu, L. Zhang, Z. Zheng, J. Zhao, *Chem. Mater.* **2003**, *15*, 2280–2286; b) D. M. Antonelli, J. Y. Ying, *Angew. Chem.* **1995**, *107*, 2202–2206; *Angew. Chem. Int. Ed. Engl.* **1995**, *34*, 2014–2017; c) Y. Ding, M. Chen, J. Erlebacher, *J. Am. Chem. Soc.* **2004**, *126*, 6876–6877; d) Y. L. Wang, X. C. Jiang, Y. N. Xia, *J. Am. Chem. Soc.* **2003**, *125*, 16176–16177.
- [10] a) X. D. Wang, C. J. Summers, Z. L. Wang, *Adv. Mater.* **2004**, *16*, 1215–1218; b) C. X. Ji, P. C. Searson, *J. Phys. Chem. B* **2003**, *107*, 4494–4499; c) F. Li, J. He, W. L. Zhou, J. B. Wiley, *J. Am. Chem. Soc.* **2003**, *125*, 16166–16167; d) D. G. Shchukin, R. A. Caruso, *Chem. Mater.* **2004**, *16*, 2287–2292; e) J. Jiang, A. Kucernak, *Chem. Mater.* **2004**, *16*, 1362–1367; f) K. Suzuki, K. Ikari, H. Imai, *J. Am. Chem. Soc.* **2004**, *126*, 462–463.
- [11] Z. Zhang, C. C. Wang, R. Zakaria, J. Y. Ying, *J. Phys. Chem. B* **1998**, *102*, 10871–10878.
- [12] a) Y. Zhao, Y. Zhang, H. Zhu, G. C. Hadjipanayis, J. Q. Xiao, *J. Am. Chem. Soc.* **2004**, *126*, 6874–6875; b) J. Nanda, S. Sapra, D. D. Sarma, N. Chandrasekharan, G. Hodes, *Chem. Mater.* **2000**, *12*, 1018–1024.

Cover Picture

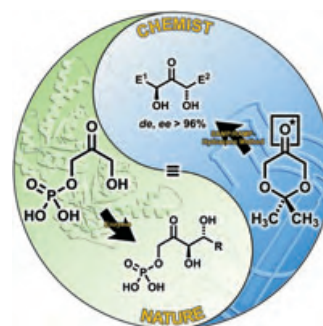
Emma J. Brown, Anne-K. Duhme-Klair,* Matthew I. Elliott, Jane E. Thomas-Oates, Phillipa L. Timmins, and Paul H. Walton*

Peroxide is frozen in perfect symmetry, which if viewed down the principle axis, resembles that of the snowflake in the cover-picture background. An unprecedented μ_6 peroxide coordination mode is found in an octanuclear nickel complex with near S_6 symmetry (core shown in foreground; green Ni, red O). The encapsulation of the peroxide by the nickel cage stabilizes this reactive species. For more details see the Communication by A.-K. Duhme-Klair, P. H. Walton, and co-workers on page 1392 ff. (Background picture reproduced with permission from Prof. K. G. Libbrecht, Caltech.)



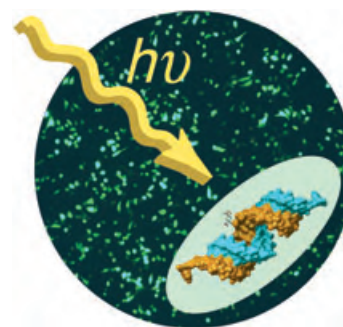
Synthetic Methods

In their Review on page 1304 ff., D. Enders et al. show how broad the scope of application of the biologically important dihydroxyacetone unit has become in organic synthesis through the development of synthetic equivalents of the natural building block.



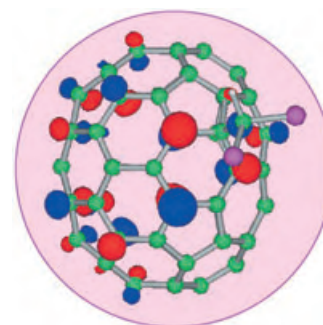
RNA Interference

S. H. Friedman and co-workers demonstrate in their Communication on page 1328 ff. that the process of RNA interference can be controlled by using light. Irradiation of siRNAs modified with photolabile groups deprotects them and releases fully active siRNA.



Fullerenes

In their Communication on page 1398 ff., T. Kitagawa, K. Komatsu, and co-workers report the generation and spectroscopic observation of the first functionalized C_{70} cation, $[\text{CHCl}_2\text{-}C_{70}]^+$, and a quantitative evaluation of its thermodynamic stability.





The following Communications have been judged by at least two referees to be “very important papers” and will be published online at www.angewandte.org soon:

Paul J. Goldsmith, Simon J. Teat, Simon Woodward*
Enantioselective Preparation of β,β -Disubstituted α -Methylenepropionates by Methylaluminoxane Promotion of the Zinc Schlenk Equilibrium

Holger Braunschweig,* Krzysztof Radacki, David Scheschkewitz, George R. Whittell
Boron as a Bridging Ligand

Rimane Aoun, Jean-Luc Renaud, Pierre H. Dixneuf, Christian Bruneau*
Concomitant Monoreduction/Hydrogenation of Unsaturated Cyclic Imides to Lactams Catalyzed by Ruthenium Precursors

M. Maue, T. Schrader*
A Color Sensor for Catecholamines

Stuart L. Schreiber,* Chuo Chen, Xiaodong Li, Christopher S. Neumann, Michael M.-C. Lo
Convergent Diversity-Oriented Synthesis of Small-Molecule Hybrids

Ralf Haiges,* Jerry A. Boatz, Robert Bau, Stefan Schneider, Thorsten Schroer, Muhammed Yousufuddin, Karl O. Christe
Polyazide Chemistry: The First Binary Group 6 Azides, $\text{Mo}(\text{N}_3)_6$, $\text{W}(\text{N}_3)_6$, $[\text{Mo}(\text{N}_3)_7]^-$, and $[\text{W}(\text{N}_3)_7]^-$ and the $[\text{NW}(\text{N}_3)_4]^-$ and $[\text{NMo}(\text{N}_3)_4]^-$ Ions

Web Sites

<http://www.scirus.com>

Search Engines for Publications on the Internet

R. Wallenwein _____ 1292 – 1293

Books

Polymer Brushes

Rigoberto C. Advincula, William J. Brittain, Kenneth C. Caster, Jürgen Rühle

reviewed by J. v. Hest _____ 1294

Homogeneous Catalysis

Piet W. N. M. van Leeuwen

reviewed by A. Zapf _____ 1295

Multimetallic Catalysts in Organic Synthesis

Masakatsu Shibasaki
 Yoshinori Yamamoto

reviewed by B. Kreidler _____ 1295

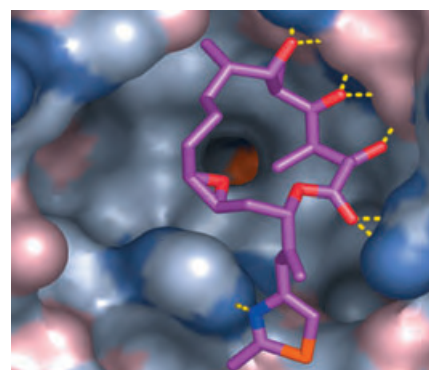
Highlights

Epothilone

D. W. Heinz,* W.-D. Schubert, G. Höfle* _____ 1298 – 1301

Much Anticipated—The Bioactive Conformation of Epothilone and Its Binding to Tubulin

Filled pockets: Epothilones initiate apoptosis in eukaryotic cells by inducing extensive polymerization of $\alpha\beta$ -tubulin. Until recently, little was known about the binding mode of epothilones within the tubulin binding cavity. The structure of the epothilone A/tubulin complex (see picture) determined by electron crystallography has dramatically reversed the situation.

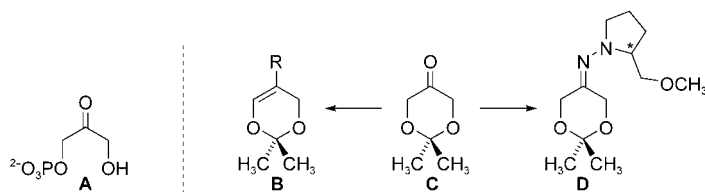


Reviews

Asymmetric Synthesis

D. Enders,* M. Voith,
A. Lenzen _____ 1304–1325

The Dihydroxyacetone Unit—A Versatile
C₃ Building Block in Organic Synthesis



Dihydroxyacetone phosphate (DHAP, A) plays a pivotal role in nature as a C₃ building block. Synthetic equivalents of DHAP, such as **C** and **D**, have been developed in recent years and applied

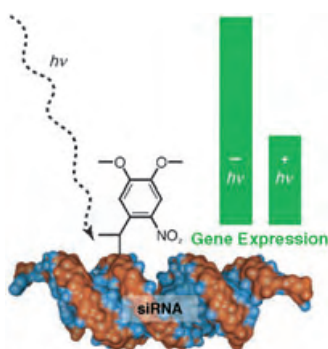
successfully in synthesis. Furthermore, 1,3-dioxins **B** derived from **C** can be used as equivalents of 2-substituted acrolein derivatives.

Communications

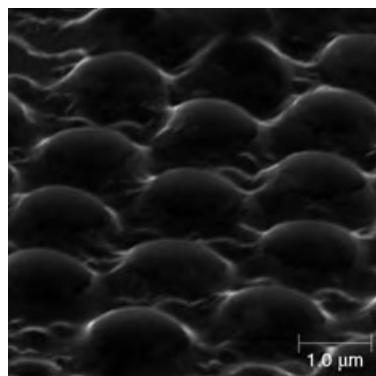
Gene Expression

S. Shah, S. Rangarajan,
S. H. Friedman* _____ 1328–1332

Light-Activated RNA Interference



Light-controlled gene expression: Cellular mRNA levels that are regulated by the RNA interference pathway can now be controlled with light. The modification of small interfering RNA (siRNA) with photolabile moieties can partially or fully block RNA interference, depending on the extent of siRNA modification. Upon irradiation, siRNA is released (see picture). Now in its active state, it is able to suppress target gene expression.



Light through a lens: 2D microlens arrays composed of temperature- and pH-responsive poly(*N*-isopropylacrylamide-co-acrylic acid) microgels assembled on Au nanoparticles have been prepared (see SEM image). Optical properties of the arrays can be modulated locally and reversibly in response to illumination with a Nd:YAG laser.

Micro-optics

J. Kim, M. J. Serpe,
L. A. Lyon* _____ 1333–1336

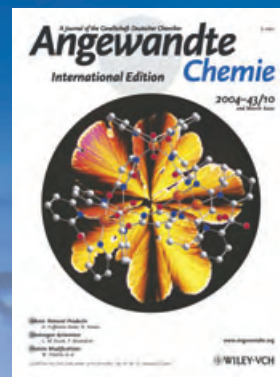
Photoswitchable Microlens Arrays

For the USA and Canada:
ANGEWANDTE CHEMIE International Edition (ISSN 1433-7851) is published weekly by Wiley-VCH PO Box 191161, D 69451 Weinheim, Germany. Air freight and mailing in the USA by Publications Expediting Inc. 200 Meacham Ave., Elmont, NY 11003. Periodicals

postage paid at Jamaica NY 11431. US POSTMASTER: send address changes to *Angewandte Chemie*, Wiley-VCH, 111 River Street, Hoboken, NJ 07030. Annual subscription price for institutions: US\$ 4948.00/4498.00 (valid for print and electronic / print or electronic delivery); for individuals who are personal members of a

national chemical society, or whose institution already subscribes, or who are retired or self-employed consultants, print only: US\$ 394.00. Postage and handling charges included. All Wiley-VCH prices are exclusive VAT.

The best in chemistry – for more than a hundred years



A Journal of the Gesellschaft Deutscher Chemiker
**Angewandte
Chemie**
International Edition

www.angewandte.org

1888: The beginning
of a success story

Constant Innovations

- 1962:** First issue of the International Edition
- 1976:** Graphical abstracts
- 1979:** Cover pictures
- 1988:** Centenary of Angewandte
- 1989:** Routine use of color
- 1991:** New section: Highlights
- 1992:** Computerized editorial tracking system
- 1995:** Internet service for readers
- 1998:** Regular press service; full-text online
- 2000:** New section: Essays; EarlyView: Communications available online ahead of the printed version
- 2001:** New section: Minireviews
- 2002:** Online submission of manuscripts
- 2003:** Weekly publication; new section: News; new layout
- 2004:** Backfiles (1962-1997); ManuscriptXpress: Online system for authors and referees



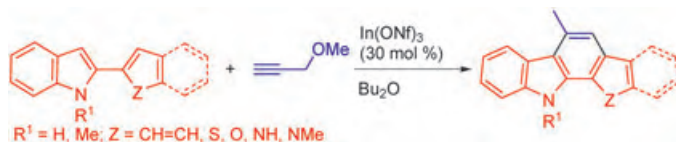
Angewandte's advisors...

Daniel Bellus
Ciba Specialty Chemicals,
Basel

» For the past thirty years **Angewandte Chemie** has continued to be my primary source of inspiration and self-education. In each new issue I find a real gem of chemistry, capable of further nurturing the innovation process. It is my pleasure to inject my industrial R&D experience into the International Advisory Board.«

Angewandte Chemie International Edition is
a journal of the German Chemical Society (GDCh)





Indoles and indium: An indium salt catalyzes the assembly of 2-arylindoles and propargyl ethers into diverse aryl- and heteroaryl-annulated[*a*]carbazoles in a

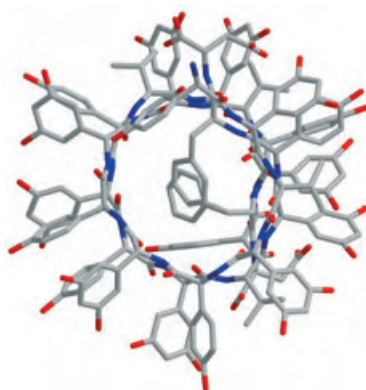
highly regioselective manner, in which two different modes of carbon–carbon bond-forming reactions are successfully incorporated in one step (see scheme).

Synthetic Methods

T. Tsuchimoto,* H. Matsubayashi,
M. Kaneko, E. Shirakawa,*
Y. Kawakami _____ **1336–1340**

Easy Access to Aryl- and Heteroaryl-Annulated[*a*]carbazoles by the Indium-Catalyzed Reaction of 2-Arylindoles with Propargyl Ethers

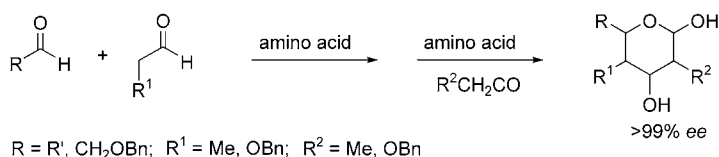
The double-helical structure adopted by the antiviral peptide feglymycin (see picture) is reminiscent of that of gramicidin, but feglymycin is more likely to function as an ion carrier than as a membrane channel. With more than 1000 unique atoms this is the largest equal-atom crystal structure solved by ab initio direct methods.



Peptide Structure Elucidation

G. Bunkóczi, L. Vértessy,
G. M. Sheldrick* _____ **1340–1342**

The Antiviral Antibiotic Feglymycin: First Direct-Methods Solution of a 1000+ Equal-Atom Structure



Back to the future: In a biomimetic asymmetric synthesis of sugars (see scheme) sequential cross-aldol reactions of simple aldehydes were catalyzed by amino acids. Deoxysugars were obtained with excellent chemoselectivity and up to

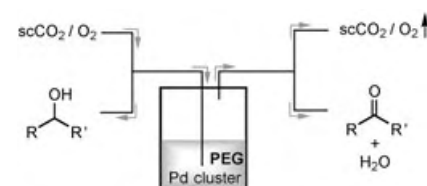
> 99% *ee*. This transformation may implicate a prebiotic catalytic pathway in which amino acids transferred their stereochemical information to carbohydrates.

Carbohydrate Synthesis

J. Casas, M. Engqvist, I. Ibrahim,
B. Kaynak, A. Córdova* _____ **1343–1345**

Direct Amino Acid Catalyzed Asymmetric Synthesis of Polyketide Sugars

Active, selective, and stable: The combination of poly(ethylene glycol) (PEG) as a catalyst phase and supercritical carbon dioxide (scCO₂) as a mobile phase provides a “green” approach to the continuous-flow aerobic oxidation of primary and secondary alcohols by catalytically active palladium nanoparticles (see scheme). The activity of the system even slightly increases with reaction time,



because CO₂ appears to improve the dispersion of the Pd particles in the PEG matrix.

Multiphase Catalysis

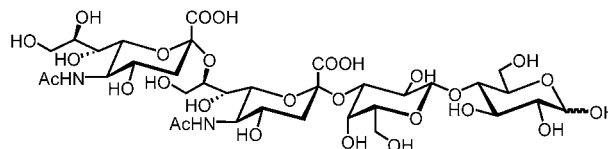
Z. Hou, N. Theyssen, A. Brinkmann,
W. Leitner* _____ **1346–1349**

Biphasic Aerobic Oxidation of Alcohols Catalyzed by Poly(ethylene glycol)-Stabilized Palladium Nanoparticles in Supercritical Carbon Dioxide

Oligosaccharide Biosynthesis

T. Antoine, A. Heyraud, C. Bosso,
E. Samain* 1350–1352

Highly Efficient Biosynthesis of the Oligosaccharide Moiety of the GD3 Ganglioside by Using Metabolically Engineered *Escherichia coli*



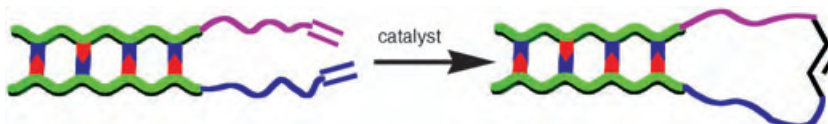
Express order for oligosaccharides: A microbiological process for the synthesis of the carbohydrate portion of gangliosides GD3 and GT3 is described (see structure). Lactose and sialic acid are

used as exogenous precursors by a metabolically engineered *Escherichia coli* strain that overexpresses the bifunctional sialyltransferase *cstII* gene from *Campylobacter jejuni*.

Olefin Metathesis

X. Yang, B. Gong* 1352–1356

Template-Assisted Cross Olefin Metathesis



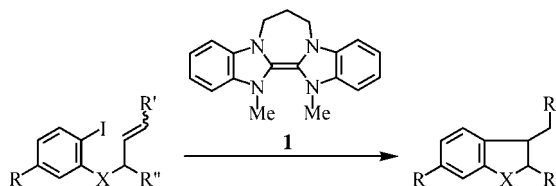
Making ends meet: Alkene units tethered to two complementary oligoamide strands, which pair sequence-specifically into hydrogen-bonded duplexes, undergo

intermolecular cross-metathesis when the two alkene moieties are in close proximity upon heating in the presence of Grubbs' catalyst (see graphic).

Synthetic Methods

J. A. Murphy,* T. A. Khan, S.-z. Zhou,
D. W. Thomson, M. Mahesh 1356–1360

Highly Efficient Reduction of Unactivated Aryl and Alkyl Iodides by a Ground-State Neutral Organic Electron Donor



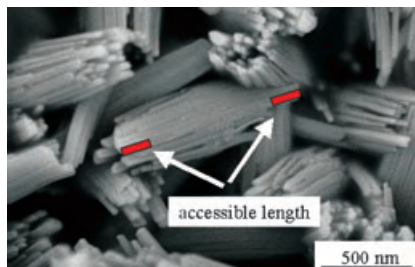
Electron-transfer reductions of unactivated aryl and alkyl iodides with a neutral ground-state organic molecule are reported. The reducing agent **1** is formed in two

steps from *N*-methylbenzimidazole using very simple chemistry, and subsequent treatment of the iodoalkane or -arene with **1** affords cyclized products (see scheme).

Zeolites

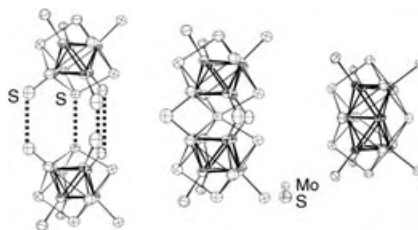
S. van Donk, J. H. Bitter,*
A. Verberckmoes, M. Versluijs-Helder,
A. Broersma, K. P. de Jong 1360–1363

Physicochemical Characterization of Porous Materials: Spatially Resolved Accessibility of Zeolite Crystals



Blocked pores: Hydrocarbon diffusion and coke profile measurements were used to study zeolite pore accessibility. For mordenite crystals the accessible length of the micropores (red bars in picture) is as low as 30% of the value expected from the crystal size. New analysis strategies are advocated for micro- and mesoporous materials, for which the performance in adsorption, separation, and catalysis is strongly affected by accessibility.

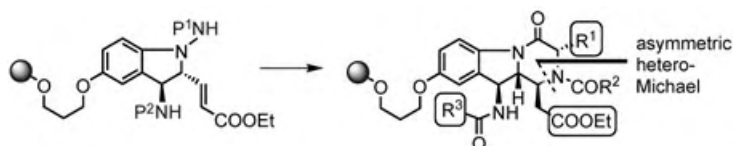
New structural type: The three-dimensional Mo–S framework of the solid-state compound $\text{Ba}_4\text{Mo}_{12}\text{S}_{18}$ contains the novel dimeric $(\text{Mo}_6)_2\text{S}_{24}$ unit (picture, middle). This can be regarded as the result of fusing two octahedral Mo_6S_{14} units (left) and as the intermediate step towards formation of the bi-octahedral Mo_9S_{17} unit (right). $\text{Ba}_4\text{Mo}_{12}\text{S}_{18}$ was found to be a superconductor with a transition temperature of 7 K.



Ternary Molybdenum Sulfide

D. Salloum, R. Gautier, M. Potel,
P. Gougeon* 1363–1365

$\text{Ba}_4\text{Mo}_{12}\text{S}_{18}$: A Superconductor Containing the Dimeric Unit $(\text{Mo}_6)_2\text{S}_{24}$, the Missing Link between the Mo_6S_{14} and Mo_9S_{17} Units



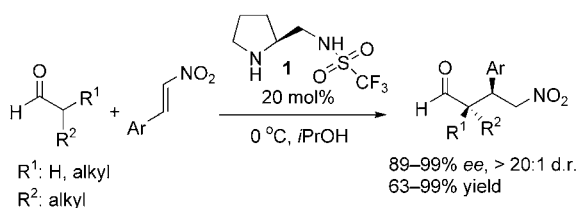
A library of tricyclic derivatives, similar to indoline alkaloids, has been generated by using a stereocontrolled, conjugate hetero-Michael approach in both the solution and the solid phase (see scheme;

P = protecting group, R = functional group). The mild reaction conditions that lead to the tricyclic derivatives, which contain β -amino acid functionalities, are highly attractive.

Combinatorial Chemistry

Z. Gan, P. T. Reddy, S. Quevillon,
S. Couve-Bonnaire, P. Arya* 1366–1368

Stereocontrolled Solid-Phase Synthesis of a 90-Membered Library of Indoline-Alkaloid-like Polycycles from an Enantioenriched Aminoindoline Scaffold



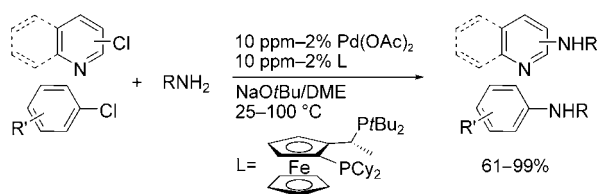
Just can't get enough: The highly versatile pyrrolidine sulfonamide organocatalyst **1**, which has been used in α -aminooxylation and Mannich-type reactions, also medi-

ates diastereo- and enantioselective Michael addition reactions of aldehydes and ketones to nitroolefins (see scheme).

Asymmetric Organocatalysis

W. Wang,* J. Wang, H. Li 1369–1371

Direct, Highly Enantioselective Pyrrolidine Sulfonamide Catalyzed Michael Addition of Aldehydes to Nitroolefins



Resisting pathways for decomposition followed by palladium complexes of monodentate ligands is one characteristic of the highly reactive but long-lived catalyst generated from the Josiphos ligand L

and palladium. It catalyzes under mild conditions the coupling of primary amines with chloropyridines and chloroarenes in high yield with low catalyst loadings (see scheme).

Arene–Amine Coupling

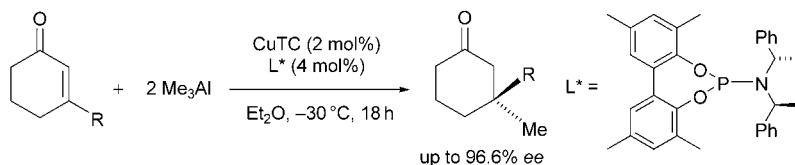
Q. Shen, S. Shekhar, J. P. Stambuli,
J. F. Hartwig* 1371–1375

Highly Reactive, General, and Long-Lived Catalysts for Coupling Heteroaryl and Aryl Chlorides with Primary Nitrogen Nucleophiles

Asymmetric Synthesis

M. d'Augustin, L. Palais,
A. Alexakis* _____ **1376–1378**

Enantioselective Copper-Catalyzed
Conjugate Addition to Trisubstituted
Cyclohexenones: Construction of
Stereogenic Quaternary Centers



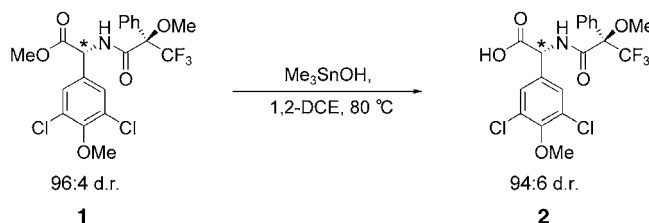
Trimethyl- and triethylaluminum undergo enantioselective conjugate addition to 3- and 2-substituted cyclohexenones in the presence of catalytic amounts of a Cu salt and a phosphoramidite ligand L^* (see

scheme). Thus, chiral quaternary centers can be built with up to 96.6% *ee*. Functionalized enones lead to bicyclic structures by a subsequent aldol reaction.

Synthetic Methods

K. C. Nicolaou,* A. A. Estrada, M. Zak,
S. H. Lee, B. S. Safina _____ **1378–1382**

A Mild and Selective Method for the
Hydrolysis of Esters with Trimethyltin
Hydroxide



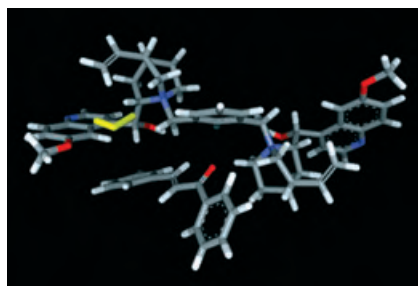
Mild, selective, and efficient: A new method that involves the use of trimethyltin hydroxide for the hydrolysis of specific ester groups allows chemists to steer clear of unwanted elimination reactions and epimerizations. For example,

the conversion of ester **1** into carboxylic acid **2** takes place under mild conditions, with nearly complete retention of stereochemical integrity. 1,2-DCE = 1,2-dichloroethane.

Phase-Transfer Catalysis

S.-s. Jew,* J.-H. Lee, B.-S. Jeong, M.-S. Yoo,
M.-J. Kim, Y.-J. Lee, J. Lee, S.-h. Choi,
K. Lee, M. S. Lah,
H.-g. Park* _____ **1383–1385**

Highly Enantioselective Epoxidation of
2,4-Diarylenones by Using Dimeric
Cinchona Phase-Transfer Catalysts:
Enhancement of Enantioselectivity by
Surfactants

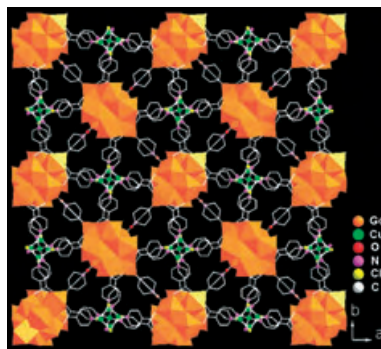


Dramatic increases in reaction rates and enantioselectivities can be effected by the use of surfactants for the phase-transfer catalytic epoxidation of aromatic enones. Based on the X-ray crystal structure of the most effective catalyst—a modified cinchona alkaloid—a plausible transition state of the reaction has been modeled (see picture; HOO^- yellow, C gray, H white, N blue, O red).

Coordination Network

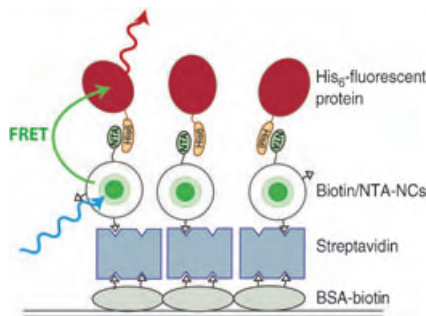
M.-B. Zhang, J. Zhang, S.-T. Zheng,
G.-Y. Yang* _____ **1385–1388**

A 3D Coordination Framework Based on
Linkages of Nanosized Hydroxo
Lanthanide Clusters and Copper Centers
by Isonicotinate Ligands



Lanthanide oxides as sources of lanthanides provided 3D coordination polymers under hydrothermal conditions in which distinct $[\text{Ln}_{14}(\mu_6\text{-O})(\mu_3\text{-OH})_{20}(\text{H}_2\text{O})_8]^{20+}$ ($\text{Ln} = \text{Y}, \text{Gd}, \text{Dy}$) clusters are linked to two different types of copper centers through isonicotinate ligands. The unprecedented 3D network topology of these isostructural compounds is exemplified for $\text{Ln} = \text{Gd}$ in the picture, which reveals the presence of 1D channels along the c axis.

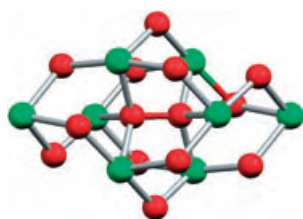
Nanometer light source: Interaction between high-affinity binding sites on lipid-coated nanocrystals (NCs) and different proteins enables the controlled formation of supramolecular nanostructures on micropatterned surfaces (see picture; FRET = fluorescence resonant energy transfer, NTA = nitrilotriacetic acid, His₆ = hexahistidine). The NCs serve as local light sources emitting light over distances from 1 to more than 10 nm.



Supramolecular Assemblies

I. Geissbuehler, R. Hovius, K. L. Martinez, M. Adrian, K. R. Thampi, H. Vogel* — 1388 – 1392

Lipid-Coated Nanocrystals as Multifunctionalized Luminescent Scaffolds for Supramolecular Biological Assemblies

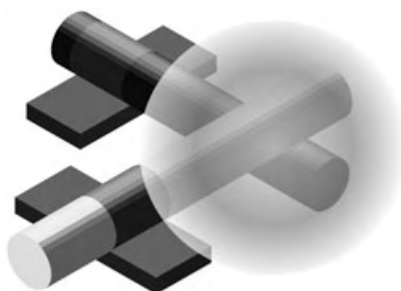


Caged peroxide: An octanuclear nickel complex, which exhibits peroxide in an unprecedented $\mu_6(\eta^1)_3$ coordination mode, was prepared (see structure: only the Ni₈ unit with the central peroxo ligand and the bridging oxygen atoms is shown; green Ni, red O). This mode of binding finally completes the series of symmetrical $\mu_n(\eta^1)_{n/2}$ peroxide binding modes in complexes.

Cluster Compounds

E. J. Brown, A.-K. Duhme-Klair,* M. I. Elliott, J. E. Thomas-Oates, P. L. Timmins, P. H. Walton* — 1392 – 1395

The First μ_6 -Peroxide Transition-Metal Complex: $[\text{Ni}_8(\text{L})_{12}(\text{O}_2)]^{2+}$

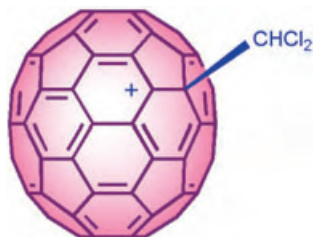


NanoLEDs constructed from crossed silicon and cadmium sulphide nanowires emit light at 514 nm (see picture). These integrated light sources have been used for the imaging of single quantum dots both in solution and in cells.

Nanodevices

O. Hayden,* C. K. Payne* — 1395 – 1398

Nanophotonic Light Sources for Fluorescence Spectroscopy and Cellular Imaging



Positively charged: The cation of a monoalkylated C₇₀ fullerene, $[\text{CHCl}_2\text{-C}_{70}]^+$ (see picture), has been generated as a long-lived species in an isomerically pure form by ionization of the corresponding fullerenol in $\text{CF}_3\text{SO}_3\text{H}$. The thermodynamic stability of the new carbocation is comparable to that of the C₆₀ analogue, $[\text{CHCl}_2\text{-C}_{60}]^+$, according to kinetic studies for the solvolysis of the parent chloride $\text{CHCl}_2\text{-C}_{70}\text{-Cl}$.

Fullerenes

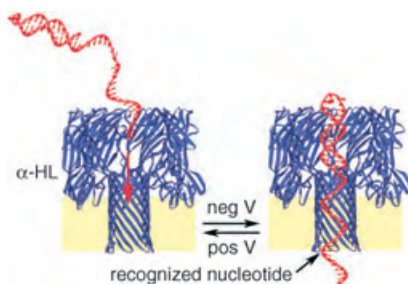
T. Kitagawa,* Y. Lee, N. Masaoka, K. Komatsu* — 1398 – 1401

Generation and Properties of an Alkylated C₇₀ Cation

Molecular Recognition

N. Ashkenasy, J. Sánchez-Quesada,
H. Bayley, M. R. Ghadiri* — 1401 – 1404

Recognizing a Single Base in an Individual
DNA Strand: A Step Toward DNA
Sequencing in Nanopores

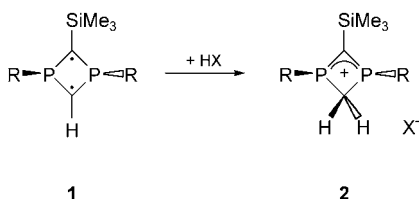


The capture of single strands of DNA inside the α -hemolysin (α -HL) transmembrane pore protein upon application of a positive potential leads to single α -HL-DNA pseudorotaxane species (see picture). By monitoring the characteristic decreases in the ion conductance of α -HL, a single adenine nucleotide can be identified at a specific location on a strand of DNA.

Stable Carbenium Ions

M. Sebastian, A. Hoskin, M. Nieger,
L. Nyulászi,* E. Niecke* — 1405 – 1408

Cyclic Bis(phosphanyl)carbenium Ion
by Protonation of a
1,3-Diphosphacyclobutane-2,4-diyl



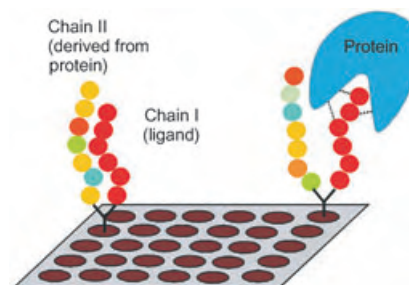
Strong interactions with the lone pairs of the neighboring, pyramidalized phosphorus atoms stabilize the cyclic carbenium ion **2**. The 1,3-bis(phosphanyl)carbenium unit was obtained by protonation of a 1,3-diphosphacyclobutane-2,4-diyl **1** ($R = 2,4,6\text{-tBu}_3\text{C}_6\text{H}_2$, $\text{HX} = \text{trifluoromethanesulfonic acid}$).

Protein–Ligand Interactions

C. Yu, M. Malesevic, G. Jahreis,
M. Schutkowski, G. Fischer,*
C. Schiene-Fischer — 1408 – 1412

The Architecture of Protein–Ligand
Binding Sites Revealed through
Template-Assisted Intramolecular
Peptide–Peptide Interactions

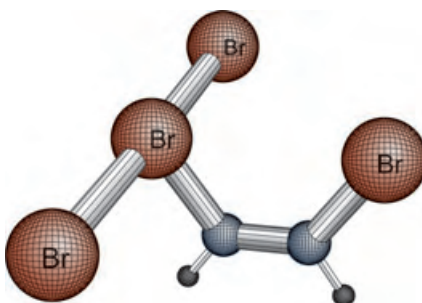
Matching Pairs: The interactions between template-immobilized peptide pairs can provide a picture of ligand-binding sites in proteins. If the members of a given peptide pair do not interact, a soluble protein can bind its ligand (picture, right). If the pair interacts, the peptide ligand is masked from protein binding (left).



Reaction Mechanisms

R. Herges,* A. Papaflippopoulos, K. Hess,
C. Chiappe, D. Lenoir,*
H. Detert* — 1412 – 1416

cis-Bromination of Alkynes without
Cationic Intermediates



Surprising insight into a classical mechanism is provided by theoretical and experimental investigations on the bromination of alkynes. In nonpolar solvents the bromination of acetylene via a covalent tribromide adduct is strongly favored over the textbook mechanism via a bridged bromirenium ion. The structurally interesting intermediate explains the *syn* selectivity of the bromination of strained cycloalkynes.

The issues for February 2005 appeared online on the following dates
Issue 5: January 18. • Issue 6: January 25. • Issue 7: February 1. • Issue 8: February 4.

Sources

Product and Company Directory

You can start the entry for your company in "Sources" in any issue of *Angewandte Chemie*.

If you would like more information, please do not hesitate to contact us.

Wiley-VCH Verlag – Advertising Department

Tel.: ☎ 62 01 - 60 65 65

Fax: ☎ 62 01 - 60 65 50

E-Mail: MSchulz@wiley-vch.de

Service

Keywords _____ 1418

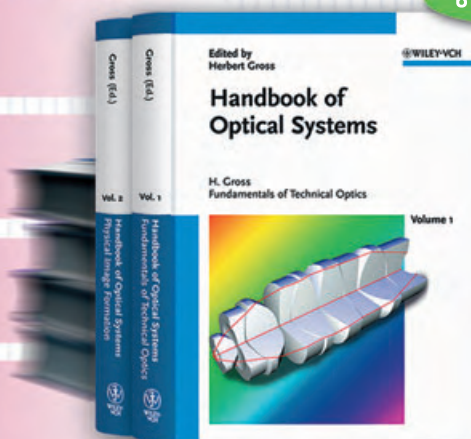
Authors _____ 1419

Angewandte's
Sister Journals _____ 1420–1421

Preview _____ 1423

Unique series on Optical Design

- gives a unique overview for both newcomers and professionals in academia and industry
- balances comprehensive introduction with latest research results in a uniform style
- features over 3,000 color illustrations that facilitate access to complex problems
- written by experts at the world's leading manufacturer of optical systems



6 Volume Set

Price of each volume if purchased as part of the set:

€ 248.00 / £ 175.00 / US\$ 335.00

Each volume will be invoiced and despatched upon publication.

Single volume price:

Approx € 298.00 / £ 210.00 / US\$ 400.00

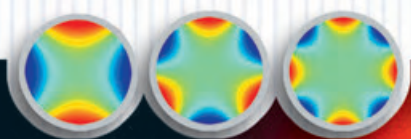
Publication dates:

Volumes 1 and 2: Spring 2005

Volumes 3 and 4: Spring 2006

Volumes 5 and 6: Fall 2007

ISBN 3-527-40382-5



Wiley-VCH • Tel.: +49 (0) 6201 - 606 400
Fax: +49 (0) 6201 - 606 184
e-Mail: service@wiley-vch.de • www.wiley-vch.de

 **WILEY-VCH**

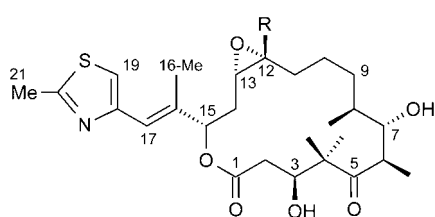
Much Anticipated—The Bioactive Conformation of Epothilone and Its Binding to Tubulin

Dirk W. Heinz,* Wolf-Dieter Schubert, and Gerhard Höfle*

Keywords:

conformation analysis · electron crystallography · macrocycles · molecular modeling · natural products

Amere ten years ago, Bollag et al. demonstrated that cytotoxicity of epothilones is a result of their ability to



epothilone A: R = H
B: R = CH₃

disrupt the intrinsic dynamics of microtubules. This recognition initiated intense chemical and biological analyses of this previously neglected class of substances, the momentum of which continues to this day.^[2] Apart from Taxol, the epothilones were the first natural products known to stabilize microtubules, triggering apoptosis.^[1,3] This mechanism, resulting in extensive polymerization of $\alpha\beta$ -tubulin, is assumed to hold for the clinically highly successful cytostatic drugs Taxol and

Taxotere and for epothilones, as well.^[4] Furthermore, their significantly higher activity and their undiminished effectiveness against multiresistant tumor cells^[1,3,5] have raised the possibility that epothilones could potentially replace taxanes. A major advantage of epothilones is that essentially unlimited quantities can be produced from cultures of the myxobacterium *Sorangium cellulosum*.^[6] Several natural, semisynthetic, and fully synthetic epothilones are currently undergoing clinical trials. Of these, epothilone B lactam^[7] (Ixabepilone) has been most successful (phase III).^[8] There has been much speculation on the binding mode of epothilone, but very little hard evidence had been forthcoming. This situation changed abruptly following the publication of the electron-crystallographic structure of the epothilone A/tubulin complex—the centerpiece of this highlight.

The early observation that epothilones can displace tubulin-bound Taxol suggested that both are bound by the same or by overlapping binding sites.^[1] Structural similarities, such as epoxide and oxetane rings, geminal dimethyl groups, and flexible aromatic side chains, inspired many a mind, and soon a series of models had been proposed for a common pharmacophore for both groups of compounds. These speculations were based on the crystal structure of epothilone B crystallized from dichloromethane,^[10] known since 1995, and the later structures of epothilones A and B crystallized from methanol/water (Figure 1a).^[11] Whereas the macrolide moiety conformation is extraordinarily similar in all these structures, those of the thiazole side chain are very different, presumably due to its high rota-

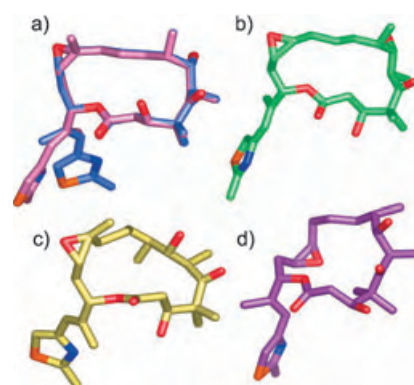


Figure 1. Three-dimensional structures of epothilones in different physical environments: a) Molecular structure of epothilone B from dichloromethane/petroleum ether determined by X-ray crystallography^[10] (pink), superimposed upon that of epothilone A from methanol/water^[11] (blue); b) structure of epothilone A in the presence of tubulin in aqueous medium determined by NMR spectroscopy;^[22] c) conformation of epothilone B in a complex with cytochrome P450epoK;^[26] d) conformation of epothilone A in a complex with $\alpha\beta$ -tubulin in Zn²⁺-stabilized layers.^[9] This Figure was produced using Pymol (<http://pymol.sourceforge.net>).

tional freedom. This was confirmed by NMR spectroscopy in DMSO/water. In addition, the preferred conformation of the macrocycle in organic solvents was found to correspond to that in the crystal.^[10] A refined analysis and the molecular model developed by Taylor and Zajicek indicated a secondary conformation for the C3–C9 ring segment, in which the 7-OH and 8-methyl groups are axial and the 3-OH group assumes an equatorial position.^[12]

In the search for a common pharmacophore by modeling experiments, the epothilone thiazolyl side chain was

[*] Prof. Dr. D. W. Heinz, Dr. W.-D. Schubert

Division of Structural Biology
Gesellschaft für Biotechnologische
Forschung (GBF)
38124 Braunschweig (Germany)
Fax: (+49) 531-618-763
E-mail: dih@gbf.de

Prof. Dr. G. Höfle
Department of Natural Product Chemistry
Gesellschaft für Biotechnologische
Forschung (GBF)
38124 Braunschweig (Germany)
Fax: (+49) 531-618-1515
E-mail: g.höfle@gbf.de

mostly associated with one of three phenyl or even the 10-acetyl side chain of Taxol.^[13–16] Once it emerged that the C13 side chain of Taxol is not strictly required for recognition by tubulin, the models were narrowed down to those sharing homologous thiazole and 2-benzoyl fragments, as well as the taxane framework and macrolide ring.^[17] Conclusive evidence for common binding sites in tubulin was provided by cross-resistant tubulin mutants, especially Thr274, Arg282, Gln292, and Ala231.^[18–20] Nevertheless, an unequivocal model of epothilone bound to tubulin remained elusive, despite the publication of the electron-crystallographic structure of the Taxol/tubulin complex.^[21]

In an alternative approach, Carluccio et al. set out to determine the conformation of tubulin-bound epothilone by NMR spectroscopy.^[22] Under the assumption of a rapid exchange of free and bound epothilone A, transfer nuclear Overhauser effects (transfer-NOEs) and torsion angles were determined by a transfer cross-correlated relaxation experiment. The results were used for a force-field calculation to determine the epothilone A conformation. Overall, the derived conformation of the macrolide ring in this tubulin-associated epothilone is similar to the crystal structures of free epothilone. Only the C2–C3 segment deviates significantly; the 3-OH group is placed in an equatorial orientation, as proposed by Taylor et al. and observed in the crystal structure of epothilone A *N*-oxide.^[12,23] In the side chain, 19-H and 16-Me adopt a *syn* orientation analogous to that in the crystal structure obtained from methanol/water (Figure 1). This is also in agreement with the structure–activity investigations of pyridine and benzimidazole analogues. In a control experiment the authors demonstrate that the observed NMR effects can indeed be ascribed to the protein-associated epothilone A. They found that epothilone B, due to its twofold higher affinity for tubulin, permanently displaces epothilone A from the binding sites, canceling the observed effects. Nevertheless, the small difference in binding affinity does not explain how small amounts of epothilone B in solution could induce such strong re-

sponses. Furthermore it remains unclear why a hundredfold excess of epothilone A does not in itself lead to the polymerization of the tubulin.^[24] Yet despite these uncertainties, the conformation described appears to be induced by the presence of tubulin, and this is clearly different from those of free epothilone A in solution.

Crystal structures of epothilone B and D in complex with cytochrome P450epoK, which catalyzes the last step in the biosynthesis of epothilones A and B, have been refined at 1.9 and 2.7 Å, respectively.^[25] Both epothilone B (Figure 1c) and D are found to adopt conformations quite distinct from those discussed before. Apart from the flexible thiazolyl side chain, the conformations bear some resemblance to the “minor conformer B” proposed by Taylor and Zajicek.^[12a] Nevertheless, these epothilone conformations could not be modeled into the Taxol-binding pocket of tubulin with confidence.

With their recent publication of the electron-crystallographic structure of the epothilone A/tubulin complex, Nettles et al. were able to solve the puzzle of the bioactive conformation of epothilone A.^[9] As reported for the electron-crystallographic structure determination of the Taxol/ $\alpha\beta$ -tubulin complex, two-dimensional crystals of tubulin heterodimers were obtained by adding Zn^{2+} in the presence of an excess of epothilone A. The protofilaments are oriented antiparallel in the Zn^{2+} -induced tubulin layers, rather than parallel as in true microtubules. The 2D crystals diffract electrons to a resolution of 2.9 Å parallel to the crystal plane and 4.2 Å perpendicular to it. Due to the limited resolution, the conformation of the epothilone A was derived with the help of NMR-generated structure ensembles and molecular dynamics modeling procedures. The structure of the complex is an important breakthrough as it allows the interactions of epothilone A with β -tubulin to be described in detail for the first time. At a stroke, it also provides answers to many previously vexing questions: How can known resistance mutants in β -tubulin be explained? How do structural modifications of epothilone affect the interaction with β -tubulin? How does the binding of epothilone compare to that of Taxol?

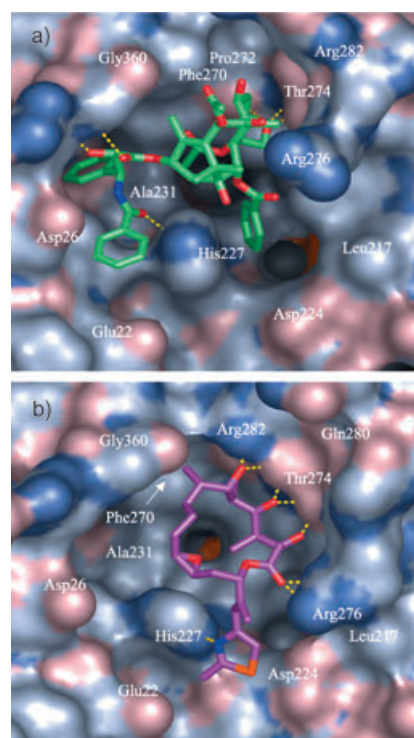


Figure 2. The Taxol/epothilone binding cavity in β -tubulin from the corresponding electron-crystallographically obtained structures with bound a) Taxol and b) epothilone. For β -tubulin the surface of the molecule is depicted (C: gray, O: dark pink, N: gray-blue). Taxol (C: green, O: red, N: blue) and epothilone A (C: violet, O: red, N: blue) are represented as stick models. This Figure was produced using Pymol (<http://pymol.sourceforge.net>).

As expected, epothilone binds within a cavity on the surface of β -tubulin (Figure 2b). This binding site, overlapping with that of Taxol, is partly constituted by the so-called M-loop, which is also essential for lateral contacts between protofilaments in the Zn^{2+} -induced tubulin layers and in microtubules.^[21a] Stabilization of the M-loop, and hence of lateral contacts between protofilaments, ultimately stabilizes growing microtubules, preventing their depolymerization once formed. Through modeling studies, Nettles et al. were able to elucidate the influence of known epothilone modifications on the interaction with β -tubulin. For example, an unexpected *endo* orientation of the epoxide places the large C12 substituent (including N-acyl groups of aziridine analogues) into the extensive hydrophobic indentation below the epothilone macrolide ring, explaining why larger

substituents at C12 and a 9,10-*trans* double bond in epothilone can be tolerated. Because of this hydrophobic indentation, however, the model does not explain why epothilones of the B series, which have a methyl substituent at C12, are generally more active than those of the A series. It is also not obvious how the high-energy *syn*-pentane orientation of the C6 and C8 methyl groups comes about and why removal of the C8 methyl group leads to a reduction in activity by a factor of 200.^[26] Furthermore the influence of additional methyl groups at C10 and C14 is difficult to follow, in particular as the accepted configuration of the biologically active C14-methyl analogue^[27] is depicted in Figure 4B of ref. [9] incorrectly. The structure of the complex is in agreement with some, but not all, of the known resistance mutation in β -tubulin. As expected, however, mostly amino acids that interact directly or indirectly with epothilone are affected.

Direct comparison of epothilone binding with Taxol binding is particularly interesting (Figure 2). Not surprisingly, the smaller epothilone molecule fills only about half of the Taxol-binding cavity in β -tubulin. One striking aspect of this is that the binding cavity adjusts to the substrate by reorienting amino acid side chains, optimizing the interactions with epothilone and Taxol ("induced fit"). The Taxol/ β -tubulin interactions differ fundamentally from those in the epothilone A/tubulin complex. The hypotheses concerning a common pharmacophore can thus finally be laid to rest. With the exception of the hydrogen bond from 7-OH to Arg282, there are no interactions of structurally homologous groups in Taxol and epothilone with β -tubulin. Furthermore, the amino acids in the binding cavity are involved in entirely unrelated interactions with the two natural products. The adaptable binding cavity in β -tubulin is known to also bind further cytostatic effectors other than taxanes and epothilones, including Eleutherobin/Sarcodictyn, that bear little structural resemblance either to each other or to taxanes and epothilones.

How does the conformation of epothilone A observed in the presence of tubulin (Figure 1b) as determined by Carlomagno et al. by NMR spectroscopy

fit into this picture? The two conformations are clearly profoundly different such that an intermediate structure that fits both forms at least to some extent is not readily conceivable. Instead, it is more likely that each of the two conformations exists in the specific environment in which it was studied. Ultimately, both the Zn^{2+} -stabilized tubulin layers and the undefined tubulin present in the NMR experiments are artificial systems. The biologically relevant conformation and binding site of epothilones could thus still differ appreciably from both of these proposed forms.

What experiments could dispel any remaining doubts? Due to the intermediate resolution of the epothilone/tubulin structure, the proposed conformation and orientation of epothilone in the tubulin-binding cavity must be corroborated by independent methods. An obvious approach would be photoaffinity labeling with epothilone derivatives having photolabile substituents at the methyl group of the thiazolyl fragment or, in the case of aziridine analogues, on the aziridine nitrogen atom. Both these positions can be modified without affecting the binding to tubulin.^[28,29] Also conceivable is a solid-state NMR spectroscopic investigation (MAS-NMR) of microtubules loaded with ^{13}C - and ^{19}F -labeled epothilones. This would allow the conformation of the bound molecule to be determined as well as individual distance measurements (REDOR-NMR).

Clearly, attempts will be undertaken to develop novel epothilones that not only support the postulated structure but also have a higher affinity for tubulin and thus possibly exhibit a more pronounced cytotoxicity. Epothilones developed along these lines will, however, presumably not be of therapeutic value, as a clinical application would instead require the pharmacological properties to be optimized to achieve higher selectivity and lower sensitivity toward the development of resistance. This would result in drugs with an improved efficiency and fewer side effects.

[1] D. M. Bollag, P. A. McQueney, J. Z. Zhu, O. Hensens, L. Koupal, J. Liesch,

M. Goetz, E. Lazarides, C. M. Woods, *Cancer Res.* **1995**, 55, 2325–2333.

- [2] a) K. C. Nicolaou, F. Roschangar, D. Vourloumis, *Angew. Chem.* **1998**, 110, 2120–2153; *Angew. Chem. Int. Ed.* **1998**, 37, 2014–2045; b) R. M. Borzilleri, G. D. Vite, *Drugs Future* **2002**, 27, 1149–1163; c) K.-H. Altmann, *Med. Chem.* **2003**, 3, 149–158.
- [3] R. J. Kowalski, P. Giannakakou, E. Hamel, *J. Biol. Chem.* **1997**, 272, 2534–2541.
- [4] a) P. B. Schiff, J. Fant, S. B. Horwitz, *Nature* **1979**, 277, 665–667; b) P. B. Schiff, S. B. Horwitz, *Biochemistry* **1981**, 20, 3247–3252.
- [5] A. Wolff, A. Technau, G. Brandner, *Int. J. Oncol.* **1997**, 11, 123–126.
- [6] a) K. Gerth, N. Bedorf, G. Höfle, H. Irschik, H. Reichenbach, *J. Antibiot.* **1996**, 49, 560–563; b) K. Gerth, S. Pradella, O. Perlova, S. Beyer, R. Müller, *J. Biotechnol.* **2003**, 106, 233–253.
- [7] R. M. Borzilleri, X. Zheng, R. J. Schmidt, J. A. Johnson, S.-H. Kim, J. D. DiMarco, C. R. Fairchild, J. Z. Gougoutas, F. Y. F. Lee, B. H. Long, G. D. Vite, *J. Am. Chem. Soc.* **2000**, 122, 8890–8897.
- [8] S. Goodin, M. P. Kane, E. H. Rubin, *J. Clin. Oncol.* **2004**, 22, 2015–2025.
- [9] J. H. Nettles, H. Li, B. Cornett, J. M. Krahn, J. P. Snyder, K. H. Downing, *Science* **2004**, 305, 866–869.
- [10] G. Höfle, N. Bedorf, H. Steinmetz, D. Schomburg, K. Gerth, H. Reichenbach, *Angew. Chem.* **1996**, 108, 1671–1673; *Angew. Chem. Int. Ed. Engl.* **1996**, 35, 1567–1569. The crystal structure data have been available to interested research groups since October 1995.
- [11] H.-J. Hecht, G. Höfle, unpublished results; CCDC 241333 and CCDC 241334 contain the supplementary crystallographic data for this paper. These data can be obtained free of charge via www.ccdc.cam.ac.uk/conts/retrieving.html (or from the Cambridge Crystallographic Data Centre, 12, Union Road, Cambridge CB21EZ, UK; fax: (+44) 1223-336-033; or deposit@ccdc.cam.ac.uk).
- [12] a) R. E. Taylor, J. Zajicek, *J. Org. Chem.* **1999**, 64, 7224–7228; b) R. E. Taylor, Y. Chen, G. M. Galvin, P. K. Pabba, *Org. Biomol. Chem.* **2004**, 2, 127–132.
- [13] J. D. Winkler, P. H. Axelsen, *Bioorg. Med. Chem. Lett.* **1996**, 6, 2963–2966.
- [14] I. Ojima, S. Chakravarty, T. Inoue, S. Lin, L. He, S. B. Horwitz, S. D. Kuduk, S. J. Danishefsky, *Proc. Natl. Acad. Sci. USA* **1999**, 96, 4256–4261.
- [15] M. Wang, X. Xia, Y. Kim, D. Hwang, J. M. Jansen, M. Botta, D. C. Liotta, J. P. Snyder, *Org. Lett.* **1999**, 1, 43–46.

- [16] F. Manetti, S. Forli, L. Maccari, F. Corelli, M. Botta, *Il Farmaco* **2003**, 58, 357–361.
- [17] L. He, P. G. Jagtap, D. G. I. Kingston, H.-J. Shen, G. A. Orr, S. B. Horwitz, *Biochemistry* **2000**, 39, 3972–3978.
- [18] P. Giannakakou, R. Gussio, E. Nogales, K. H. Downing, D. Zaharevitz, B. Bollbuck, G. Poy, D. Sackett, K. C. Nicolaou, T. Fojo, *Proc. Natl. Acad. Sci. USA* **2000**, 97, 2904–2909.
- [19] N. M. Verrills, C. L. Flemming, M. Liu, M. T. Ivery, G. S. Cobon, M. D. Norris, M. Haber, M. Kavallaris, *Chem. Biol.* **2003**, 10, 597–607.
- [20] L. He, C.-P. H. Yang, S. B. Horwitz, *Mol. Cancer Ther.* **2001**, 1, 3–10.
- [21] a) E. Nogales, S. G. Wolf, K. H. Downing, *Nature* **1998**, 391, 199–203; b) J. Löwe, H. Li, K. H. Downing, E. Nogales, *J. Mol. Biol.* **2001**, 313, 1045–1057; c) J. P. Snyder, J. H. Nettles, B. Cornett, K. H. Downing, E. Nogales, *Proc. Natl. Acad. Sci. USA* **2001**, 98, 5312–5316.
- [22] T. Carlomagno, M. J. J. Blommers, J. Meiler, W. Jahnke, T. Schupp, F. Petersen, D. Schinzer, K.-H. Altmann, C. Griesinger, *Angew. Chem.* **2003**, 115, 2615–2619; *Angew. Chem. Int. Ed.* **2003**, 42, 2511–2515.
- [23] G. Höfle, N. Glaser, M. Kiffe, H.-J. Hecht, F. Sasse, H. Reichenbach, *Angew. Chem.* **1999**, 111, 2090–2093; *Angew. Chem. Int. Ed.* **1999**, 38, 1971–1974.
- [24] According to HPLC analysis, a solution in D₂O, saturated at room temperature, contains 0.5 mg mL⁻¹ epothilone A and 0.06 mg mL⁻¹ epothilone B; G. Höfle, unpublished results.
- [25] S. Nagano, H. Li, H. Shimizu, C. Nishida, H. Ogura, P. R. Ortiz de Montellano, T. L. Poulos, *J. Biol. Chem.* **2003**, 278, 44886–44893.
- [26] A. Balog, P. Bertinato, D.-S. Su, D. Meng, E. Sorensen, S. J. Danishefsky, Y.-H. Zheng, T.-C. Chou, L. He, S. B. Horwitz, *Tetrahedron Lett.* **1997**, 38, 4529–4532.
- [27] R. E. Taylor, Y. Chen, A. Beatty, D. C. Myles, Y. Zhou, *J. Am. Chem. Soc.* **2003**, 125, 26–27.
- [28] N. Glaser, PhD Thesis, Technische Universität Braunschweig, **2001**.
- [29] A. Regueiro-Ren, R. M. Borzilleri, X. Zheng, S.-H. Kim, J. A. Johnson, C. R. Fairchild, F. Y. F. Lee, B. H. Long, G. D. Vite, *Org. Lett.* **2001**, 3, 2693–2696.

Quality counts...

The best of chemistry every week



Wiley-VCH

P.O. Box 10 11 61
69451 Weinheim
Germany
Phone +49 (0) 6201–606-400
Fax +49 (0) 6201–606-184
e-mail: angewandte@wiley-vch.de

www.angewandte.org

Angewandte Chemie International Edition is a journal of the GDCh, the German Chemical Society

GDCh



WILEY-VCH

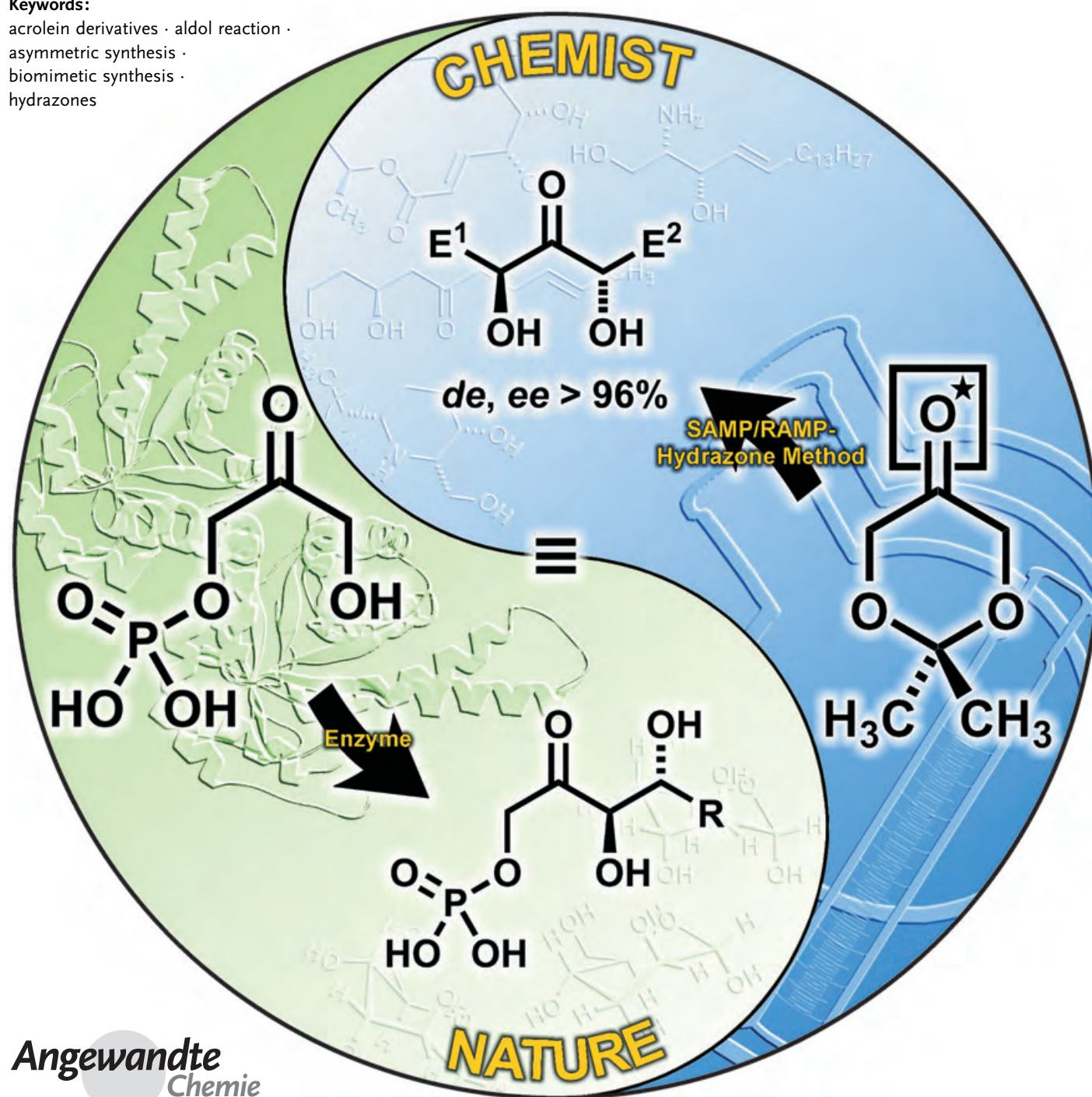
Asymmetric Synthesis

The Dihydroxyacetone Unit—A Versatile C₃ Building Block in Organic Synthesis

Dieter Enders,* Matthias Voith, and Achim Lenzen

Keywords:

acrolein derivatives · aldol reaction ·
asymmetric synthesis ·
biomimetic synthesis ·
hydrazones



Nature employs dihydroxyacetone phosphate (DHAP) as the donor component in various enzyme-catalyzed aldol reactions. Probably the most significant example in this regard is photosynthesis, in which D-glucose, the most widespread natural product, is formed in just a few steps from DHAP. In recent years a number of synthetic equivalents of DHAP have been reported that deserve particular attention, as their applicability in organic synthesis is not limited to (stereoselective) aldol reactions. The power of these reagents has also been demonstrated convincingly in numerous other asymmetric electrophilic α -substitution reactions in target-oriented syntheses. Furthermore, the related 1,3-dioxins are useful equivalents of 2-substituted acrolein derivatives.

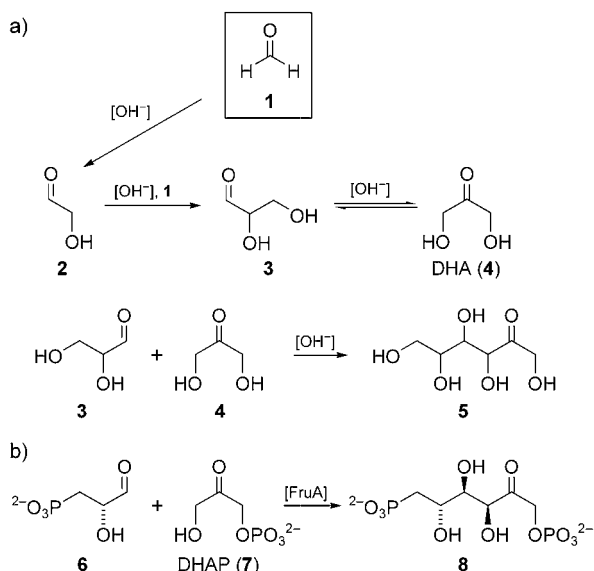
1. Introduction

About 140 years ago Butlerow first observed the formation of a sugarlike syrup, which he named “methylenitan”, when he treated paraformaldehyde with lime water.^[1,2] A few years later, Tollens^[3] and then Loew^[4] obtained similar mixtures starting from formaldehyde. Loew named his product “formose”, a term that nowadays covers all sugar syrups derived from formaldehyde. Although it was evident that these mixtures consisted mainly of sugars, 25 years passed before E. Fischer could prove the presence of small quantities of DL-fructose and DL-sorbose.^[5,6] In view of the large number of reaction products identified so far and the numerous reaction types that occur, it is not surprising that the reaction mechanism has not yet been clarified in its entirety.^[7] However, the main pathway for the formation of the hexoses can be considered to be that depicted in Scheme 1a.^[8] Glycolaldehyde (**2**)—formed from two molecules of formaldehyde (**1**)—undergoes an aldol reaction to form glyceraldehyde (**3**). A Lobry de Bruyn–van Ekenstein

rearrangement provides dihydroxyacetone (**4**, DHA), whose aldol reaction with **3** leads to the formation of the ketohexoses **5**.^[9]

It goes without saying that nature has evolved more subtle methods for the synthesis of sugars and their derivatives. The last step of the mechanism described above, for example, very much resembles the formation of D-fructose-1,6-diphosphate—the first step in the biosynthesis of the different kinds of carbohydrates (Scheme 1b).^[10] This reaction, which is catalyzed by D-fructose-1,6-diphosphate aldolase (FruA), starts from phosphorylated **3** and **4**, that is, **6** and **7** (dihydroxyacetone phosphate, DHAP), respectively, and yields diphosphorylated D-fructose **8** as the only stereoisomer.

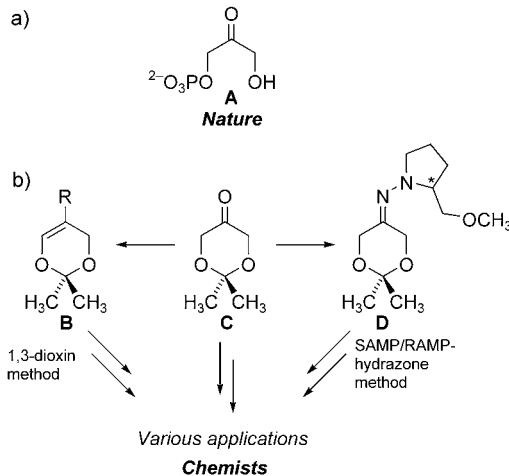
As is evident from this short discussion, DHA, as its phosphorylated analogue DHAP (**A**, Scheme 2), plays a



Scheme 1. a) Mechanism of the formose reaction leading to the ketohexoses **5**; b) formation of D-fructose-1,6-diphosphate (**8**) in the course of photosynthesis. DHA = dihydroxyacetone, DHAP = dihydroxyacetone phosphate, FruA = D-fructose-1,6-diphosphate aldolase.

From the Contents

1. Introduction	1305
2. Building Blocks Derived from DHA and Their Use in Organic Synthesis	1306
2.1. Acyclic Derivatives	1306
2.2. Cyclic Derivatives	1308
2.2.1. 2,2-Dimethyl-1,3-dioxan-5-one Derivatives	1308
2.2.2. Miscellaneous	1318
3. Conclusion and Outlook	1322



Scheme 2. a) Dihydroxyacetone phosphate (DHAP, **A**)—a very important C₃ building block in nature—and b) valuable synthetic equivalents thereof: 2,2-dimethyl-1,3-dioxan-5-one (**C**) and its SAMP/RAMP hydrazones (**D**). 1,3-Dioxins **B**, obtainable from **C**, can be regarded as equivalents of 2-substituted acroleins.

[*] Prof. Dr. D. Enders, Dr. M. Voith, Dipl.-Chem. A. Lenzen
Institut für Organische Chemie
Rheinisch-Westfälische Technische Hochschule
Professor-Pirlet-Strasse 1, 52074 Aachen (Germany)
Fax: (+49) 241-80-92-127
E-mail: enders@rwth-aachen.de

pivotal role in nature as a very important C₃ building block (as do pyruvate and phosphoenolpyruvate (PEP)). Owing to this importance and to the often undesired chemical reactivity of free DHA, it is not surprising that a lot of effort has been devoted to the development of DHA equivalents, such as **C** and **D**. Herein the developments in this area to date are summarized, with emphasis on the contributions by our research group with the SAMP/RAMP-hydrazone method. Also covered are 1,3-dioxins of type **B**, derived from **C**, and their equivalence to 2-substituted acrolein derivatives. For clarity we have divided the text into two main sections: acyclic and cyclic derivatives of DHA.

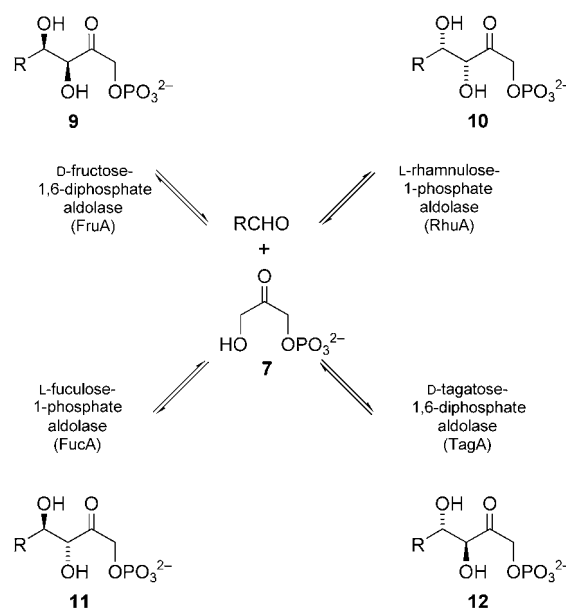
2. Building Blocks Derived from DHA and Their Use in Organic Synthesis

2.1. Acyclic Derivatives

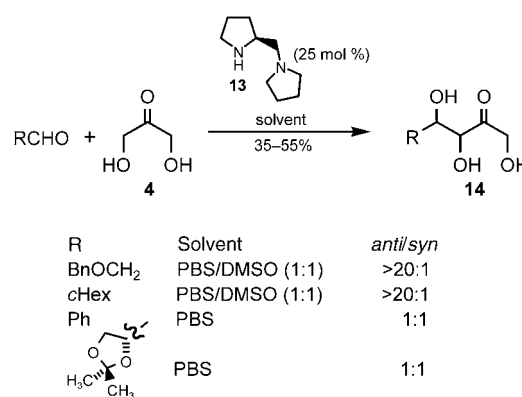
D-Fructose-1,6-diphosphate aldolase (FruA) is not the only DHAP-dependent enzyme that catalyzes aldol reactions highly stereoselectively. Nature has evolved a full set of complementary aldolases that provide access to the four stereoisomeric aldol products **9–12** (Scheme 3).^[11]

Although these enzymes accept quite a wide range of aldehydes as acceptor substrates (only aromatic, α,β -unsaturated, and sterically hindered aliphatic aldehydes are poor substrates or do not react at all), they are restricted to very few donor substrates, of which DHAP is by far the most frequently used.^[12] D-Tagatose-1,6-diphosphate aldolase (TagA) has not yet been applied in synthesis, as it does not catalyze reactions with nonnatural substrates with sufficient diastereoselectivity.^[11a,13] The three remaining enzymes have been utilized frequently—mainly for the synthesis of sugars, azasugars, and their derivatives.^[14,15] Moreover, the enzymes L-fucose-1-phosphate aldolase (FucA) and L-rhamnulose-1-phosphate aldolase (RhuA) can be employed for the efficient kinetic resolution of 2-hydroxyaldehydes.^[16]

Recently, Barbas III and co-workers reported a direct aldol reaction of DHA with different aldehydes in the presence of (*S*)-1-(2-pyrrolidinylmethyl)pyrrolidine (**13**) as the catalyst in a buffered aqueous medium (Scheme 4).^[17] This organocatalytic^[18] approach corresponds to a class I aldolase catalyzed reaction (that is, a reaction that proceeds



Scheme 3. The four DHAP-dependent aldolases.



Scheme 4. Direct organocatalytic aldol reaction of DHA (**4**). Bn = benzyl, cHex = cyclohexyl, DMSO = dimethyl sulfoxide, PBS = phosphate buffer solution.

via an enamine intermediate of DHA). Although the diastereoselectivity was excellent in some cases, the products **14** were racemic.

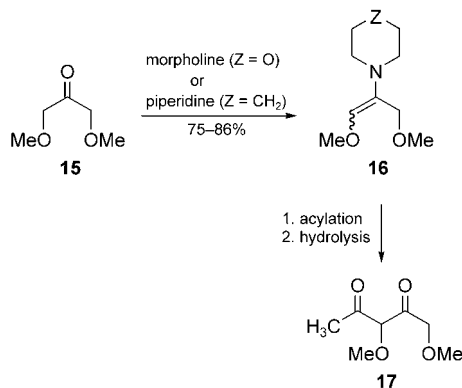


Born in 1946 in Butzbach (Germany), Dieter Enders completed his PhD at the Justus-Liebig-Universität Giessen in 1974 under the supervision of D. Seebach. After postdoctoral studies at Harvard University with E. J. Corey, he returned to Giessen and completed his habilitation there in 1979. He became associate professor at the Universität Bonn in 1980, and moved to his present position as Professor of Organic Chemistry at the RWTH Aachen in 1985. He has received many awards for his research, which focuses on the asymmetric synthesis of biologically active compounds and the development of new synthetic methods.



Matthias Voith was born in 1973 in Duisburg (Germany). He studied chemistry at the RWTH Aachen and the University of York (UK) and completed his PhD in 2003 under the guidance of D. Enders (RWTH) on the development of methodology for the asymmetric synthesis of 2-methyl-substituted 1,3-diols. He is currently a postdoctoral fellow (DAAD fellowship) in the research group of B. H. Lipshutz at the University of California, Santa Barbara (USA), where he is investigating the asymmetric synthesis of actinoidinic acid derivatives by copper-mediated stereoselective biaryl coupling reactions.

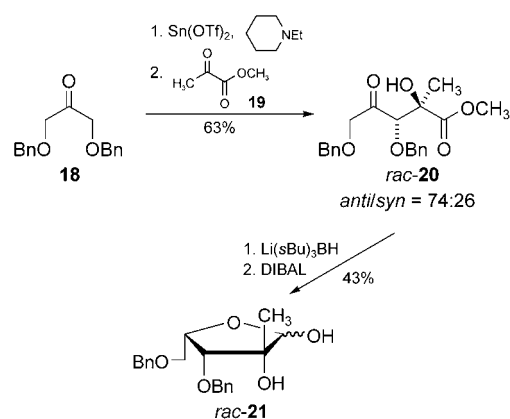
Tang et al. had already reported a similar enamine approach in 1982.^[19] Starting from the dimethylated DHA derivative **15**, the corresponding morpholine- or piperidine-derived enamines **16** were formed. After acylation and hydrolysis, the acylated 1,3-dimethoxypropanone derivative **17** was obtained (Scheme 5).



Scheme 5. The enamine approach of Tang et al.

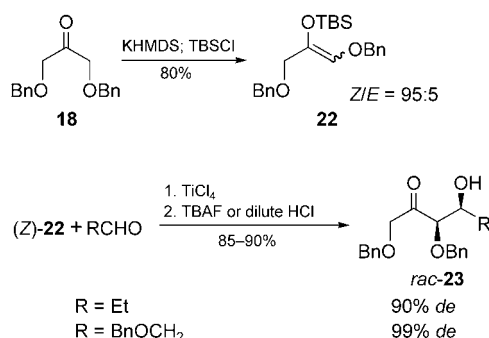
In view of the advantages of benzyl protecting groups,^[20] it is not surprising that the dibenzylated DHA derivative 1,3-dibenzylxypropanone (**18**) has been investigated much more intensively than **15**. Mukaiyama and co-workers applied their $\text{Sn}(\text{OTf})_2$ -promoted *anti*-selective aldol methodology to **18** as the donor substrate (Scheme 6).^[21] Reaction with methyl pyruvate (**19**) as the carbonyl component led to the adduct **20** with moderate diastereoselectivity. Compound **20** could be transformed further into the partially protected branched-chain sugar **21**, which is derived from 2-C-methyl-DL-lyxofuranose.

Kim and Hong used **18** in aldol reactions with aldehydes.^[22] They trapped the lithium enolate generated from **18** under standard conditions (lithium diisopropylamide (LDA), THF, -78°C) with propionaldehyde or benzyloxyacetaldehyde and obtained the corresponding aldol products in good yields (80–82 %) but only with very low stereoselectivity (*syn/anti* = 58:42). Therefore, they performed a Mukaiyama-type aldol reaction starting from the corresponding TBS-protected enol ether (*Z*)-**22**. Of the various Lewis acids tested, TiCl_4



Scheme 6. Tin-mediated aldol reaction of the dibenzylated DHA derivative **18**. DIBAL = diisobutylaluminum hydride, Tf = trifluoromethanesulfonyl.

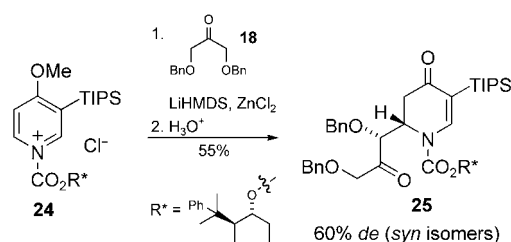
gave by far the best results: The aldol products **23** were isolated in very good yields (85–90 %) with high diastereoselectivity ($\geq 90\%$ *de*; Scheme 7).



Scheme 7. Use of **18** in Mukaiyama-type aldol reactions. HMDs = hexamethyldisilazide, TBAF = tetrabutylammonium fluoride, TBS = *tert*-butyldimethylsilyl.

The lithium enolate of **18** can also be transmetalated with ZnCl_2 , as demonstrated by Comins et al. (Scheme 8).^[23] The resulting zinc enolate underwent addition to the chiral 1-acyl pyridinium salt **24** to give the 2-substituted 1-acyl 2,3-dihydro-4-pyridinone **25** in 55 % yield and with a diastereomeric excess of 60 % *de* for the *syn* isomers.

Carda, Marco, and co-workers studied **18**, as well as the doubly silyl protected DHA derivatives **26a–c**, in aldol

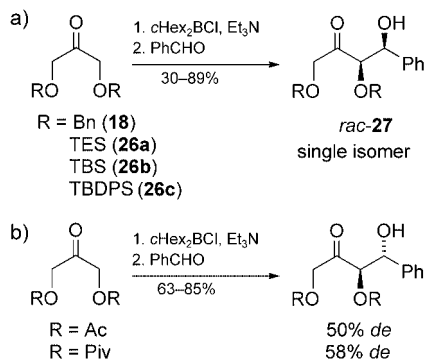


Scheme 8. Transmetalation of lithiated **18** and its addition to the chiral 1-acyl pyridinium salt **24**. TIPS = triisopropylsilyl.



Born 1977 in Geilenkirchen (Germany), Achim Lenzen studied chemistry at the RWTH Aachen and the University of Toronto (Canada). After completing his degree in 2002 he remained in the research group of D. Enders, where his current focus is the total synthesis of various natural products.

reactions via the corresponding dicyclohexylboron enolates (Scheme 9a).^[24] Only benzaldehyde was tested as the acceptor component, and in all cases only the *syn* stereoisomeric products **27** were detected. When ester protecting groups were used, the aldol products were obtained in an *anti*-selective fashion, but with significantly lower stereoselectivity (Scheme 9b).



Scheme 9. Boron-mediated aldol reactions of protected DHA derivatives. Piv = pivaloyl, TES = triethylsilyl, TBDPS = *tert*-butyldiphenylsilyl.

These results are reminiscent of the investigations by Paterson and co-workers of α -oxy-substituted diethyl ketones.^[25] A simple exchange of the Bn protecting group for Bz was accompanied by a reversal of the stereoselectivity of aldol reactions from *syn* to *anti* (see also Scheme 10). Carda, Marco, and co-workers also examined differentially protected DHA derivatives. Their results appear to contradict the chelate model with which Paterson attempted to account for the reversal of stereoselectivity in his system.^[24,25a,26,27]

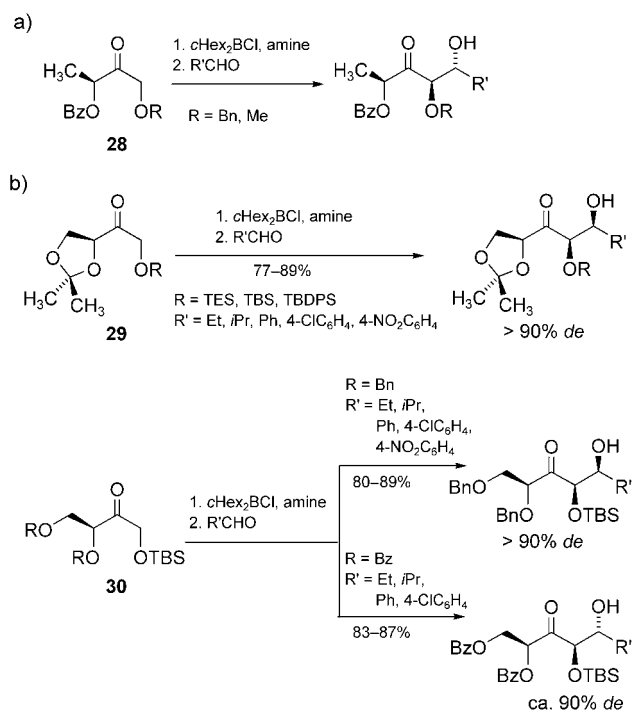
The difficulty with differentially protected DHA derivatives lies in the regioselectivity.^[24] However, at least for the formation of boron enolates, the regioselectivity is excellent if more highly substituted analogues are used. As summarized in Scheme 10, a methyl substituent is already sufficient for this purpose. Paterson and co-workers,^[28] and others,^[29] used derivatives **28** in highly *anti* selective aldol reactions. Carda, Marco, and co-workers showed that the erythrose derivatives **29** and **30** can also be used successfully in stereoselective aldol reactions.^[30] Again, the exchange of protecting groups in **30** was accompanied by a reversal of stereoselectivity (see also Scheme 9).

2.2. Cyclic Derivatives

2.2.1. 2,2-Dimethyl-1,3-dioxan-5-one Derivatives

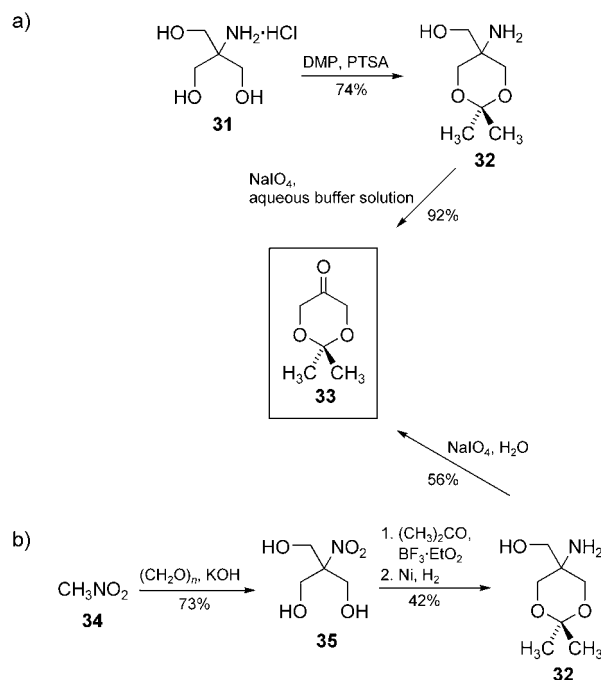
2,2-Dimethyl-1,3-dioxan-5-one (**33**) occupies an exceptional position among the DHA derivatives, as it is by far the most widely used; in the following, acetal- or ketal-protected DHA derivatives will be referred to as dioxanone derivatives.

Two closely related syntheses of **33** have been described. The first approach was developed by Hoppe et al.: It starts from the commercially available hydrochloride salt **31** of 2-amino-2-(hydroxymethyl)propane-1,3-diol, which is first



Scheme 10. Boron-mediated aldol reactions of α -substituted DHA derivatives. Bz = benzoyl.

transformed into acetal **32** in an acid-catalyzed acetalization reaction with 2,2-dimethoxypropane (Scheme 11a).^[31] Subsequent treatment with sodium periodate generates formaldehyde and 2,2-dimethyl-1,3-dioxan-5-imine, which is hydrolyzed in situ to give 2,2-dimethyl-1,3-dioxan-5-one (**33**) in



Scheme 11. The two most common approaches for the synthesis of 2,2-dimethyl-1,3-dioxan-5-one ("dioxanone", **33**). DMP = 2,2-dimethoxypropane, PTSA = *p*-toluenesulfonic acid.

68% yield over two steps. This protocol was based on unpublished results of Woodward and Vorbrüggen and is now the most established method for accessing the dioxanone **33**. Later, the original procedure of Hoppe et al. was modified slightly by different research groups.^[32]

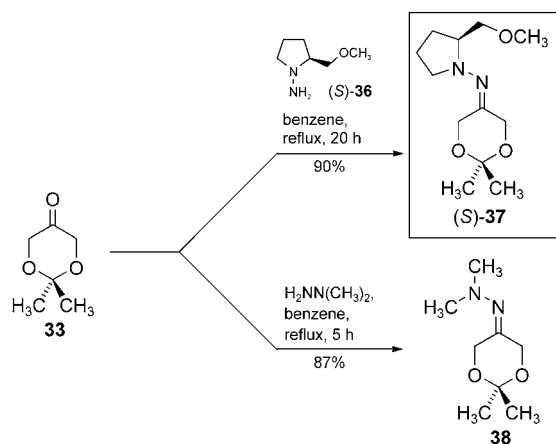
The other approach to dioxanone **33** comprises a four-step synthesis starting from nitromethane (**34**; Scheme 11 b).^[33] A base-catalyzed nitroaldol reaction with paraformaldehyde gave 2-(hydroxymethyl)-2-nitropropane-1,3-diol (**35**). After Lewis acid catalyzed acetalization and hydrogenation with Raney nickel as the catalyst, the β -amino alcohol **32** was obtained, and again subjected to sodium periodate cleavage. The overall yield of this four-step sequence was, however, significantly lower (17%).^[34,35]

Majewski et al. also investigated the possibility of a synthesis starting directly from DHA (**4**).^[35] DHA is available commercially as a dimer and can be cleaved to the monomer at elevated temperatures. However, all attempts to transform the dimer or the monomer by treatment with acetone under acidic conditions resulted in the formation of various condensation products. Hence, it was postulated that the dimer might react faster than DHA itself.

2.2.1.1. The SAMP/RAMP-Hydrazone Methodology

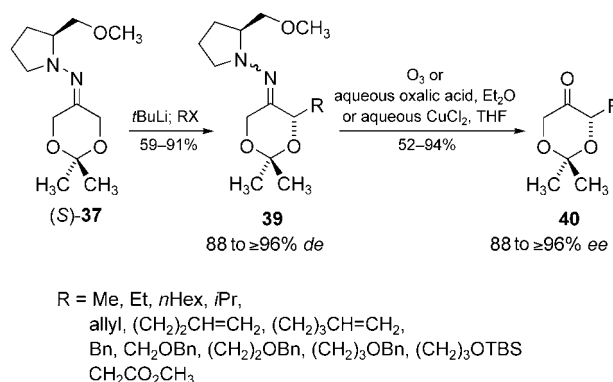
The formation of carbon–carbon or carbon–heteroatom bonds α to a carbonyl group is without a doubt one of the most powerful transformations in organic synthesis. A major contribution in this regard by our research group was the development of the SAMP/RAMP-hydrazone methodology.^[36] Its application to dioxanone **33** provides a very versatile chiral DHA equivalent for asymmetric synthesis. The reaction of dioxanone **33** with (*S*)-1-amino-2-methoxymethylpyrrolidine (SAMP, (*S*)-**36**) or its enantiomer RAMP under water-separating conditions leads to the formation of SAMP hydrazone (*S*)-**37** and its enantiomer (*R*)-**37**, respectively. The corresponding *N,N*-dimethylhydrazone **38**, which has also proven to be useful for some applications, can be obtained under similar conditions (Scheme 12).^[37]

The first effective use of hydrazone (*S*)-**37** was demonstrated in 1989 by our research group in a highly stereo-



Scheme 12. Synthesis of the SAMP hydrazone (*S*)-**37** and the *N,N*-dimethylhydrazone **38** of dioxanone **33**.

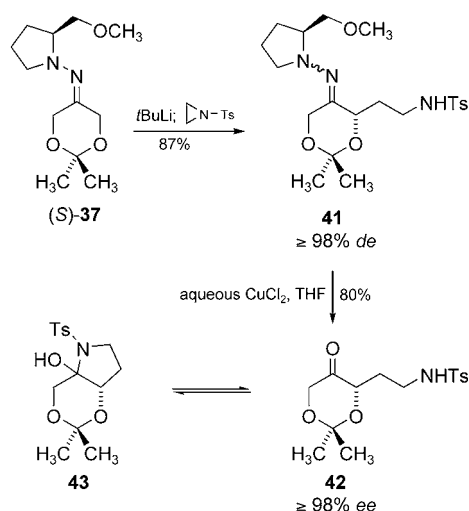
selective α -alkylation reaction.^[33a,38] This methodology was then extended much further to many different classes of electrophiles. The deprotonation of (*S*)-**37** with *tert*-butyllithium and trapping of the lithium azaenolate thus generated with a variety of electrophiles gave the α -alkylated hydrazones **39** with excellent diastereoselectivity (88 to $\geq 96\%$ *de*). The auxiliary was then cleaved (without racemization), either oxidatively with ozone at low temperature or in biphasic systems (solutions of aqueous copper(II) chloride^[39a] or oxalic acid^[39b] together with an organic cosolvent, such as Et₂O or THF). Ozonolysis is a mild and fast cleavage method, which does not affect the acetal functionality and enables recycling of the chiral auxiliary through reduction of the nitrosamine cleavage product. Only in the case of substrates with more double bonds are larger amounts of by-products formed. The biphasic cleavage methods have the advantage over oxidative cleavage that the toxic nitrosamine is not formed. Moreover, the protocol with oxalic acid enables the recovery of the chiral auxiliary through extraction of the aqueous phase after basification. The cleavage with copper(II) chloride is advantageous in the case of substrates that are not particularly stable under the conditions of the other cleavage methods (e.g. substrates that contain double bonds or acid-labile groups). Overall, a highly efficient enantioselective method was developed for accessing the DHA derivatives **40** (Scheme 13).^[33a,39]



Scheme 13. Efficient asymmetric synthesis of the α -substituted dioxanone derivatives **40** by α alkylation of (*S*)-**37**.

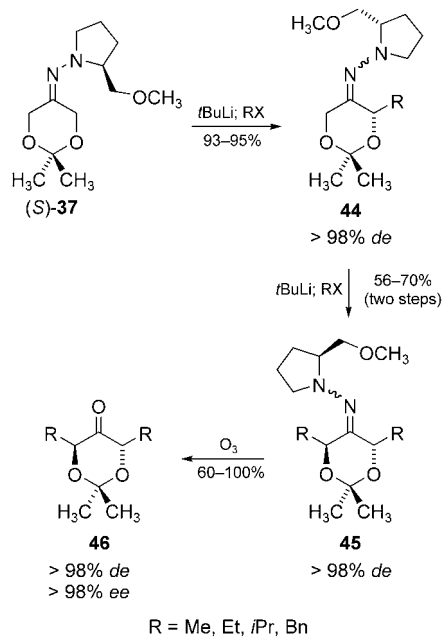
However, not only alkyl halides can be used as electrophiles for α -alkylation reactions. We could show that the reaction also proceeds with tosylaziridine (Scheme 14).^[40] The γ -amino hydrazone **41** was obtained in very high yield and virtually diastereomerically pure. The corresponding γ -amino ketone **42** formed by the copper(II) chloride mediated cleavage of **41** was in equilibrium with its *N,O*-hemiacetal **43** (as a single diastereomer; the relative configuration of the newly formed stereogenic center was not determined).

This monoalkylation concept was extended to the introduction of a second substituent in the α' position.^[41] The monoalkylated hydrazones **44** could be used in this second reaction after aqueous workup without any further purification. The alkylation in the α' position was carried out by the same procedure as described above for α alkylation. After



Scheme 14. Use of tosylaziridine as the electrophile in the α alkylation of (S)-37.

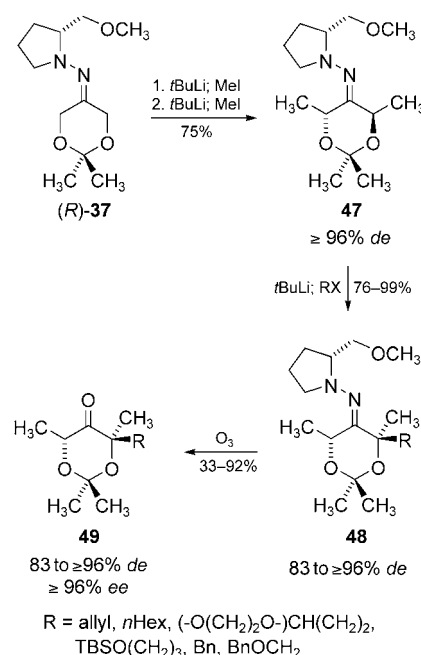
ozonolysis of the dialkylated hydrazones 45, the C_2 -symmetric ketones 46 were isolated in good overall yields with excellent diastereomeric and enantiomeric excess ($>98\%$ de, $>98\%$ ee; Scheme 15). General procedures for α alkylation



Scheme 15. Synthesis of the protected C_2 -symmetric ketodiols 46.

and α, α' dialkylation, including the ozonolytic cleavage of the auxiliary, have been described in the literature, thus providing a reliable, high-yielding, and highly stereoselective approach to a variety of α - and α, α' -substituted protected ketodiols.^[32c]

Furthermore, we were able to show that even a third alkylation step can be carried out in the case of the symmetrically substituted hydrazone 47 (Scheme 16).^[42, 43] However, hydrazones 48 bearing a quaternary stereogenic center



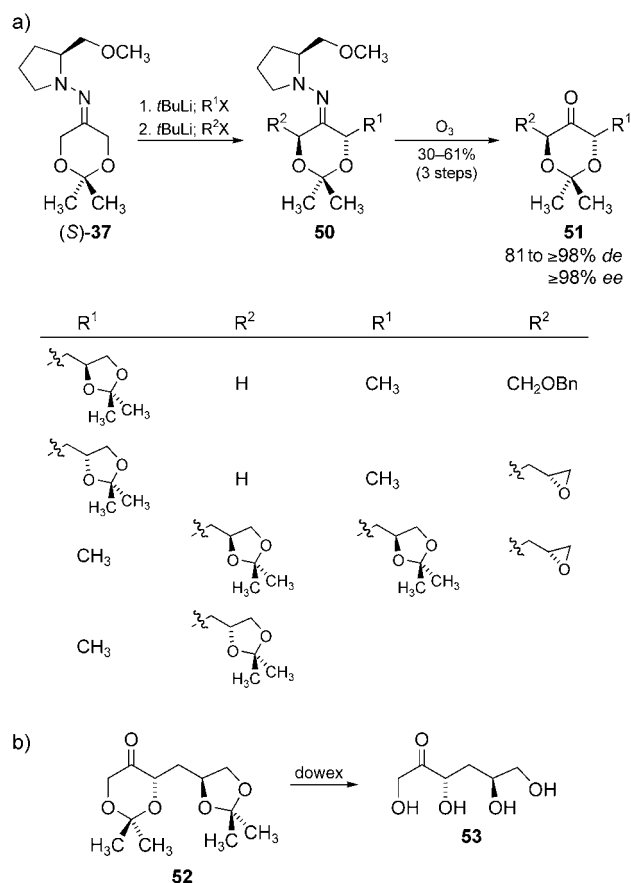
Scheme 16. Alkylation of the α, α' -dimethyl-substituted hydrazone 47.

could only be cleaved with ozone to the ketones. Sterically hindered electrophiles led to diminished stereodifferentiation ($\approx 0\%$ de in the case of $\text{RX} = i\text{PrI}$).

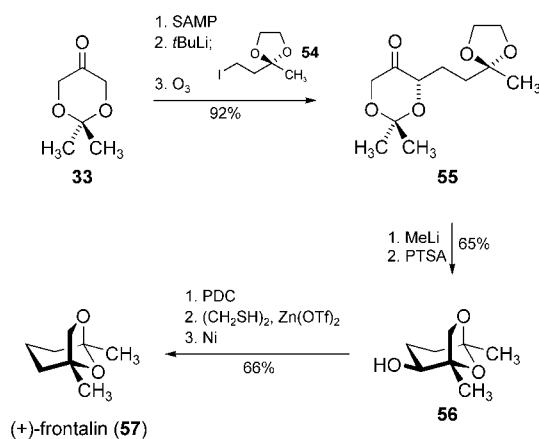
These reliable procedures for mono- and dialkylation have been applied in numerous syntheses. The first application was described by our research group in 1993 in the context of the asymmetric synthesis of C_5 to C_9 deoxy sugars.^[44] Such deoxy sugars are characteristic fragments of a number of antibiotics, such as rifamycin S,^[45] amphotericin B,^[46] and palytoxin.^[47] Moreover, they play an important role in cell-adhesion processes and reperfusion tissue damage, which often occurs after organ transplants.^[48] The deoxy sugars are accessible starting from (S)-37 by alkylation with electrophiles derived from 4-methyl-2,2-dimethyl-1,3-dioxolane or/and 2-methyloxirane. The protected ketodiols 51 were finally isolated after ozonolytic cleavage of the auxiliary in moderate yield over three steps and with excellent diastereomeric and enantiomeric excess (81 to $\geq 98\%$ de, $\geq 98\%$ ee; Scheme 17a).

Demuyne and co-workers made use of this methodology in their synthesis of 4-deoxy-D-fructose (53) for enzymatic affinity studies.^[49] The final cleavage of both acetonide protecting groups in 52 was carried out in the presence of the acid resin dowex (Scheme 17b).

Majewski and Nowak used 2-(2-iodoethyl)-2-methyl-1,3-dioxolane (54) as the electrophile in the α -alkylation step.^[50] After ozonolytic cleavage of the auxiliary they were able to isolate the alkyl dioxolane substituted dioxanone 55 in very high yield. The addition of methyllithium to the free carbonyl group, followed by protonation, gave a secondary alcohol with 95% ee. Acid-catalyzed intramolecular acetalization gave 56, the hydroxy group of which was removed in three further steps to give (+)-frontalin (57), the aggregation pheromone of *Dendroctonus* beetles (Scheme 18).

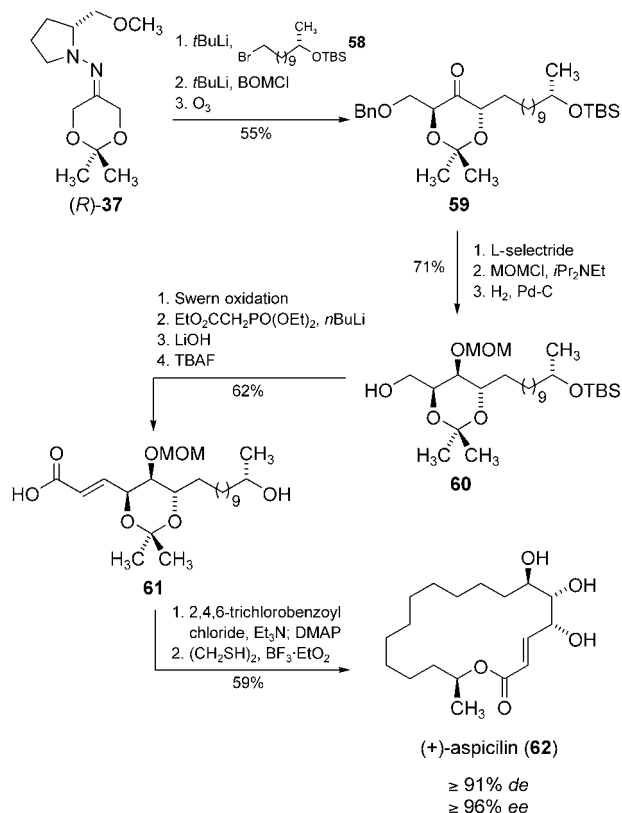


Scheme 17. a) Use of (*S*)-**37** for the synthesis of differently protected deoxy sugars **51**; b) synthesis of 4-deoxy-D-fructose (**53**) with this methodology.



Scheme 18. Asymmetric total synthesis of (+)-frontalin (**57**). PDC = pyridinium dichromate.

Another contribution from our research group in this area was the asymmetric total synthesis of the lichen macrolide (+)-aspicilin (**62**; Scheme 19).^[51] The key intermediate **59**, obtained by dialkylation of (*R*)-**37** with **58** and BOMCl and subsequent cleavage of the auxiliary, was reduced diastereoselectively with L-selectride. Protecting-group manipulations led to **60**, from which the precursor **61** for the Yamaguchi

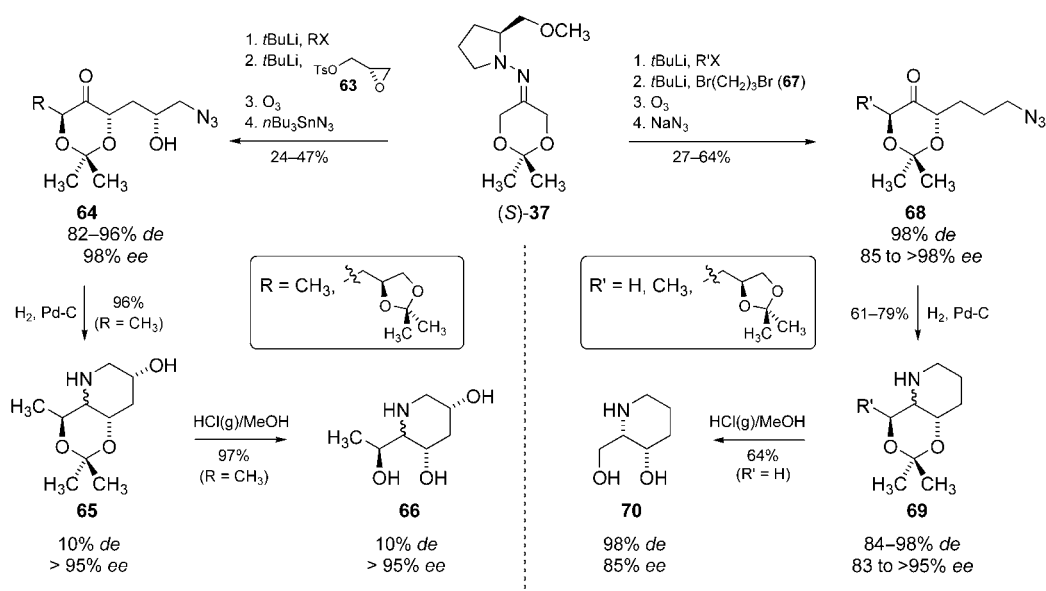


Scheme 19. Asymmetric total synthesis of (+)-aspicilin (**62**). BOM = benzyloxymethyl, DMAP = *p*-dimethylaminopyridine, MOM = methoxymethyl.

macrolactonization could be synthesized. Macrocyclization and cleavage of the remaining acetal protecting groups finally yielded the natural product **62** with the correct absolute configuration.

Cleavage of the auxiliary group of substituted SAMP/RAMP hydrazones reveals the keto group of the dioxanone again, thus opening up a wide range of further possibilities for derivatization. For example, reductive amination with concomitant ring closure led to novel aza sugars (Scheme 20).^[52] The critical electrophiles in the second alkylation step were either (*S*)-1-tosyloxy-2,3-epoxypropane (**63**) or 1,3-dibromopropane (**67**). After the auxiliary had been cleaved an azide group was introduced, either by nucleophilic ring opening of the epoxide with $n\text{Bu}_3\text{SnN}_3$ or by nucleophilic substitution of the bromide with sodium azide. The corresponding azides **64** and **68** were then reduced with hydrogen on Pd-C to the aminoketones, which immediately underwent reductive amination under the reaction conditions to give the substituted piperidines **65** and **69**. The synthesis of aza sugars from these precursors was demonstrated by treatment with gaseous HCl in methanol to give **66** and **70**.

In the case of (+)-2-*epi*-deoxoprosopinine (**73**), the N-containing electrophile **71** was used for the alkylation (Scheme 21).^[53] The hydrogenation of the protected amino-ketone **72** on Pd-C led to the cleavage of the Cbz protecting group with concomitant reductive amination. After removal of the acetal protecting group, the target compound **73**

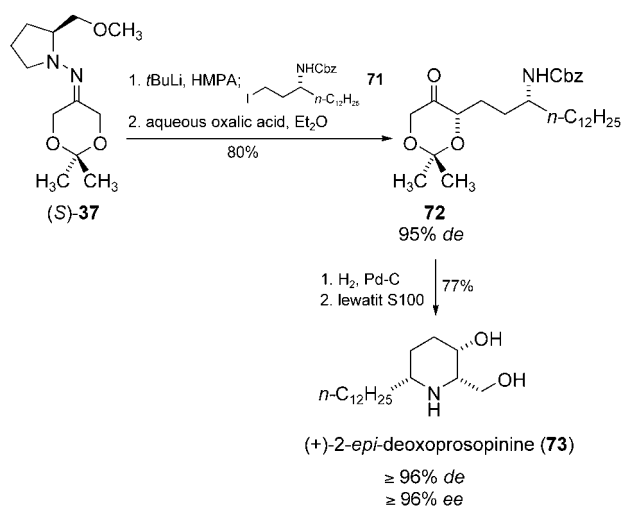


Scheme 20. Synthesis of various azasugars from hydrazone (S)-37 by a sequence consisting of α,α' alkylation, hydrazone cleavage, and reductive amination. Ts = *p*-toluenesulfonyl.

protection of the primary hydroxy group finally yielded the monoprotected double allylic alcohols **76** in very good yield.

As shown in Scheme 23, the Wittig methylenation could also be applied to the α,α' -dialkylated ketones **77**.^[56] Hydrogenation of the double bond in **78** afforded the protected 2-methyl-substituted 1,3-diols **79** in very good yield and with very high diastereomeric and enantiomeric excess. The hydrogenation step does not lead to the formation of a new stereogenic center because of the C_2 symmetry of the olefinic precursor.

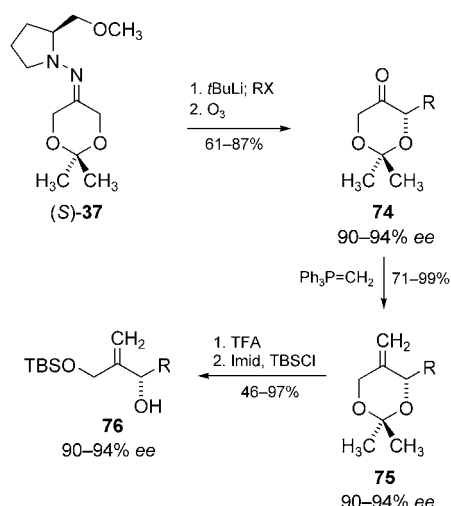
Diastereoselective reduction of the double bond in differentially substituted *exo* olefins, such as **80**, seems to be



Scheme 21. Asymmetric total synthesis of (+)-2-epi-deoxoprosopinine (**73**). Cbz = benzyloxycarbonyl, HMPA = hexamethyl phosphoramide.

was obtained with excellent stereoselectivity ($\geq 96\%$ de, $\geq 96\%$ ee).

Another possibility for hydrazone alkylation and subsequent derivatization of the regenerated carbonyl functionality was shown in the asymmetric synthesis of monoprotected “double allylic alcohols”.^[54] Double allylic alcohols are found as subunits of many natural products, for example, in metabolites with ionophoric activity isolated from marine sponges and microorganisms.^[55] Starting from the dioxanone hydrazone (S)-37, a variety of α -substituted protected ketodiols **74** could be synthesized by the procedure described (90–94% ee; Scheme 22). A racemization-free Wittig methylenation of these ketones gave the exocyclic olefins **75**. Subsequent deprotection of the acetal moiety and selective TBS

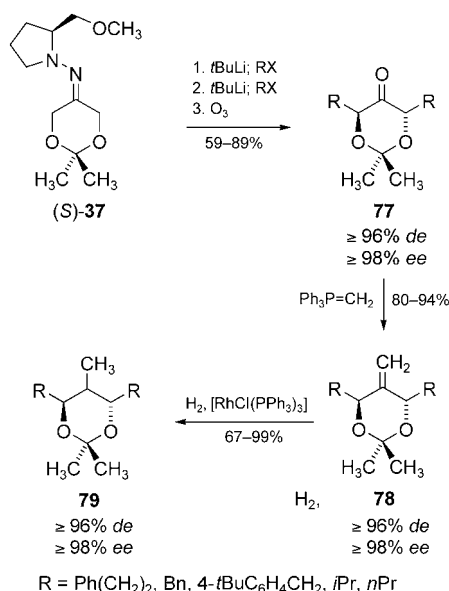


R = Ph(CH₂)₂, Bn, 4-*t*BuC₆H₄CH₂, *i*Pr, *n*Bu

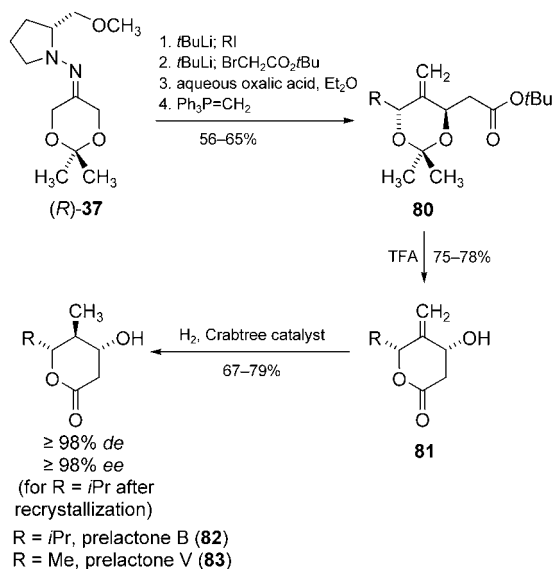
Scheme 22. Synthesis of monoprotected “double allylic alcohols” **76**. Imid = imidazole, TFA = trifluoroacetic acid.

almost impossible. However, in the course of the asymmetric synthesis of prelactones B and V we recently demonstrated that this problem can be circumvented (in a few cases) by using a little trick (Scheme 24).^[57] Intermediate **80** first underwent transesterification with TFA to yield β -hydroxy-lactone **81**. By using the Crabtree catalyst for the hydrogenation,^[58] we made use of the directing properties of the free hydroxy group. This protocol yielded prelactones B (**82**) and V (**83**) with high stereochemical purity.

The α,α' dialkylation of hydrazone **37** also allows stereoselective access to protected *anti*-1,3-diols. As 1,3-diols are important structural subunits of polyene macrolides, the efficient stereoselective synthesis of 1,3-polyol chains is still of



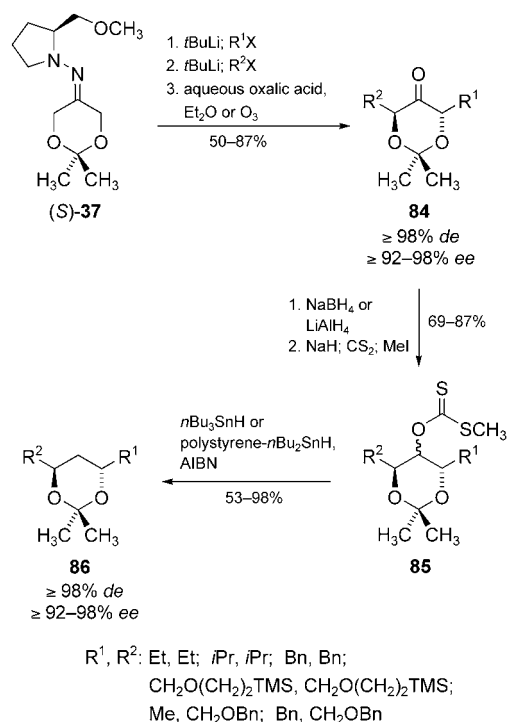
Scheme 23. Synthesis of the protected C₂-symmetric 2-methyl-1,3-diols **79**.



Scheme 24. Asymmetric synthesis of prelaetones B (**82**) and V (**83**).

enormous interest.^[59] In our approach, the α,α' -dialkylated dioxanones **84**, again obtained from (S)-37, were first reduced unselectively with LiAlH₄ or NaBH₄ (Scheme 25).^[60] The resulting secondary alcohols were then deoxygenated by xanthate formation (to give **85**) and Barton–McCombie reaction (either with *n*Bu₃SnH or its polymer-supported equivalent, polystyrene-*n*Bu₃SnH). This sequence gave the protected *anti*-1,3-diols **86** in good yield (31–69% over six steps), with almost complete diastereoselectivity and excellent enantioselectivity.

In further work it was shown that this procedure is not only applicable to simple dioxanone systems, such as **84**, but that it can also be repeated in an iterative manner

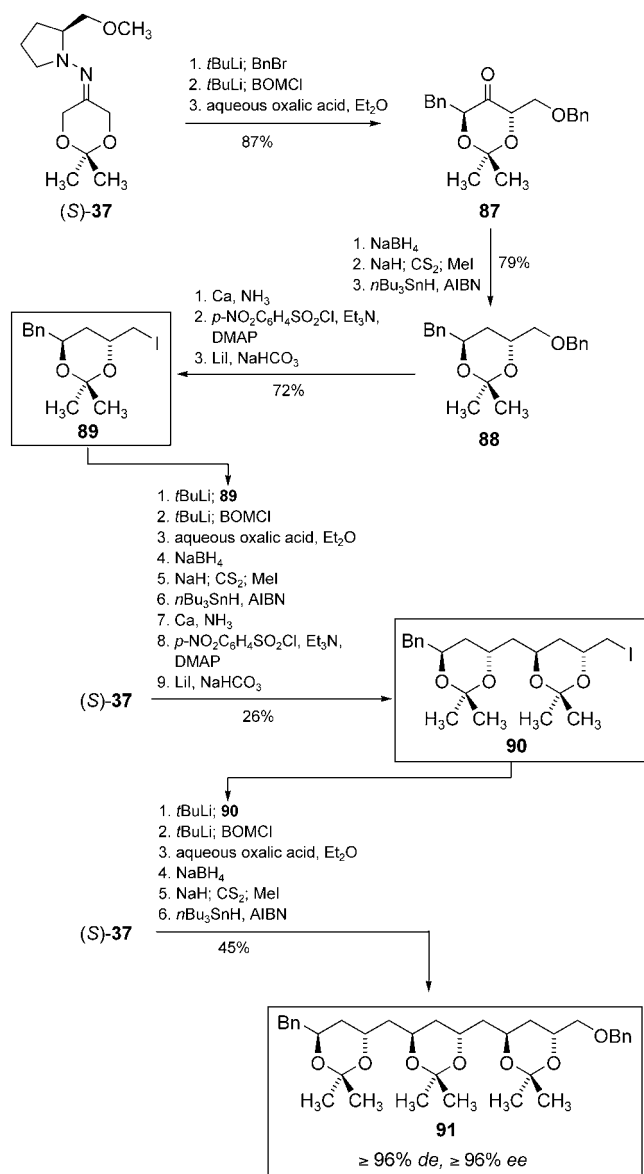


Scheme 25. Synthesis of the protected *anti*-1,3-diols **86**. AIBN = azobisisobutyronitrile, TMS = trimethylsilyl.

(Scheme 26).^[61] The underlying idea was to transform the deoxygenated dioxanones, that is, the dioxanes, into electrophiles with which (S)-37 could be alkylated. BOMCl was chosen as the electrophile for the second alkylation step, as the benzyloxy group could be transformed into the iodide through a simple three-step sequence. In this manner, the acetonide-protected all-*anti*-1,3-polyol **91** was prepared via the electrophiles **89** and **90** with excellent stereoselectivity ($\geq 96\% \text{ de}$, $\geq 96\% \text{ ee}$).

This methodology was applied to the asymmetric total synthesis of both enantiomers of streptenol A (**94**), a secondary metabolite of several *Streptomyces* species.^[62] (+)-Streptenol A is a potent inhibitor of cholesterol biosynthesis with antitumor and immunostimulating activity.^[63] In our synthesis the key intermediate **92** was synthesized starting from the dioxanone RAMP hydrazone (R)-37 through sequential α alkylation, auxiliary cleavage, and deoxygenation (Scheme 27). Removal of the TBS protecting group and TPAP-catalyzed oxidation afforded aldehyde **93**, which was then transformed into (+)-streptenol A (**94**) in three further steps. The other enantiomer was prepared in an analogous manner from (S)-37. The most recent application of this methodology enabled the asymmetric total synthesis of attenols A and B.^[64]

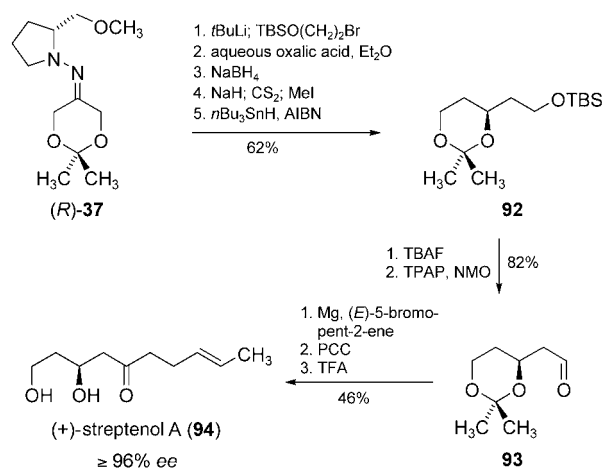
If one disregards the two big sections about dioxanone–SAMP/RAMP-hydrazone chemistry and 1,3-dioxin chemistry, the examples in this Review show that DHA derivatives have mainly been used as donor components in aldol reactions, in analogy with their reactivity in nature. With the SAMP/RAMP-hydrazone methodology we have also overcome this limitation, although the aldol reaction is not



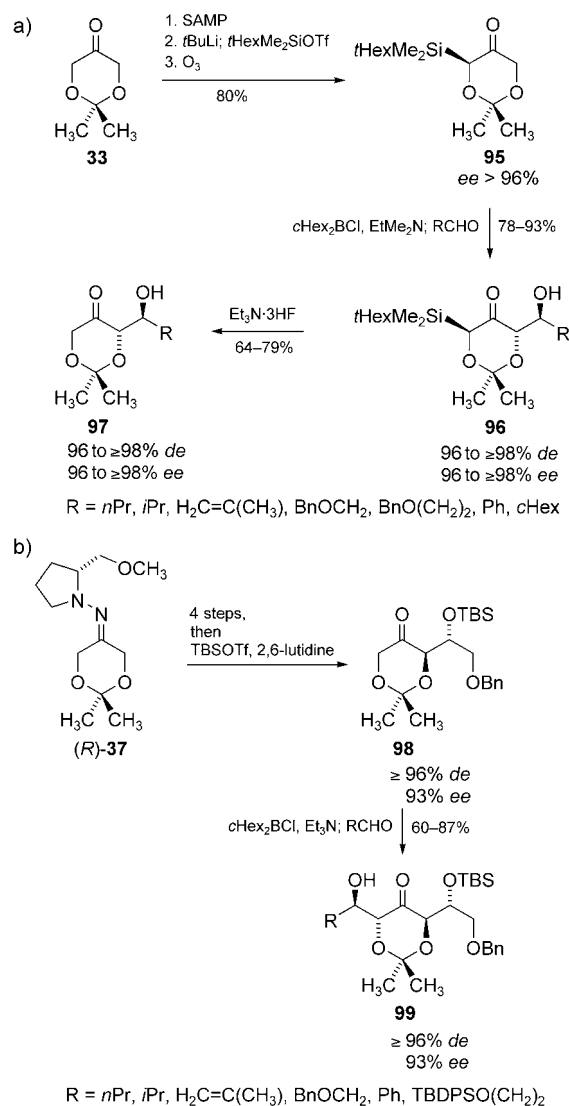
Scheme 26. Iterative synthesis of all-*anti*-1,3-polyols.

performed with hydrazone (*S*)-**37** directly. Instead, use is made of the “silyl trick”: a bulky silyl group is first introduced by α alkylation of a hydrazone.^[65] This silyl group has a directing effect in the subsequent reaction of the carbonyl compound obtained after cleavage of the auxiliary, and is then removed. The corresponding sequence for the dioxanone system is depicted in Scheme 28a. The aldol reaction itself proceeds via the dicyclohexylboron enolates.^[66] Moreover, the chirality introduced by the first aldol reaction can direct a second aldol reaction on the other side of the molecule (e.g. in the synthesis of **99**, Scheme 28b).^[67] This rapid assembly of 1,2-polyols could serve as an entry to the styryllactone family of natural products.^[68]

Majewski and Nowak investigated dicyclohexylboron enolate mediated aldol reactions of the unsubstituted dioxanone **33**, but the diastereoselectivities were somewhat lower (92% *de* for pivaldehyde and benzaldehyde).^[69,70]

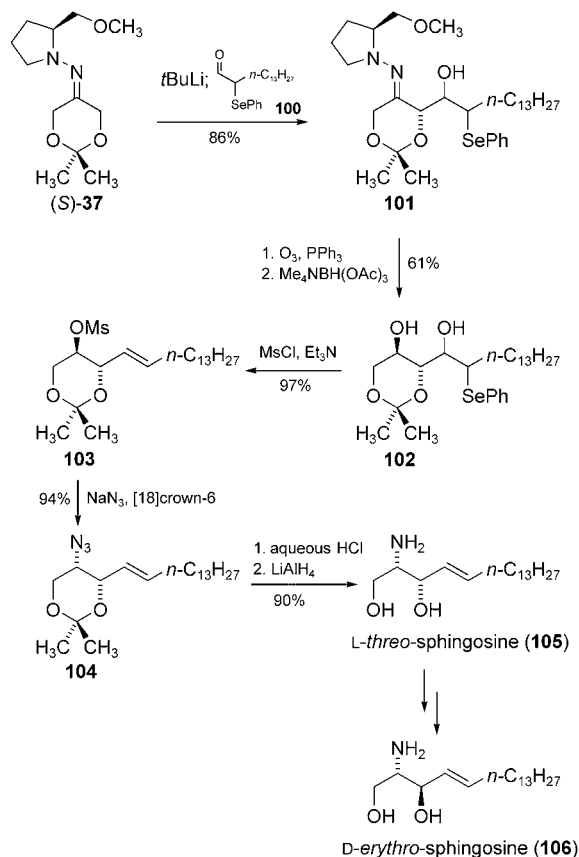


Scheme 27. Asymmetric synthesis of (+)-streptenol A (**94**). NMO = *N*-methylmorpholine *N*-oxide, PCC = pyridinium chlorochromate, TPAP = tetrapropylammonium perruthenate.



Scheme 28. a) Asymmetric aldol reaction with (*S*)-**37** utilizing the “silyl trick”; b) sequence with a second aldol reaction.

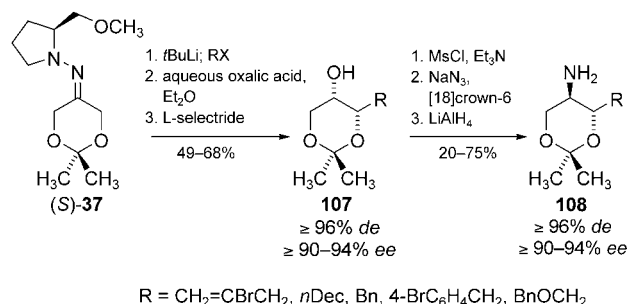
Aldol reactions can be carried out with lithiated SAMP/RAMP hydrazones directly if one is only interested in attaining a high level of asymmetric induction at the α center. The efficiency of this method was demonstrated through the enantioselective α alkylation of aldehydes and ketones by using α -phenylselenenyl aldehydes. The stereochemical information at the β center was lost afterwards through the formation of a double bond.^[71] The application of this methodology starting from hydrazone (*S*)-**37** allowed the highly stereoselective synthesis of both *L*-threo-sphingosine (**105**) and *D*-erythro-sphingosine (**106**), which are subunits of many glycosphingolipids, gangliosides, and ceramides with broad biological activity (Scheme 29).^[72] After the formation



Scheme 29. Asymmetric synthesis of *L*-threo-sphingosine (**105**) and *D*-erythro-sphingosine (**106**). Ms = methanesulfonyl.

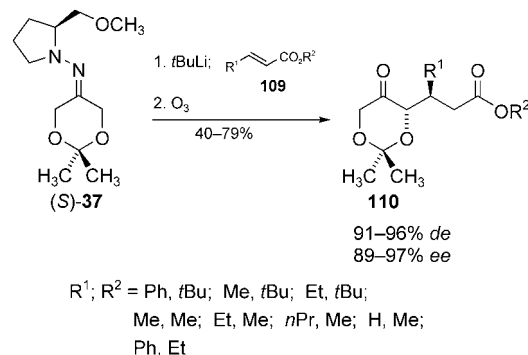
of **101** by such an aldol reaction, the auxiliary was cleaved carefully to avoid the oxidative elimination of selenoxide. The ketone thus obtained was reduced with high *anti* diastereoselectivity to **102** with tetramethylammonium triacetoxymethylborohydride. The treatment of diol **102** with methanesulfonyl chloride afforded mesylate **103** as a single diastereomer with the newly formed double bond in the *E* configuration. Mesylate **103** was then converted into the natural product *L*-threo-sphingosine (**105**) by using standard functional-group interconversions. The natural product could be converted into its epimer *D*-erythro-sphingosine (**106**) in five further synthetic steps, including a Mitsunobu inversion as a key step.

Closely related is our recently published asymmetric synthesis of *anti*-2-amino-1,3-diols (Scheme 30).^[73] In this case the reduction of the intermediate α -substituted dioxanones with *L*-selectride led to the *cis* configuration with regard to the stereocenters at C4 and C5 of the dioxanone ring. The resulting alcohols **107** were then transformed into the amines **108** by a similar method to that shown in Scheme 29.



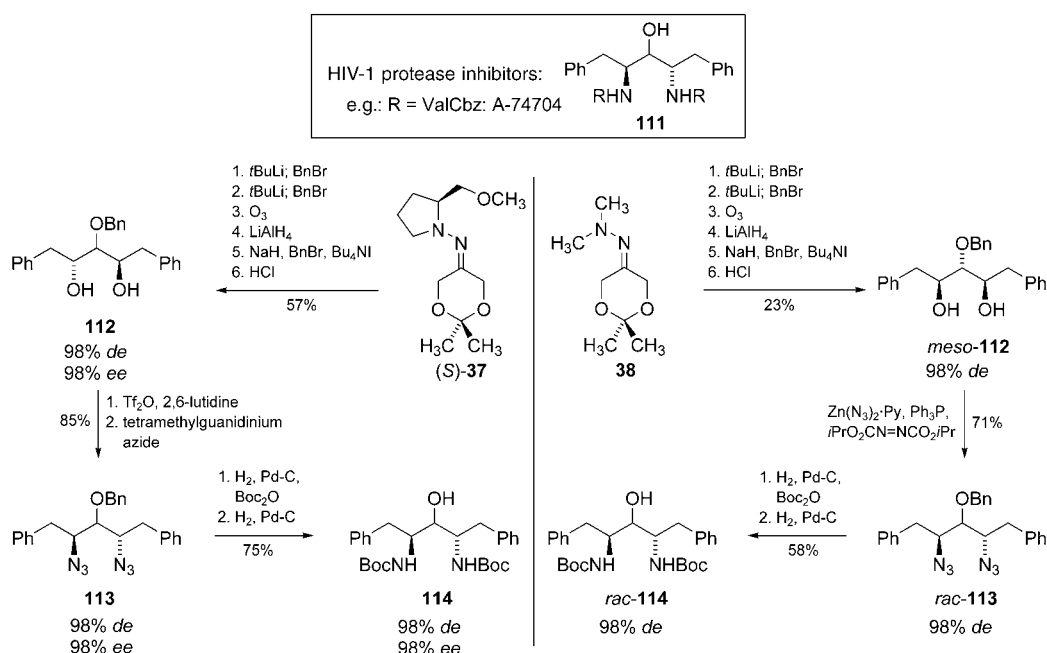
Scheme 30. Synthesis of the protected *anti*-2-amino-1,3-diols **108**. *n*Dec = *n*-decyl.

With hydrazone (*S*)-**37** not only alkylation and aldol reactions, but also Michael additions, can be conducted with a high degree of stereoselectivity.^[74] Thus, the *E*-configured α,β -unsaturated esters **109** were added to the lithium enolate of (*S*)-**37** (Scheme 31). After cleavage of the auxiliary with ozone, the protected 4,6-dihydroxy-5-oxoesters **110** were isolated in moderate to good yield and with very good diastereomeric and enantiomeric excess (91–96% *de*, 89–97% *ee*).



Scheme 31. Asymmetric Michael additions to enoates with lithiated (*S*)-**37** as a chiral nucleophile.

Finally, one last target-oriented synthesis should be presented in this section, namely, that developed us for the C_2 -symmetric HIV-1 protease inhibitors of the general formula **111**, which were introduced by Erickson, Kempf, and co-workers.^[75] Starting from hydrazone (*S*)-**37**, the monoprotected triol **112** could be obtained in a straightforward manner and excellent yield over six steps (Scheme 32).^[37] Substitution of the free hydroxy groups with concomitant inversion of both stereocenters gave diazide **113**, which could be transformed into the title compound **114** in



Scheme 32. Asymmetric (left) and symmetric (right) synthesis of HIV-1 protease inhibitors **111**. Boc = *tert*-butoxy-carbonyl, Py = pyridine.

just two further steps. The racemate of this HIV-1 protease inhibitor was synthesized starting from the dioxanone dimethylhydrazone **38**. The same sequence of steps this time afforded the *meso* monoprotected triol *meso*-**112**. Subsequent substitution of the hydroxy group with zinc azide under Mitsunobu conditions occurred with inversion of only one of the two stereogenic centers to furnish diazide *rac*-**113**. Finally, reduction, introduction of the Boc protecting group, and debenzoylation under the same conditions as described for the nonracemic product yielded the *N*-Boc-protected amino alcohol *rac*-**114** with 98% *de*.

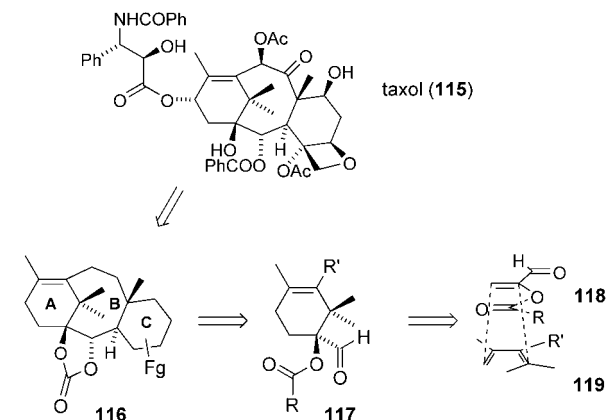
2.2.1.2. The 1,3-Dioxin Methodology

Another very useful application of dioxanone **33** in organic synthesis is the 1,3-dioxin methodology, which Funk and co-workers have developed over the last nine years. To gain access to different derivatives of taxol (**115**), a stereo-selective synthesis of a suitably functionalized taxane carbocyclic framework **116** was desired. Funk and Yost proposed that **116** could be synthesized from the A-ring fragment **117**, as shown retrosynthetically in Scheme 33. As **117** is a substituted cyclohexene, the most straightforward approach would be an intermolecular Diels–Alder cycloaddition between a diene **119** and a 2-acyloxy acrolein **118**.^[76]

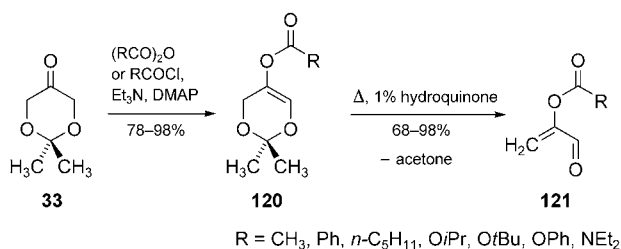
Since no mild and versatile synthesis of these dienophiles was known, Funk and co-workers developed a new strategy based on their previous discovery that 4-alkyl 4*H*-1,3-dioxins undergo facile retrocycloaddition reactions to provide 3-alkyl acroleins and formaldehyde.^[77] Starting from dioxanone **33**, O acylation upon treatment with triethylamine/DMAP and an anhydride, chloroformate, or carbamoyl halide furnished the 5-acyloxy dioxins **120**, all of which underwent smooth

retrocycloaddition to yield the desired 2-acyloxy acroleins **121** with the release of acetone (Scheme 34).^[76] The retrocycloaddition was induced by heating in the presence of hydroquinone (1 mol %).

The 2-acyloxy acroleins **121** were then subjected to Diels–Alder cycloaddition reactions—either after generation *in situ* from the corresponding 5-acyloxy dioxin precursor (Table 1, entries 1 and 2) or as pure samples (Table 1, entries 3–7). It was observed that: 1) 2-acyloxy acroleins **121** can also function as heterodienes in cycloadditions with electron-rich alkenes in the presence of lanthanide catalysts (e.g. $\text{Yb}(\text{fod})_3$; Table 1, entry 5; fod = 1,1,1,2,2,3,3-heptafluoro-7,7-dimethyloctane-4,6-dionate),



Scheme 33. Retrosynthesis of taxol (**115**) with an intermolecular Diels–Alder cycloaddition as the key step.



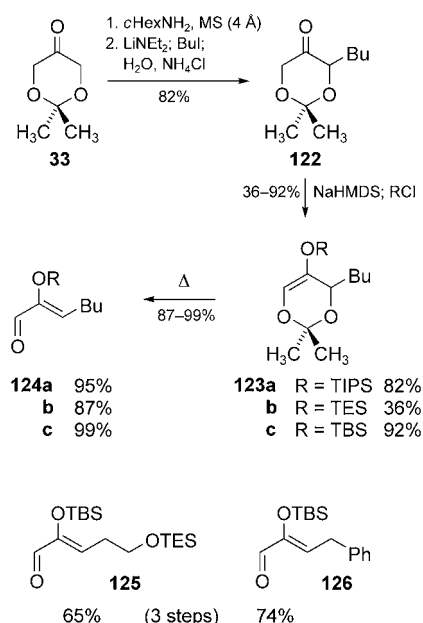
Scheme 34. Synthesis of the 2-acyloxy acrolein derivatives **121**.

and 2) the reactions with tetrasubstituted dienes could be optimized to provide access to the desired functionalized A-ring synthons in high yield (Table 1, entries 6 and 7).

The 4-alkyl 5-trialkylsiloxy 4*H*-1,3-dioxins also gave remarkably good results (Scheme 35).^[78] Dioxanone **33**,

Table 1: Diels–Alder cycloadditions of 2-acyloxy acroleins **121** with dienes.

Entry	Diene/ heterodienophile	R in 121	Adduct	Yield [%]
1		Ph		68
2		Ph		71
3		Ph		69
4		<i>n</i> -C ₅ H ₁₁		85
5		Ph		78
6		<i>n</i> -C ₅ H ₁₁		95
7		OiPr		90

**Scheme 35.** Synthesis of the 2-trialkylsiloxy acrolein derivatives **124a–c**, **125**, and **126**.

again the starting material, was alkylated in the α position with butyl iodide via the corresponding cyclohexylimine. The lithium enolate of the butylated dioxanone **122** was formed under kinetic conditions and trapped with different trialkyl

silyl chlorides to give 4-alkyl 5-trialkylsiloxy 4*H*-1,3-dioxins **123a–c**. Upon heating, the aforementioned retrocycloaddition resulted in the formation of the (*Z*)-2-trialkylsiloxy-2-enals **124a–c** as the only stereoisomers in excellent yields. The (*Z*)-2-(*tert*-butyldimethylsiloxy)-2-enals **125** and **126** were synthesized in an analogous manner.

Compounds **124–126** were tested in Sasaki-type [4+3] cycloaddition reactions with dienes in the presence of different Lewis acids. In many cases excellent regio- and/or stereoselectivity was observed (Table 2).

Funk and co-workers could also show that this retrocycloaddition reaction is not restricted to 5-oxy-substituted 1,3-dioxin substrates. To access 1,3-dioxin derivatives with substituents other than RO in the 2-position, he synthesized the vinyl triflate **127**, which was used in a range of (mainly palladium-catalyzed) coupling reactions (Scheme 36, Table 3).^[79] The results obtained demonstrate the impressive variety of derivatives accessible by this approach. The products were then subjected to retrocycloaddition to yield the 2-substituted acroleins **129**, which underwent cycloaddition reactions in the presence of dienes or electron-rich olefins. Overall, vinyl triflate **127** can be seen as a synthetic equivalent of the acrolein α^2 -synthon **128** (umpolung!).

Now that 5-acyl 1,3-dioxins were accessible, the first total synthesis of cytotoxic (\pm)-euplotin (**136**) could be realized (Scheme 37).^[80] Lewis acid mediated opening of the bicyclic acetal of the Paterno–Büchi photocycloadduct **130** and acetylation of the resulting free hydroxy group furnished **131**. This compound was then converted into iodide **132**, which was used as the electrophile for the α alkylation of the dioxanone cyclohexylimine. Dioxanone **133** was then transformed into the key intermediate **134** by triflate formation and palladium-catalyzed CO insertion (compare entry 8 in Table 3). A sequence of retrocycloaddition and intramolecular cycloaddition gave **135**, which was transformed into the natural product in three further steps.

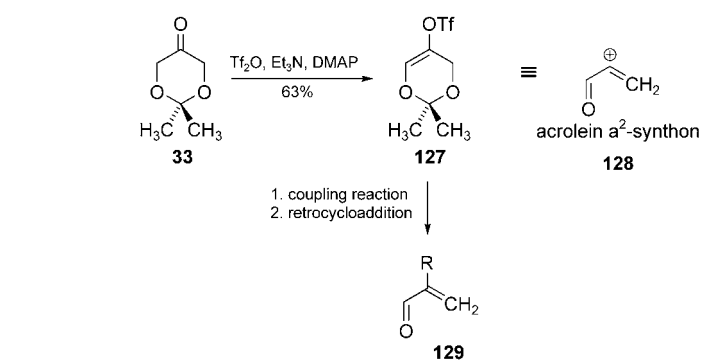
Another class of 1,3-dioxin derivatives that have proven extremely useful are the 5-amido 1,3-dioxins. Four different routes have been developed for their synthesis (Scheme 38).^[81] 5-Amido 1,3-dioxins are accessible by treatment of the dioxanone imine **137** with an anhydride (method a) or an acid chloride (method b) together with an appropriate amine base. 5-Triflamidyl 1,3-dioxins **139** are synthesized by an analogous method to method a, but in the presence of triflic anhydride (method c). Only when R³ is not stable under the reaction conditions of method c is it necessary to make a detour via **140**, which is then alkylated to yield **141** (method d).

The retrocycloaddition of 2-amido 1,3-dioxins leads to 2-amido acroleins, such as **147** (Scheme 40), which have been used by Funk and co-workers in the total synthesis of a variety of natural products. The following examples are classified according to the subsequent reaction of the 2-amido acrolein intermediate:

- a) *Intermolecular Diels–Alder cycloaddition reactions*: The first step in the total synthesis of the immunosuppressant (\pm)-FR901483 (**146**) was the formation of **142** (by method a, Scheme 39).^[82] Retrocycloaddition, followed by a cycloaddition with **143**, gave **144**. Two successive

Table 2: Use of 2-trialkylsiloxy acroleins in Sasaki-type [4+3] cycloaddition reactions.

Reactants	Lewis acid (yield)	Products	endo/exo
124c	Me ₂ AlCl (76%) R = TBS		77:23
124b	Me ₂ AlCl (78%) R = TES		92:8
124c	SnCl ₄ (73%) R = TBS		80:20
124c	Me ₂ AlCl (100%) R = TBS		100:0
124b	SnCl ₄ (70%) R = TES		90:10
126	Me ₂ AlCl (63%)		—
126	EtAlCl ₂ (65%)		—
124c	TiCl ₄ (54%) R = TBS		89:11
124b	TiCl ₄ (40%) R = TES		50:50
124c	EtAlCl ₂ (50%)		3:97
	Me ₂ AlCl (74%)		79:21
	Me ₂ AlCl (80%)		85:15

**Scheme 36.** Synthesis of 2-substituted acrolein derivatives via triflate **127**—an equivalent of the acrolein α^2 -synthon **128**.

aldol reactions afforded the tricyclic lactam **145**, from which the target molecule could be built up in 18 further steps. The similarities in the syntheses of (\pm)-lepadiformine (**150**)^[83] and (\pm)-fascicularin (**154**)^[84] are evident

(Scheme 40). The reaction of the intermediates **147** and **151** (each obtained by method c) with the dienes **148** and **152** gave **149** and **153**, respectively, which were transformed further into the target compounds in several steps.

- b) *Electrophilic aromatic substitution reactions*: Provided that the R¹ or R³ substituent (see Scheme 38) contains an appropriate aromatic moiety, the 2-amido acrolein derivatives obtained after retrocycloaddition can undergo an intramolecular electrophilic aromatic substitution in the presence of a suitable Lewis acid. Fuchs and Funk investigated this interesting reaction quite extensively (Table 4).^[81] This methodology offers a new route to a range of tetrahydroisoquinolines, tetrahydro-3-benzazepines, and hexahydro-3-benzacocines, all of which contain the pharmacologically important β -phenethylamine moiety. Finally, this methodology found application in the total syntheses of (\pm)-aphanorphone and (\pm)-lennoxamine (**158**; Scheme 41).^[85] In the total synthesis of **158**, dioxanone **33** was first transformed into dioxin **155** by method b (Scheme 38). Boron trifluoride mediated both the retrocycloaddition and the electrophilic aromatic substitution of the intermediate *N*-amido acrolein. The oxidation of aldehyde **156** to the carboxylic acid, followed by a Kochi reaction, gave enamide **157**, which underwent radical cyclization in the presence of *n*BuSn₃H and AIBN to give (\pm)-lennoxamine (**158**).

2.2.2. Miscellaneous

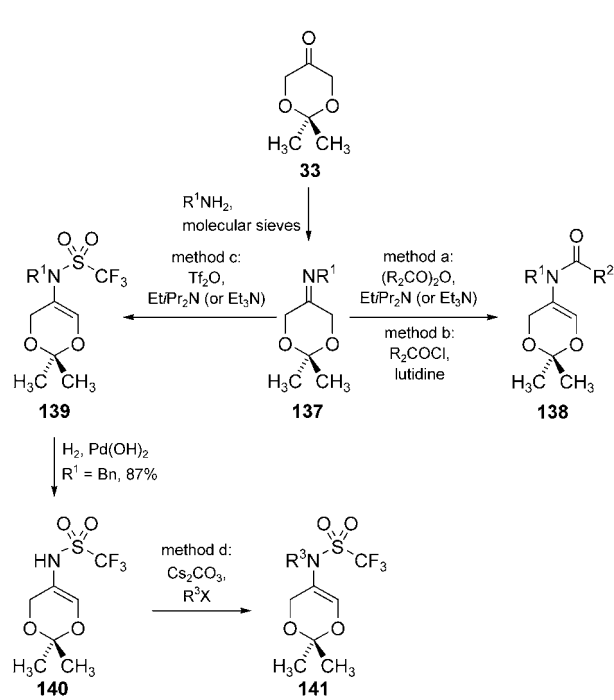
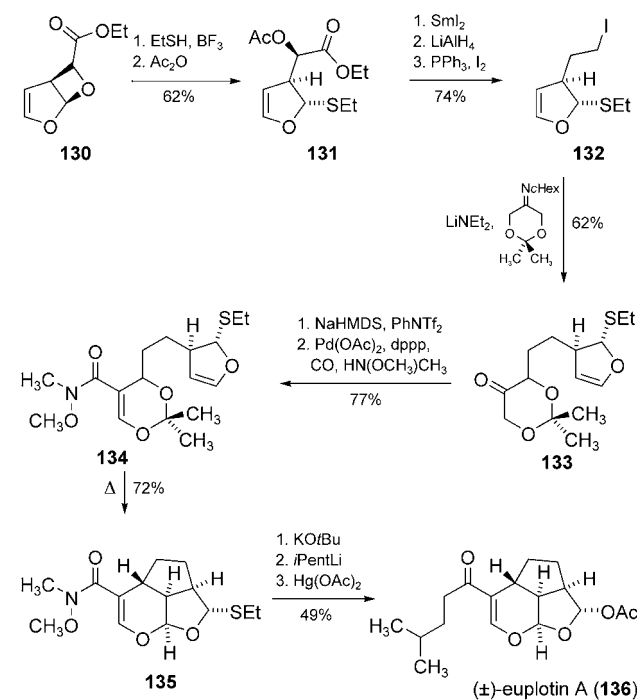
This section includes other important applications of dioxanone **33** in organic synthesis, as well as reactions of other cyclic DHA derivatives. By analogy with the work of Tang et al. (see Scheme 5), Steglich and Miltz used the cyclic enamine **161** (derived from dioxanone **33** and morpholine) in an addition reaction to *N*-benzoyl-*N*-(2,2,2-trichloroethylidene)amine (**160**), which was formed in situ through the elimination of HCl (Scheme 42).^[86] The addition product **162** was obtained with very high diastereoselectivity ($\geq 96\%$ *de*).

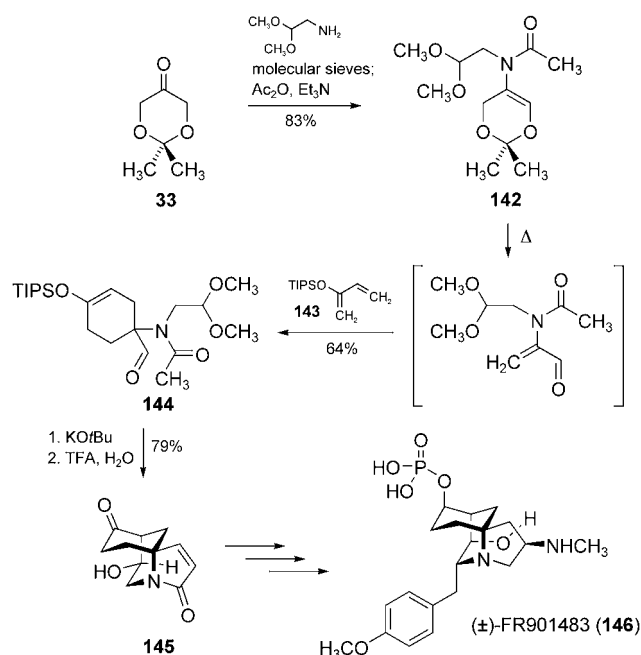
Lithium enolates derived from cyclic DHA derivatives have been investigated extensively. The first example of their use was provided by Hiram et al. (Scheme 43).^[87] In their studies directed towards the total synthesis of the avermectins and milbemycins, the lithium enolate of **163** (obtained in five steps from D-glucose) was treated with aldehyde **164** to give the aldol product **165** in modest yield and with moderate diastereoselectivity (79% *de*; only the *anti* diastereomers were observed).

Table 3: Coupling reactions of triflate **127** (see Scheme 36) to yield various 5-substituted 1,3-dioxins.

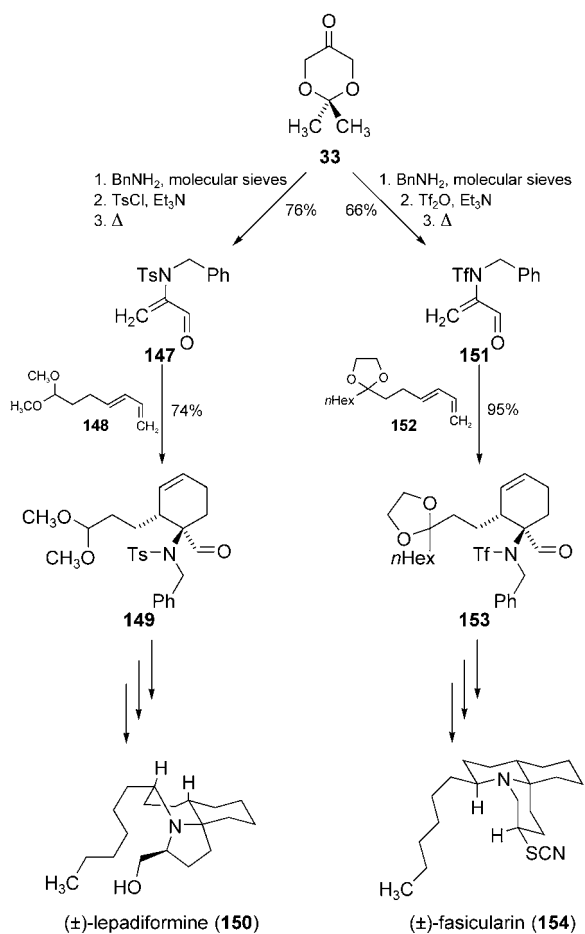
Entry	Coupling conditions	Coupling product	Yield [%]	Thermolysis conditions	Retrocycloaddition/cycloaddition product	Yield [%]
1	Hex ₂ CuLi		76	CDCl ₃ , 115 °C		79
2	[Pd ₂ (dba) ₃], AsPh ₃ , PhSnBu ₃		60	C ₇ D ₈ , 130 °C		97 (dimer)
3	[PdCl ₂ (PhCN) ₂], AsPh ₃ , ArB(OH) ₂		88	CDCl ₃ , 130 °C		88
4	product of entry 3, MeONH ₃ Cl		89	<i>o</i> -dichlorobenzene, 130 °C		96
5	[Pd(PPh ₃) ₄], CuI, TIPS-C≡CH		82	 toluene, 110 °C		100
6	ethyl vinyl ether, NEt ₃ , Pd(OAc) ₂		67	 C ₆ H ₆ , 78 °C		—
7	Pd(OAc) ₂ , PPh ₃ , CO, NEt ₃		60	<i>i</i> BuO-C≡CH 80 °C		92
8	Pd(OAc) ₂ , dppp, CO, NEt ₃ , MeONHMe		50	<i>i</i> BuO-C≡CH 80 °C		70
9	product of entry 8, 7-lithio-1,3-hexadiene		60	C ₆ D ₆ , 70 °C		80

dba = dibenzylideneacetone.

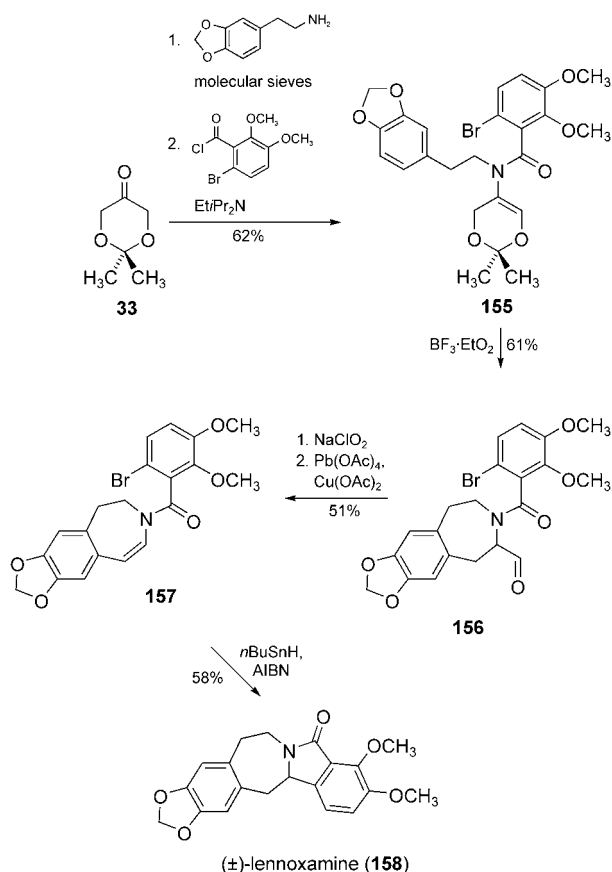




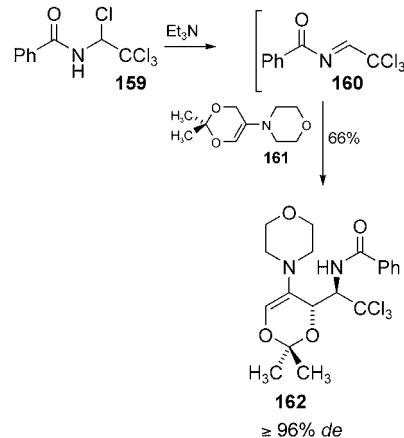
Scheme 39. Total synthesis of (±)-FR901483 (146).



Scheme 40. Total synthesis of (±)-lepadiformine (150) and (±)-fasicularin (154).



Scheme 41. Total synthesis of (±)-lennoxamine (158).

Scheme 42. Addition of enamine 161 to N -benzoyl- N -(2,2,2-trichloroethylidene)amine (160).

Later, Majewski and co-workers investigated lithium enolates, their formation and their reactions, more thoroughly.^[35,69a] Studies with derivative 166, which is monosubstituted in the 2-position, showed that LDA leads to significant reduction of the keto group. The yield of the reduction product increased significantly with diethyl ether as the solvent, thus opening up a high-yielding alternative route to the *trans* dioxanole 167 (Scheme 44a). The reduction could be suppressed sufficiently by 1) the use of the “internal quench”

Table 4: Electrophilic aromatic substitution reactions of different 5-amido-1,3-dioxins.

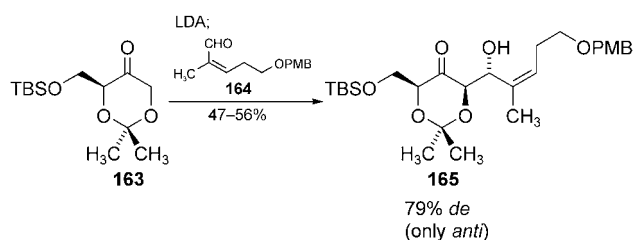
Entry	Substrate	Method, ^[a] substrate yield	Lewis acid	Product	Yield [%]
1		a, 85 %	BF ₃ ·Et ₂ O		61
2		a, 72 %	BF ₃ ·Et ₂ O		67
3		a, 65 %	AlCl ₃		67
4		b, 65 %	BF ₃ ·Et ₂ O		61
5		d, 75 %	SnCl ₄		68
6		c, 61 %	SnCl ₄		71
7		d, 80 %	SnCl ₄		75
8		b, 68 %	BF ₃ ·Et ₂ O		61
9		b, 64 %	BF ₃ ·Et ₂ O		54

[a] See Scheme 38.

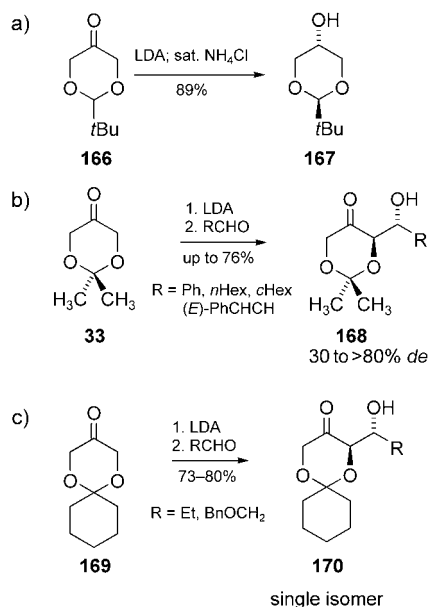
procedure developed by Corey (LDA and TMSCl are premixed to give the TMS enol ether), 2) the use of bases that lack α hydrogen atoms (e.g. LiTMP, LiHMDS; TMP = 2,2,6,6-tetramethylpiperidine), or 3) the use of ketals rather than acetals as protecting groups for the 1,3-diol functionality of DHA. On the basis of these observations, Majewski and co-workers chose dioxanone **33** for aldol reactions with aldehydes.

The aldol products **168** were obtained with up to 80 % *de* (in the case of cyclohexanecarbaldehyde; Scheme 44b). Meanwhile we successfully developed an organocatalytic variant of the aldol reaction of **33**.^[88] With this biomimetic approach protected sugars and aminosugars are readily accessible in only one step with high selectivity. Kim and Hong started instead with the lithium enolate of **169**, which seems to react much more stereoselectively than the lithium enolate of **33** in aldol reactions: With both *n*-propanal and benzylloxycetaldehyde only the *anti* diastereomers **170** of the products were detected (Scheme 44c).^[22] The TBS enol ether derived from **169** was also tested in a Mukaiyama-type aldol reaction in the presence of different Lewis acids (by analogy with Scheme 7). As expected, only the *anti* diastereomer was obtained.

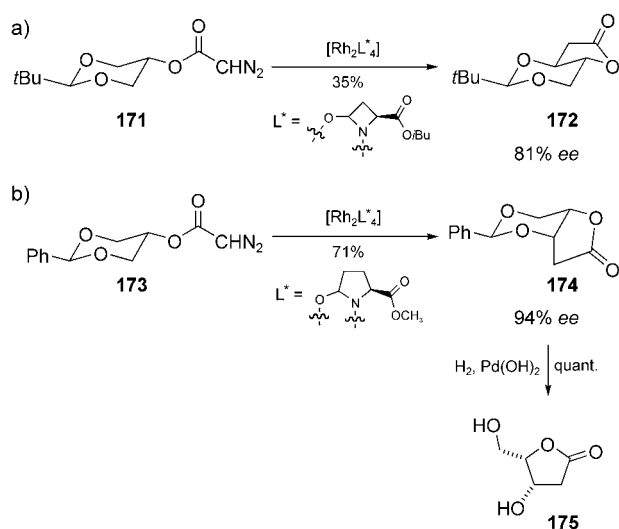
LDA has not often been used for the stereoselective reduction of ketones. More common reagents, such as LiAlH₄ and L-selectride, allow selective access to *trans* and *cis* dioxanols, respectively.^[32a] Doyle et al. used the diazoacetates of these dioxanols in stereoselective intramolecular C–H insertion reactions in the presence of dirhodium(II) carboxamidates as catalysts.^[89] In the case of the *trans* *tert*-butyl acetal **171**, catalytic decomposition of the diazo group led to insertion only into the equatorial C–H bond to give **172** with up to 81 % *ee* in modest yields (Scheme 45a). In striking contrast was the behavior of the *trans* phenyl acetal **173**. Although ligands with the same absolute configuration were used, both the diastereoselectivity and enantioselectivity observed in the formation of **174** were different from what one might expect based on the reaction of **171** (Scheme 45b): Insertion into the axial CH bond occurred and the γ -lactone ring was formed on the other side of the molecule. However, the reason for this unexpected difference remains unclear. Recrystallization of **174** provided enantiomerically pure material. Hydrogenolysis then gave 2-deoxy-L-xylono-1,4-lactone (**175**), an important precursor to carbohydrate-based and polyhydroxylated natural products.



Scheme 43. First use of a lithium enolate derived from a derivative of dioxanone **33**. LDA = lithium diisopropylamide, PMB = *p*-methoxybenzyl.



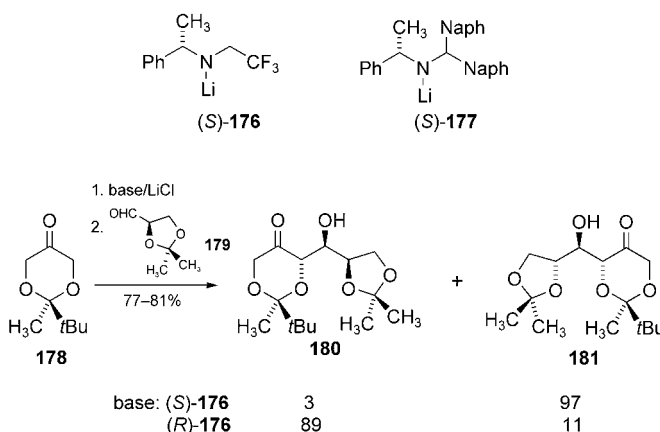
Scheme 44. Cyclic DHA derivatives and their different reactivity towards LDA. a) The acetal-protected derivative **166** undergoes stereoselective reduction. b) The ketal-protected derivatives **33** and **169** can be deprotonated cleanly and trapped with aldehydes to give the corresponding aldol products **168** and **170**.



Scheme 45. Stereoselective intramolecular insertion reactions into C–H bonds.

Cyclic DHA derivatives that are differentially substituted at C2 can be deprotonated enantioselectively. Majewski and co-workers also tackled this problem.^[35,69] The most effective bases, **176** and **177**, deprotonated ketone **178** with up to 90% *ee* (Scheme 46). This methodology was applied in the stereoselective synthesis of partially protected D-tagatose **180** and D-psicose **181** by using (*R*)-**176** and (*S*)-**176**, respectively.

Ulven and Carlsen applied the hydrazone methodology outlined in Section 2.2.1.1. to 2-phenyl-1,3-dioxan-5-one as the ketone component. Highly stereoselective α, α' -alkylation reactions enabled the synthesis of 2-deoxy-L-ribose, as well as all diastereomers of the 2-deoxypentoses and 2,6-dideoxyhexoses.^[90]



Scheme 46. Enantioselective deprotonation of dioxanone **178** and use of the resulting lithium enolate in the synthesis of the partially protected ketohexoses **180** and **181**. Naph = naphthyl.

Comins et al. also used the zinc enolate of **33** in additions to the chiral 1-acyl pyridinium salt **24** (see Scheme 8). As the *E* enolate is formed from **33** (as opposed to the *Z* enolate in the case of **18**) the configuration α to the carbonyl group was inverted.^[23] Francl, Swindell, and co-workers could alkylate **33** with MeI by using LDA as the base (71% yield). This is the only example to date of a direct alkylation of **33**.^[91]

3. Conclusion and Outlook

In this Review we have presented many different DHA derivatives, which have mainly been developed for and used in stereoselective aldol reactions. Two classes of derivatives deserve particular attention, because their applicability has been shown to be much broader: The 5-substituted 1,3-dioxins provide an elegant route to various 2-substituted acroleins, and the 2,2-dimethyl-1,3-dioxan-5-one SAMP/RAMP hydrazones (*S*)-**37**/*R*-**37** are chiral DHAP equivalents that enable stereoselective aldol reactions, as well as highly stereoselective alkylation and Michael addition reactions. Since at least two alkylations can be performed in succession, (*S*)-**37** and (*R*)-**37** can even be regarded as chiral equivalents of a double DHA d^2 -synthon. Many further

applications of the efficient methodologies described herein to the synthesis of bioactive compounds can be anticipated.

Received: February 19, 2004

Published Online: January 13, 2005

- [1] A. Butlerow, *Ann.* **1861**, 120, 295–298.
- [2] For historical overviews, see: a) J. K. N. Jones, W. A. Szarek in *The Total Synthesis of Natural Products, Vol. 1* (Ed.: J. ApSimon), Wiley, New York, **1973**, pp. 1–8; b) R. Mayer, K. Runge, H. Drechsel, *Z. Chem.* **1963**, 3, 134–142.
- [3] B. Tollens, *Ber. Dtsch. Chem. Ges.* **1882**, 15, 1629–1634; B. Tollens, *Ber. Dtsch. Chem. Ges.* **1883**, 16, 917–921.
- [4] O. Loew, *J. Prakt. Chem.* **1886**, 33, 321–351.
- [5] H. Beyer, W. Walter, *Lehrbuch der Organischen Chemie*, Hirzel, Stuttgart, **1991**, p. 435.
- [6] E. Fischer isolated DL-fructose and DL-sorbose as their phenyl-osazones, α -acrosazone and β -acrosazone, respectively. He derived these names from bromoacrolein (2,3-dibromopropionaldehyde), which upon treatment with base yields a product mixture that consists mainly of α - and β -acrose. The phenyl-osazones of these compounds were identical to those obtained by Fischer from formose. For Fischer's work, see, for example: a) E. Fischer, J. Tafel, *Ber. Dtsch. Chem. Ges.* **1887**, 20, 1088–1094; b) E. Fischer, J. Tafel, *Ber. Dtsch. Chem. Ges.* **1887**, 20, 2566–2575; c) E. Fischer, *Ber. Dtsch. Chem. Ges.* **1888**, 21, 988–991; d) E. Fischer, F. Passmore, *Ber. Dtsch. Chem. Ges.* **1889**, 22, 359–361; e) E. Fischer, *Ber. Dtsch. Chem. Ges.* **1890**, 23, 2114–2141.
- [7] For mechanistic considerations, see: a) reference [2b]; b) E. Pfeil, G. Schroth, *Chem. Ber.* **1952**, 85, 293–307; c) R. Breslow, *Tetrahedron Lett.* **1959**, 1, 22–26; d) W. P. Huskey, I. R. Epstein, *J. Am. Chem. Soc.* **1989**, 111, 3157–3163.
- [8] It should be mentioned that formose consists mainly of pentoses, and that hexoses constitute only a small fraction of the mixture; see reference [2b].
- [9] The observation that D-glyceraldehyde and 1,3-dihydroxyacetone (and even D-glyceraldehyde alone!) react in basic solution to yield D-fructose and D-sorbose as major products provided support for this pathway: H. O. L. Fischer, E. Baer, *Helv. Chim. Acta* **1936**, 19, 519–532.
- [10] M. Calvin, *Angew. Chem.* **1962**, 74, 165–175; *Angew. Chem. Int. Ed. Engl.* **1962**, 1, 65–75.
- [11] For excellent reviews, see: a) T. D. Machajewski, C.-H. Wong, *Angew. Chem.* **2000**, 112, 1406–1430; *Angew. Chem. Int. Ed.* **2000**, 39, 1352–1375; b) W.-D. Fessner, C. Walter, *Top. Curr. Chem.* **1996**, 184, 97–194.
- [12] For possible alternatives to DHAP, see: a) M. D. Bednarski, E. S. Simon, N. Bischofberger, W.-D. Fessner, M.-J. Kim, W. Lees, T. Saito, H. Waldmann, G. M. Whitesides, *J. Am. Chem. Soc.* **1989**, 111, 627–635; b) reference [11b]; c) DHA in the presence of inorganic arsenate can mimic DHAP: J. R. Durrwachter, D. G. Drueckhammer, K. Nozaki, H. M. Sweers, C.-H. Wong, *J. Am. Chem. Soc.* **1986**, 108, 7812–7818; D. G. Drueckhammer, J. R. Durrwachter, R. L. Pederson, D. C. Crans, L. Daniels, C.-H. Wong, *J. Org. Chem.* **1989**, 54, 70–77; R. Schoevaart, F. van Rantwijk, R. A. Sheldon, *J. Org. Chem.* **2001**, 66, 4559–4562.
- [13] a) A. N. Phung, M. T. Zannetti, G. Whited, W.-D. Fessner, *Angew. Chem.* **2003**, 115, 4970–4972; *Angew. Chem. Int. Ed.* **2003**, 42, 4821–4824; b) W.-D. Fessner, O. Eyrisch, *Angew. Chem.* **1992**, 104, 76–78; *Angew. Chem. Int. Ed. Engl.* **1992**, 31, 56–58.
- [14] For the synthesis of sugars and their derivatives, see: a) C.-H. Wong, G. M. Whitesides, *J. Org. Chem.* **1983**, 48, 3199–3205; b) C.-H. Wong, F. P. Mazenod, G. M. Whitesides, *J. Org. Chem.* **1983**, 48, 3493–3497; c) reference [12c]; d) J. R. Durrwachter, H. M. Sweers, K. Nozaki, C.-H. Wong, *Tetrahedron Lett.* **1986**, 27, 1261–1264; e) M. D. Bednarski, H. J. Waldmann, G. M. Whitesides, *Tetrahedron Lett.* **1986**, 27, 5807–5810; f) R. Schoevaart, F. van Rantwijk, R. A. Sheldon, *J. Org. Chem.* **2000**, 65, 6940–6943.
- [15] For the synthesis of azasugars and their derivatives, see: a) T. Ziegler, A. Straub, F. Effenberger, *Angew. Chem.* **1988**, 100, 737–738; *Angew. Chem. Int. Ed. Engl.* **1988**, 27, 716–717; b) C. H. von der Osten, A. J. Sinskey, C. F. Barbas III, R. L. Pederson, Y.-F. Wang, C.-H. Wong, *J. Am. Chem. Soc.* **1989**, 111, 3924–3927; c) R. L. Pederson, C.-H. Wong, *Heterocycles* **1989**, 28, 477–480; d) T. Kajimoto, K. K.-C. Liu, R. L. Pederson, Z. Zhong, Y. Ichikawa, J. A. Porco, Jr., C.-H. Wong, *J. Am. Chem. Soc.* **1991**, 113, 6187–6196; e) T. Kajimoto, L. Chen, K. K.-C. Liu, C.-H. Wong, *J. Am. Chem. Soc.* **1991**, 113, 6678–6680; f) K. K.-C. Liu, T. Kajimoto, L. Chen, Z. Zhong, Y. Ichikawa, C.-H. Wong, *J. Org. Chem.* **1991**, 56, 6280–6289.
- [16] a) W.-D. Fessner, J. Badía, O. Eyrisch, A. Schneider, G. Sinerius, *Tetrahedron Lett.* **1992**, 33, 5231–5234; b) W.-D. Fessner, A. Schneider, O. Eyrisch, G. Sinerius, J. Badía, *Tetrahedron: Asymmetry* **1993**, 4, 1183–1192.
- [17] A. Córdova, W. Notz, C. F. Barbas III, *Chem. Commun.* **2002**, 3024–3025.
- [18] a) B. List, *Tetrahedron* **2002**, 58, 5573–5590; b) P. I. Dalko, L. Moisan, *Angew. Chem.* **2001**, 113, 3840–3864; *Angew. Chem. Int. Ed.* **2001**, 40, 3726–3748; c) P. I. Dalko, L. Moisan, *Angew. Chem.* **2004**, 116, 5248–5286; *Angew. Chem. Int. Ed.* **2004**, 43, 5138–5175; d) E. R. Jarvo, S. J. Miller, *Tetrahedron* **2002**, 58, 2481–2495.
- [19] H. T. Tang, S. X. Cheng, P. Zhang, *Chem. Abstr.* **1983**, 98, 143347c, 160502s.
- [20] P. J. Kocienski, *Protecting Groups*, Thieme, Stuttgart, New York, **2003**.
- [21] a) R. W. Stevens, T. Mukaiyama, *Chem. Lett.* **1983**, 595–598; b) T. Mukaiyama, N. Iwasawa, R. W. Stevens, T. Haga, *Tetrahedron* **1984**, 40, 1381–1390.
- [22] K. S. Kim, S. D. Hong, *Tetrahedron Lett.* **2000**, 41, 5909–5913.
- [23] D. L. Comins, J. T. Kuethe, H. Hong, F. J. Lakner, *J. Am. Chem. Soc.* **1999**, 121, 2651–2652.
- [24] J. Murga, E. Falomir, M. Carda, F. González, J. A. Marco, *Org. Lett.* **2001**, 3, 901–904.
- [25] a) I. Paterson, D. J. Wallace, S. M. Velázquez, *Tetrahedron Lett.* **1994**, 35, 9083–9086; b) I. Paterson, D. J. Wallace, *Tetrahedron Lett.* **1994**, 35, 9087–9090; c) I. Paterson, D. J. Wallace, *Tetrahedron Lett.* **1994**, 35, 9477–9480; d) I. Paterson, D. J. Wallace, C. J. Cowden, *Synthesis* **1998**, 639–652.
- [26] a) J. M. Goodman, *Tetrahedron Lett.* **1992**, 33, 7219–7222; b) J. M. Goodman, I. Paterson, *Tetrahedron Lett.* **1992**, 33, 7223–7226.
- [27] The results of investigations into aldol reactions of α -silyloxy-3-pentanones also seem to contradict Paterson's model: M. Galobardes, M. Gascón, M. Mena, P. Romea, F. Urpí, J. Vilarrasa, *Org. Lett.* **2000**, 2, 2599–2602.
- [28] a) I. Paterson, K. Feßner, M. R. V. Finlay, M. F. Jacobs, *Tetrahedron Lett.* **1996**, 37, 8803–8806; b) I. Paterson, V. A. Doughty, M. D. McLeod, T. Trieselmann, *Angew. Chem.* **2000**, 112, 1364–1368; *Angew. Chem. Int. Ed.* **2000**, 39, 1308–1312.
- [29] For an example from another research group, see: S. Sasaki, Y. Hamada, T. Shioiri, *Tetrahedron Lett.* **1999**, 40, 3187–3190.
- [30] a) J. A. Marco, M. Carda, E. Falomir, C. Palomo, M. Oiarbide, J. A. Ortiz, A. Linden, *Tetrahedron Lett.* **1999**, 40, 1065–1068; b) M. Carda, E. Falomir, J. Murga, E. Castillo, F. González, J. A. Marco, *Tetrahedron Lett.* **1999**, 40, 6845–6848; c) M. Carda, J. Murga, E. Falomir, F. González, J. A. Marco, *Tetrahedron* **2000**, 56, 677–683.

- [31] a) D. Hoppe, H. Schmincke, H.-W. Kleemann, *Tetrahedron* **1989**, 45, 687–694; b) reference [32c].
- [32] a) D. C. Forbes, D. G. Ene, M. P. Doyle, *Synthesis* **1998**, 879–882; b) R. M. Carman, P. N. Handley, *Aust. J. Chem.* **2001**, 54, 769–776; c) D. Enders, M. Voith, S. J. Ince, *Synthesis* **2002**, 1775–1779.
- [33] a) D. Enders, B. Bockstiegel, *Synthesis* **1989**, 493–496; b) E. Schmidt, R. Wilkendorf, *Ber. Dtsch. Chem. Ges.* **1919**, 52, 389–399; c) G. B. Linden, M. H. Gold, *J. Org. Chem.* **1956**, 21, 1175–1176; d) R. A. Y. Jones, A. R. Katritzky, K. A. F. Record, R. Scattergood, J. M. Sullivan, *J. Chem. Soc. Perkin Trans. 2* **1974**, 402–406; e) Y. Araki, J.-i. Nagasawa, Y. Ishido, *J. Chem. Soc. Perkin Trans. 1* **1981**, 12–23.
- [34] Majewski et al. developed another approach for the synthesis of 2,2-dimethyl-1,3-dioxan-5-one (**33**), similar to that depicted in Scheme 11 b. As the overall yields were lower and the synthesis was less amenable to scale-up, they finally prepared **33** according to the sequence shown in Scheme 11 b (see reference [35]).
- [35] M. Majewski, D. M. Gleave, P. Nowak, *Can. J. Chem.* **1995**, 73, 1616–1626.
- [36] a) For reviews, see: A. Job, C. F. Janeck, W. Bettray, R. Peters, D. Enders, *Tetrahedron* **2002**, 58, 2253–2329; b) D. Enders in *Asymmetric Synthesis*, Vol. 3 (Ed.: J. D. Morrison), Academic Press, Orlando, **1984**, pp. 275–339; c) D. Enders, H. Kipphardt, P. Fey, *Org. Synth.* **1987**, 65, 183–202; d) D. Enders, H. Eichenauer, *Angew. Chem.* **1976**, 88, 579–580; *Angew. Chem. Int. Ed. Engl.* **1976**, 15, 549–550; e) D. Enders, H. Eichenauer, *Tetrahedron Lett.* **1977**, 18, 191–194.
- [37] D. Enders, U. Jegelka, B. Dücker, *Angew. Chem.* **1993**, 105, 423–425; *Angew. Chem. Int. Ed. Engl.* **1993**, 32, 423–425.
- [38] Parts of the work on (*S*)-**37** and (*R*)-**37** have been reviewed already: D. Enders, B. Bockstiegel, W. Gatzweiler, U. Jegelka, B. Dücker, L. Wortmann, *Chim. Oggi* **1997**, 15, 20–23.
- [39] a) D. Enders, T. Hundertmark, R. Lazny, *Synth. Commun.* **1999**, 29, 27–33; b) D. Enders, T. Hundertmark, R. Lazny, *Synlett* **1998**, 721–722.
- [40] D. Enders, C. F. Janeck, J. Runsink, *Synlett* **2000**, 641–643; D. Enders, C. F. Janeck, G. Raabe, *Eur. J. Org. Chem.* **2000**, 3337–3345.
- [41] D. Enders, W. Gatzweiler, U. Jegelka, *Synthesis* **1991**, 1137–1141.
- [42] D. Enders, A. Nührling, J. Runsink, G. Raabe, *Synthesis* **2001**, 1406–1414.
- [43] The trisubstituted hydrazones thus obtained can be subjected to a fourth alkylation reaction. These results will be published in due course.
- [44] D. Enders, U. Jegelka, *Tetrahedron Lett.* **1993**, 34, 2453–2456.
- [45] a) H. Nagaoka, Y. Kishi, *Tetrahedron* **1981**, 37, 3873–3888; b) S. Hanessian, J.-R. Pouigny, I. K. Boessenkool, *J. Am. Chem. Soc.* **1982**, 104, 6164–6166.
- [46] K. C. Nicolaou, R. A. Daines, Y. Ogawa, T. K. Chakraborty, *J. Am. Chem. Soc.* **1988**, 110, 4696–4705.
- [47] R. W. Armstrong, J.-M. Beau, S. H. Cheon, W. J. Christ, H. Fujioka, W.-H. Ham, L. D. Hawkins, H. Jin, S. H. Kang, Y. Kishi, M. J. Martinelli, W. W. McWorther, Jr, M. Mizuno, M. Nakata, A. E. Stutz, F. X. Talamas, M. Taniguchi, J. A. Tino, K. Ueda, J.-i. Uenishi, J. B. White, M. Yonaga, *J. Am. Chem. Soc.* **1989**, 111, 7530–7533.
- [48] Y. Ichikawa, Y.-C. Lin, D. P. Dumas, G.-J. Shen, E. Garcia-Junceda, M. A. Williams, R. Bayer, C. Ketcham, L. E. Walker, J. C. Paulson, C.-H. Wong, *J. Am. Chem. Soc.* **1992**, 114, 9283–9298.
- [49] C. André, J. Bolte, C. Demuyne, *Tetrahedron: Asymmetry* **1998**, 9, 3737–3739.
- [50] M. Majewski, P. Nowak, *Tetrahedron: Asymmetry* **1998**, 9, 2611–2617.
- [51] D. Enders, O. F. Prokopenko, *Liebigs Ann.* **1995**, 1185–1191.
- [52] D. Enders, U. Jegelka, *Synlett* **1992**, 999–1002.
- [53] D. Enders, J. H. Kirchhoff, *Synthesis* **2000**, 2099–2105.
- [54] D. Enders, M. Voith, *Synthesis* **2002**, 1571–1577.
- [55] a) W. A. König, H. Drautz, H. Zähler, *Liebigs Ann. Chem.* **1980**, 1384–1391; b) D. J. Faulkner, B. N. Ravi, *Tetrahedron Lett.* **1980**, 21, 23–26.
- [56] D. Enders, M. Voith, *Synlett* **2002**, 29–32.
- [57] D. Enders, M. Haas, *Synlett* **2003**, 2182–2184.
- [58] R. H. Crabtree, M. W. Davis, *J. Org. Chem.* **1986**, 51, 2655–2661.
- [59] a) S. Omura, H. Tanaka in *Macrolide Antibiotics: Chemistry, Biology, Practice* (Ed.: S. Omura), Academic Press, New York, **1984**, pp. 351–404; b) S. D. Rychnovsky, *Chem. Rev.* **1995**, 95, 2021–2040; c) T. Oishi, T. Nakata, *Synthesis* **1990**, 635–645; d) C. Schneider, *Angew. Chem.* **1998**, 110, 1445–1448; *Angew. Chem. Int. Ed.* **1998**, 37, 1375–1378.
- [60] D. Enders, T. Hundertmark, C. Lampe, U. Jegelka, I. Scharfbillig, *Eur. J. Org. Chem.* **1998**, 2839–2849.
- [61] D. Enders, T. Hundertmark, *Tetrahedron Lett.* **1999**, 40, 4169–4172.
- [62] D. Enders, T. Hundertmark, *Eur. J. Org. Chem.* **1999**, 751–756.
- [63] S. Mizutani, H. Odai, T. Masuda, M. Iijima, M. Osono, M. Hamda, H. Naganawa, M. Ishizuka, T. Takeuchi, *J. Antibiot.* **1989**, 42, 952–959.
- [64] D. Enders, A. Lenzen, *Synlett* **2003**, 2185–2187.
- [65] For the “silyl trick”, see: a) D. Enders, J. Adam, D. Klein, T. Otten, *Synlett* **2000**, 1371–1384; b) D. Enders, B. B. Lohray, F. Burkamp, V. Bhushan, R. Hett, *Liebigs Ann.* **1996**, 189–200; c) D. Enders, B. B. Lohray, *Angew. Chem.* **1987**, 99, 359–360; *Angew. Chem. Int. Ed. Engl.* **1987**, 26, 351–352.
- [66] D. Enders, O. F. Prokopenko, G. Raabe, J. Runsink, *Synthesis* **1996**, 1095–1100.
- [67] D. Enders, S. J. Ince, *Synthesis* **2002**, 619–624.
- [68] D. Enders, S. J. Ince, M. Bonnekessel, J. Runsink, G. Raabe, *Synlett* **2002**, 962–966.
- [69] a) M. Majewski, P. Nowak, *Synlett* **1999**, 1447–1449; b) M. Majewski, P. Nowak, *J. Org. Chem.* **2000**, 65, 5152–5160.
- [70] Majewski and Nowak (reference [69]) were the first to show the possibility of a double aldol reaction (compare reference [68]). The aldol adduct resulting from dioxanone **33** and benzaldehyde did not need to be protected for the second aldol reaction with cyclohexanecarbaldehyde. However, this was the only example presented, and an 83:9:6:2 mixture of diastereomers was obtained.
- [71] D. Enders, D. L. Whitehouse, *Synthesis* **1996**, 621–626.
- [72] D. Enders, D. L. Whitehouse, J. Runsink, *Chem. Eur. J.* **1995**, 1, 382–388.
- [73] D. Enders, A. Müller-Hüwen, *Eur. J. Org. Chem.* **2004**, 1732–1735.
- [74] D. Enders, D. Kownatka, T. Hundertmark, O. F. Prokopenko, J. Runsink, *Synthesis* **1997**, 649–652.
- [75] a) J. Erickson, D. J. Neidhart, J. VanDrie, D. J. Kempf, X. C. Wang, D. W. Norbeck, J. J. Plattner, J. W. Rittenhouse, M. Turon, N. Wideburg, W. E. Kohlbrenner, R. Simmer, R. Helfrich, D. A. Paul, M. Knigge, *Science* **1990**, 249, 527–533; b) D. J. Kempf, D. W. Norbeck, L. M. Codacovi, X. C. Wang, W. E. Kohlbrenner, N. E. Wideburg, D. A. Paul, M. Knigge, S. Vasavanonda, A. Craig-Kennard, A. Saldivar, W. Rosenbrock, J. J. Clement, J. J. Plattner, J. Erickson, *J. Med. Chem.* **1990**, 33, 2687–2689.
- [76] R. L. Funk, K. J. Yost III, *J. Org. Chem.* **1996**, 61, 2598–2599.
- [77] R. L. Funk, G. L. Bolton, *J. Am. Chem. Soc.* **1988**, 110, 1290–1292.
- [78] R. A. Aungst, Jr, R. L. Funk, *Org. Lett.* **2001**, 3, 3553–3555.
- [79] S. P. Fearnley, R. L. Funk, R. J. Gregg, *Tetrahedron* **2000**, 56, 10275–10281.
- [80] R. A. Aungst, Jr, R. L. Funk, *J. Am. Chem. Soc.* **2001**, 123, 9455–9456.
- [81] J. R. Fuchs, R. L. Funk, *Org. Lett.* **2001**, 3, 3349–3351.

- [82] J.-H. Maeng, R. L. Funk, *Org. Lett.* **2001**, 3, 1125–1128.
[83] T. J. Greshock, R. L. Funk, *Org. Lett.* **2001**, 3, 3511–3514.
[84] J.-H. Maeng, R. L. Funk, *Org. Lett.* **2002**, 4, 331–333.
[85] J. R. Fuchs, R. L. Funk, *Org. Lett.* **2001**, 3, 3923–3925.
[86] W. Miltz, W. Steglich, *Synthesis* **1990**, 750–752.
[87] M. Hirama, T. Noda, S. Itô, *J. Org. Chem.* **1988**, 53, 708–710.
[88] D. Enders, C. Grondal, *Angew. Chem.* **2005**, in press.
[89] M. P. Doyle, J. S. Tedrow, A. B. Dyatkin, C. J. Spaans, D. G. Ene, *J. Org. Chem.* **1999**, 64, 8907–8915.
[90] a) T. Ulven, P. H. J. Carlsen, *Synth. Commun.* **2000**, 30, 2275–2280; b) T. Ulven, P. H. J. Carlsen, *Eur. J. Org. Chem.* **2001**, 3367–3374.
[91] M. M. Franci, G. Hansell, B. P. Patel, C. S. Swindell, *J. Am. Chem. Soc.* **1990**, 112, 3535–3539.
-

Life's Simple Pleasures!



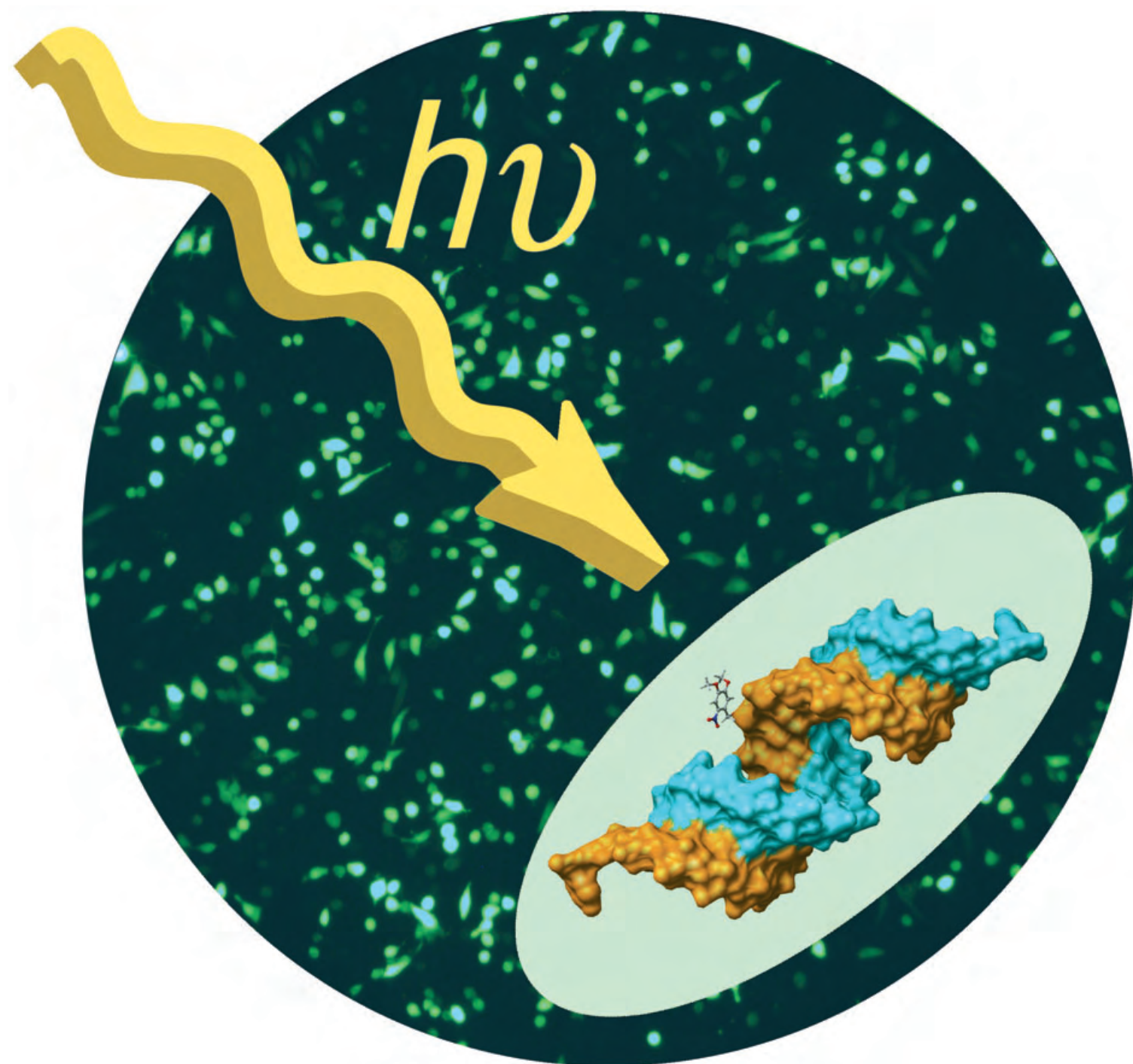
No need to waste precious time looking for the right information – Register now for the free **Wiley-VCH Alerting Service**.

It's simple – and it's fast.

To receive regular news per e-mail tailored precisely to your needs and interests, just fill in the registration form at www.wiley-vch.de/home/pas/



Communications



The process of RNA interference can be controlled with light. On the following pages, S. H. Friedman and co-workers demonstrate that siRNAs modified with photolabile groups have reduced ability to effect RNA interference until irradiation deprotects them and releases fully active siRNA.

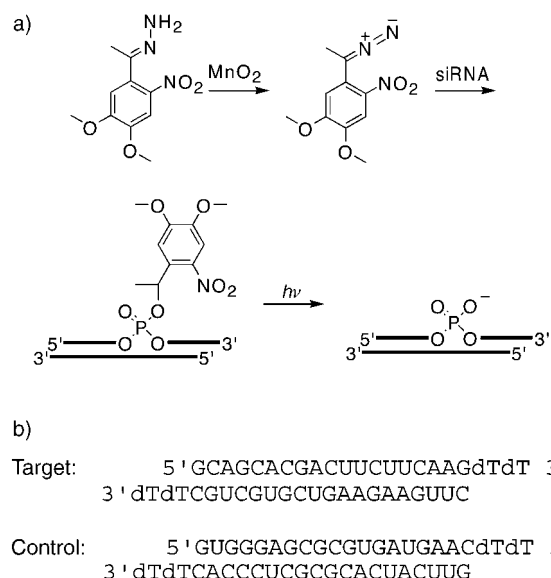
Gene Expression

Light-Activated RNA Interference**

Samit Shah, Subhashree Rangarajan, and
Simon H. Friedman*

Small interfering RNA (siRNA) molecules are 21–23 nucleotide-long duplex RNAs that are able to control gene expression through the process of RNA interference.^[1–4] RNA interference involves siRNA binding to the RNA-induced silencing complex (RISC), which then directs the destruction of messenger RNA (mRNA) that is complementary to the antisense strand of the siRNA. RNA interference directed by siRNA has proven to be a broadly applicable method for controlling gene expression and has therefore become a central tool in investigating the role of specific genes in cellular processes.

The aim of the work described herein is to develop a method to control the process of RNA interference with light (light-activated RNA interference, (LARI)). This will allow the spacing, timing, and degree of gene expression to be controlled by irradiation. This added level of control to the widely applied method of RNA interference should be particularly beneficial for the study of cell development, which is tied closely to the location, timing, and degree of expression of key proteins (i.e., morphogens). Our rationale involves the covalent attachment of a photolabile group to an siRNA duplex to sterically block the initial siRNA–RISC interaction, thus preventing the degradation of its target mRNA. Only upon irradiation would active siRNA be released. The photolabile moiety that we used for this study is the 4,5-dimethoxy-2-nitrophenylethyl (DMNPE) group previously used by Monroe, Haselton, and co-workers to cage plasmids.^[5] Caging is effected by reaction of the precursor hydrazone to create the corresponding diazo compound, which can react with phosphate groups (Scheme 1a). We have used the GFP-targeting siRNA (GFP = green fluorescent protein) developed by Chiu and Rana.^[6] This allows quantitation of gene expression through the fluorescent signal generated by GFP. A further advantage of this system is that it has been well-characterized. Therefore, potential complicating factors such as an antisense effect have been ruled out.



Scheme 1. a) Reactions to introduce photolabile groups into siRNA (see Experimental Section. b) Target and control sequences of siRNA used in the study.

To analyze the effect of caging, we used two siRNA sequences (Scheme 1b): the target siRNA that directs the degradation of GFP mRNA, and a control siRNA that has been shown to have no effect on GFP expression.^[7] RNA oligonucleotides were deprotected after automated synthesis and annealed to form duplex siRNA. Target and control duplexes (1 nmol each) were photoprotected by using a 100-fold excess of diazo reagent relative to RNA duplex. The extent of photocaging was determined with the technique of Monroe, Haselton, and co-workers by using the absorbance of the sample at $\lambda = 355$ nm.^[5] Under these conditions we obtained 1.4 photocaging groups per duplex. This 3% caging efficiency is similar to the results found in two other systems.^[5,8] Melting temperature (T_m) determination was used to characterize further the target caged and uncaged siRNA duplexes ($T_m = 65$ and 54°C , respectively). Finally, in an analysis of the modified duplex through ESI MS, we were able to observe sense and antisense strands, both with and without a photolabile group (Figure 1).

Gene expression was analyzed by using the system developed by Rana and Chiu which examines GFP expression in HeLa cells.^[6] We have modified this approach for use with 96-well plates. This allows us to quantitate GFP expression in vivo with a scanning fluorescence microplate reader equipped with a 485-nm excitation filter and a 535-nm emission filter. It also allows us to average larger numbers of experimental observations. HeLa cells were seeded in 96-well cell-culture plates at 70% confluency and allowed to grow over a period of 18–20 h. These cells were then transfected with the pEGFP-C1 plasmid and the appropriate siRNA by using lipofectamine. GFP controls were transfected with plasmid only, and mock transfection controls had neither plasmid nor siRNA. After a transfection period of 6 h, the cell culture media was removed and replaced with fresh media. The wells were then either exposed to light or masked.

[*] S. Shah, S. Rangarajan, S. H. Friedman
Division of Pharmaceutical Sciences
School of Pharmacy, University of Missouri, Kansas City
Kansas City, MO 64110 (USA)
Fax: (+1) 816-235-5190
E-mail: friedmans@umkc.edu

[**] We thank Dr. Dhananjay Pal and Professor Ashim K. Mitra for access to cell culture facilities. We also thank Dr. Scott Carter and Professor Paramjit Arora for useful discussions. Molecular graphics images were produced in part with the UCSF Chimera package from the Computer Graphics Laboratory, University of California, San Francisco (supported by NIH P41 RR-01081).^[14]

Supporting information for this article is available on the WWW under <http://www.angewandte.org> or from the author.

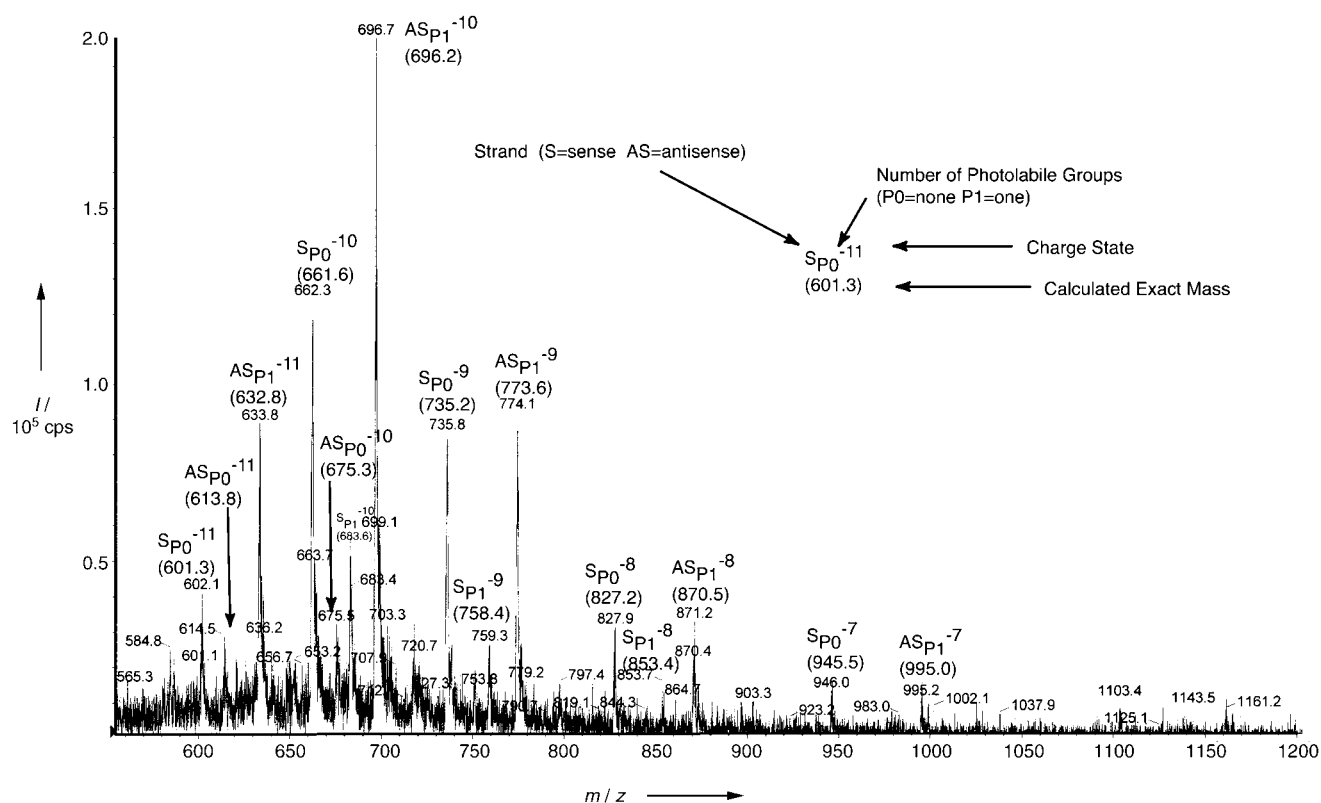


Figure 1. ESI mass spectrum of modified siRNA. Peaks are annotated to indicate the strand (AS = antisense; S = sense), the number of photolabile groups (P0 = none, P1 = one group, etc.), and the charge state (e.g., -10). Below the annotation is the expected m/z ratio in parentheses which is positioned above the actual m/z ratio. cps = counts s^{-1} .

A WG-320 longpass filter (Edmund Industrial Optics) permitted transmission of the frequencies needed for deprotection ($\lambda > 320$ nm) but blocked shorter and more-toxic wavelengths. The samples were exposed for 12 min with a Blak-Ray fluorescent UV lamp (XX-15 L, 15 W) at a distance of 10 cm. After exposure to light, the culture media were changed again, and the cells were allowed to culture for an additional 42 h. This is the period of time found by Rana and Chiu to produce an optimal decrease in GFP expression in this system.^[6] The GFP signal was then quantitated in vivo by using microplate fluorescence. We have not found it necessary to normalize for transfection efficiency with an internal standard. To accommodate variations in transfection efficiency, each experimental point represents an average of five wells. Furthermore, all the points represented in a figure come from a single 96-well plate, another factor that contributes to more consistent transfection efficiencies. This consistency is evidenced by the relatively low standard errors observed. Cells that were exposed to mock transfection (transfection agent without GFP plasmid) show auto-fluorescence signals of $< 4\%$ of the GFP control signal. This value does not change with irradiation of the cells.

The results are summarized in Figure 2. The only cells that had a significant difference in GFP expression upon exposure to light were those that had been treated with the caged target siRNA ($p < 0.005$). Selective phototoxicity can be eliminated as a mechanism of action, because light had no significant effect on GFP signal in any of the other samples. Light-

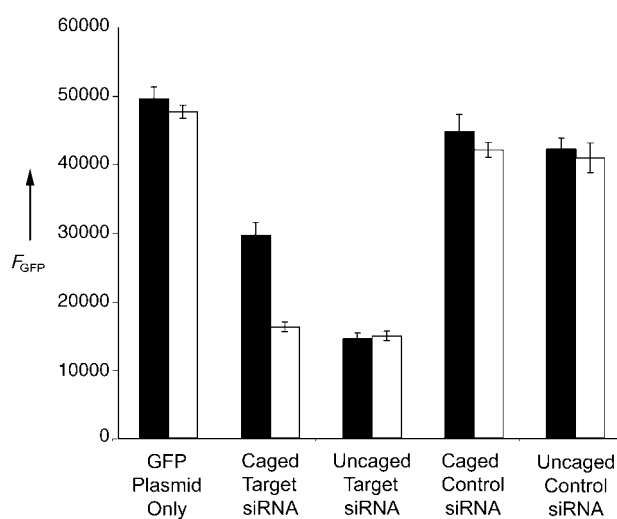


Figure 2. Influence of modified siRNA on GFP expression in HeLa cells upon exposure to and in the absence of light. Dark bars indicate signals from nonirradiated samples. Light bars indicate signals from irradiated samples. Only caged target siRNA shows a significant decrease upon irradiation ($p < 0.005$). F_{GFP} = GFP fluorescence signal.

induced damage of the RISC can also be eliminated, because the non-photoprotected target siRNA gave equivalent suppression of GFP signal with and without light. Nonspecific reduction in overall gene expression as a result of nucleic acid

transfection can be eliminated as a mechanism of action, because the control siRNA at identical concentration to target siRNA produced no significant change in GFP expression. Finally, selective toxicity of the released DMNPE group can be eliminated as a mechanism of action, because the caged control siRNA gave equivalent GFP signal with and without light. The most reasonable interpretation of the results is that the DMNPE group blocks RNA interference and that exposure to light releases active siRNA.

The lack of light-dependent changes in GFP expression in the presence of photoprotected control siRNA minimizes the possibility that the light-dependent changes observed with target siRNA are nonspecific. To further support the conclusion that the changes stem from the release of active siRNA and subsequent RNA interference, a similar experiment was performed with GFP expression normalized to red fluorescent protein (RFP) expression in which RFP-expressing plasmid was cotransfected with GFP-expressing plasmid. Again, photoprotected siRNA that targets GFP produced a light-dependent decrease in GFP signal normalized to RFP signal. Likewise, photoprotected siRNA that targets RFP produced a light-dependent decrease in RFP signal normalized to GFP signal (Figure 3).

We have also explored the ability of caged siRNA to modulate the degree of RNA interference. This is an additional potential benefit of caging, as it allows the variation of the amount of expression of a given gene in target tissue. We therefore examined the expression of GFP in cells that had been treated as before with caged target siRNA. Exposure to light during deprotection with DMNPE was varied from 0 to 12 min. Figure 4 summarizes the results of this experiment. Increasing the time of light exposure gave a gradual increase

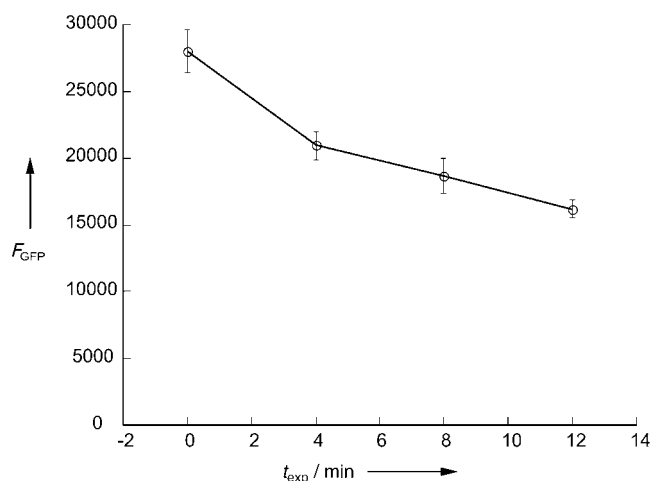


Figure 4. Decrease in GFP signal with increased time of exposure to light in cells treated with caged target siRNA.

in the RNA interference effect between the two limits established previously. In this experiment, eight wells were averaged for each time point.

The results of the experiments described herein show that RNA interference can be brought under the control of light through the use of photolabile groups. It is clear that the caging of the siRNA does not completely eradicate RNA interference. A likely reason for this is the 3% caging efficiency, which corresponds to an average of 1.4 phosphate groups modified per duplex. It is probable that some duplexes are completely unmodified, while others are modified in positions that are unable to block the siRNA–RISC interaction.

A potential solution to this problem is to increase the substitution level, which would produce a larger proportion of the siRNA duplexes that have blocked positions.

We have examined this potential solution by systematically increasing the number of DMNPE equivalents we used during caging. For this experiment we used 175, 875, and 1750 equivalents of caging (DMNPE) compound relative to duplex to modify three different samples of target siRNA. The experiments resulted in 4.8%, 10.8%, and 15.2%, respectively, of phosphate groups modified. These modified siRNAs were then transfected in a manner identical to the previously described experiment, and their effect on GFP expression determined in the presence and absence of light exposure. The results are shown in Figure 5. Again, the only samples that showed a statistically significant difference in GFP signal upon irradiation were those treated with modi-

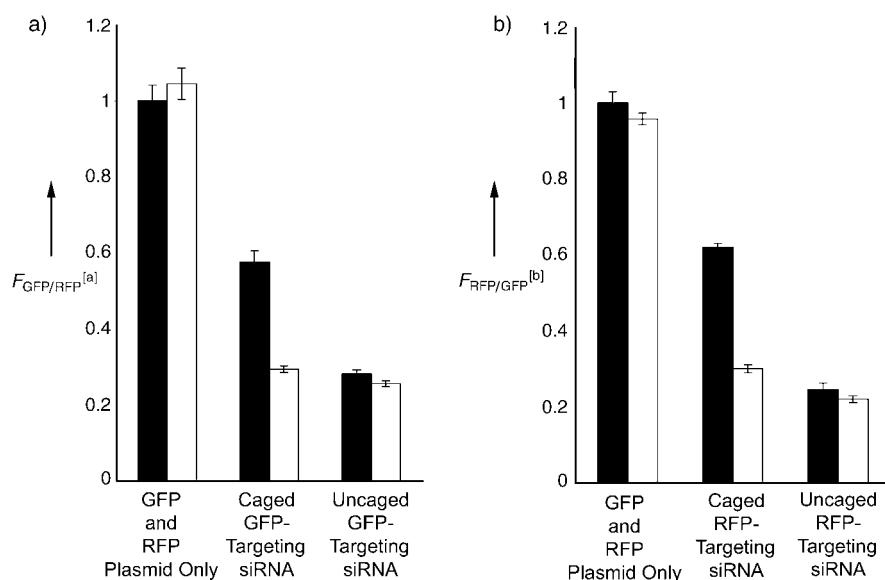


Figure 3. Normalized GFP and RFP expression in the presence and absence of modified siRNA. Dark bars indicate signals from nonirradiated samples. Light bars indicate signals from irradiated samples. a) For each set of experimental conditions, the GFP/RFP ratio was normalized to the same ratio in the nonirradiated, plasmid-only sample (far left bar). [a] $F_{\text{GFP/RFP}}$ = GFP fluorescence normalized to that of RFP. b) The same approach was taken using the RFP/GFP ratio. [b] $F_{\text{RFP/GFP}}$ = RFP fluorescence normalized to that of GFP. All signals were corrected for autofluorescence, which is typically < 4% of the total signal.

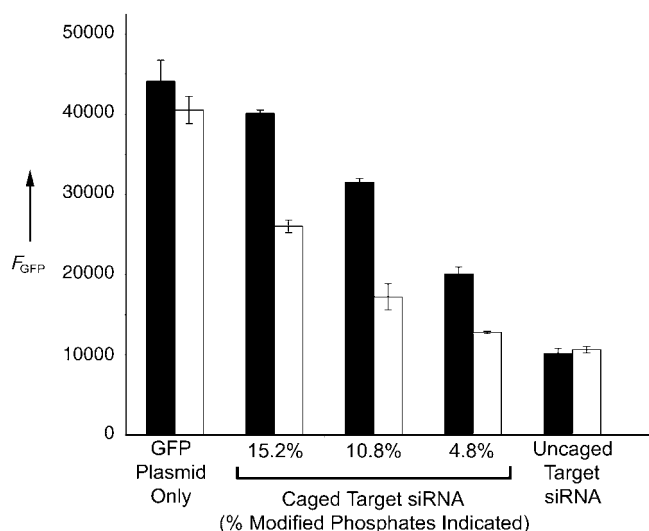


Figure 5. Influence of increasing amounts of caging compound upon blocking and release of siRNA. Dark bars indicate signal from nonirradiated samples. Light bars indicate signals from irradiated samples. Higher amounts of caging compound result in greater blocking of RNA interference before irradiation and less RNA interference upon irradiation.

fied siRNAs ($p < 0.05$). With increasing amounts of siRNA modification, there is an increased blocking of RNA interference before irradiation. This is paralleled by a greater resistance to complete release of fully active siRNA after irradiation. In theory, increasing the time of irradiation could lead to a complete release of active siRNA. We have found, however, that increasing irradiation beyond 10–12 min leads to a decrease in control GFP expression that is significant in comparison with cells that are not irradiated, which is likely a result of phototoxicity. Modification of some positions on the duplex should be more effective at blocking RNA interference than others, and we are exploring this as a possible route to complete caging of the siRNA.

These results indicate that light-mediated control of RNA interference is possible. We have demonstrated that the modification of siRNA with a photolabile group results in a species that is blocked from full RNA interference until irradiated, upon which it is as active as unprotected siRNA. We have further shown that this effect can be modulated by varying the time of photodeprotection. Finally, we have shown that increasing the number of equivalents of caging compound to siRNA increases the extent to which RNA interference is blocked, but also results in incomplete RNA interference after irradiation. Based on the growing understanding of the structural features required for effective RNA interference, we are currently exploring the positional and steric factors that may allow complete caging of siRNA.^[6,9–11] Previous efforts at light-mediated control of gene expression include the caging of hormones,^[12] mRNA,^[8] whole plasmids,^[5] and ribozymes.^[13] A potential advantage of our approach is that it utilizes the generality found in RNA interference. This allows the specific targeting of endogenous genes, something that plasmid and mRNA caging cannot do. We anticipate that this approach may be useful for a range of

biological studies, in particular studies of development, in which the spacing, timing, and amount of gene expression are key factors in determining developmental outcome.

Experimental Section

siRNA caging with DMNPE: MnO_2 (10 mg, 0.115 mmol) was added to 4,5-dimethoxy-2-nitroacetophenone hydrazone (2.5 mg, 0.011 mmol) (Molecular Probes, Inc., Eugene, OR) in DMSO (250 μL) and gently agitated for 45 min at room temperature. The solution was then filtered through Celite (Molecular Probes) supported by glass wool in a borosilicate glass pipet to remove MnO_2 from the activated caging compound. The filter pad was washed with DMSO (750 μL) to extract the activated caging compound. A volume of this filtrate appropriate to generate the required molar ratio described in the text was gently agitated with siRNA (50 μL , 20 μM) in tris-acetate EDTA buffer for 24 h at room temperature, protected from light. To remove the excess caging compound from the reaction, the caged siRNA was precipitated from EtOH in the presence of glycogen, followed by two extractions with CHCl_3 . The caged siRNA was stored in RNase-free, diethylpyrocabonate-treated water (United States Biochemical) at -20°C , protected from light. The extent of modification of the siRNA was determined through the method of Monroe, Haselton, and co-workers by using the extinction coefficient for DMNPE-ATP and absorbance at $\lambda = 355 \text{ nm}$.^[5] The stability of the caged duplex was confirmed by melting studies on the double-stranded siRNA molecule (1°C min^{-1}). The duplex was further characterized by ESI MS, which showed sense and antisense strands, with and without caging groups. See Supporting Information for detailed procedures used for cell culture, duplex formation, mass spectrometry, and normalized expression studies.

Received: July 28, 2004

Published online: January 11, 2005

Keywords: gene expression · oligonucleotides · photochemistry · photolysis · RNA recognition

- [1] T. Tuschl, *ChemBioChem* **2001**, 2, 239.
- [2] D. M. Dykxhoorn, C. D. Novina, P. A. Sharp, *Nat. Rev. Mol. Cell Biol.* **2003**, 4, 457.
- [3] S. M. Elbashir, J. Harborth, W. Lendeckel, A. Yalcin, K. Weber, T. Tuschl, *Nature* **2001**, 411, 494.
- [4] S. M. Elbashir, W. Lendeckel, T. Tuschl, *Genes Dev.* **2001**, 15, 188.
- [5] W. T. Monroe, M. M. McQuain, M. S. Chang, J. S. Alexander, F. R. Haselton, *J. Biol. Chem.* **1999**, 274, 20895.
- [6] Y.-L. Chiu, T. M. Rana, *Mol. Cell* **2002**, 10, 549.
- [7] Y.-L. Chiu, T. M. Rana, *RNA* **2003**, 9, 1034.
- [8] H. Ando, T. Furuta, R. Y. Tsien, H. Okamoto, *Nat. Genet.* **2001**, 28, 317.
- [9] A. Reynolds, D. Leake, Q. Boese, S. Scaringe, W. S. Marshall, A. Khvorova, *Nat. Biotechnol.* **2004**, 22, 326.
- [10] M. Amarzguioui, T. Hølen, E. Babaie, H. Prydz, *Nucleic Acids Res.* **2003**, 31, 589.
- [11] F. Czauderna, M. Fechtner, S. Dames, H. Aygun, A. Klippel, G. J. Pronk, K. Giese, J. Kaufmann, *Nucleic Acids Res.* **2003**, 31, 2705.
- [12] F. G. Cruz, J. T. Koh, K. H. Link, *J. Am. Chem. Soc.* **2000**, 122, 8777.
- [13] S. G. Chaulyk, A. M. MacMillan, *Nucleic Acids Res.* **1998**, 26, 3173.
- [14] E. F. Pettersen, T. D. Goddard, C. C. Huang, G. S. Couch, D. M. Greenblatt, E. C. Meng, T. E. Ferrin, *J. Comput. Chem.* **2004**, 25, 1605.

Photoswitchable Microlens Arrays**

Jongseong Kim, Michael J. Serpe, and L. Andrew Lyon*

Micro-optical structures have been of recent interest to both industrial and academic pursuits with regards to the miniaturization of optical elements and the development of novel functional materials.^[1–3] Microlens array technology has also been used recently as a route to highly parallel image projection to enable microlens-directed photolithography.^[4,5] While microlens array technology is constantly being improved with respect to fabrication methods and optical quality, these arrays are typically comprised of optical elements with fixed focal lengths, relatively large diameters, and/or slow focal length switching speeds. Furthermore, many array technologies require meticulous photolithographic processing for fabrication.^[6–9] It would be a major advancement if an array of micron-scale optical elements with dynamically tunable focal lengths could be prepared in a facile, inexpensive, and scalable fashion. Another challenge is to construct true microlens arrays for which the focal length of individual lens elements can be addressed on demand and independently of other array elements. Accomplishment of the above goals would represent an enabling technology for a new class of applications in foveated vision, parallel chemical sensing, and beam steering, as well as an expansion of the tools available to current efforts in the field.

We have previously shown by using an electrostatic self-assembly approach that ordered microlens arrays could be fabricated on glass substrates and that they effectively function as optical elements that are capable of focusing images in air and water.^[10,11] The lensing ability is mainly a result of the hemispherical shape of the particle that results from its immobilization on the solid support and the contrast in the refractive index (RI) between the deswollen microgel polymer (≈ 1.4) and the medium. Tunability of the focal length in a microlens array in water has also been demonstrated from the thermoresponsivity of pNIPAM-co-AAc (pNIPAM = poly(*N*-isopropylacrylamide), AAc = acrylic acid) microgels in aqueous solution. As the temperature of a pNIPAM microgel in solution is increased to the intrinsic lower critical solution temperature (LCST) of the polymer, the microgels undergo a phase transition from a solvent-swollen state to a deswollen state.^[12,13] Accordingly, the

thermo-responsive optical properties of the microlens arrays can be understood not only by considering the microgels to be more optically dense above the LCST but also by considering that lensing power is dependent upon the ratio of the RI of the lens material and the surrounding medium, such that a higher difference in the RI results in a shorter focal length lens.

Here we describe the first demonstration of microlens arrays comprised of fast-responding, reversible, phototunable lens elements, which are prepared using simple wet-chemical methods. These arrays are fabricated by exposing 3-aminopropyltrimethoxysilane (APTMS)-functionalized glass substrates to citrate-stabilized Au nanoparticles (16 ± 1.6 nm), which attach themselves to the glass substrate through electrostatic interactions.^[14] The presence of Au nanoparticles on the surface allows for local heating of the sample through excitation of surface plasmon modes on the Au nanoparticles with a frequency-doubled Nd:YAG laser ($\lambda = 532$ nm).^[15] Plasmon excitation results in a transfer of energy to the environment in the form of thermal dissipation through electron–phonon and phonon–phonon coupling interactions.^[16] Note that other means of heating the particles, such as by temperature-jump dyes and IR irradiation, have also been reported.^[17,18] This Au nanoparticle-coated substrate is subsequently rendered positively charged by exposure to the cationic polyelectrolyte poly(allylamine hydrochloride) (PAH). PNIPAM-co-AAc microgels are attached to the substrate by adding a drop of an aqueous solution of the microgel (10% v/v) at pH 6.5 to the APTMS–Au–PAH-modified glass substrate. In this fashion, the microgel particles coat the nanoparticle-modified glass substrate by electrostatic self-assembly. At this pH value, the microgels are anionic, which allows good adhesion to the cationic substrate. After the substrate is dried for 24 hours, it is immersed in and rinsed with deionized water to leave behind only the microgels strongly attached to the substrate through electrostatic interactions. Figure 1 shows a schematic depiction and a scanning electron microscopy (SEM) image of this structure.

For lens-tuning studies, the microlens array was then exposed to solutions at various pH values by introduction of the appropriate solution into the void space of a microlens array/silicone gasket/coverglass sandwich assembly. The temperature of this sample was controlled by a Peltier heating/cooling stage mounted on the sample holder of an optical microscope. Optical microscopy measurements were performed on this assembly to explore the phototuning of the microlens array in response to laser excitation. An Olympus IX-70 inverted optical microscope equipped with a 1.30 N.A. (N.A. = numerical aperture) oil-immersion 100 \times objective, a microscope objective heater, a Peltier-based temperature stage with an integrated thermocouple, and a black and white CCD camera (PixelFly, Cooke Corporation) was used for imaging the pattern under continuous-wave laser irradiation, and an Itronx Imaging Technologies FASTCAM DVR CCD camera was used to image the lenses exposed to pulsed laser excitation. In this arrangement, we take advantage of the conjugate focal planes in the microscope by placing a pattern near a plane conjugate to the back focal plane of the objective. When the microgels act as lens elements, they

[*] J. Kim, Dr. M. J. Serpe, Prof. L. A. Lyon
School of Chemistry and Biochemistry
Georgia Institute of Technology
Atlanta, GA 30332-0400 (USA)
Fax: (+1) 404-894-7452
E-mail: lyon@chemistry.gatech.edu

[**] L.A.L. acknowledges support from a Sloan Fellowship and a Camille Dreyfus Teacher–Scholar Award. We thank Prof. M. Srinivasarao for the fast frame rate CCD camera used in this study.

Supporting information for this article is available on the WWW under <http://www.angewandte.org> or from the author.

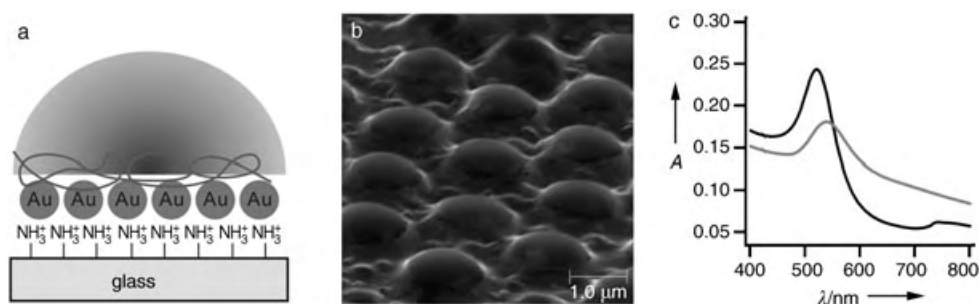
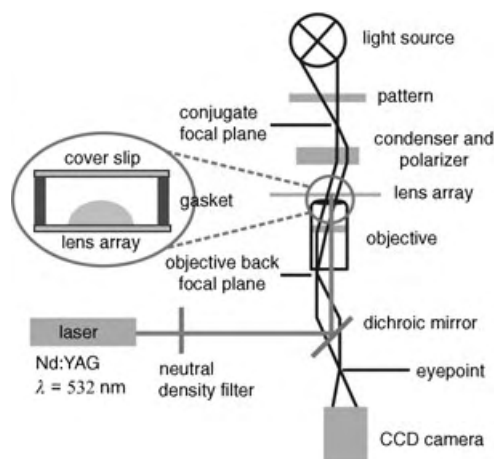


Figure 1. a) Depiction of the multicomponent film used to create photoswitchable microlens arrays. b) SEM image of the constructed microlens array at grazing angle. c) UV/Vis spectra of Au nanoparticles in solution (black) and bound to substrate (gray).

change the effective focal length of the microscope, bringing the back focal plane of the objective near the eyepoint. This is observed as a projection of the pattern through each active element in the lens array. A diagram of the microscopy setup is shown in Scheme 1.



Scheme 1. Inverted light microscopy setup used for detection of the photoswitchable behavior of microlens arrays in the liquid phase. The lenses at the imaging plane move the objective back focal plane to the eyepoint, thus bringing a pattern placed near the source into focus.

The key characteristics of the phototuning of this construction relate to the optical properties of the colloidal Au array and the thermoresponsivity of the microgel lens elements. UV/Vis spectroscopy was used to confirm the presence of Au nanoparticles on the glass substrate following assembly. Figure 1c shows the spectra of Au nanoparticles either in aqueous solution or on a substrate coated with a microlens array. The absorption spectrum of the substrate-bound Au nanoparticles is shifted to slightly higher wavelengths than that of the free Au nanoparticles in solution. A long-wavelength shoulder is also apparent in the spectrum of the lens array and is most likely caused by some aggregation of Au nanoparticles on the substrate during assembly, while the shift in the plasmon resonance results from the microlens array. The deswollen microlenses present a higher local refractive index to the surface of the Au nanoparticles, thereby shifting the plasmon resonance to lower energy.

The photoresponsivity of the microlens arrays was initially investigated by monitoring the projection of a triangle pattern through the lenses while they were exposed to a solution at pH 3.0 in response to various laser powers and bath temperatures. Figure 2a and b show the focal length tunability of the

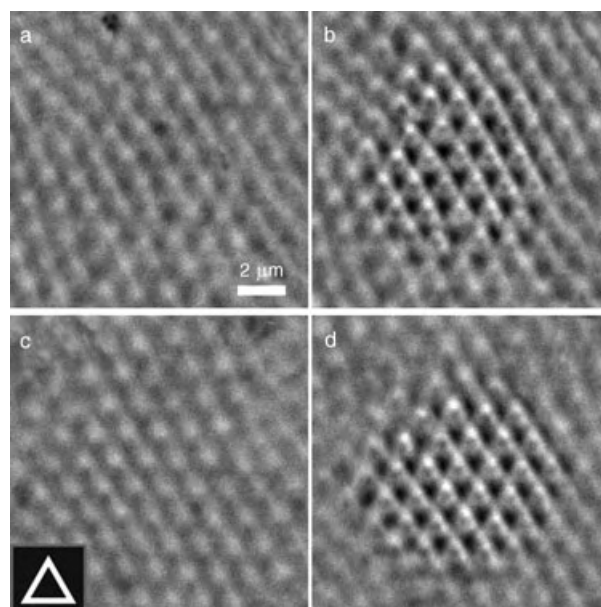


Figure 2. Photoswitching of microlens arrays as a function of laser power and solution temperature at pH 3.0. Arrays at 25 °C (a and b) and 10 °C (c and d) show laser-power-dependent optical properties by projecting a triangle pattern (c, lower left corner) only when the laser power is sufficient to produce the necessary temperature jump to above the microgel LCST. Laser powers: 10.22 mW μm⁻² (a), 38.45 mW μm⁻² (b, c), and 88.90 mW μm⁻² (d). It can also be seen that each lens is capable of projecting an image only in the region surrounding the incident laser light excitation.

microlens arrays at a bath temperature of 25 °C upon laser exposure. Each lens projects the triangle image only in the region of laser light excitation, where the effective temperature is higher than the lower critical solution temperature of the microgel. The number of lenses that display a high quality image is also tunable by varying the laser power (see Supporting Information). Similarly, Figure 2c and d show the focal length tunability of the microlens arrays at a bath temperature of 10 °C upon laser exposure. A smaller area of

the array is switched under these conditions, as the bath temperature is further from the LCST of pNIPAm (31 °C). Note that the same laser power is impinging on the array in Figure 2b and c. As a fixed laser power induces a fixed jump in temperature, decreasing the temperature of the bath to far below the LCST results in a photoinduced temperature excursion that is now below the LCST of the polymer (Figure 2c). It is also theoretically possible to control single lens elements of the array by this method. As the laser spot is essentially diffraction-limited in size (≈ 266 nm in diameter) under these illumination conditions, it is in fact smaller than an individual lens. By controlling the bath temperature and the laser intensity, one can therefore interrogate a single lens element (see Supporting Information).

Figure 3a and b show images projected through the microlens array at 25 °C at pH 6.5 as a function of laser power. A comparison of Figure 2b and Figure 3a, for which the laser powers are identical, suggests that the microlens array at pH 6.5 is less sensitive to laser irradiation than at pH 3.0. This behavior is a result of the higher LCST of the microgels at this pH, caused by deprotonation of AAc within the microgel network at pH values greater than the pK_a value ($pK_a \approx 4.25$).^[19] As expected, the lensing ability of the microlens is unaffected by temperature up to the transition temperature of approximately 48 °C, as observed by the bulk heating experiments (see Supporting Information). Figure 3b and d illustrate that the microlens array is again extremely sensitive to the bath temperature, as indicated by a decrease in the area of the modulated region at low temperature. This effect can also be confirmed by comparing the modulated area in Figure 2d to Figure 3d and is caused by the lower LCST of the microgels at pH 3.0, therefore they are able to respond to smaller jumps in temperature than the microgels at pH 6.5.

The reversibility and response rate of the microlens array are shown in Figure 4. The laser modulation frequency was controlled by passing it through an optical chopper. Figure 4

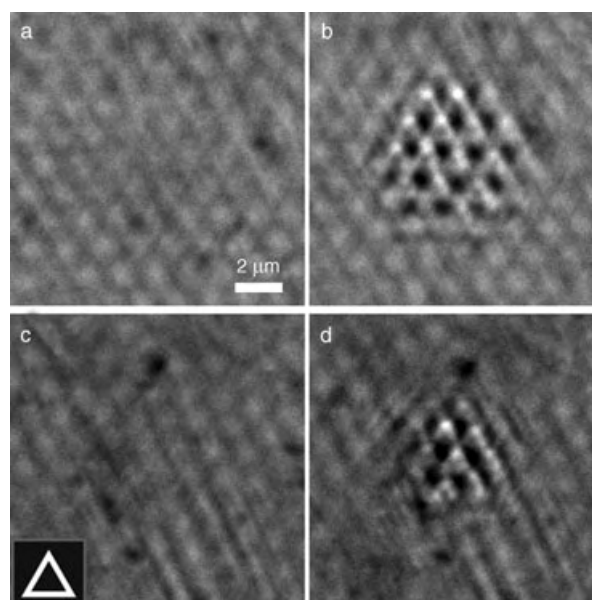


Figure 3. Photoswitching of microlens arrays as a function of laser power and solution temperature at pH 6.5. Again it can be seen that the arrays at 25 °C (a and b) and 10 °C (c and d) show laser-power-dependent optical properties by projecting a triangle pattern (c, lower left corner) only when the laser power is sufficient to produce the necessary temperature jump to above the microgel LCST. Laser powers: $38.45 \text{ mW } \mu\text{m}^{-2}$ (a), $88.90 \text{ mW } \mu\text{m}^{-2}$ (b, d), and $48.56 \text{ mW } \mu\text{m}^{-2}$ (c). By comparison to Figure 2 it can be seen that more laser power is required to modulate the micro-optical array at this pH value.

row a shows that the optical properties of the microlens array can be fully modulated in a completely reversible fashion by using laser pulses of 10 ms. This experiment was performed without the projection of a pattern through the array as the camera was not sensitive enough to detect the projected image while acquiring images at 2000 fps (frames per second).

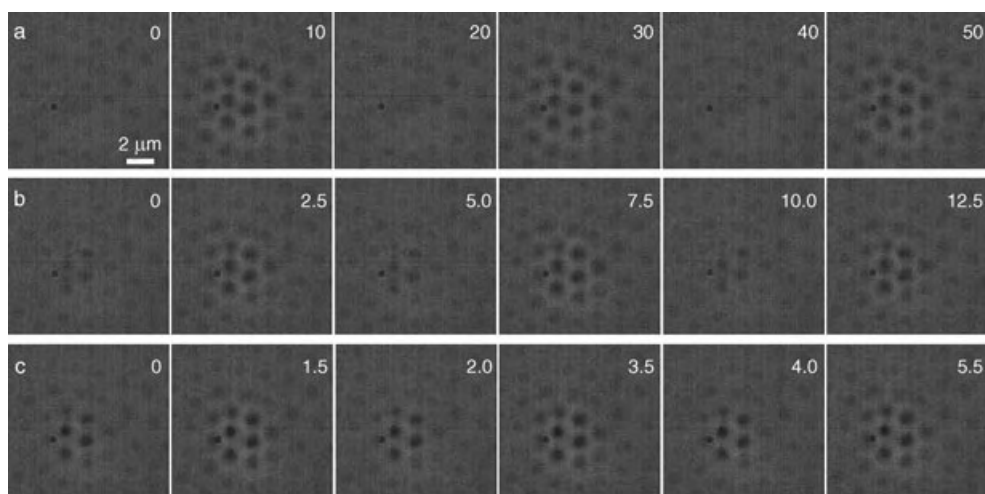


Figure 4. Images captured with a fastcam DVR CCD camera at 2000 fps while chopping the Nd:YAG laser source at 50 Hz (a), 200 Hz (b), and 500 Hz (c) in solution at pH 6.5 and at 15 °C. The optical properties of the array can be reversibly modulated in phase with laser pulses of 50 Hz (a). However, once the laser modulation frequency exceeds the rate of thermal diffusion from the microgels, the modulation of the microlens array diminishes (b and c). The laser intensity at the array surface is $184.97 \text{ mW } \mu\text{m}^{-2}$. The numbers in the upper-right corners of each image indicate the time interval Δt in milliseconds after which the image was recorded.

The apparent response time of microlenses in the array was measured at $< 500 \mu\text{s}$ as we cannot resolve intermediate stages of microgel deswelling at 2000 fps under the conditions presented in Figure 4 (see Supporting Information). In other words, individual lens elements go from a non-lensing to a lensing state within one frame at this image-capture rate. Literature reports place microgel deswelling rates on the timescale of tens to hundreds of microseconds, depending on the network density and particle size.^[18] Figure 4b and c also show that this reversibility is diminished upon increasing the laser repetition frequency from 200 to 500 Hz because, while microgel deswelling is caused by fast thermal dissipation from the laser-excited Au nanoparticles to the microlenses, the reswelling of the microgel is limited by the slow dissipation of heat away from the substrate. Thus, the microlens array appears totally deswollen at 500 Hz as the pulsing frequency is faster than the microgel reswelling rate.

In conclusion, by using simple wet-chemical methods we have fabricated a high-density microlens array that can be tuned or switched by an external laser source. The fabrication technology is inexpensive, scalable, and rapid, in contrast to traditional micromolding or photolithographic approaches. The unique characteristics of the micro-optics include the ability to confine the tunable region to the single-microlens scale, fast response rate (≈ 10 -fold faster than video rate), and highly reversible behavior under pulsed laser control. These characteristics make this system an attractive enabling technology for the future development of agile micro-optical components.

Received: August 4, 2004

Revised: November 1, 2004

Published online: January 20, 2005

Keywords: gels · gold · laser spectroscopy · nanotechnology · surface plasmon resonance

- [14] R. G. Freeman, K. C. Grabar, K. J. Allison, R. M. Bright, J. A. Davis, A. P. Guthrie, M. B. Hommer, M. A. Jackson, P. C. Smith, D. G. Walter, M. J. Natan, *Science* **1995**, 267, 1629.
- [15] C. D. Jones, M. J. Serpe, L. Schroeder, L. A. Lyon, *J. Am. Chem. Soc.* **2003**, 125, 5292.
- [16] S. Link, M. A. El-Sayed, *Int. Rev. Phys. Chem.* **2000**, 19, 409.
- [17] S. Nayak, L. A. Lyon, *Chem. Mater.* **2004**, 16, 2623.
- [18] J. Wang, D. Gan, L. A. Lyon, M. A. El-Sayed, *J. Am. Chem. Soc.* **2001**, 123, 11284.
- [19] C. D. Jones, L. A. Lyon, *Macromolecules* **2000**, 33, 8301.

-
- [1] Y. N. Xia, G. M. Whitesides, *Angew. Chem.* **1998**, 110, 568; *Angew. Chem. Int. Ed.* **1998**, 37, 551.
 - [2] P. D. Yang, G. Wirsberger, H. C. Huang, S. R. Cordero, M. D. McGehee, B. Scott, T. Deng, G. M. Whitesides, B. F. Chmelka, S. K. Buratto, G. D. Stucky, *Science* **2000**, 287, 465.
 - [3] M. H. Qi, E. Lidorikis, P. T. Rakich, S. G. Johnson, J. D. Joannopoulos, E. P. Ippen, H. I. Smith, *Nature* **2004**, 429, 538.
 - [4] H. K. Wu, T. W. Odom, G. M. Whitesides, *J. Am. Chem. Soc.* **2002**, 124, 7288.
 - [5] M. H. Wu, G. M. Whitesides, *Adv. Mater.* **2002**, 14, 1502.
 - [6] Y. N. Xia, E. Kim, X. M. Zhao, J. A. Rogers, M. Prentiss, G. M. Whitesides, *Science* **1996**, 273, 347.
 - [7] Y. Lu, Y. D. Yin, Y. N. Xia, *Adv. Mater.* **2001**, 13, 34.
 - [8] S. Yang, T. N. Krupenkin, P. Mach, E. A. Chandross, *Adv. Mater.* **2003**, 15, 940.
 - [9] H. W. Ren, Y. H. Fan, S. Gauza, S. T. Wu, *Opt. Commun.* **2004**, 230, 267.
 - [10] M. J. Serpe, J. Kim, L. A. Lyon, *Adv. Mater.* **2004**, 16, 184.
 - [11] J. Kim, M. J. Serpe, L. A. Lyon, *J. Am. Chem. Soc.* **2004**, 126, 9512.
 - [12] D. Gan, L. A. Lyon, *J. Am. Chem. Soc.* **2001**, 123, 7511.
 - [13] C. D. Jones, L. A. Lyon, *Macromolecules* **2003**, 36, 1988.

Synthetic Methods

Easy Access to Aryl- and Heteroaryl-Annulated[a]carbazoles by the Indium-Catalyzed Reaction of 2-Arylindoles with Propargyl Ethers**

Teruhisa Tsuchimoto, Hiromichi Matsubayashi, Masayoshi Kaneko, Eiji Shirakawa,* and Yusuke Kawakami*

Aryl- and heteroaryl-annulated[a]carbazoles constitute an attractive class of compounds in view of their biological and pharmacological activities that result from their special affinity toward DNA.^[1] Among them, indolo[a]carbazoles, which are found in many natural products,^[1,2] seem to be the most intriguing, and thus numerous studies on their activities^[3] and synthetic methodologies^[4] have been reported. Although other analogues are rather rare in nature,^[5] synthetic approaches to such molecules have also been developed owing to their potential as antitumor agents.^[1] However, no short synthetic route that is applicable to the various compounds has appeared in the literature despite the vast amount of work performed in this area.^[6] Thus, we

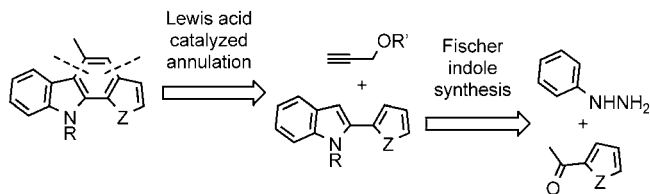
[*] Dr. T. Tsuchimoto, H. Matsubayashi, M. Kaneko,
Prof. Dr. Y. Kawakami
Graduate School of Materials Science
Japan Advanced Institute of Science and Technology
Asahidai, Tatsunokuchi, Ishikawa 923-1292 (Japan)
Fax: (+81) 761-51-1635
E-mail: tsuchimo@jaist.ac.jp
Prof. Dr. E. Shirakawa
Department of Chemistry
Graduate School of Science
Kyoto University
Sakyo-ku, Kyoto 606-8502 (Japan)
Fax: (+81) 75-753-3988
E-mail: shirakawa@kuchem.kyoto-u.ac.jp

[**] Financial support by a grant-in-aid for Scientific Research (No. 16750075) from the Ministry of Education, Culture, Sports, Science, and Technology is highly acknowledged. We are grateful to Miss Keiko Miyabayashi for the measurement of high-resolution mass spectra.



Supporting information for this article is available on the WWW under <http://www.angewandte.org> or from the author.

envisaged that Lewis acid catalyzed annulation of 2-arylindoles with propargyl ethers in a route that comprises two successive carbon–carbon bond-forming reactions should make for a short-step synthesis of aryl- and heteroaryl-annulated[*a*]carbazoles. Various 2-arylindoles are readily accessible through the Fischer indole synthesis,^[7] and an overview of our strategy is summarized in Scheme 1. Herein



Scheme 1. Retrosynthetic strategy for the synthesis of aryl- and heteroaryl-annulated[*a*]carbazoles. Z = CH=CH, S, O, NH, NMe; R = H, Me; R' = Alkyl.

we report a new method for the synthesis of a wide range of aryl- and heteroaryl-annulated[*a*]carbazoles that uses an indium-catalyzed addition–substitution sequence^[8,9] of various 2-arylindoles with propargyl ethers.

First, we investigated the reaction of 2-phenylindole (**1a**; R¹ = H, Z = CH=CH) with methyl propargyl ether (**2a**; R² = Me, R³ = H; see Equation (1) and Table 1). Treatment of **1a**

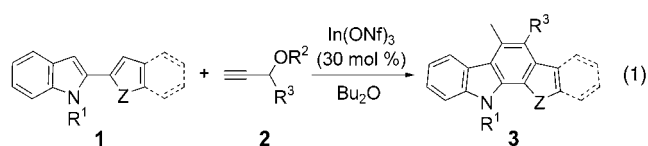


Table 1: Lewis acid catalyzed annulation of 2-phenylindole with methyl propargyl ether.^[a]

Entry	Lewis acid	<i>t</i> [h]	Conv. [%] of 1a ^[b]	Yield [%] of 3aa ^[b]
1	In(OTf) ₃	72	78	62
2	In(ONf) ₃	24	87	69
3	In(ONf) ₃	35	> 99	64
4	In(ONf) ₃ ^[c]	120	68	53
5	Sc(OTf) ₃	24	1	< 1
6	Zr(OTf) ₄	24	1	< 1
7	InCl ₃	24	1	< 1
8	BF ₃ ·Et ₂ O	24	1	< 1
9	TiCl ₄	24	14	< 1

[a] The reaction was carried out in Bu₂O (3.0 mL) at 70 °C using **1a** (0.20 mmol) and **2a** (0.22 mmol) in the presence of a Lewis acid (60 μmol). [b] Determined by GC using 1,2-dichlorobenzene as an internal standard. [c] In(ONf)₃ (20 μmol) was used.

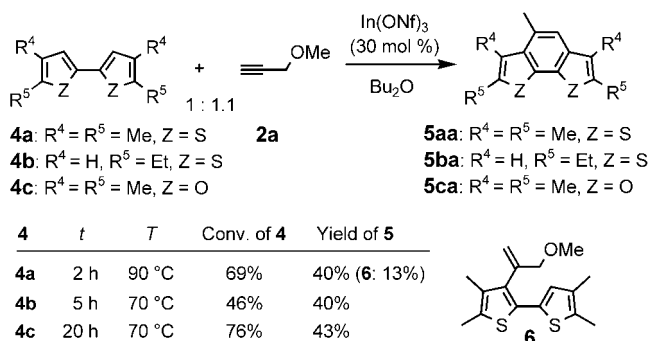
and **2a** with 30 mol % of indium triflate (triflate = CF₃SO₃), In(OTf)₃,^[10] in Bu₂O at 70 °C for 72 h gave 6-methyl-11*H*-benzo[*a*]carbazole (**3aa**) in 62 % yield (Table 1, entry 1) by a route in which two subsequent inter- and intramolecular carbon–carbon bond-forming reactions took place in one step. With the nonaflate analogue In(ONf)₃ (nonaflate = C₄F₉SO₃),^[11] which should be a stronger Lewis acid than

In(OTf)₃,^[12] as a catalyst, the yield of **3aa** was improved and the reaction rate was also increased (entry 2). Prolonging the reaction time to ensure complete consumption of **1a** led to a slight decrease in the yield (entry 3). Use of a lower loading of In(ONf)₃ gave **3aa** in an acceptable yield, but the reaction was sluggish (entry 4). Other metal triflate salts as well as metal halides were totally inactive (entries 5–9). The reliable activity of indium nonaflate may be ascribed to the soft nature of indium which renders it compatible with soft Lewis bases such as alkynes.^[13]

We next turned to other 2-arylindoles, which were prepared here by the Fischer indole synthesis^[7,14] and then subjected to the annulation reaction with **2a** in the presence of In(ONf)₃ [Eq. (1) and Table 2]. As well as **1a**, its *N*-methyl derivative **1b** and 2-phenylindoles that have a methoxy or hydroxy group on the phenyl ring reacted with **2a** to give the corresponding benzo[*a*]carbazoles (Table 2, entries 1–5);^[15] a functional group such as -OMe should be useful for further carbon–carbon bond formation through nickel-catalyzed cross-coupling reaction with Grignard reagents.^[16] The annulation of 2-thienyl- and 2-furylindoles also provided tetracyclic heteroaryl-annulated[*a*]carbazoles in moderate to good yields (entries 6–8). A series of pentacyclic analogues which comprise a heterocyclic ring such as thiophene, furan, or pyrrole were also prepared (entries 9–11). Note that the methyl group on the newly formed aromatic ring was always located next to C3 of the indole nucleus.^[17] Besides **2a**, 3-butoxy-1-butyne (**2b**) also underwent the annulation reaction (entry 12).

The strategy is also applicable to the annulation of bithiophenes and a bifuran (Scheme 2). Thus, both 4,4',5,5'-tetramethyl-2,2'-bithiophene (**4a**) and the diethyl analogue **4b** reacted with **2a** under similar conditions to afford the corresponding benzodithiophenes **5aa** and **5ba**, respectively, although in rather low yields. In the reaction of **4a**, formation of the 1:1 adduct of **4a/2a** (**6**) was observed which may be informative for a discussion of the reaction mechanism. Benzodifuran **5ca** was also produced in 43 % yield in the reaction of tetramethylbifuran **4c** with **2a** (Scheme 2).

The annulation reaction should involve three distinct steps that comprise addition of an arene to a carbon–carbon triple bond, substitution of an alkoxy group with an arene, and aromatization. Consideration of the observed perfect regioselectivity should give us insight into the order of the



Scheme 2. In(ONf)₃-catalyzed annulation of bithiophenes or a bifuran with methyl propargyl ether.

Table 2: In(ONf)₃-catalyzed annulation of 2-arylindoles **1** with propargyl ethers **2**.^[a]

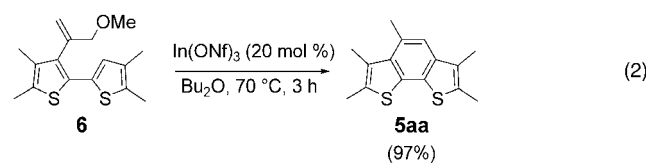
Entry	2-Arylindole (1)		<i>t</i> [h]	Conv. [%] of 1 ^[b]	Product (3)	Yield [%] of 3 ^[c]
1		1 a	24	91		3 aa 65
2 ^[d]		1 b	11	76		3 ba 52
3 ^[e]		1 c	11	78		3 ca 67
4 ^[e]		1 d	10	88		3 da 59
5 ^[e]		1 e	45	90		3 ea 48
6		1 f	50	83		3 fa 79
7		1 g	25	80		3 ga 70
8		1 h	8	61		3 ha 57
9		1 i	8	76		3 ia 61
10		1 j	40	87		3 ja 60
11		1 k	25	89		3 ka 64
12 ^[f]		1 f	110	84		3 fb 74

[a] The reaction was carried out in Bu₂O (3.0 mL) at 70 °C using **1** (0.20 mmol) and **2 a** (0.22 mmol) in the presence of In(ONf)₃ (60 μmol).

[b] Determined from recovered **1**. [c] Isolated yield based on the 2-arylindole. [d] In Bu₂O (9.0 mL). [e] In Bu₂O (9.0 mL) at 100 °C. [f] 3-Butoxy-1-butyne (**2 b**) was used instead of **2 a**.

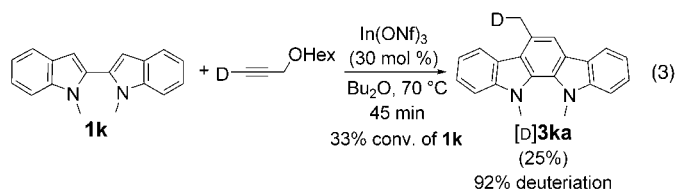
sequence. We previously demonstrated that 1-octyne, an aliphatic terminal alkyne, undergoes addition of heterocyclic arenes exclusively at the internal carbon atom of the carbon–carbon triple bond.^[8b] Therefore, considering that C3 of 2-arylindoles, which should be the most nucleophilic in **1**,^[18] added first to **2 a** in a similar manner, the position of the resulting methyl group should be rationally understood. Furthermore, formation of **6**, which should be an intermediate in the reaction of **4 a** with **2 a**, possibly suggests that the first step is not substitution but addition, though the formation of a 1:1 adduct such as **6** was not observed in the annulation of 2-arylindoles. Actually, transformation of **6** into **5 aa** in Bu₂O at

70 °C for 3 h using 20 mol % of In(ONf)₃ proceeded smoothly [Eq. (2)]. Despite two possible routes for the next cyclization, that is, S_N2 and S_N2' reactions, the fact that the reaction of **1 k** with 1-deuterio-3-hexyloxy-1-propyne afforded [D]**3 ka** which contains a deuterium atom only in the CH₃ group should

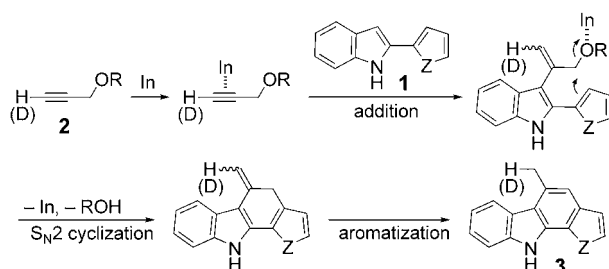


support the probability of S_N2 cyclization [Eq. (3)].^[19] Thus, coordination of the carbon–carbon triple bond of **2a** to an

Keywords: annulation · fused-ring systems · heterocycles · indium · Lewis acids



indium atom should induce regioselective addition of **1** followed by intramolecular S_N2 reaction. Finally, aromatization should give **3** (Scheme 3).



Scheme 3. Proposed mechanism for the $\text{In}(\text{ONf})_3$ -catalyzed annulation of 2-arylimidoles with propargyl ethers.

In conclusion, we have demonstrated a novel annulation reaction that allows the assembly of readily accessible building blocks into diverse aryl- and heteroaryl-annulated-[a]carbazoles with the aid of an indium catalyst. The highlight of our approach is the direct use of aromatic C–H bonds and the absence of the need to introduce reactive functional groups into the substrates. Studies on the mechanistic details as well as application of the reaction to other substrates are currently underway.

Experimental Section

General procedure for the synthesis of aryl- and heteroaryl-annulated-[a]carbazoles (see also Table 2): $\text{In}(\text{ONf})_3$ (60.7 mg, 60.0 μmol) was placed in a 20-mL Schlenk tube and heated at 150 °C in vacuo for 2 h. The tube was cooled to room temperature and filled with nitrogen. Dibutyl ether (3.0 or 9.0 mL) was added to the tube, and the contents were stirred for 10 min at room temperature. A 2-arylimidole (0.20 mmol) and a propargyl ether (0.22 mmol) were added successively to the catalyst mixture, and the resulting mixture was stirred at 70 or 100 °C. After the time specified in Table 2, the mixture was diluted with ethyl acetate (10 mL), washed with aqueous saturated NaHCO_3 solution (1 mL) and brine (1 mL), and then dried over anhydrous sodium sulfate. The mixture was filtered through a pad of Celite and the solvents were evaporated, then the residue was purified by column chromatography on silica gel to give the corresponding aryl- or heteroaryl-annulated-[a]carbazole.

Received: October 12, 2004

Published online: January 21, 2005

- [1] For recent reviews, see: a) G. H. Kirsch, *Curr. Org. Chem.* **2001**, 5, 507–518; b) J. Bergman, T. Janosik, N. Wahlstrom, *Adv. Heterocycl. Chem.* **2001**, 80, 1–71; c) H.-J. Knölker, K. R. Reddy, *Chem. Rev.* **2002**, 102, 4303–4427; For recent reviews on biological properties, see: d) U. Pindur, Y.-S. Kim, F. Mehrabani, *Curr. Med. Chem.* **1999**, 6, 29–69; e) M. Prudhomme, *Eur. J. Med. Chem.* **2003**, 38, 123–140.
- [2] For a recent example, see: K. M. Meragelman, L. M. West, P. T. Northcote, L. K. Pannell, T. C. McKee, M. R. Boyd, *J. Org. Chem.* **2002**, 67, 6671–6677.
- [3] For recent examples, see: a) C. Ho, S. J. Slater, C. D. Stubbs, *J. Photochem. Photobiol. A* **2001**, 142, 163–168; b) M. Facompre, C. Carrasco, P. Colson, C. Houssier, J. D. Chisholm, D. L. Van Vranken, C. Bailly, *Mol. Pharmacol.* **2002**, 62, 1215–1227; c) F. P. Monnet, M. P. Morin-Surun, J. Leger, L. Combettes, *J. Pharmacol. Exp. Ther.* **2003**, 307, 705–712; d) C.-H. Liao, Y.-J. Hsieh, Y.-C. Lin, *Eur. J. Pharmacol.* **2004**, 484, 29–39.
- [4] For recent examples, see: a) S. P. Gaudêncio, M. M. M. Santos, A. M. Lobo, S. Prabhakar, *Tetrahedron Lett.* **2003**, 44, 2577–2578; b) X. Cai, V. Snieckus, *Org. Lett.* **2004**, 6, 2293–2295; c) M. M. Faul, K. A. Sullivan, J. L. Grutsch, L. L. Winneroski, C. Shih, C. Sanchez-Martinez, J. T. Cooper, *Tetrahedron Lett.* **2004**, 45, 1095–1098; d) M. M. M. Santos, A. M. Lobo, S. Prabhakar, M. M. B. Marques, *Tetrahedron Lett.* **2004**, 45, 2347–2349; e) J. T. Kuethe, I. W. Davies, *Tetrahedron Lett.* **2004**, 45, 4009–4012.
- [5] For furo[a]carbazoles, see: H.-J. Knölker, M. P. Krahle, *Synlett* **2004**, 528–530, and references therein.
- [6] To the best of our knowledge, only two precedents for the synthesis of several (hetero)aryl-annulated-[a]carbazoles have been reported. For the synthesis of benzo-, thieno-, and pyrrolo[a]carbazoles using photochemical cyclization of 3-(2-styryl)indoles, see: a) E. M. Beccali, A. Marchesini, T. Pilati, *Synthesis* **1992**, 891–894. For the synthesis of benzo-, naphtho-, thieno-, and benzothienol[a]carbazoles using photochemical cyclization of 3-indolyl-4-arylmaleimides or the Mizoroki–Heck-type cyclization of 3-indolyl-4-(2-bromoaryl)maleimides, see: b) C. Sanchez-Martinez, M. M. Faul, C. Shih, K. A. Sullivan, J. L. Grutsch, J. T. Cooper, S. P. Kolis, *J. Org. Chem.* **2003**, 68, 8008–8014.
- [7] For example, see: a) R. L. Shriner, W. C. Ashley, E. Welch, *Org. Synth. Coll. Vol. 3* **1955**, 725–727; b) K. C. Joshi, R. Jain, S. Garg, *J. Indian Chem. Soc.* **1985**, 62, 388–390; c) J. Slätt, J. Bergman, *Tetrahedron* **2002**, 58, 9187–9191; For a review, see: d) B. Robinson, *Chem. Rev.* **1969**, 69, 227–250.
- [8] We recently demonstrated that a C–H bond of arenes and heterocyclic arenes adds to alkynes in the presence of a metal triflate catalyst, see: a) T. Tsuchimoto, T. Maeda, E. Shirakawa, Y. Kawakami, *Chem. Commun.* **2000**, 1573–1574; b) T. Tsuchimoto, K. Hatanaka, E. Shirakawa, Y. Kawakami, *Chem. Commun.* **2003**, 2454–2455.
- [9] We previously reported that metal triflates catalyze the substitution reaction of the C–O bond of alcohols and acetals with arenes, see: a) T. Tsuchimoto, K. Tobita, T. Hiyama, S. Fukuzawa, *Synlett* **1996**, 557–559; b) T. Tsuchimoto, T. Hiyama, S. Fukuzawa, *Chem. Commun.* **1996**, 2345–2346; c) T. Tsuchimoto, K. Tobita, T. Hiyama, S. Fukuzawa, *J. Org. Chem.* **1997**, 62, 6997–7005.
- [10] $\text{In}(\text{OTf})_3$ is commercially available from Aldrich.
- [11] $\text{In}(\text{ONf})_3$ was prepared for the first time from In_2O_3 and $\text{CF}_3\text{CF}_2\text{CF}_2\text{SO}_3\text{H}$ in an easy manner. For details, see Supporting Information.

- [12] It has been reported that gallium nonaflate exhibits higher catalytic activity than the corresponding triflate and chloride salts in the Friedel–Crafts acylation reactions, see: J. Matsuo, K. Odashima, S. Kobayashi, *Synlett* **2000**, 403–405.
- [13] Murai and co-workers have described that softness of gallium contributes to the high catalytic activity of GaCl₃ in the cycloisomerization of ω-aryl-1-alkynes. As indium is located below gallium in the periodic table, indium nonaflate should also be soft: H. Inoue, N. Chatani, S. Murai, *J. Org. Chem.* **2002**, 67, 1414–1417. For a review of hard and soft acids and bases (HSAB) principle, see: T.-L. Ho, *Chem. Rev.* **1975**, 75, 1–20.
- [14] For the synthesis of a homodimer such as 2,2'-bis(*N*-methylindolyl) (**1k**), oxidative homocoupling of *N*-methylindole is more straightforward, see: U. Pindur, Y.-S. Kim, D. Schollmeyer, *J. Heterocycl. Chem.* **1994**, 31, 377–386.
- [15] The benzo[*a*]carbazole **3ba** is known to exhibit pronounced antitumor activity against, for example, leukemia, renal tumor, and colon cancer, see: U. Pindur, T. Lemster, *Recent Res. Dev. Org. Bioorg. Chem.* **1997**, 33–53. See also reference [1c].
- [16] Alkoxy groups of alkenyl and aryl ethers have been reportedly transformed into alkyl and aryl groups by using Grignard reagents in the presence of a nickel catalyst, see: E. Wenkert, E. L. Michelotti, C. S. Swindell, M. Tingoli, *J. Org. Chem.* **1984**, 49, 4894–4899.
- [17] The position of the methyl group was determined by ¹H–¹H COSY and NOESY NMR techniques.
- [18] a) M. F. Gotta, H. Mayr, *J. Org. Chem.* **1998**, 63, 9769–9775;
b) J. A. Joule, K. Mills, *Heterocyclic Chemistry*, Blackwell Science, Oxford, **2000**, pp. 324–379.
- [19] The ²H NMR spectrum showed no incorporation of the deuterium atom at the other carbon atoms.

Peptide Structure Elucidation



The Antiviral Antibiotic Feglymycin: First Direct-Methods Solution of a 1000+ Equal-Atom Structure**

Gábor Bunkóczi, László Vértesy, and
George M. Sheldrick*

Despite all the progress in recent decades, antiviral chemotherapy is still much less effective than the treatment of bacterial infections by antibiotics. The human immunodeficiency virus (HIV) represents a particularly problematic case since its high variability is likely to reduce the effectiveness of

vaccines. Although many antiviral compounds are now available for the treatment of acquired immunodeficiency syndrome, the increasing resistance of HIV requires the constant development of new drugs. The 13-amino-acid feglymycin (Figure 1), a novel peptide isolated from *Streptomyces* cultures, was found to strongly inhibit the formation of HIV syncytia in vitro, and a weak antibacterial activity against Gram-positive bacteria has also been reported.^[1] Based on its unique amino acid sequence and biological activity, feglymycin represents a promising new class of antibiotics.

Feglymycin contains a high percentage of unusual amino acids such as 4-hydroxyphenylglycine and 3,5-dihydroxyphenylglycine. Structural relatives that contain hydroxyphenylglycine residues have also been found to inhibit diverse steps in the replication of HIV. In addition, a large percentage of anti-HIV agents isolated from natural sources also contains a 1,3-hydroxyphenyl moiety either detached or as part of a condensed ring system.^[2]

In this communication we report the crystal structures of two crystal forms (**1** and **2**) of feglymycin. Crystals of **1** diffracted to atomic resolution (1.10 Å), and the phase problem could be solved by ab initio direct methods despite (or possibly even aided by) perfect merohedral twinning.^[3] With about 1033 unique non-hydrogen atoms, this structure is about 50% larger than the largest equal-atom structure (containing no atom heavier than oxygen) previously solved by direct methods; equal-atom structures are much more resistant to solution by direct methods than structures containing a few heavier atoms. The structure of crystal form **2**, which diffracted to 1.40 Å, could be solved by molecular replacement using a feglymycin dimer (taken from **1**) as search fragment; it also exhibits perfect merohedral twinning.^[3] The X-ray sequence of the peptide confirmed that deduced from NMR and MS data, and the configurations of all chiral centers could be assigned; except for the two termini, the chirality of the residues alternates between D and L.

Although crystals of **1** grew under aqueous conditions (0.1 M Tris/Tris HCl pH 8.4, 4% PEG8000) with six antibiotic molecules in the asymmetric unit, and **2** from highly alcoholic solution (0.25 M Na₃Cit/H₃Cit pH 6.5, 30% isopropyl alcohol) with eight, both structures contain similar double-helical dimers that interact to form infinite helical chains along the crystallographic *c* axes. As observed for some other alternating D,L-peptides with bulky side chains, for example, the membrane channel peptide gramicidin, the feglymycin dimers are wide, antiparallel, double-stranded β helices. However the helical pitch of feglymycin varies around 9.0 residues per turn, while for the native gramicidin it is 5.6 and for gramicidin-Cs⁺ 7.2 residues per turn.^[4] Despite this structural homology, it is not likely that feglymycin acts as a membrane channel peptide: the channel is probably not long enough to span a biological membrane (Figure 2), and although the feglymycin channel is wider, it is blocked by phenylalanine side chains that would prevent all transport phenomena (see figure in the Table of Contents). Action as an ion carrier seems more feasible and would also suggest a mechanism for membrane penetration of feglymycin that may be important in the HIV-inhibitory activity.

[*] Dr. G. Bunkóczi, Prof. G. M. Sheldrick
Lehrstuhl für Strukturchemie
Georg-August Universität
Tammannstrasse 4, 37077 Göttingen (Germany)
Fax: (+49) 551-392-582
E-mail: gsheldr@shelx.uni-ac.gwdg.de
Dr. L. Vértesy
Aventis Pharma Deutschland GmbH
Division LG Natural Products
65926 Frankfurt am Main (Germany)

[**] Financial support from the Fonds der Chemischen Industrie and the Deutsche Forschungsgemeinschaft (SFB416) is gratefully acknowledged.

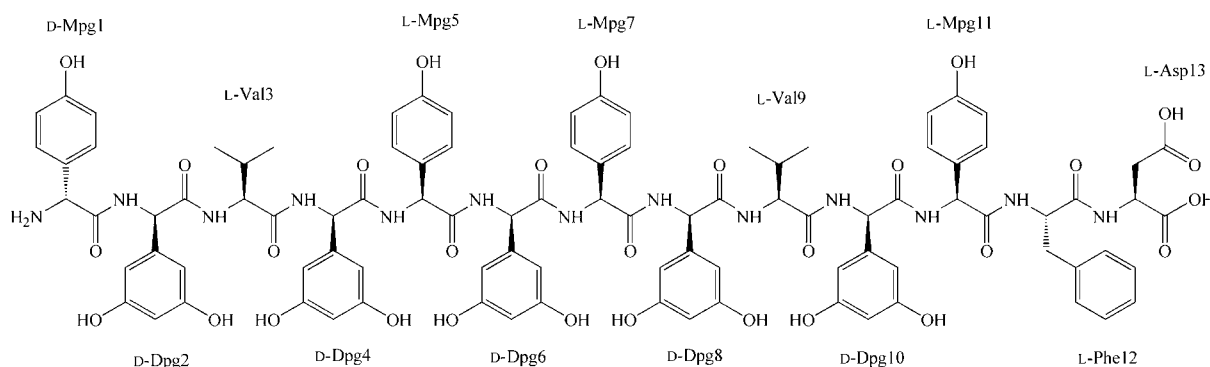


Figure 1. Chemical structure of feglymycin. The absolute configuration assignment is based on the hand of the conventional amino acids, which are all present as the L enantiomer (identified by HPLC).^[1] Mpg = 4-hydroxyphenylglycine, Dpg = 3,5-dihydroxyphenylglycine.

The feglymycin dimer is significantly less symmetric than those of gramicidin, which exhibit nearly exact twofold symmetry. This is to be expected since the chirality alternation for feglymycin is not as regular as for gramicidin. The most distinctive difference between the peptides constituting one dimer can be found at Phe12, where, to avoid collision of the two benzene rings, the main chain of one monomer takes a sudden 60° turn and the corresponding side chain also rotates by 120° (Figure 3). The dimer is stabilized by a multitude of secondary interactions involving hydrogen bonds either between main-chain amide hydrogens and carbonyl oxygens or between hydroxy groups of dihydroxyphenylglycine residues, thus creating two hydrogen-bonding shells. Hydrophobic interactions between the two Phe12 side chains and among the benzene rings of dihydroxyphenylglycine residues may also contribute substantially to the stability and result in a rather rigid structure, as indicated by the mean-square deviations between the main-chain atoms of the six independent dimers in **1** after least-squares fitting, which vary in the range 0.1–0.2 Å. Moreover, the presence of 4-hydroxyphenylglycine residues creates a well-defined hydrogen-bonding pattern on the dimer surface, since rotation of these side chains about the Cα–Cβ bond does not change the position of their hydroxy groups.

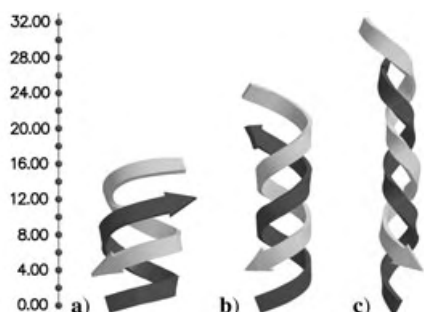


Figure 2. Schematic representation of the size and structure of dimers of a) feglymycin, b) gramicidin-Cs⁺, and c) uncomplexed gramicidin. Note that (a) and (b) are right-handed helices, while (c) is left-handed. The ruler on the left shows the scale in Å.^[5]

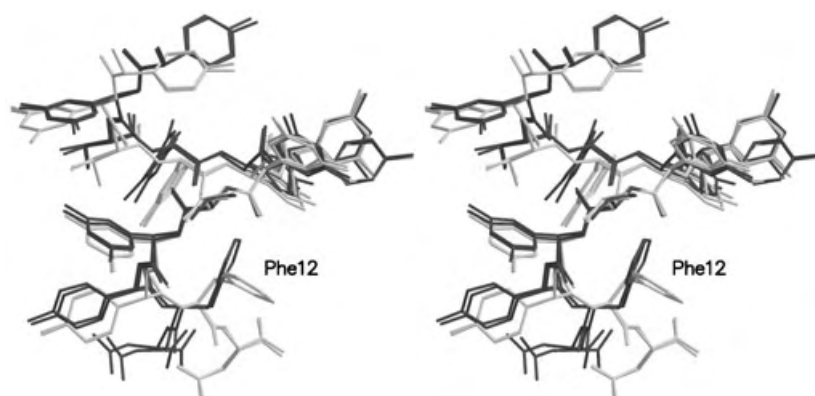


Figure 3. Stereoview of the superposition of four feglymycin molecules that constitute two dimers. Rigid fragments (corresponding to residues Mpg7–Val9) were identified with ESCET and fitted using LSQKAB.^[6] Although the rigid part comprises only three out of 13 residues, the main-chain conformations are fairly similar. A significant deviation starts at Phe12, where the main chain either continues as the helical structure would require (light color) or takes a sharp turn (dark color). A dimer is made up of a light-colored and a dark-colored monomer.^[5]

In both crystal forms, the 6₅ or 6₄ crystallographic screw axes arrange the dimers into infinite helical chains. Since the dimers are not symmetric, one can distinguish two types of interdimer interfaces. One involves the interaction of the open sides of the dimers and creates a binding pocket that binds several ethyleneglycol units of a PEG molecule in **1** and two molecules of isopropyl alcohol in **2** (Figure 4); the other, between the closed sides, lacks such properties and keeps the molecules further apart. This may suggest that the biologically active species may be a tetramer formed by the association of two dimers at their more open sides that could enclose an ionic or polar species. Apart from these interfaces, very few connections can be seen between the molecules. These are limited to a small number of hydrogen bonds and hydrophobic interactions between the benzene rings and hydroxy groups of certain dihydroxyphenylglycine residues. There are also large holes in the crystal that are filled by disordered solvent. Therefore, though the interaction within a helical chain is relatively strong, the helices are kept together by much weaker forces, and this property is most likely to be responsible for the unusual fragility exhibited by these

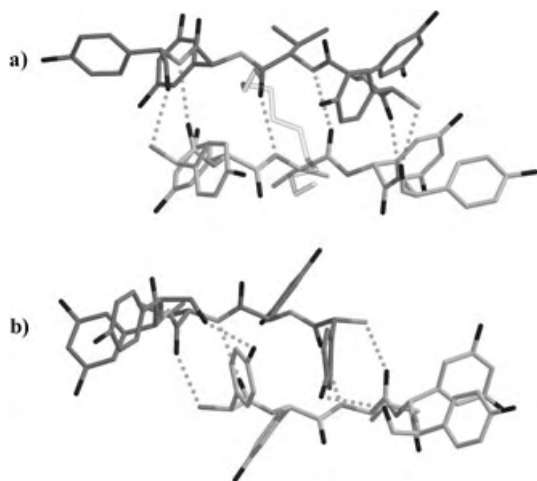


Figure 4. The packing of feglymycin dimers can either result in a) a binding pocket, when the dimers face each other with their more open sides or b) a more closed packing that does not allow anything to enter the internal cavity of the dimers. For clarity, only the residues involved in the interdimer interface are shown. In **1** the binding pocket is filled with a polyethylene glycol fragment (shown as a pale zigzag).^[5]

crystals. In both crystal forms, the twin components are related by a rotation of 180° about an axis perpendicular to *c*, simulating the higher symmetry hexagonal Laue group; this form of twinning is not unusual for trigonal and hexagonal crystals. The twin boundary involves a reversal of the helix direction, which can arise easily because of the weak lateral interactions between the helices.

Received: September 9, 2004

Published online: January 26, 2005

Keywords: antibiotics · peptides · structure elucidation · X-ray diffraction

- [1] L. Vértessy, W. Aretz, M. Knauf, A. Markus, M. Vogel, J. Wink, *J. Antibiot.* **1999**, 52, 374–382.
- [2] a) T. Asano, K. Matsuoka, T. Hida, M. Kobayashi, Y. Kitamura, T. Hayakawa, S. Iinuma, A. Kakinuma, K. Kato, *J. Antibiot.* **1994**, 47, 557–565; b) H. Tanaka, K. Matsuzaki, H. Nakashima, T. Ogino, A. Matsumoto, H. Ikeda, H. B. Woodruff, S. Ōmura, *J. Antibiot.* **1997**, 50, 58–65; c) G. Matthée, A. D. Wright, G. M. König, *Planta Med.* **1999**, 65, 493–506.
- [3] a) Crystallographic data for **1**: $6\text{C}_{95}\text{H}_{97}\text{N}_{13}\text{O}_{30} + 37\text{C}_2\text{H}_4\text{O} + 5\text{C}_2\text{H}_5\text{OH} + 79\text{H}_2\text{O}$, hexagonal, space group $P6_5$, $a = b = 83.54$, $c = 35.73$ Å, $V = 215949.7$ Å³, $Z = 6$, $F(000) = 44831$, $\lambda = 1.54178$ Å, $T = 100$ K, $\mu(\text{CuK}\alpha) = 0.45$ mm⁻¹, crystal dimensions $0.3 \times 0.3 \times 0.5$ mm³, $1.22 \leq 2\theta \leq 88.98^\circ$. In total 578199 reflections were collected, of which 57985 were independent ($R_{\text{int}} = 0.0408$, Friedel pairs merged) and employed for refinement: 9811 parameters, 13411 restraints, $R1 = \sum |F_o - F_c| / \sum F_o = 0.143$ ($I > 2\sigma(I)$), $wR2 = [\sum w(F_o^2 - F_c^2)^2 / \sum wF_o^4]^{1/2} = 0.344$ (all data); min./max. difference electron density $-0.32/0.47$ e Å⁻³. A suitable crystal was soaked in a cryoprotectant solution consisting of the crystallization medium supplemented by 25% glycerol and shock-frozen in a cold nitrogen stream. Intensity data were collected with a Bruker rotating anode, Osmic focusing mirrors, Bruker SMART6000 4K CCD detector with CuK α radiation by performing six ω -scans at different 2θ -offsets. Raw images were

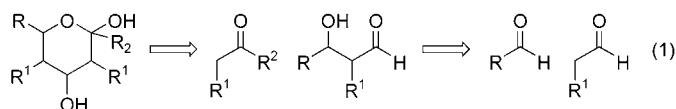
integrated using SAINT, and the resulting intensities were scaled using SADABS. The structure was solved using SHELXD^[7] employing real/reciprocal space recycling and peaklist optimization; b) Crystallographic data for **2**: $8\text{C}_{95}\text{H}_{97}\text{N}_{13}\text{O}_{30} + 4\text{C}_3\text{H}_7\text{OH} + \text{C}_6\text{H}_8\text{O}_7 + 106\text{H}_2\text{O}$, hexagonal, space group $P6_4$, $a = b = 60.30$, $c = 83.75$ Å, $V = 263724.2$ Å³, $Z = 6$, $F(000) = 52846$, $\lambda = 0.950$ Å, $T = 100$ K, $\mu(0.95 \text{ Å}) = 0.05$ mm⁻¹, crystal dimensions $0.3 \times 0.3 \times 0.5$ mm³, $1.92 \leq 2\theta \leq 39.67^\circ$. In total 484869 reflections were collected, of which 34149 were independent ($R_{\text{int}} = 0.0634$, Friedel pairs merged) and employed for refinement: 11147 parameters, 14595 restraints, $R1 = \sum |F_o - F_c| / \sum F_o = 0.155$ ($I > 2\sigma(I)$), $wR2 = [\sum w(F_o^2 - F_c^2)^2 / \sum wF_o^4]^{1/2} = 0.373$ (all data); min./max. difference electron density $-0.26/0.32$ e Å⁻³. After briefly soaking in a cryoprotectant solution consisting of the crystallization medium plus 20% 1,2-propanediol, the crystal was dipped into liquid nitrogen and mounted frozen for measurement. Data sets were collected at the BL1 beamline PSF/BESSY and processed using XDS.^[8] The molecular replacement program EPMR^[9] was employed for structure solution; c) Both structures have been found to be merohedrally twinned by a twofold rotation perpendicular to *c* (twin ratio: 0.51 and 0.50 for **1** and **2**, respectively). Both crystal forms have very low calculated densities (ca. 0.65 g cm⁻³) because they consist of 40–50% disordered aqueous solvent that is not taken into account in calculating the density; such solvent contents would be typical for protein crystals with similar unit-cell sizes. The structures were refined with no intensity cutoff using SHELXL^[10] and electron density maps displayed by XtalView,^[11] which was also employed for hand-editing of the model. Throughout the refinement, bond length, bond angle, chiral volume and planarity restraints were imposed. All non-hydrogen atoms were refined anisotropically with suitable rigid bond, similarity, and for solvent waters, approximately isotropic restraints. Hydrogen atoms were included in later stages of the refinement. The structures have been deposited in the Protein Data Bank (www.rcsb.edu/pdb) under accession codes 1w7q and 1w7r for **1** and **2**, respectively.

- [4] a) D. A. Langs, *Science* **1988**, 241, 188–191; b) B. M. Burkhart, N. Li, D. A. Langs, W. A. Pangborn, W. L. Duax, *Proc. Natl. Acad. Sci. USA* **1998**, 95, 12950–12955.
- [5] Pictures were generated using Molscript (P. J. Kraulis, *J. Appl. Crystallogr.* **1991**, 24, 946–950) and rendered with Raster3D (E. A. Merritt, D. J. Bacon, *Methods Enzymol.* **1997**, 277, 505–524).
- [6] a) T. R. Schneider, *Acta Crystallogr. Sect. D* **2002**, 58, 195–208; b) W. Kabsch, *Acta Crystallogr. Sect. A* **1976**, 32, 922–923.
- [7] G. M. Sheldrick, H. A. Hauptman, C. M. Weeks, M. Miller, I. Usón in *International Tables for Crystallography, Vol. F* (Eds.: E. Arnold, M. G. Rossmann), Kluwer Academic Publishers, Dordrecht, **2001**, pp. 333–351.
- [8] W. Kabsch in *International Tables for Crystallography, Vol. F* (Eds.: E. Arnold, M. G. Rossmann), Kluwer Academic Publishers, Dordrecht, **2001**, pp. 218–225.
- [9] C. R. Kissinger, D. K. Gehlhaar, D. B. Fogel, *Acta Crystallogr. Sect. D* **1999**, 55, 484–491.
- [10] G. M. Sheldrick, T. R. Schneider, *Methods Enzymol.* **1997**, 277, 319–343.
- [11] D. E. McRee, *J. Struct. Biol.* **1999**, 125, 156–165.

Direct Amino Acid Catalyzed Asymmetric Synthesis of Polyketide Sugars**

Jesús Casas, Magnus Engqvist, Ismail Ibrahim, Betül Kaynak, and Armando Córdova*

The directed asymmetric assembly of simple achiral building blocks into stereochemically complex molecules like carbohydrates and polyketides has long been accomplished by enzymes in nature.^[1,2] The growing interest in glycobiology^[3] and the search for novel antibiotics has led to increased activity in developing reaction designs and methods for the synthesis of sugars and polyketides.^[1,2,4,5] Among the plethora of methods, the aldol reaction is well established in carbohydrate and triketide synthesis.^[6,7] However, it usually requires protective group strategies and subsequent reduction–oxidation steps. One efficient synthetic strategy based on retrosynthetic analysis would be a two-step sugar synthesis involving two iterative aldol reactions with three carbonyl compounds [Eq. (1)]. This potential iterative double-aldol route seems simple and attractive. However, it is challenging to carry out due to the intrinsic chemoselectivity problems with enolizable aldehydes. For example, it is difficult to control whether they would act as donors or acceptors in the sequential aldol reactions.

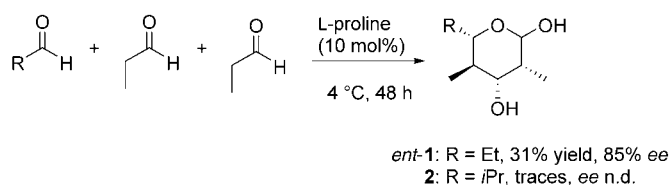


To date, only enzymes have been able to catalyze sequential one-pot direct aldol reactions with high stereoselectivity.^[8] Recently, organocatalysis has been revitalized in the area of asymmetric synthesis.^[9] The use of enamine catalysis has enabled the first step of the sequential direct

cross-aldol reaction with high stereoselectivity.^[10] However, achieving the next amino acid catalyzed aldol step to obtain hexoses with high enantioselectivity has not yet been reported. Initial attempts at conducting one-pot direct catalytic sequential aldol reactions furnished nearly racemic triketide sugars.^[10f,g]

Based on retrosynthetic analysis and our interest in developing biomimetic stereoselective transformations catalyzed by amino acids,^[11] we envisioned a potential two-step sugar synthesis based on direct amino acid catalyzed selective iterative aldol reactions with aldehydes. Herein, we report the enantioselective de novo synthesis of either enantiomer of natural and unnatural hexoses with up to > 99% *ee*. The simplicity and the high stereoselectivity of the hexose formation may support a prebiotic pathway in which amino acids transferred their chiral information to sugars.

In initial experiments we investigated the one-pot direct amino acid catalyzed sequential trimerization of propionaldehyde (Scheme 1). To our delight we were able to signifi-



Scheme 1. Direct catalytic one-pot enantioselective synthesis of **1**.

cantly increase the *ee* value of the previously reported triketide hexose *ent*-**1** from 49% to 85% *ee* by altering the reaction conditions. However, the new one-pot procedure only provided trace amounts of hexose **2**.

To improve the efficiency and selectivity of the tandem aldol process we decided to isolate the β-hydroxy aldol intermediate from the first aldol transformation prior to the second aldol reaction.^[12] The two-step synthetic protocol made it possible to investigate other amino acids as catalysts as well as change the stereochemistry of the amino acid catalyst prior to the second aldol addition. This approach would potentially improve the efficiency and selectivity of the second direct cross-aldol addition. Hence, propionaldehyde was dimerized utilizing L-proline catalysis, and the corresponding isolated β-hydroxy aldehyde was treated with propionaldehyde in the presence of a catalytic amount of D-proline (Table 1, entry 1). To our delight we were able to isolate hexose **1** as a single diastereomer in 29% yield with 99% *ee*.

Encouraged by this result we performed the iterative aldol reactions *vide infra* with a variety of aldehyde substrates (Table 1). The short synthesis of hexoses proceeded with excellent chemo-, diastereo-, and enantioselectivity. In all cases except one, the corresponding hexoses were isolated as single diastereomers in good overall yield with > 99% *ee*. Thus, out of 16 possible stereoisomers amino acid catalysis directs in some cases the creation of a single enantiomer. The yields of the hexoses **1–5** were comparable or higher than most conventional multistep sugar syntheses.^[6] In addition, this two-step synthesis of sugars is inexpensive and easy to

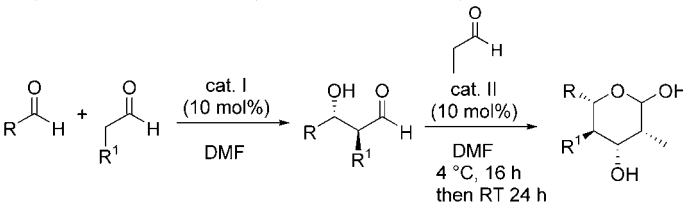
[*] Dr. J. Casas, M. Engqvist, I. Ibrahim, Prof. Dr. A. Córdova
Department of Organic Chemistry
Stockholm University
10691 Stockholm (Sweden)
Fax: (+46) 8-154-908
E-mail: acordova@organ.su.se
acordova1a@netscape.net

Dr. B. Kaynak
Department of Structural Chemistry
The Arrhenius Laboratory
Stockholm University
10691 Stockholm (Sweden)

[**] We gratefully acknowledge the Swedish National Research council and Wenner-Gren Foundation for financial support. We thank Prof. Jan-E. Bäckvall and Prof. Stefan Oscarsson for valuable discussions. We also thank the referees for suggesting the crystal structure analysis.

Supporting information for this article is available on the WWW under <http://www.angewandte.org> or from the author.

Table 1: Two-step direct amino acid catalyzed enantioselective synthesis of hexoses.

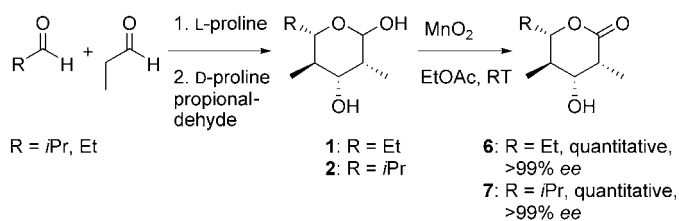


Entry	R	R ¹	Cat. I	Cat. II	Sugar	Yield [%] ^[a]	ee [%] ^[b]
1	Et	Me	L-proline	D-proline	1	29	99
2	<i>i</i> Pr	Me	L-proline	D-proline	2	42	> 99
3	<i>i</i> Pr	Me	D-proline	L-proline	<i>ent</i> - 2	40	> 99
4	<i>i</i> Bu	Me	L-proline	D-proline	3	24	> 99
5	<i>c</i> -Hexyl	Me	L-proline	D-proline	4	41	> 99
6	Et	Me	D-proline	L-4-hydroxyproline ^[c]	<i>ent</i> - 1	30	> 99
7	<i>i</i> Pr	Me	D-proline	L-4-hydroxyproline ^[c]	<i>ent</i> - 2	15	> 99
8	BnOCH ₂	OBn	L-proline	D-proline	5	39 ^[d]	> 99

[a] Overall yield of the isolated hexoses based on the two steps. [b] Determined by chiral-phase GC analyses of the peracetylated products and compared to racemic standards generated by D,L-proline catalysis. [c] 30 mol% hydroxyproline was used. [d] The overall combined yield of a 10:1 mixture of diastereomers (*anti:syn*).

conduct, and it generates minimal waste products. The sequential direct catalytic aldol reactions were also readily scaled up and performed on a gram scale. For example, we performed the two-step catalytic asymmetric synthesis of hexose **2** on a 2-g scale, and triketide sugar **2** was obtained in crystalline form in 42 % yield with > 99 % *ee*. Starting the iterative aldol reactions with D-proline as the catalyst furnished the opposite enantiomer of the hexoses without affecting the stereoselectivity of the reaction. Furthermore, performing the two-step synthesis employing sequential D-proline and L-4-hydroxyproline catalysis improved the *ee* of the triketide sugar *ent*-**1** from 99 to > 99 % *ee*. Moreover, the amino acids are able to catalyze the total synthesis of natural hexoses in one step. For example, L-4-hydroxyproline catalyzed the trimerization of α -benzyloxyacetaldehyde to yield 2,4,6-tri-*O*-benzylallose in 28 % yield as a single diastereomer with > 99 % *ee*. The hexoses obtained from the tandem direct catalytic asymmetric aldol reactions have free hydroxy groups at C1 and C3, allowing for introduction of orthogonal protective groups and selective di- or polysaccharide couplings. Furthermore, the aldehyde substrates and the amino acid catalysts can be freely varied, potentially providing access to a wide range of deoxyhexoses.

The hexoses were quantitatively converted into δ -lactones by oxidation with MnO₂. For example, lactones **6** and **7** were prepared in three steps with > 99 % *ee* (Scheme 2). Thus, the



Scheme 2. Direct catalytic enantioselective synthesis of δ -lactones **6** and **7**.

two-step aldol strategy opens up a novel route to enantiomerically pure δ -lactones from simple aldehydes. This type of compounds were previously synthesized in 11 steps by Staunton and co-workers using Evans-type aldol reactions.^[6d]

The absolute configurations of sugars **1**–**5** have been assigned based on the crystal structure of the α -anomer of sugar **2** (Figure 1) and synthesis.^[13] The crystal structure reveals that the previously suggested relative configuration of triketide sugar **2** is incorrect.^[10f] The hexose **2** obtained by proline catalysis has a mannopyranoside configuration and not the previously believed gulopyranoside configuration. Furthermore, sequential L-proline and D-proline catalysis furnished L-hexoses. Accordingly, the observed stereochemistry of the hexoses can be readily explained (Scheme 3). The initial formation of the β -hydroxyaldehyde proceeds by means of a

re-facial attack on the acceptor aldehyde by the L-proline-derived enamine, which is in accordance with previous reported proline-catalyzed aldol reactions with aldehydes.^[8] Next, the D-proline-catalyzed aldol addition proceeds in a highly *anti*-selective fashion with the *anti*- β -hydroxyaldehyde isomer to form the L-mannose structural motif.

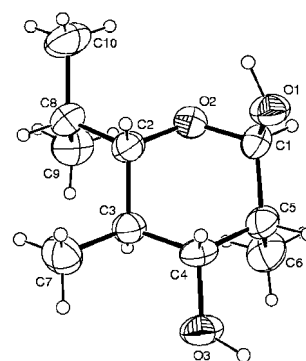
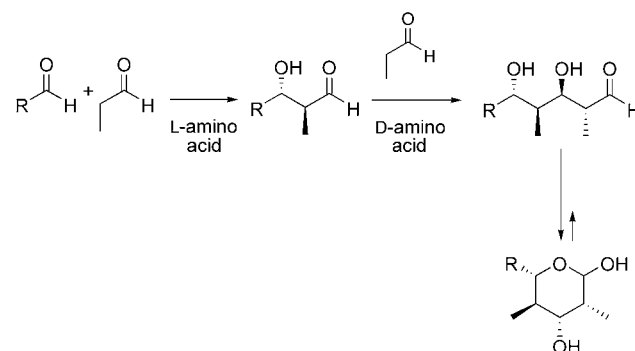


Figure 1. The crystal structure of the α -anomer of hexose **2**.



Scheme 3. The reaction pathway for the amino acid catalyzed triketide hexose synthesis.

The ability of amino acids to catalyze the asymmetric formation of sugars may have prebiotic significance. In fact, it has been reported that terrestrial and extraterrestrial amino acids catalyze the formation of tetroses under prebiotic conditions.^[14] Perhaps amino acids catalyzed asymmetric aldol reactions according to the routes presented and transferred their chiral information to hexoses,^[15] which are the building blocks of prebiotic RNA and most common polysaccharides.

In summary, we disclose the direct amino acid catalyzed asymmetric de novo synthesis of hexoses with excellent chemo-, diastereo-, and enantioselectivity. The employment of a two-step direct catalytic synthetic protocol furnished either L- or D-sugars in most cases with >99% ee. Thus, the novel synthetic approach allows for the creation of four contiguous stereocenters with excellent stereocontrol. Our hexose synthesis is inexpensive and easy to conduct, and it generates minimal waste products. The iterative aldol reaction methodology allows for variation of both the catalyst and the three carbonyl components, hence facilitating a modular enantioselective synthesis of functional sugars and isotope-labeled sugars. The ability of amino acids to mediate asymmetric formation of natural sugars may support a catalytic prebiotic homochirality pathway in which chiral amino acids transferred their stereochemical information to carbohydrates.

Received: July 22, 2004

Published online: December 28, 2004

Keywords: aldehydes · aldol reaction · asymmetric catalysis · carbohydrates · hexoses

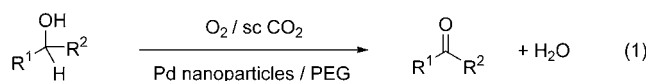
- [1] a) K. M. Koeller, C.-H. Wong, *Nature* **2001**, 409, 232; b) H. J. M. Gijzen, L. Qiao, W. Fitz, C.-H. Wong, *Chem. Rev.* **1996**, 96, 443; c) C.-H. Wong, G. M. Whitesides, *Enzymes in Synthetic Organic Chemistry*, Pergamon, Oxford, **1994**.
- [2] a) C. Khosla, *J. Org. Chem.* **2000**, 65, 8127; b) C. Khosla, P. B. Harbury, *Nature* **2001**, 409, 247; c) N. Wu, F. Kudo, C. Khosla, D. E. Cane, *J. Am. Chem. Soc.* **2000**, 122, 4847; d) C. N. Boddy, K. Hotta, M. L. Tse, R. E. Watts, C. Khosla, *J. Am. Chem. Soc.* **2004**, 126, 7436, and references therein.
- [3] *Glycochemistry: Principles, Synthesis, and Applications* (Eds.: P. Wang, C. Bertozzi), Marcel Dekker, New York, **2001**.
- [4] C. T. Walsh, *Science* **2004**, 303, 1805.
- [5] K. C. Nicolaou, H. J. Mitchell, *Angew. Chem.* **2001**, 113, 1625; *Angew. Chem. Int. Ed.* **2001**, 40, 1576.
- [6] a) D. A. Evans, E. Hu, J. S. Tedrow, *Org. Lett.* **2001**, 3, 3133; b) M. P. Sibi, J. Lu, J. Edwards, *J. Org. Chem.* **1997**, 62, 5864; c) S. G. Davies, R. L. Nicholson, A. D. Smith, *Synlett* **2002**, 10, 1637; For selected examples of the aldol reaction in assembly of triketides see: d) A. L. Wilkinson, U. Hanefeld, B. Wilkinson, P. F. Leadlay, J. Staunton, *Tetrahedron Lett.* **1998**, 39, 9827; e) J. R. Gage, D. A. Evans, *Org. Synth.* **1990**, 68, 83; f) B. C. Raimundo, C. H. Heathcock, *Synlett* **1995**, 1213.
- [7] Reviews see: a) D. A. Evans, J. V. Nelson, T. Taber in *Topics in Stereochemistry*, Vol. 13, Wiley, New York, **1982**, p. 1; b) T. D. Machajewski, C.-H. Wong, *Angew. Chem.* **2000**, 112, 1406; *Angew. Chem. Int. Ed.* **2000**, 39, 1352; c) C. Palomo, M. Oiarbide, J. M. García, *Chem. Eur. J.* **2002**, 8, 36; For examples of direct aldol reactions catalyzed by organometallic complexes see: d) Y. M. A. Yamada, N. Yoshikawa, H. Sasai, M. Shibasaki, *Angew. Chem.* **1997**, 109, 1942; *Angew. Chem. Int. Ed. Engl.* **1997**, 36, 1871; e) N. Yoshikawa, N. Kumagai, S. Matsunaga, G. Moll, T. Oshima, T. Suzuki, M. Shibasaki, *J. Am. Chem. Soc.* **2001**, 123, 2466; f) B. M. Trost, H. Ito, *J. Am. Chem. Soc.* **2000**, 122, 12003; g) B. M. Trost, E. R. Silcoff, H. Ito, *Org. Lett.* **2001**, 3, 2497; h) D. A. Evans, J. S. Tedrow, J. T. Shaw, C. W. Downey, *J. Am. Chem. Soc.* **2002**, 124, 392.
- [8] a) A. Heine, G. DeSantis, J. G. Luz, M. Mitchell, C.-H. Wong, I. A. Wilson, *Science* **2001**, 294, 369; b) H. J. M. Gijzen, C.-H. Wong, *J. Am. Chem. Soc.* **1994**, 116, 8422; c) H. J. M. Gijzen, C.-H. Wong, *J. Am. Chem. Soc.* **1995**, 117, 7585; d) H. J. M. Gijzen, C.-H. Wong, *J. Am. Chem. Soc.* **1995**, 117, 2947; e) J. Liu, C.-H. Wong, *Angew. Chem.* **2002**, 114, 1462; *Angew. Chem. Int. Ed.* **2002**, 41, 1404.
- [9] a) P. I. Dalko, L. Moisan, *Angew. Chem.* **2001**, 113, 3840; *Angew. Chem. Int. Ed.* **2001**, 40, 3726; b) B. List, *Tetrahedron* **2002**, 58, 5573; c) E. R. Jarvo, S. J. Miller, *Tetrahedron* **2002**, 58, 2481; d) R. O. Duthaler, *Angew. Chem.* **2003**, 115, 1005; *Angew. Chem. Int. Ed.* **2003**, 42, 975; e) P. I. Dalko, L. Moisan, *Angew. Chem.* **2004**, 116, 5248; *Angew. Chem. Int. Ed.* **2004**, 43, 5138.
- [10] a) A. Córdova, W. Notz, C. F. Barbas III, *J. Org. Chem.* **2002**, 67, 301; b) A. B. Northrup, D. W. C. MacMillan, *J. Am. Chem. Soc.* **2002**, 124, 6798; c) A. Bøgevig, N. Kumaragurubaran, K. A. Jørgensen, *Chem. Commun.* **2002**, 620; d) N. Mase, F. Tanaka, C. F. Barbas III, *Angew. Chem.* **2004**, 116, 2474; *Angew. Chem. Int. Ed.* **2004**, 43, 2420; e) C. Pidathala, L. Hoang, N. Vignola, B. List, *Angew. Chem.* **2003**, 115, 2474; *Angew. Chem. Int. Ed.* **2003**, 42, 2785; f) N. S. Chowdari, D. B. Ramachary, A. Córdova, C. F. Barbas III, *Tetrahedron Lett.* **2002**, 43, 9591; g) A. Córdova, *Tetrahedron Lett.* **2004**, 45, 3949; h) J. Casas, H. Sundén, A. Córdova, *Tetrahedron Lett.* **2004**, 45, 6117; i) A. B. Northrup, I. K. Mangion, F. Hettche, D. W. C. MacMillan, *Angew. Chem.* **2004**, 116, 2204; *Angew. Chem. Int. Ed.* **2004**, 43, 2152.
- [11] a) A. Córdova, H. Sundén, M. Engqvist, I. Ibrahim, J. Casas, *J. Am. Chem. Soc.* **2004**, 126, 3914; b) A. Bøgevig, H. Sundén, A. Córdova, *Angew. Chem.* **2004**, 116, 1129; *Angew. Chem. Int. Ed.* **2004**, 43, 1109; c) A. Córdova, H. Sundén, A. Bøgevig, M. Johansson, F. Himo, *Chem. Eur. J.* **2004**, 10, 3673; d) A. Córdova, *Chem. Eur. J.* **2004**, 10, 1987; e) A. Córdova, *Acc. Chem. Res.* **2004**, 37, 102; f) A. Córdova, *Synlett* **2003**, 1651, and references therein.
- [12] After the submission of this manuscript MacMillan and co-workers reported an excellent short synthesis of hexoses based on a proline-catalyzed dimerization of protected glycoaldehydes followed by Lewis acid mediated indirect tandem Mukaiyama aldol addition cyclization reactions. A. B. Northrup, D. W. C. MacMillan, *Science* **2004**, 305, 1752.
- [13] CCDC-251202 contains the crystallographic data for this paper. These data can be obtained free of charge via www.ccdc.cam.ac.uk/conts/retrieving.html (or from the Cambridge Crystallographic Data Centre, 12, Union Road, Cambridge CB21EZ, UK; fax: (+44) 1223-336-033; or deposit@ccdc.cam.ac.uk).
- [14] S. Pizzarello, A. L. Weber, *Science* **2004**, 303, 1151. For a Zn/ amino acid mediated sugar synthesis under prebiotic conditions see: J. Kofoed, M. Machuqueiro, J.-L. Reymond, T. Darbre, *Chem. Commun.* **2004**, 26, 1540.
- [15] a) L. E. Orgel, *Science* **2000**, 290, 1306; b) N. Hall, *Chem. Commun.* **2004**, 1247, and references therein.

Biphasic Aerobic Oxidation of Alcohols Catalyzed by Poly(ethylene glycol)-Stabilized Palladium Nanoparticles in Supercritical Carbon Dioxide**

Zhenshan Hou, Nils Theyssen, Axel Brinkmann, and Walter Leitner*

The aerobic oxidation of alcohols to aldehydes and ketones is a fundamental chemical transformation for the production of a large variety of important intermediates and fine chemical products. Catalytic methods for this reaction are being investigated intensively to replace stoichiometric oxidation processes that generate large amounts of heavy metal and solvent waste.^[1] Among the transition metals, palladium shows very promising catalytic properties in the form of complexes,^[2] heterogeneous metal catalysts,^[3,4] or nanoparticles.^[5] Significant progress has been made in improving activity, substrate scope, and selectivity with multifunctional substrates for the individual catalytic systems. Two of the major general limitations of the catalytic approach relate to rapid catalyst deactivation by aggregation and formation of Pd-black^[6] and the need for large amounts of organic solvents in batchwise solution-phase processes involving molecular oxygen.^[7]

Herein, we report on a new highly efficient catalytic system for the biphasic aerobic oxidation of alcohols by using palladium nanoparticles in a poly(ethylene glycol) (PEG) matrix as the catalyst and supercritical carbon dioxide (scCO₂) as the substrate- and product-phase [Eq. (1)].^[8,9] The design of this system was based on the assumption that the PEG matrix might help to prevent aggregation and deactivation of the catalytically active nanoparticles while scCO₂ could provide a safe environment for the use of molecular oxygen under essentially solvent-free conditions and could allow continuous operation, even with substrates of low volatility. The results disclosed herein confirm the feasibility of this approach, provide insight into the formation of the catalytically active particles within the matrix, and demonstrate that activity, selectivity, and substrate scope of this new system compare favorably to other catalytic approaches for selective alcohol oxidation.



In an exploratory study, the oxidation of 3-methyl-2-butene-1-ol (**1a**) to 3-methyl-2-butene-1-al (**2a**) was used as a test reaction [Eq. (2)]. The giant palladium cluster [Pd₅₆₁-phen₆₀(OAc)₁₈₀]^[5a,b,10,11] (**3**; phen = 1,10-phenanthroline) was found to lead to a particularly active and selective catalyst for aerobic oxidation of alcohols in scCO₂ when embedded in a PEG-1000 matrix (Figure 1). PEG of molecular weight 1000 is

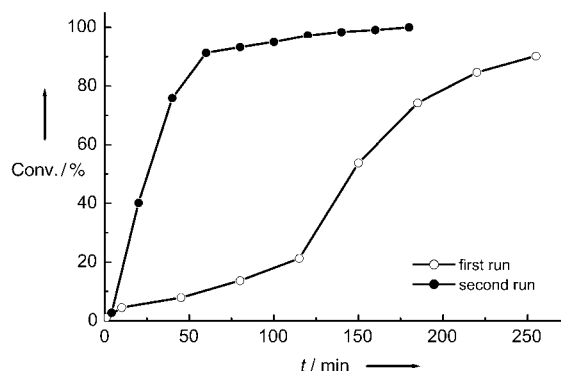
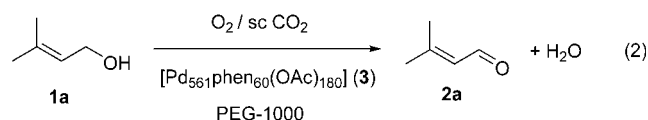


Figure 1. Conversion/time profile of the biphasic selective aerobic oxidation of 3-methyl-2-butene-1-ol (**1a**) by using a catalyst formed from [Pd₅₆₁phen₆₀(OAc)₁₈₀] (**3**) and PEG-1000 with scCO₂ as the reaction medium (*T* = 50 °C, *d*(CO₂/O₂) = 0.55 g mL⁻¹).

a waxy solid under ambient conditions but melts under CO₂ pressures at temperatures above approximately 40 °C.^[8,12] In a typical procedure, PEG-1000, cluster **3**, and substrate **1a** were charged into a window-equipped high-pressure reactor, which was then pressurized with CO₂ and O₂, either sequentially or as a preformed mixture from a high-pressure reservoir. The Pd clusters were well dispersed in the liquid PEG-1000 matrix over a period of about 1–2 h under the reaction conditions summarized in Figure 1. Substrate **1a** and product **2a** are contained preferentially in the supernatant “supercritical” CO₂ phase, as demonstrated by online GC monitoring. The conversion/time profile reveals a significant induction period in the first run, which can be associated with the dispersion process (see below). The oxidation occurs exclusively on the hydroxy function and with no significant over-oxidation to yield **2a** with selectivities well above 99 % at quantitative conversion.



After conversion is completed, the products **2a** and water can be extracted quantitatively with scCO₂ (80 °C, 14.5 MPa, 5 L h⁻¹, 7 h) with the Pd-doped PEG phase left in the reactor. Only very small amounts of PEG-1000 are extracted by scCO₂

[*] Prof. Dr. W. Leitner
Institut für Technische und Makromolekulare Chemie
Lehrstuhl für Technische Chemie und Petrochemie
RWTH Aachen, Worringerweg 1, 52064 Aachen (Germany)
Fax: (+49) 241-80-22177
E-mail: leitner@itmc.rwth-aachen.de

Dr. Z. Hou, Dr. N. Theyssen, A. Brinkmann, Prof. Dr. W. Leitner
Max-Planck-Institut für Kohlenforschung
Kaiser-Wilhelm-Platz 1, 45470 Mülheim an der Ruhr (Germany)

[**] This work was supported by the Max-Planck-Gesellschaft and the Fonds der Chemischen Industrie. We thank Axel Dreier and Dr. B. Tesche, MPI Mülheim, for the transmission electron microscopy analysis and Prof. U. Simon, RWTH Aachen, for fruitful discussions.

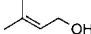
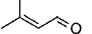
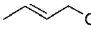
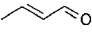
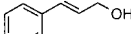
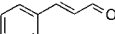
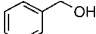
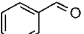
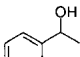
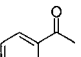
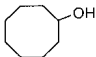
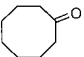
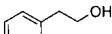
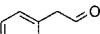
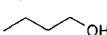
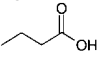
under these conditions (8 mg according to the method described in ref. [8]), and the product is contaminated with less than 2.3 ppm of Pd according to atomic absorption spectroscopy. Most notably, the reaction starts again without any noticeable induction period in the second run, thereby leading to complete conversion within less than 200 min at 50 °C (Figure 1). This high activity is fully retained or even seems to increase slightly in subsequent runs. The same qualitative behavior is observed at somewhat higher reaction temperatures and for benzyl alcohol **1d**, another prototypical substrate (Table 1).

The activity and selectivity of the catalytic system formed from **3** and PEG-1000 are remarkably higher than those of conventional heterogeneous catalysts under the same reaction conditions with scCO_2 as the reaction medium.^[4] In control experiments ($T = 65^\circ\text{C}$, $d(\text{CO}_2/\text{O}_2) = 0.55 \text{ g mL}^{-1}$), palladium on charcoal gives only 34% conversion of **1a** after 1.5 h reaction time. Higher conversion can be obtained upon prolonged reaction times, but only at the expense of significantly reduced selectivity towards the unsaturated aldehyde **2a** (5 h: conversion = 75%, selectivity = 78%). The same negative trend is even more pronounced with palladium on alumina, which gives only 45% selectivity at 88% conversion within 5 h. Interestingly, the addition of PEG-1000 results in a certain improvement of the performance of the heterogeneous catalyst, as shown for palladium on carbon (5 h: conversion = 82%, selectivity = 89%). However, neither activity nor selectivity can rival the performance of the PEG-stabilized nanoparticle catalyst.

Table 1 summarizes representative results obtained with the catalytic system **3**/PEG-1000 in scCO_2 for a variety of alcohols under a standard set of reaction conditions. Conversion and selectivity from the second run is given unless noted otherwise. Allylic alcohols **1a–c** are transformed into the corresponding α,β -unsaturated aldehydes **2a–c** in excellent yields under mild conditions. Somewhat longer reaction times are required for primary and secondary benzylic alcohols **1d** and **1e**, but selectivities remain close to 99%. The cyclic alcohol **1f** and even 2-phenylethanol (**1g**) give very high selectivities for the corresponding ketone **2f** and aldehyde **2g**, respectively, and quantitative conversion is obtained after appropriate reaction times. The only exception, so far, was found with 1-butanol (**1h**), which is oxidized rapidly but forms butyric acid **5** as the major product under the present conditions.

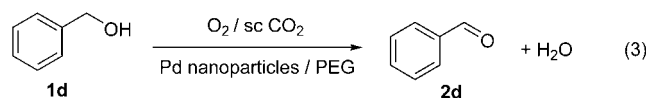
It is important to note that the giant palladium cluster **3** is known to oxidize allylic alcohols in conventional organic solvents, whereas benzylic alcohols are not effectively transformed with **3** under conventional conditions.^[11] Thus, the broad substrate scope summarized in Table 1 indicates that the catalytically active species is different in the catalytic system formed from **3**/PEG-1000 in scCO_2 . We were therefore interested in whether it is possible to generate PEG-stabilized Pd nanoparticles for the selective oxidation of alcohols from other precursors as well. Indeed, a material with almost identical catalytic properties was obtained by simply heating a mixture of $[\text{Pd}(\text{acac})_2]$ (**4**; acac = acetylacetonate; 20 mg), the commercial surfactant Brij 35 (0.8 g), and PEG-1000 (2.7 g) to 130 °C for 1 h under an argon atmosphere.

Table 1: Biphasic catalytic oxidation of alcohols **1a–h** by using PEG-stabilized palladium nanoparticles in scCO_2 .^[a]

Substrate	Product	T [°C]	t [h]	Run	Conv. [%]	Sel. [%]
		65	1.5	1	81.0	99.8
1a	2a			2	99.2	99.3
				3	100	99.1
		65	1.5	2	100	98.1
1b	2b					
		65	1.5	2	99.8	99.2
1c	2c					
		80	13	1	83.1	99.8
1d	2d			2	96.2	98.8
				3	99.8	97.5
				4	100	98.7
		80	13	2	56.9	98.8
1e	2e					
		80	26	2	99.5	98.9
1f	2f					
		80	13	2	45.8	95.5
1g	2g					
		80	4	1	65.5	57.5 ^[b]
1h	5					

[a] Reaction conditions: palladium cluster **3** (0.1 mmol Pd), PEG-1000 (2.40 g), substrate **1a–h** (1.99 mmol), $d(\text{CO}_2/\text{O}_2) = 0.55 \text{ g mL}^{-1}$. [b] Butyric acid butyl ester is formed as a second product, together with small amounts of butanal.

As we were encouraged by the promising results obtained from batchwise recycling, the aerobic oxidation of benzylic alcohol **1d** was carried out as a continuous-flow process [Eq. (3)]. The set-up was largely identical to previously described equipment,^[13] with a 36 mL stainless-steel reactor as the central part. Owing to the unique combination of gas-like mixing and liquid-like solvent properties provided by scCO_2 , a homogeneous feed of CO_2 , O_2 , and **1d/2d** can be transported through the PEG phase by using a capillary.



In the absence of CO_2 , **1d** and **2d** are liquids at the reaction temperature and are largely miscible with PEG-1500. Consequently, separation of catalysts and products would be tedious, if not impossible. Furthermore, great care would have to be taken to stay outside the explosive regime for all mixtures of the organic substrates and products and the molecular oxygen.

As judged by visual inspection, the catalyst material remains physically intact inside the reactor and no significant

extrusion of PEG or Pd is observed, even during long operation times with scCO₂ as the mobile phase. Even with the very basic reaction engineering used in these bench-scale experiments, significant single-pass conversions are achieved with substrate **1d** under the nonoptimized conditions summarized in Figure 2. The initial conversion with both Pd

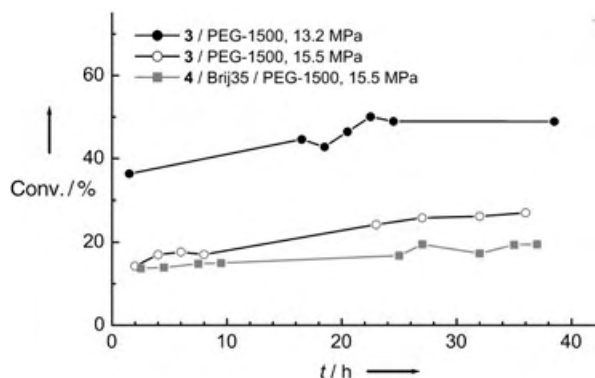


Figure 2. Continuous-flow aerobic oxidation of benzylic alcohol **1d** in scCO₂ by using PEG-stabilized Pd nanoparticles formed from [Pd₅₆₁phen₆₀(OAc)₁₈₀] (**3**) and [Pd(acac)₂] (**4**), respectively ($T = 80^\circ\text{C}$, $p(\text{CO}_2/\text{O}_2, 92:8) = 15.5\text{ MPa}$ and 13.2 MPa , respectively; flow rates: **1d**: 0.5 mL h^{-1} ; exit flow: 5 L h^{-1}).

nanoparticle/PEG-1500 catalysts reaches 15% at a total pressure of 15.5 MPa. Most notably, a small but continuous increase in activity occurs for both catalytic materials over the course of a 40 h continuous operation (Figure 2). The increase is somewhat more strongly pronounced for the system **3**/PEG-1500 where a conversion of 27% at nearly perfect selectivity is reached after 36 h.

Interestingly, the CO₂ pressure has a distinct influence on the performance of the system. A small reduction of the pressure level (13.2 MPa instead of 15.5 MPa) leads to a significant increase in conversion by a factor of almost two (Figure 2), thereby resulting in a maximum single-pass conversion of approximately 50%. Most likely, the increased conversion results from a shift of the partition coefficient of the substrate in the biphasic medium in favor of the PEG phase at lower supercritical fluid density, thus increasing substrate availability in the catalyst phase. This explanation is supported by the fact that the solubility power of scCO₂ becomes insufficiently low for continuous operation with substrate **1d** at approximately 11 MPa. In general, these results indicate the possibility for significant optimization of single-pass conversion by variation of engineering parameters such as flow rates, CO₂ density, O₂/substrate ratio, and residence time.

It seems plausible to associate the high activity and long-term stability of the new catalytic system with a high dispersion of Pd nanoparticles, which are prevented from agglomeration within the PEG matrix.^[14] This interpretation is strongly supported by transmission electron microscopy (TEM) studies of catalyst material formed from **3** and PEG-1000 before and after the reaction (Figure 3).

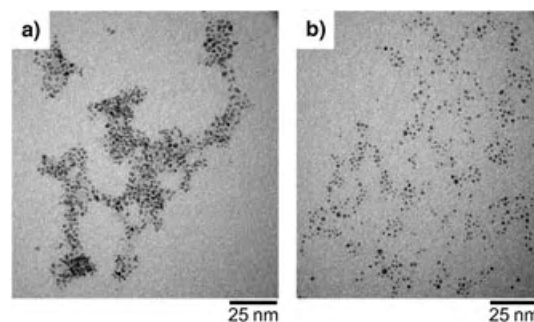


Figure 3. TEM images of the catalytically active material formed from the giant palladium cluster **3** and PEG-1000 before (a) and after (b) the selective biphasic oxidation of **1a** ($T = 65^\circ\text{C}$, $d(\text{CO}_2/\text{O}_2) = 0.55\text{ g mL}^{-1}$).

As shown in Figure 3a, the mixing of cluster **3** with PEG-1000 leads to a dispersion of particles that is far from uniform with significant agglomeration in certain areas of the matrix. In a sample taken after catalytic oxidation of **1a**, this situation has changed significantly (Figure 3b). The particles are now much more equally dispersed throughout the whole matrix. The average particle sizes were determined to be around 3.6 nm and 2.9 nm before and after the reaction, respectively. These values are consistent with values given for giant Pd clusters in other environments ($3.0\text{--}3.6\text{ nm}$,^[10] $2.6 \pm 0.35\text{ nm}$ ^[11a]). At this stage of investigation, we believe that interactions between the giant cluster and PEG are favoring dispersion of the particles within the matrix during the course of the reaction. The formation of pseudo-crown-ether structures between PEG and the nanoparticles has been suggested^[14a,c] and was recently confirmed for a ZnCl₂-PEG complex by X-ray diffraction analysis.^[15] The supercritical-phase-induced viscosity reduction may help to facilitate the necessary mass transport for the dispersion process in this multiphase approach to continuous-flow nanoparticle catalysis.

We have developed a novel catalytic system for the selective aerobic oxidation of alcohols based on highly dispersed Pd nanoparticles in a poly(ethylene glycol) (PEG) matrix with supercritical carbon dioxide (scCO₂) as the substrate and product phase. These catalytic materials show high activity, selectivity, and stability for a broad range of substrates. Catalytically active particles can be formed from various palladium sources and their dispersion appears to be aided by the presence of the supercritical reaction medium. The PEG matrix effectively stabilizes and immobilizes the catalytically active particles, whereas the unique solubility and mass-transfer properties of scCO₂ allow continuous processing at mild conditions, even with low-volatility substrates. This system nicely exemplifies the potential benefits resulting from the combination of molecular design and reaction engineering in advanced multiphase catalysis. Finally, it seems worth noting that both the catalyst matrix and the mobile phase used in this approach are toxicologically innocuous and environmentally benign materials that are applied in commercial applications in the nutrition industry, thus making this approach of general interest for “green” nanoparticle catalysis.

Experimental Section

Safety warning: Experiments using large amounts of compressed gases, especially molecular oxygen, are potentially hazardous and must only be carried out by using appropriate equipment and safety precautions.

The palladium cluster **3** was prepared under argon according to a known procedure.^[10a] [Pd(acac)₂] (**4**), Brij 35, PEG-1000, and **1a–h** were obtained from commercial suppliers. The oxidation products were identified by comparison of ¹H NMR spectra and GC data with those of authentic samples. A preformed mixture of CO₂ and O₂ (molar ratio 92:8) was prepared in a temperature-controlled 5 L autoclave at 35°C and 20.0 MPa and used throughout most of the oxidation experiments.

Batchwise catalytic oxidation of 1a–h: A solution of **3** (9.98×10^{-5} mol) in acetic acid (1 mL) was introduced into a 10 mL window-equipped stainless-steel high-pressure reactor. The solvent was evaporated; PEG-1000 (2.40 g) and then the appropriate substrate **1a–h** (2.0×10^{-3} mol) were added. The reactor was pressurized with the CO₂/O₂ mixture (5.50 g) and heated to the desired temperature under vigorous stirring for the given reaction time (see Figure 1 and Table 1). After the reaction, CO₂ at 80°C and 14.5 MPa was flushed through the liquid PEG phase for 7 h by use of a capillary with a compressor at an outlet flow-rate of approximately 5 L h⁻¹. The products were collected from the gas stream in two serial traps kept at -35°C and analyzed by ¹H NMR spectroscopy and GC. Before starting the next run, the reactor was vented to ambient pressure and then new substrate was charged, followed by the CO₂/O₂ mixture.

Continuous-flow catalytic oxidation of 1d: The catalytically active material formed from **3** or **4** and PEG-1500 (3.5 g) was charged into a 36 mL stainless-steel high-pressure reactor which was kept at 80°C. A prewarmed (50°C) continuous stream of CO₂/O₂ was passed through the liquid PEG phase at a flow rate of approximately 5 L h⁻¹ by use of a capillary (exit flow at ambient conditions, total pressure of 15.5 MPa and 13.2 MPa in the reactor, respectively; Figure 2). The substrate was fed into the CO₂ stream before it entered the reactor with an HPLC pump at a rate of 0.5 mL h⁻¹. The mixture of **1d** and **2d** was isolated in two sequential cold traps (-35°C) from the exit flow upon depressurization of the supercritical solvent. The cold traps were replaced periodically after about 2 h and their combined content was analyzed by ¹H NMR spectroscopy and GC.

Received: July 30, 2004

Revised: October 15, 2004

Published online: January 26, 2005

Keywords: aerobic oxidation · multiphase catalysis · nanoparticles · palladium · supercritical fluids

- [1] a) R. A. Sheldon, I. W. C. E. Arends, G.-J. T. Brink, A. Dijkman, *Acc. Chem. Res.* **2002**, *35*, 774–781; b) J. Muzart, *Tetrahedron* **2003**, *59*, 5789–5816; c) B.-Z. Zhan, A. Thompson, *Tetrahedron* **2004**, *60*, 2917–2935.
- [2] For recent examples, see: a) G.-J. T. Brink, I. W. C. E. Arends, M. Hoogenraad, G. Vespui, R. A. Sheldon, *Adv. Synth. Catal.* **2003**, *345*, 497–505; b) B. A. Steinhoff, S. R. Fix, S. S. Stahl, *J. Am. Chem. Soc.* **2002**, *124*, 766–767; c) N. Kakiuchi, Y. Maeda, T. Nishimura, S. Uemura, *J. Org. Chem.* **2001**, *66*, 6620–6625; d) D. R. Jensen, M. J. Schultz, J. A. Mueller, M. S. Sigman, *Angew. Chem.* **2003**, *115*, 3940–3943; *Angew. Chem. Int. Ed.* **2003**, *42*, 3810–3813; e) K. P. Peterson, R. C. Larock, *J. Org. Chem.* **1998**, *63*, 3185–3189; f) A. Haimov, R. Neumann, *Chem. Commun.* **2002**, 876–877; g) E. M. Ferreira, B. M. Stoltz, *J. Am. Chem. Soc.* **2001**, *123*, 7725–7726; h) S. Paavola, K. Zetterberg, T. Privalov, I. Csöreg, C. Moberg, *Adv. Synth. Catal.* **2004**, *346*, 237–244.

- [3] For recent examples, see: a) K. Yamaguchi, N. Mizuno, *Angew. Chem.* **2002**, *114*, 4720–4724; *Angew. Chem. Int. Ed.* **2002**, *41*, 4538–4542; b) M. Musawir, P. N. Davey, G. Kelly, I. V. Kozhevnikov, *Chem. Commun.* **2003**, 1414–1415; c) C. Keresszegi, J.-D. Grunwaldt, T. Mallat, A. Baiker, *Chem. Commun.* **2003**, 2304–2305; d) B.-Z. Zhan, M. A. White, T.-K. Sham, J. A. Pincock, R. J. Doucet, K. V. Ramana Rao, K. N. Robertson, T. S. Cameron, *J. Am. Chem. Soc.* **2003**, *125*, 2195–2199; e) R. Anderson, K. Griffin, P. Johnston, P. L. Alster, *Adv. Synth. Catal.* **2003**, *345*, 517–523; f) U. R. Pillai, E. Sahle-Demessie, *Green Chem.* **2004**, *6*, 161–165.
- [4] For the use of supercritical CO₂ with heterogeneous Pd catalysts for alcohol oxidation, see: a) G. Jenzer, D. Sœur, T. Mallat, A. Baiker, *Chem. Commun.* **2000**, 2247–2248; b) J.-D. Grunwaldt, M. Caravati, M. Ramin, A. Baiker, *Catal. Lett.* **2003**, *90*, 221–229; c) A. M. Steele, J. Zhu, S. C. Tsang, *Catal. Lett.* **2001**, *73*, 9–13; d) R. Gläser, R. Jos, J. Williardt, *Top. Catal.* **2003**, *22*, 31–39.
- [5] For recent examples, see: a) G. Kovtun, T. Kameneva, S. L. Hlady, M. Starchevsky, Y. Pazdersky, I. Stoarov, M. Vargaftik, I. Moiseev, *Adv. Synth. Catal.* **2002**, *344*, 957–964; b) K.-M. Choi, T. Akita, T. Mizugaki, K. Ebitani, K. Kaneda, *New J. Chem.* **2003**, *27*, 324–328; c) Y. Uozumi, R. Nakao, *Angew. Chem.* **2003**, *115*, 204–207; *Angew. Chem. Int. Ed.* **2003**, *42*, 194–197.
- [6] T. Iwasawa, M. Tokunaga, Y. Obora, Y. Tsuji, *J. Am. Chem. Soc.* **2004**, *126*, 6554–6555.
- [7] a) G.-J. T. Brink, I. W. C. E. Arends, R. A. Sheldon, *Science* **2000**, *287*, 1636–1639; b) K. Mori, K. Yamaguchi, T. Hara, T. Mizugaki, K. Ebitani, K. Kaneda, *J. Am. Chem. Soc.* **2002**, *124*, 11572–11573.
- [8] The immobilization of Wilkinson's catalyst in PEG for biphasic hydrogenation in scCO₂ has been described recently: D. J. Heldebrandt, P. G. Jessop, *J. Am. Chem. Soc.* **2003**, *125*, 5600–5601.
- [9] Ru and Pd nanoparticles embedded in high density polyethylene as catalysts for hydrogenations with scCO₂: H. Ohde, M. Ohde, C. M. Wai, *Chem. Commun.* **2004**, 930–931.
- [10] a) G. Schmid, M. Harms, J. O. Malm, J. O. Bovin, J. Van Ruitenbeck, H. W. Zandbergen, W. T. Fu, *J. Am. Chem. Soc.* **1993**, *115*, 2046–2048; b) G. Schmid, *Chem. Rev.* **1992**, *92*, 1709–1727.
- [11] a) M. N. Vargaftik, V. P. Zagorodnikov, I. P. Stolarov, I. I. Moiseev, *J. Mol. Catal.* **1989**, *53*, 315–348; b) M. K. Starchevsky, S. L. Hlady, Y. A. Pazdersky, M. N. Vargaftik, I. I. Moiseev, *J. Mol. Catal. A* **1999**, *146*, 229–236; c) K. Kaneda, Y. Fujie, K. Ebitani, *Tetrahedron Lett.* **1997**, *52*, 9023–9026; d) K. Ebitani, Y. Fujie, K. Kaneda, *Langmuir* **1999**, *15*, 3557–3562.
- [12] E. Kokova, M. Petermann, E. Weidner, *Chem. Ing. Tech.* **2004**, *76*, 280–284.
- [13] a) A. Bösmann, G. Franciò, E. Janssen, M. Solinas, W. Leitner, P. Wasserscheid, *Angew. Chem.* **2001**, *113*, 2769–2771; *Angew. Chem. Int. Ed.* **2001**, *40*, 2697–2699; b) M. T. Reetz, W. Wiesenhöfer, G. Franciò, W. Leitner, *Adv. Synth. Catal.* **2003**, *345*, 1221–1228.
- [14] For example: a) L. Longenberger, G. Mills, *J. Phys. Chem.* **1995**, *99*, 475–478; b) T. Bormann, H. W. Roesky, U. Ritter, *J. Mol. Catal. A* **2000**, *153*, 31–48; c) D.-H. Chen, Y.-W. Huang, *J. Colloid Interface Sci.* **2002**, *255*, 299–302.
- [15] E. Staunton, A. M. Christie, I. Martin-Litas, Y. G. Andreev, A. M. Z. Slawin, P. G. Bruce, *Angew. Chem.* **2004**, *116*, 2155–2157; *Angew. Chem. Int. Ed.* **2004**, *43*, 2103–2105.

Highly Efficient Biosynthesis of the Oligosaccharide Moiety of the GD3 Ganglioside by Using Metabolically Engineered *Escherichia coli***

Tatiana Antoine, Alain Heyraud, Claude Bosso, and Eric Samain*

GD3 (Neu5Ac α -8Neu5Ac α -3Gal β -4GlcCer; Neu5Ac = *N*-acetylneuraminic acid, Gal = D-galactose, GlcCer = glycosylceramide) is a minor ganglioside found in most normal tissues in higher vertebrates including humans. The GD3 level has been shown to increase during some pathological situations, such as cancers (glioma, melanoma), and to have an important role in tumor angiogenesis.^[1] Anti-GD3 monoclonal antibodies inhibit the growth of human melanoma cells both in vitro and in vivo.^[2,3] In normal cells, GD3 is a cell-death effector that activates the mitochondrial-dependent apoptosome in response to apoptotic stimuli.^[4] In addition, GD3 has a proapoptotic function by suppressing the nuclear factor- κ b-dependent survival pathway.^[5]

Chemical synthesis of the oligosaccharide moiety of gangliosides is difficult,^[6] but efficient biotechnological techniques have recently been developed for the synthesis of GM3, GM2, and GM1 oligosaccharides.^[7,8] The GM3 oligosaccharide (Neu5Ac α -3Gal β -4Glc; Glc = D-glucose) was synthesized by a metabolically engineered *Escherichia coli* strain which overexpressed the *Neisseria meningitidis* genes for α -3 sialyltransferase and CMP-Neu5Ac synthase (CMP = cytidine monophosphate). Lactose and the neuraminic acid were supplied as exogenous precursors and were actively internalized by the β -galactosidase and Neu5Ac permease of the *E. coli*. To prevent catabolism of the precursors, a mutant strain devoid of both β -galactosidase and Neu5Ac aldolase activities was used.

In this work, we have extended this process to the synthesis of the oligosaccharide moiety of GD3 (Neu5Ac α -8Neu5Ac α -3Gal β -4Glc, referred to later as II³(Neu5Ac)₂-lac) by using the alternative *Campylobacter jejuni* CstII sialyltransferase, which exhibited both α -3 and α -8 sialyltransferase activities.^[9] The *cstII* gene occurs as either a monofunctional or a bifunctional sialyltransferase, depending on the *C. jejuni* strain. We chose to use the ATCC 43438 version, which has both high α 3 and high α 8 activity.^[9]

The metabolically engineered pathway for the biosynthesis of the GD3 oligosaccharide is described in Figure 1. The host strain, JM107*nanA*[−], was an *E. coli* K12 JM107 strain derivative in which the Neu5Ac aldolase activity was

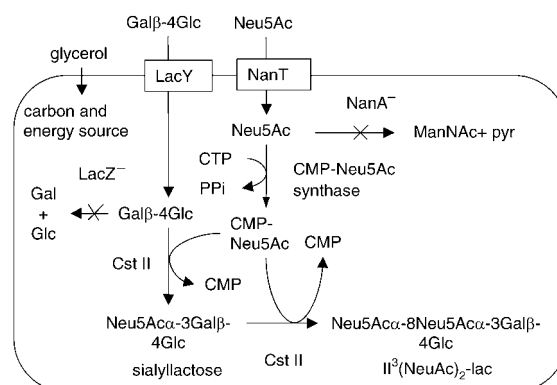


Figure 1. Metabolically engineered pathway of II³(Neu5Ac)₂-lac biosynthesis in *Escherichia coli* K12. Lactose and Neu5Ac, which were internalized by the specific β -galactoside and Neu5Ac permeases (LacY and NanT, respectively), could not be degraded because of β -galactosidase (LacZ) and aldolase (NanA) inactivation. Neu5Ac was converted into a nucleotide-activated form (CMP-Neu5Ac) by CMP-Neu5Ac synthase and then transferred onto lactose by the α -3 sialyltransferase activity of CstII to form sialyllactose. A second Neu5Ac was transferred onto the first sialic acid by the α -8 sialyltransferase activity of CstII to form II³(Neu5Ac)₂-lac. CTP = cytidine triphosphate, PPI = inorganic pyrophosphate, pyr = pyruvate.

abolished by inactivating the *nanA* gene.^[8] The *cstII* gene was amplified by PCR by using the genomic DNA of *C. jejuni* (ATCC 43438) as the template and was cloned into a pUC18 plasmid to yield pUC-*cstII*. The II³(Neu5Ac)₂-lac production strain TA15 was constructed by transforming the host strain JM107*nanA*[−] with two compatible plasmids: pUC18-*cstII* and pBBnsy,^[7] which was a pBBR1-*MCS1* derivative carrying the *N. meningitidis* gene for CMP-Neu5Ac synthase. The strain TA15 was cultured to high cell density with glycerol as the carbon source, as previously described.^[7] Lactose (3 mM) and Neu5Ac (6 mM) were added at the beginning of the fed-batch phase, as well as isopropyl- β -D-thiogalactopyranoside (IPTG), which was the inducer of the Plac promoter of the two plasmids. The oligosaccharide content in the intracellular fraction of samples withdrawn at different cultivation times was analyzed by high-performance anion-exchange chromatography (HPAEC) analysis (see Supporting Information). Lactose and Neu5Ac transiently accumulated in the intracellular fraction and were entirely consumed after 7 and 24 h of incubation, respectively (Figure 2). Concurrently two compounds, **1** and **2**, putatively II³(Neu5Ac)-lac and II³(Neu5Ac)₂-lac, were produced, with their maximal concentrations reached 7 and 9 h after induction, respectively. Concentrations of compounds **1** and **2** then decreased during the final stage of culture and this decrease correlated with the appearance of compound **3**, which had a longer retention time in the HPAEC analysis (see Supporting Information) and which was believed to be II³(Neu5Ac)₃-lac.

[*] T. Antoine, Dr. A. Heyraud, Dr. C. Bosso, Dr. E. Samain
CERMAV-CNRS
B.P. 53, 38041 Grenoble Cedex 9 (France)
Fax: (+33) 4-7654-7203
E-mail: eric.samain@cermav.cnrs.fr

[**] We thank Dr. Michel Gilbert from the Institute of Biological Science (Ottawa, Canada) for kindly providing us with the purified genomic DNA of *Campylobacter jejuni* (ATCC 43438).

Supporting information for this article is available on the WWW under <http://www.angewandte.org> or from the author.

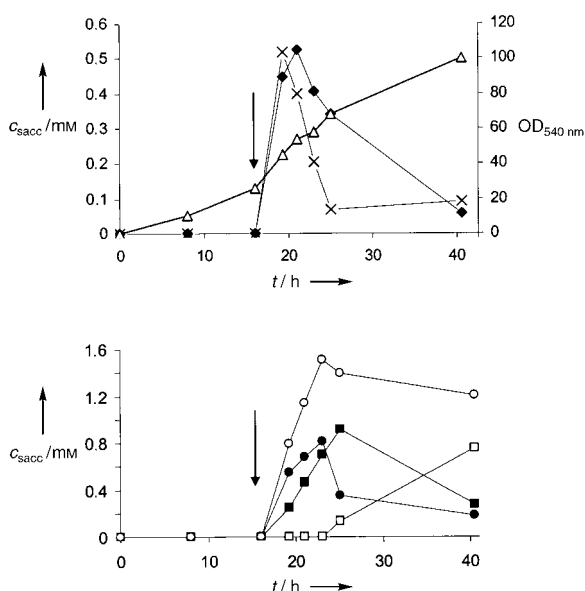
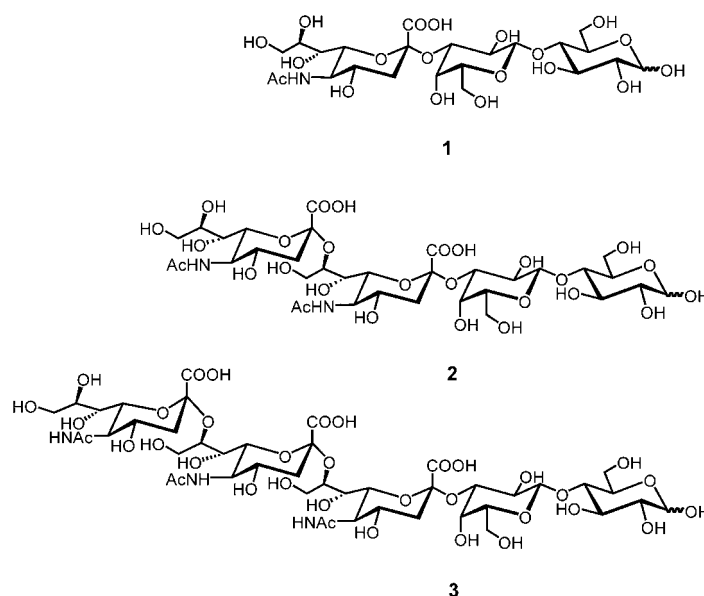


Figure 2. Production of oligosaccharides in a high-cell-density culture of strain TA15. The arrow indicates the start of induction and the addition of lactose (3 mM) and Neu5Ac (6 mM). Δ cell growth (measured by optical density, OD); \times lactose; \blacklozenge Neu5Ac; \bullet $\text{II}^3(\text{Neu5Ac})\text{-lac}$ (**1**); \blacksquare $\text{II}^3(\text{Neu5Ac})_2\text{-lac}$ (**2**); \square $\text{II}^3(\text{Neu5Ac})_3\text{-lac}$ (**3**); \circ sum of **1–3**. c_{sacc} = saccharide concentration.

The structures of compounds **1–3** were confirmed by NMR spectroscopy and mass spectrometry of purified products. The ^{13}C NMR signal assignments of **1** and **2** (see Supporting Information) were in close agreement with previously described data.^[10] The ^{13}C NMR signal assignment of **3** was made by cross-checking the ^{13}C NMR spectra of compound **2** and α -8-linked tri-Neu5Ac^[11] (see Supporting Information). In the positive mode, mass spectrometry analysis showed the presence of quasi molecular ions $[M + \text{Na}]^+$ at m/z 656 and $[(M + \text{Na} - \text{H}) + \text{Na}]^+$ at m/z 678 in the spectrum of compound **1** and quasi molecular ions $[M + \text{Na}]^+$ at m/z 969 and $[(M + \text{Na} - \text{H}) + \text{Na}]^+$ at m/z 991 in the spectrum of compound **2**. The mass spectrum of compound **3** showed one peak in the positive mode at m/z 1304, corresponding to the quasi molecular ion $[(M + 3\text{Na} - 3\text{H}) + \text{Na}]^+$, and one peak in the negative mode at m/z 1258, corresponding to the quasi molecular ion $[(M + 2\text{Na} - 2\text{H}) - \text{H}]^-$. The structures of the carbohydrate moieties of the gangliosides GM3 ($\text{II}^3(\text{Neu5Ac})\text{-lac}$; **1**), GD3 ($\text{II}^3(\text{Neu5Ac})_2\text{-lac}$; **2**), and GT3 ($\text{II}^3(\text{Neu5Ac})_3\text{-lac}$; **3**) are presented in Scheme 1.

The formation of compound **3** can be explained by a side activity of the CstII sialyltransferase, which would be able to add a third Neu5Ac onto the terminal Neu5Ac of $\text{II}^3(\text{Neu5Ac})_2\text{-lac}$. The production of compound **3** was somewhat unexpected because no such trisialylated structure has been described in the lipooligosaccharides of *C. jejuni*, and there is no report of CstII being able to use a Neu5Ac α -8Neu5Ac α -3 motif as an acceptor. However, in other species, such as humans, polysialogangliosides are synthesized by a single enzyme, GD3/GT3 synthase.^[12] GT3 is the precursor of C series gangliosides which are the major constituents in adult



Scheme 1. Structures of $\text{II}^3(\text{Neu5Ac})\text{-lac}$ (**1**), $\text{II}^3(\text{Neu5Ac})_2\text{-lac}$ (**2**), and $\text{II}^3(\text{Neu5Ac})_3\text{-lac}$ (**3**).

fish brain and are found abundantly in foetal brains of higher vertebrates.^[13] They are also found in various neuroectodermal tumors and there is thus potentially great interest in having easy access to the GT3 oligosaccharide.

By varying the lactose and Neu5Ac initial concentrations on one hand and the culture time on the other, it is possible to favor either the production of GD3 or GT3 oligosaccharides. In our culture conditions the maximal production yields of the GD3 (0.83 g L⁻¹) and GT3 (0.91 g L⁻¹) oligosaccharides were observed 9 and 24 h after induction, respectively. The yields of purified products were much lower due to the multistep purification procedure which has thus to be considerably improved if these compounds are to be used in applications that require large quantities of material. Immunoabsorbents made with the trisaccharide Neu5Ac α -8Neu5Ac α -3Gal have recently been shown to deplete anti-GQ1b antibodies in autoimmune neuropathy sera from patients suffering from the Miller–Fisher syndrome.^[14] The large-scale preparation of the GD3 oligosaccharide would thus make possible the development of effective immunoabsorption therapies for the treatment of this syndrome.

Experimental Section

The *cstII* gene was amplified by PCR from the *C. jejuni* (ATCC 43438) genome with the Pfu Turbo DNA polymerase from Stratagene. A ribosome-binding site (RBS) was inserted upstream of the original start codon in the forward primer. The PCR product was cloned into pCR4Blunt-TOPO (Invitrogen) and subcloned into the *EcoRI*-*PstI* sites of pBluescript II KS (Stratagene).

Sugars were quantified by HPAEC with a decade detector equipped with a carbopac PA10 column (Dionex). Purified compounds **1–3** were used as standards. The elution program consisted of a linear gradient of sodium acetate of 0–0.5 M over 45 minutes with an isocratic background of sodium hydroxide (100 mM). The flow rate was 0.8 mL h⁻¹.

Compounds **1** and **2** were purified from one liter of a strain TA15 culture harvested 9 h after induction. The intracellular oligosaccharides were extracted from the cells and adsorbed on activated charcoal as previously described.^[15] They were then separated by size-exclusion chromatography on a Biogel P6 column (4 × 100 cm) with NaNO₃ (50 mM) as the eluent and a flow rate of 45 mL h⁻¹ (see Supporting Information). After being desalted on a TSK HW40F/50F column (50 × 2.1 cm) with water as the mobile phase and a flow rate of 4 mL min⁻¹, pure **1** and **2** were obtained with yields of 49 mg and 98 mg, respectively.

Compound **3** was purified from one liter of a strain TA15 culture harvested 24 h after induction. The procedure was the same as for **1** and **2** except that complete purification required an additional high-performance liquid chromatography step on an ion-exchange SP250/10 nucleosil column (10 × 1 cm). Aqueous NaNO₃ (150 mM) was used as the eluent and the flow rate was 4 mL min⁻¹. After a desalting step on a TSK HW40F/50F column, pure **3** was obtained with a final yield of 15 mg.

ESI mass spectra were recorded on a ZQ Waters micromass spectrometer (capillary 3.5 kV, cone voltage 80 V). The 1D NMR spectra of II³(Neu5Ac)-lac and II³(Neu5Ac)₂-lac were recorded on a Bruker Avance 300 spectrometer as previously described.^[8]

Received: August 2, 2004

Revised: October 20, 2004

Published online: January 26, 2005

Keywords: biotechnology · carbohydrates · glycolipids · glycosyltransferases · metabolic engineering

- [1] G. Zeng, L. Gao, S. Birkle, R. K. Yu, *Cancer Res.* **2000**, *60*, 6670.
- [2] S. Birkle, G. Zeng, L. Gao, R. K. Yu, J. Aubry, *Biochimie* **2003**, *85*, 455.
- [3] P. Ruf, M. Jager, J. Ellwart, S. Wosch, E. Kusterer, H. Lindhofer, *Int. J. Cancer* **2004**, *108*, 725.
- [4] J. C. Fernandez-Checa, *Biochem. Biophys. Res. Commun.* **2003**, *304*, 471.
- [5] A. Colell, C. Garcia-Ruiz, J. Roman, A. Ballesta, J. C. Fernandez-Checa, *Faseb J.* **2001**, *15*, 1068.
- [6] J. C. Castro-Palomino, B. Simon, O. Speer, M. Leist, R. R. Schmidt, *Chem. Eur. J.* **2001**, *7*, 2178.
- [7] B. Priem, M. Gilbert, W. W. Wakarchuk, A. Heyraud, E. Samain, *Glycobiology* **2002**, *12*, 235.
- [8] T. Antoine, B. Priem, A. Heyraud, L. Greffe, M. Gilbert, W. W. Wakarchuk, J. S. Lam, E. Samain, *ChemBioChem* **2003**, *4*, 406.
- [9] M. Gilbert, M. F. Karwaski, S. Bernatchez, N. M. Young, E. Taboada, J. Michniewicz, A. M. Cunningham, W. W. Wakarchuk, *J. Biol. Chem.* **2002**, *277*, 327.
- [10] M. Gilbert, J. R. Brisson, M. F. Karwaski, J. Michniewicz, A. M. Cunningham, Y. Wu, N. M. Young, W. W. Wakarchuk, *J. Biol. Chem.* **2000**, *275*, 3896.
- [11] F. Michon, J. R. Brisson, H. J. Jennings, *Biochemistry* **1987**, *26*, 8399.
- [12] J. Nakayama, M. N. Fukuda, Y. Hirabayashi, A. Kanamori, K. Sasaki, T. Nishi, M. Fukuda, *J. Biol. Chem.* **1996**, *271*, 3684.
- [13] K. Letinic, M. Heffer-Laue, H. Rosner, I. Kostovic, *Neuroscience* **1998**, *86*, 1.
- [14] H. J. Willison, K. Townson, J. Veitch, J. Boffey, N. Isaacs, S. M. Andersen, P. Zhang, C. C. Ling, D. R. Bundle, *Brain* **2004**, *127*, 680.
- [15] E. Samain, S. Drouillard, A. Heyraud, H. Driguez, R. A. Geremia, *Carbohydr. Res.* **1997**, *302*, 35.

Template-Assisted Cross Olefin Metathesis**

Xiaowu Yang and Bing Gong*

Various strategies have been developed for the control of intermolecular association, most of which are based on the design of molecular modules that carry linear arrays of hydrogen-bond donors (D) and acceptors (A).^[1] We recently described information-storing hydrogen-bonded duplexes based on linear oligoamide strands that bear arrays of hydrogen-bond donors and acceptors.^[2] The formation of such duplexes is highly sequence-specific and involves the pairing of a single strand with another strand of a complementary hydrogen-bonding sequence. These hydrogen-bonded duplexes serve as specific, noncovalent templates for the nucleation of β -sheet structures when attached to natural oligopeptides.^[3] The sequence-specificity of our hydrogen-bonded duplexes has prompted us to explore the possibility of directing chemical reactions by using these molecules as templates. In recent years there has been intense interest in the use of duplex DNA as a template for directing chemical reactions.^[4,5] Although not yet comparable to the diverse sequence-specificity offered by duplex DNA, the hydrogen-bonded duplexes that we have developed offer some advantages: ready availability in large quantities, much lower molecular weights, and compatibility with a wide variety of organic solvents. We chose the widely utilized olefin metathesis reaction as a demonstration of principle. Specifically, olefin units attached to the same end of a duplex template should be brought into close proximity upon the formation of the hydrogen-bonded duplex in solution. Such a supramolecular event should greatly increase the effective molarity of the olefins that undergo the subsequent cross-metathesis reaction and turn an otherwise intermolecular transformation into one that is intramolecular. Here we report the highly efficient and specific intermolecular cross-metathesis reactions directed by a hydrogen-bonded duplex template.

Since the development of the well-defined catalysts by Schrock^[6] and Grubbs,^[7] olefin metathesis has become an increasingly powerful tool for carbon-carbon bond formation in organic synthesis.^[8] It has been widely used in the total synthesis of a variety of architecturally complex natural products,^[9] in polymerization,^[10] and in the construction of

[*] Dr. X. Yang, Prof. B. Gong
Department of Chemistry
University at Buffalo
The State University of New York
Buffalo, New York 14260 (USA)
Fax: (+1) 716-645-6963
E-mail: bgong@chem.buffalo.edu

[**] We thank the donors of the Petroleum Research Fund, administered by the ACS, for support of this research (37200-AC4). The NIH, NSF, and ONR are acknowledged for partial funding.

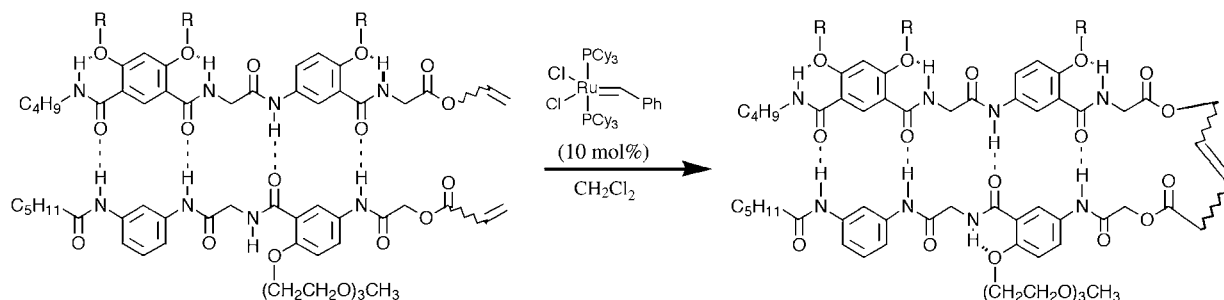


Supporting information for this article is available on the WWW under <http://www.angewandte.org> or from the author.

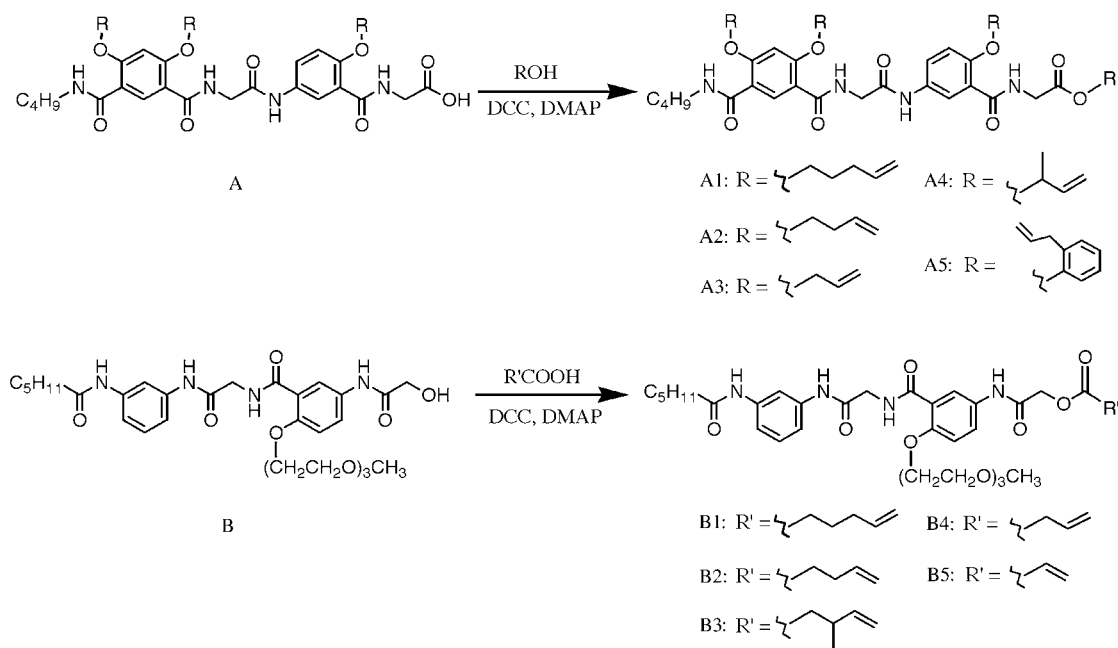
peptides.^[11] The metathesis reaction is routinely carried out for the generation of C–C double bonds by using either the cross-metathesis of two acyclic alkenes or the ring-closing metathesis (RCM) of a diene. Efforts have been made to improve the chemical selectivity of intramolecular metathesis (RCM) by controlling the concentrations of the reactants.^[12] Relative to olefin RCM, intermolecular cross-metathesis reactions, particularly those which involve two different olefins, have received less attention even though they offer great potential for a range of intermolecular C–C bond constructions. The main reason for this may be a lack of selectivity, especially because the intermolecular cross-metathesis reaction often proceeds to yield three products: two unwanted homodimeric self-metathesis products along with the desired heterodimeric product.^[13] Several methods have recently been reported in which selective cross-metathesis reactions can be achieved when olefins of high reactivity are treated with bulky, electron-deficient olefins of lower reactivity.^[14] Except for strategies that are based on intramolecular RCM,^[12] highly selective cross-metathesis reactions of olefins that exhibit similar reactivities have yet to be developed.

To test the strategy outlined above, a quadruply hydrogen-bonded duplex, which consists of two different but complementary oligoamide strands that carry the unsymmetrical hydrogen-bonding sequences ADAA and DADD, respectively, was chosen as the template (Scheme 1). Alkenyl alcohols or acids were tethered to A or B by means of DCC (dicyclohexyl carbodiimide) coupling^[15] to yield the desired strands A 1–5 and B 1–5 (Scheme 2). Combination of strands A 1–5 with strands B 1–5 should lead to 25 different A·B pairs. To demonstrate the feasibility of this approach, pair A3·B2 was first examined in detail. By using commercially available polystyrene molecular-weight standards, vapor pressure osmometry (VPO) studies at 37°C in CHCl₃ over the concentration range of 5–50 mM consistently gave an apparent molecular weight of $1471 \pm 5\%$ that corresponds to A3·B2. The presence of the dimeric A3·B2 species in solution was also supported by ¹H NMR spectroscopic studies in CDCl₃ (5 mM) that revealed significant downfield shifts of the signals of the aniline NH group ($\delta = 9.97$, 9.65, and 9.53 ppm) relative to that of the single strand 1c ($\delta = 7.62$ ppm).^[2,3]

A solution of A3·B2 in chloroform (2 mM) was then treated with Grubbs' catalyst^[7] under heating at reflux. The



Scheme 1. Cross-metathesis of oligoamide-tethered olefins. R = *n*-C₈H₁₇.



Scheme 2. Preparation of strands A 1–5 and B 1–5. R = *n*-C₈H₁₇, DCC = dicyclohexyl carbodiimide, DMAP = 4-dimethylaminopyridine.

progress of the reaction was monitored by using ESI-MS (Figure 1). Upon completion of the reaction (5 h), new peaks with m/z values of 1536 $[M+H]^+$ and 1557 $[M+Na]^+$ appeared (Figure 1b). The net loss of 28 ($CH_2=CH_2$) relative to the m/z

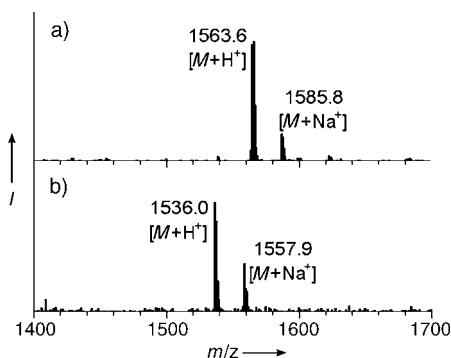


Figure 1. ESI mass spectra of a) the duplex A3-B2 and b) the product A3=B2 after the cross-metathesis reaction.

values of the starting duplex (1563 $[M+H]^+$ and 1585 $[M+Na]^+$, Figure 1a) suggested that the duplex A3-B2 underwent an intermolecular cross-metathesis reaction to afford the desired product A3=B2. Product A3=B2 was isolated in 92% yield as a mixture of *E* and *Z* isomers (*E/Z* = 8:1, determined by 1H NMR spectroscopy).^[16]

On the basis of the results obtained from the pair A3-B2, we extended this template-directed approach to the metathesis reactions of all 25 combinations (Scheme 2), the results of which are listed in Table 1. In the presence of Grubbs' catalyst, each of the 25 pairs was heated at reflux in CH_2Cl_2 during 3–6 h to afford 20 of the 25 possible products. The products formed were those expected from the cross-metathesis reactions and were all obtained as inseparable mixtures of *E* and *Z* isomers^[16] with yields ranging from 36–99%. Among the combinations, duplexes that comprised the strands A1 and B1–4 gave products A1=B1, A1=B2, A1=B3, and A1=B4 in yields ranging from 91–98%. The combinations of A2/A3/A4 with B1/B2/B3/B4 led to their products in 83–99% yields. Compared with the duplexes that contained A1, A3, and A5, those that contained A4, that is, A4-B1, A4-B2, and A4-B3, gave slightly lower yields that ranged from 83 to 87%. The two products from the cross-metathesis reactions that involved B5 were obtained in lower yields (A1=B5: 36%; A5=B5: 77%), whereas no other products were obtained from the other three combinations involving B5. Similarly, the products A3=B4 and A4=B4 that should have resulted from the cross-metathesis of pairs A3-B4 and A4-B4 were not obtained. Examination of the structures of those pairs which either did not react or which gave products in low yields revealed that the spacers between the terminal vinyl moieties and the template strands were much shorter

Table 1: Template-assisted olefin cross-metathesis.^[a]

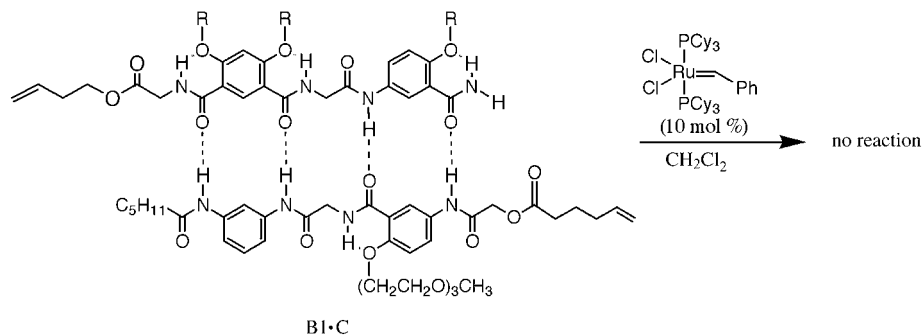
Strands	B 1	B 2	B 3	B 4	B 5
A 1	98 (1.6:1)	97 (3:1)	91 (2:1)	94 (6:1)	36 (8:1)
A 2	97 (9:1)	94 (5:1)	93 (2:1)	83 (4:1)	nr ^[b]
A 3	99 (14:1)	99 (8:1)	97 (3:1)	nr ^[b]	nr ^[b]
A 4	87 (20:1)	84 (7:1)	83 (4:1)	nr ^[b]	nr ^[b]
A 5	96 (11:1)	89 (5:1)	65 (4:1)	85 (3:1)	77 (7:1)

[a] All reactions were carried out at a concentration of 2 mM in CH_2Cl_2 in the presence of the catalyst (10 mmol%). The yields and *E/Z* ratios (quoted in brackets) were determined by 1H NMR spectroscopy. [b] No reaction.

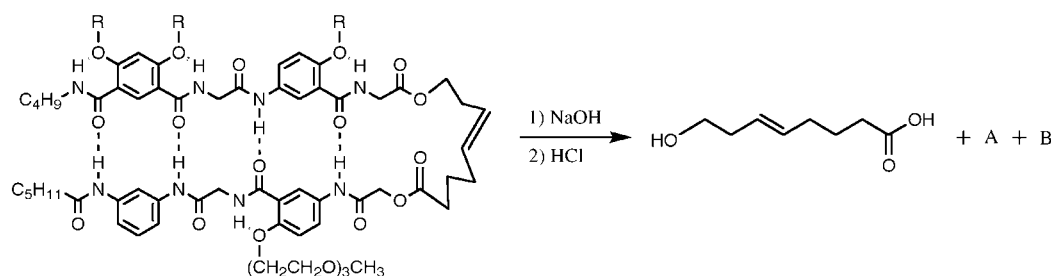
than for those combinations which resulted in efficient reactions. This suggests that for the cross-metathesis reaction to proceed, the two vinyl moieties in a duplex need to reach each other and adopt the proper orientation, which in turn requires spacers of sufficient length. Furthermore, the major stereoisomers for all transformations were consistently the thermodynamically more stable *E* isomers, which reflects the reversible nature of the metathesis reactions. The highest stereoselectivity was observed for the product A4=B1 with an *E/Z* ratio of 20:1 and a yield of 87%.^[16]

As a control, compound C, in which the olefin unit was attached to the “wrong” side of the template strand, was synthesized and then mixed with compound B1 (Scheme 3). The formation of duplex B1-C was confirmed by both NMR spectroscopy and VPO experiments. In duplex B1-C, the vinyl moieties would not be able to react with each other because they are located at the two remote ends of the duplex template. Indeed, when a solution of duplex B1-C was subjected to cross-metathesis in the presence of Grubbs' catalyst, the metathesis reaction did not occur. The hydrogen-bonded duplex B1-C was the only species detected by NMR spectroscopy or ESI-MS before and after the reaction. These results further confirmed the template-dependence of the above metathesis reactions, in which the reactions took place only when the two olefin units were brought into close proximity by the duplex template.

As shown in Scheme 1 and Scheme 2, all of the olefin units were attached to the template through an ester linkage that should be cleaved under basic conditions. To test if the desired



Scheme 3. Attempted cross-metathesis reaction of distant olefins in B1-C. R = *n*-C₈H₁₇.



Scheme 4. Cleavage of product from A2=B1. R = n -C₈H₁₇.

products could be cleaved from the template, product A2=B1 was treated with an aqueous solution of NaOH. After completion of the reaction, the insoluble residue was filtered, and the acidified aqueous layer was extracted with CH₂Cl₂ to yield the desired 8-hydroxyoct-5-enoic acid (Scheme 4).^[16]

In conclusion, we have shown that a quadruply hydrogen-bonded duplex can act as a sequence-specific template to direct the cross-metathesis of different olefins that are tethered to this duplex. These templated metathesis reactions occur with extremely high selectivity, with no homodimeric products observed. Compared to strategies that directly tether two olefin units together, our approach has the advantage of being combinatorial. By simply mixing the complementary A and B strands, a large number of A·B combinations were easily obtained. Thus, the combination (mixing) of a group of five tethered olefins with another group of five olefins lead to a total of 25 combinations. In contrast, with covalently linked olefins, all 25 possibilities have to first be synthesized before they can be tested. Obviously, the number of combinations based on our approach increases rapidly as the number of tethered olefins increases. Coupled with NMR spectroscopic and mass spectrometric methods, our template-directing method can be used to probe a large number of combinations that would otherwise be difficult to examine based on previous methods. After cleavage from the template, the desired products can be easily obtained and the template can also be recycled. It is envisaged that our current strategy will serve as a useful tool to broaden the scope of cross-metathesis reactions. The approach described here should also be generally applicable to other types of bimolecular reactions.

Received: August 24, 2004

Revised: October 5, 2004

Published online: January 20, 2005

Keywords: alkenes · C–C coupling · hydrogen bonds · noncovalent interactions · template synthesis

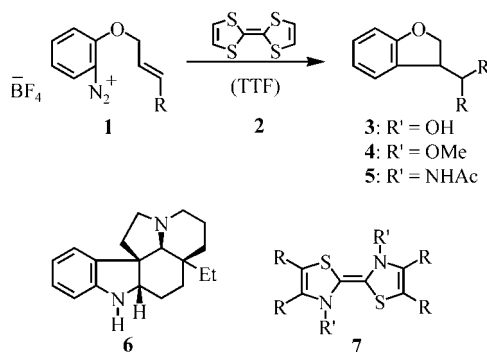
- [1] L. J. Prins, D. N. Reinhoudt, P. Timmerman, *Angew. Chem.* **2001**, *113*, 2446; *Angew. Chem. Int. Ed.* **2001**, *40*, 2382; D. C. Sherrington, K. A. Taskinen, *Chem. Soc. Rev.* **2001**, *30*, 83; S. C. Zimmerman, P. S. Corbin, *Struct. Bonding (Berlin)* **2000**, *96*, 63; C. Schmuck, W. Wienand, *Angew. Chem.* **2001**, *113*, 4493; *Angew. Chem. Int. Ed.* **2001**, *40*, 4363; E. A. Archer, H. G. Gong, M. J. Krische, *Tetrahedron* **2001**, *57*, 1139; B. Gong, *Synlett* **2001**, 582; M. S. Cubberley, B. L. Iverson, *Curr. Opin. Chem. Biol.*

- 2001**, *5*, 650; R. P. Sijbesma, E. W. Meijer, *Chem. Commun.* **2003**, *5*; C. A. Hunter, P. S. Jones, P. M. N. Tiger, S. Tomas, *Chem. Commun.* **2003**, 1642.
- [2] B. Gong, Y. Yan, H. Q. Zeng, E. Skrzypczak-Jankun, Y. W. Kim, J. Zhu, H. Ickes, *J. Am. Chem. Soc.* **1999**, *121*, 5607; H. Zeng, R. S. Miller, R. A. Flowers, B. Gong, *J. Am. Chem. Soc.* **2000**, *122*, 2635; X. W. Yang, S. Martinovic, R. D. Smith, B. Gong, *J. Am. Chem. Soc.* **2003**, *125*, 9932.
- [3] H. Q. Zeng, X. W. Yang, R. A. Flowers, B. Gong, *J. Am. Chem. Soc.* **2002**, *124*, 2903.
- [4] Z. Y. J. Zhan, J. D. Ye, X. Y. Li, D. G. Lynn, *Curr. Org. Chem.* **2001**, *5*, 885; Z. Y. Li, Z. Y. J. Zhan, R. Knipe, D. G. Lynn, *J. Am. Chem. Soc.* **2002**, *124*, 746; Z. Y. J. Zhan, D. G. Lynn, *J. Am. Chem. Soc.* **1997**, *119*, 12420.
- [5] Z. J. Gartner, D. R. Liu, *J. Am. Chem. Soc.* **2001**, *123*, 6961; Z. J. Gartner, M. W. Kanan, D. R. Liu, *Angew. Chem.* **2002**, *114*, 1874; *Angew. Chem. Int. Ed.* **2002**, *41*, 1796; C. T. Calderone, J. Q. W. Puckett, Z. J. Gartner, D. R. Liu, *Angew. Chem.* **2002**, *114*, 4278; *Angew. Chem. Int. Ed.* **2002**, *41*, 4104; Z. J. Gartner, M. W. Kanan, D. R. Liu, *J. Am. Chem. Soc.* **2002**, *124*, 10304; X. Y. Li, D. R. Liu, *J. Am. Chem. Soc.* **2003**, *125*, 10188; X. Y. Li, Z. J. Gartner, B. N. Tse, D. R. Liu, *J. Am. Chem. Soc.* **2004**, *126*, 5090.
- [6] R. R. Schrock, J. S. Murdzek, G. C. Bazan, J. Robbins, M. DiMare, M. O'Regan, *J. Am. Chem. Soc.* **1990**, *112*, 3875; G. C. Bazan, J. H. Oskam, H. N. Cho, L. Y. Park, R. R. Schrock, *J. Am. Chem. Soc.* **1991**, *113*, 6899.
- [7] S. T. Nguyen, R. H. Grubbs, J. W. Ziller, *J. Am. Chem. Soc.* **1993**, *115*, 9858; P. Schwab, M. B. France, J. W. Ziller, R. H. Grubbs, *Angew. Chem.* **1995**, *107*, 2179; *Angew. Chem. Int. Ed. Engl.* **1995**, *34*, 2039; P. Schwab, R. H. Grubbs, J. W. Ziller, *J. Am. Chem. Soc.* **1996**, *118*, 100.
- [8] For recent reviews, see: M. Schuster, S. Blechert, *Angew. Chem.* **1997**, *109*, 2124; *Angew. Chem. Int. Ed. Engl.* **1997**, *36*, 2036; R. H. Grubbs, S. Chang, *Tetrahedron* **1998**, *54*, 4413; S. K. Armstrong, *J. Chem. Soc. Perkin Trans. 1* **1998**, 371; A. Furstner, *Angew. Chem.* **2000**, *112*, 3140; *Angew. Chem. Int. Ed.* **2000**, *39*, 3012; R. Roy, S. K. Das, *Chem. Commun.* **2000**, 519; T. M. Trnka, R. H. Grubbs, *Acc. Chem. Res.* **2001**, *34*, 18.
- [9] A. Furstner, K. Radkowski, J. Grabowski, C. Wirtz, R. Mynott, *J. Org. Chem.* **2000**, *65*, 8758; I. M. Fellows, D. E. Kaelin, Jr., S. F. Martin, *J. Am. Chem. Soc.* **2000**, *122*, 10781; A. B. Smith, C. M. Adams, S. A. Kozmin, *J. Am. Chem. Soc.* **2001**, *123*, 990; P. A. Evans, J. Cui, S. J. Gharpure, A. Polosukhin, H. R. Zhang, *J. Am. Chem. Soc.* **2003**, *125*, 14702; A. Furstner, A. S. Castanet, K. Radkowski, C. W. Lehmann, *J. Org. Chem.* **2003**, *68*, 1521; T. Kawaguchi, N. Funamori, Y. Matsuya, H. Nemoto, *J. Org. Chem.* **2004**, *69*, 505; E. A. Couladouros, A. P. Mihou, E. A. Bouzas, *Org. Lett.* **2004**, *6*, 977.
- [10] T. Morita, B. R. Maughon, C. W. Bielawski, R. H. Grubbs, *Macromolecules* **2000**, *33*, 6621; C. W. Bielawski, D. Benitez, R. H. Grubbs, *Science* **2002**, *297*, 2041; C. W. Bielawski, D. Benitez, R. H. Grubbs, *J. Am. Chem. Soc.* **2003**, *125*, 8424; R. H.

- Grubbs, W. Tumas, *Science* **1989**, 243, 907; J. Feldman, R. R. Schrock, *Prog. Inorg. Chem.* **1991**, 39, 1.
- [11] H. K. Blackwell, J. D. Sadowsky, R. J. Howard, J. N. Sampson, J. A. Chao, W. E. Steinmetz, D. J. O'Leary, R. H. Grubbs, *J. Org. Chem.* **2001**, 66, 5291; P. R. Harris, M. A. Brimble, P. D. Gluckman, *Org. Lett.* **2003**, 5, 1847.
- [12] D. J. O'Leary, S. J. Miller, R. H. Grubbs, *Tetrahedron Lett.* **1998**, 39, 1689; R. M. Williams, J. W. Liu, *J. Org. Chem.* **1998**, 63, 2130; Y. Gao, P. Lane-Bell, J. C. Vederas, *J. Org. Chem.* **1998**, 63, 2133; H. Bieräugel, T. P. Jansen, H. E. Schoemaker, H. Hiemsta, J. H. van Maarseveen, *Org. Lett.* **2002**, 4, 2673.
- [13] H. E. Blackwell, D. J. O'Leary, A. K. Chatterjee, R. A. Washenfelder, D. A. Bussmann, R. H. Grubbs, *J. Am. Chem. Soc.* **2000**, 122, 58.
- [14] A. K. Chatterjee, T. L. Choi, D. P. Sanders, R. H. Grubbs, *J. Am. Chem. Soc.* **2003**, 125, 11360; A. K. Chatterjee, R. H. Grubbs, *Org. Lett.* **1999**, 1, 1751; A. K. Chatterjee, D. P. Sanders, R. H. Grubbs, *Org. Lett.* **2002**, 4, 1939; W. E. Crowe, Z. J. Zhang, *J. Am. Chem. Soc.* **1993**, 115, 10998; W. E. Crowe, D. R. Goldberg, *J. Am. Chem. Soc.* **1995**, 117, 5162; O. Brummer, A. Rckert, S. Blechert, *Chem. Eur. J.* **1997**, 3, 441; F. J. Feher, D. Soulivong, A. G. Eklund, K. D. Wyndham, *Chem. Commun.* **1997**, 1185.
- [15] See Supporting Information for details.
- [16] The conformations of double bonds were determined from the coupling constants J measured from ^1H NMR spectra, and the major *E* isomer was found to have $J > 15$ Hz (see Supporting Information).

organic molecules,^[6] or photochemically assisted electron transfer.^[7] The use of neutral ground-state organic molecules as powerful reducing agents is a novel and attractive idea. This would allow reductions to be carried out 1) under very mild conditions because of their neutrality, 2) in the absence of metal ions, a worthwhile feature as metal residues cause environmental problems, and 3) with wider applicability than in the case of photochemically assisted reactions.

Our initial studies^[8] featured the reactions between arenediazonium salts **1** and tetrathiafulvalene (TTF, **2**). TTF (**2**) reacts with diazonium salts in a radical–polar crossover reaction that leads to the formation of alcohols **3**, ethers **4**, and amides **5** (Scheme 1). This protocol has been substantially



Scheme 1. The radical–polar crossover reaction, useful in the synthesis of aspidospermidine (**6**), depends specifically on the use of tetrathiafulvalene (TTF, **2**). Conditions: **3**: acetone, water; **4**: MeOH; **5**: MeCN, then H₂O.

Synthetic Methods

Highly Efficient Reduction of Unactivated Aryl and Alkyl Iodides by a Ground-State Neutral Organic Electron Donor**

John A. Murphy,* Tanweer A. Khan, Sheng-ze Zhou, Douglas W. Thomson, and Mohan Mahesh

Reactive intermediates, namely radicals and organometallic species, can be formed by reduction of an organic substrate with an electron donor. Metals in low oxidation states^[1] frequently perform this role, and indeed, most electron-transfer reduction processes feature this route. Alternative methods include electrochemical reduction at a (usually metal) cathode,^[2,3] reduction by solvated electrons,^[4] reduction by lithium naphthalenide^[5] or related radical anions of

developed and has even been used to prepare complex products such as aspidospermidine (**6**).^[9,10] However, a limitation of this process is that only arenediazonium substrates can act as electron acceptors; attempts to extend this reaction to the much more common aryl halides or to alkyl halides have not been successful as these substrates are more difficult to reduce.^[11] It is well known that diazadithiafulvalenes **7** (see Scheme 1) are more powerful reducing agents,^[12] but we have shown that these compounds undergo a complicating side reaction when treated with arenediazonium salts^[13] and are not powerful enough electron donors to react with organic halides.

More recently, the reagent TDAE (1,1,2,2-tetra-(dimethylamine)ethane, **8**) has been reacted with very electron-deficient organic halides by Médebielle and co-workers.^[14,15] Thus, iodotrifluoromethane (**9**) was treated with TDAE and benzoyl chloride to afford the products **10** and **11**, which indicate the intermediacy of trifluoromethyl anions,^[14] and *p*-nitrobenzyl chloride (**12**) was similarly transformed to its anion^[15] upon treatment with the same reagent (Scheme 2). Accordingly, our efforts began by testing the reaction of TDAE (**8**) with unactivated aryl and alkyl halides. In all cases, we found that this reagent is not sufficiently powerful to perform the reaction.

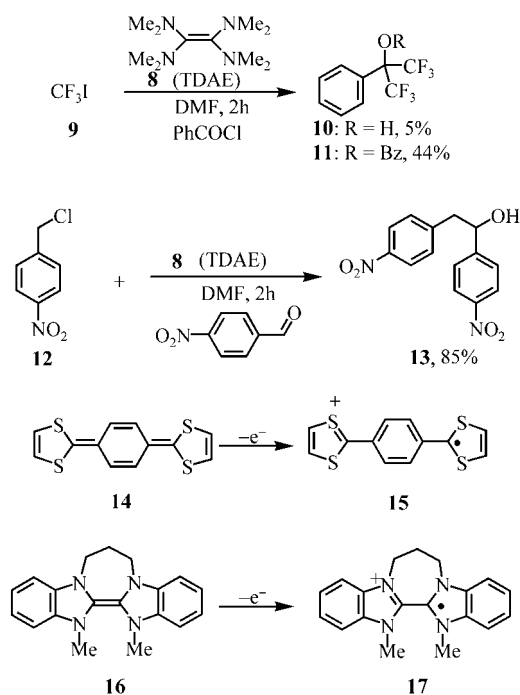
Powerful sulfur-containing organic electron donors such as **14** (Scheme 2) are available,^[16] and here the driving force for the electron donation derives from the considerable

[*] Prof. Dr. J. A. Murphy, Dr. T. A. Khan, Dr. S.-z. Zhou, D. W. Thomson, M. Mahesh

Department of Pure and Applied Chemistry
University of Strathclyde
295 Cathedral Street, Glasgow, G11 1XL (UK)
Fax: (+44) 141-548-4246
E-mail: john.murphy@strath.ac.uk

[**] We thank the EPSRC (S.Z.Z. and D.W.T.), CVCP (Universities UK), and the University of Strathclyde (T.A.K. and M.M.) for funding, and the EPSRC National Mass Spectrometry Service Centre, Swansea, for recording mass spectra.

Supporting information for this article is available on the WWW under <http://www.angewandte.org> or from the author.

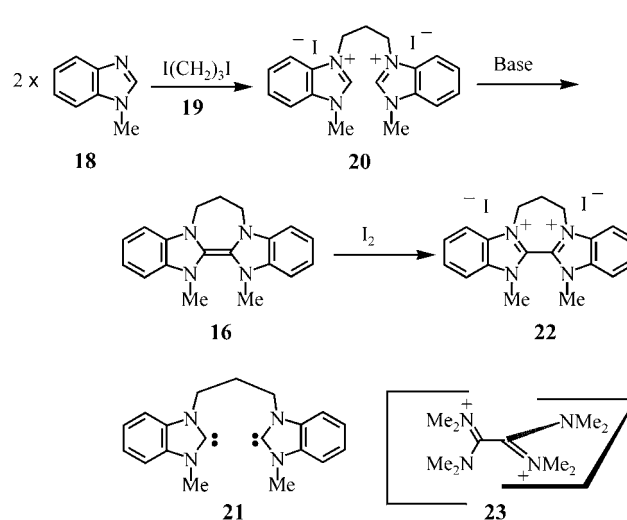


Scheme 2. Chemistry of TDAE (**8**) and structures of potentially more powerful electron donors. TDAE = 1,1,2,2-tetra-(dimethylamine)ethene, DMF = *N,N*-dimethylformamide, Bz = benzoyl.

aromatization energy residing in the corresponding radical cation, **15**. The easiest way to visualize this aromatization is by looking at the particular canonical form, **15**, in which two of the rings are represented as aromatic. However, the syntheses of such compounds are not straightforward, so it is unlikely that they could ever be used as routine reagents. Even their characterization has proved challenging. However, the message is clear: aromatic stabilization energy can greatly assist electron donation.

The presence of nitrogen is also helpful to the creation of a good electron donor, as shown by both the diazadithiafulvalenes **7** and TDAE (**8**), particularly because of the stabilization imparted to the resulting cation by the adjacent nitrogens.^[13]

These two stabilizing factors that act in concert, for example, in **16**, should therefore afford excellent electron donors. Thus, electron loss from **16** would initially afford radical cation **17**, which features the dual stabilization. Although compound **16** has not previously been prepared, a number of similar compounds, which are formally derived from the dimerization of cyclic carbenes, have been prepared^[17,18] and used in mechanistic studies of the behavior of Wanzlick carbenes^[17] or to test their ability to form carbene ligands on metals.^[18] Their reductive organic chemistry appears not to have been explored, except from an electrochemical viewpoint.^[17b,o] Reaction of benzimidazole **18** with 1,3-diiodopropane (**19**) afforded the stable crystalline salt **20**, which upon treatment with base^[17a,b,d,e,18a,18g,18h] under argon then afforded a yellow solution of the “dimer” **16**, which is highly reactive towards air (Scheme 3). The dimer was characterized upon formation in situ in deoxygenated [*D*₇]DMF (*N,N*-dimethylformamide) under argon, and the



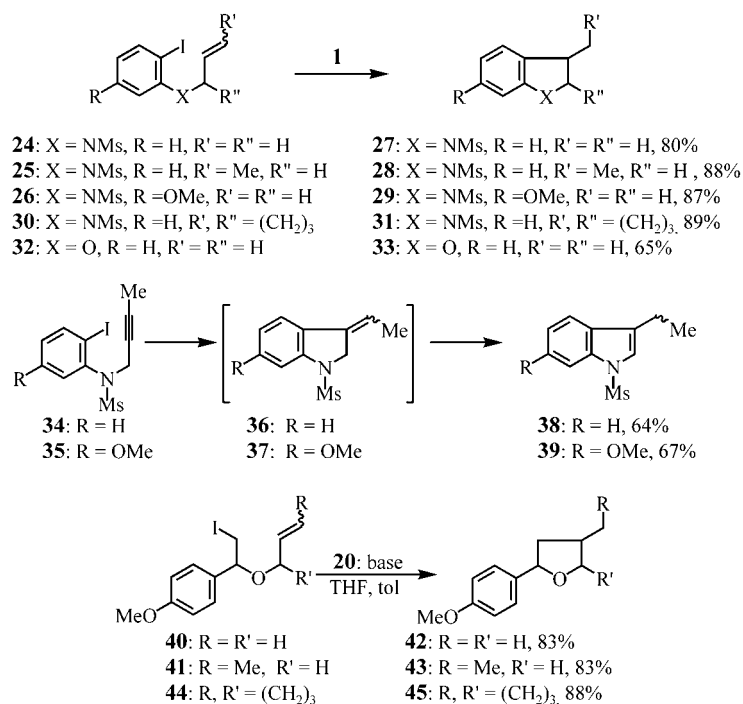
Scheme 3. Formation and reactions of tetraazaalkene **16**.

solution showed the appearance of a key signal at $\delta = 123.1$ ppm corresponding to the central quaternary carbon in the dimer. No trace^[19] of the corresponding biscarbene **21** or of a monocarbene species were evident.

To show that the dimer **16** had formed, it was treated with one equivalent of molecular iodine. With such an easily reduced compound as I_2 , we would expect that **16** would behave like TDAE in forming a dication—in this case, **22**. Molecular modeling of TDAE²⁺ indicates that the repulsion between the two positive charges would be minimized by twisting into orthogonal planes as in **23**. So the expected product **22**, being somewhat restrained by the 3-carbon strap, should subsequently undergo a helical twist to impart diastereotopicity to the protons of each of its $-NCH_2-$ groups. Indeed reaction with one equivalent of iodine led to clean formation of the disalt **22** (see Scheme 3), which was characterized by HRMS ($22-I^-$) and by ¹H and ¹³C NMR spectroscopy. As expected, the protons in the $-NCH_2-$ groups are diastereotopic. Clean formation of **22** assured us that alkene **16** had also formed cleanly. Note that a study of a bis-bridged analogue^[12d,17a] featuring 3-carbon bridges surprisingly showed no evidence for diastereotopicity.

Compound **16** was then treated with a series of aryl iodides, **24–26** and **30** (Scheme 4). All of these compounds smoothly afforded the corresponding indolines in excellent yield (81–90%). The oxygen-linked substrate **32** also showed clean transformation to the product **33**; the lower yield (65%) may reflect a greater volatility of the product relative to the nitrogen series. The alkyne-containing substrates **34** and **35** also cyclized smoothly to give the exocyclic alkenes, which were not isolated but treated with acid under mild conditions to give the corresponding indoles **38** (64%) and **39** (67%). Similarly, aliphatic iodides **40**, **41**, and **44** reacted smoothly with **16**, which was formed in situ, and gave excellent yields of cyclized products (Scheme 4).

Questions arise over the mechanisms of the observed reactions and in particular over the nature of the intermediates. Initial electron transfer to the substrate, for example, aryl iodide **24**, would afford the radical anion **46** (Scheme 5).

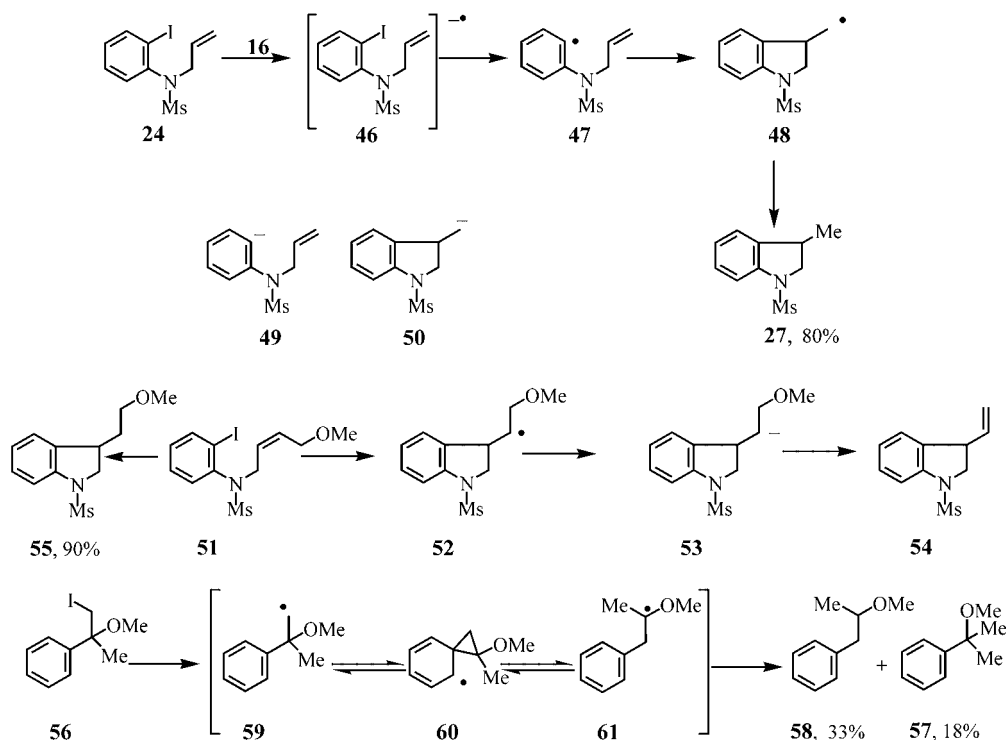


Scheme 4. Reactions of aryl iodides and aliphatic iodides with tetraazaalkene **16**. Ms = methanesulfonyl, tol = toluene.

Dissociation of **46** would then afford the aryl radical **47**. Although, in principle, **47** could be further reduced to the anion **49**, this anion would be more likely to undergo nucleophilic attack on DMF, but this reaction was not observed. The excellent yields of the products obtained preclude these pathways from our reaction. Similarly, the

cyclized radical **48** could, in principle, be reduced to the corresponding anion **50**, but again this should result in attack on DMF. No such product was seen, so we believe that the pathway featured radicals—but not anions—derived from the substrates throughout. The source of the hydrogen atom in the final hydrogen transfer, for example, in the conversion of **48** to **27**, has not yet been determined. A labeling experiment using anhydrous deuterated DMF as the exclusive solvent, sodium hydride as base rather than potassium hexamethyldisilazide (KHMDs), and **25** as substrate revealed no label in the product **28** (this point is currently under further investigation).

Similarly with the alkyl iodides **40**, **41**, and **44**, cyclization to **42**, **43**, and **45** should start with electron transfer followed by loss of iodide and formation of free-radical intermediates. In these substrates, a further opportunity exists to show the presence of carbanions prior to cyclization by the elimination of an alcoholate and the formation of a styrene product; however, in no case was such a fragmentation observed. It could be argued that the reagent has the intrinsic electron-donating power to form anions, but that the radical cyclization of these substrates occurred more rapidly than anion formation. To test further for the possibility of formation of alkyl anions, we studied the substrates **51** and **56**. Iodide **51** afforded the indoline **55** in 90% yield, presumably through quenching of radical **52**. Again, there is no evidence for formation of anion **53**, which should lead to rapid elimination to form alkene **54**. Substrate **56** also showed evidence of formation of radicals but not anions. Thus, the directly reduced product **57** was formed in 18% yield, but the major product was the ether **58**, which results from a neophyl rearrangement through radicals **59** and **60** followed by quenching.



Scheme 5. Thoughts on the mechanism of S.E.T. (single electron transfer) reactions of tetraazaalkene **16**.

In summary, the first reductions of unactivated aryl and alkyl iodides by a neutral ground-state organic molecule have been described. The reducing agent is formed in two steps from *N*-methylbenzimidazole using very simple chemistry: 1) alkylation with 1,3-diiodopropane to form a stable crystalline salt and 2) treatment of this salt with base to form the reactive reducing agent. Considerable variation of these super S.E.T. (single electron transfer) structures is now possible to afford reducing agents of greater power or to tailor reductions to particular substrates. Applications in synthesis and materials chemistry are likely to arise from this discovery.

Experimental Section

Exemplary procedures for the cyclization of aromatic and aliphatic iodide substrates are mentioned below. See Supporting Information for details of the synthesis and characterization of other compounds prepared during this research.

Cyclization of aromatic substrates: 1-Methanesulfonyl-3-ethyl-2,3-dihydro-1*H*-indole (**28**).^[21] A solution of salt **20** (202 mg, 0.36 mmol) in toluene (10 mL) and DMF (5 mL) under argon was purged with argon for 0.5 h at room temperature. Potassium bis(trimethylsilyl)amide (1.44 mL of 0.5 M solution in toluene, 0.72 mmol) was added dropwise to the mixture, and the resulting yellow solution was stirred for 1 h under argon. A solution of *N*-but-2-enyl-*N*-(2-iodophenyl)methanesulfonamide (**25**; 0.105 g, 0.3 mmol) in toluene (5 mL) was added, and the reaction mixture was heated and maintained at reflux for 18 h under Ar. The reaction mixture was then cooled and poured into diethyl ether (50 mL) and water (50 mL). The organic phase was further washed with water (3 × 50 mL) and then a saturated solution of NaCl (50 mL). The organic extract was dried over anhydrous sodium sulfate, filtered, and evaporated, and the residue was purified by column chromatography (ethyl acetate/petroleum ether 10:90) to afford the title compound as a colorless liquid (0.059 g, 88 %). FT-IR (disc): $\tilde{\nu}$ = 3016, 2963, 2930, 1599, 1478, 1342, 1232, 1161, 1051 cm⁻¹; ¹H NMR (400 MHz, CDCl₃): δ = 1.07 (3H, t, *J* = 7.3, CH₃), 1.66 (1H, m, CH₂), 1.90 (1H, m, CH₂), 2.93 (3H, s, SO₂CH₃), 3.38 (1H, m, CH), 3.69 (1H, dd, *J* = 10.2, 6.4, CH₂), 4.13 (1H, dd, *J* = 10.2, 9.2, CH₂), 7.11 (1H, dd, *J* = 7.5, 7.5, ArH), 7.27 (2H, m, ArH), 7.46 ppm (1H, d, *J* = 7.9, ArH); ¹³C NMR (100.61 MHz, CDCl₃): δ = 11.3 (CH₃), 27.5 (CH₂), 34.3 (CH₃), 41.4 (CH), 55.9 (CH₂), 113.4 (CH), 123.6 (CH), 124.7 (CH), 128.1 (CH), 135.0 (C), 141.8 ppm (C); *m/z* (EI): 225 (*M*⁺, 45 %), 196 (50), 146 (78), 130 (79), 118 (100), 91 (35); HRMS (ESI) *m/z*: Calcd for C₁₁H₁₅NO₂S: 243.1167 (*M* + NH₄⁺); found: 243.1169 (*M* + NH₄⁺).

Cyclization of aliphatic substrates: 2-(4-Methoxyphenyl)octahydrobenzofuran (**45**).^[22] A suspension of salt **20** (0.672 g, 1.20 mmol, 4.00 equiv) in dry THF (20 mL) was degassed by purging with argon at room temperature. Potassium bis(trimethylsilyl)amide (4.5 mL of 0.5 M solution in toluene, 2.25 mmol, 7.50 equiv) was added to this white suspension—the reaction mixture immediately turned bright yellow and was allowed to stir under Ar for 1 h. The solution was concentrated in vacuo, then 1-[1-(cyclohex-2-enyloxy)-2-iodo-ethyl]-4-methoxybenzene (**44**; 0.108 g, 0.30 mmol, 1.00 equiv) in dry toluene (20 mL) was added by cannula under an argon atmosphere. The reaction mixture was heated to 110 °C under Ar and was maintained at reflux for 15 h before cooling to room temperature and concentrating under reduced pressure. The residue was dissolved in diethyl ether (75 mL), and the solution was extracted with deionized water (75 mL). The aqueous phase was further extracted with diethyl ether (2 × 25 mL). The combined organic extracts were washed with a solution of brine (3 × 100 mL), separated, dried over anhydrous Na₂SO₄, filtered, and evaporated to dryness in vacuo to yield a yellow-orange semi-solid. This residue was purified by flash chromatography (diethyl ether/petroleum ether 15:85) to afford the title compound **45**

as a colorless oil as a mixture of diastereoisomers (5:8) that could not be separated (0.061 g, 88 %). FT-IR (neat): $\tilde{\nu}$ = 2931, 2854, 1613, 1513, 1458, 1443, 1302, 1246, 1172, 1036, 995, 828 cm⁻¹; ¹H NMR (400 MHz, CDCl₃): δ = 1.21–2.42 (11 H, m, CH and 5 × CH₂), 3.81 (3 H, minor, s, OCH₃), 3.82 (3 H, major, s, OCH₃), 4.02 (1 H, major, dd, *J* = 9.5, 4.8, OCH), 4.25 (1 H, minor, dd, *J* = 7.5, 3.5, OCH), 4.93 (1 H, major, t, *J* = 7.8, OCHAr), 5.15 (1 H, minor, t, *J* = 7.8, OCHAr), 6.85–6.93 (2 H, m, ArH), 7.21–7.30 (1 H, m, ArH), 7.32–7.40 ppm (1 H, m, ArH); ¹³C NMR (100.61 MHz, CDCl₃): δ = 21.1 (CH₂), 22.0 (CH₂), 24.3 (CH₂), 24.6 (CH₂), 27.9 (CH₂), 29.0 (CH₂), 29.1 (CH₂), 29.5 (CH₂), 38.7 (CH), 39.2 (CH), 41.0 (CH₂), 42.5 (CH₂), 55.8 (CH₃), 78.4 (CH), 79.1 (CH), 79.8 (CH), 114.1 (CH), 114.2 (CH), 127.2 (CH), 127.4 (CH), 136.8 (C), 137.8 (C), 159.1 (C), 159.1 ppm (C); *m/z* (CI): 250 ([*M* + NH₄]⁺, 91 %), 233 (100). HRMS (ESI) *m/z*: Calcd for C₁₅H₂₀O₂: 233.1536 (*MH*⁺); found: 233.1536 (*MH*⁺).

Received: September 18, 2004

Published online: January 26, 2005

Keywords: cyclization · electron transfer · radical reactions · reduction · synthetic methods

- a) T. Imamoto in *Comprehensive Organic Synthesis*, Vol. 8 (Ed.: B. M. Trost), Pergamon, Oxford, **1991**, chap. 4.1, pp. 795–797; b) M. Hudlicky in *Comprehensive Organic Synthesis*, Vol. 8 (Ed.: B. M. Trost), Pergamon, Oxford, **1991**, chap. 4.5, pp. 895–922.
- D. G. Peters in *Organic Electrochemistry* (Eds.: H. Lund, O. Hammerich), Marcel Dekker, New York, **1991**, p. 354.
- For indirect electrochemical reductions, see: a) M. D. Koppang, G. A. Ross, N. F. Woolsey, D. E. Bartak, *J. Am. Chem. Soc.* **1986**, *108*, 1441; b) S. Olivero, J.-P. Rolland, E. Duñach, *Organometallics* **1998**, *17*, 3747.
- a) J. M. Hook, L. N. Mander, *Nat. Prod. Rep.* **1986**, *3*, 35; b) T. J. Donohoe, R. Garg, C. A. Stevenson, *Tetrahedron: Asymmetry* **1996**, *7*, 317.
- C. J. Hollowood, S. V. Ley, *Org. Biomol. Chem.* **2003**, *1*, 3197.
- a) T. J. Donohoe, D. House, K. W. Ace, *Org. Biomol. Chem.* **2003**, *1*, 3749; b) T. J. Donohoe, D. House, *J. Org. Chem.* **2002**, *67*, 5015; c) T. J. Cleij, S. K. Y. Tsang, L. W. Jennekens, *Chem. Commun.* **1997**, 329.
- a) J. Cossy, *Bull. Soc. Chim. Fr.* **1994**, *131*, 344, and references therein; b) U. C. Yoon, Y. X. Jin, S. W. Oh, C. H. Park, J. H. Park, C. F. Campana, X. Cai, E. N. Duesler, P. S. Mariano, *J. Am. Chem. Soc.* **2003**, *125*, 10664.
- a) J. A. Murphy in *Radicals in Organic Synthesis*, Vol. 1 (Eds.: P. Renaud, M. Sibi), Wiley-VCH, Weinheim, **2001**, pp. 298–315.
- O. Callaghan, C. Lampard, A. R. Kennedy, J. A. Murphy, *J. Chem. Soc. Perkin Trans. 1* **1999**, 995.
- O. Callaghan, C. Lampard, A. R. Kennedy, J. A. Murphy, *Tetrahedron Lett.* **1999**, *40*, 161.
- A. J. Fry in *Synthetic Organic Electrochemistry*, Wiley, Chichester, **1989**, p. 95.
- a) G. V. Tormos, M. C. Bakker, P. Wang, M. V. Lakshminathan, M. P. Cava, R. M. Metzger, *J. Am. Chem. Soc.* **1995**, *117*, 8528; b) F. G. Bordwell, A. V. Satish, *J. Am. Chem. Soc.* **1991**, *113*, 985; c) V. Tormos, O. J. Neilands, M. P. Cava, *J. Org. Chem.* **1992**, *57*, 1008; d) V. Goulle, S. Chirayil, R. P. Thummel, *Tetrahedron Lett.* **1990**, *31*, 1539; e) H. H. Wanzlick, H.-J. Kleiner, I. Lasch, H. U. Fueldner, H. Steinmaus, *Justus Liebigs Ann. Chem.* **1967**, *708*, 155.
- a) T. Koizumi, N. Bashir, A. R. Kennedy, J. A. Murphy, *J. Chem. Soc. Perkin Trans. 1* **1999**, 3637; b) T. Koizumi, N. Bashir, J. A. Murphy, *Tetrahedron Lett.* **1997**, *38*, 7635.
- N. Takechi, S. Ait-Mohand, M. Médebielle, W. R. Dolbier, Jr., *Tetrahedron Lett.* **2002**, *43*, 4317.

- [15] a) G. Giuglio-Tonolo, T. Terme, M. Médebielle, P. Vanelle, *Tetrahedron Lett.* **2003**, 44, 6433; b) G. Giuglio-Tonolo, T. Terme, M. Médebielle, P. Vanelle, *Tetrahedron Lett.* **2004**, 45, 5121.
- [16] a) Y. Yamashita, Y. Kobayashi, T. Miyashi, *Angew. Chem.* **1989**, 101, 1090; *Angew. Chem. Int. Ed. Engl.* **1989**, 28, 1052; b) M. Sato, M. V. Lakshmikantham, M. P. Cava, A. F. Garito, *J. Org. Chem.* **1978**, 43, 2084.
- [17] a) Z. Shi, R. P. Thummel, *J. Org. Chem.* **1995**, 60, 5935; b) Z. Shi, V. Goulle, R. P. Thummel, *Tetrahedron Lett.* **1996**, 37, 2357; c) F. E. Hahn, L. Wittenbecher, D. LeVan, R. Froehlich, *Angew. Chem.* **2000**, 112, 551; *Angew. Chem. Int. Ed.* **2000**, 39, 541; d) Z. Shi, R. P. Thummel, *Tetrahedron Lett.* **1995**, 36, 2741; e) T. A. Taton, P. Chen, *Angew. Chem.* **1996**, 108, 1098; *Angew. Chem. Int. Ed. Engl.* **1996**, 35, 1011; f) M. K. Denk, A. Thadani, K. Hatano, A. J. Lough, *Angew. Chem.* **1997**, 109, 2719; *Angew. Chem. Int. Ed. Engl.* **1997**, 36, 2607; g) M. K. Denk, K. Hatano, M. Ma, *Tetrahedron Lett.* **1999**, 40, 2057; h) H.-W. Wanzlick, E. Schikora, *Angew. Chem.* **1960**, 72, 494; i) H.-W. Wanzlick, E. Schikora, *Chem. Ber.* **1961**, 94, 2389; j) H.-W. Wanzlick, H.-J. Kleiner, *Angew. Chem.* **1961**, 73, 493; k) H.-W. Wanzlick, *Angew. Chem.* **1962**, 74, 129; *Angew. Chem. Int. Ed. Engl.* **1962**, 1, 75; l) H.-W. Wanzlick, H. Ahrens, *Chem. Ber.* **1964**, 97, 2447; m) H.-W. Wanzlick, B. Lachmann, E. Schikora, *Chem. Ber.* **1965**, 98, 3170; n) N. Wiberg, *Angew. Chem.* **1968**, 80, 153; *Angew. Chem. Int. Ed. Engl.* **1968**, 7, 7661; o) J. R. Ames, M. A. Houghtaling, D. L. Terrian, T. P. Mitchell, *Can. J. Chem.* **1997**, 75, 28.
- [18] a) E. Çetinkaya, P. B. Hitchcock, H. Küçükbay, M. F. Lappert, S. Al-Juaid, *J. Organomet. Chem.* **1994**, 481, 89; b) F. E. Hahn, L. Wittenbacher, M. Kühn, T. Lügger, R. Fröhlich, *J. Organomet. Chem.* **2001**, 617–618, 629; c) F. E. Hahn, M. Paas, D. LeVan, T. Lügger, *Angew. Chem.* **2003**, 115, 5402; *Angew. Chem. Int. Ed.* **2003**, 42, 5243; d) D. J. Cardin, M. J. Doyle, M. F. Lappert, *J. Chem. Soc. Chem. Commun.* 1972, 927; e) M. F. Lappert, *J. Organomet. Chem.* **1988**, 358, 185; f) E. Çetinkaya, P. B. Hitchcock, M. F. Lappert, D. B. Shaw, K. Syropoulos, N. J. W. Warhurst, *J. Organomet. Chem.* **1993**, 459, 311; g) E. Çetinkaya, P. B. Hitchcock, H. A. Jasim, M. F. Lappert, K. Syropoulos, *J. Chem. Soc. Perkin Trans. 1* **1992**, 561; h) T. L. Amyes, S. T. Diver, J. P. Richard, F. M. Rivas, K. Toth, *J. Am. Chem. Soc.* **2004**, 126, 4366.
- [19] Such a carbene would be expected to display a ^{13}C chemical shift for this carbon at approximately $\delta = 235$ ppm, see Ref. [17c] and also: F. E. Hahn, L. Wittenbecher, R. Boese, D. Blaeser, *Chem. Eur. J.* **1999**, 5, 1931.
- [20] Initial experiments with aryl bromides and alkyl selenides are much more sluggish and do not lead to high extents of conversion under these conditions.
- [21] T. A. Khan, R. Tripoli, J. J. Crawford, C. G. Martin, J. A. Murphy, *Org. Lett.* **2003**, 5, 2971.
- [22] a) Y. Kita, H. Nambu, N. G. Ramesh, G. Anilkumar, M. Matsugi, *Org. Lett.* **2001**, 3, 1157; b) H. Nambu, G. Anilkumar, M. Matsugi, Y. Kita, *Tetrahedron* **2003**, 59, 77; c) L. Zhou, T. Hirao, *J. Org. Chem.* **2003**, 68, 1633.

Physicochemical Characterization of Porous Materials: Spatially Resolved Accessibility of Zeolite Crystals**

Sander van Donk, Johannes H. Bitter,
An Verberckmoes, Marjan Versluijs-Helder,
Alfred Broersma, and Krijn P. de Jong*

Zeolites and (ordered) mesoporous materials are essential building blocks of functional materials used in, for example, adsorption, separation, and catalysis.^[1] Key factors governing the performance of these materials are pore size, pore shape, surface properties, and the like. In many applications, especially for zeolites, the molecules involved either as substrate or product have similar sizes to those of the pores.^[2] This leads to molecular-sieving properties relevant for adsorption and separation processes and shape selectivity in catalysis. Likewise, the rate of access of molecules into zeolite crystals may be low or sometimes even zero if pore blocking by impurities occurs. To improve the accessibility of zeolites many different approaches have been followed, such as the synthesis of zeolites with large pores,^[3–7] small crystals,^[8] hierarchical structures,^[9] and mesoporous crystals.^[1,10,11] In all cases, however, one clearly needs reliable methods for the characterization of the accessibility of these materials. Adsorption studies,^[12] often in combination with spectroscopy,^[13–16] have been used until now to establish the average accessibility of the micropore volume of zeolite samples. Progress has been made in recent years in obtaining information on the accessibility of porous materials with techniques such as magnetic resonance imaging (MRI)^[17] or interference microscopy^[18] with a spatial resolution of millimeters and micrometers, respectively. Herein, we use adsorption and diffusion studies in combination with scanning electron microscopy/energy-dispersive X-ray (SEM/EDX) analysis, which allow us to determine quantitatively the

[*] Dr. J. H. Bitter, M. Versluijs-Helder, A. Broersma, Prof. K. P. de Jong
Department of Inorganic Chemistry and Catalysis
Debye Institute, Utrecht University
P.O. Box 80083, 3508 TB Utrecht (The Netherlands)
Fax: (+31) 30-251-1027
E-mail: j.h.bitter@chem.uu.nl

Dr. S. van Donk^[†]
Utrecht University
P.O. Box 80083, 3508 TB Utrecht (The Netherlands)
Dr. A. Verberckmoes
ExxonMobil Chemical Europe Inc.
European Technology Center, Machelen (Belgium)

[†] Current address: Albemarle Catalysts
Research Center Amsterdam (The Netherlands)

[**] Katleen Hermans (ExxonMobil) is acknowledged for performing the ICP-AES and ²⁷Al NMR measurements; Jeroen van Bokhoven (ETH Zürich) and Andrea Battiston (UU/Albemarle Catalysts) are acknowledged for helpful discussions. This work was financially supported by the Netherlands Organization for Scientific Research (NWO/CW 700-97-019).

length of the accessible micropores of zeolite crystals with a resolution of 50 nm or better. As a case in point, we will study the accessibility of the zeolite mordenite (MOR).

Mordenite is of great industrial importance in the catalytic conversion of alkanes^[19,20] and aromatic compounds.^[21] The structure of MOR is generally regarded as one-dimensional,^[22,23] with the 12-ring (12-MR) channels running parallel to the length of the crystal.^[24] Several times in the past it has been qualitatively observed that the presence of either small amounts of nonframework alumina (NFAI) or crystal-growth defects caused blockage of a large part of the micropore volume.^[12,25,26] This blockage makes it impossible for hydrocarbons to enter the micropores and consequently the catalytic action is largely hindered, which makes this system an ideal case to demonstrate the value of the new combination of techniques.

Sodium-exchanged zeolite (NaMOR) with a Si/Al ratio of 5.5:1 was synthesized by using a modified literature procedure.^[27] The Na⁺ ions were exchanged for NH₄⁺ ions to give NH₄MOR, which was subsequently calcined in air at 723 K for 6 h (ramp 1 K min⁻¹) to obtain HMOR. From the literature it is known that NFAI species that are created during synthesis or calcination can be removed by a mild treatment using oxalic acid.^[28,29] Therefore, part of the HMOR sample was treated in an aqueous solution of 0.1 M oxalic acid at 353 K for 1 h. The sample was then filtered, washed, dried at 353 K for 12 h, and calcined as described before. This treatment was executed twice to give a sample that is referred to as HMOR-ox. Both the HMOR and HMOR-ox samples were characterized by using nitrogen physisorption/t-plot analysis, elemental analysis by inductively coupled plasma atomic-emission spectrometry (ICP-AES), temperature-programmed desorption–thermogravimetric analysis (TPD-TGA) with *n*-propylamine,²⁷ Al NMR spectroscopy, and SEM.

The physicochemical characteristics of HMOR and HMOR-ox are presented in Table 1. Elemental analysis shows that the mild treatment with oxalic acid causes an increase in the Si/Al ratio from 5.6:1 to 8.0:1 (at/at). Despite the removal of aluminum by oxalic acid, the SEM images for both samples were indistinguishable, with average crystal lengths (2L) of between 1 and 2 μm. Evaluation by ²⁷Al NMR spectroscopy also indicated that upon treatment with oxalic acid, the overall amount of Al in the sample decreased. In particular, the peak at 0 ppm that is generally ascribed to octahedral NFAI species^[30,31] was lowered, which indicates

that NFAI had been removed. A minor amount of tetrahedral species was also removed; however, from the measured data it was not clear if this concerned framework Al or NFAI species. The nitrogen physisorption results presented in Table 1 suggest that no significant changes in the textural properties occurred during the oxalic acid treatment. However, the number of acid sites probed by *n*-propylamine increased by almost a factor of 3 upon leaching, while the level of aluminum was significantly lower.

Different techniques are available for studying the diffusion behavior in zeolites, such as IR spectroscopy,^[32] zero-length column (ZLC) chromatography,^[33] and pulsed field gradient (PFG) NMR spectroscopy.^[34] We chose to further investigate this discrepancy by performing transient uptake measurements for *n*-hexane in a tapered-element oscillating microbalance (TEOM; Rupprecht & Pataschnick 1500 PMA).^[35–37] The measurements were carried out at 523 K and a total pressure of 1.3 bar. The results for the uptake of *n*-hexane are shown in Figure 1, which reveals a

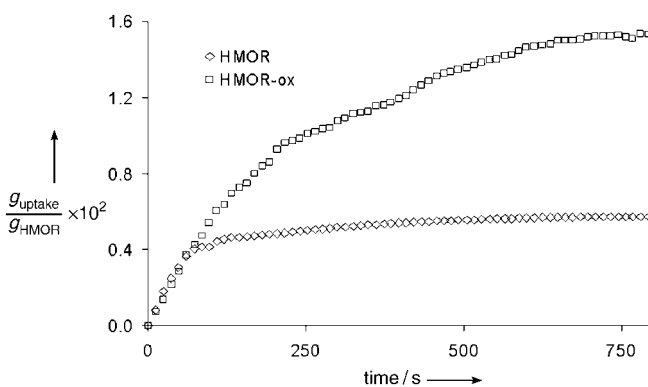


Figure 1. Experimental uptake curves for *n*-hexane over HMOR and HMOR-ox at 523 K, as monitored by a TEOM.

significant difference in the equilibrium uptake of *n*-hexane by HMOR and HMOR-ox. The amount of *n*-hexane adsorbed in the micropores almost tripled from 0.56 wt % for HMOR to 1.53 wt % for HMOR-ox (see also Table 1), which indicates a higher availability of micropore volume for HMOR-ox. Quantitative information on the nature of pore blocking could be deduced from the uptake data. The characteristic times for diffusion L^2/D [s], where D [m²s⁻¹] is the diffusion coefficient, were derived by fitting the experimental uptake curves for HMOR and HMOR-ox using a model described in an earlier study.^[35] The data presented in Table 1 clearly indicate that the acid treatment induces an almost tenfold increase in L^2/D . The accessible pore lengths for the two samples were calculated (L_{calcd} in Table 1) using a literature value^[35] for D of 3×10^{-16} m²s⁻¹. The resulting value of 0.16 μm for HMOR is much lower than one would expect from the SEM measurements. However, for HMOR-ox, the value of L_{calcd} is close to that expected.

The accessible pore lengths for HMOR and HMOR-ox were further investigated by exposing the samples to pure *n*-butene for 20 h at 623 K and 1.3 bar in the TEOM, to provoke coke formation. The coke contents were 3.7 wt % for HMOR

Table 1: Characterization data of the HMOR samples.

	HMOR	HMOR-ox
bulk Si/Al ratio, ICP-AES (at/at)	5.6	8.0
2L from SEM [μm]	1–2	1–2
micropore volume [mL g ⁻¹]	0.16	0.17
external surface area [m ² g ⁻¹]	67	52
acid sites, TPD-TGA [mmol g ⁻¹]	0.29	0.73
<i>n</i> -hexane uptake at 523 K [wt %]	0.56	1.53
L^2/D from <i>n</i> -hexane uptake [s]	85	797
L_{calcd} from <i>n</i> -hexane uptake [μm]	0.16	0.49
<i>n</i> -butene-derived coke at 623 K [wt %]	3.7	8.2
L_{coke} from SEM-EDX [μm]	≈ 0.2	≈ 1

and 8.2 wt % for HMOR-ox, which reveals a similar trend to that observed with the *n*-hexane uptake measurements (Table 1). The coked HMOR crystals were also investigated in an SEM microscope (Philips XL30FEG) equipped with an EDX detector. Line scans were taken over the HMOR samples such that the atomic carbon (C) and zeolitic oxygen (O) signals were monitored parallel to the direction of the 12-MR channels. The C/O ratio was calculated from these data to determine the penetration depth of the carbonaceous deposits into the 12-MR channels. Figure 2 shows representative

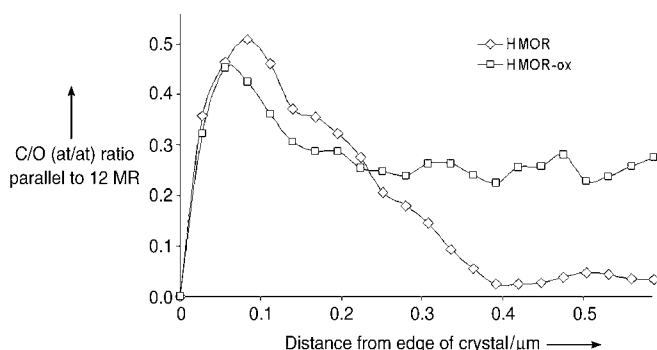


Figure 2. Coke profiles for HMOR and HMOR-ox, which show the atomic carbon to zeolitic oxygen (C/O) ratio as a function of scanning distance going from the edge to the inside of the crystal, as monitored by SEM-EDX.

line scans for HMOR and HMOR-ox crystals. The observed C/O ratios provide us with an estimate of the accessible pore length. For HMOR-ox the butene molecules have reacted throughout the pores, while for HMOR similar uptake occurs only up to 0.2 μm and total blockage is apparent beyond 0.4 μm . These data allow direct visualization of the accessible pore lengths for the two samples by their coke profiles (L_{coke} in Table 1), and clearly indicate the enhanced length of the accessible micropores for HMOR-ox in comparison with HMOR (Figure 3). In addition, the value of 0.2 μm for the accessible pore length of HMOR obtained from EDX agrees very well with the value of 0.16 μm calculated from the *n*-hexane uptake measurements. In general, the gradient of coke observed over the HMOR-ox crystal points to mass-transfer limitation of the deposition process, which has been observed before for the reaction of *n*-butene over ferrierite.^[38]

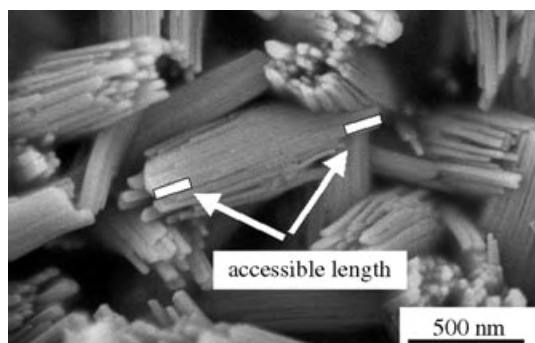


Figure 3. SEM image of HMOR. The accessible pore length is indicated by the white areas. Only 30% of the pore is accessible.

Careful selection of probe molecules allows the methods of diffusion (TEOM) and coking (SEM/EDX) to be generalized for accessibility studies of a range of microporous and mesoporous materials. If a higher spatial resolution is needed than that obtained with SEM/EDX, one can use scanning TEM/electron energy-loss spectroscopy (STEM/EELS) to detect coke profiles with about 2-nm resolution.^[38]

Received: June 15, 2004

Revised: November 23, 2004

Published online: January 20, 2005

Keywords: diffusion · mesoporous materials · microporous materials · physisorption · zeolites

- [1] A. Corma, *J. Catal.* **2003**, *216*, 298.
- [2] S. van Donk, A. H. Janssen, J. H. Bitter, K. P. de Jong, *Catal. Rev.* **2003**, *45*, 297.
- [3] A. Corma, M. J. Diaz-Cabanas, J. Martinez-Triguero, F. Rey, J. Ruis, *Nature* **2002**, *418*, 514.
- [4] J.-L. Pailloud, B. Harbuzaru, J. Patarin, N. Bats, *Science* **2004**, *304*, 990.
- [5] A. Corma, U. Diaz, M. E. Domine, V. Fornes, *Angew. Chem.* **2000**, *112*, 1559; *Angew. Chem. Int. Ed.* **2000**, *39*, 1499.
- [6] C. T. Kresge, M. E. Leonowicz, W. J. Roth, J. C. Vartuli, J. S. Beck, *Nature* **1992**, *359*, 710.
- [7] A. Corma, M. J. Diaz-Cabanas, F. Rey, S. Nicolopoulos, K. Boulahya, *Chem. Commun.* **2004**, 1356.
- [8] G. Belussi, G. Pazzuconi, C. Perego, G. Girotti, G. Terzoni, *J. Catal.* **1995**, *157*, 227.
- [9] S. S. Kim, A. Karkamkar, T. J. Pinnavaia, M. Kruk, *J. Phys. Chem. B* **2001**, *105*, 7663.
- [10] A. H. Janssen, A. J. Koster, K. P. de Jong, *Angew. Chem.* **2001**, *113*, 1136; *Angew. Chem. Int. Ed.* **2001**, *40*, 1102.
- [11] C. J. H. Jacobson, C. Madsen, J. Houzvicka, I. Schmidt, A. Carlsson, *J. Am. Chem. Soc.* **2000**, *122*, 7116.
- [12] Y. Hong, J. J. Fripiat, *Microporous Mater.* **1995**, *4*, 323.
- [13] G. Muller, T. Narbeshuber, G. Mirth, J. A. Lercher, *J. Phys. Chem.* **1994**, *98*, 7436.
- [14] T. Armadori, M. Bevilacqua, M. Trombetta, F. Milella, A. G. Alejandre, J. Ramirez, B. Notari, R. J. Willey, G. Busca, *Appl. Catal. A* **2001**, *216*, 59.
- [15] I. I. Ivanova, V. Montouillout, C. Fernandez, O. Marie, J.-P. Gilson, *Microporous Mesoporous Mater.* **2003**, *57*, 297.
- [16] N. A. Nesterenko, F. Thibault-Starzyk, V. Montouillout, V. V. Yushenko, C. Fernandez, J.-P. Gilson, F. Fajula, I. I. Ivanova, *Microporous Mesoporous Mater.* **2004**, *71*, 157.
- [17] S. P. Rigby, L. F. Gladden, *J. Catal.* **1998**, *173*, 484.
- [18] P. Kortunov, S. Vasenkov, C. Chmelik, J. Kärger, D. M. Ruthven, J. Wloch, *Chem. Mater.* **2004**, *16*, 3552.
- [19] H. W. Kouwenhoven, W. C. van Zijl-Langhout, *Chem. Eng. Prog.* **1971**, *67*, 65.
- [20] A. Corma, A. Martinez, *Catalytic Activation and Functionalization of Light Alkanes: Advances and Challenges* (Eds.: E. G. Derouane, J. Haber, F. Lemos, F. R. Ribeiro, M. Guisnet), Kluwer Academic, Dordrecht, **1998**.
- [21] G. J. Lee, J. M. Garces, G. R. Meima, M. J. M. van der Aalst, US Patent no. 325177, **1989**.
- [22] A. W. O'Donovan, C. T. O'Connor, K. R. Koch, *Microporous Mater.* **1995**, *5*, 185.
- [23] F. Eder, M. Stockenhuber, J. A. Lercher, *J. Phys. Chem. B* **1997**, *101*, 5414.
- [24] C. Baerlocher, W. M. Meier, D. H. Olson, *Atlas of Zeolite Framework Types*, 5th ed., Elsevier Science, Amsterdam, **2001**.

- [25] L. D. Fernandez, P. E. Bartl, J. L. F. Monteiro, J. G. Dasilva, S. C. Demendez, M. J. B. Cardoso, *Zeolites* **1994**, *14*, 533.
- [26] S. Moreno, G. Poncelet, *Microporous Mater.* **1997**, *12*, 197.
- [27] P. K. Bajpai, *Zeolites* **1986**, *6*, 2.
- [28] M. R. Apelian, A. S. Fung, G. J. Kennedy, T. F. Degnan, *J. Phys. Chem.* **1996**, *100*, 16577.
- [29] M. Müller, G. Harvey, R. Prins, *Microporous Mesoporous Mater.* **2000**, *34*, 135.
- [30] R. Giudici, H. W. Kouwenhoven, R. Prins, *Appl. Catal. A* **2000**, *203*, 101.
- [31] T.-H. Chen, B. H. Wouters, P. J. Grobet, *Eur. J. Inorg. Chem.* **2000**, *2*, 281.
- [32] H. G. Karge, W. Niessen, *Catal. Today* **1991**, *8*, 451.
- [33] M. Eic, D. M. Ruthven, *Zeolites* **1988**, *9*, 40.
- [34] R. Valiullin, P. Kortunov, J. Kärger, V. Timoshenko, *J. Chem. Phys.* **2004**, *120*, 11804.
- [35] S. van Donk, A. Broersma, O. L. J. Gijzeman, J. A. van Bokhoven, J. H. Bitter, K. P. de Jong, *J. Catal.* **2001**, *204*, 272.
- [36] D. Chen, H. P. Rebo, K. Moljord, A. Holmen, *Chem. Eng. Sci.* **1996**, *51*, 2687.
- [37] W. Zhu, J. M. van de Graaf, L. J. P. van den Broeke, F. Kapteijn, J. A. Moulijn, *Ind. Eng. Chem. Res.* **1998**, *37*, 1934.
- [38] S. van Donk, F. M. F. de Groot, O. Stéphan, J. H. Bitter, K. P. de Jong, *Chem. Eur. J.* **2003**, *9*, 3106.

num halides and chalcogenides;^[7] however, this occurrence in the Chevrel phases is the only one observed for the sulfides, selenides, and tellurides to date. Here we present the synthesis, crystal and electronic structures, and properties of an original reduced molybdenum sulfide, $\text{Ba}_4\text{Mo}_{12}\text{S}_{18}$, in which the $\text{Mo}_6\text{S}_8\text{S}_6^i$ units form the new dimeric unit $(\text{Mo}_6)_2\text{S}_{14}^i\text{S}_4^{i-i}-\text{S}_3^{a-a}\text{S}_6^a$, which is the missing link between the $\text{Mo}_6\text{S}_8\text{S}_6^i$ unit and the $\text{Mo}_9\text{S}_{11}\text{S}_6^a$ unit containing the biotetrahedral Mo_9 cluster.^[8]

$\text{Ba}_4\text{Mo}_{12}\text{S}_{18}$ crystallizes in a new structural type, the three-dimensional Mo–S framework of which is based on the novel dimeric unit $(\text{Mo}_6)_2\text{S}_{14}^i\text{S}_3^{i-i}\text{S}_3^{a-a}\text{S}_6^a$ (Figure 1), which can be

Ternary Molybdenum Sulfide

$\text{Ba}_4\text{Mo}_{12}\text{S}_{18}$: A Superconductor Containing the Dimeric Unit $(\text{Mo}_6)_2\text{S}_{24}$, the Missing Link between the Mo_6S_{14} and Mo_9S_{17} Units

Diala Salloum, Régis Gautier, Michel Potel, and Patrick Gougeon*

The ternary molybdenum chalcogenides $\text{M}_x\text{Mo}_6\text{X}_8$ ($\text{M} = \text{Na}, \text{K}, \text{Ca}, \text{Sr}, \text{Ba}, \text{Sn}, \text{Pb}$, lanthanide, 3d element; $\text{X} = \text{S}, \text{Se}, \text{Te}$), known as Chevrel phases, have been studied intensively in the last three decades because of their exceptional physical properties.^[1–4] Their crystal structure^[5] consists of octahedral Mo_6 clusters surrounded by fourteen chalcogen atoms, eight of which form a distorted cube (*i*-type ligands), while the remaining six cap the faces of the X_8 cube (*a*-type ligands). In the formalism of Schäfer and von Schnering,^[6] such a unit can be written as $\text{Mo}_6\text{X}_8^i\text{X}_6^a$. In the Chevrel phases, some of the chalcogen atoms of the $\text{Mo}_6\text{X}_8^i\text{X}_6^a$ unit are shared according to the developed formula $[\text{Mo}_6\text{X}_8^i\text{X}_6^{i-a}]\text{X}_{6/2}^{a-i}$ to form a three-dimensional Mo–X network. Different connectivities between the $\text{Mo}_6\text{L}_8^i\text{L}_6^a$ ($\text{L} = \text{Cl}, \text{Br}, \text{I}, \text{S}, \text{Se}, \text{Te}$) units leading to a variety of frameworks are known in reduced molybde-

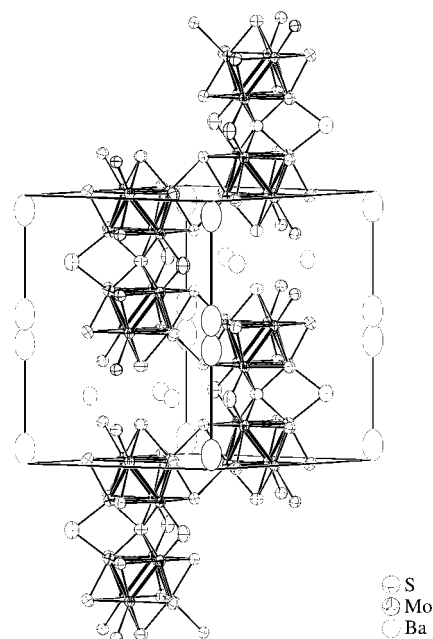


Figure 1. Crystal structure of $\text{Ba}_4\text{Mo}_{12}\text{S}_{18}$. Thick lines denote Mo–Mo bonds, and thin lines Mo–O bonds.

regarded as resulting from the fusion of two $\text{Mo}_6\text{S}_8\text{S}_6^i$ units by sharing two S^i and six S^a ligands, as shown in Figure 2 (left and middle). This new unit can be also viewed as an intermediate step towards the formation of the $\text{Mo}_9\text{S}_{11}\text{S}_6^a$ unit containing the biotetrahedral Mo_9 cluster (Figure 2, right).^[8] Halogens are well known to form *a*-*a* type ligands, however, this is the first time that sulfur atoms occupy such a position (S_3 atom in Figure 3). The Mo_6 octahedra are more

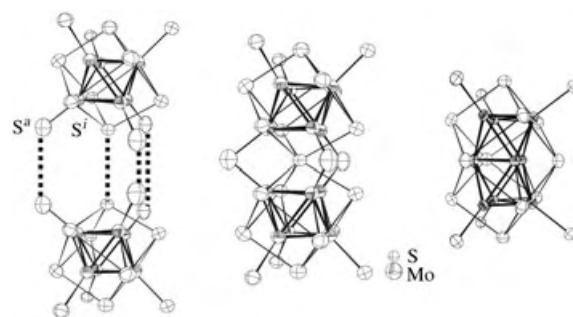


Figure 2. Process of formation of the $(\text{Mo}_6)_2\text{S}_{14}^i\text{S}_3^{i-i}\text{S}_3^{a-a}\text{S}_6^a$ unit (middle) from the fusion of two $\text{Mo}_6\text{S}_8\text{S}_6^i$ units (left). Right: the $\text{Mo}_9\text{S}_{11}\text{S}_6^a$ unit.

[*] D. Salloum, Dr. R. Gautier, Dr. M. Potel, Dr. P. Gougeon
CNRS, Université de Rennes 1, ENSC Rennes
Institut de Chimie de Rennes
Laboratoire de Chimie du Solide et Inorganique Moléculaire, UMR 6511
Avenue du Général Leclerc, 35042 Rennes Cedex (France)
Fax: (+33) 2-9963-5704
E-mail: patrick.gougeon@univ-rennes1.fr

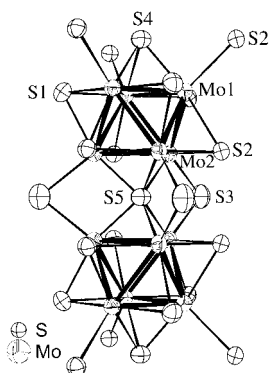


Figure 3. The $(\text{Mo}_6)_2\text{S}_{14}\text{S}_3^{i-i}\text{S}_3^{a-a}\text{S}_6^a$ unit with atomic labeling scheme. Selected distances [Å]: Mo1–Mo1 2.6921(3), Mo1–Mo2 2.6953(4), Mo2–Mo2 2.9144(4), Mo1–S1 2.4612(6), Mo1–S2 2.4655(9), Mo1–S2 2.5298(9), Mo1–S4 2.4149(11), Mo2–S1 2.4569(9), Mo2–S2 2.4691(5), Mo2–S3 2.5355(17), Mo2–S5 2.2967(3).

distorted than in the Chevrel phases with Mo–Mo distances ranging from 2.6921(3) to 2.9144(4) Å. The Mo2–Mo2 distance between the two Mo_6 clusters within the $(\text{Mo}_6)_2\text{S}_{14}\text{S}_3^{i-i}\text{S}_3^{a-a}\text{S}_6^a$ unit is 3.1264(4) Å, which is comparable to the intercluster distances observed between the Mo_6 clusters in the $\text{M}_x\text{Mo}_6\text{S}_8$ compounds. The Mo–S distances range from 2.2967(3) to 2.535(2) Å. The shortest distance occurs between the Mo2 atoms and the *i-i* type ligand S5, and the longest one between the Mo2 atoms and the *a-a* type ligands S3 (Figure 3). As observed previously in the Chevrel phases, the three-dimensional arrangement of the $(\text{Mo}_6)_2\text{S}_{14}\text{S}_3^{i-i}\text{S}_3^{a-a}\text{S}_6^a$ units arises from the sharing of the six *a*-type ligands with six *i*-type ligands. As a consequence, the connective formula of the Mo–S framework is $(\text{Mo}_6)_2\text{S}_8\text{S}_3^{i-i}\text{S}_3^{a-a}\text{S}_6^a$. The result of this arrangement is that the shortest Mo–Mo distance between the Mo_6 clusters of adjacent $(\text{Mo}_6)_2\text{S}_{14}\text{S}_3^{i-i}\text{S}_3^{a-a}\text{S}_6^a$ units is 3.0847(4) Å. As shown by the perspective view of the crystal structure along the *c* axis (Figure 4), the Ba2 ions reside in large channels extending along the *c* axis. The other barium atoms (Ba1) are located between two consecutive $(\text{Mo}_6)_2\text{S}_{14}\text{S}_3^{i-i}\text{S}_3^{a-a}\text{S}_6^a$ units around the threefold axis. The

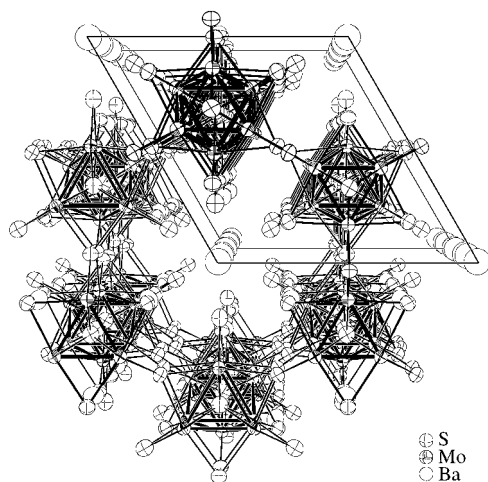


Figure 4. Perspective view of the $\text{Ba}_4\text{Mo}_{12}\text{S}_{18}$ structure down the *c* axis.

Ba1 cations are surrounded by ten sulfur atoms. The nearest four at about 3.1 Å form a distorted tetrahedron, and the remaining six at 3.3841(9)–3.4692(6) Å cap a face or bridge an edge. The Ba2 cations are located off-center of large cavities of twelve sulfur atoms forming an hexacapped trigonal antiprism. They are thus surrounded by nine sulfur atoms at distances between 3.394(1) and 3.734(3) Å.

Single-crystal electrical resistivity measurements indicate that $\text{Ba}_4\text{Mo}_{12}\text{S}_{18}$ is poorly metallic, with a room-temperature resistivity of around 1 mΩ cm, and becomes a superconductor below 7 K (Figure 5). Superconductivity was also confirmed by the Meissner effect in susceptibility measurements on powder samples.

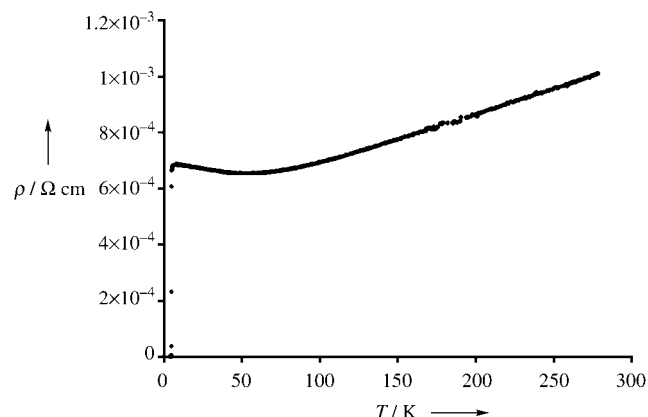


Figure 5. Temperature dependence of the electrical resistivity for a single crystal of $\text{Ba}_4\text{Mo}_{12}\text{S}_{18}$.

Metallic behavior was confirmed by periodic density functional calculations (Figure 6).^[9] The Fermi level cuts a

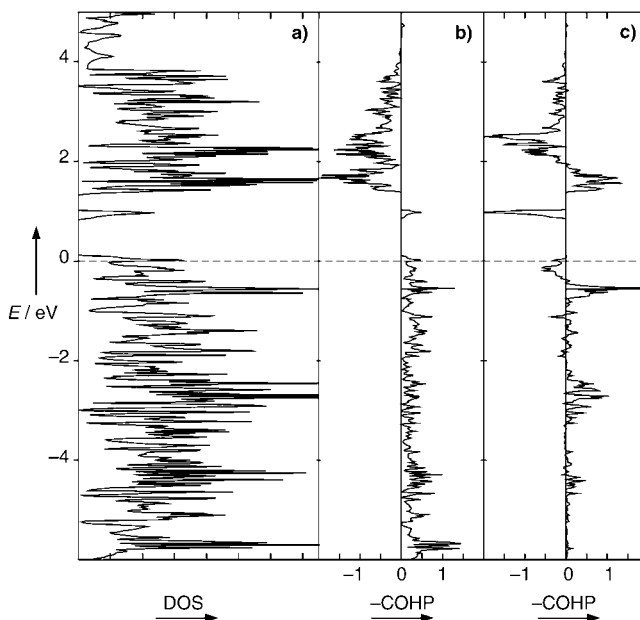


Figure 6. DFT calculations for $\text{Ba}_4\text{Mo}_{12}\text{S}_{18}$: a) total DOS, b) averaged COHP for Mo–Mo bonds of the Mo_6 unit, and c) COHP for Mo2–Mo2 bonds between the two Mo_6 clusters within the $(\text{Mo}_6)_2\text{S}_{14}\text{S}_3^{i-i}\text{S}_3^{a-a}\text{S}_6^a$ unit.

narrow peak of density of states (DOS), mainly centered on Mo atoms, that is separated by an energy gap of about 1 eV from a higher vacant DOS peak. This latter peak shows Mo₂–Mo₂ antibonding character (between the two Mo₆ clusters in the (Mo₆)₂S₁₄ⁱS₃ⁱ⁻ⁱS₆^a unit) and intra-Mo₆ Mo₂–Mo₂ bonding character. It is derived from a molecular orbital of the (Mo₆)₂S₁₄ⁱS₃ⁱ⁻ⁱS₆^a unit which is the out-of-phase combination that results from interaction of the same MO of each Mo₆ cluster among the twelve Mo–Mo bonding and nonbonding MOs.^[10] The vacancy of the band derived from this MO explains the rather long intra-Mo₆ Mo₂–Mo₂ contacts of 2.9144 Å. Since the optimal number of metallic electrons (ME) for an Mo₆S₈^a octahedral cluster is 24,^[10] that for such an (Mo₆)₂ unit is therefore 24 + 24 – 2 = 46. Analysis of the integrated crystal orbital Hamiltonian populations (COHP)^[11] indicates that the Mo₂–Mo₂ bond strength between the Mo₆ clusters is about half that of the Mo–Mo bonds within the Mo₆ unit. Therefore, the Mo₁₂ cluster must be regarded as the structural unit of this compound, and not Mo₆. Considering that the ME count for the Mo₁₂ unit in Ba₄Mo₁₂S₁₈ is 44, and because of the overall Mo–Mo non-bonding character of the DOS at the Fermi level, it should be possible to reduce this compound without altering its structural arrangement and make it semiconducting by adding two extra electrons.

Experimental Section

Preparation of Ba₄Mo₁₂S₁₈: Single-phase powder of Ba₄Mo₁₂S₁₈ was obtained from the required stoichiometric mixture of MoS₂, BaS, and Mo. These powders were mixed, ground together in a mortar, and then cold-pressed in a hand press. The pellet was loaded into a molybdenum crucible, which was sealed under a low argon pressure with an arc-welding system. The crucible was heated at 300 °C h⁻¹ to 1500 °C and held there for four days, then cooled at 100 °C h⁻¹ to 1100 °C, and finally furnace-cooled to room temperature.

Electrical resistivity and magnetic susceptibility measurements: The ac resistivity was measured out on a single crystal by a standard four-probe technique between 290 and 4.2 K. Ohmic contacts were made by attaching molten indium ultrasonically. Magnetic susceptibility data of Ba₄Mo₁₂S₁₈ were collected on a SHE-906 SQUID magnetosusceptometer under a magnetic field of 20 G.

Crystal data for Ba₄Mo₁₂S₁₈: hexagonal, space group *P*6₃/*mmc* (no. 194), *a* = 10.6985(1), *c* = 14.2264(2) Å, *V* = 1410.17(3) Å³, *Z* = 2, $\rho_{\text{calcd}} = 5.362 \text{ Mg m}^{-3}$, *F*(000) = 2032, $\lambda(\text{Mo K}\alpha) = 0.71073 \text{ Å}$, $\mu(\text{Mo K}\alpha) = 11.938 \text{ mm}^{-1}$, *T* = 20 °C. A black hexagonal crystal of approximate dimensions 0.10 × 0.08 × 0.05 mm was employed in the collection of intensity data on a Nonius KappaCCD diffractometer. Reflection indexing, correction for Lorentzian and polarization effects, peak integration, and background determination were performed by using the EvalCCD program.^[12] An absorption correction was applied by using the description of the crystal faces.^[13] Of 35551 reflections collected in the $\theta = 2.62\text{--}42.0^\circ$ range, 1877 were independent (*R*_{int} = 0.0493). The structure was solved by direct methods with the program SIR97^[14] and refined on *F* by using JANA2000.^[15] Refinement of the occupancy factor of the Ba2 atoms located along the *z* axis around the point (0,0,0.5) yielded a value of 0.502(4), which hence was fixed to 0.5. This model was refined with harmonic anisotropic atomic displacement parameters for all atoms down to *R* = 0.0275. At this stage, a difference Fourier synthesis revealed the highest residual peaks in the vicinity of the Ba2 site alternating with negative regions. Subsequently, a Gram–Charlier expansion of the nonharmonic atomic displacement parameters up to the fourth order was used in

the refinement for the Ba2 atom. Such refinement reduced the *R* factor from 0.0275 to 0.0235, and the residual peaks from 11.44 and –5.70 e Å⁻³ to 1.55 and –0.98 e Å⁻³. Because of the disorder of the Ba2 atoms, we performed reciprocal-space reconstruction of different planes, as well as long-exposure rotations about the *a* and *c* axes on a single crystal on the KappaCCD diffractometer. In both cases, we did not observe any superlattice reflection or diffuse line. Further details on the crystal structure investigations may be obtained from the Fachinformationszentrum Karlsruhe, 76344 Eggenstein-Leopoldshafen, Germany (fax: (+49) 7247-808-666; e-mail: crysdata@fiz-karlsruhe.de), on quoting the depository number CSD-414217.

Calculations: Self-consistent ab initio band-structure calculations were performed on a model compound of Ba₄Mo₁₂S₁₈ with the scalar relativistic tight-binding linear muffin-tin orbital (LMTO) method in the atomic-spheres approximation including the combined correction.^[9] Exchange and correlation were treated in the local density approximation using the von Barth–Hedin local exchange correlation potential.^[16] Charge self-consistency and the average properties were obtained from 57 irreducible *k* points.

Received: July 9, 2004

Revised: November 11, 2004

Published online: January 20, 2005

Keywords: barium · cluster compounds · molybdenum · solid-state structures · superconductors

- [1] Ø. Fischer, *Appl. Phys.* **1978**, 16, 1.
- [2] K. Yvon, *Curr. Top. Mater. Sci.* **1979**, 3, 53.
- [3] *Superconductivity in Ternary Compounds, Vols. I, II* (Eds.: Ø. Fischer, M. B. Maple), Springer, Berlin, **1982** (*Top. Curr. Phys.* **1982**, 32).
- [4] R. Flukiger in *Superconductor Materials Science* (Eds.: S. Foner, B. Schwartz), Series B, Plenum, New York, **1981**, pp. 511–604.
- [5] J. Guillelevic, O. Bars, D. Grandjean, *J. Solid State Chem.* **1973**, 7, 158.
- [6] H. Schäfer, H.-G. von Schnering, *Angew. Chem.* **1964**, 76, 833.
- [7] C. Perrin, M. Sergent, *J. Less-Common Met.* **1986**, 123, 117.
- [8] S. Picard, J.-F. Halet, P. Gougeon, M. Potel, *Inorg. Chem.* **1999**, 38, 4422.
- [9] a) O. K. Andersen, *Phys. Rev. B* **1975**, 12, 3060; b) H. L. Skriver, *The LMTO Method*, Springer, Berlin, **1984**.
- [10] T. Hughbanks, R. Hoffmann, *J. Am. Chem. Soc.* **1983**, 105, 1150.
- [11] R. Dronskowski, P. E. Blöchl, *J. Phys. Chem.* **1993**, 97, 8617.
- [12] A. J. M. Duisenberg, PhD thesis, University of Utrecht (The Netherlands), **1998**.
- [13] J. de Meulenaar, H. Tompa, *Acta Crystallogr. Sect. A* **1965**, 19, 1014.
- [14] A. Altomare, M. C. Burla, M. Camalli, G. L. Cascarano, C. Giacovazzo, A. Guagliardi, A. G. G. Moliterni, G. Polidori, R. Spagna, *J. Appl. Crystallogr.* **1999**, 32, 115.
- [15] V. Petricek, M. Dusek, Jana2000, Institute of Physics, Academy of Sciences of the Czech Republic, Prague, Czech Republic, **2000**.
- [16] U. von Barth, L. Hedin, *J. Phys. C* **1972**, 5, 1629.

Stereocontrolled Solid-Phase Synthesis of a 90-Membered Library of Indoline-Alkaloid-like Polycyclics from an Enantioenriched Aminoindoline Scaffold**

Zhonghong Gan, P. Thirupathi Reddy, Sophie Quevillon, Samuel Couve-Bonnaire, and Prabhat Arya*

With growing interest in the use of small molecules^[1] for dissecting protein–protein interactions^[2] and for understanding signaling pathways, the need for developing combinatorial methods to obtain small molecules that have stereochemical and skeletal diversity has also grown.^[3,4] Owing to their structural complexity and the diversity of their functional groups, natural products are a source of bioactive lead compounds, and it is highly likely that libraries of small molecules that also display these features would serve as valuable tools.^[5]

We initiated a combinatorial chemistry program that is aimed at providing indoline-alkaloid-like complex polycyclic compounds in a high-throughput manner.^[6] Indole and indoline alkaloids belong to an important family of bioactive natural products, and several of these derivatives (**1–3**, see Figure 1) exhibit various biological

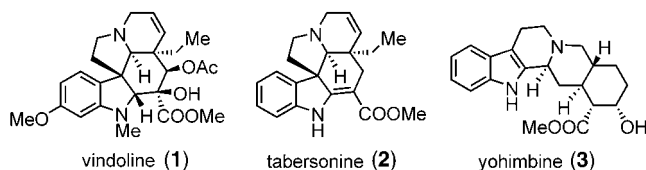


Figure 1. Examples of bioactive indole and indoline alkaloids.

[*] Dr. Z. Gan, Dr. P. T. Reddy, S. Quevillon, Dr. S. Couve-Bonnaire, Dr. P. Arya

Chemical Biology Program

Stacie Institute for Molecular Sciences

National Research Council of Canada

100 Sussex Drive, Ottawa, Ontario, K1A0R6 (Canada)

Fax: (+1) 613-952-0068

E-mail: prabhat.arya@nrc.ca

S. Quevillon, Dr. P. Arya

Department of Chemistry

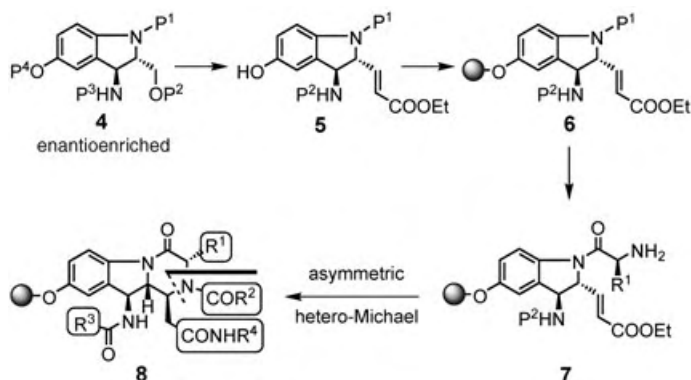
University of Ottawa

10 Marie Curie, Ottawa, K1N 6N5 (Canada)

[**] We sincerely thank Stuart Schreiber, Jared Shaw, and the DOS team members at the Broad Institute of Harvard and MIT for providing alkylsilyl-linker-based macrobeads and for their help in our solid-phase synthesis projects. This work was supported by a NRC genomics and health initiative program, special VP-NRC funds for chemical biology, the National Cancer Institute of Canada (NCIC), and the Canadian Institutes of Health Research (CIHR). Malgosia Daroszewska, Michael Barnes, and Don Leek are thanked for their technical support.

Supporting information for this article is available on the WWW under <http://www.angewandte.org> or from the author.

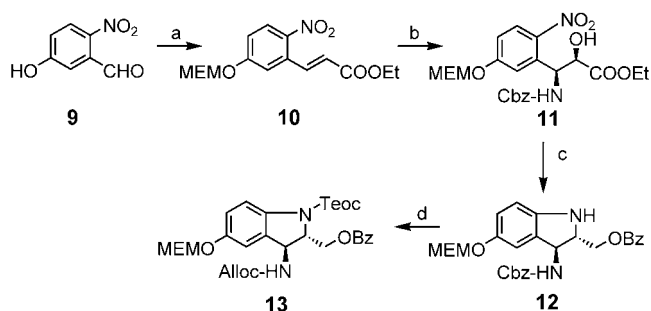
responses. An important milestone in our approach is the development of a practical, enantioselective synthesis of a functionalized aminoindoline scaffold, **4**, that could be further utilized in introducing skeletal diversity.^[7] This scaffold is highly unique and comprises four orthogonal protecting groups. Our plan was to utilize the phenolic hydroxyl group as an immobilization site in solid-phase synthesis. The remaining three functional groups could further be used in complexity-generating, diversity-oriented reactions. As shown in Scheme 1, aminoindoline **4** could be easily con-



Scheme 1. Natural-product-like and indoline-alkaloid-like complex polycyclic compounds. P = protecting group, R = diverse functional groups.

verted into **5**, which comprises a conjugated carboxylate ester. Following the immobilization of **5** through the phenolic hydroxyl group on a solid support to give **6** and upon selective removal of the indoline protecting group, the substrate could then be coupled to an amino acid to give **7**. A key step in our approach is the formation of a six-membered ring by a stereoselective, conjugate hetero (e.g. aza)-Michael reaction. This could provide the indoline-alkaloid-like tricyclic derivative **8**, in which the diversity could easily be introduced at four sites. A six-membered ring-closure strategy that involves the trapping of the primary amine by a conjugated carboxylic ester could also provide a general method to the synthesis of cyclic β -amino acids.^[8]

The enantioselective synthesis of aminoindoline derivative **13** is shown in Scheme 2. 5-Hydroxy-2-nitro-benzaldehyde (**9**) was converted into **10** in two steps that involve protection of the phenol and elongation of the carbon chain. Compound **10** was then subjected to an asymmetric amino-hydroxylation reaction to give compound **11** in 79% yield (> 92% ee).^[9] The aminoindoline **12** was obtained from **11** in several steps that involved 1) reduction of the carboxylate ester (70%), 2) benzoyl-protection of the primary alcohol (OBz, 88%), 3) tosylation of the secondary alcohol (OTs, 87%), 4) selective reduction of the nitro group, and 5) cyclization under mild basic conditions (75% for two steps). Finally, compound **13** was obtained from **12** in three steps by which the indoline nitrogen was protected (Teoc, 98%), the Cbz protecting group was removed under hydrogenation, and the benzylic amine was protected with an Alloc group (85% for two steps, see Scheme 2). The overall sequence is very clean and the desired aminoindoline **13** could be obtained in



Scheme 2. a) 1) MEMCl, DIPEA, 97%; 2) $(\text{EtO})_2\text{P}(\text{O})\text{CH}_2\text{COOEt}$, NaH, 94%; b) Sharpless aminohydroxylation, 79%; c) 1) LiBH_4 , 70%; 2) BzCl , pyridine, 88%; 3) TsCl , DMAP, 87%; 4) H_2 , Lindlar cat.; 5) K_2CO_3 , THF, 75% for two steps; d) 1) TeocCl, pyridine, 98%; 2) H_2 , 10% Pd/C, MeOH; 3) AllocCl, pyridine, 85% for two steps. MEM = Methoxyethoxymethyl, DIPEA = diisopropylethylamine, Cbz = carbobenzyloxy, Bz = benzyl, Ts = *p*-toluenesulfonyl, DMAP = 4-dimethylamino-pyridine, Teoc = (trimethylsilyl)ethoxycarbonyl, Alloc = Allyloxycarbonyl.

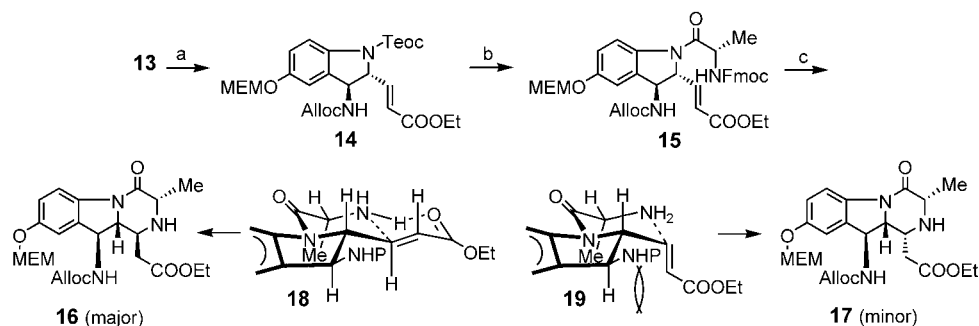
large quantities (5–10 g) in a short period. With a practical method in hand for this scaffold, the next step was to prepare **15**, a key starting material to explore the stereoselective, conjugate hetero-Michael approach.

Scheme 3 shows our model study to obtain a tricyclic derivative by use of a stereoselective, conjugate hetero-Michael approach as the key step. Conversion of **13** into the conjugated ester **14** required the removal of the protecting group at the primary alcohol (99%), oxidation of the alcohol to the aldehyde, followed by a Wittig chain extension (93% for two steps). In a test study, upon removal of the Teoc group, the indoline amine was coupled with the amino acid chloride to give *N*-Fmoc-protected derivative **15** (88% for two steps). Upon removal of the Fmoc group (20% piperidine), we were delighted that the six-membered ring formed under these mild conditions. The primary amine generated in situ was easily trapped by the conjugated carboxylate ester in a stereoselective manner to give the cyclic compounds **16** (major) and **17** (minor) in 96% overall yield ($R^1 = \text{Me}$, > 10:1 ratio of two diastereomers, 82% d.r. for the major product). The stereochemistry of the new stereogenic center was assigned by NMR spectroscopy studies. The ease of the asymmetric, conjugate hetero-Michael approach to yield the tricyclic product was a pleasant surprise and it opens a simple and very attractive approach to the synthesis of cyclic β -amino

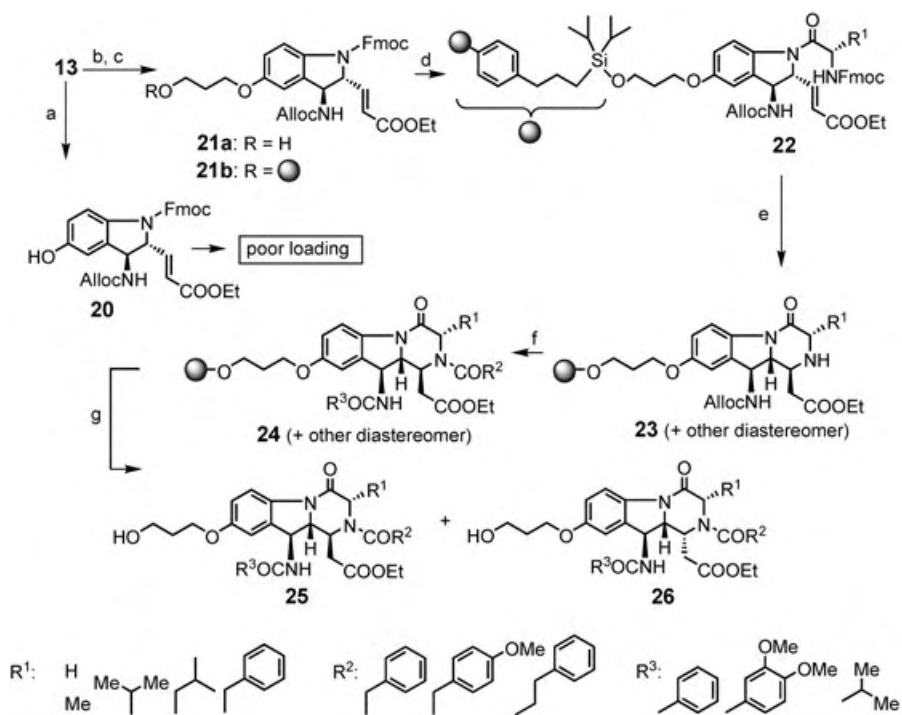
acids. The stereochemical preference of this reaction is postulated by the proposed transition states (**18** and **19**) that may account for the attack of the nucleophile from the β face. The conjugate hetero-Michael reaction is highly reproducible and gives the desired cyclic product(s) upon use of different amino acid derivatives.

The model solid-phase synthesis is shown in Scheme 4. Compound **20** was obtained from **13** in a few steps to perform solid-phase synthesis. In our hands, this scaffold gave poor loading with the use of (4-methoxyphenyl)diisopropylsilyl-propyl polystyrene beads (50–100 μm , loading 1.4 mmol g^{-1}).^[10] At this stage, we decided to work with compound **21a**, in which a three-carbon spacer was introduced between the aromatic moiety and the primary alcohol group.^[11] As expected, the loading of **21a** with commercially available silyl-linker-based beads and with the macrobeads (500–560 μm loading 1.29 mmol g^{-1})^[12,13] worked very well to give product **21b** (1.12 mmol g^{-1} , 87% upon cleavage of the product from the macrobead support).

The next series of steps were then attempted on the solid support. The indoline amine was first deprotected of its Fmoc group and then coupled with the Fmoc-protected amino acid chloride (first diversity) to give the amino acid coupled product, **22**. Several attempts were then made to optimize the conditions for the solid-phase coupling reaction, and the use of collidine as a base gave the best results. The coupled product, **22**, was then treated with piperidine, and, as observed in the synthesis carried out in solution, we were pleased that the primary amine was trapped with the conjugated carboxyl ester to give the tricyclic derivative **23** during the removal of the Fmoc group. Once again, as with the solution-state synthesis, the in situ conjugate hetero-Michael reaction was highly reproducible in the solid phase. The mild conditions for this cyclization reaction are highly appealing and attractive to explore its potential in the generation of a molecule library. The stereochemical outcome of this reaction was found to be dependent upon the choice of the amino acid, and the ratio of the two diastereomers, **25** and **26**, varied from 5:1 to 1:1.^[14] To complete the test sequence in the solid phase, **23** was then subjected to 1) an amide coupling reaction to introduce the second diversity, 2) removal of the Alloc protecting group to give the free amine, and 3) reaction with carboxylic acid chloride to introduce the third diversity and to give **24**. Finally, compounds **25** and **26** were obtained upon cleavage of the substrates from the support under



Scheme 3. a) 1) K_2CO_3 , MeOH, 99%; 2) Dess–Martin periodinane; 3) $\text{Ph}_3\text{P}=\text{CHCOOEt}$, 93% for two steps; b) 1) TBAF; 2) Fmoc alanine chloride, pyridine, 88%; c) 20% piperidine, 96%. TBAF = tetra-*n*-butylammonium fluoride, Fmoc = 9-fluorenylmethoxycarbonyl.




Scheme 4. a) and b) see Supporting Information; c) (4-methoxyphenyl)diisopropylsilyl-propyl polystyrene macrobeads (500–560 μm , loading 1.29 mmol g^{-1}), 87 % after cleavage from support; d) 1. 20% piperidine; 2. Fmoc amino acid chloride, collidine; e) 20% piperidine; f) 1. R^2COCl , pyridine; 2. $\text{Pd}(\text{PPh}_3)_4$; 3. R^3COCl , pyridine; g) pyridine–HF; 80–85 % yield of **25** and **26** over 7 steps from **21 b**.

desilylation conditions. Interestingly, compounds **25** and **26** were obtained from **21b** in seven steps in 80–85 % overall yield. The overall sequence on the solid support utilizes very mild reaction conditions that include a crucial in situ conjugate hetero-Michael reaction to give functionalized amino-indoline-based, alkaloid-like, tricyclic derivatives. With alkylsilyl-linker-based macrobeads, this method was further utilized in the generation of a test library of 90 compounds (two diastereomers per well) by an IRORI split-and-mix-type encoded method. After completion of the library synthesis, the beads were taken out of the IRORI Kans and then subjected to desilylation cleavage conditions.^[15]

To summarize, a library of indoline-alkaloid-like polycyclic compounds was synthesized on the basis of an enantiopure aminindoline scaffold. The key reaction was the stereoselective, conjugate hetero-Michael reactions with nitrogen nucleophiles to obtain cyclic β -amino acid derived compounds. Furthermore, biological studies of this library in various cellular assays are in progress and the findings will be reported in due course.

Received: October 14, 2004
Published online: January 26, 2005

Keywords: combinatorial chemistry · cyclization · indoline alkaloids · protecting groups · solid-phase synthesis

- 
- Science **2003**, 300, 294–295; d) T. U. Mayer, *Trends Cell Biol.* **2003**, 13, 270–277; e) J. R. Peterson, T. J. Mitchison, *Chem. Biol.* **2002**, 9, 1275–1285.
- [2] a) M. R. Arkin, J. A. Wells, *Nat. Rev. Drug Discovery* **2004**, 3, 301–317; b) T. Berg, *Angew. Chem.* **2003**, 115, 2566–2586; *Angew. Chem. Int. Ed.* **2003**, 42, 2462–2481; c) D. L. Boger, J. Desharnais, K. Capps, *Angew. Chem.* **2003**, 115, 4270–4309; *Angew. Chem. Int. Ed.* **2003**, 42, 4138–4176; d) R. Breinbauer, I. R. Vetter, H. Waldmann, *Angew. Chem.* **2002**, 114, 3002–3015; *Angew. Chem. Int. Ed.* **2002**, 41, 2878–2890; e) K. Hinterding, D. Alonso-Díaz, H. Waldmann, *Angew. Chem.* **1998**, 110, 716–780; *Angew. Chem. Int. Ed.* **1998**, 37, 688–749; f) A. Huwe, R. Mazitschek, A. Giannis, *Angew. Chem.* **2003**, 115, 2170–2187; *Angew. Chem. Int. Ed.* **2003**, 42, 2122–2138; g) T. Klabunde, G. Hessler, *ChemBioChem* **2002**, 3, 928–944.
- [3] a) M. D. Burke, S. L. Schreiber, *Angew. Chem.* **2004**, 116, 48–60; *Angew. Chem. Int. Ed.* **2004**, 43, 46–58; b) M. D. Burke, E. M. Berger, S. L. Schreiber, *Science* **2003**, 302, 613–618; c) S. Borman, *Chem. Eng. News* **2004**, 82, 32–40.
- [4] For a review on solution- and solid-phase library generation of natural product analogues and natural-product-like compounds, see: a) D. G. Hall, S. Manku, F. Wang, *J. Comb. Chem.* **2001**, 3, 125–150; b) P. Arya, R. Joseph, D. T. H. Chou, *Chem. Biol.* **2002**, 9, 145–156.
- [5] For selected examples of solid-phase library synthesis on benzopyrans as a privileged substructure, see: a) K. C. Nicolaou, J. A. Pfefferkorn, G.-Q. Cao, *Angew. Chem.* **2000**, 112, 750–755; *Angew. Chem. Int. Ed.* **2000**, 39, 734–739; b) K. C. Nicolaou, G.-Q. Cao, J. A. Pfefferkorn, *Angew. Chem.* **2000**, 112, 755–759; *Angew. Chem. Int. Ed.* **2000**, 39, 739–743; c) K. C. Nicolaou, J. A. Pfefferkorn, A. J. Roecker, G.-Q. Cao, S. Barluenga, H. J. Mitchell, *J. Am. Chem. Soc.* **2000**, 122, 9939–9953; d) K. C. Nicolaou, J. A. Pfefferkorn, H. J. Mitchell, A. J. Roecker, S. Barluenga, G.-Q. Cao, R. L. Affleck, J. E. Lillig, *J. Am. Chem. Soc.* **2000**, 122, 9954–9967; e) K. C. Nicolaou, J. A. Pfefferkorn, S. Barluenga, H. J. Mitchell, A. J. Roecker, G.-Q. Cao, *J. Am. Chem. Soc.* **2000**, 122, 9968–9976.
- [6] P. Arya, C.-Q. Wei, M. L. Barnes, M. Daroszewska, *J. Comb. Chem.* **2004**, 6, 65–72.
- [7] For selected examples of combinatorial approaches to obtain skeletally diverse architectures, see: a) M. D. Burke, E. M. Berger, S. L. Schreiber, *Science* **2003**, 302, 613–618; b) M. D. Burke, E. M. Berger, S. L. Schreiber, *J. Am. Chem. Soc.* **2004**, 126, 14095–14104.
- [8] For a review on β -amino acids, see: M. Liu, M. P. Sibi, *Tetrahedron* **2002**, 58, 7991–8035.
- [9] The % ee values were determined by chiral HPLC.
- [10] The resin was purchased from Novabiochem.
- [11] For the synthesis of **21a**, see the Supporting Information.
- [12] J. A. Tallarico, K. M. Depew, H. E. Pelish, N. J. Westwood, C. W. Lindsley, M. D. Shair, S. L. Schreiber, M. A. Foley, *J. Comb. Chem.* **2001**, 3, 312–318.
- [13] The alkylsilyl-linker-based macrobeads were provided by ICCB, Harvard Medical School, Harvard University.
- [14] The explanation for the decrease in diastereoselectivity during the solid-phase conjugate hetero-Michael reaction is not clear at this stage.
- [15] For detailed information on library synthesis, see the Supporting Information.

[1] a) S. L. Schreiber, *Chem. Eng. News* **2003**, 81, 51–61; b) T. Gura, *Nature* **2000**, 407, 282–284; c) R. L. Strausberg, S. L. Schreiber,

Asymmetric Organocatalysis

Direct, Highly Enantioselective Pyrrolidine Sulfonamide Catalyzed Michael Addition of Aldehydes to Nitrostyrenes**

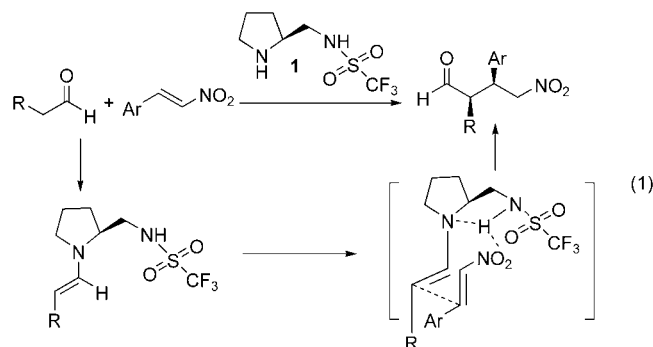
Wei Wang,* Jian Wang, and Hao Li

Dedicated to Professor Victor J. Hruby on the occasion of his 65th birthday

The Michael addition reaction is without question one of the most general and versatile methods for formation of C–C bonds in organic synthesis.^[1] Thus, it is not surprising that the development of enantioselective catalytic protocols for this cornerstone reaction has received much attention.^[2] Efforts aimed at achieving asymmetric versions of the process by using chiral organocatalysts have been explored intensively in recent years.^[3] L-Proline and other pyrrolidine-based catalytic systems for asymmetric Michael reactions have been described, but only moderate enantioselectivities are typically observed.^[4,5] As a result, the design and development of new and efficient chiral organocatalysts to achieve high levels of enantio- and/or diastereoselectivity in Michael conjugate additions remain a major challenge in synthetic organic chemistry.^[6–9] Recently, Kotsuki and his co-workers described a chiral pyrrolidine–pyridine catalyst that promoted highly enantio- and diastereoselective Michael addition reactions of ketones with nitrostyrenes.^[10] However, poor enantioselectivity (ca. 22 % *ee*) resulted when an aldehyde was used as the substrate. Herein, we describe the chiral pyrrolidine sulfonamide **1**, which catalyzes the Michael conjugate additions of aldehydes to nitrostyrenes with high levels of enantio- (89–99 % *ee*) and diastereoselectivity ($\geq 20:1$ d.r.).

As part of a program aimed at developing new organocatalysts for asymmetric organic transformations, we recently observed that the pyrrolidine sulfonamide **1** serves as an efficient catalyst for α -aminoxylation and Mannich-type reactions.^[11,12] These processes take place with exceptionally high levels of enantio- and/or diastereoselectivity. Moreover, the catalyst also shows high activity for α -sulfenylation reactions of aldehydes and ketones.^[13] Based on these observations, we envisioned that the (*S*)-pyrrolidine sulfonamide **1** would react with an aldehyde to form a chiral enamine, which could serve as a Michael donor in reactions with nitroolefins. In addition, a model inspection suggested that

the process would take place by the preferential enamine addition to the less hindered *Si* face of the nitroolefin [Eq. (1)]. Consequently, high levels of enantio- and/or diastereoselectivity are expected. In addition, the bifunctional nature of catalyst **1**, which possesses an acidic sulfonamide^[14] and a basic pyrrolidine group, could be expected to lead to high catalytic activities even in the absence of an acidic additive. Herein, we describe the results of the studies using **1** to promote highly enantio- and diastereoselective Michael addition reactions.



The reaction of isobutyraldehyde with *trans*- β -nitrostyrene in the presence of the pyrrolidine sulfonamide **1** (20 mol %) in various solvents at room temperature was investigated initially. As evident in Table 1, the reaction yields varied significantly in the solvents tested. In general, the reaction proceeded more rapidly in polar solvents. For example, in dimethyl sulfoxide (DMSO), isopropyl alcohol (*i*PrOH), *N,N*-dimethylformamide (DMF), and MeCN (Table 1, entries 1–5), high yields (64–93 %) were obtained, whereas reactions in less polar THF and 1,4-dioxane were very sluggish (Table 1, entries 7 and 8). Interestingly, regardless of the solvents used, the reactions were highly enantioselective (63–83 % *ee*). The use of *i*PrOH led to the highest *ee* value (83 %), which was further increased to 90 % *ee* when the reaction temperature was lowered to 0 °C without a significant reduction in the reaction rate (Table 1, entry 3).

Table 1: Effect of solvents on the asymmetric Michael addition reaction of isobutyraldehyde to *trans*- β -nitrostyrene.^[a]

Entry	Solv.	<i>t</i> [d]	Yield [%] ^[b]	<i>ee</i> [%] ^[c]
1	DMSO	2	93	63
2	<i>i</i> PrOH	3	89	83
3	<i>i</i> PrOH ^[d]	4.5	85	90
4	DMF	3	87	73
5	CH ₃ CN	3	64	73
6	CH ₃ NO ₂	3	37	71
7	THF	3	< 10	n.d. ^[e]
8	1,4-dioxane	3	< 10	n.d. ^[e]
9	CHCl ₃	3	43	79

[a] For reaction conditions see the Experimental Section. [b] Yield of isolated product. [c] Determined by chiral high-performance liquid chromatography (HPLC) analysis (Chiralpak AS-H). [d] Reaction conducted at 0 °C. [e] Not determined.

[*] Prof. Dr. W. Wang, J. Wang, H. Li
Department of Chemistry
University of New Mexico, MSC03 2060
Albuquerque, NM 87131-0001 (USA)
Fax: (+1) 505-277-2609
E-mail: wwang@unm.edu

[**] This research was supported by the Department of Chemistry and the Research Allocations Committee, University of New Mexico. We thank Professor Patrick S. Mariano for making critical editorial comments about the manuscript.

Supporting information for this article is available on the WWW under <http://www.angewandte.org> or from the author.

Encouraged by these results, we next probed the scope of the reaction with a variety of aldehydes and nitroolefins (Table 2). All reactions were conducted in *i*PrOH at 0 °C in the presence of 20 mol % of **1**. In each case, smooth reactions occurred to generate Michael adducts in high yields (63–99 %), high enantioselectivities (89–99 % *ee*), and excellent diastereoselectivities (*d.r.* ≥ 20:1). Variations in the nitro-

Table 2: Michael addition reactions of aldehydes to *trans*-β-nitrostyrenes catalyzed by **1**.

$\text{H}-\text{C}(\text{R}^1)(\text{R}^2)-\text{CHO} + \text{Ar}-\text{CH}=\text{CH}-\text{NO}_2 \xrightarrow[0^\circ\text{C, } i\text{PrOH}]{\text{catalyst } \mathbf{1} \text{ (20 mol\%)}} \text{H}-\text{C}(\text{R}^1)(\text{R}^2)-\text{CH}(\text{Ar})-\text{CH}_2-\text{NO}_2$					
Entry	Product	<i>t</i> [h]	Yield [%] ^[a]	<i>ee</i> [%] ^[b]	<i>d.r.</i> ^[c]
1		4.5	85	90	–
2		6	67	90	–
3		6	75	89	–
4		42	89	93	–
5		20	99	96	50:1
6		28	63	94	22:1
7		24	86	99	20:1
8		24	94	99	30:1
9		26	91	97	50:1
10		24	76	22	50:1
11		10	96	97	50:1

[a] Yield of isolated product. [b] Determined by chiral high-performance liquid chromatography analysis (Chiralpak AS-H, or AD and Chiralcel OD-H). [c] Determined by ¹H NMR spectroscopic analysis.

styrenes used in reaction with isobutyraldehyde had no effect on the enantioselectivities (Table 2, entries 1–3). Reaction of the more bulky cyclopentanecarboxaldehyde gave even higher enantioselectivity (93 % *ee*) and yield (89 %) (Table 2, entry 4). More significantly, catalyst **1** catalyzed reactions of linear chain aldehydes yielded adducts with excellent enantioselectivity (94–99 % *ee*), diastereoselectivity (≥ 20:1 *d.r.*), and high yields (63–99 %, Table 2, entries 5–9). In these processes, two adjacent stereogenic centers were generated with complete stereocontrol. Again, changes in the electronic properties of the nitroolefins (Table 2, entries 5–7) and steric demands of the aldehydes (Table 2, entries 5, 8, and 9) had only a small effect on the stereoselectivities and yields. The aliphatic nitroolefin *trans*-Ph(CH₂)₂CH=CHNO₂ provided the desired product in good yield (76 %) and high diastereoselectivity (50:1 *d.r.*), but poor enantioselectivity (22 % *ee*, Table 2, entry 10). The relative and absolute configurations of the Michael adducts were determined by comparison with ¹H NMR spectroscopic analysis and optical rotation studies of known compounds.^[15]

The results of a preliminary study demonstrated that **1** also catalyzed Michael addition reactions of ketones (Table 2, entry 11). Under the reaction conditions described above, the addition of cyclohexanone to *trans*-β-nitrostyrene resulted in the formation of the adduct in 96 % yield, 97 % *ee*, and 50:1 *d.r.*

In conclusion, we have found that the pyrrolidine sulfonamide organocatalyst **1** can be used to promote highly efficient, asymmetric Michael addition reactions of aldehydes and ketones to nitroolefins. In these transformations, **1** exhibits a high catalytic activity that takes place with excellent diastereo- and enantioselectivity. The full scope of this new catalytic reaction is currently being investigated.

Experimental Section

Typical procedure: The catalyst pyrrolidine sulfonamide **1** (10 mg, 0.044 mmol) was added to a vial containing *n*-hexanal (0.27 mL, 2.19 mmol) and *i*PrOH (1.0 mL) at 0 °C. The mixture was stirred vigorously for 15 min, and then *trans*-β-nitrostyrene (33 mg, 0.22 mmol) was added. After 24 h of stirring, the reaction mixture was concentrated in vacuo. The residue was purified by flash silica gel chromatography (ethyl acetate/hexane = 1:30) to afford 51 mg (94 %) of the adduct as a clear oil; 30:1 *d.r.* (by ¹H NMR) and 99 % *ee*, (chiral HPLC, Chiralcel OD-H column, λ = 254 nm, 20 % *i*PrOH/hexane at 1.0 mL min^{−1}, *t*_R = 10.4 min (minor) and 11.8 min (major)); [α]_D(major) = +52.4 (*c* = 0.5 in CHCl₃), ref. [5a] [α]_D = +33.4 (*c* = 1.4 in CHCl₃).

Received: September 12, 2004

Published online: January 21, 2005

Keywords: aldehydes · asymmetric catalysis · Michael addition · nitroalkenes · organocatalysts

[1] P. Perlmutter, *Conjugate Addition Reactions in Organic Synthesis*, Pergamon, Oxford, **1992**.

[2] For recent reviews of asymmetric Michael addition reactions, see: a) K. Tomioka, Y. Nagaoka, and M. Yamaguchi in *Comprehensive Asymmetric Catalysis*, Vol. III, chap. 31.1 and

- 31.2 (Eds.: E. N. Jacobsen, A. Pfaltz, H. Yamamoto), Springer, New York, **1999**, pp. 1105–1139; b) N. Krause, A. Hoffmann-Röder, *Synthesis* **2001**, 171–196; c) O. M. Berner, L. Tedeschi, D. Enders, *Eur. J. Org. Chem.* **2002**, 1877–1894; d) J. Christoffers, A. Baro, *Angew. Chem.* **2003**, *115*, 1726–1728; *Angew. Chem. Int. Ed.* **2003**, *42*, 1688–1690.
- [3] For selected reviews of organocatalysis, see: a) P. I. Dalko, L. Moisan, *Angew. Chem.* **2001**, *113*, 3840–3864; *Angew. Chem. Int. Ed.* **2001**, *40*, 3726–3748; b) B. List, *Synlett* **2001**, 1675–1686; c) B. List, *Tetrahedron* **2002**, *58*, 5573–5590; d) E. R. Jarvo, S. J. Miller, *Tetrahedron* **2002**, *58*, 2481–2495; e) B. List, *Acc. Chem. Res.* **2004**, *37*, 548–557; f) W. Notz, F. Tanaka, C. F. Barbas III, *Acc. Chem. Res.* **2004**, *37*, 580–591.
- [4] Proline-catalyzed organocatalytic Michael addition reactions, see: a) S. Hanessian, V. Pham, *Org. Lett.* **2000**, *2*, 2975–2978; b) B. List, P. Pojarliev, H. J. Martin, *Org. Lett.* **2001**, *3*, 2423–2425; c) D. Enders, A. Seki, *Synlett* **2002**, 26–28.
- [5] Pyrrolidine diamine catalyzed organocatalytic Michael addition reactions, see: a) J. M. Betancort, C. F. Barbas III, *Org. Lett.* **2001**, *3*, 3737–3740; b) J. M. Betancort, K. Sakthivel, R. Thayumanavan, C. F. Barbas III, *Tetrahedron Lett.* **2001**, *42*, 4441–4444; c) N. Mase, R. Thayumanavan, F. Tanaka, C. F. Barbas III, *Org. Lett.* **2004**, *6*, 2527–2530; d) J. M. Betancort, K. Sakthivel, R. Thayumanavan, F. Tanaka, C. F. Barbas III, *Synthesis* **2004**, 1509–1521; e) A. Alexakis, O. Andrey, *Org. Lett.* **2002**, *4*, 3611–3614; f) O. Andrey, A. Alexakis, G. Bernardinelli, *Org. Lett.* **2003**, *5*, 2559–2561; g) O. Andrey, A. Vidonne, A. Alexakis, *Tetrahedron Lett.* **2003**, *44*, 7901–7904.
- [6] MacMillan catalyst promoted organocatalytic Michael addition reactions, see: a) N. A. Paras, D. W. C. MacMillan, *J. Am. Chem. Soc.* **2001**, *123*, 4370–4371; b) J. F. Austin, D. W. C. MacMillan, *J. Am. Chem. Soc.* **2002**, *124*, 1172–1173; c) N. A. Paras, D. W. C. MacMillan, *J. Am. Chem. Soc.* **2002**, *124*, 7894–7895; d) M. T. Hechavarria Fonseca, B. List, *Angew. Chem.* **2004**, *116*, 4048–4050; *Angew. Chem. Int. Ed.* **2004**, *43*, 3958–3960.
- [7] Results of organocatalytic Michael addition reactions reported by the Jørgensen group, see: a) N. Halland, R. G. Hazell, K. A. Jørgensen, *J. Org. Chem.* **2002**, *67*, 8331–8338; b) N. Halland, P. S. Aburel, K. A. Jørgensen, *Angew. Chem.* **2003**, *115*, 685–689; *Angew. Chem. Int. Ed.* **2003**, *42*, 661–665; c) N. Halland, T. Hansen, K. A. Jørgensen, *Angew. Chem.* **2003**, *115*, 5105–5107; *Angew. Chem. Int. Ed.* **2003**, *42*, 4955–4957; d) P. Melchiorre, K. A. Jørgensen, *J. Org. Chem.* **2003**, *68*, 4151–4157; e) N. Halland, P. S. Aburel, K. A. Jørgensen, *Angew. Chem.* **2004**, *116*, 1292–1297; *Angew. Chem. Int. Ed.* **2004**, *43*, 1272–1277.
- [8] Other organocatalytic Michael addition reactions, see: a) F.-Y. Zhang, E. J. Corey, *Org. Lett.* **2000**, *2*, 1097–1100; b) T. Okino, Y. Hoashi, Y. Takemoto, *J. Am. Chem. Soc.* **2003**, *125*, 12672–12673; c) H. Li, Y. Wang, L. Tang, L. Deng, *J. Am. Chem. Soc.* **2004**, *126*, 9906–9907.
- [9] For a catalytic Mukaiyama–Michael reaction, see: D. A. Evans, K. A. Scheidt, J. N. Johnston, M. C. Willis, *J. Am. Chem. Soc.* **2001**, *123*, 4480–4491.
- [10] T. Ishii, S. Fujioka, Y. Sekiguchi, H. Kotsuki, *J. Am. Chem. Soc.* **2004**, *126*, 9558–9559.
- [11] For the preparation of organocatalyst **1**, see the Supporting Information.
- [12] a) W. Wang, J. Wang, H. Li, *Tetrahedron Lett.* **2004**, *45*, 7235–7238; b) W. Wang, J. Wang, H. Li, *Tetrahedron Lett.* **2004**, *45*, 7243–7246.
- [13] a) W. Wang, J. Wang, H. Li, *Org. Lett.* **2004**, *6*, 2817–2820; b) W. Wang, H. Li, J. Wang, *Tetrahedron Lett.* **2004**, *45*, 8229–8231.
- [14] F. G. Bordwell, *Acc. Chem. Res.* **1988**, *21*, 456–463. In DMSO, trifluoromethanesulfonamide has a greater acidity ($pK_a = 9.7$) than acetic acid ($pK_a = 12.3$).
- [15] For further details, see the Supporting Information.

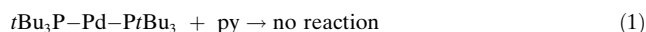
Highly Reactive, General, and Long-Lived Catalysts for Coupling Heteroaryl and Aryl Chlorides with Primary Nitrogen Nucleophiles**

Qilong Shen, Shashank Shekhar, James P. Stambuli, and John F. Hartwig*

During the past decade, the palladium-catalyzed amination of aryl halides has become a principal method to form the C–N bonds of aromatic amines.^[1–4] Although current catalysts are capable of coupling a wide range of amines with aryl halides, reactions with these catalysts have several limitations: the catalysts have short lifetimes in the reactions of primary amines with chloroarenes, even when conducted with the most recently developed, highly active catalysts containing basic, hindered alkylmonophosphines;^[5–15] the reactions of primary alkyl amines with heteroaryl chloride reagents, which are important for the synthesis of biologically active molecules, have limited scope and require large amounts of catalyst;^[7,8,11,13,15–20] and the reactions of primary alkyl amines with chloroarenes that possess common protic functional groups have not been described.

We now report on catalysts that can overcome these limitations. Our approach, which is based upon the selection of ligands that combine steric hindrance, strong electron donation, and tight chelation, leads to a catalyst that simultaneously possesses long lifetimes and displays high activity for reactions of primary nitrogen nucleophiles with chloropyridines. Many of the reactions occur with part-per-million quantities of catalyst and with turnover numbers that exceed those of previous catalysts by two or more orders of magnitude.

To identify the factors that would improve catalyst lifetime over that of current catalysts, we studied the reactions of primary amines and pyridine with aryl palladium(II) halide complexes and bisphosphine palladium(0) complexes bearing a basic, hindered alkyl monophosphine.^[21–23] Addition of benzylamine or pyridine (py) to the palladium(0) complex [Pd(PtBu₃)₂] led to no reaction [Eq. (1)]. However, addition of benzylamine or pyridine to the aryl palladium(II) halide complex [Pd(PtBu₃)(Ar)(Br)] (Ar = *o*-Tol, Ph) displaced the



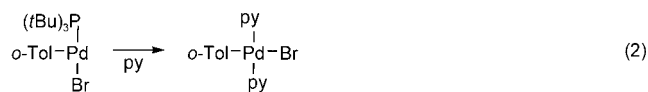
[*] Q. Shen, S. Shekhar, Dr. J. P. Stambuli, Prof. Dr. J. F. Hartwig
Department of Chemistry
Yale University
P.O. Box 208107, New Haven, CT 06520-8107 (USA)
Fax: (+1) 203-432-6144
E-mail: john.hartwig@yale.edu

[**] We thank the National Institutes of Health (GM-55382) for support of this work, Johnson-Matthey for a gift of PdCl₂, Solvias for a gift of the Josiphos ligands, and Boehringer Ingelheim for unrestricted support. We thank Leslie Bienen for assistance in manuscript preparation.



Supporting information for this article is available on the WWW under <http://www.angewandte.org> or from the author.

phosphine to form the free ligand and $[\text{Pd}(\text{PhCH}_2\text{NH}_2)_2(\text{Ph})\text{Br}]^{[24]}$ or $[\text{Pd}(\text{py})_2(o\text{-Tol})\text{Br}]$ [Eq. (2)].^[25] Although displacement of hindered aromatic phosphines occurs from aryl palladium(II) complexes,^[24,25] the



greater basicity of alkyl phosphines should make complexes of these ligands more stable toward displacement by amines and pyridines. Apparently, the higher basicity does not increase the strength of the bond between palladium(II) and a hindered alkyl phosphine enough to prevent displacement by the less hindered nitrogen donors. Displacement of the ligand from palladium accounts for the slow reactions of primary amines and pyridines because amine and pyridine

complexes do not catalyze the amination of aryl chlorides.

To prevent displacement of the phosphine ligand, while maintaining the steric and electronic properties of the hindered alkyl monophosphines, we evaluated complexes containing hindered alkyl bisphosphines as catalysts for the coupling of primary amines with heteroaryl and aryl chlorides. A series of possible structures of palladium(0) complexes of chelating phosphines are summarized in Figure 1. The unsaturated (chelate) Pd^0 fragment adds aryl halides^[26] and

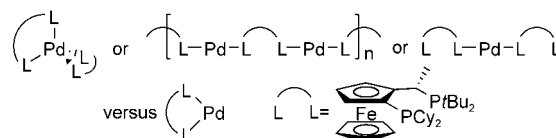


Figure 1. Potential structures of Pd^0 complexes with bisphosphine ligands and the Josiphos ligand **L** employed in this study. Cy = cyclohexyl.

Table 1: Coupling of heteroaryl chlorides with primary amines catalyzed by $\text{Pd}(\text{OAc})_2$ and **L**.^[a]

$\text{Heteroaryl-Cl} + \text{RNH}_2 \xrightarrow[25-100^\circ\text{C}]{\text{NaOtBu/DME}} \text{Heteroaryl-NHR}$					$\text{L} = \text{Ferrocene-P}(\text{tBu})_2\text{PCy}_2$				
Entry	Product	Cat. [mol %]	Cond.	Yield [%] ^[b]	Entry	Product	Cat. [mol %]	Cond.	Yield [%] ^[b]
1		1.0	25 °C, 5 h	99	15		1.0	90 °C, 12 h	85
2		0.001	100 °C, 48 h	86	16		1.0	70 °C, 16 h	85
3		0.005	70 °C, 16 h	89	17		1.0	70 °C, 16 h	99
4		0.01	70 °C, 12 h	98	18		1.0	70 °C, 8 h	93
5		1.0	70 °C, 16 h	73	19		0.01	90 °C, 24 h	83
6		1.0	70 °C, 16 h	92	20		1.0	70 °C, 10 h	99
7		1.0	70 °C, 16 h	99	21		1.0	70 °C, 24 h	75
8		1.0	70 °C, 18 h	99	22		0.005	90 °C, 48 h	94
9		0.005	90 °C, 30 h	96	23		0.01	100 °C, 48 h	60
10		0.005	70 °C, 24 h	93	24		0.001	100 °C, 48 h	89
11		0.01	100 °C, 24 h	95	25		0.005	90 °C, 15 h	91
12		0.01	100 °C, 48 h	90	26		0.005	100 °C, 16 h	82
13		0.01	100 °C, 48 h	79	27		0.05	100 °C, 24 h	91
14		1.0	70 °C, 16 h	67					

[a] Reactions conducted with a 1:1 ratio of metal to ligand, 1 mmol ArCl, 1.2 equiv amine, and 1.4 equiv NaOtBu in 1 mL 1,2-dimethoxyethane (DME).
 [b] Yield after isolation. [c] From (1-phenylethyl)amine that is stated to be 99% ee.

must be readily generated for high reactivity. Many bisphosphines form (chelate)₂Pd complexes that slowly dissociate their ligands. Because this dissociation precedes oxidative addition, these complexes tend to add aryl halides slowly.^[27] Others, such as 1,1'-ferrocenylphosphines, are flexible enough to adopt conformations that link two metals, or possess κ^1 coordination modes.^[28] Ligands that adopt κ^1 coordination modes will be more easily displaced by amines and pyridines than those that adopt chelating structures. Thus, we selected hindered alkyl bisphosphines with rigid backbones to disfavor formation of stable (chelate)₂Pd⁰ complexes containing two bidentate ligands, to disfavor formation of complexes with κ^1 structures, and to favor generation of the (chelate)Pd⁰ fragment.^[29]

The Josiphos ligand with one di-*tert*-butylphosphanyl and one dicyclohexylphosphanyl group shown in Figure 1^[30] is now commercially available, but has rarely been used successfully in catalytic chemistry. It is air-stable, both as a solid and in solution for at least 24 h, as determined by ¹H NMR and ³¹P NMR spectroscopy. The combination of the severe steric hindrance, conformational preferences of the backbone, and recent success in generating catalysts for the coupling of aryl tosylates^[31,32] led us to study complexes of this ligand as catalysts for the amination of heteroaryl and aryl chlorides.

Reactions of heteroaryl chlorides with primary nitrogen nucleophiles catalyzed by a combination of this Josiphos ligand and Pd(OAc)₂ are summarized in Table 1. Catalysts generated from Pd(OAc)₂ were more reactive than those generated from [Pd(dba)₂]. Pyridyl chlorides bearing the halogen in the 2-, 3-, or 4-position underwent reaction with a variety of primary amines and related nucleophiles in high yield at room temperature or with mild heating. In contrast, similar reactions in the presence of catalysts with hindered monodentate or aromatic bisphosphine ligands were conducted with high catalyst loadings or at high temperatures. Not only reactions of pyridyl chlorides, but reactions of quinolinyl, isoquinolinyl, and pyrazyl chlorides, occurred under mild conditions (Table 1, entries 22–26).

Reactions without catalyst were conducted in parallel with the catalyzed ones. Only reactions of quinolines and isoquinolines generated any measurable quantity of products, and conversions were below 40% in these cases. Reactions of 2- and 4-chloropyridines occur more readily in polar solvents or under high pressure but are typically conducted at temperatures closer to 150 °C.^[33] Nucleophilic substitution of 3-chloropyridines is often by a factor of

10⁴ to 10⁵ slower than that of 2- and 4-chloropyridines.^[34]

Besides the generality of the reaction, the turnover numbers are remarkable. High yields were observed for reactions between pyridyl chlorides and unhindered primary amines with loadings of metal salt and ligand between 10 and 50 ppm (Table 1, entries 2, 3, 9, 10, 22, 24–26). Some previous reactions of chloropyridines with low loadings of palladium were conducted with high loadings of ligand.^[15] This is misleading because the ligand is typically more expensive than the metal.

Hindered primary amines, such as *tert*-butylamine, as well as benzophenone hydrazone and benzophenone imine, also reacted in high yields with chloropyridines (Table 1, entries 5–7, 14, 16, 17, 20). These reactions required more catalyst, although the loading remained at or below 1 mol %. The more hindered 2-chloro-3-methylpyridine also reacted with octylamine in high yield (Table 1, entry 9). Even benzamide reacted with 2- and 4-chloropyridine with this catalyst (entries 8, 21). No coupling of amides with a pyridyl chloride has previously been reported with any catalyst. No products from coupling of primary nitrogen nucleophiles with heteroaryl chlorides to form di-heteroaryl amines were observed in any case by GC/MS.

Table 2: Coupling of aryl chlorides with primary amines catalyzed by Pd(OAc)₂ and L.^[a]

$\text{R}-\text{C}_6\text{H}_4-\text{Cl} + \text{R}'\text{NH}_2 \xrightarrow[\text{NaOtBu/DME, 70–100 °C}]{\substack{0.005\text{--}1 \text{ mol\% Pd(OAc)}_2 \\ 0.005\text{--}1 \text{ mol\% L}}} \text{R}-\text{C}_6\text{H}_4-\text{NHR}'$ $\text{L} = \text{Fe}(\text{PCy}_2)_2$								
Entry	Product	Cat. [mol %]	Cond.	Yield [%] ^[b]	Entry	Product	Cat. [mol %]	Yield [%] ^[b]
1		0.005	90 °C, 48 h	94	13		0.005	100 °C, 48 h, 99
2		0.01	100 °C, 48 h	98	14		0.005	80 °C, 20–24 h, 98
3		0.05	100 °C, 48 h	93	15		0.1	100 °C, 48 h, 90
4		0.1	100 °C, 48 h ^[c]	92	16		0.05	100 °C, 48 h, 99
5		0.1	100 °C, 36 h	97	17		0.01	80 °C, 20–24 h, 87
6		0.05	100 °C, 48 h	92	18		0.1	100 °C, 48 h, 82
7		0.05	100 °C, 48 h	83	19		1.0	80 °C, 20–24 h, 61
8		1.0	100 °C, 18–24 h	94	20		1.0	80 °C, 20–24 h, 77
9		0.005	80 °C, 20–24 h	99	21		1.0	80 °C, 20–24 h, 86
10		0.05	100 °C, 48 h	99	22		1.0	100 °C, 18–24 h, 87
11		0.5	100 °C, 36 h	99	23		1.0	80 °C, 20–24 h, 82
12		0.01	100 °C, 18–24 h	68				

[a] Reactions conducted with a 1:1 ratio of metal to ligand, 1 mmol ArCl, 1.2 equiv amine, and 1.4 equiv NaOtBu in 1 mL DME. [b] Yield after isolation. [c] 3.0 equiv of octylamine used.

The turnover numbers of 86000, 18600, and 8300 for the reactions of 2-, 3- and 4-chloropyridine with octylamine are an order of magnitude higher than those for reactions of any amine with the corresponding bromopyridine^[29,35] and about two orders of magnitude higher than those for reactions of any amine with the chloropyridine,^[7,8] and the value of 86000 is nearly three orders of magnitude greater than those reported for the reaction of a pyridyl chloride with any primary amine.^[8] To achieve such high turnover numbers with equal amounts of ligand and palladium, we mixed the dilute solutions of Pd(OAc)₂ and ligand before adding the amine or heterocyclic substrate. Presumably the combination of amine and base leads to the reduction of palladium(II) to palladium(0).

These high activities in reactions of chloropyridines led us to perform reactions of chloroarenes using the same catalyst. Results (displayed in Table 2) show similarly high yields with low catalyst loadings. Reaction of octylamine with chlorobenzene occurred to completion in 48 h and formed the coupled product in 94% yield at 90 °C, with only 50 ppm of catalyst (entry 1). This yield under these conditions corresponds to a turnover number of 18800. This value exceeds the maximum turnover numbers achieved previously for the reaction of an aryl chloride with any amine by nearly an order of magnitude and the maximum turnover numbers for the reaction of a primary alkyl amine by nearly two orders of magnitude. Reactions of several other combinations of primary amines and chloroarenes (entries 9, 13, 14) occurred in similarly high yields with the same amount of catalyst. The reactions of α -branched primary amines, for example, the reaction of cyclohexylamine with chlorobenzene, required more catalyst, but occurred in high yield with only 0.05 mol% palladium (TON = 1980, Table 2, entry 10). This loading of catalyst is more than an order of magnitude lower than that of previous reactions of α -branched primary amines with chloroarenes.^[8] In addition, reactions of *sec*-butylamine occurred in high yield with 0.01–1 mol% catalyst (entries 16–18). Reactions of benzophenone hydrazone and benzophenone imine occurred in high yield with 1.0 mol% catalyst (entries 19–23). Catalyst loadings have not yet been optimized with these reagents. Products from diarylation were observed by GC/MS only for the reaction of octylamine with 4-chloroanisole.^[36]

One benefit of the palladium-catalyzed route to *N*-aryl amines is the high tolerance of the reaction for functional

groups.^[37–41] Our results (Table 3) show that catalysts containing the hindered Josiphos ligand extend the scope of the reactions of functionalized substrates to include the coupling of primary amines with chloroarenes bearing protic functionality. This catalyst system is less reactive with weak bases than

Table 3: Coupling of functionalized aryl chlorides with primary amines catalyzed by Pd(OAc)₂ and L.^[a]

$\text{R}-\text{C}_6\text{H}_4-\text{Cl} + \text{R}'\text{NH}_2 \xrightarrow[\text{LiHMDS/DME, 70–100 } ^\circ\text{C}]{0.05–2 \text{ mol\% Pd(OAc)}_2, 0.05–2 \text{ mol\% L}} \text{R}-\text{C}_6\text{H}_4-\text{NHR}'$									
Entry	Product	Cat. [mol %]	Cond.	Yield [%] ^[b]	Entry	Product	Cat. [mol %]	Cond.	Yield [%] ^[b]
1		0.5	100 °C, 18 h	90	10		0.5	100 °C, 20 h	84
2		0.5	100 °C, 20 h	70	11		0.5	70 °C, 20 h	87
3		0.5	100 °C, 18 h	83	12		0.5	70 °C, 20 h	92
4		0.5	100 °C, 20 h	87	13		0.5	70 °C, 20 h	69
5		0.5	100 °C, 20 h	86	14		0.5	100 °C, 20 h	67
6		2.0	100 °C, 18 h	72	15		0.05	100 °C, 20 h	81
7		2.0	100 °C, 20 h	66	16		0.05	100 °C, 24 h	85
8		0.5	100 °C, 18 h	85	17		0.05	100 °C, 24 h	74
9		0.5	100 °C, 20 h	67	18		0.05	100 °C, 20 h	99

[a] Reactions conducted with a 1:1 ratio of metal to ligand, 1.0 mmol ArCl, 1.2 equiv amine, and 2.4 equiv LHMDS in 1 mL DME. [b] Yield after isolation.

those generated from monodentate ligands.^[9,10,21,38,42] However, complexes of this Josiphos ligand catalyze reactions of primary amines with chloroarenes possessing a free alcohol, phenol, carboxylic acid, amide, or enolizable ketone functionality in high yields with LHMDS (= LiN(SiMe₃)₂) as base.^[40,41] Reactions of primary alkyl amines with aryl chlorides possessing related functional groups were previously limited to electron-poor aryl chlorides containing an ester functionality.^[9,42] No examples of reactions of primary amines with chloroarenes containing the functional groups of the substrates collected in Table 3 have been published previously.

Thus far, no single combination of metal and ligand generates the most reactive catalyst for coupling of all types of amines and aryl halides. The strengths of the catalyst reported here complement those of previously reported catalysts that contain hindered monodentate ligands. The former is less, the latter more reactive toward secondary than toward primary amines. The high reactivity of catalysts containing the hindered bis(dialkyl) phosphanyl Josiphos ligand L results

from the combination of steric hindrance, strong electron donation, and tight chelation.

Experimental Section

Representative procedures: Procedure without a glovebox (Table 1, entry 2): A stock solution (100 μ L) containing Pd(OAc)₂ (1×10^{-3} mmol) and CyPF(*t*Bu) (1×10^{-3} mmol) was added to a 4-mL vial containing 2-chloropyridine (0.114 g, 1.00 mmol) and NaOtBu (0.135 g, 1.40 mmol) in 1.0 mL of DME. Octylamine (0.155 g, 1.20 mmol) was then added by syringe. The vial was sealed with a cap containing a PTFE septum, and the reaction mixture was stirred at 100 °C until the 2-chloropyridine was consumed, as determined by gas chromatography. The reaction solution was adsorbed directly onto silica gel, and the product was isolated by eluting with hexane/ethyl acetate (85:15) to give 3-(*N*-octylamino)pyridine as a yellow solid (178.1 mg, 86% yield).

Procedure with a glovebox (Table 1, entry 1): An oven-dried resealable Schlenk flask capped with a rubber septum was evacuated and backfilled with N₂. To the flask was added NaOtBu (0.135 g, 1.40 mmol) and a stirring bar. The flask was evacuated and backfilled with N₂ three times. To the flask was then added 3-chloropyridine (0.114 g, 1.00 mmol, 95.0 μ L), DME (1.0 mL), a stock solution (5.0 μ L) containing Pd(OAc)₂ (5.0×10^{-5} mmol) and L (5.0×10^{-5} mmol), and octylamine (0.155 g, 1.20 mmol). The rubber septum was wrapped with vinyl electrical tape to prevent leaking. The resulting mixture was stirred for 48 h at 100 °C until the 3-chloropyridine was consumed, as determined by gas chromatography. The reaction solution was adsorbed directly onto silica gel, and the product was isolated by eluting with hexane/ethyl acetate (85:15) to give 204.3 mg (99%) of 3-(*N*-octylamino)pyridine as a yellow solid.

Received: November 16, 2004

Published online: January 21, 2005

Keywords: amination · heterocycles · homogeneous catalysis · P ligands · palladium

- [1] J. F. Hartwig in *Modern Arene Chemistry* (Ed.: D. Astruc), Wiley-VCH, Weinheim, **2002**, p. 107.
- [2] J. F. Hartwig in *Handbook of Organopalladium Chemistry for Organic Synthesis, Vol. 1* (Eds.: E.-i. Negishi, A. de Meijere), Wiley, New York, **2002**, p. 1051.
- [3] A. R. Muci, S. L. Buchwald, *Top. Curr. Chem.* **2002**, *219*, 131.
- [4] A. J. Belfield, G. R. Brown, A. J. Foubister, P. D. Ratcliffe, *Tetrahedron* **1999**, *55*, 13285.
- [5] A. F. Littke, G. C. Fu, *Angew. Chem.* **2002**, *114*, 4350; *Angew. Chem. Int. Ed.* **2002**, *41*, 4176.
- [6] J. P. Stambuli, R. Kuwano, J. F. Hartwig, *Angew. Chem.* **2002**, *114*, 4940; *Angew. Chem. Int. Ed.* **2002**, *41*, 4746.
- [7] S. R. Stauffer, S. Lee, J. P. Stambuli, S. I. Hauck, J. F. Hartwig, *Org. Lett.* **2000**, *2*, 1423.
- [8] J. P. Wolfe, H. Tomori, J. P. Sadighi, J. Yin, S. L. Buchwald, *J. Org. Chem.* **2000**, *65*, 1158.
- [9] X. Huang, K. W. Anderson, D. Zim, L. Jiang, A. Klapars, S. L. Buchwald, *J. Am. Chem. Soc.* **2003**, *125*, 6653.
- [10] N. Kataoka, Q. Shelby, J. P. Stambuli, J. F. Hartwig, *J. Org. Chem.* **2002**, *67*, 5553.
- [11] S. Urganekar, J.-H. Xu, J. G. Verkade, *J. Org. Chem.* **2003**, *68*, 8416.
- [12] M. S. Viciu, R. M. Kissling, E. D. Stevens, S. P. Nolan, *Org. Lett.* **2002**, *4*, 2229.
- [13] G. A. Grasa, M. S. Viciu, J. Huang, S. P. Nolan, *J. Org. Chem.* **2001**, *66*, 7729.
- [14] G. Y. Li, *Angew. Chem.* **2001**, *113*, 1561; *Angew. Chem. Int. Ed.* **2001**, *40*, 1513.
- [15] F. Rataboul, A. Zapf, R. Jackstell, S. Harkal, T. Riermeier, A. Monsees, U. Dingerdissen, M. Beller, *Chem. Eur. J.* **2004**, *10*, 2983.
- [16] M. W. Hooper, M. Utsunomiya, J. F. Hartwig, *J. Org. Chem.* **2003**, *68*, 2861.
- [17] J. Yin, M. M. Zhao, M. A. Huffman, J. M. McNamara, *Org. Lett.* **2002**, *4*, 3481.
- [18] T. H. M. Jonckers, B. U. W. Maes, G. L. F. Lemiere, R. Dom-misse, *Tetrahedron* **2001**, *57*, 7027.
- [19] B. U. W. Maes, K. T. J. Loones, G. L. F. Lemiere, R. A. Dom-misse, *Synlett* **2003**, 1822.
- [20] G. Burton, P. Cao, G. Li, R. Rivero, *Org. Lett.* **2003**, *5*, 4373.
- [21] J. F. Hartwig, M. Kawatsura, S. I. Hauck, K. H. Shaughnessy, L. M. Alcazar-Roman, *J. Org. Chem.* **1999**, *64*, 5575.
- [22] J. P. Stambuli, C. D. Incarvito, M. Buehl, J. F. Hartwig, *J. Am. Chem. Soc.* **2004**, *126*, 1184.
- [23] J. P. Stambuli, M. Buehl, J. F. Hartwig, *J. Am. Chem. Soc.* **2002**, *124*, 9346.
- [24] R. A. Widenhoefer, S. L. Buchwald, *Organometallics* **1996**, *15*, 3534.
- [25] F. Paul, J. Patt, J. F. Hartwig, *Organometallics* **1995**, *14*, 3030.
- [26] L. M. Alcazar-Roman, J. F. Hartwig, A. L. Rheingold, L. M. Liable-Sands, I. A. Guzei, *J. Am. Chem. Soc.* **2000**, *122*, 4618.
- [27] C. Amatore, G. Broeker, A. Jutand, F. Khalil, *J. Am. Chem. Soc.* **1997**, *119*, 5176.
- [28] a) M. Kawatsura, J. F. Hartwig, *J. Am. Chem. Soc.* **1999**, *121*, 1473; b) Y. Ben-David, M. Portnoy, D. Milstein, *J. Am. Chem. Soc.* **1989**, *111*, 8742.
- [29] Some early reactions of pyridyl bromides with amines were reported with more flexible and aromatic bisphosphines, but the scope and activity of these catalytic reactions were limited, particularly with primary amines and chloropyridines: S. Wagaw, S. L. Buchwald, *J. Org. Chem.* **1996**, *61*, 7240.
- [30] (R)-(-)-Di-*tert*-butyl-1-[(S)-2-(dicyclohexylphosphanyl)ferrocenyl]ethylphosphine [158923-11-6], Strem catalog number 26-0975.
- [31] For early success with less hindered and less electron-donating members of the Josiphos family of ligands, see: B. C. Hamann, J. F. Hartwig, *J. Am. Chem. Soc.* **1998**, *120*, 7369.
- [32] A. H. Roy, J. F. Hartwig, *J. Am. Chem. Soc.* **2003**, *125*, 8704.
- [33] C. S. Giam in *Pyridine and Its Derivatives, Vol. 3* (Ed.: R. A. Abramovitch), Wiley, New York, **1974**, p. 41.
- [34] S. Hashimoto, S. Otani, T. Okamoto, K. Matsumoto, *Heterocycles* **1988**, *27*, 319; J. Miller in *Reaction Mechanisms in Organic Chemistry, Vol. 8* (Eds.: C. Eaborn, N. B. Chapman), Elsevier, Amsterdam, **1968**, p. 408; K. Vinter-Pasquier, B. Jamart-Gregoire, P. Caubere, *Heterocycles* **1997**, *45*, 2113.
- [35] M. Nishiyama, T. Yamamoto, Y. Koie, *Tetrahedron Lett.* **1998**, *39*, 617–620.
- [36] With 3 equiv of amine, no diarylation product was observed (Table 2, entry 4).
- [37] J. P. Wolfe, S. L. Buchwald, *Tetrahedron Lett.* **1997**, *38*, 6359.
- [38] J. P. Wolfe, S. L. Buchwald, *J. Org. Chem.* **2000**, *65*, 1144.
- [39] S. Lee, M. Jorgensen, J. F. Hartwig, *Org. Lett.* **2001**, *3*, 2729.
- [40] For the use of this base to improve functional-group tolerance with other catalysts, see: M. C. Harris, X. Huang, S. L. Buchwald, *Org. Lett.* **2002**, *4*, 2885, and reference [41].
- [41] S. Urganekar, J. G. Verkade, *Adv. Synth. Catal.* **2004**, *346*, 611.
- [42] D. W. Old, J. P. Wolfe, S. L. Buchwald, *J. Am. Chem. Soc.* **1998**, *120*, 9722.

Enantioselective Copper-Catalyzed Conjugate Addition to Trisubstituted Cyclohexenones: Construction of Stereogenic Quaternary Centers**

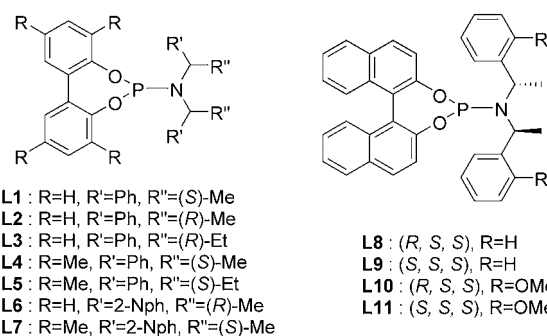
Magali d'Augustin, Laëticia Palais, and Alexandre Alexakis*

Asymmetric conjugate addition has received increasing interest during the last few years, and excellent results have been obtained, particularly for Cu^[1] and Rh-catalyzed^[2] reactions. However, one of the main drawbacks of these two systems is the lack of reactivity of β -trisubstituted enones, thus preventing the formation of chiral quaternary centers.^[3]

The Cu-catalyzed asymmetric conjugate addition of dialkylzinc reagents has been successfully applied to many substrates, including cyclic^[4] and acyclic enones,^[4a,b,5] lactones^[6] or lactams,^[7] nitro olefins,^[4b,8] amides,^[9] and malonates.^[10] However, whatever the Michael acceptor, all reactions with β -trisubstituted substrates failed, probably for steric reasons. Some examples of enantioselective addition of trialkylaluminum reagents have also been described for cyclic^[11] and acyclic enones,^[12] and nitro olefins.^[13] We reasoned that the stronger Lewis acidity of Al would effect a better activation of the substrate than Zn, thus overcoming the inherent steric hindrance of trisubstituted substrates. We report here the success of this approach.

Trialkylaluminum reagents are known to undergo Cu-catalyzed conjugate addition, even with trisubstituted enones.^[14] With these reagents stronger coordinating solvents are used than with dialkylzinc reagents (Et₂O or THF instead of toluene or CH₂Cl₂) as this allows the cleavage of the AlR₃ dimeric species, thus increasing its reactivity. We first extensively optimized experimental conditions for the conjugate addition of AlEt₃ to 3-methylcyclohexenone, and found that the reaction proceeds to completion after 18 h at –30 °C, and more rapidly at higher temperatures. Two sets of conditions were found, the choice of which depends on the copper salt used: Et₂O is best with copper thiophene carboxylate (CuTC), whereas THF is better with [Cu(CH₃CN)₄]BF₄. Although the addition of Me₃SiCl has been reported to increase the chemical yield,^[15] we found that it was detrimental in the presence of phosphorus ligands.

In a second step, we screened several biphenol- and binaphthol-based phosphoramidite ligands. The biphenol



ligands **L4** (Table 1, entries 4 and 17) and, particularly, **L7** (Table 1, entry 10) afforded the best results in terms of enantioselectivity, whatever the solvent (up to 96.6 % *ee*). In

Table 1: Addition of AlEt₃ to 3-methyl-2-cyclohexenone in the presence of various ligands.

Entry	CuX	Ligand	Solvent	Conv. [%]	<i>ee</i> [%]	Config. ^[a]
1	CuTC	L1	Et ₂ O	82	62	<i>R</i>
2	CuTC	L2	Et ₂ O	84	62	<i>S</i>
3	CuTC	L3	Et ₂ O	46	88	<i>S</i>
4	CuTC	L4	Et ₂ O	77	94	<i>R</i>
5	CuTC	L4	Et ₂ O ^[b]	85	90	<i>R</i>
6	CuTC	L4	Et ₂ O ^[c]	> 95	88	<i>R</i>
7	CuTC	L4	THF	15	94	<i>R</i>
8	CuTC	L5	Et ₂ O	91	93	<i>R</i>
9	CuTC	L6	Et ₂ O	89	78	<i>S</i>
10	CuTC	L7	Et ₂ O	> 95	96.6	<i>R</i>
11	CuTC	L8	Et ₂ O	82	72	<i>R</i>
12	CuTC	L9	Et ₂ O	51	62	<i>S</i>
13	CuTC	L10	Et ₂ O	> 95	74	<i>R</i>
14	CuTC	L11	Et ₂ O	> 95	16	<i>S</i>
15	[Cu(CH ₃ CN) ₄]BF ₄	L1	THF	76	77	<i>R</i>
16	[Cu(CH ₃ CN) ₄]BF ₄	L3	THF	46	88	<i>S</i>
17	[Cu(CH ₃ CN) ₄]BF ₄	L4	THF	64	94	<i>R</i>
18	[Cu(CH ₃ CN) ₄]BF ₄	L4	Et ₂ O	7	66	<i>R</i>
19	[Cu(CH ₃ CN) ₄]BF ₄	L7	THF	< 5	n.d. ^[d]	
20	[Cu(CH ₃ CN) ₄]BF ₄	L8	THF	66	84	<i>R</i>
21	[Cu(CH ₃ CN) ₄]BF ₄	L9	THF	65	2	<i>S</i>

[a] Product configuration. [b] Reaction was carried out at –25 °C. [c] Reaction was carried out at –15 °C. [d] n.d. = not determined.

general, the conversions are higher in Et₂O than in THF, although the enantioselectivity is unaffected. Raising the reaction temperature increases the conversion at the cost of a small drop in enantioselectivity (Table 1, entries 4, 5, and 6) from 94 % to 88 % *ee* at –15 °C. The binaphthol ligands **L8**, **L9**, **L10**, and **L11** are less efficient. It should be noted that there is a strong matched/mismatched effect (Table 1, entries 13/14 and 20/21), and that the absolute configuration of the product is dictated by the binaphthol part of the ligand.

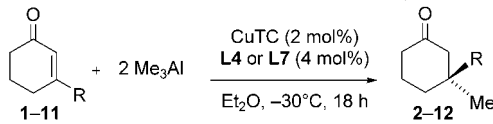
In the next step we screened various 3-substituted cyclohexenones (Table 2), which can be easily prepared by a simple protocol from commercially available 3-ethoxycyclohex-

[*] M. d'Augustin, L. Palais, Prof. Dr. A. Alexakis
 Department de chimie organique, Université de Genève
 30 quai E. Ansermet, 1211 Genève 4 (Switzerland)
 E-mail: alexandre.alexakis@chiorg.unige.ch

[**] The authors thank Stephane Rosset for help, the Swiss National Research Foundation (no. 20-068095.02), and COST action D24/0003/01 (OFES contract no. C02.0027) for financial support, and BASF for a generous gift of chiral amines.

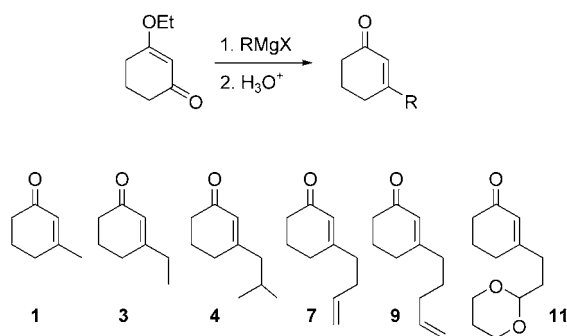
Supporting information for this article is available on the WWW under <http://www.angewandte.org> or from the author.

Table 2: Addition of AlMe_3 to various 3-substituted cyclohexenones.

						
Entry	Substrate	Ligand	Adduct	Conv. [%] ^[a]	ee [%]	Config. ^[b]
1	3	L4	2	> 95 (78)	94	S
2	3	L7	2	84	96	S
3	4	L4	5	35	93	R
4	4	L7	5	42	93	R
5	7	L4	8	> 95	91	R
6	7	L7	8	> 95 (80)	95	R
7	9	L4	10	> 95	93	S
8	9	L7	10	> 95 (76)	95	S
9	11	L4	12	> 95 (81) ^[c]	95	R

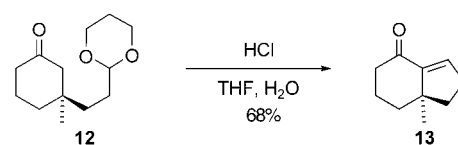
[a] Yield of isolated product in parentheses. [b] Product configuration: R/S notation may change according to the CIP priority rules. [c] 5 mol % CuTC and 10 mol % **L4**.

enone (Scheme 1). The addition of AlMe_3 to 3-ethylcyclohexenone **3** afforded excellent yields and enantioselectivities, which reached 96% ee with **L7** (Table 2, entry 2). As expected, the absolute configuration of the adduct **2** is


Scheme 1. Preparation of 3-substituted cyclohexenones.

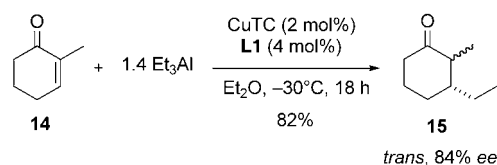
opposite to that given in Table 1 (entry 10), thus showing that the face selectivity of the addition remains the same. Although the enantioselectivity remained high (93% ee) (Table 2, entries 3 and 4), the addition of AlMe_3 to 3-isobutylcyclohexenone **4** proceeded with lower conversion owing to the increased steric demand. In this respect, isophorone **6** did not give any adduct, whereas substrates **7** and **9**, both of which contain a remote double bond, gave excellent yields and enantioselectivities (91 and 93% ee, respectively, with **L4**; Table 2, entries 5–8). Finally, an acetal functionality on **11** is tolerated, again with high yield and enantioselectivity (95% ee, Table 2, entry 9).

The absolute configuration of the conjugate adducts was determined by chemical correlation with a known compound. Thus, adduct **12**, bearing an acetal functionality, was hydrolyzed and cyclized in situ to afford the bicyclic enone **13** in 68% yield (Scheme 2). The negative optical rotation (-74.6 , $c = 1.53$, CHCl_3) corresponds to the R configuration of **13**.^[16] It is assumed that all adducts listed in Table 2 follow the same


Scheme 2. Subsequent hydrolysis of adduct **12** yields the R-configured bicyclic enone **13**.

trend. Scheme 2 also illustrates an aspect of the synthetic potential of the above conjugate addition, as such an intramolecular aldol condensation might be applied to the construction of other bicyclic structures.

In addition to 3-substituted cyclohexenones, the 2-substituted analogues are known to be difficult substrates for asymmetric conjugate addition.^[1] The present method allows such an extension, again with high yield and good enantioselectivity (84% ee for the *trans* isomer and 91% ee for the *cis* isomer; Scheme 3). The mixture of *cis* and *trans* isomers of **15** could be equilibrated (DBU, MeOH, room temperature, 20 h) to *trans/cis* ratio of 80:20. The *trans* isomer could be isolated in a pure form. The absolute configuration^[17] (2*S*,3*R*) shows that the face selectivity remains the same as usual.


Scheme 3. Conjugate addition to 2-substituted cyclohexenones.

In summary, we have discovered a new way to build chiral quaternary centers^[18] that allows the straightforward construction of chiral building blocks for more elaborate natural products.

Received: September 28, 2004

Revised: November 9, 2004

Published online: January 21, 2005

Keywords: aluminum · asymmetric catalysis · conjugate addition · enones · phosphoramidite ligands

- [1] a) A. Alexakis, C. Benhaim, *Eur. J. Org. Chem.* **2002**, 3221–3223; b) N. Krause, A. Hoffmann-Röder, *Synthesis* **2001**, 171–196; c) B. L. Feringa, *Acc. Chem. Res.* **2000**, 33, 346–353; d) M. P. Sibi, S. Manyem, *Tetrahedron* **2000**, 56, 8033–8061.
- [2] T. Hayashi, K. Yamasaki, *Chem. Rev.* **2003**, 103, 2829–2844.
- [3] a) I. Denissova, L. Barriault, *Tetrahedron* **2003**, 59, 10105–10146; b) J. Christoffers, A. Mann, *Angew. Chem.* **2001**, 113, 4725–4732; *Angew. Chem. Int. Ed.* **2001**, 40, 4591–4597.
- [4] a) A. Alexakis, D. Polet, S. Rosset, S. March, *J. Org. Chem.* **2004**, 69, 5660–5667; b) A. Alexakis, D. Polet, C. Benhaim, S. Rosset, *Tetrahedron: Asymmetry* **2004**, 15, 2199–2203; c) Z. Hua, V. C. Vassar, H. Choi, I. Ojima, *Proc. Natl. Acad. Sci. USA* **2004**, 101, 5411–5416; d) B. Breit, A. C. Laungani, *Tetrahedron: Asymmetry* **2003**, 14, 3823–3826; e) I. J. Krauss, J. L. Leighton, *Org. Lett.*

- 2003, 5, 3201–3203; f) S. J. Degrado, H. Mizutani, A. H. Hoveyda, *J. Am. Chem. Soc.* **2001**, 123, 755–756; g) L. A. Arnold, R. Imbos, A. Mandoli, A. H. M. de Vries, R. Naasz, B. L. Feringa, *Tetrahedron* **2000**, 56, 2865–2878; h) A. Alexakis, J. Burton, J. Vastra, C. Benhaim, X. Fournieux, A. van den Heuvel, J.-M. Leveque, F. Mazé, S. Rosset, *Eur. J. Org. Chem.* **2000**, 4011–4027.
- [5] a) Y. Hu, X. Liang, J. Wang, Z. Zheng, X. Hu, *Tetrahedron: Asymmetry* **2003**, 14, 3907–3915; b) H. Mizutani, S. J. Degrado, A. H. Hoveyda, *J. Am. Chem. Soc.* **2002**, 124, 779–780; c) A. Alexakis, C. Benhaim, S. Rosset, M. Humam, *J. Am. Chem. Soc.* **2002**, 124, 5262–5263.
- [6] a) L. Liang, L. Su, X. Li, A. S. C. Chan, *Tetrahedron Lett.* **2003**, 44, 7217–7220; b) M. Yan, Z. Y. Zhou, A. S. C. Chan, *Chem. Commun.* **2000**, 115–116; c) M. T. Reetz, A. Gosberg, D. Moulin, *Tetrahedron Lett.* **2002**, 43, 1189–1191.
- [7] M. Pineschi, F. Del Moro, F. Gini, A. J. Minnaard, B. L. Feringa, *Chem. Commun.* **2004**, 1244–1245.
- [8] a) A. Rimkus, N. Sewald, *Synthesis* **2004**, 135–146; b) A. Duursma, A. J. Minnaard, B. L. Feringa, *J. Am. Chem. Soc.* **2003**, 125, 3700–3701; c) C. A. Luchaco-Cullis, A. H. Hoveyda, *J. Am. Chem. Soc.* **2002**, 124, 8192–8193; d) A. Alexakis, C. Benhaim, *Org. Lett.* **2000**, 2, 2579–2581.
- [9] a) A. W. Hird, A. H. Hoveyda, *Angew. Chem.* **2003**, 115, 1314–1317; *Angew. Chem. Int. Ed.* **2003**, 42, 1276–1279.
- [10] a) J. Schuppan, A. J. Minnaard, B. L. Feringa, *Chem. Commun.* **2004**, 792–793; b) T. Watanabe, T. F. Knöpfel, E. M. Carreira, *Org. Lett.* **2003**, 5, 4557–4558; c) A. Alexakis, C. Benhaim, *Tetrahedron: Asymmetry* **2001**, 12, 1151–1157.
- [11] a) L. Su, X. Li, W. L. Chan, X. Jia, A. S. C. Chan, *Tetrahedron: Asymmetry* **2003**, 14, 1865–1869; b) L. Liang, A. S. C. Chan, *Tetrahedron: Asymmetry* **2002**, 13, 1393–1396; c) M. Diégez, S. Deerenberg, O. Pàmies, C. Claver, P. W. N. M. van Leeuwen, P. Kamer, *Tetrahedron: Asymmetry* **2000**, 11, 3161–3166; d) Y. Takemoto, S. Kuraoka, N. Hamaue, C. Iwata, *Tetrahedron: Asymmetry* **1996**, 7, 993–996.
- [12] a) P. K. Fraser, S. Woodward, *Chem. Eur. J.* **2003**, 9, 776–783; b) S. M. W. Bennett, S. M. Brown, J. P. Muxworthy, S. Woodward, *Tetrahedron Lett.* **1999**, 40, 1767–1770.
- [13] U. Eilitz, F. Lessmann, O. Seidelmann, V. Wendisch, *Tetrahedron: Asymmetry* **2003**, 14, 3095–3097.
- [14] a) J. Westermann, H. Neh, K. Nickisch, *Chem. Ber.* **1996**, 129, 963–966; b) J. Westermann, K. Nickisch, *Angew. Chem.* **1993**, 105, 1429–1431; *Angew. Chem. Int. Ed. Engl.* **1993**, 32, 1368–1370.
- [15] J. Kabarra, S. Flemming, K. Nickisch, H. Neh, J. Westermann, *Tetrahedron Lett.* **1994**, 35, 8591–8594.
- [16] T. Ohkubo, H. Akino, M. Asaoka, H. Takei, *Tetrahedron Lett.* **1995**, 36, 3365–3368.
- [17] a) B. Miller, E. R. Matjeka, *J. Am. Chem. Soc.* **1980**, 102, 4772–4780; b) A. Alexakis, S. March, *J. Org. Chem.* **2002**, 67, 8753–8757.
- [18] Typical procedure: A flame-dried Schlenk tube was charged with CuTC (3.9 mg, 2.0 mol %) and **L4** (19.8 mg, 4.0 mol %). Diethyl ether (2.0 mL) was then added and the mixture was stirred at room temperature for 30 min before being cooled to –30 °C. Trimethylaluminum (1.0 mL of a 2 M solution in heptane, 2.0 equiv) was added dropwise at such a rate that the temperature did not rise above –30 °C, and the reaction mixture was stirred at –30 °C for a further 5 min before enone **3** (124.1 mg, 1.0 mmol) in diethyl ether (0.5 mL) was added dropwise. Once the addition was complete the reaction mixture was held at –30 °C overnight. The reaction was quenched at –30 °C by addition of MeOH (0.5 mL) and then water. Workup followed by flash chromatography afforded the product as a colorless oil (109.4 mg, 78% yield). Chiral GC analysis (Lipodex E) showed an enantiomeric excess of 94% ee.

A Mild and Selective Method for the Hydrolysis of Esters with Trimethyltin Hydroxide**

K. C. Nicolaou,* Anthony A. Estrada, Mark Zak,
Sang Hyup Lee, and Brian S. Safina

The mild and selective hydrolysis of esters can often be crucial in the sequence toward a target molecule and is, therefore, an important objective in contemporary organic synthesis. Although several methods exist to accomplish this task in certain cases, a mild, generally applicable protocol remains absent. Frequent problems encountered include the concurrent hydrolysis of other ester groups present within the molecule under scrutiny, epimerization of stereocenters, and elimination reactions induced by the often basic conditions employed. Herein we report a new and selective method for the hydrolysis of esters under extremely mild conditions that avoid such side reactions and lead to high yields of the corresponding carboxylic acids.

It was during our campaign toward thioistrepton,^[1] a highly complex thiopeptide antibiotic, that we had the opportunity to search for such a method. Our sensitive intermediates proved too fragile to tolerate standard ester hydrolysis conditions. We finally came upon Me₃SnOH, which had been previously employed by Mascaretti and co-workers^[2] to cleave phenacyl ester anchored amino acids and peptides from a polystyrene resin and to hydrolyze methyl and isopropyl phenylacetate to give the corresponding acids in high yield. To our knowledge, these are the only examples in which Me₃SnOH has been previously used to carry out hydrolytic ruptures of esters.^[3] As shown in Table 1, this reagent proved extremely useful to us in attaining the high-yielding and selective hydrolysis of methyl esters within the sensitive substrates **1–4**, which were encountered en route to thioistrepton. These remarkable results prompted a second-phase investigation in which we attempted to determine systematically the generality and scope of this protocol, which involved heating the substrate with 1–10 equivalents of

[*] Prof. Dr. K. C. Nicolaou, A. A. Estrada, M. Zak, Dr. S. H. Lee,
Dr. B. S. Safina
Department of Chemistry and
The Skaggs Institute for Chemical Biology
The Scripps Research Institute
10550 North Torrey Pines Road, La Jolla, CA 92037 (USA)
Fax: (+1) 858-784-2469
E-mail: kcn@scripps.edu
and
Department of Chemistry and Biochemistry
University of California, San Diego
9500 Gilman Drive, La Jolla, CA 92093 (USA)

[**] We thank Dr. D. H. Huang and Dr. G. Siuzdak for NMR spectroscopic and mass spectrometric assistance, respectively. Financial support for this work was provided by grants from the National Institutes of Health (USA) and the Skaggs Institute for Chemical Biology, and fellowships from the National Institutes of Health (USA) (to A.A.E.), The Skaggs Institute for Research (to M.Z.), and Eli Lilly & Co. (to M.Z.).

Table 1: Trimethyltin hydroxide mediated hydrolyses used in the total synthesis of thiostrepton.^[a]

Entry	Ester	Product(s)	T [°C]	t [h]	Yield [%]
1			80	1	100
2			80	2.5	100
3			80	3	85
4			60	2.5	100

[a] Reactions were carried out in 1,2-DCE on a 0.04–0.25-mmol scale and worked up as described in the general procedure. Alloc = allyloxycarbonyl; Boc = *tert*-butoxycarbonyl; DCE = 1,2-dichloroethane; TBS = *tert*-butyldimethylsilyl; TES = triethylsilyl.

Me₃SnOH in 1,2-dichloroethane at 60–80 °C. Table 2 shows the results of this second investigation.

Whereas the successful hydrolysis of **5** (Table 2, entry 1) with LiOH had been previously reported,^[4] our attempt to reproduce these results on a larger scale resulted in significant epimerization at the azide-bearing stereocenter. Application of the Me₃SnOH conditions to substrate **5** yielded the desired product **5a** in excellent yield and without undesired epimerization. The usefulness of the mild Me₃SnOH reagent with substrates sensitive to epimerization was further illustrated in the hydrolyses of thiazolines **6** and **7** (Table 2, entries 2 and 3), in which the pure carboxylic acids were isolated in 85 and 88 % yield, respectively. Equally intriguing was the fact that the Fmoc protecting group in **6** remained intact throughout the hydrolysis, an achievement that was not attainable with other methods, and one that was further supported by the successful hydrolysis of Fmoc-D-Ala (**21**) to its corresponding

carboxylic acid (**21a**) with complete retention of the Fmoc protecting group (Table 2, entry 17). In contrast, upon treatment of **21** with LiOH, partial cleavage (≈ 33 %) of the Fmoc group was observed by the time hydrolysis of the methyl ester was complete. The hydrolyses of methyl ester **8** (Table 2, entry 4) and allyl ester **9** (Table 2, entry 5) under standard LiOH conditions revealed only decomposition, which most likely stems from side reactions with the phenyl selenium groups. In contrast, application of the new procedure generated the desired products **8a** and **9a** (physical properties, Table 4) in excellent to quantitative yields. The α,β-keto ester **10** (Table 2, entry 6) provided yet another challenging substrate for the tin reagent. Again, the use of LiOH resulted in decomposition, but when Me₃SnOH was employed the expected carboxylic acid **10a** (physical properties, Table 4) was isolated as the major component in 77 % yield, with the minor product formed from intramolecular 1,4-addition of

Table 2: Trimethyltin hydroxide mediated hydrolysis of esters and related compounds.^[a]

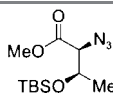
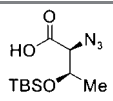
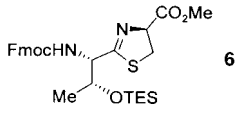
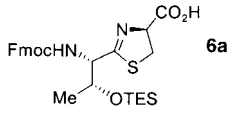
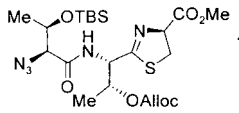
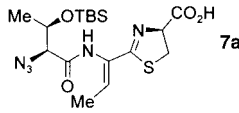
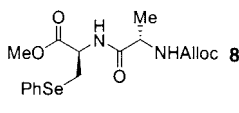
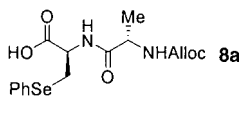
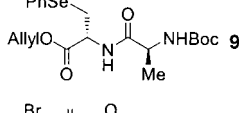
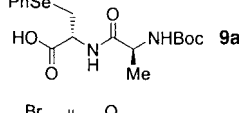
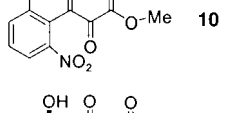
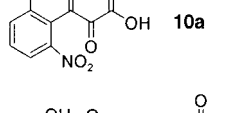
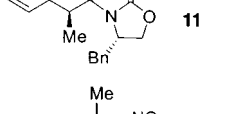
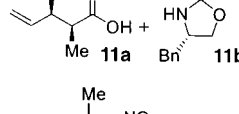
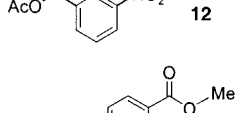
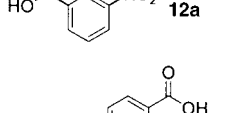
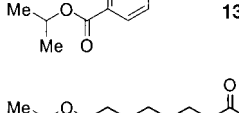
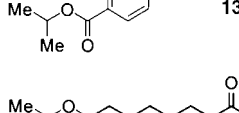
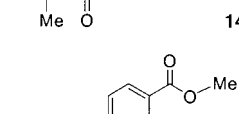
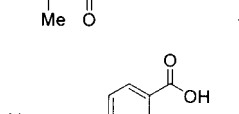
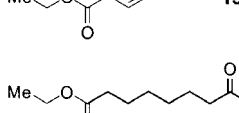
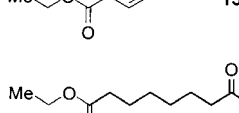
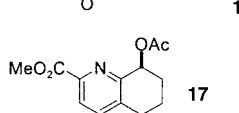
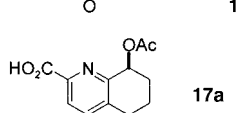
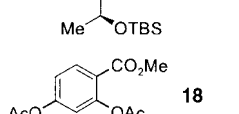
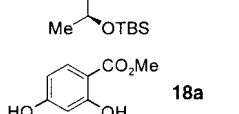
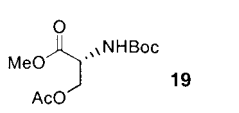
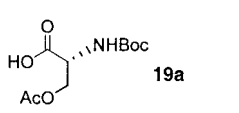
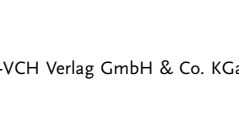

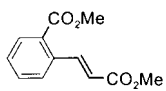
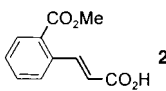
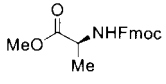
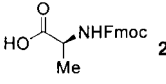
Entry	Ester	Product(s)	T [°C]	t [h]	Yield [%]	Selectivity ^[b]
1			80	3	98	—
2			70	1	85	—
3			80	2	88	—
4			80	1	87	—
5			80	2	100	—
6			80	1	77	—
7			80	7	84	—
8			80	2	100	—
9			80	5	80	≈ 90:1
10			80	7	82	≈ 10:1
11			70	9	70	≈ 10:1
12			70	10	70	≈ 3:1
13			80	2	67	—
14			80	5	100	—
15			80	2	80	—

Table 2: (Continued)

Entry	Ester	Product(s)	T [°C]	t [h]	Yield [%]	Selectivity ^[b]
16			80	9	70	≈ 7:1
17			80	5	75	–

[a] Reactions were carried out in 1,2-DCE on a 0.04–0.15-mmol scale and worked up as described in the general procedure. Bn = benzyl; Fmoc = 9-fluorenylmethoxycarbonyl. [b] For the methyl ester.

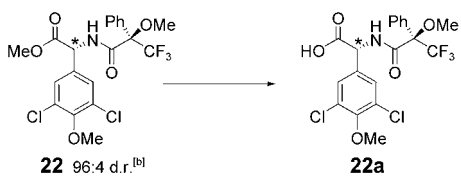
the resulting carboxylic acid group to the proximate Michael-acceptor olefin. The scope of this method was further expanded when it was discovered that Me₃SnOH could cleave the Evans oxazolidinone chiral auxiliary^[5] (**11b**) from aldol product **11** to afford carboxylic acid **11a** in good yield (Table 2, entry 7). The generality of the method with regards to other esters also proved to be quite good, as it was successful in cleaving methyl, ethyl, allyl, and benzyl esters, but ineffective toward pivalate esters. Substrate **12** (entry 8, Table 2) further illustrates the efficiency of this protocol in cleaving acetate esters in quantitative yields.

Entries 9–16 in Table 2 demonstrate the selectivity of this method. It is evident that the methyl ester is hydrolyzed preferentially over isopropyl and ethyl esters in good yield, for both aromatic and aliphatic systems. A small amount of diacid is also produced in these reactions; in these cases it is a consequence of the partial susceptibility of the isopropyl and ethyl esters to the conditions of the reaction. In testing the selectivity for benzyl versus methyl esters and allyl versus methyl esters, it was found that no significant preference prevailed. In testing the selectivity between acetate protecting groups and methyl esters, the results varied. In the activated ester **17** (Table 2, entry 13), under standard LiOH conditions, only the alcohol (arising from cleavage of the acetate) or alcohol/carboxylic acid products were obtained. In contrast, upon use of the tin reagent the methyl ester was hydrolyzed selectively in the presence of the secondary acetate. This led to further experimentation with substrates **18** and **19** (Table 2, entries 14 and 15). Compound **19** again underwent selective hydrolysis of the methyl ester in the presence of the primary acetate protecting group, whereas **18** underwent quantitative loss of its acetate protecting groups, without hydrolysis of the methyl ester. These observations can be attributed to the ease with which phenolic acetates are removed, owing to the good leaving-group nature of the phenolic moiety. Further complementing this new methodology is the ease with which the resulting carboxylic acid products are isolated. A general workup procedure involved concentration of the crude reaction mixture and redilution in ethyl acetate. The organic layer was then washed three times with

either aqueous KHSO₄ (0.01N) or HCl (5%), depending on the acid lability of the substrate. In most cases, this procedure produced a virtually pure sample of the carboxylic acid owing to the high solubility of Me₃SnOH in water^[2c,6] (typically ≤ 2 mol % of Me₃SnOH by ¹H NMR spectroscopy). When materials of higher purity were required, the remaining tin reagent could be removed by further aqueous washes or silica gel chromatography.

In a final test to demonstrate the definitive tolerance of epimerization-prone substrates to Me₃SnOH, dichlorinated phenyl glycine derivative **22**^[7] (Table 3) was prepared in four steps from commercially available (*R*)-4-hydroxyphenylglycine^[8] and (*R*)-Mosher acid chloride under standard conditions (CH₂Cl₂, pyridine, 0–25 °C).^[9] ¹H NMR spectroscopic analysis of the resulting coupled product **22** indicated a d.r. of 96:4. The attempted hydrolysis was then carried out under standard LiOH and LiOOH conditions, and with Me₃SnOH and potassium trimethylsilylanolate, a reagent reported to promote mild, epimerization-free hydrolysis of amino acid esters.^[10] After exposure of the diastereomeric mixture of methyl esters **22** (*R,R/S,R* 96:4) to 1.1 equivalents of LiOH for 20 min at 0 °C, followed by warming to room temperature for 20 min, a mixture of diastereomeric carboxylic acids was obtained in a ratio of 43:57 (*R,R/S,R*) (measured by ¹H NMR spectroscopy), while treatment with LiOOH resulted in decomposition. When the mixture of esters **22** was treated with 1.5 equivalents of KOSiMe₃ for 4 h at room temperature, a mixture of carboxylic acids (*R,R/S,R* 20:80) was isolated. However, when **22** was exposed to 3.0 equivalents of Me₃SnOH in 1,2-dichloroethane at 80 °C for 20 min, the corresponding acid was isolated in 98 % yield with only slight

Table 3: Methyl ester hydrolysis of chlorinated (*R*)-Mosher amide–(*R*)-4-hydroxyphenylglycine derivatives.^[a]

			
Entry	Substrate	Conditions	Product d.r.
1	22	Me ₃ SnOH (3.0 equiv), 1,2-DCE, 80 °C	94:6
2	22	LiOH (1.1 equiv), THF, MeOH, H ₂ O, 0–25 °C	43:57
3	22	KOSiMe ₃ (1.5 equiv), Et ₂ O, 25 °C	20:80

[a] Reactions were carried out on a 0.01–0.04-mmol scale. [b] Prepared by reaction of the corresponding amine and acid chloride in the presence of pyridine in dichloromethane at room temperature.

erosion of the stereochemical integrity (*R,R/S,R* 94:6). When the same experiments were carried out with the diastereomer of **22** obtained from the opposite enantiomer of the Mosher acid chloride (*R,S/S,S* 99:1), the results were similar but not identical (conditions of Table 3, entry 1: d.r. = 97:3; conditions of Table 3, entry 2: d.r. = 64:36; conditions of Table 3, entry 3: d.r. = 69:31).

With these final results standing as a powerful testament to the mildness of the presently introduced method, we anticipate its applicability and usefulness in chemical synthesis to be widespread.

Table 4: Selected physical properties for compounds **9a**, **10a**, **14a**, **17a**, and **22a**.

9a: R_f = 0.12 (silica gel, EtOAc/hexanes 1:1); $[\alpha]_D^{32}$ = -32.5 (CH ₂ Cl ₂ , c = 1.20); IR (film): $\tilde{\nu}_{\max}$ = 3323, 3060, 2978, 2931, 1696, 1665, 1519, 1368, 1249, 1166, 1070, 737 cm ⁻¹ ; ¹ H NMR (600 MHz, CDCl ₃): δ = 7.56–7.54 (m, 2H), 7.26–7.25 (m, 3H), 7.09 (br d, J = 7.4 Hz, 1H), 4.89 (m, 2H), 3.48 (dd, J = 13.1, 4.4 Hz, 1H), 3.34 (m, 1H), 1.46 (br s, 9H), 1.25 ppm (m, 3H); ¹³ C NMR (150 MHz, CDCl ₃): δ = 173.4, 172.9, 133.2, 129.4, 129.2, 127.4, 53.1, 50.0, 29.6, 29.2, 28.3, 18.1 ppm; HRMS (ESI-TOF): calcd for C ₁₇ H ₂₄ N ₂ O ₅ SeNa ⁺ [M+Na] ⁺ : 439.0743; found: 439.0743
10a: R_f = 0.10 (silica gel, EtOAc/hexanes 1:1); IR (film): $\tilde{\nu}_{\max}$ = 3406, 2917, 1629, 1527, 1352, 1095, 1038, 718 cm ⁻¹ ; ¹ H NMR (600 MHz, CD ₃ OD): δ = 8.03–7.99 (m, 2H), 7.51–7.48 (m, 1H), 6.89 (s, 1H), 6.22 ppm (s, 1H); ¹³ C NMR (150 MHz, CD ₃ OD): δ = 194.6, 171.0, 152.0, 144.3, 138.9, 135.4, 134.7, 131.8, 127.2, 124.8 ppm; HRMS (ESI-TOF): calcd for C ₁₀ H ₆ BrNO ₅ H ⁺ [M+H] ⁺ : 297.9357; found: 297.9354
14a: R_f = 0.30 (silica gel, EtOAc/hexanes 7:3); IR (film): $\tilde{\nu}_{\max}$ = 3460, 2980, 2934, 2859, 1731, 1714, 1467, 1374, 1181, 1109 cm ⁻¹ ; ¹ H NMR (400 MHz, CDCl ₃): δ = 5.00 (septet, J = 6.2 Hz, 1H), 2.37–2.24 (m, 4H), 1.65–1.60 (m, 4H), 1.36–1.33 (m, 4H), 1.22 ppm (d, J = 6.2 Hz, 6H); ¹³ C NMR (150 MHz, CDCl ₃): δ = 173.3, 67.4, 34.5, 28.6, 28.6, 24.7, 24.7, 24.6, 21.7 ppm; HRMS (ESI-TOF): calcd for C ₁₁ H ₂₀ O ₄ Na ⁺ [M+Na] ⁺ : 239.1254; found: 239.1255
17a: Inseparable mixture of \approx 1:1 diastereomers: R_f = 0.34 (silica gel, EtOAc/hexanes 7:3); $[\alpha]_D^{32}$ = -22.3 (CH ₂ Cl ₂ , c = 0.60); IR (film): $\tilde{\nu}_{\max}$ = 3380, 2925, 2854, 1737, 1719, 1460, 1375, 1252, 1094, 836 cm ⁻¹ ; ¹ H NMR (600 MHz, CDCl ₃): δ = 8.37 (s, 2 \times 1 H), 6.05 (m, 2 \times 1 H), 5.06–5.03 (m, 2 \times 1 H), 2.94–2.84 (m, 2 \times 1 H), 2.79–2.74 (m, 2 \times 1 H), 2.69–2.65 (m, 2 \times 1 H), 2.14 (s, 2 \times 3 H), 2.10–2.02 (m, 2 \times 2 H), 1.95 (m, 2 \times 1 H), 1.39 (d, J = 6.12 Hz, 3 H), 1.36 (d, J = 6.18 Hz, 3 H), 0.92 (s, 9 H), 0.90 (s, 9 H), 0.09 (s, 3 H), 0.07 (s, 3 H), 0.00 (s, 3 H), -0.02 ppm (s, 3 H); ¹³ C NMR (150 MHz, CDCl ₃): δ = 178.3, 170.6, 157.8, 152.4, 144.5, 134.0, 120.2, 70.3, 66.6, 66.5, 32.1, 29.9, 25.9, 25.9, 25.2, 25.0, 22.9, 21.5, 18.1, -4.6, -4.6, -4.7 ppm; HRMS (ESI-TOF): calcd for C ₂₀ H ₃₁ NO ₅ SiH ⁺ [M+H] ⁺ : 394.2044; found: 394.2049
22a: R_f = 0.34 (silica gel, MeOH/CH ₂ Cl ₂ 1:9); $[\alpha]_D^{32}$ = -62.6 (MeOH, c = 0.67); IR (film): $\tilde{\nu}_{\max}$ = 3381, 2920, 2856, 1732, 1649, 1454, 1270, 1164, 1106 cm ⁻¹ ; ¹ H NMR (600 MHz, CD ₃ OD): δ = 7.59–7.57 (m, 2H), 7.45–7.44 (m, 5H), 5.48 (br s, 1H), 3.88 (s, 3H), 3.40 ppm (m, 3H); ¹³ C NMR (150 MHz, CD ₃ OD): δ = 168.1, 153.4, 137.0, 133.7, 131.0, 130.5, 129.8, 129.5, 129.4, 126.5, 124.6, 61.3, 56.1, 55.7, 30.9 ppm; HRMS (ESI-TOF): calcd for C ₁₉ H ₁₆ Cl ₂ F ₃ NO ₅ H ⁺ [M+H] ⁺ : 466.0430; found: 466.0429
(<i>R,S</i>)-22a: R_f = 0.34 (silica gel, MeOH/CH ₂ Cl ₂ 1:9); $[\alpha]_D^{32}$ = -34.1 (MeOH, c = 0.27); IR (film): $\tilde{\nu}_{\max}$ = 3377, 2917, 2851, 1730, 1694, 1479, 1268, 1166, 1105 cm ⁻¹ ; ¹ H NMR (600 MHz, CD ₃ OD): δ = 7.46–7.44 (m, 2H), 7.41–7.37 (m, 3H), 7.29 (s, 2H), 5.52 (br s, 1H), 3.85 (s, 3H), 3.62 ppm (m, 3H); ¹³ C NMR (150 MHz, CD ₃ OD): δ = 168.1, 153.5, 136.3, 134.6, 130.9, 130.4, 129.6, 129.5, 128.5, 126.2, 124.3, 61.3, 56.6, 56.1, 30.9 ppm; HRMS (ESI-TOF): calcd for C ₁₉ H ₁₆ Cl ₂ F ₃ NO ₅ Na ⁺ [M+Na] ⁺ : 488.025; found: 488.0246

Experimental Section

General procedure: The carboxylic ester (0.01–0.15 mmol) was dissolved in 1,2-dichloroethane and after addition of trimethyltin hydroxide (1–10 equiv), the mixture was heated at 60–80 °C until TLC analysis indicated a complete reaction. After completion of the reaction, the mixture was concentrated in vacuo, and the residue was taken up in ethyl acetate (\approx 15 mL). The organic layer was washed with aqueous KHSO₄ (0.01N) or HCl (5%) (3 \times 5–15 mL). The organic layer was then washed with brine (5–15 mL) and dried over sodium sulfate. Removal of the solvent in vacuo afforded the carboxylic acid, often in > 98% purity (by ¹H NMR spectroscopy).

Received: October 5, 2004

Published online: January 26, 2005

Keywords: epimerization · hydrolysis · synthetic methods · tin

- [1] a) K. C. Nicolaou, B. S. Safina, M. Zak, A. A. Estrada, S. H. Lee, *Angew. Chem.* **2004**, *116*, 5197–5202; *Angew. Chem. Int. Ed.* **2004**, *43*, 5087–5092; b) K. C. Nicolaou, M. Zak, B. S. Safina, S. H. Lee, A. A. Estrada, *Angew. Chem.* **2004**, *116*, 5202–5207; *Angew. Chem. Int. Ed.* **2004**, *43*, 5092–5097.
- [2] a) R. L. E. Furlan, E. G. Mata, O. A. Mascaretti, *J. Chem. Soc. Perkin Trans. 1* **1998**, 355–358; b) R. L. E. Furlan, E. G. Mata, O. A. Mascaretti, C. Pena, M. P. Coba, *Tetrahedron* **1998**, *54*, 13023–13034; c) R. L. E. Furlan, O. A. Mascaretti, *Aldrichimica Acta* **1997**, *30*, 55–69; d) R. L. E. Furlan, E. G. Mata, O. A. Mascaretti, *Tetrahedron Lett.* **1996**, *37*, 5229–5232.
- [3] For a related process that employs dibutyltin oxide to induce transesterifications, see: P. Baumhof, R. Mazitschek, A. Giannis, *Angew. Chem.* **2001**, *113*, 3784–3786; *Angew. Chem. Int. Ed.* **2001**, *40*, 3672–3674.
- [4] K. C. Nicolaou, M. Nevalainen, M. Zak, S. Bulat, M. Bella, B. S. Safina, *Angew. Chem.* **2003**, *115*, 3540–3546; *Angew. Chem. Int. Ed.* **2003**, *42*, 3418–3424.
- [5] D. A. Evans, J. Bartroli, T. L. Shih, *J. Am. Chem. Soc.* **1981**, *103*, 2127–2129.
- [6] C. J. Salomon, G. O. Danelon, O. A. Mascaretti, *J. Org. Chem.* **2000**, *65*, 9220–9222.
- [7] Arylglycine derivatives such as **22** are known to be extremely prone to racemization; for examples, see: a) H. Deng, J.-K. Jung, T. Liu, K. Kuntz, M. L. Snapper, A. H. Hoveyda, *J. Am. Chem. Soc.* **2003**, *125*, 9032–9034; b) F. A. Davis, D. L. Fanelli, *J. Org. Chem.* **1998**, *63*, 1981–1985; c) A. J. Pearson, G. Bignan, P. Zhang, M. Chelliah, *J. Org. Chem.* **1996**, *61*, 3940–3941; d) A. J. Pearson, H. Shin, *J. Org. Chem.* **1994**, *59*, 2314–2323.
- [8] a) A. J. Pearson, M. V. Chelliah, G. C. Bignan, *Synthesis* **1997**, *5*, 536–540; b) L. B. Crast, US Patent 3489750, **1970** [*Chem. Abstr.* **1970**, *72*, 100725].
- [9] a) J. A. Dale, D. L. Dull, H. S. Mosher, *J. Org. Chem.* **1969**, *34*, 2543–2549; b) J. A. Dale, H. S. Mosher, *J. Am. Chem. Soc.* **1973**, *95*, 512–519.
- [10] a) I. A. Motorina, C. Huel, E. Quiniou, J. Mispelter, E. Adjadj, D. S. Grierson, *J. Am. Chem. Soc.* **2001**, *123*, 8–17; b) F. Polyak, W. D. Lubell, *J. Org. Chem.* **2001**, *66*, 1171–1180.

Phase-Transfer Catalysis

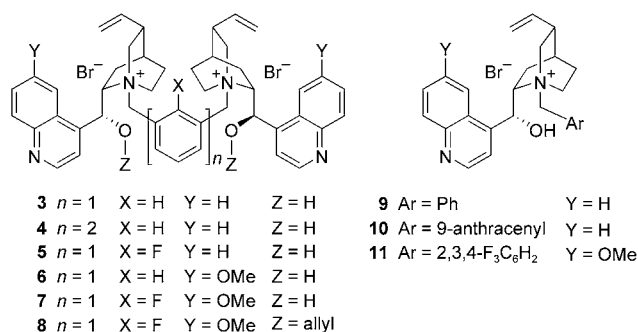
Highly Enantioselective Epoxidation of 2,4-Diarylenones by Using Dimeric Cinchona Phase-Transfer Catalysts: Enhancement of Enantioselectivity by Surfactants**

Sang-sup Jew,* Jeong-Hee Lee, Byeong-Seon Jeong, Mi-Sook Yoo, Mi-Jeong Kim, Yeon-Ju Lee, Jihye Lee, Sea-hoon Choi, Kyungjae Lee, Myoung Soo Lah, and Hyeung-geun Park*

Since the asymmetric epoxidation of allylic alcohols, which was reported by the Sharpless group in 1980, catalytic asymmetric epoxidation has been one of the most important asymmetric methodologies.^[1] A number of methods have been developed for the epoxidation of both unfunctionalized olefins and electron-deficient enones.^[2] Quite recently, catalytic asymmetric phase-transfer epoxidations by using a cinchona alkaloid-derived quaternary ammonium salt as a chiral phase-transfer catalyst (PTC) have been reported by several research groups.^[3] Despite their practical potential, several shortcomings, such as insufficient enantioselectivity, long reaction times, and low reaction temperatures, still remain. Herein we report a highly enantioselective and practical catalytic epoxidation of enones by using cinchona alkaloid-derived dimeric quaternary ammonium salts and the role of surfactants for enantioselectivity.

Recently, we reported a series of novel *meta*-dimeric catalysts, derived from cinchona alkaloids, which were successfully applied in the enantioselective synthesis of α -amino acids.^[4] As part of our research, we attempted to apply these catalysts to the asymmetric epoxidation of 2,4-diarylenones. As very versatile intermediates,^[3b] the epoxides of 2,4-diarylenones have been applied to the synthesis of various biologically active compounds such as naproxen, ibuprofen, diltiazem, the side chain of Taxol, (+)-clausenamide, as well as styryl lactones ((+)-goniotriol and (+)-goniofufurone).^[5]

We first performed the enantioselective phase-transfer epoxidation of *trans*-chalcone (**1a**) by using 5 mol % of the dimeric catalyst **3** along with 30 % aqueous H₂O₂ (30 equiv)



and 50 % aqueous KOH (3 equiv) in diisopropyl ether at 10 °C. As shown in Table 1, although the reaction time was somewhat long (48 h), the dimeric catalyst **3** showed moderate enantioselectivity (48 % *ee*) compared with the corresponding monomeric catalyst **9**, which provided virtually no enantioselectivity (Table 1, entries 1 and 8). Before we searched for an optimal catalyst for the epoxidation, we needed to reduce the long reaction time, which might cause the low enantioselectivity through non-PTC-mediated epoxidation.

Table 1: Catalytic enantioselective epoxidation of *trans*-chalcone.

$\text{Ph}-\text{CH}=\text{CH}-\text{C}(=\text{O})-\text{Ph}$ (1a) $\xrightarrow[\text{Triton X-100, } i\text{Pr}_2\text{O, } 10^\circ\text{C}]{\text{chiral PTC (5 mol \%), 30\% H}_2\text{O}_2 \text{ (30 equiv), 50\% KOH (3 equiv)}}$ $\text{Ph}-\text{CH}(\text{O})-\text{CH}(\text{O})-\text{C}(=\text{O})-\text{Ph}$ (2a)					
Entry	PTC	Triton X-100 [mol %]	<i>t</i> [h]	Yield [%]	<i>ee</i> [%] ^[a]
1	3	0	48	85	48
2	3	5	10	89	82
3	4	5	8	85	2
4	5	5	8	80	92
5	6	5	8	90	92
6	7	5	3	95	98
7	8	5	8	70	6
8	9	0	56	65	0
9	9	5	15	80	2
10	10	5	15	70	3
11	11	5	8	95	1

[a] Enantiopurity was determined by HPLC analysis with a chiral column (DAICEL Chiralpak AD), and absolute configuration was determined by comparison of the HPLC retention time with reported data.^[3]

[*] Prof. Dr. S.-s. Jew, J.-H. Lee, Dr. B.-S. Jeong, M.-S. Yoo, M.-J. Kim, Y.-J. Lee, J. Lee, S.-h. Choi, Prof. Dr. H.-g. Park
 Research Institute of Pharmaceutical Sciences and
 College of Pharmacy
 Seoul National University
 Seoul 151-742 (Korea)
 Fax: (+82) 2-872-9129
 E-mail: ssjew@plaza.snu.ac.kr
 hgpk@plaza.snu.ac.kr

K. Lee, Prof. Dr. M. S. Lah
 Department of Chemistry and Applied Chemistry
 Hanyang University
 Ansan, Kyunggi 426-791 (Korea)

[**] This research was supported by a grant (R01-2002-000-0005-0) from the Basic Research Program of the KOSEF (2004).

Supporting information for this article is available on the WWW under <http://www.angewandte.org> or from the author.

Recently, Okino and Takemoto reported a phase-transfer alkylation in a nonorganic solvent as a green chemical process;^[6] the method involved the use of a surfactant, Triton X-100. As surfactants generally increase the surface area between the two phases by the formation of micelles,^[7] we expected that the reaction would be accelerated in the presence of surfactants. Thus, we tentatively tried Triton X-100 in a phase-transfer epoxidation. Surprisingly, the use of just 5 mol % of Triton X-100 dramatically increased not only the rate of the reaction (five times) but also the enantioselectivity (82 % *ee*, Table 1, entry 2). Generally, when the nucleophile and electrophile were not in the same phase, the phase-transfer reaction was considerably slower than the reaction that occurred when both components were in the organic phase. In the case of such a slow enantioselective phase-transfer reaction, the low enantioselectivities may not

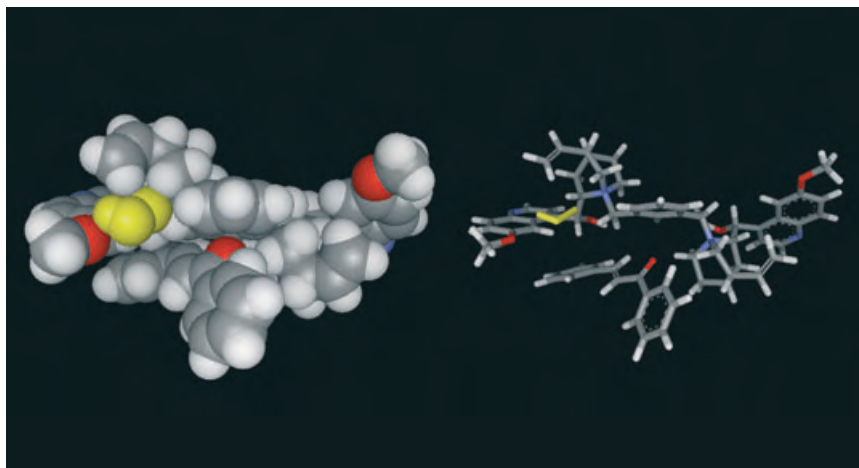


Figure 2. Plausible model of the transition state for the asymmetric epoxidation of **1a** based on the X-ray crystal structure of **7** (HOO⁻ yellow, C dark gray, H white, N blue, O red).

lectivity of phase-transfer catalytic epoxidation. The best results were obtained with Span 20. The easy preparation of the most effective catalyst, **7**, and the very mild reaction conditions make this method promising for industrial application. Further modification of the dimeric catalysts to extend the substrate scope and mechanistic studies are in progress.

Experimental Section

Aqueous hydrogen peroxide (30 %, 0.27 mL; 2.4 mmol) and 50 % aqueous KOH (0.027 mL, 0.24 mmol) were added to a mixture of chalcone **1a** (50 mg, 0.24 mmol), catalyst **7** (2.2 mg, 0.0024 mmol), and Span 20 (0.003 mL, 0.0024 mmol) in diisopropyl ether (0.8 mL), and the reaction mixture was stirred vigorously at room temperature until the starting material had been consumed. The resulting suspension was diluted with ether (10 mL), washed with water (2 × 5 mL), dried over MgSO₄, filtered, and concentrated in vacuo. Purification of the residue by flash column chromatography on silica gel (hexanes/EtOAc = 50:1) afforded the desired product **2a** (51.2 mg, 95 % yield) as a white solid. The enantioselectivity was determined by chiral HPLC analysis (DAICEL Chiralpak AD, hexanes/ethanol = 90:10, flow rate = 1.0 mL min⁻¹, 23 °C, λ = 254 nm; retention times: 16.6 min (minor), 24.0 min (major); > 99.9 % ee). The absolute configuration was determined by comparison of the HPLC retention time with reported data.^[3]

Received: October 9, 2004

Revised: November 16, 2004

Published online: January 21, 2005

Keywords: asymmetric catalysis · enantioselectivity · epoxidation · phase-transfer catalysis · surfactants

- [1] T. Katsuki, K. B. Sharpless, *J. Am. Chem. Soc.* **1980**, *102*, 5974.
- [2] For recent reviews, see: a) M. J. Porter, J. Skidmore, *Chem. Commun.* **2002**, 1215; b) C. Lauret, S. M. Roberts, *Aldrichimica Acta* **2002**, *35*, 47; c) T. Nemoto, T. Ohshima, M. Shibasaki, *J. Synth. Org. Chem. Jpn.* **2002**, *60*, 94; d) A. Gerlach, T. Geller, *Adv. Synth. Catal.* **2004**, *346*, 1247.
- [3] a) B. Lygo, P. G. Wainwright, *Tetrahedron* **1999**, *55*, 6289; b) E. J. Corey, F.-Y. Zhang, *Org. Lett.* **1999**, *1*, 1287; c) S. Arai, H. Tsuge, M. Oku, M. Miura, T. Shioiri, *Tetrahedron* **2002**, *58*, 1623; d) T. Ooi, D. Ohara, M. Tamura, K. Maruoka, *J. Am. Chem. Soc.* **2004**, *126*, 6844.

- [4] a) S.-s. Jew, B.-S. Jeong, M.-S. Yoo, H. Huh, H.-g. Park, *Chem. Commun.* **2001**, 1244; b) H.-g. Park, B.-S. Jeong, M.-S. Yoo, J.-H. Lee, B.-s. Park, M. G. Kim, S.-s. Jew, *Tetrahedron Lett.* **2003**, *44*, 3497.
- [5] a) L. Carde, D. H. Davies, S. M. Roberts, *J. Chem. Soc. Perkin Trans. 1* **2000**, 2455; b) B. M. Adger, J. V. Barkley, S. Bergeron, M. W. Cappi, B. E. Flowerdew, M. P. Jackson, R. McCague, T. C. Nugent, S. M. Roberts, *J. Chem. Soc. Perkin Trans. 1* **1997**, 3501; c) M. W. Cappi, W.-P. Chen, R. W. Flood, Y.-W. Liao, S. M. Roberts, J. Skidmore, J. A. Smith, N. M. Williamson, *Chem. Commun.* **1998**, 1159; d) W.-P. Chen, S. M. Roberts, *J. Chem. Soc. Perkin Trans. 1*, **1999**, 103.
- [6] T. Okino, Y. Takemoto, *Org. Lett.* **2001**, *3*, 1515.
- [7] D. J. Shaw, *Introduction to Colloid and Surface Chemistry*, Butterworth, Boston, **1980**.
- [8] a) H.-g. Park, B.-S. Jeong, M.-S. Yoo, J.-H. Lee, M.-k. Park, Y.-J. Lee, M.-J. Kim, S.-s. Jew, *Angew. Chem.* **2002**, *114*, 3162; *Angew. Chem. Int. Ed.* **2002**, *41*, 3036; b) S.-s. Jew, M.-S. Yoo, B.-S. Jeong, I.-Y. Park, H.-g. Park, *Org. Lett.* **2002**, *4*, 4245; c) S.-s. Jew, B.-S. Jeong, J.-H. Lee, M.-S. Yoo, Y.-J. Lee, B.-s. Park, M.-G. Kim, H.-g. Park, *J. Org. Chem.* **2003**, *68*, 4514.
- [9] For detailed crystallographic data, see the Supporting Information.

Coordination Network

A 3D Coordination Framework Based on Linkages of Nanosized Hydroxo Lanthanide Clusters and Copper Centers by Isonicotinate Ligands**

Man-Bo Zhang, Jie Zhang, Shou-Tian Zheng,
and Guo-Yu Yang*

Nanoscale clusters are of great popularity due to the novel structural characteristics and rich electronic, magnetic, optical, and catalytic properties associated with their quantum-size effects.^[1] Although the cluster chemistry of transition metals (TMs) is now well-established and many huge clusters

[*] M.-B. Zhang, Prof. J. Zhang, S.-T. Zheng, Prof. G.-Y. Yang
State Key Laboratory of Structural Chemistry
Fujian Institute of Research on the Structure of Matter
Chinese Academy of Sciences
Fuzhou, Fujian 350002 (China)
Fax: (+ 86) 591-8371-0051
E-mail: ygy@fjirsm.ac.cn

[**] This work was supported by the NNSF of China (Nos. 20271050 and 20473093), the Talents Program of Chinese Academy of Sciences, and the NSF of Fujian Province (No. E0210029). G.-Y.Y. thanks Prof. S. Gao, Peking University, for useful discussions.



Supporting information for this article is available on the WWW under <http://www.angewandte.org> or from the author.

of manganese,^[2] copper,^[3] nickel,^[4] molybdenum,^[5] and silver^[6] have been synthesized successfully, the analogous chemistry of lanthanides is less developed^[7] because the synthesis of nanosized high-nuclearity clusters is still a big challenge. At present, a common synthetic strategy for hydroxo lanthanide clusters is to control the hydrolysis of lanthanide salts in the presence of supporting ligands.^[7,8] So far, most of the reported high-nuclearity hydroxo lanthanide clusters are discrete^[7] because the presence of hydrophobic groups in the periphery of the cluster core prevents further aggregation. Recently, in an investigation on the nature of the magnetic exchange interactions between 3d and 4f metals in the solid state, some lanthanide–TM coordination polymers^[9] and clusters^[10] were reported. To date, except for four coordination polymers constructed from hydroxo lanthanide cluster cores of Dy₄,^[11] Yb₆,^[12] Ho₇, and Yb₇,^[8] no systematic investigation on lanthanide–TM coordination polymers in which high-nuclearity hydroxo lanthanide clusters and TM ions are linked by organic ligands has been carried out.

We chose isonicotinic acid (HIN) as the multifunctional bridging ligand, based on the following considerations: 1) It is a rigid ligand with oxygen and nitrogen donors on opposite sides, enabling the IN ligand to act as a linear bridge. 2) The carboxy group may induce the oxophilic lanthanide ions to undergo hydroxo lanthanide cluster aggregation, the nitrogen atoms can coordinate to TM ions, and thus extended solids containing hydroxo lanthanide cluster cores and TM ions might be obtained. Here we report the systematic syntheses and structures of three coordination polymers by using lanthanide oxide, rather than lanthanide salts, as the source of lanthanides under hydrothermal conditions: [Ln₁₄(μ₆-O)(μ₃-OH)₂₀(IN)₂₂Cu₆Cl₄(H₂O)₈·6H₂O [Ln = Y (**1**), Gd (**2**), Dy (**3**)]. These structures contain the high-nuclearity hydroxo lanthanide cluster [Ln₁₄(μ₆-O)(μ₃-OH)₂₀(H₂O)₈]²⁰⁺, which acts as a building block that combines with copper ions through linear IN ligands to form a 3D framework.

Orange rectangular-prismatic crystals of **1–3** were obtained by hydrothermal reaction of Ln₂O₃, HIN, and CuCl₂·2H₂O in water in the presence of HClO₄ (pH 2). The amount of HClO₄ used in the synthesis is a key point in the formation of **1–3**, because a chainlike Ln³⁺ polymer, which is isostructural with [Tb(IN)₃(H₂O)₂]_n,^[13] formed under weakly acidic conditions.

X-ray crystal structure analyses revealed that **1–3** are isostructural and crystallize in the high-symmetry tetragonal space group *P*₄₂/*mnm*. Therefore, only the structure of **2** is described in detail. The asymmetric unit of **2** contains four crystallographically unique Gd ions, two Cu cations, and four IN ligands (see Supporting Information). Gd1 and Gd4 are nine-coordinate: eight μ₃-OH and one μ₆-oxo for Gd1, and four μ₃-OH, one μ₆-oxo, three carboxylate oxygen (O_{COO}-) atoms from three IN ligands, and one terminal water molecule for Gd4, while Gd2 and Gd3 are eight-coordinate: three μ₃-OH, one pyridyl nitrogen (N_{PY}), and four O_{COO}- atoms from four IN for Gd2, and four μ₃-OH, one terminal water molecule, and three O_{COO}- atoms from three IN for Gd3 (see Supporting Information). The Gd³⁺ ions are linked together through hydrophilic hydroxo and oxo bridges to give the novel tetradecanuclear [Gd₁₄(μ₆-O)(μ₃-OH)₂₀]²⁰⁺ cluster

core, in which all μ₃-OH groups cap the triangular faces (Figure 1 and Supporting Information). In contrast to [Ln₁₄(μ₄-OH)₂(μ₃-OH)₁₆]²⁴⁺,^[7a,d] which contains an [Ln₆(μ₃-OH)₈]¹⁰⁺ octahedron and [Ln₅(μ₄-OH)(μ₃-OH)₄]¹⁰⁺ square

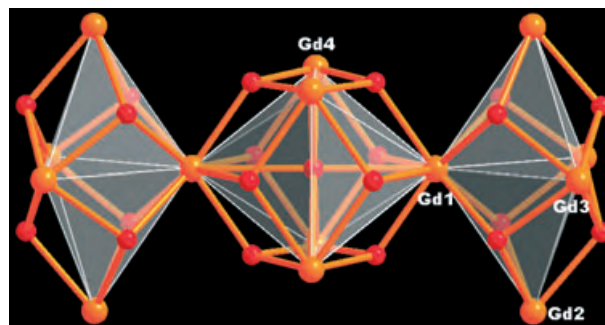


Figure 1. Polyhedral representation of the structure of the [Gd₁₄(μ₆-O)(μ₃-OH)₂₀]²⁰⁺ core, in which one octahedral [Gd₆(μ₆-O)(μ₃-OH)₈]⁸⁺ unit shares two opposing apexes (Gd1 atoms) with two trigonal-bipyramidal [Gd₅(μ₃-OH)₆]⁴⁺ units. In the octahedral Gd₆ unit: Gd1–Gd4 3.907(1), Gd4–Gd4 3.895(1)–4.033(1) Å; in the trigonal-bipyramidal Gd₅ units: Gd1–Gd2 3.894(1), Gd1–Gd3 3.802(1), Gd2–Gd3 3.888(1), Gd3–Gd3 3.859(1), and Gd2–Gd2 6.407(1) Å. Gd: orange; O: red.

pyramids, the Gd₁₄ core in **2** consists of one octahedral [Gd₆(μ₆-O)(μ₃-OH)₈]⁸⁺^[7g,h] unit that shares two opposing Gd1 apexes with two novel [Gd₅(μ₃-OH)₆]⁴⁺ trigonal bipyramids, which is a rare geometry in the reported cores of [Ln₅(μ₄-OH)(μ₃-OH)₄]¹⁰⁺,^[7a,d] [Ln₅(μ₄-O)(μ₃-OH)₄]⁹⁺,^[14] and [Ln₅(μ₃-O)(μ₃-OiPr)₄]⁹⁺.^[15]

In the structure of **2**, two Cu centers are four-coordinate, but they have different coordination environments (Cu(1)Cl₂N₂ and Cu(2)N₄). Although Cu²⁺ ions were used as starting materials, the Cu1 and Cu2 centers both have an oxidation state of +1, attributed to a reduction reaction involving the IN ligand. This observation is consistent with a tetrahedral geometry, which is common for the Cu⁺ ion,^[16] and was confirmed by magnetic measurements (see below). Whereas the Cu2 centers are bonded to four IN ligands through N_{PY} atoms, two Cu1 centers are bridged by Cl⁻ to form a Cu₂Cl₂ dimer with Cu···Cu distance of 2.662(4) Å and are coordinated to four N_{PY} atoms from IN ligands (see Supporting Information).

The linkages between the Gd₁₄ cores and two different types of copper centers through IN ligands give rise to an unusual coordination polymer with extremely complex 3D framework (Figure 2 and Supporting Information). Twenty-six IN ligands coordinate to the Gd₁₄ cores through the N_{PY} or the O_{COO}- atoms (see Supporting Information). Scheme 1 illustrates the four coordination modes of the IN ligands. Two IN ligands of mode I are terminal and only coordinate to the Gd₁₄ core through the O_{COO}- atoms (see Supporting Information). The others correspond to modes II–IV, each of which is exhibited by eight bridging IN ligands. In mode II, each IN ligand connects two Gd₁₄ cores with perpendicular orientations through the N_{PY} and O_{COO}- atoms. The coordination of the ligands is such that the pyridyl (or carboxylate) donors form a *trans* arrangement across the Gd₁₄ core (see Supporting Information). In modes III and IV, the IN ligands

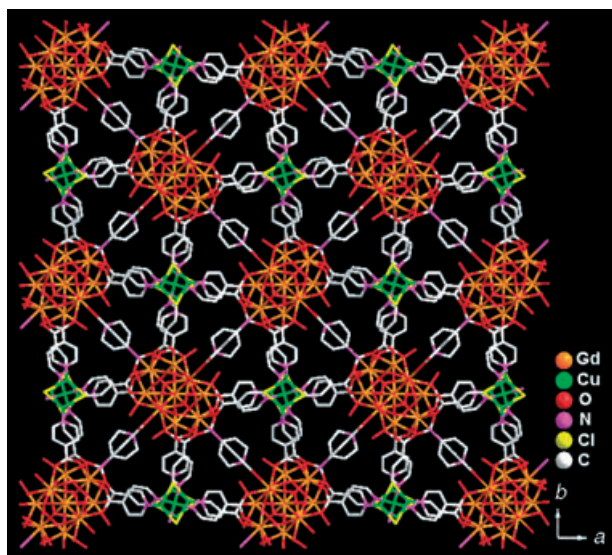
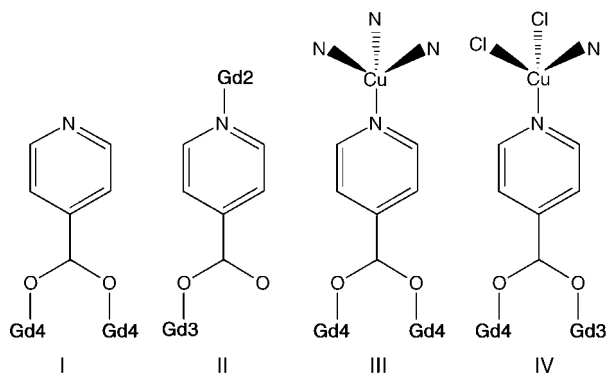


Figure 2. The overall 3D structure of **2** showing the unusual framework along the *c* axis. The lattice water molecules are omitted for clarity.



Scheme 1. Coordination modes of the IN ligands in the structure of **2**. All oxygen atoms coordinate to Gd atoms in monodentate mode.

coordinate to the Gd₁₄ core through the O_{COO}[−] atoms, leaving their N_{py} atoms to bond to Cu₂ ions and Cu₁ atoms of Cu₂Cl₂ dimers, respectively (see Supporting Information). Thus, the structure can be understood such that the strictly alternating Gd₁₄ cores, Cu₂Cl₂ dimers, and Cu ions are bridged by IN ligands of modes III and IV to form a 3D framework having 1D channels with dimensions of about 7 × 7.5 Å along the *c* axis (see Supporting Information). The channels are occupied by lattice water, coordinated water, and terminal IN ligands of mode I (see Supporting Information). Furthermore, the IN ligands belonging to mode II are also located in the channels and connect two Gd₁₄ cores to result in an overall 3D network (Figure 2 and Supporting Information).

Temperature-dependent molar susceptibility measurements on powdered samples of **1–3** were carried out at an applied field of 0.5 T in the temperature range 5–300 K. The molar magnetic susceptibility of **1** (measured on 40.2 mg) is negative and temperature-independent in the range 50–300 K, consistent with the assigned structure containing diamagnetic Cu⁺ and Y³⁺ ions. For **2**, the μ_{eff} value per molecule is 29.5 μ_{B} at room temperature, close to the

expected value of 29.7 μ_{B} for fourteen noninteracting Gd³⁺ ions^[17] ($S = 7/2$, $g = 2.0$) and remains almost constant down to about 50 K, then drops rapidly below 50 K to 25.0 μ_{B} at 5 K. The Curie–Weiss equation with $\theta = -2.1$ K fits well to the data in the range between 5 and 300 K, which suggests weak antiferromagnetic interaction between Gd³⁺ ions. Compound **3** exhibits similar temperature dependence to **2**; the μ_{eff} value of 40.3 μ_{B} at room temperature is in agreement with that expected for fourteen isolated Dy³⁺ ions (39.8 μ_{B} , ⁶H_{15/2} ground state with $g_{15/2} = 4/3$),^[17] the abrupt decrease of μ_{eff} at low temperature is mainly attributed to the splitting of the ligand field of the Dy³⁺ ion because of strong spin-orbital coupling, and some contributions from the possible antiferromagnetic interactions between the Dy³⁺ ions.^[11]

In summary, we have successfully constructed three novel 3D coordination polymers containing distinct nanosized Ln₁₄ clusters and copper centers by using lanthanide oxides as the source of lanthanides under hydrothermal conditions. The key points of the synthetic procedures have been well established.^[18] The linkages between novel nanosized Ln₁₄ cores and two different types of copper centers through IN ligands result in an unprecedented 3D network topology. These results provide a perspective towards 4f–3d mixed-metal functional materials and confirm the potential for developing new structural classes of solid-state materials by using nanosized hydroxo lanthanide clusters as building blocks.

Experimental Section

Synthesis of 1–3: A mixture of Ln₂O₃ (Y₂O₃, 0.5 mmol, 0.113 g; Gd₂O₃, Dy₂O₃, 0.181 g; 0.187 g), HIN (0.246 g, 2 mmol), CuCl₂·2H₂O (0.034 g, 0.2 mmol), H₂O (8 mL), and HClO₄ (0.385 mmol) in a molar ratio of about 2.5:10:1:2222:1.9 was sealed in a 30 mL acid digestion bomb and heated at 170 °C for 6 d. Orange rectangular prism crystals of **1–3** were collected after washing with water.

Crystal data of 1: C₁₃₂H₁₃₆Cl₄Cu₆N₂₂O₇₉Y₁₄, $M_r = 5062.41$, tetragonal, $P4_2/mnm$, $a = b = 20.284(10)$, $c = 21.344(14)$ Å, $V = 8782(8)$ Å³, $Z = 2$, $\rho = 1.914$ g cm^{−3}, $F(000) = 5004$, $\mu(\text{MoK}\alpha) = 5.434$ mm^{−1}, $2\theta_{\text{max}} = 50.06^\circ$, ($-24 \leq h \leq 11$, $-24 \leq k \leq 24$, $-22 \leq l \leq 24$), $T = 293$ K, 39645 measured reflections, 4018 independent reflections, $R1$ ($wR2$) = 0.0968 (0.2110) for 3732 reflections ($I > 2\sigma(I)$) and 321 parameters. GOF = 1.126. Crystal dimensions: 0.26 × 0.18 × 0.12 mm³.

Crystal data of 2: C₁₃₂H₁₃₆Cl₄Cu₆Gd₁₄N₂₂O₇₉, $M_r = 6019.17$, tetragonal, $P4_2/mnm$, $a = b = 20.620(3)$, $c = 21.807(4)$ Å, $V = 9272(3)$ Å³, $Z = 2$, $\rho = 2.156$ g cm^{−3}, $F(000) = 5704$, $\mu(\text{MoK}\alpha) = 5.750$ mm^{−1}, $2\theta_{\text{max}} = 50.04^\circ$, ($-24 \leq h \leq 24$, $-12 \leq k \leq 24$, $-25 \leq l \leq 22$), $T = 293$ K, 43928 measured reflections, 4348 independent reflections, $R1$ ($wR2$) = 0.0480 (0.1064) for 4231 reflections ($I > 2\sigma(I)$) and 329 parameters. GOF = 1.161. Crystal dimensions: 0.30 × 0.15 × 0.12 mm³.

Crystal data of 3: C₁₃₂H₁₃₆Cl₄Cu₆Dy₁₄N₂₂O₇₉, $M_r = 6092.67$, tetragonal, $P4_2/mnm$, $a = b = 20.540(3)$, $c = 21.650(4)$ Å, $V = 9134(3)$ Å³, $Z = 2$, $\rho = 2.215$ g cm^{−3}, $F(000) = 5760$, $\mu(\text{MoK}\alpha) = 6.481$ mm^{−1}, $2\theta_{\text{max}} = 50.04^\circ$, ($-21 \leq h \leq 24$, $-24 \leq k \leq 24$, $-18 \leq l \leq 25$), $T = 293$ K, 45652 measured reflections, 4276 independent reflections, $R1$ ($wR2$) = 0.0515 (0.1065) for 4192 reflections ($I > 2\sigma(I)$) and 329 parameters. GOF = 1.191. Crystal dimensions: 0.25 × 0.13 × 0.10 mm³.

Data were collected on a SMART-CCD diffractometer with graphite-monochromated MoK α radiation ($\lambda = 0.71073$ Å) at room temperature. The structures of **1–3** were solved by direct methods and refined on F^2 by full-matrix least-squares methods using the SHELX97 program package. All non-hydrogen atoms (except O1, C19, C20, OW3, OW4 in **1–3**) were refined anisotropically. The

positions of H atoms were generated geometrically and allowed to ride on their parent carbon atoms.

CCDC-244785–244787 (1–3) contain the supplementary crystallographic data for this paper. These data can be obtained free of charge from The Cambridge Crystallographic Data Centre via www.ccdc.cam.ac.uk/data_request/cif.

Received: July 26, 2004

Revised: November 24, 2004

Published online: January 26, 2005

Keywords: bridging ligands · cluster compounds · copper · hydrothermal synthesis · lanthanides

- [1] a) R. Sessoli, D. Gatteschi, A. Caneschi, M. A. Novak, *Nature* **1993**, 365, 141–143; b) D. Gatteschi, *Adv. Mater.* **1994**, 6, 635–645; c) A. P. Alivisatos, *Science* **1996**, 271, 933–937; d) *Clusters and Colloids: From Theory to Applications* (Ed.: G. Schmidt), VCH, Weinheim, **1994**; e) *Physics and Chemistry of Metal Cluster Compounds* (Ed.: L. J. de Jongh), Kluwer, Dordrecht, **1994**.
- [2] A. J. Tasiopoulos, A. Vinslava, W. Wernsdorfer, K. A. Abboud, G. Christou, *Angew. Chem.* **2004**, 116, 2169–2173; *Angew. Chem. Int. Ed.* **2004**, 43, 2117–2121.
- [3] H. Krautscheid, D. Fenske, G. Baum, M. Semmelmann, *Angew. Chem.* **1993**, 105, 1364–1367; *Angew. Chem. Int. Ed. Engl.* **1993**, 32, 1303–1306.
- [4] D. Fenske, J. Ohmer, J. Hachgenei, *Angew. Chem.* **1985**, 97, 993–995; *Angew. Chem. Int. Ed. Engl.* **1985**, 24, 993–995.
- [5] a) A. Müller, C. Serain, *Acc. Chem. Res.* **2000**, 33, 2–10; b) T. B. Liu, E. Diemann, H. L. Li, A. W. M. Dress, A. Müller, *Nature* **2003**, 426, 59–62.
- [6] X. J. Wang, T. Langetepe, C. Persau, B. S. Kang, G. M. Sheldrick, D. Fenske, *Angew. Chem.* **2002**, 114, 3972–3977; *Angew. Chem. Int. Ed.* **2002**, 41, 3818–3822.
- [7] a) M. R. Brügstein, P. W. Roesky, *Angew. Chem.* **2000**, 112, 559–562; *Angew. Chem. Int. Ed.* **2000**, 39, 549–551; b) R. Wang, Z. Zheng, T. Jin, R. J. Staples, *Angew. Chem.* **1999**, 111, 1929–1932; *Angew. Chem. Int. Ed.* **1999**, 38, 1813–1815; c) R. Anwender, *Angew. Chem.* **1998**, 110, 619–622; *Angew. Chem. Int. Ed.* **1998**, 37, 599–602; d) R. Wang, D. Song, S. Wang, *Chem. Commun.* **2002**, 368–369; e) R. Wang, H. D. Selby, H. Liu, M. D. Carducci, T. Jin, Z. Zheng, J. W. Anthis, R. J. Staples, *Inorg. Chem.* **2002**, 41, 278–286; f) M. R. Brügstein, M. T. Gamer, P. W. Roesky, *J. Am. Chem. Soc.* **2004**, 126, 5213–5218; g) D.-S. Zhang, B.-Q. Ma, T.-Z. Jin, S. Gao, C.-H. Yan, T. C. W. Mak, *New J. Chem.* **2000**, 24, 61–62; h) R. Wang, M. D. Carducci, Z. Zheng, *Inorg. Chem.* **2000**, 39, 1836–1837.
- [8] X.-J. Zheng, L.-P. Jin, S. Gao, *Inorg. Chem.* **2004**, 43, 1600–1602, and references therein.
- [9] a) B. Zhao, P. Cheng, Y. Dai, C. Cheng, D.-Z. Liao, S.-P. Yan, Z.-H. Jiang, G.-L. Wang, *Angew. Chem.* **2003**, 115, 964–966; *Angew. Chem. Int. Ed.* **2003**, 42, 934–936; b) A. Figuerola, C. Diaz, M. S. El Fallah, J. Ribas, M. Maestro, J. Mahia, *Chem. Commun.* **2001**, 1204–1205; c) G. B. Deacon, C. M. Forsyth, T. Behrsing, K. Konstas, M. Forsyth, *Chem. Commun.* **2002**, 2820–2821.
- [10] X. Chen, S. M. J. Aubin, Y. Wu, Y. Yang, T. C. W. Mak, D. N. Hendrickson, *J. Am. Chem. Soc.* **1995**, 117, 9600–9601.
- [11] B. Ma, D. Zhang, S. Gao, T. Jin, C. Yan, G. Xu, *Angew. Chem.* **2000**, 112, 3790–3792; *Angew. Chem. Int. Ed.* **2000**, 39, 3644–3646.
- [12] J. Liu, E. A. Meyers, S. G. Shore, *Inorg. Chem.* **1998**, 37, 5410–5411.
- [13] L. Ma, O. R. Evans, B. M. Foxman, W. Lin, *Inorg. Chem.* **1999**, 38, 5837–5840.
- [14] L. G. Hubert-Pfalzgraf, N. Miele-Pajot, R. Papiernik, J. Vaissermann, *J. Chem. Soc. Dalton Trans.* **1999**, 4127–4130.
- [15] O. Poncelet, W. J. Sartain, L. G. Hubert-Pfalzgraf, K. Folting, K. G. Caulton, *Inorg. Chem.* **1989**, 28, 263–267.
- [16] a) K. Flinzner, A. F. Stassen, A. M. Mills, A. L. Spek, J. G. Haasnoot, J. Reedijk, *Eur. J. Inorg. Chem.* **2003**, 671–677; b) P. J. Burke, K. Henrick, D. R. McMillin, *Inorg. Chem.* **1982**, 21, 1881–1886; c) Y. Shimazaki, H. Yokoyama, O. Yamauchi, *Angew. Chem.* **1999**, 111, 2561–2563; *Angew. Chem. Int. Ed.* **1999**, 38, 2401–2403; d) S. Blanchard, L. Le Clainche, M.-N. Rager, B. Chanson, J.-P. Tuchagues, A. F. Duprat, Y. Le Mest, O. Reinand, *Angew. Chem.* **1998**, 110, 2861–2864; *Angew. Chem. Int. Ed. Engl.* **1998**, 37, 2732–2735; e) M. Munakata, L. P. Wu, M. Yamamoto, T. Turoda-Sowa, M. Maekawa, *J. Am. Chem. Soc.* **1996**, 118, 3117–3124; f) J. C. Dyason, L. M. Engelhardt, P. C. Healy, C. Pakawatchai, A. H. White, *Inorg. Chem.* **1985**, 24, 1950–1957.
- [17] O. Kahn, *Molecular Magnetism*, VCH, New York, **1993**.
- [18] During preparation of this communication, other phase-pure lanthanide-TM coordination polymers, such as $[\text{Ln}_{14}(\mu_6\text{-O})(\mu_3\text{-OH})_{20}(\text{IN})_{22}\text{Cu}_6\text{X}_4(\text{H}_2\text{O})_8]\cdot 6\text{H}_2\text{O}$ (Ln = Er, Tb, X = Cl[−]; Ln = Er, Gd, Y, X = Br[−]), were obtained as single crystals. Single-crystal X-ray diffraction showed that these compounds are analogous to the present compounds. Further investigation on the fluorescent and magnetic properties of these compounds is in progress.

Supramolecular Assemblies

Lipid-Coated Nanocrystals as Multifunctionalized Luminescent Scaffolds for Supramolecular Biological Assemblies**

*Isabelle Geissbuehler, Ruud Hovius, Karen L. Martinez, Marc Adrian, K. Ravindranathan Thampi, and Horst Vogel**

Supramolecular assemblies of self-organized, functionally cooperating molecules are essential for living matter, and have broad potential to downscale and control (bio)chemical

[*] I. Geissbuehler, Dr. R. Hovius, Dr. K. L. Martinez, Prof. H. Vogel
Laboratoire de Chimie Physique des Polymères et Membranes
Ecole Polytechnique Fédérale de Lausanne
1015 Lausanne (Switzerland)
Fax: (+41) 21-693-61-90
E-mail: horst.vogel@epfl.ch

Dr. M. Adrian
Laboratoire d'Analyse Ultrastructurale
Université de Lausanne, 1015 Lausanne (Switzerland)

Dr. K. R. Thampi
Laboratoire de Photoniques et Interfaces
Ecole Polytechnique Fédérale de Lausanne
1015 Lausanne (Switzerland)

[**] This work was supported by the Swiss National Science Foundation (NRP47). We thank Dr. D. Stamou for micropatterning instructions, Dr. J. Wiedmann for plasmids encoding eqFP611-His₆, E. Guignet for help in culturing bacteria and purifying proteins, Dr. C. Duschl for discussions, and Dr. D. Abankwa for reading the manuscript.

and (bio)technological processes on the nanometer scale.^[1–3] An interesting recent development in this context is to combine semiconducting nanocrystals (NCs) of well-known, exceptional optical properties^[4,5] with various biomolecular recognition sites to produce supramolecular assemblies for *in vitro* and *in vivo* bioanalytical applications.^[6–15]

Herein, we present a general and versatile procedure to make NCs water-soluble and simultaneously decorate them with a diverse range of multiple functionalities. Our approach is based on the self-assembly of single lipid monolayers on hydrophobic NCs. The lipid coat shields the NCs perfectly from physical and chemical modification. Interestingly, it is possible to tune the physical (electrical charges, structures, entropic shielding) and chemical (reactive group, biological recognition elements) surface properties of the NCs by varying the polar head groups of the lipid. This effect can be simply controlled by the composition of the lipids used for self-assembly. We demonstrate that such multifunctionalized lipid-coated NCs can bind different proteins per particle specifically and subsequently position themselves on micro-patterned surfaces to form nanometer-sized supramolecular structures of higher complexity. Although lipids have already been used for coating (sub)micrometer containers and spheres as well as nanoparticles,^[7,16,17] their potential for multifunctionalization and formation of complex supramolecular structures have not yet been exploited in this field.

Triethylphosphine oxide (TOPO) stabilized CdSe NCs were cosolubilized with lipids in organic solvent and transferred in one step to an aqueous solution, thereby coating them with a monolayer of (functionalized) phospholipids. Aqueous solutions of these so-called lipid-NCs remain remarkably stable for several weeks. The lipid-NCs featured virtually identical spectral shape and photostability in water to those of the original NCs in organic solution, except for a twofold decrease in the fluorescence quantum yield. Lower fluorescence quantum yields of nanoparticles in water as compared to those in organic solvents have been reported before (see for example, ref [18] and references therein). However, the molecular basis of this effect is not yet understood. As shown recently, the organic coating layer can play an active role in the creation or prevention of fluorescence-quenching surface states of fluorescent NCs.^[19]

The lipid-NCs appear in cryo-TEM images as particles composed of a central black spot and a gray outer ring, which represent the dense inorganic CdSe core and the organic TOPO/lipid layer, respectively (Figure 1a). The average diameter of the lipid-NC particles is 9 nm, which corresponds to the CdSe core (3 nm) plus twice the thickness of the TOPO (1 nm^[20]) and lipid (2 nm^[21]) layers (Figure 1b and c).

The simple and versatile introduction of functional groups into the lipid coat of the NCs is demonstrated for two prototypical examples, biotin and nitrilotriacetic acid (NTA). The fluorescence resonant energy transfer (FRET) is measured upon specific interaction between the functionalized lipid-NCs, named biotin-NCs and NTA-NCs, and fluorescent streptavidin (SA) or oligohistidine-tagged proteins, respectively (Figure 2a).

First, addition of Alexa568-labeled SA (SA-A568) to a solution of biotin-NCs resulted in a progressive decrease in

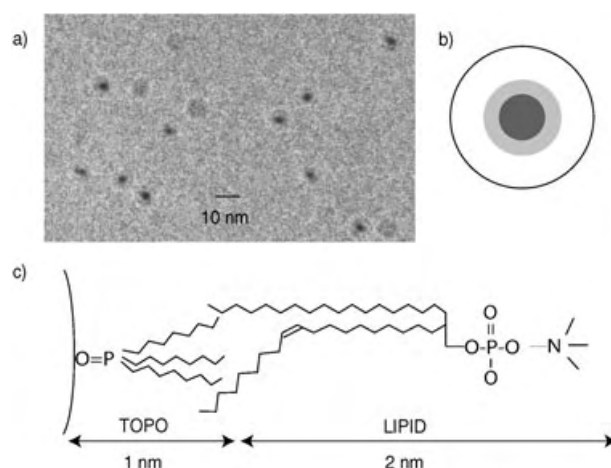


Figure 1. Composition of a lipid-NC. a) Cryogenic electron microscopy image of a vitrified solution of lipid-NCs. More than 80% of the NCs are monomeric. b) Schematic representation showing a CdSe nanocrystal (dark gray) covered by a monolayer of TOPO (light gray) which is surrounded by a self-assembled lipid monolayer (white). c) Schematic structure and orientation of TOPO and POPC with respect to the NC surface (curved line).

the fluorescence intensity of the biotin-NCs and a simultaneous increase of the SA-A568 fluorescence intensity as a result of FRET (Figure 2b). A FRET efficiency of 50% was obtained for a molar ratio of two SA units per biotin-NC. Higher concentrations of SA resulted in aggregation of the biotin-NCs because of the multivalent binding capability of SA. Control experiments performed with lipid-NC lacking biotinylated lipids did not show any change in the fluorescence intensities of the NC and SA-A568, which confirms the specific interaction between biotin-NCs and SA. Binding of SA-A568 to biotin-NCs resulted in a small blue-shift of the NC emission (also visible in Figure 3 with Alexa633-labelled SA (SA-A633)). This shift might be caused by changes in the electrostatic environment of NCs as a result of the proximity of negatively charged SA, since it is also observed for nonlabeled SA.

Second, specific binding of an oligohistidine-tagged protein to NTA-NCs was investigated using eqFP611-His₆,^[22] a red fluorescent protein with an N-terminal hexahistidine sequence. Addition of eqFP611-His₆ to NTA-NCs resulted in a saturating decrease in the NC fluorescence and a concomitant increase in the eqFP611-His₆ fluorescence intensity (Figure 2c). Subsequent addition of ethylenediamine tetraacetate (EDTA) reversed this effect. Control experiments using lipid-NCs lacking NTA did not show any interaction between the NCs and eqFP611-His₆. These findings show that eqFP611-His₆ binds specifically to NTA-NCs. A stoichiometry of four to five fluorescent proteins per NC could be estimated from the concentration dependence of the FRET efficiency. The maximal FRET efficiency obtained is determined by the optical properties of the donor–acceptor pair, and the number of accessible binding sites on the NCs.

Supramolecular assemblies of higher complexity were formed using lipid-NCs that were functionalized simultaneously with biotin and NTA in the lipid coat (biotin/NTA-

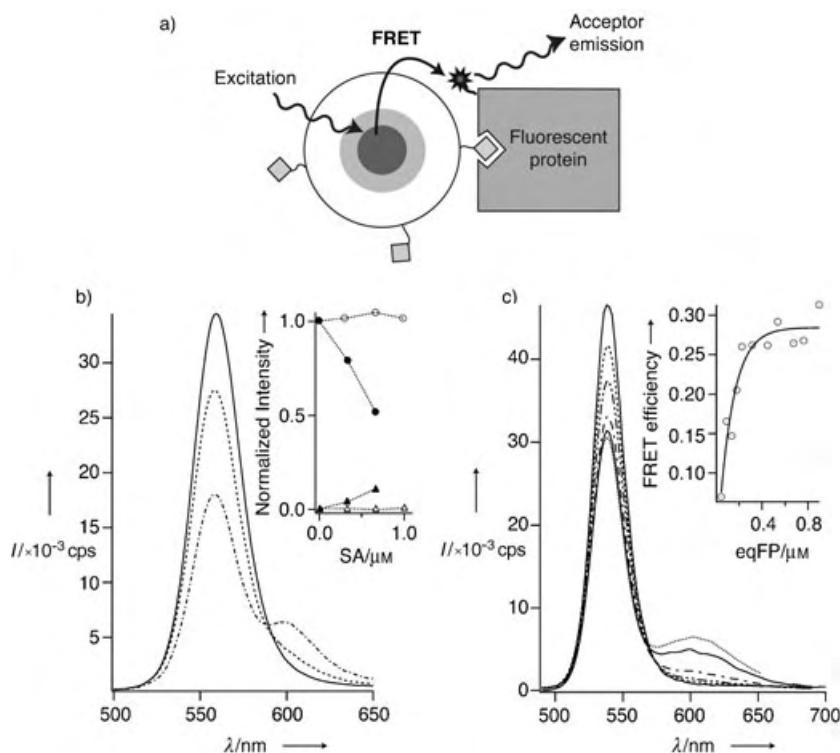


Figure 2. a) Specific interaction between a functionalized lipid-NC and a protein revealed by FRET. b) Fluorescence spectra of biotin-NCs (1 μm) in the absence (—) or presence (---- and -.-.-) of increasing concentrations of SA-A568. Excitation was at 440 nm. Insert: Intensities at the maximum of the fluorescence spectrum of biotin-NCs (560 nm, \bullet) and SA-A568 (601 nm, \blacktriangle) and for the control experiment of nonfunctionalized lipid-coated NCs (560 nm, \circ and 601 nm, \triangle) at increasing concentrations of SA-A568. The Förster distance R_0 for the couple NC/SA-A568 is 5.8 ± 0.2 nm. c) Fluorescence emission spectra of NTA-NCs (50 nm) in the absence (—) or presence (dotted and dashed lines) of increasing concentrations of eqFP611-His₆. Excitation was at 410 nm. Insert: FRET efficiency increased with the eqFP611-His₆ concentration to reach a maximum value of $E = 0.28$. The R_0 value for the couple NC/eqFP611-His₆ is 6.5 ± 0.2 nm. The distance between NC and eqFP611-His₆ is 9.7 ± 0.3 nm for 4–5 eqFP611-His₆ moieties per NC. All spectra shown were corrected for direct excitation of the fluorescent proteins.

NCs). The presence of both functionalities on the same NC could be demonstrated by sequential FRET from the NC via eqFP611-His₆ to SA-A633 upon addition of these proteins to biotin/NTA-NCs (Figure 3). Control experiments showed that eqFP611-His₆ and SA-A633 do not interact with each other or with lipid-NCs lacking both biotin and NTA. The average distances between the NC and either eqFP611 or SA, and between eqFP611 and SA, as determined by FRET are 9, 7, and 10 nm, respectively.

These results demonstrate two important features of multifunctionalized NCs. First, they can act as nanometer-sized scaffolds for the confined self-assembly of non-interacting macromolecules. Second, they serve as local excitation sources that transmit their excitation energy sequentially over distances greater than 10 nm by FRET to particular components within the supramolecular nanoassemblies.

In the next step, supramolecular nanostructures were built on top of 2D microstructured surfaces by exploiting the two

above-mentioned concepts (Figure 4a). The micro-patterning of SA on glass allowed the binding of biotin/NTA-NCs to surface areas of predefined shape (Figure 4b). Subsequent addition of eqFP611-His₆ led to the specific immobilization of this protein on the biotin/NTA-NCs areas, as demonstrated by co-localization of the fluorescence of both components and FRET between the biotin/NTA-NCs and eqFP611-His₆ (Figure 4c). The eqFP611-His₆ remained immobilized on surface-patterned nanostructures even after multiple washing with buffer, but was released after adding EDTA, which shows that the interaction between oligohistidine sequences and the NTA groups is stable and fully reversible. No binding to micro-patterned SA was observed for lipid-NCs lacking biotin or for the biotin/NTA-NCs upon preincubation of the surface with excess biotin, which confirms specific binding of the NCs to the structured surface.

Patterned nanometer-sized local light sources offer attractive applications, for example, for DNA or protein arrays, where nonspecific binding of labeled analyte molecules impairs the high sensitivity with standard illumination techniques (resolution: hundreds of nanometers). The NCs, as a

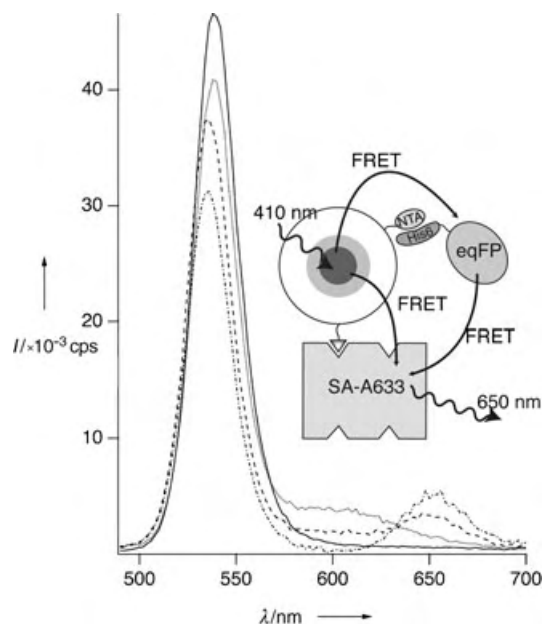


Figure 3. Schematic representation of a biotin/NTA-NC interacting with both eqFP611-His₆ and SA-A633. Fluorescence spectra of a 100-nM solution of the biotin/NTA-functionalized lipid-NCs in the absence (—) or presence of 0.4 μM eqFP611-His₆ (.....), and after subsequent addition of 47 nm (----) and 156 nm (---) SA-Alexa633 are also shown. Excitation was at 410 nm. FRET was first observed from the biotin/NTA-NCs to eqFP-His₆ and subsequently from the NCs to Alexa633, both directly and indirectly through eqFP611-His₆. The values of R_0 for the FRET couples NC/eqFP611, NC/SA-A633, and eqFP611/SA-A633 are 6.5 ± 0.2 , 5.1 ± 0.2 , and 10.2 ± 0.2 nm, respectively. The distances between these FRET couples are 8–9, 6–7, and 10–11 nm, respectively.

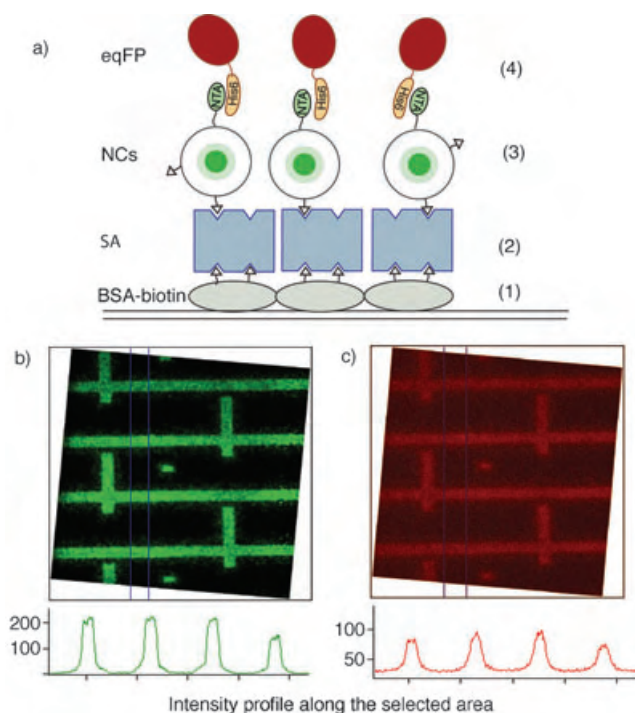


Figure 4. Directed supramolecular self-assembly on micropatterned surfaces using multifunctional NCs. a) The process is composed of the following sequential steps: 1) microcontact printing of biotinylated BSA (BSA-biotin) in 4- μm -wide lines on a glass surface; 2) binding of SA; 3) addition of biotin/NTA-NCs; and 4) incubation with eqFP611-His₆. b, c) Fluorescence confocal microscopy images and intensity profiles demonstrate specific binding of biotin/NTA-NCs to surface-patterned SA (b), step 3 (excitation: 458 nm; emission: 505–565 nm band-pass filter) and binding of eqFP611-His₆ onto surface-bound biotin/NTA-NC (c), with observation by FRET from biotin/NTA-NCs to eqFP611-His₆, step 4 (excitation: 458 nm; emission: 585 nm long-pass filter).

local light source, would only excite specifically bound analyte molecules within the FRET range (about 10 nm), thus enhancing the signal-to-noise ratio.

In summary, we have presented a versatile method to place multiple functionalities on NCs through lipid coating while minimizing nonspecific interactions. The physical and chemical long-term stability (weeks) of lipid-NCs is comparable to that of NCs covered by multilayered polymer coats.^[23] If required, the chemical stability of the lipids can be increased even further by using, for example, lipids comprising ether instead of ester groups or by using lipids isolated from thermophilic bacteria.^[24] Compared to the existing polymer-coated NCs, which are commercially available, the lipid-NCs offer complementary novel applications. Specific interaction between such NCs and different proteins through multiple high-affinity binding sites enabled site-selective controlled formation of supramolecular assemblies. The multifunctional NCs serve as local light sources which can be positioned with nanometer precision within supramolecular assemblies and can emit light over distances from 1 to more than 10 nm, again controlled with nanometer precision. Such concepts might be of importance for the development of biotechnology and bioanalytics on a nanometer and attoliter

scale. Challenging examples are the use of single NCs for investigating substrate tunneling on multienzyme complexes,^[25,26] or (bio)chemical syntheses and biomolecular reactions in submicrometer-sized containers.^[27–29]

Experimental Section

Lipid-coated NCs: TOPO-stabilized CdSe NCs, synthesized in TOPO according to Peng,^[30] were precipitated, centrifuged (4000 rpm, 5 min), and suspended in chloroform (2 volumes) containing lipids (1 mg mL^{−1}) composed of: a) 1-palmitoyl-2-oleyl-*sn*-glycerophosphatidylcholine (POPC; 90 mol %) and 1-palmitoyl-2-oleyl-*sn*-glycerophosphatidylglycerol (POPG; 10 mol %) for producing lipid-NCs; b) POPC (80 mol %), POPG (10 mol %), and either *N*-[6-(biotinoyl)amino]hexanoyl]-1,2-dihexadecanoyl-*sn*-glycero-3-phosphoethanolamine (DHPE-X-biotin, 10 mol %) or 1,2-dioleoyl-*sn*-glycero-3-[*N*-(5-amino-1-carboxypentyl)iminodiacetic acid succinyl] nickel salt (DOGS-NTA-Ni, 10 mol %), or an equimolar mixture of both, to produce biotin-, NTA-, or biotin/NTA-NCs, respectively. After adding β -octylglucopyranoside (OG, 26 mM) in water (4 volumes), the chloroform was evaporated under vacuum. The aqueous lipid-coated NC solution was dialyzed twice against 2000 volumes of water or phosphate-buffered saline (PBS) buffer to remove the detergent.

Absorbance and fluorescence spectra were recorded on a Perkin Elmer Lambda 35 spectrometer and a SPEX-fluorolog II instrument (Jobin Yvon, Stanmore, UK), respectively. Fluorescence quantum yields were determined as described elsewhere^[31] using perylene-imide as standard.^[32] The CdSe NCs exhibited fluorescence quantum yields of 20–25 % and maximal fluorescence intensities between 540 and 560 nm, which correspond to CdSe core diameters between 2.9 and 3.3 nm;^[33] the spectral halfwidths of less than 30 nm indicate that the particles are uniform with less than 10 % variation in the particle size.

Samples for cryo-TEM were prepared as described elsewhere;^[34] images from samples at -172°C were recorded at a nominal magnification of 45000 on Kodak 4489 film in a Phillips CM12 electron microscope operated at 80 kV.

The Förster distance R_0 was calculated as previously described^[31,35] assuming isotropic distribution of the transition dipoles of donor and acceptors, by taking the refractive index as 1.4 and quantum yield values of 0.1 and 0.45 for the NC and eqFP, respectively. The number n of acceptors associated with one NC and the distance r between donor and acceptor were calculated from the FRET efficiency E using the relation $E = nR_0^6/(nR_0^6 + r^6)$ ^[6] and assuming that all acceptors are equidistant to the NC donor.

Surface patterning of NCs: NCs (40 nm) in PBS were overlaid on SA, which was patterned on glass slides in 4- μm -wide line structures as described elsewhere.^[27,36,37] As a control experiment for specific binding, the surface was preincubated with biotin (1 μM) before adding the biotin/NTA-NCs. The formation and binding of molecules onto NC micropatterns were observed with a Zeiss LSM 510 confocal fluorescence microscope using appropriate laser and filter settings.

Received: July 30, 2004

Revised: November 11, 2004

Published online: January 26, 2005

Keywords: FRET (fluorescence resonant energy transfer) · lipids · luminescence · micropatterning · nanostructures

[1] H. Kuhn, H.-D. Försterling, *Principles of Physical Chemistry: Understanding Molecules, Molecular Assemblies, Supramolecular Machines*, Wiley, New York, **2000**.

[2] G. M. Whitesides, B. Grzybowski, *Science* **2002**, 295, 2418.

- [3] D. S. Goodsell, *Bionanotechnology: Lessons from Nature*, Wiley, Hoboken, NJ, **2004**.
- [4] H. Weller, *Adv. Mater.* **1993**, 5, 88.
- [5] S. V. Gaponenko, *Optical Properties of Semiconductor Nanocrystals*, Cambridge University Press, New York, **1998**.
- [6] A. R. Clapp, I. L. Medintz, J. M. Mauro, B. R. Fisher, M. G. Bawendi, H. Mattoussi, *J. Am. Chem. Soc.* **2004**, 126, 301.
- [7] B. Dubertret, P. Skourides, D. J. Norris, V. Noireaux, A. H. Brivanlou, A. Libchaber, *Science* **2002**, 298, 1759.
- [8] M. Bäuml, D. Stamou, J.-M. Segura, R. Hovius, H. Vogel, *Langmuir* **2004**, 20, 3828.
- [9] A. Sukhanova, M. Devy, L. Venteo, H. Kaplan, M. Artemyev, V. Oleinikov, D. Klinov, M. Pluot, J. H. M. Cohen, I. Nabiev, *Anal. Biochem.* **2004**, 324, 60.
- [10] M. Bruchez, M. Moronne, P. Gin, S. Weiss, A. P. Alivisatos, *Science* **1998**, 281, 2013.
- [11] W. C. W. Chan, S. M. Nie, *Science* **1998**, 281, 2016.
- [12] X. Michalet, F. Pinaud, T. D. Lacoste, M. Dahan, M. P. Bruchez, A. P. Alivisatos, S. Weiss, *Single Mol.* **2001**, 2, 261.
- [13] C. M. Niemeyer, *Angew. Chem.* **2001**, 113, 4254; *Angew. Chem. Int. Ed.* **2001**, 40, 4128.
- [14] C. M. Niemeyer, *Angew. Chem.* **2003**, 115, 5974; *Angew. Chem. Int. Ed.* **2003**, 42, 5796.
- [15] J.-M. Nam, C. S. Thaxton, C. A. Mirkin, *Science* **2003**, 301, 1884.
- [16] S. Moya, E. Donath, G. B. Sukhorukov, M. Auch, H. Baumler, H. Lichtenfeld, H. Mohwald, *Macromolecules* **2000**, 33, 4538.
- [17] F. M. Linseisen, M. Hetzer, T. Brumm, T. M. Bayerl, *Biophys. J.* **1997**, 72, 1659.
- [18] F. Pinaud, D. King, H.-P. Moore, S. Weiss, *J. Am. Chem. Soc.* **2004**, 126, 6115.
- [19] S. F. Wüster, A. Van Houselt, C. de Mello Donega, D. Vanmaekelbergh, A. Meijerink, *Angew. Chem.* **2004**, 116, 3091; *Angew. Chem. Int. Ed.* **2004**, 43, 3029.
- [20] J. E. Bowen Katari, V. L. Colvin, A. P. Alivisatos, *J. Phys. Chem.* **1994**, 98, 4109.
- [21] H. S. White, W. C. Wimley, *Annu. Rev. Biophys. Biomol. Struct.* **1999**, 28, 319.
- [22] J. Wiedenmann, A. Schenk, C. Rocker, A. Girod, K. D. Spindler, G. U. Nienhaus, *Proc. Natl. Acad. Sci. USA* **2002**, 99, 11646.
- [23] X. Wu, H. Lui, J. Lui, K. N. Haley, J. A. Treadway, J. P. Larson, G. Ge, F. Peale, M. P. Bruchez, *Nat. Biotechnol.* **2003**, 21, 41.
- [24] R. B. Gennis, *Biomembranes*, Springer, Heidelberg, **1989**.
- [25] C. Khosla, P. B. Harbury, *Nature* **2001**, 409, 247.
- [26] R. N. Perham, *Annu. Rev. Biochem.* **2000**, 69, 961.
- [27] D. Stamou, C. Duschl, E. Delamarche, H. Vogel, *Angew. Chem.* **2003**, 115, 5738; *Angew. Chem. Int. Ed.* **2003**, 42, 5580.
- [28] P.-Y. Bolinger, D. Stamou, H. Vogel, *J. Am. Chem. Soc.* **2004**, 126, 8594.
- [29] D. T. Chiu, R. N. Zare, *Science* **1999**, 283, 1892.
- [30] Z. A. Peng, X. Peng, *J. Am. Chem. Soc.* **2001**, 123, 183.
- [31] J. R. Lakowicz, *Principles of Fluorescence Spectroscopy*, 2nd ed., Kluwer, New York, **1999**.
- [32] J. Hofkens, L. Latterini, G. De Belder, T. Gensch, M. Maus, T. Vosch, Y. Karni, G. Schweitzer, F. C. De Schryver, A. Hermann, K. Müllen, *Chem. Phys. Lett.* **1999**, 304, 1.
- [33] O. Schmelz, A. Mews, T. Basche, A. Herrmann, K. Müllen, *Langmuir* **2001**, 17, 2861.
- [34] J. Dubochet, M. Adrian, J.-J. Chang, J.-C. Homo, J. Lepault, A. W. McDowell, P. Schultz, *Q. Rev. Biophys.* **1988**, 21, 129.
- [35] E. G. Guignat, R. Hovius, H. Vogel, *Nat. Biotechnol.* **2004**, 22, 440.
- [36] Y. N. Xia, G. M. Whitesides, *Angew. Chem.* **1998**, 110, 568; *Angew. Chem. Int. Ed.* **1998**, 37, 550.
- [37] A. Bernard, E. Delamarche, H. Schmid, B. Michel, H. R. Bosshard, H. Biebuyck, *Langmuir* **1998**, 14, 2225.

The First μ_6 -Peroxide Transition-Metal Complex: $[\text{Ni}_8(\text{L})_{12}(\text{O}_2)]^{2+**}$

Emma J. Brown, Anne-K. Duhme-Klair,*
Matthew I. Elliott, Jane E. Thomas-Oates,
Phillipa L. Timmins, and Paul H. Walton*

There continues to be significant attention given to the structural characterization of metal peroxide complexes.^[1] The coordination modes observed in such complexes range from peroxide coordination to a single metal center to peroxide acting as a bridging ligand between two, three, four, or six metal ions. Simple μ -peroxo complexes are common; iron, cobalt, and copper dimers are the most prevalent, with recent attention concentrated on Fe-peroxo-Cu complexes as models of the active site of cytochrome c oxidase (Figure 1 a).^[2] μ_3 -Peroxo-coordination is rare, but has

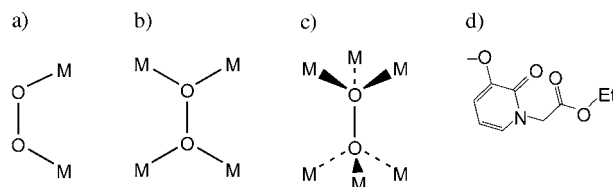


Figure 1. Peroxo binding modes: a) μ -(η^1), b) μ_4 -(η^1)₂, c) μ_6 -(η^1)₃, d) N-substituted 3-hydroxy-2-pyridinonate (L) used in this study.

been proposed as part of the laccase active site.^[3,4] Molecular species with a μ_4 -coordination mode are restricted to a handful of examples, with copper, iron, tungsten, antimony, and molybdenum complexes (Figure 1 b).^[5–13] In addition, there are two reports of a potential μ_6 -coordination mode in $[\text{Ba}_6(\text{L})_{10}(\text{H}_2\text{O})_n(\text{O}_2)]$ complexes ($n=2$ or 4), where the peroxide ion in a $[\text{Ba}_4\mu_4-(\text{O}_2)]$ moiety bridges two further barium ions in a μ - η^2 : η^2 fashion.^[14,15] As far as we can determine, however, there are no molecular examples of peroxide acting in the μ_6 -(η^1)₃ binding mode shown in Figure 1 c. This mode of binding is significant insofar as it would complete the family of possible symmetrical μ_n -(η^1) _{$n/2$} peroxide binding modes in molecular complexes.

[*] E. J. Brown, Dr. A.-K. Duhme-Klair, Dr. M. I. Elliott,
Prof. J. E. Thomas-Oates, Dr. P. L. Timmins, Prof. P. H. Walton
Department of Chemistry
University of York
York YO10 5DD (United Kingdom)
Fax: (+44) 1904-342-516
E-mail: akd1@york.ac.uk
phw2@york.ac.uk

[**] We thank Drs. Nigel A. Young (University of Hull), John N. Moore, and Laurence C. Abbott for their assistance with the Raman experiments and Prof. Robin N. Perutz and Dr. Adrian C. Whitwood for helpful discussions. E.J.B. acknowledges the Biotechnology and Biological Sciences Research Council for funding. L-H = 1-[(ethoxycarbonyl)methyl]-3-hydroxy-2-pyridinone.



Supporting information for this article is available on the WWW under <http://www.angewandte.org> or from the author.

Lately we have been investigating the preparation and reactions of metal complexes that employ N-substituted 3-hydroxy-2-pyridinones (**L**-H, Figure 1d) as ligands.^[16] Hydroxypyridinones have been used extensively as ligands designed to sequester metals.^[17] Also, the closely related 2-hydroxypyridine ligands have been used to synthesize metal complexes, including Ni₈ and Mn₁₂ clusters.^[18,19] During our study with **L** we noted the formation of an unusual peroxide-containing Ni₈ complex **1**. This complex is synthesized at room temperature from the addition of an ethanolic solution of **L**-H (2 equiv) to an ethanolic solution of Ni(NO₃)₂·nH₂O followed by addition of aqueous H₂O₂. Addition of triethylamine (2 equiv) generates a pale green precipitate of [Ni₈(**L**)₁₂(O₂)](NO₃)₂ (**1**) in approximately 80% yield. Compound **1** can be crystallized from dimethylformamide solution by vapor diffusion of diethyl ether.

Compound **1** is air-stable and was characterized by elemental analysis, UV/Vis spectroscopy, Raman spectroscopy, ES-mass spectrometry (see Supporting Information),^[20] and single-crystal X-ray diffraction.^[21–23] In addition to a satisfactory elemental analysis, the peroxide content of **1** could be determined iodometrically,^[20] giving a peroxide content of 1.15% (calcd: 1.10%), and electrospray (ES) mass spectrometry shows a series of peaks with a maximum intensity at *m/z* 1427.1 consistent with [Ni₈(**L**)₁₂(O₂)]²⁺; the isotopic distribution pattern matches that which is calculated for this elemental composition (Figure 2). Repeating the synthesis with H₂¹⁸O₂ affords the same product, which gives an ES mass spectrum containing a similar pattern of peaks now centered around *m/z* 1429.1. This pattern is consistent with the analogous [Ni₈(**L**)₁₂(¹⁸O₂)]²⁺ ion.

The structure of **1** was determined by single-crystal X-ray diffraction (Figure 3).^[20,21] The Ni₈ cage is sited on a crystallographic center of symmetry and consists of a central Ni₆(O₂) core with near-*D*_{3d} local symmetry, where the six nickel ions form the apices of an octahedron (see Figure 3; Ni···Ni separations in core, minimum = 3.234(2), maximum = 3.330(2), average = 3.291(2) Å). These separations indicate that there are no significant Ni···Ni interactions within the cage. The octahedron is end-capped by two six-coordinate nickel ions, giving an overall bicapped-octahedral arrangement of nickel ions. The eight nickel ions are held together by bridging oxygen atoms from twelve **L** ligands. The two capping nickel ions can be viewed as two Ni(**L**)₃ units, and the Ni₆ core as an Ni₆(O₂)(**L**)₆ unit.

The dipositive charge of the complex indicates that the central ligand is formally O₂²⁻. The peroxo ligand is completely caged at the center of the Ni₆ core. The peroxide axis is collinear with a threefold rotation axis of the octahedron and the principal *C*₃ axis of *D*_{3d} (Figure 3). This structural

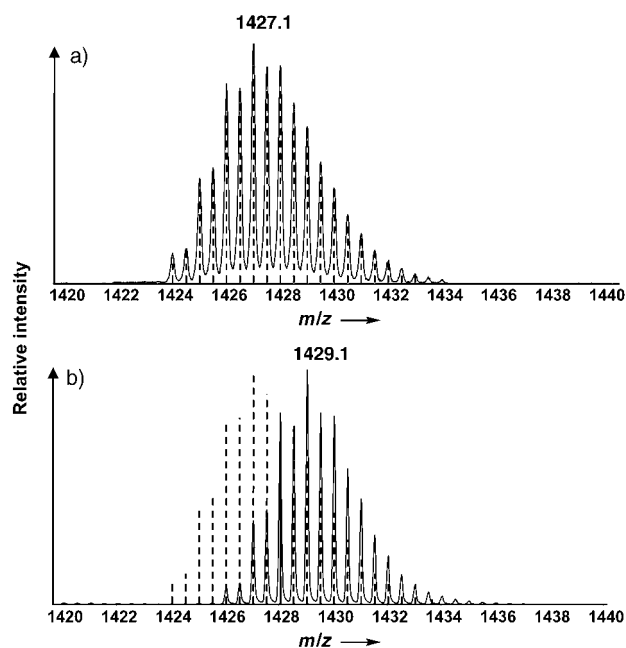


Figure 2. ES-MS analysis of a) **1** and b) [Ni₈(**L**)₁₂(¹⁸O₂)](NO₃)₂. Calculated isotopic distribution patterns for [Ni₈(**L**)₁₂(¹⁶O₂)]²⁺ are shown as broken vertical lines. In each panel, the y-axis has been normalized to the base peak in the ion cluster.

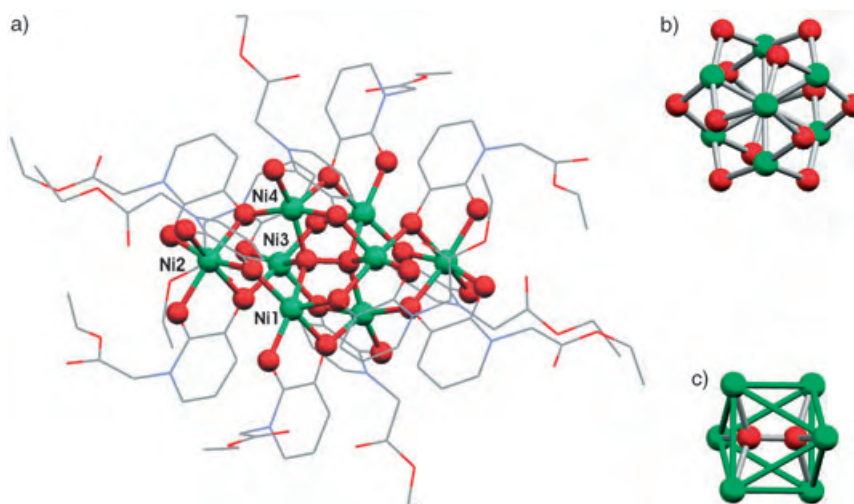


Figure 3. a) Solid-state structure of [Ni₈(**L**)₁₂(O₂)]²⁺ (hydrogen atoms are omitted for clarity),^[20] b) view of the Ni₈ unit along the peroxide O–O bond showing bridging oxygen atoms only, c) Ni₆(O₂) core; red O, green Ni.

arrangement is analogous to that observed in simple binary metal peroxides, such as Zn(O₂) and Cd(O₂), which adopt a cubic pyrites structure.^[24] The structure of a simple Ni(O₂) species is not known, although Ni(S₂) is known to adopt the pyrites structure. Assuming that the Ni₆(O₂) core is representative of the bulk structure of Ni(O₂), then it is possible to view **1** as a small fragment of Ni(O₂) surrounded by a shell of hydroxypyridinonate ligands.

In the Ni₆(O₂) unit, each nickel ion has a distorted square-pyramidal coordination geometry, with the peroxo oxygen occupying a basal coordination site. The Ni–O(peroxo) bond

lengths are 1.992(6), 1.963(8), and 2.019(6) Å. The Ni-O(peroxo)-Ni angles are 109.5(3), 112.2(3), and 109.7(3)°, and the nickel ions are in staggered conformation around the peroxide bond; adjacent Ni-O-O-Ni torsion angles range from 58.0 to 61.5°. A simple molecular orbital analysis of the σ bonding within the $\text{Ni}_6(\text{O}_2)$ unit indicates that a bonding combination of molecular orbitals can be formed between the HOMO of the peroxide and the $d_{x^2-y^2}$ orbitals of the nickel ions. The O-O bond length in the peroxide is 1.456(12) Å, which is within the range of other known peroxide bond lengths, but is at the shorter end of the expected range, possibly reflecting a nickel-peroxide interaction that is largely ionic in nature.^[25]

The Raman spectrum of **1** recorded with laser excitation at 514.5 nm shows bands in the expected region of a peroxide vibration (600–1000 cm^{-1}) at 758(s), 769(w), 817(w), 854(vs), and 881(s) cm^{-1} . None of these bands, however, was sensitive to isotopic substitution of the peroxide (see Supporting Information). Below 350 nm, the UV/Vis spectrum of **1** is dominated by strong ligand-based absorption bands (see Supporting Information). Consequently, the peroxo \rightarrow Ni^{II} charge-transfer band could not be located with certainty. Attempts to achieve resonance enhancement of the $\nu(\text{O-O})$ vibration by excitation at 350.6 and 325.0 nm were unsuccessful. The solutions of **1** in methanol or ethanol changed color upon irradiation at these wavelengths, which may indicate photodecomposition. We are, therefore, unable to determine the peroxide stretching frequency.

Notwithstanding the wide use of nickel peroxides in organic synthesis, examples of nickel peroxides that have been structurally characterized are relatively rare.^[26] A search of the Cambridge Structural Database suggests that **1** is the second molecular nickel peroxide complex to be structurally characterized; the previous example is a monomeric $[(t\text{BuNC})_2\text{Ni}(\text{O}_2)]$ complex.^[27] In addition, a bis(μ -alkylperoxo)dinickel complex was isolated and structurally characterized very recently,^[28] the synthesis of which involved a related bis(μ -superoxo)dinickel(II) complex.^[29] A monomeric Ni-O₂ adduct was also reported recently and described as Ni^{II}-superoxo species, although no single-crystal X-ray diffraction data were obtained.^[30] Despite the scarcity of nickel peroxide complexes, however, recent calculations on $[\text{L}_n\text{Ni}_2(\text{O}_2)]$ and $[\text{L}_n\text{Ni}(\text{O}_2)]$ complexes suggest that molecular nickel peroxides should be stable.^[31] Thus, the preparation and isolation of **1** in good yield is an indication of the accessibility of molecular nickel peroxide species. In contrast to most other metal peroxo species, **1** is thermally relatively stable and can be isolated and handled at room temperature. The effective encapsulation of the peroxide by the octanuclear nickel cage stabilizes the reactive species. Interestingly, an unusually high thermal stability was also reported for the tetranuclear $\mu_4-(\eta^1)_2$ -peroxocopper(II) complex.^[5]

In conclusion, we have demonstrated the preparation and characterization of a novel Ni_8 -peroxide-containing cage. The assignment of the central peroxo ligand is supported by chemical analyses, X-ray crystallography, and ES mass spectrometry. The peroxide is present in an unprecedented $\mu_6-(\eta^1)_3$ binding mode, thus completing the family of possible symmetrical $\mu_n-(\eta^1)_{n/2}$ peroxide binding modes in molecular

species. The complex can be viewed as a small fragment of solid state $\text{Ni}(\text{O}_2)_2$ surrounded by a shell of hydroxypyridinonate ligands.^[32]

Received: September 3, 2004

Revised: October 12, 2004

Published online: January 3, 2005

Please note: Minor changes have been made to this manuscript since its publication in *Angewandte Chemie* Early View. The Editor.

Keywords: cluster compounds · coordination modes · hydroxypyridinones · nickel · peroxides

- [1] See, for example: A. G. Blackman, W. B. Tolman, *Struct. Bonding (Berlin)* **2000**, 97, 179.
- [2] E. Kim, M. E. Helton, I. M. Wasser, K. D. Karlin, S. Lu, H. W. Huang, P. Moenne-Loccoz, C. D. Incarvito, A. L. Rheingold, M. Honecker, S. Kaderli, A. D. Zuberbühler, *Proc. Natl. Acad. Sci. USA* **2003**, 100, 3623, and references therein.
- [3] U. M. Sundaram, H. H. Zhang, B. Hedman, K. O. Hodgson, E. I. Solomon, *J. Am. Chem. Soc.* **1997**, 119, 12525.
- [4] N. Hakulinen, L. L. Kiiskinen, K. Kruus, M. Saloheimo, A. Paananen, A. Koivula, J. Rouvinen, *Nat. Struct. Biol.* **2002**, 9, 601.
- [5] J. Reim, R. Werner, W. Haase, B. Krebs, *Chem. Eur. J.* **1998**, 4, 289.
- [6] F. Meyer, H. Pritzkow, *Angew. Chem.* **2000**, 112, 2199; *Angew. Chem. Int. Ed.* **2000**, 39, 2112.
- [7] I. Shweky, L. E. Pence, G. C. Papaefthymiou, R. Sessoli, J. W. Yun, A. Bino, S. J. Lippard, *J. Am. Chem. Soc.* **1997**, 119, 1037.
- [8] R. Çelenligil-Çetin, R. J. Staples, P. Stavropoulos, *Inorg. Chem.* **2000**, 39, 5838.
- [9] W. Micklitz, S. G. Bott, J. G. Bentsen, S. J. Lippard, *J. Am. Chem. Soc.* **1989**, 111, 372.
- [10] T. Ozeki, T. Yamase, *Bull. Chem. Soc. Jpn.* **1997**, 70, 2101.
- [11] E. I. Tolis, M. Helliwell, S. Langley, J. Raftery, R. E. P. Winpenny, *Angew. Chem.* **2003**, 115, 3934; *Angew. Chem. Int. Ed.* **2003**, 42, 3804.
- [12] R. Stomberg, L. Trysberg, I. Larking, *Acta Chem. Scand.* **1970**, 24, 2678.
- [13] O. W. Howarth, *Dalton Trans.* **2004**, 476; H. J. Breunig, T. Krüger, E. Lork, *Angew. Chem.* **1997**, 109, 654; *Angew. Chem. Int. Ed. Engl.* **1997**, 36, 615.
- [14] N. Hovnanian, J. Galloy, P. Miele, *Polyhedron* **1995**, 14, 297.
- [15] J. Auld, A. C. Jones, A. B. Leese, B. Cockayne, P. J. Wright, P. O'Brien, M. Motevalli, *J. Mater. Chem.* **1993**, 3, 1203.
- [16] E. J. Brown, A.-K. Duhme-Klair, P. H. Walton, *Dalton Trans.* **2004**, 2458.
- [17] A. E. V. Gorden, J. D. Xu, K. N. Raymond, P. Durbin, *Chem. Rev.* **2003**, 103, 4207.
- [18] E. K. Brechin, W. Clegg, M. Murrie, S. Parsons, S. J. Teat, R. E. P. Winpenny, *J. Am. Chem. Soc.* **1998**, 120, 7365.
- [19] G. Aromi, A. R. Bell, M. Helliwell, J. Raftery, S. J. Teat, G. A. Timco, O. Roubeau, R. E. P. Winpenny, *Chem. Eur. J.* **2003**, 9, 3024, and references therein.
- [20] Full experimental and analytical details are available as Supporting Information.
- [21] Crystal data: $\text{C}_{108}\text{H}_{120}\text{N}_{14}\text{Ni}_8\text{O}_{56}$, $M_r = 2979.86$, crystal dimensions $0.40 \times 0.18 \times 0.06 \text{ mm}^3$, monoclinic, $P2_1/n$, $a = 15.0314(12)$, $b = 21.9851(17)$, $c = 19.1166(15) \text{ Å}$, $\beta = 94.453(3)^\circ$, $V = 6298.3(9) \text{ Å}^3$, $Z = 2$, $\rho_{\text{calcd}} = 1.571 \text{ g cm}^{-3}$, $2\theta_{\text{max}} = 41.68^\circ$, $T = 100(2) \text{ K}$, 8572 reflections measured, 6604 independent, $R_{\text{int}} = 0.1282$, 3920 reflections with $I \geq 2\sigma(I)$, $\mu = 1.269 \text{ mm}^{-1}$, absorption correction with SADABS^[22] (v2.03, Sheldrick),

($0.6307 \leq T \leq 0.0277$), 883 parameters, refinement against $|F^2|$, $R1 = 0.0560$ ($I = \geq 2\sigma(I)$), $wR2 = 0.1762$ (all data), $GoF = 1.072$, max shift/esd in final cycle = 0.00, largest difference peaks $0.86/-0.45 \text{ e}\text{\AA}^{-3}$, rms peak height = $0.10 \text{ e}\text{\AA}^{-3}$. Diffraction data were collected on a Bruker Smart Apex diffractometer with $\text{MoK}\alpha$ radiation ($\lambda = 0.71073 \text{ \AA}$) using a SMART CCD camera. Diffractometer control, data collection and initial unit cell determination was performed using SMART.^[22] Frame integration and unit-cell refinement software was carried out with the SAINT+^[22] software. Structures were solved by direct methods using SHELXS-97 and refined by full-matrix least squares using SHELXL-97.^[23] One of the side chains of the ligand, **L**, was assumed to be disordered over two positions. All non-hydrogen atoms were refined anisotropically, except for the disordered atoms, which were refined isotropically. Hydrogen atoms were placed using a “riding model” and included in the refinement at calculated positions. CCDC 252525 contains the supplementary crystallographic data for this paper. These data can be obtained free of charge from the Cambridge Crystallographic Data Centre via www.ccdc.cam.ac.uk/data_request/cif.

- [22] a) SMART Control software (v.5.625), Bruker-AXS Inc, Madison, USA; b) SAINT+ Integration software (v.6.22), Bruker-AXS Inc, Madison, USA; c) SADABS, G. M. Sheldrick, University of Göttingen, Germany.
- [23] a) SHELXS-97: Program for the Solution of Crystal Structures, G. M. Sheldrick, University of Göttingen, Germany, **1997**; b) SHELXL-97: Program for the Refinement of Crystal Structures, G. M. Sheldrick, University of Göttingen, Germany, **1997**.
- [24] C. W. W. Hoffman, R. C. Ropp, R. W. Mooney, *J. Chem. Soc.* **1959**, 81, 3830.
- [25] G. B. Jameson, J. A. Ibers in *Bioinorganic Chemistry* (Eds.: I. Bertini, H. B. Gray, S. J. Lippard, J. S. Valentine), University Science Books, Mill Valley, **1994**, pp. 167–252.
- [26] M. V. George, K. S. Balachandran, *Chem. Rev.* **1975**, 75, 491.
- [27] M. Matsumoto, K. Nakatsu, *Acta Crystallogr. B* **1975**, 31, 2711.
- [28] J. Cho, H. Furutachi, S. Fujinami, M. Suzuki, *Angew. Chem.* **2004**, 116, 3362; *Angew. Chem. Int. Ed.* **2004**, 43, 3300.
- [29] K. Shiren, S. Ogo, S. Fujinami, H. Hayashi, M. Suzuki, A. Uehara, Y. Watanabe, Y. Moro-oka, *J. Am. Chem. Soc.* **2000**, 122, 254.
- [30] K. Fujita, R. Schenker, W. Gu, T. C. Brunold, S. P. Cramer, C. G. Riordan, *Inorg. Chem.* **2004**, 43, 3324.
- [31] G. Aullón, M. Hamidi, A. Lledós, S. Alvarez, *Inorg. Chem.* **2004**, 43, 3702.
- [32] Note added in proof (January 12, 2005). The following article concerning peroxo-bridged nickel species has recently been published: M. T. Kieber-Emmons, R. Schenker, G. P. A. Yap, T. C. Brunold, C. G. Riordan, *Angew. Chem.* **2004**, 116, 6884; *Angew. Chem. Int. Ed.* **2004**, 43, 6716.

Nanophotonic Light Sources for Fluorescence Spectroscopy and Cellular Imaging**

Oliver Hayden* and Christine K. Payne*

*Dedicated to Professor Franz L. Dickert
on the occasion of his 60th birthday*

Herein we demonstrate a new approach to nanophotonics with the fabrication and application of nanoscale light-emitting diodes (nanoLEDs) for fluorescence spectroscopy and single-analyte detection, and as nearfield light sources for cellular imaging. The nanoLEDs have a final diameter of 50 nm and are easily integrated into microfluidic channels—a desirable property for future “lab-on-a-chip” systems. Nanophotonic devices have evolved by means of the bottom-up approach with quantum dots,^[1] carbon nanotubes,^[2] or semiconducting nanowires^[3] serving as low-dimensional building blocks. Of these devices, semiconducting nanowires offer a number of advantages for the fabrication of electrically driven nanodevices as they allow properties such as the emission wavelength^[4] of the device to be selected. Microfluidic assembly is then used to cross the semiconducting nanowires to form pn-junctions.^[5] The resulting nanowire devices can be fabricated on a variety of unconventional substrates, such as flexible plastic.^[6] We report here the first spectroscopic applications of nanoscale devices that use LEDs from crossed nanowire architectures as integrated light sources in microfluidic channels.

The nanoLEDs described here were fabricated by crossing 100-nm-diameter n-doped cadmium sulphide nanowires with 60-nm p-doped silicon nanowires (Figure 1). The nanowires have aspect ratios as high as 10^3 . The smallest diodes were prepared from 50-nm cadmium sulphide and 20-nm silicon nanowires to give a final diameter of less than 20 nm. The snapshot in Figure 2a shows the emission from the nanoLED when pulsed at 10 Hz (see Supporting Informa-

[*] Dr. O. Hayden,^[†] Dr. C. K. Payne
Department of Chemistry and Chemical Biology
Harvard University
12 Oxford Street, Cambridge, MA 02138 (USA)
E-mail: ckpayne@fas.harvard.edu

[†] Current address:
Institute of Analytical Chemistry
University of Vienna
Währingerstrasse 38, 1090 Vienna (Austria)
Fax: (+43) 1-4277-9523
E-mail: oliver.hayden@univie.ac.at

[**] O.H. is indebted to Prof. Charles M. Lieber for support of this project. C.K.P. is grateful to Prof. Xiaowei Zhuang and to a Ruth L. Kirschstein National Research Service Award (National Institutes of Health Postdoctoral Fellowship) for support. The authors would like to thank Dr. Richard Schalek and Dr. Laura Kaufman for helpful discussions.



Supporting information for this article is available on the WWW under <http://www.angewandte.org> or from the author.



Figure 1. SEM image of a crossed nanowire device assembled from a CdS nanowire (horizontal) and a silicon nanowire (vertical). Scale bar: 2 μm .

tion) with emission at $\lambda = 514\text{ nm}$ observed from the nanowire junction. End emission from the CdS nanowire can also be observed owing to the waveguide properties of this material. Leakage of light is not observed along the nanowire which indicates single-crystalline properties.

For integration in a microfluidic channel, the nanoLEDs were isolated with a 200-nm layer of Si_3N_4 (Figure 2b). Inlet and outlet connections to the microfluidic channels were formed by drilling holes into the silicon wafer substrate. The chip was then placed in either a homebuilt microscope for spectroscopy or in a laser scanning microscope. The crossed nanowire devices show the typical rectifying behavior of a diode at forward bias (Figure 3a). These LEDs emit light with a full width at half maximum (FWHM) of about 20 nm (Figure 3b), which is comparable to the photoluminescence spectrum (see Supporting Information). No emission at wavelengths larger than the bandgap of CdS was observed which indicates the absence of crystalline defects or impurities. This quality offers a large spectral window for the observation of fluorescence emission.

To test the use of nanowire light sources for fluorescence spectroscopy applications, a nanoLED was integrated into a microfluidic channel with a depth of 25 μm . This device was placed on a microscope, and a

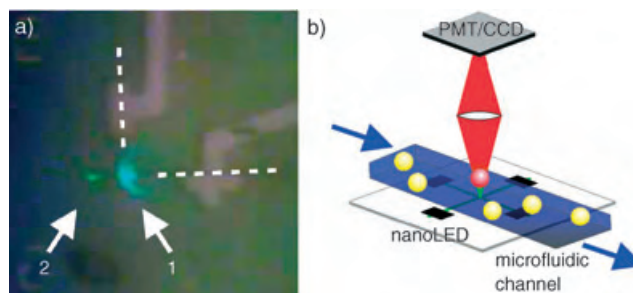


Figure 2. NanoLEDs with a crossed nanowire architecture as an integrated light source for microfluidics. a) The snapshot of a pulsed nanoLED ($13 \times 13\text{ }\mu\text{m}^2$ micrograph) shows (1) green–blue emission at the crossing point of a 60-nm p-doped silicon nanowire (vertical) and a 100-nm n-doped CdS nanowire (horizontal) and (2) red-shifted green emission from the end of the cadmium sulphide nanowire owing to the cavity properties of the nanowire. The broken lines highlight the position of the crossing nanowires. b) Schematic of the integration of a nanoLED into a microfluidic channel. Labeled analytes flow in the microchannel and cross the beam path between the nanoLED and the CCD detector (PMT=photomultiplier tube). The fluorescence emission of single analytes is spatially and spectrally resolved.

solution of quantum dots was passed into the microfluidic channel with a syringe pump. Fluorescence emission of the quantum dots from a wavelength-limited spot size was spatially resolved with a CCD. The photoluminescence

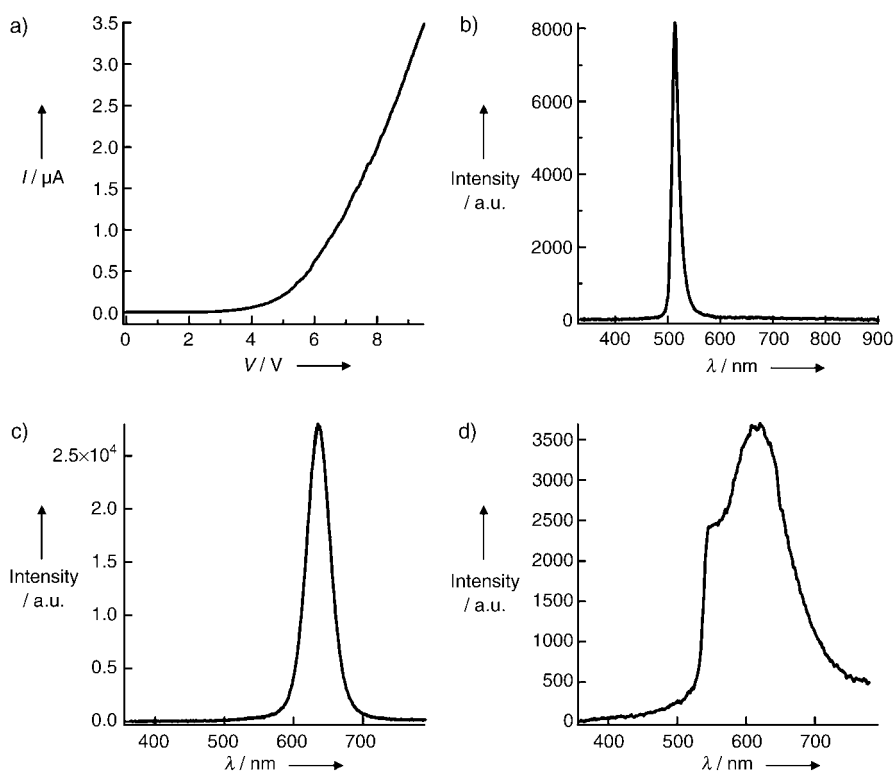


Figure 3. Physical characteristics and spectral properties of the nanoLEDs. a) The I – V curve of a Si/CdS crossed nanowire LED. The curve shows typical rectifying diode behavior. b) The electroluminescence spectrum from a crossed p-Si and n-CdS nanowire junction at room temperature. FWHM $\approx 20\text{ nm}$ for the emission peak maximum at $\lambda = 514\text{ nm}$. c) Photoluminescence of dried quantum dots on a glass slide. The fluorescence emission is red-shifted by 20 nm owing to the concentration of quantum dots (EviDots, $\lambda_{\text{em}} = 603\text{ nm}$). d) Fluorescence spectrum of the same quantum dots in a 25- μm microfluidic channel.

spectrum of the quantum dots recorded with external excitation is shown in Figure 3c for reference. The light from the nanoscale excitation source was filtered from the emission of the quantum dots with a 540-nm-long pass filter which allowed us to spectrally resolve the fluorescence emission of the quantum dots. (Figure 3d). This application demonstrates the unique nanoLED properties for highly confined fluorescence excitation.

A key challenge in modern microscopy is the excitation of a single molecule for the analysis of individual, rather than ensemble, behavior. Typically, single-molecule microscopy is carried out on a dilute solution with an excitation volume on the order of nanoliters, depending on the size of the focused laser beam. As an alternative method, an integrated nanoLED can be considered as a pointlike light source for single-analyte detection. By using a laser scanning confocal microscope, the performance of a single nanoLED as a light source for single-analyte detection was demonstrated, and movies of fluorescent beads, 1- μm diameter, flowed through a microfluidic channel were recorded.^[7] Snapshots of the movies, which were taken by either laser scanning or by excitation with the nanoLED, are shown in Figure 4.^[7] The

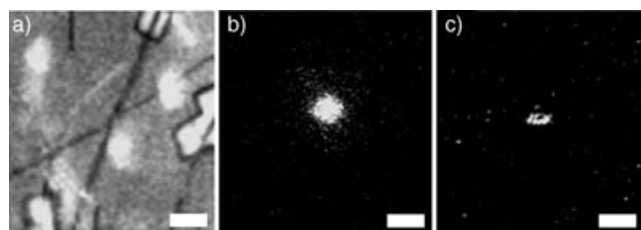


Figure 4. Single-particle detection with a nanoLED (scale bars: 2 μm).^[7] a) Laser-scanned snapshot of 1- μm -diameter microspheres flowing in the microfluidic channel over a crossed nanowire device. b) The nanoLED emission is recorded at 4-V forward bias with the pin-hole fully opened. c) Fluorescence from the microspheres is detected whenever microspheres cross the beam path between the nanoLED and the detector.

movement of single beads flowing in the microfluidic channel is shown in Figure 4a, and a crossed nanowire device can be seen in the center of the laser scanned image. The nanoLED is almost two orders of magnitude smaller in diameter than the 1-micron diameter of the fluorescent beads. The activated nanoLED is shown in Figure 4b, and the fluorescence emission of single beads upon excitation by the nanoLED is shown in Figure 4c. Fluorescence is only observed when the beads cross the beam path between the nanoLED and the detector. Furthermore, the intensity of the fluorescence depends on the distance between the nanoLED and the specimen. The light emission of the nanoLED is highly diffractive and is not a focused beam as in the case of an external light source. Also, the nanoLED excites only a small volume of the microfluidic channel, on the order of a few femtoliters ($\approx 10 \mu\text{m}^3$), depending on the LED intensity and channel height. These devices should therefore be highly suitable as light sources for highly integrated nanoflow channels.

The 50-nm diameter of the nanoLEDs makes them potential light sources for the nearfield excitation of biolog-

ical specimens. This application was demonstrated with the use of quantum dots (Qdots, CA) as cellular probes. Nearfield excitation was first tested by the direct deposition of approximately 25-nm-diameter quantum dots on the nanoLED. Given the 514-nm wavelength of light produced by the nanoLED, excitation within a distance less than this wavelength is defined as nearfield excitation. Results of the excitation by laser scanning and nanoLED are shown as Z-stacks (see Supporting Information). The strong fluorescence of the quantum dots along the CdS nanowire were recorded with a disk hole of 1.6 Airy and upon excitation at $\lambda = 543 \text{ nm}$. The same result with spatially resolved excitation was demonstrated with the nanoLED at 1.6 Airy. Nearfield and farfield cellular imaging was subsequently performed with NIH3T3 murine fibroblast cells labeled with quantum dots. The cells were grown either directly on Si_3N_4 -protected nanoLEDs or on glass coverslips, which were inverted on the nanoLEDs. Figure 5a shows a laser scanned image of cells cultivated on a chip. Quantum dots in a fibroblast cell at a distance as low as 500 nm from the nanoLED could be excited with this integrated nearfield light source as shown in Figure 5, b and c.

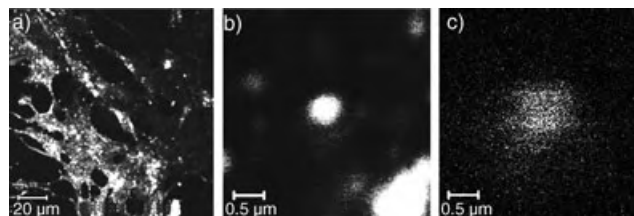


Figure 5. Comparison of cellular images collected by means of laser scanning confocal microscopy and with integrated nanoLEDs. a) Laser scanned image of fibroblast cells that are placed on top of a chip with nanoLEDs. The red spots correspond to intracellular quantum dots. b) Laser scanned image of the fluorescence from quantum dots in a fibroblast. c) NanoLED image of the same density of quantum dots within the fibroblast cell. In comparison to the laser scanned image, only quantum dots that are located on the nanoLED are excited with a vertical distance as low as approximately 500 nm. The use of a nanoLED eliminates excitation of neighboring quantum dots and reduces background fluorescence to provide an inherently confocal technique.

By using crossed Si and CdS nanowires, we have constructed a nanoLED with emission at 514 nm. These devices have been used to image single quantum dots both in solution and in cells. We believe that nanoscale optoelectronic devices could have wide applicability for integrated fluorescence spectroscopy by the use of future nanoarray-based chips as well as nearfield excitation sources for cell imaging. Furthermore, the spatially confined excitation of a few femtoliters could potentially be of use for single-molecule imaging.

Experimental Section

Nanowire synthesis: Si nanowires were synthesized catalytically by a VLS (vapor-liquid-solid) process using 60-nm gold colloids (Ted Pella) that were dispersed on an oxidized silicon substrate.^[8] CdS

wires with diameters in the range of 100 nm were synthesized by pulsed laser deposition with gold clusters for catalytic VLS growth of the target according to a reported method.^[9] *Integrated nanoLEDs and fluorescence spectroscopy*: Electrical contacts to crossed nanowires were defined by using electron-beam lithography (JEOL 6400). Electrode contacts of 100-nm Ti were deposited by using a homebuilt electron-beam evaporator system. The nanoLEDs were isolated with the deposition of 200-nm-thick Si₃N₄ by PECVD (plasma-enhanced chemical vapor deposition). Electrical transport measurements were made by using a computer-controlled homebuilt system. Room temperature electroluminescence was recorded with a homebuilt microscope (60× magnification, 0.6 NA (numerical aperture)), a liquid-nitrogen-cooled CCD (Princeton Instruments Spec-10), and a spectrometer equipped with a 1200-lines mm⁻¹ grating blazed at 500 nm (Acton Scientific 300i). True-color videos of pulsed nanoLEDs were recorded on the same setup. Water-stabilized quantum dots with an emission at $\lambda = 603$ nm were purchased from Evident Technologies. The fluorescence emission was integrated for 1 s at a flow rate of 100 $\mu\text{L h}^{-1}$ and a concentration of 25 $\mu\text{g mL}^{-1}$. The excitation of the single nanoLED was blocked with a 540-nm filter. *Single-particle detection and cell imaging*: A Zeiss LSM 510 microscope with a 60× water-immersion objective (1.2 NA) was used for confocal microscopy studies. TransFluospheres ($\lambda_{\text{ex}} = 488$, $\lambda_{\text{em}} = 605$ nm) with a diameter of 1 μm were purchased from Molecular Probes. The fluorescence of single particles was detected with a 560-nm-long pass filter in a microfluidic channel with a height of 25 μm and a flow rate of 1–5 $\mu\text{L h}^{-1}$. Movies were recorded with 10 frames s⁻¹ (see Supporting Information). Glycerol was added to the aqueous solution to control the buoyancy of the microspheres. Labeling of the cells with quantum dots was performed with a QTracker Kit from the Quantum Dot Corporation ($\lambda_{\text{em}} = 655$ nm). *Cell cultures*: NIH3T3 cells were maintained in a 5% CO₂ environment in a medium of DMEM (Dulbecco's Modified Eagle's Medium, Invitrogen) with 10% calf bovine serum and were passaged every two to three days. For imaging, cells were cultured overnight in Petri dishes with removable coverslips or were grown directly on a nanoLED, which was protected with a 200-nm-thick layer of Si₃N₄. Prior to experiments, cells were fixed with 2% formaldehyde in PBS (phosphate buffered saline) solution and permeabilized in acetone. Cells on coverslips were placed on the nanoLEDs with fixed cells facing the nanoLEDs.

Received: September 27, 2004

Revised: October 20, 2004

Published online: January 20, 2005

Keywords: analytical methods · fluorescence spectroscopy · nanotechnology · semiconductors · single-molecule studies

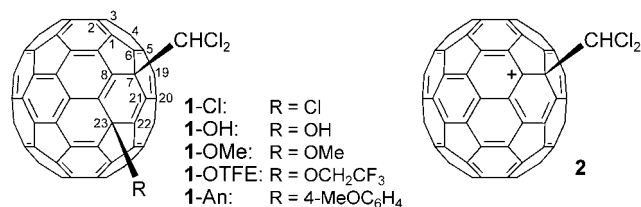
- [1] M. H. Baier, C. Constantin, E. Pelucchi, E. Kapon, *Appl. Phys. Lett.* **2004**, *84*, 1967.
- [2] J. A. Misewich, R. Martel, Ph. Avouris, J. C. Tsang, S. Heinze, J. Tersoff, *Science* **2003**, *300*, 783.
- [3] a) X. Duan, Y. Huang, Y. Cui, J. Wang, C. M. Lieber, *Nature* **2001**, *409*, 66; b) H.-M. Kim, T. W. Kang, K. S. Chung, *Adv. Mater.* **2003**, *15*, 567.
- [4] Y. Xia, P. Yang, Y. Sun, Y. Wu, B. Mayers, B. Gates, Y. Yin, F. Kim, H. Yan, *Adv. Mater.* **2003**, *15*, 353.
- [5] Y. Huang, X. Duan, Q. Wei, C. M. Lieber, *Science* **2001**, *291*, 630.
- [6] M. C. McAlpine, R. S. Friedman, C. M. Lieber, *Nano Lett.* **2003**, *3*, 443.
- [7] See Supporting Information for the movies that accompany Figure 4.
- [8] Y. Cui, C. M. Lieber, *Science* **2001**, *291*, 851.
- [9] X. Duan, Y. Huang, R. Agarwal, C. M. Lieber, *Nature* **2003**, *421*, 241.

Generation and Properties of an Alkylated C_{70} Cation**

Toshikazu Kitagawa,* Yangsoo Lee, Naoki Masaoka, and Koichi Komatsu*

Despite the widely accepted notion that fullerenes are electronegative molecules, recent studies of functionalized C_{60} cations have led to the successful generation of monoalkylated $(RC_{60})^+$ ($R = CHCl_2$,^[1] CCl_2CH_2Cl ,^[1] $CH_2P(O)(OEt)_2$,^[2]), protonated $(HC_{60})^+$,^[3] and pentaarylated $(Ar_5C_{60})^+$ ($Ar = C_6H_5$, $4-FC_6H_4$)^[4] derivatives. The fact that C_{70} is slightly more susceptible to electrochemical oxidation than C_{60} ^[5] led us to expect that a monoalkylated C_{70} cation $(RC_{70})^+$ could also be generated as a long-lived cation and that its stability would be comparable to $(RC_{60})^+$. Unlike the anionic counterpart,^[6] no derivatives of the C_{70} cation, $(RC_{70})^+$, have been prepared as directly observable species. One potential difficulty in the preparation of $(RC_{70})^+$ is the possible formation of a mixture of regioisomers owing to the presence of five different types of carbon atoms in the C_{70} cage. Here we report the generation and spectroscopic observation of the first alkylated C_{70} cation, obtained in an isomerically pure form, and a quantitative evaluation of its thermodynamic stability.

Treatment of C_{70} with $AlCl_3$ (70 equivalents) in carefully dried chloroform at 40 °C resulted in the addition of one molecule of chloroform, and the reaction reached completion within 1 hour. Separation of unconverted C_{70} (40 % recovered) by HPLC using a Buckyprep column gave the major product, **1-Cl**, in 27 % yield (45 % based on consumed C_{70}).



The FAB mass spectrum of the adduct showed a peak for the molecular ion corresponding to the monoadduct. The ^{13}C NMR spectrum showed 68 carbon signals in the sp^2

[*] Prof. T. Kitagawa, Y. Lee, N. Masaoka, Prof. K. Komatsu
Institute for Chemical Research
Kyoto University
CREST, Japan Science and Technology Agency
Uji, Kyoto 611-0011 (Japan)
Fax: (+81) 774-38-3178
E-mail: kitagawa@scl.kyoto-u.ac.jp
komatsu@scl.kyoto-u.ac.jp

[**] This work was supported by a Grant-in-Aid for Scientific Research from the Ministry of Education, Culture, Sports, Science, and Technology, Japan.



Supporting information for this article is available on the WWW under <http://www.angewandte.org> or from the author.

region ($\delta = 130\text{--}154$ ppm) and three signals in the sp^3 region ($\delta = 74.0, 61.7, \text{ and } 59.3$ ppm), whereas the ^1H NMR spectrum showed a single peak at $\delta = 6.17$ ppm. These data indicate that the product is isomerically pure and that the molecule contains no symmetry elements. On the basis of these data, as well as the more rigorous discussion on the structure of the cation $(\text{CHCl}_2\text{-C}_{70})^+$ described below, the obtained adduct was assigned to the 23-chloro-7-dichloromethyl derivative **1-Cl**, in which the two addends are positioned across a six-membered ring located at the flat region of the C_{70} core.

Adduct **1-Cl** was converted into fullereneol **1-OH** in 63 % yield by passing it through a column of 230–400-mesh silica gel using CS_2 as the eluent. The hydrolysis, which presumably occurs owing to water contained in the silica gel, is regio-specific and gives only a single isomer that shows 68 aromatic ^{13}C signals, suggesting that **1-OH** is a structural analogue of **1-Cl**.^[7] Fullereneol **1-OH** was readily soluble in $\text{CF}_3\text{SO}_3\text{H}$ and gave a reddish brown solution of $(\text{CHCl}_2\text{-C}_{70})^+$. The ^1H NMR spectrum of the solution showed a singlet at $\delta = 5.59$ ppm. In the ^{13}C NMR spectrum (Figure 1), the cationic carbon center

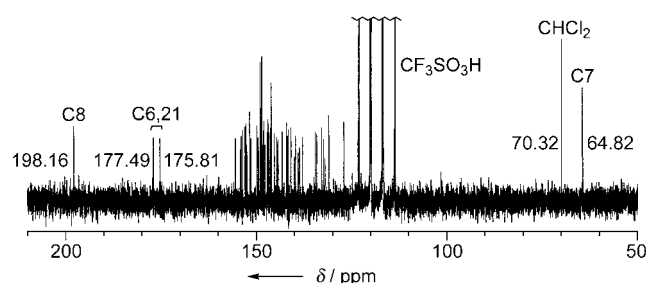


Figure 1. ^{13}C NMR spectrum of **2** (RT, 100 MHz, in $\text{CF}_3\text{SO}_3\text{H}$; $[\text{D}_{12}]$ -cyclohexane was used as an external standard). The assignment of the signal for the CHCl_2 group is based on DEPT measurements.

appears at $\delta = 198.16$ ppm, and two additional signals were observed at $\delta = 177.49$ and 175.81 ppm. The presence of 62 peaks for the other sp^2 -hybridized carbon atoms indicates C_1 symmetry for the cation. In the sp^3 region, two signals ($\delta = 70.32$ and 64.82 ppm) were observed for the carbon atom in CHCl_2 as well as the carbon atom in the cage to which this group is directly attached.

In the cation $(\text{CHCl}_2\text{-C}_{70})^+$, the CHCl_2 group is considered to be connected to one of the five types of carbon atoms (A–E) on the C_{70} cage, as illustrated in Figure 2 a). The attachment of the CHCl_2 group at carbon centers C or D produces a nonsymmetrical (C_1) cation, while isomers which have an

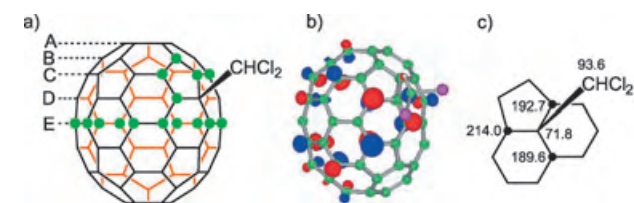


Figure 2. Results of DFT calculations for isomer D of $(\text{CHCl}_2\text{-C}_{70})^+$ (**2**): a) green dots represent carbon atoms that have a Mulliken charge greater than 0.025 (B3LYP/6-31G*); b) the LUMO (B3LYP/6-31G*); c) ^{13}C NMR chemical shifts (δ ; B3LYP/6-311G**//B3LYP/6-31G*).

addend at carbon atoms A, B, or E are C_s -symmetric. Calculation of the relative energies of the five regioisomers by the DFT method (Table 1) showed that isomer D (Figure 2 a) lies at the lowest energy and is 2.55 kcal mol $^{-1}$ more

Table 1: Molecular symmetry and calculated relative energies of the regioisomers of $(\text{CHCl}_2\text{-C}_{70})^+$.

Isomer ^[a]	Symmetry ^[b]	Relative energy ^[c] [kcal mol $^{-1}$]
A	C_s	5.58
B	C_s	0.69
C	C_1	2.55
D (2)	C_1	0.00
E	C_s	15.96

[a] Position of the CHCl_2 group. [b] Time-averaged symmetry on the assumption of rapid rotation of the CHCl_2 group around the $\text{C}_{70}\text{--C}$ bond. [c] Staggered conformations of the CHCl_2 group with respect to the $\text{C}_{70}\text{--C}$ bond were assumed. Energies were calculated at the B3LYP/6-31G* level for all possible conformers, and that of the most stable conformer is presented for each regioisomer.

stable than isomer C. The observed symmetry (C_1) and the calculated energies strongly support the conclusion that the generated cation is isomer D, that is, the 7-dichloromethylated C_{70} cation **2**.

The observed preferential electrophilic attack to carbon atom D of C_{70} under Friedel–Crafts conditions ($\text{CHCl}_3/\text{AlCl}_3$) is consistent with the large HOMO coefficient of this carbon atom (Figure 3). This is in contrast to the fact that nucleo-

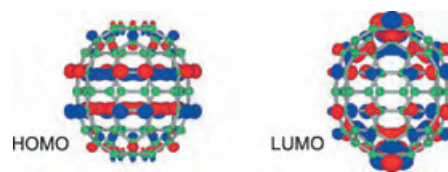


Figure 3. The HOMO and LUMO of C_{70} (B3LYP/3-21G).

philic addition^[6,8,9] and cycloaddition^[8,10] to C_{70} favors carbon atoms A and B, which have the most pyramidal shape and large LUMO coefficients (Figure 3).

A calculation of the NMR chemical shifts by the GIAO method (Figure 2 c) showed that C8 ($\delta = 214.0$ ppm) is the most deshielded, whereas C6 ($\delta = 192.7$ ppm) and C21 ($\delta = 189.6$ ppm) are considerably more deshielded than the other sp^2 -hybridized carbon atoms ($\delta = 134.4\text{--}165.0$ ppm), in qualitative agreement with the observed ^{13}C NMR spectrum. Mulliken charges are largely distributed on the carbon centers in region E and those surrounding the sp^3 -hybridized carbon atom that bears the CHCl_2 group (Figure 2 a, carbons marked by green dots), where the pyramidalization of the $\text{C}\text{--C}$ bonds is relatively small. The total charge on these carbons is $0.88e$.

Solutions of cation **2** in $\text{CF}_3\text{SO}_3\text{H}$ showed a long-wavelength band with $\lambda_{\text{max}} = 991$ nm ($\epsilon = 2020$ cm $^{-1}\text{M}^{-1}$; Figure 4), in analogy to $(\text{CHCl}_2\text{-C}_{60})^+$ (≈ 1200 nm).^[11] Quenching of a solution of **2** in $\text{CF}_3\text{SO}_3\text{H}$ by methanol yielded a single isomer of the methyl ether, $\text{CHCl}_2\text{-C}_{70}\text{-OMe}$, which has no molecular symmetry, as revealed by the observation of 72 signals in the

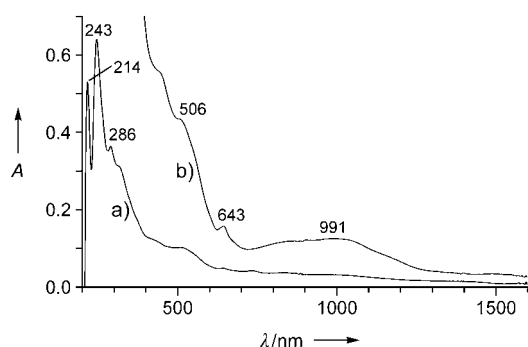


Figure 4. UV/Vis/NIR absorption spectra of **2** in $\text{CF}_3\text{SO}_3\text{H}$ at room temperature (pathlength = 1 cm); a) 1.17×10^{-5} M; b) 5.90×10^{-5} M.

^{13}C NMR spectrum. Of the three carbon atoms in **2** over which the LUMO is mainly distributed, namely C8, C21, and C23 (Figure 2b), the methoxy group appears to attack at C23 because attack at other carbon atoms would produce sterically unfavored 1,2-isomers.^[11,12] The resulting adduct, **1-OMe**,^[7] is a derivative of $7,23\text{-C}_{70}\text{H}_2$, which, on the basis of ab initio calculations, is the most stable derivative among the C_{70}H_2 isomers with nonadjacent hydrogen atoms.^[13]

Cation **2** is stable in $\text{CF}_3\text{SO}_3\text{H}$ at room temperature for over a week. The cation is also formed as a short-lived intermediate by the spontaneous ionization of the $\text{C}_{70}\text{-Cl}$ bond under solvolytic conditions. Thus, in a solution of **1-Cl** in anisole/ $\text{CF}_3\text{CH}_2\text{OH}$ (9:1 v/v), the fullerene was slowly converted according to first-order kinetics into the $\text{S}_{\text{N}}1$ products **1-An**^[7] (An = *p*-anisyl) and **1-OTFE**^[7] (TFE = 2,2,2-trifluoroethyl) in a molar ratio of 1:5. The essentially identical free energies of activation for **1-Cl** and $\text{CHCl}_2\text{-C}_{60}\text{-Cl}$ ^[14] (Table 2) indicate very similar stabilities for **2** and $(\text{CHCl}_2\text{-C}_{60})^+$.

In conclusion, the first functionalized C_{70} cation, $(\text{CHCl}_2\text{-C}_{70})^+$ (**2**), was generated as a long-lived species in isomerically pure form by ionization of the corresponding fullerene in $\text{CF}_3\text{SO}_3\text{H}$. The structure of the cation was confirmed by NMR spectroscopic analysis and DFT calculations. The thermodynamic stability of **2** was comparable to those of $(\text{CHCl}_2\text{-C}_{60})^+$ and the *tert*-butyl cation,^[15] as revealed by solvolysis rate measurements.

Experimental Section

Full details of experimental procedures and spectroscopic data for new compounds are given in the Supporting Information. **1-Cl**: AlCl_3 (1.03 g, 7.72 mmol) was added to a solution of C_{70} (97.4 mg, 0.116 mmol) in dry CHCl_3 (120 mL) at 40°C . The mixture was stirred for 50 min and quenched with cold water (100 mL). The usual workup and separation by HPLC (Buckyprep, toluene)

afforded **1-Cl** as a dark-brown solid (30.5 mg, 27%). **1-OH**: Compound **1-Cl** (30.5 mg, 31.8 μmol) was passed through a column of silica gel (230–400 mesh, 20-mm inner diameter \times 300 mm) using toluene/hexane (2:1; 20 mL min^{-1}) as eluent to give fullerene **1-OH** as a dark solid (19.0 mg, 63%). Generation of **2**: A solution of **1-OH** (13.5 mg, 14.3 μmol) in $\text{CF}_3\text{SO}_3\text{H}$ (1 mL) was placed in a 5-mm outer diameter NMR sample tube, and the ^1H and ^{13}C NMR spectra of the resulting reddish brown solution of **2** were recorded at room temperature.

Received: November 23, 2004

Published online: January 26, 2005

Keywords: carbocations · electrophilic addition · fullerenes · solvolysis · superacidic systems

- [1] T. Kitagawa, H. Sakamoto, K. Takeuchi, *J. Am. Chem. Soc.* **1999**, *121*, 4298.
- [2] Y. Murata, F. Cheng, T. Kitagawa, K. Komatsu, *J. Am. Chem. Soc.* **2004**, *126*, 8874.
- [3] a) C. A. Reed, K.-C. Kim, R. D. Bolskar, L. J. Mueller, *Science* **2000**, *289*, 101; b) L. J. Mueller, D. W. Elliott, K.-C. Kim, C. A. Reed, P. D. W. Boyd, *J. Am. Chem. Soc.* **2002**, *124*, 9360.
- [4] a) A. G. Avent, P. R. Birkett, H. W. Kroto, R. Taylor, R. M. Walton, *Chem. Commun.* **1998**, 2153; b) P. R. Birkett, M. Bühl, A. Khong, M. Saunders, R. Taylor, *J. Chem. Soc. Perkin Trans. 2* **1999**, 2037.
- [5] The oxidation potentials ($E_{1/2}$) of C_{60} and C_{70} are reported to be +1.26 and +1.20 V, respectively, versus Fc/Fc^+ (Fc = ferrocene) in $\text{Cl}_2\text{CHCHCl}_2$. Q. Xie, F. Arias, L. Echegoyen, *J. Am. Chem. Soc.* **1993**, *115*, 9818.
- [6] M. Sawamura, H. Iikura, A. Hirai, E. Nakamura, *J. Am. Chem. Soc.* **1998**, *120*, 8285.
- [7] The very similar absorption spectra for **1-Cl**, **1-OH**, **1-OMe**, **1-OTFE**, and **1-An** (see Supporting Information) suggest the same addition pattern for all of these adducts.
- [8] C. Thilgen, A. Herrmann, F. Diederich, *Angew. Chem.* **1997**, *109*, 2362; *Angew. Chem. Int. Ed. Engl.* **1997**, *36*, 2268, and references therein.
- [9] a) A. Hirsch, T. Grösser, A. Skieba, A. Soi, *Chem. Ber.* **1993**, *126*, 1061; b) Z. Wang, M. S. Meier, *J. Org. Chem.* **2003**, *68*, 3043; c) Z. Wang, M. S. Meier, *J. Org. Chem.* **2004**, *69*, 2178.
- [10] a) C. Bellavia-Lund, F. Wudl, *J. Am. Chem. Soc.* **1997**, *119*, 943; b) M. S. Meier, G.-W. Wang, R. C. Haddon, C. P. Brock, M. A. Lloyd, J. P. Selegue, *J. Am. Chem. Soc.* **1998**, *120*, 2337.
- [11] a) T. Kitagawa, T. Tanaka, Y. Takata, K. Takeuchi, K. Komatsu, *J. Org. Chem.* **1995**, *60*, 1490; b) T. Kitagawa, T. Tanaka, Y. Takata, K. Takeuchi, K. Komatsu, *Tetrahedron* **1997**, *53*, 9965; c) T. Kitagawa, T. Tanaka, H. Murakita, K. Takeuchi, *J. Org. Chem.* **1999**, *64*, 2; d) T. Kitagawa, T. Tanaka, H. Murakita, A. Nishikawa, K. Takeuchi, *Tetrahedron* **2001**, *57*, 3537.
- [12] DFT calculations (B3LYP/3-21G*) indicated that the C8-OMe and C21-OMe isomers are higher in energy by 16.9 and 5.9 kcal mol^{-1} , respectively, than the C23-OMe isomer.

Table 2: Rate constants and activation parameters for the solvolysis of **1-Cl** and $\text{CHCl}_2\text{-C}_{60}\text{-Cl}$ ^[a] in anisole/2,2,2-trifluoroethanol (9:1 v/v).

Substrate ^[b]	Intermediate	T [$^\circ\text{C}$]	k_1 ^[c] [10^{-6} s^{-1}]	ΔH^\ddagger [kcal mol^{-1}]	ΔS^\ddagger [$\text{cal mol}^{-1}\text{ K}^{-1}$]	$\Delta G^\ddagger_{25^\circ\text{C}}$ [kcal mol^{-1}]
$\text{CHCl}_2\text{-C}_{70}\text{-Cl}$ (1-Cl)	$(\text{CHCl}_2\text{-C}_{70})^+$ (2)	25.0	12.3	11.1	–44	24.1
		50.0	56.6			
$\text{CHCl}_2\text{-C}_{60}\text{-Cl}$	$(\text{CHCl}_2\text{-C}_{60})^+$	25.0	14.6	10.6	–45	24.0
		50.0	62.6			

[a] See reference [14]. [b] Initial substrate concentration: 1.5×10^{-4} M. 2,6-Lutidine (1.5 equiv) was added as a buffer to suppress the reverse reaction.

[c] Experimental error: $\pm 5\%$.

- [13] a) H. R. Karfunkel, A. Hirsch, *Angew. Chem.* **1992**, *104*, 1529; *Angew. Chem. Int. Ed. Engl.* **1992**, *31*, 1468; b) C. C. Henderson, C. M. Rohlfing, P. A. Cahill, *Chem. Phys. Lett.* **1993**, *213*, 383; c) C. C. Henderson, C. M. Rohlfing, K. T. Gillen, P. A. Cahill, *Science* **1994**, *264*, 397.
- [14] T. Kitagawa, Y. Lee, M. Hanamura, H. Sakamoto, H. Konno, K. Takeuchi, K. Komatsu, *Chem. Commun.* **2002**, 3062.
- [15] The value for ΔG^\ddagger for the solvolysis of *tert*-butyl chloride in the same solvent is 26.9 kcal mol⁻¹ at 25°C (see ref. [14]).

Molecular Recognition

Recognizing a Single Base in an Individual DNA Strand: A Step Toward DNA Sequencing in Nanopores**

Nurit Ashkenasy, Jorge Sánchez-Quesada, Hagan Bayley, and M. Reza Ghadiri*

There has been an intriguing suggestion that *Staphylococcus aureus* α -hemolysin (α -HL), a stable heptameric transmembrane protein pore,^[1] may be of use as the sensor element in a rapid, pore-mediated, single-molecule DNA sequencing process.^[2] Although there remain several requirements that must be met before such a process can be realized,^[2a,3] the most fundamental concern has been whether α -HL, or any other natural or manmade nanopore structure,^[4] is capable of recognizing DNA with single nucleobase resolution. We have probed the nucleobase resolution capacity of α -HL by threading and holding a given strand of single-stranded (ss-) DNA inside the α -HL pore in the form of a single α -HL-DNA pseudorotaxane.^[5] By using block copolymers of DNA and homopolymeric strands with position-specific single nucleotide substitutions, we have found that a single adenine nucleotide at a specific location on a strand of poly-d(C) can be distinguished by its characteristic effect on the ion conductance of α -HL. The discovery that α -HL can recognize ss-DNA with single nucleobase resolution strengthens the case for its utility in rapid single-molecule DNA sequencing.

[*] Dr. N. Ashkenasy, Dr. J. Sánchez-Quesada, Prof. Dr. M. R. Ghadiri
Departments of Chemistry and Molecular Biology and
The Skaggs Institute for Chemical Biology
The Scripps Research Institute
10550 North Torrey Pines Road, La Jolla, CA 92037 (USA)
Fax: (+1) 858-784-2798
E-mail: ghadiri@scripps.edu
Prof. Dr. H. Bayley
Department of Chemistry
University of Oxford
Chemistry Research Laboratory
Mansfield Road, Oxford, OX1 3TA (UK)

[**] This work was supported by a grant from the Office of Naval Research (Grant no. MURI-99, N000149910717). We thank W. S. Horne for his generous assistance in molecular modeling studies.

Supporting information for this article is available on the WWW under <http://www.angewandte.org> or from the author.

It has been proposed that it might be possible to rapidly establish the sequence of an individual strand of ss-DNA as it traverses through an α -HL pore by recording the perturbations in the conductance of the ion channel caused by the sequential passage of each nucleotide.^[2,6] Toward this goal, in an important early study it was shown that the transient decreases in the conductance of the ion channel could be used to distinguish homopurine from homopyrimidine ss-nucleic acid strands.^[2b,c] However, partly because of the experimental limitations imposed by the rapid rates of pore-mediated ss-nucleic acid transport, it has not yet been possible to use transient DNA transport measurements to establish the nucleobase resolution capacity of α -HL.^[2,3] We envisioned that this issue might be resolved by analyzing decreases in the conductance of the ion channel caused by a given strand of ss-DNA while it is captured and held stable inside an α -HL pore in the form of a rotaxane or pseudorotaxane.^[5]

The DNA sequences employed in our studies each have a long ss-DNA segment for threading the α -HL pore and a stable terminal hairpin structure for holding the thread in a pseudorotaxane configuration (Figure 1a).^[5b] As the hairpin duplex structure is wider than the α -HL internal lumen, a given DNA strand can only thread the pore with its free single-stranded terminus.^[5] Therefore, depending on from which end the α -HL pore is threaded and whether the hairpin structure is placed at the 3'- or 5'-terminus of the DNA thread, four distinct topoisomeric forms of α -HL-DNA pseudorotaxane

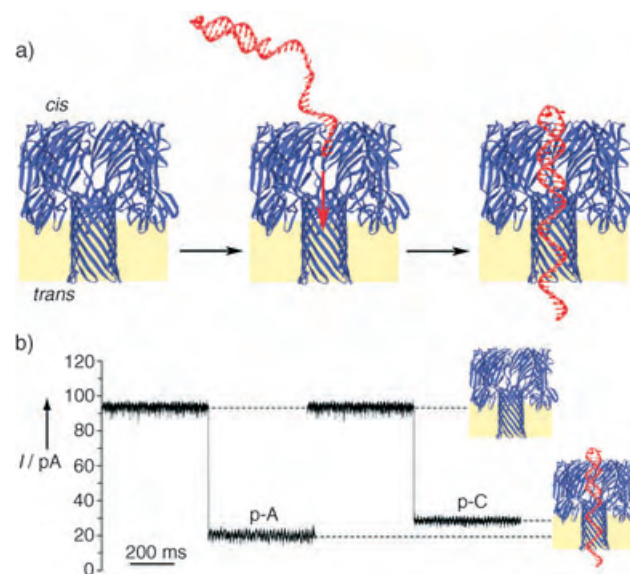


Figure 1. a) Schematic of the formation of single α -HL-DNA pseudorotaxane species. By employing a sequence with a long ss-DNA segment that has a hairpin structure at one end, the ss-DNA can thread the pore upon application of positive potentials and be held stably in a pseudorotaxane configuration by the interactions of the DNA duplex segment at the pore entrance. The heptameric transmembrane pore structure is depicted in a cutaway side view. b) Perturbations in ion current caused by the capture of poly-d(A) (p-A) and poly-d(C) (p-C) single strands (sequences 1 and 2, respectively). The events shown are typical ion-current traces recorded at 170 mV under symmetrical conditions (KCl (500 mM), MOPS (5 mM, pH 7.5), Bessel-filtered at 5 kHz, sampled at 200 μ s) with the thread molecules (1 μ m) added to the *cis* chamber.

anes can be formed.^[5b] Here we report the characteristics of the topoisomers of α -HL-DNA pseudorotaxanes that are prepared by threading DNA from the *cis* side (Figure 1 a). In a typical experiment, the DNA sample was introduced at the *cis* side of a lipid bilayer that contained a single oriented α -HL pore, and the threading process was initiated by applying positive transmembrane holding potentials (see Supporting Information for details). Formation of the α -HL-DNA pseudorotaxane was accompanied by a decrease in the conductance of the ion channel owing to the presence of the ss-DNA inside the pore (Figure 1 b).^[2,5] The DNA strand can be held stably in the pseudorotaxane configuration as long as a suitable positive transmembrane holding potential is maintained (see Supporting Information).^[5b]

Initial experiments were performed with α -HL-DNA pseudorotaxanes of poly-d(A) and poly-d(C) (sequences 1–4, Figure 2) to ascertain whether homopurine and homopyrimidine DNA strands held inside the α -HL pore give rise to distinct decreases in the ion conductance. Current versus voltage curves, measured from 10 to 170 mV, indicated that the homopurine and homopyrimidine pseudorotaxanes could be readily distinguished at applied potentials of greater than 100 mV (see Supporting Information). The residual currents I_R at 170 mV (calculated as a percentage of the current measured for the unoccupied DNA-free α -HL during the same experiment) are $22 \pm 3\%$ and $31 \pm 3\%$ for poly-d(A) (sequence 1) and poly-d(C) (sequence 2) pseudorotaxanes, respectively (Figure 2). Interestingly, topoisomeric α -HL-DNA pseudorotaxanes of poly-d(A) and poly-d(C) that differ only in the orientation of the captured DNA strand (threading from the 3'-terminus using 1 or 2 versus threading from the 5'-terminus using 3 or 4) gave similar characteristic "A-type" or "C-type" ion channel blockades, respectively (Figure 2).

As a significant portion of the ss-DNA in an α -HL-DNA pseudorotaxane is held stably inside the protein's pore,^[5] we sought to determine which part of the encased DNA thread accounted for the differences observed in the ion conductances associated with poly-d(A) and poly-d(C) oligonucleotides. Accordingly, we prepared single α -HL-DNA pseudorotaxane species from four different DNA block copolymers (sequences 5–8), each designed to place stretches of poly-d(A) and poly-d(C) at discrete locations along the DNA thread (Figure 2). The measured residual currents at 170 mV for each of the DNA block copolymer- α -HL pseudorotaxanes fall clearly into either "A-type" or "C-type" categories (Figure 2). Therefore, by a simple comparative sequence analysis, it appeared that the nucleobase(s) recognized by α -HL must be located in the region 10 to 20 nucleotides away from the edge of the hairpin structure (Figure 2). Further studies with similar DNA block copolymer threads, which have shorter poly-d(C) and poly-d(A) segments, helped to define the location of the recognition site to around nucleotide 20 (data not shown).

To address whether the α -HL pore structure could recognize DNA with single nucleobase resolution, we designed five poly-d(C) threads (sequences 9–13, Figure 3), each with a single deoxyadenosine at a unique position within the putative recognition site located 18 to 22 nucleotides away

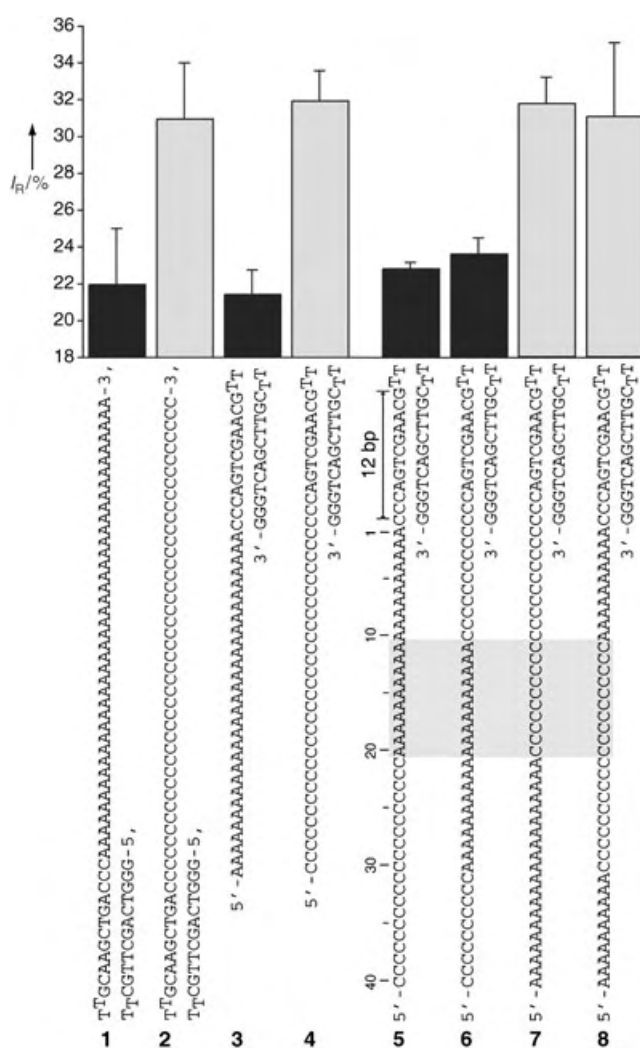


Figure 2. Averaged residual currents (I_R) for various α -HL-DNA pseudorotaxanes measured at 170 mV. Left: Bars 1–4 depict the residual currents measured for poly-d(A) and poly-d(C) threads in two topoisomeric α -HL-DNA pseudorotaxane configurations. Note that when the α -HL pore is threaded with a homopolymeric DNA segment either from the free 3'-terminus (1 or 2) or from the 5'-terminus (3 or 4), similar characteristic A-type or C-type ion-channel blockades are observed. Right: Bars 5–8 depict the observed residual currents for α -HL-DNA pseudorotaxanes prepared from four different ss-DNA block copolymer threads (5–8). A-type and C-type residual currents are shown as black and gray bars, respectively. The region of the ss-DNA segment recognized by the α -HL channel (10 to 20 nucleotides away from the edge of the hairpin segment) is shaded in gray.

from the edge of the 5'-stem-loop structure. Each DNA strand was used to prepare the corresponding single α -HL-DNA pseudorotaxane species. Furthermore, each of the pseudorotaxanes was analyzed several times to obtain statistically significant numbers of events for calculating the individual residual current values, I_R , at 170 mV (see Supporting Information). The measured I_R distributions were roughly bimodal and could be divided into two groups of events corresponding to A-type ($I_R < 27\%$) and C-type ($I_R > 27\%$) values (Figure 3). A given event displayed current characteristics similar to either poly-d(A) or poly-d(C)

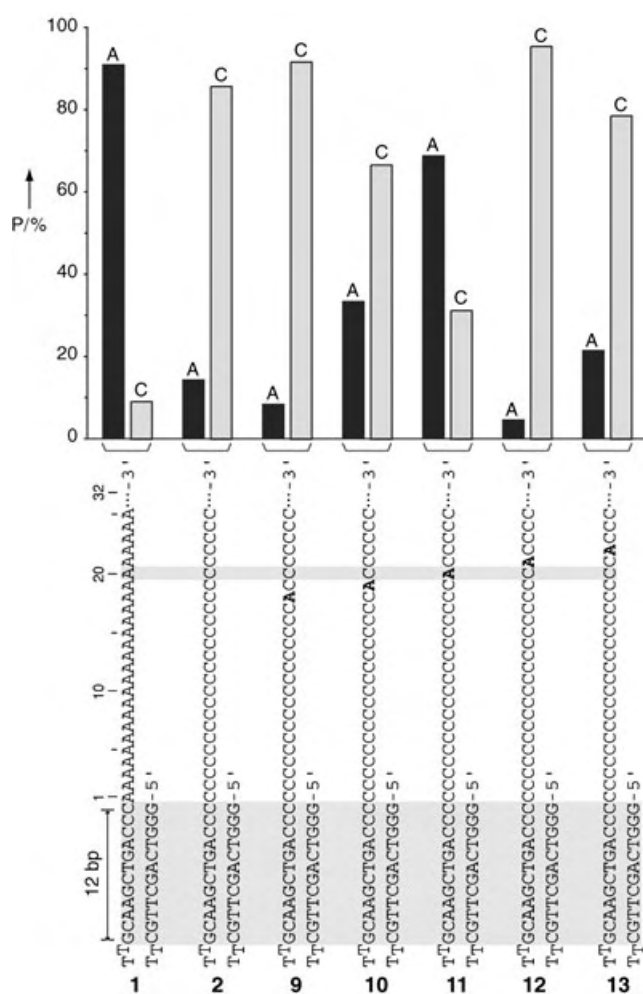


Figure 3. Percentage probability (P) of the A-type ($I_R < 27\%$) and the C-type ($I_R > 27\%$) residual currents for single deoxyadenosine-substituted poly-d(C) DNA strands captured inside the α -HL pore as a pseudorotaxane. Percentage probabilities were calculated by the number of A-type or C-type events measured at 170 mV divided by the total number of events (n) recorded for a given strand ($n = 11, 21, 22, 32, 22$, and 14 for strands **1**, **2**, **9**, **10**, **11**, **12**, and **13**, respectively). The percentage probabilities of A-type and C-type events for each strand are shown as black and gray bars, respectively.

pseudorotaxanes (Figure 1b) and did not interconvert from one type into the other during the analysis. The data clearly show that when deoxyadenosine is at positions 18, 19, 21, or 22 (sequences **9**, **10**, **12**, or **13**), the majority of the ion conductance blockades correspond to the C-type signal. However, when a single deoxyadenosine is positioned 20 nucleotides away from the edge of the stem-loop segment (sequence **11**), despite being flanked on either side by long stretches of poly-d(C), most observed events corresponded to the A-type signal (Figure 3). Therefore, these studies demonstrate that the α -HL pore structure can recognize ss-DNA site-specifically with single nucleobase resolution.

The above observations imply that in the α -HL-DNA pseudorotaxanes, the ss-DNA thread must be held in a specific conformation inside the pore to allow the correct position of the deoxyadenosine at a recognition site. Therefore, by considering how the threaded DNA hairpin is pinned

to the protein and the conformation of the ss-DNA inside the pore barrel, it should be possible to propose where on the α -HL pore the nucleobase sensing site is located. As DNA hairpins with stems longer than 8 bp can enter the vestibule and bump up against the internal pore constriction,^[7] the 12 bp stem hairpin strands used in our studies are most likely pinned to the α -HL pore constriction by the edge of their stem duplex structure (Figure 1a). This view is also consistent with a study in which covalently tethered DNA molecules were used to probe the internal pore structure and dimensions of α -HL.^[8] Therefore, in such a configuration the position of the recognized nucleotide (counting from the edge of the stem structure) should be independent of the number of stem base pairs (if > 8 bp). Consistent with this hypothesis, α -HL-DNA pseudorotaxanes prepared by using hairpin DNA strands that comprise 13 bp (strands **14** and **15**) or 10 bp (strands **16** to **18**) stem segments retained their ability to report a single deoxyadenosine placed 20 nucleotides away from the edge of the hairpin (see Figure 4 and Supporting Information). Furthermore, we speculate that the estimated length of the single DNA strand within the barrel is somewhat shorter than a DNA strand with the same number of bases within B-form ds-DNA. ss-DNA, relative to ds-DNA, is highly contractile and at forces below about 8 pN would be shortened compared to B-DNA.^[9] Such small forces seem reasonable if we take into account that the effective charge per nucleotide within the α -HL pore is only approximately $0.1 e$ as suggested by recent studies.^[5a,10] Therefore, the above rationale and observations suggest that the nucleobase recognition site is most likely located near the *trans* opening of the α -HL pore (see Figure 1a).

The precision of the single nucleobase recognition is an important factor in single-molecule DNA sequencing. Careful analysis of the data described here indicate that the precision of nucleotide sensing is not sufficiently high in the “native” α -HL pore for use in DNA sequencing. For example, whereas the observed residual currents indicate that an adenine substitution at either positions 18, 21, or 22 (sequences **9**, **12**, or **13**) is not recognized (Figure 3), the discriminating power between A and C at position 19 (by using sequence **10**) is noticeably less pronounced (see Figure 3 and Supporting Information). A number of factors may influence the precision of single nucleobase recognition, including the conformational states and structural dynamics of a single strand of DNA held inside the pore structure under the influence of an electric force^[8,11] and sequence-dependent DNA structural features that could affect the precise alignment of the recognized nucleobase with respect to the recognition site. For instance, our data indicate that variations in the hairpin structure seem to shift the alignment of the captured DNA strand with respect to the α -HL sensing site either slightly forward (strands **16** and **17**) or backward (strand **14**) relative to strand **11** (Figures 2 and 3). These small changes in apparent strand positioning could be responsible for decreased discrimination between A and C in the case of strand **14** and diminished selectivity for the C-type events in strand **17**. Factors that concern the precision of recognition arising from the base-dependent length of a ss-DNA in an electric field would be less serious for DNA that is sequenced

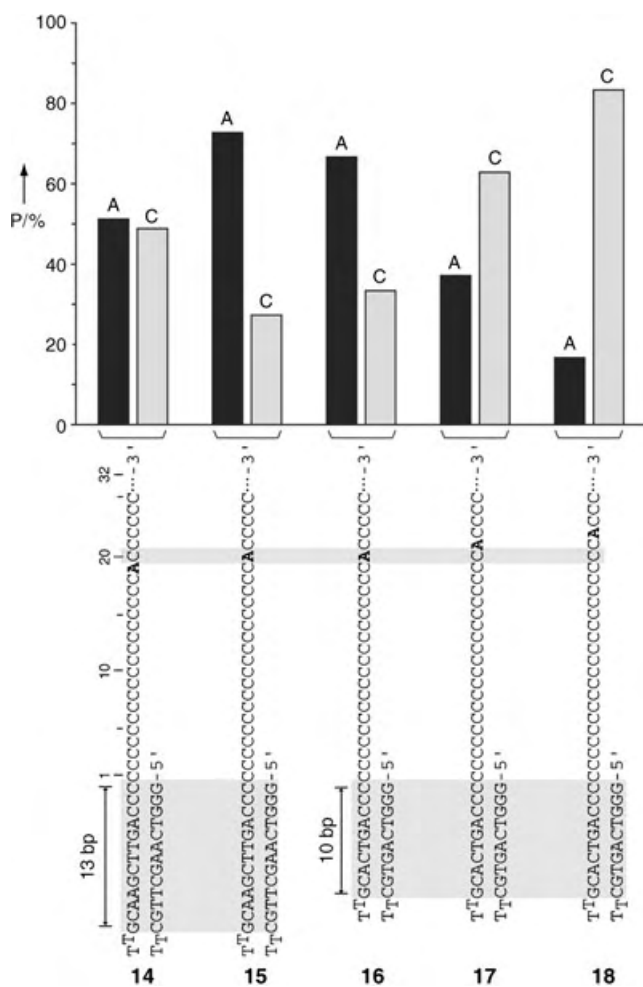


Figure 4. Percentage probability (P) of A-type and C-type events for single deoxyadenosine-substituted poly-d(C) DNA hairpin sequences that have either 13- or 10-base-pair stem duplexes (strands 14–15 and 16–18, respectively) measured at 170 mV ($n=43, 44, 69, 35$, and 66 for 14–18, respectively). The A-type ($I_R < 27\%$) and C-type ($I_R > 27\%$) events are shown as black and gray bars, respectively.

during transit through the pore, in which case the time evolution of the conductance would be monitored, or for stepwise approaches by which the DNA is fed into the pore by an enzyme or a nanoscopic device.^[3,6] In these cases, the computer that analyzes the signal would also be programmed in base recognition within the context of neighboring sequences. Approaches based on current amplitude, as demonstrated here, would have advantages over a method based on the mean dwell time of each base at a recognition site.^[3,11] Even if the mean dwell time for each of the four bases differed by an order of magnitude from the others, there would be a problematical overlap between the distributions of the four dwell times.

In conclusion, our studies support the notion that α -HL-mediated DNA sequencing might be fundamentally feasible. We believe that progress toward this goal would greatly benefit from targeted engineering of pores^[12] which could provide the means for improved positional selectivity and signal discrimination between the four DNA nucleobases.

Furthermore, the strategies for single α -HL-DNA rotaxane species described recently^[5b,c] might also be of use in enhancing the fidelity of single nucleobase recognition through multiple-pass reading.

Received: September 25, 2004

Published online: January 21, 2005

Keywords: DNA · host–guest chemistry · molecular recognition · rotaxanes · single-molecule studies

- [1] L. Song, M. R. Hobaugh, C. Shustak, S. Cheley, H. Bayley, J. E. Gouaux, *Science* **1996**, 274, 1859.
- [2] a) J. J. Kasianowicz, E. Brandin, D. Branton, D. W. Deamer, *Proc. Natl. Acad. Sci. USA* **1996**, 93, 13770; b) M. Akeson, D. Branton, J. J. Kasianowicz, E. Brandin, D. W. Deamer, *Biophys. J.* **1999**, 77, 3227; c) A. Meller, L. Nivon, E. Brandin, J. Golovchenko, D. Branton, *Proc. Natl. Acad. Sci. USA* **2000**, 97, 1079; d) S. Howorka, S. Cheley, H. Bayley, *Nat. Biotechnol.* **2001**, 19, 636.
- [3] a) H. Bayley, C. R. Martin, *Chem. Rev.* **2000**, 100, 2575; b) D. W. Deamer, M. Akeson, *Trends Biotechnol.* **2000**, 18, 147; c) D. W. Deamer, D. Branton, *Acc. Chem. Res.* **2002**, 35, 817–825; d) J. J. Nakane, M. Akeson, A. Marziali, *J. Phys. Condens. Matter* **2003**, 15, R1365.
- [4] a) K. B. Jirage, J. C. Hulteen, C. R. Martin, *Science*, **1997**, 278, 655; b) C. Schmidt, M. Mayer, H. Vogel, *Angew. Chem.* **2000**, 112, 3267; *Angew. Chem. Int. Ed.* **2000**, 39, 3137; c) J. Li, D. Stein, C. McMullan, D. Branton, M. J. Aziz, J. A. Golovchenko, *Nature* **2001**, 412, 166; d) H. Bayley, P. S. Cremer, *Nature* **2001**, 413, 226; e) P. Chen, T. Mitsui, D. B. Farmer, J. Golovchenko, R. G. Gordon, D. Branton, *Nano Lett.* **2004**, 4, 1333; f) H. Chang, F. Kosari, G. Andreadakis, M. A. Alam, G. Vasmatzis, R. Bashir, *Nano Lett.* **2004**, 4, 1551.
- [5] a) A. F. Sauer-Budge, J. A. Nyamwanda, D. K. Lubensky, D. Branton, *Phys. Rev. Lett.* **2003**, 90, 238101; b) J. Sanchez-Quesada, A. Saghatelian, S. Cheley, H. Bayley, M. R. Ghadiri, *Angew. Chem.* **2004**, 116, 3125; *Angew. Chem. Int. Ed.* **2004**, 43, 3063; c) J. Nakane, M. Wiggin, A. Marziali, *Biophys. J.* **2004**, 87, 615.
- [6] G. Church, D. W. Deamer, D. Branton, R. Baldarelli, J. Kasianowicz, US Patent 5 795 782, **1995, 1998**.
- [7] a) W. Vercoutere, S. Winters-Hilt, H. Olsen, D. Deamer, D. Haussler, M. Akeson, *Nat. Biotechnol.* **2001**, 19, 248; b) S. Winters-Hilt, W. Vercoutere, V. S. DeGuzman, D. Deamer, M. Akeson, D. Haussler, *Biophys. J.* **2003**, 84, 967; c) W. A. Vercoutere, S. Winters-Hilt, V. S. DeGuzman, D. Deamer, S. E. Ridino, J. T. Rodgers, H. E. Olsen, A. Marziali, M. Akeson, *Nucleic Acids Res.* **2003**, 31, 1311.
- [8] S. Howorka, H. Bayley, *Biophys. J.* **2002**, 83, 3202.
- [9] a) S. B. Smith, Y. Cui, C. Bustamante, *Science* **1996**, 271, 795; b) C. Bustamante, S. B. Smith, J. Liphardt, D. Smith, *Curr. Opin. Struct. Biol.* **2000**, 10, 279.
- [10] J. Mathé, H. Visram, V. Viasnoff, Y. Rabin, A. Meller, *Biophys. J.* **2004**, 87, 3205.
- [11] a) D. K. Lubensky, D. R. Nelson, *Biophys. J.* **1999**, 77, 1824; b) M. Bates, M. Burns, A. Meller, *Biophys. J.* **2003**, 84, 2366.
- [12] a) O. Braha, B. Walker, S. Cheley, J. J. Kasianowicz, L. Song, J. E. Gouaux, H. Bayley, *Chem. Biol.* **1997**, 4, 497; b) J. J. Kasianowicz, D. L. Burden, L. C. Han, S. Cheley, H. Bayley, *Biophys. J.* **1999**, 76, 837; c) L.-Q. Gu, M. Dalla Serra, J. B. Vincent, G. Vigh, S. Cheley, O. Braha, H. Bayley, *Proc. Natl. Acad. Sci. USA* **2000**, 97, 3959; d) L. Q. Gu, S. Cheley, H. Bayley, *Science* **2001**, 291, 636; e) L. Q. Gu, S. Cheley, H. Bayley, *J. Gen. Physiol.* **2001**, 118, 481; h) S. Cheley, L.-Q. Gu, H. Bayley, *Chem. Biol.* **2002**, 9, 829.

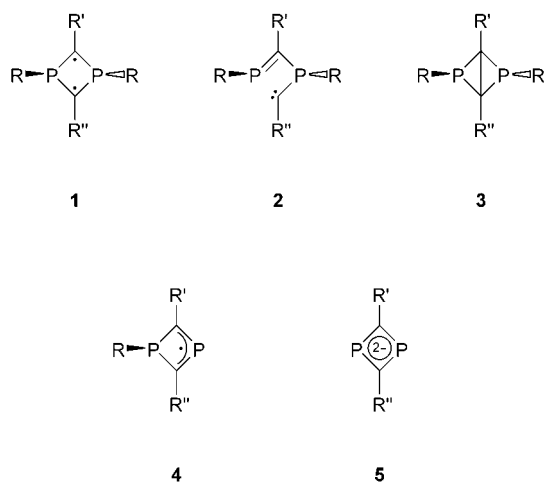
Stable Carbenium Ions

Cyclic Bis(phosphanyl)carbenium Ion by Protonation of a 1,3-Diphosphacyclobutane-2,4-diyl**

Manuel Sebastian, Aaron Hoskin, Martin Nieger, László Nyulászi,* and Edgar Niecke*

Dedicated to Professor Martin Jansen on the occasion of his 60th birthday

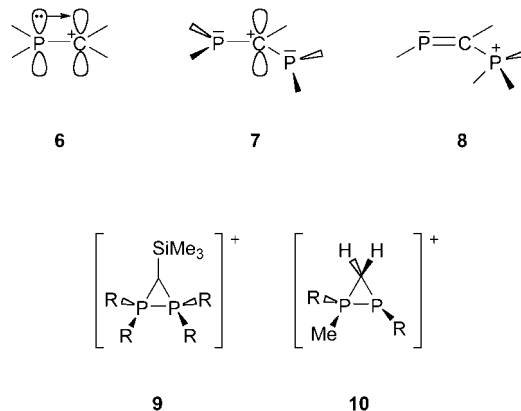
The 1,3-diphosphacyclobutane-2,4-diyl **1** is an electron-rich diradicaloid heterocycle.^[1] To reduce electron density, it undergoes valence isomerizations forming an intermediate



phosphanylcarbene (**2**, $R' = R'' = \text{Cl}$, $R = \text{Mes}^*$ (2,4,6-*i*Bu₃C₆H₂)^[1] or Tmp (2,2,6,6-Tetramethylpiperidyl)^[2] or bicyclobutane (**3**, $R' = \text{SiMe}_3$, $R'' = \text{H}$, $R = \text{Mes}^*$)^[3]). Another way to reduce the electron density is the excitation of one electron. The excited species undergoes subsequent P–aryl bond cleavage forming the radical species **4**.^[4] Alternatively, reduction of **1** leads to the formation of an intermediate radical anion, which can also undergo P–aryl bond cleavage

to give dianion **5**.^[5] We report here on a further means of reducing the electron density of **1** by the transformation of a bis(phosphanyl)methyl fragment into a bis(phosphanyl)carbenium ion.

In the phosphanyl-substituted carbenium ions **6** both the phosphorus and the carbon center have trigonal-planar

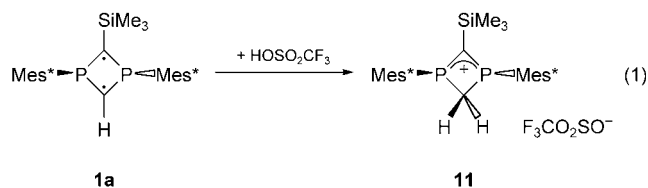


coordination,^[6] since the stabilization gained from the interaction of the carbenium ion with the good π -electron-donating phosphorus^[7] overcomes the energy required for planarization at the phosphorus center. Moiety **6** can be regarded as a highly polar alkylidene, which is a valuable building block in organophosphorus chemistry.^[8]

1,3-Bis(phosphanyl)carbenium ions **7** formally correspond to allylic anions. The stabilization of the carbenium ion, however, is insufficient to compensate for the inversion barrier of *two* phosphorus atoms. Ab initio calculations indicate that the parent **7** is nonplanar and without conjugative stabilization.^[9] Hitherto, two derivatives of **7** have been reported based on NMR evidence; however, this assignment is not completely certain owing to downfield resonances in the ³¹P NMR spectra.^[10]

Isomers of **7** such as phosphonium-substituted phosphalkenes **8**,^[6b,11] the cyclic isomers bis(phosphonium)methanide **9** ($R = \text{N}i\text{Pr}_2$),^[12] and the diphosphiranium salt **10** ($R = \text{Mes}^*$)^[9] are known. The incorporation of the parent P–C–P unit into a small ring system like **1** is beneficial since it prevents the possible formation of the P–P bond to give the three-membered ring **9**. The desired bis(phosphanyl)carbenium ion is favored, even if this would be the thermodynamically less stable species.^[13]

Herein we describe the synthesis and characterization of the bis(phosphanyl)carbenium ion **11** [Eq. (1)]. When 1,3-diphosphacyclobutane-2,4-diyl **1a** was protonated with trifluoromethanesulfonic acid, the color of the solution changed from red to yellow and the salt **11**–TfI[–] was produced, which



[*] Dr. M. Sebastian, Dr. A. Hoskin, Dr. M. Nieger, Prof. Dr. E. Niecke
Anorganisch-Chemisches Institut der Universität
Gerhard-Domagk-Strasse 1, 53121 Bonn (Deutschland)
Fax: (+49) 228-735-327
E-mail: e.niecke@uni-bonn.de

Prof. Dr. L. Nyulászi
Department of Inorganic Chemistry
Technical University of Budapest
Gellért tér 4, 1521 Budapest (Ungarn)
Fax: (+36) 1463-3642
E-mail: nyulaszi@mail.bme.hu

[**] This work was supported by the Deutsche Forschungsgemeinschaft, the Fonds der Chemischen Industrie, and the Alexander von Humboldt Stiftung (fellowship to L.N.). Generous allocation of computer time from NIIF/Hungary and support from OTKA T 034675 is also gratefully acknowledged.

was isolated as a crystalline solid. The sole signal in the ^{31}P NMR spectrum of **11**-TfI $^-$ ($\delta(^{31}\text{P}) = 0.1$ ppm) has a coupling with two protons (t, $^2J_{\text{PH}} = 14.0$ Hz), and in the ^1H NMR spectrum the resonance at $\delta(^1\text{H}) = 5.3$ also shows a triplet structure with a coupling of $^2J_{\text{PH}} = 14.0$ Hz. This indicates that the two phosphorus atoms in **11**-TfI $^-$ are equivalent and connected through a bridging CH_2 group. Thus, protonation took place at the C(H) carbon atom in **1a**. The ^{13}C NMR signals of the ring carbon atoms of **11**-TfI $^-$ ($\delta(^{13}\text{C}) = 75.8$ (t, $^1J_{\text{PC}} = 18.6$ Hz) and 123.3 ppm (t, $^1J_{\text{PC}} = 12.3$ Hz) indicate that the symmetry of the ring system is retained. The considerably downfield shift ($\Delta\delta = 10$ ppm) of the silyl group in the ^{29}Si NMR spectrum on going from **1a** to **11**-TfI $^-$ ($\delta(^{29}\text{Si}) = -3.6$, t, $^2J_{\text{PSi}} = 1.5$ Hz) indicates the electron deficiency of **11**. The ionic structure of **11**-TfI $^-$ is responsible for its poor solubility in nonpolar solvents.

Crystals of **11**-TfI $^-$ suitable for X-ray structure analysis were obtained by recrystallization from toluene/ CH_2Cl_2 (10:1) at -30°C (Figure 1).^[14] The four-membered P_2C_2 ring

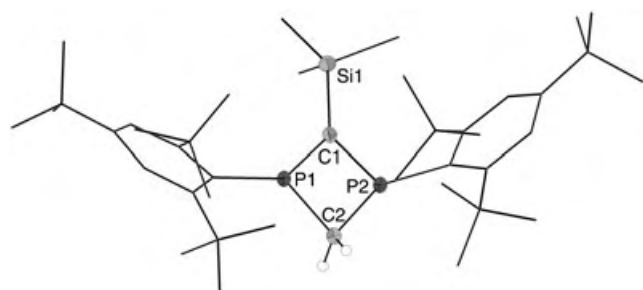


Figure 1. Molecular structure of **11**-TfI $^-$ with selected bond lengths [pm], angles [$^\circ$], and bond angle sums [$^\circ$]. (Counterion and hydrogen atoms, apart from those on the P_2C_2 ring, have been omitted for clarity.) P1–C1 173.5(3), P1–C2 185.5(3), P2–C1 172.3(3), P2–C2 183.8(3), C1–Si1 189.3(3); C1–P1–C2 90.0(1), C1–P2–C2 90.9(1), P1–C1–P2 93.2(1), P1–C2–P2 85.8(1); $\Sigma(\text{C1})$ 360, $\Sigma(\text{P1})$ 336, $\Sigma(\text{P2})$ 341.

exhibits a planar geometry. The sums of the bond angles at the phosphorus atoms ($\Sigma(\text{P1})$ 336 $^\circ$, $\Sigma(\text{P2})$ 341 $^\circ$) as well as at the tricoordinated endocyclic carbon atom ($\Sigma(\text{C1})$ 360 $^\circ$) do not differ considerably from the corresponding sums of **1a**.^[3] This holds also for the bond lengths within the bis(phosphanyl)carbenium fragment (P1–C1 173.5(3) pm, P2–C1 172.3(3) pm). The protonated carbon atom C2 exhibits a distorted tetrahedral geometry. The P–C2 bonds are significantly longer (P1–C2 185.5(3) pm, P2–C2 183.8(3) pm) and correspond to typical P–C single bonds ($\varnothing = 183$ pm).^[15] These structural motifs indicate that the moderate pyramidalization of the phosphorus atom enables the distinct delocalization of the positive charge, resulting in an allyl-like system [Eq. (1)]. The Si–C bond in **11**-TfI $^-$ (189.3(3) pm) is significantly longer than the Si–C $_{\text{ring}}$ bonds in **1a** (183.6 pm)^[3] and cation **9** ($\text{R} = \text{NiPr}_2$, 186.3 pm).^[12] Taking the lowfield ^{29}Si NMR shift (see above) into consideration, we

surmise that the electrophilic elimination of the silyl group in **11** should be facile.^[16]

Density functional calculations^[17] carried out on **11**^[18] at the B3LYP/6-31+G* level of theory provided a structure

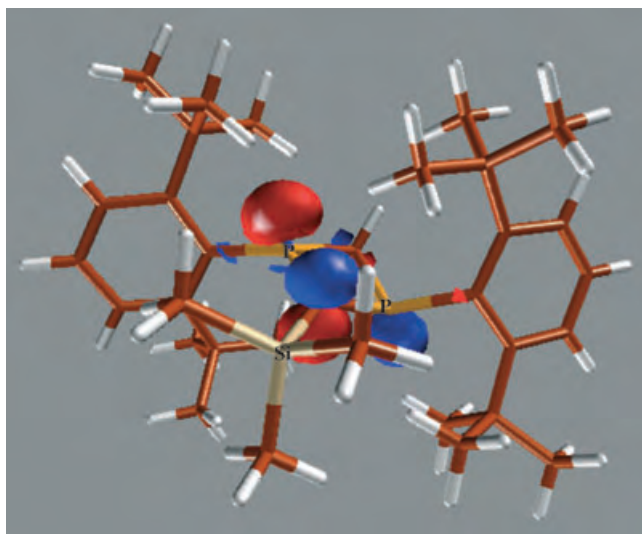


Figure 2. LUMO of the carbenium ion **11**'.

similar to that obtained by X-ray diffraction. The carbocationic character of **11**' is clearly evident in the LUMO presented in Figure 2.^[19] A carbenium ion should have a low-energy empty orbital at the tricoordinate carbon atom. In the case of **11**' the LUMO is indeed centered at the tricoordinate carbon atom but with a significant contribution from the lone-pair orbitals of the neighboring nonplanar phosphorus atoms. The aryl substituents on the two phosphorus atoms occupy a *trans* position, consequently the two "s"-type lone pairs are at opposite ends of the four-membered ring. The interaction of the two lone pairs is substantial, resulting in a bonding ($\Phi_b(\text{P})$) and an antibonding ($\Phi_a(\text{P})$) combination (Figure 3). (In the case of the saturated 1,3-diphosphacyclobutane ring, the splitting of these two Kohn–

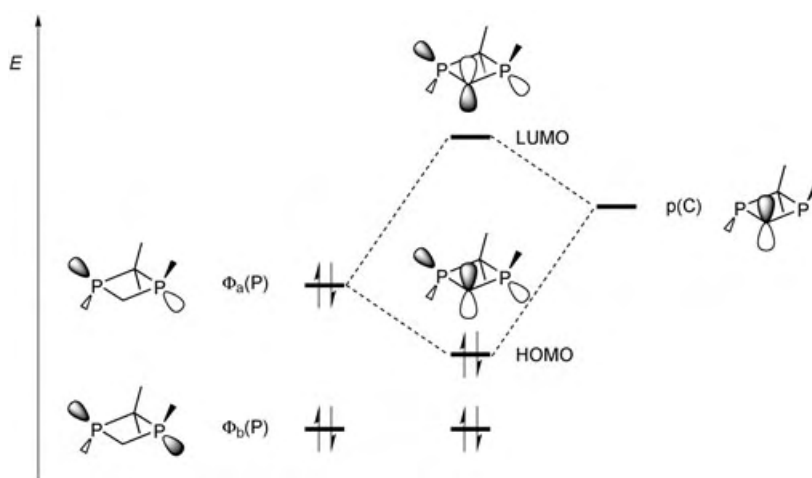
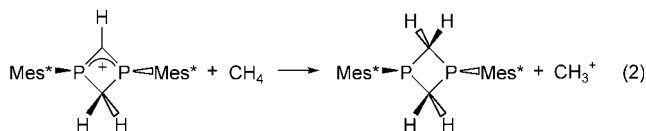


Figure 3. Stabilizing interaction between the phosphorus lone-pair orbitals and the empty p orbital of the carbenium ion **11**'.

Sham (KS) MOs is 1.1 eV, indicating a strong through-space interaction between the two n_p MOs). The antibonding combination $\Phi_a(P)$ is of suitable symmetry to overlap with the empty p orbital of the carbenium ion. The stabilization resulting from the interaction can be estimated from the isodesmic reaction (2). The calculated stabilization energy is 137.7 kcal mol⁻¹ at the B3LYP/3-21G(*) level and 132.5 kcal mol⁻¹ at the B3LYP/6-31 + G**/B3LYP/3-21G(*) level, showing the effectiveness of this interaction.



Experimental Section

11-TfI⁻: To a solution of **1a** (325 mg, 0.5 mmol) in toluene (15 mL) at room temperature was added trifluoromethanesulfonic acid (75 mg, 0.5 mmol). The reaction mixture was stirred for one hour, before a precipitate was removed from the light yellow solution by filtration. The residue was washed with toluene (5 mL). The bright yellow solid was then dissolved in a mixture of toluene (10 mL) and CH₂Cl₂ (1 mL), and the solution was stored at -30°C. Yellow crystals of **11-TfI⁻** formed over a period of two days. Yield 348 mg (87%); m.p. 185°C; NMR (CD₂Cl₂, -80°C): ³¹P{¹H} NMR: δ = 29.7 ppm (t, ²J_{PH} = 14.0 Hz); ¹H NMR: δ = -0.6 (s, Si(CH₃)₃, 9H), 1.2 (s, *p*-tBu, Mes*, 18H), 1.3 (s, *o*-tBu, Mes*, 18H), 1.7 (s, *o*-tBu, Mes*, 18H), 5.7 (t, ²J_{PH} = 14.0 Hz, PCH₂P), 7.4 (s, *m*-CH, Mes*, 2H), 7.5 ppm (s, *m*-CH, Mes*, 2H); ¹³C{¹H} NMR: δ = -2.4 (t, ³J_{PC} = 3.9 Hz, Si(CH₃)₃), 30.2 (s, *p*-CCH₃, Mes*), 30.9 (s, *o*-CCH₃, Mes*), 32.6 (s, *o*-CCH₃, Mes*), 34.2 (s, *o*-CCH₃, Mes*), 38.4 (s, *o*-CCH₃, Mes*), 38.5 (s, *p*-CCH₃, Mes*), 75.8 (t, ¹J_{PC} = 18.6 Hz, PC(H₂)P), 122.8 (pseudo t, $\Sigma(^3J_{PC} + ^5J_{PC})$ = 11.8 Hz, C_{meta}, Mes*), 123.3 (t, ¹J_{PC} = 12.3 Hz, PC(Si)P), 128.3 (pseudo t, $\Sigma(^1J_{PC} + ^3J_{PC})$ = 58.5 Hz, C_{ipso}, Mes*), 149.6 (s, C_{para}, Mes*), 157.0 (s, C_{ortho}, Mes*), 158.3 (s, C_{para}, Mes*), 160.1 ppm (pseudo t, $\Sigma(^2J_{PC} + ^4J_{PC})$ = 15.2 Hz, C_{ortho}, Mes*); ²⁹Si NMR: δ = -3.6 (t, ²J_{PSi} = 1.5 Hz).

Received: September 17, 2004

Published online: January 26, 2005

Keywords: ab initio calculations · carbenium ions · carbocations · diradicals · phosphorus heterocycles

- [1] E. Niecke, A. Fuchs, F. Baumeister, M. Nieger, W. W. Schoeller, *Angew. Chem.* **1995**, *107*, 640–642; *Angew. Chem. Int. Ed. Engl.* **1995**, *34*, 555–557.
- [2] O. Schmidt, A. Fuchs, D. Gudat, M. Nieger, W. Hoffbauer, E. Niecke, W. W. Schoeller, *Angew. Chem.* **1998**, *110*, 995–998; *Angew. Chem. Int. Ed.* **1998**, *37*, 949–952.
- [3] E. Niecke, A. Fuchs, M. Nieger, *Angew. Chem.* **1999**, *111*, 3213–3216; *Angew. Chem. Int. Ed.* **1999**, *38*, 3028–3031.
- [4] a) M. Sebastian, M. Nieger, L. Nyulászi, E. Niecke, presented at the 10th International Symposium on Inorganic Ring Systems (IRIS X), Burlington, VT, USA (August 17–22, **2003**); b) M. Sebastian, O. Schmidt, M. Nieger, L. Nyulászi, E. Niecke, unpublished results.
- [5] M. Sebastian, M. Nieger, D. Szieberth, L. Nyulászi, E. Niecke, *Angew. Chem.* **2004**, *116*, 647–651; *Angew. Chem. Int. Ed.* **2004**, *43*, 637–641.
- [6] a) O. Guerret, G. Bertrand, *Acc. Chem. Res.* **1997**, *30*, 486; C. Widauer, G. Chen, H. Grützmacher, *Chem. Eur. J.* **1998**, *4*, 1154; b) H. Grützmacher, H. Pritzkow, *Angew. Chem.* **1989**, *101*, 768–769; *Angew. Chem. Int. Ed. Engl.* **1989**, *28*, 740–741; c) H. Grützmacher, H. Pritzkow, *Angew. Chem.* **1991**, *103*, 721–722; *Angew. Chem. Int. Ed. Engl.* **1991**, *30*, 709–710; d) U. Heim, H. Pritzkow, H. Schönberg, H. Grützmacher, *J. Chem. Soc. Chem. Commun.* **1993**, 674; e) C. Boelsen, M. Nieger, E. Niecke, W. W. Schoeller, U. Zenneck, *XVth International Conference on Phosphorus Chemistry (ICPC 15)*, Sendai, Japan, **2001**, Poster Abstract PA 079.
- [7] J. Kapp, C. Schade, A. M. El-Nahasa, P. von R. Schleyer, *Angew. Chem.* **1996**, *108*, 2373–2376; *Angew. Chem. Int. Ed. Engl.* **1996**, *35*, 2236–2238.
- [8] H. Grützmacher, *Science* **2000**, *289*, 737–738.
- [9] S. Loss, C. Widauer, H. Rüegger, U. Fleischer, C. H. Marchland, H. Grützmacher, G. Frenking, *J. Chem. Soc. Dalton Trans.* **2003**, 85–91.
- [10] a) [HC(PPh₂)₂]⁺: $\delta(^{31}\text{P})$ = 67.3; H. H. Karsch, E. Witt, F. E. Hahn, *Angew. Chem.* **1996**, *108*, 2380–2382; *Angew. Chem. Int. Ed. Engl.* **1996**, *35*, 2242–2244; b) [tBu₂PC(H)P(NiPr₂)₂]⁺: $\delta(^{31}\text{P})$ = 48.6; K. S. Zawadzki, N. N. Belous, A. A. Borisenko, Z. S. Novikova, *J. Gen. Chem. USSR* **1991**, *61*, 1965.
- [11] a) H. H. Karsch, H. U. Reisacher, G. Müller, *Angew. Chem.* **1986**, *98*, 467–468; *Angew. Chem. Int. Ed. Engl.* **1986**, *25*, 455–456; b) A. Schmidpeter, G. Jochem, C. Klinger, C. Robl, H. Nöth, *J. Organomet. Chem.* **1997**, *529*, 87; c) A. Schmidpeter, *Heteroat. Chem.* **1999**, *10*, 529.
- [12] T. Kato, H. Gornitzka, A. Baceiredo, W. W. Schoeller, G. Bertrand, *Science* **2000**, *289*, 754–756.
- [13] According to ab initio calculations,^[9] **9** is more stable than **8**, if the substituents at the phosphorus atoms are amino groups, while in case of the parent compound the bis(phosphanyl) carbenium ion **8** is more stable than **9**.
- [14] X-Ray structure analysis of **11-TfI⁻**: C₄₁H₆₉P₂Si + CF₃SO₃H: yellow crystals, crystal dimensions 0.7 × 0.6 × 0.5 mm³, *M_r* = 876.10 g mol⁻¹; monoclinic, space group *P2₁/c* (No. 14), *a* = 13.7571(2), *b* = 19.6740(3), *c* = 18.1056(4) Å, β = 104.554(1)°, *V* = 4743.16(14) Å³, *Z* = 4, $\mu(\text{MoK}\alpha)$ = 0.239 mm⁻¹, *T* = 123(2) K, *F*(000) = 1876, 21 636 reflections up to $2\theta_{\text{max}}$ = 50° were measured on a Nonius KappaCCD diffractometer with MoK α radiation, 8377 of which were independent and used for all calculations. The structure was solved by direct methods and refined to *R*² anisotropically; the H atoms were refined with a riding model. *wR2*(*F*²) = 0.1692, *R*(*F*) = 0.0568 for 501 parameters and 89 restraints. CCDC-246722 (**11-TfI⁻**) contains the supplementary crystallographic data for this paper. These data can be obtained free of charge via www.ccdc.cam.ac.uk/conts/retrieving.html (or from the Cambridge Crystallographic Data Centre, 12, Union Road, Cambridge CB21EZ, UK; fax: (+44) 1223-336-033; or deposit@ccdc.cam.ac.uk).
- [15] Mean value ± 3 standard deviation as a result of a CCSD enquiry for P–C single-bond lengths in cyclic systems.
- [16] The cleavage of the silyl group from the ring is observed during different reactions of **11-TfI⁻**.
- [17] Gaussian 98 (Revision A.5), M. J. Frisch, G. W. Trucks, H. B. Schlegel, G. E. Scuseria, M. A. Robb, J. R. Cheeseman, V. G. Zakrzewski, J. A. Montgomery, R. E. Stratmann, J. C. Burant, S. Dapprich, J. M. Millam, A. D. Daniels, K. N. Kudin, M. C. Strain, O. Farkas, J. Tomasi, V. Barone, M. Cossi, R. Cammi, B. Mennucci, C. Pomelli, C. Adamo, S. Clifford, J. Ochterski, G. A. Petersson, P. Y. Ayala, Q. Cui, K. Morokuma, D. K. Malick, A. D. Rabuck, K. Raghavachari, J. B. Foresman, J. Cioslowski, J. V. Ortiz, B. B. Stefanov, G. Liu, A. Liashenko, P. Piskorz, I. Komaromi, R. Gomperts, R. L. Martin, D. J. Fox, T. Keith, M. A. Al-Laham, C. Y. Peng, A. Nanayakkara, C. Gonzalez, M. Challacombe, P. M. W. Gill, B. G. Johnson, W. Chen, M. W. Wong, J. L. Andres, M. Head-Gordon, E. S. Replogle, J. A. Pople, Gaussian, Inc., Pittsburgh, PA, **1998**. Unless otherwise

stated the geometries were optimized first at the B3LYP/3-21G(*) level of theory. At the optimized structures, second derivatives were calculated to show whether a minimum (positive eigenvalues only) had been obtained. Further optimization was performed at the B3LYP/6-31 + G* level of theory.

- [18] To decrease the computational effort, both *para-tert*-butyl groups of the 2,4,6-tri-*tert*-butylphenyl substituents were replaced by hydrogen atoms. This simplification maintains the flattening effect of the substituents on the tricoordinate phosphorus atoms.
- [19] The Kohn–Sham orbitals shown in Figure 2 are essentially identical to the canonical Hartree–Fock molecular orbitals.

Protein–Ligand Interactions

The Architecture of Protein–Ligand Binding Sites Revealed through Template-Assisted Intramolecular Peptide–Peptide Interactions**

Chao Yu, Miroslav Malesevic, Günther Jahreis,
Mike Schutkowski, Gunter Fischer,* and
Cordelia Schiene-Fischer

Many fundamental processes of life are based on protein–peptide or protein–protein interactions. An array of discontinuous polypeptide segments within a given protein may account for the specificity and free energy change of complex formation.^[1] Characterization of the polypeptide segments that compose the ligand-binding surface requires expensive structural investigations such as multidimensional NMR spectroscopy, X-ray crystallography, and phage-displayed shotgun scanning.^[2]

Herein we report a simple method for obtaining a low-resolution three-dimensional picture of protein–peptide- or protein–protein-interaction sites. The method involves the generation of a library of short oligopeptides derived from the primary sequences of interacting proteins. The peptides are spotted onto cellulose membranes as template-bound pairs. Spot synthesis^[3] of peptide pairs is followed by an assay for intramolecular interactions. We have termed this combined

technique the IANUS (induced organization of structure by matrix-assisted togetherness) spot array. Each IANUS spot is synthesized to comprise two peptide blocks. One block bears a constant peptide sequence in all spots, in which the sequence represents either the ligand peptide of a protein–peptide complex or an interacting segment of a protein–protein complex. The second block consists of variable sequences of constant length that represent overlapping regions of the entire partner protein sequence. After the synthesis is complete, the spot array includes the entire collection of linear motifs, including those of the binding cleft of the protein–ligand complex.

In aqueous solution, short peptides exist in multiple rapidly interchanging conformational states, and are expected to exhibit a full range of structural elements specific for any type of peptide–peptide, peptide–protein, or peptide–interface interaction.^[4] Peptide chain arrangements that contain multiple conformational constraints can induce a population of molecules to favor restricted conformations through mutual conformational induction. Typical constraints within IANUS spot arrays include template-assisted intramolecular interactions within the IANUS peptide pairs, high effective concentration brought about by intramolecularity, and a microenvironment of decreased polarity. In effect, matrix-assisted togetherness of peptide chains could produce a large population of binding-favorable conformations when the peptide segments originate from the interacting sites of a protein–protein complex.

Conceptually, IANUS spots that arise from protein segments distant from the active site must somehow be distinguished from those obtained from binding-site-derived peptide pairs. As the recognition site of a peptide becomes buried upon protein–peptide–ligand complexation, a similar type of masking is expected to be significant for spots containing natively interacting peptide pairs. Noninteracting IANUS peptide pairs, in contrast, leave the peptide ligands unmasked. The resulting different binding properties for the applied soluble protein allows a readout of the IANUS spot arrays and the detection of conformational induction. The result would be a collection of all protein segments that correspond to the interaction sites of the protein–peptide or protein–protein complexes.

In this study, spots were assayed by the application of soluble protein, which competes with the protein-derived peptides for binding to the matrix-bound ligand. After this treatment, IANUS peptide pairs should produce a spot pattern that reveals either: a) strong protein binding to spots of noninteracting peptide pairs, or b) diminished protein binding to spots containing peptide pairs that interact with each other through conformational induction (Figure 1).


To test the method, an IANUS spot array experiment was conducted with the complex that is formed between streptavidin and Strep-tag II (Stt II). The streptavidin homotetramer from *Streptomyces avidinii* forms a complex with the 10-residue (SNWSHPQFEK) Stt II peptide that is bound to the biotin binding pocket.^[5] Our IANUS spot array consists of variable streptavidin-derived 12-residue peptides paired with the constant Stt II peptide. Both were synthesized on the same bifunctional lysyl template at a molar ratio of 1:1 for

[*] Dr. C. Yu,^[†] Dr. M. Malesevic, Dr. G. Jahreis, Dr. M. Schutkowski,^[†,‡] Prof. G. Fischer, Dr. C. Schiene-Fischer
Max Planck Research Unit for Enzymology of Protein Folding
Weinbergweg 22, 06120 Halle/Saale (Germany)
Fax: (+49) 345-551-1972
E-mail: fischer@enzyme-halle.mpg.de

[†] Present address: Nuffield Department of Clinical Medicine
John Radcliff Hospital
Headington, Oxford, OX3 9DU (UK)

[†,‡] Present address: Jerini AG
Invalidenstrasse 130, 10115 Berlin (Germany)

[**] This work was supported by the Deutsche Forschungsgemeinschaft (SFB 610) and the Fonds der Chemischen Industrie.

 Supporting information for this article is available on the WWW under <http://www.angewandte.org> or from the author.

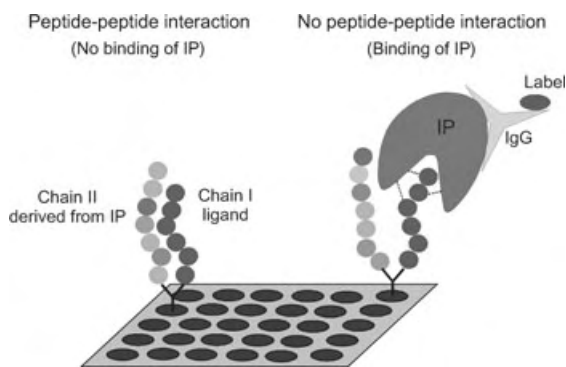
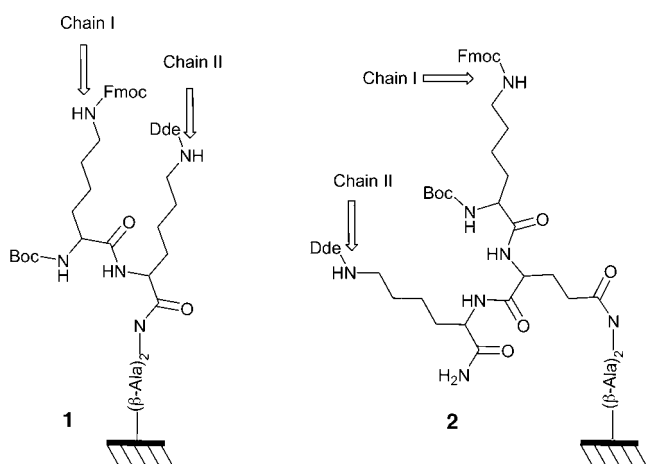


Figure 1. Treatment of spots with an interacting protein that competes with protein-derived peptides for binding to a peptide ligand. Right: noninteracting peptide pairs; strong protein binding. Left: ligand peptides are masked through conformational induction, and protein binding is weak. IP = interacting protein; IgG = protein-specific antibody.

each spot. The set of overlapping 12-mer peptides that collectively span the streptavidin sequence with a shift of three amino acid residues totals 50 individual spots, and was synthesized on the Fmoc site of the orthogonally protected template **1** (Scheme 1). The Stt II peptide was synthesized on the Dde site of the template at every spot, and both peptides were N-terminally acetylated.



Scheme 1. Templates **1** and **2** are attached to the cellulose membrane by the $(\beta\text{-Ala})_2$ spacer. Boc = *tert*-butoxycarbonyl; Fmoc = 9-fluorenylmethoxycarbonyl; Dde = 2-(4,4-dimethyl-2,6-dioxocyclohexylidene)ethyl.

To analyze the quality of the syntheses, peptide pairs of four representative spots, both with and without intramolecular interactions, were synthesized in the dark on predefined spots with a photolabile nitrobenzyl-based linker placed between each of the peptide chains and template **2**.^[6] After photolytic cleavage of the peptide pairs from the solid support, MALDI-TOF mass spectrometric analysis was performed. For every spot, each of the two peptides analyzed showed a molecular mass in agreement with calculated predictions (Supporting Information). To investigate the influence of the matrix anchoring site on the IANUS peptide pairs on template **1**, streptavidin–Stt II peptides were also

synthesized on template **2** (Scheme 1). The streptavidin peptide block of 12-mers was synthesized on the Fmoc site and spanned the streptavidin sequence with a shift of two amino acid residues, which required 75 individual spots. Conformational induction was detected by treatment of the IANUS spot array with soluble streptavidin; spots in which the binding face of Stt II was freely accessible gave rise to Stt II-mediated protein absorption, in contrast to spots in which the Stt II binding face was blocked through conformational induction. Streptavidin bound to IANUS spot arrays was detected with Western blot analysis. In fact, characteristically dark, strong Western blot signals occurred for the majority of spots prepared with template **1**. However, two regions showed weaker signals for two or more adjacent spots, which indicates a blocked Stt II binding face (Figure 2a, blue and pink underlining). These were termed IANUS-positive spots, and were quantitatively identified by the individual deviation from the reciprocal of mean spot intensity (Figure 2b). The competing streptavidin–Stt II-like interaction of the IANUS peptide pair, which precludes soluble streptavidin protein binding, can be hypothesized to account for the appearance of IANUS-positive spots. Owing to sequence overlap of the streptavidin peptides, only two or more

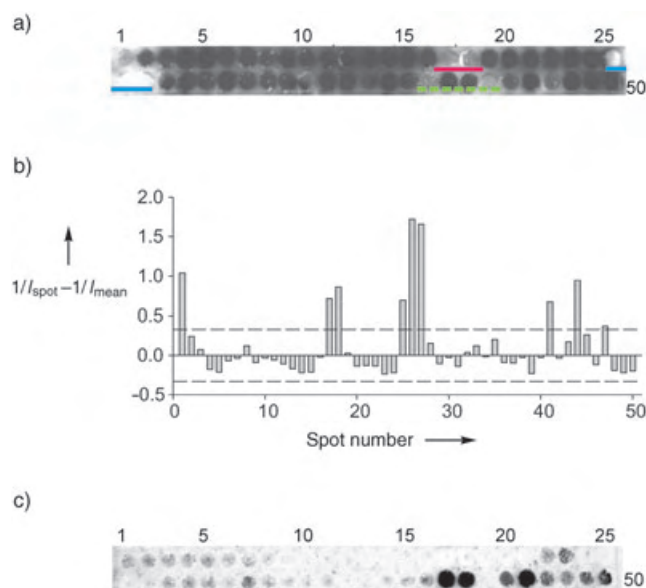


Figure 2. Binding of streptavidin to the streptavidin–Stt II peptide array attached to template **1**. The streptavidin sequence is collectively represented by 12-mer peptides that overlap with a shift of three amino acid residues. a) The cellulose membrane was probed with streptavidin (100 nM) and bound streptavidin was detected by Western blot analysis. b) Densitometry analysis of Figure 2a. The intensity of each spot was analyzed with a GS-700 imaging densitometer (Bio-Rad). The ordinate represents the reciprocal of the intensity of each analyzed spot minus the reciprocal of the average intensity of all spots tested. The large positive arbitrary unit values correspond to a weak blot signal, and indicates a potential interaction of the peptides in a pair. The dashed line represents the scatter-derived deviation 3σ manifested by the mean deviation from zero of the negative values n . c) The cellulose was probed with streptavidin (100 nM) in the presence of biotin (600 nM) and the bound streptavidin was detected by Western blot analysis. I_{spot} = intensity of each analyzed spot; I_{mean} = average intensity of all spots tested.

adjacent IANUS-positive spots were considered indicative of a nativelike interaction in the respective peptide pair. Switching Stt II attachment to the Fmoc site and streptavidin sequences to the Dde site on template **1** did not markedly alter the spot array staining patterns (Supporting Information).

When peptides were synthesized on template **2** the pattern of IANUS-positive spots was quite similar to those obtained with template **1** (Figure 3, blue and pink under-

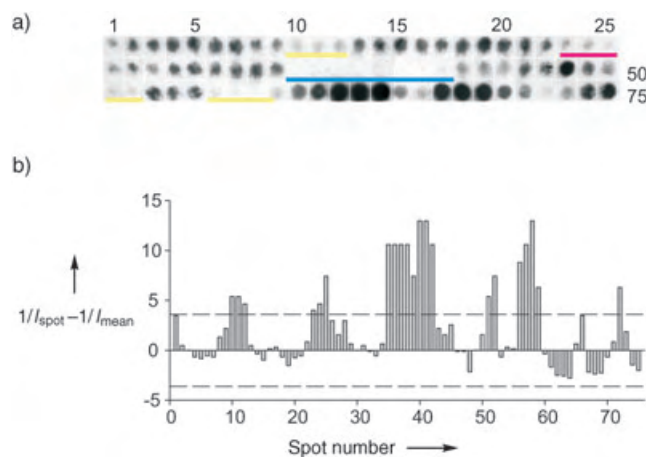


Figure 3. Binding of streptavidin to the streptavidin–Stt II peptide array attached to template **2**. The streptavidin sequence is collectively represented by 12-mer peptides that overlap with a shift of two amino acid residues. a) The cellulose was probed with streptavidin (100 nm) and the bound streptavidin was detected by Western blot analysis. b) Denitometry analysis; the intensity of each spot was analyzed as described in Figure 2b.

lining, Table 1). However, the identification of three additional interacting protein segments (Figure 3, yellow underlining) is consistent with a model in which the conformational flexibility of the template facilitates more nativelike interactions of peptide pairs. Apparently template **2** is more appropriate for the complete identification of the architecture of the streptavidin–Stt II binding site. The additional three covalent bonds in the linker region of template **2** over that of template **1** enables a majority of streptavidin-derived peptides attached to template **2** to be placed in register with the resident Stt II peptide.

Two additional IANUS-positive spots (spots 41 and 44 in Figure 2a, green underlining) indicate conformational induction but are isolated, and therefore do not fit the neighboring spot rule mentioned above. We hypothesize that a continuous stretch of four IANUS-positive spots may exist (spots 41–44). The reason behind the intense staining of spots 42 and 43 must therefore be explained. IANUS spot array assays conducted in the presence of the streptavidin ligand biotin revealed that the staining of spots 42 and 43 was a result of an interaction between soluble streptavidin and the streptavidin-derived peptide. This indicates that these spots bear a sequence region directly involved in the formation of streptavidin tetramers. The oligomerization interface is centered around H¹²⁷,^[7] and the peptides of spot 42 and 43

correspond to this region. Consequently, streptavidin retains binding affinity for both spots despite blockage of the active site with biotin. With the exception of spots 42/43, and 45/46, all other spots were unstained in the presence of biotin (Figure 2c). Consequently, the readout by Western blot analysis of the IANUS spot array bears some limitations for homooligomeric proteins, in that the intense signal for spots containing peptides of the oligomerization interface prevents the detection of some IANUS-positive spots.

Application of the potential of mean force (PMF) can generate a complete description of the binding interface of protein–ligand complexes in which direct hydrogen bonding, water bridging, and hydrophobic interactions are thought to make up the binding energy.^[8] In this model, a distance of 5.0 Å between the atoms of interacting molecules is assumed to comprise all attractive protein–ligand interactions, thus defining the binding interface. On the basis of streptavidin residues that lie within a 5.0-Å radius around the Stt II atoms (Table 1, residues in boldface), the three-dimensional binding interface of the streptavidin–Stt II complex was identified from X-ray crystallographic structure information (PDB entry: 1RSU).^[5a] Notably, the two N-terminal residues of Stt II were not localized in the crystal structure, and as a result, the unequivocal identification of their contact sites was not possible.

With the exception of the Y⁴³–E⁴⁴ segment, the streptavidin-derived peptides that correspond to the IANUS-positive spots of both templates, encompass the complete binding interface derived from the X-ray crystallographic structure. The Y⁴³–E⁴⁴ stretch, which is close to the N terminus of the IANUS-positive spot 23 (Table 1), was identified to reside within the 5.0-Å radius of Q⁷ of Stt II, but did not produce an IANUS-positive spot. Most importantly, the IANUS array did not generate false-positive regions associated with the detection of noninteracting sequences.

Critical to the appearance of some IANUS-positive spots was the sole presence of either D¹²⁸, W⁷⁹, or R⁸⁴ in the peptide pair (Table 1, spots 41–44, 25–27, 35–42, 56–59). It appears that for these amino acids, only a limited structural context was required for the intramolecular interaction with Stt II. In the case of D¹²⁸ and R⁸⁴, exceptionally strong hydrogen-bonding contacts to Stt II have already been noted.^[5a] The appearance of other IANUS-positive spots was consistent with multiple interaction sites of the peptide pairs, in which the sequence context dominates (Table 1, spots 17–18, 25–27, 23–25, 10–12, 51–52). In these cases, inspection of the three-dimensional structure of the streptavidin–Stt II complex revealed a modular arrangement of interacting residues in which both the position of the amino acid and peptide composition are necessary for an IANUS-positive spot.

Single amino acid substitutions on IANUS-positive interacting pairs provided a clear indication of the specificity of the IANUS method (Supporting Information). Positions 53 (R) and 54 (Y) were individually substituted with every other gene-coded amino acid in the streptavidin peptide segment ⁴⁹NAESRYVLTRY⁶⁰. These peptide preparations were subjected to the IANUS spot assay, and the paired peptide Stt II was held constant. Indeed, the IANUS spot array proved sensitive to single-point substitutions. Substitutions at posi-

Table 1: Sequences of peptides from IANUS-positive spots and streptavidin–Stt II contact regions derived from X-ray crystallographic data.^[a]

Spot number	Sequence
template 1	
17–18	⁴⁹ NA ESRY VLTGRYDSA ⁶³
25–27	⁷³ LGWTVAWKNNY RNAHSAT ⁹⁰
41–44 ^[b,c]	¹²¹ KSTLVGHDTFTKVKPSAASID ¹⁴¹
template 2	
23–25	⁴⁵ SAVGNA ESRY VLTGRY ⁶⁰
35–42	⁶⁹ SGTALGWTVAWKNNY RNAHSAT W ⁹⁴
10–12	¹⁹ GTWY NQLGST FIVTAG ³⁴
51–52	¹⁰¹ EARINTQ WLLT SGT ¹¹⁴
56–59 ^[c]	¹¹¹ TSGTTEANAWKSTLVGH ¹²⁸

[a] The amino acid residues identified in X-ray crystallographic data to reside in a sphere of 5.0-Å radius about the Stt II atoms in the streptavidin–Stt II complex are printed in bold face (PDB entry: 1RSU). They were considered to represent residues involved in attractive protein–ligand interactions. [b] Assuming a continuous stretch of four IANUS-positive spots (see text for details). [c] Limited information is available on the contact sites for these segments of streptavidin. This results from poorly defined atomic locations for either the streptavidin sequence S¹³⁶–Q¹⁵⁹, or the S¹ and N² residues of Stt II in the X-ray crystallographic data.

tion 53 led, in most cases, to IANUS-negative spots. Including the wild-type streptavidin peptide sequence (R⁵³), IANUS-positive spots were obtained with only K, Q, Y, and V. Substitutions at position 54, on the other hand, gave IANUS-positive results with almost all amino acid residues except E, V, and N.

The substitutional analysis of the Stt II peptide in positions 5 (H) and 9 (E) paired with a constant streptavidin peptide sequence ⁷⁵VAWKNNYRNAHS⁸⁸ was more difficult to perform, as Stt II is not only the interacting partner in the IANUS experiment, but also provides the probe for detecting IANUS-positive spots by streptavidin binding. Additional experiments showed that most Stt II variants are not able to interact with native streptavidin. In fact, an IANUS-positive spot was observed in the case of a conservatively substituted Stt II E⁹ variant that allowed streptavidin binding.

Table 1 lists the discontinuous segments of streptavidin that form the architecture of the streptavidin–Stt II binding surface, as determined by the IANUS spot array. The need for an extended sequence context in the IANUS-positive peptide pairs is variable. Modified IANUS peptide pairs were evaluated to determine the influence of reverse reading of the streptavidin sequence, starting at the C-terminal end. IANUS-positive spots were obtained with reverse streptavidin peptides containing the D¹²⁸, W⁷⁹, and R⁸⁴ residues. Given the very flexible linker regions, conformations with normal orientation may be frequently populated in the reversed-peptide arrangement (Supporting Information).

The role of template-assisted chain orientation was also investigated in two related approaches: the template assembled synthetic proteins (TASP) approach,^[9] and the modular assembly of amphiphilic helical peptides on a cyclic-peptide template for the construction of functional four-helix-bundle heme proteins.^[10] In a similar method, the identification of the Elk-1 docking domain in assisting Elk-1 phosphorylation at Ser383 was based on random distribution of two peptide

chains synthesized on monofunctional linkers.^[11] In all cases, nativelike assembly indicates the loss of conformational multiplicity of the component peptide chains in favor of freezing out interactive conformations.

The readout described herein requires a sample of biologically active streptavidin. This practical restriction on IANUS peptide arrays likely mandates the need for an alternative detection system that allows the direct observation of peptide–peptide interactions on a solid support. Examination of the streptavidin–Stt II IANUS peptide pairs involving N-terminally dansyl-labeled streptavidin peptides and N-terminally fluorescein-labeled Stt II peptide showed that IANUS-positive spots have a high fluorescence intensity at 510–530 nm. It is likely that efficient quenching of fluorescein emission is correlated to conformational flexibility of non-interacting peptide chains, and therefore occurs in IANUS-negative spots. In the presence of biotin, the fluorescence of the IANUS-positive spots is quenched to that of IANUS-negative spots. This observation indicates competition between biotin and Stt II for the interactive conformation of the streptavidin peptide of the IANUS pair (Supporting Information). The evidence presented herein suggests that the biotin ligand interferes directly with mutual conformational induction by abolishing chain togetherness with consequent alterations in the fluorescence signal. This result confirms the idea that use of a protein-free detection method for IANUS-positive spots, which would then create a powerful screen for active-site directed small-molecule ligands and inhibitors, is a promising new option for the IANUS peptide arrays.

In conclusion, a novel strategy that focuses on the induction of complementary molecular surfaces of peptide pairs has identified a complete low-resolution picture of the streptavidin–Stt II contact interface. This picture closely resembles that obtained by X-ray crystallography. IANUS peptide arrays that circumvent the need for a protein-based readout yield a low-resolution picture of protein–protein interactions on the sole basis of sequence information, thus obviating the need for native proteins in the detection step.

Experimental Section

Peptide Synthesis: Template 1 was prepared by the stepwise coupling of Fmoc-Lys(Dde)-OH and Boc-Lys(Fmoc)-OH to the (β-Ala)₂ spacer on the membrane. The amino acids were each activated with PyBOP coupling reagent (1 equiv; PyBOP = 1-benzotriazolyl-oxyl-tris(pyrrolidino)phosphonium hexafluorophosphate) and DIEA (2 equiv; DIEA = diisopropylethylamine) as base in DMF (DMF = dimethylformamide). Template 2 was prepared by solid-phase synthesis on the Rink amide MBHA resin (MBHA = 4-methylbenzhydrylamine), followed by cleavage of Fmoc-Glu-Lys(Dde)-CONH₂ from the resin by using TFA (trifluoroacetic acid). The Fmoc-Glu-Lys(Dde)-CONH₂ sequence was anchored to the (β-Ala)₂ spacer by the glutamic acid γ-carboxyl group with the coupling procedure used for template 1. After completing the synthesis of template 2 by coupling of Boc-Lys(Fmoc)-OH, the free amino and hydroxy positions were acetylated with Ac₂O (5%) and DIEA (2%) in DMF for 1 h. Peptide chains were synthesized under the standard spot synthesis protocols.^[3a] The Dde protecting group was removed with hydrazine solution (2%) in DMF, in preparation for the next peptide chain to be synthesized.

MALDI-TOF MS: Pieces of the peptide spots (4 mm²; spots 22, 29, 39, and 40; Figure 3) were irradiated with UV light for 2 min. A solution of α -cyano-4-hydroxycinnamic acid in CH₃CN/H₂O (0.1 % TFA) was then added directly onto the pieces, which were dried at room temperature. MALDI-TOF MS was carried out with the dried pieces on a Bruker Reflex II mass spectrometer (Bruker Daltonik GmbH, Bremen, Germany).

Western blots: Dry cellulose membranes were rinsed in methanol for 10 min and for 3 × 20 min in TBS buffer (Tris-HCl pH 7.6 (30 mM), NaCl (170 mM), and KCl (6.4 mM)). Streptavidin (100 nM) in MP buffer (TBS buffer supplemented with Tween (0.05 %), and sucrose (20.5 %)) was allowed to react with wet membranes overnight at 4 °C under gentle shaking. Unbound streptavidin was removed by washing with TBS buffer (4 °C), and spot-bound protein was electrotransferred onto nitrocellulose membranes (0.45 μ m, PALL Gelman, Germany) with a semi-dry blotter (Biometra, Germany). The nitrocellulose membranes were sandwiched between blotting paper soaked with transfer buffer (Tris-HCl pH 8.3 (25 mM), glycine (150 mM), and methanol (10 %)) kept at 4 °C. Electrotransfer was performed at a constant power of 0.8 mA cm⁻² with suitable time courses (first electrotransfer step for 30–45 min, second electrotransfer step for 60–90 min). Transferred streptavidin was detected with rabbit anti-streptavidin antibodies (Sigma–Aldrich) and peroxidase-conjugated anti-rabbit IgG. The final visualization was performed by using an enhanced chemiluminescence ECL system. Densitometric analysis was performed with a GS-700 imaging densitometer (Bio-Rad).^[12]

Received: June 16, 2004

Revised: October 4, 2004

Published online: January 21, 2005

Keywords: combinatorial chemistry · conformational induction · peptides · spot synthesis

- [9] a) M. Mutter, P. Dumy, P. Garrouste, C. Lehmann, M. Mathieu, C. Peggion, S. Peluso, A. Razaname, G. Tuchscherer, *Angew. Chem.* **1996**, *108*, 1588–1591; *Angew. Chem. Int. Ed. Engl.* **1996**, *35*, 1482–1485; b) S. Peluso, P. Dumy, C. Nkubana, Y. Yokokawa, M. Mutter, *J. Org. Chem.* **1999**, *64*, 7114–7120.
- [10] H. K. Rau, N. DeJonge, W. Haehnel, *Proc. Natl. Acad. Sci. USA* **1998**, *95*, 11 526–11 531.
- [11] X. Espanel, S. Walchli, T. Ruckle, A. Harrenga, M. Huguenin-Reggiani, R. H. van Huijsduijnen, *J. Biol. Chem.* **2003**, *278*, 15 162–15 167.
- [12] S. Rüdiger, B. Bukau, *Biospektrum* **1998**, *4*, 35–37.

- [1] a) P. F. Cook, J. S. Blanchard, W. W. Cleland, *Biochemistry* **1988**, *27*, 4853–4858; b) Y. Chen, D. Xu, *Curr. Protein Pept. Sci.* **2003**, *4*, 159–181.
- [2] a) S. W. Homans, *Angew. Chem.* **2004**, *116*, 292–303; *Angew. Chem. Int. Ed.* **2004**, *43*, 290–300; b) Z. Dauter, V. S. Lamzin, K. S. Wilson, *Curr. Opin. Struct. Biol.* **1997**, *7*, 681–688; c) S. K. Avrantinis, R. L. Stafford, X. Tian, G. A. Weiss, *ChemBioChem* **2002**, *3*, 1229–1234.
- [3] a) R. Frank, *Tetrahedron* **1992**, *48*, 9217–9232; b) M. Lebl, *Biopolymers* **1998**, *47*, 397–404; c) A. Kramer, U. Reineke, L. Dong, B. Hoffman, U. Hoffmüller, D. Winkler, R. Volkmer-Engert, J. Schneider-Mergener, *J. Pept. Res.* **1999**, *51*, 319–327; d) H. Wenschuh, R. Volkmer-Engert, M. Schmidt, M. Schulz, J. Schneider-Mergener, U. Reineke, *Biopolymers* **2000**, *55*, 188–206; d) R. Frank, *J. Immunol. Methods* **2002**, *267*, 13–26.
- [4] E. T. Kaiser, F. J. Kezdy, *Science* **1984**, *223*, 249–255.
- [5] a) T. G. M. Schmidt, J. Koepke, R. Frank, A. Skerra, *J. Mol. Biol.* **1996**, *255*, 753–766; b) L. A. Klumb, V. Chu, P. S. Stayton, *Biochemistry* **1998**, *37*, 7657–7663; c) I. P. Korndörfer, A. Skerra, *Protein Sci.* **2002**, *11*, 883–893; d) S. Freitag, I. Le Trong, L. Klumb, P. S. Stayton, R. E. Stenkamp, *Protein Sci.* **1997**, *6*, 1157–1166; e) A. Chilkoti, P. H. Tan, P. S. Stayton, *Proc. Natl. Acad. Sci. USA* **1995**, *92*, 1754–1758; f) S. Freitag, I. Le Trong, A. Chilkoti, L. A. Klumb, P. S. Stayton, R. E. Stenkamp, *J. Mol. Biol.* **1998**, *279*, 211–221.
- [6] F. Guillier, D. Orain, M. Bradley, *Chem. Rev.* **2000**, *100*, 2091–2158.
- [7] G. O. Reznik, S. Vajda, C. L. Smith, C. R. Cantor, T. Sano, *Nat. Biotechnol.* **1996**, *14*, 1007–1011.
- [8] L. Jiang, Y. Gao, F. Mao, Z. Liu, L. Lai, *Proteins Struct. Funct. Genet.* **2002**, *46*, 190–196.

Reaction Mechanisms

cis-Bromination of Alkynes without Cationic Intermediates**

Rainer Herges,* Andrea Papafilippopoulos,
Kirsten Hess, Cinzia Chiappe, Dieter Lenoir,* and
Heiner Detert*

*Dedicated to Professor Herbert Meier
on the occasion of his 65th birthday*

The textbook mechanism of the *trans*-bromination of alkenes and alkynes via a more or less symmetrically bridged bromonium ion does not always apply. Even in the parent system, the reaction of bromine with ethylene, this mechanism is not correct. Highly pure bromine reacts with ethylene in anhydrous dichloromethane only very slowly at room

[*] Prof. R. Herges, Dr. A. Papafilippopoulos, K. Hess
Institut für Organische Chemie
Christian-Albrechts-Universität zu Kiel
Otto-Hahn-Platz 4, 24118 Kiel (Germany)
Fax: (+49) 431-880-2440
E-mail: rherges@oc.uni-kiel.de

Prof. D. Lenoir
Institut für Ökologische Chemie
GSF-Forschungszentrum für Umwelt und Gesundheit
Postfach 1129, 85778 Neuherberg (Germany)
Fax: (+49) 89-3187-3371
E-mail: lenoir@gsf.de

Dr. H. Detert
Institut für Organische Chemie
Johannes Gutenberg-Universität
Duesbergweg 10–14, 55099 Mainz (Germany)
Fax: (+49) 6131-3925396
E-mail: detert@mail.uni-mainz.de

Prof. C. Chiappe
Dipartimento di Chimica Bioorganica e Biofarmacia
Università di Pisa
Via Bonanno 33, 56126 Pisa (Italy)

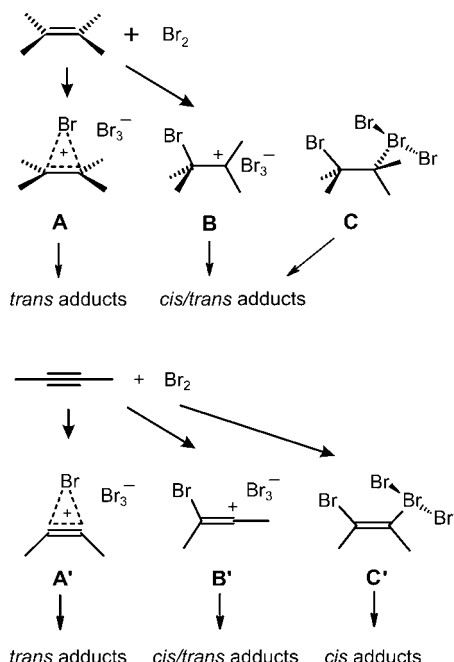
[**] We are grateful to the Fonds der Chemischen Industrie and the Deutsche Forschungsgemeinschaft for financial support.



Supporting information for this article is available on the WWW under <http://www.angewandte.org> or from the author.

temperature. Such mixtures are perfectly stable up to several days. As soon as light or traces of acids initiate the reaction, formation of 1,2-dibromoethane proceeds very rapidly and autocatalytically ($t_{1/2} < 2$ min).^[1–3]

According to the generally accepted mechanism, the stereoselective *anti* addition of bromine to alkenes and alkynes proceeds via bridged bromonium ions **A** or bromirenium ions **A'** (Scheme 1). Aberrations from *trans* selectivity are



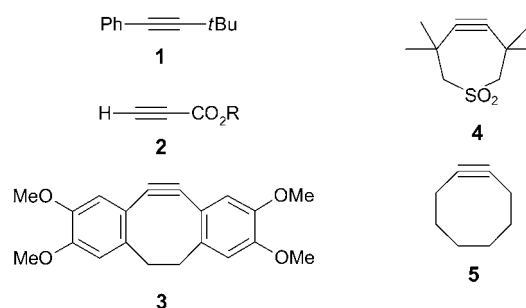
Scheme 1. Generally assumed intermediates in the addition of bromine to alkenes and alkynes **A** (bromonium ion), **A'** (bromirenium ion), **B** (β -bromocarbenium ion), **B'** (β -bromovinyl cation), and the tribromide adducts **C** and **C'** identified in the present work by theoretical calculations.

explained by the intermediacy of the nonbridged cationic species (**B**, **B'**).^[4,5] Polar solvents and cation-stabilizing substituents favor the nonstereospecific reaction by stabilization of the β -bromocarbenium ion **B** or bromovinyl cation **B'**. In extreme cases this can result in *cis/trans* ratios of 1:1. The *syn* adduct is formed after a rotation of the bromoalkyl group or by a frontside attack to the trigonal-planar cation. In alkynes only a marginal geometrical reorientation of the counterions Br^- or Br_3^- is necessary to initiate a *syn* addition to give the *cis*-dibromo adduct. There are, however, a number of halogen additions that proceed predominantly or even selectively *cis* even in nonpolar solvents. In these cases a totally different mechanism must be operative. The intermediacy of free cationic intermediates without stabilization by solvation is unlikely. A number of authors interpret the predominantly observed *syn* addition as the collapse of a contact ion pair composed of the tribromide anion and the corresponding carbocation **B** or **B'**, which is faster than the reorientation of the Br_3^- and a subsequent backside attack.^[6–9]

We now present experimental work showing that the addition of bromine to strained alkynes (cyclooctyne and

tetramethylthiacycloheptyne-1,1-dioxide) gives almost exclusively *syn* products, and we present theoretical evidence that the intermediate is not a contact ion pair of Br_3^- and the vinyl cation **B'**. Instead, in solvents of low polarity the Br_3^- anion forms a covalent bond with the cationic center (Scheme 1, **C'**). This tribromide adduct is formed from a π complex and rearranges directly to the product (dibromide) without passing through a cationic intermediate.

According to calculations of Bianchini, Lenoir, and Goldberg et al.^[10] the substituents at the alkyne determine whether the bromirenium ion **A'** or the β -bromovinyl cation **B'** will be more stable. In phenylacetylene the vinyl cation is favored because the positive charge at the benzylic position is stabilized by delocalization. Hence, the reaction proceeds in a nonstereospecific way. In *p*-nitrophenylacetylene the positive charge at the benzylic position is destabilized. Therefore the bridged bromirenium ion **A'** is more stable, and the reaction proceeds with *anti* selectivity. Apart from the *anti*-selective and the nonstereoselective additions there are a number of *syn* additions of bromine to alkynes. Uemura et al. observed the exclusive formation of the *cis*-dibromo adduct after the reaction of *tert*-butylphenylacetylene (**1**) with bromine in chloroform at -50°C (Scheme 2).^[11] Only after long reaction



Scheme 2. Alkynes that selectively add bromine in a *syn* fashion forming a *cis*-dibromoalkene.

times and higher temperatures is the thermodynamically more stable and sterically less hindered *trans*-dibromoalkene formed. Selectively *syn* additions of bromine are also observed for the reaction with alkyl propiolate **2** (which is deactivated compared to alkyl- and aryl-substituted alkynes).^[12,13] When the bromination is conducted in chloroform at 70°C and with reaction times of 1–3 h only the *cis*-dibromo adducts are formed. *trans*-Dibromopropenoates can be obtained selectively by reaction with pyridinium tribromide and bromine.

The *syn* selectivity obviously holds also for the addition of bromine to strained cycloalkynes. Krebs et al. observed the formation of only the *cis*-dibromo adducts in the bromination of dibenzocyclooctyne **3**,^[14] and 3,3,6,6-tetramethylthiacycloheptyne-1,1-dioxide (**4**)^[15] in chloroform or dichloromethane. According to our investigations, cyclooctyne (**5**) gives 25 % of the *cis*-dibromide at -40°C in CDCl_3 (detected by independent synthesis and X-ray analysis, see the Supporting Information) and only 3 % of the *trans* product. Besides that, bromocyclooctene is formed by addition of HBr (for experimental details see the Supporting Information). A single

electron transfer (SET) mechanism leading to the *cis* product is very unlikely. Kinetic measurements show that the reaction is of first order in cyclooctyne and second order in bromine. Moreover, neither the reaction rate nor the reaction order is changed upon addition of radical scavengers.^[16] The addition of tetrammonium tribromide in polar solvents yields only the *trans*-dibromide (see the Supporting Information). Wittig and Dorsch observed the formation of the *cis* product upon reaction with bromine and iron powder.^[17]

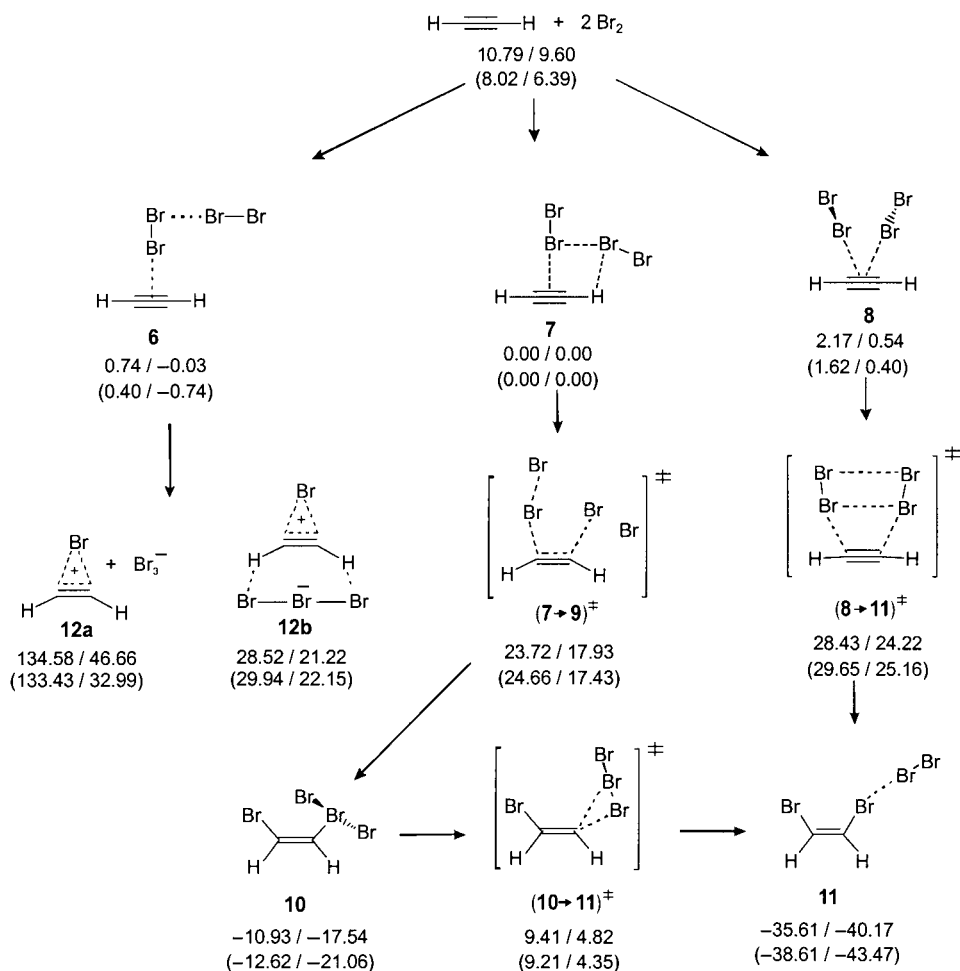
To elucidate the mechanism of the *syn* addition we performed extensive density functional theory (DFT) calculations first on the potential energy surface of the parent system acetylene+2Br₂ and also on the potential energy surface of cyclooctyne+2Br₂ at the B3LYP/6-31G*+ZPE and B3LYP/6-31G(2df)+ZPE levels of theory.^[18] The stationary points were characterized by harmonic frequency analyses, and the topology of the potential energy surface was checked by IRC calculations. To locate the stationary points, we used numerous grid calculations as well as other methods.

In agreement with experimental observations of Bianchini et al.^[10] π complexes are formed initially. As in the case of alkenes the reactive complexes have the stoichiometry

acetylene·2Br₂.^[19] According to the calculations three different 1:2 complexes are in equilibrium; these complexes are 8.62–10.79 kcal mol⁻¹ (B3LYP/6-31G*) and 6.40–8.02 kcal mol⁻¹ (B3LYP/6-31G(2df)) more stable than the separated reactants (Scheme 3). In the L-shaped complex **6**, a bromine molecule is coordinated perpendicularly to one of the π bonds and an additional bromine molecule is bound to the first at an angle of 90° (Scheme 3, Figure 1). According to our calculations this is the starting point for the formation of the bromirenium ion and the polar mechanisms.

Starting from the most stable π complex **7** and proceeding with an activation energy ((**7**→**9**)[‡]) of 23.7 kcal mol⁻¹ (B3LYP/6-31G*) or 24.7 kcal mol⁻¹ (B3LYP/6-31G(2df)), the structurally interesting tribromide adduct **10** is formed. There is a very flat minimum **9** between the transition state (**7**→**9**)[‡] and **10**, which rearranges to **10** with an activation barrier of only 0.3 kcal mol⁻¹ (B3LYP/6-31G*) or 0.1 kcal mol⁻¹ (B3LYP/6-31G(2df)) and which therefore does not have any chemically interpretable significance.

The tribromide adduct **10** diverges from the usual valence schemes of bromine in organic compounds. The central bromine atom in the Br₃⁻ unit is bound to the neighboring



Scheme 3. Comparison of the bromirenium ion with intermediates in nonionic mechanisms for the bromination of acetylene. The energies of the stationary points in a vacuum (left) and the SP solvent energies in dichloromethane (B3LYP/6-31G*+ZPE in kcal mol⁻¹, right) are relative to the most stable π complex **7**. The energies in vacuo and in dichloromethane at B3LYP/6-31G(2df) are given in parentheses (relative to the π complex **7** at the same level of theory).

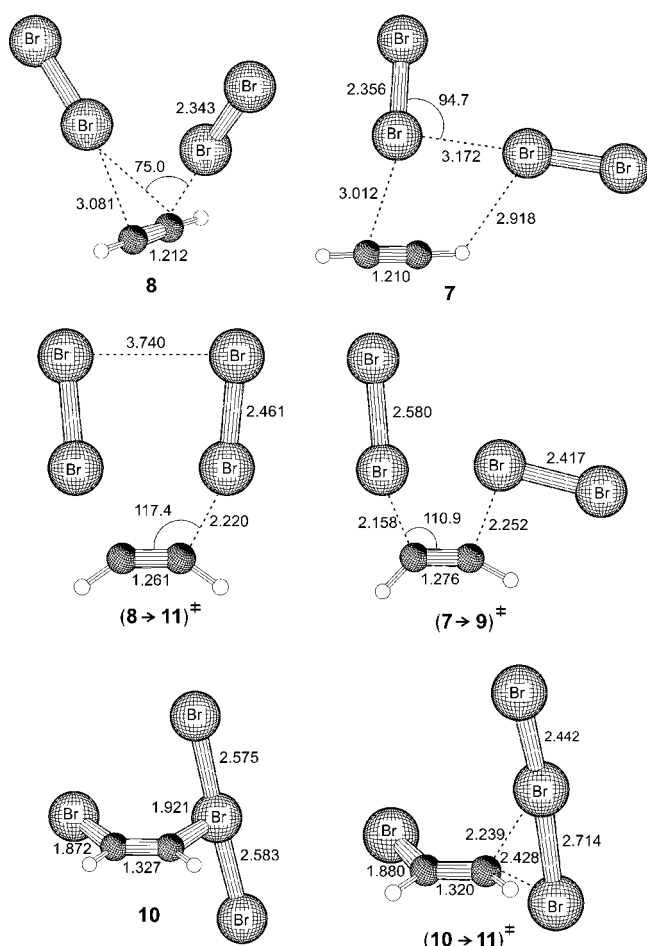


Figure 1. Geometries (B3LYP/6-31G*) of selected stationary points on the potential energy surface of the addition of bromine to acetylene.

carbon atom with a bond length of only 1.921 Å. (Figure 1). This bond is significantly shorter than that in the π complex (3.081 Å) and not much longer than a “normal” C–Br bond (≈ 1.89 Å). Also the charges (NBO analysis)^[20] indicate a covalent C–Br bond and do not support a contact ion pair. The two C atoms with a charge of -0.04 are almost neutral. The central Br bearing the C–Br bond has a positive charge of $+0.57$, which is almost compensated by the two terminal Br atoms (-0.32 and -0.31). The Br–Br bonds with 2.575 and 2.583 Å are similar in length to that in the tribromide anion (2.606 Å), and the C–C bond length of 1.327 Å corresponds that in **11** (1.330 Å). Interpreted within the simple valence bond model, the tribromide anion is a linear 22-electron species with a trigonal-planar sp^3d -hybridized central Br atom. The three lone pairs occupy the equatorial positions. The interaction of one of the lone pairs with a cation therefore generates a T-shaped molecule. Despite its unusual structure^[21] the tribromide adduct **10** is more than 10 kcal mol^{−1} more stable than

the reactants and is a well-defined minimum (also at the MP2/6-31G* level of theory).

The dibromo adduct **11** is formed from **10** by a “shift” of the Br_3^- unit and elimination of Br_2 . The activation barrier for this reaction is 20.3 kcal mol^{−1} (B3LYP/6-31G*) or 21.8 kcal mol^{−1} (B3LYP/6-31G(2df)). The product complex **11** is more stable than the isolated molecules (dibromoethene and bromine) by 6 kcal mol^{−1}. There is also a concerted six-center pericyclic transition state (**8**→**11**)[‡], which leads to the product **11**; however, with an activation barrier of $\Delta H^\ddagger = 26.3$ kcal mol^{−1} (B3LYP/6-31G*) or 28.0 kcal mol^{−1} (B3LYP/6-31G(2df)), this reaction pathway is significantly less favorable. The “textbook intermediate”, the bromirenium ion **12**, is considerably more difficult to describe theoretically than the less polar species. The relative energies given in Scheme 3 and Table 1 are therefore less reliable. The relative energy (134.6 kcal mol^{−1} (B3LYP/6-31G*) or 133.4 kcal mol^{−1} (B3LYP/6-31G(2df))) of the separated ion pair **12a** can be considered as the upper limit. As the lower limit, one can consider the twofold hydrogen-bonded ion pair **12b**^[22] with 21.2 or 22.2 kcal mol^{−1}.

Single-point energy (SP) solvent calculations using Tomasi’s Polarized Continuum Model (PCM)^[23–25] reveal that the activation barrier (**7**→**9**)[‡] leading to the tribromide adduct **10** is drastically reduced even by moderately polar media (Table 1). The same applies to the bromirenium ion **12**. The very large energy difference between **12a** and **12b** in vacuo (103.5 kcal mol^{−1}) is, as expected, drastically reduced in polar solvents (10.8 kcal mol^{−1}, B3LYP/6-31G(2df)). However, even in water the energy of **12b** is still 4.5 kcal mol^{−1} higher than the transition state (**7**→**9**)[‡] that leads to the tribromide adduct **10**. The latter is at least 40 kcal mol^{−1} more stable than the bromirenium ion **12**.

Table 1: Relative energies for the transition states and the ion pairs **12a** and **12b** in various solvents.^[a]

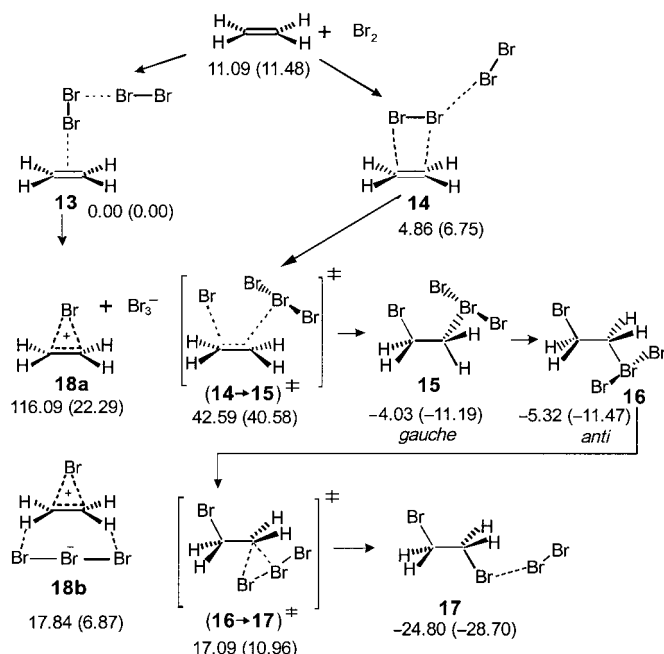
Solvent	(7 → 9) [‡]	(10 → 11) [‡]	(8 → 11) [‡]	12a	12b
cyclohexane	19.48 (20.19)	4.96 (5.15)	25.43 (27.07)	83.31 (75.45)	24.08 (25.86)
dichloromethane	17.93 (17.43)	4.82 (4.35)	24.22 (25.16)	46.66 (32.99)	21.22 (22.16)
methanol	16.02 (16.71)	3.35 (4.34)	22.50 (24.81)	26.93 (23.98)	18.89 (21.23)
DMSO	16.90 (16.04)	1.64 (3.60)	20.87 (24.16)	37.77 (22.70)	17.31 (20.58)
water	15.05 (15.74)	2.72 (3.57)	21.89 (24.09)	24.41 (22.03)	18.01 (20.17)
vacuum	23.72 (24.66)	9.41 (9.21)	28.43 (29.65)	134.58 (133.43)	28.52 (29.94)

[a] Energies relative to the π complex **7**; PCM-SP B3LYP/6-31G* in kcal mol^{−1}. The energies at the B3LYP/6-31G(2df) level of theory are given in parentheses.

Considering the relatively high barriers separating the tribromide adduct **10** from the reactants and the products, it should be possible to isolate this intermediate under suitable conditions. There is indeed evidence that a tribromide intermediate analogous to **10** is formed in the reaction of bromine with **4**. During the reaction of **4** with two equivalents of bromine at -70°C a yellow-orange precipitate formed. When the reaction mixture was allowed to warm up to 0°C , we observed the conversion of the complex to the *cis*-dibromo adduct. In the ¹³C NMR spectrum at -40°C there are only two signals at 129.79 and 135.19 ppm, which indicate olefinic rather than cationic carbon atoms. The NMR data indicate

that the observed intermediate is not symmetric, in agreement with an intermediate with a tribromide structure analogous to **10**; this is in contrast to the symmetric reactant and the product of the bromination reaction. Unfortunately, however, the spectroscopic data are not sufficient to assign the structure unambiguously. All attempts to determine a crystal structure were unsuccessful.^[26]

Because of the high stability of the tribromide adduct one could expect that this species is also an intermediate in bromination reactions of alkenes. Even in very polar solvents the two conformations of the tribromide adducts **15** and **16** are significantly more stable than the bridged bromonium ion, both as a separated ion pair **18a** as well as the contact ion pair **18b** (see Scheme 4). However, the activation barrier for the



Scheme 4. Nonionic mechanisms for the bromination of acetylene. The energies of the stationary points (B3LYP/6-31G*+ZPE in kcal mol⁻¹) are relative to the most stable π complex **13**. The SP solvent energies in dichloromethane (B3LYP/6-31G* in kcal mol⁻¹) are also relative to the π complex **13**.

formation of **15** from the π complex **14**, at least in the parent system acetylene, is too high to compete with the classical mechanism via the bromonium ion. In substituted systems like acenaphthylene, which adds bromine preferentially *cis*, however, an intermediate analogous to **15** is likely.^[7,8]

Received: August 13, 2004
Revised: November 3, 2004
Published online: January 21, 2005

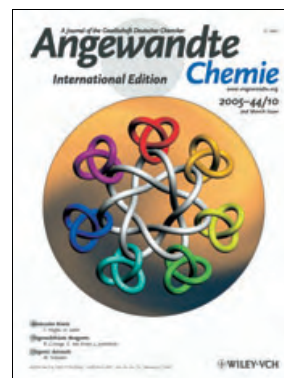
Keywords: alkynes · bromination · density functional calculations · electrophilic addition · reaction mechanisms

- [1] H. S. Davis, *J. Am. Chem. Soc.* **1928**, *50*, 2769–2780.
- [2] D. M. Williams, *J. Chem. Soc. Abstr.* **1932**, 2911–2915.
- [3] S. Kammermeier, R. Herges, unpublished results.
- [4] Review on alkenes: M.-F. Ruasse, *Adv. Phys. Org. Chem.* **1993**, *28*, 207.
- [5] Review on alkynes: G. Melloni, G. Modena, U. Tonellato, *Acc. Chem. Res.* **1981**, *14*, 227–233.
- [6] M.-F. Ruasse, G. L. Moro, B. Galland, R. Bianchini, C. Chiappe, G. Bellucci, *J. Am. Chem. Soc.* **1997**, *119*, 12492–12502.
- [7] V. F. Anikin, V. V. Veduta, A. Merz, *Monatsh. Chem.* **1999**, *130*, 681–690.
- [8] G. Bellucci, C. Chiappe, R. Bianchini, P. Lemmen, D. Lenoir, *Tetrahedron* **1997**, *53*, 785–790.
- [9] K. Zates, H. W. Leung, *J. Org. Chem.* **1980**, *45*, 1401–1406.
- [10] R. Bianchini, C. Chiappe, G. L. Moro, D. Lenoir, P. Lemmen, N. Goldberg, *Chem. Eur. J.* **1999**, *5*, 1570–1580.
- [11] S. Uemura, H. Okazaki, M. Okano, *J. Chem. Soc. Perkin Trans. 1* **1978**, 1278–1282.
- [12] F. Bellina, A. Carpita, M. de Santis, R. Rossi, *Tetrahedron Lett.* **1994**, *35*, 6913–6916.
- [13] R. Rossi, F. Bellina, A. Carpita, R. Gori, *Gazz. Chim. Ital.* **1995**, *125*, 381–392.
- [14] J. Odenthal, Dissertation, Universität Heidelberg, **1975**.
- [15] U. Höpfner, Dissertation, Universität Heidelberg, **1979**.
- [16] C. Chiappe, unpublished results.
- [17] G. Wittig, H.-L. Dorsch, *Liebigs Ann. Chem.* **1968**, *711*, 46–54.
- [18] Gaussian 98 (Revision A.11.4), M. J. Frisch, G. W. Trucks, H. B. Schlegel, G. E. Scuseria, M. A. Robb, J. R. Cheeseman, V. G. Zakrzewski, J. A. Montgomery, R. E. Stratmann, J. C. Burant, S. Dapprich, J. M. Millam, A. D. Daniels, K. N. Kudin, M. C. Strain, O. Farkas, J. Tomasi, V. Barone, M. Cossi, R. Cammi, B. Mennucci, C. Pomelli, C. Adamo, S. Clifford, J. Ochterski, G. A. Petersson, P. Y. Ayala, Q. Cui, K. Morokuma, D. K. Malick, A. D. Rabuck, K. Raghavachari, J. B. Foresman, J. Cioslowski, J. V. Ortiz, B. B. Stefanov, G. Liu, A. Liashenko, P. Piskorz, I. Komaromi, R. Gomperts, R. L. Martin, D. J. Fox, T. Keith, M. A. Al-Laham, C. Y. Peng, A. Nanayakkara, C. Gonzalez, M. Challacombe, P. M. W. Gill, B. G. Johnson, W. Chen, M. W. Wong, J. L. Andres, M. Head-Gordon, E. S. Replogle, J. A. Pople, Gaussian, Inc., Pittsburgh, PA, **2002**.
- [19] R. Bianchini, C. Chiappe, D. Lenoir, P. Lemmen, R. Herges, J. Grunenberg, *Angew. Chem.* **1997**, *109*, 1340–1343; *Angew. Chem. Int. Ed. Engl.* **1997**, *36*, 1284–1287.
- [20] A. E. Reed, L. A. Curtis, F. Weinhold, *Chem. Rev.* **1988**, *88*, 899–926.
- [21] M. L. Munzarova, R. Hoffmann, *J. Am. Chem. Soc.* **2001**, *123*, 4787–4795.
- [22] There is no minimum for a contact ion pair composed of the bromonium cation and a tribromide anion at the levels of theory that we applied (B3LYP/6-31G*, B3LYP/6-31(2d,f), MP2/6-31G*). The stationary point of lowest order that was found for such a species is the C_{2v} -symmetrical structure **12b** (saddle point). Structure **12b** is suitable as a model to estimate the lower level of the relative energy because the charges come very close to each other and hence minimize the dipole moment.
- [23] S. Miertus, J. Tomasi, *Chem. Phys.* **1982**, *65*, 239–245.
- [24] S. Miertus, E. Scrocco, J. Tomasi, *Chem. Phys.* **1981**, *55*, 117–129.
- [25] M. Cossi, M. Persico, J. Tomasi, *J. Am. Chem. Soc.* **1994**, *116*, 5373–5378.
- [26] We are grateful to Prof. Dr. R. Boese, Universität Essen, for his attempts to determine the X-ray structure of the intermediate in the bromination of **4**.

Cover Picture

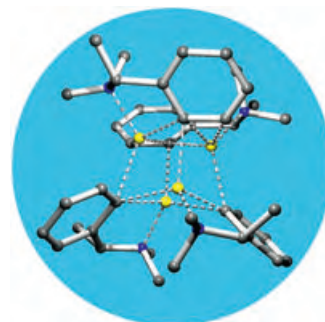
Oleg Lukin and Fritz Vögtle*

Fantasy structures such as the heptafoil knot interlocked with seven trefoil knots shown in the cover picture represents a distant goal for template synthesis. Established template strategies for the synthesis of molecular knots (knotanes) and higher assemblies with twisted architectures can lead to such structures. More on the synthesis, functionalization, and properties of knots can be found in the Review by F. Vögtle and O. Lukin on page 1456 ff.



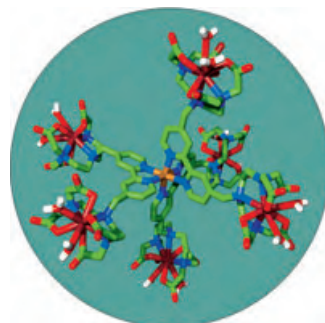
Organolithium reagents

What happens in the reactions of organolithium compounds? In their Minireview on page 1448 ff., R. Gossage, J. Jastrzebski, and G. van Koten describe the formation of hetero-aggregates with remarkable structures and reactivities.



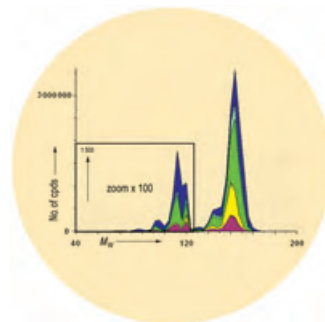
Magnetic Resonance Imaging

An Fe^{II}–Gd^{III} metallostar complex, which exhibits a remarkably high proton relaxivity and could potentially be applied in magnetic resonance imaging, is introduced by E. Tóth and co-workers in their Communication on page 1480 ff.



Chemoinformatics

In their Communication on page 1504 ff., J.-L. Reymond and co-workers describe the construction of a database that contains 13.9 million organic molecules with up to 11 atoms, under constraints for chemical stability and synthetic feasibility.





The following Communications have been judged by at least two referees to be “very important papers” and will be published online at www.angewandte.org soon:

Mark Gandelman, Eric N. Jacobsen*

Highly Enantioselective Catalytic Conjugate Addition of N Heterocycles to α,β -Unsaturated Ketones and Imides

Sang Hyuk Im, Yun Tack Lee, Benjamin Wiley, Younan Xia*

Large-Scale Synthesis of Silver Nanocubes: The Role of HCl in Promoting Cube Perfection and Monodispersity

Sridhar Narayan, John Muldoon, M. G. Finn, Valery V. Fokin, Hartmuth C. Kolb, K. Barry Sharpless*

“On Water”: Unique Reactivity of Organic Compounds in Aqueous Suspensions

Tetsuro Murahashi, Christopher R. Clough, Joshua S. Figueroa, Christopher C. Cummins*

A Ligand Comprised of Dinitrogen and Methylphenylphosphine in a Cationic Molybdenum Complex

Paul J. Goldsmith, Simon J. Teat, Simon Woodward*

Enantioselective Preparation of β,β -Disubstituted α -Methylenepropionates by Methylaluminoxane Promotion of the Zinc Schlenk Equilibrium

Holger Braunschweig,* Krzysztof Radacki, David Scheschkewitz, George R. Whittell

Boron as a Bridging Ligand

Obituary

Herbert C. Brown (1912–2004): Organoboranes

G. W. Kabalka _____ 1438

Books

Modern Fluoroorganic Chemistry

Peer Kirsch

reviewed by G. K. S. Prakash _____ 1439

Newton's Darkness

Carl Djerassi, David Pinner

reviewed by G. B. Kauffman,
L. M. Kauffman _____ 1440

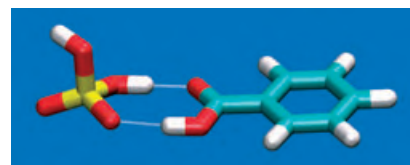
Highlights

Aerosols

W. Schrader* _____ 1444 – 1446

Atmosphere, a Chemical Reactor—
Formation Pathways of Secondary
Organic Aerosols

It's becoming clearer: The formation of atmospheric aerosols can have a distinct effect on the local climate and the radiation balance of the atmosphere. The first step in the formation of such particles can be explained, for example, by the formation of an intermediate complex composed of an aromatic acid and sulfuric acid (see picture), which occur as typical decomposition products in areas with high air pollution.



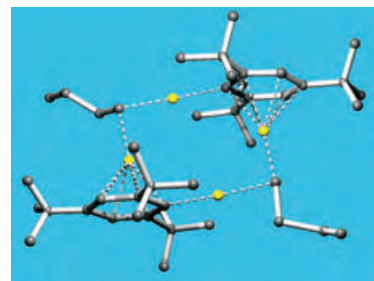
Minireviews

Organolithium Reagents

R. A. Gossage,* J. T. B. H. Jastrzebski,
G. van Koten* _____ 1448 – 1454

Hetero-Aggregate Compounds of Aryl and
Alkyl Lithium Reagents: A Structurally
Intriguing Aspect of Organolithium
Chemistry

Lithium wins on aggregate: Although often depicted as mononuclear species, organolithium compounds are in fact aggregated species and can form hetero-aggregates containing different organic groups (see structure of $[(n\text{BuLi})_2(2,4,6\text{-tBu}_3\text{C}_6\text{H}_2\text{Li})_2]$; yellow Li). The aggregation behavior of organolithium compounds is presented and the significance of the formation of such aggregates on synthesis, directed *ortho*-metalation, and the induction and formation of chiral compounds is discussed.

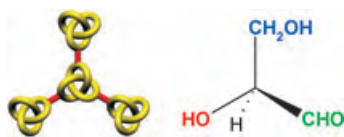


Reviews

Molecular Knots

O. Lukin, F. Vögtle* 1456–1477

Knotting and Threading of Molecules: Chemistry and Chirality of Molecular Knots and Their Assemblies



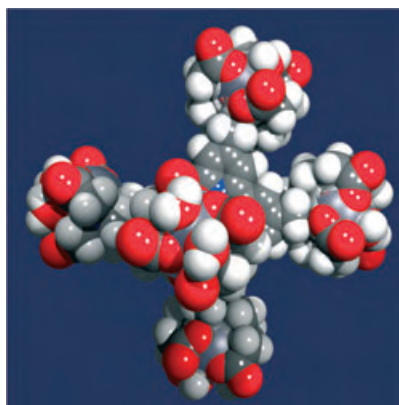
How and why do molecules thread or tangle? The answer is found in this Review, which covers the latest developments in templation techniques for the preparation of molecular knots (knotanes), their chiral resolution, their selective functionalization, and their further use as building blocks in the syntheses of higher assemblies (see picture).

Communications

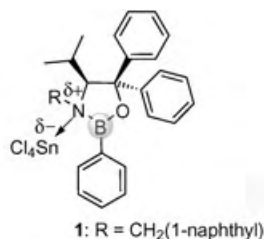
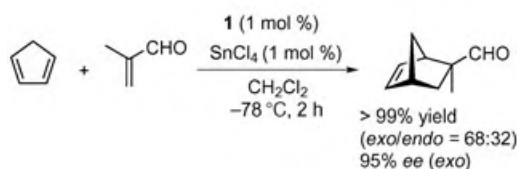
MRI Contrast Agents

J. B. Livramento, É. Tóth,* A. Sour, A. Borel, A. E. Merbach, R. Ruloff 1480–1484

High Relaxivity Confined to a Small Molecular Space: A Metallostar-Based, Potential MRI Contrast Agent



Good things come in small packages: For its moderate molecular weight, the metallostar complex $[\text{Fe}\{\text{Gd}_2\text{L}(\text{H}_2\text{O})_4\}_3]^{4-}$ (see picture; L is a bipyridine–poly(amino-carboxylate) derivative) displays exceptionally high proton relaxivity, which is explained in terms of a rigid supramolecular structure, two inner-sphere water molecules with a near-optimal exchange rate, and six efficiently relaxing Gd^{III} centers confined to a small molecular space.



Reactive, selective, and tough, the chiral Lewis acid generated from **1** and SnCl_4 catalyzes the enantioselective Diels–Alder reactions of various classes of substrates (see scheme). The reactive species pre-

serves its asymmetric induction ability even in the presence of a large excess of SnCl_4 . Importantly, this catalyst system is tolerant to a small amount of moisture, oxygen, and Lewis bases.

Asymmetric Catalysis

K. Futatsugi, H. Yamamoto* 1484–1487

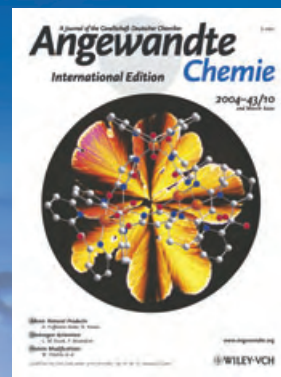
Oxazaborolidine-Derived Lewis Acid Assisted Lewis Acid as a Moisture-Tolerant Catalyst for Enantioselective Diels–Alder Reactions

For the USA and Canada: ANGEWANDTE CHEMIE International Edition (ISSN 1433-7851) is published weekly by Wiley-VCH PO Box 191161, D 69451 Weinheim, Germany. Air freight and mailing in the USA by Publications Expediting Inc. 200 Meacham Ave., Elmont, NY 11003. Periodicals

postage paid at Jamaica NY 11431. US POSTMASTER: send address changes to *Angewandte Chemie*, Wiley-VCH, 111 River Street, Hoboken, NJ 07030. Annual subscription price for institutions: US\$ 4948.00/4498.00 (valid for print and electronic / print or electronic delivery); for individuals who are personal members of a

national chemical society, or whose institution already subscribes, or who are retired or self-employed consultants, print only: US\$ 394.00. Postage and handling charges included. All Wiley-VCH prices are exclusive VAT.

The best in chemistry – for more than a hundred years



A Journal of the Gesellschaft Deutscher Chemiker
**Angewandte
Chemie**
International Edition

www.angewandte.org

1888: The beginning
of a success story

Constant Innovations

- 1962:** First issue of the International Edition
- 1976:** Graphical abstracts
- 1979:** Cover pictures
- 1988:** Centenary of Angewandte
- 1989:** Routine use of color
- 1991:** New section: Highlights
- 1992:** Computerized editorial tracking system
- 1995:** Internet service for readers
- 1998:** Regular press service; full-text online
- 2000:** New section: Essays; EarlyView: Communications available online ahead of the printed version
- 2001:** New section: Minireviews
- 2002:** Online submission of manuscripts
- 2003:** Weekly publication; new section: News; new layout
- 2004:** Backfiles (1962-1997); ManuscriptXpress: Online system for authors and referees



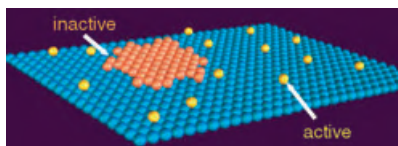
**Angewandte's
advisors...**

François Diederich
ETH Zürich

» **Angewandte Chemie** has proven over the past two decades to be the most innovative of all chemical journals, taking leadership in both quality and presentation of the published material. Rapid, high visibility of important scientific work is readily ensured. It is a true privilege to serve on the Editorial Board. «

Angewandte Chemie International Edition is
a journal of the German Chemical Society (GDCh)





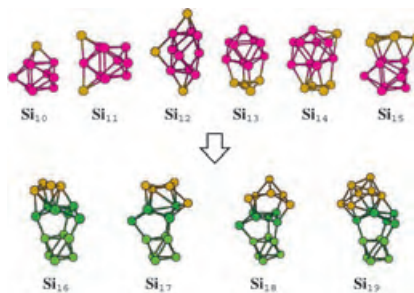
Deprotonation of the carboxy groups of 1,3,5-benzenetricarboxylic acid adsorbed on the Ag(111) surface occurs in the presence of a dilute 2D Cu adatom gas at the surface, while negligible reaction rates occur under similar conditions with Cu in the form of condensed monolayer islands. These results demonstrate that highly mobile adatoms bestow dynamic heterogeneity on materials.

Heterogeneous Catalysis

N. Lin,* D. Payer, A. Dmitriev,
T. Strunskus, C. Wöll, J. V. Barth,*
K. Kern* ————— 1488 – 1491

Two-Dimensional Adatom Gas Bestowing
Dynamic Heterogeneity on Surfaces

Generic structural motif: Small to medium-sized, energetically low-lying silicon clusters Si_n ($11 < n < 30$) are generally prolate in shape. Starting from Si_{16} , DFT calculations show that silicon clusters are most likely built on a generic structural motif consisting of an Si_6 sixfold puckered ring subunit (dark green) and a magic-number cluster such as the Si_6 tetragonal bipyramid (light green), rather than on the Si_9 tricapped trigonal prism (pink).

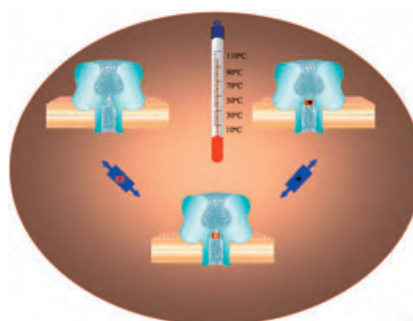


Silicon Clusters

S. Yoo, X. C. Zeng* ————— 1491 – 1494

Motif Transition in Growth Patterns of
Small to Medium-Sized Silicon Clusters

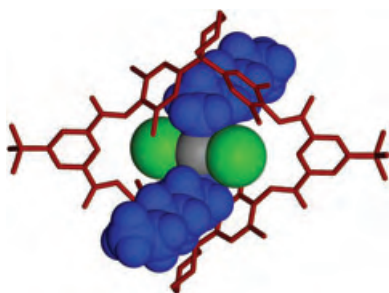
Bearing the heat: Current has been measured from individual protein pores at temperatures approaching 100°C. The molecular adapter β -cyclodextrin (red) remains bound to the α -hemolysin pore at high temperatures and retains the ability to bind guest molecules (black). Recording current at high temperatures is likely to be important for the study of single-molecule chemistry and in the development of stochastic sensors.



Biotechnology

X.-f. Kang, L.-Q. Gu, S. Cheley,
H. Bayley* ————— 1495 – 1499

Single Protein Pores Containing
Molecular Adapters at High Temperatures



A macrocyclic tetralactam and simple *trans*-palladium dihalide complexes self-assemble to form [2]pseudorotaxanes. The pseudorotaxane superstructures are formed through second-sphere coordination of the metal ligands by the macrocyclic component (see picture; red: macrocycle with hydrogen atoms removed, blue: *n*-hexylamine, green: Cl, gray: Pd).

Supramolecular Chemistry

B. A. Blight, K. A. Van Noortwyk,
J. A. Wisner,*
M. C. Jennings ————— 1499 – 1504

[2]Pseudorotaxanes through
Second-Sphere Coordination

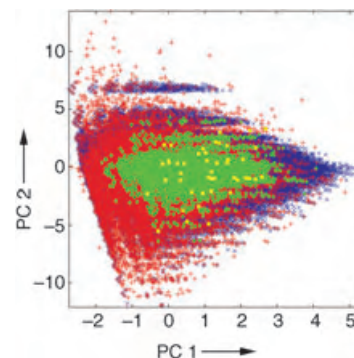


Computer Chemistry

T. Fink, H. Bruggesser,
J.-L. Reymond* 1504–1508

Virtual Exploration of the Small-Molecule
Chemical Universe below 160 Daltons

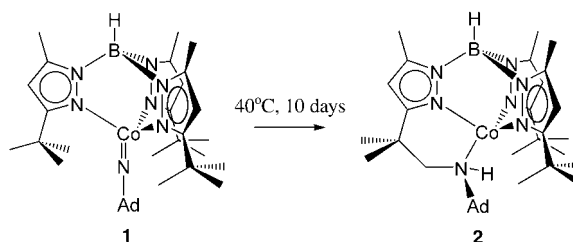
Less is more: The rules of chemical bonding allow simple elements to form a multitude of different molecules, the “chemical universe”. This space is explored by constructing a database of all molecules containing up to 11 atoms, under constraints for chemical stability and synthetic feasibility. The database which contains 13.9 million compounds (see graph; coverage of property space) can be used to identify possible new drug molecules.



C–H Activation

D. T. Shay, G. P. A. Yap, L. N. Zakharov,
A. L. Rheingold,
K. H. Theopold* 1508–1510

Intramolecular C–H Activation by an
Open-Shell Cobalt(III) Imido Complex



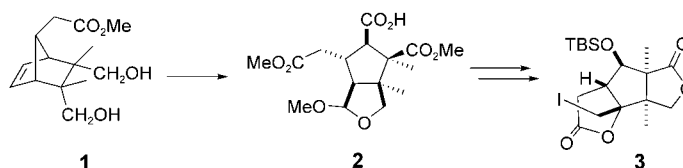
The **paramagnetic** Co^{III} imido complex **1** is stable enough to be structurally characterized by X-ray diffraction. However, in solution a primary C–H bond of the ligand

is activated and gives **2**, the product of formal insertion of the imido ligand into a methyl group (see scheme; Ad = adamantyl).

Synthetic Methods

Z. Meng, S. J. Danishefsky* 1511–1513

A Synthetic Pathway to Either Enantiomer of
Merrilactone A



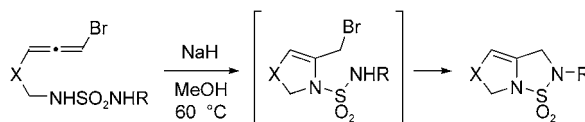
A route to enantioenriched merrilactone A was found via intermediate **3**. A degradation pathway in which *meso* compound **1** is transformed into key intermediate **2** in four steps occurs with full regiocontrol

and promising enantiocontrol. A key feature of this reaction sequence is the desymmetrization of **1** through an intramolecular asymmetric ring-opening reaction.

Cyclization Reactions

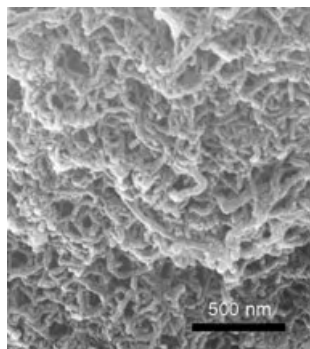
H. Hamaguchi, S. Kosaka, H. Ohno,*
T. Tanaka* 1513–1517

Bromoallenes as Allyl Dication
Equivalents in the Absence of
Palladium(0): Synthesis of Bicyclic
Sulfamides by Tandem Cyclization of
Bromoallenes



Who needs a metal? A highly regioselective synthesis of cyclic sulfamides containing a bicyclo[3.3.0]octane skeleton has been developed (see scheme). The first intramolecular nucleophilic attack of the internal sulfamide nitrogen atom takes

place at the central carbon atom of the allenic moiety, and is followed by a second intramolecular nucleophilic addition of the terminal sulfamide nitrogen atom to afford the bicyclic sulfamide.

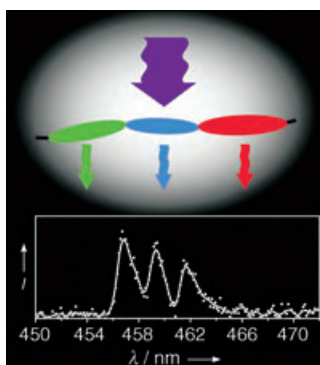


New for old: A novel catalytic combustion method to synthesize multiwalled carbon nanotubes (MWNTs, see SEM image) in situ in high yields from polypropylene as the carbon source in the presence of an organic-modified clay and a supported nickel catalyst is reported. The method allows new high-value MWNTs to be created from used polypropylene in an energy-saving and environmentally friendly process.

Nanotube Synthesis

T. Tang,* X. Chen, X. Meng, H. Chen, Y. Ding _____ 1517–1520

Synthesis of Multiwalled Carbon Nanotubes by Catalytic Combustion of Polypropylene

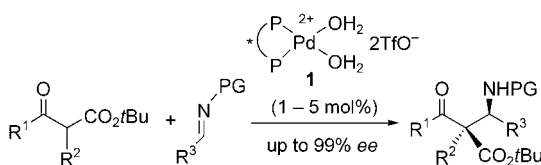


The emitting species in conjugated polymers have been studied by single-molecule spectroscopy (see picture). The number of emissive centers (chromophores) varies as a function of molecular weight and chain length. A large ladder-type undecaphenylene was used as a molecular ruler to estimate the size of chromophores in the polymer and to enable a direct assessment of the polymeric conjugation length.

Conjugated Polymers

F. Schindler, J. Jacob, A. C. Grimsdale, U. Scherf, K. Müllen, J. M. Lupton,* J. Feldmann _____ 1520–1525

Counting Chromophores in Conjugated Polymers



A highly enantioselective Mannich-type reaction of β-ketoesters was developed using a catalytic amount of the Pd-aqua complexes **1** (see scheme; PG = protecting group). A variety of imines derived

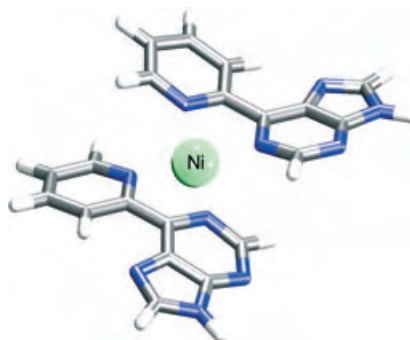
from glyoxylate, as well as simple aromatic and α,β-unsaturated aldehydes were successfully used. The corresponding Mannich adducts were obtained in high yield with excellent enantioselectivity.

Asymmetric Synthesis

Y. Hamashima, N. Sasamoto, D. Hotta, H. Somei, N. Umebayashi, M. Sodeoka* _____ 1525–1529

Catalytic Asymmetric Addition of β-Ketoesters to Various Imines by Using Chiral Palladium Complexes

Metal in the middle: A metallo base pair incorporating 6-pyridylpurine (Pur^P) was synthesized and characterized. Pur^P binds nickel(II) preferentially over other divalent ions and yields a base pair that is more stable than natural Watson–Crick pairs with high mismatch selectivity. Computational studies support a dimensional resemblance between Pur^P·Ni²⁺·Pur^P (see structure) and natural base pairs.



Nucleobases

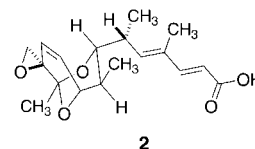
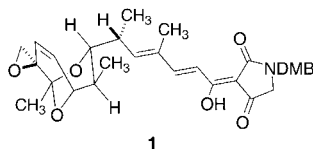
C. Switzer,* S. Sinha, P. H. Kim, B. D. Heuberger _____ 1529–1532

A Purine-like Nickel(II) Base Pair for DNA

Natural Products Synthesis

Y. Iwata, N. Maekawara, K. Tanino,
M. Miyashita* — 1532–1536

Tetramic Acid Antibiotics: Stereoselective
Synthesis of Streptolic Acid and
Tirandalydigin



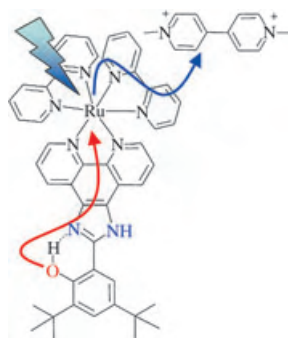
A new and promising methodology for the
synthesis of the tetramic acid family
of antibiotics was developed. The first
synthesis of *N*-2,4-dimethoxybenzyl

tirandalydigin (**1**), as well as a synthesis of
streptolic acid (**2**), was achieved in a
highly stereoselective manner.

Photosynthesis Models

F. Lachaud, A. Quaranta, Y. Pellegrin,
P. Dorlet,* M.-F. Charlot, S. Un, W. Leibl,*
A. Aukauloo* — 1536–1540

A Biomimetic Model of the Electron
Transfer between P₆₈₀ and the
TyrZ–His190 Pair of PSII



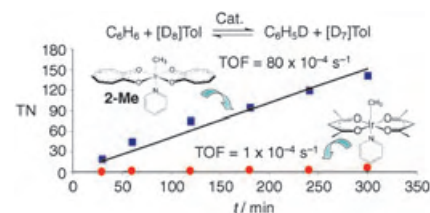
Artificial photosynthesis: The first
photoelectron trade between P₆₈₀ and the
TyrZ–His190 pair of Photosystem II was
modeled by a ruthenium(II) trisbipyridine
type complex that contains a phenol
hydrogen atom bonded to an imidazole
group. The photogenerated phenoxyl
radical has been characterized. This
opens up the way for a more complete
biomimetic model of Photosystem II.

C–H Activation Catalysis

G. Bhalla, R. A. Periana* — 1540–1543

C–H Activation of Alkanes and Arenes
Catalyzed by an O-Donor
Bis(tropolonato)iridium(III) Complex

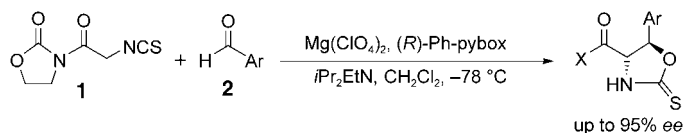
Stable and swift: The title complex is
stable to air and water under thermal
conditions. It efficiently activates the C–H
bonds of alkanes and arenes at rates
50 times higher than does the only
previously reported O-donor Ir^{III}
complex (see picture).



Enantioselective Synthesis

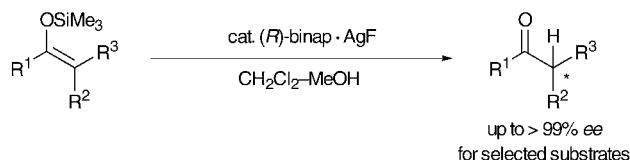
M. C. Willis,* G. A. Cutting, V. J.-D. Piccio,
M. J. Durbin, M. P. John — 1543–1545

The Direct Catalytic Enantioselective
Synthesis of Protected
Aryl β-Hydroxy-α-Amino Acids



The combination of three reagents—a
tridentate pybox ligand (pybox=pyridine
bis(oxazoline)), magnesium perchlorate,
and Hünig base (*i*Pr₂EtN)—allows the
catalytic generation of a chiral glycine
enolate from **1** that undergoes highly

enantioselective addition to a range of aryl
aldehydes **2**. The protected aryl β-hydroxy-
α-amino acid products obtained include a
protected version of one of the aryl serine
units present in the glycopeptide antibiotic
vancomycin.



Silver lining: A catalytic enantioselective protonation of trimethylsilyl enolates uses a binap/silver(I) fluoride complex as a chiral catalyst in a mixture of dichloro-

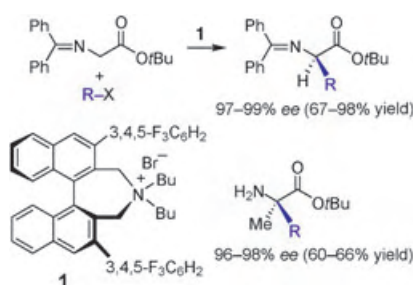
methane and methanol (see scheme). Various ketones with tertiary asymmetric carbon centers at the α position can be prepared with high enantioselectivities.

Asymmetric Catalysis

A. Yanagisawa,* T. Touge,
T. Arai _____ 1546–1548

Enantioselective Protonation of Silyl Enolates Catalyzed by a Binap-AgF Complex

The catalytic performance of the chiral phase-transfer catalyst **1** (0.1–0.01 mol %) in the asymmetric alkylation of protected glycine and alanine derivatives exceeds that of existing catalysts. The reaction is used in the enantioselective synthesis of structurally diverse natural and non-natural α -alkyl and α,α -dialkyl- α -amino acids.

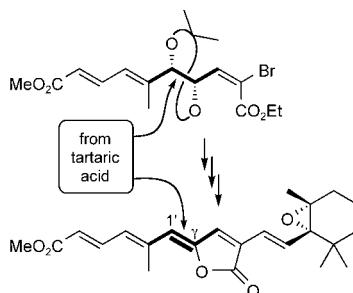


Asymmetric Synthesis

M. Kitamura, S. Shirakawa,
K. Maruoka* _____ 1549–1551

Powerful Chiral Phase-Transfer Catalysts for the Asymmetric Synthesis of α -Alkyl- and α,α -Dialkyl- α -amino Acids

Tartaric acid is the starting point for the stereoselective synthesis of the butenolide unit (see scheme) in peridinin, a marine carotenoid. Key steps were the desymmetrization of tartaric acid bis(Weinreb amide), an *E*-selective olefination by Ando-type bromophosphonates, and an *anti*-selective Mitsunobu elimination (for establishing the $C^1=C^7$ bond).

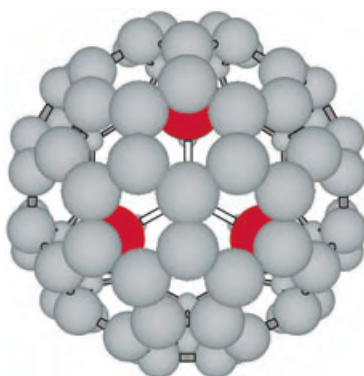


Natural Product Synthesis

T. Olpp, R. Brückner* _____ 1553–1557

Novel Strategy for the Synthesis of the Butenolide Moiety of Peridinin

Extra filling: A covalent gadolinium nitride is prepared and encapsulated as a Gd_3N cluster in fullerene cages ranging in size from C_{80} to C_{88} . The most abundant structure, $Gd_3N@C_{80}$ (**1**) (see figure; gray C, red Gd), is a large-energy-gap material based on an icosahedral cage. Gd_3N is the largest rare-earth nitride cluster to be caged in a fullerene to date. This compound has potential application as an effective contrast agent in magnetic resonance imaging.



Endohedral Fullerenes

M. Krause,* L. Dunsch _____ 1557–1560

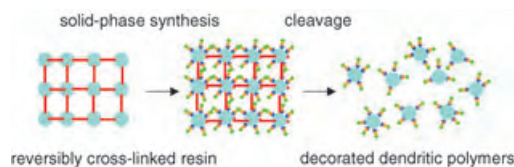
Gadolinium Nitride Gd_3N in Carbon Cages: The Influence of Cluster Size and Bond Strength

Dendritic Polymers

M. Barth, R. Fischer, R. Brock,
J. Rademann* _____ 1560 – 1563

Reversible Cross-Linking of
Hyperbranched Polymers: A Strategy for
the Combinatorial Decoration of
Multivalent Scaffolds

All decked out: Peptide-decorated dendritic polymers were synthesized on macroscopic polymer resins and then released by cleaving the reversible cross-linkers

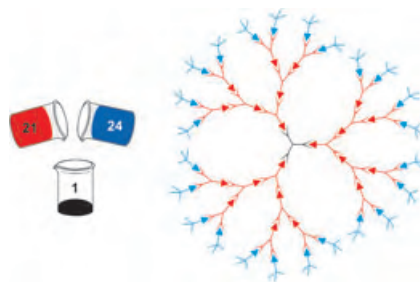


(see scheme). The released multivalent structures entered cells efficiently at low concentrations by endocytosis.

Self-Assembly

A. Franz, W. Bauer,
A. Hirsch* _____ 1564 – 1567

Complete Self-Assembly of Discrete
Supramolecular Dendrimers



Simply mixing a core (black) with defined amounts of branching units (red) and end caps (blue) leads to programmed complete self-assembly of supramolecular dendrimers through complimentary and multiple hydrogen bonding.

Sources

Product and Company Directory

You can start the entry for your company in "Sources" in any issue of *Angewandte Chemie*.

If you would like more information, please do not hesitate to contact us.

Wiley-VCH Verlag – Advertising Department

Tel.: ☎ 62 01 - 60 65 65

Fax: ☎ 62 01 - 60 65 50

E-Mail: MSchulz@wiley-vch.de

Service

Keywords _____ 1568

Authors _____ 1569

Angewandte's Sister Journals _____ 1570

Preview _____ 1571

Herbert C. Brown (1912–2004): Organoboranes

Herbert C. Brown, R. B. Wetherill Research Professor Emeritus at Purdue University, passed away on December 19, 2004 at the age of 92.



Born in London, Professor Brown came to the USA at the age of two. He attended Wright Junior College prior to enrolling at the University of Chicago, where he completed his BS in 1936 and his PhD in 1938. His graduate studies under the guidance of H. I. Schlesinger were focused on the reaction of diborane with carbonyl compounds. After studying free-radical reactions in Chicago in 1939 with M. S. Karasch, he became Schlesinger's assistant with the rank of instructor.

Brown started his independent career in 1943 at Wayne University, first as assistant professor and later as associate professor. In 1947 he moved as professor to Purdue University, where he was appointed R. B. Wetherill Professor in 1959 and R. B. Wetherill Research Professor in 1960. Emeritus professor since 1978, Brown remained actively involved in research until his death. During his career, he supervised 163 PhD students and 190 postdoctoral fellows. He also authored 8 books and nearly 1300 scientific publications.

Brown received numerous prestigious awards, including the 1979 Nobel Prize in Chemistry, the 1969 National Medal of Science, and the 1981 Priestley Medal. He was also awarded the Nichols Medal, the ACS Award for Creative Research in Synthetic Organic Chemistry, the Linus Pauling Medal, the Roger Adams Medal, the Perkin Medal, and the National Academy of Sciences Award in Chemical Sciences. He was a member of the National Academy of Sciences as well as a number of other international scientific societies.

Throughout his scientific career, Brown examined a variety of topics in physical, inorganic, and organic chemistry. At the University of Chicago, while working with Schlesinger, he codiscovered sodium borohydride. At Wayne

University, his investigation of molecular addition compounds contributed to the reacceptance of steric effects as a major factor in chemical behavior. His studies on aromatic substitution led to a quantitative theory based on the new Brown δ^+ constants.^[1a] His physical organic research continued at Purdue, where he played an active role in the "nonclassical carbonium ion" debate that polarized the physical organic community in the 1970s. Brown believed that many proposals of the existence of nonclassical carbocations at that time were not based on firm experimental foundations, and that a more traditional interpretation involving the interconversion of classical carbocations was sufficient to explain the experimental results.^[1b] In his view, the nonclassical bridged carbocation would exist as a transition state rather than as an intermediate. This viewpoint led to lively, sometimes heated, debates at scientific meetings and in the literature. In the ensuing years, NMR spectroscopic investigations at ultralow temperatures in non-nucleophilic superacid solvents provided evidence to support the existence of σ -bridged norbornyl cations. Whether or not such cations exist under solvolysis conditions remains a matter for debate.

Brown's greatest contributions, for which he won the Nobel Prize, were in the application of boron reagents in organic chemistry. The simple observation in 1956 that the reduction of ethyl oleate by sodium borohydride in the presence of aluminum chloride consumed more hydride than expected formed the basis of an entirely new area of organometallic chemistry.^[1c] Further studies established that the addition of diborane to alkenes was catalyzed by ethers and led Brown to explore the preparation and use of organoborane reagents. Indeed, his powers of observation and deductive reasoning provided the driving force for the fledgling field of organoboron chemistry. Standardized procedures for hydroboration were soon developed, exciting new hydroborating agents that generated regio- and stereochemically defined intermediates were designed, and a plethora of important new organic transformations were created.^[1d,e] Brown's development of the asymmetric hydroboration of olefins

may well have ushered in the modern era of reagent control in asymmetric synthesis.^[1f] It is nearly impossible to read a current issue of any journal devoted to organic chemistry and not encounter a boron reagent that doesn't have at least a historical tie to Brown.

Brown was a caring, calm, and optimistic man. He was not known to speak harshly of any colleague; he always endeavored to keep lines of communication open. It has been almost 40 years since I met Professor Brown and was introduced to boron chemistry. Like all his students, I benefited from his keen intellect as we learned to design and perform chemical experiments. His patience and optimism were legendary. However poor our initial chemical yields, he would encourage us by pointing out that the first one percent was the most important; he felt that it was all downhill from that point and that quantitative yields were surely on the horizon.

Brown was thankful for the love and support of his wife Sarah, a fellow student at the University of Chicago, whom he married in 1937. Later in life, he enjoyed collaborating with his son Charles, who was born in 1944. Sarah watched over everything in their lives so that her husband could focus on chemistry. Brown was especially appreciative that Sarah presented him with Alfred Stock's "Hydrides of Boron and Silicon" upon completion of their undergraduate studies at the University of Chicago. It played a role in his choice of Professor Schlesinger as his research advisor. The rest is history!

George W. Kabalka
The University of Tennessee (USA)

- [1] a) H. C. Brown, *Boranes in Organic Chemistry*, Cornell University Press, Ithaca, **1972**; b) H. C. Brown, P. von Ragué Schleyer, *The Nonclassical Ion Problem*, Plenum Press, New York, **1977**; c) H. C. Brown, *Hydroboration*, W. A. Benjamin, Inc., New York, **1962**; d) H. C. Brown, *Organic Syntheses via Boranes*, Wiley, New York, **1975**; e) H. C. Brown, M. Zaidlewicz, *Organic Syntheses via Boranes Vol. 2: Recent Developments*, Aldrich Chemical Company, Milwaukee, **2001**; f) H. C. Brown, G. Zweifel, *J. Am. Chem. Soc.* **1961**, *83*, 486–487.

Atmosphere, a Chemical Reactor—Formation Pathways of Secondary Organic Aerosols

Wolfgang Schrader*

Keywords:

aerosols · atmospheric chemistry · environmental chemistry · sulfuric acid

Dedicated to Professor Dieter Klockow on the occasion of his 70th birthday

The investigation of atmospheric processes is an extremely difficult task because of the complexity of the “chemical reactor” atmosphere. The large number of parameters that can be involved in one single observation mean that it is sometimes difficult to design laboratory experiments for finding an explanation of such processes, and often compromises are necessitated, such as higher concentrations than usually found in the natural atmosphere. The results of the experiments are then frequently criticized with regard to their significance. Nonetheless, the chemistry of the atmosphere has been an important area of research, especially since the pioneering work from Went^[1] in the early 1960s, who correlated the “blue haze” phenomenon with biogenic emission from plants. In the last few years the emissions from anthropogenic^[2] and biogenic^[3] sources, as well as their reactions in the atmosphere have been investigated. The main focus of the research has centered on the identification^[4] and determination of yields^[5] of certain products from these reactions. Recently, reactions were investigated in detail that play a role in the formation of secondary organic aerosols (SOA).^[6]

Particles in the atmosphere have different properties than their gaseous precursors. They scatter, absorb, or reflect the solar radiation and additionally, they can play an important role in cloud droplet formation.^[7] Therefore,

the study of these particles and—more importantly—their formation pathways are of great interest. The formation of the particles and their size distribution are dependent on the chemical composition of the surrounding air. Accordingly, industrial plumes or other gaseous components have an effect on the aerosol.^[8] Different low-volatile components of the atmosphere, such as biogenic compounds and their reaction products, are being discussed as having an influence on aerosol formation. Scheme 1 shows the gas-phase oxidation of α -pinene as an example for the different processes, which can lead to particle formation.

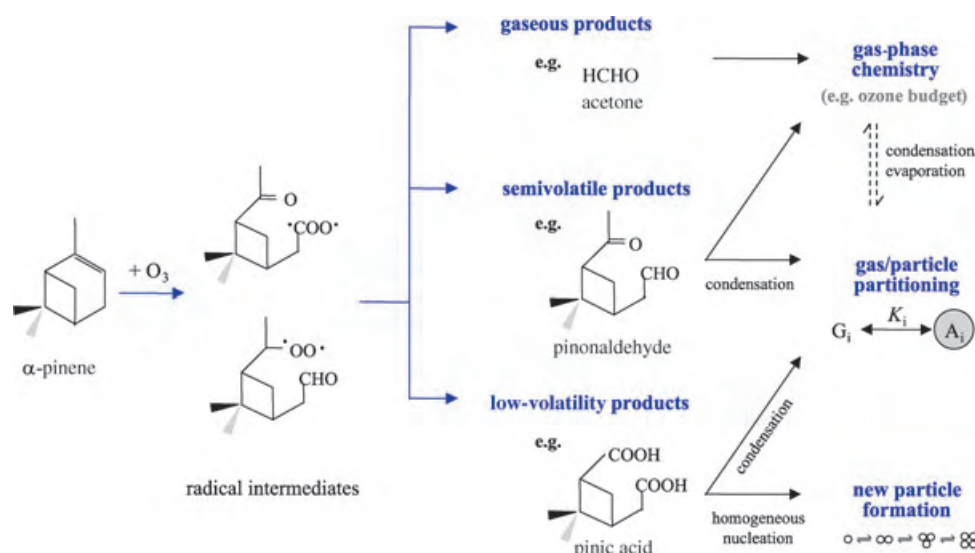
The main problem with aerosol formation is that the basic mechanisms are not yet completely understood. Different theories are discussed to explain the formation of atmospheric particles on the molecular level either directly from gaseous precursors^[12] or on the surface of already existing particles.^[9] One of these theories describes gas-phase ozonolysis of biogenic precursors, in particular monoterpenes, which lead to highly oxidized reaction products often containing carboxy groups. Experimental and theoretical studies of a number of terpenoids suggested that the formation of stable heterodimers from organic acids could be the first step of aerosol formation.^[12] Another theory of SOA formation uses a model of homogeneous nucleation in a binary system comprising water and sulfuric acid (BHN, binary homogeneous nucleation) or a ternary system comprising water, sulfuric acid, and ammonia (THN, ternary homogeneous nucleation), which each form a stable aerosol. Here, a condensation of low-volatile organic species, such as

acids, can lead to a growth of particles.^[13] The BHN model has been used to explain aerosols with a particle diameter of 5–100 nm. In some areas, local effects led to the observation of much higher particle formation rates, which was explained by using the THN model.^[14] In the THN model, which includes ammonia, the nucleation rate is much higher than in the BHN model. Still, there are a lot of uncertainties in the modeling, mainly because the classical theory of homogeneous nucleation involves the liquid drop model,^[11] which is not valid for small molecular clusters.^[10] The first step in aerosol formation still requires detailed study to clarify the major points.

Zhang et al.^[15] have recently carried out studies aimed at explaining aerosol formation. They have investigated gas-phase reactions and particle formation of anthropogenic compounds by using aromatic acids, such as benzoic acid, 4- and 3-methylbenzoic acids, in the presence of gaseous H₂SO₄. In laboratory studies, particles with a diameter of > 3 nm were produced in an aerosol chamber. The size and formation rates were dependent on the concentration of H₂SO₄ as well as on the concentration of the organic acid. It has already been proposed that sulfate possibly functions as a catalyst for aerosol formation.^[13] Zhang et al. were able to show that the influence of sulfuric acid on new particle formation seems comparable to that previously reported for ammonia.

For a better understanding of the complex processes involved, Zhang et al. performed theoretical calculations, according to which the critical step of particle formation is the generation of an embryo before the growth of the

[*] Dr. W. Schrader
Max Planck-Institut für Kohlenforschung
Kaiser Wilhelm Platz 1
45470 Mülheim/Ruhr (Germany)
Fax: (+49) 208-306-2982
E-mail: wschrader@mpi-muelheim.mpg.de



Scheme 1. The formation of a secondary organic aerosol, using α -pinene ozonolysis as an example.^[9]

particle. For the formation of such an embryo, an energy barrier has to be overcome, and thus particle growth in a single-component system only occurs under supersaturated conditions.^[15] In previous studies carried out in smog chambers, homogeneous nucleation from low-volatile compounds was reported; however, these experiments required much higher concentrations than usually found in natural environments. On the basis of their quantum-chemical calculations, Zhang et al. proposed a particle formation mechanism that involves a stable complex between the aromatic acid and sulfuric acid. The structure of this complex appears to be a planar, eight-membered-ring system connected by two hydrogen bonds, in which both the organic acid and the sulfuric acid act as a hydrogen donor and acceptor (Figure 1). The stability of the complex implies that the aromatic acid bonds irreversibly to the sulfuric acid, which subsequently reduces the barrier for continued heteromolecular nucleation.^[16]

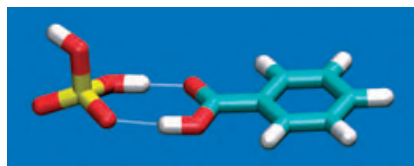


Figure 1. Possible structure of the complex between benzoic acid and sulfuric acid as the starting point for heteromolecular nucleation.^[16]

These results lead to the conclusion that homomolecular nucleation most likely does not happen under atmospheric conditions—the formation of the complex between sulfuric acid and aromatic acid rather supports heteromolecular nucleation. This mechanism explains SOA formation in polluted areas, because both organic and sulfuric acids are photochemical degradation products. It also offers a different approach to the frequently observed SOA formation than the THN model. The aromatic acid/sulfuric acid model can be related to some observations from field measurements^[17] that can explain particle growth in the presence of organic and sulfuric acids. The important first step, the formation of neutral, stable clusters could be explained by this theory.


The more aspects that become known relating to the formation of secondary organic aerosols, the better the models can be improved. Further studies are required to reveal whether aerosol formation from anthropogenic and biogenic sources proceed by the same mechanism. In this context, the direct measurement of the intermediate clusters and observation of their growth under atmospheric conditions would help to improve the understanding substantially. The formation of new particles is an essential process that has to be fully understood and incorporated into climate models.

- [1] F. W. Went, *Nature* **1960**, 187, 641.
- [2] a) I. C. Burkow, R. Kallenborn, *Toxicol. Lett.* **2000**, 112, 87; b) A. M. Hough, C. E. Johnson, *Atmos. Environ. Part A* **1991**, 25, 1819; c) J. F. Müller, *J. Geophys. Res.* **1992**, 97, 3787.
- [3] a) F. Fehsenfeld, J. Calvert, R. Fall, P. Goldan, A. Guenther, C. N. Hewitt, B. Lamb, S. Liu, M. Trainer, H. Westberg, P. Zimmerman, *Global Biogeochem. Cycles* **1992**, 4, 389; b) A. Guenther, C. N. Hewitt, D. Erickson, R. Fall, C. Geron, T. Graedel, P. Harley, L. Klinger, M. Lerdau, *J. Geophys. Res.* **1995**, 100, 8873.
- [4] a) J. Yu, D. R. Crocker III, R. J. Griffin, R. C. Flagan, J. H. Seinfeld, *J. Atmos. Chem.* **1999**, 34, 207; b) H. Hakola, J. Arey, S. M. Aschmann, R. Atkinson, *J. Atmos. Chem.* **1994**, 18, 75; c) Y. Yokouchi, Y. Ambe, *Atmos. Environ.* **1985**, 19, 1271; d) W. Schrader, J. Geiger, T. Hoffmann, D. Klockow, E. H. Korte, *J. Chromatogr. A* **1999**, 864, 299; e) W. Schrader, J. Geiger, M. Godejohann, B. Warscheid, T. Hoffmann, *Angew. Chem.* **2001**, 113, 4129; *Angew. Chem. Int. Ed.* **2001**, 40, 3998.
- [5] P. Ciccioli, E. Brancaleoni, A. Cecinato, R. Sparapani, M. Frattoni, *J. Chromatogr.* **1993**, 643, 55.
- [6] a) M. Kalberer, D. Poulsen, M. Sax, M. Steinbacher, J. Dommen, A. S. H. Prevot, R. Fisseha, E. Weingartner, V. Frankevich, R. Zenobi, U. Baltensperger, *Science* **2004**, 303, 1659; b) J. R. Odum, T. P. W. Jungkamp, R. J. Griffin, R. C. Flagan, J. H. Seinfeld, *Science* **1997**, 276, 96.
- [7] a) M. O. Andreae, P. J. Crutzen, *Science* **1997**, 276, 1052; b) A. R. Ravishankara, *Science* **1997**, 276, 1058.

- [8] M. Kulmala, *Science* **2003**, 302, 1000.
- [9] W. Schrader, J. Geiger, M. Godejohann, T. Hoffmann, B. Warscheid, U. Marggraf, *Abstr. Pap. Am. Chem. Soc.* **2001**, 221, 129-ENVR, Part 1.
- [10] S.-H. Lee, J. M. Reeves, J. C. Wilson, D. E. Hunton, A. A. Viggiano, T. M. Miller, J. O. Ballenthin, L. R. Lait, *Science* **2003**, 301, 1886.
- [11] J. H. Seinfeld, S. N. Pandis, *Atmospheric Chemistry and Physics: From Air Pollution to Climate Change*, Wiley, New York, **1998**.
- [12] a) T. Hoffmann, R. Bandur, U. Marggraf, M. Linscheid, *J. Geophys. Res.* **1998**, 103, 25569; b) U. Kückelmann, B. Warscheid, T. Hoffmann, *Anal. Chem.* **2000**, 72, 1905.
- [13] a) A. Laskin, D. J. Gaspar, W. H. Wang, S. W. Hunt, J. P. Cowin, S. D. Colson, B. J. Finlayson-Pitts, *Science* **2003**, 301, 340; b) M. Jang, N. M. Czoschke, S. Lee, R. M. Kamens, *Science* **2002**, 298, 814.
- [14] M. Kulmala, L. Pirjola, M. Mäkelä, *Nature* **2000**, 404, 66.
- [15] R. Zhang, I. Suh, J. Zhao, D. Zhang, E. C. Fortner, X. Tie, L. T. Molina, M. J. Molina, *Science* **2004**, 304, 1487.
- [16] W. Humphrey, A. Dalke, K. Schulten, *J. Mol. Graphics*, **1996**, 14, 33.
- [17] R. Gasparini, R. Li, D. R. Collins, *Atmos. Environ.* **2004**, 38, 3285.

Quality counts...

The best of chemistry every week



Wiley-VCH
 P.O. Box 10 11 61
 69451 Weinheim
 Germany
 Phone +49 (0) 6201-606-400
 Fax +49 (0) 6201-606-184
 e-mail: angewandte@wiley-vch.de
www.angewandte.org

Angewandte Chemie International Edition is a journal of the GDCh, the German Chemical Society

GDCh

WILEY-VCH

Organolithium Reagents

Hetero-Aggregate Compounds of Aryl and Alkyl Lithium Reagents: A Structurally Intriguing Aspect of Organolithium Chemistry

Robert A. Gossage,* Johann T. B. H. Jastrzebski, and Gerard van Koten*

Keywords:

aggregation · chirality · lithium · organolithium reagents · synthetic methods

Organolithium compounds are often depicted as mononuclear species. However, such compounds are in fact aggregated species and can form hetero-aggregates containing different organic groups, including heteroatom groups. In reactions involving organolithium reagents, the “pure” homo-aggregate organolithium compound can change into a hetero-aggregate, which has a different structure and reactivity to the homo-aggregate. This fact is often overlooked. When there are chiral centers in the organolithium reagent or the substrate, diastereoselective self-assembly (the preferential formation of a particular diastereoisomeric aggregate) plays a role. The importance of these contributions in understanding the structure and reactivity patterns of organolithium reagents is the focus of this Minireview.

1. Introduction

The use of organolithium compounds has evolved from what was an academic curiosity sixty years ago^[1a,b] to what is today an essential component of organic synthesis.^[1c–g] These organometallic reagents are used in a vast variety of chemical reactions from the undergraduate academic level to the large-scale applications in industry.^[2] Organolithium reagents are often depicted schematically as mononuclear species (that is, containing a single Li atom and a single “R” group: for example, *n*-butyllithium as “*n*BuLi”), however, the chemistry and structure of these compounds is much more complex.

Understanding this complexity is important for describing new reactivity patterns and for the interpretation of information related to mechanism(s). To clarify, *n*BuLi itself is a hexamer, [*n*Bu₆Li₆], in the solid state with a structure consisting of a core of alternating Li and C atoms.^[3]

This homo-aggregate is at least partially retained in solution in apolar media but in solvents such as diethyl ether, the presence of tetramers and dimers becomes predominant. It is not only the structure but also the reactivity of the various aggregated forms of even simple organolithium compounds that can be very complicated.^[1c–g] The reactivity of organolithium compounds is highly dependent on factors such as the nature of the solvent, concentration, temperature, the availability of potential donor ligands, salts (e.g., LiX) and/or other organolithium compounds.^[1c–g,4]

2. Formation of Hetero-Aggregates

The primary importance of the aggregation properties of (RLi)_x species resides in their potential for profound effect(s) on reactivity.^[5] Two primary examples of this phenomenon are the “LiX effect” and the related influence of lithium alkoxides (R'OLi)_y and amides (R'₂NLi)_y on organolithium reactivity. The “LiX effect”^[6] is a manifestation of the in situ formation of [(RLi)_x(LiX)_y] aggregates which “self-assemble” upon addition and/or formation of a salt LiX (X = Cl, Br, or I) in a solution of the RLi reagent. Hence, the hetero-aggregated form is more stable than the homo-aggregate (RLi)_n and (LiX)_n species. The formation of this type of multinuclear Li complex has indeed been known for some

[*] Prof. Dr. R. A. Gossage

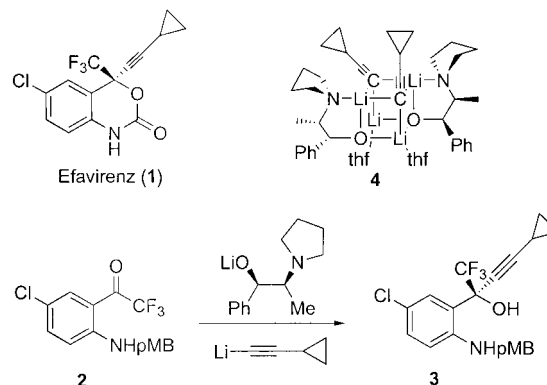
The Chester Woodleigh Small Laboratory of Organic Chemistry
Department of Chemistry
Acadia University
Wolfville, Nova Scotia B4P2R6 (Canada)
Fax: (+1) 902-585-1114
E-mail: rgossage@acadiau.ca

Dr. J. T. B. H. Jastrzebski, Prof. Dr. G. van Koten
Debye Institute
Department of Metal-Mediated Synthesis
Utrecht University
Padualaan 8, 3584 CH Utrecht (The Netherlands)
Fax: (+31) 30-252-3615
E-mail: g.vankoten@chem.uu.nl

time.^[7] Its importance lies in the fact that such hetero-aggregation leads to an observable modification (reaction rate, selectivity) of the nucleophilic properties of R relative to those demonstrated by the parent species $(\text{RLi})_x$. The addition of such salts is now common practice in yield-optimization studies in organic and polymer chemistry when organolithium reagents are involved, although the nature of the RLi-LiX interaction and the reasons for the effect on the reactivity of R, are rarely detailed.^[6] An important consequence of this chemistry is described in the following hypothetical situation. In many cases, the “quenching” of a reaction mixture involving an in situ formed organolithium is carried out using electrophilic sources E-X (e.g., $\text{E} = \text{Me}_3\text{Si}$ (TMS); $\text{X} = \text{Cl}$). The product of such an addition is LiX : a potential source of nucleation for a hetero-aggregate with residual RLi . This hetero-aggregate may now begin to modify the reaction profile because “independent” $(\text{RLi})_n$ compounds often react differently with E-X than does the $[(\text{RLi})_x(\text{LiX})_y]$ hetero-aggregate.^[8] Note that such $[(\text{RLi})_x(\text{LiX})_y]$ hetero-aggregate species can be viewed as a “resting state” that forms with E-X and hence is a kinetic intermediate from which product formation occurs. This occurrence may be a further explanation for the often spectacular improvement of yield when TMS-OTf ($\text{OTf} = \text{triflate} = \text{SO}_3\text{CF}_3$) is used to replace TMS-Cl as the electrophile. The OTf group is certainly a better leaving group than the chloride ion but in the situation where LiOTf is also forming a hetero-aggregate, this hetero-aggregate will undoubtedly have different structural features and kinetic reactivity with E-X .

Such hetero-aggregate formation is also closely mimicked by the presence of $(\text{R}'\text{OLi})_n$ or $(\text{R}'_2\text{NLi})_n$ species in solutions of RLi reagents.^[9,10] This situation occurs frequently in synthesis reactions since reagents such as lithiumdiisopropylamide (LDA ; used for RLi generation), or lithium alkoxide impurities (formed by RLi hydrolysis) are present in solution at the same time as the desired RLi compound. The hetero-aggregate $[(\text{RLi})_x(\text{R}'_2\text{NLi})_y(\text{solv})_z]$ ($\text{solv} = \text{solvent}$) can likewise have a great influence on the overall nature and reactivity of the organolithium components that are present in a reaction mixture. The effects and solution structural features of these amido adducts of organolithium reagents have been studied in some detail.^[1c-g,10] The above lithium alkoxide situation is closely related to the recent

investigations by Collum and co-workers^[11] which have demonstrated the important influence of $[(\text{RLi})_x(\text{R}'\text{OLi})_y(\text{solv})_z]$ ($\text{R}'\text{O} = \text{ephedrenato}$) hetero-aggregates on the enantioselective addition of lithium acetylides to quinazolinones.^[1c-g,4,11] A specific example of this enantioselective addition is involved in the formation of the anti-HIV drug, Efavirenz (**1**; Scheme 1) formed by a multi-step process.^[9a] A



Scheme 1. Key enantioselective step in the synthesis of Efavirenz. PMB = *p*-methoxybenzyl.

key step is the formation of intermediate **3** by the low-temperature enantioselective addition of lithium cyclopropylacetylide to quinazolinone **2**. One hetero-aggregate **4** has been specifically identified as an essential intermediate which induces the enantioselective addition of **2** to **3**; aggregate **4** is only formed after the addition of $[\text{R}'\text{OLi}]$ to lithium cyclopropylacetylide and a suitable induction period.^[4,8,10]

Much less studied (or discussed) are the structures of mixed aryl or alkyl lithium hetero-aggregates, that is, $[(\text{RLi})_x(\text{R}'\text{Li})_y(\text{solv})_z]$.^[1c-g,10f,10k,11–14] This situation is somewhat surprising since the formation of an ArLi typically either involves Li-X or Li-H exchange reactions. In Li-H exchange, the amount of ArLi formed gradually increases as the lithiating agent, such as $n\text{BuLi}$, is consumed. This is an ideal situation for the formation of hetero-aggregates. These mixed species, consisting of different alkyl and/or aryl carbanion sources, can exert a profound influence on the overall outcome of chemical syntheses that involves RLi reagents.



Gerard van Koten has been Professor of Organic Synthesis and Catalysis at the Debye Institute of Utrecht University since 1986. In 2004 he became Distinguished Professor of Utrecht University. Recently, he was appointed chairman of the committee for the Chemistry Educational Programme at the Secondary School level in the Netherlands. His research interests comprise the study of fundamental processes in organometallic chemistry and the application of organometallic complexes as homogeneous catalysts. His interest in supramolecular systems with (organometallic) catalytically active functionalities include the preparation and use of the first examples of homogeneous metallo-dendrimer catalysts.



Johann Jastrzebski was born in Maartensdijk, the Netherlands in 1954. He started his career in organometallic chemistry as a technician in 1974 at the “Organisch Chemisch Instituut TNO, Utrecht, The Netherlands (Prof. G. J. M. van der Kerk). In 1979 he moved to the Inorganic Chemistry Department of the University of Amsterdam (Prof. K. Vrieze and Prof. G. van Koten). In 1986 he joined the group of Prof. G. van Koten at the Organic Chemistry Department of Utrecht University, where he received his Ph.D. in 1991. He is interested in metal-mediated organic synthesis, main-group organometallic chemistry, and homogeneous catalysis.

For example, it has been known for some time that *t*BuLi is at least an order of magnitude more reactive in solutions containing equimolar *i*PrLi.^[5] Detailed study of this class of organolithium hetero-aggregates are quite sparse, but their formation and hence effects on chemical synthesis are probably much more common than currently realized.

The first such hetero-organolithium aggregate characterized in the solid state was not reported until 1993.^[13] The complex $[(n\text{BuLi})_2(2,4,6\text{-}t\text{Bu}_3\text{C}_6\text{H}_2\text{Li})_2]$ (**5**) results from the reaction of 2,4,6-*t*Bu₃C₆H₂Br with *n*BuLi in hexane solution. The solid-state structure is indeed unusual (Figure 1) and

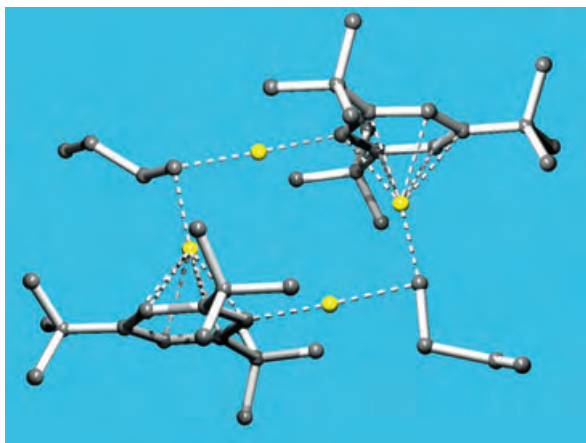


Figure 1. Structure of $[(n\text{BuLi})_2(2,4,6\text{-}t\text{Bu}_3\text{C}_6\text{H}_2\text{Li})_2]$ (**5**) in the solid state determined by X-ray diffraction. Yellow Li.^[13]

contains hydrocarbon fragments which bridge two chemically distinct lithium atoms: one lithium atom is η^6 bonding with the aromatic ring and the other is η^1 bonding with the butyl group. Apparently, this hetero-aggregate is the end product of the 1:1 molar aggregation of 2,4,6-*t*Bu₃C₆H₂Li and *n*BuLi; note that this situation leaves an equivalent of 2,4,6-*t*Bu₃C₆H₂Br in the reaction solution. The discovery of such a hetero-aggregate was a relatively new phenomenon during the course of an Li–Br exchange reaction and clearly indicates that during Li–Br exchange, stable hetero-aggregates can be formed that are kinetically inert to further reaction with aryl bromides. Hence, the formation of this hetero-organolithium

aggregate influences not only the yields of desired organolithium homo-aggregate but also leads to an unwanted product that contains residual alkyl lithium. Consequently, such species now become a topic of consideration when attempting to understand and control a reaction profile that is intended to either maximize the in situ formation of the desired RLi species^[15] and/or influence the regio- or stereochemical outcome of a synthetic procedure.^[1c–g,5,6,8–11]

The importance of this concept was first presented by us in 1989 during the course of our studies on the metalation of tertiary nitrogen donor ligands for use in organocopper chemistry.^[15] The reaction of *n*BuLi with (*R*)-[(1-dimethylamino)ethylbenzene] (**6**; dmaebH) in Et₂O solution was envisioned to yield the desired lithiated product **7** (see Scheme 1) by the well-known directed *ortho*-metalation (DoM) reaction.^[16] Analogous chemistry involving the DoM of achiral *N,N*-dimethylbenzylamine (dmbaH) was already known^[17] to yield cleanly (> 95 %) the *ortho*-lithiated product (dmbaLi).^[18] As expected, when *n*BuLi is added to **6**, selective metalation does indeed occur. Quenching of the reaction mixture after an appropriate time period with an electrophile, such as D₂O however, gives direct evidence for a disappointing 50 % yield of the *ortho*-metalated product.

This puzzling result precludes the use of such synthetic methods for further reactions with species such as CuX, owing to contamination by residual **6** and the potential presence of remaining *n*BuLi. The yields cannot be increased by the addition of excess *n*BuLi. Such a result is often attributed to ill-defined “steric effects” or the “weak” nucleophilicity of the butyl anion derived from *n*BuLi. Justification for this “weak” nucleophilicity conclusion is provided by the fact that complete *ortho*-lithiation of **6** to yield pure **7** (Figure 2) can be realized using *t*BuLi.^[19] This supports the hypothesis that the *t*Bu anion is simply a stronger or “harder” nucleophile than *n*Bu anion. However, NMR spectroscopic investigations of a 1:1 mixture of *n*BuLi and **6** revealed that in contrast to the reaction with dmbaH, the product of DoM, compound **7**, readily self-assembles with further equivalents of the reagent *n*BuLi and residual **6** to form a presumably thermodynamically stable mixed species $[(\text{dmaebLi})_2(n\text{BuLi})_2(\text{dmaebH})_2]$

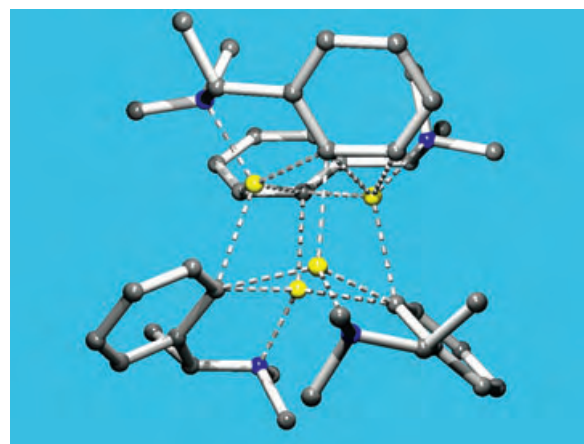
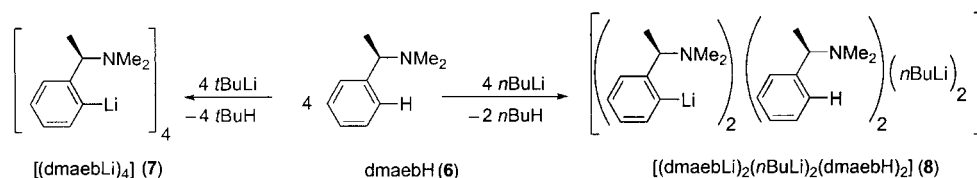


Figure 2. Structure of $(\text{dmaebLi})_4$ (**7**) in the solid state determined by X-ray diffraction. Blue N, yellow Li.^[19]



Robert A. Gossage is a native of Burlington, Ontario (Canada) and began his career in chemistry at the University of Guelph (Canada) where he completed his B.Sc. degree in 1989. After a period of employment as a technician (Prof. E. C. Alyea), he completed his Ph.D. in 1996 with Prof. Stephen R. Stobart. For the next two years he worked as a post-doctoral fellow with Prof. G. van Koten (Utrecht) on organosilicon and dendrimer chemistry. Following a period in industry (AnorMED, Inc.), he took up (1999) his current position on the faculty of Acadia University (Canada). His research interests are centered on the co-ordination, medicinal, and catalytic chemistries of oxazolines and related heterocycles.



Scheme 2.

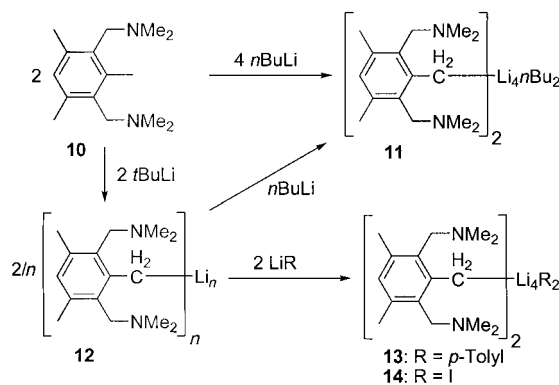
(8, Scheme 2). Hetero-aggregate **8** is so stable that in essence an equivalent of *n*BuLi and an equivalent of arene **6** have been “trapped” by each equivalent of **7** formed (compare with **5**, Figure 1).

The above observation in DoM chemistry is very likely a direct result of the stability of the in situ formed hetero-aggregate **8** and neither a consequence of steric effects nor the weak nucleophilicity of the butyl anion derived from *n*BuLi. The effectiveness of *t*BuLi can therefore be explained by invoking the idea that hetero-aggregates analogous to **8** containing sterically more demanding alkyl lithium species are significantly less stable or kinetically more disposed to initiate further DoM reactions. In other words, such hetero-aggregates are intermediates or kinetically short-lived ordered transition states (Scheme 2). Hence, *t*BuLi mediates complete DoM. The overall stability of aggregates such as **8** is highlighted by the fact that pure homo-aggregate **7** reacts cleanly in apolar solvents (yield > 90 %) with *n*BuLi to form a hetero-aggregate (free of **6**) that we have been able to isolate in pure form $[(\text{dmaebLi})_2(\text{nBuLi})_2]$ (**9**) and thereafter fully characterize by solution NMR spectroscopy, cryoscopy, and single-crystal X-ray diffraction (Figure 3).^[20]

As yield optimization is a vital aspect of synthesis involving in situ formed RLi reagents, the two above examples should serve as a caveat to those using RLi. This situation is especially true in cases where yields are “suspiciously” measured as being 50 % or 75 %; such values suggest the formation of “whole number” hetero-aggregates. For example, a 75 % yield suggests a 3:1 hetero-aggregate of the desired R/Li (3 equiv) product and the initial RLi molecule (1 equiv),

in other words, $[(\text{RLi})(\text{R}'\text{Li})_3]$ is formed. Such aggregation phenomena and their consequences, which are unexpected because we typically envision RLi reagents as mononuclear species, is of importance to synthetic organic (and organo-metallic) chemistry.

Other such hetero-aggregates can be formed with modified tertiary amine containing NCN “pincer” ligands,^[21] such as during the metalation of 1,3-bis[(dimethylamino)methyl]-2,4,6-trimethylbenzene (**10**).^[22] Reaction of **10** with 2 equivalents of *n*BuLi (in truth a 1/3 equivalent of $[\text{nBu}_6\text{Li}_6]$, see above) in hexane solution yields the hetero-aggregate **11** (Scheme 3). The solid-state structure of **11** (Figure 4) is more



Scheme 3.

typical of organolithium compounds in general than that observed earlier by Power et al. with complex **5**.^[13] The structure of **11** was at the time only the second such hetero-aggregate to be characterized by single-crystal X-ray diffraction. In relation to **6** discussed earlier, *t*BuLi will fully monodeprotonate **10** at the 2-methyl position to yield **12** (the bis-*ortho*-substituted benzyl lithium) and in a similar way, homo-aggregate **12** reacts with *n*BuLi to give back hetero-aggregate **11**. Hence, the formation of thermodynamically stable hetero-aggregates are suggested since **11** is definitely a minimum on the potential energy surface, regardless of whether its formation is approached directly from **10** or via **12**. This chemistry is not limited to the *n*BuLi aggregate, as structurally analogous and stable hetero-aggregates of **10**, each having the $[(\text{NCN})_2\text{Li}_4]^{2+}$ core structure in common, are formed from **12** with the *p*-tolyl anion (\rightarrow **13**) or an iodide anion (\rightarrow **14**; Scheme 3; LiX effect, see above).^[23] In a similar way, 1,3-bis[(dimethylamino)methyl]-2-[(trimethylsilyl)methyl]-4,6-dimethylbenzene (**15**) can be selectively deprotonated at the silylmethylene position with *n*BuLi, *t*BuLi, or *p*-tolyllithium to form lithium clusters **16a–c** and in all three

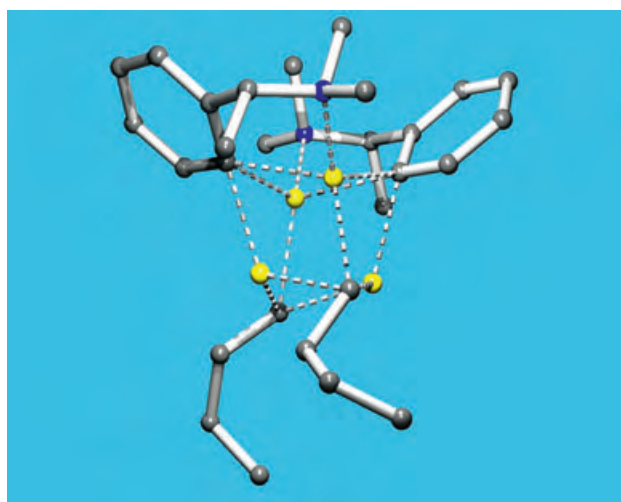


Figure 3. Structure of $[(\text{dmaebLi})_2(\text{nBuLi})_2]$ (**9**) in the solid state determined by X-ray diffraction. Blue N, yellow Li.^[20]

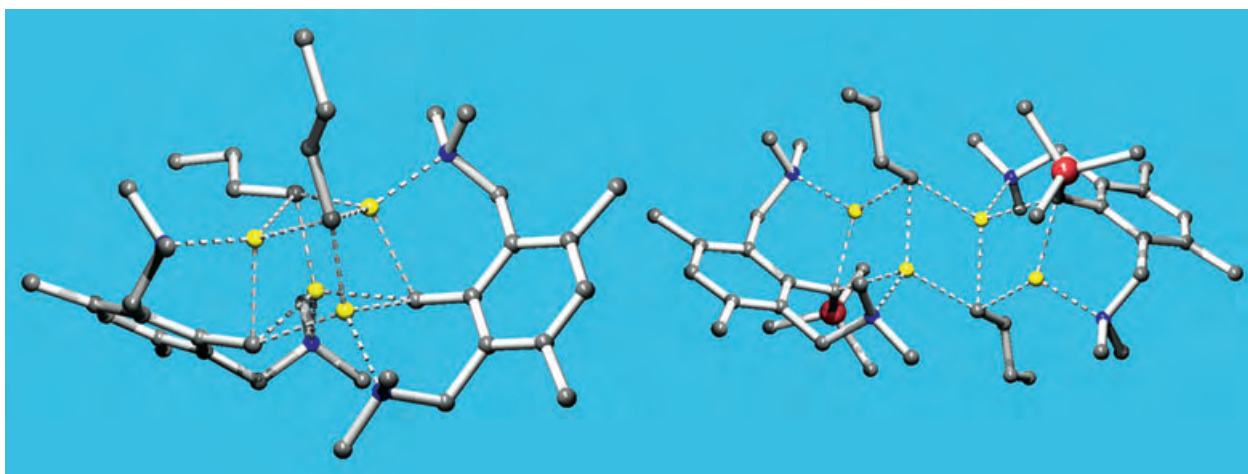
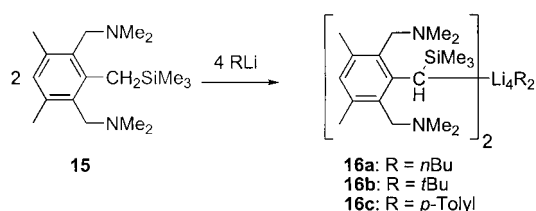


Figure 4. Structures of **11** (left) and **16a** (right) in the solid state determined by X-ray diffraction. Blue N, yellow Li, red Si.

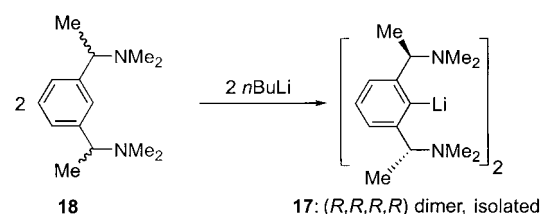
cases, 2:2 hetero-aggregates result (Scheme 4).^[24] These particular lithiated “pincer” hetero-aggregates are, in terms of the $[R_2Li_4]^{2+}$ core structure, distinct from that of **11** in the solid-state (Figure 4).^[25]



Scheme 4.

3. Diastereoselective Self-Aggregation

We have put forward the idea that alkyl/aryl lithium hetero-aggregates can have important reactivity consequences. We have yet to consider one other important feature of this concept; this is the idea of induced chiral selection during aggregate formation. The lithium atom in these (and most lithium containing) organic materials is typically tetrahedrally coordinated and hence the presence of four chemically distinct groups attached to the lithium atom infers the formation of a stereogenic lithium center. As the precursor molecules to these aggregates are typically achiral, enantioselective aggregate formation seems intuitively unlikely. This possibility has, however, been previously demonstrated. An early example of this idea was the specific formation and isolation of both complex **16a** (see Scheme 4)^[24,26] and our independent isolation of (*R,R,R,R*)- $[(NCNLi)_2]$ (NCN = 2,6- $[Me_2NCH(Me)]_2C_6H_3$) from mixtures of 1:1 *rac/ meso* 2,6-bis[1-(dimethylamino)ethyl]-1-lithiobenzene (**17**; (Scheme 5).^[27] Lithiation of arene **18**, known to exist as a 1:1 *rac/ meso* mixture, lead to the isolation of dimeric **17** (Scheme 5; Figure 5).^[27] Following lithiation, the *R,R* form of $[(NCNLi)]$ aggregates only with a second moiety of identical chirality to form selectively isolable (*R,R,R,R*)- $[(NCNLi)_2]$.^[27] In this



Scheme 5.

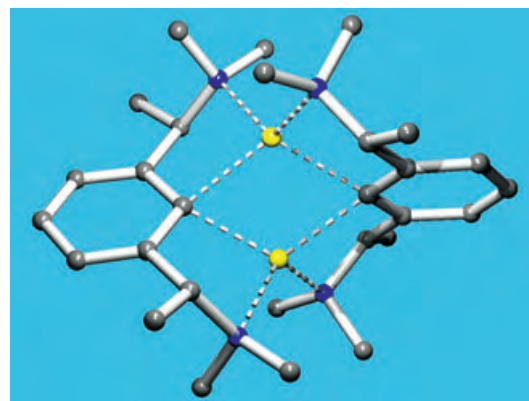
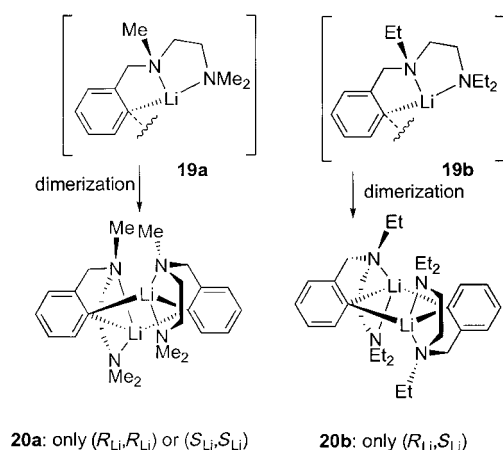


Figure 5. Structure of (*R,R,R,R*)- $[(NCNLi)_2]$ (**17**) in the solid state determined by X-ray diffraction. Blue N, yellow Li.

case, pure chiral centers (per molecule) were present at the benzylic positions before aggregate formation, although a *rac/ meso* isomeric mixture of individual molecules was present. This result suggested to us that chirality resulting only after lithiation might induce the same kind of selectivity.

The formation of fragments **19a** (R = Me) and **19b** (R = Et; Scheme 6) from Li–Br exchange of *o*- $BrC_6H_4CH_2N(R)CH_2CH_2NR_2$ results in each case in the formation of two possible stereogenic centers: one with a stable configuration at the benzylic N atom, the second stereogenic center is created at the lithium centers when two such $[(CNN)Li]$ moieties combine to form the dimeric aggregates **20a** or **20b** (Scheme 6).^[28] In the case of **19a**, the



Scheme 6.

stable species is always formed between two $[(CNN)Li]$ fragments with the same chirality at the lithium atom. Hence, selective formation of 1:1 (R_{Li}, R_{Li})- $[(CNN)_2Li_2]$ (Figure 6) and (S_{Li}, S_{Li})- $[(CNN)_2Li_2]$ is accomplished (chirality in this case being defined only at the lithium centers). The “meso” form dimer of **19a** (that is, (R_{Li}, R_{Li})- $[(CNN)_2Li_2]$) is not a thermodynamically stable aggregate and hence only enantioselective dimerization occurs. This situation is reversed, perhaps for steric reasons, when two **19b** $[(CNN)Li]$ moieties combine. This combination gives only the meso form: (R_{Li}, S_{Li})- $[(CNN)_2Li_2]$ (Figure 6). Hence, aggregate formation

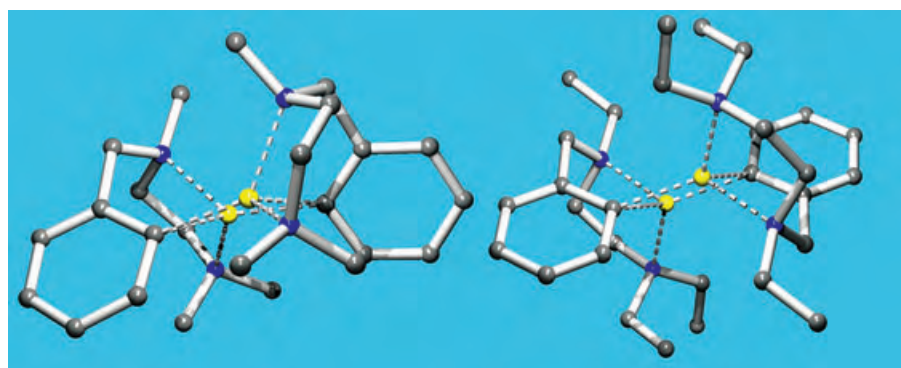


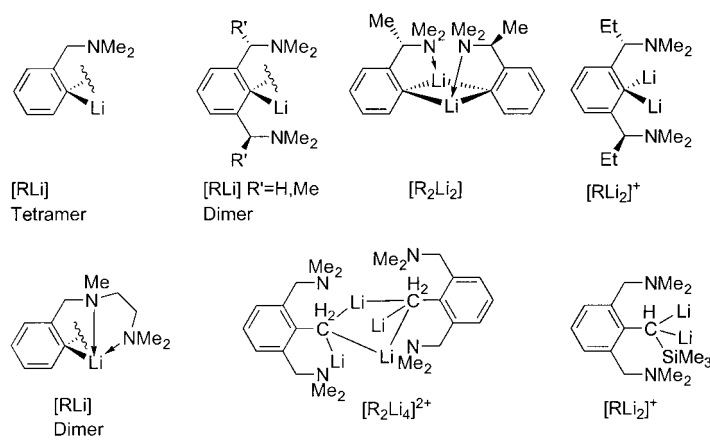
Figure 6. Structures of (R,R)- $[(CNN)_2Li_2]$ (**20a**; left) and (R,S)- $[(CNN)_2Li_2]$ (**20b**; right) in the solid state determined by X-ray diffraction. Blue N, yellow Li.

can induce and control chirality. Complex **20b** is an aryl–aryl organolithium hetero-aggregate where the only difference between two moieties that combine to form the aggregate itself is their chirality.

This concept may become important in cases of hetero organolithium aggregates that contain chiral and/or achiral fragments. Pre-defined chirality may or, more importantly, may not allow the formation of specific organolithium aggregates to be controlled in a predictable way. These species could indeed have unique (enantioselective) reaction pathways. The subtle changes in the ligands in **19a** and **19b** and their influence on the products **20a** and **20b** are a testimony to that idea.

4. Concluding Remarks

A summary of the types of fragments that can self-assemble with themselves, with each other, and with other organolithium species is shown in Scheme 7. Note that the



Scheme 7.

dimeric fragments are structurally similar to the classical “monomer” representation of an organolithium, that is, simply “RLi” and the lithium atoms act as bridges between these units. The aggregates of RLi fragments can be viewed as thermodynamically stable resting states of the reactive formal

R anion. The effect of this state on the chemical role of R in synthesis however, can be directly dictated by the relative stability of this aggregated state (or in other words, the depth of the potential energy well); this is a concept that is frequently encountered in enantioselective catalysis. This aspect of organolithium chemistry and its consequences in synthesis clearly deserve further scrutiny.

R.A.G. is indebted to NSERC (Canada) for funding. We thank the many present and former co-workers, PhD students and Post-docs who contrib-

uted over many years to our studies in organometallic chemistry.

Received: September 24, 2004

- [1] a) K. Ziegler, H. Colonius, *Justus Liebigs Ann. Chem.* **1930**, 479, 123–134; b) H. Gilman, W. Langham, F. W. Moore, *J. Am. Chem. Soc.* **1940**, 62, 2327–2335; c) “Organolithiums in Enantioselective Synthesis”: *Topics in Organometallic Chemistry*, Vol. 5 (Ed.: D. M. Hodgson), Springer, Berlin, **2003**; d) *The Chemistry of Organolithium Compounds* (Eds.: Z. Rappoport, I. Marek), Wiley, Chichester, **2004**; e) *Lithium Chemistry: A Theoretical and Experimental Overview* (Ed.: A.-M. Sapsee,

- P. v. R. Schleyer), Wiley, Chichester, **1995**; f) "Organoalkali Chemistry": M. Schlosser in *Organometallics in Synthesis: A Manual* (Ed.: M. Schlosser), Wiley, Chichester, **2002**, chap. 1; g) B. J. Wakefield, *The Chemistry of Organolithium Compounds*, Pergamon, New York, **1974**.
- [2] a) G. Fuelling, *Spec. Chem.* **1995**, *15*, 116–119; b) G. Fuelling, *Spec. Chem.* **1995**, *15*, 161–162.
- [3] T. Kottke, D. Stalke, *Angew. Chem.* **1993**, *105*, 619–621; *Angew. Chem. Int. Ed. Engl.* **1993**, *32*, 580–582.
- [4] L. M. Pratt, *Mini-Rev. Org. Chem.* **2004**, *1*, 209–217.
- [5] W. Peascoe, D. E. Applequist, *J. Org. Chem.* **1973**, *38*, 1510–1512.
- [6] a) S. K. Varshney, J. P. Hautekeer, R. Fayt, R. Jérôme, P. Teyssié, *Macromolecules* **1990**, *23*, 2618–2622; b) L. M. Jackman, F. Rakiewicz, *J. Am. Chem. Soc.* **1991**, *113*, 1202–1210; c) D. B. Collum, *Acc. Chem. Res.* **1993**, *26*, 227–234; d) J. S. Wang, R. Warin, R. Jérôme, P. Teyssié, *Macromolecules* **1993**, *26*, 6776–6781; e) R. E. Ewin, A. M. MacLeod, D. A. Price, N. S. Simpkins, A. P. Watt, *J. Chem. Soc. Perkin Trans. 1* **1997**, 401–415.
- [7] a) D. Y. Curtin, E. W. Flynn, *J. Am. Chem. Soc.* **1959**, *81*, 4714–4719; b) W. Glaze, R. West, *J. Am. Chem. Soc.* **1960**, *82*, 4437.
- [8] a) B. H. Lipshutz, M. R. Wood, C. W. Lindsley, *Tetrahedron Lett.* **1995**, *36*, 4385–4388; b) M. Majewski, R. Lazny, P. Nowak, *Tetrahedron Lett.* **1995**, *36*, 5465–5468; c) D. A. Price, N. S. Simpkins, A. M. MacLeod, A. P. Watt, *Tetrahedron Lett.* **1994**, *35*, 6159–6162; d) M. Majewski, D. M. Gleave, *J. Org. Chem.* **1993**, *58*, 3599–3605.
- [9] a) X. Fu, R. A. Reamer, R. Tillyer, J. M. Cummins, E. J. J. Grabowski, P. J. Reider, D. B. Collum, J. C. Huffman, *J. Am. Chem. Soc.* **2000**, *122*, 11212–11218; b) L. M. Pratt, A. W. Streitwieser, *J. Org. Chem.* **2003**, *68*, 2830–2838.
- [10] a) P. I. Arvidsson, P. Ahlberg, G. Hilmersson, *Chem. Eur. J.* **1999**, *5*, 1348–1354; b) C. H. Galka, D. J. M. Trösch, M. Schubart, L. H. Gade, S. Radojevic, I. J. Scowen, M. McPartlin, *Eur. J. Inorg. Chem.* **2000**, 2577–2583; c) G. Hilmersson, B. Malmros, *Chem. Eur. J.* **2001**, *7*, 337–341; d) P. I. Arvidsson, G. Hilmersson, Ö. Davidsson, *Helv. Chim. Acta* **2002**, *85*, 3814–3822; e) J. S. DePue, D. A. Collum, *J. Am. Chem. Soc.* **1988**, *110*, 5524–5533; f) A. Ramírez, E. Lobkovsky, D. B. Collum, *J. Am. Chem. Soc.* **2003**, *125*, 15376–15387; g) R. E. Mulvey, *Chem. Soc. Rev.* **1998**, *27*, 339–346; h) A. E. H. Wheatley, *New J. Chem.* **2004**, *28*, 435–443; i) J. E. Davis, P. R. Raithby, R. Snaith, A. E. H. Wheatley, *Chem. Commun.* **1997**, 1721–1722; j) R. P. Davies, P. R. Raithby, G. P. Shields, R. Snaith, A. E. H. Wheatley, *Organometallics* **1997**, *16*, 2223–2225; k) H. J. Reich, W. S. Goldenberg, A. W. Sanders, K. L. Jantzi, C. C. Tzschucke, *J. Am. Chem. Soc.* **2003**, *125*, 3509–3521.
- [11] T. F. Briggs, M. D. Winemiller, D. B. Collum, R. L. Parsons, A. H. Davulcu, G. D. Harris, J. M. Fortunak, P. N. Confalone, *J. Am. Chem. Soc.* **2004**, *126*, 5427–5435, and references therein.
- [12] C. Strohmann, B. C. Abele, *Organometallics* **2000**, *19*, 4173–4175.
- [13] K. Ruhlandt-Senge, J. J. Ellison, R. J. Wehmschulte, F. Pauer, P. P. Power, *J. Am. Chem. Soc.* **1993**, *115*, 11353–11357.
- [14] a) N. J. Hardman, B. Twamley, M. Stender, R. Baldwin, S. Hino, B. Schiemenz, S. M. Kauzlarich, P. P. Power, *J. Organomet. Chem.* **2002**, *643–644*, 461–467; b) J. Arnold, V. Knapp, J. A. R. Schmidt, A. Shafir, *J. Chem. Soc. Dalton Trans.* **2002**, 3273–3274.
- [15] G. van Koten, J. T. B. H. Jastrzebski, *Tetrahedron* **1989**, *45*, 569–578.
- [16] a) N. Sotomayor, E. Lete, *Curr. Org. Chem.* **2003**, *7*, 275–300; b) E. J.-G. Ancil, V. Snieckus, *J. Organomet. Chem.* **2002**, *653*, 150–160; c) L. Green, B. Chauder, V. Snieckus, *J. Heterocycl. Chem.* **1999**, *36*, 1453–1468; d) V. Snieckus, *Chem. Rev.* **1990**, *90*, 879–933; e) P. Beak, V. Snieckus, *Acc. Chem. Res.* **1982**, *15*, 306–312; f) I. Omae, *Chem. Rev.* **1979**, *79*, 287–321; g) H. W. Gschwend, H. R. Rodriguez, *Org. React.* **1979**, *26*, 1–360.
- [17] a) F. N. Jones, C. R. Hauser, *J. Org. Chem.* **1962**, *27*, 701–702; b) F. N. Jones, M. F. Zinn, C. R. Hauser, *J. Org. Chem.* **1963**, *28*, 663–665; c) F. N. Jones, R. L. Vaulx, C. R. Hauser, *J. Org. Chem.* **1963**, *28*, 3461–3465.
- [18] The solid-state structure of dmbaLi is actually [Li₄(dmba)₄] and this structure is retained in non-polar solvents but is broken down into a dimer in polar solvents, such as THF; see: J. T. B. H. Jastrzebski, G. van Koten, M. Konijn, C. H. Stam, *J. Am. Chem. Soc.* **1982**, *104*, 5490–5492.
- [19] C. M. P. Kronenburg, E. Rijnberg, J. T. B. H. Jastrzebski, H. Kooijman, A. L. Spek, G. van Koten, *Eur. J. Org. Chem.* **2004**, 153–159.
- [20] C. M. P. Kronenburg, E. Rijnberg, J. T. B. H. Jastrzebski, H. Kooijman, A. L. Spek, R. A. Gossage, G. van Koten, *Chem. Eur. J.* **2005**, *11*, 253–261.
- [21] a) M. Albrecht, G. van Koten, *Angew. Chem.* **2001**, *113*, 3866–3898; *Angew. Chem. Int. Ed.* **2001**, *40*, 3750–3781, and references therein; b) M. H. P. Rietveld, D. M. Grove, G. van Koten, *New J. Chem.* **1997**, *21*, 751–771; c) G. van Koten, *Pure Appl. Chem.* **1990**, *62*, 1155–1159; d) G. van Koten, *Pure Appl. Chem.* **1989**, *61*, 1681–1689.
- [22] P. Wijkens, E. M. van Koten, M. D. Janssen, J. T. B. H. Jastrzebski, A. L. Spek, G. van Koten, *Angew. Chem.* **1995**, *107*, 239–242; *Angew. Chem. Int. Ed. Engl.* **1995**, *34*, 219–222.
- [23] A related "CNN" pincer lithium complex incorporating LiBr has been structurally elucidated: I. C. M. Wehman-Ooyevaar, G. M. Kapteijn, D. M. Grove, A. L. Spek, G. van Koten, *J. Organomet. Chem.* **1993**, *452*, C1–C3.
- [24] P. Wijkens, J. T. B. H. Jastrzebski, N. Veldman, A. L. Spek, G. van Koten, *Chem. Commun.* **1997**, 2143–2144.
- [25] Complex **16a** adopts a more open ladder-type structure in contrast to complex **11** that contains a closed tetrahedral Li₄ unit. For a further discussion of such structural aspects see refs. [19, 22, 24].
- [26] Complex **16a** contains a chiral center at the methanide carbon atom, the combination of the two fragments that make up **16a** always consists of an *R* moiety combining with an *S* one and hence **16a** always has a mirror plane. The combination of chirally identical fragments is apparently not thermodynamically favored.
- [27] J. G. Donkervoort, J. L. Vicario, E. Rijnberg, J. T. B. H. Jastrzebski, H. Kooijman, A. L. Spek, G. van Koten, *J. Organomet. Chem.* **1998**, *550*, 463–467.
- [28] a) M. H. P. Rietveld, I. C. M. Wehman-Ooyevaar, G. M. Kapteijn, D. M. Grove, W. J. J. Smeets, H. Kooijman, A. L. Spek, G. van Koten, *Organometallics* **1994**, *13*, 3782–3787; b) A. M. Arink, C. M. P. Kronenburg, J. T. B. H. Jastrzebski, M. Lutz, A. L. Spek, R. A. Gossage, G. van Koten, *J. Am. Chem. Soc.* **2004**, *126*, 16249–16258.

Molecular Knots

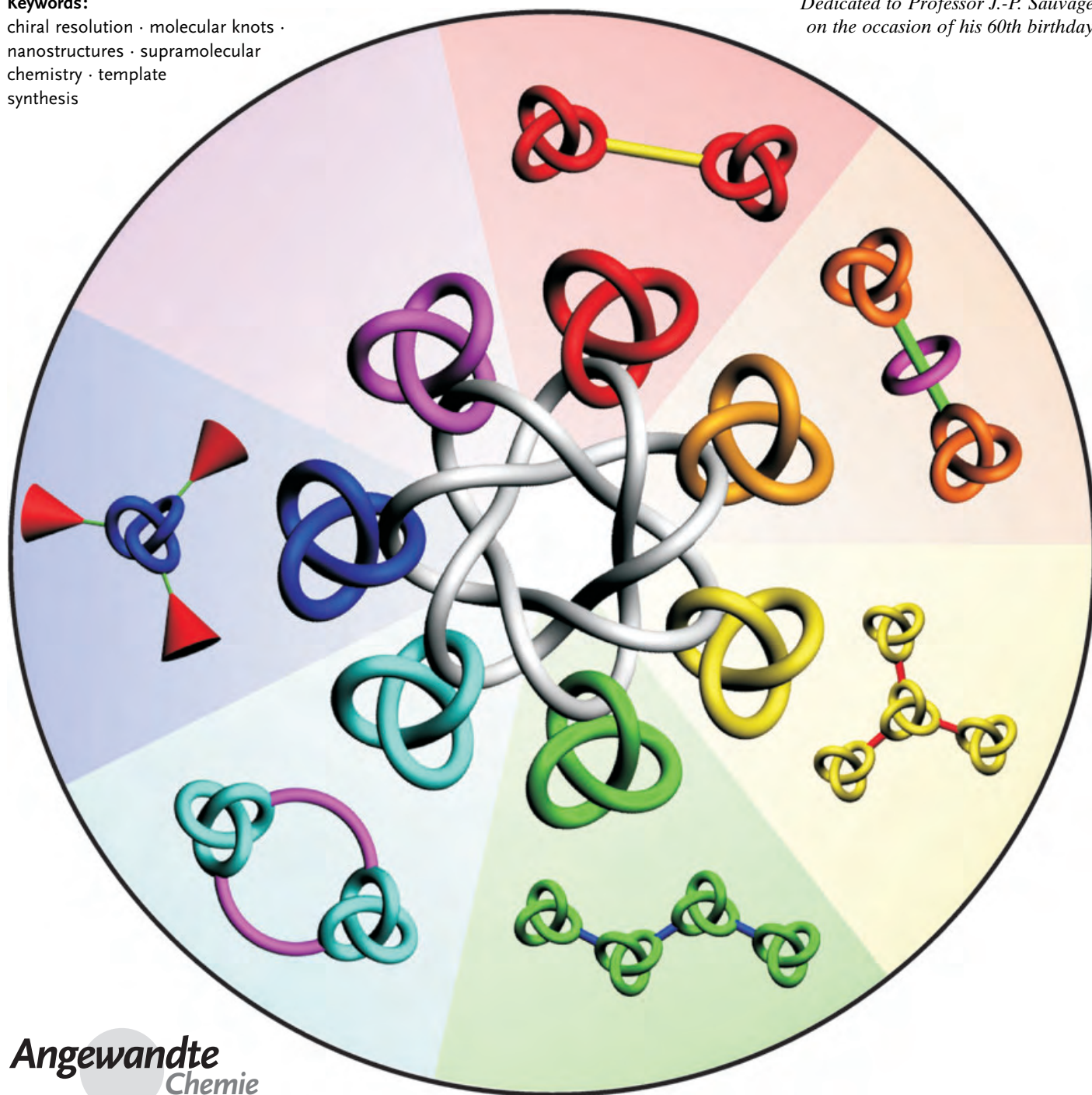
Knotting and Threading of Molecules: Chemistry and Chirality of Molecular Knots and Their Assemblies

Oleg Lukin and Fritz Vögtle*

Keywords:

chiral resolution · molecular knots · nanostructures · supramolecular chemistry · template synthesis

Dedicated to Professor J.-P. Sauvage on the occasion of his 60th birthday



Angewandte
Chemie

How and why do molecules tangle or thread? Investigations of molecular knots (knotanes) may shed some light on the mechanisms of (supra)molecular templation and the folding of molecules that result in intertwining. The topological chirality of these fascinating molecules leads to new types of isomerism and paves the way to nanosized molecular motors. Their preparation and derivatization makes high demands on modern synthetic methods and analytical separation since molecular knots are formed in a more or less planned design based on metal coordination or hydrogen-bonding patterns. This Review describes the development of templation techniques for the synthesis of knotanes and their chiral resolution as well as their selective functionalization and use as building blocks in the synthesis of higher knotane assemblies. Such assemblies can possess linear, branched, or even macrocyclic structures which, on the one hand, introduce unprecedented isomeric compositions that arise from multiple topological stereogenic units and, on the other, define new types of artificial macromolecules beyond polymers and dendritic species.

From the Contents

1. Introduction	1457
2. Amide-Based Molecular Knots	1460
3. Structure and Conformation of Knotanes: Rigidity Versus Flexibility	1464
4. Chiral Resolution, Absolute Configuration, and Chiral Induction of Molecular Knots	1467
5. Knotane Assemblies	1469
6. Conclusions and Outlook	1473

1. Introduction

1.1. Why Knots?

Knots are found everywhere in daily life (ties, shoelaces, sailors knots, sculptures, jewellery, etc; Figure 1) and are of practical use; however, molecular knots have only been known for a few years. The first scientific interest in knots was promoted by chemistry.^[1] According to the first model of the atomic structure hypothesized by Lord Kelvin, atoms consisted of knotted “ether”, wherein each knot represented a particular sort of atom. Inspired by this theory, the Scottish physicist Tait decided to list all of the possible knots to create

a table of elements. Although chemists lost interest in knots after the hypothesis of Kelvin turned out to be wrong, mathematicians immediately became interested in Tait’s knot theory and it was later integrated into the purely mathematical field of topology. Nowadays, the domain of knot theory, developed by mathematicians, is fully appreciated by researchers of different disciplines and has significant applications in chemistry and biology, thus giving rise to novel subdisciplines such as chemical topology,^[2] biochemical topology,^[3] and topological stereochemistry.^[4] Topology relates to those properties of an object that are invariant under conditions of arbitrary deformations.^[1,5]

In chemical topology^[2] the object is a molecule or a molecular assembly which is schematically represented on paper as a graph. If the graph contains crossings, then the graph and the molecule are referred to as nonplanar and topologically nontrivial, respectively. Figure 2 shows examples of both nonplanar (I and II) and planar (III) graphs. They are simplified projections of the enantiomers of the trefoil knot and a cycle, respectively. The three structures I–III are

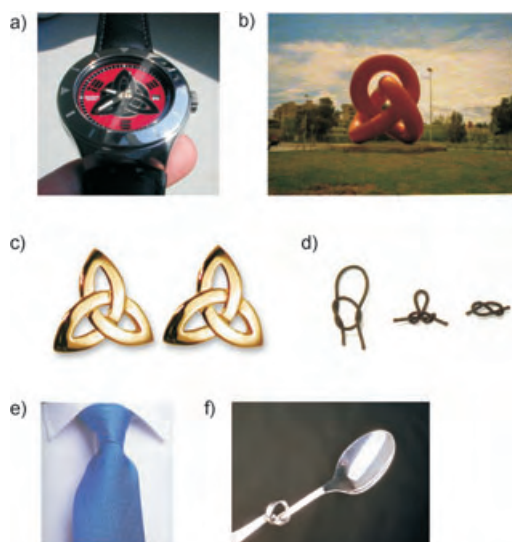


Figure 1. Knots in daily life: a) a watch with a knot symbol; b) a sculpture of a trefoil knot on Mallorca; c) celtic trinity knot earrings; d) sailor's knots; e) a necktie; f) a knotted spoon from a television commercial (Maggi).

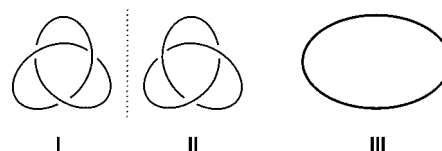


Figure 2. Projections of enantiomers of trefoil knots (I, II) and a cycle (III).

[*] Dr. O. Lukin, Prof. Dr. F. Vögtle
Kekulé-Institut für Organische Chemie und Biochemie
der Rheinischen Friedrich-Wilhelms-Universität Bonn
Gerhard-Domagk-Strasse 1, 53121 Bonn (Germany)
Fax: (+49) 228-735662
E-mail: voegtle@uni-bonn.de

topological isomers. Additionally, if a nonplanar graph such as **I** or **II** cannot be deformed to form its mirror image without cutting, then such a graph is topologically chiral. Thus, chemical topology classifies the pair **I**, **II** in Figure 2 as topological enantiomers. Liang and Mislow^[6] suggested using the molecular-graph approach to distinguish between classical and topological chirality. According to this classification, the first category includes molecules having the classical stereogenic units (points, axes, helices, and planes)^[7] while the latter refers to the chirality of the nonplanar molecular graph^[2,4,5] such as the pair **I** and **II** in Figure 2. Frisch and Wasserman^[2a] remarked in their pioneering paper on chemical topology that the essential features of molecular knots are their topological chirality and remarkable nanometer-sized dimensions. They examined molecular models and found that even the simplest possible trefoil knot made up of a hydrocarbon chain should contain more than 50 linked methylene groups and result in a nanosized globular molecule.

The later discovery of natural knotted forms of DNA^[8] and proteins^[9] justified these early expectations. The natural knots have indeed been shown to have sizes of several nanometers and possess quite unusual biochemical activities. For example, natural knotted proteins such as lactoferrin (Figure 3) and ascorbinic acid oxidase exhibit remarkable

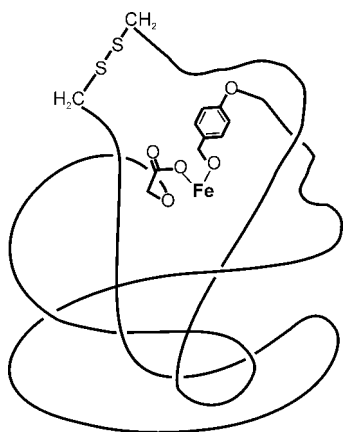


Figure 3. Schematic representation of lactoferrin, a naturally occurring knotted protein.

activities compared with linear analogues in the transport of iron(III) ions and in enzymatic oxidation, respectively.^[10] A knotted structural motif is also found in protease inhibitors and toxins, and confers a high rigidity to the overall protein structure.^[11] It is the pronounced rigidity and chirality of knotted proteins such as circulin A and B that plays the critical role in their significant antiviral activities and makes these proteins promising anti-HIV drugs.^[12]

It is now well recognized in the chemical community that the design of nanosized intertwined molecular systems of higher complexity is associated with many fundamental and practical goals, such as the quest for novel types of isomerism and chirality,^[13] the utilization of large-amplitude molecular movements of the intertwined molecular parts in molecular machinery,^[14] and the elucidation of biochemical functions of diverse nontrivial tangles in the structure of DNA^[15] and proteins.^[9] Another important aspect in this connection is the rational construction of new macromolecules from intertwined monomers.^[16] The interplay between extrinsic and intrinsic topologies of such macromolecules made up of knotted macromonomers would be of significance for materials chemistry. Additionally, when the above examples of biochemically active knotted proteins are taken into account, synthetic knots are promising as chiral heterogeneous or homogeneous catalysts for stereoselective synthesis, provided that they exhibit appreciable chiral inductions.

The methods of molecular biology that utilize the actions of specific enzymes such as topoisomerases allow for the rational construction of a range of catenated and knotted structures from DNA, RNA, and even proteins.^[3] In modern chemistry, the synthetic strategies for the preparation of such interlocked and intertwined species rely mostly on template effects associated with noncovalent interactions^[17,18] identified from the areas of coordination chemistry and supramolecular science.^[19] Despite the close similarities between the intertwined species that biologists and chemists are interested in, an essential difference lies in the goals of biology and chemistry: in molecular biology DNA molecules are usually catenated or knotted to study concentration-independent structural features and (intermolecular) interactions of DNA,^[3] while chemists first have to study molecular interactions to assemble the intertwined species.^[17]



Fritz Vögtle, born in Ehingen/Donau (Germany), in 1939, studied chemistry in Freiburg as well as chemistry and medicine in Heidelberg, where in 1965 he received his PhD for research with Prof. Heinz A. Staab on the valence isomerization of double Schiff bases. After his habilitation on steric interactions inside cyclic compounds, he became professor in Würzburg (1969). In 1975 he accepted a position as full professor and director of the Kekulé-Institut für Organische Chemie und Biochemie in Bonn. His awards include a "literature prize" from the "Fonds der Chemischen Industrie", the Lise Meitner-Alexander von Humboldt-award, and the Adolf von Baeyer medal of the German Chemical Society.



Oleg Lukin was born in 1973 in Samara (Russia) and studied chemistry in Kiev (Ukraine). In 1995 he received his MSc in chemistry with Prof. Vitaly Kalchenko at the Institute of Organic Chemistry, Kiev for his work on calixarenes. He received his PhD in 2000 for research on theoretical and experimental studies of molecular and chiral recognition by cyclodextrins with Prof. Helena Dodziuk at the Institute of Organic Chemistry, Warsaw, Poland. He then carried out postdoctoral research with Prof. Jerzy Leszczynski at Jackson State University, and in 2001 he joined the group of Prof. Fritz Vögtle in Bonn as an Alexander von Humboldt fellow. In 2004 he joined the research group of Prof. A. D. Schlüter at the ETH Zurich.

This Review covers the chemical side of the story, with a focus on so-called “small-molecule” knots obtained with the aid of supramolecular template techniques.^[18] Despite numerous reviews highlighting achievements in the preparation of molecular catenanes and rotaxanes,^[17,18] to our knowledge there is only one survey on chemical knots,^[20] in which the first synthetic phenanthroline-type knots are described from a historical perspective. The small number of reports on molecular knots definitely does not reflect a lack of interest in these species compared to other intertwined and interlocked assemblies. Molecular knots belong to the less-explored class of intertwined species that, in keeping with their higher complexity, necessitates even greater effort to control the supramolecular phenomena such as molecular recognition, folding and intertwining, and templation. Analogous to the commonly used terms “catenane” and “rotaxane” for interlocked species, we have suggested the term “knotane”^[21] for a molecular knot. The latter term is used in different combinations (for example, knotanes of the phenanthroline type, amide-knotanes, etc.) throughout this Review without further comment.

1.2. Chemical Knots (Knotanes): State of the Art

The first synthesis of a molecular knot was reported in 1989,^[22] but the earlier experimental attempts and theoretically suggested routes towards molecular knots contributed significantly to a multi-angle view of the problem of assembling synthetic knots. Since the isolation of the first [2]catenane by Wasserman^[23] in 1960, the synthesis of molecular knots has been an important topic in the chemical literature. Early designs of a molecular knot (Figure 4) invoked: a) the Möbius strip approach (Van Gülick,^[24] as well as Frisch and Wasserman^[2a]), b) a directed strategy based on a covalent template (Schill et al.^[25]), and c, d) templated strategies based on metal coordination (Walba et al.^[26] and Sokolov^[27]). A detailed discussion on these early attempts can be found in seminal reviews by Walba^[4] and Sauvage and Dietrich-Buchecker.^[20]

The first successful synthesis of a trefoil molecular knot (**1**) by a template procedure was reported by Dietrich-Buchecker and Sauvage in 1989.^[22] As illustrated in Scheme 1, the ends of a metal-templated helical dimeric complex (see also Figure 4a) composed of two bisphenanthroline ligands **2** and two Cu^I cations were linked by oligoethyleneglycol chains. The chirality of the knotane **1** was confirmed first by monitoring the separation of signals in its ¹H NMR spectrum upon addition of the chiral Pirkle reagent and subsequently by a single-crystal X-ray structure analysis.^[28] Later Sauvage and co-workers^[29] synthesized a variety of phenanthroline knotanes and showed that their yields depended critically on structural parameters such as the length and rigidity of the bridge linking the two chelating phenanthroline units and the length of the poly(ethyleneoxy) unit used in the cyclization. The best yield for knotane **3**^[29b] (76 %) was attained by combining the helical precursor composed of Cu^I-bis(phenanthroline) units with 1,3-phenylene linkers and the highly efficient ring-closing metathesis (RCM) methodology.^[30]

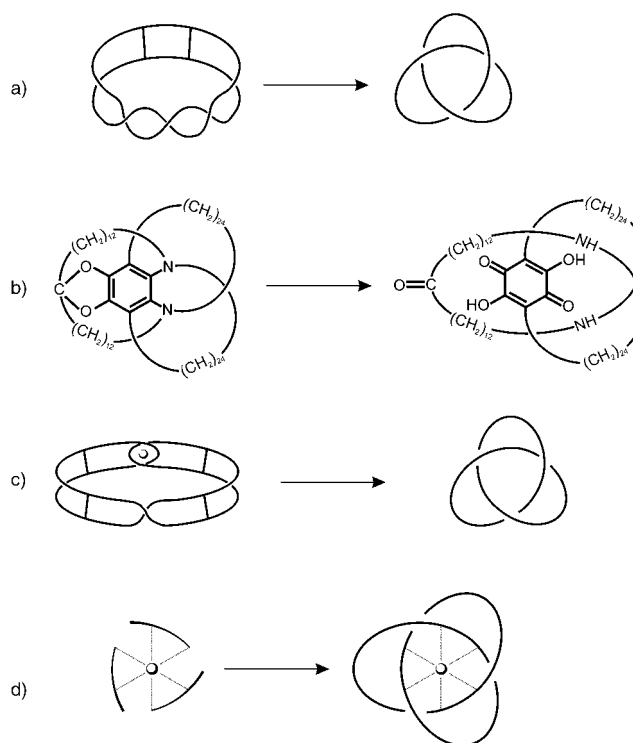
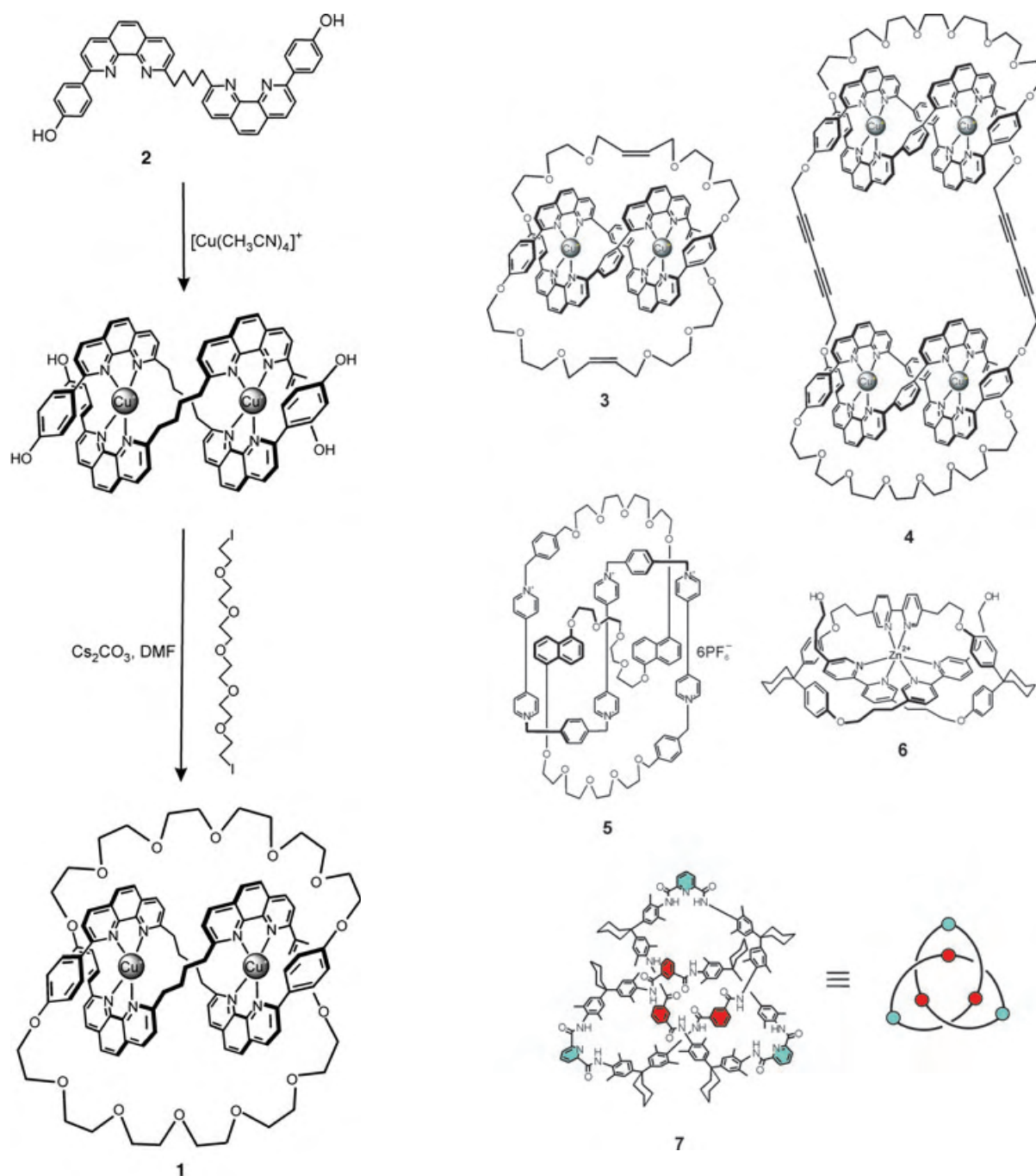


Figure 4. Early designs for the formation of the molecular knot: a) the Möbius strip approach;^[2a,24] b) application of a covalent template;^[25] c) “hook-and-ladder” proposal by Walba et al.;^[26] d) Sokolov’s application of an octahedral tris(chelate) template.^[27]

The concept of helical copper(I)-phenanthroline complexes was expanded to the preparation of molecular knots^[31] such as **4**,^[32] whose isomeric composition involves a *meso* form as well as a pair of enantiomers.

In 1997 Stoddart and co-workers^[33] isolated, in a low yield, trefoil knot **5**, which was assembled from a helical chain preorganized with the aid of a π -donor/ π -acceptor interaction between the amine units. This knotane was purified by HPLC and characterized by means of secondary-ion mass spectrometry (LSIMS). More recently Hunter and co-workers^[34] described the assembly of the “open knot” **6**. The octahedral coordination chemistry utilized in the early design developed by Sokolov^[27] (Figure 4d) was shown to be advantageous in this assembly: A molecular chain containing three moieties of 2,2'-bipyridyl ligands were octahedrally coordinated around a Zn²⁺ ion to produce the chiral open loop **6**. Unfortunately, removal of the metal ion from this loop could not be achieved.

In 2000 we reported by far the easiest synthesis of a trefoil knot **7** at that time. The synthesis made use of the folding of the loop and the intramolecular hydrogen-bonding pattern of the oligoamides.^[21] The synthesis is attractive on account of it being a one-pot procedure that affords reasonable yields and unique possibilities for further derivatizations. Of particular note is that, in comparison to the Cu^I-based template synthesis developed by Dietrich-Buchecker and Sauvage (see above),^[22] no external templating agent is necessary. Moreover, the assembly of the amide-knotanes has much in common with formation of the tertiary structural motifs in



Scheme 1. Synthesis of the first phenanthroline-knotane by using a copper(I) template.

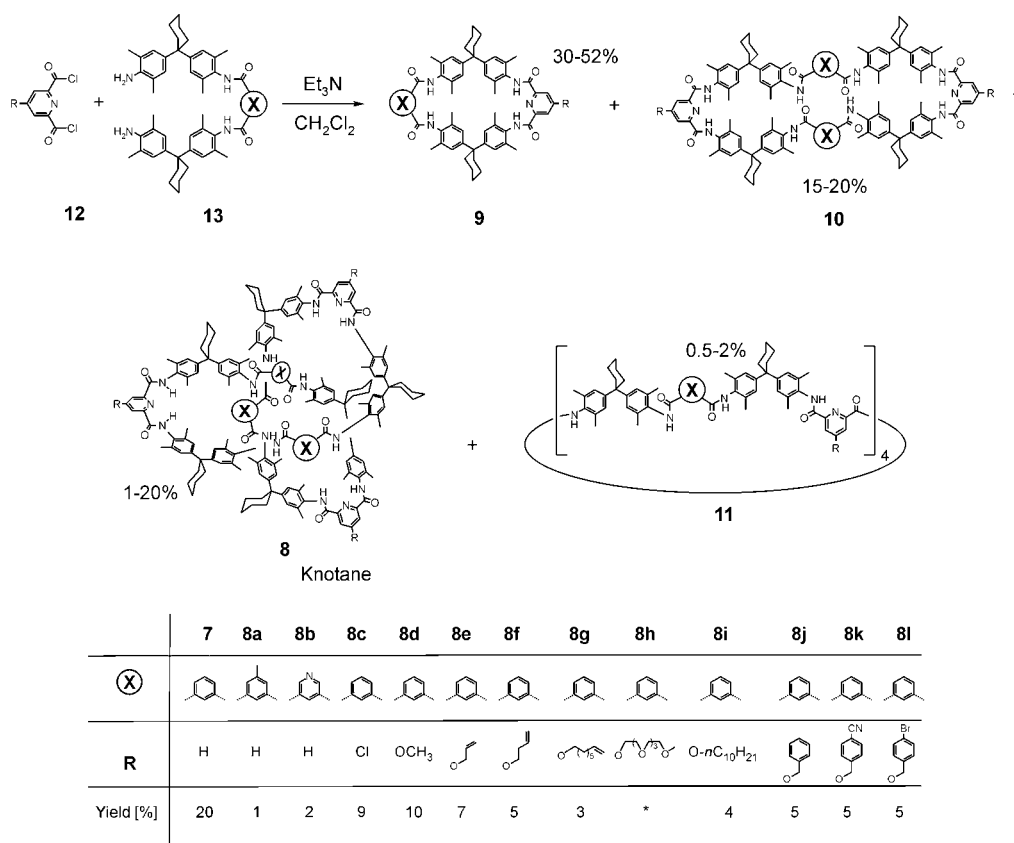
natural proteins.^[35] Our further investigations of the chemistry and topological chirality of amide-knotanes experienced an explosive growth in a relatively short time. Since the phenanthroline-type knotanes were thoroughly reviewed by Sauvage and Dietrich-Buchecker,^[20] and the knots produced by the research groups of Stoddart^[33] and Hunter^[34] have not been investigated further, the discussion presented herein concerns primarily the amide-based knots. However, comparisons of amide-knotanes with other synthetic knots are given in discussions concerning the mechanisms by which the knot

forms as well as of their conformations and topological isomerisms and chiralities.

2. Amide-Based Molecular Knots

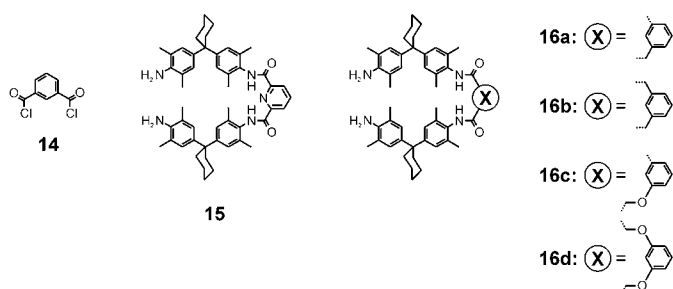
2.1. Synthesis and Mechanism of Formation

The dodecaamide-knotane of general formula **8**^[21,36–41] is one of the four isolable cyclic oligomers **8–11** formed in the course of a high-dilution macrocyclization between easily available derivatives of 2,6-pyridinedicarboxylic acid dichloride **12** and the elongated diamines **13** (Scheme 2). Useful insights into the formation of the amide-knotane were



Scheme 2. Synthesis and yields of amide-knotanes.

provided by varying the structure of the reagents and by analysing the yields of the other cyclic oligomers. Other clues to the mechanism by which the amide-knotanes formed was found from considering the solid-state structure analyses, particularly of the hydrogen-bonding patterns identified. Thus, for example, no knotane has been detected among the reaction products if 2,6-pyridinedicarboxylic acid dichloride **12** in Scheme 2 is replaced by isophthaloyl dichloride (**14**), an



observation which highlights the paramount importance of the 2,6-pyridinedicarboxylic acid dichloride for formation of the knot. [36] Furthermore, attempts to synthesize an amide-knotane from “inverted building blocks” (reaction of **15** with isophthaloyl dichloride (**14**)) also failed. Similarly, no knotanes have been isolated when the flexibility of the extended diamine is increased by the introduction of additional single

bonds between the isophthalic dicarboxamide and its two arms (as in **16**). [37] The additional degrees of freedom seem to prevent a suitable preorganization of the intermediates. In contrast, **12** can be substituted at its 4-position, even with large substituents such as *p*-bromobenzyloxy (**8l**) [38] without observing any significant reduction in the knotane yield. Any substituent present in the 5-position of **13** reduces the yield of the knotane or prevents its formation completely. [36–39] For example, a methyl group at the 5-position (as in **13a**) reduces the yield of the corresponding knotane **8a** to less than 2%, while a *tert*-butyl group in the same position results in the complete absence of knotane formation. The X-ray crystal structures of the unsubstituted and tris(allyloxy) knotanes **7** [21] and **8e**, respectively [40] (Figure 5) provide a rationalization for this finding: while the isophthalic dicarboxamide moieties are deeply buried inside the knot structure, the pyridine rings are located at the periphery. Thus, during the formation of the knot, substituents at the pyridine rings do not significantly hamper the formation of intermediates that give rise to the intertwined structure, while substituents on the isophthalic dicarboxamide moieties appear to encumber its formation. These experimental findings highlight that both the presence and the exact position of the pyridine subunits are important.

One can conclude from the X-ray structures of amide-knotanes **7** and **8e** that the specific folding of a linear precursor is most probably programmed by the pattern of hydrogen bonds, which should be strong in a noncompetitive solvent such as dichloromethane. On the other hand, the

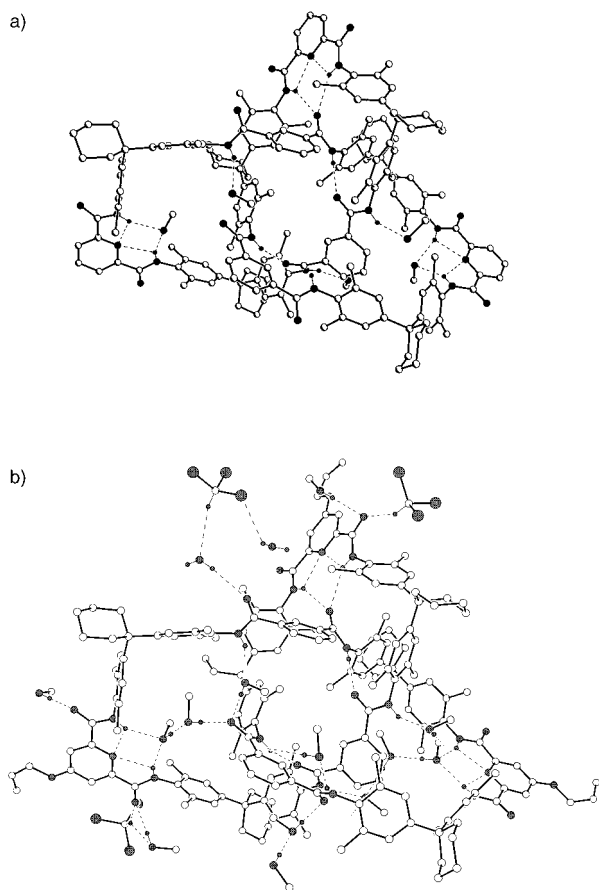


Figure 5. Single-crystal X-ray structures of: a) unsubstituted amide-knotane **7**; b) tris(allyloxy)knotane **8e**.

reaction is controlled kinetically because the formation of amides under the given conditions is irreversible, and yields the smallest cycle **9** (Scheme 2) as the main product.

We therefore attempted to control the kinetics of the reaction by changing the concentration of the reagents and thereby optimize the yields of the amide-knotanes.^[41] A concentration of **12** and **13** of 3 mM (instead of 1 mM, a concentration which is characteristic of the classical high-dilution method) and a high synchronous mixing rate were found to be optimal conditions to increase the yields of the knotanes while at the same time decreasing the yields of macrocycles **9** and **10**. Higher concentrations resulted in the formation of polycondensation products. The rationalization of those finding is that the increased reagent mixing rate, along with their higher concentration, cause an increase in the population of higher linear oligomers that can then fold, thus enhancing the probability of knotting. It is still not easy to draw a definite conclusion about the mechanism of the formation of the amide-knotane since—as with the proteins—linear oligoamides^[42] are known to adopt a vast number of stable folded conformations. A computational analysis of the knotting mechanism is also difficult because

dynamic simulations of even small rapidly folding proteins necessitate an enormous computational power.^[43]

In summary, our method for the synthesis of amide-knotanes requires no template. In contrast, in the template synthesis developed by Sauvage (Scheme 1) the Cu^{I} ions acts as an “auxiliary” which is removed from the product (“knotate”) after the C–X coupling reaction. In our case, **12** and **13** condense in an “internal templating” reaction to generate amide-knotanes. Taking into consideration the experimental data described above, including the X-ray crystal structures of amide-knotanes **7** and **8e**, the progression of the assembly seemingly begins with the fast formation of the linear diamine **17** composed of three units of **13** and two units of **12**. The diamine **17** then folds in the form of a helical loop (Figure 6a) followed by self-threading of its remaining

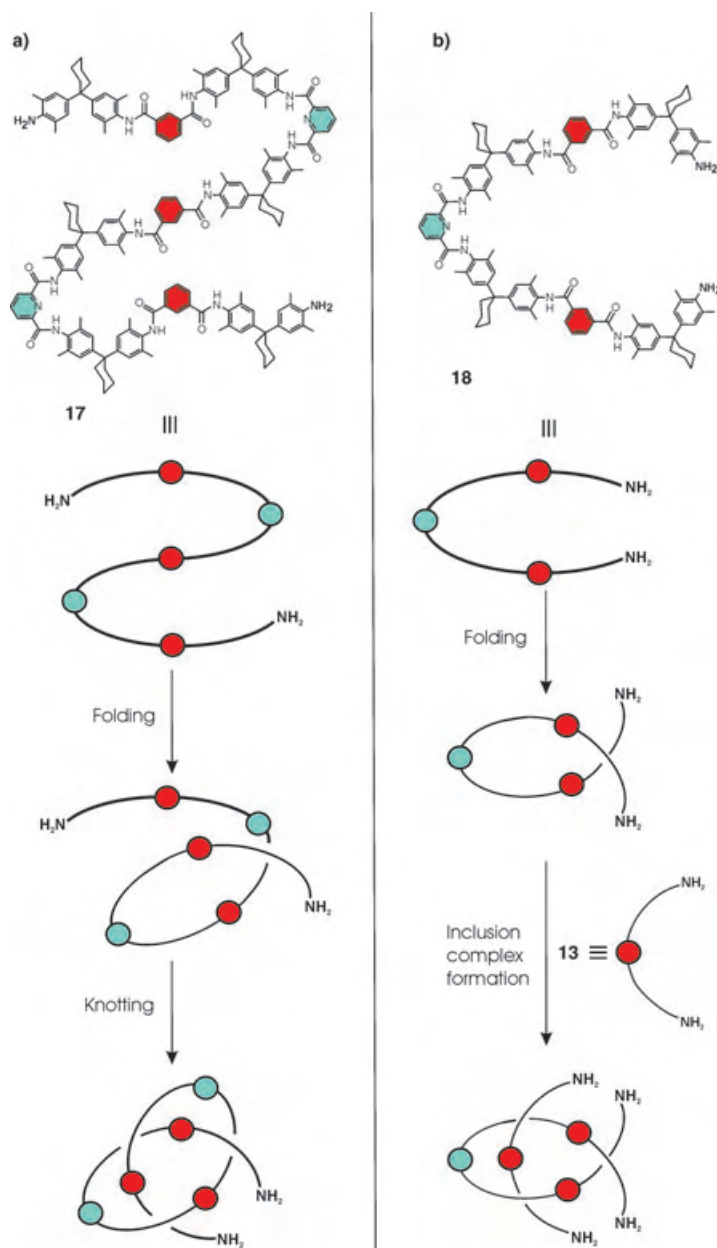


Figure 6. Proposed mechanisms for the formation of the amide-knotane.

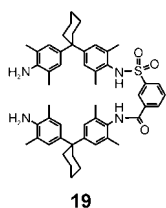
part through this loop. Finally one carboxylic acid chloride unit of **12** reacts with the terminal amino groups of the open loop to close the open knot.

Another possibility for knot formation could involve a host–guest complexation between the diamine **18** in the form of a helical loop and the diamine **13** (Figure 6b). The hydrogen-bonding pattern in this weakly bonded (supramolecular) complex resembles that found in the solid-state structures of knotanes **7** and **8e**. Although we cannot exclude the latter host–guest type of mechanism, it seems that the former version involving the folding of the long diamine **17** is more likely since the rate of the amine acylation under given conditions supercedes the rates of the folding of **18** and its complexation with **13**. Molecular modeling studies suggest that the folding pattern of **18** favors formation of macrocycle **10** rather than the helical precursor shown in Figure 6b. The latter conclusion is in line with the higher yields of **10** compared to those of knotanes. Currently, we are working on the preparation and structure elucidation of diamines **17** and **18**, which are probable oligomeric precursors of amide-knotanes and are also promising reagents for the synthesis of selectively derivatized and even more complex knotanes.

2.2. Derivatization of Amide-knotanes

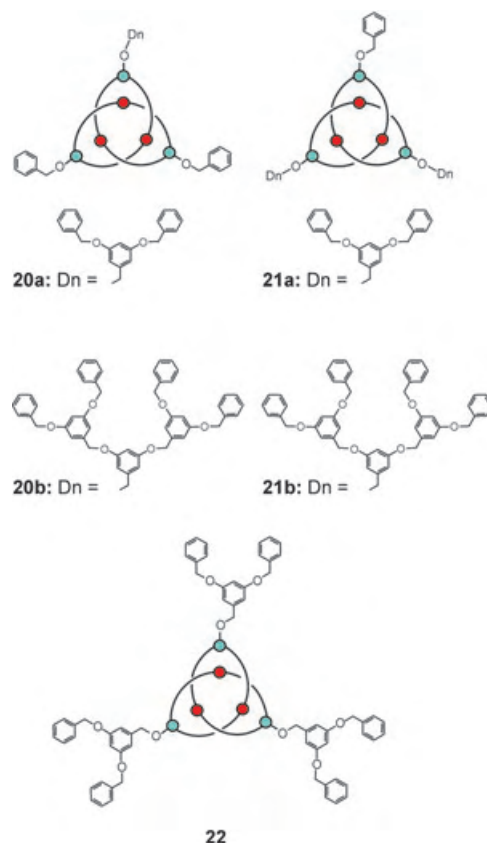
The initial interest in molecular knots arose from the elegance, symmetry, and visual power of their characteristically intertwined structure. Consequently, the first knotanes were nonfunctionalized or not intended for further reactions. The functionalization of knotanes is highly desirable: a) to improve their solubilities and thus their manageability; b) to allow their resolution by HPLC on a chiral phase; c) to study the influence of topological chirality when combining knotanes with already known functional units; and d) to prepare higher assemblies of molecular knots. In this respect amide-knotanes provide a perfect, readily available nanosized scaffold that can be modified synthetically in many different ways. As mentioned in the previous section, amide-knotanes **8** could be equipped with various small substituents at the isophthaloyl (**8a, b**) and 2,6-pyridinedicarboxamide fragments (**8c–k**)^[36–39] by means of the direct selection of suitably substituted reagents **12** and **13** prior to the assembly of the knot. Therefore, we termed the latter method the “direct”^[39] approach to functionalized knotanes.

Another interesting attempt at the monofunctionalization of amide-knotanes utilizing the direct approach was the use of a 2:1 mixture of the usual elongated diamine **13c** and the elongated diamine **19** bearing one sulfonamide arm.^[37b] The yields were low because of the statistical formation of all possible oligomers and the tedious HPLC purification.



Despite the value of its one-pot procedure, the method of direct functionalization of amide-knotanes has significant drawbacks. Firstly, large substituents are not tolerated and secondly, a rational selective derivatization is not possible. These limitations prompted us to look for other possible ways to functionalize

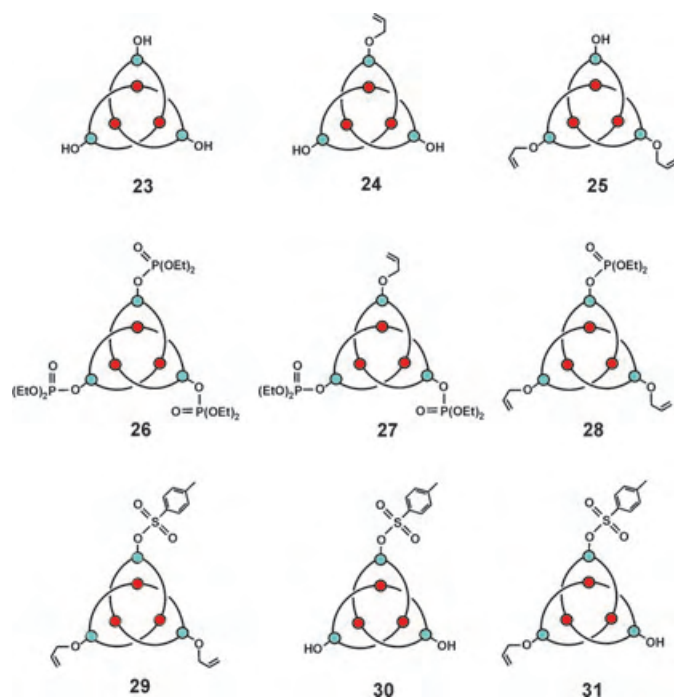
amide-knotanes. We developed the “indirect” approach^[39–41] to derivatize amide-knotanes, by taking advantage of protecting group chemistry at the 4-positions of the 2,6-pyridinedicarboxamide units which constitute the three peripheral edges of the synthesized knotanes **8**. The first synthesis in which the indirect approach was utilized was the complete and partial deprotection of tris(benzyloxy)knotane **8j**^[39] by Pd-catalyzed hydrogenation, followed by the alkylation with Fréchet-type dendrons.^[44] The isolated dendronized knotanes **20–22** (“dendroknots”) which bear one to three dendritic



wedges constituted the first examples of selectively derivatized knotanes. The main disadvantage of the latter synthesis concerns the step of deprotection which does not proceed to completion and thus gives rise to the mixture of mono-, di-, and trihydroxyknotanes which could not be separated. The excessive hydrogen pressure also seems to lead to the undesirable partial reduction of some of the amide moieties.^[45] Consequently, the mixture of hydroxyknotanes was used for the alkylation and the resulting mixtures of dendroknots were later resolved by HPLC.

The difficulty can be overcome by selecting a better protecting group whose expected reactivity will neither affect the synthesis of the amide-knotane nor its further derivatization. The 4-allyloxy group (in **12e**) seemed to be a suitably protected building block for this purpose. Tris(allyloxy)knotane **8e** is indeed readily accessible (Scheme 2) in a one-step synthesis in 8% yield. The allyl groups can be completely or selectively removed from the periphery of tris(allyloxy)-

knotane **8e** with the aid of tributyltin hydride and a Pd catalyst, thus resulting in the corresponding tri-, di-, and mono-hydroxyknotanes **23–25**.^[40,41] Unlike the above case



with tris(benzyloxy)knotane **8j**,^[39] the latter synthesis proceeds smoothly and cleanly to yield products which could be purified on a gram-scale by means of conventional column chromatography. The simple and reliable synthetic strategy for the complete and selective removal of the outer protecting groups leads to topologically chiral building blocks with unprecedented reactivity.

In our first functionalization experiment we started by introducing the biologically relevant phosphoryl groups,^[41] which offer the advantage that they have been shown to modify the stability, solubility, and binding properties of synthetic molecular hosts such as crown ethers, cryptands, calixarenes, and dendrimers.^[46] As described in Section 3, this functionalization has also allowed the analysis of conformation and dynamics of amide-knotanes in solution by means of ³¹P NMR spectroscopy. The hydroxyknotanes **23–25** react with diethylchlorophosphate to form tri-, di-, and mono-phosphorylated knotanes **26–28**, respectively.^[41] Interestingly, the phosphorylated knotanes **26–28** can be reversibly converted into the parent hydroxy derivatives **23–25** with silica gel or by hydrolysis in an ethanolic NaOH solution. Diethoxyphosphoryl groups have also been shown to be unstable under the conditions for the removal of the allyl group with Bu₃SnH, thus prohibiting possibilities for further modifications of the knotane. The latter limitation can be overcome by using chemically more-stable arylsulfonyl substituents. Sulfonation of the bis(allyloxy)hydroxyknotane **25** with *p*-toluenesulfonyl chloride in the presence of triethylamine in acetonitrile proceeds smoothly to give the monosulfonate **29** in 95 % yield.^[41] The allyl groups, in turn, can be completely or

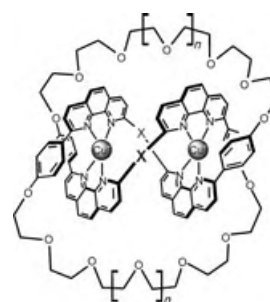
selectively removed from the periphery of **29**, thus resulting in dihydroxy- and monohydroxyknotanes **30** and **31**, respectively. The preparation of **31** with three different substituents at the loop edges constitutes a remarkable synthetic breakthrough since it allows for the preparation of amide-knotanes with a wide range of substitution patterns and affords exceptional opportunities for further synthetic variations.

3. Structure and Conformation of Knotanes: Rigidity Versus Flexibility

3.1. Conformational Dynamics of Molecular Knots in Solution

Investigation of the conformational properties of nano-sized intertwined species is of interest as a result of their potential applications in the construction of molecular switches where controlled conformational transitions might play a key role. A controllable molecular motion is usually defined as a reversible conformational transition or isomerization caused by external stimuli such as light, chemical, or electrochemical inputs etc. Numerous reports describing large-amplitude controllable motion in topologically linked interacting units of catenanes and rotaxanes have appeared in the literature,^[14] whereas there are still no examples of molecular switches involving molecular knots. Unlike catenanes and rotaxanes, molecular knots are single component molecular entities, which means they have no mechanically linked constituent parts. Therefore, reasonable questions would be: what kind of motion could be expected from a knotted topology and is it structure or topology that influences such a motion?

Sauvage and co-workers^[47] reported the first structural studies of phenanthroline knotanes in solution. They performed a comparative study of two types of knotanes in which the phenanthroline units were bridged either by oligomethylene (**32a–c**) or *m*-phenylene (**32d**) linkers. The obtained knotates with the two copper(I) cations are generally rigid in solution. Demetalation of the knotanes, which can be followed by absorption spectrophotometry, leads to molec-



32a: $n = 0$; $X = (CH_2)_6$

32b: $n = 1$; $X = (CH_2)_4$

32c: $n = 1$; $X = (CH_2)_6$

32d: $n = 1$; $X =$

ular rearrangement of the knotted skeleton. The difference between these two knotane species was found in the kinetics of their demetalation. Knotanes **32a–c** containing oligomethylene linkers release the first copper(I) cation slowly and the second one very fast. Knotane **32d** with *m*-phenylene bridges showed opposite behavior, with the first cation released much faster than the second one. The de-complexation dynamics was attributed to different structural effects of the oligomethylene and *m*-phenylene bridges in the knotted topology. ^1H NMR spectroscopic analysis showed that knotane (**32d**) had a more pronounced entwining after the release of the first cation and produced an inert monocopper(I) complex that was used subsequently for the preparation of the first heterodinuclear complexes of phenanthroline knotanes.^[48] In contrast, the mononuclear complexes of the oligomethylene-bridged phenanthroline knotanes **32a–c** exhibit much greater flexibility and the remaining copper(I) ion becomes more accessible. Fully demetalated phenanthroline knotanes containing oligomethylene bridges were shown to exhibit “worm-type” dynamics in solution, thus highlighting their unrestricted conformational mobility.^[20,22] The demetalation studies demonstrate that both geometrical (different bridges linking the chelating units) and topological (degree of entanglement) factors are responsible for the rate of cation release. Fully or partially demetalated phenanthroline knotanes/knotanes can again complex metal ions,^[22,47,48] thus restoring their conformational rigidity.

The solution behavior of amide-knotanes **8** synthesized in our research group is expected to be quite different from that of the phenanthroline knotanes, since no metal is involved. Extensive NMR spectroscopic studies were undertaken to get insights into the dynamics of amide-knotanes.^[41] We analyzed the ^1H NMR spectra of a number of amide-knotanes in different solvents and found that the spectra obtained in CDCl_3 , C_6D_6 , $[\text{D}_5]\text{pyridine}$, and $[\text{D}_{18}]\text{HMPA}$ consist of a few broad lines, thus indicating that conformational transitions occur slowly on the NMR timescale. A similar observation was reported by Sauvage and co-workers for the ^1H NMR spectroscopic analysis of the demetalated phenanthroline knotane **1**. Only the proton spectra of amide-knotanes recorded in $[\text{D}_6]\text{DMSO}$ consist of well-resolved signals at room temperature, thus enabling us to carry out signal assignments. Most of the aromatic proton signals could be assigned by using ^1H - ^1H DQF-COSY experiments. Figure 7 reveals the assignments given for the tris(allyloxy)knotane **8e**: most of the aromatic protons in the amide-knotane structure are not equivalent. The deficiency of equivalent protons in its ^1H NMR spectra indicates that, in common with the solid-state conformation (Figure 5), the knotane structure lacks symmetry and retains a relative rigid structure in DMSO solution. Figure 8 represents schematically the conceivable rigid, kinetically stable, C_1 -symmetric knotane conformation and the D_3 -symmetric averaged structure that is expected assuming that fast conformational transitions occur (in other solvents). Apart from the aromatic proton signals, only a few other signals can be unambiguously assigned in the knotane spectra. The absence of equivalent amide proton signals also proves the nonsymmetrical and relatively robust knotane conformation in solution. Moreover, our detailed investiga-

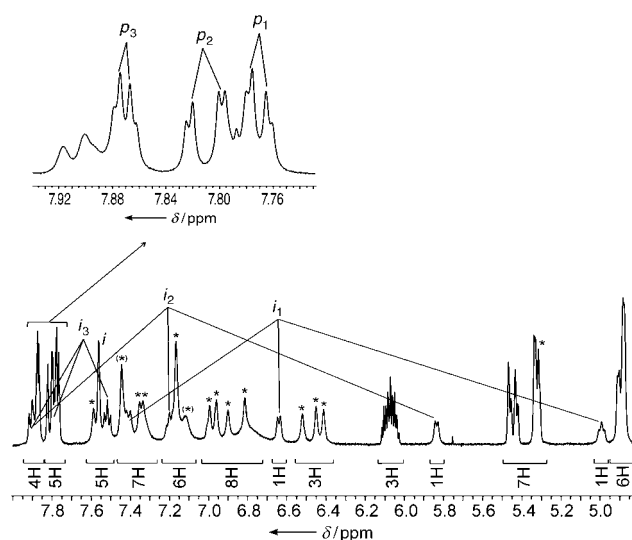


Figure 7. Signal assignments and relative integral intensities in the aromatic region of the ^1H NMR spectrum of **8e**; i_n and p_n refer to isophthaloyldiamide and 2,6-pyridinedicarboxamide units, respectively. The proton signals of 2,6-dimethylaniline residues are marked with asterisks.

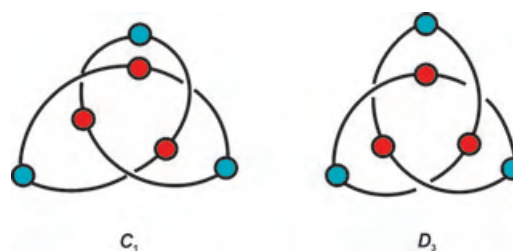


Figure 8. Schematic representation of amide-knotane conformations: a) rigid C_1 symmetry; b) average D_3 symmetry.

tions indicate that the amide proton signals of the amide-knotanes in DMSO are characteristic of the knotane substitution pattern at the 4-positions of the three 2,6-pyridinedicarboxamide rings. The amide proton region (Figure 9) of the room temperature ^1H NMR spectrum for knotane **25**, which bears two different substituent types at its 2,6-pyridinedicarboxamide edges, reveals subtle signal splittings that are not present in the spectra of the knotanes with three identical substituents such as **8e**. The corresponding spectrum for the knotane **31** with three different peripheral groups reveals even more resolved signals. If it is assumed that the amide-knotane has a stiff structure, then the signal separations of selectively substituted knotanes may originate from their equally populated and kinetically stable (in DMSO solution) nonsymmetrical conformations, for example, the ones shown in Figure 8.

Additional evidence for the relatively rigid nonsymmetrical knotane structure (Figure 8a) in DMSO solutions comes from ^{31}P NMR spectroscopic measurements of phosphorus-containing knotanes **26–28**. The room temperature ^{31}P NMR spectra of **26–28** dissolved in $[\text{D}_6]\text{DMSO}$ all exhibit three signals of equal intensity, which indicates the conformational

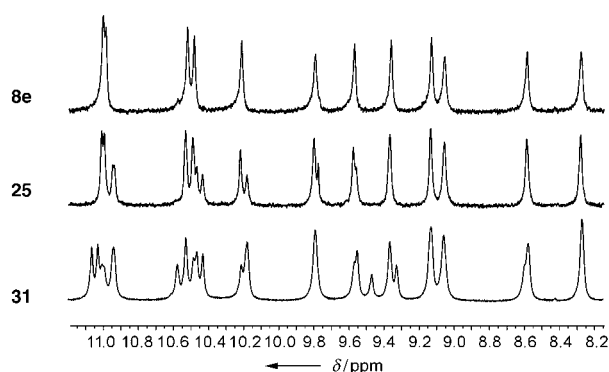


Figure 9. Amide proton areas in the $[D_6]DMSO$ 1H NMR spectra of selected amide-knotanes with different substitution patterns at the 4-positions of their three 2,6-pyridinedicarboxamide units.

rigidity of the knotane structure in solution on the NMR timescale (Figure 10). The fact that all three knotanes **26–28** give identical ^{31}P NMR spectra irrespective of the number of

phosphoryl groups on the knotane periphery is in line with their robust nonsymmetrical conformations in DMSO solution. Heating the solutions of **26**, **27**, and **28** in DMSO up to 80 °C results in the coalescence of the three signals (Figure 10), thus revealing higher conformational mobility of the knotanes at elevated temperatures. An activation energy of about 16 kcal mol $^{-1}$ can be estimated for the overall process of conformational exchange in knotanes in DMSO from the coalescence temperature.^[49] Interestingly, room temperature ^{31}P NMR spectra of **26–28** in all other solvents contain only one signal, which also reflects their averaged D_3 symmetry in solution. Further

evidence for solvent-dependent conformational transitions in amide-knotanes have been gathered from variable-temperature 1H NMR spectroscopic studies in different solvents and from comparison of H/D exchange rates for the amide protons in different solvents as well as by molecular dynamics simulations.^[41]

Furthermore, a fine tuning of the conformation of the amide-knotane backbone can be induced in mixed solvents. For example, an addition of only 10 % $[D_6]DMSO$ to the solution of **8e** in $CDCl_3$ freezes conformational motions considerably, as evident by 1H NMR spectroscopy. Similar spectral manifestations are observed when $[D_6]acetone$ is added to a solution of **8e** in $CDCl_3$. The fact that the conformations of knotanes can be instantly reinforced or made more flexible upon addition of solvent (namely, by an external chemical stimulus) has much in common with processes that generate motion in molecular shuttles.^[50]

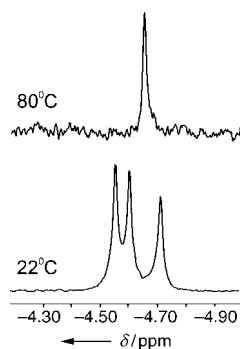


Figure 10. Variable-temperature ^{31}P NMR spectra of phosphorylated amide-knotanes **26–28** in $[D_6]DMSO$.

3.2. Inclusion Complexes of Molecular Knots

Since the template synthesis of phenanthroline-based knotanes stem from metal-coordination chemistry, it is not surprising that these types of knots form very strong complexes with metal ions. The complexes of phenanthroline knotanes were discussed in the previous section in the context of conformational transitions. From the standpoint of their synthesis, which does not require an external template, the amide-knotanes can be considered as relatively inert compounds. However, the X-ray structural analysis of tris(allyloxy)knotane **8e** (Figure 5) reveals that two of the three knotane loops form relatively big cavities, each of which includes a solvent molecule. It would be reasonable to presume that these cavity-forming loops are capable of including other molecular guests, both in solution and in the solid state. Taking into account the above discussion on solvent-dependent conformational dynamics of amide-knotanes, it might be concluded that it is solvent inclusion that regulates the conformation of the knotane. The fact that DMSO and acetone affect the conformation of amide-knotanes, whereas other polar solvents such as pyridine, hexamethylphosphoramide (HMPA), and methanol show no such effect, suggests that the former solvent molecules fit better within the knotane loops (with simultaneous formation of hydrogen bonds with amide protons of the outer 2,6-pyridinedicarboxamides). Molecular modeling studies with the MMX force field support this suggestion, and show (Figure 11) a perfect accommodation of two DMSO mole-

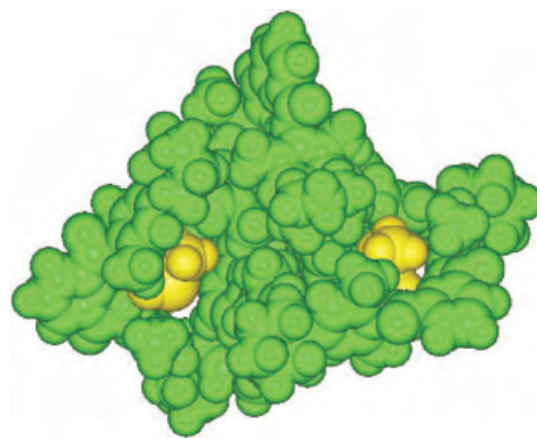


Figure 11. The energy-minimized structure of a complex composed of amide-knotane **7** and two DMSO molecules located in its loops (MMX forcefield).

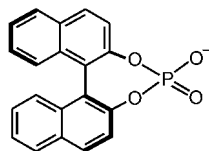
cules in the larger loops of the knotane. The stabilization energy of such a trimolecular complex, calculated from the sum of the MMX total energies of the knotane and the two DMSO molecules, is about 42 kcal mol $^{-1}$. A corresponding complex with two acetone molecules was calculated to have a stabilization energy of about 35 kcal mol $^{-1}$. Calculations carried out with other solvents reveal the volumes of the guest molecules are either too large (HMPA, pyridine,

benzene, CHCl_3) or too small (CH_3OH) to be efficiently hosted inside the knotane loops.

The interaction between guest molecules and amide-knotanes as host compounds has been studied experimentally in the solid state with the aid of a quartz microbalance technique.^[51] A layer of tris(allyloxy)knotane **8e** showed an unexpectedly high selectivity in the adsorption of octane from a gas phase, and suggests that amide-knotanes could be applied as sensing substances. It would be very interesting in the future to perform similar tests with enantiomerically pure knotanes in which the topological chirality might manifest itself as means of enantioselective sensing.

4. Chiral Resolution, Absolute Configuration, and Chiral Induction of Molecular Knots

Chiral resolution is usually performed by formation of diastereoisomeric intermediates by means of: a) chemical reaction or noncovalent association of enantiomerically pure chiral reagents (chiral auxiliaries) or b) chiral stationary phases to chromatographically separate enantiomeric mixtures. Enantiomeric separation of topologically chiral species is of special interest since, unlike centrochiral species, topological enantiomers have no closely located rigid groups that could be responsible for the enantiodifferentiation. Chiral resolution of globule-shaped molecular knots constitutes a challenge since knotanes of phenanthroline and amide types can vary their shapes upon complexation with metal ions or change of solvent, respectively. The “potato-type” chirality of molecular knots initially defied a simple method for enantiomeric separation. In 1996, the Sauvage research group introduced the unprecedented ionic combination of topological and central chiralities and reported the first enantiomeric resolution of a phenanthroline knotane by means of fractional crystallization of diastereomeric dicopper(I) complexes of the racemic phenanthroline knotane **32d**



33

with *S*-(+)-1,1'-binaphthyl-2,2'-diyl phosphate **33**.^[52] Sauvage et al.^[20] commented on the structural similarity between the rigid dicopper(I) complex of the phenanthroline knotane **32d** and known organometallic helical structures that had been separated successfully by Williams and co-workers^[53] and by Hasenknopf and Lehn.^[54]

We, in turn, have been successful in effecting the chiral resolution of topologically chiral catenanes, pretzelanes,^[55] and a cyclodiastereoisomeric [3]rotaxane^[56] of the amide type by using HPLC columns with chiral stationary phases. Our initial efforts towards enantioseparation of amide-knotanes were focused on finding an appropriate HPLC chiral stationary phase. The first racemic resolution of the amide-knotane **7**^[36a] was achieved on a noncommercial Chiralpak AD column material containing the tris(3,5-dimethylphenyl-carbamate)amylose (developed by Okamoto and co-workers) covalently linked to a silica-gel support.^[57] The unexpectedly large separation factor (α) of 2.14 obtained for the knotane **8a** leaves no doubt about the effectiveness of this resolution

method. Figure 12 shows the chromatograms for the resolution of **7** into its enantiomers. Satisfactory conditions were also found^[36a] for the separation of a number of other knotanes; for example, knotane **8b** was separated into its

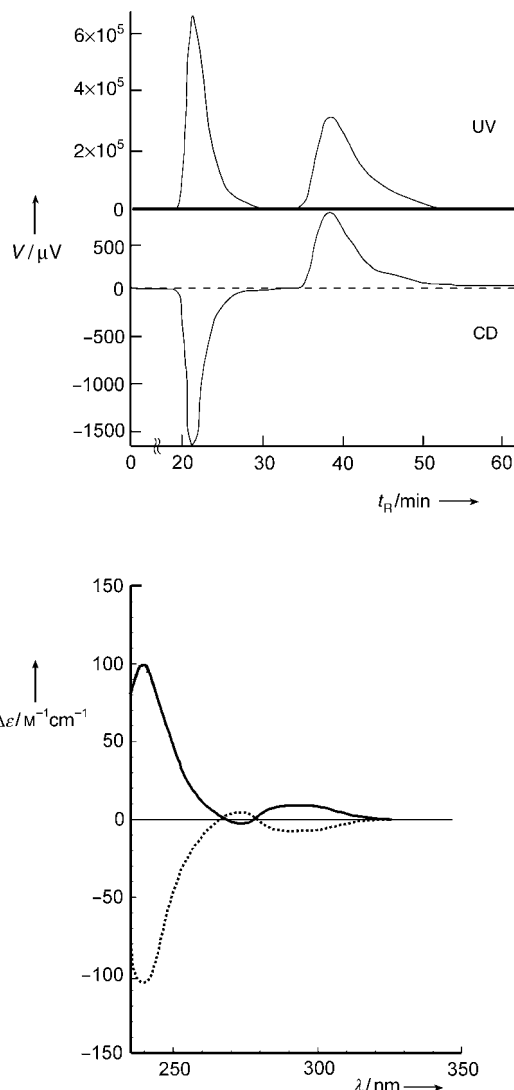


Figure 12. Resolution (chromatogram, top) and CD spectra (bottom) of separated enantiomers of amide-knotane **7** recorded in CHCl_3 . $\Delta\epsilon$ = difference in the extinction coefficient between the left- and right-polarized light ($\epsilon_L - \epsilon_R$).

enantiomers on an OD-type chiral stationary phase (CSP).^[58] In this stationary phase a branched polymeric coating is formed on the silica, thus making it solvent-resistant. Similar chromatographic separation results were obtained for **8c** by using a two-dimensional branched CSP of the AD type, which gave an α value of 1.6. Our initial efforts to use commercial HPLC columns with chiral stationary phases for the separation of amide-knotanes equipped with small substituents were unsuccessful, seemingly because of solubility problems since certain commercial materials such as noncovalent Chiralcel-1 OD^[59] can be used with a restricted number of solvents. Fortunately, as discussed in Section 2.2, our synthetic suc-

cesses in “indirect” derivatization of amide-knotanes allowed us to tune their solubilities. Thus, the dendronized knotanes **20–22** indeed showed a better solubility than the unsubstituted amide-knotane **7** or knotanes equipped with small substituents such as **8a–d**. The racemates of the dendronized knotanes were successfully separated into their enantiomers using the Chiralpak AD column material.

The isolation of milligram quantities of the enantiomers of the dendronized knotanes allowed us to study the intramolecular chiral induction of the topologically chiral knot structure into the peripheral dendron substituents. In particular, we were interested in seeing if the chirality of the knotane core would result in a preferred clockwise or counterclockwise propeller twist of the arene units in the peripheral dendrons. The CD spectra of the first-generation tridendrylated knotane **22** showed a much more pronounced Cotton effect around 240 nm than the mono- and didendrylated species **20a** and **21a**, respectively. This increase in the molar ellipticity shows clearly the emergence of certain induction effects which need to be investigated further.

Our further efforts towards simplification of the chiral resolution of amide-knotanes demonstrated that even better solubilities of amide-knotanes could be attained. For example, unlike its precursors, the triphosphorylated knotane **26** exhibits excellent solubility in almost all organic solvents, the crucial property that allowed us to achieve its unprecedented complete enantiomer separation^[41] by HPLC using the commercial noncovalent Chiralcel OD material.^[59] A mixture of hexane/isopropanol (50:50) applied as a mobile phase showed a record-breaking separation factor of $\alpha = 4.04$ for the enantiomeric resolution of **26**. Moreover, the separations showed reasonably short retention times (less than 50 min) and were carried out at room temperature, thus making the

whole process much less expensive. In earlier enantiomeric separations we cooled the HPLC column, which often resulted in the precipitation of the substance in the column material and thus significantly affected the separation. It should be stressed that the availability of the triphosphoryloxyknotane **26**, combined with its routinely achievable preparative chiral separation and the possibility of further removal of phosphoryl groups,^[41] may be used in future for the synthesis of optically active topologies which cannot be separated into enantiomers by other methods.

Further simplification of the chiral resolution can be achieved by the covalent linking of topologically chiral knotanes with centrochiral units. Therefore, we carried out acylation of tri- and monohydroxyknotanes **23** and **25** with commercially available (1*S*)-(+)-camphor-10-sulfonyl chloride to give the diastereoisomeric sulfonates **34** and **35**, respectively.^[60] The knotanes **34** and **35** are the first representatives (to our knowledge) of diastereoisomeric species produced by a covalent coupling of topologically chiral and centrochiral units. The diastereoisomeric pairs of both **34** and **35** could be resolved by standard HPLC (Figure 13).^[60] The

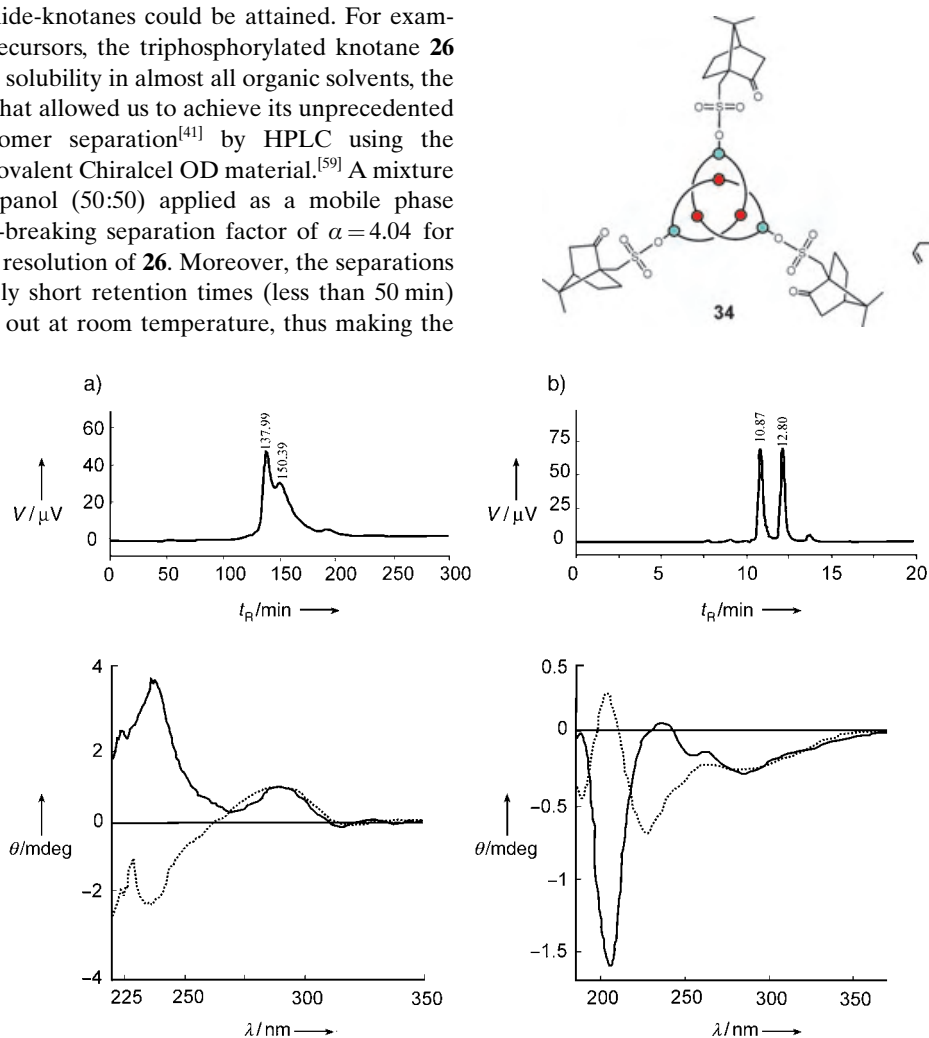


Figure 13. Separation (chromatograms, top) and CD spectra (bottom) of resolved diastereoisomers: a) of **34** (column: Chiralpak AD; material: noncovalent cellulose carbamate, hexane/isopropanol = 60/40); b) of **35** (column: Chromasil; material: silica gel, particle size 5 μm , hexane/ethanol = 60/40). θ = ellipticity.

complete separation of the diastereomers of **35** was performed on an achiral silica gel column, while the resolution of the diastereoisomeric pair of **34** was accomplished only by using an HPLC column with a commercial chiral phase (Chiralpak AD). The difficulties concerning the diastereoisomer separation of **34** can be explained in terms of its tight homochiral periphery which incorporates three camphorsulfonyl moieties that interact with the stationary phase and shield the racemic knotane cores. The chiral induction of the (1*S*)-(+)-camphor-10-sulfonyloxy moieties to the knotane centers in the diastereoisomers of both **34** and **35** breaks down the mirror-image symmetry of the CD spectra (Figure 13; in contrast with the symmetrical CD spectra of the amide-knotanes).^[36,39–41] The fact that monosulfonate **35** can be easily resolved on a silica gel column suggests the potential to utilize this process in the preparative diastereomer-mediated chiral resolution of racemic knotanes.

The determination of the absolute configuration of chiral species is of paramount importance for both basic research and industrial (for example, pharmaceutical, catalytic) applications. Assignment of the absolute configuration to a topologically chiral molecular knot seems to be an invincible challenge since, to our knowledge, it has not been done so far. The absolute configuration of a knot is assigned by determining the relative positions of the knot cross-lines. Figure 14

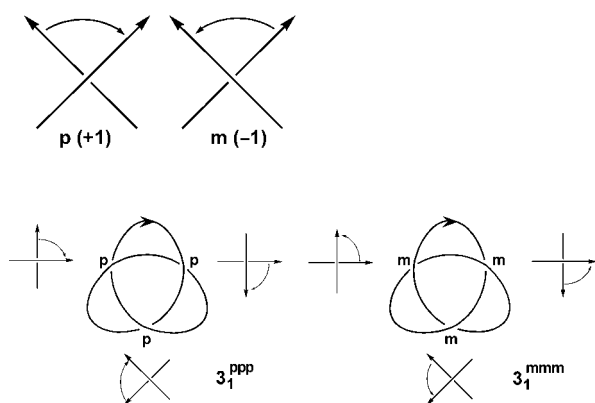


Figure 14. Description of chirality and the absolute configuration in trefoil knots.

shows, with the trefoil knot as an example, how the relative positions of these crossings are marked in the standard topology using superscripts ^[p] and ^[m]. The trefoil molecular knots can therefore be characterized as 3_1^{ppp} and 3_1^{mmm} , depending on the enantiomer. Therefore, for the purpose of assigning the absolute configuration, the CD spectra of both enantiomers of the simplest amide-knotane **7** were calculated^[36a] by applying a semi-empirical π -electron method (time-dependent Pariser–Parr–Pople, TDPPP)^[61] and accounting for all benzene rings and amide building blocks (altogether 156 π electrons, 144 atoms).

The TDPPP calculation and the subsequent simulation of the CD spectrum (Figure 15,^[36a] have been based either upon the X-ray crystal structure of **7**^[21] or upon its fully optimized AM1 geometry. Considering the simplicity of the method of calculation and the complexity of the molecule, the resulting

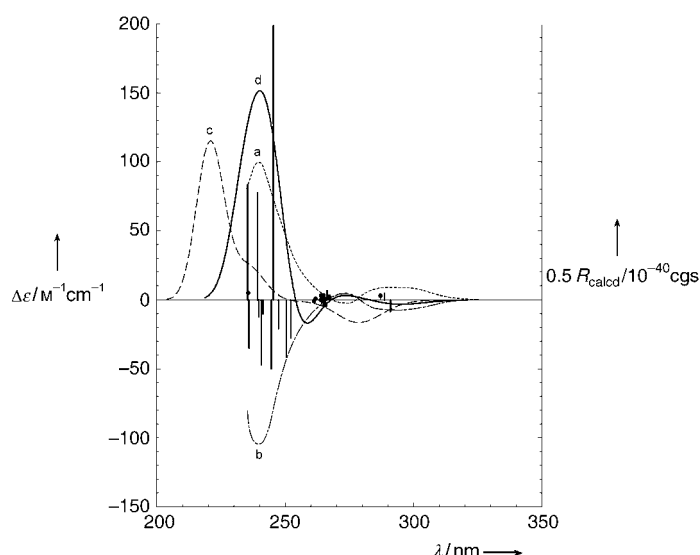


Figure 15. Experimental and theoretical CD spectra of amide-knotane **7**: a) (+) enantiomer (experimental); b) (–) enantiomer (experimental); c) calculated on the basis of the X-ray structure of **7** (non-energy minimized); d) calculated on the basis of a fully AM1-optimized geometry of **7**.

theoretical spectrum in Figure 15 represents an astonishingly close fit to the experimentally obtained spectrum. The AM1-geometry method generates quite an accurate prediction of the position and intensity of the strong band at 240 nm. The negative Cotton effect at 270 nm is also correctly predicted by the calculation. The strong band at 240 nm is stable in relation to variations in the calculations and allows a clear assignment of the absolute configuration of the laevorotatory enantiomer (with a negative Cotton effect at 270 nm) to be “ppp”. The much better agreement between the experimental CD spectra and simulated ones based on a fully AM1-optimized geometry of **7**, rather than its solid-state experimental geometry, suggests a closer fit of the AM1-optimized structure of **7** to its typical conformation in solution.

5. Knotane Assemblies

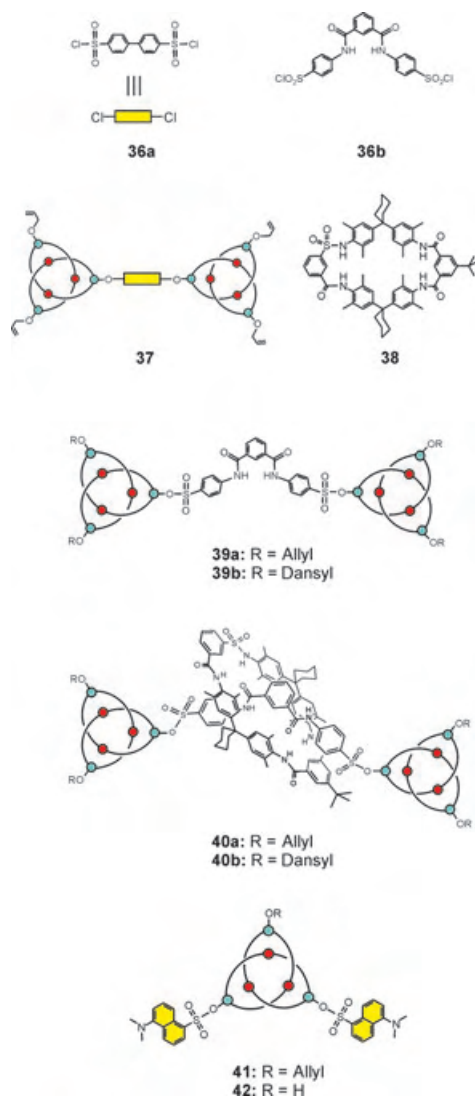
5.1. Design and Synthesis

We mentioned in the Introduction that extending the complexity of intertwined molecular assemblies invokes many fundamental and practical goals which involve the development of templation techniques and unprecedented examples of topological isomerism and chirality as well as the use of large-amplitude molecular movements of the intertwined molecular parts in molecular machinery.

Our long-standing interests in the chemistry and topological chirality of diverse intertwined species, such as catenanes,^[62] rotaxanes,^[62,63] and knotanes on the one hand, and the chemistry of dendritic molecules^[59] on the other, have emerged to formulate a more general concept of the iterative construction of unprecedented perfect macromolecular linear, branched, and cyclic topologies from intertwined and interlocked monomers. We have already reported on the

iterative^[64a] construction of $[n]$ catenanes,^[65] $[n]$ rotaxanes,^[66] and rotaxane assemblies^[67] in which rotaxanes are used as interlocked monomers. The construction of assemblies of molecular knots therefore represents a considerable challenge. The preparation of higher covalently linked knotanes necessitates the availability of selectively functionalized molecular knots, such as the monohydroxyknotane **25** that can be readily synthesized in high yield.

The reaction of the monohydroxyknotane **25** with biphenyl-4,4'-disulfonyl chloride (**36a**) in the presence of

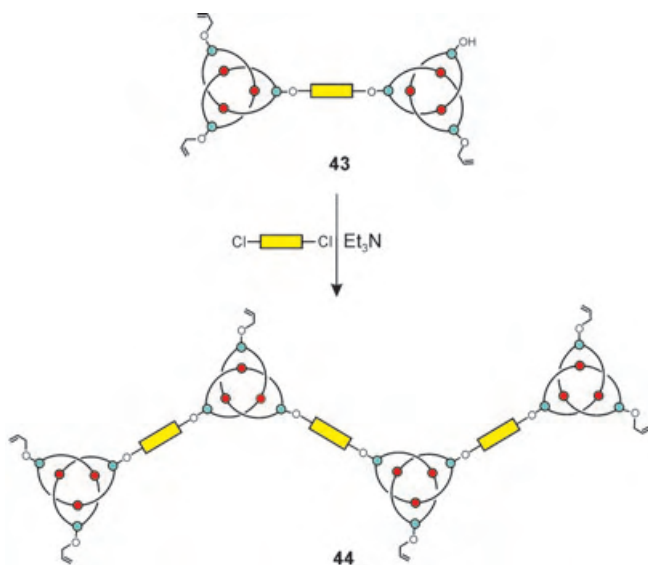


Et_3N yields a covalently linked pair of molecular knots **37**, which we term a topologically chiral dumbbell.^[40] The dumbbell **37** is a prerequisite for the construction of more elaborate assemblies of molecular knots which would have more complex isomeric compositions. Their chiralities, therefore, should be quite pronounced,^[68] and strong chiroptic effects and chiral inductions are expected. As a next step, we decided to use the rotaxane platform, with knotanes playing the role of nanosized stoppers. The rotaxane concept makes such an assembly, which we call “knotaxane”,^[69] a particularly attrac-

tive architecture in which there is the option to control the directionality^[14] of rotation or shuttling of mechanically linked constituent parts through the aid of topologically chiral knotted stoppers. Therefore, we designed an elongated axle **36b** that, according to the preliminary molecular modeling studies, could thread efficiently through the monosulfonamide macrocycle **38** and prevent noticeable overcrowding of the mechanically bound parts, both in the transition state and in the final assembly. Reaction of the monohydroxyknotane **25** with disulfonyl chloride **36b** affords the dumbbell **39a** and the desired knotaxane **40a** in 55 % and 19 % yields, respectively.^[69]

The disadvantages associated with limited solubility and, as a consequence, the purification and separation difficulties of **40a** prompted us to develop new knotted stoppers. For this purpose, we used the dihydroxyallyloxyknotane **24**, which after sulfonylation with dansyl chloride, followed by removal of the allyl group from the intermediate **41** with Bu_3SnH , readily gives the desired monohydroxy knotane **42**. The knotaxane **40b**, synthesized from **42** by the method described above for the preparation of **40a**, has been isolated in 20 % yield.^[69] The chromatographic purification of **40b** on a conventional silica-gel column was indeed found to be easier than that of **40a**. HPLC analysis along with the ^1H NMR and MALDI-TOF spectra revealed the high purity of **40b**.

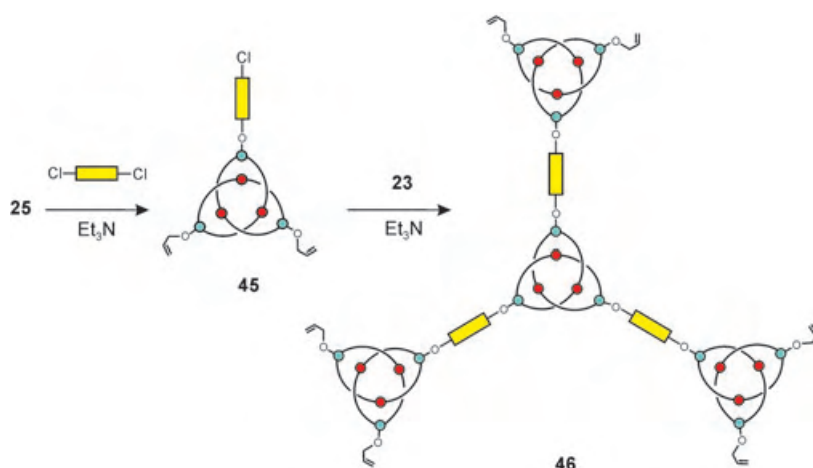
The key step in the preparation of linear knotane assemblies consists of the selective removal of the allyl groups from tris(allyloxy)knotane **8e** followed by linking with a disulfonyl chloride. Further growth of the knotted backbone can therefore be reached in an iterative way. The selective removal of one allyl group from **37** gives rise to monohydroxy dumbbell **43** which, in turn, can be sulfonylated with 4,4'-biphenyldisulfonyl chloride to afford the linear tetraknotane **44** in 55 % yield (Scheme 3).^[70] This synthetic strategy can be altered for the preparation of branched oligoknotanes, which are compounds that necessitate a multifunctional core and monofunctional branching units. Reaction of the monohy-



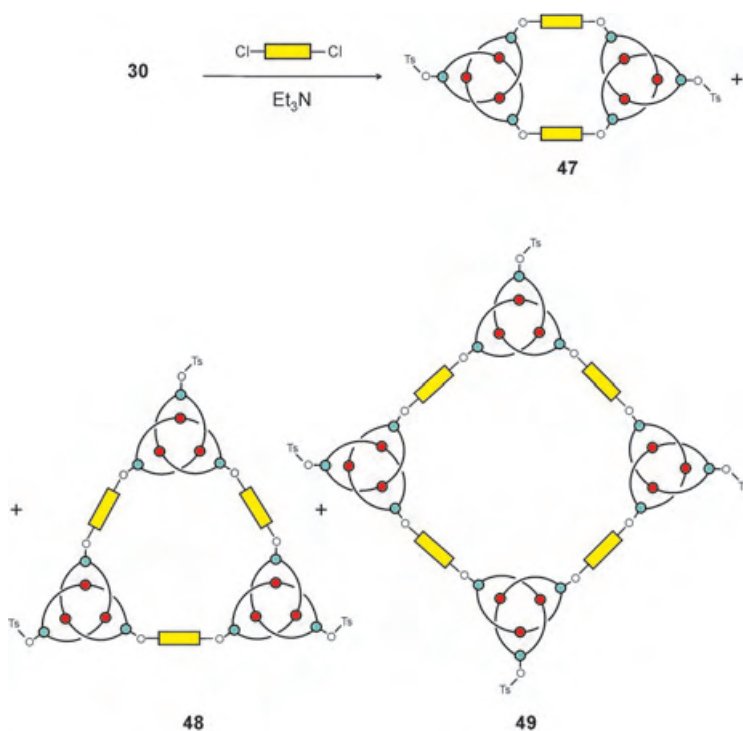
Scheme 3. Synthesis of the linear tetraknotane **44**.

droxyknotane **25** with an excess of **36a** gives sulfonated knotane **45** containing one reactive sulfonyl chloride unit (Scheme 4). The latter can be, in turn, converted by reaction with the trihydroxyknotane **23** into the branched tetraknotane **46**.^[70] The structures of the unsymmetrical dumbbell **43** and of the tetraknotanes **44** and **46** were proved by means of MALDI-TOF mass spectrometry and ¹H NMR spectroscopy.

The preparation of macrocyclic knotane oligomers implies the availability of a selectively bifunctionalized knotane, such as dihydroxyknotane **30**.^[41] The reaction of **30** with an equivalent amount of **36** under high-dilution conditions results in a mixture of the oligomeric macrocycles composed of two (**47**), three (**48**), and four (**49**) amide-knotane moieties in an overall yield of 65 % (Scheme 5).^[70]



Scheme 4. Synthesis of the branched tetraknotane **46**.



Scheme 5. Synthesis of knotanophanes **47–49**.

Following the rules of cyclophane nomenclature,^[71] we termed the latter macrocyclic knotane oligomers “knotanophanes”.^[70] The preparative isolation of the individual components **47–49** from their mixture was achieved by using a standard silica-gel HPLC column.

5.2. Topological Chirality of Knotane Assemblies

Figures 16 and 17 illustrates the expected isomeric composition of the synthesized assemblies of amide-knotanes such as **37**, **40**, **43**, **44**, and **46–49**. The analogy of the chirality designation of topologically chiral oligomeric knotanes with the description of the stereochemistry of open-chain sugar acids^[7,72] developed by Emil Fischer in 1891 is also shown. For example, if a topologically chiral stereogenic unit represented by a knotane is compared to a molecule bearing a classical carbon stereocenter, for example, glyceraldehydes, then the chirality designation of assemblies composed of two knotanes such as dumbbells **37** and **39**^[40,69] and knotaxanes **40**^[69] are analogous to the Fischer projections of tartaric and trihydroxyglutaric acids, respectively.

Further growth of the knotted chain should expand the isomeric possibilities in a manner similar to the open-chain sugars. Figure 16 depicts the relationship between the chirality designation of unsymmetrical dumbbell **43** and the linear tetraknotane **44** and the Fischer projections of erythrose/threose (two stereocenters) and hexaric acid (four stereocenters).^[7] The isomeric composition of the branched tetraknotane **46** (Figure 17a) is entirely unique since the central anchor group is itself chiral and no centrochiral analogues with such a constitution can exist (a carbon center needs to have four different substituents to be a stereocenter).

The linear and branched tetraknotanes **44** and **46** are constitutional isomers, a fact which introduces a new link between classical and topological stereochemistry. The isomerism of knotanophanes **47–49** depends on the number of amide-knotanes forming the cycle (Figure 17b). Thus, the isomerism of dimer **47** is the same type as that of dumbbell **37** (Figure 16),^[40] with the existence of one DL pair and one *meso* form. According to Figure 17b, the trimer **48** with three amide-knotanes in the cycle should consist of two DL pairs, while the largest isolated member of the knotanophane family, the tetramer **49**, should exhibit an even more complex isomeric composition. Despite the similarity of the arrangements of the stereogenic units in **48** and **49** to those in chiral trisubstituted cyclopropanes and tetrasubstituted cyclobu-

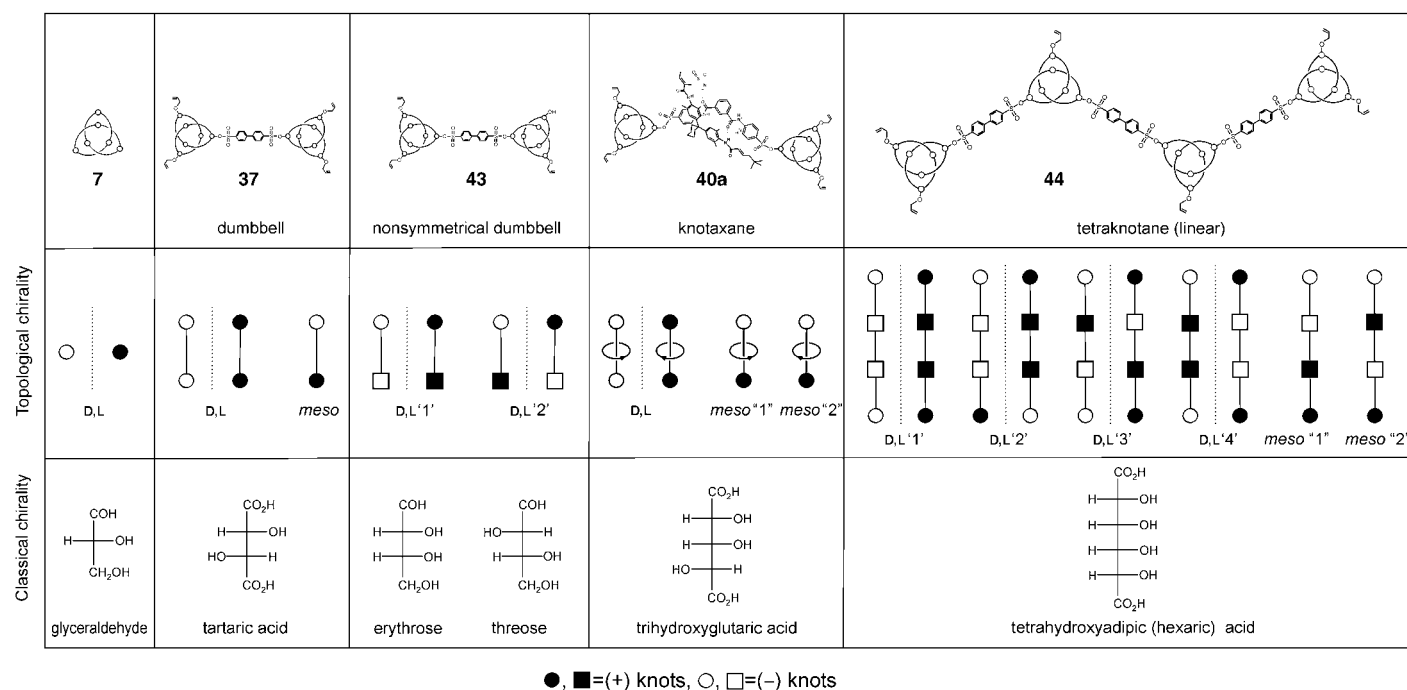


Figure 16. Isomerism of linear oligomeric amide-knotanes and the analogy of their topological descriptors to the Fischer projections of known open-chain sugars.

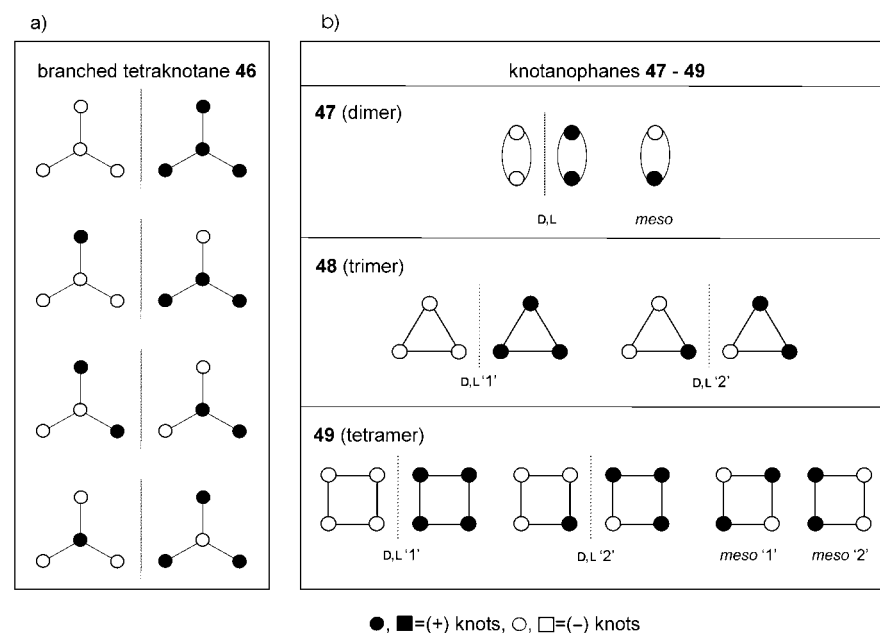


Figure 17. Isomerism of oligomeric amide-knotanes: a) expected isomeric composition of branched tetraknotane **46**; b) expected isomeric composition of knotanophanes **47–49**.

tan, respectively,^[7b] the isomerism of the former knotanophanes is essentially different on account of the impossibility of drawing additional symmetry planes through the topological stereogenic units. The isomerism of **48** and **49** can only be compared to the known chiral cyclopeptides^[7,73] which are composed of three and four equal amino acid moieties, respectively. The isomerism of **49** is also analogous to that of

cyclic forms of pentoses,^[74] but differ because of the higher symmetry of **49**.

The expected *meso* form and the DL pair of the dumbbell **37** could be completely separated^[40] on noncommercial Chiralpak AD column material.^[57] Figure 18 shows the complete and successful separation of **37**, with the *meso* form of **37** interestingly eluting between its D and L isomers. Figure 18 also shows the CD spectra of the enantiomers of **37**.

The expected DL pairs of the knotaxane **40a** and the dumbbell **39a** were also resolved^[69] on the noncommercial Chiralpak column material. The identification of the *meso* forms of both **40a** and **40b** constituted a major difficulty: in both cases, the fractions of the *meso* forms significantly overlap with those of the enantiomers. As mentioned above, unlike its analogue **40a**, the knotaxane **40b** was found to exhibit excellent solubility in alcohols, thus enabling separation of its enantiomers by HPLC on a commercial noncovalent Chiralpak material. Figure 19 shows the CD spectra of the isolated enantiomers of **40b**. As in the case of **40a**, the fractions of the *meso* forms of **40b** overlapped with those of the enantiomers.

The chiral resolution of the linear (**43**, **44**) and branched (**46**) oligomeric knotanes, as well as the knotanophanes **47–49**, was carried out on the noncommercial Chiralpak AD column material.^[70] The chromatogram of the unsymmetrical dumbbell **43** reveals not the four expected isomers from two DL pairs, but only two optically active fractions. The exper-

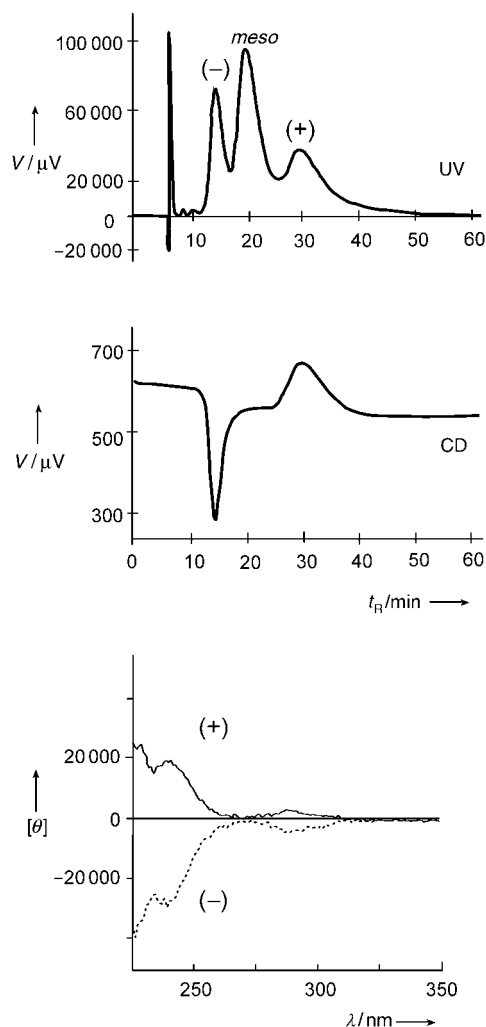


Figure 18. Chromatographic resolution (top) and CD spectra (bottom) of separated enantiomers of dumbbell **37** recorded in CHCl₃. [θ] = molar ellipticity in degrees cm² dmol⁻¹.

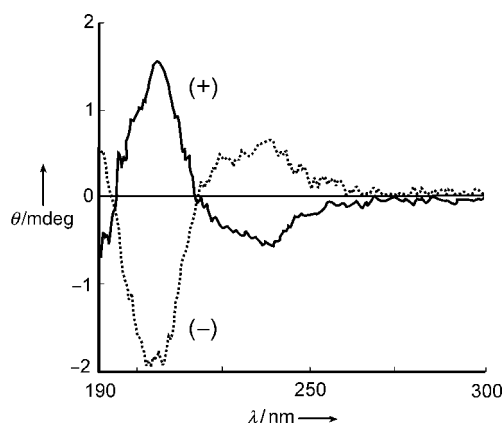


Figure 19. CD spectra of resolved enantiomers of knotaxane **40b** recorded in 2,2,2-trifluoroethanol.

imental identification of all the isomers of both **44** and **46** constitutes a major difficulty. Thus, two isomers instead of the expected eight of **44**, and only one enantiomeric pair instead

of the expected four of **46** could be detected. Chiral resolutions of knotanophanes were only successful in the case of their simplest member, dimer **47**. However, peaks for the enantiomers could only be seen in the chromatogram of **47**, whereas its *meso* form could not be detected. As in the case of the knotaxanes, the difficulties in detecting the *meso* forms are again caused by their overlap with fractions of the enantiomers. We have clearly reached the limit of complexity for separations on the currently available chiral stationary phases. Consequently, the chiral resolution of the oligomeric knotanes will require the development of new chiral stationary phases.

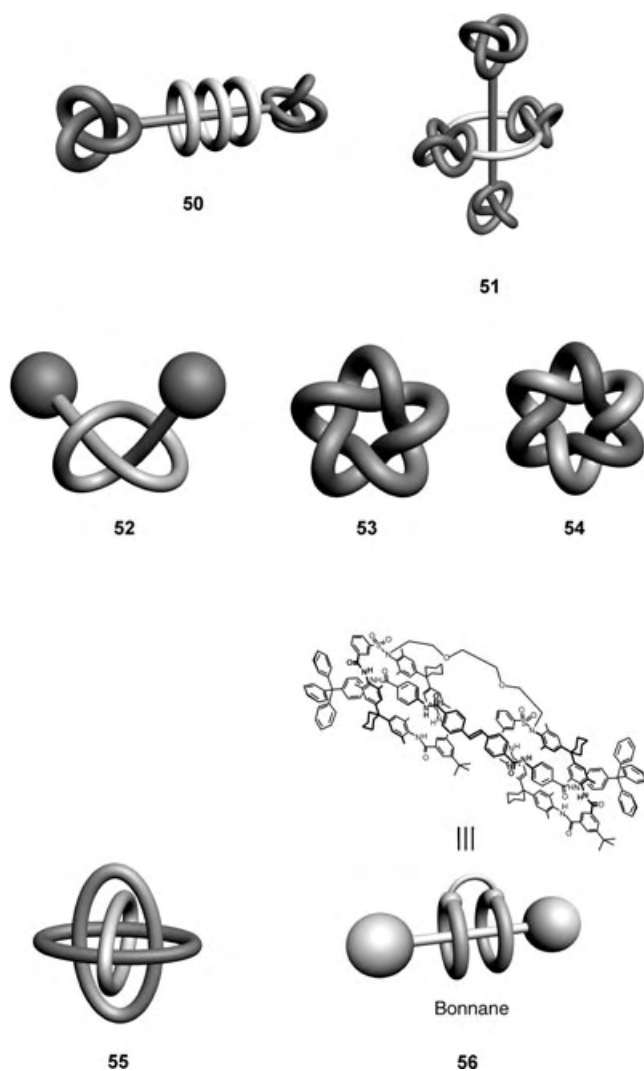
6. Conclusions and Outlook

A few years ago molecular knots could be constructed only by means of coordination chemistry; in his 1999 review^[20] Sauvage pointed out that “hopefully, chemical knots will expand to other fields than transition metal chemistry in the future”. Indeed, the chemistry of molecular knots has clearly blossomed since amide-based knotanes^[21] can be assembled not only through metal-based methods, but with the aid of reversible supramolecular templation. The successful preparation of the oligomeric amide-knotanes with linear and branched, as well as cyclic architectures, highlights the advances made in the synthesis of such topological nanostructures. We were able to construct for the first time assemblies composed of up to four covalently linked topological stereogenic units arranged in three different manners.^[70] Knotaxanes^[69] represent an even more spectacular assembly since they are made up of three topological stereogenic units held together both in an interlocked and covalent manner.

Although modern methods for enantiomeric resolution do not allow for a complete isolation of all the isomers of the synthesized topologies they have been shown to be of considerable fundamental value in regard to the chemistry of molecular knots. They have generated new knowledge about chirality, as in the case of Fischer-type designations and constitutional isomerism, and established new links between classical^[7] and topological^[2,4-6,13] stereochemistry.

Among our future projects are knotaxanes of type **50** containing more than one wheel on the axle. Our goal is to make the sugar-type skeleton longer (up to a hexose type) and to elucidate how topological chirality is tuned. In addition, monosulfonamide macrocycles, such as **38**, encircling the dumbbell in knotaxanes should induce a unidirectional rotation in the case of enantiomers around the rotaxane axis under certain conditions. Detection of such a rotation can be suggested as an interesting challenge for AFM/STM techniques.

The topological chirality of knotane assemblies combined with their remarkable sizes (greater than 6 nm) and masses (up to 12000 Da) defines a new class of artificial macromolecules beyond polymers and dendritic species, yet perfect in shape and dispersity. The chirality of knotanophanes **47–49** represents analogies to known cyclic forms of peptides or sugars with chiral centers. Additionally, knotanophanes are



topologically chiral cycles with sizes of several nanometers (nanocycles).^[75] From the phane nomenclature, these knotanophanes can be termed pyridinophanes or “phano-phanes”,^[71] in which the knotane, which is itself a phane, acts as the core and the biphenyl-4,4′-disulfonate unit as the bridge. Our intention is to use knotanophanes and linear oligomeric knotanes as the chiral wheel and axle components, respectively, in future giant rotaxanes, such as **51**, which—if properly functionalized—could mimic the naturally occurring enzyme complexes.^[76] The fascinating action of the natural molecular topologies can be the source of a future inspiration to assemble nanosized macrocycles in which the knots are not just covalently formed but also involved as intertwined parts of a macrocycle. A prerequisite for the latter goal is the assembly of a visionary open-knotted loop **52** bearing bulky stopper groups at its loose ends which prevent the loop from disentangling (for example, knotanes themselves can play the role of these bulky stoppers in the imaginary tangled dumbbell **52**).

Hopefully, the studies of the mechanisms of threading and tangling of template-preorganized molecular chains will lead to more complex topologies in the foreseeable future. In fact,

the Sauvage research group is currently completing the synthesis of five-star knotane **53** and a David star catenane **54**^[77] which can be assembled with the aid of metal-templated entangling of oligophenanthrolines. Furthermore, the research groups of Stoddart^[78] and Siegel^[79] have recently completed the supramolecular template-assisted assembly of Borromean rings compounds **55**. We have been successful in the milligram-scale preparation of a bridged diastereoisomeric [3]rotaxane **56**, which is the simplest member of a new topological family which we call “Bonnanes”.^[80] Bonnanes are expected to expand the field of rotaxane-based molecular motors in which rotary motion is controlled by link design.

These newest examples highlight the fundamental significance of intertwined and interlocked structures in chemistry. Like racing cars, from which one learns experience for everyday cars, knots and related tangled structures will provide the impetus for future synthesis, spectroscopy, chirality, and material properties.

Financial assistance by the Deutsche Forschungsgemeinschaft (Sonderforschungsbereich 624) and the Fonds der Chemischen Industrie is gratefully acknowledged. We are thankful to the CERC-3 program of the European Community (Dr. K. Schmidt, DFG) for support of the study of the topological chirality of catenanes. O.L. thanks the Alexander von Humboldt Foundation for a fellowship. We are very grateful to Professor J. F. Stoddart (UCLA) and to Dipl.-Chem. J. van Heyst (from our own research group) for their critical remarks on the manuscript. Our co-workers responsible for most of the work reported here are cited in the references and are acknowledged for their dedication, and we would particularly like to thank Priv.-Doz. Dr. C. A. Schalley, Dipl. Chem. J. Brüggemann, Dipl. Chem. A. Böhmer, Dipl. Chem. S. Müller for their stimulating discussions and support. We would also like to express our gratitude to Mr. Vadym Lukin for producing the 3D graphics.

Received: April 13, 2004

Published online: February 10, 2005

- [1] C. C. Adams, *The Knot Book*, W. H. Freeman, New York, **1994**.
- [2] a) H. L. Frisch, E. Wasserman, *J. Am. Chem. Soc.* **1961**, *83*, 3789–3795; b) J.-C. Chambron, C. Dietrich-Buchecker, J.-P. Sauvage, *Top. Curr. Chem.* **1993**, *165*, 132–162.
- [3] S. A. Wasserman, N. R. Cozzarelli, *Science* **1986**, *232*, 951–960.
- [4] D. M. Walba, *Tetrahedron* **1985**, *41*, 3161–3212.
- [5] a) E. Flapan, *A Knot Theoretic Approach to Molecular Chirality*, pp. 7–34 in Ref. [17]; b) E. Flapan, *When Topology Meets Chemistry: A Topological Look at Molecular Chirality*, Cambridge University Press, Cambridge, **2000**.
- [6] C. Liang, K. Mislow, *J. Math. Chem.* **1994**, *15*, 245–256.
- [7] a) G. Helmchen in Houben-Weyl, *Methods in Organic Chemistry*, Vol. E21, 4th ed., Thieme, Stuttgart, **1995**; b) E. L. Eliel, S. H. Wilen, L. N. Mander, *Stereochemistry of Organic Compounds*, Wiley, New York, **1994**.
- [8] a) S. A. Wasserman, N. R. Cozzarelli, *Proc. Natl. Acad. Sci. USA* **1985**, *82*, 1079–1083; b) J. D. Griffith, H. A. Nash, *Proc. Natl. Acad. Sci. USA* **1985**, *82*, 3124–3128.
- [9] a) C. Liang, K. Mislow, *J. Am. Chem. Soc.* **1994**, *116*, 11189–11190; b) W. R. Taylor, *Nature* **2000**, *406*, 916–919; c) W. R.

- Taylor, K. Lin, *Nature* **2003**, *421*, 25; d) H.-X. Zhou, *J. Am. Chem. Soc.* **2003**, *125*, 9280–9281.
- [10] M. Gross, *Chem. Unserer Zeit* **2001**, *35*, 79.
- [11] R. M. Epand, H. J. Vogel, *Biochim. Biophys. Acta* **1999**, *1462*, 11–28.
- [12] K. R. Gustafson, R. C. Sowder, L. E. Henderson, T. C. Parsons, Y. Kashman, J. H. Candellina, J. B. McMahon, R. W. Buckheit, L. K. Pannell, M. R. Boyd, *J. Am. Chem. Soc.* **1994**, *116*, 9337–9338.
- [13] O. Lukin, A. Godt, F. Vögtle, *Chem. Eur. J.* **2004**, *10*, 1878–1883.
- [14] a) V. Balzani, M. Venturi, A. Credi, *Molecular Devices and Machines. A Journey into the Nanoworld*, Wiley-VCH, Weinheim, **2003**; b) *Molecular Switches* (Ed.: B. L. Feringa), Wiley-VCH, Weinheim, **2001**; c) L. Raehm, J.-P. Sauvage, *Struct. Bonding (Berlin)* **2001**, *99*, 55–78; d) V. Bermudez, N. Capron, T. Gase, F. G. Gatti, F. Kajzar, D. A. Leigh, F. Zerbetto, S. W. Zhang, *Nature* **2000**, *406*, 608–611; e) A. M. Brouwer, C. Frochot, F. G. Gatti, D. A. Leigh, L. Mottier, F. Paolucci, S. Roffia, G. W. H. Wurpel, *Science* **2001**, *291*, 2124–2128; f) R. A. Bissell, E. Cordova, A. E. Kaifer, J. F. Stoddart, *Nature* **1994**, *369*, 133; g) B. Korybut-Daszkiewicz, A. Więckowska, R. Bilewicz, S. Domagała, K. Woźniak, *Angew. Chem.* **2004**, *116*, 1700–1704; *Angew. Chem. Int. Ed.* **2004**, *43*, 1668–1672; h) C. P. Mandl, B. König, *Angew. Chem.* **2004**, *116*, 1650–1652; *Angew. Chem. Int. Ed.* **2004**, *43*, 1622–1624.
- [15] “Synthetic DNA Topology”: N. C. Seeman in *Molecular Catenanes, Rotaxanes and Knots, A Journey Through the World of Molecular Topology* (Eds.: J.-P. Sauvage, C. Dietrich-Buchecker), Wiley-VCH, Weinheim, **1999**, pp. 323–356.
- [16] a) H. W. Gibson, M. C. Bheda, P. T. Engen, *Prog. Polym. Sci.* **1994**, *19*, 843–945; b) H. W. Gibson in *Large Ring Molecules* (Ed.: J. A. Semlyen), Wiley, New York, **1996**, pp. 191–262; c) A. Harada, *Acta Polym.* **1998**, *49*, 3–17; d) F. M. Raymo, J. F. Stoddart, *Chem. Rev.* **1999**, *99*, 1643–1663; e) J.-P. Sauvage, J. M. Kern, G. Bidan, B. Divisia-Blohorn, P. L. Vidal, *New J. Chem.* **2002**, *26*, 1287–1290; f) C.-A. Fustin, C. Bailly, G. J. Clarkson, P. De Groote, T. H. Galow, D. A. Leigh, D. Robertson, A. M. Z. Slawin, J. K. Y. Wong, *J. Am. Chem. Soc.* **2003**, *125*, 2200–2207; g) T. J. Kidd, T. J. A. Loontjens, D. A. Leigh, J. K. Y. Wong, *Angew. Chem.* **2003**, *115*, 3501–3505; *Angew. Chem. Int. Ed.* **2003**, *42*, 3379–3383; f) D. B. Amabilino, P. R. Ashton, A. S. Reder, N. Spencer, J. F. Stoddart, *Angew. Chem.* **1994**, *106*, 1316–1319; *Angew. Chem. Int. Ed. Engl.* **1994**, *33*, 1286–1290; g) F. Schwanke, O. Safarowsky, C. Heim, G. Silva, F. Vögtle, *Helv. Chim. Acta* **2000**, *83*, 3279–3290; h) T. Dünwald, R. Jäger, F. Vögtle, *Chem. Eur. J.* **1997**, *3*, 2043–2051; i) A. H. Parham, R. Schmieder, F. Vögtle, *Synlett* **1999**, *12*, 1887–1890; j) F. Osswald, E. Vogel, O. Safarowsky, F. Schwanke, F. Vögtle, *Adv. Synth. Catal.* **2001**, *343*, 303–309; k) J. W. Lee, K. Kim, *Top. Curr. Chem.* **2003**, *228*, 111–140; l) H. W. Gibson, N. Yamaguchi, L. Hamilton, J. W. Jones, *J. Am. Chem. Soc.* **2002**, *124*, 4653–4665.
- [17] a) G. Schill, *Catenanes, Rotaxanes and Knots*, Academic Press, New York, **1971**; b) *Molecular Catenanes, Rotaxanes and Knots, A Journey Through the World of Molecular Topology* (Eds.: J.-P. Sauvage, C. Dietrich-Buchecker), Wiley-VCH, Weinheim, **1999**; c) D. B. Amabilino, J. F. Stoddart, *Chem. Rev.* **1995**, *95*, 2725–2828; d) G. A. Breault, C. A. Hunter, P. C. Mayers, *Tetrahedron*, **1999**, *55*, 5265–5293.
- [18] a) *Templated Organic Synthesis* (Eds.: F. Diederich, P. J. Stang), VCH-Wiley, Weinheim, **2000**; b) J. K. M. Sanders, *Pure Appl. Chem.* **2000**, *72*, 2265–2274; c) L. M. Greig, D. Philp, *Chem. Soc. Rev.* **2001**, *30*, 287–302; d) N. V. Gerbeleu, V. B. Arion, J. Burgess, *Templated Synthesis of Macrocyclic Compounds*, Wiley-VCH, Weinheim, **1999**; e) T. J. Hubin, D. H. Busch, *Coord. Chem. Rev.* **2000**, *5*, 200–202; f) “Template or Host/Guest Relations”: F. Vögtle, R. Hoss, M. Händel in *Applied Homogeneous Catalysis with Organometallic Compounds* (Eds.: B. Cornils, W. A. Herrmann), Wiley-VCH, Weinheim, **1996**; g) R. Hoss, F. Vögtle, *Angew. Chem.* **1994**, *106*, 389–398; *Angew. Chem. Int. Ed. Engl.* **1994**, *33*, 375–384; h) R. Cacciapaglia, L. Mandolini, *Chem. Soc. Rev.* **1993**, *22*, 221–231; i) S. Anderson, H. L. Anderson, J. K. M. Sanders, *Acc. Chem. Res.* **1993**, *26*, 469–475; j) B. Dietrich, P. Viout, J.-M. Lehn, *Macrocyclic Chemistry: Aspects of Organic and Inorganic Supramolecular Chemistry*, VCH, Weinheim, **1992**.
- [19] a) J.-M. Lehn, *Supramolecular Chemistry: Concepts and Perspectives*, VCH, New York, **1995**; b) F. Vögtle, *Supramolecular Chemistry*, Wiley, Chichester, **1991**; c) *Comprehensive Supramolecular Chemistry* (Eds.: J. L. Atwood, J. E. D. Davies, D. D. MacNicol, F. Vögtle, J.-M. Lehn), Pergamon, Oxford, **1996**; d) J. W. Steed, J. L. Atwood, *Supramolecular Chemistry*, Wiley, Chichester **2000**; e) H.-J. Schneider, A. Yatsimirski, *Principles And Methods In Supramolecular Chemistry*, Wiley, Chichester, **1999**.
- [20] “Molecular Knots—From Early Attempts to High-Yield Template Synthesis”: J.-P. Sauvage, C. Dietrich-Buchecker, in *Molecular Catenanes, Rotaxanes and Knots, A Journey Through the World of Molecular Topology* (Eds.: J.-P. Sauvage, C. Dietrich-Buchecker), Wiley-VCH, Weinheim, **1999**, pp. 107–142.
- [21] O. Safarowsky, M. Nieger, R. Fröhlich, F. Vögtle, *Angew. Chem.* **2000**, *112*, 1699–1701; *Angew. Chem. Int. Ed.* **2000**, *39*, 1616–1618.
- [22] C. O. Dietrich-Buchecker, J.-P. Sauvage, *Angew. Chem.* **1989**, *101*, 192–194; *Angew. Chem. Int. Ed. Engl.* **1989**, *28*, 189–192.
- [23] E. Wasserman, *J. Am. Chem. Soc.* **1960**, *82*, 4433–4434.
- [24] N. van Gülick, *New J. Chem.* **1993**, *17*, 619.
- [25] a) G. Schill, G. Doerjter, E. Logemann, H. Fritz, *Chem. Ber.* **1979**, *112*, 3603–3615; b) J. Boeckmann, G. Schill, *Tetrahedron* **1974**, *30*, 1945–1957.
- [26] D. M. Walba, R. M. Richard, R. C. Haltiwanger, *J. Am. Chem. Soc.* **1982**, *104*, 3219–3221.
- [27] V. I. Sokolov, *Russ. Chem. Rev.* **1973**, *42*, 452–463.
- [28] C. O. Dietrich-Buchecker, J. Guilhem, C. Pascard, J.-P. Sauvage, *Angew. Chem.* **1990**, *102*, 1202–1204; *Angew. Chem. Int. Ed. Engl.* **1990**, *29*, 1154–1156.
- [29] a) C. O. Dietrich-Buchecker, J. F. Nierengarten, J.-P. Sauvage, N. Armaroli, V. Balzani, L. De Cola, *J. Am. Chem. Soc.* **1993**, *115*, 11234–11237; b) C. O. Dietrich-Buchecker, G. Rapenne, J.-P. Sauvage, *Chem. Commun.* **1997**, 2053–2054.
- [30] *Handbook of Metathesis* (Ed.: R. H. Grubbs), Wiley-VCH, Weinheim, **2003**.
- [31] In topology a knot is called a “composite knot” if it represents a composition of two nontrivial knots. Mathematically a composite knot is obtained from two prime (for example, trefoil) knots by removing a small arc from each knot projection and then connecting the four end points by two new arcs.
- [32] R. F. Carina, C. Dietrich-Buchecker, J.-P. Sauvage, *J. Am. Chem. Soc.* **1996**, *118*, 9110–9116.
- [33] P. R. Ashton, O. A. Matthews, S. Menzer, F. M. Raymo, N. Spencer, J. F. Stoddart, D. J. Williams, *Liebigs Ann.* **1997**, 2485–2494.
- [34] H. Adams, E. Ashworth, G. A. Breault, J. Guo, C. A. Hunter, P. C. Mayers, *Nature* **2001**, *411*, 763.
- [35] *Spectroscopic methods for determining protein structure in solution* (Ed.: H. A. Havel), Wiley-VCH, New York, **1995**.
- [36] a) F. Vögtle, A. Hüntel, E. Vogel, S. Buschbeck, O. Safarowsky, J. Recker, A. Parham, M. Knott, W. M. Müller, U. Müller, Y. Okamoto, T. Kubota, W. Lindner, E. Francotte, S. Grimme, *Angew. Chem.* **2001**, *113*, 2534–2537; *Angew. Chem. Int. Ed.* **2001**, *40*, 2468–2471; b) J. Recker, F. Vögtle, *J. Inclusion Phenom. Mol. Recognit. Chem.* **2001**, *41*, 3–5.

- [37] a) A. Hüntgen, PhD thesis, University of Bonn, **2000**; b) S. Buschbeck, Ph.D. thesis, University of Bonn, **2002**; c) J. Recker, PhD thesis, University of Bonn, **2002**.
- [38] J. Brüggemann, F. Vögtle, unpublished results.
- [39] J. Recker, W. M. Müller, U. Müller, T. Kubota, Y. Okamoto, M. Nieger, F. Vögtle, *Chem. Eur. J.* **2002**, *8*, 4434–4442.
- [40] O. Lukin, J. Recker, A. Böhmer, W. M. Müller, T. Kubota, Y. Okamoto, M. Nieger, F. Vögtle, *Angew. Chem.* **2003**, *115*, 458–461; *Angew. Chem. Int. Ed. Engl.* **2003**, *42*, 442–445.
- [41] O. Lukin, W. M. Müller, U. Müller, A. Kaufmann, C. Schmidt, J. Leszczynski, F. Vögtle, *Chem. Eur. J.* **2003**, *9*, 3507–3517.
- [42] I. Huc, *Eur. J. Org. Chem.* **2004**, 17–29.
- [43] C. D. Snow, B. Zagrovic, and V. S. Pande, *J. Am. Chem. Soc.* **2002**, *124*, 14548–14549.
- [44] a) C. Hawker, J. M. J. Fréchet, *J. Chem. Soc. Chem. Commun.* **1990**, 1010–1013; b) K. L. Wooley, C. Hawker, J. M. J. Fréchet, *J. Am. Chem. Soc.* **1991**, *113*, 4252–4261.
- [45] a) Y. Furusho, J. Shoji, N. Watanabe, N. Kihara, T. Adachi, T. Takata, *Bull. Chem. Soc. Jpn.* **2001**, *74*, 139–147; b) N. Watanabe, Y. Furusho, N. Kihara, T. Takata, K. Kinbara, K. Saigo, *Bull. Chem. Soc. Jpn.* **2001**, *74*, 149–155.
- [46] a) A.-M. Caminade, J.-P. Majoral, *Chem. Rev.* **1994**, *94*, 1183–1213; b) V. I. Kalchenko, D. M. Rudkevich, A. Shivanyuk, V. V. Pirozhenko, I. F. Tsybal, L. N. Markovsky, *Zh. Obshch. Khim.* **1994**, *64*, 731; [*Chem. Abstr.* **1995**, *122*, 314652u]; c) J. Lipkowski, O. I. Kalchenko, J. Slowikowska, V. I. Kalchenko, O. Lukin, L. N. Markovsky, R. Nowakowski, *J. Phys. Org. Chem.* **1998**, *11*, 426–435; d) O. Lukin, M. O. Vysotsky, V. I. Kalchenko, *J. Phys. Org. Chem.* **2001**, *14*, 468–473; e) C. Marmillon, F. Gauffre, T. Gulik-Krzywicki, C. Loup, A. M. Caminade, J. P. Majoral, J. P. Vors, E. Rump, *Angew. Chem.* **2001**, *113*, 2696–2699; *Angew. Chem. Int. Ed.* **2001**, *40*, 2626–2629; f) J.-P. Majoral, A.-M. Caminade, V. Maraval, *Chem. Commun.* **2002**, 2929–2942.
- [47] M. Meyer, A.-M. Albrecht-Gary, C. O. Dietrich-Buchecker, J.-P. Sauvage, *J. Am. Chem. Soc.* **1997**, *119*, 4599–4607.
- [48] C. O. Dietrich-Buchecker, J. P. Sauvage, N. Armaroli, P. Ceroni, V. Balzani, *Angew. Chem.* **1996**, *108*, 1190–1193; *Angew. Chem. Int. Ed. Engl.* **1996**, *35*, 1119–1121.
- [49] a) H. S. Gutowski, C. H. Holm, *J. Chem. Phys.* **1956**, *25*, 1228–1233; b) K. A. Connors, *Binding Constants: The Measurement of Molecular Complex Stability*, Wiley-Interscience, New York, **1987**.
- [50] A. S. Laine, D. A. Leigh, A. Murphy, *J. Am. Chem. Soc.* **1997**, *119*, 11092–11093.
- [51] C. Kreutz, J. Bargon, O. Lukin, F. Vögtle, unpublished results.
- [52] G. Rapenne, C. Dietrich-Buchecker, J.-P. Sauvage, *J. Am. Chem. Soc.* **1996**, *118*, 10932–10933.
- [53] L. J. Charbonnière, G. Bernardinelli, C. Pigué, A. M. Sargeson, A. F. Williams, *J. Chem. Soc. Chem. Commun.* **1994**, 1419–1420.
- [54] B. Hasenknopf, J.-M. Lehn, *Helv. Chim. Acta* **1996**, *79*, 1643–1650.
- [55] C. Yamamoto, Y. Okamoto, T. Schmidt, R. Jäger, F. Vögtle, *J. Am. Chem. Soc.* **1997**, *119*, 10547–10548.
- [56] R. Schmieder, G. Hübner, C. Seel, F. Vögtle, *Angew. Chem.* **1999**, *111*, 3741–3743; *Angew. Chem. Int. Ed.* **1999**, *38*, 3528–3530.
- [57] N. Enomoto, S. Furukawa, Y. Ogasawara, H. Akano, Y. Kawamura, E. Yashima, Y. Okamoto, *Anal. Chem.* **1996**, *68*, 2798–2804.
- [58] a) E. Francotte, *J. Chromatogr. A* **2001**, *906*, 379–397; b) N. M. Maier, P. Franco, W. Lindner, *J. Chromatogr. A* **2001**, *906*, 3–33.
- [59] a) Y. Okamoto, M. Kawashima, K. Hatada, *J. Am. Chem. Soc.* **1984**, *106*, 5357–5359; b) Y. Okamoto, M. Kawashima, K. Hatada, *J. Chromatography* **1986**, *363*, 173–186.
- [60] O. Lukin, A. Yoneva, F. Vögtle, *Eur. J. Org. Chem.* **2004**, 1236–1238.
- [61] M. Scholz, H. J. Köhler, *Quantenchemie*, Vol. 3, Hüthig, Heidelberg, **1981**.
- [62] a) F. Vögtle, T. Dünwald, T. Schmidt, *Acc. Chem. Res.* **1996**, *29*, 451–460; b) C. Yamamoto, Y. Okamoto, T. Schmidt, R. Jäger, F. Vögtle, *J. Am. Chem. Soc.* **1997**, *119*, 10547–10548; c) F. Vögtle, O. Safarowsky, C. Heim, A. Affeld, O. Braun, A. Mohry, *Pure Appl. Chem.* **1999**, *71*, 247–251.
- [63] R. Schmieder, G. Hübner, C. Seel, F. Vögtle, *Angew. Chem.* **1999**, *111*, 3741–3743; *Angew. Chem. Int. Ed. Engl.* **1999**, *38*, 3528–3530.
- [64] a) N. Feuerbacher, F. Vögtle, *Top. Curr. Chem.* **1998**, *197*, 2–18; b) G. R. Newkome, C. N. Moorefield, F. Vögtle, *Dendrimers and Dendrons: Concepts, Syntheses, Applications*, Wiley-VCH, New York, **2001**.
- [65] F. Schwanke, O. Safarowsky, C. Heim, G. Silva, F. Vögtle, *Helv. Chim. Acta* **2000**, *83*, 3279–3290.
- [66] A. Parham, R. Schmieder, F. Vögtle, *Synlett* **1999**, 1887.
- [67] a) T. Dünwald, R. Jäger, F. Vögtle, *Chem. Eur. J.* **1997**, *3*, 2043–2051; b) A. H. Parham, R. Schmieder, F. Vögtle, *Synlett* **1999**, *12*, 1887–1890; c) F. Osswald, E. Vogel, O. Safarowsky, F. Schwanke, F. Vögtle, *Adv. Synth. Catal.* **2001**, *343*, 303–309.
- [68] F. Vögtle, S. Grimme, J. Hormes, K.-H. Dötz, N. Krause in *Interactions in Molecules* (Ed.: S. D. Peyerimhoff), Wiley-VCH, Weinheim, **2003**.
- [69] O. Lukin, T. Kubota, Y. Okamoto, F. Schelhase, A. Yoneva, W. M. Müller, U. Müller, F. Vögtle, *Angew. Chem.* **2003**, *115*, 4681–4684; *Angew. Chem. Int. Ed.* **2003**, *42*, 4542–4545.
- [70] O. Lukin, T. Kubota, Y. Okamoto, A. Kaufmann, F. Vögtle, *Chem. Eur. J.* **2004**, *10*, 2804–2810.
- [71] Phane nomenclature: a) F. Vögtle, *Cyclophan-Chemie*, Teubner, Stuttgart, **1990**; *Cyclophane Chemistry*, Wiley, Chichester, **1993**; b) F. Diederich, *Monographs in Supramolecular Chemistry*, Vol. 3 (Ed.: J. F. Stoddart), Royal Society of Chemistry, Cambridge, UK, **1991**; c) *Cyclophane Chemistry for the 21st Century* (Ed.: H. Takemura), Research Singpost, Trivandrum, **2002**.
- [72] a) E. Fischer, *Ber. Dtsch. Chem. Ges.* **1891**, *24*, 1836; b) E. Fischer, *Ber. Dtsch. Chem. Ges.* **1891**, *24*, 2683; c) H. Kunz, *Angew. Chem.* **2002**, *114*, 4619–4632; *Angew. Chem. Int. Ed.* **2002**, *41*, 4439–4451.
- [73] a) M. Chorev, M. Goodman, *Acc. Chem. Res.* **1993**, *26*, 266–273; b) J. S. Fruchtel, G. Jung, *Angew. Chem.* **1996**, *108*, 19–46; *Angew. Chem. Int. Ed. Engl.* **1996**, *35*, 17–42; c) E. Graf von Roeden, E. Lohof, G. Hessler, M. Hoffmann, H. Kessler, *J. Am. Chem. Soc.* **1996**, *118*, 10151–10167; d) D. Gottschling, J. Boer, A. Schuster, B. Holzmann, H. Kessler, *Angew. Chem.* **2002**, *114*, 3133–3137; *Angew. Chem. Int. Ed.* **2002**, *41*, 3007–3011; e) D. T. Bong, T. D. Clark, J. R. Granja, M. R. Ghadiri, *Angew. Chem.* **2001**, *113*, 1016–1041; *Angew. Chem. Int. Ed.* **2001**, *40*, 988–1011; f) D. Yang, J. Qu, W. Li, Y.-H. Zang, Y. Ren, D.-P. Wang, Y.-D. Wu, *J. Am. Chem. Soc.* **2002**, *124*, 12410–12411; g) M. Amorin, L. Castedo, J. R. Granja, *J. Am. Chem. Soc.* **2003**, *125*, 2844–2845.
- [74] J. Lehmann, *Carbohydrates. Structure and Biology*, Wiley-VCH, Weinheim, **1997**.
- [75] The term “nanocycle” was introduced by us for the first time for nanometer-sized cyclic oligoamides (a) H. Schwier, F. Vögtle, *J. Inclusion Phenom. Mol. Recognit. Chem.* **2000**, *37*, 309–329; a similar term “nanoring” is also applied; see, for example: b) S.-J. Choi, S.-M. Park, *Adv. Mater.* **2000**, *12*, 1547–1549; c) T. Kawase, K. Tanaka, N. Shiono, Y. Seirai, M. Oda, *Angew. Chem.* **2004**, *116*, 1754–1756; *Angew. Chem. Int. Ed.* **2004**, *43*, 1722–1724.
- [76] a) C. A. Schalley, K. Beizai, F. Vögtle, *Acc. Chem. Res.* **2001**, *34*, 465–476; b) W. A. Breyer, B. W. Matthews, *Protein Sci.* **2001**, *10*, 1699–1711; c) S. J. Benkovic, A. M. Valentine, F. Salinas, *Annu. Rev. Biochem.* **2001**, *70*, 181–208; d) E. T. Kool, J. C. Morales, K. M. Guckian, *Angew. Chem.* **2000**, *112*, 1026–1044; *Angew. Chem. Int. Ed.* **2000**, *39*, 990–1009; e) R. G. E. Coumans,

- J. A. A. W. Elemans, P. Thordarson, R. J. M. Nolte, A. E. Rowan, *Angew. Chem.* **2003**, *115*, 674–678; *Angew. Chem. Int. Ed.* **2003**, *42*, 650–654.
- [77] J.-P. Sauvage, private communication.
- [78] K. S. Chichak, S. J. Cantrill, A. R. Pease, S.-H. Chiu, G. W. V. Cave, J. L. Atwood, J. F. Stoddart, *Science* **2004**, *304*, 1308–1312.
- [79] J. C. Loren, M. Yoshizawa, R. F. Haldimann, A. Linden, J. S. Siegel, *Angew. Chem.* **2003**, *115*, 5880–5883; *Angew. Chem. Int. Ed.* **2003**, *42*, 5702–5705.
- [80] We give the name “Bonnane” to these extendable molecules—in which two (or more) wheels are bridged by one (or more) bridges—as a symbol for the former German capital city Bonn, which formed a bridge to the current seat of government.

E. Heilbronner / F. A. Miller

A Philatelic Ramble through Chemistry

278 pages with 1025 color reproductions.

Softcover. € 79.00/ sFr 116.00.

ISBN 3-906390-31-4

A Philatelic Ramble through Chemistry is a light-hearted, historically based survey of chemistry and some related topics in physics. It is illustrated with more than 1000 beautiful color reproductions of postage stamps and covers. Many stories and anecdotes have been included. The book provides delightful personal reading and may be useful for courses on the history of chemistry. It is a source of numerous anecdotes which instructors can use to enliven their lectures.

€ -price is available only for Germany.

Wiley-VCH, Postfach 10 11 61, 69451 Weinheim, Germany
Fax: +49 (0) 6201 606-184, e-Mail: service@wiley-vch.de,
www.wiley-vch.de



Softcover edition!

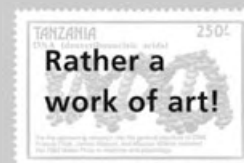
Praise for the Hardcover Edition

‘This is a gem of a book. [...] I recommend it to all those to whom chemistry means more than an academic discipline, but a multi-faceted part of human culture, as Heilbronner and Miller so beautifully demonstrated.’

Interdisciplinary Science Reviews

‘The creation of an exceptional book must be driven not only by knowledge but also by passion. This book by two chemists, Heilbronner and Miller, is clearly the product of a love for the world of postage stamps as well for chemistry in its widest sense.’

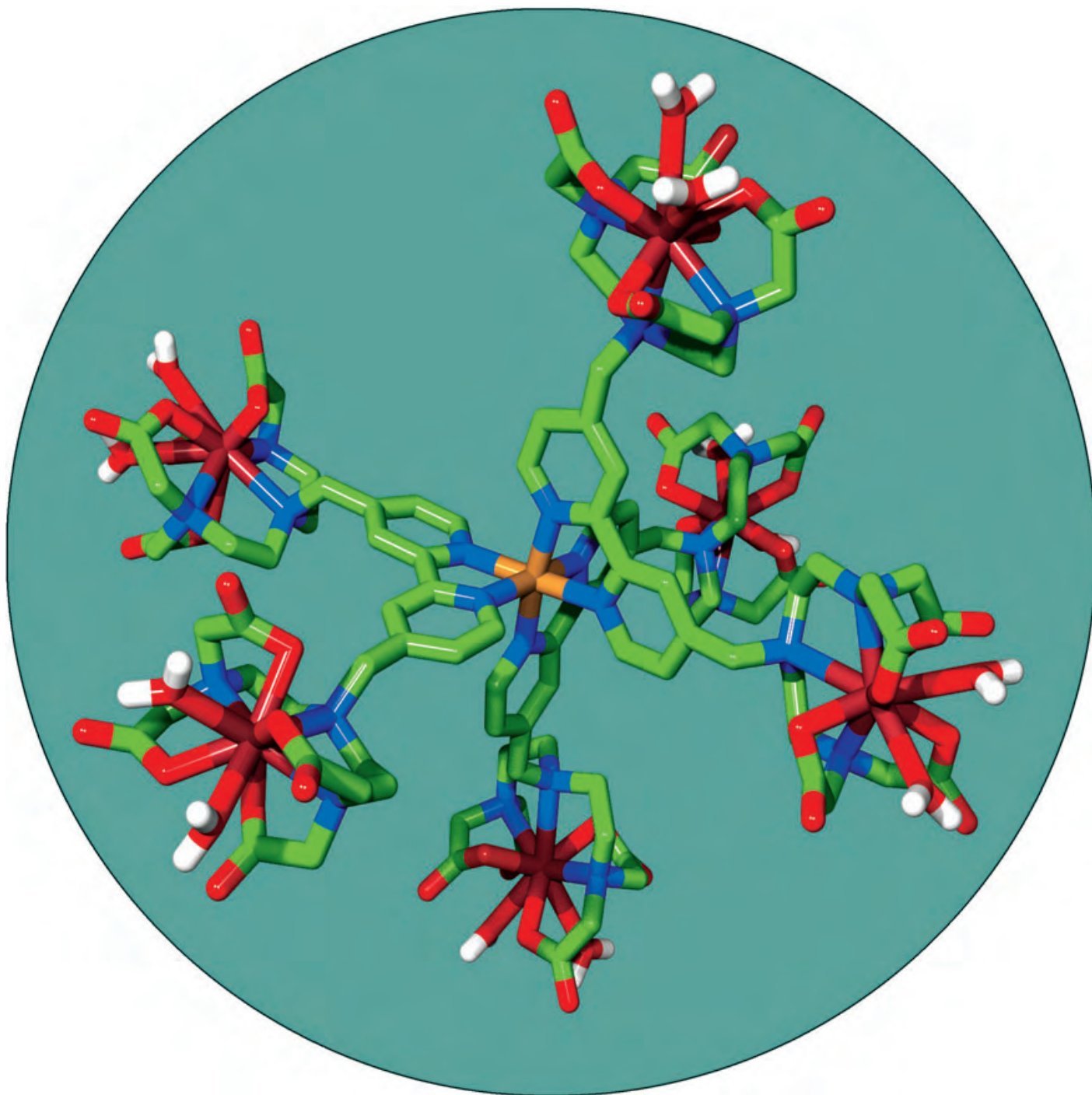
Advanced Materials



WILEY-VCH

14170409_v0

Communications



Self-assembly of a poly(aminocarboxylate)–bipyridine ligand **L** with Fe^{II} and Gd^{III} ions gives rise to a stable metallostar structure $[\text{Fe}\{\text{GdL}(\text{H}_2\text{O})_2\}_3]^{4-}$ that displays a remarkable relaxivity. In their Communication on the following pages, E. Tóth and co-workers discuss the properties of this complex with regards to its application as an MRI contrast agent.

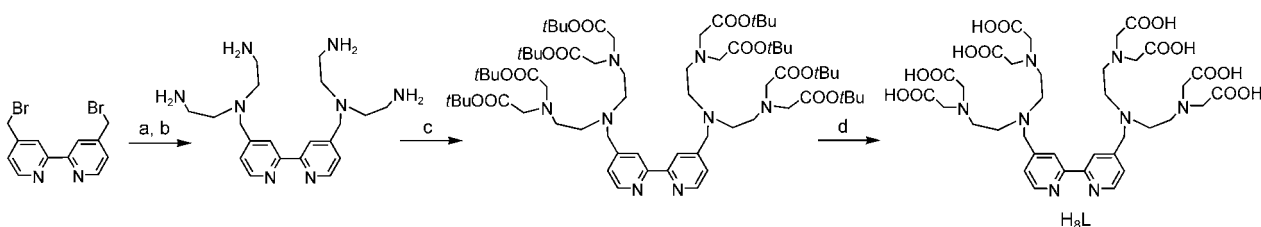
High Relaxivity Confined to a Small Molecular Space: A Metallostar-Based, Potential MRI Contrast Agent**

João Bruno Livramento, Éva Tóth,* Angélique Sour, Alain Borel, André E. Merbach, and Robert Ruloff

The 2003 Nobel Prize in medicine was awarded for discoveries concerning magnetic resonance imaging (MRI), a technique that has revolutionized medical diagnostics over the last two decades.^[1] Such spectacular developments would not have been possible without the use of paramagnetic contrast agents, the majority of which comprise Gd^{III} complexes.^[2] By reducing the relaxation time of the surrounding water protons, these agents enhance the intrinsic contrast of magnetic resonance images. The efficacy of a contrast agent is expressed by its relaxivity, r_1 , which is the enhancement of the longitudinal proton relaxation rate induced by the paramagnetic agent, referred to a concentration of Gd³⁺ of 1 mmol L⁻¹ (molar relaxivity per Gd). Theory predicts high relaxivity for a Gd^{III} complex when its rotation and electron spin relaxation are slow and when the rate of water exchange between the inner sphere and the bulk solvent is optimal. Novel applications in MRI call for very highly efficient contrast agents. It implies not only high molar relaxivity per Gd^{III} ion but high relaxivity per molecular volume/mass. For example, in cell imaging, biological constraints limit the amount of contrast agent that can be delivered into one cell without destroying it. Consequently, agents with many efficiently relaxing paramagnetic centers confined into a small space are advantageous over large macromolecules with few Gd^{III} centers.

Recently we started to exploit heterometallic assemblies in the aim of confining high relaxivity into a small molecular space. We reported a terpyridine (tpy) ligand functionalized with a poly(aminocarboxylate) group DTTA (diethylenetriamine-*N,N,N',N''*-tetraacetate), (tpy-DTTA)⁴⁻, which has distinct binding sites for Fe^{II} and Gd^{III} ions.^[3] In aqueous solution and in the presence of these metal ions, the ligand undergoes self-assembly to form a rigid supramolecular structure, [Fe^{II}(tpy-DTTA)₂Gd^{III}]. Prior to our work, Desreux and co-workers reported a [Gd(DO3A)(phen)] derivative (DO3A = 1,4,7-tri(carboxymethyl)-1,4,7,10-tetraazacyclododecane, phen = 1,10-phenanthroline) that self-assembles with Fe^{II} ions to yield a tetranuclear FeGd₃ entity.^[4]

Here we report a novel heterotritopic ligand, H₈L, which comprises a 2,2'-bipyridine moiety for specific binding to Fe^{II} ions and two poly(aminocarboxylate) groups for binding to Gd^{III} ions (Scheme 1). The ligand self-assembles with Fe^{II} and Gd^{III} into a metallostar [Fe{Gd₂L(H₂O)₄}₃]⁴⁻ structure. The rational design of H₈L consists of several key features: 1) The appropriate choice of the poly(aminocarboxylate) group, which has the same chelating unit as the previously described TTAHA (*N*-tris(2-aminoethyl)amine-*N',N'',N''',N''''*-hexaacetate) ligand,^[5] ensures sufficient thermodynamic stability for the Gd^{III} complex, an important factor for in vivo safety. It also guarantees faster water exchange than that for commercial agents, thus closer to optimal. The Gd^{III} complex has two inner-sphere water molecules to double the inner-sphere contribution to the relaxivity. Indeed, preliminary ¹⁷O NMR spectroscopy experiments on the metallostar confirmed the presence of two inner-sphere water molecules and point to a water-exchange rate which is close to that previously published for [Gd(TTAHA)-(H₂O)₂]³⁻.^[5] A complete, variable-temperature ¹⁷O NMR spectroscopic study is in progress and will be reported in due course. 2) Fe^{II} ions can accommodate three strongly



Scheme 1. Reagents and conditions: a) protected triamine, K₂CO₃, acetonitrile; b) HCl (6 M), followed by flash chromatography; c) *tert*-butyl bromoacetate, DIEA, KI, DMF; d) HCl (6 M), followed by ion-exchange chromatography. DIEA = *N,N'*-diisopropylethylamine, DMF = *N,N*-dimethylformamide.

[*] J. B. Livramento, Dr. É. Tóth, Dr. A. Sour, Dr. A. Borel, Prof. A. E. Merbach, Dr. R. Ruloff
Laboratoire de Chimie Inorganique et Bioinorganique
Ecole Polytechnique Fédérale de Lausanne
EPFL-BCH
1015 Lausanne (Switzerland)
Fax: (+41) 21-693-9875
E-mail: eva.jakabtoth@epfl.ch

[**] This work was financially supported by the FNS and OFES Switzerland and performed in the framework of COST Action D18.

Supporting information for this article is available on the WWW under <http://www.angewandte.org> or from the author.

coordinating 2,2'-bipyridine units which increases the number of Gd^{III} centers on one iron core to six. The accumulation of six Gd^{III} ions in a small space represents a clear advantage over [Fe^{II}(tpy-DTTA)₂Gd^{III}]. The negative charge of [Fe{Gd₂L(H₂O)₄}₃]⁴⁻ is also favorable for high solubility in water. 3) The linking between the Fe^{II} and Gd^{III} binding sites is designed to minimize internal flexibility that could reduce the relaxivity gained by the increased molecular size. All of these features contribute to a high relaxivity per Gd^{III} center which, for the metallostar with six Gd^{III} centers, should sum up to a remarkable relaxivity confined to a small space.

The initial step in the synthesis of the ligand is the nucleophilic substitution of 4,4'-bis(bromomethyl)-2,2'-bipyridine with two protected diethylenetriamine units (Scheme 1). The following carboxymethylation, ester hydrolysis, and ion-exchange chromatography steps are all straightforward. The ligand, which was obtained as a highly water-soluble and partially protonated ammonium salt ($\text{H}_{4.5}(\text{NH}_4)_{3.5}\text{L}$), was characterized by ^1H NMR spectroscopy, ESI-MS, and elemental analysis.^[6] The $[\text{Gd}_2\text{L}(\text{H}_2\text{O})_4]^{2-}$ complex is prepared by mixing the ligand and Gd^{3+} ions in a 1:2 molar ratio at pH 6. The metallostear $[\text{Fe}\{\text{Gd}_2\text{L}(\text{H}_2\text{O})_4\}_3]^{4-}$ (Figure 1) forms instantaneously upon addition of Fe^{2+} to a solution of $[\text{Gd}_2\text{L}(\text{H}_2\text{O})_4]^{2-}$ (convergent approach), and the formation of the complex is indicated by the appearance of an intense red color.

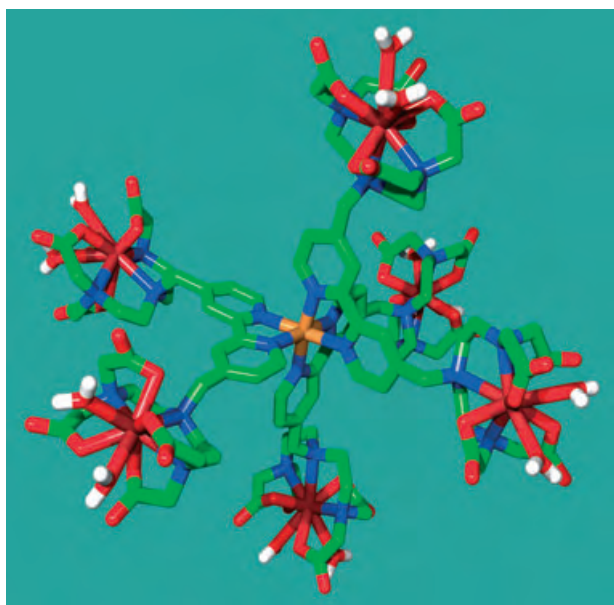


Figure 1. Framework molecular model of $[\text{Fe}\{\text{Gd}_2\text{L}(\text{H}_2\text{O})_4\}_3]^{4-}$. Hydrogen atoms have been removed for clarity. The Gd^{III} chelates, which are bound through a short spacer attached to the *para* position of the pyridyl moieties, form an octahedron around the central Fe^{II} ion that essentially reproduces the polyhedron of the bipyridine nitrogen atoms.

The dinuclear $[\text{Gd}_2\text{L}(\text{H}_2\text{O})_4]^{2-}$ species exhibits a fairly high relaxivity ($12.5 \text{ mm}^{-1} \text{ s}^{-1}$) relative to dinuclear complexes such as $[\text{pip}\{\text{Gd}(\text{DO}_3\text{A})(\text{H}_2\text{O})_2\}_2]$ (pip = piperidine) or $[\text{bisoxa}\{\text{Gd}(\text{DO}_3\text{A})(\text{H}_2\text{O})_2\}_2]$ (5.58 and $4.43 \text{ mm}^{-1} \text{ s}^{-1}$, respectively; 40 MHz, 37°C).^[7] This difference is explained by the two inner-sphere water molecules and their faster exchange, as well as the limited internal flexibility of $[\text{Gd}_2\text{L}(\text{H}_2\text{O})_4]^{2-}$. The formation of the large and rigid $[\text{Fe}\{\text{Gd}_2\text{L}(\text{H}_2\text{O})_4\}_3]^{4-}$ metallostear from $[\text{Gd}_2\text{L}(\text{H}_2\text{O})_4]^{2-}$ increases the rotational correlation time, τ_R , whereas the water-exchange rate remains unchanged. The longer τ_R value results in a substantial relaxivity gain. Consequently, the formation of the metallostear can be followed by relaxometry. Upon adding increasing amounts of Fe^{II} ions to a solution of $[\text{Gd}_2\text{L}(\text{H}_2\text{O})_4]^{2-}$, the relaxivity continuously increases until a molar ratio of $\text{Fe}^{\text{II}}/$

$[\text{Gd}_2\text{L}(\text{H}_2\text{O})_4]^{2-}$ of 1:3, after which it remains constant (Figure 2). The sharp break in the relaxometric titration curve indicates a 1:3 stoichiometry of the metallostear as expected for an Fe^{II} -2,2'-bipyridine complex. It proves that

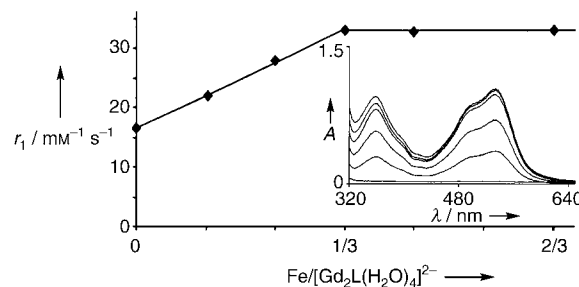


Figure 2. Relaxivity titration of $[\text{Gd}_2\text{L}(\text{H}_2\text{O})_4]^{2-}$ with Fe^{II} at pH 6.0, 25°C , $\nu = 30 \text{ MHz}$, and $c_{\text{Gd}} = 1 \text{ mM}$. Inset: UV/Vis spectra of the samples used for the relaxivity titration are shown. The absorption increases with an increasing ratio of $\text{Fe}^{\text{II}}/[\text{Gd}_2\text{L}(\text{H}_2\text{O})_4]^{2-}$.

the pending Gd^{III} -poly(aminocarboxylate) units do not sterically hinder the binding of three bipyridine units per Fe^{II} ion. Molecular modeling studies also showed that the metallostear is sterically not overcrowded (Figure 1). The invariance of the relaxivity at molar ratios of $\text{Fe}^{\text{II}}/[\text{Gd}_2\text{L}(\text{H}_2\text{O})_4]^{2-}$ higher than 1:3 points to the exclusive formation of $[\text{Fe}\{\text{Gd}_2\text{L}(\text{H}_2\text{O})_4\}_3]^{4-}$. It also shows that Fe^{II} is not oxidized to Fe^{III} which would likely replace Gd^{III} in the poly(aminocarboxylate) and the consequent release of free Gd^{3+} would decrease the relaxivity ($r_1 = 11.2 \text{ mm}^{-1} \text{ s}^{-1}$ for $\text{Gd}(\text{H}_2\text{O})_8^{3+}$ at 30 MHz and 25°C).

The formation of the metallostear was also monitored by UV/Vis spectrophotometry. Upon addition of Fe^{II} ions to a solution of $[\text{Gd}_2\text{L}(\text{H}_2\text{O})_4]^{2-}$, new absorption bands appear at 320–640 nm. Their intensity increases until a molar ratio of 1:3 $\text{Fe}^{\text{II}}/[\text{Gd}_2\text{L}(\text{H}_2\text{O})_4]^{2-}$, then it remains constant (the small further increase is due to the presence of free Fe^{II} ions; Figure 2).

Water proton relaxivities were measured for both the dinuclear $[\text{Gd}_2\text{L}(\text{H}_2\text{O})_4]^{2-}$ complex and the metallostear $[\text{Fe}\{\text{Gd}_2\text{L}(\text{H}_2\text{O})_4\}_3]^{4-}$ (25°C ; 0.01–600 MHz; Figure 3). Such nuclear magnetic relaxation dispersion (NMRD) profiles are widely used for the characterization of MRI contrast agents. As the consequence of slower tumbling, the relaxivities at almost all frequencies are considerably higher for the metal-

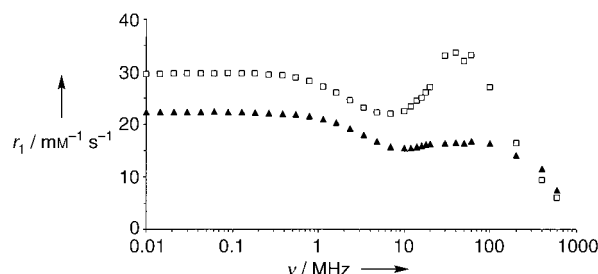


Figure 3. $1/T_1$ (T_1 = longitudinal relaxation time) NMRD profiles of solutions of $[\text{Gd}_2\text{L}(\text{H}_2\text{O})_4]^{2-}$ (▲) and $[\text{Fe}\{\text{Gd}_2\text{L}(\text{H}_2\text{O})_4\}_3]^{4-}$ (□). $c_{\text{Gd}} = 1 \text{ mM}$, pH 6.0, 25°C .

lost than for the dinuclear complex, and a maximum increase is observed at 30–60 MHz. The profile of $[\text{Fe}\{\text{Gd}_2\text{L}(\text{H}_2\text{O})_4\}_3]^{4-}$ shows the highfield peak typical of slowly rotating complexes ($r_{1\text{max}} = 33.6 \text{ mm}^{-1} \text{ s}^{-1}$ at 40 MHz). The metallostar is rather small compared to usual macro-molecular contrast agents. However, the concurrent chelation of the multifunctional ligand to Fe^{II} and Gd^{III} ions forces the rotational correlation time of the Gd^{III} –water-proton vector, which is important for relaxivity, to be close to that of the entire assembly. Thus, by strongly reducing internal flexibility, the advantage of the increased molecular size is maximized. Notably, the peak at high field is unusually broad with a relaxivity value that exceeds $16 \text{ mm}^{-1} \text{ s}^{-1}$ even at 200 MHz. Contrast agents that exhibit high relaxivities over a broad frequency range and, in particular, at high frequencies are interesting as modern clinical practice tends to use high magnetic fields ($> 60 \text{ MHz}$) to increase sensitivity.

In terms of molar relaxivity, our metallostar complex is among the best molecules reported. Its relaxivity is comparable to that of a $\text{Gd}(\text{DOTA})$ -loaded (DOTA = 1,4,7,10-tetra(carboxymethyl)-1,4,7,10-tetraazacyclododecane) Generation 10 dendrimer (relaxivity values of 27.0 and $33.2 \text{ mm}^{-1} \text{ s}^{-1}$ at 20 and 60 MHz, respectively, at 25°C for $[\text{Fe}\{\text{Gd}_2\text{L}(\text{H}_2\text{O})_4\}_3]^{4-}$ compared to 36 and $27 \text{ mm}^{-1} \text{ s}^{-1}$ at 23°C for the G10 dendrimer).^[8] This G10 dendrimer, with a molecular weight of 3000 kDa and 1860 Gd^{III} chelates on the surface, is considered to represent a high “ Gd^{III} density”. Such dendrimers have been designed for receptor targeting as they can deliver a concentrated relaxation effect to a given receptor binding site. Indeed, Wiener and co-workers used $\text{Gd}(\text{DTPA})$ (diethylenetriamine- N,N,N',N'',N'' -pentaacetic acid) dendrimers conjugated with folic acid for visualizing the folate receptor, which is overexpressed in many tumors.^[9]

The complex $[\text{Fe}\{\text{Gd}_2\text{L}(\text{H}_2\text{O})_4\}_3]^{4-}$ contains six Gd^{III} ions, each exhibiting high relaxivity, for a molecular mass of 3744 g mol^{-1} . Consequently, its efficiency by a unity mass is particularly high. Rather than determine the usual molar relaxivity per Gd , r_1 , which is not well-suited to characterize contrast agents in this respect, instead one can compare “effective” or “mass relaxivities”, which are defined as the enhancement of the relaxation rate by a unit mass (g L^{-1}) of the contrast agent (n_{Gd} is the number of Gd ions per molecule and M_w is the molecular weight of the complex; the multiplication factor of 1000 is to obtain convenient numbers) according to Equation (1).

$$\text{effective relaxivity} = \frac{r_1 n_{\text{Gd}}}{M_w} \times 1000 \quad \left(\frac{\text{mm}^{-1} \text{ s}^{-1}}{\text{g mol}^{-1}} \text{ or } (\text{g/L})^{-1} \text{ s}^{-1} \right) \quad (1)$$

High “effective relaxivities” are required for applications such as cell imaging in which a sufficient relaxation effect has to be produced by a limited mass of the agent. Figure 4 compares “effective relaxivities” for commercial and potential contrast agents and shows that the dinuclear $[\text{Gd}_2\text{L}(\text{H}_2\text{O})_4]^{2-}$ species and especially the metallostar $[\text{Fe}\{\text{Gd}_2\text{L}(\text{H}_2\text{O})_4\}_3]^{4-}$ are remarkably powerful contrast agents in terms of efficacy by unity mass.

Desreux and co-workers proposed the phenanthroline- $\text{Gd}(\text{HDO3A})$ derivative as a contrast agent responsive to Fe^{II}

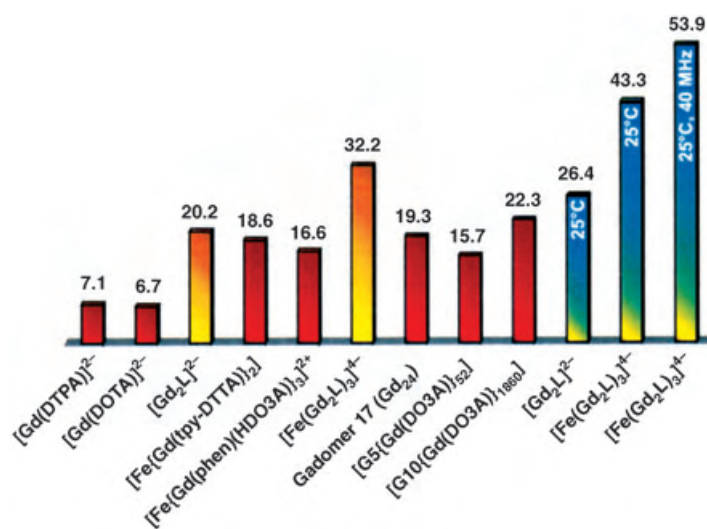


Figure 4. Comparison of the effective (mass) relaxivities (calculated according to Equation (1)) for a series of Gd^{III} complexes. The monomers $[\text{Gd}(\text{DTPA})]^{2-}$ and $[\text{Gd}(\text{DOTA})]^{2-}$ are commercial contrast agents.^[7] $[\text{Fe}\{\text{Gd}(\text{tpy-DTTA})\}_2]^{2+}$ and $[\text{Fe}\{\text{Gd}(\text{phen})(\text{HDO3A})\}_3]^{2+}$ are self-assembled structures. Gadomer 17,^[10] $[\text{G5}\{\text{Gd}(\text{DO3A})\}_{52}]^{11+}$, and $[\text{G10}\{\text{Gd}(\text{DOTA})\}_{1850}]^{8+}$ are dendrimers. The effective relaxivities were calculated at 20 MHz and 37°C , except for the last three columns which were determined at 25°C . ($r_1 = 20.17 \text{ mm}^{-1} \text{ s}^{-1}$, the molar relaxivity per Gd for $[\text{Fe}\{\text{Gd}_2\text{L}(\text{H}_2\text{O})_4\}_3]^{4-}$ at 20 MHz and 37°C used for the calculation of the “effective relaxivity”).

concentration, however, such an application did not materialize. In addition to the large increase in the relaxivity upon formation of $[\text{Fe}\{\text{Gd}_2\text{L}(\text{H}_2\text{O})_4\}_3]^{4-}$ from $[\text{Gd}_2\text{L}(\text{H}_2\text{O})_4]^{2-}$ ($\approx 100\%$ at 30–60 MHz), our system has practical advantages over $[\text{Gd}(\text{phen})(\text{HDO3A})]$. The ligand synthesis is straightforward, and the structural diversity, as it exists for $[\text{Fe}\{\text{Gd}(\text{phen})(\text{HDO3A})\}_3]$, is largely reduced by the higher symmetry of L^{8-} .

In conclusion, we have reported a heterometallic, self-assembled metallostar, $[\text{Fe}\{\text{Gd}_2\text{L}(\text{H}_2\text{O})_4\}_3]^{4-}$, which exhibits a particularly high relaxivity for its moderate molecular weight. This is explained in terms of a rigid supramolecular structure and two inner-sphere water molecules with an exchange rate that lies close to optimal. The presence of six efficiently relaxing Gd^{III} centers within one metallostar leads to an exceptionally high relaxivity confined to a small molecular space (high density of relaxivity). To our knowledge this is the highest relaxivity per molecular mass ever reported for a Gd^{III} complex. The ligand L^{8-} is also a prime candidate as a terminal ligand for constructing larger-size, Fe^{II} (or Ru^{II})-based metallostars or metal dendrimers that are loaded with Gd^{III} on the surface.

Experimental Section

$[\text{Gd}_2\text{L}(\text{H}_2\text{O})_4]^{2-}$ was prepared by adding solid L to a solution of GdCl_3 in 1:2 molar ratio (pH 6.0; 50 mM MES (2-morpholinoethanesulfonic acid) buffer). $[\text{Fe}\{\text{Gd}_2\text{L}(\text{H}_2\text{O})_4\}_3]^{4-}$ was prepared by mixing a solution of $[\text{Gd}_2\text{L}(\text{H}_2\text{O})_4]^{2-}$ with a freshly prepared solution of Fe^{II} ions ($\text{Fe}(\text{NH}_4)_2(\text{SO}_4) \times 6\text{H}_2\text{O}$) in 3:1 molar ratio (pH 6.0; 5 mM MES). ESI-MS for $[\text{Gd}_2\text{L}(\text{H}_2\text{O})_4]^{2-}$: m/z (%): 579.3 (100) $[\text{M}^{2-}]$, 1239.2 (68) $[(\text{MH}+2\text{CH}_3\text{CN})^-]$, 1180.3 (50) $[\text{MNa}^-]$, 1159.2 (23%) $[\text{MH}^-]$; ESI-MS for $[\text{Fe}\{\text{Gd}_2\text{L}(\text{H}_2\text{O})_4\}_3]^{4-}$: m/z (%): 579.3 (100)

$[M-[Fe(Gd_2L)_2]^{2-}]$, 882.3 (75) $[M^{4-}]$, 1184.7 (43%) $[MNa^{3-}]$. The isotopic peak patterns in both cases agree with simulated spectra. All manipulations with the metallostar were carried out with the exclusion of oxygen to avoid oxidation of Fe^{II} . The $1/T_1$ NMRD profiles were recorded on a Stelar Spinmaster Fast Field Cycling NMR relaxometer ($B = 2.35 \times 10^{-4}$ –0.47 T, proton Larmor frequencies 0.01–20 MHz), on Bruker Minispecs (30, 40, and 60 MHz), and on Bruker spectrometers (50, 100, 200, 400, and 600 MHz). The UV/Vis titration was performed on a Perkin-Elmer Lambda 19 spectrometer.

Received: September 2, 2004

Published online: December 6, 2004

Keywords: gadolinium · heterometallic complexes · imaging agents · NMR spectroscopy · self-assembly

-
- [1] <http://www.nobel.se/medicine/laureates/2003/press.html>, **2003**.
 - [2] É. Tóth, L. Helm, A. E. Merbach in *The Chemistry of Contrast Agents in Medical Magnetic Resonance Imaging* (Eds.: É. Tóth, A. E. Merbach), Wiley, Chichester, **2001**, pp. 45–119.
 - [3] R. Ruloff, G. van Koten, A. E. Merbach, *Chem. Commun.* **2004**, 842.
 - [4] V. Comblin, D. Gilsoul, M. Hermann, V. Humblet, V. Jacques, M. Mesbahi, C. Sauvage, J. F. Desreux, *Coord. Chem. Rev.* **1999**, 185–186, 451.
 - [5] a) R. Ruloff, R. N. Muller, D. Pubanz, A. E. Merbach, *Inorg. Chim. Acta* **1998**, 275–276, 15; b) R. Ruloff, T. Gelbrich, J. Sieler, E. Hoyer, L. Beyer, *Z. Naturforsch. B* **1997**, 52, 805.
 - [6] The synthesis and characterization of the ligand are described in detail in the Supporting Information.
 - [7] H. D. Powell, O. M. Ni Dhubhghaill, D. Pubanz, L. Helm, Y. Lebedev, W. Schlaepfer, A. E. Merbach, *J. Am. Chem. Soc.* **1996**, 118, 9333.
 - [8] L. H. Bryant, Jr., M. W. Brechbiel, W. Chuanchu, J. W. M. Bulte, V. Herynek, J. A. Frank, *Magn. Reson. Imaging* **1999**, 9, 348.
 - [9] S. D. Konda, M. Aref, M. Brechbiel, E. C. Wiener, *Invest. Radiol.* **2000**, 35, 50.
 - [10] G. M. Nicolle, É. Tóth, H. Schmitt-Willich, B. Raduchel, A. E. Merbach, *Chem. Eur. J.* **2002**, 8, 1040.
 - [11] É. Tóth, D. Pubanz, S. Vauthey, L. Helm, A. E. Merbach, *Chem. Eur. J.* **1996**, 2, 1607.
-

Oxazaborolidine-Derived Lewis Acid Assisted Lewis Acid as a Moisture-Tolerant Catalyst for Enantioselective Diels–Alder Reactions***Kentaro Futatsugi and Hisashi Yamamoto**

The Diels–Alder reaction is one of the most powerful construction processes in organic synthesis, especially for the formation of molecules containing quaternary carbon stereocenters.^[1] For this reason there has been much research on the development of enantioselective versions using chiral Lewis acid catalysis.^[2] While various kinds of chiral Lewis acid promoted reactions have been developed, these reactions must be carried out under strictly anhydrous conditions. The presence of even a small amount of water stops the reaction because most Lewis acids react immediately with water rather than with the substrate, and decompose or are deactivated.^[3] This turns out to be a serious problem when using chiral Lewis acid catalyst in organic synthesis since a large quantity of optically active product is expected to be obtained with a very small amount (> 1 mol %) of enantiopure catalyst.

Among the most useful and reactive enantioselective Diels–Alder catalysts are those reported by Corey that employ an oxazaborolidine catalyst in the presence of a Brønsted acid^[4]; this is an excellent example of a Brønsted acid assisted Lewis acid catalyst (BLA).^[5] Since we have been interested in combined acid catalysis systems for several years,^[5–7] the activity of the corresponding Lewis acid assisted Lewis acid catalyst (LLA) system^[6]—an L-proline derived oxazaborolidine as a precatalyst combined with a Lewis acid as an activator—was examined for Diels–Alder reactions. However, the resulting LLA was much less efficient (62 % *ee*) than the original BLA catalyst. Surprisingly, a simple monocyclic oxazaborolidine **1** derived from L-valine (Scheme 1) was found to be a promising chiral precatalyst for the LLA system.^[8] The resulting LLA was not only found to be a highly potent and stable chiral catalyst for the Diels–Alder reaction but it is also unusually resistant to moisture, oxygen, and Lewis bases,^[9,10] which we believe has wide implications for versatile catalyst designs in the future.

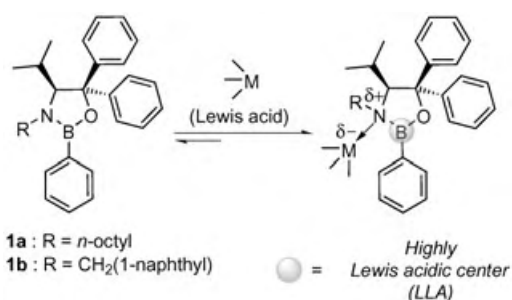
Our study commenced with a search for the most effective Lewis acid activator for the Diels–Alder reaction of 1,3-cyclopentadiene and methacrolein with the oxazaborolidine **1a** as precatalyst. LLA catalysts were typically prepared by

[*] K. Futatsugi, Prof. H. Yamamoto
Department of Chemistry
University of Chicago
5735 S. Ellis Avenue, Chicago, Illinois 60637 (USA)
Fax: (+1) 773-702-0805
E-mail: yamamoto@uchicago.edu

[**] Support for this research was provided by the SORST project of the Japan Science and Technology Agency (JST), National Institutes of Health (NIH) GM068433-01, and a starter grant from the University of Chicago.

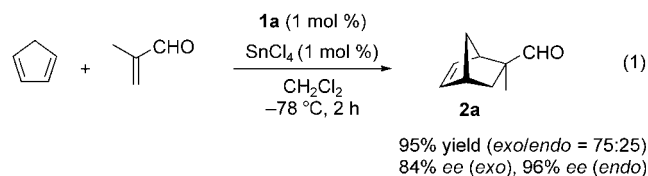


Supporting information for this article is available on the WWW under <http://www.angewandte.org> or from the author.



Scheme 1. Plausible reactive species (LLA) generated from **1** and a Lewis acid.

addition of the Lewis acid (6 mol %) to a solution of the chiral oxazaborolidine (7.2 mol %) at -78°C , followed by stirring for 15 min. Among various kinds of Lewis acids examined, AlCl_3 , Et_2AlCl , FeCl_3 , $\text{Sc}(\text{OTf})_3$, SnCl_4 , $[\text{CpTiCl}_3]$, and TiCl_4 were found to be effective activators for this reaction, and the cycloadducts were obtained in good yield (69–94 % yield, *exo/endo* = 73:27 to 77:23) at -78°C within 2 h with high enantioselectivities (80–87 % *ee* for the *exo* adduct and 95–97 % *ee* for the *endo* adduct).^[11] With these activators, both the enantioselectivity and diastereoselectivity (*exo/endo* ratio) were uniformly in the same range, and the reactivity was found to be optimal with SnCl_4 . In contrast, the use of a strong Brønsted acid, bis(trifluoromethanesulfonyl)imide gave the cycloadduct with lower enantioselectivity (67 % *ee* (*exo*), 85 % *ee* (*endo*)). Remarkably, only 1 mol % of **1a** and SnCl_4 gave the same high reactivity and enantioselectivity [Eq. (1)].^[12]



The potent reactivity of the present catalyst system was further demonstrated by changing the ratio of SnCl_4 to chiral oxazaborolidine **1a**. Surprisingly, only a slight loss of enantioselectivity was observed even in the presence of a large excess of SnCl_4 (Figure 1). This observation indicates the much higher reactivity of LLA in the Diels–Alder reaction than that of SnCl_4 . An even more attractive finding is that only a small amount of SnCl_4 (0.5 mol %) is needed to promote the reaction (86 % yield (*exo/endo* = 75:25), 85 % *ee* (*exo*), 96 % *ee* (*endo*)) using 0.5 mol % SnCl_4 and 2 mol % **1a**.

These unusual features led us to assume that such a reactive catalyst might be able to survive the presence of a small amount of a Lewis base such as water if a slight excess of SnCl_4 , which might act as both an activator of the chiral oxazaborolidine and a scavenger of Lewis basic impurities, is utilized in this combined acid system (Scheme 2).

Pursuing this hypothesis, Diels–Alder reactions were conducted with **1a** and SnCl_4 in the presence of possible deactivators for the reactive Lewis acid (Figure 2). Indeed,

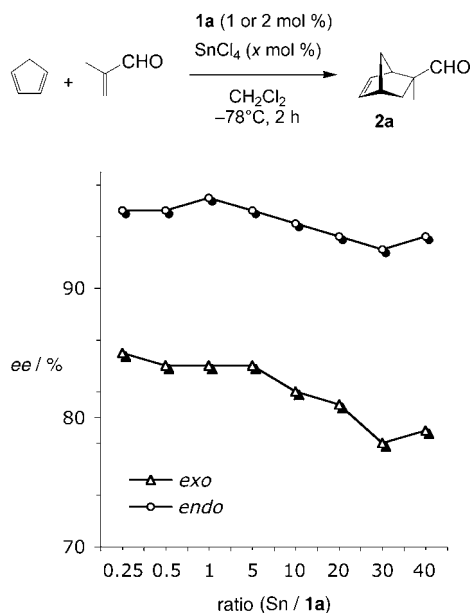
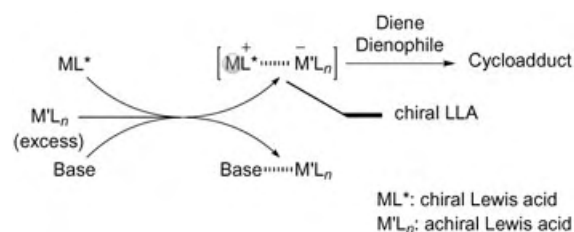


Figure 1. The effect of the amount of SnCl_4 on the enantioselectivity.



Scheme 2. Proposed working model for chiral LLA in the presence of Lewis bases.

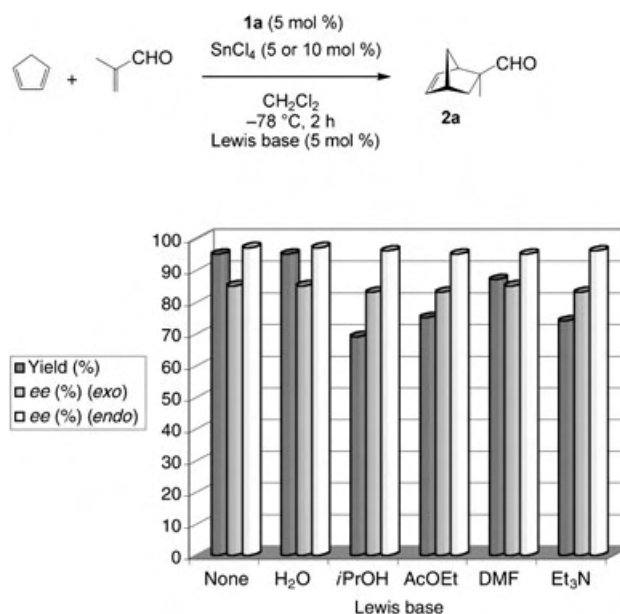


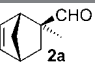
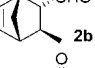
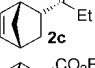
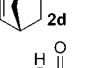
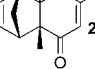
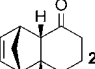
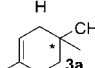
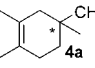
Figure 2. Diels–Alder reactions in the presence of various Lewis bases.

the LLA catalyst maintained its reactivity even in the presence of an equal amount of water to **1a** and SnCl₄ without any loss in enantioselectivity.^[13] As expected, this LLA could be utilized in nonpurified, reagent-grade dichloromethane as a reaction solvent, in air, with **1a** (5 mol %) and SnCl₄ (10 mol %). Similarly, this LLA system was found to function in the presence of a small amount of other Lewis bases (Figure 2). No significant loss of enantioselectivities was observed in any case, although the presence of these Lewis bases led to a slight diminution of the reaction rate.

Finally, a simple modification of the alkyl substituent on the nitrogen of the chiral oxazaborolidine **1a** led to a more enantioselective precatalyst **1b** (entry 1, Table 1). With this

enantioselective Diels–Alder reactions. The unique characteristics of this LLA system are as follows: 1) the enantioselectivity can be preserved even in the presence of a large amount of *achiral* Lewis acid activator, which implicates the generation of highly reactive species; 2) only 0.5 mol % of SnCl₄ is necessary to promote the reaction; 3) its inherent reactivity and asymmetric induction ability can be maintained even in the presence of a small amount of water as well as other Lewis bases by adding a slightly larger amount of SnCl₄; 4) a simple modification of the oxazaborolidine structure is possible by using commercially available chiral amino alcohols. Other applications of this LLA system are currently underway in our laboratory.

Table 1: Diels–Alder reactions catalyzed by **1b** and SnCl₄.^[a]

1b / SnCl ₄ [mol %]	T [°C]	t [h]	Product ^[b]	Yield [%] ^[c]	exo/ endo ^[d]	ee [%] ^[e]
1:1	−78	2		> 99	68:32	95 (98) ^[f]
10:10	−78	13		73	18:82	88 (34) ^[f]
10:10	−78	2		90	1:99	96
10:10	−78	16		96	1:99	95
10:10	−78	1.5		94	< 1:99	99
20:20	−20	14		93	8:92	95
5:10	−78	16		> 99		90 ^[g]
5:5	−78	16		80		93 ^[g]

[a] Unless otherwise specified, reactions were carried out with diene (5 equiv.), dienophile, **1b** (1–20 mol %), and SnCl₄ (1–20 mol %) in dichloromethane under the conditions indicated. [b] Major diastereomers are shown. For the determination of the absolute configuration, see reference [15] and Supporting Information. [c] Yield of the mixture of diastereomers isolated. [d] Determined by GC analysis or ¹H NMR analysis of the crude mixture. [e] Enantioselectivities given for the major diastereomers. For the determination of enantioselectivities, see ref. [16] and Supporting Information. [f] Enantioselectivities for the minor diastereomers. [g] The absolute configuration was not determined.

chiral unit in hand, the scope of this Diels–Alder reaction was investigated (Table 1). In every case the cycloadducts^[14] were obtained in high yield using less than 10 mol % of **1b** and SnCl₄ at −78 °C, except for the reaction between 2-cyclohexen-1-one and 1,3-cyclopentadiene. The level and the sense of asymmetric induction were found to be compatible with Corey's proline-derived BLA catalyst in most cases.

In conclusion, we have demonstrated that the combination of a chiral oxazaborolidine **1** and SnCl₄ leads to an extremely reactive chiral LLA as a promising catalyst for

Experimental Section

The synthesis of **2e** catalyzed by **1b** and SnCl₄ is given as an example. CH₂Cl₂ (35 mL) and a 1.0 M solution of oxazaborolidine **1b** in CH₂Cl₂ (1 mL, 1 mmol) were added to a dried, three-necked flask under argon. After being cooled to −78 °C, a 1.0 M solution of SnCl₄ in CH₂Cl₂ (1 mL, 1 mmol) was added dropwise. The resulting pale-yellow solution was stirred for 15 min at this temperature. A solution of 2,5-dimethyl-1,4-benzoquinone (1.4 g, 10 mmol) in CH₂Cl₂ (5 mL) was added dropwise to this mixture, and after 1–2 min a solution of cyclopentadiene (4.1 mL, 50 mmol) in CH₂Cl₂ (4.1 mL; pre-cooled to −78 °C) was added dropwise over 10 min from a syringe. The reaction mixture was stirred for 90 min at −78 °C and then quenched by addition of Et₃N (700 µL). The reaction mixture was then allowed to warm to room temperature slowly, and the solvent was removed in vacuo. The crude product was purified by silica gel chromatography (hexane/ethyl acetate, 10:1) to give **2e** in 98 % yield with > 99 % *ee*. The physical and spectroscopic data of **2e** were identical to the literature values.^[4c,14c] No signals for the *exo* adduct were detected in the NMR spectrum of the crude product. The enantioselectivity was determined by HPLC analysis (Daicel OD-H, hexane (99.4 %)/iPrOH (0.6 %), flow rate = 0.5 mL min^{−1}; *t*_R = 28.2 min (major), 30.4 min (minor).

Received: July 15, 2004

Revised: November 4, 2004

Published online: January 31, 2005

Keywords: asymmetric catalysis · cycloaddition · Diels–Alder reaction · Lewis acids

- [1] For reviews on the construction of chiral quaternary carbon stereocenters, see: a) E. J. Corey, A. Guzman-Perez, *Angew. Chem.* **1998**, *110*, 402–415; *Angew. Chem. Int. Ed.* **1998**, *37*, 388–401; b) I. Denissova, L. Barriault, *Tetrahedron* **2003**, *59*, 10105–10146.
- [2] For recent reviews on enantioselective Diels–Alder reactions, see: a) L. C. Diaz, *J. Braz. Chem. Soc.* **1997**, *8*, 289–332; b) ref. [1]; c) D. A. Evans, J. S. Johnson, in *Comprehensive Asymmetric Catalysis*, Vol. 3 (Eds.: E. N. Jacobsen, A. Pfaltz, H. Yamamoto), Springer, Berlin, **1999**, pp. 1177–1235; d) K. Ishihara, H. Yamamoto, *Eur. J. Org. Chem.* **1999**, 527–538; E. J. Corey, *Angew. Chem.* **2002**, *114*, 1724–1741; *Angew. Chem. Int. Ed.* **2002**, *41*, 1650–1667; e) Y. Hayashi, in *Cycloaddition Reactions in Organic Synthesis* (Eds.: S. Kobayashi, K. A. Jørgensen), Wiley-VCH, Weinheim, **2002**, pp. 5–55.
- [3] a) *Lewis Acids in Organic Synthesis*, Vols. 1 and 2 (Ed.: H. Yamamoto), Wiley-VCH, Weinheim, **2000**; b) *Lewis Acid*

- Reagents: A Practical Approach* (Ed.: H. Yamamoto), Oxford University Press, Oxford, **1999**.
- [4] a) E. J. Corey, T. Shibata, T. W. Lee, *J. Am. Chem. Soc.* **2002**, *124*, 3808–3809; b) D. H. Ryu, T. W. Lee, E. J. Corey, *J. Am. Chem. Soc.* **2002**, *124*, 9992–9993; c) D. H. Ryu, E. J. Corey, *J. Am. Chem. Soc.* **2003**, *125*, 6388–6390; d) G. Zhou, Q.-Y. Hu, E. J. Corey, *Org. Lett.* **2003**, *5*, 3979–3982; e) D. H. Ryu, G. Zhou, E. J. Corey, *J. Am. Chem. Soc.* **2004**, *126*, 4800–4802; f) Q.-Y. Hu, P. D. Rege, E. J. Corey, *J. Am. Chem. Soc.* **2004**, *126*, 5984–5986; g) D. H. Ryu, E. J. Corey, *J. Am. Chem. Soc.* **2004**, *126*, 8106–8107; h) Q.-Y. Hu, G. Zhou, E. J. Corey, *J. Am. Chem. Soc.* **2004**, *126*, 13708–13712.
- [5] a) K. Ishihara, H. Yamamoto, *J. Am. Chem. Soc.* **1994**, *116*, 1561–1562; b) K. Ishihara, M. Miyata, K. Hattori, T. Tada, H. Yamamoto, *J. Am. Chem. Soc.* **1994**, *116*, 10520–10524; c) K. Ishihara, H. Kurihara, H. Yamamoto, *J. Am. Chem. Soc.* **1996**, *118*, 3049–3050; d) K. Ishihara, H. Kurihara, M. Matsumoto, H. Yamamoto, *J. Am. Chem. Soc.* **1998**, *120*, 6920–6930.
- [6] a) M. Oishi, S. Aratake, H. Yamamoto, *J. Am. Chem. Soc.* **1998**, *120*, 8271–8272; b) K. Ishihara, J. Kobayashi, K. Inanaga, H. Yamamoto, *Synlett* **2001**, 394–396; c) G. Xia, K. Shibatomi, H. Yamamoto, *Synlett* **2004**, 2437–2439; for a similar activation of a chiral boron Lewis acid by another Lewis acid, see: d) H. Lachance, X. Lu, M. Gravel, D. G. Hall, *J. Am. Chem. Soc.* **2003**, *125*, 10160–10161; e) V. Rauniyar, D. G. Hall, *J. Am. Chem. Soc.* **2004**, *126*, 4518–4519; f) M. Gravel, H. Lachance, X. Lu, D. G. Hall, *Synthesis* **2004**, 1290–1302.
- [7] Lewis acid assisted Brønsted acid (LBA): a) K. Ishihara, M. Kaneeda, H. Yamamoto, *J. Am. Chem. Soc.* **1994**, *116*, 11179–11180; b) K. Ishihara, S. Nakamura, M. Kaneeda, H. Yamamoto, *J. Am. Chem. Soc.* **1996**, *118*, 12854–12855; c) K. Ishihara, H. Nakamura, S. Nakamura, H. Yamamoto, *J. Org. Chem.* **1998**, *63*, 6444–6445; d) K. Ishihara, S. Nakamura, H. Yamamoto, *J. Am. Chem. Soc.* **1999**, *121*, 4906–4907; e) S. Nakamura, M. Kaneeda, K. Ishihara, H. Yamamoto, *J. Am. Chem. Soc.* **2000**, *122*, 8120–8130; f) S. Nakamura, K. Ishihara, H. Yamamoto, *J. Am. Chem. Soc.* **2000**, *122*, 8131–8140; g) K. Ishihara, H. Ishibashi, H. Yamamoto, *J. Am. Chem. Soc.* **2001**, *123*, 1505–1506; h) K. Ishihara, H. Ishibashi, H. Yamamoto, *J. Am. Chem. Soc.* **2002**, *124*, 3647–3655; i) K. Ishihara, D. Nakashima, Y. Hiraiwa, H. Yamamoto, *J. Am. Chem. Soc.* **2003**, *125*, 24–25; j) K. Kumazawa, K. Ishihara, H. Yamamoto, *Org. Lett.* **2004**, *6*, 2551–2554; k) H. Ishibashi, K. Ishihara, H. Yamamoto, *J. Am. Chem. Soc.* **2004**, *126*, 11122–11123.
- [8] This mode of activation was speculated from the plausible active species for CBS reduction. In this process, the coordination of the electrophilic BH₃ to the nitrogen atom of the oxazaborolidine serves to increase the Lewis acidity of the endocyclic boron atom strongly. For recent reviews, see: a) E. J. Corey, C. J. Helal, *Angew. Chem.* **1998**, *110*, 2092–2118; *Angew. Chem. Int. Ed.* **1998**, *37*, 1986–2012; b) S. Itsuno in *Comprehensive Asymmetric Catalysis, Vol. 1* (Eds.: E. N. Jacobsen, A. Pfaltz, H. Yamamoto), Springer, Berlin, **1999**, pp. 290–315.
- [9] Some chiral Lewis acid catalysts have been reported to be air-stable, and even storable, see: a) S. Kobayashi, M. Ueno, S. Saito, Y. Mizuki, H. Ishitani, Y. Yamashita, *Proc. Natl. Acad. Sci. USA* **2004**, *101*, 5476–5481; b) Y. S. Kim, S. Matsunaga, J. Das, A. Sekine, T. Ohshima, M. Shibasaki, *J. Am. Chem. Soc.* **2000**, *122*, 6506–6507.
- [10] For a chiral Lewis acid catalyzed Diels–Alder reaction in water, see: a) S. Otto, G. Boccaletti, J. B. F. N. Engberts, *J. Am. Chem. Soc.* **1998**, *120*, 4238–4239; b) S. Otto, J. B. F. N. Engberts, *J. Am. Chem. Soc.* **1999**, *121*, 6798–6806.
- [11] The use of other Lewis acids (BF₃·Et₂O, tris(pentafluorophenyl)boron, [Cp₂TiCl₂], ZnCl₂) resulted in either poor reactivity or lower enantioselectivity.
- [12] For other highly enantioselective Diels–Alder reactions with less than 1 mol% of chiral Lewis acid catalyst for the same substrates, see: a) J. Bao, W. D. Wulff, A. L. Rheingold, *J. Am. Chem. Soc.* **1998**, *120*, 8271–8272; b) ref. [4c].
- [13] The addition of more than one equivalent of water to **1a** resulted in a decrease in both reactivity and enantioselectivity. This obstacle could be overcome by use of a larger amount of SnCl₄ without dramatic loss of enantioselectivity.
- [14] The physical and spectroscopic data for all cycloadducts were identical to those reported previously for these compounds. **2a**: a) Y. Hayashi, J. J. Rohde, E. J. Corey, *J. Am. Chem. Soc.* **1996**, *118*, 5502–5503; **2b**: b) S. Hashimoto, N. Komeshima, K. Koga, *J. Chem. Soc. Chem. Commun.* **1979**, 437–438 and ref. [5d]; **2c**: c) R. Kumareswaran, P. S. Vankar, M. V. R. Reddy, S. V. Pitre, R. Roy, Y. D. Vankar, *Tetrahedron* **1999**, *55*, 1099–1110 and ref. [4b]; **2d**: d) M. E. Jung, W. D. Vaccaro, K. R. Buszek, *Tetrahedron Lett.* **1989**, *30*, 1893–1896 and ref. [4b]; **2e**: e) G. Mehta, A. Srikrishna, A. V. Reddy, M. S. Nair, *Tetrahedron* **1981**, *37*, 4543–4559 and ref. [4c]; **2f**: f) S. Takano, T. Kamikubo, M. Morita, K. Ogasawara, *Synthesis* **1994**, 601–604, g) A. B. Northrup, D. W. C. MacMillan, *J. Am. Chem. Soc.* **2002**, *124*, 2458–2459, and ref. [4b]; **3a**: h) Z. Zhu, J. H. Espenson, *J. Am. Chem. Soc.* **1997**, *119*, 3507–3512 and i) J. E. Baldwin, M. J. Lusch, *J. Org. Chem.* **1979**, *44*, 1923–1927; **4a**: ref. [14i].
- [15] The absolute configurations of **2a**,^[14b] **2c**,^[4b] **2e**,^[4c] and **2f**^[4b] were assigned by comparison with optical rotation values reported in the literature. For **2b**, the absolute configuration was assigned by comparison with an authentic sample prepared separately, see a) D. Sartor, J. Saffrich, G. Helmchen, *Synlett* **1990**, 197–198. The absolute configuration of **2d** was assigned by comparison with the optical rotation value of the corresponding alcohol, see: b) O. Kitagawa, H. Izawa, K. Sato, A. Dobashi, T. Taguchi, *J. Org. Chem.* **1998**, *63*, 2634–2640.
- [16] The enantioselectivities of the cycloadducts were determined as follows. **2a**: a) K. Furuta, S. Shimizu, Y. Miwa, H. Yamamoto, *J. Org. Chem.* **1989**, *54*, 1481–1483. For a general procedure for the acetalization of Diels–Alder adducts with (–)-(2*R*,4*R*)-2,4-pentanediol, see: b) K. Furuta, Q. Gao, H. Yamamoto, *Org. Synth.* **1995**, *72*, 86–94; **2b**: ref. [5d]; for **2c–f**, see Supporting Information; **3a**: ref. [5d]; **4a**: refs. [5d] and [16b].

Two-Dimensional Adatom Gas Bestowing Dynamic Heterogeneity on Surfaces

Nian Lin,* Dietmar Payer, Alexandre Dmitriev, Thomas Strunskus, Christof Wöll, Johannes V. Barth,* and Klaus Kern*

Almost 80 years ago Taylor coined the concept of “active sites” in heterogeneous catalysis, suggesting that adsorbate bond cleavage or formation occurs preferentially at specific arrangements with low-coordinate surface atoms.^[1] The identification of such active sites is decisive for understanding surface reaction mechanisms, the corresponding rate-limiting steps, and the design of advanced catalysts with improved efficiency or selectivity.^[2–5] With the advent of modern surface science techniques, detailed insight into the features of active sites was obtained. Notably, structural defects at terraced surfaces such as steps, kinks, vacancies, and dislocations could be directly associated with centers of locally increased catalytic activity, and corresponding theoretical calculations provided much insight into the underlying chemistry.^[6–12] However, in these studies the catalyst and the active sites are generally described in terms of static configurations. This is a severe restriction in view of the generally elevated operating temperatures (ca. 400–1000 K) in industrial processes, where catalysts are frequently subject to morphological changes. Only recently an example of the dynamic formation

of active sites was conclusively demonstrated; they were encountered in the form of thermally fluctuating one-dimensional -O-Ag-O-Ag- chains that strongly accelerate the catalytic oxidation of CO on a Ag(110) surface.^[13] It is thus timely to consider the intriguing case that highly mobile adsorbed atoms, arising from evaporation at atomic step edges, may act as dynamic active sites in heterogeneous catalysis. Based on the fact that increased catalytic activity often correlates with reduced coordination number, such adatoms are in principle species of extreme efficiency. Indeed, immobilized individual metal atoms supported on various nonmetallic substrates have been proven to operate as single-site catalysts.^[14–16]

The existence of adatoms as an intrinsic property of real surfaces can be rationalized within the scope of the terrace–step–kink (TSK) model, which comprises their main defects. As illustrated in Figure 1, the arrangement of steps and kinks

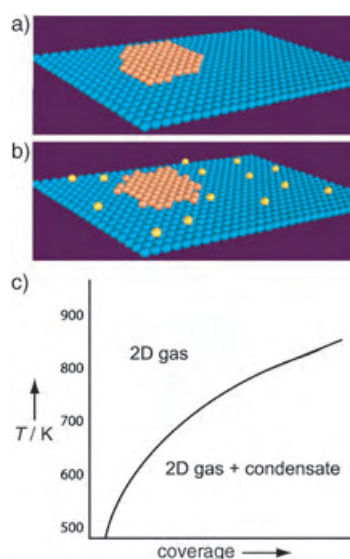


Figure 1. Island–terrace morphology of a surface covered by an island of adatoms. a) Static situation at low temperature. b) On thermal activation, island edges start fluctuating and emitting atoms from kink sites. A dilute 2D adatom lattice gas exists on the terraces. c) Schematic diagram of 2D adatom gas phase and condensed phase (islands) coexisting at elevated temperatures for metal-on-metal systems.

is static when fluctuations and atom-exchange processes are frozen, while on thermal activation adatoms start to evaporate from kink sites of the steps and are transported to terraces (Figure 1 a and b).^[17] These thermal adatoms form a two-dimensional (2D) lattice gas, whose surface concentration c_a strongly depends on temperature, chemical nature and symmetry, and step–terrace morphology of the substrate. On the basis of ultrahigh-vacuum (UHV) studies on a variety of systems,^[18–21] c_a must be appreciable for many materials at elevated temperatures. At 700 K the 2D vapor pressure of the catalytically important metals Pd, Cu, and Ag results in adatom densities ranging between 1 and 6% on the surfaces of Mo and W (Figure 1c).^[18,22] Although the decisive role of adatoms in the formation of reconstructions,^[23–25] orienta-

[*] Dr. N. Lin, D. Payer, A. Dmitriev
Max-Planck-Institut für Festkörperforschung
70569 Stuttgart (Germany)
Fax: (+49) 711-689-1662
E-mail: n.lin@fkf.mpg.de

Prof. Dr. J. V. Barth
Institut de Physique des Nanostructures
Ecole Polytechnique Fédérale de Lausanne
1015 Lausanne (Switzerland)
and
Advanced Materials and Process Engineering Laboratory
Departments of Chemistry and Physics & Astronomy
University of British Columbia
Vancouver, BC V6T 1Z4 (Canada)
Fax: (+1) 604-822-4750
E-mail: jvb@chem.ubc.ca

Prof. Dr. K. Kern
Max-Planck-Institut für Festkörperforschung
70569 Stuttgart (Germany)
Fax: (+49) 711-689-1662
and
Institut de Physique des Nanostructures
Ecole Polytechnique Fédérale de Lausanne
1015 Lausanne (Switzerland)
E-mail: klaus.kern@fkf.mpg.de

Dr. T. Strunskus, Prof. Dr. C. Wöll
Lehrstuhl für Physikalische Chemie I
Ruhr-Universität Bochum
44780 Bochum (Germany)



Supporting information for this article is available on the WWW under <http://www.angewandte.org> or from the author.

tional ordering of adsorbed organic species,^[26–28] and synthesis of metallocsupramolecular complexes^[28,29] at surfaces has been recognized, their elusive nature poses a challenge in identifying their impact as dynamic active sites.

Our combined scanning tunneling microscopy (STM) and X-ray photoelectron spectroscopy (XPS) studies aim at discriminating the chemical activity of mobile adatoms from that of substrate terraces or static surface defects, such as step edges or kinks. The experiments were conducted under well-defined conditions in two UHV systems equipped with standard facilities for surface and thin-film preparation, which incorporated a home-built STM and a photoelectron detector, respectively. The individual adatoms in the 2D gas phase are highly mobile and cannot be resolved by STM, rather they usually appear as flicker noise in the STM measurements. The XPS measurements were carried out at the HE-SGM beamline at the BESSY II synchrotron in Berlin. Specifically, we considered the deprotonation of a carboxy group by copper. For this purpose, molecules of commercially available trimesic acid (1,3,5-benzenetricarboxylic acid, $C_6H_3(COOH)_3$, TMA, see structural model in Figure 2a) were deposited on a Ag(111) substrate by organic molecular beam epitaxy (OMBE). An electron-beam evaporator was used to deposit small amounts of Cu. The controlled codeposition of Cu and TMA allows the role of Cu adatoms to be identified.

The morphology of the pure TMA molecular films is controlled by the temperature of the Ag substrate. In

particular, it is possible to fabricate hydrogen-bonded open networks by deposition on a substrate at a temperature below 340 K. This TMA supramolecular layer is illustrated by the STM image in Figure 2b, taken from a sample prepared by TMA deposition on a substrate at 120 K followed by warming to room temperature. The corresponding model in Figure 2c shows how dimerization of the self-complementary carboxylic groups accounts for the dominant planar honeycomb domains.^[27,30] The XPS data shown in Figure 2d substantiate this interpretation. In the C 1s region two well-separated peaks are identified at 285.7 and 289.9 eV, which are distinctive features of the six carbon atoms in the phenyl ring and the three carbon atoms in the carboxy groups, respectively.^[31] Accordingly, the broad O 1s signal (full width at half-maximum (fwhm) 4.0 eV at 533.3 eV) can be deconvoluted into two equal-height peaks at 532.5 and 534.0 eV, assigned to oxygen in carbonyl and hydroxy groups, respectively.^[31] These findings prove that the carboxy groups are not affected by the presence of Ag under the employed conditions (i.e., temperatures below 340 K).

To address the reactivity of coadsorbed Cu, TMA molecules were deposited on the cold Ag(111) surface (120 K), and subsequently small amounts of Cu atoms (0.05 monolayers (ML)) were added. The molecules remained unaffected at the low deposition temperature, as evidenced by the corresponding XPS measurements, where again the characteristic peaks of the carboxy groups were resolved both for the C 1s and O 1s levels. However, since regular honeycomb networks are not expected to evolve at 120 K due to the limited molecular mobility at low temperatures,^[32] the Cu atoms are highly dispersed in an irregular organic matrix, where they interact only weakly with the nearby TMA molecules.^[33] Their chemical activity becomes apparent on increasing the substrate temperature. While the details of the respective processes could not be elucidated with the present experimental means, in view of their dynamic behavior involving rapid chemical transitions and structural reorganizations in the adsorbed layer, the pertinent net outcome could be conclusively addressed, that is, the spectroscopic data show dramatic changes in the TMA carboxy groups above 200 K. The analysis of the XPS chemical shifts clearly reveals the formation of a tricarboxylate species at 300 K, that is, complete deprotonation of the carboxylic groups which is associated with the presence of Cu adatoms definitely takes place (see Figure 3a). The carboxy C 1s peak at 289.9 eV disappeared, and the new single peak at 288.7 eV is characteristic for carboxylate carbon.^[31] In the O 1s region a narrowed peak at 530.9 eV (fwhm = 1.8 eV) is detected instead of the broad peak at 533.2 eV. The symmetric peak reflects the two equivalent oxygen atoms in a carboxylate moiety. These findings are substantiated by STM topographic data (Figure 3b) showing complete inhibition of honeycomb network formation, since the underlying hydrogen-bonding motif is absent. Instead, TMA molecules aggregate in disordered agglomerates containing bright protrusions, which are Cu islands formed in the annealing process. This formation of islands reflects appreciable surface mass transport and movement of Cu adatoms. Since carboxy groups are still present after Cu deposition prior to sample annealing, it is concluded

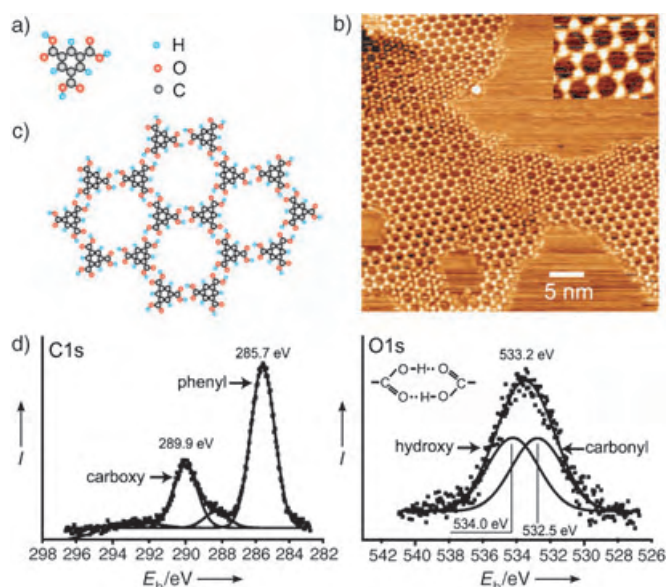


Figure 2. Hydrogen-bonded TMA supramolecular layer. a) Structural model of the TMA molecule. b) Assembly of extended hydrogen-bonded TMA honeycomb networks on Ag(111) following submonolayer deposition on the substrate at 120 K and warming to room temperature. c) Model of the hydrogen-bonded nanoporous supramolecular TMA layer with hydrogen-bond-mediated dimerization of self-complementary carboxy groups. d) XPS data to testify the integrity of the organic molecules (photon energy 400 eV for C, 670 eV for O spectrum). The C 1s position of the phenyl ring and carboxy groups and the convoluted O 1s signal with contributions from carbonyl and hydroxy groups, respectively, are indicated. E_b = binding energy.

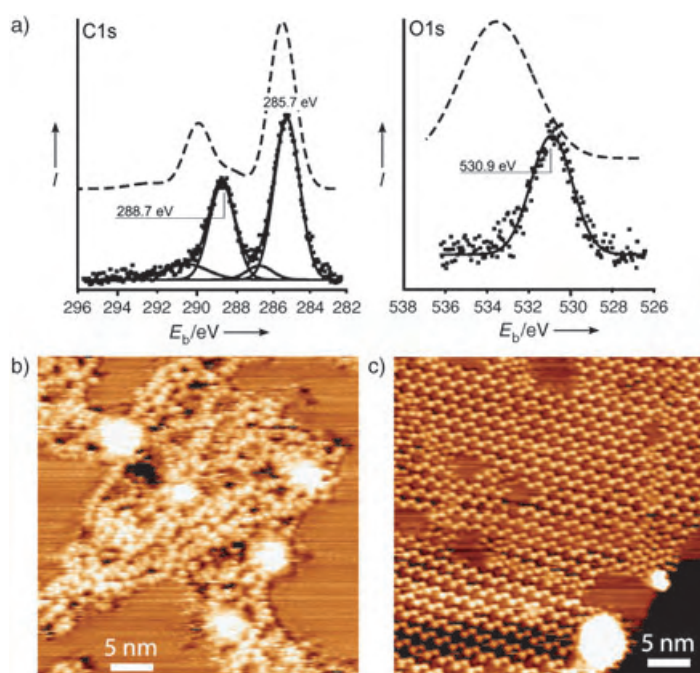


Figure 3. a) XPS data (solid curves) monitoring the chemical changes occurring during warming to 300 K of an intermixed TMA/Cu layer grown at low temperature on Ag(111) (photon energy 400 eV for C, 670 eV for O spectrum). For comparison, spectra of the protonated species are shown as dashed curves. The formation of a TMA tricarboxylate species is reflected by the distinct chemical shift of the higher energy C 1s peak and the characteristic narrowing of the O 1s peak. b) STM image of irregular TMA agglomerates coexisting with Cu islands when TMA and Cu codeposited at 120 K are annealed to room temperature. c) In the presence of predeposited condensed 2D Cu islands deprotonation on warming is negligible, and regular hydrogen-bonded TMA honeycomb networks evolve.

that the deprotonation reaction is not triggered by the impact of Cu in the deposition process; rather it must be mediated by thermal activation and Cu adatoms during warming. The corresponding temperatures are in a range for which recombinative desorption of molecular hydrogen occurs (e.g., on Ag(111) at $T = 190$ K^[34]), a process which is similarly believed to be operative in the present scenario. Furthermore, we performed a series of experiments with varying TMA coverage (0.20, 0.25, 0.40, and 0.45 ML) while keeping the Cu concentration constant. The total amount of Cu condensed in the islands proved to be independent of the TMA coverage and corresponded to the quantity of Cu deposited on a clean surface. This demonstrates the absence of formation of Cu–TMA complexes, observed under similar conditions on a Cu(100) substrate.^[29] Accordingly, no evidence for Cu^{II} species in a carboxylate is found in the Cu 2p_{3/2} XP spectrum, and high-resolution STM images reveal a homogenous character of the islands typical for metals. Consequently, the Cu active sites are not consumed in the deprotonation reaction. The resulting coupling of trimesate to the Ag(111) surface is in agreement with similar bonding schemes encountered with related systems, such as terephthalate layers on Cu(100).^[35]

To clarify whether the boosting of chemical reactivity correlates with the highly dispersed Cu adatoms, control

experiments were performed in which Cu was made available in a 2D condensed form by predepositing the same amount of Cu at room temperature on the clean Ag surface. Subsequently the substrate was cooled to 120 K and TMA was added. After warming to room temperature, the formation of perfect honeycomb structures coexisting with the Cu islands was observed, as shown by the STM image in Figure 3c. The underlying hydrogen bonding implies that TMA deprotonation does not occur in the presence of pregrown Cu islands, with the possible exception of molecules at step edges. The same behavior was encountered with pregrown Cu islands in control experiments in which TMA was codeposited at 300 K. The minute reactivity reflects the fact that the 2D adatom concentration in the presence of Cu islands at room temperature is much smaller than in the highly dispersed state obtained by low-temperature deposition in an organic matrix. Only at elevated temperatures can a 2D Cu gas with appreciable density be expected, but in the present system the chemical activity of the substrate then comes into play. Moreover, in TMA deposition at elevated temperatures both high molecular diffusivity and rotary motions may interfere.

The major difference in the scenarios is that in the first case TMA molecules experience an environment of Cu adatoms whose density is much higher than that of a 2D condensed submonolayer Cu/Ag(111) system. Hence the mobile Cu adspecies have a high probability of coming into contact with the carboxy groups during the warm-up phase, before they eventually aggregate into islands. By contrast, in the second case the Cu adatom density is in thermodynamic equilibrium with the Cu islands and thus much smaller (the 2D vapor pressure is minute at the employed temperature of 120 K); hence, the probability that deprotonation of post-deposited TMA can be mediated by mobile active sites is strongly reduced. Notably, the atomic steps of the Cu island themselves also do not interfere in a significant way. The sharp distinction between the two cases demonstrates that Cu condensation must be associated with drastically decreased chemical reactivity. Consequently, the rate of deprotonation depends on the Cu adatom density, and Cu adatoms are the decisive element mediating carboxy deprotonation, that is, this mobile species is the true active site in this surface chemical reaction.

Our findings reveal that adatom active sites interfering in a surface chemical reaction may be decisive for reaction pathways and formation of final products. Many catalytic surface reactions are run under reaction conditions for which the density of the intrinsic 2D adatom gas of a catalytically active metal is in the percent range. It is likely that these highly mobile atoms are not only the active sites in deprotonation reactions but also promote many other elementary processes. Our observations thus suggest that thermally activated formation and mobility of active sites is of general relevance in surface chemistry and may bestow a dynamic heterogeneity on catalysts.

Received: July 22, 2004

Revised: October 15, 2004

Published online: January 28, 2005

Keywords: heterogeneous catalysis · hydrogen bonds · photoelectron spectroscopy · scanning probe microscopy · surface reactions

- [1] H. S. Taylor, *Proc. R. Soc. London A* **1925**, 108.
- [2] M. Boudart, *J. Mol. Catal.* **1985**, 30, 27–38.
- [3] G. Ertl in *Catalytic Ammonia Synthesis* (Ed.: J. R. Jennings), Plenum, New York, **1991**, p. 109.
- [4] D. W. Goodman, *Chem. Rev.* **1995**, 95, 523–536.
- [5] G. A. Somorjai, K. R. McCrea, J. Zhu, *Top. Catal.* **2002**, 3–4, 157–166.
- [6] T. Zambelli, J. Wintterlin, J. Trost, G. Ertl, *Science* **1996**, 273, 1688–1690.
- [7] S. Dahl, A. Logadottir, R. C. Egeberg, J. H. Larsen, I. Chorkendorff, E. Tornqvist, J. K. Nørskov, *Phys. Rev. Lett.* **1999**, 83, 1814–1817.
- [8] P. Gambardella, Z. Sljivancanin, B. Hammer, M. Blanc, K. Kuhnke, K. Kern, *Phys. Rev. Lett.* **2001**, 87, 056103.
- [9] R. Schaub, R. Thosttrup, N. Lopez, E. Laegsgaard, I. Stensgaard, J. K. Nørskov, F. Besenbacher, *Phys. Rev. Lett.* **2001**, 87, 266104.
- [10] B. Hammer, *J. Catal.* **2001**, 199, 171–176.
- [11] J. Wintterlin, T. Zambelli, J. Trost, J. Greeley, M. Mavrikakis, *Angew. Chem.* **2003**, 115, 2956–2959; *Angew. Chem. Int. Ed.* **2003**, 42, 2850–2853.
- [12] Z.-P. Liu, P. Hu, *J. Am. Chem. Soc.* **2003**, 125, 1958–1967.
- [13] O. Nakagoe, K. Watanabe, N. Takagi, Y. Matsumoto, *Phys. Rev. Lett.* **2003**, 90, 226105.
- [14] S. Abbet, A. Sanchez, U. Heiz, W. D. Schneider, A. M. Ferrari, G. Pacchioni, N. Rösch, *J. Am. Chem. Soc.* **2000**, 122, 3435–3457.
- [15] S. Abbet, U. Heiz, H. Häkkinen, U. Landman, *Phys. Rev. Lett.* **2001**, 86, 5950–5953.
- [16] C. Nozaki, C. G. Lugmair, A. T. Bell, T. D. Tilley, *J. Am. Chem. Soc.* **2002**, 124, 13194–13203.
- [17] M. Giesen, *Prog. Surf. Sci.* **2001**, 68, 1–153.
- [18] J. Kolaczkiewicz, E. Bauer, *Surf. Sci.* **1985**, 155, 700–714.
- [19] M. Nohlen, M. Schmidt, H. Wolter, K. Wandelt, *Surf. Sci.* **1995**, 337, 294–301.
- [20] R. M. Tromp, M. Mankos, *Phys. Rev. Lett.* **1998**, 81, 1050–1053.
- [21] W. Silvestri, A. P. Graham, J. P. Toennies, *Phys. Rev. Lett.* **1998**, 81, 1034–1037.
- [22] J. Kolaczkiewicz, *Surf. Sci.* **1987**, 183, 251–262.
- [23] F. Besenbacher, J. K. Nørskov, *Prog. Surf. Sci.* **1993**, 4, 5–66.
- [24] W. W. Pai, N. C. Bartelt, M. R. Peng, J. E. Reutt-Robey, *Surf. Sci.* **1995**, 330, L67–L685.
- [25] T. Zambelli, J. V. Barth, J. Wintterlin, *Phys. Rev. B* **1998**, 58, 12663–12666.
- [26] C. C. Perry, S. Haq, B. G. Frederick, N. V. Richardson, *Surf. Sci.* **1998**, 409, 512–520.
- [27] A. Dmitriev, N. Lin, J. Weckesser, J. V. Barth, K. Kern, *J. Phys. Chem. B* **2002**, 106, 6907–6912.
- [28] J. V. Barth, J. Weckesser, N. Lin, S. Dmitriev, K. Kern, *Appl. Phys. A* **2003**, 76, 645–652.
- [29] N. Lin, A. Dmitriev, J. Weckesser, J. V. Barth, K. Kern, *Angew. Chem.* **2002**, 114, 4973–4977; *Angew. Chem. Int. Ed.* **2002**, 41, 4779–4783.
- [30] S. Griessl, M. Lackinger, M. Edelwirth, M. Hietschold, W. M. Heckl, *Single Mol.* **2002**, 3, 25–31.
- [31] a) M. Wühh, J. Weckesser, C. Wöll, *Langmuir* **2001**, 17, 7605–7612; b) F. Bournel, C. Laffon, P. Parent, G. Tourillon, *Surf. Sci.* **1996**, 350, 60–78; c) P. Aplincourt, C. Bureau, J. L. Anthoine, D. P. Chong, *J. Phys. Chem. A* **2001**, 105, 7364–7370.
- [32] J. V. Barth, J. Weckesser, G. Trimarchi, M. Vladimirova, A. De Vita, C. Cai, H. Brune, P. Gunter, K. Kern, *J. Am. Chem. Soc.* **2002**, 124, 7991–8000.
- [33] STM data showing the highly dispersed Cu atoms in an irregular TMA matrix before annealing can be found in the Supporting Information.
- [34] X.-L. Zhou, J. M. White, B. E. Koel, *Surf. Sci.* **1989**, 218, 201–210.
- [35] a) M. Lingenfelder, H. Spillmann, A. Dmitriev, S. Stepanow, N. Lin, J. V. Barth, K. Kern, *Chem. Eur. J.* **2004**, 10, 1913–1919; b) S. Stepanow, T. Strunskus, M. Lingenfelder, A. Dmitriev, H. Spillmann, N. Lin, J. V. Barth, C. Wöll, K. Kern, *J. Phys. Chem. B* **2004**, 108, 19392–19397.

Silicon Clusters

Motif Transition in Growth Patterns of Small to Medium-Sized Silicon Clusters**

Soohaeng Yoo and Xiao Cheng Zeng*

Semiconductor clusters are a special class of matter with sizes in between single atoms and semiconductor quantum dots.^[1] Small to medium-sized semiconductor clusters have received considerable attention since the 1980s, largely because of their potential relevance to and applications in the silicon-based nanoelectronics industry. It is known that geometric structures of semiconductor clusters generally bear little resemblance to those of their bulk counterparts.^[2–6] In particular, the Si₆ tetragonal bipyramid, Si₇ pentagonal bipyramid, and Si₁₀ tetracapped trigonal prism are known as magic-number clusters because, on collision or laser vaporization, medium-sized clusters dissociate mainly by loss of these Si₆, Si₇, or Si₁₀ species.^[7,8] Moreover, ion mobility measurement on cluster cations Si_n⁺ has revealed a remarkable growth-pattern transition from “sausagelike” prolate clusters to near-spherical ones over the size range of 25 ≤ *n* ≤ 30.^[9] Despite major advances in experimental characterization of semiconductor clusters in the past decade,^[5–10] the detailed morphology of silicon clusters with sizes larger than ten atoms still cannot be inferred directly from experiments. Hence, structural determination of small to medium-sized

[*] S. Yoo, Prof. X. C. Zeng
Department of Chemistry and
Center for Materials Research & Analysis
University of Nebraska
Lincoln, NE 68588 (USA)
Fax: (+1) 402-472-9402
E-mail: xczeng@phase1.unl.edu

[**] We thank Prof. T. Frauenheim, Prof. K.-M. Ho, Prof. K. A. Jackson, Prof. M. Jarrold, Prof. B. Pan, Dr. A. A. Shvartsburg, Dr. J. L. Wang, and Dr. J. J. Zhao for valuable discussions. This research was supported by grants from DOE (DE-FG02-04ER46164), NSF, Guggenheim Foundation, and Nebraska Research Initiatives (X.C.Z.) and by the Research Computing Facility and Bioinformatics Facility at University of Nebraska-Lincoln.



Supporting information for this article is available on the WWW under <http://www.angewandte.org> or from the author.

semiconductor clusters has heavily hinged on quantum-mechanical calculations in conjunction with the current global search techniques.^[11–18] To date, the global-minimum structures of small neutral silicon clusters Si_n up to $n = 12$ have been well established on the basis of ab initio calculations. Identification of true global-minimum structures for clusters beyond $n = 12$ remains a subject of current research.^[15–17]

Previous unbiased global searches using the genetic algorithm (GA) in conjunction with semiempirical tight-binding and first-principles density functional theory (DFT) have revealed a number of generic features in the growth pattern of small to medium-sized silicon clusters. For example, in the size range of $12 \leq n \leq 18$, Ho et al. reported that the clusters are mostly built up with the tricapped trigonal prism (TTP) Si_9 motif.^[11] Later, Jackson et al. performed unbiased searches using single-parent GA as well as the big-bang method^[12,17] and revealed a motif transition, starting at $n = 19$, from TTP Si_9 to a complex of the Si_6 tetragonal bipyramid and Si_6 sixfold puckered ring. The former Si_6 subunit is the magic-number cluster, whereas the latter is a part of the “adamantane” unit, a fragment of bulk diamond.^[2,5,12,17] Hereafter, we refer to the complex of the Si_6 tetragonal bipyramid and Si_6 sixfold puckered ring as the six/six (Si_6/Si_6) motif. Note that for small clusters it is well known that the addition of one more atom can often cause dramatic structural reorganization. Thus, it is not surprising that abrupt structural transition can occur in the growth pattern of small to medium-sized silicon clusters. However, what is remarkable in this particular case is that the onset of bulk fragments—the Si_6 sixfold puckered ring—occurs in clusters as small as Si_{19} , at which the growth pattern undergoes a TTP-to-six/six motif transition. Here we present a new global-minimum structure of Si_{16} obtained by using a computational approach that combines the unbiased basin-hopping (BH) global optimization method^[18] with first-principles DFT. Through this DFT-BH approach, we demonstrate that the TTP-to-six/six motif transition occurs at even a smaller size of lowest energy cluster, that is, Si_{16} . Furthermore, through high-level ab initio calculation (at the CCSD(T) level) and DFT calculations at the PBE1PBE level with two large basis sets, we show that the new isomeric structure is slightly more stable than all low-lying structures of Si_{16} reported to date. We also show that by keeping the six/six motif as the seed in the DFT-BH search, not only can we reproduce previously reported lowest energy structures of Si_{19} , Si_{20} , and Si_{21} ,^[12,17] but we also find new low-lying structures of Si_{17} , Si_{18} , and Si_{22} , all built upon the six/six motif.

First, we performed an unbiased DFT-BH search for the global-minimum structures of smaller sized silicon clusters Si_n ($12 \leq n \leq 16$), starting with several arbitrarily selected initial structures. Despite marked differences among the initial structures, the DFT-BH search indeed gives rise to the same lowest energy isomeric structure, typically, within 1000 Monte Carlo (MC) trials. We found lowest energy structures of Si_{13} and Si_{14} identical to those reported recently by Tekin and Hartke,^[15] and of Si_{12} and Si_{15} identical to those reported by Ho et al.^[11] However, we also obtained a lowest energy structure of Si_{16} (Si_{16a}) that differs from that reported (Si_{16b})^[11] (see Figure 1); the latter has a TTP motif. Note that in the

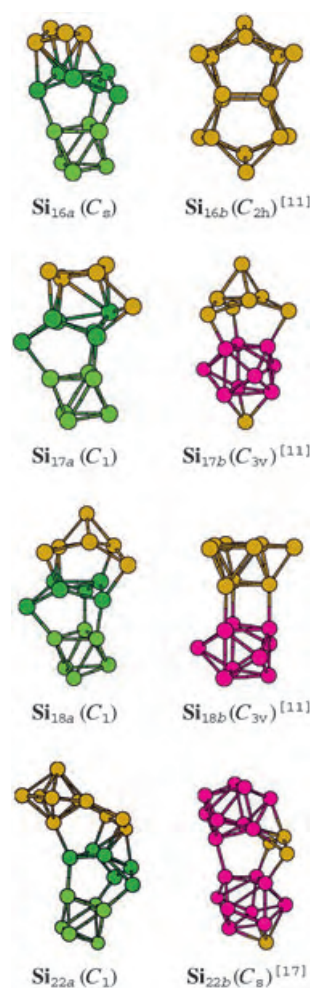


Figure 1. Lowest energy and low-lying isomers predicted in this work (left column) and those reported previously (right column).^[11,17] The Si_6 tetragonal bipyramid and the Si_6 sixfold puckered ring structural subunits (i.e., the six/six (Si_6/Si_6) structural motif) are highlighted in light green and dark green, respectively, and the Si_9 tricapped trigonal prism (TTP) motif is highlighted in pink.

DFT-BH searches we selected two types of GGA exchange-correlation functional (BLYP and PBE, see Methods). Independent of the functional selected, the unbiased searches yield the identical global-minimum structure Si_{16a} .

Next, we reoptimized the Si_{16a} and Si_{16b} structures using all-electron DFT with a modest basis set, namely, B3LYP/6-311G(2d) and PBE1PBE/6-311G(2d) implemented in the Gaussian03 code.^[19] Again, both optimizations indicate that Si_{16a} is more stable than Si_{16b} . Finally, to provide more convincing evidence that the newly obtained isomer Si_{16a} is the true global minimum, we also calculated the single-point energy of Si_{16a} and Si_{16b} using a high-level ab initio molecular orbital theory with a modest basis set (CCSD(T)/cc-PVDZ), as well as using DFT (PBE1PBE) with two large basis sets (6-311G(3df) and cc-PVTZ). All calculations are based on the optimized isomeric structures at the PBE1PBE/6-311G(2d) level/basis set. The calculated total energies, including zero-point energy corrections (see Supporting Information) are listed in Table 1. All results show that the newly obtained

Table 1: Total energies [Hartree] of the lowest energy (Si_{16a}) and low-lying (Si_{16b}) isomers of Si_{16} . The binding energies per atom [eV/atom] are shown in parentheses.^[a]

Basis set	Si_{16a}	Si_{16b}
B3LYP/6-311G(2d)	−4632.2049 (3.230)	−4632.2041 (3.228)
PBE1PBE/6-311G(2d)	−4630.1482 (3.631)	−4630.1430 (3.622)
CCSD(T)/cc-PVDZ	−4624.4528	−4624.4513
PBE1PBE/6-311G(3df)	−4630.2044	−4630.1984
PBE1PBE/cc-PVTZ	−4630.2355	−4630.2341

[a] The single-point energy calculations at CCSD(T) level with the cc-PVDZ basis set and DFT (PBE1PBE) level with both 6-311G(3df) and cc-PVTZ basis sets are all based on structures optimized at PBE1PBE/6-311G(2d) level/basis set. The zero-point energy correction (see Supporting Information) is included in the total energy and the binding energy per atom, calculated with the 6-311G(2d) basis set.

isomer Si_{16a} is slightly lower in energy than Si_{16b} , that is, Si_{16a} is the leading candidate for the global minimum of Si_{16} . More interestingly, we find that Si_{16a} contains the six/six motif, which may suggest that the TTP-to-six/six motif transition may start at an even smaller size of cluster, namely, Si_{16} instead of Si_{19} .

To confirm the above speculation, we examined, through unbiased DFT-BH global searches, whether the global-minimum structures of Si_{17} and Si_{18} contain the six/six motif. However, because the number of local minima increases exponentially with cluster size, an unbiased first-principles BH global search becomes increasingly demanding of CPU time for larger clusters (which also have many more electrons). In fact, even though the same lowest-energy structure of Si_{16} can be obtained from an unbiased DFT-BH search with less than 5000 MC trials (regardless of the initial structure), the unbiased search starts to show dependence on initial structure starting from Si_{17} , at least within a few thousand MC trials. From our previous experience of BH searches with empirical potential of silicon,^[20] the number of MC trials required to locate the true global minima for some medium sized clusters may be up to the order of 10^4 or even 10^5 . However, for a first-principles DFT-BH search, 10^5 MC trials would require more than one year CPU time on our 16-CPU AMD Athlon cluster.

We therefore undertook a more efficient (but biased) search—a DFT-BH search with a fixed seed—in order to examine the possibility of finding new low-lying structures of Si_{17} and Si_{18} that are built on the six/six motif. To this end, during the DFT-BH search, we kept the structural integrity of the six/six motif (the seed) while allowing the remaining silicon atoms to undergo the MC trial. Remarkably, this biased DFT-BH search (with the BLYP GGA functional) not only can reproduce the global-minimum structures of Si_{19} , Si_{20} , and Si_{21} reported previously,^[12,16,17] but also can produce new low-lying isomers of Si_{17} , Si_{18} , and Si_{22} (see Si_{17a} , Si_{18a} , and Si_{22a} in Figure 1). These new isomers are appreciably lower in energy than the lowest energy isomers published previously (Si_{17b} , Si_{18b} , and Si_{22b}),^[11–17] which all contain the TTP motif. We also relaxed these six isomers using all-electron DFT with modest basis sets, that is, B3LYP/6-311G(2d) and PBE1PBE/6-311G(2d).^[19] Table 2 lists the calculated total energies, including zero-point energy corrections (see Supporting Information), and the binding energies per atom. These

Table 2: Total energies [Hartree] of low-lying silicon clusters shown in Figure 1. The binding energies per atom [eV/atom] are shown in parentheses.^[a]

Si_n	B3LYP/6-311G(2d)	PBE1PBE/6-311G(2d)
Si_{17a}	−4921.7345 (3.256)	−4919.5471 (3.655)
Si_{17b}	−4921.7214 (3.235)	−4919.5443 (3.650)
Si_{18a}	−5211.2486 (3.257)	−5208.9368 (3.662)
Si_{18b}	−5211.2267 (3.224)	−5208.9318 (3.654)
Si_{22a}	−6369.3400 (3.302)	−6366.5154 (3.707)
Si_{22b}	−6369.3235 (3.281)	−6366.5128 (3.704)

[a] The zero-point energy correction (see Supporting Information) is included in the total energy and the binding energy per atom.

energy data show that the new low-lying isomers built on the six/six motif are indeed more stable than the isomers built on the TTP motif. The fact that the six/six motif emerges in all low-lying clusters of Si_{16} – Si_{22} suggests that the sixfold puckered ring plus magic-number cluster complex may be viewed as another type of generic structural motif in the growth pattern of small to medium-sized silicon cluster besides the well-known TTP motif. The latter emerges only in smaller silicon clusters starting from Si_{10} and ending at Si_{15} , and the TTP-to-six/six motif transition occurs at Si_{16} . Figure 2 graphically illustrates this TTP-to-six/six motif transition. In passing, we note that Jackson et al.^[17] have recently shown through an unbiased search that the growth pattern for medium-sized cluster cations Si_n^+ undergoes another major structural transformation, that is, the prolate-to-spherical-like structural transformation, at $n \approx 27$. Combining our theoretical results with theirs, we conclude that in the evolution of silicon clusters from small to medium size, that is, from $n \approx 16$ to $n \approx 26$, the prolate-shaped lowest energy clusters are likely to contain a sixfold puckered ring plus magic-number cluster motif, where the magic-number cluster can be Si_6 (i.e., six/six motif) or Si_{10} . The six/ten ($\text{Si}_6/\text{Si}_{10}$) motif, which can be viewed as the third type of generic structural motif, starts at $n = 23$ (see Figure 2).

In summary, we have found a new global minimum of Si_{16} as well as low-lying isomers of Si_{17} , Si_{18} , and Si_{22} using a DFT-BH computational approach. These new low-lying isomers are all built on the generic six/six (Si_6/Si_6) motif, and they are lower in energy than those built on the well-known TTP Si_9 motif. We show that the TTP-to-six/six motif transition occurs at Si_{16} . Prior to the onset of the prolate-to-spherical-like growth-pattern transformation at $n \approx 27$, all prolate-shaped clusters are likely built on generic structural motifs of the sixfold puckered ring plus a magic-number cluster, where the magic-number cluster can be Si_6 or Si_{10} .^[17] The six/six-to-six/ten motif transition appears to occur at $n \approx 23$. Finally, the prolate-to-spherical-like (e.g., endohedral silicon fullerenes^[22]) structural transition is likely to occur at $n \approx 27$.^[17]

Experimental Section

To seek lowest-energy geometric structures for small to medium-sized clusters, we adopted the basin-hopping (BH) method^[18] and combined it with first-principles DFT with two types of exchange-correlation functional (BLYP and PBE). Both types of functional are

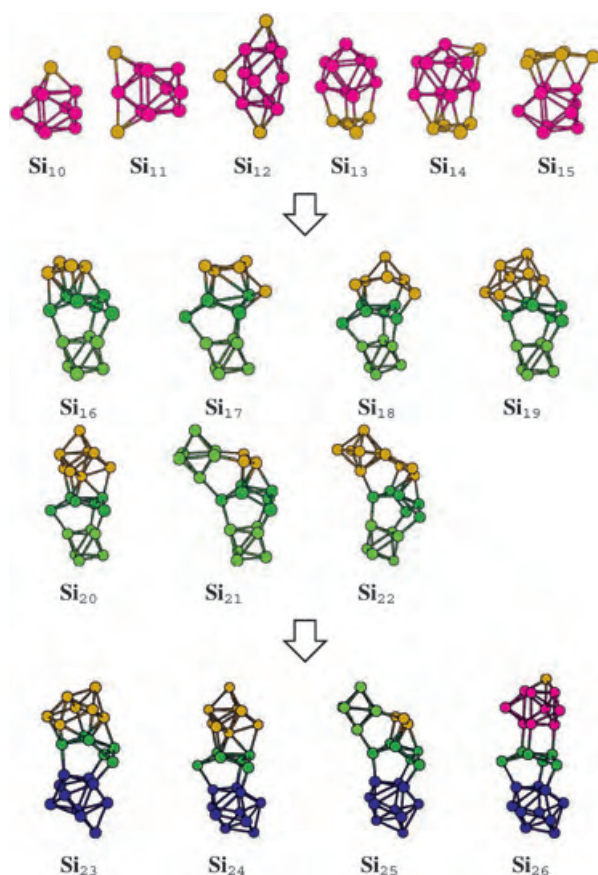


Figure 2. Lowest energy isomers (Si_{10} – Si_{15}) predicted previously,^[11,15] those reported in this work (Si_{16} – Si_{18} , Si_{22}), and those (Si_{19} – Si_{21} , and Si_{23} – Si_{26}) predicted by Jackson et al.^[12,17] The Si_9 TTP motif is high-lighted in pink. The Si_6 tetragonal bipyramid, the Si_6 sixfold puckered ring, and the Si_{10} magic-number cluster structural subunits are high-lighted in light green, dark green, and dark blue, respectively.

implemented in CPMD code.^[21] The source code of CPMD is freely available to academic researchers. Therefore, we were able to merge our BH Monte Carlo code with the CPMD code. In the DFT-BH search, we used the Monte Carlo scheme to explore the potential energy surface transformed by the DFT structural optimization, i.e., we calculated the potential energy and energy gradient using subroutines for DFT energy minimization implemented in the CPMD source code. Once the lowest energy isomers were identified, all-electron DFT calculations at the B3LYP/6-311G(2d) and PBE1PBE/6-311G(2d) levels/basis set (implemented in the Gaussian03 code^[19]) were carried out to further relax the isomers (with no symmetry constraint). Harmonic vibrational analysis at the B3LYP/6-311G(2d) and PBE1PBE/6-311G(2d) levels/basis set was also performed to assure that the isomers are local minima with no imaginary frequency. Zero-point energies are reported in the Supporting Information. For Si_{16} , all-electron ab initio molecular orbital calculations at the coupled-cluster single and double substitutions (including triple excitations) CCSD(T) theory with cc-PVDZ basis set, as well as DFT (PBE1PBE) calculations with both 6-311G(3df) and cc-PVTZ basis sets,^[19] were also carried out to confirm that the new isomer Si_{16} has a lower single-point energy than the previously reported global-minimum structure Si_{16b} .

Received: August 21, 2004
Revised: November 5, 2004
Published online: January 26, 2005

Keywords: ab initio calculations · cluster compounds · density functional calculations · silicon

- [1] A. P. Alivisatos, *Science* **1996**, *271*, 933–936.
- [2] D. Tománek, M. A. Schlüter, *Phys. Rev. Lett.* **1986**, *56*, 1055–1058.
- [3] W. L. Brown, R. R. Freeman, K. Raghavachari, M. Schlüter, *Science* **1987**, *235*, 860–865.
- [4] K. Raghavachari, C. M. Rohlfing, *J. Chem. Phys.* **1988**, *89*, 2219–2234.
- [5] M. F. Jarrold, *Science* **1991**, *252*, 1085–1092.
- [6] E. C. Honea, A. Ogura, C. A. Murray, K. Raghavachari, W. O. Sprenger, M. F. Jarrold, W. L. Brown, *Nature* **1993**, *366*, 42–45.
- [7] Q. L. Zhang, Y. Liu, R. F. Curl, F. K. Tittel, R. E. Smalley, *J. Chem. Phys.* **1988**, *88*, 1670–1677.
- [8] M. F. Jarrold, J. E. Bower, *J. Phys. Chem.* **1989**, *92*, 5702–5705.
- [9] M. F. Jarrold, V. A. Constant, *Phys. Rev. Lett.* **1991**, *67*, 2994–2997.
- [10] C. C. Arnold, D. Neumark, *J. Chem. Phys.* **1993**, *99*, 3353–3362.
- [11] K.-M. Ho, A. A. Shvartsburg, B. Pan, Z.-Y. Lu, C.-Z. Wang, J. G. Wacker, J. L. Fey, M. F. Jarrold, *Nature* **1998**, *392*, 582–585; B. Liu, Z.-Y. Lu, B. Pan, C.-Z. Wang, K.-M. Ho, A. A. Shvartsburg, M. F. Jarrold, *J. Chem. Phys.* **1998**, *109*, 9401–9409.
- [12] I. Rata, A. A. Shvartsburg, M. Horoi, T. Frauenheim, K. W. M. Siu, K. A. Jackson, *Phys. Rev. Lett.* **2000**, *85*, 546–549.
- [13] B. X. Li, P. L. Cao, S.-C. Zhan, *Phys. Lett. A* **2003**, *316*, 252–260.
- [14] S. Yoo, X. C. Zeng, X. Zhu, J. Bai, *J. Am. Chem. Soc.* **2003**, *125*, 13318–13319.
- [15] A. Tekin, B. Hartke, *Phys. Chem. Chem. Phys.* **2004**, *6*, 503–509.
- [16] A. A. Shvartsburg, M. Horoi, K. A. Jackson, *Spectroscopy of Emerging Materials*, Kluwer, Berlin, **2004**.
- [17] K. A. Jackson, M. Horoi, I. Chaudhuri, T. Frauenheim, A. A. Shvartsburg, *Phys. Rev. Lett.* **2004**, *93*, 0134011–0134014.
- [18] D. J. Wales, H. A. Scheraga, *Science* **1999**, *285*, 1368–1372.
- [19] Gaussian03 (Revision A.1), M. J. Frisch, G. W. Trucks, H. B. Schlegel, G. E. Scuseria, M. A. Robb, J. R. Cheeseman, J. A. Montgomery, Jr., T. Vreven, K. N. Kudin, J. C. Burant, J. M. Millam, S. S. Iyengar, J. Tomasi, V. Barone, B. Mennucci, M. Cossi, G. Scalmani, N. Rega, G. A. Petersson, H. Nakatsuji, M. Hada, M. Ehara, K. Toyota, R. Fukuda, J. Hasegawa, M. Ishida, T. Nakajima, Y. Honda, O. Kitao, H. Nakai, M. Klene, X. Li, J. E. Knox, H. P. Hratchian, J. B. Cross, C. Adamo, J. Jaramillo, R. Gomperts, R. E. Stratmann, O. Yazyev, A. J. Austin, R. Cammi, C. Pomelli, J. W. Ochterski, P. Y. Ayala, K. Morokuma, G. A. Voth, P. Salvador, J. J. Dannenberg, V. G. Zakrzewski, S. Dapprich, A. D. Daniels, M. C. Strain, O. Farkas, D. K. Malick, A. D. Rabuck, K. Raghavachari, J. B. Foresman, J. V. Ortiz, Q. Cui, A. G. Baboul, S. Clifford, J. Cioslowski, B. B. Stefanov, G. Liu, A. Liashenko, P. Piskorz, I. Komaromi, R. L. Martin, D. J. Fox, T. Keith, M. A. Al-Laham, C. Y. Peng, A. Nanayakkara, M. Challacombe, P. M. W. Gill, B. Johnson, W. Chen, M. W. Wong, C. Gonzalez, J. A. Pople, Gaussian, Inc., Pittsburgh, PA, **2003**.
- [20] S. Yoo, X. C. Zeng, *J. Chem. Phys.* **2003**, *119*, 1442–1450.
- [21] J. Hutter, A. Alavi, T. Deutsch, M. Bernasconi, S. Goedecker, D. Marx, M. Tuckerman, M. Parrinello, CPMD, Version 3.7.1, MPI für Festkörperforschung Stuttgart, **1997–2001**.
- [22] S. Yoo, J. Zhao, J. Wang, X. C. Zeng, *J. Am. Chem. Soc.* **2004**, *126*, 13845–13849.

Biotechnology

Single Protein Pores Containing Molecular Adapters at High Temperatures**

Xiao-feng Kang, Li-Qun Gu, Stephen Cheley, and Hagan Bayley*

Protein pores are being developed for use in biotechnology.^[1] Many applications require that pores be stable at high temperatures. Herein we report single-molecule activity measurements on three proteinaceous membrane pores at temperatures close to 100 °C. We also show that one of the pores can bind a molecular adapter, β -cyclodextrin (β CD), at elevated temperatures. The complex retains the ability to recognize small molecules which permits stochastic sensing in aqueous solution under extreme conditions (Figure 1a). The structures of many integral membrane proteins remain intact at high temperatures,^[2] and the existence of extremophiles implies that membrane proteins function at 100 °C and above.^[3] However, few measurements of membrane-protein activity have been made at temperatures above 55 °C, and none have been made for ion channels and pores. The photocycle of bacteriorhodopsin, for example, has been examined at temperatures up to 85 °C.^[4] The activity is compromised above 60 °C because the chromophore, a *trans*-retinal Schiff base, isomerizes to the 13-*cis* form. Transmembrane proton pumping was not measured directly in these experiments. Macroscopic current recordings with valinomycin, a macrocyclic antibiotic, have been carried out at up to 80 °C in bilayers comprising lipids from the hyperthermophile *Caldariella acidophila*.^[5] In the case of proteinaceous channels and pores, activity has been measured at up to 55 °C. For example, multichannel recordings of vanilloid receptors (temperature-sensitive cation channels) have been made after expression in *Xenopus* oocytes, and several subtypes of the receptor remain active at 55 °C.^[6] Recently,

single-channel recordings of the vanilloid receptor VR1 have been made at up to 55 °C.^[7] The transmembrane domains of these proteins are presumed to be largely α -helical.

Measurements on the pore-forming toxin α -hemolysin (α HL), one of the proteins examined in the present work, have been made previously at up to 50 °C.^[8–10] This protein is largely made up of β structure. Indeed, all three of the proteins examined herein contain β barrels, which are formed from either a single subunit (OmpG), seven subunits (α HL), or eight subunits (Luk). OmpG is a 280-residue polypeptide that most likely forms a β barrel of 16 antiparallel strands. Unlike most porins, which are trimeric, OmpG functions as a monomer.^[11] The homoheptameric pore formed by α HL is a mushroom-shaped structure.^[12] The stem of the mushroom is a 14-stranded transmembrane β barrel with two strands contributed by each subunit. The stem is capped by a large hollow extracellular domain. The Luk pore contains two subunit types, F and S, which are related in sequence and structure to α HL.^[13,14] The pore is a heterooctamer containing four F and four S subunits.^[15] Despite the presence of only one additional subunit, the unitary conductance of the Luk pore is more than three times that of the α HL pore.^[16]

Previous work established the electrical stability of lipid bilayers at high temperatures. For example, planar bilayers made with bipolar lipids from the hyperthermophile *Caldariella acidophila* are stable at up to 80 °C.^[5] Our experiments were carried out with planar bilayers made from 1,2-diphytanoyl-*sn*-glycero-3-phosphocholine (DPhPC), which exist as a single phase at up to 120 °C as determined by NMR spectroscopy and X-ray diffraction.^[17] In our hands, the bilayers remained stable at 98 °C as determined by capacitance measurements (Supporting Information). The saturated isoprenoid side chains of DPhPC resemble those found in certain thermophiles^[18] and may contribute to the stability of the bilayers. Multichannel current recordings in response to a temperature ramp were carried out on wild-type α HL pores incorporated as preformed heptamers into DPhPC bilayers from the *cis* chamber. In all the experiments reported herein, both chambers contained 1 M NaCl with 10 mM sodium phosphate at pH 7.5, and unless otherwise noted, recordings were made at –40 mV. The α HL pores were stable at up to 94 °C (Supporting Information), which is surprising. Wild-type α HL pores had been shown by SDS-polyacrylamide gel electrophoresis to be stable in SDS at up to 65 °C.^[19,20] The present experiments show that the pores are both stable and functional at much higher temperatures.

Single-channel current traces of wild-type α HL pores were obtained at up to 93 °C (Figure 1b). The single-channel current increased linearly from 26.4 pA at 22 °C to 91.9 pA at 93 °C. In a similar manner, single-channel recordings were obtained from the Luk and OmpG pores (Figure 1c). Again the currents increased linearly with temperature: Luk, 72.0 pA at 23 °C to 210 pA at 90 °C; OmpG, 25.5 pA at 25 °C to 101 pA at 97 °C. The highest temperatures quoted are those that were reached before technical problems were encountered (such as the insertion of a second channel), or a reverse temperature ramp was intentionally initiated; the pores may well be stable at yet higher temperatures. The occurrence of numerous spikes toward zero current^[21] dis-

[*] H. Bayley

Department of Chemistry, University of Oxford
Oxford, OX1 3TA (UK)

Fax: (+44) 1865-275-708

E-mail: hagan.bayley@chem.ox.ac.uk

X.-f. Kang, S. Cheley

Department of Medical Biochemistry and Genetics
The Texas A&M University System Health Science Center
College Station, TX 77843-1114 (USA)

L.-Q. Gu

Department of Biological Engineering, and
Dalton Cardiovascular Research Center
University of Missouri
Columbia, MO 65211 (USA)

[**] Work at Texas A&M University was supported by DARPA, the DoD Tri-Service Technology Program, DOE, NASA, NIH, and ONR. H.B. is the holder of a Royal Society–Wolfson Research Merit Award. We thank L. Jayasinghe and S. Conlan for the leukocidin and OmpG proteins.



Supporting information, including experimental details, for this article is available on the WWW under <http://www.angewandte.org> or from the author.

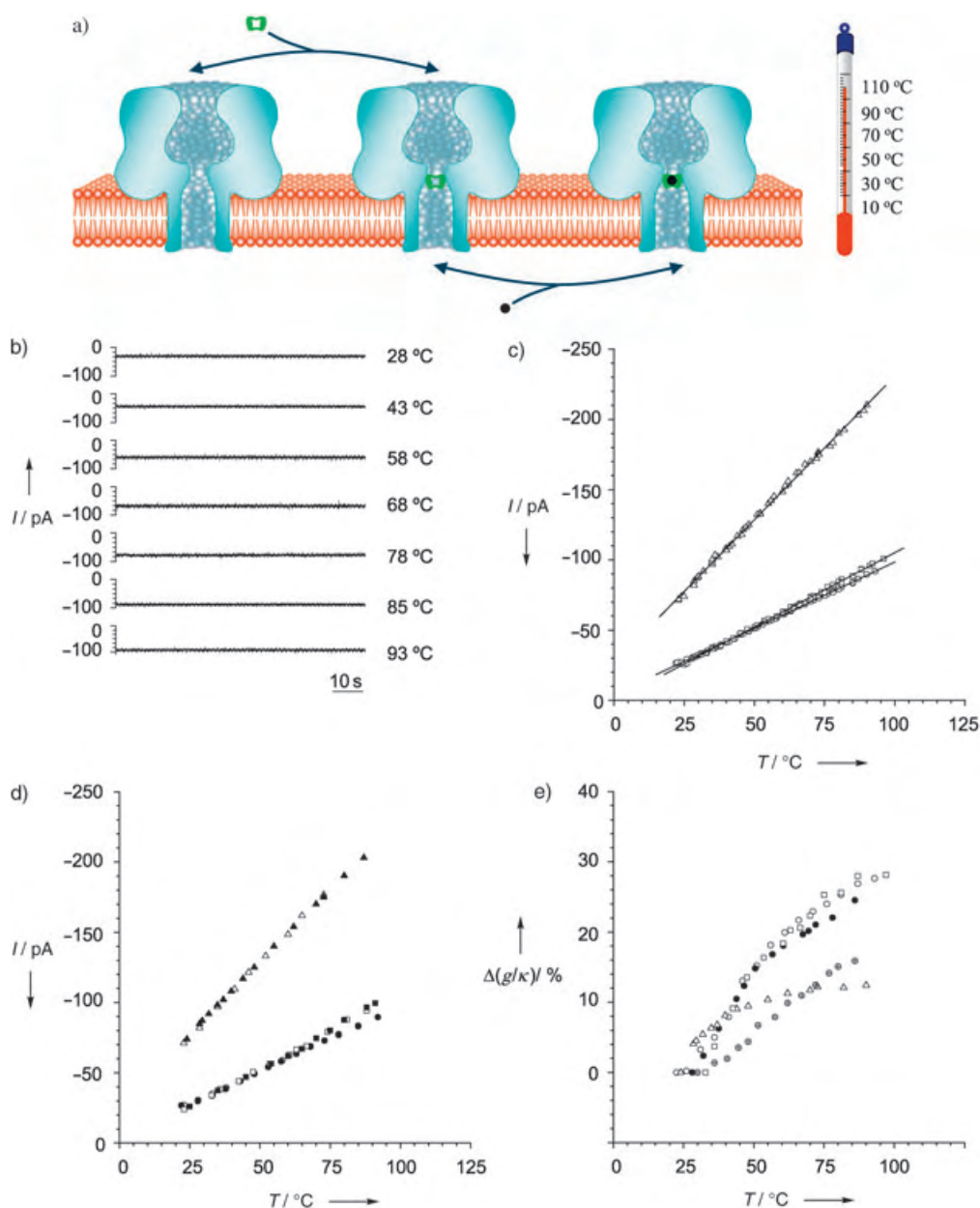


Figure 1. Single-channel currents at elevated temperatures. The buffer in both chambers was sodium phosphate (10 mM, pH 7.5), containing NaCl (1 M). Transmembrane potential was -40 mV. a) Schematic representation of one of the pores used in this work. Three states of the α HL pore in a lipid bilayer are shown. At high temperatures, the unoccupied pore (left) retains its ability to bind molecular adapters such as β CD (center, rendered in green), which can in turn bind guest molecules (right, shown in black). b) Representative single-channel current traces of unoccupied wild-type α HL pores at different temperatures. c) The variation of single-channel currents with temperature for wild-type α HL (\circ), Luk (Δ), and OmpG (\square) pores. The experimental values from four different experiments are compiled in each plot. The single-channel currents depended linearly on the temperature: wild-type α HL, $I(\text{pA}) = 4.18 + 0.944 T(^{\circ}\text{C})$ ($R = 0.999$); Luk, $I(\text{pA}) = 26.4 + 2.04 T(^{\circ}\text{C})$ ($R = 0.999$); OmpG, $I(\text{pA}) = 0.373 + 1.05 T(^{\circ}\text{C})$ ($R = 0.999$). d) The changes in single-channel currents are reversible: wild-type α HL (\circ, \bullet), Luk (Δ, \blacktriangle), and OmpG (\square, \blacksquare) pores. The data are from single representative experiments. Empty symbols represent data obtained as temperature increased, the filled symbols show data collected as temperature subsequently decreased. e) Plots of the percent change in g/κ as a function temperature for wild-type α HL (\circ), (M113N) $_7$ (\bullet), (M113N) $_7$ - β CD (\oplus), OmpG (\square) and Luk (Δ) pores. The values at 23°C were set to 0%. Single-channel conductance values (g) were from Figure 1 c, with additional data for (M113N) $_7$ and (M113N) $_7$ - β CD obtained under the same conditions (Supporting Information). Values of solution conductivity (κ) were determined from a linear fit to experimental κ values measured at different temperatures. α HL = α -hemolysin; β CD = β -cyclodextrin; Luk = leukocidin; (M113N) $_7$ = Met113-to-Asn replacement on α HL, in which all seven subunits bear the mutation.

tinguished the OmpG traces from those of the α HL pore, which has a similar conductance, thereby ruling out sample contamination. Again, the stabilities of the Luk and OmpG

pores were surprising based on their established properties in detergent solutions. Luk pores dissociate in SDS at $\approx 78^{\circ}\text{C}$,^[15b] and the OmpG protein unfolds in *n*-octyl- β -D-

glucopyranoside at 63 °C.^[11] The changes in single-channel current associated with the temperature ramp were fully reversible (Figure 1 d). Three main factors contributed to the ability to record single-channel currents at high temperatures (Supporting Information). First was the use of an aperture with a diameter of $\approx 100 \mu\text{m}$. (With a larger orifice, multiple channels were incorporated too readily and the bilayer tended to break.) Second, bilayers were formed with a large mass of DPhPC (200 μg lipid per chamber; electrolyte volume = 1.5 mL, surface area = 0.72 cm^2). Third, dilute protein samples were used (experimental details can be found in the Supporting Information).

The strong temperature dependence of the single-channel conductance values (g) of the three pores is largely a result of the variation of solution conductivity (κ) with temperature, which suggests that there is no appreciable molecular reorganization or subunit dissociation at elevated temperatures. The conductivity of the buffer was found to increase linearly with temperature from 20 to 90 °C ($\kappa = 3.74 + 0.19 T \text{ S m}^{-1}$ (T = temperature in °C; $R = 0.998$ for all data points plotted from three experiments)), which is similar to literature values for 1M NaCl.^[22] When g/κ is plotted as a function of temperature, the value increases slightly with temperature for all the pores examined (Figure 1 e). For the Luk pore, g/κ increases by $\approx 13\%$ over the 70 °C range. For wild-type αHL , the αHL mutant form (M113N)₇, and OmpG, the changes in g/κ are larger at 26%, 25%, and 24%, respectively. Because these relatively wide pores allow the passage of hydrated ions, the dominant effect of κ in determining g is reasonable. The small change in g/κ with temperature did not result from a change in the pH value of the solution nor from the development of a small electrical potential in the apparatus (Supporting Information). Therefore, the most likely explanation derives from the mechanism of ion transport through the pores. While the pores we have examined transport hydrated ions, they are weakly ion-selective. The selectivity derives from the interactions of the ions with the walls of the pore lumen. As the temperature increases, these interactions are weakened and the conductance of the pore increases to a greater extent than would be predicted from bulk conductivity measurements. By comparison with the β barrels, it is notable that the gating kinetics of several channels, including the temperature-gated vanilloid receptors, are characterized by dramatic responses to temperature (at $< 55^\circ\text{C}$).^[23]

We discovered earlier that host molecules such as cyclodextrins can become lodged within the αHL pore, where they can in turn bind guest molecules (Figure 1 a).^[24] In the work described herein, we examined the interaction of βCD with the (M113N)₇ pore at high temperatures. At room temperature, (M113N)₇ binds βCD > 10000 -fold more tightly than the wild-type protein.^[25] At 31 °C, βCD binding events with a mean duration (τ_{off}) of 14 s are observed (Figure 2). As the temperature increases, several phenomena are observed at a fixed βCD concentration:

1. The conductance values of both the unoccupied and occupied states of the pore increase.
2. Short additional blockades from the (M113N)₇ βCD level (substates) are observed. The frequency of occurrence of

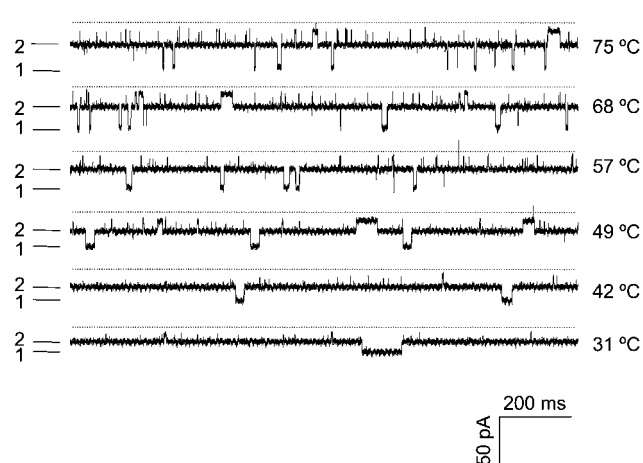


Figure 2. Interaction of βCD with (M113N)₇ pores. Representative traces obtained at various temperatures. Broken line, zero current; level 1, current through open (M113N)₇ pores; level 2, current through (M113N)₇ βCD . The conditions were as described in Figure 1 caption.

these events was independent of βCD concentration, so they do not arise from the binding of a second βCD molecule. Instead, they are assigned as a second conformation of the occupied state, (M113N)₇ βCD . Perhaps they represent the rotation of βCD at the binding site or dewetting transitions^[26] within the narrow cyclodextrin ring.

3. The dwell time of βCD (τ_{off}) and the intervals between the binding events (τ_{on}) both decrease.

In earlier work at room temperature, we showed that βCD takes part in a simple binary interaction with (M113N)₇.^[25] By a kinetic analysis, we confirmed that this was also the case at 78 °C (Supporting Information). Measurements of the mean dwell time (τ_{off}) and the mean inter-event interval (τ_{on}) were used to derive association (k_{on}) and dissociation (k_{off}) rate constants for βCD . At 25 °C, the values were $4.5 \pm 0.6 \times 10^5 \text{ M}^{-1} \text{ s}^{-1}$ and $0.031 \pm 0.01 \text{ s}^{-1}$ ($n = 3$) respectively, yielding $(k_{\text{on}}/k_{\text{off}}) = K_f = 1.5 \times 10^7 \text{ M}^{-1}$. (The literature reports a K_f value of $7.7 \times 10^6 \text{ M}^{-1}$, which was determined in a different sequence background for αHL , “RL2”, which might explain the small difference).^[25] This value is over 10000-fold greater than the value for the interaction of wild-type αHL with βCD ($K_f = 290 \text{ M}^{-1}$) reported previously.^[25] As the temperature increased, k_{on} and k_{off} increased. For example, at 85 °C, the highest temperature reached in these experiments, k_{on} increased ≈ 15 -fold to $6.5 \pm 0.8 \times 10^6 \text{ M}^{-1} \text{ s}^{-1}$ and k_{off} increased ≈ 800 -fold to $25.0 \pm 0.3 \text{ s}^{-1}$ ($n = 3$) over the values at 25 °C. Because there is a larger increase in k_{off} than with k_{on} as temperature increases, the formation constant K_f decreased to $2.6 \times 10^5 \text{ M}^{-1}$ at 85 °C.

From the slope of a linear fit to $\ln K_f$ versus $1/T$ (Supporting Information), ΔH° and ΔS° values were found to be $-60 \pm 4 \text{ kJ mol}^{-1}$ and $-62 \pm 5 \text{ J mol}^{-1} \text{ K}^{-1}$ respectively, yielding a value of $\Delta G^\circ = -41 \pm 3 \text{ kJ mol}^{-1}$ at 25 °C ($n = 4$). The value of ΔH° is close to that for the binding of βCD to glucoamylase, whereas the value of ΔS° for glucoamylase is a less favorable $-90 \text{ J mol}^{-1} \text{ K}^{-1}$,^[27–29] suggesting a more favor-

able preorganization of the binding site in (M113N)₇, which would be augmented by the matching C₇ symmetry of the αHL pore and βCD. By comparison, for the formation of an eight-nucleotide DNA duplex under similar conditions,^[10] $\Delta H^\circ = -144 \text{ kJ mol}^{-1}$, $\Delta S^\circ = -359 \text{ J mol}^{-1} \text{ K}^{-1}$, and $\Delta G^\circ = -37 \text{ kJ mol}^{-1}$. In this case, a highly favorable enthalpic contribution compensates for a far larger entropic penalty. Interestingly, binding experiments with βCD and the heteromeric^[30,31] pore containing one wild-type (WT) subunit (WT₁(M113N)₆) yielded $\Delta H^\circ = -51 \pm 2 \text{ kJ mol}^{-1}$, $\Delta S^\circ = -59 \pm 3 \text{ J mol}^{-1} \text{ K}^{-1}$, and $\Delta G^\circ = -33 \pm 2 \text{ kJ mol}^{-1}$ at 25 °C (Supporting Information). The decrease in affinity brought about by the loss of one asparagine residue is almost entirely derived from a change in ΔH° , again suggesting a preorganized binding site.

Values of ΔG^\ddagger , ΔH^\ddagger and ΔS^\ddagger for βCD and (M113N)₇ were determined by using $\ln k/\phi = -(\Delta H^\ddagger/R) \cdot 1/T + \Delta S^\ddagger/R$; ϕ is a frequency factor in a simplified transition-state theory that is useful for comparisons with related systems (Supporting Information).^[32,33] For the dissociation of βCD, $\Delta H^\ddagger = 99 \text{ kJ mol}^{-1}$ and $\Delta S^\ddagger = 130 \text{ J mol}^{-1} \text{ K}^{-1}$, with ϕ at 1 ns^{-1} .^[33] At 25 °C, $\Delta G^\ddagger = 60 \text{ kJ mol}^{-1} = 24 RT$; at 85 °C, $\Delta G^\ddagger = 53 \text{ kJ mol}^{-1} = 21 RT$. For the association of βCD, $\Delta H^\ddagger = 39 \text{ kJ mol}^{-1}$ and $\Delta S^\ddagger = 66 \text{ J mol}^{-1} \text{ K}^{-1}$ when $\phi = 1 \text{ ns}^{-1}$. Association at 25 °C gives $\Delta G^\ddagger = 19 \text{ kJ mol}^{-1} = 7.7 RT$; at 85 °C $\Delta G^\ddagger = 15 \text{ kJ mol}^{-1} = 6.1 RT$. The value of $\Delta S^\ddagger = 130 \text{ J mol}^{-1} \text{ K}^{-1}$ for dissociation can be compared with the value of $310 \text{ J mol}^{-1} \text{ K}^{-1}$ ($\phi = 1 \text{ ns}^{-1}$) for the dissociation of the duplex formed by two complementary eight-base DNA strands.^[10] In the latter case, the approach to the transition state must reflect a relatively large increase in disorder by comparison with that in βCD dissociation.

βCD is a host for a wide variety of guest molecules.^[34] Therefore, the αHL pore equipped with βCD as a molecular adapter can act as a sensor element for the stochastic detection of small organic compounds.^[24] Herein we demonstrate this approach at elevated temperatures with adamantane-1-carboxylic acid as a model analyte.^[24] Although the (M113N)₇ pore binds βCD at high temperatures, the appearance of substates (partial closures during occupancy by βCD, Figure 2), which are dependent on both temperature and the applied potential, limits its use in stochastic detection. We therefore used a homoheptameric pore made from the double mutant M113F/K147N, which has the following characteristics (unpublished work): 1. there are no substates during occupancy by βCD; 2. the binding affinity for βCD is high, with K_f (*trans*) = $1.3 \pm 0.2 \times 10^5 \text{ M}^{-1}$ at -40 mV ($n = 4$), in comparison with wild-type αHL,^[25] K_f (*trans*) = $3.0 \times 10^2 \text{ M}^{-1}$; and interestingly, 3. βCD binds from both the *cis* and *trans* sides of the bilayer. In wild-type αHL and most mutant forms, βCD binds only from the *trans* side. βCD (*cis*) bound to (M113F/K147N)₇ for extended periods ($\tau_{\text{off}} = 7.0 \pm 0.3 \text{ s}$ at -60 mV ($n = 3$)), during which an interaction with adamantane-1-carboxylic acid (*trans*) could be observed (Figure 3). At 22 and 65 °C, we ascertained that the mean residence time (τ_{off}) of the analyte was independent of analyte concentration and that $1/\tau_{\text{on}}$ (τ_{on} denotes the inter-event interval) was linearly dependent on the analyte concentration; this is diagnostic of a bimolecular interaction between the analyte

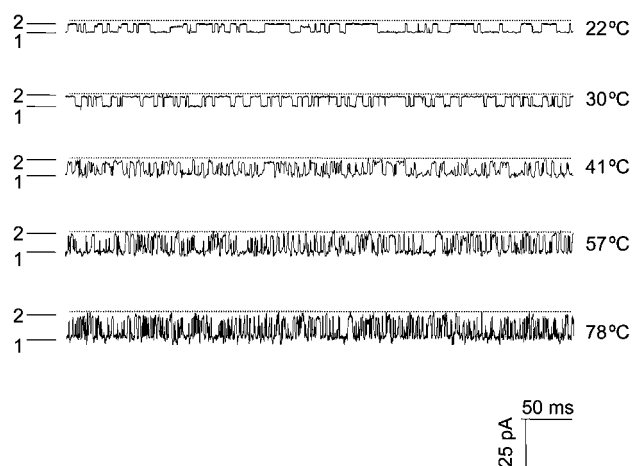


Figure 3. Interaction of the model analyte adamantane-1-carboxylic acid with βCD lodged in the (M113F/K147N)₇ pore. Representative traces showing the interaction of (M113F/K147N)₇-βCD with adamantane-1-carboxylic acid at various temperatures. βCD (40 μM) was applied to the *cis* side of the bilayer; adamantane-1-carboxylic acid (20 μM) was applied to the *trans* side. All other conditions were as described in Figure 1 caption, except the applied potential was -60 mV . Broken line, zero current; level 1, (M113F/K147N)₇-βCD; level 2, (M113F/K147N)₇-βCD blocked with adamantane-1-carboxylic acid. (M113N/K147N)₇ = mutant form of αHL, in which all seven subunits bear the double mutation Met113- and Lys147-to-Asn.

and βCD.^[25,35] Kinetic constants were determined from τ_{on} and τ_{off} values. Over the temperature range from 22 to 78 °C, k_{on} for adamantane-1-carboxylic acid increased by about sixfold from $2.5 \pm 0.2 \times 10^6 \text{ M}^{-1} \text{ s}^{-1}$ ($n = 3$) to $1.4 \pm 0.1 \times 10^7 \text{ M}^{-1} \text{ s}^{-1}$ ($n = 3$), and k_{off} increased by ≈ 43 -fold from $2.1 \pm 0.2 \times 10^2 \text{ s}^{-1}$ ($n = 3$) to $9.3 \pm 0.6 \times 10^3 \text{ s}^{-1}$ ($n = 3$) (Supporting Information). The corresponding K_f values at 22 and 78 °C, were $1.2 \pm 0.1 \times 10^4 \text{ M}^{-1}$ and $1.5 \pm 0.1 \times 10^3 \text{ M}^{-1}$, respectively. From a plot of $\ln K_f$ versus $1/T$ (Supporting Information), we obtained ΔH° and ΔS° values of $-31 \pm 2 \text{ kJ mol}^{-1}$ and $-28 \pm 1 \text{ J mol}^{-1} \text{ K}^{-1}$, respectively, yielding $\Delta G^\circ = -23 \pm 2 \text{ kJ mol}^{-1}$ at 25 °C ($n = 3$). At least seven values for the standard thermodynamic constants are available in the literature for adamantane-1-carboxylic acid as the carboxylate.^[34] They are in rough agreement with each other: $\Delta H^\circ = -22 \text{ kJ mol}^{-1}$, $\Delta S^\circ = +10 \text{ J mol}^{-1} \text{ K}^{-1}$, $\Delta G^\circ = -25 \text{ kJ mol}^{-1}$. Although the value of ΔG° is close to that obtained in our work, ΔH° and ΔS° differ. Within the αHL pore, the enthalpy change for the interaction is more favorable, but a less favorable $T\Delta S^\circ$ compensates. Perhaps the βCD presents only one face to the guest presented from the *trans* side or the βCD is in a different conformation when lodged inside the pore than it is in solution. Pore-bound βCD may form a binding site that offers more favorable noncovalent bonding interactions, but which is associated with, for example, less favorable solvent reorganization.

Our experiments show that the properties of protein pores can be examined at temperatures approaching 100 °C at the single-molecule level by planar bilayer recording. The approach we have developed will be useful in studies of the fundamental functional properties of ion channels, and how they fold and assemble. All three pores that we examined

contain transmembrane β barrels, and it will be interesting to apply this approach to channels that are predominantly α -helical. The pores we examined are functional at high temperature, although they originate in mesophilic bacteria. It will also be worth examining channels and pores from thermophiles to understand how they contribute to the physiology of these organisms.^[3] From the biotechnological point of view, the ability to observe channels and pores at high temperatures will aid our ability to engineer stable membrane proteins^[1] to act as components of devices such as sensors^[36] or DNA sequencers.^[37] In that respect, we have shown herein that an α HL pore containing a molecular adapter retains its ability to bind a model analyte at elevated temperatures. Recently, we have used the α HL pore as a nanoreactor for the examination of single-molecule chemistry.^[38–40] The ability to record at high temperatures will greatly extend the power of this methodology.

Received: September 3, 2004

Revised: October 16, 2004

Published online: January 28, 2005

Keywords: host–guest systems · ion channels · membrane proteins · sensors · single-molecule studies

- [1] H. Bayley, L. Jayasinghe, *Mol. Membr. Biol.* **2004**, *21*, 209–220.
- [2] T. Haltia, E. Freire, *Biochim. Biophys. Acta* **1995**, *1241*, 295–322.
- [3] L. J. Rothschild, R. L. Mancinelli, *Nature* **2001**, *409*, 1092–1101.
- [4] J. Wang, M. A. El-Sayed, *Biophys. J.* **2000**, *78*, 2031–2036.
- [5] A. Gliozza, R. Rolandi, M. De Rosa, A. Gambacorta, *J. Membr. Biol.* **1983**, *75*, 45–56.
- [6] M. J. Caterina, T. A. Rosen, M. Tominaga, A. J. Brake, D. Julius, *Nature* **1999**, *398*, 436–441.
- [7] B. Liu, K. Hui, F. Qin, *Biophys. J.* **2003**, *85*, 2988–3006.
- [8] G. Belmonte, L. Cescatti, B. Ferrari, T. Nicolussi, M. Ropele, G. Menestrina, *Eur. Biophys. J.* **1987**, *14*, 349–358.
- [9] A. Meller, L. Nivon, E. Brandin, J. Golovchenko, D. Branton, *Proc. Natl. Acad. Sci. USA* **2000**, *97*, 1079–1084.
- [10] S. Howorka, L. Movileanu, O. Braha, H. Bayley, *Proc. Natl. Acad. Sci. USA* **2001**, *98*, 12996–13001.
- [11] S. Conlan, H. Bayley, *Biochemistry* **2003**, *42*, 9453–9465.
- [12] L. Song, M. R. Hobaugh, C. Shustak, S. Cheley, H. Bayley, J. E. Gouaux, *Science* **1996**, *274*, 1859–1865.
- [13] R. Olson, H. Nariya, K. Yokota, Y. Kamio, E. Gouaux, *Nat. Struct. Biol.* **1999**, *6*, 134–140.
- [14] J.-D. Pédelacq, L. Maveyraud, G. Prévost, L. Baba-Moussa, A. González, E. Courcelle, W. Shepard, H. Monteil, J.-P. Samama, L. Mourey, *Structure* **1999**, *7*, 277–288.
- [15] a) G. Miles, L. Movileanu, H. Bayley, *Protein Sci.* **2002**, *11*, 894–902; b) L. Jayasinghe, personal communication.
- [16] G. Miles, S. Cheley, O. Braha, H. Bayley, *Biochemistry* **2001**, *40*, 8514–8522.
- [17] H. Lindsey, N. O. Petersen, S. I. Chan, *Biochim. Biophys. Acta* **1979**, *555*, 147–167.
- [18] V. Luzzati, A. Gambacorta, M. DeRosa, A. Gulik, *Annu. Rev. Biophys. Chem.* **1987**, *16*, 25–47.
- [19] A. C. McNiven, P. Owen, J. P. Arbuthnott, *J. Med. Microbiol.* **1972**, *5*, 113–122.
- [20] B. Walker, H. Bayley, *Protein Eng.* **1995**, *8*, 491–495.
- [21] S. Conlan, Y. Zhang, S. Cheley, H. Bayley, *Biochemistry* **2000**, *39*, 11845–11854.
- [22] V. V. M. Lobo, J. L. Quaresma, *Handbook of Electrolyte Solutions*. Part B, Elsevier, New York, **1989**.
- [23] M. Pusch, U. Ludewig, T. J. Jentsch, *J. Gen. Physiol.* **1997**, *109*, 105–116.
- [24] L.-Q. Gu, O. Braha, S. Conlan, S. Cheley, H. Bayley, *Nature* **1999**, *398*, 686–690.
- [25] L.-Q. Gu, S. Cheley, H. Bayley, *J. Gen. Physiol.* **2001**, *118*, 481–494.
- [26] O. Beckstein, M. S. P. Sansom, *Proc. Natl. Acad. Sci. USA* **2003**, *100*, 7063–7068.
- [27] B. W. Sigurskjold, B. Svensson, G. Williamson, H. Driguez, *Eur. J. Biochem.* **1994**, *225*, 133–141.
- [28] B. W. Sigurskjold, T. Christensen, N. Payre, S. Cottaz, H. Driguez, B. Svensson, *Biochemistry* **1998**, *37*, 10446–10452.
- [29] J. Sauer, T. Christensen, T. P. Frandsen, E. Mirgorodskaya, K. A. McGuire, H. Driguez, P. Roepstorff, B. W. Sigurskjold, B. Svensson, *Biochemistry* **2001**, *40*, 9336–9346.
- [30] O. Braha, B. Walker, S. Cheley, J. J. Kasianowicz, L. Song, J. E. Gouaux, H. Bayley, *Chem. Biol.* **1997**, *4*, 497–505.
- [31] S. Howorka, S. Cheley, H. Bayley, *Nat. Biotechnol.* **2001**, *19*, 636–639.
- [32] H. Gutfreund, *Kinetics for the Life Sciences*, Cambridge University Press, Cambridge, **1995**.
- [33] O. S. Andersen, *J. Gen. Physiol.* **1999**, *114*, 589–590.
- [34] M. V. Rekharsky, Y. Inoue, *Chem. Rev.* **1998**, *98*, 1875–1917.
- [35] E. Moczydlowski in *Ion Channel Reconstitution* (Ed.: C. Miller), Plenum, New York, **1986**, pp. 75–113.
- [36] H. Bayley, P. S. Cremer, *Nature* **2001**, *413*, 226–230.
- [37] D. W. Deamer, D. Branton, *Acc. Chem. Res.* **2002**, *35*, 817–825.
- [38] S.-H. Shin, T. Luchian, S. Cheley, O. Braha, H. Bayley, *Angew. Chem.* **2002**, *114*, 3859–3861; *Angew. Chem. Int. Ed.* **2002**, *41*, 3707–3709.
- [39] T. Luchian, S.-H. Shin, H. Bayley, *Angew. Chem.* **2003**, *115*, 1970–1973; *Angew. Chem. Int. Ed.* **2003**, *42*, 1926–1929.
- [40] T. Luchian, S.-H. Shin, H. Bayley, *Angew. Chem.* **2003**, *115*, 3896–3901; *Angew. Chem. Int. Ed.* **2003**, *42*, 3766–3771.

Supramolecular Chemistry

[2]Pseudorotaxanes through Second-Sphere Coordination**

*Barry A. Blight, Kevin A. Van Noortwyk,
James A. Wisner,* and Michael C. Jennings*

Interlocked compounds such as rotaxanes and catenanes have become increasingly common as synthetically accessible targets over the past two decades owing to the emergence of a number of highly effective template methods for their synthesis.^[1] Some of these strategies have employed the direct coordination of organic ligands to transition metals to achieve an interlocked geometry. The use of a metal center in this

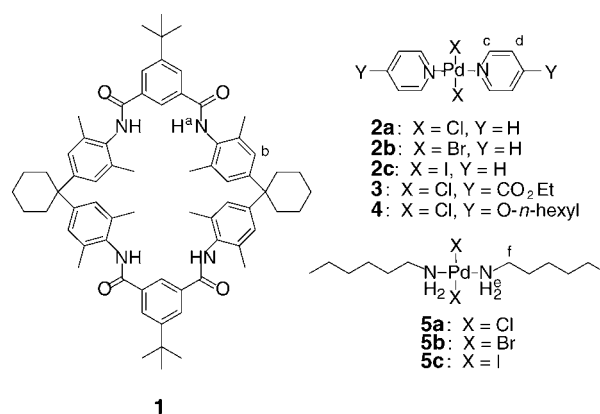
[*] B. A. Blight, K. A. Van Noortwyk, Prof. J. A. Wisner, Dr. M. C. Jennings
The University of Western Ontario
London, Ontario N6A 5B7 (Canada)
Fax: (+1) 519-661-3022
E-mail: jwisner@uwo.ca

[**] We thank the Natural Sciences and Engineering Research Council of Canada for financial support of this research.

context varies widely. Metals have been applied as an organizational template to arrange organic ligands into the appropriate topology for further covalent reaction,^[1d,f,2] coordinated to a terminal ligation point on a prethreaded axle to “stopper” a pseudorotaxane complex,^[3] or as a reversible link in the backbone of wheel-shaped components to permit their thermodynamic macrocyclization.^[4] These designs are attractive owing to the desirable properties that transition-metal complexes can impart to the interlocked structure, such as redox and photophysical activity.^[5]

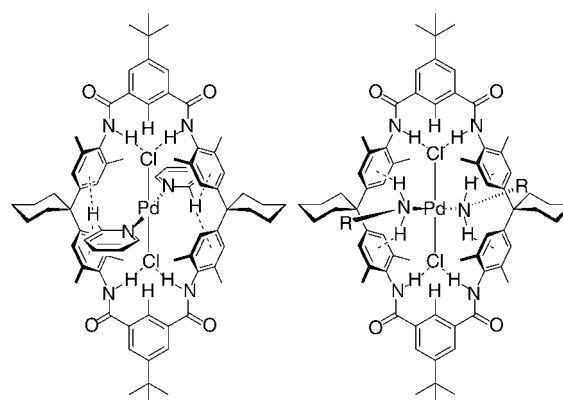
The common theme in all of these approaches is an exploitation of direct, or first-sphere, coordination of a metal atom by organic ligands. A natural extension of these strategies is the application of two or more of them in a single synthetic step. This type of integration is difficult to rationalize using first-sphere coordination alone, given the common ambiguity of multiple ligand exchanges in metal complexes of sufficient lability to be useful for thermodynamic self-assembly. However, this uncertainty may be avoided by separating the coordination spheres within which each function of the metal template is exploited. Thus, by utilizing first-sphere coordination of a metal atom to form an axle-shaped molecule and subsequent second-sphere coordination of the resulting complex by a macrocycle, the metal center may fulfill two template roles within the same supramolecular assembly. Here we demonstrate how a new template, which involves a well-known macrocyclic isophthalamide-based tetralactam system and simple preassembled *trans*-palladium dihalide complexes, produces [2]pseudorotaxanes through second-sphere coordination. Given the wide literature precedent for the thermodynamic palladium-based self-assembly of supramolecular architectures,^[6] this template should provide the foundation for the generation of a considerable range of complex interlocked compounds in a single synthetic step.

The template was based on the potential interaction of an isophthalamide subunit through hydrogen bonding to a metal-bound chloride ligand. Isophthalamide-based compounds have been shown to form complexes with chloride anions preferentially over other halides because of shape complementarity with their hydrogen-bond-donating clefts.^[7] This complexation has also been shown to template the formation of interpenetrated and interlocked compounds in an appropriately designed system.^[8] Ligation of the chloride anion to a transition metal was expected to reduce its hydrogen-bond-acceptor character significantly. However, it was anticipated that enough residual electron density would remain on the chloride ligands such that they might still interact with isophthalamide-containing compounds in a similar manner to the free anions, although less strongly. To increase the magnitude of a possible template effect, we wished to incorporate two pairs of potential chloride–isophthalamide conjugates within the design.^[9] These considerations led to the use of *trans*-palladium dihalide complexes as the axle-shaped molecules and a macrocycle with two opposing isophthalamide moieties incorporated in the ring (Scheme 1). An analysis of several spacers between the isophthalamide subunits using molecular models resulted in the choice of macrocycle **1**, which has been used in the



Scheme 1. Structures of the macrocyclic and axle-shaped components of the [2]pseudorotaxanes.

synthesis of pseudorotaxanes, rotaxanes, and catenanes for a number of years.^[10] The spacing of the isophthalamide clefts within the macrocycle was calculated by using molecular models to be a near-identical match to the spacing of the chloride ligands in the palladium complexes. Another advantage was the further possibility of attractive C–H... π and N–H... π interactions between the aromatic diphenylcyclohexyl sidewalls of **1** and acidic protons of the pyridine or hexylamine ligands of **2–5** upon interpenetration (Scheme 2).^[11]



Scheme 2. Proposed [2]pseudorotaxane structures with potential stabilizing noncovalent interactions highlighted (dashed lines).

Titration of **1** with each of the potential axles **2–5** were carried out in solution in CDCl₃, and the resulting proton shifts were monitored by NMR spectroscopy.^[12] This allowed the evaluation of the strength of any potential complexation as well as providing diagnostic information as to the nature of the complexes formed (Table 1). In all of the cases examined, except that of **2c**, there exists both a 1:1 equilibrium and a generally much weaker 2:1 (macrocycle:axle) equilibrium.^[13] The two series of axles **2a–c** and **5a–c** exhibit the same overall trends with respect to the extent of complex formation under the conditions studied. As the size of the halide ligand increases from Cl < Br < I, both the magnitude of the association constants and the proton shifts at equivalent concentrations diminish substantially. The amide protons of **1** (H^a) in all of the complexes shift downfield with respect to

Table 1: Association constants ($K_{1:1}$ and $K_{2:1}$), free energies of complexation (ΔG), and selected ^1H NMR shifts of **2–5** with **1** in CDCl_3 at 298 K.

Complex	$K_{1:1} [\text{M}^{-1}]$	$-\Delta G_{1:1} [\text{kJ mol}^{-1}]$	$K_{2:1} [\text{M}^{-1}]$	$-\Delta G_{2:1} [\text{kJ mol}^{-1}]$	H^a	H^b	H^c	H^d	H^e	H^f
1-2a	5.0×10^3	19.3	2.0×10^2	12.0	0.63	0.15	−0.63	−0.10	–	–
1-2b	7.5×10^2	15.0	1.1×10^2	10.6	0.18	0.05	−0.14	−0.04	–	–
1-2c	4.0×10^1	8.4	–	–	0.02	0.01	−0.01	−0.01	–	–
1-3	2.4×10^3	17.7	4.5×10^2	13.9	0.47	0.13	−0.49	−0.09	–	–
1-4	5.5×10^3	19.5	1.8×10^2	11.8	0.91	0.22	−0.34	−0.29	–	–
1-5a	5.0×10^4	24.6	2.0×10^1	6.8	1.21	0.16	–	–	−0.50	−0.21
1-5b	4.2×10^3	18.9	1.2×10^2	10.8	0.56	0.08	–	–	−0.47	−0.15
1-5c	4.2×10^2	13.7	1.1×10^2	10.7	0.03	0.01	–	–	−0.02	−0.06

[a] Shifts determined from 1:1 mixtures at a concentration of $5 \times 10^{-4} \text{ M}$.

their free components and this is consistent with hydrogen bonding to the halide ligands, which are the only hydrogen-bond acceptors present in these axles. These results are mirrored by previous observations involving halide anions and isophthalamide receptors which display similar selectivity owing to both the hydrogen-bond-acceptor ability of the halides and a reduction in size-complementarity between the larger anions and the hydrogen-bond-donating clefts of the receptor.^[7]

Axles **3** and **4** were investigated to determine the effect of modifying the donating ability of the pyridine ligands on the strength of complexation. An electron-withdrawing substituent at the 4-position of the pyridine rings in **3** decreases its association constant with **1** by roughly half. We interpreted this as a result of a decrease in electron density on the palladium metal center, which in turn decreases electron density on the chloride co-ligands and renders them less-effective hydrogen-bond acceptors. However, axle **4**, which incorporates an electron-donating 4-hexyloxy substituent on the pyridine rings, only increases the association constant with **1** by 10%, an amount that lies within the error margins of the values determined. While this result does not invalidate our hypothesis, it is clear that this relationship warrants a more detailed analysis to fully elicit its basis.

Upfield shifts of acidic protons H^c – H^f in both types of neutral ligands were observed which are indicative of $\text{C-H}\cdots\pi$ and $\text{N-H}\cdots\pi$ interactions with the aryl sidewalls of **1**. This is concomitant with a downfield shift of protons H^b in the macrocycle. However, the shifts of protons on the aryl sidewalls of the cavity may be a result of both interactions with the neutral ligands, as well as inductive effects from the amide $\text{N-H}\cdots\text{Cl}$ hydrogen bonds. In any case, the evidence from the NMR spectra fully supports the anticipated interpenetrated geometry of the complexes.

Confirmation of the [2]pseudorotaxane geometry of the 1:1 complexes in the solid state was obtained by single-crystal X-ray diffraction studies. Slow diffusion of isopropyl ether into solutions of **1-2a** and **1-5a** in chloroform yielded pale yellow crystals which were suitable for crystallographic analysis.^[14,15] Complex **1-2a** crystallized in space group $P\bar{1}$ to yield two conformationally different centrosymmetric pseudorotaxanes per unit cell. The two complexes have very similar interpenetrated geometries and only differ significantly in the disposition of the neutral ligands of **2a** with

respect to the aryl sidewalls of **1**. In both cases, the Cl-Pd-Cl axes are canted in relation to the least-squares planes of the macrocyclic rings by an angle of 25° and diverge from the planes that bisect the isophthalamide rings by 5 – 6° .^[16] This arrangement results in short contacts between the hydrogen atoms of the amide groups and the chloride ligands ($\text{N-Cl} = 3.30$ – 3.40 \AA , $\text{N-H-Cl} = 154$ – 159°) and reveals the hydrogen-bonding interactions anticipated in the original design. Apparently the Cl-Cl

distance of the axle is slightly too long to allow the halide ligands to completely reside within the isophthalamide clefts of **1**. Thus, the amide groups of the isophthalamide subunits deviate from coplanarity with the attached *tert*-butylphenyl rings by 10 – 25° to maintain the hydrogen-bonding contacts observed. The aryl C-H groups that further define the isophthalamide clefts also have contacts with the halide ligands ($\text{C-Cl} = 3.54$ and 3.56 \AA , $\text{C-H-Cl} = 143$ and 144°).

The two complexes present different relationships between the pyridine ligands of the axles and the aryl sidewalls of the macrocycle. In the first case (Figure 1), the

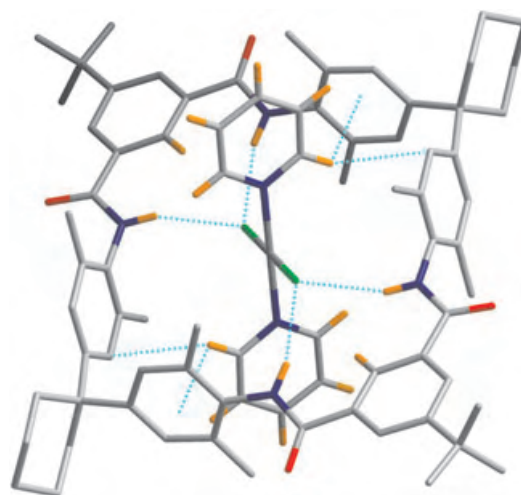


Figure 1. Stick representation of the solid-state structure of **1-2a** (conformer 1). For clarity, all hydrogen atoms have been removed from the macrocycle except those engaged in noncovalent interactions (light-blue dashed lines).

pyridine ligands are tilted into the cleft, which is defined by the sidewalls, and engage in $\text{C-H}\cdots\pi$ interactions that involve the protons at the 2-positions of the pyridine rings. The distances between the hydrogen atoms of the pyridine rings to the least-squares planes of the aryl rings are 3.03 and 2.97 \AA , and their respective $\text{C-H}\cdots\text{plane}$ angles are 152 and 150° ($\text{C}\cdots\pi(\text{least-squares plane}) = 3.47$ and 3.43 \AA , respectively). In contrast, the faces of the pyridine ligands of the second complex (Figure 2) point towards the opening of the iso-

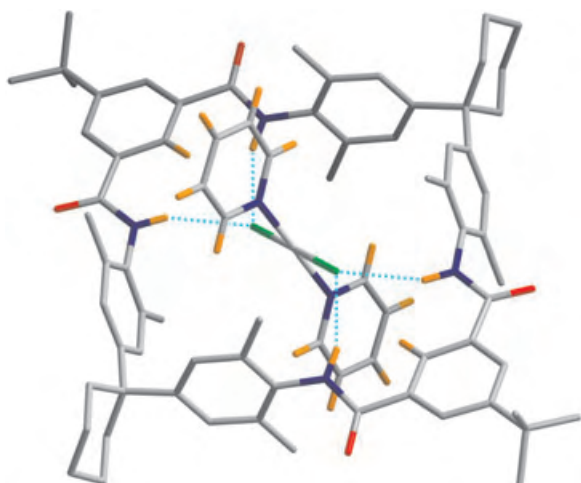


Figure 2. Stick representation of the solid-state structure of **1-2a** (conformer 2). For clarity, all hydrogen atoms have been removed from the macrocycle except those engaged in noncovalent interactions (light-blue dashed lines).

phthalamide clefts of the macrocycle. However, the protons at the 2- and 6-positions of the pyridine rings do not interact significantly with the aryl rings of **1**.

Complex **1-5a** also crystallized in space group $P\bar{1}$, but was modeled as a single centrosymmetric pseudorotaxane in the unit cell (Figure 3). The geometry is similar to **1-2a** in that the chloride ligands of the axle do not fully reside within the isophthalamide cavities. In this example, the Cl-Pd-Cl axis forms an angle with both the mean plane of the macrocyclic ring and in relation to the plane that bisects the isophthalamide ring of 14° .^[16] Only one amide hydrogen atom per isophthalamide subunit is hydrogen-bonded to the chloride ligands (N-Cl = 3.38 Å, N-H-Cl = 154°) and remains coplanar with its attached *tert*-butylphenyl ring to within 1° . The other

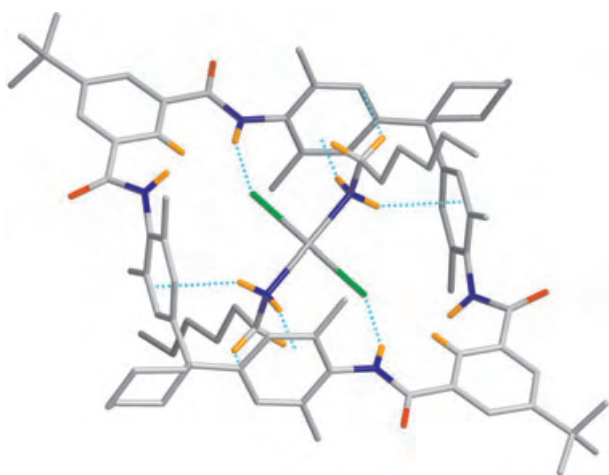


Figure 3. Stick representation of the solid-state structure of **1-5a**. All hydrogen atoms have been removed from the structure except those that define the isophthalamide cleft and the amine protons of the neutral ligands and their corresponding α protons. Noncovalent interactions between the two components have been indicated by light-blue dashed lines.

amide group deviates from coplanarity by 26° and, although it has a short contact with the chloride ligands (N-Cl = 3.40 Å), the N-H-Cl angle is too acute to provide an effective hydrogen bond (N-H-Cl = 119°). The C-H groups which complete the isophthalamide clefts of the macrocycle also display contacts with the chloride ligands (C-Cl = 3.62 Å, C-H-Cl = 172°).

The neutral hexylamine ligands engage the aryl sidewalls of **1** through four N-H $\cdots\pi$ interactions (N $\cdots\pi$ (least-squares plane) = 3.25 and 3.51 Å; NH $\cdots\pi$ = 2.36 and 2.73 Å, and N-H \cdots plane = 167° and 148° , respectively), which are augmented by two more stabilizing C-H $\cdots\pi$ interactions that involve the α protons of the hexyl chains (C $\cdots\pi$ (least-squares plane) = 3.60 Å; CH $\cdots\pi$ = 3.05 Å, C-H \cdots plane = 146°). The hexyl chains attached to the amines extend through opposite faces of the macrocycle in an extended all-*anti* conformation to give an interpenetrated complex geometry.

In summary, the results discussed here demonstrate the viability of a new template route to [2]pseudorotaxanes using second-sphere coordination to form the complexes. We are currently developing the synthesis of interlocked molecules such as rotaxanes and catenanes by this method with more-complex ligand systems.^[17] Furthermore, we believe that this approach will be amenable to other metal centers and anionic ligands, a goal we are actively pursuing.

Experimental Section

Compounds **1**,^[18a] **2a-b**,^[18b] **2c**,^[18c] **3**,^[18d] **4**,^[18e] and **5**^[18f] were prepared according to reported procedures and were characterized by ^1H and ^{13}C NMR spectroscopy as well as by high resolution ESI-MS. ^1H and ^{13}C NMR spectra were recorded on 400 MHz Varian Mercury and 600 MHz Varian Inova spectrometers, respectively, with the residual solvent peak used as reference. CDCl_3 used in the NMR titration experiments was purchased from Cambridge Isotope Laboratories and dried over 4 Å molecular sieves before use.

Received: October 20, 2004

Published online: January 31, 2005

Keywords: host-guest systems · hydrogen bonds · rotaxanes · self-assembly

- [1] See, for example: a) M. Fujita, *Acc. Chem. Res.* **1999**, 32, 53–61; b) F. G. Gatti, D. A. Leigh, S. A. Nepogodiev, A. M. Z. Slawin, S. J. Teat, J. K. Y. Wong, *J. Am. Chem. Soc.* **2001**, 123, 5983–5989; c) A. G. Johnston, D. A. Leigh, R. J. Pritchard, M. D. Deegan, *Angew. Chem.* **1995**, 107, 1324–1327; *Angew. Chem. Int. Ed. Engl.* **1995**, 34, 1209–1212; d) J.-C. Chambron, J.-P. Collin, V. Heitz, D. Jouvenot, J.-M. Kern, P. Mobian, D. Pomeranc, J.-P. Sauvage, *Eur. J. Org. Chem.* **2004**, 8, 1627–1638; e) *Molecular Catenanes, Rotaxanes, and Knots* (Eds.: J.-P. Sauvage, C. Dietrich-Buchecker), Wiley-VCH, Weinheim, **1999**; f) J.-P. Sauvage, *Acc. Chem. Res.* **1998**, 31, 611–619; g) P. R. Ashton, P. T. Glink, J. F. Stoddart, P. A. Tasker, A. J. P. White, D. J. Williams, *Chem. Eur. J.* **1996**, 2, 729–736; h) P. R. Ashton, E. J. T. Chrystal, P. T. Glink, S. Menzer, C. Schiavo, N. Spencer, J. F. Stoddart, P. A. Tasker, A. J. P. White, D. J. Williams, *Chem. Eur. J.* **1996**, 2, 709–728; i) P. L. Anelli, P. R. Ashton, R. Ballardini, V. Balzani, M. Delgado, M. T. Gandolfi, T. T. Goodnow, A. E. Kaifer, D. Philp, M. Pietraszkiewicz, L. Prodi, M. V.

- Reddington, A. M. Z. Slawin, N. Spencer, J. F. Stoddart, C. Vicent, D. J. Williams, *J. Am. Chem. Soc.* **1992**, *114*, 193–218; j) C. Seel, F. Vögtle, *Chem. Eur. J.* **2000**, *6*, 21–24; k) R. Jager, F. Vögtle, *Angew. Chem.* **1997**, *109*, 966–980; *Angew. Chem. Int. Ed. Engl.* **1997**, *36*, 930–944.
- [2] For recent examples, see: a) H. Adams, E. Ashworth, G. A. Breault, J. Guo, C. A. Hunter, P. C. Mayers, *Nature* **2001**, *411*, 763; b) A.-M. Fuller, D. A. Leigh, P. J. Lusby, I. D. H. Oswald, S. Parsons, D. B. Walker, *Angew. Chem.* **2004**, *116*, 4004–4008; *Angew. Chem. Int. Ed.* **2004**, *43*, 3914–3918; c) L. Hogg, D. A. Leigh, P. J. Lusby, A. Morelli, S. Parsons, J. K. Y. Wong, *Angew. Chem.* **2004**, *116*, 1238–1241; *Angew. Chem. Int. Ed.* **2004**, *43*, 1218–1221; d) D. A. Leigh, P. J. Lusby, S. J. Teat, A. J. Wilson, J. K. Y. Wong, *Angew. Chem.* **2001**, *113*, 1586–1591; *Angew. Chem. Int. Ed.* **2001**, *40*, 1538–1543; e) K. S. Chichak, S. J. Cantrill, A. R. Pease, S.-H. Chiu, G. W. V. Cave, J. L. Atwood, J. F. Stoddart, *Science* **2004**, *304*, 1308–1312.
- [3] For recent examples, see: a) K. Chichak, M. C. Walsh, N. R. Branda, *Chem. Commun.* **2000**, 847–848; b) K.-M. Park, D. Whang, E. Lee, J. Heo, K. Kim, *Chem. Eur. J.* **2002**, *8*, 498–508; c) K. Kim, *Chem. Soc. Rev.* **2002**, *31*, 96–107; d) E. Lee, J. Kim, J. Heo, D. Whang, K. Kim, *Angew. Chem.* **2001**, *113*, 413–416; *Angew. Chem. Int. Ed.* **2001**, *40*, 399–402; e) G. J. E. Davidson, S. J. Loeb, *Angew. Chem.* **2003**, *115*, 78–81; *Angew. Chem. Int. Ed.* **2003**, *42*, 74–77; f) G. J. E. Davidson, S. J. Loeb, N. A. Parekh, J. A. Wisner, *J. Chem. Soc. Dalton Trans.* **2001**, 3135–3136; g) S. J. Loeb and J. A. Wisner, *Chem. Commun.* **1998**, 2757–2758; h) A. J. Baer, D. H. Macartney, *Inorg. Chem.*, **2000**, *39*, 1410–1417; i) M. J. Gunter, N. Bampas, K. D. Johnstone, J. K. M. Sanders, *New J. Chem.* **2001**, *25*, 166–173; j) D. J. Cárdenas, P. Gaviña, J.-P. Sauvage, *Chem. Commun.* **1996**, 1915–1916.
- [4] For recent examples, see: a) M. E. Padilla-Tosta, O. D. Fox, M. G. B. Drew, P. D. Beer, *Angew. Chem.* **2001**, *113*, 4365–4369; *Angew. Chem. Int. Ed.* **2001**, *40*, 4235–4239; b) C. A. Hunter, C. M. R. Low, M. J. Packer, S. E. Spey, J. G. Vinter, M. O. Vysotsky, C. Zonta, *Angew. Chem.* **2001**, *113*, 2750–2754; *Angew. Chem. Int. Ed.* **2001**, *40*, 2678–2682; c) K.-J. Chang, Y.-J. An, H. Uh, K.-S. Jeong, *J. Org. Chem.* **2004**, *69*, 6556–6563; d) K.-S. Jeong, E.-J. Park, *J. Org. Chem.* **2004**, *69*, 2618–2621; e) S.-Y. Chang, K.-S. Jeong, *J. Org. Chem.* **2003**, *68*, 4014–4019; f) S.-Y. Chang, H.-Y. Jang, K.-S. Jeong, *Chem. Eur. J.* **2003**, *9*, 1535–1541; g) S.-Y. Chang, J. S. Choi, K.-S. Jeong, *Chem. Eur. J.* **2001**, *7*, 2687–2697; h) K.-S. Jeong, J. S. Choi, S.-Y. Chang, H.-Y. Chang, *Angew. Chem.* **2000**, *112*, 1758–1761; *Angew. Chem. Int. Ed.* **2000**, *39*, 1692–1695; i) F. Mohr, D. J. Eisler, C. P. McArdle, K. Atieh, M. C. Jennings, R. J. Puddephatt, *J. Organomet. Chem.* **2003**, *670*, 27–36; j) A. C. Try, M. H. Harding, D. G. Hamilton, J. K. M. Sanders, *Chem. Commun.* **1998**, 723–724; k) B. X. Colasson, J.-P. Sauvage, *Inorg. Chem.* **2004**, *43*, 1895–1901; l) C. Dietrich-Buchecker, B. Colasson, M. Fujita, A. Hori, N. Geum, S. Sakamoto, K. Yamaguchi, J.-P. Sauvage, *J. Am. Chem. Soc.* **2003**, *125*, 5717–5725.
- [5] For selected examples, see: a) B. X. Colasson, C. Dietrich-Buchecker, M. C. Jimenez-Molero, J.-P. Sauvage, *J. Phys. Org. Chem.* **2002**, *15*, 476–483; b) J.-P. Collin, C. Dietrich-Buchecker, P. Gavina, M. C. Jimenez-Molero, J.-P. Sauvage, *Acc. Chem. Res.* **2001**, *34*, 477–487; c) D. Curiel, P. D. Beer, R. L. Paul, A. Cowley, M. R. Sambrook, F. Szemes, *Chem. Commun.* **2004**, 1162–1163; d) M. J. MacLachlan, A. Rose, T. M. Swager, *J. Am. Chem. Soc.* **2001**, *123*, 9180–9181; e) M.-J. Blanco, M. C. Jimenez, J.-C. Chambron, V. Heitz, M. Linke, J.-P. Sauvage, *Chem. Soc. Rev.* **1999**, *28*, 293–305.
- [6] For representative reviews, see: a) M. Fujita, K. Umemoto, M. Yoshizawa, N. Fujita, T. Kusakawa, K. Biradha, *Chem. Commun.* **2001**, 509–518; b) M. Fujita, *Chem. Soc. Rev.* **1998**, *27*, 417–425; c) S. R. Seidel, P. J. Stang, *Acc. Chem. Res.* **2002**, *35*, 972–983; d) S. Leininger, B. Olenyuk, P. J. Stang, *Chem. Rev.* **2000**, *100*, 853–907.
- [7] a) K. Kavallieratos, C. M. Bertao, R. H. Crabtree, *J. Org. Chem.* **1999**, *64*, 1675–1683; b) K. Kavallieratos, S. R. de Gala, D. J. Austin, R. H. Crabtree, *J. Am. Chem. Soc.* **1997**, *119*, 2325–2326.
- [8] a) J. A. Wisner, P. D. Beer, M. G. B. Drew, M. R. Sambrook, *J. Am. Chem. Soc.* **2002**, *124*, 12469–12476; b) J. A. Wisner, P. D. Beer, N. G. Berry, B. Tomapatanaget, *Proc. Natl. Acad. Sci. USA* **2002**, *99*, 4983–4986; c) J. A. Wisner, P. D. Beer, M. G. B. Drew, *Angew. Chem.* **2001**, *113*, 3718–3721; *Angew. Chem. Int. Ed.* **2001**, *40*, 3606–3609.
- [9] Preliminary evaluation of this system by titration of **2a** with *N,N'*-bis-(2,6-dimethylphenyl)isophthalamide resulted in a weak 1:1 interaction with $K_a < 5 \text{ M}^{-1}$.
- [10] a) A. Affeld, G. M. Hubner, C. Seel, C. A. Schalley, *Eur. J. Org. Chem.* **2001**, 2877–2890; b) C. Fischer, M. Nieger, O. Mogck, V. Boehmer, R. Ungaro, F. Vögtle, *Eur. J. Org. Chem.* **1998**, 155–161; c) R. Jager, S. Baumann, M. Fischer, O. Safarowsky, M. Nieger, F. Vögtle, *Liebigs Ann.* **1997**, 2269–2273; d) M. Handel, M. Plevovets, S. Gestermann, F. Vögtle, *Angew. Chem.* **1997**, *109*, 1248–1250; *Angew. Chem. Int. Ed. Engl.* **1997**, *36*, 1199–1201.
- [11] a) C. Allott, H. Adams, P. L. Bernad Jr., C. A. Hunter, C. Rotger, J. A. Thomas, *Chem. Commun.* **1998**, 2449–2450; b) H. Adams, F. J. Carver, C. A. Hunter, N. J. Osborne, *Chem. Commun.* **1996**, 2529–2530; c) P. A. Brooksby, C. A. Hunter, A. J. McQuillan, D. H. Purvis, A. E. Rowan, R. J. Shannon, R. Walsh, *Angew. Chem.* **1994**, *106*, 2584–2587; *Angew. Chem. Int. Ed. Engl.* **1994**, *33*, 2489–2491; d) C. A. Hunter, *Chem. Commun.* **1991**, 749–751.
- [12] Titrations were performed with a constant concentration of the host of $5 \times 10^{-4} \text{ M}$ and the addition of appropriate aliquots of a solution of guest at $5 \times 10^{-3} \text{ M}$ (with background host concentration) using Hamilton Gastight microliter syringes. All titrations were performed three times, and the average value of the association constants obtained are reported. In all cases, the results had an estimated error of $\leq 10\%$ for $K_a > 100 \text{ M}^{-1}$ and $\leq 20\%$ for $K_a < 100 \text{ M}^{-1}$. Titrations were performed with both **1** and **2-5** as host species to verify the presence of 2:1 (with **1** as host) and 1:2 (with **2a**, **2b**, and **3-5** as hosts) equilibria where necessary. Titration data from the observation of the appropriate protons $\text{H}_a\text{--H}_f$ were analyzed with the program EQNMR (M. J. Hynes, *J. Chem. Soc. Dalton Trans.* **1993**, 311–312) and fit 1:1, 1:2, and 2:1 binding models with excellent agreement ($R_f = 0.05\%$).
- [13] While the geometries of the 2:1 complexes have not been explicitly determined, they are likely a partially interpenetrated arrangement spanning two macrocycles, similar to that of the 1:1 complex from similar ^1H NMR chemical shift behavior. Regardless, they are a minor component in the equilibria when compared to the stabilities of the prevailing 1:1 complexes.
- [14] Crystal structure data for **1-2a**: triclinic, space group $P\bar{1}$, $a = 14.9144(6)$, $b = 17.24338(6)$, $c = 19.9135(6) \text{ \AA}$, $\alpha = 105.773(2)$, $\beta = 109.268(2)$, $\gamma = 104.509(2)^\circ$, $V = 4361.4(3) \text{ \AA}^3$, $Z = 2$, $\rho_{\text{calcd}} = 1.394 \text{ g cm}^{-3}$, $2\theta_{\text{max}} = 50.00^\circ$, $\text{MoK}\alpha$ radiation ($\lambda = 0.71073 \text{ \AA}$), $T = 150 \text{ K}$. A pale yellow crystal with dimensions $0.43 \times 0.38 \times 0.16 \text{ mm}^3$ was grown by vapor diffusion of isopropyl ether into a solution of **1-2a** in CHCl_3 and mounted on a glass fiber. The 44888 unique reflections ($R_{\text{int}} = 0.060$) were integrated from frame data obtained from programmed hemisphere scan routine on a Nonius Kappa-CCD diffractometer. Lorentz and polarization corrections followed by a multiscan (HKL SCALE-PACK; Otwinowski, Minor, **1997**) absorption correction were applied to the data ($\mu = 0.692 \text{ mm}^{-1}$, min./max. transmission = $0.8973/0.7550$). The structure was solved by Patterson methods, followed by difference Fourier syntheses to find the remaining atoms. Refinement was performed with full-matrix least-squares methods against $|F^2|$ data using SHELXTL-NT

6.1 (G. M. Sheldrick, Madison, WI, **2000**) to give final R values of $R_1 = 0.0568$, $wR_2 = 0.1329$, $\text{GOF} = 1.008$, $N_o/N_v = 15\,321/967$ with $I > 2\sigma(I)$. All of the non-hydrogen atoms were refined with anisotropic thermal parameters. The hydrogen atom positions were calculated geometrically and were included as riding on their respective carbon atoms. CCDC 253083 contains the supplementary crystallographic data for this paper. These data can be obtained free of charge from the Cambridge Crystallographic Data Centre via www.ccdc.cam.ac.uk/data_request/cif.

- [15] Crystal structure data for **1-5a**: triclinic, space group $P\bar{1}$, $a = 11.9303(6)$, $b = 12.0968(9)$, $c = 15.9729(14)$ Å, $\alpha = 112.045(3)^\circ$, $\beta = 90.375(4)^\circ$, $\gamma = 105.800(5)^\circ$, $V = 2040.6(3)$ Å³, $Z = 1$, $\rho_{\text{calc}} = 1.331$ g cm⁻³, $2\theta_{\text{max}} = 50.04^\circ$, $\text{MoK}\alpha$ radiation ($\lambda = 0.71073$ Å), $T = 150$ K. A pale yellow crystal with dimensions $0.38 \times 0.13 \times 0.05$ mm³ was grown by vapor diffusion of isopropyl ether into a solution of **1-5a** in CHCl_3 and mounted on a glass fiber. The 14996 unique reflections ($R_{\text{int}} = 0.059$) were integrated from frame data obtained from programmed hemisphere scan routine on a Nonius Kappa-CCD diffractometer. Lorentz and polarization correction followed by a multiscan (HKL SCALEPACK, Otwinowski, Minor, **1997**) absorption correction were applied to the data ($\mu = 0.541$ mm⁻¹, min./max. transmission = 0.9734/0.8228). The structure was solved by Patterson methods followed by difference Fourier syntheses to find the remaining atoms. Refinement was performed with full-matrix least-squares methods against $|F^2|$ data using SHELXTL-NT 6.1 (G. M., Sheldrick, Madison, WI, **2000**) to give final R values of $R_1 = 0.0565$, $wR_2 = 0.1162$, $\text{GOF} = 1.030$, $N_o/N_v = 7071/457$ with $I > 2\sigma(I)$. All of the non-hydrogen atoms were refined with anisotropic thermal parameters. The hydrogen atom positions were calculated geometrically and were included as riding on their respective carbon atoms. CCDC 253084 contains the supplementary crystallographic data for this paper. These data can be obtained free of charge from the Cambridge Crystallographic Data Centre via www.ccdc.cam.ac.uk/data_request/cif.
- [16] The least-squares plane of the macrocycle was calculated using the four carbonyl carbon atoms. Calculation of the angle between the Cl-Pd-Cl axis and the plane that bisects the isophthalamide aryl ring was performed by calculating the angle between the planes perpendicular to the lines defined by a) the Cl-Pd-Cl axis and b) the line described by the two carbonyl-substituted carbon atoms of the isophthalamide ring. The value obtained had 90° subtracted from it to arrive at the final figure.
- [17] We very recently confirmed the synthesis of a [2]rotaxane by this method in our laboratories, the results of which will be reported in due course.
- [18] a) C. Heim, A. Affeld, M. Nieger, F. Vögtle, *Helv. Chim. Acta* **1999**, 82, 746–759; b) Z. Qin, M. C. Jennings, R. J. Puddephatt, *Inorg. Chem.* **2001**, 40, 6220–6228; G. K. Anderson, M. Lin, A. Sen, E. Gretz, *Inorg. Synth.* **1990**, 28, 60–63; c) J. W. Mellor, *A Comprehensive Treatise on Inorganic and Theoretical Chemistry*, Vol. 15, Longmans, London, **1936**, 660–680; d) P. Kong, F. D. Rochon, *Can. J. Chem.* **1981**, 59, 3293–3296; e) P. G. Hayes, S. A. M. Stringer, C. M. Vogels, S. A. Westcott, *Transition Met. Chem.* **2001**, 26, 261–266; f) P. C. L'Argentiere, E. A. Cagnola, M. E. Quiroga, D. A. Liprandi, *Appl. Catal. A* **2002**, 226, 253–263.

Virtual Exploration of the Small-Molecule Chemical Universe below 160 Daltons**

*Tobias Fink, Heinz Bruggesser, and
Jean-Louis Reymond**

The development of modern medicine largely depends on the continuous discovery of new drug molecules for treating diseases.^[1] One striking feature of these drugs is their relatively small molecular weight (M_w), which averages only 340 Da.^[2] Recently, drug discovery has focused on even smaller building blocks with M_w of 160 Da or less to be used as lead structures that can be optimized for biological activity by adding substituents.^[3] At that size it becomes legitimate to ask how many such very small molecules would be possible in total within the boundaries of synthetic organic chemistry? To address this question we have generated a database (GDB) containing all possible organic structures with up to 11 main atoms under constraints defining chemical stability and synthetic feasibility. The database contains 13.9 million molecules with an average M_w of 153 Da, and opens an unprecedented window on the small-molecule chemical universe.

Estimates have been proposed for the total number of organic molecules to be in the range of 10^{18} – 10^{200} compounds.^[4] Systematic analysis of a database of screening compounds at Novartis identified 849 574 different substituents with 12 main atoms or less, which illustrates what synthetic chemistry has achieved so far.^[5,6] To gain an insight into the size and composition of the entire small-molecule chemical universe, we set out to generate all possible organic molecules up to $M_w \approx 160$ by computer simulation from first principles.

Several programs exist to enumerate molecular structures corresponding to a given elemental formula,^[7] but they have never been implemented to carry out an exhaustive listing and their adaptation to this task would be quite cumbersome. The database was therefore constructed by a new approach, starting with a collection of mathematical graphs corresponding to saturated hydrocarbons, which were diversified to

[*] T. Fink, Prof. Dr. J.-L. Reymond
Department of Chemistry and Biochemistry
University of Berne
Freiestrasse 3, 3012 Berne (Switzerland)
Fax: (+41) 31-631-8057
E-mail: jean-louis.reymond@ioc.unibe.ch
Dr. H. Bruggesser
Institute of Mathematics
University of Berne
Sidlerstrasse 5, 3012 Berne (Switzerland)

[**] This work was financially supported by the University of Berne and the Swiss National Science Foundation. The authors thank Dr. Peter Ertl and Dr. Bernhard Rohde at Novartis for helpful discussions, Molinspiration for providing access to their virtual screening toolkit, and Molecular Networks GmbH for use of the 3D-coordinates generation program CORINA.

molecules by systematically introducing bond unsaturations and atom types using an in-house developed application written in Java.

An exhaustive library of graphs with up to 11 nodes and a maximum node connectivity of four was produced by the program NAUTY.^[8] The vast majority of these graphs (99.8%) contained three- and four-membered rings and was excluded to avoid generating a database consisting almost exclusively of such small rings.^[9] Further restrictions included the elimination of nonplanar graphs and tricyclic bridgeheads.^[10] Graph symmetry was determined in each graph using a known algorithm.^[11] Bond unsaturations were then introduced combinatorially, followed by all possible atom-type combinations by introducing carbon, nitrogen, oxygen, and fluorine (as a model halogen) at each node. The resulting collection was finally reduced by applying filters for functional groups to eliminate unstable atom-type and bond-type combinations.^[12] Each compound was stored as its USMILES representation of the structural formula.^[13] The three-dimensional structure of each compound was finally determined using CORINA, thereby generating all possible stereoisomers.^[14] A quantitative overview of the GDB construction process is shown in Table 1 and Table 2.

For comparison purposes a reference database (Rdb) of known compounds with up to 11 main atoms was assembled from ChemACX (21 698 compounds (cpds)), ChemACX-SC (10 735 cpds), NCI open database (19 438 cpds), and the Merck Index (1540 cpds), resulting in 36 227 unique structures.^[16,17] 52% of these reference compounds were present in GDB. The remaining compounds contained features which had been specifically excluded, such as elements other than C, H, N, O, or halogen (23.5%), unstable functional groups (e.g. acyl halides, peroxides, 12.0%), 3- or 4-membered rings (5.4%), triple bonds, allenes, and bridgehead olefins (4.0%), or charges (e.g. quaternary ammonium centers, 3.0%). The composition of Rdb by molecular size and graph type is shown in Table 1.

Table 2: Stereochemical composition of GDB. The 13.9 million structures in GDB give rise to approximately 44 million stereoisomers as generated by CORINA.^[14]

Contribution to GDB [%]	Stereochemical category ^[a]
24	No stereoisomers
18	<i>E/Z</i> isomers ^[b]
22	Two stereoisomers ^[c]
21	Multiple stereoisomers ^[d]
15	Mixed ^[e]

[a] Stereoisomeric diversity is mainly achieved by molecules of 11 atoms which make up 86% of GDB. [b] Single or multiple *E/Z* isomeric pairs and no stereogenic nonplanar centers (e.g. 2,4-hexadiene). [c] Enantiomeric pairs (e.g. 2-butanol) and achiral *syn/anti* pairs (e.g. 1,4-dimethyl cyclohexane) not having *E/Z* isomerism. [d] Structures with multiple independent stereogenic nonplanar centers, including *meso*-isomers, but no *E/Z* isomers (e.g. 2,3-butanediol). [e] Structures containing both nonplanar stereogenic centers and *E/Z* isomers (e.g. 3-penten-2-ol).

The 1830 graphs used for GDB generated between 4 and 79 236 different compounds per graph. There were 103 different ring types in these graphs,^[18] 50 of which did not appear in Rdb, although at least one Chemical Abstract System (CAS) entry could be found in each case for the parent hydrocarbon. In fact Rdb used only 1174 of the GDB graphs, but contained an additional 871 graphs with small rings and pentavalent nodes not used for GDB (Table 1, Figure 1). Analysis by compound type showed that heterocycles were most abundant in GDB, while aromatics were almost insignificant. By contrast, Rdb contained a relatively large proportion of acyclics and aromatics. Furthermore, GDB contained a much higher proportion of fused heterocycles than Rdb, but a smaller proportion of heteroaromatics. GDB-compounds had an average M_w of 153.2, and 87% of them had $M_w < 160$ (Table 3, Figure 2).

The databases were analyzed in terms of physicochemical and topological descriptors relevant for drug properties, including M_w , octanol/water partition coefficient (logP),^[19]

Table 1: Overview of GDB and Rdb databases.

Parameter	1	2	3	4	5	6	Atoms 7	8	9	10	11	Total
GDB												
Graphs total ^[a]	1	1	2	6	21	78	353	1929	12 207	89 402	739 335	843 335
Maximal one 3- or 4-membered ring	1	1	2	4	9	22	64	215	769	3098	13 808	17 993
No 3- or 4-membered rings	1	1	1	2	4	7	16	41	119	394	1497	2083
Planar and no tricyclic bridgeheads	1	1	1	2	4	7	16	41	116	369	1272	1830
Molecules passed filters ^[b]	4	7	16	62	251	1252	6812	40 942	258 852	1 719 366	11 864 872	13 892 436^[c]
Molecules^[d]	7	43	127	277	612	1378	2492	4304	6257	8933	11 797	36 227
Rdb												
Graphs from molecules ^[e]	1	1	2	5	11	27	66	147	270	528	988	2046
Maximal one 3- or 4-membered ring	1	1	1	4	9	22	52	125	255	500	967	1937
No 3- or 4-membered rings	1	1	1	2	4	8	18	44	111	302	683	1175
Planar and no tricyclic bridgeheads	1	1	1	2	4	8 ^[f]	18 ^[f]	44 ^[f]	111	302	682 ^[g]	1174

[a] As generated by the program NAUTY.^[8] [b] After application of filters.^[12] 0.2% of molecules passed the filters. [c] The logarithm of the number of molecules in GDB increases as a quadratic function of the number of atoms, giving 145 million compounds for 12 atoms and 3×10^{25} for 25 atoms ($R^2 = 0.999$). [d] There are more molecules with four main atoms or less in Rdb because more elements types are used. [e] Number of different graphs used in the molecules. [f] Rdb contains pentavalent phosphorus derivatives (e.g. MePCl₄) which correspond to graphs with one node of connectivity 5 not used in GDB. [g] Tricyclo[3.3.3.0]undecane is the only graph for a stable tricyclic bridgehead molecule with up to 11 main atoms but was excluded from GDB.^[15] For clarity, totals are highlighted in bold.

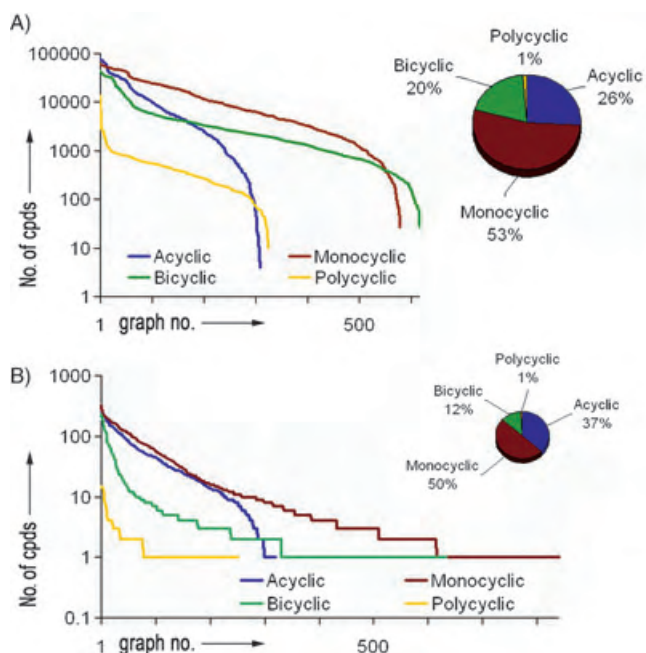


Figure 1. Composition of A) GDB and B) Rdb databases by graph type. Graphs were ordered in descending number of compounds per graph. The graphs giving the most compounds in GDB correspond to 4-ethyl-nonane (79 236 cpds, acyclic), 1-ethyl-3-propylcyclohexane (60 337 cpds, monocyclic), 5-ethylcycloheptene (42 682 cpds, bicyclic), and decahydrocyclopenta[α]pentalene (13 882 cpds, polycyclic). For Rdb, the graphs with most compounds are 2-methylpentane (249 cpds, acyclic), 1,2,4-trimethylcyclohexane (325 cpds, monocyclic), 4,6-dimethylcycloheptene (231 cpds, bicyclic), and 1-methyladamantane (15 cpds, polycyclic). There are more graph types for Rdb since 3- and 4-membered rings are also present (5.4% of Rdb, see text).

number of hydrogen-bond donors (HBD) and acceptors (HBA), fraction of rotatable bonds (FRB), and topological polar surface area (TPSA).^[20] The chemical space defined by these properties was represented in a 2-dimensional projection along the first two principal components (covering 75 % of the diversity), with PC1 reflecting the hydrophobic/hydrophilic balance and PC2 depending on molecular weight and conformational flexibility (Figure 3). GDB covered this chemical space much more densely and exhaustively than Rdb, with coverage extending in particular into high-polarity regions where no Rdb compounds were found.

The relevance of GDB for drug discovery was tested by virtual screening for bioactivity. Virtual screening uses quantitative structure–activity relationship (QSAR) methods, such as similarity searching,^[21] statistical methods (principal component regression, partial least squares),^[22] or neural networks.^[23] We used a commercial package based on Bayesian statistics (Molinspiration miscreen toolkit)^[24] trained for three important drug targets: G-protein coupled receptors (GPCR), kinases, and ion channels. The virtual screening returned a large number of high-scoring compounds in each case (GPCR ligands: 17 106; Ion-channel modulators: 7527; Kinase inhibitors: 2071). While 90 % of these virtual hits fell into regions of chemical space well covered by both databases, 10 % of these hits were found in

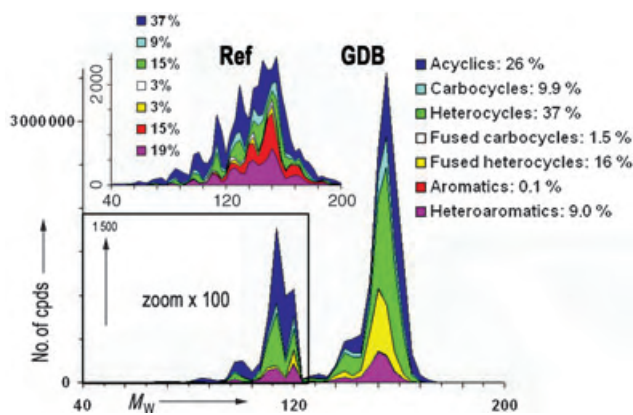


Figure 2. Database composition by structural categories and M_w . Main plot: 13.9 million GDB compounds containing up to 11 main atoms, average $M_w = 153.2$, $\sigma = 7.5$ Da, 87 % of GDB-compounds have $M_w < 160$. The lower-left portion of GDB for $M_w < 120$ has been expanded 100 \times for visibility. Inset: 36 227 Rdb compounds containing up to 11 main atoms. The M_w distribution in Rdb is broader owing to the heavier elements (P, S, Si). The maximum number of compounds occurs in the interval 155.2 ± 1.6 Da for both GDB and Rdb. For details of element composition per structural category see also Table 3.

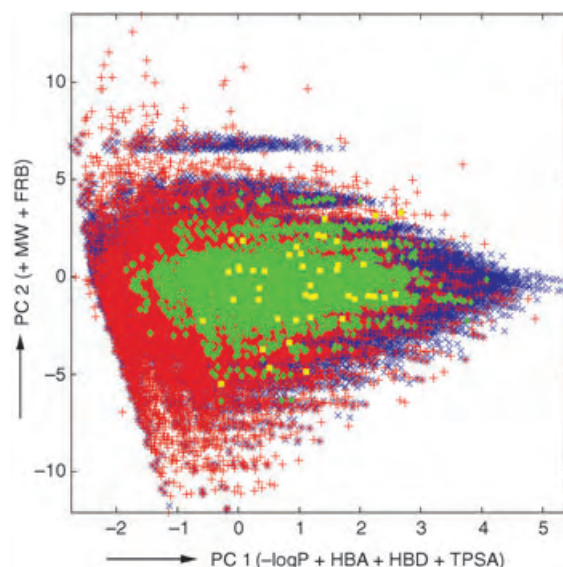


Figure 3. Coverage of property space by database compounds. \times GDB, 13.9 millions cpds; $+$ Rdb, 36 227 cpds, overlayed on GDB; \blacklozenge virtual hits from GDB, 25 676 cpds, overlayed on previous series; \blacksquare virtual hits from Rdb, 160 cpds, only the 47 hits not present in GDB are shown, overlayed on previous series. Principal component analysis (PCA) of GDB+Rdb gave: PC1: M_w 0.031, FRB 0.030, $\log P$ -0.930 , HBA 0.915, HBD 0.827, TPSA 0.943; PC2: M_w 0.756, FRB 0.775, $\log P$ 0.080, HBA 0.039, HBD 0.085, TPSA 0.098. Virtual screening was performed using the Molinspiration software.^[24] The hit rates were 0.2 % for GDB and 0.4 % for Rdb.

regions of space covered only by GDB but not by Rdb (Figure 3 and Figure 4).

The small-molecule chemical universe appears as a large yet tractable entity. Large portions of the chemical universe remain hidden as invisible “dark matter” in GDB, such as the overwhelming multitude of 3- and 4-membered ring compounds. Nevertheless, the current study reveals a wealth of

Table 3: Composition of GDB and Rdb databases by structural categories (columns) and element composition (rows).^[a]

Elements	Heteroaromatics	Aromatics	Fused Heterocycles	Structure category Fused Carbocycles	Heterocycles	Carbocycles	Acyclics	Total
GDB								
C	0	396	0	19 683	0	30 183	9364	59 626
C,F	0	1049	0	34 648	0	117 334	72 111	225 142
C,F,N	124 285	2437	174 875	19 638	453 588	170 793	377 756	1 323 372
C,F,N,O	232 910	2253	213 437	8120	866 091	177 613	746 025	2 246 449
C,F,O	22 037	2151	130 109	30 170	305 971	228 877	333 692	1 053 007
C,N	204 782	2761	435 108	29 359	723 949	143 720	352 117	1 891 796
C,N,O	648 694	5025	1 041 291	28 544	2 512 535	324 149	1 495 785	6 056 023
C,O	23 309	2273	246 184	43 477	335 434	179 018	207 323	1 037 018
No C	0	0	0	0	0	0	3	3
Total	1 256 017	18 345	2 241 004	213 639	5 197 568	1 371 687	3 594 176	13 892 436
Rdb								
C	0	269	0	352	0	457	594	1 672
C,F	0	231	0	66	0	126	388	811
C,F,N	630	291	23	6	74	37	281	1 342
C,F,N,O	510	275	10	9	241	36	508	1 589
C,F,O	33	492	34	39	181	149	971	1 899
C,N	1404	574	231	68	611	251	979	4 118
C,N,O	2509	868	305	50	2046	427	3190	9 395
C,O	159	779	301	391	850	978	2704	6 162
No C	1	0	1	2	4	1	226	235
Others ^[b]	1665	1512	168	117	1229	782	3531	9004
Total	6911	5291	1073	1100	5236	3244	13 372	36 227

[a] Compounds are assigned to one category only with the following priorities: heteroaromatics > aromatics > fused heterocycles (including spiro compounds) > fused carbocycles (including spiro compounds) > heterocycles > carbocycles > acyclics. For example furyl-benzene is classified as heteroaromatic only. [b] "Others" are C containing compounds also containing elements other than C, N, O, or halogen (e.g. S, Si, or P). For details and M_w distribution by categories, see also Figure 2. For clarity, totals are highlighted in bold.

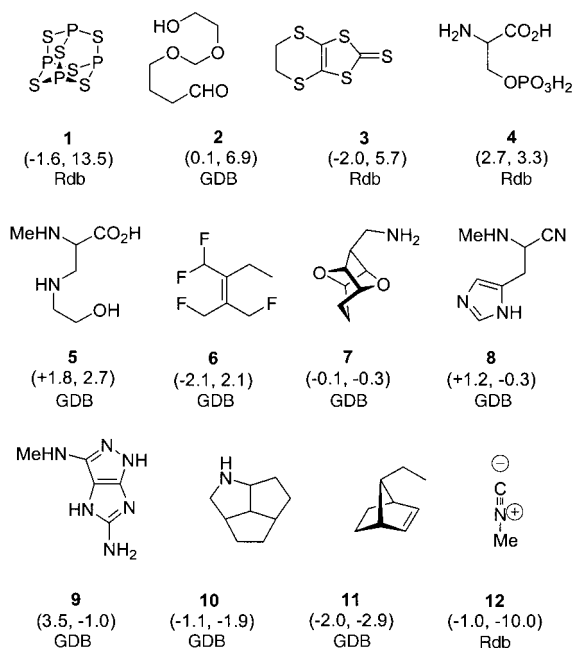


Figure 4. Examples of GDB and Rdb compounds in property space. PC-coordinates are given in parenthesis as (PC1, PC2) and the compounds are ordered by decreasing PC2. See also Figure 2 and 3. The Rdb compounds (1, 3, 4, 12) are from areas of chemical space covered only by Rdb. Compounds 5–9 are not registered in the Chemical Abstracts System (CAS) and are therefore considered as unknown. Compounds 2 and 10 are also unknown although derivatives are registered in CAS. Virtual screening^[24] gives high scores for compounds 4 (GPCR ligand), 5 (ion-channel modulator), 8 (GPCR ligand), and 9 (kinase inhibitor).

organic structures below 160 Da covering property space broadly and extensively, with many possibly bioactive compounds. The database construction strategy chosen also ensures that the majority of GDB, although presently unknown, should be synthetically accessible.

Received: October 28, 2004

Published online: January 26, 2005

Keywords: chemoinformatics · combinatorial chemistry · computer chemistry · drug design · molecular diversity

- [1] K. H. Bleicher, H.-J. Böhm, K. Müller, A. I. Alanine, *Nat. Rev. Drug Discovery* **2003**, 2, 369–378.
- [2] M. Feher, J. M. Schmidt, *J. Chem. Inf. Comput. Sci.* **2003**, 43, 218–227.
- [3] D. A. Erlanson, R. S. McDowell, T. O'Brien, *J. Med. Chem.* **2004**, 47, 3463–3482.
- [4] a) S. Petit-Zeman, Charting chemical space: finding new tools to explore biology. *4th Horizon Symposium*, Palazzo Arzaga, Italy, October 23–25, **2003**; b) R. S. Bohacek, C. McMartin, W. C. Guida, *Med. Res. Rev.* **1996**, 16, 3–50.
- [5] P. Ertl, *J. Chem. Inf. Comput. Sci.* **2003**, 43, 374–380.
- [6] Note that there are many more substituents than molecules because any one molecule gives rise to several substituents because the attachment point behaves as a virtual atom. For example toluene (methylbenzene) gives four possible substituents: *alpha*-tolyl, *ortho*-tolyl, *meta*-tolyl, and *para*-tolyl.
- [7] a) R. E. Carhart, D. H. Smith, H. Brown, C. Djerassi, *J. Am. Chem. Soc.* **1975**, 97, 5755–5762; b) R. K. Lindsay, B. G. Buchanan, E. A. Feigenbaum, J. Lederberg, *Application of Artificial Intelligence for Chemistry: The DENDRAL Project*.

New York, McGraw-Hill, **1980**; c) R. E. Carhart, D. H. Smith, N. A. B. Gray, J. G. Nourse, C. Djerassi, *J. Org. Chem.* **1981**, *46*, 1708–1718; d) C. Benecke, R. Grund, R. Hohberger, *Anal. Chim. Acta* **1995**, *314*, 141–147; e) A. Kerber, R. Laue, T. Gruner, *Commun. Math. Co.* **1998**, *37*, 205–208; f) T. Gruner, A. Kerber, R. Laue, *Commun. Math. Co.* **1999**, *39*, 135–137.

- [8] a) B. D. McKay, *Congressus Numerantium* **1981**, *30*, 45–87.
 [9] Many small-ring combinations are highly strained and unstable, such as tetrahedrane or prismane. Compounds containing multiple cyclopropanes are known, but their number is insignificant compared to the combinatorial possibilities. For a striking example of molecules with multiple cyclopropanes, see A. de Meijere, M. von Seebach, S. Zöllner, S. I. Kozhushkov, V. N. Belov, R. Boese, T. Haumann, J. Benet-Buchholz, D. S. Yufit, J. A. K. Howard, *Chem. Eur. J.* **2001**, *7*, 4021–4034.
 [10] Nonplanar graphs cannot be drawn in a plane without crossing edges (bonds) between nodes (atoms), and contain the $K_{3,3}$ graph as a subgraph. Tricyclic bridgeheads occur in tricyclo[2.2.2]decane and related compounds, and are highly distorted.



$K_{3,3}$ graph



tricyclo[2.2.2]decane

- [11] S. Bohanec, M. Perdih, *J. Chem. Inf. Comput. Sci.* **1993**, *33*, 719–726.
 [12] Unstable combinations include: bridgehead olefins, bonds between heteroatoms (except in hydrazones, oximes, nitro, and in certain aromatic heterocycles), acyl halide, enamines, acyclic imines, enols, hemiacetals, orthoesters, and similar hydrolytically labile functions. Triple bonds were not used except for nitriles, and allenes were not used.
 [13] a) D. Weininger, *J. Chem. Inf. Comput. Sci.* **1988**, *28*, 31–36; b) D. Weininger, A. Weininger, J. L. Weininger, *J. Chem. Inf. Comput. Sci.* **1989**, *29*, 97–101.
 [14] a) J. Gasteiger, C. Rudolph, J. Sadowski, *Tetrahedron Comput. Methodol.* **1990**, *3*, 537–547; b) J. Sadowski, J. Gasteiger, *Chem. Rev.* **1993**, *93*, 2567–2581; c) <http://www.mol-net.de/index.html>.
 [15] Tricyclo[3.3.3.0]undecane is present in Rdb as 1-Aza-tricyclo[3.3.3.0]undecane and 1,5-diaza-tricyclo[3.3.3.0]undecane.
 [16] <http://dtp.nci.nih.gov/index.html>
 [17] <http://www.camsoft.com>.
 [18] A ring type is a graph not containing any node of connectivity 1. The Chemical Abstracts Registry or Beilstein databases are suitable for comparison. A simple total count comparison would be of little value since many entries in these databases correspond to isotopic combinations and salts of the same compounds, and sometimes to theoretical molecules that have never been synthesized.
 [19] logP was calculated according to: A. K. Ghose, G. M. Crippen, *J. Chem. Inf. Comput. Sci.* **1987**, *27*, 21–35.
 [20] Topological polar surface area was calculated according to: P. Ertl, B. Rohde, P. Selzer, *J. Med. Chem.* **2000**, *43*, 3714–3717.
 [21] V. J. Gillet, P. Willett, J. Bradshaw, *J. Chem. Inf. Comput. Sci.* **2003**, *43*, 338–345.
 [22] a) S.-S. Liu, C.-S. Yin, Z.-L. Li, S.-X. Cai, *J. Chem. Inf. Comput. Sci.* **2001**, *41*, 321–329; b) N. Stiefl, K. Baumann, *J. Med. Chem.* **2003**, *46*, 1390–1407.
 [23] J. Gasteiger, A. Teckentrup, L. Terfloth, S. Spycher, *J. Phys. Org. Chem.* **2003**, *16*, 232–245.
 [24] Sets of active and inactive compounds for a specific drug target serve as an input for this application. After fragmentation of those compounds a pharmacophore model is created which is able to give an activity score for unknown compounds. <http://www.molinspiration.com>

Intramolecular C–H Activation by an Open-Shell Cobalt(III) Imido Complex**

Daniel T. Shay, Glenn P. A. Yap, Lev N. Zakharov, Arnold L. Rheingold, and Klaus H. Theopold*

Stable terminal imido complexes of the late transition metals (Group 9 and beyond) are rare,^[1] presumably owing to a lack of empty d orbitals available for π donation from the NR^{2-} ligand. Such complexes are of interest as intermediates in catalytic NR-group transfer reactions. Our particular interest in the chemistry of cobalt imido complexes of the type $[\text{Tp}^{\text{R,R'}}\text{Co}=\text{NR}]$ ($\text{Tp}^{\text{R,R'}} = \text{hydrotris}(3\text{-R},5\text{-R'}\text{-pyrazolyl})\text{borate}$) stems from their isoelectronic relationship to the elusive $[\text{Tp}^{i\text{Bu,Me}}\text{Co}=\text{O}]$. We have postulated the formation of $[\text{Tp}^{i\text{Bu,Me}}\text{Co}=\text{O}]$ as a reactive intermediate in the activation of O_2 and N_2O by various $\{\text{Tp}^{i\text{Bu,Me}}\text{Co}\}$ complexes.^[2] Alas, the oxo species has eluded direct observation, and to our knowledge no terminal cobalt oxo complex has ever been isolated. Herein we describe the synthesis and reactivity of stable cobalt imido analogues.

Addition of one equivalent of adamantyl azide (AdN_3) to a THF solution of $[\text{Tp}^{i\text{Bu,Me}}\text{Co}(\text{N}_2)]$ at room temperature resulted in the rapid evolution of N_2 accompanied by a color change from brown to dark green. Evaporation of the solvent followed by recrystallization from pentane afforded $[\text{Tp}^{i\text{Bu,Me}}\text{Co}=\text{NAd}]$ (**1**) as green plates in 78 % yield. A similar reaction of $[\text{Tp}^{i\text{Bu,Me}}\text{Co}(\text{N}_2)]$ with *tert*-butyl azide ($t\text{BuN}_3$) yielded a mixture of $[\text{Tp}^{i\text{Bu,Me}}\text{Co}=\text{N}t\text{Bu}]$ (**2**) (40 %) and $[\text{Tp}^{i\text{Bu,Me}}\text{CoN}_3]$. We attribute the formation of the azide side product to the greater stability of the *tert*-butyl radical. Both imido complexes have been structurally characterized by X-ray diffraction; the representative molecular structure of **1** is shown in Figure 1.^[3]

Compound **1** is a four-coordinate molecule adopting pseudo-tetrahedral coordination of cobalt by four nitrogen ligands. Of note are the short Co(1)–N(7) bond of 1.655(2) Å and the Co(1)–N(7)–C(25) angle of 178.3(2), both of which are consistent with multiple bonding between cobalt and nitrogen center N(7). The parameters of the coordination by the Tp ligand (Co–N_{av}, 2.046(7) Å; N–Co–N_{av}, 89(1)°) are not unusual; indeed, they are a testament to the rigidity of the Tp ligand and underscore the deviation of the geometry of **1** from tetrahedral coordination.

[*] D. T. Shay, Dr. G. P. A. Yap, Prof. K. H. Theopold
Department of Chemistry and Biochemistry
University of Delaware
Newark, DE 19716-2522 (USA)
Fax: (+1) 302-831-6335
E-mail: theopold@udel.edu

Dr. L. N. Zakharov, Prof. A. L. Rheingold
Department of Chemistry and Biochemistry
University of California—San Diego
La Jolla, CA 92093-0358 (USA)

[**] This research was supported by a grant from the U.S. Department of Energy (92ER14273).

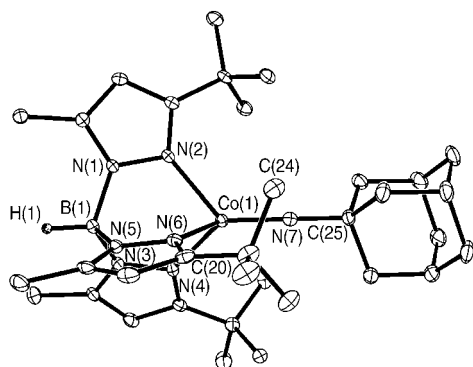


Figure 1. The molecular structure of **1** (thermal ellipsoids set at 30 % probability). Selected interatomic distances [Å] and angles [°]: Co(1)–N(7) 1.655(2), Co(1)–N(2) 2.051(2), Co(1)–N(4) 2.038(2), Co(1)–N(6) 2.049(2); Co(1)–N(7)–C(25) 178.3(2), N(2)–Co(1)–N(4) 89.54(8), N(2)–Co(1)–N(6), 88.10(8), N(4)–Co(1)–N(6) 90.09(9).

Compound **1** is thermally stable at room temperature both in solution and in the solid state. However, it decomposes upon exposure to air. At first glance its ^1H NMR spectrum seemed consistent with a closed-shell species (all resonances between $\delta = 0$ and 10 ppm), but closer inspection revealed some unusual chemical shifts, line broadening (full width at half maximum (fwhm) ≤ 14 Hz) and a significant temperature dependence. Noteworthy is that the imido complex also gave a ^{13}C NMR spectrum with sharp resonances in the range $\delta = 13$ –201 ppm, albeit with some apparent isotropic shifts. The paramagnetic nature of **1** was established by a measurement of its magnetic moment in the solid state. The value of $\mu_{\text{eff}} = 2.8(2) \mu_B$ is consistent with the presence of two unpaired electrons. Two additional observations support this notion. First, the ^{15}N NMR spectrum of a 1:1 mixture of **1** and $[\text{Tp}^{\text{tBu,Me}}\text{Co}^{15}\text{NAd}]$ (**1**- ^{15}N) did not reveal a detectable signal; this is probably due to the strong interaction between the observed nucleus and the cobalt atom housing the unpaired electrons. However, both the ^1H and ^{13}C NMR spectra of this mixture revealed some unusually large $^{15}\text{N}/^{14}\text{N}$ isotope effects on the chemical shifts of **1**.^[4] For example, $\Delta\delta$ ranged from 16 to 73 ppb in the ^1H NMR and from 28 to 410 ppb in the ^{13}C NMR spectrum. We have already observed large deuterium isotope effects on the chemical shifts of paramagnetic organometallic compounds (an effect we have termed paramagnetic isotope effect on chemical shift (PIECS));^[5] the present observations—while unprecedented for ^{15}N —are of a similar nature.

The preparation of **1**- ^{15}N was also meant to facilitate the identification of a cobalt–nitrogen stretching frequency ($\nu_{\text{Co-N}}$). Unfortunately, this proved unsuccessful; difference spectra of pure **1** and **1**- ^{15}N did not reveal any assignable features.^[6]

The high-spin configuration of the d^6 ion in this cobalt(III) complex distinguishes it from the few other known cobalt imido complexes, all of which are diamagnetic.^[1d–f] Considering the typical d-orbital splitting of a $[\text{TpCoX}]$ fragment under C_{3v} symmetry, we suggest a $1e^4a^12e^1$ (d^6 , $S = 1$) electronic configuration for **1**.^[7] We wondered whether the difference in the electronic structure would affect the

reactivity of **1**. The coupling of imido ligands with CO to form isocyanates is a common reaction of metal imido complexes.^[1,8] Monitoring the reaction of **1** with excess CO (1 atm) by ^1H NMR showed the reaction to be complete after 20 h at room temperature, with AdNCO and $[\text{Tp}^{\text{tBu,Me}}\text{Co}(\text{CO})]$ being formed exclusively. $[\text{Tp}^{\text{tBu,Me}}\text{Co}(\text{CO})]$ in turn reacted with AdN_3 to regenerate **1**, but this reaction was slow and several byproducts were detected. Protonation of **1** resulted in cleavage of the Co–N bond. Thus addition of water to **1** yielded $[\text{Tp}^{\text{tBu,Me}}\text{CoOH}]^{[2a]}$ and AdNH_2 . Similarly, reaction of **1** with one equivalent of [lutetium]BARF (BARF = tetrakis(3,5-bis(trifluoromethyl)phenyl)borate) gave $[\text{Tp}^{\text{tBu,Me}}\text{Co}(\text{NC}_5\text{Me}_2\text{H}_3)]\text{BARF}$ and AdNH_2 . The mechanism of these reactions, which involve a reduction of Co^{III} to Co^{II} has not yet been elucidated in detail. One possible pathway involves homolytic cleavage of the Co–N bond of an intermediate of the type $[\text{Tp}^{\text{tBu,Me}}\text{Co}(\text{N}(\text{H})\text{Ad})\text{BARF}]$.

Most interesting is the thermal decomposition of **1**, as it revealed a pattern related to that of the postulated reactive intermediates “ $[\text{Tp}^{\text{tBu,Me}}\text{Co}=\text{NSiMe}_3]$ ” and “ $[\text{Tp}^{\text{tBu,Me}}\text{Co}=\text{O}]$ ”.^[9,2] This reaction was discovered upon heating **1** to 40 °C for 10 days in the presence of ethylene (1 atm); however, the ethylene merely served to reversibly trap the reaction product as an ethylene complex, and the reaction product **3** can also be prepared in the absence of ethylene. The olefin is not functionalized and can be pumped off completely to leave **3**. The molecular structure of **3** was determined by X-ray crystallography and the result is shown in Figure 2.^[3]

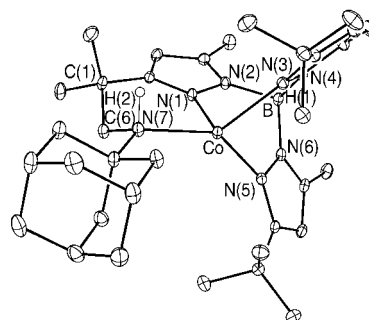


Figure 2. The molecular structure of **3** (thermal ellipsoids set at 30 % probability). Selected interatomic distances [Å] and angles [°]: Co–N(7) 2.1675(14), Co–N(1) 2.0284(13), Co–N(3) 2.1068(13), Co–N(5) 2.0771(14), C(6)–N(7) 1.501(2), N(7)–C(25) 1.5517(2); N(1)–Co–N(3) 90.99(5), N(1)–Co–N(5) 92.69(5), N(1)–Co–N(7) 89.12(5), N(3)–Co–N(5) 86.46(5), N(3)–Co–N(7) 133.41(5), N(5)–Co–N(7) 140.08(5), Co–N(7)–C(6) 107.61(10), Co–N(7)–C(25) 128.08(10) C(6)–N(7)–C(25) 112.20(12).

Compound **3**, an isomer of **1**, is a four-coordinate TpCo^{I} complex featuring binding of a tethered secondary amine nitrogen atom to cobalt. The amine is formally produced by insertion of the NAd moiety of **1** into a C–H bond of one of the *tert*-butyl groups of the Tp ligand. While the structural parameters of the Tp coordination hardly change (Co–N_{av} , 2.07 Å; $\text{N–Co–N}_{\text{av}}$, 90.0°), the Co–N(7) bond (2.1675(15) Å) is unusually long for cobalt complexes of secondary amines, which reflects the extreme steric congestion of **3**.^[10] Like other

16-electron complexes of the type $[\text{TpCo}^{\text{I}}(\text{L})]$, **3** is paramagnetic. Its coordinated amine is readily replaced by other donors; thus various derivatives containing cobalt in the oxidation states +I and +II were readily prepared.

Open-shell cobalt(III) imido complex **1** is a stable representative of a broader class of multiply bonded terminal $[\text{TpCo}=\text{X}]$ species (for example, $\text{X}=\text{NR}$); its existence suggests that other isoelectronic embodiments ($\text{X}=\text{O}$, S, PR, CR_2) may also be accessible and possess some—albeit fleeting—stability. Nevertheless, the facile transformation of **1** into **3** by a C–H activation demonstrates the inherent reactivity of compounds of this nature.

Experimental Section

1: 177 mg AdN_3 (1.0 mmol) was added in one portion to a stirred solution of $[\text{Tp}^{\text{tBu,Me}}\text{Co}(\text{N}_2)]$ (510 mg, 1.0 mmol) in THF (20 mL). Evolution of a gas (N_2) and a color change from brown to green was observed. After stirring for 60 min, the solvent was removed under reduced pressure and the resulting dark green residue was dissolved in a minimal amount of pentane and cooled to -35°C for 24 h. The resulting green crystals were collected by filtration, washed with cold pentane, and dried under vacuum to yield 523 mg (78% yield) of **1**. ^1H NMR (400 MHz, C_6D_6): δ = 7.57 (s, 3H), 6.51 (s, 3H), 3.49 (s, 9H), 2.505 (d, 3H $J_{\text{HH}} = 12$ Hz), 2.185 (d, 3H $J_{\text{HH}} = 12$ Hz), 0.79 (s, 6H), 0.63 ppm (s, 27H); IR (KBr): $\tilde{\nu}$ = 2956 (s), 2906 (s), 2513 (w, B-H), 1540 (s), 1358 (s), 1214 (s), 1063 (s), 777 (s), 646 (w), 534 cm^{-1} (w); UV/Vis (pentane): $\lambda_{\text{max}}(\epsilon)$ = 373 nm (772), 848 nm (292); m.p. decomposition above 85°C ; μ_{eff} (295 K) = 2.8(2) μ_{B} ; elemental analysis (%) calcd for $\text{C}_{34}\text{H}_{55}\text{N}_7\text{BCo}\cdot 1/2\text{C}_5\text{H}_{12}$: C 65.65, H 9.23, N 14.68; found: C 65.14, H 9.18, N 14.66.

$[\text{HB}\{\kappa^2\text{-3-CMe}_2\text{CH}_2\text{N}(\text{H})\text{Ad,5-Me-pyrazolyl}\}(\text{tBu,Me}^{\text{pz}})_2\text{Co}]$ (**3**): An NMR tube filled with **1** (25 mg, 0.04 mmol) and dry C_6D_6 (0.8 mL) was charged with dry ethylene (1 atm). The NMR tube was flame-sealed and kept in an oil bath at 40°C ; formation of $[\text{HB}\{\kappa^2\text{-3-CMe}_2\text{CH}_2\text{N}(\text{H})\text{Ad,5-Me-pyrazolyl}\}(\text{tBu,Me}^{\text{pz}})_2\text{Co}(\text{C}_2\text{H}_4)]$ was monitored by ^1H NMR spectroscopy. After 10 days the volatiles were evaporated and the solid was recrystallized from pentane at -35°C to produce 15 mg (60% yield) of lime green crystals of **3**. ^1H NMR (360 MHz, C_6D_6): δ = 51.54 (s), 3.85 (br), 2.82 (s), 2.80 (s), -1.20 (br shoulder), -2.18 (br), -3.51 (s), -9.95 ppm (s); IR (KBr, exclusion of N_2): $\tilde{\nu}$ = 2956 (s), 2912 (s), 2843 (s), 2503 (s, B-H), 1537 (s), 1422 (s), 1359 (s), 1190 (s), 1060 (m), 883 (w), 772 (s), 647 cm^{-1} (w); m.p. decomp above 85°C ; HRMS (EI): M^+/e = 631.3915 (obs) 631.3944 (calcd); μ_{eff} (295 K) = 4.6(2) μ_{B} .

Received: November 5, 2004

Revised: December 4, 2004

Published online: February 3, 2005

Keywords: C–H activation · cobalt · high-spin complexes · imido ligands · tripodal ligand

Thyagarajan, C. D. Incarvito, A. L. Rheingold, K. H. Theopold, *Chem. Commun.* **2001**, 2198; c) K. H. Theopold, O. M. Reinaud, S. Blanchard, S. Leelasubcharoen, A. Hess, S. Thyagarajan in *Advancing Sustainability through Green Chemistry* (Eds.: P. T. Anastas, R. L. Lankey), American Chemical Society, Washington, DC, **2002**, p. 75 (ACS Symposium Series 823).

- [3] Crystal data for **1**: orthorhombic, *Pccn*, $a = 15.5337(9)$, $b = 43.126(2)$, $c = 11.0273(6)$ Å, $\alpha = \beta = \gamma = 90^\circ$, $V = 7387.2(7)$ Å³, $\rho_{\text{calcd}} = 1.201$ g cm⁻³, $\theta = 1.39\text{--}28.28^\circ$, $\text{MoK}\alpha$, $\lambda = 0.71073$ Å, $T = 150(2)$ K, 43875 reflections, 8738 independent, $R(\text{int}) = 0.076$, *SADABS* absorption correction, $\mu = 0.499$ mm⁻¹, max and min transmission: 0.980 and 0.842, solved by direct methods and refined by full-matrix least-squares on F^2 , hydrogen atoms were found from the F-map and refined with isotropic thermal parameters, 608 parameters, $R = 0.0611$, $wR = 0.1309$, largest difference peak and hole: 0.970 and -0.593 e Å⁻³. A highly disordered molecule of pentane centered on a two-fold axis was resolved with Squeeze [PLATON: A. L. Spek, *J. Appl. Crystallogr.* **2003**, 36, 7–13], void space = 752.3 Å³, 158 e/cell assigned as four pentane molecules per cell (calcd: 168 e/cell). Crystal data for **3**: orthorhombic, *Pbca*, $a = 17.499(3)$, $b = 18.992(3)$, $c = 23.944(4)$ Å, $\alpha = \beta = \gamma = 90^\circ$, $V = 7957(2)$ Å³, $\rho_{\text{calcd}} = 1.185$ g cm⁻³, $\theta = 1.70\text{--}28.27^\circ$, $\text{MoK}\alpha$, $\lambda = 0.71073$ Å, $T = 120(2)$ K, 77362 reflections, 9453 independent, *SADABS* semiempirical absorption correction from equivalents, $\mu = 0.468$ mm⁻¹, max and min transmission: 0.9547 and 0.8350, solved by direct methods and refined by full-matrix least-squares on F^2 , 459 parameters, $R = 0.0433$, $wR = 0.1247$, largest difference peak and hole: 0.712 and -0.510 e Å⁻³. CDCC-253897 (**1**) and CDCC-253898 (**3**) contain the supplementary crystallographic data for this paper. These data can be obtained free of charge from the Cambridge Crystallographic Data Centre via www.ccdc.cam.ac.uk/data_request/cif.
- [4] P. E. Hansen, *Prog. Nucl. Magn. Reson. Spectrosc.* **1988**, 20, 207.
- [5] R. A. Heintz, T. G. Neiss, K. H. Theopold, *Angew. Chem.* **1994**, 106, 2389; *Angew. Chem. Int. Ed. Engl.* **1994**, 33, 2326.
- [6] W. A. Nugent, J. M. Mayer, *Metal–Ligand Multiple Bonds*, Wiley, New York, **1988**, p. 123.
- [7] J. L. Detrich, R. Konecny, W. M. Vetter, D. Doren, A. L. Rheingold, K. H. Theopold, *J. Am. Chem. Soc.* **1996**, 118, 1703.
- [8] a) D. J. Mindiola, G. L. Hillhouse, *Chem. Commun.* **2002**, 1840; b) S. D. Brown, T. A. Betley, J. C. Peters, *J. Am. Chem. Soc.* **2003**, 125, 322.
- [9] S. Thyagarajan, D. T. Shay, C. D. Incarvito, A. L. Rheingold, K. H. Theopold, *J. Am. Chem. Soc.* **2003**, 125, 4440.
- [10] A search of the Cambridge Structural Database (F. H. Allen, *Acta Crystallogr. Sect. B* **2002**, 58, 380–388) using the program Conquest (I. J. Bruno, J. C. Cole, P. R. Eddington, M. Kessler, C. F. Mcrae, P. McGabe, J. Pearson, R. Taylor, *Acta Crystallogr. Sect. B* **2002**, 58, 389–397) yielded 11 structures containing secondary amines coordinated to Co, showing a mean Co–N separation of 2.019 Å.

- [1] a) D. S. Glueck, F. J. Hollander, R. G. Bergman, *J. Am. Chem. Soc.* **1989**, 111, 2719; b) D. S. Glueck, J. X. Wu, F. J. Hollander, R. G. Bergman, *J. Am. Chem. Soc.* **1991**, 113, 2041; c) D. J. Mindiola, G. L. Hillhouse, *J. Am. Chem. Soc.* **2001**, 123, 4623; d) D. M. Jenkins, T. A. Betley, J. C. Peters, *J. Am. Chem. Soc.* **2002**, 124, 11238; e) T. A. Betley, J. C. Peters, *J. Am. Chem. Soc.* **2003**, 125, 10782; f) X. Dai, P. Kapoor, T. H. Warren, *J. Am. Chem. Soc.* **2004**, 126, 4798.

- [2] a) J. W. Egan, Jr., B. S. Haggerty, A. L. Rheingold, S. C. Sendlinger, K. H. Theopold, *J. Am. Chem. Soc.* **1990**, 112, 2445; b) S.

Synthetic Methods

A Synthetic Pathway to Either Enantiomer of Merrilactone A**

Zhaoyang Meng and Samuel J. Danishefsky*

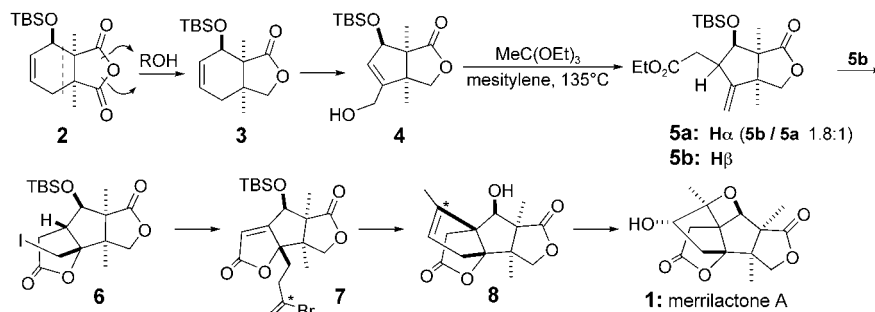
In 2002, our group reported the total synthesis of merrilactone A (racemic **1**).^[1] Aesthetically, one is attracted to this molecule by virtue of its propeller-like topology, crafted from five interlocking *cis* fusions (including two γ -lactones and an oxetane). Six stereogenic bridgehead centers serve as the anchor points of these fusions. Attempts to synthesize structures such as **1** often enrich the field of organic chemistry.

In the case of merrilactone A, additional considerations argued for a program directed to its total synthesis. Compound **1** is a member of a class of nonpeptidal neurotrophic factors. Maintenance of appropriate levels of polypeptid neurotrophic factors in the central nervous system can be critical in promoting neuronal cell viability.^[2a] Administration of polypeptid neurotrophic factors to damaged neuronal cells can lead to substantially restored phenotypes in vitro.^[2b–d] Unfortunately, however, the natural factors have performed poorly as therapeutic agents in vivo.^[2e] These failures have been ascribed to the usual transport and pharmacostability issues that beset the use of polypeptides. Thus, we have been studying the synthesis of potential nonpeptid small molecules with neurotrophic activity. Through such compounds, some of the pharmacostability issues that plague polypeptid neurotrophic factors might be overcome. Fukuyama and co-workers described promising activity for merrilactone A in a neurite growth assay.^[3] It would be of considerable interest to investigate the mechanism of this in vitro activity as well as its relevance to in vivo settings. These considerations prompted our first experiments directed toward the total synthesis of merrilactone A, which were indeed successful (Scheme 1).^[1]

There are several areas of our initial synthesis in which significant improvements would be helpful. Whereas compound **2** could be synthesized in reasonable yields through Diels–Alder cycloaddition (Scheme 1, dotted line in **2**), its conversion into γ -lactone **3** was not straightforward. Various

attempted ring openings of the anhydride were nonregio-selective; the isomeric products that arose from both modes of ring opening (Scheme 1, arrows in **2**) could be converted individually into the desired **3**.

A second difficulty arose at the level of relative stereochemistry. The transformation of **4** into **5b** by Claisen rearrangement was never realized in a selective fashion,



Scheme 1. Birman–Danishefsky synthesis of merrilactone A.

despite many attempts. At best, we could obtain only a 1.8:1 ratio of **5b/5a** favoring the desired isomer. Moreover, the synthesis produced racemic merrilactone. In the context of launching a structure–activity relationship study on this family of compounds, it would certainly be of interest to evaluate merrilactone A in its enantiomerically pure form.

As shown in Scheme 1, chirality was introduced initially in our first-generation synthesis in the Diels–Alder reaction leading to **2**. Since this reaction can only be accomplished at high temperatures, the prospects for strong margins of catalytically mediated enantioselectivity are not promising. These considerations, particularly the goal of generating the enantiopure antipodes of merrilactone A for biological assessment, led us to explore a new total synthesis route. As the previous route to merrilactone A from **6** onward is rather concise and efficient, we planned for compound **6** to be a milestone in a new route.

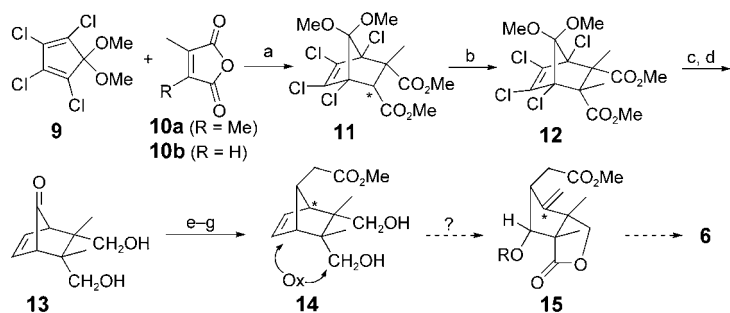
We therefore set diester **12** as our first subgoal compound. It could not be reached by Diels–Alder reaction of **10a** ($R = Me$) with **9**. A solution around this problem was required. Fortunately, cycloaddition was possible with the monomethyl compound **10b**^[4] ($R = H$) with *endo* specificity (Scheme 2). Methanolysis of the anhydride and esterification of the free acid afforded **11**. The key point was the *endo* configuration of the quaternary ester in **11**. Lithiation generated the enolate of the other ester (asterisk on **11**). In the event, stereospecific C-methylation^[5] of this enolate gave rise to **12**. The latter was advanced in a straightforward manner to *meso* structure **14**.

At this stage, the global task was the degradation of **14** to reach **15**. The latter would intersect **6** by iodolactonization. Overall, this required the oxidation of the 1,4-diol of **14** to a butyrolactone, degradation of the etheno linkage with interpolation of an oxygen function at a former bridgehead center, and attachment of an exocyclic methylene to the other (asterisks on **14** and **15**). The crux of the more subtle challenge of specificity at the regiochemical level is that the interpolated oxygen functional group appears “*ortho*” to the oxidized

[*] Prof. S. J. Danishefsky
Laboratory for Bioorganic Chemistry
Sloan-Kettering Institute for Cancer Research
1275 York Avenue, New York, NY 10021 (USA)
Fax: (+1) 212-772-8691
E-mail: s-danishefsky@ski.mskcc.org
Z. Meng, Prof. S. J. Danishefsky
Department of Chemistry, Columbia University
Havemeyer Hall, 3000 Broadway, New York, NY 10027 (USA)

[**] Support for this research was provided by the National Institutes of Health (Grant HL 25848).

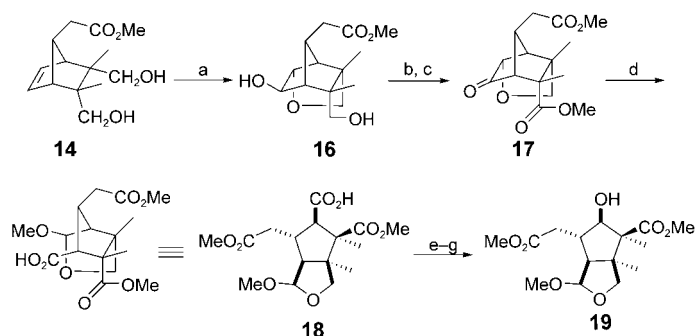
Supporting information for this article is available on the WWW under <http://www.angewandte.org> or from the author.



Scheme 2. Synthesis of key intermediate **14**: a) 180 °C, neat; then MeOH, reflux, PhH/MeOH, TMSCHN₂, 92% for one-pot reaction; b) LDA, HMPA, MeI, THF, –78 °C → RT, 95%; c) LAH, THF, reflux; d) Na, NH₃, THF/EtOH, 72% over two steps; e) 2,2-dimethoxypropane, acetone, *p*TsOH; f) NaH, (EtO)₂POCH₂CO₂Et, THF, 86% over two steps; g) Mg, MeOH, acidic workup, 77%. LAH = lithium aluminum hydride; LDA = lithium diisopropylamide; HMPA = hexamethylphosphoramide; TMS = trimethylsilyl Ts = toluenesulfonyl.

carbon of the lactone, leaving the *exo* methylene group to emerge “*ortho*” to the unoxidized hydroxymethyl equivalent (structure **15**).

Oxidation of **14** with *m*CPBA resulted, not surprisingly, in the formation of **16** (Scheme 3). Compound **16** was subjected

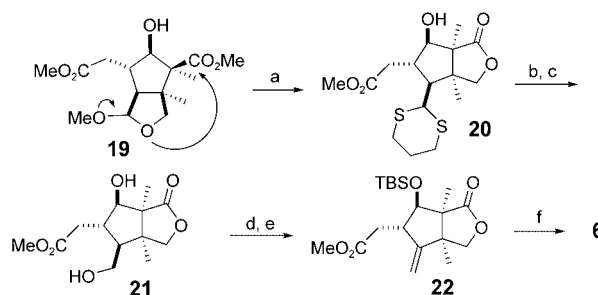


Scheme 3. Baeyer–Villiger oxidation of **17**: a) *m*CPBA, CH₂Cl₂, 90%; b) PDC, DMF; c) K₂CO₃, MeI, acetone, reflux, 70% over two steps; d) MMPP, MeOH, 0 °C → RT, 88%; e) DCC, *m*CPBA, 0 °C → RT, 83%; f) PhH, reflux; g) K₂CO₃, MeOH, 70%. DCC = *N,N*-dicyclohexylcarbodiimide; DMF = *N,N*-dimethylformamide; *m*CPBA = *meta*-chloroperoxybenzoic acid; MMPP = magnesium monoperoxyphthalate hexahydrate; PDC = pyridinium dichromate.

to oxidation with PDC, which, followed by esterification, led to the formation of ketoester **17**. As expected, Baeyer–Villiger oxidation of **17** gave rise to **18**.^[6] The resulting carboxylic acid in **18** was transformed into the requisite secondary alcohol **19** with retention of stereochemistry through carboxy inversion.^[7]

The methoxytetrahydrofuran ring moiety of **19** was opened by trapping its masked aldehyde, which prompted lactonization to produce **20** (Scheme 4, arrows). The latter was subsequently converted into **21**. In this way, the regiochemical issues delineated above had been settled in a most favorable manner.

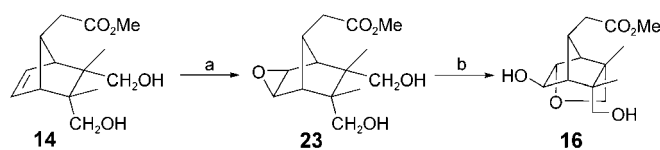
Upon exposure to the protocols of Grieco and co-workers,^[8] compound **21** underwent selective reaction at the



Scheme 4. Completion of the synthesis of racemic intermediate **6**: a) BF₃·OEt₂, HS(CH₂)₃SH, CH₂Cl₂, 50%; b) PhI(OCF₃CO₂)₂, CH₃CN/H₂O, 50%; c) NaBH₄, MeOH, 0 °C; d) *o*-NO₂C₆H₄SeCN, Bu₃P, THF, then H₂O₂ (30%), 86%; e) TBSOTf, Et₃N, CH₂Cl₂, 76%; f) LiOH, MeOH/H₂O; then I₂, saturated NaHCO₃/THF, (75%). TBS = *tert*-butyldimethylsilyl; Tf = trifluoromethanesulfonyl.

primary alcohol to provide a transient selenide, which afforded the desired exocyclic olefin after oxidative elimination. Silyl protection of the secondary alcohol gave rise to **22**. The latter was hydrolyzed and the resultant carboxylic acid underwent iodolactonization to afford the advanced intermediate **6**, whose spectroscopic properties were in complete accord with those previously reported.^[1]

With a controlled synthesis of **6** in place, we could focus on our final and most critical goal, that is, an enantioselective synthesis of merrilactone A. It was not by chance that this second-generation synthesis was built around a series of *meso* intermediates that culminated in **14**, and thence its *exo* epoxide **23** (Scheme 5). It was at this point that we hoped to



Scheme 5. Desymmetrization of *meso*-**14**: a) DMDO, CH₂Cl₂, 0.5–1 h; b) (*S,S*)-[Co^{III}(salen)]-OAc, –78 °C, two days; then –25 °C, two days, THF, 86% over two steps. DMDO = 2,2-dimethyldioxirane; salen = *N,N'*-bis(salicylidene)ethylenediamine.

make use of highly innovative asymmetric epoxide-ring-opening (ARO) methodology. Compound **14** was treated with dimethyldioxirane to form the discrete epoxide, **23**. The latter was exposed to catalytic amounts of (*S,S*)-[Co^{III}(salen)]-OAc as described by Jacobsen and co-workers^[9] (Scheme 5). We were pleased to find that this treatment led to the formation of enantioenriched **16**, with 86% ee and in 86% yield. As expected, use of the *R,R* Jacobsen catalyst led to *ent*-**16**.^[10]

One of the key teachings of this synthesis lies in the construction of **12**. Thus, we were able to compensate for the resistance of dimethyl maleic anhydride **10a** to undergo cycloaddition by performing a series of straightforward transformations with Diels–Alder adduct **11** which led to the formation of **12**. A second important feature of this synthesis is the chemical degradation pathway from **14** to **18**, which proceeded with full regiocontrol and promising enantiocontrol.

In summary, a route to the enantioenriched merrilactone antipodes has been charted. Parenthetically, the chemistry described above serves to ameliorate the regio- and diastereoselectivity awkwardness of the earlier effort,^[1] while retaining its particularly clean and convergent features. With the advances reported above, a full-scale investigation of the effects of absolute configuration on the performance of a potent, nonpeptidal neurotrophic factor will go forward.

Received: November 3, 2004

Published online: February 2, 2005

Keywords: asymmetric synthesis · enantioselectivity · natural products · regioselectivity · synthetic methods

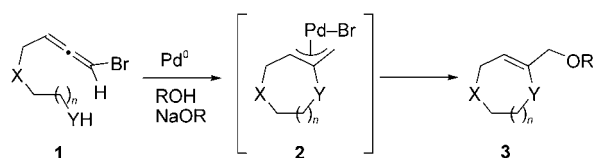
- [1] V. B. Birman, S. J. Danishefsky, *J. Am. Chem. Soc.* **2002**, *124*, 2080; another total synthesis of merrilactone A has since been reported: M. Inoue, T. Sato, M. Hirama, *J. Am. Chem. Soc.* **2003**, *125*, 10772.
- [2] a) F. Hefti, *Annu. Rev. Pharmacol. Toxicol.* **1997**, *37*, 239; b) M. R. Bennett, W. G. Gibson, G. Lemon, *Auton. Neurosci.* **2002**, *95*, 1; c) P. Lu, A. Blesch, M. H. Tuszynski, *J. Comp. Neurol.* **2001**, *436*, 456; d) M. Kaneko, Y. Saito, H. Saito, T. Matsumoto, Y. Matsuda, J. L. Vaught, C. A. Dionne, T. S. Angeles, M. A. Glicksman, N. T. Neff, D. P. Rotella, J. C. Kauer, J. P. Mallamo, R. L. Hudkins, C. Murakata, *J. Med. Chem.* **1997**, *40*, 1863; e) C. Backman, G. M. Rose, B. J. Hoffer, M. A. Henry, R. T. Bartus, P. Friden, A. C. Granholm, *J. Neurosci.* **1996**, *16*, 5437.
- [3] a) J.-M. Huang, R. Yokoyama, C.-S. Yang, Y. Fukuyama, *Tetrahedron Lett.* **2000**, *41*, 6111; b) J.-M. Huang, C.-S. Yang, M. Tanaka, Y. Fukuyama, *Tetrahedron* **2001**, *57*, 4691.
- [4] J. S. Yadav, P. K. Sasmal, *Tetrahedron* **1999**, *55*, 5185.
- [5] S. Ghosh, G. Saha, G. Mostafa, R. Siddhartha, *J. Org. Chem.* **1992**, *57*, 7344.
- [6] Y. V. S. N. Murphy, C. N. Pillai, *Synth. Commun.* **1996**, *26*, 2363.
- [7] a) D. B. Denney, N. Sherman, *J. Org. Chem.* **1965**, *30*, 3760; b) S. J. Danishefsky, K. Tsuzuki, *J. Am. Chem. Soc.* **1980**, *102*, 6891.
- [8] P. A. Grieco, S. Gilman, M. Nishizawa, *J. Org. Chem.* **1976**, *41*, 1485.
- [9] M. H. Wu, K. B. Hansen, E. N. Jacobsen, *Angew. Chem.* **1999**, *111*, 2167; *Angew. Chem. Int. Ed.* **1999**, *38*, 2012.
- [10] Compounds **16** and *ent*-**16** were converted into the corresponding benzyl esters, and the optical rotations were determined: $[\alpha]_{\text{D}}^{23} = -10.9$ (CHCl_3 , $c = 0.19$) for the benzyl ester of **16** and $[\alpha]_{\text{D}}^{23} = 7.9$ (CHCl_3 , $c = 0.34$) for the benzyl ester of *ent*-**16**. Although the HPLC data show the enantiospecificity of each reaction that arises from the antipodal catalysts to be identical, the rotations, though opposite, are not equal in magnitude. This suggests the presence of an impurity in one of the specimens. This matter is currently under investigation.

Cyclization Reactions

Bromoallenes as Allyl Dication Equivalents in the Absence of Palladium(0): Synthesis of Bicyclic Sulfamides by Tandem Cyclization of Bromoallenes**

Hisao Hamaguchi, Shohei Kosaka, Hiroaki Ohno,* and Tetsuaki Tanaka*

Reactions of bromoallenes have attracted much interest in recent years because of the interesting chemical properties associated with their cumulated double bonds and bromine atom.^[1] However, except for our recent study on ring-forming reactions,^[2,3] all the reactions of bromoallenes reported to date are intermolecular reactions, such as organocopper-mediated substitutions,^[4] palladium-catalyzed cross-coupling reactions,^[5] and formation of allenyl-metal reagents.^[6] Recently, we found that bromoallenes can act as allyl dication equivalents in the presence of palladium(0), which is an extremely useful process for the synthesis of medium-sized heterocycles (Scheme 1).^[3] Thus, reaction of bromoallene **1**



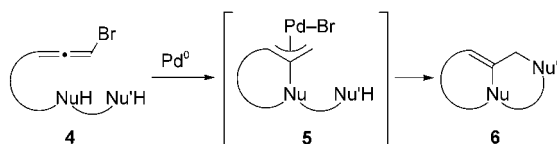
Scheme 1. Palladium(0)-catalyzed medium-ring formation from bromoallenes.

with sodium alkoxide in the presence of a palladium(0) catalyst and alcohol affords the (η^3 -allyl)palladium(II) intermediate **2** by intramolecular nucleophilic attack at the central carbon atom of the allenic moiety. A second nucleophilic reaction with alkoxide provides **3** in good to high yields. In light of this chemistry, we expected that bicyclic compounds **6** could be formed by tandem cyclization of the bromoallene **4** via (η^3 -allyl)palladium(II) intermediate **5** (Scheme 2).

In the field of medicinal chemistry, a sulfamide is one of the most important structural motifs that exist in many pharmaceutically useful compounds. For example, some sulfamides, including cyclic ones, are known to be effective HIV^[7] and serine protease inhibitors,^[8] and as both agonists

[*] H. Hamaguchi, S. Kosaka, Dr. H. Ohno, Prof. Dr. T. Tanaka
Graduate School of Pharmaceutical Sciences
Osaka University
1-6 Yamadaoka, Suita, Osaka 565-0871 (Japan)
Fax: (+81) 6-6879-8214
E-mail: t-tanaka@phs.osaka-u.ac.jp

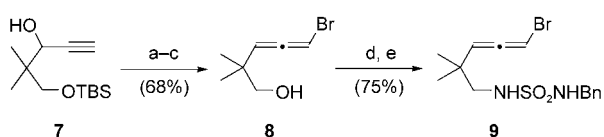
[**] This work was supported by a Grant-in-Aid for Encouragement of Young Scientists from the Ministry of Education, Culture, Sports, Science, and Technology of Japan, and the Mitsubishi Chemical Corporation Fund. H. H. is grateful to Research Fellowships from the Japan Society for the Promotion of Science (JSPS) for Young Scientists.



Scheme 2. Synthesis of bicyclic heterocycles.

and antagonists of serotonin^[9] and histamine receptors.^[10] Furthermore, cyclic sulfamides have also been used as effective chiral auxiliaries in asymmetric aldol reactions.^[11] However, most of the reported methods for the synthesis of sulfamides rely on the reaction of diamines with sulfonyl chloride or the sulfamide $\text{H}_2\text{NSO}_2\text{NH}_2$ under drastic reaction conditions.^[12] Accordingly, we planned a novel synthesis of bicyclic sulfamides by tandem cyclization of bromoallenes. We describe here a highly regioselective construction of cyclic sulfamides with a bicyclo[3.3.0]octane skeleton from bromoallenes containing a sulfamide moiety as nucleophile, and show that some bromoallenes can act as allyl dication equivalents *even in the absence of palladium(0)*.

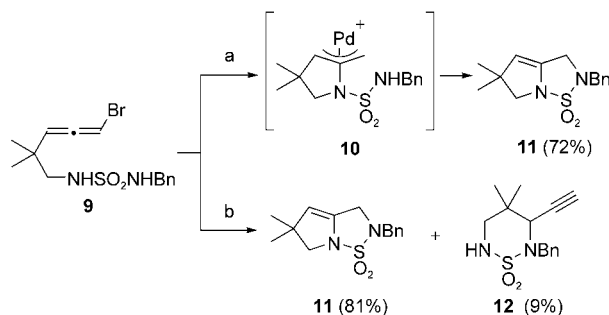
To investigate the synthesis of bicyclic sulfamides by tandem cyclization of bromoallenes, as depicted in Scheme 2, the bromoallene **9** bearing a sulfamide moiety as nucleophile was prepared from propargyl alcohol **7**^[13] as shown in Scheme 3. Thus, treatment of **7** with MsCl and Et_3N gave



Scheme 3. Synthesis of bromoallene **9** bearing a sulfamide group: a) MsCl , Et_3N ; b) $\text{CuBr}\cdot\text{SMe}_2$, LiBr ; c) 1% HCl/EtOH ; d) $\text{BocNH-SO}_2\text{NHBn}$, PPh_3 , diethylazodicarboxylate (DEAD); e) 3 N HCl , EtOAc .

the corresponding mesylate, which was then converted into the bromoallene **8** by treatment with $\text{CuBr}\cdot\text{SMe}_2/\text{LiBr}$ ^[14] followed by desilylation. Condensation of **8** with $\text{BocNH-SO}_2\text{NHBn}$ ^[15] under the Mitsunobu conditions gave the corresponding *N*-Boc bromoallene, the Boc group of which was removed by treatment with 3 N HCl to afford the desired bromoallene **9** bearing two nitrogen nucleophiles.

We next investigated the tandem cyclization of the bromoallene **9** in the presence of palladium(0). To realize the desired cyclization, selective addition of the internal sulfamide nitrogen to the central allenic carbon, followed by preferential reaction of the terminal sulfamide nitrogen over that of alkoxide, is essential. Fortunately, cyclization of the bromoallene **9** gave the bicyclic sulfamide **11** (72% yield) as the only isolable product (Scheme 4), presumably via the intermediate **10**. Surprisingly, the same reaction also proceeded in the absence of palladium(0) to afford **11** in better yield (81%) along with a small amount of the six-membered-ring product **12** (9%), although the required reaction time was longer. These results demonstrate that bromoallene **9** can act as an allyl dication equivalent in the absence of palladium(0). However, it should be clearly noted that, in

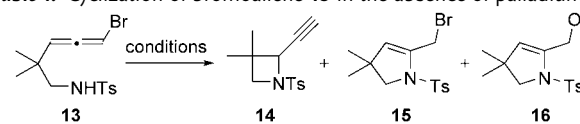


Scheme 4. Synthesis of bicyclic sulfamide **11** in the presence or absence of palladium(0): a) $[\text{Pd}(\text{PPh}_3)_4]$ (10 mol%), NaH (2.5 equiv), MeOH , 60°C , 11.5 h; b) NaH (2.5 equiv), MeOH , 60°C , 16 h.

the medium-ring formation,^[3] the palladium catalyst is essential for successful conversion.^[16] Thus, the reaction of bromoallenes as an allyl dication in the absence of a palladium catalyst can be applied to highly reactive bromoallenes which easily form cyclized products, such as five-membered rings.

Next, we investigated the effect of the solvent on the palladium-free reaction using bromoallene **13**. The results are summarized in Table 1. Treatment of bromoallene **13** with

Table 1: Cyclization of bromoallene **13** in the absence of palladium(0).^[a]



Entry	Solvent	<i>T</i>	<i>t</i> [h]	Product (yield ^[b] [%])
1	DMF ^[c]	room temp	0.5	14 (76) and 15 (13)
2	DMF ^[d]	room temp	0.5	14 (77) and 16 (7)
3	THF ^[d]	room temp	1.5	no reaction
4	THF ^[d]	50°C	2.5	14 (48) and 15 (16)
5	MeOH ^[c]	room temp	20	15 (8) ^[e]
6	MeOH ^[c]	60°C	7	16 (94)

[a] Reactions were carried out with NaH (1.5 equiv) or NaOMe (1.5 equiv) as base in the absence of $[\text{Pd}(\text{PPh}_3)_4]$. [b] Yields of isolated products. [c] NaH was used as base. [d] NaOMe was used as base. [e] 71% of **13** was recovered.

NaH in DMF gave the azetidine **14** as the major product^[17] and a small amount of dihydropyrrole **15** containing a bromomethyl group (Table 1, entry 1). Similar results were obtained when using NaOMe as the base in DMF or THF (Table 1, entries 2 and 4). Although the reaction of **13** with NaH in MeOH at room temperature gave **15** in low yield (8%; Table 1, entry 5), the reaction at 60°C gave dihydropyrrole **16**, which contains a methoxymethyl group, in high yield (94%; Table 1, entry 6). From these observations, it can clearly be seen that bromoallenes can effectively act as allyl dication equivalents in an alcoholic solvent in the absence of palladium(0).

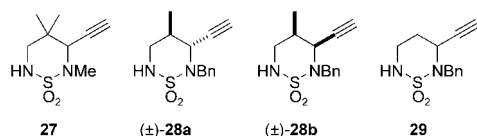
We next investigated the tandem cyclization reaction with other bromoallenes, which were prepared from the corresponding bromoallenols by a similar procedure to that shown

in Scheme 3. The results of these cyclizations are summarized in Table 2. As we expected, treatment of the bromoallene **17**, which contains a protected diol, gave the bicyclic sulfamide **22** in 91 % yield (Table 2, entry 1). Similarly, the bromoallene **18**

Table 2: Synthesis of bicyclic sulfamide in the absence of palladium(0).^[a]

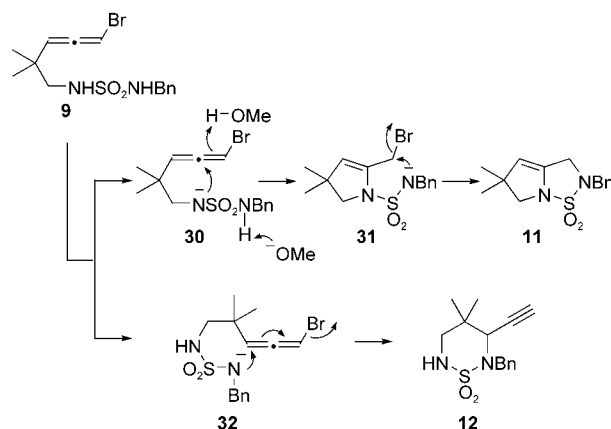
Entry	Substrate	Time [h]	Product	Yield [%] ^[b]
1		4.5		91
2		6		89
3		12		65 ^[c]
4		10		57 ^[d]
5		12		50 ^[e]

[a] Reactions were carried out with NaH (2.5 equiv) in MeOH at 60 °C. [b] Yields of isolated products. [c] Six-membered-ring product **27** was obtained in 10% yield as a minor product. [d] Six-membered-ring products **28a** and **28b** were obtained in 9% and 5% yield, respectively. [e] Six-membered-ring product **29** was obtained in 24% yield.



was converted into the tricyclic sulfamide **23** in 89% yield (Table 2, entry 2). Bicyclic sulfamides **24** and **25** were obtained as the major products from the reaction of bromoallenes **19**, which has a methyl group on the terminal nitrogen, or racemic **20**, which has a single methyl substituent on the carbon between the allenyl and sulfamide groups (Table 2, entries 3 and 4). When the bromoallene **21**, which contains an unsubstituted carbon tether, was used, bicyclic sulfamide **26** was isolated (50%) along with a considerable amount of the six-membered-ring product **29** (24%; Table 2, entry 5).

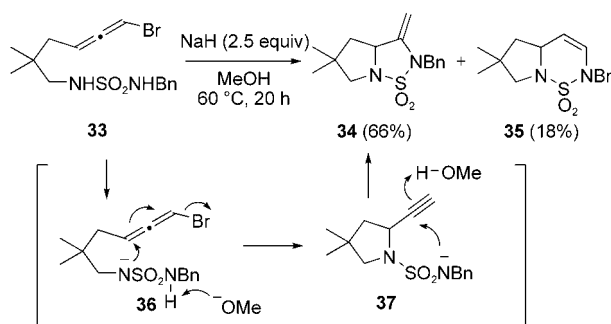
Possible reaction courses are shown in Scheme 5. In the tandem cyclization, the first intramolecular nucleophilic attack takes place at the central carbon atom of bromoallene **30** and is followed by protonation by MeOH to produce intermediate **31** bearing a bromomethyl group. The second intramolecular nucleophilic addition affords the bicyclic sulfamide **11**. This reaction pathway via the intermediate **31** is supported by the experimental results shown in Table 1: NaH-mediated cyclization of the bromoallene **13**, which



Scheme 5. Possible reaction courses.

contains a tosylamide group, in MeOH at room temperature (Table 1, entry 5), yielded the dihydropyrrole **15** (8%), which contains a bromomethyl group, along with a considerable amount of the starting bromoallene **13** (71%). In contrast, the same reaction at higher temperature (Table 1, entry 6) gave the methoxymethyl derivative **16**, which is produced by the nucleophilic substitution of **15** with methoxide. Formation of the six-membered-ring product **12** can be rationalized by an S_N2'-type intramolecular attack by the terminal nitrogen.

Finally, we investigated the synthesis of cyclic sulfamides from bromoallene **33**, which has a three-atom tether between the sulfamide and bromoallene (Scheme 6). Interestingly, the



Scheme 6. Reaction of bromoallene **33**, which has a three-atom tether between the sulfamide and bromoallene.

first cyclization occurs regioselectively at the allenic carbon close to the sulfamide group to give **34** (66%) and **35** (18%). Pyrrolidine **37** is considered to be a plausible intermediate, formed by S_N2'-type intramolecular amination of **36**.^[18] This is followed by *exo*- or *endo*-cyclization to afford **34** or **35**, respectively. This result reveals that the base-induced cyclization of bromoallenes in MeOH in the absence of palladium(0) favors five-membered-ring formation, which is in striking contrast to the palladium(0)-catalyzed reaction.^[3]

In conclusion, we have developed a novel synthesis of cyclic sulfamides containing a bicyclo[3.3.0]octane skeleton from bromoallenes having a sulfamide moiety as nucleophiles. Although the palladium-free cyclization reaction is limited to the reaction of relatively reactive substrates, we

have demonstrated for the first time that bromoallenes can act as allyl dication equivalents *even in the absence of palladium(0)*, and that the intramolecular reaction with two nucleophiles enables the direct formation of bicycles by tandem cyclization. These cyclizations are extremely useful for the synthesis of bicyclic sulfamides and could extend the potential application of sulfamides as new pharmaceutically useful agents in medicinal chemistry.

Experimental Section

General procedure for the cyclization of bromoallenes in the absence of palladium(0). Reaction of **9** (Scheme 4): NaH (60 % suspension in mineral oil; 12 mg, 0.3 mmol) was added to MeOH (0.5 mL) at room temperature under nitrogen, and the mixture was stirred for 10 min at this temperature. A solution of the bromoallene **9** (43.1 mg, 0.12 mmol) in MeOH (0.7 mL) was added at room temperature to the stirred mixture, which was stirred for 16 h at 60 °C. Concentration under reduced pressure gave an oily residue, which was purified by column chromatography over silica gel with *n*-hexane/EtOAc (3:1) to give, in order of elution, **11** (27 mg, 81 %) and **12** (3.5 mg, 9 %). **11**: colorless solid; m.p. 48 °C; IR (KBr): $\tilde{\nu}$ = 1682 (C=C–N), 1317 cm^{−1} (NSO₂); ¹H NMR (300 MHz, CDCl₃): δ = 1.21 (s, 6H; 2 × CMe), 3.32 (s, 2H; CH₂), 3.73 (d, *J* = 1.5 Hz, 2H; CH₂), 4.32 (s, 2H; CH₂Ph), 4.79 (t, *J* = 1.5 Hz, 1H; C=CH), 7.30–7.37 ppm (m, 5H; Ph); ¹³C NMR (67.8 MHz, CDCl₃): δ = 27.5 (2C), 46.1, 48.4, 51.6, 59.2, 111.6, 128.1, 128.4 (2C), 128.7 (2C), 134.7, 136.3 ppm; MS (FAB) *m/z* (%): 279 (89) [MH⁺], 91 (100); HRMS (FAB) calcd. for C₁₄H₁₉N₂O₂S [MH⁺]: 279.1167; found 279.1169. **12**: colorless crystals; m.p. 118 °C (*n*-hexane/EtOAc); IR (KBr): $\tilde{\nu}$ = 3284 (NHSO₂), 2114 (C≡C), 1336 cm^{−1} (NSO₂); ¹H NMR (300 MHz, CDCl₃): δ = 1.05 (s, 3H; CMe), 1.08 (s, 3H; CMe), 2.56 (d, *J* = 2.4 Hz, 1H; C≡CH), 2.94 (ddd, *J* = 14.4, 5.4, 1.8 Hz, 1H; CH₂H_b), 3.56 (dd, *J* = 2.4, 1.8 Hz, 1H; CH=C≡CH), 3.64 (dd, *J* = 14.4, 10.8 Hz, 1H; CH₂H_b), 4.09 (d, *J* = 14.1 Hz, 1H; PhCH₂H_b), 4.70–4.76 (m, 1H; NH), 4.78 (d, *J* = 14.1 Hz, 1H; PhCH₂H_b), 7.28–7.39 ppm (m, 5H; Ph); ¹³C NMR (75 MHz, CDCl₃): δ = 23.16, 23.22, 33.7, 49.4, 52.4, 59.5, 77.0, 77.1, 127.9, 128.6 (2C), 128.9 (2C), 135.2 ppm; elemental analysis calcd (%) for C₁₄H₁₈N₂O₂S: C 60.40, H 6.52, N 10.06; found: C 60.19, H 6.52, N 10.00.

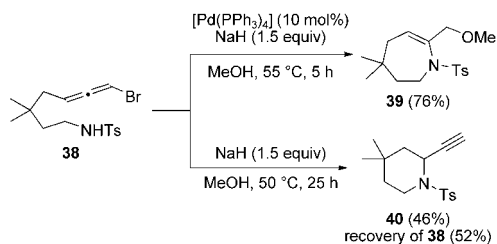
Received: November 9, 2004

Published online: January 21, 2005

Keywords: allenes · cyclization · halogen compounds · palladium · sulfamides

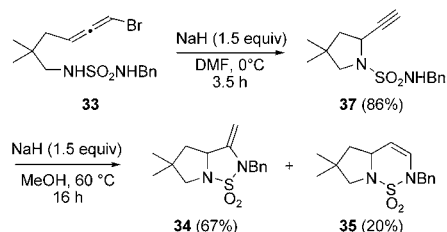
- [1] S. Ma, in *Modern Allene Chemistry, Vol. 2* (Eds.: N. Krause, A. S. K. Hashmi), Wiley-VCH, Weinheim, **2004**, pp. 614–619.
- [2] a) H. Ohno, H. Hamaguchi, T. Tanaka, *Org. Lett.* **2001**, *3*, 2269–2271; b) H. Ohno, K. Ando, H. Hamaguchi, Y. Takeoka, T. Tanaka, *J. Am. Chem. Soc.* **2002**, *124*, 15255–15266.
- [3] a) H. Ohno, H. Hamaguchi, M. Ohata, T. Tanaka, *Angew. Chem.* **2003**, *115*, 1791–1795; *Angew. Chem. Int. Ed.* **2003**, *42*, 1749–1753; b) H. Ohno, H. Hamaguchi, M. Ohata, S. Kosaka, T. Tanaka, *Heterocycles* **2003**, *61*, 65–68; c) H. Ohno, H. Hamaguchi, M. Ohata, S. Kosaka, T. Tanaka, *J. Am. Chem. Soc.* **2004**, *126*, 8744–8754.
- [4] a) E. J. Corey, N. W. Boaz, *Tetrahedron Lett.* **1984**, *25*, 3059–3062; b) A. M. Caporusso, C. Polizzi, L. Lardicci, *Tetrahedron Lett.* **1987**, *28*, 6073–6076; c) F. D'Aniello, A. Mann, A. Schoenfelder, M. Taddei, *Tetrahedron* **1997**, *53*, 1447–1456; d) F. Chemla, N. Bernard, J. Normant, *Eur. J. Org. Chem.* **1999**, 2067–2078; e) J. J. Conde, W. Mendelson, *Tetrahedron Lett.* **2000**, *41*, 811–814; f) A. M. Caporusso, S. Filippi, F. Barontini, P. Salvadori, *Tetrahedron Lett.* **2000**, *41*, 1227–1230.
- [5] a) G. Märkl, P. Attenberger, J. Kellner, *Tetrahedron Lett.* **1988**, *29*, 3651–3654; b) T. Gillmann, T. Hülsen, W. Massa, S. Wocadlo, *Synlett* **1995**, 1257–1259; c) R. W. Saalfrank, M. Haubner, C. Deutscher, W. Bauer, T. Clark, *J. Org. Chem.* **1999**, *64*, 6166–6168.
- [6] a) J. A. Marshall, N. D. Adams, *J. Org. Chem.* **1997**, *62*, 8976–8977; b) S. Ma, S. Yu, S. Yin, *J. Org. Chem.* **2003**, *68*, 8996–9002.
- [7] a) J. Hultén, N. M. Bonham, U. Nillroth, T. Hansson, G. Zuccarello, A. Bouzide, J. Åqvist, B. Classon, U. H. Danielson, A. Karlén, I. Kvarnström, B. Samuelsson, A. Hallberg, *J. Med. Chem.* **1997**, *40*, 885–897; b) K. Bäckbro, S. Löwgren, K. Österlund, J. Atepo, T. Unge, J. Hultén, N. M. Bonham, W. Schaal, A. Karlén, A. Hallberg, *J. Med. Chem.* **1997**, *40*, 898–902; c) J. Hultén, H. O. Andersson, W. Schaal, U. H. Danielson, B. Classon, I. Kvarnström, A. Karlén, T. Unge, B. Samuelsson, A. Hallberg, *J. Med. Chem.* **1999**, *42*, 4054–4061; d) W. Schaal, A. Karlsson, G. Ahlsén, J. Lindberg, H. O. Andersson, U. H. Danielson, B. Classon, T. Unge, B. Samuelsson, J. Hultén, A. Hallberg, A. Karlén, *J. Med. Chem.* **2001**, *44*, 155–169; e) P.-O. Markgren, W. Schaal, M. Hämäläinen, A. Karlén, A. Hallberg, B. Samuelsson, U. H. Danielson, *J. Med. Chem.* **2002**, *45*, 5430–5439.
- [8] a) W. C. Groutas, R. Kuang, S. Ruan, J. B. Epp, R. Venkataraman, T. M. Truong, *Bioorg. Med. Chem.* **1998**, *6*, 661–671; b) W. C. Groutas, N. M. Schechter, S. He, H. Yu, P. Huang, J. Tu, *Bioorg. Med. Chem. Lett.* **1999**, *9*, 2199–2204; c) R. Kuang, J. B. Epp, S. Ruan, H. Yu, P. Huang, R. Venkataraman, S. He, J. Tu, N. M. Schechter, J. Turbov, C. J. Froelich, W. C. Groutas, *J. Am. Chem. Soc.* **1999**, *121*, 8128–8129; d) R. Kuang, J. B. Epp, S. Ruan, L. S. Chong, R. Venkataraman, J. Tu, S. He, T. M. Truong, W. C. Groutas, *Bioorg. Med. Chem.* **2000**, *8*, 1005–1016.
- [9] J. L. Castro, R. Baker, A. R. Guiblin, S. C. Hobbs, M. R. Jenkins, M. G. N. Russell, M. S. Beer, J. A. Stanton, K. Scholey, R. J. Hargreaves, M. I. Graham, V. G. Matassa, *J. Med. Chem.* **1994**, *37*, 3023–3032.
- [10] M. J. Tozer, I. M. Buck, T. Cooke, S. B. Kalindjian, I. M. McDonald, M. J. Pether, K. I. M. Steel, *Bioorg. Med. Chem. Lett.* **1999**, *9*, 3103–3108.
- [11] a) K. H. Ahn, D. J. Yoo, J. S. Kim, *Tetrahedron Lett.* **1992**, *33*, 6661–6664; b) S. V. Pansare, A. N. Rai, S. N. Kate, *Synlett* **1998**, 623–624.
- [12] a) M. Preiss, *Chem. Ber.* **1978**, *111*, 1915–1921; b) N. Aouf, G. Dewynter, J.-L. Montero, *Tetrahedron Lett.* **1991**, *32*, 6545–6546. New methods for the synthesis of cyclosulfamides have been reported recently. For the synthesis of five-membered cyclo-sulfamides starting from amino acids, see: c) Z. Regañina, M. Abdaoui, N.-E. Aouf, G. Dewynter, J.-L. Montero, *Tetrahedron* **2000**, *56*, 381–387. For the synthesis of nonsymmetrical sulfamides using Burgess-type reagents, see: d) K. C. Nicolaou, D. A. Longbottom, S. A. Snyder, A. Z. Nalbanadian, X. Huang, *Angew. Chem.* **2002**, *114*, 4022–4026; *Angew. Chem. Int. Ed.* **2002**, *41*, 3866–3870.
- [13] M. G. Organ, J. Wang, *J. Org. Chem.* **2002**, *67*, 7847–7851.
- [14] a) M. Montury, J. Goré, *Synth. Commun.* **1980**, *10*, 873–879; b) C. J. Elsevier, J. Meijer, G. Tadema, P. M. Stehouwer, H. J. T. Bos, P. Vermeer, *J. Org. Chem.* **1982**, *47*, 2194–2196; c) C. J. Elsevier, P. Vermeer, A. Gedanken, W. Runge, *J. Org. Chem.* **1985**, *50*, 364–367.
- [15] J.-Y. Winum, L. Toupet, V. Barragan, G. Dewynter, J.-L. Montero, *Org. Lett.* **2001**, *3*, 2241–2243.
- [16] Treatment of the bromoallene **38** with NaH in MeOH in the presence of [Pd(PPh₃)₄] gave the seven-membered-ring product **39** in 76 % yield as a result of initial intramolecular nucleophilic attack on the central carbon of the allene moiety followed by a second nucleophilic attack by methoxide.^[3] However, treatment

of the bromoallene **38** with NaH in MeOH in the absence of [Pd(PPh₃)₄] gave the six-membered-ring product **40** in 46 % yield



by an S_N2'-type, intramolecular nucleophilic attack on the proximal carbon of the allene moiety.

- [17] We have already reported the formation of azetidines by NaH-mediated intramolecular amination of bromoallenes: see, ref. [2b].
- [18] To determine the intermediate of this tandem cyclization reaction, we investigated the stepwise reaction of the bromoallene **33**. Treatment of the bromoallene **33** with NaH in DMF gave the pyrrolidine **37** in 86 % yield. Reaction of **37** under the same reaction conditions as the one-pot reaction afforded the *exo*-cyclized product **34** (67 %) and *endo*-cyclized product **35** (20 %) in essentially the same product ratio. Related five-membered-ring formation by intramolecular amination of a carbon–carbon triple bond has been reported, see: a) Y. Tamaru, M. Kimura, S. Tanaka, S. Kure, Z. Yoshida, *Bull. Chem. Soc. Jpn.* **1994**, 67, 2838–2849; b) P. A. Jacobi, H. L. Brielmann, S. I. Hauck, *J. Org. Chem.* **1996**, 61, 5013–5023; c) M. M. Cid, D.



Domínguez, L. Castedo, E. M. Vázquez-López, *Tetrahedron* **1999**, 55, 5599–5610.

Synthesis of Multiwalled Carbon Nanotubes by Catalytic Combustion of Polypropylene**

Tao Tang,* Xuecheng Chen, Xiaoyu Meng, Hui Chen, and Yaping Ding

Nanostructured carbon materials^[1,2] have attracted much interest owing to their variety in structure, predicted unique properties, and potential applications.^[3–6] Carbon nanotubes (CNTs) are the most important one-dimensional nanostructured material. With progress in applications of CNTs, synthetic methods for the production of large quantities of CNTs at reasonable prices, such that the process is economically feasible, are imperative. Catalytic decomposition of hydrocarbons is a promising means to produce carbon nanotubes on a large scale.^[7,8] Recently the catalytic flame synthesis of CNTs was reported.^[9–11] This method has several advantages, for example, it is inherently easier to scale up relative to other production methods that employ electricity.^[12–17] Whatever the method of synthesizing CNTs, most of the carbon sources are usually gaseous organic molecules.^[18–20] Alternatively, and of interest here, is the much less examined possibility to use polymers as carbon sources in the flame synthesis of CNTs.

Synthesis of CNTs starting from polymers as carbon sources offers the additional advantages of energy-saving and environmental protection. Sustaining development and an increasing demand for petroleum call for the large amount of virtually nondegradable polyolefins to be recycled, in place of the current practice of incineration and landfilling. From an energetic point of view, reutilization of used polyolefins for CNTs seems to be a better choice than direct consumption of C_2H_4 , C_3H_6 , and other compounds from a petroleum source. This is also of benefit to the recycling of used polyolefins as the properties of recycled materials are usually inferior to those of the parent materials. The key question in the conversion of nondegradable polyolefins into CNTs is then whether the polyolefins can be transformed into small organic molecules to be the source of carbon in the synthesis of CNTs. Some efforts have been made in the conversion of polymers

[*] Prof. T. Tang, X. Meng, Dr. H. Chen
State Key Laboratory of Polymer Physics and Chemistry
Changchun Institute of Applied Chemistry
Chinese Academy of Sciences
Changchun, 130022 (P. R. China)
Fax: (+86) 431-568-5653
E-mail: ttang@ciac.jl.cn

X. Chen, Prof. Y. Ding
Department of Chemistry
Shanghai University
Shanghai 200436 (P. R. China)

[**] The present work was supported by the Ministry of Science and Technology of China (Project No. 2003AA302530) and the National Natural Science Foundation of China (Project No. 50473029). The authors wish to thank Prof. Baotong Huang for valuable suggestions in the preparation of this paper.

into CH_4 , C_2H_2 , C_3H_6 , and so on,^[21–25] proving the possibility of synthesizing CNTs with polymers as the carbon source. Syntheses of CNTs or other nanostructured materials in situ through thermal decomposition of polymer/catalyst or polymer/metal mixtures from polyethylene, poly(vinyl alcohol), and polytetrafluoroethylene under inert atmosphere have also been reported.^[26–29]

Herein, we demonstrate a novel catalytic combustion method of synthesizing multiwalled carbon nanotubes (MWNTs) in situ in high yield from polypropylene (PP) as the carbon source in the presence of an organic-modified clay (OMC) and a supported nickel catalyst (Ni-cat; see Experimental Section). Maleated polypropylene (PP-MA) was used as a compatibilizer to improve the dispersion of OMC and Ni-cat in the PP matrix. In preliminary experiments in the absence of OMC, although the yield of MWNTs from burning composites of PP/PP-MA/Ni-cat increased with an increasing content of Ni-cat, the yield is not yet high enough in terms of a catalyzed reaction. This mainly results from quick volatilization of pyrolytic products of PP in an open reaction system. Recent research has shown that clay in polymer/clay nanocomposites imposed gas-barrier properties and flame retardancy of polymers by creating a maze or “tortuous path” for the progress of the gas molecules through the matrix resin.^[30–34] The presence of clay in the combustion synthesis should aid in increasing the yield of MWNTs. Indeed, upon burning PP/PP-MA/OMC/Ni-cat composites, the yield of MWNTs increases with an increasing content of the OMC (Table 1).

X-ray powder diffraction (XRD) patterns of the PP/PP-MA/OMC/Ni-cat composites (Figure 1) show the XRD peaks from the OMC at angles lower than 10° and infer the

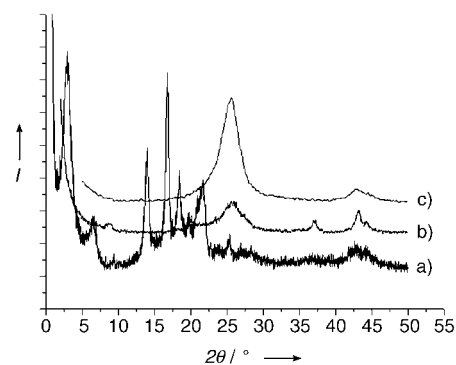


Figure 1. Powder X-ray diffraction patterns of a) PP/PP-MA/OMC/Ni-cat composite, b) its charred residue, and c) purified MWNTs (sample PCM-4).

intercalated structure of the PP/PP-MA/OMC/Ni-cat composite. After burning, the diffraction peaks of PP and OMC in the charred residue disappeared completely, whereas those of Ni-cat remained. Meanwhile two new diffraction peaks appeared, one of which is ascribed to the clay without surfactants and the other to carbon materials with graphitic structure. The charred residue was purified with nitric acid and hydrofluoric acid to remove amorphous carbon, the clay, and most of the Ni-cat, except for a part of the Ni-cat that was enwrapped by the MWNTs. Then only a strong diffraction peak at 25.7° appeared which coincides approximately with that of the (002) diffraction of graphite.

The morphology of the purified charred residue was examined by scanning electron microscopy (SEM). A large quantity of tubelike nanostructures with diameters ranging from about 20 to 40 nm were obtained (Figure 2a). To further characterize the microstructure of the synthesized nanostructure, studies were made by transmission electron microscopy (TEM). Figure 2b clearly shows that the purified charred residue comprises MWNTs with hollow centers. The MWNTs produced have a diameter of about 33 nm. The wall structure of the carbon nanotube is seen from the higher magnification image of a typical MWNT in Figure 2c. The walls are composed of graphite sheets aligned along the axis of the tube, the outer and inner diameters of which are about 33 and 12 nm.

Table 1: Effect of OMC content on the yield of the MWNTs by combustion of PP composites.

Samples	PP [wt %]	PP-MA [wt %]	OMC [wt %]	Ni-cat [wt %]	Yield of MWNTs [wt %]
PCM-0	85	10	0	5	5.24
PCM-1	82.5	10	2.5	5	7.48
PCM-2	80	10	5	5	13.75
PCM-3	77.5	10	7.5	5	32.65
PCM-4	75	10	10	5	41.16

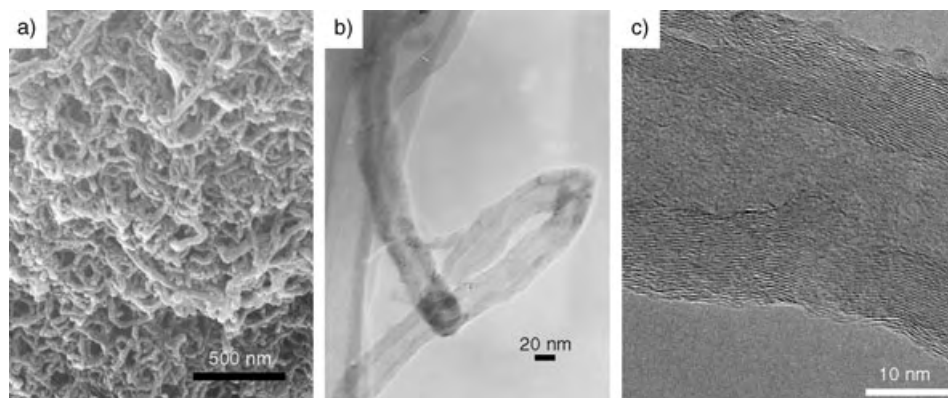


Figure 2. a) SEM image and b) TEM image of synthesized MWNTs; c) higher magnification TEM image of a typical MWNT.

Raman spectroscopy was used to further characterize graphitization of the MWNTs (Figure 3a). The peak at 1598 cm^{-1} (G-band) corresponds to an E_{2g} mode of hexagonal graphite and is related to the vibration of sp^2 -hybridized

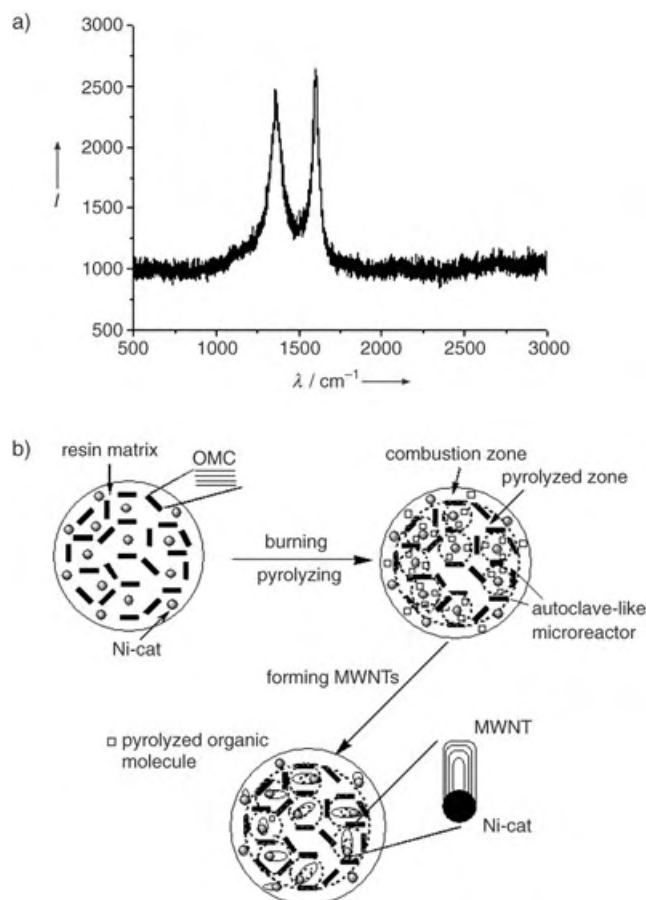


Figure 3. a) Raman spectra of the synthesized MWNTs; b) Schematic diagram of the catalytic combustion method to synthesize MWNTs from polymers as the carbon source.

carbon atoms in a graphite layer. The D-band at about 1359 cm^{-1} is associated with the vibration of carbon atoms with dangling bonds in the plane terminations of disordered graphite or glassy carbons.^[35]

The unique combination of clay and Ni-cat in the PP matrix leads to high yields of the MWNTs (Figure 3b). Under these conditions, the combustion procedure was accompanied by pyrolytic degradation of PP. In the burning zone, the presence of oxygen leads to combustion of PP with evolution of small molecules such as CO , CO_2 , C_2H_4 , and C_3H_6 .^[36] These molecules volatilize quickly and burn out, with only a few converted into MWNTs owing to a lack of contact time. However, a protective charred ceramic surface layer is formed as a result of the ablative reassembly of the clay layers on the composite surface and the charring polymer.^[34] In the pyrolytic zone in the absence of oxygen, PP chains undergo endothermic chain scission to release pyrolyzed products that mainly consist of propylene, pentane, 2,4-dimethyl-1-heptene, 2,3-dimethyl-2-heptene, and other frag-

ments, most of which are gases at 600°C , according to GC–MS analysis. Owing to the resistance of gaseous permeability of the protective charred ceramic surface layer and the inner clay layers, which act like a sealed autoclave microreactor, the pyrolytic products are sealed within a PP matrix (to allow them more time to have interactions with the catalyst particles), dehydrogenated, and aromatized to form MWNTs. With increasing clay content, the barrier properties of clay become more prominent. Note that some aspects of the mechanism of formation of MWNTs during the above synthesis await further investigation.

In summary, we have demonstrated a simple method for the synthesis of MWNTs in situ by combustion of polypropylene in air in the presence of clay and a Ni catalyst. The unique combination of clay and the Ni catalyst in a PP matrix, which resembles a sealed autoclave-like microreactor, leads to high yields of the MWNTs. This process permits an easy synthesis of MWNTs on a large scale. Furthermore, it provides a new possible avenue in the disposal of used polypropylene and its nanocomposites as carbon sources by converting them into high-value MWNTs. This process is not limited to the PP polymer system and can be applied to other polymer systems. Further investigations to improve the quality of MWNTs synthesized by this method are currently in progress in our laboratory.

Experimental Section

Polypropylene (PP; melt flow index: 0.8 g min^{-1} , Panjin Chemical Co.), was mixed with an organic-modified clay (OMC; Closite 15A, Southern Clay), Ni catalyst (Ni-cat; supported on silica–alumina, Ni content $\approx 66\%$, Alfa Aesar), and maleated polypropylene (PP-MA; acid value: 26 mg KOH g^{-1}) in a Brabender mixer at 100 rpm at 190°C for 10 min . Then a piece of the above nanocomposite was placed in a crucible and heated with the flame of a gas lamp at 600°C . The charred residue was cooled to room temperature and subsequently purified using hydrofluoric acid and nitric acid to eliminate clay, amorphous carbon, and Ni-cat. The yield of MWNTs was calculated as a ratio of the amounts of purified charred residue to polymer in the composite.

The purity and phase structure of the products were obtained by XRD using a Rigaku D/MAX-IIIB powder X-ray diffractometer. SEM (XL30EsEM FEG field emission microscope, 20 kV) and TEM (JEM-2010, 200 kV) were used to characterize the morphology and microstructure, respectively, of the products obtained. Raman spectroscopy (T6400, λ_{ex} : 514.5 nm) was used to characterize graphitization of the carbon materials.

Received: August 2, 2004

Revised: September 30, 2004

Published online: January 28, 2005

Keywords: clays · nanotubes · nickel · polymers · synthetic methods

- [1] H. Kroto, J. Heath, S. O'Brien, R. Curl, R. Smalley, *Nature* **1985**, *318*, 162.
- [2] S. Iijima, *Nature* **1991**, *354*, 56.
- [3] J. Bernholc, C. Roland, B. I. Yakobson, *Curr. Opin. Solid State Mater. Sci.* **1997**, *2*, 706.

- [4] C. Liu, Y. Y. Fan, M. Liu, H. T. Cong, H. M. Cheng, M. S. Dresselhaus, *Science* **1999**, 286, 1127.
- [5] J. Kong, N. R. Franklin, C. Zhou, M. G. Chapline, S. Peng, K. Cho, H. Dai, *Science* **2000**, 287, 622.
- [6] P. G. Collins, A. Zettl, H. Bando, A. Thess, R. E. Smalley, *Science* **1997**, 278, 100.
- [7] S. C. Lyu, B. C. Liu, S. H. Lee, C. Y. Park, H. K. Kang, C.-W. Yang, C. J. Lee, *J. Phys. Chem. B* **2004**, 108, 2192.
- [8] H. Hou, Z. Jun, F. Weller, A. Greiner, *Chem. Mater.* **2003**, 15, 3170.
- [9] L. Yuan, K. Saito, C. Pan, F. A. Williams, A. S. Gordon, *Chem. Phys. Lett.* **2001**, 340, 237.
- [10] L. Yuan, K. Saito, W. Hu, Z. Chen, *Chem. Phys. Lett.* **2001**, 346, 23.
- [11] R. L. Vander Wal, T. M. Ticich, *J. Phys. Chem. B* **2001**, 105, 10249.
- [12] D. S. Bethune, C. H. Kiang, M. S. de Vries, G. Gorman, R. Savoy, J. Vazquez, R. Beyers, *Nature* **1993**, 363, 605.
- [13] A. Thess, R. Lee, P. Nikolaev, H. Dai, P. Petit, J. Robert, C. Xu, Y. H. Lee, S. G. Kim, A. G. Rinzler, D. T. Colbert, G. E. Dcuseria, E. D. Tomanek, J. E. Fischer, R. E. Smalley, *Science* **1996**, 273, 483.
- [14] S. Amelinckx, X. B. Zhang, D. Bernaerts, X. F. Zhang, V. Ivanov, J. B. Nagy, *Science* **1994**, 265, 635.
- [15] J. F. Geng, C. Singh, D. S. Shephard, M. S. P. Shaffer, B. F. G. Johnson, A. H. Windle, *Chem. Commun.* **2002**, 2666.
- [16] Z. F. Ren, Z. P. Huang, J. W. Xu, J. H. Wang, P. Bush, M. P. Siegal, P. N. Provencio, *Science* **1998**, 282, 1105.
- [17] H. W. Zhu, C. L. Xu, D. H. Wu, B. Q. Wei, R. Vajtai, P. M. Ajayan, *Science* **2002**, 296, 884.
- [18] A. M. Cassell, J. A. Raymakers, J. Kong, H. Dai, *J. Phys. Chem. B* **1999**, 103, 6484.
- [19] G. Che, B. B. Lakshmi, C. R. Martin, E. R. Fisher, R. S. Ruoff, *Chem. Mater.* **1998**, 10, 260.
- [20] S. Huang, X. Cai, J. Liu, *J. Am. Chem. Soc.* **2003**, 125, 5636.
- [21] M. T. Sousa Pessoa De Amorim, C. Comel, P. Vermande, *J. Anal. Appl. Pyrolysis* **1982**, 4, 73.
- [22] H.-W. Wong, L. J. Broadbelt, *Ind. Eng. Chem. Res.* **2001**, 40, 4716.
- [23] R. Moliner, M. Lazaro, I. Suelves, *Energy Fuels* **1997**, 11, 1165.
- [24] S. Lovett, F. Berruti, L. A. Behie, *Ind. Eng. Chem. Res.* **1997**, 36, 4436.
- [25] E. A. Williams, P. T. Williams, *J. Chem. Technol. Biotechnol.* **1997**, 70, 9.
- [26] E. F. Kukovitskii, L. A. Chernozatonskii, S. G. L'vov, N. N. Mel'nik, *Chem. Phys. Lett.* **1997**, 266, 323.
- [27] N. I. Maksimova, O. P. Krivoruchko, G. Mestl, V. I. Zaikovskii, A. L. Chuvilin, A. N. Salanov, E. B. Burgina, *J. Mol. Catal. A* **2000**, 158, 301.
- [28] O. P. Krivoruchko, N. I. Maksimova, V. I. Zaikovskii, A. N. Salanov, *Carbon* **2000**, 38, 1075.
- [29] A. Huczko, H. Lange, G. Chojecki, S. Cudzilo, Y. Q. Zhu, H. W. Kroto, D. R. M. Walton, *J. Phys. Chem. B* **2003**, 107, 2519.
- [30] M. Alexandre, P. Dubois, *Mater. Sci. Eng. R* **2000**, 28, 1.
- [31] S. S. Ray, M. Okamoto, *Prog. Polym. Sci.* **2003**, 28, 1539.
- [32] R. K. Bharadwaj, *Macromolecules* **2001**, 34, 9189.
- [33] M. Zanetti, G. Camino, R. Thomann, R. Mulhaupt, *Polymer* **2001**, 42, 4501.
- [34] M. Zanetti, T. Kashiwagi, L. Falqui, G. Camino, *Chem. Mater.* **2002**, 14, 881.
- [35] A. M. Rao, E. Richter, S. Bandow, B. Chase, P. C. Eklund, K. A. Williams, S. Fang, K. R. Subbaswamy, M. Menon, A. Thess, R. E. Smalley, G. Dresselhaus, M. S. Dresselhaus, *Science* **1997**, 275, 187.
- [36] H. Bockhorn, M. Burckschat, H. Deusser, *J. Anal. Appl. Pyrolysis* **1985**, 7, 427.

Counting Chromophores in Conjugated Polymers**

Florian Schindler, Josemon Jacob,
Andrew C. Grimsdale, Ullrich Scherf, Klaus Müllen,
John M. Lupton,* and Jochen Feldmann

The development of novel materials for organic optoelectronics based on conjugated polymers (CPs) has been paralleled by the quest to understand the nature of the fundamental emitting species.^[1] CPs can have molecular weights of hundreds of thousands, comprising thousands of repeat units, yet the delocalization of π electrons is thought to be limited by structural and chemical defects on the chain and leads to the formation of “isolated” chromophore units on the CP. Although this idea is generally upheld, there is little direct evidence for this model; the evidence reported until now is derived mainly from site-selective fluorescence investigations.^[2] The size of the emitter has also been widely debated in the literature as the size defines the key difference between polymeric and small-molecule organic semiconductors.^[1–6] A simple way to assess the size of the chromophore is to study model oligomeric compounds and establish the critical oligomer length for which absorption and emission spectra correspond to the polymeric analogue.^[1,4] However, electron–hole correlations are very strong in conjugated systems, thus this approach only provides insight into the delocalization or coherence length of the exciton but not the so-called diagonal length; that is, the actual length of the conjugated segment over which the electron–hole pair may move.^[6] These two physical quantities can be very different, such as in the case of defect-free polydiacetylene.^[7]

Single-molecule (SM) detection and spectroscopy (SMS) are powerful tools to help to construct an understanding of the basic electronic properties of molecules.^[8] SMS has

[*] F. Schindler, Dr. J. M. Lupton, Prof. Dr. J. Feldmann
Photonics and Optoelectronics Group
Physics Department and CeNS
Ludwig-Maximilians-Universität, 80799 Munich (Germany)
Fax: (+49) 89-2180-3441
E-mail: john.lupton@physik.uni-muenchen.de
Dr. J. Jacob, Dr. A. C. Grimsdale, Prof. Dr. K. Müllen
Max Planck Institute for Polymer Research
Ackermannweg 10, 55128 Mainz (Germany)
Prof. Dr. U. Scherf
FB Chemie
Universität Wuppertal
Gauss-Str. 20, 42097 Wuppertal (Germany)

[**] The authors are grateful to W. Stadler, A. Helfrich, J. Schnee, and E. Preis for technical assistance, the Deutsche Forschungsgemeinschaft for financial support (grant nos. SFB 486 and SFB 625), as well as the Schwerpunktprogramm organische Feldeffekttransistoren, the Gottfried Wilhelm Leibniz award, and the Bundesministerium für Bildung und Forschung (project 13N8615 OLAS) for funding.



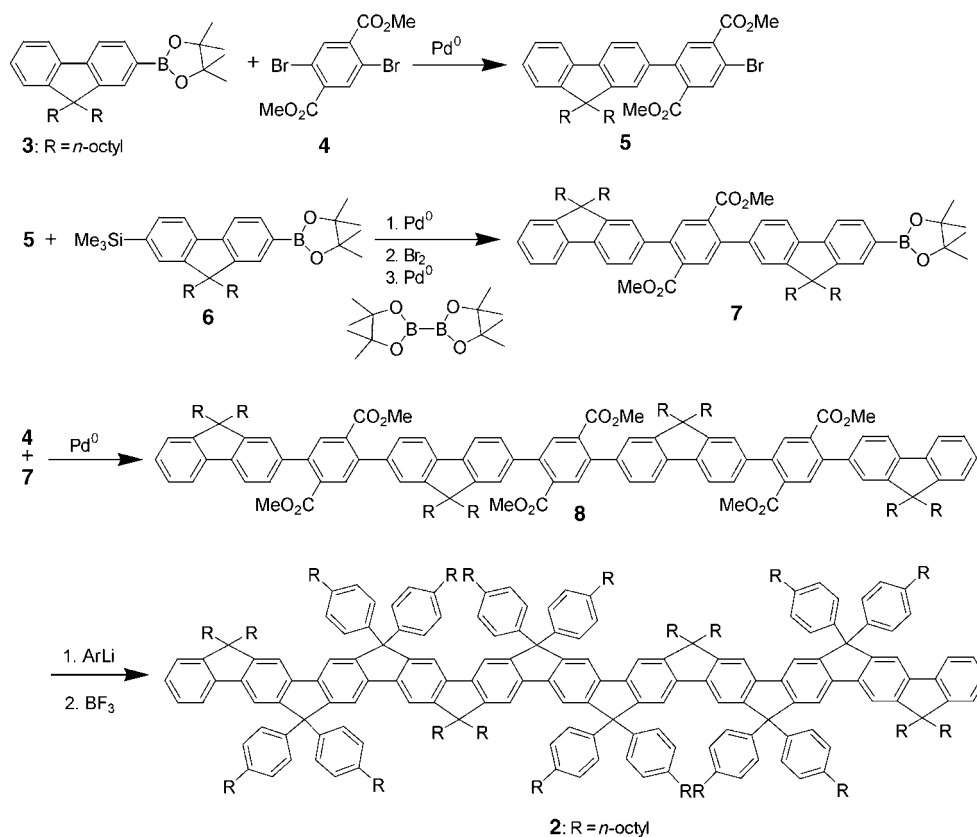
Supporting information for this article is available on the WWW under <http://www.angewandte.org> or from the author.

yielded insight into the nature of emission in a number of well-defined multichromophoric assemblies^[9–11] as well as demonstrating that the emission from CPs can occur from trap states which can be reversibly quenched.^[12–17] We recently showed that SMS can provide unique information on the presence of chromophores in CPs and may be used to investigate intramolecular interchromophoric couplings.^[18–21] Single chromophores exhibit universal photophysical properties independent of the details of the materials chemistry, thus enabling the derivation of universal structure–property relationships.^[21] Herein we address the fundamental issue of how the number of chromophores varies with molecular size (i.e. the number of repeat units) and present the first study by high-resolution SMS on model oligomeric compounds. The complexity of the SM emission spectra varies with chain length and results from the contribution of individual spectral features of single chromophores. Comparison of these data with those of oligomeric compounds allows a direct differentiation between the single-charge carrier and exciton confinement lengths. Most importantly, we demonstrate that a single CP molecule can support multichromophoric emission, which is not trap-state limited.

As a suitable polymer we chose methyl-substituted poly(*para*-phenylene) (MeLPPP, **1**), and as a model oligomer we chose a ladder-type undecaphenylene **2**, which is one of the longest poly(*para*-phenylene) oligomers reported thus far and which was specifically synthesized to clarify the nature of emission in CPs. The synthetic pathway to undecaphenylene **2** is shown in Scheme 1. The key intermediate in the preparation of **2** is a singly end-functionalized pentaphenylene

prepared by a modification of existing routes to pentaphenylenes.^[22] Starting with 2,5-dibromodimethylterephthalate **4**, two sequential Suzuki couplings generated a pentaphenylene diester bearing a trimethylsilyl group at one end. This group was converted through the bromide to a boronic ester group to produce the end-functionalized pentamer intermediate **7** in an overall yield of 14% from **3**. The corresponding deboronated compound (arising from addition of two equivalents of **3** to **4**) was present as a major (≈ 33 mol %) contaminant in all the earlier steps but could be removed by chromatography only at this stage. The problem in removing this contamination together with the low overall yield of **7** illustrate the difficulties inherent in the synthesis of defined ladder-type oligomers. Another Suzuki coupling of **7** with **4** gave the undecaphenylene hexaester **8** (68%), which upon addition of excess aryllithium followed by Lewis acid catalyzed Friedel–Crafts alkylation was converted into the undecamer **2** (56% yield from **8**, 3% overall yield based on **3**). The oligomer **2** was characterized by microanalysis, NMR, UV/Vis absorbance, and photoluminescence (PL) spectroscopy, and mass spectrometry. Full details of the synthesis and characterization of **2** are given in the Supporting Information.

We studied the PL spectra of single molecules of the rigid rod ladder-type CP **1** and the undecamer model compound **2** dispersed in a polystyrene matrix. Figure 1 shows spectra recorded both in solution at room temperature and as single molecules at 5 K. The spectra of the undecamer are blue-shifted by 8 nm with respect to the CP, but are otherwise rather similar with maxima at around 450 nm. The spectra of the SM are substantially narrower (1–2-nm width) than those



Scheme 1. Synthesis of the ladder-type undecamer **2**.

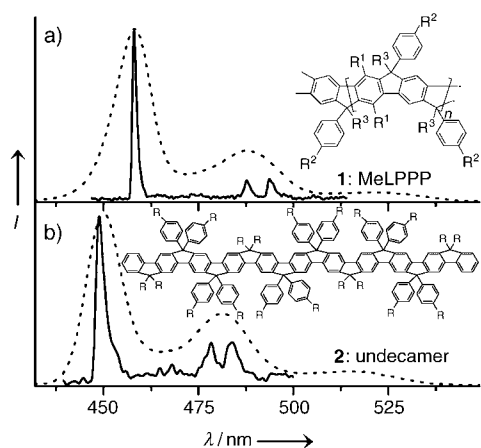


Figure 1. Single-molecule (SM) photoluminescence spectra at 5 K of a) the conjugated polymer (CP) MeLPPP (1) and b) the model oligomer 2. Dotted lines (.....) show PL spectra of the ensembles in solution at room temperature.

of the solution ensemble and reveal a distinct splitting of the vibronic 0–1 transition around 480 nm. SMS shows a significantly higher spectral resolution which allowed us to pinpoint the nature of emission on the polymer chain. To do this, the chain length of the CP was varied from approximately 62 to around 165 phenylene units ($M_r \approx 25$ kDa to $M_r \approx 67$ kDa; polydispersity ratio (PD)=1.8–4.7), with the larger CPs displaying a somewhat higher polydispersity ratio.

The different single CPs were compared directly with the undecamer model compound. Figure 2a shows the 0–0 transition of a typical PL spectrum of a single oligomer. In comparison, a characteristic PL spectrum of the short-chain CP is presented in Figure 2b. One clear peak is identified in both cases. The maximum of the short-chain CP is red-shifted by a few nm and is somewhat narrower (≈ 1 nm) relative to that of the oligomer, but otherwise they are similar in shape. The ensemble spectrum of the CP is found to be virtually independent of molecular weight (not shown). The SM spectrum of the long-chain CP in Figure 2c, however, is more complex. We identify 5 distinct peaks, all of which have the same shape and width as the single peak in panel b, and for better comparison the PL peak of the short-chain CP is superimposed on each of the 5 lines (dotted curves). We conclude that the emitting species is similar in all cases and is almost independent of chain length, which simply controls the number of emitting units. The histograms in Figure 2d show a statistical analysis of peak positions and line widths for a total of 161 SMs that exhibit resolvable peaks in the PL spectra. The distribution in peak energies is closely matched by the ensemble spectra recorded at 5 K (solid lines). The spectra of the single undecamer are on average twice as broad as the CP spectra and are blue-shifted by 10 nm. There is a certain overlap between the histograms of the CPs and the oligomers, so that a few spectra of CPs are indistinguishable from those of the oligomers. This suggests that the emitting species can indeed be identical in the undecamer and the CP; that is, a subunit on the chain which consists of 11 benzene rings makes up the conjugated segments. It should be stressed that although the line widths of the spectra of the SMs are

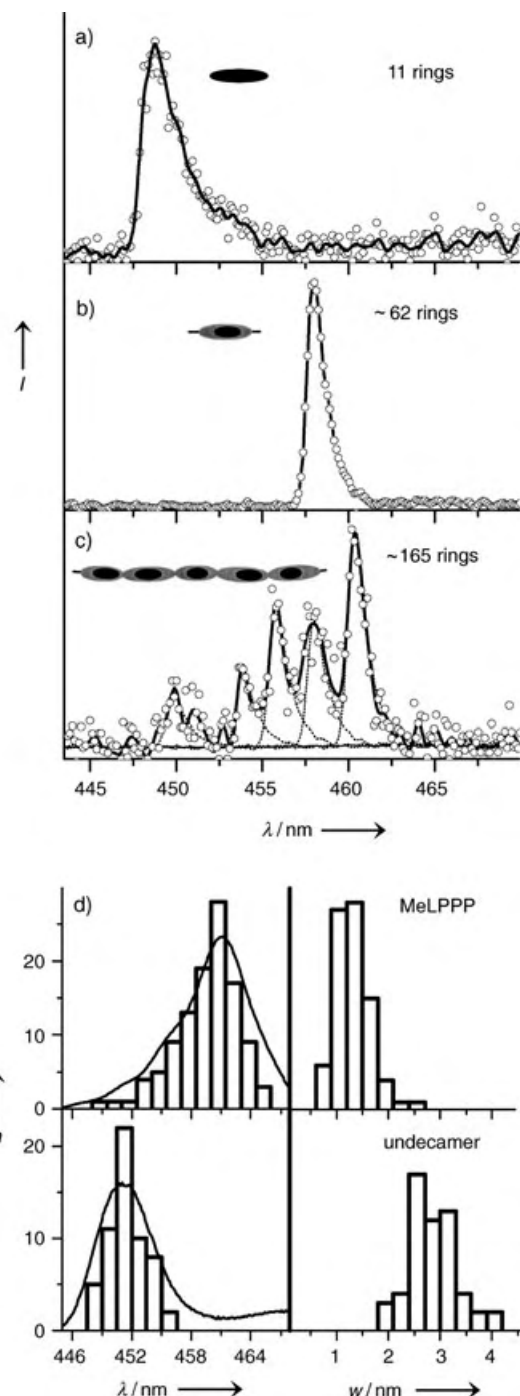


Figure 2. Single-molecule PL emission spectra at 5 K of the model oligomer and the conjugated polymer MeLPPP: a) the undecamer, b) a short-chain CP ($M_r \approx 25$ kDa), and c) a long-chain CP ($M_r \approx 67$ kDa). Each of the individual peaks in the emission from the long-chain CP is identical in shape to the single peak in the emission from the short-chain CP (this single peak is superimposed for each peak in part c;). The sketches indicate the difference between exciton size (black) and conjugation length (gray). d) The distribution of peak energies (λ) and line widths (w) for the short-chain CP and the model oligomer, with ensemble spectra overlaid (—; n =occurrence).

broader for the oligomer than those for the CP, the distribution in peak positions is considerably narrower as a direct consequence of the monodispersity of the oligomer.

Note that in contrast the spectra of the ensemble at room temperature are equally broad and thus do not provide a measure of disorder.

Evidently, segments as short as 11 rings can constitute the emitting species in CPs. The chain may be over 13 times as long as this, so that a single chain should support multiple chromophores emitting simultaneously. The number of units should therefore depend on the chain length. Figure 3 shows

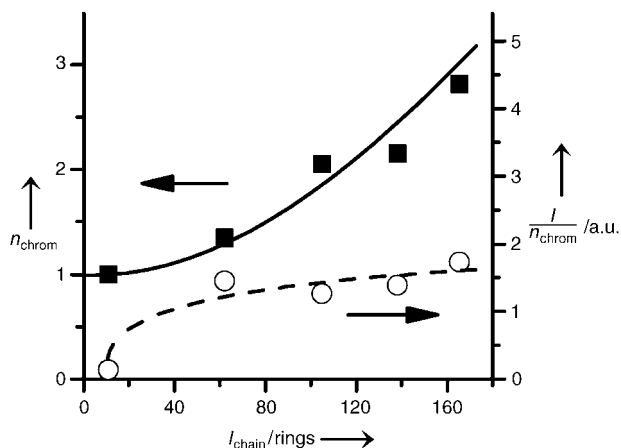


Figure 3. ■: Variation of the average number of peaks (chromophores) in the PL spectra (n_{chrom}) with chain length (l_{chain} , number of benzene rings). ○: The average intensity per peak for a total of 108 molecules (I/n_{chrom}).

the variation in the number of emission lines, that is, chromophores, with chain length which were extracted from a total of 200 SMs. Note that the data point at a chain length of 138 rings was determined for a phenyl-substituted rather than a methyl-substituted LPPP, which otherwise has identical fluorescence properties.^[23] A monotonic increase in the number of units was observed which provides clear evidence for a disruption of the π -electron system along the chain and the formation of more-or-less isolated conjugated subunits. The average PL intensity per chromophore line (circles) is also indicated. This is virtually independent of chain length, but increases almost tenfold upon going from the oligomer to the CP. The PL intensity is both a measure of the absorption and the emission efficiency. As the fluorescence yields of the ensemble are comparable for the two materials, this difference in intensity can only be an effect of a difference in absorption. The emitting unit on the CP must be comparable to the undecamer in size, but the remainder of the conjugated segment apparently leads to a substantial increase in oscillator strength and absorption.

The effective conjugation length for absorption thus increases with chain length but not the effective conjugation length for emission. This effect may in part be explicable by efficient light harvesting on the CP chain by ultrafast energy transfer between adjacent chromophore units, which we were recently able to identify by studying the polarization of absorption and emission of single chains.^[18] However, the conjugation length (marked in gray in the sketch in Figure 2)—the distance over which an excitation may move coherently—may be substantially larger than the actual size

of the excitation (black). This effect has been studied in detail by using quantum-chemical models,^[6] but has so far been hard to assess experimentally. Our data suggest that the absorbing unit should be larger than the emitting unit. Above a length of 11–12 benzene rings, the Coulombic interactions as well as phonon-mediated self-trapping are so strong that the exciton size remains independent of the length of the conjugated segment. The conjugation length may therefore substantially exceed the exciton size. For a chain length of 165 rings, we find 2.8 lines on average which provides an upper estimate of the conjugation length of 59, approximately five times the size of the exciton. Even if we account for the possibility of the chain containing structural defects that lead to a branching of the rigid rod structure and to different polarizations of the individual conjugated segments,^[18] which would not all be excited by the linearly polarized laser light used, at most 50 % of the conjugated units on the chain would escape excitation. The effective length of the optically active segment on the chain is therefore at least twice the size of the exciton. As the number of chromophores varies approximately linearly with chain length, we propose that the exciton localization length in this class of materials is generally at least twice the exciton coherence size of roughly 12 phenylene units.

This conclusion is compatible with previous observations in highly ordered and virtually defect-free polydiacetylenes.^[7] The huge optical non-linearities, which can be well-described by a phase-space-filling model of one-dimensional excitons^[7c] as well as by ultrafast intramolecular migration of excitation energy in single chains,^[7b] are signatures of extended π conjugation with limited exciton size. Evidence for conjugated units that are larger in absorption than in emission is also seen in more-disordered materials for which the red shift in fluorescence saturates considerably sooner with increasing chain length than the red shift in absorption.^[4g] This effect, which is in part related to structural relaxation (although this is very weak indeed in the ladder-type polymers^[19]), has also been investigated theoretically,^[24,25] as a precise knowledge of the size of the emitting and absorbing unit is imperative for understanding and modeling intramolecular energy transfer.^[25]

The conclusion of extended conjugations naturally raises the question of the origin of static disorder, which gives rise to a distribution in chromophore energies and the associated inhomogeneous broadening witnessed in Figure 2d. The common notion is that topological defects lead to a confinement of the excitation and thus to a modification in transition energy. Our data suggest that the origin of disorder is more subtle, although clear scissions of the π system do occur. Instead, we propose that the dielectric environment of the individual chromophores, that is, both the surrounding matrix and the remaining chain, leads to an effective potential-energy landscape, which is different for each chromophore and which slightly modifies the transition energies between different chromophores. This situation is conceptually similar to the description of energetic disorder in single dye molecules for which a comparably large degree of disorder is observed despite the absence of a distribution in conjugation lengths.^[8,9] Further evidence for this picture comes from the fact that the line widths in the PL spectra of the single-

molecule oligomer are substantially greater than those of the CP. As the undecamer is just of the length where the exciton is still slightly confined by the limited π -electron delocalization, a conclusion is that confinement of the exciton wavefunction by complete disruption of the π system leads to line broadening in similar fashion to J-aggregates, for example.^[1] The distribution in emission wavelengths in the CP is therefore most likely not a direct consequence of the distribution in conjugation lengths, which should lead to substantial line broadening.

Finally, to highlight the relevance of our conclusions to bulk materials for devices, we demonstrate that the ensemble photophysical properties of **1** and **2** are also consistent with the picture of polymeric chromophores substantially exceeding the size of oligomers. Figure 4a shows a direct comparison

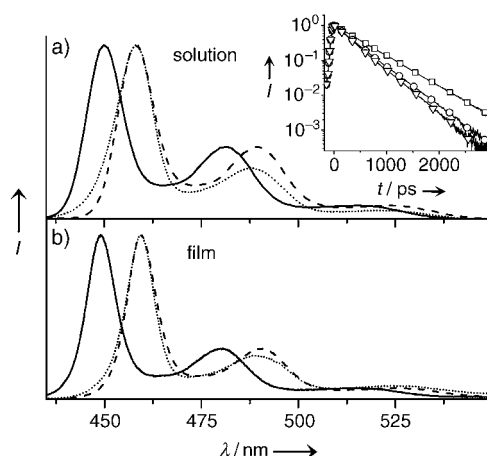


Figure 4. a) Ensemble fluorescence spectra of the undecamer (—) and polymer (.....) in dilute solution in toluene. The spectrum of the oligomer is shown as recorded as well as shifted by 8 nm to overlap that of the polymer (----) for better comparison. Inset: The PL decay of the oligomer (\square) and two conjugated polymers ($M_r \approx 25$ kDa (\circ); $M_r \approx 67$ kDa (∇)). b) Fluorescence spectra of the oligomer (—) and the polymer (.....) in the solid state, again with the spectrum of the oligomer shifted and superimposed (----).

of the PL spectra of **2** and the CP (≈ 25 kDa) in solution at room temperature. The spectra are very similar in shape. The PL spectrum of the oligomer is also shown red-shifted by 8 nm and superimposed (dashed line) on that of the CP (dotted line) for comparison. The spectral width of the monodisperse oligomer and the polydisperse CP are almost identical, in agreement with our conclusion that the CP spectrum is not primarily broadened owing to a distribution of different conjugation lengths. The CP spectrum does exhibit a slight broadening to shorter wavelengths relative to the oligomer which may indeed be an indication of the presence of conjugated segments with effective lengths equal to or shorter than the oligomer. The similarity in the PL spectra of the CP and the oligomer is even more striking in the case of spin-coated bulk films, which are compared in Figure 4b. Besides the reduced intensity of the vibronic sideband in the case of **1** and the blue shift of 10 nm, the spectra are identical to within 1 nm, thus suggesting that **2** may indeed be an excellent model for **1** in the bulk phase.

Time-resolved measurements pinpoint a substantial difference in the fluorescence from the oligomer and the CP. Figure 4 inset shows three PL lifetime measurements recorded for **2** and two CPs (with $M_r \approx 25$ kDa and $M_r \approx 67$ kDa). The oligomer has a PL lifetime of 490 ps, whereas this is reduced significantly to 360 ps in the short-chain CP. Increasing the chain length by a factor of 2.5 leads to a 10% decrease in the lifetime to 330 ps. Although the size of the π -conjugated segment occupied by the exciton in the CP must be of the order of the dimensions of the oligomer (i.e. 11 to 12 phenylene units) as the transition energies of **1** and **2** are virtually equal, the remainder of the CP chain clearly affects spontaneous emission. This is in part caused by highly efficient intramolecular energy transfer^[20] and the presence of singlet scavenging defects, which have been shown to lead to a chain-length-dependent decrease in the lifetime in polyfluorenes.^[26] However, the change in lifetime is much smaller upon increasing the length of the CP than in going from the oligomer to the CP. The conjugation length of the CP must substantially exceed the undecamer size, which in turn is a measure of the actual size of the excitation rather than of the conjugated length. Whereas the excited state on the oligomer has the nature of a molecular excitation, the emission from the CP has excitonic character^[1] as it arises from coherently coupled conjugated segments extending further than the effective spatial delocalization of the excited state. A consequence of this is that vibrational coupling is weaker in the CP than in the oligomer, which is clearly seen in the reduced intensity of the 0–1 transition. Whereas molecular excitations display very strong vibrational coupling, excitations in coherently delocalized systems such as J-aggregates or highly conjugated polydiacetylenes couple only weakly to vibrations.^[7] Furthermore, extension of the π -electron system also leads to an increase in oscillator strength and consequently to a reduction in fluorescence lifetime, in agreement with the substantial acceleration in the emission rate observed in the CP. These ensemble observations are fully consistent with our results on counting the number of chromophores in single CP chains and relating this to the dimensions of oligomers.

In summary, we have correlated the number of lines observed in the fluorescence spectra from single CP molecules directly with the average chain length. Our data suggest that the origin of disorder in CPs is not caused by a statistical distribution of defects confining the exciton but rather the polarizing influence of the local environment. Understanding the nature of the chromophores, the origin of disorder, and in particular the interactions between chromophores on a chain is absolutely vital to optimizing both electroluminescent and photovoltaic CP devices. Our results provide strong evidence that chromophoric emission is intrinsic to the nature of extended π -electron systems and not directly controlled by defects, which would be detrimental to device operation.

Received: August 25, 2004

Revised: November 3, 2004

Published online: January 31, 2005

Keywords: chromophores · luminescence · polymers · single-molecule studies

- [1] M. Pope, C. E. Swenberg, *Electronic Processes in Organic Crystals and Polymers*, 2nd ed., Oxford University Press, Oxford, **1999**.
- [2] H. Bässler, B. Schweitzer, *Acc. Chem. Res.* **1999**, 32, 173.
- [3] Y. V. Romanosvkii, H. Bässler, U. Scherf, *Chem. Phys.* **2002**, 276, 321.
- [4] a) J. Grimme, M. Kreyenschmidt, F. Uckert, K. Müllen, U. Scherf, *Adv. Mater.* **1995**, 7, 292; b) H. S. Woo, O. Lhost, S. C. Graham, D. D. C. Bradley, R. H. Friend, C. Quattrocchi, J.-L. Brédas, R. Schenk, K. Müllen, *Synth. Met.* **1993**, 59, 13; c) H. Meier, U. Stach, H. Kolshorn, *Acta Polym.* **1997**, 48, 379; d) T. Kirschbaum, P. Bäuerle, *Synth. Met.* **2001**, 119, 127; e) J. J. Apperloo, L. Groenendaal, H. Verheyen, M. Jayakannan, R. A. J. Janssen, A. Dkhissi, D. Beljonne, R. Lazzaroni, J.-L. Brédas, *Chem. Eur. J.* **2002**, 8, 2384; f) F. Wudl, S. P. Bitler, *J. Am. Chem. Soc.* **1986**, 108, 4685; g) G. Klaerner, R. D. Miller, *Macromolecules* **1998**, 31, 2007.
- [5] G. H. Gelinck, J. J. Piet, B. R. Wegewijs, K. Müllen, J. Wildeman, G. Hadzioannou, J. M. Warman, *Phys. Rev. B* **2000**, 62, 1489.
- [6] S. Mukamel, S. Tretiak, T. Wagersreiter, V. Chernyak, *Science* **1997**, 277, 781.
- [7] a) R. Lécuyer, J. Berréhar, J. D. Ganière, C. Lapersonne-Meyer, P. Lavallard, M. Schott, *Phys. Rev. B* **2002**, 66, 125205; b) T. Guillet, J. Berréhar, R. Grousson, J. Kovensky, C. Lapersonne-Meyer, M. Schott, V. Voliotis, *Phys. Rev. Lett.* **2001**, 87, 087401; c) B. I. Greene, J. Orenstein, R. R. Millard, L. R. Williams, *Phys. Rev. Lett.* **1987**, 58, 2750.
- [8] W. E. Moerner, M. Orrit, *Science* **1999**, 283, 1670.
- [9] T. Christ, F. Kulzer, T. Weil, K. Müllen, T. Basché, *Chem. Phys. Lett.* **2003**, 372, 878.
- [10] P. Tinnefeld, K. D. Weston, T. Vosch, M. Cotlet, T. Weil, J. Hofkens, K. Müllen, F. C. De Schryver, M. Sauer, *J. Am. Chem. Soc.* **2002**, 124, 14310.
- [11] T. Gensch, J. Hofkens, A. Heilmann, K. Tsuda, W. Verheijen, T. Vosch, T. Christ, T. Basché, K. Müllen, F. C. De Schryver, *Angew. Chem.* **1999**, 111, 3970; *Angew. Chem. Int. Ed.* **1999**, 38, 3752.
- [12] D. A. Vanden Bout, W. T. Yip, D. H. Hu, D. K. Fu, T. M. Swager, P. F. Barbara, *Science* **1997**, 277, 1074.
- [13] T. Huser, M. Yan, L. J. Rothberg, *Proc. Natl. Acad. Sci. USA* **2000**, 97, 11187.
- [14] J. Yu, D. Hu, P. F. Barbara, *Science* **2000**, 289, 1327.
- [15] C. W. Hollars, S. M. Lane, T. Huser, *Chem. Phys. Lett.* **2003**, 370, 393.
- [16] J. D. White, J. H. Hsu, S. C. Yang, W. S. Fann, G. Y. Pern, S. A. Chen, *J. Chem. Phys.* **2001**, 114, 3848.
- [17] W.-T. Yip, D. Hu, J. Yu, D. A. Vanden Bout, P. F. Barbara, *J. Phys. Chem. A* **1998**, 102, 7564.
- [18] J. G. Müller, J. M. Lupton, J. Feldmann, U. Lemmer, U. Scherf, *Appl. Phys. Lett.* **2004**, 84, 1183.
- [19] J. G. Müller, M. Anni, U. Scherf, J. M. Lupton, J. Feldmann, *Phys. Rev. B* **2004**, 70, 035205.
- [20] J. G. Müller, U. Lemmer, G. Raschke, M. Anni, U. Scherf, J. M. Lupton, J. Feldmann, *Phys. Rev. Lett.* **2003**, 91, 267403.
- [21] F. Schindler, J. M. Lupton, J. Feldmann, U. Scherf, *Proc. Natl. Acad. Sci. USA* **2004**, 101, 14695.
- [22] a) C. Xia, R. C. Advincula, *Macromolecules* **2001**, 34, 6922; b) J. Jacob, S. Sax, T. Piok, E. J. W. List, A. C. Grimsdale, K. Müllen, *J. Am. Chem. Soc.* **2004**, 126, 6987.
- [23] J. M. Lupton, A. Pogantsch, T. Piok, E. J. W. List, S. Patil, U. Scherf, *Phys. Rev. Lett.* **2002**, 89, 167401.
- [24] S. Tretiak, A. Saxena, R. L. Martin, A. R. Bishop, *Phys. Rev. Lett.* **2002**, 89, 097402.
- [25] D. Beljonne, G. Pourtois, C. Silva, E. Hennebicq, L. M. Herz, R. H. Friend, G. D. Scholes, S. Setayesh, K. Müllen, J. L. Brédas, *Proc. Natl. Acad. Sci. USA* **2002**, 99, 10982.
- [26] J. M. Lupton, M. R. Craig, E. W. Meijer, *Appl. Phys. Lett.* **2002**, 80, 4489.

Catalytic Asymmetric Addition of β -Ketoesters to Various Imines by Using Chiral Palladium Complexes**

Yoshitaka Hamashima, Naoki Sasamoto, Daido Hotta, Hidenori Somei, Natsuko Umebayashi, and Mikiko Sodeoka*

Addition reactions of metal enolates of carbonyl compounds to imines, the so-called Mannich-type reaction, represent an important class of carbon–carbon bond-forming reactions.^[1] Reflecting the potential utility of the Mannich adducts in the synthesis of nitrogen-containing compounds,^[2] we^[3] and others^[4] have reported efficient methods for catalytic enantioselective Mannich-type reactions.^[5] In our previous reports, however, the pre-activation of ketones to form silyl enol ethers was necessary. To meet the present need for atom-economical processes, the direct addition of pronucleophiles to imines is highly desirable.^[6]

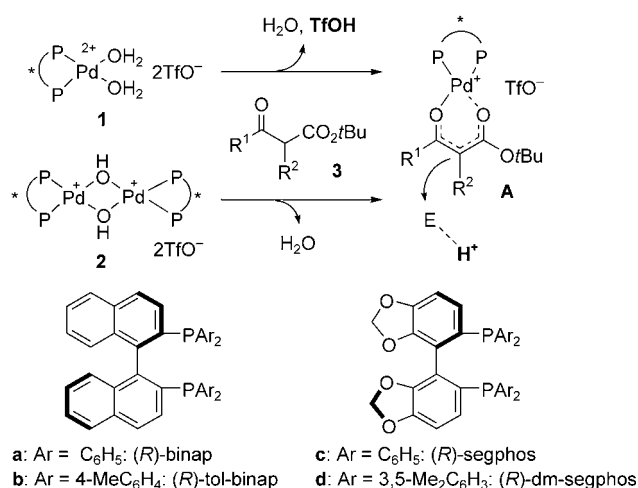
Recently we reported that chiral Pd complexes **1** and **2** reacted with 1,3-dicarbonyl compounds, such as β -ketoesters, to give chiral Pd enolates (Scheme 1).^[7] Using this Pd enolate chemistry, an efficient catalytic enantioselective Michael reaction with enones was developed.^[7a] Interestingly, the chiral enolate **A** derived from **1** underwent the Michael reaction smoothly, whereas the corresponding Pd enolate derived from **2** was completely inactive. These results indicated that the strong protic acid, trifluoromethanesulfonic acid (TfOH), formed concomitantly with the Pd enolate from **1** and activated the enone to act cooperatively with the Pd enolate **A**, thereby promoting the C–C bond-forming reaction. Provided that the reactivity of imines is greatly enhanced by protonation, the above-mentioned Pd enolate chemistry would be applicable to the Mannich-type reaction. To our knowledge there has been only one reported example of the use of β -ketoesters in a catalytic asymmetric Mannich-type reaction, where Jørgensen and co-workers^[8] achieved excellent enantioselectivities of more than 90 % *ee*. However, only the imine tested was a highly reactive *N*-*p*-toluenesulfonyl-protected imino ester and the scope of the available

[*] Dr. Y. Hamashima, N. Sasamoto, D. Hotta, Dr. H. Somei, N. Umebayashi, Prof. Dr. M. Sodeoka
Institute of Multidisciplinary Research for Advanced Materials (IMRAM)
Tohoku University
Katahira, Sendai, Miyagi 980-8577 (Japan)
and
PRESTO, Japan Science and Technology Agency (JST)
Fax: (+81) 22-217-5601
E-mail: sodeoka@tagen.tohoku.ac.jp

[**] This work was supported in part by a Grant-in-Aid for Encouragement of Young Scientists (B) from JSPS. We thank Dr. T. Saito of Takasago International Corp. for providing the chiral phosphine ligands.

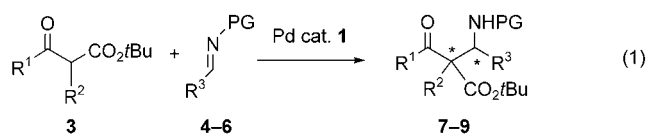


Supporting information for this article is available on the WWW under <http://www.angewandte.org> or from the author.



Scheme 1. Top: Reaction of chiral Pd complexes **1** and **2** with 1,3-dicarbonyl compounds **3** to afford chiral Pd enolates **A**. Bottom: The structures of the different PP ligands.

electrophiles was not examined. The development of such a reaction with broad generality with regard to imines would be extremely useful. Herein, we report a highly enantioselective Mannich-type reaction of β -ketoesters with various imines, including not only imino esters but also other imines derived from simple aldehydes [Eq. (1); PG = protecting group]. In these reactions, the sterically hindered vicinal tertiary and quaternary carbon centers were constructed in one step.^[9]



Initially, the reaction of β -ketoester **3a** with the *N*-*p*-methoxyphenyl-protected imino ester **4a** was chosen as a model reaction (Table 1). Using 5 mol% of **1a**, various solvents were examined, and it was found that the solvent considerably affected the reaction efficiency. The Mannich reactions in CH₃CN, EtOH, and acetone gave poor enantioselectivities (Table 1, entries 1–3). Gratifyingly, however, the enantioselectivity was greatly improved when other solvents were used (Table 1, entries 4–7). Although a relatively prolonged reaction time (72 hours) was required, the reaction in *N,N*-dimethylformamide (DMF) gave an excellent diastereoselectivity (96:4). With respect to the reaction rate, THF was the best solvent (6 hours), and **7aa** was isolated in 77% yield with 98% *ee* (major). In contrast, the reaction of **3a** with **4a** using Pd complex **2a**, in which no protic acid was produced during the generation of Pd enolate **A**,^[7a] resulted in only 23% yield of isolated product after 48 hours, and negligible asymmetric induction was observed for both diastereomers (Table 1, entry 8). These results are in accord with our initial hypothesis, which strongly indicate that cooperative activation of imines by the protic acid is essential for this reaction.

Table 1: Optimization of the reaction conditions.

Entry	Catalyst	Solvent	<i>t</i> [h]	Yield [%]	d.r. ^[a] (major:minor)	<i>ee</i> (major)/ <i>ee</i> (minor) ^[b]
1	1a	CH ₃ CN	11	73	94:6	3/9
2	1a	EtOH	12	76	96:4	15/53
3	1a	acetone	95	75	96:4	17/53
4	1a	CH ₂ Cl ₂	24	72	80:20	86/91
5	1a	toluene	20	69	75:25	98/96
6	1a	DMF	72	74	96:4	97/87
7	1a	THF	6	77	83:17	98/97
8 ^[c]	2a	THF	48	23	87:13	2/10
9	1b	THF	4	96	83:17	97/91
10	1c	THF	4	89	81:19	99/98
11	1d	THF	49	63	98:2	93/50

[a] d.r. = Diastereomeric ratio; determined by ¹H NMR spectroscopic analysis of the crude products. [b] *ee* = Enantiomeric excess. [c] The Pd complex **2a** (2.5 mol%) was used. PMP = *p*-Methoxyphenyl.

Next, we examined other bidentate chiral phosphane ligands using THF as the solvent (Table 1, entries 9–11). When tol-binap and segphos were used the chemical yields improved to 96 and 89%, respectively, maintaining the good diastereo- and excellent enantioselectivities (Table 1, entries 9, 10). On the other hand, the reaction using dm-segphos as a ligand was significantly slower, probably because of steric repulsion, although excellent diastereoselectivity was observed (Table 1, entry 11).

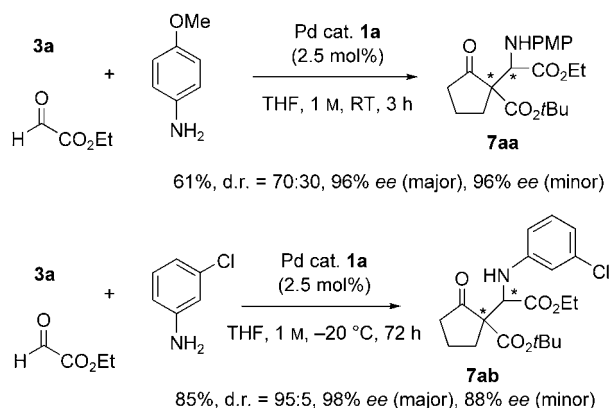
This system was applicable to other nucleophiles (Table 2). Like **3a**, six-membered cyclic and acyclic β -ketoesters **3b** and **3c** underwent the Mannich reaction to afford **7ba** and **7ca**, respectively, in good yield with high enantioselectivity, except for the minor diastereomer of **7ca** (Table 2, entries 1, 2). Moreover, as the Pd–aqua complexes are tolerant to water we envisaged that a three-component reaction would be possible, in which a stoichiometric amount of water molecules is formed during the in situ imine formation (Scheme 2). Indeed, in the presence of 2.5 mol% of **1a**, the mixture of ethyl glyoxylate, an amine component, and **3a** in THF gave rise to the corresponding Mannich adduct in good yield. Notably, in the case of 3-chloroaniline, the diastereoselectivity was found to be 95:5, and excellent enantioselectivity was observed (major: 98% *ee*; minor: 88% *ee*). Thus, an operationally convenient and highly enantioselective Mannich reaction has become feasible. In addition, our results indicate that various aromatic amines other than anisidine are potentially available for this reaction.

If imines derived from simple aldehydes could be successfully employed, the synthetic utility of this reaction would be substantially enhanced. Therefore, we examined the reaction with *N*-*tert*-butyloxycarbonyl-protected imines **5** (Table 2, entries 3–8).^[10,4f] The reaction of **3a** with **5a** was carried out in THF using 2.5 mol% of **1a** (Table 2, entry 3). The mixture was stirred for 5 hours with ice-cooling, and the corresponding product **8aa** was obtained in 93% yield with excellent enantioselectivity of more than 97% *ee* (d.r.

Table 2: Scope and limitations of the reaction.

Entry	Catalyst (x)	β -Ketoester	Imine	Product	T [°C]	t [h]	Yield [%]	d.r. ^[a]	ee ^[b]
1	1c (5)	3b	4a	7ba	RT	35	63	77:23	99/91
2 ^[c]	1a (5)	3c	4a	7ca	RT	42	70	74:26	86/55
3	1a (2.5)	3a	5a	8aa	0	5	93	88:12	99/97
4 ^[d]	1c (2.5)	3c	5a	8ca	RT	4	84	86:14	98/95
5	1a (2.5)	3a	5b	8ab	0	2	72	50:50	99/95
6 ^[d]	1a (2.5)	3c	5b	8cb	RT	5	61	69:31	95/94
7	1a (2.5)	3a	5c	8ac	0	2	75	> 95:5	86/– ^[e]
8 ^[d]	1a (2.5)	3c	5c	8cc	RT	3	71	82:18	96/99
9	1c (5)	3a	6a	9aa	RT	9	99	85:15	97/– ^[e]
10 ^[f]	1c (1)	3a	6b	9ab	–20	24	88	90:10	99/99

[a] d.r.(major:minor); determined by ¹H NMR spectroscopic analysis of the crude products. [b] ee(major)/ee(minor); determined by chiral high performance liquid chromatographic analysis. [c] Concentration = 4 M. [d] The imine (3 equiv) was used. [e] Not determined. [f] Concentration = 0.25 M. Boc = *tert*-butoxycarbonyl, Ts = *p*-toluenesulfonyl, RT = room temperature (23–25 °C).

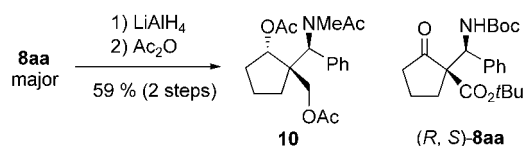

Scheme 2. Three-component coupling reactions.

= 88:12). In addition to the cyclic substrate, the less reactive acyclic substrate **3c** also reacted completely with **5a** within 5 hours and afforded **8ca** in good diastereo- and excellent enantioselectivity (major: 98% ee; Table 2, entry 4). Although the diastereoselectivity was decreased in the case of **5b**, high enantioselectivities of up to 99% ee were still maintained for both **3a** and **3c** (Table 2, entries 5, 6). A furane-ring-substituted imine **5c**, which is unstable under acidic conditions, reacted smoothly with **3a** and **3c**, with good to excellent diastereoselectivity, and the corresponding Mannich adducts **8ac** and **8cc** were formed in a highly enantioselective manner (Table 2, entries 7, 8). Furthermore, *N*-*p*-toluenesulfonyl-protected imines^[11] were also good substrates, and with **3a** as the substrate uniformly high enantioselectivities were produced (Table 2, entries 9, 10). The reaction of **6b** proceeded smoothly in the presence of as little as 1 mol% of the catalyst **1c**, and so the desired product was afforded in 88% yield with almost perfect stereocontrol (99% ee). To our knowledge, this is the first demonstration of

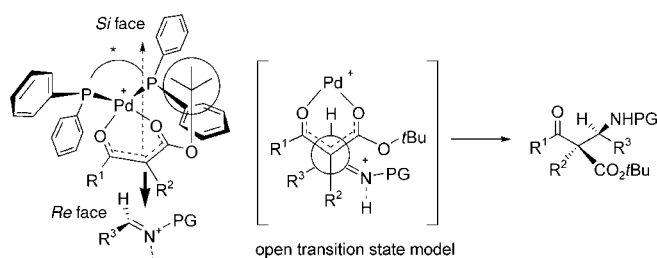
an enantioselective Mannich-type reaction of β -ketoesters with various imines. Another feature of this reaction is that the reaction can be conducted without the exclusion of air and moisture.

As shown in Scheme 3, stereoselective reduction of the major diastereomer of **8aa** with LiAlH₄ followed by acetylation afforded compound **10**, which possesses three successive chiral centers. Since the opposite enantiomer of **10** has been synthesized by Karlsson et al. through the enantioselective 1,3-dipolar cycloaddition of nitron,^[12] the absolute configuration of **10** was determined by optical rotation studies.^[13] Consequently, the absolute configuration of the quaternary carbon center in the major diastereomer of **8aa** was revealed to be *R*, and that of the tertiary carbon center was *S*. In

addition, ¹H NMR spectroscopic analysis indicated that the same Pd enolate as described in Scheme 1 was formed in this Mannich-type reaction.^[14] On the basis of these results, coupled with our previous studies on the catalytic enantioselective


Scheme 3. Conversion of **8aa** into **10**.

Michael reaction and fluorination reaction,^[7] the excellent enantioselectivity was deduced to come from face-selection of the chiral Pd enolate (Figure 1). Thus, a bulky *t*Bu group was preferentially located at one of the faces of the Pd enolate to avoid steric repulsion with the equatorial phenyl group of binap. Therefore, the imines preferentially approached the enolate from the less-crowded *Re* face. Because Pd complex **1** was superior to the Pd complex **2** as a catalyst,^[15] we speculate that protonated imines may be involved in the transition-state.^[16] On the other hand, face-


Figure 1. Proposed transition-state model.

selection of the imines was probably responsible for the relative stereochemistry. When such an iminium ion is involved, it has been proposed that the reaction proceeds through an open transition-state model.^[17,18] Thus, we speculate that C–C bond-formation in our Mannich-type reaction occurs with the appropriate geometry as described in Figure 1 to minimize steric interactions.

In summary, we have developed a highly enantioselective catalytic Mannich-type reaction of β -ketoesters. The reaction was applicable to a variety of imines derived from glyoxylate, as well as simple aromatic and α,β -unsaturated aldehydes. This method affords stereochemically elaborated β -amino carbonyl compounds in up to 99% *ee*, thus indicating that such addition reactions of β -ketoesters to various imines would be useful to provide versatile intermediates for the synthesis of chiral nitrogen-containing compounds. In this reaction, the protic acid generated during the formation of the Pd enolate would play a role in activating the imine. Since protic acids are good catalysts for the nonenantioselective Mannich reaction, it is surprising that our Mannich reaction is highly enantioselective. We think that simultaneous activation of both reactants is the key to success, and this distinctive reaction mechanism could be an important guide to the design of novel reaction systems. Further studies to elucidate the mechanism and extend the scope of the reaction are under way.

Experimental Section

Representative procedure for the synthesis of **8aa**: β -Ketoester **3a** (20 μ L, 108.6 μ mol) and palladium complex **1a** (2.9 mg, 2.5 mol%) were added successively to a solution of **5a** (33.4 mg, 162.8 μ mol) in THF (110 μ L) at 0°C. The reaction mixture was stirred for 5 hours at the same temperature. The reaction was monitored by TLC (hexane/ethyl acetate, 3:1) and after completion was quenched by addition of ethyl acetate (5 mL) and brine (3 mL). The aqueous layer was extracted with ethyl acetate (3 \times 5 mL). The combined organic layers were washed with water and brine then dried over Na₂SO₄, and the solvent was evaporated under reduced pressure. At this stage, the diastereomeric ratio was determined by ¹H NMR spectroscopic analysis of the crude products. Further purification was performed by medium pressure liquid chromatography on silica gel (hexane/ethyl acetate, 4:1; major: 35.0 mg, 82%; minor: 4.6 mg, 11%). The *ee* values of the diastereomers were determined by chiral high performance liquid chromatography analysis.

Received: October 5, 2004

Published online: January 31, 2005

Keywords: asymmetric catalysis · enolates · Mannich reaction · palladium · Schiff bases

- [1] a) E. F. Kleinman in *Comprehensive Organic Synthesis*, Vol. 2 (Eds.: B. M. Trost, I. Fleming), Pergamon, Oxford, **1991**, chap. 4.1; b) M. Arend, B. Westermann, N. Risch, *Angew. Chem.* **1998**, *110*, 1096–1122; *Angew. Chem. Int. Ed.* **1998**, *37*, 1044–1070.
- [2] For the synthesis of β -amino acids: a) *Enantioselective Synthesis of β -Amino Acids* (Ed.: E. Juaristi), Wiley, New York, **1997**; b) M. Liu, M. P. Sibi, *Tetrahedron* **2002**, *58*, 7991–8035; c) P. A. Magriotis, *Angew. Chem.* **2001**, *113*, 4507–4509; *Angew. Chem. Int. Ed.* **2001**, *40*, 4377–4379; d) J.-A. Ma, *Angew. Chem.* **2003**, *115*, 4426–4435; *Angew. Chem. Int. Ed.* **2003**, *42*, 4290–4299; e) N. Sewald, *Angew. Chem.* **2003**, *115*, 5972–5973; *Angew. Chem. Int. Ed.* **2003**, *42*, 5794–5795.
- [3] a) E. Hagiwara, A. Fujii, M. Sodeoka, *J. Am. Chem. Soc.* **1998**, *120*, 2474–2475; b) A. Fujii, E. Hagiwara, M. Sodeoka, *J. Am. Chem. Soc.* **1999**, *121*, 5450–5458; c) A. Fujii, M. Sodeoka, *Tetrahedron Lett.* **1999**, *40*, 8011–8014.
- [4] For recent examples of the catalytic enantioselective Mannich reactions using preformed metal enolates: a) H. Fujieda, M. Kanai, T. Kambara, A. Iida, K. Tomioka, *J. Am. Chem. Soc.* **1997**, *119*, 2060–2061; b) H. Ishitani, M. Ueno, S. Kobayashi, *J. Am. Chem. Soc.* **1997**, *119*, 7153–7154; c) S. Xue, S. Yu, Y. Deng, W. D. Wulff, *Angew. Chem.* **2001**, *113*, 2331–2334; *Angew. Chem. Int. Ed.* **2001**, *40*, 2271–2274; d) D. Ferraris, B. Young, C. Cox, T. Dudding, W. J. Drury III, L. Ryzhkov, A. E. Taggi, T. Lectka, *J. Am. Chem. Soc.* **2002**, *124*, 67–77; e) S. Kobayashi, T. Hamada, K. Manabe, *J. Am. Chem. Soc.* **2002**, *124*, 5640–5641; f) A. G. Wenzel, E. N. Jacobsen, *J. Am. Chem. Soc.* **2002**, *124*, 12964–12965; g) S. Kobayashi, R. Matsubara, Y. Nakamura, H. Kitagawa, M. Sugiura, *J. Am. Chem. Soc.* **2003**, *125*, 2507–2515; h) N. S. Josephsohn, M. L. Snapper, A. H. Hoveyda, *J. Am. Chem. Soc.* **2004**, *126*, 3734–3735; i) T. Akiyama, J. Itoh, K. Yokota, K. Fuchibe, *Angew. Chem.* **2004**, *116*, 1592–1594; *Angew. Chem. Int. Ed.* **2004**, *43*, 1566–1568; j) S. Kobayashi, M. Ueno, S. Saito, Y. Mizuki, H. Ishitani, Y. Yamashita, *Proc. Natl. Acad. Sci. USA* **2004**, *101*, 5476–5481.
- [5] S. Kobayashi, M. Ueno in *Comprehensive Asymmetric Catalysis*, Supplement 1 (Eds.: E. N. Jacobsen, A. Pfaltz, H. Yamamoto), Springer, Berlin, **2003**, chap. 29.5, p. 143.
- [6] Recent examples of direct catalytic asymmetric Mannich reactions: a) S. Yamasaki, T. Iida, M. Shibasaki, *Tetrahedron* **1999**, *55*, 8857–8867; b) K. Juhl, N. Gathergood, K. A. Jørgensen, *Angew. Chem.* **2001**, *113*, 3083–3085; *Angew. Chem. Int. Ed.* **2001**, *40*, 2995–2997; c) B. List, P. Pojarliev, W. T. Biller, H. J. Martin, *J. Am. Chem. Soc.* **2002**, *124*, 827–833; d) A. Córdova, W. Notz, G. Zhong, J. M. Betancort, C. F. Barbas III, *J. Am. Chem. Soc.* **2002**, *124*, 1842–1843; e) W. Notz, F. Tanaka, S.-i. Watanabe, N. S. Chowdari, J. M. Turner, R. Thayumanavan, C. F. Barbas III, *J. Org. Chem.* **2003**, *68*, 9624–9634; f) T. Itoh, M. Yokoyama, K. Miyauchi, K. Nagata, A. Ohsawa, *Org. Lett.* **2003**, *5*, 4301–4304; g) Y. Hayashi, W. Tsuboi, I. Ashimine, T. Urushima, M. Shoji, K. Sakai, *Angew. Chem.* **2003**, *115*, 3805–3808; *Angew. Chem. Int. Ed.* **2003**, *42*, 3677–3680; h) L. Bernardi, A. S. Gothelf, R. G. Hazell, K. A. Jørgensen, *J. Org. Chem.* **2003**, *68*, 2583–2591; i) B. M. Trost, L. R. Terrell, *J. Am. Chem. Soc.* **2003**, *125*, 338–339; j) S. Matsunaga, T. Yoshida, H. Morimoto, N. Kumagai, M. Shibasaki, *J. Am. Chem. Soc.* **2004**, *126*, 8777–8785; k) D. Uruguchi, M. Terada, *J. Am. Chem. Soc.* **2004**, *126*, 5356–5357; l) W. Zhuang, S. Saaby, K. A. Jørgensen, *Angew. Chem.* **2004**, *116*, 4576–4578; *Angew. Chem. Int. Ed.* **2004**, *43*, 4476–4478; m) A. J. A. Cobb, D. M. Shaw, S. V. Ley, *Synlett* **2004**, 558–560; n) A. Córdova, *Chem. Eur. J.* **2004**, *10*, 1987–1997; see also, o) A. Córdova, *Acc. Chem. Res.* **2004**, *37*, 102–112.
- [7] a) Y. Hamashima, D. Hotta, M. Sodeoka, *J. Am. Chem. Soc.* **2002**, *124*, 11240–11241; b) Y. Hamashima, K. Yagi, H. Takano, L. Támas, M. Sodeoka, *J. Am. Chem. Soc.* **2002**, *124*, 14530–14531; c) Y. Hamashima, H. Takano, D. Hotta, M. Sodeoka, *Org. Lett.* **2003**, *5*, 3225–3228; d) Y. Hamashima, M. Sodeoka, *Chem. Rec.* **2004**, *4*, 231–242.
- [8] M. Marigo, A. Kjærsgaard, K. Juhl, N. Gathergood, K. A. Jørgensen, *Chem. Eur. J.* **2003**, *9*, 2359–2367.
- [9] A report on the asymmetric synthesis of α -tetrasubstituted β -amino acids appeared during the preparation of this manuscript: N. S. Chowdari, J. T. Suri, C. F. Barbas III, *Org. Lett.* **2004**, *6*, 2507–2510.

- [10] A. M. Kanazawa, J.-N. Denis, A. E. Greene, *J. Org. Chem.* **1994**, 59, 1238–1240.
- [11] a) B. E. Love, P. S. Raje, T. C. Williams II, *Synlett* **1994**, 493–494; b) F. Chemla, V. Hebbe, J.-F. Normant, *Synthesis* **2000**, 75–77.
- [12] S. Karlsson, H.-E. Högborg, *Eur. J. Org. Chem.* **2003**, 2782–2791.
- [13] See Supporting Information.
- [14] In accord with our previous results, mixture of **1b** and **3a** (1:1) in [d₈]THF at room temperature gave an equilibrium mixture of the Pd enolate and **3a**. Upon addition of 0.6 equivalents of **4a**, rapid formation of the Mannich adduct **7aa** was observed. At that time, approximately half of the remaining **3a** was found to exist as the Pd enolate [a *t*Bu group of the Pd enolate (0.71 ppm) relative to THF (3.58 ppm) as an internal standard was observed]. Details of these ¹H NMR spectroscopy experiments will be discussed elsewhere. For details of characterization of the Pd enolate, see: Ref. [7a] and Supporting Information therein.
- [15] The reaction of **3a** with **5a** in the presence of **2a** was found to be less efficient than that in the case of **1a** under the same reaction conditions (0°C, 5 hours) [**1a** (2.5 mol %): see Table 2, entry 3; **2a** (5 mol % to Pd): 58%, d.r. = 89:11, 92% *ee* (major), 86% *ee* (minor)]. Similar diastereo- and enantioselectivities were obtained. However, the reaction rate was considerably slower in the case of **2a**, although the two-fold Pd complex was used. This clearly indicates that a proton plays a role in the acceleration of the reaction. Also, compare entries 7 and 8 in Table 1.
- [16] A recent example of the in situ generation of iminium ions by protonation of enamines: C. Koradin, K. Polborn, P. Knochel, *Angew. Chem.* **2002**, 114, 2651–2654; *Angew. Chem. Int. Ed.* **2002**, 41, 2535–2538.
- [17] An open transition-state was proposed as an important candidate. See, D. Enders, D. Ward, J. Adam, G. Raabe, *Angew. Chem.* **1996**, 108, 1059–1062; *Angew. Chem. Int. Ed. Engl.* **1996**, 35, 981–984.
- [18] The involvement of the protonated imines raises another possibility. Seebach et al. have proposed an electrostatic interaction of a Ti enolate with an iminium cation in their *anti*-selective Mannich reaction. However, in our case, such a transition-state would cause severe steric repulsion between the protecting group of the imine and the Pd catalyst. See, a) D. Seebach, C. Betschart, M. Schiess, *Helv. Chim. Acta* **1984**, 67, 1593–1597; b) D. Seebach, M. Schiess, W. B. Schweizer, *Chimia* **1985**, 39, 272–273.

A Purine-like Nickel(II) Base Pair for DNA**

Christopher Switzer,* Surajit Sinha, Paul H. Kim, and Benjamin D. Heuberger

Nucleic acids rely on complementary functionalized purine and pyrimidine heterocycles to encode genetic information as G·C and A·T(U) base pairs. Several approaches have been developed to expand the number of available base pairs beyond the two natural pairs, including the use of non-standard hydrogen-bond donor/acceptor patterns,^[1] van der Waals and hydrophobic interactions,^[2] and metal coordination.^[3] Herein we report the realization of a naturally inspired metallo base pair with a purine core whose design derives from minimal modification of adenine. The resulting base pair (Pur^P·Ni·Pur^P, Figure 1) is found to have the following novel features and properties: 1) greater stability than a G·C base pair, 2) a surprising dimensional resemblance to natural purine–pyrimidine base pairs, and 3) the potential to serve in an ion-activated switch.

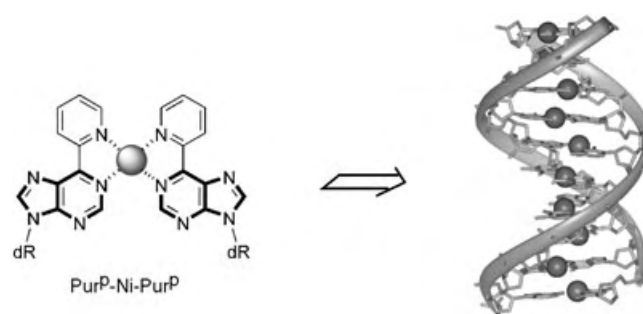
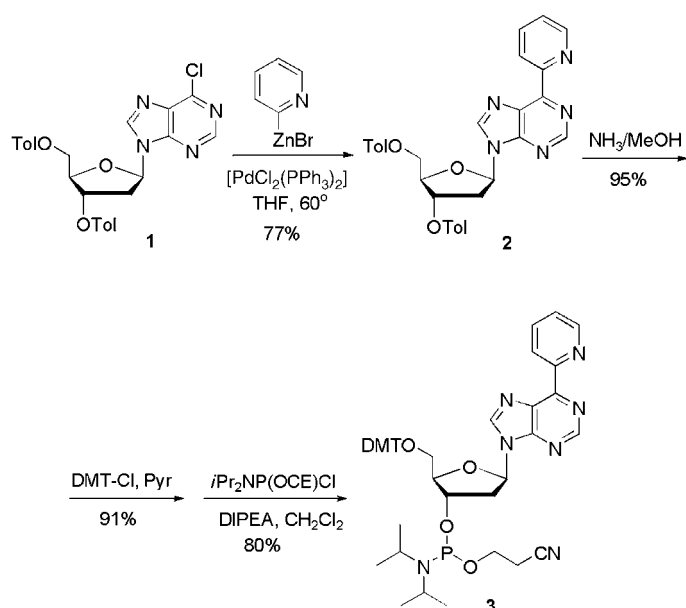


Figure 1. Left: The 6-(2'-pyridyl)-purine (Pur^P) metallo base pair. Right: A representation of a hypothetical helix composed of purely Pur^P·Ni²⁺·Pur^P base pairs.

Formally, Pur^P is derived from adenine by replacing the 6-amino group with a pyridyl group. This functional-group interchange places two Lewis basic donor atoms (the purine N1 and pyridine N1' atoms) in an optimal 1,4-relationship for coordinating metal ions. Scheme 1 summarizes the synthesis of Pur^P. The key transformation involved a modified Negishi coupling of pyridyl zinc bromide with chloropurine deoxyriboside **1**^[4] to provide pyridylpurine deoxyriboside **2**. We

[*] Prof. C. Switzer, S. Sinha, P. H. Kim, B. D. Heuberger
Department of Chemistry
University of California
Riverside, CA 92521 (USA)
Fax: (+1) 951-787-2435
E-mail: christopher.switzer@ucr.edu

[**] This work was supported by DOD/DARPA/DMEA under award no. DMEA90-02-2-0216 and the NASA exobiology program under award no. NAG5-9812.



Scheme 1. Synthesis of 2'-deoxyribosyl-N9-[6-(2'-pyridyl)-purine] phosphoramidite **3**. Tol = 4-toluoyl, THF = tetrahydrofuran, DMT = 4,4'-dimethoxytriphenylmethyl, Pyr = pyridine, OCE = cyanoethyl, DIPEA = *N,N*-diisopropylethylamine.

initially used the conditions reported for the preparation of ribosyl and acyclic analogues of **2**^[5] but found that an improved yield was possible by switching to a $[\text{PdCl}_2(\text{PPh}_3)_2]$ catalyst.^[6] Pyridylpurine nucleoside **2** was transformed in three steps into phosphoramidite **3**. DNA containing Pur^{P} was prepared by using **3** and standard phosphite triester methodology on an ABI394 synthesizer. Complementary dodecamer DNA strands were prepared, each bearing a single Pur^{P} residue: 5'-d-CTTTCT Pur^{P} TCCCT (**4**) and 5'-d-AGGGAP ur^{P} AGAAAG (**5**). These oligomers were purified by PAGE, and their identities were confirmed by MALDI mass spectrometry.

To assess the viability of Pur^{P} as the organic component of a metallo base pair, UV-monitored thermal denaturation of complementary dodecamers **4** and **5** bearing single Pur^{P} residues was performed in the presence of the divalent ions noted in Table 1. Representative denaturation profiles are shown in Figure 2. In all, nine divalent metal ions were screened for their abilities to coordinate to the $\text{Pur}^{\text{P}}\cdot\text{Pur}^{\text{P}}$ site contained in the **4/5** duplex by measuring the T_{m} value; the T_{m} value of a metal-free control with the same duplex (Table 1, entry 11) was also recorded. As is apparent from the table, only four of the seven divalent ions gave T_{m} values for **4/5** that differed significantly from the metal-free control: Ni^{2+} , Co^{2+} , Cu^{2+} , Zn^{2+} , and Ag^{+} . Of these five metals, Ni^{2+} is the most stabilizing. $\text{Pur}^{\text{P}}\cdot\text{Co}^{2+}\cdot\text{Pur}^{\text{P}}$ leads to a duplex T_{m} value roughly in between those of the **6/10** and **7/11** duplexes bearing T·A and C·G pairs, respectively. More significantly, the $\text{Pur}^{\text{P}}\cdot\text{Ni}^{2+}\cdot\text{Pur}^{\text{P}}$ base pair is more stabilizing to a double helix than a C·G base pair by a margin of 6°C under the conditions reported in Table 1, with 5 μM NiCl_2 . Importantly, the $\text{Pur}^{\text{P}}\cdot\text{Pur}^{\text{P}}$ **4/5** duplex is highly destabilized in the absence of Ni^{2+} or other

Table 1: DNA-duplex melting temperatures, T_{m} , in the presence and absence of divalent ions.^[a]

5'-d-CTTTCT Pur^{P} TCCCT
3'-d-GAAAGAP ur^{P} AGGGA

Entry	X·Y	Duplex	Metal	T_{m}	Δ ^[b]
1	$\text{Pur}^{\text{P}}\cdot\text{Pur}^{\text{P}}$	4/5	NiCl_2	46.1	+6.0
2	$\text{Pur}^{\text{P}}\cdot\text{Pur}^{\text{P}}$	4/5	$\text{Ni}(\text{NO}_3)_2$	46.6	+6.5
3	$\text{Pur}^{\text{P}}\cdot\text{Pur}^{\text{P}}$	4/5	CoCl_2	38.8	-1.3
4	$\text{Pur}^{\text{P}}\cdot\text{Pur}^{\text{P}}$	4/5	CuCl_2	31.4	-8.7
5	$\text{Pur}^{\text{P}}\cdot\text{Pur}^{\text{P}}$	4/5	ZnSO_4	30.8	-9.3
6	$\text{Pur}^{\text{P}}\cdot\text{Pur}^{\text{P}}$	4/5	AgNO_3	30.5	-9.6
7	$\text{Pur}^{\text{P}}\cdot\text{Pur}^{\text{P}}$	4/5	FeSO_4	28.8	-11.3
8	$\text{Pur}^{\text{P}}\cdot\text{Pur}^{\text{P}}$	4/5	MnCl_2	29.2	-10.9
9	$\text{Pur}^{\text{P}}\cdot\text{Pur}^{\text{P}}$	4/5	$\text{Eu}(\text{NO}_3)_3$	29.1	-11.0
10	$\text{Pur}^{\text{P}}\cdot\text{Pur}^{\text{P}}$	4/5	$\text{Pd}(\text{NO}_3)_2$	27.3	-12.8
11	$\text{Pur}^{\text{P}}\cdot\text{Pur}^{\text{P}}$	4/5	— ^[c]	28.5	-11.6
12	T· Pur^{P}	6/5	NiCl_2	27.1	-13.0
13	C· Pur^{P}	7/5	NiCl_2	26.6	-13.5
14	A· Pur^{P}	8/5	NiCl_2	27.0	-13.1
15	G· Pur^{P}	9/5	NiCl_2	29.1	-11.0
16	T·A	6/10	— ^[c]	36.8	-3.3
17	T·A	6/10	NiCl_2 ^[d]	37.4	-2.7
18	T·A	6/10	CoCl_2 ^[d]	36.7	-3.4
19	C·G	7/11	— ^[c]	40.2	+0.1
20	C·G	7/11	NiCl_2 ^[d]	40.1	0.0
21	C·G	7/11	CoCl_2 ^[d]	39.9	-0.2

[a] Samples contained 2.5 μM of each DNA strand, 5 μM divalent ion where indicated, 50 mM NaCl, and 10 mM NaH_2PO_4 (pH 7.0). All measurements were performed at least in triplicate. [b] Difference in T_{m} value relative to that of duplex **7/11** (X·Y = C·G) in the presence of NiCl_2 (entry 20). [c] No divalent metal ions were added. [d] Divalent ion was added in these cases as a control.

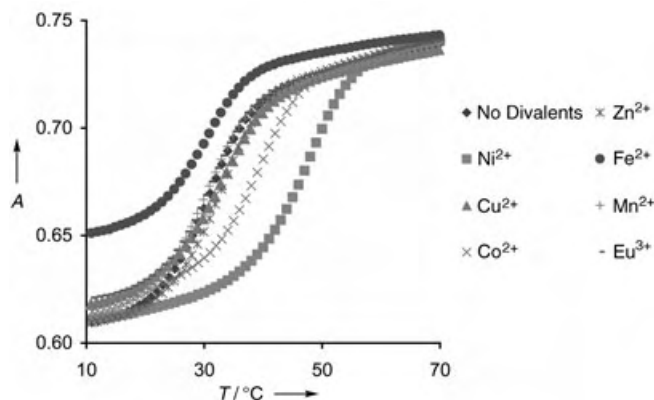


Figure 2. Absorbance versus temperature denaturation profiles. Conditions are as reported in Table 1.

divalent ions (Table 1, entry 11): there is a -17.6°C difference in T_{m} value between the $\text{Pur}^{\text{P}}\cdot\text{Ni}^{2+}\cdot\text{Pur}^{\text{P}}$ ($T_{\text{m}} = 46.1^\circ\text{C}$) and $\text{Pur}^{\text{P}}\cdot\text{Pur}^{\text{P}}$ ($T_{\text{m}} = 28.5^\circ\text{C}$) base pairs (Table 1, entry 1 versus entry 11). As a control, both the T·A **6/10** and the C·G **7/11** duplexes were denatured in the presence and absence of Ni^{2+} or Co^{2+} , and no significant changes were observed in the T_{m} values (Table 1, entries 16–21).

The stability of mismatches between the four natural bases and Pur^{P} was investigated in the presence of Ni^{2+}

(Table 1, entries 12–15). Clearly, none of the natural bases make stable pairs with $\text{Pur}^{\text{P}}\cdot\text{Ni}^{2+}$. Indeed, the ΔT_{m} values of the mismatched pairs relative to the $\text{Pur}^{\text{P}}\cdot\text{Ni}^{2+}\cdot\text{Pur}^{\text{P}}$ base pair (not the Δ values listed in Table 1 which are relative to the C-G pair) range from -17 to -19.5°C . By contrast, T-G and C-A mismatches of the parent natural duplex under the same conditions show ΔT_{m} values of -7.4 and -18.5°C under the same conditions.^[7] Thus, all four $\text{Pur}^{\text{P}}\cdot\text{Ni}^{2+}$ mismatches with natural bases are much less stable than the $\text{Pur}^{\text{P}}\cdot\text{Ni}^{2+}\cdot\text{Pur}^{\text{P}}$ match. A further point to note is that the instabilities seen for all four $\text{Pur}^{\text{P}}\cdot\text{Ni}^{2+}$ mismatches with natural bases rival the most severe natural nucleobase mismatches such as C-A.

Within the double helix, three possible geometries could be envisioned for divalent metal ion complexation by Pur_2^{P} : square planar, tetrahedral, and D_2^{d} (a geometry intermediate between square planar and tetrahedral). In the absence of a geometric preference by the metal ion, the most productive geometry for a metallo base pair in forming the double helix is expected to be square planar because this will maximize favorable nearest-neighbor stacking interactions. Low-energy square-planar geometries should be accessible for Ni^{2+} , Co^{2+} , Cu^{2+} , Ag^{+} , and Pd^{2+} ions. The first two of these five ions appreciably stabilize the Pur_2^{P} -bearing helix, whereas the latter three do not. As a result, it may be concluded that geometry alone is an insufficient predictor of metal-ion affinity for Pur^{P} . A circular dichroism spectrum of duplex **4/5** in the presence of Ni^{2+} is consistent with a B-DNA structure.

To assess the viability of a square-planar geometry for $\text{Pur}^{\text{P}}\cdot\text{Ni}^{2+}\cdot\text{Pur}^{\text{P}}$, an ab initio geometry optimization was performed on the complex by using Gaussian98^[8] at the B3LYP/6-31G*(CHN)/SDD(Ni) level of theory. Figure 3 (left panel) shows the square-planar geometry found to be a (local) minimum on the energy surface. Interestingly, this structure bears an N9–N9' (purine numbering) $\text{Pur}^{\text{P}}\text{--}\text{Pur}^{\text{P}}$ distance of 9.54 \AA , which nearly replicates the N9–N1 purine–pyrimidine distance of 9.05 \AA that occurs in natural B-DNA helices for both G-C and A-T base pairs. This suggests $\text{Pur}^{\text{P}}\cdot\text{Ni}^{2+}\cdot\text{Pur}^{\text{P}}$ is a good dimensional mimic of natural base pairs despite the fact that the metallo base pair incorporates two purine-like components. Superposition of ab initio optimized $\text{Pur}^{\text{P}}\cdot\text{Ni}^{2+}\cdot\text{Pur}^{\text{P}}$ and A-T base-pair structures (Figure 3, right panel) further supports this idea and shows that Pur^{P} coordination of Ni^{2+} is attended by rotation of the Pur^{P}

bases towards the major groove, with a corresponding shortening of the distance between interstrand N9 atoms.

The $\text{Pur}^{\text{P}}\cdot\text{Ni}^{2+}\cdot\text{Pur}^{\text{P}}$ structure in Figure 3 results from head-to-head dimerization ($\text{N1},\text{N1}'\text{--}\text{Pur}^{\text{P}}\cdot\text{Ni}^{2+}\cdot\text{N1},\text{N1}'\text{--}\text{Pur}^{\text{P}}$). An alternative head-to-tail dimerization mode of Pur^{P} ($\text{N1},\text{N1}'\text{--}\text{Pur}^{\text{P}}\cdot\text{Ni}^{2+}\cdot\text{N7},\text{N1}'\text{--}\text{Pur}^{\text{P}}$) was also investigated computationally. The geometry of this latter complex was found to be highly nonplanar due to ligand encroachment resulting from the 1,5-relationship of the nitrogen atoms ($\text{N7},\text{N1}'$) presented by the “tail”-oriented Pur^{P} . (In contrast, the opposing “head”-oriented Pur^{P} bears the optimal 1,4-relationship of nitrogen atoms, as found in bipyridine.) Therefore, the head-to-tail dimer is predicted to be less compatible with a helix than the head-to-head dimer.

Metallo base pairs could become functional elements of oligonucleotides that activate or suppress enzymatic activity (for example, transcription or translation) in the presence or absence of a metal ion. For a proof of principle, we have incorporated three consecutive Pur^{P} residues into a helix to attain “on” and “off” states (in the presence and absence of Ni^{2+} , respectively) that are sufficiently insulated from one another to be effectively binary (0 or 1). The following tetradecamer DNA strands were prepared: 5'-d-CTTCTCTPur^PPur^PPur^PTCCCT (**12**) and 5'-d-AGGGAPur^P-Pur^PPur^PAGAAAG (**13**). Gratifyingly, the T_{m} values for the **12/13** duplex under the conditions reported in Table 1 were 64.3°C in the presence of $10.0\text{ }\mu\text{M}$ NiCl_2 (1.3 equiv per Pur^{P} residue) and 20.6°C in the absence of Ni^{2+} . Thus, the T_{m} values between the “on” (Ni^{2+} present) and “off” (Ni^{2+} absent) states of this system are separated by 43.7°C , a difference sufficient to produce binary behavior at 37°C (that is, at this temperature, in the presence of Ni^{2+} the helix is present and in the absence of Ni^{2+} the helix is absent).

In summary, Pur^{P} leads to a metallo base pair with Ni^{2+} selectivity that is more stable than natural G-C and A-T base pairs. Additionally, $\text{Pur}^{\text{P}}\cdot\text{Ni}^{2+}\cdot\text{Pur}^{\text{P}}$ is orthogonal in its pairing properties relative to the four genomic nucleobases: all mismatches are highly destabilizing to the helix in comparison to the parent metallo base pair. Finally, $\text{Pur}^{\text{P}}\cdot\text{Ni}^{2+}\cdot\text{Pur}^{\text{P}}$ appears to resemble natural base pairs dimensionally and has the potential to serve as the functional component of an ion-activated switch. Given the resemblance between natural purines and Pur^{P} it is possible that enzymes, including those

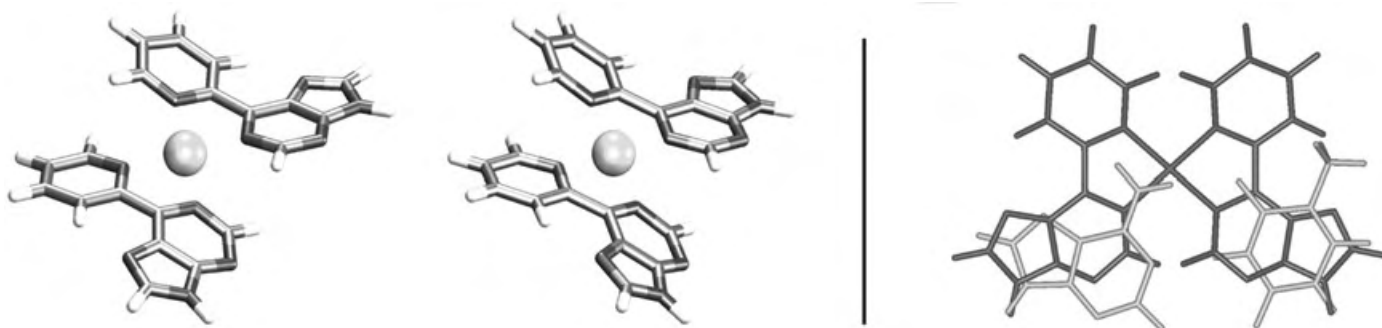


Figure 3. Left: Stereoview of the structure of $\text{Pur}^{\text{P}}\cdot\text{Ni}^{2+}\cdot\text{Pur}^{\text{P}}$ with optimized geometry obtained with Gaussian98.^[8] Right: Superposition of optimized $\text{Pur}^{\text{P}}\cdot\text{Ni}^{2+}\cdot\text{Pur}^{\text{P}}$ and A-T structures. The superposition was guided by Pur^{P} N9/A N9, Pur^{P} N9/T N1, and the hydrogen atoms attached to these nitrogen atoms.

involved in DNA replication, might recognize the $\text{Pur}^{\text{P}}\cdot\text{Ni}^{2+}$. Pur^{P} base pair. We are actively pursuing this possibility.

Received: September 21, 2004

Published online: January 28, 2005

Keywords: DNA · metallo base pairs · molecular switches · nickel · nucleobases

- [1] a) C. Switzer, S. E. Moroney, S. A. Benner, *J. Am. Chem. Soc.* **1989**, *111*, 8322–8323; b) J. A. Piccirilli, T. Krauch, S. E. Moroney, S. A. Benner, *Nature* **1990**, *343*, 33–47.
- [2] a) B. A. Schweitzer, E. T. Kool, *J. Am. Chem. Soc.* **1995**, *117*, 1863–1872; b) D. L. McMinn, A. K. Ogawa, Y. Q. Wu, J. Q. Liu, P. G. Schultz, F. E. Romesberg, *J. Am. Chem. Soc.* **1999**, *121*, 11 585–11 586.
- [3] a) E. Meggers, P. L. Holland, W. B. Tolman, F. E. Romesberg, P. G. Schultz, *J. Am. Chem. Soc.* **2000**, *122*, 10714–10715; b) H. Weizman, Y. Tor, *J. Am. Chem. Soc.* **2001**, *123*, 3375–3376; c) K. Tanaka, Y. Yamada, M. Shionoya, *J. Am. Chem. Soc.* **2002**, *124*, 8802–8803; d) T. Tanaka, A. Tengeji, T. Kato, N. Toyama, M. Shiro, M. Shionoya, *J. Am. Chem. Soc.* **2002**, *124*, 12494–12498; e) N. Zimmerman, E. Meggers, P. G. Schultz, *J. Am. Chem. Soc.* **2002**, *124*, 13684–13685; f) K. Tanaka, A. Tengeji, T. Kato, N. Toyama, M. Shionoya, *Science* **2003**, *299*, 1212–1213; g) C. Brotschi, C. J. Leumann, *Nucleosides Nucleotides Nucleic Acids* **2003**, *22*, 1195–1197.
- [4] Z. Kazimierczuk, H. B. Cottam, G. R. Revankar, R. K. Robins, *J. Am. Chem. Soc.* **1984**, *106*, 6379–6382.
- [5] M. Hocek, A. Holy, I. Vortuba, H. Dvořáková, *Collect. Czech. Chem. Commun.* **2001**, *66*, 483–499.
- [6] A. Lützen, M. Hapke, *Eur. J. Org. Chem.* **2002**, 2292–2297.
- [7] H. Hashimoto, M. G. Nelson, C. Switzer, *J. Am. Chem. Soc.* **1993**, *115*, 7128–7134.
- [8] *Gaussian 98* (Revision A.7), M. J. Frisch, G. W. Trucks, H. B. Schlegel, G. E. Scuseria, M. A. Robb, J. R. Cheeseman, V. G. Zakrzewski, J. A. Montgomery, R. E. Stratmann, J. C. Burant, S. Dapprich, J. M. Millam, A. D. Daniels, K. N. Kudin, M. C. Strain, O. Farkas, J. Tomasi, V. Barone, M. Cossi, R. Cammi, B. Mennucci, C. Pomelli, C. Adamo, S. Clifford, J. Ochterski, G. A. Petersson, P. Y. Ayala, Q. Cui, K. Morokuma, D. K. Malick, A. D. Rabuck, K. Raghavachari, J. B. Foresman, J. Cioslowski, J. V. Ortiz, B. B. Stefanov, G. Liu, A. Liashenko, P. Piskorz, I. Komaromi, R. Gomperts, R. L. Martin, D. J. Fox, T. Keith, M. A. Al-Laham, C. Y. Peng, A. Nanayakkara, C. Gonzalez, M. Challacombe, P. M. W. Gill, B. G. Johnson, W. Chen, M. W. Wong, J. L. Andres, M. Head-Gordon, E. S. Replogle, J. A. Pople, Gaussian, Inc., Pittsburgh, PA, **1998**.

Tetramic Acid Antibiotics: Stereoselective Synthesis of Streptolic Acid and Tirandalydigin**

Yasuhiro Iwata, Naomi Maekawara, Keiji Tanino, and Masaaki Miyashita*

The tetramic acid family of antibiotics have unique chemical structures composed of the 2,6-dioxabicyclononane skeleton and the characteristic dienoyl tetramic acid moiety. They exhibit potent antimicrobial activities and inhibitory activity against bacterial DNA-directed RNA polymerase.^[1] The distinctive structural features and potent pharmacological properties render this family of antibiotics worthy targets for synthetic exploration.^[2] In the tetramic acid antibiotics, two types of 2,6-dioxabicyclononane structures are known. One is the oxabicyclononane structure with an epoxy ketone moiety, as represented by tirandamycin A and B,^[3] and the other is that involving a vinyl epoxide moiety, such as that in streptolydigin (**1**)^[4] and tirandalydigin (**2**).^[5] Tirandamycin A and B, with the chemically stable 2,6-dioxabicyclononane structure, have been extensively studied and their total syntheses have already established by several groups,^[2] whereas synthetic studies of streptolydigin (**1**) and tirandalydigin (**2**), both of which bear the chemically labile vinyl epoxide moiety, are quite few. Indeed, the only synthesis of streptolic acid (**3**), the degradation product from **1** and **2** and the most potent member of the small family of 3-acyltetramic acid antibiotics, has been reported by Ireland and Smith.^[2f]

We report herein a new synthetic methodology for streptolydigin (**1**) and tirandalydigin (**2**) that culminates in the first synthesis of the latter antibiotic, as well as a highly stereoselective synthesis of streptolic acid (**3**). Synthetic challenges posed by **1** and **2** include construction of the stereochemically dense 2,6-dioxabicyclononane skeleton, including the extremely acid-labile vinyl epoxide moiety, and synthesis of the distinctive tetramic acid structures. In particular, stereoselective synthesis of the common 2,6-dioxabicyclononane system and construction of the vinyl epoxide moiety are key challenges in the synthesis, since the generally used acid-catalyzed intramolecular acetalization of keto diol precursors has been known not to be effective in the synthesis of the tetramic acid antibiotics.^[2d,h]

[*] Y. Iwata, N. Maekawara, Dr. K. Tanino, Prof. Dr. M. Miyashita
Division of Chemistry, Graduate School of Science
Hokkaido University, 060-0810 Sapporo (Japan)
Fax: (+81) 11-706-4920
E-mail: miyashita@sci.hokudai.ac.jp

[**] Financial support from the Ministry of Education, Culture, Sports, Science, and Technology, Japan, (a Grant-in-Aid for Scientific Research (A) (No. 12304042), a Grant-in-Aid for Scientific Research (B) (No. 16350049), and a Grant-in-Aid for Scientific Research on Priority Areas (A) "Exploitation of Multi-Element Cyclic Molecules" (No. 13029003)) is gratefully acknowledged.



Supporting Information for this article is available on the WWW under <http://www.angewandte.org> or from the author.

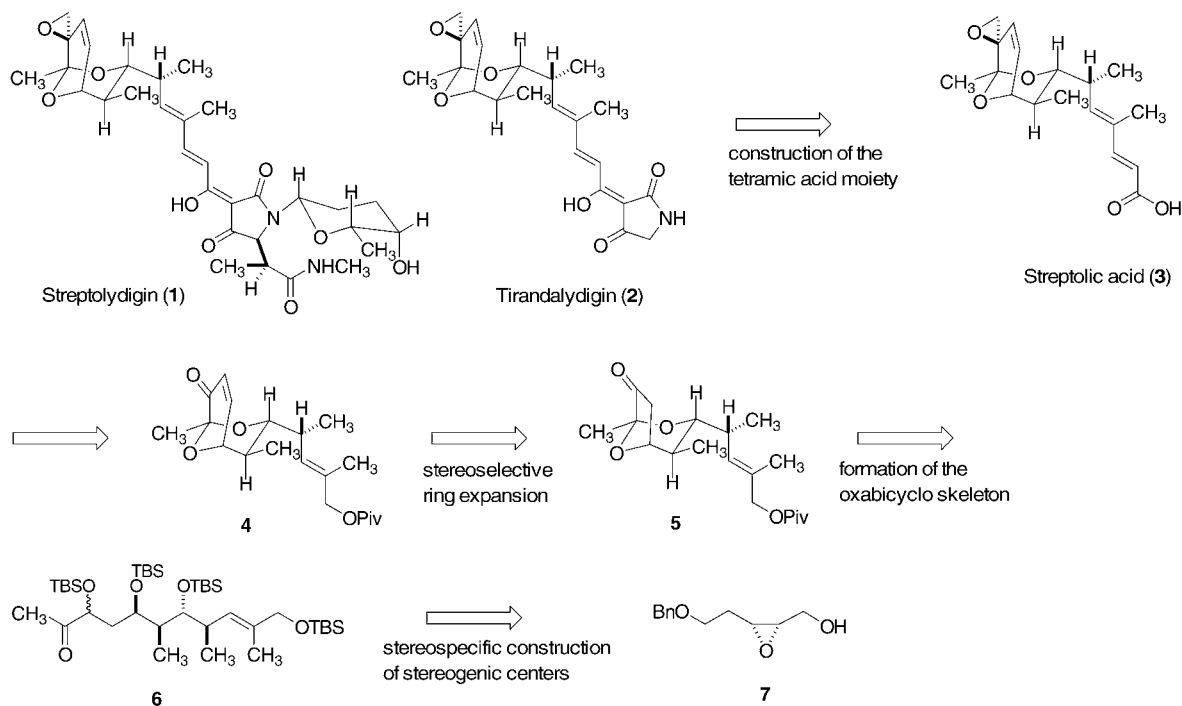
To overcome these difficulties, we designed the synthetic strategy as shown in Scheme 1. This strategy involves a key 2,6-dioxabicyclonon-7-one intermediate **4** that would be derived from a synthetically more accessible dioxabicyclooctanone **5** by a stereoselective ring expansion. We anticipated that the critical intermediate **5** could be efficiently constructed by the acid-catalyzed intramolecular acetalization of the precursor **6**.

Our first objective focused on the stereoselective synthesis of the key precursor **5** for construction of the 2,6-dioxabicyclononane skeleton. At first, the requisite acyclic compound **6** with four contiguous stereogenic centers was synthesized from the known chiral compound **7** in a highly stereoselective manner according to the method shown in Scheme 2. Thus, the epoxy alcohol **7** was converted into epoxy unsaturated ester **8** in 81% yield by a Swern oxidation followed by a Horner–Wadsworth–Emmons reaction. The crucial methylation reaction of **8** occurred stereospecifically with a Me_3Al /water system developed in our laboratory^[6] to give rise to a single product, **9**, in 96% yield. Protection of the hydroxy group in **9** with TESCl and subsequent reduction of the ester with DIBAL-H in THF furnished allyl alcohol **10** in high yield. When **10** was treated with *m*CPBA in CH_2Cl_2 , the single α -epoxy alcohol **11** was obtained as expected in 88% yield.^[7] The epoxy alcohol **11** was then transformed into epoxy unsaturated ester **12** by a three-step reaction sequence involving oxidation with PDC in $\text{ClCH}_2\text{CH}_2\text{Cl}$ to form the corresponding aldehyde, followed by a Wittig reaction in a one-pot operation, and then removal of the TES group with TBAF in THF (79% yield over three steps). The next key methylation reaction of **12** also proceeded stereospecifically upon treatment with a Me_3Al /water system,^[6] to give rise to a single product, **13**, in 90% yield. Thus, fragment **13** with four contiguous stereogenic centers was synthesized in a straight-

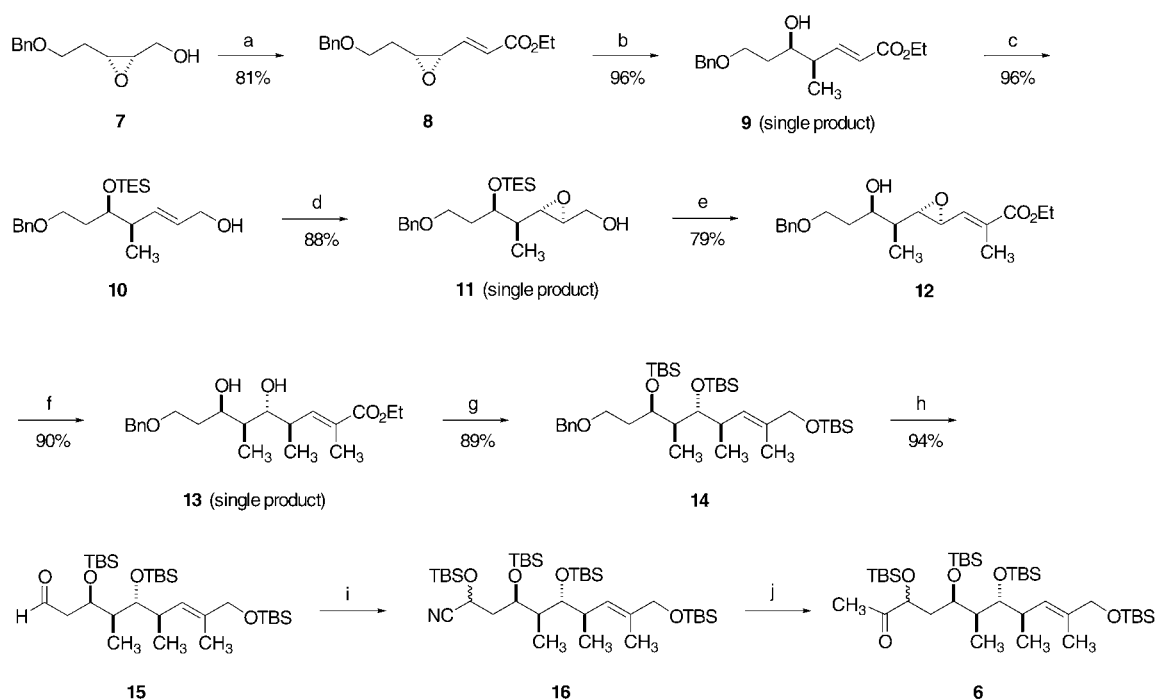
forward and highly stereoselective manner by our original strategy and methodology.

Compound **13** was readily transformed into **14** in three steps: 1) protection of the secondary hydroxy groups with TBSOTf, 2) reduction of the ester with DIBAL-H, and 3) protection of the primary alcohol with TBSCl (89% yield over three steps). When **14** was treated with LDBB in THF and then with Dess–Martin periodinane in the presence of pyridine in CH_2Cl_2 , the desired aldehyde **15** was obtained in 94% yield. The crucial acyclic precursor **6** was successfully derived from aldehyde **15** by treatment with TBSCN and ZnI_2 ,^[8] which led to cyanohydrin **16**, followed by an addition of MeLi to the nitrile group in THF. The product **6** was a diastereomeric mixture with respect to the configuration of the silyloxy group.

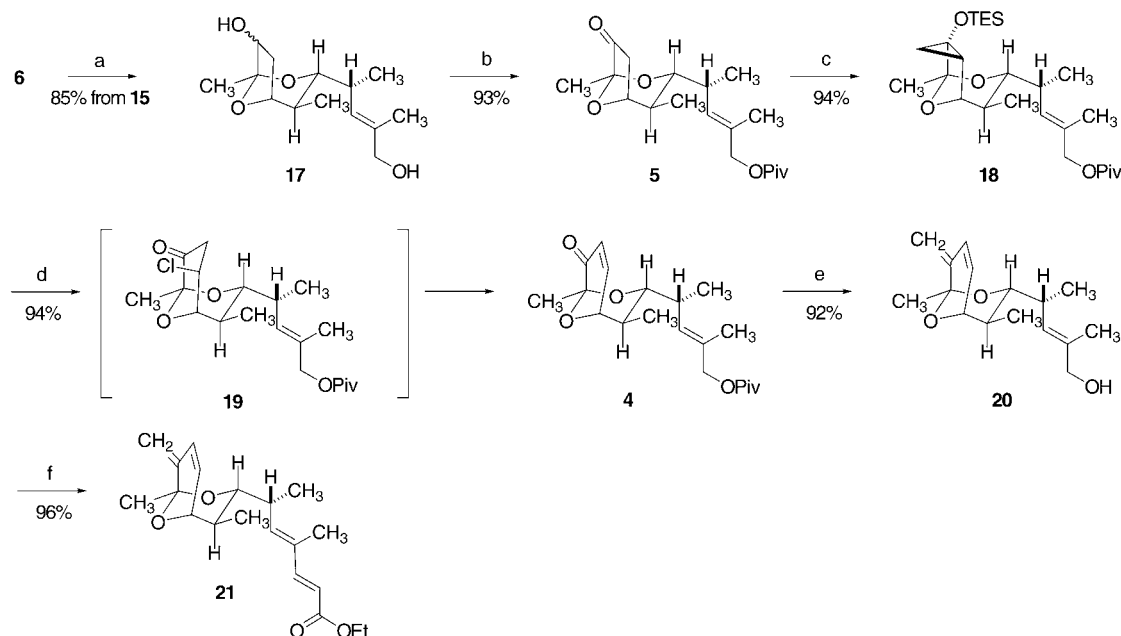
The acid-catalyzed intramolecular acetalization of **6** to form the crucial 2,6-dioxabicyclooctane skeleton proceeded very efficiently as we expected (Scheme 3). Thus, when **6** was treated with aqueous HF in CH_3CN at room temperature, the intramolecular acetalization occurred smoothly and cleanly, to give rise to **17** in 85% overall yield from **15**. After protection of the primary alcohol in **17** as a pivalate moiety, oxidation of the secondary alcohol with Dess–Martin periodinane furnished the desired 2,6-dioxabicyclooctanone **5** in 93% yield. With the critical precursor in hand, we next focused on the ring expansion of **5** to form the dioxabicyclononane skeleton **4**, the key step in the present synthesis. The key transformation was efficiently and highly stereoselectively performed by using the Ito–Saegusa method,^[9] which involves the following three-step reaction sequence: 1) preparation of the silyl enol ether by treatment of **5** with KHMDS and TESCl, 2) cyclopropanation with Et_2Zn and CH_2I_2 to form **18**, and 3) subsequent treatment of **18** with FeCl_3 (88% yield over three steps). Thus, the targeted 2,6-dioxabicyclo-



Scheme 1. Retrosynthetic analysis of streptolic acid (**3**) and tirandalydigin (**2**). Piv = pivaloyl, TBS = *tert*-butyldimethylsilyl, Bn = benzyl.



Scheme 2. Highly stereoselective synthesis of the acyclic precursor **6**. Reagents and conditions: a) 1. Swern oxidation; 2. $(\text{EtO})_2\text{P}(\text{O})\text{CH}_2\text{CO}_2\text{Et}$, NaH, THF, 0°C , 81% (2 steps); b) Me_3Al , D_2O , CH_2Cl_2 , $-30 \rightarrow -10^\circ\text{C}$, 96%; c) 1. TESCl, imidazole, DMAP, CH_2Cl_2 , room temperature; 2. DIBAL-H, THF, 0°C , 96% (2 steps); d) *m*CPBA, CH_2Cl_2 , 0°C , 88%; e) 1. PDC, MS4A, $\text{ClCH}_2\text{CH}_2\text{Cl}$, 60°C , then $\text{Ph}_3\text{P}=\text{C}(\text{CH}_3)\text{CO}_2\text{Et}$, 0°C , 79%; 2. TBAF, THF, 0°C , 100%; f) Me_3Al , D_2O , CH_2Cl_2 , $-30 \rightarrow -10^\circ\text{C}$, 90%; g) 1. TBSOTf, 2,6-lutidine, CH_2Cl_2 , 0°C , 93%; 2. DIBAL-H, THF, 0°C , 98%; 3) TBSCl, imidazole, DMAP, CH_2Cl_2 , 0°C , 98%; h) 1. LDBB, THF, $-78 \rightarrow -45^\circ\text{C}$, 99%; 2. Dess–Martin periodinane, pyridine, CH_2Cl_2 , room temperature, 95%; i) TBSCl, ZnI_2 , room temperature; j) MeLi, THF, -78°C , then aq. HCl. THF = tetrahydrofuran, TES = triethylsilyl, DMAP = 4-(dimethylamino)pyridine, DIBAL-H = diisobutylaluminum hydride, *m*CPBA = 3-chloroperoxybenzoic acid, PDC = pyridinium dichromate, MS4A = molecular sieves (4 Å), $\text{ClCH}_2\text{CH}_2\text{Cl}$ = dichloroethane, TBAF = tetrabutylammonium fluoride, OTf = trifluoromethanesulfonate, LDBB = lithium di-*tert*-butylbiphenylide.



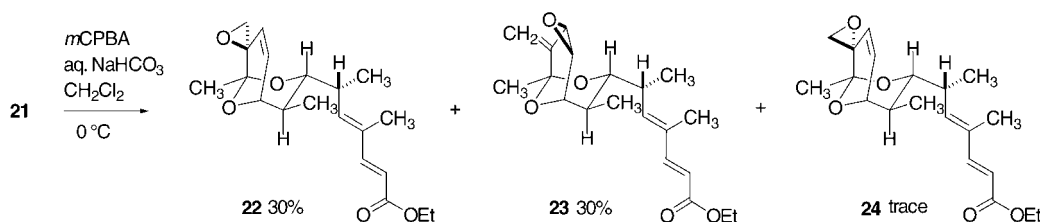
Scheme 3. Stereoselective ring expansion leading to the key dioxabicyclo compound, **4**. Reagents and conditions: a) aq. HF, CH_3CN , room temperature, 85% from **15**; b) 1. PivCl, pyridine, CH_2Cl_2 , 0°C ; 2. Dess–Martin periodinane, H_2O , pyridine, CH_2Cl_2 , room temperature, 93% (2 steps); c) 1. KHMDS, TESCl, THF, -78°C ; 2. Et_2Zn , CH_2I_2 , Et_2O , reflux, 94% (2 steps); d) 1. FeCl_3 , pyridine, DMF, 100°C , 94%; e) 1. $\text{Bu}_3\text{SnCH}_2\text{Li}$, THF, -78°C , then MeLi; 2. aq. HF, CH_3CN , room temperature, 92% (2 steps); f) 1. MnO_2 , CH_2Cl_2 , room temperature; 2. $(\text{EtO})_2\text{P}(\text{O})\text{CH}_2\text{CO}_2\text{Et}$, NaH, THF, room temperature, 96% (2 steps). Piv = pivaloyl, KHMDS = potassium hexamethyldisilazide, DMF = *N,N*-dimethylformamide, $\text{Bu}_3\text{SnCH}_2\text{Li}$ = (tributylstannyll) methylolithium.

nonane skeleton **4** could be highly efficiently and stereoselectively secured by the ring-expansion strategy. The next task was introduction of the vinyl epoxide moiety. For this purpose, the enone **4** was initially transformed into diene **20** in three steps: 1) treatment with (tributylstannyl)methyl-lithium^[10] in THF, 2) then treatment with MeLi to remove the pivaloyl group, and 3) formation of the *exo* methylene group by treatment with HF in CH₃CN (92% over three steps). Compound **20** was routinely converted into **21** in 96% yield by MnO₂ oxidation followed by a Horner–Wadsworth–Emmons reaction. Notably, every step depicted in Scheme 3 proceeded with excellent (more than 90%) yields.

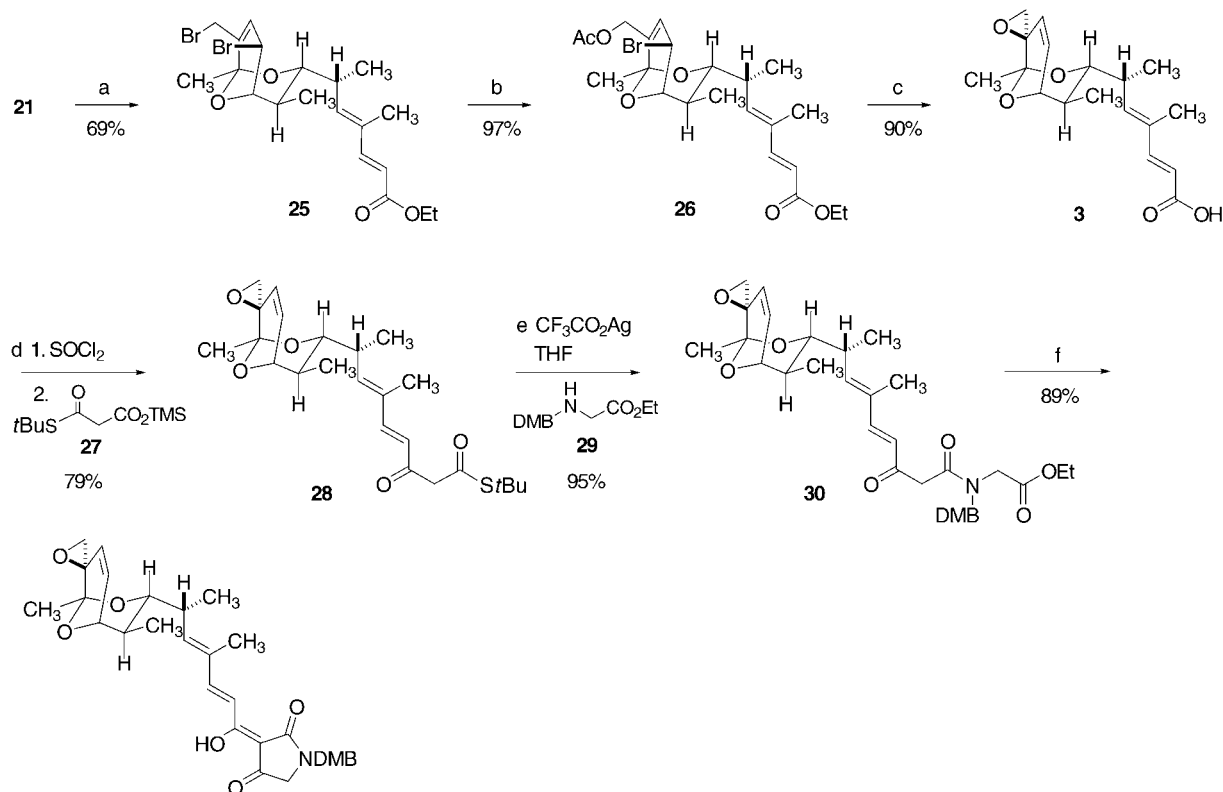
We had reached a critical stage in the total synthesis of streptolic acid (**3**) and tirandalydigin (**2**), that is, the stereoselective epoxidation of the *exo* double bond and installation of the tetramic acid moiety. To this end, we examined direct epoxidation of **21** to form **22**; however, as shown in Scheme 4,

the epoxidation of **21** with *m*CPBA only formed the desired streptolic acid ethyl ester (**22**) in low yield.

To overcome this difficulty and to secure the synthesis of **22**, we designed the synthetic route shown in Scheme 5. Thus, upon treatment of **21** with Bu₄NBr₃ and 2,6-lutidine in ClCH₂CH₂Cl, allyl dibromide **25** was produced stereoselectively in 69% yield; this compound was then transformed into acetate **26** by treatment with CsOAc in DMF in 97% yield. When compound **26** was treated with K₂CO₃ in MeOH and then with NaH in THF, streptolic acid ethyl ester (**22**) was formed almost quantitatively. Subsequent hydrolysis of **22** with aqueous NaOH in MeOH furnished streptolic acid (**3**) in 92% yield. The product was identical to natural streptolic acid in all respects, including melting point (m.p. = 163–164°C; literature value: m.p. = 168–169°C^[2f]), specific rotation ($[\alpha]_D^{24} = +139^\circ$ ($c = 1.18$, 95% EtOH); literature value:



Scheme 4. Unsuccessful epoxidation of **21** with *m*CPBA.



N-2,4-Dimethoxybenzyl tirandalydigin (31)

Scheme 5. Synthesis of streptolic acid (**3**) and *N*-2,4-dimethoxybenzyl tirandalydigin (**31**). Reagents and conditions: a) Bu₄NBr₃, 2,6-lutidine, ClCH₂CH₂Cl, room temperature, 69%; b) CsOAc, DMF, room temperature, 97%; c) 1. K₂CO₃, MeOH, 0°C; 2. NaH, THF, room temperature, 98% (2 steps); 3. aq. NaOH, MeOH, room temperature, 92%; d) 1. SOCl₂, 2,6-lutidine, CH₂Cl₂, room temperature; 2. NaH, **27**, THF, room temperature, 79% (2 steps); e) **29**, CF₃CO₂Ag, Et₃N, MS4A, THF, room temperature, 95%; f) TBAF, THF, room temperature, 89%. DMB = 2,4-dimethoxybenzyl, Bu₄NBr₃ = tetrabutylammonium tribromide, CsOAc = cesium acetate.

$[\alpha]_D^{22} = +138^\circ$ ($c = 0.55$, 95% EtOH)^[2f], and ^1H and ^{13}C NMR, IR, and mass spectra.^[2f]

The crucial construction of the tetramic acid moiety for the total synthesis of tirandalydigin was performed by employing the protocol of Ley et al.^[11] Thus, initially, streptolic acid (**3**) was converted into keto thiolester **28** in two steps: 1) treatment with SOCl_2 leading to the acid chloride and 2) condensation of the acid chloride with **27** by the use of NaH in THF (79% for two steps). Upon treatment of **28** with *N*-2,4-dimethoxybenzyl glycine ethyl ester (**29**), Et_3N , and silver trifluoroacetate in THF, the desired product **30** was obtained in 95% yield; this product was then treated with TBAF in THF to afford the target compound, *N*-2,4-dimethoxybenzyl tirandalydigin (**31**), in 89% yield.^[12] The synthesis of **31** was unambiguously confirmed by its spectral data, including the ^1H and ^{13}C NMR, IR, and mass spectra. The total yield of **31** was 9.8% (an average of 94% yield for each step) in 37 steps from the starting material **7**.

In summary, we have developed a new and promising synthetic methodology for the synthesis of the tetramic acid family of antibiotics and have completed the first synthesis of *N*-2,4-dimethoxybenzyl tirandalydigin (**31**), as well as the synthesis of streptolic acid (**3**), in a highly stereoselective manner.

Received: October 14, 2004

Published online: January 28, 2005

Keywords: antibiotics · asymmetric synthesis · methylation · natural products · stereoselectivity

39, 3775; d) K. Komatsu, K. Tanino, M. Miyashita, *Angew. Chem.* **2004**, *43*, 4441; *Angew. Chem. Int. Ed.* **2004**, *43*, 4341.

- [7] K. Maruyama, M. Ueda, S. Sasaki, Y. Iwata, M. Miyazawa, M. Miyashita, *Tetrahedron Lett.* **1998**, *39*, 4517.
- [8] a) D. A. Evans, L. K. Truesdale, *Tetrahedron Lett.* **1973**, *49*, 4929; b) D. A. Evans, L. K. Truesdale, G. L. Carrol, *J. Chem. Soc. Chem. Commun.* **1973**, 55.
- [9] Y. Ito, S. Fujii, T. Saegusa, *J. Org. Chem.* **1976**, *41*, 2073.
- [10] K. Thomas, K. Reinhard, A. Bruno, S. Fritz, *Chem. Ber.* **1982**, *115*, 1810.
- [11] S. V. Ley, S. C. Smith, P. R. Woodward, *Tetrahedron* **1992**, *48*, 1145.
- [12] Although removal of the *N*-2,4-dimethoxybenzyl group in **31**, leading to tirandalydigin (**2**), was examined under various conditions, this transformation has not been successful so far because of the susceptibility of the vinyl epoxide moiety to acidic conditions. We will discuss the removal of the protective group in detail in a full paper.

- [1] a) K. L. Rinehart, Jr., D. B. Borders, *J. Am. Chem. Soc.* **1963**, *85*, 4037; b) F. Reusser, *Antimicrob. Agents Chemother.* **1976**, *10*, 618; c) J. P. Karwowski, M. Jackson, R. J. Theriault, G. J. Barlow, L. Coen, D. M. Hensey, P. E. Humphrey, *J. Antibiot.* **1992**, *45*, 1125.
- [2] a) R. E. Ireland, P. G. M. Wutz, B. Ernst, *J. Am. Chem. Soc.* **1981**, *103*, 3205; b) R. H. Schlessinger, G. R. Bebernitz, P. Lin, *J. Am. Chem. Soc.* **1985**, *107*, 1777; c) P. DeShong, S. Ramesh, V. Elango, J. J. Perez, *J. Am. Chem. Soc.* **1985**, *107*, 5219; d) R. K. Boeckman, Jr., J. E. Starrett, Jr., D. G. Nickell, P. E. Sum, *J. Am. Chem. Soc.* **1986**, *108*, 5549; e) C. Neukom, D. P. Richardson, J. H. Myerson, P. A. Bartlett, *J. Am. Chem. Soc.* **1986**, *108*, 5559; f) R. E. Ireland, M. G. Smith, *J. Am. Chem. Soc.* **1988**, *110*, 854; g) S. F. Martin, C. Gluchowski, C. L. Campbell, R. C. Chapman, *Tetrahedron* **1988**, *44*, 3171; h) S. Ikegami, T. Katsuki, M. Yamaguchi, *Tetrahedron Lett.* **1988**, *29*, 5285; i) I. Paterson, M. A. Lister, G. R. Ryan, *Tetrahedron Lett.* **1991**, *32*, 1749.
- [3] a) C. E. Meyer, *J. Antibiot.* **1971**, *24*, 558; b) H. Hagenmaier, K. H. Jaschke, L. Santo, M. Scheer, H. Zaehner, *Arch. Microbiol.* **1976**, *109*, 65.
- [4] a) T. E. Elbe, C. M. Large, W. H. DeVries, G. F. Crum, J. W. Shell, *Antibiotics Annual 1955–56*, Medical Encyclopedia, New York, **1956**, p. 893; b) K. L. Rinehart, Jr., J. R. Beck, D. B. Borders, T. H. Kinstle, D. Krauss, *J. Am. Chem. Soc.* **1963**, *85*, 4038; c) D. J. Duchamp, A. R. Branfman, A. C. Button, K. L. Rinehart, Jr., *J. Am. Chem. Soc.* **1973**, *95*, 4077.
- [5] G. M. Brill, J. B. McAlpine, D. J. Whittern, *J. Antibiot.* **1988**, *41*, 36.
- [6] a) M. Miyashita, M. Hoshino, A. Yoshikoshi, *J. Org. Chem.* **1991**, *56*, 6483; b) M. Miyashita, T. Shiratani, K. Kawamine, S. Hatakeyama, H. Irie, *Chem. Commun.* **1996**, 1027; c) N. Ishibashi, M. Miyazawa, M. Miyashita, *Tetrahedron Lett.* **1998**,

Photosynthesis Models

A Biomimetic Model of the Electron Transfer between P_{680} and the TyrZ–His190 Pair of PSII**

Fabien Lachaud, Annamaria Quaranta, Yann Pellegrin, Pierre Dorlet, Marie-France Charlot, Sun Un, Winfried Leibl,* and Ally Aukauloo**

In memory of G. T. Babcock

The tyrosyl/tyrosine redox couple has been well established as a crucial cofactor for several enzymatic systems.^[1] In the case

[*] F. Lachaud, Y. Pellegrin, Dr. P. Dorlet, Dr. M.-F. Charlot, Prof. Dr. A. Aukauloo
Laboratoire de Chimie Inorganique
Bât. 420, Université Paris-Sud
91405 Orsay (France)
Fax: (+33) 1-6915-4754
E-mail: pierdorlet@icmo.u-psud.fr
aukauloo@icmo.u-psud.fr

Dr. A. Quaranta, Dr. S. Un, Dr. W. Leibl
Service de Bioénergétique, CEA Saclay
Bât. 532, 91191 Gif-sur-Yvette CEDEX (France)
Fax: (+33) 1-6908-8717
E-mail: leibl@dsvidf.cea.fr

Dr. A. Quaranta
Muséum National d'Histoire Naturelle
Laboratoire de Chimie et de Biochimie des Substances Naturelles
UMR 5154 CNRS/USM 0502 CNRS
63 rue Buffon, 75005 Paris (France)

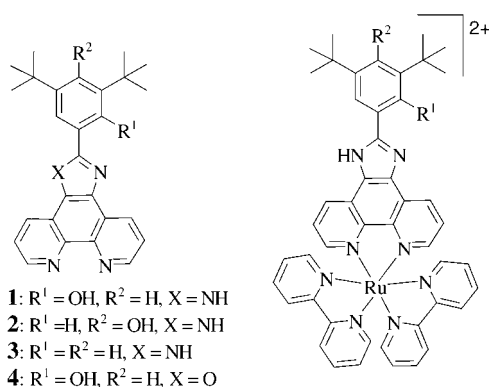
[**] This work was supported by the CNRS (Programme Energie, PRI4), the CEA for the LRC project (LRC-CEA no. 33V), and the European Commission (STRP SOLAR-H 516510). A.Q. acknowledges the European Commission for financial support (contract "Wonderfull" HPRN-CT-2002-00177). We thank the Centre Informatique National de l'Enseignement Supérieur, Montpellier, France for computation time.



Supporting information for this article is available on the WWW under <http://www.angewandte.org> or from the author.

of the photosynthetic reaction center of photosystem II (PSII) it has been argued that a histidine residue (His190) in close proximity to tyrosine Z (TyrZ) is essential to drive electron transfer from TyrZ to the P_{680}^+ primary donor ion; otherwise, the reaction would be energetically unfavorable. The decreased ionization potential of this pair is explained by hydrogen bonding and the proton coupled electron transfer process (PCET).^[2] The recently acquired X-ray crystallographic structure of PSII from the cyanobacterium *Thermosynechococcus elongatus*, shows that the TyrZ and His190 residues in the catalytic state are not coordinated to the metal ions. They are probably not involved in the proton exit from the oxygen evolving complex (OEC), as no hydrogen-bonding chain has been detected that would allow the proton from TyrZ to leave the active site.^[3] In light of the crystallographic data, it appears that the “rocking proton” mechanism between these two amino acids is favored in the electron transfer steps of the PSII catalytic cycle.

A synthetic model of PSII has recently been proposed, in which a $[Ru(bpy)_3]^{2+}$ chromophore plays the role of P_{680} .^[4] Photoinduced electron transfer from a covalently attached modified tyrosine residue to the bipyridine group has been shown, but direct evidence for the influence that both the hydrogen bond and the Ru^{II} metal ion have on the electrochemical properties of the modified tyrosine has not yet been established. Herein we report a new molecular system that serves as a closer biomimetic model for the TyrZ–His190 pair (a hydrogen-bonded phenol–imidazole interaction). The model is attached to a chelating phenanthroline group, which serves as an anchoring site for the photoactive Ru^{II} chromophore (compound **1**). Compounds **2–4** have been studied to account for the physical behavior of the parent compound **1**. The corresponding Ru-**1**–Ru-**3** complexes were prepared, and their electrochemical and photophysical properties were studied. The family of ligands was synthesized by



following the procedure of Steck and Day (Supporting Information).^[5] Compound **4** was obtained as a by-product in the synthesis of **1**.

Regardless of solvent polarity, the electronic spectrum of **1** shows a distinct structured absorption band between 300 and 380 nm, indicative of a rigid molecular framework. This supports the fact that the two aromatic rings adopt a coplanar orientation in solution through a strong intramolecular

hydrogen bond between the phenolic OH group and the imidazole nitrogen atom.^[6] This is confirmed by the 1H NMR spectrum of **1** in $[D_6]DMSO$, in which a dissymmetry of the phenanthroline protons is apparent. In the solid state, the presence of intramolecular hydrogen bonding is supported by the absence of OH group vibration characteristics in the IR spectrum of **1**; indeed these features are present in the IR spectroscopy data for **2** (Supporting Information).

Cyclic voltammograms (CV) of **1** and **4** in CH_2Cl_2 show a first oxidation process (E_{pa}) at 0.90 and 1.10 V versus standard calomel electrode (SCE) respectively, which corresponds to the process of phenoxyl radical formation from phenol. These values are lower than those observed for hydrogen-bond-free phenol,^[7] and are consistent with previous examples in which the phenolic OH group is hydrogen bonded to a nearby base.^[8] The difference in the E_{pa} values for **1** and **4** can be explained by the higher basicity of the imidazole group relative to oxazole. Under the experimental conditions reported herein, the first electron-transfer process was found to be quasireversible in nature. Cathodic shifts in the oxidation potentials were observed in CV experiments performed under basic conditions (1 equivalent NBu_4OH), which indicates the greater ease with which phenolate groups oxidize. Interestingly, a lower potential was observed for 4^{1-} (+0.18 V) than for 1^{1-} (+0.30 V), which can be rationalized by the presence of a hydrogen bond between the imidazole proton and the deprotonated phenol in 1^{1-} . Moreover, the higher values for the oxidation of 1^{1-} , 2^{1-} (0.00 V), and 4^{1-} relative to the reference compound 2,4,6-tri-(*tert*-butyl)phenolate imply a decreased electron density on the phenol ring, and thus partial delocalization on the imidazole or oxazole groups.

Ruthenium complexes Ru-**1**, Ru-**2** and Ru-**3** were synthesized and characterized by standard spectroscopic techniques (Supporting Information). The electrochemical data are given in Table 1. On the cathodic side of the CV during the scan

Table 1: Half-wave potentials for the oxidation (iE) and reduction (nE) of Ru-**1**, Ru-**2**, and Ru-**3**.^[a]

Compound	iE	iE	iE	$^nE^{[b]}$	nE
Ru- 1	−1.60	−1.40	0.58	1.08	1.29
Ru- 2	−1.63	−1.41	0.38 ^[b]	1.09	1.40
Ru- 3	−1.63	−1.41		1.10	1.40

[a] Determined by CV at 100 mVs^{-1} in CH_2Cl_2 ; $E = 1/2(E_{pa} + E_{pc})$ in V versus SCE in the presence of $TBAClO_4$. TBA = tetra-*n*-butylammonium.

[b] Nonreversible.

down to −1.9 V versus SCE, only two redox waves were observed instead of the three one-electron reduction processes that are typical for $[Ru(bpy)_3]^{2+}$ under the same conditions. This indicates that the modified phenanthroline end is less-readily reduced owing to the electron-rich imidazole ring. No electronic influence was observed on the $Ru^{III/II}$ couple at 1.26 V, a typical value for a ruthenium(II) trisbipyridine complex. However, the most interesting feature of the CV is the first reversible oxidation wave (+0.52 V versus SCE) which corresponds to the oxidation of the phenol group. The shift toward a less-positive potential for the same

process relative to the free ligand can be interpreted as a weakening of the O–H bond through an inductive effect of the Ru^{II} ion. Furthermore, the reversible nature of this wave may imply that the coordinated phenanthroline cavity cannot play the role of a proton trap, as is the case of the free ligand. Hence, as mentioned before, this is a clear example in which the presence of a divalent cation (Ru^{II} ; not directly coordinated to a phenol moiety), together with a hydrogen-bonded phenol group, lowers the oxidation potential of the phenoxyl/phenol couple by more than 300 mV. The second wave at 1.1 V was assigned to the oxidation of the imidazole ring, and was confirmed by the CV of Ru-3. The electrochemical behavior of Ru-1 is supported by density functional theory (DFT) calculations, which were carried out with the hybrid functional B3LYP^[9] as implemented in the Gaussian98 program^[10] and a LanL2DZ^[11] effective potential basis for all atoms. The geometry of the complex was optimized starting from the totally optimized geometry of the constitutive ligands. Indeed, the calculated HOMO for Ru-1 is localized primarily on the phenol ring.

The singly oxidized species of Ru-1 and Ru-2 (Ru-1^\bullet and Ru-2^\bullet , respectively) were prepared electrochemically and characterized by high-field/high-frequency EPR spectroscopy. Figure 1 shows the spectra obtained at 285 GHz for

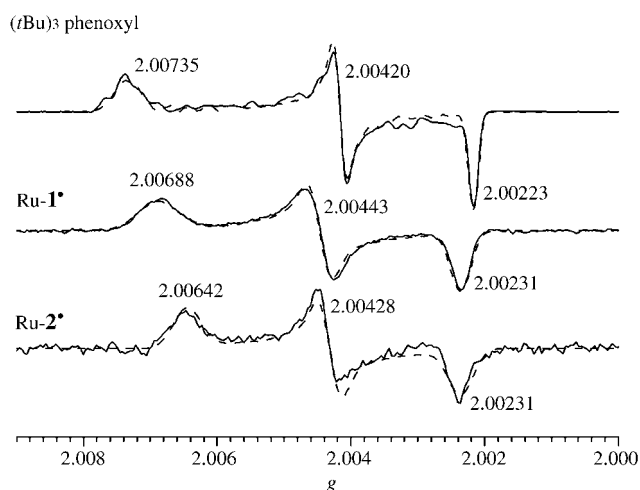


Figure 1. Experimental (solid line) and simulated (dashed line) EPR spectra (285 GHz) of the 2,4,6-tri-(*tert*-butyl)phenoxyl, Ru-1 $^\bullet$, and Ru-2 $^\bullet$ radicals. Ru-1 $^\bullet$ and Ru-2 $^\bullet$ were prepared electrochemically in dichloromethane. The 2,4,6-tri-(*tert*-butyl)phenoxyl radical was prepared by chemical oxidation of 2,4,6-tri-(*tert*-butyl)phenol in CH_3CN solution with aqueous potassium ferricyanide and sodium hydroxide. Experimental conditions: $\nu_{\text{mw}} = 285.090$ GHz, $T = 4.2$ K, modulation amplitude 0.95 mT.

the solutions of Ru-1 $^\bullet$ and Ru-2 $^\bullet$ together with the simulated spectra. As a reference, the 285-GHz spectrum of the chemically oxidized 2,4,6-tri-(*tert*-butyl)phenoxyl radicals is shown, which can be considered as a generic model for non-hydrogen-bonded 2,4,6-trisubstituted-phenoxyl radicals. The g anisotropy for these radicals is clearly resolved at 285 GHz, and the g values obtained from fitting the data are indicated. The g values for Ru-1 $^\bullet$ and Ru-2 $^\bullet$ are indeed close to those of the 2,4,6-tri-(*tert*-butyl)phenoxyl radical, and confirm that the

phenol portion of the ligand is, in fact, the locus of oxidation. The smaller g_x value observed for Ru-2 $^\bullet$ relative to Ru-1 $^\bullet$ can be attributed to the more delocalized spin density in the case of Ru-2 $^\bullet$. A more detailed HFEPR study regarding the influence of the hydrogen bond and the inductive effect of the Ru^{II} ion on the g values of the phenoxyl radical in this type of complex is currently underway.

The electronic absorption spectrum of Ru-1 is shown in Figure 2. The spectrum shows features both of the ligand and

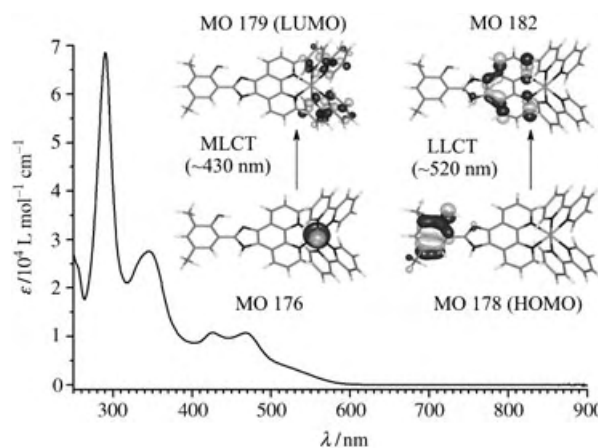


Figure 2. Electronic spectrum of Ru-1 in CH_2Cl_2 and the calculated frontier molecular orbitals involved in the calculated MLCT and LLCT transitions (see text).

the ruthenium chromophore. Preliminary results from time-dependent DFT (TD DFT) calculations^[12] confirmed that the MLCT band from the t_{2g} orbitals of Ru^{II} to the bpy^* -based MOs falls within the 450-nm wavelength range observed for $[\text{Ru}(\text{bpy})_3]^{2+}$. Through our calculations, we attribute the shoulder observed to the MLCT band that tails up to 570 nm to a ligand–ligand charge transfer from the phenol extremity (MO178: HOMO) to the coordinating phenanthroline (MO182: LUMO + 3). The MOs involved for these transitions are shown in Figure 2.

Upon excitation in the MLCT band, Ru-1, Ru-2, and Ru-3 show an emission band that peaks at ≈ 600 nm, with quantum yields and lifetimes (≈ 1 μs) similar to those for $[\text{Ru}(\text{bpy})_3]^{2+}$. In the region investigated, the transient absorption spectra of the three complexes also exhibit the typical depletion band at 450 nm, which corresponds to the absorption maximum of the MLCT band of $[\text{Ru}(\text{bpy})_3]^{2+}$. This suggests that the excited state of these complexes is similar to that of $[\text{Ru}(\text{bpy})_3]^{2+}$, despite the differences in the coordinated ligand. There is no evidence of intramolecular reactions that occur between the chromophore and the ligand, as expected from the electron-donating character of the phenol–imidazole groups.

To investigate whether the oxidized state of the chromophore is able to oxidize the ligand, electron-transfer experiments in the presence of MV^{2+} as an external electron acceptor were performed (MV = methyl viologen). The transient absorption spectra of Ru-1, Ru-2, and Ru-3 are dominated by the strong absorption of $\text{MV}^{\bullet+}$, with peaks at 390 nm and 600 nm. However, $\text{MV}^{\bullet+}$ has an absorption

minimum at 450 nm, where the recovery of the ground-state absorption of the chromophore could be monitored. The positive absorption changes that occur in the traces at 450 nm for Ru-1 and Ru-2 are reminiscent of the formation of a phenoxyl radical. The kinetics for all complexes show a recovery of the reduced state of the chromophore within 0.5 μ s (Figure 3). This is much faster than the decay of MV²⁺,

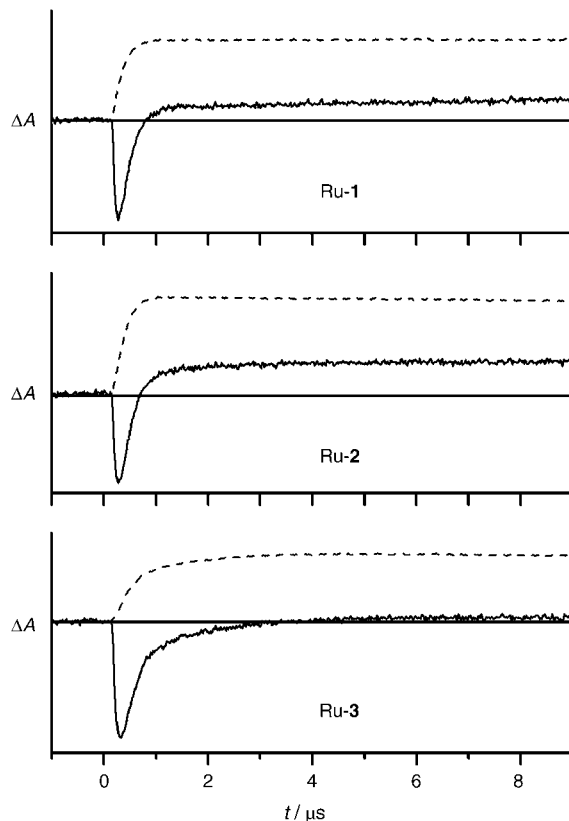


Figure 3. Time-resolved absorption changes at 600 nm (dashed lines) and 450 nm (solid lines) of complexes Ru-1, Ru-2, and Ru-3 upon excitation with nanosecond laser flashes at 355 nm in aqueous, Ar-saturated solution (HEPES, 10 mM, pH 7). MV²⁺ (10 mM) was present as an external electron acceptor.

which occurs in about 200 μ s, as monitored at 600 nm. This indicates that the reduction of Ru^{III} to Ru^{II} is the result of an electron transfer from an electron-donating group on the ligand. The apparent kinetics of the recovery phase of the absorption at 450 nm is similar to the rate of electron transfer from the chromophore to MV²⁺, which indicates that formation of the Ru^{III} oxidation state is rate limiting and that the intrinsic rate of intramolecular electron transfer is faster.

An ethanolic solution of Ru-1 was irradiated with white light in the presence of excess [Co(NH₃)₅Cl]²⁺, an irreversible electron acceptor in water. The EPR spectrum (9 GHz) of the frozen sample exhibits a single line centered at $g_{\text{iso}} = 2.004$ (Figure 4), with no resolved hyperfine structure and a peak-to-trough width of 0.9 mT. This is in good agreement with EPR spectra obtained for hydrogen-bonded phenoxyl radical^[8] and the 9-GHz spectrum of the electrolyzed sample of

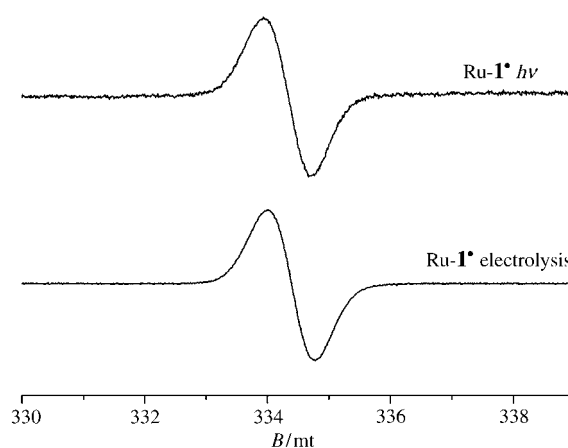


Figure 4. EPR spectra (9 GHz) of the photogenerated (top) and electrochemically prepared (bottom) Ru-1[•] radicals. Experimental conditions: $\nu_{\text{mw}} = 9.38009$ GHz (top), $\nu_{\text{mw}} = 9.38225$ GHz (bottom), $P_{\text{mw}} = 16$ μ W, modulation amplitude 0.4 mT, modulation frequency 100 kHz, $T = 100$ K.

Ru-1[•] characterized by HFEPR (Figure 1). The low concentration of the photogenerated radical did not permit the observation of the EPR signal at 285 GHz. However, the isotropic g value determined with the 9-GHz spectrum and the comparison with the spectrum of Ru-1[•] obtained by preparative electrolysis are fully consistent with a phenoxyl radical.

The EPR signature of the radical formed under photoaccumulation in conjunction with the positive absorption changes at 450 nm for times over 1 μ s clearly show a photoinduced electron transfer from a hydrogen-bonded phenol-imidazole pair to generate a phenoxyl radical. Further work with systems in which this phenol-imidazole pair is used as an electron relay between Ru^{II} and a manganese complex is underway.

Experimental Section

Typical procedure: Ru(bpy)₂Cl₂ (100 mg, 0.2 mmol) was treated with AgNO₃ (65.6 mg, 0.4 mmol) in MeOH (5 mL) for 1 h. The AgCl precipitate was filtered off, and the filtrate evaporated to dryness. Ligand **1** (85 mg, 0.2 mmol) was added to the ruthenium salt in MeOH (10 mL) and stirred at reflux for 3 h. The solvent was removed by rotary evaporation and the crude product was purified by column chromatography on neutral alumina (CH₂Cl₂/MeOH 90:10) to afford Ru-1 (102 mg, 61 %) as an orange solid. IR (KBr): $\tilde{\nu} = 2950$ (C–H), 1713 (C=N), 1360 cm^{−1} (N=O, NO₃[−]); UV/Vis (CH₂Cl₂): λ_{max} (ϵ) = 290 (68500), 345 (27800), 430 (10750), 465 (10650), 520 nm (3800); ¹H NMR (250 MHz, [D₆]DMSO): $\delta = 8.99$ (d, 2H), 8.85 (t, 4H), 8.29 (d, 1H), 8.19 (t, 2H), 8.08 (t, 2H), 7.84 (d, 2H), 7.80 (d, 2H), 7.75 (d, 1H), 7.70 (d, 1H), 7.57 (dd, 4H), 7.36 (t, 2H), 7.18 (d, 1H), 1.46 (s, 9H), 1.34 ppm (s, 9H); ESI MS: m/z (%): 419.0 (100) [M]²⁺; elemental analysis: calcd for C₄₇H₄₄N₁₀O₇Ru: C 58.7, H 4.6, N 14.6; found: C 59.3, H 4.7, N 14.9.

Received: September 10, 2004

Published online: January 28, 2005

Keywords: artificial photosynthesis · biomimetic synthesis · phenoxyl radicals · photochemistry · ruthenium

- [1] J. A. Stubbe, W. A. van der Donk, *Chem. Rev.* **1998**, 98, 705–762.
- [2] a) K. L. Westphal, C. Tommos, R. I. Cukier, G. T. Babcock, *Curr. Opin. Plant Biol.* **2000**, 3, 236–242; b) C. W. Hoganson, G. T. Babcock, *Science* **1997**, 277, 1953–1956.
- [3] K. N. Ferreira, T. M. Iverson, K. Maghlaoui, J. Barber, S. Iwata, *Science* **2004**, 303, 1831–1838.
- [4] a) M. Sjödén, S. Styring, B. Åkermark, L. Sun, L. Hammarström, *J. Am. Chem. Soc.* **2000**, 122, 3932–3936; b) D. Burdinski, K. Wieghardt, S. Steenken, *J. Am. Chem. Soc.* **1999**, 121, 10781–10787.
- [5] E. A. Steck, A. R. Day, *J. Am. Chem. Soc.* **1943**, 65, 452–456.
- [6] M. Mosquera, J. C. Penedo, M. C. Rios Rodriguez, F. Rodriguez-Prieto, *J. Phys. Chem.* **1996**, 100, 5398–5407.
- [7] F. G. Bordwell, J. P. Cheng, *J. Am. Chem. Soc.* **1991**, 113, 1736–1743.
- [8] a) L. Benisvy, A. J. Blake, D. Collison, E. S. Davies, C. D. Garner, E. J. L. McInnes, J. McMaster, G. Whittaker, C. Wilson, *Dalton Trans.* **2003**, 1975–1985; b) T. Maki, Y. Araki, Y. Ishida, O. Onomura, Y. Matsumura, *J. Am. Chem. Soc.* **2001**, 123, 3371–3372.
- [9] a) A. D. Becke, *J. Chem. Phys.* **1993**, 98, 5648–5652; b) C. T. Lee, W. T. Yang, R. G. Parr, *Phys. Rev. B* **1988**, 37, 785–789.
- [10] Gaussian98 (Revision A.7), M. J. Frisch, G. W. Trucks, H. B. Schlegel, G. E. Scuseria, M. A. Robb, J. R. Cheeseman, V. G. Zakrzewski, J. A. Montgomery, R. E. Stratmann, J. C. Burant, S. Dapprich, J. M. Millam, A. D. Daniels, K. N. Kudin, M. C. Strain, O. Farkas, J. Tomasi, V. Barone, M. Cossi, R. Cammi, B. Mennucci, C. Pomelli, C. Adamo, S. Clifford, J. Ochterski, G. A. Petersson, P. Y. Ayala, Q. Cui, K. Morokuma, D. K. Malick, A. D. Rabuck, K. Raghavachari, J. B. Foresman, J. Cioslowski, J. V. Ortiz, B. B. Stefanov, G. Liu, A. Liashenko, P. Piskorz, I. Komaromi, R. Gomperts, R. L. Martin, D. J. Fox, T. Keith, M. A. Al-Laham, C. Y. Peng, A. Nanayakkara, C. Gonzalez, M. Challacombe, P. M. W. Gill, B. G. Johnson, W. Chen, M. W. Wong, J. L. Andres, M. Head-Gordon, E. S. Replogle, J. A. Pople, Gaussian, Inc., Pittsburgh, PA, **1998**.
- [11] a) T. H. Dunning, Jr., P. J. Hay, *Modern Theoretical Chemistry*, Vol. 3, Plenum, New York, **1976**; b) P. J. Hay, W. R. Wadt, *J. Chem. Phys.* **1985**, 82, 270–283; c) P. J. Hay, W. R. Wadt, *J. Chem. Phys.* **1985**, 82, 299–310; d) W. R. Wadt, P. J. Hay, *J. Chem. Phys.* **1985**, 82, 284–298.
- [12] a) M. E. Casida, C. Jamorski, K. C. Casida, D. R. Salahub, *J. Chem. Phys.* **1998**, 108, 4439–4449; b) S. R. Stoyanov, J. M. Villegas, D. P. Rillema, *Inorg. Chem. Commun.* **2004**, 7, 838–841; c) H. Zabri, I. Gillaizeau, C. A. Bigozzi, S. Caramori, M. F. Charlot, J. Cano-Boquera, F. Odobel, *Inorg. Chem.* **2003**, 42, 6655–6666.

C–H Activation of Alkanes and Arenes Catalyzed by an O-Donor Bis(tropolonato)iridium(III) Complex**

Gaurav Bhalla and Roy A. Periana*

Catalysts based on the C–H activation reaction show potential for the development of selective hydrocarbon-oxidation reactions.^[1] One of the key challenges in this field is developing catalysts based on C–H activation that yield functionalized products such as alcohols.^[1g] We have been interested in O-ligated late-transition-metal complexes as a starting point for the development of new hydrocarbon-oxidation catalysts. Although O-donor ligands have been investigated with early and late transition metals,^[2] to our knowledge, the only well-defined O-ligated late-transition-metal complexes that activate alkane and arene C–H bonds have been reported recently by our group.^[3–5] Compared to the N-, C-, or P-donor ligands generally utilized for homogeneous catalysts,^[6] O-donor ligated complexes may have the potential for higher stability under thermal, protic, and oxidation conditions given the lower basicity and higher electronegativity of O atoms. Another important reason for the study of this class of complex is that the unique combination of the higher electronegativity with the π -donor^[7] and “hard” properties of O-donor ligands could allow access to higher oxidation states during catalysis that may be required for the C–H activation as well as for the generation of functionalized products.^[1g]

Recently, we demonstrated that the bis-bidentate O-donor complex $[\text{Ir}(\text{CH}_3)(\text{py})(\text{acac-O,O})_2]$ (acac-O,O = κ^2 -O,O-acetylacetonate, py = pyridine) catalyzes the C–H activation of alkanes^[3] and functionalization of arenes by the intermolecular anti-Markovnikov hydroarylation of olefins to selectively generate *n*-alkyl benzene derivatives.^[4] Experiments and theoretical^[5] calculations reveal that this O-donor octahedral d^6 late-transition-metal complex is stable to air and protic media under thermal conditions and activates the C–H bonds of alkanes and arenes by a transition state that has oxidative-addition or insertion character. This transition state is intriguing as the use of ligands with electronegative O-donor atoms to facilitate this mode of C–H activation may

[*] G. Bhalla, Prof. Dr. R. A. Periana
University of Southern California
Department of Chemistry
Loker Hydrocarbon Research Institute
Los Angeles, CA 90089 (USA)
Fax: (+1) 213-821-2656
E-mail: rperiana@usc.edu

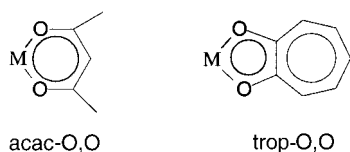
[**] This work was supported by NSF Grant CHE-0328121 and by the ChevronTexaco Energy Technology Co. We thank Dr. William Schinski of ChevronTexaco for helpful discussions. We also acknowledge Dr. Jonas Oxgaard and Prof. W. A. Goddard III for their useful insight.



Supporting information for this article is available on the WWW under <http://www.angewandte.org> or from the author.

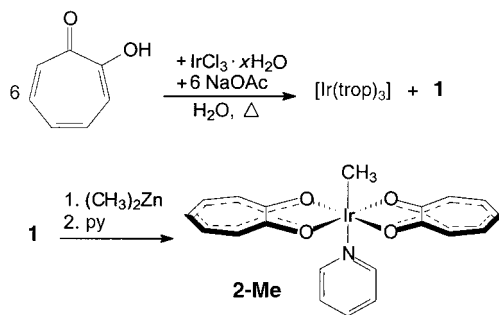
seem contrary to the common guiding principle that such reactions require electron-rich metal centers.^[8] However, one possibility is that the π -donor properties of O-donor ligands may facilitate this mode of C–H activation, whereas the σ -acceptor properties could help to stabilize the complex. This combination of stability and C–H bond reactivity is very attractive for the development of oxidation catalysts based on C–H activation and we are currently exploring the extension of this chemistry to other readily available O-donor ligands such as aryloxides,^[9] tropolones,^[10] catechols,^[11] and hydroxyacetophenones.^[11c]

The O-donor ligand, trop-O,O (trop-O,O = κ^2 -O,O-tropolonato) has often been speculated to be an analogue of the acac-O,O ligand as they share many common features. Both



ligands are bidentate, mono-anionic, and both bond through delocalized chelate rings that are formed through two oxygen atoms. Importantly, however, significant differences in reactivity could be anticipated from the smaller bite angle^[12] as well as increased delocalization over the larger tropolonato aromatic system. Thus, for example, trop-O,O complexes may more readily accommodate an increase in the coordination number at the metal center^[10] or potentially—because of changes in the extent of π donation that results from the differences in bite angle—change the reactivity of the metal center. Rate changes related to differences in ligand bite angle have been reported.^[12a,13] Herein, we report the synthesis and chemistry of the bis-bidentate, O-donor tropolonato iridium complex **2-Me** [Ir(CH₃)(py)(trop-O,O)₂]. Importantly, we find that this O-donor complex is more active for the C–H activation of alkanes and arenes than is the analogous bis-acac-O,O iridium complex.

To obtain the bis trop-O,O complex of iridium, the original synthesis of the tris complex [Ir(trop-O,O)₃] was reinvestigated in anticipation that the bis trop-O,O complex could be isolated as an intermediate in this synthesis.^[14] As reported by Griffith et al.,^[14] heating IrCl₃ with an excess of tropolone and sodium acetate in water resulted in the formation of [Ir(trop-O,O)₃] in 40% yield (Scheme 1). How-



Scheme 1. Synthesis of **2-Me**.

ever, in addition to this material a red–black solid (**1**) was also isolated, which was insoluble in dichloromethane. Attempts to purify **1** or obtain reproducible analytical data for this material were unsuccessful and we presume that the material is polymeric.^[15] The solid **1** is soluble in coordinating solvents such as THF, CH₃CN, DMSO, and pyridine, but NMR spectroscopic studies suggest that multiple species are present. Attempted separation of these species by chromatography was also unsuccessful.^[16] However, the addition of [Zn(CH₃)₂] to a solution of **1** in THF followed by the addition of pyridine, resulted in a black organometallic complex [Ir(CH₃)(py)(trop-O,O)₂] (**2-Me**), which could be obtained in 10% overall yield after column chromatography (Scheme 1). This material has been fully characterized by ¹H and ¹³C NMR spectroscopy, elemental analysis, and single-crystal X-ray diffraction.^[17] An ORTEP drawing of **2-Me** is shown in Figure 1.

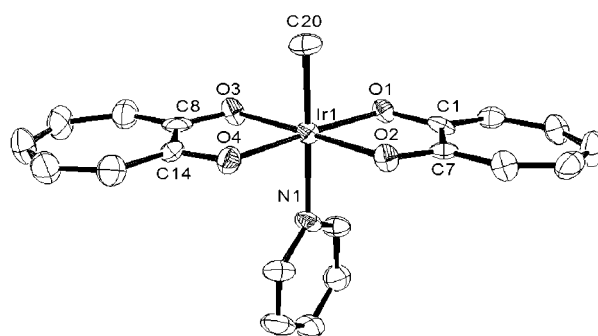
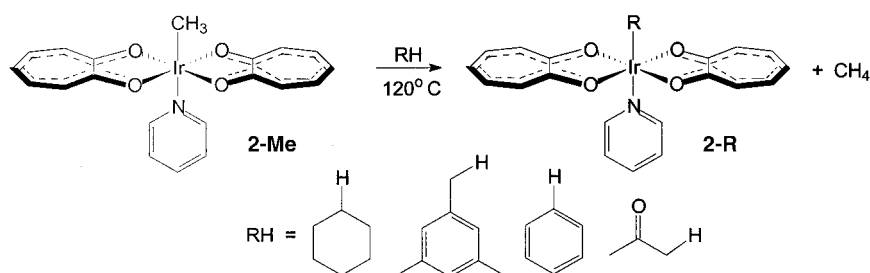


Figure 1. ORTEP drawing of **2-Me**. Thermal ellipsoids are at the 50% probability level. Hydrogen atoms omitted for clarity. Selected bond lengths [Å] and angles [°]: Ir1–C20 2.046(10), Ir1–N1 2.180(8); O1–Ir1–O2 78.4(3).

We find from ¹H NMR spectroscopic studies that the methyl group bound to the iridium center in **2-Me** (2.08 ppm, Ir–CH₃) is located downfield compared to that in the acac-O,O analogue [Ir(CH₃)(py)(acac-O,O)₂] (1.65 ppm, Ir–CH₃),^[18] which suggests possible significant electronic differences at the metal centers. A similar trend is also observed in the ¹³C NMR spectrum, with the chemical shift of the Ir–CH₃ group at –23.3 ppm for **2-Me** compared to –27.1 ppm for the acac-O,O analogue. However, the most significant difference between the two complexes can be seen in the crystal structures of these complexes. As anticipated, the bite angle O1–Ir–O2 in **2-Me** (78.4(3)°) is much smaller than that in the acac-O,O analogue (95.17(16)°). The Ir–N bond length (2.180(8) Å) is comparable to that in the analogous acac complex (2.181(4) Å).

To investigate the stoichiometric C–H activation chemistry of this new O-donor complex we examined the reaction of the complex in various hydrocarbon solvents. Thus, heating **2-Me** in neat mesitylene at 130 °C for 1 h cleanly yielded the corresponding mesityl complex **2-Mes** and methane as shown in Scheme 2. ¹H NMR spectroscopic analysis of the crude reaction mixture, after solvent removal and dissolution in CDCl₃, showed that the reaction was essentially quantitative, as in the case of the acac-O,O analogue,^[3] and only the



Scheme 2. Stoichiometric C–H activation reactions of **2-Me** with RH to generate **2-R**.

benzylic C–H bond of mesitylene was activated. Other hydrocarbon substrates that react by C–H activation with **2-Me** are shown in Scheme 2. Thus, heating a solution of **2-Me** in benzene or acetone at 120 °C for 1 h results in the formation of the corresponding hydrocarbyliridium derivatives, **2-Ph** and **2-Ace**, respectively, in almost quantitative yield. Similarly, heating **2-Me** in cyclohexane resulted in the corresponding cyclohexyliridium complex **2-Cy**, which was purified by flash chromatography and isolated in 35 % yield. All these hydrocarbyliridium derivatives, **2-R** (R = Cy, Mes, Ph, and Ace) were fully characterized by ^1H and ^{13}C NMR spectroscopy as well as by elemental analysis. Importantly, as was the case for the acac-O,O analogues, these hydrocarbyl O-donor iridium derivatives are all air, water, and thermally stable. Significantly, the stoichiometric C–H activation reactions of **2-Me** are faster than those of the acac-O,O analogue. Thus, the half-life ($t_{1/2}$) for the reaction of **2-Me** with benzene at 120 °C is less than 5 minutes versus about 50 minutes for the acac-O,O analogue.

Having established that **2-Me** can stoichiometrically activate the C–H bonds of alkanes and arenes, we examined the catalytic C–H activation of this complex as a first step towards attempting to develop stable hydrocarbon-oxidation catalysts. The relative rates of the H/D exchange reaction with a $\text{C}_6\text{H}_6/[\text{D}_8]\text{toluene}$ mixture (1:1 v/v),^[19] catalyzed at 120 °C by **2-Me** (0.1 mol %) and the acac-O,O analogue were used to compare these complexes. As can be seen in Figure 2, the trop-O,O complex, **2-Me**, is at least 50 times faster than the acac-O,O analogue. Critically, both complexes are stable over the time period studied (ca. 5 h; turnover number (TON) ca. 140 and turnover frequency (TOF) = $80 \times 10^{-4} \text{ s}^{-1}$ for **2-Me**, and TON ca. 2 and TOF = $1 \times 10^{-4} \text{ s}^{-1}$ for the acac-O,O analogue). This is an important result as it shows that: 1) the

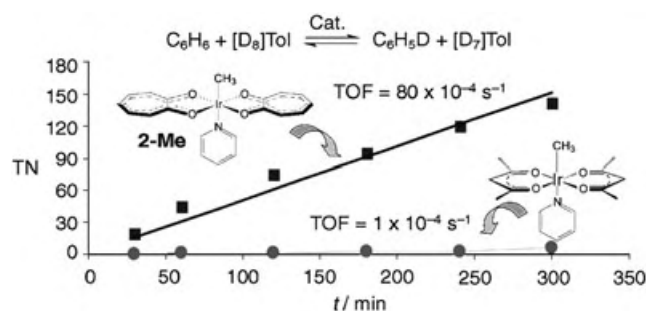


Figure 2. Comparison of catalytic C–H activation of trop-O,O and acac-O,O complexes.

C–H activation chemistry as well as the thermal stability to air and protic media of O-donor late-transition-metal complexes are not unique to the acac-O,O complex and 2) the chemistry of O-donor late-transition-metal complexes can be significantly changed by ligand modification. This observation of ligand-dependent reactivity is an important requirement for this class of O-donor ligand–metal complex to be useful. These results raise the expectation that further investigation of O-donor complexes of late-transition-metal complexes could lead to a broad class of complex with desirable stability, reactivity, and ligand control properties.

In conclusion, we have synthesized a stable O-donor late-transition-metal complex that activates the C–H bonds of alkanes and arenes more rapidly than does the only previously reported O-donor metal complex. Theoretical calculations and further experimental study of these complexes are underway to understand the basis for the increased reactivity and to determine its scope.

Received: September 21, 2004

Published online: January 26, 2005

Keywords: C–H activation · homogeneous catalysis · iridium · O ligands

- [1] a) B. A. Arndtsen, R. G. Bergman, T. A. Mobley, T. H. Peterson, *Acc. Chem. Res.* **1995**, 28, 154; b) A. E. Shilov, G. B. Shulpin, *Activation and Catalytic Reactions of Saturated Hydrocarbons in the Presence of Metal Complexes*, Kluwer, Dordrecht, **2000**; c) C. G. Jia, T. Kitamura, Y. Fujiwara, *Acc. Chem. Res.* **2001**, 34, 633; d) W. D. Jones, *Acc. Chem. Res.* **2003**, 36, 140; e) R. H. Crabtree, *J. Chem. Soc. Dalton Trans.* **2001**, 19, 2437; f) J. A. Labinger, J. E. Bercaw, *Nature* **2002**, 417, 507; g) R. A. Periana, G. Bhalla, W. J. Tenn III, K. J. H. Young, X. Y. Liu, O. Mironov, C. Jones, V. R. Ziatdinov, *J. Mol. Catal. A* **2004**, 220, 7.
- [2] a) W. P. Griffith, *Coord. Chem. Rev.* **1970**, 5, 459; b) C. J. Besecker, V. W. Day, W. G. Klemperer, *Organometallics* **1985**, 4, 564; c) R. E. LaPointe, P. T. Wolczanski, G. D. Van Duyne, *Organometallics* **1985**, 4, 1810; d) S. O. Grim, S. A. Sangokoya, I. J. Colquhoun, W. McFarlane, R. K. Khanna, *Inorg. Chem.* **1986**, 25, 2699; e) W. Klauui, A. Müller, W. Eberspech, R. Boese, I. Goldberg, *J. Am. Chem. Soc.* **1987**, 109, 164; f) M. J. Burk, R. H. Crabtree, *J. Am. Chem. Soc.* **1987**, 109, 8025; g) H. E. Bryndza, W. Tam, *Chem. Rev.* **1988**, 88, 1163; h) M. J. Burk, R. H. Crabtree, *J. Am. Chem. Soc.* **1987**, 109, 8025; i) M. D. Fryzuk, C. D. Montgomery, *Coord. Chem. Rev.* **1989**, 95, 1; j) P. P. Power, *Comments Inorg. Chem.* **1989**, 8, 177; k) B. O. West, *Polyhedron* **1989**, 8, 219; l) R. S. Tanke, R. H. Crabtree, *J. Am. Chem. Soc.* **1990**, 112, 7984; m) D. M. Lunder, E. B. Lobkovsky, W. E. Streib, K. G. Caulton, *J. Am. Chem. Soc.* **1991**, 113, 1837; n) J. T. Poulton, K. Folting, W. E. Streib, K. G. Caulton, *Inorg. Chem.* **1992**, 31, 3190; o) T. T. Johnson, J. C. Huffman, K. G. Caulton, *J. Am. Chem. Soc.* **1992**, 114, 2725; p) D. E. Wigley, *Prog. Inorg. Chem.* **1994**, 42, 239; q) R. G. Bergman, *Polyhedron* **1995**, 14, 3227; r) J. M. Mayer, *Polyhedron* **1995**, 14, 3273; s) P. R. Sharp, *J. Chem. Soc. Dalton Trans.* **2000**, 2647; t) M. A. Cinelli, G. Minghetti, *Gold Bull.* **2002**, 35, 11.
- [3] A. G. Wong-Foy, G. Bhalla, X. L. Liu, R. A. Periana, *J. Am. Chem. Soc.* **2003**, 125, 14292.

- [4] a) R. A. Periana, X. Y. Liu, G. Bhalla, *Chem. Commun.* **2002**, 3000; b) T. Matsumoto, R. A. Periana, D. J. Taube, H. Yoshida, *J. Mol. Catal. A* **2002**, 180, 1; c) T. Matsumoto, R. A. Periana, D. J. Taube, H. Yoshida, *J. Catal.* **2002**, 206, 272; d) T. Matsumoto, D. J. Taube, R. A. Periana, H. Taube, H. Yoshida, *J. Am. Chem. Soc.* **2000**, 122, 7414.
- [5] a) J. Oxgaard, R. P. Muller, W. A. Goddard III, R. A. Periana, *J. Am. Chem. Soc.* **2004**, 126, 352; b) J. Oxgaard, W. A. Goddard III, *J. Am. Chem. Soc.* **2004**, 126, 442.
- [6] a) J. R. Fulton, A. W. Holland, D. J. Fox, R. G. Bergman, *Acc. Chem. Res.* **2002**, 35, 44; b) W. D. Jones, F. J. Feher, *Acc. Chem. Res.* **1989**, 22, 91; c) T. G. P. Harper, R. S. Shinomoto, M. A. Deming, T. C. Flood, *J. Am. Chem. Soc.* **1988**, 110, 7915; d) C. M. Wang, J. W. Ziller, T. C. Flood, *J. Am. Chem. Soc.* **1995**, 117, 1647; e) M. W. Holtcamp, J. A. Labinger, J. E. Bercaw, *J. Am. Chem. Soc.* **1997**, 119, 848; f) R. A. Periana, D. J. Taube, S. Gamble, H. Taube, T. Satoh, H. Fujii, *Science* **1998**, 280, 560; g) L. Johansson, O. B. Ryan, M. Tilset, *J. Am. Chem. Soc.* **1999**, 121, 1974; h) U. Fekl, K. I. Goldberg, *Adv. Inorg. Chem.* **2003**, 5454, 259; i) F. C. Liu, E. B. Pak, B. Singh, C. M. Jensen, A. S. Goldman, *J. Am. Chem. Soc.* **1999**, 121, 4086; j) S. Nuckel, P. Burger, *Angew. Chem.* **2003**, 115, 1670; *Angew. Chem. Int. Ed.* **2003**, 42, 1632.
- [7] a) D. M. Lunder, E. B. Lobkovsky, W. E. Streib, K. G. Caulton, *J. Am. Chem. Soc.* **1991**, 113, 1837; b) T. C. Flood, J. K. Lim, M. A. Deming, W. Keung, *Organometallics* **2000**, 19, 1166.
- [8] a) F. A. Cotton, G. Wilkinson, *Advanced Inorganic Chemistry*, 5th ed., Wiley, New York, **1988**, pp. 1189–1194; b) J. P. Collman, *Acc. Chem. Res.* **1968**, 1, 136; a) D. M. Tellers, S. J. Skoog, R. G. Bergman, T. B. Gunnoe, W. D. Harman, *Organometallics* **2000**, 19, 2428; b) D. M. Tellers, R. G. Bergman, *J. Am. Chem. Soc.* **2000**, 122, 954; c) D. M. Tellers, C. M. Yung, B. A. Arndtsen, D. R. Adamson, R. G. Bergman, *J. Am. Chem. Soc.* **2002**, 124, 1400; d) H. A. Zhong, J. A. Labinger, J. E. Bercaw, *J. Am. Chem. Soc.* **2002**, 124, 1378; e) J. S. Owen, J. A. Labinger, J. E. Bercaw, *J. Am. Chem. Soc.* **2004**, 126, 8247.
- [9] D. C. Bradley, R. C. Mehrotra, I. P. Rothwell, A. Singh, *Alkoxo and Aryloxo Derivatives of Metals*, Academic Press, San Diego, **2001**.
- [10] a) E. L. Muetterties, C. M. Wright, *J. Am. Chem. Soc.* **1965**, 87, 4706; b) E. L. Muetterties, C. M. Wright, *J. Am. Chem. Soc.* **1965**, 87, 21; c) E. L. Muetterties, H. Roesky, C. M. Wright, *J. Am. Chem. Soc.* **1966**, 88, 4856; d) J. Narbutt, J. Krejzler, *Inorg. Chim. Acta* **1999**, 286, 175.
- [11] a) C. G. Pierpont, R. M. Buchanan, *Coord. Chem. Rev.* **1981**, 38, 45; b) C. G. Pierpont, C. W. Lange, *Prog. Inorg. Chem.* **1994**, 41, 331; c) Robert Martin, *Handbook of Hydroxyacetophenones*, Kluwer, Dordrecht, **1997**.
- [12] a) P. W. N. M. van Leeuwen, P. C. J. Kamer, J. N. H. Reek, P. Dierkes, *Chem. Rev.* **2000**, 100, 2741; b) P. C. J. Kamer, P. W. N. M. van Leeuwen, J. N. H. Reek, *Acc. Chem. Res.* **2001**, 34, 895; c) Z. Freixa, P. W. N. M. van Leeuwen, *Dalton Trans.* **2003**, 1890.
- [13] W. Keim, R. P. Schulz, *J. Mol. Catal. A* **1994**, 92, 21.
- [14] W. P. Griffith, C. A. Pumphrey, A. C. Skapski, *Polyhedron* **1987**, 6, 891.
- [15] M. A. Bennett, T. R. B. Mitchell, *Inorg. Chem.* **1976**, 15, 2936.
- [16] K. H. Johri, H. C. Mehra, *Separ. Sci. Technol.* **1976**, 11, 171.
- [17] Crystal data for $\text{C}_{20}\text{H}_{18}\text{IrNO}_4$: $M_r = 528.55$, monoclinic, space group $P2(1)$, $a = 8.463(2)$, $b = 11.060(3)$, $c = 9.924(3)$ Å, $\alpha = 90^\circ$, $\beta = 94.721(4)$, $\gamma = 90^\circ$, $V = 925.6(4)$ Å³, $F(000) = 508$, ρ_{calc} ($Z = 2$) = 1.896 mg m^{-3} , $\mu = 0.7236 \text{ mm}^{-1}$, approximate crystal dimensions $0.28 \times 0.06 \times 0.01 \text{ mm}^3$, θ range = $2.06\text{--}27.50^\circ$, $\text{MoK}\alpha$ ($\lambda = 0.71073$ Å), $T = 153 \text{ K}$, 5610 measured data (Bruker 3-circle, SMART APEX CCD with χ axis fixed at 54.74° by using the SMART V 5.625 program, Bruker AXS: Madison, WI, 2001), of which 3120 ($R_{\text{int}} = 0.0436$) unique. Lorentz and polarization correction (SAINT V 6.22 program, Bruker AXS: Madison, WI, 2001), absorption correction (SADABS program, Bruker AXS: Madison, WI, 2001). Structure solution by direct methods (SHELXTL 5.10, Bruker AXS: Madison, WI, 2000), full-matrix least-squares refinement on F^2 , data to parameters ratio: 13.2:1, final R indices [$I > 2\sigma(I)$]: $R1 = 0.0396$, $wR2 = 0.0676$, $R1 = 0.0511$, $wR2 = 0.0698$ (all data), GOF on $F^2 = 1.008$. CCDC 250327 contains the supplementary crystallographic data for this paper. These data can be obtained free of charge via www.ccdc.cam.ac.uk/conts/retrieving.html (or from the Cambridge Crystallographic Data Centre, 12 Union Road, Cambridge CB21EZ, UK; fax: (+44) 1223-336-033; or deposit@ccdc.cam.ac.uk).
- [18] G. Bhalla, R. A. Periana, unpublished results.
- [19] The H/D exchange rates were quantified by GC/MS analyses. This was achieved by deconvoluting the mass fragmentation pattern obtained from mass spectroscopy by using a program developed with Microsoft EXCEL. See the Supporting Information for details.

Enantioselective Synthesis

The Direct Catalytic Enantioselective Synthesis of Protected Aryl β -Hydroxy- α -Amino Acids**

Michael C. Willis,* Gary A. Cutting,
Vincent J.-D. Piccio, Matthew J. Durbin, and
Matthew P. John

β -Hydroxy- α -amino acid units are present in a significant number of biologically interesting compounds. Aryl-substituted variants are an important subclass and are responsible for a range of biological functions. For example, natural products such as vancomycin,^[1] ristocetin,^[1] and biphenomycin A^[2] display significant antibiotic activity, the cyclomarins^[3] display anti-inflammatory properties, whereas the exochelins are involved in cellular iron(III) transport.^[4] Designed molecules have also been implicated in functions such as hypotension.^[5] A variety of methods for the enantioselective synthesis of this important structural unit have been

[*] Dr. M. C. Willis, G. A. Cutting, V. J.-D. Piccio, M. J. Durbin
Department of Chemistry
University of Bath
Bath, BA2 7AY (UK)
Fax: (+44) 1225-386231
E-mail: m.c.willis@bath.ac.uk

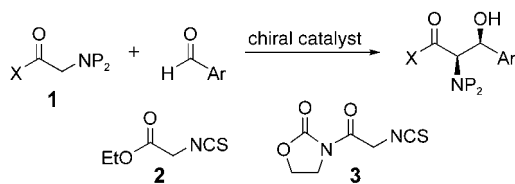
Dr. M. P. John
Chemical Development Division
GlaxoSmithKline Medicines Research Centre
Gunnels Wood Road
Stevenage, SG1 2NY (UK)

[**] This work was supported by the EPSRC, the University of Bath, and GlaxoSmithKline. The EPSRC Mass Spectrometry Service at the University of Wales, Swansea, is also thanked for their assistance.



Supporting information for this article is available on the WWW under <http://www.angewandte.org> or from the author.

reported.^[6,7] One of the most attractive routes, which involves the simultaneous formation of a C–C bond and the creation of two stereogenic centers, is the aldol addition of a glycine equivalent **1** to a suitable aldehyde (Scheme 1).



Scheme 1. The direct catalytic aldol route to aryl β-hydroxy-α-amino acids. X = OR, NR₂; P = protecting group.

A number of highly selective variants of this process are established, although in the majority of examples a preformed enolate or an enolate surrogate, such as an enol silane, is employed.^[8] Direct catalytic enantioselective variants are still scarce.^[9] We recently reported the direct addition of isothiocyanate-substituted ester **2** to a range of aryl aldehydes using an achiral catalyst generated from Mg(ClO₄)₂, bipyridine, and triethylamine.^[10] Herein we document the extension of this system into a highly enantioselective variant that employs commercially available catalyst components.

Early attempts at developing an enantioselective reaction were based on our achiral reaction and involved exchange of bipyridine for a range of enantiomerically pure bidentate ligands, which were used in combination with Mg(ClO₄)₂, Hünig base, and ester **2**. The enantioselectivities obtained were uniformly low. In the expectation of generating more-ordered enolates, we refocused on the use of oxazolidinone **3**^[11] as a glycine equivalent.^[12] The addition of **3** to benzaldehyde was selected as a test reaction, and a range of ligands, bases, and solvents were evaluated (Table 1). To aid in the determination of *ee* values of the products, the direct adducts were treated immediately with a solution of magnesium alkoxide to yield the corresponding ester derivatives.^[12a] Bidentate bis(oxazolines) used in combination with Mg(ClO₄)₂ and Hünig base generated poorly selective catalysts (entries 1 and 2),^[13] however, the switch to a pyridine bis(oxazoline) (pybox) ligand generated a catalyst that delivered the product with a much improved value of 76% *ee* (entry 3). Variation of the ligand substituents from phenyl to *tert*-butyl and benzyl resulted in decreased selectivities (entries 4 and 5). All of the reactions described so far had been conducted in methylene chloride; the use of a 1:1 mixture of CH₂Cl₂ and THF had a dramatic effect and reduced the enantioselectivity to only 10% (entry 6). Increasing the reaction temperature to ambient temperature also resulted in reduced selectivity (entry 7). As a precaution against degradation of the hygroscopic Mg(ClO₄)₂, molecular sieves were added to the system, and an increase in selectivity to 90% *ee* was observed (entry 8).^[14] Finally, variation of the base employed was also explored and Hünig base was found to be optimal (entries 9 and 10).

With optimized conditions in hand, we next explored the scope of the process with respect to the aryl aldehyde component (Table 2).^[15] A wide variety of heteroatom, alkyl,

Table 1: Catalyst evaluation and optimization for the direct addition of imide **3** to benzaldehyde.^[a]

Entry	Ligand	Base	Yield [%] ^[b]	d.r. ^[c]	<i>ee</i> [%] ^[d]
1	6	<i>i</i> Pr ₂ EtN	30	55:45	12
2	7	<i>i</i> Pr ₂ EtN	65	65:35	7
3	8	<i>i</i> Pr ₂ EtN	76	80:20	76
4	9	<i>i</i> Pr ₂ EtN	51	65:35 ^[d]	44
5	10	<i>i</i> Pr ₂ EtN	53	70:30	45
6 ^[e]	8	<i>i</i> Pr ₂ EtN	75	95:5	10
7 ^[f]	8	<i>i</i> Pr ₂ EtN	72	95:5	60
8 ^[g]	8	<i>i</i> Pr ₂ EtN	86	85:15	90
9 ^[g]	8	Et ₃ N	75	80:20	82
10 ^[g]	8	Bu ₃ N	60	85:15	80

[a] General conditions: imide (1 equiv), benzaldehyde (1.1 equiv), Mg(ClO₄)₂ (10 mol%), ligand (11 mol%), base (20 mol%), CH₂Cl₂, –78 °C. [b] Isolated yields. [c] Measured by ¹H NMR spectroscopy. [d] *ee* value of major diastereomer, measured by chiral HPLC using a Chiracel OD column. [e] 1:1 CH₂Cl₂/THF. [f] Reaction at room temperature. [g] 4 Å molecular sieves added.

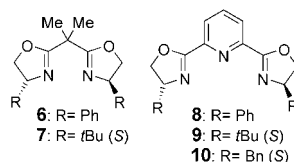


Table 2: The enantioselective addition of imide **3** to aromatic aldehydes.^[a]

Entry	Ar	Yield [%] ^[b]	d.r. ^[c]	<i>ee</i> [%] ^[d]
1	C ₆ H ₅	86	85:15	90
2	4-MeO-C ₆ H ₄	69	85:15	86
3	4-EtO-C ₆ H ₄	85	87:13	93
4	4-MeS-C ₆ H ₄	74	85:15	94
5	4-Me-C ₆ H ₄	88	88:12	92
6	4-Et-C ₆ H ₄	95	91:9	91
7	4-Ph-C ₆ H ₄	79	73:27	87
8	3-Me-C ₆ H ₄	84	82:18	86
9	2-Me-C ₆ H ₄	88	50:50	89 ^[e]
10	2-Naphthyl	64	72:28	87
11	3-Cl-4-PMBO-C ₆ H ₄	78	93:7	95

[a] General conditions: imide (1 equiv), aldehyde (1.1 equiv), Mg(ClO₄)₂ (10 mol%), **8** (11 mol%), *i*Pr₂EtN (20 mol%), CH₂Cl₂, –78 °C. [b] Isolated yields of combined diastereomers. [c] Measured by ¹H NMR spectroscopy. [d] *ee* value of major diastereomer, measured by chiral HPLC using Chiracel OD column. [e] *ee* of *anti* diastereomer; *ee* = 62% for *syn* diastereomer.

and aryl substituents were readily accommodated in the *para* position of the aldehyde with observed enantioselectivities of up to 94% *ee* (entries 1–7). In all cases the *syn*-aldol adduct was obtained as the major diastereomer with selectivities of up to 91:9. Substitution in the *meta* position was also tolerated well (entry 8), however the presence of an *ortho* substituent

resulted in a 50:50 ratio of diastereomers (entry 9). 2-Naphthaldehyde is also a good substrate with the required aldol adduct obtained in 87% *ee* (entry 10). The final entry is significant as the substitution pattern of the product matches that of one of the functionalized tyrosine residues (AA-6) of vancomycin.^[16] Reaction with 3-chloro-4-OPMB-benzaldehyde (PMB = *p*-methoxybenzyl) yielded the protected amino acid in 78% yield as a 93:7 ratio of *syn:anti* diastereomers with an impressive 95% *ee*.

In summary, a simple catalyst system assembled from an enantiomerically pure tridentate ligand, a Lewis acidic metal, and an amine base efficiently generates a chiral glycine enolate derived from oxazolidinone **3**. The enolate undergoes enantioselective addition to a range of aryl aldehydes to provide protected aryl β -hydroxy- α -amino acids in good yields with high enantioselectivities. The utility of the method has been exemplified by the preparation of a constituent amino acid of the natural product vancomycin. Importantly, all of the catalyst components are commercially available and the reactions are simple to perform. Studies to explore the addition of similar chiral enolates to alternative electrophiles and to apply these enolization conditions to alternative nucleophilic components are underway and will be reported in due course.

Experimental Section

General procedure for direct catalytic enantioselective aldol reaction, as exemplified by the preparation of (4*S*,5*R*)-ethyl 5-phenyl-2-thioxo-1,3-oxazolidine-4-carboxylate (Table 2, entry 1): Mg(ClO₄)₂ (15 mg, 0.07 mmol), 2,6-bis((*R*)-4,5-dihydro-4-phenyl-2-oxazolyl)pyridine (28 mg, 0.08 mmol), and 3-(2-isothiocyanatoacetyl)-oxazolidin-2-one (128 mg, 0.69 mmol) were stirred for 1 h in dry methylene chloride (15 mL) in the presence of activated, powdered 4 Å molecular sieves (200 mg) under nitrogen at room temperature. The temperature was then lowered to –78 °C and after 15 min, benzaldehyde (77 μ L, 0.76 mmol) and diisopropylethylamine (24 μ L, 0.14 mmol) were added, and the mixture was stirred for a further 24 h at –78 °C. The reaction was quenched with saturated aqueous ammonium chloride (5 mL). The organic layer was separated, and the aqueous layer was extracted with CH₂Cl₂ (3 \times 10 mL). The organic portions were combined, washed with brine (5 mL), dried (MgSO₄), and concentrated under reduced pressure. The residue was dissolved in dry THF (15 mL), and the solution was cooled to 0 °C. A solution of methyl magnesium bromide (3M in diethyl ether, 0.30 mL, 0.89 mmol) in ethanol (3.3 mL) at 0 °C was added through a cannula. After 3 min, the reaction was quenched by addition of aqueous phosphate buffer solution (5 mL, pH 7). The mixture was concentrated under reduced pressure, and the residue was taken up in aqueous HCl (1M, 10 mL) and CH₂Cl₂ (10 mL). The organic layer was separated, and the aqueous layer was extracted with CH₂Cl₂ (3 \times 10 mL). The organic portions were combined, dried (MgSO₄), and concentrated under reduced pressure. The residue was purified by flash chromatography (SiO₂, 98:2 CH₂Cl₂/EtOAc) to provide the title compound as colorless crystals.

Received: September 27, 2004

Published online: January 28, 2005

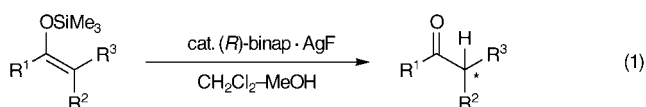
Keywords: aldol reaction · amino acids · asymmetric catalysis · Lewis acids · magnesium

- [1] *Glycopeptide Antibiotics*, (Ed.: R. Nagarajan), Marcel Dekker, New York, 1994.
- [2] M. Ezaki, M. Iwami, M. Yamashita, S. Hashimoto, T. Komori, K. Umehara, Y. Mine, M. Kohsaka, H. Aoki, H. Imanaka, *J. Antibiot.* **1985**, 38, 1453.
- [3] M. K. Renner, Y.-C. Shen, X.-C. Cheng, P. R. Jensen, W. Frankmoelle, C. A. Kauffman, W. E. Fenical, E. Lobkovsky, J. Clardy, *J. Am. Chem. Soc.* **1999**, 121, 11273.
- [4] R. Barclay, C. Ratledge, *J. Bacteriol.* **1983**, 153, 1138.
- [5] B. Herbert, I. H. Kim, K. L. Kirk, *J. Org. Chem.* **2001**, 66, 4892.
- [6] For a discussion of the different approaches used to prepare the β -hydroxy-tyrosine units found in glycopeptide antibiotics, see: K. C. Nicolaou, C. N. C. Boddy, S. Bräse, N. Winssinger, *Angew. Chem.* **1999**, 111, 2230; *Angew. Chem. Int. Ed.* **1999**, 38, 2096.
- [7] For recent examples, see: a) K. Makino, T. Goto, Y. Hiroki, Y. Hamada, *Angew. Chem.* **2004**, 116, 900; *Angew. Chem. Int. Ed.* **2004**, 43, 882, for ketone reductions; b) C. Loncaric, W. D. Wulff, *Org. Lett.* **2001**, 3, 3675, for aziridine opening; c) D. L. Boger, M. A. Patane, J. Zhou, *J. Am. Chem. Soc.* **1994**, 116, 8544; for epoxide opening; d) L. Dong, M. J. Miller, *J. Org. Chem.* **2002**, 67, 4759, for dihydroxylation; e) I. H. Kim, K. L. Kirk, *Tetrahedron Lett.* **2001**, 42, 8401, for aminohydroxylation.
- [8] Selected examples: a) H. Sugiyama, T. Shioiri, F. Yokokawa, *Tetrahedron Lett.* **2002**, 43, 3489; b) J. B. MacMillan, T. F. Molinski, *Org. Lett.* **2002**, 4, 1883; c) S. Caddick, N. J. Parr, M. C. Pritchard, *Tetrahedron* **2001**, 57, 6615; d) M. Horikawa, J. Busch-Peterson, E. J. Corey, *Tetrahedron Lett.* **1999**, 40, 3843; e) S. Kobayashi, H. Ishitani, M. Ueno, *J. Am. Chem. Soc.* **1998**, 120, 4341; f) J. Kobayashi, M. Nakamura, Y. Mori, Y. Yamashita, S. Kobayashi, *J. Am. Chem. Soc.* **2004**, 126, 9192.
- [9] a) Y. Ito, M. Sawamura, T. Hayashi, *J. Am. Chem. Soc.* **1986**, 108, 6405; b) D. A. Evans, J. M. Janey, N. Magomedov, J. S. Tedrow, *Angew. Chem.* **2001**, 113, 1936; *Angew. Chem. Int. Ed.* **2001**, 40, 1884; c) H. Suga, K. Ikai, T. Ibata, *J. Org. Chem.* **1999**, 64, 7040; d) N. Yoshikawa, M. Shibasaki, *Tetrahedron* **2002**, 58, 8289; e) T. Ooi, M. Taniguchi, M. Kameda, K. Maruoka, *Angew. Chem.* **2002**, 114, 4724; *Angew. Chem. Int. Ed.* **2002**, 41, 4542.
- [10] M. C. Willis, V. J.-D. Piccio, *Synlett* **2002**, 1625.
- [11] Oxazolidinone **3** was prepared from the corresponding azide, according to the procedure reported for a chiral derivative in Reference [12a]. See Supporting Information for details.
- [12] For examples of the use of a chiral version of **3** in diastereoselective aldol additions, see: a) D. A. Evans, A. E. Weber, *J. Am. Chem. Soc.* **1986**, 108, 6757; b) D. A. Evans, A. E. Weber, *J. Am. Chem. Soc.* **1987**, 109, 7151; c) M. A. Lago, J. Samanen, J. D. Elliot, *J. Org. Chem.* **1992**, 57, 3493; d) D. L. Boger, S. L. Colletti, T. Honda, R. F. Menezes, *J. Am. Chem. Soc.* **1994**, 116, 5607. See also Reference [5].
- [13] For the use of a Mg-bis(oxazoline) catalyst system in the direct enantioselective addition of malonate derivatives to nitroalkenes, see: J. Ji, D. M. Barnes, J. Zhang, S. A. King, S. J. Wittenberger, H. E. Morton, *J. Am. Chem. Soc.* **1999**, 121, 10215.
- [14] The addition of 20 mol% water to the reaction resulted in a significant reduction in the enantioselectivity of the process (50–60% *ee* depending on the exact reaction).
- [15] The absolute configuration of the benzaldehyde adduct (Table 2, entry 1) was established by X-ray crystallography; the remaining adducts are assigned by analogy.
- [16] N. J. Skelton, D. H. Williams, M. J. Rance, J. C. Ruddock, *J. Chem. Soc. Perkin Trans. 1* **1990**, 77.

Enantioselective Protonation of Silyl Enolates Catalyzed by a Binap-AgF Complex**

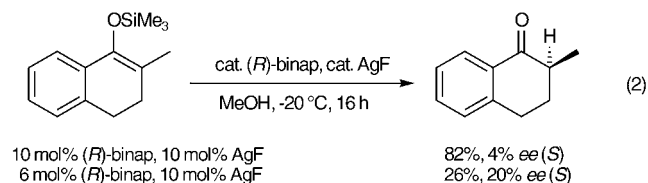
Akira Yanagisawa,* Taichiro Touge, and Takayoshi Arai

Enantioselective protonation of prochiral enolates and enantioselective alkylation of enolates are efficient methods to prepare optically active carbonyl compounds with a tertiary asymmetric carbon center at the α -position.^[1,2] The catalytic enantioselective protonation reactions of metal enolates already reported are performed either under basic or under acidic conditions. The method under basic conditions involves, for example, the protonation of a reactive metal enolate, such as lithium enolate, with a catalytic amount of a chiral acid and an excess of an achiral acid.^[3] In contrast, the method under acidic conditions uses silyl enolates or ketene silyl acetals as substrates which, in the presence of a chiral Lewis acid or a chiral Brønsted acid catalyst, are converted into optically active carbonyl compounds.^[4] Binap-AgF is an efficient chiral catalyst for the asymmetric aldol reaction of silyl enolates^[5] and also for the asymmetric allylation of aldehydes with allylsilane.^[6] Because the activation of a trimethoxysilyl group by the fluoride ion is remarkable, we envisioned that the silver fluoride complex could also act as a chiral catalyst for the asymmetric protonation of silyl enolates with an appropriate achiral proton source such as methanol. We report here a new catalytic asymmetric protonation of silyl enolates with methanol using binap-AgF as a chiral catalyst [Eq. (1)].



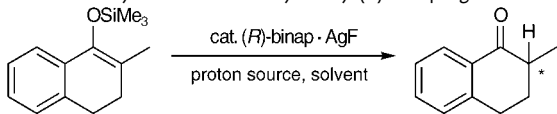
We initially examined the protonation of a 2-methyl-1-tetralone-derived trimethylsilyl enolate with methanol to find the optimal reaction conditions. We attempted the reaction employing diverse ratios of binap and AgF at -20°C and found that a 0.6:1 mixture yielded a nonracemic product with higher enantioselectivity than a 1:1 mixture [Eq. (2)]. As we

have reported previously, various ratios of binap and AgF were examined by ^1H NMR spectroscopy and the 0.6:1 mixture was found to give the desired 1:1 complex without formation of the unreactive 2:1 complex.^[5]



We then studied the influence of the solvent on yield and enantioselectivity (Table 1). Among the solvents tested, THF or chlorinated hydrocarbons gave better enantioselectivities

Table 1: Optimization of the asymmetric protonation of the trimethylsilyl enolate of 2-methyl-1-tetralone catalyzed by (R)-binap-AgF.^[a]



Entry	Solvent	Proton source	T [$^{\circ}\text{C}$]	t [h]	Yield [%] ^[b]	ee [%]	Config. ^[c]
1	MeOH	MeOH	-20	16	26	20	S
2	THF	MeOH	-40	6	87	38	S
3	DMF	MeOH	-40	5	60	30	S
4	toluene	MeOH	-20	13	18	13	S
5	Et ₂ O	MeOH	-40	6	74	26	S
6	CHCl ₃	MeOH	-20	20	47	38	S
7	CH ₂ Cl ₂	MeOH	-20	20	68	56	S
8 ^[d]	CH ₂ Cl ₂	MeOH	-20	20	44	60	S
9 ^[d]	CH ₂ Cl ₂	MeOH	-20	36	72	62	S
10	CH ₂ Cl ₂	EtOH	-20	15	75	14	S
11	CH ₂ Cl ₂	iPrOH	-20	7	97	34	R

[a] Unless otherwise noted, the reaction was carried out with (R)-binap (0.06 mmol), AgF (0.1 mmol), the trimethylsilyl enolate of 2-methyl-1-tetralone (1 mmol), and the specified proton source (0.5 mL) in the specified solvent (10 mL). [b] Yield of isolated product. [c] The enantioselectivity was determined by HPLC analysis on a chiral column (OD-H). [d] MeOH (1 mL) and CH₂Cl₂ (20 mL) were used.

than methanol, and dichloromethane was the solvent of choice. When the protonation was performed in a 20:1 mixture of dichloromethane and methanol, (S)-enriched 2-methyl-1-tetralone was obtained with 56% ee (entry 7). A further improvement in the enantiomeric ratio was achieved when twice as much solvent was used (entries 8 and 9). We also investigated the enantioselectivity of this catalytic protonation with other achiral alcohols but methanol proved most efficient (entries 7, 10, and 11).

This asymmetric protonation was applied to a variety of trimethylsilyl enolates; the results with 2-methyl-1-tetralone and related ketone derivatives are summarized in Table 2. Both the 5-methoxy and the 2-ethyl derivatives gave good optical purities similar to that of 2-methyl-1-tetralone (entries 1–3). However, to our surprise, use of the 2,2,6-trimethylcyclohexanone-derived silyl enolate resulted in a

[*] Prof. Dr. A. Yanagisawa, Dr. T. Arai
Department of Chemistry
Faculty of Science, Chiba University
Inage, Chiba 263-8522 (Japan)
Fax: (+81) 43-290-2789
E-mail: ayanagi@faculty.chiba-u.jp

T. Touge
Graduate School of Science and Technology
Chiba University
Inage, Chiba 263-8522 (Japan)

[**] We gratefully acknowledge financial support from the Novartis Foundation (Japan) for the Promotion of Science. We also thank Takasago International Corporation for a generous gift of (R)-p-Tol-binap.

Table 2: (*R*)-binap-AgF-catalyzed asymmetric protonation of various trimethylsilyl enolates.^[a]

$\text{R}^1-\text{C}(\text{OSiMe}_3)=\text{C}(\text{R}^2)-\text{R}^3 \xrightarrow[\text{CH}_2\text{Cl}_2-\text{MeOH (20:1)}]{\text{cat. (R)-binap} \cdot \text{AgF}} \text{R}^1-\text{C}(=\text{O})-\text{CH}(\text{R}^2)-\text{R}^3$						
Entry	Trimethylsilyl enolate	T [°C]	t [h]	Yield [%] ^[b]	ee [%]	Config. ^[c]
1		-20	36	72	62	S
2		-20	48	82	67	S
3		-20	48	75	64	S
4		0	48	82	87 ^[d]	S
5		-30	24	96	98	R
6 ^[e]		-30	24	75	99	R
7		-30	48	95	97	R
8		-40	48	93	> 99	R
9		-40	48	96	> 99	R
10		-40	48	89	> 99	R

[a] Unless otherwise noted, the reaction was carried out with (*R*)-binap (0.06 mmol), AgF (0.1 mmol), the trimethylsilyl enolate (1 mmol), and MeOH (1 mL) in anhydrous CH₂Cl₂ (20 mL). [b] Yield of isolated product. [c] The enantioselectivity was determined by HPLC analysis on a chiral column (OD-H). See Table 3 in the Experimental Section for details. [d] The enantioselectivity was determined by GLC analysis on a chiral column (G-TA). [e] (*R*)-*p*-Tol-binap was used.

high enantioselectivity of more than 80% *ee* (entry 4). In general, simple ketones with no aromatic substituent at the α -carbon lead to unsatisfactory results in the catalytic asymmetric protonation under acidic conditions.^[4b] Gratifyingly, a quite high enantiomeric ratio was obtained with the silyl enolate of 2-phenylcyclohexanone (entry 5), and the use of *p*-Tol-binap with the same silyl enolate afforded 99% *ee* (entry 6). 2-Arylcycloalkanones are also good substrates for the present asymmetric protonation: for instance, the trimethylsilyl enolate of 2-phenylcycloheptanone showed high enantioselectivity and reactivity (entry 7). As for *p*-methoxyphenyl, *p*-tolyl, and 2-naphthyl derivatives, almost perfect enantioselectivity was attained and *R*-enriched products were formed essentially quantitatively in every case (entries 8–10).

The reaction mechanism has not been fully elucidated; however, two mechanisms can be suggested for the catalytic asymmetric protonation (Figure 1).^[7] From the aforementioned fact that AgF obviously activates the trimethylsilyl group of the substrates, the cyclic model **A** can be postulated as an initial transition-state structure for the reaction. In this assembly, the binap-AgF complex acts as a chiral Lewis acid and MeOH coordinates to both the silver(I) complex and the silyl enolate to form a six-membered cyclic structure, which is further stabilized by the adjacent four-membered ring formed by AgF and the trimethylsilyl group. As a probable catalytic mechanism for the next stage, the binap-AgF complex is regenerated from the assembly **A** accompanied by the formation of the protonated product and methoxytrimethylsilane (route 1). However, an alternative mechanism (route 2), which generates binap-AgOMe^[8] and fluorotrimethylsilane from **A** by a transmetalation step, cannot be ruled out. In the second cycle and thereafter, binap-AgOMe is recycled and behaves as a chiral catalyst in the transition-state structure **B**.

In conclusion, we have developed a novel catalytic asymmetric protonation system. The use of a binap-AgF complex as the chiral catalyst and MeOH as the proton source allows the synthesis of various nonracemic ketones with enantioselectivities of up to 99% *ee*. Further studies on the application of this protonation to other substrates and extension of the present catalytic system to other reactions are currently underway.

Experimental Section

Typical procedure for asymmetric protonation of trimethylsilyl enolates with methanol catalyzed by (*R*)-binap-AgF.

Synthesis of (*R*)-2-phenylcyclohexanone^[2a,4b,9] (entry 5 in Table 2): A mixture of AgF (13.5 mg, 0.106 mmol) and (*R*)-binap (38.5 mg, 0.062 mmol) was dissolved in anhydrous MeOH (1 mL) under argon in the dark, and stirred at room temperature (20°C) for 10 min. After addition of anhydrous CH₂Cl₂ (20 mL) to the solution, the mixture was stirred for another 10 min at room temperature. (2-Phenylcyclohex-1-enyloxy)trimethylsilane (214.9 mg, 0.88 mmol) was added dropwise to the resulting mixture at -78°C. The mixture was stirred for 24 h at -30°C and then treated with saturated aqueous NaHCO₃ (10 mL). The aqueous layer was extracted twice with diethyl ether (10 mL each), and the

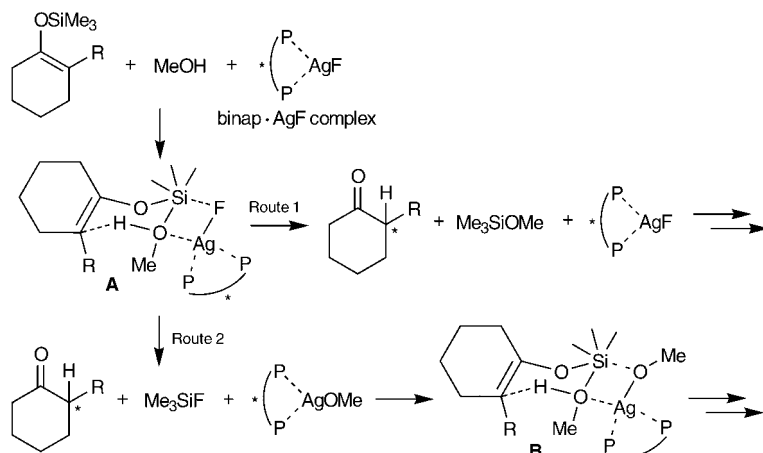


Figure 1. Plausible reaction mechanisms for the asymmetric protonation catalyzed by binap-AgF.

combined organic extracts were washed with saturated brine (20 mL), dried with anhydrous Na₂SO₄, and concentrated in vacuo after filtration. The residual crude product was purified by column chromatography on silica gel (1/7 ethyl acetate/hexane as the eluent) to give (*R*)-enriched 2-phenylcyclohexanone (146.5 mg, 96% yield) as a white solid.

Details on the products and the determination of their *ee* values are listed in Table 3.

Table 3: HPLC analysis of the chiral ketone products.^[a]

Entry	Product	<i>ee</i> [%]	hexane/ <i>i</i> PrOH	<i>t</i> _{minor} [min]	<i>t</i> _{major} [min]
1	(<i>S</i>)-3,4-dihydro-2-methyl-naphthalen-1(2 <i>H</i>)-one ^[2a, 10]	62	99:1	12.3	13.3
2 ^[b]	(<i>S</i>)-3,4-dihydro-5-methoxy-2-methylnaphthalen-1(2 <i>H</i>)-one ^[11, 12]	67	20:1	24.9	18.9
3	(<i>S</i>)-2-ethyl-3,4-dihydro-naphthalen-1(2 <i>H</i>)-one ^[11, 13]	64	99:1	13.9	14.9
4 ^[c]	(<i>S</i>)-2,2,6-trimethyl-cyclohexanone ^[3, 14]	87	–	26.3	27.1
5	(<i>R</i>)-2-phenylcyclohexanone ^[2a, 4b, 9]	98	9:1	13.9	14.8
6		99	9:1	14.0	15.0
7 ^[d]	(<i>R</i>)-2-phenylcycloheptanone ^[4b, 11, 15]	97	20:1	9.1	7.1
8	(<i>R</i>)-2-(4-methoxyphenyl)-cyclohexanone ^[4b, 9b, 16]	> 99	20:1	7.4	9.2
9	(<i>R</i>)-2- <i>p</i> -tolylcyclohexanone ^[4b, 9b, 16]	> 99	20:1	15.4	16.8
10	(<i>R</i>)-2-(naphthalen-2-yl)-cyclohexanone ^[4b, 9b, 16]	> 99	20:1	24.2	29.5

[a] HPLC analysis: Chiralcel OD-H, Daicel Chemical Industries, Ltd., flow rate = 0.5 mL min⁻¹ unless stated otherwise. The entry numbers are the same as in Table 2. [b] Chiralcel OB, flow rate = 0.5 mL min⁻¹. [c] GC analysis on a chiral column (Chiraldex G-TA, Astec, 80 °C, 50 Pa). [d] Chiralpak AS, flow rate = 1.0 mL min⁻¹.

Received: October 16, 2004

Published online: January 11, 2005

Keywords: asymmetric catalysis · ketones · protonation · silver · silyl enolates

- metry **2003**, *14*, 3851; d) L. Navarre, S. Darses, J.-P. Genet, *Angew. Chem.* **2004**, *116*, 737; *Angew. Chem. Int. Ed.* **2004**, *43*, 719; e) D. R. Carbery, T. J. Donohoe, *Chem. Commun.* **2004**, 722; f) B. M. Kim, H. Kim, W. Kim, K. Y. Im, J. K. Park, *J. Org. Chem.* **2004**, *69*, 5104; g) Y. Hamashima, H. Somei, Y. Shimura, T. Tamura, M. Sodeoka, *Org. Lett.* **2004**, *6*, 1861; h) G. Liang, D. Trauner, *J. Am. Chem. Soc.* **2004**, *126*, 9544.
- [3] A. Yanagisawa, T. Watanabe, T. Kikuchi, H. Yamamoto, *J. Org. Chem.* **2000**, *65*, 2979.
- [4] a) K. Ishihara, S. Nakamura, M. Kaneeda, H. Yamamoto, *J. Am. Chem. Soc.* **1996**, *118*, 12854; b) S. Nakamura, M. Kaneeda, K. Ishihara, H. Yamamoto, *J. Am. Chem. Soc.* **2000**, *122*, 8120. Nakai et al. have reported an asymmetric protonation of silyl enolates by water catalyzed by a chiral cationic Pd complex: c) M. Sugiura, T. Nakai, *Angew. Chem.* **1997**, *109*, 2462; *Angew. Chem. Int. Ed. Engl.* **1997**, *36*, 2366.
- [5] a) A. Yanagisawa, Y. Nakatsuka, K. Asakawa, H. Kageyama, H. Yamamoto, *Synlett* **2001**, 69; b) A. Yanagisawa, Y. Nakatsuka, K. Asakawa, M. Wadamoto, H. Kageyama, H. Yamamoto, *Bull. Chem. Soc. Jpn.* **2001**, *74*, 1477.
- [6] A. Yanagisawa, H. Kageyama, Y. Nakatsuka, K. Asakawa, Y. Matsumoto, H. Yamamoto, *Angew. Chem.* **1999**, *111*, 3916; *Angew. Chem. Int. Ed.* **1999**, *38*, 3701.
- [7] Another mechanism involving a transient silver enolate is also possible.
- [8] We attempted to generate binap-AgOMe in situ, without success.
- [9] a) G. Berti, B. Macchia, F. Macchia, L. Menti, *J. Chem. Soc. C* **1971**, 3371; b) Y. Nakamura, S. Takeuchi, Y. Ohgo, M. Yamaoka, A. Yoshida, *Tetrahedron* **1999**, *55*, 4595.
- [10] A. I. Meyers, D. R. Williams, G. W. Erickson, S. White, M. Druelinger, *J. Am. Chem. Soc.* **1981**, *103*, 3081.
- [11] The absolute configuration was assigned by analogy.
- [12] A. P. G. Kieboom, H. Van Bekkum, *Synthesis* **1970**, 476.
- [13] a) P. J. Hattersley, I. M. Lockhart, M. Wright, *J. Chem. Soc. C* **1969**, 217; b) M. Adamczyk, D. S. Watt, D. A. Netzel, *J. Org. Chem.* **1984**, *49*, 4226; c) D. D. Pathak, H. Adams, C. White, *J. Chem. Soc. Chem. Commun.* **1994**, 733; d) K. Fuji, T. Kawabata, A. Kuroda, T. Taga, *J. Org. Chem.* **1995**, *60*, 1914.
- [14] a) M. B. Eleveld, H. Hogeveen, *Tetrahedron Lett.* **1986**, *27*, 631; b) A. Yanagisawa, T. Kikuchi, T. Kuribayashi, H. Yamamoto, *Tetrahedron* **1998**, *54*, 10253.
- [15] M. W. Rathke, D. Vogiazoglou, *J. Org. Chem.* **1987**, *52*, 3697.
- [16] K. Ishihara, M. Kaneeda, H. Yamamoto, *J. Am. Chem. Soc.* **1994**, *116*, 11179.

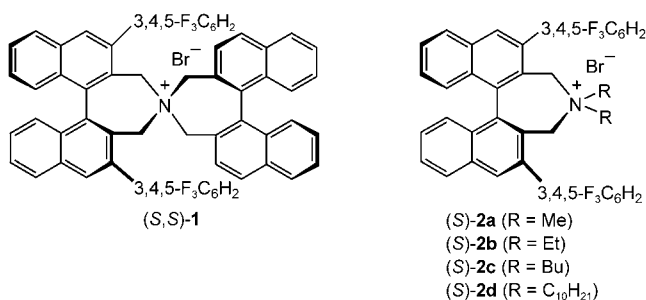
- [1] Reviews: a) S. Hünig, in *Houben-Weyl: Methods of Organic Chemistry*, Vol. E21 (Eds.: G. Helmchen, R. W. Hoffmann, J. Mulzer, E. Schaumann), Thieme, Stuttgart, **1995**, p. 3851; b) C. Fehr, *Angew. Chem.* **1996**, *108*, 2726; *Angew. Chem. Int. Ed. Engl.* **1996**, *35*, 2566; c) A. Yanagisawa, H. Yamamoto in *Comprehensive Asymmetric Catalysis III* (Eds.: E. N. Jacobsen, A. Pfaltz, H. Yamamoto), Springer, Heidelberg, **1999**, p. 1295; d) J. Eames, N. Weerasooriya, *Tetrahedron: Asymmetry* **2001**, *12*, 1; e) P. I. Dalko, L. Moisan, *Angew. Chem.* **2001**, *113*, 3840; *Angew. Chem. Int. Ed.* **2001**, *40*, 3726; f) A. Yanagisawa, in *Comprehensive Asymmetric Catalysis, Suppl. 2* (Eds.: E. N. Jacobsen, A. Pfaltz, H. Yamamoto), Springer, Heidelberg, **2004**, p. 125.
- [2] For notable recent examples of asymmetric protonation, see: a) K. Ishihara, D. Nakashima, Y. Hiraiwa, H. Yamamoto, *J. Am. Chem. Soc.* **2003**, *125*, 24; b) Y. Ohtsuka, T. Ikeno, T. Yamada, *Tetrahedron: Asymmetry* **2003**, *14*, 967; c) G. Asensio, A. Cuenca, N. Rodriguez, M. Medio-Simón, *Tetrahedron: Asym-*

Asymmetric Synthesis

Powerful Chiral Phase-Transfer Catalysts for the Asymmetric Synthesis of α -Alkyl- and α,α -Dialkyl- α -amino Acids**

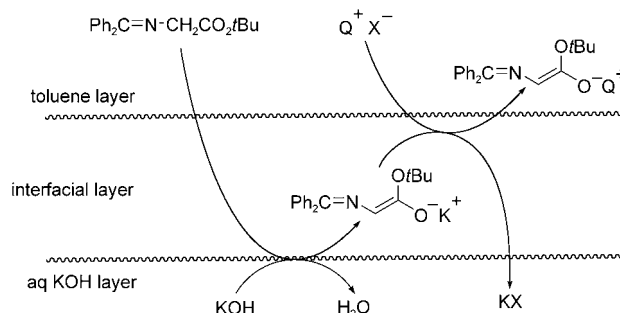
Masanori Kitamura, Seiji Shirakawa, and Keiji Maruoka*

Phase-transfer catalysis (PTC) has been recognized as a convenient and highly useful tool in academia and industry because it offers several advantages for practical organic synthesis, such as operational simplicity, mild reaction conditions in aqueous media, environmental benefits, and suitability for large-scale reactions.^[1,2] Also the development of efficient methods for the preparation of natural and non-natural α -alkyl- and α,α -dialkyl- α -amino acids, especially in their enantiomerically pure forms by asymmetric PTC, has become very important because of their high synthetic utility.^[3,4] Accordingly, several phase-transfer catalysts have been developed that lead to products with excellent enantioselectivities in high yields.^[4] However, despite numerous studies, truly efficient catalytic systems with high enantioselectivity at very low catalyst loading (e.g., < 0.1 mol %) are still rare in asymmetric carbon–carbon bond formation, and major progress in terms of catalyst loading is still desirable for practical asymmetric synthesis. Since our recently developed, chiral spiro-type (*R,R*)- or (*S,S*)-3,4,5-trifluorophenyl-NAS bromide **1** shows exceedingly high enantioselectivity in



asymmetric alkylation of α -amino acid derivatives,^[4d,e,m] our next target was the design of a very active catalyst. Consid-

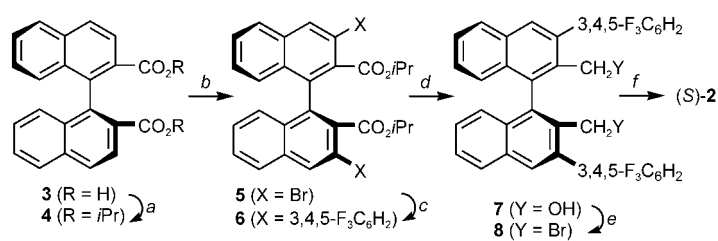
ering the highly lipophilic nature of **1** and the generation of a metal enolate in an interfacial layer,^[5] such lipophilic **1** (QX) must move to the interfacial layer to induce a facile exchange reaction with a metal enolate (Scheme 1). Based on this



Scheme 1. Proposed mechanism for the generation of chiral ammonium enolate.

assumption, our strategy was to replace the rigid binaphthyl moiety in **1** by flexible straight-chain alkyl groups to furnish a new catalyst of type **2**, which substantially accelerates the enolate exchange with **2** because of the increasing polarity of the dialkylammonium moiety. Herein, we report that such a designer chiral quaternary ammonium salt **2** behaves as a very powerful chiral phase-transfer catalyst for the highly practical, enantioselective alkylation of protected-glycine and α -alkyl- α -amino acid derivatives.

The requisite catalyst (*S*)-**2** can be readily prepared from the commercially available (*S*)-1,1'-binaphthyl-2,2'-dicarboxylic acid (**3**)^[6] in a six-step sequence as outlined in Scheme 2.^[7]



Scheme 2. a) *i*PrBr (10 equiv), Bu₄N·HSO₄ (20 mol %), KF·2 H₂O (10 equiv), THF, reflux (95 %); b) 1. Mg(TMP)₂ (4 equiv), THF, RT; 2. Br₂ (8 equiv), –78 °C → RT (91 %); c) (3,4,5-F₃C₆H₂)B(OH)₂ (2.4 equiv), Pd(OAc)₂ (5 mol %), PPh₃ (15 mol %), K₂CO₃ (3 equiv), DMF, 90 °C (94 %); d) LiAlH₄ (3 equiv), THF, 0 °C → RT; e) PBr₃ (0.5 equiv), THF, 0 °C (90 % from **6**); f) R₂NH (R = Me, Et, Bu, C₁₀H₂₁) (1.1 equiv), K₂CO₃ (2 equiv), CH₃CN, reflux (64–99 %).

Thus, (*S*)-dicarboxylic acid **3** was transformed with *i*PrBr, catalytic Bu₄N·HSO₄, and KF·2 H₂O to the corresponding diisopropyl ester **4** in 95 % yield. Treatment of **4** with freshly prepared Mg(TMP)₂ (TMP = 2,2,6,6-tetramethylpiperidine) in THF and subsequent addition of bromine gave rise to (*S*)-3,3'-dibromo-1,1'-binaphthyl-2,2'-dicarboxylic ester **5** in 91 % yield. Suzuki–Miyaura cross coupling of **5** with 3,4,5-trifluorophenylboronic acid in the presence of catalytic Pd(OAc)₂, PPh₃, and K₂CO₃ in *N,N*-dimethylformamide (DMF) afforded (*S*)-3,3'-bis(3,4,5-trifluorophenyl)-1,1'-binaphthyl-2,2'-dicarboxylic ester (**6**) in 94 % yield. Reduction of **6** with

[*] M. Kitamura, S. Shirakawa, Prof. K. Maruoka
Department of Chemistry
Graduate School of Science, Kyoto University
Sakyo, Kyoto 606-8502 (Japan)
Fax: (+81) 75-753-4041
E-mail: maruoka@kuchem.kyoto-u.ac.jp

[**] This work was partially supported by a Grant-in-Aid for Scientific Research from the Ministry of Education, Culture, Sports, Science, and Technology, Japan (21 COE on Kyoto University Alliance for Chemistry). M.K. and S.S. are grateful to the Japanese Society for the Promotion of Science for Young Scientists for a Research Fellowship.

Supporting information for this article is available on the WWW under <http://www.angewandte.org> or from the author.

LiAlH_4 in THF and subsequent treatment of the resulting crude alcohol **7** with PBr_3 in THF furnished (*S*)-dibromide **8** in 90% yield. Reaction of **8** with R_2NH ($\text{R} = \text{Me, Et, Bu, C}_{10}\text{H}_{21}$) and K_2CO_3 in acetonitrile led to the formation of the catalyst (*S*)-**2** in yields of 64–99%. The overall yields of (*S*)-**2** from the starting (*S*)-dicarboxylic acid **3** were 47–72%. The structure of (*S*)-**2c** as a PF_6^- salt determined by X-ray crystallographic analysis is shown in Figure 1.^[8]

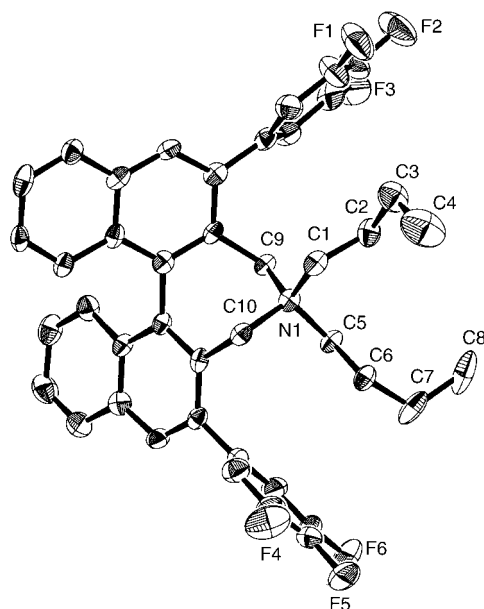


Figure 1. ORTEP drawing of (*S*)-**2c** as a PF_6^- salt. PF_6^- , solvent, and hydrogen atoms have been omitted for clarity.

The chiral efficiency of the phase-transfer catalyst (*S*)-**2** was examined by carrying out asymmetric alkylation of *N*-(diphenylmethylene)glycine *tert*-butyl ester (**9**; Table 1). (*S*)-**2a** gave a rather disappointing result in terms of reactivity, the higher homolog (*S*)-**2b** was however found to be a very active phase-transfer catalyst. Indeed, reaction of **9** with benzyl bromide (1.2 equiv) and 50% aqueous KOH in toluene was effected in the presence of only 0.05 mol % of catalyst (*S*)-**2b** under argon atmosphere at 0 °C for 3 hours to furnish the benzylation product **10** ($\text{R}' = \text{CH}_2\text{Ph}$) in 81% yield with excellent enantioselectivity (97% *ee*) (entry 2). Further acceleration of the reaction was observed by using 0.05 mol % of catalyst (*S*)-**2c** (98% yield with 99% *ee* at 0 °C for 2 hours) (entry 3).^[9] Even 0.01 mol % of catalyst (*S*)-**2c** still gave high enantioselectivity (98% *ee* at 0 °C for 9 hours) (entry 4).

Other selected examples are also listed in Table 1. There are several characteristic features of these alkylation reactions: 1) In contrast to the existing chiral phase-transfer catalysts, catalyst (*S*)-**2c** exhibited a high catalytic performance (0.01–0.1 mol %) and demonstrated the remarkable efficiency and practicality of the present approach towards the enantioselective synthesis of α -alkyl- α -amino acids. 2) The didecyl analogue (*S*)-**2d** exhibited a little less reactivity to (*S*)-**2c** without decreasing enantioselectivity (entries 5 and 6). 3) Not only benzylation and allylation, but also alkylation of **9** with a simple alkyl halide, such as ethyl iodide, proceeded

Table 1: Catalytic enantioselective phase-transfer alkylation of glycine derivative **9**.^[a]

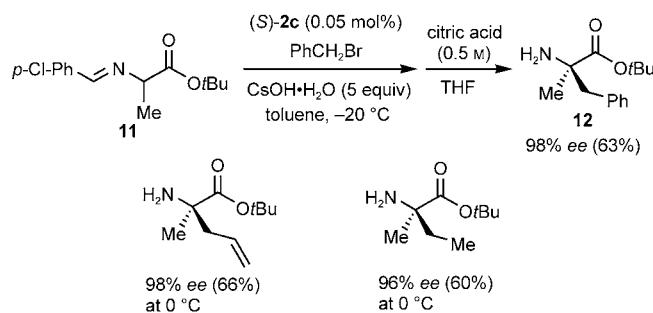
		$\text{Ph}_2\text{C}=\text{N}-\text{CH}(\text{C}(\text{O}t\text{Bu})\text{R}') + \text{R}'-\text{X} \xrightarrow[\text{toluene, 0 } ^\circ\text{C}]{\text{catalytic (S)-2c, 50\% aq. KOH}}$					
Entry	Catalyst [mol %]	R'-X	T [°C]	t [h]	Yield [%] ^[b]	ee [%] (Config) ^[c]	
1	(<i>S</i>)- 2a (0.05)	PhCH_2Br	0	4	7	33 (R)	
2	(<i>S</i>)- 2b (0.05)		0	3	81	97 (R)	
3	(<i>S</i>)- 2c (0.05)		0	2	98	99 (R)	
4 ^[d]	(<i>S</i>)- 2c (0.05)		0	12	97	99 (R)	
5	(<i>S</i>)- 2c (0.01)		0	9	92	98 (R)	
6	(<i>S</i>)- 2d (0.05)		0	4	94	99 (R)	
7	(<i>S</i>)- 2d (0.01)		0	24	79	98 (R)	
8	(<i>S</i>)- 2c (0.05)	$\text{CH}_2=\text{CHCH}_2\text{Br}$	0	3	87	98 (R)	
9	(<i>S</i>)- 2d (0.05)		0	5	75	97 (R)	
10	(<i>S</i>)- 2c (0.05)	$\text{HC}\equiv\text{CCH}_2\text{Br}$	0	4	88	98 (R)	
11	(<i>S</i>)- 2d (0.05)		0	6	83	98 (R)	
12	(<i>S</i>)- 2c (0.05)		0	64	81	97 (R)	
13	(<i>S</i>)- 2c (0.1)	$\text{CH}_3\text{CH}_2\text{I}$ ^[e,f]	−20	1	67	99 (R)	

[a] Unless otherwise specified, the reaction of **9** (0.3 mmol) was carried out with 1.2 equivalents of $\text{R}'\text{X}$ in the presence of catalytic (*S*)-**2** in 50% aqueous KOH/toluene (volume ratio = 1:1) under the given reaction conditions. [b] Yield of isolated product. [c] Enantiopurity of **10** was determined by HPLC analysis using a column with a chiral stationary phase (DAICEL Chiralcel OD) with hexane/isopropanol as the solvent. [d] Reaction scale = 3 mmol. [e] Use of 5 equivalents of alkyl halide and $\text{CsOH}\cdot\text{H}_2\text{O}$ as base. [f] Attempted reaction of **9** with EtI in the presence of (*S*)-**2c** (0.05 mol %) in 50% aqueous KOH/toluene at 0 °C for 72 hours gave **10** ($\text{R}' = \text{Et}$) in 12% yield with 91% *ee*.

smoothly under mild conditions to furnish the corresponding α -alkyl- α -amino acids in high yield and excellent enantioselectivity (entry 13).

The catalyst (*S*)-**2c** is, of course, applicable to the asymmetric alkylation of aldimine Schiff base **11** derived from D,L-alanine *tert*-butyl ester (Scheme 3). Thus, reaction of **11** with benzyl bromide (1.2 equiv) and $\text{CsOH}\cdot\text{H}_2\text{O}$ (5 equiv) in toluene in the presence of 0.05 mol % of catalyst (*S*)-**2c** under argon atmosphere at −20 °C for 1 hour gave, after acidic work-up, rise to benzylation product **12** in 63% yield with 98% *ee*. Asymmetric allylation and ethylation of **11** was carried out in a similar manner as described below.

In conclusion, we successfully designed very powerful chiral phase-transfer catalysts of type **2** to realize a general



Scheme 3. Asymmetric alkylation of Schiff base **11** by using (*S*)-**2c** as catalyst.

and useful procedure for highly practical enantioselective synthesis of α -alkyl- and α,α -dialkyl- α -amino acids.

Received: October 10, 2004

Published online: January 31, 2005

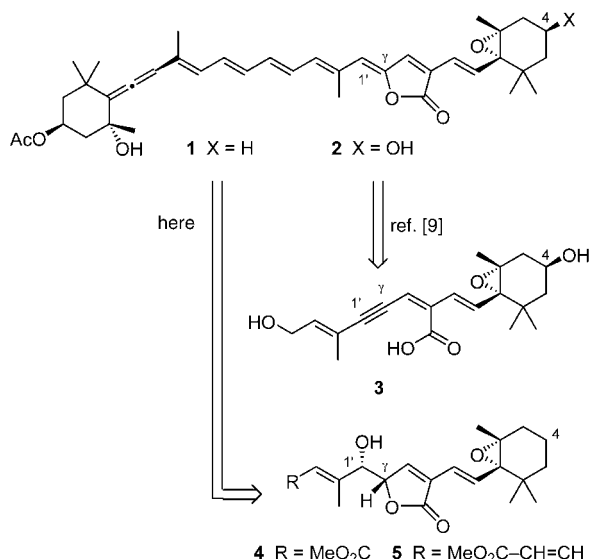
Keywords: alkylation · amino acids · enantioselectivity · glycine · phase-transfer catalysis

- [1] a) E. V. Dehmlow, S. S. Dehmlow, *Phase-transfer Catalysis*, 3rd ed., VCH, Weinheim, **1993**; b) C. M. Starks, C. L. Liotta, M. Halpern, *Phase-Transfer Catalysis*, Chapman & Hall, New York, **1994**; c) *Handbook of Phase-Transfer Catalysis* (Eds.: Y. Sasson, R. Neumann), Blackie, London, **1997**; d) *Phase-Transfer Catalysis* (Ed.: M. E. Halpern), American Chemical Society, Washington, **1997** (ACS Symposium Series 659).
- [2] Reviews: a) T. Shioiri in *Handbook of Phase-Transfer Catalysis* (Eds.: Y. Sasson, R. Neumann), Blackie, London, **1997**, chap. 14; b) M. J. O'Donnell in *Phases* (Sachem's Phase-transfer Catalysis Newsletter), **1998**, issue 4, p. 5; c) M. J. O'Donnell in *Phases* (Sachem's Phase-transfer Catalysis Newsletter), **1999**, issue 5, p. 5; d) T. Shioiri, S. Arai in *Stimulating Concepts in Chemistry* (Eds.: F. Vögtle, J. F. Stoddart, M. Shibasaki), Wiley-VCH, Weinheim, **2000**, p. 123.
- [3] Reviews: a) M. J. O'Donnell, *Aldrichimica Acta* **2001**, *34*, 3; b) K. Maruoka, T. Ooi, *Chem. Rev.* **2003**, *103*, 3013; c) M. J. O'Donnell, *Acc. Chem. Res.* **2004**, *37*, 506; d) B. Lygo, B. I. Andrews, *Acc. Chem. Res.* **2004**, *37*, 518.
- [4] a) M. J. O'Donnell, W. D. Bennett, S. Wu, *J. Am. Chem. Soc.* **1989**, *111*, 2353; b) E. J. Corey, F. Xu, M. C. Noe, *J. Am. Chem. Soc.* **1997**, *119*, 12414; c) B. Lygo, P. G. Wainwright, *Tetrahedron Lett.* **1997**, *38*, 8595; d) T. Ooi, M. Kameda, K. Maruoka, *J. Am. Chem. Soc.* **1999**, *121*, 6519; e) T. Ooi, M. Takeuchi, M. Kameda, K. Maruoka, *J. Am. Chem. Soc.* **2000**, *122*, 5228; f) S.-s. Jew, B.-S. Jeong, M.-S. Yoo, H. Huh, H.-g. Park, *Chem. Commun.* **2001**, 1244; g) H.-g. Park, B.-S. Jeong, M.-S. Yoo, M.-k. Park, H. Huh, S.-s. Jew, *Tetrahedron Lett.* **2001**, *42*, 4645; h) M. Nakoji, T. Kanayama, T. Okino, Y. Takemoto, *Org. Lett.* **2001**, *3*, 3329; i) H.-g. Park, B.-S. Jeong, M.-S. Yoo, J.-H. Lee, M.-k. Park, Y.-J. Lee, M.-J. Kim, S.-s. Jew, *Angew. Chem.* **2002**, *114*, 3162; *Angew. Chem. Int. Ed.* **2002**, *41*, 3036; j) T. Kita, A. Georgieva, U. Hashimoto, T. Nakata, K. Nagasawa, *Angew. Chem.* **2002**, *114*, 2956; *Angew. Chem. Int. Ed.* **2002**, *41*, 2832; k) T. Shibuguchi, Y. Fukuta, Y. Akachi, A. Sekine, T. Ohshima, M. Shibasaki, *Tetrahedron Lett.* **2002**, *43*, 9539; l) B. Lygo, B. Allbutt, S. R. James, *Tetrahedron Lett.* **2003**, *44*, 5629; m) T. Ooi, M. Kameda, K. Maruoka, *J. Am. Chem. Soc.* **2003**, *125*, 5139; n) Y. N. Belokon, N. B. Bespalova, T. D. Churkina, I. Císařová, M. G. Ezernitskaya, S. R. Harutyunyan, R. Hrdina, H. B. Kagan, P. Kočovský, K. A. Kochetkov, O. V. Larionov, K. A. Lyssenko, M. North, M. Poláček, A. S. Peregudov, V. V. Prisyazhnyuk, Š. Vyskočil, *J. Am. Chem. Soc.* **2003**, *125*, 12860.
- [5] For the discussion of mechanism in normal chiral phase-transfer catalyst systems: a) K. B. Lipkowitz, M. W. Cavanaugh, B. Baker, M. J. O'Donnell, *J. Org. Chem.* **1991**, *56*, 5181; b) M. J. O'Donnell, S. Wu, J. C. Huffman, *Tetrahedron* **1994**, *50*, 4507.
- [6] M. Seki, S. Yamada, T. Kuroda, R. Imashiro, T. Shimizu, *Synthesis* **2000**, 1677.
- [7] T. Ooi, Y. Uematsu, K. Maruoka, *J. Org. Chem.* **2003**, *68*, 4576.
- [8] Crystallographic data for (S)-**2c** as a PF₆⁻ salt: 0.4 × 0.3 × 0.2 mm³, monoclinic, C₂, *a* = 18.70(1), *b* = 13.80(1), *c* = 18.176(9) Å, β = 106.79(5)°, *V* = 4488(4) Å³, ρ_{calcd} = 1.403 g cm⁻³, *Z* = 4, $2\theta_{\text{max}}$ = 54.7°, μ = 0.1383 mm⁻¹, MoK α , λ = 0.7107 Å, *T* = -150 °C. A total of 20154 reflections were measured. *R* = 0.068, and *R_w* = 0.081 for 11668 observed reflections with *I* > 3.0 σ (*I*). CCDC-250335 [(S)-**2c** as a PF₆⁻ salt] contains the supplementary crystallographic data for this paper. These data can be obtained free of charge from The Cambridge Crystallographic Data Centre via www.ccdc.cam.ac.uk/data_request/cif.
- [9] Attempted asymmetric benzylation of **9** with 50 % aqueous KOH in toluene in the presence of 0.05 mol % of catalyst (S,S)-**1** under argon atmosphere at 0 °C for 24 hours resulted in formation of **10** (R' = CH₂Ph) in only 22 % yield with 85 % *ee*.

Novel Strategy for the Synthesis of the Butenolide Moiety of Peridinin**

Thomas Olpp and Reinhard Brückner*

Peridinin (**2**,^[1] Scheme 1) is one of the most common biosynthesized carotenoids on earth.^[2] Its polyene chain contains an α -alkenyl- γ -alkylidenebutenolide unit, which



Scheme 1. Strategies for the syntheses of the butenolide moieties of peridinin (**2**) and deoxyperidinin (**1**).

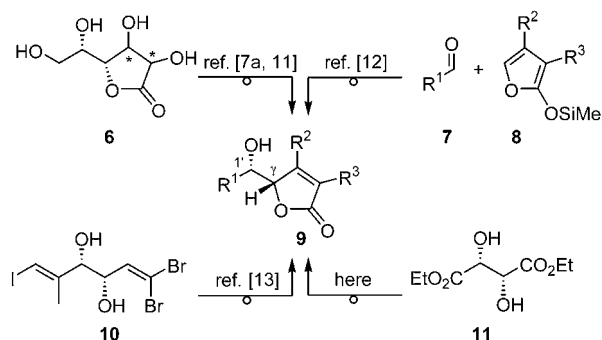
has a *Z* configuration at the C¹=C^γ bond, as is typical for naturally occurring γ -alkylidenebutenolides.^[3] Peridinin (**2**) plays a key role in marine photosynthesis^[4] and displays considerable antitumor activity.^[5] The fact that these roles are assumed solely by peridinin (**2**) and not by related carotenoids *may* be due or *supposedly*^[5] is due to its butenolide ring, which, among carotenoids, is almost unique to **2**.^[6]

As part of our study of the light-harvesting and cancerostatic properties of peridinin (**2**) and analogues such as deoxyperidinin (**1**, Scheme 1), we have developed a novel approach towards their α -alkenyl- γ -alkylidenebutenolide cores. In this communication we demonstrate this approach

with the stereoselective syntheses of compounds **36** and **37** (Scheme 5), in which the last step is the *anti*-selective dehydration of the α -alkenyl- γ -(α -hydroxyalkyl)butenolides **4** and **5**, respectively (Scheme 1). We have employed dehydrations of this type en route to a number of stereodefined γ -alkylidenebutenolides.^[7,8]

It should be possible to convert compounds **4**, **5**, **36**, and **37** into deoxyperidinin (**1**) by modification of the respective ester group. Likewise, appropriately hydroxylated analogues of compounds **4**, **5**, **36**, and **37** would be appropriate precursors for synthesizing peridinin (**2**). Two laboratory syntheses of **2** have been achieved so far. One was based on the stereocontrolled cyclization of enynic acid **3** (Katsumura et al.^[9]), the other used older, sophisticated, but stereorandom methodology (Ito et al.^[10]).

Prior to the present study, we had established three different routes to diastereomerically pure γ -(α -hydroxyalkyl)butenolides **9**, which, through *anti* elimination, furnished pure *Z*-configured γ -(alkylidene)butenolides (Scheme 2). These routes were based on: modification of sugar lactones **6**,^[7a,11] vinylogous Mukaiyama aldol additions of siloxyfurans **8** and aldehydes **7**,^[12] and sequential C-Hal→C-C conversions of trihalodienediol **10**.^[13] Here, in a fourth approach we started from (–)-diethyl tartrate (**11**; Scheme 2).

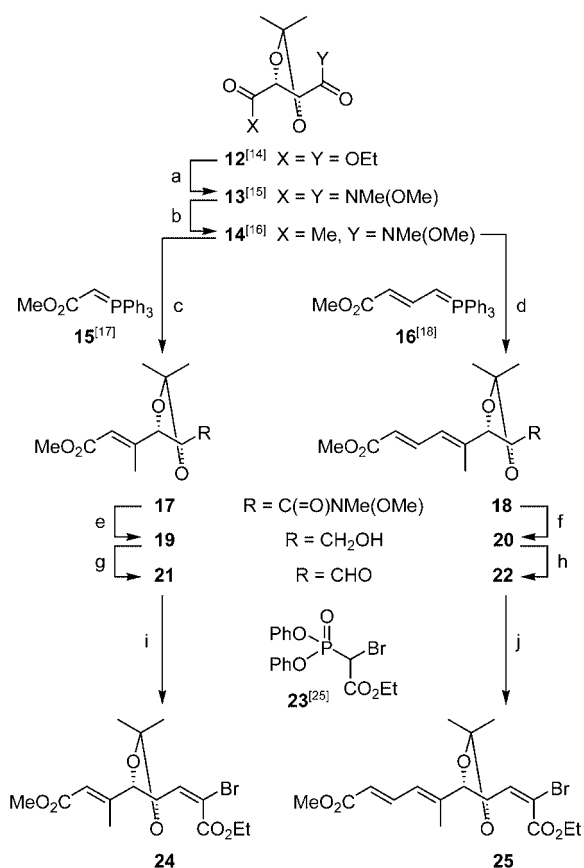


Scheme 2. Routes to γ -(α -hydroxyalkyl)butenolides **9**, which correspond to structures of type **4/5** in Scheme 1 and are precursors of γ -alkylidenebutenolides of type **1/2** structures in Scheme 1.

After acetalization of **11** (→**12**,^[14] Scheme 3), formation of the double Weinreb amide furnished **13**; the yield (99%) was better than that of the published procedure (77%),^[15] provided that the temperature was kept below –15°C throughout reaction and workup. Bis(amide) **13** thereby became available on the 40-g scale. Treatment of **13** with 1.0 equiv of MeMgBr gave rise to the monoketone **14** (66%).^[16] Wittig olefination of this compound with ylides **15**^[17] and **16**^[18] delivered the unsaturated esters **17**^[19]—as an 86:14 mixture of *E* and *Z* isomers^[20] (pure *E* isomer was obtained in 77% yield from 10-g batches after separation by flash chromatography on silica gel^[21])—and **18** (90% yield, which was isomerically pure with a *trans,E* configuration),^[22] respectively. Compounds **17** and **18** both contain C(=O)-NMe(OMe) and C(=O)OMe units but reacted exclusively at the former upon treatment with NaBH₄ (optimally 8 equiv) in methanol. To the best of our knowledge, these are the first

[*] T. Olpp, Prof. Dr. R. Brückner
Institut für Organische Chemie und Biochemie
Universität Freiburg
Albertstrasse 21, 79104 Freiburg (Germany)
Fax: (+49) 761-203-6100
E-mail: reinhard.brueckner@organik.chemie.uni-freiburg.de

[**] This work was generously supported by the Fonds der Chemischen Industrie through a Kekulé fellowship for T.O. and by the Deutsche Forschungsgemeinschaft. We thank Alexandra Müller for skilled technical assistance and Dr. Thomas Netscher (DSM Nutritional Products) for a donation of (R,R)-4-hydroxy-2,2,6-trimethyl-1-cyclohexanone.

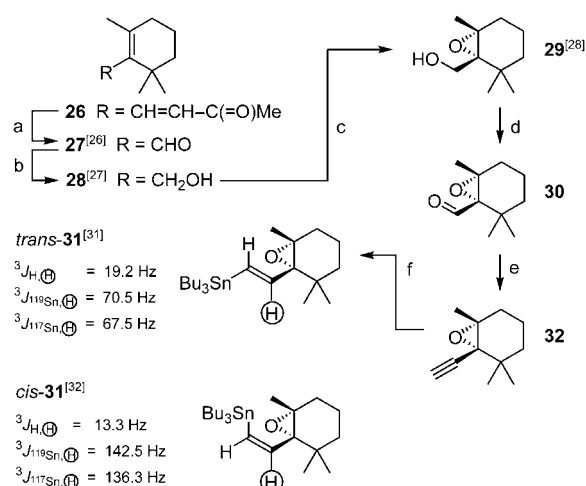


Scheme 3. Syntheses of bromoacrylate intermediates **24** and **25**.

a) HNMe(OMe)·HCl (4 equiv), Me₃Al (4 equiv), CH₂Cl₂, −15 °C, 1 h, 99%; b) MeMgBr (1.0 equiv), THF, 0 °C, 1 h, 66%; c) **15** (2.0 equiv), toluene, reflux, 27 h, 77%, *E:Z* = 86:14; d) **16** (2.0 equiv), toluene, reflux, 30 h, 90%, *E:Z* > 99:1; e) NaBH₄ (8.0 equiv), MeOH, 25 °C, 18 h, 98%; f) same as (e) but 20 h, 92%; g) (COCl)₂ (2.0 equiv), DMSO (4.0 equiv), NEt₃ (6.0 equiv), −78 °C → 0 °C, 30 min, 90%; h) same as (g) but −78 °C, 90 min, 79%; i) **23** (1.2 equiv), NaH (1.0 equiv), THF, 0 °C, 30 min, 75%, *E:Z* = 95:5; j) same as (i) but 90 min, 82%, *E:Z* = 98:2. DMSO = dimethyl sulfoxide.

reductions of Weinreb amides effected with this reagent. The resulting hydroxy esters—**19** (98% yield) and **20** (92% yield)—were oxidized under Swern conditions^[23] to afford the corresponding aldehyde esters (**21**, 90%; **22**, 79%). These were carried on to the α-bromoacrylates **24** (75%) and **25** (82%) with *E* stereoselectivities of 95:5 and 98:2, respectively, by using the Ando-type^[24] bromophosphonate **23**,^[25] which we developed to this end.

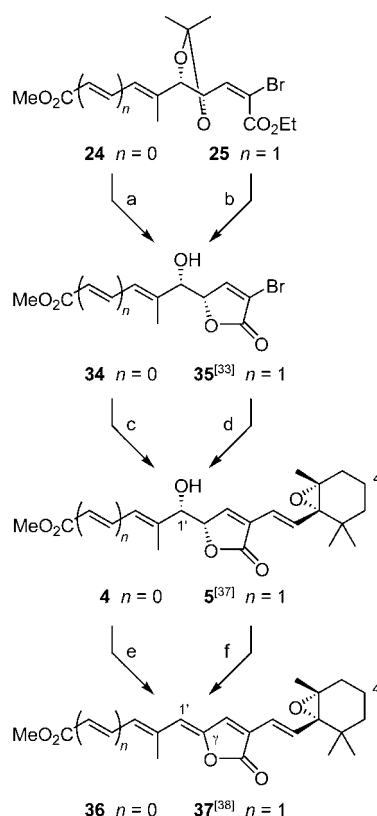
The preparation of the epoxycyclohexyl moiety of targets **4** and **5** started from β-ionone (**26**), which underwent ozonolysis and workup with Zn/HOAc to provide cyclocitral (**27**) in 93% yield (Scheme 4).^[26] Subsequent reduction with NaBH₄ led to cyclogeraniol (**28**) in 76% yield.^[27] This two-step procedure was two times more efficient than the one-step version in which the ozonolysis mixture was treated directly with NaBH₄ (→**28** in 30% yield). Asymmetric Sharpless epoxidation of **28** furnished the epoxy alcohol **29** in 67% yield.^[28a,b] The *ee* value of **29** was 99.8% according to GC analysis of the trimethylsilyl ether. This surpasses the



Scheme 4. a) O₃, MeOH, −78 °C, 2.5 h; Zn (1.5 equiv), HOAc/H₂O (1:1), 93%; b) NaBH₄ (1.5 equiv), MeOH, 0 °C, 1 h, 25 °C, 12 h, 76%; c) *t*BuOOH (2.0 equiv), Ti(O*i*Pr)₄ (0.1 equiv), (−)-DIPT (0.1 equiv), 4 Å MS, CH₂Cl₂, −25 °C, 12 h, 67%, 99.8% *ee*; d) DMSO (3.0 equiv), (COCl)₂ (1.5 equiv), NEt₃ (4.5 equiv), −78 °C, 1 h, 99%; e) Bu₃SnH (1.1 equiv), [Pd(PPh₃)₄] (0.05 equiv), THF, 25 °C, 2 h, 83%; f) Me₃SiCH=N₂ (1.2 equiv), LDA (1.2 equiv), −78 °C, 30 min, 57%. DIPT = diisopropyl tartrate, LDA = lithium diisopropylamide.

previously determined enantiopurities of **29**, regardless of whether it was synthesized in the same way (ref. [28a]: 95% *ee*; ref. [28b]: ≥ 98% *ee*) or by a different approach (ref. [28c]: 97.1% *ee*). Swern oxidation^[23] delivered aldehyde **30** (99%). Because of the tendency of **30** to decompose, it was immediately C₁-extended with Shioiri's lithiodiazomethane^[29] affording, after flash chromatography,^[21] the volatile epoxy-alkyne **32** in 57% yield. Pd-catalyzed hydrostannylation^[30] gave the desired alkenylstannane *trans*-**31**^[31] regio- and stereoselectively. The *trans* configuration of its C=C bond was deduced by comparison of the *H*–C=C–*H* and *Sn*–C=C–*H* coupling constants with those in the *cis* isomer.^[32] For the *trans* isomer the first coupling constant is larger, for the *cis* isomer the second is larger (Scheme 4).

Scheme 5 shows the concluding steps of our syntheses. The next reaction was acetal cleavage of the bromodiester acetones **24** and **25** mediated by Amberlyst 15 or preferably TsOH, which was followed by spontaneous formation of the butenolide rather than pentenolide unit. The resulting brominated γ-(α-hydroxyalkyl)butenolides **34** and **35**^[33] were obtained in nearly quantitative yields. The ensuing step, a Stille coupling^[34] with alkenylstannane *trans*-**31**, was catalyzed by bis(trifurylphosphane)palladium (generated in situ)^[35] and cocatalyzed by CuI.^[36] The final step was the *anti*-selective dehydration to form the *Z*-configured C¹=C² bond. It was realized under Mitsunobu conditions, i.e., by treatment of γ-(α-hydroxyalkyl)butenolides **4** and **5**^[37] with 2 equiv of both of PPh₃ and DEAD, at −30 °C. These conditions were gleaned from earlier experience in our group.^[12,13] While γ-alkyldenebutenolide **36** was obtained in isomerically pure form from reaction in anhydrous THF followed by aqueous workup and standard flash chromatography on silica gel,^[21] the vinologous γ-alkyldenebutenolide



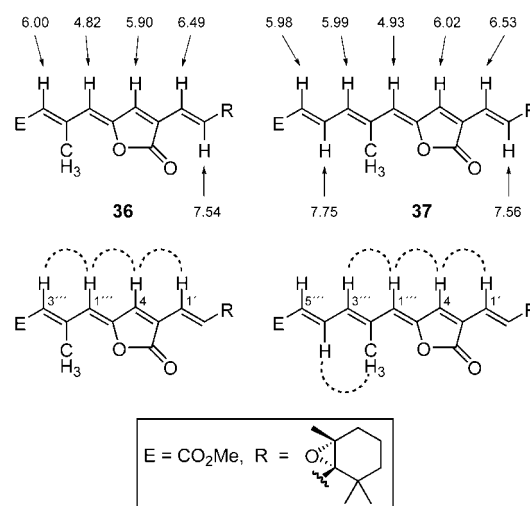
Scheme 5. Butenolide syntheses. a) MeOH, Amberlyst 15, reflux, 28 h, 95%; b) MeOH, TsOH (0.05 equiv), reflux, 1 h, 94%; c) *trans*-**31** (1.2 equiv), CuI (1.65 equiv), [Pd₂dba₃]:CHCl₃ (0.05 equiv), P(2-furyl)₃ (0.3 equiv), NMP, 25 °C, 19 h, 84%; d) same as (c), 82%; e) DEAD (2.0 equiv), PPh₃ (2.0 equiv), THF, −30 °C, 90 min, 62%; f) same as (e) except for THF (degassed, 250 ppm di-*tert*-butylcresol) and exclusion of light, 90%. DEAD = diethyl azodicarboxylate, NMP = *N*-methylpyrrolidone, Ts = *para*-toluenesulfonyl.

37 was just one constituent of a mixture of the four 1,3-diene isomers. Compound **37**^[38] could be prepared free from isomers only when:

- daylight was excluded throughout the reaction and chromatography,
- the solvent (THF) was degassed and contained di-*tert*-butylcresol as a radical scavenger,
- no aqueous workup was performed but rather the solvent was removed by vacuum distillation at −30 °C,
- and the cyclohexane/ethyl acetate mixture used as the eluent in flash chromatography was degassed. Remarkably, the yield of **37** was then 90%.^[39]

The configurational assignments of the double bonds in our target structures **36** and **37** were based on the magnitudes of the olefinic ³J_{H,H} couplings (for the configurations of the disubstituted C=C bonds) and on the NOEs indicated in Scheme 6 (for the configurations of the trisubstituted C=C bonds).

In summary, the present study establishes that diethyl tartrate is a viable precursor of stereopure *Z*-γ-alkyldienebutenolides. Moreover, extensions of this approach should make



Scheme 6. ¹H NMR experiments (500 MHz): NOEs (---); **36** in CDCl₃ and **37** in C₆D₆; characteristic chemical shifts for alkyldienebutenolides **36** and **37** (both in C₆D₆).

both deoxyperidin (1) and peridin (2) accessible by total synthesis.

Received: April 7, 2004

Revised: October 14, 2004

Published online: January 28, 2005

Keywords: *anti* elimination · butenolides · carotenoids · olefination · stereoselective synthesis

- [1] Two-dimensional structure: a) H. H. Strain, W. A. Svec, K. Aitzetmüller, M. C. Grandolfo, J. J. Katz, H. Kjösen, S. Norgård, S. Liaaen-Jensen, F. T. Haxo, P. Wegfahrt, H. Rapoport, *J. Am. Chem. Soc.* **1971**, 93, 1823–1825; three-dimensional structure: b) J. E. Johansen, G. Borch, S. Liaaen-Jensen, *Phytochemistry* **1980**, 19, 441–444; c) H. H. Strain, W. A. Svec, P. Wegfahrt, H. Rapoport, F. T. Haxo, S. Norgård, H. Kjösen, S. Liaaen-Jensen, *Acta Chem. Scand. B* **1976**, 30, 109–120.
- [2] J. A. Haugan, T. Aakermann, S. Liaaen-Jensen, *Methods Enzymol.* **1992**, 213, 231–245.
- [3] For example, a) frelingyne (revised structure): C. F. Ingham, R. A. Massy-Westropp, *Aust. J. Chem.* **1974**, 27, 1491–1503; p. 643 in D. W. Knight, G. Pattenden, *J. Chem. Soc. Perkin Trans. 1* **1975**, 641–644; b) lissoclinolide: B. S. Davidson, C. M. Ireland, *J. Nat. Prod.* **1990**, 53, 1036–1038; c) pyrrhoxanthin, two-dimensional structure: J. E. Johansen, W. A. Svec, S. Liaaen-Jensen, F. T. Haxo, *Phytochemistry* **1974**, 13, 2261–2271; three-dimensional structure: T. Aakermann, S. Liaaen-Jensen, *Phytochemistry* **1992**, 31, 1779–1782; d) Cf. also xerulic acid, xerulin, and dihydroxerulin, which, however, have no α substituent: D. Kuhnt, T. Anke, H. Besl, M. Bross, R. Herrmann, U. Mocek, B. Steffan, W. Steglich, *J. Antibiot.* **1990**, 43, 1413–1420.
- [4] E. Hofmann, P. M. Wrench, F. P. Sharples, R. G. Hiller, W. Welte, K. Diederichs, *Science* **1996**, 272, 1788–1791.
- [5] H. Nishino, *Mutat. Res.* **1998**, 402, 159–163.
- [6] γ-Alkyldienebutenolides are also part of the following carotenoids: a) peridinol: ref. [3c]; b) anhydroperidinol: D. J. Repeta, R. B. Gagosien, *Geochim. Cosmochim. Acta* **1984**, 48, 1265–1277; c) pyrrhoxanthin: ref. [3c]; d) pyrrhoxanthinol: ref. [3c]; e) hydratopyrrhoxanthinol: S. Hertzberg, V. Partali, S. Liaaen-

- Jensen, *Acta Chem. Scand. B* **1988**, 42, 495–503; f) uriolide: P. Foss, R. R. L. Guillard, S. Liaaen-Jensen, *Phytochemistry* **1986**, 25, 119–124; g) deoxyxyriolide: E. S. Egeland, S. Liaaen-Jensen, *Phytochemistry* **1995**, 40, 515–520; h) anhydrouriolide: ref. [6g]; i) 3'-dehydrouriolide: ref. [6g]; j) unnamed carotenoid: T. Maoka, K. Hashimoto, N. Akimoto, Y. Fujiwara, *J. Nat. Prod.* **2001**, 64, 578–581; k) unnamed carotenoid: M. Suzuki, K. Watanabe, S. Fujiwara, T. Kurasawa, T. Wakabayashi, M. Tsuzuki, K. Iguchi, T. Yamori, *Chem. Pharm. Bull.* **2003**, 724–727.
- [7] a) F. C. Görth, A. Umland, R. Brückner, *Eur. J. Org. Chem.* **1998**, 1055–1062; b) review: R. Brückner, *J. Chem. Soc. Chem. Commun.* **2001**, 141–152.
- [8] Other approaches to γ -alkylidenebutenolides: a) E.-I. Negishi, M. Kitora, *Tetrahedron* **1997**, 53, 6707–6738; b) R. Brückner, *Curr. Org. Chem.* **2001**, 5, 679–718; c) R. Rossi, F. Bellina in *Targets in Heterocyclic Systems: Shemistry and Properties*, Vol. 5 (Eds.: O. A. Attanasi, D. Spinelli), Società Chimica Italiana, **2002**, pp. 169–198.
- [9] a) N. Furuichi, H. Hara, T. Osaki, H. Mori, S. Katsumura, *Angew. Chem.* **2002**, 114, 1065–1068; *Angew. Chem. Int. Ed.* **2002**, 41, 1023–1026; b) N. Furuichi, H. Hara, T. Osaki, M. Takano, H. Mori, S. Katsumura, *J. Org. Chem.* **2004**, 69, 7949–7959.
- [10] a) Synthesis of a racemic mixture of diastereomers: M. Ito, Y. Hirata, Y. Shibata, K. Tsukida, *J. Chem. Soc. Perkin Trans. 1* **1990**, 197–199; b) synthesis of enantiomerically and diastereomerically pure **2**: Y. Yamano, M. Ito, *J. Chem. Soc. Perkin Trans. 1* **1993**, 1599–1610.
- [11] K. Siegel, R. Brückner, *Chem. Eur. J.* **1998**, 4, 1116–1122.
- [12] F. von der Ohe, R. Brückner, *New J. Chem.* **2000**, 24, 659–669.
- [13] I. Hanisch, R. Brückner, *Synlett* **2000**, 374–378.
- [14] M. Carmack, C. J. Kelley, *J. Org. Chem.* **1968**, 33, 2171–2173.
- [15] D. A. Nugiel, K. Jacobs, T. Worley, M. Patel, R. F. Kaltenbach III, D. T. Meyer, P. K. Jadhav, G. V. De Lucca, T. E. Smyser, R. M. Klabe, L. T. Bacheler, M. M. Rayner, S. P. Seitz, *J. Med. Chem.* **1996**, 39, 2156–2169.
- [16] J. McNulty, V. Grunner, J. Mao, *Tetrahedron Lett.* **2001**, 42, 5609–5612.
- [17] O. Isler, H. Gutmann, M. Montavon, R. Rüegg, G. Ryser, P. Zeller, *Helv. Chim. Acta* **1957**, 40, 1242–1249.
- [18] E. Buchta, F. Andree, *Chem. Ber.* **1960**, 93, 1349–1353.
- [19] All new compounds gave satisfactory ^1H and ^{13}C NMR spectra and correct combustion analyses, except aldehyde **21**, (hydroxyalkyl)butenolides **35**, **4**, and **5**, and the unstable alkylidenebutenolides **36** and **37**; all of these, however, provided correct high-resolution mass spectra.
- [20] The reaction of monoketone **14** and the sodium derivative of $(\text{EtO})_2\text{P}(=\text{O})\text{CH}_2\text{CO}_2\text{Et}$ gave the ethyl ester/Weinreb amide analogue of **17** as an *E:Z* mixture (93% yield, *E:Z* = 59:41).
- [21] W. C. Still, M. Kahn, A. Mitra, *J. Org. Chem.* **1978**, 43, 2923–2925.
- [22] Monoketone **14** and the sodium derivative of a commercial 90:10 *trans:cis* mixture of $(\text{EtO})_2\text{P}(=\text{O})\text{CH}_2\text{CH}=\text{CH}\text{CO}_2\text{Et}$ gave all four diene stereoisomers of the ethyl ester/Weinreb amide analogue of **18** in a combined yield of 49%.
- [23] A. J. Mancuso, D. Swern, *Synthesis* **1981**, 165–185.
- [24] K. Ando, T. Oishi, M. Hiramata, H. Ohno, T. Ibuka, *J. Org. Chem.* **2000**, 65, 4745–4749, and references therein.
- [25] T. Olpp, R. Brückner, *Synthesis* **2004**, 2135–2152.
- [26] N. Müller, W. Hoffmann, *Synthesis* **1975**, 781–781.
- [27] B. S. Crombie, C. Smith, C. Z. Varnavas, T. W. Wallace, *J. Chem. Soc. Perkin Trans. 1* **2001**, 206–215.
- [28] a) T. Oritani, K. Yamashita, *Phytochemistry* **1983**, 22, 1909–1912; b) A. Abad, C. Agulló, M. Arnó, A. C. Cuñat, R. Zaragoza, *Synlett* **1993**, 895–896; c) R. Okazaki, H. Kiyota, T. Oritani, *Biosci. Biotechnol. Biochem.* **2000**, 64, 1444–1447.
- [29] Method: K. Miwa, T. Aoyama, T. Shioiri, *Synlett* **1994**, 107–108.
- [30] *trans*-Selective hydrostannylation of hydroxy-**32** with Bu_3SnH and cat. $[\text{PdCl}_2(\text{PPh}_3)_2]$: M. Kuba, N. Furuichi, S. Katsumura, *Chem. Lett.* **2002**, 1248–1249.
- [31] (*trans*)-1-[(1*S*,2*R*)-1,2-Epoxy-2,6,6-trimethylcyclohexyl]-2-(tributylstannyl)ethene (*trans*-**31**): ^1H NMR (500.0 MHz, CDCl_3): δ = 0.88 (t, $J_{4',3'} = 7.3$ Hz, $3 \times 4''\text{-H}_3$), superimposed in part with 0.87–0.91 (m, $3 \times 1''\text{-H}_2$), 0.93, 1.09 and 1.15 [$3 \times$ s, $2'\text{-CH}_3$, $6'\text{-(CH}_3)_2$], 1.00–1.06 (m, $5'\text{-H}^1$), 1.30 (qt, $J_{3',4'} = J_{3'',2''} = 7.3$ Hz, $3 \times 3''\text{-H}_2$), 1.39–1.53 ppm (m, $4'\text{-H}_2$, $5'\text{-H}^2$, $3 \times 2''\text{-H}_2$), AB signal ($\delta_A = 1.72$, $\delta_B = 1.87$, $^2J_{AB} = 15.2$ Hz, additionally split by $J_{A,4'} = 5.7$ Hz and $J_{B,4'} = 7.9$ Hz, $3'\text{-H}_2$), AB signal ($\delta_A = 6.151$, $\delta_B = 6.166$, $J_{AB} = 19.2$ Hz; accompanying Sn isotope satellites as 2 d per signal branch: $^3J_{\text{H(A)},^{119}\text{Sn}} = 70.5$ Hz, $^3J_{\text{H(A)},^{117}\text{Sn}} = 67.5$ Hz, $^2J_{\text{H(B)},^{119}\text{Sn}} = 74.9$ Hz, $^2J_{\text{H(B)},^{117}\text{Sn}} = 71.7$ Hz; A: 1-H, B: 2-H).
- [32] Stannane *cis*-**31** was prepared as a racemic mixture from (2,6,6-trimethyl-1-cyclohexenyl)acetylene in two steps: radical-mediated hydrostannylation with Bu_3SnH ; epoxidation with *meta*-chloroperbenzoic acid: F. v. d. Ohe, Dissertation, Universität Freiburg, **2001**.
- [33] (5*S*)-3-Bromo-5-[(2*trans*,4*E*,1*S*)-1-hydroxy-5-(methoxycarbonyl)-2-methyl-2,4-pentadienyl]-2(5*H*)-furanone (**35**): ^1H NMR (500.0 MHz, CDCl_3): δ = 1.97 (d, $^4J_{2'\text{-Me},3'} = 1.2$ Hz, $2'\text{-CH}_3$), 2.91 (brs, OH), 3.77 (s, OCH_3), 4.30 (brd, $J_{1,5} = 5.5$ Hz, $1'\text{-H}$), 5.08 (dd, $J_{5,1'} = 5.6$ Hz, $J_{5,4} = 1.8$ Hz, 5-H), 5.94 (d, $J_{5,4'} = 15.2$ Hz, $5'\text{-H}$), 6.27 (dm, $J_{3',4'} = 11.5$ Hz, $3'\text{-H}$), 7.44 (d, $J_{4,5} = 1.9$ Hz, 4-H), 7.55 ppm (dd, $J_{4',5'} = 15.4$ Hz, $J_{4',3'} = 11.5$ Hz, $4'\text{-H}$).
- [34] V. Farina, V. Krishnamurthy, W. J. Scott, *Org. React.* **1997**, 50, 1–652.
- [35] Method: V. Farina, B. Krishnan, *J. Am. Chem. Soc.* **1991**, 113, 9585–9595.
- [36] Method: L. S. Liebeskind, R. W. Fengl, *J. Org. Chem.* **1990**, 55, 5359–5364.
- [37] (5*S*)-3-[(*E*)-2-[(1*S*,2*R*)-1,2-Epoxy-2,6,6-trimethylcyclohexyl]ethenyl]-5-[(2*E*,4*trans*,1*S*)-1-hydroxy-5-(methoxycarbonyl)-2-methyl-2,4-pentadienyl]-2(5*H*)-furanone (**5**): ^1H NMR (500.0 MHz, CDCl_3): δ = 0.93, 1.13 and 1.15 [$3 \times$ s, $2''\text{-CH}_3$, $6''\text{-(CH}_3)_2$], 1.06–1.10 (m, $5''\text{-H}^1$), ca. 1.39–1.49 (m, $4''\text{-H}^1$, $5'\text{-H}^2$), 1.61–1.68 (m, $4''\text{-H}^2$), AB signal ($\delta_A = 1.75$, $\delta_B = 1.90$, $^2J_{AB} = 15.1$ Hz, additionally split by $J_{A,4''\text{-H}(1)} = J_{A,4''\text{-H}(2)} = 5.2$ Hz, $J_{B,4''\text{-H}(1)} = J_{B,4''\text{-H}(2)} = 7.6$ Hz, $3''\text{-H}_2$), 1.99 (d, $^4J_{2''\text{-Me},3''} = 1.4$ Hz, $2''\text{-CH}_3$), 2.57 (brs, OH), 3.77 (s, OCH_3), 4.18 (d, $J_{1'',5} = 6.2$ Hz, $1''\text{-H}$), 5.01 (m, approximately interpretable as dd, $J_{5,1''} = 6.3$ Hz, $J_{5,4} = 1.9$ Hz, 5-H), 5.95 (d, $J_{5,4'} = 15.3$ Hz, $5'\text{-H}$), 6.28 (m, approximately interpretable as ddq, $J_{3'',4''} = 11.6$ Hz, $^4J_{3'',5''} \approx 1.4$ Hz, $^4J_{3'',2''\text{-Me}} \approx 0.8$ Hz, $3''\text{-H}$), 6.29 (d, $J_{1',2'} = 15.7$ Hz, $1'\text{-H}$), 6.95 (d, $J_{4,5} = 2.1$ Hz, 4-H), 7.22 (d, $J_{2',1'} = 15.6$ Hz, $2'\text{-H}$), 7.57 ppm (dd, $J_{4'',5''} = 15.1$ Hz, $J_{4'',3''} = 11.5$ Hz, $4''\text{-H}$).
- [38] (5*Z*)-3-[(*E*)-2-[(1*S*,2*R*)-1,2-Epoxy-2,6,6-trimethylcyclohexyl]ethenyl]-5-[(2*E*,4*trans*)-5-(methoxycarbonyl)-2-methyl-2,4-pentadienylidene]-2(5*H*)-furanone (**37**): To a solution of γ -(α -hydroxyalkyl)butenolide **5** (22.4 mg, 55.7 μmol) in THF (3 mL); the solvent contained 250 mg 2,6-di-*tert*-butyl-4-cresol per L and was degassed prior to use) was added DEAD (17.6 μL , 19.4 mg, 111 μmol , 2.0 equiv) at -30°C under argon atmosphere and exclusion of light. After 10 min PPh_3 (29.2 mg, 111 μmol , 2.0 equiv) was added, and the reaction mixture was stirred at -30°C for another 2 h. Two-thirds of the solvent was removed under reduced pressure at -30°C . A small portion of chromatography eluent (1 mL) was added, and this mixture was subjected to flash chromatography (cyclohexane:EtOAc 10:1 with 0.7 vol% NEt_3 ; degassed) which rendered the product (19.2 mg, 90%) as an intensely yellow solid. For selected ^1H NMR (500.0 MHz, C_6D_6) data see Scheme 6.
- [39] Following the suggestion of a referee, we also conducted the Stille coupling of the (dienoic ester)-containing bromobuteno-

lide **35** and the (4*S*)-4-hydroxy analogue of *trans*-**31**.^[30] This provided the (4*S*)-4-hydroxy analogue of **5**, a precursor of the hydroxylated butenolide moiety of natural peridinin with unaltered yield (83 %). Because of the presence of the 4-hydroxy group, which had to be conserved, the subsequent activation of the 1'-hydroxy group was best carried out under modified conditions: treatment of (4*S*)-4-hydroxy-**5** at –10 °C in THF with 9 equiv each of DEAD and PPh₃ (71 % yield). In the same way, when we processed the aldehyde analogue of the ester-substituted bromobutenolide **35**, we could swap the steps, i.e., start with the elimination and couple with the (4*S*)-4-hydroxy analogue of *trans*-**31**. The detailed results will be reported in a full paper.

Endohedral Fullerenes

Gadolinium Nitride Gd_3N in Carbon Cages: The Influence of Cluster Size and Bond Strength**

Matthias Krause* and Lothar Dunsch

Endohedral fullerenes have intriguing structural, magnetic, and electronic properties which may hold vast potential for applications in electronics and medicine.^[1,2] Among possible applications, their use as contrast agents in magnetic resonance imaging (MRI) is currently intensively discussed.^[3–6] Recently up to 20 times higher proton relaxivities were reported for $\text{Gd}@\text{C}_{82}(\text{OH})_n$ fullerenols in comparison to Gd^{3+} chelate contrast agents.^[4,5] Increased magnetic dipole–dipole relaxation was made responsible for this behavior. Hence, even higher proton relaxivities can be expected for endohedral fullerenes with two or three encaged metal ions, provided that their magnetic moments are coupled ferromagnetic. The spatial shielding of the Gd^{3+} ions by the carbon cage prevents their accumulation in human organs and tissues. Owing to this unique combination of crucial properties endohedral gadolinium fullerenes could replace current MRI agents in the future.

The discovery of $\text{Sc}_3\text{N}@\text{C}_{80}$ in 1999 opened the gate to fullerene structures with an encaged trimetal nitride cluster.^[7] The $\text{C}_{80}:7(I_h)$ ^[8] cage isomer was recognized as the most abundant fullerene cage for different trimetal nitrides, such as Sc_3N , Y_3N , and RE_3N (RE = rare-earth metals Tb, Ho, Er, Tm, Lu).^[9–14,16] No attempts to include larger nitride clusters than Tb_3N into carbon cages have been reported up to date. It is an open question, whether a stability threshold exists for C_{80}

cluster fullerenes with larger RE trimetal nitrides. Moreover it has to be addressed whether higher fullerene cages than C_{80} could be stabilized by larger RE trimetal nitrides. Therefore it is interesting whether Gd_3N cluster fullerenes can be prepared and isolated at all. From the point of medical applications, Gd_3N cluster fullerenes might yet be the precursor compounds of choice for nontoxic MRI agents with unprecedented relaxivities.

Herein the preparation of $\text{Gd}_3\text{N}@\text{C}_{2n}$ ($40 \leq n \leq 44$) cluster fullerenes and the isolation of the $\text{Gd}_3\text{N}@\text{C}_{80}(\text{I})$ isomer is reported. Its chemical identity and purity were established by mass spectrometry and high-pressure liquid chromatography (HPLC). The optical energy gap and the electronic absorptions were determined by Vis-NIR spectroscopy. Magnetic properties of $\text{Gd}_3\text{N}@\text{C}_{80}(\text{I})$ were probed by EPR spectroscopy. The cage isomer of the $\text{Gd}_3\text{N}@\text{C}_{80}(\text{I})$ was verified using Vis-NIR and FTIR spectroscopy. Raman spectroscopy was used to analyze the bonding between the caged Gd_3N cluster and the C_{80} cage. The analysis revealed two important factors that influence the abundance and stability of nitride-cluster fullerenes.

The chromatogram (Figure 1a) and the mass spectroscopic analysis of the fullerene extract, give evidence for the formation of Gd_3N cluster fullerenes with cages as small as C_{80} and as large as C_{88} . $\text{Gd}_3\text{N}@\text{C}_{80}$ is the most abundant fullerene in the extract. Its relative yield is approximately 35–40% of all fullerenes formed, which is by a factor of about two smaller than the relative yields of $\text{Sc}_3\text{N}@\text{C}_{80}$ and $\text{Tm}_3\text{N}@\text{C}_{80}$.^[15,16] The

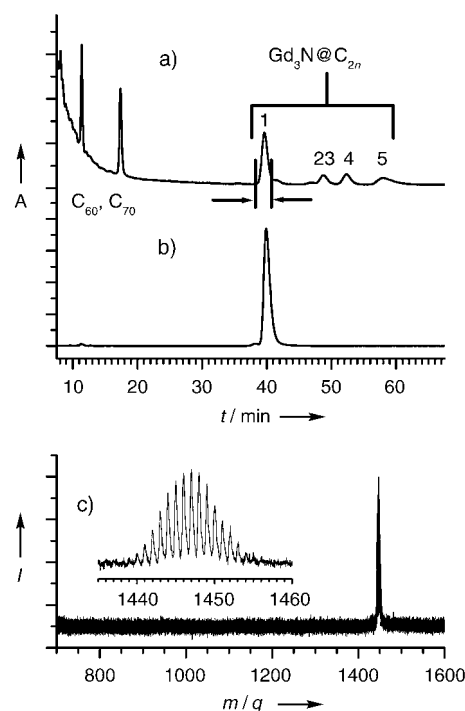


Figure 1. a) Chromatogram of the Gd_3N -fullerene extract and separation limits for $\text{Gd}_3\text{N}@\text{C}_{80}(\text{I})$, 1 = $\text{Gd}_3\text{N}@\text{C}_{80}$, 2 = $\text{Gd}_3\text{N}@\text{C}_{82}$, 3 = $\text{Gd}_3\text{N}@\text{C}_{86}$, 4 = $\text{Gd}_3\text{N}@\text{C}_{84}$, 5 = $\text{Gd}_3\text{N}@\text{C}_{88}$, flow rate 1.6 mL min^{-1} , injection volume $100 \mu\text{L}$, 30°C ; the background at low retention times is due to hydrocarbon byproducts. b) Chromatogram of isolated $\text{Gd}_3\text{N}@\text{C}_{80}(\text{I})$, conditions as for (a). c) Positive ion LD-TOF mass spectrum of isolated $\text{Gd}_3\text{N}@\text{C}_{80}(\text{I})$.

[*] Dr. M. Krause, Prof. Dr. L. Dunsch
Leibniz-Institute for Solid State and Materials Research Dresden
Institute of Solid State Research
Group for Electrochemistry and Conducting Polymers
Postfach 27 01 16, 01171 Dresden (Germany)
Fax: (+49) 351-465-9745
E-mail: m.krause@ifw-dresden.de

[**] The authors thank Mrs. H. Zöller, Ms. S. Döcke, Mrs. B. Schandert, and Dr. T. Tsend-Ayush for technical assistance in the fullerene production, HPLC separation, and spectroscopic measurements.

Gd₃N@C₈₀ HPLC fraction was composed of the Gd₃N@C₈₀ (I) isomer, whose retention time is 39.6 min, and the Gd₃N@C₈₀ (II) minor isomer giving rise to a small peak at $t = 41.5$ min. These retention times agree with those of Sc₃N@C₈₀ (I, II) and Tm₃N@C₈₀ (I, II) within a time interval of ± 1 min.^[15,16] The relative abundance of the second isomer in the entire Gd₃N@C₈₀ fraction was approximately 10% and hence only half as high as for Sc₃N@C₈₀ (II) and Tm₃N@C₈₀ (II).^[15,16] The fractions at retention times higher than 45 min were assigned to Gd₃N-cluster fullerenes with cages larger than C₈₀: Gd₃N@C₈₂, Gd₃N@C₈₆, Gd₃N@C₈₄, and Gd₃N@C₈₈. Their relative abundance was higher than within the Tm₃N@C_{2n} ($39 \leq n \leq 43$) cluster fullerene family, in which nitride-cluster fullerenes beyond C₈₀ were observed for the first time.^[16] On the other hand no Gd₃N in cages smaller than C₈₀ was detected, in contrast to the examples of Sc₃N@C₆₈,^[17] Sc₃N@C₇₈,^[18] Tm₃N@C₇₆,^[16] and Tm₃N@C₇₈.^[16] Gd₃N is the largest RE₃N cluster caged in a fullerene to date. Assuming a trigonal-planar structure and taking into account the expression $d(\text{RE}_3\text{N}) \propto 4r(\text{RE}^{3+})$ for the cluster diameter d , the Gd₃N cluster is by approximately 0.8 Å larger than Sc₃N ($r(\text{Gd}^{3+}) = 0.94$ Å, $r(\text{Sc}^{3+}) = 0.75$ Å).^[19] Apparently C₈₀ represents the size threshold for the encapsulation of the Gd₃N cluster in fullerene cages.

In the following we focus on the electronic and geometric properties of Gd₃N@C₈₀ (I), the most abundant Gd₃N structure. Its chemical identity and the purity of > 95% are shown by the chromatogram and the mass spectrum in Figure 1. Its successful isolation shows that the C₈₀ cage is large enough to form a stable Gd₃N@C₈₀ (I) cluster fullerene. The lower relative abundance of Gd₃N@C₈₀ (I) in comparison to Sc₃N@C₈₀ (I) and Tm₃N@C₈₀ (I) poses the question of whether this is due to a smaller energy gap, a different cage structure, or different bonding properties of the nitride clusters?

The Vis-NIR spectrum in Figure 2a reveals a large energy-gap electronic structure of Gd₃N@C₈₀ (I). The spectral onset is at around 780 nm. The HOMO–LUMO transition has a doublet structure with absorption maxima at 706 and 676 nm. The strongest visible absorption of Gd₃N@C₈₀ (I) is at 412 nm, and a shoulder is apparent at 555 nm. For comparison, Tm₃N@C₈₀ (I) has an onset at 780 nm, the HOMO–LUMO transitions at 705 and 675 nm, and the strongest absorptions at 540 and 407 nm.^[16] The electronic absorption spectra of Gd₃N@C₈₀ (I) and Tm₃N@C₈₀ (I) agree almost completely. Hence, neither a smaller energy gap nor the electronic structure of the C₈₀ cage can be responsible for the lower abundance of Gd₃N@C₈₀ (I) in comparison to Sc₃N@C₈₀ (I) and Tm₃N@C₈₀ (I).

Electron spin resonance of Gd₃N@C₈₀ (I) powder was studied by X-band continuous wave (cw) EPR spectroscopy at 4 and 295 K. No EPR signal for the fullerene was detected in these experiments. This result shows a diamagnetic electronic state for the C₈₀ carbon cage in Gd₃N@C₈₀ (I), similar to the cases of Sc₃N@C₈₀ (I) and Tm₃N@C₈₀ (I). On the other hand, an EPR signal from the (4f)⁷ states of the endohedral Gd³⁺ ions is expected. The g factor would be 2 and a resonance should appear at a magnetic induction of around 340 mT. The absence of this signal might be due to a strong line broadening in the powder sample. This problem can be

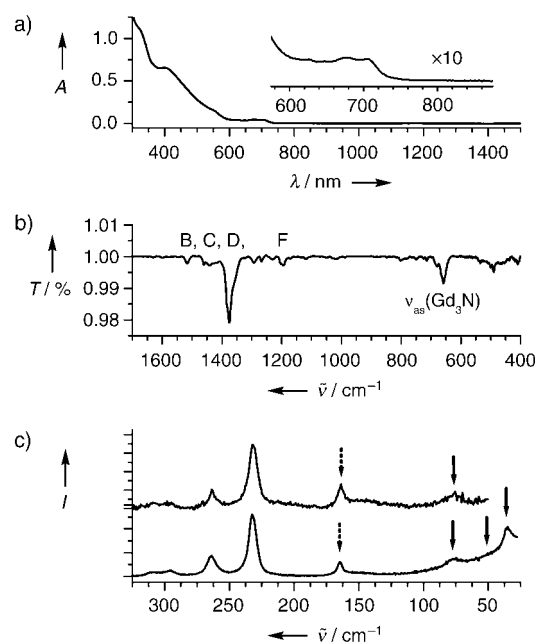


Figure 2. a) Vis-NIR spectrum of Gd₃N@C₈₀ (I) dissolved in toluene, 10-mm path length, 2 nm resolution. b) FTIR spectrum of Gd₃N@C₈₀ (I), 500 accumulations, 2 cm^{−1} resolution, capitals refer to the line-group classification introduced in refs. [15, 16]. c) Low-energy Raman spectrum of Gd₃N@C₈₀ (I), excited with 514 nm (upper trace) and 647 nm (lower trace) laser radiation, solid arrows indicate Gd₃N–C₈₀ vibrations, the broken arrows mark an internal Gd₃N cluster deformation mode.

overcome by future EPR studies in the W-band range, which have been successfully applied to detect the spin states in Gd@C₈₂.^[20]

The FTIR spectrum of Gd₃N@C₈₀ (I) in Figure 2b shows a small number of lines. This situation is characteristic for a C₈₀ cage with high symmetry. The detailed analysis revealed the same tangential cage-mode line groups as observed for the icosahedral structures Sc₃N@C₈₀ (I) and Tm₃N@C₈₀ (I).^[15,16] As for these compounds, only one strong radial cage mode was found at around 500 cm^{−1} for Gd₃N@C₈₀ (I).^[15,16] Owing to the close resemblance of its FTIR spectrum to those of Sc₃N@C₈₀ (I) and Tm₃N@C₈₀ (I), Gd₃N@C₈₀ (I) is assigned to the same carbon cage, that is, C₈₀:7 with I_h symmetry (Figure 3). This assignment is strongly supported by the HPLC and Vis-NIR analysis.

There is one major difference between the IR spectra of Gd₃N@C₈₀ (I), Tm₃N@C₈₀ (I), and Sc₃N@C₈₀ (I). The most intense low-energy IR line is at approximately 710 cm^{−1} for Tm₃N@C₈₀ (I), at 657 cm^{−1} for Gd₃N@C₈₀ (I), and at 599 cm^{−1} for Sc₃N@C₈₀ (I). Owing to its comparable intensity and the unambiguous metal-induced shift, this line is assigned to the antisymmetric M–N stretching vibration of the M₃N (M = Tm, Gd, Sc) cluster. For an explanation of the lower formation abundance of Gd₃N@C₈₀ (I) the frequency downshift of 53 cm^{−1} compared to Tm₃N@C₈₀ (I) is important. The lower vibrational energy reflects a weaker metal–nitrogen bond in Gd₃N. A mutual stabilization of the nitride cluster and the C₈₀:7(I_h) carbon cage is responsible for the unusual high abundance and stability of these structures.^[10,11] If one

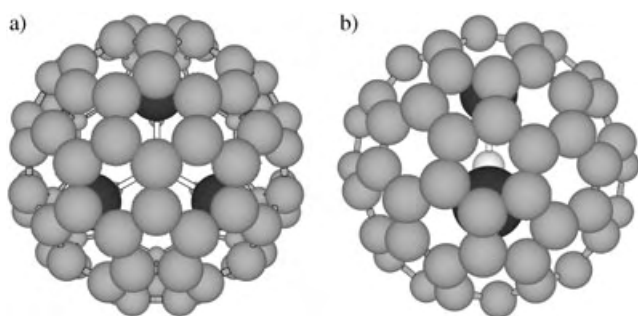


Figure 3. Schematic structure model of $\text{Gd}_3\text{N}@C_{80}$ (I_h) in orientation a) along and b) perpendicular to the C_3 axis; black Gd, gray C, white N; the geometry and orientation of the Gd_3N cluster are still to be confirmed.

component becomes less stable, the whole cluster fullerene will be destabilized and/or the formation of the structure will be suppressed. Thus, the weaker metal–nitrogen bond in Gd_3N is an important quantity in explaining the smaller yield of $\text{Gd}_3\text{N}@C_{80}$ (I). It can be rationalized by the weaker overlap of the Gd 5d and N 2p atomic orbitals, which is responsible for the chemical bond in the cluster. However, this bond-strength difference accounts only partly for the observed abundances, as the Sc_3N bond is even weaker than that of Gd_3N .

Another important factor for the overall stability of trimetal-nitride-cluster fullerenes is the interaction between the caged cluster and the carbon cage. As Figure 2c shows a typical vibrational pattern with low-energy Raman lines at 165, 77, 54, and 34 cm^{-1} is evident for $\text{Gd}_3\text{N}@C_{80}$ (I). The line at 165 cm^{-1} has counterparts in the Raman spectra of $\text{Sc}_3\text{N}@C_{80}$ at 210 cm^{-1} and at 194 cm^{-1} for $\text{Y}_3\text{N}@C_{80}$ and is attributed to a Gd_3N cluster-deformation mode. The lines below 100 cm^{-1} are assigned to frustrated Gd_3N rotations and translations. The frustration is due to $\text{Gd}_3\text{N}-C_{80}$ bond formation, which prevents a free cluster rotation as well as a cluster diffusion within the vibrational time scale of 10^{-11} – 10^{-13} s . For the alternative configurations of either a free-rotating cluster or a fast rotational diffusion, different low-energy Raman spectra are expected. For the free-rotating-cluster case, the rotation perpendicular to the cluster plane (R_x and R_y) has E'' symmetry and is Raman allowed. Therefore a multiline rotational Raman spectrum is expected. For the fast rotational-diffusion case, the rotational Raman spectrum should be broadened into a continuous background without any resolved lines.

Plotting the frequencies of the low-energy Raman modes for several $\text{M}_3\text{N}@C_{80}$ ($\text{M} = \text{Sc}, \text{Y}, \text{Gd}, \text{Tb}, \text{Ho}, \text{Er}, \text{Tm}$) versus $(1/\mu(\text{M}_3\text{N}-C_{80}))^{1/2}$ a fairly good linear correlation is obtained. Therefore, to a good approximation, the bond force constants are the same. Thus, the same type and strength of cluster–cage interaction exists in all these nitride-cluster fullerene structures. Hence, a weaker cluster– C_{80} interaction can be excluded as being significant for the lower abundance of $\text{Gd}_3\text{N}@C_{80}$ (I).

Summarizing, endohedral Gd_3N -cluster fullerenes covering cage sizes from C_{80} up to C_{88} were prepared for the first time. $\text{Gd}_3\text{N}@C_{80}$ (I) was the most abundantly formed fullerene structure in the soot, although larger Gd_3N -cluster fullerenes

were formed to a greater extent than within the $\text{Tm}_3\text{N}@C_{2n}$ ($39 \leq n \leq 43$) family. $\text{Gd}_3\text{N}@C_{80}$ (I) is based on the C_{80} cage isomer $C_{80:7}$ (I_h) and has a HOMO–LUMO energy gap of 1.75 eV. The Gd_3N cluster was found to form a bond to the C_{80} cage. The Gd_3N is the largest cluster to be caged in fullerenes to date. Two factors influence the formation abundance and distribution of nitride-cluster fullerenes: the metal-ion radius and the metal–nitrogen bond strength.

Experimental Section

The nitride-cluster fullerene preparation and isolation was described in detail elsewhere.^[10,15,16] Briefly, ammonia gas (20 mbar) was added to the helium atmosphere in the Krätschmer–Huffman arc burning reactor. Mixtures of Gd_2O_3 powder and graphite powder were pressed into the holes of graphite-rod electrodes in a molar metal/carbon ratio of 1:12.5. The fullerene soot generated was purified with acetone and subsequently extracted by CS_2 for 20 h in a soxhlet extractor. On average 100 μg fullerenes were obtained per burning. Fullerene separation was by multistage HPLC with toluene as the eluent. $\text{Gd}_3\text{N}@C_{80}$ (I) was isolated in one step using a linear combination of two analytical ($4.6 \times 250\text{ mm}$) BuckyPrep columns (Nacalai Tesque). 250 μg $\text{Gd}_3\text{N}@C_{80}$ (I) were isolated in this study. The composition of the extract and the purity of isolated $\text{Gd}_3\text{N}@C_{80}$ (I) were determined by HPLC and laser desorption time-of-flight (LD-TOF) mass spectrometry. Sample preparation and experimental details for Vis-NIR, FTIR, and Raman measurements were described elsewhere.^[15,16] Electron spin resonance (EPR) of $\text{Gd}_3\text{N}@C_{80}$ (I) powder was measured using an EMX X-band spectrometer (Bruker) with 100 kHz modulation and a microwave power of 100 mW at room temperature, and 10 mW and 100 mW at 4 K. The sample was evacuated under high vacuum and sealed in a 4-mm diameter quartz tube.

Received: July 27, 2004

Revised: October 10, 2004

Published online: January 26, 2005

Keywords: endohedral fullerenes · fullerenes · gadolinium · nitrides · spectroscopy · structure elucidation

- [1] H. Shinohara, *Rep. Prog. Phys.* **2000**, 63, 843–892.
- [2] *Endofullerenes: A New Family of Carbon Clusters* (Eds.: T. Akasaka, S. Nagase), Kluwer Academic Publishers, Dordrecht, **2002**.
- [3] L. J. Wilson, D. W. Cagle, T. P. Thrash, S. J. Kennel, S. Mirzadeh, J. M. Alford, G. J. Ehrhardt, *Coord. Chem. Rev.* **1999**, 192, 199–207.
- [4] M. Mikawa, H. Kato, M. Okumura, M. Narasaki, Y. Kanazawa, N. Miwa, H. Shinohara, *Bioconjugate Chem.* **2001**, 12, 510–514.
- [5] H. Kato, Y. Kanazawa, M. Okumura, A. Taninaka, T. Yokawa, H. Shinohara, *J. Am. Chem. Soc.* **2003**, 125, 4391–4397.
- [6] R. D. Bolskar, A. F. Benedetto, L. O. Husebo, R. E. Price, E. F. Jackson, S. Wallace, L. J. Wilson, J. M. Alford, *J. Am. Chem. Soc.* **2003**, 125, 5471–5478.
- [7] S. Stevenson, G. Rice, T. Glass, K. Harich, F. Cromer, M. R. Jordan, J. Craft, E. Hajdu, R. Bible, M. M. Olmstead, K. Maitra, A. J. Fisher, A. L. Balch, H. C. Dorn, *Nature* **1999**, 401, 55–57.
- [8] P. W. Fowler, D. E. Manolopoulos, *An Atlas of Fullerenes*, Clarendon Press, Oxford, **1995**.
- [9] L. Dunsch, P. Georgi, M. Krause, Ch. R. Wang, *Synth. Met.* **2003**, 135–136, 761–762.
- [10] L. Dunsch, M. Krause, J. Noack, P. Georgi, *J. Phys. Chem. Solids* **2004**, 65, 309–315.

- [11] M. Krause, H. Kuzmany, P. Georgi, L. Dunsch, K. Vietze, G. Seifert, *J. Chem. Phys.* **2001**, *115*, 6596–6605.
- [12] L. Feng, J. X. Xu, Z. J. Shi, X. R. He, Z. N. Gu, *Chem. J. Chin. Univ.* **2002**, *23*, 996–998.
- [13] E. B. Iezzi, J. C. Duchamp, K. R. Fletcher, T. E. Glass, H. C. Dorn, *Nano Lett.* **2002**, *2*, 1187–1190.
- [14] M. M. Olmstead, A. de Bettencourt-Dias, J. C. Duchamp, S. Stevenson, H. C. Dorn, A. L. Balch, *J. Am. Chem. Soc.* **2000**, *122*, 12220–12226.
- [15] M. Krause, L. Dunsch, *ChemPhysChem* **2004**, *5*, 1445–1449.
- [16] M. Krause, J. Wong, L. Dunsch, *Chem. Eur. J.* **2005**, *11*, 706–711.
- [17] S. Stevenson, P. W. Fowler, T. Heine, J. C. Duchamp, G. Rice, T. Glass, K. Harich, E. Hajdu, R. Bible, H. C. Dorn, *Nature* **2000**, *408*, 427–428.
- [18] M. M. Olmstead, A. de Bettencourt-Dias, J. C. Duchamp, S. Stevenson, D. Marciu, H. C. Dorn, A. L. Balch, *Angew. Chem.* **2001**, *113*, 1263–1265; *Angew. Chem. Int. Ed.* **2001**, *40*, 1223–1225.
- [19] N. N. Greenwood, A. Earnshaw, *Chemistry of the Elements*, Pergamon, Oxford, **1984**.
- [20] “Electron spin resonance spectroscopy for metallofullerenes” in: T. Kato in *Endofullerenes: A New Family of Carbon Clusters* (Eds.: T. Akasaka, S. Nagase), Kluwer Academic Publishers, Dordrecht, **2002**, pp. 153–167.

Dendritic Polymers

Reversible Cross-Linking of Hyperbranched Polymers: A Strategy for the Combinatorial Decoration of Multivalent Scaffolds**

Michael Barth, Rainer Fischer, Roland Brock, and Jörg Rademann*

Functional polymers in the nanometer range have been reported to control biomedical processes including immuni-

[*] Prof. Dr. J. Rademann
Medizinische Chemie
Forschungsinstitut für Molecular Pharmakologie
Robert-Rössle-Strasse 10, 13125 Berlin (Germany)
Fax: (+49) 30-9479-3280
E-mail: rademann@fmp-berlin.de
and
Institut für Chemie
Freie Universität Berlin
Takustrasse 3, 14195 Berlin (Germany)
Dipl.-Chem. M. Barth
Institut für Organische Chemie
Eberhard Karls Universität Tübingen
Auf der Morgenstelle 18, 72076 Tübingen (Germany)
Dipl.-Biochem. R. Fischer, Dr. R. Brock
Interfakultäres Institut für Zellbiologie
Eberhard Karls Universität Tübingen
Auf der Morgenstelle 15, 72076 Tübingen (Germany)

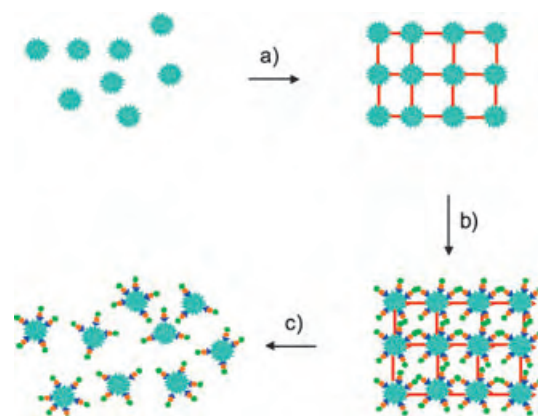
[**] This research was supported by the DFG (Graduiertenkolleg "Chemie in Interphasen, Projekt 6", fellowship for M.B.). We thank Dr. Volker Braig, BASF AG, Ludwigshafen for conducting the gel permeation chromatography.

Supporting information for this article is available on the WWW under <http://www.angewandte.org> or from the author.

zation, transfection, adhesion, and drug delivery.^[1] Multivalent scaffolds such as linear or branched polymers including dendrimers have been especially useful in these applications.^[2] They have served for the multiple presentation of single effective ligands in order to amplify low-affinity binding.^[3] In addition, dendritic structures have been found to be significantly more stable towards proteolysis in vivo than the respective monovalent ligands.^[4]

Whereas the plain, nondecorated polymers are easily accessible,^[5] the generation of chemically modified polymers with specific biological activity is much more demanding. Synthesis on soluble polymers has been studied extensively^[6] and has been inefficient in most cases due to tedious workup procedures and low yields. The one practical method to date is the conjugation of the polymer with preformed small molecules. Conjugation, however, is restricted to few coupling reactions and does not allow a flexible variation of the polymer decoration and loading. For structure–activity studies for example, during the biological optimization of polymer drugs, the preparation and variation of decorated multivalent scaffolds with increased throughput by parallel or combinatorial methods will be necessary.

Herein, we present a strategy that eliminates the problems of polymer modification and facilitates flexible access to complex decorated scaffolds (Scheme 1). Branched polymers



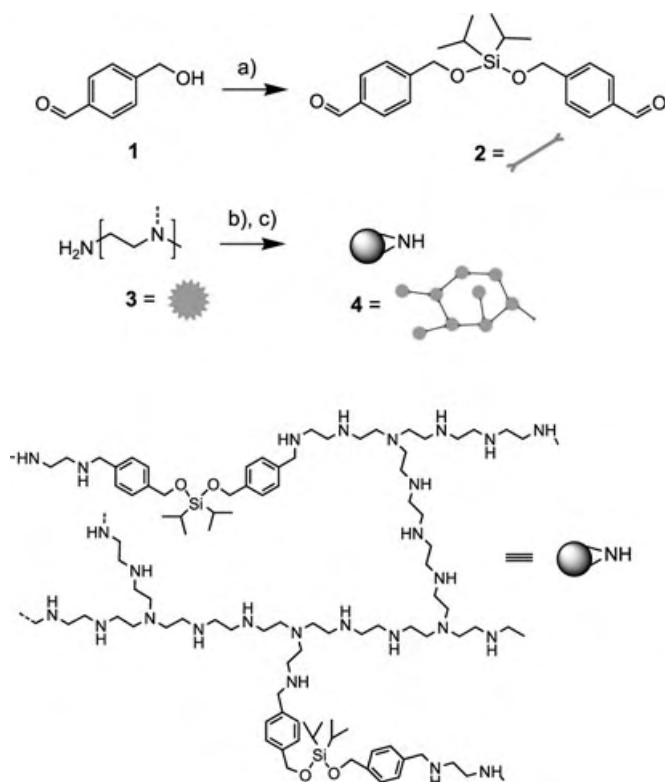
Scheme 1. Reversibly cross-linked hyperbranched polymers facilitate the multivalent decoration macromolecular structures. a) Highly branched PEI is cross-linked to yield a swellable resin that serves as a robust support in polymer-supported synthesis. b) Complex molecules can be constructed by multistep solid-phase synthesis. c) Finally, disintegration of the resin is effected by cleaving the reversible cross-linking.

were cross-linked to yield a swellable resin which served as a robust support for subsequent solid-phase synthesis (Scheme 1, top). Making use of easy-to-perform polymer-supported protocols for the multistep synthesis, we could assemble multiple copies of a target molecule on each macromolecule. Finally, the cross-linking units of the polymer support were cleaved, yielding the decorated scaffolds (Scheme 1, bottom).

Highly branched polyethylene imine (PEI) was selected as the ideal starting material for the preparation of a reversibly cross-linked resin.^[16,17] In several biological appli-

cations including in vivo transfection,^[7] PEI served as an efficient hyperbranched structure. Recently, it was demonstrated that various PEIs are well suited for the construction of ultrahigh-loaded polymer supports ("Ultraresins") useful in organic synthesis and for polymer reagents.^[8–10]

To obtain a robust solid support constructed of reversibly cross-linked hyperbranched polymers, the cross-linker must be cleaved orthogonally. Dialdehyde **2**, which contains a dialkoxysilane tether, was chosen for this purpose. Reversibly cross-linked resins were obtained by polycondensation of highly branched PEI **3** ($M_n=10\,000$; $M_w=25\,000$, polydispersity=2.5) with **2** (Scheme 2). For homogeneous cross-



Scheme 2. Cross-linker **2** was constructed from **1** and employed for construction of polymer support **4**. a) Diisopropyldichlorosilane, pyridine, 1 h, 60°C; b) **2**, THF, 4 h, RT; c) Sodium borohydride THF/MeOH 2:1, 16 h, RT.

linking in high yields, the concentrations of PEI and of the cross-linker **2** were critical. Resin **4** was characterized by ¹H MAS NMR spectroscopy, FT-ATR-IR spectroscopy, and elemental analysis (MAS=magic angle spinning, ATR=attenuated total reflection). Disintegration of resin **4** could be effected by cleaving the silicon–oxygen bonds in the cross-linker with acid (50% trifluoroacetic acid in dichloromethane, 2 h) or fluoride (1M tetrabutylammonium fluoride in THF, 2 h). Completion of the disintegration of **4** was proven by gel-permeation chromatography (GPC) yielding a PEI product with an M_n value identical to that of the starting polymer (Figure 1).

Resin **4** was employed in solid-phase synthesis (Scheme 3). Peptide synthesis could be conducted directly

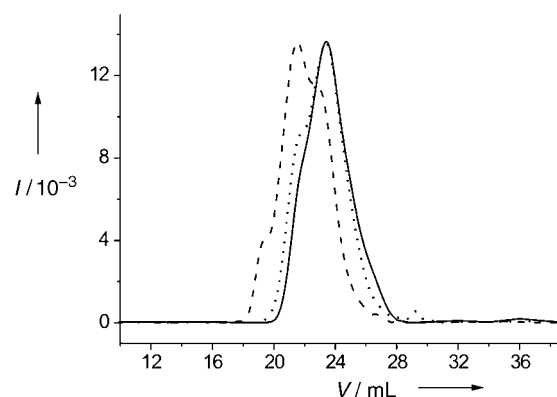
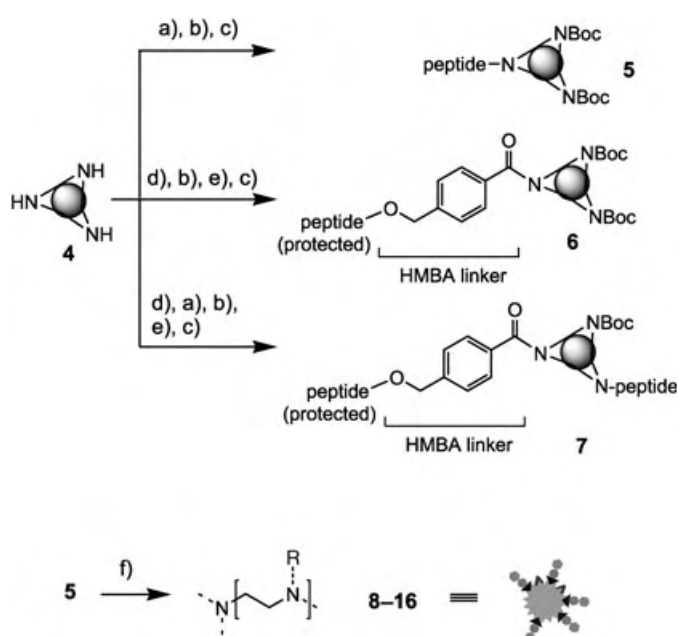


Figure 1. GPC of a) starting PEI **3** ($M_n=10\,000$, $M_w=25\,000$, continuous line), b) PEI obtained by decomposition of reversibly cross-linked resin **4** (dotted line), and c) peptide-decorated PEI polymer **8** ($M_n=24\,000$, $M_w=75\,000$, dashed line). V =elution volume, I =intensity of the detector signal.



Scheme 3. Reversibly cross-linked resin **4** was employed in the synthesis of decorated multivalent scaffolds. a) Fmoc-AA, TBTU, HOBT, DIPEA, DMF; b) di-*tert*-butyl dicarbonate, DIPEA, DMF, 2×2 h, RT; c) peptide synthesis following the Fmoc strategy; d) 4-[(acetyloxy)methyl]benzoic acid, TBTU, HOBT, DIPEA, DMF, 4 h, RT; e) NaOMe 0.1 M in MeOH, 0.5 h, RT; f) 95% trifluoroacetic acid, 2.5% triisopropylsilane, 2.5% water, 4 h, RT. R=unprotected peptide, Boc=*tert*-butoxycarbonyl, Fmoc=9-fluorenylmethoxycarbonyl.

on the secondary amines of resin **4** to yield resin **5**. Alternatively, the peptide sequences were assembled on the 4-hydroxymethyl benzoic acid linker (HMBA) (→resin **6**). This base-labile linker can be used such that orthogonal cleavage of the protected peptides from resin **6** does not affect resin integrity. In addition, the linker enables the cleavage of deprotected peptides from the released multivalently decorated scaffolds **8–16** as required for analytical purposes or as desirable for specific in vivo applications. As a third option,

only a small fraction of free amines were coupled with the HMBA linker in order to allow for the analytic monitoring of peptide synthesis by partial cleavage (\rightarrow resin **7**).

To adjust the peptide content of the resulting multivalent decorated scaffolds, a substoichiometric amount of the linker or the first amino acid was coupled on resin **4**. The remaining secondary amines of the polymer backbone were capped by reaction with Boc-anhydride. Benzotriazolyltetramethyl-uranium tetrafluoroborate (TBTU) was used to activate the Fmoc-amino acids. The success of the synthesis could be monitored by employing the Kaiser test or by cleavage and deprotection to give the final peptide product.

To demonstrate the feasibility of the concept, a selection of potentially bioactive decorated multivalent scaffolds was prepared (Table 1). The selected peptides include sequences for intracellular targeting (decorated scaffolds **8** and **9**),^[11] B and T cell epitopes for vaccination (**10–14**), and a peptide described to disrupt molecular interactions involved in the regulation of apoptosis inside the cytoplasm (**15**).^[12] This selection represents a broad spectrum of biological and biomedical applications.

Resins **5**, **6** and **7** were decomposed under acidic conditions (95 % trifluoroacetic acid, 2.5 % triisopropylsilane, 2.5 % water, 4 h), and the standard side-chain protection groups of amino acids were also removed in the same step. For workup of the decorated polymers, protocols routinely used in peptide synthesis could be employed. Repeated precipitation of the peptide-functionalized polymers in cold diethyl ether furnished pure decorated polymer scaffolds and removed the nonvolatile residues from the trityl and the 2,2,4,6,7-pentamethyldihydrobenzofuran-5-sulfonyl (Pbf) protecting groups as determined by NMR spectroscopy (see the Supplementary Information).

To evaluate the biological applicability of the peptide-decorated polymer scaffolds obtained by the novel strategy, cellular uptake was investigated by confocal microscopy of living cells. The decorated scaffold **8** bearing the fluorescein-labeled nuclear localization sequence Fluo-PKKKRKV was selected for this purpose. HeLa cells were incubated with the scaffold at a concentration of 400 nM for 2 h at 37 °C. Both a distinct vesicular staining and a homogeneous cytoplasmic and nuclear localization were observed (Figure 2). The vesicular staining colocalized with high-molecular-weight

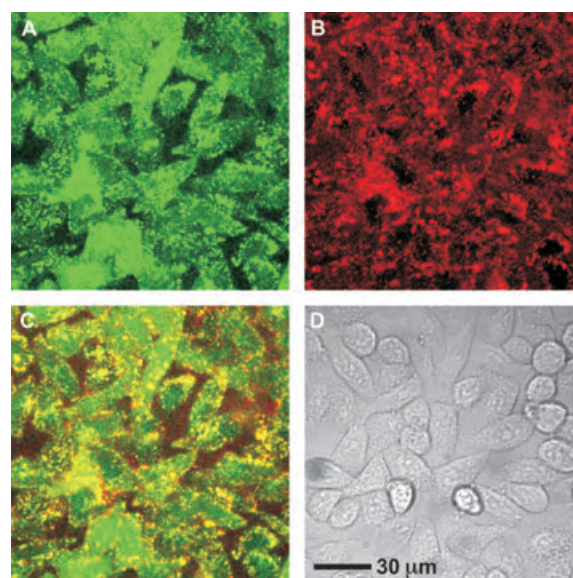


Figure 2. HeLa cells were incubated with serum-free medium containing fluorescein-labeled dendrimer (400 nM) and AlexaFluor 647-dextran (10 μ M) for 2 h, washed, and analyzed by multichannel confocal laser scanning microscopy. A) fluorescein fluorescence, B) AlexaFluor 647-dextran fluorescence, C) superposition of both fluorescence channels, D) transmission picture.

(10000 Da) dextrans, which are internalized by fluid-phase endocytosis.^[13] The observed subcellular distribution is indicative of uptake by endocytosis and subsequent escape from endocytic compartments. The cytoplasmic and nuclear localization could be inhibited by incubation with bafilomycin A1, a highly potent and selective inhibitor of vacuolar-type H⁺-ATPases (see the Supplementary Information).^[14] The homogeneity of the uptake on the level of a population of cells and the cellular toxicity of the nanoscale constructs was studied by flow cytometry. A low concentration of **8** (50 nM) was sufficient for homogeneous loading of the cell population.^[15] In addition, no toxicity was observed at concentrations up to 1 μ M (data are given in the Supplementary Information).

Reversibly cross-linked resins prepared from hyperbranched polymers are powerful new tools for the generation of decorated multivalent scaffolds. By creating a transition from solution to solid-phase methods, the concept combines the advantages of polymer-supported synthesis with the ease of conventional reaction monitoring, including on-bead and off-bead analysis. With these resins, the repertoire of combinatorial methods including parallel synthesis, automation, and split-and-mix operations is applicable to the decoration of macromolecular structures. Furthermore, the multivalent scaffolds we obtained are suitable for cellular applications. The entire cell population was affected homogeneously by scaffold **8**. In future studies the concept will be used for the development and optimization of biologically active polymers targeting the cytoplasm or specific organelles of eukaryotic cells.

Table 1: Synthesis of decorated multivalent scaffolds with potentially bioactive peptide sequences.

Decorated scaffold	Sequence	Resin	Loading [mmol g ⁻¹]	<i>M</i> _p [g mol ⁻¹] ^[a]	Purity (214 nm) [%]	<i>M</i> _n [g mol ⁻¹] ^[b]	Copies per PEI molecule
8	Fluo-PKKKRKV	5	1.6	—	—	30 000	16
9	ANWTGPKKKRKV	5	1.6	—	—	32 000	16
10	EQPRKFG	5	3.0	—	—	35 000	40
11	MAYPRISVNNG	6	1.8	1234.6	82.5	32 000	18
12	QSQPQPPHPTPYWIG	6	1.8	1745.8	84.3	41 000	18
13	KVSTLPAITLKLGGKG	6	1.8	1595.9	82.5	38 500	18
14	QSQPQPPHPTPYWIG	7	2.2	1745.8	88.3	48 000	22
15	AVPIAQKK(Fluo)G	7	2.2	1088.7 ^[c]	88.3 ^[c]	38 000	22
16	KQAIPVAK(Fluo)G	7	2.2	1088.7 ^[c]	86.6 ^[c]	38 000	22

[a] Mass of the peptide methyl ester. [b] Mass of the product. [c] Mass and purity of AVPIAQKK(Dde)G-OME and KQAIPVAK(Dde)G-OME. Fluo = 5(6)-carboxyfluorescein.

Experimental Section

Synthesis of **4**: Polyethylene imine ($M_n = 10000$, $M_w = 25000$, 1.25 g) was dissolved in THF (6.1 mL), and a solution of **2** (0.495 g, 1.29 mmol) in THF (4.6 mL) was added rapidly. After one minute the stirring bar ceased rotating. After 4 h the polymer was crushed, washed with THF, and suspended in THF/MeOH (2:1, 24 mL). Sodium borohydride (0.097 g, 2.56 mmol) was added, and the suspension was shaken for 16 h at RT. The polymer was washed with THF and MeOH, pressed through a sieve (400 μ m pores), washed again with MeOH and CH_2Cl_2 , and dried in vacuo to give resin **4** (1.5 g, 89%). Elemental analysis: C 55.6, H 9.7, N 21.0; ^1H MAS NMR (400 MHz, MeOD, rotation frequency 4500 Hz): $\delta = 0.9$ –1.2 (m, isopropyl, rel. integration 16.7), 2.2–3.0 ppm (m, PEI- CH_2 , 100), 3.72 (br.s, *sec*-N- CH_2 -aryl, 2.52), 4.56 (br.s, *tert*-N- CH_2 -aryl, 0.53) 7.2–7.5 ppm (br.s, aryl-H, 6.51); FT-ATR-IR: $\tilde{\nu} = 815$, 1063, 1090, 1461, 1572, 2815, 2932, 3277 cm^{-1} .

General procedure for the synthesis of peptide-decorated polymer scaffolds: Fmoc-glycine (446 mg, 1.5 mmol) was coupled with TBTU (482 mg, 1.5 mmol) *N*-hydroxybenzotriazole (HOBT; 230 mg, 1.5 mmol) and *N,N*-diisopropylethyl amine (DIPEA; 257 μ L, 1.5 mmol) in DMF to resin **4** (100 mg). After 4 h the resin was washed with DMF and CH_2Cl_2 and dried in vacuo. The resin was capped using di-*tert*-butyl dicarbonate (1.1 g, 5 mmol) and DIPEA (1.7 mL, 10 mmol) in DMF (2 \times 2 h) at RT. The absence of primary and secondary amines was indicated by the Kaiser test and the chloranil test, respectively. The loading of the resin was determined photometrically by cleaving the Fmoc group from the resin.

Peptides were synthesized by the Fmoc strategy using four equivalents of amino acid (based on the loading with first amino acid), TBTU, HOBT, and DIPEA in DMF for 90 min. The Fmoc group was cleaved by treatment with 20% piperidine in DMF (2 \times 8 min). Completion of the acylation was determined by the Kaiser test.

Decomposition together with removal of the amino acid side-chain protection of the peptide-decorated resin was performed by using 95% trifluoroacetic acid (TFA), 2.5% H_2O , and 2.5% triisopropylsilane for 4 h at RT. The solution was filtered, and the filter was washed with TFA. Collected solvents were evaporated. After precipitation with cold diethyl ether (4 \times) the soluble peptide-decorated polymer scaffold was lyophilized (*tert*-butanol/water 4:1).

Received: May 5, 2004

Revised: August 23, 2004

Published online: February 2, 2005

Keywords: combinatorial chemistry · drug delivery · peptides · polymers · solid-phase synthesis

- b) E. Bayer, A. Geckeler, *Justus Liebigs Ann. Chem.* **1974**, 1671–1674; c) R. Haag, A. Sunder, A. Hebel, S. Roller, *J. Comb. Chem.* **2002**, *4*, 112–119.
- [7] K. Aoki, S. Furuhashi, K. Hatanaka, M. Maeda, J.-S. Remy, J.-P. Behr, M. Terada, T. Yoshida, *Gene Ther.* **2001**, *8*, 508–514.
- [8] M. Barth, J. Rademann, *J. Comb. Chem.* **2004**, *6*, 340–349.
- [9] J. Rademann, M. Barth, *Angew. Chem.* **2002**, *114*, 3087–3090; *Angew. Chem. Int. Ed.* **2002**, *41*, 2975–2978.
- [10] M. Barth, S. T. Ali Shah, J. Rademann, *Tetrahedron* **2004**, *60*, 8703–8709.
- [11] D. A. Jans, C.-Y. Xiao, M. H. C. Lam, *Bioessays* **2000**, *22*, 532–544.
- [12] C. R. Arnt, M. V. Chiorean, M. P. Heldebrandt, G. J. Gores, S. H. Kaufmann, *J. Biol. Chem.* **2002**, *277*, 44236–44243.
- [13] C. Plank, B. Oberhauser, K. Mechtler, C. Koch, E. Wagner, *J. Biol. Chem.* **1994**, *269*, 12918–12924.
- [14] a) E. J. Bowman, A. Siebers, K. Altendorf, *Proc. Natl. Acad. Sci. USA* **1988**, *85*, 7972–7976; b) T. Merdan, K. Kunath, D. Fischer, J. Kopecek, T. Kissel, *Pharm. Res.* **2002**, *19*, 140–147.
- [15] For comparison, in a recent publication 50 μ m of a fluorophore-labeled trimeric peptide was required for detectable incorporation in HeLa cells: J. Fernandez-Carneado, M. J. Kogan, S. Castel, E. Giralt, *Angew. Chem.* **2004**, *116*, 1847–1850; *Angew. Chem. Int. Ed.* **2004**, *43*, 1811–1814.
- [16] The fragmentation of a macroscopic polymer to give a modified, multivalent structure as described in this article must be clearly distinguished from the numerous works on enzymatically or chemically cleavable dendrimers. Cleavable dendrimers are fragmented into monomeric building blocks, and thereby the multivalent character is lost. Two recent examples on triggered dendrimer cleavage are: a) F. M. H. de Groot, C. Albrecht, R. Koekkoek, P. H. Beusker, H. W. Scheeren, *Angew. Chem.* **2003**, *115*, 4628–4632; *Angew. Chem. Int. Ed.* **2003**, *42*, 4490–4494; b) J. R. Amir, N. Pessah, M. Shamis, D. Shabat, *Angew. Chem.* **2003**, *115*, 4632–4636; *Angew. Chem. Int. Ed.* **2003**, *42*, 4494–4499.
- [17] Polyethylene imine was selected as the most inexpensive commercially available starting polymer. In principle, the protocol should be applicable for other branched polyamines including amine dendrimers.

- [1] a) R. Duncan, *Nat. Rev. Drug Discovery* **2003**, *2*, 347–360; b) U. Boas, P. M. H. Heegaard, *Chem. Soc. Rev.* **2004**, *33*, 43–63; c) M. J. Cloninger, *Curr. Opin. Chem. Biol.* **2002**, *6*, 742–748; d) S.-E. Stiriba, H. Frey, R. Haag, *Angew. Chem.* **2002**, *114*, 1385–1390; *Angew. Chem. Int. Ed.* **2002**, *41*, 1329–1334.
- [2] J. P. Tam, *Proc. Natl. Acad. Sci. USA* **1988**, *85*, 5409–5413.
- [3] M. Mammen, S.-K. Choi, G. M. Whitesides, *Angew. Chem.* **1998**, *110*, 2908–2953; *Angew. Chem. Int. Ed.* **1998**, *37*, 2755–2794.
- [4] L. Bracci, C. Falciani, B. Lelli, L. Lozzi, Y. Runci, A. Pini, M. G. De Montis, A. Tagliamonte, P. Neri, *J. Biol. Chem.* **2003**, *278*, 46590–46595.
- [5] a) G. R. Newcome, C. N. Moorefield, F. Vögtle, *Dendrimers and Dendrons*, Wiley-VCH, Weinheim **2001**; b) *Dendrimers and Other Dendritic Polymers* (Eds.: J. M. J. Fréchet, D. A. Tomalia), Wiley, Chichester, **2001**.
- [6] In classic organic synthesis on dissolved polymers, various polyols were employed: a) M. Mutter, E. Bayer, *Angew. Chem.* **1974**, *86*, 101–102; *Angew. Chem. Int. Ed. Engl.* **1974**, *13*, 88–89;

Self-Assembly

Complete Self-Assembly of Discrete Supramolecular Dendrimers**

Alexander Franz, Walter Bauer, and Andreas Hirsch*

The complete self-assembly of dendrimers based on noncovalent interactions presents a great challenge. By analogy with supramolecular polymers,^[1–4] the reversible and thermodynamically controlled linkage of the basic building blocks leads to dynamic materials which are able to react to external stimuli and which are able to undergo self-healing processes. However, the hitherto presented concepts for the self-assembly of discrete and purely organic dendrimers employed preassembled dendritic systems in most cases. These entities have been linked to form discrete superstructures, for example, 1) by intermolecular hydrogen bonds with each other^[5–7] or with other molecules,^[8,9] 2) by electrostatic interactions between oppositely charged units,^[10] and 3) as a result of structural and hydrophobic effects in the case of amphiphilic dendrimers.^[11]

We here present the first approach for the complete self-assembly of discrete supramolecular dendrimers where the repetition motif is no longer based on dendritic subunits (Figure 1). We employ the homotritopic Hamilton receptor **1**,^[2,12] which can form six hydrogen bonds to cyanuric and barbituric acid derivatives. We have developed the heterotritopic AB₂ unit **2** as a branching element, which contains two Hamilton receptors as well as a complimentary cyanuric acid substrate.

The synthesis of **2** started with **4**, which was converted into the corresponding acid chloride and treated with **5** to give compound **6**. After cleavage of the ester with KOH, treatment with 0.5 equivalents of **8** led to ether formation in a twofold S_N reaction (Scheme 1). Steglich coupling of the cyanuric acid derivative **11** with compound **10** (deprotected by trifluoroacetic acid) leads to the AB₂ branching unit **2** in good yields.

A total of $3 \times 2^n - 3$ molecules of **2** (n = generation number) links the core **1** with end caps **3** in the supramolecular dendrimer. When components **1**, **2**, and **3** are mixed in a

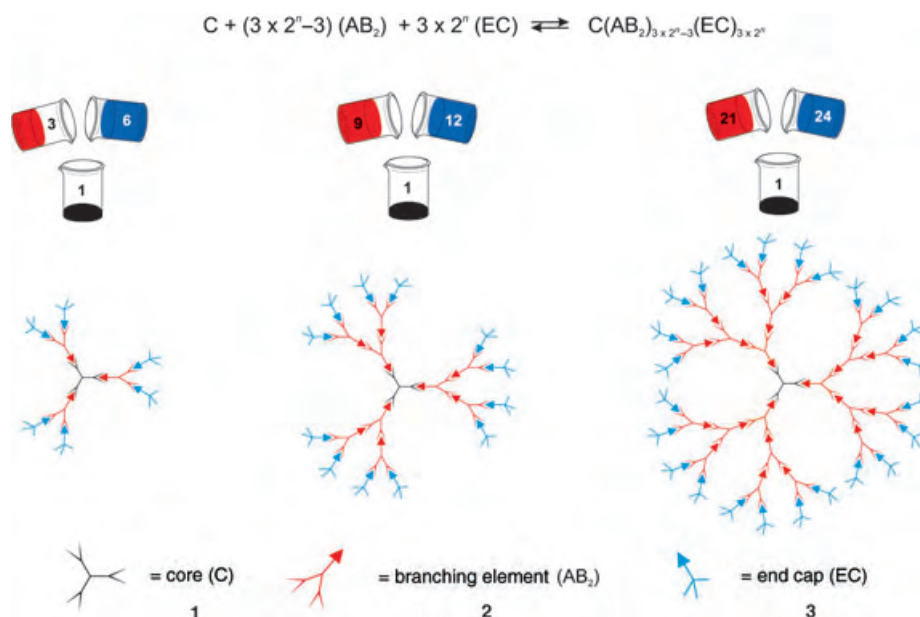
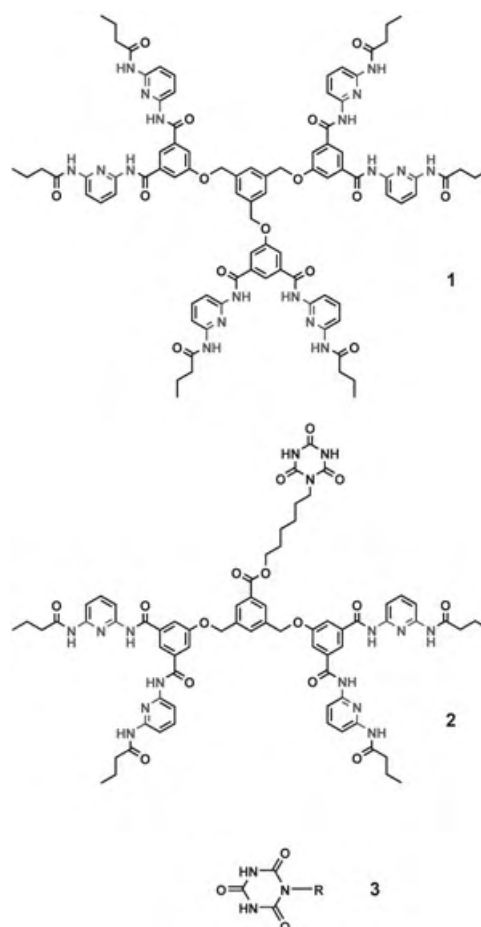
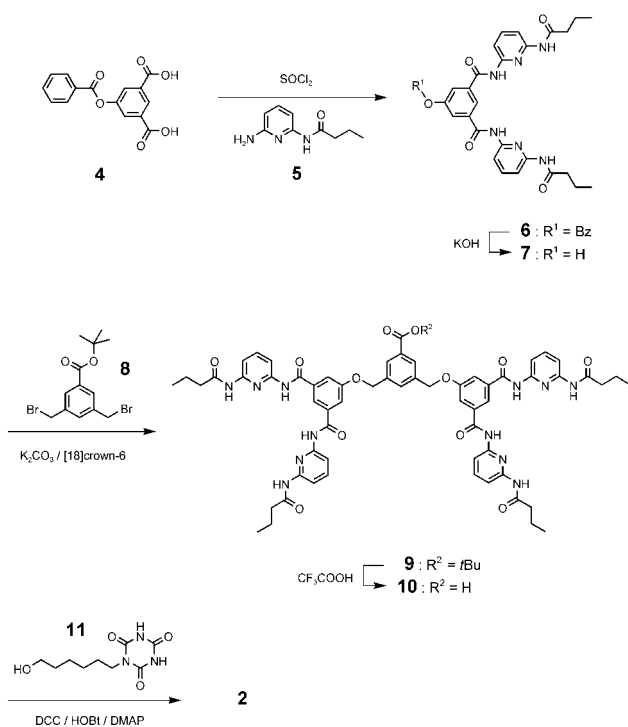


Figure 1. Supramolecular assembly of discrete dendrimers by using the homotritopic core **1**, heterotritopic AB₂ block **2**, and end caps **3**.



[*] Dipl.-Chem. A. Franz, Prof. Dr. W. Bauer, Prof. Dr. A. Hirsch
Institut für Organische Chemie
der Friedrich-Alexander-Universität Erlangen-Nürnberg
Henkestrasse 42, 91054 Erlangen (Germany)
Fax: (+49) 9131-852-6864
E-mail: andreas.hirsch@chemie.uni-erlangen.de

[**] This work was supported by the Fonds der Chemischen Industrie.
Supporting information for this article is available on the WWW
under <http://www.angewandte.org> or from the author.

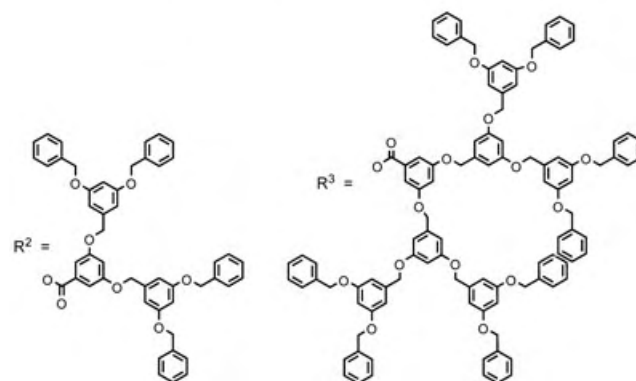
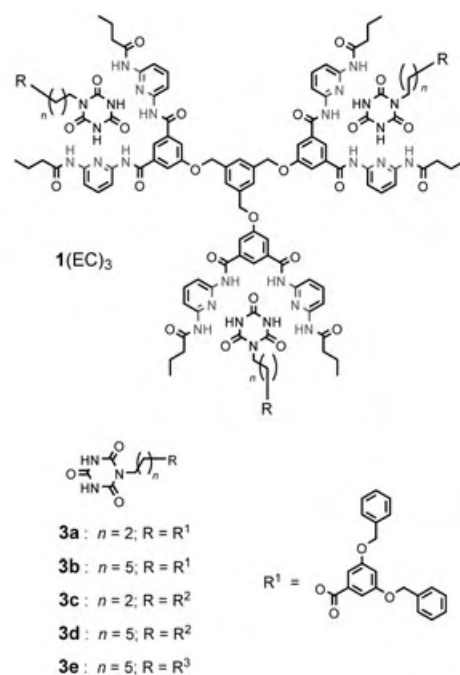


Scheme 1. Synthesis of the branching element **2**. Bz = benzoyl, DCC = dicyclohexylcarbodiimide, DMAP = 4-dimethylaminopyridine, HOBT = 1-hydroxybenzotriazole.

1:(3 × 2ⁿ−3):(3 × 2ⁿ) ratio, complete self-assembly of a supramolecular dendrimer of generation *n* can be expected, provided that all possible hydrogen bonds are formed (Figure 1).

For comparison, we first investigated the formation of **1(EC)**₃ aggregates, in which the core **1** is complexed directly by three dendritic end caps **3a–3e** (Scheme 2).^[13,14] To achieve this, end caps **3a–3e** were added by titration to core **1**. During this process the characteristic ¹H NMR chemical shifts of the NH protons to higher frequency (lower field) were monitored.^[2] From the titration curves the association constants of complexes **1(EC)**₃ were derived by using a method by Solov'ev et al.^[15] and by using the computer program Chem-Equili (Table 1). The values obtained are in good agreement with literature data for comparable systems.^[2] The Scatchard plots^[16] of these data are indicative of pronounced cooperativity in the formation of **1(EC)**₃. Due to the increase in size, the aggregation yielding dendritic complexes **1(EC)**₃ results in shorter retention times *t*_{SEC} relative to those of free **1** and **3a–3e** in size exclusion chromatography experiments. Plots of the glass transition temperatures *T*_g versus *n*_e*M*^{−1} (*n*_e = number of benzyl end groups, *M* = molecular mass) give a linear relationship for dendrons **3b**, **3d**, and **3e**, as well as for the corresponding supramolecular dendrimers **1(EC)**₃ (Table 1, Figure 2). This behavior is in complete agreement with the chain end–free volume theory for dendrimers, which is expressed as *T*_g = *T*_{g∞} − *K'* (*n*_e*M*^{−1}). On the other hand, the observed coincidence proves the existence of **1(EC)**₃ as discrete dendrimers.

Now we focus on the systems described in Figure 1 and formed by the stoichiometric mixing of core unit **1**, branching



Scheme 2. Aggregates **1(EC)**₃ with different end caps EC = **3a–e**.

Table 1: Physical properties of core **1** (C), end caps **3a–e** (EC), complexes **1(EC)**₃, and the AB₂ unit **2**.

	<i>T</i> _g [K] ^[a]	<i>n</i> _e ^[b]	<i>d</i> [nm] ^[c]	log <i>K</i> ₁ [l mol ^{−1}] ^[f]	log <i>K</i> ₂ [l mol ^{−1}] ^[g]	log <i>K</i> ₃ [l mol ^{−1}] ^[h]	<i>t</i> _{SEC} [min] ^[i]
1	418.66	—	0.82 ^[d]	—	—	—	9.74
3a	322.98	2	1.38 ^[e]	—	—	—	10.03
3b	310.20	2	2.14 ^[d]	—	—	—	10.66
3c	324.98	4	1.70 ^[e]	—	—	—	10.46
3d	317.64	4	0.66 ^[d]	—	—	—	8.75
3e	321.72	8	0.67 ^[d]	—	—	—	—
1(3a) ₃	—	6	—	1.66	1.29	26.73	8.05
1(3c) ₃	—	12	2.66 ^[d]	4.21	4.71	7.48	7.22
1(3b) ₃	312.60	6	—	3.82	2.60	8.99	7.96
1(3d) ₃	316.04	12	2.38 ^[d]	4.46	4.46	6.33	8.18
1(3e) ₃	318.34	24	—	3.51	4.51	4.09	—
2	407.07	—	2.46 ^[e]	—	—	—	9.73

[a] *T*_g = glass transition temperature. [b] *n*_e = number of terminal benzyl groups. [c] *d* = particle diameter (according to PFG NMR). [d] In CDCl₃. [e] In [D₆]DMSO. [f] *K*₁: C + EC ⇌ C(EC). [g] *K*₂: C(EC) + EC ⇌ C(EC)₂. [h] *K*₃: C(EC)₂ + EC ⇌ C(EC)₃. [i] *t*_{SEC} = retention time in size-exclusion chromatography (SEC) with MN Nucleogel GPC 500-5.

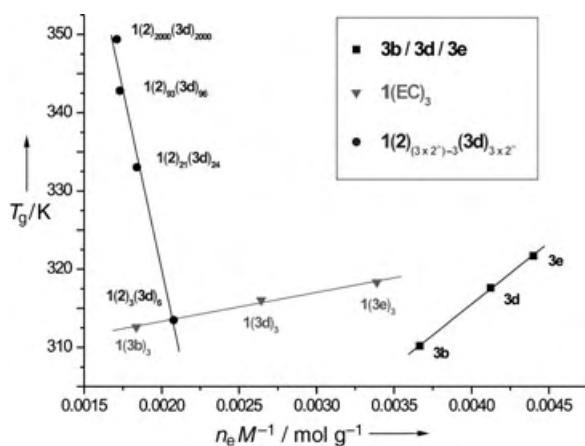


Figure 2. Plot of the glass transition temperature T_g vs. $n_e M^{-1}$, the quotient of the number of terminal benzyl groups and the molar mass, for the isolated end caps **3b**, **3d**, and **3e**, and for the complexes $1(\text{EC})_3$, and the supramolecular dendrimer $1\cdot 2\cdot 3\cdot 3d_{(3\times 2^n-3)}$.

element **2**, and end cap **3d** in a ratio of $1:(3\times 2^n-3):(3\times 2^n)$. DSC measurements of the AB_2 unit **2** afford a high glass transition temperature, indicative of aggregation to polymeric structures. As a result of the addition of core **1** and end cap **3d**, the polymer is disrupted, and a perfectly linear relationship between the glass transition temperature T_g and the $n_e M^{-1}$ ratio (and, thus, the generation number n) results (Figure 2). This demonstrates that discrete supramolecular dendrimers must be present in the solid state.

Due to the complexity of the associated exchange processes, the ^1H NMR shift of the NH proton signals during the titration of components **1**, **2**, and end cap **3a–3e** may no longer be employed to determine the various association constants. However, when one examines the determined equilibrium constants for the $1(\text{EC})_3$ complexes (Table 1) one can assume that exchange processes will take place in solution. Nonetheless, by using pulsed field gradient (PFG) NMR spectroscopy we proved the existence of discrete

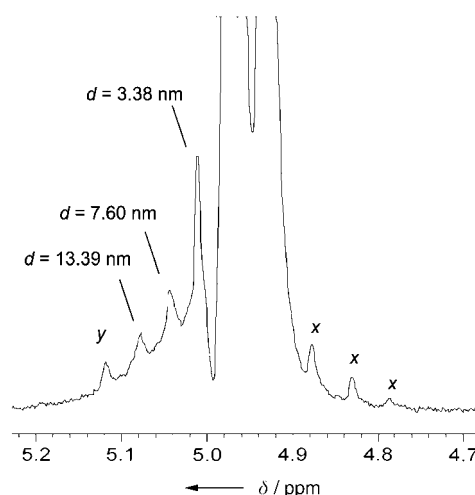


Figure 3. Section of the ^1H PFG NMR spectrum of a mixture of **1**, **2**, and **3d** in the G3 stoichiometry. The appearance of several discrete structures 3.4, 7.6, and 13.4 nm in diameter is evident. In addition, larger particles *y* are found, whose size cannot be determined due to unfavorable signal-to-noise ratio. This also holds for aggregates *x*.

dendrimers in chloroform. This method can be used to determine the diffusion constants of the dendrimers and thus, in turn, the dendrimer sizes. We employed the intensity decrease of the benzyl proton signals of core unit **1** as a probe. Components **1**, **2**, and **3d** were dissolved in CDCl_3 , in stoichiometric amounts corresponding to dendrimers of the first, third, and fifth generation. For the G1 system $1\cdot 2\cdot 3\cdot 3d_6$, aggregates of uniform size and with a diameter of 2.0 nm were found.^[17] This particle size was confirmed by dynamic light-scattering experiments (3.12 nm). For complete self assembly of the dendrimers of lower generation, the required stoichiometric ratio of branching unit **2** and end caps **3a–3e** differs more than for higher generations (where a 1:1 limit is approached). Thus, it can be assumed that comprehensive discrimination will become increasingly difficult. This expectation has been verified. Figure 3 shows the ^1H NMR spectrum

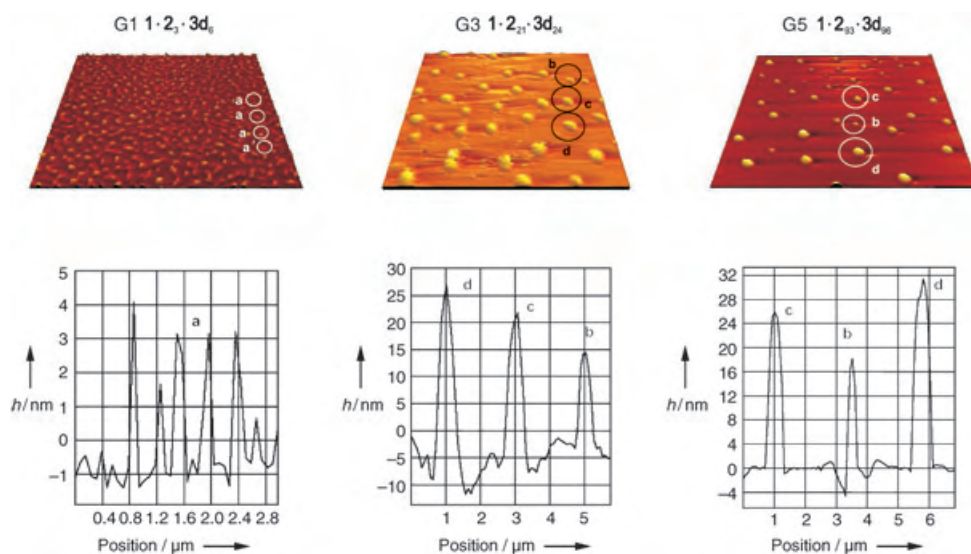


Figure 4. AFM images of supramolecular dendrimers with G1, G3, and G5 stoichiometry adsorbed on a Si wafer. Note the uniform structures with 4 nm (height profile) in the micrograph for G1. In addition, note the perfect globular shape of the higher generation aggregates.

of a mixture of components **1**, **2**, and **3d** in a stoichiometry corresponding to the G3 dendrimer. Besides the G3 dendrimer **1-2₂₁-3d₂₄** itself (3.4 nm), higher dendrimers are observed in low concentration (Figure 3). Similar observations are made for stoichiometries that correspond to even larger values of *n*. Nonetheless, all NMR experiments confirm unequivocally that discrete dendrimers are formed. Branching unit **2** exhibits very broad ¹H NMR signals in chloroform. However, these signals become sharp exactly at the point where core **1** and end cap **3** are added in amounts that correspond to a ratio of 1:(3 × 2^{*n*} – 3):(3 × 2^{*n*}) (**1:2:3**), which is the stoichiometry of a dendritic assembly. This indicates the spontaneous formation of supramolecular dendrimers, in complete agreement with DSC results.

The existence of defined dendrimers is further corroborated by AFM investigations. After adsorption of the G1 dendrimer **1-2₃-3d₆** on a Si surface, uniform and widespread distribution of completely homogeneous objects is observed with a diameter of 4 nm (Figure 4, left), which is in agreement with the expected size of **1-2₃-3d₆**. Repeated sample preparations gave completely analogous pictures. In no case were objects of different sizes observed. Similar preparations of solutions of higher generations such as **1-2₂₁-3d₂₄** (G3) and **1-2₉₃-3d₉₆** (G5) showed in a reproducible way that in addition to small discrete objects with diameters of 4, 7, and 12 nm larger objects are formed. The vast majority of these structures have diameters of 24, 28, and 32 nm (height profiles). These objects are too large to be attributed to isolated dendrimers. Presumably, these objects are clusters of higher generation dendrimers formed during an incomplete drying process in the course of the sample preparation. The discontinuity in the size distribution of aggregates is also a striking feature for the higher generation dendrimers. To summarize, the investigations presented here prove for the first time the programmed self-assembly of discrete supramolecular dendrimers from nondendritic units.

Received: September 24, 2004

Published online: January 28, 2005

Keywords: dendrimers · hydrogen bonds · scanning probe microscopy · self-assembly · supramolecular chemistry

- [1] L. Brunsfeld, B. J. B. Folmer, E. W. Meijer, R. P. Sijbesma, *Chem. Rev.* **2001**, *101*, 4071.
- [2] V. Berl, M. Schmutz, M. J. Krische, R. G. Khoury, J.-M. Lehn, *Chem. Eur. J.* **2002**, *8*, 1227.
- [3] J.-M. Lehn, *Supramolecular Polymers* (Ed.: A. Cifferi), Marcel Dekker, New York, **2000**, p. 615.
- [4] R. F. M. Lange, M. van Gurp, E. W. Meijer, *J. Polym. Sci. Polym. Chem. Ed.* **1999**, *37*, 3657.
- [5] Y. M. Ma, S. V. Kolotuchin, S. C. Zimmerman, *J. Am. Chem. Soc.* **2002**, *124*, 13757.
- [6] P. S. Corbin, L. J. Lawless, Z. Li, Y. Ma, M. J. Witmer, S. C. Zimmerman, *Proc. Natl. Acad. USA* **2002**, *8*, 5099.
- [7] D. K. Smith, F. Diederich, *Chem. Eur. J.* **1998**, *4*, 1353.
- [8] W. T. S. Huck, R. Hulst, P. Timmerman, F. C. J. M. van Veggel, D. N. Reinhoudt, *Angew. Chem.* **1997**, *109*, 1046; *Angew. Chem. Int. Ed. Engl.* **1997**, *36*, 1006.
- [9] A. Dirksen, U. Hahn, F. Schwanke, M. Nieger, J. N. H. Reek, F. Vögtle, L. De Cola, *Chem. Eur. J.* **2004**, *10*, 2036.
- [10] B. Zhishan, L. Zhang, Z. Wang, X. Zhang, J. Shen, *Mater. Sci. Eng. C* **1999**, *10*, 165.
- [11] M. Kellermann, W. Bauer, A. Hirsch, B. Schade, K. Ludwig, C. Böttcher, *Angew. Chem.* **2004**, *116*, 3019; *Angew. Chem. Int. Ed.* **2004**, *43*, 2959.
- [12] S. K. Chang, A. D. Hamilton, *J. Am. Chem. Soc.* **1988**, *110*, 1318.
- [13] Complete syntheses, characterizations, and supramolecular properties of all newly presented units will be described in a detailed forthcoming paper.
- [14] A similar system with a non-dendritic end cap was recently analyzed by Lehn and co-workers in context with investigations on supramolecular polymers (cf. ref. [2]).
- [15] V. P. Solov'ev, V. E. Baulin, N. N. Strahova, V. P. Kazachenko, V. K. Belsky, A. A. Varnek, T. A. Volkova, G. Wipff, *J. Chem. Soc. Perkin Trans. 2* **1998**, 1489.
- [16] B. Perlmutter-Hayman, *Acc. Chem. Res.* **1986**, *19*, 90.
- [17] The determination of particle sizes relies on the Stokes–Einstein relationship for globular particles. Dendrimers of low generation actually exist as disc-shaped structures. However, this method determined an average molecule size over all directions which is smaller than the true main diameter. Nonetheless, uniformity can be demonstrated clearly.

Cover Picture

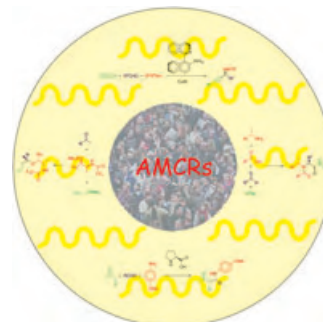
Ioannis Sapountzis, Wenwei Lin, Christiane C. Kofink, Christina Despotopoulou, and Paul Knochel*

Aryl-aryl cross-couplings are among the most important C–C bond-forming reactions. Catalysts for this reaction tend to be expensive (Pd) or toxic (Ni). Fe salts are not usually employed as they promote homocoupling of the aryl magnesium reagent. In their Communication on page 1654 ff., P. Knochel and co-workers report an efficient and environmentally benign $[\text{Fe}(\text{acac})_3]$ -catalyzed cross-coupling of organocopper species $\text{ArCu}(\text{CN})\text{MgCl}$ with aryl iodides to give a wide range of polyfunctional biphenyl compounds in 50–93 % yield.



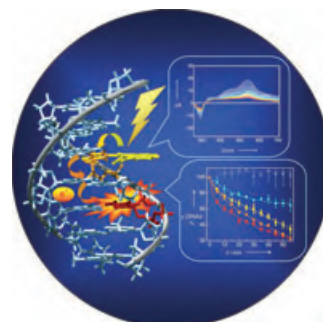
Asymmetric Synthesis

In their Review on page 1602 ff., D. J. Ramón and M. Yus discuss asymmetric multicomponent reactions, through which chiral compounds can be obtained from three or more reactants that are added simultaneously.



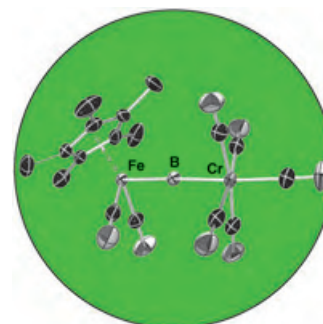
Electron Transfer

In their Communication on p. 1636 ff., H.-A. Wagenknecht, T. Fiebig, and co-workers describe investigations of reductive DNA electron transfer. With modified DNA duplexes they observed a range of electron-transfer rates.



Low-Valent Compounds

H. Braunschweig et al. present the first “naked” boron atom to linearly bridge two metal centers (Fe/Fe or Fe/Cr) in their Communication on page 1658 ff.





The following Communications have been judged by at least two referees to be “very important papers” and will be published online at www.angewandte.org soon:

Mark Gandelman, Eric N. Jacobsen*

Highly Enantioselective Catalytic Conjugate Addition of N Heterocycles to α,β -Unsaturated Ketones and Imides

Sang Hyuk Im, Yun Tack Lee, Benjamin Wiley, Younan Xia*

Large-Scale Synthesis of Silver Nanocubes: The Role of HCl in Promoting Cube Perfection and Monodispersity

Sridhar Narayan, John Muldoon, M. G. Finn, Valery V. Fokin, Hartmuth C. Kolb, K. Barry Sharpless*

“On Water”: Unique Reactivity of Organic Compounds in Aqueous Suspensions

Tetsuro Murahashi, Christopher R. Clough, Joshua S. Figueroa, Christopher C. Cummins*

A Ligand Comprised of Dinitrogen and Methylphenylphosphine in a Cationic Molybdenum Complex

Paul J. Goldsmith, Simon J. Teat, Simon Woodward*

Enantioselective Preparation of β,β -Disubstituted α -Methylenepropionates by Methylaluminoxane Promotion of the Zinc Schlenk Equilibrium

News

L. Horner Becomes Honorary Member of the GDCh _____ **1588**

C. Stubenrauch Receives Carl Duisberg Memorial Award _____ **1588**

U. Deichmann Receives Gmelin–Beilstein Medal _____ **1588**

ADUC Awards for Young Scientists **1589**

Horst Pracejus Prize to J. M. Brown _____ **1588**

Books

Bioelectrochemistry of Membranes

D. Walz, J. Teissié, G. Milazzo

reviewed by S. Terrettaz _____ **1590**

Transition Metal Arene π -Complexes in Organic Synthesis and Catalysis

E. Peter Küding

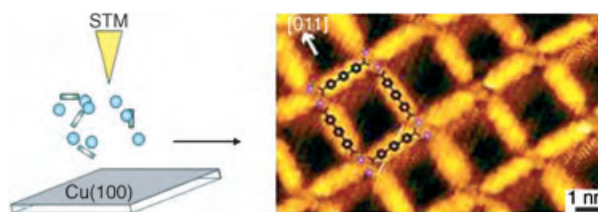
reviewed by H. Butenschön _____ **1591**

Highlights

Coordination on Surfaces

M. Ruben* _____ **1594 – 1596**

Squaring the Interface: “Surface-Assisted” Coordination Chemistry



Coming to the surface: A straightforward approach for the generation of gridlike modular structures composed of metal ions and ligands on surfaces (see picture)

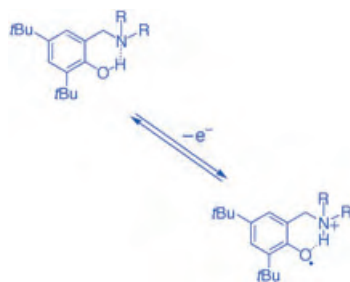
was developed by the research groups led by K. Kern, J. V. Barth, and N. Lin. This Highlight hails a novel, “surface-assisted” coordination chemistry.

Correspondence

Proton/Electron Transfer

I. J. Rhile, J. M. Mayer* — 1598–1599

Comments on “How Single and Bifurcated Hydrogen Bonds Influence Proton-Migration Rate Constants, Redox, and Electronic Properties of Phenoxyl Radicals”

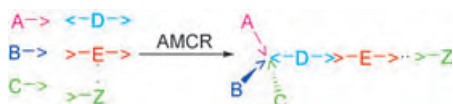


Reviews

Asymmetric Synthesis

D. J. Ramón, M. Yus* — 1602–1634

Asymmetric Multicomponent Reactions (AMCRs): The New Frontier



Some of the many advantages of asymmetric multicomponent reactions over classical divergent synthesis include superior atom economy, simple procedures, savings in solvent, time, and

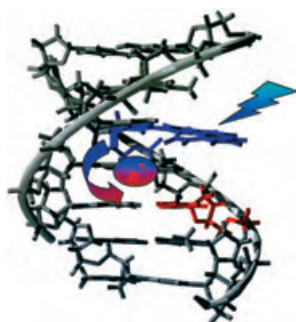
energy, simple equipment and manipulation, as well as lower costs. Besides these advantages, this new strategy has reached excellent levels of stereoselectivity in many processes.

Communications

Electron Transfer

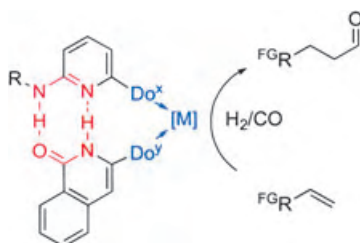
P. Kaden, E. Mayer-Enthart, A. Trifonov, T. Fiebig,*
H.-A. Wagenknecht* — 1636–1639

Real-Time Spectroscopic and Chemical Probing of Reductive Electron Transfer in DNA



Highly acceptable: DNA is a flexible medium with a range of conformational states. Thus, in investigations of the DNA-mediated reductive electron transfer using a modified DNA duplex containing 5-bromo-2'-deoxyuridine (red in picture) as the electron acceptor and pyren-1-yl-2'-deoxyuridine (blue) as the electron donor, a distribution of electron-transfer rates has been observed.

The odd couple: Inspired by the principle of DNA base pairing a conceptually new approach for the generation of a heterobidentate-ligand library based on self-assembly through hydrogen-bonding is realized. From a 4 × 4 library a catalyst that shows outstanding activity and excellent regioselectivity could be identified (see scheme; ^{FG}R = functional group, Do = donor group).



Homogeneous Catalysis

B. Breit,* W. Seiche — 1640–1643

Self-Assembly of Bidentate Ligands for Combinatorial Homogeneous Catalysis Based on an A–T Base-Pair Model

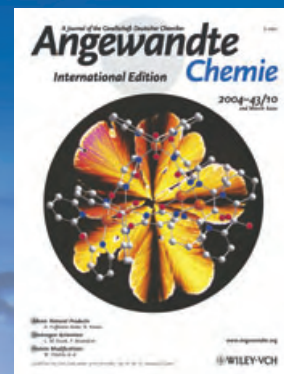
For the USA and Canada:

ANGEWANDTE CHEMIE International Edition (ISSN 1433-7851) is published weekly by Wiley-VCH PO Box 191161, D 69451 Weinheim, Germany. Air freight and mailing in the USA by Publications Expediting Inc. 200 Meacham Ave., Elmont, NY 11003. Periodicals

postage paid at Jamaica NY 11431. US POSTMASTER: send address changes to *Angewandte Chemie*, Wiley-VCH, 111 River Street, Hoboken, NJ 07030. Annual subscription price for institutions: US\$ 4948.00/4498.00 (valid for print and electronic / print or electronic delivery); for individuals who are personal members of a

national chemical society, or whose institution already subscribes, or who are retired or self-employed consultants, print only: US\$ 394.00. Postage and handling charges included. All Wiley-VCH prices are exclusive VAT.

The best in chemistry – for more than a hundred years



A Journal of the Gesellschaft Deutscher Chemiker
Angewandte
International Edition **Chemie**

www.angewandte.org

1888: The beginning
of a success story

Constant Innovations

- 1962:** First issue of the International Edition
- 1976:** Graphical abstracts
- 1979:** Cover pictures
- 1988:** Centenary of Angewandte
- 1989:** Routine use of color
- 1991:** New section: Highlights
- 1992:** Computerized editorial tracking system
- 1995:** Internet service for readers
- 1998:** Regular press service; full-text online
- 2000:** New section: Essays; EarlyView: Communications available online ahead of the printed version
- 2001:** New section: Minireviews
- 2002:** Online submission of manuscripts
- 2003:** Weekly publication; new section: News; new layout
- 2004:** Backfiles (1962-1997); ManuscriptXpress: Online system for authors and referees



Angewandte's advisors...

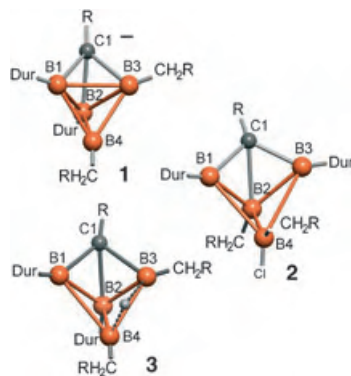
Robert Langer
Massachusetts Institute of
Technology

» **Angewandte Chemie** is one of the top chemistry journals in the world. As such, I try to publish there frequently and am honored to be a member of its International Advisory Board. «

Angewandte Chemie International Edition is
a journal of the German Chemical Society (GDCh)



Borderline aromatics: The series of compounds of composition $\text{CB}_n\text{H}_{n+1}^-$ is now completed with the simplest three-dimensional aromatic **1**. The precursor **2**, a two-dimensional aromatic, and the product of protonation, **3**, a homoaromatic, display partially nonclassical σ frameworks. $\text{R} = \text{SiMe}_3$, Dur = 2,3,5,6-tetramethylphenyl.

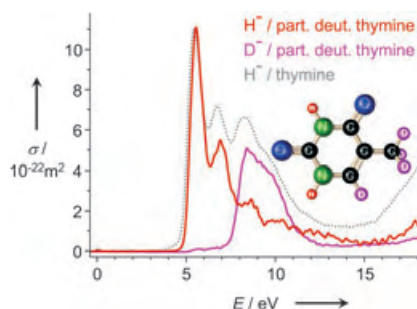


Carboranes

Y. Sahin, C. Präsang, M. Hofmann,
G. Geiseler, W. Massa,
A. Berndt* 1643–1646

Derivatives of the Simplest Polyhedral Carborane Anion: Structures at the Borderline between Two- and Three-Dimensional Aromatic Compounds

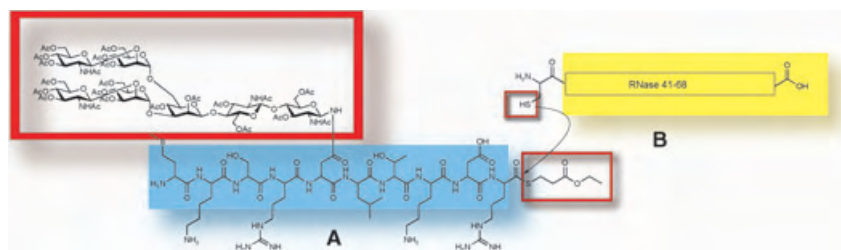
The attachment of free electrons to thymine in the gas phase leads to the abstraction of H^- ions and a broad, structured feature in the energy range between 5 and 12 eV (see picture). In experiments with partly deuterated thymine the different peaks in the H^- ion yield were shown to be associated unambiguously with abstraction from the different molecular positions. This reaction may be an important initial step towards DNA strand breaks.



Gas-Phase Reactions

S. Ptasíńska, S. Denifl, V. Grill, T. D. Märk,
P. Scheier,* S. Gohlke, M. A. Huels,
E. Illenberger 1647–1650

Bond-Selective H^- Ion Abstraction from Thymine



A safety catch combined with a Rink-amide linker allowed convenient monitoring (LC–MS) and optimization of several key reactions in a solid-phase syn-

thesis of the building block **A** for the glycoprotein RNase B. The native chemical ligation of **A** and **B** delivered the glycosylated RNase B fragment 30–68.

Glycopeptide Synthesis

S. Mezzato, M. Schaffrath,
C. Unverzagt* 1650–1654

An Orthogonal Double-Linker Resin Facilitates the Efficient Solid-Phase Synthesis of Complex-Type N-Glycopeptide Thioesters Suitable for Native Chemical Ligation



Well-matched couples: Functionalized aryl and heteroaryl copper species obtained from the corresponding magnesium derivatives undergo Fe-catalyzed cross-

coupling reactions with aryl iodides that bear keto, ester, triflate, or nitrile groups (see scheme).

Biphenyl Synthesis

I. Sapountzis, W. Lin, C. C. Kofink,
C. Despotopoulou,
P. Knochel* 1654–1658

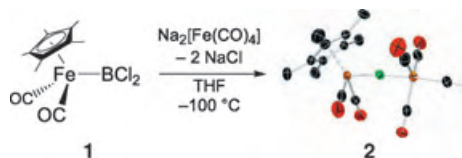
Iron-Catalyzed Aryl–Aryl Cross-Couplings with Magnesium-Derived Copper Reagents



Low-Valent Compounds

H. Braunschweig,* K. Radacki,
D. Scheschkewitz,
G. R. Whittell ————— **1658 – 1661**

Boron as a Bridging Ligand



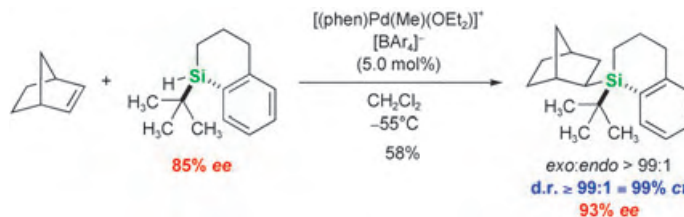
Getting boron into line: The reaction of the dichloroboryl complex **1**, with $\text{Na}[\text{Fe}(\text{CO})_4]^{2-}$ yields $[\{(\eta^5\text{-C}_5\text{Me}_5)\text{Fe}(\text{CO})_2\}(\mu_2\text{-B})\{\text{Cr}(\text{CO})_5\}]$ (**2**; see scheme green B). $\text{Na}_2[\text{Cr}(\text{CO})_5]$ reacts analogously with **1** to

give $[\{(\eta^5\text{-C}_5\text{Me}_5)\text{Fe}(\text{CO})_2\}(\mu_2\text{-B})\{\text{Cr}(\text{CO})_5\}]$ (**3**). Both compounds **2** and **3** contain an unprecedented linearly bridging “naked” boron atom.

Chirality Transfer

M. Oestreich,* S. Rendler — **1661 – 1664**

“True” Chirality Transfer from Silicon to Carbon: Asymmetric Amplification in a Reagent-Controlled Palladium-Catalyzed Hydrosilylation



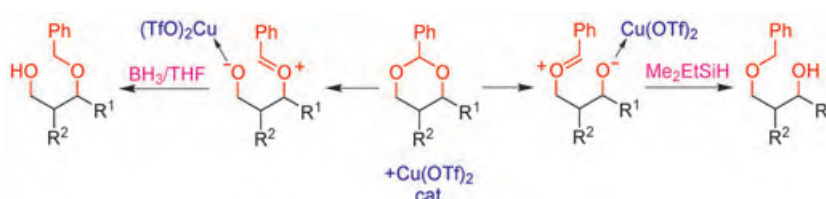
Borne by silicon: A silicon reagent with Si-centered chirality induces C-centered chirality in C–Si bond formation. All of the stereochemical information stems from the chiral silane. This first “true” chirality transfer from silicon to carbon has been

realized in a Pd-catalyzed hydrosilylation of a prochiral alkene. Moreover, this reagent-controlled process displays an unusual positive nonlinear effect (see Scheme).

Synthetic Methods

C.-R. Shie, Z.-H. Tzeng, S. S. Kulkarni,
B.-J. Uang, C.-Y. Hsu,
S.-C. Hung* ————— **1665 – 1668**

$\text{Cu}(\text{OTf})_2$ as an Efficient and Dual-Purpose Catalyst in the Regioselective Reductive Ring Opening of Benzylidene Acetals



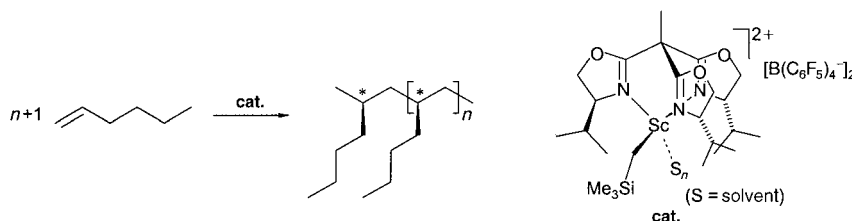
Reducing the choices. $\text{Cu}(\text{OTf})_2$ is an efficient and dual-purpose catalyst for the highly regioselective reductive ring openings of benzylidene acetals with either BH_3 or Me_2EtSiH to give the correspond-

ing primary and secondary alcohols (see scheme). Isotope studies have confirmed that both modes of ring cleavage proceed by an $\text{S}_{\text{N}}1$ reaction pathway when borane or silane attack the acetal carbon center.

Polymerization

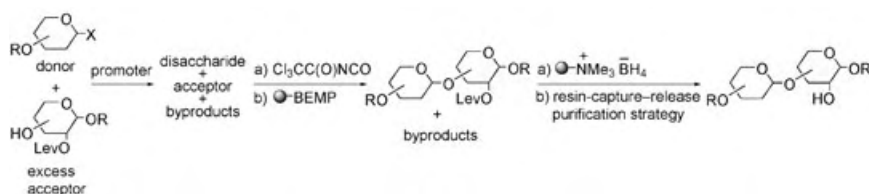
B. D. Ward, S. Bellemin-Lapponnaz,*
L. H. Gade* ————— **1668 – 1671**

C_3 Chirality in Polymerization Catalysis: A Highly Active Dicationic Scandium(III) Catalyst for the Isoselective Polymerization of 1-Hexene



A tactical approach: C_3 -chiral ancillary ligands such as tris(oxazolinyl)ethane allow stereocontrol in olefin polymerization (see scheme). An alkyl Sc^{III} catalyst

polymerizes 1-hexene with activities ranging from 2000 to 36 000 $\text{kg mol}^{-1} \text{h}^{-1}$ (at -30 to $+21$ °C) and good tacticity control at low temperatures.



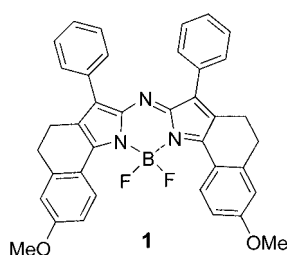
An excess of glycosyl acceptor is used in the solution-phase synthesis of oligosaccharides and any unconverted acceptor is removed by using trichloroacetyl iso-

cyanate. A levulinoyl (Lev) ester group is then used as a masked tag in the following "resin-capture–release" purification strategy (see scheme).

Carbohydrate Chemistry

A. Dondoni,* A. Marra,*
A. Massi* _____ **1672–1676**

Hybrid Solution/Solid-Phase Synthesis of Oligosaccharides by Using Trichloroacetyl Isocyanate as Sequestration-Enabling Reagent of Sugar Alcohols

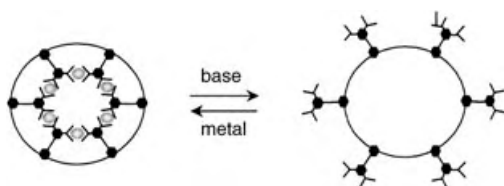


To dye for: A highly fluorescent, photo-stable aza-dipyrrromethene dye **1** ($\lambda_{em} = 751$ nm) with sharp and intense absorption (full width at half maximum height = 30.4 nm; $\epsilon = 159\,000$) in the near-infrared (NIR) region ($\lambda_{max} = 740$ nm) is reported. The dye is insensitive to solvent polarity, meets the requirements of a NIR chromophore, and has potential use in biological probes.

Fluorescent Dyes

W. Zhao, E. M. Carreira* _____ **1677–1679**

Conformationally Restricted Aza-Bodipy: A Highly Fluorescent, Stable, Near-Infrared-Absorbing Dye



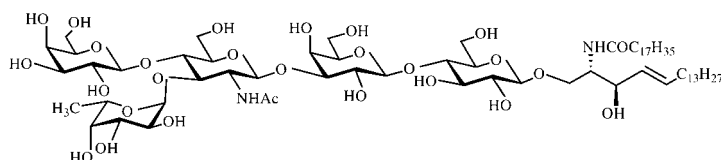
Turned inside out: The construction of a peripheral 114-membered macrocycle by a Grubbs-catalyzed metathesis reaction facilitates the self-assembly of a terpyridine-based Fe^{II} hexamer. The quantitative,

base-promoted removal of the Fe^{II} centers allows the reversible disassembly of the metalated complex (see scheme, gray metal).

Macrocycles

P. Wang, C. N. Moorefield,
G. R. Newkome* _____ **1679–1683**

Nanofabrication: Reversible Self-Assembly of an Imbedded Hexameric Metallomacrocycle within a Macromolecular Superstructure



Tight vesicles: Two glycosphingolipids, CerLLe^X (see picture) and CerLLe^a (Cer = ceramide, L = lactose, Le^X = Lewis^X determinant, Le^a = Lewis *a* determinant) are used to study the Ca^{2+} -mediated specific

adhesion of natural Le^X-bearing molecules inserted in fluid bilayer membranes. Vesicle adhesion energy experiments show that Le^X–Le^X recognition is highly sensitive to molecular structure.

Cell Adhesion

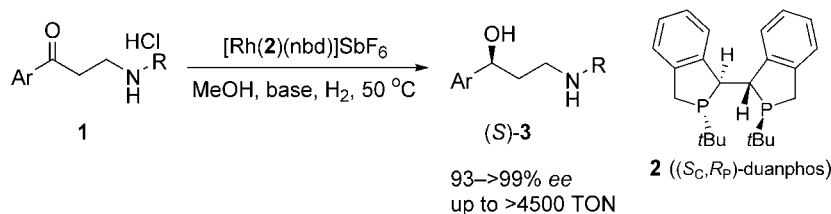
C. Gourier, F. Pincet, E. Perez,* Y. Zhang,
Z. Zhu, J.-M. Mallet,
P. Sinaÿ _____ **1683–1687**

The Natural Lewis^X-Bearing Lipids Promote Membrane Adhesion: Influence of Ceramide on Carbohydrate–Carbohydrate Recognition

Hydrogenations

D. Liu, W. Gao, C. Wang,
X. Zhang* — 1687 – 1689

Practical Synthesis of Enantiopure
γ-Amino Alcohols by Rhodium-Catalyzed
Asymmetric Hydrogenation of
β-Secondary-Amino Ketones



Another way to antidepressants: A series of β-secondary-amino ketone hydrochlorides (e.g. **1**) were hydrogenated with remarkably high enantioselectivities by using a Rh complex containing P-chiral bisphospholane **2**. These results establish

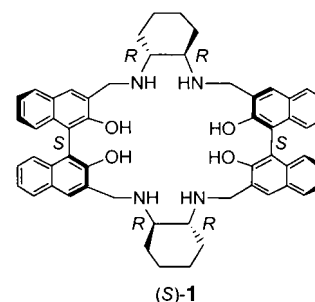
a short and practical means for the synthesis of enantiopure N-monosubstituted γ-amino alcohols (e.g. **3**), which are key intermediates in the synthesis of important antidepressants. (nbd = norbornadiene; TON = turnover number).

Fluorescent Recognition

Z.-B. Li, J. Lin, L. Pu* — 1690 – 1693

A Cyclohexyl-1,2-diamine-Derived
Bis(binaphthyl) Macrocycle: Enhanced
Sensitivity and Enantioselectivity in the
Fluorescent Recognition of Mandelic Acid

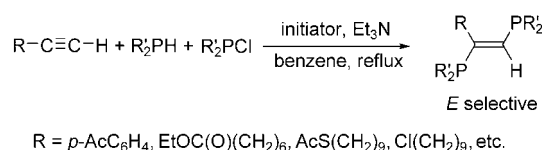
Optically active cyclohexanediamine-based bis(binaphthyl) macrocycle (*S*)-**1** shows a highly sensitive and enantioselective fluorescent recognition of mandelic acid: That is, while the *R* enantiomer of mandelic acid causes little change in the fluorescence of the macrocycle, the *S* enantiomer enhances the fluorescence by over 20-fold.



Diphosphanylethenes

A. Sato, H. Yorimitsu,
K. Oshima* — 1694 – 1696

Synthesis of (*E*)-1,2-Diphosphanylethene
Derivatives from Alkynes by Radical
Addition of Tetraorganodiphosphane
Generated In Situ



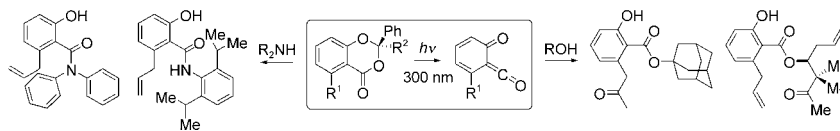
E-asyl radical addition: A tetraorgano-diphosphane, generated in situ from a diorganophosphane and a chlorodiorganophosphane in the presence of triethylamine, adds to terminal alkynes by a

radical process (see scheme) to afford (*E*)-diphosphanylethene derivatives in excellent yields. The reaction conditions are mild enough to tolerate many functional groups.

Synthetic Methods

O. Soltani,
J. K. De Brabander* — 1696 – 1699

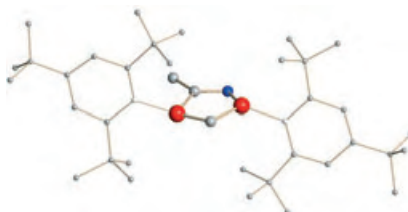
Synthesis of Functionalized Salicylate
Esters and Amides by Photochemical
Acylation



Functionalized salicylates in a flash: Photolysis of functionalized benzodioxinones in the presence of alcohols or amines is a powerful method for the synthesis of sterically hindered salicylic esters and amides (see scheme). This reaction tol-

erates a broad range of functional groups and efficiently engages a wide range of acylation substrates, including sterically hindered nucleophiles that are inert to other acylation methods.

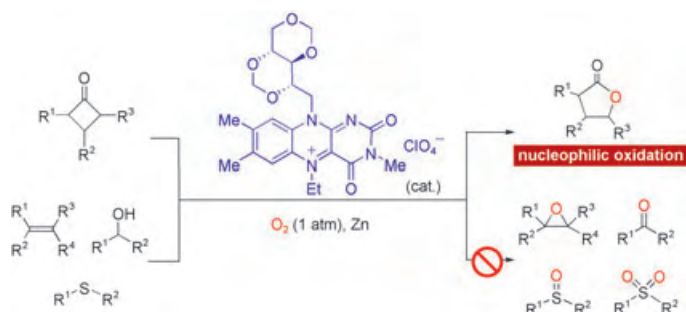
A stable diphosphorus analogue of Enders' N-heterocyclic carbene has been prepared by taking advantage of the inherent π -donor capabilities of phosphorus, which are as good as, or better than, those of nitrogen. The P-heterocyclic carbene (see figure; C gray, N blue, P red) behaves as a strong donor ligand and forms transition-metal complexes that are thermally and air stable.



Heterocyclic Carbenes

D. Martin, A. Baceiredo, H. Gornitzka, W. W. Schoeller, G. Bertrand* 1700–1703

A Stable P-Heterocyclic Carbene



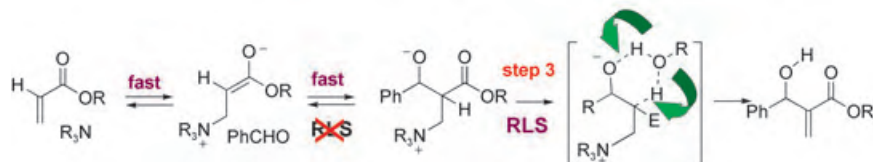
Highly chemoselective Baeyer–Villiger oxidations can be performed in the presence of other reactive functionalities such as alcohols, olefins, and sulfides, which would undergo electrophilic oxidation under conventional conditions (see

scheme). [DMRFIEt]⁺[ClO₄][−] (depicted blue) is a new class of flavin compound that catalyzes aerobic Baeyer–Villiger oxidations in the presence of Zn dust as the electron source.

Organocatalysis

Y. Imada,* H. Iida, S.-I. Murahashi,* T. Naota* 1704–1706

An Aerobic, Organocatalytic, and Chemoselective Method for Baeyer–Villiger Oxidation



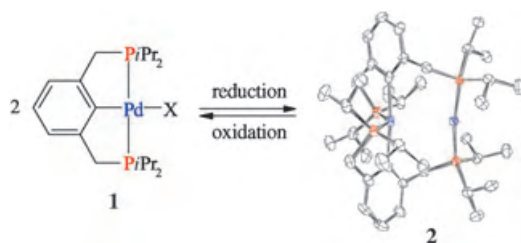
One step beyond: Proton transfer (step 3, see scheme), not C–C bond formation (step 2) as previously thought, is the rate-limiting step (RLS) in the initial stage of the Baylis–Hillman reaction, which

involves the amine-catalyzed addition of an aldehyde to an activated alkene to generate an allylic alcohol. This finding has considerable implications for asymmetric catalysis of the reaction.

Baylis–Hillman Reaction

V. K. Aggarwal,* S. Y. Fulford, G. C. Lloyd-Jones* 1706–1708

Reevaluation of the Mechanism of the Baylis–Hillman Reaction: Implications for Asymmetric Catalysis



Unequal partners: One-electron reduction of a pincer-type palladium complex **1** results in collapse of the pincer system and formation of a novel bimetallic diamagnetic complex containing a linearly

coordinated 14 e Pd⁰ center and a nonplanar Pd^{II} unit (**2**). The reaction is reversed by oxidation with Ag⁺ or organic halides. The catalytic activity of **2** is investigated for the Heck reaction.

Pincer Complexes

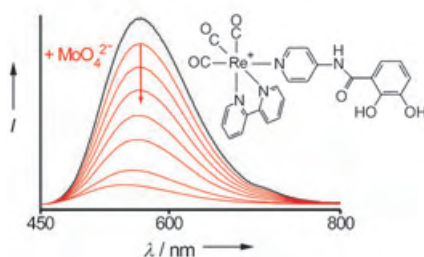
C. M. Frech, L. J. W. Shimon, D. Milstein* 1709–1711

Redox-Induced Collapse and Regeneration of a Pincer-Type Complex Framework: A Nonplanar Coordination Mode of Palladium(II)

Anion Sensors

A. F. A. Peacock, H. D. Batey, C. Raendler,
A. C. Whitwood, R. N. Perutz,*
A.-K. Duhme-Klair* — 1712–1714

A Metal-Based Lumophore Tailored To
Sense Biologically Relevant Oxometalates



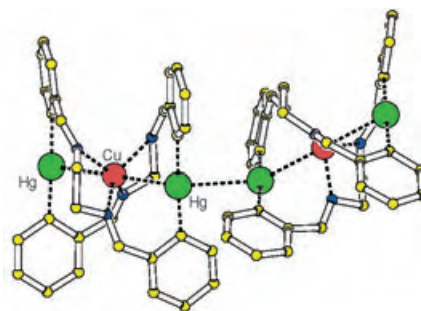
Oxometalate detection: A new catechol– $[\text{Re}^{\text{I}}(2,2'\text{-bpy})(\text{py})(\text{CO})_3]^+$ (bpy = bipyridine, py = pyridine) conjugate has been prepared which signals the presence and concentration of molybdate, vanadate, and/or tungstate ions in solution in aqueous acetonitrile by efficient quenching of the Re-based luminescence (see picture).

Metallamacrocycles

U. Patel, H. B. Singh,*
G. Wolmershäuser — 1715–1717

Synthesis of a Metallophilic
Metallamacrocycle: A
 $\text{Hg}^{\text{II}}\cdots\text{Cu}^{\text{I}}\cdots\text{Hg}^{\text{II}}\cdots\text{Hg}^{\text{II}}\cdots\text{Cu}^{\text{I}}\cdots\text{Hg}^{\text{II}}$
Interaction

Complexation of a Cu^{I} ion in a mercuramacrocyclic demonstrates the potential of metal–metal interactions in a preorganized system to trap metal ions. The molecular structure of the Cu^{I} complex is presented and shows $\text{Hg}\cdots\text{Cu}$ heterometallic and $\text{Hg}\cdots\text{Hg}$ homometallic $d^{10}\cdots d^{10}$ interactions (see figure).

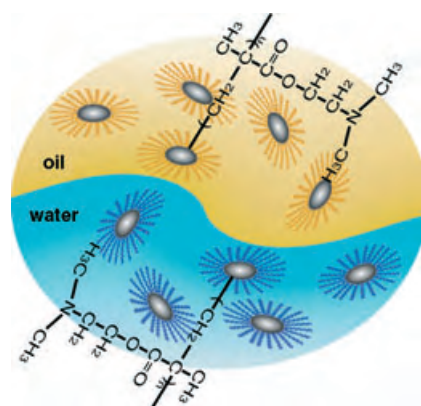


Nanotechnology

H. Duan, M. Kuang, D. Wang,*
D. G. Kurth, H. Möhwald — 1717–1720

Colloidally Stable Amphibious
Nanocrystals Derived from Poly{[2-
(dimethylamino)ethyl] Methacrylate}
Capping

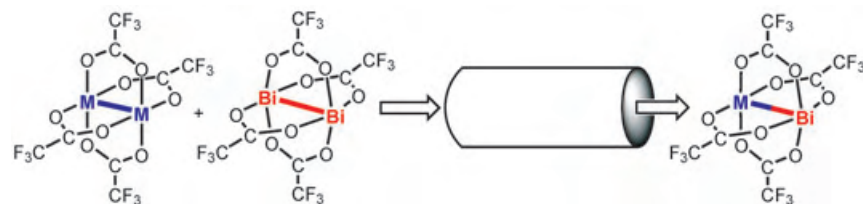
Polymer brushes are grown on both hydrophobic and hydrophilic nanocrystals by surface-initiated atom-transfer radical polymerization. The poly{[2-(dimethylamino)ethyl] methacrylate}-coated nanocrystals are well dispersed in both water and most organic solvents without detectable aggregation and deterioration of their intrinsic properties. This methodology paves a simple and efficient way to direct nanocrystals into specific media.



Mixed-Metal Complexes

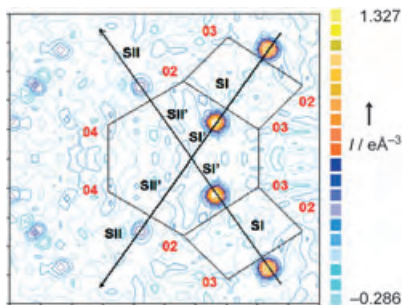
E. V. Dikarev,* T. G. Gray,
B. Li — 1721–1724

Heterobimetallic Main-Group–Transition-
Metal Paddle-Wheel Carboxylates



Bismuth(III) tetra(trifluoroacetate) acts as a metallogligand toward transition-metal units to yield heterobimetallic homoleptic carboxylates $[\text{BiM}(\text{O}_2\text{CCF}_3)_4]$ ($\text{M} = \text{Rh}, \text{Ru}$; see picture). The heterometallic mole-

cules maintain a paddle-wheel structure, with a single bond between bismuth and the transition-metal atom, and behave as one-ended Lewis acids in solution and in the solid state.

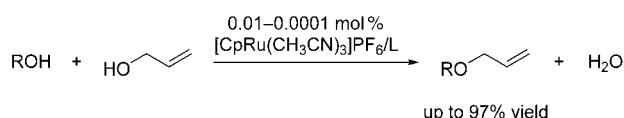


Spot on! Resonant scattering enables accurate localization of the individual cations in powders by the routine use of “anomalous differential patterns” and “dispersive difference maps” (see picture), as demonstrated for (Sr,Rb) zeolite X, a sample of potential industrial interest.

Powder Diffraction

H. Palancher, J.-L. Hodeau,* C. Pichon, J.-F. Béar, J. Lynch, B. Rebours, J. Rodriguez-Carvajal — 1725 – 1729

Direct Localization of Atoms in Mixed-Occupancy Powders by Resonant Contrast Diffraction



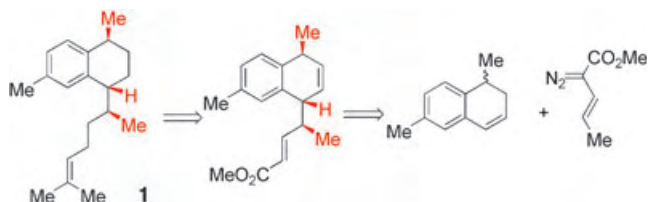
An environmentally benign synthesis of allyl ethers has been developed which can be applied to a highly chemoselective protection of hydroxyl groups. A highly efficient [CpRu]–2-quinolinecarboxylic acid (L) catalytic system was successfully

employed for the dehydrative allylation of various alcohols without additional activators and solvent (see scheme; R = alkyl, aryl, multifunctional alkyl, Cp = C₅H₅).

Synthetic Methods

H. Saburi, S. Tanaka, M. Kitamura* — 1730 – 1732

Catalytic Dehydrative Allylation of Alcohols



The combined approach of C–H activation and a Cope rearrangement catalyzed by a rhodium catalyst [Rh₂(R-dosp)₄] (dosp = (N-dodecylbenzenesulfonyl)proline) is shown to be a very effective

method for the construction of the three stereogenic centers (marked in red, see scheme) present in the diterpene erogorgiaene (1).

Natural Product Synthesis

H. M. L. Davies,* A. M. Walji — 1733 – 1735

Direct Synthesis of (+)-Erogorgiaene through a Kinetic Enantiodifferentiating Step

Looking for outstanding employees?

Do you need another expert for your excellent team?

... Chemists, PhD Students, Managers, Professors, Sales Representatives...

Place an advert in the printed version and have it made available online for 1 month, free of charge!

Angewandte Chemie International Edition

Advertising Sales Department: Marion Schulz

Phone: 0 62 01 - 60 65 65

Fax: 0 62 01 - 60 65 50

E-Mail: MSchulz@wiley-vch.de

Service

Keywords — 1736

Authors — 1737

Preview — 1739



On the occasion of the Congress of Chemistry Lecturers in Munich (Germany) from March 6 to 9, 2005, the Gesellschaft Deutscher Chemiker (GDCh, German Chemical Society) will once again present some of their internationally esteemed awards and distinctions.

L. Horner Becomes Honorary Member of the GDCh

Honorary membership is the highest distinction awarded by the GDCh. The list of honorary members includes such illustrious personalities as the Nobel Laureates Otto Hahn, Hermann Staudinger, E. O. Fischer, Jean-Marie Lehn, and Roald Hoffmann. Leopold Horner, now 93 years old, was appointed professor in 1953 at the Universität Mainz (Germany), where he remained until his retirement. His research there covered a broad range of topics in the general areas of catalytic processes and natural products, with a particular focus on



L. Horner

organophosphorus compounds: A variant of the Wittig reaction bears his name. He also devoted much time to the study of hydrogen transfer to organic systems, and published more than thirty articles on protection against corrosion. In 1963 he co-authored a Review on nitrenes.^[1a] In 1992, when he was already 81, he published a review on selectivity studies.^[1b] The GDCh awarded Horner the Liebig Memorial Medal in 1973. For some he was a candidate for the Nobel Prize in Chemistry, which was awarded in 2001 for asymmetric catalysis.

Horner was born in 1911. He began his studies in chemistry in Heidelberg, but, because of the strong influence of the national socialists there, moved to Munich in 1933. He completed his PhD in 1937 on the structure of vomicine under the guidance of Heinrich Wieland (Nobel Prize 1927) and completed his habilitation in 1942 on syntheses of oxindole derivatives. He then moved to the Deutsche Forschungsinstitut für Kunststoffe in Frankfurt am Main. From 1943 he held a lectureship at the university there concurrently. After the war he became assistant professor and finally professor at the University of Frankfurt, before taking up a position offered to him in Mainz now over 50 years ago.

U. Deichmann Receives Gmelin–Beilstein Medal

Ute Deichmann (Universität zu Köln / Leo Baeck Institute London) is to receive the Gmelin–Beilstein Medal for her book “Flüchten, Mitmachen, Vergessen—Chemiker und Biochemiker in der NS-Zeit”. The medal is awarded for outstanding services to the history of chemistry, the chemical literature, or information processing. In her book the author shows what catastrophic consequences Nazi leadership had, not only for Jewish chemists themselves, but also for the development of biochemistry, physical chemistry, and quantum chemistry in Germany.^[2]



U. Deichmann

Deichmann studied biology at the Universities of Bochum and Heidelberg (Germany), and was a high-school chemistry and biology teacher from 1975 to 1987. In 1987 she became a scientific researcher at the Institut für Genetik at the Universität zu Köln (Cologne), and she completed her PhD in 1991 with a thesis on “Biologists under Hitler”. In 2000 she completed her habilitation with her now award-winning book. She has been a visiting academic at Ben Gurion University and The Hebrew University of Jerusa-

lem (Israel), among other institutions. Deichmann has been research professor since July 2003 at the Leo Baeck Institute London for the Study of the History and Culture of German-Speaking Jewry.

Horst Pracejus Prize to J. M. Brown

John M. Brown of the University of Oxford (UK) studied chemistry at the University of Manchester and completed his PhD in 1963 under the guidance of A. J. Birch. He then spent postdoctoral periods in the research group of R. Breslow at Columbia University in New York (USA), at the Australian National University in Canberra, and in the research group of M. C. Whiting at the University of Bristol (UK). In 1966 he became a lecturer at the University of Warwick, and in 1974 took up a position as university lecturer in Oxford.



J. M. Brown

Brown has been a member of the Royal Society since 1996. He deals with problems of catalysis and catalytic mechanisms, in studies to better understand metal-catalyzed reactions: He investigates both transition-metal and Lewis acid catalysts. Recently he added solid-state synthesis to his research interests. For his research he is now to be honored by the GDCh with the Horst Pracejus Prize, which is awarded to scientists for outstanding work on chirality. He reported recently in *Angewandte Chemie* on the structure and binding of the zinc alkoxide catalyst in the asymmetric autocatalytic Soai reaction.^[3]

C. Stubenrauch Receives Carl Duisberg Memorial Award

What do a thin foam film and a real gas have in common? Cosima Stubenrauch explored this question in her habilitation research and in a minireview in *ChemPhysChem*.^[4] She studied films of alkyl glycoside tensides and thus gained insight into their stability and



C. Stubenrauch

elasticity. This work has now earned her the Carl Duisberg Memorial Award of the GDCh, which is awarded to young scientists who have completed their habilitation and excelled with original research. She

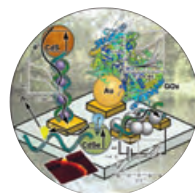
already received the ADUC Award for habilitation candidates in 2002.

Stubenrauch studied chemistry at the Universities of Münster and Freiburg, and completed her PhD in 1997 under the guidance of G. H. Findenegg at the Technische Universität Berlin on microemulsions with alkyl glycosides from a macroscopic and NMR-spectroscopic viewpoint. For her PhD research she received a Schering Award. As a postdoctoral fellow she carried out research on DNA in thin liquid films with D. Langevin at the Laboratoire de Physique des Solides in Orsay near Paris. From 1999 to 2004 she worked towards her habilitation at the Universität zu Köln in the research group of R. Strey on new concepts and perspectives of thin foam films. Stubenrauch has had research stays in Lund (Sweden) and

Yokohama (Japan), as well as at Cornell University (USA). Since the beginning of the year she has been at University College Dublin (Ireland).

ADUC Awards for Young Scientists

The recipients of this year's awards of the Arbeitsgemeinschaft Deutscher Universitätsprofessoren und -professorinnen für Chemie



(ADUC; Association of German University Professors of Chemistry) are **Dirk V. Deubel** (ETH Zürich, research group of

M. Parinello) for his theoretical studies on the role of metals in medicine,^[5]

Kai C. Hultsch (Universität Erlangen-Nürnberg, research group of J. A. Gladysz) for his studies of chiral organometallic complexes, for example, of the transition-metal-catalyzed hydroamination of alkenes,^[6] and **Martin Oestreich** (Universität Freiburg, research group of R. Brückner) for his research on stereoselective synthesis.^[7]

Most Popular Reviews 2004

The GDCh also asked faculty members at four randomly chosen German uni-

versities (Bremen, Jena, Frankfurt/M., and Karlsruhe) as well as 40 randomly chosen *Angewandte* authors and 20 referees from industry for their opinion on the reviews published in *Angewandte Chemie* in 2004. Table 1 shows the results. These reviews will be published in a special (German) issue on the occasion of the Lecturers' Congress.

- [1] a) L. Horner, A. Christmann, *Angew. Chem.* **1963**, 75, 707; *Angew. Chem. Int. Ed. Engl.* **1963**, 2, 599; b) L. Horner, *J. Prakt. Chem.* **1992**, 334, 645.
- [2] a) U. Deichmann, *Flüchten, Mitmachen, Vergessen—Chemiker und Biochemiker in der NS-Zeit*, Wiley-VCH, Weinheim, **2001**; b) U. Deichmann, *Angew. Chem.* **2002**, 114, 1364; *Angew. Chem. Int. Ed.* **2002**, 41, 1310.
- [3] I. D. Gridnev, J. M. Serafimov, J. M. Brown, *Angew. Chem.* **2004**, 116, 4992; *Angew. Chem. Int. Ed.* **2004**, 43, 4884.
- [4] C. Stubenrauch, *ChemPhysChem* **2005**, 6, 35.
- [5] D. V. Deubel, *Chem. Eur. J.* **2005**, 11, in press, DOI: 10.1002/chem.200401053.
- [6] K. C. Hultsch, *Adv. Synth. Catal.* **2005**, 347, 367.
- [7] M. Oestreich, F. Sempere-Culler, A. B. Machotta, *Angew. Chem.* **2005**, 117, 152; *Angew. Chem. Int. Ed.* **2005**, 44, 149.

Table 1: Most popular reviews published in *Angewandte Chemie* in 2004 according to a survey conducted by the German Chemical Society.

Author(s)	Title	Page
C. O. Kappe*	Controlled Microwave Heating in Modern Organic Synthesis	6250
T. Mukaiyama*	Explorations into New Reaction Chemistry	5590
E. Katz, I. Willner*	Integrated Nanoparticle–Biomolecule Hybrid Systems: Synthesis, Properties, and Applications	6042
P. I. Dalko*, L. Moisan	In the Golden Age of Organocatalysis	5138
T. Graening, H.-G. Schmalz*	Total Syntheses of Colchicine in Comparison: A Journey through 50 Years of Synthetic Organic Chemistry	3230
N. Budisa*	Prolegomena to Future Experimental Efforts on Genetic Code Engineering by Expanding Its Amino Acid Repertoire	6426
S. W. Homans*	NMR Spectroscopy Tools for Structure-Aided Drug Design	290
X. Li, D. R. Liu*	DNA-Templated Organic Synthesis: Nature's Strategy for Controlling Chemical Reactivity Applied to Synthetic Molecules	4848
I. Krossing*, I. Raabe	Noncoordinating Anions—Fact or Fiction? A Survey of Likely Candidates	2066
M. Breuer, K. Ditrach,	Industrial Methods for the Production of Optically Active Intermediates	788
T. Habicher, B. Hauer*,		
M. Keßeler, R. Stürmer,		
T. Zelinski		
P. Pyykkö*	Theoretical Chemistry of Gold	4412
D. H. Williams*, E. Stephens,	Understanding Noncovalent Interactions: Ligand Binding Energy and Catalytic Efficiency from	6596
D. P. O'Brien, M. Zhou	Ligand-Induced Reductions in Motion within Receptors and Enzymes	

Squaring the Interface: “Surface-Assisted” Coordination Chemistry

Mario Ruben*

Keywords:

coordination chemistry · grid complexes · scanning probe microscopy · self-assembly

The potential of highly ordered metal-ion arrays to be used in molecular information storage and processing devices was recently highlighted.^[1] Among the set of possible architectures, two-dimensional (2D) gridlike arrays of ion-based switchable elements have attracted particular interest due to their structural similarity to components of some of the newest information processing concepts.^[2,3] So far, the investigation of metal-ion arrays within the nanometer regime has comprised the following steps: the synthesis of the ligand molecules, the self-assembly into supramolecular entities, and the controlled deposition or anchoring of the supramolecules on or at surfaces (Figure 1, left), where the metal-ion arrays can be addressed by state-of-the-art single-molecule techniques (generally AFM- and STM-based).^[4] However, this sequence of synthesis, self-assembly, and deposition is not merely a scientific necessity, since it also reflects, at least partially, the historic background of an evolving interdisciplinary collaboration of scientific groups anchored in chemistry and physics.

A conceptually alternative route towards nanosized metal-ion arrays on surfaces was developed recently (Figure 1, right). This straightforward self-assembly protocol is based on the near-surface metal-ion coordination of simple ligand systems.^[5,7] Using such approach,

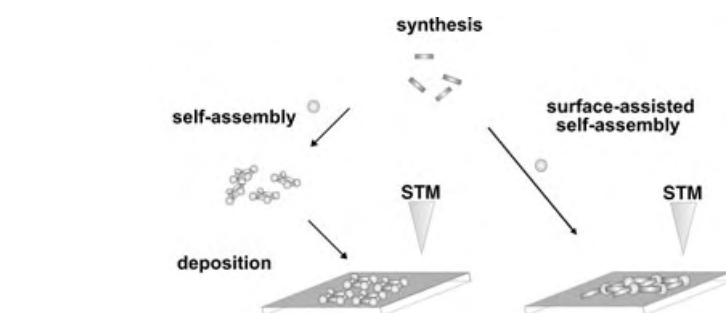


Figure 1. Schematic representation of two approaches for the construction of molecular structures on surfaces. Left: the sequence of synthesis, self-assembly, and deposition. Right: surface-assisted self-assembly.

the groups led by K. Kern, J. V. Barth, and N. Lin at the Max-Planck-Institut für Festkörperforschung in Stuttgart and at the École Polytechnique Fédérale in Lausanne generated a variety of infinite metal-ion arrays just by controlling the codeposition parameters for organic dicarboxylic acid derivatives such as terephthalic acid and iron(0) atoms on Cu(100) surfaces under ultra-high-vacuum (UHV) conditions.^[5]

In the first step the organic ligand was deposited by organic molecular beam epitaxy (OMBE) onto the Cu(100) surface. Subsequently, the metal atoms were deposited on top of the formed (and more or less complete) organic monolayer by electron beam evaporation. After a short annealing period (5 min at $T = 450$ K), during which self-assembly was initiated by the increased mobility of the molecular and ionic components on the surface, well-ordered regular structures emerged readily in domains of up to 50 nm in size (Figure 2).

The rectangular molecular assemblies shown were obtained on the copper(100) surface at an Fe/ligand ratio

of about 0.5:1. Structurally, they consist of dimeric Fe_2 nodes connected by an organic backbone of orthogonally arranged ligand linkers to form an infinite

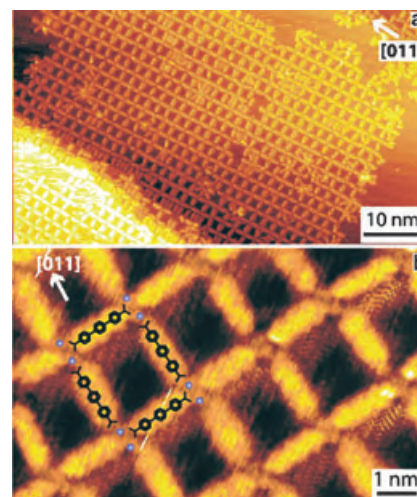


Figure 2. a) STM image showing the 2D topography of the extended gridlike Fe-ligand network; b) high-resolution image of the same network indicating the positions of the organic ligands backbone (Fe atoms of the interconnecting Fe_2 nodes are represented as blue spheres).^[5]

[*] Dr. M. Ruben
Institut für Nanotechnologie
Forschungszentrum Karlsruhe GmbH
Postfach 3640
76021 Karlsruhe (Germany)
Fax: (+49) 724-782-6434
E-mail: mario.ruben@int.fzk.de

network. The observed Fe pairs in the cross positions of the network deserve some attention due to their coordination characteristics: The two Fe centers are surrounded by two sets of two differently coordinating carboxylate groups; two of these are in a monodentate μ^2 -bridging mode and two in an apparently bidentate chelating mode (Figure 2b and Figure 3, MOCN-II). Overall, the coordination geometry of each of metal center is square-planar. However, since the resolution limits of the present STM data prevent clear distinction between the mono- and bidentate coordination modes of the two chelating carboxylate groups, the exact determination of the coordination geometry is not possible in all cases.

The Fe–O bond lengths estimated from the STM data are close to that in bulk materials ($d(\text{Fe–O}) = 1.9\text{--}2.3 \text{ \AA}$),^[6] and the metal–metal distance $d(\text{Fe–Fe})$ is about 5 Å. However, the observation of sometimes elongated Fe–O bonds might be indicative of a situation, in which both ligand and metal centers are in close contact with the Cu(100) surface, which is then apparently acting a template. Thus, the underlying crystal lattice along with the conduction band of the substrate might interfere structurally as well as electronically in the final positioning of the involved metal atoms relative to the organic ligands.

With regards to the ligands, near-edge X-ray adsorption fine structure (NEXAFS) studies have revealed that the ligand molecules are adsorbed with their phenyl rings almost parallel to the Cu(100) surface plane.^[5] This kind of metal–ligand contact is reminiscent of the donor–acceptor interaction of neutral arene rings and electron-rich metal centers, a classical coordination motif in coordination chemistry.^[8]

Since a strong interaction with the surface cannot be excluded, at least not at this stage, the discussion of the electronic properties (e.g. oxidation and spin states) of the coordination network components must involve rather unusual contributions like the electronic coupling of the metal centers to the substrate or possible counterbalancing of complex charges by mirror charges within the upper layers of the substrate. Only additional experimental data will clarify the picture and possibly

support alternative interpretations such as the formation of neutral precomplexes composed of the ligand and the Cu(100) mentioned by the same authors in two previous articles.^[9]

However, considering the distinct M_2L_4 stoichiometry of the dimeric Fe_2 nodes, it seems reasonable to assume that the principle of electroneutrality also persists under near-surface conditions. This assumption would lead to the definition of two Fe^{II} ions surrounded by four deprotonated, negatively charged carboxylate groups. The formation of such electroneutral ($4+/4-$) units will depend critically on the course of the deprotonation reaction, during which four protons are reduced to hydrogen molecules and simultaneously the two iron(0) centers are oxidized. The gaseous hydrogen could easily migrate into the UHV environment, thus driving the redox reaction to completion. The local

electroneutrality around the dimeric Fe_2 nodes may also explain the high thermal stability of the 2D networks (up to 500 K); however, they are not stable to ambient gases. Obviously, further investigations concerning the electronic nature of the metal centers and ligands are necessary, and the results will be awaited with great interest.^[5]

How the variation of the deposition parameters (e.g. ligand-to-metal ratio, annealing temperature) influences the formation of a set of different self-assembled modular structures was reported in more detail by the same authors in two further articles.^[7] Depending on the Fe^0 concentration, different network structures were formed from the same organic ligand, terephthalic acid, on the Cu(100) surface: these ranged from isolated mononuclear “cloverleaf” complexes to infinite 2D “ladder” coordination polymers to the

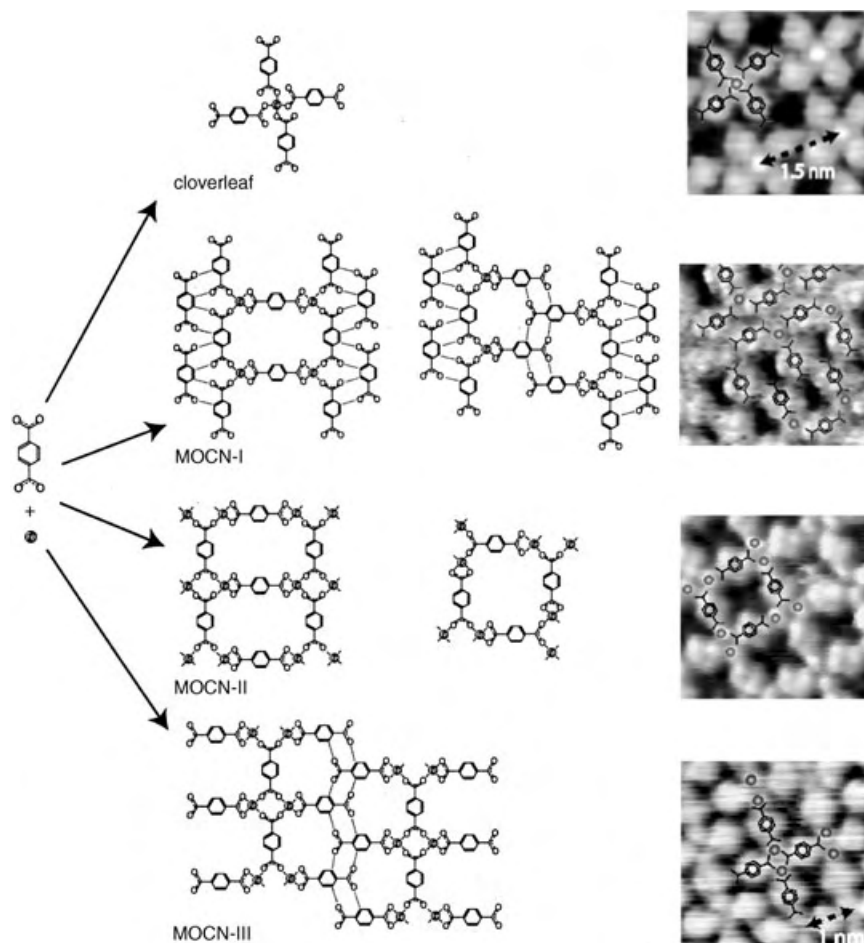


Figure 3. Structural formulas and STM images of the different network motifs (cloverleaf, MOCN-I–III) obtained on the Cu(100) surfaces by variation of the Fe/L ratio and the annealing temperature.^[7a]

previously described gridlike 2D coordination polymers (Figure 3).^[7a]

At lower Fe concentrations the connectivity of the molecular network is achieved in part by additional hydrogen bonds between the aromatic H atoms of the phenyl ring and the oxygen atoms of the carboxylate groups. At higher Fe concentrations the formation of the dimeric Fe₂-based structures predominates. In general, it was found that the amount of iron used must slightly exceed the theoretical value of the structural motif formed. This effect, which is even more pronounced at higher annealing temperatures, is attributed to the loss of Fe atoms/ions in collateral surface reactions such as decoration of substrate steps, formation of Fe islands, and Fe–Cu intermixing processes.

The further elucidation of the coordination characteristics of metal centers in close contact with metal surfaces (coordination number, redox and spin state, metal–metal interactions, mirror charges, etc.) might mark the beginning of a new branch of “surface-assisted” metal coordination chemistry (maybe as an extension of the more bulk- and solution-based, conventional “Werner-type”^[10] coordination chemistry). Together with other STM-based single-molecule surface manipulations (e.g. C–C bond formation, generation of surface chirality)^[11,12] and new approaches towards nanomagnetism (e.g. spin-polarized STM),^[13] such surface-assisted coordination chemistry might constitute part of the future tool kit needed for the construction and controlled manipulation of functional interfaces and operational surfaces.

Furthermore, the well-defined nanopores in these networks can be loaded with suitable substrates (e.g. C₆₀)^[5] which might be of importance for the design of many surface-dominated processes like heterogeneous catalysis and selective gas adsorption, and even for

the generation of optical metamaterials.^[14–16] Interestingly, the emergence of dimeric metal units is also strongly reminiscent of structural features observed around the catalytic centers of some types of enzymes.^[17]

It can be anticipated that the controlled design of functional surfaces by applying the principles of surface-assisted coordination chemistry not only opens new scientific perspectives but will also yield aesthetically appealing structures on surfaces that can be observed in real time.

- [1] a) J.-M. Lehn, *Supramolecular Chemistry. Concepts and Perspectives*, VCH, Weinheim, **1995**, chap. 9, p. 200; b) J.-M. Lehn, *Science* **2002**, 295, 2400–2403; J.-M. Lehn, *Proc. Natl. Acad. Sci. USA* **2002**, 99, 4763–4768.
- [2] M. Ruben, J. Rojo, F. J. Romero-Salguero, L. H. Uppadine, J.-M. Lehn, *Angew. Chem.* **2004**, 116, 3728–3747; *Angew. Chem. Int. Ed.* **2004**, 43, 3644–3662, and references therein; L. Thompson, O. Waldmann, Z. Xu, *Magnetism: Molecules to Materials IV* (Eds.: J. S. Miller, M. Drillon), Wiley-VCH, Weinheim, **2001**.
- [3] C. S. Lent, B. Isaksen, M. Lieberman, *J. Am. Chem. Soc.* **2003**, 125, 1056–1063; M. Lieberman, S. Chellamma, B. Varughese, Y. Wang, C. Lent, G. H. Bernstein, G. Snider, F. C. Peiris, *Ann. N. Y. Acad. Sci.* **2002**, 960, 225–239; A. O. Orlov, I. Amlani, G. H. Bernstein, C. S. Lent, G. L. Snider, *Science* **1997**, 277, 928–930.
- [4] A. Semenov, J. P. Spatz, M. Möller, J.-M. Lehn, B. Sell, D. Schubert, C. H. Weidl, U. S. Schubert, *Angew. Chem.* **1999**, 111, 2701–2705; *Angew. Chem. Int. Ed.* **1999**, 38, 2547–2550; L. Weeks, L. K. Thompson, J. G. Shapter, K. J. Pope, Z. Xu, *J. Microsc.* **2003**, 212, 102–106.
- [5] S. Stepanow, M. A. Lingenfelder, A. Dimitriev, H. Spillmann, E. Delvigne, N. Lin, X. Deng, C. Cai, J. V. Barth, K. Kern, *Nat. Mater.* **2004**, 3, 229–233.
- [6] Search in the data base of the Cambridge Crystallographic Data Centre (CCDC); minimum: C. A. Grapperhaus, B. Mienert, E. Bill, T. Weyermüller, K. Wieghardt, *Inorg. Chem.* **2000**, 39, 5306–5317; maximum: D. Coucouvanis, R. A. Reynolds III, W. R. Dunham, *J. Am. Chem. Soc.* **1995**, 117, 7570–7578.
- [7] a) M. A. Lingenfelder, H. Spillmann, A. Dimitriev, S. Stepanow, N. Lin, J. V. Barth, K. Kern, *Chem. Eur. J.* **2004**, 10, 1913–1919; b) A. Dimitriev, H. Spillmann, N. Lin, J. V. Barth, K. Kern, *Angew. Chem.* **2003**, 115, 2774–2777; *Angew. Chem. Int. Ed.* **2003**, 42, 2670–2673.
- [8] C. Eschenbroich, A. Salzer, *Organometallchemie*, Teubner, Stuttgart, **1990**.
- [9] N. Lin, A. Dimitriev, J. Weckesser, J. V. Barth, K. Kern, *Angew. Chem.* **2002**, 114, 4973–4977; *Angew. Chem. Int. Ed.* **2002**, 41, 4779–4783; P. Messina, A. Dimitriev, N. Lin, H. Spillmann, M. Abel, J. V. Barth, K. Kern, *J. Am. Chem. Soc.* **2002**, 124, 14000–14001.
- [10] G. B. Kaufman, *Inorganic Coordination Compounds*, Heyden, London, **1981**.
- [11] S. W. Hla, L. Barthels, G. Meyer, K.-H. Rieder, *Phys. Rev. Lett.* **2000**, 85, 2777–2780; W. Ho, *J. Chem. Phys.* **2002**, 117, 11033–11061.
- [12] M. Böhrringer, K. Morgenstern, W.-D. Schneider, R. Berndt, *Angew. Chem.* **1999**, 111, 823–834; *Angew. Chem. Int. Ed.* **1999**, 38, 821–823.
- [13] M. Bode, *Rep. Prog. Phys.* **2003**, 66, 523–582; R. Wiesendanger, M. Bode, A. Kubetzka, O. Pietzsch, M. Morgenstern, A. Wachowiak, J. Wiebe, *J. Magn. Magn. Mater.* **2004**, 275, 2115–2120.
- [14] J. A. van Bokhoven, A. M. J. van der Eerden, D. C. Koningsberger, *J. Am. Chem. Soc.* **2003**, 125, 7435–7442.
- [15] N. L. Rosi, J. Eckert, M. Eddaoudi, D. T. Vodak, J. Kim, M. O’Keefe, O. M. Yaghi, *Science* **2003**, 300, 1127–1129.
- [16] V. G. Veslago, *Sov. Phys. Uspekhi* **1968**, 509–515; D. R. Smith, J. B. Pendry, M. C. K. Wiltshire, *Science* **2004**, 305, 788–792.
- [17] N. Strater, W. N. Lipscomb, T. Klabunde, B. Krebs, *Angew. Chem.* **1996**, 108, 2701–2705; *Angew. Chem. Int. Ed. Engl.* **1996**, 35, 2024–2055; P. A. Karplus, M. A. Pearson, R. P. Hausinger, *Acc. Chem. Res.* **1997**, 30, 330–337; D. Lee, S. J. Lippard, *Inorg. Chem.* **2002**, 41, 2704–2719.

Comments on “How Single and Bifurcated Hydrogen Bonds Influence Proton-Migration Rate Constants, Redox, and Electronic Properties of Phenoxyl Radicals”**

Ian J. Rhile and James M. Mayer*

Keywords:

electron transfer · hydrogen bonds · oxidation · proton transfer · radicals

In a recent communication, Thomas et al. studied the oxidations of three hydrogen-bonded phenols.^[1] Such compounds serve as interesting models for hydrogen-bonded tyrosine and tyrosyl radical residues in biological systems. EPR data and DFT calculations provided strong evidence for the nature of the phenoxyl radical products of one-electron oxidation. The cyclic voltammetry (CV) data were simulated and interpreted using a model with initial interfacial electron transfer and subsequent slow proton transfer. Herein we show that this mechanistic interpretation of the CV results is problematic on both thermochemical and kinetic grounds.

Figure 1 shows the CV curve of the simplest phenol-amine studied by Thomas et al., HL^{Benz}, together with chemical structures of the various forms of the phenol and phenoxyl radical. The CV curve was modeled using DigiSim and involved transfer coefficients, redox potentials, heterogeneous electron-transfer rate constants (e.g. k_{1-2}), and subsequent proton-transfer rate constants (e.g. k_{2-3}). The peak potential of

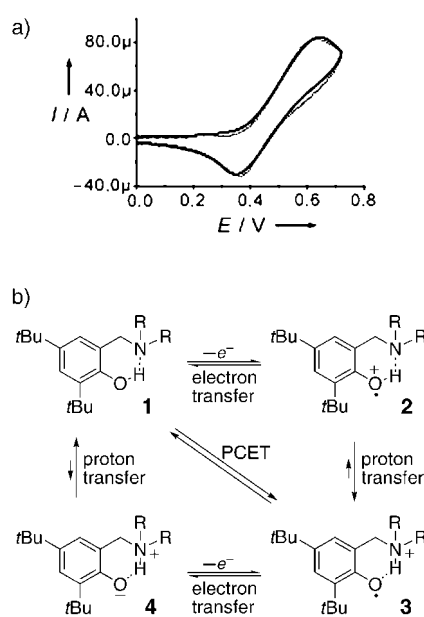
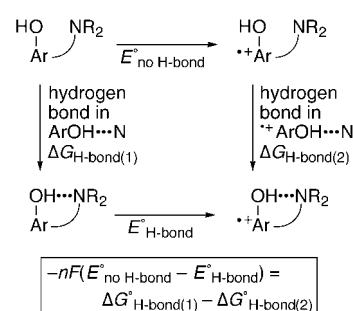


Figure 1. a) CV curve of HL^{Benz} reproduced from Reference [1]. Conditions: HL^{Benz} (2.4 mM in CH₂Cl₂), tetrabutylammonium perchlorate (0.1 M), 298 K, scan rate: 0.1 V s⁻¹; solid line: experimental; dotted line: simulation. b) Square scheme showing various pathways for oxidation of phenol-amine HL^{Benz} (R = CH₂Ph).^[1]

the oxidation wave ($E_{p(a)}$) is cited as 0.48 V less positive than that for the related 2,4,6-tri-*tert*-butylphenol, which does not contain an intramolecular hydrogen bond.^[1] The explanation for the very large difference in redox potentials between the two phenols, 0.48 V = 46 kJ mol⁻¹, was that “the hydrogen bonding increases the electron density on the phenolic oxygen making it easier to be oxidized.” A thermochemical cycle



Scheme 1. Thermochemical cycle showing the influence of hydrogen-bonding on redox potentials. R = Aryl, F = Faraday constant.

(Scheme 1) shows that the shift in potential results (in this model) from the difference in the strength of the hydrogen bond between the phenol-amine and the (phenol radical cation)-amine. A value of 46 kJ mol⁻¹ would be a large total hydrogen-bond energy and would be a very large difference between two structurally similar OH...N hydrogen bonds.

Thermochemically, it is much more likely that the electrochemical oxidation occurring at $E_{p(a)}$ forms the radical in which the proton has transferred, 1 → 3. Phenol radical cations such as 2 are extremely acidic, with pK_a values of less than 0 in aqueous solution.^[2] Ammonium cations have pK_a values of approximately 10–11 in aqueous solution.^[3] Proton transfer from a phenol radical cation to an amine, such as the intramolecular proton transfer 2 → 3, is thus very favorable. The equilibrium constant (K_{eq}) value of 10¹⁰ in water serves

[*] Dr. I. J. Rhile, Prof. J. M. Mayer
Department of Chemistry
University of Washington
Box 351700, Seattle, WA 98195-1700
(USA)
Fax: (+1) 206-543-2086
E-mail: mayer@chem.washington.edu

[**] Comments to a communication published by F. Thomas et al. Our work on proton-coupled electron transfer was funded by the US National Institutes of Health (grant no. 2 R01 GM50422-05).

as an estimate for $K_{\text{eq}}(2 \rightleftharpoons 3)$ in CH_2Cl_2 . The $K_{\text{eq}}(2 \rightleftharpoons 3)$ value of $10^{3.3}$ derived by Thomas et al. from simulation of the CV curve^[1] does not appear to be reasonable for proton transfer from a phenol radical cation to an amine.^[2b] The $K_{\text{eq}}(2 \rightleftharpoons 3)$ value of about 10^{10} implies that **3** is more stable than **2** by $\Delta\Delta G^\circ \approx -57 \text{ kJ mol}^{-1}$, which is close to the difference of -46 kJ mol^{-1} observed between the oxidation potentials of **1** and 2,4,6-tri-*tert*-butylphenol.^[4]

Besides the thermodynamic issues, the CV simulation yields remarkably slow proton-transfer rates. The model yields downhill proton-transfer rate constants for $2 \rightarrow 3$ and $4 \rightarrow 1$ of $10^{7.4 \pm 0.5} \text{ s}^{-1}$ and $10^{5.3 \pm 0.1} \text{ s}^{-1}$, respectively,^[1] equivalent to half-lives of 30 ns and 3 μs . We know of no precedent for such long timescales for simple exoergic proton transfer within a hydrogen bond between electronegative atoms, as in **2** and **4**. Proton transfers from oxygen to nitrogen are extremely facile and occur almost without a barrier.^[5] A rate constant of $10^{5.3 \pm 0.1} \text{ s}^{-1}$ would indicate a remarkably large proton-transfer energetic barrier, $\Delta G^\ddagger = 43 \text{ kJ mol}^{-1}$. Excited-state proton-transfer reactions occur on ultrafast timescales (picosecond and subpicosecond).^[6] It is not reasonable to assign the low chemical rate constants from the CV simulation to exoergic proton-transfer reactions.

Thus, for both kinetic and thermodynamic reasons, the large peak separation in the CV curve of **1** is unlikely to be a result of an electrochemical mechanism in which the chemical step is proton transfer from **2** to **3**. Similar arguments apply to the oxidations of other phenols in the communication. The electrochemistry of other hydrogen-bonded phenols in acetonitrile show various shapes of CV curves and have usually been interpreted as phenol-amine- $e^- \rightarrow$ phenoxyl-ammonium, similar to $1 \rightarrow 3$.^[7] Quasi-reversible CV curves can typically be simulated with

more than one kinetic model, so other data are required to corroborate a mechanism.^[8] A number of effects could be responsible for the shape of the CV traces reported in Reference [1]. Methylene chloride is not regarded as an ideal solvent for electrochemical measurements because of its low dielectric constant, its propensity for ion pairing, and its high resistance.^[9] Slow heterogeneous electron-transfer kinetics, owing to the solvent or other factors, could affect the shape of the CV curve.^[10] If electron transfer to the electrode is concerted with intramolecular proton transfer—a proton-coupled electron-transfer (PCET) reaction^[11]—it could display slow kinetics. Hammarström and co-workers^[12] and ourselves^[7b] have found that homogeneous electron-transfer reactions of related systems occur by concerted PCET with large intrinsic energetic barriers.

In conclusion, the oxidations of hydrogen-bonded phenols reported by Thomas et al.^[1] are very interesting models for biochemical tyrosine oxidations, but thermodynamic and kinetic arguments raise serious questions about the mechanistic interpretation of the cyclic voltammetry data.

Published online: February 11, 2005

- [1] F. Thomas, O. Jarjayes, H. Jamet, S. Hamman, E. Saint-Aman, C. Duboc, J.-L. Pierre, *Angew. Chem.* **2004**, *116*, 604; *Angew. Chem. Int. Ed.* **2004**, *43*, 594.
- [2] a) T. A. Gadosy, D. Shukla, L. J. Johnston, *J. Phys. Chem. A* **1999**, *103*, 8834; b) In the Supporting Information for reference [1], it is stated that “The phenoxyl radical cation is strongly acidic ($\text{p}K_a = -5$, see E. J. Land, G. Porter, E. Strachan, *Trans. Faraday Soc.* **1961**, *57*, 1885).”
- [3] M. B. Smith, J. March, *March's Advanced Organic Chemistry*, 5th ed., Wiley, New York, **2001**, p. 330.
- [4] Agreement between the $\Delta\Delta G^\circ$ (proton transfer) value and the shift in potential

would likely be better if $E_{1/2}$ values were used and if the $\Delta\Delta G^\circ$ values were derived from $\text{p}K_a$ values in the same solvent.

- [5] a) R. P. Bell, *The Proton in Chemistry*, Cornell University, Ithaca, New York, **1973**; b) A. J. Kresge, *Acc. Chem. Res.* **1975**, *8*, 354.
- [6] For lead references, see: a) A. Stolow, *Annu. Rev. Phys. Chem.* **2003**, *54*, 89; b) W.-S. Yu, C.-C. Cheng, Y.-M. Cheng, P.-C. Wu, Y.-H. Song, Y. Chi, P.-T. Chou, *J. Am. Chem. Soc.* **2003**, *125*, 10800; c) S. Lochbrunner, A. J. Wurzer, E. Riedle, *J. Phys. Chem. A* **2003**, *107*, 10580.
- [7] a) T. Maki, Y. Araki, Y. Ishida, O. Onomura, Y. Matsumura, *J. Am. Chem. Soc.* **2001**, *123*, 3371; b) I. J. Rhile, J. M. Mayer, *J. Am. Chem. Soc.* **2004**, *126*, 12718–12719; I. J. Rhile, T. F. Markle, J. M. Mayer, unpublished results; c) L. Benisvy, A. J. Blake, D. Collison, E. S. Davies, C. D. Garner, E. J. L. McInnes, J. McMaster, G. Whittaker, C. Wilson, *Dalton Trans.* **2003**, 1975; L. Benisvy et al. draw the product of oxidation of their phenol-imidazole as a phenol radical cation, but its EPR spectrum is “very similar” to that of the phenoxyl-ammonium reported by Maki et al.^[7a] Furthermore, stability of the oxidation product over 1 h at 0°C implies that it is in the more stable phenoxyl-imidazolium form.
- [8] a) A. W. Bott, S. W. Feldberg, M. Rudolph, *Curr. Sep.* **1996**, *15*, 67; b) Digisim 3.0 Help File, “Objectives and Comments,” Bioanalytical Systems, **2000**.
- [9] a) A. J. Fry, W. E. Britton in *Laboratory Techniques in Electroanalytical Chemistry* (Eds.: P. T. Kissinger, W. R. Heinemann), Dekker, New York, **1984**, pp. 367–382; b) K. M. Kadish, J. E. Anderson, *Pure Appl. Chem.* **1987**, *59*, 703.
- [10] A. J. Bard, L. R. Faulkner, *Electrochemical Methods: Fundamentals and Applications*, Wiley, New York, **1980**, pp. 230–231.
- [11] a) J. M. Mayer, I. J. Rhile, *Biochim. Biophys. Acta* **2003**, *1655*, 51; b) J. M. Mayer, *Annu. Rev. Phys. Chem.* **2004**, *55*, 363.
- [12] M. Sjödin, S. Styring, B. Åkermark, L. Sun, L. Hammarström, *J. Am. Chem. Soc.* **2000**, *122*, 3932.

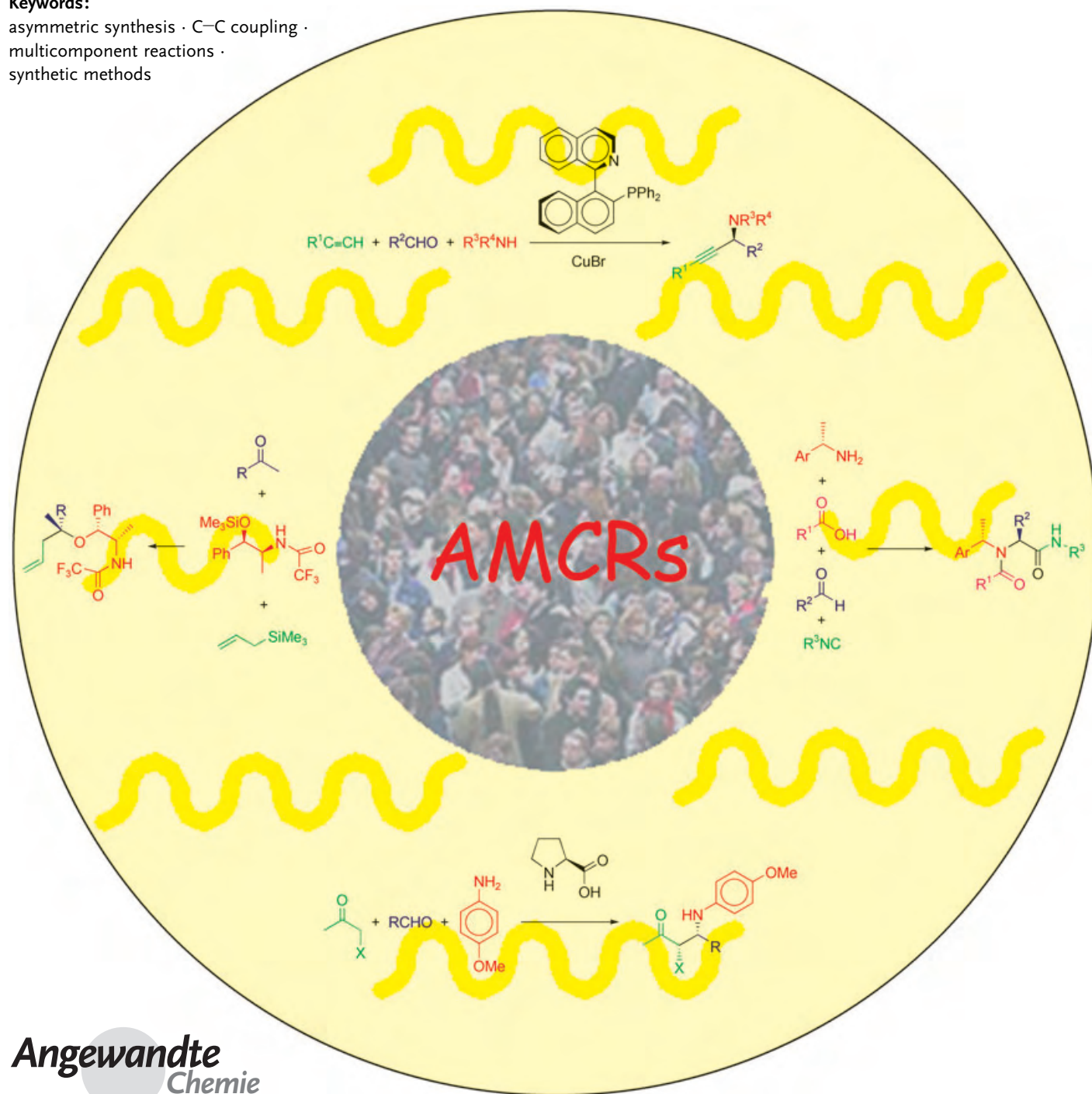
Asymmetric Synthesis

Asymmetric Multicomponent Reactions (AMCRs): The New Frontier

Diego J. Ramón and Miguel Yus*

Keywords:

asymmetric synthesis · C–C coupling ·
multicomponent reactions ·
synthetic methods



Asymmetric multicomponent reactions involve the preparation of chiral compounds by the reaction of three or more reagents added simultaneously. This kind of addition and reaction has some advantages over classic divergent reaction strategies, such as lower costs, time, and energy, as well as environmentally friendlier aspects. All these advantages, together with the high level of stereoselectivity attained in some of these reactions, will force chemists in industry as in academia to adopt this new strategy of synthesis, or at least to consider it as a viable option. The positive aspects as well as the drawbacks of this strategy are discussed in this Review.

1. Introduction and Definitions

Although asymmetric synthesis is sometimes viewed as a subdiscipline of organic chemistry, actually this topical field transcends any narrow classification and pervades essentially all chemistry.^[1] Of course, the preparation of chiral compounds impacts strongly upon pharmaceutical and agricultural chemistry owing to the possible different behavior of both enantiomers.^[2] As a result of the increased economic and ecological pressure on these industries, chemists are nowadays moving their interests to new synthetic strategies for chiral targets. In Seebach's words "for many chemists (and, too often, for those making decisions about funding research), the invention of new reactions, the development of synthetic methodology, the systematic (retrosynthetic) analysis of target structures, the investigation of reaction mechanisms, and the total synthesis of complex natural products have lost their glory. Chemists' attention has shifted to areas such as combinatorial synthesis (driven by robot, computer, and miniaturization), material sciences, supramolecular chemistry, the origin of life, the biological and even medical sciences. Yet, in all these fields chirality plays a central role".^[3]

The maximization of synthetic efficiency in the production of large collections of chiral molecules have led synthetic chemists to use extensively parallel automated synthesis^[4] or combinatorial chemistry.^[5] This fact has permitted the facile synthesis of diverse and structurally distinct compounds (diversity-oriented synthesis^[6]), and their use for the exploration of reaction pathways in cells and organisms, leading eventually to the identification of therapeutic protein targets in a systematic way (chemical genetics^[7]), as well as the ensuing emergence of the high-throughput screening^[8] of molecule candidates. However, in nearly all cases the strategy to produce a compound (or library) has been divergent, that is, only two reagents react in every step of the synthesis. As a contrast to this multistep strategy, a new concept for the synthesis of a target or library with a higher chemical efficiency is emerging. The multicomponent reactions are responsible for this higher efficiency,^[9] not only because of intrinsic aspects of the reaction such as superior atom economy,^[10] atom utilization and selectivity, as well as lower level of by-products, but also because of extrinsic aspects of

From the Contents

2. Multicomponent Reactions Based on Nucleophilic Addition to Imines	1604
3. Hantzsch Multicomponent Reaction	1611
4. Isocyanide-Based Multicomponent Reactions	1611
5. Cycloaddition-Based Multicomponent Reactions	1618
6. Asymmetric Sakurai Multicomponent Allylation Process	1624
7. Asymmetric Michael-Addition-Based Multicomponent Reactions	1625
8. Asymmetric Palladium-Based Multicomponent Reactions	1626
9. Miscellaneous Asymmetric Multicomponent Reactions	1627

the processing reaction, such as simpler procedures and equipment,^[11] lower costs, time, and energy, as well as more environmentally friendly criteria.

There are some confusing ideas among chemists about what is a multicomponent reaction (MCR). This type of process should be clearly differentiated from other one-pot processes such as domino,^[12] tandem,^[13] cascade,^[14] or zipper^[15] reactions, and in general from all those processes that involve the reaction between two reagents to yield an intermediate which is captured by the successive addition of a new reagent (sequential component reactions^[16]). Even though the history of MCRs dates back to the second half of 19th century with the reactions of Strecker, Hantzsch, and Biginelli, it was only in the last decades with the work of Ugi and co-workers that the concept of the multicomponent reaction has emerged as a powerful tool in synthetic chemistry.^[17]

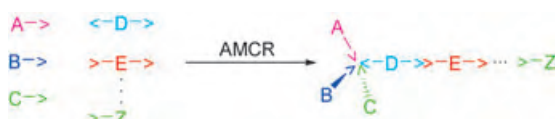
Most of the older known MCRs were found by serendipity rather than by rational planning. However, the rational design of new multicomponent reactions is possible and, to date, may be classified into three different categories: a) Combinatorial

[*] Dr. D. J. Ramón, Prof. Dr. M. Yus
Instituto de Síntesis Orgánica y Departamento de Química Orgánica
Facultad de Ciencias, Universidad de Alicante
Apdo. 99, 03080-Alicante (Spain)
Fax: (+34) 965-90-35-49
E-mail: yus@ua.es

methods: several starting materials with different functional groups are combined automatically in different vessels with different inputs and the results are tested by automated techniques (e.g. HPLC) to find new compounds; b) MCR sequences: the starting materials for a known MCR have extra functional groups (orthogonal functionalities) that do not react in the first MCR but are used in a subsequent MCR; and c) Smallest-atom connectivity: defined as the two sets, for reagents and products, with the minimum number of atom and their connections; can be used in the recognition of MCR fragments in a target molecule and can be used for planning new reactions.

The aforementioned possible designs of new MCRs imply a deep knowledge of known reactions. Several reviews on different aspects^[17] and reaction types, such as Biginelli,^[18] isocyanide-,^[19] palladium-,^[20] organometallic-,^[21] and amido-carbonylation-based^[22] multicomponent reactions have already been published. However, the asymmetric aspect of this methodology has not yet been discussed, and with this Review we would like to fill this gap.

An asymmetric multicomponent reaction (AMCR) should be defined as the reaction between three or more either chiral or achiral reagents in a single vessel which have been added together (or nearly) to form stereoselectively a new chiral compound that contains portions of all the components, forming at least one new stereogenic element (Scheme 1). According to this definition, in this Review we



Scheme 1. General scheme for an asymmetric multicomponent reaction (AMCR).

describe not only the reactions nowadays recognized as asymmetric, but also those using chiral pool strategies,^[23] excluding those processes that involve the derivatization of a reagent without creating any new stereogenic element.

2. Multicomponent Reactions Based on Nucleophilic Addition to Imines

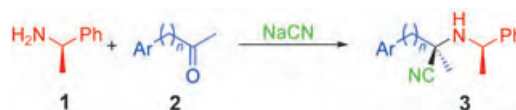
2.1. Strecker Reaction

The Strecker reaction, discovered in 1850, has been recognized as the first multicomponent reaction and has a central importance to the life sciences.^[24] The three-component coupling of an amine, a carbonyl compound (aldehyde or ketone), and hydrogen cyanide to give α -aminonitriles^[25] constitutes an important indirect route in the synthesis of α -amino acids.^[26] Earlier examples of the asymmetric Strecker-type reaction^[24,27] were not real asymmetric multicomponent reactions. What are nowadays known as asymmetric Strecker-type multicomponent reactions must be divided into two categories, according to the topological type of reaction.

2.1.1. Diastereoselective Approach

This type of reaction has always been performed with at least a chiral amine, and therefore yielded α -aminonitriles diastereoselectively.

One of the earliest examples used 1-phenylethylamine (**1**) as the chiral amine (Scheme 2). The AMCR was carried out in



Scheme 2. Diastereoselective Strecker MCR with phenylethylamine.

the presence of different arylalkyl methyl ketones **2** and sodium cyanide leading, after isolation by crystallization, to only one diastereomer in excellent yield. A careful study of the crude solution mixture by ¹H NMR spectroscopy showed that, in fact, the reaction yielded a \approx 1:1 mixture of two possible diastereomers. However, preferential crystallization of **3** under kinetic control, and reversal of the final addition reaction for the other diastereomer, gives as result only one diastereomer **3**.^[28]

The same procedure was also applied to arenecarbaldehydes,^[29] and it was found in these cases that the diastereomeric ratio in solution was dependent on the nature of the



Diego J. Ramón was born in Alicante (Spain) in 1965 and received his BSc (1988), MSc (1989), and PhD (1993) from the University of Alicante. After two years as a postdoctoral fellow at the ETH-Zürich (Switzerland) he returned to the University of Alicante, where he became Associate Professor (2000). He has been a visiting Professor at the Debye Institute (University of Utrecht, the Netherlands, 2001). In 1994 he was awarded the Prize for Young Scientists of the Spanish Royal Society of Chemistry. His research interests are focused on organometallic chemistry and asymmetric synthesis.



Miguel Yus was born in Zaragoza (Spain) in 1947 and received his BSc (1969), MSc (1971), and PhD (1973) from the University of Zaragoza. After two years as a postdoctoral fellow at the Max Planck Institut für Kohlenforschung in Mülheim (Germany) he moved to the University of Oviedo where he became Associate Professor (1977) and Professor (1987). In 1988 he moved to the University of Alicante, where he is head of the Organic Synthesis Institute. He has been a visiting Professor at several institutes (e.g. ETH-Zürich, Oxford, Harvard) and has co-authored more than 300 papers.

aldehyde (up to 98:2). The observed ratio was attributed to the stability of the corresponding conformer, which was confirmed by semiempirical (AM1) and molecular-mechanics calculations of all possible conformers.^[29b]

When the reaction was performed with α -substituted cyclic ketones, a mixture of the four possible diastereomers was isolated in different yields. In the case of cyclopropanone and cyclobutanone,^[30] the α substituent and the cyano group of the major enantiomers were placed in an *anti* configuration. However, in the case of cyclohexanone,^[31] this relationship was *syn*. On the other hand, when the reaction was performed under kinetic conditions, the relationship was *anti* as in the case of other cyclic ketones. Under typical reaction conditions these diastereomers undergo epimerization to yield those with the *syn* configuration. Therefore, the reaction pathway seems to be the same for all α -substituted cyclic ketones: After the formation of the two possible iminium cations, the nucleophilic attack is driven by the steric hindrance of the α substituent (R in Figure 1), and only in the case of cyclohexanone derivatives are these diastereomers unstable and undergo the reverse reaction to yield the thermodynamically more stable *syn* diastereomers.

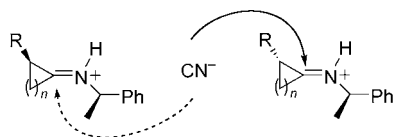
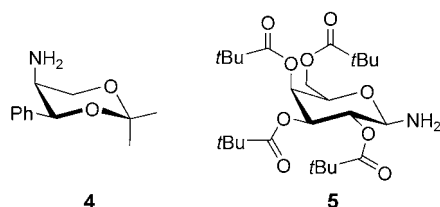


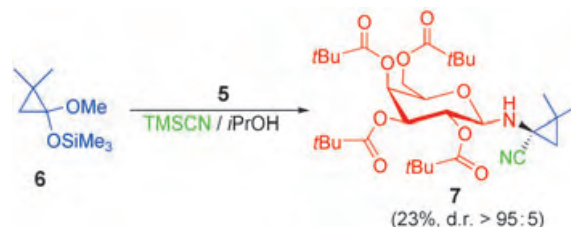
Figure 1. Proposed nucleophilic attack in α -substituted cycloketones.

Other chiral primary amines have also been used in this type of reaction. Thus, the dioxolane derivative **4**, which is



available in large quantities as an intermediate in the chloramphenicol synthesis, has been used successfully in combination with different methyl ketones **2**, yielding only one diastereomer after crystallization. Further acid hydrolysis led to the corresponding α -methyl-substituted α -amino acids.^[32] In this case, and by using benzaldehyde as the carbonyl partner, the stereochemical outcome of the addition could be deduced, implying the formation of an *exo,E* imine in which the phenyl group of the chiral amine **4** favors one of diastereotopic faces of the imine group. However, it must be pointed out that a preferential crystallization, together with an epimerization process, takes place. The galactosylamine derivative **5** could be used with aromatic and aliphatic aldehydes to give similar diastereomeric ratios of the final α -galactosylamino nitrile (up to 88:12), the final acid hydrolysis yielding the expected D amino acids.^[33]

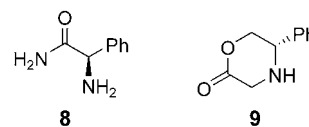
Amines **1**, **4**, and **5** were tested in the asymmetric synthesis of methanovalline (1-amino-2,2-dimethylcyclopropanecarboxylic acid), which has high potential as a plant-growth regulator and also as an enzyme inhibitor.^[34] The best results with respect to diastereoselectivity were obtained with galactosylamine derivative **5**, although the chemical yield was very poor (Scheme 3).^[35] The best yield was obtained with



Scheme 3. Diastereoselective Strecker MCR used in the synthesis of methanovalline.

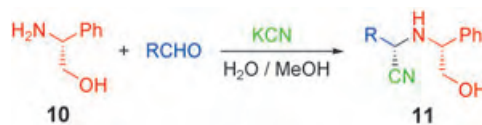
the dioxane derivative **4**, but the diastereoselectivity dropped to 82:18. Several sources of the cyanide anion were tested in these series, and it was found that trimethylsilyl cyanide in 2-propanol was the most promising.

Phenylglycine amide (**8**) has been proposed as an adequate amine in the industrial Strecker synthesis of α -



substituted α -amino acids. The MCR gave the best results in water as solvent and with pivalaldehyde. It was found that the diastereoselectivity was a function of temperature, and under these conditions the higher the temperature, the higher the diastereoselectivity; only one diastereomer was detected at 70 °C. At elevated temperatures in water, the diastereomeric outcome and yield of the process is controlled by the reversible reaction of the final aminonitrile to the intermediate imine, and also by the difference in solubilities of both diastereomers.^[36] The morpholin-2-one derivative **9** was used in the Strecker reaction in combination with aldehydes and copper(I) cyanide; the best diastereomeric ratio was obtained when aliphatic aldehydes were used (up to 94:6).^[37]

Phenylglycinol (**10**) has been proposed as the chiral amine in this AMCR.^[38] Its reaction with different aldehydes gave the expected amino nitriles **11** with modest diastereoselectivity (Scheme 4) which in turn were hydrolyzed under acidic conditions to form different 3-substituted 5-phenylmorpho-

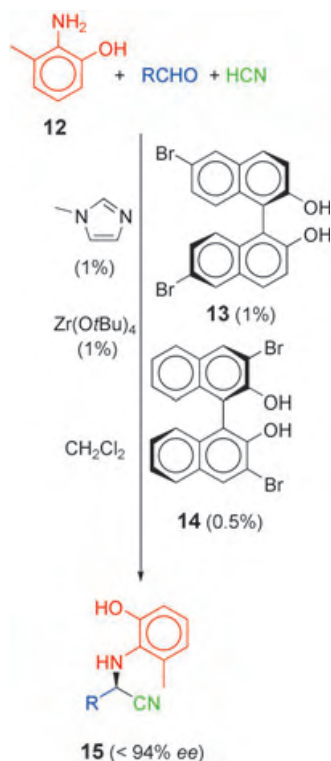


Scheme 4. Diastereoselective Strecker MCR with phenylglycinol.

lin-2-one derivatives. Alkylation of the resulting oxazinones, followed by deprotection, yielded α,α -disubstituted amino acids.^[39]

2.1.2. Enantioselective Approach

In general, enantioselective synthesis implies the preferential formation of one enantiomer of the product from achiral reagents, usually in the presence of a chiral catalyst.^[40] This synthetic approach has clear advantages and has recently been applied to the enantioselective Strecker^[41] MCR with zirconium alkoxides as catalysts in the presence of molecular sieves (Scheme 5). The chemical yield was excellent and the

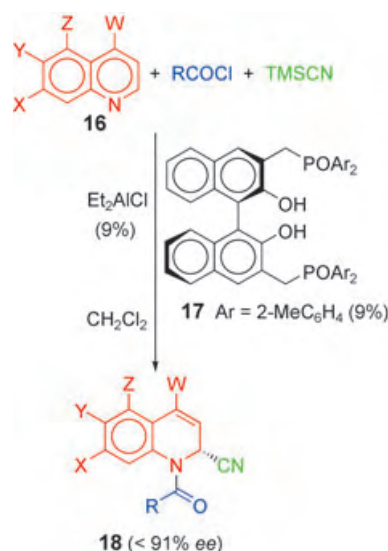


Scheme 5. Enantioselective Strecker MCR.

enantioselectivity high; the results were independent of the nature of the aldehyde (aromatic or aliphatic, including primary, secondary, and tertiary) and of the reaction scale,^[42] thus allowing the enantioselective synthesis of pipecolic acid.

The catalyst itself seems to be a binuclear species that consists of two atoms of zirconium, each bearing a binaphtholate derivative of **13**, a *tert*-butoxide group, and an *N*-methylimidazole; the binaphtholate derived from **14** bridges the two zirconium atoms. This structure appears to be very stable since the same complex was formed even when different molar ratios of starting materials were combined.

The cyanation of pyridines, the so-called Reissert–Henze reaction,^[43] may be considered as a variant of the Strecker reaction. An asymmetric multicomponent version of this reaction has been performed with different functionalized quinoline derivatives **16** and the chiral binaphthol **17** (Scheme 6).^[44] This chiral ligand reacts with diethylaluminum



Scheme 6. Enantioselective Reissert–Henze MCR.

chloride to form the corresponding chloroaluminum binaphtholate derivative. This new bifunctional intermediate can activate two substrates simultaneously: the TMSCN by the phosphorus atom and the acyl pyridine reagent through the aluminum atom. In this way, two reagents are activated and placed spatially close, thus favoring the corresponding reaction. The role of the substituent on the carbonyl chloride seems to be to control the distribution of *s-trans/s-cis* amide conformers on the acyl quinolinium intermediate prior to the enantioselective addition. The best results were obtained with the electron-rich, and therefore less-reactive electrophile, 2-furoyl chloride. The kinetic studies showed that the initial reaction rate was 1.2, 0.15, and 0 order in 2-furoyl chloride, TMSCN, and catalysts, respectively. These data indicate that the acyl quinolinium formation is the major rate-determining step and that the catalyst is not involved. A related chiral ligand of type **17** was further anchored to a solid support and employed for the efficient synthesis of a potent *N*-methyl-D-aspartate (NMDA) receptor antagonist which is a promising drug candidate for Alzheimer's disease and for reducing ischemic brain damage.^[45]

The aforementioned catalyst system (organoaluminum salt and ligand **17**) has also been used in the cyanation of different 1-substituted isoquinolines^[46] to yield the expected α,α -disubstituted aminonitriles.^[47] In this case, chloroformates resulted in higher yields and enantioselectivities than acyl chlorides. The best results were found with vinyl chloroformate (< 98% *ee*) and were practically independent of the steric hindrance of the substituent at the 1-position of isoquinoline.

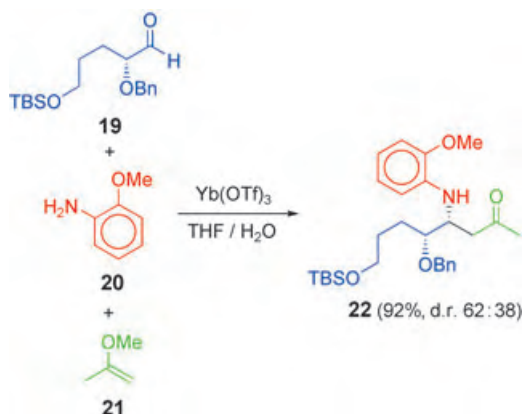
2.2. Mannich Reaction

The classic Mannich reaction, discovered in 1912, is an aminoalkylation of carbonylic compounds involving ammonia (or an amine derivative), a non-enolizable aldehyde (usually formaldehyde), and an enolizable carbonyl compound. From

a modern viewpoint, the potential of this reaction is rather modest (limited range of application, undesired by-products, unsatisfactory regio- and stereocontrol, etc.). However, the exceptional attractiveness of final products makes the challenge of overcoming these drawbacks worthwhile.^[48]

2.2.1. Diastereoselective Approach

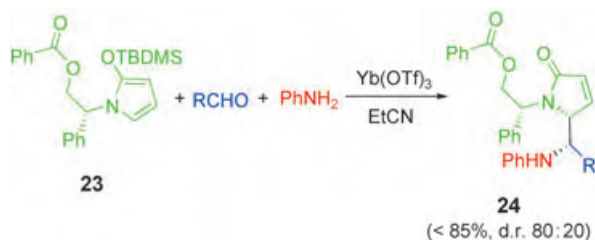
All possibilities of using chiral starting materials for this AMCR have been reported. Thus, the starting chiral compound can be the aldehyde (e.g. **19** in Scheme 7). The reaction



Scheme 7. Diastereoselective Mannich MCR with a chiral aldehyde.

catalyzed by ytterbium triflate in water afforded the expected aminoketone **22** in excellent yield, albeit with a disappointing diastereomeric ratio.^[49] Anyhow, the compound **22** was successfully used in the synthesis of isofebrifugine, an alkaloid found in common hydrangea, and allowed the correct assignment of the absolute configuration of the product.

The nucleophilic partner of the Mannich AMCR can also be chiral (**23** in Scheme 8). Its reaction with different

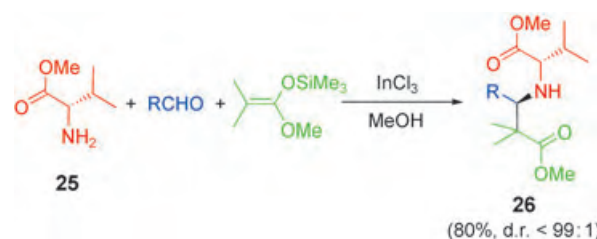


Scheme 8. Diastereoselective Mannich MCR with a chiral nucleophile. TBDMS = *tert*-butyldimethylsilyl.

aldehydes, in the presence of aniline and catalyzed by ytterbium salts, yielded the expected lactams **24**.^[50] Although two new stereocenters are created in this reaction, the diastereoselectivity for aliphatic aldehydes was high: Only two of the four possible stereoisomers were detected, and compound **24** was the major isomer. Different enamines derived from *O*-methylprolinol have also been used as chiral nucleophiles. Their corresponding reaction with benzaldehyde and morpholine in a solution of 2.5M LiClO₄ in diethyl

ether gave an unsatisfactory yield (<20%). All attempts at improving the yield led to a high decrease in the stereoselectivity.^[51]

The last possibility is to use chiral amines (Scheme 9). From the screening of several amines, valine methyl ester



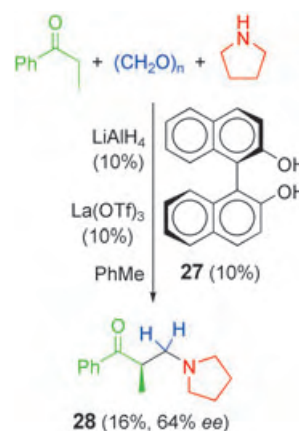
Scheme 9. Diastereoselective Mannich MCR with a chiral amine.

emerged as the best in terms of yield and diastereoselectivity. The reaction involves the condensation of the aldehyde with the amine to yield the thermodynamically more stable *E* imine derivative. The chelation of the nitrogen atom and the carbonyl group of the ester by the indium salt results in a rigid bidentate five-membered-ring conformation. The sterically demanding isopropyl group selectively shields the *Re* face of the imine derivative, and the nucleophilic addition thus takes place on the *Si* face.^[52] InCl₃ was recycled and reused without any loss of activity.

2.2.2. Enantioselective Approach

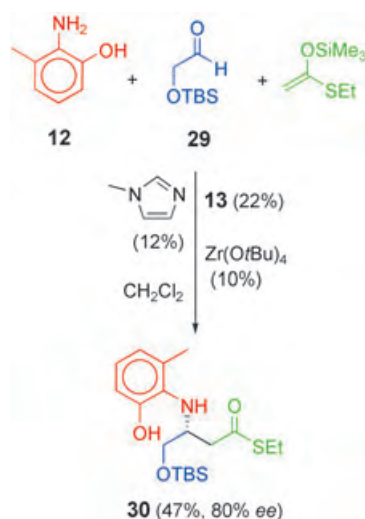
The heterobimetallic catalyst obtained by mixing binaphthol **27** with equivalent amounts of LiAlH₄ and lanthanum salts was the first system that allowed an enantioselective Mannich reaction. Although the reaction gave a very low yield, modest enantioselectivity, and seems to be limited to the reagents outlined in Scheme 10,^[53] it opened up the field for further progression.

A further evolution appeared in the synthesis of the aminic part of HPA-12, an inhibitor of ceramide trafficking from endoplasmic reticulum to the site of sphingomyelin synthesis in mammalian cells which has an important role in the cell growth, differentiation, and apoptosis.^[54] The reaction



Scheme 10. The first enantioselective Mannich MCR.

of the aniline derivative **12**, the protected hydroxyaldehyde **29**, and the silyl enol ether derived from ethyl thioacetate was catalyzed by small amounts of zirconium alkoxides in the presence of 6,6-dibromonaphthol derivative **13** to yield β -amino thioester **30** (Scheme 11) with moderate results.^[55]



Scheme 11. Enantioselective Mannich MCR catalyzed by chiral zirconium alkoxides.

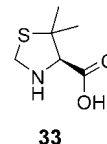
The modest results obtained in the enantioselective Mannich MCR with organometallic catalysis permitted the blossoming of the organocatalytic version.^[56] First, the reaction was successfully performed with acetone (as the source of the nucleophile), *p*-anisidine, and different aldehydes in the presence of natural L-proline (**31**) as catalyst (Scheme 12).^[57] Other substituted ketones can be used readily to furnish the desired products **32** in high yields and excellent diastereo- and enantioselectivities. Furthermore, high regioselectivities, generally favoring products that result from higher substituted α -side of ketone, were found with oxyfunctionalized ketones. The nature of the aldehyde has an important impact on the yield, which is modest for aromatic aldehydes, but not on the enantioselectivity. The amine



Scheme 12. Enantioselective Mannich MCR catalyzed by proline and the postulated transition state. DMSO = dimethyl sulfoxide

component is crucial for the further synthetic utility of Mannich products; *p*-anisidine gives excellent results compared to other amines and has the added advantage of the facile removal of the *p*-methoxyphenyl group.

The enantioselectivity attained correlates well with Hammett σ_p -values in the case of *p*-substituted benzaldehyde derivatives, and thus a linear Hammett plot was obtained. The reaction constant $\rho = 1.36$ suggests a negative charge formation in the enantioselectivity-determining step. The reaction mechanism involves both the formation of the enamine from the ketone and the catalyst and the generation of an imine from the aldehyde and *p*-anisidine. The approach between both intermediates in the transition state is governed by the steric repulsion between the anisidine and pyrrolidine moieties as well as the formation of a hydrogen bond between the nitrogen atom of the imine and the carboxy group (Scheme 12). The 5,5-dimethylthiazolidine-4-carboxylic acid (**33**) also catalyzes the aforementioned reaction. However, the enantioselectivities found are perceptively lower.^[58] β -Amino compounds **32** can readily be transformed into different chiral amine derivatives, such as 1,2-aminoalcohols, 2-aminoaldehydes, etc. The key step for these transformations is a Baeyer-Villiger oxidation with pertrifluoroacetic acid.^[59]

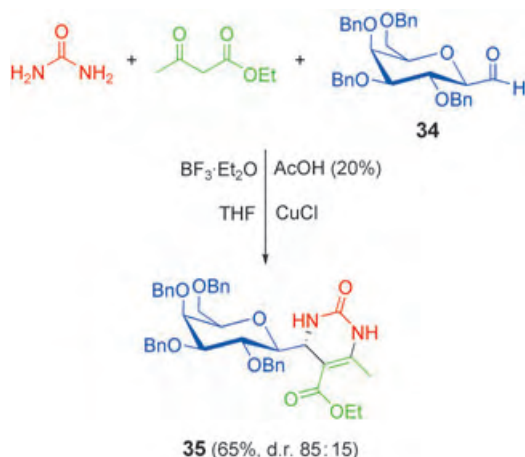


A great influence of the pressure on this three-component coupling reaction was advanced, since its activation volume is negative. In fact, when the reaction was performed in the presence of the catalyst **31** and by a new method for high pressure induced by water-freezing (≈ 200 MPa), both the yield and the enantioselectivity were improved. These good results were obtained even when using aromatic aldehydes, which gave modest results under atmospheric pressure (0.1 MPa).^[60] To facilitate the product isolation and recycling of the catalyst **31**, the reaction can be performed in an ionic-liquid solvent (*N*-butyl-*N'*-methylimidazolium tetrafluoroborate). The excellent yields and enantioselectivities are maintained, but the reaction rates increase up to 50-fold.^[61] The nucleophile source was finally no longer restricted to ketones: propanal was used as the nucleophile and different aromatic aldehydes as electrophiles in combination with amidic solvents such DMF or *N*-methyl-2-pyrrolidinone. The results obtained were excellent in terms of yield, diastereoselectivity, and enantioselectivity.^[62]

2.3. Biginelli Reaction

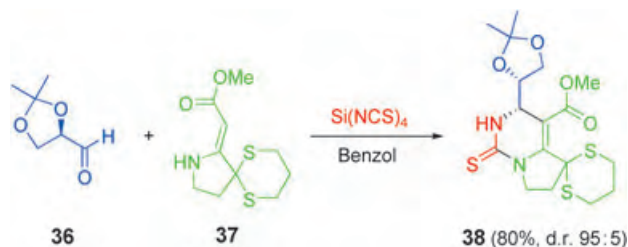
The Biginelli dihydropyrimidine synthesis,^[18] first described in 1891, consists of the condensation of urea, an aldehyde, and a 1,3-ketoester. The accepted mechanism involves, first, the condensation of urea with the aldehyde to yield an iminium intermediate, which is then trapped by an aldol-type reaction with the enol derived from the ketoester. The main drawback of this MCR is its modest yield, which has retarded its development—only a few examples of diastereoselective synthesis are known. The first example reported used different aldehydes derived from cyclic and acyclic

pentoses, which yielded only one diastereomer after purification.^[63] However, a further study with pentoses and hexoses^[64] showed that the diastereoselectivity was far superior in the case of hexose derivatives. The best result was obtained with the galactosyl derivative **34**, with 1 equivalent of CuCl and BF₃ and catalytic amounts of acetic acid (Scheme 13).



Scheme 13. Diastereoselective Biginelli MCR.

Other chiral aldehydes, such as erythrose,^[65] or α -amino^[66] derivatives did not lead to the aforementioned level of selectivity. However the use of the acetonide derived from glyceraldehyde **36**, the enamine **37**, and silicon tetraisothiocyanate as an equivalent of thiourea led to a level of diastereoselectivity up to 95:5 (Scheme 14).^[67] A plausible

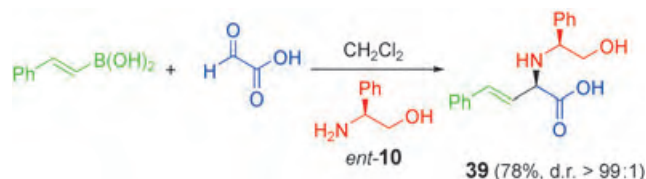


Scheme 14. Diastereoselective Biginelli MCR used in the synthesis of (–)-decarbomoylsaxitoxin.

mechanism, although not clearly established, involves the nucleophilic attack of the nitrogen atom of compound **37** at the carbon atom in the silicon derivative, thereby generating a thiourea intermediate. This thiourea could then condense with the chiral aldehyde, and the new intermediate formed could then undergo cyclization. The observed selectivity could be explained by the Felkin–Anh model. The compound **38** is an intermediate in the synthesis of decarbomoylsaxitoxin, a toxic component of the paralytic shellfish poison present in different cyanobacteria.^[68]

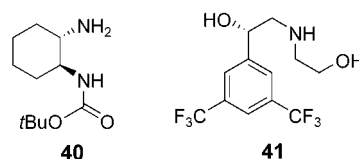
2.4. Petasis Reaction

The condensation already reported in 1993 between carbonyl compounds, amines, and aryl or vinyl boronic derivatives is recognized as the Petasis reaction.^[69a] The reaction has been performed with chiral amines, chiral carbonyl compounds, and chiral boronic acid derivatives. The use of chiral phenylglycinol (*ent*-**10**) in combination with (*E*)-2-phenylvinylboronic acid and glyoxylic acid yielded the expected amino acid derivative with excellent diastereoselectivity (Scheme 15).^[69b] Its further hydrogenolysis gave D-homophenylalanine which demonstrates the utility of this new approach in the synthesis of α -amino acids.



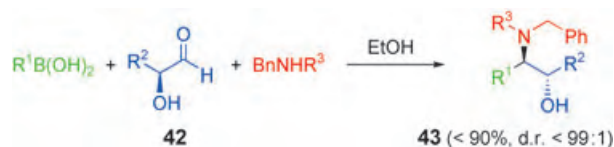
Scheme 15. Diastereoselective Petasis MCR with chiral amines.

Other chiral amines, such as phenylethylamine (**1**)^[70] and the cyclohexyl derivative **40**,^[71] have also been used in the



same reaction, but did not give better results. The morpholinone derivative **9** was, in fact, the first chiral system reported in the asymmetric Petasis MCR and gave excellent diastereoselectivity with aliphatic aldehydes and 2-furylboronic acid.^[72] Finally, the aminodiol **41** has been used as a chiral amine in this AMCR with *p*-fluorophenylboronic acid and aqueous glyoxal to give only one diastereomer, after crystallization.^[73] The product of this reaction is the key intermediate in the synthesis of several pharmaceutical compounds.

The possibility of using chiral aldehydes has also been reported. However, so far only 2-hydroxyaldehyde derivatives have been used.^[74] When the reaction is performed with benzylamine derivatives the results are excellent in terms of yield and diastereoselectivity (Scheme 16). In this case, results were practically independent of the boronic acid derivative



Scheme 16. Diastereoselective Petasis MCR with chiral aldehydes. Bn = benzyl.

(aryl or vinyl), of the substitution of benzylamine derivatives, and even of the substitution of the aldehydes (alkyl, trifluoromethyl, or difluoromethyl). The mild reaction conditions prevent the racemization of the aldehyde.

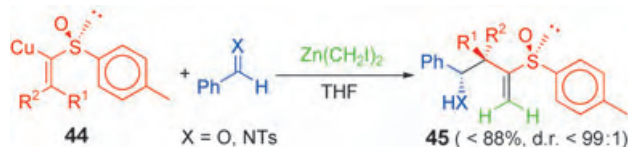
The use of chiral boronic acids has been less successful. The use of different boronic esters derived from chiral diols, such as dialkyl tartrate, together with glyoxylic acid and morpholine yielded the expected amino acid of the type **39** with poor stereoselectivity.^[75]

2.5. Organometallic 1,2-Addition Processes

In the last years, other organometallic compounds besides those used in the Petasis MCR have been used; their addition to the imine derivatives formed in situ proceed with a high level of stereoselectivity.^[76]

2.5.1. Diastereoselective Approach

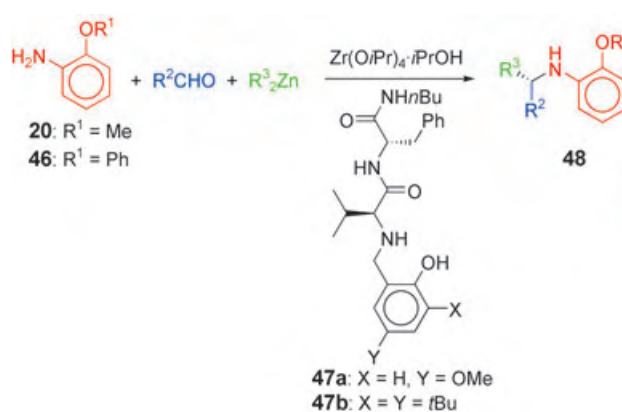
Although there is only one example in this section, it is very interesting since it allowed the preparation of molecules with two new stereocenters, one of them quaternary.^[47] The vinyl copper reagents **44** were synthesized by a *syn* carbocupration of the corresponding chiral 1-alkynyl-*p*-tolyl-sulfoxide with the appropriate organocopper reagents (R^2Cu). These organometallic reagents, as well as the carbenoid bis(iodomethyl)zinc, are not reactive enough to add to either aldehydes or to the corresponding sulfonimide derivatives. However, in the presence of a carbonyl compound, the copper reagents **44** react with the zinc carbenoid to give new chiral allylzinc intermediates, which in turn react with the carbonyl compound to yield, after hydrolysis, the corresponding sulfoxides **45**. The yields and diastereoselectivities are very good in all cases reported, even in the case of $R^1 = CH_3$ and $R^2 = CD_3$ (Scheme 17).^[77]



Scheme 17. Diastereoselective addition MCR with a chiral organometallic derivative.

2.5.2. Enantioselective Approach

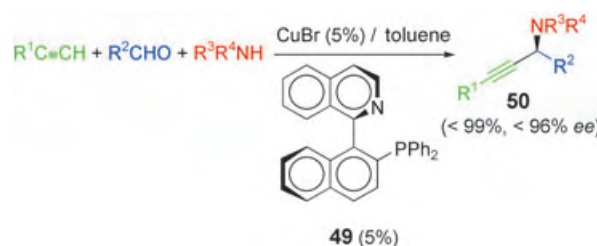
The enantioselective addition of poorly reactive dialkyl zinc reagents to imines has been performed in the presence of zirconium alkoxides.^[78] In the case of aromatic or aliphatic aldehydes in the MCR, the best results were obtained with the aniline derivative **20** and the chiral dipeptide derivative **47a** (Scheme 18). The chemical yields as well as the enantioselectivities were as high as 99% for all reported examples. Further fine tuning of the ligand allowed its use in the alkylation of alkynyl aldehydes to yield chiral propargylamines. In this case, the best aniline derivative and ligand



Scheme 18. Enantioselective dialkylzinc addition in an MCR.

catalyst were the more crowded systems **46** and **47b**, respectively.

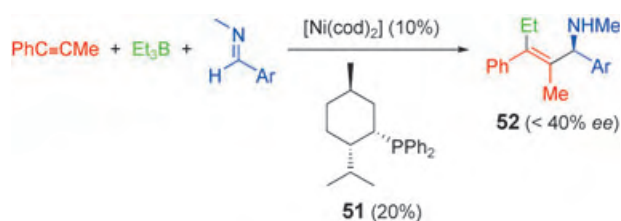
A probably more interesting approach to the synthesis of propargylamines has been developed by Knochel and co-workers which does not require previously prepared organometallic reagents (Scheme 19). In this protocol, different



Scheme 19. Enantioselective alkyne addition in an MCR.

aldehydes react with any kind of amine and 1-alkyne derivatives in the presence of catalytic amounts of a copper salt and the chiral ligand quinap (**49**). The enantioselectivity depends on the nature of the aldehyde—the best results were obtained with aliphatic aldehydes. According to X-ray crystal structures and the existence of a positive nonlinear effect, a bimetallic species bearing two quinap (**49**) units has been postulated as the starting active species in the catalytic cycle. Further complexation with the alkyne and reaction with the amine formed in situ yielded the alkynyl copper intermediate and the imine derivative. Their final reaction led to the expected propargylamines **50**, with liberation of the starting bimetallic copper complex.^[79] The diastereoselective version of this MCR reaction with chiral amines did not have any advantage.^[79,80]

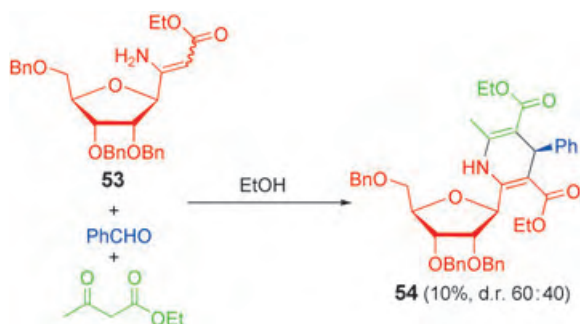
Different allylamines have been obtained by the MCR of 1-phenylpropyne, triethylborane, and *N*-methyl aryl imines catalyzed by substoichiometric amounts of a nickel complex and the chiral phosphane **51**.^[81] Although the results are still far from excellent and seem to be restricted to aryl imines, as well as to the borane and alkyne reagents shown in Scheme 20, it opens up the use of other ligands and complexes.



Scheme 20. Enantioselective organoborane addition in an MCR.
cod = cyclooctadiene.

3. Hantzsch Multicomponent Reaction

Another venerable and old MCR is the so-called Hantzsch reaction. The synthesis of 1,4-dihydropyridines by the reaction of enamines, aldehydes, and 1,3-dicarbonyl compounds was first reported in 1882.^[82,83] However, to date its enantioselective version is unknown, and in the few examples reported, the diastereoselectivity is far from acceptable. The chiral starting material used can be either the 1,3-dicarbonyl compound,^[66] the enamine derivative,^[84] or even the aldehyde.^[85] However, in all cases the diastereomeric ratio is lower than 60:40, probably due to the harsh conditions used in the standard procedures (Scheme 21) under which the chiral enamine **53** gave a very low diastereoselectivity.



Scheme 21. Diastereoselective Hantzsch MCR.

4. Isocyanide-Based Multicomponent Reactions

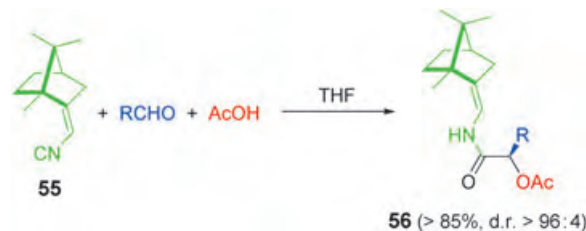
The modern concept of MCRs is intimately related to the reactions developed with isocyanide reagents.^[19] Despite this strong relationship, there are few reactions in which the use of isocyanide reagents leads to chiral compounds,^[86] the immense majority being through the diastereoselective approach.

4.1. Passerini Reaction

The Passerini MCR involves an aldehyde, an acid, and an isocyanide reagent to yield α -acyloxy carboxamides. The reaction first reported in 1921 has been used to produce chiral compounds through enantio- and diastereoselective approaches.^[87]

4.1.1. Diastereoselective Approach

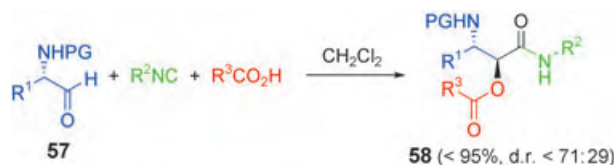
The Passerini reaction has been performed with all chiral reagent variations, with different results. The reaction can be performed with a chiral isocyanide, such as the camphor derivative **55** (Scheme 22), and the results are excellent when



Scheme 22. Diastereoselective Passerini MCR with a chiral isocyanide.

using aliphatic aldehydes. The high selectivity was rationalized as a result of the mechanism proposed, which implies the activation of the aldehyde with the carboxylic acid by hydrogen bond formation, followed by nucleophilic addition of the isocyanide to this adduct. The final intramolecular rearrangement yields the expected compounds **56**.^[88]

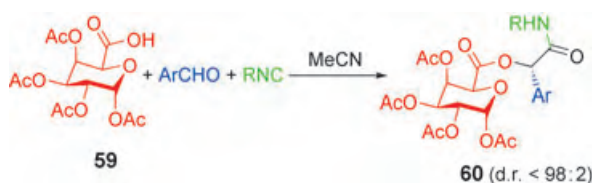
Chiral α -functionalized aldehydes^[89] have also been used in this reaction. However, the results were never as good as those in the aforementioned example. Nevertheless, chiral 2-methylglycidal has been used in combination with ethyl isocyanoacetate and 1-naphthoic acid for the preparation of the amide fragment of azinomycin (d.r. 78:22); this antibiotic^[90] has shown activity against a wide variety of tumors.^[91] A comprehensive study of the Passerini reaction has been performed with the α -aminoaldehydes **57** derived from natural amino acids.^[92] The results were very homogeneous, independently of the carboxylic acid or isocyanide reagents used, and the aldehyde side chain was found to have little influence on the diastereoselectivity (Scheme 23). This strat-



Scheme 23. Diastereoselective Passerini MCR with a chiral aldehyde.
PG = protecting group.

egy has been applied to the solid-phase synthesis of different oligopeptides by using a supported isocyanide and a chiral phenylalaninal derivative; the diastereoselectivity was appreciably lower than for the reaction in solution.^[93]

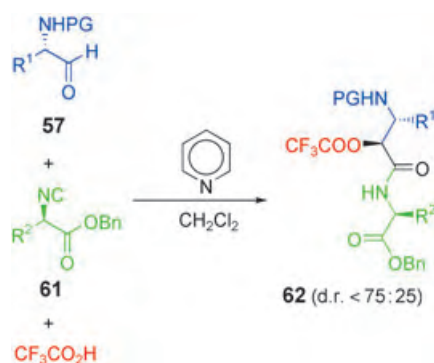
Among the different chiral acids tested for the Passerini MCR, the galacturonic derivative **59** showed the best level of diastereoselectivity.^[94] The reaction worked very well for aromatic aldehydes and aliphatic isocyanides (and even for functionalized derivatives). However, the diastereoselectivity disappeared when the reaction was performed with aromatic isocyanides (Scheme 24). Polymeric carboxymethyl cellulose



Scheme 24. Diastereoselective Passerini MCR with a chiral acid.

has been used as a chiral acid in the Passerini MCR in order to obtain transparent hydrogels, which have widespread use in diverse areas such as prosthetic materials, contact lenses, and controlled drug release.^[95]

The combination of two chiral reagents has also been studied. Thus, the reaction of different chiral natural α -amino acids and α -aminoaldehydes with isocyanides was the key step in the synthesis of inhibitors of serine proteases.^[96] The most extensively used combination of two chiral reagents has been that of chiral aldehydes and isocyanides. The reaction of an (*S*)-alaninal derivative and the isocyanide obtained by dehydration of (*S*)-*N*-formylleucinate ester with benzoic acid was the key reaction step in the synthesis of eurystatin A.^[97] However, although the yield was excellent, no diastereoselectivity was observed; the poor scope and diastereoselectivity were attributed to the vigorous reaction conditions. The use of trifluoroacetic acid in the presence of excess pyridine led to an increase in the diastereoselectivity up to 75:25 (Scheme 25).^[98] This protocol was evaluated in the synthesis

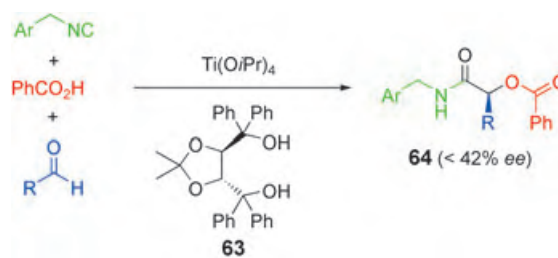


Scheme 25. Diastereoselective Passerini MCR with chiral aldehydes and isocyanides.

of bestatin, which is a potent inhibitor of aminopeptidases and prolyl endopeptidases,^[99] as well as of eurystatin A^[100] and the N10–C17 fragment of cyclotheonamides,^[101] without racemization of the α -aminoaldehyde moiety. The use of chiral isocyanides derived from glucosyl compounds and chiral aldehydes did not improve the previously mentioned stereoselectivity.^[102]

4.1.2. Enantioselective Approach

Although there is only one example of enantioselective Passerini MCR^[103] and the enantioselectivity is still far from excellent (Scheme 26), this example should encourage the search for better catalytic systems. A test with 16 metal salts



Scheme 26. Enantioselective Passerini MCR.

and 12 chiral ligands showed that the best catalytic system was that with 1 equivalent of both titanium tetraisopropoxide^[104] and the taddol ligand **63**.^[105] As expected, a decrease in the amount of catalyst produced an intensive decrease in the enantiomeric excess of compound **64**.

4.2. Ugi Reaction

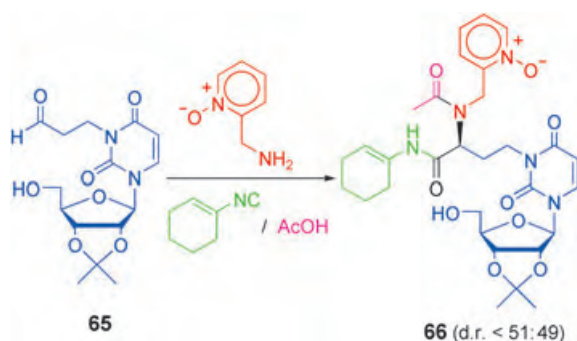
The Ugi MCR, first described in 1959, has been more widely studied and used than any other MCR.^[17] This extraordinary success is associated with the fact that it introduces a higher degree of diversity than other processes. Moreover, the two possible amide bonds that link the reagents in the final chiral product are especially suitable for the synthesis of peptidomimetics.^[24b] There are two main variants, which are usually classified according to the number of components employed. Nevertheless, an enantioselective variant of this fundamental reaction is still unknown.

4.2.1. Four-Component Approach

The Ugi four-component MCR is the reaction of a carbonyl compound (usually an aldehyde), an amine, an isocyanide, and a carboxylic acid (an alcohol can be also used instead) to yield α -amino acid derivatives. Although all four compounds may be used as chiral starting materials, the use of chiral isocyanides did not lead to any diastereoselectivity. This poor result was attributed to the possible mechanism in which, after the formation of the protonated imine derivative (by condensation of the amine and the aldehyde followed by a proton transfer from the carboxylic acid), the addition of the generated carboxylate gives a racemic α -amino α -acyloxy intermediate. The chiral isocyanide substitutes the acyloxy moiety in a pure S_N2 reaction to yield an acylimidate derivative, which after an irreversible rearrangement forms the final α -amino acid derivative as a 1:1 mixture of both diastereomers.^[88]

The results obtained with the chiral aldehyde derivative **65** were also disappointing, as no stereodiscrimination was found (Scheme 27). However, it allowed a facile entry to peptide-modified nucleoside **66**.^[106]

The results with chiral acids were no better; the final products were obtained as a 1:1 mixture of diastereomers. However, in the majority of cases the mixture of compounds were separated by flash chromatography or by recrystallization, for example, in the synthesis of different piperazine-2-



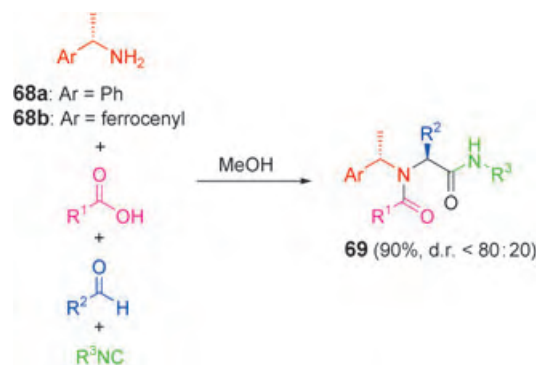
Scheme 27. Diastereoselective Ugi four-component reaction with a chiral aldehyde.

carboxamides,^[107] in which the use of different chiral acids such as camphanic, mandelic, or gulonic acid derivatives did not lead to any diastereoselectivity. In the case of α -amino acid derivatives as acid partners, the dipeptide **67** was obtained with almost no diastereoselectivity, regardless of the aldehyde, the isocyanide, or the side chain of the acid (Scheme 28).^[108] Similar results were obtained when a solution of ammonia was used instead of the amine,^[109] or when the isocyanide was bound to a solid phase.^[110] Even the use of polyfunctionalized β -amino acid derivatives did not lead to any diastereoselectivity.^[111]

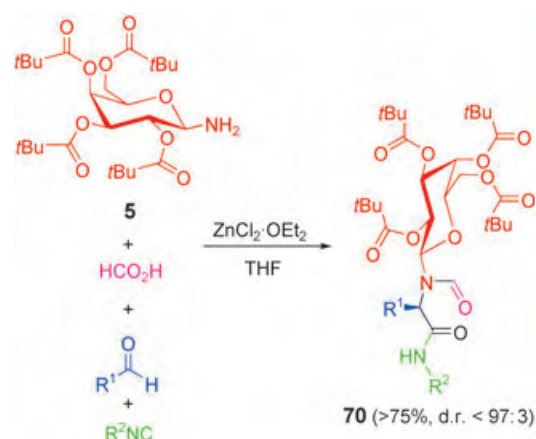


Scheme 28. Diastereoselective Ugi four-component reaction with a chiral acid. Boc = *tert*-butoxycarbonyl.

The results with chiral amines were more promising with respect to diastereoselectivity. The use of different aromatic amines **68** led to the formation of α -amino acid derivatives **69** in excellent yield and with reasonable diastereoselectivity (Scheme 29), regardless of the amine used.^[112] The use of galactosylamine **5** allowed the preparation of α -amino acid derivatives **70** with excellent results (Scheme 30), independent of the nature of both the aldehyde and the isocyanide. The reaction should be performed in the presence of 1 equivalent of zinc chloride to obtain good diastereoselectivities. The role of the Lewis acid seems to be to force the conformation of the initially formed galactosylimine by chelation with the nitrogen atom and the oxygen atom of the carbonyl group. The chiral α -amino acid can be liberated by final hydrolysis in two steps: The *N*-formyl group is first removed with hydrogen chloride in methanol, and the *N*-glycosidic bond is then cleaved by addition of water, with a 90–95 % recovery of the



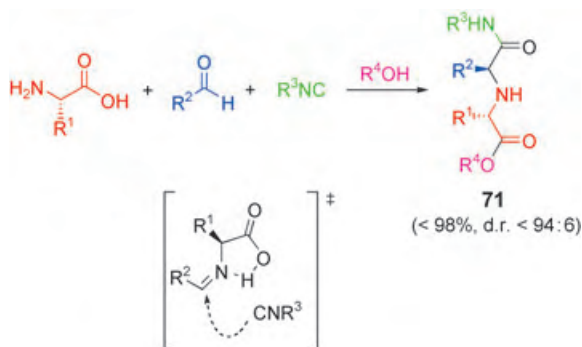
Scheme 29. Diastereoselective Ugi four-component reaction with a chiral aryl amine.



Scheme 30. Diastereoselective Ugi four-component reaction with a chiral galactosylamine.

corresponding *O*-pivaloyl galactose. The final hydrolysis of the amide moiety in aqueous hydrochloric acid yields the free α -amino acid.^[113] The galactosylamine **5** could be anchored to a Wang resin through a tetramethyl azelaic acid unit, thus allowing the reaction to be performed under solid phase conditions.^[114] However, the yield and diastereoselectivity were inferior to those under homogenous conditions. To facilitate the final hydrolysis of product **70**, 2-(*tert*-butyldimethylsilyloxymethyl)phenylisocyanide (R^2NC in Scheme 30) was introduced; the excellent results of the Ugi reaction were maintained.^[115] The related 2,3,4-tri-*O*-pivaloyl- α -D-arabinosylamine was introduced successfully instead of chiral amine **5** to obtain the amino acids with *S* configuration.^[116]

An interesting variant of Ugi four-component reaction was developed with an α -amino acid as the amine partner and with an alcohol instead of the carboxylic acid. This variant gives 1,1-iminodicarboxylic acids **71** with good diastereoselectivities (Scheme 31).^[117] The new stereocenter has the same absolute configuration as the amino acid employed (deduced on the basis of crystallographic structures). A *Z* imine was postulated as the key intermediate to explain the stereotopicity of the reaction. The nucleophilic addition takes place avoiding the more crowded face of this intermediate, rendering a cyclic *O*-acyl-amide, which after reaction with the



Scheme 31. Diastereoselective Ugi four-component reaction with a chiral α -amino acid.

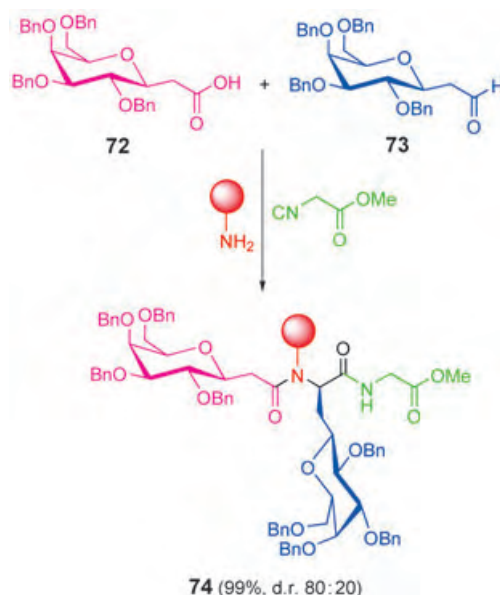
alcohol, gives compounds **71**. The use of chlorinated aldehydes permitted, in a further step, the preparation of aziridine derivatives.^[118]

On the other hand, when the reaction was performed with functionalized aromatic aldehydes the newly formed stereogenic center proved to have the *R* configuration,^[119] which contradicts the previous results. Moreover, when the reaction was performed with aliphatic alkoxy-carbonyl aldehyde derivatives the absolute configuration of the new stereocenter was deduced as *R* (according to X-ray crystallography), and the stereochemical course of the reaction was explained simply by changing the above geometry of the imine from *Z* to *E*.^[120] Therefore, a general mechanistic interpretation requires more experimental investigations.

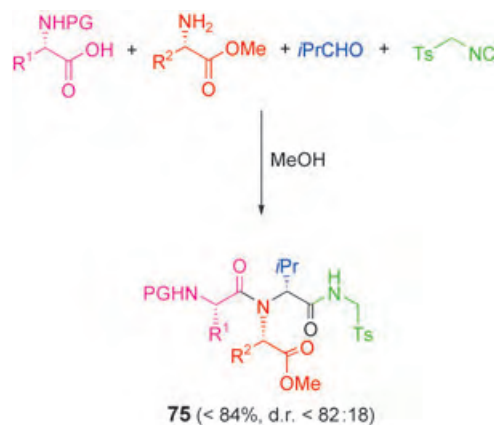
Among the six possible combinations of two chiral reagents, four have been employed in this MCR with different levels of success. The first example is the reaction between a chiral isocyanide (derived from phenylalanine), a chiral acid (in fact, a dipeptide), isobutyraldehyde, and a cinnamylamine anchored to a resin to yield, without any diastereoselectivity, the expected tetrapeptide, which was used as a β -turn mimetic.^[121]

Although the combination of chiral aldehydes and acids in the Ugi four-component reaction has been used for the synthesis of demethyldysidenin (a hexachlorinated amino acid from the marine sponge *Dysidea Herbacea*),^[122] polyoxin with *N*-methylated peptide bonds,^[123] and nodularin-V (a cyclic pentapeptide inhibitor of the serine/threonine phosphatase),^[124] the diastereoselectivity obtained was nearly zero in all cases. However, in the combinatorial solid-phase generation of a library of C-glycoside peptide ligands for cell-surface carbohydrate receptors (Scheme 32), the observed diastereomeric ratio of up to 80:20 was practically independent of the chiral acid of the type **72** used. However, the length of the side chain between the carbonyl group and the heterocyclic moiety in compounds of type **73** did influence the diastereoselectivity.^[125]

The combination of chiral amines and acids seems to be more promising. Thus, chiral, protected α -amino acids and α -amino esters have been used in the synthesis of dipeptides containing iminocarboxylic derivatives **75** (Scheme 33). As expected, the nature of the acid partner had no effect. However, the side chain of the amine derivative had a great impact on the diastereoselectivity and the best results were



Scheme 32. Diastereoselective Ugi four-component reaction with a chiral acid and a chiral aldehyde.



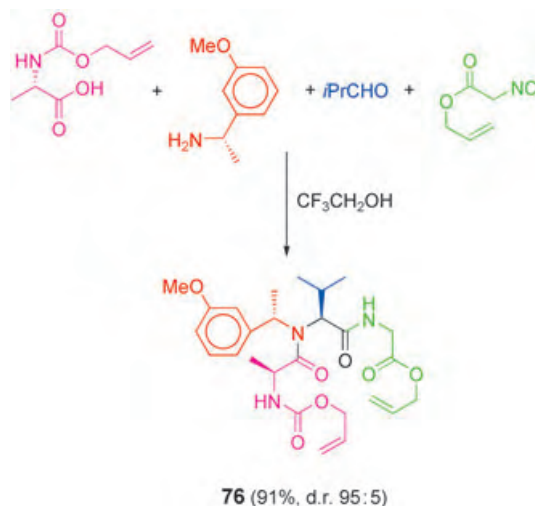
Scheme 33. Diastereoselective Ugi four-component reaction with a chiral acid and a chiral amino ester. Ts = *para*-toluenesulfonyl

obtained when aliphatic derivatives were used. The absolute configuration of the major diastereomer was the opposite of that of the amine.^[126]

The former approach has allowed anchoring of the amine partner as an ester to TentaGel polymer. The diastereoselectivities found under solid-phase conditions were the same as those under homogenous solution. The final detachment from the polymer support directly yielded different diketopiperazines.^[127] This strategy allowed the creation of a library of compounds, some of which were highly selective inhibitors of matrix metalloproteases, important therapeutic targets especially in cancer and arthritis.^[128]

The use of (*S*)-diaminopropionic acid attached to a hydroxymethyl Merrifield resin and (*R*)-2-bromoalkanoic acid derivatives as chiral components yielded the expected peptides with low diastereoselectivity (65:35). However, it allowed the rapid preparation of diketopiperazine derivatives, which are putative peptide β -turn mimetics.^[129]

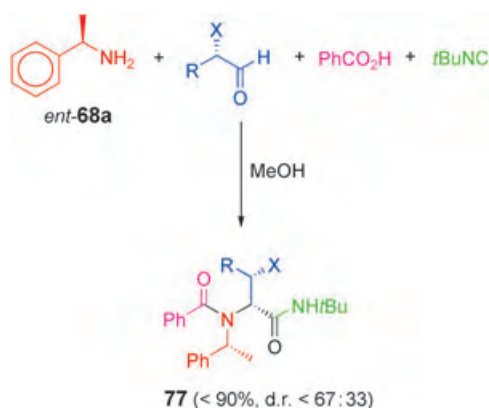
A higher diastereoselectivity was attained in the reaction outlined in Scheme 34, the choice of temperature being more crucial than the choice of aryl amine. For example the reaction carried out at room temperature gave a diastereomeric ratio of 75:25, whereas at -30°C the stereoselectivity reached 95:5. The final peptide **76** was further transformed into a conformationally fixed cyclic system by ring-closing metathesis.^[130]



Scheme 34. Diastereoselective Ugi four-component reaction with a chiral acid and a chiral aryl amine.

The combination of a chiral α -amino acid derivative and a chiral polyfunctionalized benzylamine, together with acetaldehyde and phenylisocyanide, has been used in the rapid construction of the skeleton of ecteinascidin 743,^[131] which is an extremely potent antitumor agent isolated from a marine tunicate and is currently undergoing phase II clinical trials.

The final combination of the two chiral reagents tested in the Ugi four-component reaction was the use of an aldehyde and an amine. The reaction was performed with different aldehydes bearing a stereocenter at the α position. When the substituent on the aldehyde was a methyl group ($X = \text{Me}$ in Scheme 35), a complicated mixture of four diastereomers was



Scheme 35. Diastereoselective Ugi four-component reaction with a chiral amine and a chiral aldehyde.

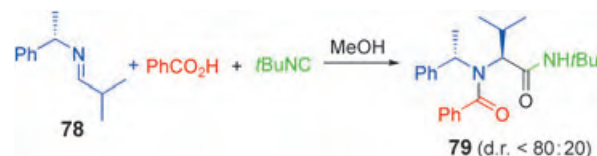
obtained. The repetition of the reaction with deuteromethanol, the amine, and the acid components yielded a final product in which deuterium appeared at the α position of the former aldehyde component. This fact indicated that racemization took place prior to condensation. However, when the reaction was carried out with α -hydroxyaldehyde derivatives, racemization did not occur and the final product **77** was isolated in excellent yield but with modest diastereoselectivity, never higher than 67:33.^[132] Despite the low diastereoselectivity, this approach has been used in the synthesis of the antibiotic furaromycin and its stereoisomers.^[133]

Not only a combination of two chiral reagents, but also combinations of three or four chiral reagents have been used in the Ugi four-component reaction. The different chiral building blocks were derived from per-*O*-benzylated- β -D-glucosyl derivatives (such as aldehydes, amines, acids, and isocyanides),^[134] and allowed facile access to glycoconjugate libraries.^[135]

4.2.2. Three-Component Approach

The Ugi three-component is a variant of the general reaction in which either two of the usual groups are included in the same reagents or the condensation of the carbonyl compound with the amine takes place before the addition of the isocyanide and acid derivatives. Even though the imine condensation could be performed in a one-pot process and its isolation was not necessary, it must be included in this category. As in the previous sections, different chiral reagents could be used alone or with others.

By far the most common approach is the use of chiral imines, which are prepared by the use of either a chiral amine or a chiral aldehyde. First we will focus on chiral imines prepared from chiral amines. One of the first examples came from the reaction of the imine **78** (formed by condensation of 1-phenylethylamine (**68a**) with isobutyraldehyde) with *tert*-butyl isocyanide and benzoic acid (Scheme 36). Although the



Scheme 36. Diastereoselective Ugi three-component reaction with a chiral imine (from a chiral aryl amine).

diastereoselectivity found was never higher than 80:20,^[136] it opened up the field for the use of other chiral imines. The mechanism of this variant was studied in the aforementioned reaction and confirmed the previously proposed Ugi four-component mechanism (see Section 4.2.1). This reaction has been utilized in the introduction of α -trifluoromethyl α -amino acid derivatives into a peptide, simply by replacing benzoic acid with the corresponding α -trifluoromethyl α -amino acid.^[136c] The stereoselectivity was improved markedly by using different 1-ferrocenylalkylamines as the chiral reagent in the imine formation, which allowed a diastereomer ratio of up to 99:1.^[137]

Problems of diastereoselectivity and stability, especially for ferrocene derivatives, were overcome by the use of triacetylglucopyranosylimine derivatives **80** (**80a** in Scheme 37). Their reaction with different isocyanides and



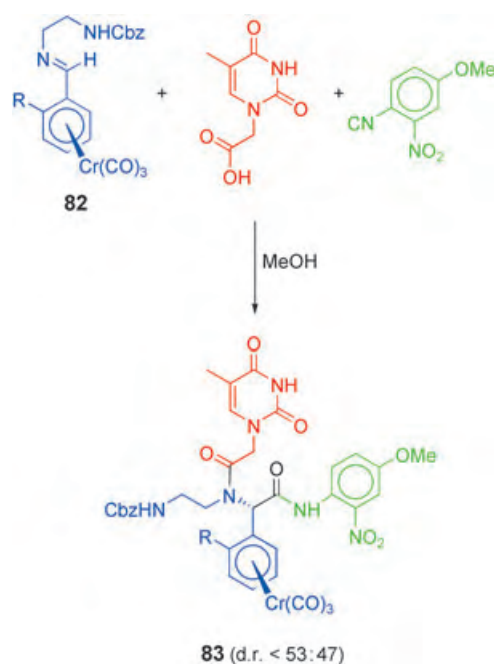
Scheme 37. Diastereoselective Ugi three-component reaction with chiral imines (from chiral 1-amino carbohydrates).

acids afforded the expected glycopeptides **81** in excellent yields and diastereoselectivities. This high stereoselectivity was attributed to the formation of a complex between zinc chloride and both the nitrogen atom of the imine moiety and the oxygen atom of the carbonyl acetamide ($R^3 = MeCO$).^[138] This complex forces the nucleophilic approach from the back side. To prove this hypothesis, other carbohydrate derivatives were tested; it was found that the presence of a carbonyl group at the 3-position has a great impact on the stereoselectivity (**80b** in Scheme 37). However, the peralkylated system **80c** gave results as good as those in the previous systems.^[139] The thiopyranosylimine derivative **80d** (Scheme 37) was introduced to facilitate the cleavage of the carbohydrate moiety from the formed α -amino acid in the final product **81**; reaction with a dilute methanolic solution of trifluoroacetic acid in the presence of mercury(II) acetate yielded the expected α -amino acid.^[140]

The use of chiral imines derived from chiral aldehydes has been less effective with respect to diastereoselectivity. For example, chiral chromium tricarbonyl imine derivatives **82** were used as starting materials for the preparation of chromium-labeled thymine peptide nucleic acid monomers **83** (Scheme 38).^[141] Recently, transition organometallic complexes have attracted attention as biomarkers owing to their facile detection (even at very low concentrations), their stability under physiological conditions, and their inertness toward the native structure of proteins and nucleic acids.^[142]

The former strategy was employed in the combinatorial synthesis of aminoglycoside antibiotics containing the neamine moiety. This class of compounds inhibited the interaction between the viral transactivator protein Rev of HIV I and the full-length target RNA sequence, and therefore they could be used in the treatment of AIDS.^[143]

Based on the results in the Ugi four-component reaction, it can be anticipated that the reaction of imines, isocyanides, and chiral acids will yield 1:1 mixtures of two possible



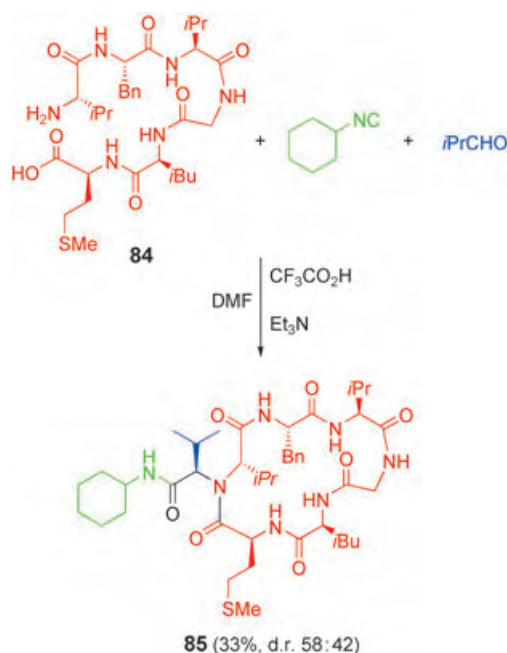
Scheme 38. Diastereoselective Ugi three-component reaction with chiral imines (from chiral aldehyde). Cbz = benzyloxycarbonyl.

diastereomers. No stereoselectivity was found, even when hydrazones were used as substitutes for imines.^[144] Nevertheless, this approach has been used in the synthesis of analogues of eldoisin; these polypeptides are stable towards α -chymotrypsin degradation and have blood-pressure-lowering activity. This strategy has also been used in the combinatorial synthesis of aspergillamides and analogues, some of which are highly active against Gram-positive bacteria and against *Candida*.^[145] The use of chiral alkylated malic acid derivatives in the Ugi three-component reaction yielded different peptide derivatives,^[146] which showed interesting properties as matrix metalloproteinase inhibitors and therefore are potentially active against certain diseases, such as arthritis and cancer.^[128]

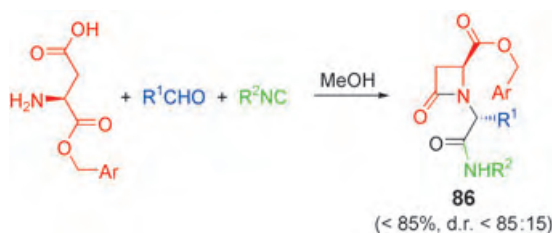
As mentioned previously, apart from the use of an imine there are other possibilities for the Ugi three-component reaction, for example, a chiral compound bearing both the amino and acid groups. This variant was employed in the cyclization of the hexapeptide **84** with isobutyraldehyde and cyclohexyl isocyanide to yield the expected cyclic system **85** (Scheme 39). Although the diastereoselectivity was very poor, both diastereomers were isolated by column chromatography. Unfortunately, against expectations, neither had any effect on the cardiovascular system.^[147]

Other systems with neighboring functional groups, such as α -benzyl aspartate, have been used. In this case, the MCR yielded β -lactams **86** (Scheme 40), which are generically speaking related to antibiotics. The diastereoselectivity influenced by the nature of both the aldehyde and the isocyanide used.^[148]

When the former reaction was carried out with (*S*)-3-amino-2-hydroxypropionic acid (isoserine) as the β -amino acid, the corresponding hydroxy- β -lactam was obtained as a



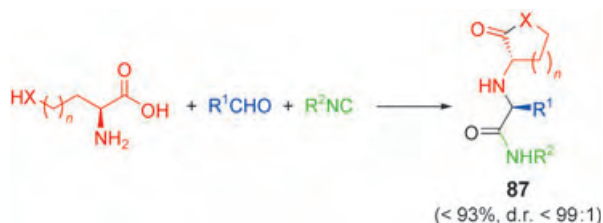
Scheme 39. Diastereoselective Ugi three-component reaction with a chiral peptide.



Scheme 40. Diastereoselective Ugi three-component reaction with a chiral β -amino acid.

1:1 mixture of diastereomers. Nevertheless, this reaction has been used in the total synthesis of nocardicin, one of the first examples of monocyclic β -lactam derivatives with potentially useful antibacterial activity.^[149]

An interesting modification of the general reaction in Scheme 40 is the use of α -amino acids with an extra functional group. A cyclization step occurs after the Ugi three-component reaction. The reaction with homoserine (Scheme 41, X = O, $n = 1$) gave the corresponding lactones **87** in excellent yields and diastereoselectivities.^[150] This reaction can be



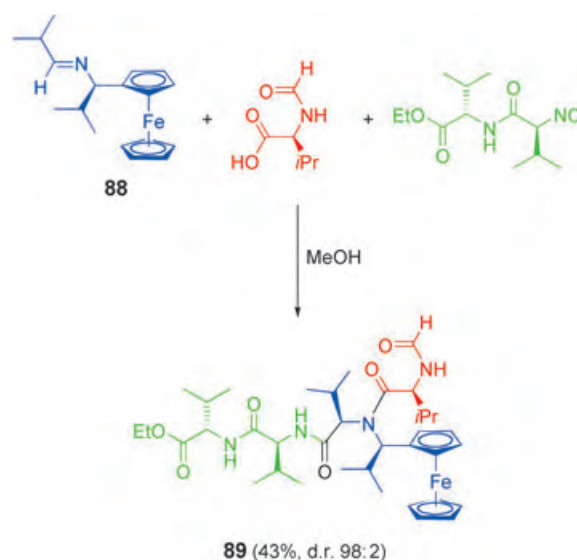
Scheme 41. Diastereoselective Ugi three-component reaction with chiral α -amino acids.

expanded to lysine (Scheme 41, X = NH, $n = 3$), giving the corresponding ϵ -lactams **87**.^[151]

Instead of using α -amino acids with an extra functional group to cyclize the intermediate, hydroxy-functionalized glycoaldehyde has been employed, leading to cyclic morpholin-2-one-5-carboxamide derivatives.^[152] The diastereoselectivity (d.r. $\leq 81:19$) depends not only on the amino acid but also on the isocyanide used.

As in the case of the Ugi four-component reaction, not only one but also two or three chiral reagents have been used in the three-component version of the reaction. Thus, the reaction between the chiral imine (3*S*)-(4-cyanophenoxy)-4,5-dihydropyrrole, and the isocyanide obtained by formylation/dehydration of isoleucine methyl ester with benzoic acid, gave the expected proline–isoleucine dipeptide derivative with a very modest diastereoselectivity.^[153] However, this mixture could be separated by column chromatography and used in the synthesis of different 14-membered cyclopeptide alkaloids related to the amphibine-B family.

An example of the use of three chiral reagents is depicted in Scheme 42. In this case, the reaction of the chiral

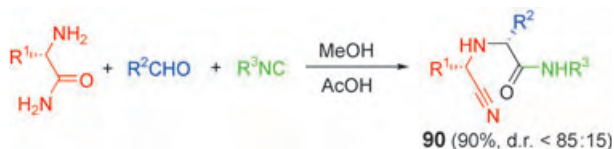


Scheme 42. Diastereoselective Ugi three-component reaction with three chiral reagents.

ferrocenylimine derivative **88** with *N*-formylvaline and the isocyanide obtained by reaction of the formylation/dehydration of the divalene dipeptide gave the expected tetrapeptide in modest yield but with excellent diastereoselectivity.^[154]

4.3. Synthesis of Chiral α -Aminonitrile Derivatives

Surprisingly, the reaction of an isocyanide, an aldehyde, a carboxylic acid, and a chiral α -amino acid amide as an amine equivalent, instead of the already shown ester, did not lead to the expected Ugi four-component reaction product but to the α -aminonitrile **90** (Scheme 43). The mechanistic pathway for the preparation of the unexpected compounds **90** partially

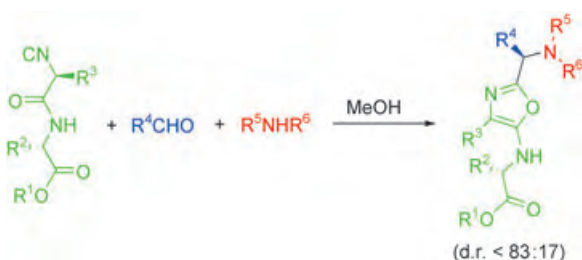


Scheme 43. Diastereoselective synthesis of α -aminonitrile derivatives.

follows the pathway already described for the Ugi four-component reaction: Reaction of the amine with the aldehyde to yield an imine and diastereoselective addition of isocyanide to the imine. At this juncture, the pathway changes: Instead of an external attack by the carboxylic acid derivative, the attack takes place by the amide moiety to form a cyclic six-membered anhydride-type intermediate, which isomerizes to yield the nitrile **90** with moderate diastereoselectivity.^[155]

4.4. Synthesis of Chiral Oxazole Derivatives

Recently, a new AMCR involving isocyanide, amine, and aldehyde derivatives was reported for the synthesis of heterocyclic oxazoles.^[156] Although the diastereoselectivity was still moderate (Scheme 44),^[157] this reaction is of impor-



Scheme 44. Diastereoselective synthesis of oxazoles.

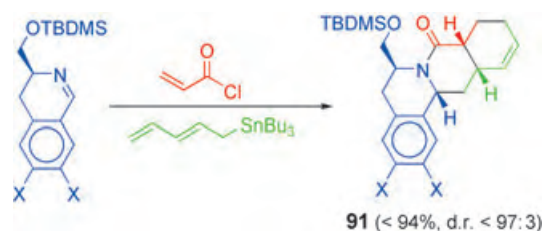
tant potential as oxazoles can be easily transformed into more-interesting compounds such as pyrrolo[3,4-*b*]pyridine and macrocyclodepsipeptide derivatives, depending on the amine used.

5. Cycloaddition-Based Multicomponent Reactions

There are several examples of AMCR in which at least one of the successive reactions involves a cycloaddition process, although authors usually do not emphasize this fact.

5.1. Diels–Alder-Based Multicomponent Reactions

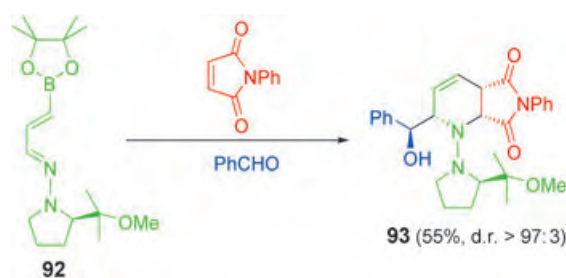
The first example illustrating the possibility of a multicomponent Diels–Alder reaction^[158] comes from the synthesis of tetracyclic protoberberine alkaloids. The three-component coupling reaction of a chiral 3,4-dihydroisoquinoline derivative with a 2,4-pentadienyltin reagent and acryloyl chloride furnished bicycloannulated products **91** (Scheme 45). The diastereoselectivity suggests that the nucleophilic attack of



Scheme 45. Diastereoselective MCR based on a Diels–Alder reaction.

the tin reagent on the *N*-acyliminium salt (Reissert–Henze reaction type; see Section 2.1.2) takes place preferentially from the axial direction, which is *anti* to the bulky (*tert*-butyldimethylsiloxy)methyl group. This intermediate then undergoes a normal Diels–Alder cyclization to yield the final product **91**.^[159] Instead of using the reagents shown in Scheme 45, the reaction could be performed with an allyltin reagent and 2,4-pentadienoyl chloride. In this way, after the final inverse-electron-demand Diels–Alder reaction, the pseudoberberine alkaloid could be obtained.

Not only typical Diels–Alder reactions intervene in asymmetric multicomponent reaction processes but also different hetero-Diels–Alder reactions. For example, an MCR based on an aza-Diels–Alder reaction was reported for the synthesis of polysubstituted piperidines. The reaction of the imine **92** with *N*-phenylmaleimide in the presence of benzaldehyde yielded the piperidine **93** in modest yield but with excellent diastereoselectivity (Scheme 46).^[160] Mecha-



Scheme 46. Diastereoselective MCR based on an aza-Diels–Alder reaction.

nistically, the pathway seems to proceed first through a [4+2] cycloaddition of diene derivative **92** with the maleimide derivative to yield the expected *endo* intermediate. The allylation step takes place subsequently.^[161] The topicity of this final step can be explained by the usual cyclic chairlike allylboration transition state involving *anti* coordination of the aldehyde to the boronyl group oriented axially on the *endo* face of the piperidine ring.

Another interesting AMCR is outlined in Scheme 47. The reaction of electron-rich dienes such as **94** with excess SO₂ in the presence of silylenol ethers (or allyl silane derivatives) catalyzed by ytterbium triflate or trifluoromethanesulfonamide, gives the corresponding sulfinate **95**. This compound was further trapped as the methyl sulfone derivative by the one-pot addition of a fluoride source and methyl iodide.^[162] The level of diastereoselectivity depends strongly on the



Scheme 47. Diastereoselective MCR based on a thia-Diels–Alder reaction.

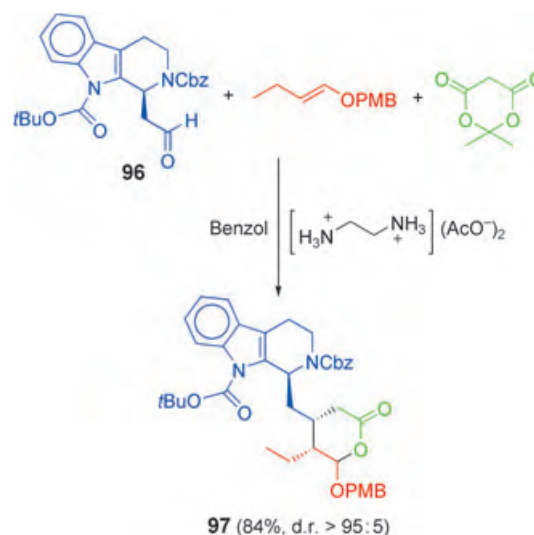
nature of the aryl moiety of the starting diene; the best diastereoselectivity was attained with **94**. The absolute configuration of final methyl sulfone derivatives was established by single-crystal X-ray crystallography. The stereochemistry of the reaction is consistent with a mechanism involving first a hetero-Diels–Alder reaction between the catalyst-activated SO_2 and the *s-cis*-conformer of the 1,3-diene, placing the C–H bond of the stereogenic center in the plane of the diene moiety. In this conformer the $A^{1,2}$ -allylic strain and *gauche* interactions are minimum. The sulfine derivative obtained after the Diels–Alder reaction is further ionized by the acidic promoter into a zwitterion oxocarbenium derivative, which reacts rapidly with the corresponding silyl enol ether derivative to yield the sulfinate **95** diastereoselectively.

5.2. Asymmetric Tietze Multicomponent Reaction

The domino Knoevenagel–Diels–Alder process is known as the Tietze multicomponent reaction. Although the first variants of this reaction were accomplished by a diastereoselective approach, enantioselective approaches have now been published.

5.2.1. Diastereoselective Approach

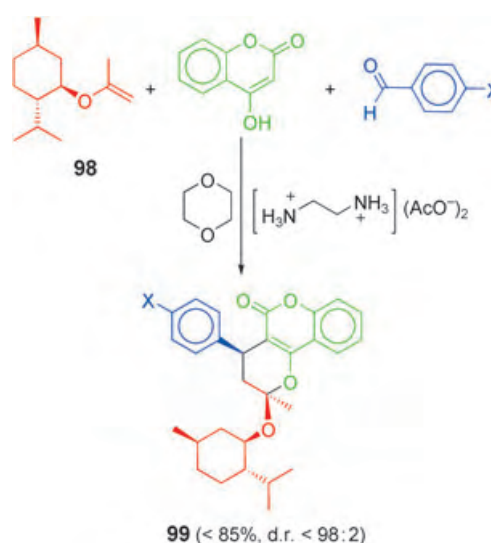
The Tietze MCR has been used extensively in the preparation of different biologically active natural products and drugs.^[163] The reaction of the chiral aldehyde **96** with Meldrum acid and 4-methoxybenzyl 1-butenyl ether (*Z/E* 1:1) catalyzed by ethylenediammonium diacetate in benzene gave the corresponding compound **97** (Scheme 48). Subsequent methanolysis deprotected all the nitrogen atoms as well as the masked aldehyde, leading to the corresponding methyl ester. Final reductive amination gave the hirsutine alkaloid, which has a strong inhibitory effect against the influenza A virus and is about 12-fold more effective than the clinically used ribavirin. The alkaloid dihydrocorynantheine was obtained by the same reaction with the enantiomer *ent*-**96**.^[164] The high diastereoselectivity refers to the two new unfunctionalized stereogenic centers, whereas the masked carbonyl center is obtained as a nearly 1:1 mixture of diastereomers, which is irrelevant in this synthesis as this stereogenic center is finally eliminated by methanolysis. The possible mechanism pathway involves the Knoevenagel reaction of Meldrum acid with the aldehyde to yield the expected α,β -unsaturated system, which



Scheme 48. Diastereoselective Tietze MCR with a chiral aldehyde. PMB = *p*-methoxybenzyl.

undergoes a hetero-Diels–Alder reaction. The elimination of CO_2 and acetone yielded the final lactone **97**. The synthesis of the ipecacua alkaloid involves the Tietze MCR as a key step (Scheme 48). However, the corresponding aldehyde with the 1,2,3,4-tetrahydro-6,7-dimethoxyisoquinoline moiety was used instead of using the 1*H*-pyrido[3,4-*b*]indole derivative **96**.^[165]

The chiral reagent can be not only the aldehyde but also the alkene derivative (Scheme 49). This strategy has been used in the synthesis of warfarin, which is the dominant coumarin anticoagulant owing to its excellent potency and good pharmacokinetic profile. While its marketed form is the racemic sodium salt, the anticoagulant activity of the *S* enantiomer is sixfold that of the *R* enantiomer. The reaction of the chiral alkene **98** with 4-hydroxycoumarin and benzaldehyde gave the corresponding ketal **99** ($X = \text{H}$) in good yield and 88:12 d.r.^[166] Final hydrolysis liberated the corresponding

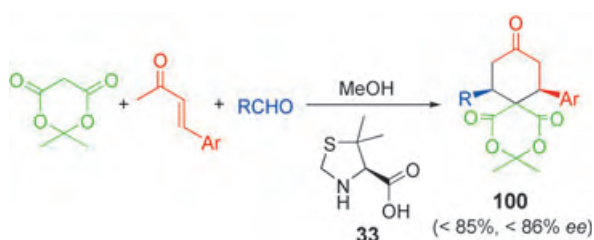


Scheme 49. Diastereoselective Tietze MCR with a chiral alkene.

methyl ketone (warfarin). The reaction with other 4-substituted benzaldehydes gave even better diastereoselectivity (up to 98:2).

5.2.2. Enantioselective Approach

The enantioselective Tietze MCR was recently reported.^[167] The reaction follows the classical pathway, that is, reaction of Meldrum acid with the aldehyde to give the corresponding alkylidene derivative, which in a second step undergoes a Diels–Alder reaction with the enol derivative of a methyl ketone. From 18 chiral pyrrolidine derivative systems, compound **33** emerged as the best catalyst. The study of solvent effect showed that in aprotic nonpolar solvents the enantioselectivity was good, whereas the yield was very low. However, both yield and enantioselectivity were improved in protic solvents (Scheme 50). It seems that the



Scheme 50. Enantioselective Tietze MCR.

rates of the Knoevenagel reaction, the formation of the enamine from chiral system **33** with the ketone, and the final Diels–Alder reactions are faster in protic solvents presumably because of the enhanced stabilization of the charged intermediates and the more-facile proton-transfer reactions.

The scope of the reaction was extended to other 1,3-dicarbonyl compounds such 1,3-indanedione;^[168] in this case the natural amino acid proline (**31**) was the best catalyst.

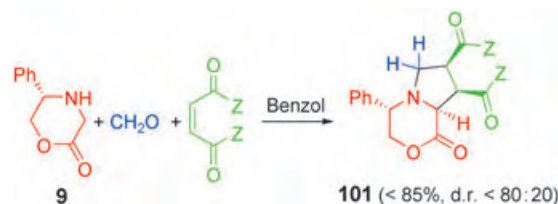
5.3. 1,3-Dipolar-Cycloaddition-Based Multicomponent Reactions

The classical 1,3-dipolar cycloaddition reaction has emerged as a powerful tool in organic chemistry, as up to four stereogenic centers can be obtained with a high level of stereocontrol in a single synthetic step.^[169] The heterocyclic compounds usually formed through this reaction are important intermediates in the preparation of different natural products, such as alkaloids and amino acids. Although the use of a multicomponent strategy in this reaction has been less popular, different examples of the two following approaches have been reported.

5.3.1. Diastereoselective Approach

The use of a chiral reagent in a multicomponent 1,3-dipolar reaction, that is, the use of a diastereoselective approach has been the most employed. The typical procedure is the reaction of a chiral amine with an aldehyde to form a chiral stabilized azomethine ylide, which is trapped in situ by

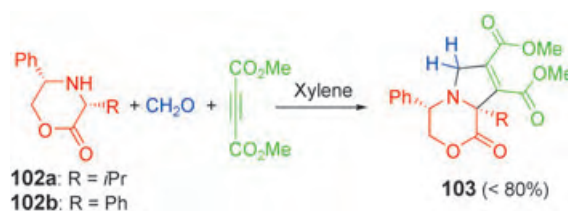
reaction with either an alkene or an alkyne dipolarophile. The first example of this class was performed with the heterocyclic amine **9**,^[170] whose thermal reaction with paraformaldehyde in the presence of electron-poor olefins, such as fumarate, maleate, and maleimide derivatives, yield the corresponding bicyclic compounds **101** (Scheme 51). In this reaction, three



Scheme 51. Diastereoselective 1,3-dipolar MCR with amine **9**.

new stereogenic centers are created, the new stereogenic center created in the heterocyclic moiety being under total control. The modest diastereoselectivity found is due to the *exo* and *endo* attack of the olefin. The reaction performed by Lewis acid catalysis improved the yield, but the diastereoselectivity remained low.

In the case of symmetric alkynes, for which there is no difference between the final products of *exo* and *endo* attack, only one diastereomer of the type **103** was isolated (Scheme 52). The regiochemistry in the cycloaddition step

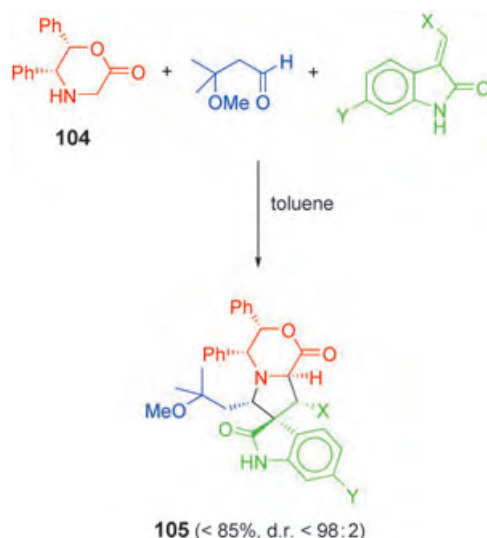


Scheme 52. Diastereoselective 1,3-dipolar MCR with amines **102**.

depends strongly on the nonsymmetrical olefin used, the chemical yield being lower than in the case of symmetric doubly activated olefins. This reaction can also be performed with aldehydes other than formaldehyde. However, the introduction of a new stereogenic center in the final product leads to a decrease in the diastereoselectivity. The stereochemistry of the major diastereomer can be rationalized by considering a trapping of the *E* ylide through an *endo* approach of the dipolarophile to the less-hindered face of the template **9**, which implies an *anti* approach to the face bearing the phenyl ring. The scope of the reaction has been expanded to other heterocyclic amines **102** derived not only from glycine but also from other α -amino acids (Scheme 52). As in the previous case of a glycine derivative, the diastereoselectivity was a function of the dipolarophile attack of the ylide, keeping the stereogenic center created in the heterocyclic moiety under strict control.^[171] The reaction with alkyne derivatives yields only one diastereomer.

The related amine **104** has been used successfully in different 1,3-dipolar MCRs.^[172] Its reaction with 3-methoxy-3-methylbutanal and different indolylidene derivatives yielded

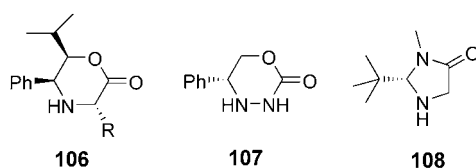
the expected compounds **105** in excellent yield and diastereoselectivity (Scheme 53). The by-products arise from the elimination of methanol and from a different regiochemistry; this regioisomer was obtained in only small amounts. This



Scheme 53. Diastereoselective 1,3-dipolar MCR used in the synthesis of (–)-spirotryprostatin A and B.

reaction has been used as the asymmetric key step in the synthesis of (–)-spirotryprostatins A and B, which belong to a promising class of antimitotic-arrest agents and inhibit microtubule assembly and therefore the progression of some mammalian cell lines. Although the diastereoselectivity shown in Scheme 53 is excellent, when the reaction was performed with other less sophisticated dipolarophiles, such as maleate derivatives, the diastereoselectivity dropped drastically and, depending on the nature of the aldehyde, was nearly zero.

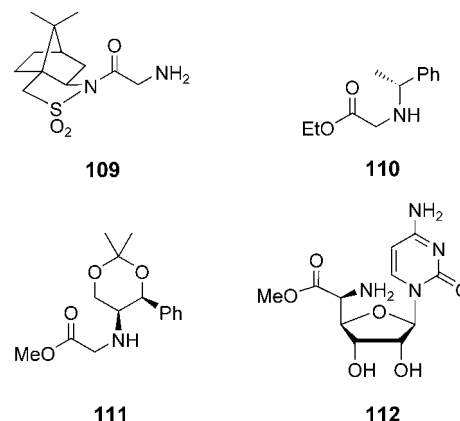
The related morpholin-2-one derivative **106** was used in combination with paraformaldehyde and different dipolarophiles,^[173] and gave similar results to those obtained with the



previous morpholinones **102** and **104**. However, when the reaction was performed with unsymmetrically substituted dipolarophiles such as ethyl acetylenecarboxylate, only one regioisomer was detected, which agrees with the expected values of the coefficients of the frontier orbitals in this stabilized ylide and the dipolarophile. Similar multicomponent 1,3-cycloadditions have been performed with the cyclic carbazate **107**^[174] and the imidazolidin-4-one **108**.^[175] In general the results were similar to those previously presented.

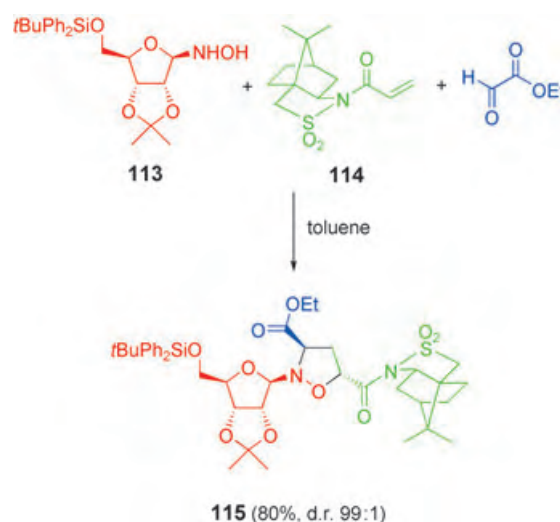
In the case of the former amine **107** and arenecarbaldehydes, the stereochemical results were excellent (d.r. up to 98:2).

Other amines whose nitrogen atom is not in a heterocyclic ring, such as systems **109**,^[176] **110**,^[177] **111**,^[178] and **112**,^[179] have



been used as chiral partners in a multicomponent 1,3-dipolar cycloaddition. Their reaction with arenecarbaldehyde or glyoxalate derivatives yields the expected proline derivatives, usually in good yields. The diastereoselectivities were a function of the nature of both the aldehyde and the dipolarophile and were generally lower than those obtained with cyclic amines.

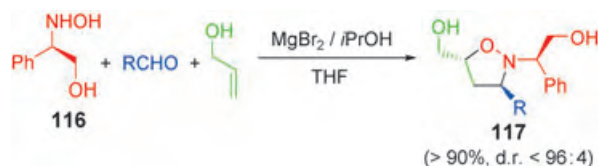
Not only amines but also hydroxyamines have been used in a multicomponent 1,3-cycloaddition. The hydroxylamine derived from D-ribofuranose **113** was used as a template in the 1,3-cycloaddition reaction with glyoxylate derivatives and different dipolarophiles, such as vinyl acetate, to obtain adequate starting materials for the production of *N,O*-nucleoside derivatives.^[180] The poor diastereoselectivity encouraged further improvement by using the chiral dipolarophile **114** (Scheme 54). In this case, the reaction afforded the expected heterocyclic compound **115** with excellent results



Scheme 54. Diastereoselective 1,3-dipolar MCR with a chiral hydroxylamine and a chiral dipolarophile.

which was used as a key compound in the synthesis of 4-hydroxypyroglutamic acid derivatives.^[181]

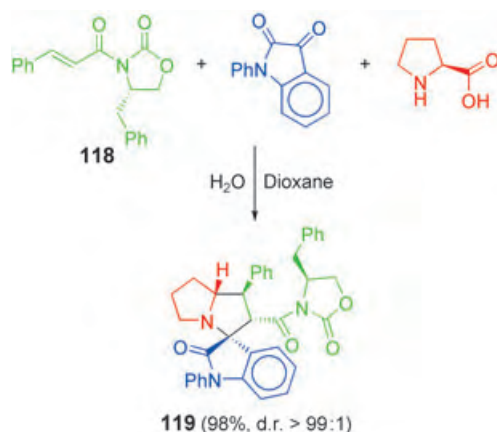
Recently, the simple hydroxylamine **116** was introduced as an excellent reagent for the 1,3-cycloaddition (Scheme 55). Its



Scheme 55. Diastereoselective 1,3-dipolar MCR with a chiral hydroxylamine.

reaction with aldehydes and allyl alcohol yielded the expected isoxazolidines **117** with excellent results.^[182] The diastereoselectivity was greatly improved by the use of anhydrous MgBr_2 and was rationalized by the formation of a magnesium complex bearing the allyl alcohol and the nitron formed in situ through coordination of the oxygen atoms. A further improvement came about by the addition of 2-propanol as additive.

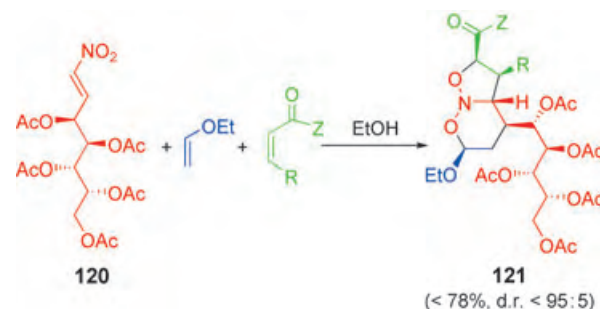
Chiral dipolarophiles can also be used in this reaction. The reaction of the cinnamyl derivative **118** with *N*-phenyl isatin and proline in aqueous dioxane yielded the corresponding spirooxindole **119** in excellent yield as a single diastereomer (Scheme 56). The structure was unambiguously assigned



Scheme 56. Diastereoselective 1,3-dipolar MCR with a chiral dipolarophile.

based on X-ray crystallographic analysis. The stereochemistry of the reaction can be explained by considering the reaction of the ketone derivative with proline to give the corresponding iminium system, which undergoes decarboxylation to form the ylide. The cycloaddition, through the classical *endo* approach, yielded the final spiro compound **119**.^[183] The same reaction can be performed through a solid-phase strategy only by using tyrosine as starting material in the synthesis of the relate system **118**. Its deprotonation and reaction with Merrifield resin permitted the attachment of the chiral system to a polymer. The results were similar to those obtained in homogenous solutions.

The example outlined in Scheme 57 could be also included in Section 5.1 as it involves two sequential cycloadditions to form five new stereogenic centers. First, a reverse-electron-demand hetero-Diels–Alder reaction between the nitrosugar



Scheme 57. Diastereoselective sequential Diels–Alder and 1,3-dipolar MCR.

120 and ethyl vinyl ether yields the corresponding cyclic nitronate, which is then trapped by a 1,3-dipolar cycloaddition with electron-poor alkenes to give the expected acetals **121**.^[184] The initial cycloaddition occurs with complete *endo* selectivity to the *Re* face of the nitroolefin **120**, whereas the following 1,3-dipolar cycloaddition takes place in the *exo* mode, which is sterically more favorable than the competitive *endo* approach. As a result of both processes, the diastereoselectivity was very good.

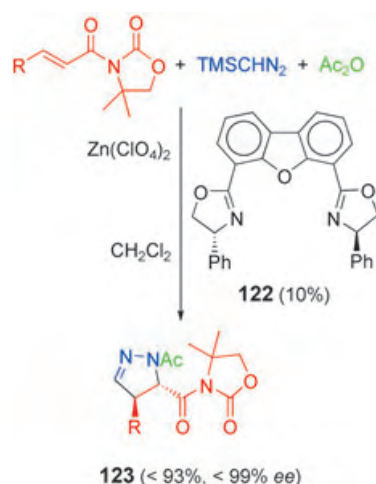
The diastereoselectivity attained in the reaction of chiral aldehydes, chlorovinylsilanes, and nitroalkanes was as good. In fact, no diastereoselectivity was observed in the nitroaldol reaction of nitroalkenes with chiral aldehydes that bear a leaving group at the α position, followed by ring closure and reaction with a chlorosilane derivative. The final 1,3-cycloaddition yielded different tricyclic systems as a 1:1 mixture of diastereomers.^[185]

5.3.2. Enantioselective Approach

There is only one example of an enantioselective MCR in which a 1,3-cycloaddition is involved: the cycloaddition of trimethylsilyl diazomethane to an α,β -unsaturated amide in the presence of acetic anhydride (Scheme 58). The reaction is catalyzed by substoichiometric amounts of the complex formed by mixing the tridentate ligand **122** with different transition-metal salts; the best results were obtained when zinc(II) perchlorate was used.^[186] The use of the 4,4-dimethyl-2-oxazolidinone moiety in the dipolarophile is crucial to maintain the high enantioselectivity. If the reaction is performed with the corresponding unsubstituted 2-oxazolidinone system, high enantioselectivity is only attained in the case of the crotonyl derivative.

5.4. Asymmetric [2+1]-Aziridination-Based Multicomponent Reactions

The aziridination^[187] of olefins is formally a [2+1] cycloaddition process in which a source of electrophilic nitrogen



Scheme 58. Enantioselective 1,3-dipolar-cycloaddition-based MCR.

atom reacts with electron-rich olefins. Nitridomanganese(IV) species have been used as source of nitrogen in several multicomponent reactions.^[188]

5.4.1. Diastereoselective Approach

In the first such reaction reported, the nitridomanganese derivative **124** reacts with trifluoroacetic anhydride to yield the corresponding acylimido complex, which in turn reacts with the olefin to yield the expected aziridine (Scheme 59).^[189]



Scheme 59. Diastereoselective multicomponent aziridination reaction.

However in this case, the final workup hydrolyzes the silyl ether and destabilizes the aziridine ring, giving the α -amino-ketone **125** in modest yield, but as a single diastereomer. The reaction was further expanded to other electron-rich olefins, such as different glycals, and as in the previous case the aziridine was unstable under the hydrolytic workup conditions, yielding the corresponding 2-trifluoroacetyl amino saccharides as final products.^[190] The chemical yield for furanoid glycals was slightly higher than for the corresponding pyranoid species; the diastereoselectivity and the absolute configuration was controlled by the proximal stereocenter.

5.4.2. Enantioselective Approach

The enantioselective version of this MCR seems to be more interesting. Different chiral salen nitridomanganese complexes were tested, and the simplest system **126** gave the

best results (Scheme 60). As in the diastereoselective approach, the *p*-toluenesulfonic anhydride activates the chiral nitridomanganese complex by formation of the corresponding tosylimido system. To improve the yield and the



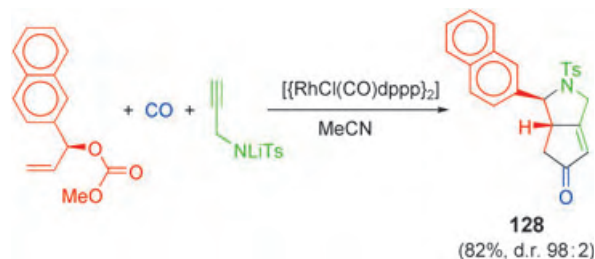
Scheme 60. Enantioselective aziridination MCR.

enantioselectivity, 1 equivalent of pyridine *N*-oxide should be added. This improvement was attributed to the stabilizing role of the oxide by complexation with the tosylimido intermediate.^[191] The reaction with a 1,3-diene system produced also a decrease in the enantioselectivity.

Oxazolines were isolated in good yield and enantioselectivity when the reaction was performed with carboxylic anhydrides.^[192] In this case, isomerization takes place after the formation of an *N*-acyl aziridine of type **127**, through the nucleophilic attack of the oxygen atom of the carbonyl moiety at the benzylic position of the aziridine. In this way, the presence of different diastereomers can be explained when *Z* olefins were used as starting materials. When the reaction was performed with silyl enol ethers as substrates, the corresponding α -acylaminoketones were isolated (see Scheme 59) with appreciable lower enantioselectivities (< 65% ee).^[193]

5.5. Pauson–Khand-Based Multicomponent Reaction

The Pauson–Khand reaction is a formal [2+2+1] cycloaddition in which an alkyne, an alkene, and CO furnish a cyclopentenone derivative.^[194] A multicomponent diastereoselective version of this reaction was described recently^[195] in which a chiral allylic carbonate reacted with lithium tosylpropargylamide under a CO atmosphere, catalyzed by a rhodium complex, to yield the expected cyclopentenone **128** with very good results (Scheme 61). First, the rhodium complex catalyzes the allylic alkylation to yield the corre-

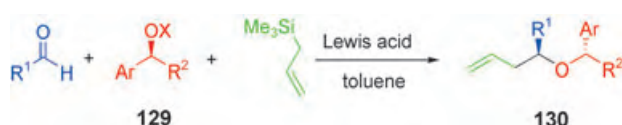


Scheme 61. Diastereoselective Pauson–Khand MCR. dppp = bis(diphenylphosphanyl)propane.

sponding enyne derivative, which then undergoes annulation. The first reaction occurs with total retention of the configuration, whereas the annulation is governed by the steric hindrance in the complex of the generated enyne and the rhodium metal atom.

6. Asymmetric Sakurai Multicomponent Allylation Process

The reaction of carbonyl compounds, as well as ketals and hemiketals, with allylsilyl derivatives catalyzed by Lewis acids to yield the corresponding homoallylic alcohol or ether derivatives, respectively, is known as the Sakurai allylation.^[161,196] The reaction was discovered in 1976, but only ten years later was the asymmetric multicomponent version published (Scheme 62). The first example used the complex



Scheme 62. Diastereoselective Sakurai MCR with chiral alcohol derivatives.

formed by reaction of titanium^[104] tetrachloride with two equivalents of lithium phenethyl alcoholate **129**: Ar = Ph, R² = Me, X = Ti[(S)-OCHMePh]Cl₂.^[197] In this way, the chiral alkoxide derivative simultaneously served as a source of the chiral alcohol moiety and as Lewis acid. The yield never exceeded 75 %, and the diastereoselectivity was consistently close to 95:5. Simple experiments showed that the reaction did not proceed by the formation of a ketal but through the corresponding hemiketal intermediate, which after elimination of titanium oxide, gave the key oxocarbenium intermediate.

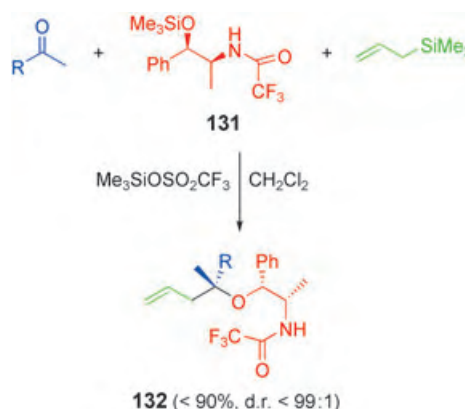
The further evolution of this process was to use chiral trimethylsilyl ethers (**129**: Ar = Ph, R² = Me, X = SiMe₃) and stoichiometric amounts of diphenylboryl triflate. Although the diastereoselectivity for some cases could be slightly improved, it was necessary also here to use 2 equivalents of the chiral alcohol derivative.^[198]

With substoichiometric amounts of trimethylsilyl triflate as catalyst, equimolar amounts of the alcohol derivative **129** (X = SiMe₃) were required.^[199] Under these new conditions, the yield and diastereoselectivity depended on the nature of both the aldehyde and the alcohol. When the reaction was performed with 1-arylethyl alcohol derivatives the diastereoselectivity never exceeded 92:8. The possible mechanism was studied in detail, and as a result, a plausible S_N2 mechanism was ruled out, confirming the S_N1 pathway, that is, the presence of an oxocarbenium intermediate. The oxocarbenium ion is very important in determining the diastereoselectivity, and although the steric effects did not have a clear influence over this intermediate, the stereoelectronic effect did. As a result, it was suggested that the reaction proceeds through a conformation of the oxocarbenium intermediate in which the aryl moiety is quasi-coplanar with the carbonyl

oxygen atom, thus allowing conjugation of the positive charge, and the alkyl group occupies an *anti* position to the nucleophilic attack.

Instead of alkyl aryl carbinol derivatives, other C-trialkylsilyl derivatives (**129**: R² = SiR₃, X = SiMe₃) have been proposed as chiral alternatives. This new system under the aforementioned protocol led to a great improvement in the yields and diastereoselectivities (up to 94 % and 99:1, respectively).^[200] This fact was attributed to the higher stability of the main oxocarbenium conformer in the silyl system relative to the alkyl species (R² = alkyl or SiR₃), because in the former, an important β-silyl effect (by the overlapping of σ C–Si and π* C=O*) is at play. However, ab initio calculations do not support this hypothesis. These silyl derivatives (**129**: R² = SiR₃, X = SiMe₃) have another advantage, apart from the high diastereoselectivity: the chiral moiety can be easily removed so that the corresponding homoallylic alcohols can be liberated simply by treatment with tetrabutylammonium fluoride.

Not only simple alcohol derivatives can be used for the Sakurai MCR but also systems derived from norpseudoephedrine such as compound **131** (Scheme 63). Its reaction with



Scheme 63. Diastereoselective Sakurai MCR with chiral pseudoephedrine derivatives.

aldehydes (Scheme 62) afforded the expected ethers **130** in good yield and with excellent diastereoselectivities (up to 85 % and 99:1, respectively).^[201] The diastereoselectivity is appreciably lower when the reaction is performed with aromatic aldehydes, whereas with chiral aldehydes the difference between matched and mismatched pairs was very low, revealing a strong reagent control. The final reduction of benzyl ethers of type **130** by using typical protocols, such as lithium catalyzed by substoichiometric amounts of arenes,^[202] yielded the expected homoallylic alcohols with excellent results.

In all the aforementioned cases, the stereochemistry of the final product **130** can be predicted and is governed by the absolute configuration of the benzylic stereocenter in either chiral system **129** or **131**. However, when the reaction was carried out with ketones (instead of aldehydes) in the presence of the chiral compound **131**, the absolute configuration of the final product **132** was the opposite (Scheme 63).

The best results were obtained when 2 equivalents of aliphatic methyl ketones were used and, as in the case of aldehydes, the presence of a stereogenic center in the ketone did not have any appreciable influence on the diastereoselectivity.^[203] Other aminoalcohols aside from norpseudoephedrine, as well as different carboxylic derivatives, were also tested to optimize the influence of the structure of type **131**. It was found that the best system was the corresponding 1,2-diphenyl-2-aminoethanol from carboxamides that bear strong electron-withdrawing groups.

Final reduction of benzylic ethers **132** liberates the corresponding tertiary alcohols which represents an indirect route to their synthesis.^[204] This strategy, consisting of a diastereoselective Sakurai MRC with ketones followed by reduction of the benzyl ether of the type **132**, has been successfully used as the stereodifferentiating key step in the synthesis of different natural products such as the chromane moiety of vitamin E,^[205] the sesquiterpene hydroxymyoporone,^[206] and the macrolide antibiotic 5,6-dihydrocineromycin B.^[207]

7. Asymmetric Michael-Addition-Based Multicomponent Reactions

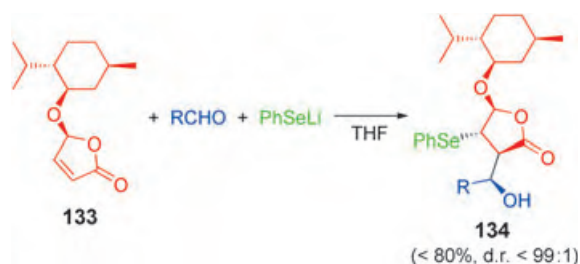
The nucleophilic 1,4-addition to electron-poor olefins, generally α,β -unsaturated carbonyl compounds, is known as the Michael addition, although it was first reported by Komnenos in 1883.^[208] Even the usual asymmetric version of this reaction^[209] employs just two reagents. In recent years, different sequences of reactions highlighted the possibility of using an asymmetric multicomponent reaction approach.

7.1. Asymmetric Michael–Aldol Multicomponent Reactions

Although the Michael–aldol reaction is really a sequential process, it is sometimes incorrectly referred to as a multicomponent reaction. However, there are some examples of asymmetric Michael–aldol processes that are genuine multicomponent reactions.

7.1.1. Diastereoselective Approach

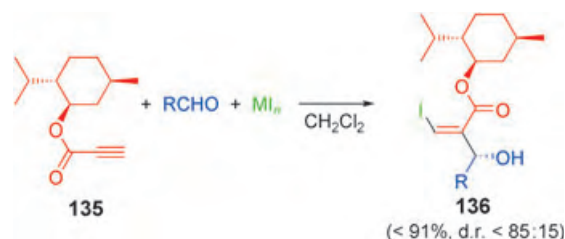
The reaction between the Michael acceptor **133**, lithium phenylselenide, and different aldehydes yielded, after hydrolysis, the expected lactones **134** (Scheme 64) in good yields and



Scheme 64. Diastereoselective Michael–aldol MCR with the chiral butenolide **133**.

with excellent diastereoselectivities.^[210] The absolute configuration was determined by X-ray crystallographic analysis. This AMCR has been used as the key asymmetric step in the synthesis of different drimane-type sesquiterpenes, such as kuehneromycin A and mniopetal F, which act as inhibitors of different reverse virus transcriptases.^[211]

A similar example is the reaction of different iodine salts (triethylaluminum iodide or magnesium iodide) and menthyl propiolate (**135**) in the presence of aldehydes to yield esters **136** (Scheme 65).^[212] According to ¹H NMR spectroscopic

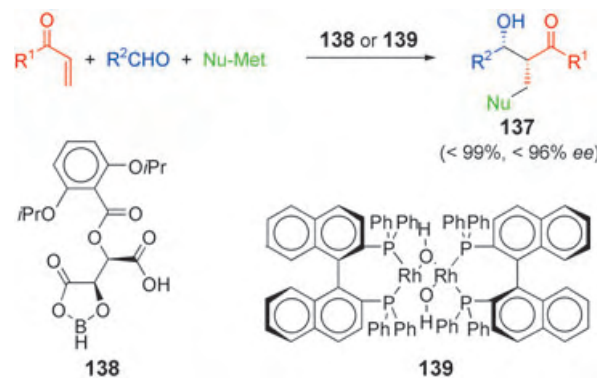


Scheme 65. Diastereoselective Michael–aldol MCR with the chiral ester **135**.

analysis, the products have predominantly the *Z* configuration and the absolute configuration of the new stereocenters was assigned by chemical correlation. The modest yields and diastereoselectivities for the majority of examples were attributed to the high flexibility of the menthyl ester moiety in the allenolate intermediate.

7.1.2. Enantioselective Approach

The enantioselective approach is generally more useful than the diastereoselective counterpart, as it permits the use of substoichiometric amounts of expensive chiral components. The Michael addition of silyl phenyl selenide or sulfide derivatives (Scheme 66, Nu-Met = PhSSiMe₃ or PhSeSiMe₃) to vinyl ketone derivatives followed by aldol condensation in situ with different aldehydes is catalyzed by the acylox-yborane **138**.^[213] The reaction proceeded smoothly to give the corresponding product **137** in good yields, which were higher for the selenium derivatives than for the sulfur species. Although the *syn/anti* diastereoselectivity was excellent



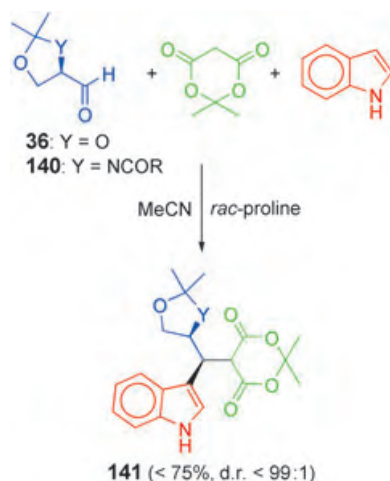
Scheme 66. Enantioselective Michael–aldol MCR.

(>95:5) and the best results were obtained with selenium derivatives, the best enantiomeric excess was attained with the corresponding sulfide derivative.

It is also possible to use different 9-aryl-9-borabicyclo[3.3.1]nonanes (Scheme 66, Nu-Met = *B*-aryl-9-BBN) as first source of nucleophile. In this case the reaction must be performed with substoichiometric amounts of rhodium complex **139**.^[214] Although the reaction was essentially non-diastereoselective, the enantioselectivity for the *anti* diastereomer **137** was as high as 94% *ee*, but modest for the *syn* diastereomer **137** (41% *ee*).

7.2. Knoevenagel–Michael Multicomponent Reactions

The Knoevenagel condensation of different chiral hydroxy- or amino-functionalized aldehydes (**36** or **140**, respectively) followed by Michael addition of indole (Scheme 67)



Scheme 67. Diastereoselective Knoevenagel–Michael MCR.

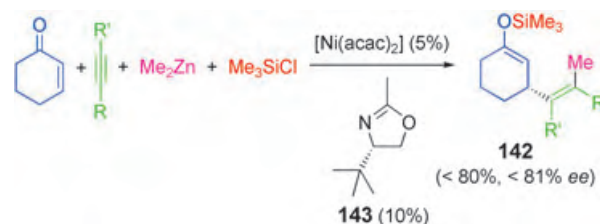
led to the corresponding compounds **141** in modest yield but with excellent diastereoselectivity, with the best result in the case of the aldehyde **36**. The absolute configuration was assigned by X-ray single-crystal structure analysis. Further hydrolysis and derivatization of compounds **141** has been used as a new approach in the synthesis of non-natural tryptophan, tryptamine, and β -carboline derivatives.^[215]

7.3. Asymmetric Double Michael Multicomponent Reaction

The double Michael reaction between nitromethane, the chiral α,β -unsaturated ketone 16-dehydropregnenolone acetate, and different alkyl acrylates was recently reported as a new AMCR.^[216] Although the yield was good, the diastereoselectivity of the 1,7-dicarbonyl compound formed was modest (maximum 70:30). Despite these disappointing initial results, it opens up the possibility of using better chiral ketones and of testing the enantioselective approach.

7.4. Asymmetric Carbometallation–Michael Multicomponent Reaction

Different complexes of nickel have been used to catalyze the four-component reaction depicted in Scheme 68. The



Scheme 68. Enantioselective carbometallation–Michael MCR. acac = acetylacetonate.

results depended strongly on the nature of the alkyne and the solvent used, the best being obtained for symmetric alkynes ($R = R'$) and poly(glycol ether)-type solvents. The nature of the chiral ligand was also important—the enantioselectivity was only high in the case of the monodentate oxazoline **143**.^[217] From a mechanistic point of view, the process begins with the *syn* carbometallation of the alkyne to yield an alkenyl metal complex, which in turn reacts with the cycloalkenone to yield the corresponding enolate. The final *O*-alkylation yields compounds **142**.

8. Asymmetric Palladium-Based Multicomponent Reactions

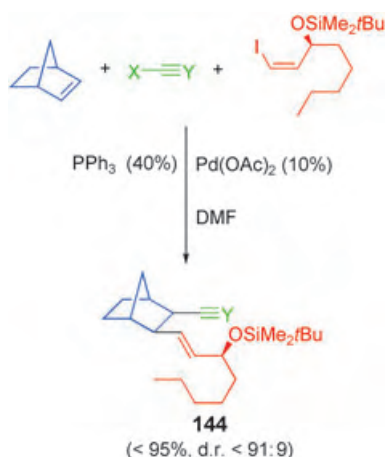
Several multicomponent reactions catalyzed by palladium complexes are known.^[20,22] However, only few involve a desymmetrization process^[218] and are encompassed in the topic of this Review.

8.1. Diastereoselective Approach

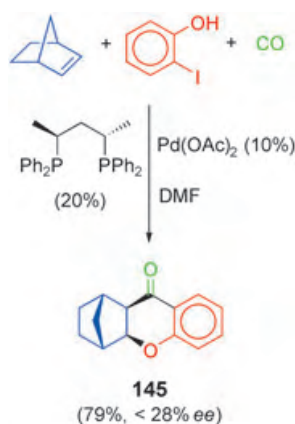
The first reported example was the diastereoselective desymmetrization of norbornene derivatives with chiral *cis*-1-iodoalkenes and potassium cyanide or 1-alkynes (Scheme 69, $X = K$, $Y = N$ or $X = H$, $Y = C$ -alkyl, respectively) catalyzed by palladium salts. The results were consistently good and were independent of the nature of the triple bond.^[219] An additional noteworthy feature was the spontaneous isomerization of the initial *cis*-1-iodoalkene derivative to give the *trans* olefin, which was rationalized on the basis of the formation of a cyclopropane intermediate that undergoes ring opening to afford the most stable olefin.

8.2. Enantioselective Approach

The related enantioselective version of the aforementioned desymmetrization has also been reported (Scheme 70). Although the results are far satisfactory, it could enlighten us



Scheme 69. Diastereoselective desymmetrization MCR. DMF = *N,N*-dimethylformamide.



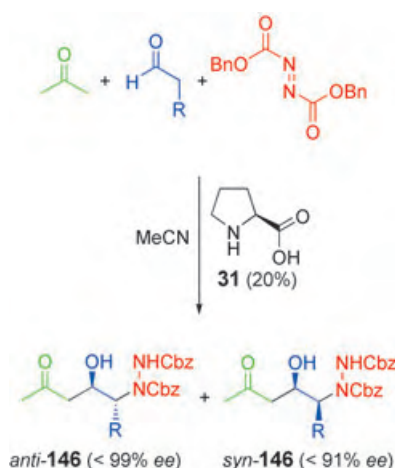
Scheme 70. Enantioselective desymmetrization MCR.

about further improvements. In this case, the mechanism is not very clear but the authors proposed that an oxidative addition of the palladium complex to the phenol derivative yields the corresponding aryl palladium complex. This complex undergoes CO insertion to give an acyl palladium intermediate, which is now asymmetrically inserted into an olefin. A β -hydride elimination leads to an α,β -unsaturated phenone, which rapidly undergoes a Michael cyclization process.^[220]

9. Miscellaneous Asymmetric Multicomponent Reactions

Although the following examples are closely related to other cases already introduced, they should be emphasized as they involve some aspects that have not yet been considered.

A multicomponent reaction between acetone, aldehydes, and azodicarboxylates catalyzed by substoichiometric amounts of natural proline (**31**) yielded a $\approx 1:1$ mixture of the corresponding diastereomers **146** (Scheme 71). The success of this assembly reaction can be attributed to the higher reactivity of aldehydes over acetone (about 100-fold) in the α -amination reaction. The disappointing *syn/anti*

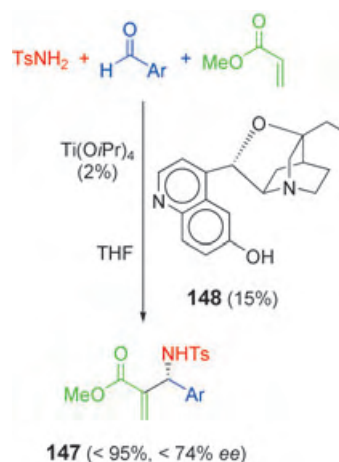


Scheme 71. Enantioselective aldol MCR.

diastereomeric ratio (never higher than 80:20) was attributed to the fact that the first α -aminoaldehyde intermediate is unstable and undergoes a racemization process catalyzed by compound **31** prior to the aldol condensation process.^[221] Despite the poor diastereomeric ratio, the overall yield ($> 80\%$), the excellent enantiomeric excess (especially for the diastereomer *anti*-**146**), and the facile isolation of both compounds make this approach very promising.^[222]

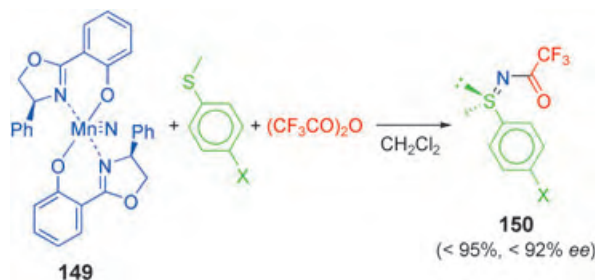
The reaction depicted in Scheme 72 is the first example of a multicomponent approach to the Baylis–Hillman reaction.^[223] The reaction takes advantage of a double activation process: a) First, the Lewis acid titanium alkoxide^[104] catalyzes the formation in situ of the corresponding imine, which is the electrophile and b) the quinidine derivative **148** is the nucleophilic base that promotes the generation of the nucleophile. The best results were obtained for electron-poor aldehydes. Similar results were observed when acrylonitrile was used instead of acrylate derivatives.^[224]

The final example of this Review is the oxidation of alkylsulfanylarenes by the nitridomanganese(V)^[188] complex **149** to yield the corresponding chiral acylsulfonimine derivatives **150** (Scheme 73). The results were excellent for both methyl and ethyl sulfanylarenes. However, the enantioselective



Scheme 72. Enantioselective aza-Baylis–Hillman MCR.

tivity was dramatically governed by the electronic character of the arene, and the best results were obtained for arenes with electron-donating groups or with weak electron-withdrawing substituents.^[225]



Scheme 73. Enantioselective nitrogenation MCR of sulfides.

10. Conclusions and Outlook

The creation of chiral molecules is still a great challenge for chemists, as the reaction of two molecules with the appropriate spatial approach for both reagents is difficult. It is generally accepted that the presence of any extra compound or impurity could alter this ideal approach, leading usually to a failure in the asymmetric synthesis. The former idea makes it more difficult to understand how it is possible to use a multicomponent reaction process to form enantiomerically enriched compounds, as it involves reactions in the presence of extra reagents. However, the increasing number of publications regarding the applications of different asymmetric multicomponent reactions paints a comprehensive picture for their real possibilities in synthetic organic chemistry. The improvements already achieved are impressive in some cases, although others are still in their early stages. Nevertheless, the asymmetric multicomponent reaction approach to synthesis should now start to be taken into account, since it shares with other multicomponent reactions the advantages of superior atom economy, simple procedures, simple equipment and manipulation, and savings in solvent, time, energy, and costs. Furthermore, as mentioned above, the level of stereoselectivity reached could be very high.

We hope that this Review will contribute to new discoveries, to the introduction of multicomponent reactions in computational methods (e.g. SMIRKS: language for reaction transformations), as well as to the continued development of this very fascinating area of research.

Addendum (January 26, 2005)

The highly topical nature of this research area results in the continuous improvements, novel applications, and new class of asymmetric multicomponent reactions (AMRs). The latest developments are described below (until January 2005).

A new monograph has just been published which covers different aspects of this subject.^[226] A recent microreview describes multicomponent reactions in which the use of 1,3-dicarbonyl derivatives is necessary.^[227] Dicarbonyl compounds are involved in different processes such as Knoeven-

nagel condensations, Michael and Mannich reactions, cyclo-dehydrations, electrocyclizations, cycloadditions, and metal-promoted transformations.

The enantioselective Reissert–Henze cyanation has been expanded to pyridine substrates with excellent enantioselectivities; the synthetic utility has been demonstrated by its application to the formal synthesis of the dopamine D₄ receptor-selective antagonist CP-293019.^[228] The Mannich AMCR has been applied for the derivatization of tyrosine residues of chymotrypsinogen, which permitted the easy modification of the protein, while preserving the native function.^[229] The enantioselective version of this reaction with L-proline has been expanded to a significant number of symmetric and nonsymmetric ketones as the source of the nucleophile, as well as different aldehydes.^[230] The problems of reproducibility and reactivity of the above organocatalyzed reaction have been partially overcome by the use of *trans*-4-*tert*-butyldimethylsiloxy-L-proline.^[231]

The diastereoselective Biginelli MCR with Si(NCS)₄ and a chiral 1,3-ketoester derivative has been used in the synthesis of the bicyclic core of batzelladine alkaloids, with a 70:30 diastereomeric ratio.^[232]

The diastereoselective Petasis MCR, with chiral aldehydes and ammonia, has been extended to the use of allylboronate derivatives, which led to the expected primary amines with excellent diastereoselectivity.^[233] The enantioselective addition of acetylene to imines formed in situ in the presence of the ligand quinap (**49**) has been used as the asymmetric key step in the synthesis of different α -aminoalkylpyridines and (*S*)-(+)-coniine.^[234] A new chiral biaryl ligand derived from phthalazine has been proposed as an alternative ligand in this acetylene addition MCR. The results were similar to those previously reported.^[235]

The enantioselectivity (89% *ee*) in MCRs with organoboranes, alkynes, and imines has improved greatly by the use of a chiral ferrocenyl monophosphane instead of ligand **51**.^[236] The diastereoselective Passerini MCR was recently performed with acyl cyanides instead of classical aldehydes, to yield a 1:1 diastereoisomeric mixture of the expected α -alkanoyloxy- α -cyanoamides.^[237] Different chiral Cu^{II}-bis(oxazolonyl)pyridine complexes have been proposed for the enantioselective version of the Passerini MCR (up to 98% *ee*).^[238]

The diastereoselectivity in the Ugi four-component reaction is highly dependent on the presence of Lewis acids. TiCl₄ gave the best results (up to 97:3 d.r.).^[239] The three-component version has been used in the preparation of different bicyclic lactams^[240] as well as of glycol- and peptidomimetics.^[241]

An AMCR based on an aza-Diels–Alder process with 2-[(*S*)-1-phenylethyl]-1,2-thiazolin-3-one-(*S*)-1-oxide as the chiral dienophile has been employed as the key step in the synthesis of (–)-methyl palustramate.^[242] The diastereoselective MCR based on a thia-Diels–Alder reaction with SO₂ has been applied to the synthesis of different polypropionate fragments and of sulfonic acid derivatives.^[243]

Different effects have been evaluated in the enantioselective Tietze MCR.^[244] Among others, the nature of the 1,3-dicarbonyl compound influences the enantioselectivity and L-

proline must be used as the organocatalyst to attain good enantioselectivities. The reaction can also be performed with a phosphorane derivative, which in turn reacts with an aldehyde in a one-pot process to form the desired α,β -unsaturated ketone.

A library of more than 3000 molecules with the spirotryprostatin structure has been obtained by the diastereoselective 1,3-dipolar MCR of chiral morpholinone **104**, isatin derivatives, and β -alkoxy aldehydes attached to a solid support. Cell-based screening showed very promising results.^[245]

The aminoalcohol derivative (*S*)-2,2,2-trifluoro-*N*-(2-phenyl-2-trimethylsilyloxyethyl)acetamide has been proposed as a more economical alternative to **131** for the diastereoselective Sakurai MCR of methyl ketones, but with no improvement in the previous results with pseudoephedrine derivatives.^[246]

A new Michael–aldol MCR has been introduced in which the addition of diethylaluminum iodide to propiolate derivatives in the presence of aldehydes was catalyzed by stoichiometric amounts of chiral salen-type ligands. The enantioselectivity was never higher than 76% ee.^[247] Finally, a novel multicomponent coupling reaction,^[248] the coupling of aryl boronic acids with allenes and aldehydes, gives rise to different homoallylic alcohols. The reaction is catalyzed by substoichiometric amounts of chiral π -allylpalladium complexes. A mechanistic pathway has been postulated in which the chiral palladium complex undergoes transmetalation to yield a chiral aryl–palladium intermediate. This intermediate inserts into the allene to yield the less-hindered σ -allylpalladium complex, which in turn reacts with the aldehyde to give the corresponding homoallylic alcoholate with high diastereoselectivity but low enantioselectivity.

This work was supported by the DGI (Project BQU2001-0538) of the Spanish Ministerio de Ciencia y Tecnología and by the Generalitat Valenciana (Project CTIDIB/2002/318). We thank Dr G. Guillena for helpful suggestions.

Received: May 4, 2004

Published online: February 18, 2005

- [1] a) *Stereoselective Synthesis (Houben-Weyl), Vols. 1–10* (Eds.: G. Helmchen, R. W. Hoffmann, J. Mulzer), Thieme, Stuttgart, **1996**; b) *Comprehensive Asymmetric Catalysis, Vols. 1–3* (Eds.: E. N. Jacobsen, A. Pfaltz, H. Yamamoto), Springer, Berlin, **1999**; c) *Comprehensive Asymmetric Catalysis, Suppl. 1* (Eds.: E. N. Jacobsen, A. Pfaltz, H. Yamamoto), Springer, Berlin, **2004**.
- [2] a) K. Mori, *Acc. Chem. Res.* **2000**, *33*, 102–110; b) E. Brenna, C. Fuganti, S. Serra, *Tetrahedron: Asymmetry* **2003**, *14*, 1–42.
- [3] R. E. Gawley, J. Aubé in *Principles of Asymmetric Synthesis*, Pergamon, Oxford, **1996**, p. xi.
- [4] a) J. F. Cargill, M. Lebl, *Curr. Opin. Chem. Biol.* **1997**, *1*, 67–71; b) D. G. Powers, D. L. Coffen, *Drug Discovery Today* **1999**, *4*, 377–383; c) A. Kirschning, H. Monenschein, R. Wittenberg, *Angew. Chem.* **2001**, *113*, 670–701; *Angew. Chem. Int. Ed.* **2001**, *40*, 650–679.
- [5] For reviews on state of the art, see: a) A. W. Czarnik, *Chemtracts* **1995**, *8*, 13–18; b) G. Lowe, *Chem. Soc. Rev.* **1995**, *24*, 309–317; c) J. C. Hogan, *Nature* **1996**, *384*, 17–19; d) A. Ganesan, *Drug Discovery Today* **2002**, *7*, 47–55; e) L. A. Marcaurelle, P. H. Seeberger, *Curr. Opin. Chem. Biol.* **2002**, *6*, 289–296; f) C. C. Tzschucke, C. Markert, W. Bannwarth, S. Roller, A. Hebel, R. Haag, *Angew. Chem.* **2002**, *114*, 4136–4173; *Angew. Chem. Int. Ed.* **2002**, *41*, 3964–4000; g) *Handbook of Combinatorial Chemistry, Vols. 1,2* (Eds.: K. C. Nicolaou, R. Hanko, W. Hartwig), Wiley-VCH, Weinheim, **2002**; h) D. Horton, G. T. Bourne, M. L. Smythe, *Chem. Rev.* **2003**, *103*, 893–930; i) H. Waldmann, *Bioorg. Med. Chem.* **2003**, *11*, 3045–3051; j) R. E. Dolle, *J. Comb. Chem.* **2003**, *5*, 693–753, and references therein.
- [6] a) S. L. Schreiber, *Science* **2000**, *287*, 1964–1969; b) H. Kubota, J. Lim, K. M. Depew, S. L. Schreiber, *Chem. Biol.* **2002**, *9*, 265–276; d) M. D. Burke, E. M. Berger, S. L. Schreiber, *Science* **2003**, *302*, 613–618; e) M. D. Burke, S. L. Schreiber, *Angew. Chem.* **2004**, *116*, 48–60; *Angew. Chem. Int. Ed.* **2004**, *43*, 46–58.
- [7] a) B. R. Stockwell, *Trends Biotechnol.* **2000**, *18*, 449–455; b) M. A. Walters, *Chemtracts* **2000**, *13*, 268–275; c) P. J. Alaimo, M. A. Shogren-Knaak, M. Shokat, *Curr. Opin. Chem. Biol.* **2001**, *5*, 360–367; d) K. M. Specht, K. M. Shokat, *Curr. Opin. Cell Biol.* **2002**, *14*, 155–159.
- [8] For recent reviews on different aspects of this topic, see: a) M. T. Reetz, *Angew. Chem.* **2001**, *113*, 292–320; *Angew. Chem. Int. Ed.* **2001**, *40*, 284–310; b) J.-L. Reymond, *Chimia* **2001**, *55*, 1049–1052; c) K. H. Bleicher, H.-J. Boehm, K. Mueller, A. I. Alanine, *Nat. Rev. Drug Discovery* **2003**, *2*, 369–378; d) P. Chen, *Angew. Chem.* **2003**, *115*, 2938–2954; *Angew. Chem. Int. Ed.* **2003**, *42*, 2832–2847; e) R. Moaddel, I. W. Wainer, *J. Pharm. Biomed. Anal.* **2003**, *30*, 1715–1724; f) H.-J. Brunnert, M. Boese, *Nachr. Chem.* **2003**, *51*, 760–761; g) G. Hoptgartner, E. Bourgoigne, *Mass Spectrom. Rev.* **2003**, *22*, 195–214; h) V. Murphy, A. F. Volpe, W. H. Weinberg, *Curr. Opin. Chem. Biol.* **2003**, *7*, 427–433; i) C. Gennari, U. Piarulli, *Chem. Rev.* **2003**, *103*, 3071–3100.
- [9] H. Bienaymé, C. Hulme, G. Oddon, P. Schmitt, *Chem. Eur. J.* **2000**, *6*, 3321–3329.
- [10] a) B. M. Trost, *Science* **1991**, *254*, 1471–1477; b) B. M. Trost, *Angew. Chem.* **1995**, *107*, 285–307; *Angew. Chem. Int. Ed. Engl.* **1995**, *34*, 259–281; c) B. M. Trost, *Acc. Chem. Res.* **2002**, *35*, 695–705.
- [11] a) M. C. Mitchell, V. Spikmans, A. Manz, A. de Mello, *J. Chem. Soc. Perkin Trans. 1* **2001**, 514–518; b) K. Jähnisch, V. Hessel, H. Löwe, M. Baerns, *Angew. Chem.* **2004**, *116*, 410–451; *Angew. Chem. Int. Ed.* **2004**, *43*, 406–446.
- [12] a) L. F. Tietze, U. Beifuss, *Angew. Chem.* **1993**, *105*, 137–170; *Angew. Chem. Int. Ed. Engl.* **1993**, *32*, 131–163; b) L. F. Tietze, *Chem. Rev.* **1996**, *96*, 115–136.
- [13] a) T.-L. Ho, *Tandem Organic Reaction*, Wiley, New York, **1992**; b) P. J. Parsons, C. S. Penkett, A. J. Shell, *Chem. Rev.* **1996**, *96*, 195–206.
- [14] a) H. M. R. Hoffmann, *Angew. Chem.* **1992**, *104*, 1361–1363; *Angew. Chem. Int. Ed. Engl.* **1992**, *31*, 1332–1334; b) K. K. Wang, *Chem. Rev.* **1996**, *96*, 207–222; c) A. Padwa, M. D. Weingarten, *Chem. Rev.* **1996**, *96*, 223–269.
- [15] For different examples, see: a) Y. Nakashita, M. Hesse, *Angew. Chem.* **1981**, *93*, 1077–1078; *Angew. Chem. Int. Ed. Engl.* **1981**, *20*, 1021; b) E. Negishi, *Pure Appl. Chem.* **1992**, *64*, 323–334; c) R. Grigg, E. Mariani, V. Sridharan, *Tetrahedron Lett.* **2001**, *42*, 8677–8680; d) D. Bourgeois, J. Prunet, A. Pancrazi, T. Prange, J.-Y. Lallemand, *J. Org. Chem.* **2002**, *67*, 4029–4036.
- [16] For recent examples of this process, see: a) J. F. Hayes, M. Shipman, H. Twin, *J. Org. Chem.* **2002**, *67*, 935–942; b) H. Shinokubo, J. Kondo, A. Inoue, K. Oshima, *Chirality* **2003**, *15*, 31–37; c) A. Fürstner, A. Leitner, *Angew. Chem.* **2003**, *115*, 320–323; *Angew. Chem. Int. Ed.* **2003**, *42*, 308–310; d) X. Gao, D. G. Hall, *J. Am. Chem. Soc.* **2003**, *125*, 9308–9309; e) C.

- Chen, X. Li, S. L. Scheiber, *J. Am. Chem. Soc.* **2003**, *125*, 10174–10175; f) A. B. Smith, S. M. Pitram, A. M. Boldi, M. J. Gaunt, C. Sfougataki, W. H. Moser, *J. Am. Chem. Soc.* **2003**, *125*, 14435–14445.
- [17] For the first account of this reaction, see: a) I. Ugi, R. Meyr, U. Fetzer, C. Steinbrückner, *Angew. Chem.* **1959**, *71*, 386; for reviews on general aspects, see: b) L. Weber, K. Illgen, M. Almstetter, *Synlett* **1999**, 366–374; c) reference [9]; d) L. Weber, *Curr. Opin. Chem. Biol.* **2000**, *4*, 295–302; e) L. Weber, *Drug Discovery Today* **2002**, *7*, 143–147; f) in reference [5g], A. Tuch, S. Wallé, *Handbook of Combinatorial Chemistry*, Vol. 2 (Eds.: K. C. Nicolaou, R. Hanko, W. Hartwig), Wiley-VCH, Weinheim, **2002**, pp. 685–705; g) R. V. A. Orru, M. de Greef, *Synthesis* **2003**, 1471–1499.
- [18] For the first account of this reaction, see: a) P. Biginelli, *Gazz. Chim. Ital.* **1891**, *21*, 497–500; for reviews, see: b) C. O. Kappe, *Acc. Chem. Res.* **2000**, *33*, 879–888; c) C. O. Kappe, *QSAR Comb. Sci.* **2003**, *22*, 630–645; d) Z. D. Aron, L. E. Overman, *Chem. Commun.* **2004**, 253–265.
- [19] a) I. Ugi, S. Lohberger, R. Karl in *Comprehensive Organic Synthesis*, Vol. 2 (Eds.: B. M. Trost, I. Fleming), Pergamon Press, Oxford, **1991**, pp. 1083–1109; b) R. W. Armstrong, A. P. Combs, P. A. Tempest, S. D. Brown, T. A. Keating, *Acc. Chem. Res.* **1996**, *29*, 123–131; c) A. Dömling, I. Ugi, *Angew. Chem.* **2000**, *112*, 3300–3344; *Angew. Chem. Int. Ed.* **2000**, *39*, 3168–3210; d) A. Dömling, *Curr. Opin. Chem. Biol.* **2000**, *4*, 318–323; e) A. Dömling, *Curr. Opin. Chem. Biol.* **2002**, *6*, 306–313; f) C. Hulme, V. Gore, *Curr. Med. Chem.* **2003**, *10*, 51–80; g) I. Ugi, B. Werner, A. Dömling, *Molecules* **2003**, *8*, 53–66; h) J. Zhu, *Eur. J. Org. Chem.* **2003**, 1133–1144.
- [20] G. Balme, E. Bossharth, N. Monteiro, *Eur. J. Org. Chem.* **2003**, 4101–4111.
- [21] K. Khanbabaee, *Nachr. Chem.* **2003**, *51*, 691–694.
- [22] A. J. von Wangelin, H. Neumann, D. Gördes, S. Klaus, D. Stübing, M. Beller, *Chem. Eur. J.* **2003**, *9*, 4286–4294.
- [23] a) W. A. Nugent, T. V. RajanBabu, M. J. Burk, *Science* **1993**, *259*, 479–483; b) G. Casiraghi, F. Zanardi, G. Rassu, P. Spanu, *Chem. Rev.* **1995**, *95*, 1677–16716; c) A. Tauss, T. M. Wrodnigg, A. E. Stutz, *Recent Res. Dev. Org. Chem.* **1999**, *3*, 319–342; d) M. Ikunaka, *Chem. Eur. J.* **2003**, *9*, 378–388.
- [24] a) A. Strecker, *Justus Liebigs Ann. Chem.* **1850**, *75*, 27–45; b) in reference [1a] H. Kunz, *Stereoselective Synthesis (Houben-Weyl)*, Vol. 3 (Eds.: G. Helmchen, R. W. Hoffmann, J. Mulzer), Thieme, Stuttgart, **1996**, pp. 1931–1952.
- [25] D. Enders, J. P. Shilvock, *Chem. Soc. Rev.* **2000**, *29*, 359–373.
- [26] R. O. Duthaler, *Tetrahedron* **1994**, *50*, 1539–1650.
- [27] K. Harada, *Nature* **1963**, *200*, 1201.
- [28] K. Weinges, K. Gries, B. Stemmlé, W. Schrank, *Chem. Ber.* **1977**, *110*, 2098–2105.
- [29] a) D. M. Stout, L. A. Black, W. L. Matier, *J. Org. Chem.* **1983**, *48*, 5369–5373; b) T. Inaba, M. Fujita, K. Ogura, *J. Org. Chem.* **1991**, *56*, 1274–1276; c) J. Tulinsky, B. V. Cheney, S. A. Mizsak, W. Watt, F. Han, L. A. Dolak, T. Judge, R. B. Gammill, *J. Org. Chem.* **1999**, *64*, 93–100.
- [30] a) A. Fadel, A. Khesrani, *Tetrahedron: Asymmetry* **1998**, *9*, 305–320; b) M. Truong, F. Lecornué, A. Fadel, *Tetrahedron: Asymmetry* **2003**, *14*, 1063–1072.
- [31] F.-J. Volk, A. W. Frahm, *Liebigs Ann.* **1996**, 1893–1903.
- [32] a) K. Weinges, G. Graab, D. Nagel, B. Stemmlé, *Chem. Ber.* **1971**, *104*, 3594–3606; b) K. Weinges, B. Stemmlé, *Chem. Ber.* **1973**, *106*, 2291–2297; c) K. Weinges, K.-P. Klotz, H. Droste, *Chem. Ber.* **1980**, *113*, 710–721.
- [33] H. Kunz, W. Sanger, D. Schanzenbach, M. Decker, *Liebigs Ann. Chem.* **1991**, 649–654.
- [34] For reviews, see: a) I. Wagner, H. Musso, *Angew. Chem.* **1983**, *95*, 827–839; *Angew. Chem. Int. Ed. Engl.* **1983**, *22*, 816–828; b) B. R. Glick, *Biotechnol. Adv.* **2003**, *21*, 383–393; c) K. Grossmann, *J. Plant Growth Regul.* **2003**, *22*, 109–122.
- [35] A. Fadel, *Synlett* **1993**, 503–505.
- [36] W. H. J. Boesten, J.-P. S. Seerden, B. de Lange, H. J. A. Dielemans, H. L. Moody, R. M. Kellogg, Q. B. Broxterman, *Org. Lett.* **2001**, *3*, 1121–1124.
- [37] L. M. Harwood, M. G. B. Drew, D. J. Hughes, R. J. Vickers, *J. Chem. Soc. Perkin Trans. 1* **2001**, 1581–1583.
- [38] a) D. Ma, K. Ding, *Org. Lett.* **2000**, *2*, 2515–2517; b) K. Ding, D. Ma, *Tetrahedron* **2001**, *57*, 6361–6366.
- [39] For reviews, see: a) C. Cativiela, M. D. Díaz de Villegas, *Tetrahedron: Asymmetry* **1998**, *9*, 3517–3599; b) C. Cativiela, M. D. Díaz de Villegas, *Tetrahedron: Asymmetry* **2000**, *11*, 645–732.
- [40] Y. Izumi, *Angew. Chem.* **1971**, *83*, 956–966; *Angew. Chem. Int. Ed. Engl.* **1971**, *10*, 837–890.
- [41] For reviews, see: a) L. Yet, *Angew. Chem.* **2001**, *113*, 900–902; *Angew. Chem. Int. Ed.* **2001**, *40*, 875–877; b) H. Gröger, *Chem. Rev.* **2003**, *103*, 2795–2827.
- [42] a) S. Kobayashi, H. Ishitani, *Chirality* **2000**, *12*, 540–543; b) H. Ishitani, S. Komiyama, Y. Hasegawa, S. Kobayashi, *J. Am. Chem. Soc.* **2000**, *122*, 762–766.
- [43] a) for the first account of this reaction, see: A. Reissert, *Ber. Dtsch. Chem. Ges.* **1905**, *38*, 3415–3435; b) for a review, see: W. K. Fife, E. F. V. Scriven, *Heterocycles* **1984**, *22*, 2375–2394.
- [44] a) M. Takamura, K. Funabashi, M. Kanai, M. Shibasaki, *J. Am. Chem. Soc.* **2000**, *122*, 6327–6328; b) M. Takamura, K. Funabashi, M. Kanai, M. Shibasaki, *J. Am. Chem. Soc.* **2001**, *123*, 6801–6808.
- [45] a) P. D. Leeson, R. W. Carling, K. W. Moore, A. M. Moseley, J. D. Smith, G. Stevenson, T. Chan, R. Baker, A. C. Foster, S. Grimwood, J. A. Kemp, G. R. Marshall, K. Hoogsteen, *J. Med. Chem.* **1992**, *35*, 1954–1968; b) R. W. Carling, P. D. Leeson, A. M. Moseley, J. D. Smith, K. Saywell, M. D. Tricklebank, J. A. Kemp, G. R. Marshall, A. C. Foster, S. Grimwood, *Bioorg. Med. Chem. Lett.* **1993**, *3*, 65–70.
- [46] K. Funabashi, H. Ratni, M. Kanai, M. Shibasaki, *J. Am. Chem. Soc.* **2001**, *123*, 10784–10785.
- [47] For reviews on the enantioselective construction of molecules with quaternary stereocenters, see: a) K. Fujii, *Chem. Rev.* **1993**, *93*, 2037–2066; b) E. J. Corey, A. Guzmán-Pérez, *Angew. Chem.* **1998**, *110*, 402–415; *Angew. Chem. Int. Ed.* **1998**, *37*, 388–401; c) J. Christoffers, A. Mann, *Angew. Chem.* **2001**, *113*, 4725–4732; *Angew. Chem. Int. Ed.* **2001**, *40*, 4591–4597; d) J. Christoffers, A. Baro, *Angew. Chem.* **2003**, *115*, 1726–1728; *Angew. Chem. Int. Ed.* **2003**, *42*, 1688–1690; e) D. J. Ramón, M. Yus, *Curr. Org. Chem.* **2004**, *8*, 149–183.
- [48] For the first account of this reaction, see: a) C. Mannich, W. Krosche, *Arch. Pharm.* **1912**, *250*, 647; for recent reviews, see: b) M. Arend, B. Westermann, N. Risch, *Angew. Chem.* **1998**, *110*, 1096–1122; *Angew. Chem. Int. Ed. Engl.* **1998**, *37*, 1044–1070; c) A. Córdova, *Acc. Chem. Res.* **2004**, *37*, 102–112.
- [49] S. Kobayashi, M. Ueno, R. Suzuki, H. Ishitani, *Tetrahedron Lett.* **1999**, *40*, 2175–2178.
- [50] B. Dudot, A. Chiaroni, J. Royer, *Tetrahedron Lett.* **2000**, *41*, 6355–6359.
- [51] A. Zarghi, M. R. Naimi-Jamal, S. A. Webb, S. Balalaie, M. R. Saidi, J. Ipaktschi, *Eur. J. Org. Chem.* **1998**, 197–200.
- [52] T.-P. Loh, S.-L. Chen, *Org. Lett.* **2002**, *4*, 3647–3650.
- [53] S. Yamasaki, T. Iida, M. Shibasaki, *Tetrahedron* **1999**, *55*, 8857–8867.
- [54] T. Kolter, K. Sandhoff, *Angew. Chem.* **1999**, *111*, 1632–1670; *Angew. Chem. Int. Ed.* **1999**, *38*, 1532–1568.
- [55] M. Ueno, H. Kitagawa, H. Ishitani, S. Yasuda, K. Hanada, S. Kobayashi, *Tetrahedron Lett.* **2001**, *42*, 7863–7865.
- [56] For reviews, see: a) P. I. Dalko, L. Moisan, *Angew. Chem.* **2001**, *113*, 3840–3864; *Angew. Chem. Int. Ed.* **2001**, *40*, 3726–3748;

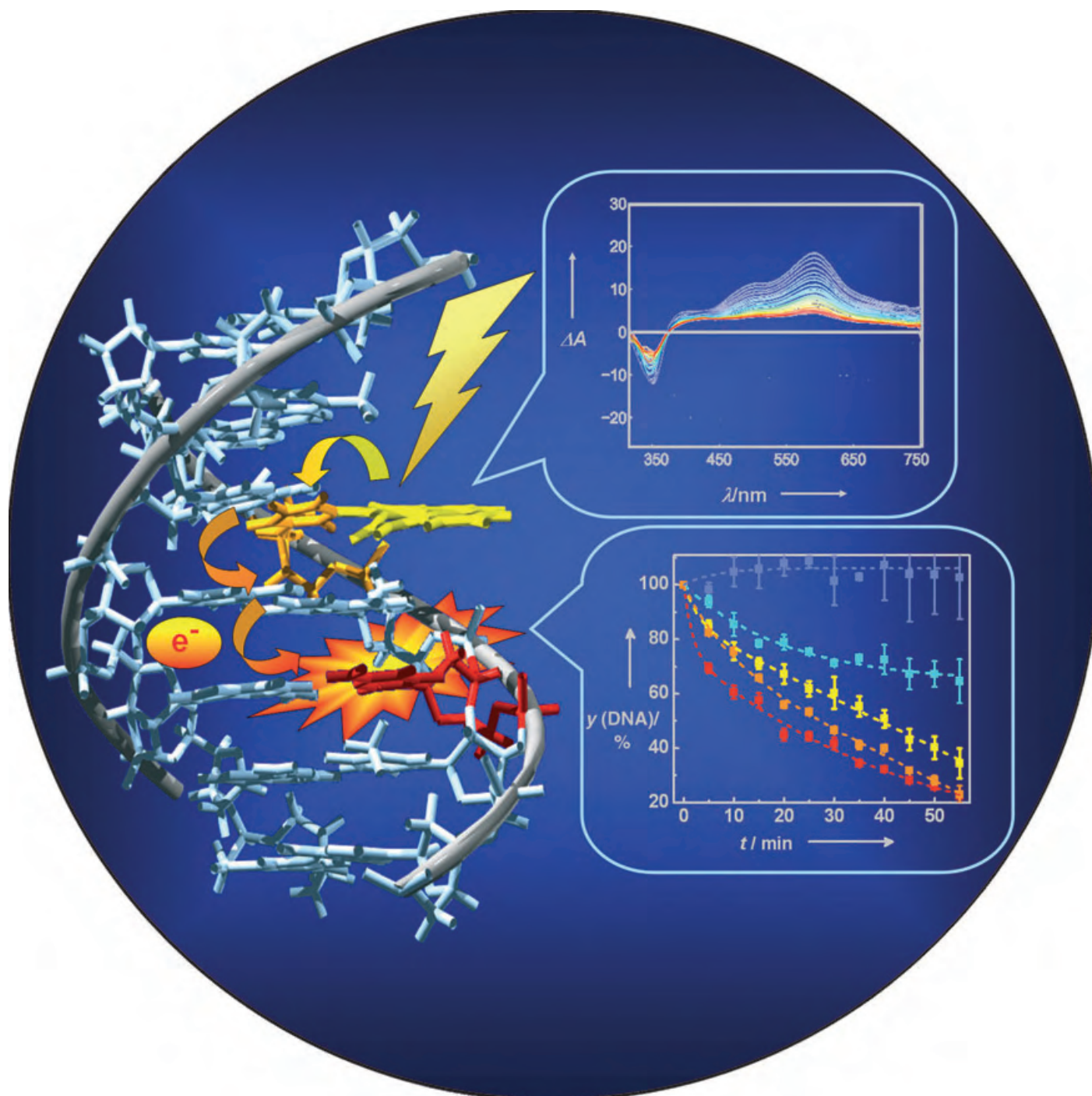
- b) B. List, *Synlett* **2001**, 1675–1686; c) B. List, *Tetrahedron* **2002**, 58, 5573–5590; d) M. Oestreich, *Nachr. Chem.* **2004**, 52, 35–38.
- [57] a) B. List, *J. Am. Chem. Soc.* **2000**, 122, 9336–9337; b) B. List, P. Pojarliev, W. T. Biller, H. J. Martin, *J. Am. Chem. Soc.* **2002**, 124, 827–833.
- [58] W. Notz, K. Sakthivel, T. Bui, G. Zhong, C. F. Barbas III, *Tetrahedron Lett.* **2001**, 42, 199–201.
- [59] P. Pojarliev, W. T. Biller, H. J. Martin, B. List, *Synlett* **2003**, 1903–1905.
- [60] Y. Hayashi, W. Tsuboi, M. Shoji, N. Suzuki, *J. Am. Chem. Soc.* **2003**, 125, 11 208–11 209.
- [61] N. S. Chowdari, D. B. Ramachary, C. F. Barbas III, *Synlett* **2003**, 1906–1909.
- [62] a) Y. Hayashi, W. Tsuboi, I. Ashimine, T. Urushima, M. Shoji, K. Sakai, *Angew. Chem.* **2003**, 115, 3805–3824; *Angew. Chem. Int. Ed.* **2003**, 42, 3677–3680; b) A. Cordova, *Synlett* **2003**, 1651–1654; c) W. Notz, F. Tanaka, S.-i. Watanabe, N. S. Chowdari, J. M. Turner, R. Thayumanavan, C. F. Barbas III, *J. Org. Chem.* **2003**, 68, 9624–9634; d) A. Cordova, *Chem. Eur. J.* **2004**, 10, 1987–1997.
- [63] F. J. López Aparicio, J. A. López Sastre, J. Molina Molina, F. J. López Herrera, *An. Quim.* **1981**, 77, 147–149.
- [64] a) A. Dondoni, A. Massi, S. Sabbatini, *Tetrahedron Lett.* **2001**, 42, 4495–4497; b) A. Dondoni, A. Massi, S. Sabbatini, V. Bertolasi, *J. Org. Chem.* **2002**, 67, 6979–6994.
- [65] M. Valpuerta Fernández, F. J. López Herrera, T. Lupión Cobos, *Heterocycles* **1988**, 27, 2133–2140.
- [66] A. Dondoni, A. Massi, E. Minghini, S. Sabbatini, V. Bertolasi, *J. Org. Chem.* **2003**, 68, 6172–6183.
- [67] C. Y. Hong, Y. Kishi, *J. Am. Chem. Soc.* **1992**, 114, 7001–7006.
- [68] J. S. Metcalf, G. A. Codd, *Chem. Res. Toxicol.* **2003**, 16, 103–112.
- [69] a) N. A. Petasis, I. Akritopoulou, *Tetrahedron Lett.* **1993**, 34, 583–586; b) N. A. Petasis, I. A. Zavialov, *J. Am. Chem. Soc.* **1997**, 119, 445–446.
- [70] N. A. Petasis, A. Goodman, I. A. Zavialov, *Tetrahedron* **1997**, 53, 16463–16470.
- [71] N. A. Petasis, Z. D. Patel, *Tetrahedron Lett.* **2000**, 41, 9607–9611.
- [72] a) L. M. Harwood, G. S. Currie, M. G. B. Drew, R. W. A. Luke, *Chem. Commun.* **1996**, 1953–1954; b) G. S. Currie, M. G. B. Drew, L. M. Harwood, D. J. Hughes, R. W. A. Luke, R. J. Vickers, *J. Chem. Soc. Perkin Trans. 1* **2000**, 2982–2990.
- [73] P. J. Pye, K. Rossen, S. A. Weissman, A. Maliakal, R. A. Reamer, R. Ball, N. N. Tsou, R. P. Volante, P. J. Reider, *Chem. Eur. J.* **2002**, 8, 1372–1376.
- [74] a) N. A. Petasis, I. A. Zavialov, *J. Am. Chem. Soc.* **1998**, 120, 11 798–11 799; b) G. K. S. Prakash, M. Mandal, S. Schweizer, N. A. Petasis, G. A. Olah, *Org. Lett.* **2000**, 2, 3173–3176; c) G. K. S. Prakash, M. Mandal, S. Schweizer, N. A. Petasis, G. A. Olah, *J. Org. Chem.* **2002**, 67, 3718–3723; Corrigendum: G. K. S. Prakash, M. Mandal, S. Schweizer, N. A. Petasis, G. A. Olah, *J. Org. Chem.* **2002**, 67, 6286.
- [75] T. Koolmeister, M. Södergren, M. Scobie, *Tetrahedron Lett.* **2002**, 43, 5969–5970.
- [76] For a review on enantioselective 1,2-additions of organometallic reagents, see: M. Yus, D. J. Ramón, *Recent Res. Dev. Org. Chem.* **2002**, 6, 297–378.
- [77] G. Sklute, D. Amsallem, A. Shabli, J. P. Varghese, I. Marek, *J. Am. Chem. Soc.* **2003**, 125, 11 776–11 777.
- [78] a) J. R. Porter, J. F. Traverse, A. H. Hoveyda, M. L. Snapper, *J. Am. Chem. Soc.* **2001**, 123, 10 409–10 410; b) L. C. Akullian, M. L. Snapper, A. H. Hoveyda, *Angew. Chem.* **2003**, 115, 4376–4379; *Angew. Chem. Int. Ed.* **2003**, 42, 4244–4247.
- [79] N. Gommermann, C. Koradin, K. Polborn, P. Knochel, *Angew. Chem.* **2003**, 115, 5941–5944; *Angew. Chem. Int. Ed.* **2003**, 42, 5763–5766.
- [80] L. Shi, Y.-Q. Tu, M. Wang, F.-M. Zhang, C.-A. Fan, *Org. Lett.* **2004**, 6, 1001–1003.
- [81] S. J. Patel, T. F. Jamison, *Angew. Chem.* **2003**, 115, 1402–1405; *Angew. Chem. Int. Ed.* **2003**, 42, 1364–1367.
- [82] For the first account of this reaction, see: a) A. Hantzsch, *Justus Liebigs Ann. Chem.* **1882**, 215, 1–82; for reviews, see: b) A. Sausins, G. Duburs, *Heterocycles* **1988**, 27, 269–289; c) G. Jones in *Comprehensive Heterocyclic Chemistry II*, Vol. 5 (Eds.: A. R. Katritzky, C. W. Rees, E. F. V. Scriven), Pergamon, Oxford, **1996**, pp. 167–243, and references therein.
- [83] For an example of a derivatization process using a Hantzsch MCR, see: S. Zehani, J. Lin, G. Gelbard, *Tetrahedron* **1989**, 45, 733–740.
- [84] a) A. Dondoni, A. Massi, E. Minghini, *Synlett* **2002**, 89–92; b) A. Dondoni, A. Massi, E. Minghini, V. Bertolasi, *Helv. Chim. Acta* **2002**, 85, 3331–3348.
- [85] A. Dondoni, A. Massi, E. Minghini, V. Bertolasi, *Tetrahedron* **2004**, 60, 2311–2326.
- [86] For an example of a derivatization process, see: P. Dumestre, L. El Kaim, A. Grégoire, *Chem. Commun.* **1999**, 775–776.
- [87] For the first account of this reaction, see: a) M. Passerini, *Gazz. Chim. Ital.* **1921**, 51, 126–129; for examples of a derivatization process with this MCR, see: b) B. Beck, M. Magnin-Lachaux, E. Hedtweck, A. Dömling, *Org. Lett.* **2001**, 3, 2875–2878; c) M. C. Pirrung, K. D. Sarma, *J. Am. Chem. Soc.* **2004**, 126, 444–445.
- [88] H. Bock, I. Ugi, *J. Prakt. Chem.* **1997**, 339, 385–389.
- [89] For a review, see: D. Gryko, J. Chalko, J. Jurczak, *Chirality* **2003**, 15, 514–541.
- [90] E. J. Moran, R. W. Armstrong, *Tetrahedron Lett.* **1991**, 32, 3807–3810.
- [91] For a review, see: T. J. Hodgkinson, M. Shipman, *Tetrahedron* **2001**, 57, 4467–4488.
- [92] L. Banfi, G. Guanti, R. Riva, *Chem. Commun.* **2000**, 985–986.
- [93] A. Basso, L. Banfi, R. Riva, P. Piaggio, G. Guanti, *Tetrahedron Lett.* **2003**, 44, 2367–2370.
- [94] R. Frey, S. G. Galbraith, S. Guelfi, C. Lamberth, M. Zeller, *Synlett* **2003**, 1536–1538.
- [95] A. E. J. de Nooy, G. Masci, V. Crescenzi, *Macromolecules* **1999**, 32, 1318–1320.
- [96] L. Banfi, G. Guanti, R. Riva, A. Basso, E. Calcagno, *Tetrahedron Lett.* **2002**, 43, 4067–4069.
- [97] U. Schmidt, S. Weinbrenner, *J. Chem. Soc. Chem. Commun.* **1994**, 1003–1004.
- [98] J. E. Semple, T. D. Owens, K. Nguyen, O. E. Levy, *Org. Lett.* **2000**, 2, 2769–2772.
- [99] For recent reviews, see: a) M. C. Koch, R. Breinbauer, H. Waldmann, *Biol. Chem.* **2003**, 384, 1265–1272; b) C. U. Nielsen, B. Brodin, *Curr. Drug Targets* **2003**, 4, 373–388.
- [100] T. D. Owens, G.-L. Araldi, R. F. Nutt, J. E. Semple, *Tetrahedron Lett.* **2001**, 42, 6271–6274.
- [101] T. D. Owens, J. E. Semple, *Org. Lett.* **2001**, 3, 3301–3304.
- [102] a) T. Ziegler, R. Schlömer, C. Koch, *Tetrahedron Lett.* **1998**, 39, 5957–5960; b) T. Ziegler, H.-J. Kaisers, R. Schlömer, C. Koch, *Tetrahedron* **1999**, 55, 8397–8408.
- [103] U. Kusebauch, B. Beck, K. Messer, E. Herdtweck, A. Dömling, *Org. Lett.* **2003**, 5, 4021–4024.
- [104] For a review on enantioselective reactions promoted by titanium derivatives, see: D. J. Ramón, M. Yus, *Recent Res. Dev. Org. Chem.* **1998**, 2, 489–523.
- [105] D. Seebach, A. K. Beck, A. Heckel, *Angew. Chem.* **2001**, 113, 96–142; *Angew. Chem. Int. Ed.* **2001**, 40, 92–138.
- [106] K. Tsuchida, Y. Mizuno, K. Ikeda, *Heterocycles* **1981**, 15, 883–887.

- [107] K. Rossen, J. Sager, L. M. DiMichele, *Tetrahedron Lett.* **1997**, 38, 3183–3186.
- [108] C. Hulme, M. M. Morrisette, F. A. Volz, C. J. Burns, *Tetrahedron Lett.* **1998**, 39, 1113–1116.
- [109] U. Kazmaier, C. Hebach, *Synlett* **2003**, 1591–1594.
- [110] B. Henkel, M. Sax, A. Dömling, *Tetrahedron Lett.* **2003**, 44, 7015–7018.
- [111] V. Gouge, P. Jubault, J.-C. Quirion, *Tetrahedron Lett.* **2004**, 45, 773–776.
- [112] a) I. Ugi, K. Offermann, *Angew. Chem.* **1963**, 75, 917; *Angew. Chem. Int. Ed. Engl.* **1963**, 2, 624; b) D. Marquarding, P. Hoffmann, H. Heitzer, I. Ugi, *J. Am. Chem. Soc.* **1970**, 92, 1969–1971; c) G. Eberle, I. Ugi, *Angew. Chem.* **1976**, 88, 509–510; *Angew. Chem. Int. Ed. Engl.* **1976**, 15, 492.
- [113] a) H. Kunz, W. Pfengle, *J. Am. Chem. Soc.* **1988**, 110, 651–652; b) H. Kunz, W. Pfengle, *Tetrahedron* **1988**, 44, 5487–5494.
- [114] K. Oertel, G. Zech, H. Kunz, *Angew. Chem.* **2000**, 112, 1489–1491; *Angew. Chem. Int. Ed.* **2000**, 39, 1431–1433.
- [115] R. J. Linderman, S. Binet, S. R. Petrich, *J. Org. Chem.* **1999**, 64, 336–337.
- [116] H. Kunz, W. Pfengle, K. Rück, W. Sager, *Synthesis* **1991**, 1039–1042.
- [117] a) A. Demharther, W. Hörl, E. Herdtweck, I. Ugi, *Angew. Chem.* **1996**, 108, 185–187; *Angew. Chem. Int. Ed. Engl.* **1996**, 35, 173–175; b) I. Ugi, A. Demharther, W. Hörl, T. Schmid, *Tetrahedron* **1996**, 52, 11 657–11 664; c) I. Ugi, W. Hörl, C. Hanusch-Kompa, T. Schmid, E. Herdtweck, *Heterocycles* **1998**, 47, 965–975.
- [118] I. Ugi, T. Schmid, *J. Prakt. Chem.* **1997**, 339, 652–655.
- [119] G. Dyker, K. Breitenstein, G. Henkel, *Tetrahedron: Asymmetry* **2002**, 13, 1929–1936.
- [120] R. Zimmer, A. Ziemer, M. Gruner, I. Brüdgam, H. Hartl, H.-U. Reissig, *Synthesis* **2001**, 1649–1658.
- [121] A. D. Piscopio, J. F. Miller, K. Koch, *Tetrahedron* **1999**, 55, 8189–8198.
- [122] S. E. de Laszlo, P. G. Williard, *J. Am. Chem. Soc.* **1985**, 107, 199–203.
- [123] J. C. Boehm, W. D. Kingsbury, *J. Org. Chem.* **1986**, 51, 2307–2314.
- [124] S. M. Bauer, R. W. Armstrong, *J. Am. Chem. Soc.* **1999**, 121, 6355–6366.
- [125] D. P. Sutherlin, T. M. Stark, R. Hughes, R. W. Armstrong, *J. Org. Chem.* **1996**, 61, 8350–8354.
- [126] T. Yamada, N. Motoyama, T. Taniguchi, Y. Kazuta, T. Miyazawa, S. Kuwata, K. Matsumoto, M. Sugiura, *Chem. Lett.* **1987**, 723–726.
- [127] a) A. Szardenings, T. S. Burkoth, H. H. Lu, D. W. Tien, D. A. Campbell, *Tetrahedron* **1997**, 53, 6573–6593; b) A. K. Szardenings, V. Antonenko, D. A. Campbell, N. DeFrancisco, S. Ida, L. Shi, N. Sharkov, D. Tien, Y. Wang, M. Navre, *J. Med. Chem.* **1999**, 42, 1348–1357.
- [128] M. Whittaker, C. D. Floyd, P. Brown, A. J. H. Gearing, *Chem. Rev.* **1999**, 99, 2735–2776; corrigendum: M. Whittaker, C. D. Floyd, P. Brown, A. J. H. Gearing, *Chem. Rev.* **2001**, 101, 2205.
- [129] a) A. Golebiowski, S. R. Klopfenstein, X. Shao, J. J. Chen, A.-O. Colson, A. L. Grieb, A. F. Russell, *Org. Lett.* **2000**, 2, 2615–2617; b) A. Golebiowski, J. Jozwik, S. R. Klopfenstein, A.-O. Colson, A. L. Grieb, A. F. Russell, V. L. Rastogi, C. F. Diven, D. E. Portlock, J. J. Chen, *J. Comb. Chem.* **2002**, 4, 584–590.
- [130] C. Hebach, U. Kazmaier, *Chem. Commun.* **2003**, 596–597.
- [131] A. Endo, A. Yanagisawa, M. Abe, S. Tohma, T. Kan, T. Fukuyama, *J. Am. Chem. Soc.* **2002**, 124, 6552–6554.
- [132] C. L. Kelly, K. W. M. Lawrie, P. Morgan, C. L. Willis, *Tetrahedron Lett.* **2000**, 41, 8001–8005.
- [133] a) M. M. Joullié, P. C. Wang, J. E. Semple, *J. Am. Chem. Soc.* **1980**, 102, 887–889; b) J. E. Semple, P. C. Wang, Z. Lysenko, M. M. Joullié, *J. Am. Chem. Soc.* **1980**, 102, 7505–7510; c) S.-Y. Chen, M. M. Joullié, *J. Org. Chem.* **1984**, 49, 1769–1772.
- [134] O. Lockhoff, *Angew. Chem.* **1998**, 110, 3634–3637; *Angew. Chem. Int. Ed.* **1998**, 37, 3436–3439.
- [135] O. Lockhoff, I. Frappa, *Comb. Chem. High Throughput Screening* **2002**, 5, 361–372.
- [136] a) I. Ugi, K. Offeremann, H. Herlinger, D. Marquarding, *Justus Liebigs Ann. Chem.* **1967**, 1–10; b) I. Ugi, K. Guenter, *Justus Liebigs Ann. Chem.* **1967**, 11–28; c) K. Burger, K. Mütze, W. Hollweck, B. Koksche, *Tetrahedron* **1998**, 54, 5915–5928.
- [137] a) R. Urban, I. Ugi, *Angew. Chem.* **1975**, 87, 67–69; *Angew. Chem. Int. Ed. Engl.* **1975**, 14, 61–62; b) F. Siglmüller, R. Herrmann, I. Ugi, *Tetrahedron* **1986**, 42, 5931–5940.
- [138] a) S. Lehnhoff, M. Goebel, R. M. Karl, R. Klösel, I. Ugi, *Angew. Chem.* **1995**, 107, 1208–1211; *Angew. Chem. Int. Ed. Engl.* **1995**, 34, 1104–1107; b) J. M. Drábik, J. Achatz, I. Ugi, *Proc. Est. Acad. Sci. Chem.* **2002**, 51, 156–168.
- [139] M. Goebel, I. Ugi, *Synthesis* **1991**, 1095–1098.
- [140] a) G. Ross, I. Ugi, *Can. J. Chem.* **2001**, 79, 1934–1939; b) G. F. Ross, E. Herdtweck, I. Ugi, *Tetrahedron* **2002**, 58, 6127–6133.
- [141] C. Baldoli, S. Maiorana, E. Licandro, G. Zinzalla, D. Perdicchia, *Org. Lett.* **2002**, 4, 4341–4344.
- [142] a) G. Guillena, G. Rodríguez, M. Albrecht, G. van Koten, *Chem. Eur. J.* **2002**, 8, 5368–5376; b) G. Guillena, K. M. Halkes, G. Rodríguez, G. D. Batema, G. van Koten, J. P. Kamerling, *Org. Lett.* **2003**, 5, 2021–2024.
- [143] W. K. C. Park, M. Auer, H. Jaksche, C.-H. Wong, *J. Am. Chem. Soc.* **1996**, 118, 10150–10155.
- [144] H. Immer, V. Nelson, W. Robinson, M. Götz, *Justus Liebigs Ann. Chem.* **1973**, 1789–1796.
- [145] B. Beck, S. Hess, A. Dömling, *Bioorg. Med. Chem. Lett.* **2000**, 10, 1701–1705.
- [146] a) C. D. Floyd, L. A. Harnett, A. Miller, S. Patel, L. Saroglou, M. Whittaker, *Synlett* **1998**, 637–639; b) S. Patel, L. Saroglou, C. D. Floyd, A. Miller, M. Whittaker, *Tetrahedron Lett.* **1998**, 39, 8333–8334.
- [147] A. Failli, H. Immer, M. Götz, *Can. J. Chem.* **1979**, 57, 3257–3261.
- [148] K. Kehagia, I. K. Ugi, *Tetrahedron* **1995**, 51, 9523–9530.
- [149] a) H. P. Isenring, W. Hofheinz, *Synthesis* **1981**, 385–387; b) H. P. Isenring, W. Hofheinz, *Tetrahedron* **1983**, 39, 2591–2597.
- [150] S. J. Park, G. Keum, S. B. Kang, H. Y. Koh, Y. Kim, D. H. Lee, *Tetrahedron Lett.* **1998**, 39, 7109–7112.
- [151] I. K. Ugi, B. Ebert, W. Hörl, *Chemosphere* **2001**, 43, 75–81.
- [152] Y. B. Kim, E. H. Choi, G. Keum, S. B. Kang, D. H. Lee, H. Y. Koh, Y. Kim, *Org. Lett.* **2001**, 3, 4149–4152.
- [153] M. M. Bowers, P. Carroll, M. M. Joullié, *J. Chem. Soc. Perkin Trans. I* **1989**, 857–865.
- [154] R. Urban, G. Eberle, D. Marquarding, D. Rehn, H. Rehn, I. Ugi, *Angew. Chem.* **1976**, 88, 644–646; *Angew. Chem. Int. Ed. Engl.* **1976**, 15, 627–628.
- [155] D. Behnke, R. Taube, K. Illgen, S. Nerdinger, E. Herdtweck, *Synlett* **2004**, 688–692.
- [156] For an example of a derivatization process through a related MCR, see: J. Sisko, A. J. Kassick, M. Mellinger, J. J. Filan, A. Allen, M. A. Olsen, *J. Org. Chem.* **2000**, 65, 1516–1524.
- [157] a) X. Sun, P. Janvier, G. Zhao, H. Bienaymé, J. Zhu, *Org. Lett.* **2001**, 3, 877–880; b) G. Zhao, X. Sun, H. Bienaymé, J. Zhu, *J. Am. Chem. Soc.* **2001**, 123, 6700–6701.
- [158] For recent reviews, see: a) B. R. Bear, S. M. Sparks, K. J. Shea, *Angew. Chem.* **2001**, 113, 864–894; *Angew. Chem. Int. Ed.* **2001**, 40, 820–849; b) P. Buonora, J.-C. Olsen, T. Oh, *Tetrahedron* **2001**, 57, 6099–6138; c) J. Yli-Kauhaluoma, *Tetrahedron* **2001**, 57, 7053–7071; d) E. M. Stocking, R. M. Williams, *Angew. Chem.* **2003**, 115, 3186–3223; *Angew. Chem. Int. Ed.* **2003**, 42, 3078–3115, and references therein.
- [159] a) R. Yamaguchi, T. Hamasaki, T. Sasaki, T. Ohta, K. Utimoto, S. Kozima, H. Takaya, *J. Org. Chem.* **1993**, 58, 1136–1143; b) Y.

- Haraguchi, S. Kozima, R. Yamaguchi, *Tetrahedron: Asymmetry* **1996**, *7*, 443–449.
- [160] a) J. Taylor, D. G. Hall, *Org. Lett.* **2000**, *2*, 3715–3718; b) B. B. Touré, H. R. Hoveyda, J. Taylor, A. Ułaczyk-Lesanko, D. G. Hall, *Chem. Eur. J.* **2003**, *9*, 466–474; c) B. B. Touré, D. G. Hall, *Angew. Chem.* **2004**, *116*, 2035–2038; *Angew. Chem. Int. Ed.* **2004**, *43*, 2001–2004.
- [161] J. W. J. Kennedy, D. G. Hall, *Angew. Chem.* **2003**, *115*, 4880–4887; *Angew. Chem. Int. Ed.* **2003**, *42*, 4732–4739.
- [162] a) V. Narkevitch, K. Schenk, P. Vogel, *Angew. Chem.* **2000**, *112*, 1876–1878; *Angew. Chem. Int. Ed.* **2000**, *39*, 1806–1808; b) V. Narkevitch, S. Megevand, K. Schenk, P. Vogel, *J. Org. Chem.* **2001**, *66*, 5080–5093; c) V. Narkevitch, P. Vogel, K. Schenk, *Helv. Chim. Acta* **2002**, *85*, 1674–1685; d) M. Turks, F. Fonquerne, P. Vogel, *Org. Lett.* **2004**, *6*, 1053–1056.
- [163] L. F. Tietze, A. Modi, *Med. Chem. Rev.* **2000**, *20*, 304–322.
- [164] L. F. Tietze, Y. Zhou, *Angew. Chem.* **1999**, *111*, 2076–2078; *Angew. Chem. Int. Ed.* **1999**, *38*, 2045–2047.
- [165] L. F. Tietze, N. Rackelmann, G. Sekar, *Angew. Chem.* **2003**, *115*, 4386–4389; *Angew. Chem. Int. Ed.* **2003**, *42*, 4254–4257.
- [166] G. Cravotto, G. M. Nano, G. Palmisano, S. Tagliapietra, *Tetrahedron Lett.* **2001**, *42*, 707–709.
- [167] D. B. Ramachary, N. S. Chowdari, C. F. Barbas III, *Angew. Chem.* **2003**, *115*, 4365–4369; *Angew. Chem. Int. Ed.* **2003**, *42*, 4233–4237.
- [168] D. B. Ramachary, N. S. Chowdari, C. F. Barbas III, *Synlett* **2003**, 1910–1914.
- [169] For a review, see: a) K. V. Gothelf, K. A. Jørgensen, *Chem. Rev.* **1998**, *98*, 863–909; For a monograph, see: b) *Synthetic Applications of 1,3-Dipolar Cycloaddition Chemistry Toward Heterocycles and Natural Products*, (Eds.: A. Padwa, W. H. Pearson), Wiley, Hoboken, **2003**.
- [170] a) A. S. Anslow, L. M. Harwood, H. Phillips, D. Watkin, *Tetrahedron: Asymmetry* **1991**, *2*, 169–172; b) L. M. Harwood, A. C. Manage, S. Robin, S. F. G. Hopes, D. J. Watkin, C. E. Williams, *Synlett* **1993**, 777–780; c) J. E. Baldwin, S. C. M. Turner, M. G. Moloney, *Synlett* **1994**, 925–928; d) L. M. Harwood, I. A. Lilley, *Tetrahedron: Asymmetry* **1995**, *6*, 1557–1560.
- [171] a) A. S. Anslow, L. M. Harwood, H. Phillips, D. Watkin, *Tetrahedron: Asymmetry* **1991**, *2*, 997–1000; b) A. S. Anslow, L. M. Harwood, H. Phillips, D. Watkin, L. F. Wong, *Tetrahedron: Asymmetry* **1991**, *2*, 1343–1358; c) A. S. Anslow, L. M. Harwood, I. A. Lilley, *Tetrahedron: Asymmetry* **1995**, *6*, 2465–2468.
- [172] a) R. M. Williams, W. Zhai, D. J. Aldous, S. C. Aldous, *J. Org. Chem.* **1992**, *57*, 6527–6532; b) P. R. Sebahar, R. M. Williams, *J. Am. Chem. Soc.* **2000**, *122*, 5666–5667; c) P. R. Sebahar, H. Osada, T. Usui, R. M. Williams, *Tetrahedron* **2002**, *58*, 6311–6322; d) T. Onishi, P. R. Sebahar, R. M. Williams, *Org. Lett.* **2003**, *5*, 3135–3137.
- [173] R. Chinchilla, L. R. Falvello, N. Galindo, C. Nájera, *Eur. J. Org. Chem.* **2001**, 3133–3140.
- [174] a) F. Roussi, A. Chauveau, M. Bonin, L. Micouin, H.-P. Husson, *Synthesis* **2000**, 1170–1179; b) F. Chung, A. Chauveau, M. Seltki, M. Bonin, L. Micouin, *Tetrahedron Lett.* **2004**, *45*, 3127–3130.
- [175] J.-F. Peyronel, S. Grisoni, B. Carboni, T. Courgeon, R. Carrié, *Tetrahedron* **1994**, *50*, 189–198.
- [176] P. Garner, O. Dogan, *J. Org. Chem.* **1994**, *59*, 4–6.
- [177] C. Wittland, N. Risch, *J. Prakt. Chem.* **2000**, *342*, 311–315.
- [178] D. Enders, I. Meyer, J. Runsink, G. Raabe, *Tetrahedron* **1998**, *54*, 10733–10752.
- [179] H. A. Dondas, C. W. G. Fishwick, R. Grigg, C. Kilner, *Tetrahedron* **2004**, *60*, 3473–3485.
- [180] U. Chiacchio, A. Corsaro, G. Gumina, A. Rescifina, D. Llanazo, A. Piperno, G. Romeo, R. Romero, *J. Org. Chem.* **1999**, *64*, 9321–9327.
- [181] P. Merino, J. Revuelta, T. Tejero, U. Chiacchio, A. Rescifina, A. Piperno, G. Romeo, *Tetrahedron: Asymmetry* **2002**, *13*, 167–172.
- [182] R. Hanselmann, J. Zhou, P. Ma, P. N. Confalone, *J. Org. Chem.* **2003**, *68*, 8739–8741.
- [183] A. K. Ganguly, N. Seah, V. Popov, C. H. Wang, R. Kuang, A. K. Saksena, B. N. Pramanik, T. M. Chan, A. T. McPhail, *Tetrahedron Lett.* **2002**, *43*, 8981–8983.
- [184] a) M. Avalos, R. Babiano, P. Cintas, J. L. Jiménez, J. C. Palacios, M. A. Silva, *Chem. Commun.* **1998**, 459–460; Corrigendum: M. Avalos, R. Babiano, P. Cintas, J. L. Jiménez, J. C. Palacios, M. A. Silva, *Chem. Commun.* **1998**, 1917; b) M. Avalos, R. Babiano, P. Cintas, J. L. Jiménez, J. C. Palacios, M. A. Silva, *J. Org. Chem.* **1999**, *64*, 1494–1502.
- [185] E. Marotta, P. Righi, G. Rosini, *Tetrahedron Lett.* **1998**, *39*, 1041–1044.
- [186] S. Kanemasa, T. Kanai, *J. Am. Chem. Soc.* **2000**, *122*, 10710–10711.
- [187] For reviews, see: a) D. Tanner, *Angew. Chem.* **1994**, *106*, 625–646; *Angew. Chem. Int. Ed. Engl.* **1994**, *33*, 599–619; b) J. B. Sweeney, *Chem. Soc. Rev.* **2002**, *31*, 247–258; c) P. Müller, C. Fruit, *Chem. Rev.* **2003**, *103*, 2905–2919.
- [188] For a review, see: J. du Bois, C. S. Tomooka, J. Hong, E. M. Carreira, *Acc. Chem. Res.* **1997**, *30*, 364–372.
- [189] J. du Bois, J. Hong, E. M. Carreira, M. W. Day, *J. Am. Chem. Soc.* **1996**, *118*, 915–916.
- [190] J. du Bois, C. S. Tomooka, J. Hong, E. M. Carreira, *J. Am. Chem. Soc.* **1997**, *119*, 3179–3180.
- [191] a) S. Minakata, T. Ando, M. Nishimura, I. Ryu, M. Komatsu, *Angew. Chem.* **1998**, *110*, 3596–3598; *Angew. Chem. Int. Ed.* **1998**, *37*, 3392–3394; b) M. Nishimura, S. Minakata, S. Thongchant, I. Ryu, M. Komatsu, *Tetrahedron Lett.* **2000**, *41*, 7089–7092; c) M. Nishimura, S. Minakata, T. Takahashi, Y. Oderaotoshi, M. Komatsu, *J. Org. Chem.* **2002**, *67*, 2101–2110.
- [192] S. Minakata, M. Nishimura, T. Takahashi, Y. Oderaotoshi, M. Komatsu, *Tetrahedron Lett.* **2001**, *42*, 9019–9022.
- [193] N. Svenstrup, A. Bøgevig, R. G. Hazell, K. A. Jørgensen, *J. Chem. Soc. Perkin Trans. 1* **1999**, 1559–1565.
- [194] For recent reviews, see: a) S. E. Gibson (née Thomas), A. Stevenazzi, *Angew. Chem.* **2003**, *115*, 1844–1854; *Angew. Chem. Int. Ed.* **2003**, *42*, 1800–1810; b) J. Blanco-Urgoiti, L. Anorbe, L. Pérez-Serrano, G. Domínguez, J. Pérez-Castells, *Chem. Soc. Rev.* **2004**, *33*, 32–42.
- [195] P. A. Evans, J. R. Robinson, *J. Am. Chem. Soc.* **2001**, *123*, 4609–4610.
- [196] a) A. Hosomi, H. Sakurai, *Tetrahedron Lett.* **1976**, *17*, 1295–1298; b) A. D. Dilmann, S. L. Ioffe, *Chem. Rev.* **2003**, *103*, 733–772.
- [197] R. Imwinkler, D. Seebach, *Angew. Chem.* **1985**, *97*, 781–782; *Angew. Chem. Int. Ed. Engl.* **1985**, *24*, 765–766.
- [198] T. Mukaiyama, M. Ohshima, N. Miyoshi, *Chem. Lett.* **1987**, 1121–1124.
- [199] a) A. Mekhalifa, I. E. Markó, *Tetrahedron Lett.* **1991**, *32*, 4779–4782; b) K. Manju, S. Trehan, *Chem. Commun.* **1999**, 1929–1930.
- [200] a) J. Cossrow, S. D. Rychnovsky, *Org. Lett.* **2002**, *4*, 147–150; b) J. R. Huckins, S. D. Rychnovsky, *J. Org. Chem.* **2003**, *68*, 10135–10145.
- [201] a) L. F. Tietze, A. Dölle, K. Schiemann, *J. Am. Chem. Soc.* **1992**, *114*, 1372–1373; b) L. F. Tietze, K. Schiemann, C. Wegner, C. Wulff, *Chem. Eur. J.* **1996**, *2*, 1164–1172; c) L. F. Tietze, C. Wulff, C. Wegner, A. Schuffenhauer, K. Schiemann, *J. Am. Chem. Soc.* **1998**, *120*, 4276–4280.
- [202] For reviews on different aspects of this reaction, see: a) M. Yus, *Chem. Soc. Rev.* **1996**, *25*, 155–161; b) D. J. Ramón, M. Yus, *Eur. J. Org. Chem.* **2000**, 225–237; c) M. Yus, *Synlett* **2001**,

- 1197–1205; d) M. Yus, D. J. Ramón, *Latv. J. Chem.* **2002**, 79–92; e) M. Yus, *Pure Appl. Chem.* **2003**, 75, 1453–1475.
- [203] a) L. F. Tietze, K. Schiemann, C. Wegner, *J. Am. Chem. Soc.* **1995**, 117, 5851–5852; b) L. F. Tietze, C. Wegner, C. Wulff, *Synlett* **1996**, 471–472; c) L. F. Tietze, K. Schiemann, C. Wegner, C. Wulff, *Chem. Eur. J.* **1998**, 4, 1862–1869; d) L. F. Tietze, C. Wegner, C. Wulff, *Eur. J. Org. Chem.* **1998**, 1639–1644; e) L. F. Tietze, B. Weigand, L. Völkel, C. Wulff, C. Bittner, *Chem. Eur. J.* **2001**, 7, 161–168; f) L. F. Tietze, L. Völkel, C. Wulff, B. Weigand, C. Bittner, P. McGrath, K. Johnson, M. Schäfer, *Chem. Eur. J.* **2001**, 7, 1304–1308.
- [204] D. J. Ramón, M. Yus, *Angew. Chem.* **2004**, 116, 286–289; *Angew. Chem. Int. Ed.* **2004**, 43, 284–287.
- [205] a) L. F. Tietze, J. Görlitzer, *Synlett* **1997**, 1049–1050; b) L. F. Tietze, J. Görlitzer, A. Schuffenhauer, M. Hübner, *Eur. J. Org. Chem.* **1999**, 1075–1084.
- [206] L. F. Tietze, C. Wegner, C. Wulff, *Chem. Eur. J.* **1999**, 5, 2885–2889.
- [207] L. F. Tietze, L. Völkel, *Angew. Chem.* **2001**, 113, 925–927; *Angew. Chem. Int. Ed.* **2001**, 40, 901–902.
- [208] a) T. Komnenos, *Justus Liebigs Ann. Chem.* **1883**, 218, 145–169; b) R. Perlmutter, *Conjugate Addition Reactions in Organic Synthesis* (Eds.: J. E. Baldwin, P. D. Magnus), Pergamon, Oxford, **1992**.
- [209] For reviews, see: a) B. E. Rossiter, N. M. Swingle, *Chem. Rev.* **1992**, 92, 771–806; b) N. Krause, A. Gerold, *Angew. Chem.* **1997**, 109, 194–213; *Angew. Chem. Int. Ed. Engl.* **1997**, 36, 186–204; c) J. Christoffers, *Chem. Eur. J.* **2003**, 9, 4862–4867.
- [210] J. Jauch, *J. Org. Chem.* **2001**, 66, 609–611.
- [211] a) J. Jauch, *Angew. Chem.* **2000**, 112, 2874–2875; *Angew. Chem. Int. Ed.* **2000**, 39, 2764–2765; b) J. Jauch, *Eur. J. Org. Chem.* **2001**, 473–476.
- [212] a) X. Du, D. Chen, H.-X. Wei, G. Li, T. L. Xiao, D. W. Armstrong, *Chirality* **2003**, 15, 139–142; b) H.-X. Wei, D. Chen, X. Xu, G. Li, P. W. Paré, *Tetrahedron Lett.* **2003**, 44, 971–974.
- [213] A. G. M. Barrett, A. Kamimura, *J. Chem. Soc. Chem. Commun.* **1995**, 1755–1756.
- [214] K. Yoshida, M. Ogasawara, T. Hayashi, *J. Am. Chem. Soc.* **2003**, 125, 10984–10985.
- [215] a) M. Boisbrun, A. Kovács-Kulyassa, L. Jeannin, J. Sapi, L. Toupet, J.-Y. Laronze, *Tetrahedron Lett.* **2000**, 41, 9771–9775; b) E. Dardennes, A. Kovács-Kulyassa, A. Renzetti, J. Sapi, J.-Y. Laronze, *Tetrahedron Lett.* **2003**, 44, 221–223; c) L. Jeannin, M. Boisbrun, C. Nemes, F. Cochard, M. Laronze, E. Dardennes, A. Kovács-Kulyassa, J. Sapi, J.-Y. Laronze, *C. R. Chim.* **2003**, 6, 517–528.
- [216] A. Chetia, C. J. Saikia, K. C. Lekhok, R. C. Boruah, *Tetrahedron Lett.* **2004**, 45, 2649–2651.
- [217] S.-i. Ikeda, D.-M. Cui, Y. Sato, *J. Am. Chem. Soc.* **1999**, 121, 4712–4713.
- [218] a) D. J. Ramón, G. Guillena, D. Seebach, *Helv. Chim. Acta* **1996**, 79, 875–894; b) M. Anstiss, J. M. Joanne, A. Nelson, J. R. Titchmarsh, *Synlett* **2003**, 1213–1220.
- [219] a) S. Torii, H. Okumoto, H. Ozaki, S. Nakayasu, T. Tadokoro, T. Kotani, *Tetrahedron Lett.* **1992**, 33, 3499–3502; b) S. Torii, H. Okumoto, T. Kotani, S. Nakayasu, H. Ozaki, *Tetrahedron Lett.* **1992**, 33, 3503–3506.
- [220] C. Moinet, J.-C. Fiaud, *Synlett* **1997**, 97–99.
- [221] For reviews, see: a) S. G. Nelson, *Tetrahedron: Asymmetry* **1998**, 9, 357–389; b) T. D. Machajewski, C.-H. Wong, *Angew. Chem.* **2000**, 112, 1406–1430; *Angew. Chem. Int. Ed.* **2000**, 39, 1352–1374; c) C. Palomo, M. Oiarbide, J. M. García, *Chem. Eur. J.* **2002**, 8, 36–44; d) B. Alcaide, P. Almendros, *Eur. J. Org. Chem.* **2002**, 1595–1601; e) C. Palomo, M. Oiarbide, J. M. García, *Chem. Soc. Rev.* **2004**, 33, 65–75.
- [222] N. S. Chowdari, D. B. Ramachary, C. F. Barbas III, *Org. Lett.* **2003**, 5, 1685–1688.
- [223] For reviews, see: a) P. Langer, *Angew. Chem.* **2000**, 112, 3177–3180; *Angew. Chem. Int. Ed.* **2000**, 39, 3049–3052; b) P. Langer in *Organic Synthesis Highlights V* (Eds.: H.-G. Schmalz, T. Wirth), Wiley-VCH, Weinheim, **2003**, pp. 165–177.
- [224] D. Balan, H. Adolfsson, *Tetrahedron Lett.* **2003**, 44, 2521–2524.
- [225] C. S. Tomooka, E. M. Carreira, *Helv. Chim. Acta* **2002**, 85, 3773–3784.
- [226] *Multicomponent Reactions* (Eds.: J. Zhu, H. Bienaymé), Wiley-VCH, Weinheim, **2005**.
- [227] C. Simon, T. Constantieux, J. Rodriguez, *Eur. J. Org. Chem.* **2004**, 4957–4980.
- [228] E. Ichikawa, M. Suzuki, K. Yabu, M. Albert, M. Kanai, M. Shibasaki, *J. Am. Chem. Soc.* **2004**, 126, 11808–11809.
- [229] N. S. Joshi, L. R. Whitaker, M. B. Francis, *J. Am. Chem. Soc.* **2004**, 126, 15942–15943.
- [230] a) W. Notz, S.-i. Watanabe, N. S. Chowdari, G. Zhong, J. M. Betancort, F. Tanaka, C. F. Barbas III, *Adv. Synth. Catal.* **2004**, 346, 1131–1140; b) I. Ibrahim, J. Casas, A. Córdova, *Angew. Chem.* **2004**, 116, 6690–6693; *Angew. Chem. Int. Ed.* **2004**, 43, 6528–6531.
- [231] Y. Hayashi, J. Yamaguchi, K. Hibino, T. Sumiya, T. Urushima, M. Shoji, D. Hashizume, H. Koshino, *Adv. Synth. Catal.* **2004**, 346, 1435–1439.
- [232] M. C. Elliot, M. S. Long, *Org. Biomol. Chem.* **2004**, 2, 2003–2011.
- [233] M. Sugiura, K. Hirano, S. Kobayashi, *J. Am. Chem. Soc.* **2004**, 126, 7182–7183.
- [234] a) H. Dube, N. Gommermann, P. Knochel, *Synthesis* **2004**, 2015–2025; b) N. Gommermann, P. Knochel, *Chem. Commun.* **2004**, 2324–2325.
- [235] T. F. Knöpfel, P. Aschwanden, T. Ichikawa, T. Watanabe, E. M. Carreira, *Angew. Chem.* **2004**, 116, 6097–6099; *Angew. Chem. Int. Ed.* **2004**, 43, 5971–5973.
- [236] S. J. Patel, T. F. Jamison, *Angew. Chem.* **2004**, 116, 4031–4034; *Angew. Chem. Int. Ed.* **2004**, 43, 3941–3944.
- [237] J. M. Oaksmith, U. Peters, B. Ganem, *J. Am. Chem. Soc.* **2004**, 126, 13606–13607.
- [238] P. R. Andreana, C. C. Liu, S. L. Schreiber, *Org. Lett.* **2004**, 6, 4231–4233.
- [239] T. Godet, Y. Bonvin, G. Vincent, D. Merle, A. Thozet, M. A. Ciufolini, *Org. Lett.* **2004**, 6, 3281–3284.
- [240] a) R. Krelaus, B. Westermann, *Tetrahedron Lett.* **2004**, 45, 5987–5990; b) L. Banfi, A. Basso, G. Guanti, R. Riva, *Tetrahedron Lett.* **2004**, 45, 6637–6640.
- [241] T. M. Chapman, I. G. Davies, B. Gu, T. M. Block, D. I. C. Scopes, P. A. Hay, S. M. Courtney, L. A. McNeill, C. J. Schofield, B. G. Davis, *J. Am. Chem. Soc.* **2005**, 127, 506–507.
- [242] B. B. Touré, D. G. Hall, *J. Org. Chem.* **2004**, 69, 8429–8436.
- [243] a) X. Huang, C. Craita, P. Vogel, *J. Org. Chem.* **2004**, 69, 4272–4275; b) L. C. Bouchez, S. Reddy, M. Turks, P. Vogel, *J. Org. Chem.* **2004**, 69, 6413–6418; c) M. Turks, X. Huang, P. Vogel, *Chem. Eur. J.* **2005**, 11, 465–476.
- [244] a) D. B. Ramachary, K. Anebuselvy, N. S. Chowdari, C. F. Barbas III, *J. Org. Chem.* **2004**, 69, 5838–5849; b) D. B. Ramachary, C. F. Barbas III, *Chem. Eur. J.* **2004**, 10, 5323–5331.
- [245] M. M.-C. Lo, C. S. Neumann, S. Nagayama, E. O. Perlstein, S. L. Schreiber, *J. Am. Chem. Soc.* **2004**, 126, 16077–16086.
- [246] L. F. Tietze, S. Hölsken, J. Adrio, T. Kinzel, C. Wegner, *Synthesis* **2004**, 2236–2239.
- [247] D. Chen, C. Timmons, J. Liu, A. Headley, G. Li, *Eur. J. Org. Chem.* **2004**, 3330–3335.
- [248] C. D. Hopkins, H. C. Malinakova, *Org. Lett.* **2004**, 6, 2221–2224.

Communications



The reductive electron transfer (ET) in DNA can be studied by ultrafast time-resolved measurements combined with chemically probed DNA-strand-cleavage experiments. Owing to the numerous conformations of DNA present the results show a variety of ET rates. For more information see the Communication by H.-A. Wagenknecht, T. Fiebig, et al. on the following pages.

Electron Transfer

Real-Time Spectroscopic and Chemical Probing of Reductive Electron Transfer in DNA**

Peter Kaden, Elke Mayer-Enthart, Anton Trifonov, Torsten Fiebig,* and Hans-Achim Wagenknecht*

Reductive electron-transfer (ET) processes in DNA have attracted considerable interest over the last 2–3 years.^[1] The injection of an excess electron into DNA initiates a type of charge transfer which is complementary to the extensively studied oxidative hole transfer.^[1,2] Recent studies^[1,3–11] support the idea that the reductive type of charge transfer has a high potential for application in new nanodevices based on DNA or DNA-inspired architectures.

Until five years ago, most knowledge about excess electrons in DNA came from γ -pulse radiolysis studies.^[3] However recent photochemical assays focus on the investigation of ET by chemical means:

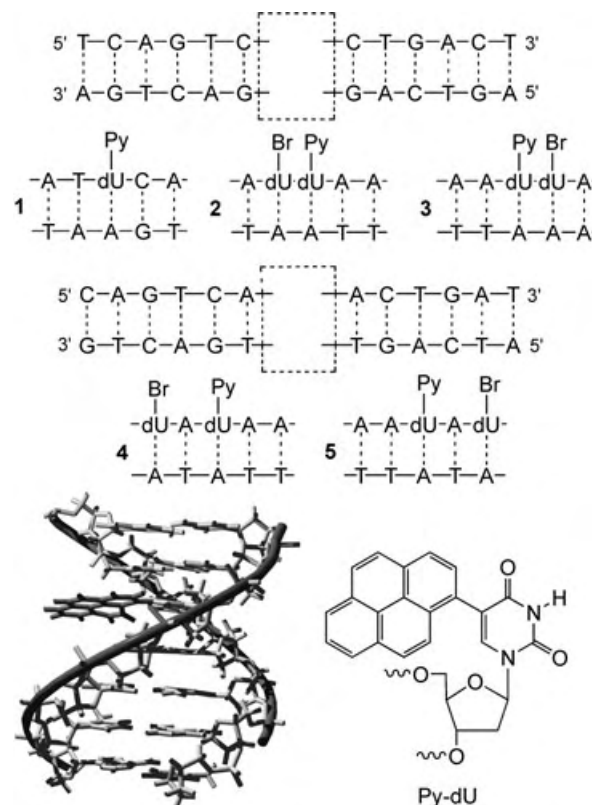
- 1) Carell et al. could show that the amount of T–T dimer cleavage depends rather weakly on the distance to the electron donor.^[4]
- 2) Giese et al. could show that a single injected electron can cleave more than one T–T dimer.^[5]
- 3) Rokita et al. detected a significant base-sequence dependence of the ET efficiency.^[6]

To date, only Lewis et al.^[7] and our groups^[8] have focused on the dynamics of ET processes. In refs. [1,3–8] a thermally activated electron hopping mechanism has been suggested with C^- and T^- as intermediates.^[9] However, we could show that proton transfer interferes with ET indicating that T^- is more likely to play a major role as an electron carrier than C^- .^[10,11]

Over the last years it has become apparent that ET phenomena in DNA cannot be understood without explicitly considering the manifold of conformational states present in DNA.^[12] Since ET rates strongly depend on the microscopic

environment, a single kinetic rate constant might not be observed for DNA-mediated ET but rather a distribution of rates.

Herein, we present our recent efforts to study the mechanism of electron injection and subsequent interbase electron shift by combining ultrafast time-resolved measurements with chemically probed strand-cleavage experiments using 5-bromo-2'-deoxyuridine (Br-dU) as the electron acceptor.^[13] Pyren-1-yl-2'-deoxyuridine (Py-dU)^[14] has been applied as the electron donor, since photoexcited Py^* allows the reduction of C and T.^[15] Using our previously published synthetic procedures, we prepared the Py-dU-modified DNA duplexes **1–5** (Scheme 1).^[8,16] The DNA **1** is a control duplex



Scheme 1. Pyrene-modified DNA duplexes **1–5** and force field (AMBER) minimized structure of a Py-dU-modified DNA duplex (bottom left).

containing only the Py-dU chromophore with adjacent C and T bases as acceptors for the subsequent electron transfer from dU^- . The DNA duplexes **2–5** contain additionally the Br-dU group which is placed either adjacent to Py-dU or separated from Py-dU by one A–T base pair.

We have applied femtosecond broadband pump-probe spectroscopy^[17] to explore the early time ET dynamics in DNAs **1–5** within a broad spectral probing window. Upon excitation at 350 nm, a pyrene-like excited state ($Py-dU^*$) is formed which undergoes ET yielding the contact ion pair (CIP) $Py^{+}-dU^-$. Since the ET process formally represents the injection of an electron into the base stack, the injection rate can be obtained from the decay of the transient

[*] P. Kaden, E. Mayer-Enthart, Dr. H.-A. Wagenknecht
Chemistry Department
Technical University Munich
Lichtenbergstrasse 4, 85747 Garching (Germany)
Fax: (+49) 89-289-13210
E-mail: wagenknecht@ch.tum.de
A. Trifonov, Prof. Dr. T. Fiebig
Eugene F. Merkert Chemistry Center
Boston College
Chestnut Hill, MA 02467 (USA)
Fax: (+1) 617-552-2201
E-mail: fiebig@bc.edu

[**] This work was supported by the Deutsche Forschungsgemeinschaft, the Volkswagen-Stiftung, Boston College, and the Fonds der Chemischen Industrie. P.K., E.M.-E., and H.-A.W. are grateful to Professor Horst Kessler, Technical University of Munich, for the generous support.

Supporting information for this article is available on the WWW under <http://www.angewandte.org> or from the author.

absorption band of (Py-dU)* at 385 nm.^[10b] In the CIP state the radical cation (Py^{•+}) and the radical anion (dU^{•-}) are electronically coupled (as a result of direct π -orbital overlap) and thus exhibit strong spectral features which extend from around 450 to approximately 750 nm. Figure 1 shows repre-

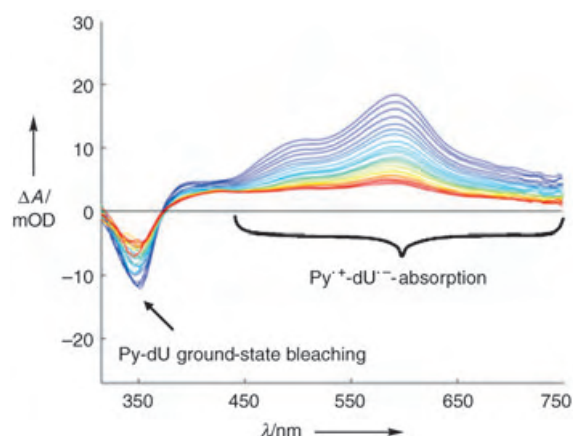


Figure 1. Time-dependent decay of the pump-probe spectra of DNA **1** (350 μ M) in buffer (10 mM Na-P, (P_i = phosphate), 250 mM NaCl, pH 7), in the time range of 150 ps (blue)–1500 ps (red) after excitation at 350 nm.

sentatively the time-dependent decay of the pump-probe spectra of DNA **1** in the time range of 150–1500 ps after excitation. While the rise time of the transient absorption signals in this spectral region is about 2–3 ps (for all five DNA duplexes) the decay times vary from 100 ps to 600 ps depending on the investigated wavelength.^[18] This strong kinetic dispersion in the lifetimes of the CIP state is consistent with multi-conformational states in a highly disordered medium such as DNA.^[12c]

To see whether subsequent ET into the base stack competes with charge recombination in the CIP state we measured the repopulation dynamics of the Py-dU ground state. The observed dynamics are very similar in all duplexes, **1**–**5**. As shown representatively for DNA **3** (Figure 2), the recovery dynamics of the ground state (530 ps (64 %), > 2 ns (36 %) at 364 nm) does not match the lifetime of the electron-injected CIP state (250 ps (55 %), > 2 ns (45 %); rise time 3 ps at 485 nm) thereby suggesting that an additional decay channel (other than charge recombination!) is present from the CIP state. This result suggests that only a fraction of CIP ensembles returns to the ground state and the remaining CIP populations are reacting through a different channel.

To identify the nature of this other channel we probed the reaction product of this multistep DNA-mediated ET process chemically. Br-dU undergoes a chemical modification after its one-electron reduction which can be analyzed by piperidine-induced strand cleavage^[13] and has been applied to quantify the efficiency of DNA-mediated ET processes.^[6,11] Based on reduction potentials, Br-dU is not a significantly better electron acceptor than C or T^[19] and thus very similar lifetimes for the CIP states were measured in DNA **1**–**3** bearing T or Br-dU directly adjacent to the Py-dU group. Hence, Br-dU is a kinetic electron trap (Scheme 2).

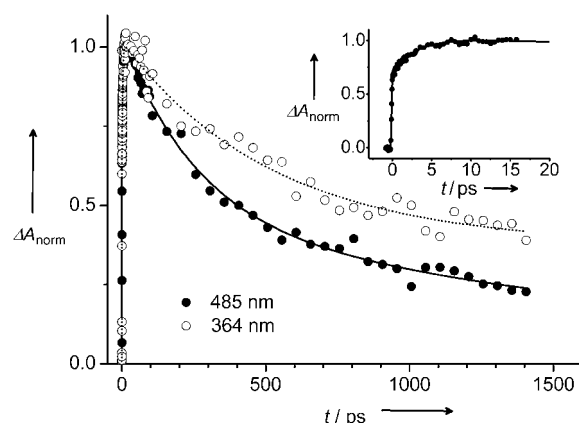
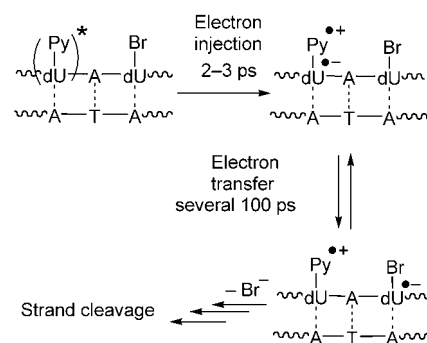


Figure 2. Pump-probe transients of DNA **3** (350 μ M) in buffer (10 mM Na-P, 250 mM NaCl, pH 7) at two different probe wavelengths. The ground-state recovery signal (\circ , 364 nm) is negative but has been inverted to be visually comparable to the (positive) transient absorption of the CIP state (\bullet , 485 nm). The inset displays the 3 ps rise of the 485 nm transient which marks the rate for electron injection.



Scheme 2. Electron injection and ET in Py-dU/Br-dU-modified duplexes.

No strand cleavage has been observed during the irradiation of DNA **1**. This result provides the important control that the observed strand cleavage in the DNA **2**–**5** can be assigned to the presence of Br-dU (Figure 3). DNAs **2** and **3** show much higher cleavage efficiency than **4** and **5**. Thus considering that strand degradation represents the chemical result of the DNA-mediated ET process, it is remarkable that just one intervening A–T base pair lowers the ET efficiency between Py-dU and Br-dU to such an extent. This result indicates that conformational control of ET in DNA becomes more dominant with increasing separations—a result which is entirely consistent with the observed dispersion of CIP lifetimes.

Several important conclusions emerge from this combined study:

- 1) DNA is a flexible medium with a manifold of conformational states exhibiting a wide range of reactivities and rate constants
- 2) As expected, the electron-injection process in our functionalized duplexes show only minor variations arising from structural inhomogeneity because it occurs between the covalently connected Py and dU moieties. Subsequent

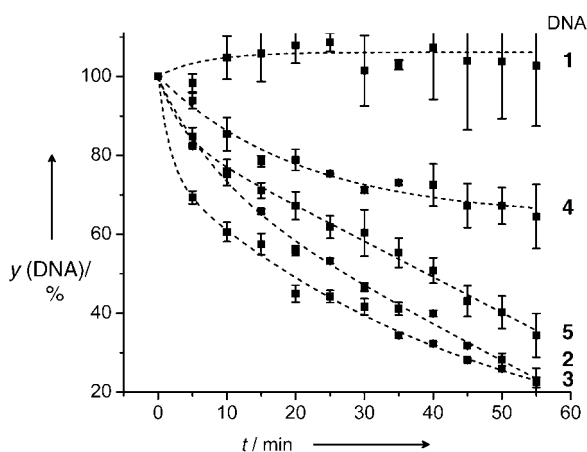


Figure 3. Analysis of the strand-cleavage experiments with DNA duplexes 1–5 (4 μM) in buffer (10 mM Na-P_i, 250 mM NaCl, pH 7). During the irradiation aliquots (30 μL) were collected after every 5 min, subsequently treated with piperidine (3 μL) at elevated temperature (90°C for 30 min), and finally analyzed by HPLC. A 75-W Xe lamp with a cut-off filter (> 305 nm) has been used.

ET into the base stack is much more sensitive to structural parameters and thereby characterized by a distribution of time constants and different strand-cleavage efficiencies

- 3) It is important to probe both the early time events and the product states for obtaining conclusive mechanistic insight. Since DNA-mediated ET is a multistep process on various time scales, the electron-injection rates may not necessarily correlate with the strand degradation as the chemical result of DNA-mediated ET
- 4) The subsequent ET in the base stack occurs on the time scale of several hundred ps, therefore competing with charge recombination in our duplexes. It is reasonable to assume that subsequent migration steps will be faster since the Coulomb interaction between the excess electron and Py^{+} decreases drastically with separation. Hence, our results provide a lower limit for the rate of reductive ET between single bases in DNA.

Received: November 12, 2004

Keywords: DNA · electron transfer · laser spectroscopy · pyrene

- [7] F. D. Lewis, X. Liu, S. E. Miller, R. T. Hayes, M. R. Wasielewski, *J. Am. Chem. Soc.* **2002**, *124*, 11280–11281.
- [8] N. Amann, E. Pandurski, T. Fiebig, H.-A. Wagenknecht, *Chem. Eur. J.* **2002**, *8*, 4877–4883.
- [9] This mechanism was first proposed in: B. Giese, *Annu. Rev. Biochem.* **2002**, *71*, 51–70.
- [10] a) R. Huber, T. Fiebig, H.-A. Wagenknecht, *Chem. Commun.* **2003**, 1878–1879; b) M. Raytchev, E. Mayer, N. Amann, H.-A. Wagenknecht, T. Fiebig, *ChemPhysChem* **2004**, *5*, 706–712.
- [11] C. Wagner, H.-A. Wagenknecht, *Chem. Eur. J.* **2005**, *11*, 1871–1876.
- [12] a) C. Wan, T. Fiebig, S. O. Kelley, C. R. Treadway, J. K. Barton, A. H. Zewail, *Proc. Natl. Acad. Sci. USA* **1999**, *96*, 6014–6019; b) Y. A. Berlin, A. L. Burin, L. D. A. Siebbeles, M. A. Ratner, *J. Phys. Chem. A* **2001**, *105*, 5666–5678; c) T. Renger, R. A. Marcus, *J. Phys. Chem. A* **2003**, *107*, 8404–8419; d) M. A. O'Neill, H. C. Becker, C. Z. Wan, J. K. Barton, A. H. Zewail, *Angew. Chem.* **2003**, *115*, 1676–1680; *Angew. Chem. Int. Ed.* **2003**, *42*, 5896–5900; e) M. A. O'Neill, J. K. Barton, *J. Am. Chem. Soc.* **2004**, *126*, 11471–11483; f) M. A. O'Neill, J. K. Barton, *J. Am. Chem. Soc.* **2004**, *126*, 13234–13235.
- [13] a) E. Rivera, R. H. Schuler, *J. Phys. Chem.* **1983**, *87*, 3966–3971; b) H. Sugiyama, Y. Tsutsumi, I. Saito, *J. Am. Chem. Soc.* **1990**, *112*, 6720–6721; c) G. P. Cook, M. M. Greenberg, *J. Am. Chem. Soc.* **1996**, *118*, 10025–10030; d) R. Tashiro, H. Sugiyama, *J. Am. Chem. Soc.* **2003**, *125*, 15282–15283.
- [14] T. L. Netzel, M. Zhao, K. Nafisi, J. Headrick, M. S. Sigman, B. E. Eaton, *J. Am. Chem. Soc.* **1995**, *117*, 9119–9128.
- [15] $E(\text{Py}^{+}/\text{Py}) = 1.5$ V (vs. normal hydrogen electrode (NHE)) and $E_{00} = 3.25$ eV, see: T. Kubota, K. Kano, T. Konse, *Bull. Chem. Soc. Jpn.* **1987**, *60*, 3865–3877; gives $E(\text{Py}^{+}/\text{Py}^{*}) = 1.85$ V; for reduction potentials of C and T see: S. Steenken, J. P. Telo, H. M. Novais, L. P. Candeias, *J. Am. Chem. Soc.* **1992**, *114*, 4701–4709.
- [16] E. Mayer, L. Valis, R. Huber, N. Amann, H.-A. Wagenknecht, *Synthesis* **2003**, 2335–2340.
- [17] The laser setup has been described elsewhere: M. Raytchev, E. Pandurski, I. Buchvarov, C. Modrakowski, T. Fiebig, *J. Phys. Chem. A* **2003**, *107*, 4592–4600.
- [18] The decay of the $\text{Py}^{+}\text{dU}^{-}$ transient absorption signals between 440 nm and 600 nm were adequately described using biexponential fit functions. In addition to the picosecond decay component there is a long time component (ca. 3 ns) which accounts for 20–40% of the decay, depending on the wavelength employed.
- [19] The reduction potential is only 0.06 eV lower than that of T, see ref. [18] in ref. [7]: V. P. Kadysh, Y. L. Kaminskii, L. N. Rumyantseva, V. L. Efimova, J. P. Strandish, *Khim. Geterotsikl. Soedin.* **1992**, *10*, 1404–1408.

- [1] Review: H.-A. Wagenknecht, *Angew. Chem.* **2003**, *115*, 2558–2565; *Angew. Chem. Int. Ed.* **2003**, *42*, 2454–2460.
- [2] See reviews in: *Top. Curr. Chem.* **2004**, 236 and 237 (whole issues).
- [3] Review: Z. Cai, M. D. Sevilla, *Top. Curr. Chem.* **2004**, 237, 103–128.
- [4] C. Haas, K. Kräling, M. Cichon, N. Rahe, T. Carell, *Angew. Chem.* **2004**, *116*, 1878–1880; *Angew. Chem. Int. Ed.* **2004**, *43*, 1842–1844.
- [5] B. Giese, B. Carl, T. Carl, T. Carell, C. Behrens, U. Hennecke, O. Schiemann, E. Feresin, *Angew. Chem.* **2004**, *116*, 1884–1887; *Angew. Chem. Int. Ed.* **2004**, *43*, 1848–1851.
- [6] Most recently: T. Ito, S. E. Rokita, *Angew. Chem.* **2004**, *116*, 1875–1878; *Angew. Chem. Int. Ed.* **2004**, *43*, 1839–1842.

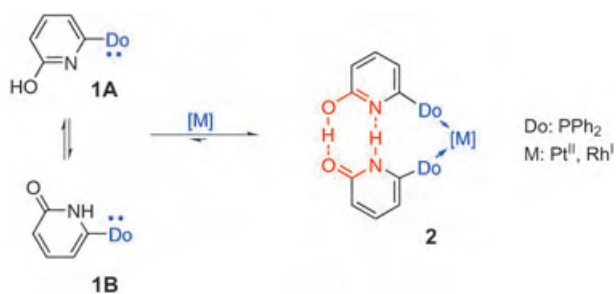
Self-Assembly of Bidentate Ligands for Combinatorial Homogeneous Catalysis Based on an A–T Base-Pair Model**

Bernhard Breit* and Wolfgang Seiche

Selectivity control in homogeneous metal complex catalysis relies in many cases on tailor-made bidentate ligands. The quest for the ultimate ligand which gives a catalyst with optimal activity and selectivity is difficult. Since rational design still does not allow the ligand of choice for a given reaction and substrate to be predicted, the combinatorial synthesis of ligand libraries and their subsequent use has become an additional strategy.^[1] However, the rate-determining step in catalyst development is in most cases the time-consuming ligand synthesis required to generate the library.

Herein we report an alternative approach to generate bidentate ligand libraries that relies on a self-assembly of bidentate ligands from monodentate ligands and is based on hydrogen-bonding. From a 4×4 library of self-assembling ligands a catalyst that shows optimal activity and regioselectivity for the hydroformylation of terminal alkenes could be identified.

We recently showed that 6-DPPon (**1**) self-assembles through hydrogen bonding of the hydroxypyridine **1A** with its pyridone tautomer **1B** in the coordination sphere of a late-transition-metal center, such as platinum(II) or rhodium(I) (Scheme 1). Compound **1** displays the typical behavior of a



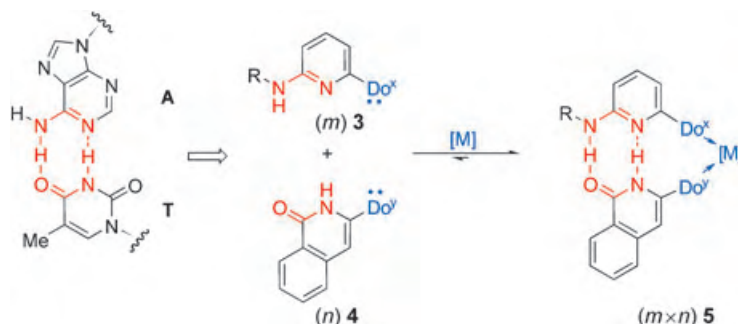
Scheme 1. Self-assembly through hydrogen bonding of the 2-pyridone/2-hydroxypyridine system **1** to generate bidentate ligand metal complexes **2** for homogeneous catalysis.

[*] Prof. Dr. B. Breit, Dipl.-Chem. W. Seiche
Institut für Organische Chemie und Biochemie
Albert-Ludwigs-Universität Freiburg
Albertstrasse 21, 79104 Freiburg (Germany)
Fax: (+49) 761-203-8715
E-mail: bernhard.breit@organik.chemie.uni-freiburg.de

[**] This work was supported by the Fonds der Chemischen Industrie, the Alfred Krupp Award for young university teachers of the Krupp foundation (to B.B.), and BASF. We thank Dr. M. Keller for the X-ray crystal structure analysis and N. Stöck and G. Leonhardt-Lutterbeck for technical assistance.

bidentate ligand, as exemplified in a highly regioselective hydroformylation of *n*-alkenes into linear aldehydes.^[2]

A potential advantage of this self-assembly approach is the possibility to form libraries of heterodimeric bidentate ligands (Scheme 2). Combining *m* different ligands equipped with donor functions Do^x with *n* different ligands equipped with donor functions Do^y should result in the formation of a set of *m* × *n* different bidentate ligands without the need for additional synthetic steps.^[3]

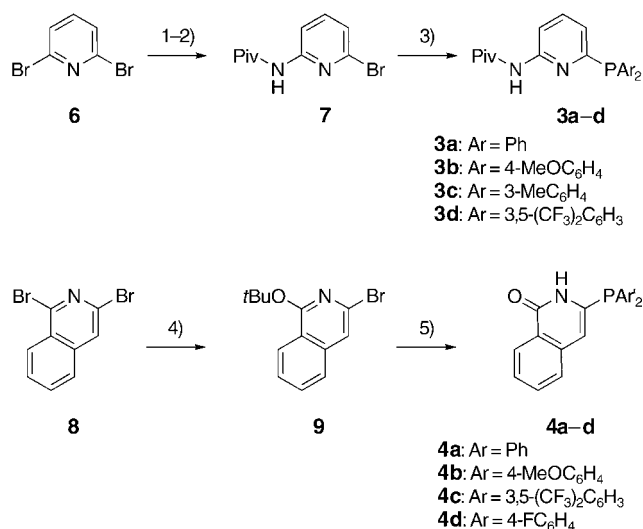


Scheme 2. An AT base-pair model (highlighted in red) as a platform for the self-assembly of monomeric to mixed bidentate ligands.

Unfortunately, this goal cannot be reached relying on the tautomeric pyridone/hydroxypyridine platform, since mixing of two pyridones with different donor functions results in a statistical mixture of the heterodimeric and the two homodimeric ligands.^[4] Our goal was to ensure the formation of single defined catalysts based on heterodimeric bidentate ligands, since this is a prerequisite for the delineation of structure–activity and structure–selectivity relations. Hence, a new template that assembles in a well-defined complementary mode giving exclusively heterodimers was required.

In fact, self-assembly of two complementary species through hydrogen bonding is possible with high precision as exemplified by DNA base pairing, for example, between adenine and thymine (Scheme 2). The physical basis for this specific complementary heterodimerization process relies on the inherent “fixation” of the adenine base as the lactim tautomeric form, and the thymine base as the lactam tautomeric form.^[5] As a model system emulating these properties of the AT base pair the aminopyridine **3**/isoquinolone **4** system was selected. Thus 2-aminopyridines exist in the lactim form^[6] whereas the isoquinolone system strongly prefers the lactam tautomeric form.^[7] As a consequence, homodimer formation similar to the 6-DPPon system should be suppressed leaving heterodimer formation (→**5**) as the exclusive alternative.

Synthesis of the phosphine functionalized aminopyridine derivatives **3a–d** is readily accomplished starting from 2,6-dibromopyridine (Scheme 3). Reaction with aqueous ammonia and protection of the amino function as the pivaloate gave pyridine **7**. The introduction of the pivaloate (Piv) protecting group proved to be beneficial for clean bromine–lithium exchange with *n*BuLi in THF at –100 °C. Diversification was achieved by trapping the thus generated lithiopyridine with



Scheme 3. Synthesis of monodentate aminopyridinyl phosphines **3** and isoquinolones **4**: 1) NH_4OH , 190°C , 5 h; 2) pivaloylchloride, NEt_3 , CH_2Cl_2 , $0^\circ\text{C} \rightarrow \text{RT}$; 3) $n\text{-BuLi}$ (2 equiv), THF, -100°C , then ClPR_2 , $-100^\circ\text{C} \rightarrow \text{RT}$; 4) KOtBu (1.1 equiv), toluene, 80°C , 1 h; 5) $n\text{-BuLi}$ (1 equiv), THF, -100°C , then ClPR_2 , $-100^\circ\text{C} \rightarrow \text{RT}$, then H_2O (1 equiv) and formic acid excess (50–75 %).

different chlorophosphines to furnish the aminopyridine type ligand set **3a–d**.

The complementary isoquinolone system **4** was obtained starting from 1,3-dibromoisoquinoline (**8**).^[8] Nucleophilic introduction of a *tert*-butoxy substituent gave bromide **9** which underwent clean bromine–lithium exchange with $n\text{BuLi}$. Trapping of the resulting lithioisoquinoline with the chlorophosphines furnished the isoquinolone ligands **4a–d**.

Mixing of one equivalent of 6-diphenylphosphino-*N*-pivaloyl-2-aminopyridine (6-DPPAP; **3a**) with one equivalent of 3-diphenylphosphinoisoquinolone (3-DPPICon; **4a**) in the presence of $[\text{PtCl}_2(1,5\text{-cod})]$ (cod = cyclooctadienyl) gave the heteroleptic *cis*-complex **5aa**- PtCl_2 in quantitative yield. From the X-ray crystal structure^[9] of **5aa**- PtCl_2 (Figure 1) it is clear that the two *cis*-coordinated phosphine ligands form the expected hydrogen-bonding network reminiscent of the Watson Crick base pairing of A and T in DNA.

NMR spectra indicate that a similar structure is found in aprotic solvents, such as CDCl_3 . The ^{31}P NMR spectrum shows an AB system with a typical $^2J(\text{P,P})$ coupling of 13 Hz which confirms the presence of two non-equivalent phosphine ligands coordinated to the same platinum center.^[10] Furthermore, the size of the $^1J(\text{P,Pt})$ coupling (3658 and 3484 Hz) is in the order expected for a *cis*-platinum(II) diphosphine complex (Figure 2).^[11] Additionally, ^1H NOE experiments in CDCl_3 show a distinct NOE between the amide NH of the pyridine ligand and the NH function of the isoquinolone unit. This result suggests that hydrogen bonding occurs in solution (CDCl_3) as well.

To explore whether the heterodimeric chelate bonding mode that results through hydrogen-bonding of the **3/4** system is operative throughout a catalytic reaction, the rhodium-catalyzed hydroformylation of terminal alkenes was chosen as

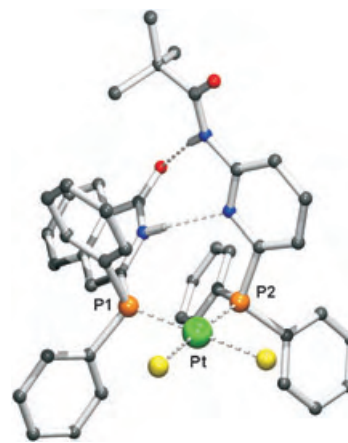


Figure 1. PLATON plot of the structure of *cis*-**5aa**- PtCl_2 in the solid state (H atoms bound to carbon are omitted for clarity). Selected interatomic distances [Å] and angles [°]: Pt-P1 2.2486(5), Pt-P2 2.2437(5), $\text{NH}\cdots\text{N}$ 2.932(2), $\text{O}\cdots\text{HN}$ 2.977(2); P1-Pt-P2 102.896(18), $\text{N-H}\cdots\text{N}$ 163(2), $\text{O}\cdots\text{H-N}$ 172(2). Green Pt, yellow Cl, orange P, blue N, red O.

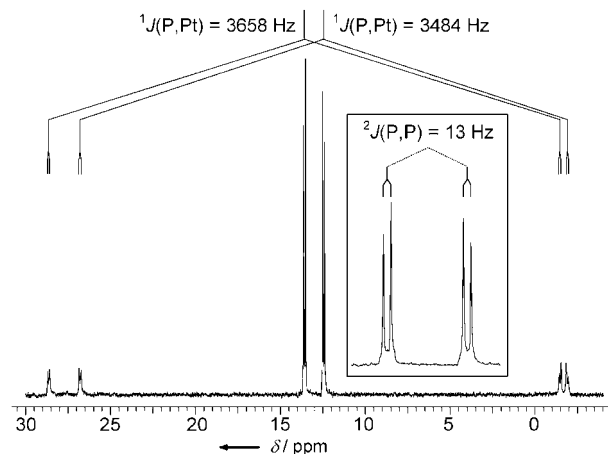


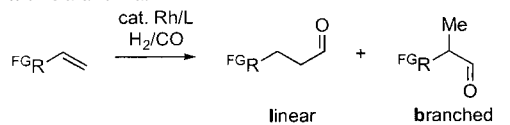
Figure 2. ^{31}P NMR spectrum of **5aa**- PtCl_2 in CDCl_3 solution.

a test reaction (see Table 1). A strong chelate effect on the regioselectivity of this reaction is well established.^[12]

Both monodentate ligands, the aminopyridine **3a** as well as the isoquinolone **4a**, furnished active rhodium catalysts for the hydroformylation of 1-octene (Table 1, entries 1 and 2). However, as expected for a monodentate phosphine ligand, regioselectivity for the linear aldehyde was rather low.^[2,13] On mixing ligands **3a** and **4a**, hydroformylation occurred with a significantly increased regioselectivity for the linear aldehyde (entries 3–6). This result indicates that the heterodimeric **3a/4a** ligand system operates as a bidentate ligand **5aa**, which is held together by hydrogen bonding, in the active rhodium catalyst.

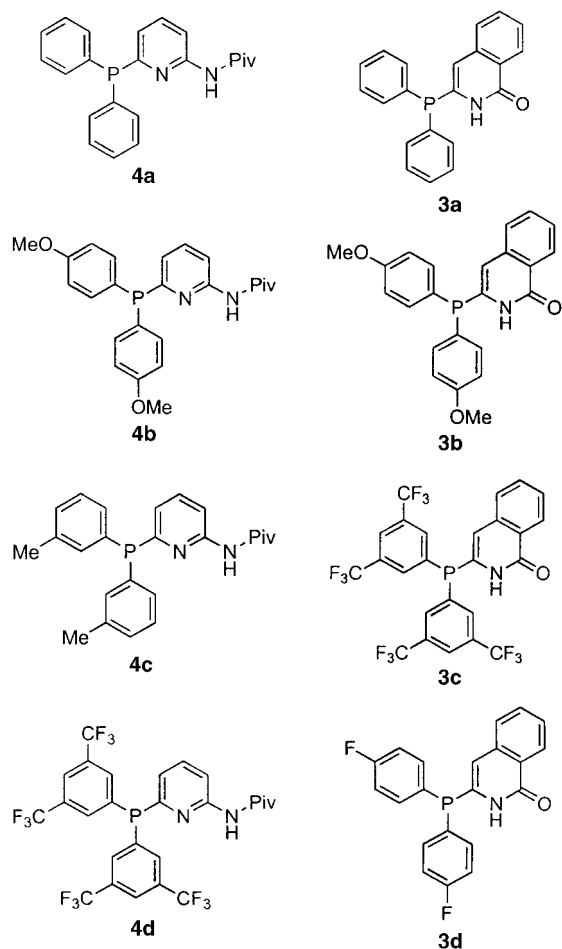
Hence, the stage was set for the generation of the first self-assembled bidentate-ligand library based on hydrogen bonding to identify a catalyst that operates with optimal activity and regioselectivity.

Table 1: Results of rhodium-catalyzed hydroformylation of terminal alkenes with **3a** and **4a**.



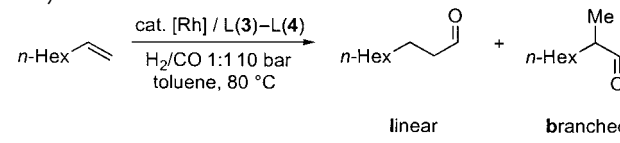
Entry ^[a]	Ligand	FGR	l:b ^[b]	Conversion ^[b]
1	3a	CH ₃ (CH ₂) ₅	72:28	quant.
2	4a	CH ₃ (CH ₂) ₅	76:24	quant.
3	3a + 4a	CH ₃ (CH ₂) ₅	94:6	quant.
4	3a + 4a	HO(CH ₂) ₉	95:5	quant.
5	3a + 4a	MeO ₂ C(CH ₂) ₈	94:6	quant.
6	3a + 4a	AcO(CH ₂) ₄	93:7	quant.

[a] Conditions: [Rh(CO)₂(acac)] : ligand : substrate 1:20:1000, 10 bar CO/H₂ (1:1), toluene (*c*₀(alkene) = 0.7 M), 70 °C, 20 h. [b] Linear versus branched (l:b). Determined by GC analysis and or ¹H NMR spectroscopy.



From four aminopyridyl phosphines **3a–d** and four phosphinoisoquinolone **4a–d** a set of 16 bidentate-ligand combinations was generated by simple mixing of the components with the catalyst precursor [Rh(CO)₂(acac)] (acac = 2,4-pentanedione). The resulting catalysts were explored with respect to their potential to catalyze the hydroformylation of 1-octene. Table 2 summarizes the results of these experiments. Some noteworthy trends are apparent. First, phosphine-substituent modification of the aminopyridines

Table 2: 4 × 4 ligand matrix of aminopyridine (**3a–d**)/isoquinolone (**4a–d**) derived self-assembled bidentate ligands in the [Rh]-catalyzed hydroformylation of 1-octene.^[a]



L(4)	L(3)			
	3a	3b	3c	3d
4a	2425 h ⁻¹ ^[b] 94:6 ^[c]	1040 h ⁻¹ 94:6	2732 h ⁻¹ 96:4	2559 h ⁻¹ 95:5
4b	2033 h ⁻¹ 93:7	1058 h ⁻¹ 92:8	1281 h ⁻¹ 96:4	1772 h ⁻¹ 94:6
4c	3537 h ⁻¹ 94:6	1842 h ⁻¹ 93:7	1808 h ⁻¹ 96:4	2287 h ⁻¹ 94:6
4d	7439 h ⁻¹ 96:4	2695 h ⁻¹ 95:5	7465 h ⁻¹ 94:6	8643 h⁻¹ 96:4

[a] Reaction conditions: [Rh(CO)₂(acac)], [Rh]:L(**3**):L(**4**):1-octene = 1:10:10:7500, 10 bar CO/H₂ (1:1), toluene (*c*₀(1-octene) = 2.91 M), 5 h. Catalyst preformation: 5 bar CO/H₂ 1:1, 30 min, RT → 80 °C. [b] Turnover frequency (TOF) was calculated as (mol aldehydes) × (mol catalyst)⁻¹ × (t h⁻¹)⁻¹ at 20–30% conversion, determined by GC analysis. [c] Regioselectivity: linear to branched determined by GC analysis. The best TOF and regioselectivity are highlighted in bold.

3a–d had the greatest impact on catalyst performance. Second, the increasing donor capability of the phosphine donors of both **3** and **4** decreased catalyst activity; correspondingly, acceptor substituents at the phosphine donors increased the catalyst activity. The most active catalyst was the **3d/4d** combination. For this catalyst a turnover frequency of 8653 h⁻¹ was noted which is exceptional for a bidentate phosphine/rhodium catalyst.^[14] Furthermore, an excellent regioselectivity of 96:4 in favor of *n*-nonanal was observed.

In conclusion, the first bidentate-phosphine-ligand library for homogeneous metal-complex catalysis, based on self-assembly through hydrogen bonding was realized. The basis for the success of this concept was the use of an AT base-pair analogous system—the aminopyridine **3**/isoquinolone **4** system. The heterodimeric ligands based on this system operate as bidentate ligands throughout the hydroformylation of terminal alkenes. From a 4 × 4 library generated by self-assembly a catalyst operating with outstanding activity and regioselectivity upon hydroformylation of terminal alkenes was identified. Application of this general principle and related libraries to asymmetric catalysis is a logical step.

Received: November 2, 2004

Published online: February 9, 2005

Keywords: combinatorial chemistry · homogeneous catalysis · hydroformylation · rhodium · self-assembly

- [1] C. Gennari, U. Piarulli, *Chem. Rev.* **2003**, 103, 3071–3100.
- [2] B. Breit, W. Seiche, *J. Am. Chem. Soc.* **2003**, 125, 6608–6609.
- [3] For alternative approaches to ligand/catalyst libraries through self-assembly see: J. M. Takacs, D. S. Reddy, S. A. Moteki, D. Wu, H. Palencia, *J. Am. Chem. Soc.* **2004**, 126, 4494–4495; V. F. Slagt, M. Röder, P. C. J. Kamer, P. W. N. M. van Leeuwen,

- J. N. H. Reek, *J. Am. Chem. Soc.* **2004**, *126*, 4056–4057; V. F. Slagt, P. W. N. M. van Leeuwen, J. N. H. Reek, *Angew. Chem.* **2003**, *115*, 5777–5781; *Angew. Chem. Int. Ed.* **2003**, *42*, 5619–5623; V. F. Slagt, P. W. N. M. van Leeuwen, J. N. H. Reek, *Chem. Commun.* **2003**, 2474–2475; K. Ding, H. Du, Y. Yuan, J. Long, *Chem. Eur. J.* **2004**, *10*, 2872–2884.
- [4] M. T. Reetz, T. Sell, A. Meiswinkel, G. Mehler, *Angew. Chem.* **2003**, *115*, 814–817; *Angew. Chem. Int. Ed.* **2003**, *42*, 790–793.
- [5] J. D. Watson, F. H. C. Crick, *Nature* **1953**, *171*, 964–967; M. D. Topal, J. R. Fresco, *Nature* **1976**, *263*, 285–289.
- [6] H. I. Abdulla, M. F. El-Bermani, *Spectrochim. Acta Part A* **2001**, *57*, 2659–2672.
- [7] G. Pfister-Guillouzo, C. Guimon, J. Frank, J. Ellison, A. R. Katritzky, *Liebigs Ann. Chem.* **1981**, 366–375.
- [8] A. R. Osborn, K. Schofield, L. N. Short, *J. Chem. Soc.* **1956**, 4191–4206.
- [9] CCDC-254720 contains the supplementary crystallographic data for this paper. These data can be obtained free of charge from the Cambridge Crystallographic Data Centre via www.ccdc.cam.ac.uk/data_request/cif. Crystal data for **5aa**-PtCl₂C₄₇H₄₉Cl₂N₃O₃P₂Pt; *M*_r = 1031.82; *T* = 100(2) K; λ = 0.71073 Å; crystal system: triclinic; space group: *P* $\bar{1}$; *a* = 11.4445(2), *b* = 12.6925(3), *c* = 16.1777(3) Å, α = 92.8636(12), β = 95.4611(11), γ = 109.5054(10)°; *V* = 2196.66(8) Å³; *Z* = 2; ρ_{calcd} = 1.560 Mg m^{−3}; absorption coefficient: 3.433 mm^{−1}; *F*(000) = 1036; crystal size: 0.3 × 0.2 × 0.1 mm; θ range for data collection: 1.71–27.49°; limiting indices: $-14 \leq h \leq 14$, $-16 \leq k \leq 16$, $-20 \leq l \leq 21$; 25457 reflections collected, 10036 reflections unique (*R*_{int} = 0.0312); completeness to θ = 25.00°: 99.9%; absorption correction: semi-empirical from equivalents; max. and min. transmission: 0.711 and 0.640; refinement method: full-matrix least-squares on *F*²; data/restraints/parameters: 10036/0/536; GoF on *F*²: 1.076; final *R* indices [*I* > 2 σ (*I*)]: *R*1 = 0.0207, *wR*2 = 0.0467; *R* indices (all data): *R*1 = 0.0239, *wR*2 = 0.0477; largest diff. peak and hole: 0.919 and −1.430 e Å^{−3}.
- [10] “³¹P and ¹³C NMR of Transition Metal Phosphine Complexes”: P. S. Pregosin, R. W. Kunz in *NMR Basic Principles and Progress*, Vol. 16 (Eds.: P. Diehl, E. Fluck, R. Kosfeld), Springer, Heidelberg, **1979**, pp. 115–122, and references therein; P. S. Pregosin, S. N. Sze, *Helv. Chim. Acta* **1978**, *61*, 1848–1855.
- [11] see “³¹P and ¹³C NMR of Transition Metal Phosphine Complexes”: P. S. Pregosin, R. W. Kunz in *NMR Basic Principles and Progress*, Vol. 16 (Eds.: P. Diehl, E. Fluck, R. Kosfeld), Springer, Heidelberg, **1979**, pp. 94–95; H. G. Alt, R. Baumgartner, H. A. Brune, *Chem. Ber.* **1986**, *119*, 1694–1703.
- [12] P. W. N. M. van Leeuwen, C. P. Casey, G. T. Whiteker in *Rhodium Catalyzed Hydroformylation* (Eds.: P. W. N. M. van Leeuwen, C. Claver), Kluwer Academic Publishers, Dordrecht, **2000**, chap. 4, pp. 76–105.
- [13] see P. W. N. M. van Leeuwen, C. P. Casey, G. T. Whiteker in *Rhodium Catalyzed Hydroformylation* (Eds.: P. W. N. M. van Leeuwen, C. Claver), Kluwer Academic Publishers, Dordrecht, **2000**, chap. 4, pp. 63–75; B. Breit, W. Seiche, *Synthesis* **2001**, 1–36.
- [14] Under identical conditions Rh/triphenylphosphine (TOF: 1312 h^{−1}, 76:24), Rh/6-DPPon (**1**; TOF: 3284 h^{−1}, 98:2), for *t*Bu-Xanthphos see ref. [2]. See also ref. [12].

Derivatives of the Simplest Polyhedral Carborane Anion: Structures at the Borderline between Two- and Three-Dimensional Aromatic Compounds**

Yüksel Sahin, Carsten Präsang, Matthias Hofmann,
Gertraud Geiseler, Werner Massa, and Armin Berndt*

Dedicated to Professor Paul von Ragué Schleyer
on the occasion of his 75th birthday

Salts of tertiary alkyl cations were recently described to be stable with carborane anions.^[1] The latter represent impressive examples of the unusual properties of three-dimensional aromatics.^[2] Characteristic for these is an increase of their aromatic stabilization energies per center with the number of framework atoms, that is also with the number of delocalized σ electrons, as shown by computations by Schleyer and Najafian.^[2] As a result, the smallest representatives of a homologous series of *three-dimensional* aromatics are the least stabilized, that is, “the weakest”. In contrast, for the *two-dimensional* aromatics, the smallest members of the series with $(4n+2)$ π electrons, that is those with the lowest number of delocalized π electrons, are “the strongest”: Two-electron ($2e$) aromatics have significantly higher aromatic stabilization energies—particularly per center—than comparable six-electron aromatics.^[3] Along the homologous series of anions $CB_nH_{n+1}^-$,^[2,4] which includes the three-dimensional aromatics **1** and **2** (Scheme 1) as well as the puckered and planar two-dimensional $2e$ aromatics **3** and **4**,^[5,6] the most weakly stabilized aromatics of one group are next to the most strongly stabilized aromatics of the other group.

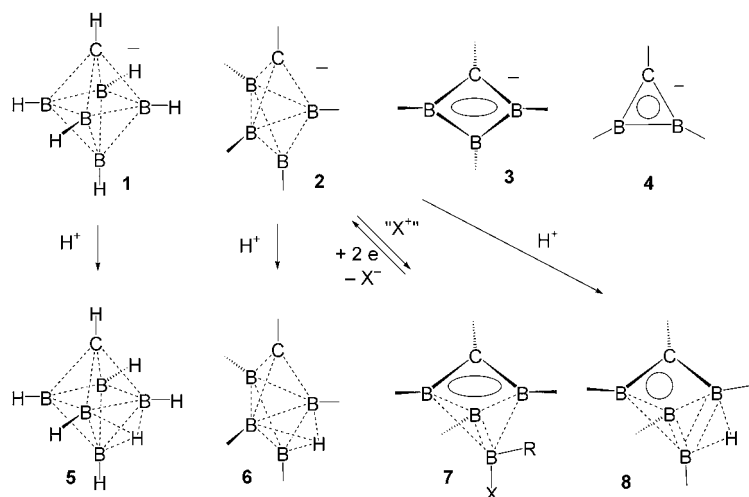
Here we report on **2a** (Scheme 2), the first derivative of the smallest anionic three-dimensional aromatic. Furthermore we describe two protonation products of **2a**, namely, **6a** and **8a**. Computations^[7] on model compounds show that the three-dimensional aromatic character—retained upon protonation of **1** and higher homologues (to give **5** and its higher homologues)^[8,9]—is lost upon protonation of anions **2**, the

[*] Dr. Y. Sahin,^[†] Dr. C. Präsang, G. Geiseler, Prof. Dr. W. Massa,
Prof. Dr. A. Berndt
Fachbereich Chemie
Universität Marburg
35032 Marburg (Germany)
Fax: (+49) 6421-282-8917
E-mail: berndt@chemie.uni-marburg.de

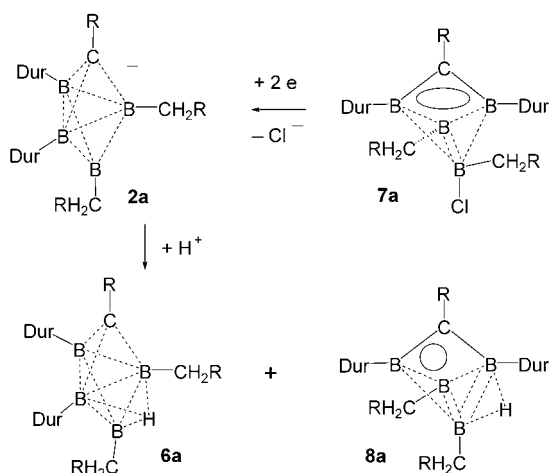
Dr. M. Hofmann
Anorganisch-Chemisches Institut
Universität Heidelberg
Im Neuenheimer Feld 270, 69120 Heidelberg (Germany)

[†] Current address:
Adnan Menderes University
Faculty of Science and Arts
Department of Chemistry
09010 Aydin (Turkey)

[**] This work was supported by the Deutsche Forschungsgemeinschaft and the Fonds der Chemischen Industrie.



Scheme 1. The carborane anion **1** and its protonated form **5**, as well as the frameworks of the smaller anions $\text{CB}_n\text{H}_{n+1}^-$ and molecules $\text{CB}_n\text{H}_{n+2}$. In the case of **7**, R may not be an H atom. The circle and the ellipsoids symbolize two cyclic delocalized electrons, dashed lines indicate multicenter bonds and, in **7** and **8**, 3c-2e σ bonds.



Scheme 2. Synthesis of the three-dimensional aromatic **2a** from the puckered 2e aromatic **7a**, and protonation of **2a** to **6a** and **8a**. Dur = 2,3,5,6-tetramethylphenyl, R = SiMe₃.

weakest three-dimensional aromatics of this series. Molecules of type **8** are two-dimensional 2e aromatics,^[10] and those of type **6** only exist in the crystal, that is, with additional stabilization by a polar medium.

The lithium salt of anion **2a** forms upon treatment of **7a**^[11] with lithium in diethyl ether at -10°C . The reaction of **2a** with $\text{HBF}_4\cdot\text{OME}_2$ provides the isomeric protonation products **6a** and **8a**, which surprisingly coexist in the crystal.

Figure 1 shows the structures of anion **2a**, as determined with a crystal of the potassium salt $[\text{K}(\text{dme})_4]\cdot\text{2a}^{[12]}$ as well as those of **6a** and **8a**.^[13] Selected structural data of these molecules as well as of **7a** are given in Table 1 along with the corresponding values computed for the model compounds **8b** and **8u** (Scheme 3).

As predicted for the prototype **2u**,^[2] compound **2a** is a trigonal bipyramid with an apical C atom. The bond lengths in

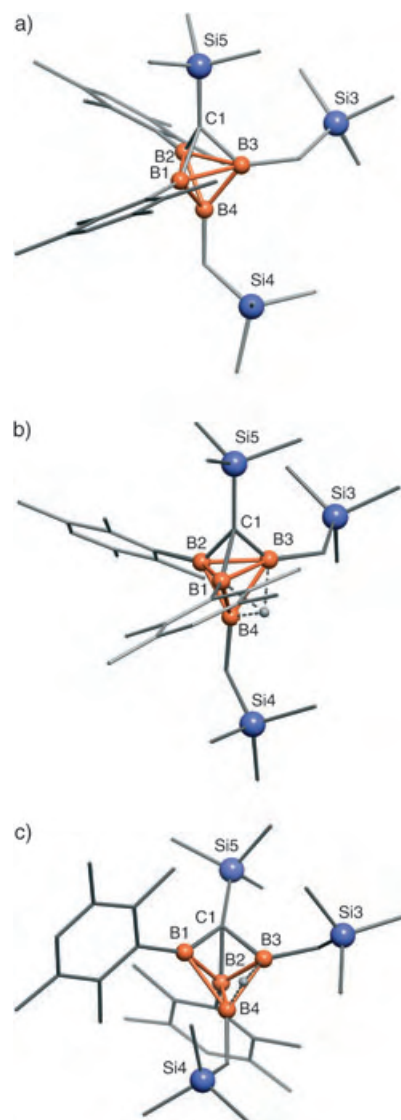
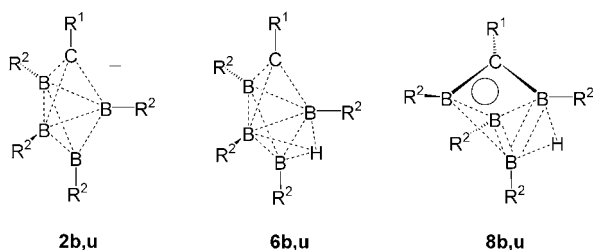


Figure 1. Structures of anion **2a** (a) as well as of **6a** (b) and **8a** (c) in the crystal. For clarity only the boron-bound H atoms are shown

Table 1: Selected distances [pm] and angles $^\circ$ for **2a** and **6a–8a** (determined experimentally) as well as for **8b** and **8u** (computed at the B3LYP/6-31G* level). Remarkable values are printed in italics.

	2a	6a	7a	8a	8b	8u
C1–B1	158.7(3)	156.1(3)	150.2(3)	148.6(3)	149.5	148.0
C1–B2	156.9(3)	158.9(3)	174.5(3)	163.6(3)	159.8	156.4
C1–B3	158.0(3)	153.9(3)	149.4(3)	160.9(3)	160.6	161.2
B1–B2	183.7(3)	179.7(3)	173.9(3)	180.6(3)	179.8	181.4
B2–B3	185.1(3)	179.5(3)	173.3(3)	175.9(3)	175.9	174.6
B1–B3	184.3(3)	208.9(3)	238.9(3)	218.8(3)	215.4	206.7
B1–B4	165.9(3)	180.0(3)	207.8(3)	198.0(3)	191.3	184.5
B2–B4	168.6(3)	166.0(3)	169.4(3)	163.6(3)	164.8	165.5
B3–B4	167.2(3)	183.4(3)	220.7(3)	175.9(3)	174.2	170.8
B1–B2–C1–B3	75.7(2)	91.8(2)	124.7(2)	99.1(2)	96.3	90.4

the framework of **2a** are in good agreement with the values computed for the model compounds (**2u**, **2b**: C–B 155.6, 157.4, B–B(basal, basal) 183.6, 184.4, B–B(basal, apical) each



Scheme 3. Molecules **2b,u**, **6b,u**, and **8b,u** computed for comparison. (b: $R^1 = \text{SiH}_3$, $R^2 = \text{CH}_3$; u: $R^1 = R^2 = \text{H}$).

166.7 pm). Substituents have only a small influence on the distances within the framework of the three-dimensional aromatics.^[14,15]

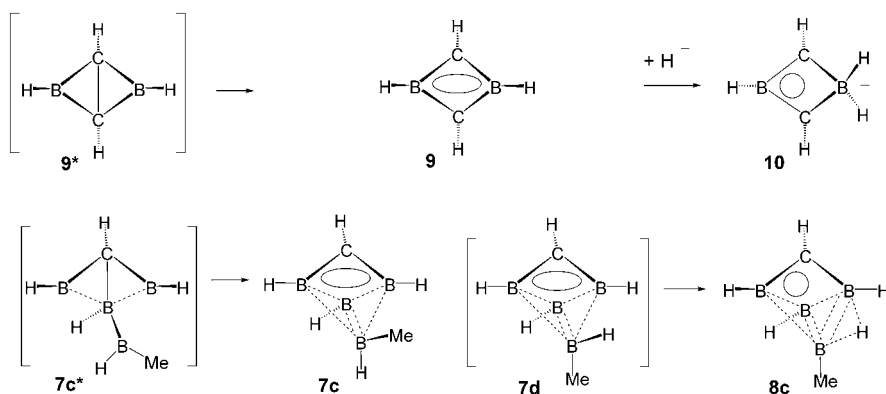
Compound **6a** derives from **2a**—just as **5**^[8] derives from **1**—by protonation of a B_3 face. The B1-B3 distance in **6a** is elongated as compared to that in **2a** by 10 pm more than in **5** with respect to **1**. However, according to calculations, the C_s -symmetrical model compounds **6u** and **6b** are transition states with energies that are very close to those of the edge-protonated minima **8u** and **8b** (0.5 and 0.0 kcal mol⁻¹, respectively). Compound **6a** exists in the crystal due to its dipole moment, which provides additional stabilization in the polar environment of the crystal.^[16] We conclude this from the free enthalpies of solvation ΔG_{solv} calculated with water as solvent.^[7] The ΔG_{solv} values are larger for **6u** and **6b** than for **8u** and **8b** (−3.1 and −9.7 compared to −0.6 and −4.5 kcal mol⁻¹).

Compound **8a** differs from **7a** mainly in the periphery: replacement of a chloride ion by a hydride ion, an additional BHB bridge, and a different substitution pattern for the boron atoms of the CB_3 ring.^[17] Similarities predominate in the framework: Remarkably short and long distances (given in italics in Table 1) are found in the framework between corresponding centers: C1-B1 in **8a** is 148.6 pm and thus relatively short, as are C1-B1,3 in **7a** (149.4, 150.2 pm). Bond lengths B1-B3 and B1-B4 in **8a** are fairly long in comparison to those in **2a** and thus are more similar to those in **7a**. The strong dependence of the elongation of the framework distances on the substituents is also striking, a feature that was not observed for the three-dimensional aromatics **2**.

To analyze the similar bond lengths in the frameworks of **7a** and **8a**, we carried out DFT calculations^[7] and NBO analyses.^[18] These showed that the initial formulation^[11] of a boryltriborabicyclobutane with an open three-center, two-electron (3c-2e) bond between the framework boron atoms does not sufficiently describe the electronic structure of **7a**. As early as 1986, through the use of isodesmic equations, Schleyer et al. demonstrated that the puckered 2e aromatic **9** is highly favored for the related bicyclobutane with two boron atoms (**9***, Scheme 4; 49.5 kcal mol⁻¹ at the level of theory used here).^[19] Calculations on boryltriborabicyclobutane **7c*** provide the analogous electronic structure **7c** with a CB_3 4c-

2e π bond and two additional 3c-2e σ bonds between the boron atoms B1,B2,B4 and B3,B2,B4 .

Compound **7d**, a stereoisomer of **7c**, does not exist. Its B-H bond at the methyl-substituted boron atom forms a BHB bridge. This leads to **8c** where the coordination number of a carbon-bound boron center is increased to five. In analogy to the tetracoordinate boron atom in **10**, this boron atom can no longer participate in the cyclic delocalization of the π electrons. As a result, this delocalization only extends over three centers. While **10** is a homoaromatic with a classical borata bridge and a classical σ skeleton, compounds **8c** and **8a**



Scheme 4. Bicyclobutanes such as **9*** and **7c*** with two boron atoms as electron-deficient centers are puckered four-membered 2e aromatics. Upon increasing the coordination number of one of the two electron-deficient centers by addition of a hydride ion (**9**→**10**) or formation of a BHB bridge (**7d**→**8c**) the cyclic delocalization of the π electrons is reduced to three centers.

are 2e homoaromatics with a partial nonclassical BH_2 bridge and a partial nonclassical σ framework. Substituents have a comparatively small influence on the geometrical parameters of the aromatic portion of molecules of type **8** as on the entire geometry of compounds of type **2**, in which all the framework atoms participate in the aromatic system.

Compound **2a** represents the first derivative of the simplest three-dimensional aromatic in the series of carborane anions $\text{CB}_n\text{H}_{n+1}^-$ to be synthesized and characterized. Upon protonation of **2a** the three-dimensional aromatic character is lost, whereas it is retained upon protonation of the more strongly stabilized higher homologues of **2**.

Received: October 22, 2004

Keywords: aromaticity · boron · carboranes · density functional calculations · multicenter bonds

- [1] T. Kato, C. A. Reed, *Angew. Chem.* **2004**, *116*, 2968; *Angew. Chem. Int. Ed.* **2004**, *43*, 2908 and references therein.
- [2] P. von R. Schleyer, K. Najafian, *Inorg. Chem.* **1998**, *37*, 3454 and references therein.
- [3] P. H. M. Budzelaar, P. von R. Schleyer, *J. Am. Chem. Soc.* **1986**, *108*, 3967, and references therein; C. S. Wannere, P. von R. Schleyer, *Org. Lett.* **2003**, *5*, 865.
- [4] Representative of the series $\text{CB}_n\text{H}_{n+1}^-$ with $n = 6$ were recently described: B. Stibr, O. L. Tok, W. Milius, M. Bakardjiev, J. Holub,

- D. Hnyk, B. Wrackmeyer, *Angew. Chem.* **2002**, *114*, 2230; *Angew. Chem. Int. Ed.* **2002**, *41*, 2126; A. Franken, D. L. Ormsby, C. A. Kilner, W. Clegg, M. Thornton-Pett, J. D. Kennedy, *J. Chem. Soc. Dalton Trans.* **2002**, 2807.
- [5] Y. Sahin, C. Präsang, P. Amseis, M. Hofmann, G. Geiseler, W. Massa, A. Berndt, *Angew. Chem.* **2003**, *115*, 693; *Angew. Chem. Int. Ed.* **2003**, *42*, 669.
- [6] A. A. Korkin, P. von R. Schleyer, U. von Arx, R. Keese, *Struct. Chem.* **1995**, *6*, 225, and references therein.
- [7] Geometry optimizations were carried out with the B3LYP hybrid functional using the 6-31G(d) basis set. The stationary points were characterized by analytical frequency calculations. Relative energies are based on energy calculations with 6-311 + G(d,p) and are corrected for zero-point vibrational energies. The energies of solvation were calculated with the conductor-like polarizable continuum model (CPCM). a) Gaussian98 (Revision A.7), M. J. Frisch, G. W. Trucks, H. B. Schlegel, G. E. Scuseria, M. A. Robb, J. R. Cheeseman, V. G. Zakrzewski, J. A. Montgomery, R. E. Stratmann, J. C. Burant, S. Dapprich, J. M. Millam, A. D. Daniels, K. N. Kudin, M. C. Strain, O. Farkas, J. Tomasi, V. Barone, M. Cossi, R. Cammi, B. Mennucci, C. Pomelli, C. Adamo, S. Clifford, J. Ochterski, G. A. Petersson, P. Y. Ayala, Q. Cui, K. Morokuma, D. K. Malick, A. D. Rabuck, K. Raghavachari, J. B. Foresman, J. Cioslowski, J. V. Ortiz, B. B. Stefanov, G. Liu, A. Liashenko, P. Piskorz, I. Komaromi, R. Gomperts, R. L. Martin, D. J. Fox, T. Keith, M. A. Al-Laham, C. Y. Peng, A. Nanayakkara, C. Gonzalez, M. Challacombe, P. M. W. Gill, B. G. Johnson, W. Chen, M. W. Wong, J. L. Andres, M. Head-Gordon, E. S. Replogle, J. A. Pople, Gaussian, Inc., Pittsburgh, PA, **1998**; b) A. D. Becke, *J. Chem. Phys.* **1993**, *98*, 1372; A. D. Becke, *J. Chem. Phys.* **1993**, *98*, 5648; c) C. Lee, W. Yang, R. G. Parr, *Phys. Rev. B* **1988**, *37*, 785.
- [8] J. Jaballas, T. Onak, *J. Organomet. Chem.* **1998**, *550*, 101, and references therein; M. L. McKee, M. Bühl, O. P. Charkin, P. von R. Schleyer, *Inorg. Chem.* **1993**, *32*, 4549.
- [9] M. McKee, *Inorg. Chem.* **2001**, *40*, 5612; I. A. Koppel, P. Burk, I. Koppel, I. Leito, T. Sonoda, M. Mishima, *J. Am. Chem. Soc.* **2000**, *122*, 5114.
- [10] Molecules of type **7** are also two-dimensional aromatics; they formally result upon reaction of the three-dimensional aromatics **2** with electrophiles (e.g. **2a** + Cl⁺ → **7a**).
- [11] Y. Sahin, C. Präsang, M. Hofmann, G. Subramanian, G. Geiseler, W. Massa, A. Berndt, *Angew. Chem.* **2003**, *115*, 695; *Angew. Chem. Int. Ed.* **2003**, *42*, 671. In that work **7a** (referred to there as **4a**) is insufficiently described as a triborabicyclobutane with an open 3c-2e BBB bond.
- [12] The potassium salt of **2a** crystallized from a solution of the lithium salt in dimethoxyethane (DME) containing small amounts of potassium/sodium alloy. Anion **2a** formed a solvent-separated ion pair with a potassium ion coordinated with four DME molecules. [K(dme)₄]-**2a**: colorless solid, m.p. > 190 °C (no decomp), yield 87%; ¹H NMR (500 MHz, [D₈]THF, -10 °C): δ = 6.42 (s, 2H, *p*-H), 2.12, 2.05 (each s, each 12H; *o*-, *m*-CH₃), 0.54, 0.35 (each s, each 2H, BCH₂), -0.01, -0.15, -0.31 ppm (each s, each 9H, Me₃Si); ¹³C NMR (125 MHz, [D₈]THF, -10 °C): δ = 149.7 (brs, 2C, *i*-C), 136.2, 130.9 (each s, each 4C; *o*-, *m*-C), 127.3 (d, 2C, *p*-C), 68.8, (brs, 1C, CB₃, confirmed by measurements in [D₁₀]DME: 69.8), 21.2 (q, 8C; *o*-, *m*-CH₃), 5.3, 3.3 (each brt, each 1C, BCH₂), 2.5, 2.1, 1.7 ppm (each q, each 3C, Me₃Si); ¹¹B NMR (96 MHz, [D₈]THF, -10 °C): δ = 36 (1B), 6 ppm (3B).
- [13] Crystal structure determination: [K(dme)₄]-**2a**: Measurements were carried out on a colorless crystal (0.35 × 0.20 × 0.20 mm) at 193 K with an IPDS-II area detector system (Stoe) with MoK_α radiation. C₄₈H₉₇B₄KO₈Si₃, *M*_r = 968.87, orthorhombic, space group *P*2₁2₁, *Z* = 4, *a* = 1233.1(1), *b* = 1394.8(1), *c* = 3557.1(2) pm, *V* = 6118.0(7) × 10⁻³⁰ m³, ρ_{calcd} = 1.052 Mg m⁻³. Of 37258 reflections to θ = 26.3°, 12166 were independent (*R*_{int} = 0.0321) and 9488 were with *I* > 2σ(*I*). The structure was solved with direct methods and refined against all *F*² data with full matrix. The hydrogen atoms of the methylene groups were refined with isotropic displacement parameters. The remaining hydrogen atoms were placed as "riding" atoms in calculated positions with displacement parameters set to 1.5 times *U*_{eq} of the bonding partner. *wR*₂ = 0.0993 for all reflections, *R* = 0.0416 for observed reflections. The correctness of the absolute structure is proved by refinement of the Flack parameter to *x* = 0.02(4). Compounds **6a** and **8a**: colorless crystal (0.54 × 0.21 × 0.07 mm), C₃₂H₅₈B₄Si₃, *M*_r = 570.29, monoclinic, space group *P*2₁/*n*, *Z* = 8, *a* = 1445.5(3), *b* = 1381.4(2), *c* = 3732.4(6) pm, β = 95.07(2)°, *V* = 7424(2) × 10⁻³⁰ m³, ρ_{calcd} = 1.020 Mg m⁻³. Measurements were carried out on an IPDS-II area detector system (Stoe) with MoK_α radiation. Of 55536 reflections to θ = 26.0°, 13828 were independent (*R*_{int} = 0.0541) and 8952 were with *I* > 2σ(*I*). The structure solution was analogous to that of [K(dme)₄]-**2a**; *wR*₂ = 0.1018 for all reflections and *R* = 0.0413 for observed reflections. The asymmetrical unit contains two isomers (**6a** and **8a**) for which the hydrogen atoms on boron and on the methylene groups were freely refined. CCDC-196908 ([K(dme)₄]-**2a**) and CCDC-196907 (**6a** and **8a**) contain the supplementary crystallographic data for this paper. These data can be obtained free of charge from The Cambridge Crystallographic Data Centre via www.ccdc.cam.ac.uk/data_request/cif.
- [14] The aromatic stabilization energy (ASE) of **2u** can be estimated as -27 kcal mol⁻¹ by interpolation of the ASEs calculated for C₂B₃H₅ and B₅H₅²⁻ (-19.8 and -34.8 kcal mol⁻¹, respectively^[15]).
- [15] P. von R. Schleyer, G. Subramanian, A. Dransfeld, *J. Am. Chem. Soc.* **1996**, *118*, 9988.
- [16] For the influence of the environment on the stabilization of polar molecules, see: V. Jonas, G. Frenking, M. T. Reetz, *J. Am. Chem. Soc.* **1994**, *116*, 8741, and references therein.
- [17] A 1:1 mixture of **7a** and **8a**: colorless solid, m.p. 132–133 °C (decomp), yield 85%. Only **8a** is present in solution: ¹H NMR (500 MHz, C₆D₆, 27 °C): δ = 6.94 (s, 2H, *p*-H), 3.09 (brs, 1H, BHB), 2.40, 2.17 (each s, each 12H; *o*-, *m*-CH₃), 0.95, 0.75 (each s, each 2H, BCH₂), 0.28, 0.23, -0.09 ppm (each s, each 9H, Me₃Si); ¹³C NMR (125 MHz, C₆D₆, 27 °C): δ = 137.5, 133.7 (each s, each 4C; *o*-, *m*-C), 132.9 (d, 2C, *p*-C), 80.3 (brs, 1C, CB₃), 22.9, 20.3 (each q, each 4C; *o*-, *m*-CH₃), 5.0, 4.9 (each brt, each 1C, BCH₂), 1.6, 0.5, 0.4 ppm (each q, each 3C, Me₃Si), the signal for the *i*-C atom was observed at 134.0 ppm in [D₈]dioxane at 70 °C; ¹¹B NMR (160 MHz, C₆D₆, 27 °C): δ = 27.0, 21.6 (2B), 15.7 ppm. In solution a rapid exchange of the two duryl-substituted boron atoms takes place for **8a**: Only one signal is observed for the *p*-H or *p*-C atoms of the duryl groups in the NMR spectra of **8a** down to -80 °C. At even lower temperature the signals broaden. This can be explained by the enantiomerization of **8a** via a C_s-symmetric transition state whose mirror plane contains the BHB bridge and bisects the B1–B2 bond. Cleavage of the B2–B3 bond and further movement of the bridging H atom towards B2 results in the enantiomer of **8a** in which the duryl-substituted boron atoms have formally switched places, in fact, however, exchanged their coordination environments. For **8b** a value of 8.2 kcal mol⁻¹ can be calculated for the energy required for the exchange to take place.
- [18] A. E. Reed, L. A. Curtiss, F. Weinhold, *Chem. Rev.* **1988**, *88*, 899.
- [19] P. H. M. Budzelaar, E. Kraka, D. Cremer, P. von R. Schleyer, *J. Am. Chem. Soc.* **1986**, *108*, 561, and references therein.

Bond-Selective H[•] Ion Abstraction from Thymine**

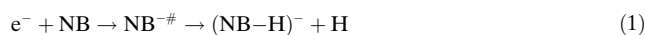
Sylvia Ptasíńska, Stephan Denifl, Verena Grill, Tilmann D. Märk, Paul Scheier,* Sascha Gohlke, Michael A. Huels, and Eugen Illenberger

It is by now well recognized that reactions in living cells induced by secondary electrons constitute an important initial step towards radiation damage.^[1,2] This notion is based on the fact that energy deposition by high-energy radiation creates electrons as the most abundant secondary species with an initial energy distribution up to a few tens of electron volts.^[3] These initially relatively fast secondary electrons are present in the medium within a short time window (femtoseconds to picoseconds), during which they are slowed down by collisions thereby initiating further ionization and excitation processes that lead to reactive species like neutral radicals, ions, and electrons. At sufficiently low energies the electrons may be captured at particular positions in the molecule to generate negatively charged transient compounds, or, alternatively, they will be trapped ultimately as solvated electrons. In the solvated stage, they may still induce genotoxic or mutagenic effects, however, on a much longer timescale (> μs). In contrast to solvated electrons, electrons with energies of up to a few tens of electron volts can immediately induce reactions, directly in DNA or its environment. Their interaction with the cellular material is hence essential to reveal the initial molecular steps in radiation damage.

Previous experiments on plasmid DNA demonstrated the ability of secondary electrons at subionization energies to effectively induce single- and double-strand breaks.^[4,5] The reaction sequence of the underlying molecular processes has not been unraveled so far. At about an electron energy of

about 10 eV the efficiency curves for the observed strand breaks show a resonant behavior that indicates the formation of a transient molecular anion. Thus it has been suggested that dissociative electron attachment (DEA) is the relevant initial molecular step towards strand breaks. In the meantime, possible low-energy pathways leading to single-strand breaks following electron attachment to DNA have been explored theoretically by ab initio calculations of the electronic structure^[6] and density functional theory (DFT) studies.^[7]

From the experimental side, efforts have been undertaken to study the effect of free-electron interaction with isolated biomolecules (DNA bases and larger building blocks) as thin multilayer films in an ultrahigh vacuum (UHV) or in the gas phase. In the UHV experiments reaction products desorbing from the film can be followed directly as a function of the energy of the bombarding electrons.^[8–10] In some cases those reaction products remaining at the surface can be characterized by X-ray photoelectron spectroscopy.^[11] In gas-phase experiments negatively charged (fragment) ions resulting from (dissociative) electron attachment to the isolated biomolecule are recorded directly by mass spectrometry. These gas-phase studies showed that all nucleobases (NBs) undergo DEA at subexcitation energies (< 3 eV) leading to dehydrogenation^[12–15] according to Equation (1). Here NB^{−#}



is the transitory negative ion (TNI) of the corresponding nucleobase, and (NB−H)[−] is the closed-shell anion formed by the ejection of a neutral hydrogen radical. The reaction is effective at subexcitation energies and driven energetically by the appreciable electron affinity of the (NB−H) radicals (3–4 eV).^[12] Experiments with partly deuterated thymine^[16] demonstrated that hydrogen abstraction is operative exclusively from the N1 position (see molecular structure in Figure 1).

In addition to the dominant low-energy feature (leading exclusively to dehydrogenation [Eq. (1)]), previous^[17] and recent^[18] gas-phase experiments on NBs identified a second resonance feature located in the energy range between 5 and 13 eV associated with various negatively charged fragments. In this energy range, desorption from the multilayer films and also the single- and double-strand breaks in DNA were observed. One of the most intense ions in this energy domain is H[•] resulting from the Equation (2), the reaction complementary to Equation (1).



Here we demonstrate for the nucleobase thymine (T) that the H[•] yield due to Equation (2) extends from ≈ 5 eV to ≈ 13 eV with pronounced peaks (structures). By using partly deuterated thymine (T_D) we could show that these structures can be correlated directly to H[•] and D[•] abstraction from the different positions in the thymine molecule. The H[•]/D[•] ion yield due to abstraction from the C positions shows a remarkable resemblance to the energy dependence of observed strand breaks in plasmid DNA and is hence considered as a possible initial reaction.

[*] Mag. S. Ptasíńska, Mag. Dr. S. Denifl, Mag. Dr. V. Grill, Prof. Dr. T. D. Märk, Prof. Mag. Dr. P. Scheier
Institut für Ionenphysik
Universität Innsbruck and
Center for Molecular Biosciences Innsbruck (CMBI)
Technikerstrasse 25, 6020 Innsbruck (Austria)
Fax: (+43) 512-507-2932
E-mail: paul.scheier@uibk.ac.at

Prof. Dr. T. D. Märk
Department of Plasma Physics
Comenius University
84248 Bratislava (Slovak Republic)

Dipl.-Chem. S. Gohlke, Prof. Dr. M. A. Huels,^[†] Prof. Dr. E. Illenberger
Institut für Chemie—Physikalische und Theoretische Chemie
Freie Universität Berlin
Takustrasse 3, 14195 Berlin (Germany)

[†] Permanent address:
Department of Nuclear Medicine and Radiobiology
Faculty of Medicine, University of Sherbrooke
Sherbrooke, QC (Canada)

[**] Financial support from the FWF, ÖAW, and ÖNB (Vienna), the EU Commission (Brussels) through the EPIC Network, and the DFG (Bonn) is gratefully acknowledged.

The present investigation was performed in a crossed electron/molecule beams device at the Innsbruck laboratory; this apparatus was described previously in detail.^[19] The electron beam was formed in a custom-built hemispherical electron monochromator, in the present experiments operated at an energy resolution of between 110 and 130 meV (FWHM) and an electron current of 5–8 nA. The molecular beam emanated from a source consisting of a temperature-regulated oven and a capillary.^[14,18] The sample was heated up to 450 K resulting in sufficient pressure to form an effusive beam, which was crossed perpendicularly by the electron beam. Negative ions formed in the collision zone were extracted by a weak electric field towards the entrance of the quadrupole mass spectrometer. The mass-selected negative ions were detected by a channeltron using a single-pulse counting technique. The intensity of a particular mass-selected negative ion was then recorded as a function of the electron energy.

The electron energy scale was calibrated using the Cl^- signal from CCl_4 yielding a very narrow peak near 0 eV. Absolute calibration of the presently measured relative partial DEA cross sections (anion yields versus electron energy) was carried out by taking the ratio of the anion current for the production of H^- from T at 5.5 eV and the anion current for the production of Cl^- from CCl_4 at the peak of the 0.8 eV resonance. With the cross section of Cl^-/CCl_4 ^[20] we derived the total DEA cross section for H^- formation (peak value at 5.5 eV) as $1.2 \times 10^{-21} \text{ m}^2$ at an accuracy within one order of magnitude. Thymine and partly deuterated thymine at a stated purity of 99.5% were purchased from Sigma–Aldrich.

In the partly deuterated thymine (T_D in Figure 1) the hydrogen atoms at the carbon positions were replaced by

deuterium. Figure 1 presents the H^-/D^- formation by dissociative electron attachment from T and T_D as a function of the electron energy E . Figure 1a shows the formation of H^- from unlabeled thymine (H^-/T), 1b indicates the generation of D^- from T_D ($\text{D}^-/\text{T}_\text{D}$), and, finally, 1c displays the formation of H^- from T_D ($\text{H}^-/\text{T}_\text{D}$). The intensity is given in arbitrary units but is comparable between the different curves. The intensity numbers can be transformed to an absolute DEA cross section by the procedure described above leading to $\sigma(\text{H}^-/\text{T}) 1.2 \times 10^{-21} \text{ m}^2$ at the dominant peak located at 5.5 eV. The H^-/T spectrum consists of three clearly separated peaks at 5.5, 6.8, and 8.3 eV and a distinct shoulder at 9.3 eV. In a simple comparison of spectra 1b and 1c it is immediately obvious that the two higher-energy features in Figure 1a and c ($> 7.5 \text{ eV}$) correspond exclusively to H^- (or D^-) formation from the C positions, while the two lower H^- peaks in Figure 1a and 1c essentially arise from abstraction at the two N positions. These are very interesting observations in view of both the associated reaction mechanism and the possible initial reactions towards strand breaks.

The pronounced site selectivity is a very remarkable observation when one considers the thermodynamics and the underlying reaction mechanism. In a recent study the binding energies for all hydrogen atoms of thymine were calculated:^[18] $D(\text{N1-H}) = 4.4$, $D(\text{N3-H}) = 5.8$, $D(\text{C6-H}) = 4.9$, and $D(\text{CH}_2\text{-H}) = 4.5 \text{ eV}$. With the electron affinity of the hydrogen atom (0.75 eV^[21]) the energy threshold for formation of H^-/D^- from the different sites becomes $E(\text{N1}) = 3.65$, $E(\text{N3}) = 5.05$, $E(\text{CH}_2) = 3.75$, and $E(\text{C6}) = 4.15 \text{ eV}$. These numbers show that H^-/D^- formation from the N and C positions cannot be separated thermodynamically and, more importantly, any H^- or D^- abstraction is accompanied by an appreciable excess energy of up to several eV.

Concerning the reaction mechanism and the electronic states involved in the process it is obvious from the ion yields that DEA is responsible for H^-/D^- abstraction. At low energy ($< 3 \text{ eV}$) transient negative ions can usually be characterized as one-particle-shape resonances; the extra electron occupies one of the normally empty molecular orbitals (MOs) thereby leaving the rest of the electronic configuration unaffected. For NBs it has been suggested very recently^[22] that in the case of the low-energy process in Equation (1) (resulting in interesting structures with a sharp peak at 1 eV) the largest contribution arises from initially formed dipole-bound (DB) states (strictly speaking, vibrational Feshbach resonances of a DB state), which couple to valence states ($\sigma^*(\text{N1-H})$) with the DB anion acting as doorway state for DEA.

In contrast to that, abstraction of H^- [Eq. (2)] occurs within an energy range where electronically excited states are accessible, and resonances in that energy domain can often be characterized as core excited resonances, in other words, TNIs with two electrons in normally unoccupied MOs. On the other hand, a quantum-dynamics scattering calculation in uracil predicts a one-particle-shape resonance at 9.1 eV with strong C5–H antibonding character.^[23] Thus from the material available so far we cannot conclude whether one-particle and/or two-particle resonances are involved in the relevant energy range. From the appreciable site selectivity, however, we can safely assume that the electronic states in the energy

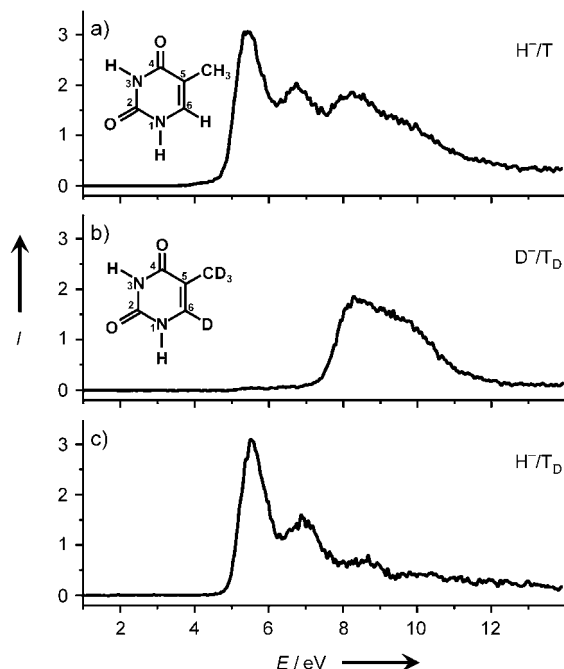


Figure 1. H^- and D^- formation from thymine (T) and partly deuterated thymine (T_D). a) H^- from T, b) D^- from T_D , and c) H^- from T_D as a function of the incident electron energy E .

range 5–7 eV must have localized N–H antibonding character and, accordingly, those in the range between about 8 and 12 eV significant C–H antibonding character. In the present case of thymine we propose to have a direct electronic dissociation along a repulsive potential energy surface, and the reaction is site selective in terms of the electron energy. In other words, due to the resonantlike structure it is possible by slightly changing the electron energy to direct the DEA reaction to different positions in the molecule.

We note that such a pronounced site selectivity by energy in a polyatomic molecule is quite remarkable. Previous experiments on methanol^[24] revealed, for example, that OH[−] and OD[−] formation (resonance peaking at 10.5 eV) was subjected to strong hydrogen/deuterium scrambling in the precursor ion. The yield function of OH[−]/OD[−] showed exactly the same pattern irrespective of the target (CH₃OH, CH₃OD, CD₃OH, CD₃OD). For the reaction mechanism this means that the (excited) TNI is subjected to effective hydrogen transfer (scrambling) (losing its original identity) prior to decomposition.

For possible relations to strand breaks we first note that in DNA the N1 position is involved in the N1–C bond connecting the nucleobase with the sugar unit while the hydrogen at the N3 position is part of the hydrogen bond to the complementary nucleobase. We can therefore assume that the resonances presently observed in isolated T associated with H[−] abstraction from the N positions (below 7 eV) will be strongly affected by these bonds and shifted to other energies.

In Figure 2 we compare D[−] formation from T_D (solid line) with the previously reported H[−] desorption yield from a thin

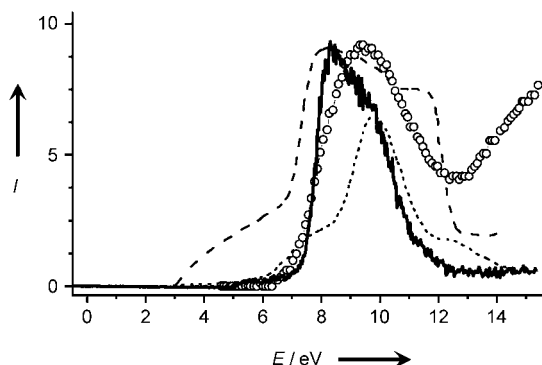


Figure 2. Comparison of D[−] formation from T_D in the gas phase (solid line) with H[−] desorption from a thin film of thymine (open circles^[25]) and with single-strand breaks (SSB; dashed line) and double-strand breaks (DSB; dotted line) observed in plasmid DNA.^[5] The intensity of SSB and DSB is arbitrarily normalized.

layer of thymine attached to a clean metal surface upon radiation with low-energy electrons.^[25] In addition the spectra corresponding to single- and double-strand breaks^[4,5] in plasmid DNA are included in this figure. A comparison with the present data shows that strand breaks are observed in the energy range in which H[−] abstraction is effective, in particular in the energy range in which H[−] abstraction from the C positions is involved. This suggests that hydrogen abstraction from the carbon atoms may represent an initial

step towards strand breaks in DNA. One has to keep in mind, however, that a single-strand break requires rupture of bonds in the sugar–phosphate moiety, and different primary events may contribute. A possible route from the attachment of a low-energy electron to a nucleobase and ultimately leading to C–O bond rupture at the sugar–phosphate units has been explored recently by ab initio structure calculations.^[6]

In conclusion, the present experiments demonstrate a remarkable site selectivity for H[−]/D[−] abstraction in thymine which is dependent on the incident electron energy. The feature due to H[−]/D[−] abstraction from the C positions resembles the energy dependence of single- and double-strand breaks observed in plasmid DNA.

Received: August 20, 2004

Published online: February 9, 2005

Keywords: anions · dissociative electron attachment · DNA damage · gas-phase reactions · nucleobases

- [1] L. Sanche, *Mass Spectrom. Rev.* **2003**, *21*, 349.
- [2] S. Gohlke, E. Illenberger, *Europhys. News* **2002**, *33*, 207.
- [3] J. A. La Verne, S. M. Pimblott, *Radiat. Res.* **1995**, *141*, 208.
- [4] B. Boudaiffa, P. Cloutier, D. Hunting, M. A. Huels, L. Sanche, *Science* **2000**, *287*, 1658.
- [5] M. A. Huels, B. Boudaiffa, P. Cloutier, D. Hunting, L. Sanche, *J. Am. Chem. Soc.* **2003**, *125*, 4467.
- [6] R. Barrios, P. Skurski, J. Simons, *J. Phys. Chem. B* **2002**, *106*, 7991.
- [7] X. Li, M. D. Sevilla, L. Sanche, *J. Am. Chem. Soc.* **2003**, *125*, 13668.
- [8] H. Abdoul-Carime, L. Sanche, *Radiat. Res.* **2001**, *156*, 151.
- [9] M.-A. Hervé du Penhoat, M. A. Huels, P. Cloutier, J.-P. Jay-Gerin, L. Sanche, *J. Chem. Phys.* **2001**, *114*, 5755. Preliminary data of D[−] ion yield from T_D were given in the cited paper; however, the present D[−] yield differs substantially from that from these earlier measurements.
- [10] X. Pan, P. Cloutier, D. Hunting, L. Sanche, *Phys. Rev. Lett.* **2003**, *90*, 208102.
- [11] D. V. Klyachko, M. A. Huels, L. Sanche, *Radiat. Res.* **1999**, *151*, 177.
- [12] G. Hanel, B. Gstir, S. Denifl, P. Scheier, M. Probst, B. Farizon, M. Farizon, E. Illenberger, T. D. Märk, *Phys. Rev. Lett.* **2003**, *90*, 188104.
- [13] S. Gohlke, H. Abdoul-Carime, E. Illenberger, *Chem. Phys. Lett.* **2003**, *380*, 595.
- [14] S. Denifl, S. Ptasińska, M. Cingel, S. Matejcek, P. Scheier, T. D. Märk, *Chem. Phys. Lett.* **2003**, *377*, 74.
- [15] R. Abouaf, J. Pommier, H. Dunet, *Int. J. Mass Spectrom.* **2003**, *226*, 397.
- [16] H. Abdoul-Carime, S. Gohlke, E. Illenberger, *Phys. Rev. Lett.* **2004**, *92*, 168103.
- [17] M. A. Huels, I. Hahndorf, E. Illenberger, L. Sanche, *J. Chem. Phys.* **1998**, *108*, 1309.
- [18] S. Denifl, S. Ptasińska, M. Probst, J. Hrusak, P. Scheier, T. D. Märk, *J. Phys. Chem. A* **2004**, *108*, 6562.
- [19] D. Muigg, G. Denifl, A. Stamatovic, O. Echt, T. D. Märk, *Chem. Phys.* **1998**, *239*, 409.
- [20] G. A. Gallup, K. Aflatoon, P. D. Burrow, *Chem. Phys.* **2003**, *118*, 2562.
- [21] *Handbook of Chemistry and Physics*, 78th ed. (Ed.: D. R. Lide), CRC, Boca Raton, FL, **1997**.
- [22] A. M. Scheer, K. Aflatoon, G. A. Gallup, P. D. Burrow, *Phys. Rev. Lett.* **2004**, *92*, 068102.

- [23] A. Grandi, F. A. Gianturco, N. Sanna, *Phys. Rev. Lett.* **2004**, 93, 048103.
- [24] A. Kühn, H.-P. Fenzlaff, E. Illenberger, *J. Chem. Phys.* **1988**, 88, 7453.
- [25] H. Abdoul-Carime, P. Cloutier, L. Sanche, *Radiat. Res.* **2001**, 155, 625.

Glycopeptide Synthesis

An Orthogonal Double-Linker Resin Facilitates the Efficient Solid-Phase Synthesis of Complex-Type N-Glycopeptide Thioesters Suitable for Native Chemical Ligation**

Stefano Mezzato, Manuela Schaffrath, and Carlo Unverzagt*

In memory of Murray Goodman

Recombinant therapeutic glycoproteins frequently bear complex oligosaccharides (N-glycans) connected to asparagine.^[1] The variability of N-glycosylation leads to glycoprotein microheterogeneity rendering the isolation of pure glycoforms extremely difficult. It has been demonstrated that the biological activity of glycoproteins depends on the nature of the attached glycans.^[2] For medicinal and pharmaceutical purposes the generation of uniform glycoproteins with a tailored glycosylation pattern is of high interest. In parallel to the creation of special expression systems,^[3] synthetic methodologies^[4] have been developed to generate homogenous natural glycoproteins by remodeling of glycans, transglycosylation, reverse proteolysis, or native chemical ligation (NCL),^[5] of which the latter promises the highest potential and flexibility. To obtain building blocks suitable for the assembly of complex-type N-glycoproteins by native chemical ligation, we have developed a high-yielding solid-phase synthesis of glycopeptide thioesters that bear complex-type N-glycans.

The native chemical ligation is based on the chemoselective reaction between a peptide α -thioester and a peptide with an N-terminal cysteine residue. Although several examples have demonstrated the use of this chemistry for synthesis of glycopeptides and glycosylated proteins,^[6] the efficient generation of glycopeptide thioesters that contain complex-type N-glycans on the solid phase has not been

reported.^[7] However, a solution to this problem was required for the envisioned synthesis of bovine RNase B as a model glycoprotein that consists of 124 amino acids with an N-glycosylation site at Asn34 and the nearest ligation site at Cys40. The glycosylated fragment 30–68 of RNase B (**C**) was selected to establish the required chemistry and was strategically split into the thioester segment **A** and the cysteine peptide **B** (Scheme 1). For the challenging solid-phase synthesis of the thioester fragment RNase 30–39 (**A**), which bears a heptasaccharide N-glycan, the sulfonamide-based safety-catch approach^[8] appeared most attractive among the methods developed for the synthesis of thioesters.^[9]

The safety-catch linker is particularly stable to nucleophiles, basic and acidic conditions,^[10] whereas, after completion of the synthesis, selective sulfonamide activation renders the linker susceptible to nucleophilic attack and allows the release of the final product. However, the inertia of the sulfonamide linker requires time-consuming two-step microcleavages to monitor the reaction efficiency by LC–MS. As a consequence, only the final products are usually checked after final release from the resin.^[11] To overcome this problem and to allow easy step-by-step control, especially for the critical glycopeptide formation, we took into consideration the attachment of an additional linker.^[12] The second handle should enable easy detachment of the peptide chain as well as be completely orthogonally stable to the safety-catch linker. These requirements are fulfilled by the Rink-amide linker,^[13] as it can be cleaved easily with trifluoroacetic acid (TFA) (Scheme 2). The peptides thus released are free of acid-labile protecting groups which therefore increases the solubility and simplifies HPLC and LC–MS analysis. A hydrophobic spacer facilitates reversed-phase HPLC detection of the products and the double-linker fragment.

As a solid support we chose an amino PEGA^[14] resin to carry the double-linker array. First, the Fmoc protected Rink-amide linker **1** was attached to the resin by using HCTU and DIPEA (Scheme 3). The Fmoc protecting group was then cleaved with piperidine in NMP to furnish compound **3**, which was elongated with Fmoc phenylalanine as a spacer. After cleavage of the Fmoc group, the safety-catch linker 3-carboxypropanesulfonamide^[8] (**4**) was coupled with DIC and HOBt to give the fully functionalized resin **5**. Reaction efficiencies were monitored by the Kaiser test^[15] and the coupling reactions went to completion.

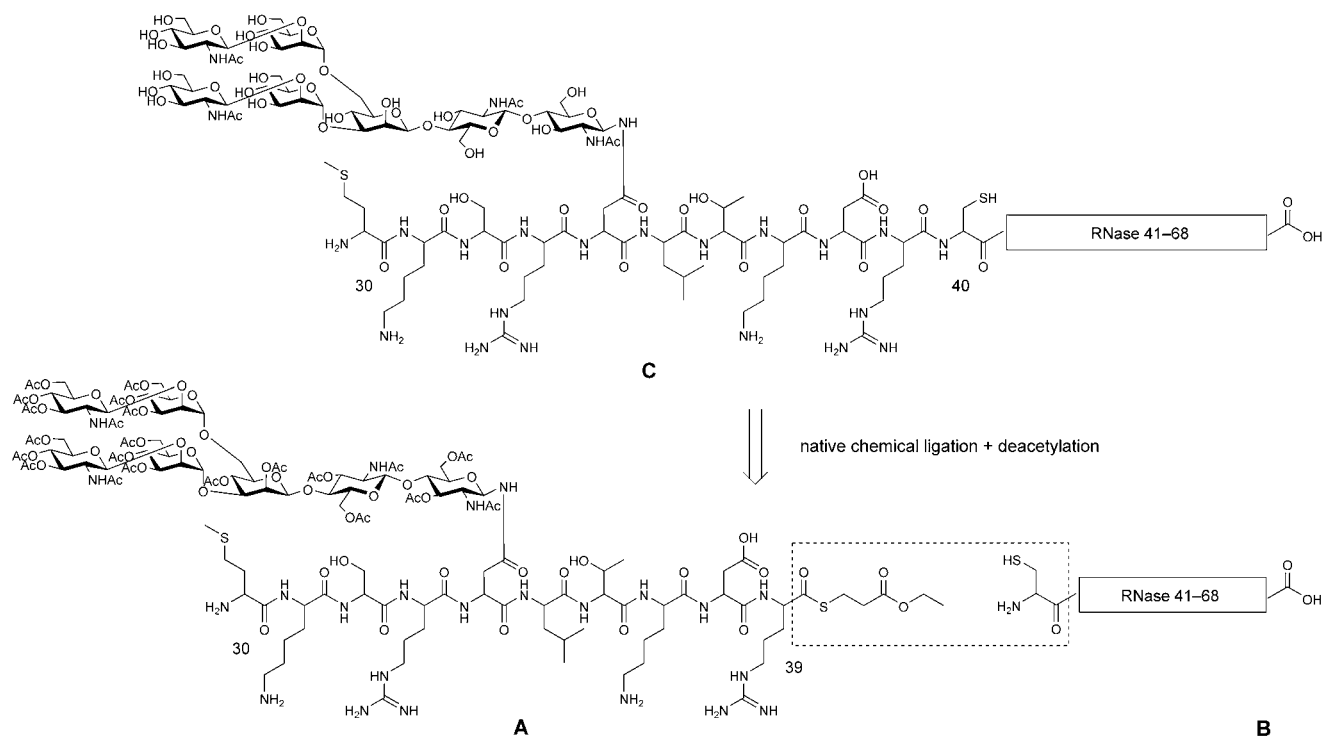
The loading of the safety-catch linker has often been a matter of concern,^[16] as poor coupling yields and racemization of the first amino acid impair further synthesis. The first amino acid loaded onto the resin was arginine by using DIC and 1-MeIm^[17] in 80 % yield as determined by UV detection of the dibenzofulvene–piperidine adduct at 290 nm.^[18] Double coupling led to nearly quantitative acylation of the sulfonamide linker. The following peptide chain elongation by four Fmoc amino acids was carried out manually under commonly used conditions,^[19] and pentapeptide **7** was obtained in high yield and purity.

From previous work it was known^[7b,20] that the coupling of Fmoc asparagine attached to complex-type N-glycans is difficult, especially on the solid phase, and tends to give low yields, presumably owing to a number of factors including the

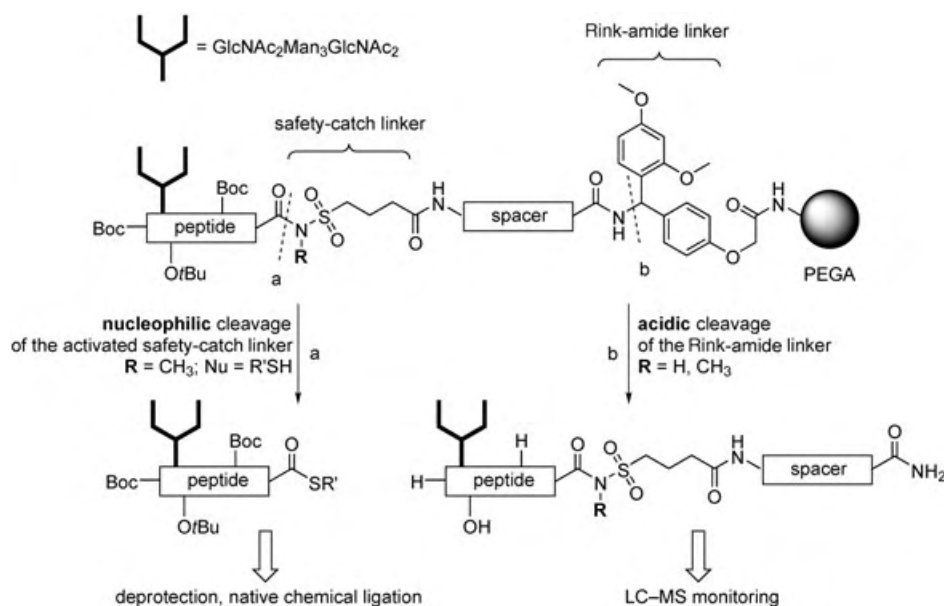
[*] S. Mezzato, Dr. M. Schaffrath, Prof. C. Unverzagt
Bioorganische Chemie, Gebäude NW1
Universität Bayreuth
95440 Bayreuth (Germany)
Fax: (+49) 921-555-365
E-mail: carlo.unverzagt@uni-bayreuth.de

[**] We thank the Deutsche Forschungsgemeinschaft and the Fonds der Deutschen Chemischen Industrie for funding.

Supporting information for this article is available on the WWW under <http://www.angewandte.org> or from the author.



Scheme 1. Retrosynthesis of complex-type glycosylated RNase B fragment 30–68.

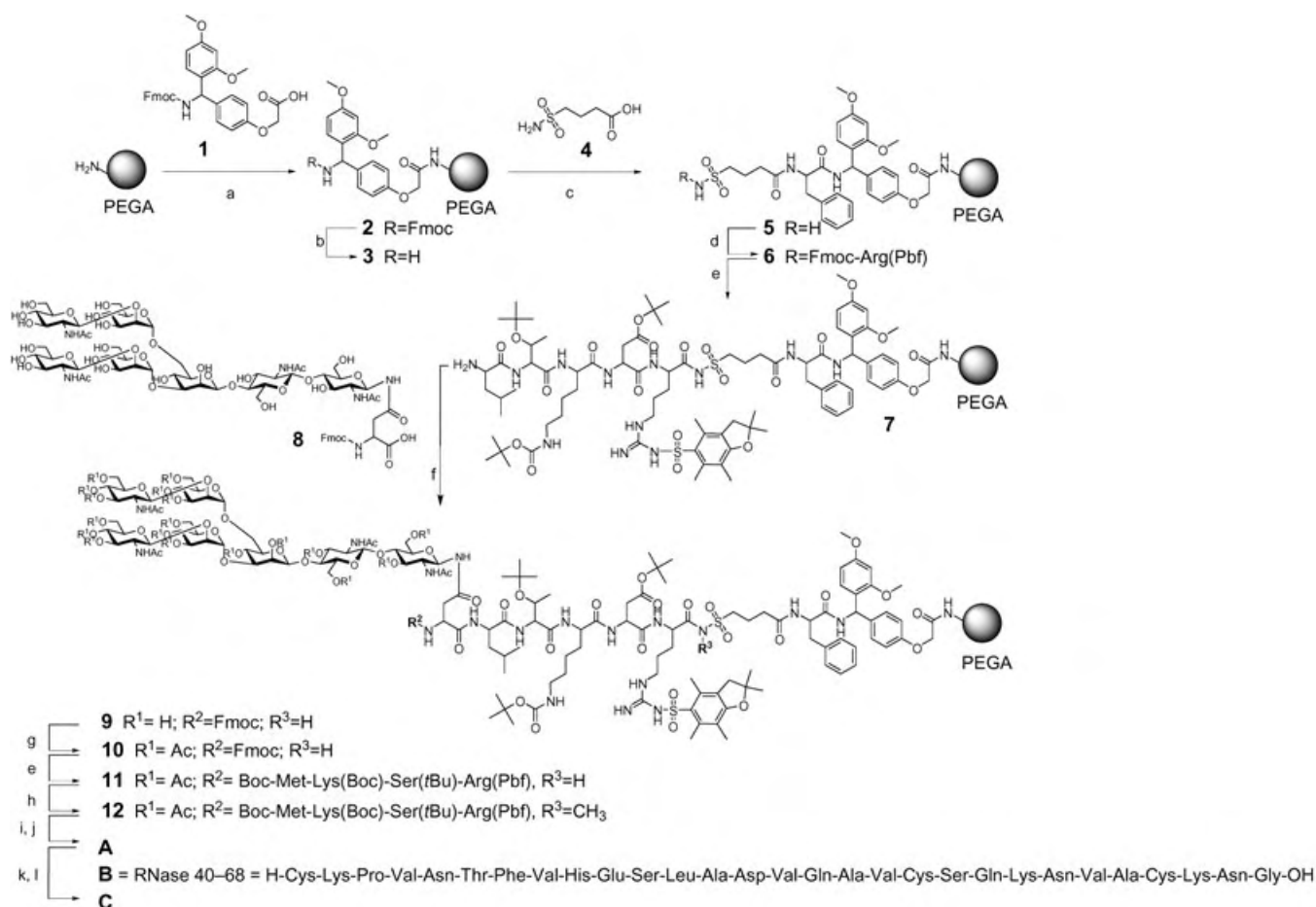


Scheme 2. The combination with the orthogonal Rink-amide linker facilitates the LC–MS monitoring of reactions based on the safety-catch linker.

resin matrix and the activation. The coupling efficiencies of the synthetic glycosyl amino acid **8**^[20b,21] carrying an unprotected biantennary complex-type heptasaccharide N-glycan were monitored under equivalent reaction conditions for different resins. The PEGA resin proved superior to other polystyrene-based matrices which may be related to the better swelling properties of PEGA. In parallel, the initially low coupling yields of **8** were optimized by comparing various activation reagents. It was found that PyBOP in the presence of DIPEA gave the best yields when using only 0.8 equiv-

alents of the precious glycosyl amino acid **8** (with respect to the loading of the resin). The glycosyl amino acid **8** was first dissolved in DMSO/NMP (1:1), added to the resin, and activated in situ with solid PyBOP and DIPEA to afford the glycopeptide **9** in excellent yield (95 %, UV detection of cleaved Fmoc).

Protection of the hydroxy groups of the carbohydrate was necessary to prevent their acylation^[20d,22] by activated amino acids during the subsequent chain elongation of **9**. Furthermore, unprotected oligosaccharides can be unstable during



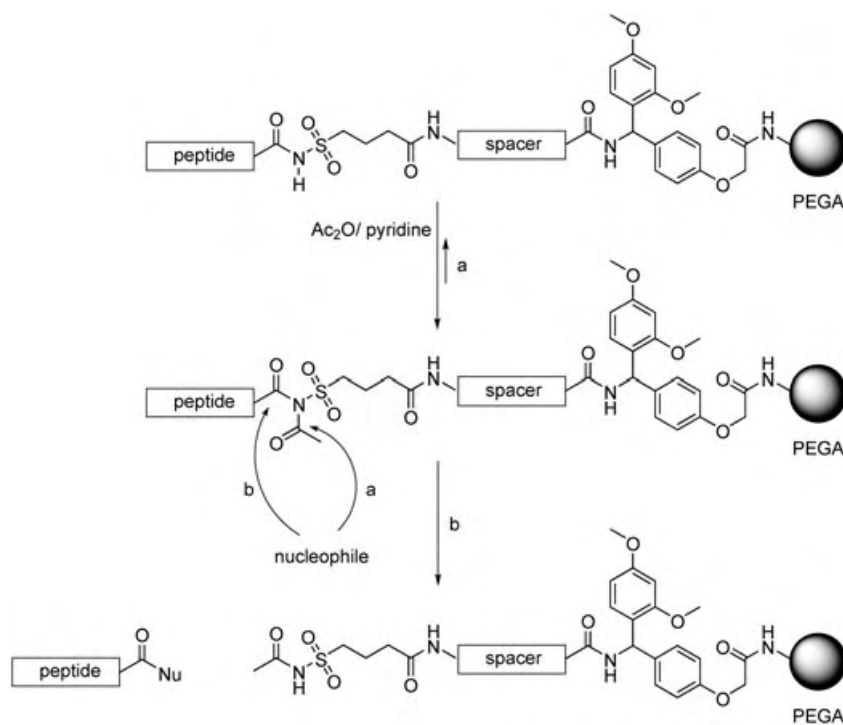
Scheme 3. Synthesis of glycopeptide thioester **A**: a) **1**, HCTU, DIPEA, DMF; b) 20% piperidine in NMP; c) **1**, Fmoc-Phe-OH, HCTU, DIPEA; d) **2**, **3**, **4**, DIC, HOBT, DMF; e) Fmoc-Arg(Pbf)-OH, DIC, 1-Melm, CH₂Cl₂, DMF; f) manual solid-phase peptide elongation by conventional Fmoc chemistry with Fmoc amino acid (4 equiv), HOBT (4 equiv), TBTU (4 equiv), DIPEA (9 equiv); g) **8** (0.8 equiv), PyBOP, DIPEA, DMSO, NMP; h) Ac₂O, pyridine, HOAc; i) TMSCHN₂, *n*-hexane, CH₂Cl₂; j) ethyl 3-sulfanypropionate, sodium thiophenolate, DMF; k) TFA, H₂O, TES, ethyl 3-sulfanypropionate, room temperature, 2 h (46% from **8**); l) **A** (1 equiv), **B** (1.3 equiv), 6 M guanidinium chloride, thiophenol (2%), phosphate buffer (pH 7.6); m) hydrazine hydrate (10%), DTT (5%). HCTU = *N*-(1*H*-6-chlorobenzotriazol-1-yl) (dimethylamino)methylene-*N*-methylmethanaminium hexafluorophosphate *N*-oxide; DIPEA = *N,N*-diisopropylethylamine; DMF = *N,N*-dimethylformamide; NMP = *N*-methylpyrrolidone; Fmoc = 9-fluorenylmethoxycarbonyl; DIC = *N,N'*-diisopropylcarbodiimide; HOBT = 1-hydroxybenzotriazole; Pbf = 2,2,4,6,7-pentamethylidihydrobenzofuran-5-sulfonyl; Melm = *N*-methylimidazole; TBTU = *N*-(1*H*-benzotriazol-1-yl) (dimethylamino)methylene-*N*-methylmethanaminium tetrafluoroborate *N*-oxide; PyBOP = benzotriazol-1-yl-*N*-oxy-tris(pyrrolidino)phosphonium hexafluorophosphate; DMSO = dimethyl sulfoxide; TMS = trimethylsilyl; TFA = trifluoroacetic acid; TES = triethylsilane; DTT = 1,4-dithiothreitol.

final deprotection of the peptide backbone with TFA,^[23a] whereas acetylation provides complete TFA stability.^[23b] Subsequently, acetylation using acetic anhydride and pyridine (1:1) protected the OH groups of the heptasaccharide and simultaneously capped the remaining N-terminal amino groups. However, after the acetylation step, the loading of the resin appeared to be significantly lower (2/3 of the peptide was cleaved within 16 h of reaction time); TFA cleavage and LC-MS showed that a major side product was identified as the *N*-acetylated sulfonamide linker completely lacking the peptide chain. Most likely, an additional *N*-acetylation of the safety-catch handle leads to this outcome (Scheme 4).

In solution the *N*-acylation of *N*-acylsulfonamides was found to occur to a small extent.^[24] Under basic conditions the *N*-acylsulfonamide ($\text{pK}_a = 2.5$ ^[25]) is easily deprotonated and the imide anion is susceptible to further acetylation. This activates the handle, which is subsequently attacked by

nucleophiles (e.g. pyridine), thus regenerating the starting material (Scheme 4, path a) or irreversibly disconnecting the peptide chain from the linker (Scheme 4, path b) with complete loss of the product. We assumed that the acylation of the acylsulfonamide should be pH-dependent, and, by avoiding the deprotonation of the *N*-acylsulfonamide, an overacylation should be precluded. Optimization studies revealed that the initial neutralization of the pyridine catalyst with acetic acid (Ac₂O/py/AcOH 5:3:2 v/v/v) afforded the fully acetylated glycopeptide without any side product being observed. The protected glycohexapeptide **10** was conveniently elongated by Fmoc solid-phase peptide synthesis to give the glycodecapeptide **11** with Boc methionine as the final residue.

The controlled release of the glycopeptide as a thioester requires the prior activation of the safety-catch linker by alkylation with iodo acetonitrile or trimethylsilyldiazome-



Scheme 4. Side-reactions of the safety-catch linker during acetylation under basic conditions.

thane (TMSCHN_2).^[8] TMSCHN_2 was selected as the more powerful and selective reagent;^[26] this commercially available and shelf-stable 2 M solution in *n*-hexane was diluted with THF (1:1) before use. In the first experiments the safety-catch linker of the PEGA resin was methylated to about 50%, whereas similar activation performed on a polystyrene matrix went to completion. We assumed that the PEGA resin did not swell enough in the nonpolar THF/*n*-hexane mixture and that peptide aggregation would further impair the activation of the linker. The use of more-polar solvent mixtures (*t*BuOH/*n*-hexane 2:1 or CH_2Cl_2 /*n*-hexane 2:1) proved very effective and furnished the methylated product **12** in quantitative yield after 2 h without side-chain modification of methionine. Activation of the safety-catch linker was conveniently monitored by LC-MS after selective TFA cleavage of the glycopeptide bound to the methylated linker. After complete activation the glycopeptide thioester was released with ethyl 3-sulfanylpropionate and catalytic sodium thiophenolate.^[11a] However, complete detachment of the peptide required 3 equivalents of sodium thiophenolate and 100 equivalents of ethyl 3-sulfanylpropionate. The displacement efficiency was indirectly monitored (LC-MS) by TFA-mediated release of the linker after treatment with thiol, which led to only the deacylated *N*-methylsulfonamide scaffold.

Subsequently, the acid-labile protecting groups were completely removed from the crude thioester at room temperature with TFA containing water (2%), TES (2%) and ethyl 3-sulfanylpropionate (2%) as scavengers. The deprotected glycodecapeptide α -thioester **A**^[27] was obtained in 46% yield (2.51 mg, 734 nmol, purity: 95% (RP18-HPLC)) after preparative reversed-phase HPLC (based on the glycosyl amino acid **8** used: 2.64 mg, 1.6 μmol).

To assure that the thioester **A** was reactive in a native chemical ligation,^[5] elongation with the synthetic RNase 40–68 peptide **B**^[28] was examined on an analytical scale. Compounds **A** and **B** were dissolved in 6 M guanidinium hydrochloride (GnHCl) buffered at pH 7.6 and the ligation was started by addition of thiophenol (final concentration of 2%).^[5b] The reaction progress was followed by LC-MS and showed that the ligation had proceeded to 50% after 1 h and was complete within 8 h. Compound **A** was completely consumed and no hydrolyzed thioester was detectable in the crude reaction mixture, thus indicating efficient ligation. The analogous reaction in aqueous 1,4-dioxane^[11a] gave rise to considerable amounts of hydrolyzed thioester. The acetate groups were then removed in a one-pot reaction with hydrazine hydrate (10%) containing DTT (5%) to prevent disulfide formation. Ester hydrolysis was finished after 1 h and yielded the desired unprotected glycopeptide **C**^[27] as the target molecule (identified by LC-MS). The glycopeptide **C** obtained by native chemical ligation represents the homogeneously glycosylated fragment 30–68 of RNase B carrying a complex-type N-glycan.

Herein we have established a general and efficient solid-phase synthesis of complex glycopeptide α -thioesters as fragments of N-glycoproteins. The orthogonal combination of a safety-catch linker with a Rink amide gave a novel analytical construct that facilitates rapid LC-MS analysis and optimization of several key reactions. It was found that activation of glycosyl-asparagine *in situ* gives the highest coupling yields and that the OH groups can be acetylated (capping) without activating the safety-catch linker. With the availability of complex-type glycopeptide thioesters the chemical synthesis of fully *N*-glycosylated glycoproteins moves closer into reach. Work is currently in progress to provide the fragments required for the synthesis of full-length RNase B.

Received: June 30, 2004

Revised: September 13, 2004

Published online: February 3, 2005

Keywords: glycopeptides · glycoproteins · native chemical ligation · oligosaccharides · solid-phase synthesis

- [1] B. Lowe, A. Varki, *Essentials in Glycobiology*, Cold Spring Harbour, 1999.
- [2] a) P. M. Rudd, H. C. Joao, E. Coghill, P. Fiten, M. R. Saunders, G. Opdenakker, R. A. Dwek, *Biochemistry* **1994**, 33, 17–22; b) A. R. Nissenson, *Am. J. Kidney Dis.* **2001**, 38, 1390–1397.
- [3] a) M. Wacker, D. Linton, P. G. Hitchen, M. Nita-Lazar, S. M. Haslam, S. J. North, M. Panico, H. R. Morris, A. Dell, B. W.

- Wren, M. Aebi, *Science* **2002**, 298, 1790–1793; b) S. R. Hamilton, P. Bobrowicz, B. Bobrowicz, R. C. Davidson, H. Li, T. Mitchell, J. H. Nett, S. Rausch, T. A. Stadheim, H. Wischniewski, S. Wildt, T. U. Gerngross, *Science* **2003**, 301, 1244–1246; c) Z. Zhang, J. Gildersleeve, Y. Y. Yang, R. Xu, J. A. Loo, S. Uryu, C. H. Wong, P. G. Schultz, *Science* **2004**, 303, 371–373.
- [4] review: B. G. Davis, *Chem. Rev.* **2002**, 102, 597–602.
- [5] a) P. E. Dawson, T. W. Muir, I. Clark-Lewis, S. B. H. Kent, *Science* **1994**, 266, 776–779; b) P. E. Dawson, M. J. Churchill, M. R. Ghadiri, S. B. H. Kent, *J. Am. Chem. Soc.* **1997**, 119, 4325–4329; c) D. W. Low, M. G. Hill, M. R. Carrasco, S. B. H. Kent, P. Botti, *Proc. Natl. Acad. Sci. USA* **2001**, 98, 6554–6559; d) T. W. Muir, *Annu. Rev. Biochem.* **2003**, 72, 249–289.
- [6] a) Y. Shin, K. A. Winans, B. J. Backes, S. B. H. Kent, J. A. Ellman, C. R. Bertozzi, *J. Am. Chem. Soc.* **1999**, 121, 11684; b) M. J. Grogan, M. R. Pratt, L. A. Marcaurelle, C. R. Bertozzi, *Annu. Rev. Biochem.* **2002**, 71, 593–634; c) J. S. Miller, V. Y. Dudkin, G. J. Lyon, T. W. Muir, S. J. Danishefsky, *Angew. Chem.* **2003**, 115, 447–450; *Angew. Chem. Int. Ed.* **2003**, 42, 431–434; d) D. Macmillan, C. R. Bertozzi, *Angew. Chem.* **2004**, 116, 1379–1383; *Angew. Chem. Int. Ed.* **2004**, 43, 1355–1359.
- [7] a) J. D. Warren, J. S. Miller, S. J. Keding, S. J. Danishefsky, *J. Am. Chem. Soc.* **2004**, 126, 6576–6578; b) H. Hojo, E. Hagnoya, Y. Matsumoto, Y. Nakahara, K. Nabeshima, B. P. Toole, Y. Watanabe, *Tetrahedron Lett.* **2003**, 44, 2961–2964.
- [8] B. J. Backes, J. A. Ellman, *J. Org. Chem.* **1999**, 64, 2322–2330.
- [9] a) J. Alsina, T. S. Yokum, F. Albericio, G. Barany, *J. Org. Chem.* **1999**, 64, 8761–8769; b) A. Sewing, D. Hilvert, *Angew. Chem.* **2001**, 113, 3503–3505; *Angew. Chem. Int. Ed.* **2001**, 40, 3395–3396; c) R. von Eggelkraut-Gottanka, A. Klose, A. G. Beck-Sickinger, M. Beyermann, *Tetrahedron Lett.* **2003**, 44, 3551–3554.
- [10] G. W. Kenner, J. R. McDermott, R. C. Sheppard, *J. Chem. Commun.* **1971**, 636–637.
- [11] a) R. Ingenito, E. Bianchi, D. Fattori, A. Pessi, *J. Am. Chem. Soc.* **1999**, 121, 11369–11374; b) R. Quaderer, D. Hilvert, *Org. Lett.* **2001**, 3, 3181–3184.
- [12] a) F. Guiller, D. Orain, M. Bradley, *Chem. Rev.* **2000**, 100, 2091–2157; b) M. S. Congreve, S. V. Ley, J. J. Scicinski, *Chem. Eur. J.* **2002**, 8, 1769–1776.
- [13] M. S. Bernatowicz, S. B. Daniels, H. Köstner, *Tetrahedron Lett.* **1989**, 30, 4645–4648.
- [14] PEGA = polyethyleneglycolacrylamide: M. Meldal, *Tetrahedron Lett.* **1992**, 33, 3077–3080.
- [15] E. Kaiser, R. L. Colescott, C. D. Bossinger, P. I. Cook, *Anal. Biochem.* **1970**, 34, 595.
- [16] R. Ingenito, D. Dreznjak, S. Guffler, H. Wenschuh, *Org. Lett.* **2002**, 4, 1187–1188.
- [17] Novabiochem, *Novabiochem Innovations* **2000**, No. 6/00, to be found on the WWW under <http://www.novabiochem.com>.
- [18] A. Dryland, R. C. Sheppard, *J. Chem. Soc. Perkin Trans. 1* **1986**, 125–137.
- [19] W. C. Chan, P. D. White, *Fmoc Solid Phase Peptide Synthesis: a Practical Approach*, Vol. 222, Oxford University, Oxford, **2000**.
- [20] a) Z.-W. Guo, Y. Nakahara, Y. Nakahara, T. Ogawa, *Angew. Chem.* **1997**, 109, 1527–1529; *Angew. Chem. Int. Ed. Engl.* **1997**, 36, 1464–1466; b) C. Unverzagt, *Tetrahedron Lett.* **1997**, 38, 5627–5630; c) E. Meinjohanns, M. Meldal, H. Paulsen, R. A. Dwek, K. Bock, *J. Chem. Soc. Perkin Trans. 1* **1998**, 549–560; d) N. Yamamoto, Y. Ohmori, T. Sakakibara, K. Sasaki, L. R. Juneja, Y. Kajihara, *Angew. Chem.* **2003**, 115, 2641–2644; *Angew. Chem. Int. Ed.* **2003**, 42, 2537–2540; e) Y. Kajihara, Y. Suzuki, N. Yamamoto, K. Sasaki, T. Sakakibara, L. R. Juneja, *Chem. Eur. J.* **2004**, 10, 971–985; f) N. Shao, J. Xue, Z. Guo, *Angew. Chem.* **2004**, 116, 1595–1599; *Angew. Chem. Int. Ed.* **2004**, 43, 1569–1573.
- [21] a) C. Unverzagt, *Carbohydr. Res.* **1997**, 305, 423–431; b) C. Unverzagt, *Chem. Eur. J.* **2003**, 9, 1369–1376.
- [22] Without the acetylation of the oligosaccharide, the subsequent peptide elongation with Fmoc-Ala and TBTU-HOBt activation was found to give substantial amounts of glycopeptides that bear multiple *O*-acyl groups.
- [23] a) J. Broddefalk, K. Bergquist, J. Kihlberg, *Tetrahedron Lett.* **1996**, 37, 3011–3014; b) H. Kunz, C. Unverzagt, *Angew. Chem.* **1988**, 100, 1763–1765; *Angew. Chem. Int. Ed. Engl.* **1988**, 27, 1697–1699.
- [24] M. T. Martin, F. Roschangar, J. F. Eaddy, *Tetrahedron Lett.* **2003**, 44, 5461–5463.
- [25] T. Wieland, H. J. Hennig, *Chem. Ber.* **1969**, 93, 1236–1246.
- [26] S. C. Fields, W. H. Dent, F. R. Green, E. G. Tromiczak, *Tetrahedron Lett.* **1996**, 37, 1967–1970.
- [27] ESI-TOF-MS ($\text{CH}_3\text{CN}/\text{H}_2\text{O}$): **A** ($\text{C}_{141}\text{H}_{219}\text{N}_{23}\text{O}_{70}\text{S}_2$): $M_{\text{calcd}} = 3418.37$, $M_{\text{found}} = 1141.14$ [$M + 3\text{H}$] $^{3+}$; **C** ($\text{C}_{230}\text{H}_{386}\text{N}_{62}\text{O}_{92}\text{S}_4$): $M_{\text{calcd}} = 5616.63$, $M_{\text{found}} = 1406.22$ [$M + 4\text{H}$] $^{4+}$.
- [28] Compound **B** was obtained by Fmoc solid-phase peptide synthesis on a TCP resin and reversed-phase HPLC purification of the deprotected peptide.

Biphenyl Synthesis

Iron-Catalyzed Aryl–Aryl Cross-Couplings with Magnesium-Derived Copper Reagents**

*Ioannis Sapountzis, Wenwei Lin, Christiane C. Kofink, Christina Despotopoulou, and Paul Knochel**

*Dedicated to Professor Michael Veith
on the occasion of his 60th birthday*

Transition-metal-catalyzed cross-coupling reactions are very powerful C–C bond-forming reactions, especially between C(sp²) centers at which typical S_N2 substitutions cannot operate.^[1] Palladium(0) catalysts are the most widely and reliably used,^[1,2] especially if appropriate ligands such as sterically hindered phosphines are present.^[3] Nickel(0) complexes have also found useful applications, but appear to have

[*] Dr. I. Sapountzis, Dipl.-Chem. W. Lin, Dipl.-Chem. C. C. Kofink, C. Despotopoulou, Prof. Dr. P. Knochel
Department Chemie
Ludwig Maximilians-Universität München
Butenandtstrasse 5–13, Haus F,
81377 München (Germany)
Fax: (+49) 89-2180-77680
E-mail: paul.knochel@cup.uni-muenchen.de

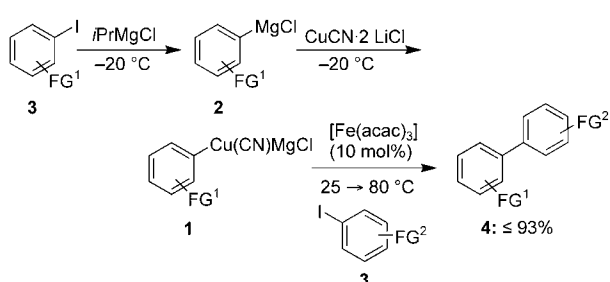
[**] We thank the Fonds der Chemischen Industrie, the Deutsche Forschungsgemeinschaft (DFG), and Merck Research Laboratories (MSD) for financial support. I.S. thanks Aventis Pharma (Frankfurt a. M.) for a fellowship. We also thank Chemetall GmbH (Frankfurt), Wacker Chemie GmbH (München), BASF AG (Ludwigshafen), and Bayer Chemicals AG for generous gifts of chemicals.



Supporting information for this article is available on the WWW under <http://www.angewandte.org> or from the author.

a less general scope.^[4] Following the pioneering work of Kochi and co-workers,^[5] iron catalysts have recently been very actively investigated for their performance in cross-coupling reactions.^[6] Although highly efficient cross-coupling reactions could be realized between a range of alkyl magnesium reagents and aryl halides or aryl sulfonates, iron-catalyzed cross-coupling between two aryl moieties remained problematic owing to extensive homo-coupling reactions of the aryl magnesium species.^[6,7] We assumed that the homo-coupling side reaction may arise by the formation of ferrate complexes with the highly reactive organomagnesium compounds.^[7] We therefore transmetalated the aryl magnesium species to the corresponding organozinc compounds, which have a lower tendency to form unstable ate complexes.^[8] Unfortunately, no iron-catalyzed cross-coupling reaction of aryl zinc reagents with aryl halides could be observed under various reaction conditions.

We therefore turned our attention to other organometallic species and found that organocopper compounds^[9] of type **1**, prepared by the reaction of functionalized aryl magnesium chlorides **2**^[10] with CuCN·2LiCl,^[11] react with functionalized aryl halides **3** in the presence of catalytic amounts of [Fe(acac)₃] (10 mol%) in DME/THF (3:2) between 25 and 80 °C, leading to polyfunctional biphenyls of type **4** (Scheme 1, Table 1 and Table 2).



Scheme 1. Fe-catalyzed cross-coupling of copper reagents **1** with aryl iodides **3**. FG¹ = CO₂Et, OMe, OTf; FG² = CO₂Et, CPh, COMe, CN, CONR₂.

Table 1: Cross-coupling of 2-substituted benzophenones with PhCu(CN)MgCl in the presence of [Fe(acac)₃].

Entry	X	Conversion [%] ^[a]
1	I	100 (< 5) ^[b] , (55) ^[c]
2	Br	86 (93) ^[d]
3	Cl	75 (77) ^[d]
4	OTf	35 (100) ^[e]
5	OTs	0

[a] Conversion after 30 min (determined by GC). [b] Conversion in the absence of [Fe(acac)₃] after 30 min. [c] Conversion after 48 h in the absence of [Fe(acac)₃]. [d] Conversion after 18 h. [e] Conversion after 2 h in THF.

Table 2: Fe-catalyzed cross-coupling between functionalized aryl copper reagents **1** and aryl iodides **3** to give **4**.

Entry	Aryl copper 1 ^[a]	Aryl iodide 3	Product 4	Yield [%] ^[b]
1	PhCu 1a	 3a	 4a	93
2	PhCu 1a	 3b	 4b	80
3	PhCu 1a	 3c	 4c	86
4	 1b	 3a	 4d	75
5	 1c	 3d	 4e	68
6	 1d	 3a	 4f	86
7	 1e	 3a	 4g	76
8	 1d	 3e	 4h	72
9	 1e	 3f	 4i	58
10	 1d	 3b	 4j	50
11	 1f	 3g	 4k	62

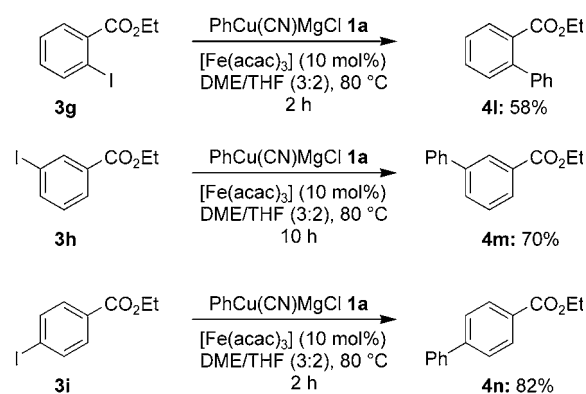
[a] The copper reagent is better represented as ArCu(CN)MgCl. [b] Yield of analytically pure products.

Remarkably, by using organocopper reagents **1**, the amount of homo-coupling is decreased, and the cross-coupling reaction occurs readily. The nature of the leaving

group of the electrophilic aromatic reagent **3** is also important (Table 1). Thus, the reaction of $\text{PhCu}(\text{CN})\text{MgCl}$ (**1a**) with 2-iodobenzophenone (**3a**) is complete within 30 min at 25 °C. In the absence of $[\text{Fe}(\text{acac})_3]$, less than 5% of biphenyl **4a** is observed after 30 min, and a conversion of approximately 54% only is observed after 48 h (Table 1, entry 1). The corresponding bromide (2-bromobenzophenone; Table 1, entry 2) also reacts fast, but after 30 min leads only to 86% conversion. A reaction time of 18 h only slightly improves the conversion (93%). Similarly, 2-chlorobenzophenone does not lead to complete conversion (75% after 30 min, but only 77% after 18 h). A significantly slower conversion is observed with a triflate substituent ($\text{X} = \text{OTf}$), but no reaction is observed with a tosylate ($\text{X} = \text{OTs}$) as leaving group. The fact that 2-chlorobenzophenone is converted indicates that the mechanism of the reaction does not involve a halogen–copper exchange reaction.^[12,13] Interestingly, the reactivity of aryl copper with aryl halides is the opposite to that observed for the Fe^{III} -catalyzed reaction with alkyl magnesium species, for which aryl iodides are poorer substrates than aryl bromides or chlorides.^[7]

We then investigated the reaction scope and noticed a remarkable functional-group compatibility and chemoselectivity. The reaction of $\text{PhCu}(\text{CN})\text{MgCl}$ (**1a**) is especially fast with 2-iodobenzophenone (**3a**) (30 min) and the corresponding ketone **4a** was obtained in 93% yield (Table 2, entry 1). 4-Iodobenzophenone (**3b**) reacts at 25 °C within 4 h to give the desired ketone **4b** in 80% yield (Table 2, entry 2). Remarkably, a methyl ketone, such as 2-iodophenyl methyl ketone (**3c**) undergoes iron-catalyzed cross-coupling without any competitive deprotonation of the methyl ketone or addition to the carbonyl function. Functionalized aryl magnesium reagents that bear an ester group at C2 or C4, such as **1b**, **1c**, or **1d** also undergo cross-coupling within a few hours, leading to the expected products **4d–f** in 68–86% yield (Table 2, entries 4–6). Thereby, the sterically hindered functionalized 2,2'-substituted biphenyl **4d** is prepared in 75% yield (Table 2, entry 4). Also, Grignard reagents that bear an electron-donating group (e.g. **1e**) react well to furnish the ketone **4g** in 76% yield (Table 2, entry 7). Various aryl iodides that bear electron-withdrawing substituents at C4 (such as a cyanide (**3e**), an amide (**3f**), or a ketone (**3b**)) undergo smooth cross-coupling and lead to the products **4h–j** in 50–70% yield (Table 2, entries 8–10). Remarkably, copper reagent **1f**, which bears a triflate group, reacts with ethyl 2-iodobenzoate **3g** to furnish biphenyl **4k** in 62% yield (Table 2, entry 11).

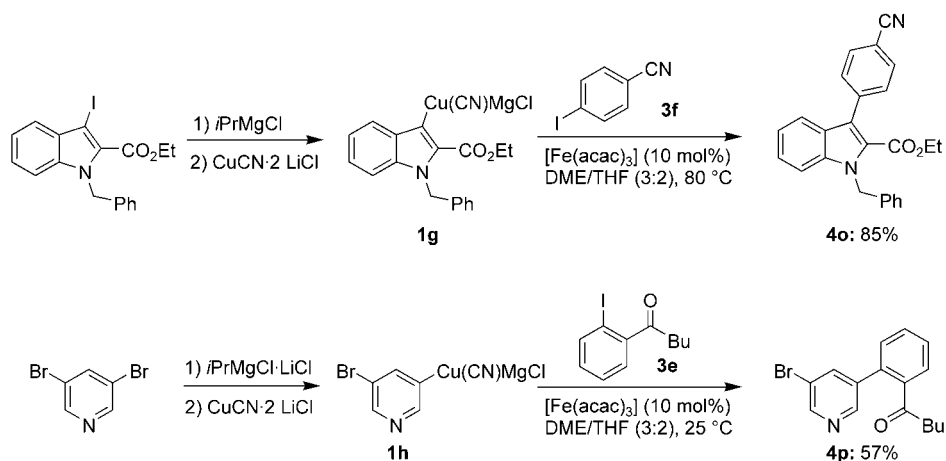
We noticed that the presence of an electron-withdrawing substituent at the aryl iodide accelerates the cross-coupling reaction and that donor substituents slow down the reaction



Scheme 2. Comparison between 2-, 3-, and 4-substituted substrates in the iron-catalyzed cross-coupling.

considerably. Thus, 4-iodoanisole leads only to some conversion at 80 °C after 12 h. We also compared the cross-coupling rate between 2-, 3-, and 4-substituted ethyl iodobenzoate (**3g–i**) with $\text{PhCu}(\text{CN})\text{MgCl}$ in the presence of $[\text{Fe}(\text{acac})_3]$ (10 mol%). Interestingly, the 2- and 4-substituted iodobenzoates **3g** and **3i** react five times faster than the 3-substituted ester **3h** (Scheme 2). This may indicate that the slow step of the cross-coupling is the nucleophilic attack of the catalytically active species to the benzoates **3g–i**.^[14]

Heterocyclic copper compounds are also suitable reagents for this cross-coupling reaction. Thus, organocopper reagents **1g** and **1h** react under standard conditions with the iodides **3f** and **3e** to furnish functionalized indole **4o** and pyridine **4p**, respectively (Scheme 3).



Scheme 3. Cross-coupling of heterocyclic copper reagents.

In summary, we have shown that the Fe-catalyzed cross-coupling reaction between functionalized heteroaryl and aryl copper reagents derived from the corresponding organomagnesium reagents proceeds readily with functionalized aryl iodides.^[15] The electron-poor electrophilic iodides undergo the cross-coupling reaction more readily. This new procedure presents an economical way (≈ 3 times cheaper than Pd-catalyzed reactions) to perform aryl–aryl cross-couplings.

Furthermore, the synergetic effect between copper and iron opens new synthetic possibilities that are being actively investigated in our laboratories.^[16]

Experimental Section

Typical procedure (4h): A 25-mL Schlenk tube equipped with a magnetic stirring bar and a septum was charged with ethyl 4-iodobenzoate (855 mg, 3.10 mmol) and DME (5 mL), and the solution was cooled to -20°C . $i\text{PrMgCl}$ (3.3 mL, 3.0 mmol, 0.90 M in THF) was then added, and the reaction mixture was stirred at this temperature for 15 min. Subsequently, a solution of $\text{CuCN}\cdot 2\text{LiCl}$ (2.8 mL, 2.8 mmol, 1.0 M in THF) was added, and the reaction mixture was stirred for an additional 10 min. A solution of 4-iodobenzonitrile (**3e**) (229 mg, 1.00 mmol) and $[\text{Fe}(\text{acac})_3]$ (35 mg, 0.10 mmol) dissolved in DME (3 mL) was added in one portion, and the reaction mixture was heated at 80°C for 3 h. The reaction mixture was quenched with saturated aqueous NH_4Cl and was extracted with CH_2Cl_2 (3×40 mL). The organic fractions were washed with saturated aqueous $\text{NH}_4\text{Cl}/\text{NH}_3$ (9:1) (50 mL) and brine (50 mL), dried over Na_2SO_4 , filtered, and the solvent was evaporated in vacuo. Purification by flash chromatography (pentane/ Et_2O 9:1) furnished **4h** as a colorless solid (181 mg, 72%).

Received: September 16, 2004

Published online: December 30, 2004

Keywords: cross-coupling · homogeneous catalysis · iron · copper · magnesium

- [1] a) *Metal-catalyzed Cross-coupling Reactions* (Eds.: F. Diederich; P. J. Stang), Wiley-VCH, Weinheim, **1998**; b) J. Tsuji, *Transition Metal Reagents and Catalysts: Innovations in Organic Synthesis*, Wiley, Chichester, **1995**; c) *Cross-Coupling Reactions. A Practical Guide* (Ed. N. Miyaura), *Top. Curr. Chem.* **2002**, 219.
- [2] *Handbook of organopalladium Chemistry for Organic Synthesis* (Ed.: E. Negishi), Wiley-Interscience, New York, **2002**.
- [3] a) C. Dai, G. C. Fu, *J. Am. Chem. Soc.* **2001**, 123, 2719; b) A. F. Littke, G. C. Fu, *J. Am. Chem. Soc.* **2001**, 123, 6989; c) A. F. Littke, L. Schwarz, G. C. Fu, *J. Am. Chem. Soc.* **2002**, 124, 6343; d) A. F. Littke, G. C. Fu, *Angew. Chem.* **2002**, 114, 4350; *Angew. Chem. Int. Ed.* **2002**, 41, 4176; e) I. D. Hills, M. R. Netherton, G. C. Fu, *Angew. Chem.* **2003**, 115, 5927; *Angew. Chem. Int. Ed.* **2003**, 42, 5749; f) A. C. Frisch, A. Zapf, O. Briel, B. Kayser, N. Shaikh, M. Beller, *J. Mol. Catal. A* **2004**, 214, 231; g) A. Tewari, M. Hein, A. Zapf, M. Beller, *Synthesis* **2004**, 935; h) F. Rataboul, A. Zapf, R. Jackstell, S. Harkal, T. Riermeier, A. Monsees, U. Dingerdissen, M. Beller, *Chem. Eur. J.* **2004**, 10, 2983.
- [4] a) M. Kumada, *Pure Appl. Chem.* **1980**, 52, 669; b) T.-Y. Luh, *Acc. Chem. Res.* **1991**, 24, 257; c) S. Sengupta, M. Leite, D. S. Raslan, C. Quesnelle, V. Snieckus, *J. Org. Chem.* **1992**, 57, 4066; d) A. F. Indolese, *Tetrahedron Lett.* **1997**, 38, 3513; e) E. Shirakawa, K. Yamasaki, T. Hiyama, *Synthesis* **1998**, 1544; f) A. Sophia, E. Karlström, K. Itami, J.-E. Bäckvall, *J. Am. Chem. Soc.* **2000**, 122, 6950; g) J. Montgomery, *Acc. Chem. Res.* **2000**, 33, 467; h) R. Giovannini, P. Knochel, *J. Am. Chem. Soc.* **1998**, 120, 11186; i) B. H. Lipshutz, *Adv. Synth. Catal.* **2001**, 343, 313; j) B. H. Lipshutz, G. Bulwo, F. Fernandez-Lazaro, S.-K. Kim, R. Lowe, P. Mollard, K. L. Stevens, *J. Am. Chem. Soc.* **1999**, 121, 11664.
- [5] a) M. Tamura, J. K. Kochi, *J. Am. Chem. Soc.* **1971**, 93, 1487; b) M. Tamura, J. K. Kochi, *Synthesis* **1971**, 93, 303; c) M. Tamura, J. K. Kochi, *J. Organomet. Chem.* **1971**, 31, 289; d) M. Tamura, J. K. Kochi, *Bull. Chem. Soc. Jpn.* **1971**, 44, 3063; e) M. Tamura, J. K. Kochi, *Synthesis* **1971**, 303; f) J. K. Kochi, *Acc. Chem. Res.* **1974**, 7, 351; g) S. Neumann, J. K. Kochi, *J. Org. Chem.* **1975**, 40, 599; h) R. S. Smith, J. K. Kochi, *J. Org. Chem.* **1976**, 41, 502; i) G. Molander, B. Rahn, D. C. Shubert, S. E. Bonde, *Tetrahedron Lett.* **1983**, 24, 5449.
- [6] a) G. Cahiez, S. Marquais, *Pure Appl. Chem.* **1996**, 68, 669; b) G. Cahiez, S. Marquais, *Tetrahedron Lett.* **1996**, 37, 1773; c) G. Cahiez, H. Avedissian, *Synthesis* **1998**, 1199; d) K. Shinokubo, K. Oshima, *Eur. J. Org. Chem.* **2004**, 2081; e) M. A. Fakhfakh, X. Franck, R. Hocquemiller, B. Figadère, *J. Organomet. Chem.* **2001**, 624, 131; f) M. Hocek, H. Dvorská, *J. Org. Chem.* **2003**, 68, 5773; g) B. Hölzer, R. W. Hoffmann, *Chem. Commun.* **2003**, 732; h) W. Dohle, F. Kopp, G. Cahiez, P. Knochel, *Synlett* **2001**, 1901; i) M. Hojo, Y. Murakami, H. Aihara, R. Sakuragi, Y. Baba, A. Hosomi, *Angew. Chem.* **2001**, 113, 641; *Angew. Chem. Int. Ed.* **2001**, 40, 621; j) M. Nakamura, A. Hirai, E. Nakamura, *J. Am. Chem. Soc.* **2001**, 123, 978; k) E. Alvarez, T. Cuvigny, C. H. du Penhoat, M. Julia, *Tetrahedron* **1998**, 54, 119; l) V. Finandane, G. Marchese, V. Martina, L. Ronzini, *Tetrahedron Lett.* **1984**, 25, 4805.
- [7] a) A. Fürstner, A. Leitner, M. Méndez, H. Krause, *J. Am. Chem. Soc.* **2002**, 124, 13856; b) A. Fürstner, A. Leitner, *Angew. Chem.* **2002**, 114, 632; *Angew. Chem. Int. Ed.* **2002**, 41, 308; c) A. Fürstner, A. Leitner, *Angew. Chem.* **2003**, 115, 320; *Angew. Chem. Int. Ed.* **2003**, 42, 308; d) G. Seidel, D. Laurich, A. Fürstner, *J. Org. Chem.* **2004**, 69, 3950; e) B. Scheiper, M. Bonnekessel, H. Krause, A. Fürstner, *J. Org. Chem.* **2004**, 69, 3943; f) A. Fürstner, D. De Souza, L. Parra-Rapado, J. T. Jensen, *Angew. Chem.* **2003**, 115, 5516; *Angew. Chem. Int. Ed.* **2003**, 42, 5355; g) M. Nakamura, K. Matsuo, S. Ito, E. Nakamura, *J. Am. Chem. Soc.* **2004**, 126, 3686; h) T. Nagano, T. Hayashi, *Org. Lett.* **2004**, 6, 1297; i) R. Martin, A. Fürstner, *Angew. Chem.* **2004**, 116, 4045; *Angew. Chem. Int. Ed.* **2004**, 43, 3955.
- [8] K. Reddy, P. Knochel, *Angew. Chem.* **1996**, 108, 1812; *Angew. Chem. Int. Ed. Engl.* **1996**, 35, 1700.
- [9] a) B. H. Lipshutz, S. Sengupta, *Org. React.* **1992**, 41, 135; b) R. J. K. Taylor, *Organocopper Reagents*, Oxford University Press, Oxford, **1994**; c) N. Krause, *Modern Organocopper Chemistry*, Wiley-VCH, Weinheim, **2002**.
- [10] a) A. Krasovskiy, P. Knochel, *Angew. Chem.* **2004**, 116, 3316; *Angew. Chem. Int. Ed.* **2004**, 43, 3333; b) for a Review, see: P. Knochel, W. Dohle, N. Gommermann, F. F. Kneisel, F. Kopp, T. Korn, I. Sapountzis, V. A. Vu, *Angew. Chem.* **2003**, 115, 4438; *Angew. Chem. Int. Ed.* **2003**, 42, 4302.
- [11] P. Knochel, M. C. P. Yeh, S. C. Berk, J. Talbert, *J. Org. Chem.* **1988**, 53, 2390.
- [12] C. Piazza, P. Knochel, *Angew. Chem.* **2002**, 114, 3397; *Angew. Chem. Int. Ed.* **2002**, 41, 3263.
- [13] In the absence of the iron catalyst, no reaction was observed for 2-chlorobenzophenone.
- [14] We submitted the substituted iodoesters **3g-i** to Pd- and Ni-catalyzed cross-coupling and found that in the case of Pd catalysis, 4-iodoester **3i** reacts significantly faster than **3g** and **3h**, whereas under Ni catalysis, the 3-iodoester **3h** is the fastest. These results indicate that the mechanism of Ni-, Pd- and Fe-catalyzed cross-coupling reactions is significantly different, as electronic and steric effects of the substituents affect them differently (see Supporting Information for details).
- [15] Interestingly, copper reagents made from aryl lithium species can also be used. The reaction proceeds at a similar rate (somewhat faster). The occurrence of an I-Cu exchange reaction is minimized with this type of copper species ($\text{ArCu}(\text{CN})\text{Li}$).
- [16] A patent application for this and related cross-coupling reactions has been filed.

Boron as a Bridging Ligand**

Holger Braunschweig,* Krzysztof Radacki,
David Scheschkewitz, and George R. Whittell

Dedicated to Professor Peter Paetzold
on the occasion of his 70th birthday

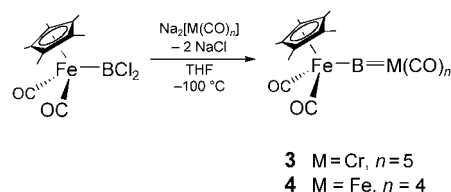
Borylenes (B–R) are highly reactive species that have only been observed at low temperatures^[1] or their presence inferred from the products of trapping reactions.^[2] The formation of an example stabilized within the coordination sphere of a transition-metal-ligand fragment thus constituted a major advance.^[3] Both bridging and terminal borylene coordination modes have now been realized, affording a comparison with common organometallic ligands.^[4] Despite these advances, however, the range of different borylenes stabilized by terminal coordination has remained somewhat narrow. The presence of bulky, π -donating substituents (η^5 -C₅Me₅,^[5] N(SiMe₃)₂,^[6] and 2,4,6-Me₃C₆H₂^[7]) would appear almost a prerequisite for stabilization, with the absence of π -donating substituents resulting in the lower thermal stability of [(OC)₅Cr{BSi(SiMe₃)₃}] (**1**).^[8] A number of theoretical studies have ventured to quantify the effects of different substituents on the nature of the transition-metal–boron bond.^[9] Experimental testing of these predictions, however, requires a wider range of examples. There would appear no reason as to why the main-group substituent at boron could not be replaced by another transition-metal–ligand fragment, as long as the steric and electronic criteria for stabilization are fulfilled. Compounds containing the heavier Group 13 elements, gallium^[10] and thallium,^[11] coordinated solely to two transition-metal–ligand fragments have been reported, these, however, partially owe their stability to the inert-pair effect.^[12] The synthesis of a boron homologue should hence pose a much more challenging problem. Such a compound represents a fundamentally new type of terminal borylene complex, but also a complex of interstitial boron^[13] containing classical (that is, electron-precise) metal–boron bonds. We report herein the syntheses, spectroscopic, and structural characterization of the first compounds to contain a boron center classically bonded solely to transition metals.

The reaction of dihaloboranes with dianionic transition-metal carbonylates has proven the most general synthetic route to terminal borylene complexes.^[4b–d] Thus, the recent realization of the dichloroboryl complex, [(η^5 -C₅H₅)Fe(CO)₂BCl₂] (**2**),^[14] afforded a starting material which could

potentially be utilized for preparation of a compound containing a μ_2 -boron bridge.

The reaction of **2** with Na₂[Cr(CO)₅] in toluene yielded a single new compound as shown by ¹¹B{¹H} NMR spectroscopy. The frequency of the signal (δ = 164 ppm), however, was shifted significantly upfield with respect to that predicted for the desired product [(η^5 -C₅H₅)Fe(CO)₂](μ_2 -B){Cr(CO)₅}, by computational methods (δ = 219.7 ppm).^[15] Although we could not isolate this compound, the formulation Na[(η^5 -C₅H₅)Fe(CO)₂](μ_2 -BCl){Cr(CO)₅} is consistent with the ¹¹B{¹H} NMR data.^[16] Furthermore, a similar species, K[(η^5 -C₅Me₅)Fe(CO)₂](μ_2 -GaCl){Fe(CO)₄}, was reportedly formed from reaction of [(η^5 -C₅Me₅)Fe(CO)₂GaCl₂] with K₂[Fe(CO)₄].^[10a] Changing the reaction solvent from toluene to THF cleanly afforded a different product, with an ¹¹B{¹H} NMR signal (δ = 199.6 ppm) at a frequency much closer to that predicted by theory. This compound, however, proved too thermally labile to be isolated.

We and others^[17] have observed that the thermal stability of the half-sandwich iron-boryl complexes, [(η^5 -C₅R₅)Fe(CO)₂BX₂], increases markedly on formal replacement of the cyclopentadienyl ligand (R = H) for pentamethylcyclopentadienyl (R = Me). Thus, when the reaction was repeated with [(η^5 -C₅Me₅)Fe(CO)₂BCl₂],^[18] the desired compound, [(η^5 -C₅Me₅)Fe(CO)₂](μ_2 -B){Cr(CO)₅} (**3**) was obtained in 35 % yield (Scheme 1).



Scheme 1. Syntheses of compounds **3** and **4**.

To demonstrate generality, the analogous reaction with Na₂[Fe(CO)₄] was attempted and this also yielded a μ_2 -boron complex, namely [(η^5 -C₅Me₅)Fe(CO)₂](μ_2 -B){Fe(CO)₄} (**4**), in comparable yield (36 %). Both compounds were extremely oxygen and moisture sensitive in the solid state and solution. However, under a dry argon atmosphere they showed no signs of decomposition in either THF or toluene solution after 24 h at room temperature.

The most striking spectroscopic feature of compounds **3** and **4** is the highly deshielded ¹¹B{¹H} NMR resonance signals (δ = 204.6 (**3**) and 190.9 ppm (**4**)). Compound **1** has a signal at a similar frequency (δ = 204.3 ppm)^[8] and the downfield shift relative to the aminoborylene, [(OC)₅Cr]BN(SiMe₃)₂ (**5**) (δ = 92 ppm),^[6a] is attributed to the absence of a π -donating substituent. It is noteworthy, however, that this region of the spectrum is normally only the domain of interstitial boron (δ = 172–226 ppm).^[19] Generally, all other spectroscopic data for **3** and **4** are as to be expected for the ancillary ligands. The only exception is that the ¹³C{¹H} NMR signal for the carbonyl ligand *trans* to boron is not observed. A similar situation, however, was reported for **1** and attributed to the high *trans* influence of the borylene ligand.^[8]

[*] Prof. Dr. H. Braunschweig, Dr. K. Radacki, Dr. D. Scheschkewitz, Dr. G. R. Whittell
Institut für Anorganische Chemie
Bayerische Julius-Maximilians-Universität Würzburg
Am Hubland, 97074 Würzburg (Germany)
Fax: (+49) 931-888-4623
E-mail: h.braunschweig@mail.uni-wuerzburg.de

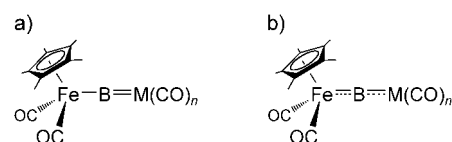
[**] This work was supported by the DFG and EPSRC.

The molecular structures of both compounds **3** and **4** were determined by single-crystal X-ray diffraction (Figure 1).^[20] The structure of **3** contains half a molecule per asymmetric unit with a crystallographic mirror plane bisecting the Cr, B, Fe atoms, and the pentamethylcyclopentadienyl ring. The structure of **4** has one molecule per asymmetric unit. In both structures the molecules are well separated and the boron center forms no close intramolecular contacts. The structures are characterized by the presence of a linear metal–boron–metal unit (Cr–B–Fe 177.75(11)° and Fe–B–Fe 175.38(12)°), confirming the bridging mode of the formally sp-hybridized boron atom. A linear bridging mode is also common to the μ_2 -Ga and μ_2 -Tl complexes, $[(\eta^5\text{-C}_5\text{Me}_5)\text{Fe}(\text{dppe})](\mu_2\text{-Ga})[\text{Fe}(\text{CO})_4]$ {dppe = 1,2-bis(diphenylphosphino)ethane},^[10a] $[(\eta^5\text{-C}_5\text{Me}_5)\text{Fe}(\text{CO})_2](\mu_2\text{-Ga})^+$,^[10b] and $[\text{Cr}(\text{CO})_5](\mu_2\text{-Tl})^-$,^[11b] that exhibit corresponding angles that are similarly close to 180° (176.01(4), 178.99(2), and 178.5(2)°, respectively). Only the μ_2 -thallium complex, $[\text{Ir}_2(\mu_2\text{-Tl})(\text{CO})_2\text{Cl}_2(\mu\text{-dmpa})_2]^+$ (dmpa = bis(diphenylphosphinomethyl)phenylarsine),^[11a] has a bridging unit which differs significantly from linearity [Ir–Tl–Ir 139.4(1)°]. This distortion, however, probably originates from the Ir...Ir separation being constrained somewhat by the bridging bidentate ligands.

For a discussion of the bonding in **3** and **4**, it is convenient to start from a formulation that depicts a single bond from boron to the half-sandwich moiety and a double bond from boron to the metal carbonyl fragment, thus affording each metal 18 valence electrons (Scheme 2a). The Fe–B bond length in **3** (1.8617(9) Å) is intermediate between those of the cationic borylene complex, $[(\eta^5\text{-C}_5\text{Me}_5)\text{Fe}(\text{CO})_2(\text{BMe}_3)]^+$ (Mes = 2,4,6-trimethylphenyl),^[7] for which an Fe–B double bond has been proposed, and **2** (1.942(3) Å),^[14] which has the shortest reported Fe–B(sp²) separation.

DFT calculations^[21] and structural studies^[14] indicate that even the Fe–B bond in **2** contains an appreciable π component, and thus the formal single bond proposed for **3** should be augmented by at least a modest π interaction. Similarly, the Cr–B bond length of 1.975(2) Å in **3** is intermediate between those of **5** (1.996(6) Å)^[6b] and **1** (1.878(10) Å).^[8] Compound **1** has a relatively strong Cr–B π interaction owing to the absence of a competing π -donor group at boron. The π contribution to the Cr–B bond in **3** is therefore less than that required for a formal double bond.

In **4**, the Fe2–B bond length (1.867(2) Å) is comparable to that in **3**, hence implying a similar π component. This



Scheme 2. Alternative bonding representations for compounds **3** (M = Cr, $n = 5$) and **4** (M = Fe, $n = 4$), see text for details.

fragment is bound to the $\{\text{Fe}(\text{CO})_4\}$ unit through the apical site and thus exhibits a similar gross structure to $[(\eta^5\text{-C}_5\text{Me}_5)\text{B}\{\text{Fe}(\text{CO})_4\}]$.^[5] However, in **4** the Fe1–B bond is significantly shorter (1.863(2) Å) than in $[(\eta^5\text{-C}_5\text{Me}_5)\text{B}\{\text{Fe}(\text{CO})_4\}]$ (2.010(3) Å) which contains only an Fe←B donor–acceptor bond. Thus, the bond lengths imply at least a degree of π bonding in the B–Fe(CO)₄ interaction of **4**. These arguments suggest that the bonding in both **3** and **4** is best described by a model in which both metal–boron bonds contain a π component (Scheme 2b). A comparable partial π -bond representation has been proposed for the μ_2 -Ga complexes on the basis of a similar structural analysis.^[10]

In conclusion, the reactions of $[(\eta^5\text{-C}_5\text{Me}_5)\text{Fe}(\text{CO})_2\text{BCl}_2]$ with either $\text{Na}_2[\text{Cr}(\text{CO})_5]$ or $\text{Na}_2[\text{Fe}(\text{CO})_4]$ affords compounds that contain a substituent-free boron center which bridges the transition metal–ligand fragments.

Experimental Section

All manipulations were conducted either under an atmosphere of dry argon or in vacuo using standard Schlenk line or glove-box techniques.

3: A solution of $\text{Na}_2[\text{Cr}(\text{CO})_5]$ ^[22] (2.354 mmol) in THF (25 mL) was prepared in a Schlenk tube and cooled to about –90 °C. This solution was then transferred, by cannula, to another Schlenk tube, similarly chilled and containing solid $[(\eta^5\text{-C}_5\text{Me}_5)\text{Fe}(\text{CO})_2\text{BCl}_2]$ ^[18] (0.702 g, 2.140 mmol). The reaction mixture was slowly allowed to warm to about –30 °C over approximately 1 h, resulting in the formation of a dark yellow/orange solution. Subsequent removal of all volatiles in vacuo, at room temperature, afforded a dark orange solid. Hexane (50 mL) was added and residual solids separated by centrifugation. The clear, orange supernatant liquors were then decanted, reduced in volume by about 50 % and cooled to –25 °C. After about 7 days, the pale orange crystals of pure **3** that had formed were isolated by removal of the mother liquors and dried in vacuo (yield 0.58 g, 31 %). IR (toluene): $\tilde{\nu}$ = 2055 (s), 2012 (s), 1976 (br s), 1932 (br s) cm^{–1}, $\nu(\text{CO})$. ¹H NMR (400 MHz, C₆D₆, 25 °C): δ = 1.40 ppm (s, 15H, C₅Me₅); ¹³C{¹H} NMR (101 MHz, C₆D₆, 25 °C): δ = 9.48 (s, C₅Me₅), 98.45(s, C₅Me₅), 210.32 (s, CO), 216.79 ppm (s,

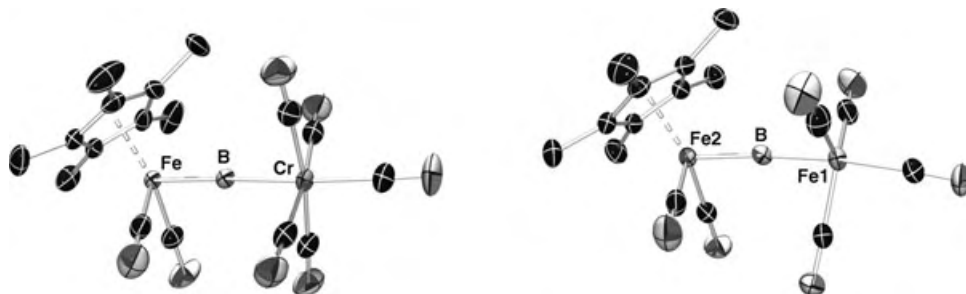


Figure 1. Molecular structures of **3** (left) and **4** (right). Selected bond lengths [Å] and angles [°]. **3**: Cr–B 1.975(2), Fe–B 1.8617(19); Cr–B–Fe 177.75(11). **4**: Fe1–B 1.863(2), Fe2–B 1.867(2); Fe1–B–Fe2 175.38(12).

CO); ^{11}B NMR (64 MHz, C_6D_6 , 25 °C): δ = 204.6 ppm ($\omega_{1/2}$ = 488 Hz). Elemental analysis (%) calcd for $\text{C}_{17}\text{H}_{15}\text{O}_7\text{BCrFe}$: C 45.38; H 3.36; found: C 45.34, H 3.41.

4: A suspension of $\text{Na}_2[\text{Fe}(\text{CO})_4]^{[23]}$ (0.329 g, 1.537 mmol) in THF (20 mL) was prepared in a 100-cm³ round-bottomed flask. This suspension was cooled to about –100 °C and then transferred, by cannula, to a similarly chilled Schlenk tube containing solid $[(\eta^5\text{-C}_5\text{Me}_5)\text{Fe}(\text{CO})_2\text{BCl}_2]^{[18]}$ (0.480 g, 1.464 mmol). The resulting brown suspension was slowly allowed to warm to around –15 °C over about 90 min affording a dark red solution. This solution was then allowed to warm to room temperature and all volatiles were removed in vacuo. Hexane (30 mL) was subsequently added to the residual dark red solid affording a cloudy, red solution. The insoluble components were separated by centrifugation and the supernatant liquors cooled to –25 °C. After about 2 days, the yellow crystals of pure **4** that had formed were isolated by removal of the mother liquors and dried in vacuo (yield 0.223 g, 36 %). IR (toluene): $\tilde{\nu}$ = 2048 (s), 2020 (s), 1979 (br s), 1929 (br s) cm^{–1}, $\nu(\text{CO})$. NMR ^1H (400 MHz, C_6D_6 , 25 °C): δ = 1.38 ppm (s, 15H, C_5Me_5); $^{13}\text{C}\{^1\text{H}\}$ NMR (101 MHz, C_6D_6 , 25 °C): δ = 9.29 (s, C_5Me_5), 98.64 (s, C_5Me_5), 209.92 (s, CO), 215.36 ppm (s, CO); ^{11}B NMR (64 MHz, C_6D_6 , 25 °C): δ = 190.9 ppm ($\omega_{1/2}$ = 521 Hz). Elemental analysis (%) calcd for $\text{C}_{16}\text{H}_{15}\text{O}_6\text{BF}_2$: C 45.13; H 3.55; found: C 45.23, H 3.65.

Received: December 22, 2004

Keywords: boron · bridging ligands · chromium · iron · low-valent compounds

- [1] B. Pachaly, R. West, *Angew. Chem.* **1984**, 96, 444; *Angew. Chem. Int. Ed. Engl.* **1984**, 23, 454.
- [2] a) P. L. Timms, *J. Am. Chem. Soc.* **1967**, 89, 1629; b) P. L. Timms, *J. Am. Chem. Soc.* **1968**, 90, 4585; c) P. L. Timms, *Acc. Chem. Res.* **1973**, 6, 118; d) P. Jutzi, A. Seufert, W. Buchner, *Chem. Ber.* **1979**, 112, 2488; e) U. Holtmann, P. Jutzi, T. Kühler, B. Neumann, H.-G. Stammer, *Organometallics* **1999**, 18, 5531; f) P. Greiwe, A. Bethäuser, H. Pritzkow, T. Kühler, P. Jutzi, W. Siebert, *Eur. J. Inorg. Chem.* **2000**, 1927; g) M. Ito, N. Tokitoh, T. Kawashima, R. Okazaki, *Tetrahedron Lett.* **1999**, 40, 5557.
- [3] H. Braunschweig, T. Wagner, *Angew. Chem.* **1995**, 107, 904; *Angew. Chem. Int. Ed. Engl.* **1995**, 34, 825.
- [4] a) H. Braunschweig, *Angew. Chem.* **1998**, 110, 1882; *Angew. Chem. Int. Ed.* **1998**, 37, 1786; b) H. Braunschweig, M. Colling, *Coord. Chem. Rev.* **2001**, 223, 1; c) H. Braunschweig, M. Colling, *Eur. J. Inorg. Chem.* **2003**, 393; d) H. Braunschweig, *Adv. Organomet. Chem.* **2004**, 51, 163.
- [5] A. H. Cowley, V. Lomeli, A. Voigt, *J. Am. Chem. Soc.* **1998**, 120, 6401.
- [6] a) H. Braunschweig, C. Kollann, U. Englert, *Angew. Chem.* **1998**, 110, 3355; *Angew. Chem. Int. Ed.* **1998**, 37, 3179; b) H. Braunschweig, M. Colling, C. Kollann, H.-G. Stammer, B. Neumann, *Angew. Chem.* **2001**, 113, 2359; *Angew. Chem. Int. Ed.* **2001**, 40, 2298; c) H. Braunschweig, M. Colling, C. Hu, K. Radacki, *Angew. Chem.* **2003**, 115, 215; *Angew. Chem. Int. Ed.* **2003**, 42, 205.
- [7] D. L. Coombs, S. Aldridge, C. Jones, D. J. Willock, *J. Am. Chem. Soc.* **2003**, 125, 6356.
- [8] H. Braunschweig, M. Colling, C. Kollann, K. Merz, K. Radacki, *Angew. Chem.* **2001**, 113, 4327; *Angew. Chem. Int. Ed.* **2001**, 40, 4198.
- [9] a) C. Boehme, J. Uddin, G. Frenking, *Coord. Chem. Rev.* **2000**, 197, 249; b) C. L. B. Macdonald, A. H. Cowley, *J. Am. Chem. Soc.* **1999**, 121, 12113.
- [10] a) K. Ueno, T. Watanabe, H. Tobita, H. Ogino, *Organometallics* **2003**, 22, 4375; b) N. R. Bunn, S. Aldridge, D. L. Coombs, A. Rossin, D. Willock, C. Jones, L. Ooi, *Chem. Commun.* **2004**, 15, 1732.
- [11] a) A. L. Balch, J. K. Nagle, M. M. Olmstead, P. E. Reedy, Jr., *J. Am. Chem. Soc.* **1987**, 109, 4123; b) B. Schiemenz, G. Huttner, *Angew. Chem.* **1993**, 105, 1840; *Angew. Chem. Int. Ed. Engl.* **1993**, 32, 1772.
- [12] F. A. Cotton, G. Wilkinson, *Advanced Inorganic Chemistry*, 5th ed., Wiley, New York, **1988**, pp. 208–209.
- [13] C. E. Housecroft, *Coord. Chem. Rev.* **1995**, 143, 297.
- [14] H. Braunschweig, K. Radacki, F. Seeler, G. R. Whittell, *Organometallics* **2004**, 23, 4178.
- [15] Gaussian03 (Revision B.04), M. J. Frisch, G. W. Trucks, H. B. Schlegel, G. E. Scuseria, M. A. Robb, J. R. Cheeseman, J. A. Montgomery, Jr., T. Vreven, K. N. Kudin, J. C. Burant, J. M. Millam, S. S. Iyengar, J. Tomasi, V. Barone, B. Mennucci, M. Cossi, G. Scalmani, N. Rega, G. A. Petersson, H. Nakatsuji, M. Hada, M. Ehara, K. Toyota, R. Fukuda, J. Hasegawa, M. Ishida, T. Nakajima, Y. Honda, O. Kitao, H. Nakai, M. Klene, X. Li, J. E. Knox, H. P. Hratchian, J. B. Cross, C. Adamo, J. Jaramillo, R. Gomperts, R. E. Stratmann, O. Yazyev, A. J. Austin, R. Cammi, C. Pomelli, J. W. Ochterski, P. Y. Ayala, K. Morokuma, G. A. Voth, P. Salvador, J. J. Dannenberg, V. G. Zakrzewski, S. Dapprich, A. D. Daniels, M. C. Strain, O. Farkas, D. K. Malick, A. D. Rabuck, K. Raghavachari, J. B. Foresman, J. V. Ortiz, Q. Cui, A. G. Baboul, S. Clifford, J. Cioslowski, B. B. Stefanov, G. Liu, A. Liashenko, P. Piskorz, I. Komaromi, R. L. Martin, D. J. Fox, T. Keith, M. A. Al-Laham, C. Y. Peng, A. Nanayakkara, M. Challacombe, P. M. W. Gill, B. Johnson, W. Chen, M. W. Wong, C. Gonzalez, J. A. Pople, Gaussian, Inc., Pittsburgh, PA, **2003**.
- [16] $^{11}\text{B}\{^1\text{H}\}$ NMR chemical shifts for three-coordinate, bridging borylene complexes range from δ = 96.5 to 170.0 ppm.^[4]
- [17] S. Aldridge, D. L. Coombs, *Coord. Chem. Rev.* **2004**, 248, 535.
- [18] H. Braunschweig, K. Radacki, D. Rais, G. R. Whittell, *Angew. Chem.* **2005**, 117, 1217; *Angew. Chem. Int. Ed.* **2005**, 44, 1192.
- [19] N. P. Rath, T. P. Fehlner, *J. Am. Chem. Soc.* **1988**, 110, 5345.
- [20] Crystal structure data for **3**: orange blocks from heptane; $\text{C}_{17}\text{H}_{15}\text{O}_7\text{BCrFe}$, orthorhombic, space group $Pnma$; a = 17.721(6), b = 12.968(4), c = 8.552(3) Å, $\alpha = \beta = \gamma = 90^\circ$, V = 1965.3(12) Å³; Z = 4, ρ_{calcd} = 1.521 g cm^{–3}; crystal dimensions: 0.25 × 0.25 × 0.2 mm; diffractometer: Bruker SMART APEX CCD; MoK_α radiation, 173(2) K; $2\theta_{\text{max}}$ = 56.56°; 19159 reflections, 2545 unique (R_{int} = 0.0261), direct methods; absorption correction SADABS (μ = 1.325 mm^{–1}); refinement (against F_o^2) with SHELXTL-97, 142 parameters, 5 restraints, R_1 = 0.0248 ($I > 2\sigma$) and wR_2 = 0.0701 (all data), Goof = 1.066, max/min residual electron density: 0.381/–0.291 e Å^{–3}. Crystal structure data for **4**: yellow plates from heptane; $\text{C}_{16}\text{H}_{15}\text{O}_6\text{BF}_2$, monoclinic, space group $P2_1/n$; a = 8.058(5), b = 14.638(10), c = 15.664(8) Å, α = 90, β = 93.87(3), γ = 90°, V = 1849(2) Å³; Z = 4, ρ_{calcd} = 1.530 g cm^{–3}; crystal dimensions: 0.05 × 0.15 × 0.15 mm; diffractometer: Bruker SMART APEX CCD; MoK_α radiation, 173(2) K; $2\theta_{\text{max}}$ = 55.78°; 18309 reflections, 4420 unique (R_{int} = 0.0312), direct methods; absorption correction SADABS (μ = 1.595 mm^{–1}); refinement (against F_o^2) with SHELXTL-97, 226 parameters, 0 restraints, R_1 = 0.0329 ($I > 2\sigma$) and wR_2 = 0.0826 (all data), Goof = 1.042, max/min residual electron density: 0.488/–0.211 e Å^{–3}. CCDC-258544 (3) and CCDC-258433 (4) contain the supplementary crystallographic data for this paper. These data can be obtained free of charge from the Cambridge Crystallographic Data Centre via www.ccdc.cam.ac.uk/data_request/cif.
- [21] A. A. Dickinson, D. J. Willock, R. J. Calder, S. Aldridge, *Organometallics* **2002**, 21, 1146.
- [22] J. M. Maher, R. P. Beatty, N. J. Cooper, *Organometallics* **1985**, 4, 1354.
- [23] H. Strong, P. J. Krusic, J. San Filippo, Jr., *Inorg. Synth.* **1990**, 28, 203.

Chirality Transfer

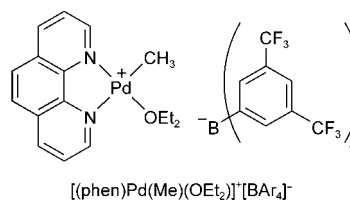
“True” Chirality Transfer from Silicon to Carbon: Asymmetric Amplification in a Reagent-Controlled Palladium-Catalyzed Hydrosilylation**

Martin Oestreich* and Sebastian Rendler

Transferring chirality from silicon to carbon has been a fundamental challenge in asymmetric synthesis since the advent of asymmetrically substituted organosilicon compounds.^[1] The expression “chirality transfer from silicon to carbon” was coined originally by Paquette to classify two categorically different stereochemical scenarios:^[2] substrate^[2a] and reagent control.^[2b] In a substrate-controlled transformation, the stereogenic silicon moiety is covalently bound to the substrate functioning as a chiral auxiliary.^[2a,3] Conversely, in a reagent-controlled reaction involving a functionalized silane with silicon-centered chirality and a prochiral substrate, a covalent bond is broken and formed at the chiral silicon center. In this case, any induced stereoselectivity stems from the stereochemical information at the silicon reagent. This “true” silicon-to-carbon chirality transfer and, therefore, the potential use of chiral silanes as reagents has not been accomplished yet^[2b,4] and still remains an unsolved problem.

In this communication, we report on the first chirality transfer from silicon to carbon with perfect stereoselectivity, which has been realized in a palladium-catalyzed hydrosilylation.^[5] Furthermore, this reaction displays an unusual positive nonlinear effect, (+)-NLE,^[6] in a transition-metal-catalyzed, reagent-controlled reaction. The observed asymmetric amplification in turn opens interesting insights into the catalytic cycle with the “chiral silicon” acting as a stereochemical probe.

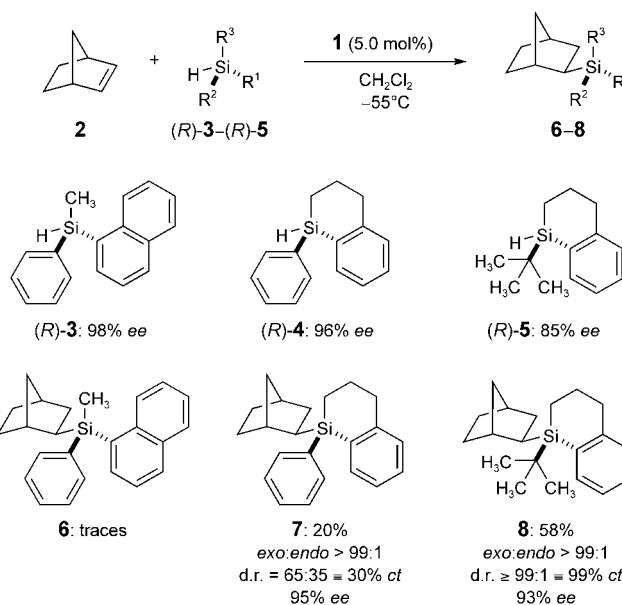
For our investigations, we selected the highly reactive catalyst **1**^[7] (phen = 1,10-phenanthroline, Ar = 3,5-bis-(trifluoromethyl)phenyl), which had been introduced to hydrosilylation chemistry by Brookhart et al.^[8] Not only does **1** catalyze the hydrosilylation of internal alkenes with triorganosilanes,^[8] its mode of reaction implies a feature of



paramount importance to our purposes. Detailed elucidation of the catalytic cycle by Brookhart et al.^[8] and Widenhoefer and Perch^[9] has revealed that carbon–silicon coupling occurs prior to carbon–hydrogen bond formation. In contrast, a reversed order of bond formations is expected for hydrosilylations following the classic Chalk–Harrod^[10] mechanism.^[5] Under these circumstances, an asymmetrically substituted silicon moiety is likely to function as a chiral monodentate ligand coordinated to the transition metal in the configuration-determining step (carbon–hydrogen bond formation/migratory insertion). This is comparable to catalyst-controlled hydrosilylations employing monodentate phosphorus-stereogenic phosphines,^[11] which are isolobal^[12] to silicon-stereogenic silyl anions. The former are known to induce low levels of stereoselection.^[11,13]

We selected norbornene (**2**) as the substrate since it is not susceptible to β -hydride elimination in the course of the catalytic cycle.^[8] The silanes (*R*)-**3**, (*R*)-**4**, and (*R*)-**5** surveyed in this study were prepared in the desired enantiomeric purities according to known procedures.^[14,15] Importantly, the oxidative addition of group VIII transition-metal centers into the silicon–hydrogen bond of silanes with silicon-centered chirality proceeds with stereoretention at silicon as verified for (*R*)-**3**.^[16,17]

The hydrosilylation of **2** catalyzed by **1** with acyclic silane (*R*)-**3** (98% *ee*) proved to be extremely sluggish (**2** \rightarrow **6**, Scheme 1). By using cyclic silane (*R*)-**4** (96% *ee*), we were able to isolate the desired product **7** (95% *ee*)^[18] in low yield



Scheme 1. Silicon-to-carbon chirality transfer in the hydrosilylation of norbornene (**2**).

[*] Dr. M. Oestreich, Dipl.-Chem. S. Rendler
Institut für Organische Chemie und Biochemie
Albert-Ludwigs-Universität
Albertstrasse 21, 79104 Freiburg (Germany)
Fax: (+49) 761-203-6100
E-mail: martin.oestreich@gmail.com; chemie.uni-freiburg.de

[**] Financial support has been provided by the Deutsche Forschungsgemeinschaft (Emmy Noether fellowship, Oe 249/2-3), the Fonds der Chemischen Industrie, and the Wissenschaftliche Gesellschaft in Freiburg im Breisgau. The authors thank Ilona Hauser for skillful technical assistance, Dr. Manfred Keller for NMR measurements as well as X-ray analysis of an intermediate silane, and Gerd Fehrenbach and Dr. Richard Krieger for performing HPLC analyses. M.O. is indebted to Prof. Reinhard Brückner for his continuous encouragement.

Supporting information for this article is available on the WWW under <http://www.angewandte.org> or from the author.

yet with “preserved” enantiomeric excess (*ee*).^[17] The diastereomeric ratio (*d.r.*) and chirality transfer (*ct*), which, in this case, corresponds to the diastereomeric excess, though only moderate exceeded any literature precedent.^[2a,4] Encouraged by this result, we employed the sterically (and electronically) modified silane (*R*)-**5** (85 % *ee*) in the hydrosilylation of **2** (**2**→**8**). We were pleased to find that **8**^[18] was formed in good yield and with perfect diastereoselection (*d.r.* ≥ 99:1 and 99 % *ct*). This constitutes the first silicon-to-carbon chirality transfer!

To our great surprise, the enantiomeric excess determined for **8** (93 % *ee*) was substantially higher than the enantiomeric purity of the starting silane (*R*)-**5** (85 % *ee*). This indicated a positive nonlinear effect,^[6] which was validated for (*R*)-**5** at several levels of enantiomeric purity (Table 1, entries 1–7, Figure 1). Asymmetric amplification in reagent-controlled

Table 1: Data for the determination of a positive nonlinear effect in (*R*)-**5**→**8** and (*R*)-**5**→**10** (see also Figure 1).^[a]

Entry (●)	<i>ee</i> [%] of (<i>R</i>)- 5 ^[b]	<i>ee</i> [%] of 8 ^[c]	Entry (▲)	<i>ee</i> [%] of (<i>R</i>)- 5 ^[b]	<i>ee</i> [%] of 10 ^[c]
1	0	0	8	0	0
2	29	38	9	16	14
3	54	69	10	40	40
4	60	76	11	65	65
5	79	85			
6	83	93			
7	85	93			

[a] All reactions were conducted with a substrate concentration of 0.1 M in CH₂Cl₂ at –55 °C and 1.2 equiv of (*R*)-**5** (see Supporting Information for a detailed procedure including full characterization of **8** and **10**). [b] HPLC analysis using a Daicel Chiralcel OJ-R column (EtOH/H₂O = 80:20 at 20 °C) provided baseline separation of enantiomers. [c] HPLC analysis using two coupled Daicel Chiralcel OD-H columns (*n*-heptane at 0 °C) for **8** and an OD-H column (*n*-heptane at 15 °C) for **10** provided baseline separation of enantiomers.

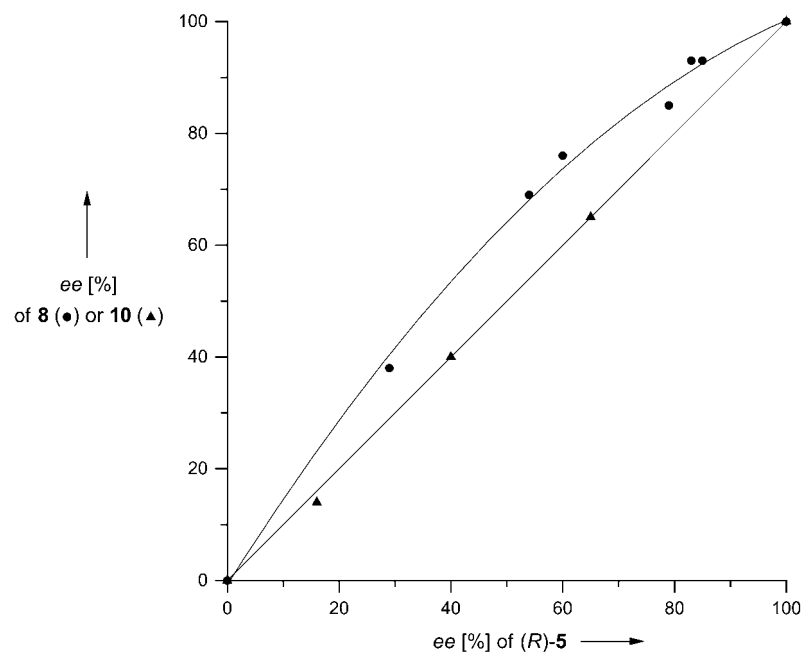
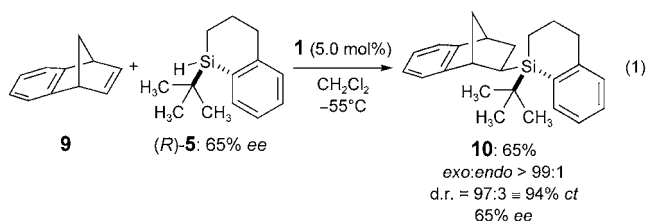


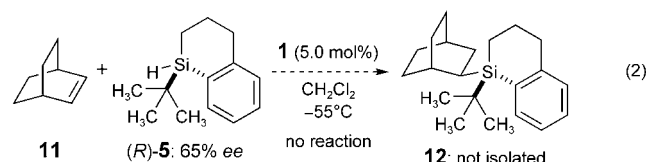
Figure 1. Positive nonlinear effect in the hydrosilylation of **2** with (*R*)-**5** (●) in comparison with the hydrosilylation of **9** with (*R*)-**5** (▲).

reactions is rare^[19] and has been described only for the reduction of a carbonyl with a chiral borane.^[20]

Interestingly, both the chiral amplification and the hydrosilylation itself are extremely sensitive to slight steric alterations within the alkene. Cognate alkene **9**, in which the ethano bridge of **2** is benzannellated, was also hydrosilylated with almost perfect chirality transfer [**9**→**10**, Eq. (1)]; how-

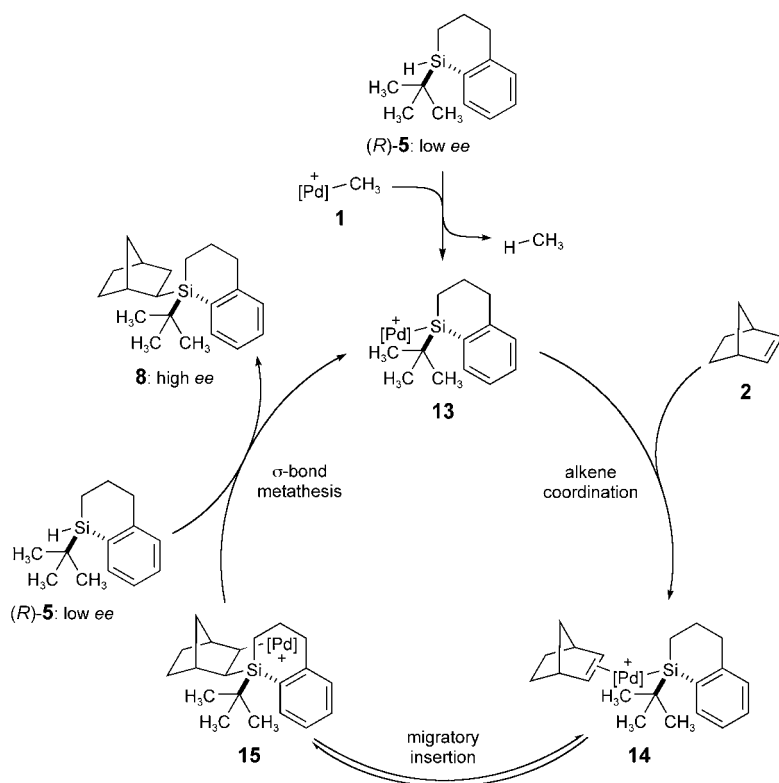


ever, no asymmetric amplification was detected in this reaction (Table 1, entries 8–11, Figure 1). Conversely, **11** incorporating two ethano bridges proved to be unreactive, and reaction under hydrosilylation conditions did not lead to any product [**11**→**12**, Eq. (2)]. It appears that the steric



requirements of alkene (and silane) must be finely balanced for a successful, chirally amplified reaction.

The observed asymmetric amplification in the hydrosilylation of **2** with (*R*)-**5** provides direct experimental insights into the mechanism as a positive nonlinear effect must arise from two molecules of (*R*)-**5**. Based on reported mechanistic investigations,^[8,9] our findings are consistent with the so-called “two-silicon cycle” depicted in Scheme 2. The stereogenic silicon center in (*R*)-**5** functions as a stereochemical probe. Reaction of (*R*)-**5** (low *ee*) with in situ generated **1**^[7,9] furnishes the cationic, mononuclear^[8] silylpalladium species **13** liberating methane.^[16,17] Electrophilic **13** coordinates norbornene (**2**) forming the alkenepalladium complex **14**. Subsequent carbon–silicon bond formation occurs during the migratory insertion furnishing **15**, which is the crucial intermediate for chiral amplification. In the final step, catalytically active **13** is regenerated by a σ -bond metathesis^[8,9] of chiral (*R*)-**5** (low *ee*) and chiral **15** (low *ee*). As there is a matched and a mismatched scenario in this transformation involving two chiral silicon moieties, one enantiomer of **8** (high *ee*) will be formed preferentially.



Scheme 2. Proposed "two-silicon cycle". Ligands at palladium are omitted for clarity.

So far, it is still unclear whether migratory insertion (**14**→**15**) or α -bond metathesis (**15**→**13**) is the crucial diastereoselectivity-determining step since the migratory insertion is potentially reversible.^[8] Future work will be devoted to clarifying the origin of stereoselection.

In summary, we have accomplished the chirality transfer from silicon to carbon accompanied by an unusual^[19] asymmetric amplification. This is the first example in which a silicon reagent with silicon-centered chirality induces carbon-centered chirality during the intermolecular formation of a carbon–silicon bond to a prochiral substrate. The exact mechanism of this reaction as well as application to other transition-metal catalysts employing silicon as a stereochemical probe are currently under investigation in our laboratories.

Received: October 19, 2004

Keywords: asymmetric amplification · asymmetric catalysis · hydrosilylation · palladium · silicon

- [1] a) L. H. Sommer, *Stereochemistry, Mechanism and Silicon*, McGraw-Hill, New York, **1965**; b) L. H. Sommer, *Intra-Sci. Chem. Rep.* **1973**, 7, 1–44; c) R. J. P. Corriu, C. Guerin, J. J. E. Moreau in *Topics in Stereochemistry*, Vol. 15 (Ed.: E. L. Eliel), Wiley, New York, **1984**, pp. 43–198; d) C. A. Maryanoff, B. E. Maryanoff in *Asymmetric Synthesis*, Vol. 4 (Eds.: J. D. Morrison, J. W. Scott), Academic Press, Orlando, **1984**, pp. 355–374.
- [2] a) Substrate control: R. G. Daniels, L. A. Paquette, *Organometallics* **1982**, 1, 1449–1453; b) Reagent control: S. J. Hath-

- away, L. A. Paquette, *J. Org. Chem.* **1983**, 48, 3351–3353; c) Reagent control using a silane with an axially chiral backbone: M. E. Jung, K. T. Hogan, *Tetrahedron Lett.* **1988**, 29, 6199–6202.
- [3] For important examples of asymmetrically substituted silicon moieties as chiral auxiliaries, see: a) G. L. Larson, V. Cruz de Maldonado, L. M. Fuentes, L. E. Torres, *J. Org. Chem.* **1988**, 53, 633–639; b) B. F. Bonini, S. Masiero, G. Mazzanti, P. Zani, *Tetrahedron Lett.* **1991**, 32, 6801–6804; c) M. Trzoss, J. Shao, S. Bienz, *Tetrahedron* **2002**, 58, 5885–5894.
- [4] For examples of attempted reagent control, see: a) J. L. Fry, M. G. Adlington, *J. Am. Chem. Soc.* **1978**, 100, 7641–7644; b) P. J. Stang, A. E. Learned, *J. Org. Chem.* **1989**, 54, 1779–1781.
- [5] a) For an excellent review on hydrosilylations including reaction mechanisms, see: I. Ojima, Z. Li, J. Zhu in *The Chemistry of Organic Silicon Compounds*, Vol. 2 (Eds.: Z. Rappaport, Y. Apeloig), Wiley, New York, **1998**, pp. 1687–1792; b) For a review on asymmetric catalyst-controlled hydrosilylations, see: T. Hayashi in *Comprehensive Asymmetric Catalysis*, Vol. 1 (Eds.: E. N. Jacobsen, A. Pfaltz, H. Yamamoto), Springer, Heidelberg, **1999**, pp. 319–333.
- [6] a) C. Girard, H. B. Kagan, *Angew. Chem.* **1998**, 110, 3088–3127; *Angew. Chem. Int. Ed.* **1998**, 37, 2923–2959; b) H. B. Kagan, *Synlett* **2001**, 888–899.
- [7] Preparation of the precatalysts of **1**: a) [(phen)PdMe₂]: W. de Graaf, J. Boersma, W. J. J. Smeets, A. L. Spek, G. van Koten, *Organometallics* **1989**, 8, 2907–2917; b) [H(OEt₂)₂]⁺[BAR₄][−]: M. Brookhart, B. Grant, A. F. Volpe, Jr., *Organometallics* **1992**, 11, 3920–3922.
- [8] A. M. LaPointe, F. C. Rix, M. Brookhart, *J. Am. Chem. Soc.* **1997**, 119, 906–917.
- [9] a) R. A. Widenhoefer, *Acc. Chem. Res.* **2002**, 35, 905–913; b) For mechanistic investigations, see: N. S. Perch, R. A. Widenhoefer, *J. Am. Chem. Soc.* **2004**, 126, 6332–6346.
- [10] For a leading reference, see: A. Magistrato, T. K. Woo, A. Togni, U. Rothlisberger, *Organometallics* **2004**, 23, 3218–3227.
- [11] K. Yamamoto, T. Hayashi, M. Kumada, *J. Am. Chem. Soc.* **1971**, 93, 5301–5302.
- [12] P. Braunstein, N. M. Boag, *Angew. Chem.* **2001**, 113, 2493–2499; *Angew. Chem. Int. Ed.* **2001**, 40, 2427–2433.
- [13] Earlier investigations from our laboratories support the assumption that formation of the carbon–hydrogen bond prior to the carbon–silicon bond is severely detrimental to efficient silicon-to-carbon chirality transfer: S. Rendler, Diploma Thesis, Albert-Ludwigs-Universität, Freiburg, **2004**.
- [14] L. H. Sommer, C. L. Frye, G. A. Parker, K. W. Michael, *J. Am. Chem. Soc.* **1964**, 86, 3271–3276.
- [15] a) For a modular and convergent approach to 1-sila-1,2,3,4-tetrahydronaphthalenes with silicon-centered chirality, see: M. Oestreich, U. K. Schmid, G. Auer, M. Keller, *Synthesis* **2003**, 2725–2739; b) HPLC analysis using a Daicel Chiralcel OD-H column (*n*-heptane at 20°C) for (*R*)-**4** provided baseline separation of enantiomers (see also Table 1).
- [16] a) Co, Ni, Pd, Ir, Pt: L. H. Sommer, J. E. Lyons, H. Fujimoto, *J. Am. Chem. Soc.* **1969**, 91, 7051–7061; b) Pt: C. Eaborn, D. J. Tune, D. R. M. Walton, *J. Chem. Soc. Dalton Trans.* **1973**, 2255–2264; c) Rh: R. J. P. Corriu, J. J. E. Moreau, *J. Organomet. Chem.* **1975**, 85, 19–33.
- [17] Oxidative addition processes might not be operating when catalyst **1** is employed. Instead, concerted σ -bond metatheses,

which very likely proceed with stereoretention at silicon, have been suggested as plausible reaction pathways.^[8]

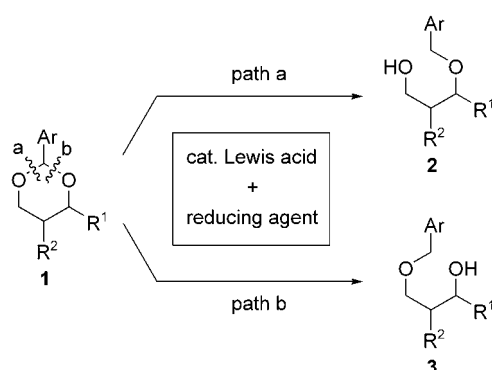
- [18] a) Not suprisingly, all attempts directed towards chemical correlation of *t*Bu-substituted cyclic silanes **8** and **10** by oxidative degradation have failed so far. Although the ROESY NMR experiments were not completely conclusive, we assigned the relative configurations of **10** and **8** (see Supporting Information for details). Based on these measurements, we suggest the relative configurations as depicted; b) HPLC analysis using two coupled Daicel Chiralcel OD-H columns (*n*-heptane at 0 °C) for **7** provided baseline separation of enantiomers (see also Table 1).
- [19] We are not aware of another example of a positive nonlinear effect in a transition-metal-catalyzed, reagent-controlled asymmetric transformation.
- [20] C. Girard, H. B. Kagan, *Tetrahedron: Asymmetry* **1997**, 8, 3851–3854.
-

Synthetic Methods

Cu(OTf)₂ as an Efficient and Dual-Purpose Catalyst in the Regioselective Reductive Ring Opening of Benzylidene Acetals**

Chi-Rung Shie, Zheng-Hao Tzeng, Suvarn S. Kulkarni, Biing-Jiun Uang, Ching-Yun Hsu, and Shang-Cheng Hung*

Regioselective ring opening of benzylidene acetals is one of the major challenges in carbohydrate and natural product syntheses.^[1] Substituted and unsubstituted benzylidene acetals are valuable protecting groups to block 1,3-diols. Arylidene acetals **1** can be opened selectively under appropriate reaction conditions (Scheme 1) to yield primary **2** (path a) or



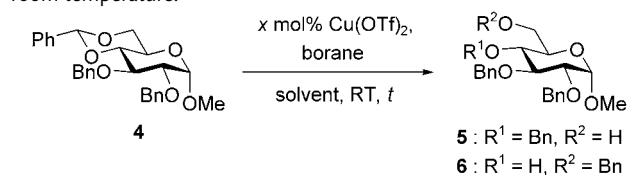
Scheme 1. Lewis acid catalyzed regioselective reductive ring opening of benzylidene acetals **1** to give primary alcohols **2** (path a) or secondary alcohols **3** (path b).

secondary alcohols **3** (path b). A number of effective reagents have been reported for the regioselective ring opening of 4,6-*O*-benzylidene acetals in hexopyranosides. Of these, AlH₃^[2] and *i*Bu₂AlH,^[3] which are commonly used to cleave at the O6

position, often lack chemoselectivity when substrates contain base-sensitive functionalities. Alternatively, traditional acid-promoted reductive cleavage has been reported to open benzylidene acetals at either the O6^[4] or O4 position.^[4a,c,f,5] However, these traditional acids have to be used stoichiometrically or in excess and can lead to hydrolysis of the acetal ring as a major side reaction. Often when these protocols have been used, a mixture of regioisomers is obtained that can be difficult to purify by chromatographic techniques. The development of new Lewis acids as efficient catalysts for ring cleavage in a highly selective manner may offer a good solution (Scheme 1). No Lewis acid catalyzed ring openings of 4,6-*O*-benzylidene acetals at the O4 position have been published to date. So far only a reductive cleavage at O6 to the give corresponding 6-alcohol using borane and with [V(O)(OTf)₂] (Tf = trifluoromethanesulfanyl) as the catalyst has been reported, and here the required amount of catalyst was 15 mol %.^[6] Herein, we have developed Cu(OTf)₂ as an efficient and dual-purpose catalyst that can be used in catalytic quantities; it effects the regioselective reductive ring opening of benzylidene acetals at the O4 or O6 position by merely altering the reactivity of the reducing agent.

Compound **4** was selected for model studies. We examined the cleavage at O6 by employing various boranes in combination with Cu(OTf)₂ at room temperature; the results are outlined in Table 1. Initially, treatment of **4** with BH₃·THF in

Table 1: Cu(OTf)₂-catalyzed regioselective borane-reductive O6-ring opening of 4,6-*O*-benzylidene acetal **4** to the corresponding 6-alcohol **5** at room temperature.



Entry	<i>x</i>	Borane	Solv.	<i>t</i> [h]	Yield [%]	
					5	6
1	15	BH ₃ ·THF ^[a]	CH ₂ Cl ₂	0.75	94	0
2	15	BH ₃ ·THF	–	0.75	92	0
3	10	BH ₃ ·THF	–	1.5	93	0
4	5	BH ₃ ·THF	–	2.5	95	0
5	1	BH ₃ ·THF	–	27	70	0
6	5	BH ₃ ·Me ₂ S ^[b]	–	10	78	3
7	5	BH ₃ ·Me ₃ N	CH ₂ Cl ₂	25	0	40
8	5	9-BBN ^[c]	–	27	40	0

[a] 1 M solution in THF. [b] 2 M solution in THF. [c] 0.5 M solution in THF, 9-BBN = 9-borabicyclo[3.3.1]nonane.

the presence of 15 mol % of catalyst in CH₂Cl₂ rapidly furnished the expected ring-opened product **5**^[7] in excellent yield (entry 1, 45 min, 94 %). Exclusion of CH₂Cl₂ gave similar results (entry 2, 92 %). Lowering the concentration of catalyst to 10 mol % and 5 mol % (entries 3 and 4) led to similar selectivity and yields, while decreasing it to 1 mol % extended the reaction time and resulted in a drop in yield (entry 5).

We then tested various borane reagents in tandem with 5 mol % of Cu(OTf)₂ to study the effect of ligation and bulk

[*] C.-R. Shie, Z.-H. Tzeng, Prof. Dr. B.-J. Uang, Prof. Dr. S.-C. Hung
Department of Chemistry
National Tsing Hua University
Hsinchu 300 (Taiwan)
Fax: (+886) 3-571-1082
E-mail: schung@chem.sinica.edu.tw

Dr. S. S. Kulkarni, Prof. Dr. S.-C. Hung
Institute of Chemistry & Genomics Research Center
Academia Sinica
128 Academia Road, Section 2
Taipei 115 (Taiwan)

Dr. C.-Y. Hsu
Department of Chemical Engineering
Cheng-Shiu University
840 Cheng-Ching Road
Kaohsiung County 833 (Taiwan)

[**] This work was supported by the National Science Council of Taiwan (NSC 92-2113M-001-028 and NSC 92-2113M-001-061).

Supporting information for this article is available on the WWW under <http://www.angewandte.org> or from the author.

on the regiochemical outcome of the reactions. In entry 6, use of the $\text{BH}_3\cdot\text{Me}_2\text{S}$ complex with **4** afforded product **5** (78%) along with a minor 4-alcohol **6** (3%). Interestingly, the mode of regioselection was markedly shifted when $\text{BH}_3\cdot\text{NMe}_3$ was used as the reductant (entry 7); compound **6** was formed in 40% yield as the sole product, and some starting material was recovered (55%). A bulkier reagent, 9-borabicyclo[3.3.1]nonane (9-BBN), was sluggish to react (entry 8), and overnight stirring was needed to furnish **5** in a modest yield (40%) together with the hydrolyzed 4,6-diol (40%) and starting material (15%).

We then proceeded to investigate the compatibility of various substrates under these optimized conditions (1M $\text{BH}_3\cdot\text{THF}$ in THF, 5 mol% $\text{Cu}(\text{OTf})_2$, without additional solvent, room temperature; Table 2). The 2-benzoyl-pro-

Table 2: Reductive ring opening of various benzylidene acetals at the O6 position using $\text{BH}_3\cdot\text{THF}$ and x mol% of $\text{Cu}(\text{OTf})_2$ as the catalyst.

Entry	Acetal	x [mol%]	t [h]	Product	Yield [%]
1	7 : R = H	5	4.5	8 : R = H	87
2	9 : R = Bz	5	23	10 : R = Bz	53
3	9	15	5	10	91
4	11 : R = Bz, R ¹ = OMe	5	4	12 : R = Bz, R ¹ = OMe	92
5	13 : R = Bn, R ¹ = STol	5	3.5	14 : R = Bn, R ¹ = STol	93
6	15 : R = Bn	5	3	16 : R = Bn	82
7	17 : R = Bz	5	21	18 : R = Bz	63
8	17	15	4.5	18	90
9	19 : R = Bn	5	6.5	20 : R = Bn	55
10	19	15	3.5	20	67
11	19	15 ^[a]	14	20	86
12	21 : R = Bz	5	5	22 : R = Bz	56
13	21	15 ^[a]	9	22	57
14	23	5	3.5	24	84
15	25	5	1.5	26	90

[a] The reaction was conducted in an ice bath. Bz = Benzoyl, Bn = benzyl, OMe = methoxy, Tol = tolyl.

ected D-glucose derivative **7** successfully furnished the expected 4-benzyl-protected product **8** (entry 1, 4.5 h, 87%), while the 2,3-dibenzoyl-protected compound **9** gave the corresponding 6-alcohol **10**^[4a] in 53% yield after 23 h (entry 2). When 15 mol% of $\text{Cu}(\text{OTf})_2$ was used, the latter transformation was carried out over a short period (5 h), affording compound **10** in a high yield (entry 3, 91%). The electron-withdrawing groups in the substrates **7** and **9** made their reaction much slower than that of the 2,3-dibenzoyl analogue **4** (0.75 h). The reaction rate is closely associated with the nucleophilicity of the oxygen atom at the C6 position and the Lewis acid catalyst. In the $\text{LiAlH}_4\text{--AlCl}_3$ system, the congestion of the protecting group at O3 in D-glucopyranosides plays an important role, and the presence of a bulkier substituent at C3 has been found to favor a higher proportion of O6-opened product.^[2b] However, no such steric dependence was observed in our system, and only O4-benzyl ethers were obtained in high yields irrespective of their nature (H, Bn, or Bz).^[4b] Similarly, the methyl β -pyranoside **11** (entry 4), β -thioglycoside **13** (entry 5), D-mannose-derived acetal **23** (entry 14), and non-sugar substrate **25** (entry 15) underwent a high-yielding facile ring fission to provide 6-OH derivatives **12**^[8] (92%), **14** (93%), **24**^[9] (84%), and **26**^[10] (90%), respectively. In the D-glucosamine series, the β -benzoyl 3-benzyl-protected **15** led to the desired product **16** in 82% yield (entry 6). Its structure was determined by single-crystal X-ray structure analysis.^[11] The 3-benzoyl analogue **17**, although sluggish to react under the optimized conditions (entry 7, 63%), did furnish the expected compound **18** rapidly and in excellent yield (90%) when 15 mol% of $\text{Cu}(\text{OTf})_2$ was used (entry 8). When the α -form 3-benzyl **19** (entry 9) and 3-benzoyl **21** (entry 12) were employed, the expected ring-opened products **20** and **22** were obtained in 55 and 56% yields, respectively. Increasing the catalyst concentration to 15 mol% and the reaction temperature to 0°C improved the yield remarkably in case of the former (entry 11, 86%), whereas a substantial amount of the 4,6-diol (30%) from hydrolysis was present in the latter (entry 13, 57%).

With success in the $\text{Cu}(\text{OTf})_2$ -catalyzed borane-induced reductive O6-ring opening of benzylidene acetals, we then explored the catalytic properties of $\text{Cu}(\text{OTf})_2$ for silane-induced reductive cleavage at the O4 position, including the effects of the solvent, silane agent, and catalyst concentration (Table 3). The catalyst was added at 0°C, and the reaction mixture was gradually warmed up to room temperature. When 1 mol% of $\text{Cu}(\text{OTf})_2$ was used together with triethylsilane in CH_2Cl_2 (entry 1), the reaction took 15 h to provide the secondary alcohol **6**^[5b] (62%) as the only regioisomer. A smaller reducing agent, Me_2EtSiH , offered a marginally improved yield of **6** in a much shorter reaction time (entry 2, 9 h, 65%). Employment of a more polar solvent like nitromethane speeded up the reaction of **4** with Et_3SiH (entry 3, 1 h) and Me_2EtSiH (entry 4, 1 h), which afforded **6** as the sole product in 60% and 68% yields, respectively. Although no other regioisomer was detected, hydrolysis of compound **4** to the corresponding 4,6-diol seemed to become a dominant factor limiting the yield. Less polar solvents, for example, THF and toluene, gave disappointing results. Nevertheless, reduction of **4** in acetonitrile using Et_3SiH (entry 5,

Table 3: Cu(OTf)₂-catalyzed reductive ring opening of compound **4** in various solvents with silanes to give the corresponding 4-alcohol **6**.

$4 \xrightarrow[\text{solvent, } 0^\circ\text{C} \rightarrow \text{RT}]{x \text{ mol } \% \text{ Cu(OTf)}_2, 2 \text{ equiv silane}} 5 + 6$						
Entry	x	Silane	Solv.	t [h]	Yield [%] 5 6	
1	1	Et ₃ SiH	CH ₂ Cl ₂	15	0 62	
2	1	Me ₂ EtSiH	CH ₂ Cl ₂	9	0 65	
3	1	Et ₃ SiH	CH ₃ NO ₂	1	0 60	
4	1	Me ₂ EtSiH	CH ₃ NO ₂	1	0 68	
5	1	Et ₃ SiH	CH ₃ CN	1	7 76	
6	1	Me ₂ EtSiH	CH ₃ CN	0.5	0 84	
7	0.5	Me ₂ EtSiH	CH ₃ CN	4	3 75	
8	5	Me ₂ EtSiH	CH ₃ CN	0.5	3 80	
9	10	Me ₂ EtSiH	CH ₃ CN	0.5	2 82	

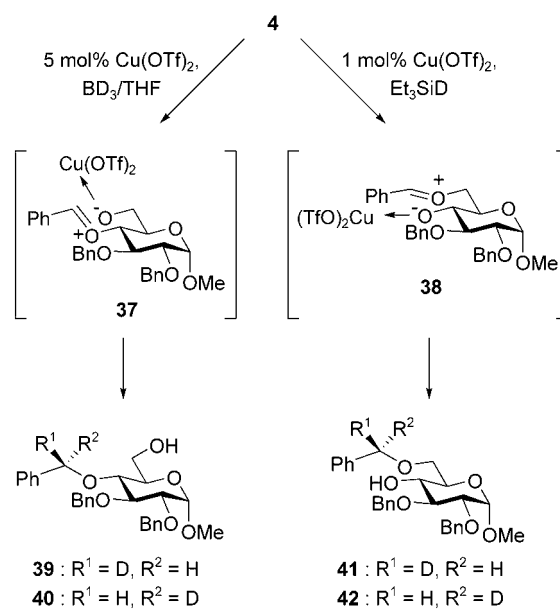
1 h) readily furnished the expected compound **6** (76 %) along with the minor isomer **5** (7 %), while Me₂EtSiH led to **6** in 84 % yield (entry 6, 0.5 h), exclusively. In these cases the hydrolyzed product was recovered in up to 10 % yield. In entry 7, when the catalyst concentration was halved, the transformation took place gradually (4 h) to afford compound **6** in 75 % yield. In contrast, increasing the concentration of catalyst to 5 mol % or 10 mol % (entries 8 and 9) did not improve the yields of **6** (80–82 %).

With these optimized reaction conditions (1 mol % Cu(OTf)₂, Me₂EtSiH, CH₃CN, 0 °C → room temperature), we examined a number of α- and β-hexopyranosides bearing different protecting groups to check the generality of this protocol (Table 4). In entries 1–8, reactions of the D-glucose-derived benzoates **7** and **9**; β-glucopyranoside **11** and β-thioglycoside **13**; D-glucosamine-derived acetals **17**, **19**, and **21**; and D-mannopyranosyl sugar **23**^[12] led to O4-opened products **27–34** in 71, 85, 74, 79, 87, 80, 83, and 70 % yield, respectively. These experiments revealed that the electron-withdrawing group at the O3 position does not affect the reactivity of substrates, in contrast to the observations of the reductive O6-opening reactions with borane. In the case of the non-carbohydrate compound **25** (entry 9), regioisomeric benzyl ethers **26** (22 %) and **35** (24 %) were generated along with 1,3-dibenzyl ether **36** (36 %) as the major product.

To examine the reaction pathway in greater depth, we performed two experiments using deuterated reducing agents (Scheme 2). Reductive ring opening of **4** with BD₃·THF furnished primary alcohols **39** and **40** in unequal proportions (5:1 ratio), as judged from the signals of the O4-benzylic protons in the ¹H NMR spectrum of the mixture with those of compound **5** (see the Supporting Information). The Cu(OTf)₂ catalyst may first coordinate with the more accessible O6 atom and lead to a zwitterionic species **37**, which can be reduced by the reactive borane reagent. The reaction essentially follows the S_N1 pathway, and the stereochemical bias is perhaps offered by the chirality at C4, which is reflected in the observed product ratio. On the other hand, the ring fission of **4** with Et₃SiD generated a 1:1 diastereomeric mixture of secondary alcohols **41** and **42**. The hindered O4-benzyl cation of the intermediate **37** cannot be reduced as the silane reagent is bulky and less reactive than borane and

Table 4: Regioselective reductive ring opening of various benzyldene acetals in acetonitrile employing Me₂EtSiH and with 1 mol % of Cu(OTf)₂ as the catalyst.

Entry	Acetal	t [h]	Product	Yield [%]
1	7	1	27 : R = H	71
2	9	1	28 : R = Bz	85
3	11	0.5	29	74
4	13	1.5	30	79
5	17	0.5	31	87
6	19	1	32 : R = Bn	80
7	21	0.5	33 : R = Bz	83
8	23	1	34	70
9	25	2	26 : R ¹ = H, R ² = Bn	22
			35 : R ¹ = Bn, R ² = H	24
			36 : R ¹ = R ² = Bn	36


Scheme 2. The treatment of **4** with deuterated reducing agents. Bn = Benzyl.

an equilibrium is soon established between the O6- and O4-coordinated complexes, which leads to another zwitterionic species **38**. The silane agent can approach the intermediate **38** at the well-exposed O6-benzyl cation from either side to generate equal amounts of diastereomers.

In conclusion, we have successfully developed Cu(OTf)₂ as an excellent dual-purpose catalyst for highly regioselective reductive ring opening of various benzyldene acetals with BH₃ and Me₂EtSiH to furnish the corresponding primary and secondary alcohols, respectively. The reaction conditions are mild, and various protecting groups in the substrates are tolerated. The isotope studies provide the first experimental evidence that neither O6- nor O4-cleavage of the benzyldene ring proceeds through the S_N2 reaction pathway when borane or triethylsilane attacks the acetal carbon center.

Received: October 1, 2004

Published online: January 31, 2005

Keywords: carbohydrates · copper · homogeneous catalysis · Lewis acids · regioselectivity

- [10] E. L. Eliel, L. Clawson, D. E. Knox, *J. Org. Chem.* **1985**, *50*, 2707–2711.
- [11] CCDC162432 (**16**) contains the supplementary crystallographic data for this paper. These data can be obtained free of charge from The Cambridge Crystallographic Data Centre via www.ccdc.cam.ac.uk/data_request/cif.
- [12] R. Madiyalakan, M. S. Chowdhary, S. S. Rana, K. L. Matta, *Carbohydr. Res.* **1986**, *152*, 183–194.

-
- [1] a) *Preparative Carbohydrate Chemistry* (Ed.: S. Hanessian), Marcel Dekker, New York, **1997**; b) T. W. Greene, P. G. M. Wuts, *Protective Groups in Organic Synthesis*, 3rd ed., Wiley, New York, **1999**, pp. 217–224.
 - [2] a) A. Lipták, I. Jodál, P. Nánási, *Carbohydr. Res.* **1975**, *44*, 1–11; b) P. Fügedi, A. Lipták, P. Nánási, *Carbohydr. Res.* **1982**, *104*, 55–67.
 - [3] T. Mikami, H. Asano, O. Mitsunobu, *Chem. Lett.* **1987**, 2033–2036.
 - [4] a) M. Ek, P. J. Garegg, H. Hultberg, S. Oscarson, *J. Carbohydr. Chem.* **1983**, *2*, 305–311; b) Y. Guindon, Y. Girard, S. Berthiaume, V. Gorys, R. Lemieux, C. Yoakim, *Can. J. Chem.* **1990**, *68*, 897–902; c) M. Oikawa, W.-C. Liu, Y. Nakai, S. Koshida, K. Fukase, S. Kusumoto, *Synlett* **1996**, 1179–1180; d) L. Jiang, T.-H. Chan, *Tetrahedron Lett.* **1998**, *39*, 355–358; e) S. Chandrasekhar, Y. R. Reddy, C. R. Reddy, *Chem. Lett.* **1998**, 1273–1274; f) M. Sakagami, H. Hamana, *Tetrahedron Lett.* **2000**, *41*, 5547–5551.
 - [5] a) P. J. Garegg, H. Hultberg, *Carbohydr. Res.* **1981**, *93*, C10–C11; b) P. J. Garegg, H. Hultberg, S. Wallin, *Carbohydr. Res.* **1982**, *108*, 97–101; c) M. P. DeNinno, J. B. Etienne, K. C. Duplantier, *Tetrahedron Lett.* **1995**, *36*, 669–672; d) N.-L. Pohl, L. L. Kiessling, *Tetrahedron Lett.* **1997**, *38*, 6985–6988; e) S. D. Debenham, E. J. Toone, *Tetrahedron: Asymmetry* **2000**, *11*, 385–387; f) B.-Z. Zheng, M. Yamauchi, H. Dei, S. Kusaka, K. Matsui, O. Yonemitsu, *Tetrahedron Lett.* **2000**, *41*, 6441–6445.
 - [6] C.-C. Wang, S.-Y. Luo, C.-R. Shie, S.-C. Hung, *Org. Lett.* **2002**, *4*, 847–849.
 - [7] The structures of all the products were assigned unambiguously through NMR spectroscopic analysis. First, a ¹H–¹³C COSY experiment was performed to mark the anomeric carbon and the doublet anomeric proton. A ¹H–¹H COSY experiment then established the correlation between all of the ring protons starting from H1. The regioselectivity was confirmed by observing the correlation between the OH and H6/H4 protons. This general protocol was followed throughout the study (see the Supporting Information).
 - [8] O. J. Plante, S. L. Buchwald, P. H. Seeberger, *J. Am. Chem. Soc.* **2000**, *122*, 7148–7149.
 - [9] V. K. Srivastava, C. Schuerch, *J. Org. Chem.* **1981**, *46*, 1121–1126.

Polymerization

C₃ Chirality in Polymerization Catalysis: A Highly Active Dicationic Scandium(III) Catalyst for the Ioselective Polymerization of 1-Hexene**

Benjamin D. Ward, Stéphane Bellemin-Laponnaz,* and Lutz H. Gade*

The possibility of controlling the tacticity and molecular-weight distribution in polymers by ligand design provides the basis for the success of Group 4 metallocene catalysis of α -olefins.^[1] Isotacticity of a poly(α -olefin) requires chirality at the active site, and the molecular shape of bent metallocenes lends itself particularly to the construction of C₂- or C₁-chiral molecular catalysts.^[2] There is no report of the use of C₃-chiral stereodirecting ligands in polymerization catalysis, although they confer an element of molecular helicity to a complex which is thought to be beneficial for face selectivity in the key migratory insertion step.^[3]

In recent years there has been a considerable effort to investigate “post-metallocene” catalysts^[4,5] with non-Cp ligand systems which has led to alternative catalyst structures. Some of these non-metallocene Group 4 catalysts were found to be highly active in the polymerization of 1-hexene and other α -olefins; several of these catalysts exhibit living behavior.^[6–13] In particular, the amine bis(phenolate) based catalysts reported by Kol and co-workers have shown remarkably high activity and may be modified to give isospecific poly(1-hexene).^[6,10,12] The ubiquitous Group 4 metal catalysts aside, the focus has very recently shifted to

[*] Dr. B. D. Ward, Dr. S. Bellemin-Laponnaz, Prof. L. H. Gade^[†]
Laboratoire de Chimie Organométallique et de Catalyse
Institut Le Bel, Université Louis Pasteur Strasbourg
4, rue Blaise Pascal, 67000 Strasbourg (France)
Fax: (+33) 390-241531

[†] new address:
Institut für Anorganische Chemie, Universität Heidelberg
Im Neuenheimer Feld 270, 69120 Heidelberg (Germany)
Fax: (+49) 6221-545609

[**] This work was supported by the CNRS and the EU (RTN Network “AC3S”). BASF as well as Degussa AG provided valuable chemicals. We thank Dr. André De Cian for collecting the X-ray crystallographic data.

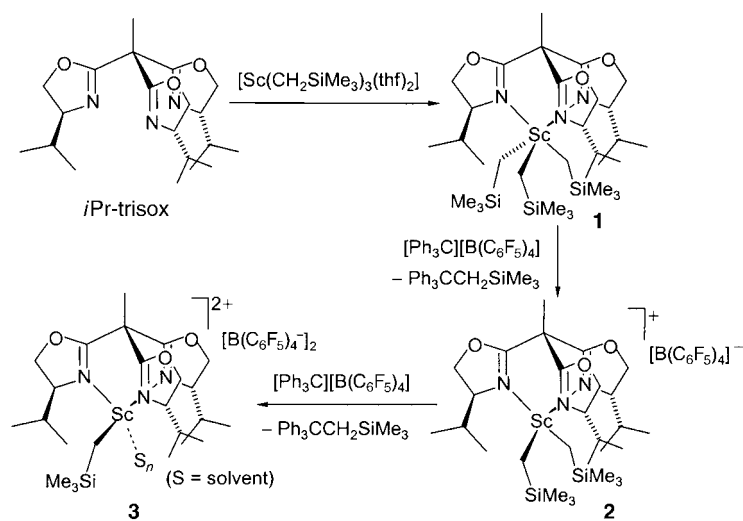


Supporting information for this article is available on the WWW under <http://www.angewandte.org> or from the author.

the use of Group 3 and lanthanide metals for olefin polymerization catalysis.^[14] Important contributions to the field were made by the groups of Hessen^[15] and Okuda,^[16] who found that the ionic radius of the metal cation plays a crucial role in determining the polymerization activity. Okuda and co-workers also noted that in the case of simple trialkyl complexes of these metals, it is most likely the monoalkyl dicationic species $[M(CH_2SiMe_3)(solvent)_n]^{2+}$ that is the catalytically active species.

The trivalent metal centers of the Group 3 elements are ideally suited for the development of C_3 -symmetric polymerization precatalysts if combined with a chiral neutral tripod spectator ligand. We recently developed a new class of chiral trisoxazoline ligands, which are capable of binding facially to d-block metals and which provide the type of C_3 -chiral complex geometry referred to above.^[17] Based on this concept, herein we report a highly active isoselective Sc catalyst. We note that, in general, scandium-based catalysts have been studied much less than those of the other Group 3 and lanthanide metals.^[18] The polymerization of ethylene with scandium complexes supported by (achiral) triazacyclononane derivatives was reported by the groups of Bercaw^[19] and Mountford.^[20]

The trialkyl complex $[Sc(iPr\text{-}trisox)(CH_2SiMe_3)_3]$ (**1**) was prepared by the reaction of the trialkyl precursor $[Sc(CH_2SiMe_3)_3(thf)_2]$ with an equimolar amount of *iPr*-trisox (Scheme 1). Complex **1** is insoluble in all common hydro-



Scheme 1. Synthesis of the Sc complex $[Sc(iPr\text{-}trisox)(CH_2SiMe_3)_3]$ (**1**) and its conversion into the mono- and dicationic catalysts **2** and **3** by alkyl abstraction.

carbon solvents and is unstable in halogenated and coordinating solvents, such that characterization by NMR spectroscopy was not possible.

Single crystals of **1** suitable for X-ray diffraction were obtained directly from the reaction mixture, and the molecular structure is shown in Figure 1. The trisoxazoline ligand is facially coordinated, with all three oxazoline moieties bound to the metal center. We are only aware of two previous examples of crystallographically characterized scandium-oxazoline complexes: the bis(oxazolinyl)pyridine-scandium

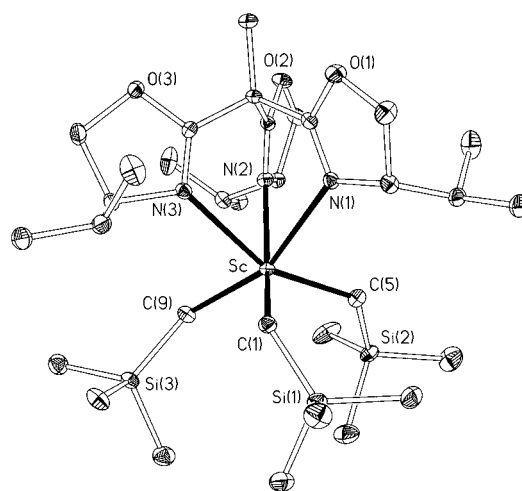


Figure 1. Structure of **1** at the 25% probability level. H atoms omitted for clarity. Principal bond lengths [Å] and angles [°]: Sc–C(1) 2.270(2), Sc–C(5) 2.272(2), Sc–C(9) 2.275(2), Sc–N(1) 2.456(2), Sc–N(2) 2.446(1), Sc–N(3) 2.464(2), C(1)–Sc–C(5) 106.69(7), C(1)–Sc–C(9) 104.38(7), C(5)–Sc–C(9) 105.51(8), N(1)–Sc–N(2) 74.90(5), N(1)–Sc–N(3) 73.95(5), N(2)–Sc–N(3) 73.81(5).

triflate complexes reported by Evans et al.^[21,22] The Sc–N_{oxaz.} bonds in complex **1** are significantly longer than expected (Sc–N 2.446(1)–2.464(2) Å)^[23,24] which suggests that the trisoxazoline ligand is less strongly bound to the metal center in this case, presumably as a result of the steric constraints imposed by the bulky trimethylsilylmethyl groups. As a whole, this strong distortion from an octahedral coordination geometry renders the N–Sc–N' angles more acute than expected for a facially coordinating tripod (N–Sc–N' 73.81(5)–74.90(5)°), whereas the C–Sc–C' angles between the sterically crowded alkyl ligands are opened up significantly (C–Sc–C' 104.38(7)–106.69(7)°). The weakly bound nature of the trisoxazoline ligand in **1** could provide an explanation for the observed instability in halogenated and coordinating solvents, in which ligand displacement may occur.

The addition of a solution of 1 equivalent of $[Ph_3C][B(C_6F_5)_4]$ in CD_2Cl_2 or C_6D_5Br to solid **1** resulted in the formation of a new species, which we tentatively assigned as $[Sc(iPr\text{-}trisox)(CH_2SiMe_3)_2][B(C_6F_5)_4]$ (**2**) based on the 1H and ^{13}C NMR spectroscopic data and the observation of 1 equivalent of $Ph_3CCH_2SiMe_3$ (Scheme 1). Solutions of **2** (prepared in situ) in chlorobenzene are active in the catalytic polymerization of 1-hexene, albeit with

rather low activity ($\approx 30 \text{ kg mol}^{-1} \text{ h}^{-1}$) and somewhat variable reproducibility with respect to tacticity control.^[25] Moreover, GPC analysis of the polymers obtained revealed bimodal molecular-mass distributions, thus indicating the presence of at least two catalytically active species.

It has been suggested by Okuda and co-workers that a dicationic species may, in fact, be the catalytically active species in certain rare-earth polymerization catalysts.^[16] We therefore investigated the reaction of **1** with 2 equivalents of

[Ph₃C][B(C₆F₅)₄]. ¹H, ¹³C, and ²⁹Si NMR tube-scale experiments indicated that in this case 2 equivalents of Ph₃CCH₂SiMe₃ were formed alongside a C₃-symmetric scandium-containing species, which we propose to be the dicationic complex [Sc(*i*Pr-trisox)(CH₂SiMe₃)][B(C₆F₅)₄]₂ (**3**). In contrast to the monocation **2**, the complex **3** generated in situ is highly active in the polymerization of 1-hexene and displayed good tacticity control. Polymerization studies were carried out at various temperatures, and the activities and polymer characteristics are provided in Table 1.

Table 1: 1-Hexene polymerization data for **3**.^[a]

<i>T</i> [°C]	<i>t</i> [min]	Yield [g]	Activity kg mol ^{−1} h ^{−1}	<i>M</i> _w	<i>M</i> _w / <i>M</i> _n
−30	3	1.01	2030	750 000	1.18
−20	1.5	1.90	7600	552 000	1.87
0	1	2.18	13080	354 000	2.36
21	0.5	3.02	36230	227 000	2.22

Yields based on 3.4 g of hexene.

Polymerization starting out at 21 °C was highly exothermic, which caused the reaction mixture to boil within 20 seconds, thus preventing control of the reaction temperature. The activity of 36200 kg mol^{−1} h^{−1} observed for **3** (Table 1) is greater by three orders of magnitude than that of the monocation **2** and comparable to the extremely high activities reported by Kol and co-workers for zirconium amine bis-(phenoxide) complexes.^[26] However, under these conditions the tacticity of the poly(1-hexene) produced was relatively low and GPC analysis of the polymer indicated a bimodal mass distribution (*M*_w/*M*_n = 2.22), which is consistent with a partial thermal degradation of the molecular catalyst. Upon decreasing the polymerization temperature to −30 °C, the activity dropped to 2030 kg mol^{−1} h^{−1}, which is still very high in absolute terms for hexene and related α-olefins.^[4] At this temperature however, the poly(1-hexene) produced was highly isotactic (*mmmm* = 90% by ¹³C{¹H} NMR spectroscopy) (Figure 2).^[27,28] GPC analysis of the polymer obtained under these conditions established a very narrow monomodal molecular-mass distribution with *M*_w = 750 000 and PDI = 1.18, thus indicating that the isoselective catalytic polymerization carried out at low temperature shows living-type behavior.

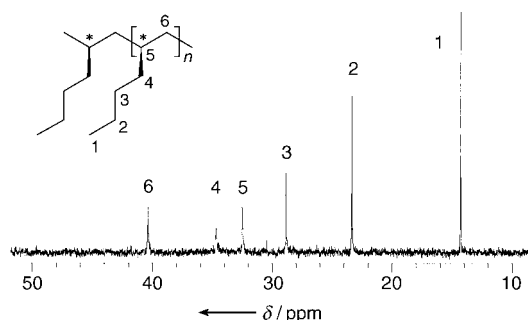


Figure 2. ¹³C{¹H} NMR spectrum of poly(1-hexene) obtained with catalyst **3** at −30 °C (recorded in CDCl₃).

The ¹H NMR spectra of all the poly(1-hexene) samples established the complete absence of olefinic end groups at all temperatures studied, indicating that chain termination by β-hydride elimination does not occur to a significant extent in this system.^[29]

In conclusion we have shown that the C₃-chiral trisoxazoline is a suitable supporting ligand for scandium-catalyzed olefin polymerization whilst invoking sufficient stereocontrol over the substrate to induce a high level of tacticity in the polymer microstructure.^[30] Studies into the mechanistic details of this system, the polymerization of other α-olefins, and the use of alternative Group 3 metals are currently underway.

Experimental Section

1: [Sc(CH₂SiMe₃)₃(thf)₂]^[31] (124 mg, 0.275 mmol) was dissolved in toluene and cooled to −78 °C for the dropwise addition of a toluene solution of *i*Pr-trisox (100 mg, 0.275 mmol) with stirring. The reaction was allowed to warm to room temperature and stirred for a further 30 min, after which a large quantity of white precipitate had formed. The precipitate was isolated by filtration and dried in vacuo to afford [Sc(*i*Pr-trisox)(CH₂SiMe₃)₃] as a white solid (113 mg, 72%). When the reaction was not stirred, slow warming to ambient temperature afforded white crystals that were suitable for X-ray diffraction studies. The compound was insoluble in all hydrocarbon solvents and decomposed in halogenated solvents and [D₈]THF; thus no NMR data could be recorded.

2: [Ph₃C][B(C₆F₅)₄] (30 mg, 0.328 mmol) was dissolved in C₆D₅Br (0.5 mL) and the resulting yellow solution was added to solid [Sc(*i*Pr-trisox)(CH₂SiMe₃)₃] (22 mg, 0.328 mmol). The white solid immediately dissolved to afford a red solution, which was added to an NMR tube, sealed, and analyzed in situ by NMR spectroscopy. The formation of Ph₃CCH₂SiMe₃ was confirmed by the ¹H and ¹³C{¹H} NMR spectra of a sample prepared from Ph₃CCl and LiCH₂SiMe₃. ¹H NMR (C₆D₅Br, 300.1 MHz, 293 K): δ = 4.50 (6H, m; OCH₂), 4.21 (3H, t, ³J = 9.6 Hz; CH*i*Pr), 2.28 (3H, sept d, ³J = 6.6 Hz, ³J = 3.4 Hz; CHMe₂), 1.72 (3H, s; Me_{apical}), 0.82 (9H, d, ³J = 6.9 Hz; CHMe₂), 0.66 (9H, d, ³J = 6.9 Hz; CHMe₂), 0.33 ppm (9H, s; SiMe₃), 0.16 (9H, s; SiMe₃); ¹³C{¹H} NMR (C₆D₅Br, 75.5 MHz, 293 K): δ = 171.1 (C=N), 148.7 (C₆F₅), ¹J(CF) = 247.4 Hz, 138.6 (C₆F₅), ¹J(CF) = 233.4 Hz, 136.2 (C₆F₅), ¹J(CF) = 241.2 Hz, 72.6 (OCH₂), 71.0 (CH*i*Pr), 57.2 (CMe_{apical}), 30.0 (CHMe₂), 18.2 (CHMe₂), 14.5 (Me_{apical}), 14.0 (CHMe₂), 3.8 (SiMe₃), 0.9 ppm (SiMe₃); ¹⁹F NMR (CD₂Cl₂, 282.4 MHz, 293 K): δ = −133.5 (8F, br s; *o*-C₆F₅), −164.1 (4F, t, ³J = 20.3 Hz; *p*-C₆F₅), −168.0 ppm (8F, br s; *m*-C₆F₅); ²⁹Si NMR (CD₂Cl₂, 79.5 MHz, 300 K): δ = −21.8 ppm.

3: [Ph₃C][B(C₆F₅)₄] (20 mg, 0.02 mmol) was dissolved in CD₂Cl₂ (0.5 mL) and the resulting yellow solution was added to solid [Sc(*i*Pr-trisox)(CH₂SiMe₃)₃] (7 mg, 0.01 mmol). The white solid immediately dissolved to afford a red solution, which was added to an NMR tube, sealed, and analyzed in situ by NMR spectroscopy. ¹H NMR (CD₂Cl₂, 300.1 MHz, 293 K): δ = 4.72–4.42 (9H, m; OCH₂, CH*i*Pr), 2.35 (3H, sept d, ³J = 6.8 Hz, ³J = 3.1 Hz; CHMe₂), 1.78 (3H, s; Me_{apical}), 0.99 (9H, d, ³J = 8.9 Hz; CHMe₂), 0.73 (9H, d, ³J = 8.9 Hz; CHMe₂), 0.19 ppm (9H, s; SiMe₃); ¹³C{¹H} NMR (CD₂Cl₂, 75.5 MHz, 293 K): δ = 168.8 (C=N), 148.7 (C₆F₅), ¹J(CF) = 247.4 Hz, 138.6 (C₆F₅), ¹J(CF) = 233.4 Hz, 136.2 (C₆F₅), ¹J(CF) = 241.2 Hz, 73.8 (OCH₂), 71.2 (CH*i*Pr), 57.2 (CMe_{apical}), 30.4 (CHMe₂), 18.4 (CHMe₂), 14.7 (Me_{apical}), 14.2 (CHMe₂), 0.3 ppm (SiMe₃); ¹⁹F NMR (CD₂Cl₂, 282.4 MHz, 293 K): δ = −133.5 (8F, s; *o*-C₆F₅), −164.1 (4F, t, ³J = 20.3 Hz; *p*-C₆F₅), −168.0 ppm (8F, s; *m*-C₆F₅); ²⁹Si NMR (CD₂Cl₂, 79.5 MHz, 300 K): δ = 8.2 ppm.

Polymerization of 1-hexene: [Ph₃C][B(C₆F₅)₄] (20 mg, 22 μmol) was dissolved in C₆H₅Cl (0.5 mL) and the resulting yellow solution

was added to solid $[\text{Sc}(\text{iPr-trisox})(\text{CH}_2\text{SiMe}_3)_3]$ (7 mg, 10 μmol). The white solid immediately dissolved to afford a red solution. The red solution was added to a Schlenk tube containing 1-hexene (5 mL), which had been precooled to the desired temperature for at least 10 min prior to the addition. The reaction was judged complete when the reaction could no longer be stirred owing to the high viscosity of the poly(1-hexene). The volatile components were removed under reduced pressure and the residue dissolved in THF. The solution was transferred into a preweighed flask, and the THF was removed under reduced pressure to yield poly(1-hexene) as a waxy solid.

Crystal data for **1**: $\text{C}_{32}\text{H}_{66}\text{N}_3\text{O}_3\text{ScSi}_3$, yellow blocks, crystal dimensions $0.20 \times 0.20 \times 0.02 \text{ mm}^3$, $M = 670.12$, monoclinic, space group $P2_1$, $a = 10.1985(2)$, $b = 19.0942(3)$, $c = 10.4478(2) \text{ \AA}$, $\beta = 102.390(5)^\circ$, $U = 1987.14(6) \text{ \AA}^3$, $Z = 2$, $\rho_{\text{calc}} = 1.12 \text{ g cm}^{-3}$, $F(000) = 732$, $\mu = 0.308 \text{ mm}^{-1}$, trans. (min/max): $0.940/0.999$, $T = 173 \text{ K}$, $\text{MoK}\alpha$, $-14 < h < 14$, $-25 < k < 26$, $-14 < l < 14$, 11 123 reflections collected ($2.5 < \theta < 30.05^\circ$) on a Nonius Kappa CCD diffractometer, 8316 ($I > 3\sigma(I)$) used in the structure refinement (378 parameters refined); $R = 0.035$, $R_w = 0.040$, $\text{GOF} = 1.050$; largest peak 0.407 e \AA^{-3} . CCDC-257336 contains the supplementary crystallographic data for this paper. These data can be obtained free of charge from the Cambridge Crystallographic Data Centre via www.ccdc.cam.ac.uk/data_request/cif.

Received: December 3, 2004

Published online: February 14, 2005

Keywords: homogeneous catalysis · polymerization · polymers · scandium · stereocontrol

- [1] For selected review articles, see: a) W. Kaminsky, A. Laban, *Appl. Catal. A* **2001**, 222, 47; b) M. Bochmann, *J. Chem. Soc. Dalton Trans.* **1996**, 255; c) M. Bochmann, *J. Organomet. Chem.* **2004**, 689, 3982; for examples of olefin polymerization by Group 4 metallocenes, see: d) C. Sishta, R. M. Hathorn, T. J. Marks, *J. Am. Chem. Soc.* **1992**, 114, 1112; e) H. Sinn, W. Kaminsky, H. J. Vollmer, R. Woldt, *Angew. Chem.* **1980**, 92, 396; *Angew. Chem. Int. Ed. Engl.* **1980**, 19, 390; f) R. F. Jordan, W. E. Dasher, S. F. Echols, *J. Am. Chem. Soc.* **1986**, 108, 1718; g) M. Bochmann, S. J. Lancaster, *J. Organomet. Chem.* **1992**, 434, C1; h) M. K. Leclerc, H. H. Brintzinger, *J. Am. Chem. Soc.* **1996**, 118, 9024; i) M. R. Kesti, G. W. Coates, R. M. Waymouth, *J. Am. Chem. Soc.* **1992**, 114, 9679.
- [2] H. H. Brintzinger, D. Fischer, R. Mülhaupt, B. Rieger, R. M. Waymouth, *Angew. Chem.* **1995**, 107, 1255; *Angew. Chem. Int. Ed. Engl.* **1995**, 34, 1143.
- [3] a) M. C. Keyes, W. B. Tolman, *Adv. Catal. Processes* **1997**, 2, 189; b) C. Moberg, *Angew. Chem.* **1998**, 110, 210; *Angew. Chem. Int. Ed.* **1998**, 37, 248.
- [4] V. C. Gibson, S. K. Spitzmesser, *Chem. Rev.* **2003**, 103, 283.
- [5] H. Makio, N. Kashiwa, T. Fujita, *Adv. Synth. Catal.* **2002**, 344, 477.
- [6] S. Groysman, E. Y. Tshuva, I. Goldberg, M. Kol, Z. Goldschmidt, M. Shuster, *Organometallics* **2004**, 23, 5291.
- [7] P. Mehrkhodavandi, P. J. Bonitatebus, Jr., R. R. Schrock, *J. Am. Chem. Soc.* **2000**, 122, 7841.
- [8] P. Mehrkhodavandi, R. R. Schrock, *J. Am. Chem. Soc.* **2001**, 123, 10746.
- [9] P. Mehrkhodavandi, R. R. Schrock, L. L. Pryor, *Organometallics* **2003**, 22, 4569.
- [10] E. Y. Tshuva, I. Goldberg, M. Kol, *J. Am. Chem. Soc.* **2000**, 122, 10706.
- [11] Y. Zhang, E. K. Reeder, R. J. Keaton, L. R. Sita, *Organometallics* **2004**, 23, 3512.
- [12] E. Y. Tshuva, I. Goldberg, M. Kol, *Organometallics* **2001**, 20, 3017.
- [13] Z. J. Tonzetich, C. C. Lu, R. R. Schrock, A. S. Hock, P. J. Bonitatebus, Jr., *Organometallics* **2004**, 23, 4362.
- [14] Z. Hou, Y. Wakatsuki, *Coord. Chem. Rev.* **2002**, 231, 1.
- [15] S. Bambirra, M. W. Bouwkamp, A. Meetsma, B. Hessen, *J. Am. Chem. Soc.* **2004**, 126, 9182.
- [16] S. Arndt, T. P. Spaniol, J. Okuda, *Angew. Chem.* **2003**, 115, 5229; *Angew. Chem. Int. Ed.* **2003**, 42, 5075.
- [17] a) S. Bellemin-Laponnaz, L. H. Gade, *Angew. Chem.* **2002**, 114, 3623; *Angew. Chem. Int. Ed.* **2002**, 41, 3473; b) C. Dro, S. Bellemin-Laponnaz, R. Welter, L. H. Gade, *Angew. Chem.* **2004**, 116, 4579; *Angew. Chem. Int. Ed.* **2004**, 43, 4479.
- [18] P. Mountford, B. D. Ward, *Chem. Commun.* **2003**, 1797.
- [19] S. Hajela, W. P. Schaefer, J. E. Bercaw, *J. Organomet. Chem.* **1997**, 532, 45.
- [20] S. L. Lawrence, B. D. Ward, S. R. Dubberley, C. M. Kozak, P. Mountford, *Chem. Commun.* **2003**, 2880.
- [21] D. A. Evans, Z. K. Sweeney, R. Tomislav, J. S. Tedrow, *J. Am. Chem. Soc.* **2001**, 123, 12095.
- [22] D. A. Evans, K. A. Scheidt, K. R. Fandrick, H. W. Lam, J. Wu, *J. Am. Chem. Soc.* **2003**, 125, 10780.
- [23] F. H. Allen, O. Kennard, *Chemical Design Automation News* **1993**, 8, 1 & 31.
- [24] D. A. Fletcher, R. F. McMeeking, D. J. Parkin, *J. Chem. Inf. Comput. Sci.* **1996**, 36, 746.
- [25] The highest tacticity control is observed at $+40^\circ\text{C}$ while the tacticity is lower at ambient temperature and below, which is probably in part due to aggregation of the catalyst (and manifest in the bimodal GPC traces). This observation is only consistent with enantiomorphic tacticity control.
- [26] S. Groysman, I. Goldberg, M. Kol, E. Genizi, Z. Goldschmidt, *Inorg. Chim. Acta* **2003**, 345, 137.
- [27] G. N. Babu, R. A. Newmark, J. C. W. Chien, *Macromolecules* **1994**, 27, 3383.
- [28] T. Asakura, M. Demura, Y. Nishiyama, *Macromolecules* **1991**, 24, 2334.
- [29] The catalyst displays living-type behavior at low temperatures with negligible chain termination. However, chain termination and catalyst decomposition occur concurrently at elevated temperatures at which the reaction cannot be controlled owing to the high exothermicity. This seems to entail homolytic M–C cleavage under these conditions, and there is much literature precedent for the thermal instability of scandium alkyl complexes.^[18] It is thus not surprising that we observe decomposition under the highly exothermic conditions employed in this study. However, the exact nature of this process remains unknown. In the ^1H NMR spectra of all the polymer samples produced by the dicationic species, no signals attributable to olefinic end groups were observed to within the detection limits of the instrument. Therefore, although we cannot rule out β -hydride elimination altogether, it is certainly not a significant contributor.
- [30] An additional control experiment to distinguish enantiomorphic from chain-end tacticity control would entail the use of an achiral trisox ligand. We previously reported such a ligand that is dimethyl-substituted in the 4-position of the oxazolines: S. Bellemin-Laponnaz, L. H. Gade, *Chem. Commun.* **2002**, 1286; however, we found that for steric reasons, this substitution pattern normally precludes the coordination of this ligand as a tripod to a single metal center, and this also seems to be the case for the scandium complexes. Since the unsubstituted oxazoline derivatives were unstable and thus inaccessible, we are unable to perform this experiment.
- [31] M. F. Lappert, R. Pearce, *J. Chem. Soc. Chem. Commun.* **1973**, 126.

Hybrid Solution/Solid-Phase Synthesis of Oligosaccharides by Using Trichloroacetyl Isocyanate as Sequestration-Enabling Reagent of Sugar Alcohols

Alessandro Dondoni,* Alberto Marra,* and
Alessandro Massi*

In recent years there has been a steady increase in interest in glycoscience with particular emphasis toward programs at the chemistry/biology interface. Current studies are mainly directed toward the understanding at molecular level of the key role exerted by glycoconjugate-derived oligosaccharides in beneficial or detrimental events that occur in living organisms.^[1] In most, if not all, of these studies, organic synthesis is required to provide meaningful quantities of native oligosaccharides and their analogues in a pure state with well-defined structures to be used as biological, biochemical, and biophysical probes. Pure oligosaccharides are very difficult to access from natural sources owing to the complexity and microheterogeneity of glycosylated proteins^[2] and their instability to many isolation procedures. Enormous progress has been made in the area of oligosaccharide synthesis especially in the last decade, and a plethora of synthetic methods in either the solution or solid phase have been reported.^[3,4] However both techniques present their own limitations. For instance, solution-phase reactions require a laborious workup and time-consuming product isolation by chromatography after each glycosidation trail. On the other hand, the solid-phase approach does not entail the above problems and lends itself to automation, however, the polymer-bound substrate suffers an attenuated reactivity for entropic and steric reasons, and monitoring the progress of the reaction and estimating the yield of coupled product by TLC or standard NMR and MS analyses is more difficult. A number of sophisticated analytical methods have therefore been developed as a result.^[5] Another serious concern in the solid-phase approach is the need for robust linkers that tolerate various reaction conditions but can be easily cleaved to retrieve the product without affecting its functionalities, especially the labile and stereomutable *O*-glycosidic bond. Even in the face of spectacular advances in the field of automated solid-phase synthesis of oligosaccharides up to nine-member constructs,^[4] the main way to access complex oligosaccharides that feature a great structural diversity still

appears to be the convergent solution-phase approach by coupling tri- or tetrasaccharide building blocks.^[6]

Hence the search for innovative and practical methods based on recent synthetic techniques is actively pursued. Notable is the tag-assisted solution-phase strategy developed by Hindsgaul and co-workers,^[7] Pozgay,^[8] and Ito and co-workers^[9] in which a suitable group (tag) installed in one of the reactants serves to selectively remove the coupled product from the complex reaction mixture. An oligosaccharide synthesis centered on the use of a highly fluorinated tag was reported by Inazu and co-workers^[10] following an earlier approach by Curran et al. based on the fluorous-tag method^[11] which, however, was quite limited in scope. We envisaged a novel approach to oligosaccharide synthesis based on a solid-supported sequestering or scavenging technique,^[12] which involves executing the reaction in solution in the presence of an excess of one reactant and then removing the residue with a polymer-bound reagent. This approach is referred to as polymer-assisted solution-phase (PASP) synthesis and offers all the advantages associated with solution-phase chemistry and those which are intrinsic to classical solid-phase techniques, such as the use of a large excess of one reagent to drive the reaction to completion followed by a simple filtration step for the isolation of the product. Quite surprisingly there are few examples of the PASP technique applied to oligosaccharide synthesis, and unfortunately the reported methods are not free of substantial shortcomings. In one instance Kirschning et al. reported a route that was limited to the preparation of 2-deoxyglycoconjugates,^[13] while Ley and co-workers developed a method that operated only with primary sugar alcohols as acceptors.^[14] Herein we report our own strategy in which the coupling of the sugar is carried out by the use of a twofold excess of a primary or secondary sugar alcohol. Once the reaction is completed, as shown by the total consumption of the glycosyl donor, the unreacted acceptor is selectively derivatized by trichloroacetyl isocyanate, which is a powerful detecting reagent of alcohols and is widely employed as an analytical tool in NMR spectroscopy.^[15] The resultant trichloroacetyl urethane is removed from the solution mixture by a suitable solid-supported base. The free sugar alcohol is recovered from the sequestered material and reused as an acceptor in a subsequent glycosylation cycle.

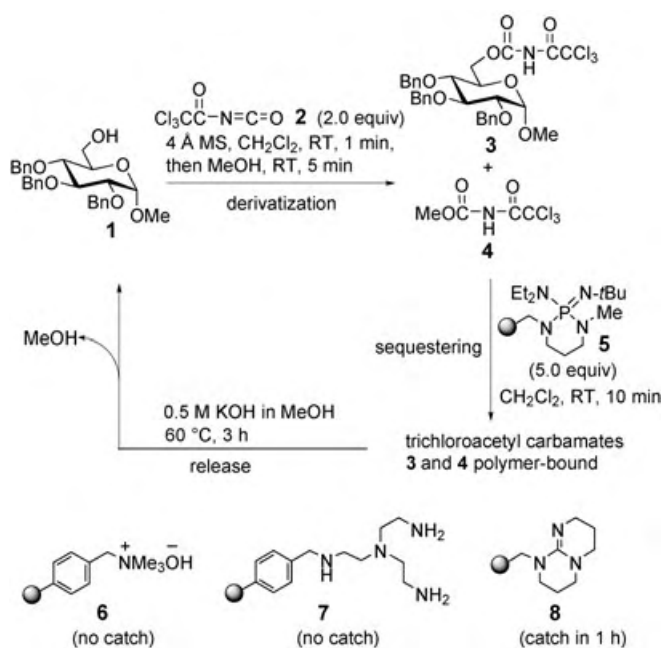
Before developing our method, we made several (unsuccessful) attempts to sequester the model secondary sugar alcohol **9** (Scheme 2) with commercially available polymer-supported reagents such as PS-benzenesulfonyl chloride (PS = polystyrene), PS-phenylisocyanate, and the dichlorotriazine developed by Masala and Taddei.^[16] Discouraging results were also obtained in an attempt to modify the capture strategy of **9** by the use of tetrafluorophthalic anhydride as a sequestration-enabling reagent (SER).^[17] This anhydride failed to provide the expected ester (see Supporting Information). To develop an efficient strategy for sequestering both primary and secondary sugar alcohols in a PASP synthesis of oligosaccharides, our study commenced by examining the capture–release sequence of the primary sugar alcohol **1** using trichloroacetyl isocyanate (**2**, TAI) as the hitherto unemployed SER.^[18] Thus treatment of **1** with **2**

[*] Prof. A. Dondoni, Prof. A. Marra, Dr. A. Massi
Laboratorio di Chimica Organica
Dipartimento di Chimica
Università di Ferrara
Via L. Borsari 46, 44100 Ferrara (Italy)
Fax: (+39) 0532-291-167
E-mail: adn@dns.unife.it
mra@dns.unife.it
msslsn@dns.unife.it



Supporting information for this article is available on the WWW under <http://www.angewandte.org> or from the author.

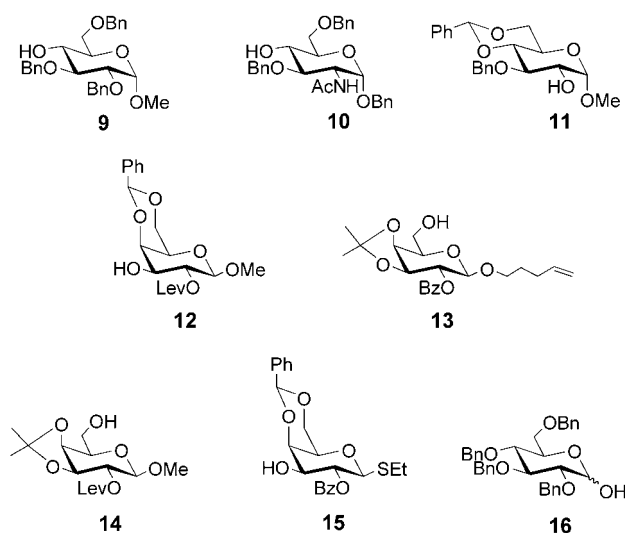
(ratio 1:2) under neutral conditions afforded the sugar urethane **3** almost instantaneously as shown by TLC analysis (Scheme 1, derivatization step). Then, the reaction mixture was quenched with a large excess of MeOH that transformed



Scheme 1. Use of trichloroacetyl isocyanate (**2**, TAI) as a new sequestration-enabling reagent (SER). Also shown are other polymer-supported bases (**6**–**8**) tested in the sequestering step. Bn = benzyl.^[19]

unconverted TAI **2** into methyl urethane **4**. The exclusion of water in this operation is recommended to avoid the decomposition of **2** into trichloroacetamide whose removal would require purification by column chromatography. The solid-phase sequestering of **3** and **4** was carried out using the highly basic, non-nucleophilic polymer-supported BEMP (2-*tert*-butylimino-2-diethylamino-1,3-dimethyl-perhydro-1,3,2-diazaphosphorine on polystyrene, **5**) to give urethanes bound to the polymer as ion pairs.^[19] Filtration of the resin and subsequent treatment with KOH in MeOH followed by neutral aqueous workup released the starting sugar alcohol **1** in high yield (95 %) and purity (95 %).

The wide scope of this derivatization–sequestering–release (DSR) sequence was demonstrated by successful application to primary and secondary sugar alcohols **9**–**15**, which feature diverse protecting groups of the hydroxy group (Scheme 2). In all cases the starting compound or a partially deprotected derivative was recovered in high yield (95 %) and purity (> 95 %) with unaltered anomeric configuration. Note that the methodology was compatible with the presence of the NHAc group (see compound **10**) which allowed *N*-acetyl amino sugars to be included as substrates in the TAI-mediated capture–release sequence.^[20] Efficient sequestering of the sugar hemiacetal **16** was also demonstrated, although in this case the polymer-bound product decomposed under the strongly basic conditions of the release step. Nevertheless, a means for removing hemiacetal side products from glycosidation mixtures is a useful tool, as these compounds may be



Scheme 2. Other representative sugar alcohols and a hemiacetal subjected to the derivatization–sequestering–release (DSR) sequence. Note compounds **12**–**15** were recovered as deacylated derivatives. Bz = benzoyl, Lev = levulinoyl (4-oxopentanoyl).

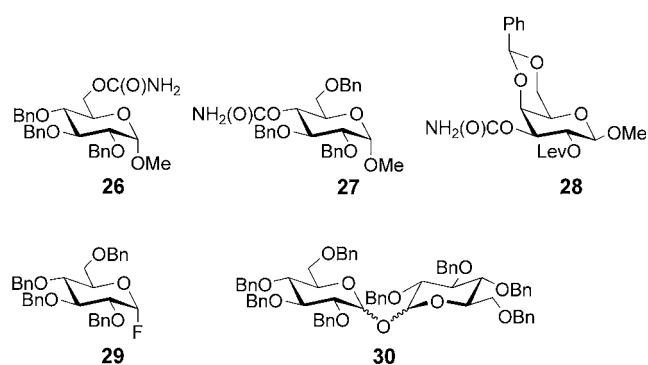
easily formed by the hydrolysis of a large variety of activated glycosyl donors.

With an efficient solid-phase sequestering methodology of sugar alcohols in hand, the solution-phase synthesis of various disaccharides and their isolation was conducted as outlined in Table 1. Once the glycosidation of the donor was completed in the presence of a twofold excess of acceptor, filtration of the reaction mixture was followed by aqueous workup and evaporation of the solvent to afford the target disaccharide along with the unconverted acceptor and other carbohydrate-containing byproducts. This reaction mixture was essentially free of impurities arising from the glycosyl donor-activation system. In fact, the accurate choice of anomeric leaving groups (thioethyl, pentenyl, phosphates, and phosphites; see Table 1 and Scheme 5) and the relevant promoters ($\text{Cu}(\text{OTf})_2$ (OTf = trifluoromethanesulfonate), MeOTf, NIS (*N*-iodosuccinimide), TMSOTf (TMS = trimethylsilyl), $\text{BF}_3 \cdot \text{OEt}_2$) led to byproducts that could be removed by filtration, evaporation, or by aqueous workup.^[21] Only in the case of succinimide, which formed in the NIS activation system, did removal of this byproduct take place in the next step upon treatment of the reaction mixture with polymer-supported BEMP (**5**). The unconverted acceptor was scavenged and recovered by the above DSR sequence, and the desired disaccharide was isolated as a mixture of anomers. Excellent yields and high purities were registered for all crude products **18**, **19**, **21**, and **23** obtained in this way. The purities estimated in the ^1H NMR spectra were confirmed by means of chromatographic purification, which also allowed the identification of the residual (4–5 %) sugar carbamates **26** and **27** byproducts (Scheme 3). The yields of the two analytically pure products **18** and **19** were much higher than those obtained when equimolar amounts of reaction partners were used in the same solution-phase synthesis, thus substantiating the effectiveness of the glycosidation reaction under the conditions employed. Nevertheless, we observed that our improved glycosidation con-

Table 1: Application of the proposed methodology to the synthesis of disaccharides.

<div> <div>donor + acceptor</div> <div>(1.0 equiv) (2.0 equiv)</div> </div> <div> <div>promoter</div> <div>disaccharide</div> <div>excess acceptor</div> </div> <div> <div>a) $\text{Cl}_3\text{CCl}(\text{O})\text{NCO}$ (2), then MeOH</div> <div>b) BEMP 5</div> </div> <div> <div>disaccharide</div> <div>polymer-bound derivatized acceptor</div> <div>0.5 M KOH in MeOH</div> <div>acceptor</div> </div>					
Glycosidation	Yield [%]	Purity [%] ^[a]	Isolated yield [%] ^[b]	Ratio α/β	Recovered excess acceptor [%]
	quant.	95	96 (83) ^[c]	1:2	92
	98	95	91 (59) ^[c]	1:1	95
	92	95	87	0:1	97
	quant.	95	96	0:1	92
	94 ^[d]	80 ^[d]	73	1:3	98 ^[e]

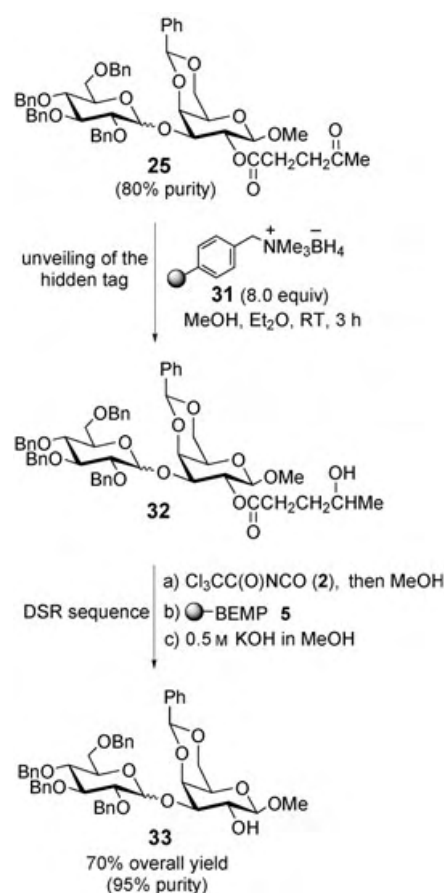
[a] From ^1H NMR analysis. [b] After column chromatography on silica gel. [c] Yield of isolated disaccharide when the glycosidation reaction is carried out with an equimolar ratio of donor and acceptor. [d] Disaccharide **25** was obtained in 88 % yield with 90 % purity using TMSOTf (trimethylsilyl trifluoromethanesulfonate) as the promoter under the same reaction conditions. [e] Acceptor recovered as deacylated derivative.



Scheme 3. Sugar byproducts formed during the glycosidations described in Table 1.

ditions did not always protect the donor from its partial degradation, thus giving unsatisfactory results especially in terms of purity of the isolated target glycoconjugate. This was the case with disaccharide **25**, which was obtained in good yield (94 %) but with quite low purity (80 %), as confirmed by

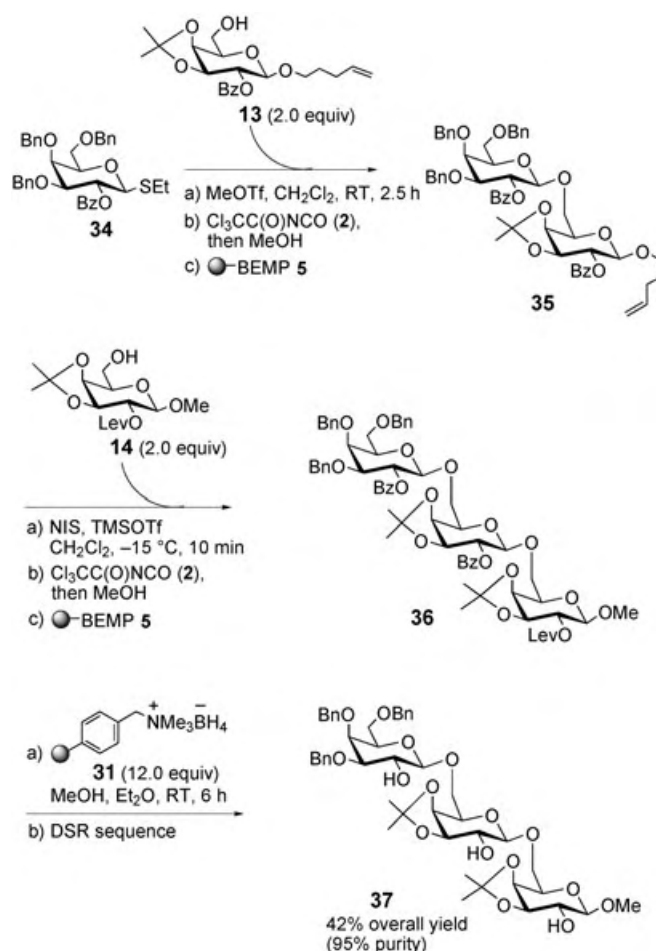
isolation of its contaminants—the carbamate **28**, glycosyl fluoride **29**, and trehaloses **30**—by chromatography (Scheme 3). Evidently, the side products **29** and **30** arise from the initial decomposition of the phosphite-activated donor **24**. To overcome this limitation, we refined the proposed methodology by considering a second cycle of purification for disaccharide **25** which exploits the benefits of both a tag-assisted and a “resin-capture–release” purification strategy.^[22] The key element in this improved protocol was the levulinoyl (4-oxopentanoyl) ester group which serves as a hidden tag (Scheme 4) and was earlier installed on the glycosyl acceptor **12**. Thus, the crude disaccharide **25**, which results from the first TAI-based purification sequence (80 % purity, Table 1), was treated with polymer-supported borohydride **31** to unveil the C2 hydroxy group.^[23] Instead, the γ -hydroxyester **32** was obtained as a single product. This product was derivatized with TAI (**2**), trapped as an activated polymer intermediate onto PS-BEMP, and finally, after washing to remove soluble byproducts **28–30**, was released in solution by means of KOH in MeOH (Scheme 4). This new hybrid solution/solid-phase approach afforded the disaccharide **33** in 70 % overall yield (starting from **24**) and with 95 %



Scheme 4. Use of the levulinoyl group as a hidden tag in the “resin-capture–release” purification strategy.

purity (determined by chromatography and ^1H NMR spectroscopy).

As a demonstration of the power of our strategy, the assembly of trisaccharide **37** was conducted by iterative glycosidation (Scheme 5). Efficiency relied on the nontrivial task to select reaction partners with suitable hydroxy group protection and anomeric activation to ensure good reactivity and stereo- and chemoselectivity in each cycle. Thus, under methyl triflate activation, the 2-benzoyl-directed β glycosidation of thioethyl galactoside **34** with an excess of primary alcohol **13** followed by derivatization with TAI (**2**) and sequestration of the urethane with PS-BEMP (**5**) afforded β -D-(1,6)-disaccharide **35**. This crude compound under *O*-pentenyl activation by NIS–TMSOTf was subjected to glycosidation by the sugar alcohol **14**, which bears the levulinoyl ester group at C2. The trisaccharide **36** obtained was isolated by workup of the reaction mixture with the standard TAI-based sequestering technique. The crude trisaccharide **36** was finally purified by reduction of the levulinate carbonyl group using the polymer-supported borohydride **31** followed by sequestration with the DSR sequence as described in Scheme 4. The benzoyl- and levulinoyl-free trisaccharide **37** was isolated in 42% yield and 95% purity according to NMR spectral analysis. In two separate experiments, the coupled products **35** and **36** were isolated (89 and 55% yield, respectively) by column chroma-



Scheme 5. Synthesis of a trisaccharide; chromatographic purification not required.

tography and were duly characterized by NMR spectroscopy, thus confirming the formation of the β -D-glycosidic linkage in both solution-phase glycosidations.

Overall, the efforts made herein were directed to find conditions that would allow an automated synthesis of oligosaccharides by the merging of the polymer-support technology with solution-phase chemistry. The results obtained so far are quite promising and indicate that this goal can be pursued. The effectiveness of TAI as a new SER for scavenging both primary and secondary sugar alcohols and the exploitation of the levulinoyl group as a hidden tag for hybrid solution/solid-phase synthesis represent the major novelties and key operations in this new strategy. However, more research is required to provide examples that allow the scope of this strategy to be extended to the synthesis of more-complex oligosaccharides than those described above. This work is currently underway in our laboratory.

Received: October 25, 2004

Revised: December 10, 2004

Published online: February 3, 2005

Keywords: chemoselectivity · glycosylation · solid-phase synthesis · synthetic methods

- [1] a) A. Varki, *Glycobiology* **1993**, *3*, 97; b) A. Kobata, *Acc. Chem. Res.* **1993**, *26*, 319; c) R. A. Dwek, *Chem. Rev.* **1996**, *96*, 683; d) *Essentials of Glycobiology* (Eds: A. Varki, R. Cummings, J. Esko, H. Freeze, G. Hart, J. Marth), Cold Spring Harbor, Plainview, New York, **1999**.
- [2] a) T. W. Rademacher, R. B. Parekh, R. A. Dwek, *Annu. Rev. Biochem.* **1988**, *57*, 785; b) R. S. Rush, P. L. Derby, D. M. Smith, C. Merry, G. Rogers, M. F. Rhode, V. Katta, *Anal. Chem.* **1995**, *67*, 1442.
- [3] For recent reviews, see: a) *Modern Methods in Carbohydrate Synthesis* (Eds: S. H. Khan, R. A. O'Neil), Harwood, Amsterdam, **1996**; b) *Preparative Carbohydrate Chemistry* (Ed.: S. Hanessian), Marcel Dekker, New York, **1997**; c) *Carbohydrates in Chemistry and Biology* (Eds.: B. Ernst, G. W. Hart, P. Sinaÿ), Wiley-VCH, Weinheim, **2000**; d) *Solid Support Oligosaccharide Synthesis and Combinatorial Libraries* (Ed.: P. H. Seeberger), Wiley-Interscience, New York, **2001**; e) G.-J. Boons, *Tetrahedron* **1996**, *52*, 1095; f) H. M. I. Osborn, T. Q. Khan, *Tetrahedron* **1999**, *55*, 1807; g) F. Schweizer, O. Hindsgaul, *Curr. Opin. Chem. Biol.* **1999**, *3*, 291; h) P. M. St. Hilaire, M. Meldal, *Angew. Chem.* **2000**, *112*, 1210; *Angew. Chem. Int. Ed.* **2000**, *39*, 1162; i) P. H. Seeberger, W.-C. Haase, *Chem. Rev.* **2000**, *100*, 4349; j) K. M. Koeller, C.-H. Wong, *Chem. Rev.* **2000**, *100*, 4465; k) H. Herzner, T. Reipen, M. Schultz, H. Kunz, *Chem. Rev.* **2000**, *100*, 4495; l) P. Sears, C.-H. Wong, *Science* **2001**, *291*, 2344; m) K. C. Nicolaou, H. J. Mitchell, *Angew. Chem.* **2001**, *113*, 1624; *Angew. Chem. Int. Ed.* **2001**, *40*, 1576; n) A. V. Demchenko, *Synlett* **2003**, 1225; o) P. H. Seeberger, *Chem. Commun.* **2003**, 1115; p) D. Crich, L. B. L. Lim, *Org. React.* **2004**, *64*, 115.
- [4] For selected recent papers (2000–2004), see: a) X.-S. Ye, C.-H. Wong, *J. Org. Chem.* **2000**, *65*, 2410; b) K. Egusa, K. Fukase, Y. Nakai, S. Kusumoto, *Synlett* **2000**, 27; c) F. Burkhart, Z. Zhang, S. Wacowich-Sgarbi, C.-H. Wong, *Angew. Chem.* **2001**, *113*, 1314; *Angew. Chem. Int. Ed.* **2001**, *40*, 1274; d) O. J. Plante, E. R. Palmacci, P. H. Seeberger, *Science* **2001**, *291*, 1523; e) T. Zhu, G.-J. Boons, *Org. Lett.* **2001**, *3*, 4201; f) H. M. Nguyen, J. L. Poole, D. Y. Gin, *Angew. Chem.* **2001**, *113*, 428; *Angew. Chem. Int. Ed.* **2001**, *40*, 414; g) S. Yamago, T. Yamada, O. Hara, H. Ito, Y. Mino, J. Yoshida, *Org. Lett.* **2001**, *3*, 3867; h) F. Roussel, M. Takhi, R. R. Schmidt, *J. Org. Chem.* **2001**, *66*, 8540; i) J. D. C. Codée, L. J. van den Bos, R. E. J. N. Litjens, H. S. Overkleeft, J. H. van Boom, G. A. van der Marel, *Org. Lett.* **2003**, *5*, 1947; j) T. K. Ritter, K.-K. T. Mong, H. Liu, T. Nakatani, C.-H. Wong, *Angew. Chem.* **2003**, *115*, 4805; *Angew. Chem. Int. Ed.* **2003**, *42*, 4657; k) D. Majumdar, T. Zhu, G.-J. Boons, *Org. Lett.* **2003**, *5*, 3591; l) K. Routenberg, P. H. Seeberger, *Angew. Chem.* **2004**, *116*, 612; *Angew. Chem. Int. Ed.* **2004**, *43*, 602; m) S. Yamago, T. Yamada, T. Maruyama, J. Yoshida, *Angew. Chem.* **2004**, *116*, 2197; *Angew. Chem. Int. Ed.* **2004**, *43*, 2145; n) X. Huang, L. Huang, H. Wang, X.-S. Ye, *Angew. Chem.* **2004**, *116*, 5333; *Angew. Chem. Int. Ed.* **2004**, *43*, 5221; o) X. Wu, R. R. Schmidt, *J. Org. Chem.* **2004**, *69*, 1853.
- [5] a) T. Kanemitsu, C.-H. Wong, O. Kanie, *J. Am. Chem. Soc.* **2002**, *124*, 3591; b) M. Mogemark, M. Elofsson, J. Kihlberg, *J. Org. Chem.* **2003**, *68*, 7281; c) M. Mogemark, F. Gårdmo, T. Tengel, J. Kihlberg, M. Elofsson, *Org. Biomol. Chem.* **2004**, *2*, 1770.
- [6] Among the numerous examples which can be cited, the most convincing case is the work recently reported by Danishefsky and co-workers targeted to carbohydrate-based HIV vaccines. See: a) M. Mandal, V. Y. Dudkin, X. Geng, S. J. Danishefsky, *Angew. Chem.* **2004**, *116*, 2611; *Angew. Chem. Int. Ed.* **2004**, *43*, 2557; b) X. Geng, V. Y. Dudkin, M. Mandal, S. J. Danishefsky, *Angew. Chem.* **2004**, *116*, 2616; *Angew. Chem. Int. Ed.* **2004**, *43*, 2562.
- [7] a) M. M. Palcic, L. D. Heeze, M. Pierce, O. Hindsgaul, *Glycoconjugate J.* **1988**, *5*, 49; b) Y. Ding, J. Labbe, O. Kanie, O. Hindsgaul, *Bioorg. Med. Chem.* **1996**, *4*, 683; c) U. J. Nilsson, E. J.-L. Fournier, O. Hindsgaul, *Bioorg. Med. Chem.* **1998**, *6*, 1563.
- [8] a) V. Pozsgay, *Org. Lett.* **1999**, *1*, 477; b) V. Pozsgay, *Tetrahedron: Asymmetry* **2000**, *11*, 151.
- [9] a) H. Ando, S. Manabe, Y. Nakahara, Y. Ito, *J. Am. Chem. Soc.* **2001**, *123*, 3848; b) Y. Ito, S. Manabe, *Chem. Eur. J.* **2002**, *8*, 3077.
- [10] a) T. Miura, Y. Hirose, M. Ohmae, T. Inazu, *Org. Lett.* **2001**, *3*, 3947; b) T. Miura, K. Goto, H. Varagai, H. Matsumoto, Y. Hirose, M. Ohmae, H. Ishida, A. Satoh, T. Inazu, *J. Org. Chem.* **2004**, *69*, 5348.
- [11] D. P. Curran, R. Ferritto, Y. Hua, *Tetrahedron Lett.* **1998**, *39*, 4937.
- [12] a) J. J. Parlow, R. V. Devraj, M. S. South, *Curr. Opin. Chem. Biol.* **1999**, *3*, 320; b) S. J. Shuttleworth, S. M. Allin, R. D. Wilson, D. Nasturica, *Synthesis* **2000**, 1035; c) L. A. Thompson, *Curr. Opin. Chem. Biol.* **2000**, *4*, 324; d) S. V. Ley, I. R. Baxendale, R. N. Bream, P. S. Jackson, A. G. Lezach, D. A. Langbottom, M. Nesi, J. S. Scott, R. I. Storer, S. J. Taylor, *J. Chem. Soc. Perkin Trans. 1* **2000**, 23, 3815; e) A. Kirschning, H. Monenschein, R. Wittenberg, *Angew. Chem.* **2001**, *113*, 670; *Angew. Chem. Int. Ed.* **2001**, *40*, 650.
- [13] a) A. Kirschning, M. Jesberger, A. Schönberger, *Org. Lett.* **2001**, *3*, 3623; b) J. Jaunzems, D. Kashin, A. Schönberger, A. Kirschning, *Eur. J. Org. Chem.* **2004**, 3435.
- [14] R. N. MacCoss, P. E. Brennan, S. V. Ley, *Org. Biomol. Chem.* **2003**, *1*, 2029.
- [15] a) V. W. Goodlett, *Anal. Chem.* **1965**, *37*, 431; b) M. Meyer zur Heyde, *Fresenius Z. Anal. Chem.* **1979**, 295, 125; c) G. H. P. Roos, M. C. Watson, *S. Afr. J. Chem.* **1991**, *44*, 95.
- [16] S. Masala, M. Taddei, *Org. Lett.* **1999**, *1*, 1355.
- [17] J. J. Parlow, W. Naing, M. S. South, D. L. Flynn, *Tetrahedron Lett.* **1997**, *38*, 7959.
- [18] To the best of our knowledge TAI (2) has not been used so far in PASP synthetic strategies. However, the use of benzenesulfonyl isocyanate as a SER was announced, see: W. Naing, S. Yang, J. J. Parlow, D. L. Flynn, R. V. Devras in *Book of Abstracts*, 216th ACS National Meeting, Boston, August 23–27, **1998**. We are not aware of any article in follow-up to that communication.
- [19] The sequestering of urethanes **3** and **4** failed with other polymer-supported bases, namely Ambersep 900 OH **6** and trisamine **7**, whereas the rigidified guanidine-type compound **8** was quite effective but required a much longer reaction time than the diazaphosphorine **5**.
- [20] The DSR sequence shown in Scheme 1 was successfully applied to a sugar primary amine and, with some limitations, to an anomeric sugar thiol (see Supporting Information). Work in this area is in progress.
- [21] In earlier PASP glycosidation approaches, Kirschning and Ley and their co-workers used thiophenyl and selenophenyl glycosides, respectively, as donors. The removal of sulphur- and selenium-containing byproducts required suitable scavenging procedures. See: a) J. Jaunzems, G. Sourkouni-Argirusi, M. Jesberger, A. Kirschning, *Tetrahedron Lett.* **2003**, *44*, 637; b) J. Jaunzems, E. Hofer, M. Jesberger, G. Sourkouni-Argirusi, A. Kirschning, *Angew. Chem.* **2003**, *115*, 1198; *Angew. Chem. Int. Ed.* **2003**, *42*, 1166, and ref. [14].
- [22] For a definition of “resin-capture-release” hybrid technique, see: A. Kirschning, H. Monenschein, R. Wittenberg, *Chem. Eur. J.* **2000**, *6*, 4445.
- [23] It is well known that the reduction by NaBH₄ of sugars protected as *O*-levulinates induces the cleavage of the ester group by removal of methyl γ -butyrolactone.

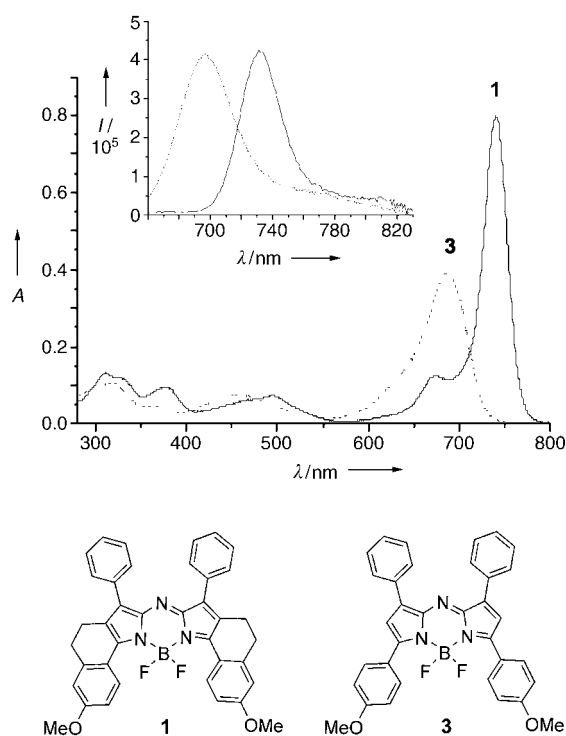


Figure 1. Absorption spectra of **1** and reference **3** (5.0×10^{-6} M CHCl_3). The inset shows corrected fluorescence spectra of **1** and **3** (in CHCl_3) at 298 K upon illumination at 670 nm.

tion ($\epsilon = 159000$; $\Phi = 0.28$). The dye meets the necessary requirements of a NIR chromophore: 1) peak fluorescence at 700–900 nm; 2) high quantum yield; 3) narrow excitation/emission spectrum; and 4) high chemical stability and photostability, as well as a convenient commercially viable synthesis for the generation of useful quantities. Additionally, the sharp fluorescence of the dye is insensitive to solvent polarity. Efforts are currently under way to develop nonsymmetrically substituted, water-soluble versions to allow conjugation for biosensing experiments.

Received: September 2, 2004

Revised: November 15, 2004

Published online: February 3, 2005

Keywords: dyes/pigments · fluorescence · fluorescent probes · imaging agents

- [1] a) J. Fabian, H. Kakazumi, M. Matsuoka, *Chem. Rev.* **1992**, 92, 1197; b) M. Matsuoka, *Infrared Absorbing Dyes*, Plenum Press, New York, **1990**; c) *Near-Infrared Dyes for High Technology Applications*, NATO Series 3, Vol. 52 (Eds.: S. Dähne, U. Resch-Genger, O. S. Wolfbeis), Kluwer, Dordrecht, **1998**.
- [2] a) J. V. Frangioni, *Curr. Opin. Chem. Biol.* **2003**, 7, 626; b) E. M. Sevick-Muraca, J. P. Houston, M. Gurfinkel, *Curr. Opin. Chem. Biol.* **2002**, 6, 642; c) C. Sun, J. Yang, L. Li, X. Wu, Y. Liu, S. Liu, *J. Chromatogr. B* **2004**, 803, 173; d) M. Funovics, R. Weissleder, C. H. Tung, *Anal. Bioanal. Chem.* **2003**, 377, 956; e) R. P. Haugland, *Handbook of Fluorescent Probes and Research Chemicals*, 6th ed., Molecular Probes, Eugene, **1996**.

- [3] a) S. R. Mujumdar, R. B. Mujumdar, C. M. Grant, A. S. Waggoner, *Bioconjugate Chem.* **1996**, 7, 356; b) M. Kasha, H. R. Rawis, M. A. El-Bayoumi, *Pure Appl. Chem.* **1965**, 11, 371; c) E. G. McRae, M. Kasha, *J. Chem. Phys.* **1958**, 28, 721.
- [4] a) A. Mishra, R. K. Behera, P. K. Behera, B. B. Mishra, G. B. Behera, *Chem. Rev.* **2000**, 100, 1973; b) M. Fabian, H. Nakazumi, M. Matsuoka, *Chem. Rev.* **1992**, 92, 1197.
- [5] M. Casalboni, F. De Matteis, P. Proposito, A. Quatela, F. Sarcinelli, *Chem. Phys. Lett.* **2003**, 373, 372.
- [6] V. Ntziachristos, J. Ripoll, R. Weissleder, *Opt. Lett.* **2002**, 27, 333.
- [7] J. Sowell, L. Strekowski, G. Patonay, *J. Biomed. Opt.* **2002**, 7, 571.
- [8] J. C. McGrath, C. J. Daly, *Br. J. Pharmacol.* **2003**, 139, 187.
- [9] R. Reents, M. Wagner, J. Kuhlmann, H. Waldmann, *Angew. Chem.* **2004**, 116, 2765; *Angew. Chem. Int. Ed.* **2004**, 43, 2711.
- [10] S. C. Hung, R. M. Mathies, A. N. Glazer, *Anal. Biochem.* **1997**, 252, 78.
- [11] H. Maas, G. Calzaferri, *Angew. Chem.* **2002**, 114, 2389; *Angew. Chem. Int. Ed.* **2002**, 41, 2284.
- [12] a) A. Burghart, L. H. Thoresen, J. Chen, K. Burgess, F. Bergström, L. B.-Å. Johansson, *Chem. Commun.* **2000**, 2203; b) A. Burghart, L. H. Thoresen, J. Chen, K. Burgess, F. Bergström, L. B.-Å. Johansson, *J. Am. Chem. Soc.* **2004**, 126, 10619.
- [13] G. Ulrich, R. Ziessel, *Synlett* **2004**, 3, 439.
- [14] F. S. Wouters, P. J. Verveer, P. I. H. Bastiaens, *Trends Cell Biol.* **2001**, 11, 203.
- [15] A. Costela, I. García-Moreno, C. Gómez, R. Sastre, F. Amat-Guerri, M. Liras, F. L. Arbeloa, J. B. Prieto, I. L. Arbeloa, *J. Phys. Chem. A* **2002**, 106, 7737.
- [16] G. Beer, C. Niederalt, S. Grimme, J. Daub, *Angew. Chem.* **2000**, 112, 3385; *Angew. Chem. Int. Ed.* **2000**, 39, 3252.
- [17] J. Karolin, L. B.-Å. Johansson, L. Starndberg, T. Ny, *J. Am. Chem. Soc.* **1994**, 116, 7801.
- [18] A. Burghart, H. Kim, M. B. Welch, L. H. Thoresen, J. Reibenspies, K. Burgess, F. Bergström, L. B.-Å. Johansson, *J. Org. Chem.* **1999**, 64, 7813.
- [19] a) H. Kim, A. Burghart, M. B. Welch, J. Reibenspies, K. Burgess, *Chem. Commun.* **1999**, 1889; b) J. Chen, J. Reibenspies, A. Derecskei-Kovacs, K. Burgess, *Chem. Commun.* **1999**, 2501; c) J. Chen, A. Burghart, A. Derecskei-Kovacs, K. Burgess, *J. Org. Chem.* **2000**, 65, 2900.
- [20] a) K. Rurack, M. Kollmannsberger, J. Daub, *New J. Chem.* **2001**, 25, 289; b) K. Rurack, M. Kollmannsberger, J. Daub, *Angew. Chem.* **2001**, 113, 396; *Angew. Chem. Int. Ed.* **2001**, 40, 385.
- [21] There have been reports of structurally rigidified bodipy dyes absorbing up to 766 nm. However, the efficiency of these systems is unclear as no fluorescence quantum yield has been documented. Notably, fusion and 3,5-diaryl substitution in these systems can result in a decreased fluorescence quantum yield (see ref. [19]); a) M. Wada, S. Ito, H. Uno, T. Murashima, N. Ono, T. Urano, Y. Urano, *Tetrahedron Lett.* **2001**, 42, 6711; b) K. Tan, L. Jaquinod, R. Paolesse, S. Nardis, C. D. Natale, A. D. Carlo, L. Prodi, M. Montalti, K. M. Smith, *Tetrahedron* **2004**, 60, 1099; c) Y. Wu, D. H. Klaubert, H. C. Kang, Y. Z. Zhang, US patent 6005113, **1999**.
- [22] a) J. Killoran, L. Allen, J. F. Gallagher, W. M. Gallagher, D. F. O'Shea, *Chem. Commun.* **2002**, 1862; b) A. Gorman, J. Killoran, C. O'Shea, T. Kenna, W. M. Gallagher, D. F. O'Shea, *J. Am. Chem. Soc.* **2004**, 126, 10619.
- [23] S. Sato, H. Kato, M. Ohta, *Bull. Chem. Soc. Jpn.* **1967**, 40, 2936.
- [24] Fluorescence quantum yield measurements were performed on a Fluorolog-3 instrument (Model FL-3-22) equipped with an R928P photomultiplier tube which is sensitive up to ≈ 850 nm. To obtain accurate excitation spectra, the excitation monochromator was calibrated by a xenon-lamp scan. The emission monochromator was calibrated using a water Raman scan. The response of the detector was calibrated with a standard

tungsten-halogen lamp. Fluorescence quantum yield determination was performed following the method recommended by the manufacturer of the fluorometer (see: www.jobinyvon.com/usadivisions/Fluorescence/applications/quantumyieldstrad.pdf), and was compared with other reported methods (S. Fery-Forgues, D. Lavabre, *J. Chem. Educ.* **1999**, 76, 1260). Compound **3** was used as standard, and the measurements were performed under identical conditions to those with **1**. Nondegassed, spectroscopic-grade chloroform and a 10-mm quartz cuvette were used. Very dilute solutions ($A \leq 0.010$) were used to minimize reabsorption effects. The optical densities of solutions of **1** and **3** were adjusted to 0.200 at 670 nm, and these solutions were diluted by factors of 20, 40, 60, 80, and 100. The excitation wavelength was 670 nm for both compound **1** and reference **3**, and a 510-nm cutoff optical filter was placed between the excitation monochromator and sample cuvette to eliminate UV (335 nm) excitation. The fluorescence quantum yield of compound **1** was calculated to be 0.278 relative to the reference (0.36), which is comparable to the data obtained by the traditional method (0.284 ± 0.006).

- [25] S. Reindl, A. Penzkofer, S. H. Gong, M. Landthaler, R. M. Szeimies, C. Abel, W. Bauml, *J. Photochem. Photobiol. A* **1997**, 105, 65.

Macrocycles

Nanofabrication: Reversible Self-Assembly of an Imbedded Hexameric Metallomacrocycle within a Macromolecular Superstructure**

Pingshan Wang, Charles N. Moorefield, and George R. Newkome*

Molecular imprinting^[1] processes widely occur in complex biosystems, thus, selective and specific guests bound by antibodies, such as hormones, are vital for basic cell–cell communication. Experimental simulation of cell imprinting^[2,3] has been predominately developed by using bulk polymerizations in which guests, or templates, are used to create a molecular “impression” through incorporation

within the infrastructure of appropriately juxtaposed ionic, hydrogen-bonding, or other noncovalent loci.^[4,5] Typically organic guests are used as the template from which, after its removal, the cavity, the shape, and the directivity of the host’s binding site are frozen for subsequent re-recognition of structurally related guests. Zimmerman et al.^[6] developed a novel monomolecular imprinting process,^[7] whereby porphyrin-cored dendrimers^[8] having terminal alkene units were initially created, and subsequent alkene cross-linking gave the host–guest combination; porphyrin removal thus created the desired cavity possessing the desired recognition sites. van Koten and co-workers^[9] employed this technique for the creation of a 69-membered macrocycle that reversibly accepts a pre-assembled platinum triad. Such host–guest molecular recognition generally relies on intermolecular assembly of components. Can the self-assembly process occur by an intramolecular mechanism in which a macromolecular skeleton has multiple ligands capable of reversible assembly–disassembly^[10] which is triggered by the presence of metal ions? We herein describe a simple method allowing molecular nanofabrication by such a procedure.

Based on our previous work^[11–13] concerning the hexameric self-assembly of *meta*-bis(terpyridinyl)arenes having the critical 120° angle with respect to the two ligating moieties, we noted that the Fe^{II} hexamer is more sensitive to basic conditions^[14] compared to the more robust Ru^{II} analogue; thus under basic conditions, demetalation quantitatively regenerated the starting bis-ligand. Colasson and Sauvage^[15] have similarly shown that the related [tpy₂Cu] (tpy = terpyridine) complex can also be destroyed by KCN. Such a facile disassembly process coupled with the high-yield hexamer macrocyclization suggested the possibility of reversible assembly in an appropriate molecular nanotemplate. Herein, we describe a reversible, assembly–disassembly procedure involving a hexametallomacrocycle containing twelve terpyridine groups enclosed within a 114-membered macrocyclic structure (Figure 1).

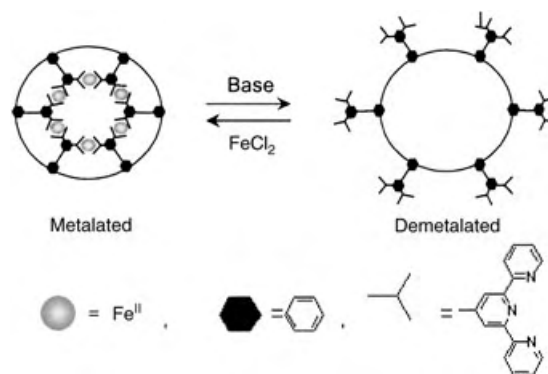


Figure 1. Reversible metalation–demetalation facilitates templated hexamer formation.

The design of the initial bis(terpyridine) ligand was facilitated by molecular modeling simulations (Figure 2) which were used to optimize the requisite alkyl chain length and thus the final ring circumference. Subsequently, oct-7-

[*] Dr. P. Wang, Prof. Dr. G. R. Newkome
Departments of Polymer Science and Chemistry
Goodyear Polymer Center
The University of Akron
Akron, OH 44325-4717 (USA)
Fax: (+1) 330-972-2413
E-mail: newkome@uakron.edu

Dr. C. N. Moorefield, Prof. Dr. G. R. Newkome
Maurice Morton Institute of Polymer Science

[**] The authors are very thankful for financial support from the Air Force Office of Scientific Research (F49620-02-1-0428), the National Science Foundation (DMR-0196231, DMR-0401780, INT-0405242, CHE-0341701, DMR-0414599, CHE-0420987), the Korea Research Foundation (KRF-2003-042-C00069), and the Ohio Board of Regents.

Supporting information for this article is available on the WWW under <http://www.angewandte.org> or from the author.

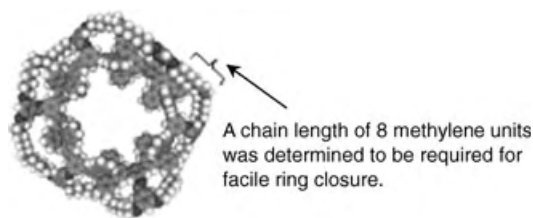
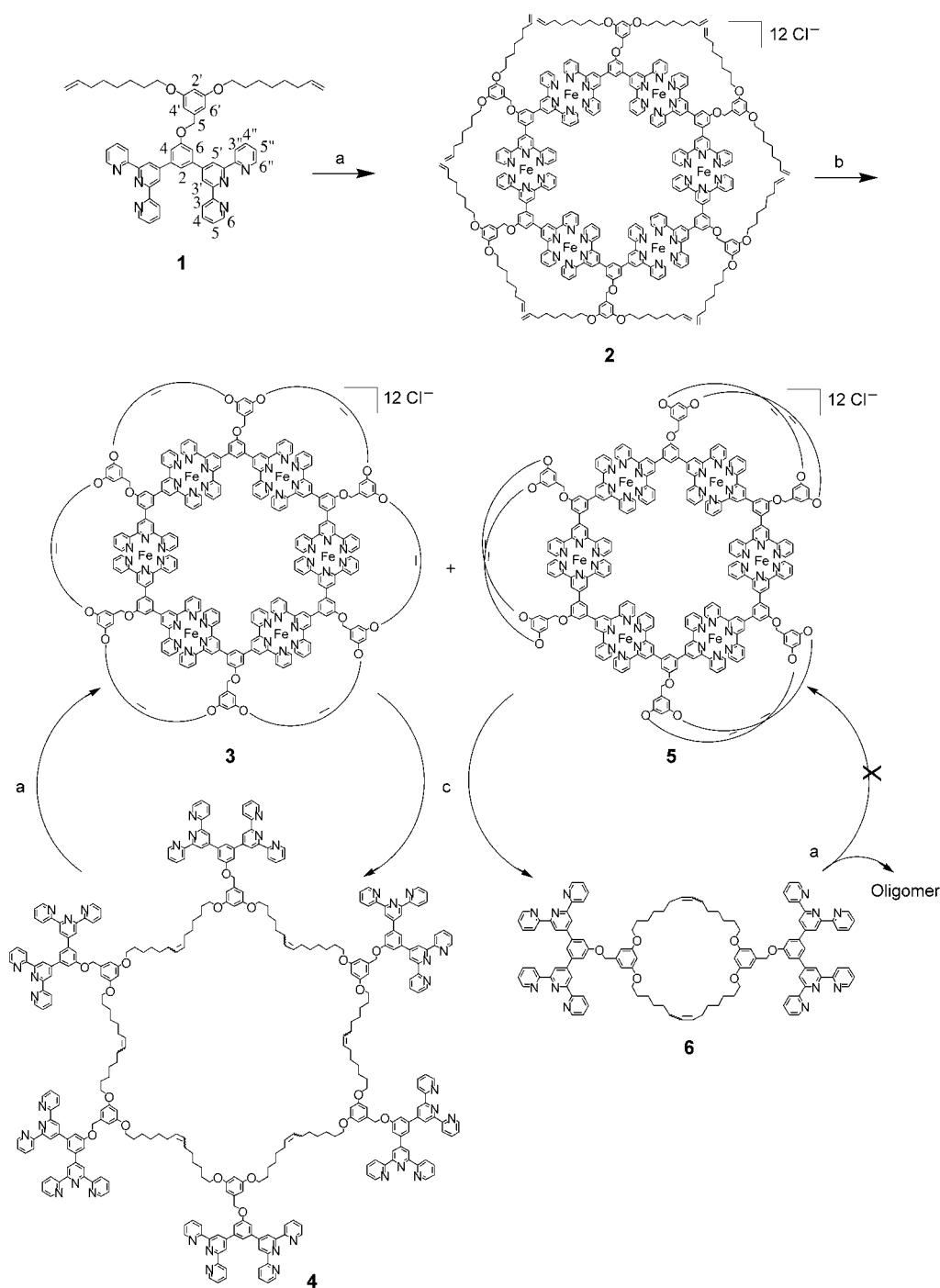


Figure 2. Computer generated molecular model of the templated hexamer **3**.

enyl groups were attached to a bis(terpyridinylphenol) to yield (82%) the alkene-modified ligand **1**.^[16] This ligand was then treated (Scheme 1) with FeCl_2 in MeOH to form a deep purple solution, from which the heliotrope, microcrystalline hexamer **2** was isolated (91%) and confirmed (^1H NMR spectroscopy) by the downfield shift of the 3',5'-tpyH (s; $\delta = 9.79$, $\Delta\delta = +0.96$ ppm), an upfield shift for the 6,6''-tpyH (d $J = 4.8$ Hz; $\delta = 7.33$, $\Delta\delta = -1.44$ ppm), and the shift of 4,6-ArH positions (s; $\delta = 8.27$, $\Delta\delta = +0.66$ ppm) upon complexation. The distinct singlets for the external 4',6'-BnH and



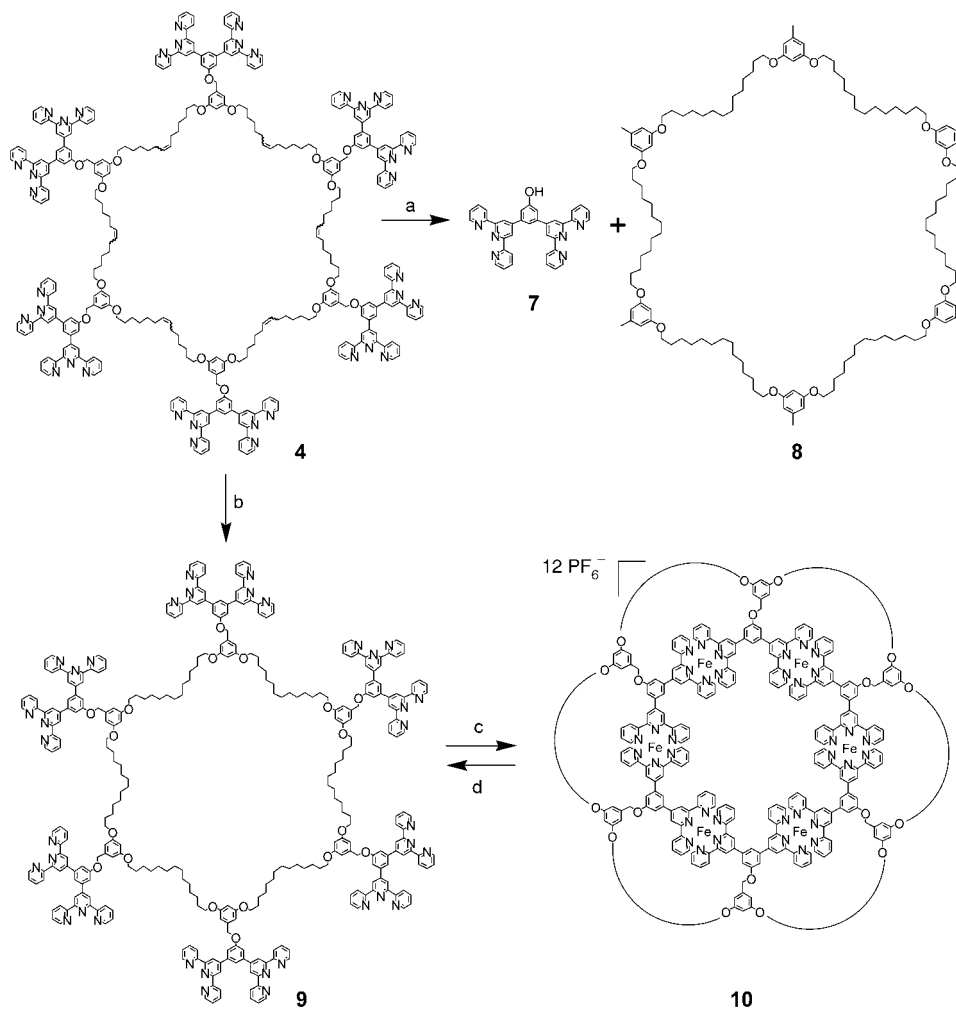
Scheme 1. a) FeCl_2 , MeOH; b) $[\text{PhCH}=\text{Ru}(\text{PCy})_2\text{Cl}_2]$ (Grubbs' catalyst), CH_2Cl_2 ; c) K_2CO_3 , DMF.

benzylic protons support the symmetric, homogenous hexamer **2**, which was completely soluble in most of the common organic solvents.

Hexamer **2** was subsequently cross-linked using Grubbs' catalyst^[6,9,17,18] to generate two major products: the desired purple, microcrystalline, inner macrocyclic complex **3**, which has the 114-membered, hexaolefinic etheral outer superstructure, as well as the isomeric by-product **5** (Scheme 1). Success of the cross-linking reaction was demonstrated (¹H NMR spectroscopy) by the disappearance of the terminal alkene signals at $\delta = 5.80\text{--}5.71$ and $4.98\text{--}4.73$ ppm along with the appearance of a new signal at $\delta = 5.62$ ppm for the formation of a new double bond as a mixture of *E* and *Z* isomers. Owing to the isomeric nature of **3** and **5**, quantitative demetalation (with K_2CO_3 , DMF) of this crude mixture was initially confirmed by the total loss of coloration, indicative of the disassembly of the hexameric core. The resultant white solid, comprised the two major components **4** and **6**, which could be readily separated by preparative thin layer chromatography (TLC; Al_2O_3) eluting with a 3:1 mixture of EtOAc and hexane. In the ¹H NMR spectrum, the expected macrocycle **4** gave rise to a triplet at $\delta = 5.36$ ppm confirming the

presence of the double bonds as well other signature resonance signals and in the mass spectrum **4** gave a definite peak at m/z 2612.8 (ESI-MS) for $(M+2\text{H})^{2+}$. The nominal dimeric byproduct **6**, generated from **5**, was also separated and confirmed by NMR spectroscopy and ESI-MS. The cross-linking reaction greatly depends upon the concentration of hexamer **2**; in general, it was found that concentrations greater than 10^{-4}M generated more complex mixtures.^[19] Subsequent treatment of pure hexa-bis(terpyridine) macrocycle **4** with Fe^{II} regenerated the purple microcrystalline **3**, which was readily demetalated (K_2CO_3 , DMF) again to recover the original ligand **4** in a respectable overall conversion (85%; after chromatography).

To remove the structural complexity caused by the mixture of *cis* and *trans* olefinic configurations, the macrocycle ligand **4** was hydrogenated (Pd/C (5 or 10%), EtOH, THF (2/1, v/v)); however, olefin reduction was accompanied with the unwanted debenzylation affording (100%) the macrocycle **8**, as a viscous oil, and hydroxybis(terpyridine) **7**^[16] that was identical to the original starting material **1** (Scheme 2). Whereas, the use of Raney-Ni^[20] with hydrazine in EtOH gave rise to smooth reduction of the olefinic centers



Scheme 2. a) Pd/C (10%), H_2 , EtOH, THF; b) 1. Raney-Ni, NH_2NH_2 , EtOH, 2. K_2CO_3 , EtOH; c) 1. FeCl_2 , MeOH, 2. NH_4PF_6 , MeOH; d) K_2CO_3 , DMF.

and circumvented the unwanted debenzoylation. The resulting a pale blue-green solution may get its color from traces of terpyridine-nickel complexes; refluxing this solution in ethanolic K_2CO_3 for 1 h subsequently afforded (> 90 %) the pure terpyridine-modified, ethereal macrocycle **9** after chromatography (Al_2O_3 , EtOAc, hexane (3:1)). The reduced superstructure was confirmed (1H NMR spectroscopy) by the disappearance of the resonance signal arising from olefinic protons. The structure was further supported by the mass peak at m/z 2641.5 (ESI-MS) for $(M+2Na)^{2+}$.

Treatment of **9** with $FeCl_2$ in MeOH gave a deep purple solid, which after column chromatography (SiO_2), eluting with a mixture of $H_2O:MeCN:KNO_3$ (1:7:1), and subsequent counterion exchange with PF_6^- gave hexamer **10** (80 %). Characteristic of this transformation, the 3' and 5' signals exhibited a 0.7 ppm downfield shift while the 6' and 6'' signals resonate 1.4 ppm upfield relative to their positions in the free ligand (Figure 3). Quantitative disassembly of **10** with K_2CO_3

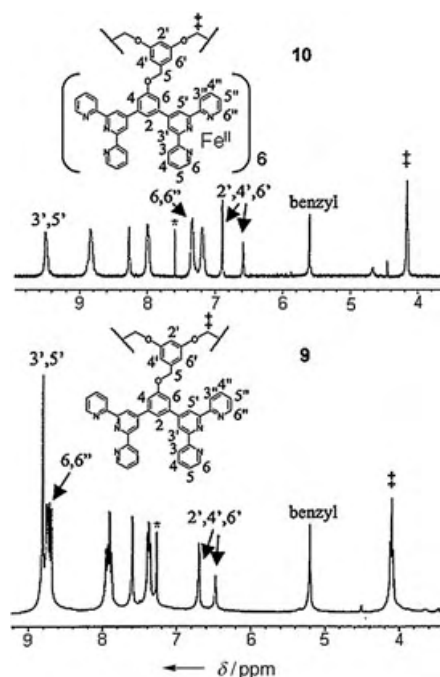


Figure 3. 1H NMR spectra of the metalated hexamer template **10** (top; 750 MHz, $CDCl_3^*$ in CD_3CN) and the demetalated, polyterpyridine-modified, 114-membered cycloalkane **9** (bottom; 300 MHz, $CDCl_3^*$).

in DMF resulted in the reformation of the metal-free **9**, which was then again transformed back to complex **10**; assembled and disassembled samples were identical in all aspects to the original materials. Since there are no opportunities for structural repair in this assembly process through this mode of construction, there is a minor (ca. 3–5 %) loss in each re-assembly phase. After removal of the pure regenerated hexamer by simple chromatography, all defective materials were simply treated with base to recover the original ligand. By using this recyclozation procedure, overall yields can approach 100 %.

In conclusion, it was shown that the assembly–disassembly of appropriately designed complexes within a macromolecu-

lar superstructure can readily occur by the use of a semilabile metal center. This nanofabrication would appear to be applicable to related high conversion complexation processes^[21] by metal-ion driven imprinting procedures. The potential to craft nanoscale components that can repetitively self-assemble has ramifications for self-repairing mechanisms and architectural molecular morphism allowing access to new smart, tailored macromolecular materials.

Experimental Section

1: 3,5-di(octenyloxy)benzyloxybisterpyridine, see ref. [16].

2: m.p. > 300 °C; 1H NMR (300 MHz; $CDCl_3/CD_3OD$ (1/1): δ = 9.79 (s, 4H, $ArH^{3,5}$), 9.11 (s, 5H, $ArH^2 + PyH^{3,3'}$), 8.27 (s, 2H, $ArH^{4,6}$), 8.01 (s, 4H, $PyH^{4,4'}$), 7.33 (d, J = 4.8 Hz, 4H, $PyH^{6,6'}$), 7.25 (s, 4H, $PyH^{5,5'}$), 6.86 (s, 2H, BnH), 6.53 (s, 1H, BnH), 5.80–5.71 (m, 2H, $CCH=C$), 5.59 (s, 2H, OCH_2Ar), 4.98–4.73 (m, 4H, $C=CH_2$), 4.04 (t, J = 11.7 Hz, 4H, OCH_2), 2.02 (m, 4H, CH_2), 1.80 (m, 4H, CH_2), 1.49–1.25 ppm (m, 16H, CH_2); ESI-MS (7469.42; $C_{354}H_{348}F_{72}Fe_6N_{36}O_{18}P_{12}$): m/z : 1722.6 [$M-4PF_6$] $^{4+}$, 1349.5 [$M-5PF_6$] $^{5+}$, 1100.3 [$M-6PF_6$] $^{6+}$, 922.1 [$M-7PF_6$] $^{7+}$, 789.0 [$M-8PF_6$] $^{8+}$, 685.1 [$M-9PF_6$] $^{9+}$, 602.3 [$M-10PF_6$] $^{10+}$.

3: 1H NMR (300 MHz; CD_3CN): δ = 9.48 (s, 4H, $ArH^{3,5}$), 8.83 (s, 5H, $ArH^2 + PyH^{3,3'}$), 8.29 (s, 2H, $ArH^{4,6}$), 8.02 (s, 4H, $PyH^{4,4'}$), 7.34 (s, 4H, $PyH^{6,6'}$), 7.24 (s, 4H, $PyH^{5,5'}$), 6.90 (s, 2H, BnH), 6.62 (s, 1H, BnH), 5.62 (m, 2H, $CH=CH$), 5.43 (s, 2H, OCH_2Ar), 4.18 and 4.07 (m, 4H, OCH_2), 1.85 (m, 4H, CH_2), 1.48–1.01 ppm (m, 16H, CH_2).

4: m.p. 82–85 °C; 1H NMR (300 MHz; $CDCl_3$): δ = 8.80 (s, 4H, $ArH^{3,5}$), 8.76 (d, 4H, $PyH^{6,6'}$), 8.71 (d, 4H, $PyH^{3,3'}$), 7.94 (s, 1H, ArH^2), 7.90 (t, 4H, $PyH^{4,4'}$), 7.58 (s, 2H, $ArH^{4,6}$), 7.39 (t, 4H, $PyH^{5,5'}$), 6.71 (2 s, 2H, BnH), 6.45 (m, 1H, BnH), 5.36 (t, J = 3.9 Hz, 2H, $CH=CH/trans$ and cis), 5.19 (s, 2H, OCH_2Ar), 4.07 (t, 4H, OCH_2), 2.02 (m, 4H, CH_2), 1.80 (m, 4H, CH_2), 1.47 (m, 4H, CH_2), 1.38 (m, 4H, CH_2), 0.89 ppm (m, 4H, CH_2); ^{13}C NMR (75 MHz; $CDCl_3$) δ = 160.4, 160.1, 156.4, 156.2, 150.4, 149.4, 141.2, 139.2, 137.1, 130.8, 130.3, 124.1, 121.6, 119.5, 114.7, 108.1, 107.6, 100.5, 70.5, 68.4, 32.2, 29.9, 29.1, 28.0, 27.6, 25.4 ppm; ESI-MS: (5226.46, $C_{342}H_{324}N_{36}O_{18}$), m/z 2612.8 [$M+2H$] $^{2+}$, 2635.3 [$M+2Na$] $^{2+}$, 2643.2 [$M+K+Na$] $^{2+}$, 1742.9 [$M+3H$] $^{3+}$, 1764.9 [$M+3Na$] $^{3+}$, 1774.2 [$M+Na+K$] $^{3+}$.

6: m.p. 80–83 °C; 1H NMR (300 MHz; $CDCl_3$): δ = 8.78 (s, 4H, $ArH^{3,5}$), 8.74 (d, 4H, $PyH^{6,6'}$), 8.70 (d, 4H, $PyH^{3,3'}$), 7.93 (s, 1H, ArH^2), 7.89 (t, 4H, $PyH^{4,4'}$), 7.57 (s, 2H, $ArH^{4,6}$), 7.35 (t, 4H, $PyH^{5,5'}$), 6.67 (2 s, 2H, BnH), 6.44 (m, 1H, BnH), 5.38 (t, 2H, $CH=CH/trans$ and cis), 5.18 (s, 2H, OCH_2Ar), 3.98 (t, 4H, OCH_2), 1.98 (m, 4H, CH_2), 1.77 (m, 4H, CH_2), 1.45 (m, 4H, CH_2), 1.36 (m, 4H, CH_2), 0.86 ppm (m, 4H, CH_2). ESI-MS: (1746.19, $C_{114}H_{112}N_{12}O_6$), m/z 1743.2 [$M+H$] $^{+}$, 1765.0 [$M+Na$] $^{+}$.

9: m.p. 75–78 °C; 1H NMR (300 MHz; $CDCl_3$): δ = 8.81 (s, 4H, $ArH^{3,5}$), 8.76 (d, 4H, $PyH^{6,6'}$), 8.72 (d, 4H, $PyH^{3,3'}$), 7.95 (s, 1H, ArH^2), 7.91 (t, 4H, $PyH^{4,4'}$), 7.60 (s, 2H, $ArH^{4,6}$), 7.37 (t, 4H, $PyH^{5,5'}$), 6.70 (2 s, 2H, BnH), 6.47 (m, 1H, BnH), 5.21 (s, 2H, OCH_2Ar), 4.10 (t, 4H, OCH_2), 1.78 (m, 4H, CH_2), 1.49 (m, 4H, CH_2), 1.38 (m, 4H, CH_2), 1.29 ppm (m, 8H, CH_2). ^{13}C NMR (75 MHz; $CDCl_3$): δ = 160.7, 156.4, 156.3, 150.4, 149.4, 141.2, 139.2, 137.1, 124.1, 121.6, 119.5, 114.7, 114.7, 106.9, 102.0, 100.2, 68.4, 28.7, 28.4, 28.2, 27.9, 25.2 ppm. ESI-MS: (5238.56, $C_{342}H_{336}N_{36}O_{18}$), m/z 2623.8 [$M+2H$] $^{2+}$, 2641.5 [$M+2Na$] $^{2+}$, 2652.5 [$M+K+Na$] $^{2+}$, 2659.7 [$M+2K$] $^{2+}$.

10: m.p. > 300 °C; 1H NMR (750 MHz; CD_3CN): δ = 9.51 (s, 4H, $ArH^{3,5}$), 8.83 (s, 5H, $ArH^2 + PyH^{3,3'}$), 8.27 (s, 2H, $ArH^{4,6}$), 7.99 (s, 4H, $PyH^{4,4'}$), 7.33 (s, 4H, $PyH^{6,6'}$), 7.18 (s, 4H, $PyH^{5,5'}$), 6.89 (s, 2H, BnH), 6.58 (s, 1H, BnH), 5.60 (s, 2H, OCH_2Ar), 4.16 (t, 4H, OCH_2), 1.77 (m, 4H, CH_2), 1.48 (m, 4H, CH_2), 1.30 ppm (m, 12H, CH_2). ESI-MS: data obtained using BF_4^- counterions; (6615.28, $C_{342}H_{336}B_{12}F_{48}Fe_6N_{36}O_{18}$), m/z 2118.5 [$M-3BF_4$] $^{3+}$, 1567.2 [$M-4BF_4$] $^{4+}$, 1236.5 [$M-5BF_4$] $^{5+}$, 1015.8 [$M-6BF_4$] $^{6+}$, 858.5 [$M-7BF_4$] $^{7+}$, 740.1 [$M-8BF_4$] $^{8+}$, 648.1

$[M-9BF_4]^{9+}$, 574.8 $[M-10BF_4]^{10+}$, 514.7 $[M-11BF_4]^{11+}$, 464.3 $[M-12BF_4]^{12+}$.

Received: October 20, 2004

Published online: January 31, 2005

Keywords: iron · macrocycles · metathesis · self-assembly · terpyridine

- [1] M. Komiyama, T. Takeuchi, T. Mukawa, H. Asanuma, *Molecular Imprinting: from fundamentals to applications*, Wiley-VCH, New York, **2002**.
- [2] C. Alexander, L. Davidson, W. Hayes, *Tetrahedron* **2003**, *59*, 2025–2057.
- [3] K. Haupt, K. Mosbach, *Chem. Rev.* **2000**, *100*, 2495–2504.
- [4] K. Mosbach, Y. Yu, J. Andersch, L. Ye, *J. Am. Chem. Soc.* **2001**, *123*, 12420–12421.
- [5] M. Subat, A. S. Borovik, B. König, *J. Am. Chem. Soc.* **2004**, *126*, 3185–3190.
- [6] J. B. Beil, S. C. Zimmerman, *Chem. Commun.* **2004**, 488–489.
- [7] S. C. Zimmerman, I. Zharov, M. S. Wendland, N. A. Rakow, K. S. Suslick, *J. Am. Chem. Soc.* **2003**, *125*, 13504–13518.
- [8] Y. Kim, M. F. Mayer, S. C. Zimmerman, *Angew. Chem.* **2003**, *115*, 1153–1158; *Angew. Chem. Int. Ed.* **2003**, *42*, 1121–1126.
- [9] A. V. Chuchurjukin, H. P. Dijkstra, B. M. J. M. Suijkerbuijk, R. J. M. K. Gebbink, G. P. M. van Klink, A. M. Mills, A. L. Spek, G. van Koten, *Angew. Chem.* **2003**, *115*, 238–240; *Angew. Chem. Int. Ed.* **2003**, *42*, 228–230.
- [10] M. C. Jiménez, C. Dietrich-Buchecker, J.-P. Sauvage, *Angew. Chem.* **2000**, *112*, 3422–3425; *Angew. Chem. Int. Ed.* **2000**, *39*, 3284–3287.
- [11] G. R. Newkome, T. J. Cho, C. N. Moorefield, G. R. Baker, M. J. Saunders, R. Cush, P. S. Russo, *Angew. Chem.* **1999**, *111*, 3899–3903; *Angew. Chem. Int. Ed.* **1999**, *38*, 3717–3721.
- [12] G. R. Newkome, T. J. Cho, C. N. Moorefield, R. Cush, P. S. Russo, L. A. Godínez, M. J. Saunders, *Chem. Eur. J.* **2002**, *8*, 2946–2954.
- [13] G. R. Newkome, T. J. Cho, C. N. Moorefield, P. P. Mohapatra, L. A. Godínez, *Chem. Eur. J.* **2004**, *10*, 1493–1500.
- [14] B. G. G. Lohmeijer, U. S. Schubert, *Macromol. Chem. Phys.* **2003**, *204*, 1072–1078.
- [15] B. X. Colasson, J.-P. Sauvage, *Inorg. Chem.* **2004**, *43*, 1895–1901.
- [16] P. Wang, C. N. Moorefield, G. R. Newkome, *Org. Lett.* **2004**, *6*, 1197–1200.
- [17] A. F. M. Kilbinger, S. J. Cantrill, A. W. Waltman, M. W. Day, R. B. Grubbs, *Angew. Chem.* **2003**, *115*, 3403–3407; *Angew. Chem. Int. Ed.* **2003**, *42*, 3281–3285.
- [18] V. Martinez, J.-C. Blais, D. Astruc, *Angew. Chem.* **2003**, *115*, 4502–4505; *Angew. Chem. Int. Ed.* **2003**, *42*, 4366–4369.
- [19] A simple alternative approach to separation was treatment of the **4** and **6** mixture with $FeCl_2$, which regenerated the hexameric core (**3**) from **4**; whereas, **6** generated an intractable polymer.
- [20] X. A. Dominguez, I. C. Lopez, R. Franco, *J. Org. Chem.* **1961**, *26*, 1625.
- [21] M. Ruben, J. Rojo, F. J. Romero-Salguero, L. H. Uppadine, J.-M. Lehn, *Angew. Chem.* **2004**, *116*, 3728–3747; *Angew. Chem. Int. Ed.* **2004**, *43*, 3644–3662.

The Natural Lewis^X-Bearing Lipids Promote Membrane Adhesion: Influence of Ceramide on Carbohydrate–Carbohydrate Recognition

Christine Gourier, Frédéric Pincet, Eric Perez,*
Yongmin Zhang, Zhenyuan Zhu, Jean-Maurice Mallet,
and Pierre Sinaÿ

Carbohydrate–carbohydrate recognition has recently emerged as a potentially important interaction in cell adhesion processes.^[1] One carbohydrate, the Lewis^X determinant (Le^X), is involved in murine embryogenesis,^[2] although the precise mechanism underlying this role is as yet unclear. Ca²⁺-mediated homotypic interaction between two Le^X determinants has been proposed to initiate cell adhesion during the compaction stage of the embryo.^[3,4] Several recent studies support the existence of such calcium-mediated homotypic recognition^[5,6] and have also provided a body of information on the geometry, structural requirements,^[7–9] and energetics^[10–12] of a Le^X–Le^X interaction. However, in these studies the local environment of the Le^X was always very different from that existing at a typical cell surface. In cells, the Le^X-bearing molecules are usually composed of a ceramide connected to the Le^X trisaccharide through a lactose group. This geometry considerably restricts the possible orientations of the Le^X^[13] compared to those of soluble forms,^[5,7,8] or to the large freedom in orientation provided by long flexible spacers.^[5,7–9,14] The ceramide in the natural Le^X-bearing molecules may therefore have a very strong influence on the recognition of Le^X borne by opposite cells, by inhibiting or enhancing the recognition. To test more directly the hypothesis that Le^X could serve as a promoter for cell adhesion, the challenge is to determine if the natural Le^X-bearing molecules allow the Le^X–Le^X recognition between two membranes. Two natural glycosphingolipids have been synthesized for this purpose.

The first one, called CerLLe^X, is composed of a Le^X trisaccharide (Galβ1→4[Fucα1→3]GlcNAc) attached to a ceramide (Cer) unit (two hydrophobic tails: one sphingosine and one stearic acid) through a lactose (L) group (Figure 1 a). The second one, CerLLe^a, is used as a control and is composed of the same ceramide and lactose moieties, but has a Lewis *a* (Le^a) trisaccharide as headgroup instead of a Le^X determinant. Le^a is an isomer of Le^X, and the only difference between the two determinants is the position of the

[*] Dr. C. Gourier, Dr. F. Pincet, Dr. E. Perez
Laboratoire de Physique Statistique
de l'Ecole Normale Supérieure
UMR 8550 associée au CNRS
et aux Universités Paris 6 et Paris 7
24 rue Lhomond, 75231 Paris Cedex 05 (France)
Fax: (+33) 1-4432-3433
E-mail: perez@lps.ens.fr

Dr. Y. Zhang, Z. Zhu, Dr. J.-M. Mallet, Prof. Dr. P. Sinaÿ
Département de Chimie de l'Ecole Normale Supérieure
24 rue Lhomond, 75231 Paris Cedex 05 (France)

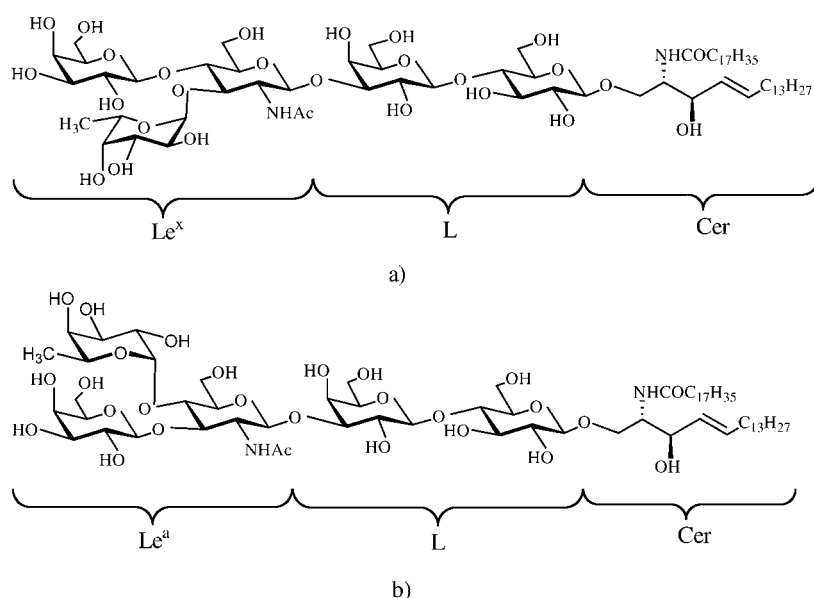


Figure 1. a) CerLLe^X: the Le^X determinant is a trisaccharide (Galβ1→4[Fucα1→3]GlcNAc). In a classical natural sphingolipid, it is attached to the ceramide (Cer) through a lactose (L) group. b) CerLLe^A: the Le^A determinant differs from the Le^X trisaccharide in the position of the fucose and galactose groups which are inverted. In these molecules the ceramide moieties impose an orientation on the headgroup that is perpendicular to the axis of the sphingosin.

fructose and galactose residues (Galβ1→3[Fucα1→4]GlcNAc) which are permuted (see Figure 1b). Both molecules are neutral.

This study involves two vesicles in tight contact, to simulate the geometry of two cells at the compaction stage. They are composed of a 1:9 mixture of glycosphingolipid and stearyl-oleoylphosphatidylcholine (SOPC) and are referred to by the name of the glycolipid that they bear (CerLLe^X or CerLLe^A). CerLLe^X and CerLLe^A have two saturated chains, so one can expect the formation of domains in the vesicle membrane. We performed monolayer compression isotherm measurements of pure CerLLe^X, pure CerLLe^A, pure SOPC,

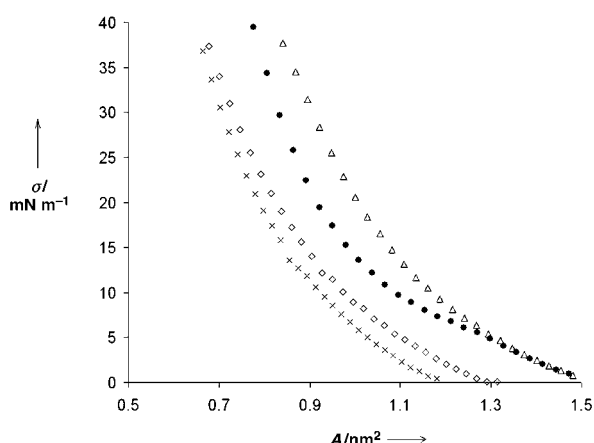


Figure 2. Isotherm compression measurements of lipid monolayers at an air/water interface. σ is the surface tension and A is the molecular area; pure SOPC (x), 1:9 SOPC/CerLLe^X (or CerLLe^A) mixture (◇), pure Le^X neoglycolipid (△),^[11] and pure CerLLe^X or CerLLe^A (●).

and pure Le^X neoglycolipid,^[11] which has three ramified chains (Figure 2). The ceramide moiety causes pure CerLLe^X and CerLLe^A monolayers at an air/water interface to undergo a phase transition upon compression, which indicates that clustering of glycolipids can occur at the membrane surface that influences Le^X–Le^X recognition.^[15] By contrast, we observed that monolayers composed of a 1:9 ratio of CerLLe^X or CerLLe^A and SOPC show the same liquid shape as SOPC or Le^X neoglycolipid. This result is consistent with an NMR study on the effect of ceramide on phosphatidylcholine membranes, in which no phase separation was observed at either ambient or physiological temperatures for ceramide concentrations smaller than 15 mol %.^[16] In the 1:9 glycosphingolipid/SOPC vesicles, the two components are therefore homogeneously mixed.

The adhesion energies of CerLLe^X–CerLLe^X and CerLLe^X–CerLLe^A vesicle pairs were measured in NaCl and CaCl₂ aqueous solutions using a micropipette manipulation technique. This technique and the experimental conditions have been extensively described elsewhere.^[11] Briefly, two vesicles (either both CerLLe^X, or one CerLLe^X and one CerLLe^A) in separate micropipettes are aspirated and brought into contact by displacement of the pipettes (Figure 3). The aspiration pressure in the pipettes

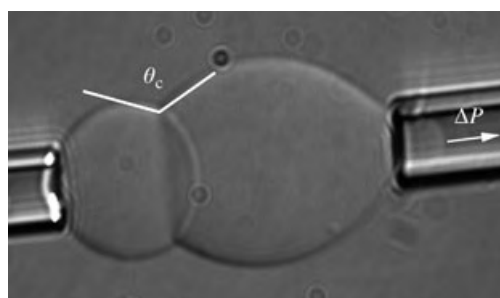


Figure 3. The two osmotically controlled vesicles held in micropipettes by aspiration are observed by interference contrast microscopy. The suction pressure applied to the micropipettes allows control of the tension of the vesicle bilayers. One of them (left) is pressurized into a tight, rigid sphere with large bilayer tension, whereas the adherent vesicle (right) is held with low pressure and remains deformable. The adhesion energy W_{adh} is obtained by determining the contact angle θ_c of the two vesicles and the tension τ_m of their membrane.^[11]

controls the mechanical tension of the vesicle membrane. Conditions are set such that one of the vesicles is pressurized into a tight, rigid sphere with large bilayer tension, whereas the other is held with low pressure and remains deformable. The adhesion energy W_{adh} ^[17] is obtained by determining the contact angle θ_c of the two vesicles (Figure 3) when equilibrium is reached. The appropriate relationship can be written as: $\Delta P = C W_{\text{adh}}$, where ΔP is the pressure applied in the pipette controlling the flaccid vesicle and parameter C depends only on the radius of the micropipette (r_p), the radius of the vesicle (r_v), which can both be measured, and θ_c . The value of θ_c was numerically deduced from geometrical

parameters^[18] and was measured for several tension values of the flaccid vesicle membrane by decreasing and then increasing the aspiration to check the reversibility of the adhesion. The adhesion results for CerLLe^X–CerLLe^X and CerLLe^X–CerLLe^a pairs are displayed in Figure 4 as plots of ΔP versus C ; W_{adh} is the slope of the linear regression. The adhesion energy values are reported in Table 1.

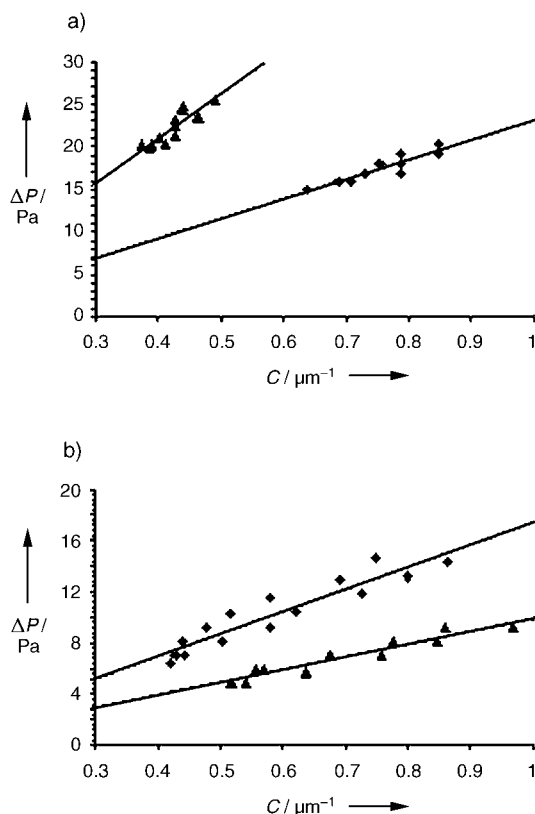


Figure 4. Aspiration pressure (ΔP) as a function of parameter C : a) CerLLe^X–CerLLe^X experiment (two vesicles with SOPC/CerLLe^X, 9:1); b) CerLLe^X–CerLLe^a experiment (one vesicle is SOPC/CerLLe^X, 9:1, and the other is SOPC/CerLLe^a, 9:1); CaCl₂ solution (▲) and NaCl (◆). The straight lines are least-squares fits.

Table 1: Adhesion energy of vesicle pairs in CaCl₂ or NaCl aqueous medium.

Left vesicle–right vesicle	Adhesion energy [$\mu\text{J m}^{-2}$]	
	in CaCl ₂ (0.11 M)	in NaCl (0.2 M)
CerLLe ^X –CerLLe ^X	67.8 ± 24.0	26.6 ± 2.1
CerLLe ^X –CerLLe ^a	15.1 ± 6.6	21.4 ± 5.8

CerLLe^a differs from CerLLe^X by only a structural isomeric change of the sugar headgroup, so interactions between two CerLLe^X vesicles or one CerLLe^X and one CerLLe^a vesicle should be equal unless there are specific effects. Nonspecific interactions (van der Waals attraction, Helfrich undulations, steric repulsions etc.) for the two systems are similar, as confirmed by the results obtained in a NaCl environment (Table 1) where, as expected, the substitution of the Le^X by Le^a has no significant effect on adhesion. By

contrast, the adhesion energy of the CerLLe^X–CerLLe^X pair increases significantly in the presence of calcium ions, whereas that of the CerLLe^X–CerLLe^a pair actually decreases slightly. The strong specific enhancement obtained for the CerLLe^X–CerLLe^X pair proves that two Le^X determinants borne by natural molecules inserted in lipid bilayers can indeed recognize each other and produce additional adhesion.

The specific adhesion energy (W_{spe}) caused exclusively by Le^X–Le^X recognition can be extracted from the measured adhesion energies for the vesicular interactions. As shown in Equation (1), W_{spe} is given by the difference between the

$$W_{\text{spe}}^{\text{(Le}^{\text{X}}\text{–Le}^{\text{X}}\text{)}} = W_{\text{adh}}^{\text{(Le}^{\text{X}}\text{–Le}^{\text{X}}\text{)}_{\text{CaCl}_2}} - \left[W_{\text{adh}}^{\text{(Le}^{\text{X}}\text{–Le}^{\text{X}}\text{)}_{\text{NaCl}}} + \left(W_{\text{adh}}^{\text{(Le}^{\text{X}}\text{–Le}^{\text{a}}\text{)}_{\text{CaCl}_2}} - W_{\text{adh}}^{\text{(Le}^{\text{X}}\text{–Le}^{\text{a}}\text{)}_{\text{NaCl}}} \right) \right] \quad (1)$$

adhesion energy measured with calcium ions and that contributed by all other (nonspecific) interactions. The specific adhesion energy is about $47.5 \mu\text{J m}^{-2}$. In similar experiments performed on vesicles made of SOPC and a Le^X neoglycolipid mixed in the same 9:1 proportion,^[11] the specific adhesion energy was only one-fifth ($\approx 9.5 \mu\text{J m}^{-2}$) of the value reported here with the natural molecule. What could be the explanation for such a large discrepancy?

The surface density (ρ) of molecules involved in Le^X–Le^X recognition can be determined directly from $W_{\text{spe}}^{\text{[19]}}$ $\rho = W_{\text{spe}}/k_{\text{B}}T$. In this expression, ρ depends not only on the surface density of the glycolipids on each vesicle, but also on the Le^X accessibility and therefore on the architecture of the Le^X-bearing molecule. The surface densities were equal for both natural (CerLLe^X) and neoglycolipid systems. However, these glycolipids present some differences in their aliphatic tails. The natural molecule is based on a ceramide, whereas the neoglycolipid used in the previous study was composed of three alkyl chains linked to a long flexible spacer.^[20] In the latter case the spacer provides the Le^X group with a high orientational freedom, whereas in CerLLe^X the rigid connection between the sugar headgroup and the ceramide restricts the possible conformations of the Le^X group.^[13] The affinity of two Le^X groups for calcium ions depends strongly on their relative positions.^[8] Therefore, the relative orientation of two Le^X groups is a predominant factor in Le^X–Le^X recognition. The specific adhesion energies experimentally obtained show that although the ceramide restricts the number of spatial orientations accessible to the Le^X group, the proportion of those suitable for Le^X–Le^X recognition is higher. This is possible only if the orientations provided by the ceramide chains in the natural molecule enhance Le^X–Le^X recognition.

The choice of the Le^a determinant as a control highlighted both the specificity of Le^X–Le^X interaction and the very high sensitivity of the recognition to structural changes. The weak adhesion energy obtained for the CerLLe^X–CerLLe^a pair with CaCl₂ salt shows clearly that the permutation of the fucose and galactose residues in the trisaccharide headgroup effectively prevents specific adhesion (Table 1) and therefore demonstrates that the molecular recognition involved is

highly specific. In another carbohydrate couple, lactose–GM3, some hints on the high sensitivity of recognition to molecular structure were obtained through surface tension measurements.^[21] Taken together, these results illustrate the wealth of specific interactions that carbohydrates can provide through their wide variety of structures and spatial orientations.

In summary, Ca^{2+} -dependent specific adhesion was firmly established for natural Le^{X} -bearing molecules inserted in fluid bilayer membranes. The choice of the Le^{a} determinant as the control molecule underscored the high sensitivity of Le^{X} – Le^{X} recognition to molecular structure. Moreover, the vesicle adhesion energy experiments demonstrate that in a geometry akin to that of a cell membrane, the possible orientations provided by natural Le^{X} -bearing molecules not only allow but also strongly favor Le^{X} – Le^{X} recognition.

Experimental Section

The synthesis of CerLLe^{X} is depicted in Scheme 1. The previously prepared trisaccharide **1**^[22] was condensed with the known diol **2**^[23] to give regio- and stereoselectively the pentasaccharide **3** in 90% yield. After a sequence of deprotection and protection reactions, the obtained imidate **4** was coupled with azidosphingosine **5**^[24] to afford a glycoside in 57% yield. Selective reduction of the azide group, followed by condensation with octadecanoic acid, gave an acylated Le^{X} compound, which was *O*-deacylated to provide the CerLLe^{X} in 95% yield.

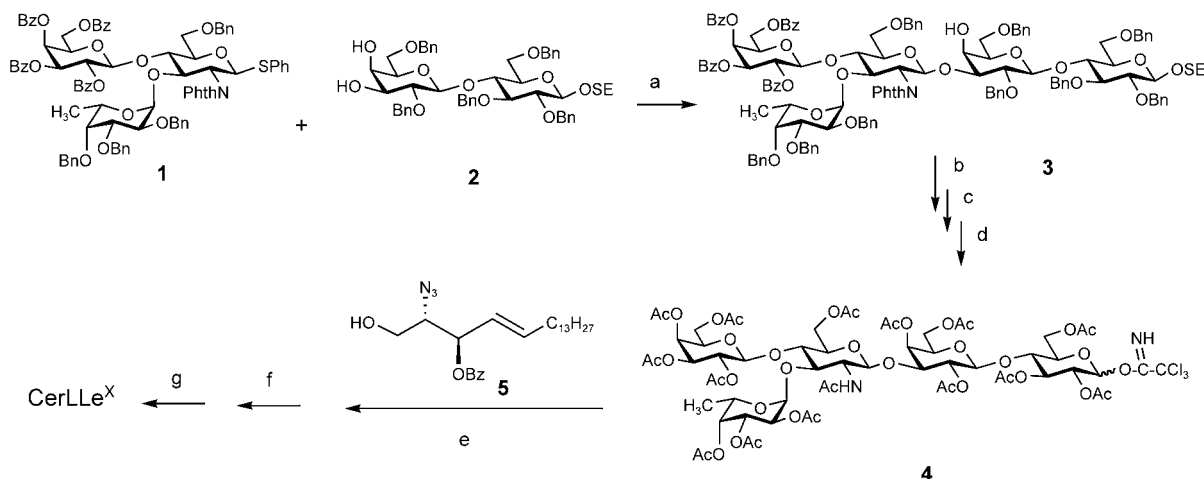
Similarly, CerLLe^{a} was synthesized using the donor **6** instead of compound **1**. This trisaccharide was prepared in 82% yield by condensation of **7** and **8** (Scheme 2).

Received: July 7, 2004

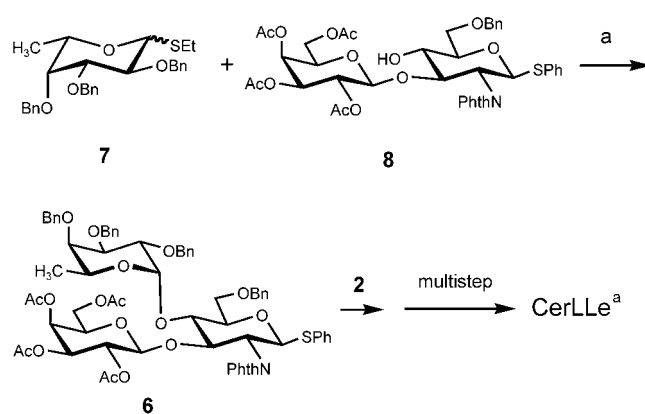
Revised: October 15, 2004

Published online: February 3, 2005

Keywords: carbohydrates · cell adhesion · Lewis^X determinant · lipids · vesicles



Scheme 1. Reagents: a) NIS/TfOH, CH_2Cl_2 , 90%; b) 1. NH_2NH_2 , EtOH, 2. Ac_2O , CH_2Cl_2 , MeOH 78%; c) 1. H_2 , Pd/C (10%), MeOH, EtOAc, 2. Ac_2O /Py, DMAP, 74%; d) 1. $\text{CF}_3\text{CO}_2\text{H}$, CH_2Cl_2 , 2. CCl_3CN , DBU, CH_2Cl_2 , 80%; e) TMSOTf, CH_2Cl_2 , 57%; f) 1. PPh_3 , benzene, H_2O , 2. octadecanoic acid, WSC, CH_2Cl_2 , 72%; g) NaOMe, MeOH, 95%. Bz = benzoyl, Bn = benzyl, Phth = phthaloyl, SE = trimethylsilylethyl, NIS = *N*-iodosuccinimide, Tf = triflate, DMAP = 4-dimethylaminopyridine, DBU = 1,8-diazabicyclo[5.4.0]undec-7-ene, TMS = trimethylsilyl, WSC = 1-(3-dimethylamino-propyl)-3-ethylcarbodiimide hydrochloride.

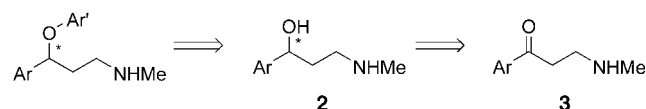


Scheme 2. Reagent: a) NIS/TfOH, toluene, 82%.

- [1] a) N. V. Bovin, *Biochemistry (Moscow)* **1996**, 61, 694–704; b) D. Spillmann, M. M. Burger in *Carbohydrates in Chemistry and Biology*, Vol. 2 (Eds.: B. Ernst, G. W. Hart, P. Sinaÿ), Wiley-VCH, Weinheim, **2000**, pp. 1061–1091; c) J. Rojo, J. C. Morales, S. Penadès, *Top. Curr. Chem.* **2002**, 218, 45–92.
- [2] a) D. Solter, B. B. Knowles, *Proc. Natl. Acad. Sci. USA* **1978**, 75, 5565–5569; b) R. Kannagi, E. Nudelman, S. B. Levery, S. Hakomori, *J. Biol. Chem.* **1982**, 257, 14865–14974.
- [3] I. Eggens, B. A. Fenderson, T. Toyokuni, B. Dean, M. Stroud, S. Hakomori, *J. Biol. Chem.* **1989**, 264, 9476–9484.
- [4] N. Kojima, B. A. Fenderson, M. R. Stroud, R. I. Goldberg, R. Habermann, T. Toyokuni, S. Hakomori, *Glycoconjugate J.* **1994**, 11, 238–248.
- [5] A. Geyer, C. Gege, R. R. Schmidt, *Angew. Chem.* **1999**, 111, 1569–1571; *Angew. Chem. Int. Ed.* **1999**, 38, 1466–1468.
- [6] M. Boubelik, D. Floryk, J. Bohata, L. Draberoova, J. Macak, F. Smid, P. Draber, *Glycobiology* **1998**, 8, 139–146.
- [7] A. Geyer, C. Gege, R. R. Schmidt, *Angew. Chem.* **2000**, 112, 3381–3383; *Angew. Chem. Int. Ed.* **2000**, 39, 3246–3249.
- [8] A. Geyer, C. Gege, R. R. Schmidt, *Eur. J. Org. Chem.* **2002**, 2475–2485.

- [9] G. Siuzdak, Y. Ivhikawa, T. J. Caulfield, B. Munoz, C.-H. Wong, K. C. Nicolaou, *J. Am. Chem. Soc.* **1993**, *115*, 2877–2881.
- [10] M. J. Hernáiz, J. M. de la Fuente, A. G. Barrientos, S. Penadès, *Angew. Chem.* **2002**, *114*, 1624–1627; *Angew. Chem. Int. Ed.* **2002**, *41*, 1554–1557.
- [11] F. Pincet, T. Le Bouar, Y. Zhang, J. Esnault, J.-M. Mallet, E. Perez, P. Sinaÿ, *Biophys. J.* **2001**, *80*, 1354–1358.
- [12] C. Tormas, R. García, *Top. Curr. Chem.* **2002**, *218*, 115–132.
- [13] a) I. Pascher, S. Sundell, *Chem. Phys. Lipids* **1977**, *20*, 175–191; b) T. Kaizu, S. B. Levery, E. Nudelman, R. E. Stenkamp, S. Hakomori, *J. Biol. Chem.* **1986**, *261*, 11254–11258.
- [14] C. Tormas, J. Rojo, J. M. de la Fuente, A. G. Barrientos, S. Penadès, *Angew. Chem.* **2001**, *113*, 3142–3145; *Angew. Chem. Int. Ed.* **2001**, *40*, 3052–3055.
- [15] R. J. Stewart, J. M. Boggs, *Biochemistry* **1993**, *32*, 10666–10674.
- [16] Y.-W. Hsueh, R. Giles, N. Kitson, J. Thewalt, *Biophys. J.* **2002**, *82*, 3069–3095.
- [17] E. Evans, *Colloids Surf.* **1990**, *43*, 327–347.
- [18] E. Evans, *Biophys. J.* **1980**, *31*, 425–432.
- [19] a) G. I. Bell, M. Dembo, P. Bongrand, *Biophys. J.* **1984**, *45*, 1051–1064; b) E. Evans, *Biophys. J.* **1985**, *48*, 175–183.
- [20] J. Esnault, J.-M. Mallet, Y. Zhang, P. Sinaÿ, T. Le Bouar, F. Pincet, E. Perez, *Eur. J. Org. Chem.* **2001**, 253–260.
- [21] P. V. Santacroce, A. Basu, *Angew. Chem.* **2003**, *115*, 99–102; *Angew. Chem. Int. Ed.* **2003**, *42*, 95–98.
- [22] Y.-M. Zhang, J. Esnault, J.-M. Mallet, P. Sinaÿ, *J. Carbohydr. Chem.* **1999**, *18*, 419–427.
- [23] K. Jansson, S. Ahlfors, T. Frejd, J. Kihlberg, G. Magnusson, *J. Org. Chem.* **1988**, *53*, 5629–5647.
- [24] a) R. R. Schmidt, P. Zimmermann, *Tetrahedron Lett.* **1986**, *27*, 481–484; b) Y. Ito, M. Kiso, A. Hasegawa, *J. Carbohydr. Chem.* **1989**, *8*, 285–294.

selective reduction of β -amino ketones with a secondary amino group, an unsolved class of substrates in asymmetric hydrogenation. To our knowledge, no Ru catalytic system has successfully been used for the asymmetric hydrogenation of amino ketones with a secondary amino group. A Rh-MCCPM (MCCPM = (2*S*,4*S*)-4-dicyclohexylphosphino-2-diphenylphosphinomethyl-1-(*N*-methylcarbamoyl)pyrrolidine) catalyst has been reported for the hydrogenation of one β -secondary-amino ketone substrate with only moderate efficiency (80 % *ee*, turnover number (TON) = 1000).^[2e] Given the importance of chiral γ -amino alcohols **2** as key intermediates for the synthesis of pharmaceutical products **1**^[4] (Scheme 1), an efficient enantioselective reduction of β -



- 1a:** Ar = Ph, Ar' = 4-CF₃-Ph (fluoxetine)
1b: Ar = Ph, Ar' = 2-Me-Ph (tomoxetine)
1c: Ar = Ph, Ar' = 2-OMe-4-CF₃-Ph (nisoxetine)
1d: Ar = thiophenyl, Ar' = 1-naphthyl (duloxetine)

Scheme 1. A retrosynthesis of fluoxetine and related compounds by asymmetric hydrogenation.

secondary-amino ketones **3** into **2** would be of great significance, not only for pharmaceutical development but also as a generally useful organic transformation. Herein, we report a Rh-catalyzed highly efficient hydrogenation of a series of β -secondary-amino ketones with *ee* values of up to > 99 % and with turnover numbers of more than 4500; this hydrogenation provides a potentially practical synthesis of key pharmaceutical intermediates.

γ -Secondary amino alcohols **2** are of particular interest to synthetic chemists as they are key intermediates for the synthesis of an important class of antidepressants, **1a–d**.^[4] Owing to the different biological activities exhibited by individual enantiomers of **1**, a number of enantioselective syntheses of **1**, as well as of **2**, have been developed in recent years.^[5] Although highly enantioselective hydrogenation of β -tertiary-amino ketones, catalyzed by a chiral [RuCl₂(diphosphine)(1,2-diamine)] complex, provides an effective route for the enantioselective syntheses of **1**,^[1c–e] subsequent selective removal of one *N*-methyl group is needed to afford the desired amino alcohols **2**.^[5b] A direct hydrogenation of β -secondary-amino ketones **3** would be a more attractive and economic strategy for the syntheses of **2**. However, Ru systems have not been effective for the latter reduction so far. Recently, we revealed the synthesis of a highly electron-donating P-chiral trialkylbisphospholane ligand, **4** (duanphos, see Scheme 2), in both enantiomeric forms.^[6] The high reactivities and enantioselectivities observed in the Rh-duanphos-catalyzed hydrogenation of various types of functionalized C=C bonds^[6] suggest the feasibility of using the Rh-duanphos system for the reduction of the C=O bond in amino ketones, provided a proper metal–substrate chelate forms through coordination of the nitrogen atom to the metallic center.

Hydrogenations

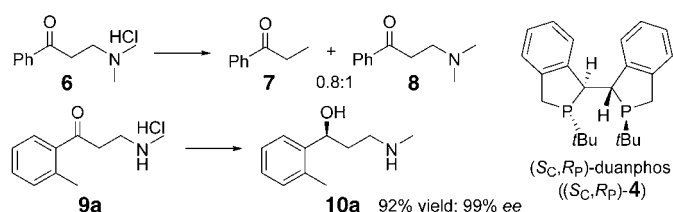
Practical Synthesis of Enantiopure γ -Amino Alcohols by Rhodium-Catalyzed Asymmetric Hydrogenation of β -Secondary-Amino Ketones

Duan Liu, Wenzhong Gao, Chunjiang Wang, and Xumu Zhang*

Enantioselective hydrogenation of amino ketones catalyzed by Ru^[1] or Rh–phosphine^[2] complexes provides an efficient method for the synthesis of enantiomerically active amino alcohols, a class of chiral compounds of great importance in pharmaceutical products. A recent challenging target^[3] inspired us to look for a practical solution for the enantio-

[*] D. Liu, W. Gao, C. Wang, Prof. X. Zhang
 Department of Chemistry
 The Pennsylvania State University
 University Park, PA 16802 (USA)
 Fax: (+1) 814-865-3292
 E-mail: xumu@chem.psu.edu

Supporting Information for this article is available on the WWW under <http://www.angewandte.org> or from the author.



Scheme 2. Asymmetric hydrogenation of β -amino ketone hydrochlorides with $[\text{Rh}\{(\text{S}_\text{C},\text{R}_\text{P})\text{-4}\}(\text{nbd})]\text{SbF}_6$ (**5a**) as the catalyst. Reaction conditions: **5a** (0.5 mol %), MeOH, K_2CO_3 (0.5 equiv), H_2 (10 bar), 50°C , 12 h. nbd = norbornadiene.

Initially, the commercially available substrate **6** was examined with $[\text{Rh}\{(\text{S}_\text{C},\text{R}_\text{P})\text{-4}\}(\text{nbd})]\text{SbF}_6$ (**5a**) as the catalyst in the presence of K_2CO_3 (0.5 equiv) in MeOH under H_2 (10 bar) at 50°C for 12 h. Unfortunately, none of the desired amino alcohol product was obtained, but a mixture of a deamination byproduct **7**^[7] and unconverted free amino ketone **8** was recovered. When isolated **8** was employed without a base under otherwise the same reaction conditions, a similar mixture of **7** and unconverted **8** was obtained. However, we were pleased to find that a β -secondary-amino ketone hydrochloride **9a**^[8] was readily hydrogenated to give γ -amino alcohol **10a** in 92% yield with 99% *ee* (< 5% deamination byproduct indicated by ^1H NMR spectroscopy) after isolation. These observations strongly support our hypothesis that, unlike the situation in the Ru-catalyzed hydrogenation of amino ketones,^[1c] an effective ligation of the nitrogen atom to the metallic center to form a metal–substrate chelate is probably critical for achieving high enantioselectivity and reactivity in this hydrogenation. A secondary amino group is a better ligand than a tertiary amino group to coordinate to a Rh center to form a chelate, owing to less steric interaction, and this, in turn, facilitates the reaction rate of C=O bond reduction relative to deamination. Further screening of reaction conditions for the hydrogenation of **9a** (Table 1) resulted in the following observations: 1) A higher temperature or H_2 pressure has little effect on the enantioselectivity but does accelerate the relative rate of hydrogenation, thereby leading to a higher yield of **10a** (Table 1, entries 1–4); 2) although there is no significant solvent effect on the enantioselectivity, the hydrogenation rates differ dramatically with diverse solvents (reflected by the yields of **10a**), and MeOH is found to be the solvent of choice (Table 1, entries 1 and 5–10); 3) both inorganic bases, such as K_2CO_3 and KHCO_3 , and organic bases, such as triethylamine, can promote the hydrogenation of **9a** with comparable yields and stereoselectivities (Table 1, entries 1, 11, and 12).

Under the conditions optimized for the hydrogenation of **9a**, the hydrogenation of a series of β -secondary-amino ketone hydrochlorides **9a–i** were explored with Rh-complex **5a** and its antipodal complex $[\text{Rh}\{(\text{R}_\text{C},\text{S}_\text{P})\text{-duanphos}\}(\text{nbd})]\text{SbF}_6$ (**5b**). As shown in Table 2, entries 1–7, all the hydrogenations proceeded to completion and afforded the corresponding amino alcohols **10** in high yields (90–93%) with excellent enantioselectivities (93–99% *ee*); these results indicate a high tolerance to the pattern and electronic properties of the substituent on the phenyl ring in terms of

Table 1: Screening of reaction conditions for the Rh-catalyzed asymmetric hydrogenation of β -amino ketone hydrochloride **9a**.^[a]

Entry	Solvent ^[b]	Base	<i>P</i> (H_2) [bar]	<i>T</i> [$^\circ\text{C}$]	Yield [%] ^[c]	<i>ee</i> [%] ^[d]
1	MeOH	K_2CO_3	10	50	> 95 (92%)	99
2	MeOH	K_2CO_3	50	50	> 95	99
3	MeOH	K_2CO_3	2	50	75	98
4	MeOH	K_2CO_3	10	23	95	97
5	EtOH	K_2CO_3	10	50	65	98
6	<i>i</i> PrOH	K_2CO_3	10	50	45	94
7	MeCN	K_2CO_3	10	50	50	96
8	CH_2Cl_2	K_2CO_3	10	50	75	94
9	DMF	K_2CO_3	10	50	< 10	–
10	THF	K_2CO_3	10	50	< 10	–
11	MeOH	KHCO_3	10	50	95	98
12	MeOH	NEt_3	10	50	> 95	99

[a] The hydrogenations were carried out under the described conditions for each entry with 0.5 mol % of **5a** as the catalyst precursor, according to the general procedure given in the Supporting Information. [b] DMF = *N,N*-dimethylformamide. [c] Estimated yields based on ^1H NMR spectroscopy of the crude products. The yield after isolation is given in parenthesis. [d] The *ee* values of **10a** were determined by chiral HPLC with an OD-H column after the product had been converted into the *N*-acyl derivative **11a** (see Supporting Information).

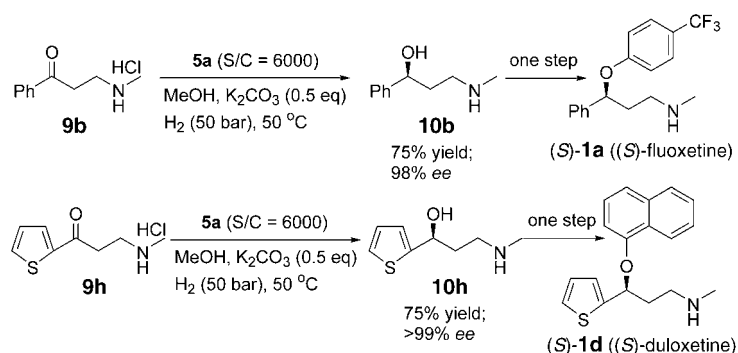
Table 2: Rh-catalyzed asymmetric hydrogenation of β -secondary-amino ketone hydrochlorides.^[a]

Entry	9	Ar	R	Yield [%] ^[b]	<i>ee</i> [%]	Configuration ^[c]
1	a	2-Me-phenyl	Me	92	99 ^[d]	S
2	b	phenyl	Me	90	98 ^[d]	S
3	c	3-Br-phenyl	Me	90	96 ^[d]	S
4	d	4-Br-phenyl	Me	93	> 99 ^[d]	S
5	e	2-OMe-phenyl	Me	93	93 ^[d]	S
6	f	4-OMe-phenyl	Me	93	> 99 ^[d]	S
7	g	2-naphthyl	Me	92	99 ^[e]	S
8	h	2-thienyl	Me	93	> 99 ^[e]	S
9	h	2-thienyl	Me	93	> 99 ^[e]	<i>R</i> ^[f]
10	i	phenyl	Bn ^[g]	90	96 ^[d]	S

[a] The hydrogenations were carried out with 0.5 mol % of **5a** (entries 1–8 and 10) or **5b** (entry 9) as the catalyst precursor for 12 h. Complete conversions were indicated by ^1H NMR spectroscopy in all runs. See Supporting Information for the general procedure. [b] Yield after isolation. [c] The absolute configurations of **10b** and **10h** were determined by comparing the sign of the optical rotations with reported data. For the other compounds, the absolute configurations were assumed to be S when **5a** was used. [d] The *ee* values were determined by chiral HPLC with an OD-H column after the product had been converted into the *N*-acyl derivative (see Supporting Information). [e] The *ee* values were determined directly by chiral HPLC with an OD-H column (see Supporting Information). [f] The Rh complex **5b** was used. [g] Bn = benzyl.

both reactivity and enantioselectivity. In the hydrogenation of a more interesting amino ketone, **9h**, with a heteroaromatic function, (*S*)-**10b** and (*R*)-**10b** were obtained in 93% yield with > 99% *ee* by using **5a** and **5b** as the catalyst, respectively (Table 2, entries 8 and 9). An *N*-benzyl-amino ketone, **9i**, was also hydrogenated to afford amino alcohol **10i** in 90% yield and 96% *ee* (Table 2, entry 10).

To demonstrate the potential Rh–duanphos-catalyzed asymmetric hydrogenation of β -secondary-amino ketones as a practical means for the enantioselective synthesis of γ -secondary-amino alcohols, two particularly interesting substrates, **9b** and **9h**, which are readily available from the corresponding ketones in one step, were explored with a low catalyst loading of the Rh complex **5a** (Scheme 3). When **9b**



Scheme 3. Enantioselective synthesis of pharmaceutical intermediates by a practical Rh-catalyzed asymmetric hydrogenation. S/C = substrate/catalyst ratio.

(1.42 g) was hydrogenated with of **5a** (1 mg) as the catalyst precursor (S/C = 6000) and K_2CO_3 (0.5 equiv) as the base in MeOH (10 mL) under H_2 (50 bar) at 50 °C for 12 h, γ -amino alcohol (*R*)-**10b** was isolated in 75% yield (TON > 4500) with 98% *ee*. When **9h** (1.52 g) was hydrogenated with **5a** (1 mg; S/C = 6000) under the same reaction conditions, (*S*)-**10b** was also isolated in 75% yield (TON > 4500) and > 99% *ee*. Therefore, the described catalytic system is highly efficient for the reduction of β -secondary-amino ketones in terms of both enantioselectivity and reactivity. According to literature procedures,^[5a,9] (*S*)-**10b** and (*S*)-**10h** can be subsequently converted into (*S*)-**1a** and (*S*)-**1d** in one step, respectively. Thus, these results provide one of the shortest (three steps overall) and most highly enantioselective (> 98% *ee* without further recrystallization) syntheses of fluoxetine and duloxetine.

In conclusion, a series of β -secondary-amino ketone hydrochlorides were hydrogenated with remarkably high enantioselectivity, for the first time, with a Rh complex containing a highly electron-donating P-chiral bisphospholane ligand, **4**. For two substrates of particular interest, **9b** and **9h**, high turnover numbers were also achieved. These results established one of the shortest and most potentially practical means for the synthesis of enantiopure *N*-monosubstituted γ -amino alcohols, which are important pharmaceutical intermediates.

Received: October 1, 2004
Published online: February 3, 2005

Keywords: amino alcohols · asymmetric catalysis · hydrogenation · P ligands · rhodium

- [1] a) M. Kitamura, T. Ohkuma, S. Inoue, N. Sayo, H. Kumobayashi, S. Akutagawa, T. Ohta, H. Takaya, R. Noyori, *J. Am. Chem. Soc.* **1988**, *110*, 629; b) K. Mashima, K. Kusano, H. Sato, Y. Matsu-mura, K. Nazaki, H. Kumobayashi, N. Sayo, Y. Hori, T. Ishizaki, S. Akutagawa, H. Takaya, *J. Org. Chem.* **1994**, *59*, 3064; c) T. Ohkuma, D. Ishii, H. Takeno, R. Noyori, *J. Am. Chem. Soc.* **2000**, *122*, 6510; d) T. Ohkuma, M. Koizumi, M. Yoshida, R. Noyori, *Org. Lett.* **2000**, *2*, 1749; e) T. Ohkuma, M. Koizumi, K. Muniz, G. Hilt, C. Kabuto, R. Noyori, *J. Am. Chem. Soc.* **2002**, *124*, 6508.
- [2] a) T. Hayashi, A. Katsumura, M. Konishi, M. Kumada, *Tetrahe-dron Lett.* **1979**, *20*, 425; b) H. Takeda, T. Tachinami, M. Aburatani, H. Takahashi, T. Morimoto, K. Achiwa, *Tetrahedron Lett.* **1989**, *30*, 363; c) H. Takahashi, S. Sakuraba, H. Takeda, K. Achiwa, *J. Am. Chem. Soc.* **1990**, *112*, 5876; d) H. Takeda, S. Hosokawa, M. Aburatani, K. Achiwa, *Synlett* **1991**, 193; e) S. Sakuraba, K. Achiwa, *Synlett* **1991**, 689; f) S. Sakuraba, N. Nakajima, K. Achiwa, *Synlett* **1992**, 829; g) S. Sakuraba, N. Nakajima, K. Achiwa, *Tetrahedron: Asymmetry* **1993**, *4*, 1457; h) S. Sakuraba, H. Takahashi, H. Takeda, K. Achiwa, *Chem. Pharm. Bull.* **1995**, *43*, 738; i) A. Roucoux, M. Devocelle, J.-F. Carpentier, F. Agbossou, A. Mortreux, *Synlett* **1995**, 358; j) M. Devo-celle, F. Agbossou, A. Mortreux, *Synlett* **1997**, 1306; k) C. Pasquier, S. Naili, L. Pelinski, J. Brocard, A. Mortreux, F. Agbossou, *Tetrahedron: Asymmetry* **1998**, *9*, 193.
- [3] Innocent Inc. (www.innocentive.com) has posted the following target transformation: .



- [4] a) D. T. Wong, J. S. Horong, F. P. Bymaster, K. L. Hauser, B. B. Molloy, *Life Sci.* **1974**, *15*, 471; b) D. T. Wong, F. P. Bymaster, J. S. Horong, B. B. Molloy, *J. Pharmacol. Exp. Ther.* **1975**, *193*, 804; c) B. J. Foster, E. R. Lavagnino, *Drugs Future* **1986**, *11*, 134; d) S. I. Ankier, *Prog. Med. Chem.* **1986**, *26*, 121; e) D. W. Robertson, J. H. Krushinski, R. W. Fuller, J. D. Leander, *J. Med. Chem.* **1988**, *31*, 1412; f) D. T. Wong, D. W. Robertson, F. P. Bymaster, J. H. Krushinski, L. R. Reid, *Life Sci.* **1988**, *43*, 2049.
- [5] For enantioselective synthesis of **1a–c**, see: a) V. Ratovelomana-Vidal, C. Girard, R. Touati, J. P. Tranchier, B. B. Hassine, J. P. Genet, *Adv. Synth. Catal.* **2003**, *345*, 261, and references therein; for enantioselective synthesis of **1d**, see: reference [5a]; b) J. Deeter, J. Frazier, G. Staten, M. Staszak, L. Weiget, *Tetrahedron Lett.* **1990**, *31*, 7101; c) H. Liu, B. H. Hoff, T. Anthonsen, *Chirality* **2000**, *12*, 26; d) A. Kamal, G. B. R. Khanna, R. Ramu, T. Krishnaji, *Tetrahedron Lett.* **2003**, *44*, 4783.
- [6] a) D. Liu, X. Zhang, *Eur. J. Org. Chem.* **2005**, in press; b) patent application: X. Zhang, W. Tang (The Penn State Research Foundation), WO 2003042135, **2003**.
- [7] The same deamination by-product was previously observed in a Rh-catalyzed hydrogenation of **6**; see: reference [2j].
- [8] For syntheses of **9a–i**, see Supporting Information.
- [9] Y. Gao, K. B. Sharpless, *J. Org. Chem.* **1988**, *53*, 4081.

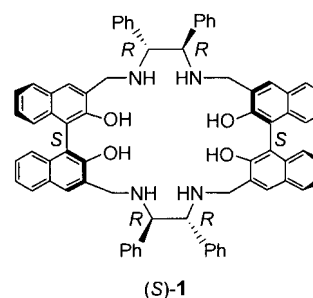
Fluorescent Recognition

A Cyclohexyl-1,2-diamine-Derived Bis(binaphthyl) Macrocycle: Enhanced Sensitivity and Enantioselectivity in the Fluorescent Recognition of Mandelic Acid**

Zi-Bo Li, Jing Lin, and Lin Pu*

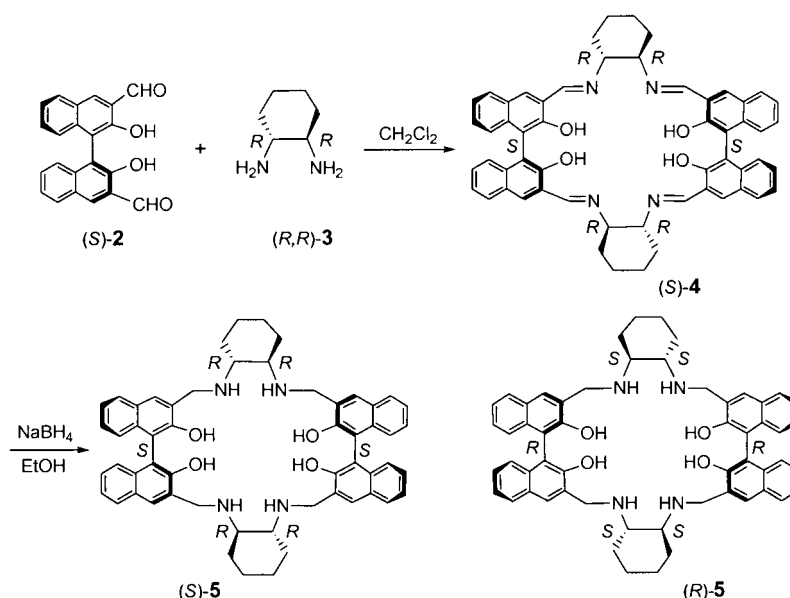
Separation-based techniques such as HPLC and GC equipped with chiral columns are the main analytical tools used today in both academy and industry for the determination of the enantiomeric composition of chiral compounds. With the development of the combinatorial chemistry technique, a large number of organic compounds including those with chirality can be synthesized very rapidly.^[1] This presents a great challenge to analyze the chiral composition of these compounds because of the inherently slow separation techniques. A number of techniques such as mass spectrometry, electrophoresis, IR thermography, and UV absorption, circular dichroism, and fluorescence spectroscopies^[2–6] are being developed for the fast assay of chiral compounds. We are particularly interested in the application of fluorescence spectroscopy in chiral recognition because it not only provides a real-time analysis but also offers high sensitivity and diverse sensing modes. With the use of a fluorescence microplate reader or a fluorescence imaging technique, hundreds of samples can be analyzed very quickly.

Application of fluorescence spectroscopy in chiral recognition has received growing attention in recent years.^[4–6] Among these studies, significant work has been conducted with 1,1'-binaphthyl molecules.^[5,6] This is because the unique chiral and aromatic structure of the 1,1'-binaphthyl unit could provide both excellent chiral recognition capability and interesting fluorescence signals. For example, we recently found that the macrocyclic compound (S)-1, with two 1,1'-binaphthyl and two 1,2-diphenylethylenediamine units, is capable of enantioselective fluorescent recognition.^[6c,d] This compound shows emissions both from the monomer as well as an excimer. The enantioselective fluorescent response of (S)-1 in the presence of mandelic acid was high for the emission of the excimer, but much



smaller for that of the monomer. Herein we report a modified bis(binaphthyl) macrocycle that exhibits an extremely high enantioselective fluorescent response in the emission from the monomer in the presence of mandelic acid.

Similar to the reaction reported by Brunner and Schiesling,^[7] a remarkable four-component condensation of (S)-2 and (R,R)-3 occurred at room temperature in CH₂Cl₂ to form the chiral macrocyclic Schiff base (S)-4 (Scheme 1). Reduc-



Scheme 1. Synthesis of the bis(binaphthyl) macrocycle (S)-5.

tion of (S)-4 with NaBH₄ in ethanol gave (S)-5. Although compound (S)-5 is structurally similar to (S)-1, purification of (S)-5 proved to be much more difficult. There was always approximately 5% impurity persistent in (S)-5 when purified either by column chromatography or by recrystallization. Finally, we found that (S)-5 formed a gel-like material in water when its solution in CH₂Cl₂ was treated with aqueous HCl. After the organic phase was removed, neutralization (NaHCO₃) and extraction (CH₂Cl₂) of the aqueous phase, followed by removal of the solvent led to analytically pure (S)-5.^[8] The specific optical rotation of (S)-5 was [α]_D = –86.3 (*c* = 0.22, C₆H₆). The ¹H NMR spectrum of (S)-5 shows two signals at δ = 4.27 and 4.43 ppm (AB, 8H, *J* = 14.4 Hz) for the diastereotopic methylene protons at the 3,3'-positions of the

[*] Z.-B. Li, Dr. J. Lin, Prof. L. Pu
Department of Chemistry
University of Virginia
Charlottesville, VA 22904-4319 (USA)
Fax: (+1) 434-924-3710
E-mail: lp6n@virginia.edu

[**] We are very grateful for the support of this work from the US National Institutes of Health (R01M58454 and R01EB002037-05). We also thank Dr. Jeff Ellena at the University of Virginia for assistance with the NMR spectroscopic study.

binaphthyl units. Compound (*R*)-**5**, the enantiomer of (*S*)-**5**, was synthesized similarly starting from (*R*)-**2** and (*S,S*)-**3**.

Although the concentration of (*S*)-**5** had little effect on the positions of the peaks and the shapes of the absorption spectra, a large concentration dependence was observed for the fluorescence spectra of the macrocycle. As the concentration increased from 1.0×10^{-6} to 1.0×10^{-4} M in benzene, the emission intensity of the macrocycle (*S*)-**5** at the long-wavelength band ($\lambda = 435$ nm) increased greatly (Figure 1).

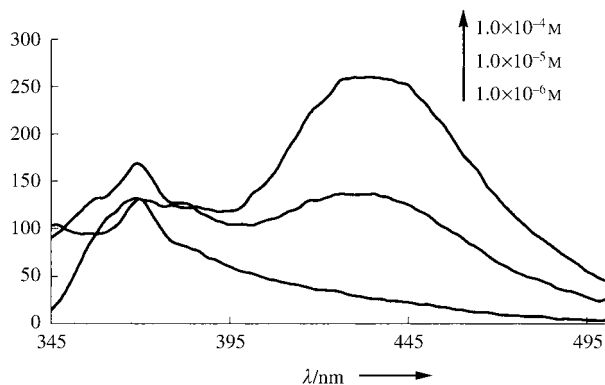


Figure 1. Concentration effect on the fluorescence spectra of (*S*)-**5** in benzene ($\lambda_{\text{ex}} = 332$ nm, ex/em slits = 3.5/6.5 nm).

At 1.0×10^{-4} M, the long-wavelength emission dominated. The change at the short-wavelength emission band ($\lambda = 370$ nm) with respect to the concentration was much smaller. According to our previous study on the macrocycle (*S*)-**1**,^[6d] we attribute the long-wavelength band of (*S*)-**5** to emission from its excimer and the short-wavelength band to emission from the monomer.

The interaction of the macrocycle (*S*)-**5** with the enantiomers of mandelic acid was studied. The UV/Vis spectrum of the macrocycle showed only a slight decrease in the absorbance intensity when treated with mandelic acid, but no changes in the shape or position of the peak and almost no difference between the effects of (*R*)- and (*S*)-mandelic acid were observed. In contrast, a dramatic difference was observed for the fluorescence responses of the macrocycle towards (*R*)- and (*S*)-mandelic acid.^[9] As shown in Figure 2a, (*R*)-mandelic acid (5.0×10^{-4} M) had almost no effect on the fluorescence of (*S*)-**5** (1.0×10^{-5} M in benzene containing 0.05 % 1,2-dimethoxyethane (DME)). However, under the same conditions, (*S*)-mandelic acid caused an increase in the fluorescence intensity of monomeric (*S*)-**5** by over 20-fold.

To ascertain that the observed large difference in the fluorescence responses of (*S*)-**5** toward (*R*)- and (*S*)-mandelic acid is the result of inherent chiral recognition, we studied the interaction of (*R*)-**5**, the enantiomer of (*S*)-**5**, with (*R*)- and (*S*)-mandelic acid. Figure 2b presents the fluorescence emission spectra of (*R*)-**5** (1.0×10^{-5} M in benzene/0.05 % DME) in both the presence and absence of (*R*)- and (*S*)-mandelic acid (5.0×10^{-4} M). Whereas (*S*)-mandelic acid caused little change in the fluorescence of (*R*)-**5**, (*R*)-mandelic acid greatly enhanced its fluorescence emission. Thus, there is a mirror-image relationship in the results of Figure 2a and Figure 2b.

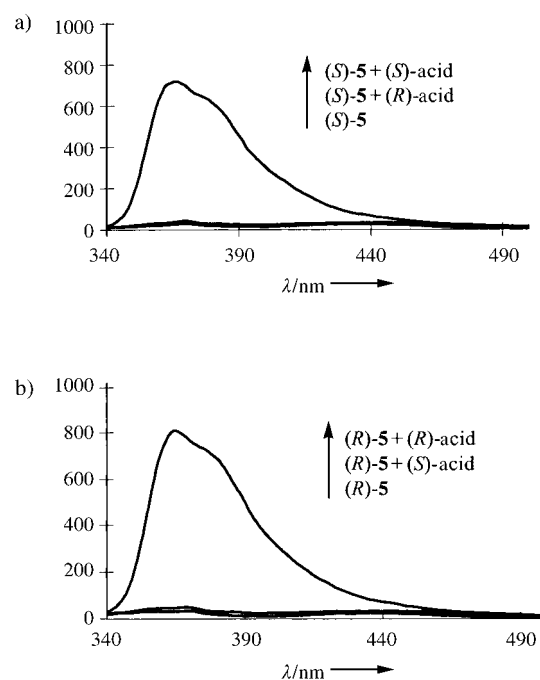


Figure 2. Fluorescence emission spectra of a) (*S*)-**5** and b) (*R*)-**5** in the absence/presence of (*R*)- and (*S*)-mandelic acid ($\lambda_{\text{ex}} = 332$ nm, ex/em slits = 3.5/3.5 nm).

This demonstrates that the fluorescence interaction of the macrocycle with mandelic acid is indeed highly enantioselective.

The fluorescence enhancement (I/I_0) of (*S*)-**5** as a function of the concentrations of (*R*)- and (*S*)-mandelic acid is plotted in Figure 3a. As the concentration of the acid increased, the

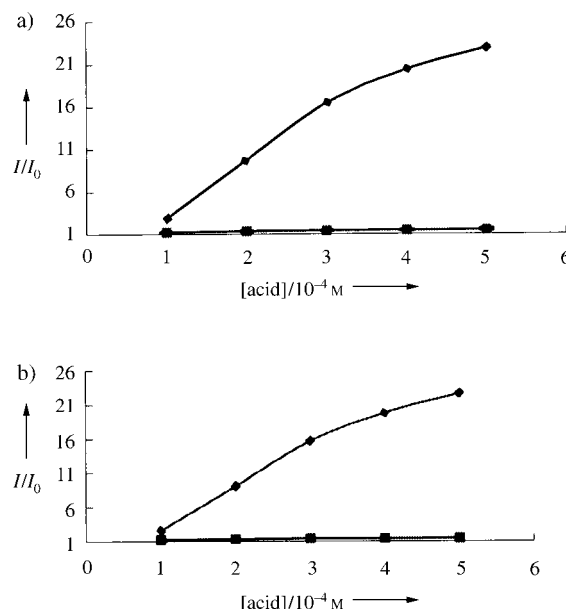


Figure 3. Fluorescence enhancement of a) (*S*)-**5** and b) (*R*)-**5** (1.0×10^{-5} M in benzene/0.05 % DME) versus concentrations of (*R*)- and (*S*)-mandelic acid ($\lambda_{\text{ex}} = 332$ nm). a) The average of four experiments are presented; av (*S*):♦; av (*R*):■. b) (*R*) acid:♦; (*S*) acid:■.

(*S*) enantiomer greatly enhanced the fluorescence of (*S*)-**5**, but the *R* enantiomer did not. At a concentration of acid of 5.0×10^{-4} M, the enantiomeric fluorescence difference ratio, $ef = (I_S - I_0)/(I_R - I_0)$, was as high as 46. Figure 3b shows the fluorescence enhancement of (*R*)-**5** versus the concentration of (*R*)- and (*S*)-mandelic acid. The fluorescence response shown in Figure 3b mirrors that shown in Figure 3a.

The fluorescence enhancement of (*S*)-**5** reached a maximum as the concentration of (*S*)-mandelic acid increased to around 7.0×10^{-4} M. A further increase in the concentration of (*S*)-mandelic acid led to a small decrease in the fluorescence intensity. Over the concentration range 1.0×10^{-4} to 2.0×10^{-3} M, (*R*)-mandelic acid caused little change on the fluorescence of (*S*)-**5**.

The effect of the enantiomeric purity of mandelic acid on the fluorescence of (*R*)-**5** was also studied. Figure 4 curve a

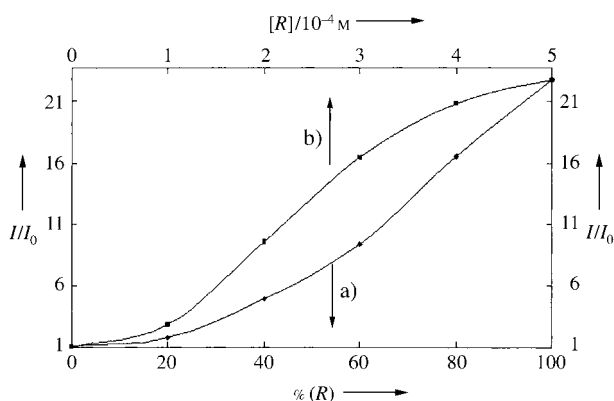
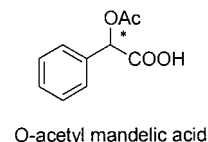


Figure 4. Fluorescence enhancement of (*R*)-**5** in the presence of samples containing either the optically pure (*R*)-mandelic acid or various enantiomeric compositions (% *R*) values of the total acid concentration: 5×10^{-4} M).

shows the fluorescence enhancement of (*R*)-**5** (1.0×10^{-5} M in benzene/0.05 % DME) in the presence of mandelic acid (5.0×10^{-4} M) at various compositions of the *R* and *S* enantiomers. Figure 4 curve b shows the fluorescence enhancement of (*R*)-**5** (1.0×10^{-5} M in benzene/0.05 % DME) when treated with the optically pure (*R*)-mandelic acid at concentrations that correspond to those of (*R*)-mandelic acid in the enantiomeric mixture. Thus, at the same amount of the *R* enantiomer, the optically pure (*R*)-mandelic acid caused a greater enhancement in fluorescence emission than the mixture containing both the *R* and *S* enantiomers. That is, even though (*S*)-mandelic acid could not increase the fluorescence intensity of the sensor (*R*)-**5**, it might be still in competition with (*R*)-mandelic acid in binding with the sensor which reduced the effective concentration of (*R*)-mandelic acid. Apparently, the binding of (*R*)-mandelic acid with (*R*)-**5** was much stronger than that of (*S*)-mandelic acid, and the racemic mixture of mandelic acid still led to a large fluorescence enhancement. For samples containing less than 20 % (*R*)-mandelic acid, the fluorescent enhancement of (*R*)-**5** was small because of the large amount of (*S*)-mandelic acid (> 80 %). However, this sample could be analyzed by using the enantiomeric sensor

(*S*)-**5** and should show a large fluorescence enhancement. Thus, by using both enantiomers of the sensor and by measuring the difference between their fluorescence responses toward the substrate under the same conditions will allow the determination of any enantiomeric composition of the chiral acid.

We also studied the interaction of (*S*)-**5** with *O*-acetyl mandelic acid. Under the same conditions employed with mandelic acid, almost no enhancement in the fluorescence emission was observed with either (*R*)- or (*S*)-*O*-acetyl mandelic acid. This demonstrates that both the α -hydroxy group and its chiral configuration are very important for the binding of the acid with the macrocyclic receptor. Under similar conditions, (*S*)-**5** showed various degrees of chiral recognition toward other chiral acids such as $\text{PhCH}(\text{NHCO}_2\text{CH}_2\text{Ph})\text{CO}_2\text{H}$ ($ef = 6.7$), $\text{PhCH}_2\text{CH}(\text{NHCO}_2\text{CH}_2\text{Ph})\text{CO}_2\text{H}$ ($ef = 2.1$), and $\text{PhCH}_2\text{CH}(\text{OH})\text{CO}_2\text{H}$ ($ef = 3.0$).



We previously reported that the highest enantioselectivity of (*S*)-**1** ($ef \approx 12$) in the fluorescent recognition of mandelic acid was observed with the emission of excimeric (*S*)-**1** which required high concentrations of both (*S*)-**1** (1.0×10^{-4} M) and the acid (2.0×10^{-2} M).^[6c,d] At the emission of the (*S*)-**1** monomer, the enantioselectivity was lower with $ef = 3.2$. With the newly synthesized sensor (*S*)-**5**, we have observed the highly enantioselective fluorescent recognition of mandelic acid (*S*)-**5** with $ef \approx 46$. Furthermore, as this high enantioselectivity is observed at the emission of the (*S*)-**5** monomer, it decreases the working concentrations of the sensor and mandelic acid by one and two orders of magnitude, respectively. Even at the greatly decreased concentrations of both the sensor and substrate, the fluorescence enhancement of (*S*)-**5** in the presence of (*S*)-mandelic acid can be over 10-times greater than that of (*S*)-**1** in the presence of (*S*)-mandelic acid. Therefore, (*S*)-**5** is a sensor of greatly increased enantioselectivity and sensitivity over (*S*)-**1**.

An NMR spectroscopic study on the interaction of the bis(binaphthyl) macrocycle with mandelic acid was also conducted. We found that a 1:1 mixture of (*S*)-**5** and (*S*)-mandelic acid dissolved in a solvent system of $[\text{D}_6]\text{acetone}$ (4 %) in $[\text{D}_6]\text{benzene}$ caused a large upfield shift ($\Delta\delta = 1.0$ – 1.1 ppm) for the signal of the α proton of (*S*)-mandelic acid; that is, from $\delta = 5.20$ to $\delta = 4.1$ – 4.2 ppm. However, under the same conditions, the chirality-mismatched mixture of (*S*)-**5** and (*R*)-mandelic acid led to only a small upfield shift ($\Delta\delta = 0.25$ ppm) for the α proton of (*R*)-mandelic acid. This proton only showed an upfield shift of 0.02 ppm when mandelic acid was treated with dibenzylamine. These observations suggest that in the macrocycle–mandelic acid complex, (*S*)-mandelic acid is probably located much deeper inside the chiral cavity of (*S*)-**5** than (*R*)-mandelic acid which significantly shields the α proton of (*S*)-mandelic acid by the aromatic rings of the macrocycle. This could be the origin of the dramatic difference in the fluorescence responses of (*S*)-**5** toward the two enantiomers of mandelic acid. The ^1H NMR spectroscopic study also indicates that (*S*)-**5** probably binds more than one

equivalent of (*S*)-mandelic acid. Further studies on the structure of the sensor–substrate complex are in progress in our laboratory.

Received: October 29, 2004

Revised: December 1, 2004

Published online: February 2, 2005

Keywords: chirality · enantioselectivity · fluorescent probes · macrocycles · molecular recognition

- [1] For a special issue on combinatorial chemistry, see: *Chem. Rev.* **1997**, 97, 347–510.
- [2] For reviews, see: a) M. G. Finn, *Chirality* **2002**, 14, 534–540; b) M. T. Reetz, *Angew. Chem.* **2002**, 114, 1391–1394; *Angew. Chem. Int. Ed.* **2002**, 41, 1335–1338; c) M. Tsukamoto, H. B. Kagan, *Adv. Synth. Catal.* **2002**, 344, 453–463.
- [3] a) UV/Vis spectroscopy: M. T. Reetz, A. Zonta, K. Schimossek, K. Liebeton, K.-E. Jaeger, *Angew. Chem.* **1997**, 109, 2961–2963; *Angew. Chem. Int. Ed. Engl.* **1997**, 36, 2830–2832; L. Zhu, E. V. Anslyn, *J. Am. Chem. Soc.* **2004**, 126, 3676–3677; b) IR thermography: M. T. Reetz, M. H. Becker, K. M. Kuhling, A. Holzwarth, *Angew. Chem.* **1998**, 110, 2792–2795; *Angew. Chem. Int. Ed.* **1998**, 37, 2647–2650; c) CD spectroscopy: K. Ding, A. Ishii, K. Mikami, *Angew. Chem.* **1999**, 111, 519–523; *Angew. Chem. Int. Ed.* **1999**, 38, 497–501; d) Capillary electrophoresis: M. T. Reetz, K. M. Kuhling, A. Deege, H. Hinrichs, D. Belder, *Angew. Chem.* **2000**, 112, 4047–4049; *Angew. Chem. Int. Ed.* **2000**, 39, 3891–3893; e) Mass spectrometry: J. Guo, J. Wu, G. Siuzdak, M. G. Finn, *Angew. Chem.* **1999**, 111, 1868–1871; *Angew. Chem. Int. Ed.* **1999**, 38, 1755–1758; M. T. Reetz, M. H. Becker, H.-W. Klein, D. Stockigt, *Angew. Chem.* **1999**, 111, 1872–1875; *Angew. Chem. Int. Ed.* **1999**, 38, 1758–1761; f) Immunoassay: F. Taran, C. Gauchet, B. Mohar, S. Meunier, A. Valleix, P. Y. Renard, C. Créminon, J. Grassi, A. Wagner, C. Mioskowski, *Angew. Chem.* **2002**, 114, 132–135; *Angew. Chem. Int. Ed.* **2002**, 41, 124–127; g) Enzyme assay: P. Abato, C. T. Seto, *J. Am. Chem. Soc.* **2001**, 123, 9206–9207; h) Electrochemistry: A. P. Abbott, G. W. Barker, D. L. Davies, G. A. Griffiths, A. J. Walter, P. Kočovský, *Anal. Chem.* **2002**, 74, 4002–4006.
- [4] a) For a review on the use of fluorescence in chiral recognition, see: L. Pu, *Chem. Rev.* **2004**, 104, 1687–1716; b) G. A. Korbel, G. Lalic, M. D. Shair, *J. Am. Chem. Soc.* **2001**, 123, 361–362; c) M. Matsushita, K. Yoshida, N. Yamamoto, P. Wirsching, R. A. Lerner, K. D. Janda, *Angew. Chem.* **2003**, 115, 6166–6169; *Angew. Chem. Int. Ed.* **2003**, 42, 5984–5987; d) G. Klein, J. -L. Reymond, *Helv. Chim. Acta* **1999**, 82, 400–407; e) X. F. Mei, C. Wolf, *Chem. Commun.* **2004**, 2078–2079.
- [5] a) T. D. James, K. R. A. S. Sandanayake, S. Shinkai, *Angew. Chem.* **1996**, 108, 2038–2050; *Angew. Chem. Int. Ed. Engl.* **1996**, 35, 1911–1922; b) T. D. James, K. R. A. S. Sandanayake, S. Shinkai, *Nature* **1995**, 374, 345–347; c) M. Takeuchi, S. Yoda, T. Imada, S. Shinkai, *Tetrahedron* **1997**, 53, 8335–8348; d) J. -Z. Zhao, T. M. Fyles, T. D. James, *Angew. Chem.* **2004**, 116, 3543–3546; *Angew. Chem. Int. Ed.* **2004**, 43, 3461–3464.
- [6] a) J. Lin, Q.-S. Hu, M.-H. Xu, L. Pu, *J. Am. Chem. Soc.* **2002**, 124, 2088–2089; b) M.-H. Xu, J. Lin, Q. -S. Hu, L. Pu, *J. Am. Chem. Soc.* **2002**, 124, 14239–14246; c) J. Lin, H.-C. Zhang, L. Pu, *Org. Lett.* **2002**, 4, 3297–3300; d) Z.-B. Li, J. Lin, H.-C. Zhang, M. Sabat, M. Hyacinth, L. Pu, *J. Org. Chem.* **2004**, 69, 6284–6293; e) V. Pugh, Q.-S. Hu, L. Pu, *Angew. Chem.* **2000**, 112, 3784–3787; *Angew. Chem. Int. Ed.* **2000**, 39, 3638–3641; f) L.-Z. Gong, Q.-S. Hu, L. Pu, *J. Org. Chem.* **2001**, 66, 2358–2367; g) V. Pugh, Q.-S. Hu, X.-B. Zuo, F. Lewis, L. Pu, *J. Org. Chem.* **2001**, 66, 6136–6140; h) J. Lin, Z.-B. Li, H.-C. Zhang, L. Pu, *Tetrahedron Lett.* **2004**, 45, 103–106; i) J. Lin, A. R. Rajaram, L. Pu, *Tetrahedron* **2004**, 60, 11277–11281.
- [7] a) H. Brunner, H. Schiessling, *Angew. Chem.* **1994**, 106, 130–130.; *Angew. Chem. Int. Ed. Engl.* **1994**, 33, 125–126; b) H. Brunner, H. Schiessling, *Bull. Soc. Chim. Belg.* **1994**, 103, 119–126.
- [8] Preparation and characterization of (*S*)- and (*R*)-**5**: Aldehyde (*S*)-**2** (274 mg, 0.80 mmol) and cyclohexane-1,2-diamine ((*R,R*)-**3**, 93 mg, 0.80 mmol) were dissolved in dry CH₂Cl₂ under N₂, and the mixture was stirred at RT for 2 days. After evaporation of the solvent, the resulting Schiff base (*S*)-**4** was purified by passing through a short column of silica gel. Compound (*S*)-**4** was then combined with NaBH₄ (88 mg, 2.32 mmol) and ethanol (25 mL), which was degassed with nitrogen, and heated at reflux for 4 h. After removal of the solvent, the residue was dissolved in CH₂Cl₂ (10 mL) and aqueous HCl (0.4 N, 30 mL) was added. The organic layer was separated from the gel-like aqueous layer and discarded. The aqueous layer was neutralized with NaHCO₃ and then extracted with CH₂Cl₂ (3 × 20 mL). Removal of the solvent gave pure (*S*)-**5** as a white solid (170 mg, 55 %). m.p. > 230 °C (dec.); [α]_D = –86.30 (*c* = 0.22, C₆H₆); ¹H NMR ([D₆]acetone, 300 MHz): δ = 0.86–1.16 (m, 8H), 1.48–1.60 (m, 4H), 2.01–2.18 (m, 4H), 2.18–2.32 (m, 4H), 4.27 and 4.43 (AB, 8H, *J* = 14.4 Hz), 7.08–7.28 (m, 12H), 7.67(s, 4H), 7.76–7.83 ppm (m, 4H); ¹³C NMR ([D₆]acetone, 75 MHz): δ = 24.86, 32.34, 51.58, 61.55, 117.36, 122.65, 124.82, 125.46, 126.94, 127.35, 127.92, 128.54, 134.45, 154.82 ppm; HRMS (MALDI): *m/z* calcd for C₅₆H₅₇N₄O₄ [*MH*⁺]: 849.4374; found: 849.4382; Elemental analysis (%) calcd for C₅₆H₅₆N₄O₄: C 79.22, H 6.65, N 6.60; found: C 79.18, H 6.77, N 6.45.
- [9] Preparation of samples for fluorescence measurements: The enantiomers of mandelic acid were purchased from Aldrich and recrystallized from methanol. All of the solvents were HPLC grade. The stock solutions of the sensors in benzene were freshly prepared for each measurement. For the fluorescence enhancement study, a solution of the sensor was mixed with a solution of mandelic acid at RT in a 5-mL volumetric flask, and the mixture was diluted to the desired concentration. The resulting solution was allowed to stand at RT for 2–4 h before measurement of the fluorescence emission.

Diphosphanylethenes

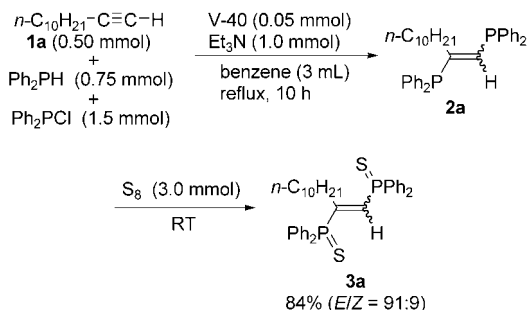
Synthesis of (*E*)-1,2-Diphosphanylene Derivatives from Alkynes by Radical Addition of Tetraorganodiphosphane Generated In Situ**

Akinori Sato, Hideki Yorimitsu, and Koichiro Oshima*

Organophosphorus compounds serve as reagents, ligands for transition metals, biologically active substances, and building blocks of nanoarchitectures, and thus play vital roles in organic chemistry. Among them, (*E*)-1,2-bis(diphenylphosphanyl)ethene has recently attracted increasing attention in the field of self-assembly.^[1] Construction of hierarchical structures for use as new functional materials^[2] calls for derivatives of (*E*)-1,2-bis(diphenylphosphanyl)ethene that have functional groups to induce further assembly. However, there are a limited number of methods for the synthesis of such peculiar diphosphanylene skeletons; these syntheses are always carried out under harsh and/or strongly basic conditions.^[3] Highly efficient and mild reactions affording (*E*)-1,2-bis(diphenylphosphanyl)ethene derivatives are therefore required.

Here we report a general, facile, and reliable synthesis of (*E*)-diphosphanylene derivatives starting from an alkyne and a tetraorganodiphosphane. Radical addition of a tetraorganodiphosphane across a C–C triple bond seems to be a straightforward strategy for the synthesis of 1,2-diphosphanylenes.^[4,5] However, tetraorganodiphosphanes are so sensitive to oxygen that their preparation, purification, and handling are quite difficult and must be carried out under a strictly inert atmosphere.^[6] The inherent instability of diphosphanes in the presence of oxygen poses a serious problem in their synthetic use. The present diphosphanylation reaction employs a tetraorganodiphosphane that is cleanly generated in situ prior to the reaction. The high efficiency of this method will allow the 1,2-diphosphanylenes synthesized to be applicable in organic materials science.

A mixture of 1-dodecyne (**1a**), diphenylphosphane,^[7] chlorodiphenylphosphane, triethylamine, and 1,1'-azobis(cyclohexanecarbonitrile) (V-40)^[8] was heated in boiling benzene for 10 h (Scheme 1). The product was isolated as a 91:9 mixture of *E* and *Z* isomers of phosphane sulfide **3a** in 84 % yield. These two stereoisomers were separable from each other by thorough chromatographic purification on silica gel.



Scheme 1.

The presence of an excess of chlorodiphenylphosphane is essential for the success of the reaction: the use of a smaller amount (1.0 mmol) of chlorodiphenylphosphane gave (1-dodecyl)diphenylphosphane sulfide (**4**, 9 %, *E/Z* = 18:82) along with **3a** (78 %, *E/Z* = 90:10). Complete conversion of diphenylphosphane to tetraphenyldiphosphane is important to avoid contamination by monoadduct **4**.

Tetraphenyldiphosphane is commercially available. However, the reaction of **1a** (0.75 mmol) with the purchased tetraphenyldiphosphane^[9] (1.5 mmol) yielded both **3a** (60 %, *E/Z* = 88:12) and **4** (27 %, *E/Z* = 37:63). It is worth noting that addition of chlorodiphenylphosphane to the reaction mixture suppressed the generation of **4**, and generated **3a** (87 %, *E/Z* = 89:11) selectively.

A variety of terminal alkynes undergo this radical diphosphanylation reaction (Table 1). Aryl-substituted acetylenes react with tetraphenyldiphosphane prepared in situ to yield 1-aryl-1,2-bis(diphenylthiophosphanyl)ethenes in excellent yield with high stereoselectivity (entries 1–5). The *E* configuration of the major isomer of **3c** was determined by X-ray crystallographic analysis (see the Supporting information). Purification of **2b** under argon allowed us to isolate this compound in 78 % yield (*E/Z* = 92:8). Ester (entries 3 and 7), iodo (entry 4), keto (entry 5), and thioester (entry 8) moieties remained unchanged under the reaction conditions; these groups are not tolerated in the conventional incorporation of a diphenylphosphanyl group which requires the use of a highly nucleophilic and basic metal diphenylphosphide.^[3] Gratifyingly, a carbon(sp³)–halogen bond was also stable during the reaction, although **1j** is prone to form the corresponding Wittig salt (entry 9). Tetracyclohexyldiphosphane, prepared in situ from dicyclohexylphosphane^[7] and chlorodicyclohexylphosphane, added to **1b** in a similar fashion to afford (*E*)-**3b'** in excellent yield after careful separation from contaminants such as (*Z*)-**3b'** (Scheme 2).

The reactions with *tert*-butylacetylene failed to yield the desired product, and internal alkynes such as diphenylacety-

[*] A. Sato, Dr. H. Yorimitsu, Prof. Dr. K. Oshima
Department of Material Chemistry
Graduate School of Engineering
Kyoto University
Kyoto-daigaku Katsura, Nishikyo-ku, Kyoto 615-8510 (Japan)
Fax: (+81) 75-383-2438
E-mail: oshima@orgxn.mbox.media.kyoto-u.ac.jp

[**] This work was supported by Grants-in-Aid for Scientific Research, Young Scientists, and COE Research from the Ministry of Education, Culture, Sports, Science, and Technology, Japan. We thank Prof. Masaki Shimizu (Department of Material Chemistry, Kyoto University) and Dr. Yasuyuki Ura (Department of Energy and Hydrocarbon Chemistry, Kyoto University) for generous help with the X-ray crystallographic analysis and for teaching us how to purify air-sensitive compounds, respectively. We also acknowledge Mr. Hiroshi Hata and Prof. Naoki Aratani and Prof. Hiroshi Shinokubo (Department of Science, Kyoto University) for measuring UV/Vis and fluorescence spectra. Chlorodicyclohexylphosphane was a gift from Hokko Chemical Industry Co., Ltd.

Supporting information for this article is available on the WWW under <http://www.angewandte.org> or from the author.

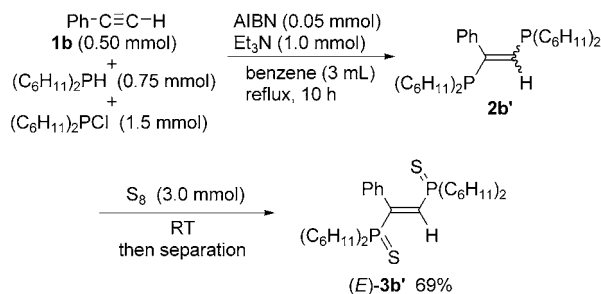
Table 1: Radical diphosphanylation of terminal alkynes.

$$\begin{array}{ccc}
 \text{R}-\text{C}\equiv\text{C}-\text{H} & \xrightarrow[\text{Et}_3\text{N (1.0 mmol)}]{\text{V-40 (0.05 mmol)}} & \text{R}-\text{C}=\text{C}-\text{PPh}_2 \\
 \textbf{1 (0.50 mmol)} & & \textbf{2} \\
 + & & \text{benzene (3 mL)} \\
 \text{Ph}_2\text{PH (0.75 mmol)} & & \text{reflux, 10 h} \\
 + & & \\
 \text{Ph}_2\text{PCI (1.5 mmol)} & &
 \end{array}$$

$$\begin{array}{ccc}
 & \xrightarrow[\text{RT}]{\text{S}_8 \text{ (3.0 mmol)}} & \\
 & & \text{R}-\text{C}=\text{C}-\text{P}(\text{SPh})_2 \\
 & & \textbf{3}
 \end{array}$$

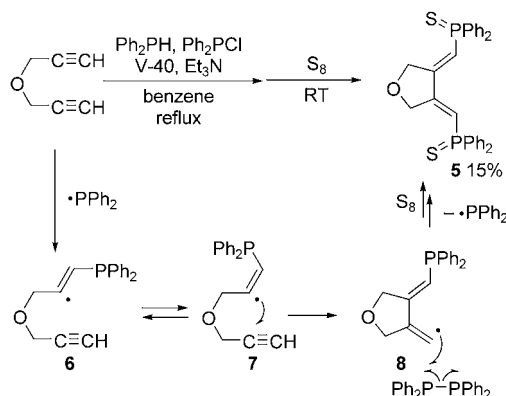
Entry	3	R	Yield [%] ^[a]	E/Z ^[a]
1	3b	Ph	87 (96) ^[b]	93:7
2	3c	<i>p</i> -MeOC ₆ H ₄	89	94:6
3	3d	<i>p</i> -MeOC(O)C ₆ H ₄	95	94:6
4	3e	<i>p</i> -IC ₆ H ₄	83	94:6
5	3f	<i>p</i> -AcC ₆ H ₄	96	95:5
6	3g	PhCH ₂ OCH ₂ CH ₂ CH ₂	78	90:10
7	3h	EtOC(O)(CH ₂) ₆	86	90:10
8	3i	AcS(CH ₂) ₉	80	90:10
9	3j	Cl(CH ₂) ₉	86	91:9

[a] Determined by ³¹P NMR spectroscopy with (MeO)₃P=O as internal standard. [b] Performed on a 5.0-mmol scale.


Scheme 2.

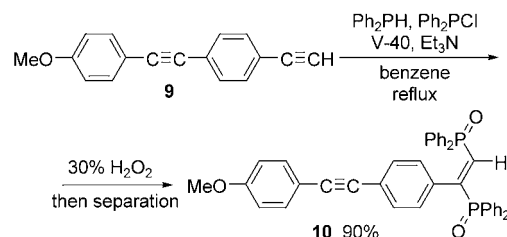
lene and 6-dodecyne also remained intact. Under the same reaction conditions 4-pentyn-1-ol or 3-butyne-2-one gave complex mixtures containing small amounts of the desired products.

The reaction clearly proceeds via a radical pathway, as demonstrated in Scheme 3. The formation of **5** necessitates


Scheme 3.

addition of a phosphorus-centered radical^[10] followed by 5-*exo-dig* radical cyclization. Isomerization of **6** to **7** reduces the steric hindrance in the cyclization, and subsequent radical S_H2 substitution^[11] affords the doubly phosphinated diene.^[12]

The high efficiency of this reaction might offer a reliable method for the synthesis of organic compounds for use in single-molecule devices, self-assembled monolayers (Table 1, entry 8), or optically intriguing organic materials. Scheme 4 illustrates the synthesis of a new fluorescent compound **10** which exhibits a couple of intense absorption bands in the UV region ($\lambda_{\text{max}} = 302, 320 \text{ nm}$; $\epsilon = 2.0 \times 10^4 \text{ M}^{-1} \text{ cm}^{-1}$ for both) and blue fluorescence ($\lambda_{\text{max}} = 469 \text{ nm}$) upon irradiation at 302 or 320 nm.


Scheme 4.

In summary, we have developed a highly efficient and concise diphosphanylation reaction for terminal alkynes. The radical addition of a tetraorganodiphosphane to an alkyne affords 1,2-diphosphanylenes in good yield with high *E* selectivity. The required tetraorganodiphosphane was readily prepared by mixing a diorganophosphane and a chlorodiorganophosphane in situ in the presence of triethylamine, which allowed us to avoid the troublesome isolation of tetraorganodiphosphane. The mild reaction conditions offer excellent functional-group compatibility and hence provide a powerful tool for the synthesis of important compounds by introducing two phosphorus atoms in one shot.

Received: November 14, 2004

Published online: February 2, 2005

Keywords: alkenes · alkynes · diphosphanylenes · radical reactions · synthetic methods

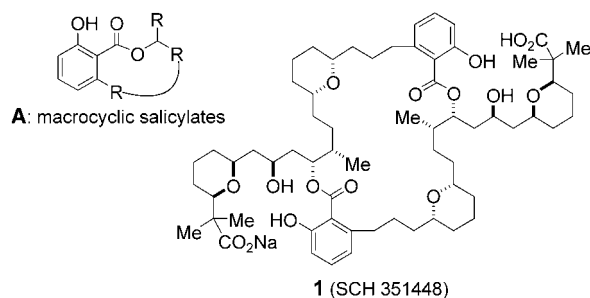
- [1] a) M.-C. Brandys, R. J. Puddephatt, *J. Am. Chem. Soc.* **2001**, *123*, 4839–4840; b) M.-C. Brandys, R. J. Puddephatt, *J. Am. Chem. Soc.* **2002**, *124*, 3946–3950; c) W. J. Hunks, J. Lapierre, H. A. Jenkins, R. J. Puddephatt, *J. Chem. Soc. Dalton Trans.* **2002**, 2885–2889; d) E. Lozano, M. Nieuwenhuyzen, S. L. James, *Chem. Eur. J.* **2001**, *7*, 2644–2651; e) A. S. DelNegro, S. M. Woessner, B. P. Sullivan, D. M. Dattelbaum, J. R. Schoonover, *Inorg. Chem.* **2001**, *40*, 5056–5057.
- [2] J. A. A. W. Elemans, A. E. Rowan, R. J. M. Nolte, *J. Mater. Chem.* **2003**, *13*, 2661–2670.
- [3] a) S. Hietkamp, O. Stelzer, *Inorg. Chem.* **1984**, *23*, 258–260; b) A. M. Aguiar, D. Daigle, *J. Am. Chem. Soc.* **1964**, *86*, 2299–2300; c) R. B. King, P. N. Kapoor, *J. Am. Chem. Soc.* **1971**, *93*, 4158–4166; d) W. Hewertson, H. R. Watson, *J. Chem. Soc.* **1962**,

- 1490–1494; e) K. K. Chow, W. Levason, C. A. McAuliffe, *J. Chem. Soc. Dalton Trans.* **1976**, 1429–1432.
- [4] A couple of reports underscore the difficulty of achieving this strategy—the attempted reactions suffered from very low yields and lack generality. a) J. G. Morse, J. J. Mielcarek, *J. Fluorine Chem.* **1988**, *40*, 41–49; b) V. A. Tzschach, S. Baensch, *J. Prakt. Chem.* **1971**, *313*, 254–258.
- [5] Dichalcogenides underwent similar radical-addition reactions to alkynes. For disulfides, see: a) E. I. Heiba, R. M. Dessau, *J. Org. Chem.* **1967**, *32*, 3837–3840. For diselenides, see: b) T. G. Back, M. V. Krishna, *J. Org. Chem.* **1988**, *53*, 2533–2536; c) A. Ogawa, H. Yokoyama, K. Yokoyama, T. Masawaki, N. Kambe, N. Sonoda, *J. Org. Chem.* **1991**, *56*, 5721–5723; d) A. Ogawa, N. Takami, M. Sekiguchi, H. Yokoyama, H. Kuniyasu, I. Ryu, N. Sonoda, *Chem. Lett.* **1991**, 2241–2242. For ditellurides, see: e) A. Ogawa, K. Yokoyama, H. Yokoyama, R. Obayashi, N. Kambe, N. Sonoda, *J. Chem. Soc. Chem. Commun.* **1991**, 1748–1750; f) A. Ogawa, K. Yokoyama, R. Obayashi, L.-B. Han, N. Kambe, N. Sonoda, *Tetrahedron* **1993**, *49*, 1177–1188. For a review of radical addition of dichalcogenides across C–C triple bonds, see: g) A. Ogawa, *J. Synth. Org. Chem. Jpn.* **1995**, *53*, 869–880.
- [6] a) W. Kuchen, H. Buchwald, *Chem. Ber.* **1958**, *91*, 2871–2877; b) E. J. Spanier, F. E. Caropreso, *J. Am. Chem. Soc.* **1970**, *92*, 3348–3351; c) A. H. Cowley, *Chem. Rev.* **1965**, *65*, 617–634.
- [7] Caution: Liquid diorganophosphanes undergo very rapid oxidation in air. They are highly pyrophoric, especially when wiped with a tissue in air.
- [8] Use of AIBN decreased the yield slightly by 10%.
- [9] Obtained from Aldrich. Diphosphane from Acros Co. led to a similar result. Note that ¹H NMR analysis of the purchased Ph₂P–PPh₂ revealed no detectable amount of HPPPh₂ in the commercial material.
- [10] a) C. M. Jessop, A. F. Parsons, A. Routledge, D. Irvine, *Tetrahedron Lett.* **2003**, *44*, 479–483, and references therein; b) H. Yorimitsu, H. Shinokubo, K. Oshima, *Bull. Chem. Soc. Jpn.* **2001**, *74*, 225–235; c) T. N. Mitchell, K. Heesche, *J. Organomet. Chem.* **1991**, *409*, 163–170.
- [11] R. Okazaki, Y. Hirabayashi, K. Tamura, N. Inamoto, *J. Chem. Soc. Perkin Trans. 1* **1976**, 1034–1036. See also ref. [10c].
- [12] Along with **5**, the crude mixture contained several byproducts, which could not be exactly identified. 2,3-Bis(diphenylthiophosphanyl)-2-propenyl propargyl ether seemed to be the main byproduct.

Synthesis of Functionalized Salicylate Esters and Amides by Photochemical Acylation**

Omid Soltani and Jef K. De Brabander*

Ortho-substituted salicylate esters (**A**) are an integral subunit of various important natural products.^[1] Often, their formation through acylation poses a problem for which no general solution has been formulated.^[1] Indeed, acylation is impeded by a combination of increased electron density and steric hindrance (*ortho*-substitution) at the acyl carbon center. This problem is circumvented through reactivity umpolung with Mitsunobu-type chemistry, but is limited to relatively unhindered alcohol substrates.^[2] Alternative approaches include alcohol activation by alkoxide formation,^[3,4] high-temperature trans-esterification with salicylate cyanomethyl esters,^[5] Trost–Chisholm lactonization,^[6] or late-stage de novo aryl synthesis.^[7] However, numerous failed attempts to introduce an *ortho*-functionalized salicylate ester during our synthetic program for **1** (SCH351448) required us to address the limitations of current methodology and formulate alternative approaches.^[8]



In search of useful reactivity patterns, we settled on the exploration of quinoketenes as potential highly reactive electrophilic salicylate equivalents. Quinoketene **C** ($R = H$) has been implicated as a reactive intermediate during various thermolytic and photochemical processes and was spectroscopically characterized at low temperatures in glassy or argon matrices.^[9] Of the various reaction manifolds to quinoketene,^[9] we were most inspired by the photolysis of 2-phenyl-benzo[1,3]dioxin-4-one (**B**, $R = H$) which has led to the first observation of quinoketene **C** ($R = H$) in solution at

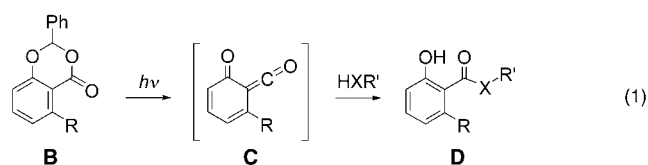
[*] O. Soltani, Prof. Dr. J. K. De Brabander
Department of Biochemistry
University of Texas Southwestern Medical Center at Dallas
5323 Harry Hines Blvd
Dallas, TX 75390-9038 (USA)
Fax: (+1) 214-648-6455
E-mail: jdebra@biochem.swmed.edu

[**] Financial support was provided by the Robert A. Welch Foundation and the National Institutes of Health (CA 90349). J.K.D.B. is a fellow of the Alfred P. Sloan Foundation.



Supporting information for this article is available on the WWW under <http://www.angewandte.org> or from the author.

room temperature [Eq. (1)].^[10] In the same report, Tidwell and co-workers also detailed quantitative reactivity studies

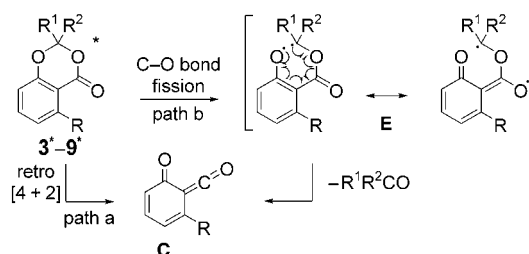


and proposed a pseudopericyclic transition state for the capture of **C** ($R=H$) with water, methanol, and diethylamine.^[10a] Despite this theoretical and mechanistic interest, and contrary to the situation with α -oxoketenes,^[9b] the synthetic exploitation of quinoketenes for the formation of salicylate esters and amides remains largely unexplored.^[11] Herein we report a general and high-yielding protocol for the synthesis of sterically hindered *ortho*-substituted salicylates through photolysis of previously unexplored *ortho*-substituted benzodioxinones in the presence of sterically hindered alcohols, phenols, and anilines [Eq. (1), $R \neq H$], and for the first time we shed some light on the mechanism and structural requirements for the photochemical decomposition of benzodioxinones.

Initial efforts to develop the photochemical acylation as a preparative method for the formation of salicylate esters were promising. Using a set of optimized conditions, we found that irradiating ($\lambda = 300$ nm) a solution that contained the parent 2-phenyl-benzo[1,3]dioxin-4-one (**3**) and 1-adamantanol (**2**) provided 1-adamantyl salicylate (**10**) in 76 % yield (Table 1, entry 1).^[12] More importantly, *ortho*-substituted salicylate esters **11–12** are similarly accessible in high yields through photochemical acylation with *ortho*-substituted benzodioxinones **4–6** (entries 2–4). In contrast, heating a mixture of benzodioxinone **4** and 1-adamantanol (**2**) in toluene at 110 °C for 3 hours resulted in complete recovery of starting materials, whereas reaction of benzodioxinone **9** with the adamantanyl-derived sodium alkoxide (**2**, sodium hexamethyldisilazide (NaHMDs), THF) gave a 1:1.5 mixture of the desired salicylate **11** and the corresponding styryl double-bond isomer (not shown) in 25 % combined yield. Particularly noteworthy

is the formation of the *ortho*-(2-oxopropyl)-substituted salicylate **13** in 80 % yield which occurs without a trace of formation of isocoumarin (entry 5)—a reaction pathway that is difficult to avoid with more conventional acylation methods, underscoring the mild conditions of the photochemical alternative.^[13]

Two alternative pathways can be formulated for the photochemical fragmentation of benzodioxinones to quinoketenes **C** (Scheme 1). One potential pathway features a



Scheme 1. Mechanistic considerations.

concerted photochemical [4+2] cycloreversion to generate **C** directly from an excited singlet state (path a). Alternatively, a homolytic C–O bond fission from an excited triplet state would produce a biradical intermediate **E**, followed by a thermal fragmentation to **C** (path b). The following observation provided some insight: 2,2-dialkyl-substituted benzodioxinones **8** ($R^1 = R^2 = (CH_2)_4$) and **9** ($R^1 = R^2 = Me$) were very poor photolysis substrates (Table 1, entries 6–7), despite exhibiting UV/Vis absorbance spectra that were virtually indistinguishable from **6** and **4/5** respectively.^[14] These results are best explained by invoking biradical intermediate **E** (path b), which is significantly better stabilized by phenyl substitution than by alkyl substitution.^[15] The relative quantum yields (ϕ) for the disappearance of benzodioxinone **4** and concomitant appearance of benzaldehyde at 300 nm were estimated as 0.64 and 0.58, respectively, relative to a benzophenone/benzhydrol actinometer ($\phi = 0.68$) under identical conditions.^[14,16] Our structure–photoactivity studies described above are revealing and provide a guiding principle for the orthogonal exploitation of photoactive and photo-silent benzodioxinones.^[17]

The results presented in Table 2 demonstrate the broad scope of the photochemical acylation reaction. A wide range of sterically hindered alcohols (**14a–i**) are acylated with *ortho*-allyl-substituted benzodioxinones **4** and **5** to provide acceptable yields of salicylate esters **15a–i** with broad functional group compatibility (silyl and *p*-methoxybenzyl ethers, ester, aryl, ketone, and olefin functionality). Particular examples include the formation of salicylate esters **15h** and **i** (Table 2), a key transformation in our approach^[8a] to SCH 351448 (**1**) that has eluded us with other methodologies. The efficient photochemical acylation of *anti*- β -isopropanoyloxy alcohol (**14g**) represents an alternative approach to a key fragment **15g** in our synthesis of salicylhalamides.^[18] On the basis of these results and in line with the proposed pseudopericyclic transition state,^[10a] this reaction appears to be less sensitive to steric bulk in the alcohol than classical acylation reactions.^[19]

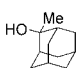
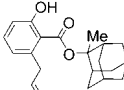
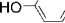
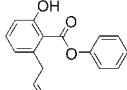
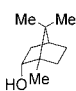
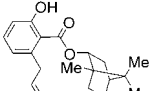
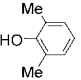
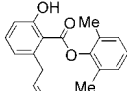
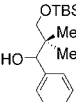
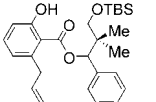
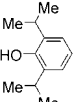
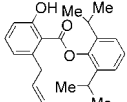
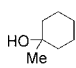
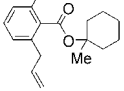
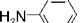
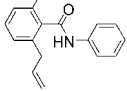
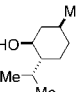
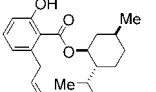
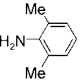
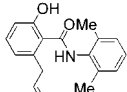
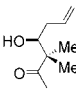
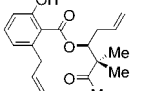
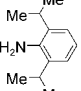
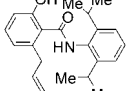
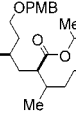
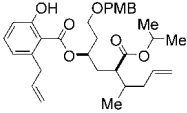
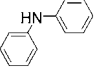
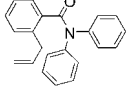
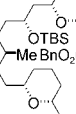
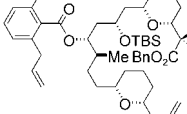
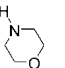
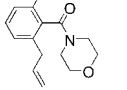
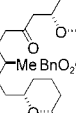
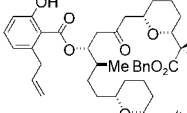
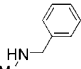
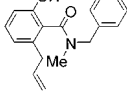
Table 1: Photochemical acylation of 1-adamantanol (**2**) with benzodioxinones **3–9**.

Entry	Substrate	$R/R^1/R^2$	Product	Yield [%]
1	3	H/H/Ph	10	76
2	4	$CH_2CHCH_2/H/Ph$	11	81
3	5	$CH_2CHCH_2/Ph/Ph$	11	85
4	6	OMe/Ph/Ph	12	77 ^[a]
5	7	$CH_2COMe/H/Ph$	13	80
6	8	OMe/-(CH_2) ₄ -	12	6 ^[b]
7	9	$CH_2CHCH_2/Me/Me$	11	< 5 ^[b]

[a] Yield after stirring the reaction mixture with $K_2CO_3/MeOH$.^[20]

[b] Benzodioxinones **8** and **9** were recovered in $\geq 80\%$ yield.

Table 2: Photochemical acylation of alcohols **14a–i**, phenols **16a–c**, anilines **18a–d**, and amines **20a** and **b** with benzodioxinones **4** and/or **5**.^[a]

Substrate	Benzodioxinone	Product	Yield [%] ^[b]	Substrate	Benzodioxinone	Product	Yield [%] ^[b]
	4		72 ^[c]		4		81
	5		62		5		85
	4		76 ^[d]		4		82
	5		73		5		79
	4		47 ^[d]		5		80
	5		61		5		83
	5		61 (72) ^[e]		5		70 ^[e]
	5		75 ^[e,f]		5		73 ^[e]
	4		48		5		64 ^[e]
	5		45				
	5		65 ^[f]				

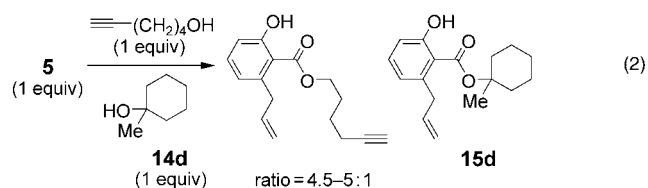
[a] Photolysis ($\lambda = 300$ nm) of benzodioxinone (2 equiv) in the presence of alcohol/amine (1 equiv, 0.25 M) in CH_2Cl_2 at RT for 4 h. See Experimental Section and Supporting Information for details. TBS = *tert*-butyldimethylsilyl, PMB = *p*-methoxybenzyl, Bn = benzyl. [b] Isolated yields of chromatographically pure material. [c] Twofold excess of alcohol. [d] 3 equivalents of **4**. [e] Yield obtained after stirring the reaction mixture with $\text{K}_2\text{CO}_3/\text{MeOH}$.^[20] [f] Alcohol was recovered in 17%.

For more quantitative information, we performed a competition experiment between 5-hexyn-1-ol and 1-methylcyclohexanol (**14d**) for photoacylation with benzodioxinone **5** [Eq. (2)]. ^1H NMR spectral analysis of the crude reaction mixture revealed an approximately 5:1 mixture of primary/tertiary alcohol derived salicylate esters.

Phenols (**16a–c**) and anilines (**18a–d**) are particularly good substrates for photoacylation, providing substituted

salicylate esters **17a–c** and anilides **19a–d** which are not accessible by Mitsunobu methodology (Table 2): this is dramatically illustrated by the efficient formation of *o,o'*-substituted benzoates of 2,6-(*i*Pr)₂PhOH (**16c**), 2,6-(*i*Pr)₂PhNH₂ (**18c**), and Ph₂NH (**18d**; Table 2, products **17c** and **19c** and **d**, respectively) under essentially neutral conditions. In a control experiment, heating a solution of aniline and benzodioxinone **5** or **9** in toluene in a sealed vial at 110°C for 3 h resulted in complete recovery of unconverted starting materials. Finally, secondary amines (**20a** and **b**) also participate as nucleophiles in the photoacylation (Table 2, products **21a** and **b**).^[20]

In conclusion, we have developed a general method for the synthesis of functionalized salicylic esters and amides by photolysis of *ortho*-functionalized 2-phenyl-benzo[1,3]dioxin-4-ones in the presence of alcohols, phenols, amines, and



anilines. This reaction occurs under essentially neutral conditions, yet efficiently engages a very wide range of acylation substrates, including sterically hindered nucleophiles that are inert to other acylation methods.^[21] The present study also defines the structural requirements for efficient photolysis of benzodioxinones to quinoketenes. Applications toward natural product synthesis and exploration of other reactivity modalities of quinoketenes generated in situ will be reported in due course.

Experimental Section

Procedure A (Table 1, entries 1–3 and 5–7; Table 2, **15a–c**, **15h** and **i**, and **17a–c**): An oven-dried borosilicate test tube was charged with alcohol/phenol and benzodioxinone at the ratios indicated in Table 1 and Table 2. The tube was sealed with a rubber septum, and freshly distilled CH₂Cl₂ (alcohol/phenol concentration: 0.25 M) was added under nitrogen. The nitrogen inlet was removed and the reaction vessel was sealed with parafilm. This reaction solution was then placed in a Rayonett RPR-100 reactor fitted with a test tube carousel and 300-nm bulbs and photolyzed for 4 h at 300 nm. The solution was then concentrated and purified by flash chromatography (silica gel, EtOAc/Hex).

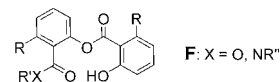
Procedure B (Table 1, entry 4; Table 2, **15f** and **g**, **19a–d**, and **21a** and **b**): Same procedure as above but with degassed solvent. After photolysis, the crude reaction mixture was concentrated and redissolved in anhydrous methanol, then anhydrous K₂CO₃ (1.5 equiv) was added. After stirring for 0.5–2 h at RT, the mixture was poured into H₂O and extracted with EtOAc (3 ×). The organic phase was dried (MgSO₄) and concentrated, and the residue was purified by flash chromatography (silica gel, EtOAc/Hex).

Received: November 11, 2004

Published online: January 31, 2005

Keywords: acylation · natural products · photochemistry · synthetic methods

- [1] For reviews, see: a) L. Yet, *Chem. Rev.* **2003**, *103*, 4283–4306; b) J. A. Beutler, T. C. McKee, *Curr. Med. Chem.* **2003**, *10*, 787–796.
- [2] a) O. Mitsunobu, *Synthesis* **1981**, 1–28; b) For a modification applied to the formation of resorcinyl esters, see: R. M. Garbaccio, S. J. Stachel, D. K. Baeschlin, S. J. Danishefsky, *J. Am. Chem. Soc.* **2001**, *123*, 10903–10908.
- [3] For selected examples, see: a) A. Bhattacharjee, J. K. De Brabander, *Tetrahedron Lett.* **2000**, *41*, 8069–8073; b) K. C. Nicolaou, D. W. Kim, R. Baati, A. O'Brate, P. Giannakakou, *Chem. Eur. J.* **2003**, *9*, 6177–6191; c) F. Hilli, J. M. White, M. A. Rizzacasa, *Org. Lett.* **2004**, *6*, 1289–1292; d) Q. Su, J. S. Panek, *J. Am. Chem. Soc.* **2004**, *126*, 2425–2430.
- [4] See also citations [32, 34, 37–38, and 46] in reference [1 a].
- [5] R. Shen, C. T. Lin, E. J. Bowman, B. J. Bowman, J. A. Porco, Jr., *J. Am. Chem. Soc.* **2003**, *125*, 7889–7901.
- [6] a) A. F. Petri, A. Bayer, M. E. Maier, *Angew. Chem.* **2004**, *116*, 5945–5947; *Angew. Chem. Int. Ed.* **2004**, *43*, 5821–5823; b) B. M. Trost, J. D. Chisholm, *Org. Lett.* **2002**, *4*, 3743–3745.
- [7] a) For an elegant route to benzo-fused resorcinyl macrolides by de novo aryl synthesis from ynolides, see: Z.-Q. Yang, X. Geng, D. Solit, C. A. Pratilas, N. Rosen, S. J. Danishefsky, *J. Am. Chem. Soc.* **2004**, *126*, 7881–7889; b) For an elegant route to apicularen through de novo aryl synthesis by an intramolecular Diels–Alder/oxidative aromatization sequence, see: B. R. Graetz, S. D. Rychnovsky, *Org. Lett.* **2003**, *5*, 3357–3360.
- [8] a) A. Bhattacharjee, O. Soltani, J. K. De Brabander, *Org. Lett.* **2002**, *4*, 481–484; b) Isolation: V. R. Hedge, M. S. Puar, P. Dai, M. Patel, V. P. Gullo, P. R. Das, R. W. Bond, A. T. McPhail, *Tetrahedron Lett.* **2000**, *41*, 1351–1354; c) For a total synthesis, see: E. J. Kang, E. J. Cho, Y. E. Lee, M. K. Ji, D. M. Shin, Y. K. Chung, E. Lee, *J. Am. Chem. Soc.* **2004**, *126*, 2680–2681.
- [9] For reviews, see: a) C. Simion, I. Costea, F. Badea, F. Iordache, *Rouv. Chem. Q. Rev.* **2000**, *8*, 131–143; b) C. Wentrup, W. Heilmayer, G. Kollenz, *Synthesis* **1994**, 1219–1248.
- [10] a) R. C.-Y. Liu, J. Luszyk, M. A. McAllister, T. T. Tidwell, B. D. Wagner, *J. Am. Chem. Soc.* **1998**, *120*, 6247–6251; b) O. L. Chapman, C. L. McIntosh, *J. Am. Chem. Soc.* **1970**, *92*, 7001–7002.
- [11] For the photolysis of coumarandione to quinoketene, and its capture by H₂O, PhOH, and PhCO₂H, see: W. M. Horspool, G. D. Khandelwal, *J. Chem. Soc. Chem. Commun.* **1970**, 257–258.
- [12] The reaction can be performed in several solvents with varying ratios of substrates. Optimal yields are obtained by irradiating a 1:2 or 2:1 mixture of reactants in benzene or CH₂Cl₂ at RT for 2–4 h. See Supporting Information for details.
- [13] Formation of isocoumarin is a common problem associated with *ortho*-(2-oxo-alkyl)-substituted resorcinylates, requiring the use of masked ketones in synthetic sequences. For selected examples, see: a) R. M. Garbaccio, S. J. Stachel, D. K. Baeschlin, S. J. Danishefsky, *J. Am. Chem. Soc.* **2001**, *123*, 10903–10908; b) J. A. Elix, V. K. Jayanthi, *Aust. J. Chem.* **1987**, *40*, 1851–1859; c) J. A. Elix, J. H. Wardlaw, *Aust. J. Chem.* **1997**, *50*, 479–486.
- [14] See the Supporting Information for UV/Vis absorbance spectra and the determination of relative quantum yields.
- [15] Intermediates similar to **E** have been proposed previously during the photolysis of 3,1-benzoxathian-4-ones (A. O. Pedersen, S.-O. Lawesson, P. D. Klemmensen, J. Kolc, *Tetrahedron* **1970**, *26*, 1157–1161) and 2-phenyl-benzoxan-4-one (flavanone; P. O. L. Mack, J. T. Pinhey, *J. Chem. Soc. Chem. Commun.* **1972**, 451–452).
- [16] a) M. S. Sigman, C. E. Kerr, B. E. Eaton, *J. Am. Chem. Soc.* **1993**, *115*, 7545–7546; b) W. M. Moore, M. Ketchum, *J. Am. Chem. Soc.* **1962**, *84*, 1368–1371.
- [17] They also explain a previous fruitless photolysis of a 2,2-dimethyl-substituted benzodioxinone, see reference [5].
- [18] Y. Wu, X. Liao, R. Wang, X.-S. Xie, J. K. De Brabander, *J. Am. Chem. Soc.* **2002**, *124*, 3245–3253. In this study, we were forced to prepare a salicylate ester similar to **15g** through a Mitsunobu esterification reaction with an epimeric alcohol precursor as all attempts to prepare this compound by acylation failed.
- [19] A similar observation was reported for acylations with acyclic α -oxoketenes: R. Shelkov, M. Nahmany, A. Melman, *J. Org. Chem.* **2002**, *67*, 8975–8982.
- [20] In some cases, but more pronounced with aniline/amine substrates, further acylation of the phenol product leads to varying amounts (5–15 %) of **F**. These can be converted into the desired salicylates **12**, **15f** and **g**, **19a–d**, and **21a** and **b** by treatment with K₂CO₃ in MeOH.



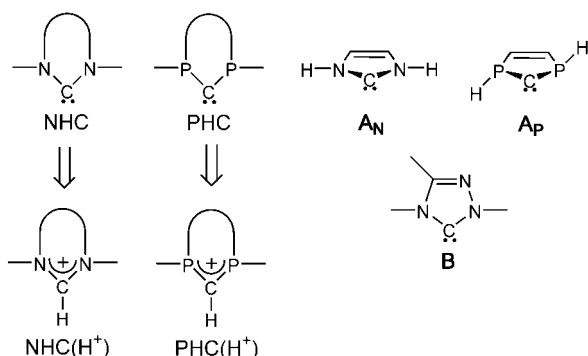
- [21] For those cases examined, alternative procedures failed to deliver the corresponding esters/amides in yields higher than 0–36 %. See Supporting Information for examples.

Heterocyclic Carbenes

A Stable P-Heterocyclic Carbene**

David Martin, Antoine Baceiredo, Heinz Gornitzka, Wolfgang W. Schoeller, and Guy Bertrand*

The availability of catalysts that can perform specific transformations is critical for both industry and academia. Over the years, the success of homogeneous catalysis can be attributed largely to the development of a diverse range of ligand frameworks that have been used to tune the behavior of a variety of systems. Recently, spectacular achievements have been made using cyclic diaminocarbenes, usually called N-heterocyclic carbenes (NHCs; Scheme 1), as ligands for



Scheme 1. N- and P-Heterocyclic carbenes and their classical precursors.

transition-metal-based catalysts,^[1–3] and even as catalysts in their own right.^[4,5] Compared to most classical ligands, such as phosphanes, NHCs bind more strongly to metal centers (thus avoiding the necessity for the use of excess ligand), and the resulting NHC-based catalysts are less sensitive to air and moisture, and have proven remarkably resistant to oxidation.^[6]

It is noteworthy that although NHC–transition-metal complexes have been known since the Sixties,^[7–9] the recent developments in their application as scaffolds in catalysis

have only been made possible because of the availability of isolable NHCs.^[10,11] The unusual stability of NHCs (for a long time carbenes were considered as prototypical reactive intermediates, their instability being due to their six-valence-electron shell that defies the octet rule)^[12] results from the ability of nitrogen to act as a π -donor, which decreases the electron deficiency at the adjacent carbene center. This electronic stabilization produces the strong σ -donor and weak π -acceptor properties of NHCs that explain their efficiency as ligands for transition-metal-based catalysts.

In a seminal paper, Schleyer et al.^[13] concluded that the inherent π -donor capabilities of the heavier elements (such as phosphorus) are as large as, or larger than, those of their second-row counterparts (such as nitrogen), and that their apparently inferior donor ability is due to the difficulty in achieving the optimum planar configuration. Therefore, one of the obvious interesting candidates to compete with and/or complement NHCs as ligands for transition-metal-based catalysts are P-heterocyclic carbenes (PHCs),^[14–18] providing that there is a driving force for the planarization of the phosphorus centers. Previous calculations have shown that the nitrogen centers of the parent NHC **A_N** (Scheme 1) are in a perfectly planar environment,^[19,20] whereas the phosphorus centers of the corresponding PHC **A_P** are strongly pyramidalized, as expected.^[21,22] Consequently, the singlet–triplet gap drops from 79 kcal mol^{–1} for **A_N**^[19] to 21 kcal mol^{–1} for **A_P**^[22] although the latter is predicted to be highly unstable with respect to dimerization.^[21] However, there are several ways to decrease the inversion barrier at phosphorus, as discussed recently in a comprehensive review,^[23] the simplest being to use bulky substituents. Here, we report the synthesis and ligand properties of a stable diphosphorus analogue of Enders' NHC **B**.^[24]

The classical precursors for NHCs are the well-known corresponding protonated species NHC(H⁺) (Scheme 1). In contrast, the phosphorus analogues of such species, PHC(H⁺), are unknown.^[25–28] Moreover, the synthetic methods used in the nitrogen series cannot be extended to compounds of its heavier congener. We therefore designed an original synthetic approach: a formal [3+2] cycloaddition of the transient diphosphaallylic cation **2** with a dipolarophile (Scheme 2). Addition of silver trifluoromethanesulfonate or gallium trichloride to a dichloromethane solution of the readily available phosphalkene **1**,^[29,30] at –78 °C, in the presence of a large excess of acetonitrile (30–45 equiv) afforded the desired salts **3a** and **3b**, respectively. They were isolated after recrystallization as white crystals (see Experimental Section). Deprotonation of derivative **3a** was then carried out in THF at –78 °C with lithium bis(trimethylsilyl)amide. The resulting carbene **4** was isolated after recrystallization from a concentrated THF/toluene solution at –30 °C as light-yellow crystals.

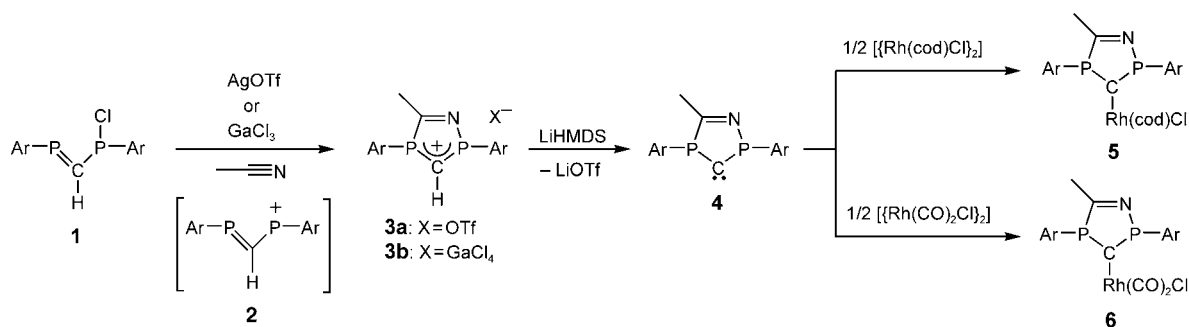
The X-ray diffraction analyses of compounds **3b** and **4** (Figure 1 and 2) revealed the almost planar environment of the phosphorus centers in both molecules (sum of the angles, **3b**: 354° and 348°; **4**: 353° and 348°).^[31] However, the slight deviation from planarity (*trans* arrangement of the 2,4,6-*tert*-butylphenyl substituents) makes **3b** and **4** chiral in the solid state. In solution both ¹H and ¹³C NMR spectroscopy showed the equivalency of the diastereotopic *tert*-butyl

[*] D. Martin, G. Bertrand
UCR-CNRS Joint Research Chemistry Laboratory (UMR 2282)
Department of Chemistry
University of California
Riverside, CA 92521-0403 (USA)
Fax: (+1) 909-787-2725
E-mail: gbertran@mail.ucr.edu

D. Martin, A. Baceiredo, H. Gornitzka, G. Bertrand
Laboratoire Hétérochimie Fondamentale et Appliquée (UMR 5069)
Université Paul Sabatier
118, route de Narbonne, 31062 Toulouse Cedex 04 (France)

W. W. Schoeller
Fakultät für Chemie der Universität
Postfach 10 01 31, 33615 Bielefeld (Germany)

[**] We are grateful to the ACS/PRF (38192-AC4), RHODIA, and the DFG for financial support of this work.



Scheme 2. Synthesis and complexation of P-heterocyclic carbene **4**. Ar = 2,4,6-tri-*tert*-butylphenyl, cod = cycloocta-1,5-diene, HMDS = hexamethyldisilazide, Tf = trifluoromethanesulfonyl.

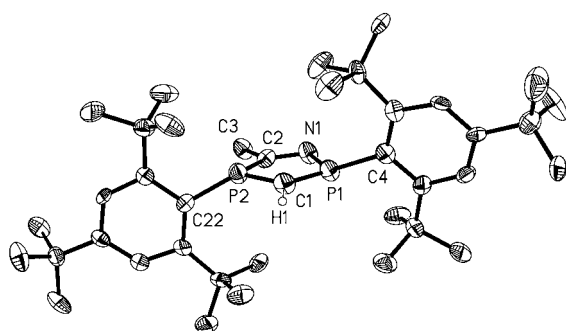


Figure 1. Molecular view of **3b** in the solid state. Selected bond lengths [Å] and angles [°]: P1–C1 1.693(11), P2–C1 1.720(11), P1–N1 1.662(8), P2–C2 1.799(10), C2–N1 1.318(12); P1–C1–P2 106.2(5), C1–P1–N1 106.2(5), C1–P1–C4 126.2(5), C4–P1–N1 121.7(4), C1–P2–C2 99.2(5), C1–P2–C22 129.6(5), C22–P2–C2 119.5(5), P1–N1–C2 112.6(7), P2–C2–N1 114.7(8).

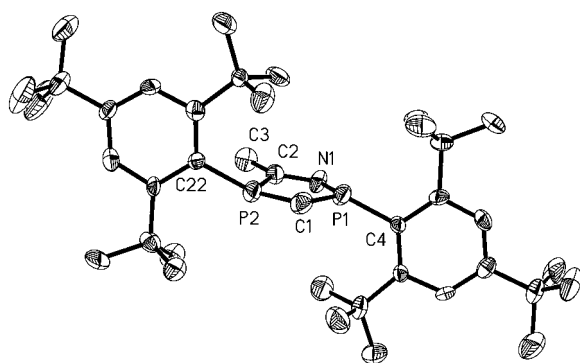


Figure 2. Molecular view of **4** in the solid state. Selected bond lengths [Å] and angles [°]: P1–C1 1.673(6), P2–C1 1.710(6), P1–N1 1.708(5), P2–C2 1.796(6), C2–N1 1.306(6); P1–C1–P2 98.2(3), C1–P1–N1 113.9(3), C1–P1–C4 124.9(3), C4–P1–N1 114.1(3), C1–P2–C2 105.7(3), C1–P2–C22 128.7(3), C22–P2–C2 113.4(3), P1–N1–C2 107.3(4), P2–C2–N1 113.7(4).

groups, even at -100°C , thereby suggesting that the two enantiomers are in rapid equilibrium, in agreement with the expected low inversion barriers at the phosphorus centers. The strong donation of the phosphorus lone-pairs to the electron-deficient carbene center is clearly apparent from the P–C1 bond lengths (1.693(11) and 1.720(11) Å (**3b**); 1.673(6)

and 1.710(6) Å (**4**)), which are significantly shorter than normal P–C single bonds (>1.80 Å). Since the N1–C2 and the P1–N1 and P2–C2 bonds are only marginally longer and shorter than typical double and single bonds, respectively, the interaction between the N1–C2 unit and the P1–C1–P2 fragment is weak for both **3b** and **4**. The same conclusions have been drawn for the Enders-type carbene **B**.^[24] Interestingly, the same differences that are observed between NHCs and their NHC(H⁺) precursors can be found between **3b** and **4**. The P1–C1–P2 bond angle for **4** (98.2°) is more acute than in its cationic precursor (106.2°), and is in fact very similar to the carbene bond angle recently reported for a four-membered NHC (96.7°).^[32] The ^{13}C NMR signal for the carbene carbon ($\delta = 184$ ppm) of **4** is strongly deshielded compared to that of **3** ($\delta = 119$ ppm), and is observed at a slightly higher field than those of NHCs ($\delta = 205$ – 244 ppm).

Ab initio calculations^[33] were performed on carbene **4** and on its derivatives **4a** and **4b**, which feature hydrogen and phenyl substituents, respectively, instead of 2,4,6-tri-*tert*-butylphenyl substituents. As expected, the sum of the angles around P increases significantly as the steric demand of the substituent increases (**4a**: 328° and 342° ; **4b**: 341° and 341° ; **4**: 351° and 352°). As a consequence of the enforced planarization of the phosphorus centers, the singlet–triplet energy gap increases strongly (**4a**: 22.6; **4b**: 26.7; **4**: 41.4 kcal mol^{−1}) as does the energy of the HOMOs (Kohn–Sham (KS) orbital energies) (**4a**: -5.9 ; **4b**: -5.3 ; **4**: -5.0 eV). Interestingly, the HOMO of the experimentally observed carbene **4** is even higher in energy than that calculated at the same level of theory for Enders' NHC **B** (-5.1 eV); this can be regarded as a first indication of the strongly basic character of **4**.

In initial attempts to evaluate the ligand properties of **4**, we prepared the [RhCl(cod)(**4**)] complex **5** and compared its geometric parameters with those of corresponding NHC complexes.^[34–38] Complex **5** was isolated as highly thermally stable single crystals (78% yield; m.p.: 187 – 189°C). Notably, no significant decomposition was observed when a dichloromethane solution of **5** was stirred for several hours in air. As observed for NHCs, the complexation induces a very small lengthening of the P–C bonds, which, however, stay shorter than those in the corresponding cation **3b** (Figure 3).^[31] Importantly, the phosphorus centers are not pyramidalized, the sum of the angles around phosphorus (350° and 351°) being essentially identical to those observed for the free PHC

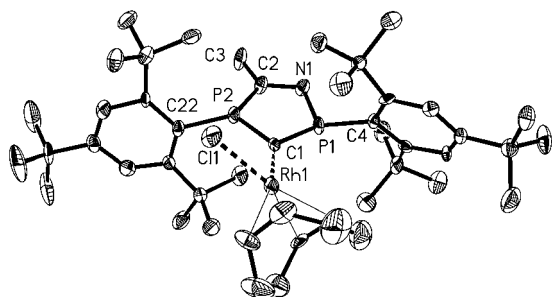


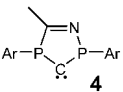
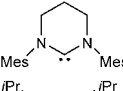
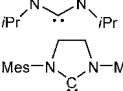
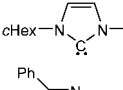
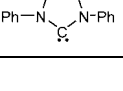
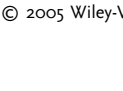
Figure 3. Molecular view of **5** in the solid state. Selected bond lengths [Å] and angles [°]: C1–Rh 2.064(8), P1–C1 1.730(7), P2–C1 1.701(8), P1–N1 1.657(6), P2–C2 1.782(8), C2–N1 1.325(10); P1–C1–P2 100.7(4), C1–P1–N1 109.2(4), C1–P1–C4 124.5(4), C4–P1–N1 116.2(3), C1–P2–C2 104.6(4), C1–P2–C22 131.7(4), C22–P2–C2 114.4(4), P1–N1–C2 111.5(5), P2–C2–N1 112.6(6).

4. These data suggest a very weak π -donation from the metal to the carbene ligand. This is confirmed by the $C_{\text{carbene}}\text{--Rh}$ bond length (2.064(8) Å), which is at the upper limit of those observed for [RhCl(cod)(NHC)] complexes (2.00–2.06 Å), and distinctly longer than that found for the analogous complex with Enders' NHC **B** as ligand (2.004 Å).^[36]

The carbonyl stretching frequencies of *cis*-[RhCl(CO)₂(L)] complexes are recognized as an excellent measure of the σ -donor and π -acceptor properties of the carbene ligand L.^[38,39] Complex **6** was easily prepared by addition of half an equivalent of [[RhCl(CO)₂]₂] to the free PHC **4**. The values of the carbonyl stretching frequencies for complex **6** are lower than those observed for the analogous complex with Enders' NHC **B** as ligand (Table 1). In fact, the observed values for **6** are as low as those reported for complexes featuring the most basic NHC and even acyclic diaminocarbene ligands.^[40,41]

PHC **4** is an analogue of one of the less-basic NHCs, although its basicity already appears to be comparable to those of saturated five- and six-membered NHCs. Therefore, it is quite likely^[42] that saturated PHCs will push upward the electronic parameter scale characterizing NHC-type ligands.

Table 1: IR carbonyl stretching frequencies $\tilde{\nu}$ [cm^{−1}] for *cis*-[RhCl(CO)₂(L)] complexes.

L	$\nu(\text{CO})$ I	$\nu(\text{CO})$ II	Ref.
	2059	1985	this work
	2062	1976	[39]
	2057	1984	[40]
	2081	1996	[42]
	2076	2006	[42]
	2089	2009	this work

Any catalytic application requiring electron-rich ligands might benefit from the use of PHC ligands.

Experimental Section

All manipulations were performed under an inert atmosphere of argon using standard Schlenk techniques. Dry, oxygen-free solvents were employed. ¹H, ¹³C, and ³¹P NMR spectra were recorded on Bruker AC80, AC200, Avance 300, or AMX400 spectrometers. ¹H and ¹³C chemical shifts are reported in ppm relative to SiMe₄ as external standard. ³¹P NMR downfield chemical shifts are expressed with a positive sign, in ppm, relative to external 85% H₃PO₄.

3a: A solid mixture of 3-chloro-1,3-bis(2,4,6-*tert*-butylphenyl)-1,3-diphosphaprop-1-ene (**1**; 1.06 g, 1.7 mmol) and silver triflate (0.453 g, 1.7 mmol) was cooled to −78 °C. Acetonitrile (4 mL, 76 mmol) and dichloromethane (10 mL) were then added with vigorous stirring and the reaction mixture was warmed to room temperature. After 30 min the mixture was filtered and the solvent removed under vacuum. The crude product was crystallized from a CH₂Cl₂/Et₂O mixture at −30 °C to give the title compound as white needles (yield: 80 %); m.p.: 157–159 °C; ¹H NMR (300 MHz, CDCl₃, 298 K): δ = 1.39 (s, 18H; CCH₃), 1.45 (s, 36H; CCH₃), 2.63 (dd, J_{PH} = 20 and 2 Hz, 3H; NCCH₃), 7.73 (d, J_{PH} = 4 Hz, 2H; CH_{arom}), 7.75 (d, J_{PH} = 3 Hz, 2H; CH_{arom}), 8.60 ppm (dd, J_{PH} = 16 and 7 Hz, 1H; PCHP); ¹³C{¹H} NMR (75 MHz, CDCl₃, 298 K): δ = 22.2 (dd, J_{PC} = 25 and 30 Hz, NCCH₃), 30.8 (s, CH_{3para}), 30.9 (s, CH_{3para}), 33.0 (s, CH_{3ortho}), 33.4 (s, CH_{3ortho}), 38.5 (d, J_{PC} = 3 Hz, C_qCH₃), 38.6 (d, J_{PC} = 8 Hz, C_qCH₃), 119.3 (dd, J_{PC} = 51 and 44 Hz, PCHP), 124.4 (d, J_{PC} = 16 Hz, C_{aromH}), 124.8 (d, J_{PC} = 14 Hz, C_{aromH}), 159.8 (d, J_{PC} = 3 Hz, C_{arom}), 160.3 (d, J_{PC} = 4 Hz, C_{arom}), 160.6 (dd, J_{PC} = 3 and 13 Hz, C_{arom}), 160.6 (d, J_{PC} = 10 Hz, C_{arom}), 172.2 ppm (dd, J_{PC} = 7 and 29 Hz, NCCH₃); ³¹P{¹H} NMR (81 MHz, CDCl₃, 298 K): δ = 104 and 85 ppm (J_{PP} = 266 Hz).

3b: Compound **1** (0.8 g; 1.3 mmol) was dissolved in a mixture of dichloromethane (10 mL) and acetonitrile (2 mL, 38 mmol). One equivalent of GaCl₃ (0.235 g) in 2 mL of dichloromethane was added, with vigorous stirring, at −78 °C. The reaction mixture was then warmed up to room temperature. The solvents were removed under vacuum and the crude product was crystallized from a CH₂Cl₂/Et₂O mixture at −30 °C. White needles (yield: 67 %); m.p.: 173–175 °C.

4: A solution of **3a** (1 g, 1.4 mmol) in THF (5 mL) was cooled to −78 °C. A solution of lithium hexamethyldisilazide (0.335 g, 1.4 mmol) in THF (3 mL) was added dropwise. After warming up to room temperature, the reaction was complete. The solvent was removed under vacuum, and the solid was extracted with pentane. The resultant solution was concentrated and cooled to −30 °C to afford a yellow powder, which was dried under vacuum. Single crystals suitable for X-ray analysis were obtained from a concentrated solution in THF/toluene cooled to −30 °C. Yellow crystals (yield: 72 %); m.p.: 123–127 °C; ¹H NMR (400 MHz, [D₈]THF; 263 K): δ = 1.35 (s, 18H; CCH₃), 1.40 (s, 18H; CCH₃), 1.41 (s, 18H; CCH₃), 2.26 (dd, J_{PH} = 13 and 3 Hz, 3H; NCCH₃), 7.61 (d, J_{PH} = 4 Hz, 2H; CH_{arom}), 7.63 ppm (d, J_{PH} = 4 Hz, 2H; CH_{arom}); ¹³C{¹H} NMR (100 MHz, [D₈]THF, 263 K): δ = 19.8 (dd, J_{PC} = 30 and 34 Hz, N=CCH₃), 30.6 (s, CH₃), 32.0 (s, CH₃), 32.5 (s, CH₃), 35.3 (s, CCH₃), 38.3 (s, CCH₃), 121.1 (d, J_{PC} = 34 Hz, C_{arom}), 121.3 (d, J_{PC} = 34 Hz, C_{arom}), 122.3 (d, J_{PC} = 12 Hz, HC_{arom}), 122.5 (d, J_{PC} = 11 Hz, HC_{arom}), 153.8 (d, J_{PC} = 4 Hz, C_{arom}), 153.9 (d, J_{PC} = 3 Hz, C_{arom}), 157.8 (m, C_{arom}), 179.1 (dd, J_{PC} = 16 and 31 Hz, C=N), 184.4 ppm (pseudo t, J_{PC} = 147 Hz, PCP); ³¹P{¹H} NMR (162 MHz, [D₈]THF, 263 K): δ = 85 and 73 ppm (J_{PP} = 135 Hz).

5 and 6: A solution of **4** in THF was added to a solution of 0.5 equivalents of the corresponding chlororhodium(II) dimer ([{Rh(cod)Cl}₂] for **5**, [{Rh(CO)₂Cl}₂] for **6**) in THF at −78 °C. After the mixture had been warmed up to room temperature, the solvent was removed under vacuum and the product extracted with pentane.

Single crystals suitable for X-ray analysis were obtained from a pentane/toluene solution cooled to -30°C .

5: Deep red crystals (yield: 78%); m.p.: $187\text{--}189^{\circ}\text{C}$; ^1H NMR (300 MHz, C_6D_6 , 298 K): $\delta = 1.21$ (s, 18H; CH_3), 1.31 (s, 18H; CH_3), 1.66 (s, 18H; CH_3), 1.74 (s, 18H; CH_3), 1.0–2.0 (m, 6H; $\text{H}_2\text{C}_{\text{allyl}}$), 2.31 (dd, $J_{\text{PH}} = 13$ and 8 Hz, 3H; $\text{N}=\text{CCH}_3$), 3.17 (br, 2H; $\text{H}_2\text{C}_{\text{allyl}}$), 4.29 (br, 2H; HC_{vinyl}), 5.14 (br, 2H; HC_{vinyl}), 7.74 ppm (m, 4H; HC_{arom}); ^{13}C NMR (75 MHz, C_6D_6 , 298 K): $\delta = 21.4$ (dd, $J_{\text{PC}} = 25$ and 27 Hz, $\text{N}=\text{CCH}_3$), 29.1 (s, $\text{H}_2\text{C}_{\text{allyl}}$), 30.7 (s, $\text{H}_2\text{C}_{\text{allyl}}$), 30.8 (s, CH_3), 31.0 (s, CH_3), 33.2 (s, $\text{H}_2\text{C}_{\text{allyl}}$), 33.9 (s, CH_3), 34.4 (s, CH_3), 35.0 (s, CCH_3), 35.3 (s, CCH_3), 39.3 (d, $J_{\text{PC}} = 4$ Hz, CCH_3), 40.2 (d, $J_{\text{PC}} = 2$ Hz, CCH_3), 69.3 (d, $J_{\text{C,Rh}} = 14$ Hz, CH_{vinyl}), 78.2 (d, $J_{\text{C,Rh}} = 14$ Hz, CH_{vinyl}), 93.8 (d, $J_{\text{C,Rh}} = 8$ Hz, CH_{vinyl}), 117.0 (dd, $J_{\text{PC}} = 16$ and 28 Hz, C_{arom}), 119.0 (dd, $J_{\text{PC}} = 14$ and 33 Hz, C_{arom}), 123.5 (dd, $J_{\text{PC}} = 3$ and 9 Hz, HC_{arom}), 125.2 (dd, $J_{\text{PC}} = 6$ and 9 Hz, HC_{arom}), 153.9 (d, $J_{\text{PC}} = 3$ Hz, C_{arom}), 155.1 (d, $J_{\text{PC}} = 3$ Hz, C_{arom}), 157.7 (dd, $J_{\text{PC}} = 5$ and 8 Hz, C_{arom}), 159.2 (dd, $J_{\text{PC}} = 5$ and 8 Hz, C_{arom}), 170.9 (ddd, $J_{\text{PC}} = 61$ and 72 Hz, $J_{\text{C,Rh}} = 41$ Hz, CRh), 176.8 ppm (pseudo t, $J_{\text{PC}} = 14$ Hz, $\text{N}=\text{C}$); ^{31}P NMR (81 MHz, C_6D_6 , 298 K): $\delta = 89$ and 88 ppm (AB system, $^2J_{\text{PP}} = 173$ Hz).

6: Yellow crystals (yield: 69%); m.p.: $175\text{--}178^{\circ}\text{C}$; IR (KBr): $\tilde{\nu} = 1985$ and 2059 cm^{-1} (CO); ^1H NMR (300 MHz, C_6D_6 , 298 K): $\delta = 1.23$ (s, 9H; CCH_3), 1.26 (s, 9H; CCH_3), 1.60 (s, 18H; CCH_3), 1.62 (s, 18H; CCH_3), 2.33 (dd, $J_{\text{PH}} = 17$ and 4 Hz, 3H; NCCCH_3), 7.71 (d, $J_{\text{PH}} = 5$ Hz, 2H; CH_{arom}), 7.74 ppm (d, $J_{\text{PH}} = 6$ Hz, 2H; CH_{arom}); ^{13}C NMR (75 MHz, C_6D_6 , 298 K): $\delta = 22.2$ (dd, $J_{\text{PC}} = 25$ and 330 Hz, $\text{N}=\text{CCH}_3$), 31.5 (s, CH_3), 31.8 (s, CH_3), 34.6 (s, CH_3), 34.8 (s, CH_3), 36.2 (s, CCH_3), 36.0 (s, CCH_3), 40.0 (d, $J_{\text{PC}} = 4$ Hz, CCH_3), 40.6 (d, $J_{\text{PC}} = 4$ Hz, CCH_3), 116.3 (dd, $J_{\text{PC}} = 11$ and 39 Hz, C_{arom}), 118.6 (dd, $J_{\text{PC}} = 4$ and 58 Hz, C_{arom}), 124.6 (d, $J_{\text{PC}} = 14$ Hz, HC_{arom}), 125.7 (dd, $J_{\text{PC}} = 1$ and 14 Hz, HC_{arom}), 156.2 (d, $J_{\text{PC}} = 4$ Hz, C_{arom}), 157.1 (d, $J_{\text{PC}} = 3$ Hz, C_{arom}), 159.0 (dd, $J_{\text{PC}} = 5$ and 9 Hz, C_{arom}), 159.9 (dd, $J_{\text{PC}} = 3$ and 9 Hz, C_{arom}), 175.9 (ddd, $J_{\text{PC}} = 2$ and 8 Hz, $J_{\text{C,Rh}} = 24$ Hz, CRh), 183.9 (ddd, $J_{\text{C,Rh}} = 75$ Hz, $J_{\text{PC}} = 3$ and 6 Hz, RhCO), 185.9 ppm (dt, $J_{\text{C,Rh}} = 86$ Hz, $J_{\text{PC}} = 3$ Hz, RhCO); ^{31}P NMR (81 MHz, C_6D_6 , 298 K): $\delta = 101$ and 93 ppm ($^2J_{\text{PP}} = 187$ Hz).

Received: October 8, 2004

Published online: February 11, 2005

Keywords: carbene ligands · carbenes · heterocycles · phosphorus · rhodium

- [1] W. A. Herrmann, *Angew. Chem.* **2002**, *114*, 1342; *Angew. Chem. Int. Ed.* **2002**, *41*, 1290.
- [2] L. Jafarpour, S. P. Nolan, *Adv. Organomet. Chem.* **2001**, *46*, 181.
- [3] T. M. Trnka, R. H. Grubbs, *Acc. Chem. Res.* **2001**, *34*, 18.
- [4] D. Enders, T. Balensiefer, *Acc. Chem. Res.* **2004**, *37*, 534.
- [5] G. A. Grasa, R. Singh, S. P. Nolan, *Synthesis* **2004**, 971.
- [6] E. Peris, R. H. Crabtree, *C. R. Chim.* **2003**, *6*, 33.
- [7] K. Öfele, *J. Organomet. Chem.* **1968**, *12*, 42.
- [8] H. W. Wanzlick, H. J. Schönherr, *Angew. Chem.* **1968**, *80*, 154; *Angew. Chem. Int. Ed. Engl.* **1968**, *7*, 141.
- [9] D. J. Cardin, B. Centinkaya, M. F. Lappert, *Chem. Rev.* **1972**, *72*, 545.
- [10] D. Bourissou, O. Guerret, F. P. Gabbaï, G. Bertrand, *Chem. Rev.* **2000**, *100*, 39.
- [11] A. J. Arduengo III, *Acc. Chem. Res.* **1999**, *32*, 913.
- [12] *Reactive Intermediate Chemistry* (Eds.: M. Jones, R. A. Moss), Wiley-Interscience, Hoboken, **2004**.
- [13] J. Kapp, C. Schade, A. M. El-Nahasa, P. von R. Schleyer, *Angew. Chem.* **1996**, *108*, 2373; *Angew. Chem. Int. Ed. Engl.* **1996**, *35*, 2236.
- [14] A titanocene and a zirconocene complex of a PHC have been characterized spectroscopically.^[15] A trimethylalane adduct of a cyclic anion with a diphosphanylcarbene unit has also been isolated.^[16] Metalladiphosphanyl carbenes^[17] are known as transient species, whereas several bis(iminophosphoranyl)carbene $[(\text{R}_2\text{P}=\text{NSiMe}_3)_2\text{C}]$ complexes have been isolated.^[18]
- [15] T. Cantat, N. Mezailles, N. Maigrot, L. Ricard, P. Le Floch, *Chem. Commun.* **2004**, 1274.
- [16] E. Niecke, A. Fuchs, M. Nieger, O. Schmidt, W. W. Schoeller, *Angew. Chem.* **1999**, *111*, 3216; *Angew. Chem. Int. Ed.* **1999**, *38*, 3031.
- [17] J. Ruiz, M. E. G. Mosquera, G. García, E. Patrón, V. Riera, S. García-Granda, F. van der Maelen, *Angew. Chem.* **2003**, *115*, 4915; *Angew. Chem. Int. Ed.* **2003**, *42*, 4767.
- [18] N. D. Jones, G. Lin, R. A. Gossage, R. McDonald, R. G. Cavell, *Organometallics* **2003**, *22*, 2832.
- [19] D. A. Dixon, A. J. Arduengo III, *J. Phys. Chem.* **1991**, *95*, 4180.
- [20] C. Boehme, G. Frenking, *J. Am. Chem. Soc.* **1996**, *118*, 2039.
- [21] A. Fekete, L. Nyulászi, *J. Organomet. Chem.* **2002**, *643–644*, 278.
- [22] W. W. Schoeller, D. Eisner, *Inorg. Chem.* **2004**, *43*, 2585.
- [23] L. Nyulászi, *Tetrahedron* **2000**, *56*, 79.
- [24] D. Enders, K. Breuer, G. Raabe, J. Runsink, J. H. Teles, J.-P. Melder, K. Ebel, S. Brode, *Angew. Chem.* **1995**, *107*, 1119; *Angew. Chem. Int. Ed. Engl.* **1995**, *34*, 1021.
- [25] Acyclic diphosphaallyl cations $>\text{P-C(R)}-\text{P}<$ are unstable towards rearrangement,^[26] and only one C-substituted derivative ($\text{R} = \text{SiMe}_3$) is known with four-^[27] and five-membered-ring systems.^[28]
- [26] T. Kato, H. Gornitzka, A. Baceiredo, W. W. Schoeller, G. Bertrand, *J. Am. Chem. Soc.* **2002**, *124*, 2506.
- [27] M. Sebastian, O. Schmidt, A. Fuchs, M. Nieger, D. Szieberth, L. Nyulaszi, E. Niecke, *Phosphorus, Sulfur Silicon Relat. Elem.* **2004**, *179*, 779.
- [28] A. Fuchs, M. Nieger, E. Niecke, L. Nyulaszi, O. Schmidt, W. Schoeller, M. Sebastian, *Phosphorus, Sulfur Silicon Relat. Elem.* **2002**, *177*, 1605.
- [29] H. H. Karsch, H.-U. Reisacher, G. Müller, *Angew. Chem.* **1986**, *98*, 467; *Angew. Chem. Int. Ed. Engl.* **1986**, *25*, 454.
- [30] H. H. Karsch, H. Reisacher, T. Ruprich in *Synthetic Methods of Organometallic and Inorganic Chemistry*, Vol. 3 (Ed.: W. A. Hermann), Thieme, Stuttgart, **1996**, pp. 140.
- [31] CCDC-252550 (**3b**), -252551 (**4**) and -252552 (**5**) contain the supplementary crystallographic data for this paper. These data can be obtained free of charge from the Cambridge Crystallographic Data Centre via www.ccdc.cam.ac.uk/data_request/cif.
- [32] E. Despagne-Ayoub, R. H. Grubbs, *J. Am. Chem. Soc.* **2004**, *126*, 10198.
- [33] RI-DFT with the BP86 density functional and the SVP basis set. Turbomole program systems. R. Ahlrichs et al.: www.turbomole.com.
- [34] A. W. Coleman, P. B. Hitchcock, M. F. Lappert, R. K. Maskell, J. H. Müller, *J. Organomet. Chem.* **1985**, *296*, 173.
- [35] W. A. Herrmann, M. Elison, J. Fischer, C. Kocher, G. R. J. Artus, *Chem. Eur. J.* **1996**, *2*, 772.
- [36] D. Enders, H. Gielen, J. Runsink, K. Breuer, S. Brode, K. Boehn, *Eur. J. Inorg. Chem.* **1998**, 913.
- [37] P. Bazinet, G. P. A. Yap, D. S. Richeson, *J. Am. Chem. Soc.* **2003**, *125*, 13314.
- [38] M. Mayr, K. Wurst, K.-H. Ongania, M. Buchmeiser, *Chem. Eur. J.* **2004**, *10*, 1256.
- [39] W. A. Herrmann, K. Öfele, D. von Preysing, E. Herdweck, *J. Organomet. Chem.* **2003**, *684*, 235.
- [40] R. W. Alder, P. R. Allen, M. Murray, A. G. Orpen, *Angew. Chem.* **1996**, *108*, 1211; *Angew. Chem. Int. Ed. Engl.* **1996**, *35*, 1121.
- [41] K. Denk, P. Sirsch, W. A. Herrmann, *J. Organomet. Chem.* **2002**, *649*, 219.
- [42] A. M. Magill, K. J. Cavell, B. F. Yates, *J. Am. Chem. Soc.* **2004**, *126*, 8717.

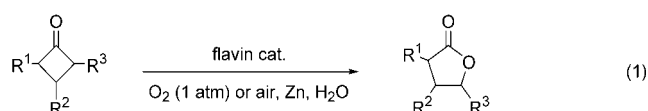
An Aerobic, Organocatalytic, and Chemoselective Method for Baeyer–Villiger Oxidation**

Yasushi Imada,* Hiroki Iida, Shun-Ichi Murahashi,* and Takeshi Naota*

Direct incorporation of molecular oxygen into organic substrates has recently attained widespread interest as a forward-looking technology for mild and green molecular transformations.^[1] One subject of great urgency is the development of organocatalytic methods.^[2] These methods should facilitate new strategies that provide an alternative to the conventional unsustainable processes, which use oxygenated transition-metal complexes.^[3] A limited number of organocatalytic aerobic oxidations has been reported. These reactions involve a multistep radical-transfer process from O₂ by using semi-stable organic radicals^[4] and photoinduced electron-transfer systems.^[5]

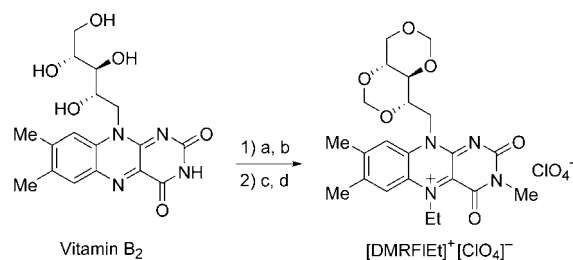
A new method for organocatalytic aerobic oxidation of heteroatomic organic compounds^[6] was recently developed by simulating the enzymatic function of microsomal FAD-containing monooxygenase.^[7] As this new system includes the direct conversion of molecular oxygen into synthetic flavin hydroperoxides, which are highly reactive towards various organic substrates,^[8,9] the principle of the reaction should enable sustainable aerobic oxidation chemistry with high selectivity and controllability. As a variation on this system, we describe herein the first organocatalytic aerobic method of the Baeyer–Villiger oxidation, which exhibits rare and high chemoselectivity for this nucleophilic oxidation [Eq. (1)].

The Baeyer–Villiger oxidation is a special class of nucleophilic oxidative transformation that proceeds specifically with peroxides and peracids through noncatalytic^[10] and



catalytic reactions.^[9a,b,11,12] The aerobic method for Baeyer–Villiger oxidations is limited to reactions that involve the in situ generation of peracids from aldehydes by a transition-metal-mediated radical-chain process with molecular oxygen.^[12] Thus, there has been no exploitation of organocatalytic methods and no molecular design of the catalysts. Furthermore, one of the unsolved problems of catalytic Baeyer–Villiger oxidations is the lack of chemoselectivity for nucleophilic oxidations over electrophilic oxidations. There is no report of a chemoselective catalytic method in the presence of heteroatomic moieties. This omission is due to the strong electrophilic character of their peroxo intermediates. Although catalytic methods that resist epoxidation have been reported,^[13] the strength of the oxidant usually results in electrophilic oxidation of heteroatomic compounds.^[14] The application of our new strategy has meant that we can overcome these long-unsolved problems to produce a selective, sustainable, and highly practical method.

The catalytic activity of a series of flavin compounds was examined for the aerobic oxidation of 3-(2-naphthyl)cyclobutanone (**1**) with zinc dust (1.5 equiv) in CH₃CN/EtOAc/H₂O (8:1:1, v/v) under oxygen (1 atm). Unlike electrophilic oxidations that need specific flavins,^[6] the present nucleophilic oxidation exhibits high catalytic activities for a variety of 5-ethylisoalloxazinium perchlorates that bear 3,10-dimethyl, 3,7,8,10-tetramethyl, or 3-methyl-10-phenyl functionalities. A new type of flavin catalyst—5-ethyl-3-methyl-2',4':3',5'-di-*O*-methyleneriboflavinium perchlorate ([DMRFIEt]⁺[ClO₄][−]), which can be readily derived from commercially available vitamin B₂ (Scheme 1)—also shows



Scheme 1. Synthesis of [DMRFIEt]⁺[ClO₄][−]: a) HCHO, HCl, 60 °C, 3 days; b) CH₃I, K₂CO₃, DMF, RT, overnight; c) CH₃CHO, NaBH₃CN, Na₂S₂O₄, DMF, 60 °C, 2 h; d) NaNO₂, HClO₄, NaClO₄, 0 °C.

high catalytic activity, comparable with that of 3,7,8,10-tetramethyl flavins. The preparation is quite easy compared with the multistep methods that are required for conventional flavin catalysts.^[15] Zinc dust acts as an efficient reductant for the activation of the flavin catalysts. Water is an essential proton source for this system, and the use of water-containing solvent mixtures, such as CH₃CN/EtOAc/H₂O, results in the production of the corresponding lactones.

Representative results for the aerobic Baeyer–Villiger oxidation catalyzed with [DMRFIEt]⁺[ClO₄][−] are summar-

[*] Prof. Dr. Y. Imada, H. Iida, Prof. Dr. S.-I. Murahashi,^[†] Prof. Dr. T. Naota
Department of Chemistry
Graduate School of Engineering Science
Osaka University
Machikaneyama, Toyonaka, Osaka 560-8531 (Japan)
Fax: (+81) 6-6850-6222
E-mail: imada@chem.es.osaka-u.ac.jp
murahashi@high.ous.ac.jp
naota@chem.es.osaka-u.ac.jp

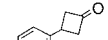
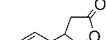
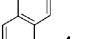
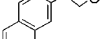
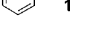
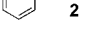

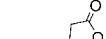
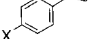
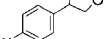


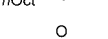
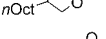



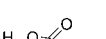
Prof. Dr. T. Naota
PRESTO, Japan Science and Technology Agency (JST)
Machikaneyama, Toyonaka, Osaka 560-8531 (Japan)
Fax: (+81) 6-6850-6224

[†] Present address:
Department of Applied Chemistry
Okayama University of Science
1-1, Ridaicho, Okayama 700-0005 (Japan)

[**] This work was supported by a Grant-in-Aid for Scientific Research, the Ministry of Education, Science, Sports, and Culture of Japan, and JSPS Research Fellowship for Young Scientists.

Supporting information for this article is available on the WWW under <http://www.angewandte.org> or from the author.

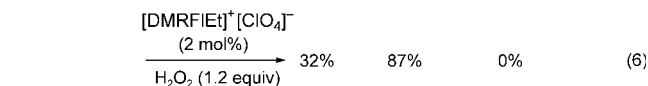
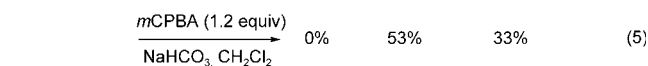
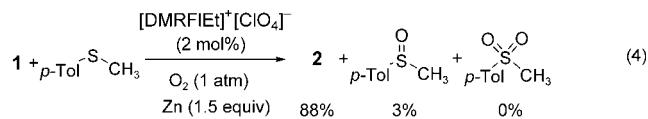
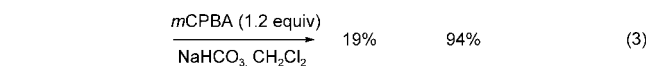
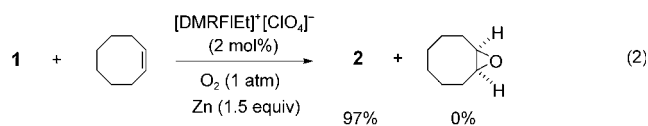
Table 1: Aerobic Baeyer–Villiger oxidation of ketones with [DMRFIEt]⁺[ClO₄][−].

Entry	Substrate	Product	t [h]	Yield [%]
1			7	94
2			7	91 ^[a]
3			12	88 ^[b]
4 (X=H)			4	78
5 (X=F)			4	80
6 (X=Cl)			6	84
7			4	95 ^[c]
8			8	86 (72:28) ^[d]
9			4	83 ^[e] (57:43) ^[e]

[a] 5-Ethyl-3,7,8,10-tetramethylisalloxazin-2-one perchlorate (2 mol %) was used instead of [DMRFIEt]⁺[ClO₄][−]. [b] The reaction was performed in air. [c] Zinc dust (2.0 equiv) was used. [d] [DMRFIEt]⁺[ClO₄][−] (4 mol %) was used. [e] Regioselectivities of the expected and unexpected lactones were determined by ¹H NMR spectroscopy.

ized in Table 1. Various substituted cyclobutanones can be converted into the corresponding lactones efficiently when a 1.0 M solution of the substrate is stirred in a mixture of CH₃CN/EtOAc/H₂O (8:1:1 v/v) at 60 °C in the presence of the catalyst (2 mol %), zinc dust (1.5 equiv), and oxygen (1 atm). The products can be isolated simply by filtration and extraction because the reactions are generally clean and are accompanied only by the formation of insoluble Zn(OH)₂. The reaction can be also conveniently performed in air (Table 1, entry 3). Similar treatment of bicyclic ketones gave a mixture of expected and unexpected lactones (Table 1, entries 8 and 9), both of which are important synthetic intermediates for various biologically active compounds such as prostaglandins and pheromones.^[16b] Baeyer–Villiger monooxygenase, which is also an important class of flavoenzyme, also exhibits similar selectivity,^[16] whereas conventional synthetic methods generally give an expected lactone by the ordinary electronic limitations of the Criegee rearrangement.^[10,11]

One important feature of the new method is the chemoselective oxidation of ketones in the presence of other reactive functionalities. Indeed, the flavin-catalyzed reaction of an equimolar mixture of **1** and cyclooctene gave exclusively the Baeyer–Villiger product **2**, without the formation of cyclooctene oxide [Eq. (2); Scheme 2]. Similar treatment with methyl *p*-tolyl sulfide also afforded **2** with extraordinarily high selectivity [Eq. (4)]. The intramolecular version of such a preference is also exhibited in entries 8 and 9 of Table 1, in which highly reactive cyclopentanol and cyclopentene moieties are completely tolerated under the stated conditions, as they are with an enzymatic oxidation.^[16b] This selectivity is rare under artificial oxidative conditions,^[14] and this is the first



Scheme 2. Performance of [DMRFIEt]⁺[ClO₄][−] in Baeyer–Villiger reactions of **1**. *m*CPBA = *meta*-chloroperbenzoic acid.

chemoselective catalytic method for nucleophilic oxidation in preference to oxidation at the heteroatom. Even the use of *m*CPBA, a specific oxidant for the Baeyer–Villiger oxidation, shows unsatisfactory results, as exemplified in Equations (3) and (5) (Scheme 2). Furthermore, the flavin-catalyzed Baeyer–Villiger oxidation with H₂O₂^[9a,b] does not exhibit chemoselectivity for nucleophilic oxidations, as shown in the preferential formation of the sulfoxide [Eq. (6)].

The reaction can be rationalized by the formation and subsequent oxidative transformation of the reactive 4a-peroxyflavin intermediate, as already described for the aerobic oxidation of heteroatomic compounds.^[6] The flavin cation, FIEt⁺, undergoes a two-electron reduction with zinc to afford the reduced flavin, FIEt[−].^[17] The FIEt[−] intermediate and its semiquinone radical precursor, FIEt[•], have been confirmed by the UV/Vis analysis of the control experiments of [DMRFIEt]⁺[ClO₄][−] with zinc dust.^[18] Incorporation of molecular oxygen into FIEt[−] affords the flavin 4a-peroxy anion FIEtOO[−],^[19] which effects nucleophilic oxidation of ketones to afford the corresponding lactones. Dehydrogenation of the resulting FIEtOH regenerates FIEt⁺ to complete the catalytic cycle. Chemoselective Baeyer–Villiger oxidations in this process can be ascribed to the neutrality of the reaction media and the highly nucleophilic character of the anionic peroxy intermediate,^[20] which forms under the influence of the zinc counterion. Indeed, dramatic loss of the chemoselectivity has been observed when acidic CF₃CH₂OH was employed as one component of the solvent mixture. Research is currently underway to elucidate the mechanism and to apply the reaction to other systems.

Received: October 26, 2004

Published online: February 3, 2005

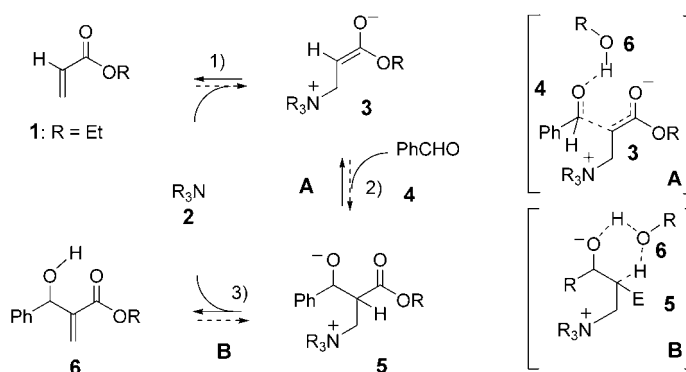
Keywords: chemoselectivity · green chemistry · lactones · organocatalysis · oxidation

- [1] a) *Advances in Catalytic Activation of Dioxygen by Metal Complexes* (Ed.: L. I. Simándi), Kluwer, Dordrecht, **2003**; b) *Biomimetic Oxidations Catalyzed by Transition Metal Complexes* (Ed.: B. Meunier), Imperial College Press, London, **2000**.
- [2] W. Adam, C. R. Saha-Möller, P. A. Ganeshpure, *Chem. Rev.* **2001**, *101*, 3499–3548.
- [3] a) *Metal-oxo and Metal-peroxo Species in Catalytic Oxidations* (Ed.: B. Meunier), Springer, Berlin, **2000**; b) *Organic Syntheses by Oxidation with Metal Compounds* (Eds.: W. J. Mijs, C. R. H. I. de Jonge), Plenum, New York, **1986**.
- [4] Y. Ishii, S. Sakaguchi in *Modern Oxidation Methods* (Ed.: J.-E. Bäckvall), Wiley-VCH, Weinheim, **2004**, pp. 119–163.
- [5] K. Ohkubo, K. Suga, K. Morikawa, S. Fukuzumi, *J. Am. Chem. Soc.* **2003**, *125*, 12850–12859.
- [6] Y. Imada, H. Iida, S. Ono, S.-I. Murahashi, *J. Am. Chem. Soc.* **2003**, *125*, 2868–2869.
- [7] *Chemistry and Biochemistry of Flavoenzymes* (Ed.: F. Müller), CRC, Boston, **1991**.
- [8] S.-I. Murahashi, T. Oda, Y. Masui, *J. Am. Chem. Soc.* **1989**, *111*, 5002–5003, and references therein.
- [9] a) S.-I. Murahashi, S. Ono, Y. Imada, *Angew. Chem.* **2002**, *114*, 2472–2474; *Angew. Chem. Int. Ed.* **2002**, *41*, 2366–2368; b) C. Mazzini, J. Lebreton, R. Furstoss, *J. Org. Chem.* **1996**, *61*, 8–9; c) K. Bergstad, J.-E. Bäckvall, *J. Org. Chem.* **1998**, *63*, 6650–6655.
- [10] a) G. R. Krow, *Org. React.* **1993**, *43*, 251–798; b) M. Renz, B. Meunier, *Eur. J. Org. Chem.* **1999**, 737–750.
- [11] For reviews, see: a) G. Strukul, *Angew. Chem.* **1998**, *110*, 1256–1267; *Angew. Chem. Int. Ed.* **1998**, *37*, 1198–1209; b) J. Le Paih, J.-C. Frison, C. Bolm in *Modern Oxidation Methods* (Ed.: J.-E. Bäckvall), Wiley-VCH, Weinheim, **2004**, pp. 253–294.
- [12] a) T. Mukaiyama, T. Yamada, *Bull. Chem. Soc. Jpn.* **1995**, *68*, 17–35; b) S.-I. Murahashi, Y. Oda, T. Naota, *Tetrahedron Lett.* **1992**, *33*, 7557–7560.
- [13] a) A. M. F. Phillips, C. Romao, *Eur. J. Org. Chem.* **1999**, 1767–1770; b) C. Bolm, O. Beckmann, *Chirality* **2000**, *12*, 523–525; c) C. Bolm, O. Beckmann, C. Palazzi, *Can. J. Chem.* **2001**, *79*, 1593–1597; d) M. Renz, T. Blasco, A. Corma, V. Fornés, R. Jensen, L. Nemeth, *Chem. Eur. J.* **2002**, *8*, 4708–4717.
- [14] M. Hudlický, *Oxidations in Organic Chemistry*, American Chemical Society, Washington, **1990**.
- [15] F. Yoneda, Y. Sakuma, M. Ichiba, K. Shinomura, *J. Am. Chem. Soc.* **1976**, *98*, 830–835, and references therein.
- [16] a) V. Alphand, R. Furstoss in *Enzyme Catalysis in Organic Synthesis* (Eds.: K. Drauz, H. Waldmann), VCH, New York, **1995**, pp. 745–772; b) M. D. Mihovilovic, B. Müller, P. Stanetty, *Eur. J. Org. Chem.* **2002**, 3711–3730; c) C. T. Walsh, Y.-C. J. Chen, *Angew. Chem.* **1988**, *100*, 342–352; *Angew. Chem. Int. Ed. Engl.* **1988**, *27*, 333–343.
- [17] E. J. Nanni, D. T. Sawyer, S. S. Ball, T. C. Bruice, *J. Am. Chem. Soc.* **1981**, *103*, 2797–2802.
- [18] Addition of zinc dust to a solution of [DMRFIEt]⁺[ClO₄][−] in CH₃CN/H₂O (9:1 v/v) results in an increase in the corresponding semiquinone radical (DMRFIEt•; λ_{max} = 598 and 631 nm) and the anion (DMRFIEt[−]; 328 nm) along with the consumption of the equilibrated mixture of [DMRFIEt]⁺[ClO₄][−] (558 nm) and DMRFIEtOH (311, 345 nm).
- [19] C. Kamel, T. W. Chan, T. C. Bruice, *J. Am. Chem. Soc.* **1977**, *99*, 7272–7286.
- [20] It was suggested that flavin 4a-peroxy anion is an active species during the enzymatic catalysis of Baeyer–Villiger monooxygenase: D. Sheng, D. P. Ballou, V. Massey, *Biochemistry* **2001**, *40*, 11156–11167.

Reevaluation of the Mechanism of the Baylis–Hillman Reaction: Implications for Asymmetric Catalysis**

Varinder K. Aggarwal,* Sarah Y. Fulford, and
Guy C. Lloyd-Jones*

The Baylis–Hillman reaction^[1] (BHR, see Scheme 1) involves the amine- (or phosphine-)^[2] catalyzed addition of an aldehyde to an activated alkene, such as an acrylate, **1**, to generate an allylic alcohol of type **6**.^[3] The commonly accepted mechanism^[4] for this process involves reversible conjugate addition of the nucleophilic amine catalyst to the activated alkene to generate an enolate (step 1), nucleophilic attack of the enolate on the aldehyde to generate a second zwitterionic intermediate (step 2), and then elimination (step 3) to generate the product and liberate the amine catalyst (Scheme 1). The reaction shows pseudobimolecular kinetics, and the rate-limiting step (RLS) of the reaction has been determined as step 2 on the basis that no primary kinetic isotope effect (KIE) was observed.^[4a] Protic solvents are known to accelerate the BHR, and it has been proposed^[5] that this acceleration occurs through activation of the aldehyde by hydrogen bonding to thereby promote step 2 (see intermediate **A**, Scheme 1). However, hydrogen bonding to the aldehyde would have to compete with the enolate, which is a much better hydrogen-bond acceptor. Indeed, this more thermodynamically favorable interaction will stabilize the enolate and render it less reactive and so should slow down



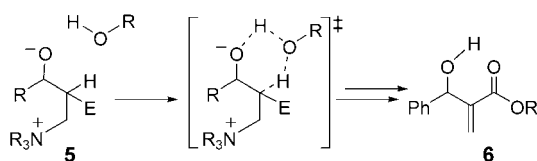
Scheme 1. Proposed mechanism of the Baylis–Hillman reaction with potential for autocatalysis through **A** or **B**.

[*] Prof. V. K. Aggarwal, S. Y. Fulford, Prof. G. C. Lloyd-Jones
School of Chemistry
Bristol University
Cantock's Close, Bristol BS8 1TS (UK)
Fax: (+44) 117-929-8611
E-mail: v.aggarwal@bristol.ac.uk
guy.lloyd-jones@bristol.ac.uk

[**] We thank Bristol University and the EPSRC for financial support
Supporting information for this article is available on the WWW
under <http://www.angewandte.org> or from the author.

the reaction, albeit with an accumulation of the hydrogen-bonded enolate. Interestingly, in the absence of proton donors the reaction shows autocatalysis, presumably because the product can act as a hydrogen-bond donor and promote the reaction.^[6] These issues made us consider an alternative hypotheses for the role of the protic solvent, including the possibility that it could accelerate formal proton transfer from the α -keto methine to the alkoxide in the zwitterion **5** to facilitate liberation of the product and regeneration of the catalyst through elimination (see intermediate **B**, Scheme 1). We now show that step 3 is the RLS in the initial phase of the reaction and that once the concentration of product has built up, step 2 becomes the RLS. The consequences of these findings with respect to asymmetric catalysis are also discussed.

First, we examined the profile of the reaction of ethyl acrylate with benzaldehyde catalyzed by quinuclidine in which the onset of significant autocatalysis was readily apparent between 0 and 20 % conversion.^[6] Study of the reaction mixture by ¹H NMR spectroscopy (600 MHz) showed that there were no species (< 1 %) other than the substrates, catalyst, and product throughout the entire reaction. Thus all equilibria prior to thermodynamically favorable liberation of **6** must lie predominantly on the side of the starting materials (see Scheme 2).^[4b]



Scheme 2. Proton-transfer mechanism.

The rate acceleration was confirmed to arise from autocatalysis owing to the protic nature of the product **6** by the absence of such an induction period in control reactions with catalytic quantities of 1) the product or 2) MeOH.^[7] The

kinetics of the reaction were readily simulated^[8] by the use of two simple models, one (see **A**, Scheme 1) that follows the conventional mechanism in which the product catalyzes the addition of the enolate **3** to the aldehyde **4**, and the second (see **B**, Scheme 1) in which the product catalyzes a rate-limiting breakdown of the zwitterionic intermediate **5**, for example, by proton transfer.

The two mechanistic scenarios (**A** and **B**) can, in principle, be distinguished on the basis that upon employing α -deuterated acrylate ($2\text{-}[^2\text{H}_1]\text{-1}; = d_1\text{-1}$), a primary KIE should be completely absent in **A** but evident in **B** prior to the autocatalyzed breakdown of zwitterion **5** becoming more efficient than its generation. As the latter condition might only be fulfilled very early in the reaction, the comparison of absolute rates over a number of half-lives, as performed by Isaacs and co-workers with deuterated (> 99 %) acrylonitrile,^[4a] is unlikely to be informative. In fact, a competition experiment between $d\text{-1}$ and **1** would clearly identify the RLS because we would expect a primary KIE to increase the mole fraction of $d\text{-1}$ in the acrylate (x_{d-1}) if step 3 is rate-limiting and a secondary KIE to decrease x_{d-1} if step 2 is rate-limiting.^[9] We thus analyzed the effect of C(2)-deuteration by ¹H NMR spectroscopic analysis of the BHR of approximately equimolar mixtures of $d\text{-1}$ and **1** ($x_{d-1} = 0.505 \pm 0.005$, Figure 1). As evident from Figure 1b, in the early stages of reaction (up to $\approx 20\%$ conversion), the mole fraction of $d\text{-1}$ increases substantially. As reaction proceeds further into the phase where autocatalysis is by far the dominant process, the ratio then stabilizes ($x_{d-1\text{max}} = 0.55$).^[9] This shows that in the early phase (< 20 % conversion), step 3 is rate-limiting (primary KIE evident). By using model **B** as a starting point, we were able to simulate the kinetics of the competition experiments,^[8,9] for example, see the comparison of the predicted (lines) and observed (circles) kinetics in Figure 1, graphs a and c. For satisfactory simulation, the model required incorporation of a substantial primary KIE ($k_{\text{H}}/k_{\text{D}} = 5 \pm 2$) for the noncatalyzed step 3. The fact that the simplification of $k_{\text{H}}/k_{\text{D}} = 1$ for autocatalysis of step 3 allows a satisfactory simulation suggests that the autocatalysis causes a change in the RLS from step 3 to step 2 early in the reaction.^[9]

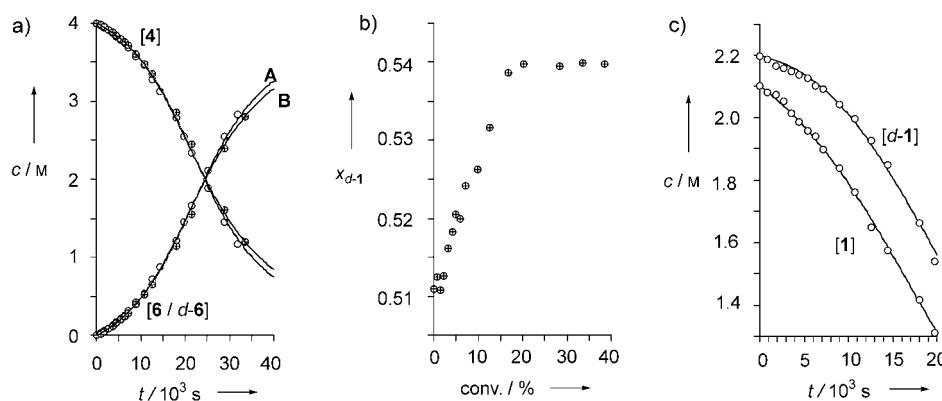
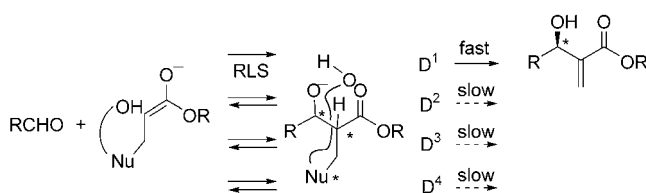


Figure 1. a) Evolution of the Baylis–Hillman reaction of PhCHO (**4**, 4.0 M) with $\text{C}(2)\text{-}^2\text{H}_{0.51}$ -ethyl acrylate ($1/d\text{-1}$, 4.3 M) catalyzed by quinuclidine (**2**, 1.0 M) at room temperature to give a mixture of $O\text{-}d\text{-6}$ and **6**. Lines through data points are kinetic simulations based on models **A** and **B** with refinement for contraction^[7] (see Supporting Information for full details). b) Relationship between conversion (based on PhCHO) and the mole fraction $d\text{-1}$ ($x_{d-1} = [d\text{-1}]/[1 + d\text{-1}]$). c) Simulated variation of the concentrations of **1** and $d\text{-1}$ (**1** and $[d\text{-1}]$) in the first 40 % of the reaction by employing model **B** with $k_{\text{H}}/k_{\text{D}} = 4.8$ for step 3 (non-autocatalyzed).

The efficient autocatalysis of step 3 by a simple hydroxyl moiety is easily accommodated by the model outlined in Scheme 2 which involves a six-membered proton transfer from ROH to the alkoxide with concomitant deprotonation of the α -methine to give an enolate, followed by elimination of the amine (E1cB).^[10] The intramolecular four-membered direct proton transfer is presumably disfavored owing to strain induced in attaining the appropriate eclipsed conformation of the C(O)–C(H) bond and the transfer angle between O–H–C which is far from optimal. Moreover, the approximately 90° transfer angle between O–H–C in the transition state is expected to limit the primary KIE to roughly 2.3, a much lower value than that observed in the non-autocatalytic phase of the reaction.^[11]

In summary, these studies have shown that in the absence of added protic species, the initial stage of the BHR involves rate-limiting proton transfer (step 3). As the product concentration builds, proton transfer becomes increasingly efficient and the RLS step is then step 2, as in the conventional model. This finding has considerable implications for asymmetric catalysis of the BHR. The successful catalysts to date (> 80 % ee) have hydrogen-bond donors appended at some point to the nucleophile.^[12] It is quite likely that all four diastereomers of the intermediate alkoxide are formed, but only one has the hydrogen-bond donor suitably positioned to allow fast proton transfer.^[13] The other diastereomers revert back to starting materials and eventually the reaction filters through the pathway that leads to fast elimination (Scheme 3). The low



Scheme 3. Likely origin of enantioselection in the Baylis–Hillman reaction. D^{1–4} are diastereomers of the alkoxide adduct.

success rate in the design of chiral catalysts for the BHR could be because the focus has been on controlling the stereochemistry of the C–C bond in the RLS (step 2) of the reaction. On the basis of the above study, we now believe that the positioning of suitable hydrogen-bond donors for selective proton transfer of one of the alkoxide diastereoisomers, and not the others, is likely to more successful. The alkoxide diastereomer that undergoes the fast, selective proton-transfer reaction may also be the diastereomer that is preferentially formed, but this is not a prerequisite. As a caveat, the use of an aprotic solvent may be crucial for attaining high enantioselectivity, and enantiomeric excesses could be decreased by competitive nonselective autocatalysis.^[14]

Received: October 29, 2004

Published online: February 3, 2005

Keywords: asymmetric catalysis · autocatalysis · kinetics · proton transfer · reaction mechanisms

- [1] A. B. Baylis, M. E. D. Hillman, *Offenlegungsschrift* 2155113, U.S. Patent 3,743,669, **1972**, [Chem. Abstr. **1972**, 77, 34174q].
- [2] K. Morita, Z. Suzuki, H. Hirose, *Bull. Chem. Soc. Jpn.* **1968**, *41*, 2815.
- [3] For reviews, see: a) D. Basavaiah, A. J. Rao, T. Satyanarayana, *Chem. Rev.* **2003**, *103*, 811–892; b) P. Langer, *Angew. Chem.* **2000**, *112*, 3177–3180; *Angew. Chem. Int. Ed.* **2000**, *39*, 3049–3052; c) E. Ciganek, *Org. React.* **1997**, *51*, 201–350; d) D. Basavaiah, P. D. Rao, R. S. Hyma, *Tetrahedron* **1996**, *52*, 8001–8062; e) S. E. Drewes, G. H. P. Roos, *Tetrahedron* **1988**, *44*, 4653–4670.
- [4] a) J. S. Hill, N. S. Isaacs, *J. Phys. Org. Chem.* **1990**, *3*, 285–288; b) L. S. Santos, C. H. Pavam, W. P. Almeida, F. Coelho, M. N. Eberlin, *Angew. Chem.* **2004**, *116*, 4430–4433; *Angew. Chem. Int. Ed.* **2004**, *43*, 4330–4333.
- [5] a) F. Ameer, S. E. Drewes, S. Freese, P. T. Kaye, *Synth. Commun.* **1988**, *18*, 495–500; b) I. E. Markü, P. R. Giles, N. T. Hindley, *Tetrahedron* **1997**, *53*, 1015–1024; c) Y. M. A. Yamada, S. Ikegami, *Tetrahedron Lett.* **2000**, *41*, 2165–2169.
- [6] V. K. Aggarwal, I. Emme, S. Y. Fulford, *J. Org. Chem.* **2003**, *68*, 692–700.
- [7] The reactions display a noticeable contraction in volume as they proceed. However, the nonlinear relationship between the conversion and the concentrations of all components is not the origin of the induction period. See Supporting Information for a full discussion.
- [8] The kinetics were simulated using MacKinetics (Leipold Associates, USA); see Supporting Information for full discussion.
- [9] The magnitude of the secondary KIE on any individual step in the reaction of **1/d-1** would be small—typically $1.15 \geq k_H/k_D \geq 0.87$ —but the net effect across equilibria may be larger and for steps 1 and 2 is expected to favor the reaction of **d-1** (i.e. $k_H/k_D < 1$) owing to a change in hybridization at C(2) from sp² in **1** to sp³ in the zwitterion **5**. However, control experiments (see Supporting Information) revealed a slow background exchange of H and D between **1/d-O-6** and **d-1/6** catalyzed by quinuclidine and presumably through the enolate **3/d-3**. This observation compromises any meaningful analysis of the decrease in x_{d-1} observed in the later phase of the reaction when significant **6/d-O-6** has accumulated.
- [10] The question remains as to what mediates step 3 in the absence of significant quantities of product. The possibility that a second molecule of quinuclidine acts as a base was eliminated by a study of the effect of doubling the catalyst loading which caused only an approximately 1.75-fold increase in rate in the crucial early stages of reaction—exactly as would be predicted on the basis of first-order dependency on each of the three reaction components when the dilution of aldehyde and alkene caused by increased catalyst loading is taken into account. We therefore suggest that traces of protic species, for example, water, enol, etc., may well be sufficient to initiate reaction. A hemiacetal anion intermediate (derived from **5** and **4**) has been proposed by McQuade and co-workers to effect proton transfer. See Reference [14].
- [11] R. A. More O'Ferrall, *J. Chem. Soc. B* **1970**, 785.
- [12] a) Y. Iwabuchi, M. Nakatani, N. Yokoyama, S. Hatakeyama, *J. Am. Chem. Soc.* **1999**, *121*, 10219–10220; b) K.-S. Yang, W.-D. Lee, J.-F. Pan, K. Chen, *J. Org. Chem.* **2003**, *68*, 915–919; c) M. Shi, L.-H. Chen, *Chem. Commun.* **2003**, 1310–1311; d) N. T. McDougal, S. E. Schaus, *J. Am. Chem. Soc.* **2003**, *125*, 12094–12095; e) J. E. Imbriglio, M. M. Vasbinder, S. J. Miller, *Org. Lett.* **2003**, *5*, 3741–3743.
- [13] Such a model to account for asymmetric induction has been suggested by Hatakeyama, see Reference [12a].
- [14] Note added in proof: McQuade and co-workers have independently found a substantial kinetic isotope effect during the initial phase of the Baylis–Hillman reaction (< 10 % conversion). See: K. E. Price, S. J. Broadwater, H. M. Jung, D. T. McQuade, *Org. Lett.* **2005**, 147–150.

Pincer Complexes

Redox-Induced Collapse and Regeneration of a Pincer-Type Complex Framework: A Nonplanar Coordination Mode of Palladium(II)**

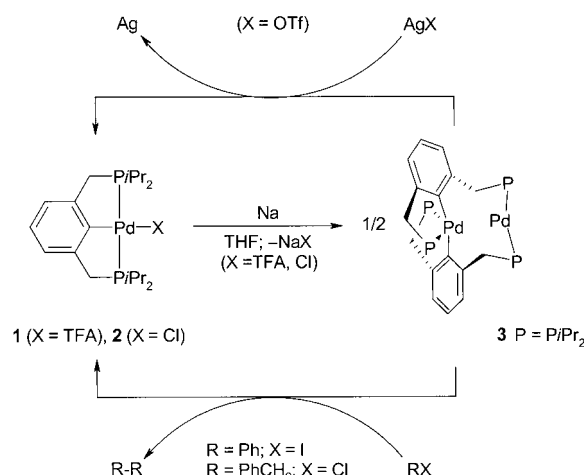
Christian M. Frech, Linda J. W. Shimon, and David Milstein*

Pincer-type complexes constitute a large family of compounds that have attracted much recent interest.^[1] Such complexes play important roles in organometallic reactions and mechanisms, catalysis, and the design of new materials. High stability of pincer-type complexes is often invoked as a key feature, which permits their use as catalysts at elevated temperatures. PCP-type d⁸ metal complexes (PCP = phosphorous-carbon-phosphorous pincer ligand) have been utilized in various catalytic applications, such as efficient iridium(I)-catalyzed alkane dehydrogenation reactions and C–C bond-forming reactions in which PCP-Pd^{II} complexes were utilized,^[1b,2] such as the synthetically important Heck coupling of aryl halides with alkenes.^[3] We present herein an unprecedented process resulting in the facile collapse of a thermally very stable d⁸ (Pd^{II}) pincer system under reducing conditions. This process leads to the formation of a novel binuclear Pd⁰/Pd^{II} complex incorporating a 14e linear Pd⁰ moiety and a completely nonplanar, “butterfly” type Pd^{II} 16e moiety. The complex is diamagnetic. Large deviations from planarity are totally unexpected for low-spin d⁸ ML₄ systems. Remarkably, the original PCP-Pd^{II} mononuclear framework can be regenerated upon direct oxidation of the binuclear complex, or upon its reaction with organic halides.

We anticipated that reduction of a square-planar, PCP-type d⁸ ML₄ complex to a d¹⁰ complex might lead to unprecedented transformations, since a d¹⁰ ML₄ complex is expected to be tetrahedral, thus rendering a meridional PCP arrangement unfavorable. This situation is of relevance to various catalytic reactions, such as Heck reactions catalyzed by PCP-Pd^{II} complexes. The traditional mechanism accepted for Heck reactions involves a Pd⁰/Pd^{II} cycle, which would

require reduction of the Pd^{II} center. Mechanisms based on Pd^{II}/Pd^{IV} have been postulated as well.^[3a,4–6] Reduction of PCP-Pd^{II} complexes has been postulated also in the catalytic electrochemical reduction of CO₂, although the nature of the reduced species is unknown.^[7]

When the palladium(II) complex **1** (Scheme 1) was reduced with sodium in THF at room temperature overnight, a color change from colorless to bright yellow took place.



Scheme 1. Reduction of complexes **1** and **2** to form the binuclear complex **3** and its oxidation with silver cation or organic halides to regenerate pincer complexes (in which X can be Cl, I, or OTf depending on the reagent used); OTf = trifluoro methanesulfonate ([CF₃SO₃][−]).

Monitoring the reaction by ³¹P NMR spectroscopy, two new signals with the same intensity were observed at δ = 55.89 and 36.96 ppm while the signal corresponding to the PCP-Pd-TFA complex (TFA = trifluoroacetate) decreased. The ratio between these two new signals did not change during reaction progress, or on modification of the reaction conditions, which suggests formation of a binuclear complex. The ¹H NMR as well as ¹³C NMR spectra of the reaction product are complex but nevertheless support formation of a dinuclear product involving two pincer ligands coordinated in an unsymmetrical manner. The signals in the ¹H and ¹H{³¹P} NMR spectra of the methylene groups at δ = 3.55 and 2.82 ppm appear as doublets (*J*_{HH} = 11.6 Hz) consistent with *cis* coordinated phosphine ligands, while those at δ = 3.51 and 3.00 ppm appear in ¹H NMR spectrum as a doublet (*J*_{HH} = 15.9) and a doublet of virtual triplets (*J*_{HH,PH} = 15.9, 4.9 Hz), respectively, and as doublets (*J*_{HH} = 15.9 Hz) in ¹H{³¹P} NMR, consistent with *trans* coordinated phosphine groups.^[8] The corresponding ¹³C{¹H} NMR spectrum shows a broad singlet at δ = 42.37 ppm, which correlates with the methylene protons signals at δ = 3.55 ppm and 2.82 ppm, as well as a triplet resonance at δ = 38.36 ppm (vt, *J*_{PC} = 23 Hz) which correlates with the methylene protons signals at δ = 3.51 ppm and 3.00 ppm and hence is consistent with the assignments.

The pentane-soluble pure reaction product was isolated as a yellow powder. Crystals of this complex were obtained by slow evaporation of its concentrated pentane solution at room

[*] Dr. C. M. Frech, Prof. D. Milstein
Department of Organic Chemistry
Weizmann Institute of Science
76100 Rehovot (Israel)
Fax: (+972) 8-934-4142
E-mail: david.milstein@weizmann.ac.il

Dr. L. J. W. Shimon
Chemical Research Support
Weizmann Institute of Science
76100 Rehovot (Israel)

[**] This research was supported by the Israel Science Foundation and the Helen and Martin Kimmel Center for Molecular Design. D.M. holds the Israel Matz Professorial Chair of Organic Chemistry.

Supporting information for this article (procedures for the preparation and characterization of complexes **2**, **3** and [PdX{2,6-C₆H₃(CH₂P*i*Pr₂)₂}] (X = OTf, I), procedure for X-ray crystallographic determination of **3**) is available on the WWW under <http://www.angewandte.org> or from the author.

temperature. An X-ray diffraction study (Figure 1) revealed that a novel binuclear palladium complex **3** was formed, incorporating a very rare, nonplanar diamagnetic Pd^{II} moiety

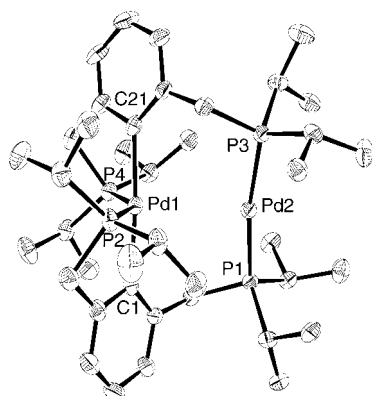


Figure 1. ORTEP diagram of a molecule of **3** (thermal ellipsoids set at 50% probability). Hydrogen atoms are omitted for clarity. Selected interatomic distances [Å] and angles [°]: Pd1–C21 2.126(4), Pd1–C1 2.130(4), Pd1–P4 2.2878(13), Pd1–P2 2.2947(12), Pd1...Pd2 3.0389(11), Pd2–P3 2.2447(12), Pd2–P1 2.2492(12); C21–Pd1–C1 175.66(14), P4–Pd1–P2 144.82(4), P3–Pd2–P1 170.48(4).^[15]

and a 14e Pd⁰ center.^[9] Thus, in an unprecedented process, the pincer system opened up and the aryl anchor was transferred from one palladium center to the other (Scheme 1). Complex **3** was formed in similar yield by the reduction of the complex PCP–Pd–Cl (**2**) under identical conditions.^[10]

The solid-state structure of **3** shows a four-coordinate Pd^{II} center with a distorted butterfly environment (C21–Pd1–C1 175.66(14)°; P4–Pd1–P2 144.82(4)°) and a palladium(0) center complexed in a linear manner by two phosphine arms (P3–Pd2–P1 170.48(4)°) from different PCP ligands. The extremely rare butterfly environment of the palladium(II) center is probably mostly a consequence of steric effects and the rigidity of the PCP units resulting from the almost-linearly coordinated phosphine arms on the palladium(0) center.

A butterfly-type geometry is reported for the four-coordinate d⁸ Ru⁰ and Re^{–1} complexes [Ru(CO)₂(PR₃)₂], [Ru(CO)(NO)(PR₃)₂]⁺ and [Re(NO)₂(PR₃)₂]⁺. However, in these cases the large deviation from planarity is due mainly to the strong back bonding to the carbonyl and nitrosyl ligands.^[11]

The observed P3–Pd–P1 angle (170.48(4)°) is slightly distorted from linearity, as compared with perfectly linear P–Pd–P angles reported for the few other structurally characterized 14e Pd⁰ complexes,^[12] except when steric factors are involved.^[12c] The distance between the metal centers of 3.0389(11) Å in **3** seems too long for a Pd–Pd bond, although there are instances where Pd–Pd separations of approximately 3.0 Å are treated as bonding.^[13] This distance, together with the slight distortion from linearity of the Pd⁰ moiety, which is pointed towards the Pd^{II} atom, might indicate a weak electronic interaction between the metal centers which might provide additional stabilization to the butterfly environment of the Pd^{II} center.

Complex **3** is significantly less thermally stable than **1**, undergoing decomposition in aromatic solvents within hours at room temperature. Heating **3** in NMP (*N*-methylpyrrolidone) up to 140°C led to a mixture of products, in contrast to **1** which shows exceptional thermal stability.

Although mechanistic studies were not performed, a possible scenario for formation of **3** might include a single electron transfer from sodium to Pd^{II} with precipitation of NaX and formation of a tri-coordinate Pd^I intermediate which is likely to undergo dimerization, subsequent disproportionation to Pd⁰ and Pd^{II}, and rearrangement involving the pincer ligands.

If complex **3** is involved in the Heck reaction catalyzed by **1**, following a classical Pd^{II}/Pd⁰ mechanism, then **3** should be at least as active as **1**. However, the dinuclear complex **3** exhibits lower activity. Using Heck coupling of iodobenzene and methyl acrylate as an example, under the reported conditions,^[3a] after 60 h a turnover number (TON) of 142 900 and quantitative conversion were obtained with **1** while a TON of 54 300 (based on Pd atom) and 38% yield were obtained with **3**. This result indicates that **3** is not an intermediate in the catalysis by **1**. Moreover, formation of biphenyl (approximately one equivalent relative to **3**) was observed in the reaction catalyzed by **3**, unlike when **1** was the catalyst.^[3a]

When complex **3** was treated with an excess of benzyl chloride, quantitative formation of the monomeric PCP–Pd–Cl complex was observed within minutes. A corresponding amount of dibenzyl was detected by GC. Similarly, adding iodobenzene to a THF solution of complex **3** led to formation of the PCP–Pd–I complex and biphenyl but at a much slower reaction rate. These reactions indicate electron transfer from the Pd⁰ center to the organic halide.^[14] Supporting the electron-transfer reaction, addition of two equivalents of AgOTf to a THF solution of **3** resulted in immediate and clean formation of the monomeric PCP–Pd–OTf complex as well as silver metal. This complex was independently prepared by addition of an equimolar amount of AgOTf to a THF solution of complex **2**. The relatively high catalytic activity of the binuclear **3** in Heck reactions is probably based on formation of the corresponding monomeric PCP–Pd–I complex upon reaction with iodobenzene. Indeed, when an NMP solution of **3** was heated for several minutes before the olefin and iodobenzene were added, the catalytic activity dramatically decreased, owing to the thermal instability of **3** under the reaction conditions. These results are in line with a mechanism of the Heck catalysis by PCP–Pd^{II} which might be different than the traditional Pd⁰/Pd^{II} catalytic sequence.

In summary, reduction of a PCP-type palladium(II) complex results in an unprecedented process leading to a novel dinuclear complex **3**, incorporating a very rare, diamagnetic nonplanar “butterfly” type palladium(II) moiety and a 14e Pd⁰L₂ unit. This process can be reversed upon mild oxidation, regenerating the PCP system. The Pd^{II}–Pd⁰ complex **3** is unlikely to be an intermediate in the Heck catalysis by the more active Pd^{II} pincer complex **1**. Thus, despite the high thermal stability of pincer systems they may not retain their structural integrity under reducing conditions and can open up, giving rise to unusual structures, and can be regenerated

upon reaction with potential oxidants, including organic halides, which are often used as substrates in catalytic reactions.

Received: October 21, 2004

Published online: February 11, 2005

Keywords: Heck reaction · homogeneous catalysis · palladium · pincer complexes · reduction

- [1] Reviews: a) M. Albrecht, G. van Koten, *Angew. Chem.* **2001**, *113*, 3866; *Angew. Chem. Int. Ed.* **2001**, *40*, 3750; b) M. E. van der Boom, D. Milstein, *Chem. Rev.* **2003**, *103*, 1759; c) B. Rybtchinski, D. Milstein, *Angew. Chem.* **1999**, *111*, 918; *Angew. Chem. Int. Ed.* **1999**, *38*, 870; d) J. T. Singleton, *Tetrahedron* **2003**, *59*, 1837; e) A. Vigalok, D. Milstein, *Acc. Chem. Res.* **2001**, *34*, 798; f) D. Milstein, *Pure Appl. Chem.* **2003**, *75*, 2003; g) C. M. Jensen, *Chem. Commun.* **1999**, 2443.
- [2] a) M. Gupta, C. Hagen, R. Flesher, W. C. Kaska, C. M. Jensen, *Chem. Commun.* **1996**, 2083; b) W. W. Xu, G. P. Rosini, M. Gupta, C. M. Jensen, A. S. Goldman, *Chem. Commun.* **1997**, 2273; c) F. Liu, A. S. Goldman, *Chem. Commun.* **1999**, 655; d) K. B. Renkema, Y. V. Kissin, A. S. Goldman, *J. Am. Chem. Soc.* **2003**, *125*, 7770; e) D. Morales-Morales, D. W. Lee, Z. Wang, C. M. Jensen, *Organometallics* **2001**, *20*, 1144; f) M. W. Haenel, S. Oevers, K. Angermund, W. C. Kaska, H. J. Fan, M. B. Hall, *Angew. Chem.* **2001**, *113*, 3708; *Angew. Chem. Int. Ed.* **2001**, *40*, 3596; g) I. Gottker-Schnetmann, P. S. White, M. Brookhart, *J. Am. Chem. Soc.* **2004**, *126*, 1804.
- [3] a) M. Ohff, A. Ohff, M. E. van der Boom, D. Milstein, *J. Am. Chem. Soc.* **1997**, *119*, 11687; b) K. Kiewel, Y. Liu, D. E. Bergbreiter, G. A. Sulikowski, *Tetrahedron Lett.* **1999**, *40*, 8945; c) F. Miyazaki, K. Yamaguchi, M. Shibasaki, *Tetrahedron Lett.* **1999**, *40*, 7379; d) D. Morales-Morales, R. Redon, C. Yung, C. M. Jensen, *Chem. Commun.* **2000**, 1619; e) D. Morales-Morales, C. Grause, K. Kasaoka, R. Redon, R. Cramer, C. M. Jensen, *Inorg. Chim. Acta* **2000**, *300–302*, 958; f) S. Sjövall, M. H. Johansson, C. Anderson, *Eur. J. Inorg. Chem.* **2001**, 2907; g) S. Sjövall, O. P. Wendt, C. Anderson, *J. Chem. Soc. Dalton Trans.* **2002**, 1396; h) D. Morales-Morales, R. E. Cramer, C. M. Jensen, *J. Organomet. Chem.* **2002**, *654*, 44; i) I. P. Beletskaya, A. V. Chuchuryukin, G. van Koten, H. P. Dijkstra, G. P. M. Klink, S. E. Nefedov, I. L. Eremenko, *Russ. J. Org. Chem.* **2003**, *39*, 1268; j) H. Alper, R. Chanthateyanonth, *J. Mol. Catal. A* **2003**, *201*, 23; k) M. R. Eberhard, *Org. Lett.* **2004**, *6*, 2125; l) C. Herrera-Alvarez, V. Gomez-Bnitez, R. Redon, J. J. Garcia, S. Hernandez-Ortega, R. A. Toscano, D. Morales-Morales, *J. Organomet. Chem.* **2004**, *689*, 2464.
- [4] Reviews that include catalysis of the Heck reaction by palladacycles: a) refs [1a,b]; b) P. L. Beletskaya, A. V. Cheprakov, *Chem. Rev.* **2000**, *100*, 3009; c) M. Dupont, M. Pfeffer, J. Spencer, *Eur. J. Inorg. Chem.* **2001**, 1917; d) R. B. Bedford, *Chem. Commun.* **2003**, 1787.
- [5] a) W. A. Herrmann, V. P. W. Böhm, C.-P. Reisinger, *J. Organomet. Chem.* **1999**, *576*, 23; b) B. L. Shaw, S. D. Perera, E. A. Staley, *Chem. Commun.* **1998**, 1362.
- [6] Active metallic palladium is proposed to be involved when phosphinite PCP-type Heck catalysts are utilized (see ref [3k]). While the PCP phosphinite system might decompose at elevated temperatures under the basic Heck conditions (probably by P–O bond cleavage) this is not necessarily true for a phosphine-based PCP system.
- [7] B. D. Steffey, A. Miedaner, M. L. Maciejewski-Farmer, P. R. Bernatis, A. M. Herring, V. S. Allured, V. Carperos, D. L. DuBois, *Organometallics* **1994**, *13*, 4844.
- [8] No J_{PH} coupling is observed for the methylene protons of the *cis* phosphine groups or for one of the geminal protons of the *trans* phosphine groups. COSY and HMQC NMR experiments confirmed the assignments of these protons.
- [9] We are aware of two examples of completely nonplanar (rather than distorted square planar) $\text{Pd}^{\text{II}}\text{L}_4$ complexes, only one of them being diamagnetic: a) M. Bröring, C. D. Brandt, *J. Chem. Soc. Dalton Trans.* **2002**, 1391; b) J. S. L. Yeo, J. J. Vittal, T. S. A. Hor, *Chem. Commun.* **1999**, 1477 (paramagnetic).
- [10] Complex **2** was prepared in 74% yield by reaction of 2,6- $(\text{CH}_2\text{P}i\text{Pr}_2)_2\text{C}_6\text{H}_4$ with $[\text{PdCl}_2(\text{cod})]$ (cod = cyclooctadiene), in analogy to published methods. See for example, ref [3e].
- [11] a) M. Ogasawara, S. A. Macgregor, W. E. Streib, K. Folting, O. Eisenstein, K. G. Caulton, *J. Am. Chem. Soc.* **1996**, *118*, 10189; b) M. Ogasawara, D. Huang, W. E. Streib, J. C. Huffman, N. Gallego-Planas, F. Maseras, O. Eisenstein, K. G. Caulton, *J. Am. Chem. Soc.* **1997**, *119*, 8642; c) H. Jacobsen, K. Heinze, A. Llamazares, H. W. Schmalke, G. Artus, H. Berke, *J. Chem. Soc. Dalton Trans.* **1999**, 1717.
- [12] a) A. Immirzi, A. Musco, *J. Chem. Soc. Chem. Commun.* **1974**, 400; b) S. Otsuka, T. Yoshida, M. Mastumoto, K. Nakatsu, *J. Am. Chem. Soc.* **1976**, *98*, 5850; c) F. Paul, J. F. Hartwig, *J. Am. Chem. Soc.* **1994**, *116*, 5969; d) G. Mann, C. Incarvito, A. L. Rheingold, J. F. Hartwig, *J. Am. Chem. Soc.* **1999**, *121*, 3224; e) H. Weissman, L. J. W. Shimon, D. Milstein, *Organometallics* **2004**, *23*, 3931.
- [13] a) T. Murahashi, H. Kurosawa, *Coord. Chem. Rev.* **2002**, *231*, 207; b) Y. Yamamoto, T. Ohno, K. Itoh, *Organometallics* **2003**, *22*, 2267.
- [14] A mechanism involving organic halide oxidative addition to generate dibenzyl or biphenyl is also possible. See, for example, H.-B. Kraatz, M. E. van der Boom, Y. Ben-David, D. Milstein, *Isr. J. Chem.* **2001**, *41*, 16.
- [15] CCDC-252736 (complex **3**) contains the supplementary crystallographic data for this paper. These data can be obtained free of charge from the Cambridge Crystallographic Data Centre via www.ccdc.cam.ac.uk/data_request/cif.

A Metal-Based Lumophore Tailored To Sense Biologically Relevant Oxometalates**

Anna F. A. Peacock, Helen D. Batey, Claudia Raendler, Adrian C. Whitwood, Robin N. Perutz,* and Anne-K. Duhme-Klair*

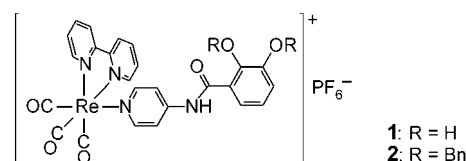
Catechol–lumophore conjugates are attracting increasing interest as supramolecular photochemical devices, with potential applications as sensors,^[1] redox switches,^[2] and photo- and electrocatalysts.^[3] The versatility of the conjugates results from the redox activity of the catechol moiety, the oxidation potential of which can be modulated by pH control and metal ion coordination.^[4] Once deprotonated, the negatively charged catecholate oxygen donors are well suited to chelate chemically hard metal ions in high oxidation states.^[5]

As metal ions in high oxidation states typically form oxometalate anions in aqueous media, a selective analytical technique must be directed at anions. There is interest in the analysis of oxometalate ions, such as molybdate, for several types of application. Environmental monitoring of molybdate is required as excessive soil molybdate causes molybdenosis in ruminants;^[6] biochemical monitoring is needed to understand molybdate uptake^[7] and the recently discovered link between MoO_4^{2-} and Cu^{2+} metabolism.^[8] Medical analysis is of interest as deficiency of Mo cofactor causes neurological disorders.^[9] A sensor that is selective for oxometalates must not only compete successfully with other oxoanions, such as SO_4^{2-} and HPO_4^{2-} , but also with metal cations, such as Fe^{3+} and Cu^{2+} .

Although the development of luminescent sensors and probes for anions is an emerging field,^[10] as yet, no selective chemosensors for biologically important oxometalates are available on the market,^[11] and studies that target these oxometalates are rare.^[12] Promising approaches to molybdate sensing include catalytic fluorometric methods^[12b] and the quenching of the fluorescence of organic ligands by Mo^{VI} .^[12a,c] Furthermore, heteroditopic ion-pair receptors were recently designed for the sequestration of environmentally deleterious oxometalates, such as ReO_4^- and TcO_4^- , which were bound as Na^+ salts through a combination of hydrogen-bonding and electrostatic interactions.^[13]

In pursuit of an optical detection method for early-transition-metal ions in high oxidation states, we have recently taken a supramolecular two-component approach in the development of a catechol– $[\text{Ru}^{\text{II}}(2,2'\text{-bpy})_3]^{2+}$ (bpy = bipyridine) conjugate, which signals the presence and concentration of molybdate (MoO_4^{2-}) in solution through luminescence quenching.^[1c,d] In this prototype sensor, the metal-binding catechol unit is separated from the lumophore by an alkyl chain. In principle, the long excitation and emission wavelengths and large Stokes shifts of metal-based lumophores, such as Ru- and Re-polypyridyl complexes, are advantageous for measurements in biological media, provided that the compatibility of the complexes with water is improved.

Here we report the design, synthesis, and luminescent properties of a second-generation sensor **1** based on a



$[\text{Re}^{\text{I}}(2,2'\text{-bpy})(\text{py})(\text{CO})_3]^+$ chromophore (py = pyridine). In **1**, the catechol unit is linked directly to the monodentate pyridyl ligand of the chromophore. The electron-withdrawing effect of the π -deficient pyridyl group which is enhanced by the coordinated positively charged chromophore increases the acidity of the phenolic OH groups. This has two main advantages: First, the affinity of the sensor for Mo at low pH values is increased, and second, the system is stabilized against air oxidation. Furthermore, the amide linker facilitates electron transfer from the catecholate quencher to the photoexcited chromophore as it ensures the planarity of the ligand. The $[\text{Re}^{\text{I}}(\text{bpy})(\text{py})(\text{CO})_3]^+$ chromophore was selected for the ease with which it is derivatized, its long-lived luminescence, and its photochemical stability.^[14]

The benzyl (Bn)-protected pyridine ligand Bn_2L (2,3-dibenzyloxybenzoyl-4-aminopyridine) was synthesized by condensation of 2,3-dibenzyloxybenzoic acid chloride^[15] with 4-aminopyridine by an analogous procedure to that reported by MacQueen and Schanze.^[14a] Bn_2L was then heated at reflux with rhenium tricarbonyl bipyridyl bromide and silver triflate in THF to form the benzyl-protected complex, which was isolated as the PF_6^- salt **2**, upon addition of NH_4PF_6 , in 60% yield. Complex **2** was characterized by ES mass spectrometry, IR and NMR spectroscopy, as well as X-ray crystallography (Figure 1).^[16] The coordination geometry of the rhenium center in **2** is distorted octahedral and typical for bipyridine-coordinated $\text{fac-Re}^{\text{I}}(\text{CO})_3$ units.^[17] The crystal structure confirms that the core of **L** is held essentially planar by an intramolecular hydrogen bond between the amide proton and the adjacent 2-benzyloxy donor (distance $\text{N}(4)\cdots\text{O}(5) = 2.64(1) \text{ \AA}$). The dihedral angle between the catechol moiety and the pyridine ring deviates by $7.6(2)^\circ$ from an ideal coplanar orientation.

Complex **2** was debenzylated by catalytic hydrogenolysis to give **1** and the product was identified by TLC, mass spectrometry, and NMR spectroscopy. The solubility of **1**, and

[*] A. F. A. Peacock, H. D. Batey, C. Raendler, Dr. A. C. Whitwood, Prof. R. N. Perutz, Dr. A.-K. Duhme-Klair
Department of Chemistry
University of York
York YO10 5DD (United Kingdom)
Fax: (+44) 190-443-2516
E-mail: akd1@york.ac.uk

[**] We thank the EPSRC and the EU for financial support and Dr. Nicole Reddig for experimental assistance.

Supporting information for this article is available on the WWW under <http://www.angewandte.org> or from the author.

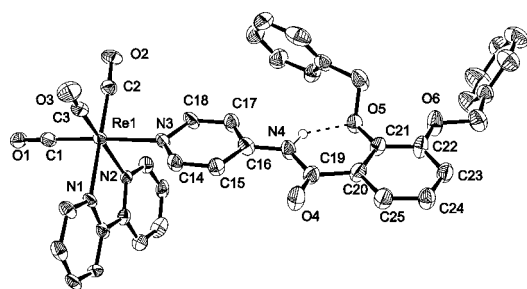


Figure 1. ORTEP plot of $[\text{Re}(\text{2,2'}\text{-bpy})(\text{Br}_2\text{L})(\text{CO})_3]^+$ (50% probability ellipsoids). Hydrogen atoms, except that at the amine (N4), are omitted for clarity. Selected bond lengths [Å]: Re–C1 1.917(8), Re–C2 1.921(8), Re–C3 1.926(8), Re–N1 2.168(5), Re–N2 2.160(6), Re–N3 2.219(6).

in particular **2**, in water is limited. To allow a comparison of the spectroscopic properties of **1** and **2**, the solvent system used throughout the studies consisted of 95:5 acetonitrile/water. In studies with **1**, however, the water content of the solvent mixture can be increased up to 20% without apparent precipitation or loss of sensor activity (see Supporting Information).^[18] As acetonitrile is miscible with water, it is possible to detect metal ions that are added in aqueous solution. Furthermore, the pH range for the detection can be established and adjusted by using standard buffer solutions.

Excitation at 370 nm into the $\text{Re}(\text{d}\pi) \rightarrow \text{bpy}(\pi^*)$ charge-transfer bands^[14,17] of **1** and **2** gives rise to broad emission bands around 565 nm. Whereas the emission spectrum of **2** is pH-independent between pH 0.1 and 10, the emission of the “free” sensor **1** shows a sigmoidal decrease in intensity due to the deprotonation of the OH group in the *ortho* position (Figure 2). The pH dependence of luminescence gives an apparent $\text{p}K_{\text{a}}$ value of around 4.9 for **1**, which is comparatively low for a catecholamide.^[1c,19] The maximum emission intensity of **1** observed at low pH, however, is still approximately 30% lower than that of **2**.

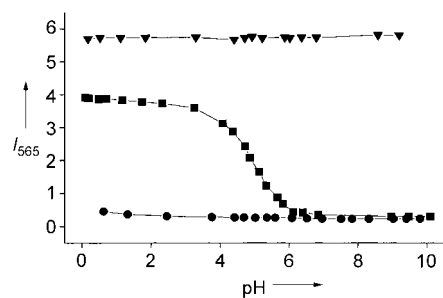


Figure 2. Intensity of emission at maximum ($\lambda_{\text{em}} = 565$ nm) versus pH for **2** (▼), **1** (■), and **1** in the presence of molybdate (0.5 equiv; ●). $\lambda_{\text{ex}} = 370$ nm, solutions in aqueous acetonitrile.

The addition of 0.5 equivalents of molybdate^[20] results in quenching of the emission, indicating strong binding of the analyte. To gain further insight into the stoichiometry of the molybdenum complex formed, a solution of **1**, buffered at pH 4, was titrated with molybdate (Figure 3). Upon addition of molybdate, the emission intensity decreased gradually.

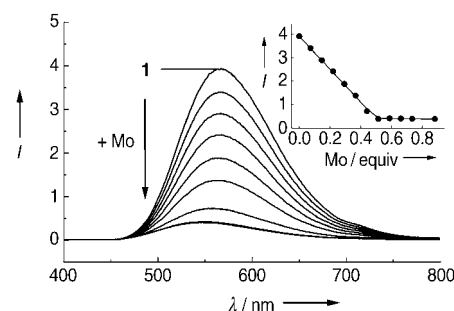
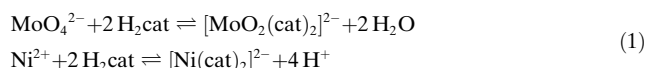


Figure 3. Emission spectra (uncorrected) of **1** (10^{-4} M) in the presence of increasing concentrations of molybdate (in aqueous acetonitrile at pH 4.0, buffer: 2,6-lutidine, $\lambda_{\text{ex}} = 370$ nm). Inset: Emission intensity at 565 nm as a function of molar equivalents of MoO_4^{2-} .

Apart from a slight shift of the emission maximum toward shorter wavelengths at high levels of molybdate, no other spectral changes were observed. The emission intensity decreases linearly up to a clear break at a ratio of Mo/**1** of 0.5, consistent with the formation of a 1:2 molybdenum/catecholate complex. The response fits^[21] to an apparent overall binding constant of $\log \beta'_2 = 13(\pm 1)$. Under these conditions, the detection limit was determined to be $55 \mu\text{g L}^{-1}$.^[18]

Next, the selectivity of **1** was investigated by repeating the titration of the solution of the acidic sensor with standard base in the presence of potentially interfering ions. The pH profiles obtained in the presence of metal cations, such as Co^{2+} , Ni^{2+} , Cu^{2+} , Zn^{2+} , and Fe^{3+} , do not differ significantly from that obtained for the titration of **1** alone (see Supporting Information). The lack of quenching in the low pH region may be rationalized by the stronger pH dependence of the reaction of metal cations with catechols [Eq. (1), cat = catechol]. The pH profiles obtained in the presence of oxoanions, such as sulfate or phosphate, are almost identical to the pH profile of **1** (see Supporting Information). This absence of interference is particularly advantageous for biological applications, where high concentrations of sulfate and phosphate ions are likely to be present.



In the presence of tungstate,^[20] the initial emission intensity at low pH values decreases slightly, probably owing to the heavy-atom effect; the $\text{p}K_{\text{a}}$ value, however, is not shifted significantly (Figure 4). As the coordination chemistry of Mo is very similar to that of W, the unexpectedly high selectivity for molybdate over tungstate under acidic conditions merited further investigations. We therefore examined the reversibility of the titrations in detail. Whereas the response of **1** in the absence and in the presence of most of the ions tested was independent of the direction of the titration (low to high pH, or high to low pH), the pH profile obtained in the presence of tungstate revealed hysteresis-type behavior. The lack of quenching during the forward titration (low to high pH) may be related to the formation of polyoxometalates. Both W and Mo form polyoxometalates

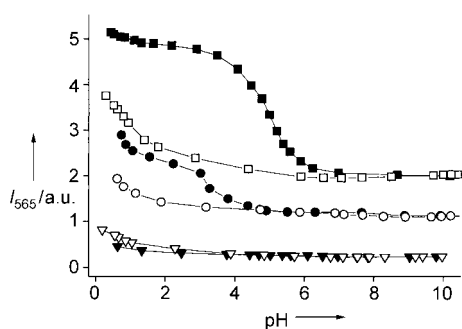


Figure 4. Reversibility studies with solutions containing **1** in the presence of the following oxometalates (0.5 equiv): tungstate (■, □), vanadate (●, ○), and molybdate (▼, ▽). Titrations from low to high pH: solid symbols; from high to low pH: hollow symbols. Offset: 0.8 a.u. each.

in acidic solutions; however, the Mo-containing species react quickly, whereas the W-containing species are known to be more inert.^[22] This allows kinetic differentiation of the two analytes.

As molybdenum is diagonally related to vanadium as well as rhenium, vanadate and perrhenate ions were also tested. Whereas perrhenate gave no response (see Supporting Information), vanadate^[20] was found to be the only other biologically relevant ion investigated that also quenches the emission of **1**. During the forward titration, the emission intensity of **1** decreases significantly in the low pH region, indicating a moderate binding affinity toward vanadate. The pH profile obtained is more complicated in shape, and the back titration reveals hysteresis-type behavior. Further studies are required to identify the vanadium-containing species that are involved in the underlying equilibria.

In conclusion, we have developed a new selective high-affinity chemosensor for the most biologically relevant oxometalates: molybdate, tungstate, and vanadate. The sensor system operates in up to 20% (v/v) H₂O in CH₃CN in the pH range 0.1–4.5 and indicates binding of the analyte by efficient quenching of the (Re–bipyridyl)-based luminescence.

Received: October 14, 2004

Published online: February 3, 2005

Keywords: luminescence · molybdenum · oxo ligands · sensors

- [1] a) P. D. Beer, *Chem. Commun.* **1996**, 689; b) I. Costa, L. Fabbrizzi, P. Pallavicini, A. Poggi, A. Zani, *Inorg. Chim. Acta* **1998**, 275–276, 117; c) S. B. Jedner, R. J. James, R. N. Perutz, A.-K. Duhme-Klair, *J. Chem. Soc. Dalton Trans.* **2001**, 2327; d) S. B. Jedner, R. N. Perutz, A.-K. Duhme-Klair, *Z. Anorg. Allg. Chem.* **2003**, 629, 2421; e) L. O'Brien, M. Duati, S. Rau, A. L. Guckian, T. E. Keyes, N. M. O'Boyle, A. Serr, H. Görls, J. G. Vos, *Dalton Trans.* **2004**, 514.
- [2] V. Goulle, A. Harriman, J.-M. Lehn, *J. Chem. Soc. Chem. Commun.* **1993**, 1034.
- [3] a) B. Whittle, N. S. Everest, C. Howard, M. D. Ward, *Inorg. Chem.* **1995**, 34, 2025; b) A. D. Shukla, B. Whittle, H. C. Bajaj, A. Das, M. D. Ward, *Inorg. Chim. Acta* **1999**, 285, 89; c) G. D. Storrier, K. Takada, H. D. Abruna, *Inorg. Chem.* **1999**, 38, 559.

- [4] D. E. Wheeler, J. H. Rodriguez, J. K. McCusker, *J. Phys. Chem. A* **1999**, 103, 4101.
- [5] a) C. G. Pierpont, R. M. Buchanan, *Coord. Chem. Rev.* **1981**, 38, 45; b) C. G. Pierpont, C. W. Lange, *Prog. Inorg. Chem.* **1994**, 41, 331.
- [6] J. Mason, *Toxicology* **1986**, 42, 99.
- [7] R. N. Pau, D. M. Lawson in *Metal Ions in Biological Systems* (Eds.: H. Sigel, A. Sigel), Marcel Dekker, New York, **2002**, 32.
- [8] J. Kuper, A. Llamas, H.-J. Hecht, R. R. Mendel, G. Schwarz, *Nature* **2004**, 430, 803.
- [9] a) V. E. Shih, I. F. Abrams, J. L. Johnson, M. Carney, R. Mandell, R. M. Robb, J. P. Cloherty, K. V. Rajagopalan, *N. Engl. J. Med.* **1977**, 297, 1022; b) C. Kisker, H. Schindelin, A. Pacheco, W. A. Wehbi, R. M. Garrett, K. V. Rajagopalan, J. H. Enemark, D. C. Rees, *Cell* **1997**, 91, 973.
- [10] P. D. Beer, P. A. Gale, *Angew. Chem.* **2001**, 113, 503; *Angew. Chem. Int. Ed.* **2001**, 40, 486.
- [11] R. P. Haugland, *Handbook of Fluorescent Probes and Research Products*, Molecular Probes, <http://www.probes.com>, **2004**.
- [12] a) B. K. Pal, K. A. Singh, K. Dutta, *Talanta* **1992**, 39, 971; b) S. Kawakubo, H. Suzuki, M. Iwatsuki, *Anal. Sci.* **1996**, 12, 767; c) C. Jiang, J. Wang, F. He, *Anal. Chim. Acta* **2001**, 439, 307, and references therein.
- [13] P. D. Beer, P. K. Hopkins, J. D. McKinney, *Chem. Commun.* **1999**, 1253.
- [14] a) D. B. MacQueen, K. S. Schanze, *J. Am. Chem. Soc.* **1991**, 113, 6108; b) K. S. Schanze, D. B. MacQueen, T. A. Perkins, L. A. Cabana, *Coord. Chem. Rev.* **1993**, 122, 63.
- [15] W. H. Rastetter, T. J. Erickson, M. C. Venuti, *J. Org. Chem.* **1981**, 46, 3579.
- [16] X-ray crystallography: Diffraction data were collected on a Bruker Smart Apex diffractometer using a SMART CCD camera. Structures were solved by direct methods using SHELXS-97 and refined by full-matrix least squares using SHELXL-97 (G. M. Sheldrick, University of Göttingen, Germany, **1997**). All non-hydrogen atoms were refined anisotropically. Hydrogen atoms were placed using a "riding model" and included in the refinement at calculated positions. Crystal data: C_{40.5}H₃₀F₆N₄O_{6.5}PRe, *M* = 1007.85, yellow crystals, size 0.13 × 0.08 × 0.03 mm³, monoclinic, *P*2₁/c, *a* = 19.8498(11), *b* = 9.4358(6), *c* = 21.1502(12) Å, β = 95.111(1)°, *U* = 3945.7(4) Å³, *Z* = 4, ρ_{calcd} = 1.697 g cm⁻³, θ_{max} = 25°, MoKα radiation, λ = 0.71073 Å, φ- and ω-scans, *T* = 115 K, 21 632 reflections collected, 6970 independent (*R*_{int} 0.0654). Absorption correction was applied using SADABS (v2.03, Sheldrick), μ = 3.203 mm⁻¹, 0.797 < *T* < 1.000, multiscan, final *R* = 0.0407 (for *I* ≥ 2σ(*I*)), *wR*(*F*²) 0.1114 (all data). CCDC 248500 contains the supplementary crystallographic data for this paper. These data can be obtained free of charge from The Cambridge Crystallographic Data Centre via www.ccdc.cam.ac.uk/data_request/cif.
- [17] a) V. W.-W. Yam, S. H.-F. Chong, C.-C. Ko, K.-K. Cheung, *Organometallics* **2000**, 19, 5092; b) K. K.-W. Lo, D. C.-M. Ng, W.-K. Hui, K.-K. Cheung, *J. Chem. Soc. Dalton Trans.* **2001**, 2634; c) M. Busby, D. J. Liard, M. Motevalli, H. Toms, A. Vlcek, Jr., *Inorg. Chim. Acta* **2004**, 357, 167.
- [18] See Supporting Information for supplementary figures and experimental details.
- [19] K. N. Raymond, G. Mueller, B. F. Matzkanke, *Top. Curr. Chem.* **1984**, 123, 49.
- [20] The oxometalates were added in the form of concentrated aqueous standard solutions of Na₂MoO₄·2H₂O, Na₂WO₄·2H₂O, NH₄ReO₄, and NH₄VO₃.
- [21] J. Huskens, H. van Bekkum, J. A. Peters, *Comput. Chem.* **1995**, 19, 409.
- [22] K.-H. Tytko, O. Glemser, *Adv. Inorg. Chem. Radiochem.* **1976**, 19, 239; J. J. Cruywagen, *Adv. Inorg. Chem.* **2000**, 49, 127.

Metallamacrocycles

Synthesis of a Metallophilic Metallamacrocycle: A Hg^{II}...Cu^I...Hg^{II}...Hg^{II}...Cu^I...Hg^{II} Interaction**

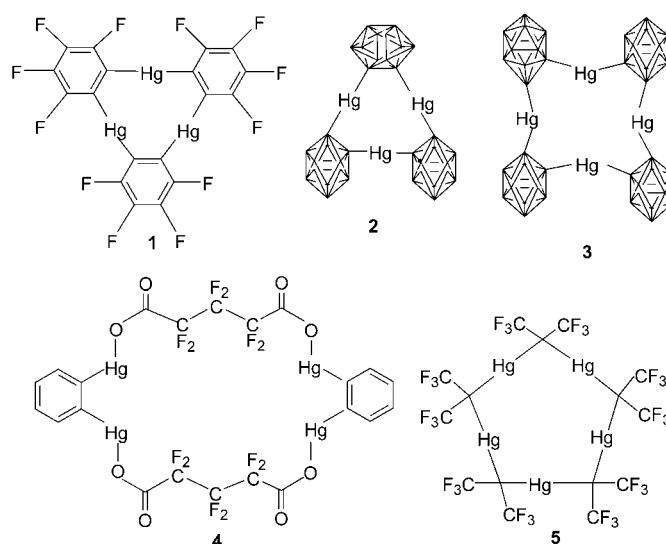
Upali Patel, Harkesh B. Singh,* and
Gotthelf Wolmershäuser

Macrocyclic multidentate Lewis acids have attracted considerable interest as electrophilic hosts in supramolecular chemistry. The electrophilic hosts generally use tin,^[1] silicon,^[2] boron,^[3] germanium,^[4] and mercury^[5–8] atoms as binding sites for neutral and anionic electron-rich guests. Polydentate organomercurials are the most investigated series of all the multidentate Lewis acids and have applications as catalysts^[9] and sensors.^[10] These organomercurials include trimeric perfluoro-*o*-phenylenemercury (**1**),^[6a] [9]mercuraborand-3 (**2**), [12]mercuracarborand-4 (**3**),^[7] the 24-membered macrocyclic perfluoroglutarate **4**,^[8b] and the cyclic pentameric [(CF₃)₂CHg]₅ macrocycle **5**.^[6b] Some of these compounds exhibit short intermolecular Hg...Hg metallophilic interactions in the solid state, and these metallophilic interactions are often associated with unusual luminescent properties.^[5b,c,11]

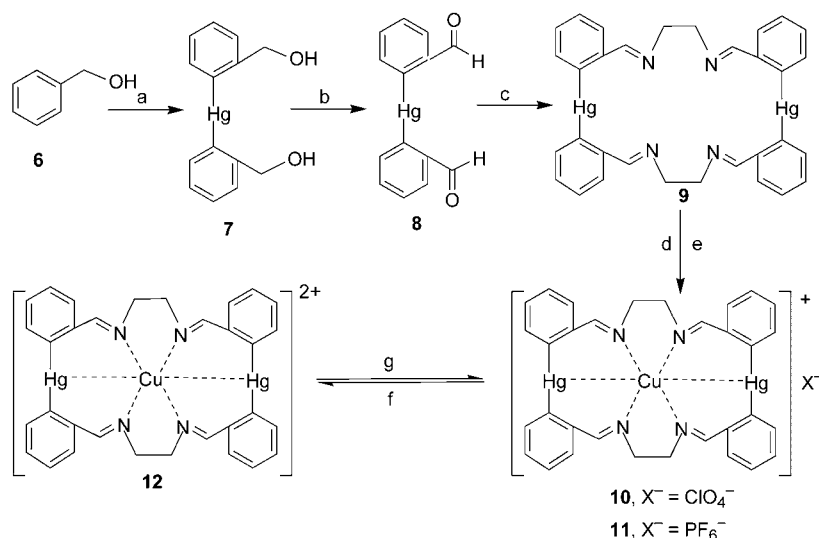
Whereas the interaction of metallamacrocycles with electron-rich species has been studied extensively, their coordination through short metal–metal interactions with cations is still largely unexplored. However, the work of Catalano et al. on mixed-metal metallocryptands^[12] formed by self-assembly is a notable exception. Severin and co-workers also reported a similar metallamacrocycle, an organo-metallic [12]metallacrown-3 species, that was obtained by self-assembly.^[13]

Herein, we present a metallamacrocycle that contains both a Lewis acidic mercury center and basic nitrogen atoms in a preorganised macrocycle and a cation complex of a mercuramacrocycle that exhibits metallophilic interactions between the coordinated Cu^I and Hg^{II} centers.

The white and air-stable, novel 22-membered metallamacrocycle **9** was prepared by [2+2] cycloaddition of **8**^[14] with ethylenediamine in high yield without recourse to a template. The precursor **8** was synthesized from benzyl alcohol by lithiation.



Ortho-lithiation of benzyl alcohol, followed by treatment with mercuric chloride, afforded compound **7**, which was oxidized with pyridinium chlorochromate (PCC) to give **8** in good yield (Scheme 1). The Hg...O intramolecular interaction



Scheme 1. Synthetic route to the 22-membered mercuramacrocycle **9** and its Cu^I complexes: a) *n*BuLi (2 equiv), –78 °C, THF, HgCl₂; b) PCC, CH₂Cl₂; c) H₂NCH₂CH₂NH₂, MeOH; d) [Cu(CH₃CN)₄]ClO₄, MeOH; e) Cu(CH₃COO)₂, NH₄PF₆, MeOH; f) coulometry; g) left to stand.

in **8** presumably plays a role in macrocyclization. To synthesize the Cu^I complex, ligand **9** was treated with one equivalent of [Cu(CH₃CN)₄]ClO₄ in methanol to afford an orange–yellow-colored complex **10**. In an attempt to prepare a Cu^{II} complex, **9** was treated with Cu(OCOCH₃)₂, followed by an excess of ammonium hexafluorophosphate. An orange–yellow-colored Cu^I complex **11** was produced unexpectedly with PF₆[–] as the counter ion (Scheme 1). Both complexes were characterized by IR, ¹H NMR, and ¹³C NMR spectroscopic analysis, as well as MS(ESI) and elemental analysis. The reduction of the Cu^{II} ion without a reducing agent is not

[*] U. Patel, Prof. H. B. Singh
Department of Chemistry
Indian Institute of Technology Bombay
Powai, Mumbai 400 076 (India)
Fax: (+91) 22-2572-3480
E-mail: chhbsia@chem.iitb.ac.in
Dr. G. Wolmershäuser
Universität Kaiserslautern
Postfach 3049, 67653 Kaiserslautern (Germany)

[**] This work was supported by DST and DRDO. We are grateful to Prof. G. K. Lahiri for providing access to coulometric equipment.

Supporting information for this article is available on the WWW under <http://www.angewandte.org> or from the author.

unprecedented. Lai and co-workers^[15] observed a similar reduction of a Cu^{II} ion when treated with a quinquedentate macrocycle, and they suggested that the autoreduction occurred because of the electron-donating properties of the ligand or the geometry of the complex formed.

Single crystals of **10** were isolated as orange needles from a solution in acetonitrile/ether for X-ray diffraction studies.^[16] The structure confirms the novel coordination of the Cu^I center to all four nitrogen atoms and to the two mercury atoms to give a distorted octahedral geometry (Figure 1). The

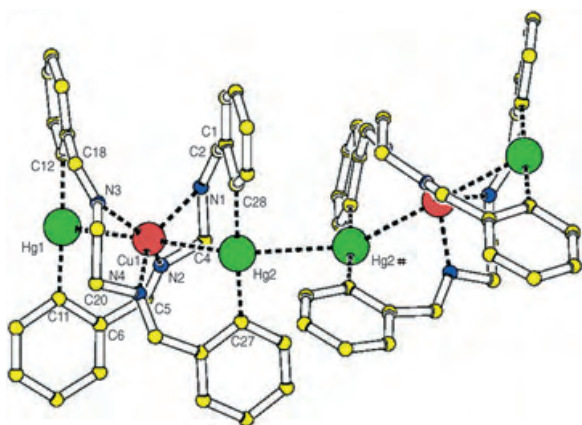


Figure 1. PLATON view of compound **10** that shows the dimerization of compound **10** through a Hg...Hg intermolecular homometallic d¹⁰...d¹⁰ interaction and Hg...Cu d¹⁰...d¹⁰ heterometallic interactions. Hydrogen atoms and anions are omitted for clarity. Selected bond lengths [Å] and angles [°]: Cu1–Hg1 2.921(7), Cu1–Hg2 2.919(7), Hg2–Hg2# 3.203(4), Hg1–Cu1–Hg2 177.88(3), Cu1–Hg2–Hg2# 154.40(17), C11–Hg1–C12 177.80(18), C27–Hg2–C28 177.21(18), Hg2–Cu1–N1 69.70(12), Hg2–Cu1–N4 71.03(10), Cu1–Hg2–Hg2# 154.40(17).

Cu...Hg interatomic distances (Cu1–Hg1 2.921 Å and Cu1–Hg2 2.919 Å) are shorter than the sum of the van der Waals radii of the copper and mercury atoms ($r_{\text{vdw}} = 1.40$ and 1.75 Å, respectively).^[17] However, this Cu...Hg distance is longer than the Cu...Hg distance found in the polymetallic mesocycle [Hg{Fe[Si(OMe)₃](CO)₃(μ-dppm)}₂Cu]⁺.^[18] Further inspection of the crystal packing revealed that two cations of **10** are linked by a Hg...Hg intermolecular interaction of 3.20 Å to give a chain of six d¹⁰ ions. The Hg...Hg distance is longer than the Hg...Hg distance in metallic mercury (3 Å)^[19] but much shorter than those observed in other structures with Hg...Hg interactions^[5b,c,d,g,20] and the calculated value for the perpendicular HgMe₂ dimer (3.50 Å).^[17b] However, this distance in **10** is slightly longer than that observed for bis(trimethylsilyl)mercury.^[21] The important feature of this molecule is the presence of two types of d¹⁰...d¹⁰ metallophilic interaction: a homometallic Hg^{II}...Hg^{II} interaction and a heterometallic Hg^{II}...Cu^I interaction.

Complexes **10** and **11** show a well-defined reversible redox wave with $E_{1/2}$ values of 0.55 and 0.57 V versus the saturated calomel electrode (SCE) and ΔE values of 0.078 and 0.080 V with $I_{\text{pc}}/I_{\text{pa}}$ values of 1.06 and 1.03, respectively. The green-colored solution of the Cu^{II} complex **12** could be generated by coulometric oxidation of the orange-colored solution of **10** in

acetonitrile at 0.725 V in a cyclic-voltammetry cell. The Cu^{II} complex could be stabilized for a short time by quenching the solution at 77 K. The ESR spectrum of **12** shows $g_{\text{II(av)}}$ at 2.54 with $A_{\text{(av)}} = 190$ G and $g_{\perp(\text{av})}$ at 2.09 with $A_{\perp(\text{av})} = 67.50$ G. The green-colored Cu^{II} complex is reduced again to the orange-colored Cu^I complex within half an hour when left to stand in solution.

The electronic absorption spectrum of **9** in acetonitrile solution exhibits a strong absorption band at 292 nm ($\epsilon = 6400 \text{ M}^{-1} \text{ cm}^{-1}$). Complex **10** shows a low-energy band at 410 nm ($\epsilon = 800 \text{ M}^{-1} \text{ cm}^{-1}$) and a strong peak at 292 nm in the same solvent. The band at 410 nm is attributed to a metal-to-ligand charge transfer. Cu^I complexes **10** and **11** were found to be luminescent at room temperature and also at 77 K both in acetonitrile solution and in the solid state. The acetonitrile solution of **10** shows a very weak emission at $\lambda_{\text{max}} = 445$ nm. Upon cooling to 77 K and in the solid state, the emission spectrum becomes more intense. Upon excitation at $\lambda_{\text{max}} = 450$ nm in the solid state, the emission spectra exhibited a sharp band at $\lambda_{\text{max}} = 485$ nm, along with weaker bands at 530 and 545 nm. Detailed photophysical studies are in progress.

Successful trapping of a Cu^I ion in a mercuramacrocycle demonstrates that a metallamacrocycle can be used to entrap suitably sized metal ions with metal–metal interactions in a preorganized system. This approach can be extended to prepare various mixed-metal systems, in particular those with d¹⁰...d¹⁰ interactions, with interesting structural and luminescent properties.

Received: November 1, 2004

Published online: February 3, 2005

Keywords: copper · heterometallic complexes · mercury · metallacycles · metal–metal interactions

- [1] a) M. Newcomb, J. H. Homer, M. T. Blanda, *J. Am. Chem. Soc.* **1987**, *109*, 7878–7879; b) M. Newcomb, M. T. Blanda, *Tetrahedron Lett.* **1988**, *29*, 4261–4264; c) K. Jurkschat, K. G. Kuivila, S. Liu, J. A. Zubietta, *Organometallics* **1989**, *8*, 2755–2759; d) K. Jurkschat, A. Ruhlemann, A. Tzschach, *J. Organomet. Chem.* **1990**, *381*, C35–C56.
- [2] E. J. Michael, X. Haiji, *Tetrahedron Lett.* **1988**, *29*, 297–300.
- [3] a) S. Aoyagi, K. Tanaka, L. Zicmane, Y. Takeuchi, *J. Chem. Soc. Perkin Trans. 2* **1992**, 2217–2220; b) S. Aoyagi, K. Tanaka, Y. Takeuchi, *J. Chem. Soc. Perkin Trans. 2* **1994**, 1549–1553.
- [4] a) M. T. Reetz, C. M. Niemeyer, K. Harms, *Angew. Chem.* **1991**, *103*, 1515–1517; *Angew. Chem. Int. Ed. Engl.* **1991**, *30*, 1472–1474.
- [5] a) M. Tsunoda, F. P. Gabbai, *J. Am. Chem. Soc.* **2000**, *122*, 8335–8336; b) J. B. King, M. R. Haneline, M. Tsunoda, F. P. Gabbai, *J. Am. Chem. Soc.* **2002**, *124*, 9350–9351; c) M. R. Haneline, M. Tsunoda, F. P. Gabbai, *J. Am. Chem. Soc.* **2002**, *124*, 3737–3742; d) M. A. Omary, R. M. Kassab, M. R. Haneline, O. Elbjairami, F. P. Gabbai, *Inorg. Chem.* **2003**, *42*, 2176–2178; e) M. Tsunoda, F. P. Gabbai, *J. Am. Chem. Soc.* **2003**, *125*, 10492–10493; f) M. R. Haneline, J. B. King, F. P. Gabbai, *Dalton Trans.* **2003**, *13*, 2686–2690; g) M. R. Haneline, F. P. Gabbai, *Angew. Chem.* **2004**, *116*, 5587–5590; *Angew. Chem. Int. Ed.* **2004**, *43*, 5471–5474.
- [6] a) P. Sartori, A. Golloch, *Chem. Ber.* **1968**, *101*, 2004–2009; b) M. Yu. Antipin, Yu. T. Struchkov, A. Yu. Volkonsky, E. M.

- Rokhlin, *Izv. Akad. Nauk SSSR Ser. Khim.* **1983**, 2, 452–455; b) I. A. Tikhonova, F. M. Dolgushin, A. I. Yanovsky, Yu. T. Struchkov, A. N. Gavrilova, L. N. Saitkulova, E. S. Shubina, L. M. Epstein, G. G. Furin, V. B. Shur, *J. Organomet. Chem.* **1996**, 508, 271–273; c) *J. Organomet. Chem.* **1991**, 418, C29–C32; d) I. A. Tikhonova, F. M. Dolgushin, K. I. Tugashova, P. V. Petrovskii, G. G. Furin, V. B. Shur, *J. Organomet. Chem.* **2002**, 654, 123–131; e) V. B. Shur, I. A. Tikhonova, F. M. Dolgushin, A. I. Yanovsky, Yu. T. Struchkov, A. Yu. Volkonsky, E. V. Solodova, S. Yu. Panov, P. V. Petrovskii, M. E. Vol'pin, *J. Organomet. Chem.* **1993**, 443, C19–C21.
- [7] T. J. Wedge, M. F. Hawthorne, *Coord. Chem. Rev.* **2003**, 240, 111–128, and references therein.
- [8] a) J. D. Wuest, *Acc. Chem. Res.* **1999**, 32, 81; b) J. D. Wuest, B. Zacharie, *J. Am. Chem. Soc.* **2000**, 122, 4714–4715.
- [9] H. Lee, M. Diaz, M. F. Hawthorne, *Tetrahedron Lett.* **1999**, 40, 7651–7655.
- [10] I. H. Badr, R. D. Johnson, M. Diaz, M. F. Hawthorne, L. G. Bachas, *Anal. Chem.* **2000**, 72, 4249–4254.
- [11] W. Y. Wong, G. L. Lu, L. Liu, J. X. Shi, Z. Lin, *Eur. J. Inorg. Chem.* **2004**, 2066–2077.
- [12] a) V. J. Catalano, B. L. Bennett, R. L. Yson, B. C. Noll, *J. Am. Chem. Soc.* **2000**, 122, 10056–10062; b) V. J. Catalano, L. Byron, *Chem. Commun.* **2000**, 1413–1414; c) V. J. Catalano, M. A. Malwitz, B. C. Noll, *Chem. Commun.* **2001**, 6, 581–582; d) V. J. Catalano, M. A. Malwitz, B. C. Noll, *Inorg. Chem.* **2002**, 41, 6553–6559; e) V. J. Catalano, M. A. Malwitz, *J. Am. Chem. Soc.* **2004**, 126, 6560–6561.
- [13] a) H. Piotrowski, K. Polborn, G. Hilt, K. Severin, *J. Am. Chem. Soc.* **2001**, 123, 2699–2700; b) H. Piotrowski, G. Hilt, A. Schulz, P. Mayer, K. Polborn, K. Severin, *Chem. Eur. J.* **2001**, 7, 3197–3208; c) M. L. Lehaire, A. Schulz, R. Scopelliti, K. Severin, *Inorg. Chem.* **2003**, 42, 3576–3581.
- [14] a) C. E. F. Rickard, W. R. Roper, F. Tutone, S. D. Woodgate, L. J. Wright, *J. Organomet. Chem.* **2001**, 619, 293–298; b) K. R. Flower, V. J. Howard, S. Naguthney, R. G. Pritchard, J. E. Warren, *Inorg. Chem.* **2002**, 41, 1907–1912.
- [15] M. Vetrichelvan, Y. Lai, K. F. Mok, *Dalton Trans.* **2003**, 295–303.
- [16] Crystal structure data for **10**: $C_{32}H_{28}ClHg_2N_4O_4$, $M_w = 1032.75$. Monoclinic, space group $I2/a$ with $a = 18.6441(10)$, $b = 10.3912(8)$, $c = 31.9312(18)$ Å, $\alpha = 90^\circ$, $\beta = 95.741(7)^\circ$, $\gamma = 90^\circ$, $V = 6155.1(10)$ Å³, $Z = 8$, $\rho_{\text{calc}} = 2.229$ mg m⁻³, $2.64 < \theta < 26.73^\circ$, crystal dimensions $0.24 \times 0.16 \times 0.08$ mm, $\mu = 10.768$ mm⁻¹, $T = 293(2)$ K. A total of 46961 reflections were measured in the range $2.64 < \theta < 26.73^\circ$ ($-23 < h < 23$, $-13 < k < 13$, $-40 < l < 40$) with 6500 unique reflections ($R_{\text{int}} = 0.1056$). Full-matrix least-squares refinement on F^2 $R1 = 0.0229$, ($I > 2\sigma(I)$) $R1 = 0.0577$ (all data); $wR2 = 0.0311$ ($I > 2\sigma(I)$), $wR2 = 0.0355$. Further details are given in the Supporting Information. CCDC 253481 contains the supplementary crystallographic data for this paper. These data can be obtained free of charge from The Cambridge Crystallographic Data Centre via www.ccdc.cam.ac.uk/data_request/cif.
- [17] a) A. Bondi, *J. Phys. Chem.* **1964**, 68, 441–451; b) P. Pykkö, M. Straka, *Phys. Chem. Chem. Phys.* **2000**, 2, 2489–2493, and references therein.
- [18] M. Benard, U. Bodensieck, P. Braunstin, M. Knorr, M. Strampfer, C. Strohmam, *Angew. Chem.* **1997**, 109, 2890–2893; *Angew. Chem. Int. Ed. Engl.* **1997**, 36, 2758–2761.
- [19] J. Donohue, *The Structure of the Elements*, Wiley, New York, **1947**, p. 233.
- [20] P. Pykkö, *Chem. Rev.* **1997**, 97, 597–636.
- [21] N. L. Pickett, *Acta Crystallogr. C* **2000**, 56, 412–413.

Colloidally Stable Amphibious Nanocrystals Derived from Poly[[2-(dimethylamino)ethyl] Methacrylate] Capping**

Hongwei Duan, Min Kuang, Dayang Wang,*
Dirk G. Kurth, and Helmuth Möhwald

We present a general protocol for the capping of nanocrystals (NCs) with poly[[2-(dimethylamino)ethyl] methacrylate] (PDMA) brushes to render NCs soluble in both water and organic solvents. The PDMA-capped NCs are not amphiphilic and do not absorb at interfaces but remain in bulk phases in water/oil two-phase systems. We therefore refer to them as amphibious NCs. Recently, NCs have been extensively investigated because of their unique size-dependent, electronic, magnetic, and optical properties.^[1] A number of wet-chemical strategies have been well established to generate NCs in either aqueous or organic phases. One of the problems of water-based NCs is their tendency to agglomerate on changing the pH value, the temperature, and/or the ionic strength of the aqueous solution.^[2] Their stability may be improved by capping with hydrophilic ligands as stabilizers, but the excess stabilizer is generally difficult to remove. One can transfer hydrophilic NCs to organic solutions with the aid of surfactants with long hydrocarbon chains based on direct covalent bonding or electrostatic interactions to improve the colloidal stability or to organize particles into ordered arrays.^[3] The efficiency of the phase transfer, however, is generally low. High-quality NCs, with well-defined size, shape, and crystallinity, can be prepared in organic media.^[1c,4] Nevertheless, their water immiscibility limits their usage in aqueous milieu. Such hydrophobic NCs may be transferred into aqueous phases by replacing surface capping agents with multi- or monolayers of surfactants with short hydrocarbon chains.^[5] However, the colloidal stability of the transferred NCs remains poor. Although the coating by hydrophilic polymers and silica can improve the colloidal stability, there are difficulties in avoiding aggregation of NCs during the coating procedures.^[6] Overall it remains a challenge to direct NCs into specific physicochemical environments without the loss of properties and colloidal stability.

Herein, we present a new, efficient and versatile process to transfer hydrophobic or hydrophilic NCs into a specific milieu by coating them with shells of PDMA brushes. These brushes

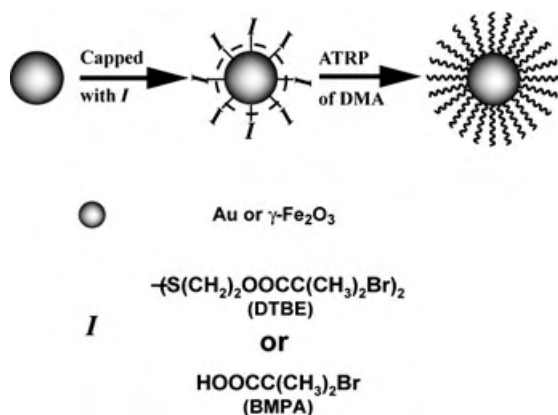
[*] H. Duan, M. Kuang, Dr. D. Wang, Dr. D. G. Kurth, Prof. H. Möhwald
Max Planck Institute of Colloids and Interfaces
14424 Potsdam (Germany)
Fax: (+49) 331-567-9202
E-mail: dayang.wang@mpikg-golm.mpg.de

[**] This work is supported by the Max Planck Society. We thank J. Hartmann and R. Pitschke for assistance with TEM experiments. G. Goll (MPI of Metals Research) is acknowledged for help with magnetic measurements.



Supporting information for this article is available on the WWW under <http://www.angewandte.org> or from the author.

were capped on organic $\gamma\text{-Fe}_2\text{O}_3$ and aqueous Au NCs through surface-initiated atom-transfer radical polymerization (ATRP). Because of the unique solubility of PDMA, the coated NCs can be well dispersed in both water and organic solvents. This report is the first step towards the fabrication of amphibious NCs. We were encouraged by the success of surface-initiated ATRP on colloidal particles.^[7] A number of hydrophobic polymers such as polystyrene and poly(methyl methacrylate) have been recently grafted onto colloidal particles of sizes ranging from nanometers to submicrometers.^[7a-e] Armes and co-workers have created hydrophilic brushes on silica spheres.^[7f] All these reports mainly focus on the synthesis and structural characterization of polymer grafted NCs. So far there are few reports on the use of surface-initiated ATRP as a phase-transfer means to direct NCs into specific physicochemical media. Our protocol benefits from several recent developments in both polymer chemistry and materials synthesis. First, surface-initiated ATRP provides a “grafting-from” strategy to coat NCs, thus preventing their aggregation during the growth of polymer brushes. Second, ATRP allows the coating of NCs with shells of dense polymer brushes, so the stability and solubility of the resulting coated NCs should be dominated by the polymer brushes rather than by the NCs themselves. Third, PDMA can be dissolved in common organic solvents (except alkanes), including methanol, ethanol, acetone, toluene, carbon tetrachloride, chloroform, dichloromethane, THF, and *N,N*-dimethylformamide (DMF). Because of its $\text{p}K_{\text{a}}$ of 7.0 ± 0.5 , PDMA can be partially protonated in water and is therefore water-soluble. The capped PDMA brushes render NCs soluble in both aqueous and organic phases, thus providing the freedom to disperse the coated NCs in either aqueous or organic solvents. This differs from traditional phase-transfer methods used to one-way direct NCs from the aqueous to the organic phase or vice versa with the aid of amphiphilic ligands. Fourth, PDMA chains are weak cationic polyelectrolytes that allow for the conjugation of other functional materials, such as biomolecules, through electrostatic interactions. Scheme 1 depicts our method of generating amphibious NCs. First, ATRP initiators were capped on NCs by ligand exchange. Second, PDMA brushes were formed on NCs by surface-initiated ATRP.



Scheme 1. Generation of PDMA brushes on NCs by surface-initiated ATRP.

$\gamma\text{-Fe}_2\text{O}_3$ NCs of 4 nm were prepared in toluene by using a method based on that reported by Sun and Zeng.^[4c] The surface stabilizers of the NCs were replaced with 2-bromo-2-methylpropionic acid (BMPA), as described by Yang and co-workers.^[7a,8] In our work, little variation was observed by transmission electron microscopy (TEM) and UV/Vis absorption spectroscopy when $\gamma\text{-Fe}_2\text{O}_3$ NCs were compared before and after ligand exchange. Over a period of 2 h of BMPA-initiated ATRP, PDMA brushes were generated on $\gamma\text{-Fe}_2\text{O}_3$ NCs in toluene, marked as $\gamma\text{-Fe}_2\text{O}_3\text{@PDMA}$. The capped NCs could be isolated as a solid, which could be redispersed in either water or common organic solvents. A typical TEM image of $\gamma\text{-Fe}_2\text{O}_3\text{@PDMA}$ nanoparticles reveals cores of $\gamma\text{-Fe}_2\text{O}_3$ of 4 nm (Figure 1a). Figure 1b shows typical absorption spectra of $\gamma\text{-Fe}_2\text{O}_3\text{@PDMA}$ nanoparticles, dispersed in water (black), chloroform (red), and toluene (blue); there is little difference between the spectra and they are similar to that of the initial $\gamma\text{-Fe}_2\text{O}_3$ NCs (black dotted). The absorption spectra prove that the PDMA shell renders $\gamma\text{-Fe}_2\text{O}_3$ NCs soluble in both water and organic solvents. Our experiments indicate that $\gamma\text{-Fe}_2\text{O}_3\text{@PDMA}$ nanoparticles can be well

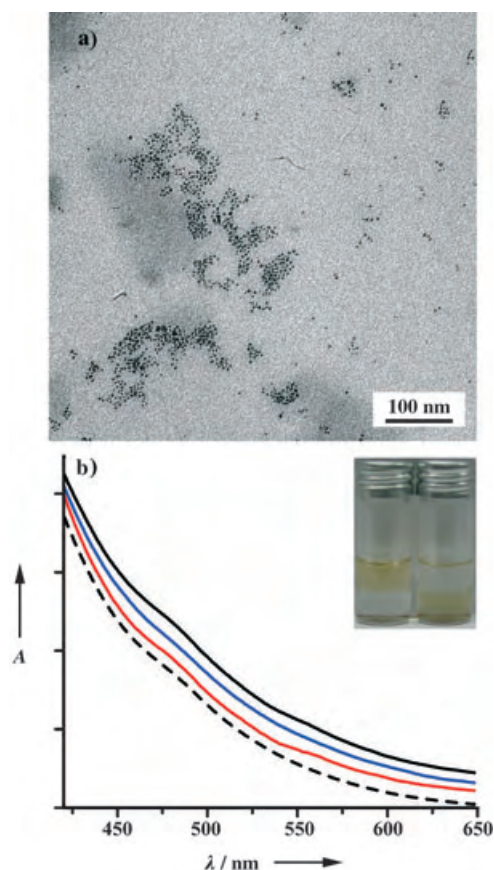


Figure 1. a) TEM image of $\gamma\text{-Fe}_2\text{O}_3\text{@PDMA}$ nanoparticles consisting of 4 nm $\gamma\text{-Fe}_2\text{O}_3$ cores. b) UV/Vis absorption spectra of $\gamma\text{-Fe}_2\text{O}_3\text{@PDMA}$ nanoparticles dispersed in water (black), toluene (blue), and chloroform (red) as well as of 4-nm $\gamma\text{-Fe}_2\text{O}_3$ NCs dispersed in toluene (black dashed). The inset shows photographs of an aqueous solution of pH 7 above chloroform. In the left sample the $\gamma\text{-Fe}_2\text{O}_3\text{@PDMA}$ nanoparticles were initially dissolved in water and in the right sample in chloroform.

dispersed in water and common organic solvents (except alkanes such as hexane). The inset in Figure 1 b shows that γ -Fe₂O₃@PDMA nanoparticles prefer to reside in the bulk water of pH 7 (left) or chloroform phase (right) and no nanoparticles are observed at the water/chloroform interface, which demonstrates their amphibious nature. Because water solubility depends on the protonation of the ternary amine groups of the PDMA chains, the transfer from the aqueous phase to organic phase is expected to be slow in chloroform and deprotonation is expected to be slow in water. Hence, we do not observe phase transfer within a few days. This transfer is accelerated by reducing the pH and subjecting the sample to sonification. Even after sonification and a further wait of over two weeks, more than 90 % of the particles remained in the phase in which they were initially dissolved, as determined by absorption spectroscopy (see the Supporting Information). As determined by dynamic light scattering (DLS), the hydrodynamic diameter of the resulting γ -Fe₂O₃@PDMA nanoparticles is approximately 8 nm, which suggests that the PDMA shell has a thickness of about 2 nm. Furthermore, DLS does not reveal any sign of aggregation. Due to the living character of ATRP, the thickness of the PDMA shell can be controlled by varying the polymerization time (see the Supporting Information).

The γ -Fe₂O₃@PDMA nanoparticles remain magnetic. In their aqueous or organic dispersions, we observe the accumulation of γ -Fe₂O₃@PDMA nanoparticles on the wall of a glass vial by applying an external magnetic field (see the Supporting Information). Our preliminary measurements with a superconducting quantum interference device (SQUID) indicate that these γ -Fe₂O₃@PDMA nanoparticles become superparamagnetic at about 20 K. The study of the magnetic property of γ -Fe₂O₃@PDMA nanoparticles as a function of their PDMA shell thickness is underway.

To generalize our method and to investigate the solvent effect on properties of NCs, we employed Au NCs as cores to grow PDMA brushes as their plasmon absorption band is sensitive to their environment.^[9] Au NCs of 12 nm were synthesized by citrate reduction of chloroauric acid in the aqueous phase.^[2a] To prevent Au NCs from aggregating during ligand exchange, 2,2'-dithiobis[1-(2-bromo-2-methylpropionyloxy)ethane] (DTBE) was synthesized as an ATRP initiator.^[8] During DTBE-initiated aqueous ATRP, PDMA brushes were grown on Au NCs. PDMA-capped Au nanoparticles are denoted as Au@PDMA. DLS data reveal that the hydrodynamic diameter of Au@PDMA nanoparticles was about 32 nm, which corresponds to a PDMA shell of 10 nm in thickness. Figure 2a shows a typical TEM image of Au@PDMA nanoparticles in which individual nanoparticles with 12 nm Au cores are discernable. Due to the high electron density of the central Au core, it is not possible to detect the PDMA shell. During TEM measurement, drying may reduce the PDMA shell thickness considerably as the brushes collapse under vacuum.^[7f] Thus, in some cases the core-to-core distance is smaller than the shell thickness in Figure 2a. As with the γ -Fe₂O₃@PDMA nanoparticles, those of Au@PDMA can be dispersed in both water and common organic solvents. The inset in Figure 2b demonstrates the amphibious nature of Au@PDMA nanoparticles. In comparison with that

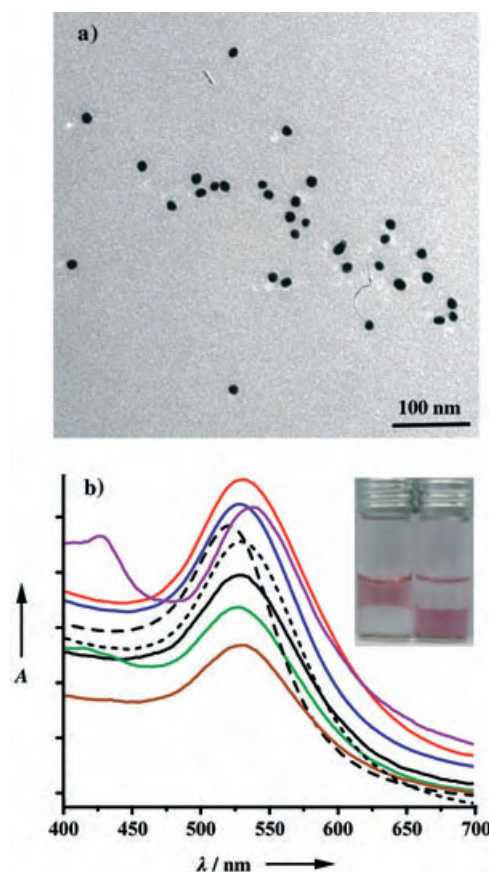


Figure 2. a) TEM image of Au@PDMA nanoparticles consisting of 12 nm Au cores. b) UV/Vis absorption spectra of Au@PDMA nanoparticles dispersed in water (black), methanol (green), DMF (brown), toluene (blue), chloroform (red), and 0.5 M NaCl aqueous solution (black dotted), and of quaternized Au@PDMA nanoparticles (purple) as well as of 12-nm Au NCs dispersed in water (black dashed). The inset in (b) shows photographs of a water solution of pH 7 above chloroform. In the left sample the Au@PDMA nanoparticles were initially dissolved in water and in the right sample in chloroform.

of Au NCs (520 nm, black dotted, Figure 2b), the plasmon absorbance band of Au@PDMA nanoparticles is red-shifted to 530 nm due to an increase of the refractive index of the surrounding of the Au cores,^[9] which is induced by the PDMA brushes. Figure 2b verifies that the plasmon absorbance band of Au@PDMA nanoparticles has little dependence on the dispersion solvents (water black; methanol green; DMF brown; chloroform red; toluene blue). Turning neutral PDMA brushes into cationic brushes by quaternization, one observes a red-shift of the plasmon absorbance band (purple line, Figure 2). This shift suggests that the plasmon absorbance of Au cores is mainly determined by the capping PDMA brushes. Furthermore, we noted that an aqueous dispersion of Au@PDMA nanoparticles that contain 0.5 M NaCl remains stable for at least 3 months without any visible precipitation. The dotted line in Figure 2b indicates that the introduction of NaCl causes little change of the plasmon absorbance band of Au NCs. These data prove an absence of aggregates and a high colloidal stability of Au@PDMA nanoparticles in the aqueous phase.

In summary, we have demonstrated a new and efficient approach—coating with PDMA brushes—to pull both hydrophobic and hydrophilic NCs into specific media without detectable aggregation, while their intrinsic magnetic and optical properties are maintained. PDMA brushes have been formed on hydrophobic $\gamma\text{-Fe}_2\text{O}_3$ and hydrophilic Au NCs by surface initiated ATRP. The capping PDMA brushes render NCs an amphibious character; the coated NCs can be dispersed in both aqueous and common organic solvents except alkanes without sticking to the aqueous/oil interfaces. The PDMA-capped NCs exhibit long-term colloidal stability in aqueous and organic media. Our approach provides interesting opportunities for the exploitation of different NCs in aqueous media for biological applications. Our preliminary results demonstrate the potential of forming NC bioconjugates through electrostatic interactions between proteins and PDMA brushes (see the Supporting Information). Clearly, our approach can be extended to other NCs, such as CdTe and CoPt, which is ongoing research in our laboratory. Moreover, such amphibious NCs provide functional building blocks for other existing assembly strategies.

Experimental Section

The toluene dispersion of 4 nm $\gamma\text{-Fe}_2\text{O}_3$ NCs was prepared based on the method of Sun and Zeng.^[4c] The aqueous dispersion of citrate-stabilized Au NCs of 12 nm was synthesized as described elsewhere.^[2a] BMPA was purchased from Aldrich. DTBE was obtained by acrylation of bis-(2-hydroxyethyl) disulfide with 2-bromoisobutryl bromide in the presence of triethylamine by using a procedure described elsewhere.^[10] The $\gamma\text{-Fe}_2\text{O}_3$ @BMPA and Au@DTBE NCs were prepared as described previously.^[8] ATRP of DMA on $\gamma\text{-Fe}_2\text{O}_3$ @BMPA nanoparticles was carried out in toluene at 40°C, triggered by adding CuBr/(–)-sparteine (SP) complex. Aqueous ATRP of DMA on Au@DTBE nanoparticles was started by adding the CuBr/2,2'-bipyridine (BPy) catalyst at room temperature. The initial DMA concentration based on toluene or water was 50 vol %; the molar ratio of initiator/CuBr/SP or BPy was 1:1:2. After 2 h ATRP under Ar, the PDMA-capped NCs were collected by repeating the cycle of centrifugation/THF wash/redispersion for three times.

UV/Vis absorption spectra were recorded by using a Cary 50 UV/Vis spectrophotometer. TEM images were obtained by a Zeiss EM 912 Omega microscope at an acceleration voltage of 120 kV. DLS measurements were implemented by a Malvern HPPS 500.

Received: June 21, 2004

Revised: December 13, 2004

Published online: January 31, 2005

Keywords: colloids · nanostructures · nanotechnology · phase transfer · polymerization

- [3] a) S. Underwood, P. Mulvaney, *Langmuir* **1994**, *10*, 3427–3430; b) L. M. Liz-Marzan, I. Lado-Tourino, *Langmuir* **1996**, *12*, 3585–3589; c) K. V. Sarathy, G. U. Kulkarni, C. N. R. Rao, *Chem. Commun.* **1997**, 537–538; d) B. Kim, S. L. Tripp, A. Wei, *J. Am. Chem. Soc.* **2001**, *123*, 7955–7956; e) N. Gopanik, D. V. Talapin, A. L. Rogach, A. Eychmüller, H. Weller, *Nano Lett.* **2002**, *2*, 803–806; f) K. Mayya, F. Caruso, *Langmuir*, **2003**, *19*, 6987–6993.
- [4] a) Z. Peng, X. Peng, *J. Am. Chem. Soc.* **2001**, *123*, 183–184; b) E. V. Shevchenko, D. V. Talapin, A. L. Rogach, A. Kornowski, M. Haase, H. Weller, *J. Am. Chem. Soc.* **2002**, *124*, 11480–11485; c) S. Sun, H. Zeng, *J. Am. Chem. Soc.* **2002**, *124*, 8204–8205; d) L. Manna, D. J. Milliron, D. Meisel, E. C. Scher, A. P. Alivisatos, *Nat. Mater.* **2003**, *2*, 382–385.
- [5] a) M. Bruchez, M. Moronne, P. Gin, S. Weiss, A. P. Alivisatos, *Science* **1998**, *281*, 2013–2016; b) W. C. Chan, S. Nie, *Science* **1998**, *281*, 2016–2018; c) A. C. Templeton, W. P. Wuelfing, R. W. Murray, *Acc. Chem. Res.* **2000**, *33*, 27–36; d) J. Simard, C. Briggs, A. K. Boal, V. M. Rotello, *Chem. Commun.* **2000**, 1943–1944; e) D. Gittins, F. Caruso, *Angew. Chem.* **2001**, *113*, 3089–3092; *Angew. Chem. Int. Ed.* **2001**, *40*, 3001–3004.
- [6] a) D. Gerion, F. Pinaud, S. C. Williams, W. J. Parak, D. Zanchet, S. Weiss, A. P. Alivisatos, *J. Phys. Chem. B* **2001**, *105*, 8861–8871; b) B. Dubertret, P. Skourides, D. J. Norris, V. Noireaux, A. H. Brivanlou, A. Libchaber, *Science* **2002**, *298*, 1759–1762; c) X. Wu, H. Liu, J. Liu, K. N. Haley, J. A. Treadway, J. P. Larson, N. Ge, F. Peale, M. P. Bruchez, *Nat. Biotechnol.* **2003**, *21*, 41–46.
- [7] a) Y. Wang, X. Teng, J. Wang, H. Yang, *Nano Lett.* **2003**, *3*, 789–793; b) K. Ohno, K. Koh, Y. Tsujii, T. Fukuda, *Angew. Chem.* **2003**, *115*, 2857–2860; *Angew. Chem. Int. Ed.* **2003**, *42*, 2751–2754; c) T. K. Mandal, M. S. Fleming, D. R. Walt, *Nano Lett.* **2002**, *2*, 3–7; d) K. Kamata, Y. Lu, Y. Xia, *J. Am. Chem. Soc.* **2003**, *125*, 2384–2385; e) S. Nuß, H. Böttcher, H. Wurm, M. L. Hallensleben, *Angew. Chem.* **2001**, *113*, 4137–4139; *Angew. Chem. Int. Ed.* **2001**, *40*, 4016–4018; f) X. Chen, D. P. Randall, C. Perruchot, J. F. Watts, T. E. Patten, T. von Werne, S. P. Armes, *J. Colloid Interface Sci.* **2003**, *257*, 56–64.
- [8] H. Duan, D. Wang, D. G. Kurth, H. Möhwald, *Angew. Chem.* **2004**, *116*, 5757–5760; *Angew. Chem. Int. Ed.* **2004**, *43*, 5639–5642.
- [9] P. Mulvaney, *Langmuir* **1996**, *12*, 788–800.
- [10] R. R. Shah, D. Merrecyces, M. Husemann, I. Rees, N. L. Abbott, C. J. Hawker, J. L. Hedrick, *Macromolecules* **2000**, *33*, 597–605.

[1] For reviews, see: a) H. Weller, *Angew. Chem.* **1993**, *105*, 43–55; *Angew. Chem. Int. Ed. Engl.* **1993**, *32*, 41–53; b) A. P. Alivisatos, *Science* **1996**, *271*, 933–937; c) C. B. Murray, C. R. Kagan, M. G. Bawendi, *Annu. Rev. Mater. Sci.* **2000**, *30*, 545–610.

[2] For reviews, see: a) *Colloidal Gold: Principles, Methods, and Applications* (Ed.: M. A. Hayat), Academic Press, San Diego, **1991**; b) A. N. Shipway, E. Katz, I. Willner, *ChemPhysChem* **2000**, *1*, 18–52; c) L. M. Liz-Marzan, P. Mulvaney, *J. Phys. Chem. B* **2003**, *107*, 7312–7326; d) H. Weller, *Philos. Trans. R. Soc. London Ser. A* **2003**, *361*, 229–239.

Heterobimetallic Main-Group–Transition-Metal Paddle-Wheel Carboxylates**

Evgeny V. Dikarev,* Thomas G. Gray, and Bo Li

“Main group elements and transition metal fragments interact with one another in interesting and often unexpected fashions”

K. H. Whitmire

Heterometallic carboxylates along with alkoxides are of great interest as they can be used as single-source precursors for binary or multimetallic oxides.^[1] Bismuth-containing oxide materials cover a broad range of high-technology applications, including high T_c superconductivity,^[2] oxide-ion conductivity,^[3] nonlinear optics,^[4] catalysis,^[5] and ferroelectrics.^[6] Of all heavy metals, bismuth has the greatest potential for applications within the context of green chemistry.^[7] The first heterometallic precursor for bismuth-containing inorganic materials was reported only in 1996^[8] and several others have been isolated since then.^[9] However, none of these materials are homoleptic carboxylates. Recently we described a rational synthesis of the first bismuth(II) carboxylate, $[\text{Bi}_2(\text{O}_2\text{CCF}_3)_4]$, which forms a dimeric tetrabridged structure (Figure 1 a).^[10] Owing to the high reactivity of this unusual complex and its potential Lewis base character, we decided to study its reactions with Lewis acidic transition-metal carboxylates to obtain mixed-metal complexes of the general formula $[\text{BiM}(\text{O}_2\text{CR})_4]$. Heterometallic carboxylates can assemble in two different ways: 1) through formation of Lewis acid–base adducts (Figure 1, b and c) to give an ordered arrangement of homonuclear units in infinite chains, and 2) through formation of a “true” heterobimetallic unit bridged by carboxylate ligands and further supported by direct metal–metal bonding (Figure 1 d) to provide homogenization at the molecular level. Herein we report the synthesis and characterization of the first two bismuth-

containing heterobimetallic carboxylates that indeed adopt the paddle-wheel structure shown in Figure 1 d, $[\text{BiRh}(\text{O}_2\text{CCF}_3)_4]$ (**1**) and $[\text{BiRu}(\text{O}_2\text{CCF}_3)_4]$ (**2**).

Compounds **1** and **2** were obtained by heating stoichiometric mixtures of $[\text{Bi}_2(\text{O}_2\text{CCF}_3)_4]$ and unligated $[\text{M}_2(\text{O}_2\text{CCF}_3)_4]$ (**1**: $\text{M} = \text{Rh}$; **2**: $\text{M} = \text{Ru}$) in the solid state in

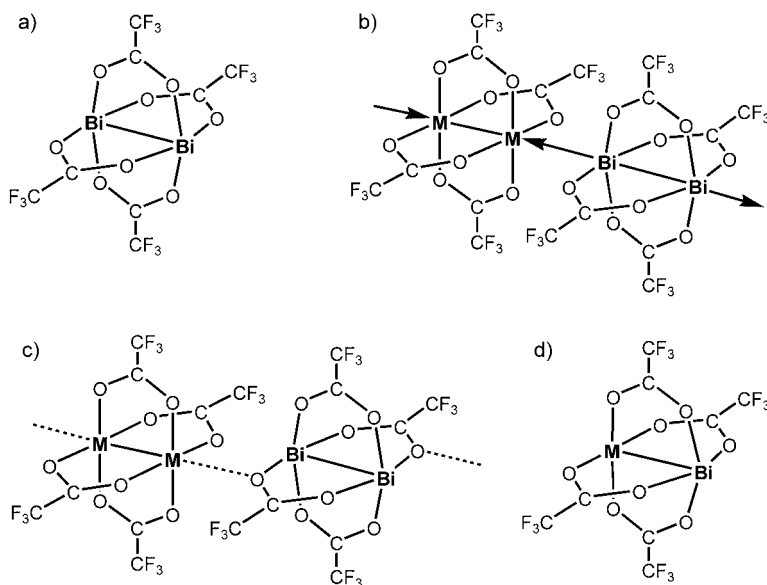


Figure 1. a) Dimeric tetrabridged structure of $[\text{Bi}_2(\text{O}_2\text{CCF}_3)_4]$; b), c) Lewis acid–base adducts formed by homonuclear units; d) paddle-wheel structure of “true” heterobimetallic unit $[\text{BiM}(\text{O}_2\text{CCF}_3)_4]$.

a sealed ampoule. While the formation of **1** proceeds well, the yield of **2** is far from quantitative. Our attempts to prepare these heterometallic compounds by heating in toluene at reflux failed. The use of Bi^{III} trifluoroacetate instead of Bi^{II} results in the same products with lower yields; this finding can be explained by our previous observation^[10] that Bi^{III} trifluoroacetate partially disproportionates in the vapor phase to give Bi^{II} species.

Bismuth rhodium tetra(trifluoroacetate) (**1**) is volatile and can be quantitatively resublimed upon heating. It shows fair thermal stability in a sealed ampoule, decomposing at around 250°C. In open air, crystals of **1** are more stable than both parent homometallic species. Compound **1** is soluble in anhydrous, deoxygenated toluene, acetone, ether, ethyl alcohol, and THF and can be kept in these solutions for prolonged times. It is also partially soluble in CHCl_3 , CH_2Cl_2 , and DMSO. The infrared and mass spectra indicate that the dimeric molecules remain intact in solution.

The structures of **1** and **2**^[11] consist of heterobimetallic paddle-wheel units (Figure 2). Each bismuth atom maintains a distorted square-pyramidal coordination geometry composed of one Rh(Ru) and four O atoms. In contrast, the similar coordination around the transition-metal ion is less distorted. The distances between the bismuth and transition-metal atoms are 2.5493(3) and 2.5487(4) Å for **1** and **2**, respectively. Table 1 shows that these distances are significantly shorter than the average values of metal–metal

[*] Prof. Dr. E. V. Dikarev, B. Li
Department of Chemistry
University at Albany
Albany, NY 12222 (USA)
Fax: (+1) 518-442-3462
E-mail: dikarev@albany.edu

Prof. Dr. T. G. Gray
Department of Chemistry
Case Western Reserve University
Cleveland, OH 44106 (USA)

[**] This work was supported by the University at Albany, SUNY. E.V.D. also thanks the National Science Foundation for the CCD X-ray diffractometer (NSF-01300985). T.G.G. acknowledges a National Institutes of Health postdoctoral fellowship. The authors are grateful to Professor D. G. Nocera (MIT) for computer time, Professor R. Clérac (CRPP, University Bordeaux 1) for magnetic measurements, Dr. M. Shatruk (Texas A&M University) for mass spectrometry experiments, and Dr. I. Novozhilova (SUNY Buffalo) for technical assistance.

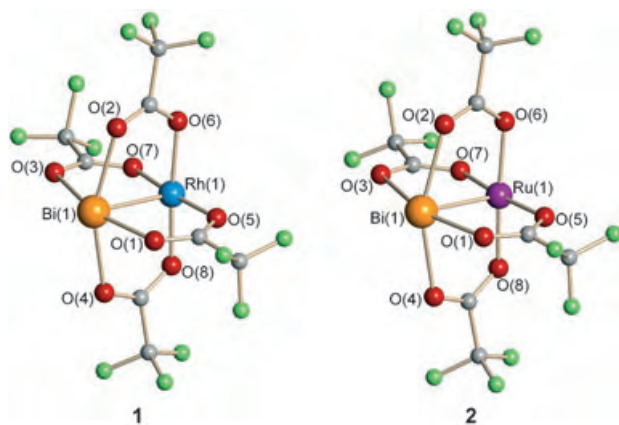


Figure 2. Paddle-wheel heterobimetallic carboxylates $[\text{BiM}(\text{O}_2\text{CCF}_3)_4]$ (1: $\text{M} = \text{Rh}$; 2: $\text{M} = \text{Ru}$). 1: $\text{Bi}-\text{Rh}$ 2.5493(3), $\text{Bi}-\text{O}$ 2.315(3)–2.575(3), $\text{Rh}-\text{O}_{\text{av}}$ 2.018(3) Å; 2: $\text{Bi}-\text{Ru}$ 2.5487(4), $\text{Bi}-\text{O}$ 2.347(3)–2.691(3), $\text{Ru}-\text{O}_{\text{av}}$ 2.022(3) Å.

Table 1: Metal–metal bond distances [Å] in homo- and heterometallic paddle-wheel carboxylates

metal–metal bonds	$\text{M} = \text{Rh}$	$\text{M} = \text{Ru}$
$\text{Bi}-\text{Bi}^{[a]}$	2.9462(3)	2.9462(3)
$\text{M}-\text{M}^{[b]}$	2.3813(8)	2.2645(6)
$1/2\Sigma$	2.664	2.606
$\text{Bi}-\text{M}$	2.5493(3)	2.5487(4)

[a] See Reference [10]. [b] See Reference [12].

distances in the corresponding homometallic trifluoroacetates. Importantly, the $\text{M}-\text{O}$ ($\text{M} = \text{Bi}$, Rh , Ru) distances in heterometallic units **1** and **2** are essentially the same as the corresponding distances in the homometallic molecules $[\text{M}_2^{\text{II}}(\text{O}_2\text{CCF}_3)_4]$.^[10,12]

The bimetallic molecules **1** and **2** act as one-end Lewis acids. In the solid state they form extended chain structures

(Figure 3 a) through axial coordination of the transition-metal center to one of the Bi-bound carboxylate oxygen atoms from a neighboring unit. When **1** was treated with excess $(\text{C}_2\text{H}_5)_2\text{O}\cdot\text{BF}_3$, the monoadduct $[\text{BiRh}(\text{O}_2\text{CCF}_3)_4]\cdot\text{O}(\text{C}_2\text{H}_5)_2$ (**3**) was the only product isolated from the solution. The structure of **3** reveals that the ether molecule is coordinated to the Rh end of the heterometallic unit (Figure 3 b), while the Bi end exhibits neither Lewis acidic nor basic properties.

The examples of heterobimetallic carboxylates with direct metal–metal bonding are by far limited to quadruply-bonded Group 6 transition metals,^[13] $[\text{MoM}(\text{O}_2\text{CR})_4]$ ($\text{M} = \text{Cr}$, $\text{R} = \text{Me}$; $\text{M} = \text{W}$, $\text{R} = t\text{Bu}$). Several other heterometallic carboxylates,^[14] that also contain main group–transition-metal species, $[\text{PdTi}(\text{O}_2\text{CCH}_3)_5]$, $[\text{Au}_2\text{M}(\text{O}_2\text{CCH}_3)_8]$ ($\text{M} = \text{Pb}$, Sr), and $[\text{M}_2\text{Ca}(\text{O}_2\text{CR})_6]$ ($\text{M} = \text{Zn}$, $\text{R} = \text{Et}$; $\text{M} = \text{Co}$, $\text{R} = t\text{Bu}$), are reported to maintain no metal–metal bonding interactions. To understand better the bonding character between bismuth and transition metals,^[15] scalar relativistic density functional theory calculations were carried out for **1** and **2**. The rhodium complex, which is experimentally diamagnetic, was calculated in a spin-restricted manner; the calculation for the ruthenium compound was spin-unrestricted. As metal–metal bond lengths are especially sensitive to crystal-packing effects,^[16] all calculations were run on the experimental geometries.

Figure 4 shows a diagram of the calculated energies of one-electron (Kohn–Sham) orbitals that display significant d-metal character. Images of selected orbitals are inset. Irreducible representations of the metal d orbitals in C_{4v} symmetry are indicated; however, the crystallographic structure departs from this idealized symmetry, and d_{xz} and d_{yz} orbitals (i.e. in C_{4v}) are only approximately degenerate. In both complexes, the Bi–M bonding combination lies below the frontier in energy and is doubly occupied. The highest-occupied molecular orbitals (HOMOs) are predominantly transition-metal d orbitals (d_{xy} , **1**; d_{yz} , **2**) that are effectively nonbonding with respect to bismuth. One consequence is that

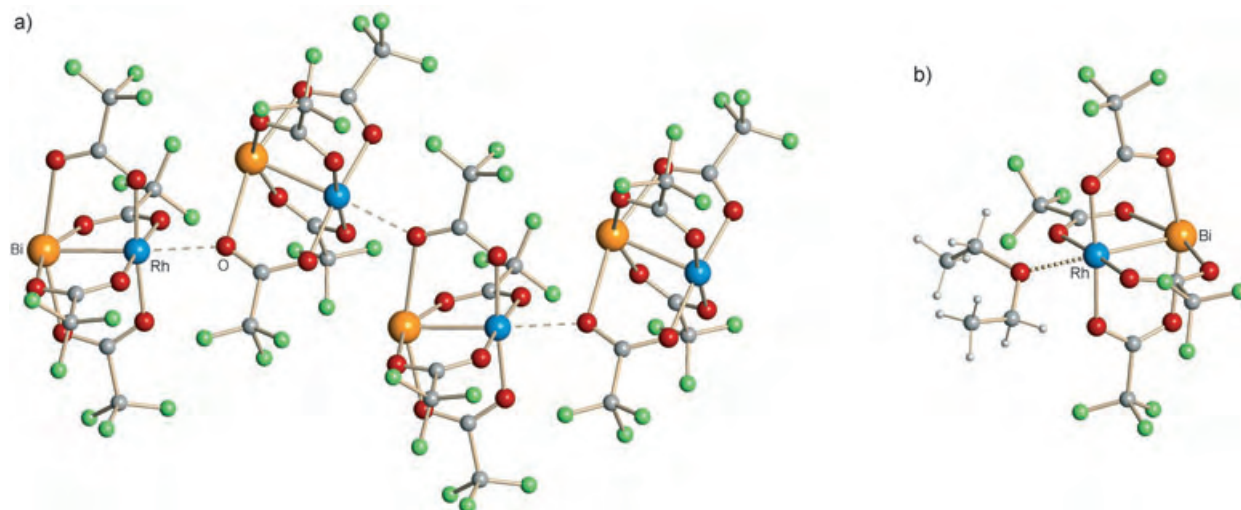


Figure 3. a) A fragment of a 1D infinite chain in the structure of **1**. Intermolecular contacts $\text{Rh}\cdots\text{O}$ 2.413(3) Å, $\text{Bi}\cdots\text{Rh}\cdots\text{O}$ 175.83(7)°. For **2** (chain structure not shown): $\text{Ru}\cdots\text{O}$ 2.369(3) Å, $\text{Bi}\cdots\text{Ru}\cdots\text{O}$ 176.34(8)°. b) Crystal structure of the $[\text{BiRh}(\text{O}_2\text{CCF}_3)_4]\cdot\text{ether}$ adduct **3**. $\text{Bi}-\text{Rh}$ 2.5519(3), $\text{Rh}\cdots\text{O}$ 2.291(3) Å, $\text{Bi}\cdots\text{Rh}\cdots\text{O}$ 179.60(8)°.

the program MOLEKEL;^[24] default isodensity values were applied. Mayer bond orders were calculated with the program MAYER.^[17a,25]

Received: October 26, 2004

Revised: December 3, 2004

Published online: February 3, 2005

Keywords: bismuth · carboxylate ligands · density functional calculations · heterometallic complexes · transition metals

- [1] a) L. G. Hubert-Pfalzgraf, *Inorg. Chem. Commun.* **2003**, 6, 102; b) V. G. Kessler, *Chem. Commun.* **2003**, 1213; c) K. G. Caulton, L. G. Hubert-Pfalzgraf, *Chem. Rev.* **1990**, 90, 969.
- [2] a) P. Majewski, *J. Mater. Res.* **2000**, 15, 854; b) M. L. Norton in *Chemistry of Superconductor Materials* (Ed.: T. A. Vanderah), Noyes, New Jersey, **1992**, pp. 347–379.
- [3] a) J. H. Thurston, T. Ould-Ely, D. Trahan, K. H. Whitmire, *Chem. Mater.* **2003**, 15, 4407; b) N. M. Sammes, G. A. Tompsett, H. Nafe, F. Aldinger, *J. Eur. Ceram. Soc.* **1999**, 19, 1801.
- [4] A. Sharan, I. An, C. Chen, R. W. Collins, J. Lettieri, Y. Jia, D. G. Schlom, V. Gopalan, *Appl. Phys. Lett.* **2003**, 83, 5169.
- [5] a) E. M. Slavinskaya, S. A. Veniaminov, P. Notte, A. S. Ivanova, A. I. Boronin, Yu. A. Chesalov, I. A. Polukhina, A. S. Noskov, *J. Catal.* **2004**, 222, 129; b) B. Mazumder, J. C. Vedrine, *Appl. Catal. A* **2003**, 245, 87; c) R. Rangel, P. Bartolo-Perez, A. Gomez-Cortes, G. Diaz, S. Fuentes, D. H. Galvan, *J. Mater. Synth. Process.* **2001**, 9, 207; d) E. Mamedov, *Catal. Rev. Sci. Eng.* **1994**, 36, 1.
- [6] a) R. C. Mehrotra, A. Singh, *Chemtracts* **2003**, 16, 734; b) L. E. Cross, R. C. Pohanka, *Mater. Res. Bull.* **1971**, 6, 939.
- [7] P. C. Andrews, G. B. Deacon, W. R. Jackson, M. Maguire, N. M. Scott, B. W. Skelton, A. H. White, *J. Chem. Soc. Dalton Trans.* **2002**, 4634.
- [8] J. W. Pell, W. C. Davis, H. C. zur Loye, *Inorg. Chem.* **1996**, 35, 5754.
- [9] a) J. H. Thurston, D. Trahan, T. Ould-Ely, K. H. Whitmire, *Inorg. Chem.* **2004**, 43, 3299; b) J. H. Thurston, K. H. Whitmire, *Inorg. Chem.* **2003**, 42, 2014; c) R. E. Bachman, K. H. Whitmire, J. H. Thurston, A. Gulea, O. Stavila, V. Stavila, *Inorg. Chim. Acta* **2003**, 346, 249; d) J. H. Thurston, K. H. Whitmire, *Inorg. Chem.* **2002**, 41, 4194; e) M. Hunger, C. Limberg, E. Kaifer, P. Rutsch, *J. Organomet. Chem.* **2002**, 641, 9.
- [10] E. V. Dikarev, B. Li, *Inorg. Chem.* **2004**, 43, 3461.
- [11] X-ray crystal data for **1**: BiRhC₈F₁₂O₈, *M_r* = 763.97, light brown block, 0.26 × 0.11 × 0.07 mm³, orthorhombic, space group *Pbca*, *a* = 9.7378(4), *b* = 16.8545(8), *c* = 20.9850(10) Å, *V* = 3444.2(3) Å³, *Z* = 8, *T* = 173(2) K, ρ_{calcd} = 2.947 g cm⁻³, $2\theta_{\text{max}}$ = 56.62°. For **2**: BiRuC₈F₁₂O₈, *M_r* = 762.13, red block, 0.15 × 0.08 × 0.08 mm³, orthorhombic, space group *Pbca*, *a* = 9.7061(5), *b* = 16.8655(9), *c* = 21.1527(12) Å, *V* = 3462.7(3) Å³, *Z* = 8, *T* = 173(2) K, ρ_{calcd} = 2.924 g cm⁻³, $2\theta_{\text{max}}$ = 56.48°. For **3**: BiRhC₁₂F₁₂O₉H₁₀, *M_r* = 838.09, orange plate, 0.19 × 0.19 × 0.04 mm³, monoclinic, space group *C2/c*, *a* = 31.0308(19), *b* = 10.0341(6), *c* = 16.2637(10) Å, β = 116.7220(10)°, *V* = 4523.1(5) Å³, *Z* = 8, *T* = 173(2) K, ρ_{calcd} = 2.461 g cm⁻³, $2\theta_{\text{max}}$ = 56.56°. Bruker SMART APEX CCD diffractometer, MoK α radiation (λ = 0.71073 Å). The structures were solved by direct methods and refined using the Bruker SHELXTL (version 6.1) Software Package. Data were corrected for absorption effects using the empirical methods SADABS (min./max. apparent transmission are 0.311, 0.608, and 0.401 for **1**, **2**, and **3**, respectively). All non-hydrogen atoms were refined anisotropically except the disordered fluorine atoms. Hydrogen atoms in **3** were included in idealized positions for structure factor calculations. The fluorine atoms of some CF₃ groups were disordered over two or three different rotational orientations. This disorder was modeled individually in each case. In the structure of **3** both ethyl groups of ether were found to be disordered over two orientations. For **1** full-matrix refinement on *F*² converged at *R*1 = 0.0225 and *wR*2 = 0.0511 for 310 parameters and 72 restraints and 3785 reflections with *I* > 2σ(*I*) (*R*1 = 0.0257, *wR*2 = 0.0523 for 4171 unique reflections) and a goodness-of-fit of 1.056. For **2** full-matrix refinement on *F*² converged at *R*1 = 0.0266 and *wR*2 = 0.0626 for 298 parameters and 54 restraints and 3570 reflections with *I* > 2σ(*I*) (*R*1 = 0.0342, *wR*2 = 0.0653 for 4179 unique reflections) and a goodness-of-fit of 1.039. For **3** full-matrix refinement on *F*² converged at *R*1 = 0.0215 and *wR*2 = 0.0527 for 325 parameters and 25 restraints and 4926 reflections with *I* > 2σ(*I*) (*R*1 = 0.0237, *wR*2 = 0.0536 for 5310 unique reflections) and a goodness-of-fit of 1.051. CCDC 252670, CCDC 252671, and CCDC 252672 (**1**, **2**, and **3**) contain the supplementary crystallographic data for this paper. These data can be obtained free of charge from the Cambridge Crystallographic Data Centre via www.ccdc.cam.ac.uk/data_request/cif.
- [12] a) F. A. Cotton, E. V. Dikarev, X. Feng, *Inorg. Chim. Acta* **1995**, 237, 19; b) E. V. Dikarev, A. S. Filatov, M. A. Petrukhina, unpublished results.
- [13] a) C. D. Garner, R. G. Senior, T. J. King, *J. Am. Chem. Soc.* **1976**, 98, 3526; b) V. Katovic, R. E. McCarley, *J. Am. Chem. Soc.* **1978**, 100, 5586.
- [14] a) S. Adam, A. Bauer, O. Timpe, U. Wild, G. Mestl, W. Bensch, R. Schlogl, *Chem. Eur. J.* **1998**, 4, 1458; b) A. L. Balch, B. J. Davis, E. Y. Fung, M. M. Olmstead, *Inorg. Chim. Acta* **1993**, 212, 149; c) P. G. Jones, R. Schelbach, E. Schwarzmann, C. Thone, A. Vielmader, *Z. Naturforsch. B* **1988**, 43, 807; d) P. G. Jones, *Acta Crystallogr. Sect. C* **1984**, 40, 804; e) Y. Cui, X. Zhang, F. Zheng, J. Ren, G. Chen, Y. Qian, J. Huang, *Acta Crystallogr. Sect. C* **2000**, 56, 1198.
- [15] T. R. Cundari, *Chem. Rev.* **2000**, 100, 807.
- [16] A. Martin, A. G. Orpen, *J. Am. Chem. Soc.* **1996**, 118, 1464.
- [17] a) A. J. Bridgeman, G. Cavigliasso, L. R. Ireland, J. Rothery, *J. Chem. Soc. Dalton Trans.* **2001**, 2095; b) I. Mayer, *Chem. Phys. Lett.* **1983**, 97, 270.
- [18] F. A. Cotton, R. A. Walton, *Multiple Bonds between Metal Atoms*, Oxford University Press, New York, **1993**.
- [19] a) G. te Velde, F. M. Bickelhaupt, E. J. Baerends, C. Fonseca Guerra, S. J. A. van Gisbergen, J. G. Snijders, T. Ziegler, *J. Comput. Chem.* **2001**, 22, 931; b) C. Fonseca Guerra, J. G. Snijders, G. te Velde, E. J. Baerends, *Theor. Chem. Acc.* **1998**, 99, 391; c) ADF2003.01, SCM, Theoretical Chemistry, Vrije Universiteit, Amsterdam, The Netherlands, <http://www.scm.com>.
- [20] S. H. Vosko, L. Wilk, M. Nusair, *Can. J. Phys.* **1980**, 58, 1200.
- [21] A. D. Becke, *Phys. Rev. A* **1988**, 38, 3098.
- [22] J. P. Perdew, *Phys. Rev. B* **1986**, 33, 8822.
- [23] a) E. van Lenthe, E. J. Baerends, J. G. Snijders, *J. Chem. Phys.* **1993**, 99, 4597; b) E. van Lenthe, E. J. Baerends, J. G. Snijders, *J. Chem. Phys.* **1994**, 101, 9783; c) E. van Lenthe, J. G. Snijders, E. J. Baerends, *J. Chem. Phys.* **1996**, 105, 6505; d) E. van Lenthe, R. van Leeuwen, E. J. Baerends, J. G. Snijders, *Int. J. Quantum Chem.* **1996**, 57, 281.
- [24] a) MOLEKEL 4.3, P. Flükiger, H. P. Lüthi, S. Portmann, J. Weber, Swiss Center for Scientific Computing, Manno (Switzerland), **2000–2002**; b) S. Portmann, H. P. Lüthi, *Chimia* **2000**, 54, 766.
- [25] A. J. Bridgeman, C. J. Empson, MAYER, The University of Hull, Hull, UK, **2003**.

Direct Localization of Atoms in Mixed-Occupancy Powders by Resonant Contrast Diffraction

Herve Palancher, Jean-Louis Hodeau,*
Christophe Pichon, Jean-François Béar, John Lynch,
Bernadette Rebours, and Juan Rodriguez-Carvajal

Presently, one challenge in structural determination is to describe the detailed atomic order in complex powders such as natural samples or materials involved in industrial processes (cement manufacturing, production of chemicals, mineral extraction). Classical X-ray powder diffraction is a key technique for this investigation but it has intrinsic limitations, especially the difficulty in discriminating between elements with similar atomic numbers or occupying neighboring sites.

In the study of complex samples (structures with large cell parameters), an “acceptable” fit can correspond to a false local minimum, with inappropriate attribution of electron density to a given element compensated by an inaccurate localization or quantification of other atoms in the unit cell. A common and difficult problem in powdered samples is the detailed study of mixed powders (with either several phases or a range of atomic occupancies in the same phase), as occurs in minerals and in industrial preparations. Furthermore, chemical or physical properties are generally driven (or at least affected) by the localization of some specific atoms in a mixture.

Two different methods are used to enhance the chemical contrast between elements in powder diffraction techniques. The first one uses neutron diffraction, since the nuclear scattering length is not related to the atomic number. The efficiency of this technique for contrast studies is, in general, satisfactory, but it requires large samples, and the high resolution obtained with synchrotron radiation cannot be achieved in current neutron diffractometers. This last point is primordial for powder diffraction, where reflections may overlap on the one-dimensional diffraction pattern. The second method uses resonant X-ray diffraction. The variation of the resonant scattering contribution near the edge of a given atom affects the contribution of this specific atom to the

diffracted intensities.^[1] Based on this effect, a site-selective technique, namely diffraction anomalous fine structure (DAFS) has been developed that combines diffraction and spectroscopic measurements.^[2–5] Moreover, the anomalous effect provides an elegant and efficient way of solving the structure factor phase problem in bio-crystallography by the so-called multiwavelength anomalous diffraction (MAD)^[6–8] and single-wavelength anomalous diffraction (SAD) methods.^[9,10] The software and the experimental developments dedicated to these studies, as well as the worldwide availability of synchrotron radiation, have made this a well-established method that is routinely used by structural biologists.^[11] A third type of application uses the chemical sensitivity of resonant diffraction to extract the contribution of a single element in a given crystallographic site and this resonant contrast diffraction (RCD) is the focus of the present contribution.

The specificities of the RCD method were demonstrated on powders in the 1990s.^[12–15] Thanks to partial Patterson density maps and maximum entropy methods (MEMs) it was possible to use resonant diffraction for ab initio structure determination.^[16] However, this ab initio structure solution method can become inefficient for complex powder samples due to the small number of non-overlapping reflections, and direct space methods such as those based on genetic algorithms and simulated annealing^[17] are generally used to solve the structure of organic samples of high interest for the pharmaceutical industry.^[18] It has been shown that differential anomalous scattering and partial structure factor analysis are efficient for studying amorphous-like materials such as glasses, liquids, nanoparticles, and also crystallized catalysts.^[19,20] They have also been used for quantitative analysis of minority phases such as Pt-metal inclusions in amorphous or crystalline substrates. Nevertheless, this resonant technique is still not widely used in powder diffraction, probably due to its relative complexity. Herein, we make use of recent advances in both MAD methods used in bio-crystallography and DAFS methods used for site-selective spectroscopy to show that accurate localization of atoms in powders is possible by the routine use of “anomalous differential patterns”. The gain in the multi-wavelength powder data refinement allows a direct visualization of these atoms by “dispersive difference maps”.

Owing to the superposition of (*hkl*) and ($-h-k-l$) reflections in powder diffraction diagrams, the SAD method (based on f' variation and calculations of Bijvoet difference maps) cannot be used. In powder diffraction, the intensity difference is mainly a function of $\Delta f'$ ($\Delta f'$ is the difference between the two f' values for the same resonant element at the two data collection energies) and can allow the calculation of “dispersive difference maps”, as performed currently by bio-crystallographers: the scattering contrast for a defined element is obtained by collecting data at two different photon energies. The Bragg intensities in powder diffraction data are much weaker than in single-crystal studies, and the relative weakness of the anomalous f' and f'' contribution (-8 to -5 electron unit (eu) for transition metals) compels us to collect patterns with very good statistics and to eliminate systematic errors.

[*] H. Palancher, Dr. J.-L. Hodeau, Dr. J.-F. Béar
Laboratoire de Cristallographie (CNRS)
25, avenue des Martyrs, 38042 Grenoble Cedex (France)
Fax: (+33) 4-7688-1038
E-mail: hodeau@grenoble.cnrs.fr
H. Palancher, Dr. C. Pichon, Dr. J. Lynch, B. Rebours
Institut Français du Pétrole
BP3, 69390 Vernaison (France)
Dr. J.-F. Béar
French CRG BM2 - ESRF
6, rue Jules Horowitz, 38049 Grenoble Cedex 9 (France)
Dr. J. Rodriguez-Carvajal
Laboratoire Léon Brillouin (CEA-CNRS)
CEA/Saclay
91191 Gif/Yvette (France)

Herein, this multiwavelength approach using resonant scattering is developed and validated by the analysis of a well-crystallized solid of industrial interest: hydrated SrRbX zeolite.^[21] This sample, in which both Sr^{2+} and Rb^{+} ions have the same number of electrons ($Z=36$ eu), is a particularly difficult case for conventional X-ray diffraction. Neutron diffraction is also unable to discriminate between the two nuclei because their scattering lengths are too close: $b(\text{Sr})=0.702 \times 10^{-14}$ m and $b(\text{Rb})=0.709 \times 10^{-14}$ m. In X-type zeolites the cations compensate the negatively charged

framework. In a first step, SrX was prepared by aqueous ion-exchange from NaX.^[22] The dicationic SrRbX sample was then obtained from SrX by the same chemical process. Its composition ($\text{Sr}_{24}\text{Rb}_{15}\text{Na}_4\text{Al}_{79}\text{Si}_{113}\text{O}_{384} \cdot 211\text{H}_2\text{O}$) was determined by elemental and thermogravimetric analyses. Diffraction measurements were performed on the BM2 beamline at the European Synchrotron Radiation Facility (ESRF).

To validate our methodology, diffraction patterns with a $s=1/d=2\sin\theta/\lambda$ range up to at least 1.0 \AA^{-1} , were collected in Debye–Scherrer geometry on the hydrated SrRbX sample at

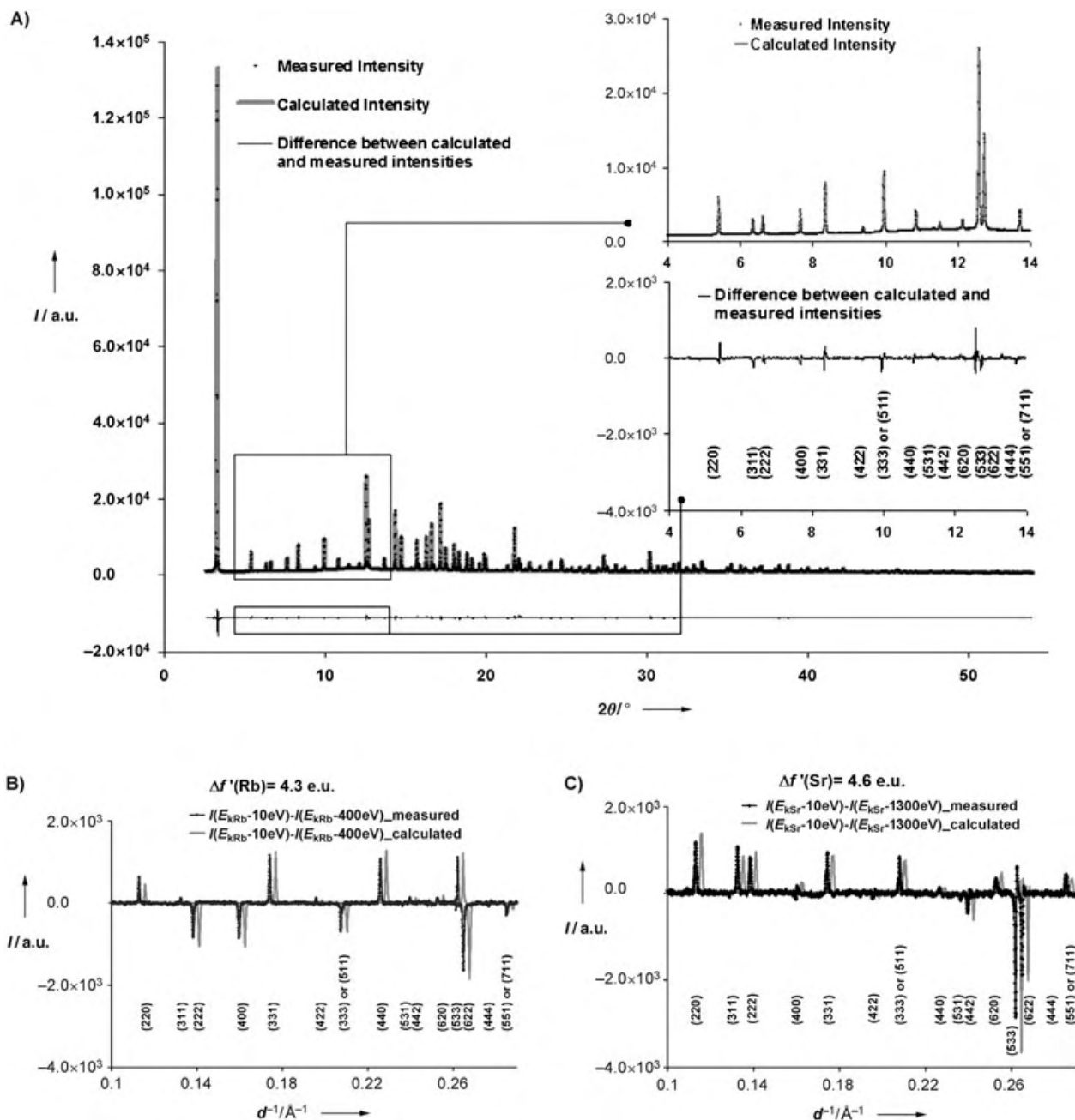


Figure 1. Influence of anomalous effects at the strontium and rubidium edges on the intensity of various reflections of diffraction patterns collected for hydrated SrRbX: A) Measured diffraction data and calculated diagram recorded for a hydrated SrRbX sample at $E_{\text{K Sr}} - 1300 \text{ eV}$; insert: zoom of diffracted and conventional difference diagram for $0.10 \text{ \AA}^{-1} < 1/d < 0.29 \text{ \AA}^{-1}$. B) Comparison of the measured and calculated “anomalous differential patterns” at the rubidium K absorption edge (difference between diagrams obtained at $E_{\text{K Sr}} - 10 \text{ eV}$ and $E_{\text{K Sr}} - 1300 \text{ eV}$). The calculated pattern is shifted along the x axis for better visualization of the intensity variations, C) Same figure as (B) but performed at the strontium K absorption edge. For (B) and (C) the same intensity normalization was applied.^[34]

three energies: about 10 eV below the rubidium and the strontium K absorption edges ($E_{\text{K}_{\text{Rb}}} = 15.192$ and $E_{\text{K}_{\text{Sr}}} = 16.096$ keV, respectively) and at 14.800 keV, far below both edges. Figure 1 A shows the diffraction pattern collected at $E_{\text{K}_{\text{Sr}}} - 1300$ eV. The high quality of the diffraction patterns enables the observation of intensity variations with energies exceeding the background noise. The anomalous effect can be clearly seen in the two anomalous difference patterns calculated from data collected at $E_{\text{K}_{\text{Sr}}} - 10$ eV and $E_{\text{K}_{\text{Sr}}} - 1300$ eV at the strontium absorption edge (and at $E_{\text{K}_{\text{Rb}}} - 10$ eV and $E_{\text{K}_{\text{Rb}}} - 400$ eV at the rubidium absorption edge), so that they can be taken into account in the pattern refinement (Figure 1B,C).

This data set has been refined with FULLPROF, a multipattern profile refinement software that uses the Rietveld method.^[23,24] As it is very often the case in industrial or mineral compounds, where the framework structure is roughly known, we do not need ab initio methods: in X-type zeolites we can introduce the basic framework atomic

positions in the refinement. The initial relative intensities of the different peaks that contribute to overlapped reflections, and the rough initial phases determined by these positions, allow us to calculate an initial Fourier map from the amplitude of the “observed” structure factors and the calculated phases. These Fourier maps are proportional to the electron density of the structure and already give a rough and non-element-selective localization of all extra-framework atoms (cations, molecules such as water, etc.). In X-type zeolites the cations and water are normally located at the well-known sites I, I', II, II', and III (Figure 2A). However, they can be introduced in the refinement only as electron densities, with no assumption of the atom type. Figure 2B shows the electron density calculated for the hydrated SrRbX sample in a plane (hereafter labelled *P*) containing the two $\langle 111 \rangle$ axes shown schematically in Figure 2A. The occupancies of the different atoms (cations, water) are normally differentiated only by a chemical knowledge of the usual atom-to-framework distances. By using resonant diffraction

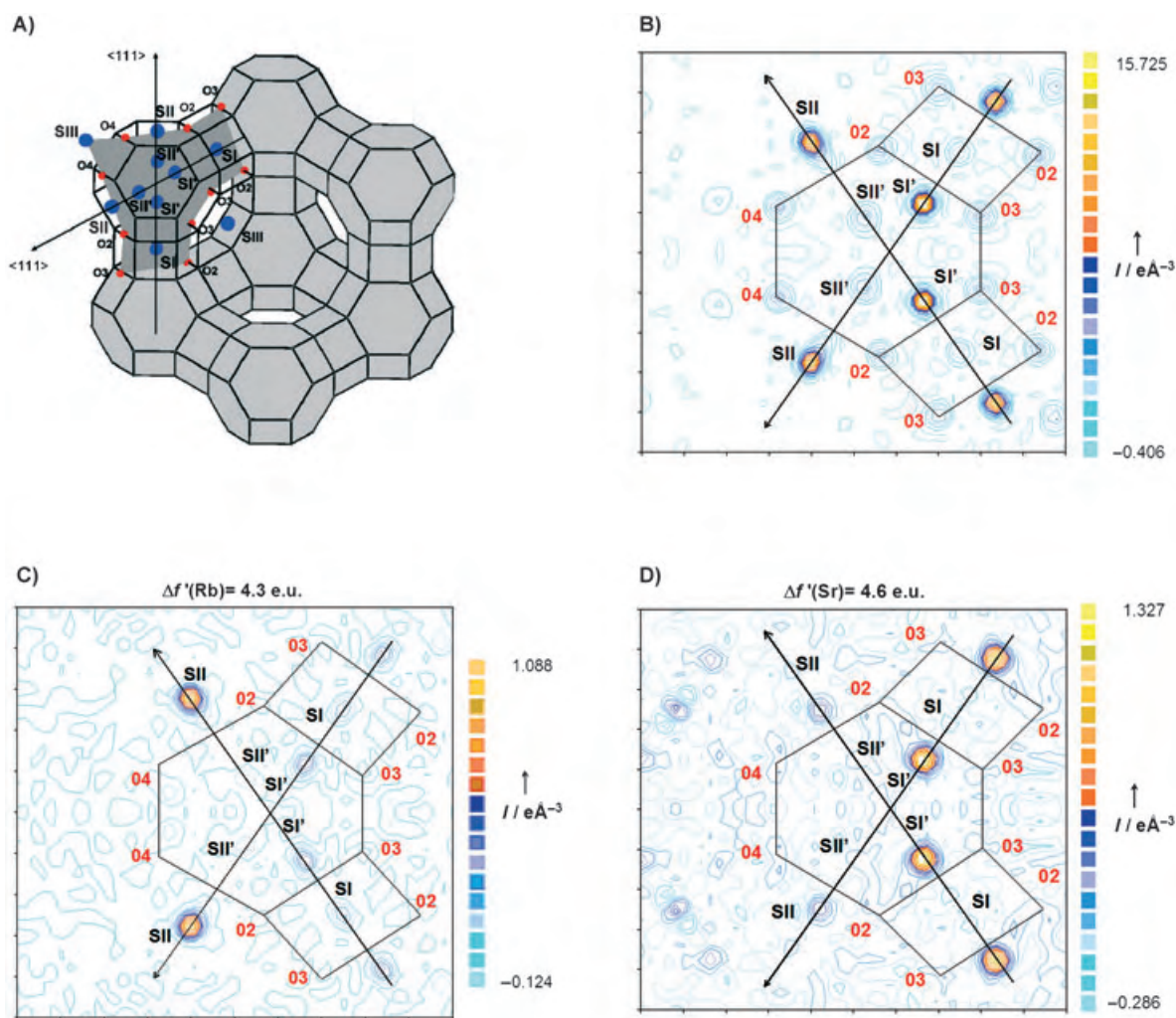


Figure 2. Strontium and rubidium cation localization in a water-saturated SrRbX sample: A) Localization of the main cationic sites in the unit cell of X-type zeolite. Sites I, I', II, II', and III are labeled SI, SI', SII, SII', SIII, and SIII', respectively. Plane *P*, defined by the intersection of two $\langle 111 \rangle$ axes, is represented in dark gray. B) Fourier map in the *P* plane calculated from diffraction data measured at $E_{\text{K}_{\text{Sr}}} = -1300$ eV. Electronic densities appear at sites I, I', II', and II. C) Dispersive difference electron-density maps calculated at the rubidium K absorption edge ($\Delta f'(\text{Rb}) = 4.3$ e.u.). D) Same figure as (C) but performed at the strontium K absorption edge ($\Delta f'(\text{Sr}) = 4.6$ e.u.). Electronic density at site II' cannot be attributed to rubidium or strontium cations.

at the edge of one of these atoms, we can calculate the difference between the electron densities determined from patterns collected at various energies. This corresponds to Fourier maps (“dispersive difference maps”) in which the amplitude of the Fourier coefficients is proportional to the difference of the structure factors of both energies, so that the corresponding density is proportional to the variation of the real anomalous term of the resonant scatterers ($\Delta f'$) (this has been confirmed by an RCD study of a hydrated SrX sample at the Sr^{2+} K absorption edge).^[25] “Dispersive difference maps” (P plane) have been obtained at both the Rb^+ and Sr^{2+} absorption edges on hydrated SrRbX (Figure 2C,D): no noticeable intensity appears at the localization of the framework atoms. These results show that the use of “dispersive difference maps” enables not only resonant cation localization but also their quantification.

It is obvious that accurate values for the anomalous scattering factors f' and f'' are needed. For each data collection energy, values for the cation anomalous terms f' and f'' were determined experimentally. At energies far from the absorption edges of the considered element they are not influenced by the chemical environment; tabulated values for the free atoms are therefore satisfactory.^[26] For energies close to an absorption edge, the f' and f'' values have to be determined directly for the sample studied since absorption edge displacements due to valence variations and fine-structure oscillations can strongly modify their values. When performing diffraction measurements, the easiest method consists in collecting absorption spectra in fluorescence or transmission mode. Values for f' and f'' can then be obtained with the Kramers–Kronig relationship.^[27] As shown in Figure 3, corrections of f' and f'' values close to the absorption edge may reach 10 %, and accuracy is directly related to the quality of the experimental determination of f' and f'' .

Both types of information (cation localization and anomalous scattering factors) were introduced into a structural model, thereby enabling the calculation of diffraction diagrams at $E_{\text{K Sr}} - 10$ eV and at $E_{\text{K Rb}} - 10$ eV. A comparison of the calculated and measured “anomalous differential patterns” at both the rubidium and strontium absorption edges shows a close agreement between the two (Figure 1B,C). Such “anomalous difference patterns” are extremely sensitive to

resonant atom location and occupancy, and are a key agreement test for various atom occupancies in sites occupied by chemically different cations.^[28]

The high resolution of our data collection enables a mixed population of site II to be detected in the initial Fourier map derived from the data collected at $E_{\text{K Sr}} - 1300$ eV (Figure 2B) from the weak splitting of the peak at site II. Each extra framework species (Sr^{2+} , Rb^+ , Na^+ , H_2O) has a given radius and its position depends on the bond length between the cations and the oxygen atoms of the framework. Here also the occupancies of the different atoms corresponding to such a splitting can be determined independently by the use of “dispersive difference maps” obtained at both the Rb^+ and Sr^{2+} absorption edges (Figure 2C,D). It appears that Sr^{2+} ions occupy sites I' and II, whereas Rb^+ ions are located mainly at site II but also at sites I and I'. The presence of both cations at sites II and I' is thus proven and can be directly seen in these differential electron-density maps.

The accuracy of this methodology can also be illustrated by a study of the population in sites I and II'. Classical refinement of the diffraction patterns of the hydrated SrRbX sample leads to identical results irrespective of whether these sites are considered as being occupied solely by residual, non-exchanged sodium cations or by a combination of sodium and rubidium cations. The difference anomalous Fourier map at the rubidium edge simulated for both site I occupation possibilities confirms the presence of Rb^+ cations at this site. Moreover, using the same strategy, anomalous diffraction at the rubidium K absorption edge shows the unique presence of water molecules in site II' (Figure 2C).^[29]

Based on the experimental improvement of data collection achieved with DAFS spectroscopy and applied by using the MAD principles, a methodology has been developed for powder-sample analysis that optimizes the use and the interpretation of anomalous information. Our aim was to validate, using a real-world example, the resonant scattering method for contrast studies in complex powders with mixed-occupancy sites. We have shown that, even in powder samples with considerable reflection overlap and with a basically known framework, the use of “dispersive difference” electron density maps allows an easy localization of the resonant atoms. The use of “anomalous difference patterns” enables good agreement factors to be achieved for accurate localization. These two specific difference tools can also be used with powders containing several phases. The application of these methods can be extended to numerous materials in geology, industry, and environmental studies to localize transition metals or heavy atoms. It can also give their valence by the use of diffraction anomalous near-edge structure (DANES) spectroscopy^[3,5,30] with powders; that is, refinement of the f' value to extract the chemical shift in the resonant-atom absorption edge. The extension of resonant contrast diffraction to measurements in situ can also be foreseen for the analysis of the evolution of atomic order during chemical reactions.

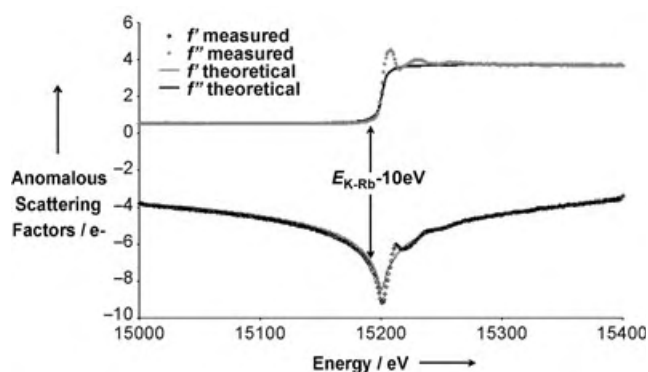


Figure 3. Rubidium f' and f'' values determined as a function of energy by using the Kramers–Kronig transformation of strontium K absorption data measured on a hydrated SrX sample in transmission mode.

Received: August 13, 2004

Published online: February 11, 2005

Keywords: anomalous scattering · cation distribution · powder diffraction · resonant contrast diffraction · structure elucidation · zeolites

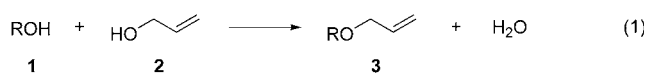
- [1] For X-ray diffraction, the expression for the atomic scattering factor, f , consists of three terms: $f = f_0 + f' + if''$, where f_0 defines classical Thomson scattering, and the resonant (or anomalous) f' and f'' represent dispersion and absorption processes, respectively. Their values vary strongly with energy when the incoming photon energy is close to an absorption edge. The structure factor F_{hkl} is derived from the atomic scattering factors of the elements constituting the unit cell weighted by their localization in the cell. Therefore, since the diffracted intensity is proportional to $|F_{hkl}|^2$, it also depends on the resonant scattering factors of the elements.
- [2] H. Stragier, J. O. Cross, J. J. Rehr, L. B. Sorensen, C. E. Bouldin, J. C. Woicik, *Phys. Rev. Lett.* **1992**, *69*, 3064–3067.
- [3] I. J. Pickering, M. Sansone, J. Marsch, G. N. George, *J. Am. Chem. Soc.* **1993**, *115*, 6302–6311.
- [4] L. B. Sorensen, J. O. Cross, M. Newville, B. Ravel, J. J. Rehr, H. Stragier, C. E. Bouldin, J. C. Woicik, in *Resonant Anomalous Diffraction X-ray Scattering* (Eds.: G. Materlik, C. J. Sparks, K. Fischer), Elsevier Science B.V., Amsterdam, **1994**, pp. 389–420.
- [5] J. L. Hodeau, V. Favre-Nicolin, S. Bos, H. Renevier, E. Lorenzo, J. F. Berar, *Chem. Rev.* **2001**, *101*, 1843–1867.
- [6] In the MAD method, the variation of intensity reflections with energy, caused by the energy fluctuation of anomalous scattering factors, is interpreted to locate the anomalous scatterers.
- [7] W. A. Hendrickson, M. M. Teeter, *Nature* **1981**, *290*, 107–113.
- [8] W. A. Hendrickson, *Science* **1991**, *254*, 51–58.
- [9] The SAD method is based on the study of intensity differences for (hkl) and $(-h-k-l)$ reflections at a given energy due to the contribution of anomalous scattering factors.
- [10] J. M. Bijvoet, *Proc. Acad. Sci. Amsterdam B* **1949**, *52*, 313–314.
- [11] CCP4: *Acta Crystallogr. Sect. D* **1994**, *50*, 760–763.
- [12] R. S. Howland, T. H. Geballe, S. S. Laderman, A. Fischer-Colbrie, M. Scott, J. M. Tarascon, P. Barboux, *Phys. Rev. B* **1989**, *39*, 9017–9027.
- [13] J. P. Attfield, *Nature* **1990**, *343*, 46–49.
- [14] G. H. Kwei, R. B. Von Dreele, A. Williams, J. A. Goldstone, A. C. Lawson II, W. K. Warburton, *J. Mol. Struct.* **1990**, *223*, 383–406.
- [15] D. E. Cox, A. P. Wilkinson in *Resonant Anomalous Diffraction X-ray Scattering* (Eds.: G. Materlik, C. J. Sparks, K. Fischer), Elsevier Science B.V., Amsterdam, **1994**, pp. 195–219.
- [16] K. Burger, D. Cox, R. Papoular, W. Prandl, *J. Appl. Crystallogr.* **1998**, *31*, 789–797.
- [17] For a review see: K. D. M. Harris, M. Tremayne, B. M. Kariuki, *Angew. Chem.* **2001**, *113*, 1674–1700; *Angew. Chem. Int. Ed.* **2001**, *40*, 1626–1651.
- [18] S. Pagola, P. W. Stephens, D. S. Bohle, A. D. Kosar, S. K. Madsen, *Nature* **2000**, *404*, 307–310.
- [19] E. Matsubara, Y. Waseda, in *Resonant Anomalous Diffraction X-ray Scattering* (Eds.: G. Materlik, C. J. Sparks, K. Fischer), Elsevier Science B.V., Amsterdam, **1994**, pp. 345–364.
- [20] C. Meneghini, S. Mobilio, L. Lusvarghi, F. Bondioli, A. M. Ferrari, T. Manfredini, C. Siligardi, *J. Appl. Crystallogr.* **2004**, *37*, 890–900.
- [21] SrRbX stands for zeolite NaX highly exchanged with Sr^{2+} and Rb^+ cations.
- [22] This sample was prepared by aqueous ion-exchange at 353 K from a NaX zeolite and a 1 mol L^{-1} solution of $\text{Sr}(\text{NO}_3)_2$.^[31] After activation at 573 K under nitrogen flow the sample was slowly rehydrated.
- [23] H. M. Rietveld, *J. Appl. Crystallogr.* **1969**, *2*, 65–71.
- [24] J. Rodríguez-Carvajal, *Physica B* **1993**, *192*, 55–69. For a recent version see: Juan Rodríguez-Carvajal, *Recent Developments of the Program FULLPROF* in, Commission on Powder Diffraction (IUCr), Newsletter **2001**, *26*, 12–19, available at <http://journals.iucr.org/iucr-top/comm/cpd/Newsletters/>. The complete program and documentation can be obtained from the anonymous ftp-site: <ftp://ftp.ccea.fr/pub/llb/divers/fullprof.2k>.
- [25] Powder-diffraction measurements were performed with a hydrated SrX sample following the same strategy (as detailed for SrRbX in the text) at three energies: 16.196 keV ($E_{\text{K Sr}} - 10 \text{ eV}$), 16.041 keV ($E_{\text{K Sr}} - 65 \text{ eV}$), and 15.192 keV ($E_{\text{K Sr}} - 904 \text{ eV}$). At the Sr^{2+} absorption edge, two “dispersive difference” maps were calculated from diagrams collected at $E_{\text{K Sr}} - 904 \text{ eV}$ and $E_{\text{K Sr}} - 65 \text{ eV}$ (for the first), and at $E_{\text{K Sr}} - 904 \text{ eV}$ and $E_{\text{K Sr}} - 10 \text{ eV}$ in the second case. The maximum intensities on these maps obtained for sites I' and II are 0.775/1.421 and 0.664/1.217, respectively, with energy variations corresponding to $\Delta f = 2.6 \text{ e.u./4.8 e.u.}$
- [26] For calculated values, see, for example: S. Sasaki, *Anomalous Scattering Factors for Synchrotron Radiation Users Calculated Using Cromer Liberman's method*, National Laboratory for High-Energy Physics, Tsukuba (Japan), **1984**.
- [27] f' and f'' are linked by the Kramers–Kronig relationships: $f'\omega_0 = \frac{2}{\pi} P \int_0^\infty \frac{\omega f''(\omega)}{\omega^2 - \omega_0^2} d\omega$ and $f''\omega_0 = \frac{2}{\pi} P \int_0^\infty \frac{\omega f'(\omega)}{\omega^2 - \omega_0^2} d\omega$. To apply the Kramers–Kronig relationship, f' or f'' must be known over a very large energy range (ranging from $\sim 30 \text{ eV}$ up to $\sim 200 \text{ keV}$ for an absorption edge near 10 keV). Thus, for such a calculation theoretical values are generally used far from the edge and merged to experimental values. We applied the Kramers–Kronig relationship to the difference spectrum (experimental factor minus the theoretical one), the final resonant factor being the sum of the result and the tabulated theoretical factor.^[32,33]
- [28] In the current version of FULLPROF (version 2.70) the use of “anomalous differential patterns” and a direct plot of normalized near-edge minus far-from-edge difference patterns is possible.
- [29] The distinction between cations and water molecules in zeolites X or Y is of high importance regarding the influence of water molecules in hydrocarbon adsorption processes.
- [30] S. Bos, PhD thesis, University of Grenoble (France), **1999**.
- [31] H. S. Sherry, *J. Phys. Chem.* **1968**, *72*, 4086–4094.
- [32] L. K. Templeton, D. H. Templeton, *J. Appl. Crystallogr.* **1988**, *21*, 558–561.
- [33] G. Evans, R. Pettifer, *J. Appl. Crystallogr.* **2001**, *34*, 82–86.
- [34] With the $Fd\bar{3}m$ space group, the elements situated on the $\langle 111 \rangle$ axis contribute to all reflections. In consequence, no reflection can, in principle, be used for intensity normalization between diagrams collected at different energies below a cation absorption edge. The reflection (1086), which is less sensitive to cations, was chosen as a reference.

Synthetic Methods

Catalytic Dehydrative Allylation of Alcohols**

Hajime Saburi, Shinji Tanaka, and Masato Kitamura*

Allyl ethers are not only recognized as important starting materials for a wide range of organic reactions, including the 1,3 hydrogen shift, [3.3]-sigmatropic rearrangement, and polymerization,^[1] but also constitute one of the most useful protecting groups for alcohols.^[2] In contrast to the extensively studied allyl ether cleavage, the formation of allyl ethers is still under development and relies mainly on a Williamson-type ether synthesis that uses metal alkoxides and allyl halides or their equivalents.^[3] Salt waste-free allylation of alcohols is desirable, and several catalytic methods utilizing allyl esters have been reported.^[4] Ideally, the catalysis should directly convert a 1:1 mixture of alcohols **1** and 2-propen-1-ol (**2**) into allyl ethers **3** [Eq. (1)] in a solvent-free system without the

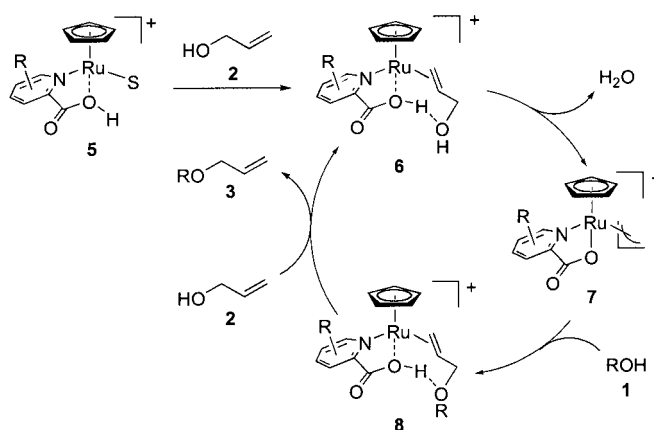


- | | |
|---|---|
| a: C ₆ H ₅ CH ₂ CH ₂ | g: geranyl |
| b: c-C ₆ H ₁₁ | h: C ₆ H ₅ CH ₂ O(CH ₂) ₆ |
| c: 2-indanyl | i: C ₆ H ₅ COO(CH ₂) ₆ |
| d: C ₆ H ₅ CH ₂ C(CH ₃) ₂ | j: CH ₃ OCH ₂ O(CH ₂) ₆ |
| e: CH ₂ =CHCH ₂ CH ₂ CH ₂ CH ₂ | k: (t-C ₄ H ₉)(C ₆ H ₅) ₂ SiO(CH ₂) ₆ |
| f: C ₆ H ₅ | |

need for any additional stoichiometric activators. As water should be the only co-product this dehydrative allylation is efficient, environmentally friendly, and simple to operate. However, the poor leaving ability of the hydroxy group as well as the low nucleophilicity of the alcoholic oxygen presents major difficulties.^[5] Pioneering research in this area has been carried out by the Showa Denko company. As it is assumed that the reaction involves a π -allyl mechanism, various combinations of palladium or platinum compounds with mono- and bidentate phosphanes or phosphites were systematically examined.^[6] Several similar approaches have been reported,^[7] but to date none of them have been

sufficiently developed to be useful from a generic synthetic perspective.^[8] Herein, we report a highly efficient catalytic system for the direct dehydrative allylation of alcohols, which is effective even with only 1.0 equivalents of **2**.

We have developed a new catalytic system that consists of a cationic [CpRu] (Cp = cyclopentadienyl) complex and 2-pyridinecarboxylic acid derivatives for direct allyl ether cleavage in alcoholic solvents.^[2] Taking into account the reversibility of the cleavage reaction, the catalytic cycle shown in Scheme 1 is assumed to operate during the



Scheme 1. Supposed catalytic cycle for allyl ether formation.

allylation. In the formation of **6** the catalyst precursor **5** captures **2** through an Ru–olefin interaction together with a hydrogen bond interaction between the COOH moiety and the OH group. In this catalyst–substrate complex, the hydrogen bond interaction and the strong coordination of the σ -donating sp² nitrogen atom of the pyridine moiety and the monoanionic η^5 -Cp ligand to the Ru atom synergistically enhance the electrophilicity of **2** and the nucleophilicity of the Ru center. This effect accelerates the oxidative addition of the Ru^{II} center onto **2** to generate a cationic [CpRu^{IV}(C₃H₅)]⁺ carboxylate species **7**. Nucleophilic attack of **1** onto the π -allyl carbon, assisted by the good leaving ability of the carboxylate ligand, gives a catalyst–product complex **8**. Liberation of the product **3** revives the chain carrier **6**. All the elementary steps are essentially reversible, but the phase separation of water from the reaction system together with water's poor nucleophilicity may force the equilibrium to the allyl ether side.

Based on the above concept, the reaction conditions for the allylation of 2-phenylethan-1-ol (**1a**) with **2** were examined. Representative results of screening reactions are listed in Table 1. The allylation proceeds at 70 °C with 1.0 equivalents of **2** and 0.0005 equivalents of [CpRu(CH₃CN)₃]PF₆ (**9**)^[9] and 2-quinolinecarboxylic acid (**10**) each to give **3a** in 90 % yield after 6 hours. Formation of the 1,3-hydrogen shifted isomer, 1-propenyl ether, was not observed. The substrate/catalyst (S/C) ratio of 10000 is acceptable, which approaches a turnover number (TON) of 6500 and a turnover frequency (TOF) of 5200 at 26 % conversion. At 50 °C, it requires 42 hours to attain 90 % yield. When heated to reflux, the shift of the equilibrium to the product side is retarded. The ligand acceleration efficiencies of 1-isoquinolinecarboxylic

[*] H. Saburi, S. Tanaka, Prof. Dr. M. Kitamura
Research Center for Materials Science
Department of Chemistry, Nagoya University
Chikusa, Nagoya 464-8602 (Japan)
Fax: (+81) 52-789-2261
E-mail: kitamura@os.rcms.nagoya-u.ac.jp

[**] This work was aided by a Grant-in-Aid for Scientific Research (No. 14078212) from the Ministry of Education, Science, Sports, and Culture, Japan. We are grateful to T. Noda, K. Oyama, Y. Maeda, and T. Okuno for their technical support in the production of reaction vessels, NMR spectroscopic analysis, and X-ray diffraction crystallographic analysis.

Supporting information for this article (preparation and characterization of all substrates and products, general procedures for allylations, ¹H NMR spectroscopic analysis, and X-ray crystallographic analysis) is available on the WWW under <http://www.angewandte.org> or from the author.

Table 1: Direct allylation of various monoalcohols with 2-propen-1-ol (**2**) catalyzed by [CpRuPF₆]-2-pyridinecarboxylic acid derivative combined systems [cf. Eq. (1)].^[a]

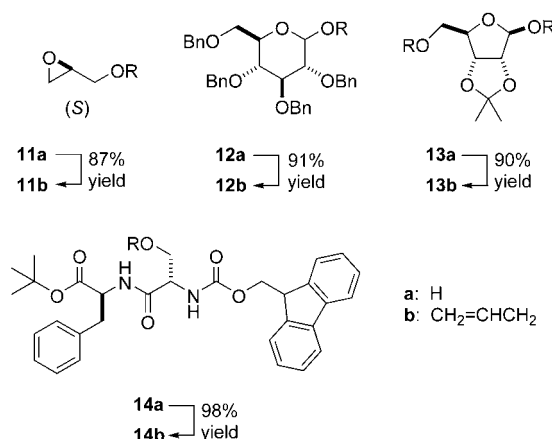
Entry	Alcohol	Ligand	<i>t</i> [h] ^[b]	Yield [%] ^[b]
1	1a		6 (3)	90 (93)
2	1a	10	0.5 (0.5)	66 (58 ^[c])
3	1a		0.5 (0.5)	16 (11 ^[c])
4	1a		0.5 (0.5)	20 (1.3 ^[c])
5	1a		0.5 (0.5)	21 (5.7 ^[c])
6	1a		0.5 (0.5)	2 (0 ^[c])
7	1b	10	24 (24)	76 (90)
8	1c	10	12 (5)	84 (92)
9	1d	10	3 (24)	29 (30)
10	1e	10	12 (5)	90 ^[d] (97)
11	1f	10	12 (5)	24 (62)
12	1g	10	12 (3)	92 (91)
13	1h	10	10 (6)	90 (94)
14	1i	10	3 (6)	92 (94)
15	1j	10	12 (6)	93 (92)
16	1k	10	12 (6)	91 (97)

[a] Reactions were performed at 70 °C without solvent in a 2000:2000:1:1 ratio of **1**/**2**/[CpRu(CH₃CN)₃]PF₆(**9**)/ligand. The yields were determined by GC analysis, see the Supporting Information for details. [b] The values in parentheses are those obtained at reflux temperature in CH₂Cl₂ ([**1**] = [**2**] = 500 mM; [**9**] = [ligand] = 1 mM). [c] S/C = 100. [d] S/C = 1000.

acid, 3-isoquinolinecarboxylic acid, and 2-pyridinecarboxylic acid are 3–10 times lower than that of **10** in comparison to the initial rates (entries 2–5). Saturation of the pyridine ring retards catalytic activity (entry 6). Replacement of the COOH group of 2-pyridinecarboxylic acid with COOCH₃ or CH₂OH groups also abolishes the activity. Diphenylphosphanyl acetic acid gave an undesired 1,3-hydrogen shift-derived compound, 1,1-di(2-phenylethoxy)propane, in 27% yield after 24 hours. Secondary alcohols, such as **1b** and **1c**, are allylated in high yields (entries 7 and 8). Alcohol **1e**, which has a C=C bond at the 5-position, was converted into the corresponding allyl ether without any isomerization (entry 10). With geraniol (**1g**), only geranyl allyl ether (**3g**) was produced among many other possible diallyl ethers (entry 12). The low yields in the allylation of tertiary alcohol **1d** and aryl alcohol **1f** (entries 9 and 11) may be ascribed to the low nucleophilicity and the reversibility of the present catalysis. The chemoselectivity of the reaction was high; allylation was attained in > 90% yield without modifying the benzyl, benzoyl, methoxymethyl, and *tert*-butyldiphenylsilyl protecting groups (entries 13–16).

Furthermore, the present catalytic system is even more effective with a solvent and can be applied to the synthesis of multifunctional compounds, such as carbohydrates and peptides, where solvents are essential. For example, (*S*)-glycidol

(**11a**) in 98% *ee* was allylated with 1.2 equivalents of **2** to give (*S*)-allyl glycidyl ether (**11b**) in 98% *ee* and in 87% yield (S/C = 100/1, CH₂Cl₂, reflux). No racemization was detectable by



high performance liquid chromatographic (HPLC) analysis. Optically active **11b** is widely used as a chiral unit not only for the synthesis of functionalized epoxy resins but also for a variety of natural products. However, there are problems associated with the preparation of (*S*)- or (*R*)-**11b**. The Williamson-type allylation often causes a Payne rearrangement, which decreases the optical purity.^[10] Transformation from chiral glycerol derivatives involves several steps.^[11] The hydroxy group at the anomeric C1 of **12a** was also smoothly allylated to give the allyloxy compound in 91% yield of isolated product, and 1,5-free furanose **13a** was diallylated in 90% yield of isolated product. *tert*-Butyl Fmoc-protected phenylalanyl serine **14a** was converted in a 98% yield to the corresponding allyl ether, leaving the Fmoc and *tert*-butyl ester intact (**12a**, **13a**, or **14a** = 100 mM, 2 equivalents of **2** for each OH group, CH₂Cl₂, reflux).

Consistent with the proposed catalytic cycle in Scheme 1, **9** was mixed with **10** in a 1:1 ratio in [D₆]acetone (each 10 mM) at 27 °C. A new set of signals was observed [δ = 8.01 (t, 1H, *J* = 7.57 Hz), 8.15 (t, 1H, *J* = 7.57 Hz), 8.32 (m, 2H), 8.84 (d, 1H, *J* = 8.26 Hz), 9.14 ppm (d, 1H, *J* = 8.26 Hz)] that could be assigned to **5** (S = CH₃CN, R = 5,6-(CH)₄).^[12] The signals immediately disappeared when 1 equivalent of **2** was introduced at 27 °C to give another new set of signals characteristic of **7** [R = 5,6-(CH)₄] [π -allyl moiety: δ = 4.40 (dd, 1H (*syn*), *J* = 2.75, 5.85 Hz), 4.44 (dd, 1H (*syn*), *J* = 2.75, 6.20 Hz), 4.75 (d, 1H (*anti*), *J* = 9.64 Hz), 4.96 (d, 1H (*anti*)), 4.96–5.20 ppm (m, 1H (*center*))]. In solution, the complex is assumed to have an *endo* π -allyl structure with a narrowed dihedral angle φ defined by the coordination plane and the π -allyl plane.^[13] This is supported by three observations: 1) the clear A₂B₂X allyl signal pattern, 2) the two H_{*syn*} protons resonating at a higher magnetic field than H_{*anti*} protons, and 3) the observation of 2–5% and approximately 8% enhancements of the two H_{*anti*} signals and the H_{*syn*} signal on irradiating CpH protons and C(8)H of the quinoline ring, respectively. Under the reaction conditions described herein no catalyst–substrate complex **6** was detected, which demonstrates the efficiency of

the bifunctional property of **6** to form **7**. The signals for **7** were unaffected by the introduction of 10 mole amounts each of **1a** and **2** at reflux while the allylation proceeded.^[14] This indicates that the π -allyl species **7** is at the resting state in the catalysis. Complex **7** [R = 5,6-(CH)₄] was isolated as a single pale yellow crystal. The characteristic feature of the *endo* π -allyl conformation at a small value of φ is also seen in the X-ray crystallographic measurements (Figure 1). The

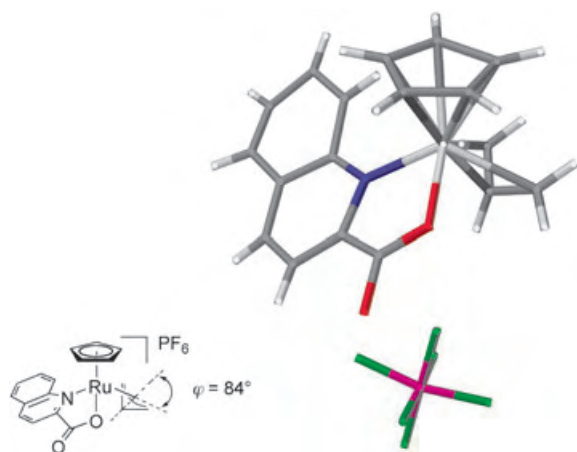


Figure 1. Molecular structure of [CpRu(π -C₃H₅)(2-quinolinecarboxylato)]PF₆ [**7**; R = 5,6-(CH)₄] determined by X-ray crystallographic analysis.^[15]

isolated Ru^{IV} complex acted as the allylation catalyst with higher reactivity than that of the corresponding 2-pyridinecarboxylic acid complex. The rate-determining reductive elimination of Ru^{IV} to a Ru^{II} center could be accelerated by a quinoline ring, which has a higher π -accepting ability than pyridine.

In conclusion, we have developed an efficient catalytic system for the dehydrative allylation of alcohols. The new methodology is superior to conventional synthetic routes^[3–8] in many respects, and it increases the importance of allyl ethers not only as basic compounds but also as protecting groups in organic synthesis. Furthermore, a series of NMR spectroscopic and X-ray crystallographic studies on a key π -allyl intermediate has given insight into the probable reaction mechanism.

Received: November 4, 2004

Published online: February 3, 2005

Keywords: allyl ethers · allylation · homogeneous catalysis · quinolinecarboxylic acid · ruthenium

- [3] A. W. Williamson, *J. Chem. Soc.* **1852**, 4, 229.
- [4] Pd: a) R. Akiyama, S. Kobayashi, *J. Am. Chem. Soc.* **2003**, 125, 3412–3413; b) A. Yamamoto, *Adv. Organomet. Chem.* **1992**, 34, 111–147; c) R. C. Larock, N. H. Lee, *Tetrahedron Lett.* **1991**, 32, 6315–6318; d) R. Lakhmiri, P. Lhoste, D. Sinou, *Tetrahedron Lett.* **1989**, 30, 4669–4672; e) J. Muzart, J.-P. Genêt, A. Denis, *J. Organomet. Chem.* **1987**, 326, C23–C28; f) I. Minami, I. Shimizu, J. Tsuji, *J. Organomet. Chem.* **1985**, 296, 269–280; g) F. Gübbe, Y. S. M'leux, *Tetrahedron Lett.* **1981**, 22, 3591–3594; h) K. Takahashi, A. Miyake, G. Hata, *Bull. Chem. Soc. Jpn.* **1972**, 45, 230–236; Ir: i) H. Nakagawa, T. Hirabayashi, S. Sakaguchi, Y. Ishii, *J. Org. Chem.* **2004**, 69, 3474–3477.
- [5] For a recent example of Pd-catalyzed allylation of metal alkoxides with allyl esters, see: H. Kim, C. Lee, *Org. Lett.* **2002**, 4, 4369–4371.
- [6] a) J. Qü, Y. Ishimura, N. Nagato, *Nippon Kagaku Kaishi* **1996**, 9, 787–791; b) Y. Ishimura, J. Qü, *Jpn. Kokai Tokkyo Koho Jpn. Pat.* 05306246, **1993**.
- [7] Pd: Y. Kayaki, T. Koda, T. Ikariya, *J. Org. Chem.* **2004**, 69, 2595–2597; Ru: R. C. van der Drift, M. Vailati, E. Bouwman, E. Drent, *J. Mol. Catal. A* **2000**, 159, 163–177; Ni: H. Bricout, J.-F. Carpentier, A. Mortreux, *J. Mol. Catal. A* **1998**, 136, 243–251.
- [8] For acid-catalyzed direct allylation, see: a) E. Moffett, *J. Am. Chem. Soc.* **1934**, 56, 2009; b) M. J.-B. Senderens, *Compt. Rend.* **1925**, 181, 698–701; for oxymetalation–dehydroxymetalation using Cu, Pd, and Hg, see: c) W. Oguchi, H. Uchida, WO Patent 03/106024, **2003**; d) C. M. Dumlao, J. W. Francis, P. M. Henry, *Organometallics* **1991**, 10, 1400–1405; e) W. H. Watanabe, L. E. Conlon, J. C. H. Hwa, *J. Org. Chem.* **1958**, 23, 1666–1668.
- [9] T. P. Gill, K. R. Mann, *Organometallics* **1982**, 1, 485–488; for a recent efficient synthesis, see: E. P. Kündig, F. R. Monnier, *Adv. Synth. Catal.* **2004**, 346, 901–904.
- [10] G. Uray, N. M. Maier, W. Lindner, *J. Chromatogr. A* **1994**, 666, 41–53.
- [11] a) R. L. Pederson, K. K.-C. Liu, J. F. Rutan, L. Chen, C.-H. Wong, *J. Org. Chem.* **1990**, 55, 4897–4901; b) A. B. Mikkilineni, P. Kumar, E. Abushanab, *J. Org. Chem.* **1988**, 53, 6005–6009.
- [12] About 10% of unassignable signals were also observed, see Supporting Information for details.
- [13] a) E. Rüba, W. Simanko, K. Mauthner, K. M. Soldouzi, C. Slugovc, K. Mereiter, R. Schmid, K. Kirchner, *Organometallics* **1999**, 18, 3843–3850; b) T. Kondo, H. Ono, N. Satake, T. Mitsudo, Y. Watanabe, *Organometallics* **1995**, 14, 1945–1953; c) H. Nagashima, K. Mukai, Y. Shiota, K. Yamaguchi, K. Ara, T. Fukahori, H. Suzuki, M. Akita, Y. Moro-oka, K. Itoh, *Organometallics* **1990**, 9, 799–807.
- [14] The ratio of **3a**, **2**, and diallyl ether after 30 minutes was approximately 40:20:20.
- [15] Crystallographic analysis of **7** (R = 5,6-(CH)₄) pale yellow prism; *P* $\bar{1}$, *a* = 7.94(6), *b* = 8.3(1), *c* = 14.3(1) Å, α = 106.2(5)°, β = 89.95(2)°, γ = 90.0(3)°, *V* = 906.7(19) Å³, *Z* = 2, *R* = 0.136, *R*_w = 0.163. CCDC 251818 contains the supplementary crystallographic data for this paper. These data can be obtained free of charge from the Cambridge Crystallographic Data Centre via www.ccdc.cam.ac.uk/data_request/cif.

[1] a) J. Tsuji in *Handbook of Organopalladium Chemistry for Organic Synthesis*, Vol. 5 (Ed.: E. Negishi), Wiley, New York, **2002**, pp. 1669–1687; b) B. M. Trost, D. L. VanVranken, *Chem. Rev.* **1996**, 96, 395–422; c) S. A. Godleski in *Comprehensive Organic Synthesis*, Vol. 4 (Eds.: B. M. Trost, I. Fleming), Pergamon, Oxford, **1991**, pp. 585–661.

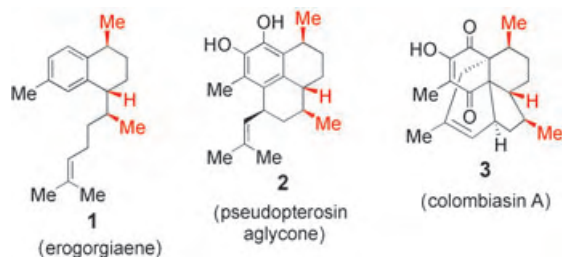
[2] S. Tanaka, H. Saburi, Y. Ishibashi, M. Kitamura, *Org. Lett.* **2004**, 6, 1873–1875, and references therein.

Natural Product Synthesis

Direct Synthesis of (+)-Erogorgiaene through a Kinetic Enantiodifferentiating Step**

Huw M. L. Davies* and Abbas M. Walji

(+)-Erogorgiaene is a member of the marine diterpenes isolated from the West Indian sea whip *Pseudopterogorgia elisabethae* and displays promising activity against *Mycobacterium tuberculosis* H37Rv.^[1] Several important biologically active secondary metabolites have been isolated from the *Pseudopterogorgia* corals.^[2] Consequently, there has been extensive activity directed towards the synthesis of these natural products.^[3] Even though these compounds are not especially complex, a major challenge associated with their synthesis has been the control of the three stereocenters (marked in red, **1–3**, Scheme 1), common to all of them. The

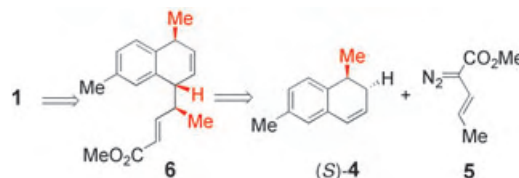


Scheme 1. Diterpenes isolated from *Pseudopterogorgia elisabethae*.

stereocontrol has been challenging because of the lack of functional groups near to the stereogenic centers. This has meant that many of the syntheses have been very lengthy with considerable functional group interconversions, and even then the stereocontrol has been less than satisfactory.^[3] The only reported synthesis of (+)-erogorgiaene (**1**), described by Hoveyda and co-workers, employed a chiral-catalyst-controlled conjugate addition in a sequential manner to set up the desired stereocenters.^[4]

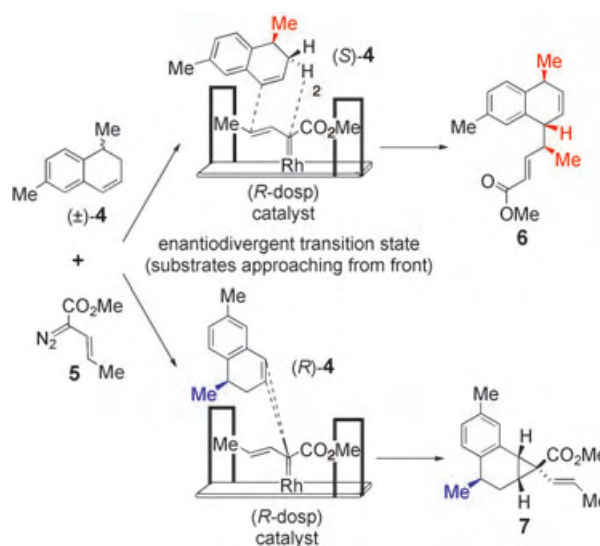
Here we illustrate through the enantioselective synthesis of (+)-erogorgiaene (**1**) a potentially general strategy to the synthesis of this class of diterpenes. The key step is our recently discovered combined C–H activation/Cope rearrangement catalyzed by dirhodium tetraproline [Rh₂(dosp)₄] (dosp = (*N*-dodecylbenzenesulfonyl)proline),

a reaction that is notable for its very high diastereoselectivity and enantioselectivity.^[5] Application of this methodology to the retrosynthetic analysis of (+)-erogorgiaene revealed that the unsaturated ester **6** would be a very desirable precursor to **1**. Reaction of the vinyl diazoacetate **5** with the dihydronaphthalene (*S*)-**4** would be expected to readily form **6** with the desired relative stereochemistry (Scheme 2).



Scheme 2. Retrosynthetic analysis of (+)-erogorgiaene (**1**).

During the analysis of this synthetic problem, we recognized that the synthesis offered a very exciting opportunity for enantiomer differentiation, such that the racemic dihydronaphthalene (\pm)-**4** could be used as starting material. Even though the exact mechanism of these carbenoid reactions is not known, we have developed models that are excellent at predicting the stereochemical outcome of this chemistry.^[5b,6] Applying these models to the [Rh₂(*R*-dosp)₄]-catalyzed reaction of (\pm)-**4** with **5**, it was revealed that only (*S*)-**4** would be capable of a matched combined C–H activation/Cope rearrangement to form **6** whereas (*R*)-**4** would be matched for a cyclopropanation to form **7** (Scheme 3). This



Scheme 3. Stereochemical prediction for combined C–H activation/Cope rearrangement strategy.

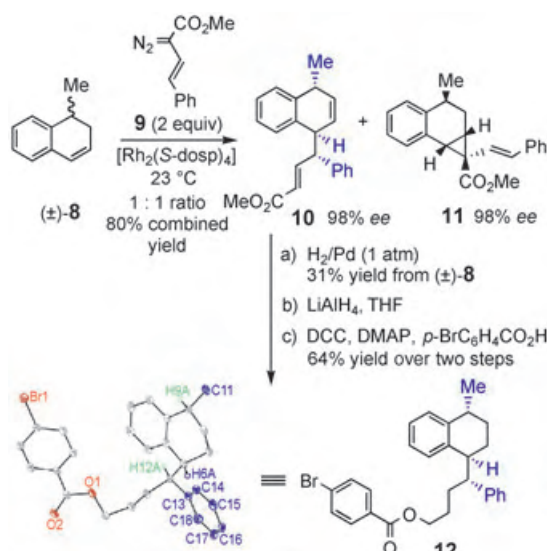
would be a very exciting outcome because the dihydronaphthalene (\pm)-**4** could potentially be used as the limiting agent, as both enantiomers would be consumed but would form different products.

To test this possibility, the reaction of dihydronaphthalene **8** with the phenylvinyl diazoacetate **9** was used as a model reaction (Scheme 4). We were delighted that the reaction

[*] Prof. H. M. L. Davies, A. M. Walji
Department of Chemistry
University at Buffalo
The State University of New York
Buffalo, NY 14260-3000 (USA)
Fax: (+1) 716-645-6547
E-mail: hdavies@acsu.buffalo.edu

[**] This work was supported by the National Science Foundation (CHE-0092490). We thank Oksana O. Gerlits for the X-ray crystallographic analysis.

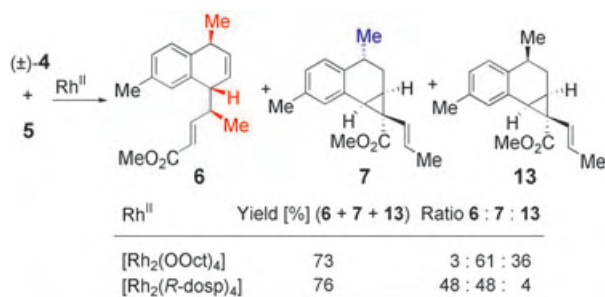
Supporting information for this article is available on the WWW under <http://www.angewandte.org> or from the author.



Scheme 4. Preliminary modeling studies and determination of absolute configuration: ORTEP drawing of **12**. DCC = dicyclohexyl carbodiimide, DMAP = 4-dimethylaminopyridine.

catalyzed by $[\text{Rh}_2(\text{S-dosp})_4]$ gave a 1:1 mixture of the combined C–H activation/Cope rearrangement product **10** and the cyclopropane **11** in a combined yield of 80%. Remarkably, both products were produced in 98% *ee* and essentially as single diastereomers. The relative and absolute stereochemistry of **10** was confirmed by conversion of **10** into the crystalline *p*-bromobenzoate **12** whose configuration was confirmed by X-ray crystallography.^[7]

Having successfully completed the model studies, attention was then directed towards the total synthesis of erogorgiaene. The key step is the rhodium-catalyzed reaction between the vinyl diazoacetate **5** and the dihydronaphthalene (\pm)-**4** (Scheme 5). A comparison between the reaction of **5**

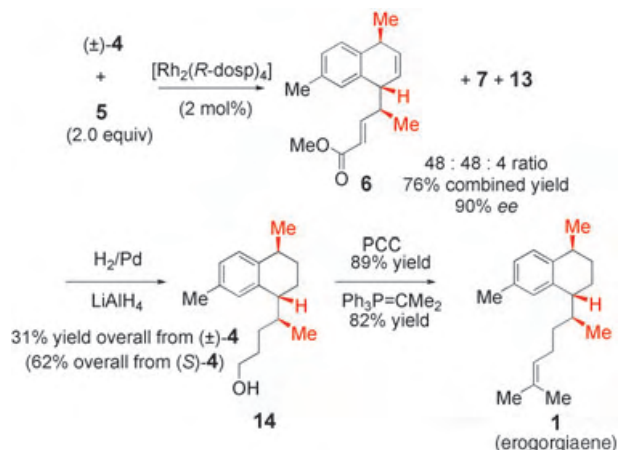


Scheme 5. Influence of catalyst $[\text{Rh}_2(\text{R-dosp})_4]$ on product distribution.

with (\pm)-**4** catalyzed by either rhodium octanoate or $[\text{Rh}_2(\text{R-dosp})_4]$ is very informative because it demonstrates the important role of $[\text{Rh}_2(\text{R-dosp})_4]$ not only to induce the enantioselectivity but also to achieve an effective C–H transformation. The reaction between **5** and (\pm)-**4** catalyzed by rhodium(II) octanoate results in the formation of only a trace of the combined C–H activation/Cope rearrangement product **6**. The major products are the diastereomeric cyclopropanes **7** and **13** (as racemic mixtures). In contrast, the

reaction catalyzed by $[\text{Rh}_2(\text{R-dosp})_4]$ is truly exceptional and results in a 1:1 mixture of the combined C–H activation product **6** and the cyclopropane **7** with just a trace of the diastereomer **13**. Furthermore, **6** was formed in 90% *ee*.

The synthesis of (+)-erogorgiaene (**1**) was readily completed as illustrated in Scheme 6. Owing to the tendency of **6**



Scheme 6. Total synthesis of (+)-erogorgiaene (**1**). PCC = pyridinium chlorochromate.

to undergo a retro-Cope rearrangement, the combined mixture of **6** and **7** was globally hydrogenated, and the ester was reduced to the alcohol **14**, which was isolated in 31% overall yield from the dihydronaphthalene (\pm)-**4** (62% yield from the matched enantiomer (*R*)-**4**). Oxidation of **14** to the aldehyde with pyridinium chlorochromate (PCC) followed by a Wittig reaction completed the total synthesis of (+)-erogorgiaene (**1**).

In summary, we have demonstrated that the combined C–H activation/Cope rearrangement protocol is an exceptional method for the construction of the three stereogenic centers common to the numerous diterpenes isolated from *Pseudopterogorgia elisabethae*. The synthetic potential of this chemistry was demonstrated by means of a very direct synthesis of erogorgiaene. Further studies are in progress to apply this methodology to other members of this class of diterpenes.

Received: October 6, 2004


Revised: December 8, 2004

Published online: February 11, 2005

Keywords: C–H activation · enantioselectivity · natural products · terpenoids · total synthesis

- [1] A. D. Rodriguez, C. Ramirez, *J. Nat. Prod.* **2001**, *64*, 100–102. Erogorgiaene displayed 96% inhibition of *Mycobacterium tuberculosis* H37Rv at 12.5 $\mu\text{g mL}^{-1}$.
- [2] a) S. A. Look, W. Fenical, R. S. Jacobs, J. Clardy, *Proc. Natl. Acad. Sci. USA* **1986**, *83*, 6238–6240; b) A. D. Rodriguez, Y.-P. Shi, *Tetrahedron* **2000**, *56*, 9015–9023; c) A. D. Rodriguez, *Tetrahedron* **1995**, *51*, 4571–4618, and references therein.
- [3] Selected examples: Pseudopterogens: E. J. Corey, S. E. Lazerwith, *J. Am. Chem. Soc.* **1998**, *120*, 12777–12782; Pseudopteroxazole:

- J. P. Davidson, E. J. Corey, *J. Am. Chem. Soc.* **2003**, *125*, 13486–13489; Elisabethins: T. J. Heckrodt, J. Mulzer, *J. Am. Chem. Soc.* **2003**, *125*, 4680–4681; Colombiasin A: a) K. C. Nicolaou, S. A. Synder in *Classics in Total Synthesis II*, Wiley-Interscience, Weinheim, **2003**, pp. 423–442; b) K. C. Nicolaou, G. Vassiliko-
giannakis, W. Magerlein, R. Kranich, *Chem. Eur. J.* **2001**, *7*, 5359–5371; Colombiasin A and Elisapterosin B: A. I. Kim, S. D. Rychnovsky, *Angew. Chem.* **2003**, *115*, 1305–1308; *Angew. Chem. Int. Ed.* **2003**, *42*, 1267–1270.
- [4] R. R. Cesati, J. De Armas, A. H. Hoveyda, *J. Am. Chem. Soc.* **2004**, *126*, 96–101.
- [5] a) H. M. L. Davies, Q. Jin, *Proc. Natl. Acad. Sci. USA* **2004**, *101*, 5472–5475; b) H. M. L. Davies, Q. Jin, *J. Am. Chem. Soc.* **2004**, *126*, 10862–10863.
- [6] a) D. T. Nowlan III, T. M. Gregg, H. M. L. Davies, D. A. Singleton, *J. Am. Chem. Soc.* **2003**, *125*, 15902–15911; b) H. M. L. Davies, R. E. J. Beckwith, *Chem. Rev.* **2003**, *103*, 2861–2904.
- [7] O. O. Gerlits, P. Coppens, Private Communication, **2004**. CCDC-242585 contains the supplementary crystallographic data for this paper. These data can be obtained free of charge from the Cambridge Crystallographic Data Centre via www.ccdc.cam.ac.uk/data_request/cif.


WILEY InterScience®
 DISCOVER SOMETHING GREAT
 Access some of the finest full text journals, reference works, books, and databases from around the globe. It's just what you need to make some important discoveries of your own.

ABOUT US
 VIEW DEMO
 CONTACT US
 HELP


Access your saved titles, articles, queries and alerts in My Profile.
 USER NAME: PASSWORD:
☐ Remember Me
[Register Now](#) | [Forgot My Password](#)


Manage your access easily with “MY PROFILE”

Key features available to registered users include:

Easy Access	Enhanced Tools
● Save Titles, Articles & Queries for quick access	● Set E-Mail Alerts when new content is available
● Setup roaming access to access content outside of your institutions network	● Purchase individual articles online with Pay-Per-View
● Get free online sample copies	● Purchase Article Select Tokens online
● Get free online trial subscriptions	● Track your manuscripts
● View a complete list of your subscriptions and accessible products	

Register now and sign up for “MY PROFILE”! Registration is fast and free!

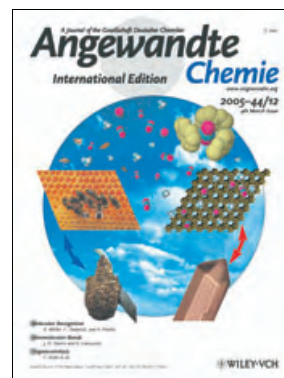
 www.interscience.wiley.com


WILEY InterScience®
 DISCOVER SOMETHING GREAT

Cover Picture

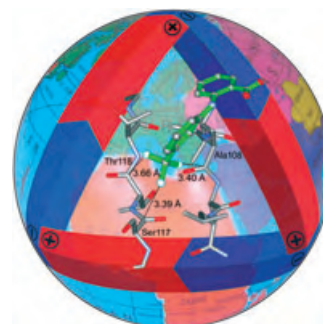
P. Sozzani,* S. Bracco, A. Comotti, L. Ferretti, and R. Simonutti

Like a swarm of bees who find shelter in the hexagonal cells of the beehive, CH₄ and CO₂ molecules are stabilized by weak CH... π interactions within the open-pore van der Waals crystals of tris-*o*-phenylenedioxy-cyclotriphosphazene. The supramolecular network is sufficiently robust to store a large number of gas molecules. In their Communication on page 1816 ff., P. Sozzani et al. describe the absorption properties of the crystals and the spectroscopic observation of gases trapped in the nanochannels.



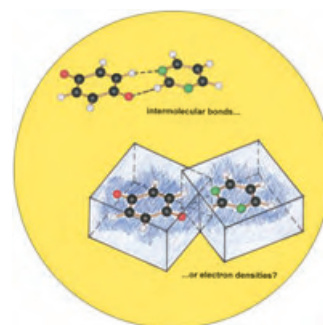
Multipolar Interactions

Based on the results of database mining, K. Müller, F. Diederich, and R. Paulini give an overview of the significance of multipolar (in particular, orthogonal) interactions in crystal structures of small molecules and the stabilization of receptor–ligand complexes in their Review on p. 1788 ff.



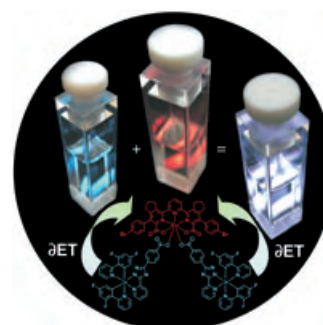
Molecular Recognition

In their Review on page 1766 ff., J. D. Dunitz and A. Gavezzotti take a critical look at classical bonding concepts for describing intermolecular interactions in crystal structures and propose an alternative model based on nonlocalized interactions between electron densities.



Luminescent Assemblies

De Cola and co-workers describe in their Communication on page 1806 ff. how the sensitization of red-emitting Eu^{III} ions through partial energy transfer from the excited state of a blue-emitting Ir^{III} center leads to the observation of white light.





The following Communications have been judged by at least two referees to be “very important papers” and will be published online at www.angewandte.org soon:

Kendric J. Nelson, Ian D. Giles, William W. Shum, Atta M. Arif,
Joe S. Miller*

**The Myth of Cyanide Always Being a Strong Field Ligand:
Synthesis and Structural Characterization of Homoleptic S = 2
Pentacyanochromate(II), [Cr^{III}(CN)₅]³⁻ and
Nonacyanodichromate(II), [Cr^{III}₂(CN)₉]⁵⁻**

Andrew J. Wilson, Mitsutoshi Masuda, Rint P. Sijbesma,*
E. W. Meijer*

**Chiral Amplification in the Transcription of Supramolecular
Helicity into a Polymer Backbone**

Mark Gandelman, Eric N. Jacobsen*

**Highly Enantioselective Catalytic Conjugate Addition of
N Heterocycles to α,β -Unsaturated Ketones and Imides**

Sang Hyuk Im, Yun Tack Lee, Benjamin Wiley, Younan Xia*

**Large-Scale Synthesis of Silver Nanocubes: The Role of HCl in
Promoting Cube Perfection and Monodispersity**

Sridhar Narayan, John Muldoon, M. G. Finn, Valery V. Fokin,
Hartmuth C. Kolb, K. Barry Sharpless*

**“On Water”: Unique Reactivity of Organic Compounds in
Aqueous Suspensions**

Tetsuro Murahashi, Christopher R. Clough, Joshua S. Figueroa,
Christopher C. Cummins*

**A Ligand Comprised of Dinitrogen and
Methyldiphenylphosphine in a Cationic Molybdenum Complex**

Obituary

Walter Hugo Stockmayer (1914–2004): Macromolecules

W. Burchard _____ 1754–1755

Books

Kinetic Processes

Kenneth A. Jackson

reviewed by A. G. Munoz _____ 1756

Energy Landscapes

David J. Wales

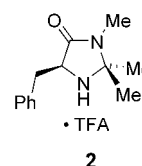
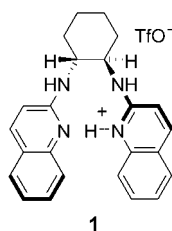
reviewed by A. Heuer _____ 1756

Highlights

Organocatalysis

C. Bolm,* T. Rantanen, I. Schiffrers,
L. Zani _____ 1758–1763

Protonated Chiral Catalysts: Versatile
Tools for Asymmetric Synthesis

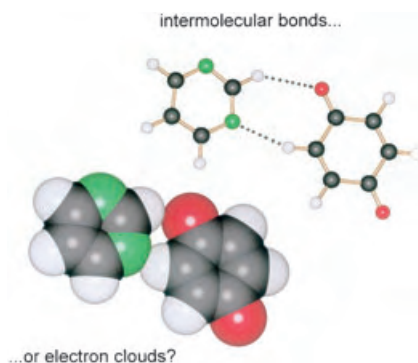


Acid treatment: Exposure of catalytically inactive (neutral) molecules to strong Brønsted acids generates cationic species (e.g. **1** and **2**) that catalyze a wide range of

synthetically powerful transformations. These reactions give products with excellent *ee* values. TfO⁻ = trifluoromethanesulfonate; TFA = trifluoroacetic acid.

Reviews

Recognising recognition: In describing intermolecular recognition, conventional wisdom often relies on weak bonds between individual atoms in different molecules, rather than considering less-localized interactions between molecular electron densities (see picture). A proposal is made to abandon the traditional view of a molecule as an array of atoms, in favor of an electron-cloud picture. The new computational tool pixel is used to calculate the intermolecular energies from the electron density of the isolated molecules.

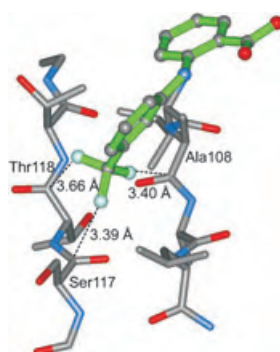


Intermolecular Bonding

J. D. Dunitz,*
A. Gavezzotti* _____ 1766–1787

Molecular Recognition in Organic Crystals: Directed Intermolecular Bonds or Nonlocalized Bonding?

Types and structural features of non-covalent, multipolar interactions between intrinsically polar molecular functional groups are analyzed by using crystallographic-database mining. The results are discussed on the basis of scatterplot correlations of geometrical parameters. The picture shows a section of a complex of human transthyretin with flufenamic acid which displays three noncovalent polar C–F...C=O contacts.

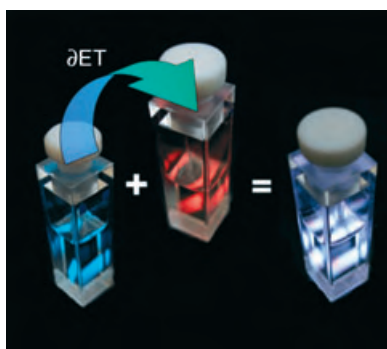


Molecular Recognition

R. Paulini, K. Müller,*
F. Diederich* _____ 1788–1805

Orthogonal Multipolar Interactions in Structural Chemistry and Biology

Red, white, and blue: White light was obtained by partial energy transfer (∂ ET) between a blue-emitting Ir^{III}–phenylpyridine complex and a red-emitting Eu^{III}–terpyridine chelate through excitation of the assembly that is formed from the two metal complexes (see picture).



Communications

Luminescent Assemblies

P. Coppo, M. Duati, V. N. Kozhevnikov,
J. W. Hofstraat, L. De Cola* 1806–1810

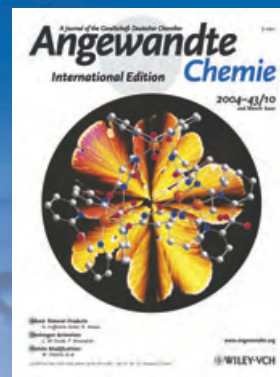
White-Light Emission from an Assembly Comprising Luminescent Iridium and Europium Complexes

For the USA and Canada:
ANGEWANDTE CHEMIE International Edition (ISSN 1433-7851) is published weekly by Wiley-VCH PO Box 191161, D 69451 Weinheim, Germany. Air freight and mailing in the USA by Publications Expediting Inc. 200 Meacham Ave., Elmont, NY 11003. Periodicals

postage paid at Jamaica NY 11431. US POSTMASTER: send address changes to *Angewandte Chemie*, Wiley-VCH, 111 River Street, Hoboken, NJ 07030. Annual subscription price for institutions: US\$ 4948.00/4498.00 (valid for print and electronic / print or electronic delivery); for individuals who are personal members of a

national chemical society, or whose institution already subscribes, or who are retired or self-employed consultants, print only: US\$ 394.00. Postage and handling charges included. All Wiley-VCH prices are exclusive VAT.

The best in chemistry – for more than a hundred years



A Journal of the Gesellschaft Deutscher Chemiker
Angewandte Chemie
International Edition

www.angewandte.org

1888: The beginning
of a success story

Constant Innovations

- 1962:** First issue of the International Edition
- 1976:** Graphical abstracts
- 1979:** Cover pictures
- 1988:** Centenary of Angewandte
- 1989:** Routine use of color
- 1991:** New section: Highlights
- 1992:** Computerized editorial tracking system
- 1995:** Internet service for readers
- 1998:** Regular press service; full-text online
- 2000:** New section: Essays; EarlyView: Communications available online ahead of the printed version
- 2001:** New section: Minireviews
- 2002:** Online submission of manuscripts
- 2003:** Weekly publication; new section: News; new layout
- 2004:** Backfiles (1962-1997); ManuscriptXpress: Online system for authors and referees



Angewandte's advisors...

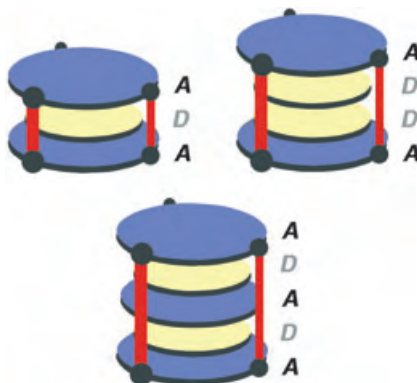
Jean-Marie Lehn
Université Strasbourg
Collège de France

» **Angewandte Chemie** provides timely reviews of great depth and wide interest together with short reports of top quality frontier research. Creative work remains creative wherever it is published! However, **Angewandte Chemie** brings high visibility while keeping restraint and rigor. Finally, it is also supranational, as science is. «

Angewandte Chemie International Edition is
a journal of the German Chemical Society (GDCh)



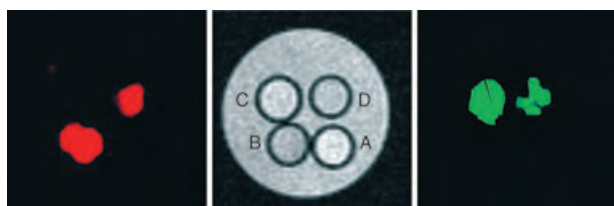
Metal-hinged, organic-pillared cages accommodate a limited number (n) of π -stacked molecules in the cavity (see scheme): Discrete $n+2$ aromatic stacking occurs by the accommodation of n large aromatic guests ($n=1-3$). Owing to efficient donor-acceptor (D-A) interactions, A-D-A ($n=1$), A-D-D-A ($n=2$), and A-D-A-D-A ($n=3$) stacks are observed, which bring about even-odd-number effects in the UV/Vis absorption spectra.



Stacking Interactions

M. Yoshizawa, J. Nakagawa, K. Kumazawa, M. Nagao, M. Kawano, T. Ozeki, M. Fujita* — 1810–1813

Discrete Stacking of Large Aromatic Molecules within Organic-Pillared Coordination Cages



Cell-tracking experiments by MRI are possible with a novel class of Tb and Eu paramagnetic imaging agents, with which contrast is generated upon irradiation at a specific frequency (see picture). Middle:

A) unlabeled; B) Tb-labeled; C) Eu-labeled; D) Tb- and Eu-labeled cells. Left: irradiation at ± 180 kHz (Tb-agent-specific). Right: irradiation at ± 15 kHz (Eu-agent-specific).

Cell Imaging

S. Aime,* C. Carrera, D. Delli Castelli, S. Geninatti Crich, E. Terreno — 1813–1815

Tunable Imaging of Cells Labeled with MRI-PARACEST Agents



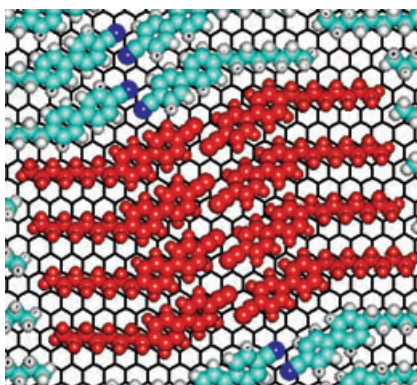
Molecular gas jars: Methane and carbon dioxide can be stored in open-pore van der Waals crystals of tris-*o*-phenylene-dioxycyclotriphosphazene at low partial pressure, whereas hydrogen, nitrogen, and oxygen are selectively excluded. Gas molecules participate in the supramolecular network of weak interactions and reside in the tight nanochannels in close contact with the surrounding aromatic rings (see picture).

Inclusion Compounds

P. Sozzani,* S. Bracco, A. Comotti, L. Ferretti, R. Simonutti — 1816–1820

Methane and Carbon Dioxide Storage in a Porous van der Waals Crystal

Chiral control without chirality: The adsorption of achiral liquid-crystal molecules to graphite substrates can generate surfaces with controlled enantiomeric excess and absolute chirality in the presence of a magnetic field, which assists in orienting the molecules. Unlike conventional approaches for chiral control, no chiral inputs are needed.



Surface Chemistry

A. M. Berg, D. L. Patrick* — 1821–1823

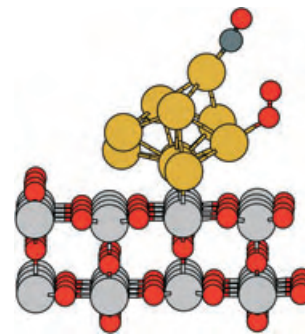
Preparation of Chiral Surfaces from Achiral Molecules by Controlled Symmetry Breaking

Heterogeneous Catalysis

I. N. Remediakis,* N. Lopez,
J. K. Nørskov — 1824 – 1826

CO Oxidation on Rutile-Supported Au Nanoparticles

What makes inert gold active? The answer lies in controlling the structure of Au particles at the nanoscale: Either many interface sites or many low-coordinate Au atoms need to be present in the particles. This principle is demonstrated by modeling the oxidation of CO on a rutile (TiO₂)-supported Au nanocluster, the transition state of which does not involve the titania support (see picture: Au yellow, Ti light gray, C dark gray, O red).



Heterogeneous Catalysis

S. Huh, H.-T. Chen, J. W. Wiench,
M. Pruski, V. S.-Y. Lin* — 1826 – 1830

Cooperative Catalysis by General Acid and Base Bifunctionalized Mesoporous Silica Nanospheres



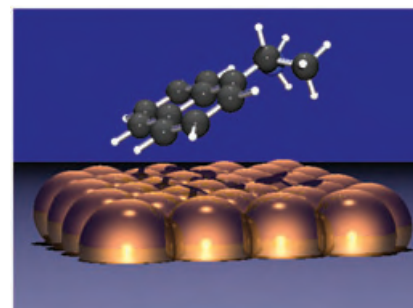
A team effort: Mesoporous silica nanosphere (MSN) materials bifunctionalized with a general acid group and a base group in various relative concentrations are described and shown to function as cooperative catalytic systems. The turnover numbers observed indicate that the acid groups can activate substrates in cooperation with the base groups to catalyze reactions that involve carbonyl activation (see picture).

Surface Chemistry

A. Mulligan, I. Lane, G. B. D. Rousseau,
S. M. Johnston, D. Lennon,
M. Kadodwala* — 1830 – 1833

Going Beyond the Physical: Instilling Chirality onto the Electronic Structure of a Metal

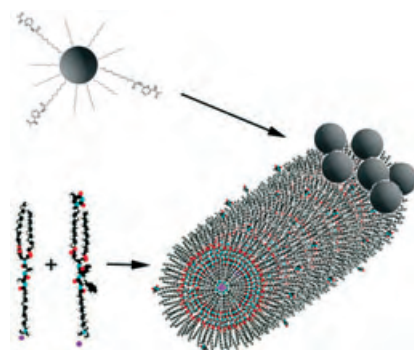
Look below the surface: An adsorbed chiral molecule, 1-(1-naphthyl)ethylamine, reversibly instills chirality onto the electronic structure of a copper surface (see picture), a previously unobserved phenomenon. Conveying chirality onto the electronic structure of a metal surface is a possible mechanism by which chemical reactivity and electrical properties may be made chirally dependent.



Self-Assembled Nanoparticles

L.-s. Li, S. I. Stupp* — 1833 – 1836

One-Dimensional Assembly of Lipophilic Inorganic Nanoparticles Templated by Peptide-Based Nanofibers with Binding Functionalities



Good as gold: Nanofibers with surface hydrogen-bonding motifs co-assembled from peptide-based amphiphilic molecules were used to template one-dimensional assemblies of preformed lipophilic inorganic nanoparticles in apolar organic solvents (see figure).

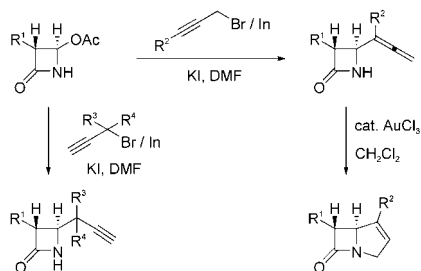


Axial ligation of the heme moiety by a proximal imidazole group is observed in a novel cytochrome *c* oxidase (CcO) active-site model **1** in which the copper ion is bound to a *N*-(2-hydroxyphenyl)imidazole moiety. Spectroscopic observations of **1** suggest the unique transformation of an initial heme- μ -peroxo-Cu^{II} species into a heme-superoxide/Cu^I intermediate in the course of the CcO oxygenation reaction at low temperature.

Active-Site Modeling

J.-G. Liu, Y. Naruta,* F. Tani **1836–1840**

A Functional Model of the Cytochrome *c* Oxidase Active Site: Unique Conversion of a Heme- μ -peroxo-Cu^{II} Intermediate into Heme-superoxide/Cu^I



Bicyclic β lactams are obtained by the two-step procedure shown in the scheme. Alternatively, with the help of organotin reagents, allenyl and propargyl groups are introduced at the C4-position of 2-azetidinones. $R^1 = \text{H}$, 1*R*-(*tert*-butyldimethylsilyloxy)ethyl (TBSO(CH₃)CH); $R^2 = \text{H}$, methyl, ethyl, *n*-butyl, phenyl, THPOCH₂, trimethylsilyl, 2-naphthyl; $R^3 = \text{H}$, methyl, phenyl; $R^4 = \text{H}$, methyl.

Synthetic Methods

P. H. Lee,* Heechul Kim, K. Lee, M. Kim, K. Noh, Hyunseok Kim, D. Seomoon **1840–1843**

The Indium-Mediated Selective Introduction of Allenyl and Propargyl Groups at the C4-Position of 2-Azetidinones and the AuCl₃-Catalyzed Cyclization of 4-Allenyl-2-azetidinones



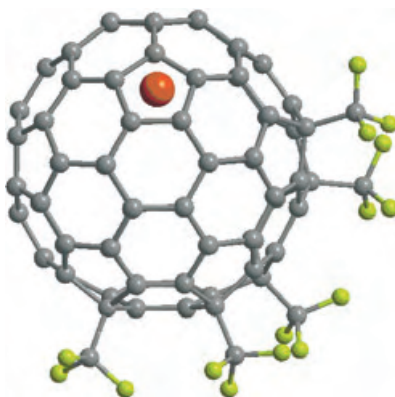
Global currents: Quantum chemical methodology has been used to investigate the magnetically induced currents of both neutral Buckminsterfullerene and its spherically aromatic +10 ion and has allowed quantitative measurement of the current strengths. Global sphere currents (see picture), instead of local ring currents, are found to be the defining feature of fullerene aromaticity.

Density Functional Calculations

M. P. Johansson, J. Jusélius, D. Sundholm* **1843–1846**

Sphere Currents of Buckminsterfullerene

Quantum chemical calculations and NMR spectroscopic data suggest that the two isomers of Y@C₈₂(CF₃)₅ prepared by trifluoromethylation of the endohedral metallofullerene (EMF) contain chains of four 1,4-C₆(CF₃)₂ edge-sharing hexagons (see picture). In striking contrast to the empty fullerenes, which form complex mixtures with up to 22 CF₃ groups, EMF Y@C₈₂ only forms products with one, three, and five CF₃ groups.



Fullerenes

I. E. Kareev,* S. F. Lebedkin, V. P. Bubnov, E. B. Yagubskii, I. N. Ioffe, P. A. Khavrel, I. V. Kuvychko, S. H. Strauss, O. V. Boltalina* **1846–1849**

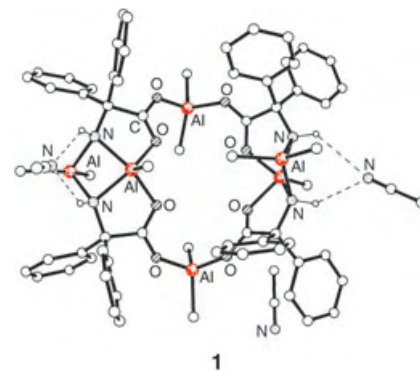
Trifluoromethylated Endohedral Metallofullerenes: Synthesis and Characterization of Y@C₈₂(CF₃)₅

Inorganic Ring Systems

C. Redshaw,* M. R. J. Elsegood,
A. E. Holmes ————— **1850 – 1853**

Synthesis of Hexa- and Dodecanuclear
Organoaluminum Ring Structures
Incorporating the “Magic” $\text{Ph}_2\text{C}(\text{X})$ Group
($\text{X} = \text{O}^-, \text{NH}^-$)

The magic touch! By using the “magic” group $\text{Ph}_2\text{C}(\text{X})$ ($\text{X} = \text{O}^-, \text{NH}^-$), aluminum ring systems such as **1** have been synthesized from trimethylaluminum. For diphenylglycine ($\text{X} = \text{NH}^-$), both six- and twelve-membered rings have been structurally identified.

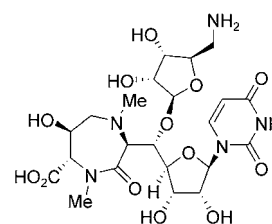


Antibiotics

S. Hirano, S. Ichikawa,
A. Matsuda* ————— **1854 – 1856**

Total Synthesis of Caprazol, a Core
Structure of the Caprazamycin
Antituberculosis Antibiotics

TB and anti-TB: Two key steps in the synthesis of caprazol (**1**), a core structure of the antituberculosis antibiotics, are the introduction of an aminoribose moiety by β -selective ribosylation without the use of neighboring-group participation and the construction of the diazepanone moiety.

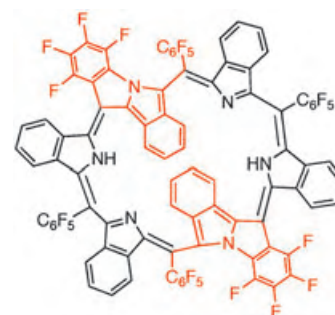


Expanded Porphyrins

Y. Inokuma, T. Matsunari, N. Ono,*
H. Uno,* A. Osuka* ————— **1856 – 1860**

A Doubly N-Fused Benzohexaphyrin and
Its Rearrangement to a Fluorescent
Macrocycle upon DDQ Oxidation

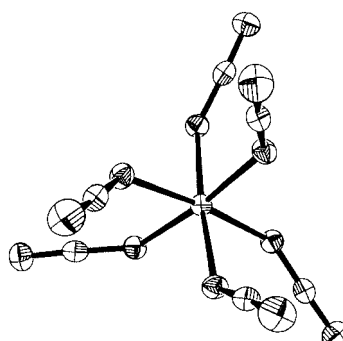
A retro-Diels–Alder reaction of a β -bicyclo[2.2.2]octadiene-fused precursor yields the doubly N-fused β -benzo[28]-hexaphyrin(1.1.1.1.1.1) shown, which undergoes oxidative rearrangement upon treatment with 2,3-dichloro-5,6-dicyano-1,4-benzoquinone (DDQ) to yield a macrocycle that emits fluorescence in the visible/near-IR region.



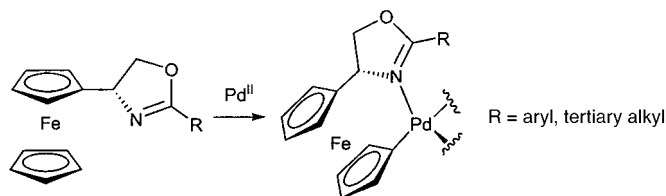
Azides

R. Haiges,* J. A. Boatz, R. Bau,
S. Schneider, T. Schroer, M. Yousufuddin,
K. O. Christe* ————— **1860 – 1865**

Polyazide Chemistry: The First Binary
Group 6 Azides, $\text{Mo}(\text{N}_3)_6$, $\text{W}(\text{N}_3)_6$,
 $[\text{Mo}(\text{N}_3)_7]^-$, and $[\text{W}(\text{N}_3)_7]^-$, and the
 $[\text{NW}(\text{N}_3)_4]^-$ and $[\text{NMo}(\text{N}_3)_4]^-$ Ions



Bang on target: The highly explosive Group 6 azides $\text{Mo}(\text{N}_3)_6$ and $\text{W}(\text{N}_3)_6$ are prepared by the reaction of Me_3SiN_3 with MoF_6 and WF_6 , respectively. The structure of $\text{W}(\text{N}_3)_6$ has perfect rhombohedral C_3 symmetry (see picture). The reaction of $\text{Mo}(\text{N}_3)_6$ and $\text{W}(\text{N}_3)_6$ with ionic azides leads to the formation of $[\text{Mo}(\text{N}_3)_7]^-$ and $[\text{W}(\text{N}_3)_7]^-$, respectively, the first binary heptaazides. Controlled decomposition of these anions produces $[\text{NMo}(\text{N}_3)_4]^-$ and $[\text{NW}(\text{N}_3)_4]^-$.



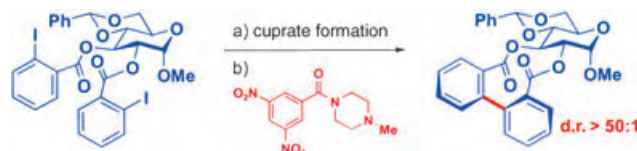
Formation of a carbon–palladium bond to the unsubstituted cyclopentadiene ring occurs during the cyclopalladation of 4-ferrocenyl-1,3-oxazolines and leads to a

new type of metalated ferrocene (see scheme). These chiral complexes catalyze the asymmetric aza-Claisen rearrangement of allylic imidates.

Asymmetric Catalysis

A. Moyano,* M. Rosol, R. M. Moreno, C. López, M. A. Maestro — **1865–1869**

Oxazoline-Mediated Interannular Cyclopalladation of Ferrocene: Chiral Palladium(II) Catalysts for the Enantioselective Aza-Claisen Rearrangement



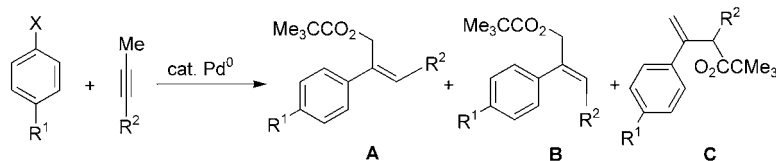
A biaryl banquet! Biphenyls with four *ortho* substituents, heteroaromatic compounds, iodinated biaryls, and medium rings containing biaryls are all readily synthesized by organocuprate oxidation.

The utility of this new methodology is illustrated by the efficient synthesis of the medium-ring core of sanguin H-5 (see scheme).

C–C Coupling

D. S. Surry, X. Su, D. J. Fox, V. Franckevicius, S. J. F. Macdonald, D. R. Spring* — **1870–1873**

Synthesis of Medium-Ring and Iodinated Biaryl Compounds by Organocuprate Oxidation



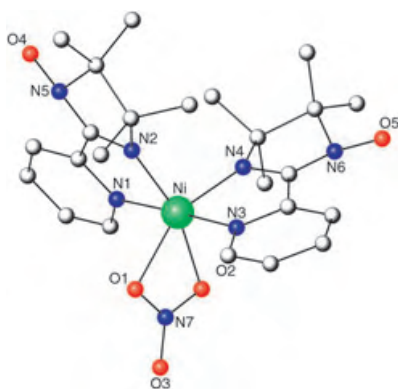
“Through-space” migration of palladium between remote carbon atoms appears to take place in the generation of π -allyl–palladium complexes, which are useful intermediates in organic synthesis. The

reaction of halogenated arenes with alkynes under Pd-migration conditions provides the mixture of allylic esters **A–C** (see reaction shown; X = Br, I; R¹ = H, OMe, CO₂Et, Cl; R² = Ph, *t*Bu).

Palladium Migration

J. Zhao, M. Campo, R. C. Larock* — **1873–1875**

Consecutive Vinylic to Aryl to Allylic Palladium Migration and Multiple C–H Activation Processes



Complementarity between different techniques (magnetization, HF-HFEPR, FDMRS) and angular-overlap-model calculations allow the precise determination of the spin-Hamiltonian parameters in an isolated octahedral Ni^{II} complex (see structure), which exhibits the largest easy axis magnetic anisotropy reported to date ($D = -10.1 \text{ cm}^{-1}$, $E/|D| = 0.02$).

Magnetic Properties

G. Rogez,* J.-N. Rebilly, A.-L. Barra, L. Sorace, G. Blondin, N. Kirchner, M. Duran, J. van Slageren, S. Parsons, L. Ricard, A. Marvilliers, T. Mallah* — **1876–1879**

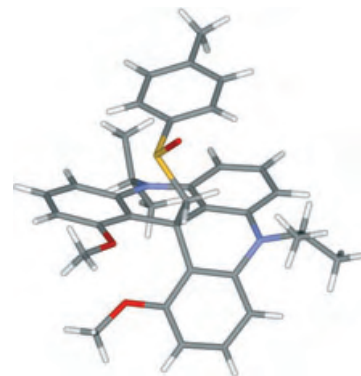
Very Large Ising-Type Magnetic Anisotropy in a Mononuclear Ni^{II} Complex

Pummerer-like Reactions

B. Laleu, P. Mobian, C. Herse,
B. W. Laursen, G. Hopfgartner,
G. Bernardinelli, J. Lacour* **1879–1883**

Resolution of [4]Heterohelicenium Dyes
with Unprecedented Pummerer-like
Chemistry

Addition of an enantiopure sulfoxide
auxiliary is the key to the resolution of
highly stable [4]helicenium dyes. This
transformation allows a facile chromato-
graphic separation of the diastereomers
(the structure of one such diastereomer is
shown; S yellow, O red, N blue). Then an
unprecedented Pummerer-like C–C bond
fragmentation takes place to release the
enantiopure cations.

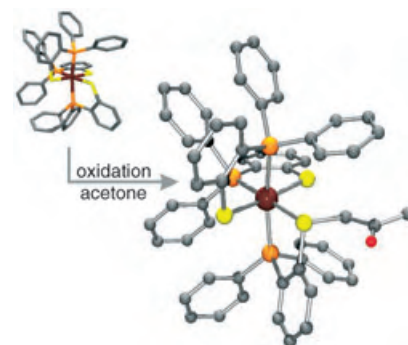


C–S Bond Formation

S. Poturovic, M. S. Mashuta,
C. A. Grapperhaus* **1883–1887**

Carbon–Sulfur Bond Formation between a
Ruthenium-Coordinated Thiyl Radical and
Methyl Ketones

A metal-coordinated thiyl radical was
revealed by the electrochemical oxidation
of a ruthenium(III)–thiolate in acetone
(and related ketones). The subsequent
reaction between the radical intermediate
and acetone resulted in C–S bond for-
mation and ultimately a ruthenium(III)–
thioether product (see picture). A
mechanism that involves reaction of the
enol tautomer of acetone with the radical
is proposed.



Angewandte
WILEY
InterScience®
DISCOVER SOMETHING GREAT

“Hot Papers” are chosen by the Editors for their importance in a rapidly evolving field of high current interest. A preview with the graphical abstracts of these articles can be found on the *Angewandte Chemie* homepage in Wiley InterScience at www.angewandte.org.

“VIPs” are Communications which are identified by two referees as being very important. They are published online up to several weeks ahead of print. A preview with short summaries of these articles can also be found on the journal's homepage.

Angewandte

Service

Keywords **1888**

Authors **1889**

**Angewandte's
Sister Journals** **1890–1891**

Preview **1893**

Walter Hugo Stockmayer (1914–2004): *Macromolecules*

After many years in science Professor Walter Hugo Stockmayer passed away peacefully on May 9, 2004, at his home in Norwich VT, just one month after his 90th birthday. This fact may have escaped our attention were it not for the informative obituary by Marshall Fixman and Ronald Koningsveldt in *Macromolecules*. *Macromolecules* was founded by Stockmayer together with Frank Bovey and Field Winslow, and he was Associate Editor from 1968 to 1994. Any author who interacted with him will remember his kind and stimulating suggestions.

Walter Hugo Stockmayer was born on April 7, 1914, in Rutherford, NJ. His father was a chemist who worked for a dye company in Stuttgart (Germany) and moved to the USA in 1909 to work in the New York branch. His mother, who in 1890 emigrated to the USA from Estonia, brought an artistic atmosphere into the family and took care of her son's musical training. Later on in life, Stocky (as he liked to be called) played the piano in private and in open concerts. His grandfather on his mother's side, who had fought in the Civil War and returned to Estonia, finally found a position on Ellis Island as an interpreter for immigrants from Eastern Europe.

In 1931 Stocky started his college training at MIT in Boston. The transition from school to college at first came as a shock, but he soon developed discipline and learnt to cope with the workload. He escaped from his routine by taking on advanced extra courses by outstanding professors in mathematics and modern physics. In 1935 he applied for the prestigious Cecil Rhodes Scholarship for training at Oxford University. He received the grant and spent two years at Jesus College. He was not very happy with the English style of research, which in those days was mainly empirical; Stocky was more interested in really understanding phenomena. His research on the “*Poisoning of a Palla-*

dium Catalyst by Carbon Monoxide” was published in 1940. Stocky was an active sportsman all his life, and when asked about his time in Oxford, his response was always: “*Rowing on the river was number one!*”. But he did train himself intensively in modern fields of research.

Stocky left Oxford in 1937 a little disappointed. He was not yet sure what to do next. He began a PhD at MIT and graduated in 1940. His work was concerned with the thermodynamics of real gases, and his main contribution was the induction of dipoles in molecules and the derivation of the interaction potential between such polar gas molecules (Stockmayer potential), which already brought him fame at a young age.

Stockmayer then left MIT for Columbia University, New York. He wished to be close to Joseph E. and Maria G. Mayer. Even then he was not sure which direction to take, until he came across the work by Paul J. Flory on the gelation of multifunctional polyesters. Stocky himself described this revelation as a “*bombshell*”, and it changed everything for him. Flory was already well-known for his derivation of molar-mass distributions from polymerization kinetics and he derived a simple mathematical equation for the conditions for gel formation. Stocky immediately tried to extend this theory, but his work did not proceed as easily as he anticipated. It was Maria Goeppert Mayer who noticed his difficulties; she was often at his side and followed his work keenly. She finally said, “*Stocky, why don't you try the way we did with the real-gas theory?*”. And this was the breakthrough. Flory was excited by this approach, and this was the beginning of a life-long steadfast friendship. In the meantime the USA had entered the war, and although most scientific activities were delayed, the paper was published in 1943.^[1] This and his consecutive paper made Stocky famous overnight. It was with this theory that Stockmayer introduced strict mathematical argumentation into macromolecular chemistry. The path he was to follow was now clear to him. He returned to MIT and subsequently developed theories on ring formation, on excluded-volume interaction, and on conforma-

tional properties of chains and branched clusters. He also made the first decisive steps in unraveling problems in copolymers.

Although Professor Stockmayer was considered by most as a pure theoretician, this impression is misleading. In the first years of his career he did a considerable amount of experimental work. Inspired by Bruno Zimm, he became interested in light scattering (LS). Together with his student E.-H. Stanley, he built an improved version of Zimm's LS instrument and carried out one of the first measurements on copolymers. However, the theory of light scattering first had to be solved for multicomponent systems. It transpired that Kirkwood was working on this problem at the same time. He was so impressed with Stocky's design that he delayed his own publication until Stocky had finished his work.^[2]

At the peak of his career at MIT, Stocky unexpectedly left in 1961 to take a chair at Dartmouth College (Hanover, NH). He felt his research had become a little stale and he wished to return to teaching. Stocky was an enthusiastic mountain climber and enjoyed the proximity of the White Mountains. In his first years at Dartmouth he felt somewhat isolated from the world. Soon, however, his interest in science was revitalized by J.E. Hearst, a young professor in biochemistry at Berkley who was on sabbatical leave at Dartmouth. Hearst sought a quantitative interpretation for his results from sedimentation analysis of DNA molecules. The collaboration reawoke Stocky's creativity and led to significant work on chain stiffness of open and cyclic stiff macromolecules, with which he was fascinated until the end of his life. In this second creative phase Stocky made significant contributions to theory of local chain dynamics, and he carried out experimental work on the dielectric relaxation of long polar chains to test the theories.^[3]

Stocky remained very interested in the ideas and progress of other people, and he was an impressively attentive listener. He was careful in choosing suitable places and stimulating people for sabbatical leaves. The first was at the Centre de Recherches sur les Macromolécules in Strasbourg (1954/55), another



at Tokyo Kyoiku and Kyoto University (1966), and the last two were at the DSM in the Netherlands with Ronald Koningsveldt (1972) and at the Institute of Macromolecular Chemistry in Freiburg, Germany (1978/79). Ron Koningsveldt shared a love of music with Stocky and they enjoyed playing together on different pianos. Their combined research projects led to a comprehensive monograph on phase-separation phenomena with polymers. Stocky stimulated Ron to write his own music, which led to the now often recited Polymer Music.

Stocky bore fond memories of his last sabbatical leave in Freiburg (1978). There he came into contact with the rapidly developing field of dynamic LS, which completed his knowledge of chain dynamics. He was overwhelmed by the wealth of cultural life in Germany, especially the opera and chamber music, and he enjoyed hiking in the nearby Black Forest. However, he was particularly touched by the young PhD students, who felt deeply ashamed of

Germany's regrettable history. He later confessed that he was not willing to return to Germany, but when he left he said: "*I am glad I came to Freiburg and I don't regret my decision. I now know, Germany has changed.*" I am grateful to my students for instilling this feeling in him.

Professor Stockmayer received numerous honors, and only a few can be mentioned here. He received the highest honors from the US Government and the American Chemical and Physical Societies. Several universities abroad bestowed honorary doctorates on him. In Germany he received the Humboldt Award for Senior Scientists (1978) and the Hermann Staudinger Prize of the German Chemical Society (2001). Stockmayer felt especially honored by the latter prize, which was awarded to a non-German scientist for the first time.

The long list impressively shows Walter Hugo Stockmayer as a great scientist. His main impact was probably the introduction of precise mathematics into

polymer science, which decisively incorporated macromolecular chemistry into polymer science and made it an exact science. His knowledge in science was always accompanied by a warm and considerate human side. Anyone who met him will always remember his ability to concentrate on the person in front of him. We all, colleagues and friends, will miss him.

Walther Burchard

Institut für Makromolekulare Chemie
Hermann-Staudinger-Haus
Albert-Ludwigs-Universität Freiburg
(Germany)

-
- [1] W. H. Stockmayer, *J. Chem. Phys.* **1943**, *11*, 45; W. H. Stockmayer, *J. Chem. Phys.* **1944**, *12*, 125.
 - [2] W. H. Stockmayer, *J. Chem. Phys.* **1950**, *18*, 58; J. G. Kirkwood, J. Goldberg, *J. Chem. Phys.* **1950**, *18*, 54.
 - [3] J. E. Hearst, W. H. Stockmayer, *J. Chem. Phys.* **1962**, *37*, 1425.

Protonated Chiral Catalysts: Versatile Tools for Asymmetric Synthesis

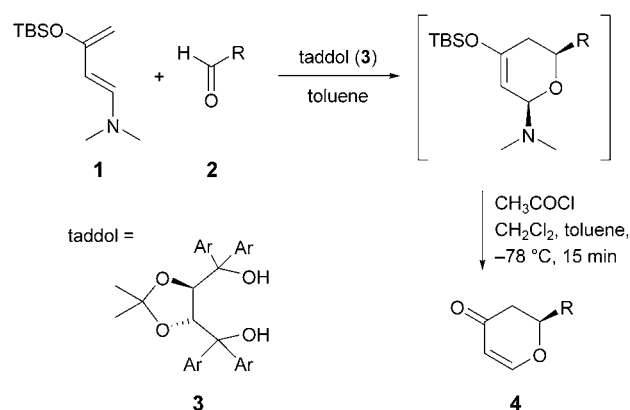
Carsten Bolm,* Toni Rantanen, Ingo Schiffrs, and Lorenzo Zani

Keywords:

asymmetric catalysis · Brønsted acids · hydrogen bonds · organocatalysis · protonation

Asymmetric catalysis of organic reactions is one of the main research fields in chemistry.^[1] Although for many years asymmetric catalysis was conceptually linked to the use of chiral transition-metal complexes, processes catalyzed by metal-free species have recently received significant attention.^[2,3] In many cases, the effectiveness of these catalysts relies on the formation of strictly oriented hydrogen bonds.^[4] The substrate(s) are then activated by noncovalent interactions, and in this manner synthetically highly valuable enantioselective transformations are possible by applying well-defined low-molecular-weight nonmetallic catalysts.^[5–7] A particularly elegant example of this concept is the taddol-catalyzed asymmetric hetero-Diels–Alder reaction developed by Rawal and co-workers.^[8] In this cycloaddition, a simple chiral alcohol complexes to a carbonyl group, thus accelerating the enantioselective C–C bond-forming process, which gives the cyclic product with > 92% *ee* (Scheme 1).

In the cycloaddition reaction of Rawal and co-workers, a rather small, uncharged, (purely) organic molecule activates the carbonyl compound and leads to excellent enantioselectivities. Conceptually different is the use of a chiral Brønsted base,^[9] which on its own is catalytically inactive and requires the addition of an acid to give an active catalyst. The Brønsted base and acid do



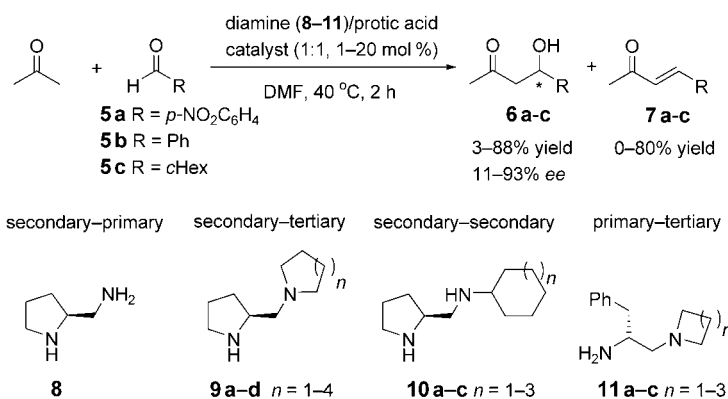
Scheme 1. Hydrogen-bond catalysis according to Rawal and co-workers. TBS = *tert*-butyldimethylsilyl.

not act independently, but their combination leads to a cationic species that is a potent catalyst with remarkable activity and (stereo)selectivity.^[10] Very recently, a number of highly exciting developments in this field have been reported and some of them are highlighted herein.

In 2001, Yamamoto and co-workers described the development and use of

protic acid–diamine catalysts for the direct asymmetric aldol reaction between acetone and some aromatic and aliphatic aldehydes.^[11] Guided by earlier observations,^[12,13] they screened several diamines, mostly bearing a pyrrolidine backbone, in combination with various sulfonic acids (Scheme 2).

Among the tested diamines, which served as Brønsted bases, those contain-

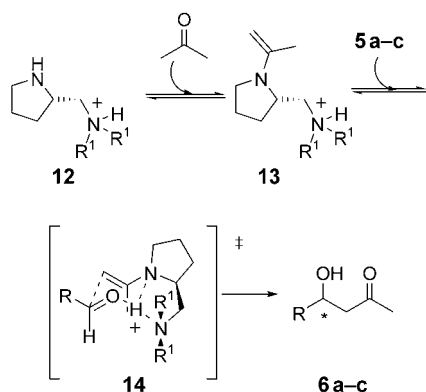


Scheme 2. Asymmetric direct aldol reaction according to Yamamoto and co-workers. DMF = *N,N*-dimethylformamide.

[*] Prof. Dr. C. Bolm, Dipl.-Chem. T. Rantanen, Dr. I. Schiffrs, Dipl.-Chem. L. Zani
Institut für Organische Chemie
RWTH Aachen
Landoltweg 1, 52056 Aachen (Germany)
Fax: (+49) 241-8092-391
E-mail: carsten.bolm@oc.rwth-aachen.de

ing a secondary and a tertiary nitrogen atom, such as **9a–d**, were found to be excellent catalysts for the direct aldol reaction. However, the formation of dehydration products **7** occasionally posed problems. The formation of such dehydration products was avoided by using the primary–tertiary diamine series **11a–c**, but unfortunately the reaction rate was much lower than with the secondary–tertiary diamine series. The best results were obtained with the secondary–secondary diamines **10a–c**, albeit that considerable amounts of **7** were still formed. Diamine **8**, which bears a secondary and a primary amine group, proved to be totally ineffective.

Various sulfonic acids were used in the early experiments, but trifluoromethanesulfonic acid (triflic acid) was later found to give optimal results. The role of the acid is probably twofold: First, it increases the rate of enamine formation, and second, it orients the substrates by hydrogen bonding (Scheme 3). Later, isolated salts such as $[9a\text{--}HOTf]_2$ (**15**) were employed in-



Scheme 3. Proposed mechanism of the direct aldol reaction in the presence of protonated diamine **12** as catalyst.

stead of the chiral diamine–triflic acid catalysts generated *in situ*.^[14] This new protocol had the advantage that the enantioselectivities in the direct aldol reaction were slightly higher and that the handling of the corrosive and hygroscopic triflic acid could be avoided in the catalytic reaction.

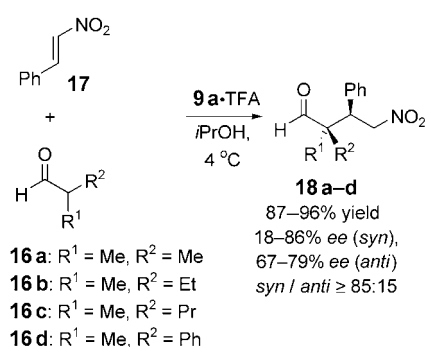
Barbas and co-workers described the use of proline and various proline derivatives in asymmetric Mannich reactions as well as in enantioselective

direct aldol and Michael reactions. In the Mannich reaction between acetone or unmodified aldehydes and preformed aldimines, surprisingly, the best catalyst was proline itself.^[15] The diamine used by Yamamoto and co-workers only led to moderate yields and enantiomeric excesses, even with the help of a protic acid.^[16]

In contrast, in direct asymmetric aldol reactions the combination of diamine **9a** and trifluoroacetic acid was highly efficient, whereas proline itself gave only moderate yields and enantioselectivities.^[17] Outstanding results were obtained by the use of this catalyst in organocatalytic direct asymmetric aldol reactions with α,α -disubstituted aldehydes as aldol donors which led to β -hydroxyaldehydes with quaternary stereogenic carbon centers.^[18] The same catalyst was also effective in the direct asymmetric Michael reaction between isobutyraldehyde and β -nitrostyrene (Scheme 4).^[19]

Comparably moderate enantioselectivities and yields were observed in 1,4-additions of acetone and various benzyl malonates to β -nitrostyrene. Interestingly, proline catalyzed these reactions as well, but the resulting products had only low *ee* values.^[19]

The direct asymmetric Michael reaction was also studied by Kotsuki and co-workers, who used cyclohexanones and β -nitroolefins as reactants.^[20] Chiral pyrrolidine–pyridine bases in combination with protic acids were applied as catalysts. Especially the results with styrene-type nitroolefins were excellent. Interestingly, when isovaleraldehyde

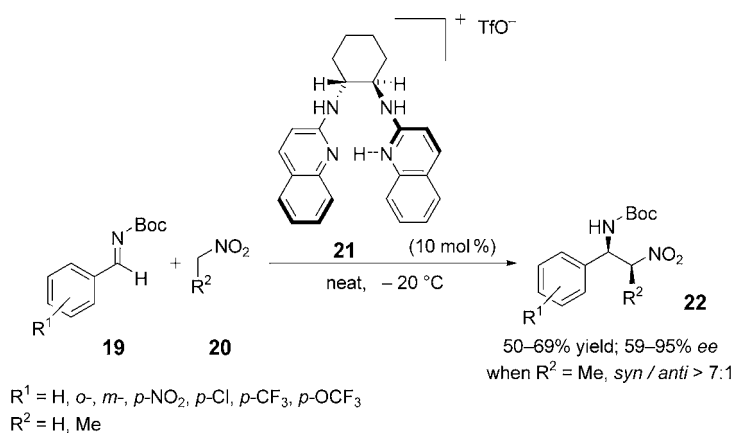


Scheme 4. Organocatalytic direct Michael additions of aldehydes to β -nitrostyrene. TFA = trifluoroacetic acid.

was used instead of a ketone, the enantioselectivity was very low.^[21]

Perhaps the most striking application of a protonated diamine-type catalyst is the so-called “chiral proton catalysis”, a strategy recently reported by Johnston and co-workers.^[22] In this approach, a chiral catalyst is generated by coordinating a proton, which stems from the strong Brønsted acid TfOH, to an axially chiral diamine (the Brønsted base). The resulting bench-stable salt **21** is then an excellent catalyst for the asymmetric aza-Henry reaction, and affords the corresponding products **22** in good yields with up to 95% *ee* (Scheme 5). Although mechanistic details have not yet been disclosed, initial experiments clearly show that the proton plays a key role in both substrate activation and orientation, thus leading to the observed selectivities.^[23]

Of particular synthetic interest are the organocatalysts developed by MacMillan and co-workers. They found that



Scheme 5. A “chiral proton catalyst” in asymmetric aza-Henry reactions. TfO^- = trifluoromethanesulfonate; Boc = *tert*-butoxycarbonyl.

chiral imidazolidinones in combination with strong Brønsted acids catalyze important organic transformations such as cycloadditions,^[24] Friedel–Crafts alkylations,^[25] Mukaiyama–Michael reactions,^[26] α -chlorination of aldehydes,^[27] aldehyde–aldehyde couplings,^[28] and hydride reductions.^[29,30] Scheme 6 shows two representative reactions, which proceed under catalysis with imidazolidinones **25** (20 mol %) and **29** (5 mol %). The chiral imidazolidinones can be synthesized readily in a few steps from commercially available enantiopure amino acids. The Brønsted acid adducts are then either prepared as salts prior to the reaction or generated in situ by premixing equimolar amounts of the two components in the reaction solvent.

Mechanistically, most transformations mentioned above proceed via iminium ions **31**,^[31] and to attain high enantioselectivities, the chiral imidazolidinone must efficiently control the formation of only one of the two possible iminium ion stereoisomers and effectively shield one of its faces, thus forcing the reaction partner to approach from the other side. Interestingly, both catalytic efficiency and stereoselectivity depend on the Brønsted acid used which suggests that the proton itself as well as its counterion play a decisive role in the process.

For the α chlorination (Scheme 6) the authors proposed an enamine-type mechanism similar to that of proline-

catalyzed reactions. In this case, the protonation of the imidazolidinone-based enamine leads to a more ordered transition state (**32**) owing to the presence of an additional hydrogen bond (Figure 1).^[27]

All catalysts described so far stem from the combination of a purely organic molecule with a strong Brønsted acid. Corey and co-workers elaborated a different concept of catalyst activation by protonation based on their previous investigations of cationic super Lewis acid catalysts in enantioselective Diels–Alder reactions^[32] and their studies of

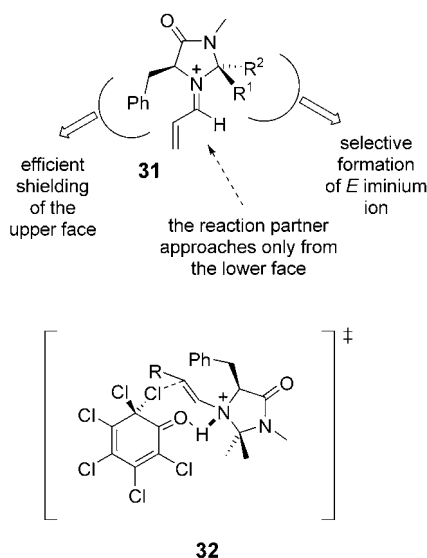


Figure 1. Proposed intermediates in reactions with imidazolidinone/Brønsted acid catalysts.

the formyl C–H...O hydrogen bond as an organizing element therein.^[33] Proline-derived oxazaborolidines **33** are especially useful catalysts for the asymmetric reduction of ketones with $\text{BH}_3\cdot\text{THF}$ or catecholborane as stoichiometric reducing agent.^[34] In Diels–Alder reactions of α,β -unsaturated aldehydes, however, they show no catalytic activity. When **33** is treated with 1 equivalent of anhydrous triflic acid, an equilibrium mixture of two *N*-protonated species **34** and **35** results, in which the latter is “highly Lewis acidic at the boron owing to its cationic character” (Scheme 7).^[35]

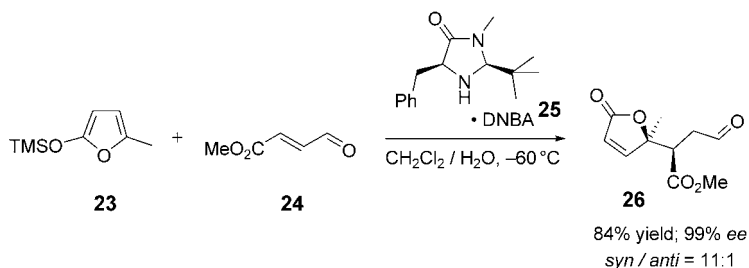
α,β -Unsaturated carbonyl compounds are efficiently activated by these protonated oxazaborolidines and even relatively unreactive dienes, such as butadiene and 1,3-cyclohexadiene, undergo rapid cycloaddition reactions at low temperatures to afford products with high enantioselectivities (Scheme 8).^[36]

The nature of the aryl boron substituent is of major importance for the enantioselectivity, and the best results are obtained with catalysts that bear an *o*-tolyl group. The authors suggested a pretransition state **46**, in which the coordinated aldehyde is fixed by a formyl C–H...O hydrogen bond and attractive π – π donor–acceptor interactions between the electron-deficient α,β -enal subunit and the *cis* aryl group of the oxazaborolidine ring (Figure 2).

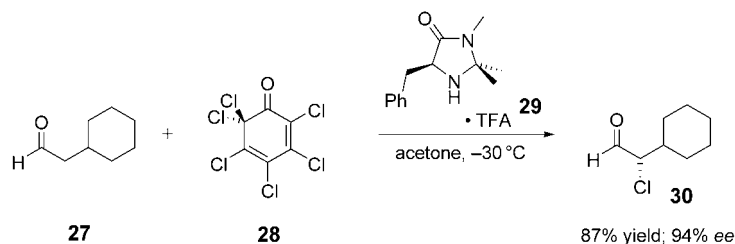
This proposal is consistent with the stereochemical result of the catalysis and the observation that a catalyst with (Ar =) 3,5-dimethylphenyl groups leads to better *ee* values than one with unsubstituted phenyl groups. The fact that an opposite face selectivity was observed in reactions with α,β -unsaturated esters and α,β -enones was attributed to a preferred coordination of such molecules, which lack a formyl hydrogen atom, by formation of a hydrogen bond between the α -olefinic hydrogen atom and the oxazaborolidine oxygen atom as shown in **47** (Figure 2).^[37]

In the context of this overview it is interesting that a simple change of the counterion from triflate (TfO^-) to triflimide (TF_2N^-) has a remarkably beneficial effect on the catalyst stability without lowering its potency.^[38] This increased thermal stability results in a superior catalytic efficacy in enantiose-

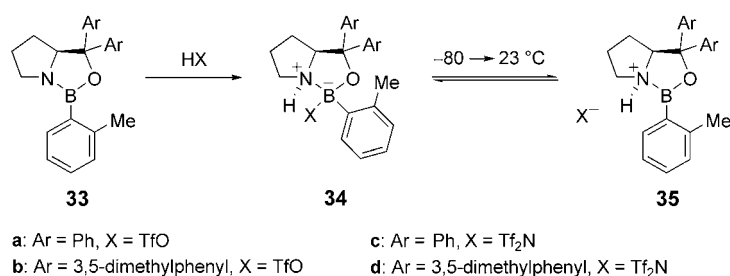
Mukaiyama–Michael reactions



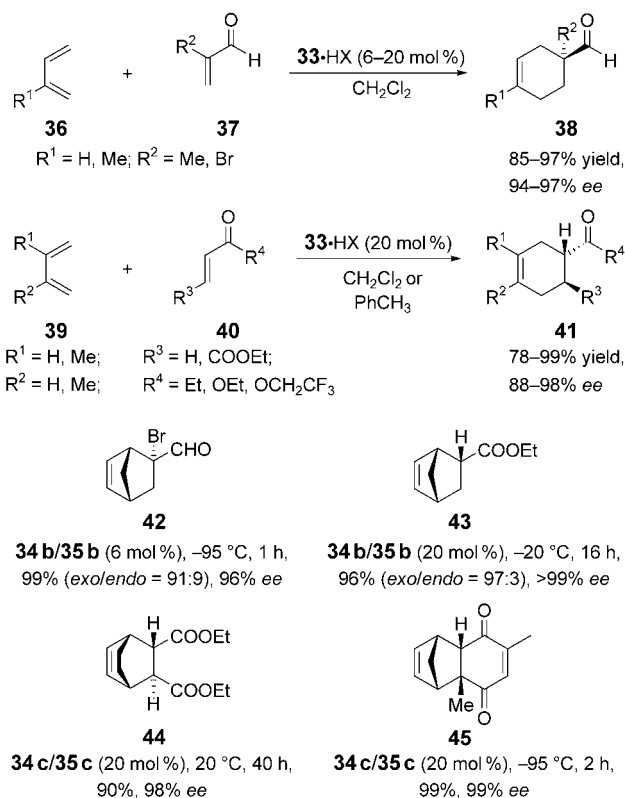
α chlorination of aldehydes



Scheme 6. Two representative applications of chiral organocatalysts by MacMillan and co-workers. TMS = trimethylsilyl; DNBA = 2,4-dinitrobenzoic acid.



Scheme 7. Oxazaborolidines and related protonated species.



Scheme 8. Protonated oxazaborolidines as catalysts for cycloaddition reactions.

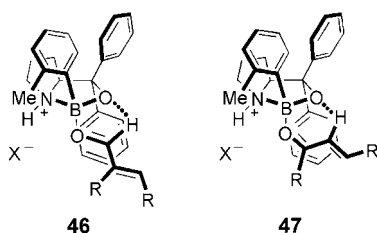
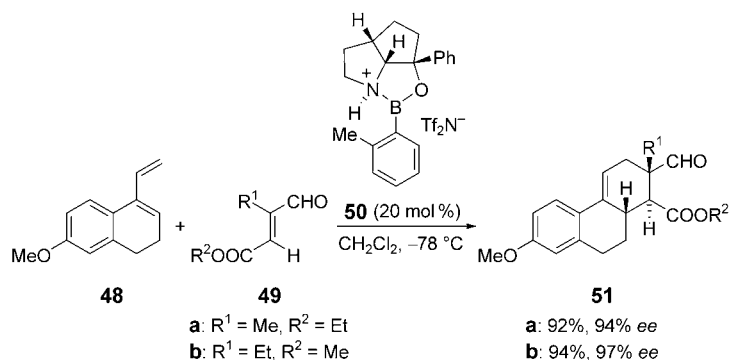


Figure 2. Preferred coordination modes of enals and other α,β -unsaturated carbonyl compounds to protonated oxazaborolidines.

lective Diels–Alder reactions between dienes of low reactivity, such as 2,3-dimethylbutadiene, and dienophiles that are unreactive in the presence of the triflate-based catalyst.



Scheme 9. Use of an oxazaborolidinium catalyst in steroid syntheses.

The preparative opportunities of these new catalyst systems were impressively demonstrated in the syntheses of the steroids estrone and desogestrel,^[39] which is an important third-generation oral contraceptive. In this case, oxazaborolidinium triflimide **50** was the most effective catalyst in the preparation of key intermediates **51** in 92–94% yield with 94–97% ee (Scheme 9). It is thus one of the most efficient synthetic methodologies in this area at the present time.^[40]

In a comprehensive study, it was shown that Diels–Alder reactions between unsymmetrical 1,3-dienes and substituted 1,4-quinones catalyzed by oxazaborolidinium salts generally afford only a single highly enantiomerically enriched regioisomer.^[35c,41] The enantioselectivity, orientational selectivity (mode of coupling the ends of the diene and the dienophile), and site selectivity (only one of the two C=C subunits of the quinone underwent reaction) were in accordance with the mechanistic model and enabled the authors to develop a reliable set of selection rules that allow the prediction of the structure and the absolute configuration of the principal reaction product. With this powerful tool in hand, Corey and co-workers modified a number of classic natural product syntheses into enantioselective versions and published an impressive contribution on the use of the oxazaborolidinium catalysts in Sarett's total synthesis of cortisone, Kende's dendrobine synthesis, the preparation of (+)-myrocin C, and the synthesis of a highly enantiomerically enriched (+)-hirsutene and (–)-coriolin precursor (**45** in Scheme 8).^[42] Recently, they showed that oxazaborolidinium cations can also

be applied in enantioselective cyanosilylations to generate cyanohydrins with 90–97% *ee* in excellent yields. Also in this case, the absolute configurations of the products were correctly predicted by the mechanistic model.^[43,44]

In conclusion, we have described the use of new chiral catalysts, which have already proved to be valuable for asymmetric synthesis. By combining catalytically inactive (neutral) molecules with strong Brønsted acids, cationic species are generated that catalyze a wide range of synthetically powerful transformations in a highly enantioselective manner. Considering the relative youth of this concept, we foresee many other applications of such cationic entities and predict a bright future for newly designed protonated chiral catalysts.^[45]

- [1] a) R. Noyori, *Asymmetric Catalysis in Organic Synthesis*, Wiley, New York, **1994**; b) *Comprehensive Asymmetric Catalysis* (Eds.: E. N. Jacobsen, A. Pfaltz, H. Yamamoto), Springer, Berlin, **1999**; c) *Catalytic Asymmetric Synthesis*, 2nd ed. (Ed.: I. Ojima), Wiley-VCH, New York, **2000**; d) *Transition Metals for Organic Synthesis*, 2nd ed. (Eds.: M. Beller, C. Bolm), Wiley-VCH, Weinheim, **2004**.
- [2] For leading reviews, see: a) P. I. Dalko, L. Moisan, *Angew. Chem.* **2001**, *113*, 3840; *Angew. Chem. Int. Ed.* **2001**, *40*, 3726; b) B. List, *Synlett* **2001**, 1675; c) E. R. Jarvo, S. J. Miller, *Tetrahedron* **2002**, *58*, 2481; d) B. List, *Tetrahedron* **2002**, *58*, 5573; e) P. I. Dalko, L. Moisan, *Angew. Chem.* **2004**, *116*, 5248; *Angew. Chem. Int. Ed.* **2004**, *43*, 5138.
- [3] Two major journals have recently dedicated special issues to organocatalysis, see: a) *Acc. Chem. Res.* **2004**, *37*(8); b) *Adv. Synth. Cat.* **2004**, *346*(9–10).
- [4] a) T. Steiner, *Angew. Chem.* **2002**, *114*, 50; *Angew. Chem. Int. Ed.* **2002**, *41*, 48; b) G. A. Jeffrey, *An Introduction To Hydrogen Bonding*, Oxford University, New York, **1997**; c) M. Meot-Ner (Mautner), *Chem. Rev.* **2005**, *105*, 213.
- [5] For selected examples, see: a) M. S. Sigman, E. N. Jacobsen, *J. Am. Chem. Soc.* **1998**, *120*, 5315; b) E. J. Corey, M. J. Grogan, *Org. Lett.* **1999**, *1*, 157; c) P. Vachal, E. N. Jacobsen, *J. Am. Chem. Soc.* **2002**, *124*, 10012; d) T. Okino, S. Nakamura, T. Furukawa, Y. Takemoto, *Org. Lett.* **2004**, *6*, 625; e) T. Okino, Y. Hoashi, Y. Takemoto, *J. Am. Chem. Soc.* **2003**, *125*, 12672.
- [6] For the use of chiral Brønsted acid type catalysts, see: a) N. T. McDougal, S. E. Schaus, *J. Am. Chem. Soc.* **2003**, *125*, 12094; b) D. Uraguchi, M. Terada, *J. Am. Chem. Soc.* **2004**, *126*, 5356; c) T. Akiyama, J. Itoh, K. Yakota, K. Fuchibe, *Angew. Chem.* **2004**, *116*, 1592; *Angew. Chem. Int. Ed.* **2004**, *43*, 1566; d) D. Uraguchi, K. Sarimachi, M. Terada, *J. Am. Chem. Soc.* **2004**, *126*, 11805.
- [7] Reviews: a) P. R. Schreiner, *Chem. Soc. Rev.* **2003**, *32*, 289; b) M. Oestreich, *Nachr. Chem.* **2004**, *52*, 35; c) P. M. Pihko, *Angew. Chem.* **2004**, *116*, 2110; *Angew. Chem. Int. Ed.* **2004**, *43*, 2062, and references therein.
- [8] a) Y. Huang, A. K. Unni, A. N. Thadani, V. H. Rawal, *Nature* **2003**, *424*, 146; for recent advances in this field, see: b) A. N. Thadani, A. R. Stankovic, V. H. Rawal, *Proc. Natl. Acad. Sci. USA* **2004**, *101*, 5846; c) A. K. Unni, N. Takenaka, H. Yamamoto, V. H. Rawal, *J. Am. Chem. Soc.* **2005**, *127*, 1336.
- [9] According to a definition proposed by Brønsted in 1923, bases are compounds that are able to accept a hydrogen ion: J. N. Brønsted, *Recl. Trav. Chim. Pays-Bas* **1923**, *42*, 718.
- [10] This scenario parallels “ligand-accelerated catalysis” (LAC). By combining the proton (stemming from the Brønsted acid) and the (catalytically inactive) chiral molecule, an equilibrium mixture results in which the active catalyst formed consists of a proton bound to a chiral ligand; for a review on LAC, see: D. J. Berrisford, C. Bolm, K. B. Sharpless, *Angew. Chem.* **1995**, *107*, 1159; *Angew. Chem. Int. Ed. Engl.* **1995**, *34*, 1059.
- [11] a) S. Saito, M. Nakadai, H. Yamamoto, *Synlett* **2001**, 1245; b) M. Nakadai, S. Saito, H. Yamamoto, *Tetrahedron* **2002**, *58*, 8167; c) S. Saito, H. Yamamoto, *Acc. Chem. Res.* **2004**, *37*, 570.
- [12] Reference [11c] gives an excellent background to the current studies and highlights the many contributions published by other researchers, which finally led to the development of the present asymmetric acid–base catalysts; for further details, this review is highly recommended.
- [13] In this context, it is also noteworthy that an enantioselective Diels–Alder reaction catalyzed by a chiral amidinium cation was reported as early as 2000: T. Schuster, M. Bauch, G. Dürner, M. W. Göbel, *Org. Lett.* **2000**, *2*, 179. Subsequently, the applicability of a C₂-symmetric bis(amidinium) catalyst was demonstrated: S. B. Tsogoeva, G. Dürner, M. Bolte, M. W. Göbel, *Eur. J. Org. Chem.* **2003**, 1661. In both studies, however, the turnover numbers of the catalysts as well as the enantioselectivities were low or moderate at best.
- [14] The salts were prepared by first reacting diamine **9a** with excess (> 2 equiv) TfOH. The resulting diammonium salt was then mixed with an additional equimolar amount of diamine **9a** to yield the desired amine–acid of composition **15**. Any variation of this ratio resulted in a decrease of the reaction rate. For example, a salt with a 1:2 (amine/acid) stoichiometry did not show any catalytic activity.
- [15] a) W. Notz, F. Tanaka, S.-I. Watanabe, N. S. Chowdari, J. M. Turner, R. Thayumanavan, C. F. Barbas III, *J. Org. Chem.* **2003**, *68*, 9624; b) N. S. Chowdari, J. T. Suri, C. F. Barbas III, *Org. Lett.* **2004**, *6*, 2507.
- [16] W. Notz, K. Sakthivel, T. Bui, G. Zhong, C. F. Barbas III, *Tetrahedron Lett.* **2001**, *42*, 199.
- [17] B. List, R. A. Lerner, C. F. Barbas III, *J. Am. Chem. Soc.* **2000**, *122*, 2395.
- [18] N. Mase, F. Tanaka, C. F. Barbas III, *Angew. Chem.* **2004**, *116*, 2474; *Angew. Chem. Int. Ed.* **2004**, *43*, 2420.
- [19] N. Mase, R. Thayumanavan, F. Tanaka, C. F. Barbas III, *Org. Lett.* **2004**, *6*, 2527.
- [20] T. Ishii, S. Fujioka, Y. Sekiguchi, H. Kotsuki, *J. Am. Chem. Soc.* **2004**, *126*, 9558.
- [21] A protonated chiral pyrrolidine has also been used in catalyzed asymmetric epoxidations. In this case, however, it appears to only serve as carrier and activator of the peroxymonosulfate anion, and no additional interaction with the olefinic substrate has been described: V. K. Aggarwal, C. Lopin, F. Sandrinelli, *J. Am. Chem. Soc.* **2003**, *125*, 7596, and references therein.
- [22] B. M. Nugent, R. A. Yoder, J. N. Johnston, *J. Am. Chem. Soc.* **2004**, *126*, 3418.
- [23] The authors report that the use of the chiral ligand alone furnished a result comparable to the uncatalyzed reaction (less than 5% yield at –20°C after 5 days).
- [24] a) K. A. Ahrendt, C. J. Borths, D. W. C. MacMillan, *J. Am. Chem. Soc.* **2000**, *122*, 4243; b) W. S. Jen, J. J. M. Wiener, D. W. C. MacMillan, *J. Am. Chem. Soc.* **2000**, *122*, 9874; c) A. B. Northrup, D. W. C. MacMillan, *J. Am. Chem. Soc.* **2002**, *124*, 2458.
- [25] a) N. A. Paras, D. W. C. MacMillan, *J. Am. Chem. Soc.* **2001**, *123*, 4370; b) J. F. Austin, D. W. C. MacMillan, *J. Am. Chem. Soc.* **2002**, *124*, 1172; c) N. A. Paras, D. W. C. MacMillan, *J. Am. Chem. Soc.* **2002**, *124*, 7894.
- [26] S. P. Brown, N. C. Goodwin, D. W. C. MacMillan, *J. Am. Chem. Soc.* **2003**, *125*, 1192.
- [27] M. P. Brochu, S. P. Brown, D. W. C. MacMillan, *J. Am. Chem. Soc.* **2004**, *126*, 4108.

- [28] I. K. Mangion, A. B. Northrup, D. W. C. MacMillan, *Angew. Chem.* **2004**, *116*, 6890; *Angew. Chem. Int. Ed.* **2004**, *43*, 6722.
- [29] S. G. Ouellet, J. B. Tuttle, D. W. C. MacMillan, *J. Am. Chem. Soc.* **2005**, *127*, 32.
- [30] After the reports by MacMillan, imidazolidinone catalysts were also applied by other groups; for examples, see: a) -[4+3] cycloadditions: M. Harmata, S. K. Ghosh, X. Hong, S. Wacharasindhu, P. Kirchhöfer, *J. Am. Chem. Soc.* **2003**, *125*, 2058; b) intramolecular Michael reactions: M. T. Hechavarria Fonseca, B. List, *Angew. Chem. Int. Ed.* **2004**, *43*, 3958; c) transfer hydrogenations: J. W. Yang, M. T. Hechavarria Fonseca, N. Vignola, B. List, *Angew. Chem.* **2005**, *117*, 110; *Angew. Chem. Int. Ed.* **2005**, *44*, 108.
- [31] The activation of the unsaturated carbonyl compound is suggested to originate from a lowering of the LUMO upon conversion of the substrate into the corresponding, and much more reactive, iminium ion.
- [32] a) Y. Hayashi, J. J. Rohde, E. J. Corey, *J. Am. Chem. Soc.* **1996**, *118*, 5502; b) E. J. Corey, *Angew. Chem.* **2002**, *114*, 1724; *Angew. Chem. Int. Ed.* **2002**, *41*, 1650.
- [33] E. J. Corey, T. W. Lee, *Chem. Commun.* **2001**, 1321.
- [34] For a review, see: E. J. Corey, C. J. Helal, *Angew. Chem.* **1998**, *110*, 2092; *Angew. Chem. Int. Ed.* **1998**, *37*, 1986.
- [35] a) E. J. Corey, T. Shibata, T. W. Lee, *J. Am. Chem. Soc.* **2002**, *124*, 3808; b) D. H. Ryu, T. W. Lee, E. J. Corey, *J. Am. Chem. Soc.* **2002**, *124*, 9992; c) D. H. Ruy, E. J. Corey, *J. Am. Chem. Soc.* **2003**, *125*, 6388.
- [36] Triflic acid was more effective than the weaker methanesulfonic acid in generating an active Diels–Alder catalyst.
- [37] Evidence for this hypothesis stems from X-ray crystal-structure investigations of the BF₃ complexes of methyl cinnamate, benzylidene acetone, and dibenzylidene acetone, in which the short distances between the α -olefinic hydrogen atom and the nearest fluorine atom suggests such an attractive interaction.
- [38] Catalyst **35a** is too unstable to be used above 4°C, whereas species **35c** functions well at 25°C.^[35c]
- [39] In this context, a stereoselective Diels–Alder reaction as key step in the synthesis of the steroid skeleton of norgestrel by Göbel and co-workers^[13] should be mentioned again.
- [40] Q.-Y. Hu, P. D. Rege, E. J. Corey, *J. Am. Chem. Soc.* **2004**, *126*, 5984.
- [41] D. H. Ryu, G. Zhou, E. J. Corey, *J. Am. Chem. Soc.* **2004**, *126*, 4800.
- [42] Q.-Y. Hu, G. Zhou, E. J. Corey, *J. Am. Chem. Soc.* **2004**, *126*, 13708.
- [43] D. H. Ryu, E. J. Corey, *J. Am. Chem. Soc.* **2004**, *126*, 8106.
- [44] For a recent extension of this study involving a combination of an alkaloid-derived ligand and a strong Brønsted acid, see: J. Huang, E. J. Corey, *Org. Lett.* **2004**, *6*, 5027.
- [45] For a recent demonstration of the ability of protons to conformationally reorient chiral ligands, see: M. Düggele, T. Christen, A. von Zelewsky, *Chem. Eur. J.* **2005**, *11*, 185.

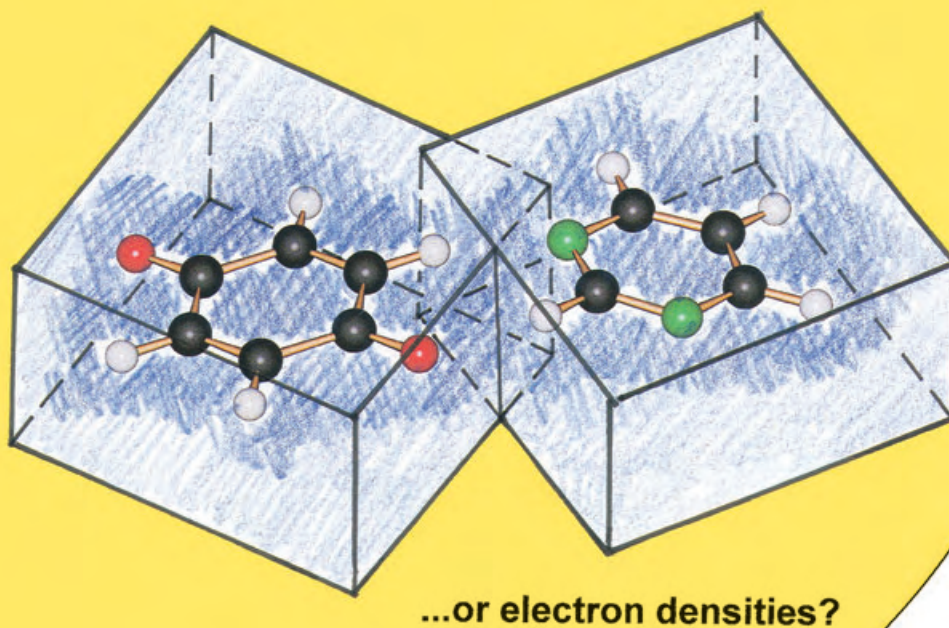
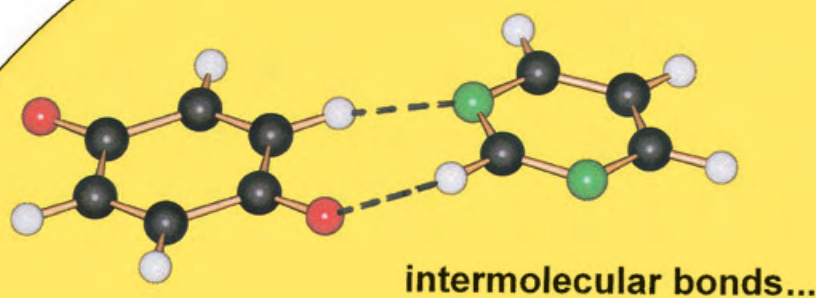
Intermolecular Bonding

Molecular Recognition in Organic Crystals: Directed Intermolecular Bonds or Nonlocalized Bonding?

Jack D. Dunitz* and Angelo Gavezzotti*

Keywords:

hydrogen bonds · intermolecular bonding · molecular recognition · pixel calculations



Molecules are held together mainly by forces acting between individual atoms. Does the same apply to molecular clusters? Does intermolecular cohesion depend on weak bonds between individual atoms in different molecules or on less localized, more diffuse interactions between molecules? We discuss these questions from several viewpoints and in particular compare interpretations based on the extension of Bader's atoms in molecules (AIM) theory to cover closed-shell intermolecular interactions with interpretations based on the new pixel method for the calculation of coulombic, polarization, dispersion, and repulsion energies from the electron density of molecular clusters.

“
Quorum ita texturae ceciderunt mutua contra,
ut cava convenient plenius haec illius illa
huiusque inter se, iuntura haec optima constat.^[+]”
Lucretius, De Rerum Natura, Book VI, 1085–1088.

1. How Well Do We Understand Crystal Packing?

How often have we heard a visiting lecturer, pointing to a projected ball-and-stick picture of a molecule, announce that this is the crystal structure of the compound? Of course, the picture we are shown is frequently not that of the crystal structure, more often it is that of the molecular structure as determined by X-ray analysis of the crystalline compound, and, apart from possible conformational and tautomeric changes, it serves to characterize the molecule in question. But it is not the crystal structure. This is at a higher level of complexity. The crystal structure is the arrangement of such molecules in a supramolecular pattern that repeats itself throughout the macroscopic lump of matter that is the crystal (Figure 1).

Even if we do have a picture of the crystal structure we can look at it in several ways. Some people might ask about the space group—a question that can often embarrass the visiting lecturer who may have to confess ignorance. The space group provides a shorthand description of the symmetry operations that interconnect all the molecules in the crystal. Another way of looking at the structure is in terms of the closest distances between atoms in different molecules. From this kind of information, hydrogen bonding and other types of characteristic intermolecular contact can be identified. Still another way is to look at the way in which a reference molecule is surrounded by neighboring molecules—the crystal packing.

Most organic crystals are held together by interactions that are much weaker than those acting between atoms in organic molecules or in minerals and inorganic crystals. How

[+] (Bodies) whose textures have fallen against one another so that empty spaces fit full spaces, this of that and that of this, such a junction between them appears the best. (Line numbers vary in different editions of the book.)

From the Contents

1. How Well Do We Understand Crystal Packing?	1767
2. Simple Models	1769
3. What is a Chemical Bond?	1770
4. Computational Models	1770
5. Determining Bond Paths from Electron Densities	1771
6. Hydrogen–Hydrogen Bonding?	1772
7. Intermolecular Bond Paths	1774
8. The Semi-Classical Density Sums (SCDS-Pixel) Approach	1775
9. Calculations versus Models and Simplifications	1777
10. Summary and Outlook	1785

does the molecular structure determine the crystal structure—or crystal structures, because many compounds occur not in a unique crystal structure but in several distinct and isolable structures, known as polymorphs? How does one molecule of a given compound “recognize” another molecule of that same compound, or a molecule of another specific compound, as in a co-crystal built from more than a single component?

The crystallization process appears to involve the phenomenon of molecular recognition, or rather molecular self-recognition, at an amazingly high degree of reliability. Indeed, crystallization has been used since time immemorial as a method of purification of mixtures of dissolved substances that may be quite similar in their chemical properties, and most organic crystals consist of identical, symmetry-related molecules. The periodic nature of a crystal does not in itself require that the constituent molecules must be identical or enantiomorphic (mirror-images) although this condition is

[*] Prof. J. D. Dunitz
Organic Chemistry Laboratory
Swiss Federal Institute of Technology
ETH-Hönggerberg HCI H333, 8093 Zurich (Switzerland)
Fax: (+41) 16322892
E-mail: dunitz@org.chem.ethz.ch
Prof. A. Gavezzotti
Dipartimento di Chimica Strutturale e Stereochimica Inorganica
Università di Milano
via Venezian 21, 20133 Milano (Italy)
Fax: (+39) 0250314454
E-mail: angelo.gavezzotti@unimi.it

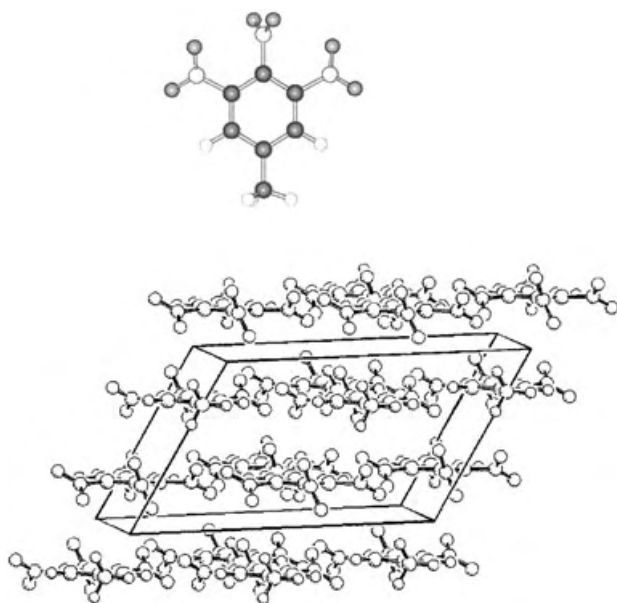


Figure 1. The molecule depicted at the top (3,4,5-trinitrotoluene; N and H atoms in white) is held together by localized bonds, indicated by the conventional connections drawn between bonded atoms. The crystal packing shown below is held together by much weaker interactions between molecular charge distributions. To what extent is it useful to describe the intermolecular bonding in terms of localized bonds between the atoms in the different molecules?

usually fulfilled. Indeed, in most crystals the molecules are all symmetry related. Nevertheless, it is interesting to note that in a small but ever increasing proportion of crystal structures the asymmetric unit consists of two or more symmetry-independent molecules.^[1] Co-crystals, crystals containing more than one component, are usually obtained not by the sheer accidents of crystallization from a mixed solution, but by design, by careful selection of molecules that are chosen to interact specifically with one another, or else they involve inclusion of small molecules within the interstices between large molecules that form the main framework of the crystal.^[2] A better understanding of these molecular recognition processes among comparatively simple molecules seems an absolute necessity if we are ever to understand the

enormously efficient and specific molecular recognition processes involved in enzyme–co-enzyme–substrate complexes or in the reconstitution of ribosomal particles from their dissociated proteins and nucleic acids.^[3]

“Molecular recognition” in its modern parlance implies that when two molecules approach one another in a particular way, the potential energy of the pair decreases significantly more than it would for a different manner of approach because of some specific interaction between the molecules. The importance of hydrogen bonding in molecular recognition and in crystal formation was recognized many years ago. In contrast, early diagrams of the crystal structures of naphthalene or anthracene, for example, did not show the positions of the hydrogen atoms, so that there appeared to be large gaps between the molecules in the crystal. It was Kitaigorodskii’s books^[4,5] that opened our eyes to the fact that organic molecules in crystals are close packed and tend to fill space as tightly as possible. As tightly as possible means that the packing coefficients of molecular crystals are about 0.7–0.8, roughly the same as for close-packed identical spheres ($\pi/\sqrt{18} = 0.7405$), and this is achieved when the “bumps” of one molecule fit into the “hollows” of adjacent molecules. Kitaigorodskii considered that for a given molecule, the actual crystal structure corresponds to one of the most densely packed of all conceivable structures. Structures held together by hydrogen bonds may be exceptions because the strongly directional nature of such bonds can lead to more open arrangements. More recent studies based on data from the Cambridge Crystallographic Database confirm Kitaigorodskii’s estimate; for a group of 164 hydrocarbons with 12–20 carbon atoms the average value of the packing coefficient was 0.721 with a standard deviation of 0.022.^[6] On melting, organic crystals typically expand by 10% or more. Hence, packing coefficients in organic liquids tend to be in the range 0.55–0.65. With packing coefficients below about 0.5 the cohesive forces between organic molecules are not strong enough to counter the entropic drive towards the gaseous state; the compounds vaporize. As far as packing energy is concerned, empty space is wasted space.

Intermolecular bonding energies are relatively weak compared to covalent bond energies. For example, the sublimation enthalpy of a 30-atom organic molecule is of



Jack Dunitz (b. 1923) studied chemistry at Glasgow University. After a decade of research at Oxford University, Caltech, National Institute of Health, and the Royal Institution in London, in 1957 he was appointed Professor of Chemical Crystallography at the ETH in Zurich, a position he held until his retirement in 1990. As a survivor of the heroic age of X-ray crystallography before the advent of computers, automatic diffractometers, and direct methods, he has witnessed how the subject has developed over the last half-century. He has written more than 360 scientific papers and is the author of “X-Ray Analysis and the Structure of Organic Molecules” (1979, 1995) and, with E. Heilbronner, “Reflections on Symmetry in Chemistry...and Elsewhere” (1993).



Angelo Gavezzotti graduated in chemistry in 1968 at the University of Milano. Except for brief research terms in France and the United States, his career developed entirely at Milano, where he is now professor of Physical Chemistry. His research concerns the theoretical and structural chemistry of organic crystals, a field to which he has contributed about 100 papers and some popular computer program packages for crystal-packing analysis, potential energy calculations, and crystal structure prediction.

the order of 100 kJ mol^{-1} , only about 20 % of the energy of a single typical covalent bond. In keeping with their relative weakness, intermolecular forces are less well defined—and in many cases perhaps less well definable—than their stronger intramolecular counterparts. If weaker than intramolecular bonding, intermolecular bonding is nevertheless persistent and reproducible—naphthalene sublimates readily at room temperature, but its crystal structure is immutable in the many tons purified and handled as the main ingredient of mothballs over the years.

2. Simple Models

With the rise of interest in intermolecular matters brought about by potential applications in materials chemistry and crystal engineering, the topic of intermolecular bonding in organic crystals has come to the fore. Similar issues arise in the design of supramolecular complexes at all levels, and especially in the structural interpretation of enzyme–substrate and enzyme–inhibitor complexes. What is the nature of the interactions between neighboring chemical entities that contribute significantly to intermolecular forces and energies? How should such interactions be named? This is not merely a nominal question, because a clear and unequivocal nomenclature for a specific physical effect is an enormous aid to understanding, and vice versa, confusion of terms can lead to misunderstanding of the underlying physics.

The chemical community soon discovered that an established language for intermolecular interactions was missing. To fill the gap, atom–atom terms borrowed from the intramolecular regime were the first choice. Hydrogen bonds of the type $\text{O(N)}\cdots\text{H}\cdots\text{O(N)}$, with directionality imposed by approximate co-linearity of the three atoms involved and by lone-pair orientation at the acceptor atom, had early been recognized as important intermolecular linkages. As an extrapolation of this type of interaction, the involvement of weak or “unconventional” hydrogen bonds has been invoked and widely discussed. From the perception of these and other frequently occurring patterns and their assumed importance as mediators of intermolecular interactions has come the concept of supramolecular synthons, “*structural units within supermolecules [e.g. crystals] which can be formed and/or assembled by known or conceivable intermolecular interactions*”^[7] The most obvious sites for localization of attractions among these units are the familiar “atoms”. Thus, it has become almost routine to discuss and analyze intermolecular interactions in terms of $\text{C}\cdots\text{H}\cdots\text{O}$, $\text{C}\cdots\text{H}\cdots\text{N}$, $\text{C}\cdots\text{H}\cdots\text{F}$, $\text{C}\cdots\text{H}\cdots\text{Cl}$, $\text{C}\cdots\text{H}\cdots\pi$, $\text{Cl}\cdots\text{Cl}$ intermolecular “bonds”.^[8]

It is clear that the atoms that come into contact in these intermolecular interactions are not those in the molecular interiors but those on the peripheries. The interior regions can contribute to the mutual intermolecular attraction but not to the repulsion. Thus, at equilibrium, the molecules in a crystal are drawn together by their mutual attraction and kept apart by their mutual repulsion, that is, by resistance to compression of the parts that come into mutual contact, the atoms on the peripheries—the very atoms that are supposed to be involved in intermolecular bonds.

At a deeper level, intermolecular energies depend on the electric charge distributions of the molecules and the way they interact. This is a quantum mechanical problem that can be solved computationally for not too complicated cases. As chemists, however, we feel the need for explanations of the crystal packing of organic molecules in more familiar terms. As far as the coulombic energy is concerned, the molecular charge distribution can be expressed in various ways. Its most simple expression is in terms of localized charges concentrated at the nuclear positions—at least X-ray crystallography tells us exactly where the nuclei are situated. However, there is already a problem with this approach. Although the charge distribution of not too complicated molecules can be calculated by quantum mechanical methods or obtained experimentally by X-ray diffraction measurements on crystals, there is no rigorous or even consensual procedure to define atomic charges, that is, no agreement about how much of the total electronic charge should be associated with each atomic nucleus. We can choose between Mulliken charges, Hirshfeld (or stockholder recipe) charges, or Bader charges, each based on a different way of allocating local electronic charge among adjacent atoms; alternatively, atomic charges can be assigned to fit the electrostatic potential produced by the molecular charge distribution over some selected region of space (we call these charges ESP charges; ESP = electrostatic potential). All of these methods yield different values for the atomic charges, sometimes very different. An alternative description of the influence of the molecular charge distribution can be made in terms of its electric central moments—monopole, dipole, quadrupole, etc. However, elementary electrostatics teaches us that the multipole expansion of a charge distribution is valid only at distances that are large compared with the spatial extension of the distribution itself. At distances comparable to the dimensions of the molecules concerned, low-order central multipole models fail to give the correct energy and high-order central multipole expansions are divergent.^[9] In summary, when an electric charge distribution, extending over a volume of some hundreds of \AA^3 and reaching out a few \AA beyond the atomic nuclei, is treated as being localized at some ten or twenty atomic positions or is restricted to a few central multipoles, the resulting electrostatic field cannot be trusted, except at long distances from the charge distribution itself. Moreover, and in particular, the electrostatic effects arising from the overlap between the charge distributions of neighboring molecules (the penetration effects) are completely lost. At very short intermolecular distances, neglect of penetration effects has an adverse influence on the reliability of the estimated electrostatic interaction energy, so the use of atomic point charges or of central multipoles for the discussion of details of molecular recognition at distances such as those found in close-packed crystals or in liquids, can hardly be expected to give reliable results. Somewhat better results can be expected as the model becomes more delocalized, as in the distributed multipole approach^[10,11] (see also Section 9.2), but an explicit inclusion of penetration effects is clearly needed when molecules come into very close contact.

3. What is a Chemical Bond?

In his *Nature of the Chemical Bond*, Pauling defined a chemical bond as follows: “We shall say that there is a chemical bond between two atoms or two groups of atoms in case that the forces acting between them are such as to lead to the formation of an aggregate with sufficient stability to make it convenient for the chemist to consider it as an independent chemical species.”^[12] Pauling explained that this definition was meant to include not only the directed valence bond of the organic chemist but also such bonds as those between sodium cations and chloride anions in the sodium chloride crystal, those between the aluminum ions and the six surrounding water molecules in the hydrated aluminum ions in solution or in crystals, and even the weak bond which holds together the two O₂ molecules in O₄. He did not consider the weak van der Waals forces between molecules as leading to chemical bonding. According to his definition, this amounts to saying that he did not find it convenient to do so. Pauling’s definition is more than 60 years old. It was written at a time when only very few crystal structures of organic compounds were known. In the meantime we have accumulated a vast and still expanding library of organic crystal structures and we also possess the theoretical and computational ability to estimate intermolecular forces and energies by several different methods. Our main aim herein is a critical comparison of the concept of chemical bonds within molecules and between molecules. When does one stop finding it convenient to draw or to talk about a chemical bond?

One speaks of a C–C bond in the ethane molecule because the change in molecular energy when the C–C distance is varied depends to a good approximation on this distance alone. Similarly, one can speak of the C–C bond-stretch vibration of ethane, even though this is strictly a particular combination of the normal vibrations of the molecule. A corresponding analogy hardly extends to intermolecular interactions. For an interaction between a methyl group in one molecule and an oxygen atom in another, for example, the best coordinate to describe the energy dependence might be the sum of three H···O distances, or some other combination of parameters, rather than just a single C–H···O bond length. In such intermolecular situations, it is a gross over-simplification to imagine that the interaction energy depends on a single internuclear distance.

While the bonding in most organic molecules can be adequately and convincingly described in terms of electron-pair bonding between atoms, this is not always the case. Pauling’s definition very wisely includes the possibility of bonds between groups of atoms. For example, the structure and stability of the ferrocene molecule is best explained in terms of bonding between the d orbitals of the iron atom and the combination of empty π molecular orbitals of the pair of cyclopentadienyl rings. One can, of course, draw a set of ten bonds between the iron atom and the individual carbon atoms but there are not enough valence electrons to make ten electron pairs. As with many other organometallic molecules involving transition metals and unsaturated organic moieties, the bonding is better described in terms of interactions between polycentric molecular orbitals, rather than by simple

overlap of atomic orbitals. Turning to intermolecular interactions, the modern bestiary includes, for, example, the X–H··· π bond, between a hydrogen atom and a group of atoms bearing π electrons which are allocated the role of acceptors in something that resembles a hydrogen bond. Another example is the stacking (or π – π) interaction between polyatomic aromatic cores. These descriptions of bonding interactions are on the way to a view of intermolecular bonding as existing not between atoms but between molecular regions, if not entire molecules. We shall return to this theme in Section 9.

On the experimental side, the most obvious criterion for the strength of a chemical bond between two atoms is the energy required to pull them apart—the depth of the potential energy well associated with the bond. For an intramolecular bond this energy is typically about 400 kJ mol^{–1}, which is orders of magnitude greater than the energy needed to remove a typical organic molecule from a crystal or a liquid. How should we appraise the putative C–H··· π bond in the acetylene crystal structure, which is broken by warming the substance to its melting point at 171 K? Another measure of bond strength is the corresponding vibration frequency, which depends on the force that restrains motion of the atoms or molecules from their equilibrium positions and on their masses. Bond vibration frequencies in molecules are 1000 to 3500 cm^{–1}; those for the lattice modes of crystals (collective molecular vibrations) are of the order of 100 cm^{–1} or less. Intermolecular bonding is clearly orders of magnitude weaker than that of typical chemical bonds.

4. Computational Models

By the late 1960s, the joint availability of direct methods, diffractometers, and adequate computational facilities had begun to produce accurate X-ray structure determinations for organic crystals at an unprecedented and ever increasing rate. Roughly in pace with this development, force fields began to be developed for the computer simulation of conformational equilibria in organic molecules—molecular mechanics. These force fields were usually developed as sums of potential energy terms centered on the atomic nuclei and involving changes in bond lengths, bond angles, and torsion angles from their assumed equilibrium values, with appropriate cross-terms, as considered necessary; further interactions were called nonbonded interactions and treated as such. Following Kitaigorodskii’s example,^[13] modelers of intermolecular interactions in the organic solid state were also looking for suitable potentials, and the most obvious thing to do was to take over the mechanical model and assume that atomic nuclei could function as reference centers for a rough evaluation of dispersion, coulombic, and repulsion effects. Indeed, one cannot deny the efficiency and consequent popularity of modern intermolecular force fields of the Buckingham type that explicitly involve atom–atom interaction terms depending on the internuclear distance, such as $E(R_{ij}) = A \exp(-BR_{ij}) - CR_{ij}^{-6} + q_i q_j R_{ij}^{-1}$, where A , B , C are parameters that depend on the atom types involved, q_i and q_j are charges assigned to the atoms, and R_{ij} is the distance between any two

atoms i and j in different molecules. Such force fields contain many adjustable parameters that have been calibrated against observed structures and sublimation enthalpies of collections of crystals of organic compounds.^[14] They are widely used and their success in correlating structures and lattice energies of organic crystals from a knowledge of the atom arrangements within the constituent molecules cannot be denied. Even in the competitive demands of crystal-structure prediction tests they are found to be about as successful, or as unsuccessful, as any other method.^[15]

When we inquire into the deeper reason for the success of this simple model we encounter a problem. The very success of the simple atom–atom force field stands in the way of a more realistic representation of the physical effects involved, as none of these effects has anything to do with nuclear positions. For example, in simulating the charge distribution of a molecule, the location of point charges at atomic nuclei is about as far from reality as the description of a molecular model can be. Insofar as the intermolecular attraction is due to dispersion forces, as expressed by the R^{-6} term in the above expression, these forces involve interactions between the molecules themselves, as aggregates, and not between the separate atoms of which they are composed. As an alternative to atom–atom interactions, Rae and Mason showed many years ago that the intermolecular attractive energy in crystals of benzene and s-triazine could just as well be expressed as a sum of pairwise interactions between bonds rather than between atoms.^[16] On the other hand, one could argue that since dispersion forces fall off with R^{-6} , any dissection of the total dispersion force or energy must concentrate on interactions between molecular regions (call them atoms or bonds) that approach one another most closely. The contributions of more distant regions are less important and can be neglected.

On the quantum chemical side, density functional theory (DFT) has promise for a correct representation of all intermolecular effects, but its application to crystals of sizeable molecules is still restricted by computational power.^[17] Moreover, even state-of-the-art DFT methods appear to be incapable of accounting for dispersion effects in a quantitative manner, as indicated by calculations for dimers of rare-gas atoms.^[18] Another quantum mechanical approach, intermolecular perturbation theory (IMPT), is based on a partitioning of total energy into coulombic, polarization, dispersion, and repulsion terms.^[19] In this method, too, benzene already counts as a large molecule if a reassuringly large basis set is desired. Recently, the semi-classical density sums (SCDS) or pixel method has been proposed^[20,21] as an intermediate solution to the problem. It easily handles the partitioned intermolecular energies in crystals of a 30-atom molecule or in dimers of even larger molecules. It requires only four empirical parameters, although their calibration still leaves something to be desired. All of these methods allow an estimation of total binding energies but they differ with respect to how this is most usefully partitioned. None of them has a direct answer to the question: are there chemical bonds between atoms in a molecular recognition system, and if so, where are they? On the other hand, as we shall discuss, an extension of Bader's Atoms in Molecules (AIM) approach makes a direct appeal

to the idea of intermolecular bond paths between atoms and suggests how they may be identified.^[22,23] Clearly there is a lack of consensus about how far the sphere of influence of an atom can usefully be extended.

5. Determining Bond Paths from Electron Densities

If the exact distribution of electrons and nuclei were known, all bonding in molecules and crystals could be analyzed as a result of the lowering of potential energy and balancing of Feynman forces at nuclei, caused by accumulation of electron density between the nuclei. Bader's atoms in molecules (AIM) theory^[22] provides a rigorous and exact space and energy partitioning, defining atomic basins and bonds between them in terms of the topological properties of the charge density $\rho(\mathbf{r})$, its gradient vector $\nabla\rho(\mathbf{r})$, and the matrix of second derivatives, its Laplacian $\nabla^2\rho(\mathbf{r})$. Points where $\nabla\rho(\mathbf{r})=0$ are called critical points (Figure 2). For a

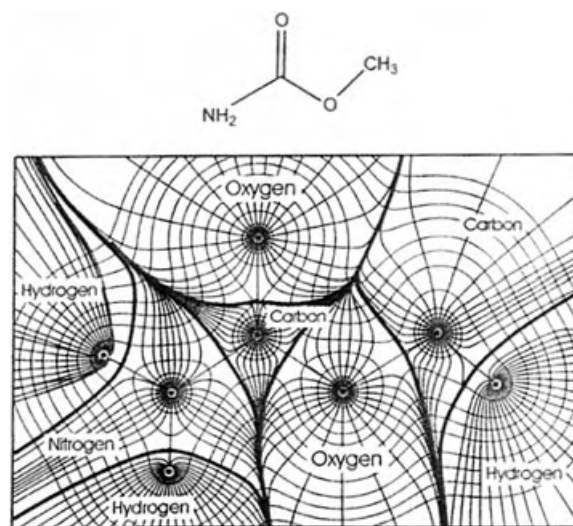


Figure 2. Acetamide trajectories of the gradient vector $\nabla\rho(\mathbf{r})$, superimposed on the charge-density contours of $\rho(\mathbf{r})$. Zero-flux surfaces defining the atomic basins Ω and bond paths are indicated by bold lines. Their intersections correspond to the bond critical points. Reproduced with permission from ref. [24].

three-dimensional density distribution, there are four types of critical point, depending on the signature (the algebraic sum of the signs of the eigenvalues of the matrix of second derivatives):

(3,−3): All curvatures negative, corresponding to a local maximum in the electron-density distribution; in a molecule, these occur only at the nuclear positions.

(3,−1): Two curvatures negative, one positive, corresponding to saddle points in the electron-density distribution; these occur between each pair of nuclei linked by a chemical bond.

(3,+1): Two curvatures positive, one negative; these occur inside a ring of bonded atoms.

(3,+3): All curvatures positive, corresponding to a local minimum in the electron-density distribution.

According to the AIM theory, $\rho(\mathbf{r})$ can be partitioned uniquely into subsystems Ω bounded by specific surfaces, the zero-flux surfaces in the gradient field $\nabla\rho(\mathbf{r})$. At any point in $\rho(\mathbf{r})$ the associated gradient vector $\nabla\rho(\mathbf{r})$ points along the direction of greatest increase in $\rho(\mathbf{r})$ and so defines a path that terminates at a (3,−3) or (3,−1) critical point, that is, at a local maximum or saddle point in the density distribution. The zero-flux surface perpendicular to this path at its saddle point is common to two subsystems and effectively defines their boundaries. The subsystems (atomic basins) defined in this way correspond to the atoms in the quantum system and show many properties associated with the traditional atoms of the chemist. An atomic property is obtained by integrating the corresponding property density over the atomic basin and any physical property of the molecule, for example, its energy, is the sum of the properties of the so-defined component atoms. Thus an atom in a molecule becomes a quantum subsystem.

Two nuclei are considered to be linked by a chemical bond if the corresponding (3, −3) critical points are connected by a line along which $\rho(\mathbf{r})$ is a maximum with respect to any neighboring line: a bond path. The nature of the bonded interaction can then be characterized by the values of the electron density ρ_b and its Laplacian $\nabla^2\rho_b$ at the bond critical point. A negative value of $\nabla^2\rho_b$ means that charge is concentrated in the internuclear region (covalent bonding), while a positive value corresponds to local depletion of charge (closed-shell interaction). A reliable calculation of atomic and bonding properties requires that $\rho(\mathbf{r})$ and its space derivatives be known with very high accuracy. This requirement is not a problem for molecules containing a modest number of atoms. Nowadays, the exact charge density can be computed and the problem of bonding thereby solved for such systems. Computational limits are certain to become less and less of a problem as time passes, but for very large systems, such as molecular clusters, the exact charge density is not yet easily available because of limitations in the size of the basis set and other approximations. For the molecules in such clusters, this does not represent a serious difficulty as their bond paths are so well defined that little ambiguity is possible. For intermolecular regions, however, where the charge density is low, it is another matter, and computations may fail to yield a clear-cut answer to the question whether there is a significant intermolecular bond path or not, and if there is one, the identification and description of its critical point(s) may not be obvious.

Bond paths can also be recognized in experimental electron densities obtained from X-ray diffraction data.^[24] However, the success of the pro-molecule density model (built from simple superposition of spherically averaged, ground-state atomic densities) as reference density in producing low “R-factors” in routine structure analyses of organic crystals emphasizes that any density deformations from this model resulting from chemical bonding are small and require highly accurate experimental data and elaborate refinement techniques for their detection and description. The effect of random measurement errors in the intensities on the standard uncertainty in the electron density can be

estimated reasonably well by standard formulae, but this is only one of many sources of error. The effect of termination-of-series error, a consequence of calculating the electron density with a finite number of Fourier terms, is mainly to produce false density ripples surrounding the atomic density peaks. Interference between such ripples produces peaks and troughs between the atomic positions, and these spurious features may well be of the same order of magnitude as the density expected for intermolecular bond paths. There are also systematic errors from a variety of sources including crystal absorption, extinction, multiple reflection, thermal diffuse scattering, whose influences on the calculated electron density are difficult to estimate. Then there are details of the refinement procedure that affect the calculated electron density—number and type of multipoles used in the refinement, treatment of thermal motion, to name a few. Even with the best experimental data, the static electron-density distribution is convoluted with vibrational motion and it is hard to separate the two.^[25] For all these reasons it is extremely difficult to reduce the uncertainty in the experimental electron density below about $0.05 \text{ e } \text{\AA}^{-3}$.^[24] This level is perfectly adequate for the description of bond-path critical points in molecules but is just about the same order of magnitude expected for crystal-field effects. Clearly, the uncertainty in the gradient and curvature of the electron density required for the description of the behavior at the critical point is even greater than in the electron density itself.

For these reasons, when the density at critical points is small, as it is between atoms in neighboring molecules in a crystal, the estimation of its exact value and that of its derivatives is fraught with uncertainties, which make reliable interpretation difficult. It is unfortunate that in many publications in this area, the information provided about experimental details and refinement procedures is insufficient for the reader to make an informed critical judgment about the reliability of the results. For atoms on molecular peripheries (such as, hydrogen, halogen, carbonyl oxygen, cyano nitrogen) some portions of the atomic basins extend to infinity. Atomic basins belonging to such atoms in neighboring molecules must therefore overlap and thereby produce bond paths. Thus it is not a question of whether we can find intermolecular bond paths, say between hydrogen atoms of neighboring phenyl groups in experimental density distributions. The question is whether and to what extent the information contained in such paths can be distinguished from experimental noise, from electron-density features inherent in the mere proximity of the atoms concerned, and from inadequacies in the multipole refinement model.

6. Hydrogen–Hydrogen Bonding?

Consider the closed-shell interaction between a pair of adjacent “nonbonded” hydrogen atoms in the equilibrium conformation of a sterically “overcrowded” molecule or between neighboring hydrogen atoms of different molecules in the crystal structure of some hydrocarbon. The distance between these atoms, between their nuclei, corresponds to the equilibrium between attractive and repulsive forces. Forces

between what? Although it is not always obvious how to resolve the individual components of these forces, the repulsive force between the hydrogen atoms, that is, their resistance to compression, is usually invoked as one of the main components of “steric nonbonded repulsion”. A recent paper by Bader and his associates raises questions about this interpretation.^[26] To take one example, the relevant electron-density distributions in the “bay areas” of phenanthrene and chrysene show a significant bond path between the two opposing hydrogen atoms, and the corresponding H...H interactions are calculated to produce stabilizing contributions of the order of 10 kcal mol⁻¹ (!) rather than destabilizing ones. The concept of “hydrogen–hydrogen bonding” is offered as an explanation for the relative thermodynamic stability of phenanthrene over anthracene and of chrysene over tetracene. This is clearly an unorthodox and challenging proposal because chemists have their own way of deciding which atoms are bonded to which in a molecule, and it clashes seriously with the chemist’s picture. Besides, there are alternative explanations of the relative stability of phenanthrene and anthracene, based on qualitative comparison of the resonance stabilization of the two molecules.

Hydrogen–hydrogen bonding is to be distinguished from what has been called a “dihydrogen bond” between hydrogen atoms of opposite charge, one hydridic, typically attached to a metal atom, the other acidic.^[27] The dihydrogen bond is dominated by electrostatic interactions, whereas hydrogen–hydrogen bonding results from a quite different type of interaction that is dominated by the attraction between each proton and the electron density of the other hydrogen atom. On passing from the linear benzenoids to their bent isomers, electronic charge is transferred from the carbon atoms to the hydrogen atoms, leading to an increase in the energy of the carbon atoms and a lowering in the energy of the hydrogen atoms, especially those in the bay area, the net result being a stabilizing change in the total molecular energy. Repulsion between the two hydrogen atoms involved does not come into this picture. In a quantum mechanical description, the only repulsive forces are the coulombic forces acting between atomic nuclei and between electrons, the only attractive forces those between atomic nuclei and electrons.

Similar considerations apply to the close approach of the two pairs of *ortho*-hydrogen atoms in the planar structure of the biphenyl molecule, in which each H...H bond path is again associated with a stabilizing energy contribution, in opposition to the simple view involving a repulsive interaction between these two atoms. On passing from the twisted equilibrium structure (torsion angle about 45°) to the metastable planar geometry there is an increase of about 2 kcal mol⁻¹ in the molecular energy and a small lengthening of the central C–C bond, attributed to the “accommodation of the approach of the *ortho*-hydrogen atoms”.^[26] Such “accommodation” might suggest adaptation to repulsion between the *ortho*-hydrogen atoms but it is emphasized that this is not what is meant.

The H...H distances in the bay areas of condensed benzenoid hydrocarbons are much shorter than 2.4 Å, the standard van der Waals diameter of a hydrogen atom. Distances estimated from crystal structure analyses of C₁₈H₁₂

isomers are 2.01 Å in benzanthracene, with one such H...H interaction,^[28] 1.91 Å in chrysene, with two,^[29] and 1.88 Å in triphenylene, with three^[30] (Figure 3). Notably, the three molecules are virtually planar although it is clear that suitable

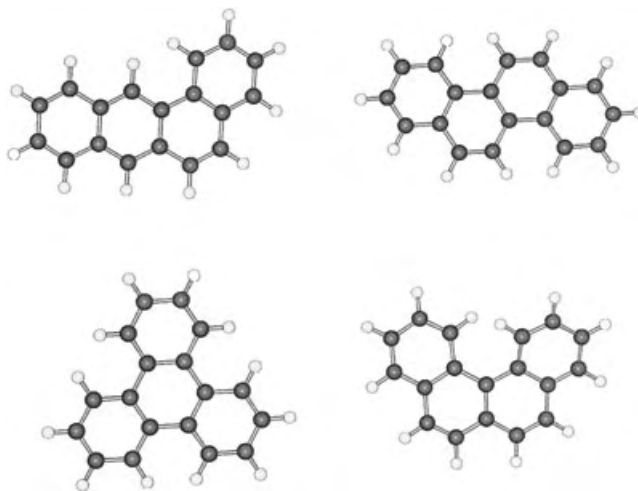


Figure 3. Short hydrogen–hydrogen distances in the sterically crowded isomeric molecules of (left to right, top to bottom) benzanthracene (2.01 Å), chrysene (1.91 Å), triphenylene (1.88 Å), and benz[*c*]phenanthrene (1.88 Å). Only in benz[*c*]phenanthrene is there any appreciable out-of-plane deformation attributable to the short H...H contacts. Hydrogen–hydrogen distances were calculated from the molecular structures determined by X-ray diffraction (Cambridge Crystallographic Database refcodes BEANTR, CRYSEN, TRIPHE12, BZPHAN01, respectively), by using renormalized hydrogen atom positions (Hcal option).

out-of-plane deformations could increase these short H...H distances towards more normal values.^[31] In contrast, the benz[*c*]phenanthrene molecule with an H...H distance of 1.88 Å is markedly helical with an angle of about 27° between the planes of the two outer rings.^[32] In this case the hydrogen atoms involved are not attached to a 1,4 carbon pair on next-nearest benzene rings but to a 1,5 pair on the outer rings. In the planar molecule the H...H distance would be even shorter than 1.88 Å but there is in this isomer an additional degree of freedom available for out-of-plane deformation. In biphenyl, although the distance between the *ortho*-hydrogen atoms increases from about 2.0 Å in the planar conformation to about 2.4 Å in the twisted equilibrium structure, the energy surface must be rather flat as the energy difference amounts only to a few kJ mol⁻¹.

Thus, even if nonbonded repulsion between hydrogen atoms in these sterically overcrowded hydrocarbons is invoked as a structural influence, its effect on their structures and energies does not seem to be determinative. In force-field language, the hydrogen atoms are surely under compression, but the force pushing them apart is countered by restraining forces so there is no net force. The H...H distance is not an independent parameter and any change in it would be coupled to changes in other structural parameters: bond

lengths, bond angles, torsion angles. The relative stiffness of these parameters, resulting in the rigidity of the planar geometry of benzenoid hydrocarbons, restricts such changes. In a language based on the AIM energy-partitioning scheme, the description is quite different. There is no repulsion between the hydrogen atoms because such repulsion does not come into the picture; there is an H \cdots H bond path, the corresponding interaction makes a stabilizing contribution to the energy, and that is all there is to be said.

7. Intermolecular Bond Paths

By extension of the concept outlined above, one should in principle be able to find bond paths whenever the charge densities of two molecules are close enough to have non-zero overlap—which, by definition, is always the case since wave functions vanish only at infinity. Some of the problems in the validation and critical interpretation of such paths, especially those derived from experimental charge-density distributions, have been mentioned in Section 5. Despite these difficulties, many papers dealing with the description and interpretation of experimental charge densities of organic crystals have appeared in the last few years. With the easier availability of high-intensity X-ray sources for measuring crystal diffraction patterns and of computer programs for interpreting the experimental data in terms of atomic multipole models and for analysis of the topological properties of the resulting density distributions, it has become practicable to undertake studies that would have previously required many years of work and to complete them in a relatively short time. We do not attempt herein to cover this area in a complete or systematic manner; the task would be beyond us. Rather, we concentrate on a few selected papers dealing mainly with aspects of weak intermolecular hydrogen bonding, a topic that never seems to become exhausted or to go out of fashion.

Criteria for recognizing C–H \cdots X hydrogen bonds from features of charge-density distributions were proposed by Koch and Popelier.^[33] These include primarily the existence of an H \cdots X bond path with a low value of ρ_b and a positive value of the Laplacian $\nabla^2\rho_b$ at the bond critical point (CP), the latter condition being required as indicator of a closed-shell interaction. Only very strong, short hydrogen bonds, such as those in the symmetric hydrogen maleate anion (H \cdots O 1.21 Å), have negative values of $\nabla^2\rho_b$, which are taken to indicate covalent character of the bonding.^[34] A further requirement is interpenetration of the H and O atom electron-density shells, judged by the difference between the bonded radius (distance from atomic nucleus to bond CP) and the nonbonded (van der Waals) radius of the two atoms concerned. Since the nonbonded radius of an atom is a rather poorly defined quantity, this requirement may strike one as being rather nebulous. Other authorities have recommended that no cut-off radius should be set in the criteria for recognizing hydrogen bonds.^[8g]

Recent studies of bond paths have made use of an equation suggested by Abramov [Eq. (1)]^[35] relating the local electronic kinetic energy density $G(\mathbf{r}_{\text{BCP}})$ with bond-path

critical points (BCP) properties where ρ and $\nabla^2\rho$ are measured in atomic units (a.u.).

$$G(\mathbf{r}_{\text{BCP}}) = (3/10)(3\pi^2)^{2/3}\rho^{5/3}(\mathbf{r}_{\text{BCP}}) + (1/6)\nabla^2\rho(\mathbf{r}_{\text{BCP}}) \\ = 2.871\rho^{5/3}(\mathbf{r}_{\text{BCP}}) + 0.167\nabla^2\rho(\mathbf{r}_{\text{BCP}}) \quad (1)$$

The corresponding potential energy density $V(\mathbf{r}_{\text{BCP}})$ can then be estimated by making use of Equation (2), which is an expression of the local virial theorem.

$$2G(\mathbf{r}_{\text{BCP}}) + V(\mathbf{r}_{\text{BCP}}) = (1/4)\nabla^2\rho(\mathbf{r}_{\text{BCP}}) \quad (2)$$

Since $G(\mathbf{r}_{\text{BCP}})$ is necessarily positive, it follows that where $\nabla^2\rho(\mathbf{r}_{\text{BCP}})$ is negative, $V(\mathbf{r}_{\text{BCP}})$ must also be negative. Thus, the charge density is locally concentrated which is characteristic for the CP behavior of a covalent bond. For closed-shell interactions, $\nabla^2\rho(\mathbf{r}_{\text{BCP}})$ is positive, the kinetic energy dominates, and charge is locally depleted. Thus the kinetic energy density $G(\mathbf{r}_{\text{BCP}})$ is a measure of the tendency of electronic charge to leave the volume element in question, while the potential energy density $V(\mathbf{r}_{\text{BCP}})$ is the tendency of electronic charge to concentrate there. In applying the above relationships to experimental charge distributions, it must not be overlooked that Equation (1) is an approximation and that the local virial theorem, the underlying basis of Equation (2), holds only for the correct charge density and not necessarily for the experimental one.

In a study of the CP properties of 83 experimentally observed bond paths for X–H \cdots O (X = O, N, C) interactions in crystals, Espinosa, Molins, and Lecomte^[36] found that $G(\mathbf{r}_{\text{BCP}})$ and $V(\mathbf{r}_{\text{BCP}})$ both followed a negative exponential dependence on the H \cdots O distance over the examined range of approximately 1.6 Å to 3.0 Å (Figure 4, left). The $V(\mathbf{r}_{\text{BCP}})$ values were found to be closely proportional to theoretical hydrogen-bond dissociation energies. Thus, in the given range, the H \cdots O distance appeared to be sufficient to determine the charge density $\rho(\mathbf{r}_{\text{BCP}})$ and its Laplacian $\nabla^2\rho(\mathbf{r}_{\text{BCP}})$ at the bond CP and hence yield a good approximation to the bond energy. In this range the Laplacian was positive throughout, characteristic of closed-shell interactions; extrapolation of the $G(\mathbf{r}_{\text{BCP}})$ and $V(\mathbf{r}_{\text{BCP}})$ values to the point where $V(\mathbf{r}_{\text{BCP}}) = -2G(\mathbf{r}_{\text{BCP}})$ and hence $\nabla^2\rho(\mathbf{r}_{\text{BCP}}) = 0$ gave an H \cdots O distance of 1.33 Å, corresponding to the transition from covalent to closed-shell character of the hydrogen bond. These were truly remarkable results.

Since the electron density in intermolecular regions should be close to that produced by simple superposition of pro-molecule electron densities, Spackman^[37] compared the above results for the $G(\mathbf{r}_{\text{BCP}})$ and $V(\mathbf{r}_{\text{BCP}})$ dependence on H \cdots O distance with those obtained from a simple model of non-interacting overlapping spherical atom electron densities and found remarkably close agreement, especially for H \cdots O distances greater than 2.2 Å, the region of mainly weak C–H \cdots O interactions (Figure 4, right). The Spackman pro-molecule was chosen to be as simple as possible; it consisted of atom densities only for the H and O atoms engaged in the hydrogen bond. A more elaborate model would be based not merely on overlap of the separate atom densities (that is, the electron densities associated with the unperturbed ground

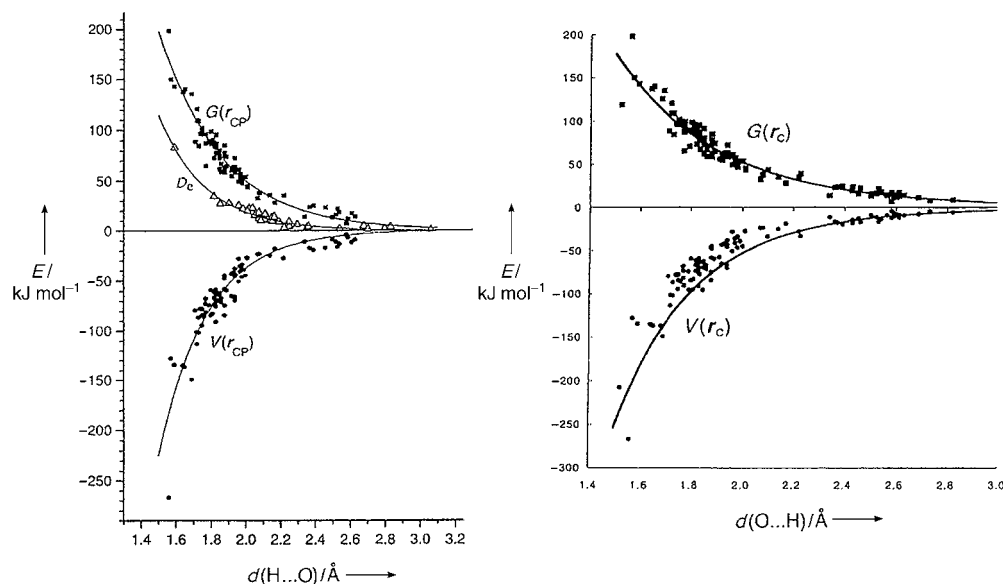


Figure 4. Left: dependence of kinetic energy density $G(r_{\text{BCP}})$, potential energy density $V(r_{\text{BCP}})$ and dissociation energy D_e on $d(\text{H}\cdots\text{O})$ distance from experimentally observed bond paths in 83 crystal structures. Energy densities in kJ mol^{-1} per atomic unit volume. Reproduced with permission from ref. [36]. Right: Same data as left, but with solid lines derived from a simple model of overlapping spherical atoms. Reproduced with permission from ref. [37].

state of individual atoms) of the atoms directly engaged but on the electron densities of the separate molecules—a pro-crystal rather than a pro-molecule model. Spackman's calculation raises the question of whether or not the bond paths from the experimental studies are providing anything more than noise about the trend determined by the pro-molecule or pro-crystal electron distribution. This question has been critically analyzed by Gatti et al.^[38] who conclude that for $\text{C-H}\cdots\text{O}$ interactions, even although charge rearrangements may occur within the atomic basins (thus changing their atomic properties), no significant information is added by experimental or theoretical studies to that contained in the pro-molecule densities for large $\text{H}\cdots\text{O}$ distances. Nevertheless, in several analyses of experimental electron densities in crystals, intermolecular bond paths are emphasized more or less irrespective of the size and significance of $\rho(r_{\text{BCP}})$ and its Laplacian. The extension of such analyses to intermolecular $\text{H}\cdots\text{H}$ bond paths and their possible significance seems inevitable. We are concerned about the uncritical assessment of such results in Pauling's pragmatic sense: is it convenient to stretch the relevance of these analyses to the point of granting the character of a significant chemical bond to every intermolecular $\text{C-H}\cdots\text{O}$ or $\text{H}\cdots\text{H}$ proximity in the crystal for which a bond path can be ascertained? Such an attitude presupposes a localization of intermolecular bonding that may neglect the interactions of surrounding regions and may therefore lead to incorrect or at least incomplete views about molecular recognition modes in general.

It is all very well to attempt to simplify complexity, but in the context of intermolecular bonding such simplistic explanations may be putting the cart before the horse: it is not the atom–atom bond path that produces the intermolecular bonding, but the intermolecular bonding that produces the

atom–atom bond path. In a condensed phase, once a pair of hydrogen atoms are drawn into sufficiently close proximity through generalized intermolecular forces to achieve close packing of molecules with a comparatively rigid framework, this proximity will lead to overlap of the electron-density distributions and hence to a bond path between the atoms. From experimental charge-density difference maps we know that the difference density between atoms in different molecules is barely measurable, that is to say, the charge density between the atoms is hardly different from the sum of the pro-molecule densities. Spackman's results^[37] indicate that this is largely true also for theoretical charge densities of weak $\text{X-H}\cdots\text{O}$ hydrogen-bonded systems. Thus, it is the intermolecular attraction that may produce the intermolecular bond paths, not the other way round. With suitable rephrasing and qualification, a similar statement could apply to intramolecular bond paths, especially those for $\text{H}\cdots\text{H}$ and other “nonbonding” interactions.

8. The Semi-Classical Density Sums (SCDS-Pixel) Approach

If localization of intermolecular bonding in terms of atom–atom interactions is sometimes questionable, a view that considers a fully delocalized electron-density cloud may offer an alternative approach. A possibility is provided by the newly developed SCDS (semi-classical density sums) or pixel method.^[20,21] The calculation of intermolecular energies starts by obtaining the electron density for the separate molecule(s) by standard quantum mechanical programs, for example, Gaussian, using a step of 0.08 \AA to produce a grid that usually contains about 10^6 points (the original pixels). This grid is

then condensed into $n \times n \times n$ super-pixels, where n is usually 3, 4, or 5; super-pixels containing less than 10^{-6} electrons are discarded as insignificant, and the electronic charge is renormalized to balance the total nuclear charge. The molecular electron density is thus usually described by some 10000–15000 pixels (Figure 5). To form a multi-molecular

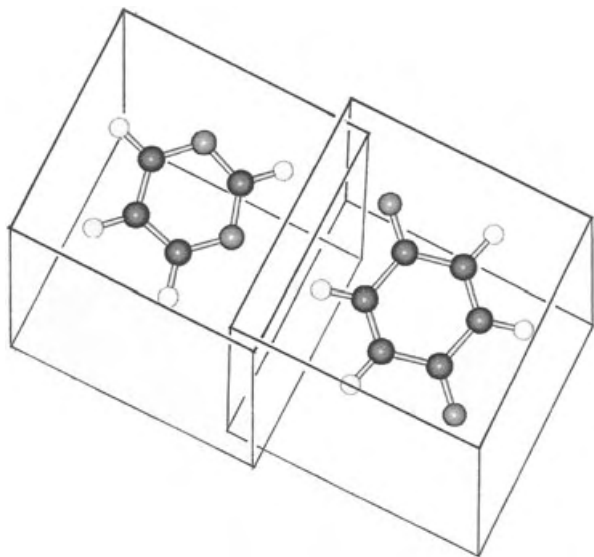


Figure 5. In the traditional atom–atom model, a molecule is described by just a few point charges located at each nuclear position. In the delocalized pixel description, of which this is a pictorial view, each molecule is represented by a box containing atomic nuclear charges and many thousands of electron-pixels. The two boxes overlap to some extent, and this accounts for repulsion and penetration energies.

ensemble, the positions of all pixels and all nuclei are repeated in space by rotation and/or translation operations, or by space-group symmetry operations if a crystal is considered. Thus, the method assumes a juxtaposition of rigid, undistorted electron densities of separated molecules in a supramolecular array.

The coulombic energy between any two molecules is calculated simply as a sum over $q_i q_j / r_{ij}$ contributions from each pair of electron-density pixels, or of pixels and nuclei, in the separate molecules. Thus, it is completely parameter-free, and it does not depend on any assignment of point charges or distributed multipoles, so that, at the short distances between adjacent molecules in condensed phases, the coulombic energy calculated by the pixel method is much more reliable than that based on electrostatic interactions among any localized distributions of point charges or multipoles. This reliability has been shown in detailed comparisons with the results of elaborate quantum mechanical calculations or of experimental electron-density measurements for glycine.^[39] The repulsion energy is taken to be proportional to the overlap integral of the electron densities (calculated by numerical integration over the original uncondensed pixel grid), elevated to a power slightly smaller than one. This procedure requires at least two empirical parameters, the proportionality constant and the exponent, which are not always easy to determine. For the estimation of the polar-

ization energy, each electron-density pixel is allotted to an atom (the one to whose nucleus the distance is the smallest fraction of the atomic radius), and the pixel polarizability is taken as the corresponding atom polarizability, scaled by the ratio of the pixel charge to the atomic number. The polarization energy is then calculated (by the induced dipole and the linear polarization formula, summed over all pixels) as a many-body effect resulting from the action of the total electric field from all surrounding molecules at each pixel. The dispersion energy is obtained as a sum of pixel–pixel terms by a London-type formula, by using the pixel polarizabilities and the overall molecular ionization potential, taken as the energy of the highest occupied molecular orbital (HOMO). Polarization and dispersion energies are multiplied by an appropriate damping function to avoid singularities, and this introduces two more empirical parameters. The total interaction energy is then the sum of the coulombic, polarization, dispersion, and repulsion terms.

The whole formulation requires no more than four fully adjustable parameters for all organic molecules, as compared to tens of parameters for even the simplest atom–atom methods. The results are scarcely sensitive to the level of the molecular orbital calculation, with MP2/6-31G** being more than satisfactory. To give an idea of feasibility and efficiency, the calculation of the dimerization energy for a guanine–cytosine base pair takes a few seconds of computer time, and the results are comparable with those of high-level quantum mechanical calculations. The calculation of the lattice energy of naphthalene takes about one hour; the heats of sublimation of organic crystals are well reproduced. The partitioned view of the interaction—coulombic, polarization, dispersion, and repulsion terms—may not be rigorous, and yet in some ways it provides an additional interpretative bonus, because it is relatively easy to connect each of these terms with the chemical structure and conformation of a particular molecule or molecular moiety.

The essence of the pixel method is to use the interaction between unperturbed molecular electron densities to obtain cluster cohesion energies, or crystal-lattice energies that can be compared with experimental heats of sublimation. The method is only in part *ab initio*, and the parameter optimization is still open to improvement,^[40] especially in the treatment of repulsion. As with many methods based on computations, its application (at least for the moment) is not immediate for the general chemical public and its results lack the visual appeal of simpler geometrical inference. In any event, the main merit of the pixel approach to intermolecular interactions is to shift the focus of the analysis from the nuclear positions to the molecular charge distributions. This change can be taken as an improvement with regard to describing the underlying physics. For a crystal, the sublimation energy concerns the separation of individual molecules from their ordered arrangement in the solid into the gaseous state, and the most appropriate breakdown of total energies is into molecule–molecule energies. This follows naturally in the pixel approach. In further justification of this molecule–molecule viewpoint, it must be conceded that a molecule is a less controversial entity than an atom in a molecule (despite the undisputed merits of Bader's AIM Theory^[22]). At the

same time, the pixel and the bond-path views can be viewed as different languages, different ways of describing the physical phenomena accompanying the aggregation of molecules into condensed matter. In one language we speak of bond paths and critical points, in the other of intermolecular coulombic, polarization, dispersion, or repulsion energies that result from confrontation and overlap of electron densities vis-à-vis the nuclear positions.

9. Calculations versus Models and Simplifications

Any discussion of structural effects in molecular recognition should ideally be based on accurately calculated molecule–molecule interaction energies. But it goes without saying that most organic and solid-state structural chemists are neither willing nor able to turn themselves into practicing theoretical chemists. At least, not yet. As suitable computer programs with simplified inputs become more readily available and user-friendly, more and more practical chemists will undoubtedly be tempted into extending their repertoire by calculating the energies of molecules and of molecular aggregates more or less routinely. In any case, the results of such calculations can only be a beginning; chemistry, like all natural sciences, proceeds by conceptual frameworks, models that rationalize the observations and predict the unobserved without recourse to the involved mathematical physics. It should now be realized that the factors that promote intermolecular bonding and select among different structures are just too complex to be described in terms of atom–atom bonds and/or central multipole–multipole models. In discussing the structures that result from the assemblage of molecules into supramolecular clusters and crystals, one feels the need for a language based on recognition modes of entire molecules or of polyatomic groupings, rather than merely on the search for atom–atom contacts or on naive electrostatic reasoning. This goal is not around the corner and we have no instant recipes, but we have at least some sobering advice against the attraction of appealingly simple but fallacious ideas.

In the following, we compare localized and delocalized electrostatic models and provide a few examples where the atom–atom viewpoint leads to wrong interpretations, or gets in the way of sensible predictions; where possible, we propose alternative views based on delocalized models, using pixel results, also in comparison with deductions from Bader's AIM method.

9.1. The Crystal Structure of Cl_2 , $\text{Cl}\cdots\text{Cl}$ "Bonds", and "Chloro-Effects"

As a first example, the crystal structure of molecular chlorine (Figure 6)^[41] may serve as basis for a comparison of the different ways of analyzing supramolecular ensembles and crystals. This structure has long been regarded as somewhat problematic because of an intermolecular $\text{Cl}\cdots\text{Cl}$ contact distance of 3.27 Å, considerably shorter than the sum of standard van der Waals radii, 3.60 Å. In the isostructural

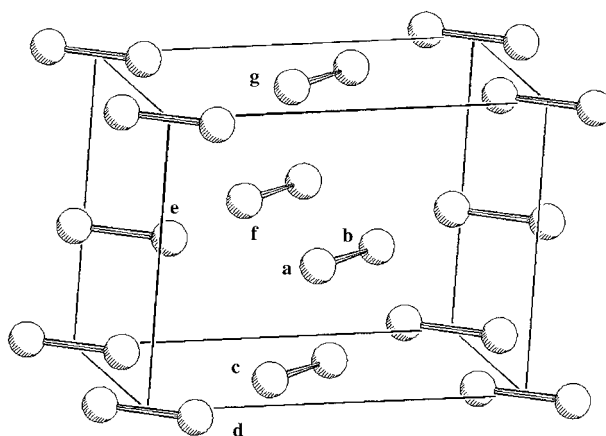


Figure 6. Crystal structure of solid chlorine.^[41] $\text{Cl}\cdots\text{Cl}$ distances [Å] are: a–c 3.82, a–d 3.92, a–e 3.27, b–f 3.74, b–g 3.70.

crystals of bromine and iodine, the corresponding intermolecular $\text{Br}\cdots\text{Br}$ and $\text{I}\cdots\text{I}$ distances are also short, and, at least in the iodine crystal, the intramolecular covalent bond length is significantly longer than in the gas phase. A corresponding bond lengthening has not been conclusively established for solid chlorine (or bromine), but the structural evidence has been interpreted by Williams and co-workers in terms of weak intermolecular $\text{Cl}\cdots\text{Cl}$ bonds.^[42] Bader and co-workers have recently proposed an interpretation of this structure in terms of intermolecular bond paths.^[43] In the topological analysis of the theoretical and experimental electron densities, bond paths were found from each Cl atom in the crystal to twelve others, including the Cl atom in the same molecule. The agreement between theoretical and experimental values for ρ_b and $\nabla^2\rho_b$ was stated to be "fair". Since no estimate of the accuracy of the experimental density was provided and since the experimental values of ρ_b for the intermolecular paths were about 0.05 e Å^{-3} it is difficult to judge the mutual consistency of the theoretical and experimental results. In any case, the weak intermolecular bond postulated earlier for the short $\text{Cl}\cdots\text{Cl}$ contact was regarded as established by the existence of a corresponding bond path in both the theoretical and experimental electron density distributions.

Table 1 gives the pixel description of this solid, with the interaction energies of a central molecule to its fourteen nearest neighbors, which among them involve the eleven $\text{Cl}\cdots\text{Cl}$ intermolecular bond paths, together with the calculated total lattice energy. This energy somewhat exceeds the measured sublimation enthalpy (32 kJ mol^{-1}), owing to a still imperfect parameterization of repulsion energies, a flaw already noted for other chlorinated compounds.^[44] In place of the emphasis on the bond-path properties of the short $\text{Cl}\cdots\text{Cl}$ interaction, the stability of the chlorine crystal is quite naturally described by the pixel calculation in terms of the ordinary ingredients of molecular interaction, all fourteen molecule–molecule pair contributions being stabilizing through coulombic and dispersion effects. The most stabilizing interaction is between parallel pairs of molecules related by the C-centering translation. The interaction between glide-plane related molecules, those with the unusually short $\text{Cl}\cdots\text{Cl}$ distance, has indeed the most stabilizing coulombic contribu-

Table 1: Cohesion energies [kJ mol^{-1}] of molecular pairs occurring in the crystal structure of chlorine^[41] (Figure 6), as calculated by the pixel method.

Symmetry ^[a]	Distance ^[b]		$E_{\text{coul}}^{[c]}$	$E_{\text{pol}}^{[c]}$	$E_{\text{disp}}^{[c]}$	$E_{\text{rep}}^{[c]}$	$E_{\text{tot}}^{[c]}$
$x, 1+y, z$	4.44; 2	3.74; 1	-1.0	-0.5	-6.4	3.9	-4.0
$1/2+x, 1/2+y, z$	3.82; 4	3.82; 4	-3.0	-1.2	-11.4	8.0	-7.6
		3.70; 2					
$x, 1/2-y, 1/2+z$	4.63; 4	3.27; 2	-5.8	-3.5	-9.7	12.8	-6.0
$1/2+x, -y, 1/2+z$	5.11; 4	3.93; 2	-0.6	-0.2	-3.6	1.6	-2.8
full crystal	—	—	-19.8	-10.2	-59.9	48.7	-41.2

[a] Symmetry operation between molecular pair. [b] Distance between molecular centers [\AA]; multiplicity, shortest distances between chlorine atoms [\AA]; multiplicity (multiplicity is the number of such symmetry-related molecules per reference molecule). [c] Coulombic, polarization, dispersion, repulsion and total molecule-molecule energies.

tion, but this is more than offset by a large repulsion term. (In general, repulsion energy tends to increase as the coulombic energy becomes more stabilizing, since both depend on overlap or penetration effects). As a result, the total interaction energy between these glide-plane-related molecules is moderately stabilizing but in no way exceptional (Table 1). When molecular interaction energies are properly evaluated over charge distributions, it appears that “short” atom–atom contacts, far from being the decisive bonding factors, may be energetically irrelevant.

For another example, we consider the dichlorobenzenes. With net negative charges on the chlorine atoms, the atom–atom standpoint has problems in explaining the short $\text{Cl}\cdots\text{Cl}$ distances that are found to occur in many crystals. For example, in the β -polymorph of 1,4-dichlorobenzene, the molecules line up in a parallel end-to-end chain with $\text{C}\cdots\text{Cl}\cdots\text{Cl}\cdots\text{C}$ distances of 3.38 \AA , much less than the sum of standard van der Waals radii (Figure 7). Such a contact might



Figure 7. Molecular motif from the end-to-end chain of molecules in the crystal structure of the β -polymorph of 1,4-dichlorobenzene. The $\text{Cl}\cdots\text{Cl}$ distance is markedly shorter than the sum of the van der Waals radii. A pixel calculation shows that the interaction energy of a pair of molecules related in this way is close to zero.^[44]

be expected to be associated with a strongly repulsive interaction, but even in the localized point-charge picture, a calculation leads to only about 1 kJ mol^{-1} destabilization.^[44] As we have no charge-density distribution at hand for this crystal structure, we cannot describe the bond path, but from the known qualitative dependence on internuclear distance and by analogy with results for the Cl_2 crystal, we can expect a bond path with a $(3,-1)$ critical point of low ρ_b with positive Laplacian, characteristic of a weakly stabilizing closed-shell interaction. A pixel calculation^[44,45] confirms that the interaction energy of a pair of molecules related in this way is close to zero: this particular molecule–molecule arrangement is thus not especially relevant in terms of stabilization or destabilization. The overall lattice energy in the crystal structures of the dichlorobenzene derivatives results mainly

from dispersion interactions between whole molecules, and the preferences among rival structures are dictated by a complex balance between dispersion and coulombic terms, whose identification is far from simple, and which involve very small energy differences.^[44] No understanding of the relative stability of these structures can be achieved through consideration of the mutual positions of particular atoms or orientations of particular bonds. The application of atom–atom reasoning to intermolecular matters can raise artificial problems. While the large polarizability of Cl relative to C and H is

certainly an important factor in the crystal packing of chlorinated compounds, one wonders how many of the models proposed over the years about the presumed importance of fine geometrical aspects of $\text{Cl}\cdots\text{Cl}$ interactions are likely to survive.

9.2. Localized versus Delocalized Electrostatic Models

From a detailed and careful survey of the performance of electrostatic atom–atom point-charge models versus distributed multipole models in the reproduction of organic crystal structures,^[46] it was found that multipole models were not on average superior to point-charge ones, although for rigid molecules the multipole models gave some improvement. Figure 8 shows coulombic energies calculated with electrostatic point charges ($E_{\text{p.c.}}$) and by the pixel method with molecular charge distributions (E_{pix}) for many virtual crystal structures of naphthalene and of benzoic acid. While there is a general correlation, the absolute magnitudes differ widely, and, for naphthalene, even the signs disagree. The E_{pix} values are much larger than $E_{\text{p.c.}}$ values and their spread is about twice as great, indicating a higher resolving power. This property may be useful, as the scatter about the correlation line is of the order of 5 kJ mol^{-1} , that is, comparable to differences in total lattice energies between rival polymorphs, real or virtual. The larger the coulombic energies, the greater is the spread (compare Figure 8a and b). These results refer to crystal structures built from completely rigid molecules and to ESP point charges, that is, those of the best possible quality. In most other calculations of intermolecular interactions, point-charge models are based on much cruder atomic charge parameters (e.g., from Mulliken population analysis or empirical partitioning schemes) and used for flexible molecules, where the electron-density distribution varies with conformation.

At intermediate intermolecular distances, point-charge models may give a reasonable estimate of energy trends, but the absolute values may still be widely off the mark. At the short intermolecular distances typical of crystals (or liquids), the use of localized or delocalized descriptions of the charge distribution may even yield opposite signs in the energy balance: stabilization versus destabilization. Thus the power of localized models to discriminate between rival structures seems very limited. Indeed, one may wonder whether there is

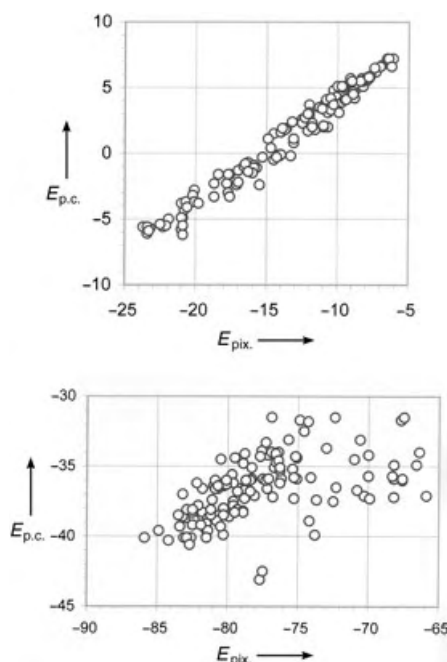


Figure 8. Pixel (E_{pix}) versus point-charge ($E_{p.c.}$) coulombic energies (kJ mol^{-1}) in many computer-generated virtual crystal structures of naphthalene (top) and benzoic acid (bottom).

any hope of constructing a reliable atom–atom force field for the prediction of crystal structures of organic compounds. And, to take matters further, it seems at least prudent to question the reliability of atom–atom models in molecular docking studies, which require delicate discrimination among sites in biological macromolecules with a large number of torsional degrees of freedom. Broderson et al. suggest that the use of multipole models can be expected to improve the description of intermolecular interactions “as the electrostatic interaction is the most prominent contribution to the intermolecular potential”.^[46] For non-hydrogen-bonded crystals, as far as “prominent” means “large”, this statement is no more than an echo of a widespread misunderstanding, because, as pixel calculations for crystals show,^[40,47] coulombic energies are no more than 20–30 % of the sublimation energy, even in crystals of strongly polar compounds. If “prominent” means “important for structural detail”, then this statement is more open to discussion.

9.3. Benzene and Its Derivatives

Because of the central place of benzene in both practical and theoretical organic chemistry, its crystal structure has been discussed in innumerable papers and at innumerable symposia. At normal pressures, liquid benzene crystallizes at about 5 °C in the structure shown in projection in Figure 9a (space group $Pbca$);^[48] at about 25 kbar, benzene has a more densely packed monoclinic $P2_1/c$ structure^[49] (Figure 9b) which is the first member of the series of homologous structures comprising the linear benzenoid aromatics: naphthalene, anthracene, tetracene, pentacene.

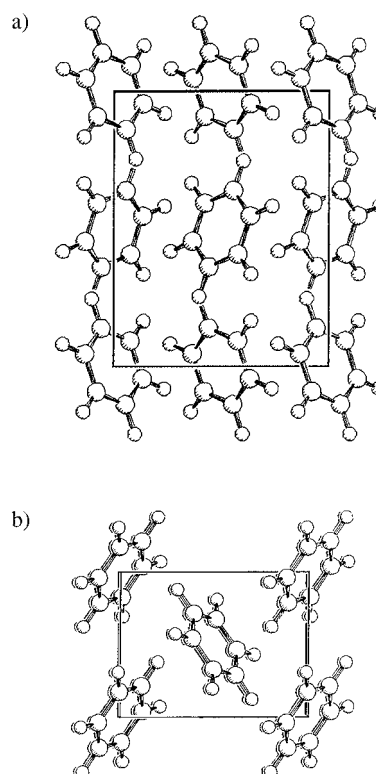


Figure 9. a) The normal-pressure orthorhombic crystal structure of benzene. b) The high-pressure monoclinic crystal structure of benzene.

From one point of view, the $Pbca$ crystal structure can be described simply as the close packing of oblate ellipsoids. Each molecule in the crystal structure is surrounded by twelve other molecules in a somewhat distorted cubic-close-packed arrangement. The molecule sits on an inversion center and thus has three non-equivalent hydrogen atoms with different environments. The $Pbca$ space group requires that neighboring pairs of molecules are tilted to varying degrees with respect to one another (Figure 10), and since the short intermolecular contacts necessarily involve hydrogen and carbon atoms one can discern $\text{C–H}\cdots\text{H}$ and $\text{C–H}\cdots\text{C}$ interactions and discuss their possible significance. In one of these neighboring pairs (Figure 10, **A**), an H atom of one molecule is approximately equidistant from the six C atoms of its neighbor so one might consider this as evidence for a $\text{C–H}\cdots\pi$ interaction. Again, one can regard the occurrence of this pair as evidence for the importance of molecular electric quadrupole interactions. All these interpretations have been proposed, compared, contrasted, and argued about.

The relative stability of parallel and T-shaped arrangements for benzene dimers has been the subject of endless discussion from the computational viewpoint. The energy difference varies and can even change sign, depending on the computational method. The only safe conclusion is that the energy difference between the two arrangements is marginal. The flexibility and modest computational demands of the pixel method (one energy point costs about 10 seconds of computer time on a 3 GHz personal computer) allow us to study the potential energy hypersurface of the benzene dimer as a function of distance between centers of mass and

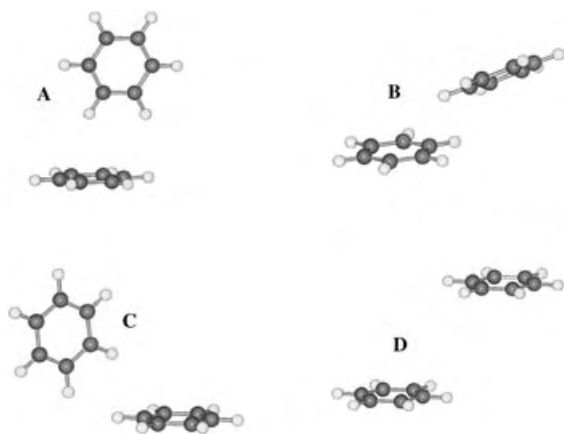


Figure 10. The four closest molecular pairs in the normal crystal structure of benzene (see Table 2 for corresponding energies).

interplanar angle. The main minima are shown in Figure 11 while Table 2 shows the energies for these computational dimers together with those for the closest molecular pairs observed in the crystal.

The structures **A–D** listed in Table 2 and illustrated in Figure 10 represent pairs of neighboring benzene molecules related by symmetry operations of the crystal (three glide planes and the *c*-axis translation). Although each of these pairs is part of an infinite repeating pattern, our calculations

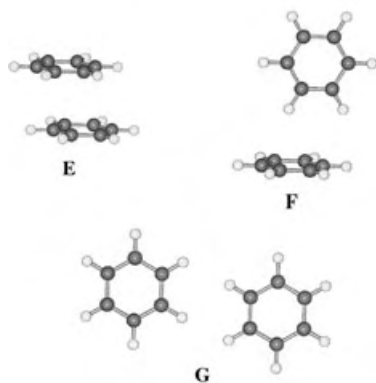


Figure 11. Selected minima in the potential energy hypersurface for the gas-phase benzene dimer (see Table 2 for corresponding energies).

Table 2: Cohesive energies [kJ mol^{-1}] of molecular pairs **A–D** (Figure 10), in the *Pbca* crystal structure of benzene, and optimized energies of selected benzene dimers **E–G** (Figure 11), as calculated by the pixel method.

Molecular pair	$E_{\text{coul}}^{[a]}$	$E_{\text{pol}}^{[a]}$	$E_{\text{disp}}^{[a]}$	$E_{\text{rep}}^{[a]}$	$E_{\text{tot}}^{[a]}$	Distance ^[b]	Angle ^[c]
A: $1/2+x, y, 1/2-z$	−3.4	−1.3	−12.2	6.6	−10.3	5.08	85
B: $x, 1/2-y, 1/2+z$	−2.0	−0.6	−7.6	3.6	−6.6	5.90	28
C: $1/2-x, 1/2+y, z$	−1.2	−0.6	−6.4	3.2	−5.0	6.05	88
D: $x, y, 1+z$	−0.4	0.0	−1.0	0.0	−1.4	6.92	0
Dimer E	−7.3	−6.7	−37.6	34.5	−17.0	3.41	0
Dimer F	−5.4	−2.5	−15.4	11.0	−12.3	4.90	90
Dimer G	−0.4	−1.5	−7.0	5.3	−3.6	6.48	0

[a] Coulombic, polarization, dispersion, repulsion, and total molecule–molecule energies. [b] Distance between centers of mass [Å]. [c] Angle [°] between mean benzene molecular planes.

refer to the interaction energy of the molecular pairs in isolation. The pixel total lattice energy of benzene, $-47.7 \text{ kJ mol}^{-1}$, corresponds well with the observed heat of sublimation, 44.4 kJ mol^{-1} .^[45]

The calculated dimer **F** shows a strong resemblance to the nearest-neighbor pair **A** in the crystal. This is about the only point of close similarity between the crystal pairs and the isolated dimers. According to the pixel calculation, the stacked dimer **E** is the best (most stable) with regard to dispersion energy and, rather surprisingly, also coulombic-polarization energy, but it does not occur in the crystal. The closest analogue to **E** is the **D** pair related by the *c*-axis translation but with more than double the interplanar spacing. The **D** pair can be described as partially stacked but not overlapping. There is not much to be said about the **C** pair; left on its own it would possibly fall into the local energy minimum represented by the **F** dimer. These observations are not easily brought into line with interpretations of the electrostatic interactions in the benzene crystal. However, our calculations confirm that although nearest-neighbor pairs, being pushed and pulled by other molecules, do not necessarily correspond to local minima in the energy landscape, they can safely be assumed to correspond to low-lying regions of the energy landscape. Thus, the **A**, **B**, and **C** nearest-neighbor pairs have been used as a basis for designing molecules with special affinity for specific aromatic guests.^[50]

The computational results inform us about how a given molecule in the benzene crystal structure interacts with its neighbors but they do not explain why benzene adopts the particular crystal structure that it does and not some other structure. Indeed, the main lesson to be drawn is that the observed benzene crystal structure depends on a subtle balance of long-range, cooperative effects, and that to describe it as being driven by favorable contacts between positively charged H atoms and negatively charged C atoms is a vast oversimplification. According to extensive force-field calculations by van Eijck et al. there are at least thirty virtual structures with lattice energies within a 10 kJ mol^{-1} window.^[51] The observed *Pbca* structure is indeed the one with the largest lattice energy but only by a very small margin, less than the uncertainty in the calculated energies, and the densest calculated structure is close to the structure of high-pressure benzene (Figure 9b). There are no known benzene polymorphs to match any of the remaining low-energy virtual structures. Thus, we do not really understand why benzene adopts the *Pbca* structure and not one of the other low-energy virtual structures.

More generally, rigid aromatic molecules can be divided schematically into a core region (the carbon atoms) and a rim region (the hydrogen atoms and/or the substituents). Such molecules can then dimerize in three basic motifs (Figure 12 and 13): parallel stacking (core–core interaction, interplanar angle 0°), bent-planes or T-shaped approach (rim–core interaction, variable interplanar angle), and coplanar approach (rim–rim interaction). We have calculated the pixel interaction energies of

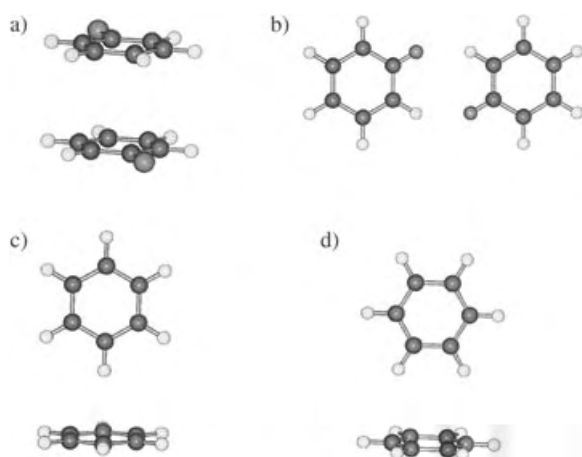


Figure 12. Some dimerization modes in benzene and substituted benzenes. a) Parallel stacking (PS), substituents pointing in the same direction, and antiparallel stacking (APS), substituents pointing in opposite directions, interring distance 3.4 Å. b) Coplanar arrangement (see details in Figure 13). c), d) T-dimers (T-1, and T-2), interplanar angle 90°, distance between ring centers 5.0 Å. For T-1 fluorobenzene (Table 3), C...F distances were set at the sum of van der Waals radii.

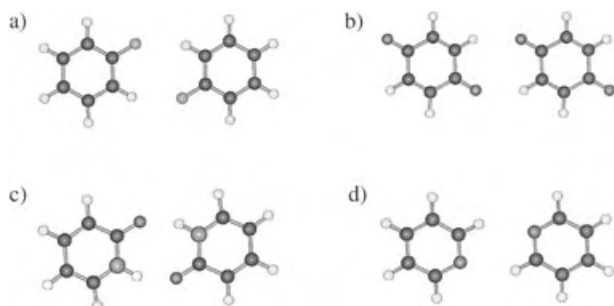


Figure 13. In-plane dimers: a) fluoro- and chlorobenzene, b) benzoquinone, c) pyridone cyclic hydrogen-bonded dimer, d) pyridine. For energies see Table 4.

dimers of benzene derivatives where one C–H group has been replaced by C–F (fluorobenzene), by C–Cl (chlorobenzene), and by N (pyridine), or two C–H groups have been replaced by two C=O groups (benzoquinone). To illustrate classical hydrogen bonding, we have also included the six-membered cyclic unsaturated amide, pyridone (Tables 3 and 4). Molecular geometries were standardized for the benzene derivatives (C–C bonds 1.40 Å, all angles 120°) and have been taken as in previous work^[45,47] for the other molecules. The dimer geometries have not been fully optimized, as the calculations are intended merely to show relative orders of magnitude.

The stacking energy of substituted benzene rings comes out as 13–18 kJ mol^{−1}, remarkably constant over the chosen derivatives (Table 3), a result mainly of the

Table 3: Interaction energies [kJ mol^{−1}] of molecular dimers of benzene derivatives, as calculated by the pixel method.

	$E_{\text{coul}}^{[a]}$	$E_{\text{pol}}^{[a]}$	$E_{\text{disp}}^{[a]}$	$E_{\text{rep}}^{[a]}$	$E_{\text{tot}}^{[a]}$	$E_{\text{p.c.}}^{[b]}$
benzene PS ^[c]	−0.7	−4.0	−31.5	23.3	−12.9	5.9
benzene T-1	−5.0	−2.2	−13.1	11.0	−9.3	−1.9
benzene T-2	−4.0	−1.6	−12.6	7.6	−10.6	−1.3
fluorobenzene PS	−2.3	−3.1	−31.8	23.1	−14.1	5.8
fluorobenzene APS	−4.4	−3.3	−31.8	23.1	−16.4	3.2
fluorobenzene T-1	−1.8	−2.2	−8.6	19.9	7.4	3.6
chlorobenzene PS	−3.0	−3.9	−35.3	29.7	−12.6	5.6
chlorobenzene APS	−3.5	−2.5	−32.1	21.5	−16.7	2.8
benzoquinone PS	4.3	−3.0	−37.6	18.4	−17.9	10.7
pyridine PS	0.7	−2.7	−28.8	19.1	−11.6	8.5
pyridine APS	−5.4	−2.7	−28.6	19.0	−17.7	−1.1
pyridone PS	10.6	−3.2	−26.8	19.9	0.4	16.5
pyridone APS	−9.5	−3.5	−27.4	20.8	−19.6	−3.3

[a] Coulombic, polarization, dispersion, repulsion, and total molecule–molecule energies. [b] Point-charge coulombic energy calculated with ESP charges. [c] Labels in this column denote: PS parallel stack, APS anti-parallel stack, T-1 and T-2 T-shaped dimers (see Figure 12).

nearly constant dispersion contribution of about 35 kJ mol^{−1}. (Note that the parallel stack (PS) dimer in Figure 12a is not quite the same as the energy-minimized slipped dimer **E** in Figure 11.) With polar substituents there is a preference for antiparallel over parallel stack dimers, but this preference is large only in the very polar molecule, pyridone. In the fluorobenzene dimer the preference stems from a coulombic effect but in the chlorobenzene dimer from a steric effect (increased repulsion between bulky chlorine atoms in the parallel dimer). Table 3 also includes point-charge coulombic energies calculated with ESP charges for comparison with the pixel coulombic energies. There is no agreement whatsoever.

Lateral interactions are only marginally stabilizing in the benzene, fluorobenzene, and chlorobenzene dimers, in spite of the more favorable coulombic contribution in the fluorobenzene, and chlorobenzene dimers (Table 4). A change in the mutual orientation of the molecules in the planar dimers has little effect on the cohesion energy. Thus, replacement of electropositive H by electronegative atoms does not lead to a major stabilizing effect in the lateral dimers.^[71] The small due to electronegative atoms additional coulombic stabilization is cancelled by the loss in dispersion energy that results from the longer intermolecular distance. Only in the benzoquinone and pyridine dimers do lateral coplanar interactions become much larger. For the pyridone dimer, the pixel energy of

Table 4: Interaction energies [J mol^{−1}] of coplanar molecular dimers,^[a] as calculated by the pixel method.

Dimer	H...X Distance [Å]	$E_{\text{coul}}^{[b]}$	$E_{\text{pol}}^{[b]}$	$E_{\text{disp}}^{[b]}$	$E_{\text{rep}}^{[b]}$	$E_{\text{tot}}^{[b]}$	$E_{\text{p.c.}}^{[c]}$
benzene	2.20	−0.3	−2.0	−6.7	7.3	−1.7	1.0
fluorobenzene	2.50	−4.4	−1.1	−3.8	7.7	−1.7	−3.2
chlorobenzene	2.84	−2.2	−2.5	−10.7	14.2	−1.3	−1.2
benzoquinone	2.50	−13.1	−3.1	−7.8	10.8	−13.2	−10.7
pyridine	2.61	−12.1	−4.0	−7.7	12.5	−11.3	−3.7
pyridone	1.80	−104	−39.6	−12.7	104.6	−51.3	−70.0

[a] See Figure 13 for the mutual orientations of the molecules; [b] Coulombic, polarization, dispersion, repulsion, and total molecule–molecule energies. [c] Point-charge coulombic energy calculated with ESP charges.

-50 kJ mol^{-1} confirms the overwhelming dominance of hydrogen bonding over all other intermolecular recognition energies. An upper limit for the energy of “weak” hydrogen bonds of the $\text{C-H}\cdots\text{O}$ or $\text{C-H}\cdots\text{N}$ type can be estimated as the difference between the lateral dimerization energy of benzoquinone or pyridine and that of benzene, that is, about 5 kJ mol^{-1} for each $\text{C-H}\cdots\text{X}$ bond (more on these bonds in Section 9.4). This value is about one fifth of the energy of a “normal” hydrogen bond as found in pyridone. Again, except for the hydrogen-bonded pyridone dimer, there is no correlation between coulombic energies calculated by pixel and those from ESP charges.

Even for benzene itself, the concept of rim-to-core interactions is probably better than that of a $\text{C-H}\cdots\pi$ “bond”. The results for the T-1 and T-2 dimers in Table 3 show that in addition to the already noted translational floppiness of all benzene dimers, there is also a relatively large freedom in the mutual orientation of the two rings, so a presumed $\text{C-H}\cdots\pi$ bond would have the unusual property of allowing one of the partners, the H atom, to be almost anywhere. The status of a “bond” seems more justified for the $\text{C-H}\cdots\pi$ interaction in the crystalline benzene–acetylene complex,^[52] where the acetylenic C-H group points directly at the center of the benzene ring, thereby producing a symmetric and highly efficient packing of the rod-like and disk-like component molecules. The optimal $\text{C-H}\cdots\pi$ bond, involving the best C-H donor and the best π acceptor, should occur in the T-shaped acetylene dimer. A pixel calculation gives an interaction energy of about 10 kJ mol^{-1} .

As already mentioned, the $\text{C-H}\cdots\text{F}$ interaction in the centrosymmetric lateral fluorobenzene dimer yields a relatively small stabilization compared with the $\text{C-H}\cdots\text{H}$ interaction in the analogous benzene dimer (Table 4). The crystal structures of a series of fluorinated benzenes have been determined and discussed in considerable detail in terms of $\text{C-H}\cdots\text{F}$ interactions.^[53] It was concluded, for example, that the crystal structure of 1,3,5-trifluorobenzene (Figure 14) is extensively stabilized by $\text{C-H}\cdots\text{F}$ interactions. This crystal structure actually consists of stacks in which alternate molecules separated by interplane distance of about 3.6 \AA are related by inversion centers; the stacks are then packed in such a way that fluorine atoms in one stack approach hydrogen atoms in adjacent stacks with $\text{H}\cdots\text{F}$ distances of $2.50\text{--}2.63 \text{ \AA}$. Table 5 lists the closest molecular pairs in this crystal structure with energies as calculated by pixel. What one sees there, as already noted in previous work,^[54] is the predominance of the stacking interaction between antiparallel molecules with offset aromatic cores, H above F. Weaker lateral interactions lead to formation of a roughly hexagonal pattern with inevitable $\text{H}\cdots\text{F}$ contacts. Although the calculated energies could easily change by a few kJ mol^{-1} on altering several computational conditions (see above), the message from the pixel analysis is clear: each lateral cohesive energy contribution is smaller

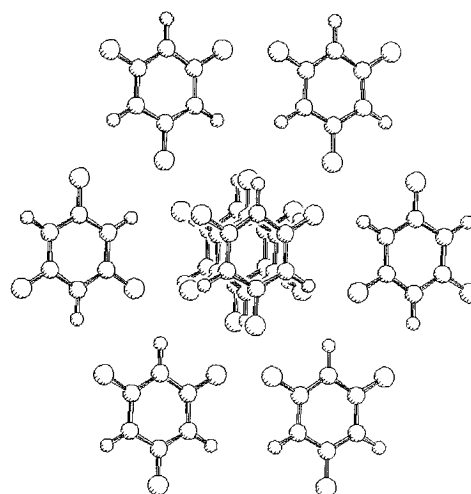


Figure 14. Schematic view of molecular packing in the 1,3,5-trifluorobenzene crystal (large spheres denote fluorine atoms): the central motif consists of a stack of overlapping molecules (H atoms over F atoms); each molecule is then surrounded by six neighbors forming a pseudo-hexagonal layer (the molecules are parallel but not strictly coplanar). Close $\text{F}\cdots\text{H}$ distances are around 2.5 \AA (the exact value depending on the C-H distance and C-C-H angle renormalization method). The sum of standard atomic radii in crystals for H and F atoms is 2.56 \AA .^[69]

Table 5: Interaction energies [kJ mol^{-1}] of closest molecular pairs in the 1,3,5-trifluorobenzene crystal structure^[53] (Figure 14), as calculated by the pixel method.

Pair type and symmetry operation	Distance [\AA]	$E_{\text{coul}}^{[a]}$	$E_{\text{pol}}^{[a]}$	$E_{\text{disp}}^{[a]}$	$E_{\text{rep}}^{[a]}$	$E_{\text{tot}}^{[a]}$	$E_{\text{p.c.}}^{[b]}$
stack, inversion	3.75	−4.0	−1.3	−26.4	11.8	−19.9	−0.6
in-plane, inversion	6.59	−4.8	−1.1	−5.6	7.7	−3.8	−2.9
in-plane, inversion	6.82	−3.2	−0.6	−4.4	4.4	−3.8	−2.6
in-plane, translation	6.16	+0.2	−0.2	−5.1	1.1	−4.0	0.4

[a] Coulombic, polarization, dispersion, repulsion, and total molecule–molecule energies. [b] Point-charge coulombic energy calculated with ESP charges.

than the stacking energy, and can be either coulombic or dispersive in nature. Thus, it is safer to say that this crystal structure arises primarily from molecular stacking that is then propagated by the cooperation of less-stabilizing, diffuse lateral interactions to form a layered structure. These lateral interactions help to explain the difference between the crystal structure of 1,3,5-trifluorobenzene and the herringbone arrangement in crystalline benzene, the second reason being the reluctance of fluorine molecular regions to come into contact with π -electron clouds. The T-shaped fluorobenzene dimer is destabilized by more than 15 kJ mol^{-1} with respect to the corresponding benzene dimer (Table 3). Of course, in a crystal, the space above the π -electron cloud must be filled by something, and if only F atoms are available then one of them must occupy this space. Thus, it is not too surprising that in the crystal structure of hexafluorobenzene^[55] one of the six F atoms in one molecule sits above the ring center of another, with $\text{F}\cdots\text{C}$ distances of $3.3\text{--}3.5 \text{ \AA}$.

On the whole, the results in Table 5 do not encourage the promotion of diffuse lateral interactions to the rank of $\text{C-H}\cdots\text{F}$ bonds and thus confirm our earlier comments about $\text{C-H}\cdots\text{F}$

H...F interactions. Since the atom–atom viewpoint is already controversial in fluorobenzenes, where H and F constitute all there is to the crystal structures, one wonders about its predictive or even descriptive use for crystals of more chemically diversified molecules. As far as prospective topological analyses of the corresponding charge densities are concerned, studies of analogous systems^[56] lead us to expect the detection of intermolecular bond paths of the closed-shell type for the H...F interactions, with ρ_b close to background-noise level (about $0.05 \text{ e } \text{\AA}^{-3}$) and a small positive Laplacian. However, with the longer intrastack distances of about 3.6 \AA , it is by no means certain that significant bond paths will be detectable for the much stronger stacking interaction. We see a danger that topological studies of the intermolecular charge density in crystals may put the emphasis in the wrong place; they will ascribe the intermolecular cohesion to interactions between pairs of atoms for which bond paths can be discerned, even if only weakly, rather than to interactions between the charge density distributions. The bond paths for such intermolecular contacts should be regarded as a secondary phenomenon (an epiphenomenon) accompanying the intermolecular attraction and caused by it.

9.4. Hydrogen-Bonded Systems

The questions of distinguishing intermolecular atom–atom bonds from more delocalized types of interaction are less problematic in “normal” or “classical” X–H...Y (X, Y = O, N) hydrogen bonds, with energies of $20\text{--}40 \text{ kJ mol}^{-1}$, and even less to “strong” charge-assisted or resonance-assisted X–H...Y hydrogen bonds, with energies up to 150 kJ mol^{-1} .^[57] Such bonds have considerable covalent character (negative Laplacian operator at the bond path CP) and are thus to a large extent describable in atom–atom terms. But even for these classical hydrogen bonds, some of the traditional atom–atom simplifications may not apply. The picture of a simple, attractive coulombic $\text{H}(\delta+) \cdots \text{O}(\delta-)$ interaction is too reductive, because in the same terms one should also take account of the repulsive $\text{O}(\delta-) \cdots \text{O}(\delta-)$ or $\text{H}(\delta+) \cdots \text{H}(\delta+)$ interactions that arise, for example, in cyclic carboxylic acid or amide dimers.

Table 6 shows some pixel results for hydrogen-bonded systems (see Figure 15). Calculated total hydrogen-bonding energies are in good agreement with estimates from quantum chemical calculations and in reasonable agreement with experimental values. On the other hand, the calculated equilibrium O...H separation of about 1.8 \AA for carboxylic acid dimers and 2.2 \AA for amides are slightly too long compared with typical experimental values (see the discussion in ref.^[45]). Since pixel uses unperturbed molecular charge distributions, large polarization energies are introduced to substitute for the bonding energy associated with development of some covalent character of the bond. In the pixel

Table 6: Interaction energies [kJ mol^{-1}] in hydrogen-bonding dimers, as calculated by the pixel method.

System ^[a]	$R(\text{O} \cdots \text{H})$ or $R(\text{N} \cdots \text{H})$ [\AA]	$E_{\text{coul}}^{[b]}$	$E_{\text{pol}}^{[b]}$	$E_{\text{disp}}^{[b]}$	$E_{\text{rep}}^{[b]}$	$E_{\text{tot}}^{[b]}$	$E_{\text{p.c.}}^{[c]}$
acetic acid	1.80	−100.1	−42.8	−15.5	100.9	−57.5	−59.0
formic acid	1.80	−92.4	−49.1	−18.1	102.1	−57.5	−44.8
benzoic acid	1.80	−106.0	−45.9	−12.4	91.5	−72.8	−68.0
formamide	2.23	−63.4	−18.6	−11.9	44.1	−49.7	−48.2
urea	2.07	−53.7	−16.5	−9.9	41.0	−39.2	−42.3
guanine–cytosine	—	−106.3	−37.3	−17.2	71.3	−89.5	−80.0
water	2.1	−24.3	−6.2	−4.3	16.1	−18.8	−18.8
acetylene, T-dimer	2.34 ^[d]	−12.7	−7.3	−7.8	18.1	−9.7	−6.5
acetylene–water	2.10	−21.8	−6.8	−4.8	21.9	−11.5	−14.6

[a] See Figure 15 for the geometries. [b] Coulombic, polarization, dispersion, repulsion, and total molecule–molecule energies. [c] Point-charge coulombic energy calculated with ESP charges. [d] Distance between hydrogen and the triple-bond midpoint.

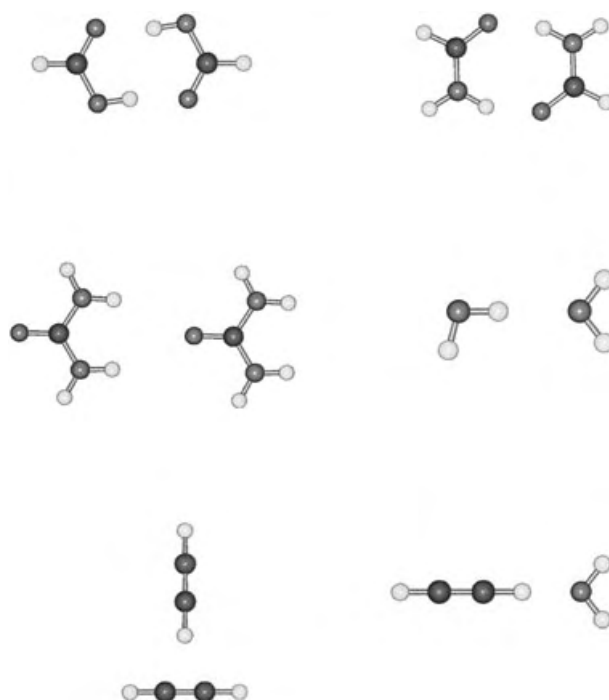


Figure 15. Hydrogen-bonded dimers whose energies are reported in Table 6: left to right, top to bottom, formic acid (also representative of the acetic and benzoic acid dimers), formamide, urea, water, acetylene, and acetylene–water.

partitioning scheme, coulombic and polarization components dominate. At O–H...O distances close to equilibrium the dispersion contribution is only about one tenth of the sum of the corresponding coulombic and polarization terms, while at O...H distances over 2.5 \AA the coulombic term is the only component that survives (see Figure 16). Remarkably, the energy components are very similar for formic, acetic, and benzoic acids, thus confirming a certain localized character of the hydrogen bond (compare also the values for formamide and urea). At the equilibrium distances the point-charge coulombic energies, calculated with good quality (ESP) point-charge parameters, are astonishingly close to the total pixel

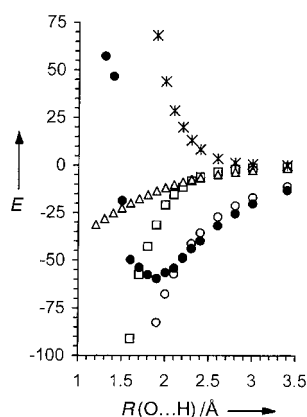


Figure 16. Pixel energy curves [kJ mol^{-1}] for the formic acid dimer; coulombic (\circ), polarization (\square), dispersion (\triangle), repulsion ($+$) and total energy (\bullet) as a function of O...H distance [\AA].

energies, a result that can only be attributed to coincidence, arising from cancellation of errors.

The pixel energies show that the formation of a single O...H or N...H...O bond is worth about twice the stacking energy of the benzene dimer, about three times the energy of the strongest C-H... π or C-H...O "bond" in the acetylene dimers or acetylene-water dimers, and more than twenty times the energy of the two C-H...F interactions in the lateral fluorobenzene dimer. These numbers confirm—if any confirmation were needed—that the traditional hydrogen bond, when present, is indeed the principal driving force in intermolecular recognition.

Nevertheless, the concept of weak C-H...O and C-H...N interactions as structure-defining, hydrogen-bonding entities still enjoys widespread popularity in the chemical literature.^[58] The problem of categorizing such interactions has of course been tackled by high-level quantum chemical methods, using small test molecules (water, ammonia, acetylene, methane, with benzene already being classed as a "large" system), but the results have a margin of indeterminacy. As a typical example, recent calculations for the fluoroform-water complex give an interaction energy ranging from 12.6 to 22.8 kJ mol^{-1} .^[59] The almost 100 % variation depends on the choice of the basis set, on exclusion or inclusion of an electron correlation, and on treatment of the basis-set superposition error, about which there does not yet seem to be general consensus.

The question of whether the C-H...O interaction is a true hydrogen bond has been explicitly posed and examined in great detail.^[60] One problem is that in many cases the putative C-H...O bond is associated with a slight shortening of the C-H bond, rather than the typical lengthening. Whereas on hydrogen-bond formation an O-H bond stretches and undergoes a red shift in its vibrational frequency, the C-H bond in many C-H...O interactions contracts slightly and shows a blue shift. Such C-H...O interactions have been called "improper blue-shifting (or blue-shifted) hydrogen bonds".^[61] The phenomenon has been studied by high-level quantum mechanical calculations and does not seem amenable to explanation in

terms of a simple model. On the one hand, it has been concluded that there is no fundamental distinction between the two types of interaction since the same sets of forces are acting in both,^[60] on the other hand the detailed balance among these forces must clearly be different. While different kinds of theoretical analysis lend themselves to different types of explanation, the basic distinction between normal red-shifting and "improper" blue-shifting hydrogen bonds is perhaps best expressed in terms of a change in the nature of the charge-transfer involved.^[61b] In contrast to normal X-H...Y hydrogen bonding, where charge density is transferred from Y lone pairs to the X-H σ^* antibonding orbital, the blue-shifting bond is characterized by charge transfer from Y to a more remote part of the acceptor molecule, for example, in the fluoroform-water dimer from the oxygen lone pairs to the C-F σ^* antibonding orbitals. The contraction of the C-H bond is a result of the induced structural reorganization. Expressed in terms of electron transfer between molecular orbitals, the matter may appear unduly intricate, but we note that such an explanation invokes diffuse, delocalized electronic effects, similar to our approach to the description of intermolecular interactions in general. The debate about the "improper blue-shifting" hydrogen bond exposes the limitations of the atom-atom viewpoint. Clearly, the interpretation of the entire binding energy of a complex such as the fluoroform-water dimer exclusively in terms of a C-H...O hydrogen bond is inadequate and can sometimes be misleading.

Indeed, the C-H...O and C-H...N interactions are borderline cases. On the one hand, we have a crystal structure of a hydrated tricyclic orthoamide^[62] where the unusual occurrence of an eclipsed C(sp³)-CH₃ group can be attributed to the presence of three stabilizing C-H...OH₂ interactions that overcome the methyl torsional barrier, normally about 10–15 kJ mol^{-1} . As discussed earlier, from the pixel calculations for the benzoquinone and pyridine lateral dimers (Table 4) the upper limit of the binding energy associated with each C-H...OH₂ interaction can be estimated as about 5 kJ mol^{-1} . On the other hand, there does not seem to be much point in ascribing significant bonding character to every short C-H...O and C-H...N interaction observed in a crystal structure. Polymorph energy landscape studies have demonstrated that 100 out of 100 virtual crystal structures for naphthoquinone contain short C-H...O contacts, with virtually no correlation between their number or length and the lattice energy.^[47] Given the molecular structure, one can hardly be surprised by such an outcome. Yet, the mere presence of short intermolecular C-H...O contacts in similar crystal structures is still being taken as evidence of a significant structure-driving contribution towards the stability of those particular structures. In the bio-structural context, the energy stabilization owing to putative C-H...O bonds has been questioned with considerable input of effort and ingenuity,^[63] but such is the persistence of the hydrogen-bonding doctrine that even in situations where such interactions are recognized as being devoid of any stabilizing contribution they are still being described as "hydrogen bonds".

10. Summary and Outlook

To what extent do intermolecular recognition and cohesion depend on weak “bonds” between individual atoms in the separate molecules and to what extent on more diffuse, delocalized interactions? That is the main question we have tried to address herein. The analysis of intermolecular (supramolecular) interactions has been conducted to date mainly in terms of localized “bonds” between individual atoms. The evidence for such weak bonds has come mainly from studies of the geometry of crystal structures, especially from the recognition of patterns of close contacts between peripheral atoms in different molecules. With the help of chemical intuition or theoretical calculations, these bonds were associated with energies extending all the way from strong hydrogen bonds (each contributing upward of 20 kJ mol^{-1}) to weak interactions that are barely above thermal noise level (recall that RT (R = gas constant, T = temperature (K)) amounts to 2.5 kJ mol^{-1} at 300 K). A vast library of information about atom–atom contacts in crystal structures has thus been amassed, categorized, classified, and analyzed in terms of noncovalent interactions and possible molecular recognition factors, especially in protein–ligand and other bio-structural complexes.^[64] With the help of the 3×10^5 organic and organometallic crystal structures in the Cambridge Structural Database (www.ccdc.cam.ac.uk/products/csd/) and the 2.5×10^4 structures of biological macromolecules in the Protein Data Bank (www.rcsb.org/pdb/) one can find examples of just about any proposed intermolecular interaction involving peripheral atoms.

Such interpretations of close intermolecular atom–atom contacts in terms of weak bonding interactions would now seem to be supported by bond-path analyses of theoretical and experimental electron-density distributions, as discussed in Section 7. From these studies, there is indeed a continuum from strong to weak (or virtually non-existent) hydrogen bonds. To a good approximation, the electron density at bond critical points follows a negative exponential dependence on the $\text{H}\cdots\text{X}$ distance until it merges with the background density at an $\text{H}\cdots\text{X}$ distance of about 2.5 \AA .^[36,56,65] For short, strong, hydrogen bonds of the $\text{O}-\text{H}\cdots\text{O}$ or $\text{O}\cdots\text{H}-\text{O}$ type, for example, as in carboxylic acid dimers or the hydrogen maleate anion^[34,66] the Laplacian operator $\nabla^2\rho_{\text{BCP}}$ is negative, indicative of some covalent character in the bond, whereas for longer hydrogen bonds the Laplacian operator is positive, indicative of a closed-shell interaction. The crossing point seems to occur at an $\text{H}\cdots\text{O}$ distance of about 1.33 \AA ,^[36] which may be regarded as the approximate boundary between electron-sharing and closed-shell interactions. As mentioned earlier, for $\text{H}\cdots\text{O}$ interactions, critical point densities ρ_{BCP} and their distance dependence are closely similar to those calculated for the overlap of the unperturbed atomic charge densities (the pro-molecule electron density)^[37] so that great care in the interpretation of experimental and theoretical intermolecular charge densities is called for.

When molecules are drawn together under their mutual attraction into condensed phases, they approach one another until mutual repulsion just balances the intermolecular attraction to produce an equilibrium structure. Since the

peripheral and protruding atoms in typical organic molecules are mostly H and otherwise F, Cl, O, N, and π -electron systems are also often easily accessible molecular regions, it is hardly surprising that $\text{C}-\text{H}\cdots\text{F}$, $\text{C}-\text{H}\cdots\text{Cl}$, $\text{C}-\text{H}\cdots\text{O}$, $\text{C}-\text{H}\cdots\text{N}$, and $\text{C}-\text{H}\cdots\pi$ contacts have been identified, sought for in databases, catalogued, and analyzed in terms of various geometric parameter distributions. The interpretation of such contacts as extensions or extrapolations of hydrogen bonds is natural and has been followed by many students of intermolecular interactions in terms of “weak” or “unconventional” hydrogen bonds^[8] or hydrogen “bridges”, as expressed in a crystal engineering context.^[67] One cannot deny that these weak intermolecular atom–atom bonds can be neatly categorized on the basis of geometrical, spectroscopic, and even energetic criteria and are thus according to these criteria existent rather than non-existent, provided one is prepared to accept a continuum of energies all the way to nearly zero. The question is not whether weak hydrogen bonds “exist” but rather to what extent are they relevant in distinguishing one possible crystal structure from another?

Whatever the answer to this question, there is no doubt that the description and analysis of molecular cohesion in terms of atom–atom interactions is probably here to stay. The desire to decompose the result of a complex interaction between molecular charge distributions into simple ingredients is irresistible. The atom–atom representation has an undeniable descriptive value and can hardly be avoided at the level of ball-and-stick models or, their modern equivalent, graphical displays of complex molecular systems such as enzyme–substrate complexes on computer screens. There is no simple alternative to these ways of analyzing large amounts of structural data. What, then, should one do about distinguishing genuine intermolecular bonds from indiscriminate atom–atom contacts? Where should one stop talking and thinking about bonds? At a certain threshold distance? At a certain threshold energy? We have no easy recipe and there probably is none. Whatever the boundaries of the definition, it amounts to a matter of existence versus relevance.

Atom–atom categories are to some extent unavoidable but on the other hand they should not be taken too seriously, and, above all, it should be realized that they are not the ideal medium through which significant progress in the understanding of the physics of intermolecular interactions will be coded. One must be distrustful about the seductive barter of physics for appearances, of energy for geometry. Protein folding and crystal growth, two great outstanding problems of modern chemistry, proceed by steps of marginal stability increment towards a final structure which is also only marginally more stable than its competitors—and, one may suspect, often barely if at all surviving the kinetic demands of a complex environment such as a molecular solution. Enzyme–substrate and enzyme–inhibitor recognition hangs on delicate energy requirements at structurally complex sites in large bio-molecules. To expect that such fine-tuned processes can be described in terms of gross simplifications as atom–atom distance and angle schemes is close to wishful thinking. Indeed, strict adherence to the atom–atom viewpoint may even be a liability in trying to understand the specificity of molecular recognition and self-recognition

because it puts the emphasis on the wrong place. Energy differences between molecular packing arrangements do not easily sort themselves out in terms of atom–atom contacts; they depend on the way in which molecules as aggregates, or at least substantial parts of molecules, approach and interact with one another. One should weigh postulated structure-directing weak atom–atom interactions, each of the order of 5 kJ mol^{-1} or less, against the total lattice energy of a medium-size organic molecule, whose order of magnitude is $E = 1.2Z_v + 20 \text{ kJ mol}^{-1}$, where Z_v is the number of its valence electrons.^[68]

Approaching the conclusion of this Review, a reader might feel quite unhappy after having invested precious time in reading mostly destructive criticism and comments, apparently without any constructive pointer towards readily applicable rules. However, we hope to have shown that the problem of molecular recognition is in general not usefully reducible to the level of atom–atom interactions. At least, we have indicated how to avoid making wrong inferences and reaching conceptual dead ends. The gist of our presentation can, perhaps, be summarized in a few final sentences. Thinking in terms of atoms in molecules, and therefore also in crystals or in supramolecular ensembles, is unavoidable. Nevertheless, it is the interaction between charge distributions, and not between point atoms, that is responsible for molecular recognition at all levels of complexity. Modern chemical thinking and modeling cannot sidestep this crucial issue. For the time being, the pixel method, involving interaction between rigid charge-density distributions of the separate molecules and with its simplified energy-partitioning scheme, offers an affordable possibility for a deeper, more quantitative picture in which the intermolecular links are not drawn between single atoms.

In writing this essay, we have benefited greatly from discussions with Richard Bader (McMaster University, Hamilton, Ontario), Albert Eschenmoser (ETH, Zurich), Carlo Gatti (CNR-ISTM, Milan), Artem Oganov (ETH, Zurich), Dieter Schwarzenbach (EPF-Lausanne), and Mark Spackman (University of New England, Armidale, New South Wales), who are not necessarily in full agreement with all the opinions expressed herein. We are also grateful to Dr. B. Schweizer (ETH, Zurich) for assistance in the preparation of the manuscript. Figures with structural diagrams have been drawn with the help of program SCHAKAL.^[70]

Received: March 30, 2004

Published online: January 31, 2005

- [1] J. W. Steed, *CrystEngComm* **2003**, *5*, 169–179.
- [2] L. R. Nassimbeni, *Acc. Chem. Res.* **2003**, *36*, 631–637.
- [3] For example: M. Nomura, V. A. Erdmann, *Nature* **1970**, *228*, 744–748; M. Nomura, *Trends Biochem. Sci.* **1997**, *22*, 275–279.
- [4] A. I. Kitaigorodskii, *Organic Chemical Crystallography*, Consultants Bureau, New York, **1961**.
- [5] A. I. Kitaigorodskii, *Molecular Crystals and Molecules*, Academic Press, New York, **1973**.
- [6] J. D. Dunitz, G. Filippini, A. Gavezzotti, *Tetrahedron* **2000**, *56*, 6595–6601.
- [7] G. R. Desiraju, *Angew. Chem.* **1995**, *107*, 2541–2558; *Angew. Chem. Int. Ed. Engl.* **1995**, *34*, 2311–2327.
- [8] a) J. Bernstein, M. D. Cohen, L. Leiserowitz in *The Chemistry of Quinonoid Compounds* (Hrsg.: S. Patai), Wiley, London, **1974**; b) R. Taylor, O. Kennard, *J. Am. Chem. Soc.* **1982**, *104*, 5063–5070; c) Z. Berkovitch-Yellin, L. Leiserowitz, *Acta Crystallogr. Sect. B* **1984**, *40*, 159–165; d) G. R. Desiraju, *Acc. Chem. Res.* **1991**, *24*, 290–296; e) G. R. Desiraju, *Acc. Chem. Res.* **1996**, *29*, 441–449; f) T. Steiner, *Crystallogr. Rev.* **1996**, *6*, 1–57; g) G. R. Desiraju, T. Steiner, *The Weak Hydrogen Bond*, IUCr Book Series, Oxford University Press, Oxford, **1999**; h) T. Steiner, *Angew. Chem.* **2002**, *114*, 50–80; *Angew. Chem. Int. Ed.* **2002**, *41*, 48–76.
- [9] P. W. Fowler, A. D. Buckingham, *Chem. Phys. Lett.* **1991**, *176*, 11–18.
- [10] a) Z. Berkovitch-Yellin, L. Leiserowitz, *J. Am. Chem. Soc.* **1980**, *102*, 7677–7690; b) Z. Berkovitch-Yellin, L. Leiserowitz, *J. Am. Chem. Soc.* **1982**, *104*, 4052–4064.
- [11] a) A. J. Stone, *The Theory of Intermolecular Forces*, Clarendon, Oxford, **1996**, chap. 7; b) S. L. Price, *J. Chem. Soc. Faraday Trans.* **1996**, *92*, 2997–3008.
- [12] L. Pauling, *The Nature of the Chemical Bond*, 2. Aufl., Cornell University Press, Ithaca, **1939**, chap. 1.
- [13] A. J. Pertsin, A. I. Kitaigorodskii, *The Atom–Atom Potential Method*, Springer, Berlin, **1987**, p. 74.
- [14] For a very recent compilation of experimental sublimation enthalpies see J. S. Chickos, W. E. Acree, Jr., *J. Phys. Chem. Ref. Data* **2002**, *31*, 537–698.
- [15] J. P. M. Lommerse, W. D. S. Motherwell, H. L. Ammon, J. D. Dunitz, A. Gavezzotti, D. W. M. Hofmann, F. J. J. Leusen, W. T. M. Mooij, S. L. Price, B. Schweizer, M. U. Schmidt, B. P. van Eijck, P. Verwer, D. E. Williams, *Acta Crystallogr. Sect. B* **2000**, *56*, 697–714; W. D. S. Motherwell, H. L. Ammon, J. D. Dunitz, A. Dzyabchenko, P. Erk, A. Gavezzotti, D. W. M. Hofmann, F. J. J. Leusen, J. P. M. Lommerse, W. T. M. Mooij, S. L. Price, H. Scheraga, B. Schweizer, M. U. Schmidt, B. P. van Eijck, P. Verwer, D. E. Williams, *Acta Crystallogr. Sect. B* **2002**, *58*, 647–661.
- [16] a) A. I. M. Rae, R. Mason, *Proc. R. Soc. London Ser. A* **1968**, *304*, 487–499; b) R. Mason, A. I. M. Rae, *Proc. R. Soc. London Ser. A* **1968**, *304*, 501–502.
- [17] “Molecular Crystals”: C. Pisani in *Handbook of Molecular Physics* (Eds.: S. Wilson, R. McWeeny), Wiley, Chichester, **2001**.
- [18] T. van Mourik, R. J. Gdanitz, *J. Chem. Phys.* **2002**, *116*, 9620–9623.
- [19] A. J. Stone, *The Theory of Intermolecular Forces*, Clarendon, Oxford, **1996**, chap. 4 and 6.
- [20] A. Gavezzotti, *J. Phys. Chem. B* **2002**, *106*, 4145–4154.
- [21] A. Gavezzotti, *J. Phys. Chem. B* **2003**, *107*, 2344–2353.
- [22] R. F. W. Bader, *Atoms in Molecules: A Quantum Theory*, Oxford University Press, Oxford, **1990**.
- [23] R. F. W. Bader, S. G. Anderson, A. J. Duke, *J. Am. Chem. Soc.* **1979**, *101*, 1389–1395.
- [24] T. S. Koritsanszky, P. Coppens, *Chem. Rev.* **2001**, *101*, 1583–1627.
- [25] R. Restori, D. Schwarzenbach, *Acta Crystallogr. Sect. A* **1996**, *52*, 369–378.
- [26] C. F. Matta, J. Hernandez-Trujillo, T.-H. Tang, R. F. W. Bader, *Chem. Eur. J.* **2003**, *9*, 1940–1951.
- [27] R. Custelcean, J. E. Jackson, *Chem. Rev.* **2001**, *101*, 1963–1980.
- [28] P. H. Friedlander, D. Sayre, *Nature* **1956**, *178*, 999–1000.
- [29] T. M. Krygowski, A. Ciesielski, B. Swirska, P. Leszczynski, *Pol. J. Chem.* **1994**, *68*, 2097–2107.
- [30] J. C. Collings, K. P. Roscoe, R. L. Thomas, A. S. Batsanov, L. M. Stimson, J. A. K. Howard, T. B. Marder, *New J. Chem.* **2001**, *25*, 1410–1417.
- [31] On the other hand, in the 1:1 triphenylene:perfluorotriphenylene co-crystal, the hydrocarbon is slightly non-planar (H⋯H,

- 1.94–1.96 Å) and the perfluorocarbon with the larger F atoms (F...F, 2.37–2.38 Å) markedly non-planar.
- [32] M. K. Lakshman, P. L. Kole, S. Chaturvedi, J. H. Saugier, H. J. C. Yeh, J. P. Glusker, A. K. Katz, C. E. Afshar, W.-M. Dashwood, G. Kenniston, W. M. Baird, *J. Am. Chem. Soc.* **2000**, *122*, 12629–12636.
- [33] U. Koch, P. L. A. Popelier, *J. Phys. Chem.* **1995**, *99*, 9747–9754.
- [34] D. Madsen, C. Flensburg, S. Larsen, *J. Phys. Chem. A* **1998**, *102*, 2177–2188.
- [35] Yu. Abramov, *Acta Crystallogr. Sect. A* **1997**, *53*, 264–272.
- [36] E. Espinosa, E. Molins, C. Lecomte, *Chem. Phys. Lett.* **1998**, *285*, 170–173.
- [37] M. A. Spackman, *Chem. Phys. Lett.* **1999**, *301*, 425–429.
- [38] C. Gatti, E. May, R. Destro, F. Cargoni, *J. Phys. Chem. A* **2002**, *106*, 2707–2720.
- [39] A. Volkov, P. Coppens, *J. Comput. Chem.* **2004**, *25*, 921–934.
- [40] A. Gavezzotti, *Z. Kristallogr.* in press.
- [41] E. D. Stevens, *Mol. Phys.* **1979**, *37*, 27–45.
- [42] a) L.-Y. Hsu, D. E. Williams, *Inorg. Chem.* **1979**, *18*, 79–82; b) S. R. Cox, L.-Y. Hsu, D. E. Williams, *Acta Crystallogr. Sect. A* **1981**, *37*, 293–301.
- [43] V. G. Tsirelson, P. F. Zou, T.-H. Tang, R. F. W. Bader, *Acta Crystallogr. Sect. A* **1995**, *51*, 143–153.
- [44] J. D. Dunitz, A. Gavezzotti, *Helv. Chim. Acta* **2002**, *85*, 3949–3964.
- [45] A. Gavezzotti, *CrystEngComm* **2003**, *5*, 429–438.
- [46] S. Brodersen, S. Wilke, F. J. J. Leusen, G. Engel, *Phys. Chem. Chem. Phys.* **2003**, *5*, 4923–4931.
- [47] A. Gavezzotti, *CrystEngComm* **2003**, *5*, 439–446.
- [48] G. E. Bacon, N. A. Curry, S. A. Wilson, *Proc. R. Soc. London Ser. A* **1964**, *279*, 98–110.
- [49] a) G. J. Piermarini, A. D. Mighell, C. E. Weir, S. Block, *Science* **1969**, *165*, 1250–1255; b) R. Fourme, D. Andr , M. Renaud, *Acta Crystallogr. Sect. B* **1971**, *27*, 1275–1276.
- [50] G. Klebe, F. Diederich, *Philos. Trans. R. Soc. London Ser. A* **1993**, *345*, 37–48.
- [51] B. P. van Eijck, A. L. Spek, W. T. M. Mooij, J. Kroon, *Acta Crystallogr. Sect. B* **1998**, *54*, 291–299.
- [52] R. Boese, T. Clark, A. Gavezzotti, *Helv. Chim. Acta* **2003**, *86*, 1085–1100.
- [53] V. R. Thalladi, H.-C. Weiss, D. Bl ser, R. Boese, A. Nangia, G. R. Desiraju, *J. Am. Chem. Soc.* **1998**, *120*, 8702–8710.
- [54] J. D. Dunitz, A. Gavezzotti, W. B. Schweizer, *Helv. Chim. Acta* **2003**, *86*, 4073–4092.
- [55] N. Boden, P. P. Davis, C. H. Stam, G. A. Wesselink, *Mol. Phys.* **1973**, *25*, 81–86.
- [56] E. Espinosa, I. Alkorta, J. Elguero, E. Molins, *J. Chem. Phys.* **2002**, *117*, 5529–5542.
- [57] G. Gilli, P. Gilli, *J. Mol. Struct.* **2000**, *552*, 1–15.
- [58] Recent review: R. K. Castellano, *Curr. Org. Chem.* **2004**, *8*, 845–865.
- [59] S. K. Rhee, S. H. Kim, S. Lee, J. Y. Lee, *Chem. Phys.* **2004**, *297*, 21–29; zit. Lit.
- [60] Y. Gu, T. Kar, S. Scheiner, *J. Am. Chem. Soc.* **1999**, *121*, 9411–9422.
- [61] a) P. Hobza, V. Špirko, Z. Havlas, K. Buchhold, B. Reimann, H.-D. Barth, B. Brutschy, *Chem. Phys. Lett.* **1999**, *299*, 180–186; b) P. Hobza, Z. Havlas, *Chem. Rev.* **2000**, *100*, 4253–4264.
- [62] P. Seiler, G. R. Weisman, E. D. Glendining, F. Weinhold, V. B. Johnson, J. D. Dunitz, *Angew. Chem.* **1987**, *99*, 1216–1218; *Angew. Chem. Int. Ed. Engl.* **1987**, *26*, 1175–1177.
- [63] S. Yohannan, S. Faham, D. Yang, D. Grosfeld, A. K. Chamberlain, J. U. Bowie, *J. Am. Chem. Soc.* **2004**, *126*, 2284–2285.
- [64] For example: E. A. Meyer, R. K. Castellano, F. Diederich, *Angew. Chem.* **2003**, *115*, 1244–1287; *Angew. Chem. Int. Ed.* **2003**, *42*, 1210–1250.
- [65] P. R. Mallinson, G. T. Smith, C. C. Wilson, E. Grech, K. Wozniak, *J. Am. Chem. Soc.* **2003**, *125*, 4259–4270.
- [66] C. Flensburg, S. Larsen, R. F. Stewart, *J. Phys. Chem.* **1995**, *99*, 10130–10141.
- [67] G. R. Desiraju, *Acc. Chem. Res.* **2002**, *35*, 565–573.
- [68] A. Gavezzotti, *Synlett* **2002**, 201–214.
- [69] R. S. Rowland, R. Taylor, *J. Phys. Chem.* **1996**, *100*, 7384–7391.
- [70] E. Keller, SCHAKAL92, *A program for the graphic representation of molecular and crystallographic models*, Universit t Freiburg, **1993**.
- [71] Note added in proof (December 21, 2004). As pointed out by a referee, energies of molecular clusters calculated by pixel are subject to many uncertainties that also affect other quantum chemical calculations. For an example, see the recent thorough analysis of the benzene dimer energy surface: M. O. Sinnokrot, E. F. Valeev, C. D. Sherrill, *J. Am. Chem. Soc.* **2002**, *124*, 10887–10893. In our case, as already discussed at length (see for example ref. [45]), cohesive energies of stacked aromatic dimers are overestimated, probably owing to an inadequate treatment of overlap repulsion. Since our Review was submitted, attempts at improving this aspect of the problem have been made (A. Gavezzotti, unpublished results, see also, for example, ref. [40]), together with extensive quantum chemical calculations (MP2/6-31G** counterpoise). In particular, the effects of calculating pixel energies from electron densities obtained with larger basis sets (cc-pVDZ and D95(d,p)) have been studied. It appears that some of the lateral interactions could be slightly underestimated by pixel. For an impression of what the changes in the stabilization energy estimates could be, the following examples can be offered: dimer E (Table 2) should be around 12 instead of 17 kJ mol^{−1}; benzene PS (Table 3), around 8 instead of 13 kJ mol^{−1}, and similarly the PS dimers in Table 3 and the 1,3,5-trifluorobenzene stacked dimer in Table 5 might be less stabilizing by 3–4 kJ mol^{−1}. On the other hand, the benzoquinone coplanar dimer in Table 4 and the 1,3,5-trifluorobenzene inversion dimers in Table 5 might be more stable by 3–4 kJ mol^{−1}. These are the largest differences that appear between results of pixel calculations and more extensive quantum chemical calculations, and they all concern extreme cases (exactly overlapping rings, double contacts between H and electronegative atoms at close range). For less extreme situations, the performance of pixel is astonishingly good in comparison with much more expensive procedures. In any case, we still do not see compelling evidence for considering C–H...X interactions (X = N, O, F) as the prime definers of crystal structure. Taking into account the above uncertainties, our calculations show that the stabilization energy due to C–H...X interactions is typically less than that owing to stacking interactions or at most on a par with them, even with such 'extreme' molecules as benzoquinone and trifluorobenzene.

Molecular Recognition

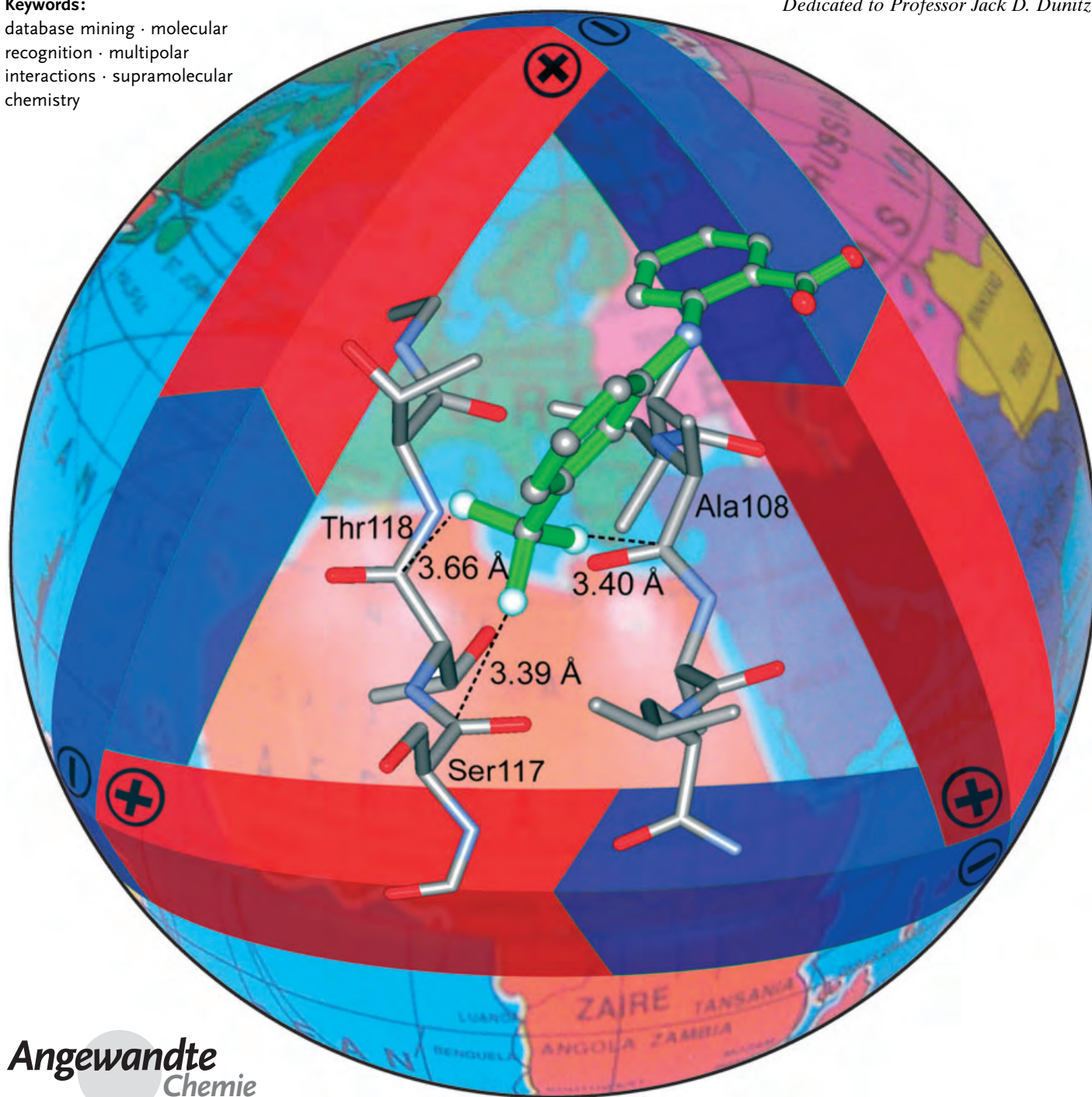
Orthogonal Multipolar Interactions in Structural Chemistry and Biology

Ralph Paulini, Klaus Müller,* and François Diederich*

Keywords:

database mining · molecular recognition · multipolar interactions · supramolecular chemistry

Dedicated to Professor Jack D. Dunitz



Angewandte
Chemie

The past few decades of molecular recognition studies have greatly enhanced our knowledge on apolar, ion–dipole, and hydrogen-bonding interactions. However, much less attention has been given to the role that multipolar interactions, in particular those with orthogonal dipolar alignment, play in organizing a crystal lattice or stabilizing complexes involving biological receptors. By using results from database mining, this review attempts to give an overview of types and structural features of these previously rather overlooked interactions. A number of illustrative examples of these interactions found in X-ray crystal structures of small molecules and protein–ligand complexes demonstrate their propensity and thus potential importance for both, chemical and biological molecular recognition processes.

From the Contents

1. Introduction	1789
2. Multipolar Interactions of Small Molecules	1790
3. Multipolar Protein–Ligand and Protein–Protein Interactions	1797
4. Quantification of Dipolar Interactions	1803
5. Summary and Conclusions	1803

1. Introduction

Among the noncovalent interactions that govern molecular recognition processes ranging from crystal growth to the formation of protein–ligand and protein–protein complexes, apolar (hydrophobic) interactions, ion–ion and ion–dipole interactions, and hydrogen-bonding association have been the preferred subjects for a large number of investigations during the past few decades.^[1] A wealth of information on the nature and energetics of these interactions has greatly enhanced our ability to use them for crystal structure prediction,^[2] crystal engineering,^[3] supramolecular synthesis,^[4] and structure-based ligand design.^[5] However, much less attention has been given to the role that multipolar interactions play in molecular recognition events, although a number of crystal structure analyses and database searches by Gavezzotti,^[6] Allen et al.,^[7] Lee et al.,^[8] and others have highlighted the main types of interaction geometries for participating dipoles, particularly the head-to-tail and antiparallel orientations.

In a recent fluorine scan of a family of tricyclic thrombin inhibitors to map favorable environments for organofluorine groups in an enzyme active site, we identified a H–C_α–C=O fragment of the peptide that provides a pronounced fluorophilic entity. A C–F residue of a potent inhibitor participated in short multipolar C–F...H–C_α and C–F...C=O interactions with Asn98 in the hydrophobic distal (D) pocket of the protein. In the latter contact, the F atom approaches the electrophilic C atom in a nearly orthogonal way, along the pseudotrigonal axis of the carbonyl unit (Figure 1).^[9] This preferred geometry for organofluorine...carbonyl interactions was further corroborated by crystal structure analyses of fluorine-containing small molecules^[9–11] and database searches in the Protein Data Bank (PDB) and the Cambridge Structural Database (CSD).^[12] The latter furnished numerous cases of C–F...C=O contacts with F...C distances below the sum of the van der Waals radii and an F...C=O angle tending toward 90°. ^[9,13] A similar directional interaction motif was also uncovered in small-molecule X-ray crystal structure analyses and subsequent CSD searches for C–F...C≡N contacts.^[11,14] Anticipating a more general importance of such

orthogonal multipolar interactions, the database mining has now been extended to explore such contacts between other dipoles, revealing a list of various cases such as C–X...C=O (X = halogen), C=O...C=O, C≡N...C=O, S=O...C=O, C–OH...CO, and H₂O...C=O. (Table 1).

This review attempts to illustrate the structural features of these previously rather overlooked interactions, with the objective of demonstrating their propensity and thus importance particularly for small-molecule crystal packing and protein–ligand assemblies. Of course, we are aware that “atoms in crystals need to go somewhere” as stated by Dunitz^[15] and that not every short contact may be an attractive one.^[16] We provide an overview over the contributions to the intricate task of putting the energetics of these weak noncovalent contacts into hard quantitative numbers, either experimentally or by using computational tools. It becomes clear that orthogonal multipolar interactions might well be an important structural contributor to both stability and selectivity in chemical and biological molecular and

[*] R. Paulini, Prof. Dr. F. Diederich
Laboratorium für Organische Chemie
ETH-Hönggerberg, HCI
8093 Zürich (Switzerland)
Fax: (+41) 01-632-1109
E-mail: diederich@org.chem.ethz.ch
Prof. Dr. K. Müller
Pharma Research Basel
Discovery Chemistry
F. Hoffmann-La Roche Ltd
4070 Basel (Switzerland)
Fax: (+41) 61-688-0986
E-mail: klaus.mueller@roche.com



Supporting information for this article (scatterplots correlating geometrical parameters of nonbonding polar interactions as retrieved from the Cambridge Structural Database (CSD) for all discussed pairs of interacting polar groups except C–F...C=O, details of additional examples of ligand–protein multipolar interactions as retrieved from the Protein Data Bank (PDB), and a detailed overview of ligand–protein dipolar interactions as found by PDB database mining) is available on the WWW under <http://www.angewandte.org> or from the author.

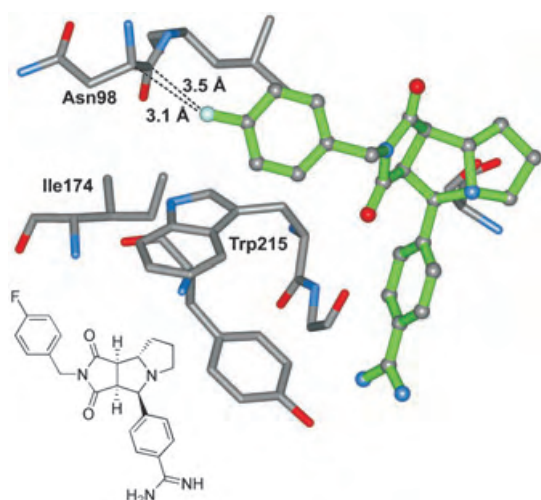


Figure 1. X-ray crystal structure (PDB code: 1OYT) showing close contacts in the distal (D) pocket between the F atom of the shown tricyclic inhibitor of thrombin and the protein backbone of the enzyme.^[9] Color code: inhibitor skeleton: green; C: gray; O: red; N: blue; F: cyan.

supramolecular structures. We also wish to emphasize that such multipolar interactions rarely exist alone, but are often complemented by additional multipolar interactions to C–H units in the vicinity of “recipient” dipolar units. However, these additional interactions will not be discussed here.



François Diederich, born in 1952 in the Grand-Duchy of Luxembourg, studied chemistry at the University of Heidelberg (1971–1977), and received his PhD there in 1979 for work on the synthesis of kekulene in the group of Prof. Heinz A. Staab. Following postdoctoral studies with Prof. Orville L. Chapman at UCLA (1979–1981), he returned to Heidelberg for his Habilitation at the Max-Planck-Institut für Medizinische Forschung (1981–1985). Subsequently, he joined the faculty in the Department of Chemistry and Biochemistry at UCLA where he became Full Professor of Organic and Bioorganic Chemistry in 1989. In 1992, he returned to Europe, joining the Department of Chemistry and Applied Biosciences at the ETH Zürich.



Ralph Paulini was born in Mühlbach, Romania in 1977. He studied chemistry at the University of Konstanz and the University of Massachusetts Amherst where he received a M.Sc. in chemistry under the supervision of Prof. Vincent M. Rotello in 2001. Currently he is a graduate student in the group of Prof. François Diederich working on the design and synthesis of bisubstrate inhibitors of catechol-O-methyltransferase.

2. Multipolar Interactions of Small Molecules

2.1. A Survey of the Literature

Short, nonbonding interatomic contacts that are indicative of attractive intermolecular forces have always been of key interest to chemists in their search for the “glue” that holds solid matter together.^[3b] In particular, contacts that are realized in crystals preferentially to other, equally possible interactions may indicate important types of such forces. As a remarkable example, the crystal structure of alloxan (pyrimidine-2,4,5,6-tetraone)^[17] (Figure 2) features an array of short, almost orthogonal intermolecular C=O⋯C=O contacts with distances of about 2.8 Å and C=O⋯C angles in the range between 155° and 163°, rather than form the hydrogen-bonded structure one would expect, given the existence of two acidic NH units per molecule.

Several other examples of similar short C=O⋯C=O contacts were observed by Bolton and others for crystalline triketoindane (indane-1,2,3-trione),^[18] parabanic acid (imidazolidine-2,4,5-trione),^[19] tetrachloro-*p*-benzoquinone (chloranil),^[20] and anhydrous barbituric acid.^[21] These contacts were later reviewed by Bent in a seminal overview of donor–acceptor interactions.^[22] The orthogonal interaction motif of carbonyls was also reported by Leiserowitz and co-workers for a series of chlorinated benzoquinones such as 2,6-dichloro-*p*-benzoquinone in a study on quinone packing modes.^[23] These authors conclude that the nature of the C=O⋯C=O interaction is best described as dipolar electrostatic, where the partial positive charge residing on the C atom of the intrinsically polar C=O unit represents an electrostatic center of attraction for the partially negatively charged O atom of an adjacent C=O fragment. Indeed, such electrostatic interactions between intrinsically dipolar molecular units can be highly directional and may be the cause of very short contact distances, bearing some structural resemblance to interactions between nucleophiles and carbonyl groups as investigated by Bürgi and Dunitz.^[24] Such purely electrostatic dipolar interactions, however, do not exhibit significant displacements of the electrophilic carbon center from the plane defined by the carbonyl unit and its two substituents and do not involve partial transfer of electron density from nucleophile to electrophile.



Klaus Müller is Head of Science and Technology Relations in Pharmaceutical Research at F. Hoffmann-La Roche AG, Basel. He is an organic chemist by training (ETH Zürich), but got also involved in theoretical and physical organic as well as biostructural chemistry. He joined F. Hoffmann-La Roche Basel in 1982 where he set up molecular modeling, biostructural research, bioinformatics, and was involved in the development of automated and miniaturized key technologies in discovery research. Since 1990 he is Extraordinary Professor for Chemo- and Bioinformatics at the University of Basel.

Table 1: Overview of dipolar interactions in small molecule crystal structures as retrieved from the CSD (version 5.25, November 2003).^[a]

A–B	E–Y	d_{vdW} [Å]	Search range [Å]	Number of structures	Number of occurrences	Number of occurrences within d_{vdW}
C–F	C=O	3.30	2.30–3.80	599	1028	243
C–Cl	C=O	3.65	2.65–4.15	1742	2968	816
C–Br	C=O	3.80	2.80–4.30	1105	1770	547
C–I	C=O	4.00	3.00–4.50	228	399	143
C–OH	C=O	3.25	2.25–3.75	587	775	144
C=O	C=O	3.25	2.25–3.75	16 546	> 10 000	1888
R ₂ C=O	R ₂ C=O	3.25	2.25–3.75	2614	4031	966
H ₂ O	C=O	3.25	2.25–3.75	814	1122	48
H ₂ O	R ₂ C=O	3.25	2.25–3.75	35	36	1
C ₂ O	C=O	3.25	2.25–3.75	1093	1358	330
C ₂ O	R ₂ C=O	3.25	2.25–3.75	197	223	48
C ₃ N	C=O	3.35	2.35–3.85	59	71	6
CN	C=O	3.35	2.35–3.85	476	664	201
C ₂ N	C=O	3.35	2.35–3.85	1405	2360	204
C ₂ N	R ₂ C=O	3.35	2.35–3.85	124	162	22
R ₂ N–O	C=O	3.25	2.25–3.75	87	114	25
C ₂ S	C=O	3.70	2.70–4.20	349	485	134
C ₂ S=O	C=O	3.25	2.25–3.75	10	19	3
C ₂ SO ₂	C=O	3.25	2.25–3.75	85	110	38
R ₃ P	C=O	3.75	2.75–4.25	14	19	3
R ₃ P–O	C=O	3.25	2.25–3.75	214	290	27
C–F	C–NO ₂	2.95	1.95–3.45	38	51	5
C–Cl	C–NO ₂	3.30	2.30–3.80	154	198	9
C–Br	C–NO ₂	3.45	2.45–3.95	77	98	5
C–I	C–NO ₂	3.65	2.65–4.15	34	59	7
C=O	CN	3.25	2.25–3.75	443	626	130
C–OH	CN	3.25	2.25–3.75	27	35	1
C ₂ O	CN	3.25	2.25–3.75	140	273	84
C ₂ S (C: C _{sp} ²)	CN	3.70	2.70–4.20	30	57	16
CN	CN	3.35	2.35–3.85	2080	5912	448
C–F	CN	3.30	2.30–3.80	110	247	58
C–Cl	CN	3.65	2.65–4.15	180	404	97
C–Br	CN	3.80	2.80–4.30	100	227	66
C–I	CN	4.00	3.00–4.50	34	73	32
C–F	R ¹ –CN ₂	3.30	2.30–3.80	19	28	7
C–Cl	R ¹ –CN ₂	3.65	2.65–4.15	74	109	33
C–Br	R ¹ –CN ₂	3.80	2.80–4.30	33	50	18
C–I	R ¹ –CN ₂	4.00	3.00–4.50	10	12	9
C=O	R ¹ –CN ₂	3.25	2.25–3.75	561	861	90
H ₂ O	R ¹ –CN ₂	3.25	2.25–3.75	190	258	17
C ₂ S	R ¹ –CN ₂	3.70	2.70–4.20	38	46	17
C ₂ O	R ¹ –CN ₂	3.25	2.25–3.75	68	96	18
C–F	C–F	3.30	2.30–3.80	1989	> 10 000	2111
C–F (C: C _{sp} ²)	C–F (C: C _{sp} ²)	3.30	2.30–3.80	926	> 10 000	2581
C–F (C: C _{sp} ³)	C–F (C: C _{sp} ²)	3.30	2.30–3.80	102	488	149
C–F (C: C _{sp} ²)	C–F (C: C _{sp} ³)	3.30	2.30–3.80	76	154	5
C–F (C: C _{sp} ³)	C–F (C: C _{sp} ³)	3.30	2.30–3.80	1077	3128	117

[a] Searches were performed without using any restrictive constraints (except for interactions involving C–OH, see text). Shown are the structures of interacting nucleophilic (A–B) and electrophilic (E–Y) polar units, van der Waals contact distances d_{vdW} [Å], search ranges [Å], total number of structures and occurrences, and number of occurrences within van der Waals distance. R = C, H; R¹ = C, N; R² = C, N, O. “C” in C₂O and C₃N denotes sp³-hybridized carbon centers; “C₂N” denotes an imine nitrogen.

With the rapidly growing X-ray structural databases and the availability and further development of effective search tools, database mining has become a powerful tool for the investigation of intermolecular interactions. In particular, the use of the Cambridge Structural Database (CSD) for research applications has been emphasized and reviewed.^[25]

In an early crystallographic database search Taylor et al. examined the composite crystal field environments of carbonyl and nitro groups and showed that the two functional groups engage in many short intermolecular contacts.^[26] The authors identified as the major interaction motifs the perpendicular and the antiparallel alignment between nitro and carbonyl groups, classifying them as favorable electrostatic interactions. Somewhat diverging from these results, Gavezzotti reported the results of a packing analysis of 80 crystal structures of organic molecules containing a carbonyl group and of 13 structures containing a cyano group, finding parallel and antiparallel orientations of carbonyl and nitrile dipoles (orthogonal orientations were absent in this search).^[6] The author concluded that dipole–dipole interactions are often “feeble” and their contribution to crystal packing “negligible”. In contrast, Allen et al. presented a more recent database search of C=O⋯C=O contacts, concluding that this type of nonbonding interaction is important in stabilizing the packing modes of small organic molecules and that it can be as effective in doing so as medium-strength hydrogen bonds.^[7] The authors describe three preferred interaction geometries: a slightly sheared antiparallel, a highly sheared parallel, and a perpendicular motif with occurrences decreasing in the order of mentioning. The two diverging interpretations of the role and the importance of dipolar C=O⋯C=O interactions were revisited very recently by Lee and co-workers, who published a more detailed CSD search on the crystal packing of molecules containing C=O, C≡N, and C(sp²)–F groups, which revealed a good correspondence between the orientation of nitrile and (to a lesser extent)

carbonyl groups with predictions of a bond dipole model.^[8] Analysis of the structural data and computational results led to the conclusion that, for large dipole moments and short contact distances, electrostatic energies are important in determining total interaction energies and geometries, whereas other intermolecular forces must also be considered

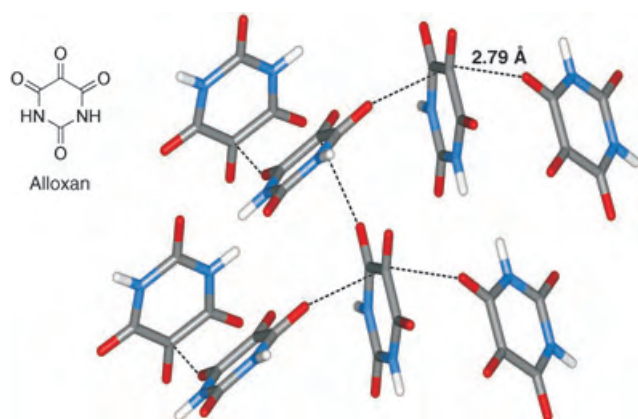


Figure 2. Crystal structure of alloxan (CSD-code: ALOXAN) featuring orthogonal intermolecular $\text{C}=\text{O}\cdots\text{C}=\text{O}$ contacts.^[18] Color code: C: gray; O: red; N: blue; H: white.

to obtain accurate distance dependencies. The authors point out that this fact explains the contrasting results of Gavezzotti, who implicitly considered the distance dependence law, and Allen et al., who directed their attention more to orientational effects.

Further reports on intra- and intermolecular short contacts between dipolar units include the case of $\text{NO}_2\cdots\text{NO}_2$ interactions in crystalline *N,N*-dipicrylamine and its ionic complexes that were published by Wozniak et al.^[27] The authors conclude that besides being engaged in the formation of hydrogen bonds, nitro groups interact as electrostatic dipoles in geometries corresponding to the antiparallel and the orthogonal motif discussed above. A later thorough investigation of dipolar contacts involving the nitro group as the recipient pole of the interaction relied on database mining and statistical analyses to conclude that there exists a preference of partially negatively charged atoms (especially oxygen) to be located above or/and below the plane of the nitro group leading to pyramidal and bipyramidal three-dimensional patterns.^[27b] Another example of the same type of dipolar orthogonal interaction, this time designated as a $\text{N}\cdots\text{O}=\text{C}$ interaction occurring between a carbonyl and a nitro group, was described by Yin et al. for the crystal structure of *N*-methyloxalyl 2,4-dinitroanilide (methyl *N*-(2,4-dinitrophenyl)oxalamate).^[28] These contacts have also been classified as electrostatic interactions and this categorization has been confirmed by ab initio calculations.

A different type of highly directional polar interactions much discussed in the literature are close $\text{C}-\text{X}\cdots\text{Z}$ contacts where X is a halogen and Z denotes electronegative atoms such as N, O, S, or halogens. These interactions have a high tendency to occur along the extension of the $\text{C}-\text{X}$ axis and have been attributed small attractive energies. We shall give a brief overview on these contacts, which are more distant from the notion of interacting dipolar vectors, in Section 2.4.

In our project aimed at the investigation of organofluorine interactions, we presented CSD searches of orthogonal $\text{C}-\text{F}\cdots\text{C}=\text{O}$ and $\text{C}-\text{F}\cdots\text{C}\equiv\text{N}$ interactions, in which we identified a considerable number of these contacts and convincingly demonstrated the importance of these dipolar intermolecular

interactions as crystal packing forces.^[9,11] To validate the generality of this interaction motif and to provide a more complete overview over types and geometries of interacting dipoles, we have now undertaken more comprehensive CSD and PDB searches^[29] including a greater number of dipolar units as potentially interacting partners, the results of which are displayed in Tables 1 and 2, and in Table 1SI in the Supporting Information. For the CSD searches, correlations of geometrical parameters are exemplarily shown as scatterplots for the $\text{C}-\text{F}\cdots\text{C}=\text{O}$ interaction (Figure 3; more plots are included in the Supporting Information).

2.2. CSD Searches I: $\text{A}-\text{B}\cdots\text{O}$, $\text{A}-\text{B}\cdots\text{C}\equiv\text{N}$, and $\text{A}-\text{B}\cdots\text{RCN}_2$ Interactions^[29]

In our previous reports of $\text{C}-\text{F}\cdots\text{C}=\text{O}$ contacts, we used scatterplots correlating the contact angle $\alpha_1(\text{F}\cdots\text{C}=\text{O})$ with the corresponding distance $d_1(\text{F}\cdots\text{C}(\text{C}=\text{O}))$ and plots linking d_1 with the distance d_2 of the F atom to the plane of the carbonyl unit (Figure 3b,d).^[9] These representations are maintained here, albeit in more general terms, such that α_1 denotes the contact angle $\text{B}\cdots\text{E}-\text{Y}$ of any negative pole B to a polar unit $\text{E}-\text{Y}$, d_1 symbolizes the nonbonded distance $\text{B}\cdots\text{E}$, and d_2 the distance of the polar atom B to the average plane p defined by the positively polarized atom E and its three ligands (where applicable). Furthermore, two additional types of correlation plots are added: a plot correlating d_1 with the angle α_2 between the vector $\text{E}\rightarrow\text{B}$ and the norm of the plane p displays the deviation of the negative pole B from the pseudotrigonal axis of the $\text{E}-\text{Y}$ unit (Figure 3c). Moreover, the plot of the angle α_3 between the bond vectors $\text{A}\rightarrow\text{B}$ and $\text{E}\rightarrow\text{Y}$ versus the torsional angle $\tau_1(\text{A}-\text{B}\cdots\text{E}-\text{Y})$ helps to better assess the orientation of the $\text{A}-\text{B}$ bond with respect to the $\text{E}-\text{Y}$ unit (Figure 3e,f).

For the $\text{C}-\text{F}\cdots\text{C}=\text{O}$ interactions (Figure 3b–f, 1028 occurrences, 243 thereof within van der Waals interaction cutoff), the d_1 versus α_1 scatterplot nicely shows a narrow cone of points converging to an angle α_1 of 90° at short distances. The sharp tip displayed in the d_1 versus d_2 graph at close contacts suggests a pronounced preference of the F atom to approach the $\text{C}=\text{O}$ unit along or close to its pseudotrigonal axis. In this plot, points significantly below the $d_1 \approx d_2$ boundary indicating deviations from the pseudotrigonal axis only become numerous at middle to longer-ranged contact distances. This picture is further substantiated by a wedge-like representation of hits in the α_2 versus d_1 plot, which displays an opening angle of about 40° for contact distances $d_1 = 3.3 \text{ \AA}$ (van der Waals distance) that rapidly narrows for shorter contacts. Indeed, a superimposition of 43 crystal structures with short $\text{F}\cdots\text{C}=\text{O}$ contact distances ($2.77 < d_1 < 3.09 \text{ \AA}$) graphically proves this preference (Figure 3g). The τ_1 versus α_3 plot divides the $\text{C}-\text{F}\cdots\text{C}=\text{O}$ interactions into four main groups: clusters at $0^\circ \leq \alpha_3 \leq 25^\circ$ and $160^\circ \leq \alpha_3 \leq 180^\circ$ denote parallel and antiparallel orientations of the $\text{C}-\text{F}$ and $\text{C}=\text{O}$ bond vectors, respectively. Further clusters include cases in which the C-end of the $\text{C}-\text{F}$ bond vector is tilted towards the oxygen hemisphere of the $\text{C}=\text{O}$ bond ($110^\circ \leq \alpha_3 \leq 140^\circ$) or the carbon hemisphere ($40^\circ \leq \alpha_3 \leq 70^\circ$). Orthogonal cases are displayed

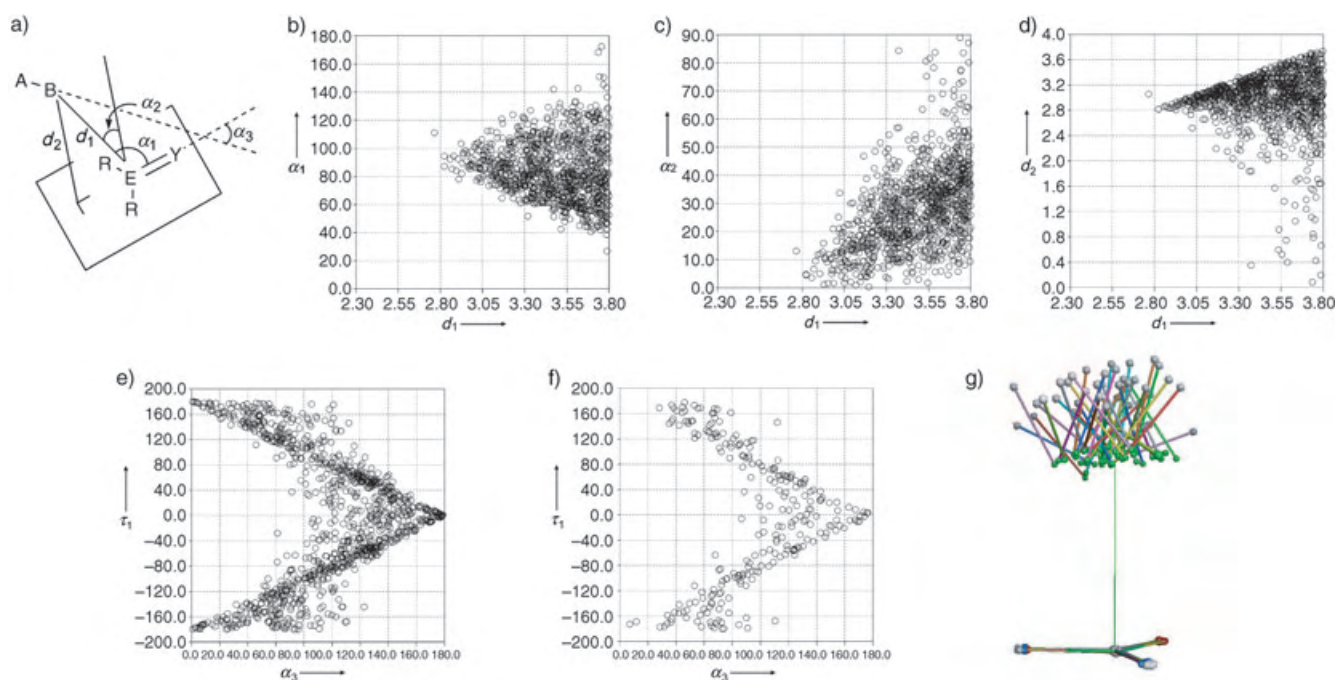


Figure 3. a) General graphical representation of the geometrical parameters used for the CSD searches. b)–f) Scatterplots correlating pairs of geometrical parameters for the C–F...C=O interaction: plots b)–e) contain the complete set of occurrences as indicated in Table 1; plot f) represents a repetition of e) for the subset of structures for which the interacting dipoles lie within the van der Waals contact distance ($2.30 \text{ \AA} < d_1 < 3.30 \text{ \AA}$). τ_1 denotes the torsional angle A–B...E–Y. g) Superposition of the carbonyl unit extracted from 43 crystal structures with intermolecular C–F...C=O contacts with $2.77 \text{ \AA} < d_1 < 3.09 \text{ \AA}$ (the carbonyl function pointing backwards to the right). The vertical line marks the pseudotrigonal axis of the carbonyl system. Color code: C: gray; F: green; O: red; N: blue.

for angles in the range of $70^\circ \leq \alpha_3 \leq 110^\circ$. In this range, the scattering of torsional angles deviating from the $\tau_1 \approx \pm (180^\circ - \alpha_3)$ -agglomeration of the plot is most pronounced, yet narrowing down to the horizontal V-shape with few exceptions for cases within van der Waals contact. The disappearance of orthogonal examples exhibiting large torsional angles with decreasing contact distances indicates that in some cases there might be a steric factor involved in orienting the two bond vectors with respect to each other in addition to the dipolar interaction forces. More precisely, for cases where the C–F bond vector is significantly tilted away from the pseudotrigonal axis towards the C-end of the C=O element, a steric clash between C_α substituents of the carbonyl unit and substituents adjacent to the C–F group of the molecule may prevent a close approach. Other clusters of hits deviating from the overall horizontal V-shape are found for $\pm (150^\circ \leq \tau_1 \leq 180^\circ)$ and $40^\circ \leq \alpha_3 \leq 70^\circ$ as well as for $\pm (0^\circ \leq \tau_1 \leq 40^\circ)$ and $110^\circ \leq \alpha_3 \leq 140^\circ$. Finally, no systematic change of the C–F or C=O bond length correlating with contact distances d_1 could be observed, additionally supporting the classification of these interactions as purely “multipolar” with no covalent character.

Among the possible interactions between the polar units considered in this search, cases involving C–X (X = halogen) bonds seem to exhibit a high probability to lie within the van der Waals distance of the nonbonding X...E contact or below (24–36% of the total number of occurrences for C–X...C=O interactions; Table 1). Interestingly, whereas the number of close contacts increases with the increasing atomic mass of the

halogens, the directional preferences become less pronounced, although the tendency of the halogen atom to lie close to the pseudotrigonal axis of the carbonyl group for C–X...C=O contacts, remains. While C–Cl...C=O interactions still display a narrow cone in the α_1 – d_1 plot and a sharp tip in the d_2 – d_1 graph, indicating the preferential alignment mentioned before, these indicators tend to broaden and to become more diffuse when going to the heavier halogens. However, the onsets of this broadening of plot shapes do not occur below the corresponding van der Waals contact distances, except for the case of C–I...C=O, where the plots are almost evenly distributed (see Figure 1SI–3SI in the Supporting Information).^[*]

In one of our previous reports^[11] we highlighted details on the phenomenological resemblance of short C–F...C≡N contacts to the C–F...C=O interactions described above (Figure 4). The occurrence of this interaction had previously been mentioned by Nishide et al. for an intramolecular case.^[14] In our CSD search, we found a good number (247, 404, 227, and 73 occurrences for C–F, C–Cl, C–Br, and C–I, respectively) of close C–X...C≡N contacts, a high proportion of which exhibit contact distances at or below the corresponding van der Waals distance (24–44% of the total number of occurrences; percentages increase with increasing atomic mass of the halogens, similar to the C–X...C=O case). The scatterplots show a pronounced preference of these

[*] The suffix SI here and in subsequent figures refers to those in the Supporting Information.

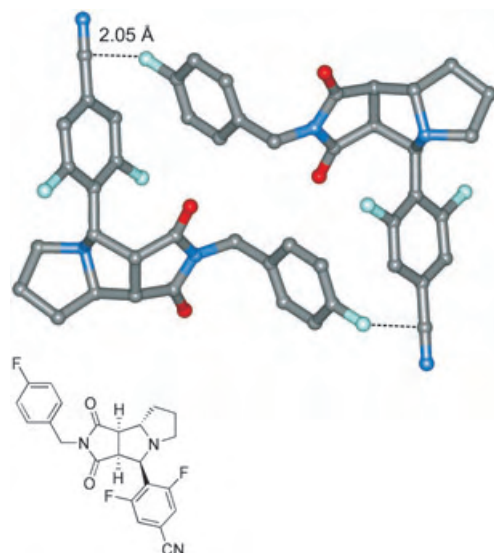


Figure 4. Short intermolecular $C_{\text{aryl}}-F \cdots C \equiv N$ contact observed in the crystal packing of a nitrile precursor to a thrombin inhibitor.^[11] Color code: C: gray; O: red; N: blue; F: cyan.

contacts to occur in an orthogonal alignment at short distances, in which the halogen atoms occupy a position close to the carbon center of the cyano group with values of α_1 converging to 90° for close contacts (Figure 30SI–33SI). Clusterings of hits in the $\tau_1-\alpha_3$ plot for bond vector angles in the range of $100^\circ \leq \alpha_3 \leq 140^\circ$ indicate that the C–F bond is often inclined towards the part of the molecule carrying the cyano group. In addition, we can identify the usual perpendicular relationship of bond vectors as well as the parallel and antiparallel alignments.

As expected, a consistent picture with these results is maintained when moving to $R-CN_2$ ($R = C, N$: amidinium/guanidinium) as the electrophilic fragment of the interaction (strictly speaking, these contacts should be referred to as ion–dipole rather than dipole–dipole interactions; Figure 34SI–37SI). Despite the smaller number of available crystal structures (Table 1) and consequently also of occurrences and hits, the data clearly show the same trends: halogen atoms prefer to be positioned orthogonally above or below the electrophilic center, close to the pseudotrigonal axis of the $R-CN_2$ unit. For this type of interaction, geometrical preferences are even more stringent with less broadening of plot shapes in the whole series of halogens, although hit numbers decrease almost below statistical significance for the $C-I \cdots R-CN_2$ case. Nevertheless, it may be stated that the perpendicular interaction motif in which both α_1 and α_3 angles display values close to 90° is statistically even more relevant for this type of contacts.

Interestingly, a somewhat different behavior is found for dipolar $C-X \cdots NO_2$ interactions (Figure 21SI–24SI). Whereas the plots generated by using data on $C-F \cdots NO_2$ contacts show the typical shapes described above for other $C-X \cdots E-Y$ interactions, contacts of the heavier halogens to the nitro group exhibit a significant number of cases in which the geometrical arrangement deviates substantially from the orthogonal positioning of the X atom close to the pseudo-

trigonal axis passing the electrophilic center. This fact is graphically illustrated by a desymmetrization of the cone in the α_1-d_1 plot, which displays an unprecedented clustering of hits for small α_1 values at longer contact distances, a rather even distribution of hits in the α_2-d_1 plot, as well as a clustering of hits for small d_2 values in the d_2-d_1 plot. Taken together, these data suggest that besides the orthogonal arrangement expected from extrapolation of the previous interaction types there exists a second geometrical preference for the halogen to be located “side-on”, close to the plane defined by the nitro group, and thereby presumably establishing close contacts to both the nitrogen and one of the oxygen atoms of the nitro group. This finding is in full agreement with studies of $C-X \cdots O(\text{nitro})$, $C-X \cdots N(C \equiv N)$ and $C-X \cdots O(C=O)$ contacts in the literature, where a certain preference of an in-plane approach of the halogen atom with $C-X-(O,N)$ arrangements tending to linearity has been observed for Cl, Br, and I (but not F).^[31–33] The directionality of this interaction has been explained by the anisotropic distribution of electron density around the halogen atom leading to a smaller radius along the C–X axis compared to the radius perpendicular to this axis (so-called “polar flattening”). In view of the remarkable capability of organic iodine, and to a lesser extent also bromine, to engage in hypervalent coordination, the in-plane approach of organic iodides (bromides) with close-contact nonbonded interactions to the terminal oxygen poles could be seen as dipolar interactions along a trajectory towards hypervalent behavior of the halogen.

Molecular units possessing large dipole moments such as the C=O and the C≡N group are represented by numerous examples in the CSD, and it is therefore informative to compare statistical data on dipolar interactions between the possible combinations of these groups. In accordance with trends observed in the literature^[8] we find the strictest correlations of geometrical parameters for contacts involving the C≡N unit, which also exhibits the larger dipole moment. The scatterplots (Figure 12SI and 29SI) indicate an exceptionally strong preference for the nitrogen end of the cyano group to be positioned close to the C atom and perpendicular to the bond vector of the interacting partner (the cone in the α_1-d_1 plots has an opening angle of less than 30° for contacts below the van der Waals contact distance). Clusters of hits deviating from orthogonality are only seen for $C=O \cdots C=O$ interactions (Figure 5SI), for which a substantial grouping of hits with angles α_1 approaching 180° indicate an aligned, almost collinear arrangement of dipoles. In addition, clusters of hits for α_2 values approaching 90° paired with small d_2 values indicate interaction geometries, in which the oxygen atom of one C=O unit is coplanar with the other (“side-on”). Note, however, that these cases contain (primary and secondary) amides, urea derivatives and, in particular lactams which can form favorable hydrogen bonds in-plane with a coplanar contacting C=O unit. Indeed, this dense in-plane cluster obtained for C=O approaching the Q–CO–Q unit ($Q = H, C, N, O$) is very narrow for the corresponding R–CO–R ($R = H, C$) case (aldehydes and ketones, Figure 6SI), for which the in-plane approach would be stabilized only by weak, but potentially still favorable short $C=O \cdots H-C$ contacts. It is remarkable that the bulk of the $C=O \cdots C=O$ cases

follows the trends outlined for all other $A-B\cdots C=O$ interactions. This is equally true for the $S=O$ unit of sulfoxides and sulfones as an interaction partner, albeit at a more limited statistical significance due to a smaller number of examples (Figure 17SI and 18SI). For $C=O\cdots R-CN_2$ contacts, the possibility of hydrogen bonding within the plane of the recipient dipolar system leads to a somewhat distorted picture, exemplified by a majority of short $O\cdots C$ contacts occurring in a geometrical arrangement, in which the O atom deviates little from coplanarity with the CN_2 unit (Figure 38SI). It is nevertheless remarkable, that a significant number of cases, particularly in the very short-contact range, adopts the orthogonal dipolar contact.

2.3. CSD Searches II: $A-B\cdots C=O$, $A-B\cdots C=N$, and $A-B\cdots RCN_2$ Interactions ($A-B = H_2O$, $R-OH$, C_2O , C_2S , C_2N (Imine), R_3N , R_3P)

In Section 2.1, we mentioned the structural similarities of dipolar contacts to nucleophile–electrophile interactions between nitrogen or oxygen nucleophiles and carbonyl groups as investigated by Bürgi and Dunitz, while at the same time highlighting the differences in nature between the two interaction types. As these authors pointed out, contact distance is the parameter of choice to distinguish between the two sorts of interactions, although the transition might be far from sharp. It is therefore interesting to extend the survey of dipolar interactions to the cases involving the typical weak nucleophiles such as water, alcohols, ethers, sulfides, and imines interacting with electrophilic centers such as in the carbonyl or the amidinium/guanidinium group, particularly because these types of interactions might play an important role in biological recognition events (e.g. between and within proteins, peptides, protein-DNA, and enzyme-inhibitor complexes). For the cases considered in our CSD search, displacements of the carbonyl-carbon atom from the plane defined by its three substituents are small and exhibit no pronounced distance dependence for middle to longer-ranged contacts; contacts significantly below van der Waals distances only show a hint of a displacement increase with decreasing d_1 for C_2O as the nucleophilic part.

Overall, the geometrical preferences of these types of (di)polar contacts included in this section are consistent with the trends observed for their previously described counterparts, although there exist interesting differences for some combinations of interacting partners. $R-OH\cdots C=O$, $C_2O\cdots C=O$, and $C_2S\cdots C=O$ interactions are generally well-behaved and exhibit the typical preference of the nucleophilic center to be located close to the pseudotrigonal axis above or below the plane defined by the $R_2C=O$ system (Figure 4SI, 9SI, 10SI, and 16SI). In the vast majority of cases, in which the O or S atom is bonded to $C(sp^3)$ centers, the two planes defined by the carbonyl system on one hand and the oxygen or sulfur atom with its two substituents on the other are oriented in a near to orthogonal fashion (here steric reasons may also play an important role). The parallel arrangement of planes is adopted preferentially for cases in which the chalcogen is part of an aromatic system, such as for furans and thiophenes; for

these cases the orthogonal alignment is scarce. Especially in the case of alcohols and sulfides, the horizontal V-shape of the τ_1 versus α_3 plot is prominent, whereas imines and H_2O show the most distinctive features. For water as a polar interaction partner, contacts at distances $d_1 \geq 3.25$ Å are dominated by a nearly coplanar arrangement of the nucleophilic oxygen atom on the C-side of the carbonyl unit, indicated by large angles α_1 ($\geq 150^\circ$), angles α_2 tending to 90° , and small distances d_2 of the O atom to the carbonyl plane (Figure 7SI and 8SI). However, these arrangements are found for the set of generalized Q-CO-Q systems, in which there are many cases of attractive $H_2O\cdots H-N$ hydrogen bonds formed in the plane. Expectedly, the dense cluster at $\alpha_2 \approx 90^\circ$ and short contact distances d_1 (Figure 7SI) disappears for the corresponding aldehyde and ketone systems ($R-CO-R$; $R = C, H$, Figure 8SI). In these cases, the H_2O molecule is seen to approach the carbonyl group within a reasonably narrow cone around the pseudo-trigonal axis of the recipient carbonyl system. The perpendicular geometrical arrangement denotes cases of exceptional importance especially for structure-based design of protein ligands, since π -exposed amide units in hydrophobic domains offer good anchor points for the introduction of polar interactions by displacement of the crystal-bound water molecule.

Illustrative examples of orthogonal $H_2O\cdots C=O$ interactions are displayed in the crystal structures of 5-azauracil monohydrate and α -L-aspartylglycine monohydrate (Figure 5a,b).^[34,35] In the former, the crystal-bound water molecules extensively engage in hydrogen bonding by donating two and accepting one hydrogen bond, yet at the same time establishing short orthogonal, polar contacts ($d_1 = 3.14$ Å, angle (O-C-O) = 98°) to adjacent 5-azauracil molecules located on both sides of the H-O-H plane. Perpendicular short $H_2O\cdots C=O$ contacts are also seen between water molecules that traverse crystals of α -L-aspartylglycine monohydrate forming channels of hydrogen-bonded chains and the amide carbonyl of the dipeptides ($d_1 = 3.05$ Å, angle (O-C-O) = 91°).

Ketones and aldehydes, on the other hand, prefer a close to perpendicular positioning of imine nitrogen atoms with respect to the plane of the $C=O$ unit for the establishment of dipolar contacts (Figure 14SI), which is equally true with some exceptions for all carbonyl systems at short distances (Figure 13SI). The majority of the latter exhibit a parallel arrangement of planes containing either the $C=O$ or both C-N bond vectors (similar to the furan and thiophene cases), probably due to the stacking of π systems in an antiparallel orientation of bond dipoles, with a small subset of “real” orthogonal examples (π systems orthogonal, $\alpha_1 \approx 90^\circ$).

In this context, it should not go unmentioned, that weak attractive $C=O\cdots SC_2$ interactions between a divalent sulfur (or selenium) as electrophilic partner and a carbonyl group have been identified in inter- and intramolecular cases for small molecules and in protein–ligand complexes. It was found that negatively polarized O atoms (and nucleophilic centers in general) prefer to approach sulfides or disulfides along the extension of the C-S (S-S) bond (σ^* direction), whereas $S\cdots O=C$ arrangements can be either perpendicular (similar to the $C_2S\cdots C=O$ interactions described above) or linear (for the case of amide carbonyls as observed in proteins

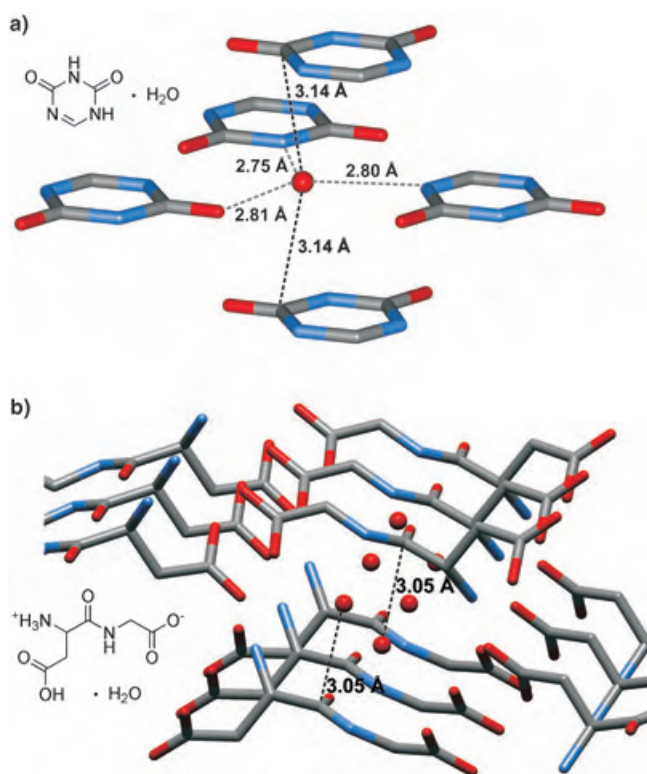


Figure 5. Crystal structures of a) 5-azauracil monohydrate^[34] and b) α -L-aspartylglycine monohydrate^[35] featuring short orthogonal intermolecular $\text{H}_2\text{O}\cdots\text{C}=\text{O}$ contacts. Color code: C: gray; O: red; N: blue.

the perpendicular arrangement was preferred significantly).^[36] These interactions have been held responsible for determining the molecular conformations of a series of angiotensin II receptor antagonists,^[37] the antitumor antibiotic leinamycin,^[38] and thiazole (selenazole) nucleosides.^[39] In proteins, these polar interactions have been statistically characterized^[40] and identified as important contributors to the mechanism of disulfide bond cleavage, which is the primary function of agonist binding to G-protein-coupled receptors.^[41]

Nitriles prefer to form contacts with ethers, sulfides, and alcohols at short distances with $\text{B}(\text{O}, \text{S})\cdots\text{C}\equiv\text{N}$ angles α_1 close to 100° ; the O or S atom is therefore displaced by about 10° toward the C–C bond (Figure 26SI–28SI). A similar inclination of the C–O(S)–C plane is manifested by a main cluster of hits for $100^\circ \leq \alpha_3 \leq 120^\circ$ with angles centroid(COC)–O–C–(C \equiv N) scattering between 130° and 160° , and the main orientation of the C \equiv N bond vector with respect to the plane of the ether unit approaching orthogonality ($\geq 60^\circ$).

A somewhat different picture is seen when exchanging the electrophilic unit for $\text{R}-\text{CN}_2$ ($\text{R} = \text{C}, \text{N}$; Figure 40SI and 41SI). Whereas the small number of contacts that are found at distances below the sum of the van der Waals radii show the typical geometrical preferences, a considerable subset of ether O atoms lie in the plane of the $\text{R}-\text{CN}_2$ group, at the same time exploring the possibility of hydrogen bonding to N–H protons. Here, the higher tendency of oxygen to undergo hydrogen-bonding interactions compared to its sulfur counterpart becomes evident, as the mentioned subset of cases is

absent for sulfides. A further piece of evidence for this assumption can be drawn from the $\text{H}_2\text{O}\cdots\text{R}-\text{CN}_2$ case, in which the majority of contacts occur in a coplanar arrangement of heavy atoms, confirming that water is a better hydrogen-bond acceptor than an ether (Figure 39SI).

2.4. CSD Searches III: $\text{C}-\text{X}\cdots\text{C}-\text{X}$ and $-\text{X}\cdots\text{X}-$ Interactions

Nonbonded interactions between $\text{C}(\text{sp}^2)\text{-F}$ groups have been surveyed recently using structural data retrieved from the CSD.^[8] Analysis of packing modes revealed that the preferred arrangement of these dipolar units exhibits a coplanar, yet shifted antiparallel orientation of C–F dipoles with an optimal value for angles α_1 of about 70° . This result could be rationalized based on a model combining dipole–dipole interaction contributions and steric effects. It was emphasized, that in contrast to the case of cyano groups, which possess a larger dipole moment, the requirements of a dense crystal packing might overrule some of the biases imposed by dipole–dipole interaction forces for weaker dipoles.

In agreement with these results, our α_1 – d_1 scatterplot for $\text{C}(\text{sp}^2)\text{-F}\cdots\text{C}(\text{sp}^2)\text{-F}$ interactions shows values of the (F–C–F) angle converging to about 70 – 80° for short $\text{F}\cdots\text{C}$ contact distances and a considerable number of search hits clustering for values of α_3 in the range of $160^\circ \leq \alpha_3 \leq 180^\circ$ (Figure 43SI). Nevertheless, at short contact distances a significant proportion of examples exhibit either an orthogonal orientation of bond vectors ($\alpha_3 \approx 90^\circ$) or cluster around geometries in which one of the C–F vectors is somewhat inclined to either the carbon or the fluorine end of the interacting bond ($\alpha_3 \approx 70^\circ$ or $\alpha_3 \approx 120^\circ$). Changing the hybridization of the fluorine-carrying carbon atom to $\text{C}(\text{sp}^3)$, which interacts as the A–B unit, does not alter the plot shapes considerably, although the (F–C–F) contact angle α_1 appears to re-increase by about 10° at short distances. However, moving to an E–Y unit bearing a sp^3 -hybridized carbon center notably increases the probability of randomly selected examples to show the “nucleophilic” fluorine atom approaching this center from the back side of the C \rightarrow F bond vector (Figures 44SI–46SI).

In addition to the notion of the whole C–X bond interacting as a dipole, in which the C-end represents the positively and the X-end the negatively polarized center of the pole, interactions between C–X units have also been regarded in terms of $-\text{X}\cdots\text{X}-$ interactions, that is, the halogen atoms constituting both, the δ^- and the δ^+ of the polar contact. The nature and importance of these interactions have been a matter of debate.^[42,43] Particularly the nature of $-\text{Cl}\cdots\text{Cl}-$ interactions has repeatedly been addressed and despite the unclear picture of whether these type of contacts are the reason or the resulting effect of an anisotropy of van der Waals radii along and perpendicular to the C–X bond axis, there seems to exist agreement upon the fact that $-\text{X}\cdots\text{X}-$ contacts are evoked by weak, attractive forces. Nevertheless, the large number of these contacts in highly halogenated aliphatic and aromatic hydrocarbons gives rise to a “steering effect” that determines crystal packing^[44,45] and may determine mutual orientations of molecules in the crystal

state even in cases where only few (or a single) halogen atoms are present in the molecule. This viewpoint has been supported by the observation that there exists a Cl_2 dimer^[46] in the gas phase and that interhalogen contacts provide good explanations of geometrical arrangements observed in crystal structures of different halogenated compounds. Subsequently, CSD analyses of symmetrical and unsymmetrical $\text{X}\cdots\text{X}$ interactions (i.e. the interacting halogen atoms are of the same or of different kind, respectively) have been used to statistically underpin this position.^[42c]

It is without doubt that $\text{C-X}\cdots\text{X-C}$ interactions mainly adopt two types of preferred geometrical arrangements, which could be characterized as essentially linear and orthogonal, that is, with angles ($\text{C-X}\cdots\text{X}$) clustering at 165° and 100° , respectively.^[47] Desiraju and co-workers found that the perpendicular geometry becomes more prevalent with increasing polarizability of the X atom and that for unsymmetrical $\text{X}\cdots\text{X}$ contacts there exists a preference of the heavier halogen atom to constitute the recipient ("hypervalent") pole of the interaction (the angle $\text{C-X}_{\text{heavy}}\cdots\text{X}_{\text{light}}$ approaches 180° and the angle $\text{C-X}_{\text{light}}\cdots\text{X}_{\text{heavy}}$ 90°).^[42c] This is particularly true for $\text{I}\cdots\text{F}$ interactions and becomes less significant for combinations of lighter halogen atoms, for which anisotropy and close packing affects might be of importance in addition to the polar interaction.

Among others, two interesting structural patterns have been highlighted as important driving forces for the assembly of a particular crystal packing motif. On the one hand, the array of simultaneous halogen \cdots halogen and hydrogen \cdots halogen interactions formed by aromatic compounds carrying a halogen substituent *ortho* to an unsubstituted position, has been shown to build up molecular chains, ladders, and two-dimensional sheets in the crystal state.^[48] On the other hand, a triangular interaction motif, in which three halogen atoms are located in short contact distance with respect to each other forming an equilateral triangle has been repeatedly reported as a useful synthon for the engineering of crystals or the assembly of host-guest complexes.^[49]

3. Multipolar Protein-Ligand and Protein-Protein Interactions

When compared to small molecules, much less is known about the role dipolar interactions play in biological assemblies, that is, in stabilizing the secondary structure of proteins or protein-ligand complexes or even about their possible functions in enzymatic mechanisms. The importance of $\text{C=O}\cdots\text{C=O}$ interactions in influencing the conformation of α -helices and antiparallel β -sheets was shown for the first time by MacCallum et al., who demonstrated that in proteins, attractive dipolar electrostatic interactions between backbone carbonyl groups of adjacent amino acid residues distort $\text{C=O}\cdots\text{H-N}$ hydrogen bonds from linearity and give rise to a preference in favor of the right-twisted β -strand conformation compared to its left-twisted counterpart.^[50] The authors estimated the strength of this dipolar interaction at about 80 % of that of a hydrogen bond and consequently developed a new method for examining interactions between hydrogen-

bonded groups in proteins integrating this new type of dipolar interaction. Carbonyl-carbonyl interactions have also been held responsible for the stabilization of conformations of asparagine and aspartic acid residues in the left-handed α -helical region and other partially allowed regions of the Ramachandran plot.^[51] These amino acid residues were found to statistically exhibit a far greater number of $\text{C=O}\cdots\text{C=O}$ interactions between their side-chain carbonyl groups and backbone C=O units than glutamine and glutamic acid residues, which elegantly explains the preference of the former to more readily adopt partially allowed conformations when compared to all other non-glycine counterparts. Despite this evident importance for protein secondary structure, the occurrence of $\text{C=O}\cdots\text{C=O}$ interactions has only recently been statistically surveyed by searching the PDB for protein-ligand interaction patterns and internal contacts in proteins.^[52] It was found that ligand-protein complexes containing a ketone moiety adopt antiparallel and orthogonal arrangements, whereas no example of the (sheared) parallel motif could be observed. The authors concluded, that contributions from this type of dipolar interaction are relevant for the structure-based design and optimization of ligands to proteins.

During a recent study of fluorinated thrombin inhibitors, we added the $\text{C-F}\cdots\text{C=O}$ interaction to the list of attractive dipolar contacts observed in protein-ligand complexes (Figure 1).^[9] Using a rigid tricyclic scaffold with a well-defined binding geometry, a single-point mutation, namely the exchange of hydrogen for fluorine, led to an increase in inhibitor potency by a factor of 5, paralleled by an increase in selectivity. This effect could be partly attributed to the establishment of an orthogonal, dipolar interaction between the newly introduced C-F bond and a backbone amide carbonyl group. These results show that the well-placed introduction of dipolar interactions into a protein-ligand binding event may substantially contribute to the optimization of both activity and selectivity of small molecule inhibitors. A search of the PDB has now furnished a considerable number of short, highly directional contacts including a variety of intrinsically dipolar units, thereby convincingly proving the generality of this type of nonbonded interactions (Table 2 and Table 1SI).

The results of this search suggest that the backbone or side chain carbonyl groups of proteins provide a "halogenophilic" environment, since short $\text{C-X}\cdots\text{C=O}$ contacts are over-represented in relation to all contacts retrieved within the respective search range of an interaction, compared to other pairs of dipoles. Consistent with the results of the CSD search, further types of prevalent dipoles interacting with protein C=O groups include C=O , $\text{C}\equiv\text{N}$, NO_2 , S=O , and weak nucleophiles such as ethers, sulfides, alcohols, imines, and water.

Interestingly, for many types of these dipolar interactions a statistically significant number of cases, particularly at short contact distances, exhibit near to orthogonal arrangements with angles $(\text{A-B}\cdots\text{E}) \geq 140^\circ$ and $70^\circ \leq \text{angle}(\text{B}\cdots\text{E-Y}) \leq 110^\circ$. In fact, a reduction of the upper limit for the contact distance d_i in the PDB search can be used as a constraint to select for these geometrical arrangements, as illustrated for the case of $\text{C-X}\cdots\text{C=O}$ interactions (Figure 6). In the following, we shall examine some illustrative cases more closely (a

Table 2: Overview of dipolar interactions of small molecule ligands bound to proteins as retrieved from the PDB.^[a]

A–B	E–Y	d_{vdW} [Å]	Search range [Å]	Number of structures	Number of occurrences	Number of occurrences within d_{vdW}
C–F	C=O	3.30	2.30–3.80	498	177 (152)	66 (43)
C–Cl	C=O	3.65	2.65–4.15	591	174 (163)	56 (46)
C–Br	C=O	3.80	2.80–4.30	220	68 (63)	22 (20)
C–I	C=O	4.00	3.00–4.50	160	61 (52)	42 (37)
C ₂ C=O (L)	C=O (P)	3.25	2.25–3.75	1454	251 (182)	42 (35)
R ₂ C=O (L)	C=O (P)	3.25	2.25–3.75	30 104	8616	1442
CN	C=O	3.35	2.35–3.85	74	24 (21)	5 (4)
NO ₂	C=O	3.25	2.25–3.75	273	71 (65)	16 (14)
R ₂ NO	C=O	3.25	2.25–3.75	344	48 (16)	13 (2)
C ₂ S=O (with DMSO)	C=O	3.25	2.25–3.75	1579	538 (502)	102 (93)
C ₂ S=O (without DMSO)	C=O	3.25	2.25–3.75	63	20 (19)	2 (2)
R ₃ N	C=O	3.35	2.35–3.85	1479	135 (26)	42 (0)
H ₂ O	C=O	3.25	2.25–3.75	496	202 (109)	78 (32)
C ₂ O	C=O	3.25	2.25–3.75	15 520	3385 (3142)	1408 (1363)
C ₂ S (L)	C=O (P)	3.7	2.70–4.20	4241	858 (670)	162 (110)
C–C–OH	C=O	3.25	2.25–3.75	38 943	14 084	3119
R ₂ C–S–CR	C=O	3.7	2.70–4.20	466	44 (31)	14 (7)
C ₂ N	C=O	3.35	2.35–3.85	13 648	1729 (1484)	147 (116)
C ₂ C=O	R–CN ₂	3.25	2.25–3.75	1454	54	10
C–F	R–CN ₂	3.30	2.30–3.80	498	27	16
C–Cl	R–CN ₂	3.65	2.65–4.15	591	10	3
C–Br	R–CN ₂	3.80	2.80–4.30	220	3	2
C–I	R–CN ₂	4.00	3.00–4.50	160	11	0
H ₂ O	R–CN ₂	4.00	3.00–4.50	496	22	0
C=O (P)	C ₂ C=O (L)	3.25	2.25–3.75	1454	80 (63)	17 (14)
C=O (P)	R ₂ C=O (L)	3.25	2.25–3.75	30 104	7435 (6379)	1282 (1062)
C ₂ S (P)	R ₂ C=O	4.00	3.00–4.50	30 104	574	156
C=O (P)	R–CN ₂ (L)	3.25	2.25–3.75	4442	790 (599)	–
C ₂ S (P)	R–CN ₂ (L)	4.00	3.00–4.50	4442	14	3
C=O (P)	CN	3.25	2.25–3.75	74	21 (17)	5 (3)
C–OH (P)	CN	4.00	3.00–4.50	74	20	7
C ₂ S (P)	CN	4.00	3.00–4.50	74	1	0

[a] The table contains the structures of interacting nucleophilic (A–B) and electrophilic (E–Y) polar units, van der Waals contact distances d_{vdW} [Å], search ranges [Å], total number of structures and occurrences, and number of occurrences within the van der Waals distance. R denotes any atom except H, C₂N denotes an imine nitrogen (may be part of an aromatic heterocycle), (P) and (L) classify the polar unit as being part of a protein or a ligand, respectively. Hit numbers of searches limited to amide carbonyl units are given in parentheses.

greater number of examples is included in the Supporting Information; Figure 47SI–64SI).

A representative example of a very short orthogonal C–F⋯C=O interaction can be found in the complex of the potent serine protease inhibitor ZK-807834 bound to the active site of its biological target, factor Xa (Figure 7a, PDB-code: 1FJS).^[53] In this complex, one fluorine atom of the central pyridine core establishes a close contact ($d(\text{F}⋯\text{C}) = 2.90$ Å, angle (F–C–O) = 91°, angle (C–F–C) = 153°) to the side chain amide carbonyl unit of Gln 192, at the same time entering into a second intramolecular close contact with almost ideal sheared parallel geometry ($d(\text{F}⋯\text{C}) = 3.0$ Å, angle (F–C–O) = 88°, angle (C–F–C) = 90°) with a nearby carboxyl unit present in the inhibitor. It therefore comes as no surprise, that for CF₃ groups having the theoretical possibility of establishing at least three C–F⋯C=O contacts, examples can be found, where a CF₃ group indeed engages in three or more close contacts to surrounding π -exposed peptide carbonyl units.^[54] One such example is displayed in the crystal structure of a trifluoroacetyl dipeptide anilide inhibitor complexed with its biological receptor elastase (Figure 7b, PDB-code: 2EST).^[54a]

Structural analysis of the complex reveals two C–F⋯C=O contacts below van der Waals distance between the CF₃ group and the backbone carbonyls of Ser214 and Phe215 ($d(\text{F}^1⋯\text{C}) = 2.97$ Å, $d(\text{F}^2⋯\text{C}) = 3.11$ Å) and a third, somewhat longer-ranged contact to the amide C=O unit of Cys191 ($d(\text{F}^3⋯\text{C}) = 3.51$ Å). In addition, one of the fluorine atoms (F¹) establishes a second contact to the backbone C=O unit of Thr213 ($d(\text{F}^1⋯\text{C}) = 3.66$ Å). In all cases, the F atom is located in close proximity to the pseudotrigonal axis of the carbonyl systems (angles (F–C–O) with values of 74°, 103°, 59°, and 87° respectively). Further examples of ligands bearing CF₃ groups that establish all three possible C–F⋯C=O contacts are seen in the case of another trifluoroacetyl dipeptide elastase inhibitor and in the complex of flufenamic acid bound to human transthyretin (prealbumin) (PDB-codes: 1ELE and 1BM7).^[54b,c]

An exceptionally short, orthogonal C–Cl⋯C=O contact may also contribute to the binding affinity of the antimalarial drug quinacrine to its target, the enzyme histamine *N*-methyltransferase.^[55] In the enzyme–ligand complex, the C–Cl bond points in a perpendicular orientation to the C atom of

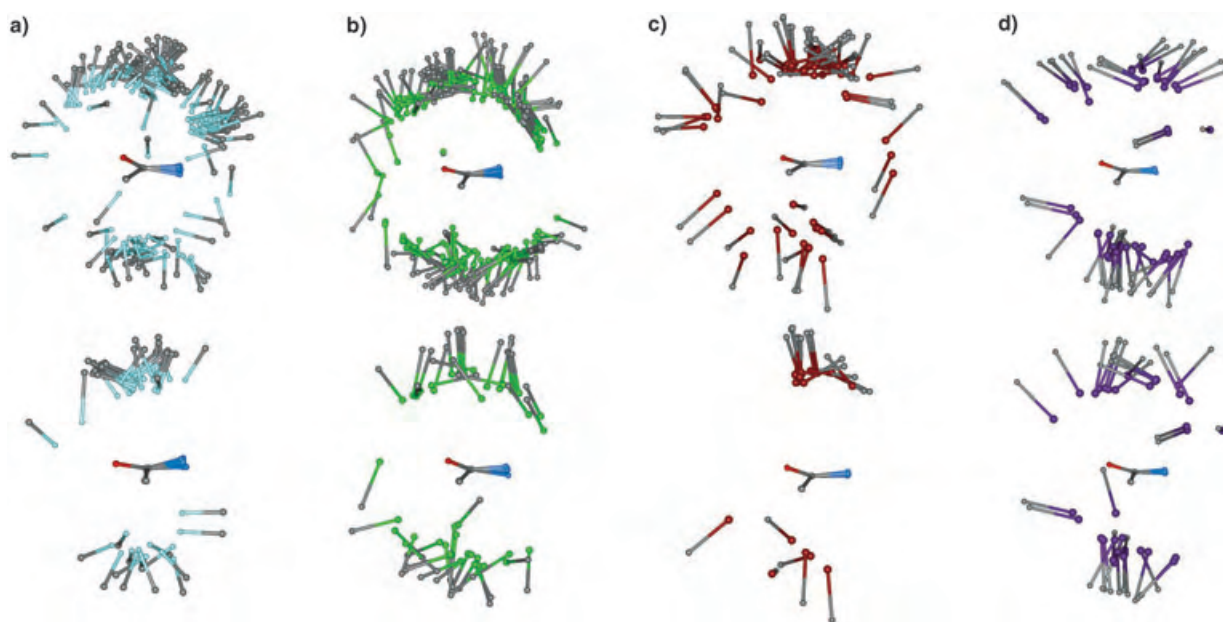


Figure 6. Superposition of carbonyl units extracted from sections of crystal structures with intermolecular $\text{C}\cdots\text{X}\cdots\text{C}=\text{O}$ (amide) contacts as retrieved from PDB-searches (see Table 2, numbers of occurrences in parentheses) for $\text{X}=\text{F}$ (a), Cl (b), Br (c), and I (d) (carbonyl function pointing backwards to the left). For the upper series of four $\text{C}\cdots\text{X}\cdots\text{C}=\text{O}$ superpositions the $\text{X}\cdots\text{C}$ contact distance d_1 ranges between $2.30\text{ \AA} < d_1 < 3.80\text{ \AA}$ (a), $2.65\text{ \AA} < d_1 < 4.15\text{ \AA}$ (b), $2.80\text{ \AA} < d_1 < 4.30\text{ \AA}$ (c), $3.00\text{ \AA} < d_1 < 4.50\text{ \AA}$ (d); the lower series of four plots displays superimposed cases for which the d_1 -cut-off equals the respective $\text{X}\cdots\text{C}$ van der Waals distance (i.e. $2.30\text{ \AA} < d_1 < 3.30\text{ \AA}$ (a), $2.65\text{ \AA} < d_1 < 3.65\text{ \AA}$ (b), $2.80\text{ \AA} < d_1 < 3.80\text{ \AA}$ (c), $3.00\text{ \AA} < d_1 < 4.00\text{ \AA}$ (d)). Color code: C: gray; O: red; N: blue; F: cyan; Cl: green; Br: brown; I: purple.

the side chain carboxyl group of Asp193 ($d(\text{Cl}\cdots\text{C}) = 3.21\text{ \AA}$, angle ($\text{Cl}-\text{C}-\text{O}$) = 84° , angle ($\text{C}-\text{Cl}-\text{C}$) = 164° ; Figure 8, PDB-code: 1JQE). Not unexpectedly, further $\text{C}\cdots\text{X}\cdots\text{C}=\text{O}$ contacts are also found in enzyme-inhibitor assemblies of fungicides, since halogenated compounds constitute the active ingredient of many crop-protecting agents. Very illustrative examples are the complexes formed by scytalone dehydratase, an enzyme involved in the fungal melanin production, and two of its inhibitors, bearing either a 4-Cl-phenyl or a 4-Br-phenyl residue (PDB-codes: 7STD and 4STD, Figures 48SI, 49SI).^[56] In the crystal structures, both the Cl and the Br atoms are in close contact to the same backbone $\text{C}=\text{O}$ group of Gly165, adopting an approximately orthogonal arrangement ($d(\text{Cl}\cdots\text{C}) = 3.35\text{ \AA}$, angle ($\text{Cl}-\text{C}-\text{O}$) = 78° , angle ($\text{C}-\text{Cl}-\text{C}$) = 154° and $d(\text{Br}\cdots\text{C}) = 3.71\text{ \AA}$, angle ($\text{Br}-\text{C}-\text{O}$) = 78° , angle ($\text{C}-\text{Br}-\text{C}$) = 161°).

There is a striking similarity between the scatterplots for $\text{C}\cdots\text{F}\cdots\text{C}=\text{O}$ (Figure 3) and those of $\text{R}-\text{OH}\cdots\text{C}=\text{O}$ (Figure 4SI). Note that for the latter the search in the CSD was done with the constraint that the OH group is intramolecularly hydrogen-bonded to a nearby lone-pair-donating oxygen or nitrogen center (Q; distance ($\text{Q}\cdots\text{O}$) $< 2.9\text{ \AA}$; angle ($\text{Q}\cdots\text{H}-\text{O}$) between 90° – 180°). This is important, since a neighboring OH and $\text{C}=\text{O}$ unit immediately provokes us to think in terms of hydrogen-bonding contacts. However, if the hydrogen-bond donating capability of an OH group is taken care of by its local environment, the OH group may act in the same dipolar fashion as, for example, a covalent F atom. The analogy between aliphatic $\text{C}-\text{F}$ and $\text{C}-\text{O}$ units has been discussed by DiMaggio and co-workers.^[57]

Such $\text{R}-\text{OH}\cdots\text{C}=\text{O}$ interactions are beautifully borne out by the well-known cases of peptide inhibitor complexes with serine proteases, in which the serine residue of the catalytic triad is intramolecularly hydrogen-bonded “back” to the nearby histidine side chain, thus disposing the polar OH group towards the π -exposed carbonyl unit of the amide group of a bound peptide inhibitor, almost exactly along the pseudo-trigonal axis of the peptide-carbonyl group. Not reported to date, to our knowledge, are the cases represented by aspartyl proteases and their complexes with statins or α,α -difluoro-ketone hydrates, as exemplified by the X-ray structure of the penicillopepsin-inhibitor complex (Figure 9a, PDB-code: 1APV).^[58] In this complex, each of the two OH groups of the tetrahedral ketone hydrate is tightly hydrogen-bonded to one of the aspartyl groups (Asp33 and Asp213) of the catalytic center. Remarkably, each of the OH groups may then interact in a dipolar fashion with an adjacent π -exposed peptide $\text{C}=\text{O}$ unit of the flanking Gly215–Thr216 and Gly35–Ser36 loops, albeit at somewhat large distances ($d_1 = 3.63$ and 3.64 \AA , respectively; angles ($\text{O}-\text{C}-\text{O}$) = 84° and 82°). However, it should be pointed out, that these two active-site-flanking peptide units are highly conserved and characteristic for aspartyl proteases. It remains to be seen to what extent dipolar interactions of the OH groups in the tetrahedral intermediate during the peptide substrate hydrolysis may be a key element in the catalytic mechanism of this family of enzymes. A remarkable inhibitor complex with a HIV aspartyl protease was reported by Silva et al. (Figure 9b, PDB-code: 1DIF).^[59] In this case, the peptidic α,α -difluoro-ketone hydrate inhibitor is bound in a strikingly different

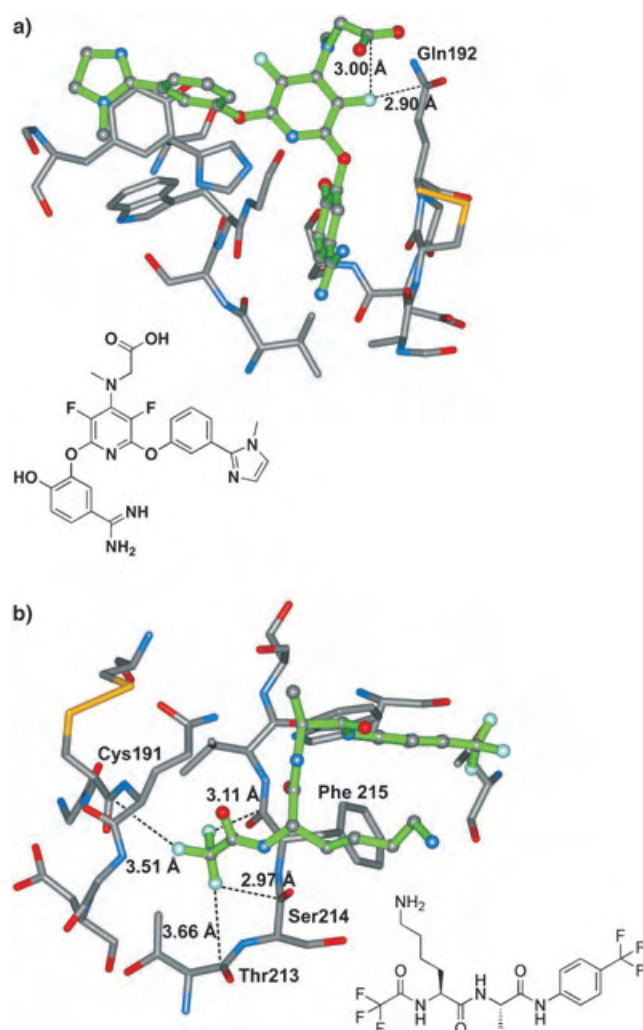


Figure 7. a) X-ray crystal structure (PDB code: 1FJS) showing a short, orthogonal C-F...C=O contact between the serine protease inhibitor ZK-80784 and factor Xa as well as another intramolecular C-F...C=O close contact of the inhibitor with sheared parallel geometry.^[53] b) The CF₃ group of a trifluoroacetyl dipeptide anilide inhibitor establishes three close C-F...C=O contacts to elastase, as shown in the X-ray crystal structure (PDB code: 2EST) of the complex.^[54a] Color code: inhibitor skeletons: green; C: gray; O: red; N: blue; S: yellow; F: cyan.

conformation extending its ketone hydrate moiety essentially to one aspartyl group (Asp25B) forming two chelating hydrogen bonds. One (“inner”) OH group then interacts in an orthogonal dipolar fashion and at a very short O...C=O distance of 3.1 Å with the flanking peptide C=O unit of Gly27B–Ala28B (angle (O–C–O) = 91°). The other (“outer”) OH group forms an ideal intramolecular dipolar interaction with a flanking peptide-carbonyl unit of the inhibitor again with a very short contact distance (d_1 = 3.0 Å, angle (O–C–O) = 96°). The binding conformation of this inhibitor disposes the two F atoms likewise into an “inner” and “outer” position. Most remarkably, both F atoms engage in close dipolar interactions with π -exposed peptide-carbonyl units: the “inner” F atom points towards the C=O carbon atom of the flanking peptide unit of Gly27A–Ala28A (d_1 = 3.1 Å, angle (F–C–O) = 93°), whereas the “outer” F atom is engaged in a

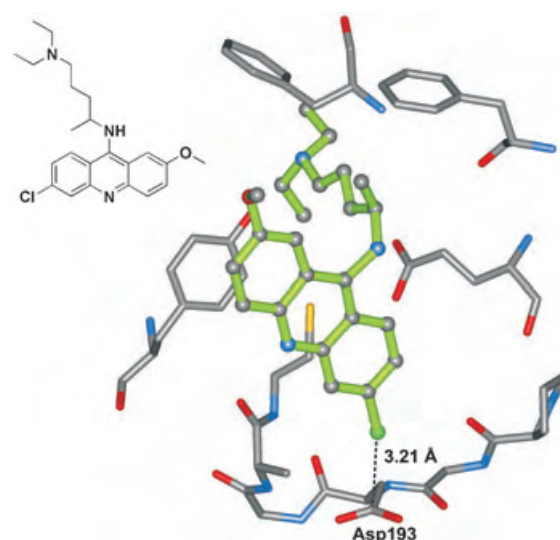


Figure 8. Section of the X-ray crystal structure (PDB code: 1JQE) of the histamine *N*-methyltransferase–quinacrine enzyme–inhibitor complex, which displays an exceptionally short, intermolecular orthogonal C–Cl...C=O contact.^[55] Color code: inhibitor skeleton: green; C: gray; O: red; N: blue; S: yellow; Cl: dark green.

tight intramolecular dipolar interaction to a nearby inhibitor peptide unit (d_1 = 3.0 Å, angle (F–C–O) = 95°). It is most instructive to witness in one single protein–inhibitor complex the completely analogous dipolar interaction patterns of two OH groups and two F atoms with nearby π -exposed peptide-carbonyl units, which underscores our findings from the scatterplots obtained from small-molecule X-ray structures.

For the establishment of orthogonal C=O...C=O contacts between proteins and small molecule ligands, two different pairings can be envisioned, in which the ligand carbonyl group interacts either at the negatively polarized O-center (C=O_{ligand}...C=O_{protein}) or at the positively polarized C-center (C=O_{protein}...C=O_{ligand}). As expected, examples of both combinations can be found in the PDB. X-ray crystal structure analysis shows that balanol analogues, which are inhibitors of the cyclic 3',5'-adenosine monophosphate dependent kinase (PKA), establish short orthogonal contacts of the ester carbonyl group to the protein backbone C=O functionality of Gly50. Figure 10a illustrates this interaction for the complex of one of the inhibitors (named BD1 by the authors) with PKA ($d(\text{O}...C)$ = 3.05 Å, angle (O_{ligand}–C–O) = 88°, angle (C_{ligand}–O_{ligand}–C) = 170°, PDB-code: 1REJ).^[60] A second corresponding combination of interacting C=O units is found when examining the X-ray crystal structure of ketobis(5-amidino-2-benzimidazolyl)methane bound to the serine protease trypsin (Figure 10b, PDB-code: 1XUI).^[61] In this complex, the side chain carbonyl group of Gln192 is ideally positioned to interact with the inhibitor keto group forming a short dipolar orthogonal contact ($d(\text{O}...C)$ = 3.00 Å, angle (O_{protein}–C–O) = 87°, angle (C_{protein}–O_{protein}–C) = 166°).

An example of an orthogonal NO₂...C=O interaction is manifested in the enzyme–inhibitor complex of the potent ATP-competitive inhibitor Alsterpaullone bound to the serine/threonine glycogen synthase kinase GSK-3 β (Figure 11, PDB-code: 1Q3W).^[62] In the crystal structure,

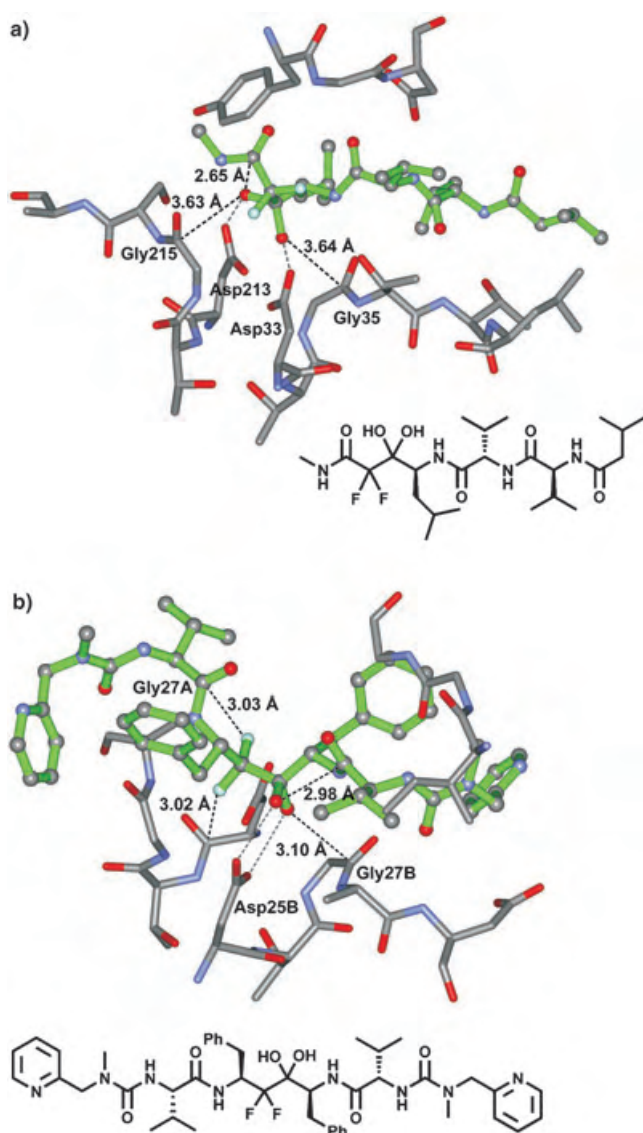


Figure 9. Examples of short inter- and intramolecular polar C=O...C=O contacts observed in the X-ray crystal structures of peptidic α,α -difluoroketone hydrate inhibitors complexed to penicillopepsin (a, PDB-code: 1APV)^[58] and HIV aspartyl protease (b, PDB-code: 1DIF).^[59] Note the additional intramolecular HO...C=O interaction in the penicillopepsin-bound inhibitor complementing the intermolecular ones mentioned in the text. Color code: inhibitor skeletons: green; C: gray; O: red; N: blue; F: cyan.

the plane of the inhibitor nitro group is positioned perpendicular to the plane of the carboxylate functionality of Asp200 thus allowing one of the NO₂ O atoms to interact with the carbonyl C atom of the amino acid side chain carboxylate ($d(\text{O}\cdots\text{C}) = 3.10$ Å, angle (O-C-O) = 87° and 103°, angle (N-O-C) = 148°). This arrangement is further stabilized by a hydrogen bond between Lys85 and an O atom of the nitro group ($d(\text{O}\cdots\text{N}) = 2.77$ Å).

Short C₂O...C=O and C₂S...C=O contacts between ligand ether and sulfide groups and protein carbonyls are displayed in the extraordinary five-bladed β -propeller structure of the enzyme tachylectin-2, which contains N-acetylglucosamine (GlcNAc) bound to the carbohydrate recognition sites, and in

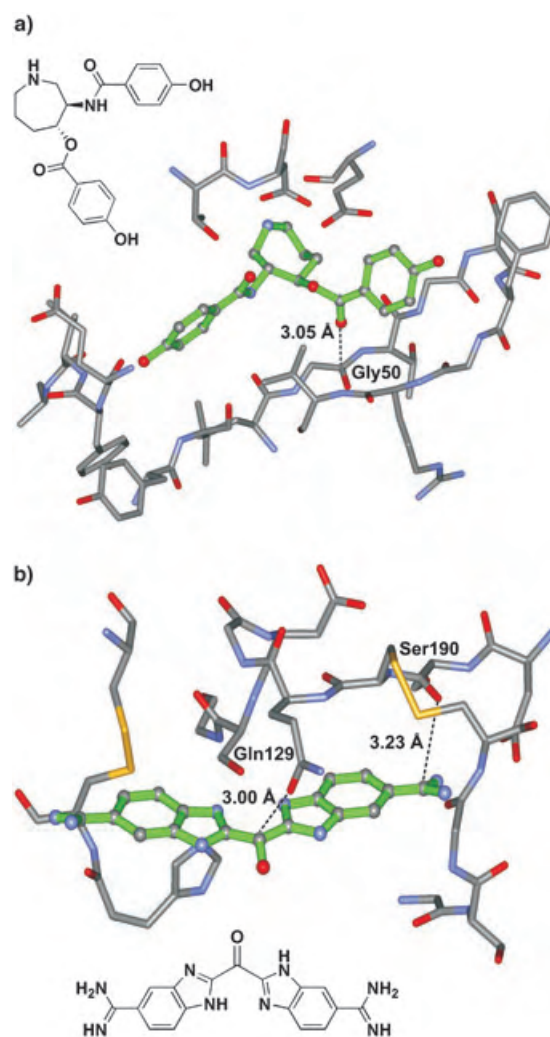


Figure 10. a) Short intermolecular, orthogonal C=O(ligand)...C=O(protein) contact observed in the X-ray crystal structure (PDB code: 1REI) of a balanol analogue inhibitor complexed with PKA.^[60] b) Ketobis(5-amidino-2-benzimidazolyl)methane establishes a short, orthogonal C=O(protein)...C=O(ligand) contact when binding to the serine protease trypsin, as observed in the X-ray crystal structure (PDB-code: 1XUI) of the complex.^[61] Color code: inhibitor skeletons: green; C: gray; O: red; N: blue; S: yellow.

the complex of acetolactate synthase with 2-hydroxyethylthiohydrothiacromediphosphate (Figure 12, PDB-codes: 1TL2 and 1OZH).^[63,64] In the former structure, the ether O atom of the sugar is positioned in an almost perfect perpendicular position above the C atom of the side chain amide functionality of Asn215 ($d(\text{O}\cdots\text{C}) = 3.21$ Å, angle (O-C-O) = 90°, angle (O-O-N) = 94°). A similar arrangement is observed for the positioning of the inhibitor S atom above the C=O unit of the backbone amide bond of Met394 in the acetolactate synthase complex ($d(\text{S}\cdots\text{C}) = 3.90$ Å, angle (S-C-O) = 67°).

Crystal-bound water molecules often play an important role in protein–ligand molecular recognition by effectively modifying the shape of the binding site or by bridging interactions between small molecules and proteins (e. g. water-mediated hydrogen bonding).^[65] Therefore, displacing or using tightly bound water molecules can be of considerable

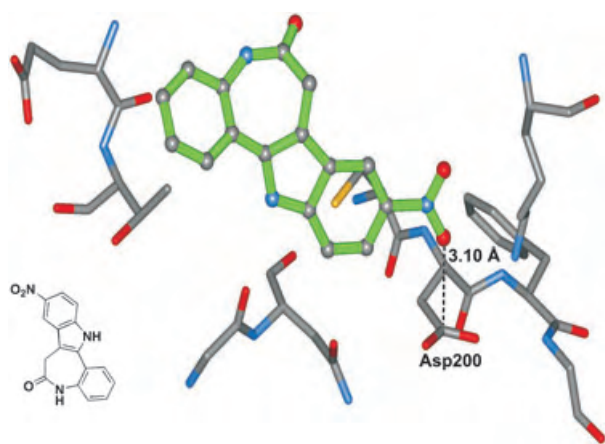


Figure 11. Example of an orthogonal $\text{NO}_2 \cdots \text{C}=\text{O}$ interaction manifested in the crystal structure (PDB-code: 1Q3W) of Alsterpaullone bound to the serine/threonine glycogen synthase kinase GSK-3 β .^[62] Color code: inhibitor skeleton: green; C: gray; O: red; N: blue.

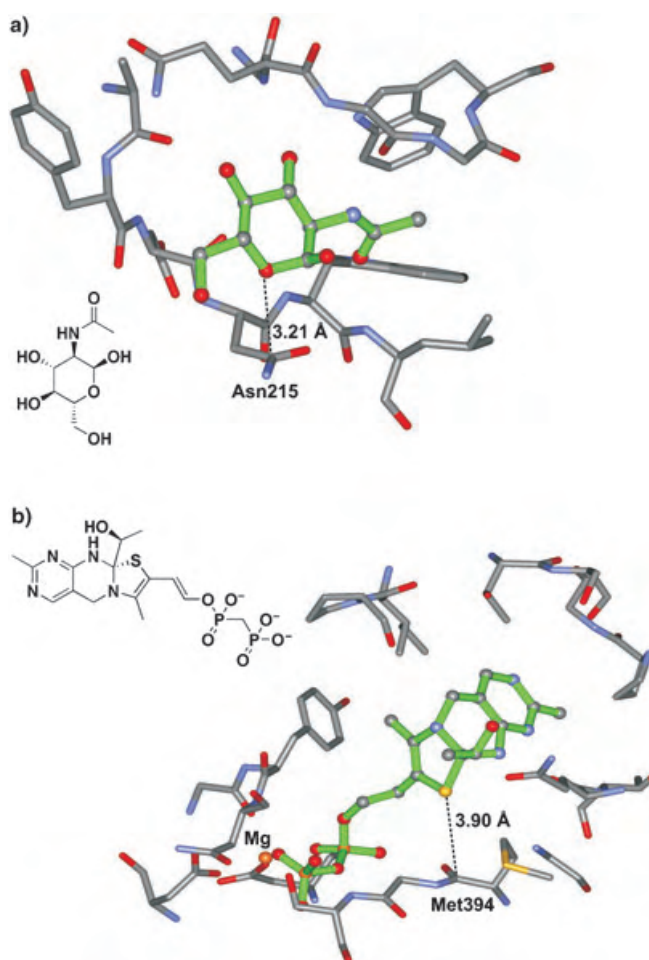


Figure 12. Short $\text{C}_2\text{O} \cdots \text{C}=\text{O}$ and $\text{C}_2\text{S} \cdots \text{C}=\text{O}$ contacts displayed in the crystal structures of tachylectin-2 containing *N*-acetylglucosamine (GlcNAc) bound to the carbohydrate recognition sites (PDB-code: 1TL2)^[63] (a) and the complex of acetolactate synthase binding 2-hydroxyethyl-dihydrothiacrome-diphosphate (PDB-code: 1OZH)^[64] (b). Color code: inhibitor skeleton: green; C: gray; O: red; N: blue; S: yellow; Mg: orange.

advantage in the structure-based design of protein ligands. The success of this strategy strongly depends on the accurate estimation of the free energy of binding and consequently of the strength of the individual noncovalent interactions between H_2O molecule and protein.^[66] Thus, polar $\text{H}_2\text{O} \cdots \text{C}=\text{O}$ interactions may be important contributors to this estimate.

Illustrative examples of $\text{H}_2\text{O} \cdots \text{C}=\text{O}$ contacts are displayed in the X-ray crystal structures of monomeric hemoglobin from the common marine bloodworm *Glycera dibranchiata* and of a formyltransferase from *Archaeoglobus fulgidus* (Figure 13, PDB-codes: 2HBG and 1M5H).^[67,68] In the hemoglobin structure (Figure 13a), the protein backbone wraps around H_2O 97 engaging its two protons in the formation of hydrogen bonds to the amide carbonyl O atoms of Tyr93 and Lys96. Concurrently, the two lone pairs of H_2O 97 establish short polar $\text{H}_2\text{O} \cdots \text{C}=\text{O}$ contacts to the amide $\text{C}=\text{O}$ units of Gly94 ($d(\text{O} \cdots \text{C}) = 2.41 \text{ \AA}$, angle ($\text{O}-\text{C}-\text{O}) = 95^\circ$) and Asn95 ($d(\text{O} \cdots \text{C}) = 3.06 \text{ \AA}$, angle ($\text{O}-\text{C}-\text{O}) = 134^\circ$). In the latter structure, H_2O 936 is encapsulated by the side chains of Asn294 and Glu295 turning back on the amide backbone and thus displays four short contacts to surrounding $\text{C}=\text{O}$ units. A very short, orthogonal contact is established to the side chain

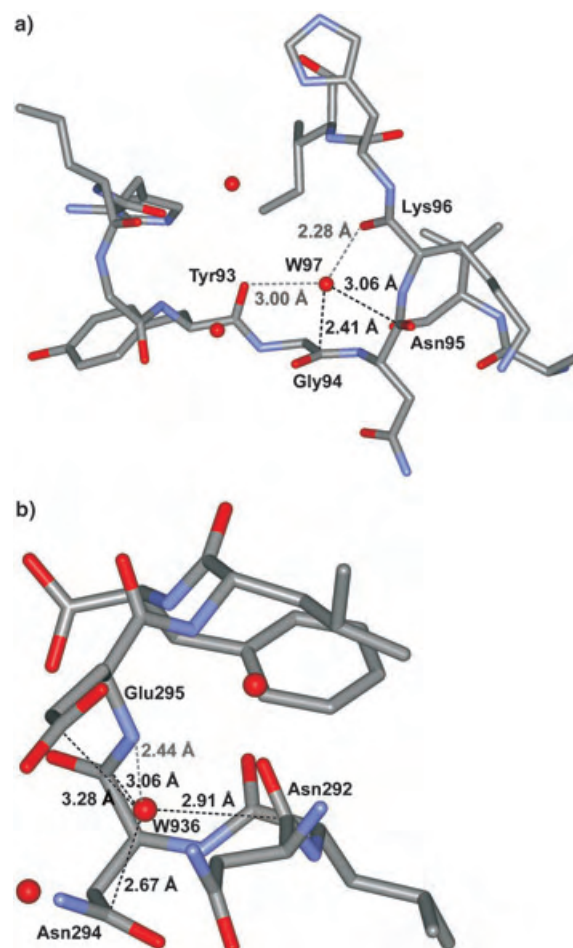


Figure 13. Examples of short orthogonal intermolecular $\text{H}_2\text{O} \cdots \text{C}=\text{O}$ contacts observed in the X-ray crystal structures of monomeric hemoglobin (PDB-code: 2HBG)^[67] (a) and a formyltransferase (PDB-code: 1M5H)^[68] (b). Color code: C: gray; O: red; N: blue.

carbonyl group of Asn294 ($d(\text{O}\cdots\text{C})=2.67\text{ \AA}$, angle ($\text{O}-\text{C}-\text{O})=89^\circ$); further polar interactions include contacts to the backbone $\text{C}=\text{O}$ of Asn292 ($d(\text{O}\cdots\text{C})=2.91\text{ \AA}$, angle ($\text{O}-\text{C}-\text{O})=63^\circ$), the side chain carboxyl-C atom of Glu295 ($d(\text{O}\cdots\text{C})=3.28\text{ \AA}$, angle ($\text{O}-\text{C}-\text{O})=106^\circ$), and the backbone carbonyl group of the same amino acid residue ($d(\text{O}\cdots\text{C})=3.06\text{ \AA}$, angle ($\text{O}-\text{C}-\text{O})=136^\circ$).

These examples demonstrate the potential of multipolar interactions to contribute to the stabilization of protein-ligand complexes and thus to enhance the affinity of small molecule inhibitors for their protein targets. It is therefore obvious, that structure-based ligand design will highly benefit from a more profound knowledge of these weak, but nevertheless in their sum important contacts.

4. Quantification of Dipolar Interactions

Dipolar interactions are directional, but short-ranged; the potential energy of interaction between two dipoles is a function of the angle between them and decreases rapidly with increasing distance (for freely rotating dipoles, the potential energy of interaction is proportional to $1/r^6$, where r denotes the distance between the centroids of the dipoles). Owing to the generally small energetic contributions of dipolar contacts to overall intermolecular interaction energies, experimental data assigning numerical energies to these types of nonbonded interactions is extremely scarce. Somewhat more often, computational methods have been used to substantiate the findings from structural analysis and to energetically quantify proposed types of interactions.

In an effort to characterize and quantify fluorine-carbonyl interactions experimentally, we have recently employed a novel combination of the Wilcox torsion balance^[69] and a double-mutant cycle^[70] together with a linear free energy relationship to assess the magnitude of the nonbonded interaction between the C-F bond dipole present in a CF_3 substituent and the $\text{C}=\text{O}$ functionality of an amide functional group.^[71] The study provided an initial measurement of this attractive interaction for the orthogonal arrangement of dipoles present in the experiment of about -0.8 to -1.5 kJ mol^{-1} in nonpolar solvents such as chloroform or benzene.

Ab initio based molecular orbital calculations at the 6-31G* basis set level using intermolecular perturbation theory (IMPT) were performed by Allen et al., yielding a somewhat larger attractive interaction energy of about -6 kJ mol^{-1} for $\text{Cl}\cdots\text{O}$ interactions in the nitromethane/1-chloro-2-methylacetylene model dimer.^[31d] However, the interaction occurs in an "in plane" arrangement of the nitro group and the halogen atom. $\text{X}\cdots\text{O}(\text{nitro})$ interactions of the heavier halogen atoms are calculated to be more attractive with an overall energy of -6 to -10 kJ mol^{-1} .

The average contribution of $\text{C}=\text{O}\cdots\text{C}=\text{O}$ interactions to intermolecular interaction energies was estimated by Gavazzotti to be weakly attractive in nature and to amount to about -8 kJ mol^{-1} .^[6] However, ab initio calculations (using 6-31G** basis sets and IMPT) applied to a propanone dimer model, yielded a somewhat larger value of -22.3 kJ mol^{-1} for

a perfect rectangular antiparallel dimer with $d(\text{C}\cdots\text{O})=3.02\text{ \AA}$ and -7.6 kJ mol^{-1} for the perpendicular motif with $d(\text{C}\cdots\text{O})$ distances again of 3.02 \AA .^[7] Interaction energies for intermediate geometries and $\text{C}\cdots\text{O}$ distances covering a wider range are generally estimated to be less favorable than -20 kJ mol^{-1} .

These values correspond roughly to $\text{O}(\text{nitro})\cdots\text{N}(\text{nitro})$ interaction energies that were calculated (MP2/6-31++G** level) to be at least -10 to -13 kJ mol^{-1} with an optimal $\text{N}\cdots\text{O}$ distance of 2.85 \AA .^[72] The consistency of this value with own computational results were noted by Yin et al. who reported a value of -13.3 kJ mol^{-1} for the attractive energy of a $\text{O}(\text{carbonyl})\cdots\text{N}(\text{nitro})$ interaction.^[28]

Despite these results—and it is without doubt that more efforts are currently underway—it can be stated that the quantitative approach to nonbonded dipolar interactions, particularly with regard to experimental model studies is still in its infancy and important contributions to this field can be anticipated.

5. Summary and Conclusions

For more than two decades supramolecular chemistry has greatly impacted many areas ranging from materials science to biomedicine. Intermolecular multipolar interactions have, however, undeservedly been looked at as being too weak, uninteresting, and less important than other nonbonding interactions. Whereas this perception may hold true for a single interaction, their general importance for a number of recognition events in chemistry and biology has been clearly underestimated and overlooked in the past. The rapid growth of structural databases and the more recent availability of powerful search and analysis tools provide opportunities for a more quantitative assessment of the occurrence and the geometrical preferences of multipolar contacts and has allowed us to gain valuable insight into previously unclear matters. More recently, the contributions of orthogonal dipolar interactions to the secondary structure of proteins and to molecular recognition in biochemical systems have been recognized and an increasing number of such cases are now being identified. Nevertheless, the experimental quantification and the theoretical treatment of these interactions are still underdeveloped and require further elaborate research efforts. It is evident, that molecular recognition studies in both small molecule model systems and in the biological protein-environment will remain important future contributors to the advancement and progress of this field.

We are grateful to F. Hoffmann-La Roche, Basel, and the ETH Research Council for continuing support of this work. Special thanks go to Dr. Jacob Olsen (now Sanofi-Aventis) who initiated the fluorine scan in our group leading to the recognition of the major role of orthogonal multipolar interactions in chemical and biological systems.

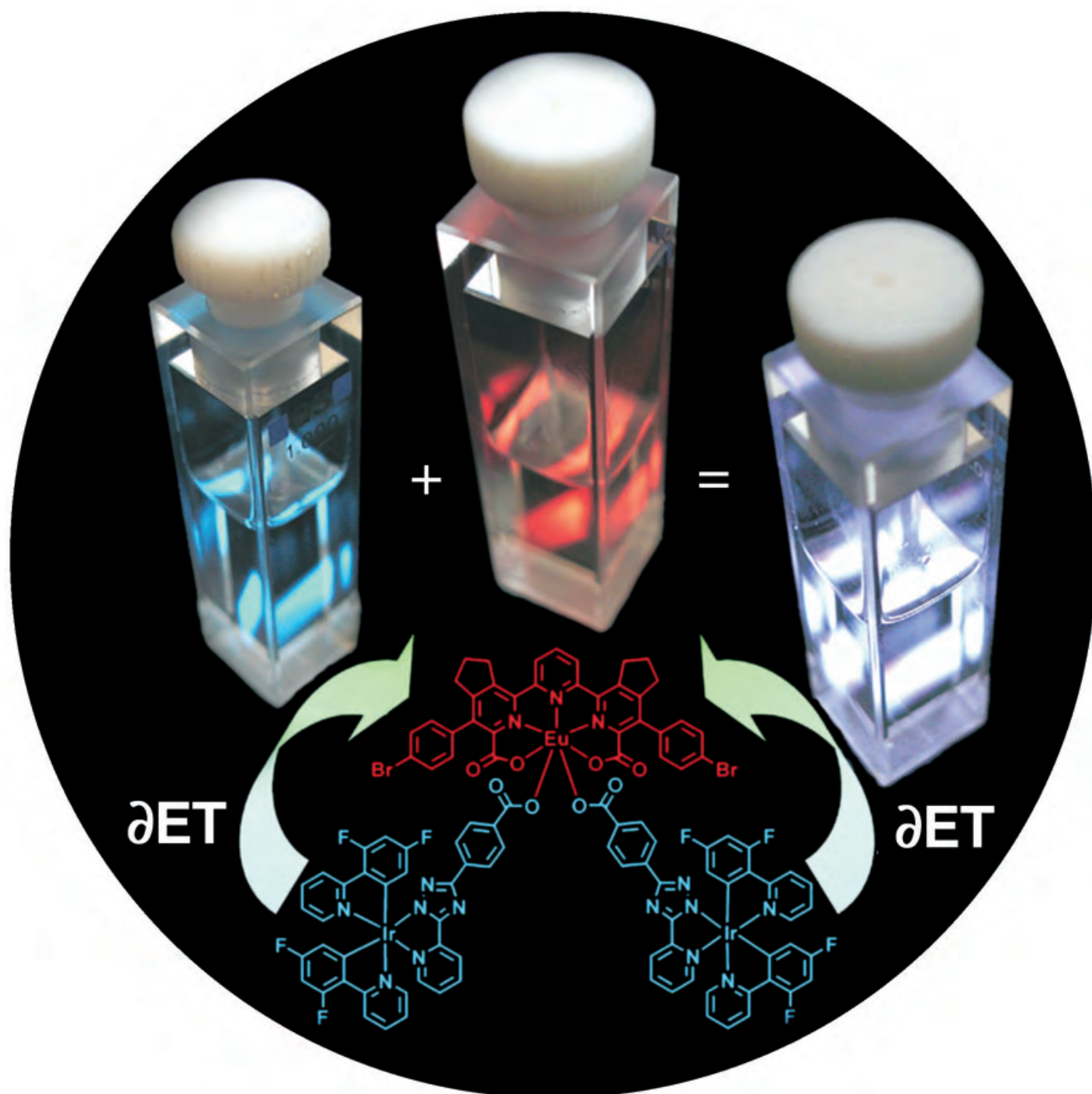
Received: October 6, 2004

Published online: February 11, 2005

- [1] For selected reviews and monographs on these topics see, for example: a) J.-M. Lehn, *Angew. Chem.* **1988**, *100*, 91–116; *Angew. Chem. Int. Ed. Engl.* **1988**, *27*, 90–112; b) J. Rebek, Jr., *Acc. Chem. Res.* **1990**, *23*, 399–404; c) H.-J. Schneider, A. Yatsimirsky, *Principles and Methods in Supramolecular Chemistry*, Wiley, Chichester, **1999**; d) T. Steiner, *Angew. Chem.* **2002**, *114*, 50–80; *Angew. Chem. Int. Ed.* **2002**, *41*, 48–76; e) E. A. Meyer, R. K. Castellano, F. Diederich, *Angew. Chem.* **2003**, *115*, 1244–1287; *Angew. Chem. Int. Ed.* **2003**, *42*, 1210–1250.
- [2] J. D. Dunitz, *Chem. Commun.* **2003**, 545–548, and references therein.
- [3] a) G. R. Desiraju, *Angew. Chem.* **1995**, *107*, 2541–2558; *Angew. Chem. Int. Ed. Engl.* **1995**, *34*, 2311–2327; b) C. B. Aakeröy, *Acta Crystallogr. B* **1997**, *53*, 569–586.
- [4] D. N. Reinhoudt, M. Crego-Calama, *Science* **2002**, *295*, 2403–2407.
- [5] a) H.-J. Böhm, G. Klebe, *Angew. Chem.* **1996**, *108*, 2750–2778; *Angew. Chem. Int. Ed. Engl.* **1996**, *35*, 2588–2614; b) “Protein-Ligand Interactions”: H.-J. Böhm in *Methods and Principles in Medicinal Chemistry* (Eds.: R. Mannhold, H. Kubinyi, G. Folkers), Wiley-VCH, Weinheim, **2003**, 3–20.
- [6] A. Gavezzotti, *J. Phys. Chem.* **1990**, *94*, 4319–4325.
- [7] F. H. Allen, C. A. Baalham, J. P. M. Lommerse, P. R. Raithby, *Acta Crystallogr. B* **1998**, *54*, 320–329.
- [8] S. Lee, A. B. Mallik, D. C. Fredrickson, *Cryst. Growth Des.* **2004**, *4*, 279–290.
- [9] a) J. A. Olsen, D. W. Banner, P. Seiler, U. Obst-Sander, A. D’Arcy, M. Stihle, K. Müller, F. Diederich, *Angew. Chem.* **2003**, *115*, 2611–2615; *Angew. Chem. Int. Ed.* **2003**, *42*, 2507–2511; b) J. A. Olsen, D. W. Banner, P. Seiler, B. Wagner, T. Tschopp, U. Obst-Sander, M. Kansy, K. Müller, F. Diederich, *ChemBioChem* **2004**, *5*, 666–675.
- [10] For an earlier crystallographic investigation, see: S. Larsen, K. Marthi, *Acta Crystallogr. B* **1994**, *50*, 373–381.
- [11] J. Olsen, P. Seiler, B. Wagner, H. Fischer, T. Tschopp, U. Obst-Sander, D. W. Banner, M. Kansy, K. Müller, F. Diederich, *Org. Biomol. Chem.* **2004**, *2*, 1339–1352.
- [12] a) H. M. Berman, J. Westbrook, Z. Feng, G. Gilliland, T. N. Bhat, H. Weissig, I. N. Shindyalov, P. E. Bourne, *Nucleic Acids Res.* **2000**, *28*, 235–242; b) F. H. Allen, *Acta Crystallogr. B* **2002**, *58*, 380–388.
- [13] a) A. Bondi, *J. Phys. Chem.* **1964**, *68*, 441–451; b) R. S. Rowland, R. Taylor, *J. Phys. Chem.* **1996**, *100*, 7384–7391; c) A.-J. Li, R. Nussinov, *Proteins Struct. Funct. Genet.* **1998**, *32*, 111–127.
- [14] For intramolecular C–F...C≡N contacts, see: K. Nishide, Y. Hagimoto, H. Hasegawa, M. Shiro, M. Node, *Chem. Commun.* **2001**, 2394–2395.
- [15] J. D. Dunitz, personal communication.
- [16] For a particularly well-studied example of short C–H...O contacts that are repulsive rather than attractive, see: P. Seiler, L. Isaacs, F. Diederich, *Helv. Chim. Acta* **1996**, *79*, 1047–1058.
- [17] W. Bolton, *Acta Crystallogr.* **1964**, *17*, 147–152.
- [18] W. Bolton, *Acta Crystallogr.* **1965**, *18*, 5–10.
- [19] D. R. Davies, J. J. Blum, *Acta Crystallogr.* **1955**, *8*, 129–136.
- [20] S. S. C. Chu, G. A. Jeffrey, T. Sakurai, *Acta Crystallogr.* **1962**, *15*, 661–671.
- [21] W. Bolton, *Acta Crystallogr.* **1963**, *16*, 166–173.
- [22] H. A. Bent, *Chem. Rev.* **1968**, *68*, 588–648.
- [23] J. Bernstein, M. D. Cohen, L. Leiserowitz in *The Chemistry of the Quinoid Compounds* (Ed.: S. Patai), Wiley, London, **1974**, pp. 83–110.
- [24] a) H. B. Bürgi, J. D. Dunitz, E. Shefter, *J. Am. Chem. Soc.* **1973**, *95*, 5065–5067; b) H. B. Bürgi, J. D. Dunitz, E. Shefter, *Acta Crystallogr. B* **1974**, *30*, 1517–1527; c) H. B. Bürgi, J. D. Dunitz, *Acc. Chem. Res.* **1983**, *16*, 153–161.
- [25] a) F. H. Allen, W. D. S. Motherwell, *Acta Crystallogr. B* **2002**, *58*, 407–422; b) “Structure-Based Drug Design”: J. C. Cole, J. P. M. Lommerse, R. S. Rowland, R. Taylor, F. H. Allen, *NATO ASI Ser. Ser. E* **1998**, 352, 113–124; c) R. Taylor, *Acta Crystallogr. D* **2002**, *58*, 879–888.
- [26] a) R. Taylor, A. Mullale, G. W. Mullier, *Pestic. Sci.* **1990**, *29*, 197–213; b) For a very recent example of a C₂N...NO₂ interaction, see: G. P. A. Yap, I. Alkorta, N. Jagerovic, J. Elguero, *Aust. J. Chem.* **2004**, *57*, 1–6.
- [27] a) K. Wozniak, H. He, J. Klinowski, W. Jones, E. Grech, *J. Phys. Chem.* **1994**, *98*, 13755–13765; b) K. Wozniak, *Pol. J. Chem.* **1997**, *71*, 779–791; c) K. Wozniak, P. R. Mallison, C. C. Wilson, E. Hovestreydt, E. Grech, *J. Phys. Chem. A* **2002**, *106*, 6897–6903.
- [28] Z. Yin, L. Jiang, J. He, J.-P. Cheng, *Chem. Commun.* **2003**, 2326–2327.
- [29] CSD search: CSD version 5.25, November 2003, containing about 300000 entries. All searches were performed for structures with R-factor < 10% (no error, no partial disorder), excluding polymeric, powder, or metalorganic compounds. In cases, where no direct torsion angles τ_1 or angles α_3 between bond vectors can be defined (e.g. H₂O, R₃N as the nucleophilic part) suitable centroids between topologically equal atoms are used to characterize structural parameters. PDB search: Searches were performed by using Relibase 1.2.1 (March 2003) (see ref. [30]) and the PDB-update of June 27, 2004, containing 26403 structures. All searches were limited to a resolution of protein crystal structures ≤ 2.5 Å.
- [30] a) M. Hendlich, A. Bergner, J. Günther, G. Klebe, *J. Mol. Biol.* **2003**, *326*, 607–620; b) J. Günther, A. Bergner, M. Hendlich, G. Klebe, *J. Mol. Biol.* **2003**, *326*, 621–636.
- [31] a) P. Murray-Rust, W. D. S. Motherwell, *J. Am. Chem. Soc.* **1979**, *101*, 4374–4376; b) G. R. Desiraju, V. R. Pedireddi, J. A. R. P. Sarma, D. E. Zacharias, *Acta Chim. Hung.* **1993**, *130*, 451–465; c) J. P. M. Lommerse, A. J. Stone, R. Taylor, F. H. Allen, *J. Am. Chem. Soc.* **1996**, *118*, 3108–3116; d) F. H. Allen, J. P. M. Lommerse, V. J. Hoy, J. A. K. Howard, G. R. Desiraju, *Acta Crystallogr. B* **1997**, *53*, 1006–1016.
- [32] G. R. Desiraju, R. L. Harlow, *J. Am. Chem. Soc.* **1989**, *111*, 6757–6764.
- [33] J. N. Moorthy, P. Venkatkrishnan, P. Mal, S. Dixit, P. Venugopalan, *Cryst. Growth Des.* **2003**, *3*, 581–585.
- [34] B. S. Potter, R. A. Palmer, R. Withnall, B. Z. Chowdhry, *New J. Chem.* **1999**, *23*, 117–122.
- [35] D. S. Eggleston, E. J. Valente, D. J. Hodgson, *Acta Crystallogr. B* **1981**, *37*, 1428–1430.
- [36] a) R. E. Rosenfield, Jr., R. Parthasarathy, J. D. Dunitz, *J. Am. Chem. Soc.* **1977**, *99*, 4860–4862; b) M. Iwaoka, S. Takemoto, S. Tomoda, *J. Am. Chem. Soc.* **2002**, *124*, 10613–10620.
- [37] Y. Nagao, T. Hirata, S. Goto, S. Sano, A. Kakehi, K. Iizuka, M. Shiro, *J. Am. Chem. Soc.* **1998**, *120*, 3104–3110.
- [38] S. Wu, A. Greer, *J. Org. Chem.* **2000**, *65*, 4883–4887.
- [39] a) F. T. Burling, B. M. Goldstein, *J. Am. Chem. Soc.* **1992**, *114*, 2313–2320; b) F. T. Burling, B. M. Goldstein, *Acta Crystallogr. B* **1993**, *49*, 738–744.
- [40] a) M. Iwaoka, S. Takemoto, M. Okada, S. Tomoda, *Chem. Lett.* **2001**, 132–133; b) D. Pal, P. Chakrabarti, *J. Biomol. Struct. Dyn.* **2001**, *19*, 115–128; c) M. Iwaoka, S. Takemoto, M. Okada, S. Tomoda, *Bull. Chem. Soc. Jpn.* **2002**, *75*, 1611–1625.
- [41] W. Brandt, A. Golbraikh, M. Täger, U. Lendeckel, *Eur. J. Biochem.* **1999**, *261*, 89–97.
- [42] a) G. R. Desiraju, *Crystal Engineering: The Design of Organic Solids*, Elsevier, Amsterdam, **1989**, pp. 175–201; b) G. R. Desiraju, R. Parthasarathy, *J. Am. Chem. Soc.* **1989**, *111*, 8725–8726; c) V. R. Pedireddi, D. S. Reddy, B. S. Goud, D. C. Craig, A. D. Rae, G. R. Desiraju, *J. Chem. Soc. Perkin Trans. 2* **1994**, 2353–2360.

- [43] S. L. Price, A. J. Stone, J. Lucas, R. S. Rowland, A. E. Thornley, *J. Am. Chem. Soc.* **1994**, *116*, 4910–4918.
- [44] J. A. R. P. Sarma, G. R. Desiraju, *Chem. Phys. Lett.* **1985**, *117*, 160–164.
- [45] J. A. R. P. Sarma, G. R. Desiraju, *Acc. Chem. Res.* **1986**, *19*, 222–228.
- [46] a) S. J. Harris, S. E. Novick, J. S. Winn, W. Klemperer, *J. Chem. Phys.* **1974**, *61*, 3866–3867; b) K. C. Jando, W. Klemperer, S. E. Novick, *J. Chem. Phys.* **1976**, *64*, 2698–2699.
- [47] a) T. Sakurai, M. Sundaralingam, G. A. Jeffrey, *Acta Crystallogr.* **1963**, *16*, 354–363; b) N. Ramasubbu, R. Parthasarathy, P. Murray-Rust, *J. Am. Chem. Soc.* **1986**, *108*, 4308–4314.
- [48] a) O. Navon, J. Bernstein, V. Khodorkovsky, *Angew. Chem.* **1997**, *109*, 640–642; *Angew. Chem. Int. Ed. Engl.* **1997**, *36*, 601–603; b) H. F. Lieberman, R. J. Davey, D. M. T. Newsham, *Chem. Mater.* **2000**, *12*, 490–494.
- [49] a) R. K. R. Jetti, F. Xue, T. C. W. Mak, A. Nangia, *Cryst. Eng.* **1999**, *2*, 215–224; b) C. K. Broder, J. A. K. Howard, D. A. Keen, C. C. Wilson, F. H. Allen, R. K. R. Jetti, A. Nangia, G. R. Desiraju, *Acta Crystallogr. B* **2000**, *56*, 1080–1084; c) R. K. R. Jetti, A. Nangia, F. Xue, T. C. W. Mak, *Chem. Commun.* **2001**, 919–920; d) E. Bosch, C. L. Barnes, *Cryst. Growth Des.* **2002**, *2*, 299–302.
- [50] a) P. H. Maccallum, R. Poet, E. J. Milner-White, *J. Mol. Biol.* **1995**, *248*, 361–373; b) P. H. Maccallum, R. Poet, E. J. Milner-White, *J. Mol. Biol.* **1995**, *248*, 374–384.
- [51] C. M. Deane, F. H. Allen, R. Taylor, T. L. Blundell, *Protein Eng.* **1999**, *12*, 1025–1028.
- [52] A. Bergner, J. Günther, M. Hendlich, G. Klebe, M. Verdonk, *Biopolymers* **2002**, *61*, 99–110.
- [53] M. Adler, D. D. Davey, G. B. Phillips, S.-H. Kim, J. Jancarik, G. Rumennik, D. R. Light, M. Whitlow, *Biochemistry* **2000**, *39*, 12534–12542.
- [54] a) D. L. Hughes, L. C. Sieker, J. Bieth, J. L. Dimicoli, *J. Mol. Biol.* **1982**, *162*, 645–658; b) C. Mattos, D. A. Giammona, G. A. Petsko, D. Ringe, *Biochemistry* **1995**, *34*, 3193–3203; c) S. A. Peterson, T. Klabunde, H. A. Lashuel, H. Purkey, J. C. Sacchettini, J. W. Kelly, *Proc. Natl. Acad. Sci. USA* **1998**, *95*, 12956–12960.
- [55] J. R. Horton, K. Sewada, M. Nishibori, X. Zhang, X. Cheng, *Structure* **2001**, *9*, 837–849.
- [56] Z. Wawrzak, T. Sandalova, J. J. Steffens, G. S. Basarab, T. Lundqvist, Y. Lindqvist, D. B. Jordan, *Proteins Struct. Funct. Genet.* **1999**, *35*, 425–439.
- [57] J. C. Biffinger, H. W. Kim, S. G. DiMagno, *ChemBioChem* **2004**, *5*, 622–627.
- [58] M. N. G. James, A. R. Sielecki, K. Hayakawa, M. H. Gelb, *Biochemistry* **1992**, *31*, 3872–3886.
- [59] A. M. Silva, R. E. Cachau, H. L. Sham, J. W. Erickson, *J. Mol. Biol.* **1996**, *255*, 321–346.
- [60] P. Akamine, Madhusudan, L. L. Brunton, H. D. Ou, J. M. Canaves, N.-H. Xuong, S. S. Taylor, *Biochemistry* **2004**, *43*, 85–96.
- [61] B. A. Katz, J. M. Clark, J. S. Finer-Moore, T. E. Jenkins, C. R. Johnson, M. J. Ross, C. Luong, W. R. Moore, R. M. Stroud, *Nature* **1998**, *391*, 608–612.
- [62] J. A. Bertrand, S. Thieffine, A. Vulpetti, C. Cristiani, B. Valsasina, S. Knapp, H. M. Kalisz, M. Flocco, *J. Mol. Biol.* **2003**, *333*, 393–407.
- [63] H.-G. Beisel, S.-I. Kawabata, S. Iwanaga, R. Huber, W. Bode, *EMBO J.* **1999**, *18*, 2313–2322.
- [64] S. S. Pang, R. G. Duggleby, R. L. Schowen, L. W. Guddat, *J. Biol. Chem.* **2004**, *279*, 2242–2253.
- [65] D. G. Lloyd, A. T. García-Sosa, I. L. Alberts, N. P. Todorov, R. L. Mancera, *J. Comput.-Aided Mol. Des.* **2004**, *18*, 89–100.
- [66] a) J. D. Dunitz, *Science* **1994**, *264*, 670; b) S. M. Tschampel, R. J. Woods, *J. Phys. Chem. A* **2003**, *107*, 9175–9181; c) D. Hamelberg, J. A. McCammon, *J. Am. Chem. Soc.* **2004**, *126*, 7683–7689; d) M. Fornabaio, F. Spyraakis, A. Mozzarelli, P. Cozzini, D. J. Abraham, G. E. Kellogg, *J. Med. Chem.* **2004**, *47*, 4507–4516.
- [67] G. Arents, W. E. Love, *J. Mol. Biol.* **1989**, *210*, 149–161.
- [68] B. Mamat, A. Roth, C. Grimm, U. Ermler, C. Tziatzios, D. Schubert, R. K. Thauer, S. Shima, *Protein Sci.* **2002**, *11*, 2168–2178.
- [69] a) S. Paliwal, S. Geib, C. S. Wilcox, *J. Am. Chem. Soc.* **1994**, *116*, 4497–4498; b) E.-I. Kim, S. Paliwal, C. S. Wilcox, *J. Am. Chem. Soc.* **1998**, *120*, 11192–11193.
- [70] See, for example: a) H. Adams, F. J. Carver, C. A. Hunter, J. C. Morales, E. M. Seward, *Angew. Chem.* **1996**, *108*, 1628–1631; *Angew. Chem. Int. Ed. Engl.* **1996**, *35*, 1542–1544; b) F. J. Carver, C. A. Hunter, P. S. Jones, D. J. Livingstone, J. F. McCabe, E. M. Seward, P. Tiger, S. E. Spey, *Chem. Eur. J.* **2001**, *7*, 4854–4862; c) C. A. Hunter, C. M. R. Low, J. G. Vinter, C. Zonta, *J. Am. Chem. Soc.* **2003**, *125*, 9936–9937.
- [71] F. Hof, D. M. Scofield, W. B. Schweizer, F. Diederich, *Angew. Chem.* **2004**, *116*, 5166–5169; *Angew. Chem. Int. Ed.* **2004**, *43*, 5056–5059.
- [72] J. A. Platts, S. T. Howard, K. Wozniak, *Chem. Phys. Lett.* **1995**, *232*, 479–485.

Communications



Partial transfer of excited-state energy from the Ir^{III} center to the Eu^{III} center in a d-f bimetallic assembly leads to the observation of white-light emission. For a more-detailed photophysical study on the energy-transfer processes involved with this assembly, see the Communication by L. De Cola and co-workers on the following pages.

Luminescent Assemblies

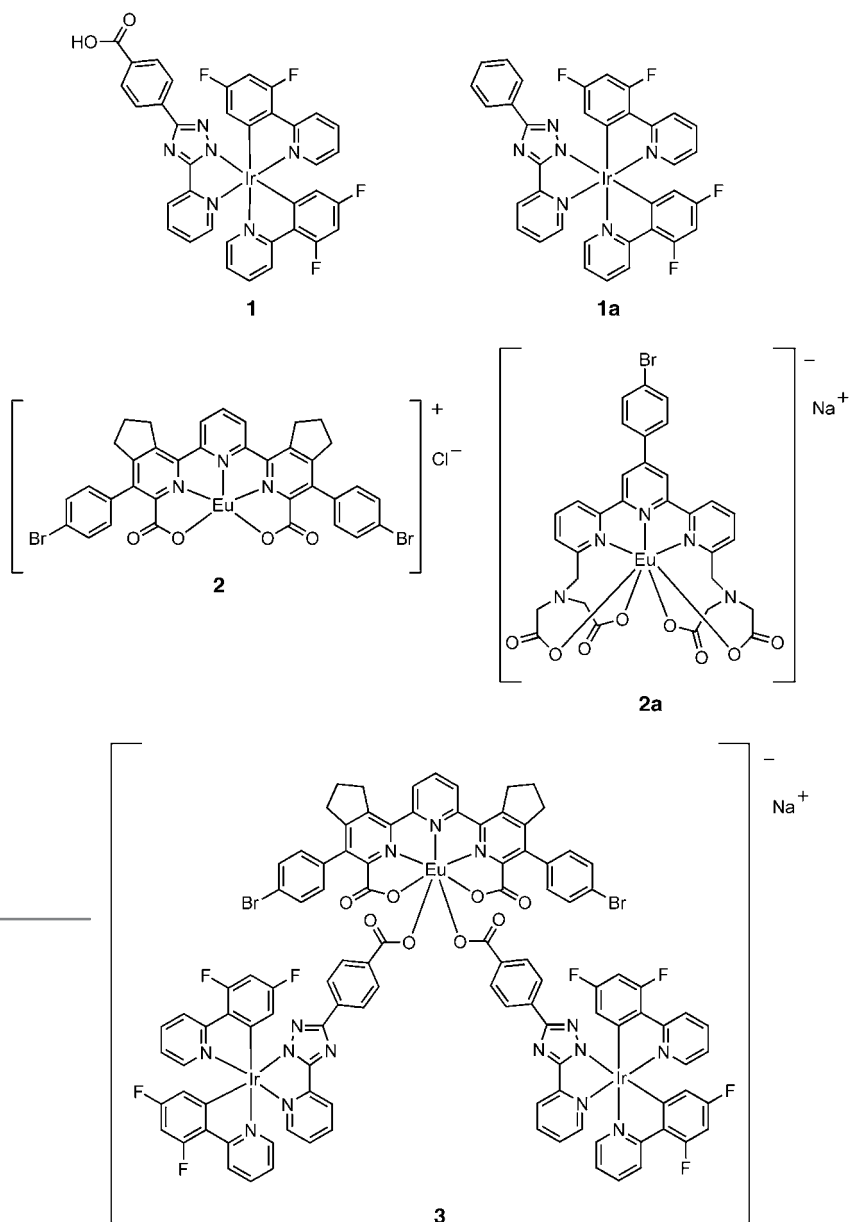
White-Light Emission from an Assembly
Comprising Luminescent Iridium and Europium
Complexes**

Paolo Coppo, Marco Duati, Valery N. Kozhevnikov,
Johannes W. Hofstra, and Luisa De Cola*

Europium(III) red emission receives increasing attention for application in bioassays and in sensors where its long-lived luminescence enables sensitive time-resolved or “gated” detection of the emission without interference from background or scattered excitation light.^[1] Furthermore, the use of Eu^{III} complexes for applications in light-emitting devices has been described.^[2] Eu^{III} complexes show little or no absorption in the visible region of the spectrum and often require the application of strongly absorbing “antennae” for light harvesting to obtain efficient photoluminescence.^[3] Recently, energy transfer from transition metals to lanthanides to obtain near-IR (NIR) emission from Yb, Nd, and Er was reported.^[4] The use of a light-harvesting unit based on a transition metal is extremely appealing for applications in luminescence and electro(che)mioluminescence owing to the addressability of the coordination-metal-based unit by both light and redox reactions. To the best of our knowledge, no transition-metal-based antennae have been reported for the photoexcitation of Eu^{III}. This absence is most likely due to the high triplet energy level required for the sensitization of this lanthanide which few metal complexes can provide. We have recently reported on the tuning of light emission in iridium(III) complexes in the

“almost-blue” region of the visible spectrum.^[5] Herein we discuss the application of such systems for the photoexcitation of a Eu^{III}—terpyridine-based complex. Emission of white light can be observed by the application of carefully designed systems that allow a partial transfer of energy from the excited Ir^{III} moiety to the Eu^{III} complex.

Complex **1** (see Scheme 1) was prepared according to procedures reported previously for similar systems, purified



Scheme 1. Structures of the investigated complexes.

by column chromatography, and obtained as an amorphous yellow powder.^[5,6] The UV/Vis absorption spectrum was consistent with the unsubstituted analogue **1a** and showed a MLCT (metal-to-ligand charge transfer) transition in the visible region and π – π^* bands that are attributed to transitions in the ligand in the UV region (see Figure 1). Complex **1** shows blue emission in CH₂Cl₂, MeOH, or CH₃CN with

[*] Dr. P. Coppo, Dr. M. Duati, Prof. Dr. L. De Cola
HIMS, Molecular Photonic Materials
University of Amsterdam
Nieuwe Achtergracht 166
1018 WV Amsterdam (The Netherlands)
Fax: (+31) 20-525-6456
E-mail: ldc@science.uva.nl
Dr. V. N. Kozhevnikov
Urals State Technical University
620002, Ekaterinburg (Russia)
Prof. Dr. J. W. Hofstra
Philips Research
Prof. Holstlaan 4
5656 AA Eindhoven (The Netherlands)

[**] The authors acknowledge Roche Diagnostics, Philips Research, and the Dutch Foundation for Scientific Research (SENTER, Project No. TSGE3140) for funding the project. Dr. R. Williams and Dr. B. Götz are acknowledged for their help with time-resolved and gated experiments. Dr. C. A. Schalley, Prof. F. Vögtle, and J. van Heyst are acknowledged for mass spectrometry analyses.

Supporting information for this article is available on the WWW under <http://www.angewandte.org> or from the author.

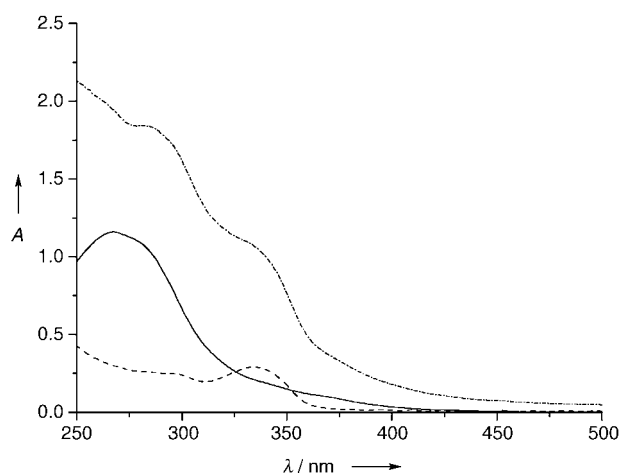


Figure 1. Absorption spectra of solutions (5×10^{-5} M in methanol) of complexes **1** (—), **2** (---), and **3** (-·-·-).

maxima centered at 460 nm and 491 nm (see Table 1) in similar fashion to the unfunctionalized analogue **1a**. The quantum yield of emission, Φ , of a deaerated solution of **1** in methanol is 17 %, which is significantly lower than that for the unsubstituted analogue **1a** ($\Phi = 27\%$). The lifetime, τ , of the emitting species **1** is 1.4 μ s.

Table 1: Emission maxima (λ_{em}), quantum yields of emission (Φ),^[a] and lifetimes (τ) of the emitting species.^[b]

Complex	λ_{em} [nm]	Φ	τ [μ s]
1 ^[c]	460, 491	0.17	1.4
1a ^[d]	461, 490	0.27	1.4
2 ^[e]	615	0.33	1900
2a ^[c]	615	0.12	1900
3 ^[c]	460, 491, 615	0.07	0.48 (Ir) 1900 (Eu)

[a] Quantum yields of complexes **1** and **1a** were measured by using quinine bisulfate in 0.5 M H_2SO_4 as a reference, whereas those of **2**, **2a**, and **3** were measured by using $[Ru(bpy)_3]Cl_2$ in distilled water as a reference (bpy = bipyridine). [b] A concentration of 5×10^{-5} M was used for steady-state experiments. A concentration of 10^{-4} M was used for time-resolved measurements. [c] Measurements performed in CD_3OD . [d] Measurements performed in dichloromethane. [e] Measurements performed in D_2O .

Complex **2** was prepared and purified according to reported procedures^[7] and was isolated as a white powder. The complex shows absorption bands in the UV region (see Figure 1) and the characteristic, well-structured emission of Eu^{III} complexes (see Figure 2). Emission is mainly observed from the $^5D_0 \rightarrow ^7F_2$ transition, centered at 615 nm (see Figure 2). This hypersensitive transition is an electric-dipole emission that is forbidden in the free ion. However, when the Eu^{III} ion experiences a strongly asymmetric or strongly interacting ligand field, this transition may be greatly enhanced.^[1a] The quantum yield of emission of **2** in an air-equilibrated solution in D_2O was 33 %. As can be seen by the schematic formula and as confirmed by spectroscopic investigation in water by comparing the excited-state lifetimes of **2**

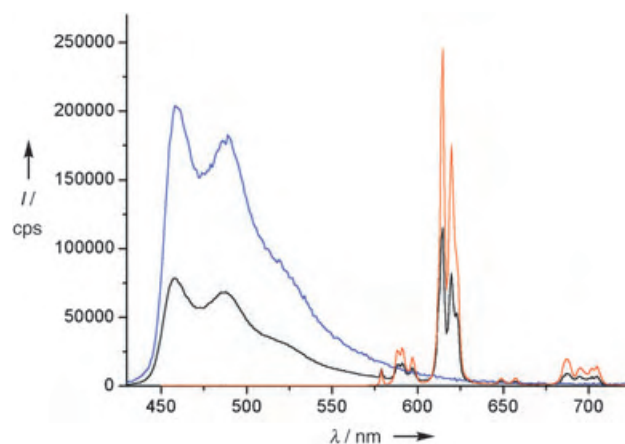


Figure 2. Relative steady-state emission spectra of solutions of complexes **1** (blue), **2** (red; $I/6$), and **3** (black) in CD_3OD upon excitation at $\lambda = 400$ nm (complex **2** was excited at $\lambda = 350$ nm as it shows negligible absorption at $\lambda = 400$ nm; cps = counts per second). The solutions all have identical absorption values at the excitation wavelength.

in D_2O ($\tau = 1.9$ ms) and in H_2O ($\tau = 0.25$ ms), the europium complex in which the Eu^{III} center is coordinated to a pentadentate cage-type ligand has a hydration number $q = 3.9$. Hence, complex **2** can bind up to 4 molecules of water or solvent to fill the coordination sphere. Such a situation is ideal for the assembly of a second metal complex through carboxylate or chelating units. Indeed, when complexes **1** and **2** were stirred in methanol at room temperature, the formation of an assembly of Eu^{III} and Ir^{III} moieties was established by spectroscopic investigations (see below). Its structure could not be determined by NMR spectroscopy owing to the paramagnetic properties of Eu^{III} and to the low solubility of the product. However, FT-IR spectroscopy of the sample in KBr matrix proved to be effective to highlight the formation of complex **3** (see Figure 3). The disappearance of the band at 1685 cm^{-1} in complex **3** which is associated with the stretch of the C=O bond in the Ar-COOH moiety of complex **1** suggests that the acid is coordinated to the europium ion. Indeed, the C=O stretching band in complex **3** can be detected at 1409 cm^{-1} , which is consistent with previous reports on Eu^{III} coordinated to four carboxylate groups.^[8] Furthermore, the disappearance for complex **3** of the broad band at 3380 cm^{-1} , which is associated with the OH stretch of coordinated methanol molecules in the neat complex **2**, suggests that the solvent molecules have been displaced by the insertion of **1** as a coordinating unit. ESI-mass spectrometry confirmed **3** to be the main product with an Ir-Eu adduct and traces of Ir_3 -Eu as byproducts (see Supporting Information).

Evidence of the formation of the adduct and of the absence of different equilibria in solution resulted from photophysical characterization. Irradiation of the assembly (diluted in CD_3OD) with monochromatic light at $\lambda = 400$ nm, where only the iridium moiety has appreciable absorption bands ($\epsilon_{400} \approx 1000\text{ M}^{-1}\text{ cm}^{-1}$), resulted in the emission of almost-white light (Commission Internationale d'Eclairage, CIE coordinates: X: 0.28 Y: 0.30) owing to the combined

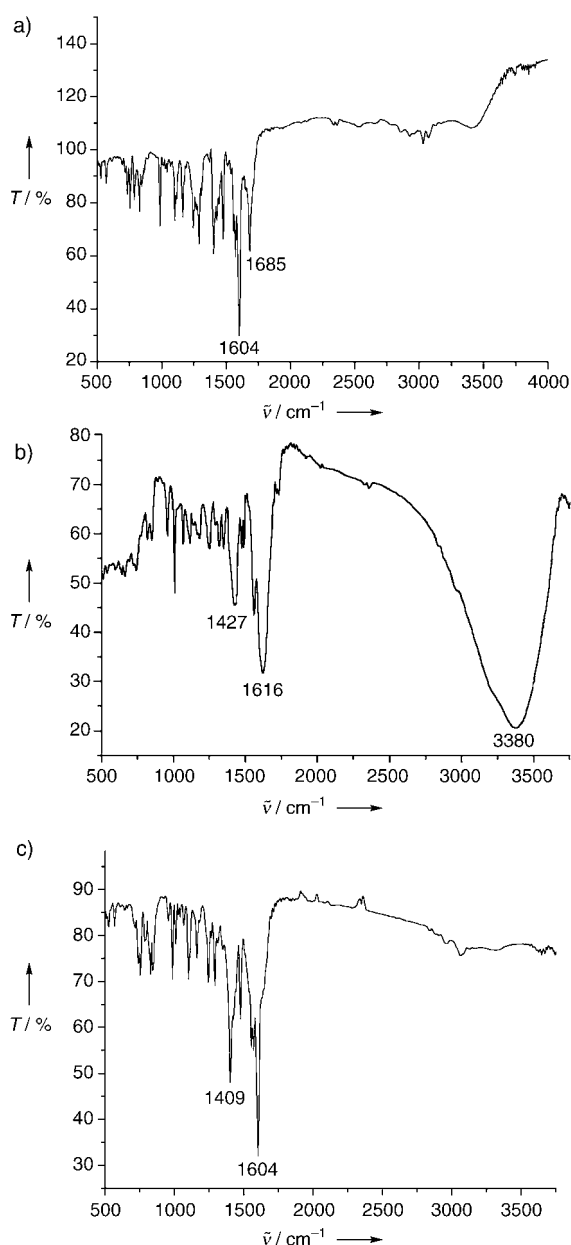


Figure 3. FT-IR spectra of complexes a) **1**, b) **2**, and c) **3** in KBr pellets.

presence of residual emission of the blue–green emitting Ir^{III} complex and the sensitized red emission of the Eu^{III} complex (see Figure 2). Measurement of the quantum yields of emission and time-resolved spectroscopy show that the excited-state lifetime of the Ir^{III} emitting species is strongly reduced ($\tau = 480$ ns, see Table 1) as compared to a deaerated solution of complex **1** alone in CD₃OD ($\tau = 1400$ ns). The sensitization of the Eu^{III} moiety suggests an energy-transfer process from the excited iridium moiety, which is the only component that absorbs light at $\lambda = 400$ nm, to the low-lying excited state (⁵D₀) of the Eu^{III} center. If the emission of the bimetallic system is detected with a long delay on a millisecond scale by means of a streak camera, only the characteristic emission of the Eu^{III}-containing moiety is observed. By comparison of the steady-state emissions of complexes **1** and

3, the efficiency of the energy transfer was determined to be 38%. This value was calculated by assuming that the quantum yield of emission of the europium complex does not change upon coordination of the iridium moiety. By comparison of the lifetime of Eu^{III} emission in complex **3** in CD₃OD ($\tau = 1.9$ ms) and CH₃OH ($\tau = 0.7$ ms), a hydration number of $q = 0.78$ was calculated for complex **3** which is significantly lower than the q value for complex **2**.

The shape of the hypersensitive emission band of **2** at 615 nm changes slightly upon coordination of the Ir^{III} moiety and indicates a lower degree of symmetry. To establish the optimal stoichiometry of the adduct in solution through the carboxylate group that belongs to the iridium complex **1**, a titration of **1** against **2** was performed. It was immediately clear that the maximum intensity of the Eu^{III} moiety upon excitation of the Ir^{III}-based moiety at 400 nm was observed for a 1:2 stoichiometry of **1/2**. When the number of Ir^{III} centers in solution exceeds twice that of Eu^{III}, the emission is dominated by the blue–green signals that originate from the Ir^{III} complex.

To confirm that such a stable adduct can occur only with complexes with an unsaturated coordination sphere, complex **2a**^[8] (see Scheme 1) was treated with complex **1** under analogous conditions. The resulting solution showed only Ir^{III}-based emission upon excitation at $\lambda = 400$ nm which suggests that no energy transfer to the europium moiety occurred. The difference in behavior is consistent with the hypothesis that the carboxylate group of **1** coordinates to the Eu^{III} ion in complex **2**, whereas for complex **2a** in which the Eu^{III} ion is already fully coordinated by the cage-type ligand ($q < 1$) no such assembly can be formed. Further evidence came by adding the unfunctionalized Ir^{III} complex **1a** (see Scheme 1), which lacks the carboxylate group, to a solution of complex **2**: Also in this case, no Eu^{III} emission was detected upon irradiation at $\lambda = 400$ nm.

In conclusion, we have reported the first example of sensitization of a Eu^{III} complex through the use of a transition-metal complex in a d–f bimetallic assembly which gives almost-white light emission. White electrophosphorescence is interesting for applications in electroluminescent displays and in lighting devices, both for illumination purposes and for backlights.^[9] Investigations on electrically generated white-light emission from complex **3** are currently in progress as well as attempts to optimize the energy transfer process and improve the solubility.

Received: September 11, 2004

Revised: October 11, 2004

Published online: December 13, 2004

Keywords: energy transfer · europium · iridium · luminescence · time-resolved spectroscopy

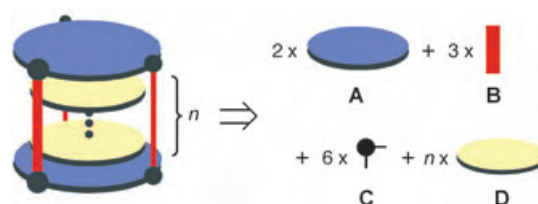
- [1] a) F. S. Richardson, *Chem. Rev.* **1982**, 82, 541; b) H. Takalo, V.-M. Mukkala, H. Mikola, P. Liitti, I. Hemmilä, *Bioconj. Chem.* **1994**, 5, 278; c) S. Petoud, S. M. Cohen, J.-C. G. Bünzli, K. N. Raymond, *J. Am. Chem. Soc.* **2003**, 125, 13324; d) G. Bobba, J. C. Frias, D. Parker, *Chem. Commun.* **2002**, 890; e) A. Beeby, S. W. Botchway, I. M. Clarkson, S. Faulkner, A. W. Parker, D. Parker, J. A. G. Williams, *J. Photochem. Photobiol. B: Biol.* **2000**, 57, 83.

- [2] a) M. A. Baldo, M. E. Thompson, S. R. Forrest, *Pure Appl. Chem.* **1999**, *71*, 2095; b) P.-P. Sun, J.-P. Duan, J.-J. Lih, C.-H. Cheng, *Adv. Funct. Mater.* **2003**, *13*, 683; c) T. Oyamada, Y. Kawamura, T. Koyama, H. Sasabe, C. Adachi, *Adv. Mater.* **2004**, *16*, 1082; d) J. W. Verhoeven, M. H. V. Werts, J. W. Hofstraat, US Pat. 2003012979.
- [3] a) M. H. V. Werts, R. T. F. Jukes, J. W. Verhoeven, *Phys. Chem. Chem. Phys.* **2002**, *4*, 1542; b) C. Yang, L.-M. Fu, Y. Wang, J.-P. Zhang, W.-T. Wong, X.-C. Ai, Y.-F. Qiao, B.-S. Zou, L.-L. Gui, *Angew. Chem.* **2004**, *116*, 5120; *Angew. Chem. Int. Ed.* **2004**, *43*, 5010.
- [4] a) T. A. Miller, J. C. Jeffery, M. D. Ward, H. Adams, S. J. A. Pope, S. Faulkner, *Dalton Trans.* **2004**, *10*, 1524; b) D. Imbert, M. Cantuel, J.-C. G. Bünzli, G. Bernardinelli, C. Piguet, *J. Am. Chem. Soc.* **2003**, *125*, 15698; c) S. J. A. Pope, B. J. Coe, S. Faulkner, *Chem. Commun.* **2004**, 1550; d) S. J. A. Pope, B. J. Coe, S. Faulkner, E. V. Bichenkova, X. Yu, K. T. Douglas, *J. Am. Chem. Soc.* **2004**, *126*, 9490; e) N. M. Shavaleev, L. P. Moorcraft, S. J. A. Pope, Z. R. Bell, S. Faulkner, M. D. Ward, *Chem. Eur. J.* **2003**, *9*, 5283; f) S. I. Klink, H. Keizer, H. W. Hofstraat, F. C. J. M. van Veggel, *Synth. Met.* **2002**, *127*, 213; g) S. I. Klink, H. Keizer, F. C. J. M. van Veggel, *Angew. Chem.* **2000**, *112*, 4489; *Angew. Chem. Int. Ed.* **2000**, *39*, 4319.
- [5] P. Coppo, E. A. Plummer, L. De Cola, *Chem. Commun.* **2004**, 1774.
- [6] a) M. Santus, *Polish J. Chem.* **1980**, *54*, 1067; b) M. Santus, *Polish J. Chem.* **1980**, *54*, 661.
- [7] V. N. Kozhevnikov, D. N. Kozhevnikov, V. L. Rusinov, O. N. Chupakhin, B. König, *Synthesis* **2003**, *15*, 2400.
- [8] a) V.-M. Mikkala, M. Helenius, I. Hemmilä, J. Kankare, H. Takalo, *Helv. Chim. Acta* **1993**, *76*, 1361; b) H. Takalo, V.-M. Mikkala, H. Mikola, P. Liitti, I. Hemmilä, *Bioconjugate Chem.* **1994**, *5*, 278.
- [9] a) B. W. D'Andrade, J. Brooks, V. Adamovich, M. E. Thompson, S. R. Forrest, *Adv. Mater.* **2002**, *14*, 1032; b) B. W. D'Andrade, S. R. Forrest, *Adv. Mater.* **2004**, *16*, 1585; c) J. Slinker, D. Bernerds, P. L. Houston, H. D. Abruna, S. Bernhard, G. G. Malliaras, *Chem. Commun.* **2003**, 2392.

Discrete Stacking of Large Aromatic Molecules within Organic-Pillared Coordination Cages**

Michito Yoshizawa, Junichi Nakagawa, Kazuhisa Kumazawa, Muneki Nagao, Masaki Kawano, Tomoji Ozeki, and Makoto Fujita*

Aromatic stacking of π -conjugated planar molecules leads to the exhibition of unique chemical and physical properties. Discotic liquid crystals are, for example, a columnar assembly of aromatic compounds that contain long alkyl chains,^[1] and organic electroconductive materials involve alternate charge-transfer stacking of electron-donating and -accepting π -conjugated compounds.^[2] Whereas such infinite assemblies have been thoroughly studied, precisely controlled discrete assemblies composed of more than two π -conjugated molecules have been explored much less frequently.^[3–6] As discrete assemblies of a limited number of π -stacked molecules are expected to show new properties different from those of isolated or infinitely stacked π -systems, a general method for constructing such structures has to be developed. Here, we report the self-assembly of a metal-hinged, organic-pillared cage with a large cavity that can accommodate two or more large π -conjugated molecules. The cage consists of two large organic panels (A), three rodlike pillars (B), and six metal hinges (C; Scheme 1). The large, box-shaped cavity accom-



Scheme 1. Schematic representation of the organic-pillared cage accommodating two or more π -conjugated guests. The ensemble self-assembles from components A–D (A: aromatic panel; B: rodlike pillar; C: metal hinge; D: aromatic guest).

[*] Dr. M. Yoshizawa, J. Nakagawa, K. Kumazawa, M. Nagao, Prof. M. Kawano, Prof. M. Fujita
Department of Applied Chemistry
School of Engineering
The University of Tokyo
Hongo, Bunkyo-ku, Tokyo 113-8656 (Japan)
Fax: (+81) 3-5841-7257
E-mail: mfujita@appchem.t.u-tokyo.ac.jp

Prof. T. Ozeki
Department of Chemistry and Materials Science
Tokyo Institute of Technology
O-okayama, Meguro-ku, Tokyo 152-8551 (Japan)

[**] This work was supported by a CREST (Core Research for Evolution Science and Technology) project from the Japan Science and Technology Agency. We thank Prof. S. Adachi (KEK) for performing the X-ray crystallographic measurements.



Supporting information for this article is available on the WWW under <http://www.angewandte.org> or from the author.

moderates a limited number of π -conjugated molecules (**D**); this number is strictly controlled by the length of the pillar molecules.

To realize such a multistacked aromatic host–guest system, we have designed the self-assembly of prismlike cage **1**¹²⁺ from tridentate panel-like ligand **2**, bidentate pillar ligand **3**, and end-capped Pd^{II} complex **4**²⁺ (Figure 1 a). The

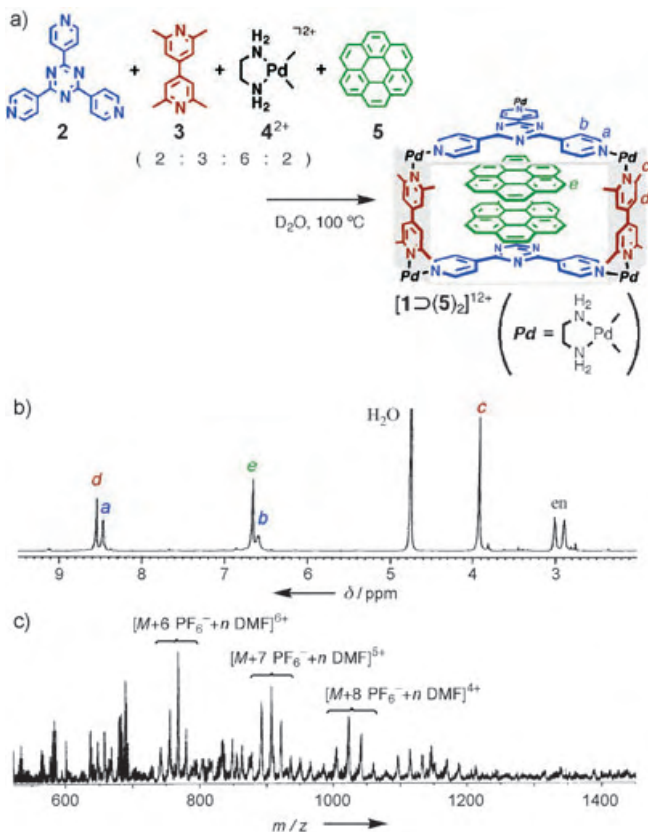


Figure 1. a) Schematic representation of the self-assembly of [1D(5)₂]¹²⁺; b) ¹H NMR (500 MHz, D₂O, RT) spectrum after the combination of **2**, **3**, **4**²⁺, and **5** in a 2:3:6:2 ratio at 100 °C for 2 h (en = ethylenediamine); c) CSI mass spectrum of [1D(5)₂]¹²⁺ after anion exchange with PF₆⁻.

resulting cage, as estimated by molecular modeling, can accommodate two large aromatic compounds. The space between the “floor” and the “roof” of the prism cage (≈ 7.5 Å) is approximately twice the thickness of planar aromatic compounds.^[7] In fact, in the presence of coronene (**5**), we observed the quantitative self-assembly of a quadruple-stacking structure [1D(5)₂]¹²⁺. Four components, **2**, **3**, **4**²⁺, and **5**, were combined in a 2:3:6:2 ratio in D₂O ([Pd^{II}] = 60 mM).^[8] After stirring at 100 °C for 2 h the suspension became clear and the color changed from pale yellow to deep red. ¹H NMR analysis of the solution indicated the formation of [1D(5)₂]¹²⁺ as a single product (Figure 1 b). The NMR spectrum agreed with the *D*_{3h} symmetry of **1**¹²⁺ and with the stoichiometry of the components. The signal of **5** (H_c) is shifted strongly upfield due to encapsulation in the cavity of **1**¹²⁺. Remarkably, the [1D(5)₂]¹²⁺ structure is stable even under CSI-MS conditions.^[9] After anion exchange with PF₆⁻,

the CSI mass spectrum shows a series of peaks for [1D(5)₂ + (12−*m*)PF₆⁻ + *n*DMF]^{*m*+} (e.g., *m/z* = 767.7 (*m* = 6, *n* = 12), 906.2 (*m* = 5, *n* = 9), and 1023.3 (*m* = 4, *n* = 1)), Figure 1 b. Guest-free **1**¹²⁺ was hardly detected, which suggests strong π – π interactions between the host and the guest.

The selective formation of [1D(5)₂]¹²⁺ from thirteen components ($2 \times 2 + 3 \times 3 + 6 \times 4^{2+} + 2 \times 5$) is due to two dominant factors: the template effect of the aromatic guests and ligand steric hindrance. Without the guests **5**, the assembly of cage **1**¹²⁺ occurs with considerable amounts of a homotopic M₆L₄ cage^[10] (composed of **2** and **4**²⁺) and some oligomeric products (composed of **3** and **4**²⁺). The α -methyl groups on the pyridyl pillars **3** provide a steric bulk that prevents the coordination of two pillar ligands to the same Pd^{II} center.^[11,12]

X-ray crystallographic analysis provided concrete evidence for the quadruple-stacking structure of [1D(5)₂]¹²⁺. When pyrene (**6**) was used as a large planar guest,^[13] a dark-reddish single crystal of [1D(6)₂]¹²⁺ was obtained after a few weeks at room temperature by the slow diffusion of ethanol vapor into an aqueous solution containing [1D(6)₂]¹²⁺. The diffraction data were collected by synchrotron X-ray radiation (KEK, PF-AR beamline NW2) at −184 °C.^[14] Despite severe disorder of the solvents and counterions, the prismlike structure of **1**¹²⁺ accommodating two molecules of **6** in the cavity was successfully solved (Figure 2). The cage is twisted by 36°, which results in efficient quadruple aromatic stacking. The interplane distances 2···6 and 6···6 are 3.4 and 3.3 Å, respectively.

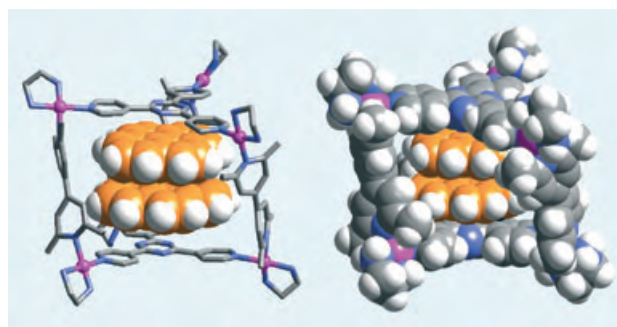


Figure 2. X-ray crystal structure of [1D(6)₂]¹²⁺ (**6**: pyrene).

The use of elongated pillar ligand **7** increased the size of the cavity (Figure 3 a). Indeed, the expanded prismlike cage **8**¹²⁺ was successfully assembled when the components **2**, **7**, and **4**²⁺ were combined in the presence of guest **5**. Surprisingly, cage **8**¹²⁺ binds two molecules of **5** and one molecule of ligand **2** within the cavity. The uncoordinated **2** is sandwiched by two coronene guests such that an [8D(5·2·5)]¹²⁺ structure is formed. The yield of this assembly was optimal when **2**, **7**, and **4**²⁺ were combined in a 3:3:6 ratio in the presence of an excess amount of **5** (Figure 3 a).^[8]

The unique structure involving quintuple stacking (2···5···2···5···2) was strongly supported by NMR spectroscopy and CSI mass spectrometry. Simple ¹H NMR spectroscopy (Figure 3 b) showed that the two Pd^{II}-coordinated panel

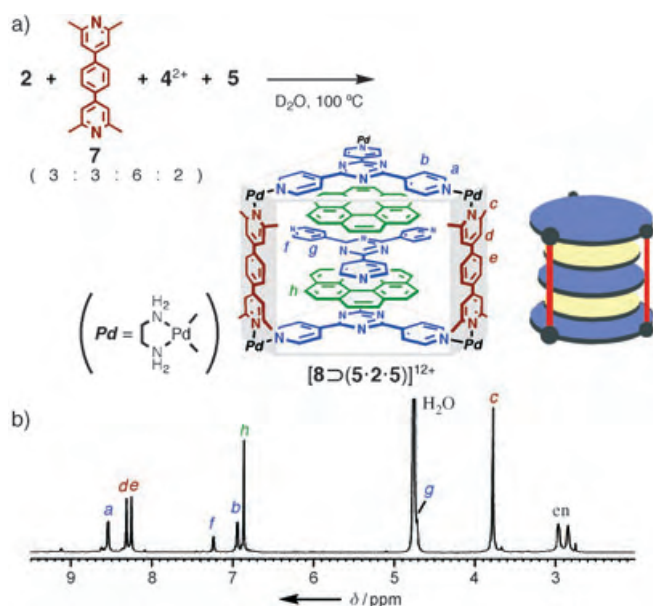


Figure 3. a) Quintuple-stacked, prismatic structure of $[8\supset(5\cdot2\cdot5)]^{12+}$ which self-assembles from **2**, **7**, **4**²⁺, and **5** in a 3:3:6:2 ratio; b) ¹H NMR (500 MHz, D₂O, RT) spectrum of $[8\supset(5\cdot2\cdot5)]^{12+}$.

ligands (**2**, signals H_a and H_b) and two coronene guests (**5**, signal H_h) are equivalent. These results are in good agreement with the expected *D*_{3h} symmetry of the system. The middle panel **2** is shifted significantly upfield (signals H_f and H_g at δ = 7.23 and 4.71 ppm, respectively) due to intercalation between two molecules of **5**. After counteranion exchange, the CSI mass spectrum showed clear peaks for $[8\supset(5\cdot2\cdot5)]^{12+} + (12-m)\text{PF}_6^- + n\text{DMF}]^{m+}$. Note that the noncovalently associated $[8\supset(5\cdot2\cdot5)]^{12+}$ structure is still stable under the CSI-MS conditions.^[8]

The efficient π -stacking in the $[8\supset(5\cdot2\cdot5)]^{12+}$ structure is ascribed to donor–acceptor charge-transfer (CT) interactions throughout the aromatic components. The Pd^{II}-coordinated ligand **2** is highly electron deficient due to metal coordination at the three pyridyl sites. Even the guest molecule of **2** possesses an electron-deficient triazine core because of the electron-withdrawing effect of the pyridyl groups. Therefore, electron-rich coronenes are apt to form a CT complex with both coordinated and free molecules of **2** such that the $[8\supset(5\cdot2\cdot5)]^{12+}$ structure is stabilized by A–D–A–D–A aromatic stacking (A: acceptor; D: donor).

The even–odd-number effect of the stacking aromatic rings was clearly demonstrated by UV/Vis absorption spectroscopy (Figure 4). The pyrazine-pillared prismatic cage **9**¹²⁺ was found to bind coronene (**5**) to form an A–D–A stack with a $[9\supset5]^{12+}$ structure.^[4] A weak CT band (shoulder) was observed for the A–D–A stack at around 450 nm. In contrast, a stronger CT absorption at around 475 nm (ϵ = 3500 M^{−1} cm^{−1}) was observed for $[1\supset(5)_2]^{12+}$, which involves A–D–D–A stacking. As the HOMO level of the stacked (**5**)₂ dimer is higher than that of **5**, the charge transfer band is red-shifted. For $[8\supset(5\cdot2\cdot5)]^{12+}$, the absorption moves back to around 450 nm because of A–D–A-type stacking similar to that of $[9\supset5]^{12+}$.

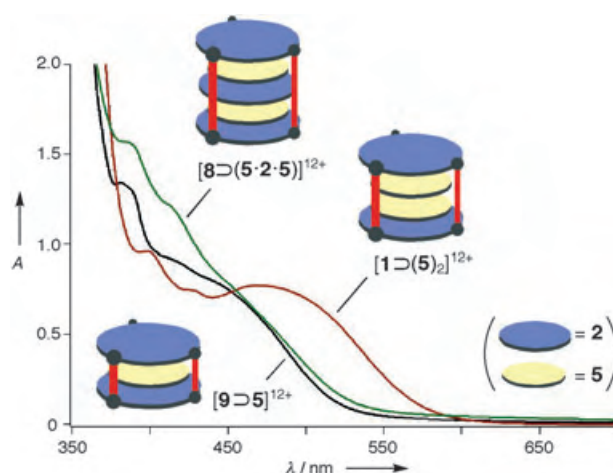
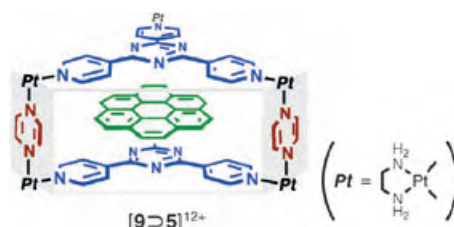


Figure 4. UV/Vis spectra (H₂O, RT) of the multistacked aromatic assemblies $[1\supset(5)_2]^{12+}$, $[8\supset(5\cdot2\cdot5)]^{12+}$, and $[9\supset5]^{12+}$.



In summary, we have achieved quadruple and quintuple stacking of large π -conjugated molecules by self-assembly. Our strategy can, in principle, be extended to multiply stacking π -systems. Such discrete stacking should produce unique photochemical and electrochemical properties that are uncommon for isolated or infinitely stacked π -systems. Further investigations in these areas are now in progress.

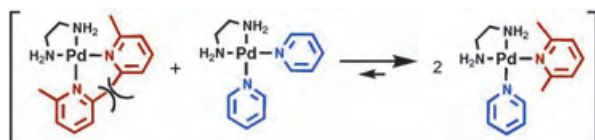
Received: October 1, 2004

Published online: February 16, 2005

Keywords: charge transfer · host–guest systems · palladium · π interactions · self-assembly

- [1] For a recent review of discotic liquid crystals, see: R. J. Bushby, O. R. Lozman, *Curr. Opin. Colloid Interface Sci.* **2002**, *7*, 343.
- [2] a) J. Ferraris, D. O. Cowan, V. Walatka, J. H. Perlstein, *J. Am. Chem. Soc.* **1973**, *95*, 948–949; b) L. B. Coleman, M. J. Cohen, D. J. Sandman, F. G. Yamagishi, A. F. Garito, A. J. Heeger, *Solid State Commun.* **1973**, *12*, 1125–1132.
- [3] a) L. D. Costanzo, S. Geremia, L. Randaccio, R. Purrello, R. Lauceri, D. Sciotto, F. G. Gulino, V. Pavone, *Angew. Chem.* **2001**, *113*, 4375–4377; *Angew. Chem. Int. Ed.* **2001**, *40*, 4245–4247; b) G. Moschetto, R. Lauceri, F. G. Gulino, D. Sciotto, R. Purrello, *J. Am. Chem. Soc.* **2002**, *124*, 14536–14537.
- [4] K. Kumazawa, K. Biradha, T. Kusukawa, T. Okano, M. Fujita, *Angew. Chem.* **2003**, *115*, 4039–4043; *Angew. Chem. Int. Ed.* **2003**, *42*, 3909–3913.
- [5] a) S.-S. Sun, A. Lees, *Chem. Commun.* **2001**, 103–104; b) J. D. Crowley, A. J. Goshe, B. Bosnich, *Chem. Commun.* **2003**, 2824–

- 2825; c) J. M. C. A. Kerckhoffs, F. W. B. A. van Leeuwen, A. L. Spek, H. Kooijman, M. Crego-Calama, D. N. Reinhoudt, *Angew. Chem.* **2003**, *115*, 5895–5900; *Angew. Chem. Int. Ed.* **2003**, *42*, 5717–5722; d) K. Kumazawa, Y. Yamanoi, M. Yoshizawa, T. Kusakawa, M. Fujita, *Angew. Chem.* **2004**, *116*, 6062–6066; *Angew. Chem. Int. Ed.* **2004**, *43*, 5936–5940.
- [6] M. Fujita, N. Fujita, K. Ogura, K. Yamaguchi, *Nature* **1999**, *400*, 52–55.
- [7] Molecular modeling of $[1\text{D}(5)_2]^{12+}$ was optimized by MM2 calculations with Cerius² 3.5 (see Supporting Information).
- [8] Physical data of $[1\text{D}(5)_2]^{12+}$ and $[8\text{D}(5\cdot2\cdot5)]^{12+}$ are given in the Supporting Information.
- [9] CSI-MS analysis: K. Yamaguchi, *J. Mass Spectrom.* **2003**, *38*, 473–490.
- [10] a) M. Fujita, D. Oguro, M. Miyazawa, H. Oka, K. Yamaguchi, K. Ogura, *Nature* **1995**, *378*, 469–471; b) M. Yoshizawa, M. Tamura, M. Fujita, *J. Am. Chem. Soc.* **2004**, *126*, 6846–6847; c) M. Yoshizawa, S. Miyagi, M. Kawano, K. Ishiguro, M. Fujita, *J. Am. Chem. Soc.* **2004**, *126*, 9172–9173; d) K. Nakabayashi, M. Kawano, M. Yoshizawa, S. Ohkoshi, M. Fujita, *J. Am. Chem. Soc.* **2004**, *126*, 16694–16695.
- [11] Side-chain-directed assembly: M. Yoshizawa, M. Nagao, K. Umemoto, K. Biradha, M. Fujita, S. Sakamoto, K. Yamaguchi, *Chem. Commun.* **2003**, 1808–1809.
- [12] The following equilibrium is pushed toward the right-hand side because of steric repulsion that arises on the left-hand side.



- [13] Other large π -aromatic guests (e.g., pyrene and perylene) were also efficiently incorporated within 1^{12+} to afford the corresponding quadruple-stacking structures. See also the Supporting Information.
- [14] X-ray crystallographic data of $[1\text{D}(6)_2]^{12+}$: $\text{C}_{244}\text{H}_{272}\text{N}_{66}\text{O}_{80}\text{Pd}_{12}$, $M = 6602.02$, crystal dimensions $0.48 \times 0.04 \times 0.04 \text{ mm}^3$, orthorhombic space group $C222_1$, $a = 20.4596(14) \text{ \AA}$, $b = 35.453(3) \text{ \AA}$, $c = 53.544(6) \text{ \AA}$, $V = 38839(6) \text{ \AA}^3$, $Z = 4$, $\rho_{\text{calcd}} = 1.129 \text{ g cm}^{-3}$, $F(000) = 13392$, $\lambda(\text{synchrotron radiation}) = 0.6890 \text{ \AA}$, $T = 89(2) \text{ K}$, reflections collected/unique $56652/25550$ ($R_{\text{int}} = 0.1703$). The structure was solved by direct methods (SHELXL-97) and refined by full-matrix least-squares methods on F^2 with 1376 parameters. $R_1 = 0.1579$ ($I > 2\sigma(I)$), $wR_2 = 0.3822$, GOF 1.122; max/min. residual density $0.621/-0.549 \text{ e \AA}^{-3}$. The counterions and water molecules were severely disordered. CCDC-251181 contains the supplementary crystallographic data for this paper. These data can be obtained free of charge from the Cambridge Crystallographic Data Centre via www.ccdc.cam.ac.uk/data_request/cif.

Tunable Imaging of Cells Labeled with MRI-PARACEST Agents**

Silvio Aime,* Carla Carrera, Daniela Delli Castelli, Simonetta Geninatti Crich, and Enzo Terreno

Magnetic resonance imaging (MRI) modality is ideally suited to monitor cell tracking in vivo, as it exhibits superb spatial resolution.^[1] Two classes of MRI probes are currently used in cell-labeling procedures: iron oxide nanoparticles and Gd^{III} chelates, both of which act as relaxation enhancers of water protons. The use of the former class in cell-tracking studies is well established.^[2–5] Until now, the latter class has enjoyed only limited use in cell labeling, although it has been shown that incubation of stem cells in the presence of stable Gd^{III} chelates can give good internalization results.^[6–8] The metal chelate units are usually confined inside endosomes in the perinuclear region; in this form, they do not affect cell viability. Moreover, it has been found recently that stem cells labeled with [Gd(hpdo3A)] (a clinically approved agent) are MRI-detectable up to two weeks after implantation.^[8] The main drawback of both classes of agents is that visualization of more than one ensemble of labeled cells in each cell-tracking experiment is not possible.

Recently, a new class of MRI contrast agents has been proposed: the so-called CEST (chemical exchange saturation transfer) agents.^[9] These systems contain at least one pool of exchangeable protons, which upon irradiation at their absorption frequency, transfer saturated magnetization to the bulk water signal (Figure 1). Thus, members of this class of agent act as negative agents (analogous to iron oxide particles) by decreasing the intensity of the water signal through the transfer of saturated magnetization. Interestingly, these agents display their effect in MRI only when the irradiation frequency is set at the value that corresponds to the absorption frequency of their mobile protons. The use of lanthanide(III) paramagnetic chelates (PARACEST agents) has been shown to be particularly beneficial, as the paramagnetic ion induces a large shift in the resonance of nuclei surrounding it.^[10] In fact, a large chemical-shift difference between the exchangeable protons and bulk water resonances allows the exploitation of larger values of exchange rates (k_{ex}) which, in turn, results in a more efficient transfer of saturated magnetization. Moreover, the use of PARACEST agents endowed with markedly different chemical-shift values of the

[*] Prof. S. Aime, Dr. C. Carrera, Dr. D. Delli Castelli, Dr. S. Geninatti Crich, Dr. E. Terreno
Dipartimento di Chimica I.F.M.
Via P. Giuria 7, 10125 Torino (Italy)
Fax: (+39) 011-670-7855
E-mail: silvio.aime@unito.it

[**] Financial support from Bracco Imaging S.p.A., and MIUR (FIRB) are gratefully acknowledged. This work has been carried out under the framework of the EU-COST D 18 Action and EMIL-NoE.

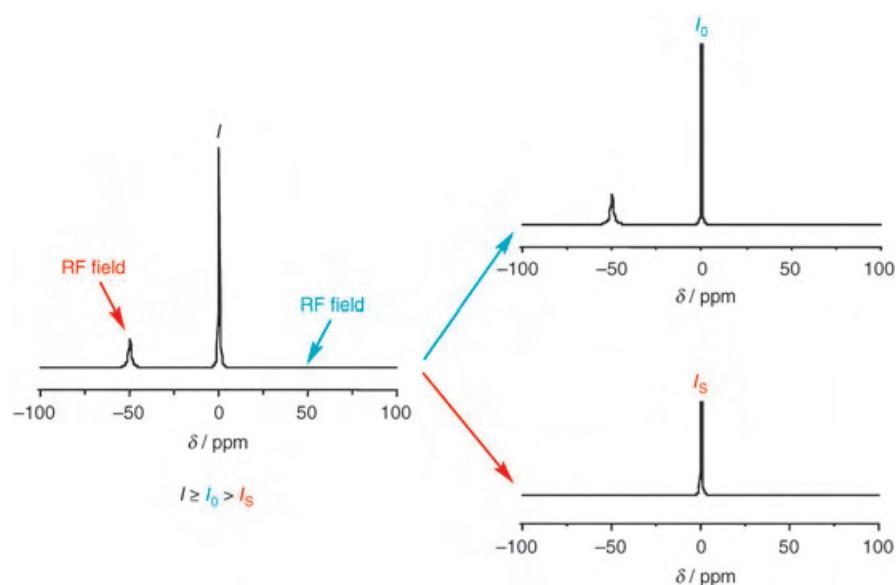
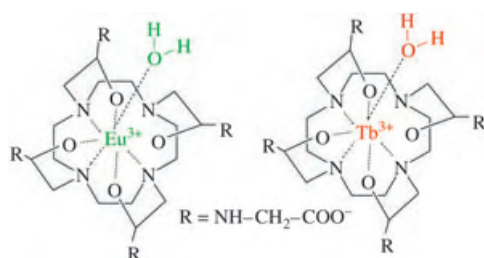


Figure 1. A given RF field is applied at the resonance frequency of the exchangeable protons of the CEST agent (red). The saturation of this resonance is transferred to the resonance of the bulk water protons ($I_S < I$). As the RF field may perturb the intensity of the signal of water protons, the same RF field is applied at a frequency symmetrically opposite to that of the CEST agent (blue). Therefore, the net saturation transfer is calculated as $ST = 1 - (I_S/I_0)$.

exchangeable protons allows them to be visualized at will by a selection of the proper irradiation frequency.

The PARACEST agents used in the study reported herein are shown below. The two metal complexes share the same



ligand (dotamGly) and therefore have the same chemical and biological behavior, whereas their ^1H NMR spectra are markedly different, as expected from the different magnetic characteristics of the two lanthanide(III) ions.^[11] Both complexes contain two pools of exchangeable protons: the metal-coordinated water protons and the amide protons.^[12] Herein, the presence of both PARACEST agents was visualized by using the water resonances that were the most dramatically shifted. Thus, by irradiation 50 ppm downfield from the resonance of bulk water protons, it is possible to detect the response from the Eu^{III} complex, whereas a switch to an irradiation frequency of -600 ppm from bulk water permits detection of the Tb^{III} complex instead.

Figure 2 shows the results obtained from a phantom that comprises four capillaries: A) phosphate buffer, B) $[\text{Tb}(\text{dotamGly})]$ (2 mM), C) $[\text{Eu}(\text{dotamGly})]$ (2 mM), and D) a mixture of the two complexes at a concentration of 1 mM. The CEST-MR images represent the subtraction of two images

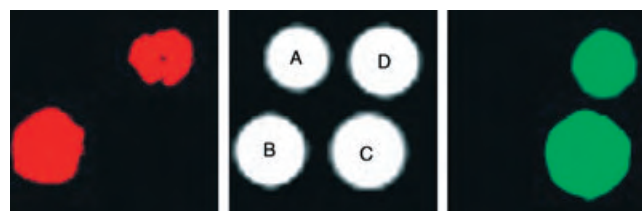


Figure 2. Middle image: MRI (7 T) of a phantom made of four capillaries that contain: A) PBS buffer, B) $[\text{Tb}(\text{dotamGly})]$ (2 mM), C) $[\text{Eu}(\text{dotamGly})]$ (2 mM), D) $[\text{Tb}(\text{dotamGly})]$ and $[\text{Eu}(\text{dotamGly})]$ (1 mM each). Right and left: CEST-MR difference images obtained by irradiation of the metal-bound water protons of $[\text{Tb}(\text{dotamGly})]$ (left) and $[\text{Eu}(\text{dotamGly})]$ (right); the contrast has been arbitrarily colored in red and green, respectively; dotamGly = the tetraglycineamide derivative of dota: 1,4,7,10-tetraazacyclododecane-1,4,7,10-tetraacetic acid.

(spot A)). The reverse result occurs upon irradiation at 50 ppm (absolute value), in which case only the presence of the Eu^{III} complex is detected (green spots). The extent of the saturation transfer is proportional to the concentration of the PARACEST agent. Consequently, tubes containing solution concentrations of 2 mM are more intense. Quantitatively, the decrease in the intensity of the water signal upon irradiation of the water bound to the Eu^{III} complex was 4% (1 mM) and 12% (2 mM), whereas the corresponding values for Tb^{III} analogue were 8% (1 mM) and 12% (2 mM).

Cell labeling with the two PARACEST probes was carried out by incubation of $\approx 10^6$ HTC (rat hepatoma) tumor cells in the presence of each complex (40 mM) in the incubation medium for 6 h. A rough estimate of the amount of internalized complex was determined by performing the same incubation procedure with the $[\text{Gd}(\text{dotamGly})]$ com-

plex. After incubation, the cells were washed three times and the amount of internalized Gd^{III} was determined by relaxometric measurement of the cell lysates obtained after mineralization with HCl (3 M) in a sealed vial at 120°C overnight.^[8] The amount of Gd^{III} complex internalized upon incubation at 40 mM, $\approx 8 \times 10^9$ molecules/cell, is a good parallel to the results reported for the internalization of $[\text{Gd}(\text{hpd}3\text{A})]$ into endothelial progenitor cells.^[8]

Cells incubated in the presence of $[\text{Eu}(\text{dotamGly})]$ and $[\text{Tb}(\text{dotamGly})]$ were collected as pellets after three wash steps with DMEM (DMEM = Dulbecco modified Eagle medium). Next, a phantom similar to that shown in Figure 2 was prepared, in which spot A) contained a pellet of unlabeled HTC cells, B) a pellet of Tb^{III} -labeled cells, C) pelleted cells labeled with the Eu^{III} complex, and D) a pellet obtained from a mixture of cells of spots B) and C). As described above for the aqueous solutions, the irradiation frequency was initially set at 600 ppm and then at 50 ppm (absolute values). Again, by irradiation at 600 ppm, cells that contained Tb^{III} complex were detected exclusively, whereas a switch of the irradiation frequency to 50 ppm showed a response only from Eu^{III} -complex-containing cells (Figure 3). The decrease in the intensity of the water signal was 4% (pellet D)) and 12% (pellet C)) upon irradiation at ± 50 ppm, and 3.5% (pellet D)) and 11.2% (pellet B)) upon irradiation at ± 600 ppm.

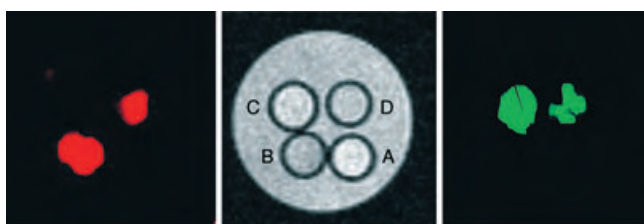


Figure 3. Middle image: MRI (7 T) of a phantom made of four capillaries that contain: A) unlabeled HTC cells, B) HTC cells labeled with $[\text{Tb}(\text{dotamGly})]$, C) HTC cells labeled with $[\text{Eu}(\text{dotamGly})]$, D) cellular pellet obtained from a mixture of pellets of spots B) and C). Right and Left: CEST-MR difference images obtained by irradiation of the metal-bound water protons of $[\text{Tb}(\text{dotamGly})]$ (left) and $[\text{Eu}(\text{dotamGly})]$ (right); the contrast has been arbitrarily colored in red and green, respectively.

In summary, these studies establish and validate a novel and powerful tool for the detection of different ensembles of labeled cells, and provide a rationale for the development of analogous procedures for detection *in vivo*. Internalization of the PARACEST agents by pinocytosis appears to be a safe and efficient route for cellular labeling, as it allows entrapment of high quantities of the agent, sufficient for CEST-MRI detection. Furthermore, as it has been shown that PARACEST agents can be designed to respond to a specific parameter of the microenvironment in which they are distributed,^[13–15] a number of applications can be envisaged that expand the potential of MRI techniques in the field of cell tracking. Finally, this approach may provide useful insight for the evaluation of novel cell-based therapies *in vivo*, as the fates of differently labeled cells that are administered serially can be followed.

Experimental Section

Chemicals: $[\text{Eu}(\text{dotamGly})]$ and $[\text{Tb}(\text{dotamGly})]$ were synthesized according to literature protocol.^[11]

Cells: HTC cells (rat tumor hepatoma cells) were provided by the ICLC (National Institute for Cancer Research, Genova, Italy) and were labeled with $[\text{Eu}(\text{dotamGly})]$ or $[\text{Tb}(\text{dotamGly})]$ probes according to methods previously described.^[8] Briefly, $\approx 5\text{--}6 \times 10^6$ cells were incubated at 37°C for 6 h in a culture medium containing the labeling probe (40 mM). The cells were then washed three times with ice-cold PBS (phosphate-buffered saline) (10 mL) and detached by the addition of trypsin and EDTA (ethylenediaminetetraacetic acid).

MRI: All CEST-MR images were acquired on a Bruker Avance 300 spectrometer equipped with a MICRO 2.5 microimaging probe (resonator ID: 10 mm). Each CEST-MR image is the difference of two spin echo images ($\text{TR}/\text{TE}/\text{NE} = 6 \text{ s}/3.5 \text{ ms}/1$) that differ in the offset of the irradiation pulse ($I_s - I_0$, Figure 1). The total irradiation time was 2 s. The irradiation pulse consisted of a train of sinc3 pulses (irradiation power $\approx 250 \mu\text{T}$) with a duration of 1 ms for the Eu^{III} complex and $250 \mu\text{s}$ for the Tb^{III} complex. The interpulse delay was 10 μs . Other parameters: 64×64 isotropic matrix; FOV $6 \times 6 \text{ mm}$; slice thickness = 2 mm.

Received: November 10, 2004

Published online: February 21, 2005

Keywords: imaging agents · lanthanides · magnetic properties · proton exchange · saturation transfer

- [1] P. A. Rinck, *Magnetic Resonance in Medicine*, ABW Wissenschaftsverlag GmbH, Berlin, **2003**.
- [2] P. Jendelova, V. Herynek, L. Urdzikova, K. Glogarova, J. Kroupova, B. Andersson, V. Bryja, M. Burian, M. Hajek, E. Sykova, *J. Neurosci. Res.* **2004**, *76*, 232–243.
- [3] J. A. Frank, B. R. Miller, A. S. Arbab, H. A. Zywicke, E. K. Jordan, B. K. Lewis, L. H. Bryant, J. W. M. Bulte, *Radiology* **2003**, *228*, 480–487.
- [4] K. A. Hinds, J. M. Hill, E. M. Shapiro, M. O. Laukkanen, A. C. Silva, C. A. Combs, T. R. Varney, R. S. Balaban, A. P. Koretsky, C. E. Dunbar, *Blood* **2003**, *102*, 867–872.
- [5] M. Hoehn, E. Kustermann, J. Blunk, D. Wiedermann, T. Trapp, S. Wecker, M. Focking, H. Arnold, J. Hescheler, B. K. Fleischmann, W. Schwindt, C. Buhle, *Proc. Natl. Acad. Sci. USA* **2002**, *99*, 16267–16272.
- [6] M. Rudelius, H. E. Daldrup-Link, U. Heinzmann, G. Piontek, M. Settles, T. M. Link, J. Schlegel, *Eur. J. Nucl. Med. Mol. Imaging* **2003**, *30*, 1038–1044.
- [7] M. Modo, K. Mellodew, D. Cash, S. E. Fraser, T. J. Meade, J. Price, S. C. R. Williams, *Neuroimage* **2004**, *21*, 311–317.
- [8] S. Geninatti Crich, L. Biancone, V. Cantaluppi, G. Esposito, S. Russo, G. Camussi, S. Aime, *Magn. Reson. Med.* **2004**, *51*, 938–944.
- [9] K. M. Ward, A. H. Aletras, R. S. Balaban, *J. Magn. Reson.* **2000**, *143*, 79–87.
- [10] S. Zhang, M. Merritt, D. E. Woessner, R. E. Lenkinski, A. D. Sherry, *Acc. Chem. Res.* **2003**, *36*, 783–790.
- [11] S. Aime, A. Barge, D. Delli Castelli, F. Fedeli, A. Mortillaro, F. U. Nielsen, E. Terreno, *Magn. Reson. Med.* **2002**, *47*, 639–648.
- [12] E. Terreno, D. Delli Castelli, G. Cravotto, L. Milone, S. Aime, *Invest. Radiol.* **2004**, *39*, 235–243.
- [13] S. Aime, D. Delli Castelli, E. Terreno, *Angew. Chem.* **2002**, *114*, 4510–4512; *Angew. Chem. Int. Ed.* **2002**, *41*, 4334–4336.
- [14] S. Aime, D. Delli Castelli, F. Fedeli, E. Terreno, *J. Am. Chem. Soc.* **2002**, *124*, 9364–9365.
- [15] S. Zhang, R. Trokowski, A. D. Sherry, *J. Am. Chem. Soc.* **2003**, *125*, 15288–15289.

Methane and Carbon Dioxide Storage in a Porous van der Waals Crystal**

P. Sozzani,* S. Bracco, A. Comotti, L. Ferretti, and R. Simonutti

The absorption properties of materials are emerging as a forefront issue of present-day research boosted by strategic industrial and environmental applications such as gas storage, selective gas recognition, and separation.^[1] Molecular self-assembled materials and organic zeolites^[2] are still to be explored extensively as a competing alternative in the field, although they are promising as a result of their unique features. In fact, they can be prepared simply by exploiting soft interactions: the ease of formation results in a surprising modularity of the preparation approach. The available space for absorbates can be engineered in the shape of nanochannels lined with an infinite number of receptors for targeted and selective physisorption. Selectivity is provided not only by the channel opening, as in conventional zeolites, but also by organic groups that focus specific interactions on the channel core and fabricate supramolecular structures that cooperatively stabilize gases that diffuse in. Relatively narrow channels with interacting walls provide greater stability and thus milder absorption conditions than those necessary in the widely reported large-cavity systems, as in the case of metal–organic frameworks.^[3] Moreover, the network of soft interactions is often amenable to switching properties and to fabricating actuators, as reversible changes from an absorbing state to a close-packed inactive polymorph can be triggered by thermal, mechanical, or radiative stimuli.^[4]

Herein we show the remarkable sorption properties of molecular crystals of tris-*o*-phenylenedioxy-cyclotriphosphazene (**1**; TPP)^[5] with respect to important gases that participate in a network of soft interactions. In fact, methane and carbon dioxide, key gases in the global economy, could be incorporated with high efficiency in the novel adducts (60% and 100% occupation, respectively, of the available sites, guest–host molar fraction of up to 1.25) with neat selectivity over other gases. Unprecedented observations of the gases in van der Waals crystals and their topology could be provided by fast MAS NMR spectroscopy.

The empty-pore hexagonal structure was solved for the first time after isolation of diffraction-quality single crystals and showed no residual electron density in the large

unoccupied volume, shaped as straight nanochannels with a minimum diameter of 4.6 Å (Supporting Information). Weak intermolecular interactions consolidate molecular stacks along the *c* axis (repeat period of 10.16 Å) and layers on the *a*–*b* plane (*a* = 11.45 Å), ensuring the stability of the assembly (Figure 1). The crystal density is low ($\rho_{\text{calcd}} = 1.321 \text{ g cm}^{-3}$) and 25% of the volume is available to guests in the noncovalent architecture.

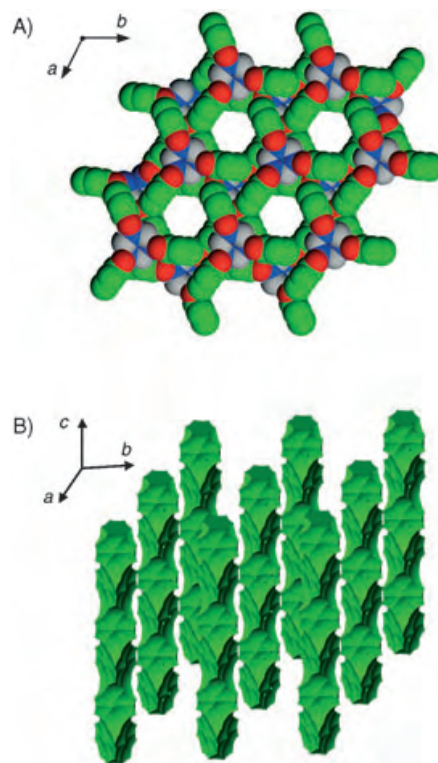


Figure 1. A) Crystal structure of **1** in the nanoporous hexagonal modification viewed along the channel axis: a double layer of molecules is presented; no residual electron density along the nanochannels is shown by Fourier difference maps, indicating the permanent porosity of the structure. B) Portion of the space described by the center of a sphere of 2.5 Å diameter exploring the empty nanochannels ($3 \times 3 \times 3$ array of unit cells).

The absorption capacity of the nanoporous crystal was measured for a few gases, including Ar, N₂, O₂, H₂, CH₄, and CO₂, under isothermal conditions both by precision microbalance and pressure measurements (see Experimental Section). The molecular structure shows the highest sorption values with methane and carbon dioxide (Figure 2).

The isotherm for methane at 195 K traces a typical type I curve that at 1 atm has not yet reached the saturation value. The nanoporous crystal can store up to 0.7 mol of CH₄ per mol of **1** under these conditions. Based on a limit storage value of about 1.2 mol per mol (58 cm³ g^{−1} at STP), beyond which the gas molecules interact directly with each other in the nanochannels by van der Waals close contacts,^[6] we can conclude that a large part of the space available for guests is occupied at equilibrium, indicating a high storage capacity

[*] Prof. P. Sozzani, Dr. S. Bracco, Dr. A. Comotti, Dr. L. Ferretti, Dr. R. Simonutti
Department of Materials Science
Università degli Studi di Milano-Bicocca
Via R. Cozzi 53, 20125 Milan (Italy)
Fax: (+39) 02-6448-5400
E-mail: piero.sozzani@mater.unimib.it

[**] This work was partially supported by MIUR and FISIR projects.
Supporting information for this article is available on the WWW under <http://www.angewandte.org> or from the author.

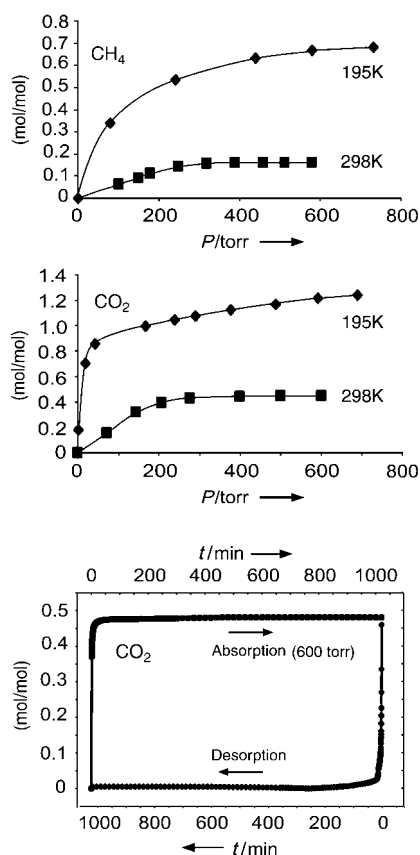


Figure 2. Absorption isotherms of CH₄ and CO₂ expressed as moles of gas per mole of **1** at 195 K and room temperature and microbalance measurements showing the absorption/desorption kinetics of CO₂ at room temperature.

and a large host–guest interaction. The uptake value of methane at 195 K is 2.4 wt %, which corresponds to 33.2 cm³ g^{−1} (at STP), and is comparable with, or exceeds, the values of inorganic zeolites containing 1D channels with a similar diameter.^[7] Even under the mild conditions of ambient pressure and temperature, the efficiency of organic zeolite for methane storage (0.6 wt %) is as high as in conventional zeolites (e.g. in silicalite)^[7b] and in metal complexes of comparable channel size (\approx 0.8 wt % at 1 atm, 298 K).^[8] The system appears to be very competitive, especially at low pressures, with respect to other recently proposed van der Waals crystals, in which high pressure (100 atm) is required to reach the saturation of the crystals.^[9] This may be due to the peculiar open-pore structure of the hexagonal crystals of **1**, as was shown by single-crystal X-ray analysis.

The nanoporous architecture of **1** presents a surprisingly high storage capacity for CO₂, even at low pressures. In fact, it reaches 1.24 mol of CO₂ absorbed per mol of host at 195 K and 1 atm (12 wt % and 60.5 cm³ g^{−1} at STP), indicating the virtually complete filling of the available volume in the structure and more than two gas molecules per unit cell.^[10] The storage capacity is also considerably high at ambient temperature, setting values of about 0.5 mol mol^{−1}: with a single CO₂ molecule occupying, on the average, the unit cell. The values match the absorption capacity of the most

valuable materials of comparable channel size described in the literature.^[11] Interestingly, the kinetics of absorption are very fast: after 14 min of contact between CO₂ and crystals of **1** at 600 torr, the saturation limit (4.3 wt %) is reached, as shown by precision microbalance measurements (Figure 2). The desorption process is equally fast and no hysteresis is present. CO₂ is rapidly absorbed by the crystals of **1** because of the small kinetic diameter of 3.3 Å and as a result of the loose steric fitting of the gas molecules inside the channels. Superior properties are shown especially under mild conditions, as the initial slopes of the sorption isotherms are very steep at low pressure, owing to the considerable stabilization in the organic zeolite.^[7b,11a] Carbon dioxide absorption values are considerably higher at room temperature than those recently reported for a molecular crystal of *tert*-butylcalixarene containing aromatic groups.^[12]

The direct observation of gas molecules diffused to nanochannels is a challenge for solid-state NMR spectroscopy. The remarkable stability of the gases stored in the host allowed the easy manipulation of the samples and detection the spectra of the gases in the crystals under ambient conditions and in natural isotope abundance. The resonance of stored methane appears in the ¹³C MAS NMR spectrum as a sharp signal at −9.4 ppm relative to TMS, notably upfield to any known resonance of methane (Figure 3a). Host signals are limited to three, as the high-symmetry arrangement of the hexagonal crystal cell is not lost upon gas loading.

Rare reports of methane observed by NMR spectroscopy have appeared in the literature, with ¹³C NMR chemical shifts ranging from $\delta = -5$ up to -8 ppm.^[13] In particular, methane stored in inorganic zeolites with channel diameters comparable to ours resonates at $\delta_C = -8$ ppm. The exceptional upfield shift to -9.4 ppm determined here is explained by the large magnetic susceptibility effect of the aromatic matrix, showing unequivocally that methane is filled into narrow crystal pipes lined with aromatic groups (Figure 3). Even more impressively, the upfield shift was apparent in the 30 ppm total range of the ¹H NMR spectrum, which was notably resolved at the high spinning speed of 15 kHz:^[14] in this case an intense signal of the stored methane is detected at $\delta_H = -2.0$ ppm along with a weak signal for the gas-phase methane loaded in the sealed rotor at $\delta_H = -0.3$ ppm.^[15] A direct comparison of the resonances of methane in the two states of free and included gas precisely measures the nucleus-independent upfield shift of $\Delta\delta_H = -1.7$ ppm ($\Delta\delta_H = \delta_{H(\text{stored gas})} - \delta_{H(\text{free gas})}$) as a result of the magnetic susceptibility of the aromatic groups directly surrounding the hydrogen atoms.^[16] The quantitative analysis of the ¹H NMR spectrum could give, independently, the amount of the gas absorbed in the zeolite, confirming the high storage values obtained by the sorption isotherms (Figure 3b).

The ¹³C MAS NMR spectrum of the sample containing CO₂ shows, in addition to the matrix carbon atoms, a signal for CO₂ stored in the nanoporous crystals (Figure 3d). However, the resonance is very close to that of one of the carbon atoms of the matrix, namely C₃; this drawback was overcome by performing a so-called Non Quaternary Suppression (NQS) experiment in which suitable irradiation conditions were found to suppress the protonated carbon atoms of the matrix.

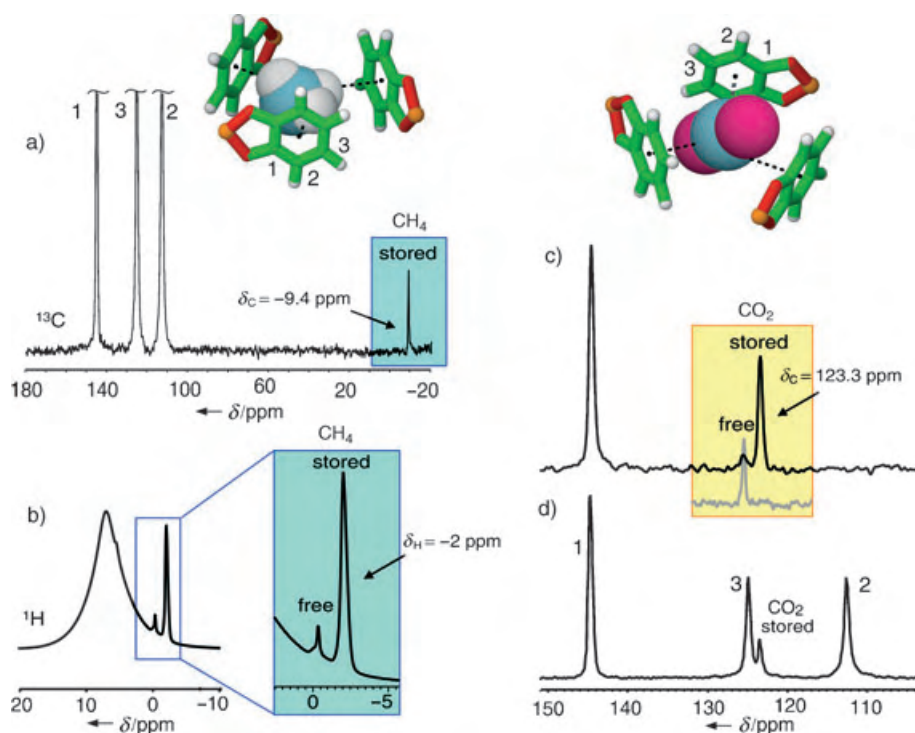


Figure 3. Fast magic-angle spinning (MAS) NMR spectra of gases stored in the van der Waals crystals. Methane stored in **1**: a) ^{13}C MAS NMR spectrum; b) ^1H MAS NMR spectrum showing the stored and free gas resonances (enlarged in the insert); the aromatic hydrogen atoms of the matrix appear as a wide signal centered at $\delta = 6.8$ ppm. Carbon dioxide stored in **1**: c) ^{13}C MAS NMR spectrum obtained by applying the Non Quaternary Suppression (NQS) filter compared with the free gas detected separately and d) single-pulse Excitation ^{13}C MAS NMR spectrum showing also the three matrix signals.

The filtered spectrum presents a neat signal at $\delta = 123.3$ ppm, which was assigned to the unprotonated carbon of CO_2 (Figure 3c). The resonance of carbon dioxide stored in the nanochannels is found at the highest field thus far reported in the literature: in particular, it appears much further upfield ($\delta = 133$ ppm) than the signals for bulk solid CO_2 , CO_2 associated with calixarenes and cucurbit[5]uril, and free CO_2 gas.^[15b,17] We measured the value of $\delta = 125.4$ ppm for pure gas-phase CO_2 under ambient conditions (insert of Figure 3c) and established, therefore, the remarkable upfield shift of $\Delta\delta_{\text{C}} = -2.1$ ppm for the stored gas with respect to the gas phase. The shift denotes the tight proximity of the gas molecules to the walls in the restricted aromatic environment and, in particular, reveals that the gas carbon atoms are located as closely as possible to the “sticky” walls.

Based on a detailed XRD single-crystal analysis of the architecture of the porous crystal, it was concluded that the aromatic paddles of **1** are aligned parallel to the channel axis at 4.0 \AA distance, so that the π electrons of the phenylenedioxy units are prone to interactions with the gas species diffusing in (Figure 4).

NMR spectroscopy provides the guest arrangement by the spatial dependence of the magnetic susceptibility on the aromatic ring coordinates.^[16] In the case of methane, a shielding effect of $\Delta\delta_{\text{H}} = -1.7$ ppm in the hydrogen spectrum corresponds to an accurate distance measurement of 2.9 \AA

from the center of an aromatic ring to the nucleus of one of the methane hydrogen atoms (Figure 4). The carbon nucleus of methane experiences a smaller shielding effect and is displaced a further 1.1 \AA apart, falling at the center of the channel. Thus, methane is located at an equilibrium distance in close contact with the π -electron clouds that protrude for about 1.7 \AA from the host paddles (Supporting Information).

The distance determinations are consistent with models of benzene/ CH_4 dimers for which the energy minimum falls at 3.8 \AA (from the methane carbon atom to the center of the aromatic ring) and indicate the formation of $\text{CH}\cdots\pi$ interactions accounting for an attractive energy of 6 kJ mol^{-1} .^[18] The distances also match a large number of examples of $\text{CH}\cdots\pi$ interactions with energies of about 8.5 kJ mol^{-1} .^[19] However, the elaboration of the absorption isotherms at variable temperatures to obtain the isosteric heat of absorption at a low pressure estimates a larger enthalpy per mol of gas of 11 kJ mol^{-1} .^[20] In fact, the tetrahedron of methane placed at the center of the channel behaves as a polydentate structure with a favorable topology for setting multiple interactions with the channel walls: $\text{CH}\cdots\pi$ interactions can be established with two or even three host paddles at a time, designing a few stable configura-

tions.^[21] Nuclear magnetic relaxation rates in the extreme narrowing limit indicate that the configurations are explored dynamically. Indeed, given the properties of scarce directionality, $\text{CH}\cdots\pi$ interactions generate shallow and proximal energy minima that do not fix methane to a single configuration, but trace easy ways for diffusion.^[18] Thus, the zeolitic modification of **1** provides considerable stabilization to the

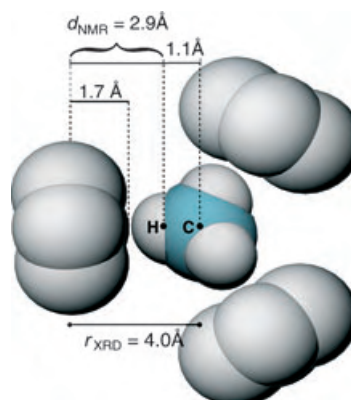


Figure 4. A single methane molecule at a particular site along the nanochannel of **1**, creating close contact interactions with the surrounding π receptors. The host–guest distances are determined by the effect of magnetic susceptibility on methane NMR resonances.

lightest of alkanes without sacrificing diffusivity in the crystal. Other kinds of local interactions are set with CO₂ for which the carbon nucleus comes closer to the aromatic groups, as proven by the large NMR upfield shift of $\Delta\delta_{\text{C}} = -2.1$ ppm. The carbon atom of CO₂ is pushed towards the walls at an equilibrium distance as short as 3.3 Å, with a stabilization energy amounting to 10.5 kJ mol⁻¹ for a single interaction of CO₂ arranged parallel to the benzene plane.^[22] This distance, shorter than the channel radius of 4.0 Å, explains the fast absorption/desorption rate and allows carbon dioxide to explore multiple aromatic receptors along the nanochannel walls.

Sorption/desorption cycles can be repeated many times in the porous molecular crystals as in conventional zeolites because, after the gas release, the open framework does not collapse to a close-packed structure, as commonly happens in molecular materials.^[2h,23] The absorbing state of **1** can be switched off by thermal treatment at high temperature, and no absorption was observed for the closed-packed polymorph after prolonged exposure to the gases. However, the molecular system can be switched back to the active nanoporous form after exposure to benzene and mild evacuation.

O₂, N₂, and Ar are absorbed in amounts below 0.04 mol of gas per mol of **1** at 400 torr and room temperature. Also, hydrogen gas is not appreciably retained by the crystal at 77 K and 1 atm even if it probably explores the interior of the porous crystal. This selectivity is an attractive property since CO₂ and/or CH₄ can be removed from the gas phase by our molecular zeolite at low partial pressures and stimulates interesting perspectives for the purification of H₂. It was recently emphasized that the removal of small amounts of contaminant gases, primarily CO₂ and CH₄, from H₂ is a determining challenge for the real use of hydrogen as a fuel.^[12] It is interesting to note that **1** can capture CH₄ as much as CO₂, contrary to other systems that cannot absorb CH₄ in comparable amounts.^[24]

In conclusion, the molecular crystal of **1**, which exhibits permanent nanoporosity, can store large amounts of carbon dioxide and methane selectively over nitrogen, oxygen, and hydrogen, suggesting intriguing applications for fuel storage, hydrogen purification, and carbon dioxide removal from the air. In fact, by exploiting the weakly directional interactions borrowed by supramolecular chemistry, we discovered that the gases were bound by the soft molecular lattice to fabricate new gas–solid adducts. This represents a still rare case of gas sorption, as until recently, molecular systems were neglected relative to metal-organic or traditional zeolites. The novel frameworks with gases could be described in-depth by NMR spectroscopy, which accurately measures intermolecular distances and recognizes the specific interactions that contribute to the overall stabilization. The impressive upfield shifts caused by the aromatic ring currents on gas molecules at the van der Waals contacts provided an unconventional tool for understanding the preferred topology of the gases interacting with the inner surface of a porous crystal. The multiple receptors lining the channel walls and the tight fit with the guests recall the specificity of biological nanochannels.^[25] Also, the relevant gas sorption capacity of the van der Waals crystals even at low pressures opens up applications to new

generations of sensing materials that contain a variety of suitably engineered functional groups.

Experimental Section

X-ray structure determination: The single-crystal X-ray data collection of the nanoporous TPP was performed on an Oxford Xcalibur automated 4-circle diffractometer with κ geometry equipped with a CCD detector and a Mo-target X-ray tube operating at 50 kV and 30 mA with a radiation wavelength λ of 0.71073 Å. The frames were integrated with the CrysAlis RED software package of Oxford Diffraction. Absorption correction was applied by using the program SADABS. The structure was solved by direct methods, and the subsequent difference Fourier synthesis and refinement was carried out with the JANA2000 software package. Crystal data of TPP: C₁₈H₁₂N₃O₆P₃, $M_r = 459.23$, crystal size 80 × 80 × 100 μm³, hexagonal, space group $P6_3/m$, $a = b = 11.454(4)$, $c = 10.160(4)$ Å, $\gamma = 120^\circ$, $Z = 2$, $V = 1154(1)$ Å³, $\rho_{\text{calcd}} = 1.321$ g cm⁻³, $F(000) = 444$, $\lambda(\text{MoK}\alpha) = 0.71073$ Å, $3.56^\circ < \theta < 28.14^\circ$, a total of 460 frames were collected with a scan width of 1 deg in ω and ϕ with an exposure time of 60 s per frame, $T = 298$ K, 8029 measured reflections, 922 ($R_{\text{int}} = 0.170$) independent reflections, $R_1 = 0.0882$, $wR_2 = 0.0128$ for 2167 observed reflections with ($I > 3\sigma$), GOF = 1.70, refinement method: full-matrix least-squares on F^2 . CCDC-253392 (**1**) contains the supplementary crystallographic data for this paper. These data can be obtained free of charge via www.ccdc.cam.ac.uk/conts/retrieving.html (or from the Cambridge Crystallographic Data Centre, 12, Union Road, Cambridge CB2 1EZ, UK; fax: (+44) 1223-336-033; or deposit@ccdc.cam.ac.uk). The simulated powder profile derived from single-crystal data reproduces the experimental X-ray powder pattern (Supporting Information).

Gas absorption: The preparation of adducts of **1** with gases and absorption isotherms were obtained by using the following instruments: a) a precision quartz microbalance system and b) gas adsorption manometry apparatus. The gravimetric apparatus is constituted by a quartz microbalance (Cahn 2000 balance) enclosed in a vessel (overall volume: 2000 cm³) connected to a vacuum pump with a gas inlet and a pressure gauge. The nanoporous crystals of **1** (50 mg) were placed on the microbalance and the apparatus was evacuated at 10⁻³ torr. The system was pressurized at the desired gas pressure and the mass of the sample was monitored over time. The sensitivity is 0.1 μg. In the manometry apparatus, samples were degassed to below 10⁻³ torr. The gas pressure was determined by an active strain gauge (Edwards ASG) with a sensitivity of 0.1 torr. Adsorption equilibrium was usually reached within 150–200 min. The measurements were carried out at room temperature and 195 K. The determination of the maximum loadings in the case of methane was checked by ¹H MAS NMR.

Solid-state NMR spectroscopy measurements: ¹H and ¹³C MAS NMR spectra were recorded at 7.04 Tesla static magnetic field on a Bruker Avance 300 apparatus at 300.13 and 75.5 MHz, respectively, and at a spinning speed of 15 kHz obtained with 4-mm zirconia rotors. Single-pulse excitation was applied; the application of the cross-polarization pulse sequence was found to be ineffective for recording the signals of gases. Spin-lattice relaxation times were measured by the inversion recovery method.

Received: August 18, 2004

Published online: January 20, 2005

Keywords: adsorption · gas storage · inclusion compounds · nanostructures · pi interactions

- [1] a) H. K. Chae, D. Y. Siberio-Perez, J. Kim, Y. Go, M. Eddaoudi, A. J. Matzger, M. O’Keeffe, O. M. Yaghi, *Nature* **2004**, 427, 523–

- 527; b) M. D. Ward, *Science* **2003**, *300*, 1104–1105; c) S. M. Kuznicki, V. A. Bell, S. Nair, H. W. Hillhouse, R. M. Jacobinas, C. M. Braunbarth, B. H. Toby, M. Tsapatsis, *Nature* **2001**, *412*, 720–724.
- [2] a) W. J. Blau, A. J. Fleming, *Science* **2004**, *304*, 1457–1458; b) G. M. Whitesides, B. Grzybowski, *Science* **2002**, *295*, 2418; c) “Organic Zeolites”: T. Hertzsch, J. Hulliger, E. Weber, P. Sozzani, *Encyclopedia of Supramolecular Chemistry*, Marcel Dekker, New York, **2004**, pp. 996–1005; strictly speaking, organic zeolites are open-channel systems that can absorb and desorb vapors or gases without structural changes, but can also refer to other systems that undergo structural changes upon absorption and revert to the former structure upon removal of the guest absorbates: d) P. Brunet, M. Simard, J. D. Wuest, *J. Am. Chem. Soc.* **1997**, *119*, 2737–2738; e) R. M. Barrer, V. H. Shanson, *J. Chem. Soc. Chem. Commun.* **1976**, 333–334; f) A. T. Ung, D. Gizachew, R. Bishop, M. L. Scudder, I. G. Dance, D. C. Craig, *J. Am. Chem. Soc.* **1995**, *117*, 8745–8746; g) T. Tanka, T. Tasaki, Y. Aoyama, *J. Am. Chem. Soc.* **2002**, *124*, 12453–12462; h) K. Endo, T. Sawaki, M. Koyanagi, K. Kobayashi, H. Masuda, Y. Aoyama, *J. Am. Chem. Soc.* **1995**, *117*, 8341–8352.
- [3] M. Eddaoudi, J. Kim, N. Rosi, D. Vodak, J. Wackter, M. O’Keeffe, O. M. Yaghi, *Science* **2002**, *295*, 469.
- [4] a) M. E. Brown, M. D. Hollingsworth, *Nature* **1995**, *376*, 323; b) R. Kitaura, K. Seki, G. Akiyama, S. Kitagawa, *Angew. Chem. Int. Ed.* **2003**, *42*, 428–431; c) K. Uemura, S. Kitagawa, K. Fukui, K. Saito, *J. Am. Chem. Soc.* **2004**, *126*, 3817–3828.
- [5] A number of tris-*o*-phenylenedioxycyclotriphosphazene inclusion compounds have been described in the literature, some of which were of high interest as macromolecular nanocomposites, electrooptically active adducts, or conductive crystals: a) T. Kobayashi, S. Isoda, K. Kubono in *Comprehensive Supramolecular Chemistry*, Vol. 6 (Eds.: J. L. Atwood, J. E. D. Davies, D. D. MacNicol, F. Vögtle), Pergamon, Oxford, **1996**, pp. 399–419; b) A. Comotti, R. Simonutti, G. Catel, P. Sozzani, *Chem. Mater.* **1999**, *11*, 1476–1483; c) P. Sozzani, A. Comotti, S. Bracco, R. Simonutti, *Chem. Commun.* **2004**, 768–769; d) P. Sozzani, A. Comotti, S. Bracco, R. Simonutti, *Angew. Chem.* **2004**, *116*, 2852–2857; *Angew. Chem. Int. Ed.* **2004**, *43*, 2792–2797; e) T. Hertzsch, F. Budde, E. Weber, J. Hulliger, *Angew. Chem.* **2002**, *114*, 2385–2388; *Angew. Chem. Int. Ed.* **2002**, *41*, 2281–2284; the inclusion compound with water and the close-packed monoclinic structures are reported in: f) H. R. Allcock, M. L. Levin, R. R. Whittle, *Inorg. Chem.* **1986**, *25*, 41–47; Xe NMR spectroscopic analysis suggested the existence of nanochannels: g) P. Sozzani, A. Comotti, R. Simonutti, T. Meersmann, J. W. Logan, A. Pines, *Angew. Chem.* **2000**, *112*, 2807–2810; *Angew. Chem. Int. Ed.* **2000**, *39*, 2695–2699; h) H. Kobayashi, T. Ueda, K. Miyakubo, T. Eguchi, *Z. Naturforsch. B* **2003**, *58*, 727–734.
- [6] The maximum sorption capacity of 58 cm³ g^{−1} (STP) can be evaluated by the intercept of the linear fitting of the Dubinin–Radushkevich plot and, independently, by van der Waals encumbrance of methane compared with the *c*/2 of 5.08 Å for the pitch of **1** along the nanochannel.
- [7] a) D. W. Breck, *Zeolite Molecular Sieves. Structure, Chemistry and Use*, Wiley, New York, **1974**, pp. 593–699; b) V. R. Choudhary, S. Mayadevi, *Zeolites* **1996**, *17*, 501–507.
- [8] K. Seki, *Chem. Commun.* **2001**, 1496–1497.
- [9] J. L. Atwood, L. J. Barbour, A. Jerga, *Science* **2002**, *296*, 2367–2369.
- [10] A microporous volume of 60 cm³ g^{−1} at STP was evaluated by the linear fitting of the Dubinin–Radushkevich plot.
- [11] a) L. Pan, K. M. Adams, H. E. Hernandez, X. Wang, C. Zheng, Y. Hattori, K. Kaneko, *J. Am. Chem. Soc.* **2003**, *125*, 3062–3067; b) M. Eddaoudi, H. Li, O. M. Yaghi, *J. Am. Chem. Soc.* **2000**, *122*, 1391–1397.
- [12] J. L. Atwood, L. J. Barbour, A. Jerga, *Angew. Chem.* **2004**, *116*, 3008–3010; *Angew. Chem. Int. Ed.* **2004**, *43*, 2948–2950.
- [13] a) J. Yang, D. Ma, F. Deng, Q. Luo, M. Zhang, X. Bao, C. Ye, *Chem. Commun.* **2002**, 3046–3047; b) H. Lee, Y. Seo, Y.-T. Seo, I. L. Moudrakovski, J. A. Ripmeester, *Angew. Chem.* **2003**, *115*, 5202–5205; *Angew. Chem. Int. Ed.* **2003**, *42*, 5048–5051; c) F. Fleyfel, K. Y. Song, A. Kook, R. Martin, R. Kobayashi, *J. Phys. Chem.* **1993**, *97*, 6722–6725; d) A. K. Jameson, C. J. Jameson, *Chem. Phys. Lett.* **1987**, *134*, 461.
- [14] The high spinning speed of 15 kHz reduces the hydrogen homonuclear couplings in the solid state, thereby allowing the notable resolution.
- [15] a) N. Branda, R. Wyler, J. Rebek, Jr., *Science* **1994**, *263*, 1267–1268; b) Y. Miyahara, K. Abe, T. Inazu, *Angew. Chem.* **2002**, *114*, 3146–3149; *Angew. Chem. Int. Ed.* **2002**, *41*, 3020–3023.
- [16] a) P. Von Ragué Schleyer, C. Maerker, A. Dransfeld, H. Jiao, N. J. R. Van Eikema Hommes, *J. Am. Chem. Soc.* **1996**, *118*, 6317–6318; b) S. Waugh, R. W. Fessenden, *J. Am. Chem. Soc.* **1957**, *79*, 846–849; c) C. W. Haigh, R. B. Mallion, *Prog. Nucl. Magn. Reson. Spectrosc.* **1980**, *16*, 303.
- [17] a) A. J. Beeler, A. M. Orendt, D. M. Grant, P. W. Cutts, J. Michi, K. W. Zilm, J. W. Downing, J. C. Facelli, M. S. Schindler, W. Kytzelnigg, *J. Am. Chem. Soc.* **1984**, *106*, 7672–7676; b) B. F. Graham, J. M. Harrowfield, R. D. Tengrove, A. F. Lagante, T. J. Bruno, *J. Inclusion Phenom. Mol. Recognit. Chem.* **2002**, *43*, 179–182.
- [18] S. Tsuzuki, K. Honda, T. Uchamaru, M. Mikami, K. Tanabe, *J. Am. Chem. Soc.* **2000**, *122*, 3746–3756.
- [19] a) M. Nishio, *CrystEngComm* **2004**, *6*, 130–158; b) G. R. Desiraju, T. Steiner in *The Weak Hydrogen Bond: Applications to Structural Chemistry and Biology*, Oxford University Press, Oxford, **1999**.
- [20] F. Rouquerol, J. Rouquerol, K. Sing, *Adsorption by Powders & Porous Solids*, Academic Press, London **1999**.
- [21] Some configurations are favored by symmetry, as three hydrogen atoms of a methane molecule are related by a C₃-symmetry element as the three host-paddles at a channel cross-section.
- [22] S. Sun, E. R. Bernstein, *J. Phys. Chem.* **1996**, *100*, 13348–13366.
- [23] a) M. R. Caira, L. R. Nassimbeni, F. Toda, D. Vujovic, *J. Am. Chem. Soc.* **2000**, *122*, 9367–9372; b) O. Saied, T. Maris, J. D. Wuest, *J. Am. Chem. Soc.* **2003**, *125*, 14956–14957.
- [24] D. N. Dybtsev, H. Chun, S. H. Yoon, D. Kim, K. Kim, *J. Am. Chem. Soc.* **2004**, *126*, 32–33.
- [25] D. M. Rudkevich, *Angew. Chem.* **2004**, *116*, 568–581; *Angew. Chem. Int. Ed.* **2004**, *43*, 558–571.

Preparation of Chiral Surfaces from Achiral Molecules by Controlled Symmetry Breaking**

Ava M. Berg and David L. Patrick*

For over 150 years understanding and controlling chirality has been an important objective in natural science.^[1] Chirality, the property of an object being nonsuperimposable on its mirror image, affects the performance of many chemical, biochemical, and physical systems, and therefore chiral control has widespread application.^[2] Surfaces, as with fully three-dimensional objects, can be chiral and such systems have been the focus of much recent attention.^[3] Herein we report a fundamentally new method for the preparation of chiral organic films which allows control over both the absolute handedness and enantiomeric excess of adsorbed molecules, yet unlike other approaches to the formation of chiral surfaces, our method involves no chiral inputs. Instead, mirror symmetry is broken in a layer of achiral molecules by controlling their arrangement on a single-crystal substrate with a liquid-crystal solvent and a magnetic field.

We studied films of the compound 4-cyano-4'-octylbiphenyl (8CB) on graphite, a room-temperature smectic-A liquid crystal (LC). When placed in contact with graphite, 8CB forms a single polycrystalline monolayer at the interface between the substrate and bulk fluid supernate.^[4] Molecules in the monolayer organize as shown in Figures 1 a–c, with the long molecular axis in the substrate plane. The unit cell contains eight molecules in registry with the substrate. They are aligned in an antiparallel configuration, which results in a cancellation of dipoles. Registry is driven by an interaction between the alkyl tails and graphite; tails always orient along one of the three graphite $\langle 1100 \rangle$ directions of a form.^[5] In three-dimensional space 8CB is achiral, but when the molecule is confined to two dimensions upon adsorption, its conformational mobility is hindered. This breaks the mirror symmetry of the adsorbed molecules; in combination with the graphite substrate the resulting monolayer sur-

face is chiral.^[6] The two enantiomorphs undergo phase separation into purely left- or right-handed domains measuring a few hundred nanometers in size.

8CB is an example of a compound that is achiral in three dimensions but that can form a chiral surface when adsorbed as a two-dimensional film. More generally, any molecule that

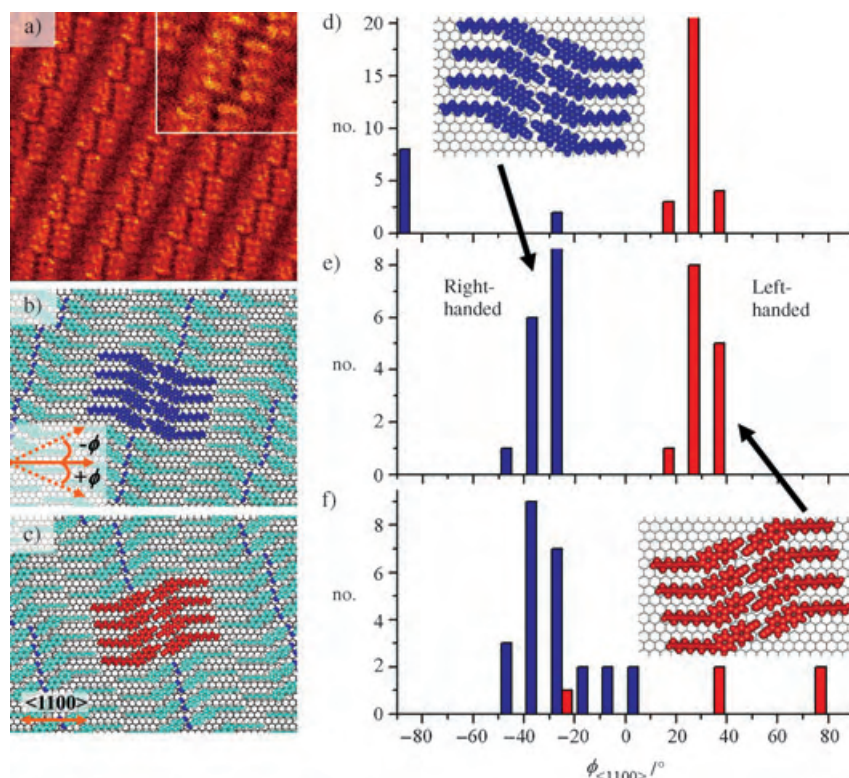


Figure 1. Monolayers of 8CB on graphite: a) STM image of a right-handed domain ($20 \times 20 \text{ nm}^2$, $I_{\text{tunn}} = 1.33 \text{ nA}$, $V_b = -1.2 \text{ V}$) (The inset is at the scale of the models in parts b) and c) ($6 \times 6 \text{ nm}^2$, $I_{\text{tunn}} = 0.60 \text{ nA}$, $V_b = -1.87 \text{ V}$)). b) Model illustration of right-handed and c) left-handed forms, which represent two of the six possible arrangements of molecules in the monolayers; note that the two are mirror images. The remaining four possible configurations are simple rotations by $\pm 60^\circ$ of the two shown. The chirality and relative orientation illustrated in part b) is the same as the STM images in part a). d)–f) Histograms of molecular headgroup orientations ($\phi_{\langle 1100 \rangle}$) determined by STM for samples prepared with three representative field alignments: d) field at -19° from $\langle 1100 \rangle$; e) field at 0° (parallel to $\langle 1100 \rangle$); and f) field at $+19^\circ$ from $\langle 1100 \rangle$. The sign convention is shown in the inset of part b). Blue bars indicate right-handed molecules, red bars indicate left-handed molecules. Part e) shows two degenerate molecular configurations that correspond to the two models shown in parts b) and c), with the cyanobiphenyl headgroups oriented at approximately $\pm 22^\circ$. More generally, other field orientations break the degeneracy which leads to an excess of one chiral population over the other, as in parts d) and f). I_{tunn} = tunneling current; V_b = bias voltage.

belongs to the C_{nh} , C_s , or C_i point groups (which are achiral in three dimensions) has the potential to form a chiral surface if restricted to two-dimensional space with the proper orientation.^[7,8] Furthermore, compounds with other symmetries can form chiral supramolecular patterns even if the individual adsorbates are not themselves chiral.^[9] This adsorption-induced breakage of chiral symmetry always leads to the formation of pairs of energetically equivalent enantiomorphs or mirror images. Consequently, surfaces covered by multiple microscopic molecular domains are racemic on a macroscopic scale, as left- and right-handed regions form in equal numbers.

[*] A. M. Berg, Dr. D. L. Patrick

Department of Chemistry, Western Washington University
516 High St., Bellingham, WA 98225 (USA)
Fax: (+1) 360-650-2826
E-mail: patrick@chem.wvu.edu

[**] The authors thank A. Kositsky, T. Fegurger, and J. Jaszczak for their assistance, T. Rayment for insightful discussions, and The Camille and Henry Dreyfus Foundation, the American Chemical Society Petroleum Research Fund (37549-B7), and the National Science Foundation (PECASE-9985428) for funding.

To produce a film with a net excess of one enantiomorph over the other—a prerequisite for many applications of chiral surfaces—a further decrease in symmetry is required. Until now, such homochiral surfaces have always been produced by the introduction of a chiral component of some kind, such as a chiral adsorbate, reactant, or catalyst, or by the cleavage of crystals along high-index faces.^[3] Herein we introduce a method which, for the first time, allows the preparation of macroscopically homochiral films without any chiral inputs; instead, the chiral symmetry of 8CB films is systematically broken by the use of a LC solvent and a magnetic field to induce a preferred in-plane orientation of adsorbed molecules on an achiral single-crystal substrate. The absolute chirality and enantiomeric excess of the resulting film can be selected and controlled so that surfaces covered by predominately left-handed, right-handed, or a mixture of left- and right-handed molecules can be prepared.

Crystallization of an 8CB monolayer on graphite yields six energetically equivalent configurations, as observed with scanning tunneling microscopy (STM): (three distinguishable orientations) \times (two enantiomorphs). All six configurations occur with equal frequency; hence in the absence of an external perturbation, 8CB films are racemic.^[5] Figures 1b and 1c show two of the six possible configurations; the other four are derived from these by a rotation of $\pm 60^\circ$ in the surface plane.

To break the degeneracy among configurations, samples were prepared by applying a magnetic field (1.2 T) parallel to the substrate as a droplet of 8CB was placed on the surface, heated at 100°C for 2 min, then gradually cooled to room temperature. We call this technique “liquid-crystal imprinting” because orientational order in the bulk LC supernate becomes imprinted on the monolayer, producing a molecular film with macroscopic uniform in-plane alignment.^[10,11c] Although strong enough to produce well-aligned films, the orientational energy of the magnetic field was small compared with the strength of intermolecular and molecule–substrate interactions. Thus, the arrangement of 8CB molecules within the unit cell, and the registry of molecules with the surface were unaltered from reference samples prepared in the absence of any field. The outcome of applying a magnetic field was therefore to select for some of the six possible configurations as being most favored. Afterward, samples were removed from the field and imaged by STM.^[12] The STM tip plunged through the thick, nonconducting 8CB-LC supernate covering the sample to image molecules in the polycrystalline monolayer. 30–40 STM images were acquired at widely separated locations (millimeter distances) to observe molecular orientation, with no more than ten measurements taken from any one sample specimen. Naturally occurring single-crystal graphite substrates, which possessed uniform crystallographic orientation over a macroscopic area, were used in all cases.^[13]

Figures 1d–f present molecular orientational distributions measured by STM for three representative magnetic field directions. The abscissa indicates the angle $\phi_{(1100)}$ between the 8CB headgroup and the substrate $\langle 1100 \rangle$ direction, with color indicating molecular chirality (blue = right-handed, red = left-handed).^[14] The distributions were nonuniform; different

field orientations favored different monolayer configurations. The preferred configuration for a particular field direction was generally observed to be one that oriented the cyanobiphenyl headgroups as nearly parallel to the field as possible, yet maintained registry of the alkyl tails along one of the graphite $\langle 1100 \rangle$ directions of a form.

A special case is shown in Figure 1e, in which the field was parallel to $\langle 1100 \rangle$. In this case, two configurations that correspond to the two shown as models (Figures 1b and 1c), occurred with equal frequency. More generally, one configuration could be made more favored—and the others less favored—by changing the field orientation. This is evident in the data from example experiments in which the magnetic field was rotated by -19° and $+19^\circ$ from $\langle 1100 \rangle$ (Figures 1d and 1f, respectively). The symmetry between configurations was broken, producing a film with a net excess of one enantiomorph over the other.^[15]

The outcome of this effect is summarized in Figure 2, which shows the overall enantiomeric excess ($ee = (P_R - P_L) / (P_R + P_L)$) for several field orientations measured by STM.

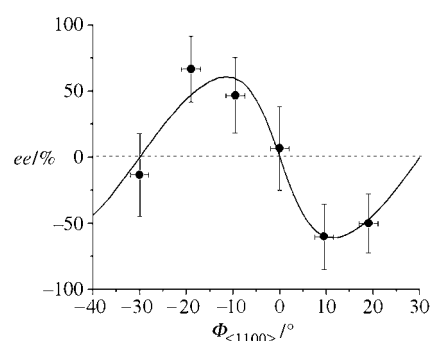


Figure 2. Absolute chirality and enantiomeric excess in polycrystalline 8CB monolayers on graphite were both adjustable by preparing samples in a magnetic alignment field oriented along different directions. Each point was determined from 30–40 STM observations on at least three different samples. The solid line is a prediction from the model described in the text. $\phi_{\langle 1100 \rangle}$ = magnetic field orientation with respect to $\langle 1100 \rangle$.

The value P_X is the experimental probability of observing a right- or left-handed domain. The enantiomeric excess oscillates between right- and left-handed surfaces with a repeat period of 60° . At the extrema the enantiomeric excess is greater than 60%, meaning that more than 80% of the surface is covered by a single enantiomorph. By simply changing the orientation of the field the absolute chirality and enantiomeric purity of the film can be engineered over a wide range of values.

To explain the trend in Figure 2 we note as discussed in reference [10] that the alignment energy of a molecular monolayer domain deposited from a LC solvent in a magnetic field can be expressed approximately as $U = A \sin^2 \theta$, in which θ represents the angle between the field and the preferred azimuthal anchoring direction at the film–LC interface, and A is a constant that depends on the properties of the LC supernate, strength of the magnetic field, domain size, and the anchoring energy. Comparison of STM images and polarizing

optical microscopy observations of the bulk director alignment showed that the preferred anchoring axis was nearly parallel to the cyanobiphenyl headgroup, establishing the reference for measuring θ , and in reference [10], A was measured to be 25 kJ mol^{-1} . The probability of observing a given configuration can therefore be estimated by assuming an equilibrium population distribution:

$$P_i = \frac{e^{(-U_i/kT)}}{\sum_{i=1}^6 e^{(-U_i/kT)}}$$

in which $\sum_{i=1}^6 e^{(-U_i/kT)}$ is the partition function, k is the Boltzmann constant, and T is the absolute temperature. The enantiomeric excess can then be calculated directly from P , with the predicted (not fitted) result shown by the solid line in Figure 2.

For the system studied herein, the LC solvent and film-forming adsorbate were both the same compound, 8CB. However, LC solvents have been effective in the control of orientational order in thin films composed of a variety of organic compounds, polymers, and small particles, including the unrestricted case in which the identity of the adsorbate building block and LC solvent were not the same.^[10,11] This method should therefore be applicable to a broad class of surfaces and films, provided a single crystal substrate is used with adsorbates of symmetry C_{nh} , C_s , or C_i .

More generally, one can view these findings in terms of the classical three-point model for chirality, which states that three unique points, or constraints, are needed to recognize a chiral object. Adsorption defines two effective constraints by inhibiting rotation and breaking mirror symmetry perpendicular to the adsorption plane. The LC-orienting influence provides a third constraint by the restriction of molecules to a single orientation within the confinement plane. The former two constraints break the mirror symmetry of individual molecules, whereas the latter breaks the mirror symmetry of molecular ensembles. This suggests that the symmetry-breaking role played by the LC solvent need not be unique, but could, in principle, be replaced by a different uniaxial influence, such as a laminar-solvent-flow field.

In summary, we report a fundamentally new way to prepare chiral surfaces that allows continuous control over absolute handedness and enantiomeric excess without incorporation of any chiral inputs. Further increases in the maximum enantiomeric excess are likely possible, as are applications of the principle to other systems in which optimization of experimental parameters can be guided by the proposed model. The findings reported herein may be applicable to a variety of fundamental problems and technologies in chiral control, ranging from the formation of chiral surfaces for use in optics, enantioselective adsorption, and chiral separations, to the preparation of orienting films in ferroelectric LC displays.

Received: August 31, 2004

Published online: February 14, 2005

Keywords: chirality · liquid crystals · monolayers · scanning probe microscopy · thin films

- [1] L. Pasteur, *Ann. Chim. Phys.* **1848**, 24, 442.
- [2] *Chirality in Natural and Applied Science* (Eds.: W. J. Lough, I. W. Wainer), CRC, Boca Raton, USA, **2002**.
- [3] a) G. P. Lopinski, D. J. Moffatt, D. D. M. Wayner, R. A. Wolkow, *Nature* **1998**, 392, 909; b) C. J. Eckhardt, N. M. Peachy, D. R. Swanson, J. M. Takacs, M. A. Khan, X. Gong, J.-H. Kim, J. Wang, R. A. Uphaus, *Nature* **1993**, 362, 614; c) A. Kühnle, T. R. Linderoth, B. Hammer, F. Besenbacher, *Nature* **2002**, 415, 891; d) J. A. Switzer, H. M. Kothari, P. Poizot, S. Nakanishi, E. W. Bohannon, *Nature* **2003**, 425, 463; e) L. C. Giancarlo, G. Flynn, *Acc. Chem. Res.* **2000**, 33, 491.
- [4] J. S. Foster, J. E. Frommer, *Nature* **1988**, 333, 542.
- [5] D. P. E. Smith, *J. Vac. Sci. Technol. B* **1991**, 9, 1119.
- [6] Note that the molecules by themselves are not chiral, insofar as a free-standing film would still possess mirror symmetry. It is the combined surface (molecular monolayer + substrate) that is chiral.
- [7] a) X. Qiu, J. Ruiz-Garcia, K. J. Stine, C. M. Knobler, J. V. Selinger, *Phys. Rev. Lett.* **1991**, 67, 703; b) R. Viswanathan, J. A. Zasadzinski, D. K. Schwartz, *Nature* **1994**, 368, 440.
- [8] P. B. Kohl, D. L. Patrick, *J. Phys. Chem. B* **2001**, 105, 8203.
- [9] F. Charra, J. Cousty, *Phys. Rev. Lett.* **1998**, 80, 1682.
- [10] J. D. Mougous, A. J. Brackley, K. Foland, R. T. Baker, D. L. Patrick, *Phys. Rev. Lett.* **2000**, 84, 2742.
- [11] a) J. F. Hulvat, S. I. Stupp, *Angew. Chem.* **2003**, 115, 802; *Angew. Chem. Int. Ed.* **2003**, 42, 778; b) M. D. Lynch, D. L. Patrick, *Chem. Mater.* **2004**, 16, 762; c) S. Hickman, A. Hamilton, D. L. Patrick, *Surf. Sci.* **2003**, 537, 113; d) M. D. Lynch, D. L. Patrick, *Nano Lett.* **2002**, 2, 1197.
- [12] Once crystallized, molecules in the monolayer did not rotate; samples removed from the magnet retained their chirality and orientation indefinitely.
- [13] Millimeter-sized crystals were extracted from graphitic calcite mineral specimens obtained from the Lead Hill Mine, Ticonderoga, NY by dissolving the calcite matrix in HCl (12M) (R. J. Lauf, A. E. Pasto, *The Mineralogical Record* **1983**, Jan.-Feb., 25). Specimens were purchased from the Mineralogical Research Company, San Jose, CA.
- [14] The left- and right-handed designations used herein conform to the convention adopted in most previous studies of 8CB on graphite, but it should be noted these designations are arbitrary and not based on CIP nomenclature rules.
- [15] The spread in the distributions of molecular orientations shown in the histograms arises principally from three factors: 1) measurement error associated with thermal drift during STM imaging and angular alignment of the samples; 2) imperfections on the single crystal substrates; and 3) alternative packing motifs in the 8CB monolayer. 8CB is known to crystallize into a family of closely related polymorphs, of which the STM image and models in Figure 1 are the most common. In some minority structures the cyanobiphenyl heads possess slightly different orientations in the unit cell. (D. L. Patrick, T. P. Beebe, Jr., *Langmuir* **1994**, 10, 298.)

CO Oxidation on Rutile-Supported Au Nanoparticles**

Ioannis N. Remediakis,* Nuria Lopez, and Jens K. Nørskov

Gold is usually catalytically inert in chemical processes.^[1] On the other hand, nanometric gold particles supported on oxides have been found to be catalytically active, even at low temperatures.^[2,3] A number of effects may contribute to the enhanced reactivity of small gold clusters: an odd or even number of electrons, a metal–insulator transition below a certain cluster size,^[3,4] charge transfer from the support,^[5,6] strain,^[7] or the presence of undercoordinated step and corner atoms.^[4,7–11] The catalytic properties of gold are also reported to be affected by the supporting oxide and the method of preparation, which suggests that atoms near the boundary between the gold cluster and the oxide may have a key role in the oxidation of CO.^[12,13] In addition, defects in the support can stabilize the metal particles and may change their catalytic properties.^[10]

In a pioneering work, Molina et al. calculated the energetics of CO oxidation on an infinite array of Au rods supported on TiO₂.^[14] They found that in the minimum-energy oxidation path, CO and O₂ are adsorbed near the gold/support interface. Similar results, for a two-layer gold strip were found by Liu et al.^[15] Herein, we take one further step and present the first theoretical study of CO oxidation on a finite gold nanoparticle supported on rutile (TiO₂). On this basis, we propose an additional mechanism for the oxidation of CO that takes place on corner Au atoms and does not directly involve the gold/support interface. The [Au₁₀] cluster that we have studied has a size of approximately 0.7 nm, which is at the lower end of the size-range for active nanoparticles reported in experiments.^[3] This model system has most of the important features that have been suggested to contribute to the catalytic activity of gold: it has a 3D structure with two layers, it contains the characteristic (111) and (100) facets of gold clusters, and, most importantly, it takes into account both the finite size of the cluster and the redox character of the support.

The relaxed structure of the [Au₁₀] cluster supported on rutile TiO₂(110) is shown in Figure 1. CO binds above the highest Au atom (labeled 1 in Figure 1) with an adsorption energy of −0.95 eV. Adsorption is significantly more exo-

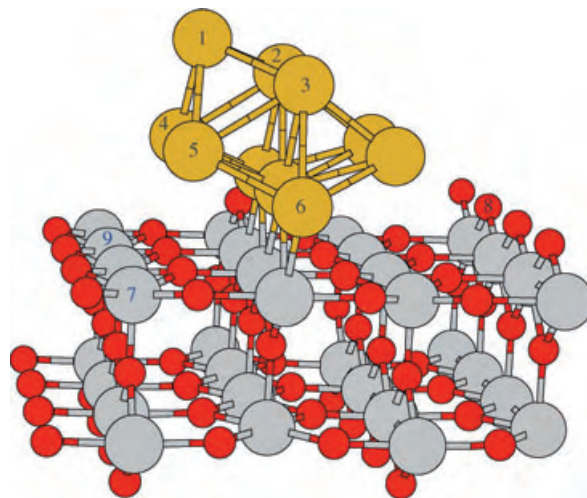


Figure 1. Relaxed geometry for an [Au₁₀] cluster supported on reduced rutile TiO₂(110). Au, Ti, and O atoms are represented by yellow, gray, and red spheres, respectively. The structure is periodic in both lateral dimensions.

thermic compared with that calculated for a free, disk-shaped gold cluster (−0.6 eV).^[8] This difference is mainly due to the decrease in the coordination number of the Au atom in the supported cluster.^[10] Recently, Meier and Goodman^[16] reported a binding energy of 0.8 eV for CO on TiO₂-supported Au bilayer clusters and 0.5 eV for CO on unsupported Au clusters. Within the error range associated with experimental and calculated values, these results are essentially the same as those calculated. For co-adsorbed CO and O₂, the minimum-energy structure (−1.59 eV, relative to gas-phase CO and O₂) involves CO adsorbed on top of Au(1) (Figure 1) and O₂ bonded between Au(5) and Ti(7). This structure is 0.4 eV lower in energy than the best co-adsorption geometry for CO and O₂ that involves Au atoms only (see below).

The ensemble, which gives rise to such strong bonding for O₂, is a corner gold atom in the basal plane of the gold particle and a neighboring “bare” Ti atom of the support. The energy of co-adsorbed CO and O₂ does not seem to be affected by redox conditions. We repeated the calculation for two different cases, one in which an extra oxygen vacancy was formed by removing O(8), and another in which an O₂ molecule is adsorbed above Ti(9). In both cases, the co-adsorption energy of CO and O₂ changed by less than 0.05 eV. Co-adsorbed CO₂ and O have an energy of −3.95 eV relative to gas-phase CO and O₂. The energy of the transition state for the reaction CO + O₂ → CO₂ + O is −1.19 eV relative to gas-phase reactants and yields an energy barrier of 0.40 eV. The relaxed structures and energies associated with this CO oxidation path are shown in Figure 2.

We then considered a second oxidation pathway, which does not directly involve the support and is similar to that

[*] Dr. I. N. Remediakis, Prof. Dr. J. K. Nørskov
Center for Atomic-Scale Materials Physics
Department of Physics
Technical University of Denmark
2800 Lyngby (Denmark)
Fax: (+45) 4593-2399
E-mail: remed@fysik.dtu.dk
Dr. N. Lopez
Departament de Química Física
Universitat de Barcelona
C/Marti i Franques 1, 08028 Barcelona (Spain)

[**] We acknowledge support from the Danish Center for Scientific Computing through grant no. HDW-1101-05. N.L. acknowledges MCYT for financing her work through the RyC program.

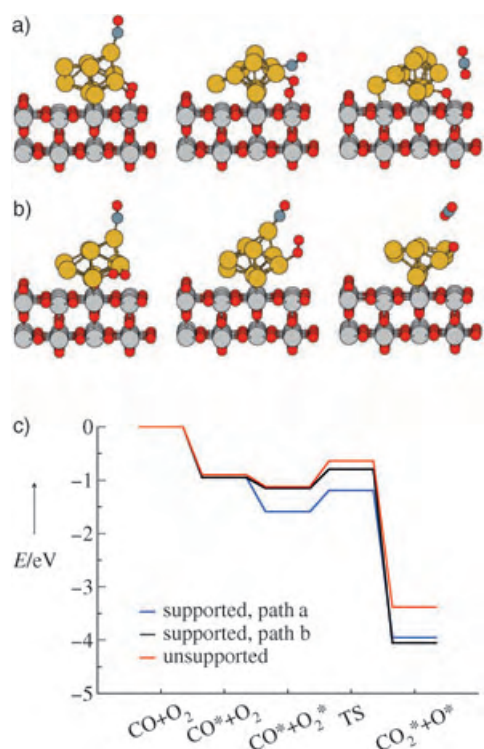


Figure 2. a, b) Relaxed geometries of the initial, transition, and final states, and c) energy profiles for CO oxidation on a $[\text{Au}_{10}]$ cluster. Blue line: $[\text{Au}_{10}]$ supported on $\text{TiO}_2(110)$, CO oxidation takes place at the Au/ TiO_2 interface (path a); black line: $[\text{Au}_{10}]$ supported on $\text{TiO}_2(110)$, CO oxidation takes place solely on the Au particle (path b); red line: unsupported cluster with the bottom three atoms kept fixed at the positions as they would be if the oxide were present.

proposed for a model $[\text{Au}_{10}]$ cluster.^[8] To obtain an adsorption energy for co-adsorbed CO and O_2 on the low-coordinated gold atoms without any direct bonding to the oxide, we performed a calculation with O_2 bonded to the bridge site between the Au atoms 5 and 6 (Figure 1) in a geometry that is very similar to the minimum-energy geometry described by Lopez and Nørskov,^[8] but with the extra constraint so that the z coordinate of the O atom bonded above the bare Ti(7) is kept within a range of 0.5 Å to Au(5). This configuration is metastable, but can still contribute to the kinetics. It has an energy of -1.15 eV relative to gas-phase CO and O_2 , which is in agreement with -0.9 eV calculated for a stand-alone $[\text{Au}_{10}]$ cluster.^[8] The use of a constraint to get a realistic configuration is necessary, because for such a small particle it is difficult to have a co-adsorption geometry that involves low-coordinated Au atoms and no interaction with the support. Co-adsorbed CO_2 and O have an energy of -4.06 eV relative to gas-phase CO and O_2 . The transition-state energy is -0.79 eV relative to gas-phase CO and O_2 and yields an oxidation barrier of 0.36 eV. The relaxed structures and energies associated with this oxidation pathway of CO are also shown in Figure 2. As can be seen from this figure, in both oxidation pathways, the cluster changes its shape slightly to minimize the total energy.

To gain insight into the role of the oxide in this pathway, we repeated the same calculations, this time without the

presence of TiO_2 , and with the bottom three Au atoms fixed at the positions they would have if the oxide were present. The comparison between the unsupported and the supported cluster is shown in Figure 2. The energy of co-adsorbed CO and O_2 is -1.12 eV, only 0.03 eV higher than the energy of the same configuration for the supported cluster. The transition-state energy is 0.15 eV higher for the unsupported cluster and yields an energy barrier of 0.48 eV. There is a significant difference in the final state (CO_2 and O) energy. This difference is an artifact related to the restructuring of the supported cluster induced by the O atom, as can be seen in Figure 2. The binding energy of the O atom is -0.9 eV, relative to gas-phase O_2 , which is 0.6 eV lower than the binding energy of the O atom to the unsupported cluster, where relaxation is not fully allowed.

The conclusion from the density functional calculations is that there are two possible reaction mechanisms for CO oxidation on a $[\text{Au}_{10}]$ cluster that is supported on rutile TiO_2 . The first pathway is similar to those previously reported,^[14,15] and can only take place at a specific ensemble at the edge of the Au/ TiO_2 interface. The other pathway takes place solely on the gold particle, with the support having a small effect on the energetics. Both pathways involve low-coordinated Au atoms to stabilize the reactants. The two pathways show similar activation energies for CO oxidation in the range 0.36–0.40 eV, which is very close to the activation energy of 0.36 eV measured by Haruta et al.,^[17] close to the range of 0.15–0.25 eV reported by Valden et al. for STM-characterized catalysts,^[18] and within the range of values between 0.16 and 0.60 eV reported by Bamwenda et al.^[12] and Choudary et al.^[19]

Our findings give further support to the notion that low-coordinated Au sites are essential to the reactivity of Au nanoparticles, as suggested in other theoretical and experimental works.^[4,7–11] In addition, our results show why some experiments may uncover effects due to interface sites. Most importantly, the finding of the pure Au pathway shows that there is at least one reaction channel open for all supports, independent of the ability of the support to provide O_2 or to stabilize intermediates. This result explains why activities of several different gold catalysts have been found to depend mainly on the size of the gold particle or, equivalently, the concentration of corner atoms on the gold particle.^[10] Finally, we note that oxygen-atom vacancies are clearly important in stabilizing Au atoms on the surface. Without them the Au particle hardly binds to the support.^[20]

Our results suggest that the art of making Au atoms reactive can be reduced to the question of controlling the structure of Au particles at the nanoscale. One has to create many interface sites or maximize the number of low-coordinate Au atoms in the particles.

Experimental Section

The calculations were carried out by using density functional theory (DFT); the DACAPO package was employed.^[21] The ionic cores and their interactions with valence electrons were described by ultrasoft pseudopotentials.^[22] Exchange and correlation effects were taken into account by using the generalized gradient approximation (GGA) and

the revised Perdew–Burke–Ernzerhof (RPBE) functional.^[23] The wave function was expanded in a plane-wave basis with a kinetic-energy cutoff of 25 Ry. The ionic degrees of freedom were relaxed by using a conjugate-gradient minimization until the root of the mean squared-force component was smaller than 0.2 eV \AA^{-1} . Further relaxation of selected structures resulted in insignificant changes in the calculated energies. The rutile $\text{TiO}_2(110)$ substrate was modeled by a two-layered slab, with a (4×2) surface unit cell. The TiO_2 slabs are separated by 15 Å of vacuum. First, we obtain a relaxed geometry for the supported cluster by allowing all Au and topmost Ti and O atoms to relax. In the calculations for adsorbed molecules on the cluster, only the coordinates of adsorbate and gold atoms were optimized. Three oxygen vacancies were placed on one of the bridging oxygen rows, with the cluster on top connected by three Au atoms of the basal plane. We used a ratio of about three Au atoms per vacancy as a consequence of experimental STM results.^[20]

To find the activation energy for the first CO oxidation pathway, which involves the Au/ TiO_2 interface, we located the transition state by decreasing the distance between the C atom of the CO molecule and the O atom of the O_2 molecule until we found a maximum in the energy at a C–O interatomic distance of 1.8 Å. To ensure that the actual transition state was reached, we repeated the series of calculations. We started this time from CO_2 and stretched the C–O bond until it started to break at 1.8 Å, which was at a very similar geometry to that of the reverse reaction. For the second CO oxidation pathway, which does not directly involve support atoms, we placed CO and O_2 on the cluster in a configuration similar to that found in the transition state reported in reference [8] and kept the C–O bond length fixed at 2.8 Å. All other degrees of freedom of the adsorbate and the gold atoms were allowed to relax. We validated this approximation in retrospect by checking that the forces on the atoms were very small, thus verifying that the system is at a saddle point. For both oxidation paths, we tried several initial geometries for the system to ensure that for each instance (initial, transition, or final state) the minimum-energy structure was found.

Received: August 18, 2004

Revised: October 21, 2004

Published online: February 14, 2005

Keywords: density functional calculations · gold · heterogeneous catalysis · nanostructures · titanium oxide

- [1] B. Hammer, J. K. Nørskov, *Nature* **1995**, 376, 238.
- [2] M. Haruta, N. Yamada, T. Kobayashi, S. Iijima, *J. Catal.* **1989**, 115, 301.
- [3] M. Valden, X. Lai, D. W. Goodman, *Science* **1998**, 281, 1647.
- [4] G. Mills, M. S. Gordon, H. Metiu, *Chem. Phys. Lett.* **2002**, 359, 493.
- [5] A. Sanchez, S. Abbet, U. Heiz, W.-D. Schneider, H. Häkkinen, R. N. Barnett, U. Landman, *J. Phys. Chem. A* **1999**, 103, 9573.
- [6] Q. Fu, H. Saltsburg, M. Flytzani-Stephanopoulos, *Science* **2003**, 301, 935.
- [7] M. Mavrikakis, P. Stoltze, J. K. Nørskov, *Catal. Lett.* **2000**, 64, 101.
- [8] N. Lopez, J. K. Nørskov, *J. Am. Chem. Soc.* **2002**, 124, 11262.
- [9] C. Lemire, R. Meyer, S. Shaikhutdinov, H.-J. Freund, *Angew. Chem.* **2004**, 116, 121; *Angew. Chem. Int. Ed.* **2004**, 43, 118.
- [10] N. Lopez, T. V. W. Janssens, B. S. Clausen, Y. Xu, M. Mavrikakis, T. Bligaard, J. K. Nørskov, *J. Catal.* **2004**, 123, 232; N. Lopez, J. K. Nørskov, T. V. W. Janssens, A. Carlsson, A. Puig-Molina, B. S. Clausen, J.-D. Grunwaldt, *J. Catal.* **2004**, 125, 86.
- [11] R. Meyer, C. Lemire, S. K. Shaikhutdinov, H.-J. Freund, *Gold Bull.* **2004**, 37, 72.
- [12] G. R. Bamwenda, S. Tsubota, T. Nakamura, M. Haruta, *Catal. Lett.* **1997**, 44, 83.
- [13] S. Carrettin, P. Concepcion, A. Corma, J. M. L. Nieto, V. F. Puentes, *Angew. Chem.* **2004**, 116, 2592; *Angew. Chem. Int. Ed.* **2004**, 43, 2538.
- [14] L. M. Molina, M. D. Rasmussen, B. Hammer, *J. Chem. Phys.* **2004**, 120, 7673.
- [15] Z.-P. Liu, X.-Q. Gong, J. Kohanoff, C. Sanchez, P. Hu, *Phys. Rev. Lett.* **2003**, 91, 266 102.
- [16] D. C. Meier, D. W. Goodman, *J. Am. Chem. Soc.* **2004**, 126, 1892.
- [17] M. Haruta, S. Tsubota, T. Kobayashi, H. Kageyama, M. J. Genet, B. Delmon, *J. Catal.* **1993**, 144, 175.
- [18] M. Valden, S. Pak, X. Lai, D. W. Goodman, *Catal. Lett.* **1998**, 56, 7.
- [19] T. V. Choudary, C. Sivadinarayana, C. C. Chusuei, A. K. Darye, J. P. Fackler, D. W. Goodman, *J. Catal.* **2002**, 207, 247.
- [20] E. Wahlström, N. Lopez, R. Schaub, P. Thosttrup, A. Rønnau, C. Africh, E. Lægsgaard, J. K. Nørskov, F. Besenbacher, *Phys. Rev. Lett.* **2003**, 90, 026 101.
- [21] The DACAPO plane wave/pseudopotential DFT code is available as open-source software at <http://www.fysik.dtu.dk/CAMPOS/>.
- [22] D. Vanderbilt, *Phys. Rev. B* **1990**, 41, 7892.
- [23] B. Hammer, L. B. Hansen, J. K. Nørskov, *Phys. Rev. B* **1998**, 59, 7413.

Heterogeneous Catalysis

Cooperative Catalysis by General Acid and Base Bifunctionalized Mesoporous Silica Nanospheres**

*Seong Huh, Hung-Ting Chen, Jerzy W. Wiench, Marek Pruski, and Victor S.-Y. Lin**

Enzymes engaged in carbonyl chemistry often employ both general acid and general base catalytic residues in the active sites to activate specific substrates cooperatively.^[1] Recently, several synthetic catalytic systems have utilized the double hydrogen-bonding capability of a urea or thiourea functionality as a general acid catalyst to activate carbonyl compounds in homogeneous reactions.^[2] However, to our knowledge, the cooperation of general acid and base groups has yet to be demonstrated in any synthetic heterogeneous catalyst. Clearly, an important prerequisite for the construction of

[*] S. Huh, H.-T. Chen, Dr. J. W. Wiench, Dr. M. Pruski,
Prof. Dr. V. S.-Y. Lin
Department of Chemistry and
U.S. DOE Ames Laboratory
Iowa State University
Ames, IA 50011 (USA)
Fax: (+1) 515-294-0105
E-mail: vsylin@iastate.edu

[**] We thank the US DOE, Office of Basic Energy Sciences, for the financial support of this research through the Catalysis Science Grant No. AL-03-380-011 and the US National Science Foundation Grant No. CHE-0239570.



Supporting information for this article is available on the WWW under <http://www.angewandte.org> or from the author.

such a cooperative catalytic system would be the multifunctionalization of a solid support with control of the relative concentrations and proper spatial arrangements between these functional groups. Many monofunctionalized mesoporous silica catalysts have been reported;^[3] however, we and others have focused on multifunctionalized mesoporous catalysts.^[4]

Herein, we report a new cooperative catalytic system comprising a series of bifunctionalized mesoporous silica nanosphere (MSN) materials with various relative concentrations of a general acid, the ureidopropyl (UDP) group, and a general base, the 3-[2-(2-aminoethylamino)ethylamino]propyl (AEP) group (Figure 1). Three bifunctional AEP/UDP-MSN catalysts, which are described by their initial molar ratio of the organoalkoxysilane precursors as AEP/UDP = 2/8, 5/5, and 8/2, were synthesized by using our previously reported cocondensation method.^[5,6] The synthesis and characterization of the monofunctionalized MSNs with either AEP or UDP functionality were reported previously.^[5a] All of the mono- and bifunctionalized MSNs exhibited spherical particle shapes with similar particle sizes (0.6 μm).^[5a,6] The actual concentrations of the two functional

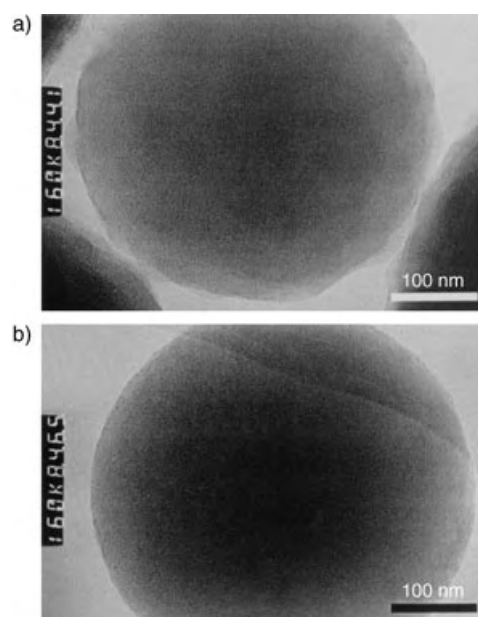


Figure 2. TEM micrographs of a) 2/8 AEP/UDP-MSN and b) 8/2 AEP/UDP-MSN materials (Philips CM-30 at 300 kV).

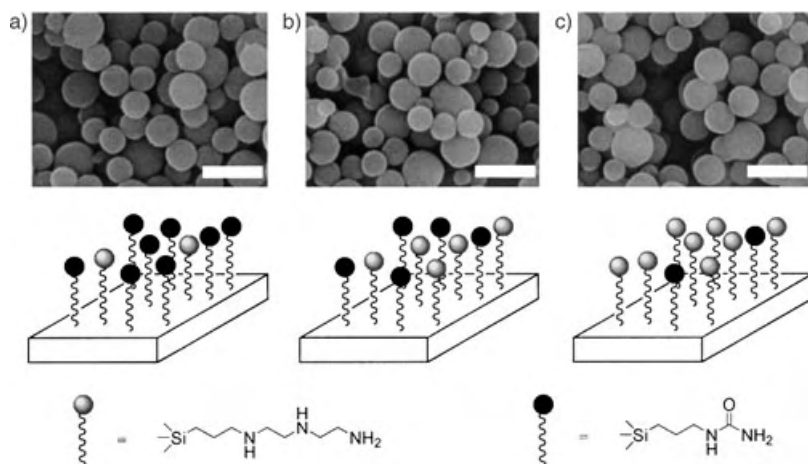
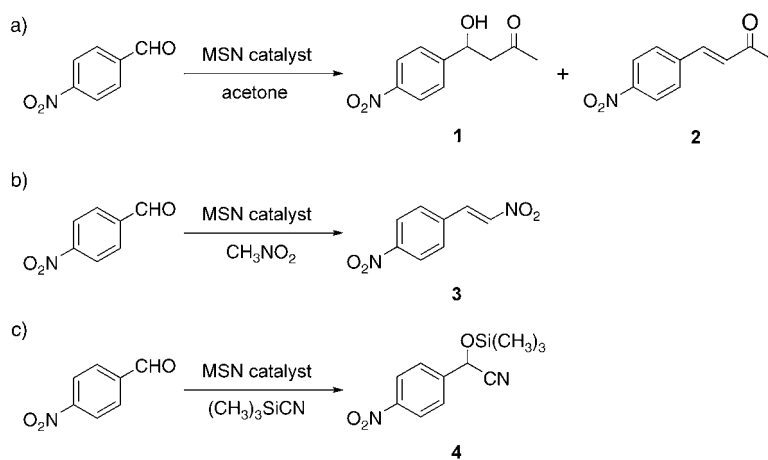


Figure 1. Scanning electron micrographs (SEM, top) and schematic drawings (bottom) of the bifunctional MSNs: a) 2/8 AEP/UDP-MSN, b) 5/5 AEP/UDP-MSN, and c) 8/2 AEP/UDP-MSN. Scale bar: 2.0 μm .

groups (AEP and UDP) were measured with the previously described solid-state ^{13}C CP MAS and ^{29}Si MAS NMR spectroscopic methods (CP MAS is cross-polarized magic-angle spinning).^[5b,6] The total surface concentrations of the organic functional groups (AEP+UDP) in the 2/8, 5/5, and 8/2 AEP/UDP-MSNs were determined to be 1.3, 1.0, and 1.5 mmol g^{-1} , respectively, and the concentration ratios of AEP/UDP were 2.5/7.5, 5.4/4.6, and 6.7/3.3, respectively.^[6] The XRD measurements of these materials showed large (100) peaks and broad higher diffraction patterns, which are typical of a disordered pore structure.^[5] The observed d_{100} values were 37.8, 41.7, and 38.1 \AA for sample 2/8, 5/5, and 8/2 AEP/UDP-MSNs, respectively. The TEM micrographs of these materials also confirmed their disordered pore structure (Figure 2).

The N_2 surface sorption analyses of these bifunctionalized MSNs revealed typical type-IV BET (Brunauer–Emmett–Teller) isotherms. The measured BET surface areas of 2/8, 5/5, and 8/2 AEP/UDP-MSNs were 938.7, 759.6, and 830.4 $\text{m}^2 \text{g}^{-1}$, respectively. The corresponding BJH (Barret–Joyner–Halenda) average pore diameters of these MSNs were 27.8, 22.9, and 25.9 \AA .

To investigate how UDP and AEP could catalyze cooperatively different reactions involving carbonyl activation, the aforementioned AEP/UDP-MSN materials were employed as catalysts for aldol, Henry, and cyanosilylation reactions. As shown in Scheme 1, a common electrophile, 4-nitro-



Scheme 1. Three model reactions catalyzed by the MSN catalysts: a) aldol reaction, b) Henry reaction, c) cyanosilylation.

benzaldehyde, and different nucleophiles, acetone, nitromethane, and trimethylsilyl cyanide, were used as reactants. In these reactions, the secondary amines of the AEP group were shown to be responsible for the enamine formation with acetone (aldol reaction),^[7] the deprotonation of CH_3NO_2 (Henry reaction),^[4] and the generation of a potential nucleophile from $(\text{CH}_3)_3\text{SiCN}$ through hypervalent silicate formation (cyanosilylation).^[8] On the other hand, a general acid group (UDP) could activate the carbonyl group of 4-nitrobenzaldehyde to nucleophilic attack through double hydrogen bonding.^[2] Therefore, the presence of both AEP and UDP groups in close proximity could activate cooperatively the electrophile and nucleophile to enhance the reaction rates of the desired catalytic reactions (Scheme 2). Indeed, the observed turnover numbers (TONs) of the catalysts in these reactions (Table 1) are consistent with this hypothesis. In the case of the aldol reaction, the monofunctionalized AEP–MSN catalyzed the conversion of 4-nitrobenzaldehyde (0.5 mmol) into compound **1** (0.091 mmol) and a small amount of the dehydrated product, compound **2** (0.018 mmol), in the presence of acetone (10 mL). In contrast, UDP–MSN did not show any catalytic activity under the same reaction conditions. This result suggested that the presence of the AEP functionality is crucial for the conversion of acetone solvent molecules into the active enamine species.^[7] However, a synergistic effect between the AEP and UDP groups was observed in the case of the bifunctionalized AEP/UDP–MSN catalysts.

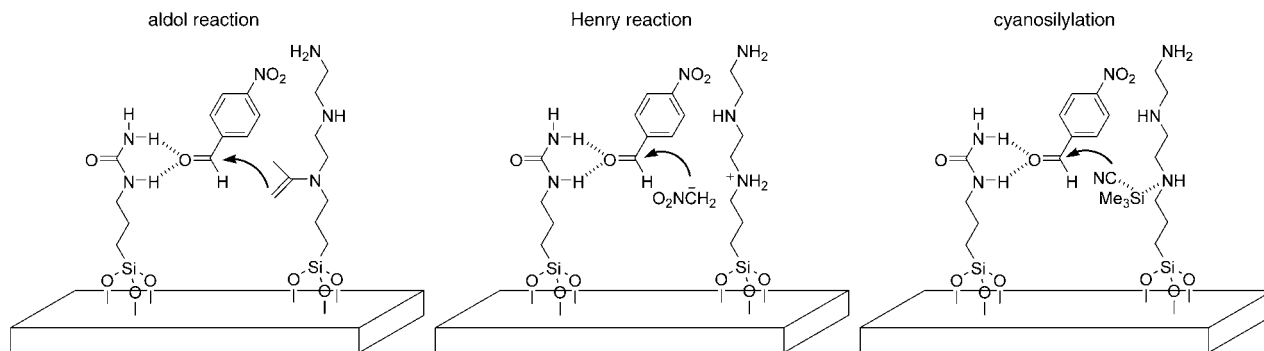
As shown in Table 1 and Figure 3, the TONs of all three AEP/UDP–MSNs were always higher than those of AEP–MSN. The largest TONs were observed in the case of the 2/8 AEP/UDP–MSN catalyst. For example, in the Henry and cyanosilylation reactions catalyzed by 2/8 AEP/UDP–MSN, the observed high TONs (125.0 and 276.1, respectively) indicate a genuine and superior catalytic performance in comparison with those of other bifunctional AEP/UDP–MSNs. In the aldol reaction, the largest TON (22.6) was also observed with 2/8 AEP/UDP–MSN as the catalyst. Furthermore, the TON (6.4) of a 1:1 mixture of the monofunctionalized AEP–MSN and UDP–MSN was clearly lower than that of the 5/5 AEP/UDP–MSN (11.9). The TONs of the bifunctionalized MSNs decreased significantly as the ratio of the surface concentrations of the AEP and UDP groups increased from 2.5/7.5 to 5.4/4.6 to 6.7/3.3. According to our

Table 1: TONs for the MSN-catalyzed reactions.^[a]

Reaction	MSN catalyst	T [°C]	Product	TON
aldol	2/8 AEP/UDP	50	1, 2	22.6
	5/5 AEP/UDP	50	1, 2	11.9
	8/2 AEP/UDP	50	1, 2	8.6
	AEP	50	1, 2	5.4
	physical mixture ^[b]	50	1, 2	6.4
	UDP	50	1, 2	0.0 ^[d]
	pure MSN ^[c]	50	1, 2	0.0 ^[d]
	2/8 AEP/CP	50	1, 2	12.4
	5/5 AEP/CP	50	1, 2	9.3
Henry	2/8 AEP/UDP	90	3	125.0
	5/5 AEP/UDP	90	3	91.1
	8/2 AEP/UDP	90	3	65.8
	AEP	90	3	55.9
	physical mixture ^[b]	90	3	79.2
	UDP	90	3	5.8
	pure MSN ^[c]	90	3	0.0 ^[d]
	2/8 AEP/CP	90	3	78.0
	5/5 AEP/CP	90	3	71.0
cyanosilylation	2/8 AEP/UDP	50	4	276.1
	5/5 AEP/UDP	50	4	170.5
	8/2 AEP/UDP	50	4	109.4
	AEP	50	4	111.4
	physical mixture ^[b]	50	4	126.9
	UDP	50	4	45.9
	pure MSN ^[c]	50	4	43.0 ^[d]

[a] TON = mmol product per mmol catalyst during 20-h reaction time for aldol and Henry reactions and 24 h for the cyanosilylation reaction with 20 mg of MSN. [b] Physical mixture = AEP–MSN (20 mg) + UDP–MSN (20 mg). [c] Nonfunctionalized MCM-41. [d] Yield [%].

solid-state NMR spectroscopic data, the total numbers of organic functional groups (AEP+UDP) in these bifunctionalized MSNs were similar; only the relative concentrations between the AEP and UDP groups varied. The recyclability of each of the bifunctional AEP/UDP–MSN catalysts was examined by isolating the catalysts from the reaction mixtures after 20 h by centrifugation. The catalysts were reused three times without purification. The TEM images^[6] of the recycled MSN materials showed some surface depositions of amorphous substances, which presumably arose from physisorbed reactants or products. Nonetheless, in all three reactions catalyzed by these recycled bifunctional MSNs, the TONs



Scheme 2. AEP and UDP groups may activate the electrophile and nucleophile cooperatively to enhance the reaction rates of the desired catalytic reactions.

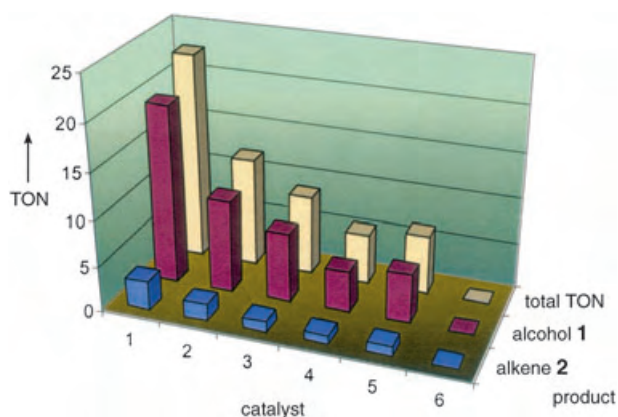


Figure 3. Diagram showing the TONs for the aldol reaction with the catalysts 2/8 AEP/UDP-MSN (1), 5/5 AEP/UDP-MSN (2), 8/2 AEP/UDP-MSN (3), AEP-MSN (4), physical mixture of AEP-MSN and UDP-MSN (5), and UDP-MSN (6).

were no more than 10% lower than those of the freshly prepared catalysts.

To examine whether this activity enhancement was due to the “surface dilution effect” of the AEP group, we investigated the catalytic performance of two bifunctional MSN materials (2/8 and 5/5 AEP/CP-MSN) that have the AEP group and a cyanopropyl (CP) functionality. CP cannot activate the electrophiles through a double hydrogen-bonding interaction. The synthesis and characterization of these two materials were reported previously.^[5b] As shown in Table 1, the TONs of the 2/8 and 5/5 AEP/CP-MSNs are 12.4 and 9.3, respectively. Indeed, the TON increased slightly as the AEP/CP ratio decreased. However, the large difference in TONs between the AEP/CP-MSN and the AEP/UDP-MSN catalysts, which have similar surface concentrations of the AEP group, can not be explained by the surface dilution effect. These results strongly indicate that the rate of the aldol reaction is accelerated as the surface concentration of UDP groups increases. Given that the UDP group can only activate the electrophile, the observed rate acceleration in the UDP-abundant MSN catalysts suggested that the activation of the carbonyl group of 4-nitrobenzaldehyde might be the rate-determining step in our cooperative catalysts. Such a “cooperative dual catalysis” effect in a homogeneous system, in which one catalyst activates the nucleophile and the other catalyst is responsible for the activation of the electrophile, was reported recently by Jacobsen and co-workers.^[9] In their study, the best molar ratio between the two catalysts was 0.67 and not 1, which indicates that the best ratio between the cooperative catalytic groups greatly depends on the kinetic nature of the reaction of interest. A similar trend in catalytic reactivity was also observed in the Henry and cyanosilylation reactions. A pronounced cooperative effect was manifested by a twofold increase in the TON of 2/8 AEP/UDP-MSN relative to that of 8/2 AEP/UDP-MSN in both reactions (Table 1). As the surface concentration of the primary catalytic group (AEP) in 2/8 AEP/UDP-MSN (AEP = 0.32 mmol g⁻¹) is only a third that of 8/2 AEP/UDP-MSN (AEP = 1.00 mmol g⁻¹), these unusual catalytic enhancements are strong indications of the existence of cooperation

between the general acid (UDP) and base (AEP) groups in our system. The control experiment with the physical mixture of AEP-MSN and UDP-MSN exhibited a slightly higher reaction rate in the cyanosilylation than AEP-MSN alone owing to the increased number of surface silanol groups, which can also moderately catalyze the reaction.

In conclusion, we have demonstrated that a general acid group, UDP, can activate substrates in cooperation with a general base group, AEP, to catalyze various reactions that involve carbonyl activation. By fine-tuning the relative concentrations and proper spatial arrangement of different cooperative functional groups, we envisage that our multifunctionalized MSNs could serve as new selective catalysts for many important reactions.

Experimental Section

The functionalized materials were synthesized by using the previously described cocondensation reaction.^[5] Typical procedure (2/8 AEP/UDP-MSN): A mixture of cetyltrimethylammonium bromide (CTAB; 2.0 g, 5.49 mmol), NaOH (2.0 M, aqueous; 7.0 mL, 14.00 mmol), and H₂O (480 g, 26.67 mol) was heated to 80 °C for 30 min. Tetraethoxysilane (TEOS; 9.34 g, 44.8 mmol), 3-[2-(2-aminoethylamino)ethylamino]propyltrimethoxysilane (AEPTMS; 0.305 g, 1.15 mmol), and ureidopropyltrimethoxysilane (UDPTMS; 1.023 g, 4.60 mmol) were added rapidly and sequentially to the resulting solution to yield an opaque reaction mixture. White precipitates were observed after vigorous (550 rpm) stirring of the reaction mixture for about 2 min. After an additional 2 h of heating at 80 °C, the as-synthesized bifunctionalized 2/8 AEP/UDP-MSN material was isolated by hot filtration, washed with copious amounts of water and methanol, and dried under vacuum. The CTAB surfactant molecules were extracted from the mesopores of the MSN by placing the as-synthesized material (1.0 g) in a mixture of methanol (100 mL) and hydrochloric acid (0.6 mL) for 2.5 h at 60 °C. The resulting solid product, which was free of surfactant, was filtered and washed with water and methanol, then dried under vacuum for 3 h at 90 °C. The non-functionalized MSN was prepared according to a reported method.^[5a]

Aldol reaction: All chemicals were purchased from Aldrich and used without further purification. Reagent-grade acetone was used without further purification. A mixture of the MSN catalyst (20 mg) and 4-nitrobenzaldehyde (0.076 g, 0.5 mmol) in acetone (10 mL) was heated at 50 °C with constant stirring for 20 h. The reaction mixture was then filtered through a glass frit, and the solids were washed with chloroform and acetone. The solvent was removed from the filtrate by rotary evaporation, and the product was dried under high vacuum. The residue was completely dissolved in CDCl₃, and THF (≈ 10 mmol) was added as an internal standard to the CDCl₃ solution. Analysis of the product mixture was performed by measuring ¹H NMR spectra on a Bruker DRX400 spectrometer. Distinctive chemical shifts were observed for the hydrogen atoms of the two products. The signals were assigned by comparing the chemical shifts observed in the spectra of the products with literature values.

Henry (nitroaldol) reaction: Reagent-grade nitromethane was used without further purification. A mixture of the MSN catalyst (20 mg) and 4-nitrobenzaldehyde (0.453 g, 3.0 mmol) in nitromethane (10 mL) was heated at 90 °C with constant stirring for 20 h. The reaction mixture was filtered through a glass frit, and the solids were washed with chloroform and acetone. The solvent was removed from the filtrate by rotary evaporation, and the residue was dried under high vacuum then completely dissolved in [D₆]acetone (10 mL). THF (≈ 10 mmol) was added as an internal standard to the [D₆]acetone solution. The product was analyzed by ¹H NMR spectroscopy on a Bruker DRX400 spectrometer. Distinctive chemical shifts were

observed for the vinylic hydrogen atoms of the product. The signals were assigned by comparing the chemical shifts observed for the product with literature values.

Cyanosilylation: A mixture of the MSN catalyst (20 mg), 4-nitrobenzaldehyde (0.453 g, 3.0 mmol), and $(\text{CH}_3)_3\text{SiCN}$ (0.298 g, 3.0 mmol) in dry toluene (10 mL) was heated at 50 °C with constant stirring for 24 h. The reaction mixture was then filtered through a glass frit, and the solids were washed with chloroform and acetone. The solvent was removed from the filtrate by rotary evaporation, and the residue was dried under high vacuum then completely dissolved in CDCl_3 . THF (≈ 10 mmol) was added as an internal standard to the CDCl_3 solution. The product was analyzed by ^1H NMR spectroscopy on a Bruker DRX400 spectrometer. A distinctive chemical shift of 5.6 ppm was observed for the silyl ether product. The signals were assigned by comparing the chemical shifts observed for the products with literature values.

Solid-state NMR spectra were obtained at 100.59 (^{13}C) and 79.47 MHz (^{29}Si) on a Varian/Chemagnetics Infinity spectrometer equipped with a doubly tuned 5-mm MAS probe. Direct polarization (DP) and variable-amplitude CP MAS methods were used under the conditions described in our previously published studies.^[4a,5b] These measurements provided quantitative evidence for functionalization of the mesopores with the organic moieties and confirmed the structure of the bifunctionalized materials. For AEP-MSNs, UDP-MSNs, and AEP/UDP-MSNs, the ^{29}Si and ^{13}C NMR spectra were assigned as described for our earlier study (see the Supporting Information).^[4a,5a] The methods used for quantitative measurements of the ^{29}Si and ^{13}C signal intensities are detailed below. All NMR spectroscopic results are summarized in the Supporting Information,^[6] which contains the relative concentrations of T^n and Q^n groups (silicon groups $(=\text{SiO})_n\text{Si}(\text{OH})_{(4-n-m)}\text{R}_m$ are designated as T^n for $m = 1$ and as Q^n for $m = 0$), the molar concentrations of organic functional groups, and the corresponding average molecular formulae.

Relative concentrations of T^n and Q^n silicon groups^[10] were obtained from the analysis of ^{29}Si DPMAS spectra. In agreement with our earlier results,^[5a] the measurements of the T_1 relaxation in functionalized MSNs yielded T_1 values in the order of 50–65 s for T^n groups and 30–45 s for Q^n groups. Therefore, a delay of 300 s between scans was used during the acquisition of ^{29}Si NMR spectra. The accumulation of 270 scans yielded intensities that were accurate within $\pm 10\%$. Although direct polarization is the preferred method for quantitative measurements, relative intensities of ^{13}C signals were measured by using a CP MAS based method. The strategy, developed in our earlier study,^[5b] was also successfully used for the AEP/UDP-MSN system in our previous report.^[4a] The procedure uses differences in values of T_{ρ}^H and τ_{CH} times between AEP and UDP.^[5b] The bifunctionalized samples could be characterized quantitatively without tedious measurements of the ^{13}C build-up curves^[4a,5b] by properly measuring and processing the CP MAS spectra with two different contact times (i.e., 0.4 and 1.5 ms) with known physical mixtures of monofunctionalized samples as intensity standards.^[4a,5a]

Received: October 26, 2004

Published online: February 11, 2005

Keywords: cooperative phenomena · heterogeneous catalysis · mesoporous materials · organic–inorganic hybrid composites · silicon

- 1999, 111, 2288–2309; *Angew. Chem. Int. Ed.* **1999**, 38, 2154–2174; c) A. Corma, *Chem. Rev.* **1997**, 97, 2373–2419.
- [4] a) S. Huh, H.-T. Chen, J. W. Wiench, M. Pruski, V. S.-Y. Lin, *J. Am. Chem. Soc.* **2004**, 126, 1010–1011; b) J. Liu, Y. Shin, Z. Nie, J. H. Chang, L. -Q. Wang, G. E. Fryxell, W. D. Samuels, G. J. Exarhos, *J. Phys. Chem. A* **2000**, 104, 8328–8339; c) F. Gelman, J. Blum, D. Avnir, *Angew. Chem.* **2001**, 113, 3759–3761; *Angew. Chem. Int. Ed.* **2001**, 40, 3647–3649.
- [5] a) S. Huh, J. W. Wiench, J.-C. Yoo, M. Pruski, V. S.-Y. Lin, *Chem. Mater.* **2003**, 15, 4247–4256; b) S. Huh, J. W. Wiench, B. G. Trewyn, S. Song, M. Pruski, V. S.-Y. Lin, *Chem. Commun.* **2003**, 2364–2365.
- [6] See Supporting Information for details.
- [7] a) Y. Kubota, K. Goto, S. Miyata, Y. Goto, Y. Fukushima, Y. Sugi, *Chem. Lett.* **2003**, 32, 234–235; b) B. List, *Acc. Chem. Res.* **2004**, 37, 548–557.
- [8] M. L. Kantam, P. Sreekanth, P. L. Santhi, *Green Chem.* **2000**, 2, 47–48.
- [9] G. M. Sammis, H. Danjo, E. N. Jacobsen, *J. Am. Chem. Soc.* **2004**, 126, 9928–9929.
- [10] G. E. Maciel in *Encyclopedia of Nuclear Magnetic Resonance*, Vol. 7 (Eds.: D. M. Grant, R. K. Harris), Wiley, Chichester, **1996**, pp. 4370–4386.

[1] For a review, see: T. Nakayama, H. Suzuki, T. Nishino, *J. Mol. Catal. B* **2003**, 9, 117–132.

[2] For a review, see: P. M. Pihko, *Angew. Chem.* **2004**, 116, 2110–2113; *Angew. Chem. Int. Ed.* **2004**, 43, 2062–2064.

[3] a) A. P. Wight, M. E. Davis, *Chem. Rev.* **2002**, 102, 3589–3613; b) E. Lindner, T. Schneller, F. Auer, H. A. Mayer, *Angew. Chem.*

Surface Chemistry

Going Beyond the Physical: Instilling Chirality onto the Electronic Structure of a Metal**

*Andrew Mulligan, Ian Lane, Gilles B. D. Rousseau, Shona M. Johnston, David Lennon, and Malcolm Kadodwala**

Conveying chirality onto the electronic structure of a metal surface is a possible mechanism by which chemical reactivity and electrical properties may be made chirally dependent. Here we report for the first time, to the best of our knowledge, that an adsorbed chiral molecule, 1-(1-naphthyl)ethylamine,

[*] A. Mulligan, Dr. G. B. D. Rousseau, S. M. Johnston, Dr. D. Lennon, Dr. M. Kadodwala
Department of Chemistry
Joseph Black Building
University of Glasgow
Glasgow G12 8QQ (UK)
Fax: (+44) 141-3304-888
E-mail: malcolmk@chem.gla.ac.uk

Dr. I. Lane
Department of Chemistry
David Keir Building
Queen's University of Belfast
Belfast, BT9 5AG (UK)

[**] Dr. L. Hecht is thanked for his help with the design of the laser system. A.M., S.M.J., and G.B.D.R. thank the EPSRC for the provision of studentships, and M.K. thanks the EPSRC and the University of Glasgow for funding.



Supporting information for this article is available on the WWW under <http://www.angewandte.org> or from the author.

can reversibly instill chirality onto the electronic structure of a metal surface, a previously unobserved phenomenon. We further demonstrate that although all chiral adsorbates physically convey chirality onto a surface at a local level, not all have the ability to further instill chirality onto the electronic structure of the underlying metal surface. This observation has strong implications for the chiral technologies that are governed by the functionality of these metal surfaces.

On the nanoscale, naturally occurring metal surfaces exhibit planes of mirror symmetry. This mirror symmetry can be lifted and chirality can be “physically” conveyed onto a surface through adsorption of a chiral molecule.^[1] Metal surfaces that have been functionalized in this way have applications in emerging chiral technologies, such as enantioselective metal-based heterogeneous catalysis, chiral recognition, and sensing.^[2] Until now it has been unclear whether the instilling of chirality by an adsorbate is limited to just the physical structure or whether it goes deeper and the electronic structure of the underlying surface can be imbued with chiral character.^[3] To establish that the electronic structure of a metal can be reversibly instilled with chirality is highly significant because it offers an alternative view of how chiral adsorbates can induce chiral dependencies in the physical and chemical properties of interfaces. Current understanding of chirally dependent processes is based on purely geometric arguments, and the effects of a “chiral” perturbation on the electronic structure of the interface are not considered.^[3]

We investigated single layers of (*R*)- and (*S*)-1-(1-naphthyl)ethylamine (NEA) adsorbed on a Cu(111) surface. NEA was chosen for the study because it has been shown to modify the reactivity of particles of metal catalyst in such a way that they selectively produce a particular enantiomer in hydrogenation reactions.^[4] Previous studies of NEA and related cinchona alkaloids on Pt^[5] and Cu^[6] surfaces have shown that they bind to the surface predominantly through the aromatic ring, which is slightly inclined with respect to the surface. In the case of NEA, the aromatic ring is attached to the asymmetric carbon atom, which also has a methyl group, an amine group, and a hydrogen atom attached to it. In the adsorption geometry adopted by NEA, two of these three groups, as well as the aromatic naphthalene ring, are in close vicinity to the surface (Figure 1).

NEA interacts weakly with Cu(111) through adsorption, without forming strong chemical bonds, and it thermally desorbs from the surface without dissociation below 300 K. The combination of the weak interaction and the cryogenic temperatures at which the layers of NEA are deposited preclude the possibility of the adsorbate inducing chiral restructuring (etching) of the copper surface. Adsorbate-induced chiral restructuring of copper has been observed previously^[7] and involves the formation of chiral facets, which have associated chiral electronic states that remain on the surface after the removal of the adsorbate and are stable up to the annealing temperature of the metal (≈ 900 K for Cu).

To determine whether NEA instills chirality onto the surface electronic structure of copper, optically active second-harmonic generation (SHG) measurements are performed; these have been shown to be highly flexible probes of surface chirality.^[8] SHG is a nonlinear optical response of an interface

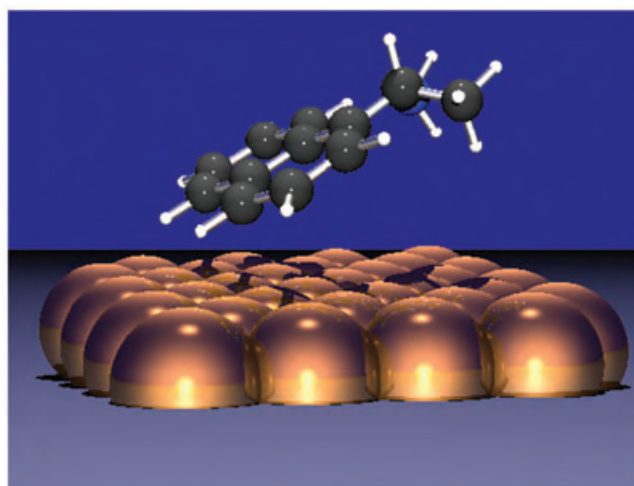


Figure 1. The adsorption geometry of NEA, taken from reference [5], on Cu(111).

which involves the frequency doubling of incident radiation. The SHG response is determined by the second-order susceptibility tensor $\chi^{(2)}$ of the surface. In the optically active variant of SHG that was used in this study, elliptically polarized SHG light (532 nm) was generated from a chiral interface by incident linearly polarized pulsed laser radiation (1064 nm, 8-ns duration). The ellipticity in the SHG light can be viewed as resulting from an optical rotation, the sense of which depends upon the handedness of the chiral interface. Hence the technique can be considered a nonlinear analogue of traditional polarimetry measurements.

The overall $\chi^{(2)}$ value of the NEA/copper interface has two contributions, one from the metal–adsorbate interface ($\chi_{\text{Cu}}^{(2)}$) which is governed by the electronic structure of the metal, and a second from the adsorbate–vacuum interface ($\chi_{\text{NEA}}^{(2)}$). If $\chi_{\text{Cu}}^{(2)} \gg \chi_{\text{NEA}}^{(2)}$, then the SHG signal is only sensitive to the electronic structure of the metal, and an optically active response would be observed only if chirality had been instilled on the surface electronic structure. The $\chi_{\text{NEA}}^{(2)}$ value is governed by the hyperpolarizability (β) of each single molecule, and the number density of surface molecules (N_s). The β value for NEA has not been measured, however, there is considerable experimental data on other monosubstituted aromatic compounds, such as benzenes, stilbenes, and polyphenyls,^[9,10] which all display $\beta \leq 10^{-30}$ esu (electrostatic unit). Theoretical work has also shown the polarizability properties of naphthalene are of the same order of magnitude as for benzene.^[11] β values of greater than 10^{-28} are only observed in aromatic systems that contain electron-donating and -withdrawing groups: NEA is not of this type. Enhancements of an order of magnitude in $\chi^{(2)}$ values have been reported from chiral films of molecules which have a resonant electronic transition that coincide with the frequency of the second-harmonic (SH) radiation.^[12] However, such enhancements are not expected for NEA, which is transparent at the wavelengths of both the incident and SH radiation. This indicates that 10^{-30} esu is an upper limit for the β value of NEA. As a saturated monolayer of NEA has a surface molecule density of approximately

10^{14} cm^{-2} ,^[5] then $\chi_{\text{NEA}}^{(2)} \leq 10^{-16} \text{ esu}$, which compares with $\chi_{\text{Cu}}^{(2)} \approx 10^{-12} \text{ esu}$.^[13]

To further increase the relative contribution that $\chi_{\text{Cu}}^{(2)}$ makes to the overall SH signal, p-polarized (electric field perpendicular to the surface) incident radiation was used. With p-polarized incident radiation the contribution of $\chi_{\text{Cu}}^{(2)}$ to the overall $\chi^{(2)}$ value of the interface is maximized,^[14] while the $\chi_{\text{NEA}}^{(2)}$ contribution will be reduced. This reduction in the contribution of $\chi_{\text{NEA}}^{(2)}$ is caused by the fact that the incident electric field is not parallel to the highly polarizable π system of the naphthalene. Given that $\chi_{\text{Cu}}^{(2)} \gg \chi_{\text{NEA}}^{(2)}$, the observation of optical activity in SH measurements will signal the instilling of chirality onto the electronic structure of the metal.

Figure 2 depicts plots of SHG intensity as a function of detection polarization for incident p-polarized light from a

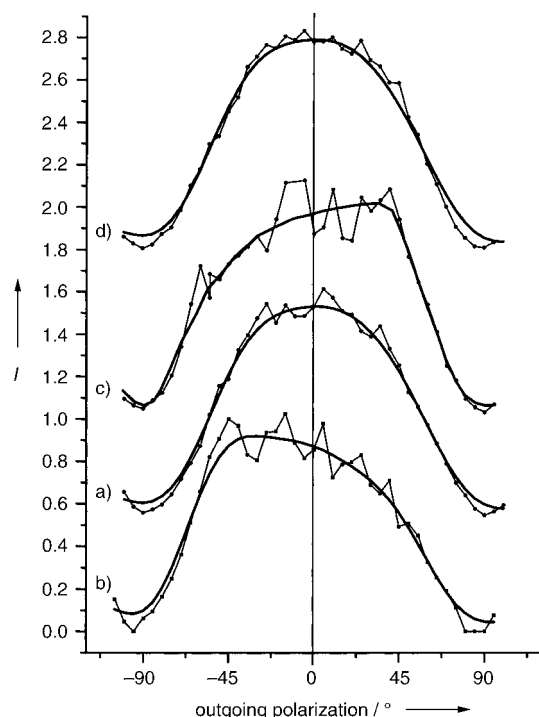


Figure 2. Representative profiles showing second-harmonic (SH, $\lambda = 532 \text{ nm}$) intensity generated by incident p-polarized laser pulses (duration: 8 ns; wavelength: 1064 nm) from a) a clean Cu(111) surface, b) and c) Cu surface with monolayers of (S)- (b) and (R)-NEA (c), and d) a surface after the desorption of a monolayer of NEA. The horizontal axis is the detection polarization angle with respect to the p-polarization direction.

clean Cu(111) surface and for overlayers of (R)- and (S)-NEA (both have identical submonolayer coverages). A symmetrical profile is observed for the clean surface, with maximum intensity observed for p-polarization and minimum intensities for outgoing s-polarization. This behavior is consistent with that expected for an achiral Cu(111) surface. However, there is a dramatic change in profiles for (R)- and (S)-NEA monolayers. Both are asymmetric about the p-polarization direction, but in the profile for (R)-NEA the maximum in SHG intensity peaks close to 45° , while for (S)-NEA it is located at -45° . The asymmetry of the two profiles has been

parameterized in two ways: the first method uses the ratio I_{45}/I_{-45} , while the second method involves the ratio of the integrated area at negative (I_-) and positive (I_+) angles. All of the measured ratios are listed in Table 1. Both types of ratio

Table 1: Parameters showing the asymmetry of SH profiles obtained from monolayers of (S)- and (R)-NEA.^[a]

	I_{45}/I_{-45}	I_{-45}/I_{45}	I_+/I_-	I_-/I_+
(R)-NEA	1.50 ± 0.10	0.67 ± 0.07	1.14 ± 0.06	0.88 ± 0.05
(S)-NEA	0.75 ± 0.07	1.33 ± 0.13	0.90 ± 0.06	1.11 ± 0.07

[a] The tabulated values are averages obtained from five freshly prepared surfaces; the quoted errors correspond to one standard deviation in ratios.

show that the profiles for the R and S isomers are asymmetric and they are those expected for an optically active measurement: I_{45}/I_{-45} for one enantiomer is equal to I_{-45}/I_{45} ratio of the other. SHG polarimetry measurements have also been collected after the NEA layers were removed from the surface through desorption by heating to 273 K. The obtained profiles are once again symmetric about the p-polarization direction.

The results from SHG polarimetry clearly show that NEA reversibly instills chirality onto the surface electronic structure of Cu(111). The fact that the surface returns to achirality after the desorption of the adsorbate below 300 K rules out, as expected, the possibility of chiral etching by NEA. So, chirality must be instilled onto the surface electronic structure of the metal by the adsorbate without induction of a significant physical chiral rearrangement of the surface itself. The instilling of chirality onto the electronic structure of a metal by an adsorbate is not a generic phenomenon. In previous work,^[14] we have found that another chiral molecule, 2-butanol, does not instill the surface electronic structure of Cu(111) with chirality. 2-Butanol, like NEA, interacts weakly with Cu(111) desorbing from the surface below 300 K. We believe that the ability of NEA to instill chirality is associated with its adsorption geometry. NEA adopts a geometry that results in a “chiral footprint”, in which three different chemical groups are in close proximity to the surface. In contrast, 2-butanol does not have a chiral footprint, as it adopts a geometry where only a single group, the hydroxyl, is close to the surface.^[15] An analogy can be drawn between our hypothesis and the observed behavior of chiral inorganic metal complexes. The electronic structure of a metal ion that is in a chiral ligand environment has chiral character, which is revealed by the observation of circular dichroism (CD) in UV/Vis absorption bands associated with transitions localized to the metal center. This observation suggests that the chiral footprint plays the same role as the chiral ligand environment and reduces the symmetry of the surface electronic states from C_{3v} to a chiral point group. On the basis of this mechanism, we predict that a prerequisite for the instilling of chirality is an adsorption geometry that displays a chiral footprint on the surface.

The conveyance of chirality onto the surface electronic structure of a metal challenges the established view of the mechanisms by which chiral adsorbates induce enantioselectivity.

tivity in surface reactions. Current models for the mechanism are based on solely geometric arguments,^[16–18] in which the adsorbed chiral modifier interacts with the achiral reactants to control the stereochemistry of the surface transition state and, consequently, of the reaction products. The models can explain some but not all of the features of enantioselective reactions, and in particular they cannot predict in a meaningful way the effect of structural variations of the modifier on enantioselectivity.^[19] We suggest that to fully model the action of a chiral modifier, its ability to instill chirality on the surface electronic structure should be taken into account. In the case where a modifier instills chirality onto the electronic structure, the absolute configurations of a chiral transition state and chiral product would be expected to govern how strongly they interact with the metal surface, which will influence directly the thermodynamics of the reaction and consequently enantioselectivity. Similar “chiral” electronic effects on the thermodynamics of the adsorbed state have clear implications for the mechanisms of chiral separation and recognition, which are currently also understood by using solely geometric arguments.^[2] In summary, this new insight pushes forward the boundaries of the understanding of chiral adsorption phenomena and consequently should aid in the future development of lucrative chiral technologies.

Experimental Section

For optimal control of the NEA/copper interface, experiments were performed under ultrahigh vacuum (UHV) conditions (base pressure: 1×10^{-10} mbar) using an atomically clean well-ordered Cu(111) single-crystal surface. Single layers of (*R*)- and (*S*)-NEA were deposited from the vapor phase onto Cu(111) at 100 K. SHG measurements were performed using pulses (8–12 ns) of fundamental Nd:YAG laser (Spectra Physics Quanta Ray) 1064-nm radiation at a repetition rate of 10 Hz and around 3.6 mJ pulse⁻¹. The beam was defocused (10-mm diameter) and was incident on the crystal at 60° with respect to the surface normal, the incident polarization was varied by using a $\lambda/2$ plate. The SH signal was monitored at 60° with respect to the surface normal: it first passed through a polarizer before being focused into a spectrograph and then detected on an intensified CCD camera.

Received: October 11, 2004

Revised: November 2, 2004

Published online: February 16, 2005

Keywords: adsorption · chirality · copper · electronic structure · surface chemistry

- [8] S. Sioncke, T. Verbiest, A. Persoons, *Mater. Sci. Eng. R* **2003**, *42*, 115–150.
- [9] L. T. Cheng, W. Tam, S. R. Marder, A. E. Stiegman, G. Rikken, C. W. Spangler, *J. Phys. Chem.* **1991**, *95*, 10631–10643.
- [10] L. T. Cheng, W. Tam, S. R. Marder, A. E. Stiegman, G. Rikken, C. W. Spangler, *J. Phys. Chem.* **1991**, *95*, 10643–10652.
- [11] P. Norman, D. Jonsson, H. Ågren, *Chem. Phys. Lett.* **1997**, *268*, 337–344.
- [12] T. Verbiest, S. van Elshocht, M. Kauranen, L. Hellemans, J. Snauwaert, C. Nuckolls, T. J. Katz, A. Persoons, *Science* **1998**, *282*, 913–915.
- [13] H. W. K. Tom, G. D. Aumiller, *Phys. Rev. B* **1986**, *33*, 8818–8821.
- [14] J. E. Sipe, D. J. Moss, H. M. van Driel, *Phys. Rev. B* **1987**, *35*, 1129–1141.
- [15] A. Mulligan, I. C. Lane, G. B. D. Rousseau, L. Hecht, S. M. Johnston, D. Lennon, M. Kadodwala, *Chem. Commun.* **2004**, 2492–2493.
- [16] A. J. Baiker, *J. Mol. Catal. A* **1997**, *115*, 473–493.
- [17] J. L. Margitfalvi, E. Tfirst, *J. Mol. Catal. A* **1999**, *139*, 81–95.
- [18] R. L. Augustine, S. K. Tanielyan, L. K. Doyle, *Tetrahedron: Asymmetry* **1993**, *4*, 1803–1827.
- [19] H. U. Blaser, H. P. Jalett, W. Lottenbach, M. Bacher, *J. Am. Chem. Soc.* **2000**, *122*, 12675–12682.

[1] M. O. Lorenzo, C. J. Baddeley, R. Muryn, R. Raval, *Nature* **2000**, *404*, 376–379.

[2] R. A. Sheldon, *Chirality*, Marcel Dekker, New York, **1993**.

[3] W. A. Hofer, V. Humbolt, R. Raval, *Surf. Sci.* **2004**, *554*, 141–149.

[4] T. Heinz, G. Z. Wang, A. Pfaltz, A. Minder, M. Schuch, T. Mallat, A. Baiker, *J. Chem. Soc. Chem. Commun.* **1993**, 1421–1422.

[5] J. M. Bonella, F. J. Williams, R. M. Lambert, *J. Am. Chem. Soc.* **2003**, *125*, 2723–2729.

[6] Q. M. Xu, D. Wang, L. J. Wan, C. L. Bai, Y. Wang, *J. Am. Chem. Soc.* **2000**, *122*, 14300–14301.

[7] X. Zhao, *J. Am. Chem. Soc.* **2000**, *122*, 12584–12585.

Self-Assembled Nanoparticles

One-Dimensional Assembly of Lipophilic Inorganic Nanoparticles Templated by Peptide-Based Nanofibers with Binding Functionalities**

*Liang-shi Li and Samuel I. Stupp**

Spatially controlled assemblies of inorganic nanoparticles are of fundamental interest because of their unique electronic and optical properties.^[1–3] To prepare one-dimensional systems, biological substrates^[4] such as peptides,^[5] viruses,^[6]

[*] Dr. L.-s. Li, Prof. Dr. S. I. Stupp

Department of Chemistry

Northwestern University

Evanston, IL 60208 (USA)

Fax: (+1) 847-491-3010

E-mail: s-stupp@northwestern.edu

Prof. Dr. S. I. Stupp

Department of Materials Science and Engineering

Northwestern University

Evanston, IL 60208 (USA)

Prof. Dr. S. I. Stupp

Feinberg School of Medicine

Northwestern University

Evanston, IL 60208 (USA)

[**] We thank Dr. John D. Tovar and Dr. Keisuke Tajima for helpful discussions. This work was supported by the US Department of Energy (DE-FG02-00ER45810/A005), the Air Force Office of Scientific Research AFOSR-MURI (F49620-00-1-0283), and the National Science Foundation (NSEC EEC-0118025).



Supporting information for this article is available on the WWW under <http://www.angewandte.org> or from the author.

fungi,^[7] and DNA^[8] have been used recently as scaffolds for the assembly or growth of nanoparticles. Previous work has been limited to water-soluble nanoparticles because the templates used require water as a solvent. Thus, a large variety of well-characterized lipophilic nanocrystals that have been synthesized with excellent size and shape control have been excluded from these strategies. These include nanocrystals of II–VI^[9] or III–V semiconductors,^[10] metals,^[11] and oxides.^[12] We report herein a strategy for the creation of one-dimensional assemblies of lipophilic inorganic nanoparticles in apolar solvents by using peptide-based nanofibers with surface-binding motifs.

Nanofiber structures based on peptide β -sheet motifs have been widely studied^[4,13,14] in analogy to physiological amyloid fibrils, the insoluble protein deposits related to Alzheimer's disease and other illnesses.^[15] In our laboratory, we have been working on peptide amphiphiles that self-assemble in water to form supramolecular nanofibers containing β sheets for biomedical applications.^[5a,16] To assemble nanofibers in apolar organic solvents capable of binding lipophilic nanoparticles, we started the study described herein with a tripeptide amphiphilic molecule of the type developed by Yamada and co-workers,^[13] such as molecule **1**. It was previously demonstrated^[13] that these molecules self-assemble into nanofibers in both water and apolar solvents such as benzene and carbon tetrachloride (CCl₄). For nanocrystals to bind specifically to the surfaces of the nanofibers, we designed molecule **2**, which contains a thymine moiety, and used it along with **1** in our previously described strategy of mixing two molecules to co-assemble nanofibers bearing two biological signals.^[17] These surface-modified nanofibers of **1** and **2** formed in CCl₄ and were then mixed with lipophilic gold nanoparticles decorated with diaminopyridine (DAP) (Figure 1). The thymine–DAP base pairing was chosen in this case because of its chemical simplicity and high binding efficiency in aprotic environments.^[18]

Molecules **2** and **1** (1:10 molar ratio) were dissolved in a mixture of methanol and chloroform to ensure mixing, and the solution was subsequently dried. Excess of CCl₄ was then added, and the mixture was heated. A semitransparent gel

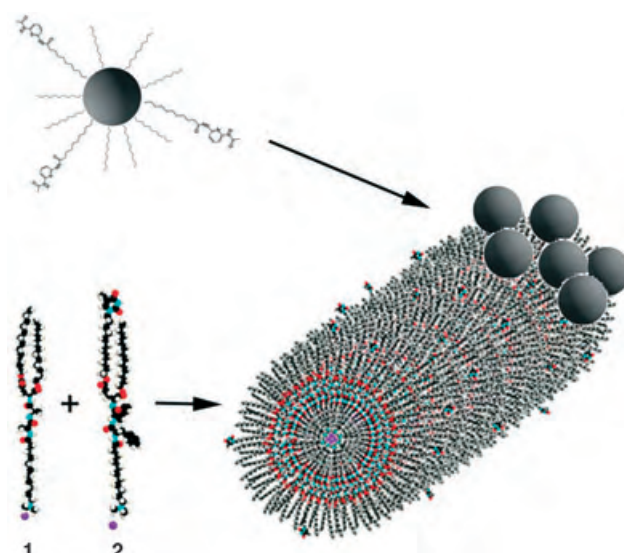
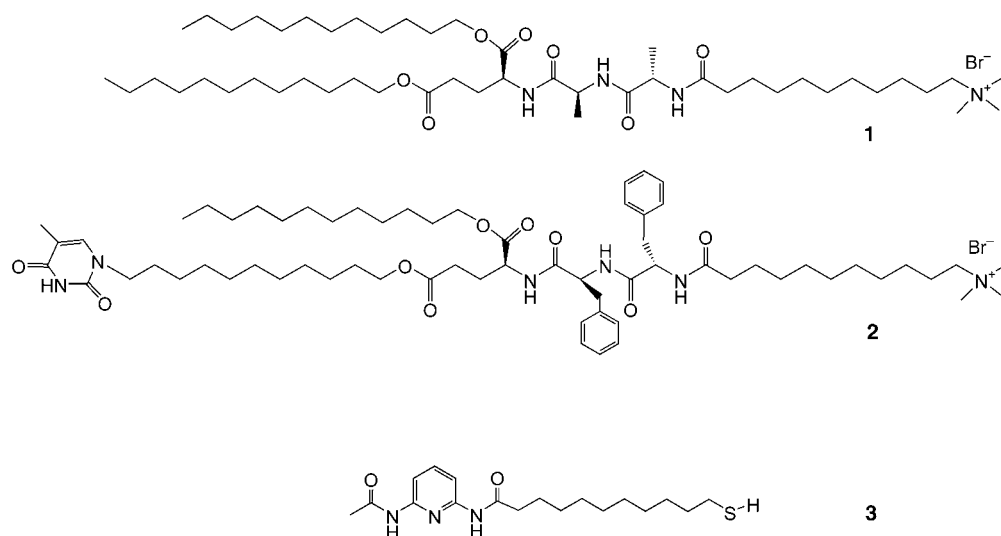


Figure 1. Schematic representation of the co-assembled nanofibers and binding of surface-modified nanoparticles. Molecules of **2** with a thymine moiety co-assemble into nanofiber matrices with a large excess of molecule **1**, providing binding sites on the surfaces of the fibers for its complementary base-pairing molecules, such as diaminopyridine functionalized molecules (e.g. DAP-SH **3**), which are bound to the nanoparticle surfaces.

formed when the mixture was cooled, and transmission electron microscopy (TEM) confirmed the formation of bundled nanofibers with diameters of ≈ 8 nm (see Supporting Information). Molecule **2** does not dissolve or cause gelation in CCl₄, but for entropy reasons, its mixing with a much larger amount of **1** should result in nanofibers that trap molecules of **2** and thus provide binding sites on their surfaces.

Lipophilic gold nanoparticles (≈ 3 nm diameter) were synthesized through the two-phase method developed by Brust et al.^[11a] with octanethiol as the surface-stabilizing ligands. We then modified the gold nanoparticle surfaces with DAP-functionalized alkyl thiol **3**^[18b] (DAP-SH) by stirring the nanoparticles in a DAP-SH/octanethiol solution (1:10 molar ratio) in dichloromethane at room temperature for 48 h^[19] (NMR spectroscopy confirmed the attachment of the DAP-SH molecules on gold particles). When a solution of DAP-SH-coated gold particles (≈ 0.1 mg mL⁻¹) in CCl₄ (1.0 mL) was added to the thymine-modified nanofiber suspension (1.0 mL, ≈ 0.5 mg mL⁻¹), the aggregation of gold nanoparticles could be seen with the naked eye within 30 minutes at room temperature.

The observed aggregates were diluted and collected with carbon-coated TEM grids. Under a transmission electron microscope, large numbers of linear arrays of gold nanoparticles were observed along



with isolated particles. Figure 2A shows a representative micrograph. The arrays of gold nanoparticles may extend for lengths of up to a few microns (Figure 2C) and are made up of densely packed gold nanoparticles with an interparticle distance comparable to twice the length of the surface ligands (≈ 1 nm).

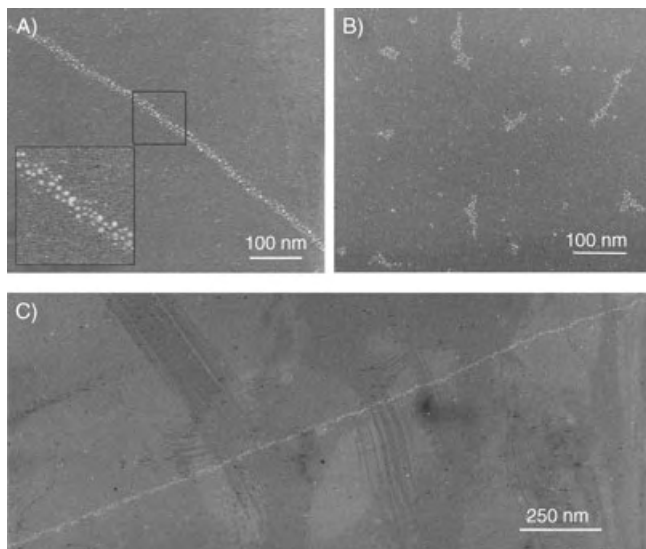


Figure 2. A) and C) Linear arrays of surface-modified gold nanoparticles in the presence of surface-modified peptide amphiphile nanofibers observed under TEM. B) For comparison, a typical image of gold nanoparticles when the surfaces of either the nanofibers or the nanoparticles are not modified. The inset (in A) is a zoom-in of the 100×100 nm² area enclosed in by the square.

To establish the relationship between the formation of the linear arrays of gold nanoparticles and chemical modifications on the surfaces of the nanoparticles and nanofibers, a series of control experiments were performed. Mixtures of gold nanocrystals and nanofibers without modification on either reagent did not show any precipitation in solution, nor were linear arrays of gold nanoparticles with a long persistence length observed by TEM (see Figure 2B for a representative micrograph). In addition, a decrease in the molar ratio of thymine-functionalized amphiphile **2** in the fiber suspension or a decrease in the amount of DAH-SH on the gold particles results in a lower yield of the linear arrays and a longer incubation time required to observe precipitation from solution. These results indicate that formation of the linear arrays of gold nanoparticles is the result of specific binding between the nanoparticles and nanofibers.^[20] The observations also prove indirectly the expected presence of trapped molecules of **2** in the nanofibers.

Whereas the long persistence length of the gold nanoparticle arrays is consistent with that of the nanofibers,^[13a] their widths vary from a few (Figure 3A) to tens of nanometers (e.g. Figure 2A). In some cases the width is not uniform, even within the same array (Figure 3B). This can be attributed to the strong tendency of nanofibers to bundle, which has been demonstrated in TEM and AFM studies.^[13]

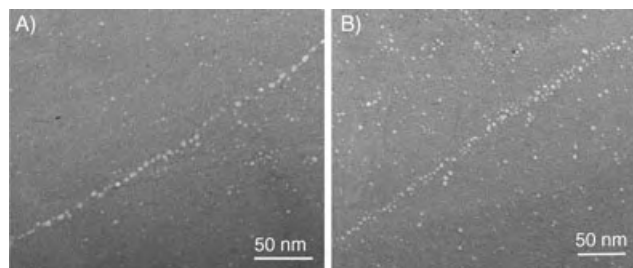


Figure 3. Variation in the width of nanoparticle arrays. A) An array made of a single file of gold nanoparticles. B) An array with variable width, presumably as a result of either bundling of the nanofibers or that of linear arrays.

Furthermore, the modified gold nanoparticles can link nanofibers through their binding to thymine sites, and therefore may also result in width variation of the arrays.

We have shown that peptide-based nanofibers can serve as scaffolds for the 1D assembly of lipophilic inorganic nanoparticles in apolar solvents. The method is simple and very general, and therefore could be extended to other surface-modified inorganic nanoparticles as well. In addition, because the scaffold molecules can be further modified with various organic functional groups such as chromophores and conducting oligomers, these nanofibers may prove to be a versatile scaffold for constructing various functional one-dimensional hybrid nanostructures.

Experimental Section

Molecule **1** and **2** were synthesized through the procedure described in reference [13a], except that 1-[3-(dimethylamino)propyl]-3-ethylcarbodiimide hydrochloride (EDCI) and 1-hydroxybenzotriazole hydrate (HOBT) were used as coupling reagents in all the ester and amide formation, and that all the intermediates were purified by silica gel chromatography with dichloromethane/methanol (95:5 v/v) as eluent. To synthesize heterodiesters of glutamic acid, Boc-Glu(OBzl)-OH was used as one of the starting materials.

The intermediate 1-(ω -hydroxy-undecyl) thymine for molecule **2** was synthesized through a published procedure^[18c] to make dodecyl uracil except that thymine and 11-bromo-1-undecanol were used instead. Yield: 50%. ¹H NMR (400 MHz, CDCl₃): δ = 8.24 (s, 1H), 6.97 (s, 1H), 3.65 (m, 4H), 1.92 (s, 3H), 1.70–1.45 (m, 4H), 1.40–1.20 ppm (m, 14H); ESI MS (*m/z*): 297.5 [*M* + 1].

Molecule **2** was recrystallized from ethyl acetate as a white powder. ¹H NMR (500 MHz, CDCl₃): δ = 7.58 (b, 1H), 7.25 (m, 10H), 6.97 (s, 1), 4.60 (m, 2H), 4.46 (m, 1H), 4.06 (m, 4H), 3.67 (m, 2H), 3.46 (m, 2H), 3.33 (s, 9H), 3.05 (m, 4H), 2.40–2.20 (m, 2H), 2.20–2.00 (m, 4H), 1.91 (s, 3H), 1.72 (m, 2H), 1.60 (m, 6H), 1.45 (m, 2H), 1.40–1.10 (b, 44H), 0.87 ppm (t, *J* = 6.8 Hz, 3H); ESI MS (*m/z*): 1113.8.

TEM was performed on a Hitachi H-8100 microscope operating at 200 kV.

Received: September 28, 2004

Published online: February 18, 2005

Keywords: gold · nanostructures · peptides · self-assembly · template synthesis

- [1] A. N. Shipway, E. Katz, I. Willner, *ChemPhysChem* **2000**, *1*, 18; C. P. Collier, T. Vossmeier, J. R. Heath, *Annu. Rev. Phys. Chem.* **1998**, *49*, 371; and references therein.
- [2] W. L. Barnes, A. Dereux, T. W. Ebbesen, *Nature* **2003**, *424*, 824; M. Quinten, A. Leitner, J. R. Krenn, F. R. Aussenegg, *Opt. Lett.* **1998**, *23*, 1331; S. A. Maier, P. G. Kik, H. A. Atwater, S. Meltzer, E. Harel, B. E. Koel, A. A. G. Requicha, *Nat. Mater.* **2003**, *2*, 229.
- [3] C. M. Lieber, *Sci. Am.* **2001**, Sept, 59.
- [4] C. M. Niemeyer, *Angew. Chem.* **2001**, *113*, 4254; *Angew. Chem. Int. Ed.* **2001**, *40*, 4128; S. G. Zhang, *Nat. Biotechnol.* **2003**, *21*, 1171; and references therein.
- [5] a) J. D. Hartgerink, E. Beniash, S. I. Stupp, *Science* **2001**, *294*, 1684; J. D. Hartgerink, E. Beniash, S. I. Stupp, *Proc. Natl. Acad. Sci. USA* **2002**, *99*, 5133; b) R. Djalali, Y. Chen, H. Matsui, *J. Am. Chem. Soc.* **2002**, *124*, 13660; c) M. Rechtes, E. Gazit, *Science* **2003**, *300*, 625.
- [6] C. Mao, D. J. Solis, B. D. Reiss, S. T. Kottmann, R. Y. Sweeney, A. Hayhurst, G. Georgiou, B. Iverson, A. M. Belcher, *Science* **2004**, *303*, 213.
- [7] Z. Li, S. W. Chung, J. M. Nam, D. S. Ginger, C. A. Mirkin, *Angew. Chem.* **2003**, *115*, 2408; *Angew. Chem. Int. Ed.* **2003**, *42*, 2306.
- [8] M. G. Warner, J. E. Hutchison, *Nat. Mater.* **2003**, *2*, 272; H. Nakao, H. Shiigi, Y. Yamamoto, Y. Yamamoto, S. Tokonami, T. Nagaoka, S. Sugiyama, T. Ohtani, *Nano Lett.* **2003**, *3*, 1391.
- [9] See, for example: C. B. Murray, D. J. Norris, M. G. Bawendi, *J. Am. Chem. Soc.* **1993**, *115*, 8706; M. Hines, P. Guyot-Sionnest, *J. Phys. Chem. B* **1998**, *102*, 3655; X. G. Peng, L. Manna, W. D. Yang, J. Wickham, E. Scher, A. Kadavanich, A. P. Alivisatos, *Nature* **2000**, *404*, 59.
- [10] O. I. Micic, J. R. Sprague, C. J. Curtis, K. M. Jones, J. L. Machol, A. J. Nozik, H. Giessen, B. Fluegel, G. Mohs, N. Peyghambarian, *J. Phys. Chem.* **1995**, *99*, 7754; A. A. Guzelian, J. E. B. Katari, A. V. Kadavanich, U. Banin, K. Hamad, E. Juban, A. P. Alivisatos, R. H. Wolters, C. C. Arnold, J. R. Heath, *J. Phys. Chem.* **1996**, *100*, 7212.
- [11] See, for example: a) M. Brust, M. Walker, D. Bethell, D. J. Schiffrin, R. Whyman, *J. Chem. Soc. Chem. Commun.* **1994**, 801; b) S. Sun, C. B. Murray, D. Weller, L. Folks, A. Moser, *Science* **2000**, *287*, 1989; c) V. F. Puentes, D. Zanchet, C. K. Erdonmez, A. P. Alivisatos, *J. Am. Chem. Soc.* **2002**, *124*, 12874.
- [12] See, for example: a) T. J. Trentler, T. E. Denler, J. F. Bertone, A. Agrawal, V. L. Colvin, *J. Am. Chem. Soc.* **1999**, *121*, 1613; b) J. Rockenberger, E. C. Scher, A. P. Alivisatos, *J. Am. Chem. Soc.* **1999**, *121*, 11595; c) Y. W. Jun, M. F. Casula, J. H. Sim, S. Y. Kim, J. Cheon, A. P. Alivisatos, *J. Am. Chem. Soc.* **2003**, *125*, 15981.
- [13] a) N. Yamada, K. Ariga, M. Naito, K. Matsubara, E. Koyama, *J. Am. Chem. Soc.* **1998**, *120*, 12192; b) N. Yamada, E. Koyama, T. Imai, K. Matsubara, S. Ishida, *Chem. Commun.* **1996**, 2297; c) N. Yamada, K. Ariga, *Synlett* **2000**, *5*, 575.
- [14] A. Aggeli, M. Bell, N. Boden, J. N. Keen, P. F. Knowles, T. C. B. McLeish, M. Pitkeathly, S. E. Radford, *Nature* **1997**, *386*, 259.
- [15] J. D. Harper, P. T. Lansbury, Jr., *Annu. Rev. Biochem.* **1997**, *66*, 385–407; M. Sunde, C. C. F. Blake, *Q. Rev. Biophys.* **1998**, *31*, 1–30; M. Sunde, L. C. Serpell, M. Bartlam, P. E. Fraser, M. B. Pepys, C. C. F. Blake, *J. Mol. Biol.* **1997**, *273*, 729.
- [16] G. A. Silva, C. Czeisler, K. L. Niece, E. Beniash, D. A. Harrington, J. A. Kessler, S. I. Stupp, *Science* **2004**, *303*, 1352.
- [17] K. L. Niece, J. D. Hartgerink, J. J. J. Donners, S. I. Stupp, *J. Am. Chem. Soc.* **2003**, *125*, 7146.
- [18] a) A. D. Hamilton, D. Van Engen, *J. Am. Chem. Soc.* **1987**, *109*, 5035; A. K. Boal, F. Ilhan, J. E. DeRouchey, T. Thurn-Albrecht, T. P. Russell, V. M. Rotello, *Nature* **2000**, *404*, 746; b) A. K. Boal, V. M. Rotello, *J. Am. Chem. Soc.* **2002**, *124*, 5019; c) G. M. Credo, A. K. Boal, K. Das, T. H. Galow, V. M. Rotello, D. L. Feldheim, C. B. Gorman, *J. Am. Chem. Soc.* **2002**, *124*, 9036.
- [19] R. S. Ingram, M. J. Hostetler, R. W. Murray, *J. Am. Chem. Soc.* **1997**, *119*, 9175.
- [20] As suggested by one of the reviewers of this manuscript, we treated DAP-SH modified gold nanoparticles with excess 1-[ω -(*N*-Boc-phenylalanyl)-undecyloxy]thymine in CCl₄, and then mixed them with a thymine-modified nanofiber suspension. We found that the binding affinity between the nanoparticles and the nanofibers decreased significantly.

Active-Site Modeling

A Functional Model of the Cytochrome *c* Oxidase Active Site: Unique Conversion of a Heme- μ -peroxo- Cu^{II} Intermediate into Heme-superoxo/ Cu^{I} ***Jin-Gang Liu, Yoshinori Naruta,* and Fumito Tani*

Cytochrome *c* oxidase (CcO), the terminal enzyme of the respiratory chain, catalyzes the four-electron reduction of molecular oxygen to water at a low overpotential without the release of the toxic reactive intermediates superoxide and peroxide.^[1] The active site of the enzyme at which dioxygen reduction takes place is composed of heme $\text{a}_3/\text{Cu}_\text{B}$ dinuclear center. Heme a_3 is ligated axially by a histidinyl imidazole, and Cu_B is coordinated with tridentate chelation by three histidine ligands, one of which (His240) is linked to a tyrosine residue (Tyr244) by a covalent bond (in the bovine enzyme sequence).^[2] The function of this unprecedented Tyr-His cross-link has provoked considerable interest, and it has been proposed to function either as an electron and proton donor to dioxygen bound to heme a_3 or to provide a means to fix Cu_B in an optimal configuration at an optimal distance from heme a_3 during the catalytic reduction of O_2 .^[3]

The reduction of dioxygen by CcO has been proposed to proceed via various intermediates; oxyheme (a heme-superoxide complex) and oxoferryl intermediates have been observed spectroscopically.^[1c] A peroxide species $[\text{Fe}^{\text{III}}-\text{O}_2-\text{Cu}^{\text{II}}]^+$ has been proposed as a possible intermediate in the catalytic cycle, but has yet to be observed in the enzyme.^[4]

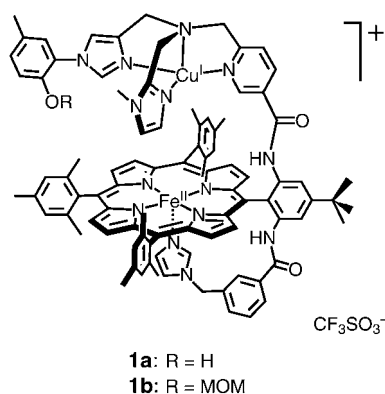
[*] Dr. J.-G. Liu, Prof. Dr. Y. Naruta, Dr. F. Tani
Institute for Materials Chemistry and Engineering
Kyushu University
Higashi-ku, Fukuoka, 812-8581 (Japan)
Fax: (+81) 92-642-2715
E-mail: naruta@ms.ifoc.kyushu-u.ac.jp

[**] This work was supported financially by the Grant-in-Aid for Scientific Research on Priority Areas (#11228207 and #16033247) from the MEXT, and for Scientific Research (A) (#14204073) from the JSPS. This research was supported in part by the Takeda Science Foundation and the P&P project, Green Chemistry, of Kyushu University. J.-G.L. gratefully acknowledges the JSPS for providing a research fellowship for foreign researchers.



Supporting information for this article is available on the WWW under <http://www.angewandte.org> or from the author.

Thus, the exact role of the Cu_B center in the binding and activation of dioxygen are not yet well defined. The construction of functional biomimetic molecules that closely resemble the native enzyme active site is crucial for the elucidation of the CcO catalytic mechanism. Considerable progress has been made in the creation of heme/copper model compounds that provide further understanding of the enigmatic heme a₃/Cu_B dinuclear center in CcO.^[5] Few of the previously reported synthetic models, however, bear a mimic of the Tyr–His cross-link, a feature which appears to play an important role in the mechanism of dioxygen reduction catalyzed by CcO.^[6–8] Recently, a heme-containing CcO-active-site model was reported which lacks the axial imidazole ligand and contains covalently appended copper-chelating groups and a cross-linked Tyr–His mimic. It reacts with dioxygen to form a stable peroxide species at low temperature.^[9] Toward the construction of closer structural analogues of the CcO active site, a fully integrated model [(L^{N4-OH})Cu^I/Fe^{II}(TMPIm)] (**1a**) was prepared. We report



herein spectroscopic evidence that the formation of a heme-μ-peroxo-Cu^{II} species is followed by conversion into a heme-superoxo/Cu^I intermediate during the oxygenation reaction with this new model compound. The unique conversion of the transiently formed μ-peroxide into the corresponding superoxide species revealed by this synthetic model may provide some clarification of the ill-defined mechanism of dioxygen reduction by CcO.

The oxygenation reaction of **1a** was monitored by UV/Vis spectroscopy. Exposure of **1a** to O₂ in CH₃CN/THF (20%) at –70°C leads to distinctive spectral changes with clear isosbestic points, as shown in Figure 1. The Soret band shifts from 426 nm ($\epsilon = 88\,500\text{ M}^{-1}\text{ cm}^{-1}$) to 429 nm ($\epsilon = 81\,600\text{ M}^{-1}\text{ cm}^{-1}$) with a slight decrease in intensity, whereas the Q band at 533 nm ($\epsilon = 12\,000\text{ M}^{-1}\text{ cm}^{-1}$) disappears, and a new band at 538 nm ($\epsilon = 9\,300\text{ M}^{-1}\text{ cm}^{-1}$) develops. This species formed at low temperature, intermediate **A**, is unstable ($t_{1/2} = 0.5\text{ h}$, –70°C), and its gradual transformation into intermediate **B** is marked by a shift in the Soret band at 429 nm to 425 nm, whereas the Q band shifts from 538 nm to 550 nm (Figure 2). Intermediate **B** is observable in the temperature range of –70 to –30°C, and its UV/Vis spectral characteristics resemble those of the copper-free heme-superoxide species, observed with the same system under similar experimental conditions.

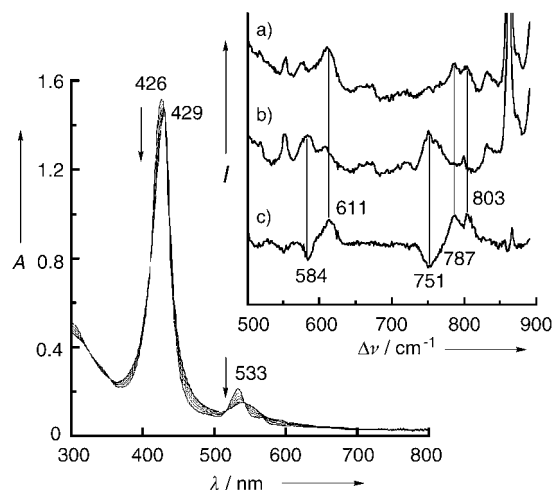


Figure 1. UV/Vis spectral changes of **1a** upon exposure to dioxygen in 20% CH₃CN/THF at –70°C. Spectral interval is 1 min. Inset: resonance Raman spectra of intermediate **A** formed from a) ¹⁶O₂ and b) ¹⁸O₂; c) difference spectra of a) minus b); conditions: 20% CH₃CN/THF, –70°C, excitation at 413 nm, 20 mW.

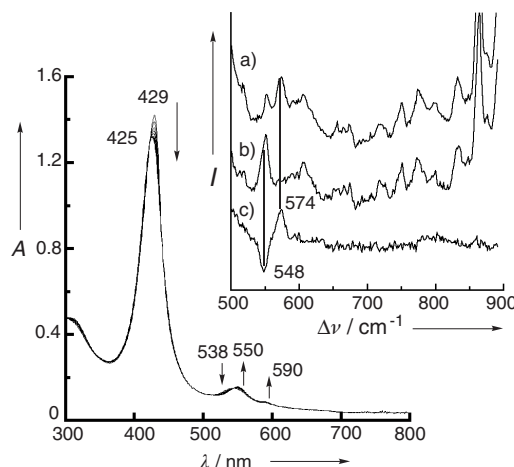


Figure 2. Absorption spectral changes of intermediate **A** in the course of decay in 20% CH₃CN/THF at –70°C. Spectral interval is 20 min. Inset: resonance Raman spectra of intermediate **B** derived from a) ¹⁶O₂ and b) ¹⁸O₂; c) difference spectra of a) minus b); conditions: 20% CH₃CN/THF, –35°C, excitation at 413 nm, 20 mW.

Resonance Raman spectroscopy was used to probe the binding of dioxygen to **1a** under the same experimental conditions used for UV/Vis spectroscopic measurements. Raman spectra of intermediate **A** exhibit two groups of isotope-sensitive bands, one at 787, 803 cm^{–1} (¹⁶O₂)/751 cm^{–1} (¹⁸O₂), and the other at 611 cm^{–1} (¹⁶O₂)/584 cm^{–1} (¹⁸O₂) (Figure 1, inset). Bands at both 787 and 803 cm^{–1} are assigned to the O–O stretch ($\nu_{\text{O-O}}$) vibration. The appearance of two bands near 800 cm^{–1} with ¹⁶O₂ may be caused by vibrational coupling between the bound O₂ molecule and the internal vibration mode of the porphyrin (799 cm^{–1}), which produces the spectral split.^[10] In the case of ¹⁸O₂, however, the two original bands disappear, and only one band at 751 cm^{–1} is observed. This observation rules out the existence of two

potentially bound O_2 species. The observed $\nu_{\text{O-O}}$ value is comparable to those of our previously reported peroxide compounds^[9,11] (for example, $[(\text{TMP})\text{Fe}^{\text{III}}-\text{O}_2-\text{Cu}^{\text{II}}(5\text{-MeTPA})]^+$: 790 cm^{-1} ($^{16}\text{O}_2$)/ 746 cm^{-1} ($^{18}\text{O}_2$)) and is also similar to those of the reported dioxygen adducts in the peroxy state ($\text{TMP-5-MeTPA} = N\text{-}[2\text{-}[10,15,20\text{-tris}(2,4,6\text{-trimethylphenyl})\text{porphyrin-5-yl}]\text{phenyl}]\text{-6-}[\text{bis}(5\text{-methylpyridin-2-ylmethyl})\text{amino}]\text{methyl}]\text{nicotinamide}$).^[5] The band at 611 cm^{-1} is assigned to the $\nu_{\text{Fe-O}_2}$ mode of a peroxo species. The value of the $\nu_{\text{Fe-O}_2}$ band observed herein is quite similar to those reported for peroxo-myoglobin^[12a] (617 cm^{-1}) and low-spin iron-peroxide model compounds ($617\text{--}632\text{ cm}^{-1}$).^[12b,c] Thus, the Raman bands for the O–O stretch and the Fe–O stretch are observed simultaneously for the initially formed intermediate **A**.

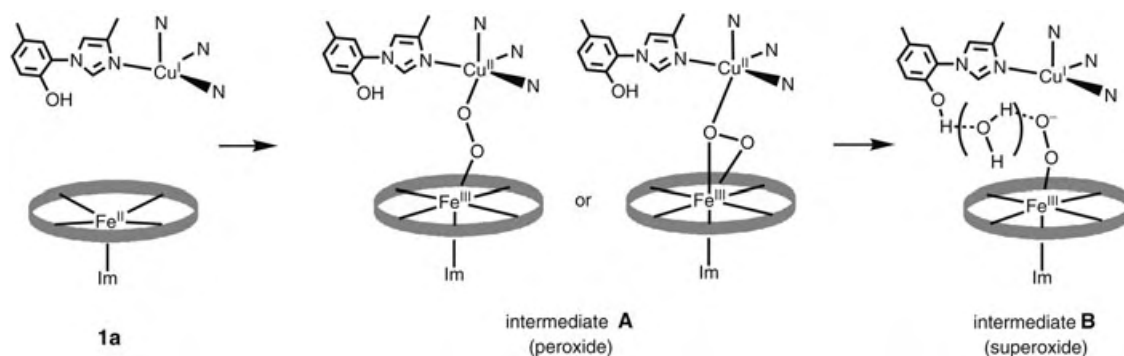
Raman spectra of intermediate **B**, however, do not exhibit an oxygen-isotope-sensitive band in the region near 800 cm^{-1} or above. Instead, an isotope-sensitive band is observed at 574 cm^{-1} ($^{16}\text{O}_2$)/ 548 cm^{-1} ($^{18}\text{O}_2$) (Figure 2, inset). The observed isotopic frequency shift ($\Delta\nu_{^{16}\text{O}_2/^{18}\text{O}_2} = 26\text{ cm}^{-1}$) matches well with the expected value for the $\nu_{\text{Fe-O}_2}$ mode in the diatomic harmonic approximation. Oxy-myoglobin^[13] (570 cm^{-1}), oxyCcO^[14] (572 cm^{-1}), the reported CcO model compound^[15] $\text{Fe-O}_2/[\text{Cu}(\text{NMePr})]^+$ (570 cm^{-1}), and all well-characterized examples of heme-superoxide complexes manifest similar Fe– O_2 stretch vibrations.^[16] Accordingly, the Raman band at 574 cm^{-1} is assigned to the Fe– O_2 stretch vibration of a superoxide species. More importantly, upon oxygenation of the copper-free complex with the same system, an oxygen-isotope-sensitive band appears at 576 cm^{-1} ($^{16}\text{O}_2$)/ 549 cm^{-1} ($^{18}\text{O}_2$), which indicates formation of the expected heme-superoxide species and is consistent with the UV/Vis spectroscopic results. Furthermore, the oxidation marker band (ν_4) of the porphyrin in resonance Raman exhibits a clear frequency shift from 1357 cm^{-1} for the reduced Fe^{II} -heme unit of **1a** to 1365 cm^{-1} for the Fe^{III} -heme moiety of the superoxide-like intermediate **B**, via 1361 cm^{-1} for the initially formed peroxide intermediate **A**. The ν_4 band, which can be clearly identified without interference from other modes, is sensitive to the extent of π back-donation from iron to the π^* antibonding orbitals of porphyrin.^[17] Consequently, when the π back-donation decreases, an increased frequency of ν_4 is observed. The spin-state marker band (ν_2) of the porphyrin ring appears at $\approx 1563\text{ cm}^{-1}$ for both intermediates **A** and **B**, consistent with the presence of a

six-coordinated low-spin ferric heme. By comparison with these values, the ν_2 band appears at 1552 cm^{-1} for the high-spin dioxygen-heme/Cu adduct with the parent model compound,^[9] which lacks the axially bound imidazole.

Further evidence comes from EPR spectroscopic experiments. Frozen samples of both intermediates **A** and **B** are EPR silent. The EPR-silent character of the former is ascribed to the strong antiferromagnetic coupling between the Cu^{II} and Fe^{III} ions through a peroxo (O_2^{2-}) bridge as observed in other examples.^[5,9,11] It also rules out the presence of a side-on η^2 -peroxo-heme/ Cu^{I} or Cu^{II} adduct, because the side-on η^2 -peroxo-heme moiety produces a strong EPR marker signal at $g = 4.2$.^[18] In the case of intermediate **B** it may be understood that the Cu^{I} complex sits just above, or is directed away from the superoxide $\text{Fe}^{\text{III}}-\text{O}_2^-$ moiety without direct contact between the two metal ions. Therefore we conclude that the dioxygen adduct intermediate **A**, initially formed from the heme/Cu model compound **1a**, is an imidazole-ligated low-spin heme- μ -peroxo- Cu^{II} species ($\mu\text{-}1,2$ or $\mu\text{-}\eta^2\text{:}\eta^1$), which is subsequently transformed into a more stable superoxide intermediate **B**.

The preferred formation of a heme-superoxo/ Cu^{I} intermediate derived from its precursor, heme-peroxo- Cu^{II} , rather than from the direct oxygenation of **1a** tempts us to postulate the scenario of dioxygen binding to this heme/Cu model compound. Exposure of the reduced $\text{Fe}^{\text{II}}/\text{Cu}^{\text{I}}$ form to dioxygen may initially result in a transient end-on $\text{Cu}^{\text{II}}-\text{O}_2^-$ species en route to the heme- μ -peroxo- Cu^{II} intermediate.^[19] The μ -peroxo intermediate thus formed is quite unstable owing to the electron-push effect of the axial imidazole,^[20] and as a result, the bound peroxide breaks away from the cupric ion to form the thermodynamically more stable heme-superoxo/ Cu^{I} intermediate. The redox couples of the two metal centers integrated in **1a** (heme-superoxo/heme-peroxo and $(\text{L}^{\text{N4-OH}})\text{Cu}^{\text{I}}/\text{Cu}^{\text{II}}$) are likely to be responsible for this unique transformation. When the potential of the former couple is more negative than that of the latter, the conversion of heme-peroxo- Cu^{II} into heme-superoxo/ Cu^{I} becomes thermodynamically allowed.^[21] The nearby cross-linked cresolyl OH group could facilitate the conversion of the newly formed peroxide into the superoxide by hydrogen-bonding stabilization, possibly by water molecules (Scheme 1).^[22]

Notably, a similar bridged peroxo complex is also generated through the oxygenation of an analogous model compound **1b**, in which the cross-linked phenolic hydroxy



Scheme 1. Dioxygen binding and subsequent transformation proposed for the model compound **1a**. Im = imidazole group.

function is protected by a methoxymethyl (MOM) group. Its O–O stretch ($\nu_{\text{O-O}}$) mode appears at 788 and 804 cm^{-1} ($^{16}\text{O}_2$)/752 cm^{-1} ($^{18}\text{O}_2$), and the $\nu_{\text{Fe-O}}$ stretch mode appears at 617 cm^{-1} ($^{16}\text{O}_2$)/589 cm^{-1} ($^{18}\text{O}_2$). All oxygen-sensitive Raman bands of the peroxide formed with **1b** shift slightly to higher wavenumbers relative to those of **1a**. The UV/Vis spectroscopic features of the MOM-protected peroxide in solution are quite similar to those of the peroxide initially generated (intermediate **A**) from **1a**; the thermal decay of the MOM-protected peroxide, however, gives a heme- μ -oxo- Cu^{II} species, and quite unlike that of the superoxide species associated with **1a**.

The heme-superoxide intermediate **B** from **1a** is stable below -30°C and does not revert to the deoxy state even under vacuum. On the other hand, the process of dioxygen binding to the corresponding distal copper-free complex in the same ligand system is reversible, and the oxy species reverts to its deoxy form when argon is bubbled through the solution, a vacuum is applied, or the temperature is increased. The evident difference between these two complexes may suggest that a copper complex in the distal site avoids the superoxide-releasing autoxidation of the heme-superoxide intermediate, thereby enhancing the binding of dioxygen to iron, possibly in cooperation with hydrogen bonding with the phenolic OH group.

In summary, a novel heme/Cu CcO model has been prepared in which the heme iron center is axially ligated by a proximal imidazole group and the copper is bound to a cross-linked *N*-(2-hydroxyphenyl)imidazole ligand; these moieties represent two important residues around the heme $\text{a}_3/\text{Cu}_\text{B}$ as observed in the enzyme active site. Spectroscopic evidence demonstrates the unique transformation of the heme- μ -peroxo- Cu^{II} intermediate into the heme-superoxo/ Cu^{I} species in the course of the oxygenation reaction at low temperature. The superoxide intermediate is thermodynamically more stable than its precursor in the presence of a trace amount of water. With this heme/Cu model compound, initial binding of the copper ion to dioxygen en route to the heme- μ -peroxo- Cu^{II} species is proposed. These results imply that during the process of dioxygen binding and activation as catalyzed by this model compound, the copper center not only plays a role as a redox center but also stabilizes the heme-superoxide intermediate; the phenolic hydroxy group plays a dominant role in the generation of the corresponding superoxide intermediate. This synthetic model study also suggests that after one-electron reduction of the oxyheme unit in CcO under physiological conditions, O–O bond cleavage could occur through a heme-hydroperoxy rather than a heme-peroxo- Cu species.

Experimental Section

The UV/Vis electronic spectra were recorded on a Hamamatsu PMA-11 CCD spectrophotometer with a D_2/W_2 light source. O_2 gas previously dried with molecular sieves was introduced with an O_2 line to a degassed solution of **1a** or **1b** ($1.0 \times 10^{-4} \text{ mol L}^{-1}$) in 20% $\text{CH}_3\text{CN}/\text{THF}$ in a 0.2-cm quartz cuvette at -70°C .

Resonance Raman spectra were obtained on a SpectraPro-300i spectrometer (Acton Research) with a 2400-groove grating, a Beamlok 2060 Kr ion laser (Spectra-Physics), a holographic super-

notch filter (Kaiser Optical Systems), and a LN-1100PB CCD detector (Princeton Instruments) cooled with liquid N_2 . Spectra were collected in spinning cells (2.0-cm diameter, 1500 rpm) at -70°C for intermediate **A** and -35°C for intermediate **B**, at an excitation wavelength $\lambda = 413.1 \text{ nm}$ (20 mW), 90° scattering geometry, and 5-min data accumulation. Peak frequencies were calibrated relative to indene and CCl_4 standards (accurate to $\pm 1 \text{ cm}^{-1}$). During each Raman experiment, UV/Vis spectra were collected simultaneously.

Received: November 11, 2004

Published online: February 18, 2005

Keywords: copper · heme proteins · iron · metalloenzymes · oxidoreductases

- [1] a) S. Ferguson-Miller, G. T. Babcock, *Chem. Rev.* **1996**, 96, 2889; b) G. T. Babcock, *Proc. Natl. Acad. Sci. USA* **1999**, 96, 12971; c) T. Kitagawa, *J. Inorg. Biochem.* **2000**, 82, 9.
- [2] a) S. Yoshikawa, K. Shinzawa-Itoh, R. Nakashima, R. Yaono, E. Yamashita, N. Inoue, M. Yao, M. J. Fei, C. P. Libeu, T. Mizushima, H. Yamaguchi, T. Tomizaki, T. Tsukihara, *Science* **1998**, 280, 1723; b) C. Ostermeier, A. Harrenga, U. Ermler, H. Michel, *Proc. Natl. Acad. Sci. USA* **1997**, 94, 10547.
- [3] a) P. E. M. Siegbahn, M. R. A. Blomberg, *Biochim. Biophys. Acta* **2004**, 1655, 45; b) D. A. Proshlyakov, M. A. Pressler, C. DeMaso, J. F. Leykam, D. L. DeWitt, G. T. Babcock, *Science* **2000**, 290, 1588; c) E. Pinakoulaki, U. Pfizner, B. Ludwig, C. Varotsis, *J. Biol. Chem.* **2002**, 277, 13563.
- [4] a) G. T. Babcock, M. Wikstrom, *Nature* **1992**, 356, 301; b) M. Fabian, G. Palmer, *Biochemistry* **1995**, 34, 13802; c) D. A. Proshlyakov, M. A. Pressler, G. T. Babcock, *Proc. Natl. Acad. Sci. USA* **1998**, 95, 8020; d) H. Michel, J. Behr, A. Harrenga, A. Kannt, *Annu. Rev. Biophys. Biomol. Struct.* **1998**, 27, 329; e) T. L. Poulos, H. Li, C. S. Raman, *Curr. Opin. Chem. Biol.* **1999**, 3, 131.
- [5] a) E. Kim, E. E. Chufan, K. Kamaraj, K. D. Karlin, *Chem. Rev.* **2004**, 104, 1077; b) J. P. Collman, R. Boulatov, C. J. Sunderland, L. Fu, *Chem. Rev.* **2004**, 104, 561; c) J. P. Collman, R. Boulatov, C. J. Sunderland in *The Porphyrin Handbook*, Vol. 11 (Eds.: K. M. Kadish, K. M. Smith, R. Guilard), Academic Press, San Diego, **2003**, pp. 1–49.
- [6] Cross-linked phenol-imidazole compounds: a) J. P. Collman, Z. Wang, M. Zhong, L. Zeng, *J. Chem. Soc. Perkin Trans. 1* **2000**, 1217; b) K. M. McCauley, J. M. Vrtis, J. Dupont, W. A. van der Donk, *J. Am. Chem. Soc.* **2000**, 122, 2403; c) J. A. Cappuccio, I. Ayala, G. I. Elliott, I. Szundi, J. Lewis, J. P. Konopelski, B. A. Barry, O. Einarsdottir, *J. Am. Chem. Soc.* **2002**, 124, 1750; d) M. Aki, T. Ogura, Y. Naruta, T. H. Le, T. Sato, T. Kitagawa, *J. Phys. Chem. A* **2002**, 106, 3436.
- [7] Crosslinked phenol-imidazole copper complexes: K. Kamaraj, E. Kim, B. Galliker, L. N. Zakharov, A. L. Rheingold, A. D. Zuberbuhler, K. D. Karlin, *J. Am. Chem. Soc.* **2003**, 125, 6028.
- [8] Metal-free dinucleating ligands bearing a Tyr244 mimic: a) J. P. Collman, R. A. Decreau, S. Costanzo, *Org. Lett.* **2004**, 6, 1033; b) J. P. Collman, R. A. Decreau, C. Zhang, *J. Org. Chem.* **2004**, 69, 3546.
- [9] J.-G. Liu, Y. Naruta, F. Tani, T. Chishiro, Y. Tachi, *Chem. Commun.* **2004**, 120.
- [10] The vibrational coupling phenomenon in the resonance Raman spectra of dioxygen adducts of heme proteins and other model compounds has been reported previously: L. M. Proniewicz, J. R. Kincaid, *Coord. Chem. Rev.* **1997**, 161, 81.
- [11] a) Y. Naruta, T. Sasaki, F. Tani, Y. Tachi, N. Kawato, N. Nakamura, *J. Inorg. Biochem.* **2001**, 83, 239; b) T. Chishiro, Y. Shimazaki, F. Tani, Y. Tachi, Y. Naruta, S. Karasawa, S. Hayami,

- Y. Maeda, *Angew. Chem.* **2003**, *115*, 2894; *Angew. Chem. Int. Ed.* **2003**, *42*, 2788.
- [12] a) M. Ibrahim, I. G. Denisov, T. M. Makris, J. R. Kincaid, S. G. Sligar, *J. Am. Chem. Soc.* **2003**, *125*, 13714; b) R. Y. N. Ho, G. Roelfes, B. L. Feringa, L. Que, Jr., *J. Am. Chem. Soc.* **1999**, *121*, 264; c) A. J. Simaan, S. Dopner, F. Banse, S. Bourcier, G. Bouchoux, A. Boussac, P. Hildebrandt, J. J. Girerd, *Eur. J. Inorg. Chem.* **2000**, *2000*, 1627.
- [13] E. A. Kerr, N.-T. Yu, D. E. Bartnicki, H. Mizukami, *J. Biol. Chem.* **1985**, *260*, 8360.
- [14] C. Varotsis, W. H. Woodruff, G. T. Babcock, *J. Biol. Chem.* **1990**, *265*, 11131.
- [15] J. P. Collman, C. J. Sunderland, K. E. Berg, M. A. Vance, E. I. Solomon, *J. Am. Chem. Soc.* **2003**, *125*, 6648.
- [16] a) K. Nakamoto, I. R. Paeng, T. Kuroi, T. Isobe, H. Oshio, *J. Mol. Struct.* **1988**, *189*, 293; b) J. P. Collman, J. I. Brauman, T. R. Halbert, K. S. Suslick, *Proc. Natl. Acad. Sci. USA* **1976**, *73*, 3333; c) E. A. Kerr, H. C. Mackin, N.-T. Yu, *Biochemistry* **1983**, *22*, 4373; d) M. A. Walters, T. G. Spiro, K. S. Suslick, J. P. Collman, *J. Am. Chem. Soc.* **1980**, *102*, 6857.
- [17] a) T. G. Spiro, J. M. Burke, *J. Am. Chem. Soc.* **1976**, *98*, 5482; b) J. M. Burke, J. R. Kincaid, S. Peters, R. R. Gagne, J. P. Collman, T. G. Spiro, *J. Am. Chem. Soc.* **1978**, *100*, 6083.
- [18] a) E. E. Chufan, K. D. Karlin, *J. Am. Chem. Soc.* **2003**, *125*, 16160; b) M. Selke, M. F. Sisemore, J. S. Valentine, *J. Am. Chem. Soc.* **1996**, *118*, 2008; c) J. N. Burstyn, J. A. Roe, A. R. Miksztal, B. A. Shaevitz, G. Lang, J. S. Valentine, *J. Am. Chem. Soc.* **1988**, *110*, 1382.
- [19] The very fast binding of O₂ to copper complexes with tetradentate tripodal ligands, and dioxygen association with Cu^I_B prior to binding to heme a₃ during the reaction of O₂ with reduced CcO have been proposed: a) K. D. Karlin, S. Kaderli, A. D. Zuber-buhler, *Acc. Chem. Res.* **1997**, *30*, 139; b) R. S. Blackmore, C. Greenwood, Q. H. Gibson, *J. Biol. Chem.* **1991**, *266*, 19245; c) M. Oliveberg, B. G. Malmstrom, *Biochemistry* **1991**, *30*, 7053; d) M. Oliveberg, B. G. Malmstrom, *Biochemistry* **1992**, *31*, 3560; e) M. I. Verkhovsky, J. E. Morgan, M. Wikstrom, *Biochemistry* **1994**, *33*, 3079; f) J. A. Bailey, C. A. James, W. H. Woodruff, *Biochem. Biophys. Res. Commun.* **1996**, *220*, 1055.
- [20] a) K. Yamaguchi, Y. Watanabe, I. Morishima, *J. Chem. Soc. Chem. Commun.* **1992**, 1709; b) S.-I. Ozaki, M. P. Roach, T. Matsui, Y. Watanabe, *Acc. Chem. Res.* **2001**, *34*, 818.
- [21] For the analogous complexes, the redox potentials of (TPP)Fe^{II}-O₂/(TPP)Fe^{III}-O₂²⁻ (-0.73 V versus SCE, DMF) and (TMPA)-Cu^I/Cu^{II} (-0.61 V versus SCE, DMF) have been reported; TPP = *meso*-tetraphenylporphinate, TMPA = tris(2-pyridylmethyl)amine; see: a) S. E. Jones, G. S. Srivatsa, D. T. Sawyer, T. G. Traylor, T. C. Mincey, *Inorg. Chem.* **1983**, *22*, 3903; b) N. Wei, N. N. Murthy, Q. Chen, J. Zubieta, K. D. Karlin, *Inorg. Chem.* **1994**, *33*, 1953.
- [22] Addition of a trace amount of water to the reaction mixture at low temperature greatly enhances the conversion of the peroxy into the superoxy intermediate.

The Indium-Mediated Selective Introduction of Allenyl and Propargyl Groups at the C4-Position of 2-Azetidinones and the AuCl₃-Catalyzed Cyclization of 4-Allenyl-2-azetidinones**

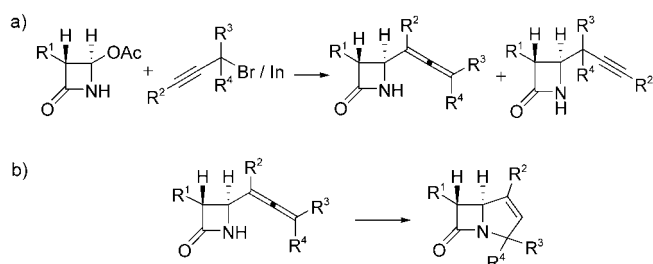
Phil Ho Lee,* Heechul Kim, Kooyeon Lee, Misook Kim, Kwanghyun Noh, Hyunseok Kim, and Dong Seomoon

The 2-azetidinone nucleus is the central building block of β -lactam antibiotics, so functionalization of the 2-azetidinone framework is pivotal for the development of new β -lactam antibiotics.^[1] The selective introduction of ethynyl,^[2] allyl,^[3] allenyl,^[4] and propargyl^[5] groups at the C4-position of 2-azetidinones is an especially intriguing and fundamental problem in the field of carbapenem synthesis because further functionalization of these groups could potentially lead to the construction of the bicyclic nucleus.^[6] Therefore, considerable effort has been devoted to the selective introduction of these groups by reaction of 4-acetoxy-2-azetidinones with various organometallic reagents. Although a variety of allylations at the C4-position of 4-acetoxy-2-azetidinone has been reported,^[3] there are relatively few methods for selective nucleophilic allenylation or propargylation.^[4] Also, it remains a formidable challenge to control the regioselectivity of the reaction of propargyl-metal compounds with 4-acetoxy-2-azetidinones when, for example, applied to the synthesis of either 4-allenyl or 4-propargyl-2-azetidinones. These aspects led us to develop a facile, efficient method for the direct and selective introduction of allenyl or propargyl groups at the C4-position of 4-acetoxy-2-azetidinones.^[7] Herein, the selective introduction of allenyl and propargyl groups at the C4-position of 4-acetoxy-2-azetidinones by using organoindium reagents generated in situ from propargyl bromides and indium powder as well as cyclizations of 4-allenyl-2-azetidinones catalyzed by AuCl₃ is presented (Scheme 1).

Initially, the optimum conditions for indium-mediated allenylation at the C4-position of 2-azetidinones were examined by the reaction of [3*R*(1'*R*,4*R*)]-(+)-4-acetoxy-3-[1'-(*tert*-butyldimethylsilyloxy)ethyl]-2-azetidinone (**1**) with organoindium reagents generated from indium and 1-bromo-2-butyne (**2**) (Table 1). Treatment of **1** with 1.5 equivalents of

[*] Prof. Dr. P. H. Lee, H. Kim, Dr. K. Lee, M. Kim, K. Noh, H. Kim, D. Seomoon
Department of Chemistry
Kangwon National University
Chunchon 200-701 (Republic of Korea)
Fax: (+82) 33-253-7582
E-mail: phlee@kangwon.ac.kr

[**] This work was supported by Grant No. R02-2003-000-10023-0 of the Basic Research Program of the Korea Science and Engineering Foundation and the Center for Molecular Design and Synthesis (CMDS) at the Korea Advanced Institute of Science and Technology (KAIST). We thank Professor Lanny S. Liebeskind of Emory University for providing spectroscopic data of the bicyclic β -lactams and Professor Tom Livinghouse of Montana State University for proof-reading this manuscript.



Scheme 1. a) The use of organoindium reagents to selectively introduce allenyl and propargyl groups at the C4-position of 4-acetoxy-2-azetidinones. b) The AuCl_3 -catalyzed cyclization of 4-allenyl-2-azetidinones.

Table 1: Optimization of allenylation reactions at the C4-position of 2-azetidinone **1**.

Entry	Equivalents 2	In	KI	T [°C]	t [h]	Yield [%] ^[a]
1	1.5	1.0	–	60	4	69
2	1.5	1.0	1.5	25	9	73
3	1.5	1.0	3.0	25	3.5	91
4	3.0	2.0	3.0	25	3	95

[a] Yield of isolated product.

2 and 1.0 equivalents of indium powder selectively produced the allenic product **3** in 69% yield at 60°C in *N,N*-dimethylformamide (DMF; entry 1). No propargylic product was obtained in this reaction. When 1.5 equivalents of KI were used as an additive, compound **3** was obtained in 73% yield at 25°C (entry 2). The best results among the several reaction conditions examined were obtained with the organoindium reagent that was generated in situ from the reaction of 2.0 equivalents of indium with 3.0 equivalents of **2** in the presence of 3.0 equivalents of KI; this combination produced **3** in 95% yield (entry 4). DMF was found to be the best solvent from those that were screened (DMF, THF, C_6H_6 , and $\text{C}_6\text{H}_5\text{CH}_3$).

We applied the optimum conditions to numerous propargyl bromides to demonstrate the efficiency and scope of this procedure (Table 2). Although treatment of **1** with indium powder and propargyl bromide produced a mixture of 4-allenyl- and 4-propargyl-2-azetidinone derivatives in 14 and 78% yields, respectively (entry 1), propargyl bromides with substituents such as methyl, ethyl, *n*-butyl, THPOCH_2 (THP = tetrahydropyran), phenyl, and 2-naphthyl at the γ -position

gave 4-allenyl-2-azetidinones selectively in excellent yields (85–97%, entries 2–5, 7, and 8). The reaction of indium powder and 3-bromo-1-propynyltrimethylsilane afforded 4-(1'-trimethylsilylallenyl)-2-azetidinone in 88% yield as the major product (entry 6). 4-Propargyl-2-azetidinone derivatives were produced selectively in excellent yields (entries 9–11) by using propargyl bromides with methyl, phenyl, and 1,1-dimethyl substituents at the α position. Organoindium reagents generated from indium powder and 1-phenyl-3-bromo-1-butyne gave rise to a mixture of 4-allenyl- and 4-propargyl-2-azetidinones in 32 and 48% yields, respectively (entry 12). Treatment of 4-acetoxy-2-azetidinone with organoindium reagents generated from indium powder and various propargyl bromides that had γ -substituents gave 4-allenyl-2-azetidinones selectively in good yields (entries 13–17).

Next, we turned our attention to the cyclization of 4-(1'-methylallenyl)-2-azetidinone derivatives with a variety of catalysts (Table 3). Although many catalysts such as $\text{Pd}(\text{OAc})_2$, PdCl_2 , $[\text{Pd}(\text{PPh}_3)_4]$, and $[\text{Pd}_2(\text{dba})_3]\cdot\text{CHCl}_3$ failed to give the desired cyclized products, exposure of 4-(1'-methylallenyl)-2-azetidinone to 5 mol % AuCl_3 in CH_2Cl_2 produced the bicyclic β -lactam product in 65% yield (entry 1).^[4,8] The desired products were produced in good yields (entries 2–5) for 2-azetidinones with *n*-butyl, THPOCH_2 , phenyl, and 2-naphthyl substituents.

Although the mechanism of the cyclization reaction has not been established, a possible reaction pathway is described in Scheme 2. AuCl_3 activates the allenyl group of **A** and subsequent cyclization affords **B**, which then gives a vinyl gold intermediate **C**.^[8] Subsequent protonation of the transient

Table 2: Reactions of 4-acetoxy-2-azetidinones with organoindium reagents.^[a]

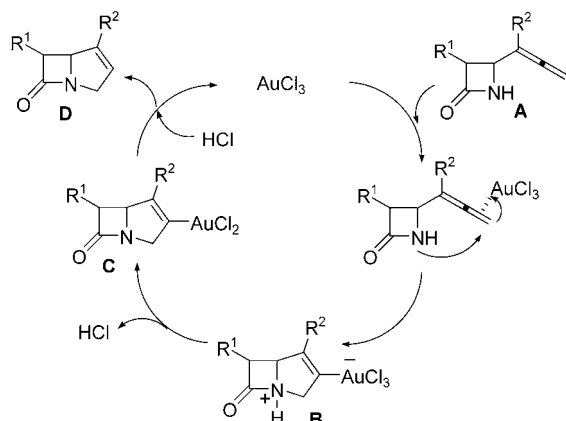
Entry	R^1	R^2	R^3	R^4	T [°C]	t [h]	Yield [%] ^[b]	I	II
1	(TBSO)(CH_3)CH	H	H	H	30	2	14	78	
2	(TBSO)(CH_3)CH	Me	H	H	30	2	95	0	
3	(TBSO)(CH_3)CH	Et	H	H	30	4	93	0	
4	(TBSO)(CH_3)CH	<i>n</i> Bu	H	H	30	3	95	0	
5	(TBSO)(CH_3)CH	THPOCH_2	H	H	30	3	97 ^[c]	0	
6	(TBSO)(CH_3)CH	TMS	H	H	30	6	88	9	
7	(TBSO)(CH_3)CH	Ph	H	H	30	4	95	0	
8	(TBSO)(CH_3)CH	2-naph ^[d]	H	H	30	4	85	0	
9	(TBSO)(CH_3)CH	H	Me	H	80	4	0	87 ^[e]	
10	(TBSO)(CH_3)CH	H	Ph	H	80	5	0	93 ^[f]	
11	(TBSO)(CH_3)CH	H	Me	Me	80	5	0	81	
12	(TBSO)(CH_3)CH	Ph	Me	H	30	3	32 ^[g]	48 ^[h]	
13	H	Me	H	H	30	3	84	0	
14	H	Et	H	H	30	3	88	0	
15	H	<i>n</i> Bu	H	H	30	4	84	0	
16	H	TMS	H	H	30	3	85	0	
17	H	Ph	H	H	30	5	84	0	

[a] Reaction performed in the presence of 1.0 equivalents of 4-acetoxy-2-azetidinone, 3.0 equivalents of propargyl bromide, 2.0 equivalents of indium powder, and 3.0 equivalents of KI in DMF. [b] Yield of isolated product. [c] d.r. = 1.1:1. [d] 2-naph = 2-naphthyl. [e] d.r. = 3.1:1. [f] d.r. = 1.4:1. [g] d.r. = 1.5:1. [h] d.r. = 11.1:1.

Table 3: Cyclization of 4-allenyl-2-azetidinone catalyzed by AuCl₃.^[a]

Entry	R	t [min]	Yield [%] ^[b]
1	Me	15	65
2	nBu	20	81
3	THPOCH ₂	60	80
4	Ph	15	85
5	2-naph ^[c]	60	71

[a] Reaction performed in the presence of 5 mol% of AuCl₃ in CH₂Cl₂.
[b] Yield of isolated product. [c] 2-naph = 2-naphthyl.



Scheme 2. A possible reaction pathway for the AuCl₃-catalyzed cyclization of 4-allenyl-2-azetidinones.

vinyl gold intermediate **C** produces **D** and regenerates AuCl₃ to continue the catalytic cycle.

In summary, we have demonstrated that the reaction of 4-acetoxy-2-azetidinones with organoindium reagents generated in situ from indium powder and γ -substituted propargyl bromides in the presence of KI in DMF selectively produced 4-allenyl-2-azetidinones in good to excellent yields and that α -substituted propargyl bromides gave 4-propargyl-2-azetidinones selectively. Furthermore, treatment of 4-(1-substituted allenyl)-2-azetidinone derivatives with 5 mol% AuCl₃ in CH₂Cl₂ produced the corresponding bicyclic β -lactams in good yields.

Experimental Section

Typical experimental procedures for allenylation and cyclization reactions: The allenylindium reagent was prepared by the addition of indium powder (99.99% (Aldrich); 92.0 mg, 0.8 mmol) to a solution of 3-bromo-1-phenyl-1-propyne (234.0 mg, 1.2 mmol) and KI (199.0 mg, 1.2 mmol) in DMF (1.5 mL) and the mixture was stirred for 1 h at 30 °C. [3*R*(1'*R*,4*R*)]-(+)-4-Acetoxy-3-[1'-(*tert*-butyldimethylsilyloxy)ethyl]-2-azetidinone (115.0 mg, 0.4 mmol) was added to the reaction mixture, and after stirring the mixture for 4 h, it was poured into saturated ammonium chloride solution (20 mL), extracted with CH₂Cl₂ (3 \times 20 mL), and washed with brine (20 mL). The organic layer was dried over anhydrous MgSO₄ and evaporated in vacuo. The crude product was purified by column chromatography

on silica gel with EtOAc/hexane (1:3, *R*_f = 0.4) as the eluant to afford [3*R*(1'*R*,4*S*)]-4-(1'-phenylallenyl)-3-[(1'-(*tert*-butyldimethylsilyloxy)ethyl]-2-azetidinone (131.0 mg, 95%). ¹H NMR (400 MHz, CDCl₃): δ = 7.40–7.35 (m, 4H), 7.29–7.28 (m, 1H), 5.91 (s, 1H), 5.24 (d, *J* = 2.00 Hz, 2H), 4.72 (q, *J* = 2.53 Hz, 1H), 4.30–4.28 (m, 1H), 3.23–3.22 (m, 1H), 1.16 (d, *J* = 6.27 Hz, 3H), 0.91 (s, 9H), 0.1 ppm (s, 6H); ¹³C NMR (100 MHz, CDCl₃): δ = 207.6, 168.7, 134.0, 128.8, 127.5, 126.3, 106.2, 80.6, 65.0, 64.7, 48.3, 25.8, 22.7, 18.0, –4.3, –4.9 ppm; IR (film) 3054, 2956, 1758, 1265 cm^{–1}; HRMS (EI) calcd for C₂₀H₂₉NO₂Si [*M*⁺]: 343.1968, found: 343.1967.

AuCl₃ (99% (Au = 99.9%; Strem Chemicals); 3.0 mg, 0.01 mmol) was added to a solution of [3*R*(1'*R*,4*S*)]-4-(1'-phenylallenyl)-3-[(1'-(*tert*-butyldimethylsilyloxy)ethyl]-2-azetidinone (69.0 mg, 0.2 mmol) in CH₂Cl₂ (1.0 mL). After stirring the mixture for 15 min, it was poured into saturated ammonium chloride solution (15 mL), extracted with CH₂Cl₂ (3 \times 15 mL), and washed with brine (15 mL). The organic layer was dried over anhydrous MgSO₄ and evaporated in vacuo. The crude product was purified by column chromatography on silica gel using EtOAc/hexane (1:5, *R*_f = 0.35) as the eluant to afford [6*R*(1'*R*,5*S*)]-1-aza-6-[(1'-(*tert*-butyldimethylsilyloxy)ethyl]-4-phenylbicyclo[3.2.0]-3-hepten-7-one (60.0 mg, 85%). ¹H NMR (400 MHz, CDCl₃): δ = 7.55 (d, *J* = 7.02 Hz, 2H), 7.36–7.28 (m, 3H), 6.32 (s, 1H), 4.66 (t, *J* = 1.81 Hz, 1H), 4.53 (dt, *J* = 16.09, 5.76 Hz, 1H), 4.31 (quint, *J* = 6.12 Hz, 1H), 3.74 (dd, *J* = 15.99, 2.61 Hz, 1H), 3.17 (dd, *J* = 7.93, 2.04 Hz, 1H), 1.36 (d, *J* = 6.11 Hz, 3H), 0.97 (s, 9H), 0.16 ppm (d, *J* = 2.57 Hz, 6H); ¹³C NMR (100 MHz, CDCl₃): δ = 180.7, 142.1, 132.9, 129.1, 128.7, 126.8, 126.4, 68.1, 66.5, 62.6, 53.9, 26.3, 23.5, 18.5, –4.0, –4.02 ppm; IR (film) 3061, 2929, 1770, 1256 cm^{–1}; HRMS (EI) calcd for C₂₀H₂₉NO₂Si [*M*⁺]: 343.1968, found: 343.1965.

Received: November 4, 2004

Published online: February 16, 2005

Keywords: allenylation · cyclization · gold · indium · lactams

- [1] a) M. S. Manhas, D. R. Wagle, J. Chiang, A. K. Bose, *Heterocycles* **1988**, 27, 1755; b) G. I. Georg, *The Organic Chemistry of β -Lactams*, VCH, New York, **1992**; c) I. Ojima, *Adv. Asymmetric Synth.* **1995**, 1, 95; d) I. Ojima, F. Delalogue, *Chem. Soc. Rev.* **1997**, 26, 377; e) C. Palomo, J. M. Aizpurua, I. Ganboa, M. Oiarbide, *Amino Acids* **1999**, 16, 321; f) B. Alcaide, P. Almendros, *Chem. Soc. Rev.* **2001**, 30, 226; g) B. Alcaide, P. Almendros, *Org. Prep. Proced. Int.* **2001**, 33, 315; h) C. Palomo, J. M. Aizpurua, I. Ganboa, M. Oiarbide, *Synlett* **2001**, 1813; i) B. Alcaide, P. Almendros, *Synlett* **2002**, 381.
- [2] S. Mori, H. Iwakura, S. Takechi, *Tetrahedron Lett.* **1988**, 29, 5391.
- [3] a) M. Aratani, H. Hirai, K. Sawada, M. Hashimoto, *Heterocycles* **1985**, 23, 1889; b) H. Fliri, C.-P. Mak, *J. Org. Chem.* **1985**, 50, 3438; c) K. Fujimoto, Y. Iwano, K. Hirai, *Bull. Chem. Soc. Jpn.* **1986**, 59, 1363; d) L. C. Blaszcak, H. K. Armour, N. G. Halign, *Tetrahedron Lett.* **1990**, 31, 5693; e) C. A. Tarling, A. B. Holmes, R. E. Markwell, N. D. Pearson, *J. Chem. Soc. Perkin Trans. 1* **1990**, 1695; f) S.-K. Kang, T.-G. Baik, X.-H. Jiao, K.-J. Lee, C. H. Lee, *Synlett* **1999**, 447.
- [4] a) J. S. Prasad, L. S. Liebeskind, *Tetrahedron Lett.* **1988**, 29, 4253; b) J. S. Prasad, L. S. Liebeskind, *Tetrahedron Lett.* **1988**, 29, 4257.
- [5] a) M. Shibasaki, A. Nishida, S. Ikegami, *J. Chem. Soc. Chem. Commun.* **1982**, 1324; b) J.-I. Haruta, K. Nishi, K. Kikuchi, S. Matsuda, Y. Tamura, Y. Kita, *Chem. Pharm. Bull.* **1989**, 37, 2338.
- [6] a) T. Kobayashi, N. Ishida, T. Hiraoka, *J. Chem. Soc. Chem. Commun.* **1980**, 736; b) D. H. Hua, A. Verma, *Tetrahedron Lett.* **1985**, 26, 547.
- [7] a) B. Alcaide, P. Almendros, C. Aragoncillo, *Chem. Eur. J.* **2002**, 8, 1719; b) B. Alcaide, P. Almendros, C. Aragoncillo, *Org. Lett.* **2003**,

- 5, 3795; c) B. Alcaide, P. Almendros, J. M. Alonso, *J. Org. Chem.* **2004**, 69, 993.
- [8] a) G. Dyker, *Angew. Chem.* **2000**, 112, 4407; *Angew. Chem. Int. Ed.* **2000**, 39, 4237; b) A. Hoffmann-Roder, N. Krause, *Org. Lett.* **2001**, 3, 2537; c) A. S. K. Hashmi, *Gold Bull.* **2004**, 37, 51; d) A. Arcadi, S. Di Giuseppe, *Curr. Org. Chem.* **2004**, 8, 795; e) A. S. K. Hashmi, P. Sinha, *Adv. Synth. Catal.* **2004**, 346, 432; f) N. Morita, N. Krause, *Org. Lett.* **2004**, 6, 4121.

Density Functional Calculations

Sphere Currents of Buckminsterfullerene**

Mikael P. Johansson, Jonas Jusélius, and
Dage Sundholm*

The aromatic character of Buckminsterfullerene has been a matter of debate since the remark by Kroto et al.^[1] that C_{60} “appears to be aromatic”. Since then, various studies of the aromaticity of C_{60} have been reported. All studies on aromaticity are of course challenged by the elusive nature of the property; although age-old as a concept, a final, clear-cut definition of aromaticity has not emerged. However, aromatic systems tend to behave in a characteristic manner in a magnetic field. Traditional aromatic species, such as the arch-example benzene, contain rings and are more or less planar, two-dimensional molecules. Also, they usually follow the $4N + 2$ Hückel rule for annulene aromaticity. Exposure of the molecules to a magnetic field perpendicular to the plane induces ring currents, with the electrons circling the rings or even larger areas. The magnetic view of aromaticity has usually been employed in the study of fullerene aromaticity, and more often than not the focus has been on local currents of, and shieldings near, the constituent rings. The endohedral magnetic shielding has also been used as a measure of the strength of the ring currents of the individual rings,^[2] and ^3He NMR spectroscopy has been used to estimate the chemical shifts of the endohedral carbon atoms of fullerenes.^[3,4]

The charge state is known to alter the electronic structure of fullerenes significantly, and thereby also their magnetic properties.^[4–7] This strong dependence on charge was ration-

alized when Hirsch et al.^[8] devised a rule for a three-dimensional (3D) form of aromaticity for fullerenes of icosahedral symmetry. Like 2D aromaticity, this spherical aromaticity depends on the number of delocalized π electrons present, but instead follows a $2(N+1)^2$ rule that corresponds to closed-shell configurations of pseudoatoms with spherical shell potentials.^[9] Spherically aromatic fullerenes exhibit many of the usual characteristics of aromatic species, such as enhanced stability, bond-length equalization, and high diamagnetic shielding at the cage centers.

As discussed above, the magnetically induced currents can provide valuable information about potentially aromatic species such as fullerenes. Although it is a real physical effect, a method for direct experimental observation of these currents has yet to be devised. Quantum chemical calculations can, however, provide insight into the electronic pathways.^[10–12] With the newly developed gauge-including magnetically induced currents (GIMIC) method,^[13] it is possible to not only visualize these currents, but also to get a quantitative measure of their strength, a property previously unattainable. Herein, we investigate by using GIMIC the magnetic properties of both the neutral C_{60} and the spherically aromatic, though still unsynthesized, C_{60}^{10+} ion, which fulfills the $2(N+1)^2$ rule with $N=4$.

The currents induced by a magnetic field are visualized in Figures 1 and 2 by using vector plots of the current strength at various parts of the surfaces. Figure 1 shows a side view of the fullerenes, with the magnetic field oriented vertically from above, perpendicular to the pentagons positioned at the

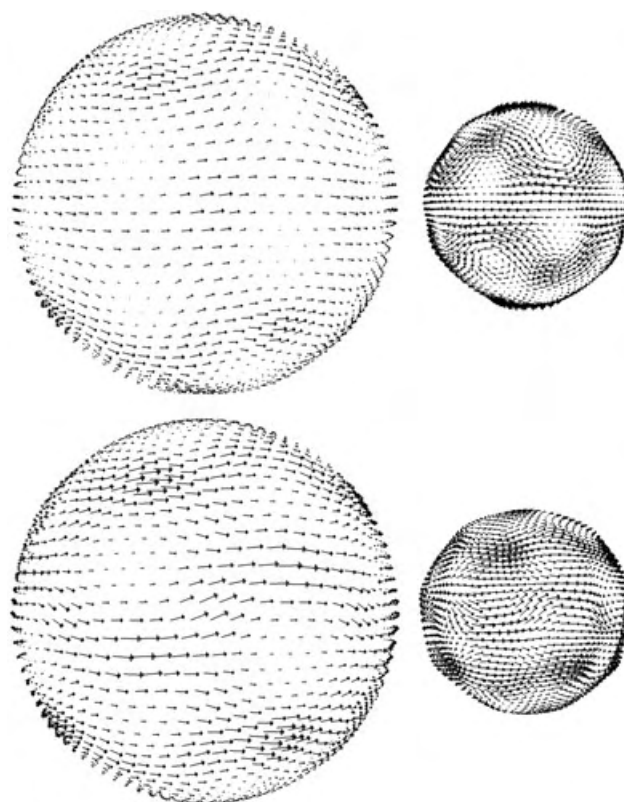


Figure 1. The induced currents in neutral (top) and +10 charged (bottom) fullerene 1 Å above (left) and below (right) the surface. The magnetic field is directed along the plane from top to bottom.

[*] M. P. Johansson, J. Jusélius, Dr. D. Sundholm
Laboratory for Instruction in Swedish
Department of Chemistry
University of Helsinki
P.O. Box 55, 00014 Helsinki (Finland)
Fax: (+358) 9-191-50169
E-mail: sundholm@chem.helsinki.fi

[**] This work was supported by The Academy of Finland (FA 53915, 200903, 206102), the Magnus Ehrnrooth foundation, and Waldemar von Frenckells Stiftelse. We thank Prof. Reinhart Ahlrichs for a copy of Turbomole and Sampo Smolander for helpful suggestions. CSC—Scientific Computing Ltd provided computer resources.

Supporting information for this article is available on the WWW under <http://www.angewandte.org> or from the author.

“poles”. The plots show the currents 1 Å above and below the surfaces. The currents are seen to move around the whole pseudosphere roughly perpendicularly to the magnetic field. The wavy nature^[10] of the currents is quite pronounced. For the neutral fullerene, the currents on either side of the surface predominantly move in opposite directions: the current is diamagnetic on the outside, but paramagnetic on the inside. The diamagnetic outside current was noted already in the work by Zanasi and Fowler.^[10] The field lines are diamagnetic throughout for C_{60}^{10+} . The currents in C_{60} and C_{60}^{10+} are, perhaps a bit surprisingly, nearly indistinguishable at the surface (see the Supporting Information). It can be noted that the currents of neutral fullerene, especially on the inside, are much more twisted and nonuniform than in C_{60}^{10+} . The ring currents under the pentagons can, in particular, be discerned. The π electrons also move quite freely over, and under, the entire surface in neutral C_{60} .

Figure 2 shows the currents, looking out from the centers of the fullerenes, along the magnetic field towards one of the pentagons. Again, plots 1 Å above and below the surfaces are shown. The currents for C_{60}^{10+} are seen to move in a clockwise, diamagnetic manner on both sides of the surface. A weak counterclockwise, paramagnetic current circulates the pentagon. The strength of this current 1 Å above the plane is, however, too weak to be seen from the figure. This is in stark contrast to the currents in neutral C_{60} ; for this species, the outside current is again diamagnetic, with the exception of the area occupied by the pentagon. On the inside, however, the currents are mostly paramagnetic.

The vector plots reveal the main feature of the induced currents, that is, their large uniformity as they traverse the fullerene. This uniformity of the currents persists through the fullerenes, with the largest deviations seen just on the surface of the carbon framework. Here, the bond and ring currents of the individual pentagons and hexagons dominate the picture. However, these local currents are obscured just beyond the surface by the sphere currents of the fullerene. The global currents seem predominant, even in neutral C_{60} . The strengths of the currents decrease significantly when moving away from the atomic cage and fall to zero at the center (a view of the currents in a plane through the equator is available in the Supporting Information).

Although the pictures are descriptive and provide a qualitative view, they give no accurate information about the strengths of the currents. Quantitative measurement of the strengths were obtained by numerically integrating the current passing a plane from the central axis out through half the fullerene. The magnetic field can of course be directed at any angle with respect to the fullerene. Here, we chose two different orientations: perpendicular to a pentagon (along a C_5 axis) and perpendicular to a hexagon (C_6 axis). The total net current along with the diamagnetic and paramagnetic components are tabulated in Table 1. The net current for neutral C_{60} is actually paramagnetic when the field is

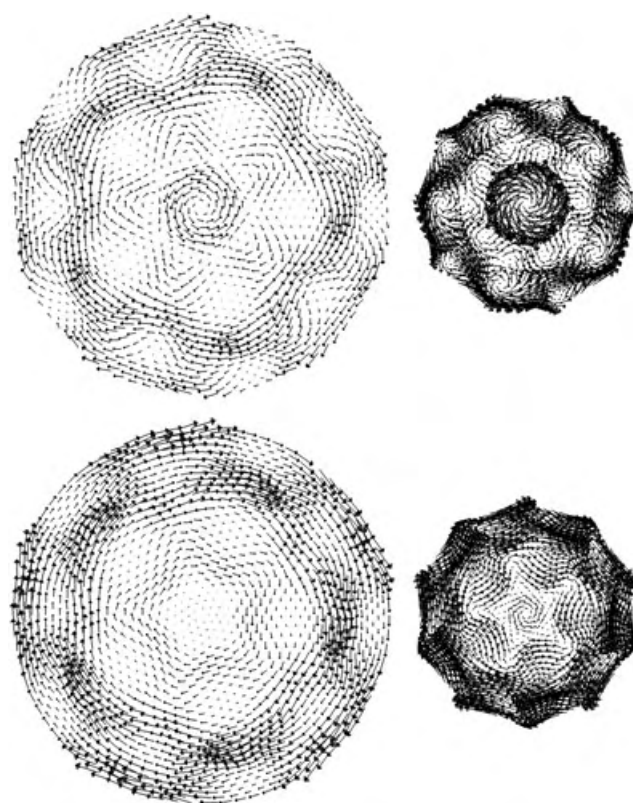


Figure 2. The induced currents in neutral (top) and +10 charged (bottom) fullerene 1 Å above (left) and below (right) the surface. The magnetic field is directed perpendicularly out of the plane.

directed through a pentagon and only very slightly diamagnetic with hexagons at the poles. This observation is in line with the previously noted strong paramagnetism of the pentagons.^[6,7,14] The currents in C_{60} are thus somewhat sensitive to the orientation of the molecule in the magnetic field, but the net current is always small. The case of the spherically aromatic C_{60}^{10+} ion is very different: with the direction of the currents the same on both sides of the surface, the net current is significantly stronger than in the neutral counterpart. The currents show only a slight dependence on the direction of the magnetic field, thus indicating the much weaker paramagnetism of the pentagons.

The integration shows that neutral C_{60} is best described as globally non-aromatic. Thus, the “ambiguous character” of fullerene aromaticity^[15,16] appears to be a mirage; local ring currents induce an association between them and the aromaticity of the annulene. However, when assessing the

Table 1: Integrated induced global currents for the icosahedral fullerenes C_{60} and C_{60}^{10+} [nAT^{-1}].^[a]

	C_{60}		C_{60}^{10+}		chd		Benzene
	5R	6R	5R	6R	DB	SB	
total current	−15	3	57	60	−1	−1	12
positive part	36	42	78	81	10	7	17
negative part	−51	−39	−21	−21	−11	−8	−5

[a] Values with the magnetic field perpendicular to both a pentagon (5R) and a hexagon (6R) are shown. The results for cyclo-1,4-hexadiene (chd) and benzene are reported for comparison; for chd, currents over both the double (DB) and single (SB) bonds are shown. The positive (diamagnetic) and negative (paramagnetic) contributions are reported together with the total current.

aromaticity of three-dimensional pseudospherical molecules, such as fullerenes, one should primarily consider global currents, and only ascribe secondary importance to local currents. The one-dimensional bond currents are not decisive for traditional, two-dimensional aromaticity either. The difference between C_{60} and C_{60}^{10+} can be compared to that between non-aromatic cyclo-1,4-hexadiene and benzene. From Table 1 it can be seen that the total gross current, determined by adding together both the absolute diamagnetic and paramagnetic contributions, is of comparable magnitude for cyclohexadiene and benzene. The same is true for C_{60} and C_{60}^{10+} . Benzene and C_{60}^{10+} are aromatic because the global currents cancel only to a small extent, while cyclohexadiene and C_{60} are non-aromatic because the currents almost completely cancel. So, contrary to common belief, the reason for the global non-aromaticity of C_{60} is not directly related to the paramagnetism of the pentagons, although they do contribute to the decrease in net current. Instead, the main reason is the oppositely directed exterior and interior sphere currents of the π electrons. This finding is also consistent with the low magnetic susceptibility of C_{60} .

This view is corroborated by studying the equatorial region, where the currents are quite independent of the nature of the ring and sphere currents near the polar caps of the fullerenes. In this region, the oppositely directed sphere currents of C_{60} in effect cancel each other: integration of the net current through a slab 1 Å thick at the equator gives essentially a zero result. For the C_{60}^{10+} ion, with its concurrent sphere currents, the same integration yields a value of 9 and 13 nAT⁻¹, with the magnetic field perpendicular to a pentagon and hexagon, respectively. Over two thirds of this current is endohedral. The endohedral magnetic shielding originates from the induced currents in the surrounding carbon shell.^[2,16,17] For a fullerene with a finite thickness of the carbon network, the magnetic shielding inside the molecule depends both on the current strengths and on the radius of the system.^[18] A spherical, infinitely thin and magnetically susceptible shell is in effect a perfect magnetic Faraday cage; the magnetic shielding inside is constant. Whereas neutral fullerene has been found to behave as an electric Faraday cage,^[19] spherical aromaticity indeed makes the fullerenes behave like miniature magnetic Faraday cages.^[20] The magnetic shielding inside C_{60}^{10+} is quite constant, but much more irregular and weaker inside C_{60} (see the Supporting Information). It can be noted that the negative value at the origin corresponds to the nucleus-independent chemical shift (NICS) value^[21] at the center of the fullerenes. As observed from the initial studies,^[8] the shielding at the center of C_{60}^{10+} is high—ten times larger than in C_{60} .

In summary, we have described the extraordinary behavior of both neutral and spherically aromatic fullerene in a magnetic field. In both, the π electrons move uniformly around the fullerene on both sides of the surface. The currents mainly move in opposite directions in neutral C_{60} . However, the current is unidirectional in C_{60}^{10+} and leads to a strong induced electric current around the molecule as well as a remarkably homogeneous and large endohedral magnetic shielding. These truly three-dimensional sphere currents are, in our opinion, the defining feature of global aromaticity in

fullerenes. While the currents of the 60 π electrons in neutral C_{60} compete in moderate discord, the 50 π electrons of the spherically aromatic fullerene are beautifully in accord.

Experimental Section

The molecular structures were optimized at the density functional theory (DFT) level,^[22,23] using the hybrid, semilocal gradient-corrected density functional B3LYP.^[24,25] The calculations were performed with the Turbomole program suite,^[26] version 5.6, modified to provide the perturbed densities required for the calculation of the induced currents. Turbomole's standard doubly polarized basis sets of triple-zeta quality (TZVPP)^[27,28] was used for the geometries, while the magnetic calculations were performed using the smaller polarized split-valence basis set (SVP).^[29] This has been shown to be adequate for organic aromatic systems.^[13] Turbomole's standard m4 grid was used.

A quantitative measure of the induced ring current can be obtained by using the newly developed GIMIC method.^[13] The various components of the magnetically induced current-density tensor are calculated using gauge-including atomic orbitals (GIAO). The current-density tensor is independent of the direction of the magnetic field. The tensor is contracted with an explicit magnetic field, thus making the induced current density direction-dependent. The magnetically induced current density was obtained at selected points in space. A scheme for obtaining quantitative values for induced currents by numerical integration over the current flow was developed. The net current flow through a plane could be determined by defining suitable cut planes.

Received: October 18, 2004

Published online: February 11, 2005

Keywords: aromaticity · density functional calculations · fullerenes · magnetic properties · quantum chemistry

- [1] H. W. Kroto, J. R. Heath, S. C. O'Brien, R. F. Curl, R. E. Smalley, *Nature* **1985**, *318*, 162–163.
- [2] M. Bühl, *Chem. Eur. J.* **1998**, *4*, 734–739.
- [3] M. Saunders, H. A. Jiménez-Vázquez, R. J. Cross, S. Mroczkowski, D. I. Freedberg, F. A. L. Anet, *Nature* **1994**, *367*, 256–258.
- [4] E. Shabtai, A. Weitz, R. C. Haddon, R. E. Hoffman, M. Rabinovitz, A. Khong, E. J. Cross, M. Saunders, P.-C. Cheng, L. T. Scott, *J. Am. Chem. Soc.* **1998**, *120*, 6389–6393.
- [5] V. Elser, R. C. Haddon, *Nature* **1987**, *325*, 792–794.
- [6] A. Pasquarello, M. Schlüter, R. C. Haddon, *Science* **1992**, *257*, 1660–1661.
- [7] A. Pasquarello, M. Schlüter, R. C. Haddon, *Phys. Rev. A* **1993**, *47*, 1783–1789.
- [8] A. Hirsch, Z. Chen, H. Jiao, *Angew. Chem.* **2000**, *112*, 4079–4081; *Angew. Chem. Int. Ed.* **2000**, *39*, 3915–3917; .
- [9] M. Reiher, A. Hirsch, *Chem. Eur. J.* **2003**, *9*, 5442–5452.
- [10] R. Zanasi, P. W. Fowler, *Chem. Phys. Lett.* **1995**, *238*, 270–280.
- [11] P. Lazzeretti, *Prog. Nucl. Magn. Reson. Spectrosc.* **2000**, *36*, 1–88.
- [12] J. A. N. F. Gomes, R. B. Mallion, *Chem. Rev.* **2001**, *101*, 1349–1383.
- [13] J. Jusélius, D. Sundholm, J. Gauss, *J. Chem. Phys.* **2004**, *121*, 3952–3963.
- [14] M. Prato, T. Suzuki, F. Wudl, V. Lucchini, M. Maggini, *J. Am. Chem. Soc.* **1993**, *115*, 7876–7877.
- [15] R. C. Haddon, *Science* **1993**, *261*, 1545–1550.
- [16] M. Bühl, A. Hirsch, *Chem. Rev.* **2001**, *101*, 1153–1183.
- [17] M. Bühl, W. Thiel, H. Jiao, P. von R. Schleyer, F. A. L. Anet, *J. Am. Chem. Soc.* **1994**, *116*, 6005–6006.
- [18] J. Lounila, M. Ala-Korpela, J. Jokisaari, M. J. Savolainen, Y. A. Kesäniemi, *Phys. Rev. Lett.* **1994**, *72*, 4049–4052.

- [19] P. Delaney, J. C. Greer, *Appl. Phys. Lett.* **2004**, *84*, 431–433.
- [20] M. P. Johansson, D. Sundholm, J. Vaara, *Angew. Chem.* **2004**, *116*, 2732–2735; *Angew. Chem. Int. Ed.* **2004**, *43*, 2678–2681; .
- [21] P. von R. Schleyer, C. Maerker, A. Dransfeld, H. Jiao, N. J. R. van Eikema Hommes, *J. Am. Chem. Soc.* **1996**, *118*, 6317–6318.
- [22] P. Hohenberg, W. Kohn, *Phys. Rev.* **1964**, *136*, B864–B871.
- [23] W. Kohn, L. J. Sham, *Phys. Rev.* **1965**, *140*, A1133–A1138.
- [24] A. D. Becke, *J. Chem. Phys.* **1993**, *98*, 5648–5652.
- [25] C. Lee, W. Yang, R. G. Parr, *Phys. Rev. B* **1988**, *37*, 785–789.
- [26] R. Ahlrichs, M. Bär, M. Häser, H. Horn, C. Kölmel, *Chem. Phys. Lett.* **1989**, *162*, 165–169.
- [27] A. Schäfer, C. Huber, R. Ahlrichs, *J. Chem. Phys.* **1994**, *100*, 5829–5835.
- [28] T. H. Dunning, Jr., *J. Chem. Phys.* **1989**, *90*, 1007–1023.
- [29] A. Schäfer, H. Horn, R. Ahlrichs, *J. Chem. Phys.* **1992**, *97*, 2571–2577.

Fullerenes

Trifluoromethylated Endohedral Metallofullerenes: Synthesis and Characterization of $Y@C_{82}(CF_3)_5^{**}$

Ivan E. Kareev,* Sergey F. Lebedkin,
Vyacheslav P. Bubnov, Eduard B. Yagubskii,
Ilya N. Ioffe, Pavel A. Khavrel, Igor V. Kuvychko,
Steven H. Strauss, and Olga V. Boltalina*

In contrast to the exohedral modification of empty fullerenes, which has been well-established, the development of regioselective reactions for endohedral metallofullerenes (EMFs) is

[*] I. E. Kareev, Dr. V. P. Bubnov, Prof. E. B. Yagubskii
Institute of Problems of Chemical Physics
Russian Academy of Sciences
Chernogolovka, 142432, Moscow Region (Russia)
Fax: (+7) 096-515-5420
E-mail: kareev@hotmail.ru

I. V. Kuvychko, Prof. S. H. Strauss, Prof. O. V. Boltalina
Department of Chemistry
Colorado State University
Fort Collins, CO 80523 (USA)
Fax: (+1) 970-491-1801
E-mail: ovbalt@lamar.colostate.edu

I. E. Kareev, Dr. S. F. Lebedkin
Forschungszentrum Karlsruhe
Institute for Nanotechnology
Postfach 3640, 76021 Karlsruhe (Germany)

Dr. I. N. Ioffe, P. A. Khavrel, Prof. O. V. Boltalina
Chemistry Department
Moscow State University
Moscow 119992 (Russia)

[**] This work was supported by the Volkswagen Foundation (I-77/855), the RFBR (Project No. 02-03-33352), an INTAS Young Scientist Fellowship (No YSF 2002-327/F3 to I.E.K.), President of Russia Grant (MK-2734.2004.03 to I.N.I.), an AvH Foundation Friedrich Bessel Award (to O.V.B.), and the US NSF (Grant No. CHE-9905482). We thank Prof. M. M. Kappes for his generous support of this work. The assistance of Mr. A. A. Goryunkov with the algorithm for the generation of isomers is appreciated.

still in its infancy. This is because of the following factors: 1) their limited availability to most synthetic chemists, 2) their difficult purification to homogeneity from fullerene soots, 3) the difficulty in characterizing EMFs (many EMFs are paramagnetic, thus precluding routine NMR spectroscopic characterization), and 4) the paucity of theoretical studies on hypothetical chemically modified EMFs that would guide synthetic chemists to investigate productive but not immediately apparent reaction schemes.

The cycloaddition of disilacyclopropane to $La@C_{82}$ was the first chemical modification of an EMF and was reported in 1995.^[1] Several other research groups also reported cycloadducts of EMFs,^[2,3] but unambiguous structural characterization has only been achieved in one study.^[4] More recently, water-soluble EMFs, such as the cycloadduct $Gd@C_{60}-(C(COOH)_2)_{10}$ reported by Bolskar et al.,^[5] have been prepared to explore their potential use as magnetic resonance imaging (MRI) contrast agents.^[5,6] Also Shinohara et al. used fluororous biphasic techniques to prepare $La@C_{82}(C_8F_{17})_2$.^[7] However, until now $La@C_{82}(C_8F_{17})_2$ was the only reported exohedral derivative of an EMF with atomic substituents, such as H, F, Cl, or Br, or with organic substituents (R) having only $R-C_{EMF}$ single bonds.

Herein, we applied our recently developed chemical derivatization of the rare, unstable, small-band-gap fullerene C_{74} ^[8] to a rare (but stable) EMF. The reaction of interest, the first trifluoromethylation of an EMF, was carried out on crude EMF material and was followed by exhaustive chromatographic separation and characterization of the purified isolated products. This approach ensures that no EMF (mg or sub-mg quantities) is wasted during purification of the starting material or during synthetic investigations. In addition, many underivatized EMFs have low solubilities and tend to oxidize and/or polymerize in air during their separation and purification from crude EMF-containing soots.^[9] Therefore, a derivatized EMF may not only be more soluble than the parent EMF, it may also be more stable, further aiding the laborious but necessary purification by chromatography (compare unstable C_{74} ^[10] with stable $C_{74}F_{38}$ ^[8]).

Despite our extensive experience with regioselective fluorination reactions of fullerenes,^[11,12] we chose to study EMF trifluoromethylation because CF_3 derivatives are less prone to hydrolysis than fluorofullerenes and are more soluble in common organic solvents.^[13–15] Figure 1 shows the MALDI mass spectrum of the crude product of the high-temperature reaction between the $Y@C_{82}$ -enriched EMF starting material and silver(i) trifluoroacetate ($AgCF_3CO_2$). In addition to the main product, $Y@C_{82}(CF_3)_5$, ions corresponding to $Y_2@C_{80}$ derivatives with one and three CF_3 groups were observed. It is interesting to note that no EMF derivative with more than five CF_3 groups was formed, since similar high-temperature reactions of $AgCF_3CO_2$ and empty fullerenes yielded $C_{60/70}(CF_3)_n$ products where n as high as 22.^[13,14,16] Figures 2 and 3 show the subsequent multiple-stage, two-column HPLC separation that afforded two isomers of $Y@C_{82}(CF_3)_5$. The FTIR and MALDI mass spectra of isomer **II** are shown in Figure 4.

The addition of an odd number of CF_3 groups to paramagnetic $Y@C_{82}$ rendered the two isomers of $Y@C_{82}$ -

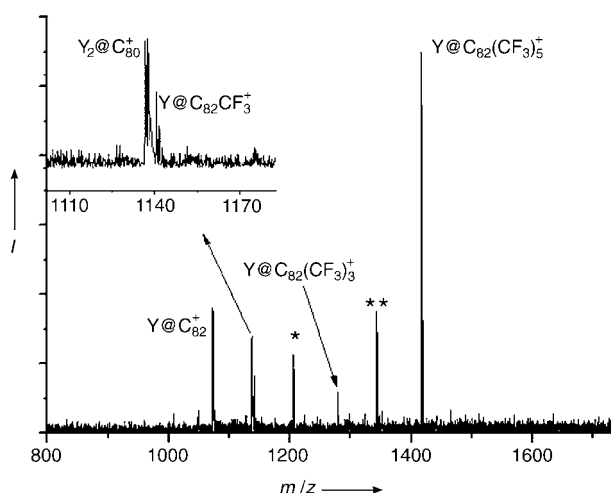


Figure 1. Positive-ion S_8 -MALDI mass spectrum of the crude reaction product. Signals marked with one or two asterisks are assigned to $Y_2@C_{80}(CF_3)^+$ and $Y_2@C_{80}(CF_3)_3^+$, respectively. The inset shows the expanded mass range 1100–1170 Da (note the characteristic isotope distributions for the mono- and dimetallic EMF species $Y@C_{82}$ and $Y_2@C_{80}$). Matrix S_8 suppresses fragmentation and enhances the yields of molecular ions.

$(CF_3)_5$ diamagnetic, thus allowing 1D and 2D ^{19}F NMR spectroscopic analysis to be used for structure elucidation. Previously reported EMF cycloaddition products retained the paramagnetic nature of the parent EMFs, and routine NMR spectroscopic characterization was not possible.^[17] Both isomers of $Y@C_{82}(CF_3)_5$ exhibited a ^{19}F NMR spectrum with five resonances having a 1:1:1:1:1 intensity pattern. The δ values for isomer **II** ranged from $\delta = -53$ to -69 ppm, which is similar to the δ values for $C_{60}(CF_3)_{2/4/6}$ (which ranged from $\delta = -66$ to -72 ppm).^[13] Figure 5 shows the 2D COSY ^{19}F NMR spectrum of isomer **II** and the labeling of resonances a–e. The topology of the 2D spectrum, the simple 1:3:3:1 splitting of resonances d and e, and the similar J_{FF} values for all of the resonances of both isomers (12–14 Hz) indicate that 1) the distances between pairs of J -coupled CF_3 groups are similar and 2) the d-a-c-b-e groups are located on a chain of 1,3- or 1,4- $C_6(CF_3)_2$ hexagons on the surface of the C_{82} cage. The second conclusion is based on the fact that the J_{FF} values for resonances d and e of 13.8(3) and 11.9(3) Hz, respectively, for isomer **I** and 13.6(3) and 12.7(3) Hz, respectively, for isomer **II** are virtually the same as the J_{FF} values for the end-of-chain CF_3 groups in $C_{1-}C_{60}(CF_3)_4$ and $C_{1-}C_{60}(CF_3)_6$, which ranged from 12.3(3) to 14.5(3) Hz.^[13] DFT calculations have shown that 1,2-additions of CF_3 groups in those two trifluoromethylated [60]fullerenes, as well as in $C_{60}(CF_3)_2$, do not lead to stable structures.^[13] Instead, 1,4-additions, which led to the occasional 1,3 arrangement of CF_3 groups in the

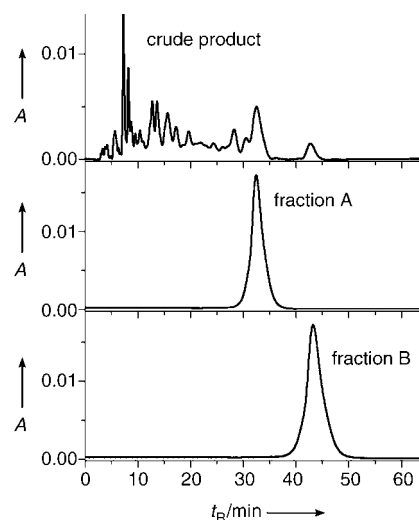


Figure 2. HPLC traces (Cosmosil Buckyprep column) of the crude reaction product (a) as well as isolated fractions A (b) and B (c).

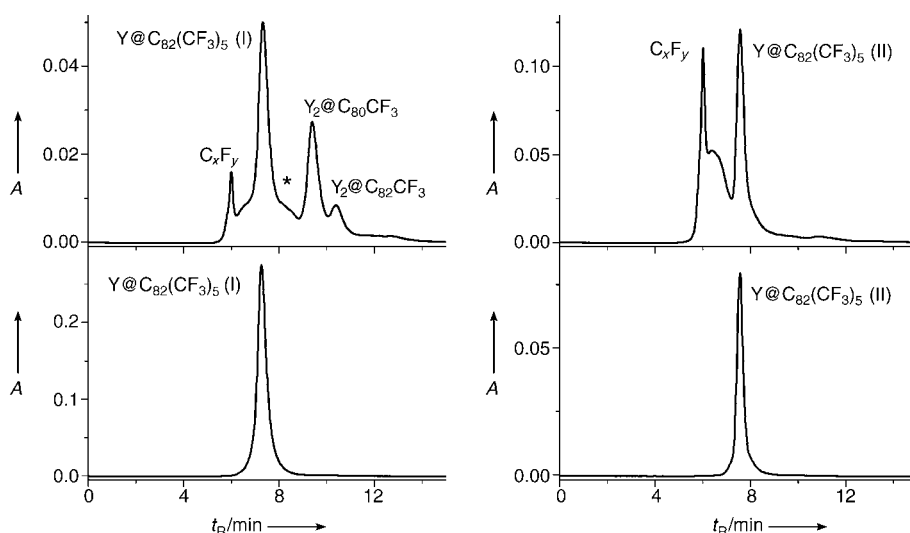


Figure 3. HPLC traces (Buckyclutcher column) of fraction A (top left), purified sample of $Y@C_{82}(CF_3)_5$ isomer **I** (bottom left), fraction B (top right), and purified sample of $Y@C_{82}(CF_3)_5$ isomer **II** (bottom right). The signal marked with an asterisk in the upper left trace corresponds to $Y@C_{82}(CF_3)_3$.

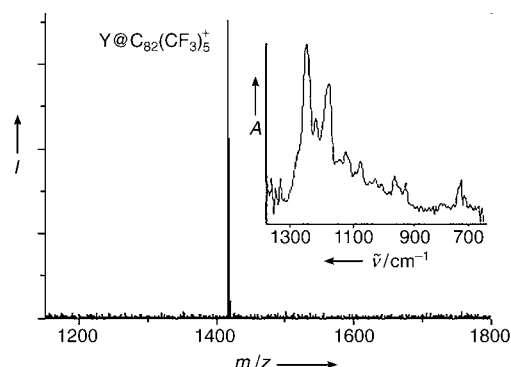


Figure 4. Positive-ion S_8 -MALDI mass spectrum of HPLC-purified $Y@C_{82}(CF_3)_5$ isomer **II**. The inset shows the ATR-FTIR spectrum of $Y@C_{82}(CF_3)_5$ isomer **II**.

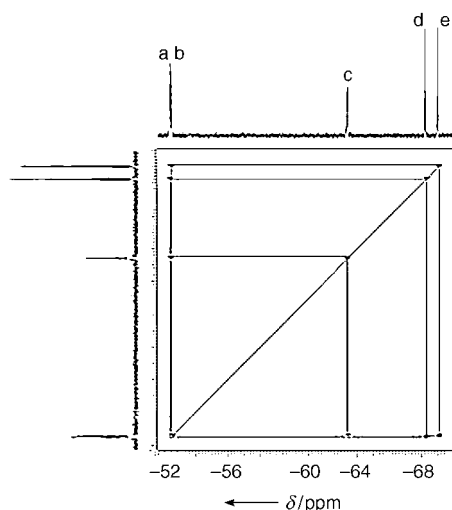


Figure 5. 376.5 MHz 1D and 2D COSY ^{19}F NMR spectra of $\text{Y}@\text{C}_{82}(\text{CF}_3)_5$ isomer II in $[\text{D}_6]\text{benzene}$.

interior of a chain of $\text{C}_6(\text{CF}_3)_2$ edge-sharing hexagons, led to the most stable structures.^[13]

New DFT calculations^[18] of structures, relative energies, and chemical shifts for a large group of $\text{Y}@\text{C}_{82}(\text{CF}_3)_5$ isomers support this interpretation of the NMR spectroscopic data for isomers **I** and **II** of $\text{Y}@\text{C}_{82}(\text{CF}_3)_5$. For simplicity, we chose the C_{2v} isomer of $\text{Y}@\text{C}_{82}$ as the basis for our calculations because this particular cage structure has been proven for the related compounds $\text{Sc}@\text{C}_{82}$ and $\text{La}@\text{C}_{82}$.^[9] For isomers with a chain of four 1,4- $\text{C}_6(\text{CF}_3)_2$ hexagons, the first, third, and fifth CF_3 groups were found to have a staggered conformation with respect to the C–C bonds of the carbon cage which forces the two remaining CF_3 groups to exhibit eclipsed conformations because of F...F steric repulsions. The calculated differences between the δ values for the ^{19}F atoms for these two types of conformations were found to be in good agreement with the experimentally observed values irrespective of the position of the 1,4- $\text{C}_6(\text{CF}_3)_2$ hexagons on the C_{2v} - C_{82} cage. On the contrary, steric interactions in 1,2- $\text{C}_6(\text{CF}_3)_2$ or 1,3- $\text{C}_6(\text{CF}_3)_2$ hexagons forced all of the CF_3 groups to exhibit similar

conformations (all staggered or all nearly staggered, respectively) and, as a result, the δ values of the ^{19}F atoms were nearly the same.

The structures of 56 1,4 isomers of $\text{Y}@\text{C}_{82}(\text{CF}_3)_5$ in which the 1,4- $\text{C}_6(\text{CF}_3)_2$ edge-sharing hexagons had various arrangements and locations on the C_{2v} - $\text{Y}@\text{C}_{82}$ cage were computationally studied. The two almost isoenergetic structures shown in Figure 6a and b were calculated to be approximately 14 kJ mol^{-1} more stable than the third isomer (Figure 6c) and at least 50 kJ mol^{-1} more stable than the other 53 isomers.

We propose that isomers **I** and **II** of $\text{Y}@\text{C}_{82}(\text{CF}_3)_5$ have 1,4 chain structures similar to those shown in Figure 6. Significantly, the two structures in Figure 6 are also predicted to be more than 100 kJ mol^{-1} more stable than the hypothetical structures with a closed loop of 1,4-additions that would result in the formation of an isolated, six-electron, aromatic cyclopentadienyl (Cp) ring, such as those observed in $\text{Ti}(\text{C}_{60}\text{Ph}_5)^{[19]}$ and related organometallic compounds that contain Cp-like $\text{C}_{60}\text{R}_5^-$ ligands.^[20] Although such a structure might be the most stable isomer for a hypothetical EMF $\text{M}@\text{C}_{82}(\text{CF}_3)_5$ in which the metal atom can donate only one electron to the C_{82} cage, the calculated lowest energy structures shown in Figure 6 are apparently the most stable isomers when the metal atom donates three electrons to the cage.

In summary, we have 1) demonstrated an efficient method for the exohedral derivatization of the EMF $\text{Y}@\text{C}_{82}$, 2) isolated and characterized two diamagnetic stable isomers of $\text{Y}@\text{C}_{82}(\text{CF}_3)_5$, 3) used a combination of 2D ^{19}F NMR spectroscopic analysis and DFT calculations to elucidate the most probable type of CF_3 addition pattern of these isomers, and 4) isolated and characterized by mass-spectrometric analysis $\text{Y}@\text{C}_{82}(\text{CF}_3)_n$ ($n = 1, 3$) and $\text{Y}_2@\text{C}_{80}(\text{CF}_3)$. Further studies on other EMFs will show if particular compositions and addition patterns depend on the nature of the encapsulated metal atom(s).

Experimental Section

EMF-containing soot was prepared by burning composite graphite electrodes with metallic yttrium in an arc-discharge reactor. The

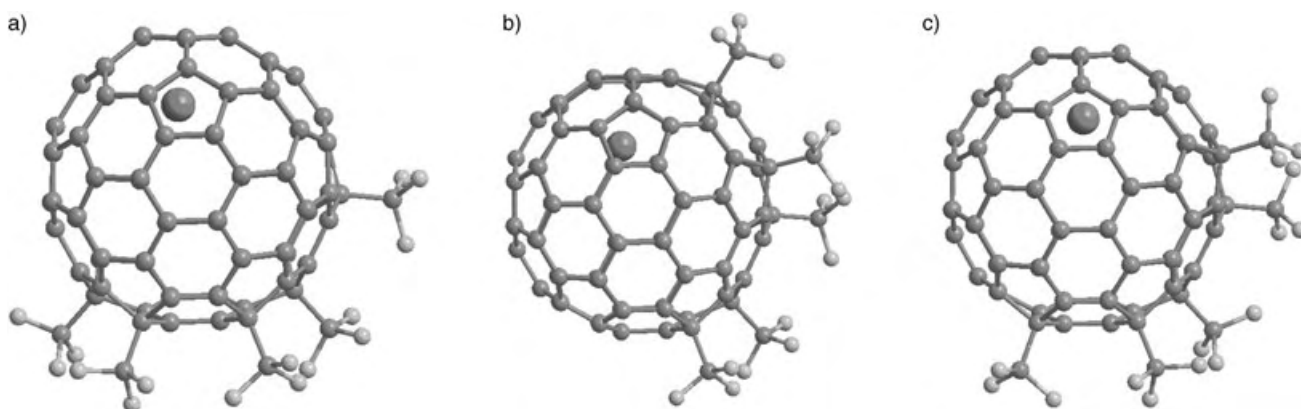


Figure 6. Three low-energy structures of $\text{Y}@\text{C}_{82}(\text{CF}_3)_5$ chains of 1,4- $\text{C}_6(\text{CF}_3)_2$ edge-sharing hexagons calculated at the DFT level of theory. Structures (a) and (b) were found to be 14 kJ mol^{-1} more stable than structure (c) and at least 50 kJ mol^{-1} more stable than the other 53 calculated isomers (see text).

EMFs $Y_m@C_{2n}$ were extracted in a two-stage procedure under an atmosphere of argon (using *ortho*-dichlorobenzene followed by *N,N*-dimethylformamide (DMF), both heated to reflux),^[21,22] which resulted in an extract enriched in $Y@C_{82}$, as evidenced by mass-spectrometric analysis.^[21] The isomeric composition of the EMFs in DMF extract is not known. However, ESR analysis of the *ortho*-dichlorobenzene extract of the same soot showed the presence of two main isomers of $Y@C_{82}$ in an approximate 3:1 ratio, which agreed with literature data on $Y@C_{82}$ -containing soots.^[23–25]

In a typical synthetic experiment, $Y@C_{82}$ -enriched extract (100 mg) was thoroughly mixed with $AgCF_3CO_2$ (Aldrich, 500 mg). The reaction mixture was placed in a quartz reactor under dynamic vacuum (10^{-6} Torr) and heated to 400 °C (at 40 °C min⁻¹) for 10 h. An IR spectrum of the cooled product mixture showed that no $AgCF_3CO_2$ remained. Increasing the $AgCF_3CO_2$ /EMF extract ratio above 25:1 did not yield products with more than five CF_3 groups per cage. A MALDI mass spectrum of the crude product mixture (MALDI Voyager-DE PRO Biospectrometry Workstation, Applied Biosystems, USA, with 0.5 ns radiation pulses at 3 Hz from a 337 nm N_2 laser) and HPLC analysis (HP-1050, Hewlett Packard Co.) showed that the main product was $Y@C_{82}(CF_3)_5$. The following two-stage HPLC purification procedure was used: 1) Cosmosil Buckyprep column (20 mm i.d. \times 250 mm, Nacalai Tesque Inc., 9 mL injections, 18 mL min⁻¹ flow rate, toluene eluent) for separation of the two major $Y_m@C_{80/82}(CF_3)_n$ -containing fractions A (28 min) and B (38 min; cf. C_{60} : 8.8 min); 2) Regis Buckyclutcher column (20 mm i.d. \times 250 mm, Regis Chemical Co., 1.2 mL injections, 12 mL min⁻¹ flow rate, toluene eluent) for isolation of the pure compounds from fraction A: $Y@C_{82}(CF_3)_5$ (isomer **I**, 6.2 min), $Y@C_{82}(CF_3)_3$ (6.8 min), $Y_2@C_{80}(CF_3)_3$ (8 min), $Y@C_{82}(CF_3)_3$ (9.8 min); and from fraction B: $Y@C_{82}(CF_3)_5$ (isomer **II**; 6.8 min; Figure 3). The 99% purity of $Y@C_{82}(CF_3)_5$ (isomers **I** and **II**) was determined by HPLC and MALDI-MS analysis. The main IR bands were (ReactIR-1000 ATR-FTIR, Applied Systems Inc., 4 cm⁻¹ resolution): isomer **I**, $\tilde{\nu}$ = 1248(s), 1223(m), 1179(s), 733(w), and 675(w) cm⁻¹; isomer **II**, $\tilde{\nu}$ = 1256(s), 1225(m), 1181(s), and 720(w) cm⁻¹. ¹⁹F NMR spectra (376.5 MHz, C_6D_6 , 25 °C, J_{FF} values \pm 0.3 Hz) showed five equal-intensity resonances for isomer **I** (δ = -52.8 (sept, J = 12.4 Hz, 1 F, a), -53.1 (sept, J = 11.3 Hz, 1 F, b), -63.6 (sept, J = 12.0 Hz, 1 F, c), -66.9 (quint, J = 13.8 Hz, 1 F, d), -69.1 ppm (quint, J = 11.9 Hz, 1 F, e)) and for isomer **II** (δ = -52.8 (2 \times sept, J = 12.8 Hz, 2 F, a, b), -63.5 (m, J \approx 12 Hz, 1 F, c), -68.3 (quint, J = 13.6 Hz, 1 F, d), -69.1 ppm (quint, J = 12.7 Hz, 1 F, e)).

Received: July 31, 2004

Revised: December 6, 2004

Published online: February 18, 2005

Keywords: 1,4-addition · density functional calculations · fullerenes · NMR spectroscopy · trifluoromethylation

- [7] N. Tagmatarchis, A. Taninaka, H. Shinohara, *Chem. Phys. Lett.* **2002**, 355, 226.
- [8] A. A. Goryunkov, V. Y. Markov, I. N. Ioffe, R. D. Bolskar, M. D. Diener, I. V. Kuvychko, S. H. Strauss, O. V. Boltalina, *Angew. Chem.* **2004**, 116, 1015; *Angew. Chem. Int. Ed.* **2004**, 43, 997.
- [9] H. Shinohara, *Rep. Prog. Phys.* **2000**, 63, 843.
- [10] M. D. Diener, J. M. Alford, *Nature* **1998**, 393, 668.
- [11] O. V. Boltalina, A. A. Goryunkov, V. Y. Markov, I. N. Ioffe, L. N. Sidorov, *Int. J. Mass Spectrom.* **2003**, 228, 807.
- [12] O. V. Boltalina, S. H. Strauss in *Dekker Encyclopedia of Nanoscience and Nanotechnology* (Eds.: J. A. Schwarz, C. Contescu, K. Putyera), Marcel Dekker, New York, **2004**, pp. 1175.
- [13] A. A. Goryunkov, I. V. Kuvychko, I. N. Ioffe, D. L. Dick, L. N. Sidorov, S. H. Strauss, O. V. Boltalina, *J. Fluorine Chem.* **2003**, 124, 61.
- [14] P. J. Fagan, P. J. Krusic, C. N. McEwen, J. Lazar, D. H. Parker, N. Herron, E. Wasserman, *Science* **1993**, 262, 404.
- [15] A. Darwish, A. K. Abdul-Sada, A. G. Avent, Y. Lyakhovetsky, E. A. Shilova, R. Taylor, *Org. Biomol. Chem.* **2003**, 1, 3102.
- [16] I. S. Uzkikh, E. I. Dorozhkin, O. V. Boltalina, A. I. Boltalin, *Dokl. Akad. Nauk* **2001**, 379, 344.
- [17] B. Cao, T. Wakahara, Y. Maeda, A. Han, T. Akasaka, T. Kato, K. Kobayashi, S. Nagase, *Chem. Eur. J.* **2004**, 10, 716.
- [18] D. N. Laikov, *Chem. Phys. Lett.* **1997**, 281, 151.
- [19] M. Sawamura, H. Iikura, E. Nakamura, *J. Am. Chem. Soc.* **1996**, 118, 12850.
- [20] Y. Kuninobu, Y. Matsuo, M. Toganoh, M. Sawamura, E. Nakamura, *Organometallics* **2004**, 23, 3259.
- [21] V. P. Bubnov, E. E. Laukhina, I. E. Kareev, V. K. Koltover, T. G. Prokhorova, E. B. Yagubskii, Y. P. Kozmin, *Chem. Mater.* **2002**, 14, 1004.
- [22] I. E. Kareev, V. P. Bubnov, E. E. Laukhina, A. F. Dodonov, V. I. Kozlovski, E. B. Yagubskii, *Fullerenes Nanotubes Carbon Nanostruct.* **2004**, 12, 65.
- [23] E. Nishibori, M. Takata, M. Sakata, M. Inakuma, H. Shinohara, *Chem. Phys. Lett.* **1998**, 298, 79.
- [24] K. Kobayashi, S. Nagase, *Chem. Phys. Lett.* **1998**, 282, 325.
- [25] Z. Slanina, K. Kobayashi, S. Nagase, *Chem. Phys. Lett.* **2004**, 388, 74.

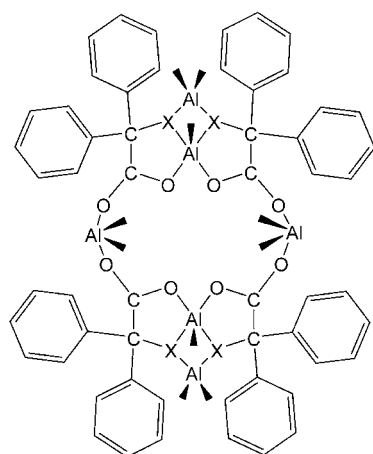
- [1] T. Akasaka, S. Nagase, K. Kobayashi, T. Kato, K. Yamamoto, H. Funasaka, T. Takahashi, *J. Chem. Soc. Chem. Commun.* **1995**, 1343.
- [2] T. Akasaka, T. Kato, S. Nagase, K. Kobayashi, K. Yamamoto, H. Funasaka, T. Takahashi, *Tetrahedron* **1996**, 52, 5015.
- [3] L. Feng, X. Zhang, Z. Yu, J. Wang, Z. Gu, *Chem. Mater.* **2002**, 14, 4021.
- [4] E. B. Lezzi, J. C. Duchamp, K. Harich, T. E. Glass, H. M. Lee, M. M. Olmstead, A. L. Balch, H. C. Dorn, *J. Am. Chem. Soc.* **2002**, 124, 524.
- [5] R. D. Bolskar, A. F. Benedetto, L. O. Husebo, R. E. Price, E. F. Jackson, S. Wallase, L. Wilson, J. M. Alford, *J. Am. Chem. Soc.* **2003**, 125, 5471.
- [6] H. Kato, Y. Kanazawa, M. Okumura, A. Taninaka, T. Yokawa, H. Shinohara, *J. Am. Chem. Soc.* **2003**, 125, 4391.

Synthesis of Hexa- and Dodecanuclear Organoaluminum Ring Structures Incorporating the "Magic" $\text{Ph}_2\text{C}(\text{X})$ Group ($\text{X} = \text{O}^-$, NH^-)**

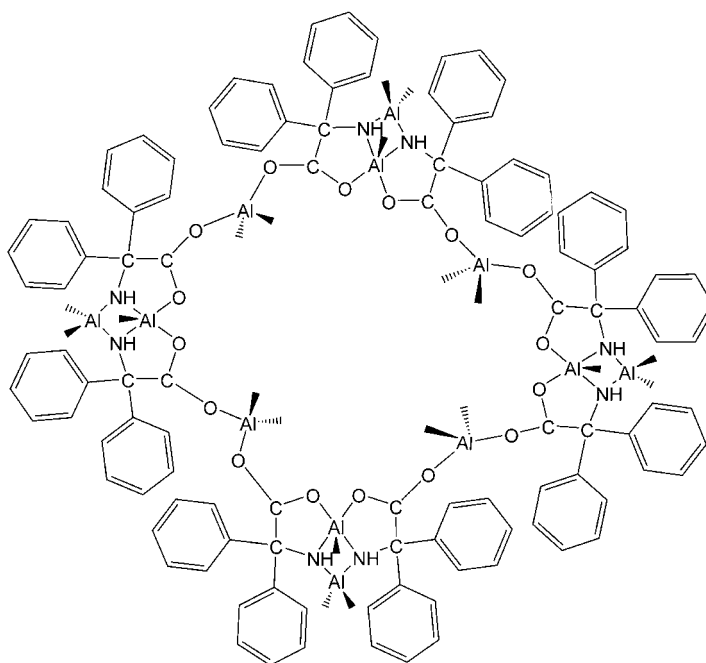
Carl Redshaw,* Mark R. J. Elsegood, and Kathryn E. Holmes

Organoaluminum carboxylates are attracting attention owing to their biological relevance^[1] and their usefulness as precursors in materials science.^[2] Bifunctional carboxylic acid ligation has been extensively studied by Lewiński and co-workers. A number of adducts, both bi- and tetranuclear, were isolated and structurally characterized and a preference for *anti* binding of aluminum at a carboxylic acid group was identified.^[3–6] We have been intrigued by the ring formation of a number of *N,N'*- and *N,O*-chelate ligands on treatment with Group 13 alkyl derivatives. In our work, we have previously

structurally characterized rings containing two, four, six, and eight Group 13 metal centers. For example, anthranilic acid, 1,2-(H_2N) $\text{C}_6\text{H}_4\text{CO}_2\text{H}$, afforded a macrocyclic deca-ring system $[\{\text{Me}_2\text{Al}(\text{MeAl})(\mu_3\text{-O})(\mu_2\text{-O})\text{L}\}_3]$ (L = quinazoline heterocycle), whilst the Schiff-base ligand 3,5-*t*Bu₂-2-(OH) $\text{C}_6\text{H}_2\text{CHNC}_6\text{H}_4$ -2-(CO_2H) affords the tetrameric systems $[\{\text{M}[3,5\text{-}t\text{Bu}_2\text{-2-(O)}\text{C}_6\text{H}_2\text{CHNC}_6\text{H}_4\text{-2-(CO}_2\text{)}]\}_2]_2$ ($\mu\text{-MMe}_2$) ($\text{M} = \text{Al, Ga}$; $\text{X} = \text{Me, Cl}$).^[7] In our search for related ligand systems containing both amino and carboxylic acid functionalities, we have turned our attention to amino acids and related ligands. In the present work, the reaction of Me_3Al with the amino acid 2,2-diphenylglycine as well as with the closely related benzilic acid (diphenylglycolic acid) is studied. The products are the remarkable 16-membered macrocyclic structures **1** and **2**, each of which contains six aluminum centers (in three different environments), and a nonsymmetric 32-membered ring complex **3** containing twelve aluminum centers. Despite being recrystallized from acetonitrile, none of the products **1–3** are the result of MeCN insertion into aluminum–nitrogen bonds, which we have



1 ($\text{X}=\text{NH}$), **2** ($\text{X}=\text{O}$)



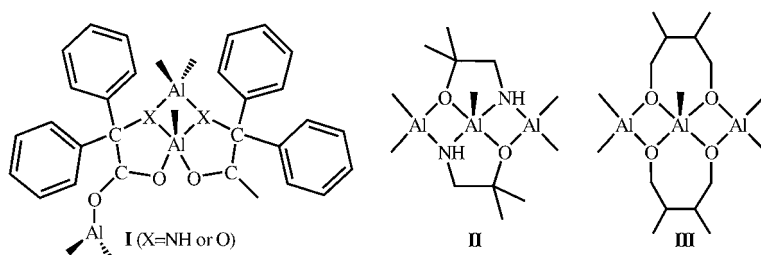
3

[*] Dr. C. Redshaw
Wolfson Materials and Catalysis Centre
School of Chemical Sciences and Pharmacy
The University of East Anglia
East Anglia NR4 7TJ (UK)
Fax: (+44) 1603-592-003
E-mail: carl.redshaw@uea.ac.uk
Dr. M. R. J. Elsegood, K. E. Holmes
Chemistry Department
Loughborough University
Loughborough, Leicestershire, LE11 3TU (UK)

[**] The University of East Anglia is thanked for financial support. The EPSRC is thanked for the award of beamtime at Daresbury and a studentship (K.E.H.). We also thank the EPSRC Mass Spectroscopy Service Centre, Swansea.

previously observed for a number of anilines and hydrazines.^[7a] All three structures contain the common structural motif $\{[\text{Ph}_2\text{C}(\text{X})(\text{CO}_2)]_2(\text{Me}_2\text{Al})(\text{MeAl})\}(\text{AlMe}_2)$ ($\text{X} = \text{O}$ or NH) (**I**). The structure **II** has recently been postulated for a glycine-derived product,^[6] and a closely related motif **III** has been characterized following reaction of Me_3Al with a number of sterically hindered diols.^[8]

Addition of 1.5 molar equivalents of Me_3Al to diphenylglycine, 2,2'- $\text{Ph}_2\text{C}(\text{NH}_2)(\text{CO}_2\text{H})$, in refluxing toluene results in rapid evolution of methane and formation of a colorless solution. Following workup, small colorless prisms of **1**, suitable for an X-ray analysis using synchrotron radiation,^[9] were grown from solutions in acetonitrile on prolonged



standing at ambient temperature in about 55% yield. The molecular structure of the acetonitrile solvate is shown in Figure 1. The structure is made up of two of the subunits **I**

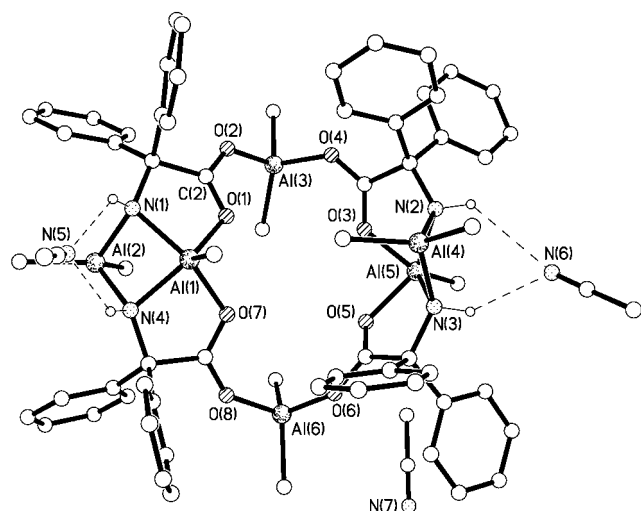


Figure 1. Molecular structure of **1**.^[15] Selected bond lengths [Å] and angles [°]: Al(1)–N(1) 2.0010(12), Al(1)–O(1) 1.8964(10), Al(1)–N(4) 1.9816(12), Al(1)–O(7) 1.9108(10), Al(2)–N(1) 1.9632(12), Al(2)–N(4) 1.9598(12), Al(3)–O(2) 1.8580(11), Al(3)–O(4) 1.8295(12); O(7)–Al(1)–O(1) 84.79(4), N(4)–Al(1)–N(1) 81.37(5), O(1)–Al(1)–N(1) 80.69(4), N(4)–Al(1)–O(7) 81.73(4), N(4)–Al(2)–N(1) 82.88(5), Al(1)–O(1)–C(2) 120.01(9), C(2)–O(2)–Al(3) 130.11(9).

(X=NH) linked by the Me₂Al bridges to form a 16-membered macrocyclic ring system; there is no overall symmetry for the molecule (Figure 1). The six aluminum centers possess three very different environments. The five-coordinate Al(1)-type centers are square-based pyramids with an apical methyl group and basal O and N atoms each derived from two diphenylglycine ligands. For the latter, the N atoms are bridged by a pseudo-tetrahedral Al(2)-type center with angles in the range of 82.9–121.2°. The Al(1)⋯Al(2) distance of 2.84 Å is not indicative of any metal–metal interaction. The geometries at the bridging aluminum centers (Al(3)-type) are only slightly distorted from tetrahedral, with angles ranging between 100.2 and 123.9°. Throughout the structure the carboxylate groups bind in an *anti/syn* fashion and in each case the aluminum centers pretrude somewhat out of the plane of the carboxylate group (0.02–0.15 Å for type 1, 0.06–0.66 for type 3) resulting in an overall puckering of the macrocycle. The presence of the inwardly directed methyl groups results in an essentially self-filling macrocycle

with no obvious cavity. The ¹H NMR spectrum supports this formulation with peaks in the region $\delta = -0.25$ to -1.46 ppm integrating to 30 H for the Al–Me groups. The NH groups are observed at $\delta = 2.41$ ppm and 3313 cm^{−1} in the ¹H NMR and IR spectra, respectively.

Encouraged by the synthesis of the ring complex **1**, we then investigated the related ligand benzoic acid, 2,2′-Ph₂C(OH)(CO₂H). A similar procedure to that employed for **1** yielded small colorless prisms suitable for X-ray crystallography using synchrotron radiation^[9] in about 17% yield. The product here was remarkably similar to **1**, incorporating two of the subunits (X=O) bridged by the Me₂Al units to afford an Al₆-containing 16-membered macrocyclic ring. Figure 2 empha-

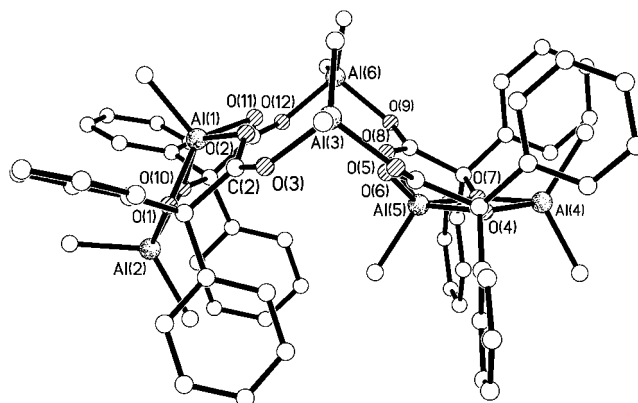


Figure 2. Molecular structure of **2**.^[15] Selected bond lengths [Å] and angles [°]: Al(1)–O(2) 1.8582(17), Al(1)–O(11) 1.8679(18), Al(1)–O(10) 1.8788(17), Al(1)–O(1) 1.8974(17), Al(2)–O(1) 1.8519(17), Al(2)–O(10) 1.8612(18), Al(3)–O(3) 1.8392(18), Al(3)–O(6) 1.8469(18); O(2)–Al(1)–O(1) 82.62(7), Al(3)–O(3)–C(2) 134.90(17).

sizes the folded geometry adopted by the asymmetric rings **1** and **2**; the asymmetry is best highlighted by the Al(1)/Al(2) and Al(4)/Al(5) vectors which are almost vertical and horizontal, respectively. The rings **1** and **2** differ in the degree of associated solvent (**1**·3 MeCN and **2**·MeCN), doubtless due to H-bonding interactions with the NH groups in **1**.

Unsuspectingly, on increasing the ratio of Al to ligand for the diphenylglycine reaction from 1.5:1 to 2:1, we selectively crystallized the 32-membered ring system shown in Figure 3. The homogeneity of the sample was verified by measuring the unit cell dimensions of eight crystals picked at random from several different reactions and crystallizations. The molecule has no overall symmetry and can be viewed as a “doubling-up” of the complex **1**, such that we now have four subunits **I** each linked through the Me₂Al bridges. Overall the macrocycle adopts a bowl-like conformation with aluminum centers 2, 5, 8, and 11 forming the rim of the bowl. The Al–N, Al–O, and Al–C bond lengths in **3** are all similar to those observed in **1**. In total for **3**, there are about 15.5 MeCN of crystallization, four of which are involved in bifurcated hydrogen bonding to NH groups as observed in **1**·3 MeCN.

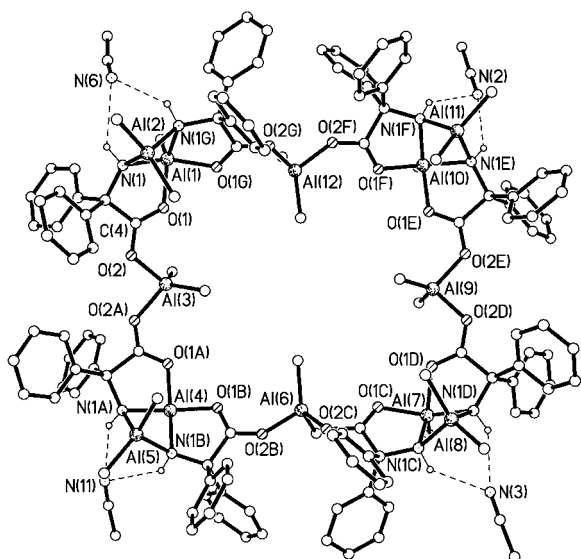
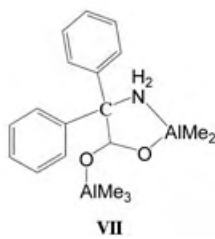
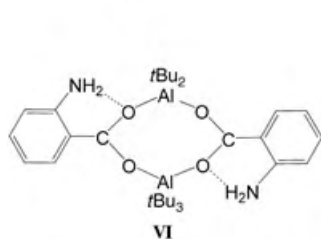
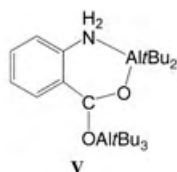
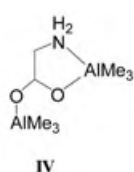


Figure 3. Molecular structure of **3**. Selected bond lengths [Å] and angles [°]: Al(1)–O(1) 1.877(4), Al(1)–O(1G) 1.901(4), Al(1)–N(1G) 1.986(4), Al(1)–N(1) 1.990(4), Al(2)–N(1G) 1.961(4), Al(2)–N(1) 1.965(4), Al(3)–O(2A) 1.842(4), Al(3)–O(2) 1.855(4); O(1)–Al(1)–O(1G) 85.54(16), Al(3)–O(2)–C(4) 123.9(4).

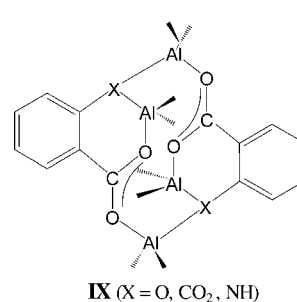
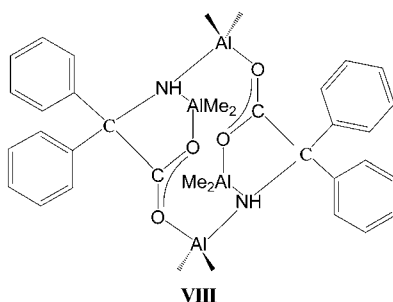
Unfortunately, cryoscopic molecular weight measurements (in benzene) proved to be uninformative with these systems.

The formation of the products **1** or **3** is dependent on the ligand to aluminum ratio employed in the reaction. Recent work by Lewiński and co-workers on both anthranilic acid and glycine has shown how quite different products can arise through the use of differing amounts of Me_3Al . In particular, for the amino acid glycine, use of two equivalents of Me_3Al affords the adduct **IV**, in which only the carboxylate is deprotonated.^[6] Adduct **IV** can either be further deprotonated at the amine functionality or can



monoalkylation of the carboxylate occur. A related adduct **V** has been isolated (and structurally characterized) from the reaction of $\text{Al}i\text{Bu}_3$ and anthranilic acid.^[3] Interestingly, mechanical grinding of **V** results in expulsion of $\text{Al}i\text{Bu}_3$ and

formation of the dimeric carboxylate **VI**. Clearly, in our case (diphenylglycine), subsequent C alkylation (as in the formation of **II**) does not occur. It is possible that the formation of **1** and **3** involves the initial formation of the adduct **VII**—the diphenylglycine analogue of **IV** and **V**. Two molecules of this adduct **VII** would then need to combine in the presence of a further equivalent of Me_3Al with concomitant loss of methane to afford the motif **I**. Alternatively, a tetranuclear adduct **IX**, similar to those (**VIII**) reported for salicylic acid and phthalic acid,^[4,5] and proposed for anthranilic acid^[6] is plausible, which can rearrange to the motif **I** with concomitant loss of Me_3Al . It is also possible that rapidly equilibrating species are present in solution and that an increase in the aluminum to ligand ratio promotes (or induces) the crystallization of **3**.^[10] Equilibria involving polynuclear species have been observed previously, most notably for palladium-based molecular triangles and squares.^[11] With this in mind, peaks in the electrospray mass spectra^[12] of **3** can tentatively be assigned to both Al_6 - and Al_9 -containing species. However, we have not carried out any mechanistic studies and as yet have not observed any intermediates prior to isolation of **1–3** (^1H NMR spectra for **1–3** show little change over the range $+20^\circ\text{C}$ to -50°C). It is noteworthy that **1–3** contain the



“magic” diarylhydroxy(or amino)methyl group, the ability of which to enhance selectivity in asymmetric synthesis is now well documented.^[13]

The use of only one equivalent or an excess (three equivalents) of Me_3Al under similar conditions repeatedly failed to yield any crystalline material, whilst reactions between diphenylglycine and Me_3Ga yielded the known complex $[(\text{Me}_2\text{Ga})_4(\text{MeGa})_2\{\text{HNC}(\text{Me})\text{C}(\text{CN})\text{CH}(\text{NCMe})_2\}]_2$ as the only crystalline product.^[14] Attempts to convert ring system **1** into the larger ring system **3** by using varying amounts of Me_3Al were also unsuccessful; on each occasion unreacted **1** was retrieved.

In conclusion, we have identified a structural motif, which is the building block for a number of new organoaluminum macrocycles, and observed that subtle changes in reaction stoichiometry can lead to the isolation of quite different products. Here, for example, we have shown that both 16- and 32-membered macrocycles are readily accessible from diphenylglycine and Me_3Al . The reasons why excess Me_3Al should promote increased ring size are as yet unclear; however, further work is now in progress to explore this chemistry in more detail.

Experimental Section

All manipulations were performed under N₂ by using standard Schlenk techniques and dried, deoxygenated solvents.

Complexes **1–3** were prepared by heating Me₃Al (5 mL, 2.0 M, 0.01 mol) and the appropriate acid (0.01 or 0.005 mol) under reflux for 12 h. Volatile components were then removed in vacuo, and the products were obtained by extraction into hot acetonitrile (40–50 mL). Colorless prisms were obtained on prolonged standing at ambient temperature.

1: Yield 56%; elemental analysis calcd (%) for C₆₆H₇₄N₄O₈Al₆·3-MeCN: C 61.8, H 6.0, N 7.0; found: C 61.9, H 5.9, N 6.4 (sample dried in vacuo for 12 h); IR: $\tilde{\nu}$ = 3337 (ν(NH)), 1576 (ν(CO) (broad)) cm⁻¹; ¹H NMR ([D₈]toluene, 400 MHz, 298 K): δ = 7.48 (m, 16H; aryl-H), 7.05 (overlapping m, 24H; aryl-H), 2.39 (s, 4H; NH), 0.73 (s, 15H; MeCN), -0.25 (s, 6H; Me₂Al), -0.36 (s, 12H; Me₂Al), -0.81 (s, 6H; Me₂Al), -1.46 ppm (s, 6H; MeAl); ES-MS: 689 (I-2MeCN); m.p. > 350 °C (decomp).

2: Yield 17%; elemental analysis calcd (%) for C₆₆H₇₀O₁₂Al₆·MeCN: C 65.3, H 6.1, N 0.6; found: C 65.2, H 5.8, N 0.8% (sample dried in vacuo for 24 h); IR: $\tilde{\nu}$ = 1632 (ν(CO)), 1613 (ν(CO)) cm⁻¹; ¹H NMR (C₆D₆, 400 MHz, 298 K): δ = 6.68–8.21 (5 × m, 40H; aryl-H), 0.50 (s, 15H; MeCN), 0.09 (s, 6H; Me₂Al), 0.02 (s, 12H; Me₂Al), 0.00 (s, 6H; Me₂Al), -2.21 ppm (s, 6H; MeAl); m.p. > 350 °C (darkens at 285 °C).

3: Yield 49%; elemental analysis calcd (%) for C₁₃₂H₁₄₈N₈O₁₆Al₁₂·12MeCN: C 64.1, H 6.4, N 9.6; found: C 63.6, H 6.4, N 9.5 (sample dried in vacuo for 24 h); IR: $\tilde{\nu}$ = 3313 (ν(NH)), 1603 (ν(CO)) cm⁻¹; ¹H NMR (C₆D₆, 400 MHz, 298 K): δ = 7.48 (m, 32H; aryl-H), 7.01 (m, 48H; aryl-H), 2.43 (s, 8H; NH), 0.63 (s, 16.5H; MeCN), -0.23 (s, 12H; Me₂Al), -0.32 (s, 24H; Me₂Al), -0.80 (s, 12H; Me₂Al), -1.41 ppm (s, 12H; MeAl); ES-MS: 1213 (I), 1861 (3I-MeCN), 1943 (3I-3MeCN); m.p. > 350 °C (decomp).

Received: August 12, 2004

Revised: November 3, 2004

Published online: February 18, 2005

Keywords: aluminum · amino acids · macrocycles

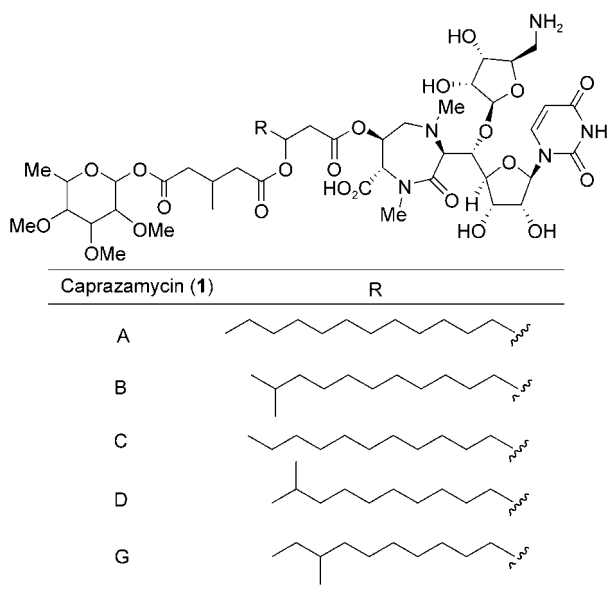
- [1] a) A. K. Powell, S. L. Heath, *Coord. Chem. Rev.* **1996**, *149*, 59; b) A. Salifoglou, *Coord. Chem. Rev.* **2002**, *228*, 297.
- [2] a) M. Rajendran, A. K. Bhattacharya, *Mater. Lett.* **1999**, *39*, 188; b) Y. Liu, R. M. Laine, *J. Eur. Ceram. Soc.* **1999**, *19*, 1949; c) Z. Flojańczyk, E. Zygadlo-Monikowska, E. Rogalska-Jońska, F. Krok, J. R. Dygas, B. Misztal-Faraj, *Solid State Ionics* **2002**, *152/153*, 227; d) K. A. Defriend, A. R. Barron, *J. Mater. Sci.* **2003**, *38*, 927; e) C. Clar, A. N. Scian, E. F. Aglietti, *Thermochim. Acta* **2003**, *34*, 407.
- [3] C. S. Branch, J. Lewiński, I. Justyniak, S. G. Bott, J. Lipkowski, A. R. Barron, *J. Chem. Soc. Dalton Trans.* **2001**, 1253.
- [4] J. Lewiński, J. Zachara, I. Justyniak, *Organometallics* **1997**, *16*, 3859.
- [5] J. Lewiński, J. Zachara, I. Justyniak, *Inorg. Chem.* **1998**, *37*, 2575.
- [6] J. Lewiński, I. Justyniak, J. Zachara, E. Tratkiewicz, *Organometallics* **2003**, *22*, 4151.
- [7] a) V. C. Gibson, C. Redshaw, A. J. P. White, D. J. Williams, *Angew. Chem.* **1999**, *111*, 1014; *Angew. Chem. Int. Ed.* **1999**, *38*, 961; b) V. C. Gibson, C. Redshaw, A. J. P. White, D. J. Williams, *Chem. Commun.* **2001**, 79; c) C. Redshaw, M. R. J. Elsegood, *Chem. Commun.* **2001**, 2016.
- [8] W. Ziemowska, S. Pasynekiewicz, T. Glowiak, *J. Organomet. Chem.* **1998**, *562*, 3.
- [9] a) W. Clegg, M. R. J. Elsegood, S. J. Teat, C. Redshaw, V. C. Gibson, *J. Chem. Soc. Dalton Trans.* **1998**, 3037; b) W. Clegg, *J. Chem. Soc. Dalton Trans.* **2000**, 3223.
- [10] We would like to thank a referee for this suggestion.
- [11] a) M. Fujita, O. Sasaki, T. Mitsuhashi, T. Fujita, J. Yazaki, K. Yamaguchi, K. Ogura, *Chem. Commun.* **1996**, 1535; b) S. B. Lee, S. Hwang, D. S. Chung, H. Yun, J.-I. Hong, *Tetrahedron Lett.* **1998**, *39*, 873. For a recent review of self-assembly see: G. F. Swiegers in *Comprehensive Coordination Chemistry II* (Eds.: J. A. McCleverty, T. J. Meyer), Elsevier Pergamon, Oxford, **2004**, p. 747.
- [12] S. Leininger, B. Olenyuk, P. Stang, *Chem. Rev.* **2000**, *100*, 853.
- [13] M. Braun, *Angew. Chem.* **1996**, *108*, 565; *Angew. Chem. Int. Ed. Engl.* **1996**, *35*, 519.
- [14] M. R. Kopp, T. Kräuter, A. Dashti-Mommertz, B. Neumüller, *Organometallics* **1998**, *17*, 4226.
- [15] Crystal data for **1**·3MeCN: C₆₆H₇₄Al₆N₄O₈·3CH₃CN, *M*_r = 1336.34, orthorhombic, space group *Pbca*, colorless, 0.19 × 0.12 × 0.06 mm³, *a* = 24.1743(6), *b* = 19.2565(5), *c* = 31.6425(8) Å, *V* = 14730.0(6) Å³, *T* = 160(2) K, *Z* = 4, ρ_{calcd} = 1.205 g cm⁻³, *2* θ_{max} = 56.98°, synchrotron, λ = 0.6928 Å, ω scans with narrow frames, 102 505 data measured on a Bruker SMART 1K CCD diffractometer (Bruker SMART software), 18 684 independent, (*R*_{int} = 0.047), *Lp* and absorption corrections applied (based on symmetry equivalent and repeated measurements), μ = 0.144 mm⁻¹, min and max trans: 0.97, 0.99, solved by direct methods (Bruker SHELXTL software), *wR*₂ = 0.123 (all data), *R*₁ = 0.044 (14 097 unique data with *I*² > 2σ(*I*²)) refined on *F*² (SHELXTL), for 851 parameters with H atoms constrained, largest difference map features within ±0.37 e Å⁻³. Crystal data for **2**·MeCN: details as above except C₆₆H₇₀Al₆O₁₂·CH₃CN, *M*_r = 1258.15, triclinic, space group *P* $\bar{1}$, 0.06 × 0.05 × 0.01 mm³, *a* = 10.8136(10), *b* = 13.7496(13), *c* = 23.423(2) Å, α = 92.891(2), β = 97.964(2), γ = 92.453(2)°, *V* = 3440.2(6) Å³, *T* = 150(2) K, *Z* = 2, λ = 0.6861 Å, 27 917 data measured, 13 310 independent, (*R*_{int} = 0.050), μ = 0.152 mm⁻¹, min and max trans: 0.99, 1.00, *wR*₂ = 0.125, *R*₁ = 0.049 (8859 unique), 795 parameters, largest difference map features within ±0.35 e Å⁻³. Crystal data for **3**·15.5MeCN: details as above except C₁₃₂H₁₄₈Al₁₂N₈O₁₆·15.5CH₃CN, *M*_r = 3068.69, monoclinic, space group *P*2₁/*n*, 0.80 × 0.21 × 0.16 mm³, *a* = 21.9995(18), *b* = 25.854(2), *c* = 31.963(3) Å, β = 94.131(2), *V* = 18 133(3) Å³, *T* = 160(2) K, *Z* = 4, $\mu_{\text{K}\alpha}$ λ = 0.71073, 92 789 data measured, 23 712 independent (*R*_{int} = 0.131), μ = 0.126 mm⁻¹, min and max trans: 0.91, 0.98, *wR*₂ = 0.176, *R*₁ = 0.068 (11 627 unique), 1854 parameters, largest difference map features within ±0.48 e Å⁻³. A total of 4.5MeCN were badly disordered and were modeled as diffuse electron density with the Platon “Squeeze” procedure.^[16] CCDC-244038—CCDC-244040 contain the supplementary crystallographic data for this paper. These data can be obtained free of charge from The Cambridge Crystallographic Data Centre via www.ccdc.cam.ac.uk/data_request/cif.
- [16] A. L. Spek, *Acta Crystallogr. A* **1990**, *46*, C34.

Antibiotics

Total Synthesis of Caprazol, a Core Structure of the Caprazamycin Antituberculosis Antibiotics**

Shinpei Hirano, Satoshi Ichikawa, and Akira Matsuda*

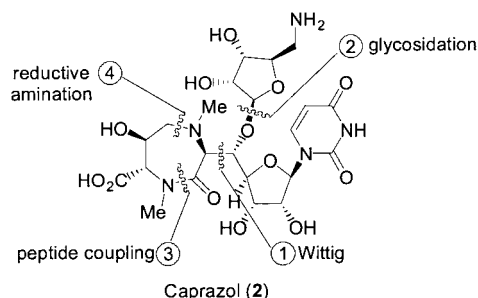
Tuberculosis (TB) is a disease, primarily of the respiratory system, from which two million people die each year. With resistant strains continuing to emerge, the development of new anti-TB agents with new mechanisms of action is of critical importance. The caprazamycins (CPZs; **1**, Scheme 1),^[1] which were isolated from a culture broth of the Actinomycete strain *Streptomyces* sp. MK730-62F2 in



Scheme 1. Structures of the caprazamycins.

2003, have shown excellent antimycobacterial activity in vitro against drug-susceptible and multidrug-resistant *Mycobacterium tuberculosis* strains and exhibit no significant toxicity in

mice. Caprazol (**2**, Scheme 2), the deacylated CPZ whose stereochemical structure (5'S,6'S,2'''S,3'''S) was recently revealed through X-ray crystal analysis,^[2] consists of a uridine, an aminoribose, and a characteristic diazepanone. Liposido-



Scheme 2. Structure of caprazol (**2**) and the synthetic strategy.

mycins (LPSs), which are related nucleoside antibiotics, are also known to exhibit antibacterial activity similar to that of CPZs.^[3] LPSs prevent the formation of one of the components of bacterial cell walls, peptidoglycan, by inhibiting Mra Y, a key enzyme for peptidoglycan biosynthesis.^[4] It has been suggested that CPZs might follow the same mode of action as LPSs because of their complex structural and biological similarities. Consequently, they have become intriguing, challenging synthetic targets.^[5] We report herein the first synthesis of caprazol (**2**).

One of the major difficulties posed by the synthesis is the introduction of the 5-aminoribose moiety found in **2** after construction of the uridyldiazepanone moiety, because the tertiary amines contained in the diazepanone structure inhibit the usual ribosylation promoted by Lewis acid,^[6] and the 5'-hydroxy group is presumed to be in a highly sterically hindered position.^[7] Furthermore, compound **2**, which contains a β -heterosubstituted carboxyl moiety, would be sensitive to basic conditions.^[3c] Although a general method exists for the construction of β -glycosides through neighboring-group participation by using a glycosyl donor protected with a 2-O-acyl group, which is then usually deprotected under basic conditions, we planned to introduce the aminoribose protected with an acid-labile protecting group at an early stage of the synthesis. In so doing, we hoped to control the β -selective introduction by steric hindrance of a group installed on the α face of the ribofuranoside.^[8]

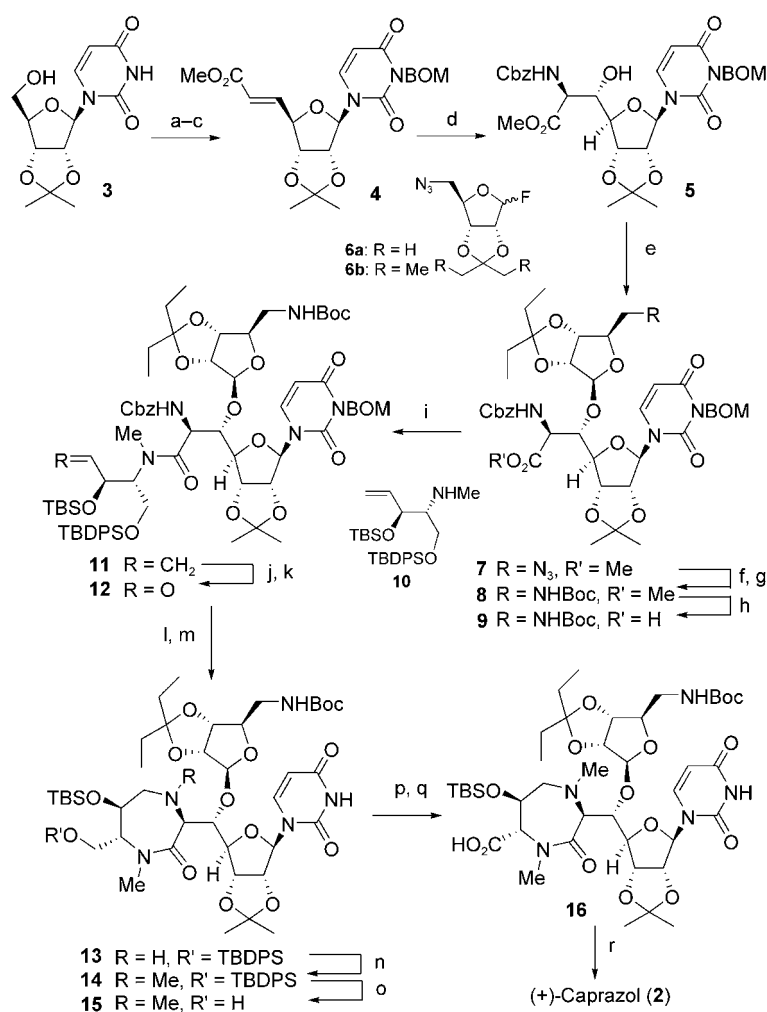
Oxidation of 2',3'-O-isopropylideneuridine (**3**) with IBX^[9] followed by a two-carbon elongation with $\text{Ph}_3\text{P}=\text{CHCO}_2\text{Me}$ and BOM protection of the NH group at position 3 of the uracil moiety provided **4** (*trans/cis* = 37:1) over three steps (Scheme 3). Sharpless aminohydroxylation^[10] of **4** with $(\text{DHQD})_2\text{AQN}$ as a chiral ligand afforded **5**^[11] with a 5'S,6'S/5'R,6'R ratio of 86:14. In the absence of the chiral ligand, the diastereoselectivity was reversed to give **5** in a ratio of 40:60 with a decrease in yield.

When the ribosyl fluoride **6a**^[12] protected with an isopropylidene group was activated with $\text{BF}_3\cdot\text{Et}_2\text{O}$ ^[13] at -30°C , the corresponding ribosides were obtained in 79% yield and the stereoselectivity at the anomeric position was 27:73 (α/β). The use of AgOTf and Cp_2HfCl_2 ^[14] (OTf = tri-

[*] S. Hirano, Dr. S. Ichikawa, Prof. A. Matsuda
Graduate School of Pharmaceutical Sciences
Hokkaido University
Sapporo 060-0812 (Japan)
Fax: (+81) 11-706-4980
E-mail: matuda@pharm.hokudai.ac.jp

[**] This work was supported financially by a Grant-in-Aid from the Ministry of Education, Science, Sports, and Culture. We thank Dr. Masayuki Igarashi (Bioresources Unit, Bioactive Molecular Research Group, Microbial Chemistry Research Center) for providing us with a sample of natural caprazol and the coordinate data of its X-ray crystal-structure analysis. Nucleosides and Nucleotides, Part 230; for Part 229, see reference [22].

Supporting information for this article (experimental details and characterization data for **3–16** and synthetic **2**) is available on the WWW under <http://www.angewandte.org> or from the author.



Scheme 3. Total synthesis of caprazol (**2**). Reagents and conditions: a) IBX, MeCN, 80 °C; b) Ph₃P=CHCO₂Me, CH₂Cl₂, -30 °C; c) BOMCl, Na₂CO₃, Bu₄NI, CH₂Cl₂/H₂O, room temperature, 70% over 3 steps; d) CbzNH₂, K₂OsO₂(OH)₄, (DHQD)₂AQN, NaOH, *t*BuOCl, *n*PrOH/H₂O, 5 °C → RT, 61%; e) **6**, BF₃·OEt₂, MS4A, CH₂Cl₂, -30 °C, 80%; f) Ph₃P, H₂O, benzene/THF, 50 °C; g) (Boc)₂O, 95% over 2 steps; h) Ba(OH)₂, THF/H₂O, room temperature, 50%; i) **10**, DEPBT, NaHCO₃, THF, 0 °C → RT, 81%; j) OsO₄, NMO, *t*BuOH, acetone/H₂O, room temperature; k) NaIO₄, acetone/H₂O, room temperature, 61% over 2 steps; l) H₂, Pd/C, *i*PrOH, room temperature; m) NaBH(OAc)₃, AcOH, AcOEt, room temperature, 34% of **13** and 24% of **14** over 2 steps; n) (CH₂O)_{*n*}, NaBH(OAc)₃, AcOH, AcOEt, room temperature, 65%; o) NH₄F, MeOH, room temperature, 60%; p) Dess–Martin periodinane, CH₂Cl₂, room temperature; q) NaClO, NaH₂PO₄, *t*BuOH/H₂O, 56% over 2 steps; r) HF, THF/H₂O, 50%. Boc = *tert*-butoxycarbonyl, BOM = benzyloxymethyl, Cbz = benzyloxycarbonyl, DEPBT = 3-(diethoxyphosphoryloxy)-1,2,3-benzotriazin-4(3H)-one, (DHQD)₂AQN = 1,4-bis(dihydroquinidiny)anthraquinone, IBX = 1-hydroxy-1,2-benziodoxol-3-(1H)-one 1-oxide, MS4A = molecular sieves (4 Å), NMO = 4-methylmorpholine *N*-oxide, TBDPS = *tert*-butyldiphenylsilyl, TBS = *tert*-butyldimethylsilyl, THF = tetrahydrofuran.

fluoromethanesulfonate, Cp = cyclopentyl) as Lewis acids at -40 °C resulted in a loss of stereoselectivity. Further exploration with the ribosyl fluoride **6b**,^[12] which possesses a more sterically hindered 3-pentylidene group, afforded the desired **7**^[15] with good β selectivity ($\alpha/\beta = 4:96$) when activation was conducted with BF₃·Et₂O at -30 °C. Notably, a decrease in β selectivity was again observed in the presence of a trifluoromethanesulfonate ion (that is, with AgOTf and

Cp₂HfCl₂, when $\alpha/\beta = 11:89$). Presumably, the β -*O*-trifluoromethanesulfonyl riboside intermediate^[16] might be formed, and subsequent S_N2 attack of the alcohol would give the undesired α -riboside. Our simple and effective method can be considered an alternative for the construction of β -ribosides without neighboring-group participation.

The azide group in **7** was reduced to the corresponding amine, which was protected with a Boc group to give **8**. Basic hydrolysis of the methyl ester in **8** was troublesome^[17] and the desired carboxylic acid **9** was obtained only when **8** was treated with Ba(OH)₂ in aqueous THF. Thus, treatment with base should be avoided in the synthesis to prevent β elimination followed by decomposition. Coupling of **9** with the secondary amine **10** by using DEPBT^[18] gave the amide **11**. Compound **11** was treated with OsO₄, and the resulting mixture of the diastereomeric diols was oxidatively cleaved to provide the aldehyde **12**.

The next step involved the construction of the characteristic seven-membered diazepanone system, the system on which most of the synthetic studies for LPSs have focused.^[5] Initial attempts to construct the diazepanone by deprotection of the Cbz group in **12** and reductive amination of the aldehyde, both promoted by catalytic hydrogenation with Pd/C, were unsuccessful because of the difficulty in hydrogenating the cyclic imine to give **13**. Additional forcing conditions under medium pressure gave the 5,6-dihydrouridine derivative owing to overreduction. After extensive efforts to overcome this problem, reductive amination was abandoned in favor of hydride reduction with NaBH(OAc)₃, and the desired diazepanone **13** was obtained along with its *N*-methylated compound **14**.^[19] Compound **13** was methylated by using (CH₂O)_{*n*} and NaBH(OAc)₃ to give **14**. Treatment of **14** with NH₄F in MeOH resulted in selective cleavage of the TBDPS protecting group at the primary hydroxy group to form **15**, which was then transformed into carboxylic acid **16** by a two-step sequence with Dess–Martin periodinane^[20] and NaOCl^[21] oxidation. Finally, global deprotection of **16** with aqueous HF provided (+)-**2** ($[\alpha]_D^{25} = +23.8$ ($c = 0.24$, dimethyl sulfoxide); literature value:^[2] $[\alpha]_D^{19} = +28^\circ$ ($c = 0.5$, dimethyl sulfoxide)), the properties of which were identical in all respects with those reported for the natural material.^[2]

In conclusion, the first total synthesis of (+)-**2** in a highly concise manner over 18 steps, with uridine as the starting material, is reported. This work confirms the stereochemical assignments for the LPS core structure that were suggested by earlier synthetic studies.

Received: October 27, 2004

Published online: February 18, 2005

Keywords: antibiotics · glycosylation · heterocycles · natural products · total synthesis

- [1] a) M. Igarashi, N. Nakagawa, S. Doi, N. Hattori, H. Naganawa, M. Hamada, *J. Antibiot.* **2003**, *56*, 580–583; b) T. Takeuchi, M. Igarashi, H. Naganawa, JP P2003-12687A, **2003**.
- [2] T. Miyake, M. Igarashi, T. Shidara, Y. Takahashi, JP WO 2004-067544A1, **2004**.
- [3] a) K. Isono, M. Uramoto, H. Kusakabe, K. Kimura, K. Izaki, C. C. Nelson, J. A. McCloskey, *J. Antibiot.* **1985**, *38*, 1617–1621; b) K. Kimura, Y. Ikeda, S. Kagami, M. Yoshihama, K. Suzuki, H. Osada, K. Isono, *J. Antibiot.* **1998**, *51*, 1099–1104; c) M. Ubukata, K. Kimura, K. Isono, C. C. Nelson, J. M. Gregson, J. A. McCloskey, *J. Org. Chem.* **1992**, *57*, 6392–6403; d) K. Kimura, Y. Ikeda, S. Kagami, M. Yoshihama, M. Ubukata, Y. Esumi, H. Osada, K. Isono, *J. Antibiot.* **1998**, *51*, 647–654; e) K. Kimura, S. Kagami, Y. Ikeda, H. Takahashi, M. Yoshihama, H. Kusakabe, H. Osada, K. Isono, *J. Antibiot.* **1998**, *51*, 640–646.
- [4] K. Kimura, T. D. H. Bugg, *Nat. Prod. Rep.* **2003**, *20*, 252–273.
- [5] a) S. Knapp, G. J. Morriello, S. R. Nandan, T. J. Emge, G. A. Doss, R. T. Mosley, L. Chen, *J. Org. Chem.* **2001**, *66*, 5822–5831; b) M. R. Spada, M. Ubukata, K. Isono, *Heterocycles* **1992**, *34*, 1147–1167; c) N. Nakajima, T. Isobe, S. Irida, M. Ubukata, *Heterocycles* **2003**, *59*, 107–113; d) S. Knapp, G. J. Morriello, G. A. Doss, *Org. Lett.* **2002**, *4*, 603–606; e) K. S. Kim, Y. H. Ahn, *Tetrahedron: Asymmetry* **1998**, *9*, 3601–3605; f) C. Gravier-Pelletier, M. Milla, Y. L. Merrer, J. Depezay, *Eur. J. Org. Chem.* **2001**, 3089–3096; g) F. Sarbia, L. Martin-Ortiz, F. J. Lopez-Herrera, *Org. Lett.* **2003**, *5*, 3927–3930.
- [6] Introduction of uracil by the Vörruggen method following the construction of the ribosyl diazepanone was reported to have some drawbacks.^[5a]
- [7] During the course of our synthetic studies on nucleoside antibiotics, it was revealed that the introduction of a protecting group or substituent on this type of alcohol was quite difficult: S. Ichikawa, S. Shuto, M. Matsuda, *J. Am. Chem. Soc.* **1999**, *121*, 10270–10280.
- [8] A similar concept was reported in *N*-glycosidation to synthesize nucleoside derivatives: T. Kusumi, T. Fukushima, I. Ohtani, H. Kakisawa, *Tetrahedron Lett.* **1991**, *32*, 2939–2942.
- [9] J. D. More, N. S. Finny, *Org. Lett.* **2002**, *4*, 3001–3003.
- [10] a) B. Tao, G. Schlingloft, K. B. Sharpless, *Tetrahedron Lett.* **1998**, *39*, 2507–2510; b) A. J. Morgan, C. E. Masse, J. S. Panek, *Org. Lett.* **1999**, *1*, 1949–1952.
- [11] The stereochemistry of the 5' position of **5** was determined to be the *R* configuration by the modified Mosher method with the amide derivatives, which were prepared by deprotection of the Cbz protecting group of **5** and subsequent acylation of the liberated amine with 2-methoxy-2-trifluoromethylphenylacetic acid (see the Supporting Information); T. Kusumi, T. Fukushima, I. Ohtani, H. Kakisawa, *Tetrahedron Lett.* **1991**, *32*, 2939–2942.
- [12] Details for the preparation and characterization may be found in the Supporting Information.
- [13] K. C. Nicolaou, A. Chucholoeski, R. E. Dolle, J. L. Randall, *J. Chem. Soc. Chem. Commun.* **1984**, 1155–1158.
- [14] K. Suzuki, H. Maeta, T. Matsumoto, G. Tsuchihashi, *Tetrahedron Lett.* **1988**, *29*, 3571–3574.
- [15] The stereochemistry of the 1'' position was confirmed by the NOESY correlations between 1''-H and 4''-H for the β -riboside and by the typical coupling constant ($J_{1,2}=0$ Hz) for a 2,3-*O*-alkylidene-protected ribofuranoside that was observed in the ¹H NMR spectrum.
- [16] D. Crich, S. Sun, *J. Am. Chem. Soc.* **1997**, *119*, 11217–11223.
- [17] Extensive efforts to obtain the acid **9** have been conducted with **8** by hydrolysis under other conditions (that is, LiOH in THF/MeOH/H₂O, NaOH in CH₂Cl₂/H₂O, or lipase in aq. CH₃CN) and demethylation (PhSH, Cs₂CO₃, *N,N*-dimethylformamide).
- [18] H. Li, X. Jiang, Y. Ye, C. Fan, T. Romoff, M. Goodman, *Org. Lett.* **1999**, *1*, 91–94.
- [19] It was presumed that the methyl source was the formaldehyde generated upon cleavage of the BOM protecting group from the 3 position.
- [20] D. B. Dess, J. C. Martin, *J. Org. Chem.* **1988**, *53*, 4155–4156.
- [21] J. M. Andres, N. D. Elena, R. Pedrosa, *Tetrahedron* **2000**, *56*, 1523–1531.
- [22] S. Hikishima, N. Minakawa, K. Kuramoto, Y. Fujisawa, M. Ogawa, A. Matsuda, *Angew. Chem.* **2005**, *117*, 602–604; *Angew. Chem. Int. Ed.* **2005**, *44*, 596–598.

Expanded Porphyrins

A Doubly N-Fused Benzo-hexaphyrin and Its Rearrangement to a Fluorescent Macrocycle upon DDQ Oxidation**

Yasuhide Inokuma, Takahiro Matsunari, Noboru Ono,*
Hidemitsu Uno,* and Atsuhiko Osuka*

Over the past decade, much progress has been made in the expansion of π -conjugated porphyrinic electronic systems because of their potential applications as conductive materials, near-infrared (NIR) dyes, nonlinear optical materials, and photosensitizers for photodynamic therapy.^[1–3] Representative examples include *meso*-ethynyl-substituted porphyrin oligomers^[1] and multiply connecting porphyrin oligomers

[*] Prof. Dr. N. Ono

Department of Chemistry, Faculty of Science
Ehime University
Bunkyo-cho 2-5, Matsuyama 790-8577 (Japan)
Fax: (+81) 89-927-9670
E-mail: ononbr@dpc.ehime-u.ac.jp

Prof. Dr. H. Uno

Integrated Center for Science
Ehime University
Bunkyo-cho 2-5, Matsuyama 790-8577 (Japan)
Fax: (+81) 89-927-9670
E-mail: uno@dpc.ehime-u.ac.jp

Y. Inokuma, T. Matsunari, Prof. Dr. A. Osuka
Department of Chemistry, Graduate School of Science
Kyoto University, and
Core Research for Evolutional Science and Technology (CREST)
Japan Science and Technology Agency
Sakyo-ku, Kyoto 606-8502 (Japan)
Fax: (+81) 75-753-3970
E-mail: osuka@kuchem.kyoto-u.ac.jp

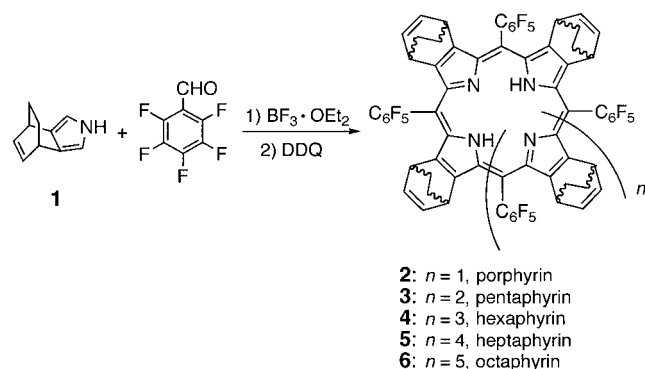
[**] This work was partly supported by a grant-in-aid from the Ministry of Education, Culture, Sports, Science, and Technology, Japan (No. 15350022, and 21st Century COE on Kyoto University Alliance for Chemistry). DDQ = 2,3-dichloro-5,6-dicyano-1,4-benzoquinone.



Supporting information for this article is available on the WWW under <http://www.angewandte.org> or from the author.

exemplified by *meso-meso*, β - β , β - β -triple-linked porphyrin arrays.^[2,3] Another effective and promising synthetic strategy is the fusion of aromatic rings at the β -pyrrolic positions which can lead to a significant alternation in the electronic and optical properties through expansion of the π -electronic system as well as a change in the orbital symmetry.^[4,5] This synthetic transformation has been made more feasible by using 4,7-dihydro-4,7-ethano-2*H*-isoindole (**1**, Scheme 1)^[5a] as most of the synthetic steps can be performed without serious problems of solubility and a final retro-Diels–Alder reaction provides a benzoporphyrin quantitatively. Accordingly, various aromatic-fused porphyrins have been explored by this strategy.^[5] Elsewhere, expanded porphyrins have recently emerged as a new class of oligopyrrolic macrocycle that exhibit unique optical and electrochemical properties as a result of their enlarged π -conjugated networks, which are larger than those of porphyrins.^[6] Among these, we reported a series of *meso*-aryl expanded porphyrins prepared from the condensation reaction of pentafluorobenzaldehyde and pyrrole under modified Rothemund–Lindsey conditions.^[7] Herein we report our attempts to apply the retro-Diels–Alder strategy to the synthesis of β -benzohexaphyrin-(1.1.1.1.1.1) using **1** as a key building block.

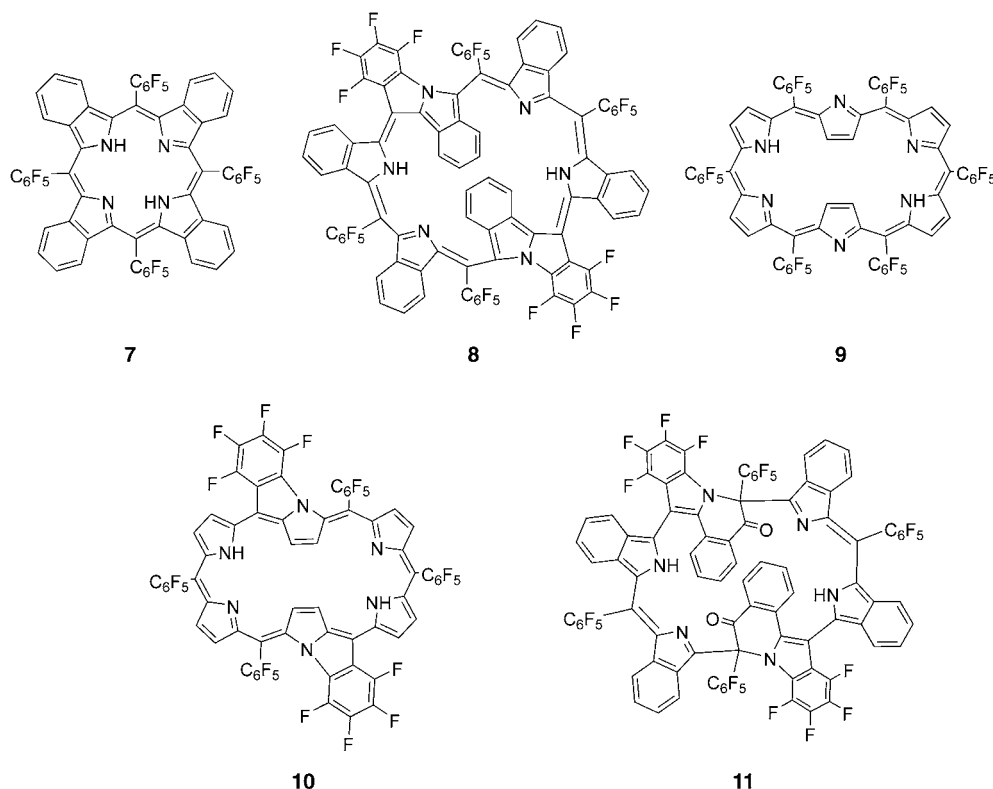
Following our protocol of *meso*-aryl-substituted expanded porphyrins,^[7] a solution of **1** and pentafluorobenzaldehyde in CH_2Cl_2 (67 mM each) was treated with a catalytic amount of $\text{BF}_3 \cdot \text{OEt}_2$ for 2 h, and the resulting mixture was oxidized with 2,3-dichloro-5,6-dicyano-1,4-benzoquinone (DDQ) overnight (Scheme 1). Analysis by MALDI-TOF mass spectrometry of the reaction mixture revealed the formation of expanded porphyrins **3–6** as well as porphyrin **2**, each as products of retro-Diels–Alder reactions.



Scheme 1. Synthesis of porphyrins and expanded porphyrins.

Purification by column (silica gel) and gel-permeation chromatography led to the isolation of porphyrin **2**, pentaphyrin **3**, and hexaphyrin **4** in 18, 11, and 9.4% yield, respectively, as atropisomeric mixtures with respect to the orientation of the bicyclic rings.^[8]

We then attempted retro-Diels–Alder reactions of **2** and **4**. Under the standard conditions (200 °C, 0.1 mm Hg, 10 min), porphyrin **2** was quantitatively converted into tetrabenzoporphyrin **7**, which is green in color ($\lambda_{\text{max}} = 458 \text{ nm}$ in CH_2Cl_2) and displays a parent-ion peak at $m/z = 1175.1288$ in its high



resolution electrospray-ionization time-of-flight (HR ESI-TOF) mass spectrum (calcd for $\text{C}_{60}\text{H}_{18}\text{N}_4\text{F}_{20}$: 1175.1285 $[M+H]^+$). Good-quality crystals of **7** in its diprotonated form were obtained which were suitable for analysis by X-ray diffraction.^[9] The crystal structure shows a highly distorted saddle conformation with a dihedral angle between two opposite isoindole planes of 108.6° (Figure 1).

Under the same retro-Diels–Alder reaction conditions, the hexaphyrin **4** gave an intractable complicated mixture, which contained multiply fluorine-eliminated products, as judged from MALDI-TOF mass spectra. But under milder retro-Diels–Alder conditions (170 °C, 0.1 mmHg, 30 min), **4** afforded a red–violet solid as the major product in 47% which has been assigned to the doubly N-fused β -benzo-[28]hexaphyrin(1.1.1.1.1.1) **8**. The HR ESI-TOF mass spectrum of **8** revealed a parent peak at $m/z = 1722.1767$ (calcd for $\text{C}_{90}\text{H}_{26}\text{N}_6\text{F}_{28}$: 1722.1766 $[M]^+$), and its ^1H NMR spectrum exhibited six doublets and six triplets in the range $\delta = 8.68$ –6.16 ppm which are attributed to the peripheral protons at the fused benzo moieties, and a broad signal at $\delta = 17.87 \text{ ppm}$ for

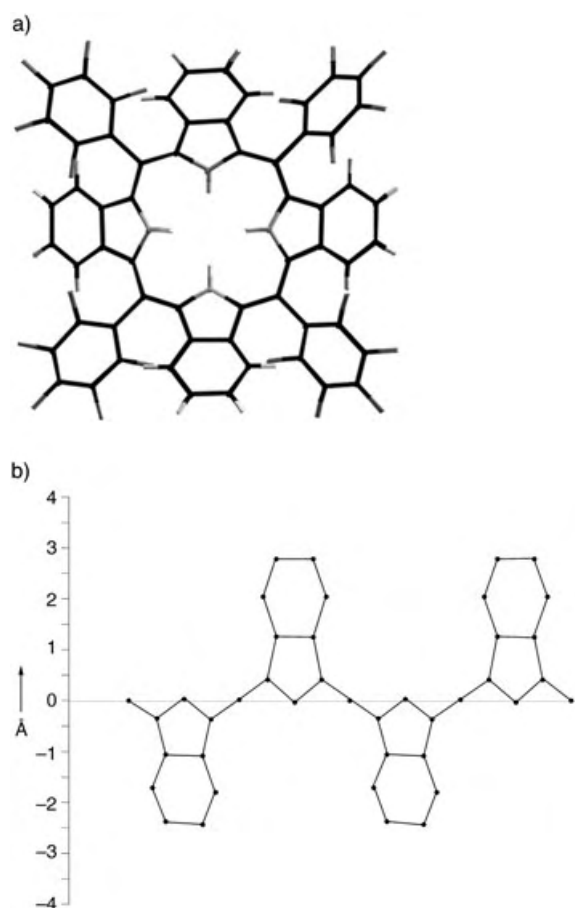


Figure 1. a) Crystal structure and b) skeletal deviation of tetrabenzoporphyrin **7**. Solvent molecules and counteranions (trifluoroacetate) are omitted for clarity.

the inner NH protons. The down-field-shifted NH signal suggests hydrogen-bonding interactions. Overall these ^1H NMR data suggest nonaromatic character for **8**. The structure of **8** was confirmed by single-crystal X-ray diffraction analysis to be an *anti* doubly N-fused product from the expected benzohexaphyrin(1.1.1.1.1.1) (Figure 2),^[10] which reveals a very strained structure that consists of two planar diindomethene and 11*H*-isoindolo[2,1-*a*]indole moieties with C_2 symmetry. The 11*H*-isoindolo[2,1-*a*]indole moieties are arranged in a near-parallel and face-to-face manner with an interplanar distance of 3.78 Å and a small dihedral angle of 16.5°, and are connected with diindomethene units with dihedral angles of 33.4° and 49.2°. The two planar diindomethene moieties are arranged in an almost perpendicular manner with a dihedral angle of 81.0°, despite the fully conjugated electronic system. As *anti* dou-

ble-N-fusion of hexaphyrin can be effected upon heating a solution of hexaphyrin **9** in the presence of $[\text{Fe}(\text{acac})_3]$ (acac = acetylacetonate),^[11] the thermal reaction of **9** (170 °C, 0.1 mmHg, 30 min) was carried out and merely gave a complicated mixture that contained a trace amount of **10**. This result suggests that the smooth *anti* double-N-fusion reaction observed for **4** is not general for hexaphyrins, but characteristic for β -benzohexaphyrin.

Next, the oxidation of **8** with DDQ was attempted to explore its two-electron-oxidized form. Addition of DDQ to a solution of **8** in CH_2Cl_2 led to clear spectral changes with isosbestic points (see Supporting Information) which suggest the formation of a complex between **8** and DDQ, but **8** was recovered quantitatively after the above solution was passed through a short column of alumina. A relatively low oxidation potential for **8** ($E_1 = 0.17$ V and $E_2 = 0.35$ V versus the ferrocene/ferrocenium (Fc/Fc^+) ion couple, as determined by cyclic voltammetry in acetonitrile) suggests a charge-transfer interaction for **8** and DDQ. This reaction was also monitored by ^1H NMR spectroscopy by using concentrated solutions of **8** (≥ 1 mM) and DDQ. Upon addition of 5 equivalents of DDQ to **8**, the ^1H NMR spectrum of **8** broadened and remained without substantial change for several hours. However, after 3 days, a clear and sharp spectrum was obtained from this sample which featured a single set of signals that indicate formation of a single major product. This change was accompanied by a distinct change in the color of the solution from red–purple to navy blue.

This oxidation reaction was then carried out on a preparative scale in the presence of a small amount of water to afford **11** in 48% yield. The X-ray crystal structure of **11** was measured (Figure 3) and shows a C_2 -symmetric structure that consists of two planar diindomethene and isoindolo[2,1-

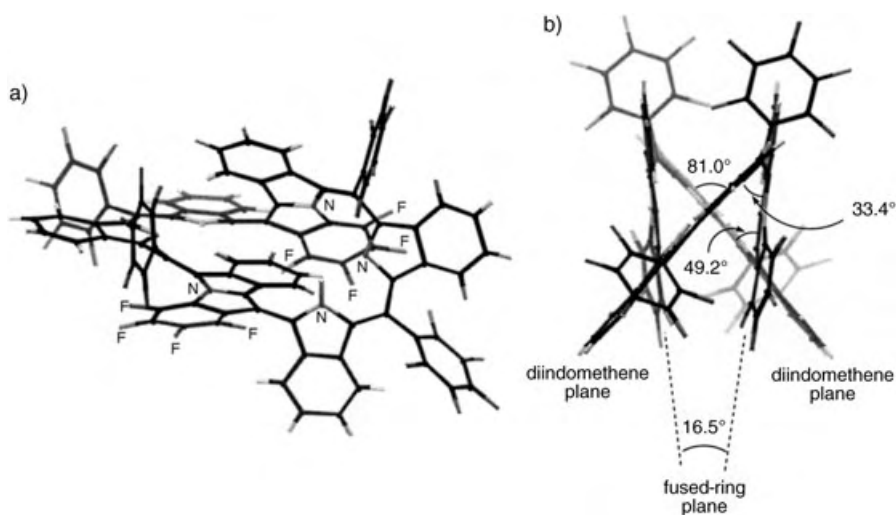


Figure 2. Crystal structure of **8**: a) top view, b) side view.

*anti*isoquinolin-5-one subunits.^[12] Interestingly, the resulting two sp^3 -hybridized carbon atoms that connect these two subunits serve to interrupt the conjugation of the macrocycle. In the structure of **11**, the two diindomethene moieties are

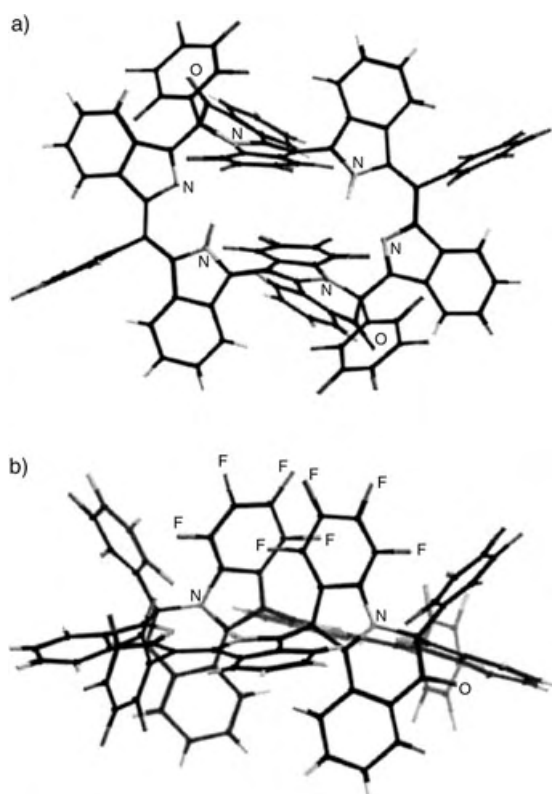


Figure 3. Crystal structure of **11**: a) top view, b) side view.

arranged in a roughly coplanar arrangement (dihedral angle 30.8°) to which the isoindolo[2,1-*a*]isoquinolin-5-one moieties are placed with dihedral angles of 69.2° and 81.4° . The spectral data for **11** are fully consistent with this unique structure: HR ESI-TOF mass spectroscopy revealed a parent ion peak at $m/z = 1755.1732$ (calcd for $H_{90}H_{27}N_6F_{28}O_2$: 1755.1743 $[M+H]^+$), and ^{13}C NMR spectroscopy showed signals at $\delta = 186.2$ and 37.3 ppm which correspond to carbonyl and sp^3 -hybridized carbon atoms, respectively. When this oxidation was performed in the presence of $H_2^{18}O$, the oxygen atoms of the carbonyl group were enriched with ^{18}O , which suggests adventitious water as a source of oxygen atoms. A similar oxidation reaction was attempted for *anti* double-N-fused hexaphyrin **10** under the same conditions. Although similar spectral changes were observed upon addition of DDQ in CH_2Cl_2 , **10** was recovered quantitatively from the reaction mixture at high concentration, which suggests that this oxidative rearrangement is unique to a doubly N-fused benzohexaphyrin substrate, plausibly being triggered by its severe strain.

The absorption spectra of **8** and **11** differ significantly from each other (Figure 4), which reflect skeletal rearrangements and disruption of the electronic conjugation. Whereas **8** is virtually nonfluorescent in most of the solvents examined, **11** emits relatively strong fluorescence in nonpolar solvents. As shown in Figure 4, the fluorescence emission of **11** is observed at $\lambda = 718$ nm ($\lambda_{ex} = 578$ nm), with a large Stokes shift and a quantum yield of $\Phi_F = 0.034$ in CH_2Cl_2 with respect to that of methylene blue ($\Phi_F = 0.035$ in methanol).^[13] The

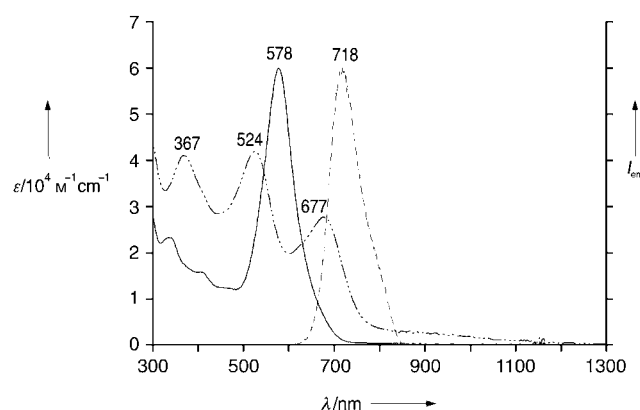


Figure 4. UV/Vis absorption spectra of **8** (---) and **11** (—), and the fluorescence emission spectrum of **11** (---, $\lambda_{ex} = 578$ nm) in CH_2Cl_2 .

fluorescence of **11** can be thought to originate from a diindomethene subunit, according to a recent report on a series of related boron-diindomethene dyes,^[14] but its substantial shift to longer wavelengths is noteworthy and can be accounted for in terms of conjugation with an isoquinolin-5-one subunit. The relatively high quantum yield of fluorescence for **11** is attractive as fluorescence in this near-IR region (650–900 nm) is quite useful for a variety of applications including biochemical fluorescence imaging and sensing,^[15] despite a limited number of fluorescent dyes in this region known.^[16] Furthermore, the fluorescence of **11** is quite dependent on solvent polarity and its fluorescent quantum yield decreases with increasing solvent polarity: $\Phi_F = 0.056$ in chlorobenzene, 0.054 in toluene, 0.048 in benzene, 0.033 in ethyl acetate, 0.029 in tetrahydrofuran, 0.013 in pyridine, 0.008 in benzonitrile, 0.004 in acetone, 0.002 in methanol, and less than 10^{-3} in nitromethane, *N,N*-dimethylformamide, and acetonitrile, in parallel to the reported trend of polar diindomethene dyes.^[14] The quenching of the fluorescence of **11** is indeed dependent on the polarity of the bulk solvent, but not on specific molecular interaction with polar solvent molecules, as revealed by experiments in mixed solvent systems, CH_2Cl_2 /acetonitrile and toluene/nitromethane. These results are encouraging for the potential use of **11** as a polarity indicator in complicated environments.

In summary, doubly N-fused β -benzo[28]hexaphyrin-(1.1.1.1.1.1) **8** was synthesized as the first example of a β -benzo-expanded porphyrin through the retro-Diels–Alder reaction of a β -bicyclo[2.2.2]octadiene-fused hexaphyrin. The molecule **8** undergoes an oxidative rearrangement to macrocycle **11**, which emits fluorescence that is dependent on the polarity of the solvent. Extension of this synthetic strategy to larger expanded porphyrins is currently in progress in our laboratory.

Received: December 6, 2004

Published online: February 21, 2005

Keywords: fluorescence · macrocycles · oxidation · porphyrinoids · retro reactions

- [1] a) V. S.-Y. Lin, S. G. DiMaggio, M. Therien, *Science* **1994**, *264*, 1105; b) M. L. LeCours, H.-W. Guan, S. G. DiMaggio, C. H. Wang, M. J. Therien, *J. Am. Chem. Soc.* **1996**, *118*, 1497; c) H. L. Anderson, *Chem. Commun.* **1999**, 2323; d) T. E. O. Screen, J. R. G. Thorne, R. G. Denning, D. G. Bucknall, H. L. Anderson, *J. Am. Chem. Soc.* **2002**, *124*, 9714. For the first example of ethynyl-conjugated porphyrins: see, D. P. Arnold, A. W. Johnson, M. Mahendran, *J. Chem. Soc. Perkin Trans. 1* **1978**, 366.
- [2] a) M. J. Crossley, L. J. Govenlock, J. K. Prashar, *J. Chem. Soc. Chem. Commun.* **1995**, 2379; b) L. Sendt, L. A. Johnson, W. A. Hough, M. J. Crossley, N. S. Hush, J. R. Reimers, *J. Am. Chem. Soc.* **2002**, *124*, 9299; c) M. G. H. Vicente, L. Jaquinod, K. M. Smith, *Chem. Commun.* **1999**, 1771; d) R. Paolesse, L. Jaquinod, F. D. Sala, D. J. Nurco, L. Prodi, M. Montalti, C. D. Natale, A. D'Amico, A. D. Carlo, P. Lugli, K. M. Smith, *J. Am. Chem. Soc.* **2000**, *122*, 11295.
- [3] a) A. Tsuda, A. Osuka, *Science*, **2001**, *293*, 79; b) A. Tsuda, H. Furuta, A. Osuka, *J. Am. Chem. Soc.* **2001**, *123*, 10304.
- [4] a) J. Martinsen, L. J. Pace, T. E. Phillips, B. M. Hoffman, J. A. Ibers, *J. Am. Chem. Soc.* **1982**, *104*, 83; b) K. Murata, K. Liou, J. A. Thompson, E. M. McGhee, D. E. Rende, D. E. Ellis, R. L. Musselman, B. M. Hoffman, J. A. Ibers, *Inorg. Chem.* **1997**, *36*, 3363; c) R. Cheng, Y. Chen, S. L. Wang, C. Y. Cheng, *Polyhedron* **1993**, *12*, 1353.
- [5] a) S. Ito, T. Murashima, N. Ono, *J. Chem. Soc. Perkin Trans. 1* **1997**, 3161; b) S. Ito, T. Murashima, H. Uno, N. Ono, *Chem. Commun.* **1998**, 1661.
- [6] a) A. Jasat, D. Dolphin, *Chem. Rev.* **1997**, *97*, 2267; b) T. D. Lash, *Angew. Chem.* **2000**, *112*, 1833; *Angew. Chem. Int. Ed.* **2000**, *39*, 1763; c) H. Furuta, H. Maeda, A. Osuka, *Chem. Commun.* **2002**, 1795; d) J. L. Sessler, D. Seidel, *Angew. Chem.* **2003**, *115*, 5292; *Angew. Chem. Int. Ed.* **2003**, *42*, 5134; e) A. Ghosh, *Angew. Chem.* **2004**, *116*, 1952; *Angew. Chem. Int. Ed.* **2004**, *43*, 1918.
- [7] a) J.-Y. Shin, H. Furuta, K. Yoza, S. Igarashi, A. Osuka, *J. Am. Chem. Soc.* **2001**, *123*, 7190; b) J.-Y. Shin, H. Furuta, A. Osuka, *Angew. Chem.* **2001**, *113*, 639; *Angew. Chem. Int. Ed.* **2001**, *40*, 619.
- [8] MALDI-TOF mass spectrometry revealed the formation of heptaphyrin **5** ($m/z = 2055$, calcd for $C_{105}H_{32}F_{35}N_7$:2055.2) and octaphyrin **6** ($m/z = 2353$, calcd for $C_{120}H_{38}F_{40}N_8$:2350.3). A retro-Diels–Alder reaction occurred under laser-irradiation to produce a benzo skeleton from a bicyclo one. These products could not be isolated owing to low yields and overlapping R_f values in TLC.
- [9] Crystal data for the diprotonated form of tetrabenzoporphyrin **7**: monoclinic, space group $C2/c$ (no. 15), $a = 20.91(3)$, $b = 20.76(3)$, $c = 15.87(2)$ Å, $\beta = 102.26(6)^\circ$, $V = 6732(17)$ Å³, $Z = 4$, $\rho_{\text{calcd}} = 1.690$ g cm⁻³, $T = 123$ K, crystal size $0.50 \times 0.40 \times 0.20$ mm³, $R = 0.085$, $R_w = 0.241$, GOF = 1.363 with $I > 2.00\sigma(I)$. CCDC 257492 contains the supplementary crystallographic data for this paper. These data can be obtained free of charge from the Cambridge Crystallographic Data Centre via www.ccdc.cam.ac.uk/data_request/cif.
- [10] Crystal data for **8**: orthorhombic, space group $C22_1$ (no. 20), $a = 20.06(3)$, $b = 26.20(2)$, $c = 16.36(1)$ Å, $V = 8595(14)$ Å³, $Z = 4$, $\rho_{\text{calcd}} = 1.398$ g cm⁻³, $T = 123$ K, crystal size $0.25 \times 0.10 \times 0.05$ mm³, $R = 0.061$, $R_w = 0.085$, GOF = 0.861 with $I > 3.00\sigma(I)$. CCDC 257493 contains the supplementary crystallographic data for this paper. These data can be obtained free of charge from the Cambridge Crystallographic Data Centre via www.ccdc.cam.ac.uk/data_request/cif.
- [11] M. Suzuki, R. Taniguchi, A. Osuka, *Chem. Commun.* **2004**, 2682.
- [12] Crystal data for **11**: orthorhombic, space group $Pbcn$ (no. 60), $a = 22.78(2)$, $b = 21.31(1)$, $c = 20.26(1)$ Å, $V = 9837(11)$ Å³, $Z = 4$, $\rho_{\text{calcd}} = 1.547$ g cm⁻³, $T = 123$ K, crystal size $0.60 \times 0.20 \times 0.10$ mm³, $R = 0.069$, $R_w = 0.105$, GOF = 0.839 with $I > 3.00\sigma(I)$.
- CCDC 257494 contains the supplementary crystallographic data for this paper. These data can be obtained free of charge from The Cambridge Crystallographic Data Centre via www.ccdc.cam.ac.uk/data_request/cif.
- [13] J. Olmsted III, *J. Phys. Chem.* **1979**, *83*, 2581.
- [14] Z. Shen, H. Röhr, K. Rurack, H. Uno, M. Spieles, B. Schulz, G. Reck, N. Ono, *Chem. Eur. J.* **2004**, *10*, 4853.
- [15] R. Weissleder, *Nat. Biotechnol.* **2001**, *19*, 316; A. Becker, C. Hessenius, K. Kicha, B. Ebert, U. Sukowski, W. Semmler, B. Wiedenmann, C. Grötzinger, *Nat. Biotechnol.* **2001**, *19*, 327.
- [16] J. Fabian, H. Nakazumi, M. Matsuoka, *Chem. Rev.* **1992**, *92*, 1197.

Polyazide Chemistry: The First Binary Group 6 Azides, $\text{Mo}(\text{N}_3)_6$, $\text{W}(\text{N}_3)_6$, $[\text{Mo}(\text{N}_3)_7]^-$, and $[\text{W}(\text{N}_3)_7]^-$, and the $[\text{NW}(\text{N}_3)_4]^-$ and $[\text{NMo}(\text{N}_3)_4]^-$ Ions**

Ralf Haiges,* Jerry A. Boatz, Robert Bau, Stefan Schneider, Thorsten Schroer, Muhammed Yousufuddin, and Karl O. Christe*

Dedicated to Professor Kurt Dehnicke

Whereas numerous binary transition-metal azido complexes have been reported,^[1] no binary Group 6 azides are known. Only a limited number of partially azide-substituted molybdenum and tungsten compounds have been reported.^[2–30] Furthermore, no heptaazido compounds have been described.

Herein, we report the synthesis and characterization of the first binary Group 6 azides, $\text{Mo}(\text{N}_3)_6$, $\text{W}(\text{N}_3)_6$, $[\text{Mo}(\text{N}_3)_7]^-$, and $[\text{W}(\text{N}_3)_7]^-$. The last two ions represent the first examples of heptaazides. We also report the crystal structure of $\text{W}(\text{N}_3)_6$ and the controlled nitrogen loss from the heptaazido anions to

[*] Dr. R. Haiges, Prof. Dr. R. Bau, Dr. S. Schneider, Dr. T. Schroer, M. Yousufuddin, Prof. Dr. K. O. Christe
Loker Research Institute and Department of Chemistry
University of Southern California
Los Angeles, CA 90089-1661 (USA)
Fax: (+1) 213-740-6679
E-mail: haiges@usc.edu, kchriste@usc.edu

Dr. J. A. Boatz
Space and Missile Propulsion Division
Air Force Research Laboratory (AFRL/PRSP)
10 East Saturn Boulevard
Edwards Air Force Base, CA 93524 (USA)

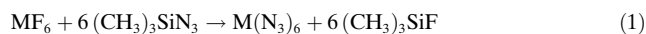
[**] This work was funded by the Air Force Office of Scientific Research and the National Science Foundation. We thank Prof. Dr. G. A. Olah and Dr. M. Berman, for their steady support, and Dr. R. Wagner for his help and stimulating discussions. Dedicated to Professor Kurt Dehnicke for his lifelong contributions to azide chemistry.



Supporting information for this article is available on the WWW under <http://www.angewandte.org> or from the author.

give nitrido-terazido anions. The $[\text{NMo}(\text{N}_3)_4]^-$ ion is already known but had been obtained by a different method.^[25]

The reactions of MoF_6 or WF_6 with excess $(\text{CH}_3)_3\text{SiN}_3$ in acetonitrile solution at -25 to -30°C result in complete fluoride–azide exchange and yield clear, dark-red solutions of $\text{Mo}(\text{N}_3)_6$ or $\text{W}(\text{N}_3)_6$, respectively [Eq. (1), ($\text{M} = \text{Mo}, \text{W}$)].



Removal of the volatile compounds $(\text{CH}_3\text{CN}, (\text{CH}_3)_3\text{SiF}$, and excess $(\text{CH}_3)_3\text{SiN}_3$) at -25°C results in the isolation of the neat hexaazides in quantitative yield.

As expected for covalently bonded, neutral, high-oxidation-state polyazides,^[31] $\text{Mo}(\text{N}_3)_6$ and $\text{W}(\text{N}_3)_6$ are extremely shock sensitive and can explode violently even at low-temperature, when either touched with a metal spatula or by rapid change in temperature, such as freezing with liquid nitrogen. $\text{W}(\text{N}_3)_6$ was isolated as a dark red solid, and ruby-red single crystals were obtained by recrystallization from its CH_3CN solution. Neat $\text{W}(\text{N}_3)_6$ must be handled with extreme care and at reduced temperature. Warming the compound to ambient temperature results in violent decomposition and can cause serious damage. For example, when a Teflon ampule, containing a small amount of single crystals, was allowed to warm to room temperature inside a stainless steel can, an explosion resulted which not only destroyed the ampule but also blew a hole of 5-cm diameter through the wall of the steel can. $\text{Mo}(\text{N}_3)_6$ was obtained as a dark red solid. It is even more sensitive than $\text{W}(\text{N}_3)_6$ and explodes violently upon the slightest provocation, such as a rapid change in the pressure of the inert gas in the vacuum line.

Tungsten hexaazide was characterized by its crystal structure^[32] and vibrational spectroscopy. It crystallizes in the trigonal space group $P\bar{3}$ and contains isolated $\text{W}(\text{N}_3)_6$ molecules (Figure 1), as shown by the closest $\text{W}\cdots\text{N}$ and $\text{N}\cdots\text{N}$ contacts between neighboring molecules of 4.02 \AA and

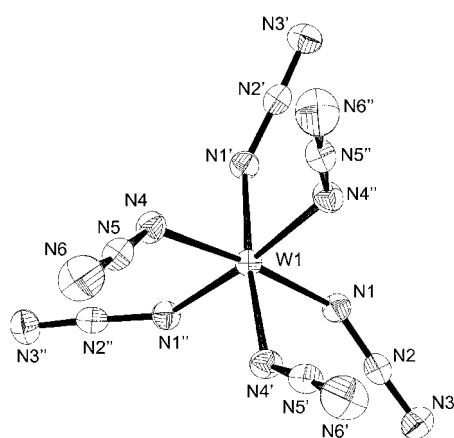


Figure 1. ORTEP diagram of $\text{W}(\text{N}_3)_6$. Thermal ellipsoids are set at 50% probability. The tungsten atom is situated on a crystallographic site of S_6 symmetry. Selected bond lengths [Å] and angles [°]: W1-N1 1.949 (2), W1-N4 2.006 (2), N1-N2 1.224 (2), N2-N3 1.123 (2), N4-N5 1.216 (2), N5-N6 1.129 (2); N1-N2-N3 176.7 (2), N4-N5-N6 176.7 (2), N1-W1-N1' 92.42 (6), N1-W1-N4 172.84 (5), N1-W1-N4' 94.68 (5), N1-W1-N4'' 86.38 (6), N4-W1-N4' 86.69 (6), W1-N1-N2 138.31 (11), W1-N4-N5 134.34 (12).

2.95 \AA , respectively. The structure of the $\text{W}(\text{N}_3)_6$ unit is only slightly distorted from perfect S_6 symmetry and closely resembles those of $[\text{As}(\text{N}_3)_6]^-$,^[33] $[\text{Sb}(\text{N}_3)_6]^-$,^[34] $[\text{Si}(\text{N}_3)_6]^{2-}$,^[35] $[\text{Ge}(\text{N}_3)_6]^{2-}$,^[36] and $[\text{Ti}(\text{N}_3)_6]^{2-}$,^[1a] but contrasts that of $[\text{Te}(\text{N}_3)_6]^{2-}$ ^[37] which possesses a sterically active free valence electron pair on its central atom. $\text{W}(\text{N}_3)_6$ consists of an asymmetric $\text{W}(\text{N}_3)_2$ unit with two azido groups covalently bonded in a bent fashion to the tungsten. The remaining four coordination positions at the metal center are occupied by four symmetry related azido groups (symmetry operations $-y+1, x-y+1, z$ and $-x+y, -x+1, z$). The observed W-N bonds of $1.949(2) \text{ \AA}$ and $2.006(2) \text{ \AA}$ are significantly longer than that of $1.85(2) \text{ \AA}$ found for $[\text{WF}_5\text{N}_3]$.^[13a]

The observed low-temperature Raman spectrum of $\text{W}(\text{N}_3)_6$ (Figure 2) was assigned (see Supporting Information) by

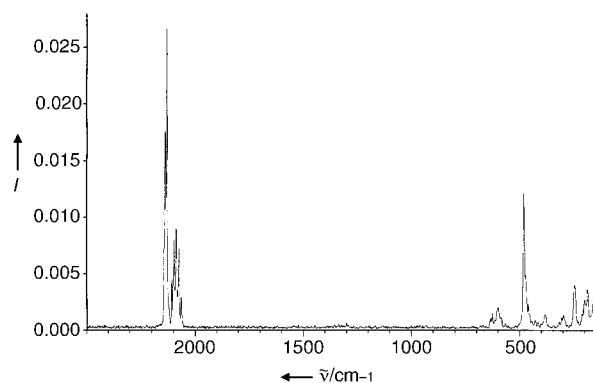


Figure 2. Low-temperature Raman spectrum of solid $\text{W}(\text{N}_3)_6$.

comparison with the spectra calculated at the MP2^[38] and B3LYP^[39] levels of theory using a SBKJ+(d) basis set.^[40] Although the calculated frequencies and intensities vary somewhat with the method used, their overall agreement with the experiment is very satisfactory. The internal modes of the azido ligands are separated into groups of six, owing to in-phase (one mode) and out-of-phase (five modes) coupling, with the in-phase mode resulting in the highest polarizability change and Raman intensity. For example, the antisymmetric N_3 stretching modes exhibit two very intense bands at 2139 and 2130 cm^{-1} , which represent the in-phase coupled mode, split by either Fermi resonance or site symmetry effects, and a cluster of five less intense bands between 2107 and 2064 cm^{-1} which represents the five out-of-phase coupled modes. The $\{\text{WN}_6\}$ skeleton is approximately octahedral with the deviations from right angles being 7° or less. Therefore, the skeletal vibrations can be derived from O_h symmetry, allowing for a splitting into the degenerate components (two for the E modes and three for the F modes). It should be noted that there is no clear preference for using either the MP2 or the B3LYP set for fitting the entire spectrum. There is considerable variation in the relative intensities and sequences of the modes within a given group, and both sets should be used for a comparison with the observed spectrum.

Because of its extreme sensitivity, the identity of molybdenum hexaazide could only be established by its low-temperature Raman spectrum in CH_3CN solution (Figure 3 and Supporting Information). The agreement between

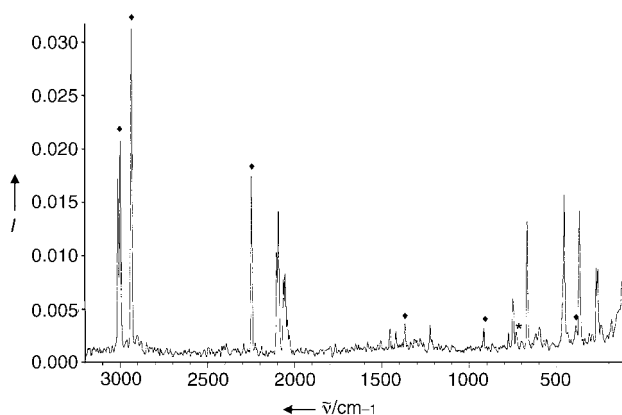
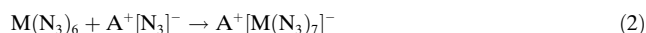


Figure 3. Low-temperature Raman spectrum of $\text{Mo}(\text{N}_3)_6$ dissolved in CH_3CN . The band marked by an asterisk (*) is due to the Teflon-FEP sample tube. Bands marked by ◆ are from CH_3CN .

observed and calculated spectra is again satisfactory. All attempts failed to obtain single crystals of diffraction quality. Additional proof for the presence of $\text{Mo}(\text{N}_3)_6$ was obtained by its conversion into $[\text{Mo}(\text{N}_3)_7]^-$ and the known^[25] $[\text{NMo}(\text{N}_3)_4]^-$ ion.

The reactions of $\text{M}(\text{N}_3)_6$ ($\text{M} = \text{Mo}$ or W) with ionic azides, such as $[\text{NMe}_4]^+[\text{N}_3]^-$ or $[\text{PPh}_4]^+[\text{N}_3]^-$, produce the corresponding $[\text{M}(\text{N}_3)_7]^-$ salts [Eq. (2), ($\text{A} = \text{PPh}_4$, NMe_4)].



Salts of both heptaazido anions were isolated at low temperature as extremely shock-sensitive red solids that explode violently when warmed towards room temperature. Not surprisingly, they are less stable and more difficult to handle than hexaazido salts, thus preventing us from obtaining their crystal structures. These salts were characterized by low-temperature Raman spectroscopy and represent the first known examples of covalent heptaazides. The spectra of $[\text{PPh}_4][\text{Mo}(\text{N}_3)_7]$ and $[\text{PPh}_4][\text{W}(\text{N}_3)_7]$ are shown in Figure 4 and 5, respectively (the observed and calculated frequencies and intensities are listed in the Supporting Information). Three different ligand arrangements are possible for hepta-coordinated transition-metal complexes which differ only little in energy.^[41] They are derived from a pentagonal bipyramid (1/5/1 arrangement), a monocapped trigonal prism (1/4/2 arrangement), and a monocapped octahedron (1/3/3 arrangement). Therefore, we have explored the possibility of these three arrangements for $[\text{W}(\text{N}_3)_7]^-$ at the B3LYP(3)/SBKJ+(d) level of theory. Two stable minimum energy structures, a 1/5/1 and a 1/4/2 structure (Figure 6 and Supporting Information), were located, the 1/5/1 structure being favored by 3.3 kcal mol⁻¹. When monocapped octahedral structures were used as starting points, the calculations always converged to the pentagonal bipyramidal structure. This result was somewhat unexpected because $[\text{WF}_7]^-$ and $[\text{MoF}_7]^-$ exhibit monocapped octahedral structures in their cesium salts.^[41h] In view of the small energy difference, the similarity of their calculated vibrational spectra, and the sensitivity of the calculated spectra to the level of theory used (Supporting Information), it was not possible to distinguish

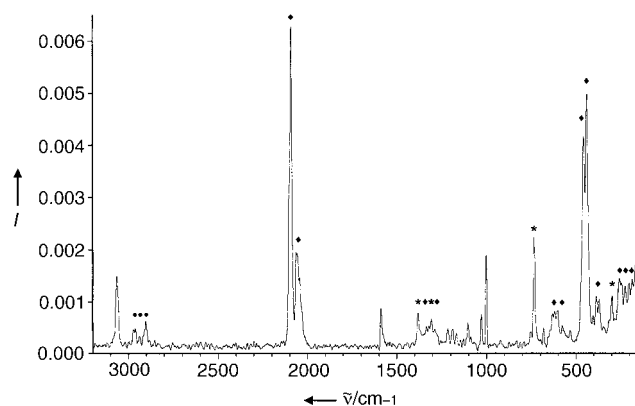


Figure 4. Low-temperature Raman spectrum of $[\text{PPh}_4][\text{Mo}(\text{N}_3)_7]$. The bands marked by an asterisk (*) are due to the Teflon-FEP sample tube. Bands marked by ◆ are from the $[\text{Mo}(\text{N}_3)_7]^-$ ion. The three bands marked by ● arise from excess Me_3SiN_3 .

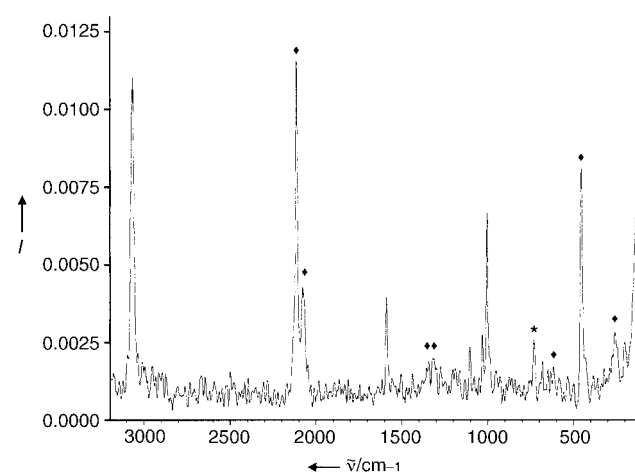


Figure 5. Low-temperature Raman spectrum of $[\text{PPh}_4][\text{W}(\text{N}_3)_7]$. The band marked by an asterisk (*) is due to the Teflon-FEP sample tube. Bands marked by ◆ are from the $[\text{W}(\text{N}_3)_7]^-$ ion.

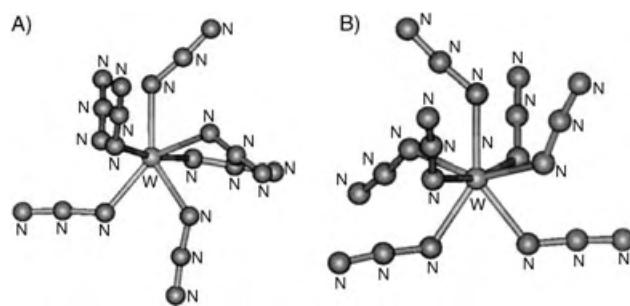
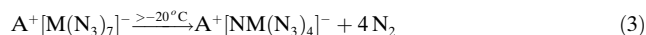


Figure 6. B3LYP/SBKJ+(d) optimized geometries of $[\text{W}(\text{N}_3)_7]^-$. A) Pentagonal bipyramid (1/5/1), B) monocapped trigonal prism (1/4/2).

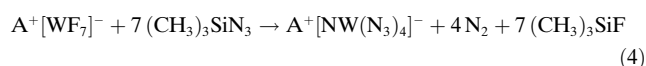
between the 1/5/1 and 1/4/2 structures based on the observed Raman spectra. Additional evidence for the formation of heptaazido anions is derived from the observed frequencies. Compared to the neutral hexaazides, the addition of a negatively charged $[\text{N}_3]^-$ ion increases the ionicity of the metal-azide bonds and the ionic character of the azide ligands.

This effect should cause decreases in the antisymmetric N_3 ligand and $\{MN_6\}$ skeletal stretching frequencies and increases in the symmetric N_3 ligand frequencies, and is clearly observed in our spectra.

Solutions of either heptaazido anion in SO_2 or CH_3CN decompose on warming to room temperature with nitrogen evolution and formation of the tetraazido nitrido molybdate(vi)^[25] and tetraazido nitrido tungstate(vi) anion, respectively [Eq. (3) ($M = Mo, W$)].



The $[NW(N_3)_4]^-$ salts can also be prepared in a single step from the corresponding $[WF_7]^-$ salt and $(CH_3)_3SiN_3$ in CH_3CN solution [Eq. (4) ($A = PPh_4, NMe_4$)].



The identity of $[NW(N_3)_4]^-$ and $[NMo(N_3)_4]^-$ was established by vibrational spectroscopy and for $[PPh_4][NMo(N_3)_4]$ also by its crystal structure (see Supporting Information).^[42] The structure of the $[NMo(N_3)_4]^-$ ion and its vibrational spectra were in excellent agreement with those reported by Dehnicke and co-workers for $[AsPh_4]^+[NMo(N_3)_4]^-$, which was prepared from the $[NMoCl_4]^-$ salt and AgN_3 in a CH_2Cl_2 suspension,^[25] and, therefore require no further discussion. The observed Raman spectrum of $[NMe_4][NW(N_3)_4]$ is shown in Figure 7. The observed frequencies and assignments, based on the calculated spectra, are listed for both tetraazido nitrido anions in the Experimental Section.

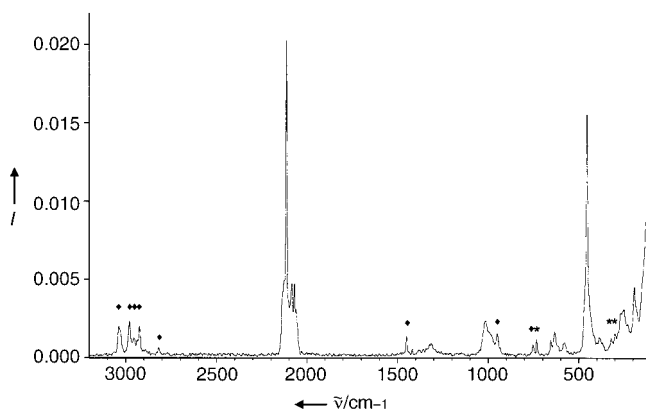


Figure 7. Low-temperature Raman spectrum of $[NMe_4][NW(N_3)_4]$. The bands marked by an asterisk (*) are due to the Teflon-FEP sample tube. Bands marked by ♦ are from the $[NMe_4]^+$ ion.

Experimental Section

Caution! Covalent azides are potentially hazardous and can decompose explosively under various conditions! The polyazides of this work are extremely shock-sensitive and can explode violently upon the slightest provocation. They should be handled only on a scale of less than 1 mmol and can cause, even on a 1-mmol scale, significant damage. During the handling of $W(N_3)_6$ and $Mo(N_3)_6$, rapid changes in temperature or pressure can result in violent explosions. The use of appropriate safety precautions (safety shields, face shields, leather gloves, protective clothing, such as heavy leather welding suits and ear

plugs) is mandatory.^[1a] Ignoring safety precautions can lead to serious injuries!

Materials and Apparatus: All reactions were carried out in Teflon-FEP ampules (FEP = perfluoro ethylene propylene polymer) that were closed by stainless steel valves. Volatile materials were handled in a Pyrex glass or stainless steel/Teflon-FEP vacuum line.^[43] All reaction vessels and the stainless steel/Teflon-FEP vacuum line were passivated with ClF_3 prior to use. Nonvolatile materials were handled in the dry argon atmosphere of a glove box.

Raman spectra were recorded in the range 4000–80 cm^{-1} on a Bruker Equinox 55 FT-RA spectrophotometer using a Nd-YAG laser at 1064 nm with power levels less (!) than 50 mW. Teflon-FEP tubes with stainless steel valves that were passivated with ClF_3 were used as sample containers.

The starting materials WF_6 , MoF_6 (both Ozark Mahoning) and $[PPh_4]I$ (Aldrich) were used without further purification. $(CH_3)_3SiN_3$ (Aldrich) was purified by fractional condensation prior to use. Solvents were dried by standard methods and freshly distilled prior to use. $[PPh_4]F$ and $[PPh_4]N_3$ were prepared from $[PPh_4]I$ and AgF and AgN_3 , respectively. $[NMe_4][WF_7]$ and $[PPh_4][WF_7]$ were obtained from WF_6 with $[NMe_4]F$ and $[PPh_4]F$, respectively.^[44] $[NMe_4]F$ ^[45] and $[NMe_4]N_3$ ^[46] were prepared by literature methods.

Preparation of $W(N_3)_6$: On the stainless steel vacuum line, WF_6 (0.463 mmol) was condensed at $-196^\circ C$ into a Teflon-FEP ampule. The ampule was then attached to a glass vacuum line and after evacuation, CH_3CN (50 mmol) was condensed in at $-196^\circ C$. The mixture was allowed to warm to ambient temperature forming a colorless solution. After re-cooling to $-196^\circ C$, $(CH_3)_3SiN_3$ (4.43 mmol) was condensed onto the frozen solution, and the mixture was warmed to $-25^\circ C$. Within minutes, the mixture turned orange-red and the color intensified while the reaction proceeded. After 1 h, the reaction mixture was dark red. All volatile material was pumped off at $-25^\circ C$, leaving behind a dark red solid (yield: 0.215 g, expected for 0.463 mmol of $W(N_3)_6$, 0.202 g). Ruby-red single crystals were grown from a solution in CH_3CN by slow evaporation of the solvent in vacuo.

Preparation of $Mo(N_3)_6$: The reaction was carried out as described above for $W(N_3)_6$ using MoF_6 (0.133 mmol), CH_3CN (30 mmol), and $(CH_3)_3SiN_3$ (1.07 mmol). After keeping the mixture for 1 h at $-30^\circ C$, a Raman spectrum of the reaction mixture was recorded. The removal of all material volatile at $-30^\circ C$ resulted in the formation of a dark red, extremely explosive solid.

Preparation of $[M(N_3)_7]^-$ salts ($M = Mo, W$): Cold solutions of $M(N_3)_6$ (0.20 mmol) in SO_2 (60 mmol) were added to mixtures of PPh_4N_3 (0.20 mmol) and SO_2 (25 mmol) at $-64^\circ C$. The mixtures were kept at this temperature for 30 min and occasionally agitated. All volatiles were removed at $-64^\circ C$ in a dynamic vacuum, leaving behind dark red solids; weight expected for 0.20 mmol of $[PPh_4][Mo(N_3)_7]$: 0.146 g; found 0.158 g; weight expected for 0.20 mmol of $[PPh_4][W(N_3)_7]$: 0.163 g; found: 0.171 g.

Preparation of $[NM(N_3)_4]^-$ salts ($M = Mo, W$): Cold solutions of the $[M(N_3)_7]^-$ salts (0.25 mmol) in SO_2 (100 mmol) were warmed from $-64^\circ C$ to $-25^\circ C$. After about 30 min at $-25^\circ C$, the temperature was raised over a period of 2 h to $25^\circ C$. All volatiles were slowly removed in a dynamic vacuum, leaving behind dark red solids.

$[P(C_6H_5)_4][NMo(N_3)_4]$: weight found: 0.145 g; weight expected for 0.25 mmol: 0.154 g; Raman of the $[NMo(N_3)_4]^-$ ion (50 mW, $-80^\circ C$): $\tilde{\nu} = 2109(10.0)$, $2098(2.2)$, $2070(1.5)$, $2064(1.9)$, $2055(1.8)$, $2047(1.1)$, $2040(1.1)$, $2025(0.5)$ ($\nu_{as}N_3$); $1331(0.7)$, $1319(0.7)$, $1285(0.5)$, $1259(0.3)$ (ν_sN_3); $1034(2.2)$ ($\nu_{Mo\equiv N}$); $657(0.6)$, $639(0.6)$, $626(0.5)$, $596(0.4)$, $589(0.4)$, $568(0.3)$ (δN_3); $443(4.1)$, $429(4.1)$, $405(0.8)$, $384(0.9)$, $357(1.1)$ ($\nu_{MoN_{azide}}$); $292(1.2)$, $273(1.1)$, $258(1.5)$ (δMoN_{azide}); $216(1.2)$, $183(2.7)$, $161(1.7)$ cm^{-1} .

$[N(CH_3)_4][NW(N_3)_4]$: weight found: 0.117 g, weight expected for 0.25 mmol: 0.110 g; Raman of the $[NW(N_3)_4]^-$ ion (50 mW, $-80^\circ C$): $\tilde{\nu} = 2114(10.0)$, $2083(2.2)$, $2069(2.2)$, $2060(1.4)$, ($\nu_{as}N_3$); $1324(0.4)$, $1315(0.4)$, $1259(0.2)$ (ν_sN_3); $1010(1.0)$, ($\nu_{W\equiv N}$); $655(0.6)$, $632(0.7)$,

611(0.3), 579(0.5) (δN_3); 452(7.1), 416(0.7), 321(0.6) (νWN_{azide}); 266(1.3), 262(1.3), 253(1.4), 247(1.4), 226(1.0) (δWN_{azide}); 189(2.0), 118(4.0), 110(4.0), 100(4.1) cm^{-1} .

Theoretical Methods: The molecular structures and harmonic vibrational frequencies were calculated using second-order many-body perturbation theory^[38] (denoted as MP2, but also known as MBPT(2)) and also density functional theory (DFT) level using the B3LYP hybrid functional,^[39a-c] which included the VWN5 correlation functional.^[39d] The Stevens, Basch, Krauss, and Jaisan effective core potentials and the corresponding valence-only basis sets were used.^[40a-b] The basis set for nitrogen was augmented with a d polarization function (exponent of 0.8^[40c]) and a diffuse s + p shell (exponent of 0.0639^[40d]), denoted as SBKJ + (d). Hessians (energy second derivatives) were calculated for the final equilibrium structures to determine if they are minima (positive definite hessian) or *n*th-order transition states ("*n*" negative eigenvalues). All calculations were performed using the electronic structure code GAMESS.^[47]

Received: November 27, 2004

Published online: February 21, 2005

Keywords: azides · molybdenum · nitrides · structure elucidation · tungsten

- [1] a) R. Haiges, J. A. Boatz, S. Schneider, T. Schroer, K. O. Christe, *Angew. Chem.* **2004**, *116*, 3210; *Angew. Chem. Int. Ed. Angew. Chem. Int. Ed. Engl.* **2004**, *43*, 3148; b) B. Busch, E. Hellner, K. Dehnicke, *Naturwissenschaften* **1976**, *63*, 531; c) H. Willner, K. Höslér, K. Dehnicke, *Z. Anorg. Allg. Chem.* **1989**, *574*, 7; d) W. Beck, T. M. Klapötke, J. Knizek, H. Nöth, T. Schütt, *Eur. J. Inorg. Chem.* **1999**, 523; e) K. Steiner, W. Willing, U. Müller, K. Dehnicke, *Z. Anorg. Allg. Chem.* **1987**, *555*, 7; f) W. Beck, H. Nöth, *Chem. Ber.* **1984**, *117*, 419; g) G. F. Platzler, H. Krischner, *Z. Kristallogr.* **1975**, *141*, 363; h) A. C. Brunner, H. Krischner, *Z. Kristallogr.* **1975**, *142*, 24; i) H. Krischner, O. Baumgartner, H. E. Maier, A. I. Saracoglu, *Z. Kristallogr.* **1983**, *164*, 89; j) F. A. Mautner, H. Krischner, *Monatsh. Chem.* **1990**, *121*, 91; k) W. P. Fehlhammer, L. F. Dahl, *J. Am. Chem. Soc.* **1972**, *94*, 3377; l) G. De Munno, T. Poerio, G. Viau, M. Julve, F. Lloret, *Angew. Chem.* **1997**, *109*, 1531; *Angew. Chem. Int. Ed. Engl.* **1997**, *36*, 1459; m) M. A. S. Goher, N. A. Al-Salem, F. A. Mautner, K. O. Klepp, *Polyhedron* **1997**, *16*, 825; n) D. Fenske, K. Steiner, K. Dehnicke, *Z. Anorg. Allg. Chem.* **1987**, *553*, 57; o) F. A. Mautner, H. Krischner, C. Kratky, *Monatsh. Chem.* **1988**, *119*, 509; p) F. A. Mautner, S. Hanna, R. Cortes, L. Lezama, M. G. Barandika, T. Rojo, *Inorg. Chem.* **1999**, *38*, 4647; q) W. Clegg, H. Krischner, A. I. Saracoglu, G. M. Sheldrick, *Z. Kristallogr.* **1982**, *161*, 307; r) H. Krischner, C. Kratky, H. E. Maier, *Z. Kristallogr.* **1982**, *161*, 225; s) F. A. Mautner, R. Cortes, L. Lezama, T. Rojo, *Angew. Chem.* **1996**, *108*, 96; *Angew. Chem. Int. Ed. Engl.* **1996**, *35*, 78; t) J. Drummond, J. S. Wood, *Chem. Commun.* **1969**, 1373.
- [2] K. Wieghardt, G. Backes-Dahmann, W. Swiridoff, J. Weiss, *Inorg. Chem.* **1983**, *22*, 1221 ([Mo(NO)(H₂NO)(N₃)₄]²⁻).
- [3] K. Dehnicke, R. Dübgen, *Z. Anorg. Allg. Chem.* **1978**, *444*, 61 ([M(CO)₂(N₃)₂] (M = Mo, W)).
- [4] a) S. P. Anand, *J. Inorg. Nucl. Chem.* **1974**, *36*, 925; b) M. K. Rastogi, R. K. Multani, *J. Inorg. Nucl. Chem.* **1975**, *37*, 1995 ([$(\pi-C_5H_5)_2Mo(N_3)_2$] (M = Mo, W)).
- [5] a) J. Chatt, J. R. Dilworth, *J. Indian Chem. Soc.* **1977**, *54*, 13; b) J. Chatt, J. R. Dilworth, *J. Chem. Soc. Chem. Commun.* **1975**, 983; c) P. C. Bevan, J. Chatt, J. R. Dilworth, R. A. Henderson, G. J. Leigh, *J. Chem. Soc. Dalton Trans.* **1982**, 821 (*trans*-[MN(N₃)L₂], [W(NEt)(N₃)L₂]⁺ (M = Mo, W; L = 1,2-ethanedithiolbis-(diphenyl)phosphine) (dppe)).
- [6] D. L. Hughes, M. Y. Mohammed, C. J. Pickett, *J. Chem. Soc. Dalton Trans.* **1990**, 2013 (*trans*-[MoN(N₃)L₂], [[μ -MoN(N₃)₂]₂][NMo(N₃)L₂]₂ (L = dppe)).
- [7] S. J. N. Burgmayer, J. L. Templeton, *Inorg. Chem.* **1985**, *24*, 2224 ([M(CO)₂(S₂CNEt₂)₂N₃]⁻ (M = Mo, W)).
- [8] D. Sellmann, W. Weber, G. Liehr, H. P. Beck, *J. Organomet. Chem.* **1984**, *269*, 155 ([$\{(\mu-N_3)_3[M(CO)_3]_2\}_3$] (M = Mo, W), [W(CO)₅N₃]⁻).
- [9] C. T. Kan, P. B. Hitchcock, R. L. Richards, *J. Chem. Soc. Dalton Trans.* **1982**, 79 (*trans*-[M(N₃)(NO)(dppe)₂] (M = Mo, W)).
- [10] J. A. Broomhead, J. R. Budge, *Aust. J. Chem.* **1979**, *32*, 1187 ([Mo(NCO)(N₃)(NO)L₂]⁻, [W(N₃)₂(NO)L₂]⁻, [W(N₃)(NO)-(Me₂SO)L₂] (L = S₂CNEt₂)).
- [11] H. Behrens, E. Lindner, G. Lehnert, *J. Organomet. Chem.* **1970**, *22*, 665 ([M(CO)₃(N₃)L]⁻ (M = Mo, W; L = 2,2'-bipyridine (bipy), ethylenediamine)).
- [12] G. Hoch, R. Panter, M. L. Ziegler, *Z. Naturforsch. B* **1976**, *31*, 294 ([$(\pi-C_7H_7)M(CO)_2(N_3)$] M = Mo, W)).
- [13] a) J. Fawcett, R. D. Peacock, D. R. Russell, *J. Chem. Soc. Dalton Trans.* **1980**, 2294; b) B. Glavincevski, S. Brownstein, *Inorg. Chem.* **1981**, *20*, 3580 ([WF₅N₃]).
- [14] B. Glavincevski, S. Brownstein, *J. Inorg. Nucl. Chem.* **1981**, *43*, 1827 ([WF₅N₃], [WF₆N₃]⁻).
- [15] R. G. W. Gingerich, R. J. Angelici, *J. Organomet. Chem.* **1977**, *132*, 377 ([W(CO)₅N₃]).
- [16] a) W. Palitzsch, C. Beyer, U. Böhme, B. Rittmeister, G. Roewer, *Eur. J. Inorg. Chem.* **1999**, 1813; b) R. M. Dahlgren, J. I. Zink, *J. Chem. Soc. Chem. Commun.* **1978**, 20, 863; c) H. Werner, W. Beck, H. Engelmann, *Inorg. Chim. Acta* **1969**, *3*, 331 ([W(CO)₅N₃]⁻).
- [17] P. Dabas, R. Saxena, M. K. Rastogi, *Asian J. Chem.* **1997**, *9*, 453 ([W(N₃)₃(OR)₂] (R = Alkyl)).
- [18] S. M. Musleh, P. Dabas, R. K. Multani, M. Katyal, *Curr. Sci.* **1985**, *54*, 138 ([WO(N₃)₂(OR)₂] (R = Alkyl)).
- [19] S. M. Musleh, M. K. Rastogi, R. K. Multani, *Orient. J. Chem.* **1986**, *2*, 11 ([WS₂(N₃)₂]).
- [20] D. Fenske, A. Frankenau, K. Dehnicke, *Z. Anorg. Allg. Chem.* **1989**, *579*, 27 ([WCl₃(NCl)(CH₃CN)(N₃)], [WCl₄(NCl)(N₃)⁻]).
- [21] I. Walker, J. Strähle, P. Ruschke, K. Dehnicke, *Z. Anorg. Allg. Chem.* **1982**, *487*, 26 ([WCl₃HN₃]₄]).
- [22] H.-w. Lam, G. Wilkinson, B. Hussain-Bates, M. B. Hursthouse, *J. Chem. Soc. Dalton Trans.* **1993**, 781 ([{W(NrBu)₂(N₃)-(NH₂BU)₂}(μ -N₃)₂]).
- [23] E. O. Fischer, D. Wittmann, D. Himmelreich, R. Cai, K. Ackermann, D. Neugebauer, *Chem. Ber.* **1982**, *115*, 3152 ([$(\mu-N_3)_2(CO)_3WCNEt_2$]).
- [24] T.-Y. Cheng, M. R. Smith, III, J. M. Dysard, J. Y. Ali, G. L. Hillhouse, *Polyhedron* **1996**, *15*, 2551 (*trans*, *trans*-[W-(NHNHPh)(N₃)₂(NO)(PPh₃)₂]).
- [25] K. Dehnicke, J. Schmitte, D. Fenske, *Z. Naturforsch. B* **1980**, *35*, 1070; [AsPh₄][MoN(N₃)₄].
- [26] J. Beck, E. Schweda, J. Strähle, *Z. Naturforsch.* **1985**, *40b*, 1073; [MoN(N₃)₂Cl(terpy)] (terpy = 2,2':6',2''-terpyridine).
- [27] E. Schweda, J. Strähle, *Z. Naturforsch. B* **1980**, *35*, 1146; [MoN(N₃)₃(bipy)].
- [28] E. Schweda, J. Strähle, *Z. Naturforsch. B* **1981**, *36*, 662; [MoN(N₃)₃(NC₃H₅)].
- [29] K. Jansen, J. Schmitte, K. Dehnicke, *Z. Anorg. Allg. Chem.* **1987**, *552*, 201; ([PPh₄]₂[MoN(N₃)₂]).
- [30] C. G. Young, J. Fotini, M. A. Bruck, P. A. Wexler, J. H. Enemark, *Aust. J. Chem.* **1990**, *43*, 1347; ([{HB(3,5-Me₂C₃H₂H)₃}[MoN(N₃)Cl]₂]).
- [31] A. M. Golub, H. Köhler, V. V. Stopenko, *Chemistry of Pseudo-halides*, Elsevier, Amsterdam, **1986**.
- [32] Further details on the crystal structure investigations may be obtained from the Fachinformationszentrum Karlsruhe, 76344 Eggenstein-Leopoldshafen, Germany (fax: (+49) 7247-808-666;

- e-mail: crysdata@fiz-karlsruhe.de), on quoting the depository number CSD-413860.
- [33] a) K. Karaghiosoff, T. M. Klapötke, B. Krumm, H. Nöth, T. Schütt, M. Suter, *Inorg. Chem.* **2002**, *41*, 170; b) T. M. Klapötke, H. Nöth, T. Schütt, M. Warchhold, *Angew. Chem.* **2000**, *112*, 2197; *Angew. Chem. Int. Ed.* **2000**, *39*, 2108.
 - [34] R. Haiges, A. Vij, V. Vij, J. A. Boatz, M. Gerken, S. Schneider, T. Schroer, M. Yousufuddin, K. O. Christe, *Angew. Chem.* **2004**, *116*, 6844; *Angew. Chem. Int. Ed.* **2004**, *43*, 6676.
 - [35] A. C. Filippou, P. Portius, G. Schnakenburg, *J. Am. Chem. Soc.* **2002**, *124*, 12396.
 - [36] A. C. Filippou, P. Portius, D. U. Neumann, K.-D. Wehrstedt, *Angew. Chem.* **2000**, *112*, 4524; *Angew. Chem. Int. Ed.* **2000**, *39*, 4333.
 - [37] R. Haiges, J. A. Boatz, A. Vij, M. Gerken, S. Schneider, T. Schroer, K. O. Christe, *Angew. Chem.* **2003**, *115*, 6027; *Angew. Chem. Int. Ed.* **2003**, *42*, 5847.
 - [38] a) C. Moller, M. S. Plesset, *Phys. Rev.* **1934**, *46*, 618; b) J. A. Pople, J. S. Binkley, R. Seeger, *Int. J. Quantum Chem. S10* **1976**, 1; c) M. J. Frisch, M. Head-Gordon, J. A. Pople, *Chem. Phys. Lett.* **1990**, *166*, 275; d) R. J. Bartlett, D. M. Silver, *Int. J. Quantum Chem. Symp.* **1975**, *9*, 1927.
 - [39] a) A. D. Becke, *J. Chem. Phys.* **1993**, *98*, 5648; b) P. J. Stephens, F. J. Devlin, C. F. Chablowski, M. J. Frisch, *J. Phys. Chem.* **1994**, *98*, 11 623; c) R. H. Hertwig, W. Koch, *Chem. Phys. Lett.* **1997**, *268*, 345; d) S. H. Vosko, L. Wilk, M. Nusair, *Can. J. Phys.* **1980**, *58*, 1200.
 - [40] a) W. J. Stevens, H. Basch, M. Krauss, *J. Chem. Phys.* **1984**, *81*, 1626; b) W. J. Stevens, M. Krauss, H. Basch, P. G. Jansen, *Can. J. Chem.* **1992**, *70*, 612; c) P. C. Hariharan, J. A. Pople, *Theor. Chim. Acta* **1973**, *28*, 213; d) T. Clark, J. Chandrasekhar, G. W. Spitznagel, P. v. R. Schleyer, *J. Comput. Chem.* **1983**, *4*, 294.
 - [41] a) R. J. Gillespie, I. Hargittai, *The VSEPR Model of Molecular Geometry*, Allyn and Bacon, Needham Heights, MA, **1991**; b) R. Hoffmann, B. F. Beier, E. L. Muetterties, A. R. Rossi, *Inorg. Chem.* **1977**, *16*, 511; c) D. Kepert, *Inorganic Stereochemistry*, Springer, Berlin, **1982**; d) T. A. Claxton, G. C. Benson, *Can. J. Chem.* **1966**, *44*, 157; e) H. Bradford Thompson, L. S. Bartell, *Inorg. Chem.* **1968**, *7*, 488; f) H. K. McDowell, H.-L. Chiu, J. F. Geldard, *Inorg. Chem.* **1988**, *27*, 1674; g) G. W. Drake, D. A. Dixon, J. A. Sheehy, J. A. Boatz, K. O. Christe, *J. Am. Chem. Soc.* **1998**, *120*, 8392, and references therein; h) S. Giese, K. Seppelt, *Angew. Chem.* **1994**, *106*, 473; *Angew. Chem. Int. Ed. Engl.* **1994**, *33*, 461.
 - [42] [PPh₄][NM_o(N₃)₄]: CCDC 249712 contains the supplementary crystallographic data for this paper. These data can be obtained free of charge from the Cambridge Crystallographic Data Centre via www.ccdc.cam.ac.uk/data_request/cif.
 - [43] K. O. Christe, W. W. Wilson, C. J. Schack, R. D. Wilson, *Inorg. Synth.* **1986**, *24*, 39.
 - [44] K. O. Christe, J. C. P. Sanders, G. J. Schrobilgen, W. W. Wilson, *J. Chem. Soc. Chem. Commun.* **1991**, 837.
 - [45] K. O. Christe, W. W. Wilson, R. D. Wilson, R. Bau, J. Feng, *J. Am. Chem. Soc.* **1990**, *112*, 7619.
 - [46] K. O. Christe, W. W. Wilson, R. Bau, S. W. Bunte, *J. Am. Chem. Soc.* **1992**, *114*, 3411.
 - [47] M. W. Schmidt, K. K. Baldrige, J. A. Boatz, S. T. Elbert, M. S. Gordon, J. H. Jensen, S. Koseki, N. Matsunaga, K. A. Nguyen, S. J. Su, T. L. Windus, M. Dupuis, J. A. Montgomery, *J. Comput. Chem.* **1993**, *14*, 1347.

Oxazoline-Mediated Interannular Cyclopalladation of Ferrocene: Chiral Palladium(II) Catalysts for the Enantioselective Aza-Claisen Rearrangement**

Albert Moyano,* Malgorzata Rosol, Rosa M. Moreno,
Concepción López, and Miguel A. Maestro

Cyclopalladated complexes derived from organic molecules bearing N-donor groups were first described by Cope et al. almost forty years ago.^[1] Since then, the study of these complexes has become a fundamental area of research in organometallic chemistry.^[2] Cyclopalladated ferrocene derivatives are particularly interesting,^[3] as they are planar chiral compounds with increasing applications in materials chemistry, asymmetric synthesis, and catalysis.^[4–6] Up until now, the cyclopalladation of ferrocene compounds with nitrogen-containing substituents, such as amines, imines, and oximes, has invariably led to the formation of *ortho*-palladated derivatives,^[7] although very few of these chiral complexes have been obtained in the optically active form.^[8] On the other hand, the direct cyclopalladation of 2-ferrocenyl-1,3-oxazolines, which are compounds of special relevance in asymmetric synthesis,^[3,9,10] is not successful because of concurrent oxidation of the ferrocene ligand by Pd^{II} salts, and for this reason the corresponding *ortho*-palladated derivatives either have been obtained by indirect methods or have been replaced in some applications by cobaltocene complexes.^[11] 4-Ferrocenyl-1,3-oxazoline derivatives form a new class of chiral ferrocene compounds that are easily available in both enantiomeric forms and with excellent optical purities. We report herein the cyclopalladation of several 4-ferrocenyl-1,3-oxazoline derivatives that takes place in good yield to furnish a hitherto unknown type of metalated ferrocenes in which the carbon–palladium bond is formed by using a carbon atom in the unsubstituted cyclopentadiene ring (we have coined the term “interannular cyclometalation” for this reaction).^[12]

[*] Prof. A. Moyano, M. Rosol, R. M. Moreno
Departament de Química Orgànica
Universitat de Barcelona, Facultat de Química
C. Martí i Franquès, 1–11, 08028-Barcelona (Spain)
Fax: (+34) 93-339-78-78
E-mail: amoyano@ub.edu

Prof. C. López
Departament de Química Inorgànica
Universitat de Barcelona, Facultat de Química
C. Martí i Franquès, 1–11, 08028-Barcelona (Spain)

Prof. M. A. Maestro
Àrea de Química Orgànica
Departamento de Química Fundamental, Facultade de Ciencias
Universidade da Coruña, 15071 A Coruña (Spain)

[**] The authors thank the DGI (grant BQU2003-03426) and the Generalitat de Catalunya (DURSI) (grant 2001SGR50) for financial support. M.R. and R.M.M. are grateful to the DURSI for predoctoral fellowships.

The initial impetus for this research came from the reasoning that in 4-ferrocenyl-1,3-oxazoline compounds, in contrast to what happens in the regioisomeric 2-ferrocenyl-1,3-oxazolines, the conformation in which the carbon–nitrogen heterocyclic bond would be coplanar with the cyclopentadiene ring is strongly destabilized by steric hindrance between the C5 oxazoline carbon atom and the ferrocenyl moiety. Therefore, the most stable conformer would be that in which the C4–H bond is coplanar with the upper cyclopentadiene ring, thus directing the nitrogen atom towards the lower one. Simple quantum-mechanical calculations^[13] support this hypothesis by showing that 2-(*tert*-butyl)-4-ferrocenyl-1,3-oxazoline had only one stable conformer (Figure 1).

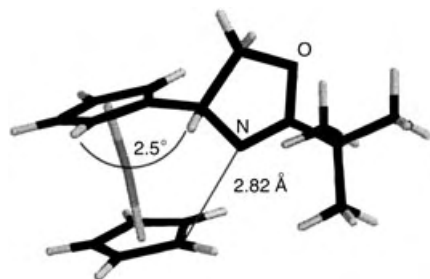
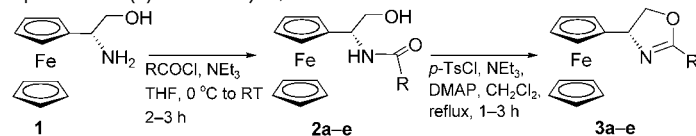


Figure 1. Energy-minimized geometry of (*R*)-2-(*tert*-butyl)-4-ferrocenyl-1,3-oxazoline, as determined by PM3 calculations.

This observation prompted us to synthesize a series of 4-ferrocenyl-1,3-oxazolines with different C2 substituents and study their cyclopalladation. Highly enantiopure (98% *ee*) (*S*)-2-amino-2-ferrocenylethanol (**1**)^[14] was readily converted into the target oxazolines **3a–e** by standard procedures (Table 1).

Table 1: Preparation of (*S*)-4-ferrocenyl-1,3-oxazolines.^[a]



Entry	R	Yield of 2 [%] ^[b]	Yield of 3 [%] ^[b]
1	<i>tert</i> -butyl	71 (2a)	77 (3a)
2	1-adamantyl	77 (2b)	68 (3b)
3	phenyl	78 (2c)	80 (3c)
4	isopropyl	78 (2d)	60 (3d)
5	ethyl	81 (2e)	64 (3e)

[a] Ts = *para*-toluenesulfonyl, DMAP = 4-dimethylaminopyridine. [b] Yield of product isolated after purification by chromatography.

We were pleased to find that after the oxazoline **3a** and 1.5 equivalents of Pd(OAc)₂ had been stirred together overnight at room temperature in benzene a palladated derivative **4a** was obtained in 78% yield after recrystallisation. Both the ¹H and ¹³C NMR spectra indicated that the unsubstituted cyclopentadiene ring of **3a** had been palladated, which was in agreement with our hypothesis. Moreover, both the NMR spectroscopic and the mass-spectrometric analysis clearly

showed the presence of two ferrocenyloxazoline units, three palladium atoms, and four acetate bridges in this compound. Finally, the unprecedented structure of **4a** was unequivocally established by X-ray diffraction analysis (Figure 2).

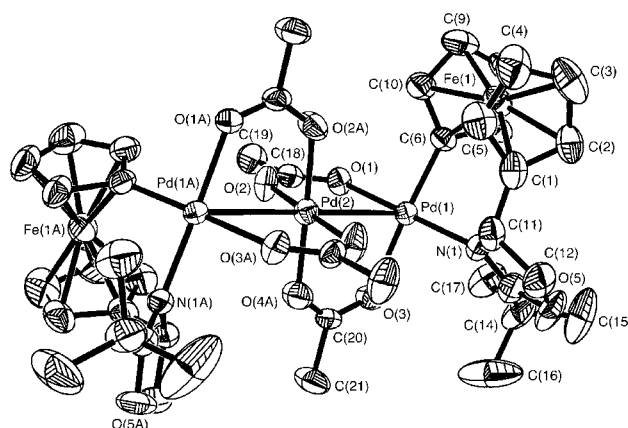
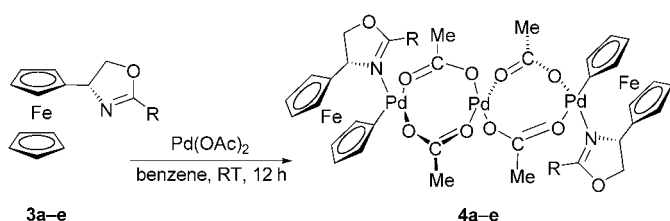


Figure 2. ORTEP representation of the crystal structure of **4a**. Hydrogen atoms have been omitted for clarity.

Several structural features of **4a** deserve some comment: The three palladium atoms show a very small departure (less than 1.1°) from linearity. Although the formation of linear trinuclear cyclopalladated complexes has been reported in a few cases starting from C(sp³) donors,^[15] **4a** represents the first example of this type of complex with C(sp²)–Pd bonds and also the only one whose geometry has been determined by X-ray diffraction analysis. The Pd–Pd bond of 3.0457(5) Å is somewhat shorter than that observed in the palladium diacetate trimer (ca. 3.15 Å),^[16] but clearly beyond the upper value (ca. 2.87 Å) reported for neutral bimetallic complexes with weak bonding interactions between the two palladium atoms.^[17] The Pd–C distance at 1.961(7) Å is appreciably longer than that reported for dimeric cyclopalladated ferrocenylimines with acetate bridges, but the Pd–N bond length at 2.021(6) Å falls in the range observed in these compounds.^[18]

We submitted the other 4-ferrocenyl-1,3-oxazolines **3b–e** to the same reaction conditions used for **3a** (Scheme 1) to study the scope of this new cyclopalladation reaction. Both the spectral and analytical data of the cyclopalladated complexes **4b** and **4c** revealed that they were structurally analogous to **4a**. It is worth noting that cyclopalladation did not take place at the phenyl ring in the case of **3c**, which is in accordance with the preferences observed in the *ortho* palladation of imine derivatives of benzoyl ferrocene.^[17d] On the other hand, the cyclopalladation of both **3d** and **3e** led to complex mixtures of unidentified products. Clearly, the presence of C–H bonds in the α position of the oxazoline substituent at C2 has a deleterious effect in this reaction.

Electrochemical studies of **3a** and **4a** were performed^[18] to elucidate the effect of interannular palladation upon the



Scheme 1. Interannular cyclopalladation of ferrocenyloxazoline derivatives **3**. Yields: **4a** 78%, **4b** 78%, **4c** 64%, **4d** < 2%, **4e** 0%. R = *tert*-butyl (**4a**), 1-adamantyl (**4b**), phenyl (**4c**), isopropyl (**4d**), ethyl (**4e**).

proclivity of the iron(II) center towards oxidation. The cyclic voltammogram (CV) of **3a** exhibits an anodic signal with a directly associated cathodic signal in the reverse scan (Figure 3). The value of the half-wave potential ($E_{1/2}$) for **3a**

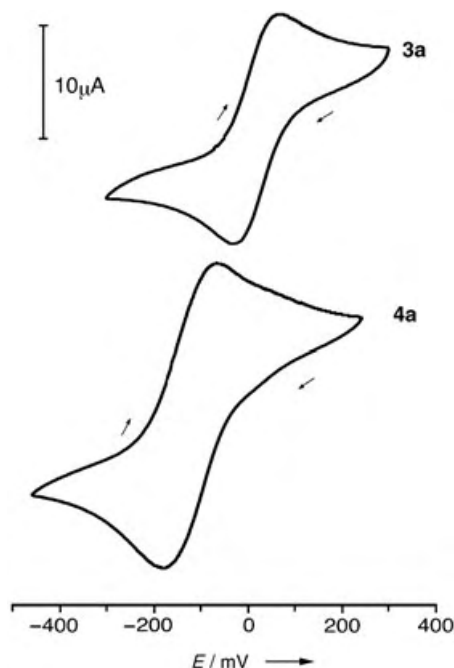
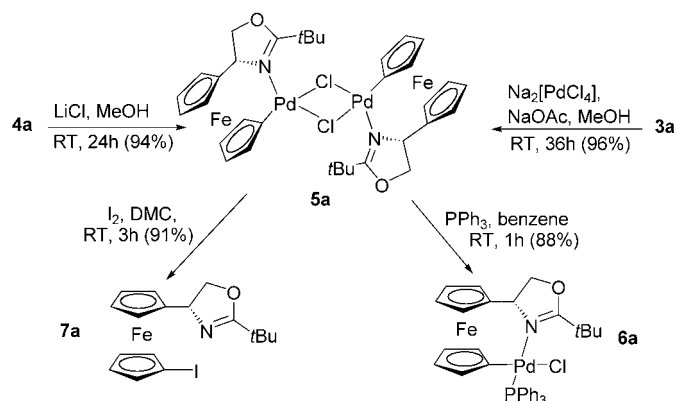


Figure 3. Cyclic voltammograms of 10^{-3} M solutions of **3a** or **4a** in CH_3CN at 20°C and at a scan speed of $v = 100 \text{ mVs}^{-1}$ (electrochemical data: anodic (E_{pa}), cathodic (E_{pc}), and half-wave potentials ($E_{1/2}$) potentials (in mV) referred to ferrocene $E_{pa} = 54$ (for **3a**) and -52 (for **4a**), $E_{pc} = -33$ (for **3a**) and -184 (for **4a**), and $E_{1/2} = 10$ and -123 for **3a** and **4a**, respectively).

is smaller than those reported for $[(\eta^5\text{-C}_5\text{H}_5)\text{Fe}\{(\eta^5\text{-C}_5\text{H}_4)\text{-C(R}^1\text{)=N-R}^2\}]$ (in the range of 85–200 mV) but greater than those of the ferrocenylamines $[(\eta^5\text{-C}_5\text{H}_5)\text{Fe}\{(\eta^5\text{-C}_5\text{H}_4)\text{-(CH}_2)_n\text{-NH}_2\}]$ ($n = 1$ or 2) and the Schiff bases $[(\eta^5\text{-C}_5\text{H}_5)\text{Fe}\{(\eta^5\text{-C}_5\text{H}_4)\text{-CH}_2\text{-N=CH(R}^3)\}]$ with $E_{1/2}$ values varying from -30 to -5 mV .^[19] These findings suggest that the electron-withdrawing character of the 4'-oxazoline moiety is between those of the $-\text{CH}_2\text{-N=CH(R}^3\text{)}$ and the $-\text{C(R}^1\text{)H=N-R}^2$ substituents.^[20] Only one wave was observed for **4a**, thus indicating that the two ferrocene moieties in **4a** do not interact electronically with each other. Moreover, the wave

was shifted to a more cathodic potential (Figure 3). This finding agrees with the results reported for the ferrocenyl-imines $[(\eta^5\text{-C}_5\text{H}_5)\text{Fe}\{(\eta^5\text{-C}_5\text{H}_4)\text{-C(R}^1\text{)=N-R}^2\}]$ and their cyclopalladated derivatives where a $\sigma(\text{Pd-C(sp}^2\text{)})$ bond is held in the adjacent position to the functional $>\text{C=N}$ group.^[19] However, the magnitude of the shift was greater (ca. 130 mV) for **4a** than for the previously reported systems (in the range of 40–80 mV).

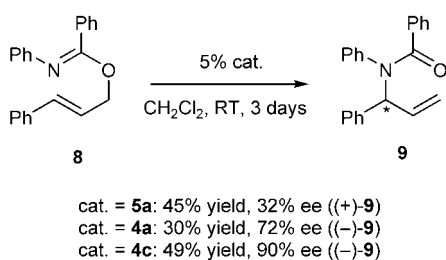
The chemical behavior of these novel complexes appears to be similar to that of previously known *ortho*-palladated ferrocene derivatives (Scheme 2). Thus, the treatment of **4a**



Scheme 2. Preparation and reactivity of the di- μ -chloro complex **5a**. DMC = dimethylaminoethyl chloride hydrochloride.

with lithium chloride produces a di- μ -chloro complex **5a**. The same compound is obtained when **3a** is treated with $\text{Na}_2\text{[PdCl}_4\text{]}$ in the presence of NaOAc . In turn, **5a** is readily converted into the mononuclear complex **6a** by cleavage with triphenylphosphine. Finally, iodination of **5a** affords (*S*)-2-(*tert*-butyl)-4-(1'-iodoferrocenyl)-1,3-oxazoline (**7a**) in high yield and provides conclusive evidence of the high reactivity of the $\sigma(\text{Pd-C(sp}^2\text{)})$ bond in **5a**. This reaction paves the way for the preparation of 1,1'-disubstituted ferrocenes.

These new chiral cyclopalladated complexes hold significant promise as catalysts for asymmetric transformations and are far from being a mere chemical curiosity. In particular, preliminary results show that the trinuclear complexes **4a–c** and the di- μ -chloro complex **5a** are able to catalyze the enantioselective rearrangement of allylic imidates to allylic amides. This Pd^{II} -catalyzed aza-Claisen reaction offers convenient access to various allylic amides from the corresponding allylic alcohols. Some *ortho*-palladated complexes derived from ferrocene and which combine both central and planar chirality have also been shown to give high yields and enantioselectivities in the rearrangement of imidates derived from alkyl-substituted allylic alcohols.^[6,21] The reaction of imidates derived from aryl-substituted allylic alcohols is, however, much less stereoselective. In the light of these precedents, we investigated the performance of our 1'-palladated complexes in the [3,3]-sigmatropic rearrangement of (*E*)-3-phenylallyl (*N*-phenyl)benzimidate (**8**) (Scheme 3).^[22]



Scheme 3. Asymmetric catalysis of the aza-Claisen rearrangement by complexes **4a**, **4c**, and **5a**.

The di- μ -chloro complex **5a** afforded the dextrorotatory allylic amide (+)-**9** in 45% yield and with low, but significant, optical purity (32% *ee* according to HPLC analysis) whereas the mononuclear complex **6a** did not show any catalytic activity in this reaction. We found that the opposite levorotatory enantiomer of **9** became the major rearranged product (with a 72% *ee*) when the trinuclear cyclopalladated complex **4a** was used. This unexpected change in enantioselectivity is certainly surprising when it is considered that the only chirality element present in **4a** and in **5a** is the C4 oxazoline stereogenic carbon atom (which is of *S* absolute configuration). Finally, the use of the (*S*)-2-phenyl-4-ferrocenyloxazoline-derived trinuclear complex **4c** gave (–)-**9** in 49% yield and with an unprecedented high optical purity (90% *ee*).^[23] These reactions constitute the first examples of an asymmetric transformation catalyzed by a cyclopalladated ferrocene derivative that exhibits only central chirality.

In summary, the rational design of a ferrocenyloxazoline ligand that allows a direct interannular cyclopalladation of ferrocene derivatives^[24] for the first time has led to a new structural type of chiral palladium-bridged heteropolynuclear complexes of potential interest in several fields of chemistry.

Experimental Section

3a: M.p. 50–51 °C; $[\alpha]_D^{20} = -85$ ($c = 0.47$, CH_2Cl_2). IR (KBr): $\tilde{\nu} = 3080$, 2980, 1650, 1489, 1120, 1020, 810 cm^{-1} ; ^1H NMR (200 MHz, CDCl_3): $\delta = 1.26$ (s, 3H, $3 \times \text{CH}_3$), 4.15 (m, 9H, Fe), 4.36 (m, 1H, CHOH), 4.50 (m, 1H, CHOH), 4.86 ppm (dd, $^1J = 9.6$ Hz, $^2J = 7.4$ Hz, 1H, CHN); ^{13}C NMR (50.3 MHz, CDCl_3): $\delta = 27.9$ ($3 \times \text{CH}_3$), 35.2 (*t*Bu-Cq (quaternary carbon center)), 64.7 (CH-N), 66.2 (CH-Fc), 67.2 (CH-Fc), 67.8 (CH-Fc), 7.9 (CH-Fc), 68.3 (CH-Fc), 73.4 (CH₂-O), 90.8 (Cq-Fc), 172.8 ppm (C=O); HRMS (CI, NH_3): m/z calcd for $\text{C}_{17}\text{H}_{21}\text{FeNO}$: 312.1006, found: 312.1001.

4a: A solution of **3a** (0.15 g, 0.48 mmol) and $\text{Pd}(\text{OAc})_2$ (1.5 equiv) in dry benzene (7 mL) was stirred overnight at room temperature. The resulting dark brown solution was filtered through a small pad of celite with CHCl_3 and evaporated. The resulting dark residue was dissolved in a minimal amount of CH_2Cl_2 and hexane was added. The solution was filtered to remove impurities that had precipitated after heating. Recrystallization from dichloromethane/hexane afforded the red-brown pentametallic complex **4a** as a crystalline solid (0.22 g, 78% yield). M.p. 160 °C (decomp); $[\alpha]_D^{20} = +463$ ($c = 0.26$, CH_2Cl_2); IR (KBr): $\tilde{\nu} = 3100$, 2971, 1626, 1578, 1408, 1342, 1167, 1024, 1034, 804 cm^{-1} ; ^1H NMR (200 MHz, CDCl_3): $\delta = 1.80$ (s, 6H, $2 \times \text{CH}_3$ bridge), 1.92 (s, 18H, $6 \times \text{CH}_3$), 2.01 (s, 6H, $2 \times \text{CH}_3$ bridge), 3.97 (m, 1H, CH-Fc), 3.99 (m, 1H, CH-Fc), 4.01 (m, 1H, CH-Fc), 4.03 (m, 1H, CH-Fc), 4.10 (m, 1H, CH-Fc), 4.30 (m, 1H, CH-Fc), 4.44 (m, 1H, CH-Fc), 4.47 (m, 2H, CH₂-O), 4.80 (m, 1H, CH-Fc), 6.18 ppm (dd, $^1J = 4.6$ Hz, $^2J = 2.2$ Hz, 1H, CH-N); ^{13}C NMR

(50.3 MHz, CDCl_3): $\delta = 23.7$ (CH_3 bridge), 23.8 (CH_3 bridge), 28.7 ($3 \times \text{CH}_3$), 34.3 (*t*Bu-Cq), 64.7 (CH-Fc), 65.8 (CH-N), 66.2 (CH-Fc), 66.7 (CH-Fc), 67.3 (CH-Fc), 69.0 (CH-Fc), 72.6 (CH-Fc), 72.7 (CH-Fc), 73.4 (CH-Fc), 73.4 (CH₂-O), 84.7 (Cq-Fc-Pd), 87.9 (Cq-Fc-ox), 175.3 (C=N), 181.7 (C=O), 184.4 ppm (C=O); MS (FAB+): m/z (%) 1176.0 (9.9) [M^+], 475.1 (100). HRMS: m/z calcd for $\text{C}_{19}\text{H}_{23}\text{FeNO}_3\text{Pd}$: 474.0078; found: 474.0072. **5a**: **3a** (85 mg, 0.27 mmol) was added to a solution of $\text{Na}_2[\text{PdCl}_4]$ (81 mg, 0.27 mmol) and NaOAc (23 mg, 0.27 mmol) in dry methanol (2 mL) at room temperature and stirring was maintained for 36 h. The resulting dark brown solution was filtered through a sintered glass frit and washed with methanol. The filtrate was concentrated and the crude product was purified by dissolving in a minimal amount of CH_2Cl_2 followed by the addition of hexane. The solution was filtered to remove impurities that had precipitated after heating and the tetrametallic complex **5a** was obtained as an orange solid (118 mg, 96%). M.p. 156 °C (decomp); $[\alpha]_D^{20} = +436$ ($c = 0.15$, CH_2Cl_2); IR (KBr): $\tilde{\nu} = 3100$, 2927, 1624, 1578, 1458, 1400, 1362, 1169, 1032, 806, 733 cm^{-1} ; ^1H NMR (200 MHz, CDCl_3): $\delta = 1.72$ (s, 18H, $6 \times \text{CH}_3$), 3.85 (m, 1H, CH-Fc), 3.93 (m, 1H, CH-Fc), 3.99 (m, 1H, CH-Fc), 4.02 (m, 1H, CH-Fc), 4.08 (m, 1H, CH-Fc), 4.35 (m, 1H, CH-Fc), 4.39 (m, 1H, CH-Fc), 4.46 (m, 2H, CH₂-O), 4.47 (m, 1H, CH-Fc), 5.04 ppm (m, 1H, CH-N); ^{13}C NMR (50.3 MHz, CDCl_3): $\delta = 28.8$ ($6 \times \text{CH}_3$), 34.3 (*t*Bu-Cq), 64.9 (CH-Fc), 66.0 (CH-Fc), 66.3 (CH-Fc), 67.0 (CH-N), 67.8 (CH-Fc), 69.5 (CH-Fc), 71.7 (CH-Fc), 72.1 (CH-Fc), 73.2 (CH-Fc), 73.2 (CH₂-O), 87.9 (Cq-Fc-Pd), 88.9 (Cq-Fc-ox), 175.3 ppm (C=N); MS (MALDI-TOF) m/z (%): 903.5 (100) [$M+1$]⁺; HRMS: m/z calcd for $\text{C}_{34}\text{H}_{40}\text{Cl}_2\text{Fe}_2\text{N}_2\text{O}_2\text{Pd}_2$: 901.9241; found: 901.9230.

General experimental procedure for the aza-Claisen rearrangement of **8**: A solution of (*E*)-3-phenylallyl (*N*-phenyl)benzimidate (**8**) (45 mg, 0.14 mmol) and the cyclopalladated complex (**4a**, **4c**, or **5a**; 0.007 mmol) in anhydrous CH_2Cl_2 (1 mL) was stirred at room temperature under nitrogen for 3 days. The solution was concentrated and the residue was purified by column chromatography on silica gel with ethyl acetate/hexanes (4:96) as the eluant to afford the optically active **9** (30–49% yield). Conditions for the HPLC determination of the enantiomeric purity of **9**: chiralpak AS column, hexane/isopropyl alcohol (96:4), $\Phi = 0.5 \text{ mL min}^{-1}$, $\lambda = 254 \text{ nm}$, $t_R(+)$ = 28.1 min, $t_R(-)$ = 34.1 min.

Received: October 26, 2004

Published online: February 18, 2005

Keywords: allylic compounds · asymmetric catalysis · metalation · metallocenes · palladium

- [1] a) A. C. Cope, R. W. Siekman, *J. Am. Chem. Soc.* **1965**, 87, 3272–3273; b) A. C. Cope, E. C. Friedrich, *J. Am. Chem. Soc.* **1968**, 90, 909–913.
- [2] Reviews: a) J. Dupont, M. Pfeffer, J. Spencer, *Eur. J. Inorg. Chem.* **2001**, 1917–1927; b) S. B. Wild, *Coord. Chem. Rev.* **1997**, 166, 291–311; c) G. R. Newkome, W. E. Puckett, V. K. Gupta, G. E. Fieffer, *Chem. Rev.* **1986**, 86, 451–489; d) D. W. Evans, G. R. Baker, G. R. Newkome, *Coord. Chem. Rev.* **1989**, 93, 155–183; e) A. D. Ryabov, *Chem. Rev.* **1990**, 90, 403–489.
- [3] a) *Ferrocenes. Homogeneous Catalysis, Organic Synthesis and Materials Sciences* (Eds.: A. Togni, T. Hayashi), VCH, Weinheim, **1995**; b) I. R. Whittall, A. M. Mc Donagh, M. C. Humphrey, M. Samoc, *Advances in Organometallic Chemistry*, Vol. 42, Academic Press, San Diego, **1998**, p. 291.
- [4] Heck reactions: a) S. Iyer, A. Jayanthi, *Tetrahedron Lett.* **2001**, 42, 7877–7878; b) F. Yang, Y. Zhang, R. Zheng, J. Tang, M. He, *J. Organomet. Chem.* **2002**, 651, 146–148.
- [5] Suzuki–Miyaura couplings: D. A. Alonso, C. Nájera, M. C. Pacheco, *J. Org. Chem.* **2002**, 67, 5588–5594.

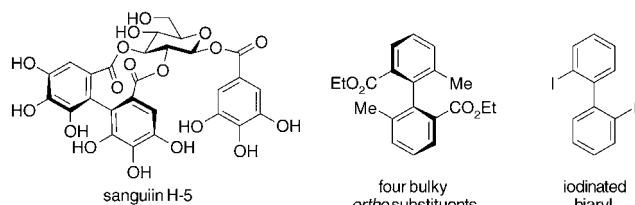
- [6] Asymmetric aza-Claisen rearrangements of allylic imidates and related reactions: a) F. Cohen, L. E. Overman, *Tetrahedron: Asymmetry* **1998**, 9, 3213–3222; b) T. K. Hollis, L. E. Overman, *J. Organomet. Chem.* **1999**, 576, 290–299; c) Y. Donde, L. E. Overman, *J. Am. Chem. Soc.* **1999**, 121, 2933–2934; d) J. Kang, K. H. Yew, T. H. Kim, D. H. Choi, *Tetrahedron Lett.* **2002**, 43, 9509–9512; e) L. E. Overman, T. P. Remarchuk, *J. Am. Chem. Soc.* **2002**, 124, 12–13.
- [7] For some leading references, see: a) M. Pfeffer, M. A. Rotteveel, J. Pascal, A. De Cian, J. Fischer, *J. Organomet. Chem.* **1989**, 371, C21–5; b) W. Tao, L. J. Silverberg, A. L. Rheingold, R. F. Heck, *Organometallics* **1989**, 8, 2550–2559; c) M. Nonoyama, K. Hamamura, *J. Organomet. Chem.* **1991**, 407, 271–277; d) R. Bosque, C. López, J. Sales, X. Solans, *J. Organomet. Chem.* **1994**, 483, 61–71; e) C. López, A. Caubet, X. Solans, M. Font-Bardía, *J. Organomet. Chem.* **2000**, 598, 87–102; f) S. Pérez, C. López, A. Caubet, R. Bosque, X. Solans, M. Font-Bardía, A. Roig, E. Molins, *Organometallics*, **2004**, 23, 224–236.
- [8] a) K. Takao, M. Nonoyama, J. Fujita, *Bull. Chem. Soc. Jpn.* **1981**, 54, 186–189; b) L. L. Troitskaya, N. S. Khrushova, V. I. Sokolov, O. A. Reutov, *Zh. Obshch. Khim.* **1982**, 2606–2608; c) G. Zhao, F. Xue, Z.-Y. Zhang, T. C. W. Mak, *Organometallics* **1997**, 16, 4023–4026; d) Z. Gang, Q.-C. Yang, T. C. W. Mak, *Organometallics* **1999**, 18, 3623–3636; e) C. López, R. Bosque, X. Solans, M. Font-Bardía, *Tetrahedron: Asymmetry* **1996**, 7, 2527–2530.
- [9] Reviews: a) C. J. Richards, A. Locke, *Tetrahedron: Asymmetry* **1998**, 9, 2377–2407; b) L.-X. Dai, T. Tu, S.-L. You, W.-P. Deng, K. L. Hou, *Acc. Chem. Res.* **2003**, 36, 659–667; c) P. J. Guiry, C. P. Saunders, *Adv. Synth. Catal.* **2004**, 346, 497–537.
- [10] Recent references: a) C. Bolm, N. Hermanns, A. Classen, K. Muñoz, *Bioorg. Med. Chem. Lett.* **2002**, 12, 1795–1798; b) T. Tu, X.-L. Hou, L.-X. Dai, *Org. Lett.* **2003**, 5, 3651–3653; c) Y. Nishibayashi, A. Yamauchi, G. Onodera, S. Uemura, *J. Org. Chem.* **2003**, 68, 5875–5880.
- [11] a) L. E. Overman, C. E. Owen, M. M. Parvan, C. J. Richards, *Org. Lett.* **2003**, 5, 1809–1812; b) C. E. Anderson, L. E. Overman, *J. Am. Chem. Soc.* **2003**, 125, 12412–12413; c) J. Kang, T. H. Kim, H. Y. Kyoung, W. K. Lee, *Tetrahedron: Asymmetry* **2003**, 14, 415–418; d) S. F. Kirsch, L. E. Overman, M. P. Watson, *J. Org. Chem.* **2004**, 69, 8101–8104.
- [12] A few examples of interannular lithiation of ferrocenes can be found in the literature, see: a) G. Iftime, C. Moreau-Bossuet, E. Manoury, G. G. A. Balavoine, *Chem. Commun.* **1996**, 527–528; b) G. Iftime, J.-C. Daran, E. Manoury, G. G. A. Balavoine, *Organometallics* **1996**, 15, 4808–4815; c) M. Tsukazaki, M. Tinkl, A. Roglans, B. J. Chapell, N. J. Taylor, V. Snieckus, *J. Am. Chem. Soc.* **1996**, 118, 685–686.
- [13] Optimization of the geometry was performed with the semi-empirical PM3(tm) procedure, as implemented in the SPARTAN package of programs.
- [14] Obtained as described in: a) M. Catasús, A. Bueno, A. Moyano, M. A. Maestro, J. Mahía, *J. Organomet. Chem.* **2002**, 642, 212–226. (*R*)-**1** is also obtained in high enantiomeric purity by the same method or by the alternative procedure of: b) A. Patti, M. Lotz, P. Knochel, *Tetrahedron: Asymmetry* **2001**, 12, 3375–3380.
- [15] a) Y. Fuchita, K. Hisaki, T. Uchiyama, *J. Organomet. Chem.* **1985**, 280, C51–C54; b) M. Pfeffer, E. Wehman, G. van Koten, *J. Organomet. Chem.* **1985**, 282, 127–131; c) G. G. A. Balavoine, J. C. Clinet, *J. Organomet. Chem.* **1990**, 390, C84–C88; d) M. T. Alonso, O. Juanes, J. de Mendoza, J. Rodríguez-Ubis, *J. Organomet. Chem.* **1992**, 430, 349–356.
- [16] A. C. Skapshi, M. L. Smart, *Chem. Commun.* **1970**, 658–659.
- [17] T. Murahashi, H. Kurosawa, *Coord. Chem. Rev.* **2002**, 231, 207–228.
- [18] Electrochemical data for **3a** and **4a** were obtained by cyclic-voltammetric analysis under nitrogen gas at approximately 20 °C using HPLC-grade acetonitrile as the solvent, tetrabutylammonium hexafluorophosphate (0.1M) as the supporting electrolyte, and a potentiostat from EG&G instruments. The half-wave potentials $E_{1/2}$ were referenced to an Ag/AgNO₃ (0.1M in acetonitrile) electrode separated from the solution by a medium-porosity fritted disk. A platinum-wire auxiliary electrode was used in conjunction with a platinum disk working TACUSSEL-EDI rotatory electrode (3.14 mm²). Cyclic voltammograms of ferrocene were recorded before and after each sample to ensure the reproducibility of the results, in particular to test and monitor the stability of the Ag/AgNO₃ electrode (for the Fc/Fc⁺ couple $E_{1/2}$ = 50 ± 2 mV). Three consecutive scans of freshly prepared solutions (10^{−3} M) of the samples in acetonitrile were run and the average $E_{1/2}$ values measured were then referred to the Fc/Fc⁺ couple ($E_{1/2}$ (Fc)) which was used as the internal reference. No additional waves were observed up to 2 V. The standard error of the measured potentials was ± 5 mV in these experimental conditions and the cyclic voltammograms were registered using scan speeds varying from v = 10 to 100 mV s^{−1} in all experiments.
- [19] a) R. Bosque, C. López, J. Sales, *Inorg. Chim. Acta* **1996**, 244, 141–145; b) C. López, R. Bosque, X. Solans, M. Font-Bardía, D. Tramuns, G. Fern, J. Silver, *J. Chem. Soc. Dalton Trans.* **1994**, 3039–3046.
- [20] a) P. Zanello, A. Cinquantini, S. Mangani, G. Opro-molla, L. Pardi, C. Janiak, M. D. rausch, *J. Organomet. Chem.* **1994**, 471, 171–177; b) P. Zanello, G. Opro-molla, L. Pardi, K. H. Panell, K. H. Sharma, *J. Organomet. Chem.* **1993**, 450, 193–196; c) W. F. Little, C. N. Reilley, J. D. Johnson, A. P. Sanders, *J. Am. Chem. Soc.* **1964**, 86, 1382–1386; d) G. L. Hoh, W. E. McEwen, J. Kleinberg, *J. Am. Chem. Soc.* **1961**, 83, 3949–3953.
- [21] a) M. Calter, T. K. Hollis, L. E. Overman, J. Ziller, G. G. Zipp, *J. Org. Chem.* **1997**, 62, 1449–1445; b) Y. Jiang, J. M. Langmire, X. Zhang, *Tetrahedron Lett.* **1999**, 40, 1449–1450.
- [22] Prepared from (*E*)-cinnamyl alcohol in 84 % yield according to the literature procedure: L. Engman, *J. Org. Chem.* **1993**, 58, 2394–2401.
- [23] The asymmetric rearrangement of **8** to (−)-**9** catalyzed by a dimeric (di-μ-trifluoroacetate)palladium complex derived from (*R*)-*N,N*-dimethyl-2-(ferrocenyl)ethylamine occurred in 47 % yield with 47 % *ee*; see: T. K. Hollis, L. E. Overman, *Tetrahedron Lett.* **1997**, 38, 8837–8840.
- [24] The low-yield, multistep-formation of metallaferrocenophanes by insertion of Pd⁰ and Pt⁰ complexes into silicon- or phosphido-bridged ferrocenophanes has been described; see: T. Mizuta, M. Onishi, T. Nakazono, H. Nakazawa, K. Miyoshi, *Organometallics* **2002**, 21, 717–726.

C–C Coupling

Synthesis of Medium-Ring and Iodinated Biaryl Compounds by Organocuprate Oxidation**

David S. Surry, Xianbin Su, David J. Fox, Vilius Franckevicius, Simon J. F. Macdonald, and David R. Spring*

The importance of the biaryl motif is illustrated by its presence in an extensive range of natural products, pharmaceuticals, agrochemicals, dyes, and chiral catalysts. A variety of reactions are available to construct biaryls,^[1] mostly through palladium-,^[2,3] nickel-,^[4] or copper-mediated processes.^[5] Unfortunately, only a limited number of these methods is suitable for the synthesis of medium-ring compounds,^[6] sterically hindered systems, and iodinated biaryls (Scheme 1). Biaryl-containing medium-ring compounds are



Scheme 1. Biaryl-containing medium-ring compounds, sterically hindered biaryls, and iodinated biaryls are all difficult synthetic targets using existing methodology.

difficult to synthesize because of their associated torsional, transannular, and large angle strain; nevertheless, there are thousands of potent bioactive natural products that contain this motif, such as the ellagitannin class of natural products, of which sanguin H-5 is one of over 500 members.^[7] In addition, the synthesis of biaryls that contain four *ortho* substituents is often challenging, and palladium-catalyzed reactions that accomplish this goal have only recently been developed.^[8] Moreover, iodinated biaryls are powerful synthetic intermediates, yet they are only formed by a relatively small

number of reactions.^[9] New methodology that can overcome these caveats will allow efficient access to largely unexploited classes of biaryls.

Oxidation of organocuprates allows the formation of both intermolecular^[10] and intramolecular^[11] biaryl bonds; however, extreme reaction conditions and poor functional-group tolerance means that this reaction is not seen as being widely useful. We have endeavored to change this opinion. Herein, we report the optimization of organocuprate oxidation, which involves the design and utilization of a new oxidant, the exploitation of the iodine–magnesium exchange procedure developed by Knochel and co-workers,^[12] and the cross-coupling of different aryl units by an intramolecular process. The utility of the new methodology is illustrated by the efficient synthesis of the biaryl-containing medium-ring core of sanguin H-5.

Initial optimization studies revealed that a range of copper(I) salts could be used in the organocuprate oxidation reaction (Table 1), with the copper(I) bromide/dimethyl

Table 1: Substoichiometric amounts of dinitroarenes, such as **3**, could be used as effective oxidants.

Entry	Oxidant	Oxidant [equiv]	Yield [%]
1		1	68
2	3	0.2	62
3	3	0.1	31
4	CuCl ₂	0.2	12
5	CuCl ₂	1	60
6		1.5	57

sulfide complex proving the most convenient.^[13] In contrast, the choice of oxidant was crucial to the success of the reaction. Initially, *meta*-dinitrobenzene^[14] was the most successful oxidant examined,^[15] but it was difficult to obtain the pure product free of oxidant-derived by-products. Therefore, the new oxidant **3** was synthesized, which could be completely removed by an aqueous acid wash during the work up or by passage through silica gel.^[16] Under the reaction conditions employed, molecular oxygen as the oxidant caused significant formation of phenols, whilst none were detected when **3** was employed. Interestingly, as few as 0.2 equivalents of **3** (with respect to the aryl magnesium species formed) may be used without significant depreciation of yield (Table 1, entries 1 and 2). Further lowering of the quantity of dinitroarene to 0.1 equivalents, drastically decreased the yield of isolated product (entry 3). This “substoichiometric” effect was not observed for the inorganic, single-electron oxidant CuCl₂ (entries 4 and 5). A likely explanation of these findings is that the dinitroarene **3** can accept more than one electron during the oxidation process.^[17] Support for this hypothesis

[*] D. S. Surry, X. Su, Dr. D. J. Fox, V. Franckevicius, Dr. D. R. Spring
Department of Chemistry
University of Cambridge
Lensfield Road, Cambridge, CB21EW (UK)
Fax: (+44) 1223-336362
E-mail: drspring@ch.cam.ac.uk

Dr. S. J. F. Macdonald
GlaxoSmithKline
Centre for Excellence in Drug Discovery
Stevenage, SG1 2NY (UK)

[**] We gratefully acknowledge financial support from the EPSRC and GSK (D.S.S.), Cambridge Trusts (X.S.), Pfizer UK (V.F.), and the BBSRC. We would also like to acknowledge the EPSRC National Mass Spectrometry Service Centre, Swansea, UK, for providing mass-spectrometric analysis.

Supporting information for this article is available on the WWW under <http://www.angewandte.org> or from the author.

comes from the fact that the radical anion of *meta*-dinitrobenzene (available by reduction of *meta*-dinitrobenzene with one equivalent of potassium) may itself be used to perform the oxidation (entry 6).^[18]

The optimized methodology can be used for the preparation of a wide range of functionalized biaryls (Table 2). The

Table 2: Intermolecular biaryl formation by using the optimized organocuprate oxidation methodology.^[a]

Entry	Substrate (1)	Product (2)	Yield [%]
a			88
b			75
c			82
d			67
e			72
f			66
g			75
h			53

[a] Conditions: a) **1** (1 mmol), *i*PrMgCl (1 equiv), THF (3 mL), -20°C , 10 min; b) CuBr-SMe₂ (0.5 equiv); c) **3** (1 equiv) in THF (3 mL).

reaction does not seem to be significantly influenced by steric interactions, thus allowing the synthesis of a biaryl bond with multiple *ortho* substituents (**2a** and **2b**). Iodinated aromatic heterocycles are also suitable substrates, which makes the synthesis of the corresponding dimer **2c** possible.^[19] The iodine–magnesium exchange can be performed in the presence of an aryl bromide,^[20] which allows the formation of brominated biaryls (**2d**). Furthermore, the ability to regioselectively perform a single iodine–magnesium exchange on multiply iodinated substrates permits the synthesis of iodinated biaryls **2e–h**, which are often extremely difficult to form directly by other methods because of oligomerization.

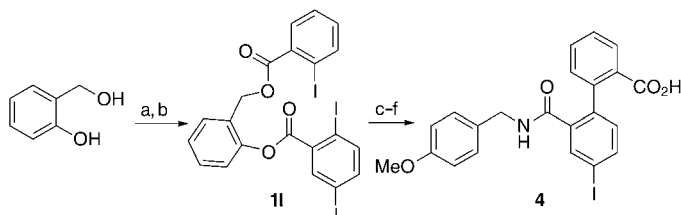
The reaction is equally successful when performed intramolecularly (Table 3) so that strained medium-ring compounds with 10- and 11-membered rings (**2i,j** and **2k**, respectively) can be constructed without the need for high-dilution conditions (approximately 0.3 M in THF).

Table 3: Intramolecular biaryl formation using the optimized organocuprate oxidation methodology.^[a]

Entry	Substrate (1)	Product (2)	Yield [%]
i			82
j			70
k			85

[a] Conditions: a) **1** (1 mmol), *i*PrMgCl (2 equiv), THF (3 mL), -20°C , 10 min; b) CuBr-SMe₂ (1 equiv); c) **3** (1 equiv) in THF (3 mL).

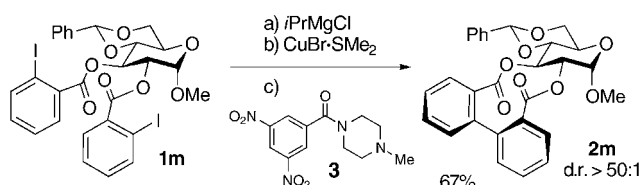
The success of this cyclization allows cross-coupling of different aryl units (Scheme 2). Two different aryl units can be



Scheme 2. Formal cross-coupling of aryl units by intramolecular biaryl formation followed by selective aminolysis: a) 2-iodobenzoyl chloride, Et₃N, DMAP, DMA, -20°C , 6 h; b) 2,5-diiodobenzoyl chloride, Et₃N, DMAP, DMA, -20°C , 6 h, 90%; c) *i*PrMgCl (2 equiv), THF, -20°C ; d) CuBr-SMe₂ (1 equiv); e) **3** (1 equiv), 79% from **11**; f) 4-methoxybenzylamine, 1,4-dioxane, 60°C , 6 h, 84%. DMAP = 4-(dimethylamino)pyridine, DMA = *N,N*-dimethylacetamide.

tethered with 2-hydroxybenzyl alcohol to give **11**,^[21] which can be readily cyclized in 79% yield by using our methodology. The 11-membered ring product readily undergoes aminolysis with concomitant loss of the tether to give **4** directly, thus, allowing an overall cross-coupling of two aryl iodides. This procedure could be readily exploited for the generation of a library of functionalized biaryls derivatives, which could then be further modified.

Most importantly, this methodology was used to form **2m**, a model for the highly strained medium-ring core of sanguin H-5 in 67% yield and with complete diastereoselectivity (Scheme 3).^[22] This significant result represents a high-yielding synthesis of bisester biaryl-containing medium rings that can be applied to the preparation of the ellagitannin



Scheme 3. Synthesis of **2m**, a model for the highly strained, medium-ring core of sanguini H-5.

family of natural products. The success of this reaction in forming biaryl bonds in hindered systems and strained rings may be because the two aryl moieties that eventually bond in the intermediate organocuprate are a considerable distance apart. The C–Cu–C bond angle is approximately 180° and the C–Cu bond is somewhat long at 1.9 \AA ,^[23] thereby reducing unfavorable interactions.

In summary, we report a new functional-group-tolerant methodology for the synthesis of sterically hindered biaryls, including highly strained medium-ring-containing biaryls, which are key structural units within the ellagitannin family of natural products. The methodology can also be used to cross-couple different aryl units by use of a tether. We are currently working towards exploiting this methodology in the synthesis of ellagitannin natural products.

Experimental Section

General procedure for the biaryl bond-forming reaction: Titrated *i*PrMgCl (1 mmol, 2.0 M solution in THF) was added to a solution of an aryl iodide (1 mmol) in THF (3 mL) at -20°C . The reaction mixture was then stirred for 10 min at -20°C and then transferred by cannula onto freshly recrystallized, solid CuBr·SMe₂ (0.5 mmol). After stirring the reaction mixture for 30 s, a solution of **3** (1 mmol) in THF (3 mL) was added and the resulting solution was warmed to ambient temperature. The reaction mixture was then filtered through a plug of silica by using a mixture of hexane and EtOAc (1:1) as the eluant. The filtrate was concentrated under reduced pressure and the residue purified by flash column chromatography on silica gel.

3: 3,5-Dinitrobenzoic acid (21.2 g, 0.1 mol) was dissolved in thionyl chloride (100 mL), heated at reflux for 10 h, and then cooled to ambient temperature. Excess thionyl chloride was removed under reduced pressure and by azeotropic distillation with toluene. The residue was dissolved in CHCl₃ (200 mL) and added dropwise to a stirred slurry of 1-methylpiperazine (12.0 g, 0.12 mol) and K₂CO₃ (14 g, 0.1 mol) in CHCl₃ (200 mL) at 0°C . The reaction mixture was warmed to ambient temperature over 1 h, washed with water (4 × 400 mL), dried over K₂CO₃, filtered, and the solvent removed under reduced pressure. The residue was recrystallized from hexane as yellow needles (20.4 g, 70 %); m.p. $138\text{--}141^\circ\text{C}$; IR (film): $\tilde{\nu} = 1633, 1531, 1435, 1339, 1295, 1277, 1133, 995, 917, 908, 720, 681 \text{ cm}^{-1}$; ¹H NMR (500 MHz; [D₆]DMSO; 120°C): $\delta = 8.87$ (t, $J = 2.0 \text{ Hz}$, 1 H), 8.56 (d, $J = 2.0 \text{ Hz}$, 2 H), 3.54 (br, 4 H), 2.42 (t, $J = 5.0 \text{ Hz}$, 4 H), 2.27 ppm (3 H, s); ¹³C NMR (125 MHz; [D₆]DMSO; 120°C): $\delta = 165.5, 149.1, 139.8, 127.6, 119.4, 54.7, 45.7 \text{ ppm}$; HRMS (ESI) [MH]⁺ $m/z = 295.1042$, [C₁₂H₁₅N₄O₅]⁺ calcd $m/z = 295.1043$.

Received: November 17, 2004

Published online: February 9, 2005

Keywords: biaryls · C–C coupling · medium-ring compounds · organocuprates · oxidation

- [1] J. Hassan, M. Sévignon, C. Gozzi, E. Sculz, M. Lemaire, *Chem. Rev.* **2002**, *102*, 1359.
- [2] For the palladium-catalyzed dimerization of aryl halides, see: a) D. D. Hennings, T. Iwama, V. H. Rawal, *Org. Lett.* **1999**, *1*, 1205; b) J. Hassan, V. Penalva, L. Lavenot, C. Gozzi, M. Lemaire, *Tetrahedron* **1998**, *54*, 13793; c) F.-T. Luo, A. Jeevanandam, M. K. Basu, *Tetrahedron Lett.* **1998**, *39*, 7939.
- [3] For palladium-catalyzed cross-coupling reactions, see: a) T. N. Mitchell in *Metal-Catalyzed Cross-Coupling Reactions* (Ed.: F. Diederich, P. J. Stang), Wiley-VCH, New York, **1998**, chap. 4; b) N. Miyaura, A. Suzuki, *Chem. Rev.* **1995**, *95*, 2457; c) E. Negishi, *Acc. Chem. Res.* **1982**, *15*, 340.
- [4] a) R. Hong, R. Hoen, J. Zhang, G. Lin, *Synlett* **2001**, 1527; b) M. F. Semmelhack, P. Helquist, L. D. Jones, L. Keller, L. Mendelson, L. S. Ryono, J. G. Smith, R. D. Stauffer, *J. Am. Chem. Soc.* **1981**, *103*, 6461.
- [5] a) P. E. Fanta, *Synthesis* **1974**, 9; for a recent application, see: b) A. I. Meyers, T. D. Nelson, H. Moorlag, D. J. Rawson, A. Meier, *Tetrahedron* **2004**, *60*, 4459.
- [6] a) Oxidative coupling, for example: B. Kramer, A. Averhoff, S. R. Waldvogel, *Angew. Chem.* **2002**, *114*, 3103; *Angew. Chem. Int. Ed.* **2002**, *41*, 2981; b) Ullmann-type coupling, for example: S. Zhang, D. Zhang, L. S. Liebeskind, *J. Org. Chem.* **1997**, *62*, 2312; c) radical coupling: H. Tanaka, M. Doi, H. Shimizu, H. Etoh, *Heterocycles* **1999**, *51*, 2415; d) reductive coupling: S. Miyake, A. Sasaki, T. Ohta, K. Shudo, *Tetrahedron Lett.* **1985**, *26*, 5815.
- [7] K. Khanbabaee, T. van Ree, *Synthesis* **2001**, 1585.
- [8] a) W. Su, S. Urgaonkar, P. M. McLaughlin, J. G. Verkade, *J. Am. Chem. Soc.* **2004**, *126*, 16433; b) G. Altenhoff, R. Goddard, C. W. Lehmann, F. Glorius, *J. Am. Chem. Soc.* **2004**, *126*, 15195; c) J. E. Milne, S. L. Buchwald, *J. Am. Chem. Soc.* **2004**, *126*, 13028; d) A. N. Cammidge, K. V. L. Crépy, *Tetrahedron* **2004**, *60*, 4377; e) C. Dai, G. C. Fu, *J. Am. Chem. Soc.* **2001**, *123*, 2719.
- [9] a) Direct iodination: P. C. Anelli, M. Brochetta, C. Maffezzoni, P. Paoli, P. Rossi, F. Uggeri, M. Visigalli, *Perkin Trans. 1* **2001**, 1175; b) from a diazonium salt: B. Ghebremariam, S. Matile, *Tetrahedron Lett.* **1998**, *39*, 5335; c) from an aryne: H. Hart, K. Harada, C.-J. F. Du, *J. Org. Chem.* **1985**, *50*, 3104; d) oxidative coupling: D. Mirk, A. Willner, R. Frölich, S. R. Waldvogel, *Adv. Synth. Catal.* **2004**, *346*, 675, and references therein.
- [10] a) For the first detailed studies, see: G. M. Whitesides, J. SanFilippo, Jr., C. P. Casey, E. P. Panek, *J. Am. Chem. Soc.* **1967**, *89*, 5302; b) for an example of their use as an aggregation probe, see: W. H. Mandeville, G. M. Whitesides, *J. Org. Chem.* **1974**, *39*, 400; c) for the oxidation of organocuprates under “kinetic” conditions, see: B. H. Lipshutz, K. Siegmann, E. Garcia, F. Kayser, *J. Am. Chem. Soc.* **1993**, *115*, 9276, and references therein; e) for a recent application in crystal engineering, see: Y. Morita, T. Murata, S. Yamada, M. Tadokoro, A. Ichimura, K. Nakasuji, *J. Chem. Soc. Perkin Trans. 1* **2002**, 2598.
- [11] a) B. H. Lipshutz, F. Kayser, Z.-P. Liu, *Angew. Chem.* **1994**, *106*, 1962; *Angew. Chem. Int. Ed. Engl.* **1994**, *33*, 1844; b) D. R. Spring, S. Krishnan, H. E. Blackwell, S. L. Schreiber, *J. Am. Chem. Soc.* **2002**, *124*, 1354; c) T. Sugimura, H. Yamada, S. Inoue, A. Tai, *Tetrahedron: Asymmetry* **1997**, *8*, 649; d) A.-C. Carbonnelle, E. G. Zamora, R. Beugelmans, G. Roussi, *Tetrahedron Lett.* **1998**, *39*, 4471; e) S. M. H. Kabir, M. Iyoda, *Chem. Commun.* **2000**, 2329.
- [12] A. E. Jensen, W. Dohle, I. Sapountzis, D. M. Lindsay, V. A. Vu, P. Knochel, *Synthesis* **2002**, 565, and references therein.
- [13] CuCN, CuSCN, and CuI gave comparable but lower yields.
- [14] S. H. Bertz, C. P. Gibson, *J. Am. Chem. Soc.* **1986**, *108*, 8286.
- [15] Other oxidants, such as FeCl₃, [Fe(acac)₃] (acac = acetylacetonate), CuCl₂, LiCuCl₃, CrCl₂, LiNO₃, CeSO₄, 2,3-dichloro-5,6-

- dicyano-1,4-benzoquinone (DDQ), and potassium nitrosodisulfonate (Fremy's salt), gave unsatisfactory yields.
- [16] This compound is readily synthesized in high yield on a large scale from commercially available starting materials (see the Supporting Information) and can be stored indefinitely at room temperature.
- [17] The dianion of dinitrobenzene has been studied electrochemically; for an example see: H. Wang, V. D. Parker, *Acta Chem. Scand.* **1994**, *48*, 933.
- [18] An alternative possibility is that the biphenyl product can itself act as a single-electron oxidant; however, this possibility was ruled out as biphenyl did not act as an oxidant in control reactions.
- [19] It has recently been found that this dimerization proceeds in only moderate yield in a palladium-catalyzed system, see: C. F. Nising, U. K. Schmid, M. Nieger, S. Bräse, *J. Org. Chem.* **2004**, *69*, 6830.
- [20] The halogen–metal exchange has recently been extended to allow the formation of aryl magnesium compounds from the corresponding aryl bromides: A. Krasovskiy, P. Knochel, *Angew. Chem.* **2004**, *116*, 3396; *Angew. Chem. Int. Ed.* **2004**, *43*, 3333. Our preliminary investigations suggest that Grignard reagents formed in this way may also be used to form organocuprates, which may be successfully oxidized under our conditions.
- [21] a) M. Takahashi, T. Ogiku, K. Okamura, T. Da-te, H. Ohmizu, K. Kondo, T. Iwasaki, *J. Chem. Soc. Perkin Trans. 1* **1993**, 1473; b) M. Takahashi, T. Kuroda, T. Ogiku, H. Ohmizu, K. Kondo, T. Iwasaki, *Heterocycles* **1993**, *36*, 1867; c) M. Takahashi, T. Kuroda, T. Ogiku, H. Ohmizu, K. Kondo, T. Iwasaki, *Heterocycles* **1992**, *34*, 2061; d) M. Takahashi, T. Kuroda, T. Ogiku, H. Ohmizu, K. Kondo, T. Iwasaki, *Tetrahedron Lett.* **1991**, *32*, 6919.
- [22] The axial configuration of **2m** was assigned by comparison to literature data: G. Capozzi, C. Ciampi, G. Delogu, S. Menichetti, C. Nativi, *J. Org. Chem.* **2001**, *66*, 8787.
- [23] G. van Koten, S. L. James, J. T. B. H. Jastrzebski in *Comprehensive Organometallic Chemistry II* (Ed.: E. W. Abel, F. G. A. Stone, G. Wilkinson, J. L. Wardell), Pergamon, Oxford, **1995**, chap. 2.

Consecutive Vinylic to Aryl to Allylic Palladium Migration and Multiple C–H Activation Processes**

Jian Zhao, Marino Campo, and Richard C. Larock*

The rearrangement of a Pd moiety along a saturated hydrocarbon chain by a sequence involving Pd–H elimination and subsequent readdition has been extensively explored and developed into a very useful synthetic process.^[1] On the other hand, there are few reports of the “through-space” migration of Pd between remote carbon atoms. The facile 1,4-migration of Pd between a vinylic position and an arene^[2] and between the *ortho* positions of biaryl compounds^[3] have recently been reported. Aryl to benzylic^[4] and alkyl to aryl Pd migrations^[5] are also known. Herein we report a novel, consecutive vinylic to aryl to allylic Pd migration that involves multiple C–H bond activations, which provides a new route to π -allyl palladium intermediates of great interest in organic synthesis.^[6]

The reaction of *p*-iodoanisole and 1-phenyl-1-propyne with CsO₂CCMe₃ as the base provides a 1:1 mixture of (*E*)- and (*Z*)-2-(4-methoxyphenyl)-3-phenyl-2-propenyl pivalate in 20% yield (**1A/B**; Table 1, entry 1). Different aryl halides and alkynes were then used in this reaction, and most combinations give allylic esters in respectable yields. Three isomers are usually obtained when R² = *t*Bu, and only two isomers are generated when R² = Ph. The ratio of the various isomers is dependent on the reaction time and temperature. It appears that longer reaction times and higher temperatures generally favor the formation of isomer C.

Although these reactions proceed in relatively low yields, the mechanism of this unique transformation is quite interesting. This process appears to involve Pd migration from a vinylic to an aryl to an allylic position and subsequent displacement by a pivalate anion (Scheme 1). Intermediate **5**, generated by oxidative addition of the aryl halide to Pd⁰, adds to the alkyne to produce the vinylic Pd intermediate **6**. Insertion of Pd into the neighboring C–H bond forms palladacycle **7**, and subsequent reductive elimination affords

[*] J. Zhao, Prof. Dr. R. C. Larock

Department of Chemistry

Iowa State University

Ames, IA 50011 (USA)

Fax: (+1) 515-294-0105

E-mail: larock@iastate.edu

Dr. M. Campo

University of Geneva

Laboratoire de Pharmacie Galénique et de Biopharmacie

Section de Pharmacie

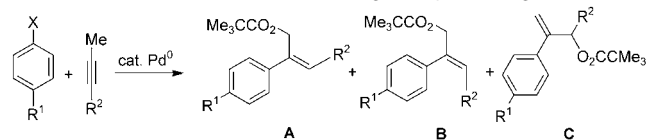
Quai Ernest-Ansermet 30, 1211 Genève 4 (Switzerland)

[**] This work was supported by the National Science Foundation. We thank Johnson Matthey, Inc. and Kawaken Fine Chemical Co. for donations of Pd(OAc)₂.



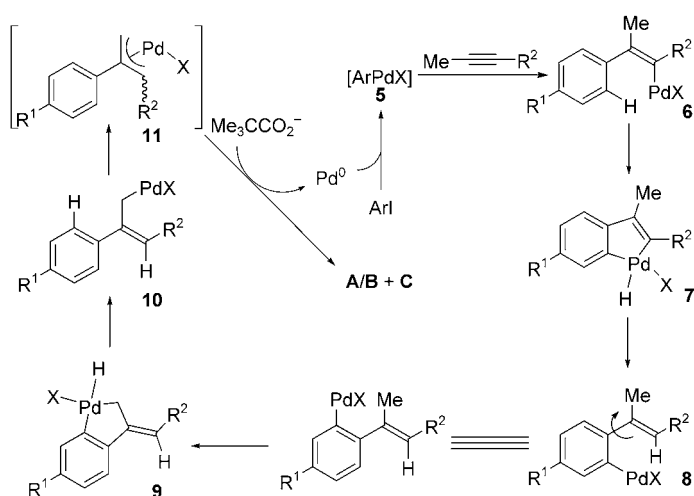
Supporting information for this article is available on the WWW under <http://www.angewandte.org> or from the author.

Table 1: Results of the reactions involving multiple Pd migrations.^[a]



Entry	X	R ¹	R ²	Products	Yield [%] (A:B:C)
1	I	OMe	Ph	1A/B	20 (1:1:0) ^[b]
2	Br	H	<i>t</i> Bu	2A/B, 2C	35 (1:2:7) ^[c]
3	I	H	<i>t</i> Bu	2A/B, 2C	44 (1:2:12) ^[c]
4	Br	CO ₂ Et	<i>t</i> Bu	3A/B, 3C	50 (1:2:18) ^[c]
5	Br	Cl	<i>t</i> Bu	4A/B, 4C	42 (1:2:20) ^[c]

[a] All reactions were conducted on a 0.5-mmol scale for 24 h, and the ratio of ArX to alkyne was 1:1 (sealed vial, under Ar). [b] This reaction was run with 5 mol % Pd(OAc)₂ and 5 mol % dppe at 100 °C, along with DMF (10 mL) and Cs₂CO₃ (2 equiv). [c] This reaction was run with 10 mol % Pd(OAc)₂ and 10 mol % dppe at 125 °C, as well as *N,N*-dimethylacetamide (DMA, 5 mL) and Cs₂CO₃ (2 equiv).



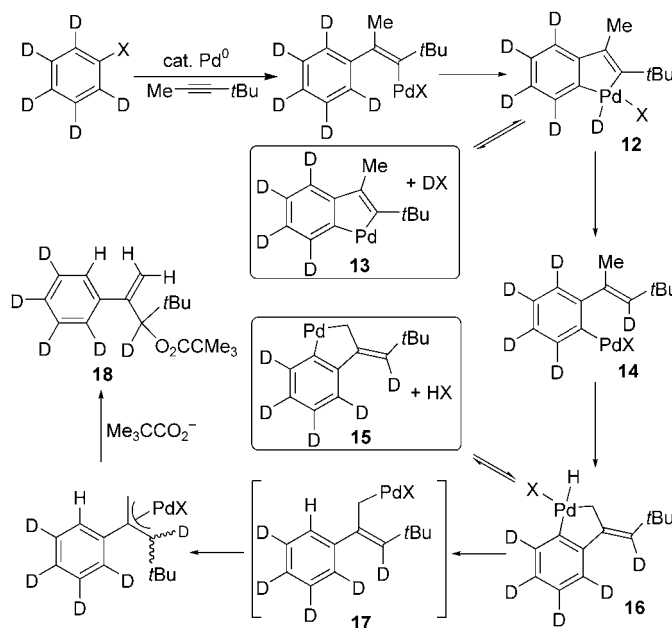
Scheme 1. Proposed mechanism of the Pd migration.

8. This results in Pd migration from a vinylic to an aryl position by C–H bond activation, a process we have reported earlier.^[2]

To initiate a second C–H bond activation, the Pd moiety apparently rotates into the vicinity of the methyl group. Insertion of Pd into the neighboring C–H bond affords palladacycle **9**, which undergoes reductive elimination with transfer of the Pd moiety to the allylic position. This unprecedented migration generates Pd intermediate **10**, which rapidly isomerizes to the corresponding π -allyl palladium species **11**. This unusual process provides a new route for preparing π -allyl palladium compounds, which have proven very versatile as intermediates in organic synthesis.^[6] The three isomeric ester products are presumed to arise by attack of the pivalate anion on the Pd intermediate **11**.

This proposed mechanism indicates that the migration of Pd is always accompanied by a simultaneous migration of hydrogen in the opposite direction. Thus, the observation of a hydrogen or deuterium shift should provide convincing evidence for the Pd migration. [D₅]Bromobenzene (99%

deuterium) and 4,4-dimethyl-2-pentyne were allowed to react with $\text{Pd}(\text{OAc})_2$ (10 mol %), dppm (1,2-bis-(diphenylphosphino)methane; 10 mol %), and $\text{CsO}_2\text{CCMe}_3$ (2 equiv) in DMA at 125°C (Scheme 2). The *E* and *Z* isomers



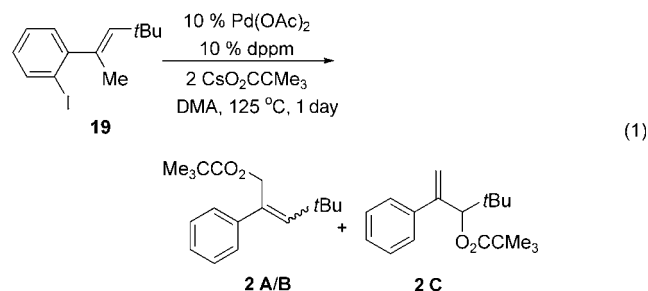
Scheme 2. Proposed formation of the deuterium-labeled product.

of 4,4-dimethyl-2-phenylpent-2-enyl pivalate and 1-*tert*-butyl-2-phenyl-2-propenyl pivalate (**18**) were obtained in a ratio of 1:2:7. Ester **18** was isolated in 20 % yield and found to contain 40 % deuterium in the allylic position and 95 % hydrogen in one of the two *ortho* positions of the phenyl moiety (GC–MS data indicate that hydrogen is only incorporated at one of the two *ortho* positions). This result, except for the relatively low allylic deuterium content, is consistent with the proposed mechanism. However, the deuterium content can be increased by adding 10 equivalents of D₂O to the reaction mixture. The three products were again obtained in a similar ratio, and the resulting ester **18** contained 55 % hydrogen in one *ortho* position of the arene and 75 % deuterium in the allylic position.

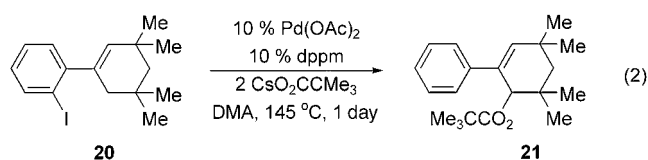
The loss of deuterium in the allylic position probably arises by deuterium/hydrogen exchange through an equilibrium between organopalladium(IV) intermediate **12** and palladacycle **13** or direct exchange of the metal hydride/deuteride in intermediate **12**. Incorporation of deuterium in the allylic position is dependant on the competition between H/D exchange and Pd migration, and it appears that neither is dominant in this case. This reaction was repeated in the presence of 10 equivalents of H₂O, and the three esters obtained incorporate approximately the same ratio of allylic deuterium as the reaction conducted in the absence of H₂O. A similar exchange of hydrogen and deuterium has been observed in aryl norbornyl palladacycles.^[7] When nondeuterated bromobenzene and 4,4-dimethyl-2-pentyne were allowed to react in the presence of 10 equivalents of D₂O, the ester **18** that was obtained had incorporated 40%

deuterium in one of the *ortho* positions of the arene and 40 % deuterium in the allylic position. Although the experimental data is consistent with the proposed mechanism, an alternative mechanism involving an organopalladium(II) palladacycle^[8] and a Pd- π -arene complex^[9] is also possible. Further studies to better understand the mechanism of this process are underway.

We also carried out a Pd migration reaction with the aryl iodide **19**, which would be expected to generate intermediate **8** directly [Eq. (1)]. This species might then undergo Pd



migration to produce the same mixture of pivalate esters formed by the consecutive rearrangement. Under the same reaction conditions, we obtained the anticipated product mixture (**2A**:**2B**:**2C** = 1:2:20) in 65 % yield. Although the ratio of the regioisomer **2C** to **2A/B** is a little higher than in the consecutive migration process, the results are still consistent with our proposed mechanism. We also examined the reaction of aryl iodide **20** under the usual reaction conditions, but at 145 °C [Eq. (2)]. This reaction affords the allylic pivalate **21** in 45 % yield. Thus, it appears that the aryl palladium intermediate corresponding to **20** is able to undergo migration to a secondary allylic position.



In terms of mechanism, an intermediate such as **17** could also be generated by carbopalladation of the allene 4,4-dimethyl-1,2-pentadiene, which might arise by isomerization of 4,4-dimethyl-2-pentyne. However, when carried out with [D₅]bromobenzene, this process would not introduce a hydrogen atom into the *ortho* position of the arene or a deuterium atom into the allylic position of the final ester product, unless the Pd moiety could reversibly migrate from the allylic to the aryl to the vinylic position. Only then could we observe a hydrogen atom in the *ortho* position of the arene and a deuterium atom in the vinylic position, as well as deuterium incorporation into the allylic position. To better understand this process, the reaction shown in Equation (1) was conducted in the presence of 10 equivalents of D₂O. The isolated product **2C** contained 40 % deuterium in one of the *ortho* positions of the arene (according to GC-MS analysis,

see Supporting Information), but no deuterium in the vinylic or allylic positions. This suggests that the vinylic to aryl migration is not a reversible process. Because no deuterium incorporation in the methylene or allylic positions was observed, we can also rule out reversible Pd migration from the allylic to the aryl position.

In conclusion, we have discovered a novel consecutive vinylic to aryl to allylic Pd migration, which affords a unique way to generate π -allyl palladium complexes. This migration process appears to involve an equilibrium between organopalladium(IV) hydrides and organopalladium(II) intermediates, which undergo facile exchange with a hydrogen source in the solution. However, we cannot rule out direct exchange of the Pd^{IV} hydride. We are continuing to study this process in order to better understand the mechanism and its synthetic potential.

Received: October 16, 2004

Published online: February 14, 2005

Keywords: C–H activation · deuterium · palladium · rearrangement · synthetic methods

- [1] a) Y. Wang, X. Dong, R. C. Larock, *J. Org. Chem.* **2003**, *68*, 3090–3098, and references therein; b) R. C. Larock, Y. Lu, A. C. Bain, C. E. Russell, *J. Org. Chem.* **1991**, *56*, 4589–4590; c) R. C. Larock, Y. Wang, Y. Lu, C. E. Russell, *J. Org. Chem.* **1994**, *59*, 8107–8114.
- [2] R. C. Larock, Q. Tian, *J. Org. Chem.* **2001**, *66*, 7372–7379.
- [3] a) G. Karig, M. T. Moon, N. Thasana, T. Gallagher, *Org. Lett.* **2002**, *4*, 3115–3118; b) M. A. Campo, R. C. Larock, *J. Am. Chem. Soc.* **2002**, *124*, 14326–14327; c) M. A. Campo, Q. Huang, T. Yao, Q. Tian, R. C. Larock, *J. Am. Chem. Soc.* **2003**, *125*, 11506–11507.
- [4] L. Wang, Y. Pan, X. Jiang, H. Hu, *Tetrahedron Lett.* **2000**, *41*, 725–727.
- [5] a) M. Catellani, F. Cugini, G. Bocelli, *J. Organomet. Chem.* **1999**, *584*, 63–67; b) M. Catellani, L. Ferioli, *Synthesis* **1996**, 769–772; c) Q. Huang, A. Fazio, G. Dai, M. A. Campo, R. C. Larock, *J. Am. Chem. Soc.* **2004**, *126*, 7460–7461.
- [6] For a recent review, see: a) B. M. Trost, M. L. Crawley, *Chem. Rev.* **2003**, *103*, 2921–2944; for a brief overview, see b) J. Tsuji in *Handbook of Organopalladium Chemistry for Organic Synthesis*, Vol. 2 (Eds.: E. Negishi, A. de Meijere, J. E. Backvall, S. Cacchi, T. Hayashi, Y. Ito, M. Kosugi, S. I. Murahashi, K. Oshima, Y. Yamamoto), Wiley-Interscience, New York, **2002**, pp. 1663–2305.
- [7] B. A. Markies, P. Wijkens, H. Kooijman, A. L. Spek, J. Boersma, G. Van Koten, *J. Chem. Soc. Chem. Commun.* **1992**, 1420–1423.
- [8] a) M. Catellani, E. Motti, S. Ghelli, *Chem. Commun.* **2000**, 2003–2004; b) for a recent review, see M. Catellani, *Synlett* **2003**, 298–313; c) G. Dyker, *Angew. Chem.* **1999**, *111*, 1808–1822; *Angew. Chem. Int. Ed.* **1999**, *38*, 1699–1712; d) G. Dyker, *Angew. Chem.* **1994**, *106*, 117–119; *Angew. Chem. Int. Ed. Engl.* **1994**, *33*, 103–105; e) G. Dyker, *Angew. Chem.* **1992**, *104*, 1079–1081; *Angew. Chem. Int. Ed. Engl.* **1992**, *31*, 1023–1025.
- [9] J. Campora, J. A. Lopez, P. Palma, V. Pedro, S. Edzard, C. Ernesto, *Angew. Chem.* **1999**, *111*, 199–203; *Angew. Chem. Int. Ed.* **1999**, *38*, 147–151, and references therein.

Magnetic Properties

Very Large Ising-Type Magnetic Anisotropy in a Mononuclear Ni^{II} Complex**

Guillaume Rogez,* Jean-Noël Rebilly,
Anne-Laure Barra, Lorenzo Sorace,
Geneviève Blondin, Nadeschda Kirchner, Marc Duran,
Joris van Slageren, Simon Parsons, Louis Ricard,
Arnaud Marvilliers, and Talal Mallah*

Magnetic anisotropy is one of the crucial parameters governing the magnetic behavior of large spin-clusters. Single-molecule magnetism (SMM) and quantum tunneling of the magnetization in clusters are mainly governed by the nature and the magnitude of the magnetic anisotropy in their ground spin state.^[1] One of the main sources of magnetic anisotropy in polynuclear clusters is single-ion anisotropy.^[2]

In this respect Ni^{II} complexes are particularly interesting and are frequently used as building blocks of single-molecule magnets.^[3] Nonetheless, few studies have been devoted to the magnetic anisotropy of isolated Ni^{II} complexes,^[4] with the

most recent report concerning a family of pseudotetrahedral dihalobis(triphenylphosphite) complexes.^[5]

We report here the preparation, structure, and magnetic properties of a mononuclear octahedral Ni^{II} complex [Ni-(HIM2-py)₂NO₃]₂NO₃ (**1**) with the bidentate ligand HIM2-py. Magnetization versus field measurements at different temperatures, high-field and high-frequency EPR (HF-HFEPR) studies, and frequency domain magnetic resonance spectroscopy (FDMRS) studies indicated the presence of a very large Ising-type anisotropy ($D = -10.1 \pm 0.1 \text{ cm}^{-1}$ and $E/|D| = 0.02 \pm 0.01$) never before reported for an isolated Ni^{II} complex.

The structure of **1** shows that the coordination sphere of the Ni^{II} center contains the four nitrogen atoms of the two HIM2-py ligands in the *cis* positions and the two oxygen atoms of the *O,O'*-chelating nitrate (Figure 1). The geometry

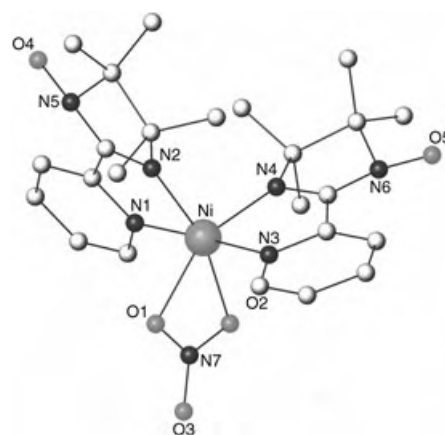
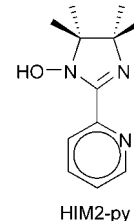


Figure 1. View of the molecular structure of **1**.

around the nickel atom is highly distorted. The Ni–N bond lengths are all different and range from 204.3(9) to 208.9(9) pm, whereas the Ni–O distances are 213.3(8) and 219.4(9) pm. The O1–Ni–O2 angle is very small (59.0°) and is similar to that found in other Ni^{II} complexes that bear an *O,O'*-bound nitrate.^[6] The bite angles of the other bidentate ligands are 79.6(4)° and are, as expected, far from 90°. We can thus consider that **1** has a symmetry close to *C*_{2v} with a pseudoprincipal symmetry *C*₂-rotation axis that bisects the O–Ni–O angle along which it is elongated.

Magnetization versus field measurements between 0 and 5.5 T were performed at different temperatures with a SQUID magnetometer. The $M = f(H/T)$ plots for $T = 2, 4, 6$, and 8 K are not superimposable owing to the presence of magnetic anisotropy within the complex (Figure 2). For $T = 2 \text{ K}$ and $H = 5.5 \text{ T}$ the observed magnetization value of 1.65 BM ($9.22 \times 10^{-3} \text{ m}^3 \text{ Oe mol}^{-1}$) is well below the theoretical saturation for an $S = 1$ system ($M_{\text{sat}} = 2.2 \text{ BM}$ ($12.29 \times 10^{-3} \text{ m}^3 \text{ Oe mol}^{-1}$) for $g = 2.2$), as expected in the case of appreciable magnetic anisotropy. The experimental data were fitted by exact diagonalization of the energy matrices corresponding to the spin Hamiltonian $\mathcal{H} = \mu_B \mathbf{B} [g] \hat{\mathbf{S}} +$

[*] Dr. G. Rogez, J.-N. Rebilly, Dr. G. Blondin, Dr. A. Marvilliers, Prof. T. Mallah

Laboratoire de Chimie Inorganique, UMR CNRS 8613

Université Paris-Sud, Bât 420, 91405 Orsay (France)

Fax: (+33) 1-6915-4754

E-mail: guillaume.rogez@ipcms.u-strasbg.fr
mallah@icmo.u-psud.fr

Dr. G. Rogez

IPCMS-GMI, UMR CNRS 7504

23, rue du Loess, B.P. 43, 67034 Strasbourg Cedex 2 (France)

Fax: (+33) 3-8810-7247

Dr. A.-L. Barra

Laboratoire des Champs Magnétiques Intenses, UPR CNRS 5021
25, avenue des Martyrs, B.P. 166, 38042 Grenoble Cedex 9 (France)

Dr. L. Sorace

UdR INSTM and Department of Chemistry

University of Florence, Polo Scientifico Universitario

Via della Lastruccia 3, 50019 Sesto Fiorentino (Italy)

N. Kirchner, Dr. M. Duran, Dr. J. van Slageren

1. Physikalisches Institut, Universität Stuttgart

Pfaffenwaldring 57, 70550 Stuttgart (Germany)

Dr. S. Parsons

Department of Chemistry, The University of Edinburgh

West Mains Road, Edinburgh EH9 3JJ (UK)

Dr. L. Ricard

Laboratoire "Hétéroéléments et Coordination", UMR CNRS 7653

Ecole Polytechnique

91128 Palaiseau (France)

[**] We thank the CNRS, the Université Paris XI, and the EPSRC for funding, the LCMI for provision of magnet time, and the EC for financial support (MRTN-CT-2003-504880/RTN Network "QuE-MolNa"). The work at Stuttgart was supported by the DFG priority program on molecular magnetism (SPP1137). M.D. acknowledges a NANOTEC fellowship from the Catalan Government. We thank H. Weihe for provision of the SimEPR program and A. Bencini for provision of the AOM program.

Supporting information for this article is available on the WWW under <http://www.angewandte.org> or from the author.

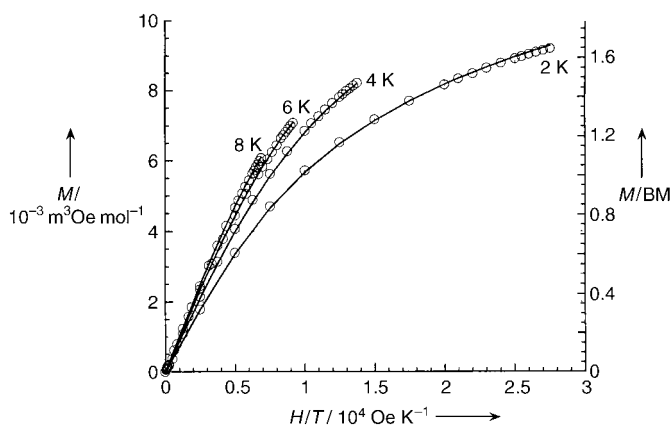


Figure 2. $M=f(H/T)$ plots for complex **1**. The lines correspond to the best fit (see text).

$D[\hat{S}_x^2 - S(S+1)/3] + E[\hat{S}_x^2 - \hat{S}_y^2]$, where D and E are the axial and rhombic anisotropy parameters, respectively, averaged over 120 orientations of the magnetic field.^[7] The fitting was performed simultaneously for the four experimental temperatures. The best fit was obtained with $D = -11.2 \text{ cm}^{-1}$, $E/|D| = 0.0$, and $g_{\text{iso}} = 2.16$ ($R = 3.7 \times 10^{-5}$). To reduce the variable parameters during the fitting procedure, the $[g]$ tensor was constrained to be isotropic. Generally, it is not possible to determine the sign of the axial parameter D from the magnetization data as it is possible to find different sets of values for D and $E/|D|$, in which D may be positive or negative, that yield equally satisfactory agreement factors. However, in the case of large D values, low rhombicity, and when the fit is made for different temperatures simultaneously, only one set of parameters is obtained, as in the present case.^[8b] All attempts to fit the experimental data using a positive value for D were, indeed, unsuccessful.

Owing to the very large anisotropy of the compound, only a few transitions are visible in the HF-HFEPR spectra. The main feature of the spectra is a very intense transition at low field, denoted B_{min} , the others being much weaker and difficult to assign precisely (the assignments reported in Figure 3 were made on the basis of the best simulation

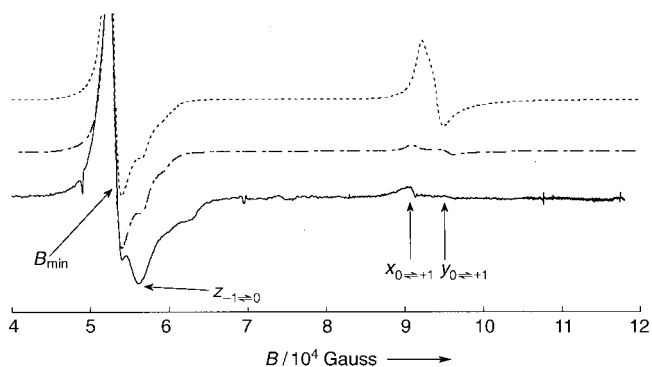


Figure 3. Experimental HF-EPR spectra of **1** at 475 GHz, $T = 5 \text{ K}$ (—) and simulated with $E/|D| = 0.01$, $g_{\text{iso}} = 2.17$, and $D = -10.15 \text{ cm}^{-1}$ (---) or $D = +10.15 \text{ cm}^{-1}$ (----). The transitions are identified by the m_s value of the levels between which they occur, considering the quantization axis parallel to the external field.

parameters). Assuming an axial symmetry, the zero-field signal at the lowest frequency provides a direct determination of $|D|$ of about 10 cm^{-1} . On this basis, B_{min} , which occurs at 5.3 T for an incident radiation of 475 GHz, can be assigned to an off-axis turning-point-allowed transition.^[5a] No clear evolution of the intensity of the allowed transitions was observed when changing the temperature, which prevents direct determination of the sign of D ; nevertheless, the spectra were better reproduced with $D < 0$ (Figure 3). The very high anisotropy of the zero-field splitting tensor prevents determination of the g anisotropy, although the $[g]$ tensor is most probably strongly axial. We thus used an isotropic value for g ($g_{\text{iso}} = 2.17$), which is in the range expected for Ni^{II} . The HF-HFEPR spectra are well reproduced at all frequencies, and the best simulations were obtained with the following values: $g_{\text{iso}} = 2.17$, $D = -10.15 \text{ cm}^{-1}$, and $E/|D| = 0.01$ (see Supporting Information).

The most important feature in the FDMRS spectra (Figure 4) is a narrow line at about 10.5 cm^{-1} , which decreases

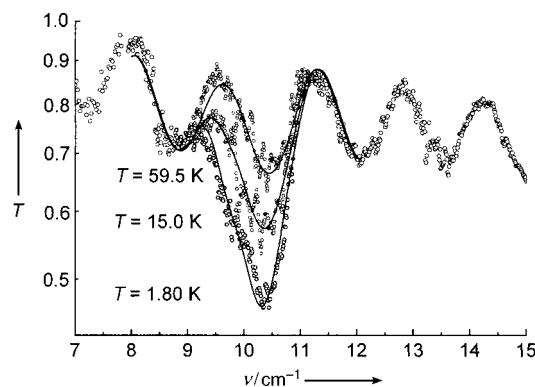


Figure 4. FDMRS spectra of **1** at various temperatures (experimental (○), simulation (—)).

in intensity on raising the temperature. This line is due to magnetic resonance transitions between the m_s levels of the $S = 1 \text{ Ni}^{\text{II}}$ ion. The resonance frequencies were obtained from the normalized spectra (i.e. all spectra were divided by the spectrum recorded at the highest temperature). From the line shape it was clear that the resonance line must consist of two overlapping lines owing to the transitions between the $|1\rangle$ and $|0\rangle$ and the $|-1\rangle$ and $|0\rangle$ m_s states, respectively. In an $S = 1$ system the resonance frequencies of these transitions correspond to $|D| - E$ and $|D| + E$, respectively. The resonance frequencies were found to be $\nu_1 = 9.7 \pm 0.1$ and $\nu_2 = 10.3 \pm 0.1 \text{ cm}^{-1}$, respectively. Therefore, it immediately follows that $|D| = 10.0 \pm 0.1 \text{ cm}^{-1}$ and $E = 0.3 \pm 0.1 \text{ cm}^{-1}$. The simulated spectra are also shown in Figure 4. The best fit was obtained using Gaussian line shapes, which means that the line width is determined by distributions in the sample rather than by spin-lattice relaxation.

The sign of D can be obtained from the temperature dependence of the spectra. When $D > 0$, both resonance lines should retain the same intensity. However, if $D < 0$, the intensity of the lowest frequency line should tend to zero upon decreasing the temperature because it is a transition from an excited state.

Figure 5 shows the line intensities in terms of the mode contributions to the magnetic permeability, obtained from the spectral fit, as a function of temperature, together with the calculated behavior using $D < 0$ and $D > 0$ values. Note that

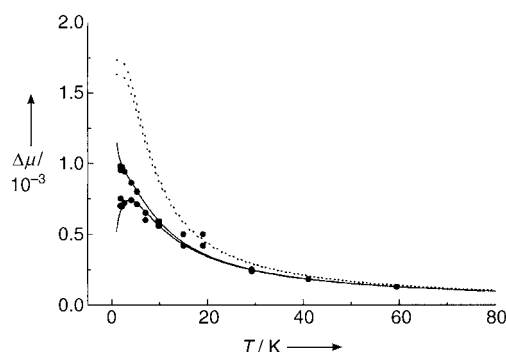


Figure 5. Dependence of the resonance mode contribution to the magnetic permeability $\Delta\mu$ on temperature (experimental $\Delta\mu$ (●); calculations with $D < 0$ (—); calculations with $D > 0$ (·····)).

these values are absolute numbers, and that the calculated temperature dependence of the mode contribution is not scaled. Thus, not only does the intensity of the low-frequency line decrease at the lowest temperatures, but the absolute intensities of the mode contributions are also in much better agreement with a negative D parameter. From these calculations it is clear that D must be negative, and therefore $D = -10.0 \pm 0.1 \text{ cm}^{-1}$ and $E = 0.3 \pm 0.1 \text{ cm}^{-1}$. These values correspond very well to those found from magnetization and HF-HFEPR measurements. Moreover, this FDMRS experiment confirms unambiguously the negative sign of the D parameter. This is also in agreement with ligand-field-based, second-order-perturbation calculations, which show that a Ni^{II} complex bearing six identical ligands and elongated along a C_2'' axis should possess an Ising-type magnetic anisotropy ($D < 0$ and $E/|D| = 0$).^[8]

To go beyond this qualitative assertion, we used a computer program based on the angular-overlap model that enables the calculation of the spin Hamiltonian parameters if the structure of the complex and the angular-overlap parameters of each ligand are known.^[9] However, as the exact parameters for the ligand HIM2-py are not known, we extrapolated them from the data of the literature on similar ligands^[10] whilst neglecting the anisotropy of the π -overlap as a first approximation. We checked that assuming a completely anisotropic π -interaction for pyridine did not significantly modify the results. We obtained values of $D = -10.1 \text{ cm}^{-1}$ and $E/|D| = 0.10$,^[11] in good agreement with the experimental values, even though the estimated rhombic parameter is much larger than the experimental value, as already observed for other systems.^[5] Varying the angular overlap parameters slightly does not significantly alter the results of the calculation, although a variation of $\pm 10\%$ around the above-mentioned values of e_σ and e_π leads to proportional changes in the D values (ranging from -9.0 to -11.5 cm^{-1}) and almost no change in the rhombic parameter.

To the best of our knowledge, **1** shows the largest Ising-like magnetic anisotropy ($D < 0$) ever reported for an isolated octahedral Ni^{II} complex, thus making it a suitable candidate for use as a building block in polynuclear clusters showing SMM behavior, even though the relative orientation of the local anisotropy axis within the cluster is also crucial.^[12] Data obtained from HF-HFEPR spectra, field-dependent magnetization, and FDMRS are in very good agreement (within 10%) and show the complementarity between these techniques for the study of highly anisotropic integer-spin systems, especially for the unambiguous determination of the sign of the D parameter. Moreover, we have shown in this study that careful examination of the molecular structure by relatively easy to perform AOM calculations could allow us to perform a good estimation of the zero field splitting (ZFS) parameters. This may serve as a very useful “prediction tool” in order to help to design complexes with a desired magnetic anisotropy, which could be of great use for the so-called “rational approach” to single-molecule magnets.

Experimental Section

Synthesis of 1: HIM2-py was synthesized according to published procedures.^[13] A deaerated solution of $[\text{Ni}(\text{H}_2\text{O})_6](\text{NO}_3)_2$ (1.4 g, 4.8 mmol) in a mixture of acetonitrile and methanol (70:30 v/v, 40 mL) was added, under an inert atmosphere, to a deaerated solution of HIM2-py (2.1 g, 9.5 mmol) in the same mixture of solvents (50 mL). Crystals of **1** were isolated by slow diffusion of diethyl ether vapor into the mixture (yield = 17%). Elemental analysis calcd (%) for **1**, $\text{C}_{24}\text{H}_{34}\text{N}_8\text{NiO}_8$: C 46.40, H 5.51, N 18.03, Ni 9.44; found: C 46.47, H 5.51, N 18.42, Ni 9.13.

X-ray crystallographic data: Nonius KappaCCD diffractometer, ϕ and ω scans, $\text{MoK}\alpha$ radiation ($\lambda = 0.71073 \text{ \AA}$), graphite monochromator, $T = 150 \text{ K}$, structure solution with SIR97,^[14] refinement against F^2 (SHELXL97)^[15] with anisotropic thermal parameters for all non-hydrogen atoms; hydrogen positions calculated with riding isotropic thermal parameters. Data collection for **1**: crystal dimensions $0.20 \times 0.18 \times 0.16 \text{ mm}^3$, orthorhombic, $P2_12_12_1$, $a = 10.9890(10)$, $b = 13.2620(10)$, $c = 20.2230(10) \text{ \AA}$, $V = 2947.2(4) \text{ \AA}^3$, $Z = 4$, $\rho_{\text{calcd}} = 1.400 \text{ g cm}^{-3}$, $\mu = 0.717 \text{ cm}^{-1}$, $F(000) = 1304$, $\theta_{\text{max}} = 30.03^\circ$, hkl ranges: -15 to 15 ; -18 to 18 ; -28 to 28 , 8518 data collected, 8518 unique data, 7020 data with $I > 2\sigma(I)$, 379 parameters refined, $\text{GOF}(F^2) = 1.015$, final R indices ($R1 = \sum ||F_o| - |F_c|| / \sum |F_o|$, $wR2 = [\sum w(F_o^2 - F_c^2)^2 / \sum w(F_o^2)^2]^{1/2}$, $R1 = 0.0378$, $wR2 = 0.0971$, Flack parameter $0.027(9)$, max/min residual electron density $0.541(0.057) / -0.463(0.057) \text{ e \AA}^{-3}$. CCDC-251946 contains the supplementary crystallographic data for this paper. These data can be obtained free of charge via www.ccdc.cam.ac.uk/conts/retrieving.html (or from the Cambridge Crystallographic Data Centre, 12, Union Road, Cambridge CB2 1EZ, UK; fax: (+44) 1223-336-033; or deposit@ccdc.cam.ac.uk).

Magnetization measurements were performed on a Quantum Design MPMS5 SQUID magnetometer. The powder obtained from ground crystals of **1** was sealed in parafilm to avoid any orientation of the sample. Data were corrected for the parafilm contribution, and diamagnetism was estimated from Pascal constants.

HF-HFEPR experiments were performed at the High Magnetic Field Laboratory, Grenoble, France, using a previously described apparatus.^[16] We used ground crystals (about 30 mg) pressed to form a pellet to reduce torquing effects under high magnetic fields. A simulation program is available from Dr. H. Weihe; for more information see <http://sophus.kiku.dk/software/epr/epr.html>.^[17]

Frequency domain magnetic resonance spectroscopic (FDMRS) measurements were performed on a homebuilt spectrometer described in the literature.^[18] Spectra were recorded at various temper-

atures on a pressed powder pellet of 155 mg with a diameter of 1 cm and a thickness of 1.82 mm.

Received: October 13, 2004

Published online: February 11, 2005

Keywords: angular-overlap model · EPR spectroscopy · FDMR spectroscopy · magnetic properties · nickel

- [1] R. Sessoli, D. Gatteschi, *Angew. Chem.* **2003**, *115*, 278; *Angew. Chem. Int. Ed.* **2003**, *42*, 268, and references cited therein.
- [2] a) A.-L. Barra, A. Caneschi, A. Cornia, F. Fabrizi de Biani, D. Gatteschi, C. Sangregorio, R. Sessoli, L. Sorace, *J. Am. Chem. Soc.* **1999**, *121*, 5302; b) G. L. Abbati, L.-C. Brunel, H. Casalta, A. Cornia, A. C. Fabretti, D. Gatteschi, A. K. Hassan, A. G. M. Jansen, A. L. Maniero, L. Pardi, C. Paulsen, U. Segre, *Chem. Eur. J.* **2001**, *7*, 1796; c) D. Gatteschi, L. Sorace, *J. Solid State Chem.* **2001**, *159*, 253; d) D. Collison, M. Murrie, V. S. Oganessian, S. Piligkos, N. R. J. Poolton, G. Rajaraman, G. M. Smith, A. J. Thomson, G. A. Timco, W. Wernsdorfer, R. E. P. Winpenny, E. J. L. McInnes, *Inorg. Chem.* **2003**, *42*, 5293.
- [3] a) N. Vernier, G. Bellessa, T. Mallah, M. Verdager, *Phys. Rev. B* **1997**, *56*, 75; b) C. Cadiou, M. Murrie, C. Paulsen, V. Villar, W. Wernsdorfer, R. E. P. Winpenny, *Chem. Commun.* **2001**, 2666; c) S. T. Ochsenbein, M. Murrie, E. Rusanov, H. Stoeckli-Evans, C. Sekine, H. U. Güdel, *Inorg. Chem.* **2002**, *41*, 5133; d) M. Moragues-Cánovas, M. Helliwell, L. Ricard, E. Rivière, W. Wernsdorfer, E. Brechin, T. Mallah, *Eur. J. Inorg. Chem.* **2004**, 2219.
- [4] a) B. E. Myers, L. G. Polgar, S. A. Friedberg, *Phys. Rev. B* **1972**, *6*, 3488; b) Y. Ajiro, S. A. Friedberg, N. S. VanderVen, *Phys. Rev. B* **1975**, *12*, 39; c) R. L. Carlin, C. J. O'Connor, S. N. Bhatia, *J. Am. Chem. Soc.* **1976**, *98*, 3523; d) L. A. Pardi, A. K. Hassan, F. B. Hulsbergen, J. Reedijk, A. L. Spek, L.-C. Brunel, *Inorg. Chem.* **2000**, *39*, 159; e) J. Mroziński, A. Skorupa, A. Pochaba, Y. Dromzée, M. Verdager, E. Goovaerts, H. Varcammen, B. Korybut-Daszkiewicz, *J. Mol. Struct.* **2001**, *559*, 107; f) A. Mašlejová, R. Boča, L. Dlháň, R. Herchel, *J. Magn. Magn. Mater.* **2004**, *272–276*, 380; g) R. Boča, *Coord. Chem. Rev.* **2004**, *248*, 757.
- [5] a) J. Krzystek, J.-H. Park, M. W. Meisel, M. A. Hitchman, H. Strateimer, L.-C. Brunel, J. Telser, *Inorg. Chem.* **2002**, *41*, 4478; b) S. Vongtragool, B. Gorshunov, M. Dressel, J. Krzystek, D. M. Eichhorn, J. Telser, *Inorg. Chem.* **2003**, *42*, 1788.
- [6] T. Astley, M. A. Hitchman, B. W. Skelton, A. H. White, *Aust. J. Chem.* **1997**, *50*, 145.
- [7] O. Horner, E. Rivière, G. Blondin, S. Un, A. W. Rutherford, J.-J. Girerd, A. Boussac, *J. Am. Chem. Soc.* **1998**, *120*, 7924.
- [8] a) F. E. Mabbs, D. Collison, *Electron Paramagnetic Resonance of d Transition Metal Compounds*, Elsevier, Amsterdam, **1992**; b) G. Rogez, PhD thesis, Université Paris-Sud, Orsay (France), **2002**.
- [9] A. Bencini, I. Ciofini, M. G. Uytterhoeven, *Inorg. Chim. Acta* **1998**, *274*, 90.
- [10] a) A. B. P. Lever, *Inorganic Electronic Spectroscopy*, 2nd ed., Elsevier, Amsterdam, **1984**; b) A. Bencini, C. Benelli, D. Gatteschi, *Coord. Chem. Rev.* **1984**, *60*, 131.
- [11] The parameters for aromatic polyamines were estimated by considering that in these systems e_o and e_π and the ratio e_o/e_π are slightly higher than for the corresponding monoamine.^[10b] For the O,O'-bound nitrate, we used the values reported for another complex with similar structure.^[6] We used $B = 860\text{ cm}^{-1}$, $C/B = 3.9$, and $\xi = 630\text{ cm}^{-1}$ for the Racah parameters and the spin-orbit constant, and $e_o(N1_{\text{pyr}}) = e_o(N3_{\text{pyr}}) = 4400\text{ cm}^{-1}$, $e_\pi(N1_{\text{pyr}}) = e_\pi(N3_{\text{pyr}}) = 400\text{ cm}^{-1}$, $e_o(N2_{\text{im}}) = e_o(N4_{\text{im}}) = 4600\text{ cm}^{-1}$, $e_\pi(N2_{\text{im}}) = e_\pi(N4_{\text{im}}) = 500\text{ cm}^{-1}$, $e_o(O1_{\text{nitrate}}) = 3300\text{ cm}^{-1}$, $e_\pi(O1_{\text{nitrate}}) = 400\text{ cm}^{-1}$, $e_o(O2_{\text{nitrate}}) = 3200\text{ cm}^{-1}$, and $e_\pi(O2_{\text{nitrate}}) = 300\text{ cm}^{-1}$ for the angular-overlap parameters.
- [12] J. van Slageren, R. Sessoli, D. Gatteschi, A. A. Smith, M. Helliwell, R. E. P. Winpenny, A. Cornia, A.-L. Barra, A. G. M. Jansen, E. Rentschler, G. A. Timco, *Chem. Eur. J.* **2002**, *8*, 277; b) D. Collison, V. S. Oganessian, S. Piligkos, A. J. Thomson, R. E. P. Winpenny, E. J. L. McInnes, *J. Am. Chem. Soc.* **2003**, *125*, 1168.
- [13] J. N. Helbert, P. W. Kopf, E. H. Pointdexter, B. E. Wagner, *J. Chem. Soc. Dalton Trans.* **1975**, 998.
- [14] A. Altomare, M. C. Burla, M. Camalli, G. Cascarano, C. Giacovazzo, A. Guagliardi, A. G. G. Moliterni, G. Polidori, R. Spagna, SIR97, an integrated package of computer programs for the solution and refinement of crystal structures using single crystal data.
- [15] G. M. Sheldrick, SHELXL-97, Universität Göttingen, Germany, **1997**.
- [16] A.-L. Barra, L.-C. Brunel, J. B. Robert, *Chem. Phys. Lett.* **1990**, *165*, 107.
- [17] J. Glerup, H. Weihe, *Acta Chem. Scand.* **1991**, *45*, 444.
- [18] J. van Slageren, S. Vongtragool, B. Gorshunov, A. A. Mukhin, N. Karl, J. Krzystek, J. Telser, A. Müller, C. Sangregorio, D. Gatteschi, M. Dressel, *Phys. Chem. Chem. Phys.* **2003**, *5*, 3837.

Pummerer-like Reactions

**Resolution of [4]Heterohelicenium Dyes with
Unprecedented Pummerer-like Chemistry****

*Benoît Laleu, Pierre Mobian, Christelle Herse,
Bo W. Laursen, Gérard Hopfgartner,
Gérald Bernardinelli, and Jérôme Lacour**

Helicenes and heterohelicenes, which present fascinating left-
and right-handed chiral helical structures (of *M* and *P*

[*] B. Laleu, Dr. P. Mobian, C. Herse, Prof. J. Lacour
Department of Organic Chemistry
University of Geneva
quai Ernest Ansermet 30, 1211 Genève 4 (Switzerland)
Fax: (+41) 22-379-3215
E-mail: jerome.lacour@chiorg.unige.ch
Dr. G. Bernardinelli
Laboratory of Crystallography
University of Geneva
quai Ernest Ansermet 24, 1211 Genève 4 (Switzerland)
Prof. G. Hopfgartner
School of Pharmacy
University of Geneva
20, Bd d'Yvoy, 1211 Genève 4 (Switzerland)
Dr. B. W. Laursen
Nano-Science Center
Department of Chemistry
Universitetsparken 5, 2100 Copenhagen (Denmark)

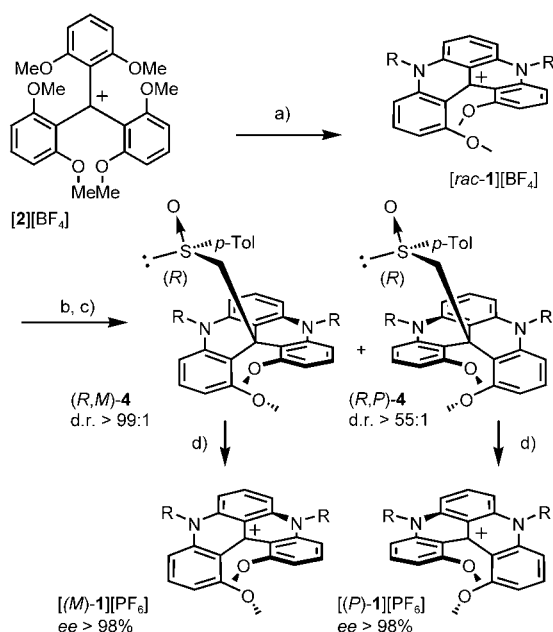
[**] We are grateful for financial support of this work by the Swiss
National Science Foundation, the Federal Office for Education and
Science (COST), and the Sandoz Family Foundation (J.L.).



Supporting information for this article is available on the WWW
under <http://www.angewandte.org> or from the author.

configuration, respectively),^[1] have been intensively studied owing to their excellent ability to self-assemble^[2] as well as their chiroptical, photochromic, nonlinear optical,^[3] and DNA-intercalating properties.^[4] Furthermore, they are useful for applications in asymmetric molecular recognition^[5] and synthesis^[6] as well as in polymer and material sciences.^[7,8] For many of these applications, the (hetero)helicenes must be isolated with high enantiomeric purity. The most efficient syntheses of nonracemic helicenes reported to date are based on resolutions of racemic derivatives.^[9,10] Several enantio- or diastereoselective approaches have also been described, and in some cases high levels of asymmetric inductions have been achieved.^[1d,11]

The 1,13-dimethoxyquinacridinium cation **1a** has previously been reported (Scheme 1, R = *n*Pr).^[12] This cationic dye



Scheme 1. Synthesis of [(*M*)-**1**][PF₆] and [(*P*)-**1**][PF₆]. a) RNH₂ (R = *n*Pr (a), *n*Oct (b), *i*Pr (c), *c*Hex (d)), *N*-methylpyrrolidine (NMP), 1.5 h, 110 °C; b) (+)-(*R*)-**3**, LDA, THF, 0 °C, 1:1 mixture of diastereomers; c) column chromatography (SiO₂); d) aq. HPF₆, acetone. Tol = tolyl.

is prepared in one step and with good yield by the reaction of primary propylamine and the readily available salt of **2**. The molecular framework of **1** contains four *ortho*-condensed aromatic rings. Owing to the steric repulsion between the two methoxy substituents, these derivatives adopt a twisted helical conformation. As such, compounds of type **1** may be regarded as [4]heterohelicinium derivatives.^[13,14]

Recently it was shown that cation **1a** demonstrates high configurational stability, even more so than [6]helicene.^[15] The hexafluorophosphate salt of **1a** was obtained in enantioenriched form (*ee* > 96 %) by ion-pairing association with enantiopure BINPHAT (BINPHAT = bis-(tetrachlorobenzenediolato)mono([1,1']binaphthalenyl-2,2'-diolato)-phosphate(v)) anion,^[16] selective precipitation of one diastereomeric salt (benzene/THF), and ion metathesis with KPF₆. However, the moderate yields at the precipitation stage

(30 %), the low diastereomeric purity in the mother liquor (*de* = 41 %), and the fact that the process cannot be applied to lipophilic cations such as **1b** (R = *n*Oct) prompted us to look for a more effective resolution procedure. Herein we report a short and general protocol for the resolution of cationic dyes of type **1** using 1) the addition of an enantiopure sulfoxide moiety,^[17] 2) a facile chromatographic separation of the neutral diastereomers ($\Delta R_f \approx 0.3$), and 3) an unprecedented Pummerer-like C–C bond-fragmentation reaction that generates both enantiomers with high enantiomeric purity (*ee* > 98 %).

Procedures involving preparative chromatographic resolution have often freed chemists from being dependent on crystallization.^[18] These procedures are usually performed with covalent diastereomer mixtures prepared by reactions of racemic substrates with classical enantiopure resolving agents (acids, alcohols, amines, etc.). In helicene chemistry, several such examples make use of aminohydroxybornane^[10a] and camphanates.^[10b,c,19] However, as cations **1** are devoid of functional handles for attaching these resolving agents, an alternative procedure had to be found.

Siegel, Krebs, Laursen, and co-workers have shown that reactive carbanions can attack the center of structurally related carbenium ions to generate rigid neutral molecular cavities by the formation of a covalent C–C bond between the reactants.^[20] In the case of [**1a**][PF₆], reaction with acetonitrile in the presence of NaH was documented, and the product of CH₂CN addition was isolated.^[15] For the resolution of cations of type **1**, we expected that the addition of a reactive enantiopure carbanionic moiety would result in two neutral diastereomeric structures, which could then be separated by chromatography.

(+)-(*R*)-Methyl-*p*-tolylsulfoxide ((+)-(*R*)-**3**) was selected for its ready availability,^[21] known carbanionic chemistry,^[22] and, once introduced, efficiency in chromatographic separation of diastereomers.^[23] Treatment of (+)-(*R*)-**3** with lithium diisopropylamide (LDA) at 0 °C in THF and subsequent addition of [*rac*-**1a**][BF₄] resulted in the formation of two neutral diastereomeric adducts, (*R,M*)-**4a** and (*R,P*)-**4a**, in good overall yield (Scheme 1, Table 1).^[24,25]

Thin layer chromatographic plates (SiO₂, Et₂O) of the 1:1 mixture of (*R,M*)-**4a** and (*R,P*)-**4a** displayed two spots with very different *R_f* values ($\Delta R_f = 0.36$). Preparative chromatography under analogous conditions afforded two separated fractions in good yields (Table 1). The electronic circular dichroism spectra of the first and second eluted compounds, [α]_D²⁰ = –700 and +820, respectively (CH₂Cl₂, *c* = 0.056 g/100 mL), displayed symmetrical curves except in the region below 250 nm due to the contribution from the CD-active (*R*)-tolylsulfoxide (Figure 1). At higher wavelengths, only negative or positive Cotton effects were observed for (–)-**4a** and (+)-**4a**, respectively; this spectral region is only related to valence transitions in the helical chromophore of compounds **4a**.

The next question concerned the removal of the chiral auxiliary. Sulfoxide groups are usually removed by treatment with Raney nickel to cleave C–S bonds adjacent to the sulfoxide moiety.^[22b] In the case of **4a**, this would mean leaving an extra methyl group on the skeleton of the addition

Table 1: Synthesis of the sulfoxide diastereomers **4**: Results of the Pummerer-like reaction and resulting enantiopure carbenium ions **1**.

compound	R	$R_f^{[a]}$	Sulfoxides yield [%]	d.r. ^[b]	$[\alpha]_D^{20}$	config.	Derived carbenium salts			
							compound	yield [%]	config.	$[\alpha]_{365}^{20}$ [c]
(-)- 4a	<i>n</i> Pr	0.63	39	> 99:1	-710	<i>R,M</i>	(-)-[1a][PF ₆]	94	<i>M</i>	-12 500
(+)- 4a	<i>n</i> Pr	0.27	39	55:1	+820	<i>R,P</i>	(+)-[1a][PF ₆]	92	<i>P</i>	+13 200
(-)- 4b	<i>n</i> Oct	0.92	44	> 99:1	-680	<i>R,M</i>	(-)-[1b][PF ₆]	92	<i>M</i>	-12 200
(+)- 4b	<i>n</i> Oct	0.59	44	> 99:1	+800	<i>R,P</i>	(+)-[1b][PF ₆]	92	<i>P</i>	+12 200
(-)- 4c	<i>i</i> Pr	0.56	43	> 99:1	-610	<i>R,M</i>	(-)-[1c][PF ₆]	80	<i>M</i>	-10 000
(+)- 4c	<i>i</i> Pr	0.28	41	> 99:1	+880	<i>R,P</i>	(+)-[1c][PF ₆]	82	<i>P</i>	+10 200
(-)- 4d	<i>c</i> Hex	0.82	44	> 99:1	-480	<i>R,M</i>	(-)-[1d][PF ₆]	88	<i>M</i>	-7500
(+)- 4d	<i>c</i> Hex	0.43	43	61:1	+550	<i>R,P</i>	(+)-[1d][PF ₆]	94	<i>P</i>	+8700

[a] Et₂O as eluent. [b] Determined by HPLC (see Supporting Information). [c] Cations **1** are dyes that absorb light efficiently in most of the visible region. Very dilute solutions and restricted wavelengths were required to measure the specific optical rotations.

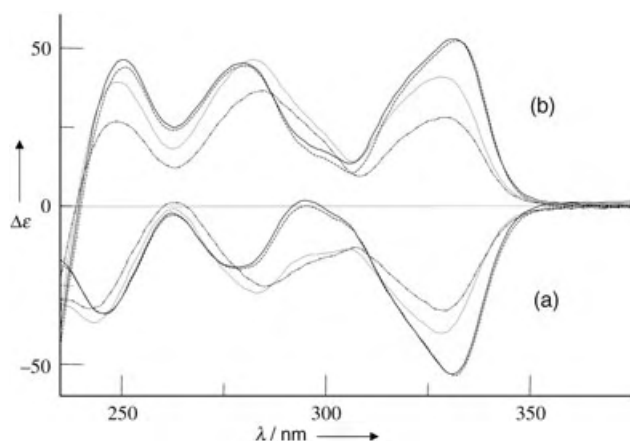
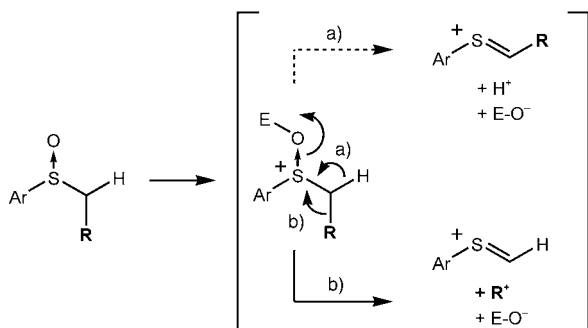


Figure 1. Superposition of the CD spectra of the first (a) and second (b) eluted diastereomers—that is, compounds of (-)-(*R,M*) and (+)-(*R,P*) configuration, respectively—for derivatives **4a** (—), **4b** (-----), **4c** (.....), and **4d** (-.-.-).

adducts, and then carbenium ion **1a** would not be generated. However, it is known that treatment of aryl alkyl sulfoxides with strong acids or anhydrides results in aldehyde moieties and/or derivatives.^[26] This Pummerer reaction proceeds by protonation or esterification of the oxygen atom of the sulfoxide (Scheme 2). Subsequent cleavage of the S–O and β–C–H bonds results in the formation of a thionium moiety that can be trapped to generate a variety of functional groups (route a). To our knowledge, β–C–C bond fragmentation



Scheme 2. The Pummerer reaction of a branched aryl alkyl sulfoxide with an electrophile E⁺ along the classical (a) and nonclassical pathways (b).

(route b) instead of β–C–H bond cleavage has not been reported. This is probably due to the strong electrofugal character of H⁺. As nitrogen-containing carbenium ions obtained by the reaction of amines with cation **2** show high chemical stability ($pK_{R^+} \geq 19$),^[12] we considered that the traditional pathway of the Pummerer reaction could be overcome as cation **1a** could be a better leaving group than H⁺ (route b).

The colorless compounds (-)-**4a** and (+)-**4a** were treated with aqueous HPF₆ in acetone at room temperature. The immediate formation of a deep green color indicated the presence of cation **1a**. Addition of water and partial concentration under vacuum resulted in the precipitation of salts (-)-[**1a**][PF₆] and (+)-[**1a**][PF₆]. Further purification of the isolated salts on SiO₂ afforded the compounds in good overall yields and with high enantiomeric purity (Table 1).^[27]

The generality of the resolution procedure was then tested on derivatives from linear (**1b**, R = *n*Oct) and branched (**1c**, R = *i*Pr; **1d**, R = *c*Hex) primary amines (Scheme 1). These compounds were prepared by the addition of *n*OctNH₂, *i*PrNH₂, and *c*HexNH₂ to [2][BF₄] in NMP at 110 °C (yield: 80, 58, and 48 %, respectively). Addition of (+)-(*R*)-**3** to the BF₄⁻ salts of *rac*-**1b**, *rac*-**1c**, and *rac*-**1d** proceeded as for *rac*-**1a** and formed compounds **4b**, **4c**, and **4d** in good yields (78–88 %). In all cases, 1:1 mixtures of diastereomers were obtained (as determined by ¹H NMR spectroscopy and HPLC), which were separated by column chromatography (SiO₂) in satisfying yields and with good diastereomeric excess (Table 1). The first and second eluted fractions were all levogyre and dextrogyre, respectively, and presented CD spectra similar to that of (-)-**4a** and (+)-**4a** (Figure 1). In the case of [*rac*-**1a**][BF₄], the addition of (+)-(*R*)-**3** was scaled-up to 10 mmol of cation **1a** (5.0 g); the addition and separation proceeded with no loss of efficiency.

X-ray-quality crystals of diastereomerically pure (+)-**4c** were obtained, and the absolute *R,P* configuration was determined from the crystal structure analysis (Figure 2).^[28] As all the second eluted chromatographic fractions of diastereomeric compounds **4a–d** demonstrate analogous chiroptical properties (Figure 1), the *R,P* configuration determined for (+)-**4c** can also be assigned to (+)-**4a**, (+)-**4b**, and (+)-**4d**. Consequently, the first eluted derivatives (-)-**4a–d** are all of *R,M* configuration. Previously, an absolute *M* configuration was determined for (-)-[**1a**][PF₆] by vibrational circular dichroism analysis.^[15] Evidently, upon removal

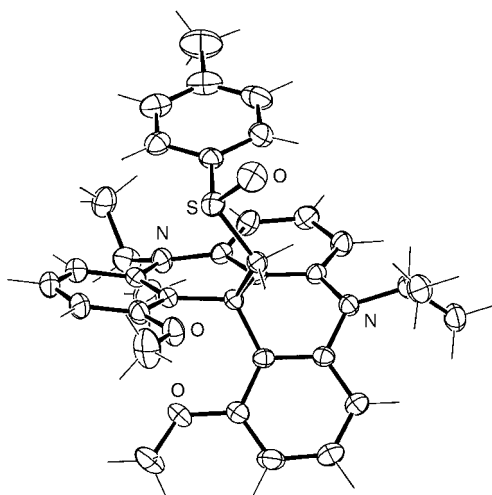


Figure 2. X-ray crystal structure of (+)-(R,P)-4c. Ellipsoids are represented at the 40% probability level.

of the central sulfoxide moiety, the sense of helicity of the skeleton remains. This means that the fragmentation occurs with retention of configuration, for example, from (–)-(R,M)-4a to (–)-[(M)-1a][PF₆].

Finally, treatment of (R,M)-4b–d with HPF₆ in acetone afforded salts (–)-[1b][PF₆], (–)-[1c][PF₆], and (–)-[1d][PF₆] in excellent yields. Analogous results were obtained for the diastereomeric (R,P) series in favor of the dextrogyre salts (Table 1). In the case of the more hindered compounds 4c and 4d, simply increasing the reaction times and the amount of Brønsted acid (50.0 equiv) was sufficient for the reactions to proceed to completion. Interestingly, a comparison of the CD spectra of salts (–)-[1][PF₆] showed that the CD properties of the carbenium ions depend on the nature of the side-chain residues. The branched compounds (–)-1c and (–)-1d display stronger Cotton effects (4×, Δε₆₂₀ ≈ 7.5) at higher wavelength than the linear derivatives (–)-1a and (–)-1b. This result opens interesting prospects for future applications.^[19]

Received: October 15, 2004

Published online: February 11, 2005

Keywords: carbocations · chiral auxiliaries · chiral resolution · dyes · helicenes

- [1] For general references, see a) W. H. Laarhoven, W. J. C. Prinsen, *Top. Curr. Chem.* **1984**, *125*, 63–130; b) K. P. Meurer, F. Vögtle, *Top. Curr. Chem.* **1985**, *127*, 1–76; c) T. J. Katz, *Angew. Chem.* **2000**, *112*, 1997–1999; *Angew. Chem. Int. Ed.* **2000**, *39*, 1921–1923; d) A. Urbano, *Angew. Chem.* **2003**, *115*, 4116–4119; *Angew. Chem. Int. Ed.* **2003**, *42*, 3986–3989; e) C. Diedrich, S. Grimme, *J. Phys. Chem. A* **2003**, *107*, 2524–2539; f) S. D. Peyerimhoff, *Interactions in Molecules: Electronic and Steric Effects*, Wiley-VCH, Weinheim, **2003**, pp. 363.
- [2] Y. Kitahara, K. Tanaka, *Chem. Commun.* **2002**, 932–933.
- [3] C. Wachsmann, E. Weber, M. Czugler, W. Seichter, *Eur. J. Org. Chem.* **2003**, 2863–2876; J. E. Field, T. J. Hill, D. Venkataraman, *J. Org. Chem.* **2003**, *68*, 6071–6078; T. Verbiest, S. Sioncke, A. Persoons, L. Vyklicky, T. J. Katz, *Angew. Chem.* **2002**, *114*, 4038–

- 4040; *Angew. Chem. Int. Ed.* **2002**, *41*, 3882–3884; T. B. Norsten, A. Peters, R. McDonald, M. T. Wang, N. R. Branda, *J. Am. Chem. Soc.* **2001**, *123*, 7447–7448; F. Furche, R. Ahlrichs, C. Wachsmann, E. Weber, A. Sobanski, F. Vögtle, S. Grimme, *J. Am. Chem. Soc.* **2000**, *122*, 1717–1724.
- [4] Y. Xu, Y. X. Zhang, H. Sugiyama, T. Umano, H. Osuga, K. Tanaka, *J. Am. Chem. Soc.* **2004**, *126*, 6566–6567; S. Honzawa, H. Okubo, S. Anzai, M. Yamaguchi, K. Tsumoto, I. Kumagai, *Bioorg. Med. Chem.* **2002**, *10*, 3213–3218.
- [5] L. Owens, C. Thilgen, F. Diederich, C. B. Knobler, *Helv. Chim. Acta* **1993**, *76*, 2757–2774; E. Murguly, R. McDonald, N. R. Branda, *Org. Lett.* **2000**, *2*, 3169–3172.
- [6] I. Sato, R. Yamashima, K. Kadowaki, J. Yamamoto, T. Shibata, K. Soai, *Angew. Chem.* **2001**, *113*, 1130–1132; *Angew. Chem. Int. Ed.* **2001**, *40*, 1096–1098; M. T. Reetz, S. Sostmann, *Tetrahedron* **2001**, *57*, 2515–2520; M. T. Reetz, E. W. Beuttenmuller, R. Goddard, *Tetrahedron Lett.* **1997**, *38*, 3211–3214; A. Terfort, H. Grls, H. Brunner, *Synthesis* **1997**, 79–86.
- [7] M. Miyasaka, A. Rajca, *Synlett* **2004**, 177–181.
- [8] See also: R. El Abed, B. Ben Hassine, J.-P. Genêt, M. Gorsane, A. Marinetti, *Eur. J. Org. Chem.* **2004**, 1517–1522; P. M. Donovan, L. T. Scott, *J. Am. Chem. Soc.* **2004**, *126*, 3108–3112; M. C. Carreño, S. García-Cerrada, A. Urbano, *Chem. Eur. J.* **2003**, *9*, 4118–4131; F. Teplý, I. G. Stará, I. Starý, A. Kollárovic, D. Saman, S. Vyskocil, P. Fiedler, *J. Org. Chem.* **2003**, *68*, 5193–5197; T. Sooksimuang, B. K. Mandal, *J. Org. Chem.* **2003**, *68*, 652–655; K. Paruch, L. Vyklicky, D. Z. Wang, T. J. Katz, C. Incarvito, L. Zakharov, A. L. Rheingold, *J. Org. Chem.* **2003**, *68*, 8539–8544; M. d. M. Real, J. Pérez Sestelo, L. A. Sarandeses, *Tetrahedron Lett.* **2002**, *43*, 9111–9114; D. C. Harrowven, M. I. T. Nunn, D. R. Fenwick, *Tetrahedron Lett.* **2002**, *43*, 7345–7347; M. C. Carreño, S. García-Cerrada, A. Urbano, *Chem. Commun.* **2002**, 1412–1413; F. Teplý, I. G. Stará, I. Starý, A. Kollárovic, D. Saman, L. Rulisek, P. Fiedler, *J. Am. Chem. Soc.* **2002**, *124*, 9175–9180; S. D. Han, A. D. Bond, R. L. Disch, D. Holmes, J. M. Schulman, S. J. Teat, K. P. C. Vollhardt, G. D. Whitener, *Angew. Chem.* **2002**, *114*, 3357–3361; *Angew. Chem. Int. Ed.* **2002**, *41*, 3223–3227; M. C. Carreño, S. García-Cerrada, A. Urbano, *J. Am. Chem. Soc.* **2001**, *123*, 7929–7930; F. Dubois, M. Gingras, *Tetrahedron Lett.* **1998**, *39*, 5039–5040.
- [9] M. S. Newman, D. Lednicher, *J. Am. Chem. Soc.* **1956**, *78*, 4765–4770; H. Wynberg, M. B. Groen, H. Schadenberg, *J. Org. Chem.* **1971**, *36*, 2797–2809; D. A. Lightner, D. T. Hefelfinger, T. W. Powers, G. W. Frank, K. N. Trueblood, *J. Am. Chem. Soc.* **1972**, *94*, 3492–3497; R. H. Martin, M. J. Marchant, *Tetrahedron* **1974**, *30*, 343–345; F. Mikes, G. Boshart, E. Gil-Av, *J. Chem. Soc. Commun.* **1976**, 99–100; C. Stammel, R. Fröhlich, C. Wolff, H. Wenck, A. de Meijere, J. Mattay, *Eur. J. Org. Chem.* **1999**, 1709–1718; K. Tanaka, H. Osuga, H. Suzuki, Y. Shogase, Y. Kitahara, *J. Chem. Soc. Perkin Trans. 1* **1998**, 935–940.
- [10] a) K. Tanaka, Y. Kitahara, H. Suzuki, H. Osuga, Y. Kawai, *Tetrahedron Lett.* **1996**, *37*, 5925–5928; b) T. Thongpanchang, K. Paruch, T. J. Katz, A. L. Rheingold, K.-C. Lam, L. Liable-Sands, *J. Org. Chem.* **2000**, *65*, 1850–1856; c) D. Nakano, R. Hirano, M. Yamaguchi, C. Kabuto, *Tetrahedron Lett.* **2003**, *44*, 3683–3686.
- [11] A. Sudhakar, T. J. Katz, *J. Am. Chem. Soc.* **1986**, *108*, 179–181; T. J. Katz, A. Sudhakar, M. F. Teasley, A. M. Gilbert, W. E. Geiger, M. P. Robben, M. Wuensch, M. D. Ward, *J. Am. Chem. Soc.* **1993**, *115*, 3182–3198; K. Tanaka, H. Osuga, H. Suzuki, *Tetrahedron: Asymmetry* **1993**, *4*, 1843–1856; I. G. Stará, I. Starý, M. Tichý, J. Závada, V. Hanus, *J. Am. Chem. Soc.* **1994**, *116*, 5084–5088; H. Osuga, H. Suzuki, K. Tanaka, *Bull. Chem. Soc. Jpn.* **1997**, *70*, 891–897; Y. Ogawa, M. Toyama, M. Karikomi, K. Seki, K. Haga, T. Uyehara, *Tetrahedron Lett.* **2003**, *44*, 2167–2170; R. El Abed, B. Ben Hassine, J.-P. Genêt, M. Gorsane, J. Madec, L. Ricard, A. Marinetti, *Synthesis* **2004**, 2513–2516.

- [12] B. W. Laursen, F. C. Krebs, *Angew. Chem.* **2000**, *112*, 3574–3576; *Angew. Chem. Int. Ed.* **2000**, *39*, 3432–3434; B. W. Laursen, F. C. Krebs, *Chem. Eur. J.* **2001**, *7*, 1773–1783.
- [13] The [4]helicene derivatives can be configurationally stable if correctly substituted; see M. S. Newman, R. M. Wise, *J. Am. Chem. Soc.* **1956**, *78*, 450–454; M. C. Carreño, S. García-Cerrada, M. J. Sanz-Cuesta, A. Urbano, *Chem. Commun.* **2001**, 1452–1453; Y. Saiki, K. Nakamura, Y. Nigorikawa, M. Yamaguchi, *Angew. Chem.* **2003**, *115*, 5348–5350; *Angew. Chem. Int. Ed.* **2003**, *42*, 5190–5192; Y. Saiki, H. Sugiura, K. Nakamura, M. Yamaguchi, T. Hoshi, J. Anzai, *J. Am. Chem. Soc.* **2003**, *125*, 9268–9269, and references therein.
- [14] Nitrogen-containing cationic heterohelicenes have been described: K. Sato, S. Okazaki, T. Yamagishi, S. Arai, *J. Heterocycl. Chem.* **2004**, *41*, 443–447, and references therein.
- [15] C. Herse, D. Bas, F. C. Krebs, T. Bürgi, J. Weber, T. Wesolowski, B. W. Laursen, J. Lacour, *Angew. Chem.* **2003**, *115*, 3270–3274; *Angew. Chem. Int. Ed.* **2003**, *42*, 3162–3166.
- [16] J. Lacour, A. Londez, C. Goujon-Ginglinger, V. Buß, G. Bernardinelli, *Org. Lett.* **2000**, *2*, 4185–4188; J. Lacour, V. Hebbe-Viton, *Chem. Soc. Rev.* **2003**, *32*, 373–382.
- [17] I. Fernández, N. Khiar, *Chem. Rev.* **2003**, *103*, 3651–3705.
- [18] J. Jacques, A. Collet, S. H. Wilen, *Enantiomers, Racemates, and Resolutions*, 2nd ed., Krieger, Melbourne, USA, **1994**.
- [19] J. E. Field, G. Muller, J. P. Riehl, D. Venkataraman, *J. Am. Chem. Soc.* **2003**, *125*, 11808–11809.
- [20] M. Lofthagen, R. V. Clark, K. K. Baldridge, J. S. Siegel, *J. Org. Chem.* **1992**, *57*, 61–69; B. W. Laursen, F. C. Krebs, M. F. Nielsen, K. Bechgaard, J. B. Christensen, N. Harrit, *J. Am. Chem. Soc.* **1998**, *120*, 12255–12263.
- [21] K. K. Andersen, *Tetrahedron Lett.* **1962**, 93–95; K. K. Andersen, *J. Org. Chem.* **1964**, *29*, 1953–1956; P. Pitchen, H. B. Kagan, *Tetrahedron Lett.* **1984**, *25*, 1049–1052; P. Pitchen, E. Dunach, M. N. Deshmukh, H. B. Kagan, *J. Am. Chem. Soc.* **1984**, *106*, 8188–8193; G. Solladié, J. Hutt, A. Girardin, *Synthesis* **1987**, 173.
- [22] a) G. Solladié, *Synthesis* **1981**, 185–196; b) M. C. Carreño, *Chem. Rev.* **1995**, *95*, 1717–1760; c) C.-C. Wang, H.-C. Huang, D. B. Reitz, *Org. Prep. Proced. Int.* **2002**, *34*, 271–319, and references therein.
- [23] M. R. Naimi-Jamal, J. Ipaktschi, M. R. Saidi, *Eur. J. Org. Chem.* **2000**, 1735–1739, J. Yoon, D. J. Cram, *J. Am. Chem. Soc.* **1997**, *119*, 11796–11806; A. Albinati, P. Bravo, F. Ganazzoli, G. Resnati, F. Viani, *J. Chem. Soc. Perkin Trans. 1* **1986**, 1405–1415; J. G. Hansen, M. Johannsen, *J. Org. Chem.* **2003**, *68*, 1266–1274; P. Macours, J. C. Braekman, D. Daloz, *Tetrahedron* **1995**, *51*, 1415–1428.
- [24] (*R,P*) and (*R,M*) indicate that the diastereomers contain a sulfoxide moiety of *R* configuration and are derived from the *P* and *M* enantiomers of compounds **1**, respectively.
- [25] The ¹H NMR spectrum of the crude reaction mixture showed two sets of related signals in a 1:1 ratio; this ratio was confirmed by chiral stationary phase (CSP) HPLC analysis (Chiralpak AD-H, Daicel, *n*-hexane/*i*PrOH). See Supporting Information for details.
- [26] K. Bur Scott, A. Padwa, *Chem. Rev.* **2004**, *104*, 2401–2432; A. Padwa, A. G. Waterson, *Curr. Org. Chem.* **2000**, *4*, 175–203.
- [27] The high enantiomeric purity of (–)-[**1a**][PF₆] and (+)-[**1a**][PF₆] was verified by ¹H NMR spectroscopy using [Bu₄N][Δ-BIN-PHAT] as an NMR chiral solvating agent. The enantiomeric ratio (e.r.) of [**1a**][PF₆] to [**1d**][PF₆] is therefore assumed to be identical to the diastereomeric ratios of the precursors **4a–d**.
- [28] Crystal data for (+)-(*R,P*)-**4c** (C₃₅H₃₈N₂O₃S): *M*_r = 566.8, *μ* = 0.148 mm^{–1}, *d*_x = 1.273 g cm^{–3}, monoclinic space group *P*2₁, *Z* = 2, *a* = 11.2301(10), *b* = 10.5366(7), *c* = 12.5563(10) Å, *β* = 95.509(10)°, *V* = 1478.9(2) Å³. A colorless prism (0.19 × 0.22 × 0.34 mm³) was mounted on a quartz fiber with protection oil. The cell dimensions and intensities were measured at 200 K on a

Stoe IPDS diffractometer with graphite-monochromated Mo_{Kα} radiation (*λ* = 0.71073 Å). Of 20736 measured reflections, 6497 were unique and 3869 were observed (*|F_o|* > 4σ(*F_o*)); *R*_{int} for 14219 equivalent reflections 0.058. Data were corrected for Lorentz and polarization effects and for absorption (*T*_{min,max} = 0.9629, 0.9745). The structure was solved by direct methods (SIR97), all other calculations were performed with XTAL system and ORTEP programs. Full-matrix least-squares refinement based on *F* using weight of 1/(σ²(*F_o*) + 0.00025(*F_o*)²) gave final values *R* = 0.040, *ωR* = 0.036, and *S* = 1.46(2). The maximum *Δ*/σ on the last cycle was 0.91 × 10^{–4}. Flack parameter *x* = 0.01(12). Hydrogen atoms were placed in calculated positions. The ECD spectrum of the crystal analyzed by X-ray diffraction was totally superposable to the spectrum of bulk (+)-**4c**. CCDC-252698 contains the supplementary crystallographic data for this paper. These data can be obtained free of charge from The Cambridge Crystallographic Data Centre via www.ccdc.cam.ac.uk/data_request/cif.

C–S Bond Formation

Carbon–Sulfur Bond Formation between a Ruthenium-Coordinated Thiyl Radical and Methyl Ketones**

Selma Poturovic, Mark S. Mashuta, and
Craig A. Grapperhaus*

The oxidation of metal–thiolate complexes to yield disulfides is well-known.^[1–4] This process may be irreversible, as with the oxidation of $[\text{Fe}(\text{SPh})(\text{CO})(\text{PPh}_3)(\eta^5\text{-C}_5\text{H}_5)]\text{PF}_6$ to form the disulfide-bridged binuclear product $[(\text{Fe}(\text{CO})(\text{PPh}_3)(\eta^5\text{-C}_5\text{H}_5)_2(\mu\text{-SSPh}_2)]^{2+}$,^[5] or reversible, as with the oxidation of $[\text{Ru}^{\text{III}}\text{L}]$, $\text{L} = 1,4,7\text{-tris}(4\text{-tert-butyl-2-mercaptobenzyl})\text{-}1,4,7\text{-triazacyclononane}$, which yields an isolable, intermolecular disulfide complex.^[6] In both cases, the oxidation is consistent with a metal–thiyl radical intermediate. Recent efforts have focused on stabilizing metal-coordinated thiyl radicals.^[7–10] Wieghardt and co-workers synthesized and compared phenylthiyl and phenoxyl radicals coordinated to Co^{III} centers (and other metal centers) with tacn-based ligands (tacn = 1,4,7-triazacyclononane).^[7] The phenylthiyl radical displays increased reactivity compared with the phenoxyl analogue. In the former the unpaired electron is localized on the sulfur

[*] S. Poturovic, Dr. M. S. Mashuta, Prof. Dr. C. A. Grapperhaus
Department of Chemistry
University of Louisville
Louisville, KY 40292 (USA)
Fax: (+1) 502-852-8149
E-mail: grapperhaus@louisville.edu

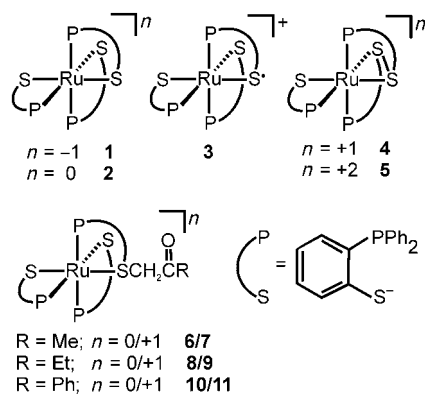
[**] This research was supported by the National Science Foundation (CHE-0238137). CCD X-ray equipment was purchased through funds provided by the Kentucky Research Challenge Trust Fund.



Supporting information for this article is available on the WWW under <http://www.angewandte.org> or from the author.

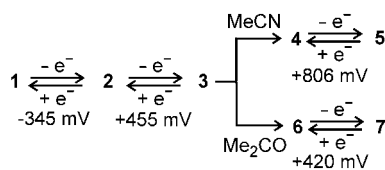
atom, whereas in the latter the electron delocalizes over the phenyl ring. Earlier Hückel molecular orbital (MO) calculations by Darensbourg and co-workers for $\text{RS} \cdot [\text{Cr}(\text{CO})_5]_2$, in which R is a *tert*-butyl group, also conclude that the singly occupied molecular orbital (SOMO) is concentrated largely on the 3p orbital of the sulfur atom.^[11] Moreover, the unpaired electron in noncoordinated thiyls is also localized on the sulfur atom as confirmed by recent density functional theory (DFT) calculations of the cysteine-derived radical.^[12] As expected, localization leads to enhanced reactivity. For example, phenylthiyl radicals decay at a rate of approximately $10^9 \text{ M}^{-1} \text{ s}^{-1}$ to disulfide.^[13]

Herein, we report the novel reactivity of an electrophilic, oxidized metal–thiolate (metal-coordinated thiyl radical) with ketones that results in C–S bond formation. Electrophilic behavior contrasts the well-studied reactivity of nucleophilic metal–thiolates and presents a new method for the synthesis of metal–sulfur complexes.^[14] Previously, we reported the oxidation of $[\text{Ru}(\text{dppbt})_3]$ (**2**; dppbt = 2-diphe-



nylphosphinobenzenethiolate) in acetonitrile to form the observable metal-coordinated Ru^{III} –thiyl radical complex **3**.^[15] In this case, complex **3** is short-lived and decays to form the proposed Ru^{II} –disulfide complex **4**. The overall oxidation of **2** to **4** proceeds by a coupled two-electron ligand oxidation and one-electron metal-centered reduction. At an applied potential of 620 mV, an EC mechanism (EC is short for electrode step–chemical step) is observed. Complex **4** can be further oxidized to its Ru^{III} derivative, **5**, but only at more positive potentials (+806 mV).

Oxidation of **2** at 620 mV in acetone or related ketones also initially yields **3**. At this point, the pathways in acetonitrile and ketones diverge as shown in Scheme 1. Decay of **3** in ketones results in C–S bond formation between the thiyl radical and the solvent molecule to yield the Ru^{II} –



Scheme 1. Oxidation pathways for **1** in acetonitrile (top) and acetone (bottom).

thioether product **6** (in acetone). Further oxidation to Ru^{III} (formation of **7**) occurs at the potential applied to the cell. Thus, the oxidation of **2** to **7** is a two-electron ECE (electrode–chemical–electrode) process with no change in the formal oxidation state of the metal center and C–S bond formation.

The oxidation of **2** in acetone was performed by bulk electrolysis in a controlled-temperature electrochemical cell ($T = -17^\circ\text{C}$) equipped with a quartz window for in situ UV/Vis monitoring. On the basis of coulometric measurements and UV/Vis spectroscopy (Figure 1), the oxidation is unequiv-

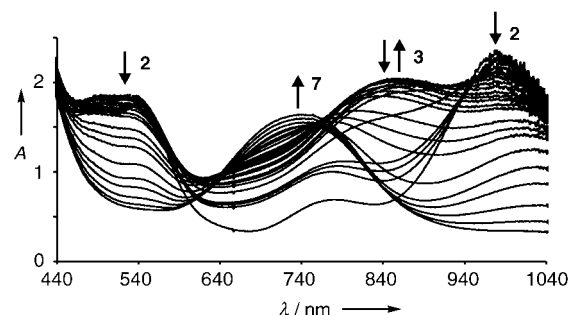


Figure 1. Electronic spectra obtained during bulk oxidation of **2** to **7** at 620 mV in acetone at -17°C . Data were collected every 50 mC (0.10 electron equivalents).

ocally assigned as two electrons per metal center, which is in contrast to the one-electron oxidation of **2** in acetonitrile to give **4**. During initial stages of the oxidation in acetone, the charge-transfer bands of **2** at 540 and 1041 nm decrease in intensity with a concomitant increase in intensity at 850 nm, which is attributed to the formation of **3**. This observation for the oxidation in acetone is identical to that for the oxidation in acetonitrile.^[15] However, upon decay of the band at 850 nm, a new band at 735 nm, which is assigned to complex **7**, emerges in stark contrast to the silent visible spectrum in acetonitrile associated with **4**.

Square-wave voltammograms recorded after bulk oxidation of **2** in acetonitrile and acetone are consistent with the assignments of **4** as Ru^{II} –disulfide and **7** as Ru^{III} –thioether (Figure 2). UV/Vis-monitored spectroelectrochemistry confirms a reversible one-electron reduction of **7** to give **6** at an applied potential of +200 mV (see Supporting Information). The $\text{Ru}^{\text{III}}/\text{Ru}^{\text{II}}$ couple of **7/6** is shifted by +813 mV relative to the thiolato precursors **2/1**, consistent with previously reported shifts associated with S alkylation.^[16] In contrast, a shift of +1151 mV in the $\text{Ru}^{\text{III}}/\text{Ru}^{\text{II}}$ potential for the disulfide complexes **5/4** indicates the modification of two anionic thiolates to form two neutral sulfur donors. All complexes assigned as Ru^{III} display rhombic electron paramagnetic resonance (EPR) spectra with *g* values near 2 as shown in Table 1. The notable exception is the metal-coordinated radical **3**, which is EPR-silent, consistent with the coupling of the ruthenium spin ($S = 1/2$) with that of the thiyl radical ($S = 1/2$).

The electrospray-ionization mass spectrum (ESI-MS) of complex **7** displays a parent ion with $m/z = 1038$, which is consistent with the proposed structure (see Supporting

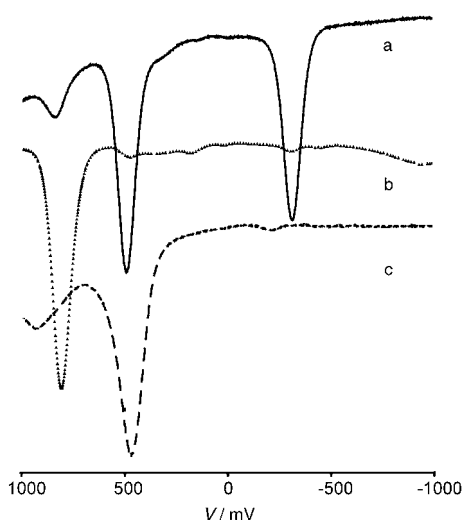


Figure 2. Comparison of square-wave voltammograms for solutions of a) **1/2** (1 mM) in acetonitrile, b) **4/5** (1 mM) in acetonitrile, and c) **6/7** (1 mM) in acetone. Voltammograms were obtained at a glassy carbon electrode referenced versus Ag^+/Ag^0 .

Table 1: Formal oxidation-state assignments, charge-transfer (CT) band energies, and EPR *g* values for **1–11**.

Complex	Formal oxidation state	CT absorbance λ_{max} (e)	<i>g</i> values ^[a]
1	II	—	—
2	III	1041 (3020) ^[b]	2.12, 2.06, 2.04
3	III	850 (4800)	—
4	II	—	—
5	III	688 (2338)	2.09, 2.05, 2.03
6	II	—	—
7	III	735 (1921) ^[c]	2.09, 2.04, 2.01
8	II	—	—
9	III	707 (557) ^[d]	2.15, 2.04, 2.02
10	II	—	—
11	III	697 (106) ^[e]	2.15, 2.06, 2.01

[a] Obtained from frozen solution at 77 K. [b] Acetonitrile solution at -17°C . [c] Acetone solution at -17°C . [d] 2-Butanone solution at -17°C . [e] Acetophenone solution recorded at 19°C .

Information). Complex **6**, the Ru^{II} derivative of **7**, was also prepared chemically by alkylation of **1** with chloroacetone in acetonitrile. The ESI-MS, UV/Vis, spectroelectrochemical, and EPR measurements of **7/6** from the two routes are indistinguishable, which is consistent with the oxidation-induced C–S bond formation and the proposed structures given above.

The X-ray crystal structure of **6**^[17–22] (Figure 3)^[23] confirms the alkylation of a single sulfur site to yield a neutral ruthenium complex in a triphosphine-dithiolate-thioether donor set. The chelating ligands arrange in a meridional fashion as seen in **1** and its methylene-bridged dialkylated derivative $[\text{Ru}(\text{dppbt})\{\text{CH}_2(\text{dppbt})_2\}]^+$ (**14**).^[24] The ketone functional group of the thioether donor is directed away from the metal center. The Ru–P bond lengths range from 2.2939(11) to 2.3626(10) Å, similar to the bonds in **1** and **14**. The Ru–S_{thiolate} bond lengths for Ru–S1, 2.3971(10) Å, and Ru–S2, 2.3826(10) Å, in **6** are not significantly shorter than

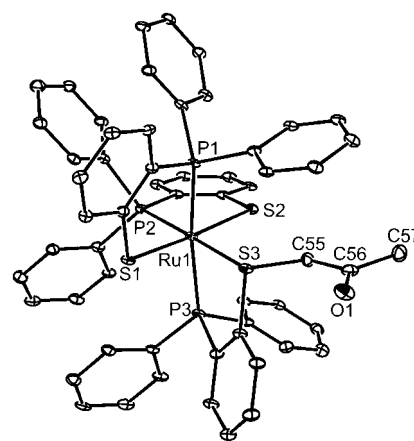
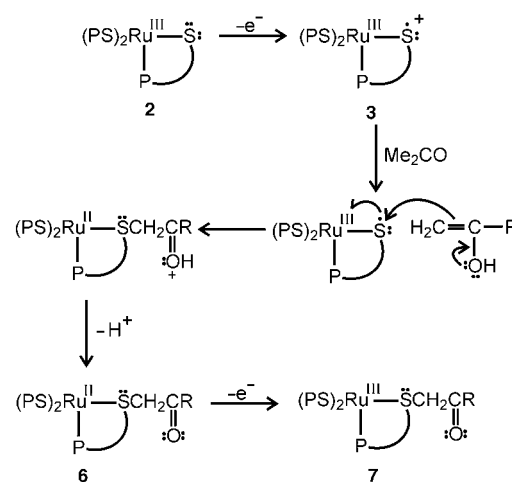


Figure 3. ORTEP representation of **6** (thermal ellipsoids are set at the 40% level of probability).^[23] Chlorobenzene molecules have been omitted. Selected bond lengths [Å] and angles [°]: Ru–P1 2.3545(10), Ru–P2 2.2939(11), Ru–P3 2.3626(10), Ru–S1 2.3971(10), Ru–S2 2.3826(10), Ru–S3 2.4151(10), S3–C55 1.813(4); P2–Ru–P1 95.00(4), S2–Ru–P1 90.16(4), S2–Ru–S1 175.57(4), C55–S3–Ru 108.98(13).

the Ru–S_{thioether} bond length for Ru–S3, 2.4151(10) Å, as is the case in **14**.

Scheme 2 details a proposed pathway for the reaction of **3** with acetone.^[25] The enol tautomer of acetone acts as a



Scheme 2. Proposed pathway for the oxidation of **2** in acetone.

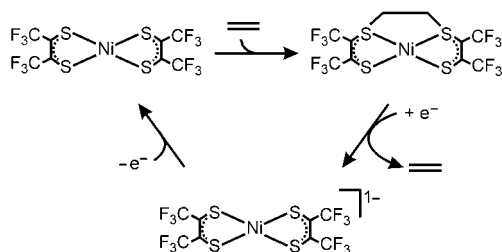
nucleophile and attacks the metal-coordinated thiyl radical to result in the reduction of the Ru^{III} center to Ru^{II} . Deprotonation of the Ru^{II} species yields the Ru^{II} –thioether product **6**. At the potentials necessary for oxidation of **2** to form **3**, **6** is further oxidized to the observed product **7**. To support this pathway, **2** was oxidized in the presence of the trimethylsilyl enol ether derivative of acetone. The oxidation is a two-electron process and yields a product identified spectroscopically as **7**. Notably, no thiyl radical intermediate is observed that is consistent with the expected rate increase with increased enol concentration.

To support the pathway proposed in Scheme 2, **3** was generated under a variety of conditions. Similar ketones (2–

butanone and acetophenone) generate products that are closely related to **6** and **7** (see complexes **8–11**; Ph = phenyl). Acetonitrile, malononitrile, or THF, which have C–H bond enthalpies similar to or lower than that of acetone, but are not enolizable, yield only Ru^{II}–disulfide **4** and there is no C–S bond formation.^[26] Thus, a pathway that involves an initial hydrogen atom abstraction step is not consistent with the observed data.

The reaction of **3** with ketones resembles the previously noted reactivity of disulfide-bridged metal clusters with acetone.^[27,28] C–S bond formation was observed at the bridging disulfide upon addition of acetone. It was suggested that the enol tautomer of acetone acts as a nucleophile and attacks the disulfide, whereas the cluster is reduced by two electrons. This reduction is spread over two metal centers.

Finally, the C–S bond formation between the enol tautomer of acetone and **3** is reminiscent of the reaction between ethylene and nickel dithiolene reported by Stiefel and co-workers (Scheme 3).^[29] In both cases, an oxidized



Scheme 3. Reversible ethylene binding to nickel dithiolene.^[29]

mononuclear metal–sulfur complex is attacked by an ene nucleophile, which results in reduction at the metal center and C–S bond formation. Reduction of the nickel center promotes C–S bond cleavage and release of ethylene. Further studies by Geiger on related systems revealed that reductive dissociation of the olefin proceeds by a two-electron ECE mechanism.^[30] Current efforts are focusing on the reaction of **3** with additional substrates.

Experimental Section

Physical and Spectroscopic Methods: IR spectra were obtained by using a Thermo Nicolet Avatar 360 spectrometer with a 4 cm^{−1} resolution. X-band EPR spectra were collected on a Bruker EMX EPR spectrometer at 77 K in a Suprasil quartz dewar. Spectra were simulated with SimFonia. An Agilent 8453 diode array spectrometer was used for electronic absorption spectroscopy. Elemental analyses were performed by Midwest Microlab (Indianapolis). Mass spectra were recorded at the University of Louisville Mass Spectrometry Core Laboratory. All electrochemical experiments were performed with an EG&E273 potentiostat/galvenostat. Electrochemical and spectroelectrochemical measurements were carried out in the 10 mL cell designed by E. Böhle of the Max Planck Institute für Bioanorganische Chemie, Mülheim (Germany), as described previously.^[15]

Synthetic Methods: Syntheses of complexes **1–5** have been previously reported.^[15,24] 2-Butanone, and acetophenone were purchased from Aldrich and were freshly distilled immediately prior to use. Syntheses were performed under a N₂ atmosphere by using

standard Schlenk techniques unless otherwise stated. Chloroacetone, chlorotrimethylsilane, sodium iodide, and triethylamine were obtained from Aldrich and used as received. (Isopropenyloxy)tri-methylsilane was prepared according to published methods.^[31]

6: Chloroacetone (0.015 g, 16 mmol) was added with a micro-syringe to a yellow solution of **1** (0.188 g, 12.4 mmol) in acetonitrile (100 mL). The reaction solution was stirred for 1 hour. Removal of solvent under reduced pressure yielded a yellow residue. The crude product was dissolved in THF and gravity filtered to remove residual PPNCl. Removal of solvent from the filtrate yielded **6** in 43 % yield. X-ray-quality needle-like crystals were obtained from liquid diffusion of chlorobenzene/ether. Elemental analysis (%) calcd for C₅₇H₄₇OP₃S₃Ru: C 65.94, H 4.56, found: C 63.48, H 4.37; IR (KBr pellet): $\tilde{\nu}$ 3047(m), 1707(m), 1429(m), 1082(s), 693(s), 518 cm^{−1} (s). Compound **6** can also be prepared by electrochemical reduction of **7** in acetone (1 mM, −17 ± 3 °C) at an applied potential of +200 mV.

7: Bulk oxidation of **3** in acetone at 620 mV (−17 °C) yields **7** by a two-electron oxidation. The product was characterized by UV/Vis and EPR spectroscopy, and square-wave voltammetry. Electronic absorption: λ_{max} = 735 nm (ϵ = 1921 cm^{−1}M^{−1}).

Received: November 24, 2004

Published online: February 11, 2005

Keywords: ketones · radicals · ruthenium · sulfur

- [1] M. T. Ashby, J. H. Enemark, D. L. Lichtenberger, *Inorg. Chem.* **1988**, 27, 191.
- [2] C. A. Grapperhaus, M. Y. Darensbourg, *Acc. Chem. Res.* **1998**, 31, 451.
- [3] L. E. Maelia, M. Millar, S. A. Koch, *Inorg. Chem.* **1992**, 31, 4594.
- [4] J. C. Noveron, R. Herradora, M. M. Olmstead, P. K. Mascharak, *Inorg. Chim. Acta* **1999**, 285, 269.
- [5] P. M. Treichel, L. D. Rosenhein, *Inorg. Chem.* **1984**, 23, 4018.
- [6] B. Albela, E. Bothe, O. Brosch, K. Mochizuki, T. Weyhermüller, K. Wieghardt, *Inorg. Chem.* **1999**, 38, 5131.
- [7] S. Kimura, E. Bill, E. Bothe, T. Weyhermüller, K. Wieghardt, *J. Am. Chem. Soc.* **2001**, 123, 6025.
- [8] D. Herebian, E. Bothe, E. Bill, T. Weyhermüller, K. Wieghardt, *J. Am. Chem. Soc.* **2001**, 123, 10012.
- [9] P. Ghosh, E. Bill, T. Weyhermüller, F. Neese, K. Wieghardt, *J. Am. Chem. Soc.* **2003**, 125, 1293.
- [10] C. H. Hsieh, I. J. Hsu, C. M. Lee, S. C. Ke, T. Y. Wang, G. H. Lee, Y. Wang, J. M. Chen, J. F. Lee, W. F. Liaw, *Inorg. Chem.* **2003**, 42, 3925.
- [11] J. Springs, C. P. Janzen, M. Y. Darensbourg, J. C. Calabrese, P. J. Krusic, J. N. Verpeaux, C. Amatore, *J. Am. Chem. Soc.* **1990**, 112, 5789.
- [12] M. van Gastel, W. Lubitz, G. Lassmann, F. Neese, *J. Am. Chem. Soc.* **2004**, 126, 2237.
- [13] G. N. R. Tripathi, Q. Sun, D. A. Armstrong, D. M. Chipman, R. H. Schuler, *J. Phys. Chem.* **1992**, 96, 5344.
- [14] E. C. Constable, *Metals and Ligand Reactivity*, 2nd ed., VCH, Weinheim, **1996**.
- [15] C. A. Grapperhaus, S. Poturovic, *Inorg. Chem.* **2004**, 43, 3292.
- [16] P. J. Farmer, J. H. Reibenspies, P. A. Lindahl, M. Y. Darensbourg, *J. Am. Chem. Soc.* **1993**, 115, 4665.
- [17] Crystal data for **6**: yellow needle, orthorhombic, space group *Pbca*, $a = 24.832(2)$, $b = 10.9955(10)$, $c = 41.949(4)$ Å, $V = 11453.7(18)$ Å³, $\rho_{\text{calcd}} = 1.465$ g cm^{−3}, $Z = 8$. Data were collected on a Bruker SMART APEX CCD using Mo $\text{K}\alpha$ radiation. For all 13702 unique reflections ($R(\text{int}) = 0.056$), the final anisotropic full-matrix least-squares refinement on F^2 for 713 variables data converged at $R1 = 0.06$ and $wR2 = 0.11$ with a GOF of 1.09. CCDC-256671 contains the supplementary crystallographic data for this paper. These data can be obtained free of charge from

- The Cambridge Crystallographic Data Centre via www.ccdc.cam.ac.uk/data_request/cif.
- [18] SHELXL-97. Program for the Refinement of Crystal Structures, University of Göttingen, Germany, **1997**.
- [19] SHELXTL (v6.12), Program Library for Structure Solution and Molecular Graphics, Bruker Advanced X-ray Solutions, Inc., Madison, WI, **2001**.
- [20] SMART (v5628), Bruker Advanced X-ray Solutions, Inc., Madison, WI, **2002**.
- [21] SAINT (v6.36), Bruker Advanced X-ray Solutions, Inc., Madison, WI, **2002**.
- [22] SADABS (v2.02), Area Detector Absorption Correction, University of Göttingen, Germany, **2001**.
- [23] ORTEP-3 for Windows: L. J. Farrugia, *J. Appl. Crystallogr.* **1997**, *30*, 565.
- [24] C. A. Grapperhaus, S. Poturovic, M. S. Mashuta, *Inorg. Chem.* **2002**, *41*, 4309.
- [25] An alternate pathway in which complex **3** is regarded as a Ru^{IV}-thiolate would yield the same product. Attack by the enol tautomer at sulfur would result in the two-electron reduction of the metal. The radical pathway is favored based on the spectroscopic assignment of **3** as a metal-coordinated thiyl radical^[15] and the high sulfur character in the HOMO of nucleophilic metal thiolates.^[1]
- [26] J. A. Kerr, *Chem. Rev.* **1966**, *66*, 465.
- [27] A. Venturelli, T. B. Rauchfuss, A. K. Verma, *Inorg. Chem.* **1997**, *36*, 1360.
- [28] K. Matsumoto, H. Sugiyama, *Acc. Chem. Res.* **2002**, *35*, 915.
- [29] K. Wang, S. E. Stiefel, *Science* **2001**, *291*, 106.
- [30] W. E. Geiger, *Inorg. Chem.* **2002**, *41*, 1360.
- [31] P. Cazeau, F. Duboudin, F. Moulines, O. Babot, J. Dunogues, *Tetrahedron* **1987**, *43*, 2075.